

# Talanta

The International Journal of Pure and Applied Analytical Chemistry

---

## Aims & Scope

**Talanta** provides a forum for the publication of original research papers, preliminary communications, and reviews in all branches of pure and applied analytical chemistry. Analytical data should be submitted only if they are clearly related to new analytical measurements. Original research papers on fundamental studies and novel sensor and instrumentation development are especially encouraged. Novel or improved applications in areas such as clinical chemistry, environmental analysis, geochemistry, and materials science and engineering are welcome. Methods should be validated by comparison with a standard method or analysis of a certified reference material, and relevant literature should be cited. Since classical spectrophotometric measurements and applications, solvent extraction, titrimetry, chemometrics, etc. are well established, studies in such areas should demonstrate a unique and substantial advantage over presently known systems. New reagents or systems should demonstrate clear advantage, and their presentation should be comprehensive rather than generating a series of similar papers for several analytes. Modifications of reagents should demonstrate significant improvements. Solvent extraction methods in particular, but others as well, should focus on the use of non-hazardous material substitutes and the minimization of waste generation. But obvious application of known chemistries or methods to established techniques are discouraged. Application of classical analytical approaches to relatively sample matrices having no major interferences, such as pharmaceutical preparations or reconstituted samples, are discouraged unless considerable improvements over other methods in the literature are demonstrated. Papers dealing with analytical data such as stability constants,  $pK_a$  values, etc. should be published in more specific journals, unless novel analytical methodology is demonstrated, or important analytical data are provided which could be useful in the development of analytical procedures.

## Editors-in-Chief

**Professor G.D. Christian**, University of Washington, Department of Chemistry, 36 Bagely Hall, P.O. Box 351700, Seattle, WA 98195-1700, U.S.A.

**Professor J.-M. Kauffmann**, Université Libre de Bruxelles, Institut de Pharmacie, Campus de la Plaine, C.P. 205/6, Boulevard du Triomphe, B-1050 Bruxelles, Belgium

## Associate Editors

**Professor J.-H. Wang**, Research Center for Analytical Sciences, Northeastern University, Box 332, Shenyang 110004, China

**Professor J.L. Burguera**, Los Andes University, IVAQUIM, Faculty of Sciences, P.O. Box 542, 5101-A Mérida, Venezuela.

## Assistant Editors

**Dr R.E. Synovec**, Department of Chemistry, University of Washington, Box 351700, Seattle, WA 98195-1700, U.S.A.

**Professor J.-C. Vire**, Université Libre de Bruxelles, Institut de Pharmacie, Campus de la Plaine, C.P. 205/6, Boulevard du Triomphe, B-1050 Bruxelles, Belgium

## Talanta

R. Apak (Istanbul, Turkey)  
E. Bakker (Auburn, AL, U.S.A.)  
D. Barceló (Barcelona, Spain)  
B. Birch (Luton, UK)  
K. S. Booksh (Tempe, AZ, U.S.A.)  
J.-L. Capelo-Martinez (Caparica, Portugal)  
Z. Cai (Kowloon, Hong Kong)  
O. Chailapakul (Thailand)  
S. Cosnier (Grenoble, France)  
D. Diamond (Dublin, Ireland)  
W. Frenzel (Berlin, Germany)  
A.G. Gonzales (Seville, Spain)  
P. de B. Harrington (OH, U.S.A.)

A. Ho (Hsin-chu, Taiwan)  
P. Hubert (Liège, Belgium)  
J. Kalivas (Pocatella, ID, U.S.A.)  
B. Karlberg (Stockholm, Sweden)  
A.A. Karyakin (Moscow, Russia)  
J.-M. Lin (Beijing, China)  
Y. Lin (Richland, WA, U.S.A.)  
M.D. Luque de Castro (Cordoba, Spain)  
I.D. McKelvie (Victoria, Australia)  
S. Motomizu (Okayama, Japan)  
J.-M. Pingarron (Madrid, Spain)  
E. Pretsch (Zürich, Switzerland)  
W. Schuhmann (Bochum, Germany)

M. Shamsipur (Kermanshah, Iran)  
M. Silva (Porto Alegre, Brazil)  
P. Solich (Hradec Králové, Czech Republic)  
K. Suzuki (Yokohama, Japan)  
D.G. Themelis (Thessaloniki, Greece)  
D.L. Tsalev (Sofia, Bulgaria)  
B. Walzac (Katowice, Poland)  
J. Wang (Tempe, AZ, U.S.A.)  
J.D. Winefordner (Gainesville, U.S.A.)  
Xiu-Ping Yan (Tianjin, China)  
E.A.G. Zagatto (Piracicaba, SP, Brazil)  
X. Zhang (Beijing, China)



# Bismuth film electrodes for the study of metal thiolate complexation: An alternative to mercury electrodes

Arístides Alberich, Núria Serrano, Cristina Ariño\*, José Manuel Díaz-Cruz, Miquel Esteban

Departament de Química Analítica, Facultat de Química, Universitat de Barcelona, Martí i Franquès 1-11, E-08028 Barcelona, Spain

## ARTICLE INFO

### Article history:

Received 25 September 2008

Received in revised form 2 December 2008

Accepted 9 January 2009

Available online 20 January 2009

### Keywords:

Heavy metals complexation  
Phytochelatin  
Bismuth film electrode (BiFE)  
Signal splitting  
Anodic signals

## ABSTRACT

A comparative study of the usual static mercury drop electrode (SMDE) and the bismuth film electrode (BiFE) as applied to the analysis of metal complexation by thiol-rich peptides is done. Preliminary experiments on BiFE by differential pulse voltammetry showed that Cd(II) and Pb(II)-ions behave in a similar way as using stripping voltammetry and stripping chronopotentiometry with regard to some splitting effects of the signals. Additionally, on BiFE glutathione (GSH) and some phytochelatin ( $PC_n$ ) produce quite irregular signals related to the anodic oxidation of bismuth, which restricted the studies to a narrower concentration range than on SMDE. In the presence of both metal ion and peptide the same characteristic signals were observed on BiFE and SMDE, but better resolution was achieved in the first one, allowing a qualitative analysis of the complexation process for the Pb–GSH system which was not possible on SMDE. This suggests that BiFE may be a complementary tool to Hg electrodes, if not a valuable alternative, in the study of metal complexation.

© 2009 Elsevier B.V. All rights reserved.

## 1. Introduction

Bioaccumulation of heavy metals by chronic exposure can cause serious diseases and irreversible side effects to human beings. To avoid their entry in the food chain, ecosystems polluted with metals can be returned to their original condition using plants that synthesize peptides that sequester and remove metal ions [1]. Among these peptides, the oligomers of glutathione (GSH) named phytochelatin ( $PC_n$ ) play a key role. With the generic structure  $(\gamma\text{-Glu-Cys})_n\text{-Gly}$ , in which  $n$  generally ranges between 2 and 6,  $PC_n$  form complexes of extraordinary stability with metal ions mainly via thiolate coordination, although N- and C-terminus of free peptides could take part in important functions [2,3].

Sequence of formation of PC–metal complexes, their stoichiometries and the function of the different chelating groups have already been studied analyzing voltammetric titrations in Hg electrodes by multivariate curve resolution by alternating least squares (MCR-ALS) [4,5]. This approach has proved to be useful for Cd(II) and Zn(II) complexes [6,7], but Pb(II)– $PC_n$  systems present the problem that thiol facilitates the oxidation of the mercury of the electrode, producing many anodic signals that appear in the reduction region of Pb(II) [8]. These signals – provided by  $PC_n$  in its free form as well as complexed [4–9] – strongly overlap with the one of free Pb(II), making more difficult to achieve satisfactory results.

The use of electrodes based in other materials than mercury [10–12] offers the chance of minimizing the presence of anodic signals. Among the alternative electrodes, bismuth film electrode (BiFE) [13] presents the advantage of being environmentally friendly and nowadays is considered, from an electrochemical point of view, a good alternative to the prevalent use of mercury electrodes [14,15].

The present work evaluates the applicability of the methodology previously developed by using mercury electrodes in the study of the complexation of Pb(II) by  $PC_n$  and GSH using a bismuth film electrode instead. The expected improvements should come from a simplification of the electrochemical data, due either to a lower number of species providing signals or to a weaker signal overlapping. Recently, Cd(II)- or Zn(II)-cysteine side chain reduction signals in metallothioneins (MTs) were studied using Bi electrodes [16,17], but in these systems neither free metal nor anodic signals of free MTs appear. Due to this lack of previous knowledge, and in order to assign accurately every species to its corresponding signal in the subsequent voltammetric titrations, firstly we study one by one the electrochemical behavior of each chemical species involved in complexation process; then, the study of Pb–GSH (a system not satisfactorily solved using a mercury drop electrode) is carried out on BiFE.

## 2. Experimental

### 2.1. Chemicals

A standard Bi(III) solution ( $996\ \mu\text{g mL}^{-1}$ , atomic absorption standard solution) was purchased from Aldrich. Phytochelatin

\* Corresponding author. Tel.: +34 93 402 15 45; fax: +34 93 402 12 33.  
E-mail address: [cristina.arino@ub.edu](mailto:cristina.arino@ub.edu) (C. Ariño).

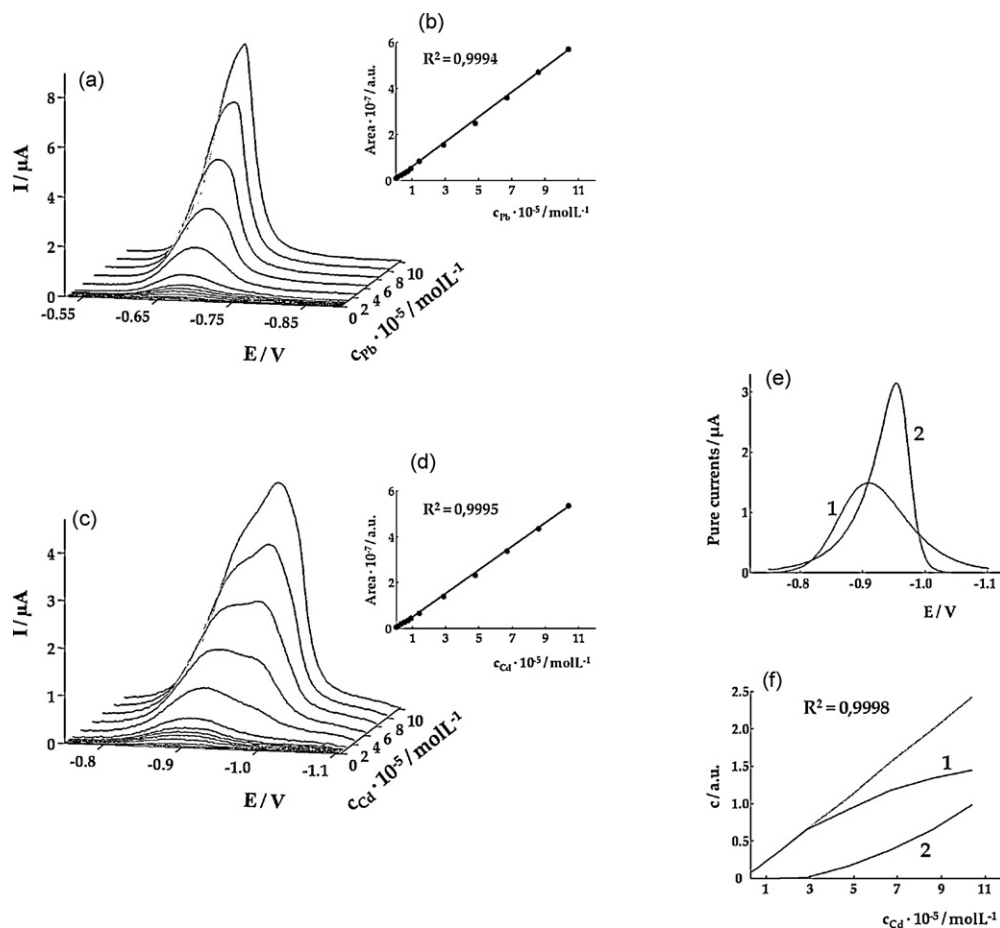


**Fig. 1.** Series of differential pulse voltammograms obtained for increasing concentrations of Pb(II) (a) and Cd(II) (c) at pH 6.4 in  $0.01 \text{ mol L}^{-1}$  maleic–maleate buffer and  $0.05 \text{ mol L}^{-1} \text{ KNO}_3$  on BiFE with their resulting calibration plots (b) and (d), respectively. (e) and (f) correspond to the normalized pure signals and the concentration profiles, respectively, obtained in the MCR-ALS decomposition of data matrix shown in (c): (1) represents the component at less negative potential and (2) represents the component at more negative potential.

with  $n=2-4$  were provided as trifluoroacetate salt by Diver-Drugs S.L. (Barcelona, Spain) with a purity of *ca.* 90% and Glutathione (GSH), in the reduced form, was provided by Merck with a purity greater than 99%. All other reagents used were Merck and Sigma/Aldrich analytical grade. Cd(II) and Pb(II) stock solutions  $10^{-2} \text{ mol L}^{-1}$  were prepared from  $\text{Cd}(\text{NO}_3)_2 \cdot 4\text{H}_2\text{O}$  and  $\text{Pb}(\text{NO}_3)_2$ , respectively, and standardized complexometrically. Maleic acid–KOH buffer solution was used for pH control and  $\text{KNO}_3$  was employed as supporting electrolyte. Ultrapure water (Milli-Q plus 185 system, Millipore) was used in all experiments.

## 2.2. Apparatus and electrochemical parameters

Differential pulse voltammetric (DPV) measurements were performed on a static mercury drop electrode (SMDE, drop area  $0.6 \text{ mm}^2$ ) using a 757VA Computrace (Metrohm) and on a bismuth film electrode (BiFE) using a Metrohm 663 VA Stand (Metrohm) attached to an Autolab System PGSTAT12 (EcoChemie).

The BiFE was prepared from a glassy carbon rotating disk electrode (RDE) of 2 mm diameter (Metrohm). The parameters used for were a pulse time of 50 ms, pulse amplitude of 50 mV, potential step of 2 mV and, in the case of SMDE, a drop time of 0.8 s. Note that DPV in SMDE is in fact differential pulse polarography (DPP).

The reference electrode (to which all potentials are referred) and the auxiliary electrode were  $\text{Ag}/\text{AgCl}/\text{KCl}$  ( $3 \text{ mol L}^{-1}$ ) and a Pt wire, respectively.

All the measurements were carried out in a glass cell at room temperature ( $20^\circ \text{C}$ ) under a purified nitrogen atmosphere (Linde N50).

## 2.3. Ex situ preparation of the bismuth film on the BiFE–RDE

The RDE was polished using a suspension of alumina particles of 300 nm diameter, and then rinsed with deionized water and sonicated in absolute ethanol and deionized water. After that, three electrodes were connected to the stand and immersed into 20 mL of a  $0.2 \text{ mol L}^{-1}$  acetate buffer solution (pH 4.5) containing 100 ppm Bi(III). After deaeration of the solution for 10 min,  $E_d = -0.60 \text{ V}$  was applied for 300 s with a RDE rotation speed of 500 rpm, followed by a rest period (without rotation) of 20 s. Once bismuth was deposited as a film, all electrodes were rinsed with water and the Bi(III) solution was replaced in the cell by the one to be measured.

## 2.4. Procedures

Measurements of free metals or ligands started by placing in the cell 20 mL of  $0.01 \text{ mol L}^{-1}$  maleic/maleate buffer (pH 6.4) and  $0.05 \text{ mol L}^{-1} \text{ KNO}_3$ . Then, the sample was deaerated with pure nitrogen for 20 min and a blank scan was recorded. Further, aliquots of metal or ligand solutions were added and the respective curves were recorded.

In voltammetric titrations of Pb(II) with ligands, 20 mL of a  $2 \times 10^{-5} \text{ mol L}^{-1}$  Pb(II) solution were placed into the cell and purged

with nitrogen for 20 min. DPV curves were then recorded. After recording reproducible curves, aliquots containing  $8 \times 10^{-4} \text{ mol L}^{-1}$  of ligand solution were added and the respective DPV curves recorded. After every addition, solutions were purged and mechanically stirred for 1 min. Titrations were also performed in the opposite way: 20 mL of a  $2 \times 10^{-5} \text{ mol L}^{-1}$  ligand solution were titrated with a  $8 \times 10^{-4} \text{ mol L}^{-1}$  Pb(II) solution following the same procedure.

### 3. Results and discussion

#### 3.1. Study of the signals observed on a BiFE in the presence of metal-thiolate

##### 3.1.1. Reduction signal of free metal ions

In a previous work, the electrochemical behavior of different metal ions was studied by stripping techniques on a BiFE [18]. Some splitting of the oxidation signals was observed, which depended on the metal (its solubility in Bi), the concentration and the deposition parameters. However, splitting did not hinder the possibility of quantitative analysis or the application of MCR-ALS, since the total area was still linear with respect to metal concentration.

Here, the behavior of some free metal ions by DPV, the technique commonly used for complexation studies, is checked. Pb(II) and Cd(II) have been considered as examples of metals whose solubility in bismuth is relatively high and quite low, respectively [19].

In the case of Pb(II) only one peak is observed in all the range considered (Fig. 1a), whereas Cd(II) presents an unique or two overlapping peaks depending on the metal concentration range (Fig. 1c), which is in agreement with the experiments done by stripping techniques in the aforementioned work [18]. Now, for both metals, the total area of voltammograms is again linear with the metal concentration over the range  $5 \times 10^{-7}$  to  $1 \times 10^{-4} \text{ mol L}^{-1}$  (Fig. 1b and d). It must be noted that the area under a DPV signal is a pure operational parameter, since pulse potential and potential step are not coincident, and this is why arbitrary units are given to that. Anyway, this area is expected to be proportional to the current that would be measured in a more “direct” technique like direct current (DC) voltammetry.

With regards to the MCR-ALS application to subsequent voltammetric titrations with ligands, this split of the free metal signal would be assumed with two components – referred to the same chemical species (Fig. 1e) – given that the sum of their concentration profiles is again linear with cadmium concentration (Fig. 1f, dashed line). The MCR-ALS analysis of the experimental data matrix (lack of fit 5.3%) has been carried out with constraints of non-negativity (for both concentrations and signals) and signal-shape

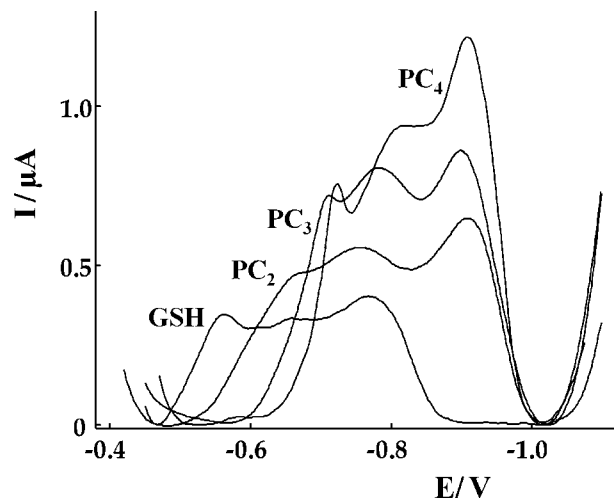


Fig. 2. Differential pulse voltammograms of a  $2 \times 10^{-5} \text{ mol L}^{-1}$  GSH and different phytochelatin solutions ( $\text{PC}_2$ ,  $\text{PC}_3$  and  $\text{PC}_4$ ) measured at pH 6.4 in  $0.01 \text{ mol L}^{-1}$  maleic–maleate buffer and  $0.05 \text{ mol L}^{-1} \text{ KNO}_3$  on BiFE.

for both components. From a qualitative point of view, this behavior is similar to that observed when analyzing free Cd(II)-ion by means of stripping voltammetry and stripping chronopotentiometry [18], where two peaks were observed and where successive additions of Cd(II)-ion produced first an increase of the peak at less negative potentials and, at higher concentration, a stabilization of this signal followed by a progressive increase of the signal at more negative potentials.

##### 3.1.2. Signals of free ligands

To analyze the signals related with anodic oxidation of the electrode material when  $\text{PC}_n$  and GSH are present, voltammograms of different peptide solutions were measured (Fig. 2). Signals of the ligands in their free form extend over a large potential range and lack of the typical DP-shape. Moreover, the current values increase with the number of thiol groups of the peptide, maybe due to a higher adsorption onto BiFE, as the presence of the characteristic peak-counterpeak shape in elimination voltammetry with linear scan (EVLS) measurements suggests (data not shown) [20,21]. The complex shape of these signals contrasts with those obtained using a mercury electrode [8,22] and could represent an additional difficulty in the further MCR-ALS analysis of data matrices [4].

In order to go into the behavior of these signals, DPV measurements of increasing GSH concentrations were made on SMDE (Fig. 3a) and BiFE (Fig. 3c). In both experiments the shapes of the sig-

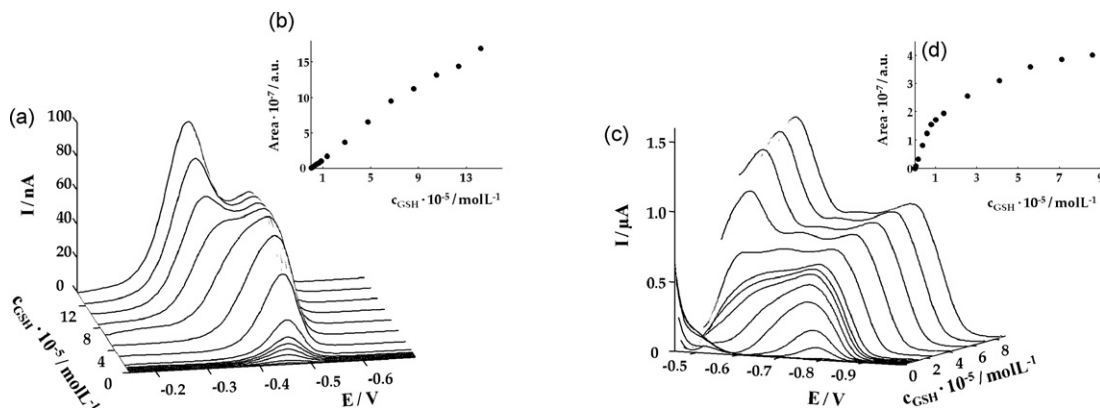
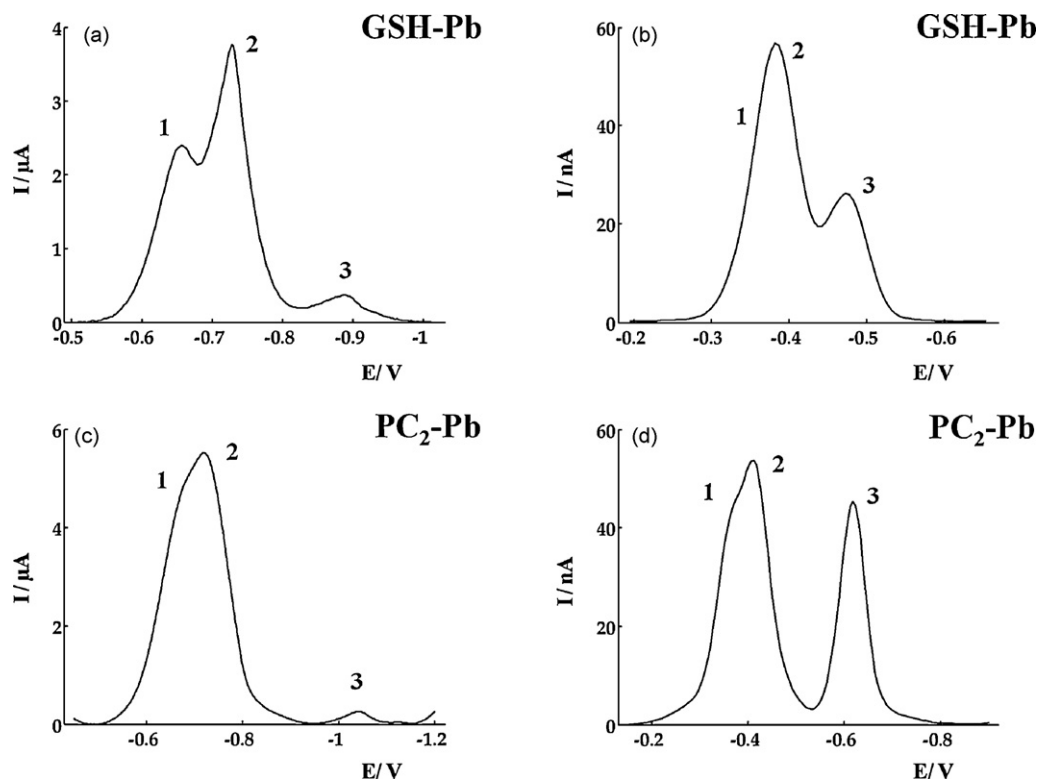


Fig. 3. Differential pulse voltammograms obtained for increasing concentrations of GSH on SMDE (a) and BiFE (c) at pH 6.4 in  $0.01 \text{ mol L}^{-1}$  maleic–maleate buffer and  $0.05 \text{ mol L}^{-1} \text{ KNO}_3$  with their resulting calibration plots (b) and (d), respectively.



**Fig. 4.** Differential pulse voltammograms of a  $2 \times 10^{-5} \text{ mol L}^{-1}$  Pb(II) solution in the presence of GSH or PC<sub>2</sub>, at the ligand-to-metal ratios of 1.5:1, measured on BiFE (a, c) and SMDE (b, d) at pH 6.4 in 0.01 mol L<sup>-1</sup> maleic-maleate buffer and 0.05 mol L<sup>-1</sup> KNO<sub>3</sub>.

nals change with GSH concentration, but there are some important differences between them. In SMDE, the shape change (respect to a simple peak) takes place at high concentrations, while for BiFE, the evolution of the GSH signal is quite intricate during all the concentrations range. Regarding linearity between the total peak areas and GSH concentration, it is fulfilled inside the full range on SMDE, but only at low GSH concentrations on BiFE (Fig. 3b and d, respectively). This would prevent MCR-ALS application to BiFE data because of the appearance of additional components without electrochemical meaning, unless voltammetric titrations are carried out in the proper GSH concentration range (where changes in the anodic signal are less pronounced and linearity is still observed):  $2 \times 10^{-7}$  to  $7.5 \times 10^{-6} \text{ mol L}^{-1}$  GSH.

### 3.1.3. Signals of the Pb-thiolate complexes

In order to analyze the signals concerning complexation, additions of Pb(II) over GSH or PC<sub>n</sub> ( $n=2-4$ ) solutions – and *vice versa* – have been carried out on BiFE and SMDE. Fig. 4 shows, as example of these experiments, the voltammograms obtained at ligand-to-metal ratio 1.5:1. At this ratio the formation of 1:2 Pb:GSH and 1:1 Pb:PC<sub>2</sub> complexes are reached completely – as previous studies in mercury electrodes confirmed [8,22] – and, therefore, some of the Pb(II) added remains as free cation.

The analysis of the different experiments suggests some general conclusions that can be visualized in Fig. 4: (i) in both electrodes, all systems provide the reduction signal of the complex (signal 3) and the signal related with the anodic oxidation of the electrode material (signal 1) which overlaps with the signal of free Pb(II) (signal 2); (ii) for BiFE the separation between signals 1 and 2 varies with the complex formed, and for SMDE it is relatively fixed; (iii) separation between signals 3 and 2 is larger on BiFE than on SMDE; (iv) comparing the heights of signal 3, it can be noticed that the reduction process of the complexes presents a marked electrochemically inert character on BiFE (reduction is faster than association–dissociation

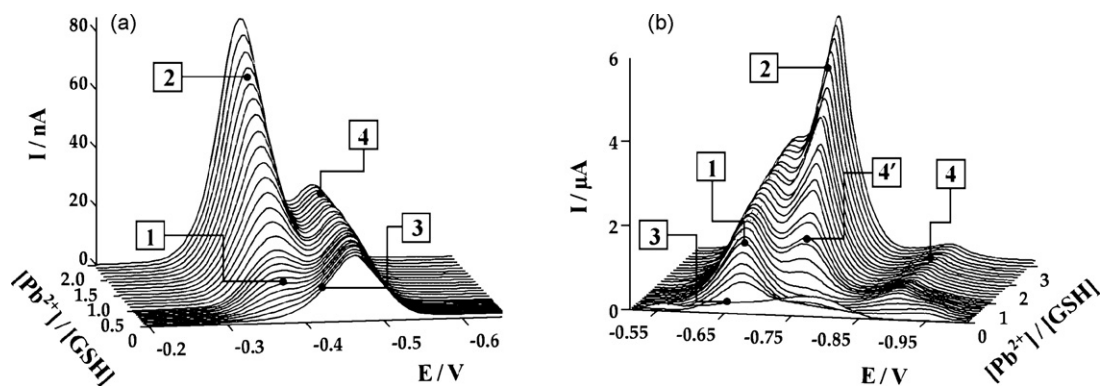
of the complex) which prevents us from doing experiments with initial concentrations of metal or ligand below  $2 \times 10^{-5} \text{ mol L}^{-1}$ .

To conclude this preliminary study, we can state that all the signals produced on SMDE by the species involved in the complexation of Pb(II) by PC<sub>n</sub> or GSH are also present on BiFE, where some of these signals become less important or undergo a weaker overlapping. In addition, due to the low sensitivity of BiFE regarding the reduction signal of complexes, voltammetric titrations have to be done at a minimum initial concentration of metal or ligand of  $2 \times 10^{-5} \text{ mol L}^{-1}$ , a range of concentrations where the shape of free ligand signals dramatically changes and can undergo an important loss of linearity, hindering a correct application of MCR-ALS.

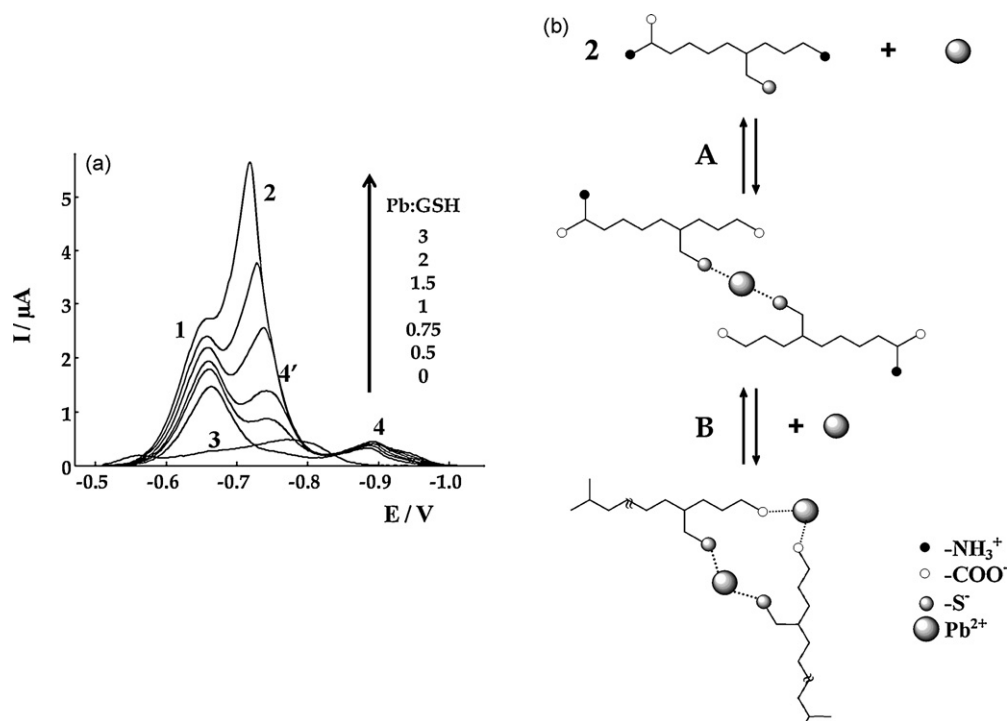
### 3.2. Study of the Pb(II)–GSH system on BiFE

Fig. 5 shows the evolution of the voltammograms corresponding to a titration of GSH with Pb(II) measured in both electrodes. Confirming our previous experience [8], experimental data on SMDE (Fig. 5a) show a very strong overlapping between the signal of free GSH (signal 3) and its complex (signal 4), in such a way that a slight shift between them is noticed but their evolution is very uncertain. Still more indistinguishable are the anodic signal related with the complex formation (signal 1) and the reduction of free Pb(II) ion (signal 2). These facts hinder any reliable proposal of a complexation sequence, from both a MCR-ALS and qualitative visual analysis of voltammograms evolution. In fact, to avoid the nearly complete overlapping between signals, Pb(II)–GSH system was already studied [23] at more extreme pH conditions where free Pb(II) ion were partially hydrolyzed, and therefore its peak potential shifted.

In contrast with SMDE, titration on BiFE (Fig. 5b) shows a much weaker overlapping of signals (1)–(2) and (3)–(4) allowing us to achieve good results from a qualitative viewpoint, since MCR-ALS cannot be applied for GSH case due, as it has been reasoned before, to the lack of linearity between the concentration of free GSH and



**Fig. 5.** Experimental data matrix containing the differential pulse voltammograms measured for a  $2 \times 10^{-5} \text{ mol L}^{-1}$  Pb(II) solution when titrated with GSH on SMDE (a) and BiFE (b) at pH 6.4 in  $0.01 \text{ mol L}^{-1}$  maleic–maleate buffer and  $0.05 \text{ mol L}^{-1} \text{ KNO}_3$ . Signals are due to: anodic of  $\text{Pb}(\text{GSH})_2$  (1),  $\text{Pb}^{2+}$ -ion (2), GSH (3), reduction of  $\text{Pb}(\text{GSH})_2$  (4) and  $\text{Pb}_2(\text{GSH})_2$  (4').



**Fig. 6.** Selected differential pulse voltammograms from Fig. 5b with the metal-to-ligand ratios marked as inset (a) and the complexation sequence inferred (b).

its signals. Furthermore, different Pb(II) bonds are well established – signals 4 and 4' – which supports BiFE as a suitable alternative to mercury electrodes in speciation studies.

The evolution of this titration can be seen in Fig. 6a – where the chosen values of metal-to-ligand ratio are specified – and its qualitative study allows us to propose a complexation sequence shown in Fig. 6b. At the beginning of the titration, only the anodic signal related to free GSH (signal 3) is observed. When Pb(II) is added over the large excess of GSH, it forms very stable bonds with two thiol groups, as the increase of signal 4 (at *ca.*  $-0.88 \text{ V}$ ) until a maximum ratio of 0.5 (two peptides per metal) indicates. Moreover, an anodic signal associated to the formation of this 1:2 Pb:GSH complex (signal 1, at *ca.*  $-0.67 \text{ V}$ ) appears and free GSH signal seems to disappear, although its evolution is unclear due to the constant changes that this signal undergoes (as Fig. 3c showed). This  $\text{Pb}(\text{GSH})_2$  complex is electrochemically inert (redox process is faster than equilibrium A) since its signal holds at a fixed potential.

As the M:L ratio increases, signals 1 and 4 associated with  $\text{Pb}(\text{GSH})_2$  complex stabilize and free metal appears (signal 2).

During its increase we can observe a noticeable shift towards less negative potentials from *ca.* metal-to-ligand ratio 1, indicating that a fraction of the Pb(II) added would be weakly bound to GSH, probably to carboxylate groups (signal 4') that are still free in the complex already formed. This  $\text{Pb}_2(\text{GSH})_2$  complex seems to be electrochemically labile (equilibrium B dissociates inside the DPV time-window) as signal 2 moving towards more positive potentials on the free Pb(II) addition indicates.

#### 4. Conclusions

It can be concluded that BiFE is a good alternative to Hg electrodes for complexation studies in the presence of thiol-rich peptides, since measures provide the same type of signals for both electrodes, and therefore, similar or even complementary information could be extracted. Moreover, some good features of mercury electrodes as the low concentration of ligands closer to the real one in cells and the strong dependence of the signals on the metal speci-

ation are maintained using bismuth electrode, with the important benefit of being non-toxic.

Certainly, MCR-ALS cannot be applied for complexation studies of GSH and PC<sub>n</sub> on BiFE, due to the electrochemically inert character of their complexes and the loss of linearity of the free ligand signals. However, this does not mean necessarily the inapplicability of MCR-ALS in complexation studies of heavy metals by other ligands of biological or environmental interest on BiFE. On the other hand, the low sensitivity of BiFE with respect to the reduction signal of complexes can simplify the voltammograms in the study of the evolution of the free metal signal, although it can also make more difficult the direct study of the evolution of every complex through its signal.

Finally, some Pb(II)–thiolate systems that present an excessive signal overlapping in mercury electrodes can be solved using a BiFE. Thus, Pb(II)–GSH system has been analyzed and a complexation sequence proposed, which can help to understand the role of low molecular weight PC-related thiols in the heavy metal detoxification procedures.

### Acknowledgements

The authors acknowledge support of the Spanish Ministry of Education and Science (project CTQ2006-14385-C02-01/BQU). This research is part of the activities of SIBA-TEQ group, which is recognized as consolidated group by the Generalitat of Catalonia (2005SGR00186).

### References

- [1] M. Mejare, L. Bulow, Trends Biotechnol. 19 (2001) 67.
- [2] E. Grill, E.L. Winnacker, M.H. Zenk, Science 230 (1985) 674.
- [3] M.H. Zenk, Gene 179 (1996) 21.
- [4] M. Esteban, C. Ariño, J.M. Díaz-Cruz, M.S. Díaz-Cruz, R. Tauler, Trends Anal. Chem. 19 (2000) 49.
- [5] M. Esteban, C. Ariño, J.M. Díaz-Cruz, Trends Anal. Chem. 25 (2006) 86.
- [6] E. Chekmeneva, R. Prohens, J.M. Díaz-Cruz, C. Ariño, M. Esteban, Environ. Sci. Technol. 42 (2008) 2860.
- [7] B.H. Cruz, J.M. Díaz-Cruz, C. Ariño, M. Esteban, Environ. Sci. Technol. 39 (2005) 778.
- [8] A. Alberich, C. Ariño, J.M. Díaz-Cruz, M. Esteban, Talanta 71 (2007) 344.
- [9] M. Heyrovsky, P. Mader, V. Veselá, M. Fedurco, J. Electroanal. Chem. 369 (1994) 53.
- [10] J. Wang, Stripping Analysis: Principles, Instrumentation and Applications, VCH, Deerfield Beach, FL, 1985.
- [11] B. Yosypchuk, L. Novotný, Crit. Rev. Anal. Chem. 32 (2002) 141.
- [12] E.P. Achterberg, C. Braungardt, Anal. Chim. Acta 400 (1999) 381.
- [13] J. Wang, J. Lu, S.B. Hocevar, P.A.M. Farias, B. Ogorevc, Anal. Chem. 72 (2000) 3218.
- [14] J. Wang, Electroanalysis 17 (2005) 1341.
- [15] A. Economou, Trends Anal. Chem. 24 (2005) 334.
- [16] M. Yang, Z. Zhang, Z. Hu, J. Li, Talanta 69 (2006) 1162.
- [17] M. Xu, Y. Wu, J. Wang, F. Zhou, Electroanalysis 18 (2006) 2099.
- [18] N. Serrano, A. Alberich, J.M. Díaz-Cruz, C. Ariño, M. Esteban, Electrochim. Acta 53 (2008) 6616.
- [19] ASM Handbook, 10th ed., vol. 3, Alloy phase diagrams Section 2, Ohio, USA, 1992.
- [20] O. Dracka, J. Electroanal. Chem. 402 (1996) 19.
- [21] L. Trnkova, O. Dracka, J. Electroanal. Chem. 413 (1996) 123.
- [22] J.M. Séquaris, Compr. Anal. Chem. 27 (1992) 115.
- [23] B.H. Cruz, J.M. Díaz-Cruz, M.S. Díaz-Cruz, C. Ariño, M. Esteban, R. Tauler, J. Electroanal. Chem. 516 (2001) 110.



## Short communication

## *In-situ* detection of single particles of explosive on clothing with confocal Raman microscopy

Esam M.A. Ali\*, Howell G.M. Edwards, Ian J. Scowen

University of Bradford, Raman Spectroscopy Group, University Analytical Centre, Division of Chemical and Forensic Sciences, Bradford, BD7 1DP, United Kingdom

## ARTICLE INFO

## Article history:

Received 14 August 2008

Received in revised form 9 December 2008

Accepted 16 December 2008

Available online 25 December 2008

## Keywords:

Explosives

Confocal Raman microscopy

Textiles

Forensic

## ABSTRACT

Confocal Raman microscopy is shown to detect picogram quantities of explosives *in-situ* on undyed natural and synthetic fibres, and coloured textile specimens leaving potentially evidential materials unaltered. Raman spectra were obtained from pentaerythritol tetranitrate (PETN), trinitrotoluene (TNT), and ammonium nitrate particles trapped between the fibres of the specimens. Despite the presence of spectral bands arising from the natural and synthetic polymers and dyed textiles, the explosive substances could be identified by their characteristic Raman bands. Furthermore, Raman spectra were obtained from explosive particles trapped between highly fluorescent clothing fibres. Raman spectra were collected from explosive particles with maximum dimensions in the range 5–10  $\mu\text{m}$ . Spectra of the explosives on dyed and undyed clothing substrates were readily obtained *in-situ* within 90 s and without sample preparation.

© 2008 Elsevier B.V. All rights reserved.

The development of new rapid and direct analytical chemistry methods for detection of explosives is of increasing importance for security and counter-terrorism issues, and for establishing criminal evidence [1]. Sensitivity and specificity in the detection of explosives is a crucial attribute and a number of recent high-profile reports have highlighted the application of desorption mass spectrometric approaches for direct analysis (i.e. without sample preparation) that allow detection of explosive residues down to picogram quantities of analyte [2]. The detection of explosive particulates is powerful indicator for linking individuals to contact with these materials as this will almost inevitably cause contamination of premises, clothing and other possessions [3,4]. There have been several high-profile cases in the public domain where the identification of minute amounts of particulate matter has formed a significant part of the forensic evidence [5]. In the wider context, a variety of analytical methods have been established for the identification of explosives under various conditions including gas chromatography [6], X-ray powder diffraction [7], thermal neutron analysis [8], ion mobility spectrometry [9,10]. However, each of these approaches requires isolation and/or destruction of the analyte and these techniques therefore alter or destroy the evidential material during analysis. Similarly, desorption mass spectrometry although direct is an inherently destructive technique.

In this paper, we will demonstrate that confocal Raman microscopy offers an alternative technique for direct analysis with advantages over other methods for explosives identification. The

Raman technique is molecular-specific and, when applied with confocal microscopy, non-destructive analysis of minute explosive particulates can be achieved *in-situ*. This is particularly important with regard to prevention of sample contamination and preservation of evidential material [11]. Several studies have appeared in the literature addressing the application of Raman spectroscopy to the detection and identification of explosives [12–16] but this is the first application of confocal Raman microscopy to the *in-situ* identification of explosives particulates on clothing. In this study, we have investigated the application of confocal Raman microscopy to the *in-situ* detection and identification of PETN, TNT and ammonium nitrate on a variety of textiles (Fig. 1). Pentaerythritol tetranitrate (PETN), trinitrotoluene (TNT), and ammonium nitrate samples were supplied by the Home Office Scientific Development Branch. A set of natural (wool, silk and cotton) and synthetic fibres (polyester) was used in this study in an attempt to cover the wide range of textile materials used in real life. In addition, pieces of blue denim and an orange-coloured T-shirt were used in this study as examples of commonly encountered dyed clothing. Bundles of fibres or textile pieces were contaminated with few crystals of each explosive prior to analysis. After identification with optical microscopy, Raman spectra were collected from explosive particles with edge dimensions in the range 5–10  $\mu\text{m}$ . Raman spectra were collected using a Renishaw *InVia* dispersive Raman microscope with a 785 nm near-infrared diode laser and a 50 $\times$  objective lens giving a laser spot diameter of 5  $\mu\text{m}$ . Spectra were obtained at 2  $\text{cm}^{-1}$  resolution for a 10 s exposure of the CCD detector in the wavenumber region 100–1800  $\text{cm}^{-1}$ . With 90.8 mW laser power, one accumulation was collected for the explosives reference spectra and for confocal experiments with contaminated textiles. Reference spectra for the

\* Corresponding author. Tel.: +44 1274 233787; fax: +44 1274 235350.  
E-mail address: [E.M.A.Ali@bradford.ac.uk](mailto:E.M.A.Ali@bradford.ac.uk) (E.M.A. Ali).



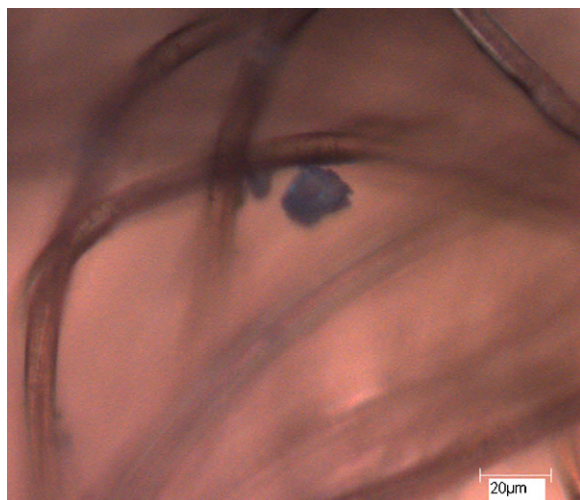


Fig. 1. PETN particle trapped between polyester fibres.

textile samples were collected with five accumulations. The total acquisition time of the spectra of the explosives on fibres was about 90 s.

Comparison of the Raman spectra collected from PETN, TNT and ammonium nitrate particles trapped between cotton fibres (Fig. 2) with the reference spectra showed that the explosives could be easily identified by their Raman spectra which comprise strong sharp features in the spectral wavenumber region 1800–100  $\text{cm}^{-1}$ . The Raman spectrum of PETN has several characteristic features of nitrate ester explosives which can be used to identify it; the symmetric ( $\text{NO}_2$ ) stretching mode at 1290  $\text{cm}^{-1}$ , the (O–N) stretch mode at 871  $\text{cm}^{-1}$ , and the (CCC) deformation mode at 622  $\text{cm}^{-1}$  [17]. Also, the Raman spectrum of TNT contains several diagnostic features such as the ( $\text{NO}_2$ ) asymmetric stretch at 1532  $\text{cm}^{-1}$ , the ( $\text{NO}_2$ ) symmetric stretch at 1357  $\text{cm}^{-1}$  and the ( $\text{NO}_2$ ) scissoring mode at 822  $\text{cm}^{-1}$  [18]. Similarly, the Raman spectrum of ammonium nitrate comprise two characteristic features: the ( $\text{NO}_3$ )<sup>-</sup> symmetric stretch at 1040  $\text{cm}^{-1}$  and the ( $\text{NO}_3$ )<sup>-</sup> in-plane bending mode at 712  $\text{cm}^{-1}$  [19]. The explosives could be identified from these characteristic bands and, through careful confocal sampling; no significant peaks in the spectra appear from the cotton fibres. Further illustrations of the applicability of this approach were obtained from PETN, TNT and ammonium nitrate particles trapped between silk and wool fibres. The spectra obtained contain some bands attributable

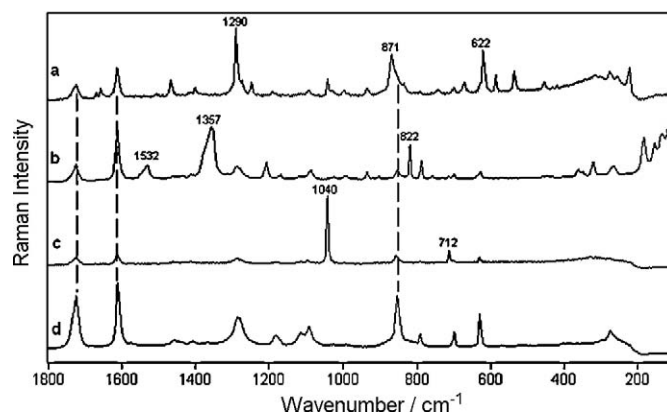


Fig. 3. Raman spectra of: (a) PETN particle on polyester fibres, (b) TNT on polyester fibres, (c) Ammonium nitrate on polyester fibres, (d) Polyester fibres. 785 nm, 90.8 mW, 10 s exposure, one accumulation for (a–c), five accumulations for (d).

to the fibre substrate. However, these bands do not overlap with the characteristic signature bands of the explosives, allowing the explosives to be readily identified. The spectra obtained from explosives particles trapped between polyester fibres also allow the presence of the explosive contaminant to be readily established (Fig. 3). In addition to the explosives diagnostic bands (vide supra), the resulting spectra also contain several peaks assigned to polyester fibres (marked with dashed lines in Fig. 3). These polyester bands do not overlap with the characteristic features of the explosives which can be clearly observed.

The previous results were acquired from explosives particles trapped between fibres of undyed natural and synthetic fibres. Of course, many real textile samples are dyed and it is necessary to determine how this will affect the Raman spectra of the explosive particles trapped between fibres of dyed clothing specimens. In particular, fluorescence background and the functional group features, arising from the dye molecules, may conceal diagnostic Raman spectral features of the explosives. The spectra obtained from explosives particles trapped between blue-dyed denim fibres again show the characteristic Raman features of the explosives. While a band corresponding with the strongest band in the Raman spectrum of the denim substrate (attributable to blue indigo dye) at 1570  $\text{cm}^{-1}$  is also present in the spectra, this band did not interfere with the identification of the explosives (Fig. 4). Raman spectra were successfully collected from crystals of PETN, TNT, and ammonium

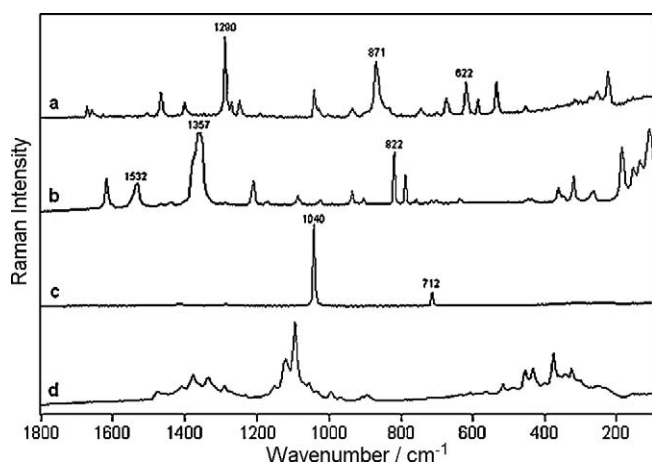


Fig. 2. Raman spectra of: (a) PETN particle on cotton fibres, (b) TNT on cotton fibres, (c) Ammonium nitrate on cotton fibres, (d) Cotton fibres. 785 nm, 90.8 mW, 10 s exposure, one accumulation for (a–c), five accumulations for (d).

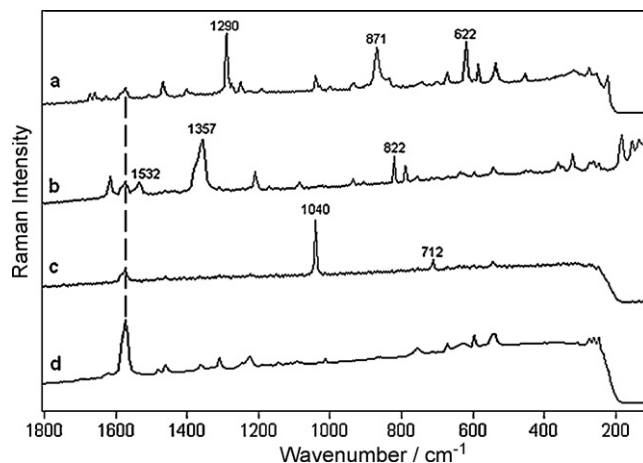
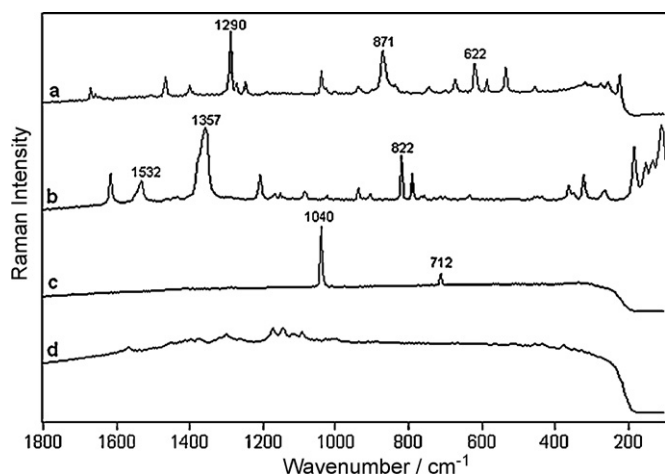


Fig. 4. Raman spectra of: (a) PETN particle on denim fibres, (b) TNT on denim fibres, (c) Ammonium nitrate on denim fibres, (d) Denim fibres. 785 nm, 90.8 mW, 10 s exposure, one accumulation for (a–c), five accumulations for (d).



**Fig. 5.** Raman spectra of: (a) PETN particle between orange T-shirt fibres, (b) TNT particle between orange T-shirt fibres, (c) ammonium nitrate particle between orange T-shirt fibres, (d) Orange T-shirt fibres. 785 nm, 90.8 mW, 10 s exposure, one accumulation for (a–c), five accumulations for (d).

nitrate trapped between fibres of an orange-coloured T-shirt. This substrate is fluorescent and this gives rise to a slight fluorescence background in the spectra. However, the Raman spectral bands of the explosives are clearly identifiable above the background and in all cases the presence of the contaminants was easily recognized (Fig. 5).

The ability of this approach to easily discriminate between contaminant and substrate lies in the ability of the confocal system to focus the incident laser radiation directly on the contaminant particles without sampling substantial areas of the substrate. This discrimination is highly desirable for automated database recognition algorithms as the spectra obtained are relatively simple and are predominantly of a single component in the mixture – an important consideration for future application with ‘non-expert’ implementation of the technique. Also, confocal Raman microscopy provides an efficient way to obtain Raman spectra of small specimens selectively even when embedded within strong Raman scattering or highly fluorescent media. Furthermore, The NIR excitation wavelength at 785 nm is an added advantage as it allows Raman spectra of the explosives to be acquired with fast acquisition times, high observable Raman intensity, and a significantly reduced fluorescence. The most difficult aspect of the analysis was the visual identification and location of the particles on the fibres prior to the acquisition of the Raman spectra. These results show that with the application of confocal techniques, interpretable Raman spec-

tra can be obtained directly from explosive particles as small as  $5 \mu\text{m}^3$  – approximately 180 pg in mass – and hence the technique has a sensitivity comparable to ionization desorption mass spectrometric techniques [2]. In addition, our approach leaves the particle unaltered and in its original environment. Thus, a clear application of the confocal Raman experiment is as a screen for identification of particulates during initial inspections of clothing prior to further examination.

### Acknowledgements

The authors would like to thank the Egyptian Government for providing the financial support to Esam M.A. Ali, and the Home Office Scientific Development Branch and the Forensic Science Service for providing the explosive samples.

### References

- [1] W.D. Smith, *Anal. Chem.* 74 2002 462a; BCS Technology Existing and Potential Standoff Explosive Detection Techniques, The National Academy Press, Washington, DC, 2004.
- [2] D.R. Justes, N. Talaty, I. Rodriguez, R.G. Cooks, *Chem. Commun.* 21 (2007) 2142; N. Na, C. Zhang, M. Zhao, S. Zhang, C. Yang, X. Fang, X. Zhang, *J. Mass Spectrom.* 42 (2007) 1079; I. Rodríguez, H. Chen, R.G. Cooks, *Chem. Commun.* 9 (2006) 953; I. Rodríguez, R.G. Cooks, *Chem. Commun.* 28 (2006) 2968; Z. Takáts, I. Rodríguez, N. Talaty, H. Chen, R.G. Cooks, *Chem. Commun.* 15 (2005) 1950; R.B. Cody, J.A. Laramée, H.D. Durst, *Anal. Chem.* 77 (2005) 2297.
- [3] C.A. Crowson, H.E. Cullum, R.W. Hiley, A.M. Lowe, *J. Forensic Sci.* 41 (1996) 980.
- [4] H.E. Cullum, C. McGavigan, C.Z. Uttley, M.A.M. Stroud, D.C. Warren, *J. Forensic Sci.* 49 (2004) 1.
- [5] E. Locard, *Am. J. Police Sci.* 1 (1930) 276.
- [6] M.E. Walsh, *Talanta* 54 (2001) 427.
- [7] M. Herrmann, *Part. Part. Syst. Charact.* 22 (2005) 401.
- [8] T.J. Shaw, D. Brown, J. D’Arcy, F. Liu, P. Shea, M. Sivakumar, T. Gozani, *Appl. Radiat. Isot.* 63 (2005) 779.
- [9] T. Keller, A. Keller, E. Tutsch-Bauer, F. Monticelli, *Forensic Sci. Int.* 161 (2006) 130.
- [10] T. Khayamian, M. Tabrizchi, M.T. Jafari, *Talanta* 59 (2003) 327.
- [11] W.E. Smith, P.C. White, C. Rodger, G. Dent, *Handbook of Raman Spectroscopy From The Research Laboratory To The Process Line*, Marcel Dekker, Inc., New York, 2001, p. 733.
- [12] J. Akhavan, *Spectrochim. Acta* 47A (1991) 1247.
- [13] I.R. Lewis, N.W. Daniel, N.C. Chaffin, P.R. Griffith, M.W. Tungol, *Spectrochim. Acta A* 51 (1995) 1985.
- [14] I.P. Hayward, T.E. Kirkbride, D.N. Batchelder, R.J. Lacey, *J. Forensic Sci.* 40 (1995) 883.
- [15] M.L. Lewis, I.R. Lewis, P.R. Griffiths, *Vib. Spectrosc.* 38 (2005) 17.
- [16] C. Cheng, T.E. Kirkbride, D.N. Batchelder, R.J. Lacey, T.G. Sheldon, *J. Forensic Sci.* 40 (1995) 31.
- [17] Y.A. Gruzdkov, Y.M. Gupta, *J. Phys. Chem. A* 105 (2001) 6197.
- [18] I.R. Lewis, N.W. Daniel, P.R. Griffiths, *Appl. Spectrosc.* 51 (1997) 1854.
- [19] G. Herzberg, *Molecular Spectra and Molecular Structure*, D. Van Nostrand Company, Inc., New York, 1945, p. 179; I.A. Degen, G.A. Newman, *Spectrochim. Acta* 49A (1993) 859.



## Determination of primary amino acids in wines by high performance liquid magneto-chromatography

E. Barrado<sup>a,\*</sup>, J.A. Rodriguez<sup>b</sup>, Y. Castrillejo<sup>a</sup>

<sup>a</sup> QUIANE/Departamento de Química Analítica, Facultad de Ciencias, Universidad de Valladolid, Prado de la Magdalena s/n, 47005 Valladolid, Spain

<sup>b</sup> Centro de Investigaciones Químicas, Universidad Autónoma del Estado de Hidalgo, Carr. Pachuca-Tulancingo Km. 4.5, C.P. 42076 Pachuca, Hidalgo, Mexico

### ARTICLE INFO

#### Article history:

Received 3 September 2008

Received in revised form 3 December 2008

Accepted 11 December 2008

Available online 24 December 2008

#### Keywords:

Magneto chromatography

Amino acids

Wines

Principal components

### ABSTRACT

Eight amino acids (ethanolamine, glycine, alanine,  $\beta$ -aminobutyric acid, leucine, methionine, histidine and asparagine) were identified and quantified in Spanish wines by high performance liquid magneto-chromatography (HPLMC) with UV-V spectrophotometry. For this method, the amino acids are first complexed with mono(1,10-phenanthroline)-Cu(II) to confer them paramagnetic properties, and then separated by application of a low magnetic field intensity (5.5 mT) to the stationary phase contained in the chromatographic column. Principal components analysis of the results obtained grouped together the wine samples according to their denomination of origin: "Ribera del Duero", "Rueda" or "Rioja" (Spain). Through cluster analysis, a series of correlations was also observed among certain amino acids, and between these groupings and the type of wine. These clusters were found to reflect the role played by the amino acids as primary or secondary nutrients for the bacteria involved in alcoholic and malolactic fermentation.

© 2008 Elsevier B.V. All rights reserved.

### 1. Introduction

Early determinations of amino acids in wines and musts relied upon the use of microbiological techniques. This was followed by methods based on paper chromatography, ninhydrin for visualization and densitometry at 570 nm for quantification [1,2]. These early works revealed that grape musts contained 20 amino acids of plant origin representing 20–30% of their total nitrogen contents [3].

The qualitative and quantitative composition of free amino acids in wine is determined by the type of grape. Hence, several authors have used the free amino acids profile to differentiate wines according to the species of grape from which they are derived [4], and even to ascertain the origin of the wine in question [5]. However, despite its specificity the grape species is not the only factor determining the amino acid composition of wines. Effectively, contents of amino acids corresponding to a single species can vary intensely according to the conditions of climate, maturity of the grapes, region of origin, etc. Low molecular weight amino acids or peptides are the most significant nitrogen source for the growth of lactic bacteria during wine production. However, it seems that heterofermenting cocci, such as *Oenococcus oeni*, have greater amino acid requirements than those of other lactic bacteria species [6]. The changes that occur in the amino acid contents of musts during malolactic fermentation have been well documented in the literature. These

studies have revealed that the concentrations of some amino acids are drastically reduced and that these affected amino acids are the main nutrients consumed during malolactic fermentation [7].

Vasconcelos and das Neves [8] used amino acid profiles to distinguish among different varieties of Portuguese wines (four white and four red) over a 7-year period. Data obtained through gas chromatography were analyzed using methods of pattern recognition, principal components analysis and discriminant analysis. Using these chemometric tools, the authors were able to classify the wines according to type and were also able to correlate their results with the grape variety. Soufleros et al. [9] performed a study on white wines from six different regions, seven grape varieties and 3 harvest years using HPLC and precolumn derivatization with o-phthalaldehyde (OPA) followed by fluorescence detection. Through discriminant analysis of amino acid profiles, the authors classified the wines according to the varieties examined. Péter et al. [10] managed to differentiate between Hungarian wines (red and white) of different denominations of origin and year based on biogenic amine, polyphenol and even amino acid profiles.

High performance liquid magneto-chromatography (HPLMC) is a new chromatography technique with two distinctive features: a high surface area stationary phase with paramagnetic properties ( $\text{SiO}_2/\text{Fe}_3\text{O}_4$ ) and a magnetic field intensity (variable from 0 to 5.5 mT) that selectively retains paramagnetic substances in the stationary phase depending on their magnetic susceptibility. The system can also be used to separate diamagnetic compounds such as biologically active organic molecules, but these first need to be complexed with Fe and Cu compounds to render them paramag-

\* Corresponding author. Fax: +34 983 423013.

E-mail address: [ebarrado@qa.uva.es](mailto:ebarrado@qa.uva.es) (E. Barrado).

netic. In a previous paper [11], we derived a theoretical expression describing the effect of the magnetic field on the analyte retention time and illustrated its use by determining the magnetic susceptibility of copper-complexed amino acids. In the present study, we demonstrate the use of the method for identifying and quantifying eight amino acids in samples of Spanish red and white wines. In addition, through principal components and cluster analyses, we were able to classify the wines according to their denomination of origin.

## 2. Experimental

### 2.1. Reagents

Stock 1.00 g l<sup>-1</sup> amino acid solutions were prepared by dissolving the appropriate amount of ethanolamine (Etn), glycine (Gly), alanine (Ala), β-aminobutyric acid (βABA), leucine (Leu), methionine (Met), histidine (His) and asparagine (Asp) (all from Aldrich) in phosphate buffer (NaH<sub>2</sub>PO<sub>4</sub>·2H<sub>2</sub>O and Na<sub>2</sub>HPO<sub>4</sub>·H<sub>2</sub>O (Fluka) 0.1 M, pH 7). The working standard solutions (1.0–30.0 mg l<sup>-1</sup>) were prepared daily by dilution of the corresponding stock solution. These solutions were stored at 4 °C. All solutions were prepared by dissolving the corresponding analytical grade reagent in filtered, deionised water with a resistivity of 18.3 MΩ cm, and used without further purification.

To confer the amino acids paramagnetic properties, they were reacted with a complexing solution prepared by dissolving CuCl<sub>2</sub>·2H<sub>2</sub>O and 1,10-phenanthroline in stoichiometric amounts (20 mmol l<sup>-1</sup>) [12] in phosphate buffer (0.10 mol l<sup>-1</sup>). Wine samples were prepared by mixing 1.0 ml of the wine and 1.0 ml of the complexing solution and then were filtered through a 0.45 μm membrane filter (Millipore) before their injection in the HPLC system. The sample solutions were stable for 1 week.

### 2.2. Preparing the magnetic stationary phase

The magnetic stationary phase is prepared as follows: magnetite synthesized hydrochemically according to Barrado et al. [13] is added to the reactor containing 20.0 ml of tetraethoxysilane (TEOS), 21.5 ml of water and 16.7 ml of ethanol. After the mixture has been stirred, the pH is adjusted to 10 using NH<sub>3</sub>. Once the gel has formed, it is stirred for 24 h to complete the condensation process. The gel is then filtered, washed and dried at 50 °C for 48 h [14,15]. The solid synthesized is ferrimagnetic, that is, it possesses magnetic properties in presence of an external magnetic field and its magnetization is proportional to the magnetic field intensity applied.

A steel column (4.6 mm × 10 cm) was filled with a SiO<sub>2</sub>/Fe<sub>3</sub>O<sub>4</sub> suspension in phosphate buffer solution (0.1 mol l<sup>-1</sup>, pH 7), which was then suctioned using a vacuum pump. The column was conditioned by passing phosphate buffer through the column at a constant flow rate of 1.0 ml min<sup>-1</sup>.

### 2.3. Equipment and experimental conditions

The experimental set-up for liquid chromatography comprised: a container for the mobile phase, a Gilson model 302 pressure pump, a Rheodyne mod. 7525 injection valve; a column as specified above and a UV-vis diode-array HP8453 spectrophotometer as detector. The column was wrapped with a copper coil (300 turns) such that the external magnetic field intensity (B) could be adjusted (from 0 to 5.5 mT) by varying the current applied to the coil by a power supply (SCIE-PLAS, mod. PSU 400/200). The magnetic field intensity was calculated using the expression  $H = nI/l_c$ , where  $H$  is the magnetic field strength (A m<sup>-1</sup>),  $n$  is the number of turns in the coil,  $I$  the current applied (A) and  $l_c$  is the coil length (m). The paramagnetic complexes prepared were detected at a wavelength of 266 nm. The mobile phase used was methanol:phosphate buffer (25:75, v/v), pH 7. The flow rate was 1.0 ml min<sup>-1</sup> and the injection volume was 25 μl.

Statistical analysis of data was performed using MINITAB 13.1 software (Minitab, Inc., PA, USA).

## 3. Results and discussion

### 3.1. Optimal conditions and reproducibility

Fig. 1 shows a chromatogram obtained under the optimal experimental conditions proposed, fixing the intensity of the external magnetic field at 5.5 mT. Once a blank had been injected, this was followed by the injection of 25 μl solutions of 5.0 mg l<sup>-1</sup> of each amino acid. Retention times for each amino acid are provided in Table 1. A lineal dependence of the peak height with the injected concentration of each amino acid was found in the concentration range 0.3–30.0 mg l<sup>-1</sup> with a practical limit of detection (LD) of 0.1 mg l<sup>-1</sup> and a limit of quantification (LQ) of 0.3 mg l<sup>-1</sup> for all the analytes. The analytical parameters were calculated according to the IUPAC criteria as 3.3 and 10.0 times the value of  $s_e/b_1$ , where  $s_e$  is the square root of the residual variance of the standard curve and  $b_1$

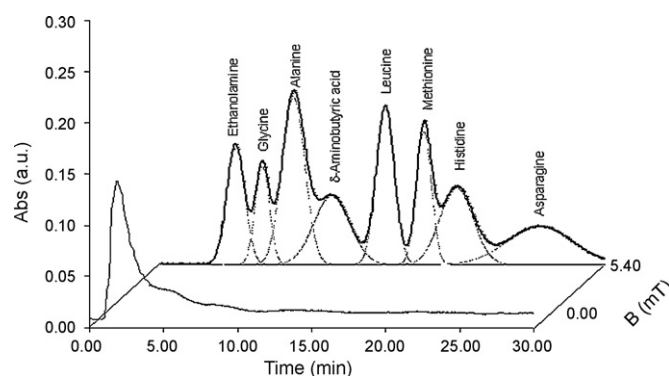


Fig. 1. Peak composition analysis and chromatogram of standard 5 mg l<sup>-1</sup> solutions of each amino acid.

**Table 1**  
Means and %RSD ( $n=3$ ) of the retention times of the paramagnetic amino acid complexes.

Analyte	Molecular weight (g mol <sup>-1</sup> )	Retention time (s)	Peak height (a.u.)	
			Repeatability	Reproducibility
Etn	61.1	324 (0.06)	0.1219 (0.43)	0.1157 (4.67)
Gly	75.1	500 (0.13)	0.1056 (1.94)	0.1110 (4.27)
Ala	89.1	640 (0.06)	0.1680 (1.48)	0.1720 (2.20)
β-ABA	103.1	826 (0.05)	0.0702 (2.49)	0.0680 (5.73)
Leu	131.2	917 (0.03)	0.1583 (2.18)	0.1662 (4.61)
Met	149.2	1067 (0.02)	0.1489 (4.30)	0.1432 (3.46)
His	155.2	1208 (0.03)	0.0762 (3.13)	0.0773 (1.37)
Asp	132.1	1514 (0.01)	0.0388 (4.24)	0.0375 (7.35)

**Table 2**  
Amino acid contents (mg l<sup>-1</sup>) recorded for the different wine samples (in three replicate determinations).

Origin	Etn	Gly	Ala	β-ABA	Leu	Met	His	Asp
Ribera Duero 1	<d.l.	5.34	9.91	12.03	<d.l.	<d.l.	<d.l.	3.15
Ribera Duero 2	<d.l.	7.62	7.57	9.66	7.76	<d.l.	<d.l.	2.57
Ribera Duero 3	<d.l.	3.24	8.97	12.54	<d.l.	<d.l.	<d.l.	2.84
Rueda 1	3.35	6.15	3.51	12.86	16.76	10.78	4.02	3.52
Rueda 2	1.47	3.46	2.31	4.84	4.68	5.63	<d.l.	<d.l.
Rueda 3	2.41	3.10	<d.l.	3.71	5.25	5.32	4.77	2.20
Rueda 4	1.22	2.89	2.28	4.19	4.74	5.41	4.28	2.26
Rueda 5	1.81	2.74	2.16	3.92	7.41	<d.l.	4.90	2.59
Rueda 6	1.91	4.47	2.64	5.93	8.91	6.06	6.05	1.59
Rueda 7	2.51	3.46	2.65	5.33	6.67	4.11	3.73	2.10
Rueda 8	2.30	3.26	1.36	2.37	4.42	<d.l.	2.89	1.64
Rueda 9	2.64	3.19	2.41	4.08	7.50	3.97	3.93	0.46
Rueda 10	2.56	5.54	1.55	2.43	3.66	1.67	1.71	1.91
Rioja 1	<d.l.	2.98	1.33	3.67	<d.l.	3.83	3.84	<d.l.

is the slope. The concentrations intervals are adequate for the analysis of the samples and the limits of detection obtained are similar to those obtained with OPA [9] and diethyl ethoxymethylenemalonate (DEEMM) [17].

Finally, a wine sample of each region was injected to check that the factors of repeatability, retention time and peak height variability for the eight amino acids identified were acceptable (<5%) and would not appreciably affect the final results.

### 3.2. Analysing the wine samples

Table 2 shows the concentrations of the different amino acids in mg l<sup>-1</sup> in the young wine samples of different origin. In the first column, the origin of each analyzed sample is indicated: “Ribera del Duero”, “Rueda” and “Rioja”, three different Spanish denominations of origin (DO). The area labelled “Ribera del Duero” is located on the northern plains of Spain, in the region of “Castilla y León”, being the Douro River the axe. The main variety of grape which gives colour, aroma and body to their red wines is the “Tempranillo”, also known as “Tinta del País”. “Tempranillo” produces soft supple wines, with aromas of soft red summer fruits like strawberries and raspberries. “Cabernet Sauvignon”, “Merlot”, “Malbec” and “Garnacha Tinta” are other grape varieties used. “La Rioja” is located in Northern Spain and dissected by the Ebro River. The wines of “Rioja” are elaborated principally with the “Tempranillo” grapes, but it can also be mixed with “Mazuelo”, “Garnacha” and “Graciano”. “Rueda”, located also in Castilla y León, is one of the few European winegrowing regions specialised in making white wine and in the preservation and development of the “Verdejo”, the autochthonous grape variety. “Rueda” wines are marked by the personality of the Verdejo grape, the incorporation of other varieties (“Sauvignon blanc”, “Viura” and “Palomino”), and the vineyards themselves, which have learned to survive in a tough environment.

It may be observed that for some amino acids, concentrations were below the method’s detection limit; these amino acids can be correlated, as mentioned earlier, with their availability as nutrients during malolactic fermentation [16]. Although on simple inspection of the table it may be noted for example that the different samples show considerable differences in their β-ABA concentrations, further information was gained by subjecting the data matrix to statistical analysis. The tools principal component analysis (PCA) and cluster analysis and have proved useful in the analysis of similar data [18,19].

### 3.3. Principal component analysis (PCA)

The objective of PCA is to reduce the dimensionality of the original data matrix by reducing the number of variables so that the

**Table 3**  
Correlation matrix of the variables.

	Etn	Gly	Ala	β-ABA	Leu	Met	His	Asp
Etn	1.000							
Gly	<b>-0.092</b>	1.000						
Ala	-0.655	0.471	1.000					
β-ABA	-0.353	<b>0.535</b>	<b>0.840</b>	1.000				
Leu	<b>0.676</b>	0.366	-0.255	0.155	1.000			
Met	<b>0.538</b>	0.008	-0.432	0.049	<b>0.641</b>	1.000		
His	<b>0.557</b>	-0.402	<b>-0.692</b>	-0.454	0.444	0.482	1.000	
Asp	0.013	0.440	0.508	<b>0.636</b>	0.275	-0.098	-0.086	1.000

Number of observations: 14;  $r_{critical}(0.05,12) = 0.532$ .

**Table 4**  
Loadings for each of the variables examined.

Factor	1	2
Etn	<b>-0.753</b>	0.451
Gly	0.492	<b>0.617</b>
Ala	<b>0.953</b>	0.152
β-ABA	<b>0.729</b>	<b>0.562</b>
Leu	-0.408	<b>0.853</b>
Met	<b>-0.567</b>	<b>0.559</b>
His	<b>-0.809</b>	0.171
Asp	0.450	<b>0.631</b>
Eigenvalue	<b>3.5957</b>	<b>2.3901</b>
Explained variance	0.449	0.299
Cumulative variance	0.449	0.748

Bold numbers: contributions greater than the critical value.

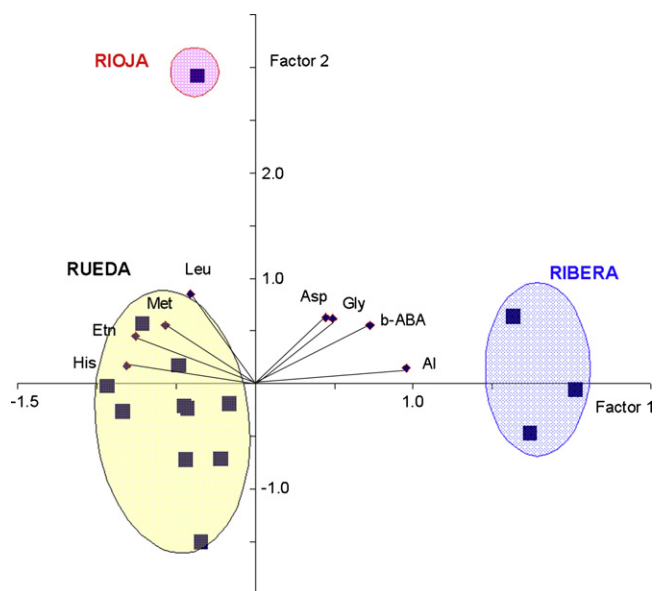
results can be better interpreted. The first step is to construct a Pearson’s correlation matrix to identify any correlations among the variables (Table 3). Since it is symmetrical, only the lower half of this table is provided. The absolute value of “*r*” for 12 degrees of freedom and  $\alpha = 0.05$  was 0.532, meaning that the coefficients indicated in bold in the Pearson’s correlation matrix are significant. These high correlations and Bartlett’s sphericity test indicate that effectively we can obtain new variables by combining some of the original variables. Since we are dealing with fewer variables it is easier to construct graphs to visualize the relationships among the objects (wine samples).

Table 4 shows the eigenvalues for the correlation matrix along with the percentages of variance explained by each one. The number of principal components can be selected according to different criteria, the most appropriate being to consider significant only those values higher than unity, that is, those that provide more information than that offered separately by each variable. Hence, in the table we indicate only the first two components, which fulfil this criterion and explain 74.8% of the total variance of the original table. The composition of the new variables (loadings) and the component values (scores) that each object (wine sample) takes for each new variable renders the plot in Fig. 2.

In this figure, we can clearly observe the differentiation of three groups of points, each one corresponding to a different denomination of origin of the wines. In the right-hand section, in the quadrant predominated by asparagine, glycine, β-aminobutyric acid and alanine appear the samples of “Ribera del Duero”. On the left-hand side of the figure, the nine “Rueda” wine samples appear in the quadrant predominated by leucine, methionine, histidine and ethanolamine and finally in the upper quadrant of this left section, clearly differentiated from the rest, appears the wine sample from the region of “La Rioja”. Accordingly, the amino acid composition of the wines serves to group the samples according to their origin.

### 3.4. Cluster analysis

Cluster analysis is basically a graphic method in which objects are separated to form clusters. There are several ways of doing



**Fig. 2.** Graphical representation of the first two scores of a PCA conducted on the amino acid contents of the wines. Denomination of origin: (■) Rivera de Duero; (○) Rioja; (●) Rueda.

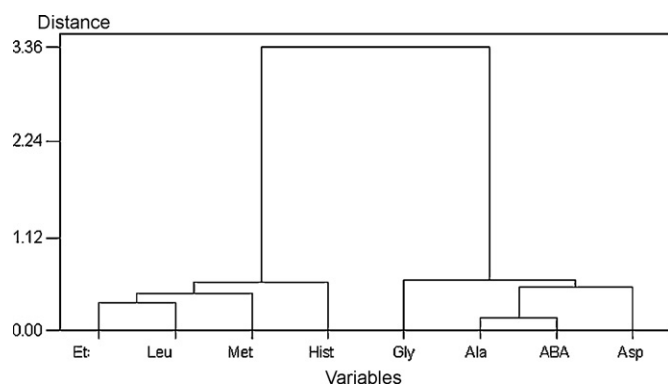


**Fig. 3.** Cluster analysis of the variable examined (amino-acid contents) in which two well-differentiated groups can be clearly observed.

this depending on how the distance between points is measured. In this study, we selected correlation as a measure of similarity among variables, and Euclidean distances as a measure of similarity among samples. Ward's method was used to generate the clusters by variable, i.e., amino acids or by object, i.e., wine samples.

In the dendrogram obtained from the cluster analysis of the variables (amino acids), two clusters can be clearly observed (Fig. 3). To the left, we find a cluster comprising ethanolamine, leucine, methionine and histidine; these amino acids are easily assimilated by the bacteria responsible for alcoholic and malolactic fermentation [7]. To the right, another group of variables can be distinguished: glycine, alanine,  $\beta$ -aminobutyric acid and asparagine. These last four amino acids are consumed by bacteria only when the primary nutrients have been exhausted. These groupings confirmed those obtained in the PCA.

In the clusters obtained for the wine samples shown in Fig. 4, three groupings can be clearly distinguished corresponding to the different denominations of origin: "Ribera del Duero" (left), "Rioja" (centre) and "Rueda" (right). These findings also confirm the PCA results.

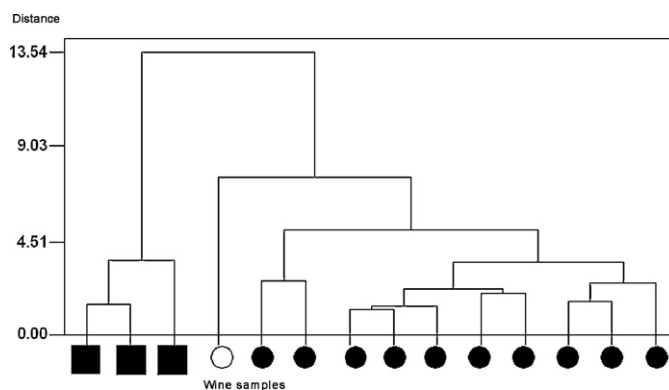


**Fig. 4.** Cluster analysis of the wine samples examined. Denominations of origin: (■) Rivera de Duero; (○) Rioja; (●) Rueda.

#### 4. Conclusions

HPLMC was used to establish amino acid profiles in Spanish wines. The experimental set up comprised a  $\text{SiO}_2/\text{Fe}_3\text{O}_4$  column as the stationary phase, a magnetic field intensity of 5.5 mT, a 0.1 M phosphate buffer:methanol solution (75:25) as the mobile phase ( $\text{pH} \approx 7.0$ ), and a UV-visible detector (273 nm). The method proposed was used to identify eight amino acids (ethanolamine, glycine, alanine,  $\beta$ -aminobutyric acid, leucine, methionine, histidine and asparagine) in several samples of wines. Both sample processing and analysis times were short compared to those needed for other techniques. The method also shows good signal reproducibility and repeatability. Finally, through principal components analysis the wines could be classified according to their denomination of origin.

#### Acknowledgements

The authors wish to thank the CONAcYT (project 61310), and the Consejería de Educación y Cultura de la Junta de Castilla y León (project VA029A07) for financial support.

#### References

- [1] J.G. Heathcote, C. Haworth, *Biochem. J.* 114 (1969) 667.
- [2] I. Smith, J.G. Feinberg, *Paper & Thin Layer Chromatography and Electrophoresis*, Shandon Scientific Company, Ltd., 1965.
- [3] C. Poux, A. Ournac, *Ann. Technol. Agric.* 19 (1970) 217–237.
- [4] S.E. Spayd, J. Andersen-Bagge, *Am. J. Enol. Viticult.* 47 (1996) 389.
- [5] C.S. Ough, Z. Huang, D. An, D. Stevens, *Am. J. Enol. Viticult.* 41 (1991) 26.
- [6] C. Flanzky, *Enología: Fundamentos Científicos y Tecnológicos*, AMV Ediciones, Madrid, 2000.
- [7] P. Ribéreau-Gayon, Y. Glories, A. Maujean, D. Dubourdieu, *Handbook of Enology*, vol. 2, John Wiley & Sons, England, 2001.
- [8] A.M.P. Vasconcelos, H.J.C. das Neves, *J. Agric. Food Chem.* 37 (1989) 931.
- [9] E.H. Soufleros, E. Boulompasi, C. Tsarchopoulos, C.G. Biliaderis, *Food Chem.* 80 (2003) 261.
- [10] A. Péter, G. Török, P. Somós, M. Péter, G. Bernáth, F. Fülöp, *J. Chromatogr. A* 761 (1997) 103.
- [11] E. Barrado, J. Rodríguez, *J. Chromatogr. A* 1128 (2006) 189.
- [12] M. Chikira, Y. Tomizawa, D. Fukita, T. Sugizaki, N. Sugawara, T. Yamazaki, A. Sasano, H. Shindo, M. Palaniandavar, W.E. Antholine, *J. Inorg. Biochem.* 89 (2002) 163.
- [13] E. Barrado, F. Prieto, M. Vega, F. Fdez-Polanco, *Water Res.* 32 (10) (1998) 3055.
- [14] A. Yasumori, H. Matsumoto, S. Hayashi, K. Okada, *J. Sol-Gel Sci. Technol.* 18 (2000) 249.
- [15] E. Barrado, J.A. Rodríguez, F. Prieto, J. Medina, *J. Non-Cryst. Solids* 351 (2005) 906.
- [16] M.C.M.M. Fernández, E.B. Paniago, S. Carvalho, *J. Braz. Chem. Soc.* 8 (1997) 537.
- [17] S. Gomez-Alonso, I. Hermosin-Gutierrez, E. Garcia-Romero, *J. Agric. Food Chem.* 55 (2007) 608.
- [18] R. Seeber, G. Sferlazzo, R. Leardi, A. Dalla Serra, G. Versini, *J. Agric. Food Chem.* 39 (1991) 1764.
- [19] H.K. Yildirim, Y. Elmaci, G. Ova, T. Altug, U. Yucel, *Int. J. Food Prop.* 10 (2007) 93.



## Separation of tyrosine enantiomer derivatives by capillary electrophoresis with light-emitting diode-induced fluorescence detection

Weiwen Bi<sup>a</sup>, Shaorong Lei<sup>b</sup>, Xiupei Yang<sup>a</sup>, Zemin Xu<sup>a</sup>, Hongyan Yuan<sup>b</sup>, Dan Xiao<sup>a,b,\*</sup>, Martin M.F. Choi<sup>c,\*\*</sup>

<sup>a</sup> College of Chemistry, Sichuan University, Chengdu 610065, PR China

<sup>b</sup> College of Chemical Engineering, Sichuan University, Chengdu 610065, PR China

<sup>c</sup> Department of Chemistry, Hong Kong Baptist University, Kowloon Tong, Hong Kong SAR, PR China

### ARTICLE INFO

#### Article history:

Received 25 September 2008

Received in revised form 20 January 2009

Accepted 20 January 2009

Available online 30 January 2009

#### Keywords:

Capillary electrophoresis

Light-emitting diode

Tyrosine

Enantiomers

Fluorescence detection

Oral solution

### ABSTRACT

Capillary electrophoresis (CE) coupled with fiber-optic light-emitting diode-induced fluorescence detection has been developed for the separation of tyrosine (Tyr) enantiomers. *R*(-)-4-(3-isothiocyanatopyrrolidin-1-yl)-7-(*N,N*-dimethylaminosulfonyl)-2,1,3-benzoxadiazole was used as a chiral fluorescence tagged reagent for derivatization of Tyr. The effect of pH, running buffer concentration and applied voltage on enantioselectivity has been investigated. The optimum CE conditions are 15 mmol/L borate running buffer (pH 10.5) and 14-kV applied voltage. Good reproducibility was obtained with coefficient of variation ( $n = 7$ ) of migration time and peak area less than 0.2 and 2.0%, respectively. The limits of detection of *D*- and *L*-Tyr derivatives were 2.9 and 2.2  $\mu\text{mol/L}$  ( $S/N = 3$ ), respectively. The proposed method has been successfully applied to the determination of Tyr in a commercial amino acid oral solution.

© 2009 Elsevier B.V. All rights reserved.

### 1. Introduction

Chiral resolution of racemic compounds has become attractive since the US FDA (Food and Drug Administration) declared that manufacturer should explain clearly the mechanism of each enantiomer when applied for chiral pharmaceuticals [1]. To date many drugs contain amino acid enantiomers or their derivatives. It is well known that many amino acids have one or more asymmetric centers. Each enantiomer of different optical activities may have different interactions with our body such that chiral drugs can present different activity, toxicity, transport mechanism and metabolic route. Thus, the development of a single enantiomer and the control of its purity are of great importance not only to avoid unwanted pharmaceutical and toxicological side effects but also to assure its therapeutic efficacy and safety. As such, chiral resolution of enantiomers plays an important role in the pharmaceutical industry. It is well known that the aromatic amino acid *L*-tyrosine is a semi-essential, geneti-

cally coded amino acid for many animals and humans, which is often added to food products and pharmaceutical formulations such as soybean cheese and amino acid oral solution. However, if ingested excessively, it will exert atherogenic effects. On the other hand, *D*-tyrosine has been the precursor of many different anti-inflammatory [2]. Thus, a simple and reliable method for determining *D*- and *L*-tyrosines in pharmaceutical formulations is highly desirable.

So far, high-performance liquid chromatography is regarded as the standard analytical method for determination of amino acids [3–5]. Despite its good reproducibility, there are some disadvantages that hinder its development, for instance, high cost, large solvent consumption and complicated operations. On the contrary, capillary electrophoresis (CE) is especially suitable for analysis of biological compounds in terms of its higher separation efficiency, shorter analysis time, simpler instrumentation, smaller sample consumption, and lower operation cost. Since the sensitivity of CE is restricted by small volume sample injection, improvement in sensitivity is highly essential. Up to now, several sensitive detectors for CE have been developed including UV/vis absorption [6], electrochemical [7], mass spectrometric [8,9] and chemiluminescence [10,11] detectors. As more commercial fluorescence tagging reagents are available in market, laser-induced fluorescence (LIF) [12–14] detection has become popular for analysis of biological assay because of its higher sensitivity of detection. However, the

\* Corresponding author at: College of Chemical Engineering, Sichuan University, Chengdu 610065, PR China. Tel.: +86 28 85415029; fax: +86 28 85416029.

\*\* Corresponding author.

E-mail addresses: [xiaodan@scu.edu.cn](mailto:xiaodan@scu.edu.cn) (D. Xiao), [mfchoi@hkbu.edu.hk](mailto:mfchoi@hkbu.edu.hk) (M.M.F. Choi).

laser source possesses drawbacks of large size, high cost, high power consumption and limited lifetime. Thus, in the past two decades, many researchers turn to other alternative light sources for fluorescence detection [15–17].

To our knowledge, light-emitting diode (LED) is probably one of the best choices for CE with fluorescence detection [18]. The emission wavelengths of LED cover much of the UV/vis and some near-infrared (NIR) regions (280–1300 nm). It has been used for analyzing riboflavin [19,20], drug [21] and amino acids [22,23]. Currently three typical configurations of CE with fluorescence detection based on LEDs have been developed: right-angle light-emitting diode-induced fluorescence (LED-IF) detector [24], collinear LED-IF detector [25], and in-column fiber-optic LED-IF detector [26]. The former two configurations have lower sensitivity due to light reflecting and scattering on capillary surface, while the latter, in-column fiber-optic LED-IF detector, can avoid these drawbacks and thus has lower background noise and higher sensitivity.

In this work, we propose to employ fiber-optic LED-IF detection for analysis of a racemic mixture of tyrosine labeled with *R*(-)-4-(3-isothiocyanatopyrrolidin-1-yl)-7-(*N,N*-dimethylamino-sulfonyl)-2,1,3-benzoxadiazole (DBD-PyNCS). As tyrosine (Tyr) does not possess native fluorescence in the visible light region, it has to be derivatized with a fluorescence reagent before it can be detected by CE-LED-IF method. The conditions affording the best resolution were optimized and the proposed CE-LED-IF method was successfully applied to determine *D*- and *L*-Tyr in a commercial amino acid oral solution.

## 2. Experimental

### 2.1. Chemicals

DBD-PyNCS was purchased from Tokyo Kasei (Tokyo, Japan). Tyr enantiomers were obtained from Biochemical Reagents Company (Shanghai, China). HPLC-grade acetonitrile was from Luzhong Industrial and Commercial Ltd. (Shanghai, China). Purified water from a Milli-Q-RO4 water purification system (Millipore, Bedford, MA, USA) with a resistivity higher than 18 MΩ cm was used to prepare all solutions. All other chemicals and organic solvents of analytical-reagent grade or above were used as received. All running buffers and NaOH solutions were filtered through 0.45-μm cellulose membrane filters (Heshi Technology Development Co. Ltd., Tianjin, China) before CE analysis.

### 2.2. Apparatus

The separations were conducted on a laboratory-built CE system equipped with a high-voltage (0–30 kV) supply (Beijing Cailu Science Instrument Company, Beijing, China). An uncoated fused-silica capillary was purchased from Yongnian County Ruifeng Chromatogram Equipment Co. Ltd. (Hebei, China). The design of the fiber-optic LED-IF detection system was reported previously [27]. In essence, a blue LED (Shifeng Optic and Electronics Ltd., Shenzhen, China; applied voltage, +4.5 V; power, ~3 mW; peak wavelength, 460 nm; and spectral half-width, ~25 nm) was employed as the excitation light source. A bare 20 cm × 40 μm o.d. optical fiber (Beijing Glass Institute, Beijing, China) was used to transmit the excitation light beam. All microscope objectives and filters were from Olympus (Tokyo, Japan). The fluorescence signal was captured by a Hamamatsu CR105 photomultiplier tube (PMT) (Beijing, China). The output signal was recorded and processed with a computer and in-house written software.

### 2.3. Sample preparation

A Dongcheng amino acid oral solution (Jiangxi Dongcheng Health Care Products Co. Ltd., Nanchang, China) was purchased

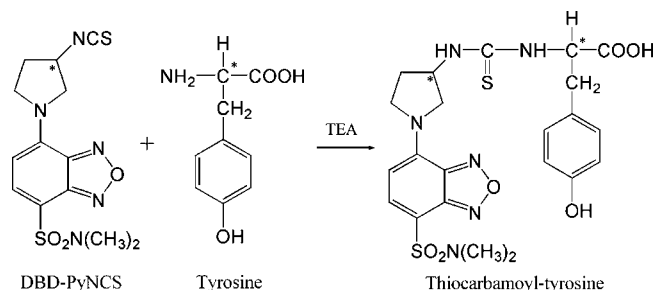


**Fig. 1.** Structure of the chiral fluorescence tagging reagent, DBD-PyNCS and its reaction with tyrosine.

from a local drugstore. 100 μL of the amino acid oral solution was transferred into a 5-mL microcentrifuge tube, diluted with 880 μL of acetonitrile–water (1:1, v/v) and 20 μL of triethylamine (TEA) and shaken vigorously. The mixture was then sonicated for 20 min and centrifuged at 10,000 × *g* for 10 min. The supernatant was transferred into a 1.5-mL vial and kept in dark at 4 °C prior to derivatization by DBD-PyNCS.

### 2.4. Chiral derivatization with DBD-PyNCS

10 μL of Tyr enantiomers in acetonitrile–water (1:1, v/v) containing 2% TEA and 10 μL of 10 mmol/L DBD-PyNCS in acetonitrile were mixed in a 0.5-mL microcentrifuge tube. The tube was tightly capped, shaken and heated at 55 °C for 20 min [28]. The derivatization reaction of Tyr with DBD-PyNCS is illustrated in Fig. 1. After cooling, 30 μL of 1.0 mol/L CH<sub>3</sub>COOH in acetonitrile–water (1:1) was added to the mixture. The derivatized solution was then kept in dark at 4 °C. Reagent blanks without amino acids and samples of 10% amino acid oral solution were also treated in the same manner.

### 2.5. CE procedure

For the first use, the capillary was preconditioned with a 1.0-mol/L NaOH solution. Prior to sample injection, the capillary was flushed sequentially with 1.0 mol/L NaOH, water and running buffer for 5, 2, and 5 min, respectively. The sample solution was injected into the capillary by hydrodynamic flow with one end of the capillary in the sample solution hoisted to a height difference of 20 cm for 8 s. The applied voltage was 12–16 kV. The running buffer was 15 mmol/L borate at pH 10.5. After each sample analysis, the capillary was rinsed with water for 2 min ready for the next injection. The total length of the i.d. 75 μm capillary used in this study was 55 cm (53 cm effective length). All CE separations were conducted at room temperature.

## 3. Results and discussion

### 3.1. Choice of LED and spectral filter

Fig. 2 displays the fluorescence excitation and emission spectra of free DBD-PyNCS, DBD-PyNCS-labeled *L*-tyrosine (DBD-PyNCS-*L*-Tyr) and DBD-PyNCS-labeled *D*-tyrosine (DBD-PyNCS-*D*-Tyr). All DBD-PyNCS, DBD-PyNCS-*L*-Tyr and DBD-PyNCS-*D*-Tyr show strong fluorescence at excitation maxima of 460 nm and emission maxima of 580 nm. Since the blue LED has maximum emission wavelength at 460 nm (curve 4, Fig. 2) which exactly matches the excitation maxima of DBD-PyNCS, DBD-PyNCS-*L*-Tyr and DBD-PyNCS-*D*-Tyr, it was chosen in our work in order to obtain the highest excitation efficiency and strongest emission intensity.

A full-width at half-maximum of a blue LED is approximately 25 nm. It implies that LED emission is not monochromatic. To a cer-



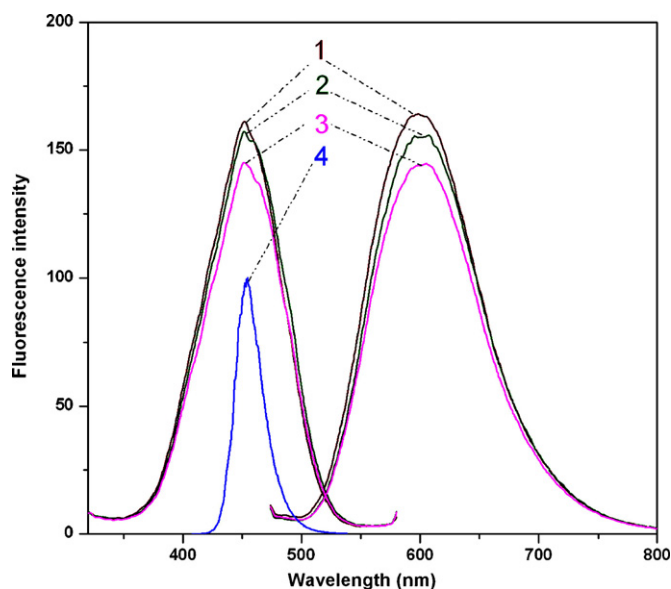


Fig. 2. Fluorescence excitation and emission spectra of (1) DBD-PyNCS, (2) DBD-PyNCS-L-Tyr and (3) DBD-PyNCS-D-Tyr, and (4) emission spectrum of the blue LED.

tain extent, it will partially overlap with the fluorescence emission from the analytes. For this reason, before reaching the PMT, fluorescence emission light should pass through a cut-off filter, which cut off most excitation light. It can reduce the background noise and obtain low detection limit and high sensitivity of detection. Thus, a red cut-off filter (570 nm) was used to reduce the background from the LED.

### 3.2. Effect of running buffer pH

Since the running buffer pH strongly affects the resolution ( $R_s$ ) and migration time, its effect on enantiomeric resolution was investigated under constant buffer concentration at pH 9.5–12.0 with a step change of 0.5. As shown in Fig. 3A, the  $R_s$  of DBD-PyNCS-Tyr increase sharply at pH 9.5–10.5. The  $R_s$  was calculated according to  $R_s = [2(t_2 - t_1)/(w_1 + w_2)]$ , where  $t_1$  and  $t_2$  are the migration times, and  $w_1$  and  $w_2$  are the peak widths at the baseline of solutes 1 and 2, respectively. We presume that since DBD-PyNCS-Tyr is negatively charged under the alkaline buffer conditions, it migrate toward the anode under the cathodic flow conditions of CE. However, the electrophoretic mobility ( $\mu_{EP}$ ) of DBD-PyNCS-Tyr is smaller than the electroosmotic mobility of the buffer ( $\mu_{EO}$ ). As a result, DBD-PyNCS-Tyr will reach the detector after the neutral molecule DBD-PyNCS (*vide infra*). The effect of pH on the  $\mu_{EP}$  of DBD-PyNCS-L-Tyr and DBD-PyNCS-D-Tyr is depicted in Fig. 3B. DBD-PyNCS-D-Tyr has higher  $\mu_{EP}$  than DBD-PyNCS-L-Tyr, attributing to the higher charge-to-size ratio of DBD-PyNCS-D-Tyr. It is well known that the  $\mu_{EP}$  of charged solute in CE is related as

$$\mu_{EP} = \frac{|Z|q}{6\pi\eta r}$$

where  $z$  is the ionic charge,  $q$  is the charge of an electron,  $\eta$  is the viscosity of the solution, and  $r$  is the radius of the ion. Since both DBD-PyNCS-L-Tyr and DBD-PyNCS-D-Tyr carry the same charges under the experimental conditions, it is possible that DBD-PyNCS-D-Tyr is smaller than DBD-PyNCS-L-Tyr, resulting in higher  $\mu_{EP}$  of DBD-PyNCS-D-Tyr. It is worth to mention that L-Tyr and D-Tyr cannot be separated in capillary zone electrophoresis (CZE) without derivatization as they have the same charge-to-size ratio. However, once they have been derivatized by DBD-PyNCS, they show different

$\mu_{EP}$ , allowing their separation in CZE with fluorescence detection. Thus, the main functions of DBD-PyNCS are to provide fluorescence tag to Tyr and distinguish the overall size of the DBD-PyNCS-Tyr derivatives. The  $\mu_{EP}$  of DBD-PyNCS-L-Tyr and DBD-PyNCS-D-Tyr increase with the increase in pH. They turn to the doubly charged anion when the pH is above 10.1. The largest difference in their  $\mu_{EP}$  is at pH 10.5, demonstrating that this is the optimal pH for their separation. When the pH was 11.0, the current reached 52  $\mu\text{A}$  which produced excessive Joule heating and poor reproducibility and thus eventually ruined the resolutions due to broadening of the solute peaks. According to the equation of  $R_s$  (*vide supra*), when  $w_1$  and  $w_2$  increase,  $R_s$  decreases. Therefore, the  $R_s$  of DBD-PyNCS-Tyr was not good at pH 11.0–12.0. The best  $R_s$  obtained at pH 10.5 was then chosen for subsequent experiments.

### 3.3. Effect of running buffer concentration

Fig. 4A shows the influence of running buffer concentration at pH 10.5 on the  $R_s$  of DBD-PyNCS-Tyr. The  $R_s$  increases with

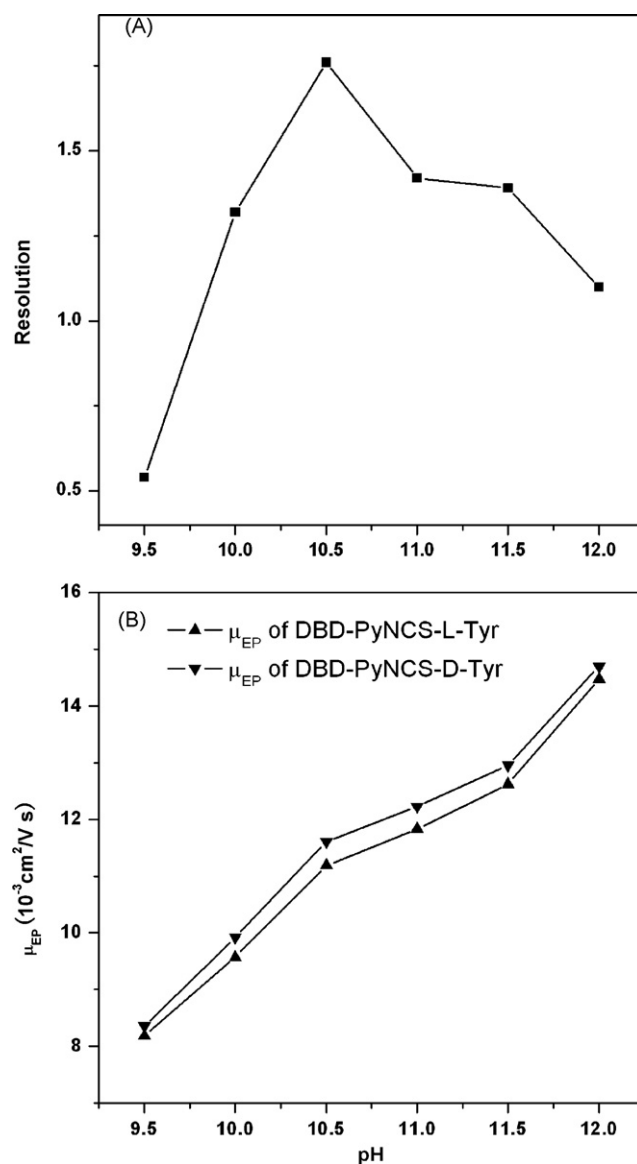


Fig. 3. Effect of running buffer pH on (A) resolution of DBD-PyNCS-labeled tyrosine enantiomers and (B) electrophoretic mobility of DBD-PyNCS-D-Tyr and DBD-PyNCS-L-Tyr. Electrolyte was 15 mmol/L borate running buffer at pH 9.5, 10.0, 10.5, 11.0, 11.5, and 12.0. The applied voltage was 14 kV.

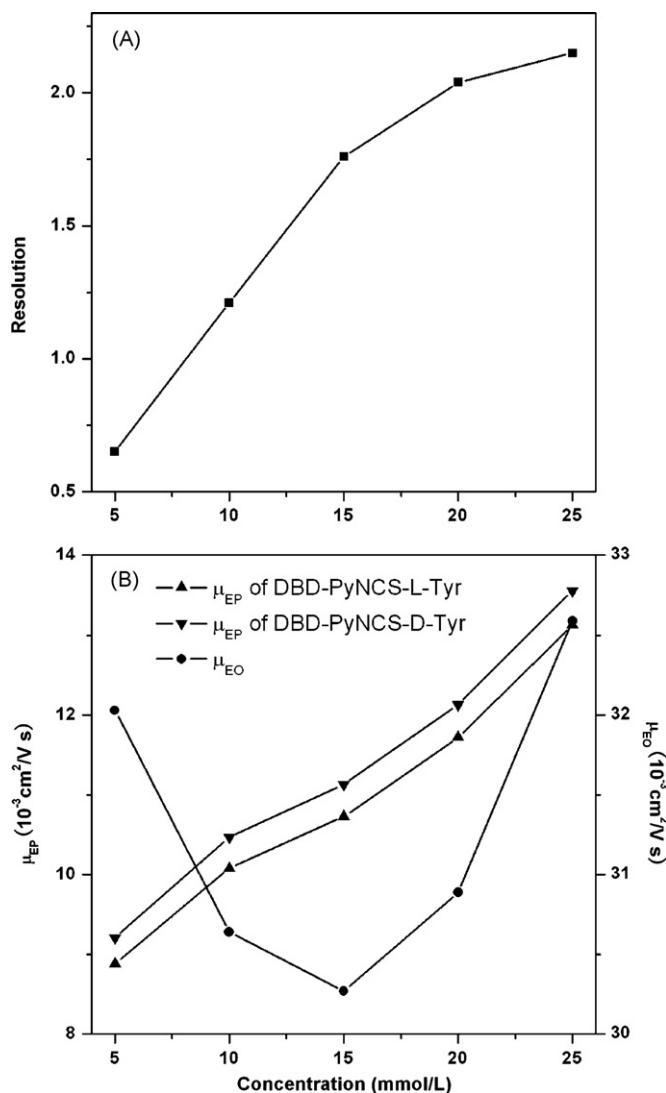


Fig. 4. Effect of running buffer concentration on (A) resolution of DBD-PyNCS-labeled tyrosine enantiomers and (B) electrophoretic mobility of DBD-PyNCS-D-Tyr and DBD-PyNCS-L-Tyr, and electroosmotic mobility at various concentrations of borate running buffer (pH 10.5). The applied voltage was 14 kV.

the increase in the borate concentration. It is well known that an increase in the ionic strength of the electrolyte results in compression of the thickness of the double layer, followed by a decrease in the absolute value of zeta potential and electroosmotic mobility ( $\mu_{EO}$ ) (at 5–15 mmol/L borate) as depicted in Fig. 4B. Simultaneously, higher buffer concentration can increase the  $\mu_{EP}$  of both DBD-PyNCS-L-Tyr and DBD-PyNCS-D-Tyr but the difference in their  $\mu_{EP}$  does not change much. Therefore, lower  $\mu_{EO}$  results in longer migration time which in turn produces better resolution. However, the improvement in resolution was less pronounced when the electrolyte concentration was increased from 15 to 25 mmol/L. This suggests that in addition to the above-mentioned effect, Joule heating also affects resolution since current rises quickly at this buffer concentration range. Joule heating raises the buffer temperature, leading to a smaller viscosity and an increase in  $\mu_{EO}$ . Consequently, the migration times of the analytes are shorter and the resolutions decrease slightly. High buffer concentration improves resolution to some extent but at the expense of reproducibility and separation efficiency. In brief, the optimal buffer concentration was chosen as 15 mmol/L borate for further studies.

### 3.4. Effect of applied voltage

In order to determine the optimal applied voltage for the CE separation, a series of operating voltages was examined with a running buffer containing 15 mmol/L borate (pH 10.5). Fig. 5A displays the resolution of the amino acid enantiomer derivatives which decreases with the increase in applied voltage from 12 to 16 kV. Fig. 5B shows that both  $\mu_{EO}$  and  $\mu_{EP}$  increase with the increase in the applied voltage. The increase in  $\mu_{EO}$  is larger than  $\mu_{EP}$  with the increasing applied voltage, leading to the decrease in migration times of both DBD-PyNCS-L-Tyr and DBD-PyNCS-D-Tyr. The difference in the  $\mu_{EP}$  between DBD-PyNCS-L-Tyr and DBD-PyNCS-D-Tyr is more or less the same and the overall resolution is degraded with the increase in applied voltage. To summarize, lower applied voltage can improve resolution with the sacrifice of analysis time. When the applied voltage is too high, it can cause excessive Joule heating which eventually ruin the resolution and repeatability. As a compromise, 14 kV was chosen as the optimal applied voltage for our work as it produced satisfactory resolution, reasonable migration time and low Joule heating.

In summary, the optimal CE conditions for separation of the Tyr enantiomer derivatives are 15 mmol/L borate solution, pH 10.5

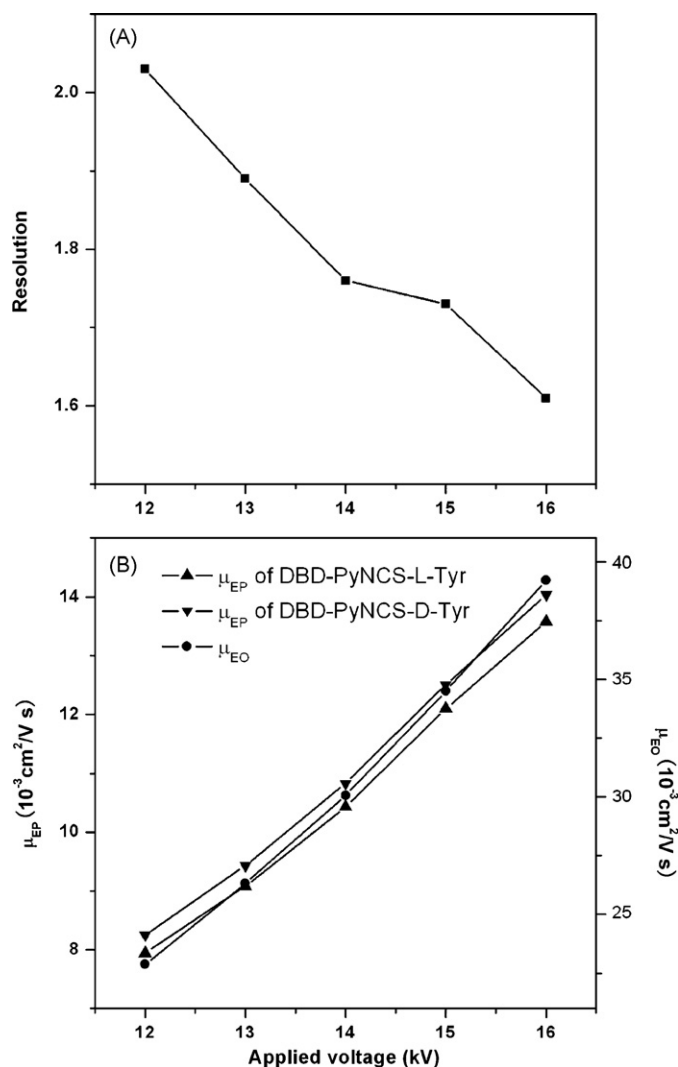
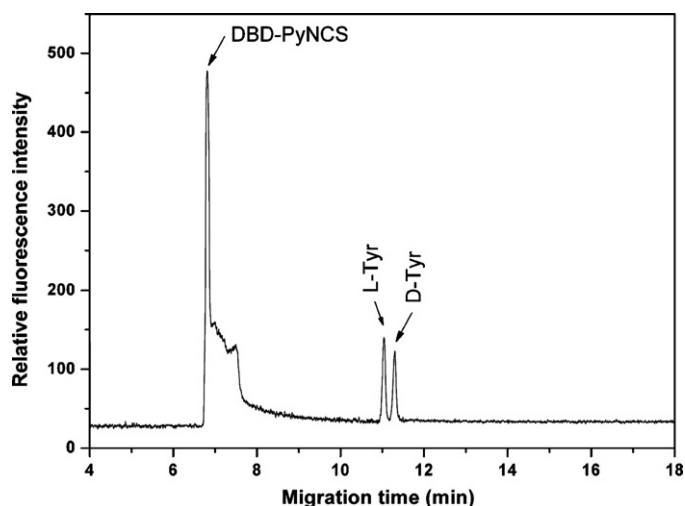


Fig. 5. Effect of applied voltage on (A) resolution of DBD-PyNCS-labeled tyrosine enantiomers and (B) electrophoretic mobility of DBD-PyNCS-D-Tyr and DBD-PyNCS-L-Tyr, and electroosmotic mobility. Electrolyte was 15 mmol/L borate running buffer (pH 10.5).



**Fig. 6.** Electrophoretic separation of D/L-tyrosine mixture derivatized with DBD-PyNCS. Concentration of each enantiomer in the mixture was 80.00  $\mu\text{mol/L}$ . Electrolyte was 15 mmol/L borate running buffer (pH 10.5). The applied voltage was 14 kV.

and 14-kV applied voltage. These conditions were successfully applied to the separation of DBD-PyNCS-L-Tyr and DBD-PyNCS-D-Tyr as depicted in Fig. 6. High sensitivity and good resolution was achieved. A large solute peak, i.e., the excess DBD-PyNCS reagent, migrated before DBD-PyNCS-Tyr peaks. The Tyr enantiomers derivatives were baseline separated with an  $R_s$  of 1.76, demonstrating that our CE-LED-IF method can separate and analyze Tyr enantiomers.

### 3.5. Linearity, limits of detection, reproducibility and interfering test

In order to validate our proposed CE method for analysis of D/L-Tyr, the reproducibility of migration time and peak area were studied. The relationship between D/L-Tyr concentration and CE-LED-IF signal was determined by a series of D/L-Tyr standard solutions. The regression equations and correlation coefficients showed that an excellent linear relationship at 5–500  $\mu\text{mol/L}$  D/L-Tyr. The limits of detection for L- and D-Tyr were estimated to be 2.2 and 2.9  $\mu\text{mol/L}$  ( $S/N=3$ ), respectively. The reproducibility and analytical figures of merit are summarized in Table 1. Excellent reproducibility was obtained with coefficient of variation ( $n=7$ ) of migration time and peak area less than 0.2 and 2.0%, respectively. In order to evaluate the potential interferent effect, several other amino acids including L-lysine (L-Lys), L-histidine (L-His), L-valine (L-Val), glycine (Gly), L-glutamic acid (L-Glu) and L-aspartic acid (L-Asp) were added into D/L-Tyr solutions and analyzed by our proposed method. Fig. 7 depicts the electropherogram of the separation of the amino acid DBD-PyNCS derivatives. DBD-PyNCS-L-Lys, -L-His,

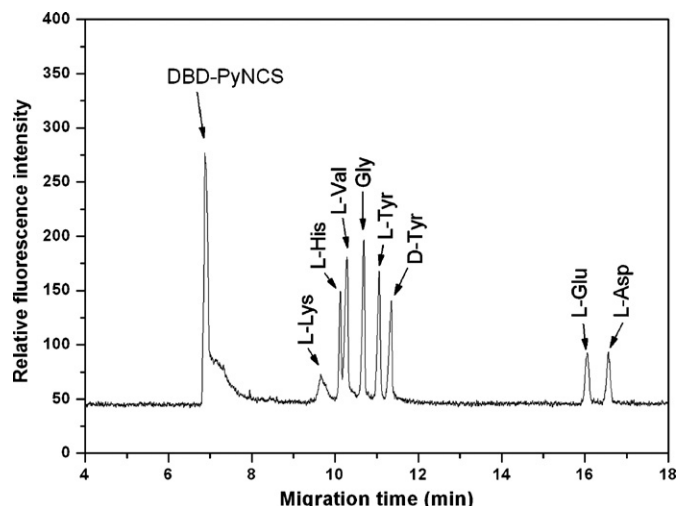


**Fig. 7.** Electrophoretic separation of D/L-tyrosine and other amino acids mixture derivatized with DBD-PyNCS. CE conditions are the same as in Fig. 6.

-L-Val, and -Gly derivatives migrated faster than DBD-PyNCS-D/L-Tyr while DBD-PyNCS-L-Glu and -L-Asp derivatives migrated far later than the DBD-PyNCS-D/L-Tyr peaks, demonstrating that these amino acids are well-separated from D/L-Tyr and should not pose any interference on Tyr determination.

### 3.6. Real samples analysis

A commercial pharmaceutical preparation (amino acid oral solution) was purchased to analyze its Tyr content. A typical electropherogram obtained from CE separation of this sample is depicted in Fig. 8. The DBD-PyNCS-L-Tyr peak is well resolved with no interference from other amino acids in the sample matrix under the optimal CE conditions. To verify the DBD-PyNCS-L-Tyr peaks, 13.00  $\mu\text{mol/L}$  of D/L-Tyr were added to the sample and analyzed again. The results are shown in the inset of Fig. 8. The solid trace was the sample and the dotted trace was the spiked sample with equal amounts of D- and L-Tyr. The sample (2% amino acid oral solution) was found to contain 12.75  $\mu\text{mol/L}$  L-Tyr and no D-Tyr. The concentration of L-Tyr in the sample and the recovery test are summarized in Table 2. The results are satisfactory with 93.04–106.3% recovery.

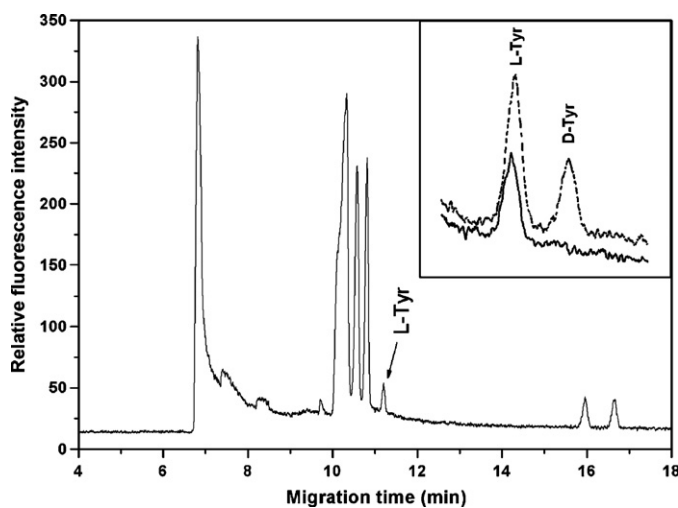


**Fig. 8.** Electrophoretic separation of an amino acid oral solution derivatized by DBD-PyNCS. The inset displays the electropherograms of the sample (solid trace) and spiked sample with 13.00  $\mu\text{mol/L}$  of DBD-PyNCS-D- and L-Tyr (dotted trace). CE conditions are the same as in Fig. 6.

**Table 1**

Coefficient of variation of migration time and peak area, and analytical figures of merit of the proposed CE-LED-IF method.

Enantiomer	L-Tyr	D-Tyr
Coefficient of variation (%)		
Migration time	0.13	0.12
Peak area	1.01	1.67
Linear range ( $\mu\text{mol/L}$ )	5–500	5–500
Regression equation <sup>a</sup>	$y = 1.29x + 1.12$	$y = 0.95x + 1.28$
Correlation coefficient	0.9997	0.9995
Limit of detection ( $\mu\text{mol/L}$ )	2.2	2.9

<sup>a</sup>  $x$ : concentration of DBD-PyNCS-labeled Tyr ( $\mu\text{mol/L}$ ) and  $y$ : fluorescence intensity.

**Table 2**  
Determination and recovery of tyrosine in a commercial amino acid oral solution using the proposed CE-LED-IF method.

Enantiomer	Sample	Initial ( $\mu\text{mol/L}$ )	Added ( $\mu\text{mol/L}$ )	Found ( $\mu\text{mol/L}$ )	Recovery (%)
L-Tyrosine	2% oral solution	12.75	13.00	26.57	106.3
		12.75	26.00	38.82	100.3
D-Tyrosine	2% oral solution	–	13.00	12.92	99.42
		–	26.00	24.19	93.04

In addition, the same amino acid oral solution sample was also analyzed by a Hitachi L-8800 amino acid auto-analyzer (Tokyo, Japan) and this method is conformed to the National Standard Method of China (GB/T 14965-1994) for analysis of amino acid [29]. The sample was found to contain 13.34  $\mu\text{mol/L}$  L-Tyr. The results obtained by the standard and the proposed CE methods only differed by 4.42%, indicating that our novel CE technique can provide reliable and accurate analysis of Tyr in real sample.

#### 4. Conclusion

Our developed fiber-optic LED-IF detection system coupled with CE has been successfully employed for the chiral separation of Tyr enantiomers labeled with DBD-PyNCS. The quantitative determination of Tyr in a commercial amino acid oral solution was demonstrated with good reproducibility, accuracy and recovery. Compared to the conventional UV/vis absorption, right-angle LED-IF and collinear LED-IF detectors, our system provides better sensitivity. The exciting light beam was directly introduced to the detection window via an inserted optical fiber, thus the light reflection and scattering effects on the capillary surface was much reduced. Our proposed apparatus is much cheaper and more compact than LIF detectors since inexpensive LED is used. Although the sensitivity of detection is not as good as LIF detection, it is adequate for most routine analysis. In essence, our proposed method can be employed as a rapid, efficient, simple and inexpensive tool for separation and determination of amino acid enantiomers.

#### Acknowledgements

This work was supported by the National Natural Science Foundation of China (20575042 and 20775050).

#### References

- [1] S.C. Stinson, Chem. Eng. News 75 (1997) 28.
- [2] K.A. Hansford, R.C. Reid, C.I. Clark, J.D.A. Tyndall, M.W. Whitehouse, T. Guthrie, R.P. McGeary, K. Schafer, J.L. Martin, D.P. Fairlie, Chem. Biochem. 4 (2003) 181.
- [3] K. Kurata, J. Ono, A. Dobashi, J. Chromatogr. A 1080 (2005) 140.
- [4] T. Suzuki, T. Watanabe, T. Toyooka, Anal. Chim. Acta 352 (1997) 357.
- [5] D.R. Jin, K. Nagakura, S. Murofushi, T. Miyahara, T. Toyooka, J. Chromatogr. A 822 (1998) 215.
- [6] S.L. Zhao, R.C. Zhang, H.S. Wang, L.D. Tang, Y.M. Pan, J. Chromatogr. B 833 (2006) 186.
- [7] Z.H. He, W.R. Jin, Anal. Biochem. 313 (2003) 34.
- [8] C.L. Schultz, M. Moini, Anal. Chem. 75 (2003) 1508.
- [9] T. Soga, D.N. Heiger, Anal. Chem. 72 (2000) 1236.
- [10] X.Y. Huang, J.C. Ren, Trends Anal. Chem. 25 (2006) 155.
- [11] K. Tsukagoshi, K. Sawanoi, R. Nakajima, J. Chromatogr. A 1143 (2007) 288.
- [12] V. Lavigne, A. Pons, D. Dubourdieu, J. Chromatogr. A 1139 (2007) 130.
- [13] Q. Yang, X.L. Zhang, X.H. Bao, H.J. Lu, W.J. Zhang, W.H. Wu, H.N. Miao, B.H. Jiao, J. Chromatogr. A 1201 (2008) 120.
- [14] Y.F. Lin, Y.C. Wang, S.Y. Chang, J. Chromatogr. A 1188 (2008) 331.
- [15] S.L. Wang, X.J. Huang, Z.L. Fang, P.K. Dasgupta, Anal. Chem. 73 (2001) 4545.
- [16] S.J. Chen, M.J. Chen, H.T. Chang, J. Chromatogr. A 1017 (2003) 215.
- [17] M.M. Hsieh, S.M. Chen, Talanta 73 (2007) 326.
- [18] D. Xiao, S.L. Zhao, H.Y. Yuan, X.P. Yang, Electrophoresis 28 (2007) 233.
- [19] A.K. Su, C.H. Lin, J. Chromatogr. B 785 (2003) 39.
- [20] A.K. Su, Y.S. Chang, C.H. Lin, Talanta 64 (2004) 970.
- [21] Q.L. Yu, S.L. Zhao, F.G. Ye, S.T. Li, Anal. Biochem. 369 (2007) 187.
- [22] C.L. Wang, S.L. Zhao, H.Y. Yuan, D. Xiao, J. Chromatogr. B 833 (2006) 129.
- [23] S.L. Zhao, B. Wang, M. He, W.L. Bai, L. Chen, Anal. Chim. Acta 569 (2006) 182.
- [24] S. Hillebrand, J.R. Schoffen, M. Mandaji, C. Termignoni, H.P.H. Grieneisen, T.B.L. Kist, Electrophoresis 23 (2002) 2445.
- [25] B.C. Yang, F. Tan, Y.F. Guan, Talanta 65 (2005) 1303.
- [26] X.P. Yang, H.Y. Yuan, C.L. Wang, X.D. Su, L. Hu, D. Xiao, J. Pharm. Biomed. Anal. 45 (2007) 362.
- [27] S.L. Zhao, H.Y. Yuan, D. Xiao, Electrophoresis 27 (2006) 461.
- [28] T. Toyooka, Y.M. Liu, J. Chromatogr. A 689 (1995) 23.
- [29] W.G. Mu, X.H. Ding, A.N. Liu, S.Y. Zhao, T.H. Wang, L.J. Qu, Amino Acids Biotic Resour. 18 (1996) 16.



## A new approach to determine $^{147}\text{Pm}$ in irradiated fuel solutions

René Brennetot\*, Guillaume Stadelmann, Céline Caussignac, Clémentine Gombert, Michèle Fouque, Christine Lamouroux

Commissariat à l'Energie Atomique, Département de Physico Chimie, Service d'Etude du Comportement des Radionucléides, Laboratoire d'Analyses Nucléaires Isotopiques et Élémentaires, Bât 391, PC 33, Centre d'étude de Saclay, 91191 Gif sur Yvette cedex, France

### ARTICLE INFO

#### Article history:

Received 12 September 2008

Received in revised form 5 December 2008

Accepted 11 December 2008

Available online 24 December 2008

#### Keywords:

$^{147}\text{Pm}$  measurement

ICP-MS

Nuclear fuel

### ABSTRACT

Developments carried out in the Laboratory of Isotopic, Nuclear and Elementary Analyses in order to quantify  $^{147}\text{Pm}$  in spent nuclear fuels analyzed at the CEA within the framework of the Burn Up Credit research program for neutronic code validation are presented here. This determination is essential for safety-criticality studies.

The quantity and the nature of the radionuclides in irradiated fuel solutions force us to separate the elements of interest before measuring their isotopic content by mass spectrometry. The main objective of this study is to modify the separation protocol used in our laboratory in order to recover and to measure the  $^{147}\text{Pm}$  at the same time as the other lanthanides and actinides determined by mass spectrometry.

A very complete study on synthetic solution (containing or not  $^{147}\text{Pm}$ ) was undertaken in order to determine the yield of the various stages of separation carried out before obtaining the isolated Pm fraction from the whole of the elements present in the spent fuel solutions. With the lack of natural tracer to carry out the measurement with the isotope dilution technique, the great number of isotopes in fuel, the originality of this work rests on the use of another present lanthanide in fuel to define the output of separation. The yields were measured at the conclusion of each stage of separation with two others lanthanides in order to show that one of them could be used as a tracer to correct the measurement of the  $^{147}\text{Pm}$  with the separation yield. The total yield (at the conclusion of the two stages of separation) was measured at the same time by ICP-MS and liquid scintillation. This last determination made it possible to validate the use of the  $^{147}\text{Sm}$  (natural) to measure the  $^{147}\text{Pm}$  in ICP-MS since the outputs determined in liquid scintillation and ICP-MS (starting from the radioactive decrease of the source having been used to make the synthetic solution) were equivalent. It is the first time that such measurement is performed in ICP-MS.

The measurement of the  $^{147}\text{Pm}$  was finally taken on fuels UOx and MOx by using the  $^{153}\text{Eu}$  like a tracer of the separation yield. The results obtained are in very good agreement with those obtained from neutronic calculation code.

© 2008 Elsevier B.V. All rights reserved.

### 1. Introduction

Promethium is a product of uranium fission. Among all Pm isotopes, measurement of isotope 147 of promethium in irradiated fuel is of prime interest (1) because this isotope contributes to the formation of samarium isotopes [1] which are retained as strong neutron absorber in Burn Up Credit studies and it is retained among the 15 fission products of interest retained by OECD for criticality studies, (2) for calculation of fuels after power. Its measurement would make it possible to raise uncertainties concerning a possible undervaluation of the fission yields.

Different methods are reported in the literature for  $^{147}\text{Pm}$  separation and measurement (principally by liquid scintillation counting) in various matrices such as urine, environmental samples and nuclear fuel [2–5]. For urine samples, Eichuk describes a method using dynamic ion exchange chromatography to separate  $^{147}\text{Pm}$  from urine matrix and a measurement of the Pm fraction by liquid scintillation counting. For environmental samples, Yoshida et al. reported a rapid separation method using HPLC with HIBA (Alpha-hydroxyisobutyric acid) stepwise eluent method for separation of lanthanides Sm, Pm, Eu, Nd with liquid scintillation counting for  $^{147}\text{Pm}$  and  $^{151}\text{Sm}$  determination and inductively coupled plasma mass spectrometry for Eu, Nd and Sm measurements. Jerome used a co precipitation method for Pm determination. The lanthanides are first co precipitated and then separated by cation exchange chromatography in HIBA medium.  $^{147}\text{Pm}$  measurement is then performed by liquid scintillation counting. This procedure has been

\* Corresponding author. Tel.: +33 169 08 56 23; fax: +33 169 08 54 11.  
E-mail address: [rene.brennetot@cea.fr](mailto:rene.brennetot@cea.fr) (R. Brennetot).

used for various matrices such as sediments, power station effluent discharges, silt, . . . G Seeber et al synthesized a new coated silica material for separation of radioactive lanthanides  $^{147}\text{Pm}$  and  $^{152}\text{Eu}$ , both measured by liquid scintillation counting. In irradiated fuel matrix, only one method has been previously reported and developed by Adriansen [6]. They first separate  $^{147}\text{Pm}$  from other lanthanides using the Ln resin and a  $^{146}\text{Nd}$  spike to obtain the separation yield.  $^{147}\text{Pm}$  measurement is performed with liquid scintillation counting.

Isotopic and elementary measurements of radionuclides in spent nuclear fuel samples are principally done with mass spectrometry techniques including thermal ionisation mass spectrometry (TIMS) [7,8], multi collector inductively coupled plasma mass spectrometry (MC-ICP-MS) [9–11], sector field inductively coupled plasma mass spectrometry (SF-ICP-MS) [12] and quadrupole inductively coupled plasma mass spectrometry (Q-ICP-MS) [13–18]. In all cases, when separation steps are needed for isotopic content determination, isotopic dilution technique is used with double spike in order to be independent of separation yields. Several works compared the ICP-MS with radiometric techniques like alpha spectrometry or gamma spectrometry for radionuclide measurements [19–21]. The goal of this work is to obtain a new protocol allowing the measurement of  $^{147}\text{Pm}$  by quadrupolar ICP-MS without adding stages.

Protocols available in our laboratory allow the separation of the various fission products as well as the determination of their concentration and isotopic content by mass spectrometry techniques. Beta-decay of  $^{147}\text{Pm}$  leads to formation of isobaric  $^{147}\text{Sm}$ . The resolution necessary to separate these two peaks (735,000), is higher than the resolution usually accessible by mass spectrometry. Thus, the determination of the  $^{147}\text{Pm}$  by mass spectrometry can consequently be done, only after chemical separation of these two elements. The goal of this work is to adapt the available protocols, in order to be able to measure  $^{147}\text{Pm}$ .

Initially, fission products (FP) are separated from uranium and plutonium, which are the two major components of irradiated fuels, using a previously described method involving ion exchange resin [6,7]. The fission products collected fraction FP which contains elements such as samarium and promethium is then injected in HPLC in order to separate the various components. Finally, the Pm fraction obtained from HPLC will be analyzed by ICP-MS by external calibration. It is obvious that we need to follow exactly the compartment of Pm during the separation steps in order to correct the ICP-MS measurement with the separation yield. The originality of this work rests on the use of another lanthanide isotope present in fuel, thus making it possible to define the yield of all the separation steps. In this work, different lanthanides such as Eu and Gd were studied to verify if they can be used as a tracer of the separation steps (Fig. 1).

The resin classically used to carry out the first U/Pu/FP separation is an anion resin AG1X4 (Biorad) in nitric medium. However, and as clearly explained by Marhol [22], lanthanides do not have the same distribution coefficients for a given acidity on AG1X4 resin in nitric medium precluding therefore the use of these conditions. The lanthanides interaction of an anion resin AG1X10 seems similar in hydrochloric medium according to the literature [3]. Consequently, the output of the first separation on resin AG1X10 in hydrochloric medium was studied in order to determine if europium and gadolinium had the same retention under these conditions according to the strategy presented in Fig. 1. The final goal of this work is to develop a new protocol for  $^{147}\text{Pm}$  measurement in nuclear fuel samples (using the actual protocol for separation yield measurement at the same time).

A complete study on synthetic solution (containing or not Pm) was undertaken in order to determine the yield of the various separation steps carried out before obtaining the pure Pm fraction. This

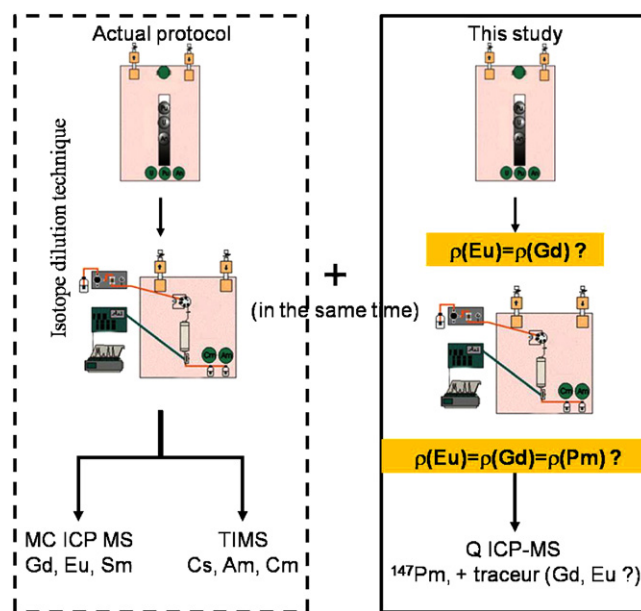


Fig. 1. Synoptic of this study.

study shows that the separation yield can be followed by the use of another lanthanide used as a tracer of the separation steps. The total yield (at the conclusion of the two separation stages) was measured at the same time by ICP-MS and liquid scintillation counting. Finally, the results obtained for the  $^{147}\text{Pm}$  measurement in two types of fuel with high burn up (70 GWd/t) UOx and MOx type are shown.

## 2. Experimental

All the concentrations reported in this paper are expressed in  $\text{ng g}^{-1}$ . Activity concentrations measured by liquid scintillation counting are expressed in  $\text{Bq g}^{-1}$ .

### 2.1. Reagents and standards

All dilutions have been performed in nitric acid at 2% (v/v). This acid is obtained by dilution of nitric acid (65% Normatom Prolabo) in deionised water (conductivity  $18.2 \text{ M}\Omega$ ) obtained from a Milli Q system (Millipore).

Sub-boiling nitric acid is manufactured at the laboratory starting from 65%  $\text{HNO}_3$  (Normatom Prolabo).

Hydrochloric acid (33–36% Optima Prolabo) is used for gravimetric separations and ICP-MS experiments.

A multi-element Tuning Solution (Spex) at  $1 \mu\text{g/L}$  was used every day for the instrument optimization and short-term stability tests.

All calibration curves have been performed using SPEX solutions ( $1 \text{ mg/L}$ ) of samarium, gadolinium and europium and uranium ( $10 \text{ mg/L}$ ) for matrix matching.

A solution of  $^{147}\text{Pm}$  certified in activity was obtained from CERCA (LEA, AREVA). The initial activity was  $800 \pm 16 \text{ kBq/g}$ . This solution has been used for experiments performed with fuel simulated solutions and calibration of the liquid scintillation counting.

$^{115}\text{In}$  (SPEX) is used as internal standard for ICP-MS measurements.

2-Hydroxy-methylbutyric acid (HMB) is used as eluent for HPLC lanthanide separation (Sigma–Aldrich). pH of the mobile phase was adjusted with a 25% ammonia solution (Normatom, Prolabo).

Arsenazo III (Sigma–Aldrich) is used as a post-column reactant for samarium detection with UV detector.

## 2.2. Ion exchange resins

An anion exchange Dowex AG1X10 (Bio Rad Laboratories) resin, 50–100 mesh, was used for U/Pu/FP separation. For conditioning, the dry resin is placed in an eco column provided by Eichrom, the height of resin must be of  $2.5 \text{ cm} \pm 1 \text{ mm}$  in the column. The resin is then washed with concentrated hydrochloric acid (10M). 15 mL of the same acid is sufficient to wash and condition the resin.

The selected protocol is the one already used at the laboratory for the separations carried out on resin in hydrochloric medium. Aliquot of solution is taken and dried in a Teflon beaker. 1 mL of OPTIMA HCl 33–36% is used to rinse the beaker, this aliquot is deposited on the head column. 4 mL of HCl 10M is necessary to elute completely the FP fraction containing the  $^{147}\text{Pm}$ ; under these conditions U and Pu are trapped on the resin.

Only the first fraction containing the fission products was recovered in a container out of Teflon and weighed precisely. This fraction, in 10 M HCl medium, was diluted in 0.5 M  $\text{HNO}_3$  for measurement by ICP-MS.

## 2.3. Samples

Simulated solutions were used for all separation yield determination of lanthanides. They are prepared by weight of SPEX standards solutions and contain only U, Sm, Eu, Gd and Pm for yield studies including HPLC separation.

The spent fuel samples were UOx and MOx types. They were dissolved in hot cells at CEA Marcoule in the ATALANTE facility. After complete dissolution, the samples are diluted and sent to CEA Saclay for elementary and isotopic analysis.

## 2.4. Analytical techniques

### 2.4.1. ICP-MS

The experiments were carried out on a quadrupole ICP-MS X series (Thermo Fischer Scientific).

This ICP-MS was the first X7 modified in order to work with radioactive materials as previously described [23].

Sample introduction to the plasma was made via a quartz concentric nebulizer (0.4 mL/min) and a quartz bead impact spray chamber. A CETAC ASX 260 auto-sampler was used in order to minimize exposure to radioactive materials.

All of the experimental parameters are daily optimized with a Test solution containing several elements in order to obtain the maximum count rates on  $^{115}\text{In}$  and  $^{238}\text{U}$  for this tuning.

After acquisition of a short-term stability test in standard mode (sensitivity, stability and oxide level test), the instrument is ready to perform measurements by external calibrations.

**Table 1**  
ICP-MS operating parameters.

Forward rf power	1400 W
Reflected rf power	<2 W
Coolant gas flow rate	15 $\text{L min}^{-1}$
Nebulizer gas flow rate	0.95 $\text{L min}^{-1}$
Auxilliary gas flow rate	0.8 $\text{L min}^{-1}$
Nebulizer type	Quartz concentric
Spray chamber	Bead impact cooled with peltier effect at $3^\circ\text{C}$
Detection mode	Pulse counting
Dwell time	10 ms
Sweeps	300
Sampling and skimmer cones	Ni

Experimental parameters for mass spectrometric measurements are summarized in Table 1.

The external calibration was carried out with multi elementary standards prepared with SPEX solutions. Indium was selected as internal standard for measurement in ICP-MS because it is the only one which can be used for the analysis of fuel. The dilution medium, 0.5 M  $\text{HNO}_3$  is selected in order to make sure that the standards, the simulated solution and FP fractions can be measured using the same calibration (absence of matrix effect).

### 2.4.2. HPLC

The chromatographic system used consists of several modules. A principal chromatographic pump (Merck-Hitachi) delivering the mobile phase made up of HMB in gradient mode (in quantity and pH) with a flow of 0.8 mL/min. A Rhéodyne valve six ways in peek is used with a 100  $\mu\text{L}$  injection loop in peek. The column used is a cation exchange column NUCLEOSIL SA of length and internal diameter respectively 250 and 4.6 mm, thermostated at  $25^\circ\text{C}$ . A secondary pump (Gilson) is used for delivery of arsenazo III necessary for the UV/vis detection of Sm at 658 nm (Jasco). A radiometric detector (PerkinElmer) is used for radio elements detection.

### 2.4.3. Liquid scintillation counting

Measurement of  $^{147}\text{Pm}$  by liquid scintillation counting were performed with two instruments: TriCarb 2900TR and Wallac Oy 1414 Guardian. The dilutant used is selected to be close to the final medium which will be used to count on the solutions resulting from the HPLC and analyzed by ICP-MS.

## 3. Results and discussion

The measurement of  $^{147}\text{Pm}$  suffers from an isobaric interference with  $^{147}\text{Sm}$  implying therefore separations steps. The main objective of this work is to find a tracer of the separation steps in order to correct the obtained value for Pm concentration in ICP-MS of the

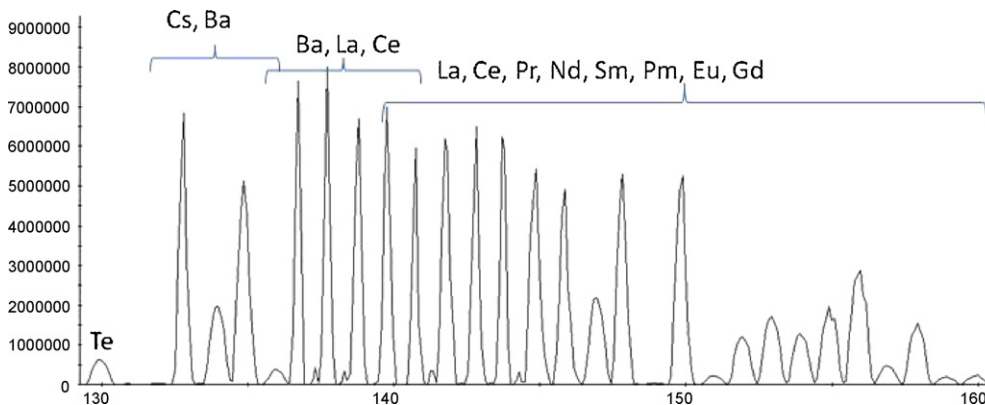


**Fig. 2.** Mass spectrum of spent fuel from 130 u to 160 u.

**Table 2**

Yield obtained for Gd and Eu for an aliquot of 1 mL of synthetic solution after gravimetric separation by AG1X10 resin in HCl medium.

	Eu yield	Gd yield
Aliquot 1	99 ± 2	99 ± 2
Aliquot 2	99 ± 2	99 ± 2
Aliquot 3	98 ± 2	98 ± 2

separation yield to be able to measure  $^{147}\text{Pm}$  in spent fuels taking into account all the separation steps to correct the final measurement. It was decided to study the separation yield at each step of the analytical process used for  $^{147}\text{Pm}$  measurement in order to find a marker of the separation to correct the final result of the separation yield.

- (1) Gravitational separation on resin: FP, U, Pu.
- (2) HPLC separation of actinides and lanthanides.
- (3) Measurement of the  $^{147}\text{Pm}$  fraction free from  $^{147}\text{Sm}$  by ICP-MS with a calibration curve at mass 147 with natural samarium.

Ideally a double spike with the use of the isotope dilution technique would be optimal to overcome the measurement of the separation yields, but such a tracer is not available.

It could be interesting to use another isotope of Pm as the  $^{148}\text{Pm}$  but its lifetime is too much short to be used.

Consequently, we decided to use a chemical analogue which would have the same chemical behaviour as Pm. The irradiated fuel is a complex solution which comprises many elements including lanthanides like shown in Fig. 2. Consequently, it is possible to use other lanthanides after ensuring that they have the same chemical behaviour as Pm with respect to the separation stages considered. Europium and gadolinium have been tested with respect to the separation stages (gravimetric separation + HPLC) in order to check their potential as tracer of the separation. We have chosen these two lanthanides for their proximity in mass and because they can be measured with a very small uncertainty, using the isotope dilution technique. This technique, well described in the literature [24] allows the determination of isotopic ratios and radionuclide concentrations with a very small uncertainty.

### 3.1. Gravimetric separation

In order to analyze and to determine the content of  $^{147}\text{Pm}$  in a spent nuclear fuel, it is necessary to separate the  $^{147}\text{Pm}$  from the other elements such as fission products, U and Pu. This separation is carried out in two stages: the first separation is performed with an ion exchange resin in order to separate rapidly FP from the U and Pu matrix. Then, FP are separated by HPLC.

In order to minimize the dose rate received by the experimenters, the yield of the first separation step for two selected lanthanides (Eu and Gd) was measured using a synthetic solution including only uranium, gadolinium and europium (natural) in proportions similar to those of spent nuclear fuels. This synthetic solution contains around 680  $\mu\text{g/g}$  U, 210  $\text{ng/g}$  Eu and 390  $\text{ng/g}$  Gd.

Three tests were carried out. An aliquot of 1 mL of this synthetic solution is used, in order to make sure that a sufficient quantity of matter is able at the end of the first separation stages, to determine the yield by ICP-MS. Eu, and Gd concentrations are perfectly known as the synthetic solution is made by weighting. Concentrations in Eu and Gd were measured before and after gravimetric separation in order to determine the yield of separation and to prove that it could be considered as equivalent.

The yields were measured for isotopes 151 and 153 of europium and 157 and 158 of gadolinium. The results from these three separations on resin are presented in Table 2. Error bars correspond to

reproducibility observed (4 calibrations ICP-MS with each time two test specimens of the fraction).

At this stage, it can be considered that europium and gadolinium could be used like a tracer of the first separation stage since the separation yields are equivalent, very reproducible and close to 100%, suggesting therefore that no fractionation is induced by the gravimetric separation with the protocol chosen here.

### 3.2. HPLC

A new synthetic solution containing  $^{147}\text{Pm}$  at the concentration of 9  $\text{ng/g}$  has been prepared.

The 5 mL solution thus recovered at the end of the first separation previously described is put in a Teflon beaker and dried. The residue is then reconditioned in nitric medium with 5 mL of 0.2N Sub-boiling nitric acid compatible with HPLC.

It is then injected on a HPLC chain confined in a glove box to separate Sm/Pm/Eu/Gd.

The separation yield for Pm is obtained by calculation of the true concentration to date. The concentration in  $^{147}\text{Pm}$  is measured by ICP-MS by using the  $^{147}\text{Sm}$  as standard (it is supposed that Sm and Pm have the same response in ICP-MS). The results obtained on the three tests carried out in glove box are presented in Table 3. To ensure that the response of Pm and Sm could be expected equivalent in ICP-MS, the yield of separation for Pm is measured in the same solution by liquid scintillation counting, an independent measurement technique without any interference since the only beta emitter in the synthetic solution is  $^{147}\text{Pm}$ .

The results presented in Table 3 show that the same yields are obtained by liquid scintillation counting and by ICP-MS with samarium 147 used as a standard for external calibration for Pm measurement. This indicates at this stage, that europium and gadolinium could be used as tracer of the whole separation steps envisaged.

### 3.3. Analysis of spent fuels

Previous developments with synthetic solutions show that the yield at the end of the separation stages with selected conditions are equivalent for selected lanthanides Pm, Eu, Gd. Thus  $^{153}\text{Eu}$  and  $^{157}\text{Gd}$  could be used as tracers of the separation yield. In addition it has been shown that  $^{147}\text{Sm}$  could be used to carry out the range of calibration to measure  $^{147}\text{Pm}$ . Two spent fuel solutions were analyzed.

Separations were carried out on the MOx and UOx fuels. Two aliquots of 250  $\mu\text{l}$  for each fuel were taken for separation steps. Chromatogram of one of the aliquot of UOx sample is presented in Fig. 3. As shown in Fig. 2, there is lots of peaks in the lanthanide zone for a spent fuel what results in to create interferences which were not taken into account up to now. Finally  $^{153}\text{Eu}$  was chosen as the tracer of the separation, because of the presence of some oxides (BaO, CeO, PrO) that induce an over estimation of the absolute content of gadolinium in the fuel without separation step. For this purpose, it has been experimentally verified that caesium do not produce a sufficient oxide quantity to interfere at mass 149,

**Table 3**

Yield obtained for Gd, Eu and Pm for an aliquot of 1 mL of synthetic solution after gravimetric separation and HPLC. The first column for Pm is the yield determined by ICPMS with Sm external calibration, the second one is the determination by liquid scintillation counting.

	Eu yield	Gd yield	Pm yield	
Aliquot 4	81 ± 3	80 ± 3	81 ± 3	79 ± 3
Aliquot 5	71 ± 3	73 ± 3	70 ± 3	70 ± 3
Aliquot 6	81 ± 3	83 ± 3	77 ± 3	78 ± 3



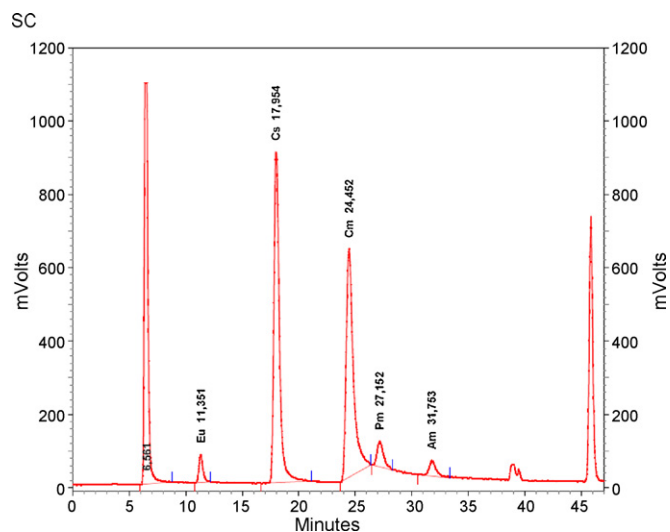


Fig. 3. Chromatogram obtained with radiometric detection for separation of the Pm fraction obtained at the first gravimetric separation of UOx GGU1 fuel.

150, 151, 153 when barium, praseodymium and cerium produces a large amount of oxides that interferes all the isotopes of gadolinium.

The results are presented in Table 4.

Uncertainties were given on several levels in order to try to take into account all stages leading to the final result. The analytical uncertainty given in ICP-MS takes into account all the analytical stages, of the preparation of the sample received at the laboratory with its analysis: preparation of the standards by weighing, uncertainty on the concentrations of the standards (calculated starting from the certificates of analysis of the standard solutions), uncertainty on the calibration, stability of the apparatus, estimate of the accuracy of the analyzes starting from standards whose concentration is known, variation of measurements on two distinct test specimens, derives possible from the apparatus over the duration of measurements.

Uncertainties on the concentrations determined in ICP-MS were given starting from LANI, homemade software which integrates the sources of uncertainties such as dilutions, uncertainty on the standards and the hyperboles of confidence of the calibration line. The values of concentrations in  $^{153}\text{Eu}$  obtained before and after separations are compiled in order to obtain the output of the stages of separation. Resulting uncertainty is given with the method described by Kragten [25].

Combined uncertainty is calculated starting from the law of propagation of uncertainties like defined in EURACHEM/CITAC guide [26].

The result obtained on the absolute concentration of  $^{153}\text{Eu}$  was first of all compared with the concentration returned by isotopic dilution (ID) in June 2006 (taken as reference value). As can be seen in Table 4, europium concentration is coherent with the result

Table 4

Results obtained for  $^{153}\text{Eu}$  and  $^{147}\text{Pm}$  concentration in spent fuels. Separation yields applied for  $^{147}\text{Pm}$  concentration are calculated from  $^{153}\text{Eu}$  concentration measured by Q-ICP-MS before and after separation steps.

$^{153}\text{Eu}$ (ng/g sol)	$^{153}\text{Eu}$ (ng/g sol) reference value	$^{147}\text{Pm}$ (ng/g sol)
UOx		
Before sep steps: 161.7	163.3 ± 3.2	27.5 ± 2.7
After sep steps: 128.3		
MOx		
Before sep steps: 266.4	273.2 ± 5.9	40.14 ± 4.06
After sep steps: 217.5		

returned by isotopic dilution with a variation observed lower than 1% for UOx sample and less than 3% for MOx sample.

The  $^{147}\text{Pm}$  concentration obtained were then compared with prediction calculation according to DARWIN 2.2 code with JEFF 2.2 library. Less than a 10% variation is obtained between the measurement and the result obtained starting from the computer code. However this variation is covered by the uncertainty of measurement which validates this protocol.

#### 4. Conclusion

With an aim of determining the concentration in  $^{147}\text{Pm}$  in UOx and MOx spent fuel solutions, a durable method was developed in order to validate the separation stages necessary to this measurement (exchange resin and HPLC). This new measurement was optimized to complete a method previously used for lanthanides determination by isotope dilution technique. These tests made it possible to show that lanthanides Eu, Gd and Pm had a similar behaviour with respect to the selected resin (AG1X10) in hydrochloric medium in this type of matrix.

We have shown that Eu and Gd had the same behaviour during all the separations steps, making it possible their use as a tracer of the separation for Pm measurement. Checking of the yield at the conclusion of the stages of separation by liquid scintillation made it possible to validate on the one hand the yields determined by ICP-MS, but also to validate the use of the natural  $^{147}\text{Sm}$  to measure the  $^{147}\text{Pm}$  after separation. The yield thus determined for the  $^{153}\text{Eu}$  could be applied to the measurement of the  $^{147}\text{Pm}$  in fuel.

These results also were validated by ICP-MS with a difference lower than 2% compared to the results resulting from the determinations by isotopic dilution in May and October 2006 to the measurements of absolute concentrations of the isotope  $^{153}\text{Eu}$  used for the follow-up and the determination of the yield on the totality of the experiment.

The measurements obtained in ICP-MS for the  $^{147}\text{Pm}$  and measurements of output of  $^{153}\text{Eu}$  made it possible to calculate the concentrations in  $^{147}\text{Pm}$  in fuel. These results are completely coherent with the values returned by calculation code with a difference less than 10% and totally covered by uncertainty measurement.

#### Acknowledgments

The authors wish to thank Cecile Riffard (CEA Cadarache, DER/SPRC/LECY) for its support for calculation codes. Authors wish to thank also Carole frechou (DEN/DANS/DPC/SECR/LANIE) for her advices and Pascal Fichet (DEN/DANS/DPC/SECR/LANIE) for his uncertainty determination program.

#### References

- [1] B. Roque, N. Thiollay, P. Marimbeau, A. Barreau, A. Tsilanizara, C. Garzenne, F. Marcel, H. Toubon, C. Garats, Park, MG, (Ed.), Proceedings PHYSOR-2002, Seoul, Korea, 7–10 October 2002.
- [2] S.M. Jerome, Sci. Total Environ. 70 (1988) 275.
- [3] M. Yoshida, S.H. Sumiya, H. Watanabe, K. Tobita, J. Radioanal. Nucl. Chem. 197 (1995) 219.
- [4] G. Seeber, P. brunner, M.R. Buchmeiser, G.K. Bonn, J. Chromatogr. A 848 (1999) 193.
- [5] S. Eichuk, C.A. Lucy, K.I. Burns, Anal. Chem. 64 (1992) 2339.
- [6] L. Adriaensen, M. Gysemans, C. Hurtgen, D. Boulanger, ENC 2007 Conference, Brussels, September 16–20, 2007.
- [7] F. Chartier, M. Aubert, M. Salmon, M. Tabarant, B.H. Tran, J. Anal. Atom. Spectrom. 14 (1999) 1661.
- [8] F. Chartier, M. Aubert, M. Pilier, Fresenius J. Anal. Chem. 364 (1999) 320.
- [9] H. Isnard, R. Brennetot, C. Caussignac, N. Caussignac, F. Chartier, Int. J. Mass Spectrom. 246 (2005) 66.
- [10] I. Gunther Leopold, N. Kivel, J. Kobler, B. Wernli, Anal. Bioanal. Chem. (2008) 503.
- [11] H. Isnard, M. Aubert, P. Blanchet, R. Brennetot, F. Chartier, V. Geertsens, F. Manuguerra, Spectrochim. Acta 61B (2006) 150.

- [12] J.S. Becker, W. Kerl, H.J. Dietze, *Anal. Chim. Acta* 387 (1999) 145.
- [13] D. Solatie, P. Carbol, M. Betti, F. Bocci, T. Hiernaut, V.V. Rondinella, J. Cobos, *Fresenius J. Anal. Chem.* 368 (2000) 88.
- [14] C.S. Kim, C.K. Kim, P. Martin, U. Sansone, *J. Anal. Atom. Spectrom.* 22 (2007) 827.
- [15] J.I. Garcia Alonso, F. Sena, P. Arbore, M. Betti, L. Koch, *J. Anal. Atom. Spectrom.* 10 (1995) 381.
- [16] J. Comte, P. Bienvenu, E. Brochard, J.M. Fernandez, G. Andreoletti, *J. Anal. Atom. Spectrom.* 18 (2003) 702.
- [17] J.I. Garcia Alonso, J.F. Babelot, J.P. Glatz, O. Cromboom, L. Koch, *Radiochim. Acta* 62 (1993) 71.
- [18] J.S. Becker, R.S. Soman, K.L. Sutton, J.A. Caruso, H.J. Dietze, *J. Anal. Atom. Spectrom.* 14 (1999) 933.
- [19] S.F. Boulyga, C. Testa, D. Desideri, J.S. Becker, *J. Anal. Atom. Spectrom.* 10 (1995) 381.
- [20] N. Baglan, C. Bouvier Capely, C. Cossonnet, *Radiochim. Acta* 90 (2002) 267.
- [21] P. Roos, H. Xiaolin, *Anal. Chim. Acta* 608 (2008) 105.
- [22] M. Marhol, *Ion Exchangers in Analytical Chemistry. Their Properties and Use in Inorganic Chemistry*, vol. XIV, Elsevier Scientific Publishing Company, 1982, 585 p.
- [23] G. Favre, R. Brennetot, F. Chartier, P. Vitorge, *Int. J. Mass Spectrom.* 265 (2007) 15.
- [24] K.G. Heumann, *Int. J. Mass Spectrom.* 118/119 (1995) 575.
- [25] J. Kragten, *Analyst* 119 (1994) 2161.
- [26] EURACHEM Secretariat, *EURACHEM/CITAC Guide Quantifying Uncertainty in Analytical Measurement*, second ed., EURACHEM Secretariat, BAM, Berlin, 2000.



# Quantitative analysis of volatile selenium metabolites in normal urine by headspace solid phase microextraction gas chromatography–inductively coupled plasma mass spectrometry

Maité Bueno, Florence Pannier\*

Laboratoire de Chimie Analytique Bio Inorganique et Environnement, IPREM, Université de Pau et des Pays de l'Adour, UMR CNRS 5254, Hélioparc, Avenue du Président Angot, 64000 Pau., France

## ARTICLE INFO

### Article history:

Received 17 June 2008

Received in revised form 12 December 2008

Accepted 17 December 2008

Available online 30 December 2008

### Keywords:

Selenium

Urine

Volatile metabolites

SPME

Headspace

GC–ICPMS

## ABSTRACT

The combination of headspace–solid phase microextraction (HS–SPME) and gas chromatography–inductively coupled plasma mass spectrometry (GC–ICPMS) was evaluated for the determination of volatile selenium metabolites in normal urine samples, *i.e.* without selenium supplementation. HS–SPME operating conditions were optimised and a sampling time of 10 min was found to be suitable for simultaneous extraction of dimethylselenide (DMSe) and dimethyldiselenide (DMDS<sub>2</sub>). The amount of DMSe and DMDS<sub>2</sub> extracted onto fibre coating was calculated in clean matrix, *i.e.* Milli-Q water, on the basis of depletion experiments. When applied to normal urine samples, the developed method allowed the detection of four volatile selenium containing species, among which DMSe and DMDS<sub>2</sub> could be quantified by standard additions.

© 2008 Elsevier B.V. All rights reserved.

## 1. Introduction

Selenium is an essential micronutrient for humans and animals that is found ubiquitously in the environment, being released from both natural and anthropogenic sources. Depending on its form and level of intake, selenium can have nutritional or negative health effects. The current recommended dietary allowance for selenium, established by the Food and Nutrition Board of the US National Research Council (National Academy of Sciences), is 55 µg/day for male and female adults (approximately 0.8 µg/kg/day) [1].

People are exposed to low levels of selenium daily through food, and in lesser importance through water and air. Selenium is primarily eliminated in the urine and feces in both humans and laboratory animals. Urinary Se has been shown to be a good indicator of total Se absorbed from all sources [2]. Mean urinary selenium concentrations vary between 22 and 58 µg(Se)l<sup>-1</sup> [1]. A recent review critically detailed all Se-species detected and identified in urine so far [3]. Study of selenium metabolism has been usually assessed based on the analysis of dissolved urinary metabolites. Methylation is an important pathway of selenium metabolism, and volatile dimethylselenide has been identified as major metabolite excreted

in human breath [4–6]. Relatively little attention was paid to volatile selenium species excreted in the urine. First indication of volatile selenium constituents in urine was reported in 1970 by Palmer et al. [7] that mentioned losses of spiked radiolabeled selenium after administration to rats. Kresimon et al. [8] detected volatile selenium species in human urine after derivatisation with sodium borohydride, such pretreatment does not warrant identification of species originally present in the urine. Recent studies on selenium urinary metabolites have shown the presence of volatile Se species either in long term stability studies of selenosugar (methyl 2-acetamido-2-deoxy-1-seleno-β-D-galactopyranoside) spiked urine sample [9], or in reconstituted urine CRM (NIES CRM 18) [10]. Unfortunately volatile selenium species quantification was not reported in these studies.

First systematic study of volatile substances of urine was reported in 1914 by Dehn and Hartman [11], four major fractions were separated as (1) acids (principally benzoic acid, hydrogen sulfide, fatty acids), (2) bases, (3) phenols (principally phenol and p-cresol) and (4) neutral substances appearing as the greatest contributors to the odor of urine. More recent investigations of urine profiling for volatile compounds have been undertaken with the object of linking profiles to metabolic disorders [12–15]. Selected volatile components have also been analysed to assess individual exposure to environmental pollutants, *i.e.* volatile chlorinated hydrocarbons [16], volatile halogenated species [17,18] or

\* Corresponding author.

E-mail address: [Florence.pannier@univ-pau.fr](mailto:Florence.pannier@univ-pau.fr) (F. Pannier).

**Table 1**  
GC–ICPMS operating parameters.

GC	
Injection port temperature	270 °C <sup>a</sup>
Carrier gas flow rate	2 ml min <sup>-1</sup> He
Oven programme	40 °C (3 min)/30 °C min <sup>-1</sup> /220 °C (2 min)
Transfer line temperature	250 °C
ICP MS	
Sampling and skimmer cones	Platinum
Forward power	1070 W
Sampling depth	8 mm
Plasma gas flow rate	15 l min <sup>-1</sup>
Auxiliary gas flow rate	0.9 l min <sup>-1</sup>
Carrier gas flow rate	0.52 l min <sup>-1</sup>
Optional gas (O <sub>2</sub> ) flow rate	5% relative to carrier gas
QP Bias	–16.5 V
Octopole Bias	–18 V
Isotopes monitored (dwell time)	76, 78, 82 (80 ms/point) <sup>b</sup> 34, 81, 124 (10 ms/point)

<sup>a</sup> Injection port temperature for SPME desorption, set at 220 °C for liquid injections.

<sup>b</sup> As no interferences were observed between *m/z* 76, 78, 82, the results are reported only for *m/z* 78.

BTX solvents [19]. The sampling techniques used in these studies include urine sparge with an inert gas followed by concentration of volatile compounds on a cryogenic trap or on porous polymer (usually Tenax) [13,14,17] or headspace solid phase microextraction [15,16,19].

This work focuses on quantitative determination of volatile selenium components in normal urine samples, *i.e.* without selenium supplementation. Optimisation of headspace solid phase microextraction (HS–SPME) conditions followed by gas chromatography–inductively coupled plasma mass spectrometry (GC–ICPMS) is described for dimethylselenide (DMSe) and dimethyldiselenide (DMDSe) quantification. Applications of the developed method to human urine samples are presented.

## 2. Experimental

### 2.1. Reagents and samples

DMSe (>99%, Strem, Bischheim, Strasbourg, France) and DMDSe (98%, Aldrich, St. Quentin Fallavier, France) were used without further purification. Individual stock standard solutions containing ≈5000 μg (Se) g<sup>-1</sup> in methanol (Normapur, >99%, Prolabo) were stored in the dark at –4 °C. Working standard solutions were prepared by successive dilutions in dichloromethane (99.9%, Aldrich, St. Quentin Fallavier, France) for direct injection calibration, or in Milli-Q water (Millipore, 18.2 MΩ cm) for SPME sampling. All standards solutions were prepared in 10 ml headspace vials sealed with polytetrafluoroethylene (PTFE)-coated silicone rubber septa (20 mm diameter) (Supelco, St. Quentin Fallavier, France).

After collection, the morning urine samples of two volunteers were immediately transferred to 38 ml headspace vials sealed with PTFE–silicone rubber septa. Samples, hereafter called F and M, were allowed to cool at room temperature before storage at 4 °C in the dark for 21 days stability study.

### 2.2. Instrumentation for ICP–MS and GC systems

The ICPMS instrument was the 7500ce from Agilent technologies (Tokyo, Japan), equipped with on-line octopole collision/reaction cell. H<sub>2</sub> of 99.995% purity (Air Liquide, Paris, France) was used as the cell gas in the octopole cell (1.5 ml min<sup>-1</sup>). Operating conditions, listed in Table 1, were optimised daily using 50 ppm Xe in Ar.

An Agilent 6890 gas chromatograph with He carrier gas (99.995% purity, Air Liquide, Paris, France) was used. Separation was obtained with SPB1–sulfur column (30 m, 0.32 mm id, 4 μm film thickness) (Supelco, St. Quentin Fallavier, France) previously used for analogous sulfur species [20]. A detailed description of GC parameters is provided in Table 1. Coupling of GC with ICPMS was accomplished through the use of Agilent GC–ICPMS interface.

### 2.3. SPME procedure

SPME was carried out manually with the appropriate SPME holder and a 75 μm carboxen–polydimethylsiloxane (CAR–PDMS) fibre (Supelco, St. Quentin Fallavier, France). Such coating is recommended for volatile analytes and has been previously shown to be well adapted for volatile selenium species [21]. CAR–PDMS was pre-conditioned by inserting it into the GC injector according to the manufacturer's instructions, *i.e.* 2 h at 300 °C.

Solid phase microextraction was performed in headspace mode, in 38 ml headspace vials with 20 ml sample volume at ambient temperature, *i.e.* 22 ± 2 °C. The effect of sampling time was investigated with Milli-Q water spiked at ≈100 ng (Se) l<sup>-1</sup>, in the range 5 min–40 min. Samples were shaken with an orbital shaker with the agitation speed adjusted to 350 rev min<sup>-1</sup>. Once the sampling was completed, the analytes were desorbed in the GC injection port using a 0.75 mm i.d. inlet liner (Supelco, St. Quentin Fallavier, France). The fibre was held in the inlet liner for the entire chromatographic run (including first 3 min in splitless mode) to assure complete analyte desorption and avoid any memory effects. Each exposure time was sampled twice.

## 3. Theoretical considerations

In HS–SPME sampling, the amount of analyte sorbed by the porous fibre coating, *n<sub>f</sub>*, can be expressed as [22]:

$$n_f = \frac{K_H K_h V_f V_s C_0 (C_{f_{\max}} - C_f^\infty)}{K_H K_h V_f (C_{f_{\max}} - C_f^\infty) + K_H V_h + V_s} \quad (1)$$

where *V<sub>f</sub>* is the fibre coating phase volume, *V<sub>s</sub>* is the aqueous phase volume, *V<sub>h</sub>* is the headspace phase volume, *C<sub>0</sub>* is the initial concentration of the analyte in the aqueous phase, *K<sub>H</sub>* is the Henry's constant of analyte between the headspace and aqueous phases, *K<sub>h</sub>* is the equilibrium constant for adsorption of the analyte from the headspace phase to the fibre coating in experimental conditions, *C<sub>f<sub>max</sub></sub>* is the maximum concentration of active sites on the coating, *C<sub>f</sub><sup>∞</sup>* is the equilibrium concentration of the analyte on the fibre.

Assuming that *C<sub>f</sub><sup>∞</sup>* is much lower than *C<sub>f<sub>max</sub></sub>*, *i.e.* in the case of diluted samples, it comes from Eq. (1):

$$n_f = \frac{K' V_f V_s C_0 C_{f_{\max}}}{K' V_f C_{f_{\max}} + K_H V_h + V_s} \quad (2)$$

with *K'* the product of *K<sub>H</sub>* and *K<sub>h</sub>*.

Eq. (2) is then very similar to the developed theory with liquid polymeric phases where the amount of analyte extracted by the fibre is directly proportional to the initial concentration of analyte in the solution [23].

Eq. (2) can be rewritten as:

$$n_f = \alpha n_0 \quad (3)$$

where *n<sub>0</sub>* is the initial amount of analyte in the aqueous phase, and *α* is the "sorption" coefficient in experimental conditions,

$$i.e. \quad \alpha = \frac{K' V_f C_{f_{\max}}}{K' V_f C_{f_{\max}} + K_H V_h + V_s}$$

If successive extractions are performed from the same sample and with the same fibre, the variation of the sample amount in the

**Table 2**  
Slopes and regression coefficients obtained for direct injection calibration.

	From peak area signal		From peak height signal	
	Slope (area unit/pg)	R <sup>2</sup>	Slope (counts/pg)	R <sup>2</sup>
DMSe	169.23	0.9994	108.46	0.9997
DMDSe	111.66	0.9994	70.46	0.9995

aqueous phase, corresponding to extracted amount, is proportional to the amount left by the previous extraction [24]:

$$n_{x-1} - n_x = n_{f,x} = \alpha n_{x-1} \quad (4)$$

where  $n_{x-1}$  and  $n_x$  are analyte amounts in the aqueous phase respectively before and after extraction number  $x$ ,  $n_{f,x}$  is extracted amount during extraction number  $x$ .

Eq. (4) can be rewritten as:

$$n_x = n_{x-1}(1 - \alpha) \quad (5)$$

Eq. (5) gives by extension:

$$n_x = n_0(1 - \alpha)^x \quad (6)$$

Moreover  $n_{f,x}$  and  $n_{x-1}$  can be correlated from observed detector signal,  $\sigma_x$ :

$$\sigma_x = sn_{f,x} = s\alpha n_{x-1} \quad (7)$$

where  $s$  is the detector response coefficient, *i.e.* the slope of calibration curve.

Combining Eqs. (6) and (7) gives:

$$\frac{\sigma_{x+1}}{\sigma_1} = \frac{n_x}{n_0} = (1 - \alpha)^x \quad (8)$$

The sorption coefficient  $\alpha$  can thus be obtained from the plotting of observed ratios  $\sigma_{x+1}/\sigma_1$  as a function of  $x$ , the extraction number. Resulting values can thus be compared with  $\alpha$  value obtained from Eq. (7) generally used to determine sorption coefficients.

## 4. Results and discussion

### 4.1. Direct injection calibration

For direct injection calibration, standard mixture solutions containing DMSe and DMDSe at concentrations of 2 ng, 4 ng, 8 ng, 13 ng and 40 ng(Se)g<sup>-1</sup> were prepared by mixing individual stock solutions and diluting them in CH<sub>2</sub>Cl<sub>2</sub>. Injections (1  $\mu$ l) were made in triplicate. Results of calibration curves, *i.e.* signal =  $f$ (amount of analyte injected), are listed in Table 2. The detection limits were evaluated according to the IUPAC specifications [25] as:

$$DL = \frac{3SD}{s} \quad (9)$$

where SD is the height standard deviation calculated from ten blank injections, *i.e.* CH<sub>2</sub>Cl<sub>2</sub>,  $s$  is the calibration curve slope, *i.e.* count/pg(Se).

Calculated absolute detection limits are respectively 0.13 pg and 0.26 pg(Se) respectively for DMSe and DMDSe.

### 4.2. Extraction time profiles

Extraction time profiles were obtained by plotting the observed signals (area counts) as a function of fibre exposure duration. Results are presented as the mean obtained from two samplings for each exposure time. Relative standard deviation varied from 1% to 14.3% depending on species and sampling time. Error bars included in Fig. 1 represent the mean relative standard deviation obtained considering all sampling time range for each species, *i.e.*

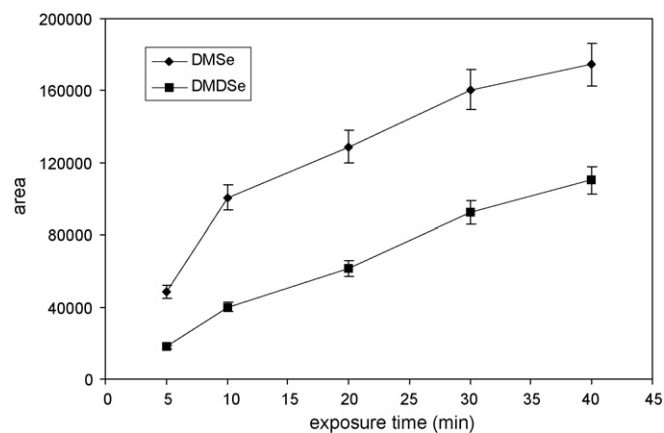


**Fig. 1.** HS-SPME time profiles for simultaneous extraction of DMSe (75 ng(Se)l<sup>-1</sup>) and DMDSe (113 ng(Se)l<sup>-1</sup>).

7.5% for DMSe and 6.7% for DMDSe. Corresponding curves are shown in Fig. 1.

Extraction time profiles show that equilibrium is not reached even after 40 min of sampling, and that DMSe is better extracted than DMDSe. As a compromise between sensitivity and extraction time adapted to GC analysis (11 min), an exposure time of 20 min was first chosen. However when applied to urine samples, it appeared that an exposure time of 20 min did not give higher signals than those of 10 min sampling (data not shown). Exposure time was then fixed at 10 min for subsequent experiments.

### 4.3. Depletion experiments

In order to approach the amount of analyte sorbed on fibre coating during HS-SPME, a depletion experiment was realised by running successive extractions from the same sample. Up to 16 HS-SPME runs were performed from the same 20 ml Milli-Q water spiked at  $\approx 50$  ng(Se)l<sup>-1</sup> of each species. For each analyte, the ratio  $\sigma_{x+1}/\sigma_1$  was plotted as a function of extraction number  $x$  (Fig. 2). Results of corresponding exponential regression curves fitting and outgoing  $\alpha$  sorption coefficients are given in Table 3. Ratios  $\sigma_1/sn_0$  calculated from the first extraction signals are also listed for comparison. It appears that extracted amounts are overestimated if calculated from calibration curve slopes and that sorption coefficients calculated from depletion curves fitting give a better estimation of analytes extracted amounts with defined experimental conditions.

A similar depletion experiment was performed with one of the urine samples. 13 successive HS-SPME runs were realised and observed ratio  $\sigma_{x+1}/\sigma_1$  was plotted as a function of extraction number  $x$ . Results are reported only for DMSe as DMDSe peak was too small when detected. Corresponding experimental curve is shown in Fig. 3 and compared with predicted regression curve calculated from  $\alpha$  coefficient determined previously, *i.e.* from HS-SPME of spiked Milli-Q water. It appears clearly that calculated regression curve does not provide a correct representation of analyte extracted amounts in real samples. In fact, in urine samples, calculated relative standard deviation from the first five HS-SPME runs is 5.2% for DMSe. It was thus assumed for subsequent experiments that two

**Table 3**  
Depletion curves fitting. Comparison between  $\alpha$  coefficients and estimation of extracted amounts from calibration curve slopes.

	$(1 - \alpha)^x$	R <sup>2</sup>	$\alpha$	$\sigma_1/sn_0$
DMSe	$e^{-0.1639x}$	0.9632	0.15	0.24
DMDSe	$e^{-0.1747x}$	0.9811	0.16	0.25

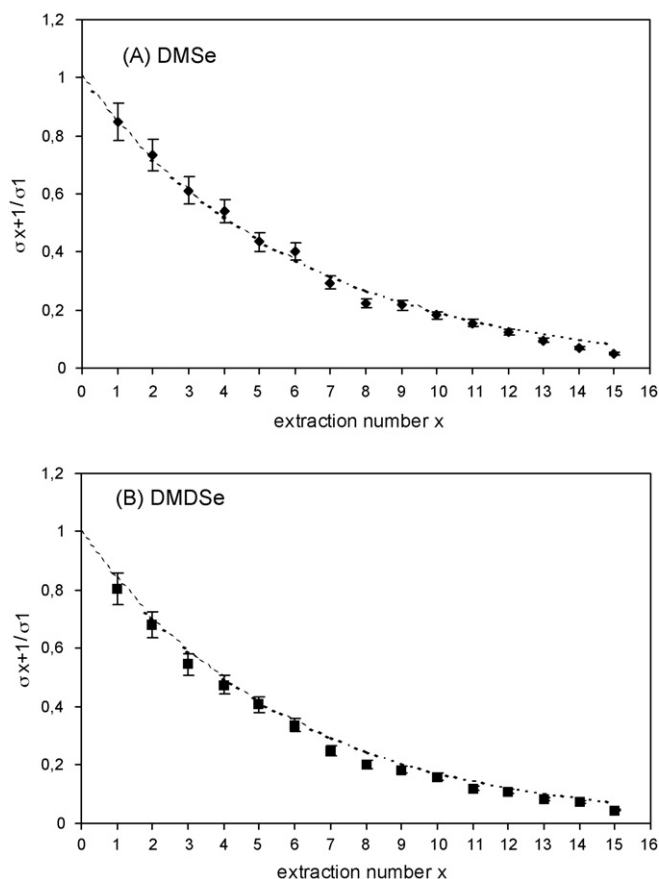


Fig. 2. Depletion curves from successive extractions of the same sample (MilliQ water), (A) DMSe  $35 \text{ ng (Se) l}^{-1}$ , and (B) DMDSe  $50 \text{ ng (Se) l}^{-1}$ .

successive HS-SPME runs can be performed from the same sample without significant evolution of analyte concentration in the sample.

#### 4.4. Quantification of volatile selenium in unspiked urine samples

Example chromatograms obtained after HS-SPME of the two urine samples are shown in Fig. 4. Profiles obtained monitoring  $m/z$  78 are quite similar for both samples, i.e. DMSe is always detected, small DMDSe peak, and up to two significant selenium-containing

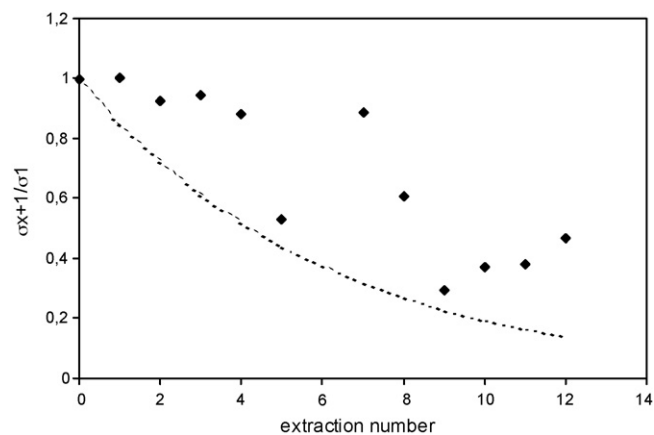


Fig. 3. Depletion curves from successive extractions of the same urine sample for DMSe. Comparison with predicted regression curve from calculated  $\alpha$  sorption coefficient (dotted line).

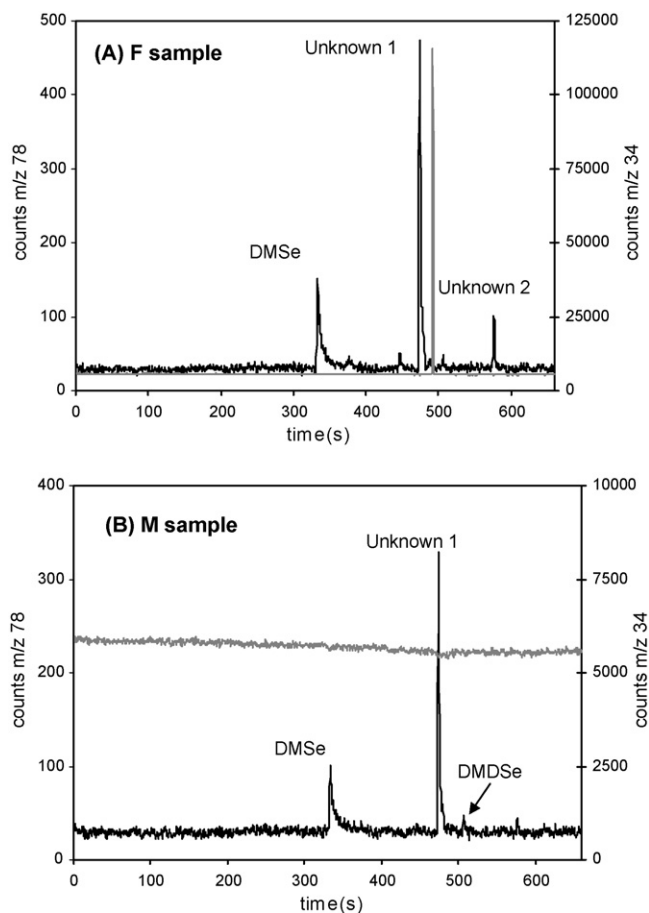


Fig. 4. Example GC-ICPMS chromatograms obtained from 10 min HS-SPME of (A) F and (B) M urine samples.

peaks were present (retention times  $t_R = 7.9$  and  $9.6$  min). For F sample an important sulfur-containing peak ( $t_R = 8.2$  min) was also detected on  $m/z$  34. Neither of the unknown selenium-containing peaks correspond to unknown sulfur-containing peak based on  $m/z$  34 monitoring.

DMSe quantification was obtained by standard additions, results are reported in Table 4 for the day of sampling ( $t = 0$ ) and after 21 days storage at  $4^\circ\text{C}$ . The two samples differ in their DMSe content, and for each sample, measured concentrations are quite constant from 0 to 21 days storage indicating that DMSe was not formed during storage. These values are in complete agreement with those previously measured in our lab with other selenium-specific detector in mixed urines sample from 11 volunteers [21].

Standard additions method was also attempted to quantify DMDSe. In sample F we observed that DMDSe peak was only slightly increased after standard addition in comparison with sample M for which the slope of standard addition curve was in the range of that previously calculated for DMSe (at  $t = 21$  days, slope =  $655.3 \text{ area unit/ng (Se) l}^{-1}$ ,  $R^2 = 0.994$ ). Corresponding DMDSe concentrations were then calculated to be  $0.6 \pm 0.1 \text{ ng (Se) l}^{-1}$  in sample M and  $0.8 \pm 0.1 \text{ ng (Se) l}^{-1}$  in sample F, i.e. no different DMDSe content between samples.

To explain the particular behaviour of DMDSe standard additions in sample F, the evolution of unknown selenium-containing peaks signals was carefully examined. We found that the signal of 7.9 min peak was stable considering 7 HS-SPME successive runs including 4 unspiked and 3 spiked urine samplings (RSD 8.9%). For the last HS-SPME sampling performed in DMDSe ( $60 \text{ ng (Se) l}^{-1}$ ) spiked urine three hours after previous standard addition, the sig-

**Table 4**  
DMSe quantification in urine samples.

	$t = 0$			$t = 21$ days		
	Slope <sup>a</sup>	$R^2$	[DMSe] <sup>b</sup> (ng(Se)l <sup>-1</sup> )	Slope <sup>a</sup>	$R^2$	[DMSe] <sup>b</sup> (ng(Se)l <sup>-1</sup> )
F sample	599.6	0.995	10.3 ± 1.5	1014.6	0.999	7 ± 1
M sample	584.2	0.965	4.5 ± 1.5	980.9	0.996	3.3 ± 0.5

<sup>a</sup> Slope in area unit/ng(Se)l<sup>-1</sup>

<sup>b</sup> Uncertainty represents the standard deviation of three replicates.

nal of 7.9 min peak was doubled in comparison with mean initial signal obtained from first 7 HS–SPME runs. Selenium-containing peak with  $t_R = 7.9$  min is thus likely formed in sample F from added DMDSe and urine component. On the basis of isotopes monitored in this work, samples F and M differ by their sulfur content. Our assumption is that sulfur-containing compound detected in sample F may react with DMDSe to form dimethyl selenyl sulfide (DMSeS) detected at  $t_R = 7.9$  min. Indeed mechanisms proposed in the literature for DMSeS formation involve reaction between DMDSe and either dimethyldisulfide or dimethyltrisulfide [26,27], compounds which have been already detected in urine [13–15]. Moreover from linearisation of retention times as a function of boiling points of known analytes, an estimation of 7.9 min peak boiling point is 136 °C which is in complete agreement with literature data for DMSeS boiling point (132 °C in [28], 135 ± 5 °C in [26]).

## 5. Conclusion

The presence of volatile selenium species at their natural occurrence level is reported for the first time in urine samples. Using HS–SPME in conjunction with GC/ICP-MS, four selenium-containing species were detected in the headspace of unspiked urines. DMSe, the most abundant of the selenium-containing species, and DMDSe were quantified by standard additions method. While DMSe was quantified with similar response slopes between the two studied samples, DMDSe quantification was more problematic as standard additions response was only obtained in urine with no significant sulfur content. For quantification purpose it appears necessary to check the presence of sulfur compounds such as DMDS or DMTS to not overestimate DMDSe content.

Concerning the two unknown selenium-containing peaks, one is probably dimethyl selenyl sulfide, based on literature and first experimental data. Further work is now needed to confirm the identity of DMSeS and of the late-eluting peak.

## References

- [1] Agency for Toxic Substances and Disease Registry (ATSDR), Toxicological Profile for Selenium, ATSDR, Atlanta, Georgia, 1998.
- [2] Y. Shiobara, T. Yoshida, K.T. Suzuki, Toxicol. Appl. Pharmacol. 152 (1998) 309.
- [3] K.A. Francesconi, F. Pannier, Clin. Chem. 50 (2004) 2240.
- [4] H.E. Ganther, J.R. Lawrence, Tetrahedron 53 (1997) 12299.
- [5] D. Kremer, G. Ilgen, J. Feldmann, Anal. Bional. Chem. 383 (2005) 509.
- [6] Y. Ohta, K.T. Suzuki, Toxicol. Appl. Pharmacol. 226 (2008) 169.
- [7] I.S. Palmer, R.P. Gunsalus, A.W. Halverson, O.E. Olson, Biochim. Biophys. Acta 208 (1970) 260.
- [8] J. Kresimon, U.M. Gruter, A.V. Hirner, Fresenius J. Anal. Chem. 371 (2001) 586.
- [9] D. Juresa, J. Darrouzès, N. Kienzl, M. Bueno, F. Pannier, M. Potin-Gautier, K.A. Francesconi, D. Kuehnelt, J. Anal. At. Spectrom. 21 (2006) 684.
- [10] D. Juresa, D. Kuehnelt, K.A. Francesconi, Anal. Chem. 78 (2006) 8569.
- [11] W. Dehn, F.A. Hartman, J. Am. Chem. Soc. 36 (1914) 2118.
- [12] A. Zlatkis, H.M. Liebich, Clin. Chem. 17 (1971) 592.
- [13] A. Zlatkis, W. Bertsch, H.A. Lichtenstein, A. Tishbee, F. Shunbo, H.M. Liebich, A.M. Coscia, N. Fleischer, Anal. Chem. 45 (1973) 763.
- [14] H.G. Wahl, A. Hoffmann, D. Luft, H.M. Liebich, J. Chromatogr. A 847 (1999) 117.
- [15] G.A. Mills, V. Walker, J. Chromatogr. B 753 (2001) 259.
- [16] D. Poli, P. Manini, R. Andreoli, I. Franchini, A. Mutti, J. Chromatogr. B 820 (2005) 95.
- [17] L.C. Michael, M.D. Erickson, S.P. Parks, E.D. Pellizzari, Anal. Chem. 52 (1980) 1836.
- [18] Z. Polkowska, K. Kosłowska, Z. Mazerska, T. Górecki, J. Namieśnik, Chemosphere 62 (2006) 626.
- [19] T. Kråmer Alkalde, M. do Carmo Ruaro Peralba, C. Alcaraz Zini, E. Bastos Caramão, J. Chromatogr. A 1027 (2004) 37.
- [20] F. Lestremay, V. Desauziers, J.C. Roux, J.L. Fanlo, J. Chromatogr. A 999 (2003) 71.
- [21] M. Bueno, F. Pannier, 7th International Conference on Environmental and Biological Aspects of Main-Group Organometallics, Heraklion, Crete, Greece, 2006.
- [22] T. Gorecki, in: J. Pawliszyn (Ed.), Applications of Solid Phase MicroExtraction, Royal Society of Chemistry, Hertfordshire, 1999, pp. 92–108.
- [23] J. Pawliszyn, J. Chromatogr. Sci. 38 (2000) 270.
- [24] L. Urruty, M. Montury, J. Chromatogr. Sci. 37 (1999) 277.
- [25] G.L. Long, J.D. Winefordner, Anal. Chem. 55 (1983) 712A.
- [26] J. Meija, J.M. Bryson, A.P. Vonderheide, M. Montes-Bayón, J.A. Caruso, J. Agric. Food Chem. 51 (2003) 5116.
- [27] J.W. Swearingen, D.P. Frankel, D.E. Fuentes, C.P. Saavedra, C.C. Vásquez, T.G. Chasteen, Anal. Biochem. 348 (2006) 115.
- [28] T.G. Chasteen, in: W.T. Frankenberger Jr., R.A. Engberg (Eds.), Environmental Chemistry of Selenium, Marcel Dekker, New York, 1998, pp. 589–612.



# Molecularly imprinted polymers: An analytical tool for the determination of benzimidazole compounds in water samples

Carmen Cacho<sup>a</sup>, Esther Turiel<sup>b</sup>, Concepción Pérez-Conde<sup>a,\*</sup>

<sup>a</sup> Departamento de Química Analítica, Facultad de Ciencias Químicas, Universidad Complutense de Madrid, Ciudad Universitaria s/n, 28040 Madrid, Spain

<sup>b</sup> Departamento de Medio Ambiente. INIA. Carretera de A Coruña Km. 7.5. 28040 Madrid, Spain

## ARTICLE INFO

### Article history:

Received 3 October 2008

Received in revised form

23 December 2008

Accepted 9 January 2009

Available online 20 January 2009

### Keywords:

Molecularly imprinted polymers

Benzimidazole compounds

Water samples

Multiresidual determination

Solid phase extraction

## ABSTRACT

Molecularly imprinted polymers (MIPs) for benzimidazole compounds have been synthesized by precipitation polymerization using thiabendazole (TBZ) as template, methacrylic acid as functional monomer, ethyleneglycol dimethacrylate (EDMA) and divinylbenzene (DVB) as cross-linkers and a mixture of acetonitrile and toluene as porogen. The experiments carried out by molecularly imprinted solid phase extraction (MISPE) in cartridges demonstrated the imprint effect in both imprinted polymers. MIP-DVB enabled a much higher breakthrough volume than MIP-EDMA, and thus was selected for further experiments. The ability of this MIP for the selective recognition of other benzimidazole compounds (albandazole, benomyl, carbendazim, fenbendazole, flubendazole and fuberidazole) was evaluated. The obtained results revealed the high selectivity of the imprinted polymer towards all the selected benzimidazole compounds.

An off-line analytical methodology based on a MISPE procedure has been developed for the determination of benzimidazole compounds in tap, river and well water samples at concentration levels below the legislated maximum concentration levels (MCLs) with quantitative recoveries. Additionally, an on-line preconcentration procedure based on the use of a molecularly imprinted polymer as selective stationary phase in HPLC is proposed as a fast screening method for the evaluation of the presence of benzimidazole compounds in water samples.

© 2009 Elsevier B.V. All rights reserved.

## 1. Introduction

Benzimidazole compounds (Fig. 1) have been widely used both as anthelmintic drugs in the treatment of parasitic infections and as fungicide agents to prevent spoilage of crops during their transport and storage. Their massive use in the last years has led into their accumulation in the environment, thus contaminating the water streams. European Water Framework Directive [1] has established a maximum concentration level (MCL) of  $0.1 \mu\text{g L}^{-1}$  for most benzimidazole compounds present in natural waters, and a total concentration of all pesticides of  $0.5 \mu\text{g L}^{-1}$ .

The development of highly sensitive methods for the multiresidue determination of benzimidazole compounds in water samples is thus highly desirable, and for that purpose a preconcentration step of the water samples is usually required. In recent years, solid phase extraction has widely been applied for the analysis of different pesticides in water samples, owing to the high enrichment factors achievable by this methodology. Thus, different sorbents ( $\text{C}_{18}$  [2–4], PS-DVB [5] or micelles adsorbed in alumina

[6,7]) have been used for benzimidazole preconcentration in water samples. However, the selection of an adequate sample treatment protocol allowing to carry out a multiresidue determination of benzimidazole compounds is currently a challenge, due to their quite different chemical properties. In this sense, extensive sample clean-up or preconcentration procedures can rarely be applied to the determination of a wide variety of benzimidazole compounds, and the use of highly selective detection methods (i.e. tandem mass spectrometry) is usually required for multiresidue analysis [8].

As an alternative, molecularly imprinted polymers have proven to be a very valuable technique for selective solid-phase extraction of the template molecule and structurally related compounds. The inherent selectivity of the molecular recognition of these materials allows a high degree of sample clean-up to be achieved [9,10]. Additionally, molecularly imprinted polymers have also been used for sample enrichment for the determination of a wide range of analytes, such as 2,4,5-trichlorophenoxyacetic acid [11], 4-nitrophenol [12,13], bentazon [14], bisphenol A [15], chloroguaiacol [16], diethylstilbestrol [17] or pirimicarb [18]. Application of molecularly imprinted polymers for the determination of benzimidazole compounds is however rather scarce. In this sense, they have been recently applied for the analysis of benzimidazole compounds in beef liver [19]. In our previous work, we investigated the

\* Corresponding author. Fax: +34 913944329.

E-mail address: [cpconde@quim.ucm.es](mailto:cpconde@quim.ucm.es) (C. Pérez-Conde).



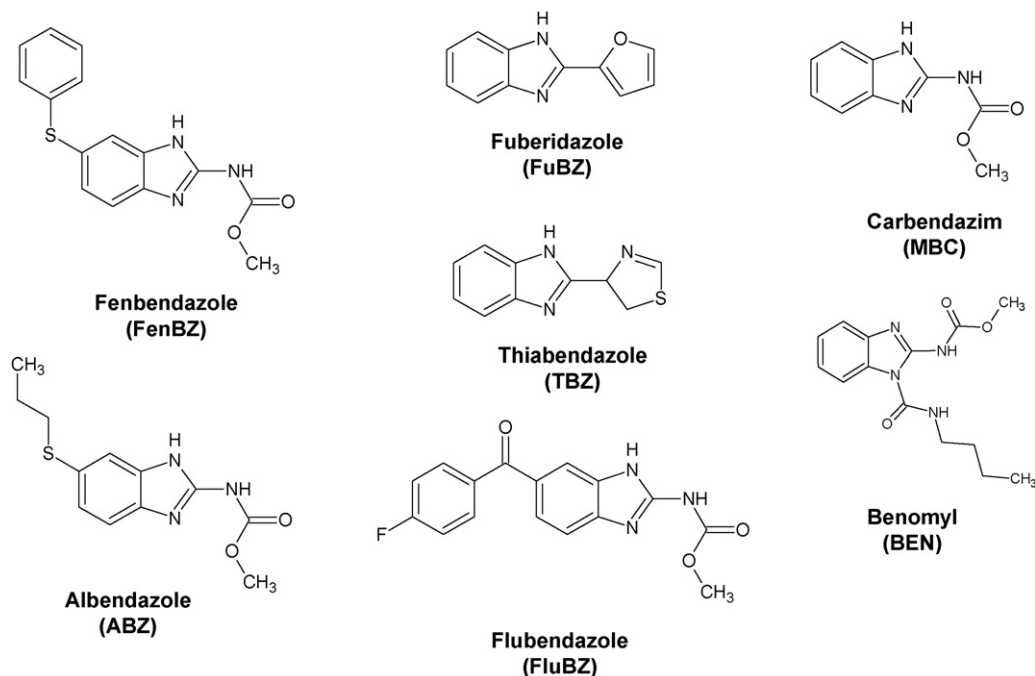


Fig. 1. Chemical structure of the evaluated benzimidazole compounds.

ability of molecularly imprinted polymers to act as selective stationary phases for the determination of benzimidazole compounds in fruits both by HPLC [20] and capillary electrochromatography [21]. Working in an organic media, the imprinted polymers did not only selectively rebind the template molecule, but other benzimidazole compounds as well, thus making them interesting materials for multiresidue determination of benzimidazoles.

Taking all these comments in mind, the main aim of the present work was the synthesis of different MIPs able of selectively rebinding benzimidazole compounds in an aqueous solution. The developed MIPs will then be used for the selective enrichment of tap, river and well water samples, thus enabling the multiresidual determination of a wide variety of benzimidazole compounds at concentration levels below the legislated MCLs.

## 2. Experimental

### 2.1. Reagents

Analytical grade benzimidazole fungicides (albendazole (ABZ), benomyl (BEN), carbendazim (MBC), fenbendazole (FenBZ), flubendazole (FluBZ), fuberidazole (FuBZ) and thiabendazole (TBZ)) were purchased from Sigma–Aldrich. The corresponding stock standard solutions ( $0.5 \text{ g L}^{-1}$ ) were prepared in acetonitrile and stored at  $-18^\circ\text{C}$ . Purum methacrylic acid (MAA, 98%), ethyleneglycol dimethacrylate (EDMA, 98%) and 2,2'-azo-bis-isobutyronitrile (AIBN,  $\geq 98\%$ ) were purchased from Sigma–Aldrich. Technical grade divinylbenzene (DVB, 80%) was purchased from Sigma–Aldrich and purified by filtration through alumina. AIBN was recrystallized in methanol prior to use. All other reagents were used as supplied without a further purification step. HPLC grade solvents (toluene, acetonitrile, methanol, dimethylsulfoxide and acetic acid) were purchased from Scharlab.

### 2.2. Preparation of polymers

TBZ imprinted polymers were prepared by adapting a procedure previously developed by Turiel et al. [20]. In this sense, TBZ

(0.17 mmol), MAA (0.68 mmol), EDMA or DVB (3.40 mmol) and AIBN (0.25 mmol) were dissolved in a mixture of acetonitrile and toluene (12.5 mL, 75:25 v/v). The solutions were deoxygenated with oxygen-free argon for 10 min while cooling on an ice bath. Polymerization was carried out in a thermostated bath at  $60^\circ\text{C}$  for 24 h, and the flasks were slowly rotated (24 rpm) around their long axis. The polymer particles were separated from the reaction mixture by vacuum filtration on a nylon membrane filter and were washed with 200 mL of a methanol/acetic acid solution (50:50 v/v) to remove both the template molecule and residual monomers. Non-imprinted polymers were prepared in the same manner, but without the addition of the template molecule.

### 2.3. Chromatographic separation of benzimidazole fungicides

All measurements were performed in an HPLC system from Thermo Separation Products consisting of a ConstaMetric 4100 Series high pressure pump, a SpectroMonitor 5000 photo diode-array detector and a Rheodyne 7725i injection valve equipped with a  $100 \mu\text{L}$  loop. The analytes were separated on a  $\text{C}_{18}$ -Kromasil column ( $250 \text{ mm} \times 4.6 \text{ mm}$  i.d.,  $5 \mu\text{m}$ ) purchased from Scharlab. In order to separate all the benzimidazole compounds, an initial isocratic elution with a mixture containing 70% of a water/acetic acid solution (96:4, v/v) (mobile phase A) and 30% of acetonitrile (mobile phase B) was firstly applied for 7 min, after which, a gradient to 100% mobile phase B was performed for 5 min, keeping these conditions constant for another 6 min. Benzimidazole fungicides were monitored at 200 and 240 nm and quantified by external calibration using peak area measurements.

### 2.4. Off-line enrichment of benzimidazole compounds

#### 2.4.1. MISPE

1000 mg of MIP–DVB were placed in an empty solid-phase extraction cartridge from Scharlab and conditioned with 50 mL of acetonitrile and 50 mL of MilliQ water. A conditioning step consisting in 25 mL of acetonitrile and 25 mL of MilliQ water was applied between samples. Next, 500 mL of spiked river, tap and well water

samples were loaded onto the polymer, and washed with  $5 \times 1$  mL of an acetonitrile solution containing 2% of dimethylsulfoxide. Subsequently, the analytes were eluted with 12 mL of a methanol/acetic acid (50:50, v/v) mixture. The obtained extracts were evaporated to dryness and redissolved in 0.3 mL of acetonitrile for HPLC analysis.

#### 2.4.2. SPE ( $C_{18}$ )

Two  $C_{18}$  discs from Sigma–Aldrich were conditioned with 20 mL of methanol, 20 mL of methanol:water (50:50, v/v) and 20 mL of water. 500 mL of benzimidazole-spiked river, tap and well water samples were loaded on the discs. Benzimidazoles were subsequently eluted with 10 mL of methanol. The extracts were evaporated to dryness and redissolved in 0.3 mL of acetonitrile for HPLC analysis.

#### 2.5. On-line enrichment of benzimidazole compounds

Around 400 mg of MIP–DVB were packed into stainless steel HPLC column (50 mm  $\times$  4.6 mm i.d.). The column was then connected to an HPLC system from Thermo Separation Products.

50 mL of spiked river, tap and well water samples were loaded on the MIP-column at a flow rate of  $1 \text{ mL min}^{-1}$ . Subsequently, the mobile phase was switched to pure methanol. After 3 min, the mobile phase was switched to a methanol/acetic acid (80:20, v/v) mixture, which was pumped at a constant flow rate of  $1 \text{ mL min}^{-1}$  during 12 min. A conditioning step with 25 mL of MilliQ water was applied between run cycles. Benzimidazole fungicides were monitored at 200 and 240 nm and quantified by external calibration using peak area measurements.

### 3. Results and discussion

#### 3.1. Characterization of the imprinted polymers

Precipitation polymerization is a convenient method for the routine preparation of imprinted polymers, as spherical imprinted polymer beads can be obtained in a simple manner. A rational design and control of the polymerization conditions have proven essential for the preparation of imprinted polymer beads of the desired particle size. In this sense, an adequate match between the solubility parameters of the developing polymer network and the polarity of the porogenic solvent enables the preparation of polymer beads with permanent pore structures and high average particle sizes.

TBZ imprinted polymers were prepared under the optimized conditions described in Section 2.2. The obtained imprinted polymer particulates had been previously characterized by scanning electron microscopy [20]. Spherical polymer beads with a narrow size distribution were obtained, being the average particle diameter of  $3.5 \mu\text{m}$ .

#### 3.2. Optimization of the MISPE procedure

As has been previously stated in Section 1, the aim of this work was the development of MIP-based procedures for the multiresidue determination of benzimidazole fungicides in water samples, at concentration levels below the legislated maximum residue limits. In this sense, two different thiabendazole-imprinted polymers, synthesized using either EDMA or DVB as cross-linkers, have been evaluated for the selective recognition of benzimidazole compounds under aqueous media. In order to evaluate the presence of imprinted sites on the obtained MIPs, the performance of both imprinted polymers has been compared with that of their respective non-imprinted polymers.

Accordingly, different rebinding experiments onto SPE cartridges containing 200 mg of the different MIPs were carried out,

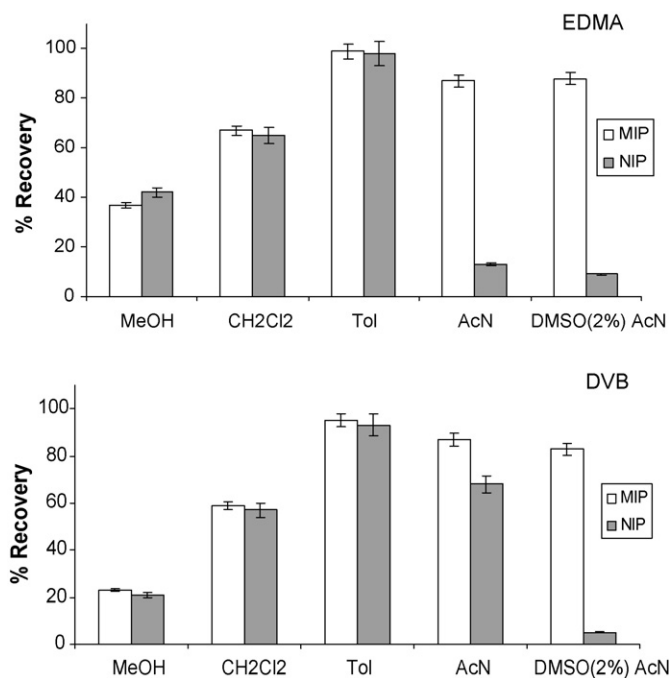


Fig. 2. Effect of the washing solvents on the recoveries obtained for EDMA and DVB polymers.  $n = 5$ .

working always in parallel with the corresponding NIPs. For this purpose, 2 mL of an aqueous solution containing  $1 \text{ mg L}^{-1}$  of thiabendazole were loaded onto the cartridges, and the effect of the addition of different organic solvents (i.e. acetonitrile, methanol, dichloromethane and toluene) has been evaluated as possible washing solutions for the removal of non-specifically bound benzimidazole compounds on both imprinted polymers.

Fig. 2 shows the recoveries obtained after washing both the imprinted and non-imprinted polymers cartridges with  $5 \times 1$  mL of the different washing solvents tested. As can be seen, a different performance of the imprinted and non-imprinted polymers was obtained when acetonitrile was used as washing solution for both imprinted polymers. In this sense, non-specifically bound compounds are completely removed from MIP–EDMA when the cartridges are washed with 5 mL of acetonitrile, while the addition of 2% dimethylsulfoxide is required to completely disrupt the non-specifically bonds between benzimidazole compounds and MIP–DVB, due to the much higher solubility of benzimidazole compounds in this solvent mixture. The differences observed for the performance of each imprinted polymer and their corresponding non-imprinted polymers under these conditions clearly demonstrate the imprint effect of both MIP–EDMA and MIP–DVB.

Taking into account the basic properties of the NH group in the benzimidazole ring, and considering that its protonation could impel the recognition of benzimidazole compounds by the imprinted polymers, the influence of the pH on the selective rebinding has been evaluated. In this sense, different thiabendazole solutions containing  $1 \text{ mg L}^{-1}$  at pH values in the range 3–7 were loaded on both MIP–EDMA and DVB–MIP. Results from these experiments demonstrated that the pH did not have any influence on the recognition process of the benzimidazole compounds, as similar recoveries were obtained in all cases.

An enrichment step of the water samples is required in order to achieve the low benzimidazole concentration levels legislated. Thus, and considering that a good degree of selectivity was achieved for both imprinted polymers, selection of the best MIP for the determination of benzimidazole compounds in spiked water samples was done in terms of their respective breakthrough volumes.

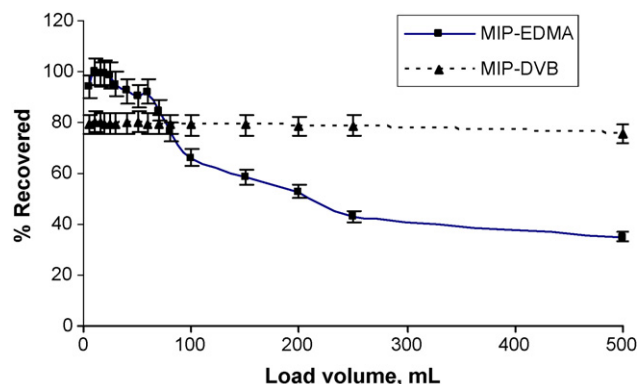


**Fig. 3.** Evaluation of the breakthrough volume obtained for the off-line enrichment of an aqueous solution containing 1 µg of thiabendazole on 1 g of MIP-EDMA and MIP-DVB.  $n = 5$ .

For this purpose, increasing volumes of aqueous TBZ solutions (containing a total amount of 1 µg) were loaded onto 1000 mg of both MIP-EDMA and MIP-DVB. The cartridges were subsequently washed with the optimized conditions for each of the imprinted polymers and eluted with  $16 \times 1$  mL (MIP-EDMA) or  $12 \times 1$  mL (MIP-DVB) of a methanol:acetic acid (50:50, v/v) mixture. Extracts were evaporated to dryness and redissolved in 0.3 mL of acetonitrile for HPLC analysis.

As can be observed in Fig. 3, a much higher breakthrough volume was achieved in the case of MIP-DVB (higher than 500 mL, compared to the 150 mL of MIP-EDMA), and thus this polymer was selected for further studies.

The recognition properties of MIP-DVB against other benzimidazole compounds (albendazole, benomyl, carbendazim, fenbendazole, flubendazole and fuberidazole) were then evaluated. With this purpose, 500 mL of solutions containing  $2 \mu\text{g L}^{-1}$  of each benzimidazole compound were independently solid phase extracted onto the MIP-DVB cartridge under the conditions previously optimized. As can be observed in the results shown in Table 1, the MIP is able to selectively rebind all the evaluated benzimidazole compounds. These results suggest that recognition between the benzimidazole compounds and the imprinted polymer takes place through the benzimidazole substructure regardless of the imidazole substituents (see Fig. 1), thus enabling the multiresidue determination of benzimidazole compounds.

Under these experimental conditions, an enrichment factor as high as 1300 times was achieved for the different benzimidazole compounds, thus enabling their determination in water samples at concentration levels below the legislated MCLs.

### 3.3. Optimization of the MIP-LC procedure

An imprinted LC column was prepared by following the experimental procedure described in Section 2.5. In this sense, around

**Table 1**  
Recoveries obtained (%) and RSD ( $n = 5$ ) for different benzimidazoles on MIP-DVB and NIP-DVB under the optimum SPE procedure.

Benzimidazole compound	MIP-DVB		NIP-DVB	
	% Rec	RSD	% Rec	RSD
Albendazole	83.6	3.9	7.1	7.3
Benomyl	75.9	2.5	3.8	4.3
Carbendazim	78.2	2.4	5.1	4.5
Fenbendazole	81.3	2.6	1.8	5.2
Flubendazole	79.7	3.3	n.d.	6.2
Fuberidazole	81.3	2.7	2.6	6.1
Thiabendazole	79.3	1.3	2.8	4.7

**Table 2**

Peak efficiencies ( $N_{\text{sys}}$ ) obtained for the elution of the different benzimidazole compounds from the imprinted column by adding different amounts of acetic acid to a methanol-based mobile phase.

% HAc	ABZ	BEN	MBC	FenBZ	FluBZ	FuBZ	TBZ
0	51	49	56	55	57	59	59
4	129	117	126	120	124	121	125
8	276	256	268	259	264	265	267
12	543	520	552	549	556	562	560
16	798	771	801	792	813	816	813
20	908	895	912	908	917	927	919
24	911	899	917	912	922	931	925
28	914	902	920	914	924	936	930
32	915	903	922	914	924	939	940
40	915	903	925	917	926	938	942

RSD ( $n = 5$ ) < 6%.

400 mg of MIP-DVB were packed in empty HPLC columns and washed with a methanol:acetic acid mixture (50:50, v/v) overnight until a stable baseline was achieved. The remaining acetic acid was then removed by pumping 50 mL of MilliQ water through the columns. This washing procedure was enough to completely remove the template molecule. Thus, no leaking effect was observed in the subsequent blank experiments.

According to the MISPE experiments above described, quantitative elution of benzimidazole compounds from the imprinted polymer can be achieved using a methanol:acetic acid mixture (50:50, v/v). In order to avoid pump damage due to the repetitive use of such high acetic acid contents in the mobile phase, an experiment was performed in order to diminish the acetic acid content. In this sense, different methanol:acetic acid mixtures have been evaluated as mobile phase for the quantitative elution of benzimidazole compounds from the imprinted column. For this purpose, initial experiments [20] were carried out in isocratic mode elution profile with mobile phases containing methanol and increasing contents of acetic acid. As was expected, an increasing acetic acid content favoured desorption of benzimidazole compounds from the polymers, but a dramatic decrease in the imprinting factor was also observed. The optimum performance was obtained for a mobile phase of methanol:acetic acid (80:20, v/v).

Taking these into account, and in an attempt to reduce peak tailing without sacrificing the imprinting factor, a first isocratic mode elution profile with methanol (mobile phase A) was maintained for 3 min, after which the mobile phase was switched to a methanol:acetic acid mixture (mobile phase B) which is maintained until the end of the chromatogram. Thus, the first elution step with pure methanol will ensure a high enough imprinting factor, while the introduction of acetic acid in the second mobile phase will theoretically diminish peak tailing, thus increasing peak efficiency, expressed as the theoretical plate numbers,  $N_{\text{sys}}$ . These were calculated for each analyte using classical chromatographic theory assuming skewed peaks [22], according to Eq. (1):

$$N_{\text{sys}} = \frac{41.7(t_R/W_{0.1})^2}{F_{\text{ass}} + 1.25} \quad (1)$$

where  $W_{0.1}$  is the peak width at a 10% peak height fraction and  $F_{\text{ass}}$  is the asymmetry factor.

As can be observed from data shown in Table 2, peak efficiencies obtained for the different benzimidazole compounds increase with increasing acetic acid concentrations, until it reaches a plateau for a methanol:acetic acid (80:20, v/v), which was thus selected as optimum in order to maximize peak efficiency.

Fig. 4 shows the chromatograms obtained for an aqueous standard solution of 0.1 mg L<sup>-1</sup> thiabendazole on both the imprinted and non-imprinted polymer under the optimized MIP-LC procedure.

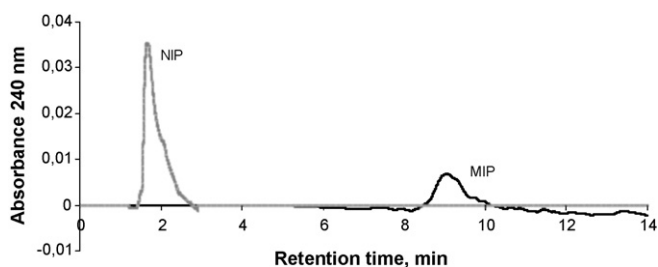


Fig. 4. Chromatograms obtained for the retention of an aqueous solution of thiabendazole ( $0.1 \text{ mg L}^{-1}$ ) on MIP-DVB (black) and NIP-DVB (grey).

Similar performance was obtained for the rest of the benzimidazole compounds, thus suggesting that the imprinted column is not only able of selectively rebinding the template molecule, but structural analogues as well. From the obtained results, it can be concluded that the on-line enrichment on a MIP-LC column is suitable for the screening of benzimidazole compounds in water samples at the concentration levels required by nowadays legislation without any other sample clean-up. However, identification and quantification of each benzimidazole compound in a mixture should be done by using the MIP cartridges for the off-line sample enrichment, combined with HPLC in reversed phase.

Since obviously the breakthrough volume is dependent on the amount of sorbent, and a lower amount of polymer was used to fill the LC column, the breakthrough volume was evaluated in a similar manner than the above described for the off-line enrichment procedure. In this sense, increasing volumes of aqueous solutions containing  $100 \mu\text{g}$  of thiabendazole were loaded on the MIP column at a flow rate of  $1 \text{ mL min}^{-1}$ . The resultant breakthrough volume for thiabendazole on the imprinted column was of 125 mL. The breakthrough volume of the rest of benzimidazoles was evaluated in a similar manner, and varied from 50 mL of albendazole or benomyl to 150 mL of carbendazim. As the developed on-line enrichment procedure is proposed as screening method for the presence of any of the studied benzimidazole compound in water samples, a volume of 50 mL was selected for the preconcentration of the different samples, to ensure the quantitative determination of all the benzimidazole compounds. Under these conditions, an enrichment factor of around 150 times was achieved.

### 3.4. Method application

Benomyl residues are known to rapidly hydrolyse into several compounds in both protic organic solvents and aqueous media. In this sense, Mallat et al. [23] evaluated the stability of benomyl residues in water samples at different pH values. These authors concluded that benomyl stability was increased with decreasing pH values, being its half-life of 3 h for samples stored at pH 7 in the dark at  $4^\circ\text{C}$ .

Table 3

Recoveries, RSD ( $n=5$ ) and detection limits<sup>a</sup> obtained after the enrichment of benzimidazole compounds present in spiked water samples ( $0.1 \mu\text{g L}^{-1}$ ) by the proposed MISPE on-line method.

Benzimidazole compound	Tap water			River water			Well water		
	% Rec	RSD	DL ( $\mu\text{g L}^{-1}$ )	% Rec	RSD	DL ( $\mu\text{g L}^{-1}$ )	% Rec	RSD	DL ( $\mu\text{g L}^{-1}$ )
Albendazole	99	5.5	0.08	102	6.3	0.09	104	6.5	0.09
Benomyl	102	4.9	0.04	103	4.6	0.05	102	6.7	0.05
Carbendazim	100	4.7	0.07	104	5.1	0.04	100	5.9	0.04
Fenbendazole	106	5.1	0.06	103	4.8	0.06	105	5.2	0.04
Flubendazole	104	3.9	0.03	99	3.6	0.04	103	4.8	0.04
Fuberidazole	99	4.2	0.06	95	5.1	0.03	89	4.7	0.03
Thiabendazole	100	2.8	0.07	102	2.1	0.05	96	4.5	0.04

<sup>a</sup> Calculated as three times the signal/noise ratio.

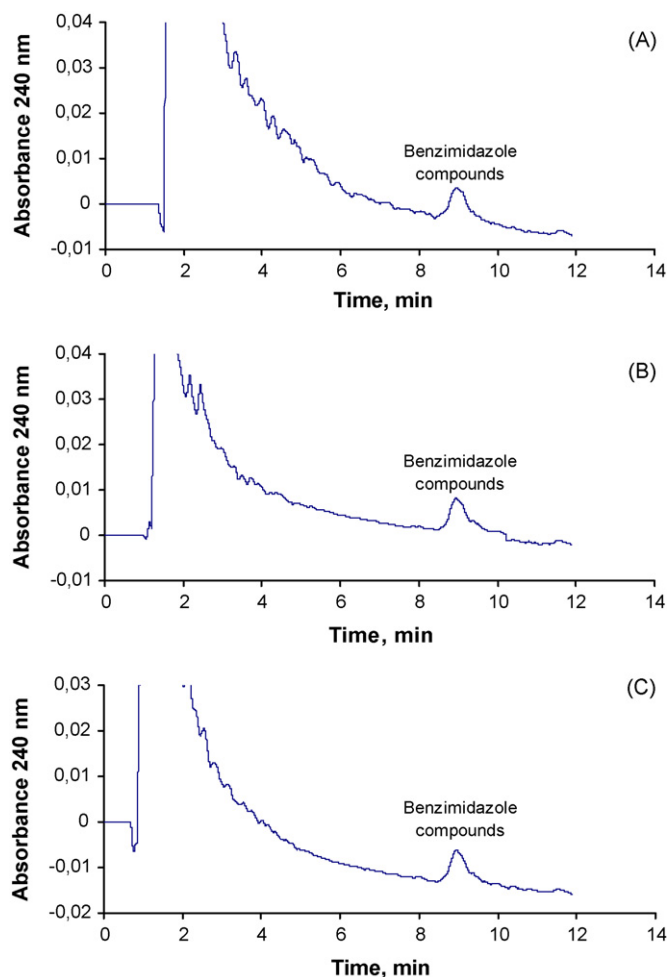
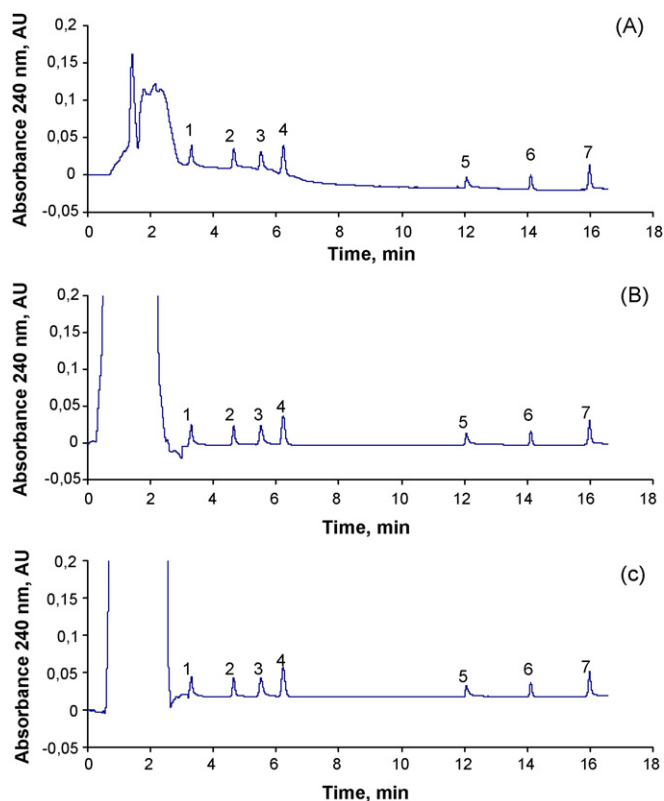


Fig. 5. Chromatogram of water samples enriched by the on-line MIP-LC procedure. [Benzimidazole] =  $0.1 \mu\text{g L}^{-1}$ . A: tap; B: river; C: well.

Taking into account that abiotic hydrolysis degradation processes are hampered by low temperatures, we evaluated the possibility of storing the samples at  $-18^\circ\text{C}$  in order to minimize degradation of benomyl. As expected, benomyl was found to be much more stable in samples stored at  $-18^\circ\text{C}$ . In this sense, a half-life of about 12 days was obtained for both standard solutions and spiked water samples.

#### 3.4.1. On-line enrichment of benzimidazole-spiked water samples

The on-line enrichment procedure based on the use of an imprinted polymer as selective stationary phase has been successfully applied to the screening determination of benzimidazole



**Fig. 6.** Chromatogram of water samples enriched by the off-line MISPE. [Benzimidazole] =  $0.1 \mu\text{g L}^{-1}$ . A: tap; B: river; C: well. 1: fenbendazole, 2: carbendazim, 3: thiabendazole, 4: fuberidazole, 5: albendazole, 6: benomyl, 7: flubendazole.

compounds in tap, river and well water samples by following the experimental procedure described in Section 2.5. Fig. 5 shows the chromatograms obtained for tap, river and well water samples spiked with  $0.1 \mu\text{g L}^{-1}$  of the different benzimidazole compounds, obtained after their enrichment by the developed on-line method. As can be observed, the high degree of selectivity of the imprinted polymer enables the separation of benzimidazoles from the interfering matrix compounds.

All the benzimidazole compounds could be quantitatively recovered with RSD values ranging from 1.7 to 5.9% ( $n=5$ ). The obtained detection limits were below the legislated MCL in all cases. Results of the recoveries and detection limits obtained for each benzimidazole compound in spiked tap, river and well water samples are summarized in Table 3. As mentioned before, the imprinted polymer is able of recognizing all the evaluated benzimidazole compounds in a similar manner. Thus, the on-line developed methodology is suitable for screening purposes, while identification and quantification of each benzimidazole compound must be

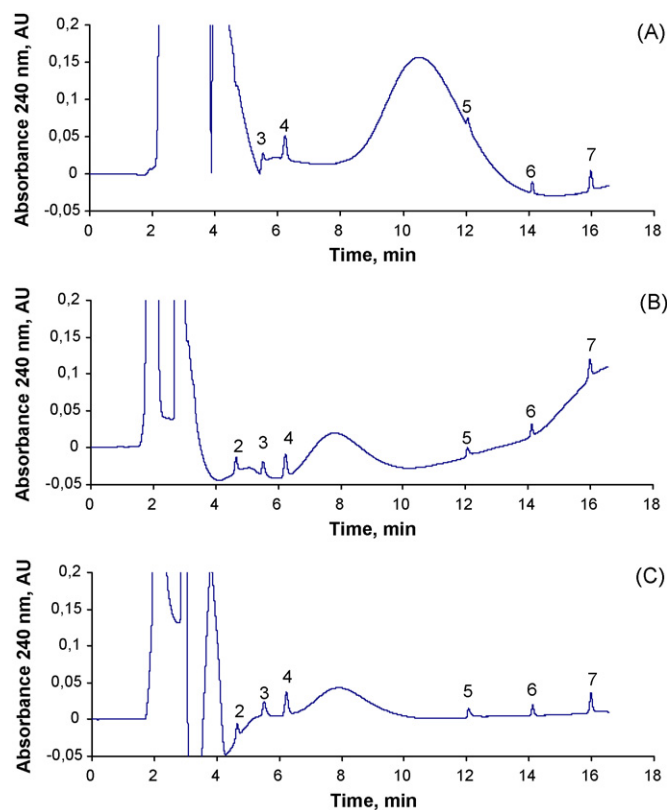


**Fig. 7.** Chromatogram of water samples enriched by off-line SPE on  $\text{C}_{18}$  discs. [Benzimidazole] =  $0.1 \mu\text{g L}^{-1}$ . A: tap; B: river; C: well. 2: carbendazim, 3: thiabendazole, 4: fuberidazole, 5: albendazole, 6: benomyl, 7: flubendazole.

carried out by the off-line enrichment procedure on MIP cartridges combined with reversed phase-HPLC.

### 3.4.2. Off-line enrichment of benzimidazole water samples

The developed MISPE procedure has been applied for the off-line enrichment of benzimidazole spiked tap, well and river water samples. In this sense, 500 mL of the standard solutions containing all the evaluated benzimidazole compounds (albendazole, benomyl, carbendazim, fenbendazole, flubendazole, fuberidazole and thiabendazole) or the water samples spiked with concentrations ranging from 0.05 to  $3 \mu\text{g L}^{-1}$  were loaded onto 1000 mg of MIP-DVB. The cartridge was then washed with  $5 \times 1 \text{ mL}$  of a DMSO:acetonitrile (2:98, v/v) solution and the benzimidazole compounds were eluted with  $12 \times 1 \text{ mL}$  of an acetic acid:methanol (50:50 v/v) mixture. The extracts were subsequently evaporated to dryness and redissolved in 0.3 mL of acetonitrile for HPLC analysis. Comparison of the obtained results with those of an external calibration proved the absence of matrix effect in all of the tested samples.

**Table 4**  
Recoveries, RSD ( $n=5$ ) and detection limits<sup>a</sup> obtained after the enrichment of benzimidazole compounds present in spiked water samples ( $0.1 \mu\text{g L}^{-1}$ ) by the proposed MISPE off-line method.

Benzimidazole compound	Tap water			River water			Well water		
	% Rec	RSD	DL ( $\mu\text{g L}^{-1}$ )	% Rec	RSD	DL ( $\mu\text{g L}^{-1}$ )	% Rec	RSD	DL ( $\mu\text{g L}^{-1}$ )
Albendazole	99	3.6	0.012	102	5.1	0.010	103	5.9	0.011
Benomyl	103	3.5	0.006	104	4.5	0.006	101	5.1	0.007
Carbendazim	100	4.2	0.008	104	2.4	0.006	100	5.2	0.005
Fenbendazole	106	2.1	0.007	102	5.2	0.005	105	4.8	0.006
Flubendazole	104	2.7	0.003	99	5.7	0.004	103	4.5	0.003
Fuberidazole	98	4.5	0.008	95	5.8	0.004	90	4.1	0.002
Thiabendazole	99	1.9	0.009	102	1.7	0.006	96	4.5	0.005

<sup>a</sup> Calculated as three times the signal/noise ratio.

Fig. 6 shows the chromatograms obtained for  $0.1 \mu\text{g L}^{-1}$  spiked tap, river and well water samples, obtained after their enrichment by the proposed off-line MISPE method. The high degree of selectivity of the divinylbenzene-imprinted polymer enables the removal of most interfering compounds in just one washing step. All the benzimidazole compounds could be quantitatively recovered by the proposed MISPE off-line enrichment method, with RSD values ranging from 2.1 to 6.7% ( $n=5$ ). The obtained detection limits were below the legislated MCL in all cases. A summary of the recoveries and detection limits obtained for each benzimidazole compound in tap, river and well water samples is shown in Table 4.

In parallel, the spiked samples were also analysed after their enrichment on  $\text{C}_{18}$  discs, following a procedure adapted from Zamora et al. [3]. Fig. 7 shows the chromatograms obtained under these conditions for  $0.1 \mu\text{g L}^{-1}$  spiked tap, river and well water samples. As can be observed from the chromatograms, a much noisier baseline was obtained when samples were preconcentrated onto  $\text{C}_{18}$  discs. Moreover, several species interfered in the determination of fenbendazole in all the evaluated water samples, and thus this compound could not be analysed by this method in any of the spiked water samples. Even if near quantitative recoveries were obtained for the rest of benzimidazole compounds, a considerable lack of reproducibility was also observed. For instance, the analysis of tap water samples yielded RSD values as high as 20% for most benzimidazole compounds.

The comparison of the obtained results by both enrichment methods (on MIP–DVB or  $\text{C}_{18}$ ) clearly demonstrate the advantage of using molecularly imprinted polymers as selective sorbents for the multiresidual determination of several benzimidazole compounds in spiked tap, river or well water samples.

#### 4. Conclusions

Two thiabendazole imprinted polymers, prepared using ethyleneglycol dimethacrylate and divinylbenzene as cross-linkers, have been synthesized and evaluated for the selective retention of benzimidazole compounds in water samples. Even if a clear imprinting effect has been obtained for both MIPs, DVB-imprinted polymer provides a much higher breakthrough volume, and thus has been selected for the enrichment of tap, river and well water samples. This imprinted polymer is able of selectively rebinding not only the template molecule, but also a wide range of benzimidazole compounds (albendazole, benomyl, carbendazim, fenbendazole, flubendazole, and fuberidazole).

An on-line enrichment procedure based on the use of a MIP–DVB column is proposed as a fast and automatic method for the screening of benzimidazole compounds present in tap, river and well water samples. A confirmatory method based on an off-line MISPE

enrichment of the water samples followed by their HPLC analysis, has also been developed. This method enables the identification and quantification of a wide range of benzimidazole compounds in a single run, thus considerably diminishing the analysis time.

The detection limits obtained for both the on-line and off-line enrichment methods are well below the legislated MRLs, thus enabling the analysis of benzimidazole compounds in tap, river and well water samples.

#### Acknowledgements

The authors wish to thank DGICYT (CTQ2005-02281), Comunidad de Madrid (S-0505/AGR/0312) and Universidad Complutense de Madrid for financial support. C. Cacho wishes to thank Comunidad de Madrid for a predoctoral fellowship.

#### References

- [1] Directive 2006/11/CE of the European Parliament and of the Council of February 15th 2006, published in the Official Journal of the European Journal on March 4th 2006.
- [2] R. Jeannot, H. Sabik, E. Sauvard, E. Gessin, J. Chromatogr. 379 (2000) 51.
- [3] D.P. Zamora, J.L.M. Vidal, M.M. Galera, A.G. Frenich, J.L.L. Gonzalez, M.R. Arahal, Talanta 60 (2003) 335.
- [4] A.G. Frenich, D.P. Zamora, J.L.M. Vidal, M.M. Galera, Anal. Chim. Acta 477 (2003) 211.
- [5] E.A. Hogendoorn, K. Westhuis, E. Dijkman, E.A.G. Eusinkweld, P. Chauvaskul, P. Biadul, R.A. Baumann, A.A. Cornelese, M.A. van der Linden, Int. J. Environ. Anal. Chem. 78 (2000) 67.
- [6] R. Halko, C.P. Sanz, Z.S. Ferrera, J.J.S. Rodríguez, Chromatographia 60 (2004) 151.
- [7] A. Moral, M.D. Sicilia, S. Rubio, D. Pérez-Bendito, Anal. Chim. Acta 569 (2006) 132.
- [8] M. Danaher, H. De Ruyck, S.R.H. Crooks, G. Dowling, M. O'Keefe, J. Chromatogr. B 845 (2007) 1–37.
- [9] C. Baggiani, L. Anfossi, C. Giovannoli, Curr. Pharm. Anal. 2 (2006) 219.
- [10] V. Pichon, K. Haupt, J. Liq. Chromatogr. Relat. Technol. 29 (2006) 989.
- [11] C. Baggiani, C. Giovannoli, L. Anfossi, C. Tozzi, J. Chromatogr. A 938 (2001) 35.
- [12] N. Masque, R.M. Marce, F. Borrull, P.A.G. Cormack, D.C. Sherrington, Anal. Chem. 72 (2000) 4122.
- [13] E. Caro, N. Masque, R.M. Marce, F. Borrull, P.A.G. Cormack, D.C. Sherrington, J. Chromatogr. A 963 (2002) 169.
- [14] C. Baggiani, F. Trotta, G. Giraudi, C. Giovannoli, A. Vanni, Anal. Commun. 36 (1999) 263.
- [15] M. Kawaguchi, Y. Hayatsu, H. Nakata, Y. Ishii, R. Ito, K. Saito, H. Nakazawa, Anal. Chim. Acta 539 (2005) 83.
- [16] C.R.T. Tarley, M.G. Segatelli, L.T. Kubota, Talanta 69 (2006) 259.
- [17] J.C. Bravo, R.M. Garcinuno, P. Fernandez, J.S. Durand, Anal. Bioanal. Chem. 388 (2007) 1039.
- [18] M.L. Mena, P. Martínez-Ruiz, A.J. Reviejo, J.M. Pingarron, Anal. Chim. Acta 451 (2002) 297.
- [19] A.G.V. de Prada, O.A. Loaiza, B. Serra, D. Morales, P. Martínez-Ruiz, A.J. Reviejo, J.M. Pingarron, Anal. Bioanal. Chem. 388 (2007) 227.
- [20] E. Turiel, J.L. Tadeo, P.A.G. Cormack, A. Martín-Esteban, Analyst 130 (2005) 1601.
- [21] C. Cacho, L. Schweitz, E. Turiel, C. Perez-Conde, J. Chromatogr. A 1179 (2008) 216.
- [22] J.P. Foley, J.G. Dorsey, Anal. Chem. 55 (1983) 730.
- [23] E. Mallat, D. Barcelo, R. Tauler, Chromatographia 46 (1997) 342.



# Sol-gel synthesized semiconducting $\text{LaCo}_x\text{Fe}_{1-x}\text{O}_3$ -based powder for thick film $\text{NH}_3$ gas sensor

G.N. Chaudhari<sup>a,\*</sup>, S.V. Jagtap<sup>a</sup>, N.N. Gedam<sup>a</sup>, M.J. Pawar<sup>a</sup>, V.S. Sangawar<sup>b</sup>

<sup>a</sup> Nano Technology Research Laboratory, Department of Chemistry, Shri Shivaji Science College, Amravati 444602, M.S., India

<sup>b</sup> P.G. Department of Physics, G.V.I.S.H., Amravati 444604, M.S., India

## ARTICLE INFO

### Article history:

Received 12 October 2008

Received in revised form 15 January 2009

Accepted 16 January 2009

Available online 24 January 2009

### Keywords:

$\text{LaCo}_x\text{Fe}_{1-x}\text{O}_3$

Electrical and sensing properties

$\text{NH}_3$  sensor

Selectivity

## ABSTRACT

Perovskite type  $\text{LaCo}_x\text{Fe}_{1-x}\text{O}_3$  nanoparticles was synthesized by a sol-gel citrate method. The structural, electrical and sensing characteristics of the  $\text{LaCo}_x\text{Fe}_{1-x}\text{O}_3$  system were investigated. The structural characteristics were performed by using X-ray diffraction (XRD) and transmission electron microscopy (TEM) to examine the phase and morphology of the resultant powder. The XRD pattern shows nanocrystalline solid solution of  $\text{LaCo}_x\text{Fe}_{1-x}\text{O}_3$  with perovskite phase. Electrical properties of synthesized nanoparticles are studied by DC conductivity measurement. The sensor shows high response towards ammonia gas in spite of other reducing gases when  $x=0.8$ . The effect of 0.3 wt.% Pd-doped  $\text{LaCo}_x\text{Fe}_{1-x}\text{O}_3$  on the response and a recovery time was also addressed.

© 2009 Published by Elsevier B.V.

## 1. Introduction

There is a need for ammonia ( $\text{NH}_3$ ) sensors in many situations including leak-detection in air-conditioning systems [1], environmental sensing of trace amounts ambient  $\text{NH}_3$  in air [2], breath analysis for medical diagnoses [3], animal housing [2], and more. Generally, because it is toxic, it is required to be able to sense low levels (~ppm) of  $\text{NH}_3$ , but it should also be sensitive too much higher levels.  $\text{NH}_3$  gas can be quiet corrosive, often causing  $\text{NH}_3$  sensors to have short lifetimes.

The gas-sensing mechanism of metal oxide materials is based on the reaction between the adsorbed oxygen on the surface of the materials and the gas molecules to be detected. The state and the amount of oxygen on the surface of materials are strongly dependent on the microstructure of the materials, namely, specific area, particle size, as well as the film thickness of the sensing film. In order to obtain gas sensors with good performance, the recent research works [4–6] were devoted to nano-materials because they have high specific area and contain more grain boundaries.

Some well-known materials for  $\text{NH}_3$  gas sensing are ZnO [7], modified-ZnO (viz. Fe-ZnO and Ru-ZnO) [8,9], indium oxide [10], molybdenum oxide [11], polyaniline [12–14], polypyrrole [15], Au and  $\text{MoO}_3$ -modified  $\text{WO}_3$  [16,17], Pt- and  $\text{SiO}_2$ -doped  $\text{SnO}_2$  [18], etc. Various ammonia sensors reported basically work at higher

temperature such as 350 °C, but it is not convenient to work at such high temperature while sensing.

There has been much interest in perovskite-structured compounds (general formula  $\text{ABO}_3$ ) because of their unique catalytic action [19] and gas-sensing properties [20–24]. Their sensitive and selective characteristics can be controlled by selecting suitable chemical dopants.

In recent studies undoped and doped  $\text{LaFeO}_3$  perovskite powder is reported to have good sensitivity to CO [21], ethanol [25] and  $\text{H}_2\text{S}$  gas [26]. We did some further studies by replace  $\text{Fe}^{3+}$  with  $\text{Co}^{2+}$ . The present work was undertaken to investigate the gas-sensing behavior of nanosized  $\text{LaCo}_x\text{Fe}_{1-x}\text{O}_3$  thick films prepared by a sol-gel citrate method. The aim of the present work is to study the evolution of structural and electrical properties of  $\text{LaCo}_x\text{Fe}_{1-x}\text{O}_3$  nanocrystalline powder in order to understand the sensor response to  $\text{NH}_3$  gas sensor based on effect of Co doping in  $\text{LaFeO}_3$ . These studies show that in perovskite structure different B-site cations exhibit significant variation in sensing properties. The structural characteristic of the material was studied by using X-ray diffraction (XRD) and transmission electron microscopy (TEM).

## 2. Experimental details

### 2.1. Preparation of $\text{LaCo}_x\text{Fe}_{1-x}\text{O}_3$

$\text{LaCo}_x\text{Fe}_{1-x}\text{O}_3$  nanocrystalline powders used in this work were synthesized by a sol-gel citrate method. The stoichiometric amount of starting material, such as lanthanum nitrate hexahydrate [ $\text{La}(\text{NO}_3)_3 \cdot 6\text{H}_2\text{O}$ ], cobalt nitrate hexahydrate [ $\text{Co}(\text{NO}_3)_2 \cdot 6\text{H}_2\text{O}$ ],

\* Corresponding author.

E-mail address: [nano.d@rediffmail.com](mailto:nano.d@rediffmail.com) (G.N. Chaudhari).

ferric nitrate polyhydrate  $[\text{Fe}(\text{NO}_3)_2 \cdot 9\text{H}_2\text{O}]$ , and citric acid were weighed and dissolved in ethylene glycol. The mixture was magnetically stirred at  $80^\circ\text{C}$  for 2 h to get homogeneous mixture. Then this mixture was heated at  $130^\circ\text{C}$  for 12 h in a closed vessel to form gel precursor. The resulting material was further heated for 3 h at  $350^\circ\text{C}$  and subsequently calcined at  $650^\circ\text{C}$  for 6 h to obtain the nanoparticles. Pd was incorporated in the nanoparticles by the process of impregnation. Appropriate quantities of  $\text{PdCl}_2$  and samples were dissolved in deionized water. This mixture was vigorously stirred and slowly dried on a water bath. The dried compound was ground to a fine powder and calcined at  $200^\circ\text{C}$  for 1 h to decompose the chloride.

## 2.2. Characterization techniques

The synthesized samples were characterized for their structure and morphology by X-ray powder diffraction (XRD; Siemens D5000) and transmission electron microscopy (TEM; Hitachi-800). The X-ray diffraction data were recorded by using  $\text{Cu K}\alpha$  radiation ( $1.5406 \text{ \AA}$ ). The intensity data were collected over a  $2\theta$  range of  $10\text{--}70^\circ$ . The average crystallite size of the samples was estimated with the help of Scherrer equation using the diffraction broadening of all prominent lines. The DC characteristics of the  $\text{LaCo}_x\text{Fe}_{1-x}\text{O}_3$  was studied in the range of  $30\text{--}350^\circ\text{C}$  with a step of  $5^\circ\text{C}$ .

## 2.3. Sensor fabrication

The  $\text{LaCo}_x\text{Fe}_{1-x}\text{O}_3$  powders prepared were mixed with a suitable amount of adhesive and then ground into paste. After that the paste was packed into a ceramic tube on which two electrodes had been installed at each end. The ceramic tube was about 10 mm in length, 2 mm in external diameter, and 1.7 mm in internal diameter. In order to improve their stability and repeatability, the gas sensors were calcined at  $400^\circ\text{C}$  for 2 h. The gas-sensing properties were measured in a temperature range of  $50\text{--}350^\circ\text{C}$ . The resistance of a sensor was measured in air and in a sample gas. Fresh air was used as a carrier gas.

The gas sensitivity ( $S$ ) is defined as the ratio of the change of resistance in presence of gas ( $R_g$ ) to that in air ( $R_a$ ) [27]. For the p-type semiconducting material following formula is used for sensitivity determination.

$$S = \frac{R_g - R_a}{R_a} = \frac{\Delta R}{R_a} \quad (1)$$

The gas-sensing properties were studied for reducing gases such as hydrogen sulphides ( $\text{H}_2\text{S}$ ), ammonia ( $\text{NH}_3$ ), liquefied petroleum gas (LPG), carbon monoxide (CO), and ethanol ( $\text{C}_2\text{H}_5\text{OH}$ ), whose concentration were fixed at 3000 ppm in air.

## 2.4. Pellet fabrication

In order to measure the electrical properties of the compound, the pellet was fabricated as: the crystalline powder was crushed into fine powder using a pestle and mortar. A quantity of 2 g powder was taken with 0.05 ml (25 mg) of an organic binder, poly vinyl alcohol (PVA) and then it was again ground to mix PVA uniformly in the powder. This powder was then used to make a dense pellet with a die of diameter 10 mm. A hand press machine was used to apply a pressure of about 8 tones on the die. The pellets prepared were then fired at  $250^\circ\text{C}$  for 1 h to remove the organic binder. Silver paint was applied at two different points on the same surface of a pellet from which contacts were drawn with very thin flexible copper wires and then it was used for electrical studies.

## 3. Results and discussion

### 3.1. X-ray diffraction

Fig. 1 shows the X-ray diffraction patterns of (a)  $\text{LaCo}_{0.8}\text{Fe}_{0.2}\text{O}_3$  and (b)  $\text{LaFeO}_3$ , calcined at  $650^\circ\text{C}$ . Definite line broadening of the diffraction peaks is an indication that the synthesized materials are in nanometer range. This is an advantage for improving the gas-sensing properties for oxide semiconductor materials. The patterns indicate that both samples have an orthorhombic distorted perovskite structure. The average particle size  $D$  was estimated by means of Scherrer formula through measuring the half-peak widths of the diffraction lines. The obtained  $D$  values were about 30 nm and 40 nm for  $\text{LaCo}_{0.8}\text{Fe}_{0.2}\text{O}_3$  and  $\text{LaFeO}_3$ , respectively, showing that the partial substitution of  $\text{Co}^{2+}$  for  $\text{Fe}^{3+}$  in the  $\text{LaFeO}_3$  lattice. The lattice parameters calculated were also in accordance with the reported value.

### 3.2. Transmission electron microscopy

The morphology of the powder sample has been observed by TEM. Fig. 2 shows the TEM micrograph of the  $\text{LaCo}_{0.8}\text{Fe}_{0.2}\text{O}_3$  pow-

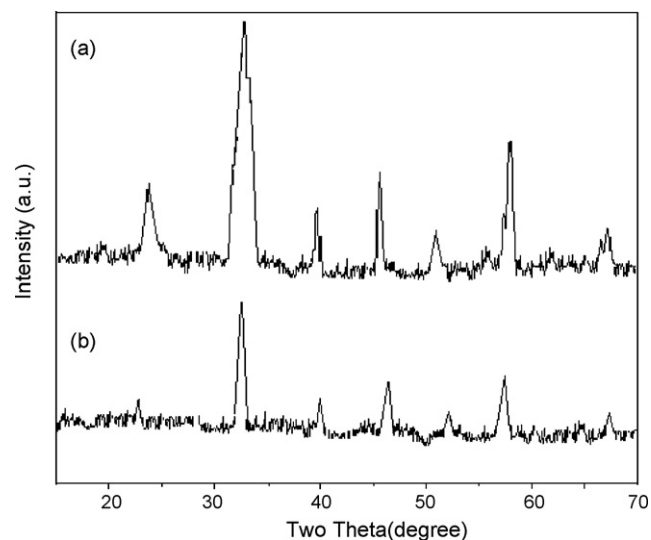


Fig. 1. X-ray diffraction patterns of (a)  $\text{LaCo}_{0.8}\text{Fe}_{0.2}\text{O}_3$  and (b)  $\text{LaFeO}_3$ , calcined at  $650^\circ\text{C}$ .

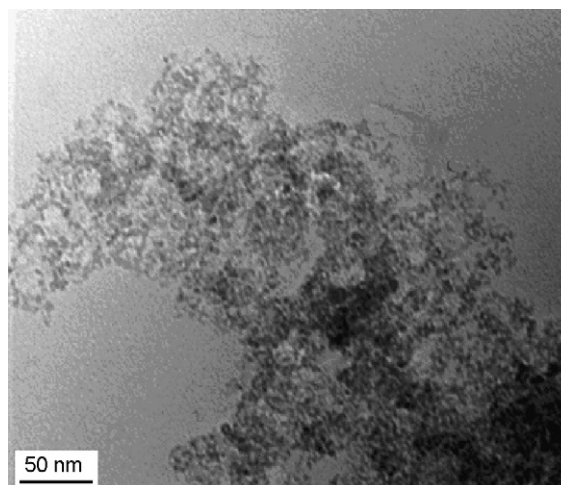


Fig. 2. TEM image of  $\text{LaCo}_{0.8}\text{Fe}_{0.2}\text{O}_3$  calcined at  $650^\circ\text{C}$ .



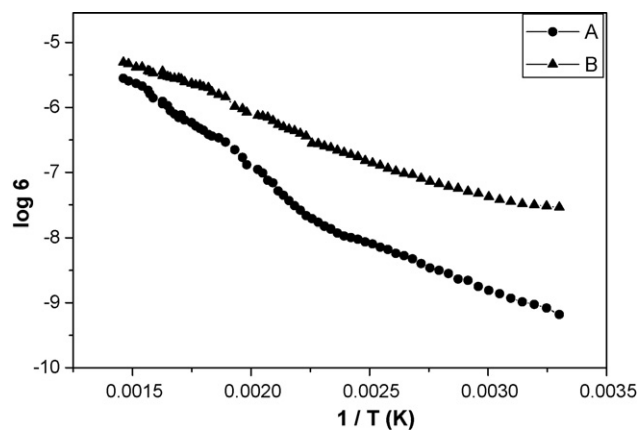


Fig. 3. Electrical conductivity of (a) LaFeO<sub>3</sub> and (b) LaCo<sub>0.8</sub>Fe<sub>0.2</sub>O<sub>3</sub> in air.

der with uniform grain size distribution having a small tendency of agglomerates formation. Due to the formation of polycrystalline material particle size are formed in the range of 30–40 nm.

### 3.3. DC conductivity

Fig. 3 shows the log  $\sigma$  versus  $1/T$  Arrhenius plot for the LaFeO<sub>3</sub> and LaCo<sub>0.8</sub>Fe<sub>0.2</sub>O<sub>3</sub> nanoparticles. As seen from the figure, the conductivity of the sample increased with an increase in temperature, following a linear dependence, as expected for a typical semiconducting material. A linear relationship of both materials could be due no change in semiconducting properties, except enhancement of conductivity. The activation energy of LaCo<sub>0.8</sub>Fe<sub>0.2</sub>O<sub>3</sub> calculated from the reciprocal of slope was about 0.5 eV.

### 3.4. Resistivity

Fig. 4 shows the resistance behavior against temperature of (a) LaFeO<sub>3</sub> and (b) LaCo<sub>0.8</sub>Fe<sub>0.2</sub>O<sub>3</sub>, respectively. It is very interesting to note that the resistance changes very sufficiently with temperature up to 200 °C and beyond this temperature the change is small. Due to incorporation of Co in LaFeO<sub>3</sub> (LaCo<sub>0.8</sub>Fe<sub>0.2</sub>O<sub>3</sub>), the resistance is considerably reduced. This reduction in resistivity may be due to rise in Fermi level by the interaction with Co to LaFeO<sub>3</sub>.

### 3.5. Gas-sensing characteristics

Fig. 5 shows the NH<sub>3</sub> gas response of undoped LaFeO<sub>3</sub>, calcined at 650 °C for various operating temperature. In general at low temperature, the gas response is restricted by the speed of chemical

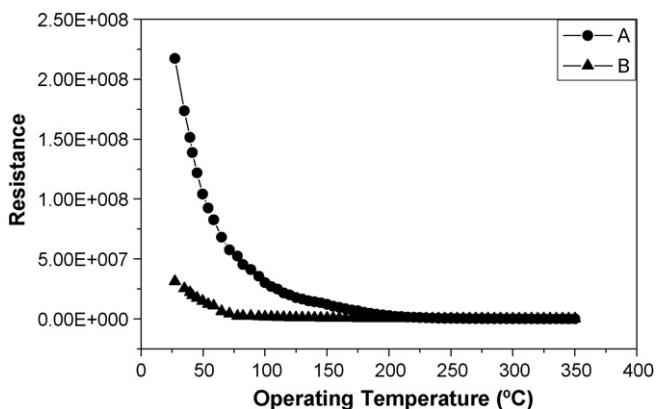


Fig. 4. Resistance behavior against temperature of (a) LaFeO<sub>3</sub> and (b) LaCo<sub>0.8</sub>Fe<sub>0.2</sub>O<sub>3</sub>.

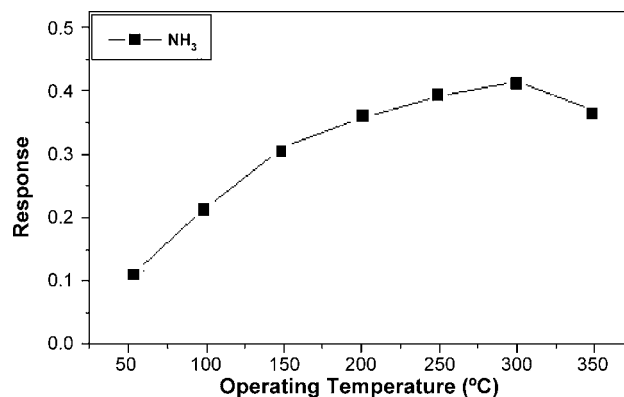


Fig. 5. Gas-sensing characteristics of undoped LaFeO<sub>3</sub> for NH<sub>3</sub> gas as a function of operating temperature.

reaction, and at higher temperature, it is restricted by the speed of diffusion of gas molecules. At some intermediate temperature, the speed value of the two processes becomes equal and at that point the sensor response reaches to its maximum. Here, the response increases with increase in operating temperature to attain maximum at 300 °C for NH<sub>3</sub>, and then decrease with further increase in operating temperature.

The samples with the composition LaCo<sub>x</sub>Fe<sub>1-x</sub>O<sub>3</sub> ( $x = 0.2, 0.4, 0.6$  and  $0.8$ ) were studied as a NH<sub>3</sub> gas sensor. It was found that response mainly depends upon operating temperature and Co content. Fig. 6 shows the gas response for different amount of  $x$  ( $x = 0.2, 0.4, 0.6$  and  $0.8$ ) at various operating temperatures. From figure it is seen that there is increase in response for LaCo<sub>0.8</sub>Fe<sub>0.2</sub>O<sub>3</sub> to maximum value at an operating temperature 260 °C, whereas the other samples show lower response to NH<sub>3</sub> gas. Compared with LaFeO<sub>3</sub>, LaCo<sub>0.8</sub>Fe<sub>0.2</sub>O<sub>3</sub> showed the large response to NH<sub>3</sub> gas. The reason may be that the partial replacement of Fe<sup>3+</sup> ions by Co<sup>2+</sup> ions at the B-sites is advantageous to adsorption and oxidation for NH<sub>3</sub> gas. Studies showed that LaFeO<sub>3</sub> is a p-type semiconductor, its charge carries are holes (h). When Fe<sup>3+</sup> in LaFeO<sub>3</sub> is replaced by Co<sup>2+</sup>, the carrier's concentration will depend on the holes produced by ionization of [Co<sub>Fe<sub>x</sub>]. In this formula, Co<sub>Fe<sub>x</sub> mean the point defect, which is produced when Co<sup>2+</sup> occupies the sites of Fe<sup>3+</sup> in the crystal. Upon the addition of Co<sup>2+</sup>, holes will be generated based on this equation. So the concentration of 'h' increases, which results in the conductivity of Co-doping samples is considerably higher than that of LaFeO<sub>3</sub>.</sub></sub>

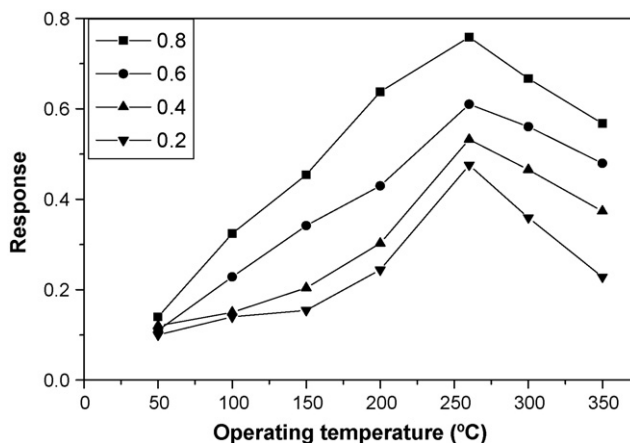


Fig. 6. Response to NH<sub>3</sub> gas of 200ppm of LaCo<sub>x</sub>Fe<sub>1-x</sub>O<sub>3</sub> doped with different amount of Co as a function of operating temperature ( $X = 0.2, 0.4, 0.6, 0.8$ ).

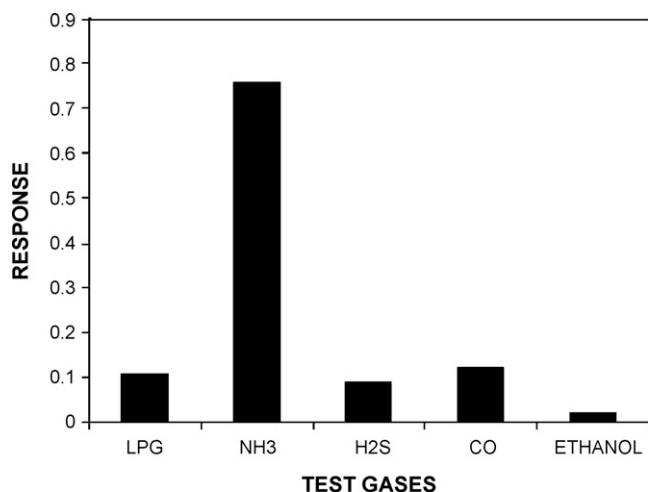


Fig. 7. Gas-sensing characteristics of  $\text{LaCo}_{0.8}\text{Fe}_{0.2}\text{O}_3$  for various reducing gases.

Iron ion are very stable in the +3 valence state, where as Co ions tend to stabilize in the +2 valence state, thus influencing the stability range of the  $\text{A}^{3+}\text{B}^{3+}\text{O}_3$  perovskite structure. It seems that, they are relatively stable under the reducing atmosphere, when Fe and Co ions exist in trivalent and divalent state, respectively [28].

Selectivity is the ability that a gas sensor to distinguishes between different kinds of gases. Fig. 7 shows the selectivity of  $\text{LaCo}_{0.8}\text{Fe}_{0.2}\text{O}_3$  sensor to various test gases such as  $\text{NH}_3$ , LPG,  $\text{H}_2\text{S}$ , CO and ethanol. The sensor shows high degree of selectivity towards  $\text{NH}_3$  gas than other reducing gases.

In order to modify and/or control the surface properties of the  $\text{LaCo}_{0.8}\text{Fe}_{0.2}\text{O}_3$ , introduction of Pd additives is usually performed. The most important effects of noble metal addition are the increase of the maximum sensitivity and the rate of response, as well as the lowering of the temperature of maximum sensitivity. All these effects arise as a consequence of the promoting catalytic activity when loading with noble metals. A great amount of additives have been studied being Pd and Pt the most used. Here Pd was incorporated into the  $\text{LaCo}_{0.8}\text{Fe}_{0.2}\text{O}_3$  by adopting the chemical wet method. Fig. 8 shows the response of  $\text{LaCo}_{0.8}\text{Fe}_{0.2}\text{O}_3$  for ammonia gas as a function of different wt.% Pd-doped. 0.3 wt.% Pd-doped  $\text{LaCo}_{0.8}\text{Fe}_{0.2}\text{O}_3$  shows higher response to ammonia gas as compare to other.

Fig. 9 shows the response of 0.3 wt.% Pd-doped  $\text{LaCo}_{0.8}\text{Fe}_{0.2}\text{O}_3$  as a function of operating temperature. Incorporation of Pd is seen to improve the response of the sensor to  $\text{NH}_3$  gas and also reduce

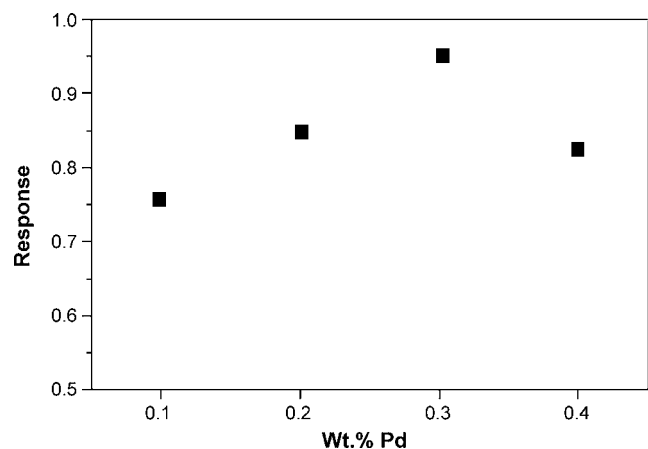


Fig. 8. Effect of Pd doping of  $\text{LaCo}_{0.8}\text{Fe}_{0.2}\text{O}_3$  on the response to  $\text{NH}_3$  gas of 200 ppm.

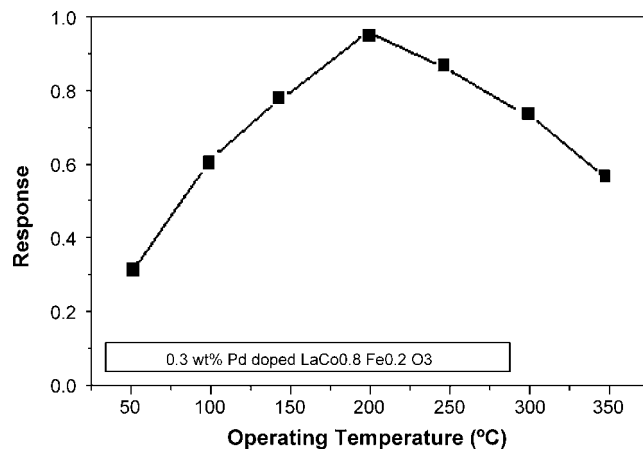


Fig. 9. Response of 0.3 wt.% Pd-doped  $\text{LaCo}_{0.8}\text{Fe}_{0.2}\text{O}_3$  as a function of operating temperature.

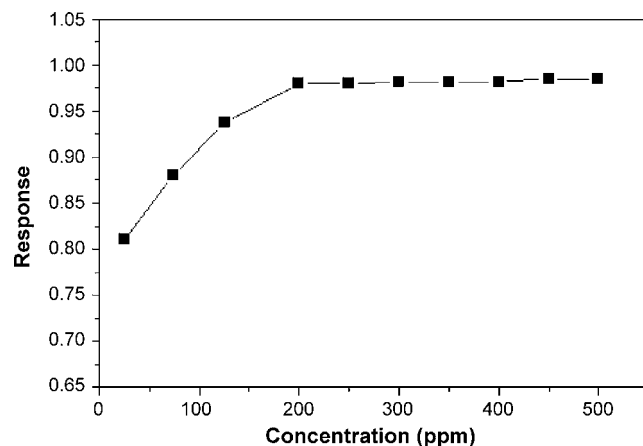


Fig. 10. Response of 0.3 wt.% Pd-doped  $\text{LaCo}_{0.8}\text{Fe}_{0.2}\text{O}_3$  to  $\text{NH}_3$  of different Concentration (in ppm).

the operating temperature. The sensor reaches its maximum value of response at an operating temperature  $200^\circ\text{C}$ .

The variation of gas response of 0.3 wt.% Pd-doped  $\text{LaCo}_{0.8}\text{Fe}_{0.2}\text{O}_3$  sample with  $\text{NH}_3$  gas concentration at  $200^\circ\text{C}$  is shown in Fig. 10. Fig. 10 shows that the response values were observed to increase continuously with increasing the gas concentration up to 200 ppm at an operating temperature  $200^\circ\text{C}$ . The rate of increase in response was relatively larger up to 200 ppm,

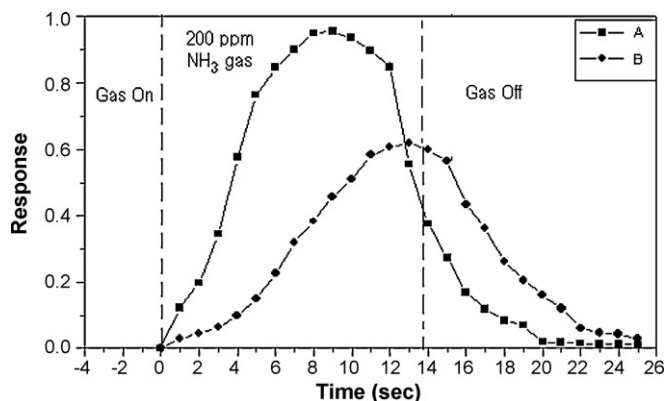


Fig. 11. Response characteristics of (a) 0.3 wt.% Pd-doped  $\text{LaCo}_{0.8}\text{Fe}_{0.2}\text{O}_3$  and (b)  $\text{LaCo}_{0.8}\text{Fe}_{0.2}\text{O}_3$ .

but smaller during 200–1000 ppm. Thus the active region of the sensors would be up to 200 ppm.

Response and recovery times, defined as the time reaching 90% of final signal, are the important parameters of the gas sensor. Fig. 11 shows the response characteristics for the  $\text{LaCo}_{0.8}\text{Fe}_{0.2}\text{O}_3$  at 260 °C and 0.3 wt.% Pd-doped  $\text{LaCo}_{0.8}\text{Fe}_{0.2}\text{O}_3$  to 200 ppm  $\text{NH}_3$  gas at 200 °C. The 0.3 wt.% Pd-doped  $\text{LaCo}_{0.8}\text{Fe}_{0.2}\text{O}_3$  sensor exhibited shorter response and recovery times (8 and 20 s, respectively) than  $\text{LaCo}_{0.8}\text{Fe}_{0.2}\text{O}_3$ . From this observation we can infer that the 0.3 wt.% Pd-doped  $\text{LaCo}_{0.8}\text{Fe}_{0.2}\text{O}_3$  responds more efficiently than  $\text{LaCo}_{0.8}\text{Fe}_{0.2}\text{O}_3$ .

#### 4. Conclusion

In the present investigation we have presented the method of synthesis and a systematic improvement in the sensing properties of  $\text{LaFeO}_3$  using two significant strategies, namely surface modification and doping with cobalt on B-site of the perovskite. The results demonstrate the development of a new class of stable and very sensitive nanostructured materials for gas sensing.  $\text{LaCo}_{0.8}\text{Fe}_{0.2}\text{O}_3$  is found to be sensitive for the detection of ammonia at 260 °C. The operating temperature was found to be reduced up to 200 °C by addition of 0.3 wt.% Pd. The fast response and recovery is the other significant properties of the sensors. Thus, the sensor is promising material for practical devices for the detection of a low concentration of  $\text{NH}_3$ .

#### References

- [1] The International Institute of Ammonia Refrigeration, <http://www.iiar.org>.  
 [2] T.T. Groot, Sense of Contact 6 Keynote, Sensor Research at Energy Research Center Netherlands (ECN), March, 2004.

- [3] B.H. Timmer, Amina-chip, Ph.D. Thesis, U. Twente, The Netherlands, 2004.  
 [4] Y. Liu, M. Liu, Adv. Funct. Mater. 15 (2005) 57–62.  
 [5] L.G. Teoh, Y.M. Hon, J. Shieh, W.H. Lai, M.H. Hon, Sens. Actuators B 96 (2003) 219–225.  
 [6] Y.G. Choi, G. Sakai, K. Shimanoe, Y. Teraoka, N. Miura, N. Yamazoe, Sens. Actuators B 93 (2003) 486–494.  
 [7] G.S. Trivikrama Rao, D. Tarakarama Rao, Sens. Actuators B 55 (1999) 166–169.  
 [8] M.S. Wagh, G.H. Jain, D.R. Patil, S.A. Patil, L.A. Patil, Sens. Actuators B 115 (2006) 128–133.  
 [9] D.R. Patil, L.A. Patil, Sens. Transducers 70 (2006) 661–670.  
 [10] A. Karthigeyan, R.P. Gupta, K. Scharnagl, M. Burgmair, S.K. Sharma, I. Eisele, Sens. Actuators B 85 (2002) 145–153.  
 [11] D. Mutschall, K. Holzner, E. Obermeier, Sens. Actuators B 36 (1996) 320–324.  
 [12] K.P. Kakke, D.J. Shirale, H.J. Kharat, P.D. Gaikwad, P.A. Savale, V.K. Gade, M.D. Shirsat, Proceedings of NSPTS-11, C 17, 2006, pp. 1–5.  
 [13] A.L. Kukla, Y.M. Shirshov, S.A. Piletsky, Sens. Actuators B 37 (1996) 135–140.  
 [14] V.V. Chabukswar, S. Pethkar, A.A. Athawale, Sens. Actuators B 77 (2001) 657–663.  
 [15] G. Lahdesmaki, A. Lewenstam, A. Ivaska, Talanta 43 (1996) 125–134.  
 [16] X. Wang, N. Miura, N. Yamazoe, Sens. Actuators B 66 (2000) 74–76.  
 [17] C.N. Xu, N. Miura, Y. Ishida, K. Matuda, N. Yamazoe, Sens. Actuators B 65 (2000) 63–165.  
 [18] Y. Wang, X. Wu, Q. Su, Y. Lee, Z. Zhou, Solid-State Electron. 45 (2001) 347–350.  
 [19] C.M. Chiu, Y.H. Chang, Mater. Sci. Eng. A 266 (1999) 93–98.  
 [20] C.M. Chiu, Y.H. Chang, Sens. Actuators B 54 (1999) 236–242.  
 [21] N.N. Toan, S. Saukko, V. Lantto, Physica B 327 (2003) 279–282.  
 [22] L.B. Kong, Y.S. Shen, Sens. Actuators B 30 (1996) 217–221.  
 [23] Y.D. Wang, J.B. Chen, X.H. Wu, Mater. Lett. 49 (2001) 361–364.  
 [24] M. Tomoda, S. Okano, Y. Itagaki, H. Aono, Y. Sadaoka, Sens. Actuators B 97 (2004) 190–197.  
 [25] L. Zhang, J. Hu, P. Song, H. Qin, K. An, X. Wang, M. Jiang, Sens. Actuators B 119 (2006) 315–318.  
 [26] S.V. Jagtap, A.V. Kadu, V.S. Sangawar, S.V. Manorama, G.N. Chaudhari, Sens. Actuators B 131 (2008) 290–294.  
 [27] P. Song, H. Qin, L. Xing, S. Huang, R. Zhang, J. Hu, M. Jiang, Sens. Actuators B 119 (2006) 415–418.  
 [28] L.W. Tai, M.M. Nasrallah, H.U. Anderson, J. Solid State Chem. 118 (1995) 117–124.



# Speciation of glyphosate, phosphate and aminomethylphosphonic acid in soil extracts by ion chromatography with inductively coupled plasma mass spectrometry with an octopole reaction system

Zuliang Chen<sup>a,b,\*</sup>, Wenxiang He<sup>a</sup>, Michael Beer<sup>a,b</sup>, Mallavarapu Megharaj<sup>a,b</sup>, Ravendra Naidu<sup>a,b</sup>

<sup>a</sup> Centre for Environmental Risk Assessment and Remediation, University of South Australia, Mawson Lakes, SA 5095, Australia

<sup>b</sup> Cooperative Research Centre for Contamination Assessment and Remediation of Environments, Mawson Lakes, SA 5095, Australia

## ARTICLE INFO

### Article history:

Received 14 September 2008

Received in revised form 9 December 2008

Accepted 22 December 2008

Available online 15 January 2009

### Keywords:

IC-ICP-MS

Octopole reaction system

Phosphorus

Soil extract

## ABSTRACT

Ion-pairing chromatography coupled with inductively coupled plasma mass spectrometry (ICP-MS) used for the speciation of phosphorus is limited as the mobile phase containing organic solvents changes in detection sensitivity and the carbon precipitates on torch and cones. To address this issue, anion-exchange chromatography with ICP-MS has been used for the speciation of glyphosate, phosphate and aminomethylphosphonic acid in soil extracts. The separation of the targets on a new column was achieved within 5 min using an eluent containing 20 mM  $\text{NH}_4\text{NO}_3$  at pH 5.1. Furthermore, since the polyatomic ions such as  $^{14}\text{N}^{16}\text{O}^1\text{H}^+$  and  $^{15}\text{N}^{16}\text{O}^+$  from a nitrogen-based ion-pairing reagent interfered with ICP-MS detection of  $^{31}\text{P}$ , an octopole reaction system was investigated to determine whether the polyatomic interferences could be reduced. The results show that addition of He to the cell can benefit analyses by reducing such interferences, but at the expense of reduced sensitivity. The detection limits in the range of 1.0–1.5  $\mu\text{g L}^{-1}$  (expressed as P) was achieved when 50  $\mu\text{L}$  was injected using He as the collision gas.

© 2009 Elsevier B.V. All rights reserved.

## 1. Introduction

Separation methods most commonly used for the determination of glyphosate and AMPA include gas chromatography (GC) and liquid chromatography (LC). Since glyphosate and AMPA lack chromophoric or fluorescent groups and are the ionizable functional groups compounds with ionizable functional groups, the derivatization of glyphosate and AMPA with different reagents is often required before GC or LC analysis. In GC-based approach, glyphosate and AMPA are usually converted into the volatile compounds and subsequently separated by GC and detection by various detection schemes [1–3]. Pre-column or post-column derivatization LC methods with various detection techniques are also commonly used for the determination of glyphosate and AMPA at trace levels. Pre-column procedures are based on derivatization with 9-fluorenylmethyl chloroformate [4–8] to allow fluorescence detection of the derivatives, while pre-column derivatization of glyphosate and AMPA is achieved directly in the native aqueous sample with 9-fluorenyl methoxycarbonyl chloride and on-line solid-phase extraction (SPE) and HPLC–ESI-MS/MS

[9]. Recently, similar works on pre-column derivatization with 9-fluorenylmethylchloroformate and LC–ESI-MS coupled with on-line SPE have been applied for the determination of glyphosate and AMPA in water samples [10,11]. Since on-line SPE was coupled with LC–ESI-MS/MS, the detection limits of 50  $\text{ng L}^{-1}$  were obtained. The reagents such as o-phthalaldehyde (OPA) and mercaptoethanol [12] in post-column derivatization react with glyphosate and AMPA to form the chromophoric or fluorescent derivatives and consequently can be detected after separation by ion chromatography. These methods are useful in real applications and provide the lower detection limit. However, the procedures of derivatization are time-consuming and tedious.

As an alternative direct method for the determination of glyphosate and AMPA, inductively coupled plasma mass spectrometry (ICP-MS) provides the advantage of high selectivity, and high sensitivity [13]. Recently, ion-pairing chromatography coupled with ICP-MS has been developed to detect glufosinate, glyphosate and AMPA in waters using a mobile phase containing tetrabutylammonium hydroxide and acetate buffer at pH 4.7 with an octopole reaction cell to reduce polyatomic ion interferences such as  $^{14}\text{N}^{16}\text{O}^1\text{H}^+$  and  $^{15}\text{N}^{16}\text{O}^+$ . Ion-pairing chromatography is useful for the separation of both ionic and non-ionic metal speciation [14]. However, the organic modifier and a nitrogen-based ion-pairing reagent in the mobile phase are not compatible with ICP plasma due to the alternation of ionisation characteristics of the Ar plasma and production of polyatomic ions [14,15]. Anion-

\* Corresponding author at: Centre for Environmental Risk Assessment and Remediation, University of South Australia, Mawson Lakes Campus, Mawson Lakes, SA 5095, Australia. Fax: +61 8 83023057.

E-mail address: [zuliang.chen@unisa.edu.au](mailto:zuliang.chen@unisa.edu.au) (Z. Chen).

exchange chromatography coupled with ICP-MS was investigated to determine trace glyphosate and phosphate in waters with a mobile phase containing a 20-mM citric acid [16], the detection limit of  $0.7 \mu\text{g L}^{-1}$  was obtained when a 500- $\mu\text{L}$  sample injection volume was injected. More recently, cation-exchange chromatography has been used for the separation of glyphosate and AMPA with 10 mM KCl and 10 mM HCl as the mobile phase, where  $P$  was measured as  $^{31}\text{P}^{16}\text{O}^+$  using oxygen as reaction gas. The lower detection limits ( $0.1 \mu\text{g L}^{-1}$ ) was obtained since the solid-phase extraction was used for the enrichment of analyte and consequently the method was successfully used for the determination of glyphosate and AMPA in various waters [17]. However, the citric acid and potassium chloride in the mobile phases resulted in high levels of carbon and potassium precipitation on the sampler and skimmer cones of ICP-MS, thus resulting in unstable plasma and considerable drift in retention time after prolonged use [15,18]. For these reasons, in this study, anion-exchange chromatography with ICP-MS was examined to determine glyphosate, AMPA and phosphate. Because phosphate is a common anion presented in water and soil samples, it could be overlapped with glyphosate and AMPA using an IC separation, and consequently it interferes in detection of glyphosate and AMPA at detection of  $m/z$   $^{31}\text{P}$ . Furthermore, to reduce the  $^{14}\text{N}^{16}\text{O}^1\text{H}^+$ ,  $^{15}\text{N}^{16}\text{O}^+$  [14] and  $\text{NOH}^+$  and  $\text{NO}^+$  [17] resulting from sample matrices; a reaction cell was used to determine whether it could reduce the polyatomic ions. The carbon and potassium residue on the sampler and skimmer cones of ICP-MS was overcome by using a mobile phase containing  $\text{NH}_4\text{NO}_3$ . To solve these issues, the following aspects were therefore systematically investigated: (1) to explore the possibility of removal polyatomic species  $^{14}\text{N}^{16}\text{O}^1\text{H}^+$  and  $^{15}\text{N}^{16}\text{O}^+$  using a collision/reaction system, (2) to separate phosphate from glyphosate and AMPA on a novel column (G3154/101A, Agilent technologies) by manipulation of mobile phase to give the reasonable resolution and (3) to demonstrate a method for the detection of these complexes in the soil extract without pre-treatment.

## 2. Experimental

### 2.1. Chemicals and solutions

All chemicals were of analytical grade reagents purchased from Sigma and Aldrich (Sydney, Australia). Milli-Q water ( $18.2 \text{ M}\Omega \text{ cm}^{-1}$ , Milli-Q Plus system, Millipore, Bedford, MA, USA) was used for preparing all solutions and standards. Eluents required for IC-ICP-MS were prepared by dissolution of an appropriate amount of ammonium salts in Milli-Q water and were filtered through a disposable  $0.45 \mu\text{m}$  cellulose acetate membrane filter (Millipore). This solution was degassed in an ultrasonic bath prior to use. Eluent pH was adjusted with 0.1 M ammonium hydroxide.

Soil samples were collected from the agricultural sites, South Australia, which were contaminated with glyphosate and AMPA. Air-dried soil samples were homogenized and 5.0 g soils were transferred to centrifuge tubes (50 mL). Samples were extracted by shaking with 0.1 M KOH (10 mL) on a mechanical shaker for 2 h, and then centrifuged at 3500 rpm for 30 min. The alkaline sample extracted was separated and neutralized by adding drops of HCl 1 M until pH 7 [10]. After that, the neutralized supernatant was 10-fold diluted with Milli-Q water prior to injection to IC-ICP-MS system.

### 2.2. IC-ICP-MS conditions

An Agilent 1100 liquid chromatography module equipped with a column oven (Agilent, Tokyo, Japan), guard column (G3154A/102)

and a separation column (G3154A/101, based on porous poly-methacrylate resin with  $10 \mu\text{m}$  particle size and an exchange capacity of  $50 \mu\text{equiv. g}^{-1}$ ) were used. The samples were injected using an 1100 auto-sampler with an injection volume of  $50 \mu\text{L}$ . The mobile phase used for separation of targets was 20 mM  $\text{NH}_4\text{NO}_3$  at pH 5.10; the flow-rate was  $1.0 \text{ mL min}^{-1}$ . The outlet of the separation column was connected directly to the Babington nebulizer of an Agilent 7500c ICP-MS by use of a 50-cm length of PEEK tubing. The conditions used for ICP-MS were RF power 1500 W, plasma gas (Ar) flow  $15 \text{ L min}^{-1}$ , auxiliary gas (Ar) flow  $1.0 \text{ L min}^{-1}$ , carrier gas (Ar) flow  $1.15 \text{ L min}^{-1}$ , sampling depth 7.5 mm, integration time 1 s, and dwell time 0.5 s. The targets were detected at  $m/z$  31 ( $^{31}\text{P}$ , 100% abundance). The IC-ICP-MS system was controlled and the data was processed using Agilent's Chemstation software package.

## 3. Results and discussion

### 3.1. Removal of the polyatomic ion by ORC

Since radio frequency (RF) forward power and carrier gas flow rate are usually the most significant parameters affecting the background and analytical signal, these are therefore needed to be optimized for an optimal signal-to-noise ratio. The solution spiked with  $20 \mu\text{g L}^{-1}$  glyphosate was directly aspirated into nebulizer with a carrier containing 20 mM  $\text{NH}_4\text{NO}_3$  at pH 5.10 at a flow rate of  $1.0 \text{ mL min}^{-1}$ . The intensities of the blank and spike solution increased with increasing carrier gas flow rate in the range of  $1.1$ – $1.25 \text{ L min}^{-1}$  with the increase of RF power in the range of 1300–1500 W. 1500 W forward power and carrier gas flow rate at  $1.15 \text{ L min}^{-1}$  were considered. Therefore, these parameters were chosen for the subsequent study.

The limitation of ICP-MS in the detection of  $^{31}\text{P}$  is interfered with the polyatomic ions such as  $^{14}\text{N}^{16}\text{O}^1\text{H}^+$  and  $^{15}\text{N}^{16}\text{O}^+$  from Ar plasma gas and matrices. In this study, the collision reaction cell technique was explored to reduce these interferences [19–22], where polyatomic interference was removed by He or  $\text{H}_2$  added to the cell. Consequently, the elimination of the isobaric interference was accomplished by either collisionally induced dissociation (CID) and kinetic energy discrimination (KED) or chemical reaction [18,19]. Since He or  $\text{H}_2$  flow rate is usually the most significant parameter affecting the background and analytical signals, it required optimization. The solution containing 20 mM  $\text{NH}_4\text{NO}_3$  at pH 5.10 and spiked with  $20 \mu\text{g L}^{-1}$  glyphosate was aspirated into nebulizer and then into plasma. Reaction gas flow rate ranged from 0 to  $5 \text{ L min}^{-1}$ . The flow rate for He was at  $3.5 \text{ L min}^{-1}$  to give the best signal-to-noise ratios. Fig. 1 shows the chromatograms obtained from IC-ICP-MS at  $m/z$  31 using no gas, He ( $3.5 \text{ L min}^{-1}$ ) and  $\text{H}_2$  ( $3.0 \text{ L min}^{-1}$ ) as the gas, respectively. The separation of the phosphorus species was performed on anion-exchange column using a mobile phase containing 20 mM  $\text{NH}_4\text{NO}_3$  at pH 5.10. It can be seen that the sensitivity for the detection of  $^{31}\text{P}$  as indicated by the counts obtained, decreased in the order of no gas >  $\text{H}_2$  > He. This indicates that the addition of He and  $\text{H}_2$  gas to the cell decreased the sensitivity, and that the no gas mode gave the greatest sensitivity. When normalised to the standard tune, the relative sensitivity expressed as a percent was in the order of no gas [AMPA, 100%; phosphate, 100%; glyphosate, 100%] >  $\text{H}_2$  [AMPA, 95.21%; phosphate, 95.91%; glyphosate, 95.44%] > He [AMPA, 53.32%; phosphate, 53.46%; glyphosate, 51.03%]. The sensitivity for the phosphorus species decreased using an octopole reaction system [14]. Compared to  $\text{H}_2$  as the reaction gas, a lower sensitivity for the phosphorus species was achieved using He as the collision gas. This can be contributed to their different mechanisms, e.g., in He cell mode, it was based on the CID, and KED and consequently reduced the sensitivity [19–22].

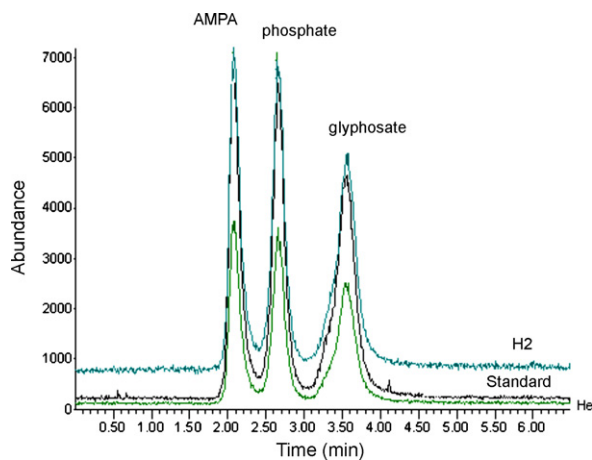


**Fig. 1.** Chromatogram obtained from standard, H<sub>2</sub> and He cell modes at  $m/z$  31. The mobile phase: 20 mM NH<sub>4</sub>NO<sub>3</sub> at pH 5.10.

It is also interesting to note the differences in the background signal were obtained using modes. The background signal and noise level were significantly reduced using He, while they were increased using H<sub>2</sub> as the reaction gas. For example, the background signal for three modes was in the order of H<sub>2</sub> (750 intensity) > no gas (250 intensity) > He (100 intensity). Compared to no gas mode, background signal increased from 100% to 300% using H<sub>2</sub> as the reaction gas resulted in forming the <sup>14</sup>N<sup>16</sup>O<sup>1</sup>H<sup>+</sup> when the H<sub>2</sub> was added to the cell based on an ion–molecule interaction [19–22]. Consequently the background signal increased. In contrast, background signal was reduced from 100% to 40% using He as the collision gas, this indicates that the addition of He did reduce the background and thus improving the detection limits. When a sufficient amount of He is added to the cell, the interfering ions such as <sup>14</sup>N<sup>16</sup>O<sup>1</sup>H<sup>+</sup> and <sup>15</sup>N<sup>16</sup>O<sup>+</sup>, which possess larger cross-sectional areas than the analyte ions, undergo more frequent collisions and lose most of their kinetic energies. As a consequence, the interfering ions with insufficient kinetic energies are unable to surmount the large energy barrier. Only the analyte ions, which have sufficient kinetic energies, eventually reach the mass detector [19,20]. He flow rate of 3.5 L min<sup>-1</sup> was found to provide the most optimal compromise when background, detection limit and sensitivity were considered. Furthermore, the detection limit of phosphorus species obtained from He as the collision gas were estimated to be 1.0 μg L<sup>-1</sup> for AMPA, 1.0 μg L<sup>-1</sup> for phosphate and 1.5 μg L<sup>-1</sup> for glyphosate, respectively.

### 3.2. IC separation of phosphorus species

Since ICP-MS is only an element-specific detector, it is impossible to detect glyphosate and AMPA when these targets are not separated by separation method such as ion chromatography. In addition, phosphate anions are commonly found in environmental samples, and thus could cause interference to ICP-MS detection of glyphosate and AMPA. For these reasons, the resolution between phosphorus species can be manipulated by the composition of mobile phase, including the mobile phase pH, the type of competing anion and its concentration [23,24], which is dependent upon the target ionic compounds. For example, AMPA (pK<sub>a1</sub>: 1.8; pK<sub>a2</sub>: 5.4; pK<sub>a3</sub>: 10.0), glyphosate (pK<sub>a1</sub>: 0.8; pK<sub>a2</sub>: 2.3; pK<sub>a</sub>: 5.3; pK<sub>a4</sub>: 11.0) and phosphate (pK<sub>a1</sub>: 2.1; pK<sub>a2</sub>: p 7.2; K<sub>a3</sub>: 12.7). It can be expected that these targets are polyvalent anions and consequently strongly retained on anion-exchange column. Therefore the addition of a strong competing anion to the mobile phase is required. Furthermore, sodium buffer deposits residue on the sampler and skimmer cones of ICP-MS causing unstable plasma unstable which results

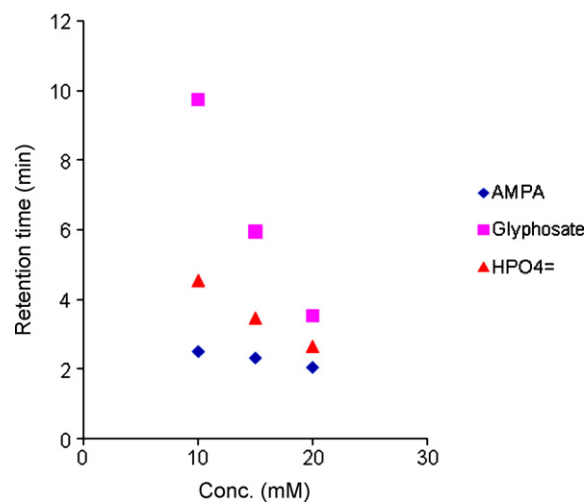


**Fig. 2.** The effect of the concentration of NH<sub>4</sub>HPO<sub>4</sub> in eluent on the retention time. The conditions as described in text.

in considerable drift in retention time after prolonged use [18]. On the basis of these points, NH<sub>4</sub>NO<sub>3</sub> was added to mobile as NO<sub>3</sub><sup>-</sup> is a strong competing anion and NH<sub>4</sub>NO<sub>3</sub> will not form residue on the cones.

The concentration of NO<sub>3</sub><sup>-</sup> in the mobile phase is one factor which influences ion-exchange retention times. Thus, the concentrations of NH<sub>4</sub>NO<sub>3</sub> at pH 6.5 in the eluent were investigated in the range of 10–20 mM. As shown in Fig. 2, the retention time decreased with increasing concentrations of NH<sub>4</sub>NO<sub>3</sub>. Thus, peak shape and resolution was improved by the manipulation of NH<sub>4</sub>NO<sub>3</sub> concentration. It was also observed that that retention times decreased as eluent concentration increased for the higher charged glyphosate than for the lower charged AMPA. The higher the concentration of NO<sub>3</sub><sup>-</sup> ions in the eluent, the more effectively displaced target ions from the stationary phase and consequently the more rapidly the target ions were eluted from anion-exchange column [23,24]. After all these factors were taken into consideration, an eluent containing 20 mM NH<sub>4</sub>NO<sub>3</sub> was determined to achieve the best peakshape with the shortest running time.

The eluent pH is also an important factor when retention times are considered since any changes in pH influence the charge of the target analyte. As shown in Fig. 3, the retention time decreased with

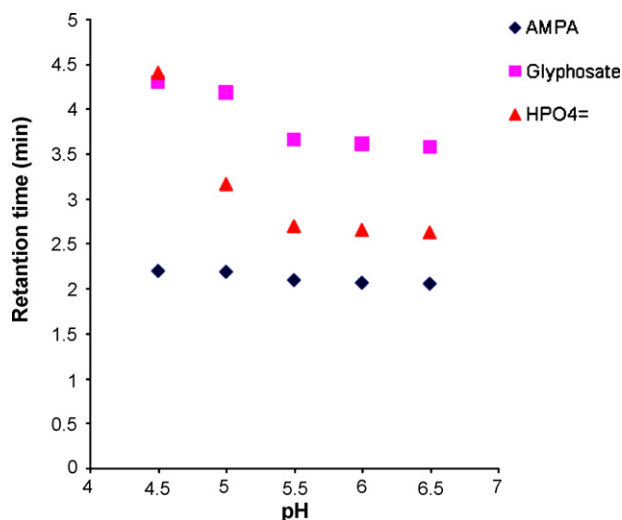


**Fig. 3.** The effect of the eluent pH on the retention time. The conditions as described in text.

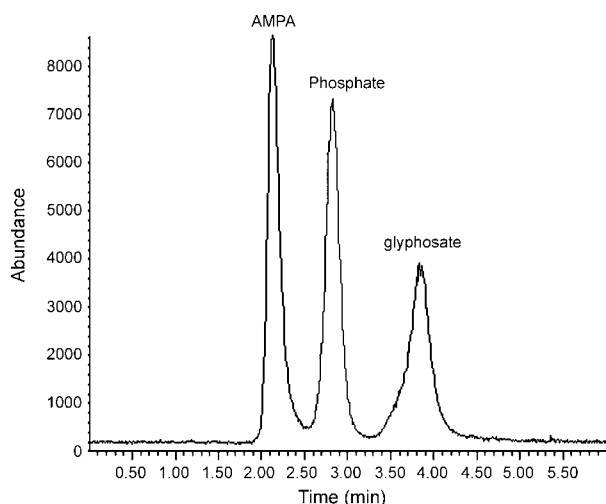


**Fig. 4.** The typical chromatogram for targets, each target concentration:  $200 \mu\text{g L}^{-1}$ ; mobile phase:  $20 \text{ mM NH}_4\text{NO}_3$  at pH 5.10. Other conditions described in text.

increasing eluent pH from 4.5 to 6.5. However, the retention time for the phosphate was significantly reduced as the eluent pH was raised because it was single charge in range of pH tested. Thus, an eluent pH at 5.10 was used to separate the phosphate from glyphosate and AMPA. Consequently, ICP-MS detection of glyphosate and AMPA was possible.

### 3.3. IC-ICP-MS analysis of AMPA, phosphate and glyphosate

Fig. 4 shows a typical chromatogram obtained from IC-ICP-MS with an eluent containing  $20 \text{ mM NH}_4\text{NO}_3$  at pH 5.10 using He cell mode. The eluted targets were in the order of AMPA, phosphate and glyphosate, a result of their mass and charge. Calibration curves for quantification were obtained by plotting peak area versus the concentration of the corresponding target compounds. All calibrations were linear over a concentration range of  $5.0\text{--}1000 \mu\text{g L}^{-1}$  with correlation coefficients greater than 0.999. Detection limits (signal-to-noise ratio of 3) ranged from  $1.0$  to  $1.5 \mu\text{g L}^{-1}$  (expressed as *P*). The reproducibility from injection of  $20 \mu\text{g L}^{-1}$  ( $n=5$ ) from a standard solution containing a mixture of the targets showed that R.S.D. was less than 2.1%. In order to test the applicability of the method for the determination of targets, soil extracts were spiked with a mixed  $20 \mu\text{g L}^{-1}$  standard. Recoveries for targets ranged from 92.7% to 101.1% as listed in Table 1. The proposed method was used to test more than 80 soil extracts. However, the data shows that the column was required to regenerate using a solution containing  $1 \text{ mM EDTA}$  after loading 50 samples. Fig. 5 shows the typical chromatogram obtained from soil extracts, a high concentration of phosphate ( $425.6 \pm 4.5 \mu\text{g L}^{-1}$ ,  $n=3$ ) was found, while a lower concentration of APMA ( $48.2 \pm 0.9 \mu\text{g L}^{-1}$ ,  $n=3$ ) and glyphosate ( $17.8 \pm 0.5 \mu\text{g L}^{-1}$ ,  $n=3$ ). The result obtained from the 200 soil extracts shows glyphosate in soil was rapidly degraded into AMPA after 10 h when the soil was spiked with glyphosate. In addition, a higher concentration of glyphosate was found in acid

**Table 1**

Analytical performance for the proposed method.

Species	DR ( $\mu\text{g L}^{-1}$ )	Coefficient	DL ( $\mu\text{g L}^{-1}$ )	R.S.D. ( $n=5$ , %)	Recovery $20 \mu\text{g}$ (%)
AMPA	1.0–1000	1.000	1.0	1.9	102.3
Phosphate	1.0–1000	0.999	1.0	2.0	95.7
Glyphosate	1.0–1000	0.999	1.5	2.1	92.7

DL: detection limit (signal/noise=3); LDR: linear dynamic range; R.S.D.: relative standard deviation.

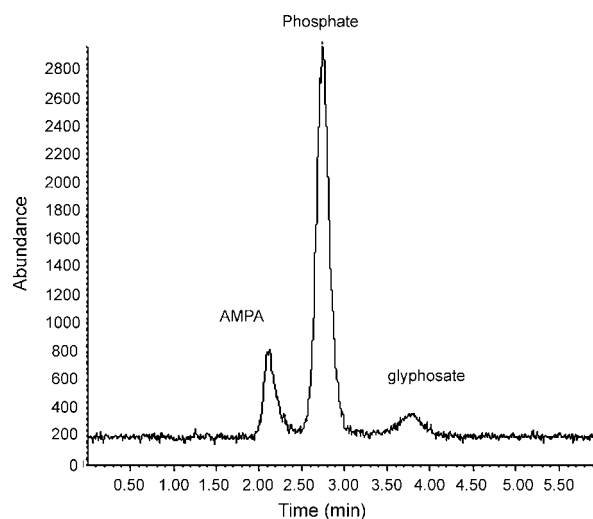


**Fig. 5.** The typical chromatograms obtained from the soil extracts. The conditions as described in Fig. 4.

soil and less in neutral soil, this is due to there is more organic matter in acid soil, and consequently a less degradation of glyphosate was observed.

## 4. Conclusions

The new anion-exchange column has been successfully applied for the speciation of AMAP, phosphate and glyphosate with an eluent containing  $20 \text{ mM NH}_4\text{NO}_3$  at pH 5.10. An eluent containing  $\text{NH}_4\text{NO}_3$  avoided clogging of the nebulizer, and the sampling and skimmer cones. In addition, the polyatomic ions such as  $^{14}\text{N}^{16}\text{O}^+\text{H}^+$  and  $^{15}\text{N}^{16}\text{O}^+$  were reduced using an octopole reaction system, while He tune was recommended with a flow rate at  $3.5 \text{ mL min}^{-1}$  to achieve a lower detection limit in the expense of loss the sensitivity. Finally, speciation was performed within 6 min low detection limits ( $\mu\text{g L}^{-1}$ ) without any chemical derivatization, sample pre-concentration and mobile phase suppressed except simple filtration.

## Acknowledgements

Dr. Wenxiang He was supported by the Natural Science Foundation of China (No. 40301022), and State Scholarship Fund. We are grateful to the anonymous reviewers for their comments which significantly improved the quality of the manuscript.

## References

- [1] C.D. Stalikas, C.N. Konidari, J. Chromatogr. A 907 (2001) 1.
- [2] E. Borjesson, L. Torstensson, J. Chromatogr. A 886 (2000) 207.
- [3] Z.H. Kudzin, D.K. Gralak, G. Andrijewski, J. Drabowicz, J. Luczak, J. Chromatogr. A 998 (2003) 183–199.
- [4] J.V. Sancho, F. Hernández, F.J. López, E.A. Hogendoorn, E. Dijkman, P. van Zoonen, J. Chromatogr. A 737 (1996) 75.
- [5] J.V. Sancho, F.J. López, F. Hernández, E.A. Hogendoorn, P. van Zoonen, J. Chromatogr. A 678 (1994) 59.
- [6] E.A. Hogendoorn, F.M. Ossendrijver, E. Dijkman, R.A. Baumann, J. Chromatogr. A 833 (1999) 67.
- [7] C. Hidalgo, C. Rios, M. Hidalgo, V. Salvadó, J.V. Sancho, F. Hernández, J. Chromatogr. A 1035 (2004) 153.
- [8] E.A. Lee, L.R. Zimmerman, B.S. Bhullar, E.M. Thurman, Anal. Chem. 74 (2002) 4937.
- [9] R.J. Vreeken, K. Speksnijder, I. Bobeldijk-Pastorova, H.M.Th. Noij, J. Chromatogr. A 794 (1998) 187.
- [10] M. Ibanez, O.J. Pozo, J.V. Sancho, F.J. López, F. Hernández, J. Chromatogr. A 1081 (2005) 145.
- [11] M. Ibanez, O.J. Pozo, J.V. Sancho, F.J. López, F. Hernández, J. Chromatogr. A 1134 (2006) 51.
- [12] E. Mallat, D. Barcelo, J. Chromatogr. A 823 (1998) 129.

- [13] M. Montes-Bayon, K. DeNicola, J.A. Caruso, *J. Chromatogr. A* 1000 (2003) 457.
- [14] B.B.M. Sadi, A.P. Vonderheide, J.A. Caruso, *J. Chromatogr. A* 1050 (2004) 95.
- [15] B. Michalke, *Trends Anal. Chem.* 21 (2002) 142.
- [16] Z.X. Guo, Q.T. Cai, Z.G. Yang, *J. Chromatogr. A* 1100 (2005) 160.
- [17] M. Popp, S. Hann, A. Mentler, M. Fuerhacker, G. Stingeder, G. Kollensperger, *Anal. Bioanal. Chem.* 391 (2008) 695.
- [18] C. B'Hymer, J.A. Caruso, *J. Liq. Chromatogr. Relat. Technol.* 25 (2002) 639.
- [19] S.D. Tanner, V.I. Baranov, D.R. Bandura, *Spectrochim. Acta B* 57 (2002) 1361.
- [20] E. McCurdy, G. Woods, *J. Anal. Atom. Spectrom.* 19 (2004) 607.
- [21] P.B. Armentrout, *J. Anal. Atom. Spectrom.* 19 (2004) 571.
- [22] J.W. Olesik, D.R. Jones, *J. Anal. Atom. Spectrom.* 21 (2006) 141.
- [23] C. Sarzanini, M.C. Bruzzoniti, *Trends Anal. Chem.* 20 (2002) 304.
- [24] J. Weiss, *Ion Chromatography*, 2nd ed., VCH, Weinheim, 1995.





# Simple and sensitive fluorometric sensing of malachite green with native double-stranded calf thymus DNA as sensing material

Dongmei Cheng, Baoxin Li\*

Key Laboratory of Analytical Chemistry for Life Science of Shaanxi Province, School of Chemistry and Materials Science, Shaanxi Normal University, Shida Road No. 1, Xi'an 710062, PR China

## ARTICLE INFO

### Article history:

Received 28 September 2008  
Received in revised form 5 January 2009  
Accepted 5 January 2009  
Available online 20 January 2009

### Keywords:

Fluorescence  
Malachite green  
Calf thymus DNA  
Intercalation binding

## ABSTRACT

A novel fluorometric sensing of malachite green is proposed in this paper. The native double-stranded calf thymus DNA was used as sensing material. In the presence of native double-stranded calf thymus DNA, malachite green could interact with the DNA, which resulted in a strong fluorescence emission. The fluorescent intensity was linear with malachite green concentration in the range of  $4.0 \times 10^{-10}$ – $1.8 \times 10^{-7}$  g ml<sup>-1</sup> and the limit of detection was  $2.0 \times 10^{-10}$  g ml<sup>-1</sup>. Before fluorescence measurement, the only required operation is the mixing of two solutions. So, this method is rather simple and rapid. The method is very safe for the analyst. Furthermore, the mechanism for fluorescence enhancing of native double-stranded calf thymus DNA on MG was proposed based on a series of experiments. The results suggest that the interaction between MG and calf thymus DNA is intercalation in nature.

© 2009 Elsevier B.V. All rights reserved.

## 1. Introduction

Malachite green (MG) is a cationic triphenylmethane dye, and its structure is shown in Fig. 1. It has been widely used around the world as a fungicide and antiseptic in the aquaculture industry [1]. Nowadays, the use of MG in aquaculture has become a matter of concern because it is suspected of being genotoxic and carcinogenic [1,2]. As a result, the use of MG has been banned in several countries. Although the use of MG has been banned in several countries including China, it is still being used in many parts of the world due to its low cost, availability, and efficacy. Thus, the searching for new MG-sensing strategies for simple, rapid and selective determination of MG is of topical interest, especially in situations where conventional techniques are not appropriate, for instance in many on-site or in situ analyses and for rapid screening applications.

Because MG has a strong chromophore at 618 nm and is positively charged, many analytical methods take advantage of the characteristic to detect MG. The methods include spectrophotometry after solid phase extraction [3] or cloud point extraction [4], liquid chromatography with visible detection [5] or mass spectrometry [6,7], surface-enhanced Raman spectroscopy [8] and enzyme-linked immunosorbent assay [9]. However, some of the problems associated with these analytical methods, such as a long sample preparation time, poor detection limit, lengthy measurement time and expensive instruments operated by well-trained

analysts, made these detection systems less attractive. Therefore, a rapid and sensitive detection method for analysis is still needed.

Fluorescence detection is now used for a wide range of quantitative applications and offers the advantages of high sensitivity, rapidity, stability, simplicity and feasibility [10]. In 2006, the fluorescent detection was used as the standard method to determine residues of MG in China [11]. In the standard method [11], MG (a nonfluorescent triphenylmethane dye) was firstly reduced to leuco malachite green with sodium borohydride, and then was detected through measuring the fluorescent intensity of the produced leuco malachite green. The method is indirect measurement, and the sample pretreatment of sample is time-consuming; it must ensure that all MG are transformed to leuco malachite green, and the operation is rather difficult.

In this paper, we interestingly observed a fluorescence phenomenon, and a strong fluorescence signal was detected when some commercial double-stranded calf thymus DNA (ct-DNA) was added into MG solution. Based this experimental phenomenon, ct-DNA is used as sensing material, and a new fluorescence detection of MG is proposed. The detection limit of the method is 0.2 ng ml<sup>-1</sup>. This method is rather simple and rapid because the only operation required before fluorescence measurement is the mixing of two solutions. Furthermore, ct-DNA is easily obtained and not poisonous, and the method is very safe for the analyst. This paper also demonstrated that nature nucleic acids could be used as tools to explore biology [12]. The experimental results showed that MG could interact with ct-DNA to form a supramolecular complex mainly by intercalation. The generated supramolecular complex showed some excellent fluorescence-property: high flu-

\* Corresponding author. Fax: +86 29 85307774.

E-mail addresses: [libx29@hotmail.com](mailto:libx29@hotmail.com), [libaoxin@snnu.edu.cn](mailto:libaoxin@snnu.edu.cn) (B. Li).

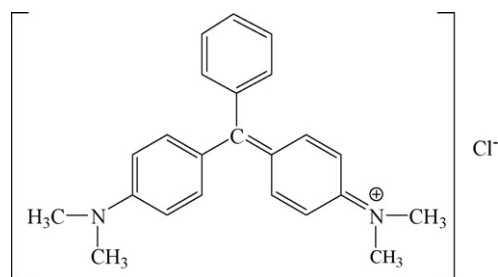


Fig. 1. Molecular structure of malachite green (MG).

orescence quantum and fluorescence emission in near infrared region ( $\lambda_{\max} = 665 \text{ nm}$ ). The proposed method was applied to detect MG in water samples of fish-farming and fish muscle.

## 2. Experimental

### 2.1. Apparatus

The fluorescence spectra and intensity were acquired on a model 970-CRT Spectrofluorimeter (Shanghai Analytical Instrument Plant, Shanghai, China) equipped with a xenon lamp. A model TU-1901 UV-vis Spectrophotometer (Beijing Purkinje General Instrument Co., Ltd., Beijing, China) was used for recording absorption spectra using 1 cm quartz cell. The pH was measured using a Model pH-3C digital pH meter (Shanghai, China).

### 2.2. Chemical and reagents

All the reagents were of analytical-reagent grade unless specified otherwise; the water used was deionized and distilled. A MG stock solution ( $1 \times 10^{-4} \text{ g ml}^{-1}$ ) was prepared by dissolving a certain amount of MG chloride salt (Tianjin Tianda Chemical Plant, Tianjin, China) in water and stored in refrigerator ( $4^\circ\text{C}$ ). A MG working solution was prepared daily by diluting the stock solution with water.

Native double-stranded ct-DNA and herring sperm DNA were purchased from Sigma. Stock solutions of nucleic acid were prepared by dissolving the DNA in  $0.1 \text{ mol l}^{-1}$  Tris-EDTA buffer solution (pH 8.0). For dissolving the DNA, 24 h or more were needed with an occasional gentle shake. The DNA solutions gave the ratios of UV absorbance at 260 and 280 nm ( $A_{260\text{nm}}/A_{280\text{nm}}$ ) of ca. 1.8–1.9, which indicated that the DNA were sufficiently free from protein. All of the stock solutions and their diluted solutions were stored in a refrigerator at  $4^\circ\text{C}$  until used.  $0.1 \text{ mol l}^{-1}$  Tris-HCl buffer solution was used to control the pH of the reaction solution.

### 2.3. Procedure

In a 5 ml volumetric flask, appropriate amount of MG,  $50 \mu\text{l}$  ct-DNA ( $5 \times 10^{-3} \text{ g ml}^{-1}$ ) and 3.0 ml Tris-HCl (pH 10.0) were successively added. The mixture was diluted with water to the scale and mixed homogeneously. The instrument excitation and emission slits were set at 10 nm, and the fluorescent spectrum and intensity were obtained with excitation wavelength of 620 nm at room temperature. The concentration of MG was quantified by the fluorescent intensity at 665 nm. Reagent blank was prepared and measured following the same procedure.

## 3. Results and discussion

### 3.1. Spectral characteristics

MG is a non-fluorescent substrate, but the strong fluorescence signal is observed when ct-DNA is added into MG solution.

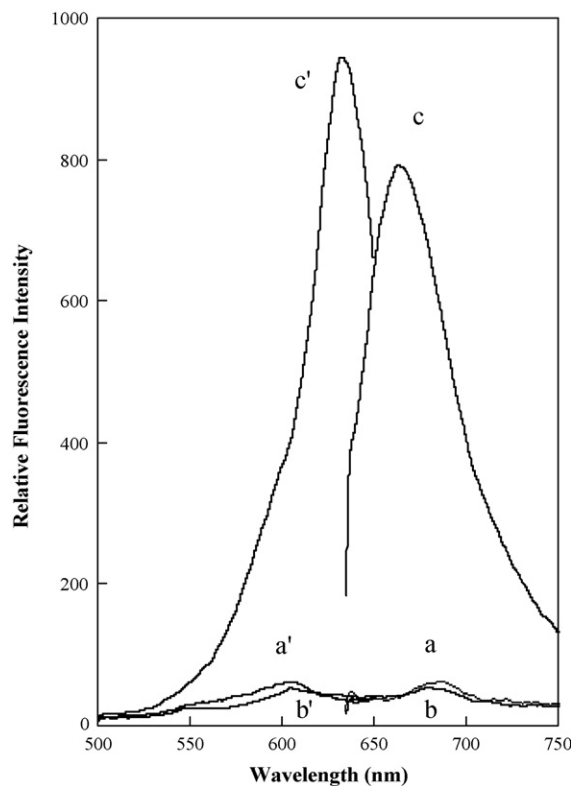


Fig. 2. Fluorescence spectra of this system. Line (a) represents emission spectrum of ct-DNA ( $50 \mu\text{g ml}^{-1} \text{ mL}^{-1}$ ) solution, line (b) represents emission spectrum of MG ( $176 \mu\text{g ml}^{-1}$ ) solution and the line (c) represents emission spectrum of MG solution in the presence of ct-DNA; Line (a'), line (b') and line (c') are the corresponding excitation spectra of MG, ct-DNA and the mixture of MG and ct-DNA in aqueous solutions, respectively.

Fig. 2 shows the fluorescence spectral of this system. It can be seen that the maxima excitation and emission wavelengths of the mixture of MG and ct-DNA are 620 and 665 nm, respectively.

### 3.2. Choice of buffer and pH

The preliminary experiments showed that this system did not emit strong fluorescence in strong acid media (pH < 5.0). The possible reason is that in strong acid media MG cannot easily interact with ct-DNA. The kind of buffer solution and pH of the buffer solution generally affect the fluorescence intensity. So, buffering systems based on carbonate, phosphate and Tris-HCl were tested in this fluorescence system. The experimental results showed that Tris-HCl was the most suitable buffer solution. Furthermore, the pH dependence of the fluorescence intensity was also investigated (Fig. 3). The weak fluorescent signal in this system was observed in strong base media (pH > 11.0), probably because of conformation change of ct-DNA (double-stranded DNA) in strong base media. In pH 10.0 media, the fluorescence system showed the maxima signal. MG has two amino groups with  $pK_a$  of 6.9 that are protonated at pH 4.0, and at pH 10.0 most molecules of MG are deprotonated. So, the pH effect is a combination of change on MG, charge on the DNA, and stability of hybridization. Then, pH 10.0 Tris-HCl buffer solution was chosen as the optimum media in this system.

### 3.3. Effect of ct-DNA concentration on the fluorescence intensity

In the absence of ct-DNA, MG is the only chromophoric reagent and is not fluorescent. In the presence of ct-DNA, a strong flu-

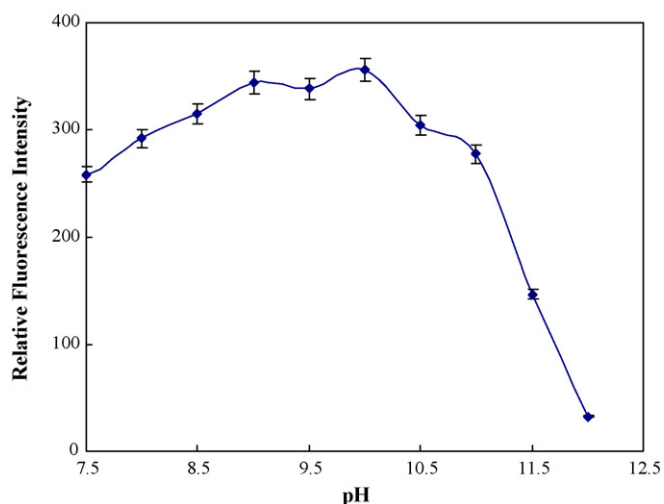


**Fig. 3.** Effect of pH on the fluorescence intensity of this system. MG:  $0.36 \mu\text{g ml}^{-1}$ ; ct-DNA:  $50 \mu\text{g ml}^{-1}$ ; Tris:  $0.1 \text{ mol l}^{-1}$ .

orescent emission is observed in the system. So, the effect of ct-NDA concentration on the fluorescence intensity was studied. The experimental result is shown in Fig. 4. It can be seen that the fluorescence intensity increased with increasing ct-NDA concentration, and above the concentration of  $50 \mu\text{g ml}^{-1}$ , the fluorescence intensity remained almost constant. The  $50 \mu\text{g ml}^{-1}$  ct-DNA was used for all subsequent experiments.

#### 3.4. Performance of the system for MG measurement

Under the optimum conditions described above, the calibration curve of the fluorescence intensity ( $F$ ) versus the MG concentration ( $C$ ) was linear in the range of  $4.0 \times 10^{-10}$  to  $1.8 \times 10^{-7} \text{ g ml}^{-1}$ , and the limit of detection was  $2 \times 10^{-10} \text{ g ml}^{-1}$ . The regression equation was  $F = 4.87C \times 10^9 + 10.3$  ( $C: \text{g ml}^{-1}$ ) with a correlation coefficient of 0.9988. Ten concentration levels in 3 replicates were used in the construction of the calibration curve. The relative standard deviation was less than 5% for the determination of  $2.0 \times 10^{-8} \text{ g ml}^{-1}$  MG ( $n=9$ ). On the other hand, the stability of the fluorescence system was tested by checking the fluorescence intensity of the same mixture solution of MG and ct-DNA every 5 min. It was found that the fluorescence intensity of this system remained almost constant for 60 min at room temperature.

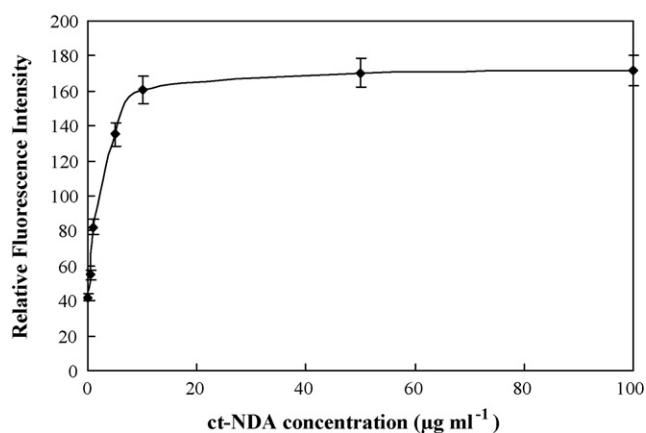


**Fig. 4.** Effect of the ct-DNA concentration on the fluorescence intensity of the MG-DNA system. MG:  $0.36 \mu\text{g ml}^{-1}$ ; Tris:  $0.1 \text{ mol l}^{-1}$ , pH 10.0.

#### 3.5. Interference study

To evaluate the selectivity of the method, the influences of other potential interfering species were investigated by analyzing a standard solution of  $1.8 \times 10^{-7} \text{ g ml}^{-1}$  MG to which increasing amounts of species was added. The tolerable limit of a foreign species was taken as a relative error not greater than 5%. The tolerated ratio of foreign substances to  $1.8 \times 10^{-7} \text{ g ml}^{-1}$  was over 10,000 for  $\text{K}^+$ ,  $\text{Na}^+$ ,  $\text{NO}_3^-$ ,  $\text{Cl}^-$  and  $\text{SO}_4^{2-}$ , 1000 for  $\text{CO}_3^{2-}$ ,  $\text{F}^-$  and EDTA, 100 for leuco malachite green,  $\text{Cu}^{2+}$  and  $\text{Mg}^{2+}$ , 50 for  $\text{Ca}^{2+}$ ,  $\text{Cr}^{3+}$ ,  $\text{Pb}^{2+}$  and  $\text{Co}^{2+}$ , 10 for  $\text{Mn}^{2+}$ ,  $\text{Zn}^{2+}$  and  $\text{Fe}^{3+}$ . It was obvious that many metal ions had some interference for determination of MG, possibly because of complexing with MG. Another reason of interference of metal ions is that some of them can cause melting of double-stranded DNA. However, the interference of the metal ions coexisting in the sample solution could be effectively eliminated by adding EDTA as a masking reagent. Leuco malachite green shows fluorescence at 360 nm ( $\lambda_{\text{ex}} = 265 \text{ nm}$ ), and in the condition for detection of MG ( $\lambda_{\text{ex}} = 620 \text{ nm}$  and  $\lambda_{\text{em}} = 665 \text{ nm}$ ), leuco malachite green could not interfere detect MG. Therefore, MG could be detected without separation of leuco malachite green.

#### 3.6. Application

The accuracy of the method was evaluated by determining the recoveries of MG after adding to fish farming water and river water samples. In order to eliminate the interference of the metal ions,  $5 \times 10^{-4} \text{ mol l}^{-1}$  EDTA was added into the samples. The results were shown in Table 1.

On the other hands, three different fish (cyprinoid, pomfret and grass carp) muscle tissues were used for making the spiked standard samples for evaluating the method performance. Fish samples were obtained from the local market. The fish was filleted, and the skin and bones were removed. The fish samples were extracted as described in reference [13] with minor modification. Five grams of fish muscle were accurately weighed into individual 50-ml Teflon centrifuge tubes. 1.5 ml of 20% hydroxylamine hydrochloride, 2.5 ml of  $1.0 \text{ mol l}^{-1}$  p-toluene sulfonic acid and 5.0 ml of acetate buffer (pH 4.5) were added to the samples. Individual sample was each spiked with 20 ng, 50 ng and 250 ng MG for the recovery tests. The sample mixtures were homogenized using a polytron homogenizer for 1 min at 10,000 rpm. 10 ml of acetonitrile was then added to the each sample, followed by shaking vigorously for 2 min. The sample was then defatted by adding 5.0 g of alumina, vigorously shaking for an additional 30 s, and then centrifuging for 10 min at 3000 rpm. The supernatant was decanted into a 250 ml separatory funnel containing water (10 ml) and diethylene glycol (2 ml). Solids were re-extracted with an additional 10 ml of acetonitrile, vortex mixed for 1 min, shaken vigorously for 1 min, and then centrifuged for 5 min. The supernatant was combined with the first extract in the separatory funnel. Dichloromethane (15 ml) was added, and after inversion to release pressure, the sample was liquid-liquid extracted for 30 s. Phases were allowed to separate for a maximum of 10 min. The lower dichloromethane layer was collected into a 100 ml glass pear-shaped boiling flask. The aqueous phase

**Table 1**  
Recovery for MG determination in fish farming and river water samples.

Sample	Added ( $\text{ng ml}^{-1}$ )	Found ( $\text{ng ml}^{-1}$ )	Recovery (%)
Fish farming water	11.0	10.5	95.4
	36.5	33.9	92.9
	100.0	103.3	103.3
River water	11.0	12.2	110.9
	25.5	24.9	97.6
	100.0	96.9	96.9

**Table 2**  
Recovery for MG determination in fish muscle at three spiked levels.

Fish sample	Spiked level (ng/g)	Found (ng/g)	Recovery (%)
Cyprinoid	4.0	3.3	82.5
	10.0	8.9	89.0
	50.0	55.0	110.0
Pomfret	4.0	3.5	85.6
	10.0	9.5	95.2
	50.0	53.2	106.4
Grass carp	4.0	3.2	79.9
	10.0	9.0	90.0
	50.0	51.2	102.3

was re-extracted with an additional 15 ml of dichloromethane, and the organic phase was combined with the first extract after 10 min of phase separation. The extract was evaporated to dryness under reduced pressure while heating the flask in a water bath set at 45 °C. 2.5 ml of acetonitrile was added to the oily residue, and the flask was swirled to dissolve the residue. The obtained sample solution was used to analysis by following the analysis procedures described in Section 2. The results were shown in Table 2.

### 3.7. Mechanism for fluorescence enhancing of ct-DNA on MG

As one kind of triphenylmethane dyes, MG displays strong absorbance and the molar extinction coefficients at 617 nm is  $9.5 \times 10^4 \text{ M}^{-1} \text{ cm}^{-1}$  in phosphate buffer (pH 5.8) [14]. Because of the propeller-like twisting of the phenyl rings with respect to the central triarylmethyl carbon, the aromatic rings of MG are forced out of the molecular plane that contains the central carbon atom. Furthermore, the twisting of the dimethylamino groups relative to the phenyl rings could contribute an additional mode of excited-state deactivation. MG normally has extremely low quantum yield of fluorescence ( $\sim 10^{-5}$ ) in low-viscosity media due to fast relaxation processes that occur via rotational motions of the aromatic rings [15,16]. So MG is often considered as a nonfluorescent compound in aqueous solution. In more viscous media or in microenvironments that could restrict such rotational relaxation processes, the fluorescence of MG tends to increase [17]. Baptista et al. [14] found that bovine serum albumin (BSA) was added into MG solution, and MG could be noncovalently bound to the protein, thereby experiencing loss of rotational degrees of freedom; the fluorescence quantum yield of BAS-bound MG increased to  $3 \times 10^{-3}$ . Babendure et al. [16] used MG aptamer RNA (5'-GGAUCCCGA CUGGCGAGAG CCAGGUAACG AAUGGAUCC-3') to bind MG, and the fluorescence of the aptamer-bound MG was tremendously enhanced (2360 times); the fluorescence characteristic of aptamer-bound MG was used to design the probe for fluorescent detection of nucleic acids [18]. Bhasikuttan et al. [19] studied the interaction of MG with guanine-rich single-stranded DNA, and found that the complex of MG with the G-quadruplex resulted in an approximately 100-fold enhancement of its fluorescence yield.

In this system, we found that the fluorescence of MG could be remarkably enhanced when ct-DNA was added into MG solution. Many organic small molecules could interact with nucleic acid [20,21]. So, we presumed that the binding of MG to ct-DNA would result in the fluorescence enhancement of this system. In order to explore the mechanism of fluorescence enhancement in the present system, a series of experiments were performed and the results are discussed as follows:

(1) Native double-stranded herring sperm DNA was used to replace of native double-stranded ct-DNA, and the same enhanced fluorescence emission for MG was observed. Furthermore, the single-stranded ct-DNA solution was prepared by heat-

ing nature double-stranded ct-NDA in boiling water bath for 8 min, and then rapidly cooling in the ice bath. When the single-stranded ct-DNA solution was added into MG solution, no significant enhancement on fluorescence emission of MG solution was observed. It is obvious from these above experimental results that the fluorescence emission of this system is dependent of binding of MG to double-stranded DNA.

- (2) Temperature is one of important factors for the interaction of small molecule and DNA. We studied the effect of temperature on the fluorescence emission in the range of 20–100 °C. The experiment results indicated that the shape and maximal emission wavelength did not change, but the fluorescence intensity decreased gradually with increasing temperature. High temperature often causes the increase of non-irradiation and thus the decrease in fluorescence intensity; higher temperature is, lower fluorescence intensity is. In this studied system, the fluorescence intensity decreased to the minimal value at 75 °C, and then remained almost constant when increasing temperature. The effect of temperature on this studied system is different from the general effect of temperature on fluorescence. In order to explain this phenomenon, we investigated the thermal stability of ct-DNA. The melting curves of ct-DNA indicated that the melting temperature ( $T_m$ ) of ct-DNA was 71 °C at the under-studied condition, which agreed with the result in the literature [22]. So, above 75 °C the native double-stranded ct-DNA would become the single-stranded ct-DNA. The experimental results further confirmed that the fluorescence emission of this system was dependent of binding of MG to double-stranded DNA.
- (3) When one organic small molecule interacts with double-stranded DNA, generally there are three different binding modes: intercalative, groove or electrostatic [18,19]. By taking MG as a cation and the negatively charged phosphate skeleton of DNA into account, there is some electrostatic interaction between MG and ct-DNA. The fluorescence of MG with ct-DNA system in presence of NaCl was studied. The result showed that when the concentration of NaCl increased from 0 to  $1 \text{ mol l}^{-1}$ , the fluorescence of the system decreased within 5%. Usually,  $\text{Na}^+$  will partly neutralize the negative charges of the DNA phosphatic backbone; if the interaction between MG and ct-DNA is electrostatic binding, the enhanced fluorescence intensity will be weaken with increasing  $\text{Na}^+$  concentration. The result indicates that there is no obvious influence on the system's fluorescence with different NaCl concentrations. Thus, the electronic binding effect between MG and ct-DNA is not the main binding mode.
- (4) The absorption spectrum of MG was measured before and after adding ct-DNA. The experimental results showed that no new peaks appeared and the maximum absorbance wavelength of MG shifted from 617 to 620 nm; the more ct-DNA added, the greater the absorption value decreased. According to Barton's results [23], the intercalation binding of small molecule with double-stranded DNA commonly results in hypochromism and a red shift of the maximum absorbance wavelength. So, we reason that the mode of MG binding to ct-DNA is intercalation. On the other hand, we also measured the fluorescence polarization of MG before and after adding ct-DNA. In the absence of ct-DNA, the fluorescence from MG was not polarized due to the rapid tumbling motion of MG in aqueous solution; in the presence of ct-DNA, the fluorescence was significantly polarized and the fluorescence polarization increased with increasing ct-DNA concentration. Generally the mere binding of organic small molecule to the phosphate backbone or to the DNA grooves does not result in enhanced fluorescence polarization. The large increase in the polarization upon binding to ct-DNA suggests the intercalation of MG into the helix of ct-DNA. The possible reason is that when MG intercalates into the helix of DNA, its rotational

motion should be restricted, and hence the fluorescence from the bound MG should be polarized. So, we could further reason that the mode of MG binding to ct-DNA is intercalation.

According to the above results, the mechanism for fluorescence enhancing of ct-DNA on MG can be summarized as follows: when ct-DNA is added into MG solution, MG intercalates into the helix of ct-DNA, thereby experiencing loss of rotational degrees of freedom; at the same time, the binding of MG to ct-DNA is very efficient in preventing fast nonradiative relaxation processes that occur via rotational motion of the aromatic rings of MG. As a result, the fluorescence quantum yield of MG could be remarkably enhanced.

#### 4. Conclusion

In this paper, we have taken full advantage of the interaction between MG and double-stranded ct-DNA, and proposed a novel and simple fluorescence system of sensing for MG. The native double-stranded ct-DNA is used as sensing material. Compared with other sensing reagents, the native ct-DNA is easily obtained and is not poisonous, and the method is very safe for the analyst.

#### Acknowledgements

This study was supported by the National Natural Science Foundation of China (Grant No. 20405009) and by the Program for New Century Excellent Talents in University (NCET-04-0956). The authors also thank Miss Lijuan Zhang (Shaanxi Normal University, China) for her helpful sample preparation.

#### References

- [1] S.J. Culp, F.A. Beland, *J. Am. Coll. Toxicol.* 15 (1996) 219.
- [2] R.A. Mittelstaedt, N. Mei, P.J. Webb, J.G. Shaddock, V.N. Dobrovolsky, L.J. McGarity, S.M. Morris, T. Chen, F.A. Beland, K.J. Greenlees, R.H. Heflich, *Mutat. Res.* 561 (2004) 127.
- [3] I. Safarik, M. Safarikova, *Water Res.* 36 (2002) 196.
- [4] N. Pourreza, Sh. Elhami, *Anal. Chim. Acta* 596 (2007) 62.
- [5] K. Mitrowska, A. Posyniak, J. Zmudzki, *J. Chromatogr. A* 1089 (2005) 187.
- [6] X. Wu, G. Zhang, Y. Wu, X. Hou, Z. Yuan, *J. Chromatogr. A* 1172 (2007) 121.
- [7] L. Valle, C. Díaz, A.L. Zanocco, P. Richter, *J. Chromatogr. A* 1067 (2005) 101.
- [8] S. Lee, J. Choi, L. Chen, B. Park, J.B. Kyong, G.H. Seong, J. Choo, Y. Lee, K.-H. Shin, E.K. Lee, S.-W. Joo, K.-H. Lee, *Anal. Chim. Acta* 590 (2007) 139.
- [9] M. Yang, J. Fang, T. Kuo, D. Wang, Y. Huang, L. Liu, P. Chen, T. Chang, *J. Agric. Food Chem.* 55 (2007) 8851.
- [10] K.A. Fletcher, S.O. Fakayode, M. Lowry, S.A. Tucker, S.L. Neal, I.W. Kimaru, M.E. McCarroll, G. Patonay, P.B. Oldham, O. Rusin, R.M. Strongin, I.M. Warner, *Anal. Chim. Acta* 590 (2007) 139.
- [11] B. Zheng, H. Zhao, K. Leng, *Determination of Malachite Green and Gentian Violet Residues in Fishery Products—High Performance Liquid Chromatography with Fluorescence Detector*, Standards Press of China, Beijing, 2006, pp. 1–6.
- [12] R.R. Breaker, *Nature* 432 (2004) 838.
- [13] W.C. Andersen, S.B. Turnipseed, J.E. Roybal, *J. Agric. Food Chem.* 54 (2006) 4517.
- [14] M.S. Baptista, G.L. Indig, *J. Phys. Chem. B* 102 (1998) 4678.
- [15] D. Ben-Amotz, C.B. Harris, *Chem. Phys. Lett.* 119 (1985) 305.
- [16] J.R. Babendure, S.R. Adams, R.Y. Tsien, *J. Am. Chem. Soc.* 125 (2003) 14716.
- [17] G. Oster, Y. Nishijima, *J. Am. Chem. Soc.* 78 (1956) 1581.
- [18] D.M. Kolpashchikov, *J. Am. Chem. Soc.* 127 (2005) 12442.
- [19] A.C. Bhasikuttan, J. Mohanty, H. Pal, *Angew. Chem. Int. Ed.* 46 (2007) 9305.
- [20] X. Hu, K. Jiao, W. Sun, J. You, *Electroanalysis* 18 (2006) 613.
- [21] S. Bi, H. Zhang, C. Qiao, Y. Sun, C. Liu, *Spectrochim. Acta Part A* 69 (2008) 123.
- [22] I. Meistermann, V. Moreno, M.J. Prieto, E. Moldrheim, E. Sletten, S. Khalid, P. Rodger, J.C. Peberdy, C.J. Isaac, A. Rodger, M.J. Hannon, *Proc. Natl. Acad. Sci. U.S.A.* 99 (2002) 5069.
- [23] E.C. Long, J.K. Barton, *Acc. Chem. Res.* 23 (1990) 271.



## A study of large-volume on-column injection GC–ECD for the ultratrace analysis of organochlorine pesticides in water

E. Concha-Graña<sup>a</sup>, G. Fernández-Martínez<sup>b</sup>, V. Fernández-Villarrenaga<sup>b</sup>, M.I. Turnes-Carou<sup>a</sup>, S. Muniategui-Lorenzo<sup>a,\*</sup>, P. López-Mahía<sup>a</sup>, D. Prada-Rodríguez<sup>a</sup>

<sup>a</sup> Department of Analytical Chemistry, University of A Coruña, Campus A Zapateira s/n, E-15071 A Coruña, Spain

<sup>b</sup> Scientific Research Support Services, University of A Coruña, Campus de Elviña s/n, E-15071 A Coruña, Spain

### ARTICLE INFO

#### Article history:

Received 24 September 2008

Received in revised form 16 December 2008

Accepted 17 December 2008

Available online 30 December 2008

#### Keywords:

Organochlorine pesticides

Large-volume on-column injection (LVOCI)

GC–ECD

Micro liquid–liquid extraction (MLLE)

Water analysis

### ABSTRACT

In this work, a large-volume on-column injection method for the analysis of 21 organochlorine pesticides, including HCH isomers, DDT derivatives and cyclodiene derivatives, was optimized. The solvent selected to carry out the study was ethyl acetate and the injection volume was 100  $\mu\text{l}$ . Some factors were introduced in a Plackett–Burman design to determine their influence in the vaporization efficiency. The significant factors were then studied by a univariate procedure and sorted according to their importance on the response. The effect of the injection conditions on the peak resolution was also noted. The conditions selected according to sensitivity and resolution were: initial oven temperature 75 °C, injection speed 20  $\mu\text{l s}^{-1}$ , solvent vapor exit (SVE) valve closure time 60 s, initial pressure 100 kPa and isothermal oven time 1 min. Analytical characteristics expressed in terms of precision, linear range, and limit of detection have been determined and compared with those obtained by splitless injection. The degradation of endrin and p,p'-DDT thermolabile pesticides was evaluated for both injection techniques. Finally the developed method was successfully applied to the ultratrace analysis of pesticides in natural waters. With this purpose a micro liquid–liquid extraction method using 2 ml of ethyl acetate to extract 10 ml of water sample was proposed. Recoveries between 69 and 107% were obtained with a very good precision (0.2–1.3%) for the studied pesticides, except for p,p'-DDD. Detection limits between 0.3 and 25  $\text{ng l}^{-1}$ , which fulfill the limits established by the new water directive 2008/105/EC, were achieved. The MLLE method was compared with the SPE method by the analysis of some water samples using both procedures, and good concordance was obtained.

© 2008 Elsevier B.V. All rights reserved.

### 1. Introduction

Organochlorine pesticides are a group of toxic and persistent organic pollutants. Most of them are included in the Stockholm convention list of priority pollutants [1]. Moreover, the European community has fixed very restrictive limits (to be achieved in 2010) for some of the organochlorine pesticides in different kinds of superficial waters in the new directive 2008/105/EC [2].

Pesticide analysis in environmental samples, where concentration levels are in the range of parts per billion, requires highly sensitive techniques. The use of large-volume injection techniques increases this sensitivity, allowing the determination of pesticides at much lower concentration levels and enabling the elimination of the re-concentration step in the extraction, which avoids a possible source of losses of the most volatile

compounds [3,4]. Different approaches are available for achieving large-volume injection in capillary gas chromatography: on-column injection [5], programmed-temperature-vaporization (PTV) injection [6–8], or splitless injection with solvent diversion [9].

Large-volume on-column injector (LVOCI) allows to introduce high volumes of sample using an uncoated precolumn with a final coated section as a retention gap [10,11]. Some advantages of automated LVOCI are injection precision, efficiency of sample transfer, elimination of inlet septum bleed, and absence of breakdown products of thermally labile compounds [12,13]. Its principal disadvantage is the difficulty to inject dirty samples without losing the efficiency and the inertness of the chromatographic system [14].

In this injection mode, the organic extract is directly injected into the precolumn, where the solvent is partially vaporized by effect of the pressure and temperature, and partially remains as a liquid causing the flooded zone. Solvent vapor is eliminated through the solvent vapor exit (SVE) valve. The coated section of the precolumn retains the analytes, while the solvent is eliminated, and then

\* Corresponding author.

E-mail address: [smuniat@udc.es](mailto:smuniat@udc.es) (S. Muniategui-Lorenzo).

the valve is closed to avoid the elimination of the volatile analytes [15]. The sensitivity is improved by two solvent effects: the solvent trapping and the phase soaking.

The vaporization efficiency is affected by several factors. A very important factor is the injection solvent, because this factor determines the values of all the variables. The solvents that are usually applied are hexane [4,14] and dichloromethane [13]. The LVOCI chromatographic software used in this work proposes standard conditions for the factors based on the solvent used and the percentage of elimination through the SVE valve; and these standard conditions are often used to carry out the analysis. Nevertheless, the complexity of this injection system, and the quantity and nature of the compounds, require an optimisation so as to achieve the best conditions of sensitivity and resolution for the compounds of interest.

Optimisation can be approached multivariately or univariately, but given to the large number of factors involved in the evaporation process, it is the multivariate procedure that will simplify the study. In this work, the classification of variables according to their influence in the response was determined by a multivariate approach that included using a Plackett–Burman design [16]. The factors were then studied by means of a univariate procedure and sorted according to their importance in the chromatographic response.

The analytical parameters obtained with the proposed LVOCI method were compared to those obtained by splitless injection. The degradation in the LVOCI of two thermolabile organochlorine pesticides was also studied and compared with the degradation caused by a splitless injector.

The low detection limits reached by the proposed LVOCI method make this suitable for application to the analysis of water samples by micro liquid–liquid extraction (MLLE). This technique allows an important reduction in the volume of sample extracted, solvent consumption, and sample handling in comparison with classical liquid–liquid extraction, or solid phase extraction (SPE) that has been widely used in the analysis of organochlorine pesticides from waters [17–19].

The EPA method 505 describes a procedure to carry out the micro liquid–liquid extraction of organohalide pesticides and PCB products in water. In this method 35 ml of water sample is extracted with 2 ml of hexane, and this extract is injected directly into the chromatograph [20]. When the split/splitless injection mode is used, a higher volume of sample is necessary to analyze the contaminants at the levels requested by the legislation, thus, 400 ml of water sample is extracted with 500  $\mu$ l of toluene to determine organic contaminants in drinking water [21]. The use of the large-volume injection techniques allows the reduction in the amount of sample extracted. The solvent more frequently used in this extraction is hexane; it was applied to the analysis of triazines [4] or organochloride and organophosphorous pesticides [14]. Other solvents that were used were tert-butylmethylether, which was applied to the analysis of triazines [22], or methylene chloride, that was applied to the analysis of semivolatiles compounds (PAH and pesticides, mainly) [13].

The main novelty in this work is the proposal of a LVOCI–GC–ECD method using ethyl acetate as solvent, which is very advantageous for the analysis of organochlorine pesticides, due to the high solubility of these compounds in this solvent. Moreover, the immiscibility of the ethyl acetate in water allows its use as extraction solvent in the MLLE, and therefore facilitates the coupling MLLE–LVOCI–GC–ECD. The very low detection limits achieved with the proposed MLLE–LVOCI–GC–ECD method allow the determination of pesticides in water samples at the levels requested by the European regulations.

The MLLE extraction process was compared with a SPE procedure [23] using C<sub>18</sub> laminar disk.

## 2. Experimental

### 2.1. Chemicals

Organochlorine pesticide mix CLP (Supelco, Bellefonte, USA), contains aldrin,  $\alpha$ -HCH,  $\beta$ -HCH,  $\gamma$ -HCH,  $\delta$ -HCH, dieldrin,  $\alpha$ -endosulfan,  $\beta$ -endosulfan, endosulfan sulfate, endrin, endrin aldehyde, heptachlor, heptachlor epoxide (B isomer), metoxichlor, p,p'-DDD, p,p'-DDE, p,p'-DDT,  $\alpha$ -chlordane,  $\gamma$ -chlordane y endrin ketone with a concentration of 2 mg ml<sup>-1</sup>, in toluene:hexane (50:50). Solid standards of  $\gamma$ -HCH,  $\alpha$ -chlordane and  $\gamma$ -chlordane were supplied by Supelco (Bellefonte, USA) and endosulfan sulfate Pestanal<sup>®</sup> was supplied by Riedel-de-Haën (Seelze, Germany). The Internal Standard (IS), 2,4,5,6-tetrachloro-m-xylene (TCMX) was supplied by Supelco.

Anhydrous sodium sulfate (Merk, Darmstadt, Germany) was for organic trace analysis and was washed with ethyl acetate prior to use. Laminar disk C<sub>18</sub> (Bakerbond Speedisk) were obtained from J.T. Baker, Deventer, Holland.

Ethyl acetate (analytical grade) for instrumental analysis was supplied by Panreac (Barcelona, Spain).

### 2.2. Instrumentation

The LVOCI experiments were performed in a Thermo Finnigan Trace GC (Austin, Texas, USA), equipped with a ECD, automatic injector AS-2000, and with a LVOCI. Data treatment software was Chrom-Card Trace-Focus GC, 2.01 version.

As precolumn a MEGA (Legnano, Italy) SE 54, 15 m length, internal diameter 0.53 mm, with 0.25  $\mu$ m film in the last 3 m was used. The capillary column was a J&W DB-XLB 60 m  $\times$  0.25 mm  $\times$  0.25  $\mu$ m (Agilent Technologies, DE, USA).

The splitless injection was done in a Perkin–Elmer Autosystem XL with ECD (PerkinElmer, Norwalk, CT, USA), equipped with a capillary column DB-35 30 m  $\times$  0.32 mm  $\times$  0.25  $\mu$ m (Agilent Technologies, DE, USA).

### 2.3. Operation conditions for LVOCI

The volume injected in the LVOCI experiments was 100  $\mu$ l. Helium was used as carrier gas at a flow of 1.5 ml min<sup>-1</sup> and the GC oven program was as follows: 70 °C hold during the isotherm time (is a factor to be studied), then 30 °C min<sup>-1</sup> to 150 °C and hold 3 min, and 3 °C min<sup>-1</sup> to 300 °C and hold 15 min. ECD temperature was 330 °C.

### 2.4. Operation conditions for splitless injection

The splitless injector conditions were: injector temperature 300 °C, split vent flow 7.7 ml min<sup>-1</sup> and splitless time 1.2 min. The oven program was 60 °C (hold 1 min) then 25 °C min<sup>-1</sup> to 220 °C, then 6 °C min<sup>-1</sup> to 280 °C (hold 5 min) and finally 30 °C min<sup>-1</sup> to 300 °C.

### 2.5. Analysis conditions for the SPE–PTV–GC–MS assay

In order to validate the proposed micro liquid–liquid extraction procedure, three water samples were analyzed by MLLE and by a solid phase extraction method previously published [8], which in summary consists in the extraction of the sample by passing 100 ml through a C<sub>18</sub> laminar disk. Pesticides were eluted with 10 ml of ethyl acetate followed by 3 ml of hexane and concentrated in rotary

evaporator and injected by PTV–GC–MS (SIM mode). The injection was done in a Thermo Finnigan gas chromatograph, equipped with a PTV injector and as detector a MS Polaris Q-IT operating in SIM mode was used. The capillary column was a DB-XLB 60 m × 0.25 mm × 0.25 μm and the oven program was 60 °C (2 min) to 300 °C (5 min) at 4.5 °C min<sup>-1</sup>. The volume injected was 10 μl and the injector program was 80 °C (hold 0.5 min) then 5 °C min<sup>-1</sup> to 255 °C (hold 10 min).

### 3. Results and discussion

#### 3.1. Selection of significant factors

Ethyl acetate was tested as solvent for LVOCl. The injection volume was 100 μl in all the experiences. In order to determine which of the factors involved in the LVOCl have more influence on the response, a randomized Plackett–Burman 2<sup>8</sup>\*3/64 design with three dummy factors was carried out. The factors and the maximum and minimum values of each factor that were selected for analysis were: system pressure during injection (100–150 kPa); initial oven temperature (80–130 °C), injection speed (5–20 μl s<sup>-1</sup>), which is directly involved in the formation of the flooded zone, SVE valve closure time (25–120 s), which affects the solvent elimination and also the more volatile pesticides, and isothermal oven time (0.47–1.5 min). The introduction of these values in the statistical program (Statgraphics Plus 4.0 for Windows) provides the Plackett–Burman matrix with the value of each factor in each experiment (Table 1). All the experiments were carried out in triplicate. Due to the high effect of the injection conditions on the peak resolution, it was difficult to carry out the design with all the pesticides; we therefore selected three representative compounds. The studied pesticides were separated in three groups according to the volatility and their behaviour in previous large-volume injection studies [24,25]. For the most volatile compounds γ-HCH was selected, and for the heaviest compound we selected endosulfan sulfate. In the intermediate zone γ-chlordane was selected. These three compounds elute in the chromatogram at very different retention times, and are eluted separately in all the experiences. α-chlordane was also introduced in order to evaluate the chromatographic resolution, and then both chlordane isomers were quantified together in all the experiences.

The response in each experiment was measured as height of peak, in order to avoid errors in the interpretation of results caused by the presence of broad and tailed peaks, in some of the experiences. For the interpretation of the results of the design, a peak with a big area but misshapen, give a favourable response in the design in terms of response but is unfavourable in terms of resolution and peak shape.

**Table 1**  
Factors of the Plackett–Burman design.

Experiment	A	B	C	D	E	F	G	H
1	75	130	20	90	0.47	–	–	–
2	180	130	1	90	2.0	–	–	–
3	180	80	20	10	0.47	–	–	–
4	75	130	20	10	2.0	–	–	–
5	180	80	1	10	2.0	–	–	–
6	75	80	1	10	0.47	–	–	–
7	75	130	1	10	0.47	–	–	–
8	75	80	1	90	2.0	–	–	–
9	180	80	20	90	0.47	–	–	–
10	180	130	1	90	0.47	–	–	–
11	75	80	20	90	2.0	–	–	–
12	180	130	20	10	2.0	–	–	–

A: initial pressure (kPa), B: oven initial temperature (°C), C: injection speed (μl s<sup>-1</sup>), D: SVE valve closure time (s), E: oven isothermal time (min), F: dummy, G: dummy, H: dummy (n = 3).

The results were analyzed by means of the representation of the first- and second-order Pareto charts (P = 95.0%) (Fig. 1). In these charts, the length of each bar is proportional to the standardized effect which is the estimated effect divided by its standard error, equivalent to computing a t-statistic for each effect. The vertical line on the plot judges the effects that are statistically significant. Bars that extend beyond this vertical line correspond to effects that are statistically significant at the 95% confidence level.

The Pareto charts show that the initial oven temperature (factor B) is the only significant factor for chlordanes and γ-HCH, and the second-order interaction between this factor and the SVE closure time is significant for γ-HCH. No significant factors were found for endosulfan sulfate. The great significance of factor B, can disguise the influence of other factors. This can be avoided by representing the normal probability plot, with and without the initial oven temperature, which allows for the identification of other significant factors (Fig. 2). Effects that are not significant have a normal distribution behaviour and are represented close to the line, whereas significant effects are distant from the line. As can be seen in Fig. 2 (b), when factor B is eliminated, factors C (injection speed) and D (SVE closure time) are distant from the line and are therefore significant factors. The plots obtained for chlordane isomers show that D and A (initial pressure) are slightly distant from the line. For endosulfan sulfate all the points are close to the line and so there are no significant factors for this compound. The sign of the estimated effect determines the influence of the variables on the response (positive or negative influence), and helps to carry out the following study of the factors.

#### 3.2. Study of the factors

Due to the influence of the injection conditions not only in the response, but also in the chromatographic resolution, the variables were studied through a univariate approach, taking into account both parameters. Moreover, the values studied for each variable were selected according to the results of the Plackett–Burman design, that is, we selected low or high values depending on the sign of the estimated effect. The results of all these experiments are shown in Fig. 3. The first factor that was studied was the initial oven temperature, assaying values between 70 and 85 °C. This experiment set the injection speed at 10 μl s<sup>-1</sup>, the initial pressure at 100 kPa, SVE closure at 90 s, and the isothermal oven time at 1.5 min. As can be seen in the fig., the variation of the initial oven temperature affects mainly the most volatile compounds (γ-HCH). There is an increase in the peak area when this temperature is set at 75 °C, but this area decreases slightly at a higher temperature. The selected initial oven temperature was therefore 75 °C.

We studied injection speeds between 5 and 30 μl s<sup>-1</sup>, setting the initial oven temperature at 75 °C and the other factors at the values cited above. The response for chlordanes and endosulfan sulfate remains almost constant when the injection speed is increased. Nevertheless, the response for γ-HCH has a critical maximum at an injection speed of 20 μl s<sup>-1</sup>. This can be due to the influence of the injection speed on the formation of the flooded zone, and then on the solvent trapping effect, which mainly affects the most volatile compounds. For this reason an injection speed of 20 μl s<sup>-1</sup> was selected.

The results that were obtained with a SVE closure time in the range from 20 to 80 s show a maximum in the response at 60 s for chlordanes and endosulfan sulfate. Nevertheless, for γ-HCH the response remains almost constant until 60 s and decreases at higher values, which is why the SVE closure time was set at 60 s.

The initial pressure was studied between 80 and 130 kPa. As can be seen in Fig. 3, there is no variation in the response for γ-HCH and endosulfan sulfate. For chlordanes the response increases slightly at 100 kPa (this factor was slightly distant from the line in the normal



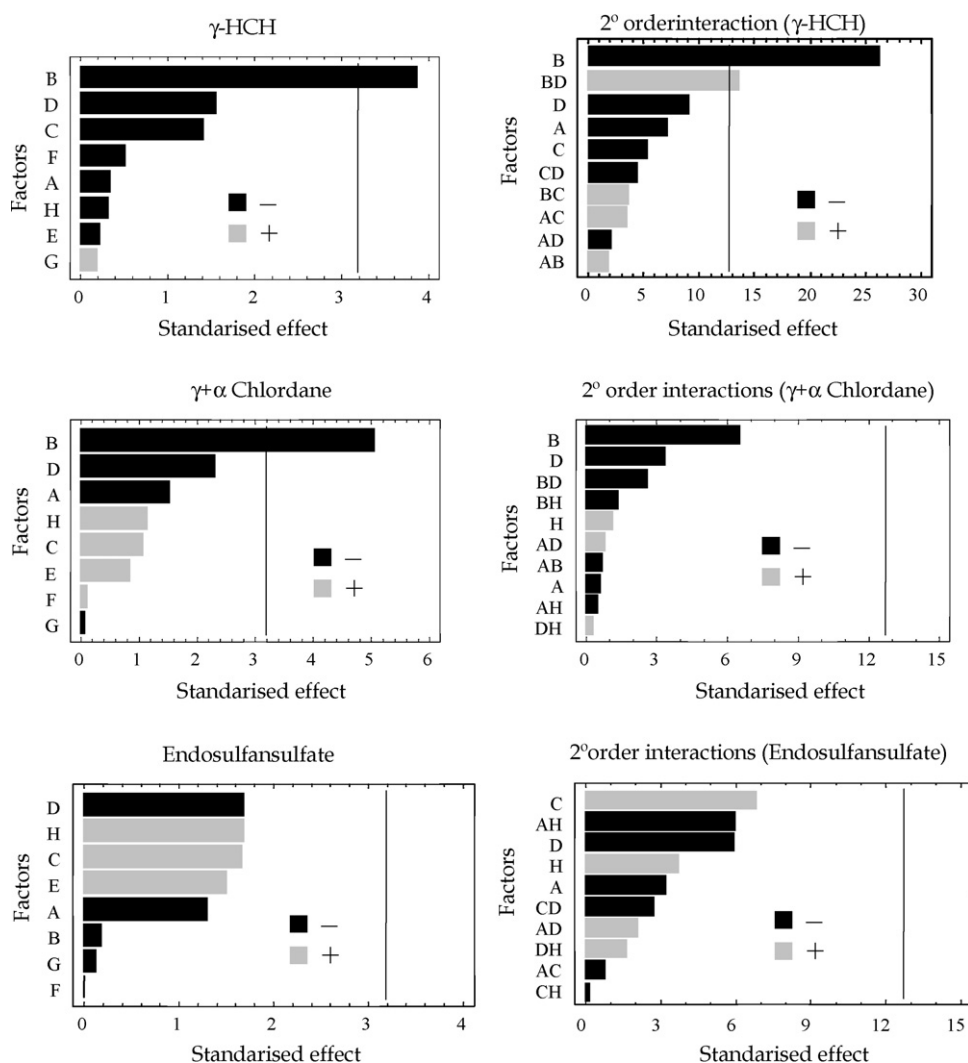


**Fig. 1.** Pareto charts (first and second order) obtained for  $\gamma$ -HCH, sumatory of chlordanes ( $\gamma + \alpha$ ) and endosulfan sulfate. A: initial pressure; B: initial oven temperature; C: injection speed; D: SVE valve closure time; E: isothermal oven time; F, G and H: Dummies.

probability plot for these compounds). A worsening in the peak resolution was observed when the pressure increased, obtaining co-eluting peaks when the pressure was set at 130 kPa. For this reason, the selected pressure was 100 kPa.

Finally, although this factor was not significant, we also studied the isothermal oven time, because this factor affects the peak resolution. As expected, an almost constant response was obtained when the isothermal oven time varied between 0.47 and 2 min with a slight increment in the response between 0.47 and 1 min, which is in concordance with the results obtained in the Plackett–Burman design. No differences in resolution were observed, so the selected isothermal oven time was 1 min.

In summary, the values selected to improve the sensitivity without affecting the peak resolution were the following: initial oven temperature 75 °C, injection speed 20  $\mu\text{l s}^{-1}$ , SVE closure time 60 s, initial pressure 100 kPa and isothermal oven time 1 min. Fig. 4A shows the chromatogram that was obtained by injecting a pesticide standards solution under these conditions.

### 3.3. Evaluation of DDT and endrin degradation

An advantage of automated LVOCI is the reduction in breakdown products of thermally labile compounds. This fact was corroborated by the evaluation of the degradation of endrin and p,p'-DDT as the

EPA methods propose [26]. The percentages of degradation were 7.4% for endrin and 3.9% for p,p'-DDT. These values are considerably lower than the percentages obtained when splitless injection is used (19% for endrin and 15% for p,p'-DDT). The degradation is also lower than that obtained with PTV injection [24] (15% for endrin and 18% for p,p'-DDT). These high values in the PTV can be due to the presence of active sites in the glass wool of the liner [27]. Thus, the LVOCI has demonstrated its suitability for the analysis of these thermolabile pesticides.

### 3.4. Figures of merit of the proposed LVOCI method

Calibration curves were made by analysing pesticide standards in ethyl acetate at 7 levels of concentration between 0.01 and 15  $\text{ng ml}^{-1}$ . Calibrations were linear up to 10  $\text{ng ml}^{-1}$  for all the pesticides. The linearity was evaluated by determining the correlation coefficients, which were higher than 0.995 in all cases. The linearity was also verified by representing the residuals plot. There is no trend in the spread of residuals with concentration.

The instrumental detection limits (LOD) were calculated as  $\bar{x}_b + 3s_b$  (average value and standard deviation of the blank, respectively) and the quantification limits (LOQ) as  $\bar{x}_b + 10s_b$ . As can be seen in Table 2, the obtained instrumental detection limits were below 0.1  $\text{ng ml}^{-1}$  for all the studied pesticides and below

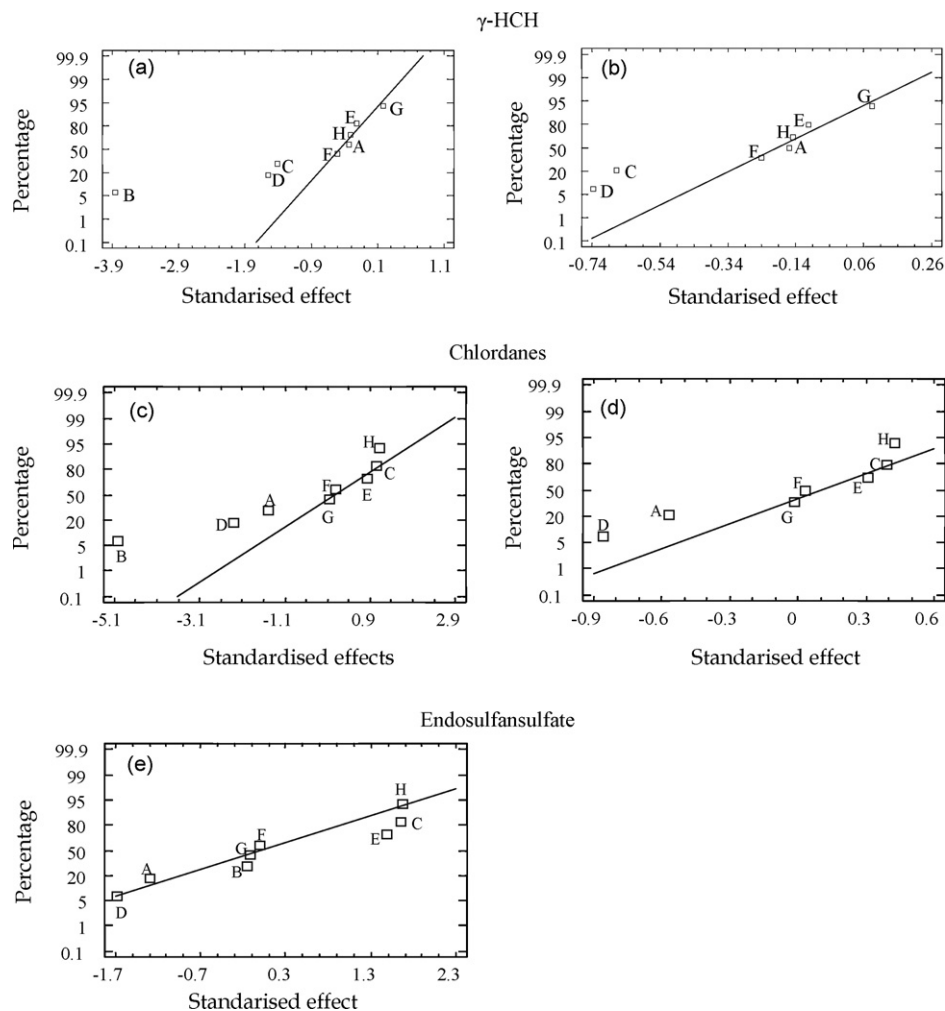


Fig. 2. Normal probability plots with initial oven temperature (a), (c), (e) and without initial oven temperature (b), (d).

**Table 2**  
Instrumental detection limits (LOD), quantitation limits (LOQ) obtained with LVOCI and splitless injection ( $\text{ng ml}^{-1}$ ).

Pesticide	LVOCI		Splitless	
	LOD	LOQ	LOD	LOQ
$\alpha$ -HCH	0.0088	0.0153	3.0	3.2
$\gamma$ -HCH	0.0087	0.0155	2.3	2.4
$\beta$ -HCH	0.1260	0.1435	0.4	0.9
Heptachlor	0.0010	0.0068	0.7	0.9
$\delta$ -HCH	0.0852	0.0903	4.1	4.3
Aldrin	0.0130	0.0147	3.5	3.6
Isodrin	0.0072	0.0137	0.7	0.9
Heptachlor epoxide	0.0026	0.0067	1.1	1.3
$\gamma$ -chlordane	0.0023	0.0080	1.8	2.0
$\alpha$ -chlordane	0.0015	0.0065	1.3	1.5
$\alpha$ -endosulfan	0.0076	0.0109	1.8	2.0
p,p'-DDE	0.0062	0.0098	3.4	3.6
Dieldrin	0.0057	0.0102	3.6	3.8
Endrin	0.0057	0.0087	3.7	4.0
p,p'-DDD	0.0141	0.0175	4.9	5.1
$\beta$ -endosulfan	0.0043	0.0078	3.0	3.2
Endrin aldehyde	0.0205	0.0385	0.2	0.5
p,p'-DDT	0.0091	0.0156	8.0	8.3
Endosulfan sulfate	0.0042	0.0128	1.0	1.3
Metoxychlor	0.0130	0.0295	5.9	6.6
Endrin ketone	0.0021	0.0077	3.5	3.7

0.013  $\text{ng ml}^{-1}$  for the majority of them. These limits were similar to those obtained by PTV injection (injection volume 100  $\mu\text{l}$ ) [28]. Also, a considerably improvement was obtained in comparison with the LODs obtained by splitless injection in the conditions described in the instrumental section (Table 2).

Regarding instrumental precision (Table 3), the repeatability was evaluated by 11 consecutive injections of a standard solution and the intermediate precision by injections of a standard solution over the course of 6 alternate days. The precision obtained was very satisfactory for all the pesticides, with repeatability below 6% and intermediate precision below 8%, for all the pesticides.

**Table 3**  
Instrumental repeatability (A) ( $n=11$ ) and intermediate precision (B) ( $n=6$ ) expressed as %RSD.

Pesticide	A% RSD	B% RSD	Pesticide	A% RSD	B% RSD
$\alpha$ -HCH	5.1	7.7	p,p'-DDE	2.7	5.2
$\gamma$ -HCH	4.9	7.8	Dieldrin	3.0	7.2
$\beta$ -HCH	4.3	5.2	Endrin	4.3	6.6
Heptachlor	4.2	5.2	p,p'-DDD	5.1	6.5
$\delta$ -HCH	4.6	5.6	$\beta$ -endosulfan	5.1	6.0
Aldrin	4.1	4.1	Endrin aldehyde	4.3	7.0
Isodrin	5.6	6.0	p,p'-DDT	3.6	7.0
Heptachlor epoxide	3.0	6.6	Endosulfan sulfate	3.0	6.2
$\gamma$ -chlordane	2.9	4.2	Metoxychlor	4.0	7.0
$\alpha$ -chlordane	2.3	6.9	Endrin ketone	3.2	4.9
$\alpha$ -endosulfan	3.4	4.1			

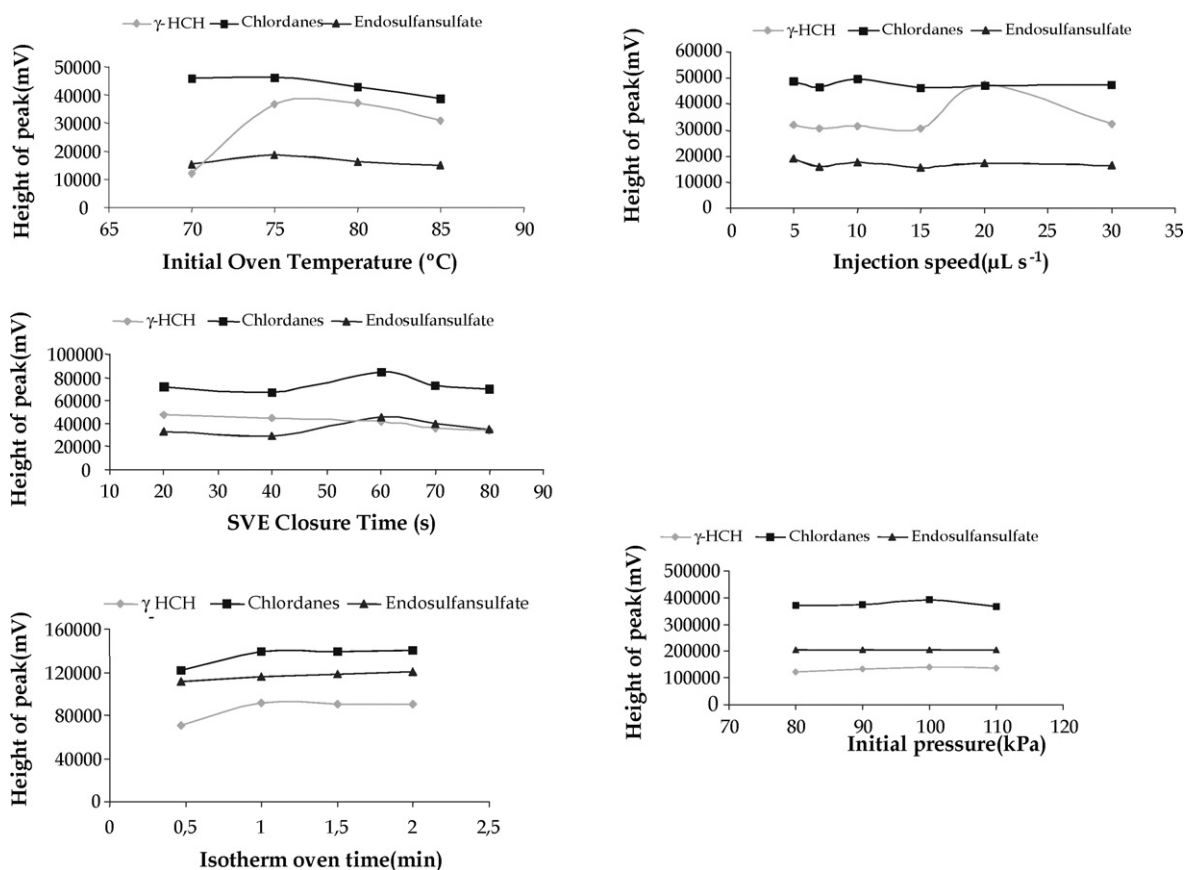


Fig. 3. Results of the study of the factors.

#### 4. Application to the analysis of water samples by micro liquid–liquid extraction

The low detection limits reached by the proposed LVOCI method make this method suitable for application to the analysis of pesticides in water samples by micro liquid–liquid extraction.

Thus, in this work 10 ml of water was extracted in a vial with 2 ml of ethyl acetate with similar conditions than those proposed by the EPA 505 method [20]. The solvent selected to carry out the extraction was ethyl acetate because of its immiscibility in water and the high solubility of the organochlorine pesticides in it.

The sample was extracted by mechanical shaking during 1 min. Then, the organic layer on the top was transferred to another vial with a Pasteur pipette. In order to eliminate all the water from the extract, anhydrous sodium sulfate was added. Finally, the extract was injected into the optimized LVOCI–GC–ECD system.

The accuracy was investigated by means of a surface water spiked at a concentration level of  $1 \mu\text{g l}^{-1}$  of pesticides standards. Analytical recoveries were assessed by comparing the results with those obtained for Milli-Q water spiked at the same level of concentration. The results ( $n=4$ ) are presented in Table 4. Except for *p,p'*-DDD (50%), the recovery values (%) were between 69 and 107%.

The detection limits obtained (Table 5) with the proposed method of MLE–LVOCI–GC–ECD were sufficient to allow the direct determination of these pesticides at the level established by the European legislation (Directive 98/83/CE) for pesticides in water for human consumption, and also the very restrictive limits established in the new Directive 2008/105/EC [2] for superficial waters.

In order to verify the effectiveness of the proposed MLE–LVOCI–GC–ECD method, four natural water samples were analyzed with this procedure and the results were compared

to those obtained through solid phase extraction (SPE) with  $\text{C}_{18}$  laminar disk and determination by PTV–GC–MS (SIM mode), as it was described in the operation conditions section. Three water samples were collected at three different points along the Louro river, and another sample was collected from As Laxes stream, both located in Porriño (Pontevedra, NW of Spain). This area is affected by contamination by hexachlorocyclohexane isomers [29].  $\beta$ -HCH was detected in As Laxes sample (Fig. 4B) at a concentration of

Table 4

Analytical relative recoveries for superficial water and relative standard deviation (RSD) ( $n=4$ ), expressed as percentages, of the microliquid–liquid extraction process.

Pesticide	% Recovery	% RSD
$\alpha$ -HCH	69	0.9
$\gamma$ -HCH	73	1.0
$\beta$ -HCH	90	0.9
Heptachlor	79	0.2
$\delta$ -HCH	97	0.6
Aldrin	98	0.9
Isodrin	103	0.4
Heptachlor epoxide	102	0.3
$\gamma$ -chlordane	99	0.7
$\alpha$ -chlordane	100	0.9
$\alpha$ -endosulfan	105	1.2
<i>p,p'</i> -DDE	107	0.9
Dieldrin	106	0.9
Endrin	86	0.8
<i>p,p'</i> -DDD	50	1.3
$\beta$ -endosulfan	75	1.0
Endrin aldehyde	100	–
<i>p,p'</i> -DDT	104	0.8
Endosulfan sulfate	90	0.9
Metoxychlor	72	0.9
Endrin ketone	100	0.9

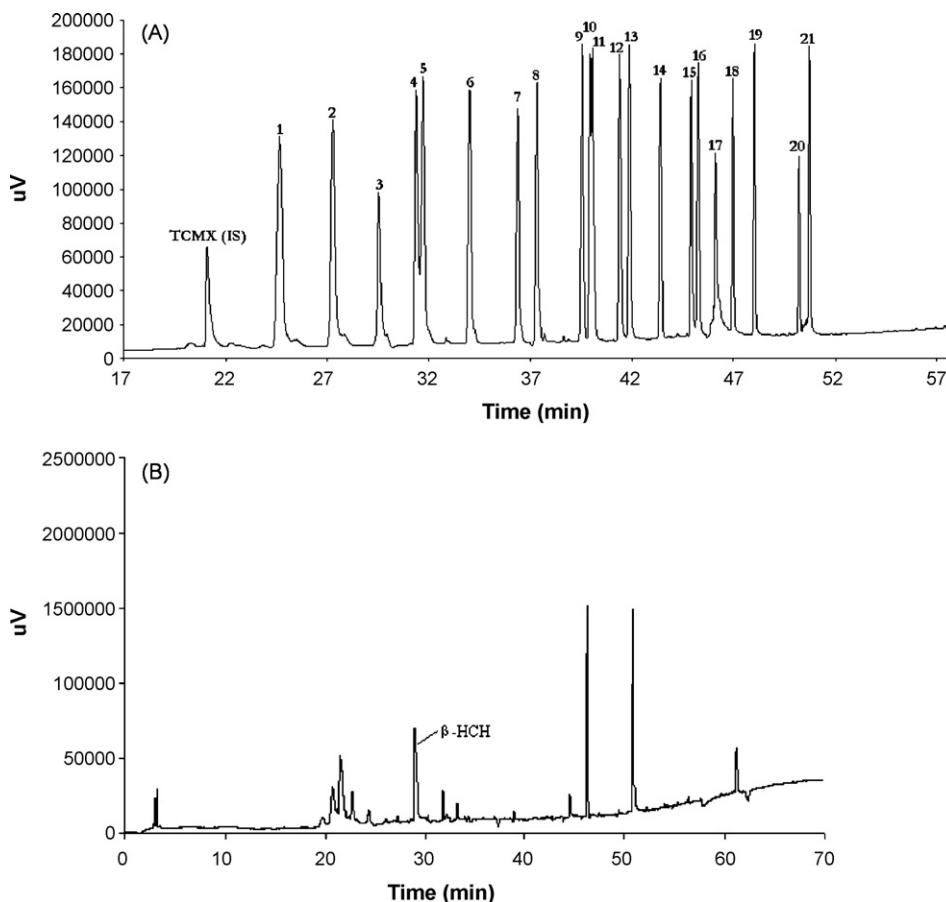


**Fig. 4.** Chromatogram obtained by injection of a standard solution ( $10 \text{ ng ml}^{-1}$ ) in the optimized conditions (A) and chromatogram of a natural water (As Laxes stream) sample analyzed (B). 1:  $\alpha$ -HCH, 2:  $\gamma$ -HCH, 3:  $\beta$ -HCH, 4: heptachlor, 5:  $\delta$ -HCH, 6: aldrin, 7: isodrin, 8: heptachlor epoxide, 9:  $\gamma$ -chlordane, 10:  $\alpha$ -chlordane, 11:  $\alpha$ -endosulfan, 12: p,p'-DDE, 13: dieldrin, 14: endrin, 15: p,p'-DDD, 16:  $\beta$ -endosulfan, 17: endrin aldehyde, 18: p,p'-DDT, 19: endosulfan sulfate, 20: metoxychlor, 21: endrin ketone. (IS): TCMX.

**Table 5**  
 Detection limits (LOD) obtained with the proposed MLE-LVOCI-GC-ECD method ( $\text{ng ml}^{-1}$ ) and values established in the Directive 2008/105/EC ( $\text{ng ml}^{-1}$ ).

Pesticide	LOD	Continental superficial waters	
		AA	MAC
$\alpha$ -HCH	0.0018		
$\gamma$ -HCH	0.0017		
$\beta$ -HCH	0.0252	HCH: 0.020	0.040
$\delta$ -HCH	0.0170		
Heptachlor	0.0002		
Aldrin	0.0026		
Isodrin	0.0014	$\Sigma = 0.010$	-
Dieldrin	0.0011		
Endrin	0.0011		
Heptachlor .epoxide	0.0005		
$\gamma$ -chlordane	0.0005		
$\alpha$ -chlordane	0.0003		
$\alpha$ -endosulfan	0.0015	0.005	0.010
$\beta$ -endosulfan	0.0009		
Endosulfan sulfate	0.0008		
p,p'-DDT	0.0041	10	-
p,p'-DDE	0.0012	Total* = 0.025	-
p,p'-DDD	0.0028		
Endrin aldehyde	-		
Metoxychlor	0.0026		
Endrin ketone	0.0004		

AA: annual average. MAC: maximum allowable concentration.

\* Total DDT:  $\Sigma$ p,p'-DDT, o,p'-DDT, p,p'-DDE and p,p'-DDD.

$4.29 \text{ ng ml}^{-1}$  when analyzed with the proposed MLE method and  $4.42 \text{ ng ml}^{-1}$  when analyzed with the SPE method. Organochlorine pesticides were not detected in the other samples when analyzed with both procedures. The good concordance of the results obtained by both analytical procedures shows the suitability of the proposed MLE-LVOCI-GC-ECD method for the direct analysis of organochlorine pesticides in water samples.

## 5. Conclusions

This work proposed the injection conditions for large-volume on-column injection for the analysis of 21 organochlorine pesticides. The selected solvent was ethyl acetate and the injection volume  $100 \mu\text{l}$ . The conditions selected according to sensitivity and resolution were the following: initial oven temperature  $75^\circ\text{C}$ , injection speed  $20 \mu\text{l s}^{-1}$ , SVE closure time 60 s, initial pressure 100 kPa and isothermal oven time 1 min. With these injection conditions a good precision and very low detection limits were achieved (below  $0.13 \text{ ng ml}^{-1}$  for all the studied pesticides and below  $0.01 \text{ ng ml}^{-1}$  for most of them) that considerably improve the LOD obtained by splitless injection. In addition, a low degradation of thermolabile pesticides was demonstrated with the proposed method.

Finally, the low detection limits achieved with the proposed LVOCI-GC-ECD method allowed its application to the pesticide analysis of extracts obtained by the micro liquid-liquid extraction of natural waters (MLE-LVOCI-GC-ECD), at ultratrace levels. This method supposes an important reduction in analysis time (1 min of extraction), solvent consumption (2 ml), sample volume (10 ml),

and sample handling in comparison with the classical liquid–liquid extraction or SPE.

### Acknowledgment

Authors wish to thank Xunta de Galicia for the financial support PGIDIT07PXIB103193PR.

### References

- [1] Official J. Eur. Union 209 (L) (2006) 3.
- [2] 2008/105/CE Directive of the European Parliament and of the Council on environmental quality standards in the field of water policy, amending and subsequently repealing Council Directives 82/176/EEC, 83/513/EEC, 84/156/EEC, 84/491/EEC, 86/280/EEC and amending Directive 2000/60/EC of the European Parliament and of the Council. Official J. Eur. Union 348 (L) (2008) 84.
- [3] F.J. López, J. Beltrán, M. Forcada, F. Hernández, J. Chromatogr. 823 (1998) 25.
- [4] J. Beltrán, F.J. López, M. Forcada, F. Hernández, Chromatographia 44 (1997) 274.
- [5] H.-G. Janssen, H. Steenbergen, J. Oomen, J. Beens, J. Microcolumn Sep. 12 (2000) 523.
- [6] J.H. Wang, Y.B. Zhang, X.L. Wang, J. Sep. Sci. 29 (2006) 2330.
- [7] Y. Saito, S. Kodama, A. Matsunaga, A. Yamamoto, J. AOAC Int. 87 (2004) 1356.
- [8] E. Korenkova, E. Matisova, J. Slobodnik, J. Sep. Sci. 26 (2003) 1193.
- [9] J. Teske, W. Engewald, TrAC 21 (2002) 584.
- [10] K. Grob, G. Karrer, M.-L. Riekkola, J. Chromatogr. 334 (1985) 129.
- [11] E.M. Kristenson, D.A. Kamminga, M.I. Catalina, C. Espiga, R.J.J. Vreuls, U.A.T. Brinkman, J. Chromatogr. A 975 (2002) 95.
- [12] R. Bailey, W. Belzer, J. Agric. Food Chem. 55 (2007) 1150.
- [13] J. Crockett-Butler, R. Anderson, J. Ragsdale, Thermo Finnigan Application Note, 1999.
- [14] L. Anelli, F. Munari, A. Trisciani, J.R. Castanho, Am. Lab. May (2001) 45.
- [15] J.C. Bosboom, H.-G. Janssen, H.G.J. Mol, C.A. Cramers, J. Chromatogr. A 724 (1996) 384.
- [16] S.N. Deming, S.L. Morgan, Experimental Design. A Chemometric Approach, Elsevier, Amsterdam, 1987.
- [17] A.A. D'Archivio, M. Fanelli, P. Mazzeo, F. Ruggieri, Talanta 71 (2007) 25.
- [18] C.C. Leandro, D.A. Bishop, R.J. Fussell, F.D. Smith, B.J. Keely, J. Agric. Food Chem. 54 (2006) 645.
- [19] S.H.G. Brondi, F.C. Spoljaric, F.M. Lancas, J. Sep. Sci. 28 (2005) 2243.
- [20] EPA-505, in: J.W. Munch (Ed.), Analysis Of Organohalide Pesticides And Commercial Polychlorinated Biphenil (Pcb) Products In Water By Microextraction And Gas Chromatography, Revision 2.1, 1995.
- [21] A. Zapf, R. Heyer, H.-J. Stan, J. Chromatogr. A 694 (1995) 453.
- [22] J. Teske, J. Efer, W. Engewald, Chromatographia 47 (1998) 35.
- [23] E. Concha-Graña, M.I. Turnes-Carou, S. Muniategui-Lorenzo, P. López-Mahía, E. Fernández-Fernández, D. Prada-Rodríguez, Chromatographia 54 (2001) 501.
- [24] E. Concha-Graña, M.I. Turnes-Carou, S. Muniategui-Lorenzo, P. López-Mahía, E. Fernández-Fernández, D. Prada-Rodríguez, Anal. Bioanal. Chem. 379 (2004) 1120.
- [25] E. Concha-Graña, M.I. Turnes-Carou, S. Muniategui-Lorenzo, P. López-Mahía, E. Fernández-Fernández, D. Prada-Rodríguez, J. Chromatogr. A 958 (2002) 17.
- [26] EPA-508, Determination of organochlorine pesticides in water by gas chromatography with an electron capture detector, 1995.
- [27] G.R.v.d. Hoff, P.v. Zoonen, J. Chromatogr. A 843 (1999) 301.
- [28] T. Rankin, Thermo Quest CE Instruments, 1998, p. 1.
- [29] E. Concha-Graña, M.I. Turnes-Carou, S. Muniategui-Lorenzo, P. López-Mahía, D. Prada-Rodríguez, E. Fernández-Fernández, Chemosphere 64 (2006) 588.



# Determination of bioavailable soluble arsenic and phosphates in mine tailings by spectrophotometric Sequential Injection Analysis

Belén E. Ramírez Cordero, María P. Cañizares-Macías\*

Facultad de Química, Departamento de Química Analítica, Universidad Nacional Autónoma de México, México D.F., 04510, Mexico

## ARTICLE INFO

### Article history:

Received 15 October 2008

Received in revised form 13 January 2009

Accepted 13 January 2009

Available online 23 January 2009

### Keywords:

Sequential Injection Analysis

Arsenic

Speciation

Phosphates

Molybdenum blue reaction

Mine tailings

## ABSTRACT

By using a simple Sequential Injection Analysis (SIA) manifold and in base to the kinetic reaction of the molybdenum with As(V) and P(V) was possible to determine As(III), As(V) and P(V) in simple, binary and ternary samples. The activation energies for the reaction between molybdenum and As(V) and P(V) were of 70.90 kJ mol<sup>-1</sup> and of 19.02 kJ mol<sup>-1</sup>, respectively, therefore it was possible to determine both analytes in mixtures by using different reaction temperature. When the analyses were carried out at room temperature, only the P(V) supplied analytical signal; with increased temperature, the kinetics of reaction for As(V) also increased, and a signal was obtained, being 55 °C the optimum temperature. In order to determine As(III), it was oxidized into As(V) with KIO<sub>3</sub>, and the reaction was carried out in the same way as for As(V). To resolve mixtures, an equations system from six calibration curves with different sequences of SIA at different temperature was performed. The lineal ranges were between 0.5 µg mL<sup>-1</sup> and 10 µg mL<sup>-1</sup> with a repeatability and reproducibility between 0.7% and 5.2% and detection limits between 0.36 µg mL<sup>-1</sup> and 0.58 µg mL<sup>-1</sup>. In binary mixtures of P(V)/As(V) the recoveries were close to 100% for both analytes at ratios lesser than 10:1. For As(V)/As(III) ratios between 1:1 and 5:1 the recoveries were ranged between 85% and 95%. The method was applied in mine tailings and in arsenopyrite. The results showed that the soluble arsenic was found oxidized as As(V). These results were compared with those obtained by atomic absorption spectrometry and both proved to be very close.

© 2009 Elsevier B.V. All rights reserved.

## 1. Introduction

Tailings are solid residues produced during primary operations in the separation and concentration of minerals, therefore, environmental concerns make tailing control extremely important. The metals and metalates' toxicity in tailings depends mostly on the extractable portion and not on the total concentration, due to the extractable portion causes environmental damage because of their mobility both water and soils. Also, the extractable portion is considered an indirect measurement for bioavailable fraction. Tailings contain residual metallic sulfides as arsenopyrite (FeAsS), galene (PbS), sphalerite (ZnS) and calcopyrite (CuFeS<sub>2</sub>), and their oxidation brings out acid drain and high concentrations of potentially toxic elements such As or Pb [1–4]. The transportation of these elements poses a serious environmental problem as they can pollute the soil and sediments, as well as superficial and underground water [5,6]. Therefore, it is necessary to carry out tests to identify the presence of potentially toxic elements under environmental conditions. Arsenic is a real cancer-causing agent, which can also damage human genetics [7–10]. The most toxic species of arsenic are arse-

nates and arsenites, and among them, As(III) is more toxic than As(V).

Arsenic solubility depends principally on Mn, Fe, and Ca concentrations in water because of the formation non-soluble salts such as Mn<sub>3</sub>(AsO<sub>4</sub>)<sub>2</sub>, FeAsO<sub>4</sub> and Ca<sub>3</sub>(AsO<sub>4</sub>)<sub>2</sub>. Therefore, the ions that compete with these metals change the mobility of the arsenic, as it is the case of phosphates, which at 0.003 mol L<sup>-1</sup> avoid arsenic precipitation. Consequently, sometimes water exposed to arsenic with high phosphates concentrations has higher amounts of dissolved arsenic than water with fewer phosphates [11].

The most used analytical methods for the arsenic determination are: electrothermal atomic absorption (AA) [12], inductively couple plasma coupled with atomic fluorescence spectrometry (ICP-AES) [13,14] and ICP coupled with mass spectrometry (ICP-MS) [15,16]. However, although these techniques are precise and accurate, their cost can be enormous.

Several colorimetric methods to determine arsenic are also used. Some of them are connected with the Gutzeit method, which is based on the generation of arsenine gas by reduction of arsenic under acid conditions, followed by the addition of zinc powder and the quantification of arsine gas on paper impregnated with mercuric bromide [17–19]. At present, the molybdenum blue method is the colorimetric method most used, and it is based on the reaction between the molybdate in acid medium and the As(V) and/or the

\* Corresponding author. Tel.: +52 55 56 22 37 88; fax: +52 55 56 22 37 88.  
E-mail address: [pilarm@servidor.unam.mx](mailto:pilarm@servidor.unam.mx) (M.P. Cañizares-Macías).

P(V), in order to form the corresponding molybdenum heteropoly acid, which is yellow, has a type cage structure and is able to be reduced or oxidized [20]. As(III) does not form complexes with molybdenum, so that arsenic can only be quantified like As(V). To determine As(V), As(III) and P(V) in a mixture, some methods have been described, such as: Johnson and Pilson [21,22] determined the three analytes in sea water and fresh water with a good precision, but colour development took up to 90 min. In a more recent paper, Dhar et al. [23] decreased the reaction time by raising the concentration of potassium antimonyl tartrate and by changing  $\text{KIO}_3$  concentration from  $0.25 \text{ mmol L}^{-1}$  (the original conditions of Johnson and Pilson), to  $2 \text{ mmol L}^{-1}$ , which caused a more efficient oxidation for As(III).

In 2002, Dasgupta et al. [24] determined As(III) and As(V) in drinking water, based on the same reaction of formation of arsenomolybdate, and by using a continuous flow manifold and an anion exchange resin column. They also used  $\text{KBrO}_3$  to oxidize As(III) into As(V) and L-cystine to reduce As(V) into As(III), so, it was possible to speciate both analytes.

Other papers determining P(V) by using molybdenum reaction with flow injection analysis have been reported [25–27], and some of them have succeeded in decreasing the interference from silicates either by using a gas segmented flow system [28] or by a Sequential Injection Analysis (SIA) system [29]. In this paper, 0.25% oxalic acid was used to avoid the molybdosilic acid formation.

Mexico has been a mining country since the Spanish colonial age and the wastes from the mines have been collected since then. Besides, Mexico produces 20% of the amount of arsenic in the whole world. Although storing and treatment methods of mine tailings have been actually improved, their study is, however, of an absolute necessity.

In this paper, an analysis by sequential injection method to quantify As(V) and P(V) in mine tailings based on its kinetic reaction to form the molybdenum blue complex at different temperatures was carried out. The SIA system also allowed to determine As(III).

## 2. Experimental

### 2.1. Instruments and apparatus

To construct the SIA manifold the following component were used: an automatic selection valve with six channels (SCIVEX), a peristaltic pump Gilson Minipuls 3 (France) which was controlled using software made in the laboratory, and Teflon and Tygon tubing of 0.5 mm I.D. One UV-VIS spectrophotometer Cary 3 (Varian, Sydney Australia) equipped with a flow cell of  $118 \mu\text{L}$  inner volume measured the absorbance.

A Lab-line thermostat water bath with an error range of  $\pm 0.2^\circ\text{C}$  was used to control temperature during the arsenic reaction. The temperature was also measured with a Fisherbrand mercury thermometer (from  $-10^\circ\text{C}$  to  $260^\circ\text{C}$ ). An orbital stirrer (Lab-line) and a Millipore filtration system were used in the samples treatment. pH and potential from sample extracts were measured with a Metrohm 620 pH-meter and a Cole Parmer 05669-20 potentiometer.

### 2.2. Reagents and solutions

All the used reagents were analytically graded, the solutions were prepared using distilled water and all glass materials were cleaned with phosphate-free detergent.

A  $500 \text{ mg L}^{-1}$  P(V) stock solution was prepared from  $\text{KH}_2\text{PO}_4$  (99.5% of purity, Sigma). The stock solutions for As(V) and As(III) were prepared from  $\text{Na}_2\text{HAsO}_4 \cdot 7\text{H}_2\text{O}$  (99% of purity, Sigma) and  $\text{NaAsO}_2$  (100% purity, Sigma) at  $500 \text{ mg L}^{-1}$  each. Standard solutions were prepared from stock solutions to suitable concentrations.

A 6% (w/v) ascorbic acid (Sigma) solution, as well as a 0.4% (w/v) tetrahydrate ammonium molybdate (Sigma) solution prepared in  $0.15 \text{ M H}_2\text{SO}_4$  (Baker), were used to carry out the derivation reaction.

To validate the method (in order to achieve reproducibility, repeatability and accuracy) certificated standards were used: phosphorous  $1000 \pm 3 \mu\text{g mL}^{-1}$  in 0.05%  $\text{HNO}_3$ , As(V)  $1000 \pm 3 \mu\text{g mL}^{-1}$  in 2% NaOH and Tr bromine, and As(III)  $1000 \pm 3 \mu\text{g mL}^{-1}$  in 2% HCl. All the standards were supplied by High Purity Standards.

A 0.5%  $\text{KIO}_3$  (Baker) solution was used as As(III) to As(V) oxidation agent.

### 2.3. Sample preparation

The proposed method was applied to mine tailings collected from three mining zones in Mexico (northern, central and southern), as well as to arsenopyrite samples. The extraction method was carried out in accordance with the ASTM D3987-85 method [30], used for lixiviation of tailings with water in equilibrium with atmospheric  $\text{CO}_2$  (pH 5.5).

#### 2.3.1. Collection and preservation

Tailings samples were collected in accordance with the Norma Oficial Mexicana NOM-141-SEMARNAT-2003 [31]. Each sample weighed approximately 2 kg, and each of one was made up of five different sub-samples. They were stored in plastic containers with no substance added to preserve them. Once the samples arrived at the laboratory, they were dried at room temperature and were stored in plastic bags until their analysis.

#### 2.3.2. Determination of pH and potential

5 g of sample were weighed and 100 mL of distilled water were added to them. The mixture was stirred for 10 min, and then the pH and the potential were measured.

#### 2.3.3. Extraction of arsenates from tailings

5 g of sample were weighed and placed into an Erlenmeyer flask, then 100 mL of distilled water were added. The mixture was stirred in an open flask, for 18 h at 200 rpm using an orbital stirrer [30]. Then, the mixture was filtered through a  $45 \mu\text{m}$  porous size Nylon membrane by using a Millipore system, and the soluble arsenic was measured using the SIA system.

#### 2.3.4. Extraction of arsenates from arsenopyrite

0.1 g of sample was weighed and 4 mL of a  $\text{HCl}/\text{HNO}_3$  (1:3) solution were added. The mixture was left to rest for 8 h. Then the sample was filtered and the extract was dissolved at 100 mL with distilled water. Later, a 1:100 dilution was carried out to measure the soluble arsenic by using the SIA system.

The extraction of soluble compounds was carried out in duplicate for all samples.

### 2.4. Sequential injection procedure

Fig. 1 shows the used SIA manifold to determine P(V), As(V) and As(III) in simple, binary and ternary solutions. The analysis sequence in Table 1 shows the sequence for single solutions. When these sequences are combined, it is also possible to resolve binary and ternary samples. The carrier was distilled water and the flow-rate was  $20 \mu\text{L s}^{-1}$  for steps A–L; for step M the flow-rate was changed into  $15 \mu\text{L s}^{-1}$  in order to improve the oxidation reaction of the As(III).

#### 2.4.1. Determination of P(V), As(V) and As(III) in single solutions

Three calibration equations for each analyte were obtained by using the sequences showed in Table 1:

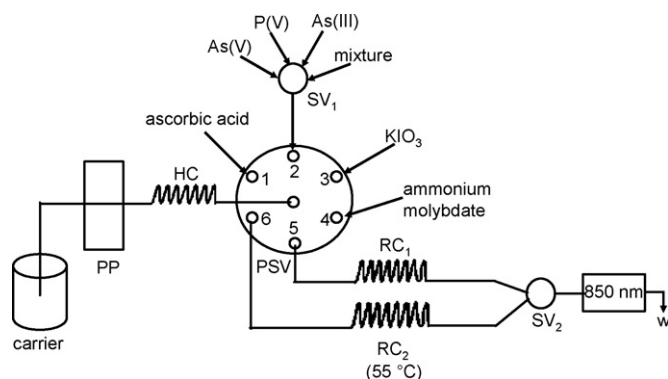


**Fig. 1.** SIA manifold for the determination of As(V), As(III) and P(V). HC: holding coil, RC: reactor coil, SV: selection valve, PSV: principal selection valve with six ways, PP: peristaltic pump, carrier: distilled water.

P(V) at room temperature (steps from A to D; sequence 1)

$$A_1 = C_{P(V)}m_1 + b_1 \quad (1)$$

where  $A$  is the absorbance signal,  $m$  is the slope and  $b$  is the intersection in zero for all the equations.

As(V) (steps from E to H; sequence 2)

$$A_2 = C_{P(V)}m_2 + b_2 \quad (2)$$

As(III) (steps from I to M; sequence 3)

$$A_3 = C_{P(V)}m_3 + b_3 \quad (3)$$

#### 2.4.2. Determination of P(V) and As(V) in binary solutions

We need a third calibration curve of P(V) at 55 °C by using sequence 2:

$$A_4 = C_{P(V)}m_4 + b_4 \quad (4)$$

Therefore, in binary solutions, when sequence 2 was used, the obtained absorbance ( $A_{55^\circ\text{C}}$ ) was the given absorbance by As(V) and by P(V) at 55 °C.

$$A_{55^\circ\text{C}} = A_2 + A_4 \quad (5)$$

So, in order to resolve binary samples, two analyses were carried out: first using sequence 1, and second, using sequence 2. The P(V) concentration was directly obtained after the first analysis and

using Eq. (1). The As(V) concentration was calculated after the second analysis, by substituting Eqs. (1) and (4) in Eq. (5) and resolving  $C_{As(V)}$ :

$$C_{As(V)} = \frac{A_{55^\circ\text{C}} - C_{P(V)}m_4 - b_4 - b_2}{m_2} \quad (6)$$

#### 2.4.3. Determination of As(V) and As(III) in binary solutions

Two analyses were carried out to resolve these mixtures: one by using sequence 2 to know the As(V) concentration, and another by using sequence 3. Consequently, with sequence 3 the dispersion changed and a new calibration curve was constructed for As(V) by using sequence 3:

$$A_7 = A_{As(V)}m_7 + b_7 \quad (7)$$

In the binary solutions, the obtained signal with this sequence was the sum of absorbance given by the original As(V) and by the oxidized As(III):

$$A_{\text{ox}} = A_3 + A_7 \quad (8)$$

The As(III) concentration was calculated by substituting Eqs. (3) and (7) in Eq. (8) and resolving  $C_{As(III)}$ :

$$C_{As(III)} = \frac{A_{\text{ox}} - C_{As(V)}m_7 - b_7 - b_3}{m_3} \quad (9)$$

#### 2.4.4. Determination of P(V), As(V) and As(III) in ternary solutions

In this case, three analyses were carried out: one by using sequence 1, another by using sequence 2 and a third one by using sequence 3. It was necessary to build a new calibration curve for P(V) using sequence 3:

$$A_{P(V)} = A_{P(V)}m_{10} + b_{10} \quad (10)$$

Therefore, in the ternary solutions, the obtained signal with sequence 3 belongs to the three analytes:

$$A_{\text{Total}} = A_3 + A_7 + A_{10} \quad (11)$$

P(V) and As(V) concentrations were obtained with their corresponding equations (Eqs. (1) and (6), respectively). To determine the As(III) concentration, Eqs. (3), (7) and (6) were substituted in Eq. (11), and  $C_{As(III)}$  was resolved:

$$C_{As(III)} = \frac{A_{\text{Total}} - C_{P(V)}m_{10} - b_{10} - C_{As(V)}m_7 - b_7 - b_3}{m_3} \quad (12)$$

**Table 1**

Sequence of analysis for P(V), As(V) and As(III) in single, binary and ternary samples by using the manifold shown in Fig. 1.

Step	Selection valve position (PSV)	Action	Time (s) <sup>a</sup>	Description
<b>Determination of P(V): sequence 1</b>				
A	1	Aspiration	5	Ascorbic acid toward HC
B	2	Aspiration	5	P(V) sample/standard toward HC (to select with SV <sub>1</sub> )
C	4	Aspiration	5	Ammonium molybdate toward HC
D	6	Delivery	120	Delivery to the RC <sub>1</sub> and detector (to select with SV <sub>2</sub> )
<b>Determination As(V): sequence 2</b>				
E	1	Aspiration	5	Ascorbic acid toward HC
F	2	Aspiration	5	As(V) sample/standard toward HC (to select with SV <sub>1</sub> )
G	4	Aspiration	5	Ammonium molybdate toward HC
H	5	Delivery	120	Delivery to the RC <sub>2</sub> (55 °C) and detector (to select with SV <sub>2</sub> )
<b>Determination of As(III): sequence 3</b>				
I	1	Aspiration	5	Ascorbic acid toward HC
J	2	Aspiration	5	As(III) sample/standard toward HC (To select with SV <sub>1</sub> )
K	3	Aspiration	2	KIO <sub>3</sub> toward HC
L	4	Aspiration	5	Ammonium molybdate toward HC
M	5	Delivery	130 <sup>b</sup>	Delivery to the RC <sub>2</sub> (55 °C) and detector (to select with SV <sub>2</sub> )

PSV: principal selection valve.

<sup>a</sup> Flow-rate: 20  $\mu\text{L s}^{-1}$ .

<sup>b</sup> Flow-rate: 15  $\mu\text{L s}^{-1}$ .



The detection limits were calculated by using the equation:

$$Y_B + 3S_B$$

where  $Y_B$  is the blank signal and  $S_B$  is the standard deviation from blank.  $S_B$  was calculated from calibration graphs for each analyte at different conditions (temperature and SIA sequence).  $S_B$  was calculated from the equation:

$$S_B = \frac{\sqrt{\sum (y_i - \hat{y}_i)^2}}{n - 2}$$

This equation utilizes the  $y$ -residuals,  $y_i - \hat{y}_i$ , where the  $\hat{y}_i$  values are the points on the calculated regression line corresponding to the individual  $X$ -values. The calculated intercept for each calibration graph was used as an estimate of  $Y_B$  [32].

### 3. Results and discussion

First, the SIA manifold was optimized for phosphates. To optimize the reagent concentrations, the aspiration sequence as well as the injection volume, a  $6 \mu\text{g mL}^{-1}$  P(V) solution was used. The optimum conditions for P(V) were the same as for As(V). However, for this analysis it was necessary to optimize the reaction temperature, because on flow conditions phosphates only form the complex with ammonium molybdate at room temperature.

#### 3.1. Optimization of SIA manifold

##### 3.1.1. Determination of P(V) and As(V)

**3.1.1.1. Study of the reagents concentration. Ascorbic acid:** The concentration used was 6% (w/v), in accordance with that mentioned by Linares et al. [33].

**Ammonium molybdate:** A range between 0.1% and 1% (w/v) was evaluated. All the tested solutions were dissolved in 0.6 M sulfuric acid. The optimum selected concentration was 0.4%.

**Reaction medium:** Different acids were also evaluated as a reaction medium, such as: nitric acid, sulfuric acid and hydrochloric acid. The analytical signal was similar for the three of them, but the blank signal when HCl or  $\text{HNO}_3$  were used was higher than  $\text{H}_2\text{SO}_4$  and, therefore, the last one was selected to perform the analysis.

**3.1.1.2. Study of the aspiration sequence.** The first step of the molybdenum blue reaction is the formation of a yellow complex (heteropoly acid), and the second one is the reduction of this to Mo(V). With the aim of increasing the overlapping zone between the sample and the reagents, six aspiration sequences were studied:

- Ammonium molybdate–sample/standard–ascorbic acid.
- Ascorbic acid–sample/standard–ammonium molybdate.
- Sample/standard–ammonium molybdate–ascorbic acid.
- Sample/standard–ascorbic acid–ammonium molybdate.
- Ascorbic acid–ammonium molybdate–sample/reagent.
- Ammonium molybdate–ascorbic acid–sample/reagent.

In sequence (a) double peaks were obtained although the RC length was increased; with the other sequences, only one peak was obtained. In sequence (b) the peaks were higher, so this sequence was selected as optimum for the analysis. In sequences (a and b), the sample was between the two reagents, allowing higher overlapping of the dispersed zones. But in these tests the order of the reagents influenced the reaction product: when the ascorbic acid was first aspirated (optimum sequence (b)), there was more contact time between it and the formed heteropoly acid, which was obtained from the reaction between the sample and the ammonium molybdate, causing a higher signal; on the contrary, when

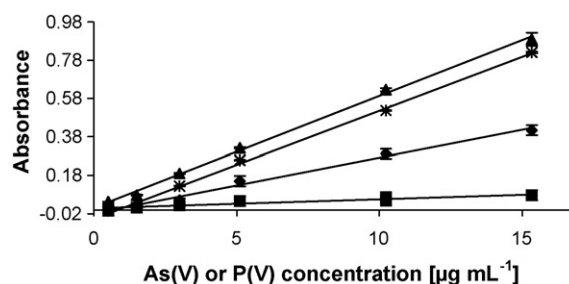


Fig. 2. Study of the sulfuric acid concentration at 0.15 M and 0.6 M for As(V) and P(V), respectively. P(V): (\*) 0.15 M, (▲) 0.6 M; As(V): (◆) 0.15 M, and (■) 0.6 M.

the ammonium molybdate was first aspirated (sequence (a)) double peaks were obtained possibly because of the refraction index gradient.

**3.1.1.3. Study of the aspiration time and the flow-rate.** A range between  $8 \mu\text{L s}^{-1}$  and  $33 \mu\text{L s}^{-1}$  to study the aspiration flow-rate for reagents and sample and the flow-rate for the complex formation was evaluated. The optimum flow-rate found was  $20 \mu\text{L s}^{-1}$ . The aspiration time was established at 5 s equivalent to  $100 \mu\text{L}$ .

**3.1.1.4. Evaluation of the holding coil (HC) and the reaction coil (RC) lengths.** The HC length was long enough to avoid the contamination of reagents and samples, and to assure the maximum overlapping between reagents and sample. The optimum length was 200 cm. In the case of RC the higher signal was obtained at 300 cm.

**3.1.1.5. Optimization of the sulfuric acid concentration.** Linares et al. [33] established that a high  $\text{H}_2\text{SO}_4$  concentration inhibited the formation of the arsenomolybdate but, in accordance with our results, the  $\text{H}_2\text{SO}_4$  was also the best acid for the reaction, therefore, we studied the effect of the sulfuric acid concentration. A concentration range between 0.1 M and 1 M was evaluated. Fig. 2 shows the obtained results when two concentrations of sulfuric acid (0.15 M and 0.6 M) are used to form the heteropolyacids of As(V) or of P(V) at different concentrations. The results show that, at lower sulfuric acid concentrations, the analytical signal for As(V) is higher and it is lower than P(V), which improves the determination of As(V). Therefore, a 0.15 M sulfuric acid concentration was selected as optimum, in order to carry out the analysis of As(V) in presence of P(V).

**3.1.1.6. Evaluation of the temperature to quantify As(V) and P(V).** When arsenates solutions were aspirated with the same concentrations as phosphates at room temperature, the reaction did not take place. Therefore, a study to evaluate the optimum reaction temperature, the rate velocity and the activation energy for As(V) and P(V) was performed. Fig. 3A shows the As(V) plots at several concentrations and at different temperatures. Fig. 3B shows the behaviour of P(V). To calculate the apparent reaction rate ( $K'$ ) some concentrations absorbance at different temperatures for each analyte were measured. The measurement was carried out by using the SIA system and the reaction time was established in the maximum of the SIA peak corresponding to 60 s. The apparent activation energy ( $E'$ ) was calculated after evaluating  $1/T(^{\circ}\text{K})$  vs  $\log K'$ . The reaction rate of each analyte at different temperatures and the activation energy are shown in Table 2. The results show that the reaction rate increases when the temperature also increases for both analytes. In the case of P(V) the kinetic of reaction is similar from room temperature to  $45^{\circ}\text{C}$  increasing to double at  $55^{\circ}\text{C}$ . On the other hand, for As(V) the  $K'$  is much increased from  $40^{\circ}\text{C}$ . Moreover, at room temperature the complex is not formed at least in the time that is evaluated. Besides, the same table shows that for As(V) form the blue complex needs a higher activation energy than P(V), so P(V) can be quantified at

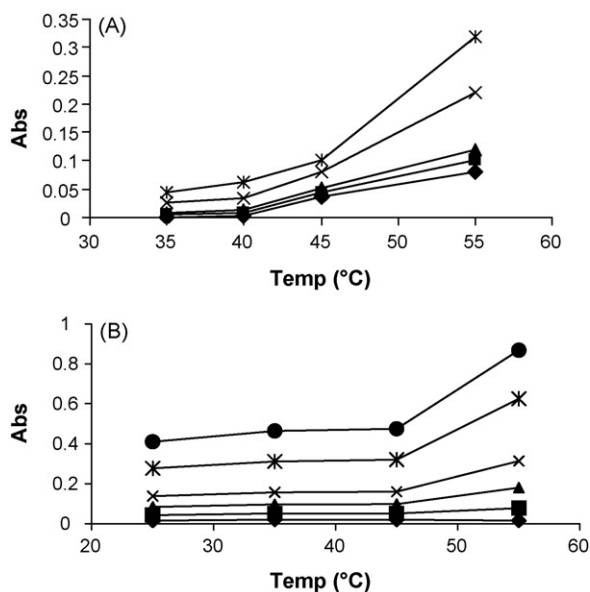


**Fig. 3.** (A) Temperature evaluation at different concentrations of As(V). (◆) 0.15  $\mu\text{g mL}^{-1}$ , (■) 1.5  $\mu\text{g mL}^{-1}$ , (▲) 3  $\mu\text{g mL}^{-1}$ , (×) 7.5  $\mu\text{g mL}^{-1}$ , and (\*) 15  $\mu\text{g mL}^{-1}$ . (B) Temperature evaluation at different concentrations of P(V). (◆) 0.5  $\mu\text{g mL}^{-1}$ , (■) 1.5  $\mu\text{g mL}^{-1}$ , (▲) 3  $\mu\text{g mL}^{-1}$ , (×) 5  $\mu\text{g mL}^{-1}$ , (\*) 10  $\mu\text{g mL}^{-1}$ , (●) 15  $\mu\text{g mL}^{-1}$ .

**Table 2**

Apparent reaction rate ( $K'$ ) and apparent activation energy ( $E'$ ) for As(V) and P(V).

Temperature ( $^{\circ}\text{C}$ )	$K'$ ( $\text{s}^{-1}$ )	
	P(V)	As(V)
25	$4.45 \times 10^{-4}$	–
35	$4.9 \times 10^{-4}$	$5 \times 10^{-5}$
40	n.d.	$6.8 \times 10^{-5}$
45	$5.1 \times 10^{-4}$	$7.2 \times 10^{-5}$
55	$9.7 \times 10^{-4}$	$2.7 \times 10^{-4}$
Activation energy ( $E'$ )	$19.02 \text{ kJ mol}^{-1}$	$70.90 \text{ kJ mol}^{-1}$

n.d.: not determined.

room temperature with no interference of As(V) and it showed the influence of the temperature on the reaction kinetic. These graphics also show that the signal for As(V) begins to increase from 35  $^{\circ}\text{C}$  but, although higher temperatures than 55  $^{\circ}\text{C}$  gave higher peaks, these were not reproducible because bubbles into SIA system appeared. Consequently, 55  $^{\circ}\text{C}$  was selected as the temperature analysis for As(V).

### 3.1.2. Determination of As(III)

To determine As(III) using the molybdenum blue method, it is necessary to oxidize it into As(V). With this aim, the concentration of  $\text{KIO}_3$ , the aspiration SIA sequences, as well as the injection volume, were optimized.

**Table 3**

Characteristics of the method for the determination of P(V), As(V) and As(III) in single standard using different SIA sequences.

Equations <sup>a</sup>	Analyte	Sequence <sup>b</sup>	Slope	Intercept	Linear range ( $\mu\text{g mL}^{-1}$ )	$r$	D.L. ( $\mu\text{g mL}^{-1}$ ) <sup>c</sup>
(1)	P(V)	1	$m_1 = 0.033 \pm 0.001^d$	$b_1 = -0.002 \pm 0.007^d$	0.5–10	0.9995	0.37
(2)	As(V)	2	$m_2 = 0.0649 \pm 0.002$	$b_2 = 0.0085 \pm 0.013$	0.5–10	0.9995	0.36
(3)	As(III)	3	$m_3 = 0.0127 \pm 0.001$	$b_3 = 0.0069 \pm 0.004$	0.6–10	0.9990	0.52
(4)	P(V)	2	$m_4 = 0.0817 \pm 0.004$	$b_4 = 0.0133 \pm 0.020$	0.6–10	0.9992	0.46
(7)	As(V)	3	$m_7 = 0.0255 \pm 0.002$	$b_7 = 0.0287 \pm 0.010$	1–10	0.9990	0.55
(10)	P(V)	3	$m_{10} = 0.0497 \pm 0.003$	$b_{10} = 0.0065 \pm 0.021$	1–10	0.9990	0.58

<sup>a</sup> In accordance with the Sections 2.4.1–2.4.4.

<sup>b</sup> See Table 1.

<sup>c</sup> Detection limit.

<sup>d</sup> Confidence limits.

**3.1.2.1. Sequence of aspiration.** Although the number of reagents was increased for this analysis, we studied only three sequences, as the  $\text{KIO}_3$  and the sample were aspirated one by one to make the oxidation easier. Ammonium molybdate was aspirated at the end, in accordance with the optimization for As(V). The studied sequences were:

- Sample– $\text{KIO}_3$ –ascorbic acid–ammonium molybdate.
- $\text{KIO}_3$ –sample–ascorbic acid–ammonium molybdate.
- Ascorbic acid–sample– $\text{KIO}_3$ –ammonium molybdate.

As the highest analytical signal was in sequence (c), this one was selected to carry out the other analyses (Table 1, sequence 3).

**3.1.2.2.  $\text{KIO}_3$  concentration.** The evaluated range of concentrations was from 0.2% to 1.3%. The optimum concentration was 0.5%. The aspiration volume was also evaluated, being the optimum value 40  $\mu\text{L}$ .

**3.1.2.3. Aspiration and reaction flow-rates.** The aspiration flow-rate was of 20  $\mu\text{L s}^{-1}$  and the reaction flow-rate (delivery step) was of 15  $\mu\text{L s}^{-1}$  to increase the reaction time with the  $\text{KIO}_3$ .

## 3.2. Calibration graphs

Six calibration curves were made by using the sequences of Table 1 to obtain Eqs. (1–4), (7) and (10). The slope and intersection in zero, the correlation coefficient, the lineal range, and the detection limit are shown in Table 3. With these equations data, and substituting them in Eqs. (5), (6), (8), (9), (11) or (12), the concentrations of As(V) and of As(III) in binary and ternary samples were obtained. P(V) was always obtained by using Eq. (1) and sequence 1.

The results show that the determination of P(V) at 55  $^{\circ}\text{C}$  has a sensibility 2.5 times higher than P(V) at room temperature, and 1.25 times higher than As(V) at 55  $^{\circ}\text{C}$ . However, the linear ranges for the six curves are practically the same. When sequence 3 was used, the slope was lower, as the system had one reagent more.

## 3.3. Validation of the method

Certificated standards of P(V), As(V) and As(III) were used to validate the method. Its precision, within-laboratory reproducibility as well as its repeatability were evaluated in a single experimental set-up in duplicate.

### 3.3.1. Simple solutions

The experiments were carried out by using two concentrations of P(V), As(V) and As(III) (2  $\text{mg L}^{-1}$  and 6  $\text{mg L}^{-1}$ ), and using the suitable SIA sequence. To carry out the study, two daily measurements for each concentration were performed for seven days. Table 4 shows the results of reproducibility and repeatability, as well as the

**Table 4**  
Results of the accuracy and precision in the determination of As(V), P(V) and As(III) in single, binary and ternary solutions.

Equation <sup>a</sup>	Analyte	Concentration ( $\mu\text{g mL}^{-1}$ )	Reproducibility (r.s.d.)	Repeatability (r.s.d.)	Accuracy (%)
1	P(V)	2	2.2	4.4	101.4
		6	3.3	3.9	102
2	As(V)	2	2.8	3.5	106.2
		6	2.0	1.7	101.3
3	As(III)	2	4.6	5.2	105.2
		6	4.2	4.5	98.9
4	P(V) at 55 °C	2	1.9	2.3	100.4
		6	0.7	1.4	102.1
7	As(V) <sup>b</sup>	2	2.8	2.6	99.8
		6	2.6	3.2	104.6
10	P(V) <sup>b</sup>	2	1.6	2.9	97.3
		6	1.3	2.1	102.4
1, 6	P(V)/As(V)	1.5/4.5	1.8/1.64	5.0/2.4	102.6/101.5
		4.5/1.5	1.3/4.03	1.7/5.3	100.4/102.1
2, 9	As(V)/As(III)	1.5/4.5	1.9/1.74	2.3/2.8	101.2/98.8
		4.5/1.5	2.2/3.59	2.8/4.9	98.6/96.2
1, 6, 12	P(V)/As(V)/As(III)	1.5/1.5/4.5	1.3/1.8/2.1	1.8/2.8/2.5	101.0/99.6/103.1
		1.5/4.5/1.5	1.5/1.6/2.6	1.8/2.1/3.2	100.2/101.0/96.8

<sup>a</sup> Used equation to determine the concentration of each analyte.

<sup>b</sup> Using sequence 3.

accuracy, in determining the three analytes when found in simple samples.

### 3.3.2. Binary and ternary solutions

In Table 4 are also shown the results of the study for two rates of P(V)/As(V), As(V)/As(III) and P(V)/As(V)/As(III). These results show a bigger error when the As(III) concentration is lower than As(V), because the slope for As(III) is lower than for As(V). Even though, the results also show that the precision and the accuracy are adequate for all the analyses.

Another study on recoveries was also performed in order to evaluate the interference between the analytes. Some ratios of P(V), As(V) and As(III) in binary and ternary mixtures were measured. The ratios were selected in accordance with the lineal range from the different calibration graphs. So, the total concentration of the mixtures could not be higher than  $9 \mu\text{g mL}^{-1}$  and the minimum concentration used for any analyte had to be higher than  $1 \mu\text{g mL}^{-1}$  because at concentrations lower than  $1 \mu\text{g mL}^{-1}$  the confidence limits from calibrations graphs are higher. In Table 5, these results

**Table 5**  
Recoveries study in binary and ternary mixtures.

Mixture	Rate	Recovery (%)		
		P(V)	As(V)	As(III)
P(V)/As(V)	1:1	102.4 ± 1.0	101.0 ± 0.4	
	1:3	104.2 ± 0.5	102.0 ± 0.8	
	1:5	95.7 ± 0.8	100.2 ± 0.5	
	3:1	101.8 ± 0.6	106.6 ± 0.3	
	5:1	98.8 ± 0.3	108.6 ± 0.2	
As(V)/As(III)	1:1		101.2 ± 1.1	94.3 ± 0.2
	1:3		99.5 ± 0.5	104.8 ± 0.6
	1:5		96.2 ± 0.2	101.6 ± 0.1
	3:1		102.2 ± 0.3	90.5 ± 1.0
	5:1		97.2 ± 0.1	85.6 ± 0.6
P(V)/As(V)/As(III)	1:1:1	106.1 ± 0.2	102.5 ± 0.2	93.3 ± 0.3
	1:1:2	107.1 ± 0.6	104.9 ± 0.6	107.6 ± 0.6
	1:1:5	102.1 ± 1.4	98.5 ± 0.2	108.4 ± 0.3
	3:3:1	99.2 ± 0.3	104.2 ± 1.1	91.6 ± 0.2
	1:5:1	105.1 ± 0.5	102.3 ± 0.5	85.3 ± 0.3
	5:1:1	97.6 ± 0.6	98.3 ± 0.3	95.1 ± 0.3

show that when As(V)/As(III) rate is 3:1 or 5:1, the recoveries for As(III) are lower than As(V) and decrease down to 85%. Therefore, although the quantification of As(III) in binary or ternary samples is acceptable, it improves when the concentration is higher than As(V). On the other hand, the determination of P(V) and of As(V) in binary and ternary samples has a higher precision.

Therefore, the SIA manifold allows the analysis of the three analytes in mixtures with a sample throughput of 27 determinations  $\text{h}^{-1}$ .

A few calibration graphs during the tests of validation were built to evaluate their stability. Standards of P(V), As(III) and As(V) at different concentrations were evaluated every week to assure the precision and accurate from the graphs. The values were always between 96% and 103% for simple solutions and between 87% and 110% for binary and ternary mixtures for ratios between 1:1 and 5:1. The slope and the intercept values from calibration equations were always into the precision range of them.

### 3.4. Analysis of samples

Samples of mine tailings and arsenopyrite were analyzed to measure bioavailable soluble arsenic. Five tailings from three mining zones in Mexico were analyzed: two samples from the southern zone (S), one sample from the northern (N) and two samples from the central one (C).

All the samples were analyzed in duplicate, and  $1.5 \mu\text{g mL}^{-1}$  As(V) and P(V) and  $2 \mu\text{g mL}^{-1}$  As(III) were added for the recovery studies. Table 6 shows the concentrations found for soluble arsenic in the analyzed tailings samples, as well as for the arsenopyrite. The pH, the colour and the redox potential of the studied tailings are also reported and, also in the same table, the obtained results by atomic absorption are shown.

As silicates are also interferences in the molybdenum blue reaction, some tests adding 0.25% oxalic acid [29] to the extracts were performed. The signals were the same when oxalic acid was not added because the silicates were not dissolved when the extraction took place.

Tailings from northern and central zones were brown and grey, and the redox potential was close to 350 mV (reported with regards to standard hydrogen electrode, HNE) with a pH between 5 and

**Table 6**  
Determination of soluble arsenic in tailings and arsenopyrite by the proposed SIA method.

Sample	Colour	pH	$E$ (mV) <sup>a</sup>	Concentration in the extracts <sup>b</sup> ( $\mu\text{g mL}^{-1}$ )		Concentration in the tailings ( $\text{mg kg}^{-1}$ )		Recoveries (%)			AA <sup>c</sup> ( $\text{mg kg}^{-1}$ )
				P(V)	As(V)	P(V)	As(V)	P(V)	As(V)	As(III)	
N <sub>1</sub>	Brown	8.0	377	0.58 ± 0.02	<D.L.	11.6	–	96.3	88.6	95.2	–
N <sub>2</sub>	Brown	7.6	396	0.46 ± 0.03	<D.L.	9.2	–	92.1	90.5	92.4	–
C <sub>1</sub>	Grey	5.3	402	1.02 ± 0.13	<D.L.	20.4	–	98.6	100.6	100.3	–
C <sub>2</sub>	Grey	5.6	415	0.96 ± 0.05	<D.L.	19.2	–	101.3	101.2	102.6	–
C <sub>3</sub>	Brown	6.2	312	0.71 ± 0.07	<D.L.	14.2	–	100.3	100.0	104.5	–
C <sub>4</sub>	Brown	6.5	320	0.59 ± 0.05	<D.L.	11.8	–	104.6	99.8	98.4	–
S <sub>1</sub>	Yellow	2.4	730	0.97 ± 0.04	2.29 ± 0.20	19.4	45.08	99.4	105.9	96.8	44.20
S <sub>2</sub>	Yellow	2.7	753	0.96 ± 0.06	2.09 ± 0.05	19.2	41.80	97.6	101.3	97.5	43.00
S <sub>3</sub>	Yellow	3	702	1.91 ± 0.10	7.46 ± 0.16	38.2	149.20	103.2	99.1	92.1	146.00
S <sub>4</sub>	Yellow	2.9	702	1.99 ± 0.15	6.98 ± 0.12	39.8	139.60	98.2	102.2	93.4	140.00
1 <sup>d</sup>	–	–	–	<D.L.	2.85 ± 0.15	–	28.50 <sup>e</sup>	100.6	100.3	96.1	30.00
2 <sup>d</sup>	–	–	–	<D.L.	2.80 ± 0.13	–	28.40 <sup>e</sup>	101.8	98.2	103.5	29.00

<sup>a</sup> Potential reported with regards to standard hydrogen electrode (ENH).

<sup>b</sup> Proposed method. The results are the average and standard deviation for three determinations by extract.

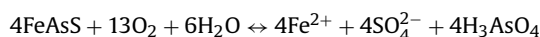
<sup>c</sup> Concentration in the extracts by absorption atomic: Varian SpectraAA 110, empty cathode lamp of arsenic, lengthwave: 193.7 nm, flame: air/acetylene.

<sup>d</sup> Arsenopyrite.

<sup>e</sup> Concentration (w/w).

8. These results indicated that tailings were fresh and, therefore, the soluble arsenic concentration should have been low. This was confirmed with the obtained results, where the soluble arsenic concentration was very low indeed. It was possible because the oxidation process was incipient, (because of the freshness of the tailings) and, besides, because they were stabilized by a high percentage of calcite.

The tailings from the southern zone were old and their colour was yellow. The pH was lower than 3, and the redox potential close to 700 mV (HNE). Therefore, they were oxidized and the soluble arsenic concentration had turned higher. In oxidized tailings the oxidation of the arsenal pyrite is made easier from As(0) to As(V) [34]:



Authors as Foster et al. [35] analyzed mine tailings using an X-ray absorption near edge structure (XANES) spectroscopy, and found that the dominating oxidation state is the As(V) in oxidized mine tailings.

The results show that soluble arsenic from extracts was found as As(V) and not as As(III), because the AAS results for total arsenic from extracts were similar to As(V), which also shows that the proposed method is suitable enough to determine bioavailable soluble arsenic in tailings. On the other hand, the extraction method also makes the oxidation from arsenic to As(V) easier, because the extraction process was carried out at room temperature in open conditions for 24 h. Moreover, when the extraction was finished, HNO<sub>3</sub> was added to the extracts to avoid the arsenic precipitation, and therefore the oxidation of the As(III) was improved. With regard to the arsenopyrite mineral, the results showed an approximate arsenic value of 30%, which is very close to the percentage of arsenic in these minerals. In this case, the mineral was digested and, therefore, all the arsenic was oxidized into As(V).

Besides, the S<sub>3</sub> and S<sub>4</sub> tailings were considered “hazardous residues” in accordance with the Official Mexican Norms NOM-052-SEMARNAT-1993 [36] and the NOM-141-SEMARNAT-2003 [31], which establish that if the extract contains  $\geq 5 \text{ mg L}^{-1}$  of arsenic, the material may be considered a “hazardous residue due to its toxicity for the environment”.

#### 4. Conclusions

The obtained results of soluble arsenic in tailings using the proposed method were very similar to those obtained by AAS.

Therefore, it is possible to state that the molybdenum blue SIA method is an excellent choice to quantify soluble arsenic without P(V) interference. On the other hand, the obtained results about the validation of the SIA method proved to be precise and accurate and, besides, it was made possible to automatize all the analysis with a simple manifold. The values found for the apparent activation energies show the relation between the temperature and the complex formation for As(V) and P(V), which allows the quantification of these in mixtures when different temperatures are used. Although it is necessary to build some calibration curves to determine both three analytes with the proposed SIA method, it is stable and reproducible and the graphs are allowed to be used for a long time, besides the analysis is fast with a sample throughput of 27 h<sup>-1</sup>. The method is not only suitable for other kinds of samples, where only one of the three analytes is measured, but also for more complex samples where one, two or the three analytes are present.

Moreover, the proposed method is a good option for determining bioavailable arsenic in mine tailings, and at the same time minimizing pollution, due to its low levels of generated waste in comparison to other methods.

#### Acknowledgements

The Facultad de Química of the Universidad Nacional Autónoma de México and the “Programa de Apoyo a Proyectos de Investigación e Innovación Tecnológica, PAPIIT” (grant no. IN209707) of the Dirección General de Asuntos del Personal Académico are gratefully acknowledged for the financial support.

#### References

- [1] Z. Lin, *Sci. Total Environ.* 198 (1997) 13.
- [2] R.H. Johnson, D.W. Blowes, W.D. Robertson, J.L. Jambor, *J. Contam. Hydrol.* 41 (2000) 49.
- [3] C.B. Rousel, H.A. Fernández, *J. Environ. Qual.* 29 (2000) 182.
- [4] M.C. Moncur, C.J. Ptacek, D.W. Blowes, J.L. Jambor, *Appl. Geochem.* 20 (2005) 639.
- [5] J.G. Bain, D.W. Blowes, W.D. Robertson, E.O. Frind, *J. Contam. Hydrol.* 41 (2000) 23.
- [6] M.A. Armienta, G. Villaseñor, R. Rodríguez, L.K. Onley, H. Mango, *Environ. Geol.* 40 (2001) 571.
- [7] H.G. Sieler, H. Sigel, *Handbook of Toxicity of Inorganic Compounds*, Marcel Dekker Inc., USA, 1988, p. 79.
- [8] D.Q.O. Hung, O. Nekrassova, R.G. Compton, *Talanta* 64 (2004) 269.
- [9] Organización Mundial de la Salud. *Guías para la calidad del agua potable*, 2<sup>o</sup> edición, vol. 1, Ginebra, 1995, pp. 37–43.
- [10] B.K. Mandal, K.T. Suzuki, *Talanta* 58 (2002) 201.

- [11] M.P. Landeros Albores, Estudio de Arsénico y Selenio en Aguas Subterráneas, Tesis.
- [12] D.Q. Hung, O. Nekrasova, R.G. Compton, *Talanta* 64 (2004) 269.
- [13] K.J. Lamble, S.J. Hill, *Anal. Chim. Acta* 334 (1996) 261.
- [14] N.V. Semenova, F.M. Bauzá de Mirabó, R. Forteza, V. Cerdá, *Anal. Chim. Acta* 412 (2000) 169.
- [15] X. Wei, C.A. Brockhoff-Schwegel, J.T. Creed, *JAAS* 16 (2001) 12.
- [16] I. Havezov, A. Datcheva, J. Rendl, *Microchim. Acta* 119 (1995) 147.
- [17] H. Gutzeit, *Pharmaz. Zeitung* 24 (1879) 263.
- [18] P. Lohmann, *Pharmaz. Zeitung* 36 (1891) 756.
- [19] D. Kinniburg, W. Kosmus, *Talanta* 58 (2002) 165.
- [20] M.T. Pope, *Heteropoly and Isopoly Oxometalates*, Spring-Verlag, Berlin, 1983.
- [21] D.L. Johnson, *Environ. Sci. Technol.* 5 (1971) 411.
- [22] D.L. Johnson, M.E.Q. Pilsen, *Anal. Chim. Acta* 58 (1972) 289.
- [23] R.K. Dhar, Y. Zheng, J. Rubrnstone, A. Van Geen, *Anal. Chim. Acta* 526 (2004) 203.
- [24] P.K. Dasgupta, H. Huang, G. Zhang, G. Cobb, *Talanta* 58 (2002) 153.
- [25] J.L. Manzoori, A. Miyazaki, H. Tao, *Analyst* 115 (1990) 1055.
- [26] R.L. Benson, Y.B. Truong, I.D. McKelvie, B.T. Hart, *Water Res.* 30 (1996) 1959.
- [27] K. Grudpan, P. Ampan, Y. Udnan, S. Jayasvati, S. Lapanatnoppakhun, J. Jakmune, G.D. Christian, J. Ruzicka, *Talanta* 58 (2002) 1319.
- [28] J.Z. Zhang, J. Charles Fischer, P.B. Ortner, *Talanta* 49 (1999) 293.
- [29] C.X. Galhardo, J.C. Masini, *Anal. Chim. Acta* 417 (2000) 191.
- [30] ASTM D 3987-85 American Society for Testing and Materials, Standard Test Method for Shake Extraction of Solid Waste with Water, ASTM, West Conshohocken, PA, 1992, 4 p.
- [31] Norma Oficial Mexicana NOM-141-SEMARNAT-2003. Requisitos para la caracterización del sitio, proyecto, construcción, operación y postoperación de presas de jales, Secretaría de Medio ambiente y Recursos Naturales, México, 2003.
- [32] J. Miller, J. Miller, *Estadística y quimiometría para química analítica*, 4ª edición, Prentice Hall, Madrid, España, 2002, 78–155.
- [33] P. Linares, M.D. Luque de Castro, M. Valcárcel, *Anal. Chem.* 58 (1986) 120.
- [34] G. Morin, G. Calas, *Elements* 2 (2006) 97.
- [35] A.L. Foster, E.B. Gordon Jr., T.N. Tingle, G. Parks, *Am. Mineral.* 83 (1998) 553.
- [36] Norma Oficial Mexicana NOM-052-SEMARNAT-1993. Características de los residuos peligrosos y el listado de los mismos y los límites que hacen un residuo peligroso por su toxicidad al ambiente. Characteristics of dangerous residues and listed of them and the limits of toxicity to the environmental. Secretaría de Medio Ambiente y Recursos Naturales, México, 1993.



# An electrochemical biosensor for $\alpha$ -fetoprotein based on carbon paste electrode constructed of room temperature ionic liquid and gold nanoparticles

Caifeng Ding<sup>a,b</sup>, Fei Zhao<sup>b</sup>, Rui Ren<sup>b</sup>, Jin-Ming Lin<sup>a,\*</sup>

<sup>a</sup> The Key Laboratory of Bioorganic Phosphorus Chemistry & Chemical Biology, Department of Chemistry, Tsinghua University, Beijing 100084, PR China

<sup>b</sup> Key Laboratory of Eco-chemical Engineering, Ministry of Education; College of Chemistry and Molecular Engineering, Qingdao University of Science and Technology, Qingdao 266042, PR China

## ARTICLE INFO

### Article history:

Received 10 October 2008

Received in revised form 15 January 2009

Accepted 18 January 2009

Available online 24 January 2009

### Keywords:

Electrochemical immunoassay

$\alpha$ -Fetoprotein (AFP)

Carbon paste electrode (CPE)

Gold nanoparticle

Room temperature ionic liquid (RTIL)

O-Aminophenol (OAP)

## ABSTRACT

A novel and effective electrochemical immunosensor for the rapid determination of  $\alpha$ -fetoprotein (AFP) based on carbon paste electrode (CPE) consisting of room temperature ionic liquid (RTIL) *N*-butylpyridinium hexafluorophosphate (BPPF<sub>6</sub>) and graphite. The surface of the CPE was modified with gold nanoparticles for the immobilization of the  $\alpha$ -fetoprotein antibody (anti-AFP). By sandwiching the antigen between anti-AFP on the CPE modified with gold nanoparticles and the secondary antibody, polyclonal anti-human-AFP labeled with horseradish peroxidase (HRP-labeled anti-AFP), the immunoassay was established. The concentration of AFP was determined based on differential pulse voltammetry (DPV) signal, which was generated in the reaction between *O*-aminophenol (OAP) and H<sub>2</sub>O<sub>2</sub> catalyzed by HRP labeled on the sandwich immunosensor. AFP concentration could be measured in a linear range of 0.50–80.00 ng mL<sup>-1</sup> with a detection limit of 0.25 ng mL<sup>-1</sup>. The immunosensor exhibited high sensitivity and good stability, and would be valuable for clinical assay of AFP.

© 2009 Elsevier B.V. All rights reserved.

## 1. Introduction

Due to the highly sensitive and selective nature of the recognition between antigens and antibodies (Ab), immunoassays are very useful in many fields such as medical detection, processing quality control and environmental monitoring [1]. Conventional methods used in immunoassays, including enzyme-linked immunosorbent assay (ELISA), immunoradiometric assay (IRMA) and single radial immunodiffusion, usually have various limitations such as relying on the label of either antigen or antibody, radiation hazards, long analysis time, expensive instruments and skillful operators [2]. New techniques, such as electrochemistry [3], chemiluminescence [4], piezoelectricity [5] and surface plasmon resonance [6], have attracted extensive interests in immunoassays due to their simple and specific characteristics. Among these techniques, electrochemical immunoassay has received much attention for its high sensitivity and low cost. In electrochemical immunoassays, the target specific ligands must be effectively immobilized on the electrode surface and the analytes must be able to access their immobilized recognition couple under satisfactory frequency without severe steric hindrance and nonspecific binding [7]. Thus, the design and implementation of a unique sensing surface for facile ligand functionalization and biospecific interaction are crucial.

Carbon paste electrode (CPE), which was made up of carbon particles and organic liquid, has been widely applied in the electroanalytical community due to its low cost, ease of fabrication, high sensitivity for detection and renewable surface [8–13]. Generally, the organic liquid, as a binder component in the pastes, is a non-conductive mineral oil, which to some extent weakens the electrochemical response of CPE, thus is especially disadvantageous for the detection. Room temperature ionic liquids (RTILs), possessing unique properties such as negligible vapor pressure, wide potential windows, high thermal stability and high viscosity and good conductivity and solubility, have been developed and received much attention in many areas in chemistry study and electrochemical industry [14–16]. Several groups have utilized RTILs as alternative medias for biocatalysis [17,18]. Our group has constructed an excellent electrochemical biosensor based on RTIL (BPPF<sub>6</sub>), sodium alginate (SA) and graphite for the determination of H<sub>2</sub>O<sub>2</sub> [19]. Electrodepositing gold nanoparticles onto the surface of the CPE was another strategy to enhance the sensitivity of the immunosensor. Many works had been conducted to construct the immunosensor using CPE modified with gold nanoparticles [20–26]. However, to the best of our knowledge, none immunosensor based on CPE modified with RTIL and gold nanoparticles has been reported.

As a well-known tumor marker,  $\alpha$ -fetoprotein (AFP) is widely used for the diagnosis of patients with germ cell tumors and hepatocellular carcinoma [27–29]. Thus, it is necessary to detect AFP for the clinical diagnosis, especially for early detection of liver carci-

\* Corresponding author. Tel.: +86 10 62792343; fax: +86 10 62792343.  
E-mail address: [jmlin@mail.tsinghua.edu.cn](mailto:jmlin@mail.tsinghua.edu.cn) (J.-M. Lin).

noma. In recent years, numerous immunological methods for AFP detection have been described [30–33]. Liu and co-workers has proposed a novel reusable electrochemical immunosensor for AFP based on phenylboronic acid monolayer on gold [34]. Yuan and co-workers has constructed some electrochemical immunosensors based on gold nanoparticles, silver nanoparticles and CdS nanoparticles with the detection limits ranging from 0.12 to 2.4 ng mL<sup>-1</sup> [35–38]. Ye et al. developed novel fluorescent Tb<sup>3+</sup> chelate-doped silica nanoparticles with surfacing amino groups for time-resolved fluoroimmunoassay of human AFP. The assay response is linear from 0.10 to about 100 ng mL<sup>-1</sup> with the detection limit of 0.10 ng mL<sup>-1</sup> [39]. Zhang et al. has developed a new voltammetric enzyme-linked immunoassay system of 3-hydroxyl-2-aminopyridine (HAP)–H<sub>2</sub>O<sub>2</sub>–horseradish peroxidase (HRP) for the assay of AFP in human serum ranging from 0.1 to 200 ng mL<sup>-1</sup> with a detection limit of 0.1 ng mL<sup>-1</sup> [40].

In this study, a novel electrochemical immunosensor based on RTIL (BPPF<sub>6</sub>), gold nanoparticles and graphite was constructed for the determination of AFP. It was expected that replacing silicone oil with BPPF<sub>6</sub> would enhance the current intensity, and the gold nanoparticles on the surface of the electrode could amplify the signal significantly. Moreover, the electrochemical immunosensor could also be renewed easily by mechanical polishing whenever needed.

## 2. Experimental

### 2.1. Materials

An AFP ELISA kit, containing a series of AFP standard solutions and polyclonal anti-human-AFP antibody labeled with horseradish peroxidase (HRP-labeled anti-AFP), was purchased from Zhengzhou Bosai Biotechnology (China). Anti-mouse-AFP monoclonal Ab (AFP-McAb) was purchased from Meiao Biotechnology (China). Bovine serum albumin (BSA)-fraction was from AiBi Chemistry Preparation (China). *O*-Aminophenol (OAP) was obtained from Beijing Hengyezhongyuan Limited (China). H<sub>2</sub>O<sub>2</sub> (Shanghai Chemical Plant, China) was of analytical grade and used as received. 1-Ethyl-3-(3-dimethylaminopropyl)carbodiimide solution (EDC) and *N*-hydroxysuccinimide solution (NHS) were purchased from Sigma. The ionic liquid *N*-butylpyridinium hexafluorophosphate (BPPF<sub>6</sub>, 97%, melting point 65 °C) was purchased from Hangzhou Chemer Chemical Limited (China). Graphite powder (average particle size 30 μm) was obtained from Shanghai Colloid Chemical (China) and used without further treatment. The supporting electrolyte solution was 0.1 M phosphate buffered saline (PBS, pH 7.5) containing 0.1 M KCl. All other reagents used were of analytical grade and doubly distilled water was used throughout.

### 2.2. Apparatus

Cyclic voltammetry (CV) was performed on a CHI 832B electrochemical analyzer (Shanghai ChenHua Instrument, China) with a three-electrode system composed of a platinum wire as auxiliary electrode, an Ag/AgCl/KCl (sat) electrode as reference electrode and the HRP-anti-AFP/CILE as working electrode. Electrochemical impedance spectroscopy (EIS) was carried out on CHI 660C electrochemical analyzer (Shanghai Chenhua Instrument Company, China) with the same three-electrode system described above. All the electrochemical experiments were performed at an ambient temperature of 25 ± 2 °C. Scanning electron microscopy (SEM) measurements were carried out on a JSM-6700F scanning electron microscope (Japan Electro Company). Gold nanoparticles deposition was made on Potentiostat/Galvanostat Model 263A (America).

### 2.3. Procedure

#### 2.3.1. Construction of CPE and CILE

The ionic liquid carbon paste electrode (CILE) was fabricated with the following procedure: 9 g graphite powder, 3 g ionic liquid BPPF<sub>6</sub> (mp 65 °C) and 3 g paraffin were hand-mixed thoroughly in a mortar and heated at a temperature of 80 °C to form a homogeneous carbon paste. A portion of the carbon paste was filled firmly into one end of a glass tube (inner diameter 0.35 cm), and a copper wire was inserted through the opposite end to establish an electrical contact. It was then left to cool to room temperature. Prior to use, a mirror-like surface was obtained by smoothing the electrode on a weighing paper.

#### 2.3.2. Electrodeposition of gold nanoparticles onto CILE

The CILE was immersed into 6 mM HAuCl<sub>4</sub> solution containing 0.1 M KNO<sub>3</sub> (prepared in doubly distilled water, and deaerated by bubbling with nitrogen). A constant potential of -0.4 V versus Ag/AgCl was applied for 400 s. Then, the modified electrode (nano-Au-CILE) was washed with doubly distilled water and dried carefully. The electrode was characterized by cyclic voltammetry in 0.1 M HCl and SEM.

#### 2.3.3. Fabrication of the immunosensor

The nano-Au/CILE was electrochemically cleaned by cyclic scanning with a potential range of 0.1–1.5 V in 0.1 M H<sub>2</sub>SO<sub>4</sub> at a scan rate of 0.1 V s<sup>-1</sup>. The nano-Au/CILE was first dipped in 5 mM thioglycolic acid (TGA) aqueous solution for 24 h to form self-assembled monolayer, and then rinsed thoroughly with doubly distilled water to remove extra TGA. The electrode was inverted and activated by being rinsed in 20 μL of solution containing EDC and NHS in 50 mM PBS (pH 7.0), and then evaporated to dryness. After rinsing, the α-fetoprotein immunosensor has developed by covalently conjugating AFP-McAb with TGA on the Nano-Au covered electrode. The unreacted TGA-activated surface groups were subsequently passivated by reaction with 1% (w/w) BSA at room temperature for 2 h.

The AFP immunosensor was based on a sandwich immunoassay method. Before measurement, it was incubated with different concentrations of AFP and excessive HRP labeled AFP antibody in turn at 37 °C for 0.5 h, and the formed immunoconjugation in the immunosensor was detected in an OAP–H<sub>2</sub>O<sub>2</sub>–HRP electrochemical system. The fabricated AFP immunosensor was stored at 4 °C when not in use. The fabrication process is shown in Scheme 1.

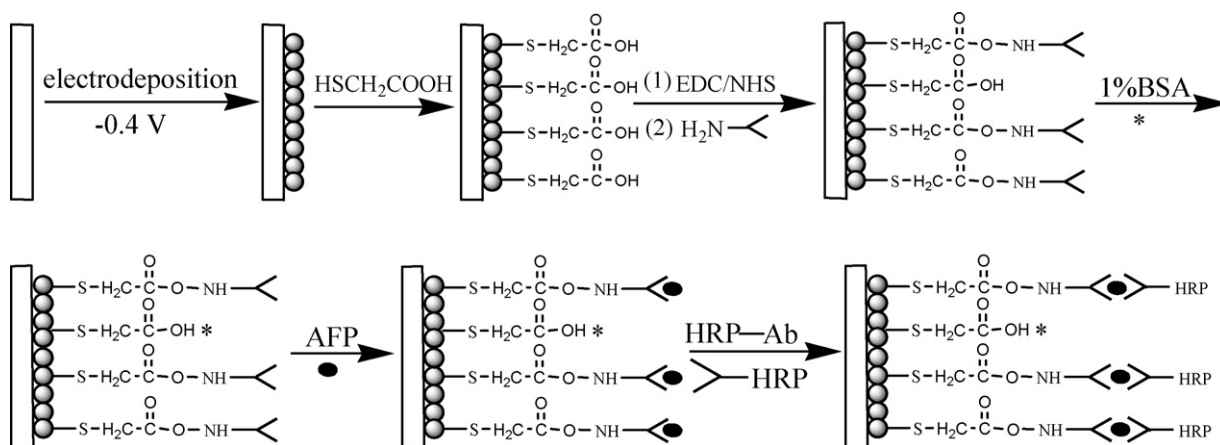
#### 2.3.4. Electrochemical measurements

The electrochemical characterizations and measurements on the modified electrode were carried out using cyclic voltammetry and differential pulse voltammetry (DPV) from -0.6 to 0.1 V (versus Ag/AgCl) in 2 mL of 0.1 M PBS containing 5 mM OAP and 1 mM H<sub>2</sub>O<sub>2</sub> at room temperature. The EIS were performed in a solution of 0.01 M PBS (7.4) containing 0.1 M KCl and 5 mM Fe(CN)<sub>6</sub><sup>3-</sup>/Fe(CN)<sub>6</sub><sup>4-</sup> with the frequencies ranging from 1 to 10<sup>4</sup> Hz.

## 3. Results and discussion

### 3.1. Morphologies of the different electrodes

The response of a biosensor is related to its physical morphology. The SEM of CPE, CILE, nano-Au/CILE and HRP-Ab/AFP/Ab/TGA/nano-Au/CILE were shown in Fig. 1. Significant differences in the surface structure of CPE and CILE are observed. The surface of the CPE was predominated by isolated and irregularly shaped graphite flakes and separated layers were seen (Fig. 1A). The SEM image of CILE showed more uniform surface and no separated carbon layers could



**Scheme 1.** Schematic illustration of the stepwise immunosensor fabrication process.

be observed in Fig. 1B. It was shown that a mass of RTIL had been embedded in carbon layers [41]. As a liquid with good conductivity and high viscosity, RTIL is capable of better dispersing the graphite powder in the paste than the conditional paraffin, thus could better bridge the graphite flakes, multilayer nanoparticles with an irregular distribution and interstices among the nanoparticles were observed in SEM image of the nano-Au/CILE (Fig. 1C), exhibiting large surface area. Quite different aggregative morphology was shown in Fig. 1D, showing HRP-Ab/AFP/Ab complex had been formed on gold nanoparticles, and the surface area of the electrode increased further.

### 3.2. Deposition of gold nanoparticles on the CILE

Nano-Au was electrochemically deposited on the surface of CILE at the potential of  $-0.4$  V. The amount of nano-Au deposited can be determined and controlled by the electric quality passing through the cell. The nano-Au film on CILE was electrochemically characterized using CV in 0.1 M HCl at a scan rate of  $0.1 \text{ V s}^{-1}$ , as shown in Fig. 2b. For comparison, the voltammogram of bare CILE with the same geometric surface area is also presented in Fig. 2a. Nano-Au reduction started at about 1.0 V, showing two reductive current peaks.

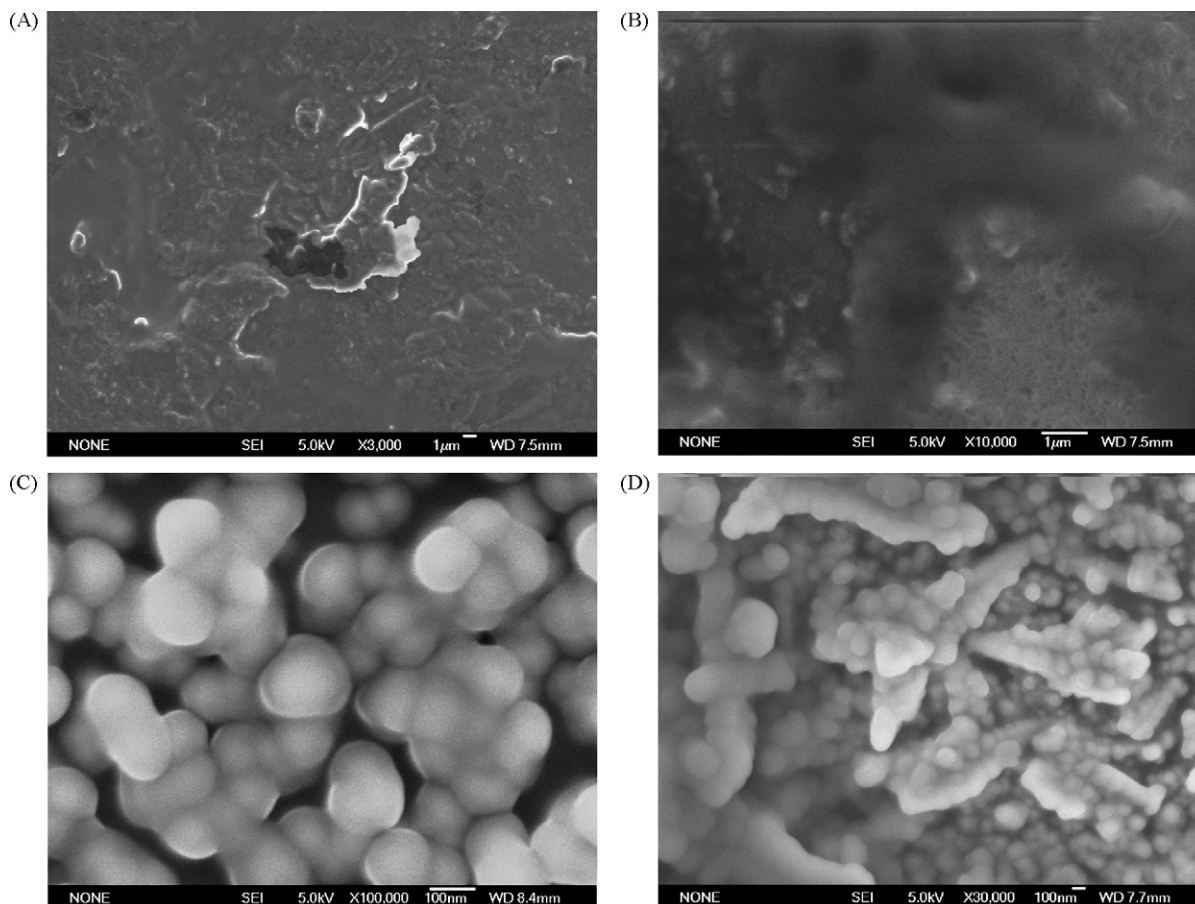


**Fig. 1.** SEM images of the different types of modified electrodes: (A) CPE; (B) CILE; (C) nano-Au/CILE; (D) HRP-Ab/AFP/Ab/TGA/nano-Au/CILE.



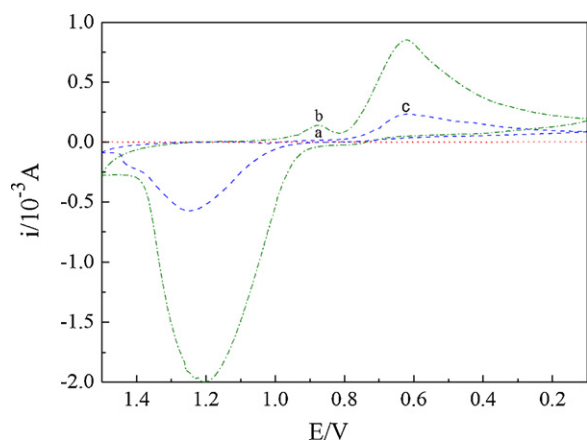
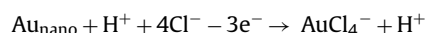


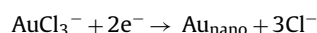
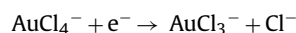
**Fig. 2.** Cyclic voltammograms (CV) for (a) bare CILE; (b) nano-Au/CILE; (c) nano-Au/CPE in 0.1 M HCl at a scan rate of 0.1 V s<sup>-1</sup>.

From experimental results and related documents [42], the following electrode mechanism can be proposed:

Oxidation process at 1.21 V



Reduction processes at 0.64 and 0.88 V



For comparison, the CV pattern of nano-Au modified CPE (i.e. without RTIL) was shown in curve c. It can be clearly seen that the peak positions were similar to those in curve b, but the peak currents was about just a quarter of the latter's, showing the conductivity of nano-Au modified CILE was much higher than that of nano-Au modified CPE.

### 3.3. Electrochemical characteristics of the CILE surface

All electrochemical measurements were performed in 0.01 M PBS solution containing 0.1 M KCl and 5 mM Fe(CN)<sub>6</sub><sup>3-/4-</sup>. The CV of ferricyanide was chosen as a marker to investigate the changes of the electrode behavior before and after each assembly step. Fig. 3A shows the CV of Fe(CN)<sub>6</sub><sup>3-/4-</sup> at the bare CILE (curve a), nano-Au/CILE (curve b), TGA/nano-Au/CILE (curve c), Ab/TGA/nano-Au/CILE (curve d), AFP/Ab/TGA/nano-Au/CILE (curve e), HRP-Ab/AFP/Ab/TGA/nano-Au/CILE (curve f), respectively. As shown in Fig. 3A, it was observed that the peak current of nano-Au/CILE greatly increased after the modification of nano-Au. Obviously, the nano-Au film increase of conductivity and stability. Moreover, three-dimensionally ordered nano-Au film electrode had a much larger effective surface area than the geometrical surface area, as a result of the efficient alignment of the McAb molecules. Stepwise modifications on the nano-Au/CILE was accompanied by decreases in amperometric response and increases in the peak-to-peak separation between the cathodic and anodic waves of the redox probe, showing that the electron-transfer of Fe(CN)<sub>6</sub><sup>3-/4-</sup> was obstructed. After the nano-Au film electrode was functionalized with TGA, the electron transfer between the electrochemical probe and electrode surface was inhibited, owing to the electrostatic repulsion between TGA with negative charges and the negatively charged electrochemical probe. When McAb, AFP and HRP-Ab were immobilized on the electrode surface in turn, the peak currents of the redox couple of Fe(CN)<sub>6</sub><sup>3-/4-</sup> decreased further.

EIS is an effective tool for studying the interface properties of surface-modified electrodes. The typical impedance spectrum

(presented in the form of the Nyquist plot) includes a semicircle portion at higher frequencies corresponding to the electron-transfer-limited process and a linear part at lower frequency range representing the diffusion limited process. The semicircle diameter in the impedance spectrum equals the electron-transfer resistance,  $R_{\text{et}}$ . This resistance controls the electron-transfer kinetics of the redox probe at the electrode interface. Therefore,  $R_{\text{et}}$  can be used to describe the interface properties of the electrode. Its value varies when different substances that are adsorbed onto the electrode surface [43]. The complex impedance was displayed as the sum of the real and imaginary components ( $z_{\text{re}}$  and  $z_{\text{im}}$ ). To obtain the detailed information of the impedance spectroscopy, a simple equivalent circuit model was used to fit the results. Fig. 3B showed the impedance spectra observed upon the stepwise modification process. The CILE revealed a very small semicircle domain (curve a), implying a very low electron-transfer resistance of the redox probe. After the CILE was modified with nano-Au, the  $R_{\text{et}}$  was a smaller semicircle domain near to linear (curve b), showing that the nano-Au/CILE promoted conductivity. When the electrode was conjugated with TGA, the  $R_{\text{et}}$  slightly increased (curve c). This was attributed to that the self-assembled layer of COO<sup>-</sup> terminal groups on the electrode surface generated a negatively charged surface, which reduced the ability of the redox probe to access the layer [44]. Subsequently, after McAb, AFP and HRP-Ab were immobilized on the electrode surface, the  $R_{\text{et}}$  increased again. The results were consistent with the CV curves shown in Fig. 3A. In comparison with CV, the EIS presented more apparent differences to multilayers deposited on the CILE, indicating better sensitivity.

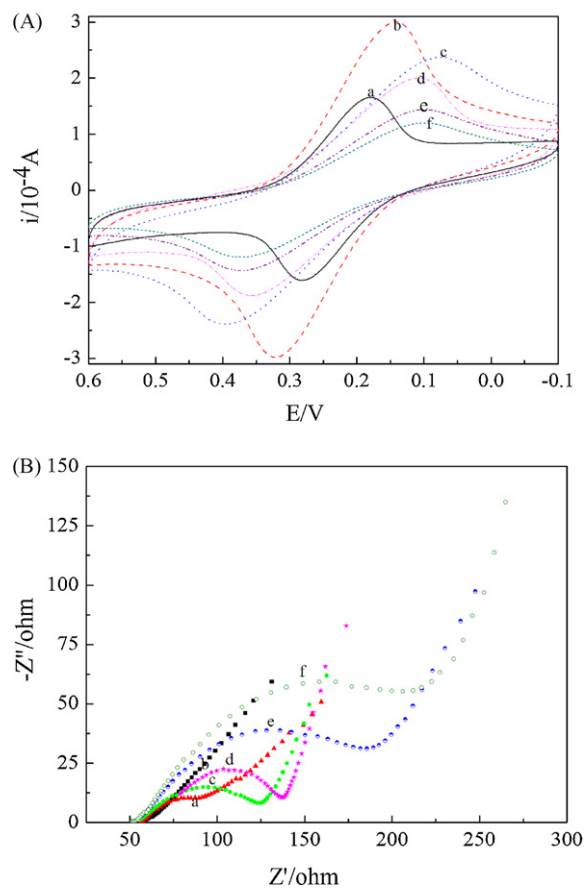
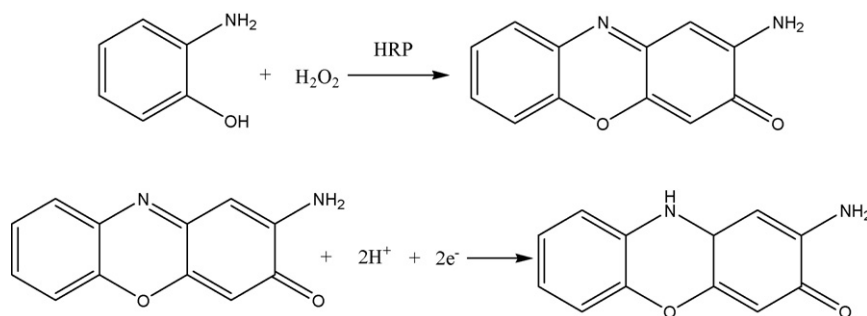


**Fig. 3.** Cyclic voltammograms (CV) curves (A) and electrochemical impedance spectroscopy (B) of different electrode in PBS (10 mM, pH 7.4) solution containing 0.1 M KCl and 5 mM Fe(CN)<sub>6</sub><sup>3-/4-</sup>; (a) bare CILE; (b) nano-Au/CILE; (c) TGA/nano-Au/CILE; (d) Ab/TGA/nano-Au/CILE; (e) AFP/Ab/TGA/nano-Au/CILE; (f) HRP-Ab/AFP/Ab/TGA/nano-Au/CILE. Scan rate: 0.1 V s<sup>-1</sup>, quiet time: 2 s.



**Scheme 2.** Response mechanism of HRP to  $\text{H}_2\text{O}_2$  and OAP.

### 3.4. CV behavior of the HRP-anti-AFP modified electrodes

It is well known that HRP can catalyze the oxidation reaction of OAP by  $\text{H}_2\text{O}_2$ . The mechanism of enzymatic catalysis and oxidation has been described previously [45]. A possible mechanism of reaction of  $\text{H}_2\text{O}_2$  catalyzed by HRP is proposed in Scheme 2. Fig. 4 showed the CV of various electrodes in different solutions. No response of the CILE was observed in the absence of OAP and  $\text{H}_2\text{O}_2$  in 0.1 M pH 7.5 PBS (curve a). Whereas, the CV of CILE showed a pair of obvious redox peaks at  $-0.25$  and  $-0.34$  V (curve b). As three-dimensionally ordered nano-Au/CILE had not only good conductivity and stability, but also a much larger effective surface area, the peak currents of the redox couple became bigger than the bare CILE. But the peak-to-peak separation between the cathodic and anodic waves increased slightly. As to the HRP-Ab/AFP/Ab/TGA/nano-Au/CILE, the redox current attributed to the catalytic process of HRP at the immunosensor increased (curve c). The increased current response indicated the direct electron-transfer of HRP with the aid of nano-Au.

### 3.5. Influence of the scan rate

Typical CV curves of the HRP-Ab/AFP/Ab/TGA/nano-Au/CILE in 0.1 M PBS (pH 7.5) containing 5.0 mM OAP and 1 mM  $\text{H}_2\text{O}_2$  at different scan rates were shown in Fig. 5. It can be seen that a pair of roughly symmetric anodic and cathodic peaks appeared with almost equal peak currents in the scan rate range from 0.03 to  $0.45 \text{ V s}^{-1}$ . The peak-to-peak separation also increased with the

scan rate. A good linear relationship was found for the peak current and scan rate, with the results shown in Fig. 5 (upper left inset). The reduction and oxidation peak currents rise linearly with the linear regression equations as  $i_{\text{pc}} (10^{-4} \text{ A}) = 7.4276v^{1/2} (\text{V s}^{-1})^{1/2} - 0.2494$  ( $n = 10$ ,  $\gamma = 0.9987$ ),  $i_{\text{pa}} (10^{-4} \text{ A}) = -10.077v^{1/2} (\text{V s}^{-1})^{1/2} - 0.6483$  ( $n = 10$ ,  $\gamma = 0.9994$ ), respectively, suggesting that the reaction is a quasi-reversible diffusion-controlled behavior with an electron transfer process.

### 3.6. Optimization of experimental conditions

The experimental conditions, which can affect the amperometric determination of AFP, including the time of electrodeposition, the pH of supporting electrolyte, the incubation temperature and time of immunoreaction were optimized.

The peak current increased with the deposition time. When the deposition time reached 400 s, at the potential of  $-0.4$  V (versus Ag/AgCl) in 6 mM  $\text{HAuCl}_4$ , the nano-Au/CILE surface was found to be best and the current response in 0.1 M HCl increased slightly. So the electrodeposition time optimum was 400 s (Fig. 6A).

The acidity of the solution greatly affects the enzyme activity. So the pH value of substrate solution was the important factor to the current response. The influence of the pH of the assay solution in 0.1 M PBS containing 5 mM OAP and 1 mM  $\text{H}_2\text{O}_2$  was investigated. The pH optimum was 7.5. Thus, pH 7.5 (Fig. 6B) was fixed for the rest of the experiments.

The influences of the antigen–antibody incubation temperature and time on the amperometric responses were also studied. The optimum conditions were  $37^\circ\text{C}$  and 0.5 h (Fig. 6C and D).

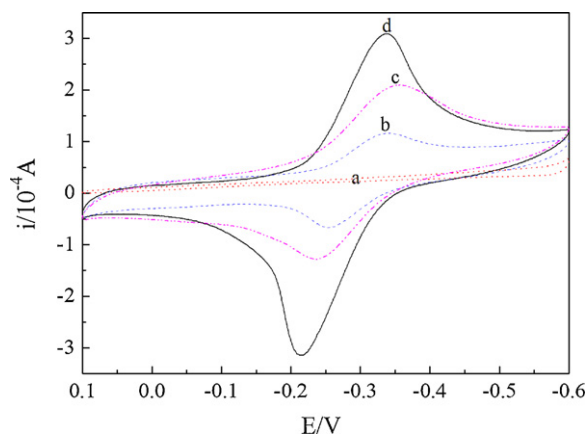


**Fig. 4.** Cyclic voltammograms (CV) of different electrodes: (a) bare CILE in PBS (0.1 M, pH 7.5); (b) bare CILE in PBS (0.1 M, pH 7.5) containing 5 mM OAP and 1 mM  $\text{H}_2\text{O}_2$ ; (c) nano-Au/CILE in PBS (0.1 M, pH 7.5) containing 5 mM OAP and 1 mM  $\text{H}_2\text{O}_2$ ; (d) HRP-Ab/AFP/Ab/TGA/nano-Au/CILE in PBS (0.1 M, pH 7.5) containing 5 mM OAP and 1 mM  $\text{H}_2\text{O}_2$ . Scan rate:  $0.10 \text{ V s}^{-1}$ , quiet time: 2 s.

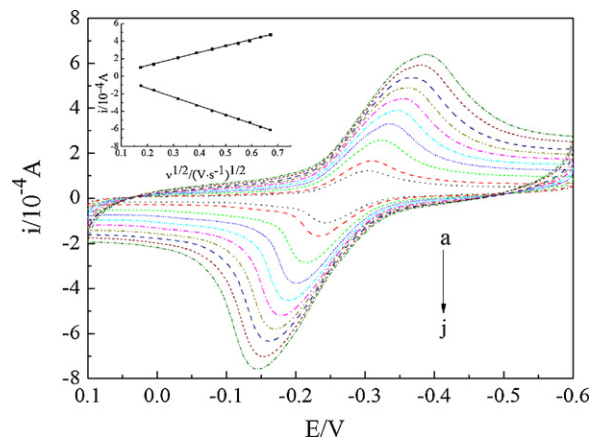


**Fig. 5.** Cyclic voltammograms (CV) of HRP-Ab/AFP/Ab/TGA/nano-Au/CILE in 0.1 M PBS (pH 7.5) containing 5.0 mM OAP and 1 mM  $\text{H}_2\text{O}_2$  at: (a) 0.03; (b) 0.05; (c) 0.10; (d) 0.15; (e) 0.20; (f) 0.25; (g) 0.30; (h) 0.35; (i) 0.40; (j)  $0.45 \text{ V s}^{-1}$ . The inset shows a calibration plot of peak current versus scan rate.

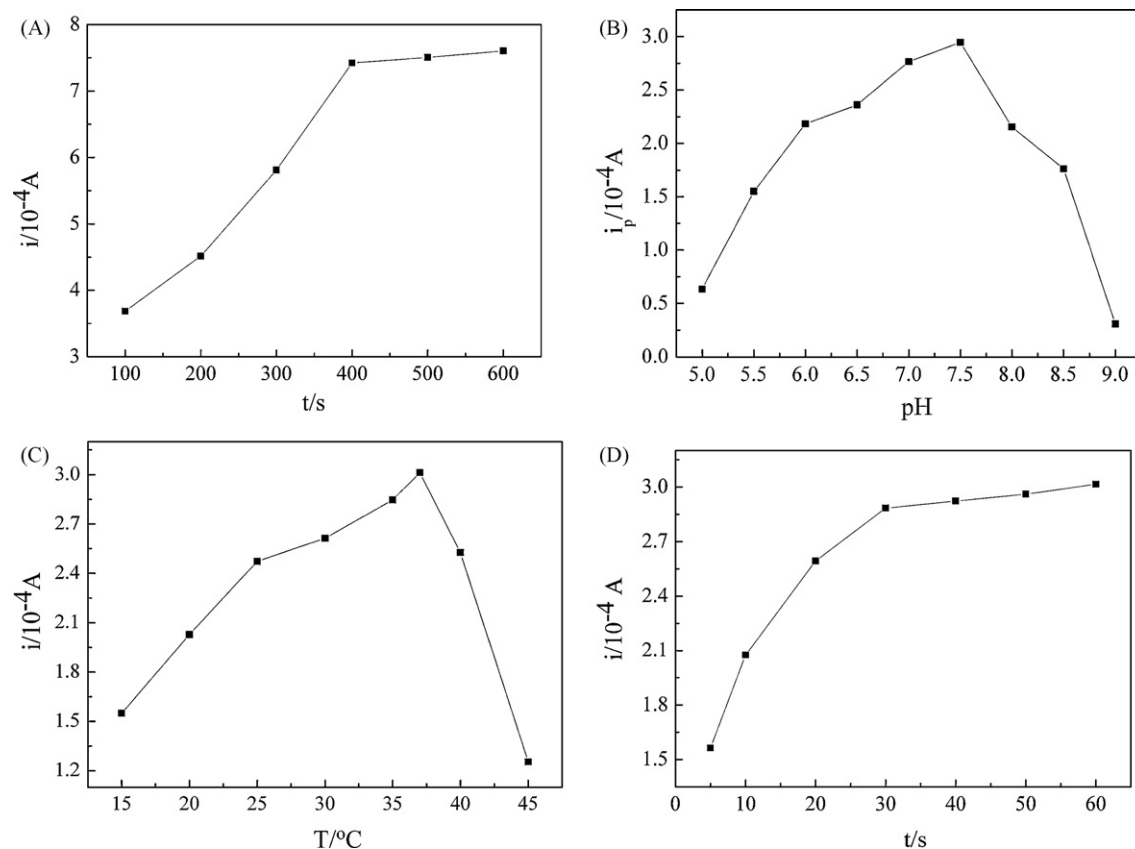


Fig. 6. Optimization of experimental conditions. (A) The time of electrodeposition; (B) the pH of supporting electrolyte; (C) the incubation temperature; (D) time.

### 3.7. Analytical performance

Under the optimized experimental conditions mentioned above, the relationship between the peak current and the concentration of AFP was investigated. As presented in Fig. 7, the amperometric response increased with the increase of AFP concentration from 0.5 to 80  $ng mL^{-1}$  with a correlation coefficient of 0.9948. The regression equation was  $\Delta i (10^{-4} A) = 0.1655C (ng mL^{-1}) + 2.1453$ , where  $i$  is the current intensity, and  $C$  is the AFP concentration. The detection limit ( $3\sigma$ ,  $n = 11$ ) is estimated to be 0.25  $ng mL^{-1}$ . A series of 11 repetitive measurements of 1.0  $ng mL^{-1}$  AFP are used for estimat-

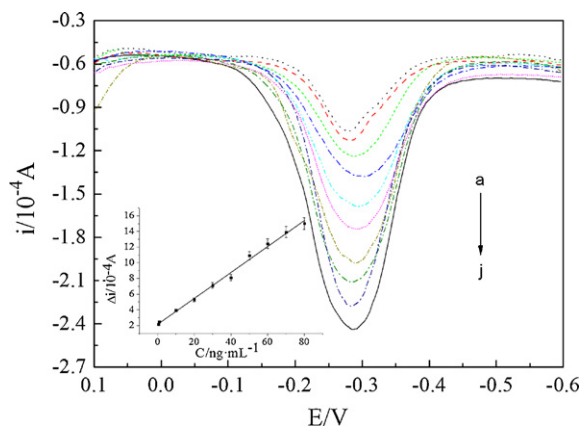


Fig. 7. The differential pulse voltammograms (DPV) of different AFP concentration obtained at HRP-Ab/AFP/Ab/TGA/nano-Au/CILE in PBS (0.1 M, pH 7.5) containing 5 mM OAP and 1 mM  $H_2O_2$ ; (a) 0.5; (b) 1; (c) 10; (d) 20; (e) 30; (f) 40; (g) 50; (h) 60; (i) 70; (j) 80  $ng mL^{-1}$ . The inset show a calibration plot of peak current versus OAP concentration.

ing the precision and the relative standard deviation (R.S.D.) is 2.3%, indicating an acceptable level of the precision for the immunoassay.

### 3.8. Selectivity and stability of immunosensor

Selectivity is also important in practical use of the biosensors. The specific analyte has to be measured in the presence of a relatively high amount of nonspecific species in diagnostic applications. In this study, four kinds of potentially interferent, including L-glutamic acid, BSA, hemoglobin and D-glucose were used to evaluate the selectivity of the immunosensor. 50  $ng mL^{-1}$  AFP was detected with the established sensor in the presence of these interferents of various concentrations ranging from 1 to 10  $\mu g mL^{-1}$  under the optimized situation. The responses, shown as the relative value to that generated by mere 50  $ng mL^{-1}$  AFP, was shown in Table 1. It can be seen that the interferents of relatively high concentrations only posed negligible affection on AFP detection, showing the established sensor had high selectivity.

The storage stability of the sensor was studied by storing it at 4  $^\circ C$  when not in use and measured intermittently. Five days later the response of the sensor still retained 96% and after two weeks the response still retained 90% of the initial. The good stability could be

Table 1

The relative responses of 50  $ng mL^{-1}$  AFP in the presence of interferent on the established sensor (compared to the response mere 50  $ng mL^{-1}$  AFP)\*.

Interferents	Concentrations ( $\mu g mL^{-1}$ )	Relative responses
L-Glutamic acid	1	0.9974
BSA	10	0.9743
Hemoglobin	140	1.003
D-Glucose	1	0.9865

\* Each value is the average of three measurements.

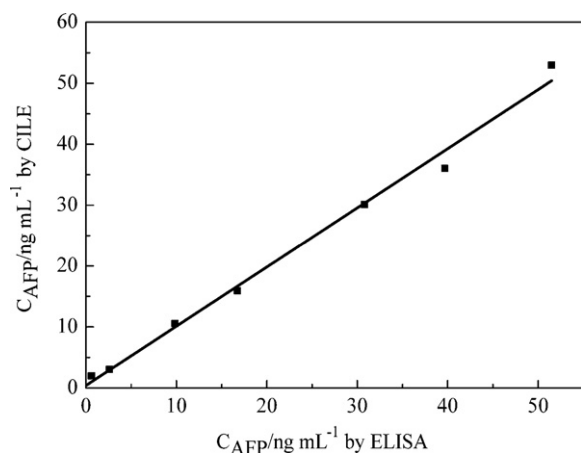


Fig. 8. Correlation of proposed electrochemical immunoassay for human serum samples against ELISA.

Table 2  
AFP concentration in clinical sera.

Sample	Proposed method (ng mL <sup>-1</sup> )	ELISA (ng mL <sup>-1</sup> )	Relative deviation (%)
1	283.4	264.3	7.2
2	13.76	14.91	-7.7
3	162.5	151.6	6.7

Higher serum AFP levels could be detected with an appropriate dilution.

due to the good biocompatibility of the nano-Au film aqueous solution. Moreover, the nanostructure of Au greatly enhances the active surface available for protein molecules binding over the geometrical area.

### 3.9. The corelationship of electrochemical immunosensor and ELISA for detection of AFP in clinical serum samples

Some clinical sera were analyzed using the electrochemical immunosensor as well as the reference ELISA. The calibration curve between proposed method and ELISA was shown in Fig. 8. The regression equation could be expressed as  $Y=0.9722X+0.3685$  ( $X$  was the concentration of AFP detected by the proposed method, ng mL<sup>-1</sup>,  $Y$  was the concentration of AFP detected by ELISA method, ng mL<sup>-1</sup>,  $n=7$ ,  $\gamma=0.9933$ ). In order to assess the accuracy and applicability of the present method, three serum samples were determined and the results were compared with the standard ELISA method (Table 2). It can be seen obviously that this developed electrochemical immunoassay may provide an alternative method for liver cancer biomarkers diagnosis in clinical analysis.

## 4. Conclusion

In the present work, novel immunosensor based on CPE constructed of RTIL and gold nanoparticles was used for electrochemical determination of human AFP. The combination of the good conductivity of RTIL and the advantages of the gold nanoparticles, including biocompatibility and amplification, enhanced the sensitivity of the immunosensor significantly. The results showed that

the method was simple and sensitive enough for determination of AFP in human serum samples with good precision and accuracy. It can be expected that the new immunoassay would be widely useful for highly sensitive clinical analysis and other biotechnology applications.

## Acknowledgments

This work was supported by the Excellent Young Scientists Encouragement Foundation of Shandong Province (No. 2008BS05004), the Educational Administration of Shandong Province (No. J07YC09) and the National Natural Science Foundation of China (No.20775038).

## References

- [1] T.C. Tang, A. Deng, H.J. Huang, *Anal. Chem.* 74 (2002) 2617.
- [2] K. Sato, A. Hibara, M. Tokeshi, H. Hisamoto, T. Kitamori, *Adv. Drug. Deliv. Rev.* 55 (2003) 379.
- [3] M.S. Wilson, *Anal. Chem.* 77 (2005) 496.
- [4] T. Konry, A. Novoa, Y. Shemer-Avni, N. Hanuka, *Anal. Chem.* 77 (2005) 1771.
- [5] B.L. Zuo, S.M. Li, Z. Guo, J.F. Zhang, C.Z. Chen, *Anal. Chem.* 76 (2004) 3536.
- [6] R. Kurita, Y. Yokota, Y. Sato, F. Mizutani, O. Niwa, *Anal. Chem.* 78 (2006) 5525.
- [7] B.Y. Won, H.G. Choi, K.H. Kim, S.Y. Byun, *Biotechnol. Bioeng.* 89 (2005) 815.
- [8] J. Wang, L. Fang, *J. Am. Chem. Soc.* 120 (1998) 1049.
- [9] J. Kulyš, *Biosens. Bioelectron.* 14 (1999) 473.
- [10] C.M.V.B. Almeida, B.F. Giannetti, *Electrochem. Commun.* 4 (2002) 985.
- [11] D. Moscone, D.D. Ottavi, D. Compagnone, G. Palleschi, A. Amine, *Anal. Chem.* 73 (2001) 2529.
- [12] N.S. Lawrence, R.P. Deo, J. Wang, *Anal. Chem.* 76 (2004) 3735.
- [13] P. Tomcik, C.E. Banks, T.J. Davies, R.G. Compton, *Anal. Chem.* 76 (2004) 161.
- [14] T. Welton, *Chem. Rev.* 99 (1999) 2071.
- [15] F. Endres, *ChemPhysChem* 3 (2002) 144.
- [16] M.C. Buzzeo, R.G. Evans, R.G. Compton, *ChemPhysChem* 5 (2004) 1106.
- [17] S. Park, R. Kazlauskas, *Curr. Opin. Biotechnol.* 14 (2003) 432.
- [18] J.A. Laszlo, D.L. Compton, *J. Mol. Catal. B: Enzym.* 18 (2002) 109.
- [19] C.F. Ding, M.L. Zhang, F. Zhao, S.S. Zhang, *Anal. Biochem.* 378 (2008) 32.
- [20] H.X. Ju, S. Liu, B. Ge, F. Lisdat, F.W. Scheller, *Electroanalysis* 14 (2002) 141.
- [21] M.B. González-García, C. Fernández-Sánchez, A. Costa-García, *Biosens. Bioelectron.* 15 (2000) 315.
- [22] M.L. Mena, P. Yáñez-Sedeño, J.M. Pingarrón, *Anal. Biochem.* 336 (2005) 20.
- [23] J. Manso, L. Agüí, P. Yáñez-Sedeño, J.M. Pingarrón, *Anal. Lett.* 37 (2004) 887.
- [24] L. Agüí, J. Manso, P. Yáñez-Sedeño, J.M. Pingarrón, *Sens. Actuators B* 113 (2006) 272.
- [25] L. Agüí, J. Manso, P. Yáñez-Sedeño, J.M. Pingarrón, *Talanta* 64 (2004) 1041.
- [26] L. Agüí, C. Peña-Farfal, P. Yáñez-Sedeño, J.M. Pingarrón, *Talanta* 74 (2007) 412.
- [27] E. Alpert, R. Hershsberg, P.H. Schur, K.J. Lsselbacher, *Gastroenterology* 61 (1971) 137.
- [28] K. Okuda, *Dig. Dis. Sci.* 31 (1986) 133.
- [29] X.W. Wang, H. Xie, *Life Sci.* 64 (1999) 17.
- [30] M. Xue, T. Haruyama, E. Kobatake, M. Aizawa, *Sens. Actuators B* 35 (1996) 458.
- [31] Y. Yamagata, H. Katoh, K. Nakamura, T. Tanaka, S. Satomura, S. Matsuura, *J. Immunol. Methods* 212 (1998) 161.
- [32] K. Ito, M. Oda, A. Tsuji, M. Maeda, *J. Pharm. Biomed. Anal.* 20 (1999) 169.
- [33] R. Wang, X. Lu, W. Ma, *J. Chromatogr. B* 779 (2002) 157.
- [34] Z. Wang, Y.F. Tu, S.Q. Liu, *Talanta* 77 (2008) 815.
- [35] Z. Qiang, R. Yuan, Y.Q. Chai, N. Wang, *Electrochim. Acta* 51 (2006) 3763.
- [36] Y. Zhuo, R. Yuan, Y.Q. Chai, D.P. Tang, *Electrochem. Commun.* 7 (2005) 355.
- [37] Y. Zhuo, R. Yuan, Y.Q. Chai, Y. Zhang, *Sens. Actuators B* 114 (2006) 631.
- [38] X.M. Miao, R. Yuan, Y.Q. Chai, Y.T. Shi, *Biochem. Eng. J.* 38 (2008) 9.
- [39] Z.Q. Ye, M.Q. Tan, G.L. Wang, J.L. Yuan, *Talanta* 65 (2005) 206.
- [40] S.S. Zhang, J. Zou, F.L. Yu, *Talanta* 76 (2008) 122.
- [41] T.E. Sutto, P.C. Trulove, H.C. DeLong, *Electrochem. Solid-State Lett.* 6 (2003) 50.
- [42] M.B.G. García, A.C. García, *Bioelectrochem. Bioenerg.* 38 (1995) 389.
- [43] Y.J. Liu, F. Yin, Y.M. Long, Z.H. Zhang, S.Z. Yao, *Colloid Interface Sci.* 258 (2003) 75.
- [44] Z.P. Li, C.H. Liu, Y.Q. Su, X.R. Duan, *Chem. J. Internet* 7 (2005) 83.
- [45] Y.N. He, H.Y. Chen, J.J. Zheng, G.Y. Zhang, Z.L. Chen, *Talanta* 44 (1997) 823.



# Application of ionic liquids in the microwave-assisted extraction of polyphenolic compounds from medicinal plants

Fu-You Du, Xiao-Hua Xiao, Xue-Jun Luo, Gong-Ke Li\*

School of Chemistry and Chemical Engineering, Sun Yat-Sen University, Guangzhou 510275, China

## ARTICLE INFO

### Article history:

Received 12 October 2008  
Received in revised form 16 January 2009  
Accepted 20 January 2009  
Available online 30 January 2009

### Keywords:

Ionic liquids  
Microwave-assisted extraction  
Polyphenolic compounds  
Medicinal plants

## ABSTRACT

Ionic liquids (ILs) solutions as solvents were successfully applied in the microwave-assisted extraction (MAE) of polyphenolic compounds from medicinal plants. ILs, its concentration and MAE conditions were investigated in order to extract polyphenolic compounds effectively from *Psidium guajava* Linn. (*P. guajava*) leaves and *Smilax china* (*S. china*) tubers. The results obtained indicated that the anions and cations of ILs had influences on the extraction of polyphenolic compounds as well as the ILs with electron-rich aromatic  $\pi$ -system enhanced extraction ability. Under the optimized conditions, the extraction yields of the polyphenolic compounds were in the range of 79.5–93.8% with one-step extraction, and meanwhile the recoveries were in the range of 85.2–103% with relative standard deviations (R.S.D.s) lower than 5.6%. Compared to conventional extraction procedures, the results suggested that the proposed method was effective and alternative for the extraction of polyphenolic compounds from medicinal plants. In addition, the extraction mechanisms and the structures of samples before and after extraction were also investigated. ILs solutions as green solvents in the MAE of polyphenolic compounds from medicinal plant samples showed a great promising prospect.

© 2009 Elsevier B.V. All rights reserved.

## 1. Introduction

Ionic liquids (ILs) are composed of organic cations and inorganic or organic anions and are liquid near room temperature (or by convention below 100 °C). They have been proposed as greener alternatives to volatile organic solvents thanks to their unique characteristics: negligible vapor pressure, good thermal stability, very wide liquidus range, good dissolving and extracting ability, excellent microwave-absorbing ability, designable structures and among others [1–4]. In recent years, ILs have been received much attention as neoteric solvents in various applications including catalysis, synthesis, industrial cleaning, extraction and separation [4–8].

Applications of ILs in sample preparation have shown great promising prospect [7–10], which includes liquid–liquid extraction, liquid–phase microextraction, solid-phase microextraction and aqueous two-phase systems extraction, for that ILs could alleviate environmental pollution and improve the selectivity and the extraction yields of interesting compounds in sample pretreatment processes in comparison to conventional organic solvents. Considered that ILs as solvents and co-solvents can efficiently absorb microwave energy [2] and at the same time microwave-assisted

extraction (MAE) is an attractive and rapid sample preparation technique [11], it is a rather interesting project that ILs solution as solvent is applied in the MAE of various useful substances from solid samples. Recently, 1-*n*-butyl-3-methylimidazolium-based ionic liquids aqueous solutions as solvents were investigated in the extraction of *trans*-resveratrol from *Rhizma Polygoni Cuspidati* [9] and alkaloids from medicinal plants [10,12], indicating that ILs had potential applications in the MAE of useful substances from medicinal plants.

Many medicinal plants contains various bioactive compounds, such as polyphenolic compounds, nitrogen compounds, vitamins, terpenoids and some other endogenous metabolites, and have been used for pharmaceutical and dietary therapy for several millennia [13]. *Psidium Guajava* Linn. (*P. guajava*) leaves and *Smilax china* (*S. china*) tubers are two popular and important herbal medicines, the extracts have multiple therapeutic effects and pharmacological activities, such as anti-oxidant, anti-inflammatory, anti-microbial, and anti-tumor effects, which were related with polyphenolic compounds including gallic acid, ellagic acid, quercetin and *trans*-resveratrol (see Fig. 1) [13–17]. They could be extracted with volatile organic solvents [17,18], and these polyphenolic compounds in samples proved to be stable under direct heating extraction (HE) and microwave-assisted heating extraction at temperatures even up to 100 °C for 20 min without degradation [9,19]. However, to our best knowledge, there are no reports on the extraction and determination of polyphenolic compounds in the two medicinal plants using ILs solution as solvent.

\* Corresponding author. Tel.: +86 20 84035156; fax: +86 20 84112245.  
E-mail address: [cesgkl@zsu.edu.cn](mailto:cesgkl@zsu.edu.cn) (G.-K. Li).

In order to study the potentiality of ILs solutions as alternative solvents in the MAE of polyphenolic compounds, including gallic acid, ellagic acid, quercetin and *trans*-resveratrol (see Fig. 1), from *P. guajava* leaves and *S. china* tubers, 11 ILs with different cations and anions were investigated (for chemical structures of ILs see Fig. S1, Supplementary Data). The influential parameters of the MAE procedure were optimized systematically. The ionic liquids-based microwave-assisted extraction (ILs-MAE) approach proposed here was compared with conventional extraction approaches. The extraction results were evaluated by the determination of the polyphenolic compounds in the extracts using high-performance liquid chromatography (HPLC) with UV detection. The extraction mechanisms and the microstructures and chemical structures of samples before and after extractions were also investigated.

## 2. Experimental

### 2.1. Reagents and samples

Gallic acid (with purity >99%) was obtained from Kemiou Chemical Reagent Company (Tianjin, China). Quercetin was purchased from Acros (Geel, Belgium). *trans*-Resveratrol and ellagic acid were purchased from Sigma (St. Louis, MO, USA) and of minimum 95% purity. HPLC grade acetonitrile used for mobile phase was purchased from Merck (Darmstadt, Germany). Sodium dicyanamide was purchased from Sigma-Aldrich Co. (St. Louis, USA). 1-Methylimidazole was received from Kaile Chemical Plant (Zhejiang, China) and of approximately 99% purity, 1-bromoethane, 1-chlorobutane, 1-bromobutane and 1-bromohexane were obtained from Sinopharm Chemical Reagent Company and of >98% purity, tetramethylammonium chloride was purchased from Shanghai Chemical Reagent Company (Shanghai, China), sodium tetrafluoroborate ( $\geq 98\%$ ) was purchased from Xiangyang Chemical Factory (Zhejiang, China), pyridine and other reagents used were supplied by Guangzhou Chemical Reagent Factory (Guangzhou, China).

*P. guajava* leaves (Guangxi, China) and *S. china* tubers (Hunan, China) were dried and then triturated to various particle sizes, respectively. The same batch of sample was used here in the experiments.

### 2.2. Apparatus

MAE experiments were performed with an MAS-I microwave oven (Sineo Microwave Chemistry Technology Company, Shanghai, China). The scheme and its illustration of the MAS-I microwave oven were described in previous work [9]. The LC-10AT (Shimadzu, Japan) HPLC system equipped with a SPD-10A UV-visible dual wavelength detector was used for analysis. A Luna C<sub>18</sub> column (250 mm  $\times$  4.6 mm I.D., 5  $\mu$ m, Phenomenex, USA) was used as LC analytical column. <sup>1</sup>H NMR and <sup>13</sup>C NMR spectra were recorded on Mercury-Plus 300 and Varian-INOVA 500 NMR spectrometry (Varian, USA). A XL-30 scanning electron microscope (Philips, Eindhoven, Netherlands) was used to observe pictures of sample before and after extraction. FTIR spectra were recorded in the region of 400–4000 cm<sup>-1</sup> on a Nicolet Avatar 300 model FTIR spectrometer (USA). The pH values were measured with an E-201 pH-meter (Shanghai Precision & Scientific Instrument Company, China).

### 2.3. Preparation of ILs and standard solutions

1-Butyl-3-methylimidazolium chloride ([bmim]Cl), 1-butyl-3-methylimidazolium bromide ([bmim]Br) and 1-butyl-3-methylimidazolium tetrafluoroborate ([bmim][BF<sub>4</sub>]) were prepared as previously described [9], the same procedure was used as for 1-ethyl-3-methylimidazolium bromide ([emim]Br), 1-hexyl-3-methylimidazolium bromide ([hmim]Br) and 1-ethyl-3-methylimidazolium tetrafluoroborate. 1-butyl-3-methylimidazolium dicyanamide ([bmim][N(CN)<sub>2</sub>]), 1-butyl-3-methylimidazolium sulfate ([bmim]<sub>2</sub>[SO<sub>4</sub>]), *N*-butylpyridinium chloride (bPyCl) and 1-butyl-3-methylimidazolium dihydrogen phosphate ([bmim][H<sub>2</sub>PO<sub>4</sub>]) were synthesized according to the experimental procedures described in the literatures [20–22]. All ILs obtained were dried at 80 °C for 12 h under vacuum and then checked by <sup>1</sup>H NMR and <sup>13</sup>C NMR spectra on Mercury-Plus 300 or INOVA 500 NMR spectrometry at room temperature in D<sub>2</sub>O and d<sub>6</sub>-acetone. The NMR spectra data obtained were described in detail in the supplementary data (see Tables S1 and S2) and the characterization of NMR spectroscopy showed that there were no organic impurities in ILs.

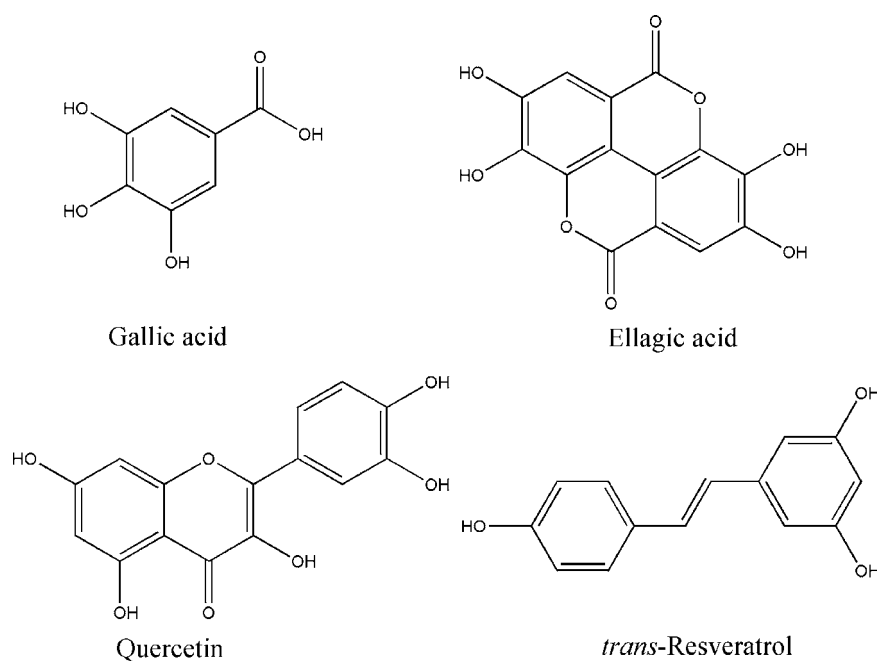


Fig. 1. Chemical structures of four polyphenolic compounds investigated.

Stock solution of gallic acid, ellagic acid and quercetin (each 200 mg/L) were prepared in 1.67 mol/L [bmim]Br acid solution (pH 2.5, adjusted with 6.0 mol/L hydrochloric acid). Stock solution of *trans*-resveratrol and quercetin (each 100 mg/L) were prepared in 1.67 mol/L [bmim]Br solution. Working standard solutions were prepared by serial dilution of the two stock solutions in the corresponding [bmim]Br solution, respectively, and then stored at 1–4 °C in darkness. Deionized water was used throughout the work.

#### 2.4. Ionic liquids-based microwave-assisted extraction (ILs-MAE)

1.0 g of accurately weighed sample was extracted with 20 mL of different ILs solution. 0.75 mol/L [bmim]<sub>2</sub>[SO<sub>4</sub>] and 1.50 mol/L other ILs aqueous solutions were used here, respectively. *P. guajava* leaves were extracted for 10 min at 70 °C. *S. china* tubers were extracted for 10 min at 60 °C.

The influences of the MAE conditions in the extraction of polyphenolic compounds were investigated by an orthogonal design L<sub>9</sub> (3<sup>4</sup>) and subsequently a factorial design experiments. All extraction experiments were repeated for three times. The extracts obtained were filtrated and then diluted to 30.0 mL with deionized water. The pH value of the extract of *P. guajava* leaves was adjusted to 2.5 with 6.0 mol/L hydrochloric acid solutions.

The extraction yield of polyphenolic compound was defined as follows:

$$\text{Yield (\%)} = \frac{\text{Mass of polyphenolic compound in one-step extraction solution}}{\text{Sum of the mass of polyphenolic compound in sample}} \times 100$$

The total mass of gallic acid, ellagic acid, quercetin or *trans*-resveratrol in sample was determined by analysis of the total extraction solutions after five consecutive extraction with fresh [bmim]Br solution under the optimized MAE conditions. In this work, our experimental results showed that the mean of total mass of gallic acid, ellagic acid and quercetin in *P. guajava* leaves was 0.608, 2.947 and 0.679 mg/g, respectively, and the mean of total mass of *trans*-resveratrol and quercetin in *S. china* tubers was 0.581 and 0.235 mg/g, respectively.

#### 2.5. Conventional reference extraction procedure

Methanol was selected as the reference solvent in the MAE of polyphenolic compounds in *P. guajava* leaves and *S. china* tubers. The extraction experiments were operated under the optimized conditions except for solvent type and extraction temperature. 65 °C (the best extraction temperature according to our preliminary experiments) was selected for *P. guajava* leaves. After extraction, the obtained extracts were cooled to ambient temperature and then diluted to 30 mL with methanol.

Heating extraction was selected as the reference method for extraction of the four polyphenolic compounds. A water-bath extraction was performed with a 1.0 g sample and 40 mL 2.50 mol/L [bmim]Br in a flask (100 mL) and the suspensions were heated for 4 h at the optimized temperature under mechanical stirring. After that, the extracts were filtrated and then diluted to 60 mL with deionized water.

#### 2.6. HPLC analysis

The filtrated extracts were collected in a graduate cuvette and then diluted to 30 mL with water. The pH of diluted solution of the extracts of *P. guajava* leaves was adjusted to 2.5. An aliquot was filtrated through a 0.45 μm microporous membrane for subsequent HPLC analysis. Injection volume was 10 μL and column temperature

was ambient. The mobile phase consisted of acetonitrile (solvent A) and 0.6% (v/v) acetic acid aqueous solution (solvent B) with a flow rate of 1 mL/min. For analysis of the extracts of *P. guajava* leaves, the gradient elution program was the following: 5–9% of solvent A from 0 to 8 min, 9–20% from 8 to 10 min, 20–30% from 10 to 25 min, 30–60% from 25 to 40 min and then held for 5 min; the UV detection wavelengths were 254 and 273 nm. The extract of *S. china* tubers was monitored at 254 and 306 nm, the corresponding gradient elution program was as follows: 28% of solvent A from 0 to 10 min, 28–50% from 10 to 20 min, 50–70% from 20 to 25 min and then held for 5 min. Registering of the detector signal and operating of the system were accomplished by the software Shimadzu Class-VP.

Gallic acid, ellagic acid, quercetin and *trans*-resveratrol in each extracts were identified by comparing their retention time and UV spectra with those of the reference standards. The external standard method was set up for quantitative determination of the analytes.

### 3. Results and discussion

#### 3.1. Optimization of ILs-MAE

##### 3.1.1. Selection of ILs

ILs have strong solvent dissolving power and can efficiently absorb microwave energy, thus they were employed as solvents and co-solvents in the MAE of analytes [9,10,12]. Moreover, the structures of ILs have significant influences on the extraction yields of analytes, owing greatly to their distinct multiple interactions with analytes [23] and their dissolving ability for polyphenolic compounds [24]. To find out the optimal ILs and evaluate its performance in the MAE of polyphenolic compounds from *P. guajava* leaves and *S. china* tubers, ILs with different cations and anions were tested in the present work.

From Table 1, it can be seen that the addition of ILs to the extraction solvent obviously improved the extraction yields of polyphenolic compounds, especially ellagic acid, quercetin and *trans*-resveratrol, from *P. guajava* leaves and *S. china* tubers compared with the extraction using water as solvent in MAE. The results have been indicated by the similar results of Du et al. [9]. On the other hand, the results of Table 1 suggested that the cations and anions of ILs influenced the extraction yields of polyphenolic compounds. For the 1-*n*-butyl-3-methylimidazolium based ionic liquids with Br<sup>-</sup>, Cl<sup>-</sup>, BF<sub>4</sub><sup>-</sup>, SO<sub>4</sub><sup>2-</sup>, N(CN)<sub>2</sub><sup>-</sup> and H<sub>2</sub>PO<sub>4</sub><sup>-</sup>, the obtained extraction yields indicated that Br<sup>-</sup> and H<sub>2</sub>PO<sub>4</sub><sup>-</sup> were more efficient than other four anions in the MAE of polyphenolic compounds from *P. guajava* leaves, and Br<sup>-</sup> and BF<sub>4</sub><sup>-</sup> were more efficient than other four anions in the MAE of *trans*-resveratrol and quercetin from *S. china* tubers. With the same anion of Br<sup>-</sup>, [emim]Br, [bmim]Br and [hmim]Br were used to investigate the effects of the alkyl chain length on the MAE of polyphenolic compounds. The results indicated that the increasing alkyl chain length has influence on the extraction, and the [bmim]Br was more efficient than the other two ILs in the MAE of polyphenolic compounds from the two medicinal plants. Although the hydrogen bond acidity for the three cations increased from ethyl to hexyl of 1-position of the 1-alkyl-3-methylimidazolium ring [24], the hydrophobicity increased with the increasing of alkyl chain length. Both the right hydrogen bonding and hydrophobic interactions of [bmim]Br resulted in the stronger solvation interactions for polyphenolic compounds and then the higher extraction yields in comparison with these of [emim]Br and [hmim]Br. For the extraction efficiency of [emim][BF<sub>4</sub>] and [bmim][BF<sub>4</sub>], there was no obvious difference in the MAE of polyphenolic compounds except for quercetin in *S. china* tubers. The above results suggested that the extraction yields of polyphenolic compounds were largely anion-dependent for the same class ILs, owing to the anion-dependency of the solubilities of analytes in ILs [24].

**Table 1**  
Results of different ILs effects on extraction yields of polyphenolic compounds<sup>a</sup> (n = 3).

Ionic liquids	<i>P. guajava</i> leaf			<i>S. china</i> tuber	
	Gallic acid (mean ± S.D., %)	Ellagic acid (mean ± S.D., %)	Quercetin (mean ± S.D., %)	<i>trans</i> -Resveratrol (mean ± S.D., %)	Quercetin (mean ± S.D., %)
[bmim]Br	88.7 (±2.2)	65.9 (±3.3)	69.5 (±3.7)	57.0 (±3.3)	59.6 (±3.7)
[bmim]Cl	91.0 (±2.3)	59.4 (±1.7)	41.5 (±1.1)	34.6 (±1.7)	21.3 (±1.1)
[bmim][BF <sub>4</sub> ]	65.6 (±2.8)	74.8 (±3.0)	59.4 (±2.7)	51.7 (±3.0)	51.5 (±2.7)
[emim][BF <sub>4</sub> ]	67.3 (±1.7)	71.5 (±2.9)	55.8 (±2.1)	47.5 (±2.9)	39.6 (±2.1)
[bmim][N(CN) <sub>2</sub> ]	76.8 (±2.1)	59.7 (±2.2)	49.2 (±1.4)	56.5 (±2.2)	30.2 (±1.4)
[bmim] <sub>2</sub> [SO <sub>4</sub> ]	75.2 (±2.4)	42.8 (±2.5)	29.9 (±2.4)	50.7 (±2.5)	47.7 (±2.4)
[bmim][H <sub>2</sub> PO <sub>4</sub> ]	90.6 (±3.8)	65.9 (±3.7)	74.5 (±3.0)	58.3 (±3.7)	45.5 (±3.0)
(CH <sub>3</sub> ) <sub>4</sub> NCl	78.0 (±2.8)	26.5 (±0.9)	21.4 (±0.3)	10.3 (±0.9)	4.3 (±0.3)
bPyCl	80.3 (±3.4)	62.2 (±2.9)	50.7 (±1.5)	52.4 (±3.8)	26.4 (±1.9)
[emim]Br	74.3 (±1.1)	59.1 (±1.9)	47.6 (±1.3)	40.3 (±1.9)	28.5 (±1.3)
[hmim]Br	77.0 (±2.6)	61.3 (±2.0)	49.7 (±1.4)	52.7 (±2.0)	46.0 (±1.4)
Water	63.3 (±0.5)	35.1 (±0.3)	15.2 (±0.2)	3.0 (±0.3)	1.8 (±0.2)

<sup>a</sup> Extraction yield values are expressed as mean and standard deviation (S.D.) calculated from three independent experiments.

For (CH<sub>3</sub>)<sub>4</sub>NCl, [bmim]Cl and bPyCl, the obtained results indicated that the extraction yields of polyphenolic compounds were greatly influenced by the cations species. ILs which have cationic moieties with an electron-rich aromatic  $\pi$ -system produced stronger interactions with solute molecules capable of undergoing polarity,  $\pi$ - $\pi$  and  $n$ - $\pi$  interactions [23,25]. ILs containing the *N*-butylpyridinium cation have a more aromatic character than the imidazolium based ionic liquids, and they had stronger solvation interactions and better dissolving ability [24,26], leading to the higher extraction yields of polyphenolic compounds. In lack of  $\pi$ - $\pi$  and  $n$ - $\pi$  interactions between ammonium cation and polyphenolic compounds, the extraction ability of (CH<sub>3</sub>)<sub>4</sub>NCl for polyphenolic compounds was lower than the other two ILs, contributed to the lower extraction yields.

Considering both the extraction yields of polyphenolic compounds and the simple synthesis of ILs, [bmim]Br was selected to simultaneously extract polyphenolic compounds from *P. guajava* leaves and *S. china* tubers in the present work.

### 3.1.2. Optimization of ILs concentration

Our previous work [9] indicated that [bmim]Br concentration had significant influence on the extraction of *trans*-resveratrol. Therefore, the concentration effect of [bmim]Br on extraction of polyphenolic compounds from *P. guajava* leaves and *S. china* tubers was studied and the results are shown in Fig. 2.

In the light of Fig. 2, it can be observed that the extraction yields of polyphenolic compounds from *P. guajava* leaves and *S. china* tubers were increased with the increase of [bmim]Br concentration.

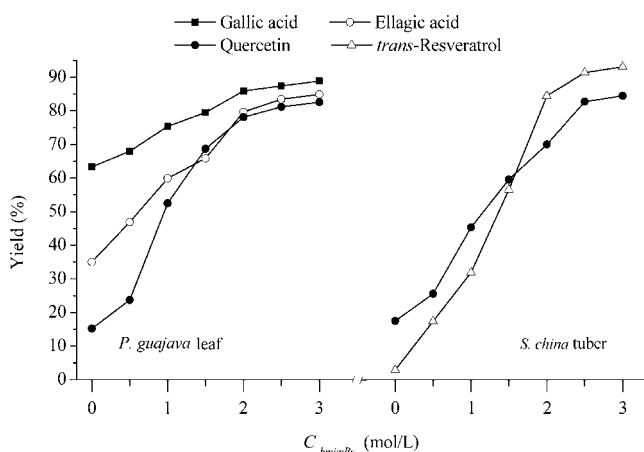


**Fig. 2.** Effect of [bmim]Br concentration on extraction yields of polyphenolic compounds from *P. guajava* leaves and *S. china* tubers.

The increasing tendency of the extraction yields of quercetin from *P. guajava* leaves and *S. china* tubers was the similar, which indicated that the influence by the nature of sample in the extraction of quercetin was not obvious. Below 2.0 mol/L [bmim]Br solution, the extraction yields of quercetin and *trans*-resveratrol increased more rapidly than that of ellagic acid, while that of gallic acid increased slowly. The reasons were related to the solubility of the polyphenolic compounds in extraction solvents. Gallic acid is soluble in water, but ellagic acid is poorly soluble, and quercetin and *trans*-resveratrol are insoluble, leading to the obvious difference in their extraction yields when water was used as extraction solvent (see Table 1). The addition of [bmim]Br improved the extraction yields of the polyphenolic compounds, especially quercetin and *trans*-resveratrol, due to the solvation power and multiple interactions of [bmim]Br. The strong interactions between imidazolium cation and phenolic compounds [23–26], especially hydrogen bonding,  $\pi$ - $\pi$ ,  $\pi$ - $n$ , ionic/charge–charge and dipolarity, contributed greatly to this increase. On the other hand, [bmim]Br changed the dissipation factor of solution and improved the transfer efficiency of microwave energy, and thus also improved the extraction yields of the targets.

When [bmim]Br concentration was between 2.5 and 3.0 mol/L, the extraction yields of the four polyphenolic compounds were nearly stable, due to that the diffusion and transfer capacity of the solutions changed a little, even though the solvation ability of the solution was slightly increased. Given the similar extraction yields, 2.5 mol/L of [bmim]Br was selected for the subsequent experiments.

### 3.1.3. Optimization of MAE conditions

In this work, the influential factors of MAE procedure, including sample particle size (A), liquid/solid ratio (B), extraction temperature (C) and time (D), were optimized by means of an orthogonal design L<sub>9</sub> (3<sup>4</sup>). The factors and the corresponding levels for the extraction of polyphenolic compounds from the two medicinal plants are shown in Table 2. Nine experimental trials were carried out according to the orthogonal array designs and the results are also shown in Table 2. The *K* and *R* values are calculated and listed in Table 3.

The differences of the extraction yields of polyphenolic compounds under different MAE conditions were obvious (see Table 2), illustrating that each of MAE factors had different influences on extraction. According to the largest donating rule, the largest value of *K* under every level of an investigating variable is the optimized value, however, the optimal MAE conditions of each polyphenolic compound presented in the same sample were not identical (see Table 3). The *R* values shown in Table 3 indicated that the influences of the investigated factors to the mean extraction yields were also not identical, and the influence of extraction time was minor



**Table 2**  
Extraction yields<sup>a</sup> extracted with the orthogonal design L<sub>9</sub> (3<sup>4</sup>) (n = 3).

Design ID number	Factor <sup>b</sup>				<i>P. guajava</i> leaf			<i>S. china</i> tuber			
	A	B	C	D	Gallic acid (%)	Ellagic acid (%)	Quercetin (%)	<i>trans</i> -Resveratrol (%)	Quercetin (%)		
	Particle size (mm)	Liquid/solid ratio (mL:g)	Temperature (°C)	Time (min)							
1	A <sub>1</sub> (0.90–0.45)	B <sub>1</sub> (10:1)	(15:1)	C <sub>1</sub> (60)	(50)	D <sub>1</sub> (5)	50.3 ± 1.0	37.1 ± 1.2	32.1 ± 1.0	71.8 ± 3.4	48.8 ± 1.6
2	A <sub>1</sub>	B <sub>2</sub> (15:1)	(20:1)	C <sub>2</sub> (60)	(60)	D <sub>2</sub> (10)	61.8 ± 3.6	64.5 ± 1.5	45.4 ± 2.3	91.4 ± 3.7	80.7 ± 3.1
3	A <sub>1</sub>	B <sub>3</sub> (20:1)	(25:1)	C <sub>3</sub> (80)	(70)	D <sub>3</sub> (15)	82.1 ± 3.5	67.0 ± 2.8	53.0 ± 2.6	85.8 ± 3.0	89.2 ± 4.3
4	A <sub>2</sub> (0.45–0.30)	B <sub>1</sub>		C <sub>2</sub>		D <sub>3</sub>	68.4 ± 1.5	42.9 ± 0.7	34.2 ± 0.9	70.8 ± 1.6	51.9 ± 3.7
5	A <sub>2</sub>	B <sub>2</sub>		C <sub>3</sub>		D <sub>1</sub>	77.3 ± 2.4	65.2 ± 1.7	56.3 ± 1.5	77.9 ± 3.9	65.0 ± 2.6
6	A <sub>2</sub>	B <sub>3</sub>		C <sub>1</sub>		D <sub>2</sub>	56.4 ± 2.6	79.1 ± 3.1	76.7 ± 2.9	73.5 ± 3.4	66.9 ± 3.3
7	A <sub>3</sub> (0.30–0.12)	B <sub>1</sub>		C <sub>3</sub>		D <sub>2</sub>	77.0 ± 2.8	38.2 ± 0.8	35.3 ± 1.5	55.6 ± 3.7	42.7 ± 2.3
8	A <sub>3</sub>	B <sub>2</sub>		C <sub>1</sub>		D <sub>3</sub>	58.2 ± 1.7	58.4 ± 1.6	52.7 ± 1.7	63.1 ± 2.3	56.5 ± 4.2
9	A <sub>3</sub>	B <sub>3</sub>		C <sub>2</sub>		D <sub>1</sub>	71.1 ± 2.9	77.4 ± 3.0	66.0 ± 2.0	63.9 ± 2.0	67.0 ± 3.5

<sup>a</sup> Each extraction yield value was the mean and standard deviation (S.D.) of three independent experiments.

<sup>b</sup> The levels of the other two factors (A and D) set were the same for *P. guajava* leaves and *S. china* tubers.

in comparison with the other three factors. The optimal extraction time was 10 min, while sample particle size, extraction temperature and liquid/solid ratio were further optimized by a factorial design experiments, respectively.

For sample particle size, Fig. 3A shows that it had remarkable effects on the extraction of polyphenolic compounds from *S. china* tubers, while it had slight effects on the extraction of polyphenolic compounds from *P. guajava* leaves contributing to their soft material which were permeated easily by solvent and ruptured easily under microwave irradiate. A particle size of 0.45–0.30 mm for *P. guajava* leaves and 0.90–0.45 mm for *S. china* tubers was adopted in the present work.

Fig. 3B shows that the extraction yields of the four polyphenolic compounds increased with the increase of temperature below 60 °C. From 60 to 80 °C, the extraction yields of gallic acid and ellagic acid kept slightly increasing. The extraction yield of quercetin extracted from *P. guajava* leaves or *S. china* tubers slightly decreased when the temperature was higher than 70 °C, while that of *trans*-resveratrol reached its maximum value at 60 °C, though our preliminary experimental results showed that the four polyphenolic compounds were not degraded below 100 °C in MAE process,

and the similar results also have been indicated by Liaizid et al. [19]. Thus, 70 °C for *P. guajava* leaves and 60 °C for *S. china* tubers were used as the optimum extraction temperature.

As for liquid/solid ratio, Fig. 3C shows that the extraction yields of the four polyphenolic compounds increased rapidly with the increase of the ratio of liquid/solid below 20:1. When the liquid/solid ratio varied from 20:1 to 30:1, the extraction yields changed a little. Thus, a liquid/solid ratio of 20:1 was selected in this study.

Under the optimized conditions, the polyphenolic compounds present in the two medicinal plants were successfully extracted out (Table 4). Namely, the extraction yields were in the range of 79.5–93.8% with one-step extraction.

### 3.2. Comparison of different extraction procedures

Methanol was used to extract polyphenolic compounds from *P. guajava* leaves and *S. china* tubers in order to compare the extraction efficiency by ILS solution with volatile organic solvents in MAE process. The results shown in Table 4 indicated that, as extraction solvent, the [bmim]Br solution and methanol had not remark-

**Table 3**  
Analysis of L<sub>9</sub> (3<sup>4</sup>) test results.

Sample	Polyphenolic compound	Factor	K <sub>1</sub> <sup>a</sup>	K <sub>2</sub>	K <sub>3</sub>	R <sup>b</sup>	Optimal level <sup>c</sup>
<i>P. guajava</i> leaf	Gallic acid (%)	A	64.7	67.4	68.8	4.1	A <sub>3</sub>
		B	65.2	65.8	69.9	4.7	B <sub>3</sub>
		C	55.0	67.1	78.8	23.8	C <sub>3</sub>
		D	66.2	65.1	69.6	4.5	D <sub>3</sub>
	Ellagic acid (%)	A	56.2	62.4	58.0	6.2	A <sub>2</sub>
		B	39.4	62.7	74.5	35.1	B <sub>3</sub>
		C	58.2	61.6	56.8	4.8	C <sub>2</sub>
		D	59.9	60.6	56.1	4.5	D <sub>2</sub>
	Quercetin (%)	A	43.5	55.7	51.3	12.2	A <sub>2</sub>
		B	33.9	51.5	65.2	31.3	B <sub>3</sub>
		C	53.8	48.5	48.2	5.6	C <sub>1</sub>
		D	51.5	52.5	46.6	5.9	D <sub>2</sub>
<i>S. china</i> tuber	<i>trans</i> -Resveratrol (%)	A	83	74.1	60.9	22.1	A <sub>1</sub>
		B	66.1	77.5	74.4	11.4	B <sub>2</sub>
		C	69.5	75.4	73.1	5.9	C <sub>2</sub>
		D	71.2	73.5	73.2	2.3	D <sub>2</sub>
	Quercetin (%)	A	72.9	61.3	55.4	17.5	A <sub>1</sub>
		B	47.8	67.4	74.4	26.6	B <sub>3</sub>
		C	57.4	66.5	65.6	9.1	C <sub>2</sub>
		D	60.3	63.4	65.9	5.6	D <sub>3</sub>

<sup>a</sup>  $K_i^F = (1/3) \sum$  the extraction yield of target compounds at F<sub>i</sub>.

<sup>b</sup>  $R_i^F = \max\{K_i^F\} - \min\{K_i^F\}$ , here F and i means extraction factor and setting level, respectively.

<sup>c</sup> For key to factors, see Table 2.

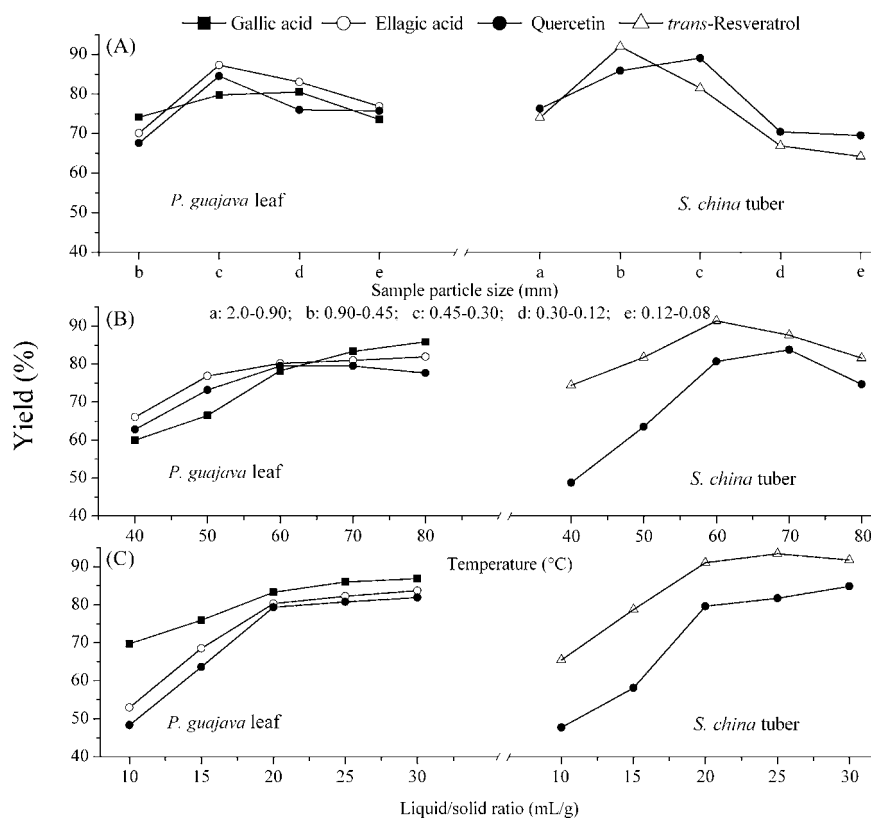


**Fig. 3.** Effect of sample particle size (A), extraction temperature (B) and liquid/solid ratio (C) on extraction yields of polyphenolic compounds from *P. guajava* leaves and *S. china* tubers.

able difference in the extraction of polyphenolic compounds from *P. guajava* leaves and *S. china* tubers, which suggested that the [bmim]Br solution was an alternative solvent to replace organic solvent in the MAE of polyphenolic compounds from the two Chinese herbs.

To evaluate the extraction efficiency of MAE with conventional extraction techniques, HE was carried out. The results in Table 4 suggested that higher ratio of liquid/solid (40:1) and longer time (4 h) in HE process were preferred in order to obtain high extraction yields compared to MAE. The diverse results between MAE and HE were mainly due to the unique extraction mechanism of MAE. Superheating, mass heating and fast heating were obtained by microwave heating but not conventional heating, so, MAE could obtain higher extraction yields with less solvent consumption and shorter time compared with conventional extraction techniques [11].

### 3.3. Method validation

The four polyphenolic compounds were identified by their corresponding chromatograms and retention time in comparison to those of the authentic standard compounds. Examples of chromatograms of standards and extracts are shown in Figs. 4 and 5.

A series of standard solutions of gallic acid, ellagic acid and quercetin at eight levels in the concentration range from 0.5 to 200 mg/L were prepared to determine the linearity of this method for analyzing polyphenolic compounds in *P. guajava* leaves. The similar process was performed for the analysis of *trans*-resveratrol and quercetin in *S. china* tubers. Each of them was analyzed in triplicate. Table 5 summarized the linear ranges and limits of detection (LODs,  $S/N = 3$ ). Good linearity was observed with the regression coefficients ( $r$ ) between 0.9990 and 0.9998. The LODs obtained were between 0.012 and 0.029 mg/L for the polyphenolic compounds.

**Table 4**  
Comparative study of extraction efficiency using different extraction methods.

Sample	Analytes	Proposed method <sup>a</sup>		Conventional method <sup>b</sup>			
		ILs-MAE ([bmim]Br)		Regular MAE (methanol)		Heating extraction ([bmim]Br)	
		Observed values (mean $\pm$ S.D., mg/g)	Recovery (mean $\pm$ S.D., %)	Observed values (mean $\pm$ S.D., mg/g)	Recovery (mean $\pm$ S.D., %)	Observed values (mean $\pm$ S.D., mg/g)	Recovery (mean $\pm$ S.D., %)
<i>P. guajava</i> leaf	Gallic acid	0.507 $\pm$ 0.024 <sup>c</sup>	103.0 $\pm$ 3.9	0.446 $\pm$ 0.017	90.5 $\pm$ 2.8	0.529 $\pm$ 0.030	107.4 $\pm$ 5.0
	Ellagic acid	2.387 $\pm$ 0.118	93.7 $\pm$ 5.6	1.930 $\pm$ 0.068	75.8 $\pm$ 2.3	2.599 $\pm$ 0.159	102.0 $\pm$ 5.4
	Quercetin	0.540 $\pm$ 0.027	98.5 $\pm$ 4.8	0.618 $\pm$ 0.032	107.2 $\pm$ 6.9	0.572 $\pm$ 0.031	104.0 $\pm$ 4.6
<i>S. china</i> tuber	<i>trans</i> -Resveratrol	0.531 $\pm$ 0.030	100.5 $\pm$ 3.7	0.545 $\pm$ 0.027	103.1 $\pm$ 4.6	0.445 $\pm$ 0.016	84.2 $\pm$ 2.7
	Quercetin	0.189 $\pm$ 0.012	85.2 $\pm$ 3.1	0.188 $\pm$ 0.010	84.5 $\pm$ 3.8	0.169 $\pm$ 0.010	75.9 $\pm$ 3.1

<sup>a</sup> Operation under optimized conditions.

<sup>b</sup> See experimental section for operation conditions.

<sup>c</sup> Each value was the mean and standard deviation (S.D.) of three independent experiments, Observed value (mg/g) = mass of polyphenolic compound in extraction solution (mg)/mass of sample (g).

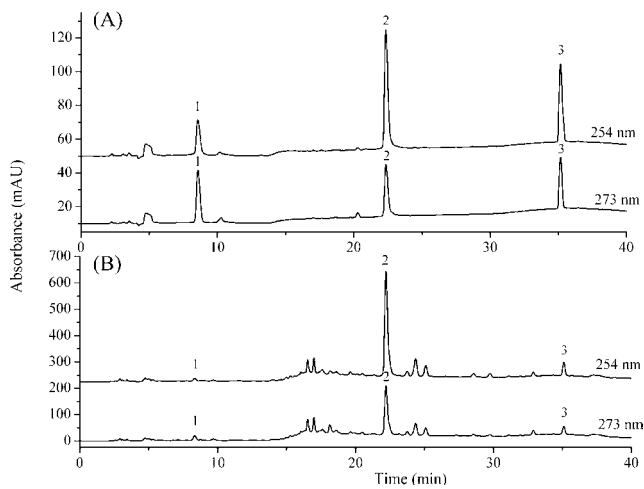


**Fig. 4.** Chromatograms of standard solution of 20 mg/L (A) and extract of *P. guajava* leaves by [bmim]Br solution (B). Peaks: (1) gallic acid, (2) ellagic acid and (3) quercetin.

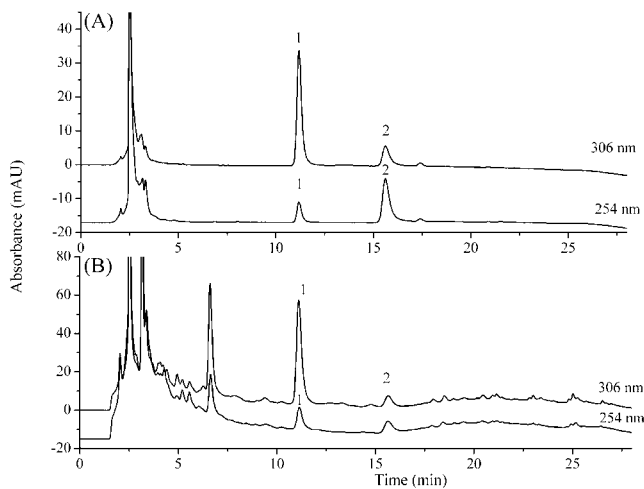


**Fig. 5.** Chromatograms of standard solution of 10 mg/L (A) and extract of *S. china* tubers by [bmim]Br solution (B). Peaks: (1) *trans*-resveratrol and (2) quercetin.

The precision of the chromatographic determination was evaluated by standard solution of 10 mg/L of the polyphenolic compounds. The reproducibility of the peak area and retention time of each polyphenolic compounds were estimated for 15 days. The relative standard deviations (R.S.D.s) of intra-day precisions for polyphenolic compounds ranged from 1.4 to 2.9%, and the corresponding R.S.D.s of inter-day precisions between 4.3% and 6.8%. Recoveries were evaluated by standard-addition method. Each polyphenolic compound was added at concentrations *ca.* 0.5, 1 and 1.5 times the observed concentration in the two original samples. Results showed that the recoveries were in the range of 85.2–103%

**Table 5**

The calibration curves, correlation coefficients (*r*), limits of detection (LODs) of the proposed analytical procedures.

Sample	Polyphenolic compound <sup>a</sup>	Calibration curve <sup>b</sup>	<i>r</i>	Linear range (mg/L)	LODs (mg/L)	RSD <sup>c</sup> ( <i>n</i> = 6)
<i>P. guajava</i> leaf	Gallic acid	$Y = 26794X + 20150$	0.9993	0.50–200	0.029	6.8
	Ellagic acid	$Y = 77004X - 25168.3$	0.9993	0.50–200	0.012	4.7
	Quercetin	$Y = 37446X - 10646.6$	0.9990	0.50–200	0.027	5.1
<i>S. china</i> tuber	<i>trans</i> -Resveratrol	$Y = 60985X - 16314$	0.9998	0.50–100	0.022	4.3
	Quercetin	$Y = 32625X - 3651$	0.9994	0.50–100	0.024	4.5

<sup>a</sup> Gallic acid was monitored at 273 nm, ellagic acid and quercetin were monitored at 254 nm, *trans*-resveratrol was monitored at 306 nm.

<sup>b</sup> *X* was compound concentration as mg/L and *Y* was peak area.

<sup>c</sup> R.S.D. was monitored with 10 mg/L polyphenolic compounds mixed standard solution in 15 separate days.

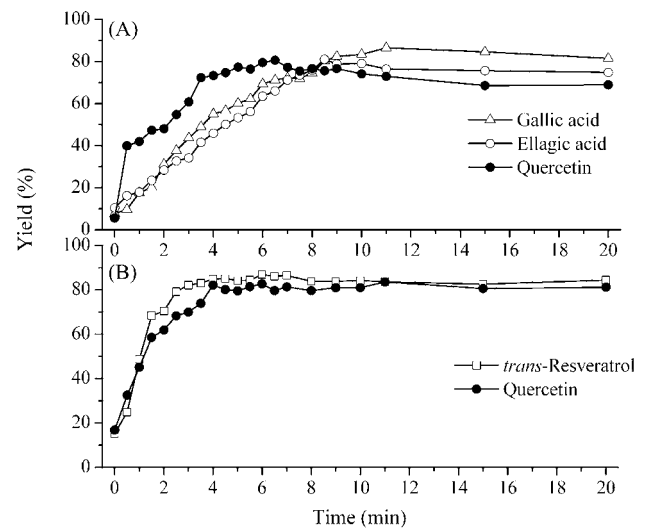


**Fig. 6.** Kinetic curves of polyphenolic compounds extracted from *P. guajava* leaves (A) and *S. china* tubers (B) using 2.50 mol/L [bmim]Br.

for the polyphenolic compounds with R.S.D.s lower than 5.6%. The reproducibility and recovery proved that the present method was credible.

The stability was investigated by determining the varieties of the polyphenolic compounds in [bmim]Br solution and extracts on 15 separate days. All the R.S.D.s of intra-day and inter-day were less than 3.7% and 8.5%, respectively. The results suggested that the polyphenolic compounds were stable in the IL solution and in the extracts.

### 3.4. Mechanism of ILS-MAE

#### 3.4.1. Study of kinetic mechanism

To investigate the changes of the extraction yields in MAE process, the ILS-MAE kinetic mechanism was studied in this study. The results of kinetic curves for the MAE of polyphenolic compounds, according to time, from *P. guajava* leaves and *S. china* tubers were shown in Fig. 6(A and B), respectively. For the polyphenolic compounds from the same sample, the extraction yields increased rapidly at first and then reached an equilibrium concentration, and all the kinetic curves obtained were similar. For *S. china* tubers, the kinetic curves of *trans*-resveratrol and quercetin were similar, the extraction yields of *trans*-resveratrol and quercetin reached the corresponding maximum values (about 90%) before 6 min, which were different from the kinetic curves of polyphenolic compounds from leaf samples. The extraction yields of polyphenolic compounds in leaves arrived to the maximum after 6 min. The above results indicated that the kinetic mechanisms were correlated with the sample structures [27]. The extraction yields of gallic acid, ellagic acid and quercetin from *P. guajava* leaves reached the maximum at 10, 11 and 6.5 min, respectively, suggesting that the structures and character-

istics of polyphenolic compounds influenced kinetic mechanisms. Moreover, the results of the MAE kinetic mechanism indicated that about 10 min of MAE time was enough to obtain high extraction yields of polyphenolic compounds from medicinal plants when ILs solutions were used as solvents.

#### 3.4.2. Structural changes after extraction

In order to further elucidate the extraction mechanism, the identification of microstructure and chemical structure of sample was carried out by SEM and FTIR spectroscopy, respectively. Compared Fig. S2A with Fig. S2B (see Supplementary Data), the microstructures of *P. guajava* leaves changed obviously after MAE. The surface of the *P. guajava* leaves was greatly destroyed and the structure of cells walls was ruptured after MAE using [bmim]Br solution as solvent, which resulted in exposing gallic acid, ellagic acid and quercetin to [bmim]Br solution which could trap them and dissolve them. The results suggested that the mechanism of MAE was based on an explosion at the cell level, which was in accord with the hypothesis investigated by Paré et al. [28,29]. The structure of *S. china* tuber sample also was severely ruptured after MAE (see Fig.S3B), which suggested that the MAE mechanism of *trans*-resveratrol and quercetin from *S. china* tubers was similar to that of polyphenolic compounds from *P. guajava* leaves. However, the microstructures of *P. guajava* leaves and *S. china* tubers were not considerably changed and ruptured after HE (Figs. S2C and S3C in Supplementary Data), indicating that the polyphenolic compounds were extracted by exuding from the two samples.

The changes in chemical structures of *P. guajava* leaves and *S. china* tubers were investigated by FTIR spectra, since FTIR spectra can provide useful information for identifying the presence of certain function groups or chemical bonds in a molecule or an interaction system, attributable to the unique energy absorption bands for specific bonding environments or interactions, it has been applied in the rapid and nondestructive identification and quantification of medicinal plants [30] and the analysis of interactions between ILs and proteins or DNA [31,32]. Generally, reflectance peaks between 1800 and 700  $\text{cm}^{-1}$  were selected as representative peaks for known carbohydrate compounds [33]. The results of FTIR spectra showed that the signal situations and intensity of absorption bands at 1622, 1447, 1318, 1035 and 780  $\text{cm}^{-1}$  for *P. guajava* leaf sample and at 1733, 1624, 1426, 1374, 1247, 1160 and 1038  $\text{cm}^{-1}$  were not obviously changed after MAE or HE with the [bmim]Br solution, which suggested that the chemical structures of carbohydrate compounds, including lignin, cellulose, hemicellulose and insoluble starch, were not destroyed in extraction process, the reasons probably were that water segregated the strong interactions between ILs and carbohydrate compounds of matrix [34–36]. The results indicated that the chemical bonding interactions between IL and sample matrix were not obvious.

*S. china* tubers samples are stiff lignocellulosic materials, *P. guajava* leaves are soft, however, the changes of microstructures and chemical structures of *P. guajava* leaves and *S. china* tubers after MAE were similar, which indicated the MAE mechanism of polyphenolic compounds from *P. guajava* leaves and *S. china* tubers was not related with the characteristics of sample.

## 4. Conclusion

In this work, ILs aqueous solution was proved to be a possible alternative solvent in the MAE of polyphenolic compounds from medicinal plants. The cations and especially anions of ILs had influences on the extraction, and the ILs with electron-rich aromatic  $\pi$ -system enhanced extraction ability. Under the optimized extraction conditions, the extraction yields of polyphenolic compounds from *P. guajava* leaves and *S. china* tubers were higher than

79.5% with 2.5 mol/L [bmim]Br solution. Compared to conventional extraction procedures, the proposed method could provide higher extraction yields and take a much shorter extraction time. The MAE kinetic mechanisms were related with the structures and characteristics of polyphenolic compounds, and the enhanced extraction was mainly based on the destruction of sample microstructures in MAE process. No obvious chemical interactions between ILs and sample matrix were identified. To alleviate environmental pressure and to develop green sample preparation techniques, ILs solutions as solvents in the MAE of polyphenolic compounds from medicinal plants showed a great promising prospect.

## Acknowledgements

This work was supported by the National Natural Science Foundation of China (No. 20375050), by the project of the National Key Technologies R&D Programme of the 11th-five-year Plan (No. 2006BAK03A08), and by the Natural Science Foundation of Guangdong Province (No. 7300594), respectively. The authors thank Sineo Microwave Chemistry Technology Company for the support of MAS-I microwave oven.

## Appendix A. Supplementary data

Supplementary data associated with this article can be found, in the online version, at doi:10.1016/j.talanta.2009.01.040.

## References

- [1] T. Welton, Chem. Rev. 99 (1999) 2071.
- [2] J. Hoffmann, M. Nüchter, B. Ondruschka, P. Wasserscheid, Green Chem. 5 (2003) 296.
- [3] C.F. Poole, J. Chromatogr. A 1037 (2004) 49.
- [4] F. van Rantwijk, R.A. Sheldon, Chem. Rev. 107 (2007) 2757.
- [5] V.I. Părvulescu, C. Hardacre, Chem. Rev. 107 (2007) 2615.
- [6] N.V. Plechkova, K.R. Seddon, Chem. Soc. Rev. 37 (2008) 123.
- [7] J.F. Liu, J.A. Jönsson, G.B. Jiang, Trends Anal. Chem. 24 (2005) 20.
- [8] A. Berthod, M.J. Ruiz-Ángel, S. Carda-Broch, J. Chromatogr. A 1184 (2008) 6.
- [9] F.Y. Du, X.H. Xiao, G.K. Li, J. Chromatogr. A 1140 (2007) 56.
- [10] F.Y. Du, X.H. Xiao, G.K. Li, Chin. J. Anal. Chem. 35 (2007) 1570.
- [11] C.S. Eskilsson, E. Björklund, J. Chromatogr. A 902 (2000) 227.
- [12] Y. Lu, W. Ma, R. Hu, X. Dai, Y. Pan, J. Chromatogr. A 1208 (2008) 42.
- [13] Y.Z. Cai, Q. Luo, M. Sun, H. Corke, Life Sci. 74 (2004) 2157.
- [14] W.K. Oh, C.H. Lee, M.S. Lee, E.Y. Bae, C.B. Sohn, H. Oh, B.Y. Kim, J.S. Ahn, J. Ethnopharmacol. 96 (2005) 411.
- [15] H.Y. Chen, G.C. Yen, Food Chem. 101 (2007) 686.
- [16] X.S. Shu, Z.H. Gao, X.L. Yang, J. Ethnopharmacol. 103 (2006) 327.
- [17] B. Shao, H.Z. Guo, Y.J. Cui, A.H. Liu, H.L. Yu, H. Guo, M. Xu, D.A. Guo, J. Pharm. Biomed. Anal. 44 (2007) 737.
- [18] J.L. Huang, Z.X. Zhang, Anal. Sci. 20 (2004) 395.
- [19] A. Liazid, M. Palma, J. Brigui, C.G. Barroso, J. Chromatogr. A 1140 (2007) 29.
- [20] Q.B. Liu, M.H.A. Janssen, F. van Rantwijk, R.A. Sheldon, Green Chem. 7 (2005) 39.
- [21] R.C. Vieira, D.E. Falvey, J. Am. Chem. Soc. 130 (2008) 1552.
- [22] G. Zhao, T. Jiang, H. Gao, B. Han, J. Huang, D. Sun, Green Chem. 6 (2004) 75.
- [23] J.L. Anderson, J. Ding, T. Welton, D.W. Armstrong, J. Am. Chem. Soc. 124 (2002) 14247.
- [24] Z. Guo, B.M. Lue, K. Thomasen, A.S. Meyer, X.B. Xu, Green Chem. 9 (2007) 1362.
- [25] L. Crowhurst, P.R. Mawdsley, J.M. Perez-Arlandis, P.A. Salter, T. Welton, Phys. Chem. Chem. Phys. 5 (2003) 2790.
- [26] C.G. Hanke, A. Johansson, J.B. Harper, R.M. Lynden-Bell, Chem. Phys. Lett. 374 (2003) 85.
- [27] H.J. Fan, G.X. Lin, X.H. Xiao, G.K. Li, Chin. J. Anal. Chem. 34 (2006) 1260.
- [28] J.R.J. Paré, M. Sigouin, J. Lapointe, US Patent, 5,002,784 (1991).
- [29] J.R.J. Paré, J.M.R. Bélanger, S.S. Stafford, Trends Anal. Chem. 13 (1994) 176.
- [30] Y. Li, R.R. Wu, B.H. Yu, J.D. Wang, Spectrosc. Spect. Anal. 26 (2006) 1846.
- [31] Z. Du, Y.L. Yu, J.H. Wang, Chem. Eur. J. 13 (2007) 2130.
- [32] J.H. Wang, D.H. Cheng, X.W. Chen, Z. Du, Z.L. Fang, Anal. Chem. 79 (2007) 620.
- [33] J. Dighton, M. Mascarenhas, G.A. Arbuckle-Keil, Soil Biol. Biochem. 33 (2001) 1429.
- [34] R.P. Swatloski, S.K. Spear, J.D. Holbrey, R.D. Rogers, J. Am. Chem. Soc. 124 (2002) 4974.
- [35] R.C. Remsing, R.P. Swatloski, R.D. Rogers, G. Moyna, Chem. Commun. 6 (2006) 1271.
- [36] D.A. Fort, R.C. Remsing, R.P. Swatloski, P. Moyna, G. Moyna, R.D. Rogers, Green Chem. 9 (2007) 63.



# The analysis of a group of acidic pharmaceuticals, carbamazepine, and potential endocrine disrupting compounds in wastewater irrigated soils by gas chromatography–mass spectrometry

Juan C. Durán-Alvarez<sup>a</sup>, Elías Becerril-Bravo<sup>a</sup>, Vanessa Silva Castro<sup>a</sup>, Blanca Jiménez<sup>a</sup>, Richard Gibson<sup>b,\*</sup>

<sup>a</sup> Instituto de Ingeniería, Universidad Nacional Autónoma de México, Ciudad Universitaria, 04510 Mexico, D.F., Mexico

<sup>b</sup> Instituto de Geografía, Universidad Nacional Autónoma de México, Ciudad Universitaria, 04510 Mexico, D.F., Mexico

## ARTICLE INFO

### Article history:

Received 20 October 2008

Received in revised form 17 January 2009

Accepted 19 January 2009

Available online 24 January 2009

### Keywords:

Pharmaceuticals

Carbamazepine

Endocrine disruptors

Wastewater

Soil

Unplanned reuse

## ABSTRACT

The analysis of pharmaceuticals and potential endocrine disruptors in the environment has rightly concentrated on their presence in wastewaters and possible contamination of receiving bodies, such as groundwaters. However, wastewater is increasingly being reused for irrigation and in order to fully understand the environmental fate of these compounds, reliable methods for their analysis in soil are required, of which there are relatively few available. This article reports a method for a range of acidic pharmaceuticals, carbamazepine, and endocrine disrupting compounds in soils with final analysis by gas chromatography–mass spectrometry. Two soil types (Phaeozom and Leptosol) and three fortification levels were used to validate the method. Recoveries of acidic pharmaceuticals varied between 62 and 102%, carbamazepine from 75 to 118%, and potential endocrine disruptors between 54 and 109%; most recoveries were between 75 and 95% and relative standard deviations were generally less than 10%. Detection limits were between 0.25 and 2.5 ng/g except for phthalates and 4-nonylphenols (25 ng/g). The method was used to analyze soils where untreated wastewaters have been used to irrigate crops for approximately 90 years. Concentrations of acidic pharmaceuticals in the soil were <1 ng/g and potential endocrine disruptors varied from below the limit of detection (estrone, 17 $\beta$ -estradiol, and 17 $\alpha$ -ethinylestradiol) to 2079 ng/L (*bis*-diethylhexyl phthalate). This data indicated that despite the continuous application of the contaminants over many years, concentrations were generally lower than those expected to be contributed by a single irrigation event. Only carbamazepine, at concentrations of 6.48 ng/g (in Phaeozem) and 5.14 ng/g (in Leptosol), showed any evidence of persistence in the soils analyzed.

© 2009 Elsevier B.V. All rights reserved.

## 1. Introduction

Over the past two decades research has shown that many classes of organic compounds that are used in our daily lives are entering the natural environment. Particular attention has been paid to their presence in wastewaters and the possibility of contamination of potential receiving bodies such as groundwater [1–3]. These as yet mostly unregulated classes of compound include a wide range of properties and environmental fates, but although most are not thought to be persistent, their continuous introduction and the biological activity of some have resulted in concerns about possible impacts on organisms and ecosystems [4,5]. There is strong evidence of biological effects caused by exposure to wastewater [6,7] and by specific compounds in laboratory studies [8,9] but the complicity of individual contaminants in the environment is complicated by the inevitable exposure to mixtures of compounds.

The analysis of these emerging contaminants has developed rapidly over the last 10–15 years, undoubtedly helped by improvements in analytical equipment, in particular the maturing of liquid chromatography coupled to mass spectrometry (LC–MS). Many of these compounds are relatively non-volatile and contain polar functional groups for which LC–MS offers the advantage of direct injection [10] whereas analysis by gas chromatography (GC) may require a derivatization step and often is unsuitable for higher molecular weight and relatively polar compounds. However, LC–MS suffers much more than GC–MS from suppression effects, particularly in complicated matrices such as wastewaters and amended soils and therefore requires a more extensive use of often expensive internal standards. This, combined with ready availability means that GC–MS is still an attractive option for the analysis of these contaminants, especially where a simple derivatization reaction is all that is required. There are now many reported analytical methods for wastewaters, which are the most common point of entry into the environment, and for surface and groundwaters [11,12]. Methods for analysis of these compounds in solid matrices are less common and have tended to focus on specific areas such as estrogens

\* Corresponding author. Tel.: +52 56224336; fax: +52 56224352.

E-mail address: [richard@igg.unam.mx](mailto:richard@igg.unam.mx) (R. Gibson).

**Table 1**  
Details of the acidic compounds and carbamazepine including use, retention time and characteristic ions (quantification ion underlined).

Analyte	Use	Retention time (min)	Characteristic ions
Clofibrac acid	Metabolite of lipid regulator clofibrate	7.88	143 243 271
Ibuprofen	Analgesic and anti-inflammatory	7.05	<u>263</u> 264
Salicylic acid	Metabolite of the analgesic aspirin	8.63	195 <u>309</u> 310
2,4-D	Pesticide	8.74	219 <u>277</u> 279
Gemfibrozil	Lipid regulator	9.68	179 <u>243</u> 307
Naproxen	Analgesic and anti-inflammatory	10.30	185 <u>287</u> 344
Ketoprofen	Analgesic and anti-inflammatory	11.00	295 <u>311</u> 312
Diclofenac	Antophlogistic	11.62	214 <u>352</u> 354
Carbamazepine	Anti-epileptic	11.38	<u>193</u> 293 180

**Table 2**  
Details of the potential endocrine disruptors including use, retention time and characteristic ions (quantification ion underlined).

Analyte	Use	Retention time (min)	Characteristic ions
4-Nonylphenols	Industrial chemical	7.40–7.75	193 207 <u>221</u>
Triclosan	Anti-septic	9.52	200 360 362
Bisphenol-A	Industrial chemical	9.82	<u>357</u> 372
Di- <i>n</i> -butylphthalate (Di- <i>n</i> -BuP)	Plasticizer	8.60	<u>149</u> 223
Butylbenzylphthalate (BuBeP)	Plasticizer	10.48	91 <u>149</u> 206
Bis-2-ethylhexylphthalate (DEHP)	Plasticizer	11.40	<u>149</u> 167 279
Estrone	Natural estrogen	12.25	218 257 <u>342</u>
17β-Estradiol	Natural estrogen	12.59	285 416
17α-Ethinylestradiol (EE2)	Artificial estrogen	13.58	285 <u>425</u> 440

in sediments [13] and antibiotics in sediments and soils [5,14–15]. There are situations where a complete view of environmental fate requires soil analysis, for example when wastewater is treated by a natural process such as infiltration through soil. The heterogeneity of soils, the different possibilities of adsorption to natural organic matter and clays in particular, and the different extraction methods available all contribute to a more complicated methodology than for waters which probably helps explain the lack of methods reported.

Soil infiltration is becoming more common for wastewater effluents in developed countries as a tertiary treatment process and a way of reusing water as resources become scarcer [16]. However, the use of wastewater, often untreated, to irrigate soils occurs widely in less developed countries and has done so for many years [17]. One of the largest, oldest, and well documented of such systems occurs in the state of Hidalgo in Mexico. Most of the water from Mexico City is sent untreated via three canals to the Tula Valley in naturally arid Hidalgo to the north east of the city at an average annual flow rate of approximately 50 m<sup>3</sup>/s. The water has helped a flourishing agricultural area to develop over the past 100 years, at present close to 80,000 hectares in size. The main crops grown are alfalfa, maize, and grazing pasture for milk production. The sheer volume of water sent to the area and the practice of flood irrigation have led to a rise in the level of the shallow aquifer under the region and in some places the appearance of new springs. These springs and many wells tapping into this and two deeper aquifers provide the water for approximately 500,000 people living in the valley. Only in the last few years has consideration been given to

the fact that as the wastewater is applied directly to fields, there is also the possibility of organic chemical contaminants reaching the aquifer. Recent work [18] has shown that there are considerable concentrations of commonly occurring organic contaminants in the wastewater, roughly equivalent to influent concentrations seen in developed countries, yet little apparent contamination of the aquifer. It appears that the soil acts as an effective barrier, and through adsorption and degradation processes, protects the aquifer from serious contamination. In order to provide a more complete picture of the fate of organic micro-pollutants in this system, it is necessary to understand better this important natural barrier. This work describes the development and validation of methodology for the analysis in soil of some acidic pharmaceuticals, carbamazepine, and a disparate group of potential endocrine disrupting compounds, all commonly found in wastewaters. GC–MS was used for the final analysis.

## 2. Experimental

### 2.1. Chemicals and reagents

All of the target acidic compounds and potential endocrine disruptors (listed in Tables 1 and 2) were available from Sigma–Aldrich (St. Louis, MO, USA). The recovery and internal standards (Table 3) were also purchased from Sigma–Aldrich except 3,4-dichlorophenoxyacetic acid (3,4-D) and 2,3-dichlorophenoxyacetic acid (2,3-D) which were obtained from Riedel-de Haën (Seelze, Germany). The derivatization agents *N*-tert-butylidimethyl-

**Table 3**  
Recovery and internal standards for the analytical method, including retention times and characteristic ions (quantification ion underlined).

Analyte	Use	Retention time (min)	Characteristic ions
3,4-D	Recovery standard	8.84	219 <u>277</u> 279
2,3-D	Internal standard	8.94	251 <u>277</u> 279
10,11-Dihydrocarbamazepine	Internal standard	11.18	<u>195</u> 295 165
4- <i>n</i> -Nonylphenol	Recovery standard	8.40	<u>179</u> 292
[ <sup>2</sup> H <sub>4</sub> ]4- <i>n</i> -Nonylphenol	Internal standard	8.39	<u>183</u> 296
[ <sup>2</sup> H <sub>16</sub> ]Bisphenol-A	Internal standard	9.80	<u>368</u> 386
[ <sup>2</sup> H <sub>4</sub> ]DEHP	Recovery standard	11.40	<u>153</u> 171
[ <sup>2</sup> H <sub>4</sub> ]Estrone	Recovery standard	12.24	<u>346</u> 261
[ <sup>2</sup> H <sub>3</sub> ]17β-Estradiol	Internal standard	12.58	<u>419</u> 285

**Table 4**  
Basic soil parameters.

Parameter	Phaeozem	Leptosol
Sand (%)	13.3	24.5
Loam (%)	38.3	30.8
Clay (%)	48.4	44.7
Density (g/cm <sup>3</sup> )	2.08	2.11
pH	5.88	6.77
cation exchange capacity (cmol/Kg)	37.9	43.4
Organic carbon (%)	3.1	2.91

silyl-*N*-methyltrifluoroacetamide (MTBSTFA) with 1% *t*-butyldimethylsilylchlorane (TBDMSCI) and *N,O*-bis(trimethylsilyl)trifluoroacetamide (BSTFA) with 1% trimethylsilylchlorane (TMSCl) were also bought from Sigma–Aldrich. All solvents used were of HPLC grade, supplied by Burdick and Jackson (Morristown, NJ, USA). Oasis HLB extraction cartridges were purchased from Waters (Milford, MA, USA).

## 2.2. Sampling

The wastewater used in the Tula Valley arrives via three drainage canals from Mexico City; a more detailed description can be found elsewhere [19]. The water is distributed via a complex series of canals, and irrigation is carried out by opening small sluice gates in the ditches that surround the fields. Typical rates are 13–15 cm per event and the process usually results in complete flooding of the field. During the growing season of the most common crops, alfalfa and maize, the fields are typically irrigated in this way every 15 to 20 days and a total of 5–6 times during each growing cycle. This equates to annual rates of between 1 and 2 m as two or three cycles are possible each year. Two soils commonly found in the Tula Valley, Phaeozem and Leptosol, were used for the validation and details of their physicochemical properties can be found in Table 4. The soil was taken to a depth of 30 cm from at least eight points in each area sampled and a composite was then prepared by mixing 50 g sub-samples after partially air-drying and sieving to 2 mm. The soils were stored at –20 °C before analysis.

## 2.3. Sample preparation strategy

Parameters affecting the extraction efficiency using the Dionex accelerated solvent extraction (ASE) system were first tested. Following this, having established that the presence of hexane aided that efficiency, the initial strategy was to remove this non-polar solvent during concentration before adding water and isolating the compounds on a reverse phase Oasis HLB cartridge. A comparison was then made between simple elution of all analytes in a single fraction with separate elution of fractions labelled as acidic compounds and endocrine disruptors. This latter approach was designed to improve the cleanliness of the samples and allow the flexibility to apply a different derivatization step to each fraction in order to improve sensitivity and permit adequate analysis of all of the compounds. A representation of the method and areas of investigations are shown in Fig. 1. The final method developed is described in the next section.

## 2.4. Extraction and isolation

The soil (10 g) was weighed accurately and mixed thoroughly with diatomaceous earth (2 g) before being added to the extraction cell; blanks consisted of 2 g of diatomaceous earth. 4-*n*-nonylphenol (500 ng) and [<sup>2</sup>H<sub>4</sub>]estrone (250 ng) were added as recovery standards and then samples were fortified with the analytes where appropriate (see Tables 5 and 6 for details). After investigation, the most efficient solvent mixture for extraction was acetone:hexane:acetic acid (50:50:2; v/v/v) and ASE conditions used in the validation were as follows: pre-heat (0 min), heating time (5 min), static time (5 min), 50% flush, 2 cycles. After extraction, 3,4-D (100 ng) was added as a recovery standard for the acids, and the samples were evaporated to a volume of approximately 3–4 mL then water (20 mL) added. Oasis HLB cartridges (200 mg) were conditioned with acetone (2 × 5 mL) followed by 5 mL of acetic acid:water (10% v/v). The samples were passed through the cartridges at a flow rate of 1–2 mL/min. After washing the cartridges with water (2 mL), acidic compounds were eluted with 5.5 mL of a 40:60 (v/v) mixture of acetone:0.10 M sodium hydrogencarbonate buffer (adjusted to pH 10 using 1.0 M sodium hydroxide

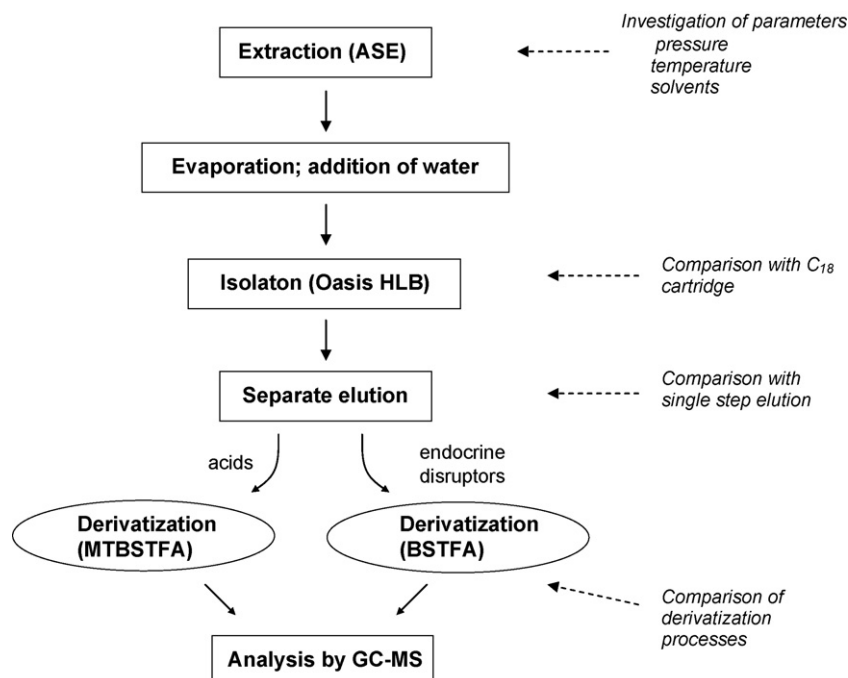


**Fig. 1.** Schematic representation of the analytical procedure and the areas where method development was concentrated.

**Table 5**  
Instrument LOD (ng), linear correlation coefficients ( $R^2$ ), and recovery data (%  $\pm$  relative standard deviation) for target acidic pharmaceuticals and carbamazepine ( $n=3$ ).

Analyte	Instrument LOD	$R^2$	Fortification (ng/g; Phaeozem)			Fortification (ng/g; Leptosol)		
			(2.5)	(10)	(50)	(2.5)	(10)	(50)
Clofibric acid	0.01	0.9999	96 $\pm$ 9	99 $\pm$ 3	88 $\pm$ 2	84 $\pm$ 13	81 $\pm$ 1	79 $\pm$ 1
Ibuprofen	0.005	0.9996	101 $\pm$ 2	102 $\pm$ 2	92 $\pm$ 3	87 $\pm$ 13	104 $\pm$ 3	93 $\pm$ 1
2,4-D	0.01	0.9997	89 $\pm$ 13	78 $\pm$ 13	62 $\pm$ 8	85 $\pm$ 20	82 $\pm$ 1	72 $\pm$ 3
Gemfibrozil	0.005	0.9997	100 $\pm$ 16	97 $\pm$ 1	84 $\pm$ 3	98 $\pm$ 14	97 $\pm$ 3	83 $\pm$ 2
Naproxen	0.005	0.9997	93 $\pm$ 11	101 $\pm$ 2	74 $\pm$ 1	80 $\pm$ 12	83 $\pm$ 6	75 $\pm$ 2
Ketoprofen	0.01	0.9998	94 $\pm$ 5	100 $\pm$ 1	74 $\pm$ 2	79 $\pm$ 7	93 $\pm$ 6	75 $\pm$ 1
Diclofenac	0.005	0.9992	79 $\pm$ 5	80 $\pm$ 2	71 $\pm$ 3	65 $\pm$ 11	69 $\pm$ 4	62 $\pm$ 4
Carbamazepine	0.01	0.9998	112 $\pm$ 8	118 $\pm$ 7	91 $\pm$ 5	75 $\pm$ 23	88 $\pm$ 8	75 $\pm$ 3

solution). The cartridge was then washed with a further 2 mL of water and dried for 60 min under vacuum. The potential endocrine disruptors were then eluted from the cartridge with 6 mL of acetone:dichloromethane (1:1).

### 2.5. Concentration and derivatization

The acid fraction was evaporated for 15 min under a stream of nitrogen to remove a proportion of the acetone present, acidified to below pH 2 with sulphuric acid (25  $\mu$ L), and then the acids and carbamazepine extracted into ethyl acetate (2  $\times$  2 mL). Remnants of water were removed with anhydrous sodium sulphate, and 2,3-D (100 ng) and 10,11 dihydrocarbamazepine (100 ng) were added as internal standards before final evaporation to dryness under a stream of nitrogen at room temperature. The residue was reconstituted in ethyl acetate (25  $\mu$ L) then MTBSTFA (50  $\mu$ L) added. *N*-tert-butyltrimethylsilyl derivatives were produced by reaction at 60  $^{\circ}$ C for 30 min then samples were diluted with ethyl acetate before injection. The blanks, unfortified samples, and samples at the lowest level of fortification were diluted to a final volume of 100  $\mu$ L while samples at the higher two fortification levels were diluted to 1000  $\mu$ L.

The acetone:dichloromethane fraction was evaporated to approximately 200  $\mu$ L then 1 mL of ethyl acetate added. Water was removed by addition of anhydrous sodium sulphate and then [ $^2$ H $_4$ ]4-*n*-nonylphenol (500 ng), [ $^2$ H $_{16}$ ]bisphenol-A (500 ng), and [ $^3$ H $_4$ ]estradiol (250 ng) were added as internal standards. The sample was evaporated to dryness under a stream of nitrogen at room temperature and the residue was reconstituted in pyridine (25  $\mu$ L). BSTFA (50  $\mu$ L) was added and *N*-trimethylsilyl derivatives were produced by reaction at 60  $^{\circ}$ C for 30 min then samples were diluted to either 100 or 1000  $\mu$ L with ethyl acetate (as described above) before injection.

### 2.6. GC-MS analysis

The samples were analyzed using a HP 6890 gas chromatograph fitted with a 30 m HP5-MS fused silica capillary column

(30 m  $\times$  0.25 mm, 0.25  $\mu$ m film thickness), and connected to an HP 5973 mass selective detector. Injection port temperature was 250  $^{\circ}$ C and 1  $\mu$ L samples were injected in splitless mode. Carrier gas was helium at a constant flow rate of 1 mL/min and the oven programme was: 100  $^{\circ}$ C for 1 min, 20  $^{\circ}$ C/min to 280  $^{\circ}$ C, 280  $^{\circ}$ C for 10 min. The electron impact source temperature of the detector was 230  $^{\circ}$ C with electron energy of 70 eV. The quadrupole temperature was 150  $^{\circ}$ C, and GC interface temperature was 280  $^{\circ}$ C. Single ion monitoring (SIM) was used for quantitative analysis while a scan range of 50–500 *m/z* was used for full scan analysis of selected samples. Ions monitored (quantification ions underlined) and retention times are detailed in Tables 1–3, and typical chromatography of standards is shown in Fig. 2.

## 3. Results and discussion

### 3.1. Extraction procedure

Pressurized liquid extraction (PLE) methods have the advantages over Soxhlet systems of shorter extraction times and reduced solvent use [20]. However, some analytes are unstable at the elevated temperatures and pressures required therefore a brief investigation of these parameters was carried out using acetone:hexane (1:1) as the extraction solvent. Poor recoveries (generally under 50%) from fortified soils were obtained for some of the acidic pharmaceuticals under the initial extraction conditions of 100  $^{\circ}$ C and 1500 psi. Similar losses were seen at extraction temperatures of 60  $^{\circ}$ C, 75  $^{\circ}$ C, and 90  $^{\circ}$ C when the pressure was maintained constant at 1500 psi. At a constant temperature of 100  $^{\circ}$ C, better recoveries of acids were obtained at 1000 psi than 1250 or 1500 psi. Recoveries of the endocrine disruptors were more or less consistent up to 1250 psi but dropped slightly at 1500 psi (data not shown). In a PLE system, increased temperature accelerates the kinetics of extraction while elevated pressures keep the solvent below its boiling point. Therefore, a pressure of 1000 psi was chosen for the method, a pressure sufficient to maintain the solvent as a liquid at 100  $^{\circ}$ C without causing degradation of the analytes. A Phaeozem soil that was known to have been irrigated with wastewater and therefore suspected to

**Table 6**  
Instrument LOD (ng), linear correlation coefficients ( $R^2$ ), and recovery data (%  $\pm$  relative standard deviation) for target potential endocrine disrupting compounds ( $n=3$ ).

Analyte	Instrument LOD	$R^2$	Fortification <sup>a</sup> (Phaeozem)			Fortification <sup>a</sup> (Leptosol)		
			Low	Medium	High	Low	Medium	High
4-Nonylphenols	0.01	0.9989	90 $\pm$ 3	98 $\pm$ 4	86 $\pm$ 8	82 $\pm$ 4	82 $\pm$ 3	79 $\pm$ 2
Triclosan	0.005	0.9985	93 $\pm$ 18	95 $\pm$ 3	92 $\pm$ 7	128 $\pm$ 4	88 $\pm$ 5	88 $\pm$ 4
Bisphenol-A	0.005	0.9975	91 $\pm$ 8	83 $\pm$ 2	88 $\pm$ 2	81 $\pm$ 3	80 $\pm$ 2	85 $\pm$ 7
Di- <i>n</i> -BuP	0.005	0.9995	–	97 $\pm$ 6	106 $\pm$ 4	–	95 $\pm$ 17	97 $\pm$ 4
BuBeP	0.01	0.9994	–	75 $\pm$ 4	94 $\pm$ 3	–	72 $\pm$ 15	109 $\pm$ 2
[ $^2$ H $_4$ ]DEHP	0.01	0.9950	76 $\pm$ 9	74 $\pm$ 4	71 $\pm$ 9	58 $\pm$ 7	73 $\pm$ 4	72 $\pm$ 1
Estrone	0.005	0.9995	63 $\pm$ 19	83 $\pm$ 2	83 $\pm$ 2	54 $\pm$ 2	86 $\pm$ 3	78 $\pm$ 4
17 $\beta$ -Estradiol	0.005	0.9994	78 $\pm$ 21	78 $\pm$ 7	70 $\pm$ 6	77 $\pm$ 4	76 $\pm$ 5	68 $\pm$ 1
EE2	0.02	0.9960	85 $\pm$ 17	85 $\pm$ 5	76 $\pm$ 2	103 $\pm$ 2	73 $\pm$ 7	54 $\pm$ 9

<sup>a</sup> Fortification concentrations: 4-Nonylphenols, Di-*n*-BuP, BuBeP, and [ $^2$ H $_4$ ]DEHP: 250 ng/g (low), 1000 ng/g (medium), and 2000 ng/g (high); Bisphenol-A, triclosan: 10 ng/L (low), 50 ng/g (medium), and 100 ng/g (high); Estrone, 17 $\beta$ -estradiol, and EE2: 2.5 ng/g (low), 10 ng/g (medium), and 50 ng/g (high)



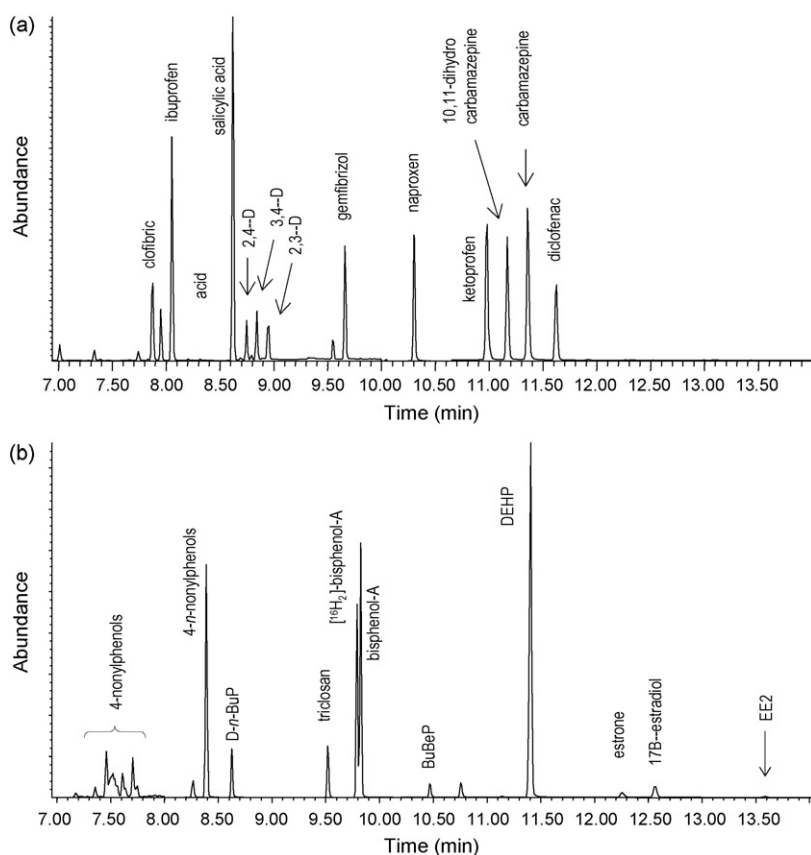


Fig. 2. Total ion chromatograms of standards of (a) the acidic pharmaceuticals and carbamazepine, and (b) the potential endocrine disruptors.

contain concentrations of the analytes of interest was used in experiments to compare different extraction solvents. This was deemed more appropriate than spiking a soil which does not take true account of aging effects. The presence of hexane in the extraction solvent mixture notably improved the recovery of ibuprofen and 4-nonylphenols compared to either a simple methanol or acetone extraction. Recoveries of triclosan, carbamazepine and bisphenol-A were either similar or slightly improved compared to the single solvents (Fig. 3). Although it has been reported that acetone alone was the most effective solvent for extraction of estrogens [21], because this is a multi-residue method, a mixture of acetone:hexane (1:1,

modified with 2% acetic acid) was chosen because of the complementary nature of the mixture, where acetone aids contact with soils in the presence of water while hexane helps the extraction of compounds adsorbed to refractory non-polar material.

### 3.2. Practical considerations

It was necessary to remove the hexane from the extraction solution and add water before passing the sample through the Oasis HLB cartridge. The addition of water resulted in the precipitation of some solids, but an extraction of this material showed a complete

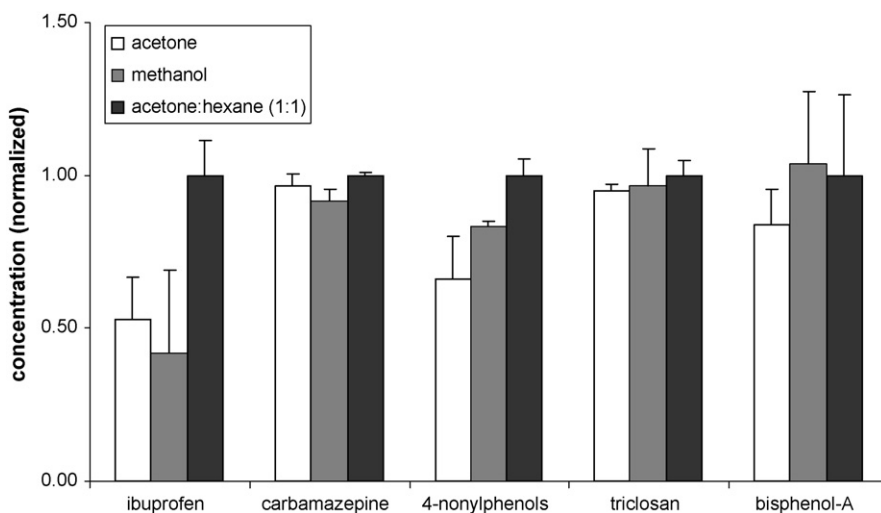


Fig. 3. Comparison of solvents used for extraction; normalized extraction data.

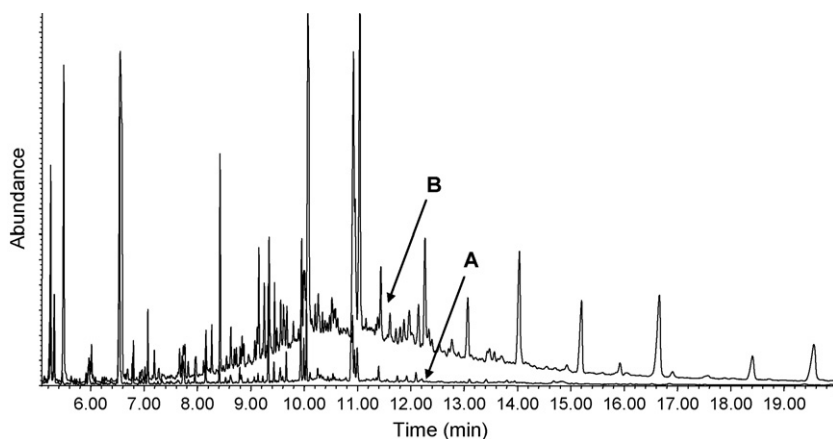


Fig. 4. Full scan chromatograms of elution with buffer solution (A) and simple elution with acetone (B).

absence of the analytes. Nevertheless, to be sure of no losses at this stage, these solids were added to the cartridge which although causing a slowing in the passage of the solution, never resulted in complete blockage.

The elution of an acidic fraction with an acetone:buffer solution had advantages over the more common single elution with a polar solvent. First, it allowed a specific derivatization of the acids with MTBSTFA and the resulting *N-tert*-butyldimethylsilyl derivatives produced improved peak shape in comparison to their trimethylsilyl equivalents from BSTFA derivatization. Second it produced a relatively much cleaner fraction, as can be seen from a comparison of full scan chromatograms in Fig. 4. This helped sensitivity in SIM mode by removing background noise and interfering peaks, and was particularly useful for the identification and quantification of later eluting acids such as naproxen and diclofenac (Fig. 5). It also allowed analysis of carbamazepine which was otherwise not possible (see Section 3.3). The chromatogram of the endocrine disruptor fraction showed little difference compared to a single elution step, but did produce a slightly cleaner sample for injection. This is in contrast to results obtained when this separation procedure was applied to waters where the acid fraction was little changed compared to the single elution and the endocrine disruptor fraction was much cleaner [18]. This difference can be explained by the nature of the natural organic material which in water is generally relatively polar and hence more likely to elute in the acidic fraction whereas in soil it is more refractory in nature and contains less acidic functional groups, is less polar and therefore less likely to be encouraged from the column by the buffer solution. A mixture

of acetone:dichloromethane (1:1) was used to elute the endocrine disruptors although it proved to be only marginally better than pure acetone, helping improve the recovery of 4-nonylphenols by a few percent.

### 3.3. The case of carbamazepine

The analysis of carbamazepine is complicated by partial degradation of the derivatized compound, resulting in two peaks in the chromatogram, the parent compound and derivatized iminostilbene (Fig. 6). This degradation in the GC inlet has been reported before [22] but it was noted in this work that the extent to which this degradation occurs and the sensitivity of response in general appears to depend on the state of the inlet, determined by previous injections as well as the matrix of the sample actually being injected. For example, injection of a standard solution produced both the parent compound and the degradation product whereas for the majority of soil samples the degradation product was not formed at all. Carbamazepine could still be quantified with the use of 10,11-dihydrocarbamazepine as an internal standard as it produced the equivalent degradation product (see Fig. 6) and in the same proportion, as indicated by the calibration curve and validation data obtained (see following two sections). The separate elution with buffer proved advantageous for the analysis because when a single elution was carried out, carbamazepine and the internal standard were entirely absent from the chromatogram, even in soils fortified at a high concentration. It is possible that this was due to the matrix material

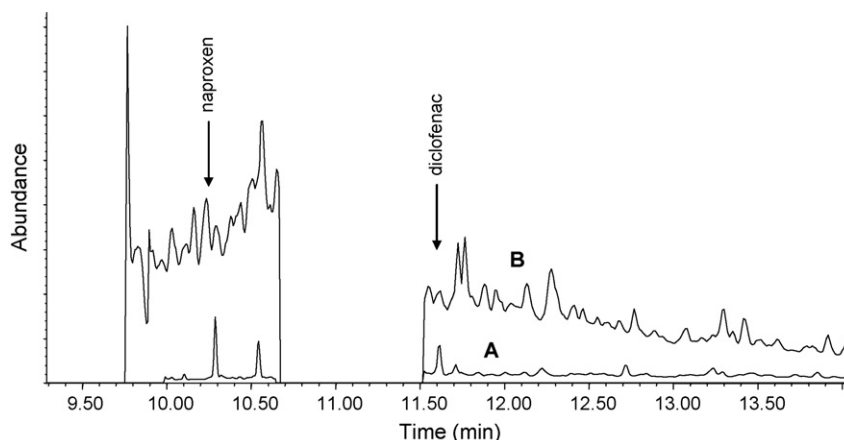


Fig. 5. SIM chromatograms of elution with buffer solution (A) and simple elution with acetone (B): naproxen (ion 287) and diclofenac (ion 352).

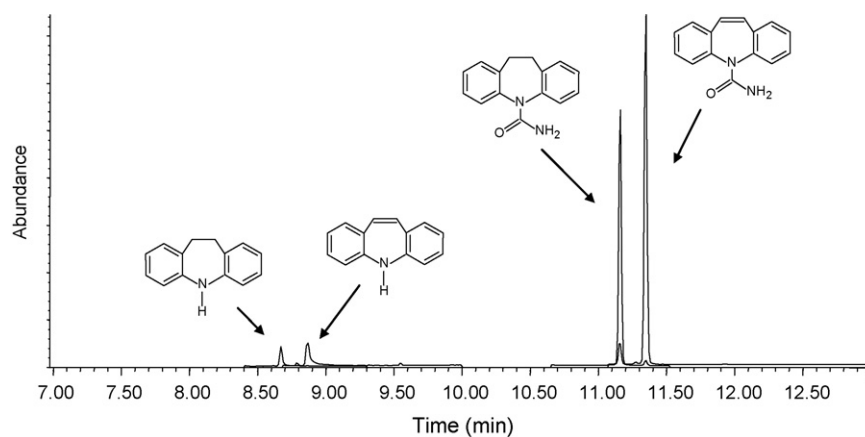


Fig. 6. Chromatogram of carbamazepine and 10,11-dihydrocarbamazepine showing the generation of degradation products.

causing a different or more complete degradation process in the inlet.

#### 3.4. Linear correlation coefficients, limits of detection, and blank concentrations

The linearity of the instrument was acceptable for all analytes with correlation coefficients always greater than 0.99 in the concentration range of the study (Tables 5 and 6). This was also true for carbamazepine despite the variable production of the degradation product, indicating an effective internal standard. The limit of detection (LOD) of the method was defined as three times background (signal to noise ratio of 3) and any peak above the LOD was quantified.

LODs for the acids (Table 8) varied between 0.10 and 2.0 ng/g and were in general dictated by the presence of matrix material. For the potential endocrine disruptors, LODs varied from 1.0 to 25 ng/g (Table 8). The limits for 4-nonylphenols and the phthalates were influenced by unavoidable contamination picked up during the procedure from solvents and cartridges. There was very little background present for the analysis of the estrogens and limits could be lowered beyond those reported here simply by further concentration of the final sample. Overall, these limits were considered practical and comparable to reported values.

Blank samples were included in each batch of the validation. The acids were generally absent from the blanks as were carbamazepine and the three estrogens. 4-nonylphenols and the phthalates were present as expected, the main sources probably being the solvents and the Oasis HLB cartridges, while very low concentrations of triclosan and bisphenol-A were noted. Blank subtraction was carried out for all samples.

#### 3.5. Recovery data

The two soil types were fortified at three different levels, the lowest of which was close to the limit of detection of the method. Mean recoveries for the acidic compounds (Table 5) at the lowest fortification level ranged from 79% to 112% (Phaeozem) and from 65% to 98% (Leptosol). At the intermediate level recoveries ranged from 78% to 118% (Phaeozem) and 69% to 104% (Leptosol), while at the highest level they were from 62% to 92% and 62% to 93% respectively. Relative standard deviations were mostly less than 10% at the two higher fortification levels but were greater at the lowest, a level deliberately close to the detection limit of most of the compounds. The data for carbamazepine was acceptable, despite the complica-

tion of partial degradation, so showing that the internal standard adequately corrected the data. Validation was also attempted for salicylic acid but it degraded almost completely during the extraction procedure.

Recoveries for the potential endocrine disruptors from soil type Phaeozem varied from 63 to 93% (lowest fortification level), 74% to 98% (intermediate) and from 70% to 106% (highest). Relative standard deviations were generally less than 10%, the notable exception being the three estrogens at the lowest fortification level. For soil type Leptosol, recoveries ranged from 54% to 128%, 72% to 95%, and 54% to 109% respectively (Table 6). Recoveries were a little lower for the estrogens than the other phenols, notably estrone at the lowest fortification and EE2 at the highest. This may be due to the use of [ $^2\text{H}_3$ ]17 $\beta$ -estradiol as the internal standard for all the estrogens or possibly because of irreversible adsorption sites in particular soil samples. Again relative standard deviations were generally less than 10%. It was not possible to obtain validation data at the lowest fortification level for the phthalates in either soil type as the fortification level was too close to or less than the amounts present in the soil. This problem was anticipated for DEHP and [ $^2\text{H}_4$ ] DEHP was used for the validation instead. Overall, recoveries were considered acceptable considering the complexity of the samples, being soils subjected to irrigation with untreated wastewater for many years. The recovery data compare favourably with a microwave extraction method that also involved a more laborious clean-up procedure [23] and were similar to those reported recently for these types of compounds in a sandy loam soil [24].

Three recovery standards were also evaluated as part of the validation process (Table 7). For the acids, the recovery of 3,4-D was generally greater than for the analytes, averaging 107% in the Phaeozem soil and 110% in the Leptosol. This probably reflects losses of analytes during extraction while 3,4-D was added after the extraction because it was found to degrade completely under the extraction conditions employed. Mean recoveries of 4-*n*-nonylphenol were slightly greater in Phaeozem (84%) than

Table 7  
Data for the recovery standards (where  $n = 12$ ); RSD = relative standard deviation.

Sample	3,4-D	4- <i>n</i> -Nonylphenol	[ $^2\text{H}_4$ ]Estrone
Phaeozem			
Recovery (%)	107	84	87
RSD (%)	14	16	13
Leptosol			
Recovery (%)	110	77	75
RSD (%)	7	5	9

**Table 8**

Concentration of the analytes in Phaeozem and Leptosol soils under irrigation with wastewater for approximately 90 years.

Analyte	LOD (ng/g)	Phaeozem	Leptosol
Clofibric acid	2.0	<LOD	<LOD
Ibuprofen	0.1	0.25 ± 0.04	<LOD
2,4-D	2.0	<LOD	<LOD
Gemfibrozil	2.0	<LOD	<LOD
Naproxen	0.2	0.55 ± 0.01	0.73 ± 0.20
Ketoprofen	1.0	<LOD	<LOD
Diclofenac	1.0	<LOD	<LOD
Carbamazepine	0.5	6.48 ± 0.59	5.14 ± 0.48
4-Nonylphenols	25	41 ± 6	123 ± 9
Triclosan	1.0	4.4 ± 0.1	18.6 ± 1.2
Bisphenol-A	2.0	<LOD	14.8 ± 3.2
Di- <i>n</i> -BuP	25	244 ± 43	552 ± 57
BuBeP	25	131 ± 23	346 ± 50
DEHP	25	820 ± 87	2079 ± 201
Estrone	1.0	<LOD	<LOD
17β-Estradiol	1.0	<LOD	<LOD
EE2	2.5	<LOD	<LOD

Leptosol (77%) and the same was true of [<sup>2</sup>H<sub>4</sub>] estrone, 87% and 75% respectively. The recoveries were considered acceptable and broadly representative of the recoveries of the analytes and therefore that these compounds were suitable recovery standards for quality control during routine analysis.

### 3.6. Concentrations of the analytes in soils

The concentration of the analytes was measured in both Phaeozem and Leptosol soil types where irrigation had been carried out for 90 years (Table 8). Ibuprofen and naproxen were present, but the concentrations (<1 ng/g) were very low, indicating no build up of these acids in the soil. The most probable explanation is degradation, probably aided by the microbial activity in the wastewater and soil, the high temperatures typical of the region, and possibly photolytic processes. The concentration of carbamazepine in the soil was 6.48 ng/g (Phaeozem) and 5.14 ng/g (Leptosol) compared to an estimated addition equivalent to approximately 0.2 ng/g for each irrigation event (data not presented), suggesting some persistence of this compound. The potential endocrine disruptors were also present in the soil, except for the estrogens which were all below the limit of detection. Concentrations were greater in the Leptosol than in the Phaeozem soil but overall, there was no compelling evidence of any build up in the soil, suggesting degradation processes in the soil prevail.

## 4. Conclusions

A simple method using GC–MS detection was developed for the analysis of a selection of acidic pharmaceuticals and potential endocrine disruptors in soils. The separate elution of an acidic

fraction permitted more sensitive detection of the acids, as well as allowing detection of carbamazepine. The endocrine disruptor fraction was physically cleaner but little difference was noted in the chromatograms. A comprehensive validation proved the robustness of the method which was used to measure the concentration of the compounds in soils that had been irrigated with untreated wastewater. The concentrations of most compounds were low, generally well below the amount that would be applied in a single application, indicating most likely that rapid degradation processes occur between irrigation events, preventing accumulation of these micro-pollutants. The only contaminant that showed signs of persistence was carbamazepine which was present in the soils at much greater concentrations than would be applied in a single irrigation event.

## Acknowledgements

We would like to acknowledge the Secretaría de Medio Ambiente y Recursos Naturales and the CONACYT of the Mexican government (No. SEMARNAT-2002-01-0519) and the European Commission (RECLAIM WATER; project number:018309) for supporting this research.

## References

- [1] T. Heberer, *J. Hydrol.* 266 (2002) 175.
- [2] K.K. Barnes, D.W. Kolpin, E.T. Furlong, S.D. Zaugg, M.T. Meyer, L.B. Barber, *Sci. Total Environ.* 402 (2008) 192.
- [3] J. Opper, G. Broll, D. Löffler, M. Meller, J. Römbke, T. Ternes, *Sci. Total Environ.* 328 (2004) 265.
- [4] K. Fent, A.A. Weston, D. Caminada, *Aquat. Toxicol.* 76 (2006) 122.
- [5] M.D. Hernandez, M. Mezcuca, A.R. Fernández-Alba, D. Barceló, *Talanta* 69 (2006) 334.
- [6] S. Jobling, M. Nolan, C.R. Tyler, G. Brighty, J.P. Sumpter, *Environ. Sci. Technol.* 32 (1998) 2498.
- [7] J.P. Sumpter, *Acta Hydroch. Hydrob.* 33 (2005) 9.
- [8] R. Triebskorn, H. Casper, V. Scheil, J. Schwaiger, *Anal. Bioanal. Chem.* 387 (2007) 1405.
- [9] F. Pomati, S. Castiglioni, E. Zuccato, R. Fanelli, D. Vigetti, C. Rossetti, D. Calamari, *Environ. Sci. Technol.* 40 (2006) 2442.
- [10] S.-C. Kim, K. Carlson, *TrAC-Trend Anal. Chem.* 24 (2005) 635.
- [11] C. Hao, X.R. Clement, P. Yang, *Anal. Bioanal. Chem.* 387 (2007) 1247.
- [12] M. Petrovic, M.D. Hernandez, M.S. Díaz-Cruz, D. Barceló, *J. Chromatogr. A* 1067 (2005) 1.
- [13] P. Labadie, E.M. Hill, *J. Chromatogr. A* 1141 (2007) 174.
- [14] M.P. Schlüsener, M. Spiteller, K. Bester, *J. Chromatogr. A* 1003 (2004) 21.
- [15] A.M. Jacobsen, B. Halling-Sørensen, F. Ingerslev, S. Honoré Hansen, *J. Chromatogr. A* 1038 (2004) 157.
- [16] S. Toze, *Agric. Water Manage.* 80 (2006) 147.
- [17] B. Jiménez, *Int. Rev. Environ. Strategies* 4 (2006) 229.
- [18] R. Gibson, E. Becerril-Bravo, V. Silva-Castro, B. Jiménez, *J. Chromatogr. A* 1169 (2007) 31.
- [19] T.J. Downs, E. Cifuentes, E. Ruth, I. Suffet Irwin, *Water Environ. Res.* 72 (2000) 4.
- [20] S. Armenta, S. Garrigues, M. de la Guardia, *TrAC-Trends Anal. Chem.* 27 (2008) 497.
- [21] J. Beck, K.U. Totsche, I. Kögel-Knabner, *Chemosphere* 71 (2008) 954.
- [22] M.J. Gómez, A. Agüera, M. Mezcuca, J. Hurtado, F. Mocholí, A.R. Fernández-Alba, *Talanta* 73 (2007) 314.
- [23] S.L. Rice, S. Mitra, *Anal. Chim. Acta* 589 (2007) 125.
- [24] J. Xu, L. Wu, W. Chena, A.C. Chang, *J. Chromatogr. A* 1202 (2008) 189.



# Cobalt phthalocyanine as a novel molecular recognition reagent for batch and flow injection potentiometric and spectrophotometric determination of anionic surfactants

Eman M. El-Nemma<sup>a</sup>, Nahla M. Badawi<sup>b</sup>, Saad S.M. Hassan<sup>b,\*</sup>

<sup>a</sup> Department of Chemistry, Faculty of Arts and Science, Qatar University, Doha, Qatar, Egypt

<sup>b</sup> Department of Chemistry, Faculty of Science, Ain Shams University, Cairo, Egypt

## ARTICLE INFO

### Article history:

Received 7 October 2008  
Received in revised form 12 December 2008  
Accepted 12 December 2008  
Available online 24 December 2008

### Keywords:

Potentiometry  
Spectrophotometry  
Anionic surfactants  
Sensors  
Chromogen  
Molecular recognition  
Flow injection analysis  
Cobalt(II)phthalocyanine

## ABSTRACT

Cobalt(II) phthalocyanine [Co(II)Pc] is used as both an ionophore and chromogen for batch and flow injection potentiometric and spectrophotometric determination of anionic surfactants (SDS), respectively. The potentiometric technique involves preparation of a polymeric membrane sensor by dispersing [Co(II)Pc] in a plasticized PVC membrane. Under batch mode of operation, the sensor displays a near-Nernstian slope of  $-56.5 \text{ mV decade}^{-1}$ , wide response linear range of  $7.8 \times 10^{-4}$  to  $8.0 \times 10^{-7} \text{ mol L}^{-1}$ , lower detection limit of  $2.5 \times 10^{-7} \text{ mol L}^{-1}$  and exhibits high selectivity for anionic surfactants in the presence of many common ions. Under hydrodynamic mode of operation (FIA), the slope of the calibration plot, limit of detection, and working linear range are  $-51.1 \text{ mV decade}^{-1}$ ,  $5.6 \times 10^{-7}$  and  $1.0 \times 10^{-3}$  to  $1.0 \times 10^{-6} \text{ mol L}^{-1}$ , respectively. The spectrophotometric method is based on the use of [Co(II)Pc] solution in dimethylsulfoxide (DMSO) as a chromogenic reagent. The maximum absorption of the reagent at 658 nm linearly decreases with the increase of anionic surfactant over the concentration range  $2\text{--}30 \mu\text{g mL}^{-1}$ . The lower limit of detection is  $1 \mu\text{g mL}^{-1}$  and high concentrations of many interfering ions are tolerated. Flow injection spectrophotometric measurements are carried out by injection of the surfactant test solution in a stream of the reagent in DMSO. The sample throughput, working range and lower detection limit are  $25\text{--}30 \text{ samples h}^{-1}$ ,  $4\text{--}60$  and  $2 \mu\text{g mL}^{-1}$ , respectively. The potentiometric and spectrophotometric techniques are applied to the batch and flow injection measurements of anionic surfactants in some commercial detergent products. The results agree fairly well with data obtained using the standard methylene blue spectrophotometric method.

© 2009 Published by Elsevier B.V.

## 1. Introduction

It is a frequent task of many analytical laboratories to determine surfactants in product formulations for quality control, in industrial samples for process control, in wastewaters for environmental control and in food products for contamination control. Although various instrumental methods have been suggested for quantification of anionic surfactants, spectrophotometry [1–10] and potentiometry [11–22] remain the easier and relatively low cost applicable techniques.

The standard method for determining anionic surfactants is based on the formation of an ion pair complex between the surfactants and methylene blue, followed by extraction into chloroform, and spectrophotometric measurements [1]. Ethyl violet [2,3], malachite green [4], methyl orange [5] and pyridinium deriva-

tives [6–9] have been similarly used. Most of these methods are time-consuming, involve multiple solvent extraction procedures [1–6,8,10], and suffer from serious interferences by organic sulfates, sulfonates, carboxylates, phenolates, thiocyanate, cyanate, nitrate, and chloride ions [1,7,8]. On the other hand, application of these methods with the flow injection systems necessitates the use of multiple stream setup [4,5,8], phase converter, segmentor, separator with porous PTFE membrane, and a special line connector to deal with the two-phase extraction process [2,4,6].

The potentiometric approach for determining anionic surfactants involves either titration with cationic species [11–13] or direct potentiometry using surfactant-sensitive sensors. Ion-selective sensors for anionic surfactants were first prepared using liquid ion exchangers dissolved in water-immiscible organic solvents [14,15]. Sensors with better selectivity and longer life time have been suggested based on the use of poly(vinyl chloride) or modified polymer matrix membranes [16–18] in the form of tubular or coated wire designs [15,19,20]. Applications of some of these sensors for flow

\* Corresponding author. Tel.: +2026822991; fax: +2026822991.  
E-mail address: [saadsmhassan@yahoo.com](mailto:saadsmhassan@yahoo.com) (S.S.M. Hassan).

injection determination of surfactants have been also described [20–22].

Metal phthalocyanines are well known commercially available dyes, with good chemical and thermal stabilities. Relatively little attention has been paid to the potential utility of these compounds as active sensing materials, molecular recognition species or a promising class of ionophores in potentiometric sensors [23–27]. Recently, methods for a batch and flow injection analysis of azide ion using cobalt(II)phthalocyanine PVC based membrane sensor have been described [28]. Potentiometric response of metal phthalocyanine-doped membrane sensors for some anions is believed to be due to coordination of the analyte anion as an axial ligand, to the metal center of the carrier molecule [29]. The literature is also scanty about the use of these compounds for spectrophotometric measurements due to their poor solubility in aqueous solutions.

In this study, new simple, selective and sensitive potentiometric and spectrophotometric methods for determining sodium dodecylsulfate (SDS) are described based on the use of cobalt(II) phthalocyanine [Co(II)Pc] as a molecular recognition reagent. A poly(vinyl chloride) matrix membrane sensor for batch and flow injection analysis (FIA) of anionic surfactants is described. The sensor has the advantages of fast response, reasonable selectivity, low detection limit, long life span and a wide pH working range. The use of [Co(II)Pc] as a chromogenic reagent offers a simple non-extraction procedure for batch and continuous monitoring of anionic surfactants with high accuracy, selectivity and sensitivity. Both the potentiometric and spectrophotometric methods are validated and satisfactorily used for the quality control assessment of anionic surfactants in some commercial detergent products.

## 2. Experimental

### 2.1. Reagents

All reagents were of analytical grade quality and used as received without further purification. Deionized doubly distilled water was used throughout. Cobalt(II) phthalocyanine [Co(II)Pc], tetrahydrofuran (THF), and high molecular weight poly(vinyl chloride) powder (PVC) were obtained from Aldrich Chemical Co. (Milwaukee, WI, USA). Dioctylsebacate (DOS), *o*-nitrophenyloctyl ether (*o*-NPOE) and a certified reference sample of sodium dodecylsulfate, SDS (BioUltra) were obtained from Fluka (Ronkonkoma, NY). Commercial detergent samples were obtained from the local market.

### 2.2. Equipment

All potentiometric measurements were conducted at  $25 \pm 1$  °C with an Orion digital pH/mV meter (Model SA 720) using cobalt(II)phthalocyanine based PVC membrane sensor in conjunction with an Orion Ag/AgCl double-junction reference electrode (Model 90-02) containing 10% (w/v) potassium nitrate in the outer compartment. Combination Ross glass electrode (Model 81-02) was used for all pH measurements. All spectrophotometric measurements were carried out at 658 nm with a double beam Shimadzu spectrophotometer (Mv model 1601) using 1.00 cm quartz cuvettes.

A single-stream flow injection (FI) system [21] consisting of a Monostat cassette pump (Junior, NY) and an Omnifit injection valve (Omnifit Cambridge, UK) with a 100  $\mu$ L sample loop was used. Slight pulsation, originating from the peristaltic pump, was avoided by grounding connection. The potentiometric and spectrophotometric signals were monitored using a home made high-impedance data acquisition 8-channel box connected to a PC through the interface ADC 16 (Pico Tech., UK) and PicoLog for windows (version 5.07) software.

### 2.3. Membrane preparation and sensor construction

A mixture of PVC (66 mg), DOS or *o*-NPOE plasticizer (131 mg) and Co(II) phthalocyanine (3 mg) was thoroughly mixed and dissolved in  $\sim 5$  mL of THF. The membrane cocktail was poured into a glass cup (30 mm i.d.), covered with a filter paper, left to stand over night at room temperature until complete evaporation of THF and formation of a thin PVC membrane. A membrane disk of  $\sim 9$  mm diameter was sectioned with a cork borer and glued to a piece of Tygon tube (5 mm i.d., 9 mm o.d.) using THF. The tube was attached to the electrode glass body as previously described [30,31]. A mixture of an equal volume of  $1.0 \times 10^{-3}$  mol L<sup>-1</sup> KCl and  $1.0 \times 10^{-3}$  mol L<sup>-1</sup> SDS solutions was used as an internal filling solution. An Ag/AgCl electrode ( $\sim 0.5$  mm diameter) was used as internal reference electrode. The sensor was conditioned before use by soaking in  $1.0 \times 10^{-4}$  mol L<sup>-1</sup> SDS for 24 h and stored in the same solution when not in use. The sensor potential was measured against an external Ag/AgCl double-junction reference electrode (Orion 90-02).

A laboratory-made flow-through tubular potentiometric cell detector, equipped with a [Co(II)Pc] PVC membrane was fabricated as described previously [21]. A coating THF solution containing PVC/*o*-NPOE/[Co(II)Pc] in the ratio of 33:65.5:1.5 wt%, respectively, was deposited 3–4 times directly in a hole wall of a Tygon tube window (1 cm length, 2 mm width) using a dropper. After each addition, the THF was allowed to evaporate slowly at room temperature to give a thin film of  $\sim 0.1$  mm thickness. The sensor was conditioned by soaking for 24 h in a  $1.0 \times 10^{-3}$  mol L<sup>-1</sup> solution of SDS and closed fitted in the FIA setup tubing at a distance of 5 cm from the injection valve. The end of the tube was placed in a Petri dish with an Orion (model 90-02) double-junction Ag/AgCl reference electrode. The cell was incorporated in the flow injection setup.

### 2.4. Sensor and detector calibration

Calibration of SDS based membrane sensor under a batch mode of operation was made by immersing the sensor in conjunction with an Orion Ag/AgCl double-junction reference electrode into a 20 mL beaker containing 10 mL of  $1.0 \times 10^{-3}$  mol L<sup>-1</sup> phosphate buffer of pH 7 background. Aliquots (100  $\mu$ L) of  $1.0 \times 10^{-7}$  to  $1.0 \times 10^{-2}$  mol L<sup>-1</sup> standard SDS solutions were successively added and the potential change after each addition was recorded. A calibration curve was constructed by plotting potential reading changes against logarithm [SDS] concentrations. The calibration plot was used for all subsequent batch potentiometric measurements of unknown concentrations of anionic surfactants under the same conditions.

Calibration of SDS tubular flow-through cell detector was made at  $25 \pm 1$  °C by pumping a stream of a  $1.0 \times 10^{-3}$  mol L<sup>-1</sup> phosphate buffer of pH 7 in the flow injection setup at a flow rate of 3.5 mL min<sup>-1</sup> by means of a peristaltic pump and Tygon tubing (0.8 mm i.d.). The length of the tube between the injection valve and detector was 10 cm in the form of a mixing coil. After a steady-state baseline stabilization within  $\pm 0.2$  mV, successive 100  $\mu$ L aliquots of standard  $1.0 \times 10^{-6}$  to  $1.0 \times 10^{-2}$  mol L<sup>-1</sup> SDS were injected in the carrier stream. The potential signals were recorded at least 3 times for each concentration using a home made high-impedance data acquisition computer system. The average peak height was plotted against SDS concentration and the calibration plot was used for all subsequent flow injection measurements of unknown test solutions.

### 2.5. Sensor selectivity

The potentiometric selectivity coefficients ( $K_{\text{SDS,B}}^{\text{Pot}}$ ) of [Co(II)Pc] based membrane sensor were measured using the separate solu-

tions (SSM) method [32,33]. Potential responses of two separate solutions, one containing  $1.0 \times 10^{-3} \text{ mol L}^{-1}$  SDS ion (A) and the other containing  $1.0 \times 10^{-3} \text{ mol L}^{-1}$  of the interfering ion (B) in  $1.0 \times 10^{-3} \text{ mol L}^{-1}$  phosphate buffer background of pH 7 were measured. Selectivity data were obtained using the equation:

$$\log K_{A,B}^{\text{Pot}} = \frac{E_B - E_A}{S} + \frac{1 - Z_A}{Z_B} \log a_A \quad (1)$$

where  $K_{A,B}^{\text{Pot}}$  is the potentiometric selectivity coefficient,  $S$  is the slope of the calibration plot,  $a_A$  is the activity or concentration of SDS and  $Z_A$  and  $Z_B$  are the charges of SDS and the interfering anions, respectively.

### 2.6. Spectrophotometric determination of anionic surfactants

For batch analysis, 2.5 mL aliquots of  $0.1 \text{ mg mL}^{-1}$  [Co(II)Pc] in DMSO solution were added to a series of 5-mL calibrated flasks containing 10–500  $\mu\text{L}$  of  $1.0 \times 10^{-3} \text{ mol L}^{-1}$  SDS (the final concentrations were 0.6–28.8  $\mu\text{g mL}^{-1}$ ). The mixtures were thoroughly mixed and the absorbances were measured at 658 nm using 1.00 cm quartz cuvettes. A blank experiment was carried out under identical conditions and the absorbance difference vs [SDS] concentration plot was made and used for all subsequent batch assay of SDS. Higher [SDS] concentrations (up to 200  $\mu\text{g mL}^{-1}$ ) can be measured by increasing the reagent concentration (ca.  $1.0 \text{ mg mL}^{-1}$ ).

For flow injection analysis, a stream of  $0.1 \text{ mg mL}^{-1}$  [Co(II)Pc] in DMSO reagent was pumped through the flow injection system. Calibrants ( $1.0$ – $20.0 \mu\text{g mL}^{-1}$ ) and unknown test solutions of SDS were injected (in triplicates) using a 100  $\mu\text{L}$  injector loop and allowed to mix at room temperature in a 10 cm long mixing coil. The absorbance of the developed color was continuously recorded at a wavelength of 658 nm. A calibration plot connecting the decrease in the absorption peak height as a function of [SDS] concentration was constructed and used for measurement of unknown test samples.

### 2.7. Determination of some commercial detergent products

A 1.00 g portion of the detergent powder or a 1.00 mL aliquot of the liquid detergent was accurately weighed, transferred to a 100-mL calibrated flask, completed to the mark with deionized water and shaken well. A test solution was prepared by transferring a 1.0-mL aliquot of the clear supernatant to a 100-mL calibrated flask, diluted to the mark with  $1.0 \times 10^{-3} \text{ mol L}^{-1}$  phosphate buffer of pH 7 and shaken well. The batch and FIA potentiometric and spectrophotometric procedures described above were followed for determination of anionic surfactants in some commercial products.

## 3. Results and discussion

Metallophthalocyanines are strong ligands for many anions with a good discriminating ability due to the specific anion axial ligation reactions with the central metal ion of the reagents. In the present study, the interaction of cobalt(II) phthalocyanine

[Co(III)Pc] reagent with anionic surfactants was spectrophotometrically examined. Since [Co(II)Pc] is poorly soluble in aqueous media, the measurements were conducted in dimethylsulfoxide (DMSO) solution. The absorption spectrum of [Co(II)Pc] displays two peak maxima at 658 ( $\epsilon = 3.9 \times 10^3 \text{ L mol}^{-1} \text{ cm}^{-1}$ ) and 598 nm ( $\epsilon = 1.2 \times 10^3 \text{ L mol}^{-1} \text{ cm}^{-1}$ ) due to monomer and dimer species, respectively. Upon addition of sodium dodecylsulfate surfactant (SDS), a significant hypochromic shift of both absorption peaks takes place probably due to the formation of an aggregate complex between (SDS) and [Co(II)Pc]. Similar behavior has been previously reported by reaction of some surfactants with metal porphyrins [34]. It has been also reported that anionic detergents at concentration levels below the critical micellization, linearly decrease the absorption intensity of cationic dyes due to the formation of dye–detergent aggregates [35,36]. The strong and fast binding of [Co(II)Pc] with (SDS) suggests the use of this system for batch and flow injection potentiometric and spectrophotometric determination of anionic surfactants.

### 3.1. Potentiometric measurements

#### 3.1.1. Sensor characteristics

Four SDS sensors with polymeric membranes consisting of 1–5 wt% [Co(II)Pc], 60–65 wt% DOS or *o*-NOPE plasticizer and 30–35 wt% PVC, were prepared and electrochemically evaluated according to IUPAC recommendations [32]. The optimum response characteristics are obtained with a membrane incorporating 1.5 wt% [Co(II)Pc], 65.5 wt% *o*-NOPE and 33 wt% PVC (Table 1). Calibration plots, made in  $1.0 \times 10^{-3} \text{ mol L}^{-1}$  phosphate buffer of pH 7 background, for sensors with membranes plasticized with DOP ( $\epsilon = 3.9$ ) and *o*-NPOE ( $\epsilon = 24$ ) are shown in Fig. 1. Results from three replicate studies on each sensor indicate sub-, and near-Nernstian slopes of  $-37.5$  and  $-56.5 \text{ mV decade}^{-1}$ , linear response range of  $6.3 \times 10^{-4}$  to  $3.2 \times 10^{-6}$  and  $7.8 \times 10^{-4}$  to  $8.0 \times 10^{-7} \text{ mol L}^{-1}$  and lower detection limits of  $1.9 \times 10^{-6}$  and  $2.5 \times 10^{-7} \text{ mol L}^{-1}$  SDS with membrane sensors incorporating DOS and *o*-NPOE plasticizers, respectively. The lower limit of detection is defined as the concentration of [SDS] corresponding to the intersection of the extrapolated linear segments of calibration graphs. Measurements of SDS at concentration levels  $>10^{-3} \text{ mol L}^{-1}$  are not possible due to the formation of critical micelle (CMC). The critical micelle concentration of SDS in water is  $1.6 \times 10^{-3} \text{ mol L}^{-1}$  [37]. A membrane sensor plasticized with *o*-NPOE gives more favorable performance characteristics. It reaches  $\sim 95\%$  of its equilibrium potential response within 20 s, and its lifetime is at least 2 months. During this period, the variation in the calibration slope does not exceed  $\pm 3 \text{ mV decade}^{-1}$ . After 2 months, the calibration slope starts to deteriorate rapidly. This sensor was used for all subsequent investigation.

The operative response mechanism of the sensor can be explained on the basis of an axial ligation of the central cobalt atom of [Co(II)Pc] by sodium dodecylsulfate (SDS) with the

**Table 1**  
Performance characteristics of batch wise and flow injection potentiometric measurements of SDS using [Co(II)Pc] as a membrane sensing material.

Parameter	Batch	FIA
Slope ( $\text{mV decade}^{-1}$ )	$-56.5$	$-51.1$
Correlation coefficient ( $r^2$ )	0.9972	0.9977
Linear range ( $\text{mol L}^{-1}$ )	$8.0 \times 10^{-7}$ to $7.9 \times 10^{-4}$	$1.0 \times 10^{-6}$ to $1.0 \times 10^{-3}$
Detection limit ( $\text{mol L}^{-1}$ )	$2.5 \times 10^{-7}$	$5.6 \times 10^{-7}$
Working range (pH)	2–7	2–7
Response time for $10^{-4} \text{ mol L}^{-1}$ (s)	$\leq 30$	$< 90$
Within-day-reproducibility (mV)	0.4	0.7
Between-day-variability (mV)	0.7	0.9
Accuracy (%)	98.7	97.9
Relative standard deviation (%)	0.4	0.7

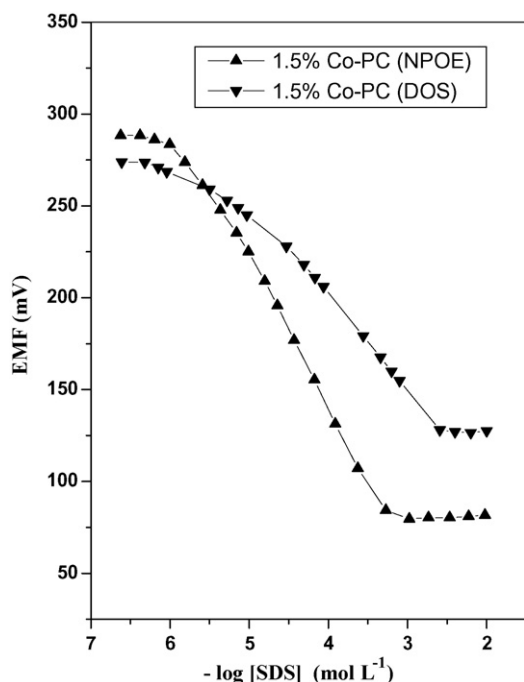


Fig. 1. Calibration of [SDS] PVC membrane sensors using cobalt phthalocyanine as ionophore and NPOE and DOS plasticizers.

formation of an aggregate at the organic membrane/aqueous sample interface. Although [Co(II)Pc] exists in monomer/dimer equilibrium [38], both forms have axial coordination sites available for interaction with SDS anion and induce potential response.

### 3.1.2. Effect of pH

The influence of pH on the potentiometric response of [Co(II)Pc] based membrane sensor was tested with  $1.0 \times 10^{-4}$  and  $1.0 \times 10^{-3}$  mol L<sup>-1</sup> SDS solutions over a pH range 2–10. The sensor shows practically no significant potential dependence over the pH range 2–7 (Fig. 2). This observation was further confirmed by calibration of the sensor with  $1.0 \times 10^{-2}$  to  $1.0 \times 10^{-6}$  mol L<sup>-1</sup> SDS solutions using  $1.0 \times 10^{-3}$  mol L<sup>-1</sup> phthalate buffer of pH 5, and  $1.0 \times 10^{-3}$  mol L<sup>-1</sup> phosphate buffer of pH 7 as backgrounds. The calibration plots obtained are almost identical in terms of slope, detection limit and linear response range. All subsequent measure-

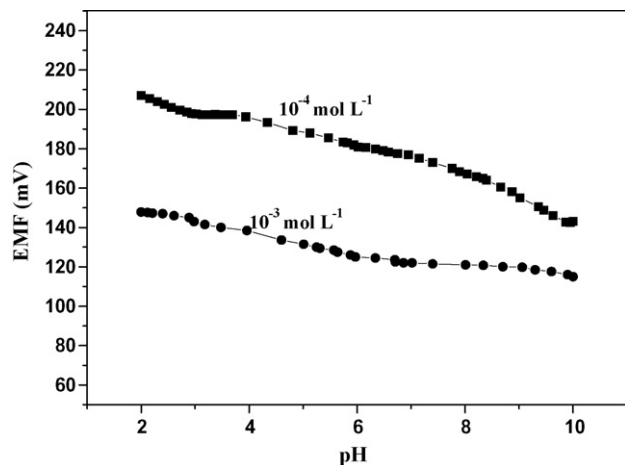


Fig. 2. Effect of pH on the response of [SDS] PVC membrane sensor based on cobalt phthalocyanine ionophore and NPOE plasticizer.

Table 2

Potentiometric selectivity coefficients and spectrophotometric tolerance of some interfering ions using [Co(II)Pc] as a membrane sensing material and chromogenic reagent.

Interferent (B)	Potentiometry selectivity coefficient $[K_{SDS,B}^{Pot}]$	Spectrophotometry, w/w tolerance ratio $[B]/[SDS]$
Cl <sup>-</sup>	$6.8 \times 10^{-4}$	425
I <sup>-</sup>	$2.6 \times 10^{-3}$	30
F <sup>-</sup>	$8.2 \times 10^{-4}$	520
SO <sub>4</sub> <sup>2-</sup>	$7.9 \times 10^{-3}$	410
SO <sub>3</sub> <sup>2-</sup>	$7.4 \times 10^{-3}$	8
PO <sub>4</sub> <sup>3-</sup>	$4.2 \times 10^{-4}$	420
SCN <sup>-</sup>	$2.2 \times 10^{-3}$	55
NO <sub>2</sub> <sup>-</sup>	$1.2 \times 10^{-3}$	320
NO <sub>3</sub> <sup>-</sup>	$1.0 \times 10^{-3}$	300
CO <sub>3</sub> <sup>2-</sup>	$5.0 \times 10^{-3}$	350
ClO <sub>4</sub> <sup>-</sup>	$7.9 \times 10^{-3}$	350
Citrate <sup>3-</sup>	$1.3 \times 10^{-3}$	380
Acetate <sup>-</sup>	$8.6 \times 10^{-3}$	435
Oxalate <sup>2-</sup>	$7.7 \times 10^{-4}$	365

ments were made in  $1.0 \times 10^{-3}$  mol L<sup>-1</sup> phosphate buffer of pH 7 as a background.

### 3.1.3. Sensor selectivity

Potentiometric selectivity coefficients ( $K_{SDS,B}^{Pot}$ ) of [Co(II)Pc] based membrane sensor were determined using the separate solutions method [SSM] at a fixed concentration of [SDS] species as a primary analyte ion in one run and the interfering species (B) in a separate run [32,33]. As can be seen in Table 2, the sensor exhibits a high selectivity towards [SDS] over many common anions. The selectivity order is: SDS<sup>-</sup> > acetate<sup>-</sup> > SO<sub>4</sub><sup>2-</sup> = ClO<sub>4</sub><sup>-</sup> > SO<sub>3</sub><sup>2-</sup> > CO<sub>3</sub><sup>2-</sup> > I<sup>-</sup> > SCN<sup>-</sup> > citrate<sup>3-</sup> > NO<sub>2</sub><sup>-</sup> > NO<sub>3</sub><sup>-</sup> > F<sup>-</sup> > oxalate<sup>2-</sup> > Cl<sup>-</sup> > PO<sub>4</sub><sup>3-</sup>. This sequence significantly differs from the hydrophobicity-based Hofmeister series (ClO<sub>4</sub><sup>-</sup> > SCN<sup>-</sup> > I<sup>-</sup> > NO<sub>3</sub><sup>-</sup> > Br<sup>-</sup> > Cl<sup>-</sup> > HCO<sub>3</sub><sup>-</sup> > CH<sub>3</sub>COO<sup>-</sup> > SO<sub>4</sub><sup>2-</sup> > HPO<sub>4</sub><sup>2-</sup>) commonly observed with ion exchanger based membrane sensors and supporting a neutral or charged carrier sensing mechanism with the present ionophore.

It has been reported that the classical ion exchanger based membrane sensors display Hofmeister selectivity order, influenced by the hydration energy or hydrophilicity of the analyte anions [39]. In this case, the electrostatic interaction plays the dominant role for the transfer of the anion across the organic/water interface and inducing the potential response. However, the potentiometric response of metallophthalocyanine-doped membrane sensors is believed to be based on the coordination of the analyte anion as an axial ligand to the central metal of the carrier molecule with little influence from anion hydration energy. Variation of coordination affinity of the various anions to the central metal of the complex strongly influences the potentiometric selectivity and alters the Hofmeister selectivity sequence of the classical liquid membrane sensors [39].

### 3.1.4. Batch and flow injection potentiometric determination of anionic surfactants

The potentiometric assay method of SDS was validated by determining the performance characteristics of the procedure using the quality control-quality assurance standards [40]. Five batches (six determinations each) of internal quality control SDS samples prepared from a certified reference material (CRM) and covering the concentration range  $1.0 \times 10^{-7}$  to  $1.0 \times 10^{-3}$  mol L<sup>-1</sup> SDS were used. The accuracy (trueness) and precision (relative standard deviation) were calculated according to Eqs. (2) and (3):

$$\text{Accuracy, \%} = \frac{X'}{\mu} \times 100 \quad (2)$$



$$\text{Precision, \%} = \frac{SD}{\bar{X}'} \times 100 \quad (3)$$

where  $\bar{X}'$ ,  $\mu$  and SD are the mean of concentration found, reference value, and standard deviation, respectively. Linear measurement range (R), lower detection limit (LOD), within-day-repeatability ( $CV_w$ ) and between-day-variability ( $CV_b$ ) were also evaluated. The results obtained are presented in Table 1. A statistical evaluation of the results indicates that the student's test ( $t$ ) at 95% confidence level shows no statistical difference between the theoretically tabulated ( $t=2.015$ ) and the practically obtained values ( $t=0.955$ ).

A tubular-type detector incorporating [Co(II)Pc] based membrane sensor was used under a hydrodynamic mode of operation for continuous SDS quantification. Factors affecting signal shape and intensity such as flow rate, injection volume and tubing diameter were optimized using a  $1.0 \times 10^{-3} \text{ mol L}^{-1}$  phosphate buffer solution of pH 7 as a carrier stream. The effects of sample injection volume (20–700  $\mu\text{L}$ ), carrier flow rate (0.2–4.5  $\text{mL min}^{-1}$ ) and tubing diameter (0.5–3.5 mm) were examined. High sample volume shows high peak height, long residence time, and long recovery time and low sample throughput. With a constant injection volume, the residence time of the sample is inversely proportional to the flow rate. As the carrier flow rate increases, the response peak becomes higher and narrower, thus resulting in an increase of the sampling frequency. Optimum performance is achieved under the conditions: flow rate: 3.5  $\text{mL min}^{-1}$ , tubing internal diameter: 2 mm, injector/detector distance: 10 cm and injection volume: 100  $\mu\text{L}$ . These conditions provide about 96–98% of the maximum peak height and compromise between sensitivity, sample rate and linear operational range.

Under the above optimum conditions, the residence time ( $T$ ) (i.e., the time span from injection until the appearance of maximum signal) ranges from 11 s for  $1.0 \times 10^{-6} \text{ mol L}^{-1}$  to 28 s for  $1.0 \times 10^{-3} \text{ mol L}^{-1}$  SDS solution. The period elapsed from injection time to the start of the signal (travel time  $t_a$ ) is 4–15 s. As SDS concentration increases, the response time increases. The period between the appearance of the maximum signal and the return to the baseline (return time,  $t$ ) is 14–35 s. Baseline-to-baseline time ( $\Delta t$ ) defined as the interval between the start of the signal and its return to the baseline is 25–60 s. These data reveal that the proposed SDS detector provides a low dead volume, fast response time, reasonable washout characteristic, and possible measurement of 25–30 samples  $\text{h}^{-1}$ .

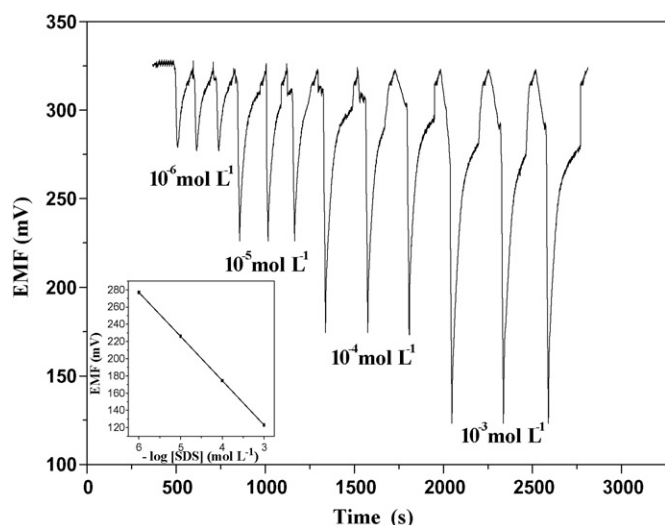


Fig. 3. Potentiometric flow injection signals of [SDS] standard solutions using cobalt phthalocyanine based membrane sensor.

It can be seen that the profile of the signals is not symmetrical, probably due to a convection diffusion mode of the flow system [41], besides a relatively slow washout of the detergent from the detector membrane. A linear relationship between SDS concentration and FIA signal intensity is obtained over the range  $1.0 \times 10^{-6}$  to  $1.0 \times 10^{-3} \text{ mol L}^{-1}$  (Fig. 3) with a calibration slope of  $-51.1 \text{ mV decade}^{-1}$ . The relative standard deviations of the FIA potential signals are 1–2% for SDS samples containing  $3.5 \times 10^{-5}$  to  $3.5 \times 10^{-4} \text{ mol L}^{-1}$  and 2.4% for the entire concentration range ( $3.5 \times 10^{-3}$  to  $3.5 \times 10^{-6} \text{ mol L}^{-1}$ ).

### 3.1.5. Method advantages

Some significant advantages are offered by the proposed SDS potentiometric sensor over many of the previously described potentiometric methods. The lower detection limit and/or linear response range of the present method are at least one or two orders of magnitude better [16–18,20] and negligible effects (low selectivity coefficient values) are caused by  $\text{ClO}_4^-$ ,  $\text{SCN}^-$ ,  $\text{Cl}^-$  and  $\text{PO}_4^{3-}$  interferences [13,19,20].

## 3.2. Spectrophotometric measurements

### 3.2.1. Method performance

Reaction of SDS with [Co(II)Pc] reagent in DMSO is associated with a significant decrease of the reagent absorbance peak at 658 nm (Fig. 4). The effect of pH on the stability of [SDS]/[Co(II)Pc] system was examined by following the absorbance intensity at 658 nm for a series of SDS solutions containing 10  $\mu\text{mol}$  ( $\sim 3 \mu\text{g mL}^{-1}$ ). The pH of each SDS aqueous test solution was adjusted at various pH values, using hydrochloric acid and/or NaOH solutions, before treatment with the chromogen solution. The absorbance-pH profile shows a reasonable color stability of the test solutions over the pH range 2–9 (Fig. 5). Internal quality control SDS samples, prepared from certified reference material (30–60  $\mu\text{g mL}^{-1}$ ), were spiked into 10.0 mL of tap and seawater samples to evaluate the method precision and recovery using Eqs. (3) and (4), respectively.

$$\text{Recovery, \%} = \left[ \frac{(X'_s - X')}{X_{\text{added}}} \right] \times 100 \quad (4)$$

where  $X'_s$ ,  $X'$  and  $X_{\text{added}}$  are the mean result of spiked samples, mean results of unspiked samples and amount of added (spiked) reference SDS samples, respectively. The results reveal average recoveries of 99.6 and 98.4% and mean precisions of 2.3 and 1.8% ( $n=6$ ) for batch and FIA mode of operations, respectively (Table 3).

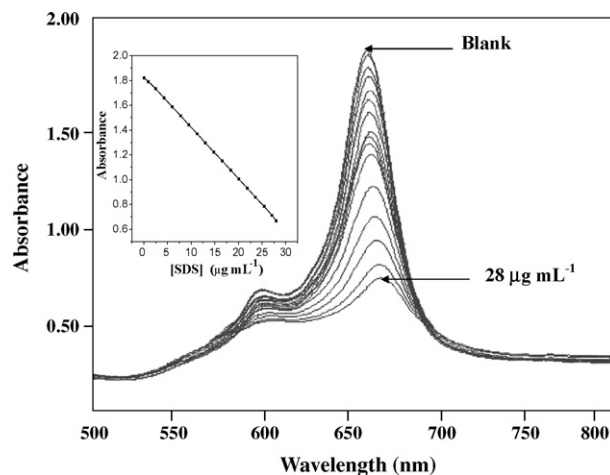


Fig. 4. Absorbance plots of different concentrations of [SDS] using cobalt phthalocyanine in DMSO as a chromogenic reagent.

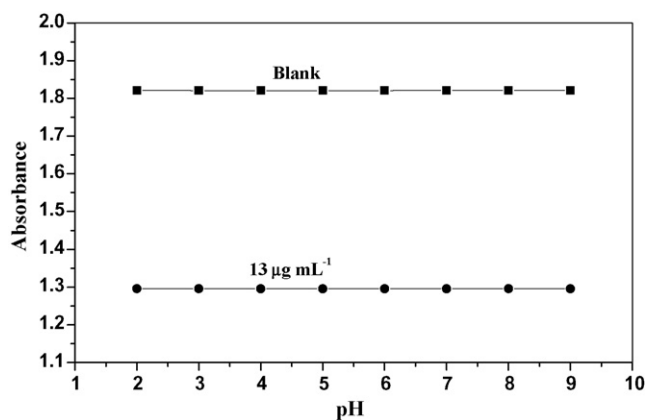


Fig. 5. Effect of pH on the absorbance of SDS/cobalt phthalocyanine reaction in DMSO.

### 3.2.2. Method selectivity

The selectivity of SDS/[Co(II)Pc] color reaction was examined, by following the absorbance response at 658 nm for a number of interfering ions with the reagent. The tolerance limits of 14 different anions, in the form of sodium or potassium salts, which commonly associated with various commercial detergent products and present in other natural matrices were evaluated. The tolerance limit was considered as the concentration of the interferent that causes a maximum of  $\pm 5\%$  deviation in the absorbance value. The results obtained (Table 2) reveal reasonable selective recognition characteristics of [Co(II)Pc] reagent for SDS. Sulfite, iodide and thiocyanate ions interfere, when present at concentration levels  $>8$ -,  $30$ - and  $55$ -fold excess, respectively, over SDS. However, these species are seldom present with SDS in real detergent samples.

### 3.2.3. Batch and flow injection spectrophotometric determination of anionic surfactants

Under batch and flow injection modes of operation, linear relationships are observed between the decrease in the absorbance of [Co(II)Pc] reagent and SDS concentration. Beer's law is obeyed over the working ranges  $2$ – $30$  and  $4$ – $60 \mu\text{g mL}^{-1}$  with average response times of  $40$  and  $60$  s under batch and FIA, respectively. The lower limit of detection was calculated according to IUPAC standards [42] using the relation:  $(\text{LOD}) = K\text{SD}/S$ , where SD is the standard deviation of the blank measurements ( $n = 6$ ),  $S$  is the slope of the calibration curve and  $K$  is a numerical factor depending on the degree of confidence level needed. With  $K = 3$  (i.e.,  $3$  SD), the detection limits are  $1$  and  $2 \mu\text{g mL}^{-1}$  for batch and FIA spectrophotometric measurements of SDS, respectively. Fig. 6 shows representative flow injection traces of  $10$ – $17 \mu\text{g mL}^{-1}$  SDS. The response time ( $t_a$ ) and baseline-to-baseline time ( $\Delta t$ ) over this range are  $12$ – $70$  and  $50$ – $230$  s, respectively. The signal shape displayed by the spectrophotometric and potentiometric detectors is almost similar.

Table 3

Performance characteristics of batch wise and flow injection spectrophotometric measurements of SDS using [Co(II)Pc] as a chromogenic reagent.

Parameter	Batch*	FIA*
Linear response range ( $\mu\text{g mL}^{-1}$ )	2–30	4–60
Lower limit of detection ( $\mu\text{g mL}^{-1}$ )	1	2
Response time for $10 \mu\text{g mL}^{-1}$ (s)	40	60
Precision (%)	2.3	1.8
Relative standard deviation (%)	0.7	1.1
Accuracy (%)	98.8	97.6
Between-day-variability (mV)	0.9	1.4
Within-day-reproducibility (mV)	0.8	1.2

\* Average of 6 measurements.

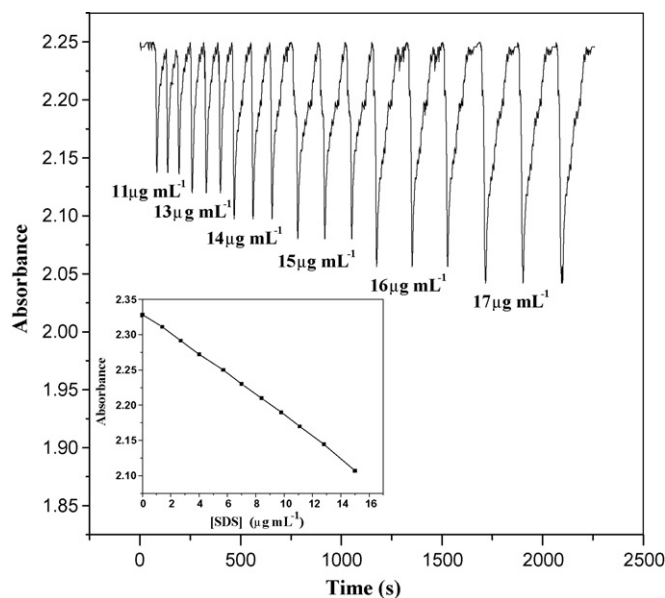


Fig. 6. Spectrophotometric flow injection signals of [SDS] standard solution using cobalt phthalocyanine in DMSO as a chromogenic reagent.

### 3.2.4. Method advantages

Many of the previously described spectrophotometric methods exhibit some significant drawbacks upon comparison with the proposed method. These are, the limited applications to acidic surfactant test solutions [3,8,10], the use of multiple stream flow injection setup [6,9], the need for special FIA instrumentation [2,4–6,8], and the time-consuming extraction procedure [2,3,6,8,10]. The present method, however, is used over a wider pH range of the test solutions (pH 3–8), requires a simple single-stream flow injection setup and involves a simple homogenous (non-extraction) procedure. On the other hand, a comparison of the performances of the proposed potentiometric and spectrophotometric methods reveals that the former method covers a wider range of SDS concentration, offers a lower detection limit, and is less affected by most common interfering ions.

### 3.3. Potentiometric and spectrophotometric determination of anionic surfactants in commercial products

Anionic surfactants in some commercial detergent samples (clothes washing powders and dish washing liquids) were potentiometrically and spectrophotometrically determined under batch and flow injection modes. Sample test solutions containing  $1.0 \text{ g L}^{-1}$  or  $1.0 \text{ mL}^{-1}$  of the powder and liquid formulations were prepared in  $1.0 \times 10^{-3} \text{ mol L}^{-1}$  phosphate buffer of pH 7 and directly measured by batch and flow injection potentiometry. Measurements were also conducted by batch and flow injection spectrophotometry after further dilution of the test solutions. The results obtained are recorded in Table 4 and compared with data obtained using the standard spectrophotometric methylene blue method [1]. The potentiometric data compare fairly well with the results of both the proposed and standard methylene blue spectrophotometric methods. The standard spectrophotometric method, however, involves time-consuming extraction step with a hazardous solvent and suffers from interferences by carboxylate, sulfonate and phenolate compounds [1]. An  $F$ -test shows no significant difference at 95% confidence level between means and variances of the potentiometric and spectrophotometric sets of results. The calculated  $F$ -values ( $n = 6$ ) are in the range  $1.1$ – $3.9$  compared with the theoretically tabulated value ( $6.39$ ).

**Table 4**

Batch and flow injection potentiometric and spectrophotometric determination of anionic surfactants in some commercial detergents ( $\text{mg g}^{-1}$ ) using [Co(II)Pc] as a membrane sensing material and chromogenic reagent, respectively.

Sample trade name and source	Potentiometry*		Spectrophotometry*		Standard spectrophotometry* [1]
	FIA	Batch	FIA	Batch	
General (Henkel)	293 ± 2.0	297 ± 2.1	294 ± 4.1	295 ± 6.1	291 ± 4.8
Lang (Henkel)	274 ± 4.4	281 ± 3.4	275 ± 5.3	277 ± 4.2	276 ± 4.3
Ariel (Procter & Gamble)	260 ± 3.1	262 ± 4.2	260 ± 4.2	264 ± 4.4	257 ± 6.5
Omo (Lever)	255 ± 5.2	252 ± 4.3	250 ± 4.1	254 ± 6.4	248 ± 5.5
Persil (Henkel)	246 ± 2.9	241 ± 2.8	240 ± 5.2	238 ± 5.2	235 ± 6.3
Tide (Procter & Gamble)	226 ± 4.2	231 ± 3.3	232 ± 4.2	230 ± 5.3	229 ± 4.9

\* Average of 6 measurements.

#### 4. Conclusions

A PVC membrane sensor with [Co(II)Pc] as an ionophore and *o*-NPOE as a plasticizer is described for direct potentiometric determination of anionic surfactants (e.g., sodium dodecylsulfate, SDS). Under batch mode of operation, the working response range is  $8.0 \times 10^{-7}$  to  $7.8 \times 10^{-4}$   $\text{mol L}^{-1}$  SDS over the pH range 4–7 with anionic slope of  $-56.5$   $\text{mV decade}^{-1}$  and lower detection limit of  $2.5 \times 10^{-7}$   $\text{mol L}^{-1}$ . Under flow injection mode of analysis, the linear response range, lower limit of detection and calibration slope are  $1.0 \times 10^{-3}$  to  $1.0 \times 10^{-6}$   $\text{mol L}^{-1}$ ,  $5.6 \times 10^{-7}$   $\text{mol L}^{-1}$  and  $-51.1$   $\text{mV decade}^{-1}$ , respectively. [Co(II)Pc] in DMSO displays an absorption maximum at 658 nm linearly decreases with the increase of SDS concentration over the ranges 2–30 and 2–20  $\mu\text{g mL}^{-1}$  for batch and flow injection analysis, respectively. Both the potentiometric and spectrophotometric techniques are satisfactorily used for determination of SDS in commercial detergent products with negligible interferences from most common associated substances.

#### References

- [1] A.E. Greenberg, L.S. Clesceri, A.D. Eaton, Standard Methods for the Examination of Water and Wastewater, 18th ed., American Public Health Association, Washington, DC, 1992, pp. 5–36.
- [2] Y. Hirai, K. Tomokuni, Anal. Chim. Acta 167 (1985) 409.
- [3] K. Yamamoto, S. Motomizu, Analyst 112 (1987) 1405.
- [4] T. Sakai, H. Harada, X. Liu, N. Ura, K. Takeyoshi, K. Sugimoto, Talanta 45 (1998) 543.
- [5] Q. He, H. Chen, Fresenius J. Anal. Chem. 367 (2000) 270.
- [6] S. Motomizu, Y. Hazaki, M. Oshima, K. Tōei, Anal. Sci. 3 (1987) 265.
- [7] Y. Shimoishi, H. Miyata, Fresenius J. Anal. Chem. 338 (1990) 46.
- [8] H. Kubota, M. Katsuki, S. Motomizu, Anal. Sci. 6 (1990) 705.
- [9] Y. Shimoishi, H. Miyata, Fresenius J. Anal. Chem. 345 (1993) 456.
- [10] I. Kasahara, K. Hashimoto, T. Kawabe, A. Kunita, K. Magawa, N. Hata, S. Taguchi, K. Goto, Analyst 120 (1995) 1803.
- [11] D.C. Cullum, Introduction to Surfactant Analysis, Blackie, London, 1994.
- [12] S. Alegret, J. Alonso, J. Bartrolí, J. Baró-Romà, J. Sánchez, M. del Valle, Analyst 119 (1994) 2319.
- [13] W. Szczepaniak, Analyst 115 (1990) 1451.
- [14] C. Gavach, C. Bertrand, Anal. Chim. Acta 55 (1971) 385.
- [15] C. Gavach, P. Seta, Anal. Chim. Acta 407 (1970) 50.
- [16] H. Fukui, A. Kaminaga, T. Maeda, K. Hayakawa, Anal. Chim. Acta 481 (2003) 221.
- [17] N. Alizadeh, H. Khodaei-Tazekendi, Sens. Actuators B 75 (2001) 5.
- [18] B. Kovács, B. Csóka, G. Nagy, A. Ivaska, Anal. Chim. Acta 437 (2001) 67.
- [19] M.J. Seguí, J.L. Sabater, R.M. Mániz, T. Pardo, F. Sancenón, J. Soto, Anal. Chim. Acta 525 (2004) 83.
- [20] J. Alonso, J. Baró, J. Bartrolí, J. Sánchez, M. del Valle, Anal. Chim. Acta 308 (1995) 115.
- [21] S.S.M. Hassan, I.H.A. Badr, H.S.M. Abd-Rabboh, Mikrochim. Acta 144 (2004) 263.
- [22] S. Martínez-Barrachina, J. Alonso, L. Matia, R. Prats, M. delValle, Anal. Chem. 71 (1999) 3684.
- [23] J. Li, X. Wu, R. Yuan, H. Lin, R. Yu, Analyst 119 (1994) 1363.
- [24] J. Li, X. Pang, D. Gao, R. Yu, Talanta 42 (1995) 1775.
- [25] S.S.M. Hassan, W.H. Mahmoud, M.A.F. Elmosallamy, M.H. Almarzooqi, J. Pharm. Biomed. Anal. 39 (2005) 315.
- [26] M.R. Ganjali, M.R. Pourjavid, M. Shamsipur, T. Poursaeri, M. Rezapour, M. Javanbakht, H. Sharghi, Anal. Sci. 19 (2003) 995.
- [27] J.R. Allen, A. Florido, S.D. Young, S. Daunert, L.G. Bachas, Electroanalysis 7 (1995) 710.
- [28] S.S.M. Hassan, A.E. Kelany, S.S. Al-Mehrezi, Electroanalysis 20 (2008) 438.
- [29] S. Shahrokian, M. Amimi, S. Solagr, S. Tangestaninejad, Microchem. J. 63 (1999) 3.
- [30] S.S.M. Hassan, F.M. Elzawawy, S.A.M. Marzouk, E.M. Elnemma, Analyst 117 (1992) 1683.
- [31] S.S.M. Hassan, S.A.M. Marzouk, Talanta 41 (1994) 891.
- [32] IUPAC Analytical Chemistry Division, Commission on Analytical Nomenclature, J. Pure Appl. Chem. 72 (2000) 1851.
- [33] T.S. Ma, S.S.M. Hassan, Organic Analysis Using Ion Selective Electrodes, vols. 1, 2, Academic Press, London, 1982.
- [34] S.C.M. Gandinia, V.E. Yushmanov, M. Tabaka, J. Inorg. Biochem. 85 (2001) 263.
- [35] H. Sato, M. Kawasaki, K. Kasatani, N. Nakashima, K. Yoshihara, Bull. Chem. Soc. Jpn. 56 (1983) 3588.
- [36] M. Oshima, S. Motomizu, H. Doi, Analyst 117 (1992) 1643.
- [37] K.G. Furton, A. Norelus, J. Chem. Educ. 70 (1993) 254.
- [38] V.N. Nemykin, V.Ya. Chernil, S.V. Volkov, N.I. Bundina, O.L. Kaliya, V.D. Li, E.A. Lukyanets, J. Porphyrins Phthalocyanines 3 (1999) 87.
- [39] E. Bakker, E. Malinowska, R.D. Schiller, M.E. Meyerhoff, Talanta 41 (1994) 881.
- [40] J.K. Taylor, Quality Assurance of Chemical Measurements, CRC Press, Boca Raton, 1987.
- [41] M. Valcarcel, M.D. Luque de Castro, Flow-Injection Analysis, Principles and Applications, Ellis Horwood, Chichester, England, 1987.
- [42] H.M.N.H. Irving, H. Freiser, T.-S. West (Eds.), IUPAC Compendium of Analytical Nomenclature, Definitive Rules, Pergamon Press, Oxford, 1981.



# Determination of ultra trace amount of enrofloxacin by adsorptive cathodic stripping voltammetry using copper(II) as an intermediate

Ali A. Ensaifi\*, T. Khayamian, M. Taei

Department of Chemistry, Isfahan University of Technology, Isfahan 84156-83111, Iran

## ARTICLE INFO

### Article history:

Received 11 December 2008

Accepted 3 January 2009

Available online 20 January 2009

### Keywords:

Enrofloxacin

Support vector machine

Copper(II)

Adsorptive cathodic voltammetry

## ABSTRACT

In this work, a simple and sensitive electroanalytical method was developed for the determination of enrofloxacin (ENRO) by adsorptive cathodic stripping voltammetry (ADSV) using Cu(II) as a suitable probe. The complex of copper(II) with ENRO was accumulated at the surface of a hanging mercury drop electrode at  $-0.10$  V for 40 s. Then, the preconcentrated complex was reduced and the peak current was measured using square wave voltammetry (SWV). The optimization of experimental variables was conducted by experimental design and support vector machine (SVM) modeling. The model was used to find optimized values for the factors such as pH, Cu(II) concentration and accumulation potential. Under the optimized conditions, the peak current at  $-0.30$  V is proportional to the concentration of ENRO over the range of  $10.0$ – $80.0$  nmol L<sup>-1</sup> with a detection limit of  $0.33$  nmol L<sup>-1</sup>. The influence of potential interfering substances on the determination of ENRO was examined. The method was successfully applied to determination of ENRO in plasma and pharmaceutical samples.

© 2009 Elsevier B.V. All rights reserved.

## 1. Introduction

Fluoroquinolones are an important group of synthetic antibacterial agents developed in recent years, widely used in human and veterinary medicine. These compounds are derived from nalidixic acid and anaphthridine derivative that was introduced for clinical application in livestock and farming industries usually to treat urinary pulmonary and digestive infection [1]. In recent years, the utilization of antibiotics in food producing animals has caused public concern due to the transfer of antibiotic-resistant bacteria to human beings [2,3]. This is an increasingly prominent problem, because antibiotics are used in animals to treat infections and to act as growth promoters. This fact would make the antibiotics treatment useless in common human infections. European Community has fixed a maximum residue limit in edible animal products for some quinolones, such as enrofloxacin (ENRO). The maximum residue limit values are in the range  $100$ – $300$   $\mu\text{g kg}^{-1}$  for the sum of ENRO in foodstuffs of animal origin [4]. Therefore, the development of rapid, simple, sensitive, and accurate methods for monitoring ENRO level is of increasing interest.

Current methods of the analysis of quinolones, especially ENRO, are based on liquid chromatography (mainly with fluorimetric detection) [5–9] with pre- or post-column reaction and/or using liquid chromatography/mass spectrometry [10], solid phase

separation/spectrophotometric determination [11], capillary electrophoresis [2], indirect atomic absorption spectrometry [12], and spectrophotometric detections [13,14].

Voltammetric methods may be an interesting alternative to separation techniques for the analysis of pharmaceutical samples. Electrochemical techniques have been used for determination of ENRO, particularly adsorptive cathodic stripping voltammetry (ADSV) that it is an effective technique for determination of fluoroquinolones, pharmaceuticals and biomolecules down to the nano molar levels [15–17]. The comparing of the proposed method with the other published papers is given in Table 1. Recently, an electrochemical method for the determination of ENRO in pharmaceutical formulation and dog urine was found based on adsorptive stripping voltammetry [18]. The studies have been carried out in a static mercury drop electrode with two different linear ranges of  $4$ – $25$  and  $18$ – $55$  ng mL<sup>-1</sup>, using 180 s as an accumulation time. However, the reported method has not been applied for analysis of ENRO in plasma samples due to its negative peak potential ( $-1.62$  V vs. Ag/AgCl electrode), whereas the peak potential of the proposed method is shifted to more positive value ( $-0.30$  V). This enhances the selectivity of the method relative to the cases where more negative potential is used. There is not any report for the determination of ENRO in tissue and plasma by electroanalytical techniques. Copper(II) makes complexes with divers drugs have been subject of numbers of researches [19–21], presumably due to the biological role of copper(II) and synergetic activity with the drugs.

Support vector machine (SVM) is an algorithm from the machine learning community, developed by Cortes and Vapnik and Lerner

\* Corresponding author. Tel.: +98 311 3912351; fax: +98 311 3912350.  
E-mail address: [Ensaifi@cc.iut.ac.ir](mailto:Ensaifi@cc.iut.ac.ir) (A.A. Ensaifi).

**Table 1**  
Comparison of the some recently methods in the determination of ENRO.

Methods	LOD* ( $\mu\text{g mL}^{-1}$ )	LDR** ( $\mu\text{g mL}^{-1}$ )	Interfering species	Time consuming (min)	Reference
HPLC <sup>a</sup> -fluorimetry	0.009	0.03–15.0	–	21	[5]
HPLC	0.06	0.20–200.0	–	23	[9]
HPLC	0.015	2.0–19.6	–	6	[6]
HPLC	–	0.005–10	–	13	[7]
LC <sup>b</sup> -fluorimetry	0.001	0.008–0.250	–	12	[8]
HPLC-UV	2.0	5–120	–	20	[11]
CE-ECL <sup>c</sup>	0.01	0.03–1	–	20	[2]
AAS <sup>d</sup>	3.3	6.0–72.0	–	3	[12]
Spectrophotometry	1.0	2.0–12.0	–	1	[14]
ADSV <sup>e</sup>	0.013	0.004–0.055	Ciprofloxacin	3	[18]
HPLC	0.01	0.001–15.0	–	3.3	[33]
FI-CL <sup>h</sup>	0.003	0.008–3.6	Tryptophan, ciprofloxacin	0.5	[34]
DDP <sup>f</sup> -DME <sup>g</sup>	0.036	14.4–18.0	–	0.2	[35]
SPF <sup>i</sup> -fluorimetry	0.004	0.02–0.39	Imipenem, Fe(III)	3	[36]
AdCdSWV <sup>j</sup>	0.0001	0.0036–0.0287	Tyrosine, cysteine, Tryptophan, ciprofloxacin	0.7	This work

\* LOD is limit of detection.

\*\* LDR is linear dynamic range.

<sup>a</sup> High-performance liquid chromatography.

<sup>b</sup> Liquid chromatography.

<sup>c</sup> Electrophoresis-electrochemiluminescence.

<sup>d</sup> Atomic absorption spectrometric.

<sup>e</sup> Differential pulse adsorptive stripping voltammetry.

<sup>f</sup> Differential pulse voltammetry.

<sup>g</sup> Dropping mercury electrode.

<sup>h</sup> Flow injection-chemiluminescence.

<sup>i</sup> Solid phase spectrofluorimetry.

<sup>j</sup> Adsorptive cathodic stripping square wave voltammetry.

[22]. Due to its remarkable generalization performance, SVM has attracted attention and gained extensive application in pattern recognition and regression problems [23–26]. Suykens and Vandewalle [24] proposed a modified version of SVM called least-squares SVM (LS-SVM), which resulted in a set of linear equations instead of a quadratic programming problem, which can extend the applications of the SVM. In the optimization of ADSV experimental conditions, chemometrics techniques are often applied to achieve a reasonable time, better peak shape, lower detection limit, higher precision, and better signal-to-noise ratio. However, the best experimental conditions can be obtained through constrained optimizations. LS-SVM model is applied to simulate the experimental responses under the combination of experimental conditional variables. The basic idea of SVM is, at first, to provide a non-linear function approximation by mapping the input vectors into high dimensional feature spaces where a special type of hyperplane is constructed, and then, to build a regression model in the hyperplane. SVR is based on a kernel substitution, in Eq. (2),  $X [n \times p]$  is replaced by an  $[n \times n]$  kernel matrix  $\kappa$  which is defined as:

$$\kappa = \begin{pmatrix} k_{1,1} & \cdots & k_{1,n} \\ \vdots & \ddots & \vdots \\ k_{n,1} & \cdots & k_{n,n} \end{pmatrix} \quad (1)$$

where  $k_{ij}$  is defined by the kernel function. In this study, the Gaussian radial basis function (RBF) kernel was used:

$$k_{i,j} = e^{-|x_i - x_j|/2\sigma^2} \quad (2)$$

where  $\mathbf{x}_i$  and  $\mathbf{x}_j$  indicate measured variables of different samples,  $\sigma$  is the kernel width parameter. The kernel width parameter,  $\sigma$ , is related to the confidence in the data; adjustment of  $\sigma$  also influences the non-linear nature of the regression. As  $\sigma$  increases, the kernel becomes wider, forcing the model toward a less complex (more linear) solution. LS-SVR proposed by Suykens is an alternate formulation of SVR. In LS-SVM, the  $\epsilon$ -insensitive loss function (defined using the significance threshold  $\epsilon$ ) is replaced by a classical squared loss function, which constructs the Lagrangian by solving

the linear Karush–Kuhn–Tucker (KKT) system:

$$\begin{bmatrix} 0 & I_n^T \\ I_n & K + \frac{1}{\gamma} \end{bmatrix} \begin{bmatrix} b_0 \\ b \end{bmatrix} = \begin{bmatrix} 0 \\ y \end{bmatrix} \quad (3)$$

where  $I_n$  is a  $[n \times 1]$  vector of ones,  $T$  means transpose of a matrix or vector,  $\gamma$  a weight vector,  $b$  regression vector and  $b_0$  is the model offset. The solution of Eq. (3) can be found by using the most standard methods of solving sets of linear equations.

In this work, Cu(II) was used as a suitable probe for determination of ENRO. Cu(II) makes a stable complex with ENRO in ammonium buffer. Then the complex was accumulated at a surface of hanging mercury drop electrode (HMDE) for a suitable period of time. Then the accumulated complex was reduced when the potential was scanned to the negative direction using square wave voltammetry (SWV). The peak potential  $-0.30\text{V}$  was used as an analytical signal.

## 2. Experimental

### 2.1. Reagents

All of the chemicals were of analytical grades, and were purchased from Sigma–Aldrich, unless stated otherwise. Doubly distilled water was used throughout

Stock solution ( $100.0 \mu\text{g mL}^{-1}$ ) of Cu(II) was prepared by dissolving 0.0384 g of copper(II) nitrate trihydrate in water in a 100-mL volumetric flask.

ENRO solution,  $1.0 \times 10^{-3} \text{ mol L}^{-1}$ , was prepared by dissolving 0.0364 g of ENRO powder in water in a 100-mL volumetric flask.

Ammonium buffer solution ( $0.05 \text{ mol L}^{-1}$  in ammonia and ammonium chloride) in the pH range of 8.0–11.5 was used, throughout.

### 2.2. Apparatus

A Corning pH-meter, Model 140, with a glass electrode (conjugated with an Ag/AgCl reference electrode, Model 6.0232.100), was used to determine pH of the solutions.

SWV were obtained using an Autolab instrument, Model PGSTAT-10 processor, with three electrodes consisting of a HMDE ( $r_0 = 0.20$  mm, 0.450 mg) as a working electrode, an Ag/AgCl ( $3.0 \text{ mol L}^{-1}$  KCl) reference electrode and a carbon counter electrode that linked to a computer (Pentium IV, 2.0 GHz). Solutions were deoxygenated with high-purity nitrogen for 3 min prior to each experiment.

All programs were run on an AMD 2000 XP and 512 MB RAM computer. The LS-SVM optimization was obtained using the LS-SVM lab toolbox (Matlab/C Toolbox for Least-Squares SVM [27]).

### 2.3. Recommended procedure

Twenty-five milliliters of a solution containing  $80.0 \text{ ng mL}^{-1}$  copper(II) and  $0.050 \text{ mol L}^{-1}$  ammonia buffer (pH 8.7) was transferred into an electrochemical cell. The solution was purged with nitrogen gas for 3 min. Then an accumulation potential of  $-0.10$  V vs. Ag/AgCl electrode was applied to a fresh HMDE during stirring the solution for a period of 40 s. Following this preconcentration stirring was stopped and after equilibration of 5 s, the square wave voltammogram was recorded from  $-0.10$  to  $-0.80$  V with a potential scan rate of  $0.25 \text{ V s}^{-1}$ . The peak current was measured and recorded as a blank signal ( $I_b$ ). After the background voltammogram was obtained, aliquots of the sample solution containing ENRO were introduced into the cell while maintaining a nitrogen atmosphere above the solution. Then the square wave voltammogram was recorded as described above to give the sample peak current. The peak current was measured and recorded as a sample signal ( $I_s$ ). All data was obtained at room temperature. The difference in current ( $I_{ps} - I_{pb}$ ) was considered as a net signal ( $\Delta I_p$ ). Calibration graphs were prepared by plotting the net peak currents vs. the ENRO concentrations in solution.

### 2.4. Preparation of real samples

Aliquots  $18.0 \mu\text{L}$  of the ENRO drugs including injectable (Enrofan 5%, Erfan Daru Co., Iran) and  $9.0 \mu\text{L}$  of oral (ENRO 10%, Damayaran Co., Iran) solutions were directly transferred into a 25 mL volumetric flask, followed by making up to volume with distilled water. Then  $20 \mu\text{L}$  of the solution plus  $20 \mu\text{L}$  of  $1.0 \times 10^{-5} \text{ mol L}^{-1}$  standard solution of ENRO was mixed in a 25 mL volumetric flask with water and were used for the analysis as recommended procedure.

Plasma samples were obtained from a healthy volunteer and were stored frozen until the assay. Into each of seven centrifugation tubes, 1.0 mL of the spiked human serum or plasma, containing various concentrations of ENRO was transferred and then mixed well with 4.0 mL of methanol to precipitate the proteins. The precipitated proteins were separated by centrifugation for 20 min at 2000 rpm. The clear supernatant layer was filtered through  $0.45 \mu\text{m}$  Milli-pore filter. A  $0.25 \text{ mL}$  of the supernatant liquor was transferred into the voltammetric cell containing  $80.0 \text{ ng mL}^{-1}$  Cu(II) and ammonia buffer (pH 8.7). Then the ENRO content was quantified by means of the proposed stripping voltammetric procedure.

## 3. Results and discussion

### 3.1. Square wave voltammetry

ENRO is a substance with acetate and keto groups. Efthimiadou et al. [28] proved that ENRO makes a complex with Cu(II) leads to the formation of the neutral complex  $\text{Cu}(\text{ENRO})_2(\text{H}_2\text{O})$  in basic solution [28] as shown in Fig. 1. We found that the ENRO-Cu(II) complex has the ability to be adsorbed at mercury electrode under appropriate conditions. In addition, ENRO can be reduced at the surface of mercury electrode at more negative potential ( $-1.6$  V vs. Ag/AgCl

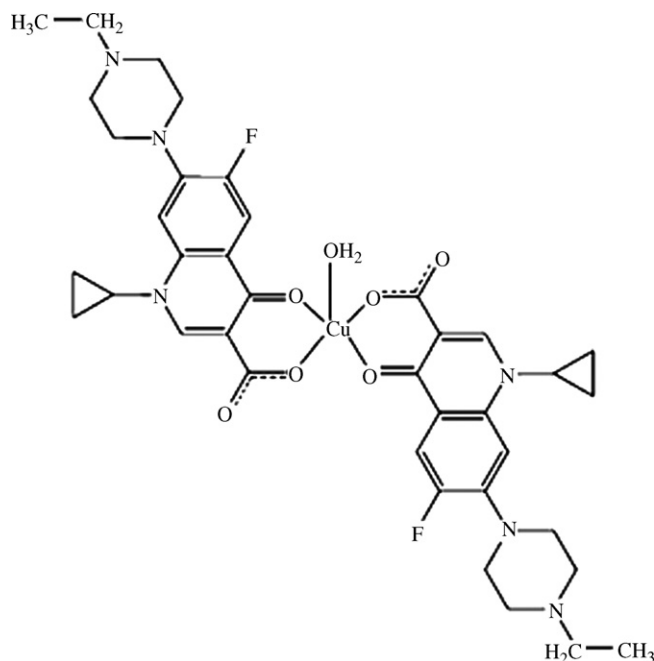


Fig. 1. Structure of complexed ENRO.

electrode). Fig. 2 displays square wave voltammograms of a Cu(II)-buffer and Cu(II)-ENRO-buffer with accumulation time of 40 s at pH of 8.7 vs. Ag/AgCl. According to those voltammograms, with the addition of ENRO to Cu(II)-buffer system and with increasing the accumulation time from 0 to 40 s, a large cathodic peak current located at about  $-0.30$  V was obtained, with a big positive shift in the peak potential from  $-1.60$  V (from pure ENRO) to about  $-0.30$  V (for the complex). Comparison of the voltammograms showed that the height of the reduction peak current of ENRO depends on the duration of the accumulation time and also presence or absence of copper(II) in the solution. Also, any change in accumulation time change the peak current of ENRO. These phenomena prove the adsorptive characteristic of the complex.

In order to obtain the coordination numbers ( $m$ ) and the formation constant ( $\beta$ ) of the complex (Cu(II)-ENRO) adsorbed at the

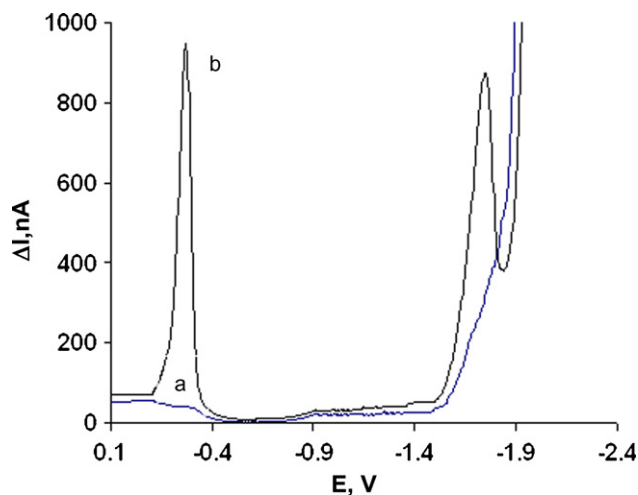
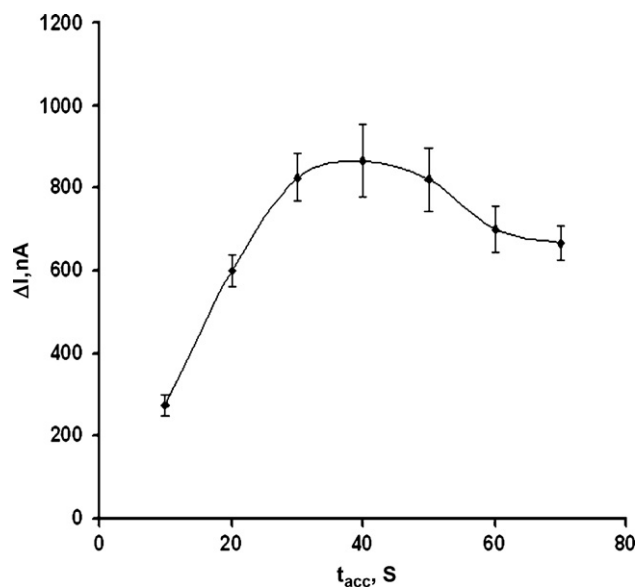


Fig. 2. Square wave voltammogram of ENRO-Cu(II) system; a)  $80.0 \text{ ng mL}^{-1}$  copper(II) in ammonium buffer (pH 8.7) after 40 s accumulation time at  $-0.10$  V; and b) is (a) plus  $80.0 \text{ ng mL}^{-1}$  ENRO.

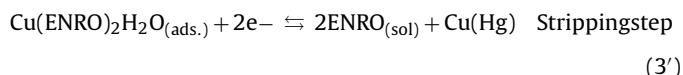
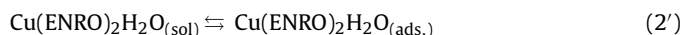


**Fig. 3.** Influence of accumulation time on the peak currents 70.0 nmol L<sup>-1</sup> ENRO. Conditions: Cu(II), 80 ng mL<sup>-1</sup>; accumulation potential, -0.10 V; pH, 8.7; scan rate, 0.25 V s<sup>-1</sup>.

surface of the electrode, the following equation can be used [29,30]:

$$\frac{1}{I_p} = \frac{1}{I_{p,\max}} + \frac{1}{I_{p,\max}\beta C^m} \quad (4)$$

where  $I_p$  is the measured peak current,  $I_{p,\max}$  is the peak current when all the metal ions form the complex,  $\beta$  is the formation constant of the complex and  $C$  is the concentration of the ligand. By plotting  $1/I_p$  vs.  $C^m$  for different  $m$  values, a straight line will be constructed for the corresponding complex. The results of our calculation shows that when  $m=2$ , a straight line with  $r=0.9870$  is obtained for ENRO. Those results indicate that the composition of the electroactive complex on the surface of the mercury electrode is 1:2 for Cu(II)/ENRO. According to the results, Cu(II) makes complexes with ENRO in the solution. The complexes were adsorbed on the surface of the electrode by applying the accumulation potential during the accumulation time. Then the adsorbed complexes were reduced by scanning the potential from -0.10 to -0.80 V. The electrode processes can be summarized as follows:



The formation constants for Cu(II)-ENRO complex was found as  $4.20(\pm 0.2) \times 10^5$ .

### 3.2. Optimization of variables

In order to find the optimum conditions with the highest sensitivity for determination of ENRO, the influence of various parameters such as pH, copper(II) concentration, accumulation potential, accumulation time and scan rate on the peak current were studied.

With increasing accumulation time and scan rate, the peak current of Cu(II)-ENRO increased. Those two variables were independent of the other variables. Thus, according to Figs. 3 and 4 and for simplicity (to reduce the variables in our model), in all experiments, 40 s and 0.25 V s<sup>-1</sup> was chosen as an accumulation time and scan rate, respectively.

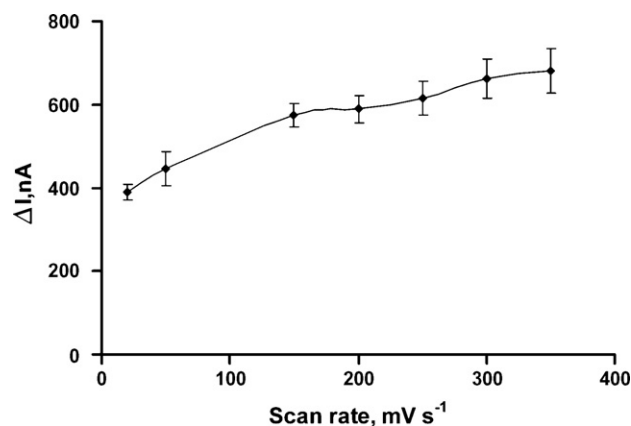


**Fig. 4.** Influence of scan rate on the peak current of 70.0 nmol L<sup>-1</sup> ENRO in the presence of 80 ng mL<sup>-1</sup> copper(II). Conditions: pH, 8.7; accumulation potential, -0.10 V; and accumulation time of 40 s.

For selection of the type of buffer solution, the influence of different buffer composition at the same concentration (such borate, ammonia, and universal buffer containing a mixture of phosphate, borate and acetate) on the peak current were studied with 70.0 nmol L<sup>-1</sup> ENRO in the presence of 80 ng mL<sup>-1</sup> copper(II), accumulation potential of -0.10 V, accumulation time of 40 s and scan rate of 250 mV s<sup>-1</sup>. The results showed that ammonium buffer was the best, because the peak current was decreased with other buffer solution drastically. Thus, for the pH study, 0.4 mol L<sup>-1</sup> ammonium chloride-ammonia solution was selected for this study to have enough buffer capacity. The influence of the three parameters including pH, copper(II) concentration and accumulation potential on the peak current were optimized using LS-SVM (Table 2). Twenty experiments were designed based on the experimental design [31]. A central composite design (CCD) was carried out for study of the chemical variables. An experimental design software design.expert 7(44), was used for the data manipulation.

#### 3.2.1. Optimization of SVR parameters

The SVR parameters  $\gamma$  and  $\sigma$  were optimized with five-fold cross-validation for the training set in terms of RMSE. During this process, first, a broad range of parameter settings is investigated with large steps. Second, after identifying a promising region, this region is searched in more detail. In a promising region, the detailed process of selecting the parameters and the effects of the two

**Table 2**

Design matrix for the central composite design.

Exp. no.	Cu(II) (ng mL <sup>-1</sup> ) (X <sub>1</sub> )	pH (X <sub>2</sub> )	E <sub>acc</sub> (X <sub>3</sub> )
1	50.0	9.75	-0.35
2	50.0	8.00	-0.35
3	50.0	9.75	-0.35
4	20.0	10.8	-0.08
5	80.0	10.8	-0.08
6	20.0	8.71	-0.08
7	50.0	9.8	-0.35
8	50.0	11.5	-0.35
9	80.0	8.71	-0.62
10	50.0	9.75	-0.35
11	20.0	10.8	-0.62
12	-	9.75	-0.35
13	80.0	8.71	-0.08
14	50.0	9.75	-0.8
15	50.0	9.75	0.1
16	50.0	9.75	-0.35
17	0.10	9.75	-0.35
18	200	8.71	-0.35
19	80.0	10.8	-0.62
20	50.0	9.75	-0.35

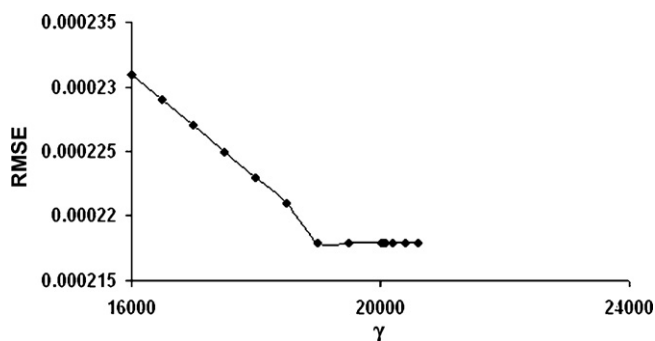


Fig. 5. RMSE error vs.  $\gamma$  of the prediction set based on five-fold cross-validation ( $\sigma = 1$ ).

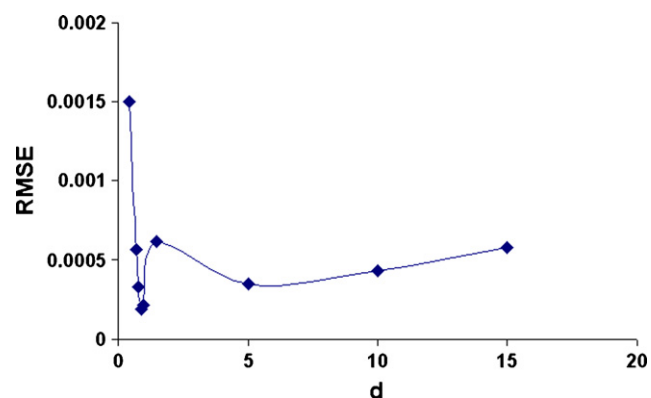


Fig. 6. RMSE error vs. sigma ( $\sigma$ ) of the training set based on five-fold cross-validation ( $\gamma = 20,600$ ).

parameters ( $\gamma, \sigma$ ) on generalization performance of the corresponding model are shown in Figs. 5 and 6, respectively [32]. Standard deviation (SD) was given for an estimate of the models' performance.

The choosing of parameter  $\gamma$  is not critical from theory; this parameter should not be too small because if  $\gamma$  is too low, the SVM regression function cannot grow enough to reach the output values. As can be seen in Fig. 5, there is a significant increase in RMSE of prediction set as the value of  $\gamma$  decreases when the value of  $\gamma$  is in an under-size range. If  $\gamma$  is too large (infinity), the objective is to minimize the empirical risk only without regarding to the complexity of the model. The Gaussian parameter  $\sigma$  is another important one. As can be seen in Fig. 6,  $\sigma$  is the most sensitive parameter to choose because it has the strongest influence on the risk. Parameter  $\gamma$  controls the amplitude of the Gaussian function and therefore controls

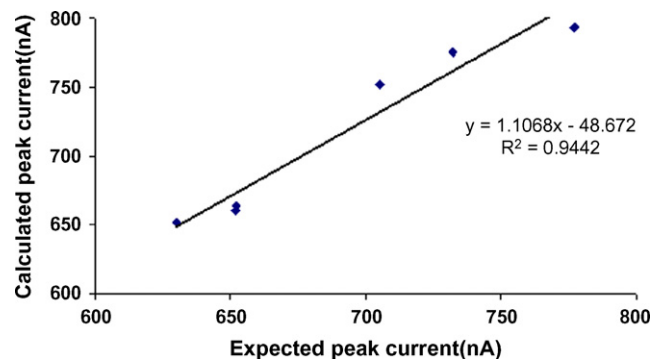


Fig. 7. Relationship between expected current of  $70.0 \text{ nmol L}^{-1}$  ENRO calculated currents of these species for the prediction set (accumulation time, 40 s; scan rate,  $0.25 \text{ V s}^{-1}$ ).

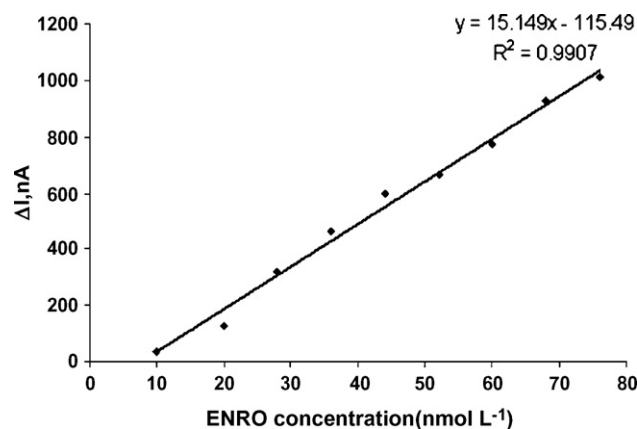


Fig. 8. Calibration curve of calculated currents of these species for the prediction set. Conditions: pH, 8.7; copper(II),  $80 \text{ ng mL}^{-1}$ ; accumulation potential,  $-0.10 \text{ V}$ ; accumulation time, 40 s; and scan rate of  $0.25 \text{ V s}^{-1}$ .

the generalization ability of SVM. The optimized values of  $\gamma, \sigma$  were 20,600 and 0.9, respectively. The expected current values and SVM computation results for the prediction set are shown in Fig. 7. The small errors ( $\text{RMSE} = 2.18 \times 10^{-4}$ ,  $r^2 = 0.944$ ) of the prediction set reveal good performance of the model.

At the optimized parameters of SVM, the peak current of Cu(II)–ENRO was calculated for different values of the inputs variables. The peak current was maximized at pH of 8.9, Cu(II) concentration of  $80.0 \text{ ng mL}^{-1}$ , and an accumulation potential of  $-0.10 \text{ V}$ . Therefore, we used pH of 8.7, Cu(II) concentration of  $80.0 \text{ ng mL}^{-1}$ , an accumulation potential of  $-0.10 \text{ V}$ , an accumulation time of 40 s and a scan rate of  $0.250 \text{ V s}^{-1}$  for determination of ENRO.

### 3.3. Figures of merit

Under the optimized conditions, the calibration graph for determination of ENRO was obtained. The calibration plot was linear over the ranges of  $10.0\text{--}80.0 \text{ nmol L}^{-1}$  with a regression equations of  $I_p = 15.149(\pm 0.680) C_{\text{ENRO}} - 115.49(\pm 0.585)$  ( $r^2 = 0.9907$ ,  $n = 9$ ), where  $I_p$  and  $C_{\text{ENRO}}$  are the net current (nA) and concentration of the ENRO in  $\text{nmol L}^{-1}$ , respectively (Fig. 8).

The limits of detection (defined as the amount of analytes which increases response to  $3S_B$  (three times of the standard deviation of the blank solution)), was  $0.33 \text{ nmol L}^{-1}$  of ENRO.

The relative standard deviation for determination of  $40.0 \text{ nmol L}^{-1}$  of ENRO ( $n = 10$ ) was 4.5%.

## 4. Interference study

Interfering species that may exist in pharmaceutical formulations and biological fluids were investigated concerning the

Table 3

Maximum tolerable concentration of interfering species in the present of  $40.0 \text{ nmol L}^{-1}$  ENRO.

Species	Tolerance limit ( $\text{mol mol}^{-1}$ )
Urea, benzoic acid, carbonate, glucose, sucrose, $\text{Pb}^{+2}$	1000 <sup>a</sup>
Leucine, glycine, fructose	800
Lactose	700
Ascorbic acid, $\text{Fe}^{+3}$ , $\text{Cd}^{+2}$	500
$\text{Zn}^{+2}$ , $\text{Co}^{+2}$	150
Valine	100
Phenylalanine	30
Tyrosine, cysteine, tryptophan, ciprofloxacin	5

<sup>a</sup> Maximum concentration of the species was tested.



**Table 4**  
Determination of ENRO in some real samples.

Sample	Added (nmol L <sup>-1</sup> )	Found <sup>a</sup> (nmol L <sup>-1</sup> )	Official method (nmol L <sup>-1</sup> )	Recovery (%)
Pharmaceutical Enrofan <sup>b</sup> 5%	–	38.1 ± (3.1)	36.9 ± (2.23)	–
	10.0	49.2 ± (1.4)	–	104.9
Enrofloxacin <sup>c</sup> 10%	30.0	69.2 ± (2.22)	–	103.4
	–	39.2 ± (5.24)	41.3 ± (5.32)	–
	10.0	47.8 ± (3.21)	–	93.2
	30.0	65.3 ± (4.21)	–	91.6
Plasma	–	<LOD	–	–
	10.0	9.5 ± 0.52	–	95.0
	30.0	28.9 ± 1.06	–	96.3
	40.0	37.92 ± 1.83	38.8 ± (6.0)	97.0

<LOD, less than limit of detection.

<sup>a</sup> Mean values of three replications.

<sup>b</sup> Each mL contains 50 mg injectable solution.

<sup>c</sup> Each mL contains 100 mg oral solution.

adsorptive stripping voltammetric determination of ENRO. Possible interferences by many substances including cations, anions and organic substances was investigated by the proposed method using addition of the potential interfering substances to a solution containing 40.0 nmol L<sup>-1</sup> ENRO under the optimized conditions. Tolerance limit was defined as the concentrations which give an error of ≤5% in the determination of ENRO. The tolerance ratio of all examined compounds at several molar ratios over ENRO concentration on the measured analytical signal is given in Table 3. The results showed that many of metal ions, anions and organic substances have not considerable effect on the ENRO signal.

## 5. Determination of ENRO in real samples

In order to evaluate the applicability of the proposed method for the determination of ENRO, the utility of the developed method was tested by determining ENRO in several samples containing pharmaceuticals and blood serum and the proposed method was also compared with the other published method for ENRO determination. The results are given in Table 4 that is in accordance with those obtained by the standard method for the pharmaceutical using the absorbance measurements at  $\lambda_{\max} = 278 \text{ nm}$  [33] and chemiluminescence method for the serum [34]. The good agreement of the results with the other reported methods and their recoveries of the spiked samples indicate the successful applicability of the proposed method for determination of ENRO in real samples.

## 6. Conclusions

The work carried out demonstrates the suitability of the adsorption of ENRO on a HMDE as an effective preconcentration step useful for its determination at low concentration levels in urine samples. Moreover, applying the appropriate dilution, the drug can be analyzed as well in commercial formulations. The method is simple, sensitive and rapid for ENRO determination. A detection limit of 0.33 nmol L<sup>-1</sup> was experimentally obtained that is compared with the reported value of 3.6 nmol L<sup>-1</sup>. Moreover some common sugars, amino acids and many ions have no significant interference effect on the determination of ENRO. In addition, this study also was demonstrated the ability of the LS-SVM as an optimization model for the electroanalytical techniques. This procedure has the advantages of simplicity and speed relative to earlier methods, thus allowing for high throughput analysis required for real samples.

## Acknowledgements

The authors gratefully acknowledge support of this work by Research Council of Isfahan University of Technology (IUT) and Center of Excellence in Sensor.

## References

- [1] J.C. Yorke, P. Froc, J. Chromatogr. A 882 (2000) 63.
- [2] X. Zhou, D. Xing, D. Zhu, Y. Tang, L. Jia, Talanta 75 (2008) 1300.
- [3] F.J. Lara, A.M. Garcia-Campana, F. Ales-Barrero, J.M. Bosque-Sendra, L.E. Garcia-Ayuso, Anal. Chem. 78 (2006) 7665.
- [4] The European Agency for the Evaluation of Medicinal Products Report, EMEA/MRL/574/99, <http://www.emea.eu.int>.
- [5] M.A. Bimazubute, E. Rozet, I. Dizier, P. Gustin, Ph. Hubert, J. Crommen, P. Chiap, J. Chromatogr. A 1189 (2008) 456.
- [6] A. Espinosa-Manisilla, A. Munoz de la Pena, D. Gonzalez Gomez, F. Salinas Lopez, Talanta 68 (2006) 1215.
- [7] C. Gonzalez, L. Moreno, J. Small, D.G. Jones, S.F. Sanchez Bruni, Anal. Chim. Acta 560 (2006) 227.
- [8] M.K. Hassouan, O. Ballesteros, A. Zafrá, J.L. Vilchez, A. Navalon, J. Chromatogr. B 859 (2007) 282.
- [9] M. Dunnett, D.W. Richardson, P. Lees, Res. Vet. Sci. 77 (2004) 143.
- [10] M.P. Hermo, E. Nemutlu, S. Kir, D. Barron, J. Barbosa, Anal. Chim. Acta 613 (2008) 98.
- [11] E. Caro, R.M. Marce, P.A.G. Cormack, D.C. Sherrington, F. Borrull, Anal. Chim. Acta 562 (2006) 145.
- [12] G.H. Ragab, A.S. Amin, Spectrochim. Acta Part A 60 (2004) 973.
- [13] S. Mostafa, M. El-Sadek, E.A. Alla, J. Pharm. Biomed. Anal. 27 (2002) 133.
- [14] S. Mostafa, M. El-Sadek, E.A. Alla, J. Pharm. Biomed. Anal. 28 (2002) 173.
- [15] A. Tamer, Anal. Chim. Acta 231 (1990) 129.
- [16] M. Rizk, F. Belal, F.A. Aly, N.M. El-Enany, Talanta 46 (1998) 83.
- [17] M. Tuncel, Z. Atkosar, Pharmazie 47 (1992) 642.
- [18] A. Navalon, R. Blanc, L. Reyes, N. Navas, J.L. Vilchez, Anal. Chim. Acta 454 (2002) 83.
- [19] D. Hodgson, Prog. Inorg. Chem. 19 (1975) 173.
- [20] M. Kato, Y. Muto, Coord. Chem. Rev. 92 (1988) 45.
- [21] J.E. Weder, C.T. Dillon, T.W. Hambley, B.J. Kennedy, P.A. Lay, J.R. Biflin, H.L. Regtop, N.M. Davies, Coord. Chem. Rev. 232 (2002) 95.
- [22] V. Vapnik, A. Lerner, Autom. Remote Control 24 (1963) 774.
- [23] D.Q. Peng, J. Liu, J.W. Tian, S. Zheng, Pattern Recognit. Lett. 27 (2006) 1397.
- [24] J.A.K. Suykens, J. Vandewalle, Neural Process. Lett. 9 (1999) 293.
- [25] H.Y. Yu, X.Y. Niu, H.J. Lin, Y.B. Ying, B.B. Li, X.X. Pan, J. Food Chem. 113 (2009) 291.
- [26] L. Adriano, I. Olivera, Neuro Comput. 69 (2006) 1749.
- [27] [www.esat.kuleuven.ac.be/sista/lssvmlab/](http://www.esat.kuleuven.ac.be/sista/lssvmlab/).
- [28] E.K. Efthimiadou, Y. Sanakis, M. Katsarou, C.P. Raptopoulou, A. Karaliota, N. Katsaros, G. Psomas, J. Inorg. Biochem. 100 (2006) 1378.
- [29] X. Gao, Handbook on the Physics on the Chemistry of Rare Earths, Elsevier, Amsterdam, 1986, p. 163.
- [30] R. Hajian, E. Shams, J. Iranian Chem. Soc. 3 (2006) 32.
- [31] R.G. Brereton, Analyst 122 (1997) 1521.
- [32] T. Zou, Y. Dou, H. Mi, J. Zou, Y. Ren, Anal. Biochem. 355 (2006) 1.
- [33] M.J.E. Souza, C.F. Bittencourt, L.M. Morsch, J. Pharm. Biomed. Anal. 28 (2002) 1195.
- [34] B. Rezaei, A. Mokhtari, Luminescence 23 (2008) 357; M.A. Garcia, C. Solans, J.J. Aramayona, S. Rueda, M.A. Bregante, A. de Jong, J. Biomed. Chromatogr. 13 (1999) 350.

- [35] M. Rizk, F. Belal, F. Ibrahim, S. Ahmed, N.M. EL-Enany, J. Pharm. Biomed. Anal. 24 (2000) 211.
- [36] O. Ballesteros, J.L. Vilchez, J. Taoufiki, A. Navalon, Microchim. Acta 148 (2004) 227.

**Ali A. Ensaifi** was graduated in Chemistry (MSc) from Shiraz University (Iran) in 1988 and received his PhD in 1991 in analytical chemistry in the same University. Then he joined the Department of Chemistry at the Isfahan University of Technology (Iran). He became full professor in 2001. His research interest comprises the development of new electrochemical, or chromogenic chemosensors and molecular probes for anions, cations and neutral chemical species.

**T. Khayamian** was graduated in Chemistry (MSc) from Sharif University (Iran) in 1980 and received his PhD in 1997 in analytical chemistry (Dalhousie University, Canada). Then he joined the Department of Chemistry at the Isfahan University of Technology (Iran). He is an Associate Professor now. His research interest is application of chemometrics methods in analytical chemistry, and also ion mobility spectrometry.

**M. Taei** received his BS degree in 2002 and MS degree in 2003 from Yazd University, Yazd (Iran). He is a PhD student in analytical chemistry in Isfahan University of Technology (Iran).



# Selective spectrophotometric determination of TNT using a dicyclohexylamine-based colorimetric sensor

Erol Erçağ, Ayşem Üzer, Reşat Apak\*

Istanbul University, Faculty of Engineering, Department of Chemistry, Avcilar 34320, Istanbul, Turkey

## ARTICLE INFO

### Article history:

Received 21 September 2008

Received in revised form 15 December 2008

Accepted 17 December 2008

Available online 30 December 2008

### Keywords:

TNT

Tetryl

Polynitro-explosives

Colorimetric sensor

Field spectrophotometry

Dicyclohexylamine

## ABSTRACT

Because of the extremely heterogeneous distribution of explosives in contaminated soils, on-site colorimetric methods are efficient tools to assess the nature and extent of contamination. To meet the need for rapid and low-cost chemical sensing of explosive traces or residues in soil and post-blast debris, a colorimetric absorption-based sensor for trinitrotoluene (TNT) determination has been developed. The charge-transfer (CT) reagent (dicyclohexylamine, DCHA) is entrapped in a polyvinylchloride (PVC) polymer matrix plasticised with dioctylphthalate (DOP), and moulded into a transparent sensor membrane sliced into test strips capable of sensing TNT showing an absorption maximum at 530 nm when placed in a 1-mm spectrophotometer cell. The sensor gave a linear absorption response to 5–50 mg L<sup>-1</sup> TNT solutions in 30% aqueous acetone with limit of detection (LOD): 3 mg L<sup>-1</sup>. The sensor is only affected by tetryl, but not by RDX, pentaerythritol tetranitrate (PETN), dinitrotoluene (DNT), and picric acid. The proposed method was statistically validated for TNT assay against high performance liquid chromatography (HPLC) using a standard sample of Comp B. The developed sensor was relatively resistant to air and water, was of low-cost and high specificity, gave a rapid and reproducible response, and was suitable for field use of TNT determination in both dry and humid soil and groundwater with a portable colorimeter.

© 2008 Elsevier B.V. All rights reserved.

## 1. Introduction

An 'explosive' is a chemically unstable molecule having a rapid rate of auto-decomposition with the accompanying evolution of large amounts of heat and gaseous products. There has been a huge increase in the development of trace explosive detection in the last decade, probably due to globalization of terrorist acts, and to reclamation of contaminated land previously used for military purposes.

A comprehensive review on explosive compounds and mixtures, chromatographic and mass spectrometric methods, environmental analysis of residual explosives, and detection of hidden explosives was given by Yinon and Zitrin [1]. Recent advances in trace explosive detection instrumentation has been reviewed by Moore [2]. In this regard, trace vapor detection methods on which most recent advances were focused continue to be plagued by the low volatility of many target analytes [2]. Additionally, the effective vapor pressure of explosives may be reduced by terrorists up to 1000-fold in plastic packages [3].

Although ion mobility spectrometry (IMS) has evolved to be a fast and mature technology for the analysis by vapor sampling and swipes [2], the limit of detection (LOD) for trinitrotoluene (TNT) using toluene as the sensitizing solvent was only 187 mg L<sup>-1</sup> [4].

Rodacy and Leslie presented an initial investigation of the use of IMS in explosives detection [5], and Avolio et al. described employing IMS technology for rapid on-site analysis of RDX together with TNT and dinitrotoluene (DNT), where the best results were obtained when acetone extracts of explosive residues were deposited on a polytetrafluoroethylene (PTFE) filter and thermally desorbed into the IMS instrument [6]. High performance liquid chromatography (HPLC) methods, though much reliable, still suffer from long analysis times at the order of tens of minutes. Examples for hyphenated use of HPLC techniques in the literature include HPLC–Ultraviolet (UV) spectroscopy [7–10], HPLC–thermal energy analysis (TEA) [11] and HPLC–mass spectrometry (MS) [12]. Although TEA responds specifically to nitro- and nitroso-compounds, the results are usually confirmed with gas chromatography (GC)–MS since unidentified peaks or false positives may appear in the GC–TEA chromatogram. MS methods show a great promise in explosive detection, but are still held back from routine portable application by their high cost and size [2]. Enzyme immunoassay (EIA) methods generally suffer from low reproducibility and interferences from most common ions [13,14]. Vibrational spectroscopy (exploiting the scissoring and out-of-plane deformation frequencies of –NO<sub>2</sub> groups in energetic compounds) has been shown to be capable of detecting nitro-explosives at stand-off distances, although much work remains to be done to improve the selectivity and differentiation from matrix effects and background clutter. Likewise, a major issue in Raman spectroscopic detection of polynitro compounds is that of

\* Corresponding author. Tel.: +90 212 4737028.

E-mail address: [rapak@istanbul.edu.tr](mailto:rapak@istanbul.edu.tr) (R. Apak).

background clutter, not only in the form of fluorescence, but also from Raman signals from matrix materials or surfaces [2]. Differential reflection spectroscopy in the ultraviolet–visible (UV–vis) region may be used to distinguish between the reflectivities of two adjacent parts of a specimen with and without adsorbed TNT [15].

Because of the extremely heterogeneous distribution of explosives in contaminated soils of abandoned and to be remediated military sites, on-site colorimetric methods are a valuable, cost-effective tool to assess the nature and extent of contamination. Because costs per sample are lower, more samples can be analyzed per unit of time. Thus, redesign of sampling or remediation scheme while in the field can be accomplished. On-site screening also facilitates more effective use of off-site laboratories [16] using more sophisticated but costly instrumental techniques. Another advantage of on-site screening is fast decision making of police criminology laboratories after terrorist attacks. For example, colorimetric screening tests for detecting tri- and di-nitrotoluenes in post-blast debris with the alcoholic KOH reagent has found application to a large number (exceeding 2000) of samples in the mobile laboratory unit of Australian Federal Police (AFP) following the 2002 Bali bombings [17]; the presence of TNT could only be later confirmed in the laboratory by IMS and GC–TEA techniques. The most important lesson learned during the investigation of the Bali bombings was the combination of portable instruments like IMS, FT-IR with classical colorimetric techniques using spot-tests for most rapid and efficient identification of the explosives actually used on the site.

Our research group has carried out extensive work on spectrophotometric determination of TNT by improving the water tolerance and color stability of the TNT-hydroxide or TNT-acetate charge-transfer (CT) complexes named as “Meisenheimer or Janowsky anions” [18,19] first used for analytical chemical purposes by Heller et al. in 1982 [20] and later improved by Jenkins and coworkers [21–24]. We also developed the electron-donating dicyclohexylamine (DCHA) as a charge-transfer reagent for the electron-withdrawing analyte, TNT, that could selectively assay TNT in the presence of other explosives, common soil ions and soil humates [25]. As opposed to the intramolecular CT complexes of TNT-hydroxide or TNT-acetate [22], the intermolecular CT complex of TNT–DCHA had an extremely high tolerance for common interferents present in soil and groundwater [25].

During the last decade, a great deal of effort was spent for chemical sensing of explosive traces or residues in soil and strategic locations (such as airports) with the use of sensors. Based on the character of signals, sensors for explosive detection may be broadly classified as electrochemical, mass-based, optical and bio-sensors [26]. Electrochemical sensors may suffer from limited sensitivity and electrode fouling, while immunosensors are good for detecting explosive residues in soil but not for airport security screening applications [26]. Optical sensors have the advantages of flexibility and miniaturization (shrinkability), and may also be used for remote sensing. Among these types of sensors, fluorescence techniques are highly sensitive but not as selective, since electron deficient interferents other than the analytes (e.g., polynitro-explosives) may quench the fluorescence of the electron-rich fluorophore polymer (which is usually of semi-conducting type). Among optical sensors, colorimetric sensors based on light absorption at a specified visible wavelength are the simplest types, and can be used for relatively rapid on-site applications. Zhang's fiber optic-based sensor in this regard made use of an amine-loaded polyvinylchloride (PVC) membrane for reacting with TNT [27]. For fixing the vapors of TNT and DNT, the polymeric semi-permeable membrane was subjected to these vapors at 50 °C for a few days, and the maximal absorption wavelengths for these two nitro-compounds were 500 and 430 nm, respectively [27]. Detection of trace amounts of nitro-explosives was also real-

ized by using cyclopentadienylmanganetricarbonyl(cymantrene) embedded in a thin polymer gel layer [28].

The authors believe that the full range of advantages such as selectivity, sensitivity, rapidity, and versatility of light absorption-based colorimetric sensors has not been sufficiently exploited. Since on-site colorimetric methods are a low-cost tool to assess the nature and extent of contamination in remediated sites and to enable on-site screening for police criminology laboratories, the aim of this work was to develop a DCHA-based colorimetric sensor (probe) for the assay of TNT on-site and in the field. This reagent (DCHA) was previously shown by the authors [25] to be basically interference-free, and useful in both acetone and water media, having a double-fold superiority over existing colorimetric methods. Now the idea is to fix this colorimetric sensing agent (DCHA) in a suitable polymer matrix, and use it as a probe for TNT detection. It was endeavoured to keep this sensor low-cost, portable, interference-free, and flexible. Additionally, the stability of the donor (D)–acceptor (A) complex (DA) (i.e., DCHA–TNT) forming the basis of the sensing reaction was investigated in several non-aqueous media. Analytical findings with the developed sensor were statistically validated against standard reference colorimetric methods, and also against HPLC [8] for the assay of TNT in composite explosives (such as Comp B). The TNT sensor thus synthesized was shown to also detect and quantify tetryl(*N*-methyl-*N*-2,4,6-tetranitroaniline), another military-purpose explosive.

## 2. Materials and methods

### 2.1. Chemicals, instruments, and solutions

The chemicals used in the investigation of optimal preparation of the colorimetric sensor were high molecular weight (HMW) polyvinylchloride (Fluka); dioctylphthalate (DOP, 99%), 2-nitrophenyloctylether (NPOE), bis(2-ethylhexyl) sebacate (DOS), potassium tetrakis-(4-chlorophenyl)borate (PTCPB), dicyclohexylamine (99%) (Aldrich). The solvents used for finding the stability constants of donor–acceptor complexes were tetrahydrofuran (THF, Riedel-deHaen, HPLC grade), acetonitrile (Sigma, HPLC grade) and acetone (Sigma, ≥99.5% extra pure), ethanol (Riedel-deHaen, extra pure), and dimethylformamide (DMF, Merck, analytical grade). The explosive materials; TNT, RDX (1,3,5-trinitro-1,3,5-triazacyclohexane), pentaerythritol tetranitrate (PETN), tetryl(2,4,6-trinitrophenyl-*N*-methylnitramine), 2,4-dinitrotoluene, and Comp B composite explosive (containing 60% RDX, 39% TNT, and 1% wax) were kindly supplied by Makine Kimya Endustrisi Kurumu (MKEK: Machinery & Chemistry Industries Institution) through the supervision of Milli Savunma Bakanligi, Teknik Hizmetler Daire Baskanligi (Ministry of National Defence, Office of Technical Services) of Turkey. A 0.01 M hydrochloric acid (HCl, Merck titrisol, factor = 1.00) solution was used to acidimetrically titrate the remaining amine in the sensor membrane left to stand in air or water, methyl orange being used as neutralization indicator. The alkali, alkaline earth, and transition metal ions were investigated as possible interferents to the developed assay as their nitrate, chloride, and sulfate salts. All other chemicals were supplied from E. Merck, and were of analytical reagent grade unless otherwise stated.

The polymer, plasticiser, and charge-transfer reagent blends in tetrahydrofuran solution were agitated with a Chiltern magnetic stirrer, and the thickness of the polymer membrane thus synthesized was measured with a Elektro-physik model minitest 1100 instrument. Spectrophotometric measurements and spectra recording were made using a Cary 1E (Varian) UV–vis spectrophotometer having a scan rate of 600 nm min<sup>-1</sup> and a spectral resolution of 1 nm, equipped with a pair of matched Helma quartz

cuvettes of 1 mm optical path length. The properly sliced polymer membranes on which the charge-transfer complex coloration of TNT or tetryl was developed were inserted in these cuvettes for absorbance measurements. The pH adjustments were made with the aid of a E512 Metrohm Herisau pH-meter using a glass electrode. For validation of the proposed assay against HPLC on a Comp B sample (containing both RDX and TNT), a Perkin Elmer Series 200 HPLC chromatographic instrument equipped with a Hypersil C<sub>18</sub> (5 μm), 250 mm × 4.6 mm ID reversed phase (RP)-column was used in conjunction with a UV (254 nm) detector, and a 40% MeOH + 60% H<sub>2</sub>O (v/v) mixture mobile phase at a flow rate of 0.8 mL min<sup>-1</sup>. The injection volume was 25 μL.

The standard stock solutions of TNT and tetryl at 250 mg L<sup>-1</sup> concentrations were prepared in pure acetone, and the working solutions to be tested with the developed sensor were prepared from these stock solutions by dilution with 30% aqueous acetone in the concentration range of 5–50 mg L<sup>-1</sup>. In interference studies, the potential interferent cation or anion was applied in the same solvent medium (30% aqueous acetone) at a mass ratio of 10, 20, and 100-fold in admixture with 20 mg L<sup>-1</sup> TNT.

## 2.2. Procedures

### 2.2.1. Preparation of the sensor

The sensor material should be prepared as transparent, and hard enough to be sliced and placed into a 1-mm spectrophotometer cuvette. The polymer blend entrapping the charge-transfer reagent DCHA should not completely fix it that would otherwise prevent the color response to TNT. These expectations required the optimization of the sensor membrane composition in regard to polymer, plasticiser, sensing reagent, and solvent. The polymer and plasticiser blend should be compatible with DCHA. Preliminary experiments (for mixtures 1–6) regarding the optimization of the sensor film composition were summarized in Table 1. Only mixtures containing high molecular weight PVC together with DOP and DCHA (in THF solution) were successful, yielding an optimal composition for mixture 4 (Table 1).

### 2.3. Optimized preparation of the polymeric sensor

In a beaker kept at 30 °C, 1 g PVC (high molecular weight) was dissolved with 11 mL THF under a magnetic stirrer. During dissolution, the beaker was covered with a watch glass to prevent

the essential part of the solvent to evaporate. Magnetic stirring was adjusted at a controlled speed so as not to include air bubbles. The PVC residues remaining on the sides of the beaker were transferred back to the main solution with the help of a glass rod. Complete dissolution took approximately three hours, and more elevated temperatures caused serious evaporation losses of the solvent (THF). After dissolution, 0.3 mL DOP and 0.6 mL DCHA were added. Stirring was maintained until a homogeneous mixture was obtained. After ascertaining that no particles or air bubbles were included in the mixture, it was poured into a 9 cm diameter petri dish placed on a flat surface previously controlled by a water balance. The excess of THF was let to evaporate under ambient conditions, and for this purpose, the mixture was covered with a petri glass and stabilized by letting to stand for 3–4 h. Every 30 min during that time, the petri dish cover was removed for 5 min to enable controlled evaporation. If these measures were not strictly followed, the relatively rapid solvent losses may give rise to a polymer film having a non-transparent, hazy surface. The rest of the solvent was evaporated in a temperature-controlled oven kept at 40 °C for 12 h. The blank (*i.e.*, without sample) films for mixtures 1–3, together with the blank and color-developed sample films of optimized composition mixture 4 (as described in Table 1) are shown in Fig. 1. The average thickness of the film was 146 μm.

The polymeric sensor should be kept away from open air (preferably kept in a vacuum desiccator) for prolonged preservation, otherwise, the sensor film may gain a hazy appearance, which would cause a high blank value in colorimetric measurements.

## 2.4. TNT and tetryl assay with the developed colorimetric sensor

### 2.4.1. Calibration curves and recommended procedure for TNT and tetryl assay

To glass tubes of 10 cm × 1.1 cm dimension, 7 mL of the analyte (TNT) solution were added into which rectangular-shaped test strips of 0.8 cm × 6 cm dimension cut from the polymeric sensor film were placed. The tubes were stoppered to prevent evaporation losses of the solvent (*i.e.*, 30% aqueous acetone), and the strips were kept inside these tubes for 15 min. The absorbances of the strips placed in 1-mm optical cuvettes were read at 530 nm with a spectrophotometer against a reagent blank strip immersed in a tube containing all reagents but the analyte. Exactly the same procedure was followed for tetryl standard solutions with the exception that the analytical wavelength was 460 nm. The calibration curves

**Table 1**  
Conditions for synthesis of sensor film<sup>a</sup>.

Mixture no.	<i>t</i> (°C)	PVC (1 g) type	Plasticiser	Sensing reagent	Results
1	Room	HMW	0.1 g PTCPB 0.3 mL DOS	0.6 mL DCHA	Very soft film of turbid appearance
2	Room	carboxylated form	0.3 mL DOP	0.6 mL DCHA	Turbid mixture stayed in homogeneous upon THF addition
3	Room	HMW	0.24 mL DOP 0.3 mL DOS 0.23 mL NPOE	0.6 mL DCHA PTCPB (twice as much of DCHA-by mole)	Blend lost transparency after air contact
4 <sup>b</sup>	30	HMW	0.3 mL DOP	0.6 mL DCHA	Homogeneous mixture under controlled evaporation (of solvent) at 40 °C for 12 h gave a transparent polymer
5	30	HMW	0.2 mL DOP	0.7 mL DCHA	DCHA excess was transferred to acetone solution instead of being entrapped in the film. The rather viscous mixture did not spread evenly in the petri dish, producing a film of inhomogeneous thickness
6	30	HMW	0.4 mL DOP	0.5 mL DCHA	Too elastic film could not be placed properly in the optical cuvette. Amount of DCHA was insufficient to obtain maximal color development

<sup>a</sup> All mixtures contained 1 g PVC and 11 mL THF (the solvent (THF) volume was selected to be 11 mL, because higher volumes caused a retardation in polymer setting while lower amounts gave rise to harder initial dissolution of PVC and a hazy appearance of the sensor film).

<sup>b</sup> Optimal composition of sensor film.

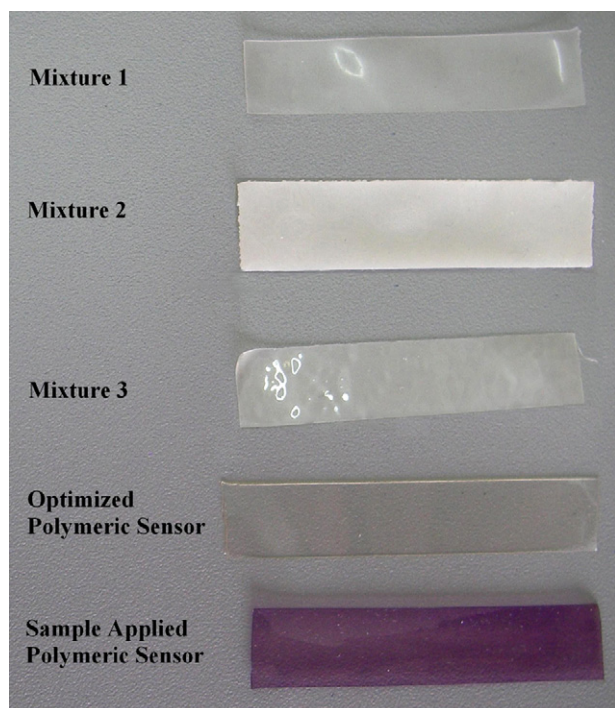


**Fig. 1.** The blank (*i.e.*, without sample) films for mixtures 1–3, together with the blank and violet color-developed sample films of optimized composition mixture 4 (as described in Table 1). (For interpretation of the references to color in this figure legend, the reader is referred to the web version of the article.)

for each analyte were constructed by recording the corresponding absorbance values of the sensor strips against analyte concentration. The unknown concentrations of TNT and tetryl were found by means of these calibration curves.

#### 2.4.2. Investigation of tetryl interference to extractive-spectrophotometric determination of TNT in acetonated aqueous solution with DCHA

Extractive-spectrophotometric determination of TNT in 50% acetonated aqueous solution with DCHA was carried out as previously described by the authors [25]. Briefly, to 5 mL of TNT solution in this solvent, 1 mL of 0.05% methyl paraben solution prepared in the same solvent was added, and extracted with 4 mL of 10:1 (v/v) DCHA–IBMK mixture solvent at room temperature. After separation of phases and filtering of the amine extract through a Whatman black-band filter paper into a quartz absorption cell containing a few crystals of anhydrous  $\text{Na}_2\text{SO}_4$ , TNT was quantified by measuring the absorbance of the red–violet complex in the DCHA–IBMK phase at 531 nm. The interference of tetryl was investigated in this system by adding increasing concentrations of tetryl to an analyte solution containing a fixed concentration ( $10 \text{ mg L}^{-1}$ ) of TNT, and applying the described method.

#### 2.4.3. Finding the association constants of donor–acceptor complexes of DCHA–TNT in different non-aqueous solvents

The association constants ( $K_{\text{ass}}$ ) of DCHA–TNT charge-transfer complexes were calculated in different non-aqueous solvents, namely dimethylformamide, ethanol, acetone, and 1:1 (v/v) acetonitrile–THF mixture by mixing in equal volumes DCHA solutions of decreasing concentration with TNT concentrations of increasing concentration in the corresponding solvents, and measuring the maximum absorbances of the violet colored complexes formed. The reason why acetonitrile–THF mixture was used (instead of a pure solvent) was that acetonitrile alone was not miscible with DCHA.

#### 2.4.4. Determination of the amount of DCHA remaining in the sensor polymer upon standing in air and water

Since the active ingredient of the polymeric sensor is DCHA capable of forming a colored charge–transfer complex with TNT and tetryl, its remaining amount in the sensor material upon standing in air and water should be periodically checked for maximum sensitivity. The weight of the polymeric sensor film peeled off from the petri dish was 1.458 g. It was sliced into four equal parts each weighing 0.3645 g, a one set was kept under water while the other in an air-containing dessicator for different periods of time. After standing in the air, each film slice was transferred to Erlenmeyer flasks containing 50 mL  $\text{H}_2\text{O}$ , waited for 10 min for equilibration, and titrated with 0.01 M HCl in the presence of methyl orange to acidimetrically calculate the amount of remaining amine, expressed as the percentage of initial amount of amine entrapped in the original sensor film. For membranes kept under water, the amount of amine leached into water after a certain standing period was directly found by acidimetric titration. For the latter, the amount of amine remaining in the sensor was calculated by difference (*i.e.*, initial–final amount). DCHA is a secondary amine of molecular weight:  $181.3 \text{ g mol}^{-1}$  and formula:  $(\text{C}_6\text{H}_{11})_2\text{NH}$ , and reacts with HCl at a mole ratio of 1:1. If the volume of HCl consumed in the acidimetric titration is  $V_{\text{HCl}}$  mL, then the weight of amine titrimetrically determined is  $0.01 \times V_{\text{HCl}} \times 0.1813 \text{ g}$ .

#### 2.4.5. Interference analysis

The non-interference of nitro-explosives and explosive related materials other than tetryl (*e.g.*, RDX, PETN, picric acid, DNT, and dinitrophenol) was basically shown in a previous work of the authors involving liquid–liquid extraction with DCHA [25]. For testing the potential interference of nitro-explosives, 5 mL of  $1000 \text{ mg L}^{-1}$  acetonated solution of the interferent (*i.e.*, 10-fold of the analyte by mass) was added to 2 mL of  $250 \text{ mg L}^{-1}$  acetonated TNT; 0.5 mL acetone and 17.5 mL  $\text{H}_2\text{O}$  were added to dilute the sample to 25 mL. The effect of the interferent was measured in a final mixture solution of 30% aqueous acetone. The tolerable concentrations of some cations ( $\text{Cu}^{2+}$ ,  $\text{Pb}^{2+}$ ,  $\text{K}^+$ ) and anions ( $\text{SO}_4^{2-}$ ,  $\text{Cl}^-$ ,  $\text{NO}_3^-$ ) in the determination of  $20 \text{ mg L}^{-1}$  TNT were found in admixtures of the potential interferent ion with TNT when the sensor response at 530 nm at the end of 15 min equilibration period varied within  $\pm 10\%$  of that of TNT alone. The recovery for TNT from (analyte + interferent) mixtures (on the basis of the percentage of pure TNT response) was calculated. The recommended procedure for TNT assay was followed in each determination.

#### 2.4.6. Validation of the proposed method against HPLC using Comp B composite explosive reference sample

For method validation, 5–100  $\text{mg L}^{-1}$  TNT standard solutions in acetone were assayed by both the recommended sensing method and HPLC to construct the calibration graphs. The HPLC calibration curve for TNT was constructed by recording the peak areas versus concentration. As the reference material, 25.0 mg samples ( $N=5$ ) of Comp B composite explosive (containing 39% TNT) were dissolved in 25 mL acetone, 2 mL of this stock solution (containing  $1000 \text{ mg L}^{-1}$  Comp B) was diluted with acetone to a final volume of 25 mL to yield  $80 \text{ mg L}^{-1}$  Comp B solutions (theoretically containing  $31.2 \text{ mg L}^{-1}$  TNT) to be assayed with HPLC. For testing the Comp B working solutions with the proposed sensor under the same conditions of the TNT standards (*i.e.*, 30% aqueous acetone), 2 mL of  $1000 \text{ mg L}^{-1}$  Comp B solution in acetone was withdrawn, 5.5 mL acetone was added, and the mixture was diluted to a final volume of 25 mL with water. The recommended procedure was followed in each determination. The statistical comparisons between the findings of the recommended and reference methods were made with the aid of *t*- and *F*-tests.

**Table 2**

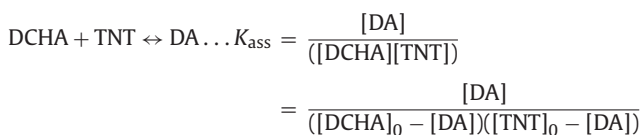
The data used for calculation of the stability constant ( $K_{\text{ass}}$ ) of DCHA–TNT donor–acceptor complex in 1:1 (v/v) acetonitrile–THF solvent (concentrations in mol L<sup>-1</sup>).

[TNT] <sub>0</sub>	[TNT] <sub>0</sub> /Abs	[DCHA] <sub>0</sub>	1/[DCHA] <sub>0</sub>	$A_{529\text{nm}}$
$5 \times 10^{-5}$	$7.17 \times 10^{-4}$	2.485	0.402	0.0697
$1.0 \times 10^{-4}$	$7.87 \times 10^{-4}$	2.39	0.418	0.1270
$1.5 \times 10^{-4}$	$7.84 \times 10^{-4}$	2.28	0.438	0.1913
$2.0 \times 10^{-4}$	$5.14 \times 10^{-4}$	2.09	0.478	0.3890
$2.5 \times 10^{-4}$	$6.38 \times 10^{-4}$	1.79	0.559	0.3919
$3.0 \times 10^{-4}$	$6.03 \times 10^{-4}$	1.25	0.80	0.4972
$3.5 \times 10^{-4}$	$6.44 \times 10^{-4}$	1.00	1.00	0.5434
$4.0 \times 10^{-4}$	$6.35 \times 10^{-4}$	0.84	1.19	0.6297
$4.5 \times 10^{-4}$	$6.87 \times 10^{-4}$	0.50	2.00	0.6546
$5.0 \times 10^{-4}$	$8.64 \times 10^{-4}$	0.36	2.78	0.5785
$1.0 \times 10^{-3}$	$1.29 \times 10^{-3}$	0.25	4.00	0.7767

### 3. Results and discussion

#### 3.1. Mathematical treatment of charge-transfer complex formation equilibria

For a 1:1 donor–acceptor complex (DA), we have the following formation equilibrium reaction with an association constant  $K_{\text{ass}}$ :



where the donor (D) is DCHA and the acceptor (A) TNT, and the subscript (0) shows the initial concentrations of the concerned species. Since the concentration of the amine donor is in excess, we have:  $[\text{DCHA}]_0 - [\text{DA}] \approx [\text{DCHA}]_0$

$$K_{\text{ass}} = \frac{[\text{DA}]}{[\text{DCHA}]_0([\text{TNT}]_0 - [\text{DA}])}$$

Reciprocating this equation yields:

$$\frac{1}{K_{\text{ass}}} = [\text{DCHA}]_0 \left( \frac{[\text{TNT}]_0}{[\text{DA}]} - 1 \right)$$

Since only the DA charge-transfer complex absorbs light in the visible range,  $[\text{DA}] = \text{Abs}/\varepsilon$  for a fixed cell thickness, where Abs is the absorbance at a specified wavelength of the charge-transfer complex, and  $\varepsilon$  is the absorptivity constant of the complex under the given conditions. Reorganizing the terms of the final equation gives:

$$(K_{\text{ass}}\varepsilon)^{-1}[\text{DCHA}]_0^{-1} + \varepsilon^{-1} = [\text{TNT}]_0\text{Abs}^{-1} \quad (1)$$

meaning that a plot of  $[\text{TNT}]_0\text{Abs}^{-1}$  versus  $[\text{DCHA}]_0^{-1}$  with respect to Eq. (1) would yield a straight line of slope  $(K_{\text{ass}}\varepsilon)^{-1}$  and intercept  $\varepsilon^{-1}$ . Then  $\varepsilon = \text{intercept}^{-1}$  and  $K_{\text{ass}} = \text{intercept}(\text{slope})^{-1}$ .

#### 3.2. Stability constants of DCHA–TNT charge-transfer complexes in non-aqueous media

The stability constants ( $K_{\text{ass}}$ ) of the donor–acceptor complexes of DCHA–TNT in different non-aqueous solvent media were calculated as: DMF:  $5.8 \pm 0.6$ , EtOH:  $0.21 \pm 0.10$ , acetonitrile–THF:  $2.6 \pm 0.2$ , and acetone:  $2.5 \pm 0.3 \text{ M}^{-1}$ . The example calculations are shown in Table 2 for acetonitrile–THF (1:1, v/v). For obtaining a recti-linear curve described in the Benesi and Hildebrand method [29], the 4th, 5th and 7th–11th (total  $N=7$  data points) experimental data were fitted to Eq. (1). The correlation coefficient:  $r$  was 0.933,  $\varepsilon$  was  $2.18 \times 10^3$ , and  $K_{\text{ass}}$  was computed as  $2.56 \text{ M}^{-1}$ . Among the solvents studied, EtOH was polar protic (dielectric constant:  $D=24.3$ ), while the other solvents were polar-aprotic (the  $D$  values were DMF: 38.3, acetonitrile: 36.6, THF: 7.52, and acetone: 20.7). It is natural that the stability constants of donor–acceptor complexes in

polar-aprotic solvents were greater than in water, in accord with the general Bjerrum theory. DMF produced a difference that could not be expected from its dielectric constant probably because its amide functional group participated in charge–transfer interaction with the analyte (TNT) along with the donor (DCHA). Preliminary experiments indeed showed that DMF was capable of forming a charge-transfer complex with TNT, the color of which was much more intensified upon addition of DCHA. On the other hand, dioxane, though having a low dielectric constant, was not a suitable solvent, because colored charge-transfer complexes did not form in dioxane.

#### 3.3. Nature of charge-transfer complex between DCHA and TNT

In general, the intensely colored product formed between aromatic-NO<sub>2</sub> compounds and amine type Lewis bases may be attributed to the partial transfer of electronic charge (*i.e.*, through overlap of orbitals of appropriate symmetry) from the Lewis base to the aromatic nucleus of the nitro-compound depleted of electron density, owing to the electron-attracting behaviour of the –NO<sub>2</sub> substituents. This phenomenon was named as charge-transfer interaction after Mulliken [30,31]. Interaction between trinitrophenols (*e.g.*, picric acid) and cyclic amines may give rise to the formation of a Lewis salt where a proton is transferred from trinitrophenol to the amine, as well as to charge-transfer interaction *via* partial transfer of charge from  $n$ -lone pair of the amine to the oxygen- $\pi^*$  of the nitro-group [32]. Modern understanding of CT interaction involves the partial transfer of charge from the highest occupied molecular orbital (HOMO) to the lowest unoccupied molecular orbital (LUMO) of the CT complex upon light absorption. Specifically, the nature of interaction between TNT and DCHA is presumed to be of charge-transfer type (*i.e.*, transfer of electronic charge—upon incident light—from the amine donor to TNT acceptor) as shown in Fig. 2.

#### 3.4. Optimal sensor composition

On the basis of 1.0 g of PVC (high molecular weight), the volume of DOP was optimized as 0.3 mL. Plasticiser volume exceeding this amount yielded a very soft sensor film that could not be sliced and placed in a spectrophotometer cuvette. When DOP volume was <0.3 mL, the plasticising effect was insufficient. The DCHA volume was optimized as 0.6 mL, because when this limit was exceeded, the surrounding solution phase instead of the polymeric sensor surface became colored due to transfer of amine between the two phases, and additionally, the sensor lost its flexibility. On the other hand, when the amine volume was <0.6 mL, the absorbance of the charge-transfer complex on the film severely decreased. The solvent (THF) volume was selected to be 11 mL, because higher volumes caused an extension in polymer setting period while lower amounts gave rise to harder initial dissolution of PVC, a hazy appearance of the sensor film, and consequently imprecise absorbance recordings.

The best amine for charge-transfer complex formation was DCHA [25]. In preliminary experiments, other amines as *o*-phenylenediamine, dipicrylamine, hexamethylenetetramine, diethylenetriamine, tributylamine, triethylamine, and Alamine-336 were observed not to produce an appreciable color with TNT. DCHA not only produced an intense color with TNT, but this color did not form with nitro-explosives and explosive related materials other than tetryl. DCHA, being a high molecular weight lipophilic amine, did not appreciably leach out into the 30% acetone-aqueous solution during TNT assay, as opposed to hydrophilic amines easily leachable into solution. The only interferent nitro-explosive, tetryl, gave an orange color on the sensor which was completely different from that of TNT, an important factor in qualitative identifications. DCHA was compatible with PVC and DOP to yield a

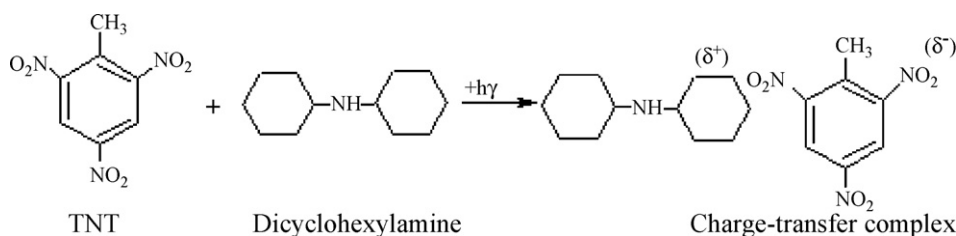


Fig. 2. The charge-transfer complex formed between DCHA donor and TNT acceptor.

transparent film, as other amines may form separate micro-areas on the sensor to yield a hazy appearance or form different layers on the PVC membrane [27].

Zhang et al. in their sensor synthesis used a PVC prepared by emulsion polymerization [27]. This type of PVC has been stated to contain traces of surfactants containing ionic functional groups. These surfactant residues may produce micro-areas of water accumulation within the membrane. Consequently, the resulting membrane, when exposed to water for several hours, may achieve hazyness. Due to these reasons, Zhang et al. preferred to use 1.8% carboxylated PVC [27], which proved to yield a non-transparent film with DCHA in our preliminary studies. Thus, high molecular weight PVC was the main choice for our sensor material. DOP was the complementary plasticiser to impart the right dose of softness and flexibility to the resulting membrane. DOP may also increase the diffusion rate of amine and TNT to rapidly obtain color as a result of charge-transfer complexation on the membrane. It is known that pure PVC yields hard membranes and is unsuitable for optical measurements, while overdoses of DOP cause turbidity in the blends [27]. In the synthesis of an azlactone-based  $\text{H}^+$ -sensitive fluorescence optical sensor in the literature, the addition of DOP to PVC was claimed to increase reproducibility of pH measurements [33].

### 3.5. Time of colored complex formation on the sensor

A time period of 15 min was optimally chosen for color development on the sensor membrane immersed in TNT solutions. Less time caused a non-linear drop of absorbance for TNT solutions more concentrated than  $10 \text{ mg L}^{-1}$ . More time significantly longer than 15 min caused an increase in turbidity on the sensor surface (especially for the blank sensor) kept in aqueous solutions. Since the observed absorbance is recorded against that of the blank, this caused a decrease in effective absorbance values.

### 3.6. Acetone–water ratio

The analyte solution composition was optimized as 30% acetone + 70% water (v/v) in this study, because higher acetone ratios gave rise to the transfer of the DCHA–TNT charge-transfer complex from the sensor surface to the solution phase, while lower ratios may cause incomplete dissolution or resuspension of the analyte (TNT has very limited solubility in water). This composition of the solvent was optimized (Fig. 3), as TNT in 30% acetone-containing aqueous solution gave the highest (net) sensor response. It is known from the literature that spectrophotometric methods of TNT assay based on the formation of Meisenheimer or Janowsky anions by the addition of hydroxide or acetate anions to the aromatic ring of TNT, respectively, are strongly affected by the presence of water, and  $\text{H}_2\text{O}$  more than 17.5% in the solvent mixture causes rapid obscuring of charge-transfer bands [18,22]. As a result, the widely used CRREL or Jenkins' method [22] is not capable of determining TNT in groundwater or humid soils. Obviously, a requirement for complete drying of humid soils containing

unknown amounts of TNT prior to analysis poses a great risk to laboratory safety, and may additionally cause some thermal degradation of TNT residues in soil. With its relative independence from excessive water (i.e., up to 70% by vol.), the proposed method is a great improvement over Meisenheimer or Janowsky anions-based spectrophotometric methods, and is capable of quantifying TNT in humid soil and groundwater without preliminary operations.

### 3.7. Sensor response to TNT solutions, and analytical figures of merit

The absorbances of the charge-transfer complexes developed on the sensor (against the blank sensor) for TNT solutions containing  $5\text{--}50 \text{ mg L}^{-1}$  TNT in 30% acetonated aqueous solution were recorded against concentration to yield a calibration line (figure not shown) with the equation:

$$A_{530\text{nm}} = 0.0124 C_{\text{TNT}(\text{mgL}^{-1})} + 0.116 (\text{correlation coefficient : } r = 0.9948)$$

with a LOD of  $3.0 \text{ mg L}^{-1}$  and a limit of quantification (LOQ) of  $10.0 \text{ mg L}^{-1}$ . Since the calibration line did not pass through the origin, unknown TNT concentrations should be calculated with the help of this calibration equation. Each data point on this line was the average of three determinations ( $N=3$ ) with a relative standard deviation (RSD) varying between 5.3 and 7.7%, depending on the concentration. Considering that the US-EPA limit of TNT decontamination for remediated sites is 50 ppm ( $\text{mg g}^{-1}$  of soil) and that the Jenkins' method extracts 20 g of contaminated soil with 100 mL acetone [24], the proposed method is sensitive enough to quantitatively analyze this limiting concentration level in soil. The CT spectra of solutions used in constructing the calibration curve are shown in Fig. 4.

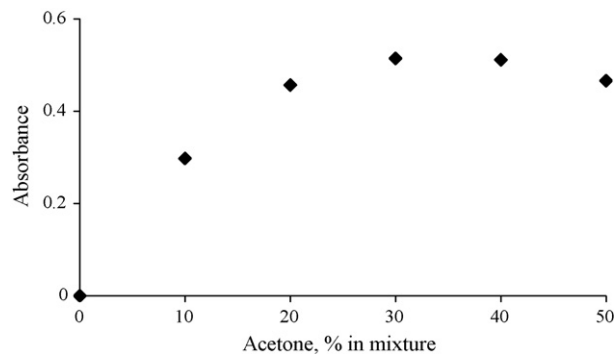


Fig. 3. Variation of the sensor absorbance (i.e., net absorbance, meaning the difference between sample and blank absorbances) as a function of acetone content of the analyte solution ( $30 \text{ mg L}^{-1}$  TNT was measured in each case at 530 nm wavelength).



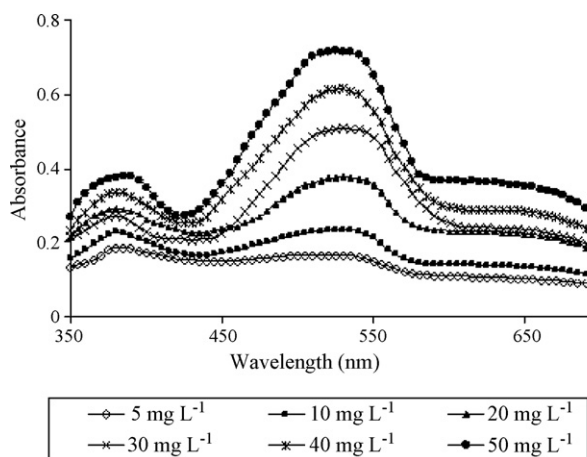


Fig. 4. The CT spectra of 5–50 mg L<sup>-1</sup> TNT solutions (recordings were made on the sensor immersed in the analyte solution against that in the blank).

### 3.8. Sensor response to tetryl solutions, and analytical figures of merit

The absorbances of the charge-transfer complexes developed on the sensor (against the blank sensor) for tetryl solutions containing 5–40 mg L<sup>-1</sup> tetryl in 30% acetonated aqueous solution were recorded against concentration to yield a calibration line (figure not shown) with the equation:

$$A_{460\text{nm}} = 0.0269 C_{\text{tetryl}(\text{mgL}^{-1})} - 0.0624 \text{ (correlation coefficient : } r = 0.9929)$$

with a LOD of 3.8 mg L<sup>-1</sup> and a LOQ of 12.6 mg L<sup>-1</sup>. Since the calibration line did not pass through the origin, unknown tetryl concentrations should be calculated with the help of this calibration equation. Each data point on this line was the average of three determinations ( $N=3$ ) with a RSD varying between 6.5 and 13.1%, depending on the concentration. The CT spectra of solutions used in constructing the calibration curve are shown in Fig. 5.

### 3.9. Magnitude of correlation coefficients for the calibration equations of TNT and tetryl

An optical sensor that has entrapped a colorimetric reagent will mainly undergo three types of interactions with incident light: absorption, scattering, and reflection. In a polymeric sensor film, the latter two interactions will play a stronger part than in a transpar-

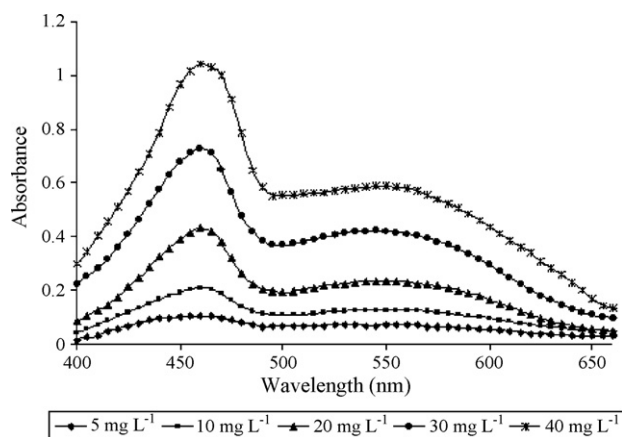


Fig. 5. The CT spectra of 5–40 mg L<sup>-1</sup> tetryl solutions (recordings were made on the sensor immersed in the analyte solution against that in the blank).

ent solution, and therefore, the absorptimetric response of a sensor film will have a less linear correlation against analyte concentration than that of a corresponding solution. Thus, the correlation coefficients obtained for TNT and tetryl in this work are perfectly acceptable. The following examples of this argument are extracted from literature sources (none of them has  $r=0.999$ ):

- (i) Bis(acetylacetonethylenediamine)-tributylphosphin Co(III) tetraphenylborate complex coated on triacetylcellulose; correlation coefficient of absorbance against ammonia concentration:  $r=0.9981$  [34].
- (ii) Pyrogallol red immobilized on cellulose acetate film; correlation coefficient of absorbance against Co(II) concentration:  $r=0.9967$  [35].
- (iii) 4-(2-Pyridylazo)-resorcinol immobilized on triacetylcellulose membrane; correlation coefficient of absorbance against log Hg(II) concentration:  $r=0.9984$  [36].
- (iv) Bis-8-hydroxyquinoline immobilized on XAD-7 resin optical fiber reflectance sensor for *p*-aminophenol detection; correlation coefficient of reflectance against *p*-aminophenol concentration:  $r=0.9934$  [37].

### 3.10. Investigation of tetryl interference to extractive-spectrophotometric determination of TNT with DCHA in aqueous solution

Using the DCHA extractive-spectrophotometric determination technique for TNT in aqueous solution [25], increasing concentrations of tetryl (2–10 mg L<sup>-1</sup>) were added to a fixed concentration (10 mg L<sup>-1</sup>) of TNT. The spectra of the charge-transfer complexes in DCHA phase extracted from 50% acetonated aqueous solution show that tetryl at comparable concentrations interfered seriously with TNT determination with the proposed assay (figure not shown). The same spectra also show that additivity of absorbances with respect to Beer's law exists within the linear concentration range, and that a mixture of TNT and tetryl (*e.g.*, in the tetryl-cyclonite composite explosive) can be analyzed using this additivity principle by recording the absorbances of the unknown mixture at the analytical wavelengths of 530 and 460 nm.

### 3.11. Percentage of amine remaining in the sensor upon standing in air and under water

The amounts of DCHA remaining in the sensor (as the percentage of originally entrapped amount) as a function of time of standing in air and under water are given in Figs. 6 and 7, respectively. It can be deduced from Figs. 6 and 7 that approximately

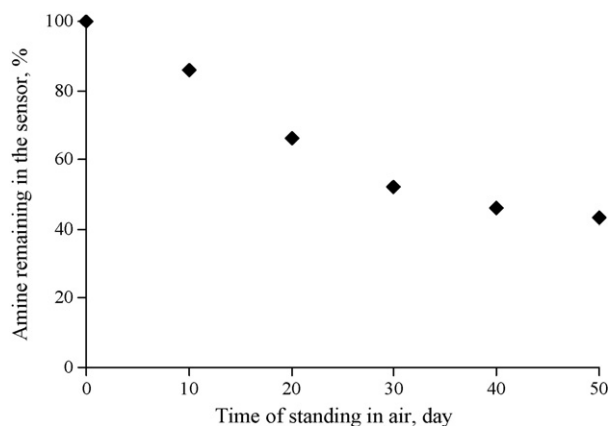
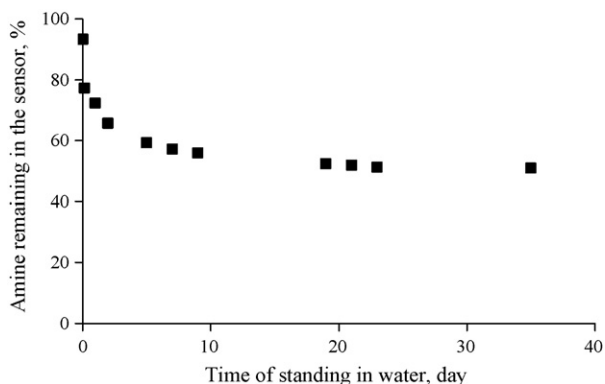


Fig. 6. The amount of DCHA remaining in the sensor (as the percentage of originally entrapped amount) as a function of time of standing in air.



**Fig. 7.** The amount of DCHA remaining in the sensor (as the percentage of originally entrapped amount) as a function of time of standing under water.

half of the original amine remains in the sensor after 35 days of standing either in air or under water. Although this amount of remaining amine would still yield a sensor response at lower sensitivity, it can be recommended that the sensor films be kept in a desiccator saturated with DCHA vapor prior to use. For mobile use on-site, the colorimetric sensors may be transferred to the site sealed in polyethylene bags. The sensor films give their optimal colorimetric response after 15 min of contact with 30% acetonated aqueous solution of TNT. For high analytical precision and accuracy, the absorbance due to charge-transfer complexation of the analyte should be read within 30 min of contact of the films with aqueous medium.

### 3.12. Tolerance levels for potential interferences

The non-interference of nitro-explosives and explosive related materials other than tetryl (e.g., RDX, PETN, picric acid, DNT, and dinitrophenol) as previously shown by the authors for liquid–liquid extraction of TNT+interferent mixture solutions with DCHA [25] was confirmed in this study at 10-fold levels of these nitro-explosives compared to 20 mg L<sup>-1</sup> TNT (table not shown). Some common oxidants (dichromate and bromate) and reductants (iodide and sulfite) at 50-fold levels were also shown not to interfere. The recoveries for TNT in the presence of a number of cations and common anions in admixture with 20 mg L<sup>-1</sup> TNT are tabulated in Table 3. As is apparent from these data, the proposed method is applicable to TNT assay in soil and groundwater containing a large variety of electrolytes, and constitutes a substantial advantage over the CRREL/Jenkins' method [22]. The method was also insensitive to small changes in initial pH of solutions, as DCHA at the sen-

**Table 3**

The recoveries for TNT in the presence of a number of cations and common anions in admixture with 20 mg L<sup>-1</sup> TNT.

Interferent ion	Interferent/analyte mass ratio	Recovery of TNT (%)
Cu <sup>2+</sup> <sup>a</sup>	10	80.9
	50	103
	100	96.7
Pb <sup>2+</sup>	50	102
	100	139
K <sup>+</sup>	100	97.9
SO <sub>4</sub> <sup>2-</sup>	100	112
Cl <sup>-</sup>	100	107
NO <sub>3</sub> <sup>-</sup>	100	108

<sup>a</sup> A small excess of Cu<sup>2+</sup> possibly consumes the amine at the sensor–solution interface by complexation, while a higher excess probably adds up to the observed absorbance by adsorption of copper-amines onto the sensor. This adsorption is reversible, as water-washed sensors retained their initial absorbance.

sor/solution interface constituted a buffering conjugate base/acid pair (e.g., R<sub>2</sub>NH/R<sub>2</sub>NH<sub>2</sub><sup>+</sup>).

### 3.13. Validation of the proposed method against HPLC

The proposed sensor determination was validated against HPLC on five different samples of Comp B (declared by the manufacturer MKEK to contain 39% TNT) diluted to a final concentration of 80 mg L<sup>-1</sup>. A typical chromatogram of Comp B composite explosive sample showed the peaks of TNT and RDX (Fig. 8). The retention time of the main peak was 6.9 min for RDX and 13.7 min for TNT.

The calibration line for HPLC determination of pure TNT in the concentration range of 5–100 mg L<sup>-1</sup> was:

$$\text{Peak area} = 6.13 \times 10^4 C_{\text{TNT(mg L}^{-1})} - 1.53 \times 10^5 \quad (r = 0.9996)$$

By means of this calibration line, the TNT content of five different samples of Comp B (each of 80 mg L<sup>-1</sup> initial concentration) were analyzed with HPLC as: 39.10, 39.15, 41.19, 42.65, and 40.84% (mean = 40.59%). On the other hand, using the recommended colorimetric sensor method, the same samples were analyzed as: 40.22, 38.51, 39.31, 45.86, and 44.55% (mean = 41.69%). Statistical analysis was made using the one-way ANOVA (ANALYSIS OF VARIANCE) approach with the aid of *t*- and *F*-tests [38].

The *t*-test of comparison of the means yielded:

Proposed method, mean and standard deviation:  $\bar{a}_1 = 41.69$ ,  $s_1 = 3.298$ ,  $N = 5$ .

Reference method, mean and standard deviation:  $\bar{a}_2 = 40.59$ ,  $s_2 = 1.497$ ,  $N = 5$ .

Pooled estimate of standard deviation:  $s = 2.561$ .

$$t = (41.69 - 40.59) / 2.561 (1/5 + 1/5)^{1/2} = 0.679$$

$$|t|_8 = 2.31 \text{ (from } t\text{-table for } P = 0.05); t_{\text{exp.}} < t_{\text{crit.}}, \text{ or } 0.68 < 2.31$$

There was no significant difference at 95% confidence level between the means of the recommended (colorimetric sensor) and reference (HPLC) methods.

The *F*-test of comparison of the variances yielded:

$$F_{\text{exp.}} = (3.298/1.497)^2 = 4.853; \text{ the critical value from } F\text{-table};$$

$$F_{4,4} = 6.388 \quad (P = 0.05)$$

$$F_{\text{exp.}} < F_{4,4}, \text{ or } 4.853 < 6.388.$$

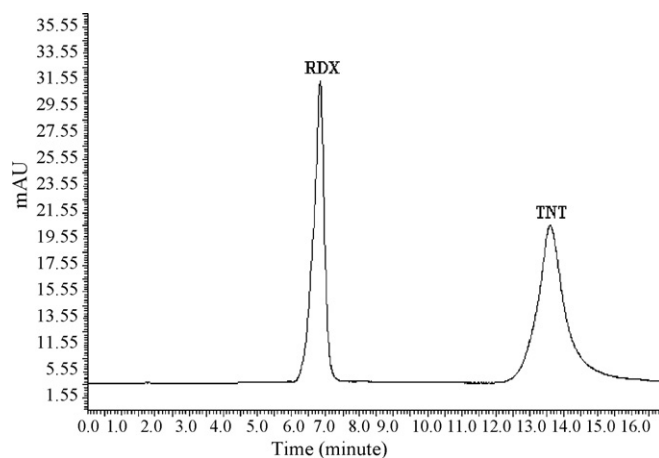


**Fig. 8.** The chromatogram of Comp B composite explosive (80 mg L<sup>-1</sup>) sample showing the peaks of TNT and RDX.

There was no significant difference at 95% confidence level between the precisions of the recommended (colorimetric sensor) and reference (HPLC) methods.

#### 4. Conclusions

Rapid and low-cost chemical sensing of explosive traces or residues in soil and post-blast debris for environmental and criminological purposes with the use of sensors has recently gained importance. Thus, an inexpensive colorimetric sensor was synthesized from PVC, DOP, and DCHA, and was effectively used in quantitative TNT and tetryl assay in 30% acetonated aqueous solutions. The sensor can also be used for qualitative identification, as it gives a violet color with TNT and an orange color with tetryl. The sensor is not affected by other nitro-explosives, such as RDX, PETN, DNT, and picric acid. As a superiority to the widely used CRREL/Jenkins' colorimetric method or other sensing methods in literature that are not tolerant towards water, the proposed TNT assay is applicable to humid soils and groundwater. The sensor is insensitive to small changes in initial pH of solution and to a wide range of common electrolytes. The sensor is suitable for field colorimeters (maximum absorption wavelength for TNT is 530 nm), and gives a fairly rapid and sensitive response (the LOD for TNT being  $3 \text{ mg L}^{-1}$ ). The sensitivity of the method (for soil leached with acetone at a liquid/solid ratio of 5, LOQ =  $50 \text{ mg kg}^{-1}$ , equivalent to US-EPA limit of decontamination) is sufficient to monitor the clean-up operations of remediated sites contaminated with TNT. The proposed method was statistically validated against the HPLC reference method using a composite explosive sample of Comp B.

#### Acknowledgements

The authors wish to express their gratitude to the Ministry of National Defence, Office of Technical Services (Milli Savunma Bakanligi, Teknik Hizmetler Daire Baskanligi) and MKEK (Makine Kimya Endüstrisi Kurumu) for the donation of TNT, tetryl and Comp B samples. Additionally, the authors thank TUBITAK (Turkish Scientific and Technical Research Council) for the research projects 105T402 and 107T698.

One of the authors (Dr. Erol Erçağ) extends his thanks to Istanbul University Bilimsel Arastirma Projeleri (BAP) Yurutucu Sekreterligi for the support given to Project UDP-510/07062005, which enabled him to present a part of this work in the 40th IUPAC Congress 2005 International Meeting in Beijing, China.

#### References

- [1] J. Yinon, S. Zitrin, *Modern Methods and Applications in Analysis of Explosives*, Wiley, New York, 1993, p. 316.
- [2] D.S. Moore, *Sense Imaging* 8 (2007) 9–38.
- [3] P. Kolla, *Angew. Chem. Int. Ed. Engl.* 36 (1997) 800.
- [4] G.A. Buttigieg, A.K. Knight, S. Denson, C. Pommier, M.B. Denton, *Forensic Sci. Int.* 135 (2003) 53–59.
- [5] P. Rodacy, P. Leslie, *Proceedings of the 1993 U.S. EPA/A&WMA International Symposium*, vol. 2, 1993, pp. 823–829.
- [6] J. Avolio, R. DeBono, P. Radwanski, *Proceedings of the International Symposium on Field Screening Methods for Hazardous Wastes and Toxic Chemicals*, Las Vegas, Nevada, February 22–24, 1995, p. 1037.
- [7] F.J. Thomas, D.C. Leggett, C.L. Grant, C.F. Bauer, *Anal. Chem.* 58 (1986) 170.
- [8] R. Bongiovanni, G.E. Podolak, L.D. Clark, D.T. Scarborough, *Am. Ind. Hyg. Assoc. J.* 45 (1984) 222–226.
- [9] K.L. Bjella, *U.S. Cold Regions Research and Engineering Laboratory ERDC/CRREL TN-05-2*, 2005.
- [10] G. Özhan, S. Topuz, B. Alpertunga, *II Farmaco* 58 (2003) 445–448.
- [11] D.H. Fine, W.C. Yu, E.U. Goff, *J. Forensic Sci.* 29 (1984) 732.
- [12] H.R. Beller, K. Tiemeier, *Environ. Sci. Technol.* 36 (2002) 2060.
- [13] C. Heiss, M.G. Weller, R. Niessner, *Anal. Chim. Acta* 396 (1999) 309–316.
- [14] B.T. Oh, G. Sarath, P.J. Shea, R.A. Drijber, S.D. Comfort, *J. Microbiol. Methods* 42 (2000) 149–158.
- [15] R.E. Hummel, A.M. Fuller, C. Schöllhorn, P.H. Holloway, *Appl. Phys. Lett.* 88 (2006) 231903.
- [16] A.B. Crockett, T.F. Jenkins, H.D. Craig, W.E. Sisk, *U.S. Army Corps of Engineers, CRREL, Special Report 98-4*, 1998.
- [17] D. Royds, S.W. Lewis, A.M. Taylor, *Talanta* 67 (2005) 262–268.
- [18] A. Üzer, E. Erçağ, R. Apak, *Anal. Chim. Acta* 505 (2004) 83–93.
- [19] A. Üzer, E. Erçağ, R. Apak, *Forensic Sci. Int.* 174 (2008) 239–243.
- [20] C.A. Heller, S.R. Grenl, E.E. Erickson, *Anal. Chem.* 54 (1982) 286.
- [21] T.F. Jenkins, *US Army Corps of Engineers, CRREL, Special Report 90-38*, 1990.
- [22] T.F. Jenkins, M.E. Walsh, *Talanta* 39 (1992) 419.
- [23] T.F. Jenkins, M.E. Walsh, in: V. Lopez-Avila (Ed.), *Current Protocols in Analytical Chemistry*, vol. 2, Wiley, New York, Unit 2D, 1998.
- [24] A.D. Hewitt, T.F. Jenkins, *U.S. Army Corps of Engineers, CRREL, Special Report 99-9*, 1999.
- [25] A. Üzer, E. Erçağ, R. Apak, *Anal. Chim. Acta* 534 (2005) 307–317.
- [26] S. Singh, *J. Hazard. Mater.* 144 (2007) 15–28.
- [27] Y. Zhang, W.R. Seitz, C.L. Grant, D.C. Sunberg, *Anal. Chim. Acta* 217 (1989) 217–227.
- [28] L.M. Dorozhkin, V.A. Nefedov, A.G. Sabelnikov, V.G. Sevastjanov, *Sens. Actuators B* 99 (2004) 568.
- [29] H.A. Benesi, J.H. Hildebrand, *J. Am. Chem. Soc.* 71 (8) (1949) 2703–2707.
- [30] R.S. Mulliken, *J. Am. Chem. Soc.* 74 (1952) 811.
- [31] E. Bunce, A.R. Norris, K.E. Russell, *Q. Rev. Chem. Soc.* 22 (1968) 123.
- [32] M. Hasani, M. Irandoust, M. Shamsipur, *Spectrochim. Acta A* 63 (2006) 377.
- [33] K. Ertekin, S. Alp, C. Karapire, B. Yenigül, E. Henden, S. İcli, *J. Photochem. Photobiol. A: Chem.* 137 (2000) 155–161.
- [34] G. Absalan, M. Soleimani, M. Asadi, M.B. Ahmadi, *Anal. Sci.* 20 (2004) 1433.
- [35] A.A. Ensafi, A. Aboutalebi, *Sens. Actuators B* 105 (2005) 479.
- [36] A.A. Ensafi, M. Fouladgar, *Sens. Actuators B* 113 (2006) 88.
- [37] H. Filik, M. Hayvalı, E. Kılıç, R. Apak, D. Aksu, Z. Yanaz, T. Çengel, *Talanta* 77 (2008) 103.
- [38] J.C. Miller, J.N. Miller, *Statistics for Analytical Chemists*, 3rd ed., Ellis Horwood and Prentice Hall, New York and London, 1993.



# Molecularly imprinted sol gel for ibuprofen: An analytical study of the factors influencing selectivity

Keith Farrington, Fiona Regan\*

School of Chemical Sciences, Dublin City University, Dublin 9, Ireland

## ARTICLE INFO

### Article history:

Received 15 April 2008  
Received in revised form  
26 November 2008  
Accepted 2 December 2008  
Available online 11 December 2008

### Keywords:

Molecularly imprinted sol gels  
Ibuprofen  
Solid phase extraction  
Swelling/shrinkage  
Shape selectivity  
 $\pi$ – $\pi$  stacking

## ABSTRACT

This paper describes the preparation and testing of a sol gel specific for the non-steroidal anti-inflammatory drug ibuprofen. Ibuprofen was selected as a model compound due to the fact that it contains a number of structural and functional analogues, in this case ketoprofen and naproxen. In order to study the specific criteria affecting selectivity in sol gels, three sol gels were prepared for ibuprofen utilising two and three functional silane systems. The relative rebinding of each of the three compounds to the sol gels was assessed by % recovery in solid phase extraction. The results of the experiments indicate that along with the functionality imparted to the sol gel by the development of template-monomer complexes a major determinant of selectivity is shape selective memory. The utilisation of a three monomer system affords the cavity recognition based on the formation of  $\pi$ – $\pi$  stacking interactions, hydrogen bonding, van der Waals forces, electrostatic interactions and shape complementarity and minimises cross reactivity. In addition real sample analysis has been performed on urine samples containing ibuprofen and metabolites showing specific preconcentration.

© 2009 Elsevier B.V. All rights reserved.

## 1. Introduction

Molecular imprinting technology is now an established technique for the production of synthetic receptors. The mechanism of imprinting is based on the prearrangement of a template–functional monomer complex in a facilitating solvent (porogen). Applications of MIPs in analytical chemistry are diverse and include solid phase extraction [1–3], binding assays [4,5] and incorporation into biosensors [6,7].

Pauling [8], first proposed the concept of prearrangement of monomer units around a chemical species (in this case an antigen) in terms of explaining the production of antibodies in mammalian systems. The arrangement of these monomer units around the antigen was achieved by weak intermolecular interactions such as electrostatic interactions, van der Waals forces and by hydrogen bonding. Although abandoned as an immunological concept, the work of Pauling resurfaced in the studies of Dickey [9]. Dickey noted that a silica gel synthesised in the presence of methyl orange exhibited selective memory for this compound when rebinding experiments were performed in the presence of related compound structures (n-butyl, n-propyl and ethyl orange). This (early) process whereby nanostructured silica based solids exhibit selective molecular recognition is now referred to as the sol gel process. Imprinted

sol gels are a rapidly developing area of synthetic receptor science. They have had application in sensor development [10], solid phase extraction or selective clean up [11] for analysis of the specific compounds propranolol [12], 2,4-dichlorophenoxyacetic acid [13], nafcillin [14], for selective discrimination of methylxanthines [15] and in protein/peptide recognition [16,17].

Sol gels are based on a silica backbone and inorganic-organic hybrid materials based on organically modified silicas (ormosils) offer an attractive alternative to molecularly imprinted polymers. Indeed imprinted sol gels possess, numerous significant advantages over MIPs, namely, ease of preparation, gelation at ambient temperatures (particularly important when preserving weak interactions). In addition to this sol gels exhibit significantly higher porosity and surface area than MIPs along with negligible swelling in organic solvents and good optical (transparent) properties [18].

Sol gel chemistry utilises mild acid- or base-catalysed conditions to achieve hydrolysis and condensation of numerous silane monomers. Gelation of the silane(s) such as tetraethyl orthosilicate (TEOS), 3-Aminopropyl triethoxysilane (APTES) and phenyltriethoxy silane (PTMOS) under aqueous conditions with alcohol (usually ethanol or ethoxyethanol) in the presence of a template molecule leads to the imprinted sol gel. The pH of the mixture will determine whether the dominant process is hydrolysis or condensation. At low pH, i.e. acid catalysed sol gels, condensation occurs at an enhanced pace in comparison to hydrolysis. The result of this being that polymer growth is favoured over cross-linking. The resultant acid catalysed gel is optically transparent with very small pores

\* Corresponding author. Tel.: +353 17005765; fax: +353 18360830.  
E-mail address: [fiona.regan@dcu.ie](mailto:fiona.regan@dcu.ie) (F. Regan).

(2–50 nm) and high surface area (>200 m<sup>2</sup>/g). Sol gels have significant potential in the development of thin films and layers. A sol gel film has been developed for the analysis of propranolol [12]. A direct comparison between the sol gel and the acrylic based molecularly imprinted polymer was performed. The findings were that the sol gels exhibited a lower total uptake of propranolol but significantly lower non-specific binding. Furthermore, the binding was found to be abrogated when aqueous solutions were replaced with organic solvents. Since it is known that sol gels do not exhibit the same degree of swelling as MIPs do, the loss of affinity may be due to shrinkage of sol gels. Sol gels in bulk form however have strong potential for use in solid phase extraction and recently these applications have been highlighted [11,19]. Given that swelling and changes in pH should not be as significant an issue as with MIPs, this means that the internal structure of the nanocavities within the sol gel should be maintained when loading in organic solvents or at lower pHs. Furthermore given that the nature of the functional interactions is non-directional in nature (hydrogen bonding, electrostatic, van der Waals) spatial complementarity is a considerable determinant of the potential of sol gel selectivity. Sol gels have been employed for the preparation of catalytic materials [20]. Here it was shown that the amorphous microporous oxide retained structural memory for the kinetic diameter of the alcohol used. This is indicative of the shape of the molecule being a determinant or at least a major component of selectivity. This phenomenon has been further characterised [21]. In this study the imprinting of amorphous bulk silicas with single aromatic rings containing up to three 3-aminopropyltriethoxysilane side groups was performed. The triethoxysilane portion of the molecules side groups was incorporated into the silica framework during synthesis. The aromatic portion is cleaved thus creating a cavity in which the aminopropyl groups are spatially orientated and covalently attached to the pore surface. Leung et al. [13] have employed a tailor made organosilane – 3-[*N,N*-bis(9-anthrylmethyl)aminopropyltriethoxysilane as a functional monomer forming an acid base ion pair with the template 2,4-dichlorophenoxyacetic acid. The resultant sol gel material displayed good selectivity for 2,4-dichlorophenoxyacetic acid over acetic acid and benzoic acid. The authors here have concentrated on selectivity achieved by the functionalities within the pores of the sol gel rather than the shape of the cavity or hydrophobic interaction. A three monomer approach to the sol gel imprinting of lisinopril dehydrate [22] and a similar approach for 2-Aminopyridine was used [23]. It is likely that both chemical functionality and spatial complementarity of the binding cavities play significant roles in the potential selectivity of an imprinted sol gel.

This paper describes the study of the individual and combined factors which are responsible for selectivity in sol gels. The template chosen was ibuprofen, a member of the class of non-steroidal anti-inflammatory drugs (NSAIDs). Ibuprofen is indicated for rheumatoid arthritis and conditions involving inflammation. It is an inhibitor of cyclooxygenase 1, which is endogenously expressed in all human cells. In order to gain an enhanced understanding of factors affecting selectivity, three sol gels each of differing complexity and functionality have been prepared and their ability to selectively discriminate between ibuprofen and its structural and functional analogues, naproxen and ketoprofen have been studied. In the choice of functionalised siloxanes (analogous to functional monomers in MIPs) important functionalities such as hydrogen bond forming ability, electrostatic interactions and potential  $\pi$ – $\pi$  stacking interactions have been considered. Furthermore, the two and three monomer systems offer an increased complexity in terms of the molecular size and shape of the resultant nanocavities in the sol gel. It is proposed that the major determinant of selectivity is the spatial complementarity of the cavity, however, there is a significant contribution from functional interactions within the cavity.

## 2. Experimental

### 2.1. Materials

Tetraethoxysilane (TEOS), 3-Aminopropyltriethoxysilane (APTES) and phenyltrimethoxysilane (PTMOS) were purchased from Sigma–Aldrich, Dublin and used as received. Ibuprofen (C<sub>13</sub>H<sub>18</sub>O<sub>2</sub>, MW 206.28 g/mol), naproxen (C<sub>14</sub>H<sub>13</sub>O<sub>3</sub>, MW 230.26 g/mol) and ketoprofen (C<sub>16</sub>H<sub>14</sub>O<sub>3</sub>, MW 254.28 g/mol) were also purchased from Sigma–Aldrich, Dublin. All organic solvents were of HPLC grade and were purchased from Labscan, Dublin, Ireland.

### 2.2. Preparation of sol gels

All of the sol gels generated contained TEOS and one or both of APTES/PTMOS. The preparation consisted of two stages: firstly the hydrolysis without ibuprofen (template) and secondly condensation in the presence of ibuprofen. A 12 ml aliquot of 2-ethoxyethanol was mixed with 12 ml of TEOS. A 400  $\mu$ l quantity of PTMOS and 600  $\mu$ l of APTES were then added. Following this 400  $\mu$ l of concentrated HCl followed by 4 ml of water were then added and the mixture left stirring for 2 h at RT. After 2 h, 206.28 mg of ibuprofen in 20 ml water (min vol. ethanol) was added to 16 ml of the imprinting mixture and stirred for 10 min. A non-imprinted sol gel was prepared under the same conditions but with the omission of ibuprofen. The components of each of the sol gels are shown in Table 1. Condensation was allowed to progress at 80 °C for 16 h and then for 1 week at room temperature. Following this the sol gel was crushed with a mortar and pestle and sieved. Particles of 75 and 25  $\mu$ m diameter were collected by sieving. The crushed sol gels were then washed to remove the template by continuous stirring in a solution of hot methanol containing 10% acetic acid. Washing was repeated until no trace of ibuprofen could be detected by HPLC.

### 2.3. Computational studies

The DS Viewer pro suite from Accelrys was used to calculate the molecular volumes of ibuprofen, ketoprofen and naproxen.

### 2.4. Physical characterisation of sol gels

The infrared absorption spectra of the three of the sol gels were obtained on a Perkin Elmer GX FTIR system. Particle size measurements were performed on a Malvern mastersizer particle size instrument by light scattering technique. A 25 mg quantity of the sol gel was exposed to 5 ml of a range of solvents for 24 h in order to examine changes in the average particle sizes of the particles.

### 2.5. Nitrogen sorption measurements

Pore size and surface areas of the washed sol gels were obtained by Brunauer–Emmett–Teller analysis. The analysis was performed on an ASAP 2010 from RMIT Applied Chemistry (Micromeritics). A 250 mg quantity of sol gel was used for the analysis. The sample

**Table 1**  
The components of each of the sol gels.

Sol gel 1	Sol gel 2	Sol gel 3
2-EtOH (12 ml)	2-EtOH (12 ml)	2-EtOH (12 ml)
TEOS (12 ml)	TEOS (12 ml)	TEOS (12 ml)
APTES (600 $\mu$ l)		APTES (600 $\mu$ l)
	PTMOS (400 $\mu$ l)	PTMOS (400 $\mu$ l)
HCl (400 $\mu$ l)	HCl (400 $\mu$ l)	HCl (400 $\mu$ l)
H <sub>2</sub> O (24 ml)	H <sub>2</sub> O (24 ml)	H <sub>2</sub> O (24 ml)

was degassed for 12 h at 70 °C before analysis. Relevant information obtained from this method included surface area, total pore volume and pore diameters.

## 2.6. Rebinding analysis

For assessing the effect of different solvents on the % uptake of ibuprofen by the sol gels a 1 ml solution of ibuprofen at 1 µg/ml was added to 50 mg of the sol gels (and controls) in a 1 ml microcentrifuge tube in the solvents as shown in Fig. 3. The solutions were shaken for 4 h at room temperature and then centrifuged. The presence of ibuprofen in the supernatant was assayed by HPLC and the amount bound was calculated as:

$$\text{Total ibuprofen} - \text{free (supernatant)} = \text{bound ibuprofen}$$

## 2.7. Solid phase extraction studies

Empty solid phase extraction cartridges were washed with methanol before use. The cartridges were then dried and 200 mg of the dry sol gel (or corresponding control) was placed in between two frits. The cartridge was washed with 10% acetic acid in methanol and then with methanol 4 times until no trace of ibuprofen could be detected by HPLC. All SPE experiments were performed on a VacMaster SPE processing station manifold. Before analyte loading, the polymer was conditioned with 1 ml methanol, 1 ml acetonitrile and 1 ml water and then conditioned to the appropriate pH (pH 4–8) with water adjusted with dilute HCl. In the loading step, 1 µg/ml Ibuprofen, naproxen and ketoprofen was loaded in water at pH 4–8. For the washing step, 1 ml of 1% triethylamine (TEA) or 1% pyridine in acetonitrile or a 50:50 ratio of toluene: acetonitrile was used. Specifically bound material was eluted with 2 ml of methanol. The experiments were repeated in triplicate. After each experiment the cartridge was regenerated by washing with 3 ml of water and 3 ml of methanol.

## 2.8. High performance liquid chromatography (HPLC) instruments

HPLC was performed on a Hewlett Packard 1050 (HP 1050) LC system (pump, injector, detector) employing Chemstation software. The variable wavelength detector was operated at 220 nm for Ibuprofen determinations. For fluorescence applications the excitation wavelength was set at 290 nm and the emission at 350 nm.

A 10 µl injection volume was used. Separations were performed on a 25 cm × 4.6 mm, 5 µm Alltech Bravda BDS C18 column.

## 2.9. HPLC measurements

For the Ibuprofen/Naproxen/Ketoprofen selectivity studies the mobile phase used was a 52:28:20 ratio of water: acetonitrile: methanol. The mobile phase was adjusted to pH 3.2 with phosphoric acid. For urine analysis, the mobile phase used was a 50:50 ratio of 50 mM phosphoric acid: acetonitrile.

## 2.10. Real sample analysis

A volunteer was given a single dose of ibuprofen (200 mg) contained in a Nurofen™ tablet. Urine samples were collected at a 6 h interval. A 1 ml aliquot of each urine sample was passed through the sol gel SPE cartridge and washed and eluted as described in Section 2.7. Free ibuprofen was quantified with reference to a standard curve. To examine conjugated ibuprofen and ibuprofen metabolites, the urine samples were hydrolysed according to the methods of [24] and [25].

## 3. Results and discussion

### 3.1. Physical and morphological characterisation of the sol gels

The three sol gels prepared were analysed by IR spectroscopy post washing. Fig. 1 shows the most distinctive infrared absorption bands related to the generation of sol gels. In the 3400–3200 cm<sup>-1</sup> region, the stretching due to residual water and Si–OH stretching is observed. The band observed in all three samples at ~1050 cm<sup>-1</sup> is indicative of Si–O [26] stretching while that at 930 cm<sup>-1</sup> and 780 cm<sup>-1</sup> can be attributed to methyl C–H stretching. Sol gels 1 and 3 both contain a small band at ~1500 cm<sup>-1</sup> and this is absent in sol gel 2. This can be attributed to the incorporation of the amine group from the APTES silane (functional monomer) into the former sol gels and not the latter. The chemical nature of the polymers is unaltered by the presence of the template as there were no observable differences between each sol gel and its individual control non-imprinted sol gel (data not shown). Furthermore as has been described [15] the spectral features are consistent with organic modified silicas.

In contrast to MIPs, sol gels do not exhibit significant swelling [18]. In order to examine the potential degree of swelling further, a 50 mg amount of sol gel 3 was placed in equal volumes of a range

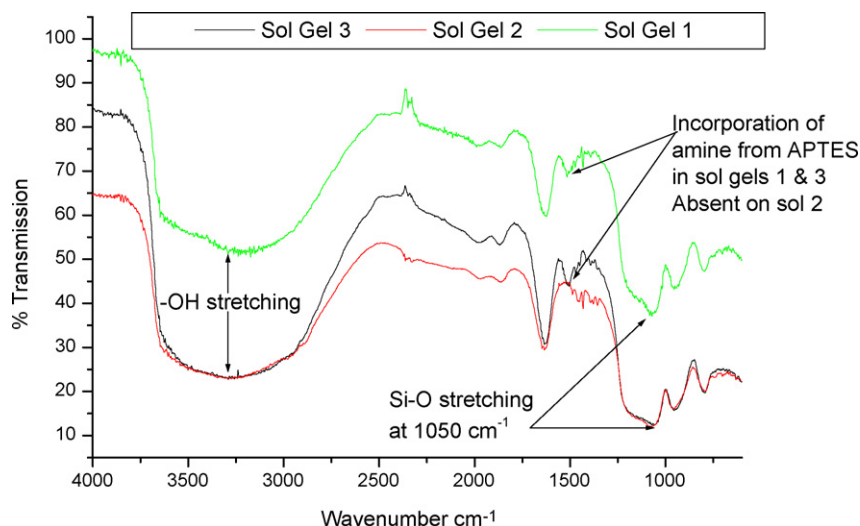
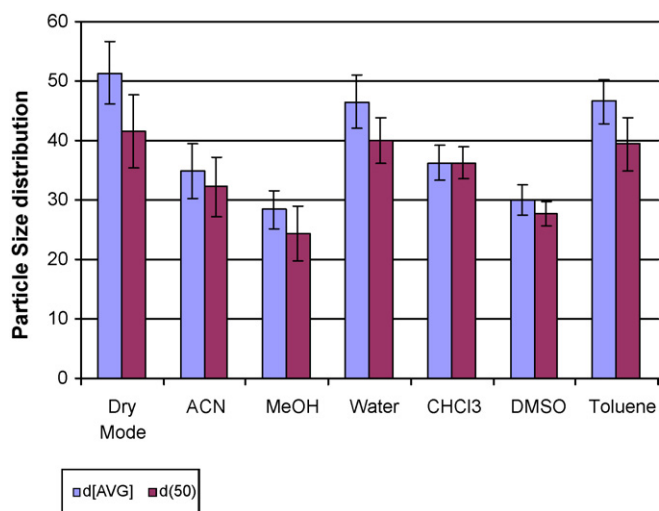


Fig. 1. FTIR absorption spectra for the three sol gels. Notable bands include the –OH at ~3250 cm<sup>-1</sup> and Si–O stretching at 1050 cm<sup>-1</sup>.



**Fig. 2.** The percentage shrinkage associated with particle size distribution measurements for sol gel 3. The sol gel was exposed to the solvents shown and the shrinking (relative to dry mode) is illustrated. Errors are based on the standard deviation of three experiments. The value  $d(50)$  is the value at which 50% of the particles in the solution lie while the value  $d[AVG]$  is the average particle size. Both can be interpreted as the mean of the particle sizes in a sample.

of organic and aqueous solvents and the average particle size of sol gel 3 was measured by particle size light scattering technology. The lack of swelling is an important characteristic in sol gels and will act to preserve the integrity of the binding cavity. However, sol gels have been reported to shrink [27] with an associated loss of sorption capacity. Fig. 2 shows the % shrinkage observed when sol gel 3 was dispersed in the relevant solvent for 4 h (stirring) followed by measurement of particle size. It was found that water caused the least reduction in average particle size and nonpolar solvents lead to only minimal shrinkage. Both polar protic (methanol) and polar aprotic (ACN and DMSO) cause greater observed shrinkage of the sol gel. It is somewhat surprising that the more polar solvents are observed to lead to greater shrinkage of the sol gel than the nonpolar solvents. Collinson [28] has reported that during drying, alcohol evaporates from the pores causing the sol gel to shrink. In this instance it is likely that the polar solvents diffuse into the pores and cavities of the sol gel replacing residual water and evaporate during the measurements leading to continued shrinking of the material. The nonpolar solvents may not diffuse into the pores as efficiently and hence their loss through evaporation has less of a shrinking effect on the pores. It is important to note that while sol gel materials do not swell to the same degree as conventional imprinted materials, their extended use at  $pH > 8$  is likely to lead to their destruction.

### 3.2. Initial rebinding studies

Fig. 3 shows the relative specific uptake of ibuprofen i.e. % rebinding in the sol gels minus that in the control sol gels for the three sol gels prepared. It was found that all three of the sol gels demonstrate enhanced rebinding in aqueous conditions. Furthermore, there is a cline of decreased rebinding given that the sol gels perform best in aqueous conditions followed by nonpolar (chloroform, toluene) then polar aprotic (acetonitrile, DMF) and then polar protic (methanol and ethanol). A similar trend has been noted by other authors [12]. In this study, it was pointed out that the increased rebinding of propranolol to the sol gel could result from the preferred solubility of the molecule in organic media relative to aqueous and this is in part justified by the partition coefficient of propranolol in the octanol/water system. Nonpolar solvents such

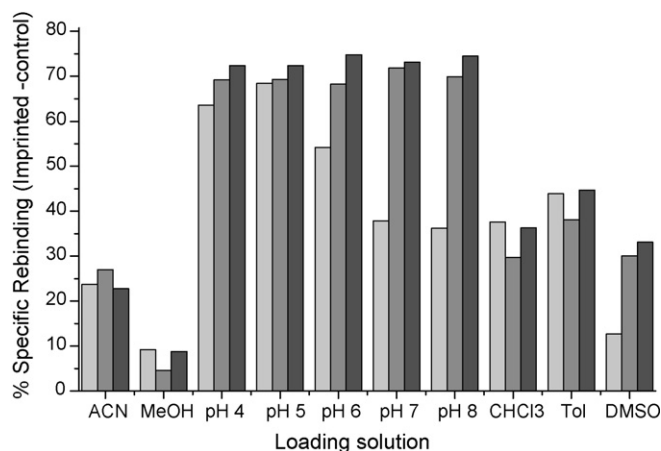
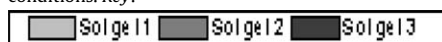


**Fig. 3.** Shows the specific rebinding of ibuprofen (uptake in imprinted sol gels minus that in non-imprinted) for the three sol gels under a range of organic and aqueous conditions. Key:



as chloroform would not be expected to interfere with hydrogen bonding whereas more polar solvents will form strong hydrogen bonds with the template thus precluding the formation of specific interactions with the functionalities in the pores [23].

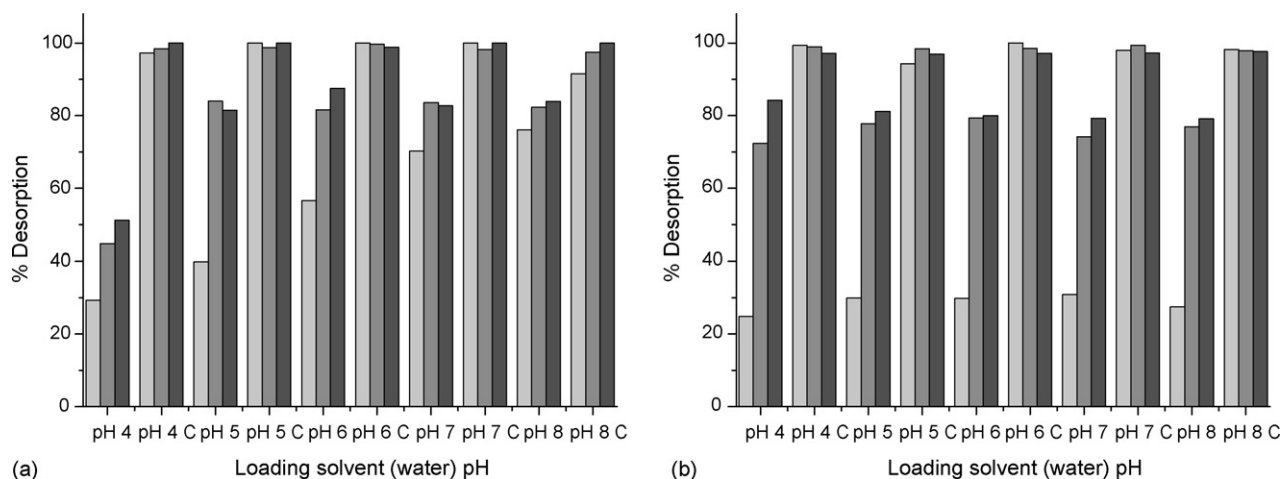
### 3.3. Effect of pH on rebinding

Fig. 3 also describes the effect of variation of pH on rebinding. Firstly, in regards to sol gel 1 (prepared with the APTES monomer), at pH 4 and 5 the rebinding is significantly greater than at pH 6–8 (>60% specific rebinding as opposed to 40–50%). Since the significant method of complex formation of ibuprofen with APTES is hydrogen bonding, a negatively charged molecule will be unable to participate in hydrogen bonding and hence this type of interaction is inhibited at higher pH where the molecule will be deprotonated. Some rebinding will still occur to the sol gel at higher pHs because of the presence of van der Waals, electrostatic forces, shape complementarity along with interactions of ibuprofen with the silanols of the sol gel. For these reasons an abrogation of rebinding will not be observed. This is further exemplified by the rebinding in aqueous conditions to sol gels 2 and 3 as shown in Fig. 4b (and sol gel 3) as shown in Fig. 5. Here the monomer used was PTMOS which will form  $\pi$ - $\pi$  stacking or hydrophobic interactions with ibuprofen and the nature of these interactions will not be significantly altered by changes in pH in the region 4–8. As such, a greater level of rebinding of ibuprofen to sol gels 2 and 3 is observed at all pHs examined.

Sol gel 3 contains both APTES and PTMOS as functionalised silane monomers. As part of the three monomer system, the significance of the hydrogen bonding interaction with APTES is reduced relative to other determinants of selectivity such as shape complementarity,  $\pi$ - $\pi$  stacking and hydrophobic interactions and hence these interactions can to a large extent compensate for the loss of the hydrogen bonding. The rebinding studies have shown that there are number of factors which combine to reach optimum binding conditions for all of the sol gels prepared which can be accounted for individually.

### 3.4. Selectivity studies using solid phase extraction

In order to analyse the individual and collective factors responsible for rebinding ibuprofen and for selectivity for ibuprofen over the structural analogues naproxen and ketoprofen, solid phase extraction (SPE) was performed utilising a range of loading and washing (desorption) conditions. Initially the desorption conditions were analysed to examine which washing conditions led to



**Fig. 4.** Selectivity study on sol gel 1 (a) and sol gel 2 (b). The % desorption from each of the sol gels was studied on washing with 1% pyridine under loading conditions ranging from pH 4–8. Key: .

optimal retention of the analyte of interest (ibuprofen) on the sol gel columns while minimising the cross reactivity.

Non-imprinted controls were also used to determine the specificity of the molecularly imprinted sol gels. For all of the sol gels and controls equal concentrations (1  $\mu\text{g/ml}$ ) of ibuprofen, naproxen and ketoprofen were loaded in under aqueous conditions at pH 4–8. A 1% solution of pyridine in water was used as the washing solvent in order to act as a competing amine for non-specifically bound material. This procedure was applied to all of the sol gels. Fig. 4a (sol gel 1), 4b (sol gel 2) and 5 (sol gel 3) shows the result of this approach. At a loading and washing pH of 5, the quantity of ibuprofen desorbed from the sol gel column is approximately 2.5 times less than both naproxen and ketoprofen. At pH 4 the effect is somewhat reduced but selectivity for ibuprofen over the analogues is still noticeable. Interestingly, as the pH of the loading and washing solutions increase, the selectivity for ibuprofen over the analogues is significantly reduced.

### 3.5. Contribution of hydrophobic interactions to selectivity

Sol gel 2 contained PTMOS as the functional monomer with the concomitant ability to form  $\pi$ – $\pi$  stacking (or hydrophobic) interac-

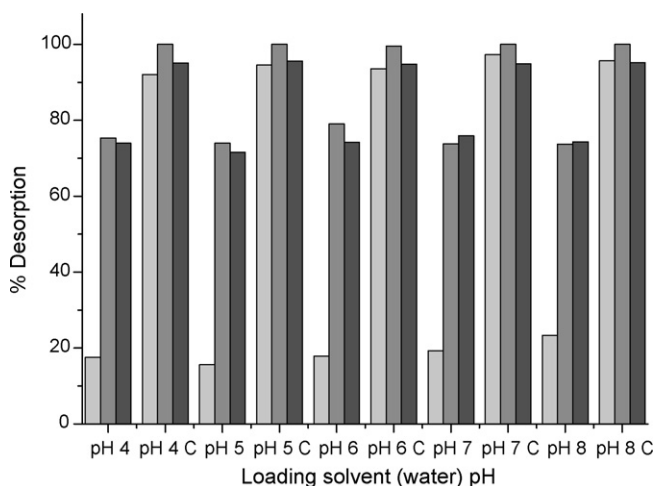


**Fig. 5.** Selectivity study on sol gel 3. The % desorption was studied on washing with 1% pyridine. Key: .

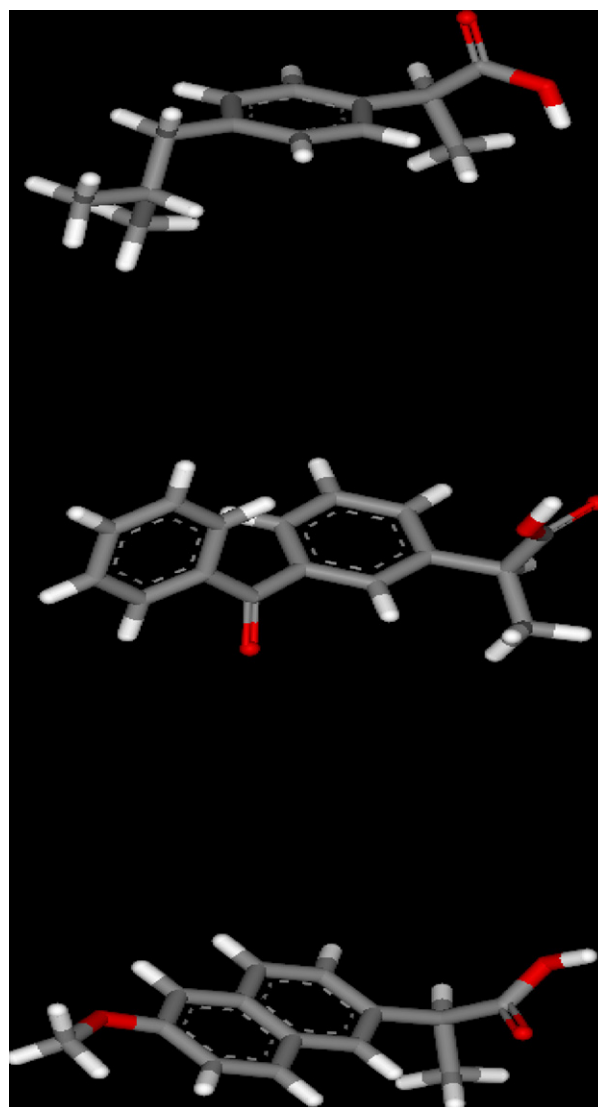


**Fig. 6.** The three-dimensional structures of the molecules used in the study: ibuprofen (above), ketoprofen (middle) and naproxen (below).



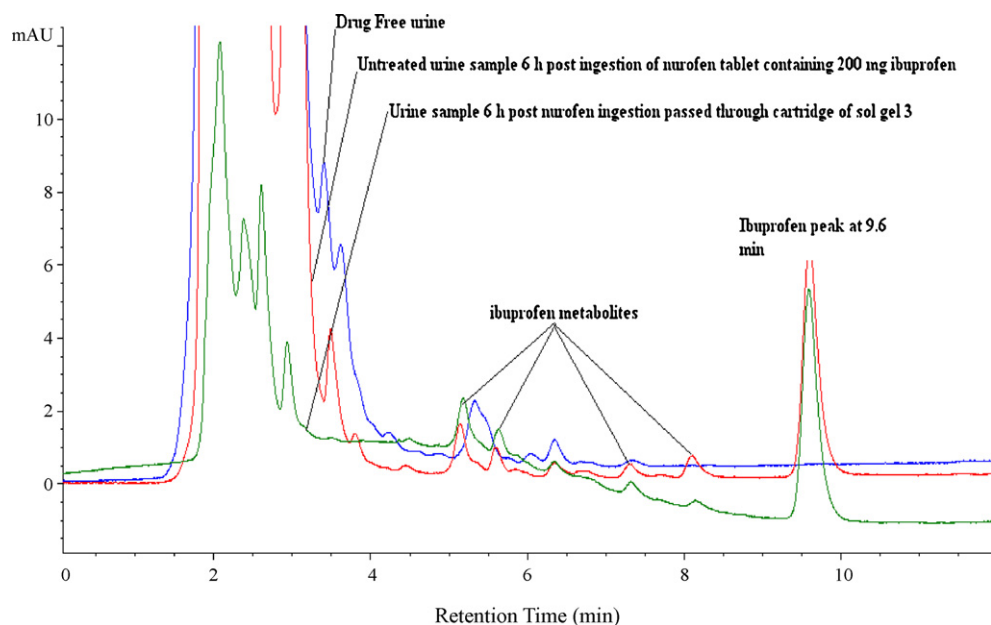


**Fig. 7.** HPLC chromatograms obtained following solid phase extraction of urine sample 6 h post ingestion of 200 mg ibuprofen using 200 mg of sol gel 3. Ibuprofen eluted at 9.6 min with the more polar unidentified species possibly the metabolites between 5.0 and 8.5 min.

tions with ibuprofen. However both naproxen and ketoprofen also contain aromatic rings, which could increase the probability of cross reactivity. Pyridine was again chosen as a component of the washing solution due to that fact that it would disrupt non-specific interactions by forming interactions with weakly bound material i.e. naproxen and ketoprofen and also to act as a competing amine for material which may be non-specifically bound. When 1% pyridine in acetonitrile was used as the washing solution, a large portion of the ibuprofen was removed from all of the sol gels. It was noticeable however that a larger proportion of the analogues were removed also. This is attributed to two reasons. Firstly as already mentioned, acetonitrile is a powerful eluting solvent but secondly, the nature of  $\pi$ - $\pi$  stacking is that it is a weak interaction (significantly weaker than hydrogen bonding). As a result of this a 1% solution of pyridine in water was applied as washing solution. For sol gel 2, Fig. 4b shows that when using this washing solution maximal selectivity for the sol gel towards ibuprofen was achieved. The relative strength of the mechanisms of interaction will differ considerably between the molecules. The three-dimensional structure of the three analogues is shown in Fig. 6. Ibuprofen contains a single aromatic ring with no electron withdrawing substituents directly on the ring. The shape of the molecule also affords steric manoeuvrability to a potential aromatic ring coming into close contact and allowing the formation of the  $\pi$ - $\pi$  electron delocalisation necessary. Regarding the three-dimensional structure of naproxen the naphthyl group will be significantly more stable than the single ring of ibuprofen. The result of this is that the electronic distribution will be more stable and hence will not participate as readily in a  $\pi$ - $\pi$  stacking arrangement. Regarding ketoprofen, the molecule possesses a carbonyl group between the two aromatic rings. The electron withdrawing nature of this substituent will adversely affect the ability of the ketoprofen aromatic rings to form  $\pi$ - $\pi$  stacking arrangements with PTMOS. Hence, the strength of  $\pi$ - $\pi$  stacking interactions between the PTMOS ring and each of the analogues will differ.

### 3.6. Shape complementarity

There is considerable difference in both size and shape between the three molecules used in this study. The Acceryls program cal-

culated the molecular volume of ibuprofen to be  $149.8 \text{ \AA}^3$  with that of naproxen at  $151.0 \text{ \AA}^3$ . Ketoprofen has a molecular volume of  $174.8 \text{ \AA}^3$ . In the field of molecularly imprinted polymers, the work of Spivak and co-workers [29] has shown the importance of shape selectivity in non-covalently imprinted polymers. For sol gels, it has been demonstrated [21] that imprinted silica could act as a shape selective base catalysts. To study this further a third sol gel (sol gel 3) was prepared using both APTES and PTMOS. It was expected that the resultant nanocavity would be even more size and shape selective for ibuprofen. As is shown in Fig. 5a, the selectivity for ibuprofen over naproxen and ketoprofen showed a marked increase over using APTES or PTMOS alone as the functional monomer. The binding of catecholamines on imprinted on silica-alumina gel shows a size selective effect [30]. Compared to norepinephrine and epinephrine, the smallest size of dopamine imprinted cavities only allowed rebinding to dopamine itself. Shape complementarity assumes an increased significance when a competing molecule to the analyte of interested is smaller in size or bulk (or at least of similar size). If the competing molecule was larger then it would be excluded from the binding cavity due to steric hindrance as is evident from the high level of desorption of ketoprofen.

Essentially, a molecule of similar size but difference shape i.e. ibuprofen will be allowed to manoeuvre within the naproxen sol gel binding cavity but with sub-maximal binding. The phenomenon is described as a "non-optimal spatial fit" with reference to MIPs. In effect, if a molecule lacks optimal shape complementarity to the spatial organisation of the binding cavity, the number of potential contact interaction points will be reduced. Since the optimal spatial fit is not achieved, rebinding will have to overcome an extra thermodynamic barrier hence a lower level of rebinding will be observed. The molecule exhibiting the optimal spatial fit, in this will demonstrate a better fit to the shape of the binding cavity and thus the sol gel (sol gel 3) shows enhanced selectivity towards ibuprofen. Despite the similar molecular volumes of ibuprofen and naproxen, the shapes of the molecules are significantly different. Hence, a molecularly imprinted sol gel prepared against ibuprofen demonstrates selective rebinding on the order of ibuprofen  $\gg$  naproxen > ketoprofen.

### 3.7. Application to real samples.

To demonstrate the applicability of the molecularly imprinted ibuprofen sol gel (sol gel 3) it was employed in a solid phase extraction procedure. A urine sample was taken from a volunteer at 6 h post ingestion of a single dose of 200 mg of ibuprofen contained in a Nurofen™ tablet. Ibuprofen undergoes extensive conjugation in the human body with the kidney being the main source of excretion. Only 1% of an ingested dose of ibuprofen is excreted as the free i.e. unconjugated molecule. Two major metabolites of ibuprofen are produced—carboxyibuprofen and hydroxyibuprofen for each of which exists stereoisomers. A 1 ml volume of urine at the above time point was loaded independently onto the sol gel column without pH adjustment. Although, selective clean up of the urine sample was achieved, a small recovery of ibuprofen along with several other peaks—most likely the analogues carboxyibuprofen and hydroxyibuprofen was obtained. This was attributed to the significant glucuronidation of ibuprofen. Given the large size of this molecule it will not be compatible with the spatial complementarity afforded by the sol gel cavity. In order to free the ibuprofen, the urine sample was subjected to a hydrolysis reaction as described [24,25]. This led to greatly increased peak areas for ibuprofen and also the unidentified peaks for the same sample which further indicates the probability of these peaks being those of the ibuprofen metabolites. The above procedure was repeated using the same loading and washing conditions as before. As can be seen from Fig. 7, quantitative clean up of the urine sample was achieved and the amount of unmetabolised ibuprofen in the sample at 6 h post ingestion was quantified at 7.07 µg/ml. Given the close structural similarity between ibuprofen and the two major metabolites, it is likely that the sol gel did not discriminate significantly between the metabolites. At a loading pH of 6–7, it was noted that the sol gel had greater retention of unidentified compounds over ibuprofen. This is likely due to the fact that both of the metabolites contain an extra hydroxyl group and will still be capable of undergoing hydrogen bonding with the APTES functionality while at pH 6–7 ibuprofen will be fully deprotonated. This is the most likely working hypothesis as the spatial differences between ibuprofen, carboxyibuprofen and hydroxyibuprofen are minimal.

### 4. Conclusion

The objective of this study was to enhance the understanding of the nature of selectivity in molecularly imprinted sol gels. This was achieved in two ways. Firstly, the physical characterisation of sol gels generated using different functional silanes and secondly by probing the selective rebinding abilities of each of the sol gels by varying experimental rebinding conditions and determining the optimum solid phase extraction procedure to extract ibuprofen from a mixture of ibuprofen, ketoprofen and naproxen. It was proposed that there are two determinants of selectivity in these sol gels. Firstly the chemical functionality imparted to the sol gel by

the functional silane e.g. APTES, PTMOS and secondly the specific geometric binding cavity which through spatial complementarity serves as a highly selective shape based exclusion cavity which allows entry of the analyte of interest (template) whilst refusing access to even analogues of the template depending on the level of spatial similarity of the analogue(s) with the template.

Furthermore, the potential applications of such highly selective sol gels have been demonstrated by solid phase extraction clean up and preconcentration of ibuprofen (and metabolites) from urine. The applications of this type of material are many and can be performed easily and economically. It is demonstrated that by understanding the nature of sol gel chemistry, specific and selective materials can be produced that can easily be used as solid phase sorbents or incorporated into analytical devices.

### Acknowledgement

The authors wish to thank the Irish Research Council for Science Engineering and Technology (IRCSET) for the funding provided.

### References

- [1] I. Ferrer, D. Barcelo, Trends Anal. Chem. 18 (1999) 180.
- [2] M.-C. Hennion, J. Chromatogr. A 856 (1999) 3.
- [3] C. Berggren, S. Bayouhd, D. Sherrington, K. Ensing, J. Chromatogr. A 889 (2000) 105.
- [4] R.J. Ansell, D. Kriz, K. Mosbach, Curr. Opin. Cell Biol. 7 (1996) 89.
- [5] B. Selligren, L. Andersson, Methods 22 (2000) 92.
- [6] Z. Cheng, E. Wang, X. Yang, Biosens. Bioelectron. 16 (2001) 179.
- [7] L. Fang, Y. Liu, Y. Tan, J. Hu, Biosens. Bioelectron. 19 (2004) 1513.
- [8] L. Pauling, J. Am. Chem. Soc. 62 (1940) 2643.
- [9] F.H. Dickey, Proc. Natl. Acad. Sci. U.S.A. 35 (1949) 227.
- [10] Z. Zhang, L. Nie, S. Yao, Talanta 69 (2006) 435.
- [11] D.-M. Han, G.-Z. Fan, X.-P. Yan, J. Chromatogr. A 1100 (2005) 131.
- [12] S. Marx, Z. Liron, Chem. Mater. 13 (2001) 3624.
- [13] M.K.-P. Leung, C.-F. Chow, M.-H. Lam, J. Mater. Chem. 11 (2001) 2985.
- [14] A. Fernandez-Gonzalez, R. Badia Laino, M.-E. Diaz Garcia, L. Guardia, A. Viale, J. Chromatogr. B 804 (2004) 247.
- [15] R.G. da Costa Silva, F. Augusto, J. Chromatogr. A 1114 (2006) 216.
- [16] Z. Zhang, Y. Long, L. Nie, S. Yao, Biosens. Bioelectron. 21 (2006) 1244.
- [17] Z. Zhang, H. Liao, H. Li, L. Nie, S. Yao, Anal. Biochem. 336 (2005) 108.
- [18] B. Selligren (Ed.), Molecularly Imprinted Polymers: Man-Made Mimics of Antibodies and their Applications in Analytical Chemistry, Elsevier, Amsterdam, 2001.
- [19] M. Cichna-Markl, J. Chromatogr. A 1124 (2006) 167.
- [20] M. Hunnius, A. Rufiska, W.F. Maier, Microporous Mesoporous Mater. 29 (1999) 389.
- [21] A. Katz, M.E. Davis, Nature 403 (2000) 286.
- [22] A. Olwill, H. Hughes, M. O'Riordain, P. McLoughlin, Biosens. Bioelectron. 20 (2004) 1045.
- [23] W. Cummins, P. Duggan, P. McLoughlin, Anal. Chim. Acta 542 (2005) 52.
- [24] S.C. Tan, S.H.D. Jackson, C.G. Swift, A.J. Hutt, J. Chromatogr. B 701 (1997) 53.
- [25] A.R.M. de Oliveira, F.J.M. de Santana, P.S. Bonato, Anal. Chim. Acta 538 (2005) 25.
- [26] R.M. Silverstein, F.X. Webster, Spectrometric Identification of Organic Compounds, sixth ed., Wiley, New York, 1997.
- [27] L. Guardia, R. Badia, M.E. Diaz-Garcia, Biosens. Bioelectron. 21 (2006) 1822.
- [28] M.M. Collinson, Cirt. Rev. Anal. Chem. 29 (1999) 289.
- [29] D.A. Spivak, R. Simon, J. Campbell, Anal. Chim. Acta 504 (2004) 23.
- [30] L. Tzong-Rong, Y.Z. Syu, Y.-C. Tasi, T.-C. Chou, C.-C. Liu, Biosens. Bioelectron. 21 (2005) 901.



# Use of ion mobility spectroscopy with an ultraviolet ionization source as a vanguard screening system for the detection and determination of acetone in urine as a biomarker for cow and human diseases

R. Garrido-Delgado<sup>a</sup>, L. Arce<sup>a</sup>, C.C. Pérez-Marín<sup>b</sup>, M. Valcárcel<sup>a,\*</sup>

<sup>a</sup> Department of Analytical Chemistry, University of Córdoba, Annex C3 Building, Campus of Rabanales, E-14071 Córdoba, Spain

<sup>b</sup> Department of Animal Medicine and Surgery, Faculty of Veterinary Medicine, University of Córdoba, Campus de Rabanales, E-14071 Córdoba, Spain

## ARTICLE INFO

### Article history:

Received 23 October 2008

Received in revised form 19 December 2008

Accepted 22 December 2008

Available online 15 January 2009

### Keywords:

Ion mobility spectrometry

Acetone

Urine samples

Screening

## ABSTRACT

An ion mobility spectrometer equipped with an ultraviolet lamp was used for the qualitative and quantitative determination of acetone in urine samples. This analyte can be used as a biomarker for some fat metabolism-related diseases in humans and cows. Samples require no pretreatment other than warming at 80 °C for 5 min, after which an N<sub>2</sub> stream is used to drive volatile analytes to the ion mobility spectrometer. The precision of the ensuing method, expressed as relative standard deviation (%RSD), is better in all cases than 6.7% for peak height and calculated at three levels of concentration. The analyte concentration range studied was from 5 to 80 mg L<sup>-1</sup>, its limit of detection in the aqueous matrix 3 mg L<sup>-1</sup> and recoveries from spiked urine samples 109 ± 3%. The calculated reduced mobility for acetone in the urine samples, 1.75 ± 0.04 cm<sup>2</sup> V<sup>-1</sup> s<sup>-1</sup>, was similar to previously reported values. Also, the results were consistent with those provided by test strips used for reference. The proposed method provides a new vanguard screening system for determining acetone in urine samples.

© 2009 Elsevier B.V. All rights reserved.

## 1. Introduction

Acetone is a highly volatile compound and a frequent object of research in biological and environmental samples [1]. This compound is harmful if swallowed or inhaled; also, it causes irritation to the skin, eyes and respiratory tract, and can affect the central nervous system. Exposure to acetone is usually assessed by measuring its concentration in urine, where its pressure is in equilibrium with pressure in the blood and alveoli [2]. Acetone can be produced *in vivo* via two different metabolic pathways, namely: decarboxylation of acetoacetate and dehydrogenation of isopropanol [3].

In this work, human and cow urine samples were used to determine acetone as a potential biomarker for some diseases in both species. In humans, an increased level of acetone in body fluids is frequently ascribed to uncontrolled diabetes—mostly diabetes mellitus or type I diabetes. Acetone levels must be carefully controlled in pregnant women with pre-existent diabetes or gestational diabetes. Acetone can also be produced during starvation, following excessive, prolonged bouts of vomiting [4]. This metabolite is not so important in humans as it is in cows. The presence of acetone in cow urine is the result of a negative energy balance in the third week post-partum [5]. During this period, cows are unable to eat

or absorb enough nutrients to meet their energy requirements for maintenance and milk production; this reduces their blood glucose levels and causes fat and protein reserves in the body to be used in the form of amino acids and triglycerides, which eventually leads to the formation of ketone bodies [6]. This can result in economic losses for the dairy industry through decreased milk production and reproductive efficiency, as well as increased involuntary culling and veterinary costs [7].

In recent years, acetone has usually been determined chromatographically (especially by Gas [8–11] and Liquid Chromatography [12], but also Electrochromatography [13] and Micellar Electrokinetic Chromatography [14]). Non-chromatographic techniques including Photometry [15], Fluorimetry [1] and Fourier Transform Infrared Spectroscopy [16,17] have also been used for this purpose. Other non-chromatographic techniques such as Ion Mobility Spectrometry (IMS) with corona-discharge [18] and UV ionization sources [19] have been assessed for the determination of acetone in synthetic and human breath samples, respectively.

Most clinical analysis laboratories use test strips to detect acetone in urine. This method allows no quantitation of acetone and exhibits a high limit of detection for the analyte. Also, the reagent in the test strips, nitroprusside, can give false positives in the presence of drugs containing SH groups and false negatives if the strips are exposed to air or the urine samples are very acidic.

IMS provides a very fast, sensitive, inexpensive tool for the efficient analysis and characterization of gaseous organic analytes [20].

\* Corresponding author.

E-mail address: [qa1meobj@uco.es](mailto:qa1meobj@uco.es) (M. Valcárcel).

The time needed to acquire a simple spectrum is typically only 10–100 ms. Although this makes IM spectrometers suitable for process control, the presence of ion–molecule reactions and relatively poor resolution of the species formed generally preclude its use to identify unknown compounds [21]. The ionization source used in this work was an ultraviolet (UV) lamp. Baim et al. [22], and Eiceman et al. [23,24], demonstrated that vacuum UV discharge lamps constitute inexpensive, non-radioactive ionization sources especially suitable for direct operation in nitrogen and air. Such lamps are commercially available with photoionization energies from 8.6 to 11.7 eV [25].

Broadly, analytical techniques can be classified as rearguard or vanguard techniques. Sample-screening systems are used in vanguard analytical strategies to classify samples into two groups (positive or negative) in a fast, reliable way [26]. The primary objectives of sample-screening systems are as follows [27]:

- To provide a rapid, reliable response about a specific characteristic of an object or system for immediate decision making.
- To minimize or avoid preliminary operations in conventional analytical processes.
- To avoid the permanent use of high cost, high maintenance instruments in routine analyses.

Therefore, IMS can be deemed a vanguard screening system inasmuch as it provides a rapid response to the presence or absence of some type of compound potentially present in a given sample.

In this work, we developed a rapid, simple method using IMS with a UV ionization source for routine measurements of acetone in biological fluids such as urine. The proposed method can be used for qualitative and quantitative analysis. For qualitative analysis, 86 urine samples from cows and humans were analysed and the results used for statistical classification. The result for each individual sample was obtained within 7 min. Therefore, UV–IMS equipment can be used as an effective screening system for classifying samples according to the presence or absence of acetone. Also, it has the potential for quantifying acetone in urine samples.

## 2. Experimental

### 2.1. Ion mobility spectrometer

Measurements were made with a portable UV–IMS instrument from Gesellschaft für analytische Sensorsysteme (Dortmund, Germany). The UV–IMS system was 350 mm × 350 mm × 150 mm in size, had a tube length 12 cm, weighed 5 kg, had a voltage of 230 V and used a constant voltage supply of 333 V cm<sup>-1</sup>. The ionization source was a 10.6 eV UV lamp. The instrument was operated at ambient pressure and temperature.

GASpector software was used to record spectra, which were acquired in the positive ion mode. A total of 25 spectra were continuously recorded for about 2 min per analysis, each spectrum being the average of 64 scans. The spectrum length was 1024 points, the grid pulse width 500 μs, the repetition rate 50 ms and the sampling frequency 30 000 Hz.

Ions in the gas phase were resolved in terms of mobility. The mobility  $K$  of an ion depends on its charge, shape and size, and can be expressed mathematically as follows:

$$K = \frac{d}{tE} \quad (1)$$

where  $d$  is the length of the drift region (cm),  $t$  the drift time (s) and  $E$  is the electric field strength (V/cm). By normalizing  $K$  to standard conditions (*viz.* 273 K and 101 kPa) the reduced mobility constant,

$K_0$  (cm<sup>2</sup> V<sup>-1</sup> s<sup>-1</sup>), was calculated from the following expression:

$$K_0 = K \left( \frac{273}{T} \right) \left( \frac{p}{101} \right) \quad (2)$$

where  $T$  (K) and  $p$  (kPa) are the temperature and pressure, respectively, of the drift region.

### 2.2. Sample introduction system

The sample introduction system (SIS, Fig. 1A) consisted of a headspace sampling unit including a vaporization container to facilitate equilibration, a heating device intended to keep the headspace container at a constant temperature and an injection device for transfer of the vapour phase from the headspace container into the IMS equipment [28]. The system is described in greater detail elsewhere [29]. The operational procedure was as follows: a volume of 100 μL of sample was placed in a 10 mL glass vial which was then sealed with a polytetrafluorethylene (PTFE)-faced septum and heated at 80 °C in an Eco 1G Thermoreactor (Velp Scientifica) for 5 min (volatilization step). Meanwhile, a stream of highly pure nitrogen (6.0) from Abelló Linde (Barcelona, Spain) was passed through the UV–IMS system for cleaning and stabilization. The flow-rates of N<sub>2</sub> (140 and 90 mL min<sup>-1</sup> for the drift gas and sample gas, respectively) were controlled via an Alltech Digital Flow Check HR<sup>TM</sup> supplied by Chromatographic Service GMBH. After 5 min of heating, two stainless-steel switching valves (Selectomite®-7177G2Y, HOKE Incorporated, Spartanburg, SC) were actuated, the headspace vapours thus formed in the vial being swept out by the N<sub>2</sub> stream and transferred to the UV–IMS equipment for measurement (injection step). Connectors were made from 1/8 in. PTFE tubes obtained from Varian (Harbor City, CA).

### 2.3. Samples and reagents

Analytical tests were conducted on human and cow urine samples. The human urine samples were obtained from 36 males and females of variable age with an empty stomach, whereas the cow urine samples were obtained from 50 cows also of variable age on a farm in Jaén (Spain). The cows were either pregnant, in their post-partum period or non-pregnant. All samples were collected in sterile plastic flasks and some stored at –18 °C in the freezer compartment of a refrigerator until analysis.

Acetone was supplied in HPLC grade by Sigma (St. Louis, MO) and used to prepare a 1000 mg L<sup>-1</sup> standard solution by diluting 0.126 mL of product to 100 mL with water in a volumetric flask. This standard solution was stored at ambient temperature and used to make others solutions on daily basis. The distilled water used to prepare the solutions was purified by passage through a Milli-Q system from Millipore (Bedford, MA).

## 3. Results and discussion

The positive-ion mobility spectrum for acetone as obtained with UV ionization was used for its qualitative and quantitative determination in human and cow urine samples. Mobility measurements took less than 7 min and required no sample pretreatment other than warming.

### 3.1. Optimization of the sample introduction system

The proposed system relies on the formation of a headspace which is created by encapsulating each liquid sample in a carefully thermostated glass vial. The resulting gas phase is then introduced into the spectrometer by actuating two switching valves (see Fig. 1A).

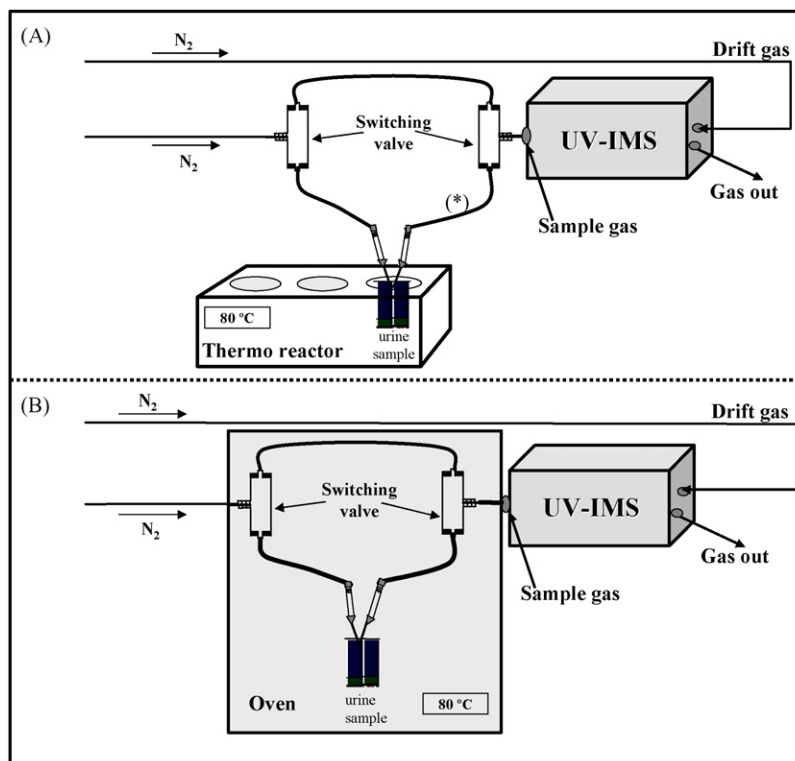


Fig. 1. Scheme of the instrumental devices used.

One other similar SIS (Fig. 1B) was also evaluated for use in order to avoid slight condensation of the samples in the tube (asterisk in Fig. 1A) connecting the samples to the measuring equipment, the whole system being heated in an oven. The spectral signal thus obtained was very poor and no peak was observed during a drift time of  $\sim 19$  ms. This may have been a result of the abrupt temperature difference between the SIS ( $80^\circ\text{C}$ ) and IMS equipment (ambient temperature). Also, this alternative configuration might facilitate condensation inside the IMS equipment and cause it to malfunction, which led us to discard it for further testing.

Rather, we used the system of Fig. 1A since slight sample condensation in the tube leading the volatile compounds to the measuring instrument was expected to have little effect on the quality of the results. This system is simple, requires little sample handling and removes non-volatile interferents. The critical point is equilibration of the aqueous phase and vapour phase; also, several factors must be optimized in order to maximize analyte recovery and sensitivity in the proposed SIS–IMS method.

The experimental variables optimized were the sample temperature, sample volume, vial volume, heating time, and sample gas and drift gas flow rates. Table 1 shows the studied range and selected value for each parameter. The optimal values chosen were taken to be those resulting in the maximum possible repeatability

Table 1  
Optimized parameter values for the sample introduction system.

	Studied range	Optimum value
Temperature, $^\circ\text{C}$	70–100	80
Sample volume, $\mu\text{L}$	50–200	100
Vial volume, mL	1.5 and 10	10
Heating time, min	1–15	5
Tube length <sup>a</sup> , cm	13 and 24	13
Sample flow-rate, $\text{mL min}^{-1}$	80–120	90
Drift flow-rate, $\text{mL min}^{-1}$	90–160	140

<sup>a</sup> See Fig. 1A.

and peak height for acetone in a urine sample spiked to  $50\text{ mg L}^{-1}$  with the analyte. All tests were performed in triplicate.

The first parameter to be optimized was the sample temperature. Tests were conducted at temperatures above the boiling point for acetone ( $56.3^\circ\text{C}$ ) and spanning the range  $60$ – $100^\circ\text{C}$ . The optimum temperature was found to be  $80^\circ\text{C}$ ; in fact, although the acetone signal was stronger at  $90^\circ\text{C}$  and  $100^\circ\text{C}$ , there was the risk of other compounds present in urine evaporating simultaneously and interfering with the analyte measurements. Also, such high temperatures could cause water in urine to evaporate and the water stream to reach the IMS equipment as a result.

The optimum sample volume was taken to be  $100\ \mu\text{L}$ , which resulted in the highest spectral repeatability. The influence of the vial volume was also studied. Initially, reducing such a volume was expected to increase the analytical signal through an increased concentration of the analyte. The two vial volumes examined (1.5 and 10 mL), however, resulted in no significant differences between spectra. This led us to use 10 mL in subsequent tests. The effect of the sample heating time was examined over the range 1–15 min and 5 min found to result in the strongest possible acetone signal and most repeatable spectrum.

One other potentially influential variable was tube length. The most critical tube in the manifold (asterisk in Fig. 1A) was that leading the analytes to the IMS instrument. Two different tube sizes were studied (13 and 24 cm) and no significant spectral differences observed. Therefore, we chose to use the shorter tube in order to expedite transfer of the analytes to the ionization region.

One of the most crucial variables affecting the acetone signal was the  $\text{N}_2$  flow rate. The sample gas flow rate was initially optimized at a constant drift gas flow rate of  $140\text{ mL min}^{-1}$ ; the maximum peak height and most repeatable signal was obtained at  $90\text{ mL min}^{-1}$ , above which peak height decreased—possibly through dilution of the sample in the ionization region. Likewise, the drift gas flow rate was optimized at a constant sample gas flow rate of  $90\text{ mL min}^{-1}$ . Peak height increased with increasing drift gas flow rate, but the

**Table 2**  
Precision values obtained for peak height and drift time at three levels of concentration.

Precision					
Urine	Acetone (mg L <sup>-1</sup> )	Within-day		Between-day	
		Peak height	Drift time (ms)	Peak height	Drift time (ms)
Male urine	5	2.0	0.9	2.5	1
Female urine	50	3.4	0.3	5.4	0.4
Cow urine	80	5.8	0.7	6.7	0.7

analytical signal was poorly repeatable above 160 mL min<sup>-1</sup>. We thus chose to use a drift gas flow rate of 140 mL min<sup>-1</sup> and hence a drift gas to sample gas flow rate ratio of ca. 3/2.

### 3.2. Calculation of the reduced ion mobility constant for acetone

The reduced ion mobility of the analyte was calculated from Eqs. (1) and (2).  $K_0$  was calculated at a drift time coinciding with the average drift time for all urine samples (86), which was  $19.0 \pm 0.4$ , and ambient temperature (298 K) and pressure (101.65 kPa). This provided a  $K_0$  value for acetone of  $1.75 \pm 0.04$  cm<sup>2</sup> V<sup>-1</sup> s<sup>-1</sup>, which is quite consistent with that previously reported by Xie et al. [19]:  $1.74 \pm 0.03$  cm<sup>2</sup> V<sup>-1</sup> s<sup>-1</sup>.

### 3.3. Analytical features of the proposed method

The analytical figures of merit used to characterize the proposed SIS-IMS method included precision, calibration curve, sensitivity (expressed as limit of detection), limit of quantification and recovery.

#### 3.3.1. Precision

The precision of the overall procedure was assessed by analysing three different urine samples spiked at three different levels of concentration of acetone (5, 50 and 80 mg L<sup>-1</sup>) on the same or three different days under identical testing conditions. The within-day precision was obtained in nine replicates on the same day and the between-day precision was obtained in three replicates within three consecutive days. The within-day and between-day precision values obtained from the acetone peak height are shown in Table 2, both as relative standard deviation (RSD). As can be seen from this table, in all cases the precision of the method was less than 6.7%.

Drift times of acetone peak was also assessed with the same spiked urine samples and within-day and between-day

**Table 3**  
Analytical parameters for standard solutions of acetone in water and urine matrix.

	Aqueous matrix	Urine matrix
Intercept	$-0.002 \pm 0.005$	$0.012 \pm 0.003$
Slope	$0.0057 \pm 0.0002$	$0.0017 \pm 0.0001$
Regression coefficient ( $r^2$ )	0.998	0.992
LOD (mg L <sup>-1</sup> )	2.63	5.30
LOQ (mg L <sup>-1</sup> )	8.77	17.65

precision was also measured. The values obtained were less than 1% in all cases. These values are also summarized in Table 2.

The precision of the method was also calculated with different urine samples spiked with different concentrations of salt (0.5, 1 and 2 g added to 10 mL of urine). The results obtained at these three levels of concentration were not different to those obtained without adding NaCl.

#### 3.3.2. Linearity and limit of detection

A calibration curve was constructed from standard solutions containing 5–80 mg L<sup>-1</sup> acetone in water and the urine matrices. The figures of merit of the proposed screening method are shown in Table 3. Each concentration used to obtain the curve was measured in triplicate and all figures were obtained from the acetone peak height.

The limit of detection (LOD) was taken to be the smallest detectable amount of acetone and calculated as three times the standard deviation of the intercept divided by the slope. This provided a value of 3 mg L<sup>-1</sup> for the aqueous matrix, and, as can be seen from Table 3, was slightly higher for the urine samples—possibly as a result of matrix effects. The limit of quantification (LOQ) was also calculated and it is also indicated in Table 3.

#### 3.3.3. Recovery

The analyte recoveries obtained in triplicate analyses of a urine sample spiked with a low concentration of acetone (5 mg L<sup>-1</sup>) was  $109 \pm 3\%$ . The same urine sample was previously analysed by IMS and found to give no signal for acetone—which does not exclude its containing the analyte at an undetectable concentration.

### 3.4. Qualitative analysis of urine samples

The proposed method provides a new vanguard screening system for detecting potential diseases in humans and cows. The screening system was designed to provide a rapid response to the presence or absence of acetone in urine. Based on the results, the method affords the analysis of 50 samples of urine in a working

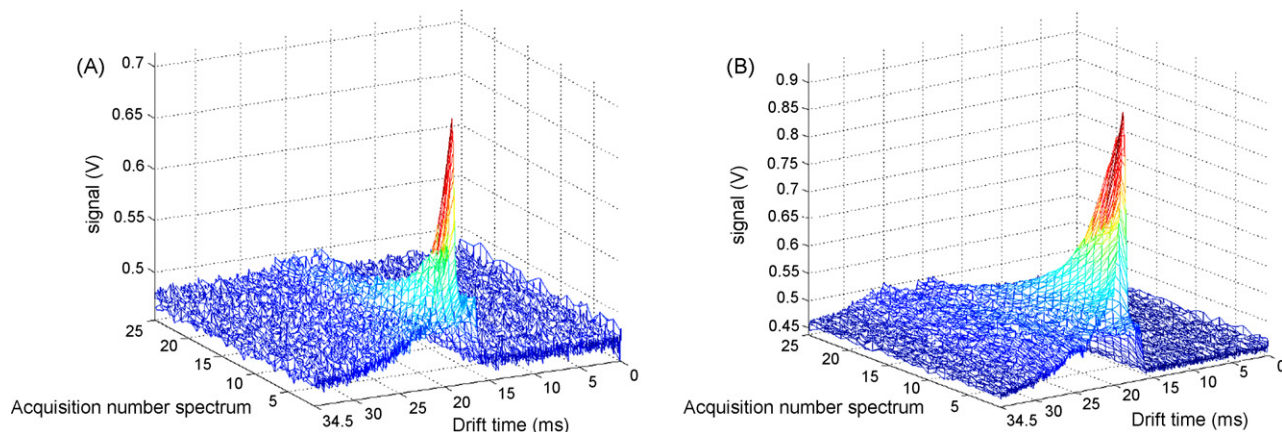


**Fig. 2.** Ion mobility spectra for a human urine sample (A) and a cow urine sample (B).

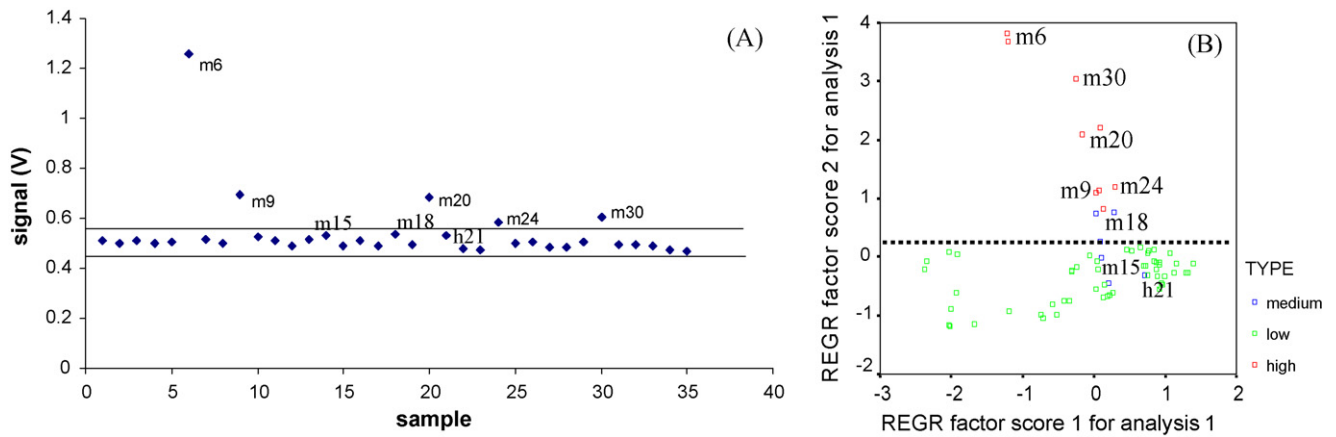


Fig. 3. Control charts (A) and PCA (B) for human urine samples.

day (8 h); also, the samples require no pretreatment other than warming.

The method was validated by using it to screen 36 human urine samples and 50 cow urine samples. Mobility measurements, which were obtained in less than 2 min, allowed a three-dimensional graph to be constructed for both types of samples (see Fig. 2). As can be seen, the 3D profiles varied little between the 25 spectra, but peak intensity changed during the acquisition time. Thus, the signal was stronger at the beginning, immediately after the valves were switched, and then decreased exponentially with increasing number of spectra. We therefore recorded 25 spectra only. Also, as can be seen from Fig. 2, the profiles for both types of samples were essentially identical; by exception, that for cow urine was broader than the profile for human urine.

For qualitative analysis, all urine samples (cow and human) were classified by using control charts. Figs. 3A and 4A show such charts for all human and cow samples studied, respectively. Based on the results for the 86 urine samples analysed, the cut-off value was set at a signal voltage of 0.55 V, corresponding to an acetone concentration lower than  $17 \text{ mg L}^{-1}$ . If acetone levels are above the cut off it would mean that the individuals are out of the normal level of a healthy population. Most of the samples studied exhibited signal voltages below 0.55 V. A principal component analysis (PCA) of all human (Fig. 3B) and cow urine samples (Fig. 4B) analysed in duplicate was performed in order to confirm the control charts. This chemometric study was based on the average of the 25 spectra used for each analysis and the 2000 data per sample used as input for the statistical software (SPSS 12.0 Inc., Chicago, IL). As can be seen, all samples containing acetone at high concentrations fell above the line (m6, m30, m20, m9, m24, v2822(1), v2822(2), v2823). Also, the PCA discriminated samples at the cut-off bound-

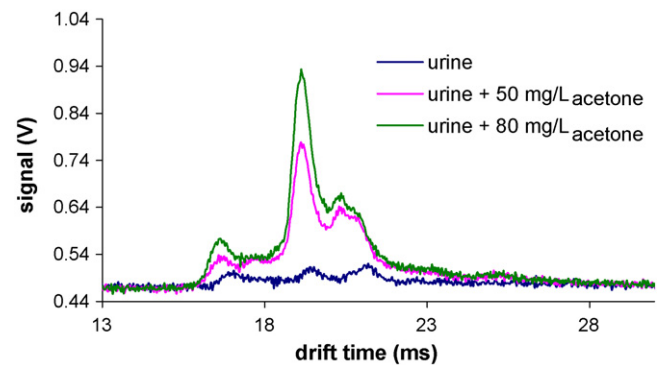


Fig. 5. IMS spectra for an unspiked urine sample and the same sample following spiking with 50 and  $80 \text{ mg L}^{-1}$  acetone.

ary (m18, v2949, vE1690, v4530). These results are consistent with those provided by the test strips used to confirm the presence of acetone. The cow urine samples with the highest concentrations of acetone came from animals in their post-partum period (1–2 weeks after birth), whereas the equivalent human urine sample (m6) was obtained from a person after excessive, prolonged vomiting. Other human urine samples with acetone concentrations above the cut-off value were from individuals on a diet.

### 3.5. Quantitative analysis of urine samples

The quantitative response of the IM spectrometer was established from the maximum peak height in the full scan at the drift time (19 ms). Fig. 5 shows the spectrum for a urine sample spiked

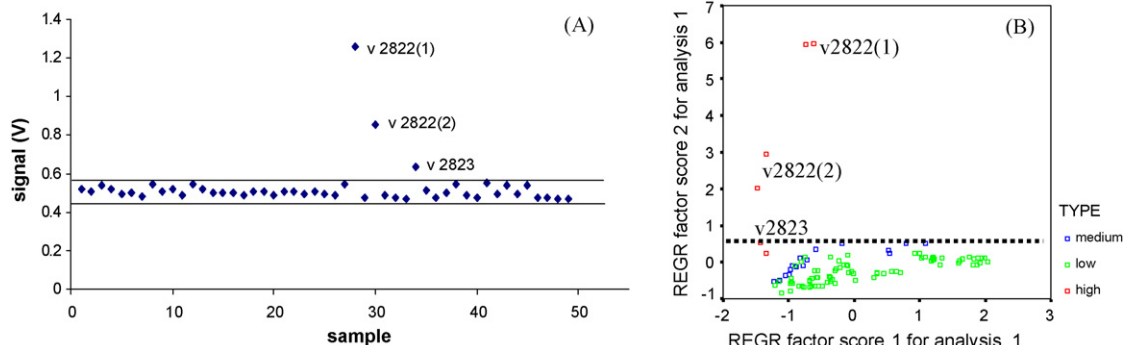


Fig. 4. Control charts (A) and PCA (B) for cow urine samples.

**Table 4**  
Amounts of acetone found in different urine samples.

Urine sample	Concentration (mg L <sup>-1</sup> )	Reference method <sup>a</sup>	
Cow 1	73.1	77 ± 5	+
	82.9		
	75.7		
Cow 2 <sup>b</sup>	98.9	104 ± 5	+
	108.2		
	104.9		
Human 1	23.2	27 ± 3	+
	30.3		
	26.8		
Human 2	32.1	28 ± 3	+
	28.2		
	26.1		

<sup>a</sup> Test strips.

<sup>b</sup> Sample diluted (50%).

at two different acetone concentration levels (50 and 80 mg L<sup>-1</sup>). As can be seen, the sample gave three peaks of which the strongest (*viz.* that at 19 ms) was used to quantify the analyte. Acetone in the urine samples was quantified with the standard addition method. Table 4 shows the results for two human and two cow urine samples analyzed by using the proposed IMS method and also by the reference method.

Other ketone bodies present in urine such as acetoacetate and β-hydroxybutyrate pose no interference with the proposed method as their ionization energy exceeds that supplied by the source.

#### 4. Conclusions and outlook

The potential of using IMS with a 10.6 eV UV-lamp as an analytical screening system for the determination of acetone in urine samples was demonstrated. Acetone can be used as a biomarker for fat metabolism-related diseases. The proposed SIS–UV–IMS method is simple, easy to use, inexpensive and expeditious (the results can be obtained within a few minutes). Also, it requires no sample pretreatment other than warming. These advantages and the goodness of the results testify to its robustness. Therefore, the proposed method can be used by clinical analysis laboratories for the routine monitoring of acetone in urine. In fact, it allows one to rapidly determine whether acetone is present above a preset concentration level in urine samples.

#### Acknowledgement

This work was supported by DGI, Spain's Ministry of Science and Technology, within the framework of Project CTQ2007-60426.

#### References

- [1] C. García de María, K.B. Hueso Domínguez, N. Martín Garrido, *Anal. Chim. Acta* 600 (2007) 172.
- [2] A. Brega, P. Villa, G. Quadri, A. Quadri, C. Lucarelli, *J. Chromatogr.* 553 (1991) 249.7.
- [3] A.A. Matin, R. Maleki, M.A. Farajzadeh, K. Farhadi, R. Hosseinzadeh, A. Jouyban, *Chromatographia* 66 (2007) 383.
- [4] I.A. McDonald, L.P. Hackett, L.J. Dusci, *Clin. Chim. Acta* 553 (1975) 249.
- [5] P. Mandevbu, C.S. Ballard, C.J. Sniffen, D.S. Tsang, F. Valdez, S. Miyoshi, L. Schlatter, *Anim. Feed Sci. Technol.* 105 (2003) 81.
- [6] The Merck Veterinary Manual, Merck & Co., New York, 2000.
- [7] C.S. Ballard, P. Mandevbu, C.J. Sniffen, S.M. Emanuele, M.P. Carter, *Anim. Feed Sci. Technol.* 93 (2001) 55.
- [8] I. Sarudi, E. Visi-Varga, *Talanta* 46 (1998) 589.
- [9] I.Z. Dong, S.C. Moldoveanu, *J. Chromatogr. A* 1027 (2004) 25.
- [10] N. Sugaya, K. Sakurai, T. Nakagawa, N. Onda, S. Onodera, M. Morita, M. Tezuka, *Anal. Sci.* 20 (2004) 865.
- [11] L. Dong, X.Z. Shen, C.H. Deng, *Anal. Chim. Acta* 569 (2006) 91.
- [12] C. Kempter, W. Pötter, N. Binding, H. Kläning, U. Witting, U. Karst, *Anal. Chim. Acta* 410 (2000) 47.
- [13] Y.S. Fung, Y. Long, *Electrophoresis* 22 (2001) 2270.
- [14] S.L. Zhao, T.Y. Dai, Z. Liu, F.S. Wie, H.F. Zou, X.B. Xu, *Chemosphere* 35 (1997) 2131.
- [15] N. Teshima, J.Z. Li, K. Toda, P.K. Dasgupta, *Anal. Chim. Acta* 535 (2005) 189.
- [16] M. Kansiz, J.R. Gapes, D. McNaughton, B. Lendl, K.C. Shuster, *Anal. Chim. Acta* 438 (2001) 175.
- [17] Y. Li, J.D. Wang, Z.H. Huang, H.Q. Xu, X.T. Zhou, *J. Environ. Sci. Health A* 37 (2002) 1453.
- [18] T. Khayamian, M. Tabrizchi, N. Taj, *Fresenius J. Anal. Chem.* 370 (2001) 1114.
- [19] Z. Xie, St. Sielemann, H. Schmidt, F. Li, J.I. Baumbach, *Anal. Bioanal. Chem.* 372 (2002) 606.
- [20] S. Bader, W. Urfer, J.I. Baumbach, *IJMS* 8 (2005) 1.
- [21] G. Walendzik, J.I. Baumbach, D. Klockow, *Anal. Bioanal. Chem.* 382 (2005) 1842.
- [22] M.A. Baim, R.L. Eatherton, H.H. Hill, *Anal. Chem.* 55 (1983) 1761.
- [23] G.A. Eiceman, V.J. Vandiver, *Anal. Chem.* 54 (1986) 38.
- [24] C.S. Leasure, M.E. Fleischer, G.K. Anderson, G.A. Eiceman, *Anal. Chem.* 58 (1986) 2142.
- [25] St. Sielemann, J.I. Baumbach, H. Schmidt, P. Pilzecker, *Anal. Chim. Acta* 431 (2001) 293.
- [26] M. Valcárcel, S. Cárdenas, M. Gallego, *Trends Anal. Chem.* 18 (1999) 685.
- [27] M. Valcárcel, S. Cárdenas, *Trends Anal. Chem.* 24 (2005) 67.
- [28] L. Arce, M. Menéndez, R. Garrido-Delgado, M. Valcárcel, *Trends Anal. Chem.* 27 (2008) 139.
- [29] R. Alonso, V. Rodríguez-Estévez, A. Domínguez-Vidal, M.J. Ayora-Cañada, L. Arce, M. Valcárcel, *Talanta* 76 (2008) 591.





# Taguchi OA<sub>16</sub> orthogonal array design for the optimization of cloud point extraction for selenium determination in environmental and biological samples by tungsten-modified tube electrothermal atomic absorption spectrometry

Mahnaz Ghambarian<sup>a</sup>, Yadollah Yamini<sup>a,\*</sup>, Abolfazl Saleh<sup>a</sup>, Shahab Shariati<sup>b</sup>, Najmeh Yazdanfar<sup>c</sup>

<sup>a</sup> Department of Chemistry, Faculty of Sciences, Tarbiat Modares University, P.O. Box: 14115-175, Tehran, Iran

<sup>b</sup> Department of Chemistry, Faculty of Sciences, Islamic Azad University, Rasht Branch, Rasht, Iran

<sup>c</sup> Iranian Research and Development Center for Chemical Industries, Academic Center for Education, Culture and Research, Tehran, Iran

## ARTICLE INFO

### Article history:

Received 6 November 2008

Received in revised form 31 December 2008

Accepted 5 January 2009

Available online 20 January 2009

### Keywords:

Cloud point extraction

Electrothermal atomic absorption spectrometry

Orthogonal array design

*o*-Phenylenediamine

## ABSTRACT

Orthogonal array design (OAD) was applied for the first time to optimize cloud point extraction (CPE) conditions for Se(IV) determination by electrothermal atomic absorption spectrometry (ETAAS) in environmental and biological samples. Selenium was reacted with *o*-phenylenediamine to form piaszelenol in an acidic medium (pH 2). Using Triton X-114, as surfactant, piaszelenol was quantitatively extracted into small volume (about 30  $\mu$ L) of the surfactant-rich phase after centrifugation. Five relevant factors, i.e. surfactant concentration, pH, ionic strength, equilibrium time and temperature were selected and the effects of each factor were studied at four levels on the extraction efficiency of Se(IV) and optimized. The statistical analysis revealed that the most important factors contributing to the extraction efficiency are ionic strength, pH and percent of surfactant. Based on the results obtained from the analysis of variance (ANOVA), the optimum conditions for extraction were established as: pH 6; vial temperature = 50 °C; extraction time = 7 min and 0.3% (w/v) of Triton X-114. The method was permitted to obtain a detection limit of 0.09 ng mL<sup>-1</sup> and two linear calibration ranges from 0.6 to 1.0 and 1.0 to 80.0 ng mL<sup>-1</sup> Se. The precision (%RSD) of the extraction and determination for the six replicates of Se at 20 ng mL<sup>-1</sup> was better than 3.6% and the enrichment factor of 63.5 was achieved. The studied analyte was successfully extracted and determined with high efficiency using cloud point extraction method in water and biological matrices.

© 2009 Elsevier B.V. All rights reserved.

## 1. Introduction

Research involving selenium has become an increasingly popular area in the research community in the last 20 years. Selenium is present in soil, water and all living organisms, and has been reported to be both toxic and essential. It plays an important role in environmental and health studies. It is necessary for the formation and function of at least 13 proteins and the component of glutathione peroxidase (GSHPx) enzyme, mainly in the form of selenocysteine [1]. Its anti-carcinogenic effect, especially in prostate cancer and some gastric cancers, has been reported in recent years [2], indicating the possible significance of food supplementation with Se species against cancer. However, the bioavailability, toxicity and chemoprotective activity of Se are species dependant. Each species is absorbed differently by the human body and has a different tendency to bioaccumulate in organisms [3]. Therefore, Se speciation is necessary for envi-

ronmental, nutritional and clinical purposes. Inorganic forms of selenium are more toxic than its organic forms, and the toxicity of Se(VI) is more severe than that of Se(IV) for humans and most of other mammals [4]. The maximum allowed tolerance limit of Se is <0.1 mg m<sup>-3</sup> in air, <0.05 g mL<sup>-1</sup> in water and  $\leq$ 80 g kg<sup>-1</sup> in soil [5].

Due to the ambivalent behavior of Se, there is an urgent need to determine its concentration in different environmental matrices. Various instruments, such as UV–vis spectrophotometry [6,7], voltammetry [8–10], X-ray fluorescence [11], high performance liquid chromatography-atomic fluorescence spectrometry (HPLC-AFS) [12,13], gas chromatography (GC) [14–16], atomic absorption spectrometry (AAS) [17–19], etc., have been applied for determination of Se in different matrices.

Monitoring of trace element concentrations in biological materials, particularly in biological fluids, might be considered as a difficult analytical task, mostly due to the complexity of the matrix and the low concentration of these elements, which requires sensitive instrumental techniques and often preconcentration step. In order to solve these problems, pre-concentration-separation techniques including liquid–liquid extraction (LLE) [20], liquid phase microextraction (LPME) [21], solid phase extraction (SPE) [22], solid

\* Corresponding author. Fax: +98 21 88006544.

E-mail address: [yyamini@modares.ac.ir](mailto:yyamini@modares.ac.ir) (Y. Yamini).

**Table 1**  
Instrumental parameters for Se determination using tungsten as a permanent modifier.

Step	Temperature (°C)	Time (s)		Ar flow rate (L min <sup>-1</sup> )
		Ramp	Hold	
Graphite atomizer				
Pre-warming	50	1.0	2.0	3.0
Inject step	Inject sample	–	–	3.0
Drying	120	15.0	10.0	3.0
Pyrolysis or ashing	900	10.0	5.0	3.0
Gas stop step	900	0	1.0	0
Atomization	2100	0.8	1.0	0
Cleaning	2300	1.0	2.0	3.0

phase microextraction (SPME) [23–25], coprecipitation [26,27], ion-exchange [28], hydride generation [29], etc., have been proposed to extract selenium ions from aqueous solutions.

Cloud point extraction (CPE) technique offers a convenient alternative to more conventional extraction systems. In this technique, small volume of the surfactant-rich phase allows the preconcentration and extraction of the analytes in one step [30,31].

The published results clearly demonstrate the usefulness of the CPE technique for quantitative extraction and concentration of a variety of metal ions. The surfactant-rich phase obtained in the extraction process is compatible with most of the mobile phases used in hydrodynamic analytical systems, while it increases atomic signal in flame atomic absorption spectrometry (FAAS) and wettability of the graphite surface in electrothermal atomic absorption spectrometry (ETAAS) techniques [31]. ETAAS could, in this sense, combine all the benefits associated with cloud point extraction to a sensitive instrumental technique. ETAAS also allows elimination of the matrix prior to the atomization stage and increases the residence time of the analyte in the atomizer, which improves the sensitivity by about 2–3 folds in comparison to FAAS [32].

The present work describes the application of cloud point extraction to determine Se in environmental and biological samples by ETAAS after reaction with *o*-phenylenediamine and preconcentration of the produced piaselelol using octyl phenoxy polyethoxy ethanol (Triton X-114) as a non-ionic surfactant. The extraction conditions were optimized using an OA<sub>16</sub> (4<sup>5</sup>) orthogonal array design.

## 2. Experimental

### 2.1. Instrumentation

All of the Se measurements were carried out on a GBC Atomic Absorption Spectrometer (Avanta PM, Australia) equipped with a GF 3000 graphite furnace atomizer and an autosampler (Pal 3000). Deuterium background correction was employed to correct non-specific absorbance. Hollow cathode lamp of Se was operated at 10 mA with the spectral bandwidth of 1 nm. The selected wavelength was 196.0 nm for Se. Argon 99.999% was used as the protected and purge gas. The details of graphite furnace temperature program for determination of Se are shown in Table 1.

**Table 2**  
Temperature program for the treatment of graphite furnace with tungsten as a permanent modifier.

Step	Temperature (°C)	Time (s)		Ar flow rate (L min <sup>-1</sup> )
		Ramp	Hold	
Pre-warming	110	10.0	20.0	3.0
Pyrolysis or ashing	160	20.0	15.0	3.0
Gas stop step	160	0	6.0	0
Atomization	1000	20.0	10.0	0
Cleaning	2000	20.0	5.0	3.0

Chromatographic separations were carried out on a Varian 9012 HPLC pump (Mulgrave Victoria, Australia) and a 9010 autosampler having a 20 µL sample loop and equipped with a Varian 9050 UV–vis detector. The separations were carried out on an ODS-3 column (100 mm × 4.0 mm, with 3 µm particle size) from MZ-Analytical Company.

A thermostated bath maintained at the desired temperature was applied for cloud point extraction experiments. A centrifuge purchased from Sepand Azma (Tehran, Iran) was employed for phase separation. The pH of the solutions was determined and adjusted using a model WTW pH meter (Inolab, Germany) equipped with a combined glass-calomel electrode.

### 2.2. Reagents and standard solutions

All of the chemicals used were of analytical reagent grade. Ultrapure water used was purified with a Milli-Q system (Millipore, Bedford, MA, USA). All of the plastics and glassware were cleaned by soaking for 24 h in 10% (v/v) HNO<sub>3</sub>. After cleaning, all the containers were thoroughly rinsed three times with ultrapure water and twice with acetone prior to use. The stock solution of selenite (1000 mg L<sup>-1</sup>) was prepared by dissolving appropriate amounts of H<sub>2</sub>SeO<sub>3</sub> (Merck, Darmsdat, Germany) in ultrapure water. The chelating agent, *o*-phenylenediamine solution, was prepared daily by dissolving appropriate amount of reagent (Fluka, Chemie AG, Switzerland) in 0.1 mol L<sup>-1</sup> HCl. The non-ionic surfactant, Triton X-114 (Fluka), was used without further purification. The pH of the solution was adjusted by dropwise addition of hydrochloric acid and sodium hydroxide (2 mol L<sup>-1</sup>).

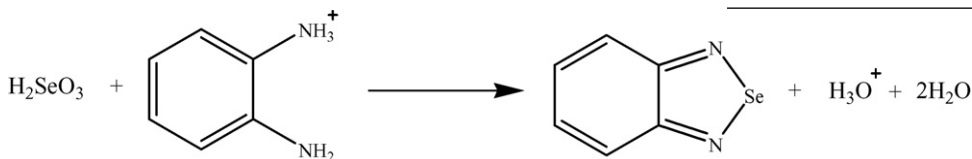
A 500 mg L<sup>-1</sup> stock palladium solution was used as a chemical modifier. It was prepared in 5% (v/v) HNO<sub>3</sub> by appropriate dilution of 10,000 mg L<sup>-1</sup> Pd(NO<sub>3</sub>)<sub>2</sub> solution (Merck). The permanent modifier (500 mg L<sup>-1</sup>) was prepared by dissolving 0.025 g of Na<sub>2</sub>WO<sub>4</sub>·2H<sub>2</sub>O (Merck) in 50 mL of ultrapure water.

### 2.3. Treatment of platforms with permanent modifiers

The permanent modifier (W) was applied to the platform by 25 consecutive injections of 40 µL aliquots of a 500 mg L<sup>-1</sup> W solution into the graphite furnace; each injection was followed by a specific temperature program given in Table 2. The procedure resulted in the deposition of 500 µg of the modifier onto the platform surface.

## 2.4. Procedure

In the previous studies, the synthesis conditions of piaszelenol were optimized [33,34]. The conversion of Se(IV) into piaszelenol complex was completed after 30 min at 90 °C and pH 2–3 according to the following reaction:



For CPE preconcentration, the pH of the solutions (10.0 mL) containing piaszelenol complex (100 µg L<sup>-1</sup>) and 0.15% (w/v) Triton X-114 was adjusted at six. Then, the solutions were heated in a thermostatted water bath at 50 °C for 7 min.

In order to separate the phases, the turbid solution was centrifuged for 10 min at 3500 rpm, and then cooled down in an ice bath for 5 min. After cooling, the surfactant-rich phase became viscous and was retained at the bottom of the tube.

The supernatant aqueous phase was removed with a pipette and 100 µL of methanol was added to decrease the viscosity of the surfactant-rich phase and facilitate sample handling. Finally, 10 µL of the final sample solution plus 10 µL of Pd(NO<sub>3</sub>)<sub>2</sub> (500 mg L<sup>-1</sup>) as chemical modifier was injected into the tungsten-modified pyrolytic tube graphite furnace by autosampler.

## 2.5. Preparation of real samples

### 2.5.1. Water samples

The original water samples collected were stored in pre-cleaned polyethylene bottles in a fridge at about 4 °C under darkness condition. The samples were filtered through a 0.45 µm pore-size cellulose acetate membrane filters prior to extraction.

### 2.5.2. Urine sample

The real urine sample obtained from a non-exposed volunteer was also analyzed without prior digestion. For preparation of human urine, 5.0 mL of the urine sample was transferred into a 50 mL volumetric flask and diluted to the mark with ultrapure water. Aliquots (10 mL) of the resulting clear solution were analyzed according to the prescribed procedure.

### 2.5.3. Human plasma sample

Frozen plasma sample were obtained from the Iranian Blood Transfusion Organization (Tehran, Iran), thawed and allowed to reach room temperature. To precipitate the protein contents of the human plasma sample, 5 mL of plasma with a small amount of trichloroacetic acid was centrifuged for 5 min at the rate of 8000 rpm. After decantation of the plasma sample, it was diluted at 1:10 ratio with ultrapure water and extracted by using the CPE procedure.

**Table 3**  
Factors and levels of an orthogonal design (A–E are the respective codes for each factor).

Levels	Factors				
	A (pH)	B (surfactant (%))	C (salt concentration (mol L <sup>-1</sup> ))	D (temperature (°C))	E (equilibrium time (min))
1	3	0.02	0	30	1
2	4	0.06	0.1	40	7
3	5	0.15	0.25	50	15
4	6	0.30	0.5	60	25

## 3. Results and discussion

### 3.1. Taguchi design

Taguchi's optimization technique is a unique and powerful optimization discipline that allows optimization with minimum

number of experiments [35]. In this work, the effect of five important factors including equilibrium temperature and time, ionic strength, surfactant concentration, pH and each factor at four levels on the CPE of Se(IV) were studied using Taguchi's method. The used level setting values of the main factors (A–E) and the OA<sub>16</sub> (4<sup>5</sup>) matrix employed to assign the considered factors are shown in Tables 3 and 4, respectively. It is noteworthy that the mean of absorbance responses ( $r_1$ ,  $r_2$ ,  $r_3$  and  $r_4$ ) for each factor at different levels was also calculated (Table 4). OA<sub>16</sub> orthogonal array scheme was adapted, which needs 16 experiments to complete the optimization process; however, all of the trials were replicated three times to obtain suitable precision. The sequence, in which the experiments were carried out, was randomized to avoid any personal or subjective bias. In the proposed method, no interaction between the variables was found in the matrix and the focus was placed on the main effects of the five most important factors. ANOVA was used to assess the OAD results [36]. The results of the sums of squares (SS) for different variables were calculated (Table 5). The error estimation of the experiments was calculated and used in ANOVA, since no dummy column was assigned in OA<sub>16</sub> (4<sup>5</sup>) matrix. The SS of error was obtained by subtracting all the SS of the items from the total SS. The ANOVA results showed that the most important factor contributing to the extraction efficiency was factor C (ionic strength, 68.25%) followed by factor A (pH, 12.68%) and lastly, factor B (percent of surfactant, 11.93%). The results also showed that, under the best conditions obtained from the OA<sub>16</sub> (4<sup>5</sup>) matrix, the normalized experimental responses were similar to the optimum responses calculated using the following expression:

$$Y_{\text{opt}} = \frac{T}{N} + \left( \bar{B} - \frac{T}{N} \right) + \left( \bar{D} - \frac{T}{N} \right) \quad (1)$$

where  $T$  is the grand total of all results,  $N$  is the total number of results,  $Y_{\text{opt}}$  is the response under the optimum conditions,  $\bar{B}$  and  $\bar{D}$  are the mean responses of the stirring speed and extraction time at optimum levels, respectively. Based on the above equation, under the best conditions, the response is estimated using only the significant factors (ionic strength, pH and the percent of surfactant). Under the optimum conditions, the confidence interval (C.I.) of the performance is calculated using the following expression:

$$\text{C.I.} = \pm \sqrt{\frac{F(1, n_2) V_e}{N_e}} \quad (2)$$

**Table 4**The OA<sub>16</sub> (4<sup>5</sup>) matrix for optimization of cloud point extraction of Se complex.

Exp. no.	Exp. order	Factor A	Factor B	Factor C	Factor D	Factor E	Response
1	16	4	4	1	3	2	1.115
2	10	3	2	4	3	1	0.104
3	5	2	1	2	3	4	0.121
4	4	1	4	4	4	4	0.136
5	2	1	2	2	2	2	0.142
6	12	3	4	2	1	3	0.275
7	3	1	3	3	3	3	0.343
8	9	3	1	3	4	2	0.042
9	7	2	3	4	1	2	0.152
10	11	3	3	1	2	4	0.807
11	14	4	2	3	1	4	0.239
12	1	1	1	1	1	1	0.449
13	8	2	4	3	2	1	0.069
14	13	4	1	4	2	3	0.174
15	15	4	3	2	4	1	0.455
16	6	2	2	1	4	3	0.540
r <sub>1</sub>		0.266	0.195	0.733	0.278	0.268	
r <sub>2</sub>		0.221	0.256	0.247	0.302	0.362	
r <sub>3</sub>		0.311	0.443	0.172	0.420	0.333	
r <sub>4</sub>		0.495	0.398	0.141	0.293	0.329	

**Table 5**ANOVA results for experimental responses in the OA<sub>16</sub> (4<sup>5</sup>) matrix.

Source	d.f.	SS	MS	F <sup>a</sup>	SS'	PC (%)
pH (A)	3	0.346	0.115	55.202	0.339	12.683
% Surfactant (B)	3	0.326	0.108	51.985	0.319	11.93
Ionic strength (C)	3	1.835	0.611	292.678	1.829	68.252
Temperature (D)	3	0.101	0.033	16.25	0.095	3.568
Time (E)	3	0.037	0.012	5.904	0.03	1.147
Error	32	0.033	0.002	–	–	2.42
Total	47	2.68	–	–	–	100.00

SS = Sum of squares; d.f. = degrees of freedom; MS = mean squares; SS' = purified sum of squares; PC = percentage contribution.

<sup>a</sup> F, Critical value is 3.26 ( $P < 0.05$ ) and 2.27 ( $P < 0.1$ ).

where  $F(1, n_2)$  is the  $F$ -value from the  $F$  table in a required confidence level at the degree of freedom (DOF) of 1 and DOF of error,  $n_2$ ;  $V_e$  is the variance of error term (from ANOVA) and  $N_e$  is the effective number of replications. Taguchi method predicted that the absorbance under the optimum conditions will be  $1.11 \pm 0.02$ . The average ( $n = 3$ ) of the obtained absorbance under the optimum conditions was  $1.11 \pm 0.04$ . Based on the obtained results there are satisfactory agreements between the results for the responses of the estimated Se(IV) based on Eq. (1) and those obtained under the optimum conditions.

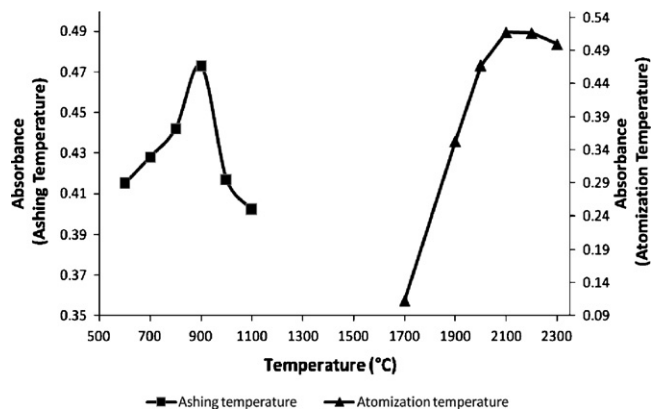
### 3.2. Optimization of ETAAS determination of Se

The main purpose of using a modifier or a modifier mixture in ETAAS is to stabilize the relatively volatile elements so that higher permissible ashing temperatures can be applied to efficiently volatilize the matrix components in a sample prior to atomization of the analyte [37,38]. By using higher ashing temperatures, less interference is encountered in the atomization step [37]. Selenium is a volatile element that is lost from the graphite atomizer at the temperatures higher than 400 °C in the absence of a chemical modifier. In the present work, Pd(NO<sub>3</sub>)<sub>2</sub> was used as conventional liquid chemical modifier in addition to W as permanent modifier for the stabilization of selenium in the biological and environmental samples.

Optimization of the furnace program focused on the ashing and atomization steps and was carried out using a single injection (10 μL). For each step, the ramp and hold times and the gas flow of Ar were studied. Integrated absorbance was used as signal in quantitative measurements.

In the ashing step, the temperatures between 600 and 1100 °C were studied at a constant atomization temperature of 2000 °C. As shown in Fig. 1, a significant change in the selenium absorption was observed over the temperature range, thus the ashing temperature was set at 900 °C to ensure maximum matrix removal without any signal loss.

The atomization temperature of Se was studied over the range of 1500–2300 °C at a constant ashing temperature of 900 °C. Within this range, the atomic absorption signal kept improving with the increasing of the atomization temperature to 2100 °C (Fig. 1). After atomization, a final cleaning step was introduced at a slightly higher temperature to avoid memory effects.

**Fig. 1.** Optimization of ashing and atomization temperatures.

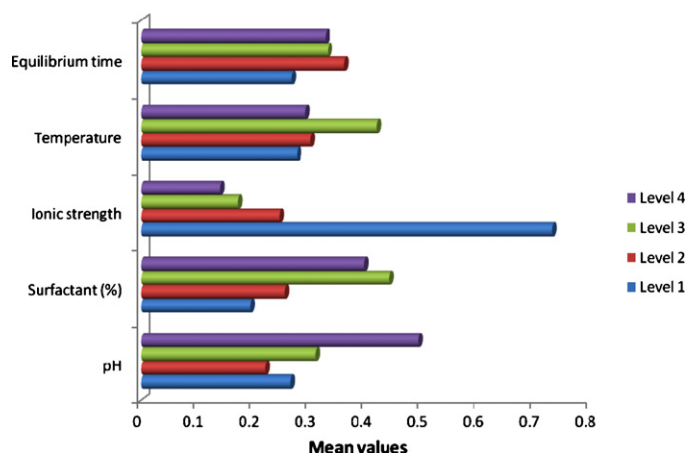


**Fig. 2.** The response graph illustrating the variation of the mean absorbance values plotted against various extraction parameters. pH [level 1 = 3, level 2 = 4, level 3 = 5, level 4 = 6]. Surfactant (%) [level 1 = 0.02, level 2 = 0.06, level 3 = 0.15, level 4 = 0.3]. Ionic strength (M) [level 1 = 0, level 2 = 0.1, level 3 = 0.25, level 4 = 0.5 of NaCl]. Temperature ( $^{\circ}\text{C}$ ) [level 1 = 30, level 2 = 40, level 3 = 50]. Equilibrium time (min) [level 1 = 1, level 2 = 7, level 3 = 15, level 4 = 25].

### 3.3. Study of the CPE system variables

To take full advantages of the procedure, various experimental parameters must be studied to obtain an optimized system. These parameters were optimized in the present research by a five-factor four-level factorial design and the experimental data were evaluated using Qualitek 4 Software. The mean values of the four levels of each factor revealed how the extraction efficiency changes when the level of that factor changes. Fig. 2 shows the mean the integrated absorbance as a function of the levels of the studied factors.

#### 3.3.1. Influence of pH on CPE

After completion of piaszelenol formation, the pHs of the solutions were adjusted by dropwise addition of HCl and/or NaOH solutions ( $2 \text{ mol L}^{-1}$ ). Then, selenium was extracted from the aqueous solutions with different pHs within the range of 3–6 using cloud point extraction method. As Fig. 2 shows, the extraction efficiency increased by increasing of the pH. The lower extraction efficiency in the acidic media might be due to the fact that ionic form of piaszelenol (from nitrogen atoms) does not normally interact with the micellar aggregate as strongly as its non-ionic form, and a smaller amount of the analyte was, therefore, extracted [39]. As a result, pH 6 was selected for the further studies.

#### 3.3.2. Influence of salt addition

Presence of salt in the solution can affect the extraction efficiency and volume of the surfactant-rich phase. The influence of salt concentration on the extraction efficiency was examined in the presence of known concentrations of NaCl ( $0\text{--}0.5 \text{ mol L}^{-1}$ ). Fig. 2 shows the variation of extraction efficiency in the presence of various concentrations of NaCl. The signal decreased considerably due to the increase in the salt concentration. This effect might be explained by the additional surface charge when the concentration of salt is increased. Consequently, it leads to a change in the molecular architecture of the surfactant and the micelle formation process as well. Further experiments were performed in the absence of NaCl.

#### 3.3.3. Influence of surfactant concentration

In CPE, the theoretical preconcentration factors depend on the volume of the surfactant-rich phase, which at the same time varies with the surfactant concentration in the solution [40]. In the present work, the non-ionic Triton X-114 surfactant was chosen for its low cloud point temperature, low toxicological properties and high den-

sity [41]. The effect of the surfactant concentration ranging from 0.02% to 0.3% (w/v) on the extraction efficiency was examined and the results are shown in Fig. 2. At 0.15% (w/v) of Triton X-114, nearly a perfect extraction of the analyte occurred. At lower concentrations of the surfactant, the extraction efficiency was low probably due to inadequacy of the assemblies to entrap the hydrophobic complex quantitatively. At higher concentrations of Triton X-114 ( $>0.15\%$  (w/v)), the signals' intensity decreased probably due to increase in the viscosity of the surfactant phase. To achieve maximum preconcentration factor, Triton X-114 concentration of 0.15% (w/v) was selected for further experiments.

Since the surfactant is fairly viscous in CPE, methanol ( $100 \mu\text{L}$ ) was added into the surfactant-rich phase after separation of the phases in order to facilitate its injection into the graphite furnace.

#### 3.3.4. Influence of equilibrium temperature and time

The effects of equilibration temperature and incubation time on the extraction efficiency of Se(IV) were the next parameters considered. It was desirable to employ the shortest incubation time and the lowest possible equilibration temperature, which compromise completion of the reaction and efficient separation of the phases.

For Triton X-114, an increase in the cloud point temperature leads to a slight decrease in the volume of the surfactant-rich phase. This can be interpreted in terms of the fact that as temperature increases, hydrogen bonds are disrupted and dehydration occurs. Thus, by increasing of temperature, the amount of water in the surfactant-rich phase will reduce; hence, the volume of that phase will decrease [39]. In this study, the effect of equilibration temperature was investigated in the range of  $30\text{--}60^{\circ}\text{C}$  (Fig. 2). The optimal temperature was found to be  $50^{\circ}\text{C}$  for the CPE of Se(IV). By studying the effect of incubation time on the extraction efficiency of Se(IV), the maximum extraction efficiency was obtained at 7–25 min. Thus, the shortest incubation time (7 min) was applied in the subsequent experiments.

A centrifugation time of 10 min at 3500 rpm was selected to get a complete phase separation and no appreciable improvements were observed for longer times. However, the centrifugation time did not have a considerable effect on the analytical characteristics of the CPE method.

### 3.4. Interferences

The effects of representative potential interfering species on complexation and extraction of selenium ( $100 \mu\text{g L}^{-1}$ ) were tested (Table 6). The results showed that As(III),  $\text{Pb}^{2+}$ ,  $\text{Ni}^{2+}$ ,  $\text{Co}^{2+}$ ,  $\text{Mn}^{2+}$  and  $\text{Fe}^{2+}$  (up to the concentration level of  $1000 \mu\text{g L}^{-1}$ ),  $\text{Na}^{+}$  (up to  $10,000 \text{ mg L}^{-1}$ ),  $\text{Mg}^{2+}$  and  $\text{K}^{+}$  (up to  $500 \text{ mg L}^{-1}$ ) did not cause any significant interference on the CPE of Se(IV). However, since  $\text{Cu}^{2+}$  interferes in the preconcentration of the Se(IV) ion, thus by

**Table 6**  
Effect of foreign ions on the preconcentration and determination of Se.

Coexisting ions	Foreign ion to analyte ratio	Relative absorbance
$\text{Na}^{+}$	10,000	0.98
$\text{K}^{+}$	10,000	0.92
$\text{Mg}^{2+}$	5,000	0.99
$\text{As}^{3+}$	10	0.93
$\text{Pb}^{2+}$	10	1.02
$\text{Ni}^{2+}$	10	1.03
$\text{Mn}^{2+}$	10	0.86
$\text{Co}^{2+}$	10	0.95
$\text{Fe}^{2+}$	10	0.87
$\text{Cu}^{2+}$	10	0.40

Relative absorbance = [absorbance of Se ( $100 \mu\text{g L}^{-1}$ ) + foreign ion]/absorbance of Se ( $100 \mu\text{g L}^{-1}$ ).

**Table 7**

Comparison of the proposed method with other methods applied for extraction and determination of Se(IV).

Tl ions	Method of extraction/detection system	DLR (ng mL <sup>-1</sup> )	LOD (ng mL <sup>-1</sup> )	Extraction time (min)	RSD%	Ref.
Se(IV)	LLE/GC-MS	–	1 ng	1	5.0	[42]
Se(IV)	LLE/UV-vis	1000–7000	166.5	–	–	[43]
Se(IV), Se(VI)	HG/ICP-MS	–	0.03 (500 mL)	–	4.2	[44]
As(III), Se(IV), Sb(III)	SPE/GF-AAS	–	0.06	>10	3.3	[22]
Se(IV), Se(VI)	SPE/GF-AAS	–	0.049 (100 mL)	>20	4.3	[45]
Se(IV)	DLLME/GF-AAS	0.1–3	0.05	2	4.5	[46]
Se(IV)	CPE/GF-AAS	0.6–80	0.09	7	3.6	Proposed method

masking Cu<sup>2+</sup> with 1 mL of 5% EDTA, its interference was eliminated completely.

### 3.5. Analytical figures of merit

The calibration curve was obtained by preconcentration of a suitable amount of Se(IV) solution under the optimized experimental conditions, using the proposed method. The calibration line exhibited a good linearity over the ranges of 0.6–1.0 and 1.0–80.0 μg L<sup>-1</sup> Se(IV) with correlation coefficients better than 0.998. The limit of detection (LOD) of the method for determination of Se(IV) was studied under the optimal experimental conditions. The LOD was obtained from  $C_{LOD} = (K_b S_b / m)$ , where  $m$  is the slope of the calibration graph,  $K_b$  is the numerical value of 3 and  $S_b$  is the standard deviation of ten replicates of the blank measurement. The LOD thus obtained (based on the first part of the calibration line) was 0.09 ng mL<sup>-1</sup> ( $V_{sample} = 10$  mL). The relative standard deviation (RSD) was 3.6% ( $n = 6$ ,  $C = 20$  ng mL<sup>-1</sup>) and the enhancement factor (that is defined as the ratio of the slopes of the calibration curves with and without preconcentration) was 63.5.

A comparison between the figures of merit of the proposed CPE method and some of the published methods for extraction and determination of Se are summarized in Table 7. It clearly shows that our proposed method has good sensitivity and precision with a wide dynamic linear range. Also, the obtained LODs by this method are better than those obtained by other methods [39–42]. Accordingly, the main advantages of our proposed method include high sensitivity with good precision, rapidity, low consumption of organic solvents, low cost and simplicity to operation.

### 3.6. Determination of selenium in real samples

The proposed CPE-ETAAS methodology was applied for determination of Se in several water, urine and plasma samples. In order to validate the proposed method, recovery experiments were also carried out by spiking the samples with different amounts of Se before any pretreatment. The urine and plasma samples were analyzed using the standard addition calibration and the percentages of recoveries were calculated (Table 8). The good agreement between the table results and the known values indicates the successful applicability of the present method for determination of Se in real samples.

Also, in order to further investigate the accuracy of the proposed method, some experiments were done on other plasma and urine samples and the results were compared with those obtained by the extraction and determination of Se(IV) using hollow fiber liquid phase microextraction-HPLC method (Table 9). One can see that a satisfactory agreement exists between the results obtained for the Se(IV) in the real samples by CPE method and those by the hollow fiber liquid phase microextraction-HPLC method [47].

## 4. Conclusions

This study demonstrated the application of fractional factorial experimental design based on Taguchi's orthogonal array for

**Table 8**

Analytical results for determination of Se(IV) in real aqueous samples.

Sample	Concentration (mean, $n = 3$ ) (ng mL <sup>-1</sup> )		
	Se(IV) added	Se(IV) found	Recovery (%)
Tap water <sup>a</sup>	0.0	0.96	–
	20.0	20.6	98.2
Well water <sup>b</sup>	0.0	0.63	–
	20.0	19.8	96.0
Plasma	0.0	42.0	–
	20.0	61.1	95.7
Urine	0.0	23.1	–
	20.0	42.1	94.9

<sup>a</sup> Tap water (Karaj, Iran).

<sup>b</sup> Obtained from Tarbiat Modares University, Tehran, Iran.

**Table 9**

Determination of selenium(IV) in plasma and urine samples.

Sample	Concentration (ng mL <sup>-1</sup> )	
	HPLC-UV	ETAAS
Plasma	46 ± 4	45 ± 5
Urine	19 ± 3	23 ± 4

screening of the significant factors of CPE for the extraction and analysis of Se in environmental and biological samples. An OA<sub>16</sub> (4<sup>5</sup>) matrix was applied to study the effects of five factors (equilibrium temperature and time, ionic strength, surfactant concentration, pH) on extraction efficiency of Se(IV). The effect of each factor was estimated using individual contributions as response functions. The results of ANOVA showed that the equilibrium temperature and time have no significant effect on the extraction efficiency. Also, better analytical characteristics, such as higher ashing temperature, lower characteristic masses, lower detection limits, longer tube lifetime and better analyte recoveries in the water and biological samples were obtained using W as permanent modifier and Pd(NO<sub>3</sub>)<sub>2</sub> as a chemical modifier.

Our findings in the present study also demonstrated that CPE-ETAAS is an effective approach for the extraction and determination of trace amount of Se (sub- to low ng mL<sup>-1</sup>) in environmental and biological samples.

## References

- [1] L. Campanella, T. Ferri, R.A. Morabito, *Analisis* 17 (1989) 507.
- [2] E. Klein, I. Thompson, S. Lippman, P. Goodman, D. Albanes, P. Taylor, C. Coltman, *Urol. Oncol.* 21 (2003) 59.
- [3] J. Zheng, Y. Shibata, N. Furuta, *Talanta* 59 (2003) 27.
- [4] B.D. Wake, A.R. Bowie, E.C.V. Butler, P.R. Haddad, *TRAC Trends Anal. Chem.* 23 (2004) 491.
- [5] G.V. Iyengar, W.E. Kollmer, H.J.M. Bowen, *The Elemental Composition of Human Tissues and Body Fluid*, Verlag Chemie, Weinheim, 1978.
- [6] Z.J. Gong, X.S. Zhang, G.H. Chen, X.F. Xiao, *Talanta* 66 (2005) 1012.
- [7] M.B. Melwanki, J. Seetharamappa, *Turk. J. Chem.* 24 (2000) 287.
- [8] F.A. Bertolino, A.A.J. Torriero, E. Salinas, R. Olsina, L.D. Martinez, J. Raba, *Anal. Chim. Acta* 572 (2006) 32.
- [9] B. Lange, C.M.G. van den Berg, *Anal. Chim. Acta* 418 (2000) 33.
- [10] B. Zhang, H. Xu, J.C. Yu, *Talanta* 57 (2002) 323.

- [11] A.C.F. Gomes, A.A. Menegário, D.C. Pellegrinotti, *Spectrochim. Acta Part B: Atom. Spectrosc.* 59 (2004) 1481.
- [12] Z. Mester, P. Fodor, *Anal. Chim. Acta* 386 (1999) 89.
- [13] I. Ipolyi, P. Fodor, *Anal. Chim. Acta* 413 (2000) 13.
- [14] A.K. Singh, T. White, T. Arendt, Y. Jiang, *J. Chromatogr. B Biomed. Sci. Appl.* 696 (1997) 324.
- [15] V. Stibilj, M. Dermelj, A.R. Byrne, *J. Chromatogr. A* 668 (1994) 449.
- [16] A. Elaseer, G. Nickless, *J. Chromatogr. A* 664 (1994) 77.
- [17] R. Manjusha, K. Dash, D. Karunasagar, *Food Chem.* 105 (2007) 260.
- [18] D. Bohrer, E. Becker, P. Cícero do Nascimento, *Food Chem.* 104 (2007) 868.
- [19] H. Bertelsmann, A. Kyriakopoulos, M. Oezaslan, *Microchem. J.* 85 (2007) 239.
- [20] M.N. Pathare, A.D. Sawant, *Anal. Lett.* 28 (1995) 317.
- [21] S. Forager, I. Lavilla, C. Bendicho, *Talanta* 68 (2006) 1096.
- [22] L. Zhang, Y. Morita, A. Sakuragawa, A. Isozaki, *Talanta* 72 (2007) 723.
- [23] C. Dietz, J.S. Landaluze, P. Ximénez-Embún, Y. Madrid-Albarrán, *Anal. Chim. Acta* 501 (2004) 157.
- [24] Z. Mester, R. Sturgeon, *Spectrochim. Acta Part B: Atom. Spectrosc.* 60 (2005) 1243.
- [25] Z. Mester, R. Sturgeon, J. Pawliszyn, *Spectrochim. Acta Part B: Atom. Spectrosc.* 56 (2001) 233.
- [26] Y. Kashiwagi, E. Kokufuta, T. Kawashima, *Anal. Sci.* 13 (1997) 623.
- [27] T.P. Rao, M. Anbu, M.L.P. Reddy, C.S.P. Iyer, A.D. Damodaran, *Anal. Lett.* 29 (1996) 2563.
- [28] S.V.K. Yathavakilla, M. Shah, S. Mounicou, J.A. Caruso, *J. Chromatogr. A* 1100 (2005) 153.
- [29] D.L. Tsalev, L. Lampugnani, A. D'Ulivo, *Microchem. J.* 70 (2001) 103.
- [30] Z.S. Ferrera, C.P. Sanz, C.M. Santana, J.J.S. Rodriguez, *Trends Anal. Chem.* 23 (2004) 469.
- [31] E.K. Paleologos, D.L. Giokas, M.I. Karayannis, *Trends Anal. Chem.* 24 (2005) 426.
- [32] D.L.G. Borges, M.A.M.S. da Veiga, V.L.A. Frescura, B. Welz, A. Curtius, *J. Anal. At. Spectrom.* 18 (2003) 501.
- [33] M. Sarkouhi, Y. Yamini, M.R. Khalili-Zanjani, A. Afsharnaderi, *Int. J. Environ. Anal. Chem.* 87 (2007) 603.
- [34] Z. Marczenko, *Separation and Spectrophotometric Determination of Elements*, John Wiley & Sons, Australia, 1986, p. 508.
- [35] L.J. Yang, *J. Mater. Process. Technol.* 113 (2001) 521.
- [36] W.G. Lan, M.K. Wong, N. Chen, *Analyst* 119 (1994) 1659.
- [37] B. He, Z.M. Ni, *J. Anal. At. Spectrom.* 11 (1996) 165.
- [38] Y. Wei-Ming, N. Zhe-Ming, *Spectrochim. Acta B* 52 (1997) 241.
- [39] R.P. Frankewich, W. Hinze, *Anal. Chem.* 66 (1994) 944.
- [40] B. Delgado, V. Pino, J.H. Ayala, *Anal. Chim. Acta* 518 (2004) 165.
- [41] F. Shemirani, M. Baghdadi, M. Ramezani, M.R. Jamali, *Anal. Chim. Acta* 534 (2005) 163.
- [42] J.L. Gomez-Ariza, J.A. Pozas, I. Giraldez, E. Morales, *Talanta* 49 (1999) 285.
- [43] J.M. Sankalia, R.C. Mashru, M.G. Sankalia, *Spec. Lett.* 38 (2005) 61.
- [44] H. Narasaki, K. Mayumi, *Anal. Sci.* 16 (2000) 65.
- [45] K. Pyrzynska, P. Drzewicz, M. Trojanowicz, *Anal. Chim. Acta* 363 (1998) 141.
- [46] A. Bidari, E. Zeini Jahromi, Y. Assadi, M.R. Milani Hosseini, *Microchem. J.* 87 (2007) 6.
- [47] A. Saleh, *Hollow fiber liquid phase microextraction and HPLC-UV determination of trace amounts of Se(IV) in natural waters and biological samples*, MSc thesis, Tarbiat Modares University, Tehran, Iran, 2007.



## Novel platinum(II) selective membrane electrode based on 1,3-bis(2-cyanobenzene)triazene

Mohammad Bagher Gholivand<sup>a,\*</sup>, Moslem Mohammadi<sup>b</sup>,  
Mehdi Khodadadian<sup>a</sup>, Mohammad Kazem Rofouei<sup>b</sup>

<sup>a</sup> Department of Chemistry, Razi University, Kermanshah, Iran

<sup>b</sup> Faculty of Chemistry, Tarbiat Moallem University, Tehran, Iran

### ARTICLE INFO

#### Article history:

Received 29 October 2008

Received in revised form

28 December 2008

Accepted 30 December 2008

Available online 22 January 2009

#### Keywords:

Platinum

Ion-selective electrode

PVC membrane

Potentiometry

1,3-Bis(2-cyanobenzene) triazene

### ABSTRACT

A plasticized poly (vinyl chloride) membrane electrode based on 1,3-bis(2-cyanobenzene)triazene (CBT) for highly selective determination of platinum(II) (in  $\text{PtCl}_4^{2-}$  form) is developed. The electrode showed a good Nernstian response ( $29.8 \pm 0.3 \text{ mV decade}^{-1}$ ) over a wide concentration range ( $1.0 \times 10^{-6}$  to  $1.0 \times 10^{-2} \text{ mol L}^{-1}$ ). The limit of detection was  $5.0 \times 10^{-7} \text{ mol L}^{-1}$ . The electrode has a response time of about 40 s, and it can be used for at least 1 month without observing any considerable deviation from Nernstian response. The proposed electrode revealed an excellent selectivity toward platinum(II) ion over a wide variety of alkali, alkaline earth, transition, and heavy metal ions, and it could be used in the pH range of 3.2–5.1. The practical utility of the electrode has been demonstrated by its use in determination of platinum ion in, alloy, tap, mineral and river water samples.

© 2009 Elsevier B.V. All rights reserved.

### 1. Introduction

The increasing use of platinum group elements (PGEs) Ru, Rh, Pd, Os, Ir and Pt in different medical and industrial fields has led to a growing need for suitable analytical tools for the reliable determination of these elements at low level concentrations. On account of two main applications of platinum such as anti-cancer drugs (such as cisplatin) [1] and Pt containing vehicle exhaust catalyst (VECs) [2–10], the determination of total Pt contents of environmental matrices gained a considerable interest in the last decade. Pt from VECs is emitted in the form of fine suspended particulate matter and; therefore, it might be inhaled and accumulated by living organisms [11–13]. The high biochemical activity of some Pt species, e.g. the cytotoxicity and mutagenicity of cisplatin or the sensitizing effect of hexachloroplatinate bears the risk of significant negative effects on human health after chronic exposure even to trace amounts of Pt species. Therefore, there are enough reasons to introduce simple and rapid methods for determination of the platinum content in various environmental samples. Several analytical techniques, such as inductively coupled plasma atomic emission spectrometry (ICP-AES) [14], inductively coupled plasma mass spectrometry (ICP-MS) [15,6] and atomic absorption

spectrometry (AAS) [16], neutron activation analysis (NAA) [17] and cathodic stripping voltammetry (CSV) [18], were applied in order to determine the platinum, palladium, and rhodium in various samples. However, these methods are either time-consuming, involving multiple sample manipulations, or too expensive for most analytical laboratories. Among the available analytical techniques, the application of carrier based ion-selective electrodes (ISEs) has become a well-established routine analytical technique. The most important properties of these electrodes are the high speed sample analysis, portability of the device, sample non-destructive, on-line monitoring, cost effectiveness and wide measuring range [19–23].

Triazene compounds, characterized by having a diazoamino group ( $-\text{N}=\text{N}-\text{N}-$ ), have been studied for over 130 years concerning their interesting structural, anticancer, and reactivity properties [24]. The first extensive investigation of the coordination chemistry of a triazene derivative (1,3-diphenyltriazene) was carried out in 1887 by Meldola [25]. The interaction of triazene derivatives with platinum metal has been studied in the past few years by several authors [26–30]. In the present study, we describe the fabrication and characterization of a new ISE based on 1,3-bis(2-cyanobenzene)triazene as a selective and lipophilic ionophore. The coordinating effect for the selective response of platinum ion was investigated by the use of PVC membrane. To the best of our knowledge, this is the first PVC-ISE which is sensitive to platinum ion concentration with specified features as Nernstian response, wide concentration range, and low detection limit.

\* Corresponding author. Tel.: +98 831 4274557; fax: +98 831 4274559.  
E-mail address: [mbgholivand@yahoo.com](mailto:mbgholivand@yahoo.com) (M.B. Gholivand).



## 2. Experimental

### 2.1. Reagents

Reagent grade chemicals were used without any further purification. Stock solutions were prepared with doubly distilled water. Potassium tetrachloroplatinate(II)  $K_2[PtCl_4]$ , dibutylphthalate (DBP), dioctylphthalate (DOP), tris(2-ethylhexyl)phosphate (TEHP), dioctylsebasate (DOS), tetrahydrofuran (THF), tetrabutylammonium perchlorate (TBAP), hexadecyltrimethylammonium bromide (HTAB), tetraoctylammonium perchlorate (TOAP) and high relative molecular weight poly (vinyl chloride) (PVC) were obtained from Merck or Sigma and used without any further purification. 2-Nitrophenyloctylether (O-NPOE) was purchased from Acros. The sodium salts of anions and all other chemicals were of the highest purity available from Merck, and they were used without further purification. The acetate buffer solution containing appropriate amount of  $0.1 \text{ mol L}^{-1}$  acetic acid and  $0.1 \text{ mol L}^{-1}$  sodium acetate was adjusted to pH 4.0 with sodium hydroxide solution and utilized to adjust pH of the test solution.

### 2.2. Synthesis and characterization of CBT

The 1,3-bis(2-cyanobenzene)triazene (CBT) was used as the ionophore, and its structure is shown in Fig. 1. It was synthesized as follows: A 1000 mL flask was charged with 100 g of ice and 150 mL of water and then cooled to  $0^\circ\text{C}$  in an ice-bath; afterwards, it was added by 11.80 g (0.10 mol) of o-cyanoaniline and 13 g (0.36 mol) of hydrochloric acid ( $d = 1.18 \text{ g mL}^{-1}$ ), and then a solution of  $\text{NaNO}_2$  containing 4.10 g (0.06 mol) in 25 mL of water was added in 15 min under stirring solution. Finally a solution containing 14.76 g (0.18 mol) of sodium acetate in 45 mL of water was added and stirred for 45 min. The yellow product was filtered and dissolved in diethyl ether. After evaporation of diethyl ether, a purified sharp yellow powder, which has a melting point of  $128\text{--}130^\circ\text{C}$ , was produced (yield, 62%). Infra red and  $^1\text{H}$  NMR spectra confirmed the CBT structure. IR (KBr): 3222, 3104, 3029, 2233, 1800–1600, 1604, 1588–1486, 1300–1000, 1064, 900–600,  $759 \text{ cm}^{-1}$ ,  $^1\text{H}$  NMR (DMSO):  $\delta$  7.2–7.8 (phenyl protons, 8); 13.4(NH, 1); 3.3–2.4 (solvent).

The crystal structure of 1,3-bis(2-cyanobenzene)triazene was solved by direct methods and refined by full-matrix least squares using the program SHELXTL-98.4. The H atoms were isotropically refined. The molecular structure of crystalline 1,3-bis(2-cyanobenzene)triazene is presented in Fig. 2. Crystal and experimental data are listed in Table 1.

### 2.3. Complex study

In order to determine the stoichiometry and stability of the resulting CBT complex with platinum(II) in acetonitrile solution,

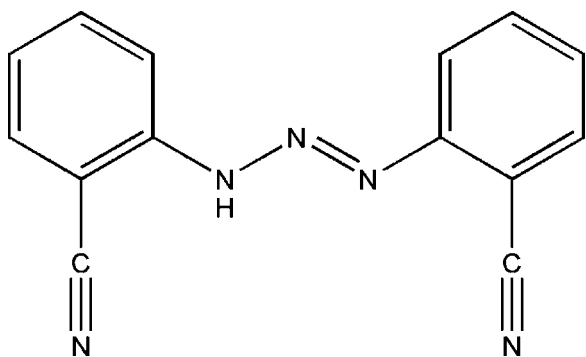


Fig. 1. Structure of 1,3-bis(2-cyanobenzene)triazene (CBT).

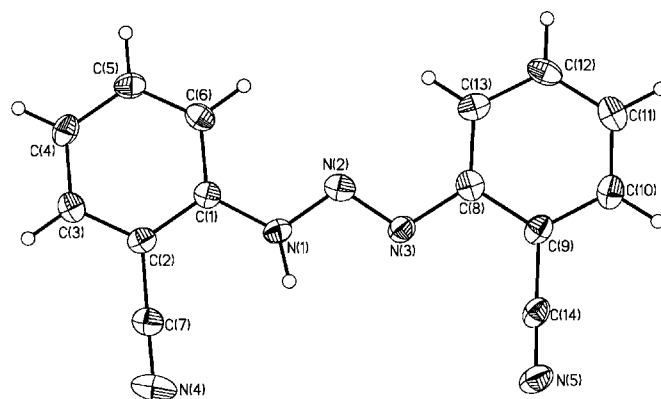


Fig. 2. ORTEP drawing of the molecule structure 1,3-bis(2-cyanobenzene)triazene (CBT).

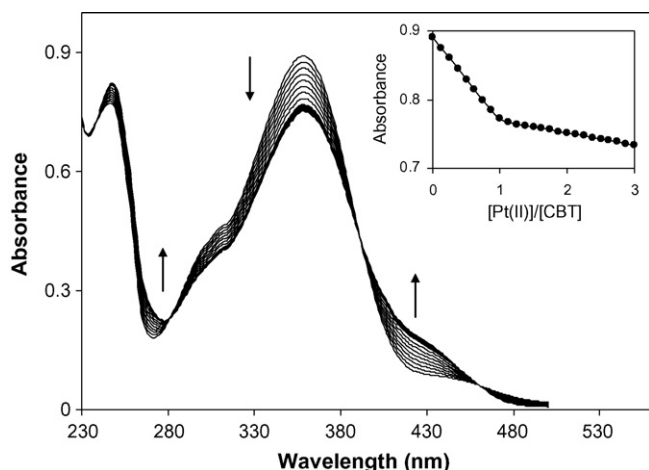
the spectra of a series of solutions containing a constant concentration of ligand ( $5.0 \times 10^{-5} \text{ mol L}^{-1}$ ) at a fixed ionic strength of  $1.0 \times 10^{-3} \text{ mol L}^{-1}$ , maintained by tetraethylammonium perchlorate (TEAP), and varying amounts of the metal ion were obtained (the spectra are shown in Fig. 3). As seen, the complexation was accompanied by a relatively strong shift of the absorption bands of the CBT. Such a pronounced effect on the electronic spectra of the complexes could be related to a large change in the conjugation of the ligands. The resulting absorbance vs.  $[\text{Pt(II)}]/[\text{CBT}]$  mole ratio plot

Table 1

Crystal data and structure refinement for 1,3-bis(2-cyanobenzene)triazene (CBT).

Empirical formula	C <sub>14</sub> H <sub>9</sub> N <sub>5</sub>	
Formula weight	247.26	
Temperature	100(2)K	
Wavelength	0.71073 Å	
Crystal system	Triclinic	
Space group	P-1	
Unit cell dimensions	$a = 6.818(3) \text{ Å}$ $b = 7.642(3) \text{ Å}$ $c = 23.848(9) \text{ Å}$	$\alpha = 90.911(8)^\circ$ $\beta = 90.983(7)^\circ$ $\gamma = 105.970(7)^\circ$
Volume	1194.3(8) E <sup>3</sup>	
Z	4	
Density (calculated)	1.375 Mg/m <sup>3</sup>	
Absorption coefficient	0.089 mm <sup>-1</sup>	
F(000)	512	
Crystal size	0.15 × 0.03 × 0.01 mm <sup>3</sup>	
Theta range for data collection	0.85–26.00°	
Index ranges	–8 < = h < = 8, –9 < = k < = 9, –26 < = l < = 29	
Reflections collected	8532	
Independent reflections	4632 [R(int) = 0.0695]	
Completeness to theta = 26.00°	98.2%	
Absorption correction	None	
Refinement method	Full-matrix least-squares on F <sup>2</sup>	
Data/restraints/parameters	4632/0/343	
Goodness-of-fit on F <sup>2</sup>	1.049	
Final R indices [for 2530 rfln with I > 2sigma(I)]	R1 = 0.0891, wR2 = 0.1653	
R indices (all data)	R1 = 0.1594, wR2 = 0.1923	
Largest diff. peak and hole	0.350 and –0.271 e Å <sup>-3</sup>	

Measurement: Bruker SMART APEX2 CCD area detector. Program system: Bruker (2005). APEX2 software package, Bruker AXS Inc, 5465, East Cheryl Parkway, Madison, WI 5317. CCDC 677843 contains the supplementary crystallographic data for this paper. Copies of the data can be obtained free of charge from the Cambridge Crystallographic Data Center via [www.ccdc.cam.ac.uk](http://www.ccdc.cam.ac.uk).



**Fig. 3.** Electronic absorption spectra of ligand (CBT) in acetonitrile ( $5.0 \times 10^{-5} \text{ mol L}^{-1}$ ) in the presence of increasing concentration of platinum(II) ion. Corresponding mole ratio plot at 358 nm is shown in the inset.

obtained at 358 nm is shown in the inset of Fig. 3. As seen, the absorbance–mole ratio plot revealed a distinct inflection point at  $[\text{Pt(II)}]/[\text{CBT}]$  molar ratio of about 1, emphasizing the formation of 1:1 complex in solution. Also, the complexation of CBT with a number of metal ions was investigated. The formation constants of the resulting 1:1 complexes are listed in Table 2. As it can be seen, the CBT with the most stable complex with Pt(II) ion is expected to act as a selective ionophore for preparation of Pt(II) ion-selective membrane electrodes. The formation constants of the resulting complex between cations and CBT were evaluated by computer fitting of the corresponding mole ratio data to a previously derived equation [31] using a non-linear curve-fitting program, KINFIT [32]. Absorbance spectra were recorded using a HP spectrophotometer (Agilent 8453) equipped with a thermostated bath (Huber polystat cc1). For complexation studies, the temperature of the cell holder was maintained at  $25 \pm 0.1^\circ \text{C}$ .

#### 2.4. Preparation of the electrode

The general procedure in order to prepare the PVC membrane was to mix thoroughly 1 mg of ionophore (CBT), 1 mg of additive (TBAP), 33 mg of powdered PVC and 65 mg of plastisizer TEHP in a glass dish of 2 cm diameter. The mixture was then completely dissolved in 5 mL of fresh THF. The solvent was slowly evaporated until an oily concentrated mixture was resulted. A Pyrex or Teflon tube (3–5 mm i.d. on top) was dipped into the mixture for 10 s, so a membrane was formed. The tube was then pulled out from the mixture and kept at room temperature for 24 h. The tube was then filled with internal filling solution of  $1.0 \times 10^{-3} \text{ mol L}^{-1}$  of  $\text{PtCl}_4^{2-}$  con-

**Table 2**  
Formation constants of different metal–CBT complexes in acetonitrile.

Metal	$\log K_f$
Pt(II)	$3.96 \pm 0.02$
Pb(II)	$2.55 \pm 0.03$
Pd(II)	$3.07 \pm 0.03$
Cd(II)	$2.75 \pm 0.02$
Hg(II)	$3.48 \pm 0.04$
Ni(II)	$2.37 \pm 0.03$
Mn(II)	$2.12 \pm 0.02$
Ag(I)	$3.22 \pm 0.03$
Cu(II)	$2.91 \pm 0.04$
Zn(II)	$2.63 \pm 0.03$
Fe(III)	$2.01 \pm 0.04$
Au(III)	$2.93 \pm 0.02$

**Table 3**

Equilibrium constants for aqualization reactions of platinum tetrachloride in water.

Reactions	Equilibrium constant
$\text{PtCl}_4^{2-} + \text{H}_2\text{O} \rightleftharpoons \text{PtCl}_3(\text{H}_2\text{O})^- + \text{Cl}^-$	$8.70 \times 10^{-3}$
$\text{PtCl}_3(\text{H}_2\text{O})^- + \text{H}_2\text{O} \rightleftharpoons \text{PtCl}_2(\text{H}_2\text{O})_2 + \text{Cl}^-$	$2.50 \times 10^{-4}$
$\text{PtCl}_2(\text{H}_2\text{O})_2 + \text{H}_2\text{O} \rightleftharpoons \text{PtCl}(\text{H}_2\text{O})_3^+ + \text{Cl}^-$	$1.76 \times 10^{-6}$
$\text{PtCl}(\text{H}_2\text{O})_3^+ + \text{H}_2\text{O} \rightleftharpoons \text{Pt}(\text{H}_2\text{O})_4^{2+} + \text{Cl}^-$	$1.55 \times 10^{-7}$

taining  $0.2 \text{ mol L}^{-1}$  NaCl. The electrode was finally conditioned for 24 h by soaking in a  $1.0 \times 10^{-3} \text{ mol L}^{-1}$  solution of  $\text{PtCl}_4^{2-}$  containing  $0.2 \text{ mol L}^{-1}$  NaCl.

#### 2.5. EMF measurements

A cell assembly of the following type was used:

Ag/AgCl, KCl ( $3 \text{ mol L}^{-1}$ ) | internal solution:  $\text{PtCl}_4^{2-}$  ( $1.0 \times 10^{-3} \text{ mol L}^{-1}$ ),  $0.2 \text{ mol L}^{-1}$  NaCl | PVC membrane | test solution | Hg/Hg<sub>2</sub>Cl<sub>2</sub>, KCl (satd.).

A Metrohm-692 pH/mV meter was used for measurements at  $25.0 \pm 0.1^\circ \text{C}$ . All measurements were carried out at  $25.0 \pm 0.1^\circ \text{C}$ . The pH of test solutions was adjusted.

### 3. Results and discussion

#### 3.1. Distribution of different platinum species in aqueous solution

When platinum tetrachloride ( $\text{PtCl}_4^{2-}$ ) dissolves in aqueous solution, its chloride ligands can be substituted by water molecules one by one leading to mono-, di-, tri- and tetra-aquo platinum complexes. Zhu and Ziegler [33] have reported the calculated equilibrium constants for aqualization reactions of platinum tetrachloride ( $\text{PtCl}_4^{2-}$ ) in water (Table 3). The concentration ratios of the different aquo platinum species depend on the concentration of chloride ions added to the solution in excess of those originating from  $\text{PtCl}_4^{2-}$ . It is shown that, at excess concentrations of chloride ion, tetrachloroplatinum ( $\text{PtCl}_4^{2-}$ ) is the dominant species.

The influence of chloride ion concentration on the slope of the electrode is shown in Fig. 4. Obviously, the electrode does not show Nernstian behavior at low chloride concentrations. This is probably due to the fact that at lower chloride concentrations a mixture of platinum species is present in the solution causing a mean response of the electrode. As chloride ion concentration increases, the slope of the electrode decreases and tends to level off at  $\sim 30.0 \text{ mV decade}^{-1}$ . As mentioned above, at higher chloride concentrations the major species is  $\text{PtCl}_4^{2-}$ , which is probably responsible for the observed slope. Therefore, in all experiments

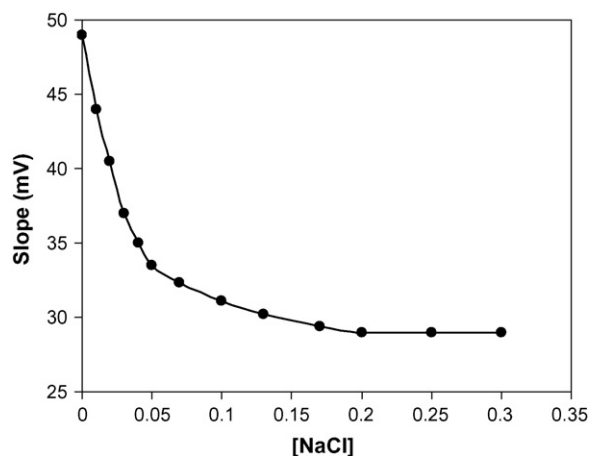


**Fig. 4.** Effect of excess chloride ions concentration on the slope of the electrode.

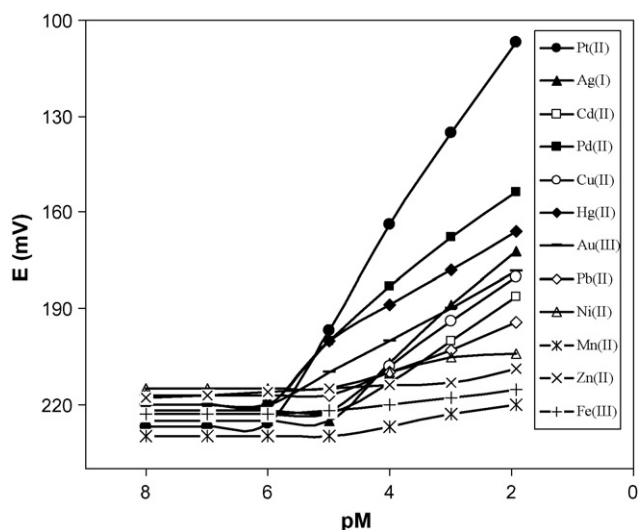


Fig. 5. Potential response of ion-selective electrode based on CBT (composition no. 8) for various metal ions.

the electrode potential was measured in the excess of chloride ion concentration ( $[Cl^-] = 0.2 \text{ mol L}^{-1}$ ).

### 3.2. Effect of electrode composition

Due to its sufficient insolubility in water and the presence of donating nitrogen atoms in its structure, ligand CBT was expected to act as a suitable ion carrier in the PVC membranes with respect to special transition and heavy metal ions of proper size and charge. Thus, in preliminary experiments, it was used as a neutral carrier to prepare PVC-based membrane electrodes for a variety of metal ions. The potential responses of the most sensitive electrodes, prepared under the same experimental conditions (except for 24 h conditioning in a  $0.001 \text{ mol L}^{-1}$  of the corresponding cations) are shown in Fig. 5. As it can be seen, among different tested cations, platinum(II) with the most sensitive response seems to be suitably determined with the PVC membrane based on CBT, and the EMF responses obtained for all other cation-selective electrodes are much lower than that predicted by the Nernst equation. This is probably due to both the selective behavior of the ionophore against platinum(II) in comparison to some other metal ions and the rapid exchange kinetics of the resulting CBT–Pt(II) complexes [34].

It is obvious that some important features of the PVC-based membranes, such as the nature and amount of ionophore, the properties of the plasticizer, the plasticizer/PVC ratio, and especially the nature of additives used significantly influence the sensitivity and selectivity of the ion-selective electrodes [35–37]. Thus, different aspects of membrane preparation based on CBT were optimized and the results are given in Table 4. Solvent polymeric membrane ion-selective electrodes are usually based on a matrix of the solvent mediator/PVC ratio about 2. Polymeric films with such a plasticizer/PVC ratio will result in optimum physical properties and high enough mobility of their constituents. In this study, a plasticizer/PVC ratio of nearly 2 was found to be the most suitable ratio. It is vivid that the selectivity and working concentration range of the membrane sensors are affected by the nature and amount of plasticizer used. This is due to the influence of plasticizer on the dielectric constant of the membrane phase, the mobility of the ionophore molecules, and the state of ligands. Among of the five different plasticizers used (Table 4), TEHP resulted in the best sensitivity. Moreover, 1% of CBT was chosen as the optimum amount of the ionophore in the PVC membrane (no. 8). Although neutral-

carrier-based ISE membranes may work properly even when they contain only a very small amount of ionic sites (e.g., as impurities), the addition of a salt of lipophilic ion is advisable and beneficial for various other reasons as well. In fact, the use of additives may catalyze the exchange kinetic at the sample-membrane surface and gives rise to significant changes in selectivity [38]. Thus, addition of a little amount of additives improves the response characteristics of the proposed electrode. From the data presented in Table 4, it is seen that the addition of TBAP increases the sensitivity of the electrode response considerably. The Use of 1% TBAP resulted in a Nernstian behavior of the electrode (no. 8). Thus, the obtained results indicate that the best sensitivity and linear range is obtained for the membrane no. 8 with a PVC: TEHP: CBT: TBAP percent ratio of 33:65:1:1 which resulted in a Nernstian behavior of the membrane electrode over a wide concentration range.

### 3.3. Effect of pH on potential response of electrode

The influence of the pH of the test solution ( $1.0 \times 10^{-3} \text{ mol L}^{-1}$   $PtCl_4^{2-}$  containing  $0.2 \text{ mol L}^{-1}$  NaCl) on the sensor potential was investigated over the pH range 2–7, where pH was adjusted with dilute  $HNO_3$  or NaOH solutions. The potential–pH plot (Fig. 6) reveals that, within the pH range 3.2–5.1, the potential do not vary by more than  $\pm 1.0 \text{ mV}$ . The change in potentials at higher pH values may be due to the hydrolysis of Pt(II) in solution. Also, a drift in the potential response is observed at pH values lower than 3.2. This is probably due to the protonation of  $PtCl_4^{2-}$  species. Thus, the pH of 4.0 was selected and kept constant using acetate buffer solution for further studies.

### 3.4. Influence of concentration of inner filling solution and condition time

The concentration of the internal platinum solution in the electrode was changed from  $1.0 \times 10^{-5}$  to  $1.0 \times 10^{-2} \text{ mol L}^{-1}$  (containing  $0.2 \text{ mol L}^{-1}$  NaCl) and the potential response of the electrode was studied. It was found that the variation of the concentration of the internal solution does not cause any significant difference in the potential response, except for an expected change in the intercept of the resulting Nernstian plots. A  $1.0 \times 10^{-3} \text{ mol L}^{-1}$  concentration of the reference platinum solution is quite appropriate for smooth functioning of the electrode system.

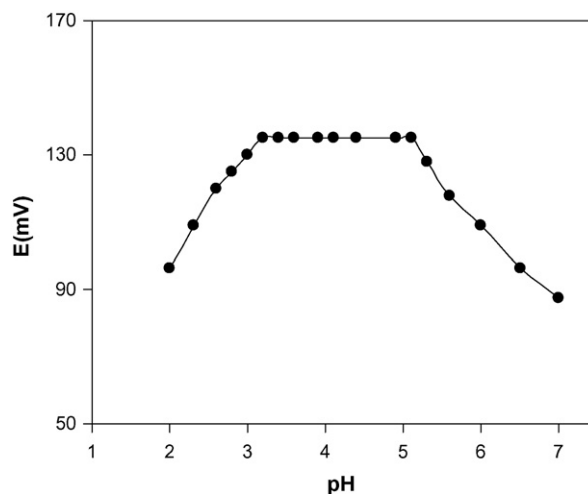
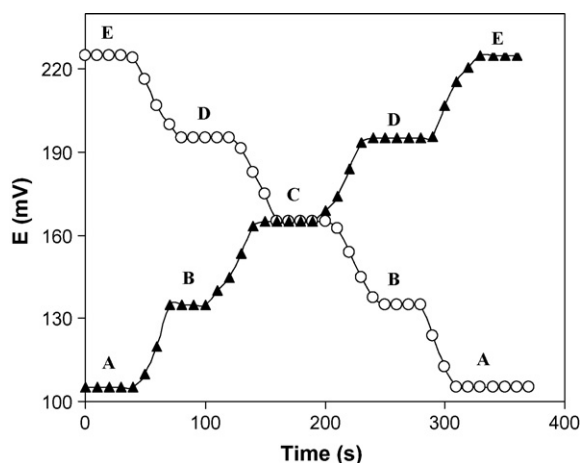


Fig. 6. Effect of pH on the response of the platinum ion-selective electrode (composition no. 8).

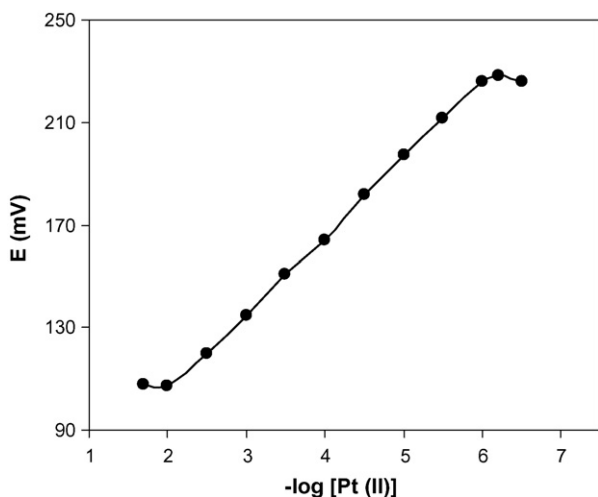
**Table 4**  
Optimization of membrane ingredients.

Membrane no.	Composition of membrane (wt%)				Slope (mV decade <sup>-1</sup> )	Linear range (mol L <sup>-1</sup> )
	PVC	Plasticizer	Additive	Ionophore		
1	33.0	66 (NPOE)	0.0	1.0	37.4 ± 0.4	1.5 × 10 <sup>-4</sup> to 1.0 × 10 <sup>-2</sup>
2	33.0	66 (DOS)	0.0	1.0	13.1 ± 0.4	4.1 × 10 <sup>-4</sup> to 1.0 × 10 <sup>-2</sup>
3	33.0	66 (DBP)	0.0	1.0	19.4 ± 0.5	4.7 × 10 <sup>-5</sup> to 1.0 × 10 <sup>-2</sup>
4	33.0	66 (DOP)	0.0	1.0	22.3 ± 0.3	8.8 × 10 <sup>-6</sup> to 1.0 × 10 <sup>-2</sup>
5	33.0	66 (TEHP)	0.0	1.0	27.1 ± 0.4	5.0 × 10 <sup>-6</sup> to 1.0 × 10 <sup>-2</sup>
6	33.0	65 (TEHP)	1.0 (TOAP)	1.0	27.9 ± 0.5	2.6 × 10 <sup>-6</sup> to 1.0 × 10 <sup>-2</sup>
7	33.0	65 (TEHP)	1.0 (HTAB)	1.0	28.3 ± 0.4	4.3 × 10 <sup>-6</sup> to 1.0 × 10 <sup>-2</sup>
8	33.0	65 (TEHP)	1.0 (TBAP)	1.0	29.8 ± 0.3	1.0 × 10 <sup>-6</sup> to 1.0 × 10 <sup>-2</sup>
9	33.5	65 (TEHP)	0.5 (TBAP)	1.0	28.5 ± 0.4	3.1 × 10 <sup>-6</sup> to 1.0 × 10 <sup>-2</sup>
10	32.5	65 (TEHP)	1.5 (TBAP)	1.0	28.1 ± 0.3	4.5 × 10 <sup>-6</sup> to 1.0 × 10 <sup>-2</sup>
11	33.5	65 (TEHP)	1.0 (TBAP)	0.5	27.4 ± 0.5	6.5 × 10 <sup>-6</sup> to 1.0 × 10 <sup>-2</sup>
12	32.5	65 (TEHP)	1.0 (TBAP)	1.5	27.8 ± 0.4	4.3 × 10 <sup>-6</sup> to 1.0 × 10 <sup>-2</sup>
13	33.0	66 (TEHP)	1.0 (TBAP)	0.0	8.7 ± 0.5	5.0 × 10 <sup>-4</sup> to 1.0 × 10 <sup>-2</sup>

**Fig. 7.** Dynamic response of the CBT membrane electrode for step changes in concentration (from low to high and vice versa): (A) 10<sup>-2</sup>, (B) 10<sup>-3</sup>, (C) 10<sup>-4</sup>, (D) 10<sup>-5</sup>, and (E) 10<sup>-6</sup> mol L<sup>-1</sup>.

### 3.5. Response time, lifetime and calibration curve

The average time required for platinum-ion-selective electrode no. 8 in order to reach a potential within ±0.5 mV of the final equilibrium value after successive immersion in the series of platinum ion solutions, each having a 10-fold difference in concentration

**Fig. 8.** Calibration graph for platinum(II) ion selective electrode based on CBT (composition no. 8).**Table 5**  
The lifetime of the Pt(II) membrane sensor.

Day	Slope (mV decade <sup>-1</sup> )	Linear range (mol L <sup>-1</sup> )
1	29.8 ± 0.3	1.0 × 10 <sup>-6</sup> to 1.0 × 10 <sup>-2</sup>
5	29.6 ± 0.3	1.5 × 10 <sup>-6</sup> to 1.0 × 10 <sup>-2</sup>
10	29.2 ± 0.4	2.6 × 10 <sup>-6</sup> to 1.0 × 10 <sup>-2</sup>
15	28.7 ± 0.5	3.0 × 10 <sup>-6</sup> to 1.2 × 10 <sup>-2</sup>
20	28.3 ± 0.4	3.9 × 10 <sup>-6</sup> to 1.6 × 10 <sup>-2</sup>
25	28.0 ± 0.5	4.7 × 10 <sup>-6</sup> to 1.8 × 10 <sup>-2</sup>
30	27.5 ± 0.5	5.5 × 10 <sup>-6</sup> to 2.1 × 10 <sup>-2</sup>

from 1.0 × 10<sup>-6</sup> to 1.0 × 10<sup>-2</sup> mol L<sup>-1</sup>, was considered. The results are given in Fig. 7. As it can be seen, in the whole concentration range the static response times of the membrane electrode were obtained in a short time (about 40 s), and potentials stayed constant for at least 5 min when the potentials recorded from low to high concentrations or vice versa. The PVC membrane electrode prepared, filled by conventional inner filling solution, and operated under optimal experimental conditions, shows a linear response to the activity (concentration) of platinum ion in the range 1.0 × 10<sup>-6</sup> to 1.0 × 10<sup>-2</sup> mol L<sup>-1</sup> ( $r^2 = 0.998$ ), with a Nernstian slope of 29.8 mV per decade of platinum ion concentration (Fig. 8). The limit of detection, as determined from the intersection of the two extrapolated segments of the calibration graph, was 5.01 × 10<sup>-7</sup> mol L<sup>-1</sup>. In order to evaluate the reproducibility of this electrode, a series of membranes with similar composition (no. 8) were prepared and filled by 1.0 × 10<sup>-3</sup> mol L<sup>-1</sup> of platinum ion solution (containing 0.2 mol L<sup>-1</sup> NaCl). The response of these electrodes to platinum ion concentrations was tested. The results showed that the average of slopes, detection limits, and linear dynamic ranges were, respectively, 29.8 ± 0.3 mV decade<sup>-1</sup>, (5.01 ± 0.30) × 10<sup>-7</sup> mol L<sup>-1</sup> and (1.0 ± 0.21) × 10<sup>-2</sup> to (1.0 ± 0.29) × 10<sup>-6</sup> mol L<sup>-1</sup>. In order to evaluate the reproducibility of the platinum ion concentration,

**Table 6**  
Selectivity coefficient of various interfering ions<sup>a</sup> (n = 5).

Interfering ion	-log K	Interfering ion	-log K
Pd <sup>2+</sup>	2.14 ± 0.31	Al <sup>3+</sup>	3.64 ± 0.24
Pb <sup>2+</sup>	2.74 ± 0.27	Mn <sup>2+</sup>	3.15 ± 0.26
Cd <sup>2+</sup>	2.62 ± 0.28	Co <sup>2+</sup>	3.08 ± 0.24
Ni <sup>2+</sup>	2.89 ± 0.26	Cr <sup>3+</sup>	3.63 ± 0.26
Au <sup>3+</sup>	2.32 ± 0.29	Zn <sup>2+</sup>	3.02 ± 0.25
Cu <sup>2+</sup>	2.71 ± 0.26	Ca <sup>2+</sup>	4.09 ± 0.24
Hg <sup>2+</sup>	2.26 ± 0.30	K <sup>+</sup>	4.71 ± 0.23
Fe <sup>3+</sup>	3.38 ± 0.24	Na <sup>+</sup>	4.53 ± 0.24
Ag <sup>+</sup>	2.43 ± 0.28	Li <sup>+</sup>	4.92 ± 0.22
NO <sub>3</sub> <sup>-</sup>	3.53 ± 0.24	IO <sub>4</sub> <sup>-</sup>	2.91 ± 0.28
CN <sup>-</sup>	3.04 ± 0.26	SO <sub>4</sub> <sup>2-</sup>	2.88 ± 0.27
IO <sub>3</sub> <sup>-</sup>	2.96 ± 0.27	SCN <sup>-</sup>	3.14 ± 0.25

<sup>a</sup> All test solutions containing 0.2 mol L<sup>-1</sup> NaCl.

**Table 7**Determination of the platinum ions in different samples<sup>a</sup> ( $n = 5$ ).

Sample	Added (mol L <sup>-1</sup> )	Found by ISE (mol L <sup>-1</sup> )	Found by AAS (mol L <sup>-1</sup> )
Tap water	$1 \times 10^{-3}$	$(1.04 \pm 0.03) \times 10^{-3}$	$(1.04 \pm 0.03) \times 10^{-3}$
	$3 \times 10^{-4}$	$(3.22 \pm 0.18) \times 10^{-4}$	$(3.25 \pm 0.20) \times 10^{-4}$
	$5 \times 10^{-5}$	$(5.52 \pm 0.35) \times 10^{-5}$	$(5.57 \pm 0.37) \times 10^{-5}$
Mineral Water	$1 \times 10^{-3}$	$(1.06 \pm 0.04) \times 10^{-3}$	$(1.06 \pm 0.04) \times 10^{-3}$
	$3 \times 10^{-4}$	$(3.25 \pm 0.20) \times 10^{-4}$	$(3.26 \pm 0.23) \times 10^{-4}$
	$5 \times 10^{-5}$	$(5.66 \pm 0.44) \times 10^{-5}$	$(5.68 \pm 0.48) \times 10^{-5}$
River water	$1 \times 10^{-3}$	$(1.06 \pm 0.05) \times 10^{-3}$	$(1.07 \pm 0.04) \times 10^{-3}$
	$3 \times 10^{-4}$	$(3.28 \pm 0.23) \times 10^{-4}$	$(3.29 \pm 0.25) \times 10^{-4}$
	$5 \times 10^{-5}$	$(5.70 \pm 0.50) \times 10^{-5}$	$(5.79 \pm 0.49) \times 10^{-5}$

<sup>a</sup> Standard addition method was used.**Table 8**Analysis of platinum in synthetic alloys by proposed sensor<sup>a</sup> ( $n = 5$ ).

Composition (%)	Concentration (%) platinum certified value	Found by ISE (%)
Mn, 0.30; Co, 0.20; Cr, 0.10; Al, 0.20; Ni, 0.15; Pt, 0.05	0.050	$0.056 \pm 0.003$
Zn, 0.25; Mn, 0.05; Sr, 0.25; Pb, 0.10; Ni, 0.10; Pt, 0.10; Al, 0.20;	0.100	$0.109 \pm 0.004$

<sup>a</sup> All test solutions containing 0.2 mol L<sup>-1</sup> NaCl.

five replicate measurements of  $3.0 \times 10^{-3}$  and  $5.0 \times 10^{-5}$  mol L<sup>-1</sup> of platinum ion were carried out by the proposed sensor. The results taken by the sensor were as  $3.11(\pm 0.09) \times 10^{-3}$  and  $5.51(\pm 0.33) \times 10^{-5}$  mol L<sup>-1</sup>.

The electrode lifetime was studied by periodically recalibrating of the platinum response in platinum solution in the range of  $10^{-6}$ – $10^{-2}$  mol L<sup>-1</sup>. The PVC membrane electrode based on ionophore CBT can be repeatedly used for at least 1 month (Table 5). This prominent feature rise from the lipophilicity of the ionophore and plasticizer ensures stable potentials and long lifetime [39–41].

### 3.6. Potentiometric selectivity

The most prominent characteristic of a membrane sensor is its response to the primary ion in the presence of other ions. This is measured in terms of the potentiometric selectivity coefficient ( $K_{A,B}^{\text{Pot}}$ ) which has been evaluated by the fixed interference method [42] that is based on the semiempirical Nikolsky–Eisenman equation

$$E_{\text{ISE}} = E^{\circ} \pm \frac{RT}{Z_A F} \ln \left[ a_A + \sum K_{A,B}^{\text{Pot}} (a_B)^{Z_A/Z_B} \right]$$

where  $E_{\text{ISE}}$  is the measured potential,  $E^{\circ}$  the standard cell potential,  $a_A$  and  $a_B$  are the activities of primary and interfering ions, and all other symbols have their usual meanings. In the fixed interference method, the concentration of the platinum ion is varied while that of the interfering ions is fixed at  $1.0 \times 10^{-2}$  mol L<sup>-1</sup>. From the plots of  $E_{\text{ISE}}$  vs.  $\log a_{\text{Pt}}$  and using the expression

$$\ln K_{A,B}^{\text{Pot}} = \ln \frac{a_A}{a_B^{Z_A/Z_B}}$$

the selectivity coefficients were determined. The value of  $a_A$  estimated by the determination of the Pt(II) activity for which the linear and rising portion of the graph deviates by  $2.303RT \log 2/F$  mV from the curved part [43] and the value of  $a_B^{Z_A/Z_B}$  ( $a_B$  and  $Z_B$  are the activity and charge of interfere ion, respectively) were used to calculate the potentiometric selectivity coefficient. The resulting selectivity coefficients are summarized in Table 6. As seen for all ions used, they would not disturb the functioning of the Pt(II) ion selective membrane. Hence, these cations are not expected to interfere with the functioning of the proposed platinum(II) selective sensor even at high concentration levels.

### 3.7. Analytical application

In order to assess the practical utility of the proposed platinum(II) sensor, it was employed well under optimum conditions. The sensor was successfully applied to the direct determination of platinum(II) ion in tap, mineral and river water sample solutions. The data taken by proposed electrode showed satisfactory agreement with those obtained by AAS (Table 7). Furthermore, the applicability of the proposed sensor was also tested to determine of platinum(II) in alloy samples, using standard addition method. The results obtained by the new sensor were quite quantitative, precise, and accurate (Table 8).

## 4. Conclusions

The results obtained from the above-mentioned study reveal that a potentiometric PVC-based membrane sensor based on 1,3-bis(2-cyanobenzene)triazene functions as an excellent platinum ion selective sensor, and it can be used for the determination of this ion in the presence of considerable concentrations of common interfering ions. Applicable pH range, lower detection limit, and potentiometric selectivity coefficients of the proposed sensor make it a superior device compared to other methods used for the determinations of this ion. It also can be employed for the estimation of platinum content in real samples.

## Acknowledgement

It is worth mentioning our grateful acknowledgment for the support of this work by the Razi University research council.

## References

- [1] K. Kümmerer, E. Helmers, P. Hubner, G. Mascart, M. Milandri, F. Reinthaler, M. Zwakenberg, Sci. Total Environ. 225 (1999) 155.
- [2] K. Ravindra, L. Bencs, R.V. Grieken, Sci. Total Environ. 318 (2004) 1.
- [3] R.R. Barefoot, Trends Anal. Chem. 18 (1999) 702.
- [4] L. Bencs, K. Ravindra, R.V. Grieken, Spectrochim. Acta B 58 (2003) 1723.
- [5] K.H. Ek, G.M. Morrison, S. Rauch, Sci. Total Environ. 334 (2004) 21.
- [6] R. Djingova, H. Heidenreich, P. Kovacheva, B. Markert, Anal. Chim. Acta 489 (2003) 245.
- [7] R. Djingova, P. Kovacheva, G. Wagner, B. Markert, Sci. Total Environ. 308 (2003) 235.
- [8] G. Köllensperger, S. Hann, G. Stinger, J. Anal. At. Spectrom. 15 (2000) 1553.
- [9] M.B. Gomez, M.M. Gomez, M.A. Palacios, J. Anal. At. Spectrom. 18 (2003) 80.

- [10] J.C. Ely, C.R. Neal, C.F. Kulpa, M.A. Schneegurt, J.A. Seidler, J. Jain, *Environ. Sci. Technol.* 35 (2001) 3816.
- [11] K. Kanitsar, G. Koellensperger, S. Hann, A. Limbeck, H. Puxbaum, G. Stinger, *J. Anal. At. Spectrom.* 18 (2003) 239.
- [12] S. Artelt, O. Creutzenberg, H. Kock, K. Levsen, D. Nachtigall, U. Heinrich, T. Rühle, R. Schlögl, *Sci. Total Environ.* 228 (1999) 219.
- [13] M. Moldovan, S. Rauch, M. Gomez, M.A. Palacios, G.M. Morrison, *Water Res.* 35 (2001) 4175.
- [14] Z. Fan, Z. Jiang, F. Yang, B. Hu, *Anal. Chim. Acta* 510 (2004) 45.
- [15] M. Niemelä, P. Perämäki, J. Piispanen, J. Poikolainen, *Anal. Chim. Acta* 521 (2004) 137.
- [16] S. Vouillamoz-Lorenz, J. Bauer, F. Lejeune, L.A. Decosterd, *J. Pharm. Biomed. Anal.* 25 (2001) 465.
- [17] X. Dai, C. Koeberl, H. Fröschl, *Anal. Chim. Acta* 436 (2001) 79.
- [18] A.A. Dalvi, A.K. Satpati, M.M. Palrecha, *Talanta* 75 (2008) 1382.
- [19] M.E. Meyerhoff, M.N. Opdyche, *Adv. Clin. Chem.* 25 (1986) 1.
- [20] G.J. Moody, B.B. Saad, J.D.R. Thomas, *Sel. Electrode Rev.* 10 (1988) 71.
- [21] K. Kimura, T. Shono, Y. Inoue, G.W. Gokel (Eds.), *Cation Binding by Macrocycles*, Marcel Dekker, New York, 1990.
- [22] E. Bakker, P. Bühlmann, E. Pretsch, *Chem. Rev.* 97 (1997) 3083.
- [23] P. Bühlmann, E. Pretsch, E. Bakker, *Chem. Rev.* 98 (1998) 1593.
- [24] D.B. Kimball, R. Herges, M.M. Haley, *J. Am. Chem. Soc.* 124 (2002) 1572.
- [25] R. Meldola, F.W. Streatfield, *J. Chem. Soc.* 52 (1887) 434.
- [26] N. Chen, M. Barra, I. Lee, N. Chahal, *J. Org. Chem.* 67 (2002) 2271.
- [27] A. Singhal, V.K. Jain, *Polyhedron* 14 (1995) 285.
- [28] S.F. Colson, S.D. Robinson, *Polyhedron* 9 (1990) 1737.
- [29] S.F. Colson, S.D. Robinson, M. Motevalli, M.B. Hursthouse, *Polyhedron* 7 (1988) 1919.
- [30] S.C. De Sanctis, L. Toniolo, T. Boschi, G. Deganello, *Inorg. Chim. Acta* 12 (1975) 251.
- [31] N. Alizadeh, S. Ershad, H. Naeimi, H. Sharghi, M. Shamsipur, *Pol. J. Chem.* 73 (1999) 915.
- [32] V.A. Nicely, J.L. Dye, *J. Chem. Educ.* 49 (1971) 443.
- [33] H. Zhu, T. Ziegler, *J. Organomet. Chem.* 691 (2006) 4486.
- [34] E. Bakker, P. Bühlmann, E. Pretsch, *Chem. Rev.* 97 (1997) 3083.
- [35] D. Ammann, E. Pretsch, W. Simon, E. Lindner, A. Bezegh, E. Pungor, *Anal. Chim. Acta* 171 (1991) 1380.
- [36] R. Eugster, P.M. Gehring, W.E. Morf, U. Spichiger, W. Simon, *Anal. Chem.* 63 (1990) 2285.
- [37] T. Rosatzin, E. Bakker, K. Suzuki, W. Simon, *Anal. Chim. Acta* 280 (1993) 197.
- [38] P.M. Gehring, W.E. Morf, M. Welte, E. Pretsch, W. Simon, *Helv. Chim. Acta* 73 (1990) 203.
- [39] P.C. Meier, D. Ammann, W.E. Morf, W. Simon, J. Koryta (Eds.), *Medical & Biological Application of Electrochemical Devices*, Wiley, 1980, p. p. 19.
- [40] T. Sokalski, A. Ceresa, T. Zwickl, E. Pretsch, *J. Am. Chem. Soc.* 119 (1997) 11347.
- [41] O. Dinten, U.E. Spichiger, N. Chaniotakis, P. Gehrig, B. Rusterholz, W.E. Morf, W. Simon, *Anal. Chem.* 63 (1991) 596.
- [42] R. Yuan, H.L. Wu, R.Q. Yu, *Sci. China* 36 (1993) 140.
- [43] P. Kane, D. Diamond, *Talanta* 44 (1997) 1847.



## Short communication

# A comparison of three analytical techniques for the measurement of steroidal estrogens in environmental water samples

D.P. Grover<sup>a,b</sup>, Z.L. Zhang<sup>a,1</sup>, J.W. Readman<sup>b</sup>, J.L. Zhou<sup>a,\*</sup>

<sup>a</sup> Department of Biology and Environmental Science, School of Life Sciences, University of Sussex, Falmer, Brighton BN1 9QG, UK

<sup>b</sup> Plymouth Marine Laboratory, Prospect Place, West Hoe, Plymouth PL1 3DH, UK

## ARTICLE INFO

## Article history:

Received 24 October 2008

Received in revised form 20 December 2008

Accepted 22 December 2008

Available online 15 January 2009

## Keywords:

Endocrine disrupting chemicals

Estrogens

Effluents

Chromatography

Mass spectrometry

## ABSTRACT

Research into the analysis and monitoring of steroidal estrogens has grown significantly over the last decade, resulting in the emergence of a range of applicable techniques. In this study, three popular techniques, gas chromatography–mass spectrometry (GC–MS), gas chromatography–tandem mass spectrometry (GC–MS–MS) and liquid chromatography–tandem mass spectrometry (LC–MS–MS) for the analysis of three highly potent steroidal estrogens in the aquatic environment have been compared. It has been observed that overall, the three techniques appear comparable in generating similar estrogen concentrations for river and effluent samples. Of the three techniques, the GC–MS technique is the simplest to operate, but fails to detect the estrogens at the lower-end of environmentally relevant concentrations. The tandem MS techniques are more selective than MS, and therefore able to detect lower concentration levels of the three steroidal estrogens of interest. However, the LC–MS–MS technique is more susceptible to matrix interferences for the analysis of samples, resulting in a reduction of the signal-to-noise ratio and a subsequent reduction in reliability and stability compared to GC–MS–MS. With the GC–MS–MS technique offering increased selectivity, the lowest limits of detection, and no false positive identification, it is recommended to be the preferred analytical technique for routine analysis of estrogens in environmental water samples.

© 2009 Elsevier B.V. All rights reserved.

## 1. Introduction

Of current concern worldwide are the so-called endocrine-disrupting chemicals (EDCs) which are broadly defined as chemicals that may interfere with the function of the endocrine system in wildlife and humans. Endocrine disruption has been shown to reduce fish fertility, to be linked to human cancers, and may also affect human fertility [1–4]. A wide diversity of compounds has been found to possess endocrine disrupting properties, including naturally occurring estrogens such as estrone (E1), 17 $\beta$ -estradiol (E2) and 16 $\alpha$ -hydroxyestrone, androgens and progestogens [5–7]. In comparison, man-made EDC suspects are more diverse in range and are produced in greater quantities than natural EDCs and include the synthetic steroid 17 $\alpha$ -ethynylestradiol (EE2; the contraceptive pill), certain pesticides and industrial chemicals such as bisphenol A and alkylphenols [7,8]. Many of such compounds are classified as priority substances in the EU's Water Framework Directive (2000/60/EC). In terms of estrogenic activity, however, the most

important EDCs are E1, E2 and EE2 as they are far more potent than other compounds such as bisphenol A or alkylphenols, and can cause fish feminisation at approximately the ng L<sup>-1</sup> level [9,10]. Due to uncertainty in their impacts on terrestrial and aerial organisms as a result of lack of data, E1, E2 and EE2 are not yet included in the list of 146 substances with endocrine disruption classification [11], nevertheless, their feminisation effects in invertebrates and fish have been confirmed worldwide. In addition, it is widely recognised that effluent discharges from sewage treatment works (STW) are the main source of EDC inputs to the aquatic environment such as rivers and streams [12,13]. Other sources include animal agriculture, aquaculture and spawning fish [14].

In order to minimise EDC impacts on fish populations, reliable and sensitive analytical methods are needed to detect EDCs in the aquatic environment. The concentrations of EDCs are generally low in aquatic systems, up to 19.4 ng L<sup>-1</sup> in surface water, although levels as high as 5400 ng L<sup>-1</sup> have been found in some STW effluents [7]. As a result, water samples are usually concentrated using solid-phase extraction (SPE). A wide variety of analytical techniques have been developed and subsequently optimised for EDC analyses, among which gas chromatography (GC) coupled with mass spectrometry (MS) and tandem MS is the first developed and still widely used [15–19]. A more recent and increasingly popular technique has been the liquid chromatography (LC) coupled with MS or MS–MS

\* Corresponding author. Tel.: +44 1273 877318; fax: +44 1273 678937.

E-mail address: [j.zhou@sussex.ac.uk](mailto:j.zhou@sussex.ac.uk) (J.L. Zhou).

<sup>1</sup> Present address: The Macaulay Institute, Craigiebuckler, Aberdeen AB15 8QH, UK.

which does not require sample derivatisation [20–24]. As EDCs are being measured at trace levels, often close to the limit of detection (LOD) of the instruments, there is a need to understand how the different techniques compare in terms of their performance. Only by knowing which technique(s) are most reliable and reproducible, can we appraise relative merits and focus on the optimisation of methodologies.

This study investigates the performance of three analytical techniques including GC–MS, GC–MS–MS and LC–MS–MS, all previously developed and validated for the analysis of emerging contaminants including E1, E2 and EE2 in environmental water samples [17,19,25]. The influence of sample matrix on analytical quality at trace levels is highly important and widely speculated, and is addressed.

## 2. Experimental

### 2.1. Chemicals and standard solution

All solvents used (methanol, ethyl acetate, acetone, dichloromethane, hexane and acetonitrile) were of distilled-in-glass grade (purchased from Rathburn Chemicals Ltd., Walkerburn, Scotland). EDC standards including E1, E2 and EE2, together with their deuterated internal standards E2-d<sub>2</sub> were purchased from Sigma, UK. In addition, other internal standards E1-d<sub>4</sub>, E2-d<sub>4</sub> and EE2-d<sub>4</sub> were obtained from Qmx Laboratories Ltd., UK, all with an isotopic purity >98%. Separate stock solutions of individual standards (1000 mg L<sup>-1</sup>) were prepared in methanol, from which working standards (10 mg L<sup>-1</sup>) of individual compounds and mixtures were prepared. All standards were stored at -18 °C. Ultrapure water was supplied by a Maxima Unit from USF Elga, UK.

### 2.2. Sampling and sample treatment

Water samples (in triplicate) were collected in pre-cleaned Winchester amber-glass bottles (2.5 L) from four sites (sites 1–4) along the River Ray, and at one control site (site 5) on the River Ock, Swindon, UK. Site 1 is approximately 3.5 km upstream from the effluent of Rodbourne STW (adjacent to site 2). Sites 3 and 4 are 1.7 and 8.3 km downstream of the effluent, respectively. Sodium azide (10 mL, 2 M) was added to each sample as a general biocide to eliminate bacteria and thus minimise biodegradation during sample storage and processing. Samples were refrigerated at 4 °C until filtration and extraction. Each sample was filtered under vacuum using pre-ashed glass fibre filters (Whatman, GF/F). The filtrates were subsequently spiked with 100 ng of the internal standards.

### 2.3. SPE

The target compounds were extracted from the filtered water samples using SPE. Oasis® SPE cartridges (0.2 g HLB, Waters) were conditioned with 5 mL of ethyl acetate to remove residual bonding agents, followed by 5 mL of methanol which was drawn through

the cartridges under a low vacuum to ensure that the sorbents were soaked in methanol for 5 min. Ultrapure water (3 × 5 mL) was then passed through the cartridges at a rate of approximately 1–2 mL min<sup>-1</sup>. Water samples (2 L) were then extracted at approximately 10 mL min<sup>-1</sup>, as this has been shown to be optimal [18]. The SPE cartridges were subsequently dried under vacuum and the extracts eluted from the sorbents into 20 mL vials with 10 mL of methanol at a flow rate of 1 mL min<sup>-1</sup>. The solvent was then blown down to 100 µL under a gentle N<sub>2</sub> flow, and transferred to 300 µL microvials ready for analysis.

### 2.4. Derivatisation

In the case of GC analyses of EDCs, the target compounds need to be derivatised to produce less polar derivatives. This enhances chromatographic performance by improving peak shape, reduces tailing and provides a better baseline. Briefly, the extracts were transferred into 3 mL reaction vials and were evaporated to dryness under a gentle stream of nitrogen. The dry residues were then derivatised by the addition of 50 µL each of pyridine (dried with KOH solid) and *N,O*-bis(trimethylsilyl)trifluoroacetamide (BSTFA), which were heated in a heating block at 60–70 °C for 30 min following a previously optimised method [18]. The derivatives were cooled to room temperature, evaporated under a gentle stream of nitrogen to dryness, reconstituted in 100 µL of hexane and transferred to 300 µL microvials ready for analysis by GC–MS and GC–MS–MS.

### 2.5. Sample analyses

#### 2.5.1. LC–MS–MS

The untreated extracts in methanol were analysed using a Waters 2695 HPLC separations module (Waters, Milford, MA, USA) fitted with a Waters Symmetry C<sub>18</sub> column (4.6 mm × 75 mm, particle size 3.5 µm). The mobile phase comprised of eluent A (0.1% formic acid in ultrapure water), solvent B (acetonitrile) and eluent C (methanol). The flow rate was 0.2 mL min<sup>-1</sup> and the elution started with 90% eluent A:10% eluent B, a 25 min gradient to 80% of eluent B, then a 3 min gradient to 100% eluent B, followed by an 8 min gradient to 100% of eluent C. This was held for 10 min and then returned back to the initial conditions within 4 min. The system re-equilibration time was 10 min and the sample injection volume was 10 µL. The MS–MS analyses were completed with a Micromass Quattro triple-quadrupole mass spectrometer equipped with a Z-spray electrospray interface. The analyses were in negative ion mode. The parameters for the analyses were: electrospray source block and desolvation temperature 100 and 300 °C, respectively; capillary and cone voltages 3.0 kV and 30 V, respectively; argon collision gas 3.6 × 10<sup>-3</sup> mbar; cone nitrogen gas flow and desolvation gas: 25 and 550 L h<sup>-1</sup>, respectively. Following the selection of the precursor ions, product ions were obtained at optimum collision energies and were selected according to the fragmentation that produced a useful abundance of fragment ions. The optimal collision energy, cone voltage and transitions chosen for the multi-

**Table 1**  
Retention times (RT) and ions used for the analysis of E1, E2 and EE2.

Compound	LC–MS–MS			GC–MS–MS			GC–MS		
	RT (min)	Precursor ion (m/z)	Product ion (m/z)	RT (min)	Precursor ion (m/z)	Product ion (m/z)	RT (min)	Quantitative ion (m/z)	Confirmation ion (m/z)
E1-d <sub>4</sub>							14.44	346	257 (100%), 285 (30%)
E1	19.50	269	183	18.10	342	257 (100%), 327 (10%)	14.51	342	257 (100%), 218 (20%)
E2-d <sub>4</sub>							17.72	289	420 (100%), 330 (35%)
E2-d <sub>2</sub>	17.75	273	186	18.50	418	287 (100%), 233 (75%)			
E2	17.70	271	145	18.50	416	285 (100%), 243 (28%)	18.08	285	416 (100%), 326 (40%)
EE2-d <sub>4</sub>							19.29	289	430 (100%)
EE2	19.05	295	145	19.70	425	193 (100%), 231 (70%)	19.42	285	425 (100%), 232 (30%)



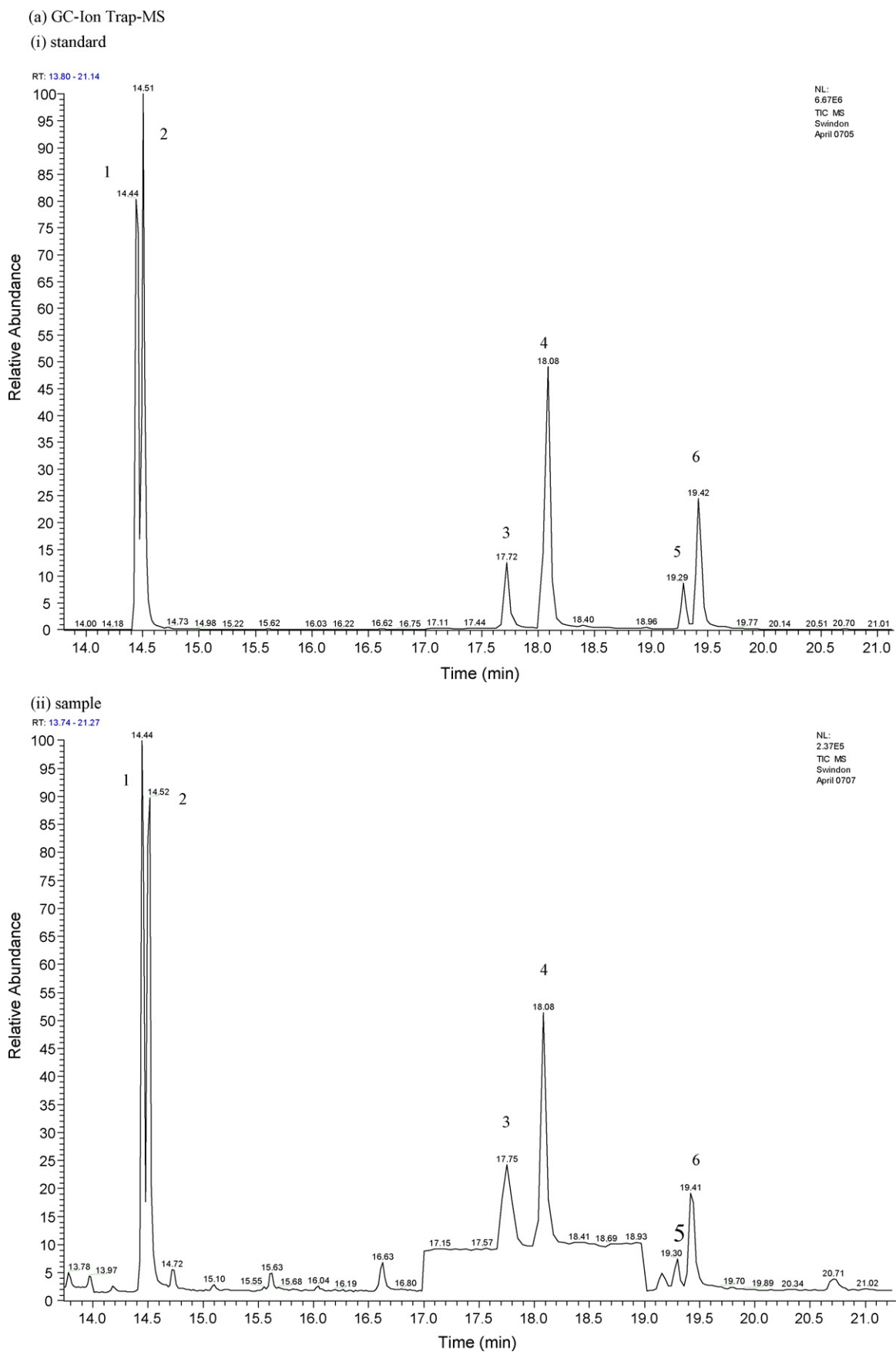
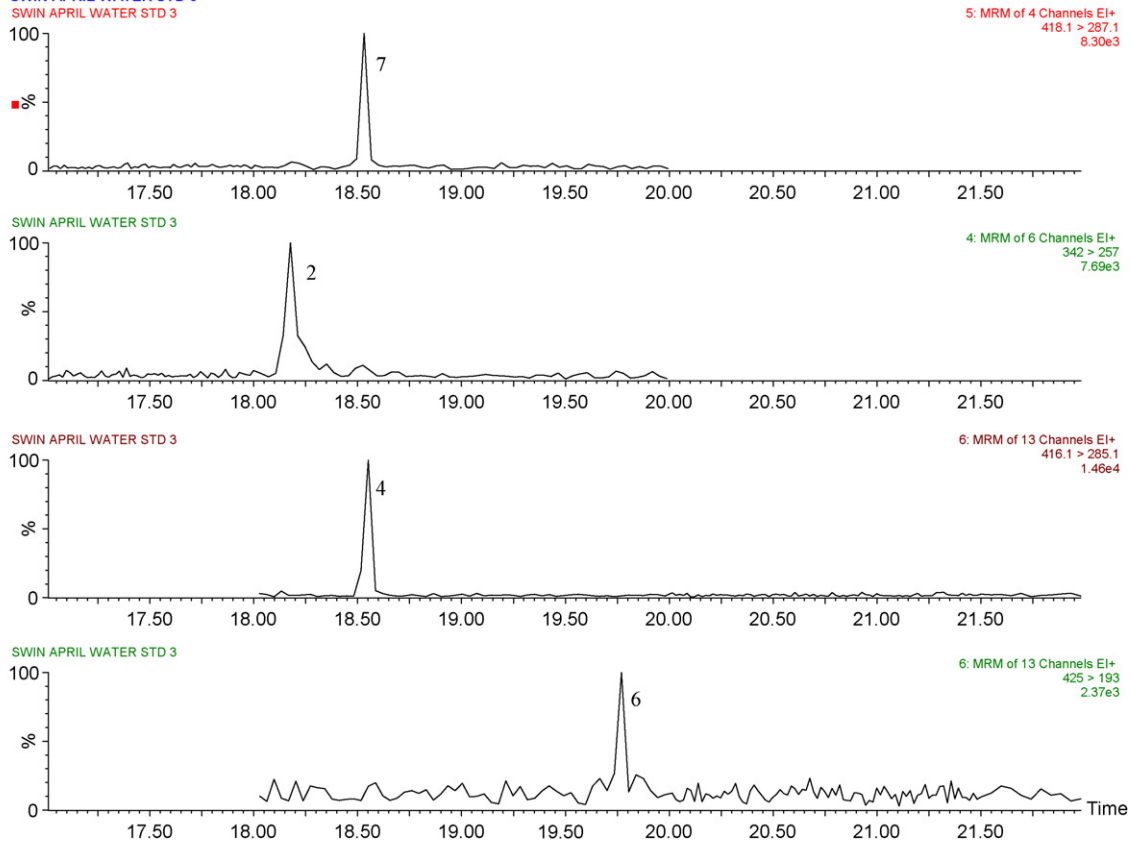


**Fig. 1.** Chromatograms of a 10-ng mL<sup>-1</sup> standard mix (i) and an effluent (site 2) sample (ii) as analysed by (a) GC-ion trap-MS, (b) GC-MS-MS and (c) LC-ESI-MS-MS. Peaks are (1) E1-d<sub>4</sub>, (2) E1, (3) E2-d<sub>4</sub>, (4) E2, (5) EE2-d<sub>4</sub>, (6) EE2 and (7) E2-d<sub>2</sub>.

(b) GC-MS-MS

(i) standard

SWIN APRIL WATER STD 3  
 SWIN APRIL WATER STD 3



(ii) sample

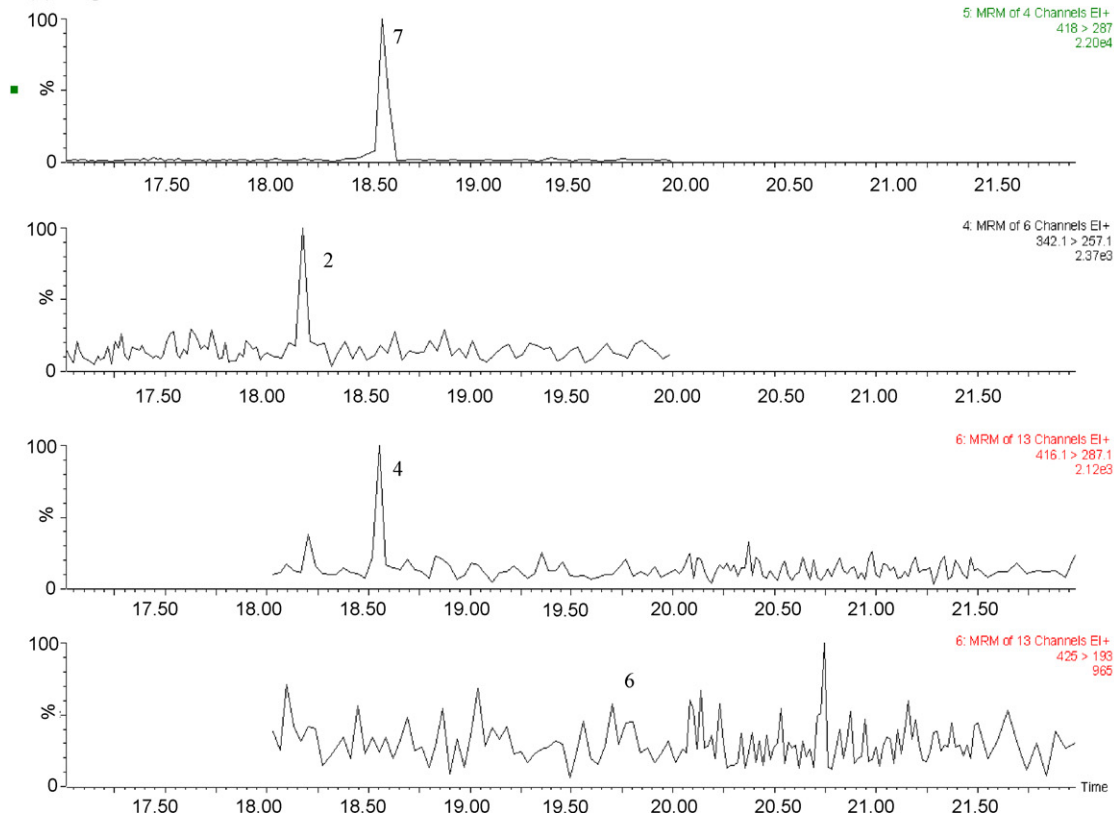
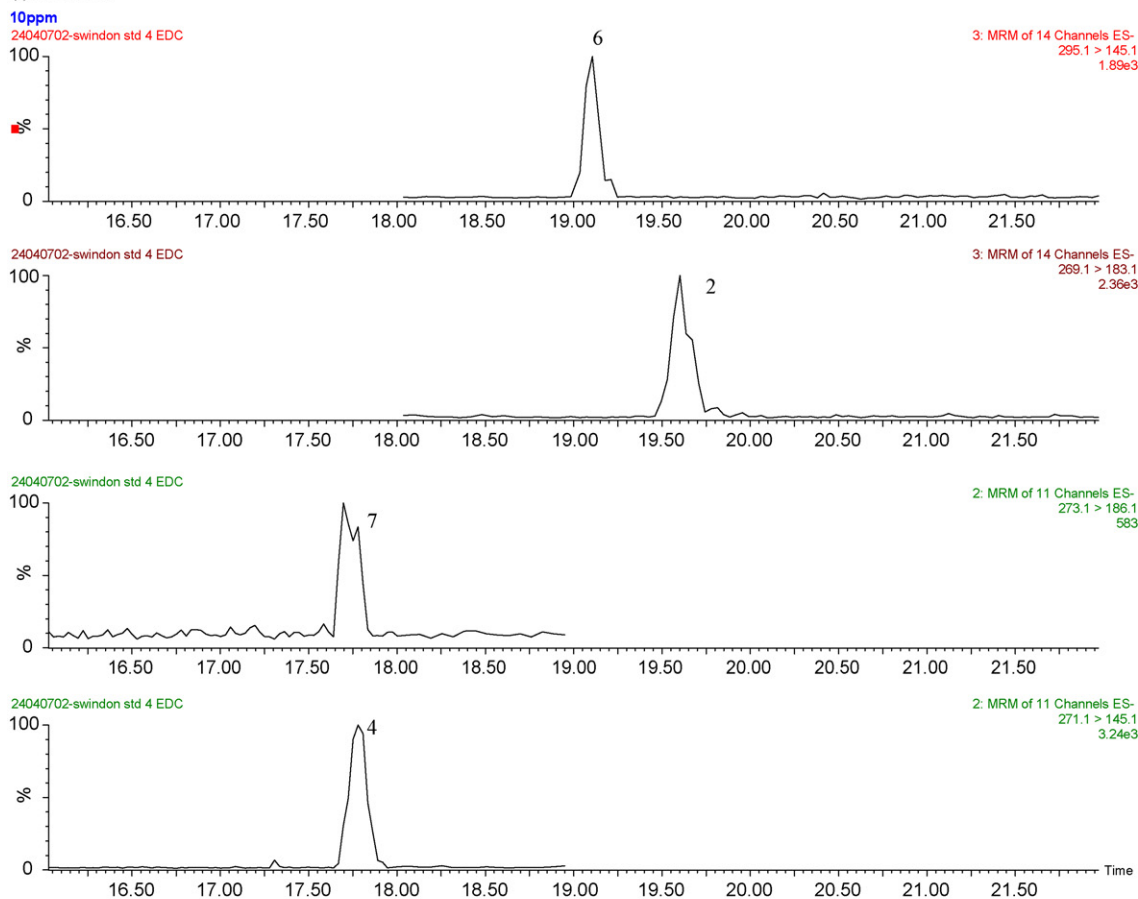


Fig. 1. (Continued)

## (c) LC-MS-MS

## (i) standard



## (ii) sample

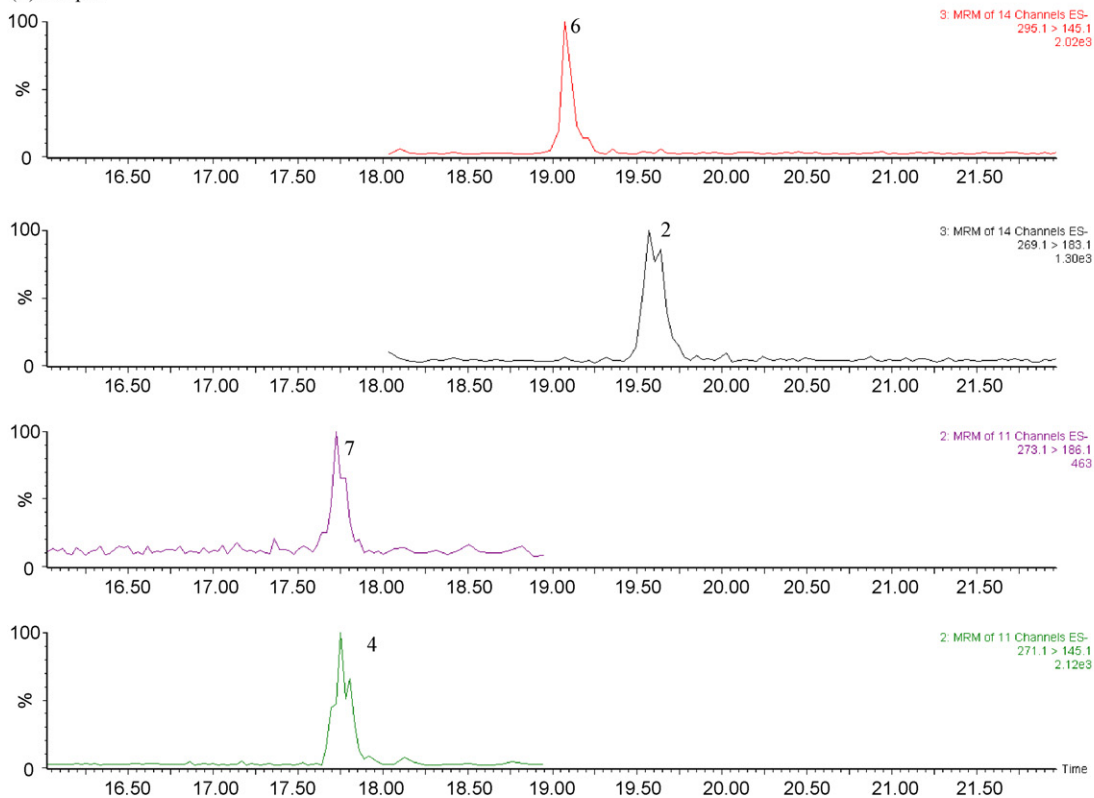


Fig. 1. (Continued).

ple reaction monitoring (MRM) experiment were optimised and a dwell time of 10 ms was used. The mass spectrometer was operated in MRM mode with unit mass resolution on both mass analysers. The precursor and product ions monitored for each compound are shown in Table 1.

### 2.5.2. GC–tandem MS

During our method development, silylated EDCs (through BSTFA) are stable for up to 120 h with the exception of TMS-EE2 which has been found to be stable for only 48 h [18]. Others [26] used *N*-methyl-*N*-(trimethylsilyl)trifluoroacetamide (MSTFA) as the derivatisation agent and obtained stable derivatives for up to 4 weeks. Consequently as a result of the limitations, all GC–MS and GC–MS–MS analyses were performed immediately and definitely within 48 h of derivatisation. To maintain the optimum performance, regular changes were made to the pre-column and injector liner in GC, together with regular cleaning of the ion source.

The GC–MS–MS analyses were performed using a 6890N network gas chromatograph (Agilent Technologies, USA) interfaced with a mass spectrometer (Quattro Micro, Micromass, USA) with a tandem quadrupole. An Agilent 30 m HP-5 capillary column with a 0.25-mm internal diameter and a 0.25- $\mu$ m film thickness was used. The carrier gas was helium, which was maintained at a constant flow of 1.0 mL min<sup>-1</sup>. The GC column temperature was programmed from 100 °C (initial equilibrium time 1 min) to 200 °C via a ramp of 10 °C min<sup>-1</sup>, 200–260 °C via a ramp of 15 °C min<sup>-1</sup>, 260–300 °C via a ramp of 3 °C min<sup>-1</sup> and was maintained at 300 °C for 2 min, with a total run time of 30.33 min. The MS was set for positive electron impact ionisation (70 eV) and was operated in MRM mode for quantitative analyses, using argon as the collision gas. The inlet and MS transfer line temperatures were both maintained at 280 °C and the ion source temperature was 250 °C. Sample injection (1  $\mu$ L) was in splitless mode. The precursor and product ions for each compound are shown in Table 1.

### 2.5.3. GC–ion trap–MS

GC–MS analyses were performed using a gas chromatograph (Trace GC 2000, Thermoquest CE Instruments, TX, USA) coupled with an ion trap mass spectrometer (Polaris Q, Thermoquest CE Instruments, Texas, USA) and an autosampler (AS 2000). A ZB5 (5% diphenyl–95% dimethylpolysiloxane) capillary column of 30 m  $\times$  0.25 mm i.d. (0.25  $\mu$ m film thickness) was used. Helium carrier gas was maintained at a constant flow rate of 1.5 mL min<sup>-1</sup>, which was found to be the optimum for the separation of target compounds. The GC column temperature was programmed from 100 °C (initial equilibrium time 1 min) to 200 °C via a ramp of 10 °C min<sup>-1</sup>, 200–260 °C via a ramp of 15 °C min<sup>-1</sup>, 260–300 °C via a ramp of 3 °C min<sup>-1</sup> and maintained at 300 °C for 2 min. The MS was adjusted for selected ion monitoring mode for quantitative analyses. The inlet and MS transfer line temperatures were both maintained at 280 °C, and the ion source temperature was 250 °C. Sample injection was in splitless mode. The ions monitored are shown in Table 1.

## 3. Results and discussion

### 3.1. Validation of the analytical methods

Chromatograms for the three steroidal estrogens and their associated internal standards are shown in Fig. 1. In GC–MS–MS or LC–MS–MS operation, E2-d<sub>2</sub> was the only deuterated internal standard found to give a satisfactory response with these instruments. A visual comparison of the three chromatograms suggests little difference in the quality of the separation of the standards. Analysis of deuterated internal standards by LC–MS–MS proved, however, to be more difficult than with the GC techniques owing to higher

**Table 2**

Limits of detection (ng L<sup>-1</sup>) for three steroidal estrogens by each method.

Compound	GC–MS	GC–MS–MS	LC–MS–MS
E1	0.7	0.3	0.6
E2	1.4	0.3	1.2
EE2	0.8	0.3	0.4

background noise (even with E2-d<sub>2</sub>). All three analytical techniques relied upon SPE as the pre-concentration step, which has been assessed extensively for EDC recovery [17,19]. Each method was then thoroughly validated for the linear range of calibration curve, sensitivity, specificity, blanks, precision and bias (through the use of recovery experiments due to lack of certified reference materials). The linear ranges of calibration curve for the GC–MS and GC–MS–MS have previously been determined, from 1 to 500 ng L<sup>-1</sup> [17,19]. The linear range for the LC–tandem MS was between 15 and 750 ng L<sup>-1</sup>. The LOD, defined as the concentration that corresponds to three times the standard deviation of blanks, was measured by integrating blank peak area for each analyte in 10 independent performances with ultrapure water as the blank. As shown in Table 2, the GC–MS–MS method offers improved performance over the two alternatives with regard to LOD. The LOD for the GC–MS technique is relatively poor among the three techniques. The analysis of procedural blanks (blanks being treated as samples) did not detect any of the three compounds in our regular sampling trips, confirming a good quality procedure. Furthermore, extensive recovery experiments were performed regularly by the spiking of the three estrogens at different levels (1, 20, 50, 100, 200 ng L<sup>-1</sup>) in different waters (e.g. river water, seawater, groundwater, wastewater), with satisfactory recoveries from 72 to 119% [17,19]. In addition, an inter-calibration exercise was undertaken recently with three other laboratories in the UK, among which a good agreement was achieved.

### 3.2. Application of the analytical methods

Once validated, the techniques were applied to the EDC analysis of environmental sample extracts. Overall, the LC–MS–MS was observed to be most heavily affected by matrix interferences in terms of elevated background noise and reduced peak area for the target compounds. Similar matrix interference effect in LC–tandem MS has been reported by Beck et al. [23], who observed a signal suppression of between 80 and 85% for the three compounds. As a result, the signal-to-noise ratio was reduced such that peaks were less clear than in either of the GC techniques. Surprisingly, a significant interference for the analysis of EE2 was noted for GC–MS–MS of some effluent sample extracts. For both standards and sample extracts, the GC–MS technique appears to offer the best baseline of the three techniques, but it lacks the robustness of the tandem MS techniques, where fragment ions are used to confirm the identity of the analytes.

As the LOD for the GC–MS technique is relatively poor, its signal quality rapidly declines with a reduction in concentration of the analytes, and as can be seen (Fig. 2), several of the environmental samples analysed were below LOD for this instrument. However, each of three techniques is operating at or near their detection limits for many of the samples for at least one of the estrogens due to matrix interferences. The three techniques used here, however, reflect LODs reported by other laboratories using similar extraction and analytical techniques, which range from 0.1 to 1 ng L<sup>-1</sup> [15,16,27] for each compound.

As is shown in Fig. 2 there is a very good agreement between the three techniques, particularly for E1 (0.1–0.2 ng L<sup>-1</sup> difference between techniques, RSD = 28%) and E2 (<0.1–0.2 ng L<sup>-1</sup>, RSD = 4%). However, it is evident that the LC–MS–MS measurements of EE2 are significantly higher than measurements by GC techniques, par-

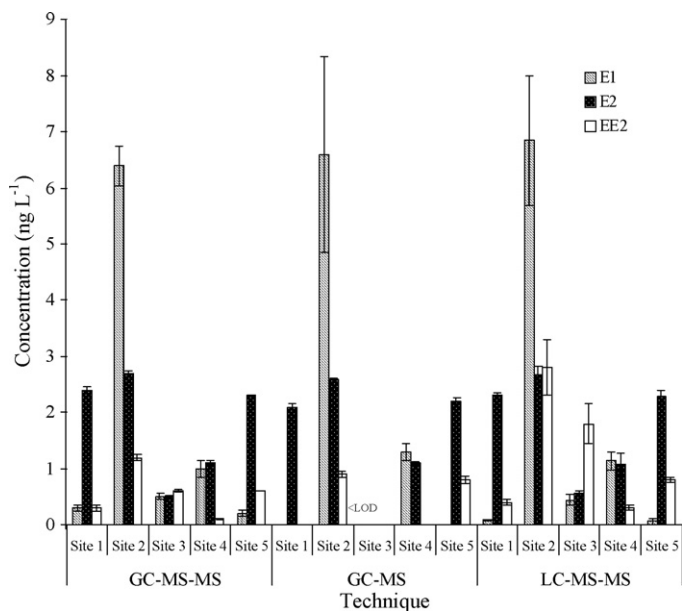


**Fig. 2.** Analysis of estrogens E1, E2 and EE2 in river and effluent samples as measured by the three analytical techniques.

ticularly in areas where matrix interferences are likely to be high (e.g. sewage effluents), as a result there is a larger variability in measured concentrations between the three techniques for EE2 (0.1–1 ng L<sup>-1</sup>, RSD = 45%). The precision for each technique which is comparable across the techniques, is the lowest for the GC–MS–MS technique.

In addition, all three techniques identify the STW effluent (site 2) as the location at which concentrations of the three estrogens are the highest. This shows that all three techniques are consistent in their identification of pollution hotspots. The results are in agreement with other studies [12,13,17,28] which identify sewage effluent as the primary source of steroidal estrogens in river waters.

#### 4. Conclusions

Three popular techniques for the analysis of steroidal estrogens in the aquatic environment have been compared. It has been observed that overall, the three techniques appear comparable, but that tandem-mass spectrometric techniques are able to detect at lower concentration levels of the three steroidal estrogens of interest. In particular, the GC–MS technique fails to detect the pollutants at the lower-end of environmentally relevant concentrations. However, the LC–MS–MS technique is more susceptible to matrix

interferences for the analysis of samples resulting in a reduction of the signal-to-noise ratio and a subsequent reduction in reliability and stability. With the GC–MS–MS offering increased selectivity, the lowest LOD, and with a good a signal-to-noise ratio for all compounds in all samples, it is regarded as the preferred analytical method for the reliable identification and analysis of estrogens in environmental water samples. However, it does require derivatisation of samples prior to injection, which can be time consuming and therefore a disadvantage for sample throughput.

#### Acknowledgements

This work was funded as part of the Endocrine Disruption in Catchments Programme (EDCAT), which is supported by the UK Department for Environment Food and Rural Affairs, and the Environment Agency of England and Wales. Funding from EU FP6 (grant number: MIF1-CT-2004-510012) is also acknowledged. We thank Andrew Hibberd for help with the GC–MS–MS analyses.

#### References

- [1] J.J. Amaral Mendes, Food Chem. Toxicol. 40 (2002) 781.
- [2] R.L. Gomes, M.D. Scrimshaw, J.N. Lester, Trends Anal. Chem. 22 (2003) 697.
- [3] L.J. Mills, C. Chichester, Sci. Total Environ. 343 (2005) 1.
- [4] E. Vulliet, L. Wiest, R. Baudot, M.-F. Grenier-Loustalot, J. Chromatogr. A 1210 (2008) 84.
- [5] S.D. Richardson, Anal. Chem. 78 (2006) 4021.
- [6] H. Chang, S. Wu, J. Hu, M. Asami, S. Kunikane, J. Chromatogr. A 1195 (2008) 44.
- [7] B. Kudlak, J. Namieśnik, Crit. Rev. Anal. Chem. 38 (2008) 242.
- [8] G. Gatidou, N.S. Thomaidid, A.S. Stasinakis, T.D. Lekkas, J. Chromatogr. A 1138 (2007) 32.
- [9] C. Desbrow, E.J. Routledge, G. Brighty, J.P. Sumpter, M.J. Waldock, Environ. Sci. Technol. 32 (1998) 1549.
- [10] K.V. Thomas, M. Hurst, P. Mattheissen, M.J. Waldock, Environ. Toxicol. Chem. 20 (2001) 2165.
- [11] <http://europa.eu.int/comm/environment/endocrine/strategy/substances.en.htm>.
- [12] A.C. Johnson, J.P. Sumpter, Environ. Sci. Technol. 35 (2001) 4697.
- [13] Y. Zhang, J.L. Zhou, Chemosphere 73 (2008) 848.
- [14] E.P. Kolodziej, T. Harter, D.L. Sedlak, Environ. Sci. Technol. 38 (2004) 6377.
- [15] C. Kelly, J. Chromatogr. A 872 (2000) 309.
- [16] H. Kuch, K. Ballschmitter, Environ. Sci. Technol. 35 (2001) 3201.
- [17] R. Liu, J.L. Zhou, A. Wilding, J. Chromatogr. A 1022 (2004) 179.
- [18] Z.L. Zhang, A. Hibberd, J.L. Zhou, Anal. Chim. Acta 577 (2006) 52.
- [19] A. Hibberd, K. Maskaoui, Z. Zhang, J.L. Zhou, Talanta 77 (2009) 1315.
- [20] T. Isobe, H. Shiraiishi, M. Yasuda, A. Shinoda, H. Suzuki, M. Morita, J. Chromatogr. A 984 (2003) 195.
- [21] A. Laganá, A. Bacaloni, I. De Ieva, A. Faberi, G. Fago, A. Marino, Anal. Chim. Acta 501 (2004) 79.
- [22] S. Rodriguez-Mozaz, M. Lopez de Alda, D. Barceló, Anal. Chem. 76 (2004) 6998.
- [23] I. Beck, R. Bruhn, J. Gandrass, W. Ruck, J. Chromatogr. A 1090 (2005) 98.
- [24] A. Salvador, C. Moreton, A. Piram, R. Faure, J. Chromatogr. A 1145 (2007) 102.
- [25] Z.L. Zhang, J.L. Zhou, J. Chromatogr. A 1154 (2007) 205.
- [26] H. Noppe, K. De Wasch, S. Poelmans, N. Van Hoof, T. Verslycke, C.R. Janssen, H.F. De Brabander, Anal. Bioanal. Chem. 382 (2005) 91.
- [27] V. Gabet, C. Miège, P. Bados, M. Coquery, Trends Anal. Chem. 26 (2007) 1113.
- [28] E.Z. Harrison, S. Rayne Oakes, M. Hysell, A. Hay, Sci. Total Environ. 367 (2006) 481.



# Measurement of oligochitosan–tobacco cell interaction by fluorometric method using europium complexes as fluorescence probes

Weihua Guo<sup>a</sup>, Zhiqiang Ye<sup>b</sup>, Guilan Wang<sup>b</sup>, Xiaoming Zhao<sup>a</sup>, Jingli Yuan<sup>b,\*</sup>, Yuguang Du<sup>a,\*</sup>

<sup>a</sup> Department of Biotechnology, Dalian Institute of Chemical Physics, Chinese Academy of Sciences, Dalian 116023, PR China

<sup>b</sup> State Key Laboratory of Fine Chemicals, Department of Chemistry, Dalian University of Technology, Dalian 116012, PR China

## ARTICLE INFO

### Article history:

Received 12 November 2008

Received in revised form 4 January 2009

Accepted 5 January 2009

Available online 20 January 2009

### Keywords:

Oligochitosan

Tobacco cells

Interaction

Europium complex

Time-resolved fluorescence

## ABSTRACT

The interaction of oligochitosan and tobacco cells has been investigated by fluorometric method using two  $\text{Eu}^{3+}$  complexes as the probes in this work. Based on the reaction of tobacco cells with oligochitosan conjugated to a strongly fluorescent  $\text{Eu}^{3+}$  complex 4,4'-bis(1'',1'',2'',3''-heptafluoro-4'',6''-hexanedion-6''-yl)chlorosulfo-*o*-terphenyl- $\text{Eu}^{3+}$  (oligochitosan–BHHCT- $\text{Eu}^{3+}$  conjugate), the binding kinetic process of oligochitosan–tobacco cells was fluorescently imaged. The results indicate that oligochitosan can be specifically bound to the walls as well as the membranes of tobacco cells. A sensitive and selective  $\text{Eu}^{3+}$  complex luminescence probe specific for singlet oxygen, [4'-(10-methyl-9-anthryl)-2,2':6',2''-terpyridine-6,6''-diyl]bis(methylenetrilo)tetrakis(acetate)- $\text{Eu}^{3+}$ , was used for developing a new time-resolved fluorescence assay method for the determinations of indole-3-acetic acid (IAA) and peroxidase produced in the cells during the interaction of oligochitosan and tobacco cells. The assays are sensitive with the detection limits of 32 nM for IAA, and 1.2 nM for peroxidase, respectively. The concentration changes of IAA and peroxidase induced by oligochitosan in tobacco cells reveal that oligochitosan can effectively induce the increase of IAA concentration, accompanied by the decrease of peroxidase concentration. These results give a primary and reliable evidence to explain the growth-promoting mechanism of oligochitosan on the plants at molecular level.

© 2009 Elsevier B.V. All rights reserved.

## 1. Introduction

In recent years, oligochitosan has become a research attraction for its various biological activities in food, biomedical and bio-pesticide applications [1–3]. Oligochitosan prepared by enzymatic hydrolysis of deacetylated chitosan polymer [4] is water-soluble, nontoxic, biodegradable and biocompatible, and possesses versatile functional properties in agriculture such as inducement of resistance of plants against disease and promotion of plant growth [5–9]. However, it is still not very clear about the interaction between oligochitosan and plant cells as well as the growth-promoting mechanism of oligochitosan on the plants.

Indole-3-acetic acid (IAA), a member of the phytohormone group called auxins that can induce cell elongation and division with all subsequent results for plant growth and development [10,11], is generally considered to be one of most important native auxins. Some sensitive methods for IAA determination in biological samples, such as GC–MS, HPLC and immunoassay, have been

established [12,13]. These methods, however, require several time-consuming steps, careful treatment to ensure purity of the sample, and/or special immunoglobulins. Therefore, to reveal the growth-promoting mechanism of oligochitosan on the plants at molecular level, the development of a rapid, simple, sensitive and accurate method for monitoring the real-time IAA generation in plant cells is of increasing interest.

Time-resolved fluorescence technique using lanthanide complexes ( $\text{Eu}^{3+}$  or  $\text{Tb}^{3+}$  complexes) as fluorescence probes provides an excellent way for developing highly sensitive bioassays [14–17], in which the short-lived background noise from both biological samples and the optical components can be effectively eliminated. Recently, a novel  $\text{Eu}^{3+}$  complex, [4'-(10-methyl-9-anthryl)-2,2':6',2''-terpyridine-6,6''-diyl]bis(methylenetrilo)tetrakis(acetate)- $\text{Eu}^{3+}$  (MTTA- $\text{Eu}^{3+}$ ), was developed as a highly sensitive and selective time-resolved fluorescence probe for singlet oxygen ( $^1\text{O}_2$ ) [18,19]. This probe can specifically react with  $^1\text{O}_2$  to form its endoperoxide (EP-MTTA- $\text{Eu}^{3+}$ ) with a high reaction rate constant at  $10^{10} \text{ M}^{-1} \text{ s}^{-1}$  level, accompanied by the remarkable increases of fluorescence quantum yield from 0.90% to 13.8%. In addition, a specific and real-time method for monitoring the kinetic process of  $^1\text{O}_2$  generation in the aerobic oxidation of IAA catalyzed by horseradish

\* Corresponding authors. Tel.: +86 411 84706293/84379061; fax: +86 411 84706293/84379061.

E-mail addresses: [jingliyuan@yahoo.com.cn](mailto:jingliyuan@yahoo.com.cn) (J. Yuan), [duyg@dicp.ac.cn](mailto:duyg@dicp.ac.cn) (Y. Du).

peroxidase (HRP) in a weakly acidic buffer was provided using MTTA–Eu<sup>3+</sup> as a probe [18]. The total reaction rate constant of IAA–HRP–MTTA–Eu<sup>3+</sup> system is reached to  $6.5 \times 10^{10} \text{ M}^{-1} \text{ s}^{-1}$ .

In the present work, a strongly fluorescent conjugate of oligochitosan covalently bound to a Eu<sup>3+</sup> complex, 4,4'-bis(1'',1'',1'',2'',2'',3'',3''-heptafluoro-4'',6''-hexanedion-6''-yl)chlorosulfo-*o*-terphenyl–Eu<sup>3+</sup> (BHHCT–Eu<sup>3+</sup>), was prepared and used to monitor the kinetic process of the interaction between oligochitosan and tobacco cells with a fluorescence imaging method, since BHHCT–Eu<sup>3+</sup> is a stable fluorescence label that can easily be conjugated to a biomolecule [20]. Furthermore, the highly specific fluorescence enhancement of MTTA–Eu<sup>3+</sup> in IAA–HRP system [18] allows the system to be used for both the IAA and HRP determinations. By using this system, a simple and sensitive time-resolved fluorescence assay method for the determinations of IAA in tobacco cell solution and IAA-related peroxidase in tobacco cells was developed. The assays are sensitive with the detection limits of 32 nM for IAA, and 1.2 nM for IAA-related peroxidase, respectively. The kinetics and correlation of the oligochitosan-induced IAA and peroxidase generations in tobacco cells were also investigated.

## 2. Experimental

### 2.1. Materials and physical measurements

The Eu<sup>3+</sup> complex MTTA–Eu<sup>3+</sup> and ligand BHHCT were synthesized by using the previous methods [18,20]. Oligochitosan was prepared by enzymatic hydrolysis of chitosan (the degree of N-acetylation <5%, average molecular weight ~1000) and purified using a previous method [21]. Tobacco (*Nicotiana tabacum* var. *sam sun* NN) tissue cells were cultured in our laboratory. Indole-3-acetic acid and horseradish peroxidase were purchased from Sigma. Unless otherwise stated, all chemicals were purchased from commercial sources and used without further purification.

Fluorescence imaging measurements were carried out on a laboratory-use fluorescence microscope [18,22]. The microscope-equipped 100 W mercury lamp, UV-2A fluorescence filters (excitation filter, 330–380 nm; dichroic mirror, 400 nm; emission filter, >420 nm) and color CCD camera system were used for the imaging measurement with an exposure time of 2.0 s. Absorption spectra were measured on a PerkinElmer Lambda 35 UV–vis spectrophotometer. Time-resolved fluorescence assays were carried out on a PerkinElmer Victor 1420 multilabel counter with the conditions of excitation wavelength, 340 nm, emission wavelength, 615 nm, delay time, 0.2 ms, and window time, 0.4 ms (FluoroNunc 96-well microtiter plates were used).

### 2.2. Preparation of the oligochitosan–BHHCT–Eu<sup>3+</sup> conjugate

Before the preparation, an amino modified ligand, BHHCT–NH<sub>2</sub>, was prepared by reacting BHHCT with ethylenediamine [20]. To a solution of ethylenediamine (30.0 mg, 0.5 mmol) and triethylamine (50  $\mu$ l) in 10 ml ethanol was added a solution of BHHCT (20 mg, 0.025 mmol) in 2 ml ethanol with stirring. After the solution was stirred at room temperature for 3 h, the solvent was evaporated and the residue was completely dried yielding the amino modified ligand, BHHCT–NH<sub>2</sub> (BHHCT–SO<sub>2</sub>–NHCH<sub>2</sub>CH<sub>2</sub>NH<sub>2</sub>), which was used in the next step without further manipulation.

The oligochitosan–BHHCT–Eu<sup>3+</sup> conjugate was prepared by a “one-pot” Schiff reaction between the end-aldehyde group of oligochitosan and amino group of BHHCT–NH<sub>2</sub> followed by NaBH<sub>4</sub> reduction [21,23] as in the following. To a solution of 10 mg BHHCT–NH<sub>2</sub> in 0.1 ml dimethyl sulfoxide (DMSO) was added a

solution of 10 mg oligochitosan in 1.0 ml H<sub>2</sub>O with stirring. After the solution was stirred for 5 h at 80 °C and 16 h at room temperature, 4.5 mg EuCl<sub>3</sub>·6H<sub>2</sub>O and 1.0 mg NaBH<sub>4</sub> were added with stirring. The solution was incubated for 2 h at room temperature, and then 1.0 ml tetrahydrofuran (THF) was added. The mixture was centrifuged at 12,000 rpm for 10 min. The precipitate of the oligochitosan–BHHCT–Eu<sup>3+</sup> conjugate was washed several times with THF until no absorption of free BHHCT–NH<sub>2</sub> was observed in supernatant, and then dissolved with 0.1 ml DMSO and 0.1 ml H<sub>2</sub>O, and stored at 4 °C before use.

### 2.3. Fluorescence imaging of oligochitosan binding to tobacco cells

Fresh tobacco cells cultured in the MX medium [24] were harvested by filtration of the cell suspension through a 200-mesh nickel screen and rinsed twice with the culture medium. An aliquot was suspended in the washing medium (an isotonic saline solution consisting of 140 mM NaCl, 10 mM glucose, and 3.5 mM KCl). The cell density was adjusted to 10<sup>5</sup> cells/ml. The oligochitosan–BHHCT–Eu<sup>3+</sup> conjugate (1  $\mu$ l) was added to the cell suspension (150  $\mu$ l). The mixture was kept in the dark at room temperature, and then centrifuged for 5 min at 400 rpm at 4 °C. The supernatant was discarded and the cells were carefully washed three times with the washing medium. The cells were spotted on a glass slide for fluorescence microscopy imaging detection. For plasmolysis analysis, the tobacco cells were treated in the aqueous solution containing 10% CaCl<sub>2</sub> for 10 min before washing, and then were reacted with the oligochitosan–BHHCT–Eu<sup>3+</sup> conjugate by the same method.

### 2.4. Time-resolved fluorescence assay for IAA in tobacco cell solution

Fresh tobacco cells were collected by filtration and washed twice with distilled water. The cells were suspended in distilled water with a density of  $1.5 \times 10^6$  cells/ml. The cell suspension mixed with an appropriate amount of oligochitosan was incubated at room temperature with slowly shaking. At different treatment times, the cells were centrifuged for 5 min at 10,000 rpm and 4 °C. To 1.0 ml supernatant was added 1.0 ml of 0.1 M sodium acetate buffer of pH 4.0 containing 0.05  $\mu$ M HRP and 0.2  $\mu$ M MTTA–Eu<sup>3+</sup>. After incubated at room temperature with shaking for 20 min, the solution was subjected to the time-resolved fluorescence measurement by using PerkinElmer Victor 1420 multilabel counter. To confirm the specificity of IAA generation in the cell solution, a control experiment in the absence of oligochitosan was also carried out with the same method.

### 2.5. Time-resolved fluorescence assay for IAA-related peroxidase in tobacco cells

The tobacco cells ( $1.5 \times 10^6$  cells/ml)–oligochitosan (0.01 mg/L) suspension was prepared as mentioned above. At different treatment times, the cells were centrifuged for 5 min at 10,000 rpm and 4 °C. The precipitate was ground with liquid nitrogen and quartz sands for 3 min, and the mixture was stirred in 0.1 M phosphate buffer of pH 7.0 for 30 min. After centrifuged for 5 min at 10,000 rpm and 4 °C, 1.0 ml of supernatant was added to 1.0 ml of 0.1 M sodium acetate buffer of pH 4.0 containing 2.0  $\mu$ M of IAA and 0.2  $\mu$ M of MTTA–Eu<sup>3+</sup>. The solution was incubated at room temperature with shaking for 20 min, and then subjected to the time-resolved fluorescence measurement by using PerkinElmer Victor 1420 multilabel counter. A control experiment in the absence of oligochitosan was carried out with the same method.

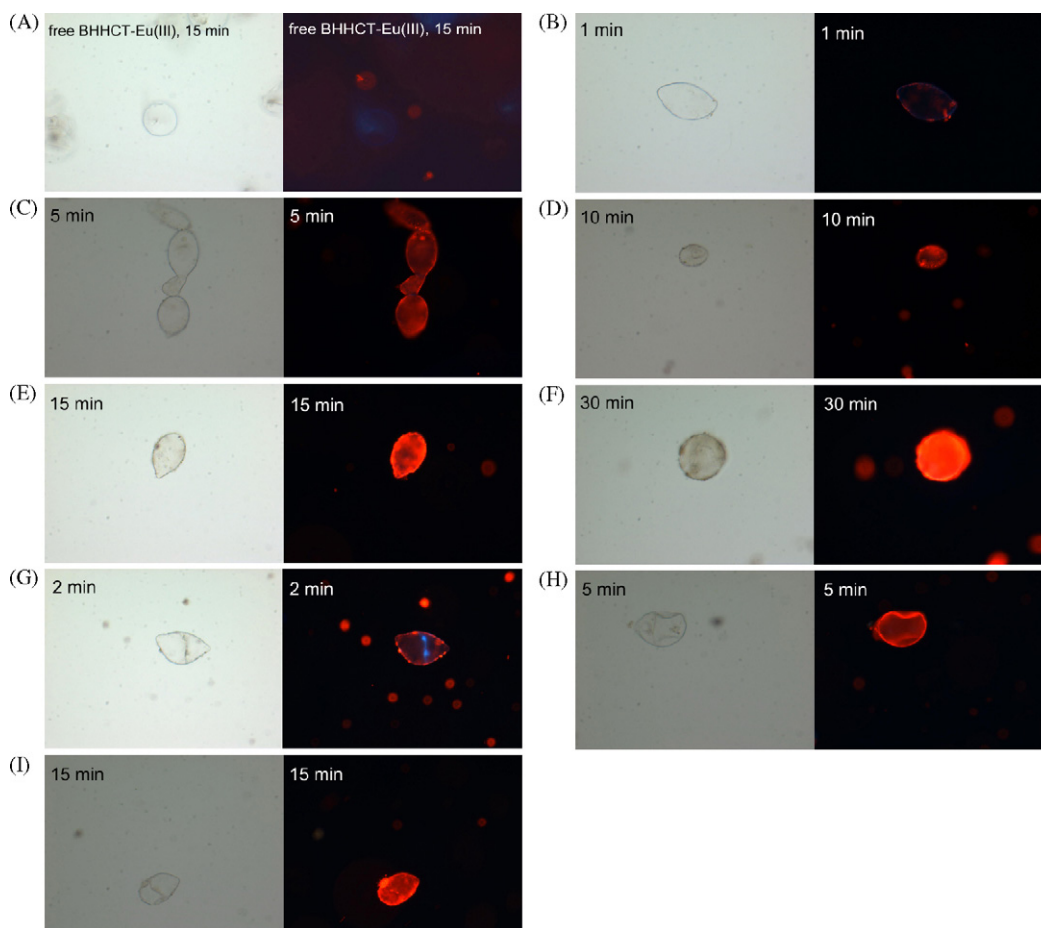


**Fig. 1.** Bright-field (left) and fluorescence (right) images of the oligochitosan–BHHCT–Eu<sup>3+</sup> conjugate binding to tobacco cells at different treatment times. (A) The cells were treated with free BHHCT–Eu<sup>3+</sup> complex for 15 min; (B–F) the cells were treated with the oligochitosan–BHHCT–Eu<sup>3+</sup> conjugate for 1, 5, 10, 15 and 30 min, respectively; (G–I) the plasmolysed cells were treated with the oligochitosan–BHHCT–Eu<sup>3+</sup> conjugate for 2, 5 and 15 min, respectively.

### 3. Results and discussion

#### 3.1. Observation of oligochitosan binding to tobacco cells

An organic fluorophore 2-aminoacridone has been used as a probe for investigating the binding of oligochitosan to tobacco cells [24]. However, the result was not convincing enough since 2-aminoacridone can freely enter the cells and its fluorescence can be easily quenched by an intense excitation source. A more photo-stable Eu<sup>3+</sup> complex, BHHCT–Eu<sup>3+</sup>, is suitable for monitoring some real-time biological processes with fluorescence imaging method. Furthermore, as shown in Fig. 1A (tobacco cells were incubated with free BHHCT–Eu<sup>3+</sup> complex for 15 min), since free BHHCT–Eu<sup>3+</sup> complex can neither enter tobacco cells nor bind to the cell surface, the binding process of oligochitosan to tobacco cells can be exactly observed without the interference of the fluorescence probe.

To investigate the kinetic process of oligochitosan binding to tobacco cells, fluorescence images of tobacco cells treated by oligochitosan–BHHCT–Eu<sup>3+</sup> conjugate were monitored at different treatment times. As shown in Fig. 1, oligochitosan begins to bind to tobacco cell walls after ~1 min treatment (Fig. 1B), and the bound oligochitosan molecules on the cell walls are increased with the increase of treatment time (Fig. 1C–F). Additionally, when the plasmolysed tobacco cells were treated with the oligochitosan–BHHCT–Eu<sup>3+</sup> conjugate, fluorescence spots on the plasma membrane can also be observed apparently (Fig. 1G–I). The above results clearly indicate that the oligochitosan binding sites

are present both on the walls and on the plasma membranes of tobacco cell.

#### 3.2. Kinetic determination of oligochitosan-induced IAA generation in tobacco cell solution

IAA is generally considered to regulate the plant growth at molecular level as an important native auxin. Duran et al. and Kanofsky have previously proposed that IAA can be catalyzed by HRP at lower pH to produce <sup>1</sup>O<sub>2</sub> [25,26]. Recently, we have demonstrated that a Eu<sup>3+</sup> complex, MTTA–Eu<sup>3+</sup>, can be used as a specific probe to monitor <sup>1</sup>O<sub>2</sub> generation in the aerobic oxidation of IAA catalyzed by HRP in a weakly acidic buffer based on the formation of strongly fluorescent endoperoxide EP–MTTA–Eu<sup>3+</sup> (Fig. 2) [18]. Based on this reaction, a highly sensitive and selective time-resolved fluorescence assay method for the determination of IAA in the tobacco cell solution was developed by using IAA–HRP–MTTA–Eu<sup>3+</sup> aerobic oxidation system.

The calibration curve for IAA is shown in Fig. 3. The calibration curve shows a good straight line, which can be expressed as  $\log(\text{signal}) = 0.751 \log[\text{IAA}] + 9.963$  ( $r = 0.992$ ), in IAA concentration range of 10–1000 nM. The detection limit, defined as the concentration corresponding to 3SD (standard deviation) of background signal, is 32 nM.

Fig. 4 shows the concentration changes of IAA induced by oligochitosan in tobacco cell solution at different treatment times. In the presence of oligochitosan, the IAA concentration increases gradually from 0 to 8 h to reach the maximum value of ~0.24 μM, which is



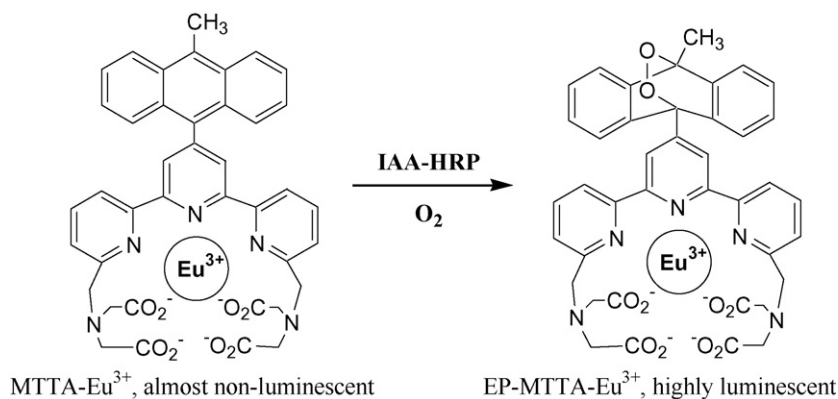


Fig. 2. Aerobic oxidation reaction of IAA-HRP-MTTA-Eu<sup>3+</sup> system accompanied by the remarkable fluorescence enhancement.

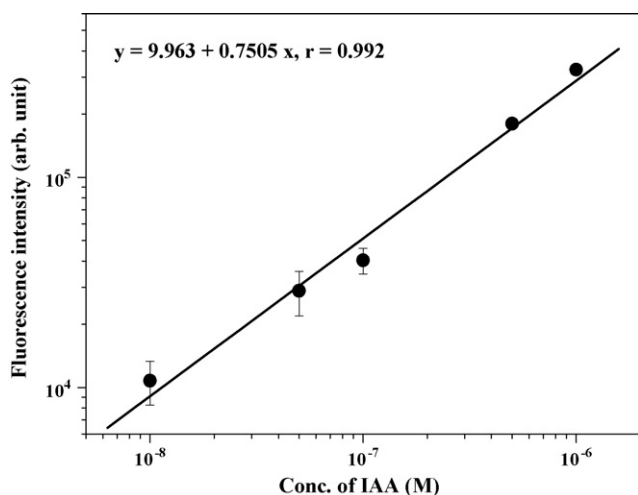


Fig. 3. Calibration curve for IAA. The curve was derived from the fluorescence intensity of the IAA-HRP-MTTA-Eu<sup>3+</sup> reaction in 0.05 M sodium acetate buffer of pH 4.0 with 0.1 μM of MTTA-Eu<sup>3+</sup>, 0.025 μM of HRP and a series of standard IAA solutions.

approx. six times higher than the original concentration. After 8 h, the IAA concentration begins to decrease gradually and returns to original concentration at ~18 h. This phenomenon can be explained as follows. In general, the production and degradation of IAA in

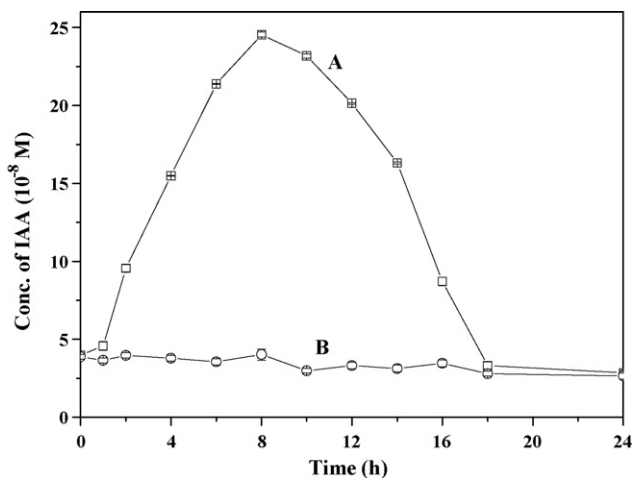


Fig. 4. The concentration changes of IAA in the presence (A) and absence (B) of oligochitosan in tobacco cell solution at different treatment times.

plant cells are in a dynamic balance. When the tobacco cells were induced by oligochitosan, the IAA concentration in tobacco cells was increased. At the same time, the tobacco cells could adjust the IAA concentration to return to the normal level by a series of physiological and biochemical processes, such as the change of the IAA-related peroxidase concentration, facilitating the degradation of the IAA in the cells. Thus, after 8 h reaction, the IAA concentration begins to decrease and gradually recovers to original level. The control experiment result in the absence of oligochitosan shows that the IAA concentration in the solution does not change with the increase of treatment time, which clearly demonstrates that oligochitosan can effectively induce the tobacco cells to produce IAA beneficial for plant growth and development.

The effect of oligochitosan concentration on the IAA concentration in tobacco cell solution was also investigated. After the tobacco cells were treated by different concentrations of oligochitosan for 4 h, the IAA concentrations were assayed. As shown in Fig. 5, the IAA concentration is remarkably depending on the oligochitosan concentration. The highest IAA concentration can be obtained when the oligochitosan concentration is 0.01 mg/L, while higher or lower oligochitosan concentration is unfavorable for the IAA production. This result perfectly matches the result in a planting experiment, in which 0.01 mg/L of oligochitosan has been demonstrated to be the best concentration to promote the growth of tobacco plants in comparison with the other oligochitosan concentrations (unpublished result).

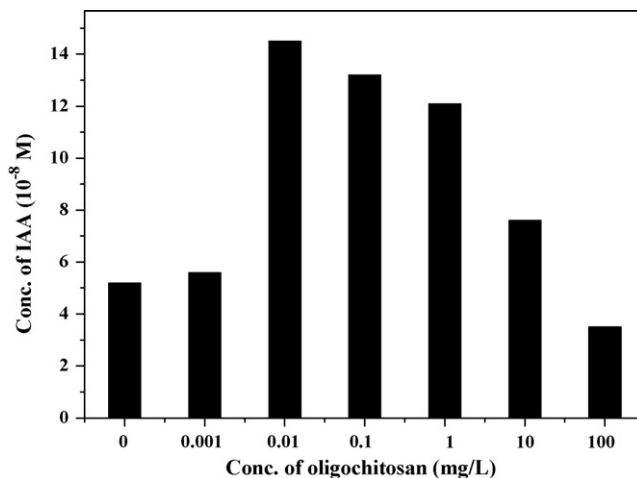
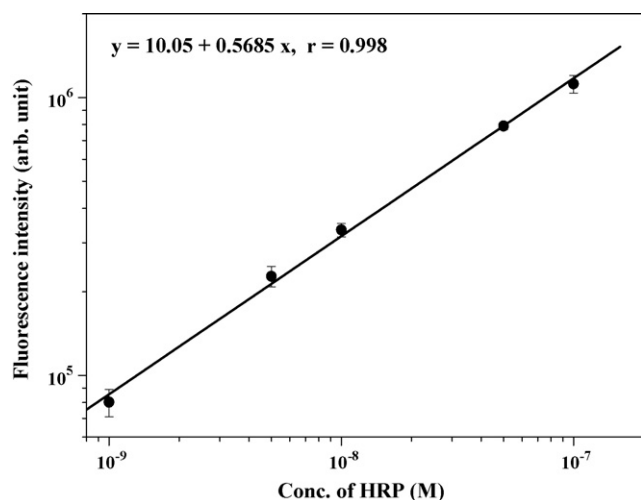


Fig. 5. IAA concentration in tobacco cell solution treated with different concentrations of oligochitosan for 4 h.



**Fig. 6.** Calibration curve for HRP. The curve was derived from the fluorescence intensity of the IAA–HRP–MTTA–Eu<sup>3+</sup> reaction in 0.05 M sodium acetate buffer of pH 4.0 with 0.1 μM of MTTA–Eu<sup>3+</sup>, 1.0 μM of IAA and a series of standard HRP solutions.

### 3.3. Kinetic determination of IAA-related peroxidase in tobacco cells

To investigate the effect of oligochitosan on the concentration of IAA-related peroxidase in tobacco cells, the IAA–HRP–MTTA–Eu<sup>3+</sup> system was also used for the time-resolved fluorescence assay of IAA-related peroxidase in tobacco cells. In the method, HRP was used as a standard to determine the total IAA-related peroxidases in the cells. As shown in Fig. 6, the calibration curve for HRP shows a good straight line that can be expressed as  $\log(\text{signal}) = 0.568 \log[\text{HRP}] + 10.05$  ( $r = 0.998$ ), in HRP concentration range of 1.0–100 nM. The detection limit, defined as the concentration corresponding to 3SD of background signal, is 1.2 nM.

The concentration changes of IAA-related peroxidase in tobacco cells induced by oligochitosan at different treatment times are shown in Fig. 7. In the presence of oligochitosan, the peroxidase concentration in the cells decreases dramatically with the increase of treatment time, giving the minimum value of ~1.7 nM at ~8 h, and then gradually recovers to its original level. The control experiment result in the absence of oligochitosan shows that the peroxidase concentration in the cells is almost unchanged with the increase of treatment time, indicating the specificity of the method.

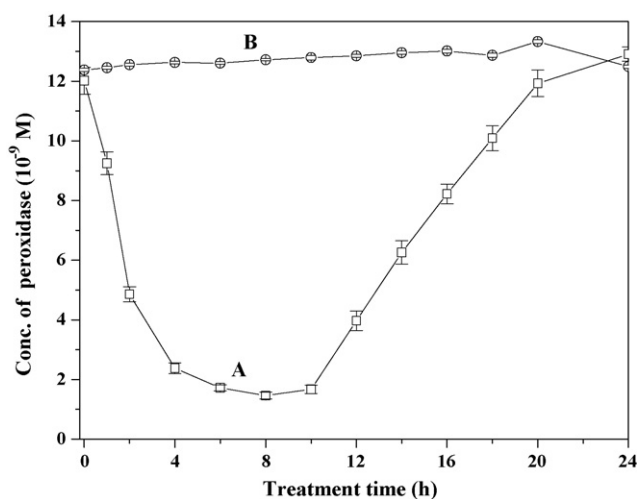


**Fig. 7.** The concentration changes of IAA-related peroxidase in the presence (A) and absence (B) of oligochitosan in tobacco cells at different treatment times.

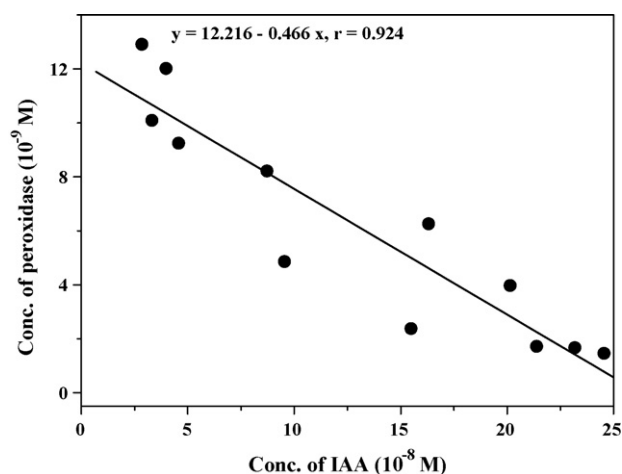


**Fig. 8.** Correlation of IAA concentration in the cell solution and peroxidase concentration in the cells induced by oligochitosan at different treatment times.

The correlation of IAA concentration in the cell solution and peroxidase concentration in the cells induced by oligochitosan in the period of 0–24 h was analyzed. As shown in Fig. 8, the concentration changes of IAA and peroxidase in the period show a good correlation with a correlation coefficient of 0.924. This result suggests that the IAA concentration in the solution should be significantly correlated with the peroxidase concentration in the cells, which reveals the key role of peroxidase in controlling the IAA concentration in tobacco cells to regulate the cell growth.

## 4. Conclusion

In the present work, the interaction of oligochitosan and tobacco cells was investigated by the fluorometric method using two Eu<sup>3+</sup> complexes as the probes. The fluorescence imaging results of oligochitosan–tobacco cell binding indicate that oligochitosan can be rapidly bound to the cells, and the binding sites are present on the walls and plasma membranes of the tobacco cells. A highly selective and sensitive time-resolved fluorescence assay method for the determinations of IAA in the cell solution and IAA-related peroxidase in the cells was established by using the IAA–HRP–MTTA–Eu<sup>3+</sup> aerobic oxidation system. The kinetic monitoring results of the IAA and peroxidase generations demonstrate that oligochitosan can effectively induce tobacco cells to produce IAA, accompanied by the decrease of peroxidase. In addition, the IAA concentration in the cell solution is well-correlated with the peroxidase concentration in the cells, providing a primary and reliable evidence at molecular level to reveal the growth-promoting mechanism of oligochitosan on the plants.

## Acknowledgements

The present work was supported by the National Natural Science Foundation of China (No. 20575069, 20835001), Hi-tech Research and Development Program of China (No. 2007AA091601), and the Innovation Program of the Chinese Academy of Sciences (No. KSCX2-YW-N-007, KSCX2-YW-G-041).

## References

- [1] J. Dou, C. Tan, Y. Du, Carbohydr. Polym. 69 (2007) 209.
- [2] Q. Xu, J. Dou, P. Wei, Carbohydr. Polym. 71 (2007) 509.
- [3] A.I. Ussov, Russ. Chem. Rev. 62 (1993) 1119.
- [4] H. Zhang, Y. Du, X. Yu, Carbohydr. Res. 320 (1999) 257.
- [5] F. Côté, M.G. Hahn, Plant Mol. Biol. 26 (1994) 1397.
- [6] D. Kenda, D. Christian, L.A. Hadwiger, Physiol. Mol. Plant Pathol. 35 (1989) 215.
- [7] Y. Heng, S. Li, X. Zhao, Y. Du, X. Ma, Plant Physiol. Biochem. 44 (2006) 910.

- [8] W. Wang, S. Li, Y. Du, B. Lin, *Pestic. Biochem. Physiol.* 90 (2008) 106.
- [9] J. Xu, X. Zhao, X. Han, Y. Du, *Pestic. Biochem. Physiol.* 87 (2007) 220.
- [10] A. Woodward, B. Bartel, *Ann. Bot. (Lond.)* 95 (2005) 707.
- [11] X. Ding, Y. Cao, L. Huang, J. Zhao, C. Xu, X. Li, S. Wang, *Plant Cell* 20 (2008) 228.
- [12] R. Horgan, *Plant Hormones: Physiology, Biochemistry Molecular Biology*, Kluwer Academic Publishers, Netherlands, 1995, p. 415.
- [13] H. Gao, T. Jiang, W. Heineman, H. Halsall, J. Caruso, *Fresenius J. Anal. Chem.* 364 (1999) 170.
- [14] J. Yuan, G. Wang, *TrAC-Trends Anal. Chem.* 25 (2006) 490.
- [15] G. Wang, J. Yuan, X. Hai, K. Matsumoto, *Talanta* 70 (2006) 133.
- [16] Z. Ye, M. Tan, G. Wang, J. Yuan, *Talanta* 65 (2005) 206.
- [17] I. Hemmilä, V.-M. Mikkilä, *Crit. Rev. Lab. Sci.* 38 (2001) 441.
- [18] B. Song, G. Wang, M. Tan, J. Yuan, *J. Am. Chem. Soc.* 128 (2006) 13442.
- [19] B. Song, G. Wang, J. Yuan, *Talanta* 72 (2007) 231.
- [20] J. Yuan, K. Matsumoto, H. Kimura, *Anal. Chem.* 70 (1998) 596.
- [21] X. Zhao, X. She, Y. Du, X. Liang, *Pestic. Biochem. Physiol.* 87 (2007) 78.
- [22] J. Wu, Z. Ye, G. Wang, J. Yuan, *Talanta* 72 (2007) 1693.
- [23] G. Okafo, J. Langridge, S. North, A. Organ, A. West, M. Morris, P. Camilleri, *Anal. Chem.* 69 (1997) 4985.
- [24] X. Zhao, X. She, W. Yu, X. Liang, Y. Du, *J. Plant Pathol.* 89 (2007) 55.
- [25] M.P. De Mello, S.M. De Toledo, M. Haun, G. Cilento, N. Duran, *Biochemistry* 19 (1980) 5270.
- [26] J.R. Kanofsky, *J. Biol. Chem.* 263 (1988) 14171.



# Silica-based monolithic columns versus conventional particle-packed columns for liquid chromatographic analysis of tetracycline, oxytetracycline and chlortetracycline

Erik Haghedooren, Liesbeth Peeters, Sanja Dragovic, Jos Hoogmartens, Erwin Adams\*

Katholieke Universiteit Leuven, Laboratorium voor Farmaceutische Analyse, O&N 2, PB 923, Herestraat 49, B-3000 Leuven, Belgium

## ARTICLE INFO

### Article history:

Received 27 August 2008  
Received in revised form 5 December 2008  
Accepted 11 December 2008  
Available online 24 December 2008

### Keywords:

Monolithic columns  
Liquid chromatography  
Tetracycline  
Oxytetracycline  
Chlortetracycline

## ABSTRACT

The rise of monolithic stationary phases offers to routine and research laboratories several advantages. In spite of their recent discovery, they have rapidly become highly popular separation media for liquid chromatography. Time reduction and economic reasons like e.g. a diminished use of mobile phase are the most important ones. At the same time, it was reported that these columns offer a faster and better separation. The aim of this article was to investigate the transferability of methods originally developed on conventional particle-packed  $C_{18}$  columns (XTerra RP18 and Zorbax RX), onto the more recent monolithic columns. Both types, conventional particle-packed and monolithic columns, were able to separate tetracycline, oxytetracycline and chlortetracycline from their respective impurities with sufficient resolution, but showed remarkably shorter analysis times and lower backpressures, improving the lifetime of the column.

© 2009 Elsevier B.V. All rights reserved.

## 1. Introduction

In the early 70s, chromatography made a giant leap forward with the advent of the 'high pressure liquid chromatography' (HPLC), which became nowadays one of the most widely spread analytical techniques. HPLC offers the possibility to analyse qualitatively and quantitatively many kinds of components in a non-destructive way.

Since, many improvements in pumping systems, sample introduction, detectors and column design have carried HPLC far from its infancy. The evolution of column packing materials has allowed increased selectivity, better and faster separations, and in many cases greater longevity. This column evolution can be divided up into four distinct generations.

The first columns consisted of *irregular, porous* silica with a particle size of 5–10  $\mu\text{m}$  and alkali silicates as starting material. A fast evolution led to the production of *spherical porous* material, called the second generation. These spherical particles were assembled to a higher density packing, generating better separations. In the mid-80s, spherical silica with a *high purity* were used, i.e. with a low amount of metal contamination (third generation). Hence, non-selective reactions like complex formation or ion effects, leading to less good separations, could be prevented. However, one large disadvantage of all particle-based silica columns was the relatively

high backpressure. Other disadvantages were the inevitable internal shift of particles and the slow degradation of the stationary phase, causing problems like peak tailing and splitting [1,2].

A new sol-gel technology was developed, resulting in a new kind of stationary phase, consisting of silica rods with a bimodal structure. This technique was based on the acid catalyzed hydrolysis and polycondensation of tetramethoxysilane, tetraethoxysilane or n-alkyltrialkoxysilanes in the presence of water soluble polymers such as polyethyleneglycols and polyacrylic acid and surfactants as additives, producing particles with nanometer size called sols. These sols aggregated to a three-dimensional complex, forming a gel [1,3,4]. This strongly porous material consisted of macropores (2  $\mu\text{m}$ ), responsible for a low column resistance and a high flow rate, and mesopores (about 12 nm) creating a large surface area, ensuring plenty of contact area needed for an efficient separation. These so called monolithic columns are the fourth generation [1,5,6]. Although these columns are known for their fast separations, only a limited number of pharmaceutical separations were described on these columns until now.

In order to compare the performance of particle-based conventional stationary phases like XTerra RP18 and Zorbax RX with monolithic columns, three pharmaceutical separations were selected: tetracycline (TC), oxytetracycline (OTC) and chlortetracycline (CTC). For each of these, the main compound has to be separated from its respective impurities. Chemical structures of those molecules and their impurities can be found in Refs. [7,8,9], respectively. These separations were first performed as described in

\* Corresponding author. Tel.: +32 16 323444; fax: +32 16 323448.  
E-mail address: [erwin.adams@pharm.kuleuven.be](mailto:erwin.adams@pharm.kuleuven.be) (E. Adams).

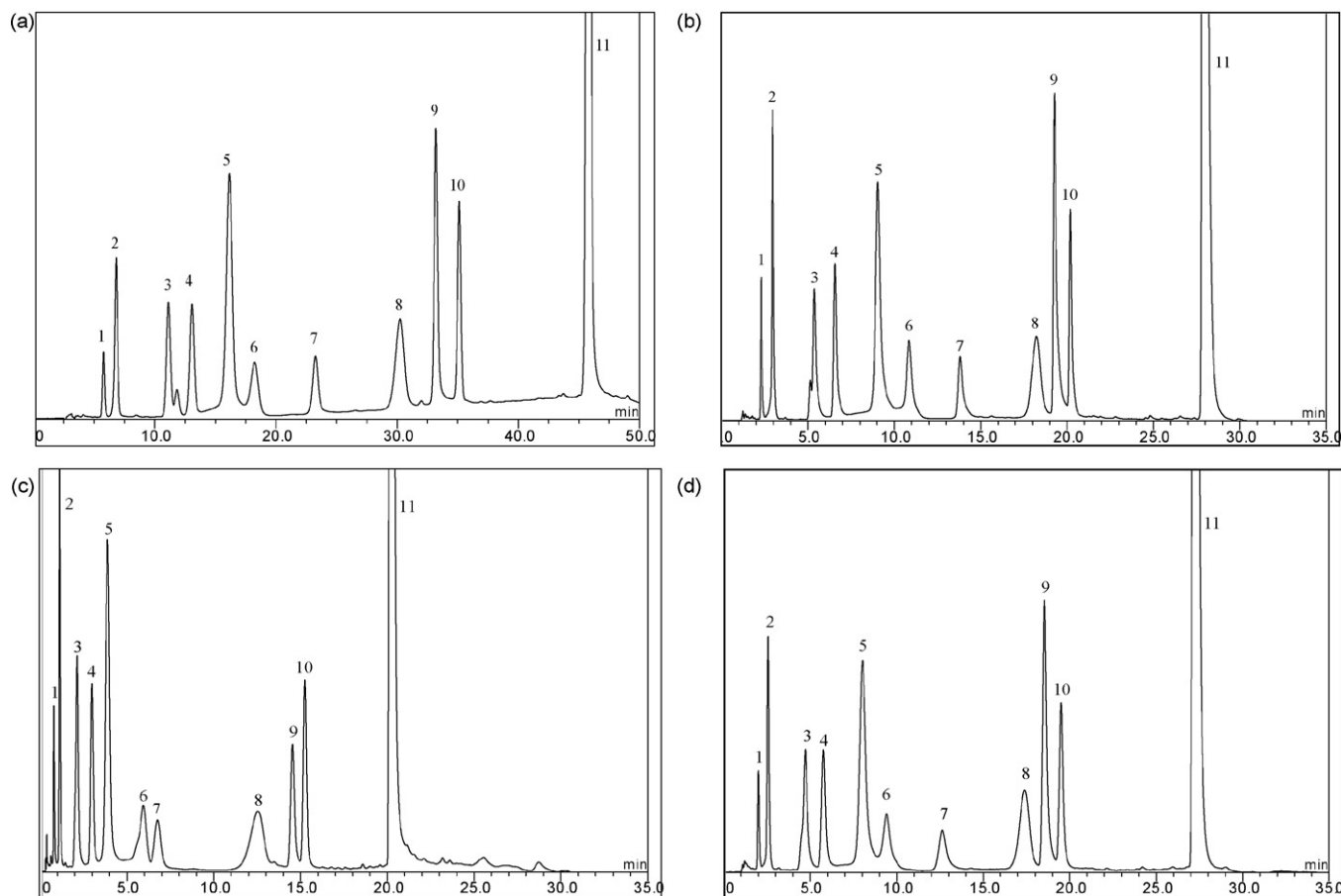


**Fig. 1.** Separation of TC and its impurities on: (a) XTerra RP18; (b) Chromolith Performance; (c) Chromolith Flash; (d) Onyx: (1) EDMTC, (2) ETC, (3) DMTC, (4) EDMTC, (5) TC, (6) ElsoCTC, (7) DMCTC, (8) CTC, (9) EATC, (10) IsoCTC and (11) ATC.

the references cited and additionally, onto  $C_{18}$  monolithic columns. Two brands of the same type of silica-based monolithic columns were available: Onyx and Chromolith. The latter was available as Performance and Flash, which differ only in length. The applicability will be compared based on three criteria: (a) the analysis speed: retention time, (b) the separation efficiency: the apparent number of theoretical plates and the plate height and (c) the separation quality: resolution between peak pairs.

## 2. Experimental

### 2.1. Chemicals and reagents

HPLC grade acetonitrile (ACN) was purchased from Biosolve Ltd. (Valkenswaard, The Netherlands), tetrabutylammonium hydrogen sulphate 98% (TBA), ethylenediaminetetraacetic acid (EDTA) and dimethyl sulphoxide (DMSO), analytical grade, were from Acros Organics (Geel, Belgium). Concentrated ammonia 25% was from Riedel-de Haën (Seelze, Germany). Perchloric acid was acquired from Ferak GMBH (Berlin, Germany). Water was purified with a Milli-Q50 (Millipore, Billerica, MA, USA).

Reference substances of 4-epi-tetracycline (ETC), CTC, isochlortetracycline (IsoCTC), TC, OTC, 4-epi-oxytetracycline (EOTC),  $\alpha$ -apooxytetracycline ( $\alpha$ -APOTC),  $\beta$ -apooxytetracycline ( $\beta$ -APOTC), 4-epi-chlortetracycline (ECTC), anhydrochlortetracycline (ACTC), 4-epi-anhydrochlortetracycline (EACTC), anhydro-tetracycline (ATC) and 4-epi-anhydrotetracycline (EATC) are available from Acros Organics (Geel, Belgium). Demethylchlortetracycline (DMTC), 4-epidemethylchlortetracycline (EDMTC), demethylchlortetracycline (DMCTC), 4-epiisochlortetracycline

(ElsoCTC), 2-acetyl-2-decarboxamidotetracycline (ADTC) and anhydroxytetracycline (AOTC) were available in-house.

### 2.2. Chromatographic apparatus

#### 2.2.1. Tetracycline

The LC apparatus consisted of a Varian 9010 LC-pump (Walnut Creek, CA, USA), a SpectraSeries AS100 auto injector (20  $\mu$ L injection) and a UV-vis detector (Merck-Hitachi, Darmstadt, Germany) at 280 nm. The columns were maintained at 40 °C in a water bath, heated by means of a Julabo EC thermostat (Julabo, Seelbach, Germany). The columns used were XTerra RP18 (4.6 mm  $\times$  250 mm, 5  $\mu$ m, Waters, Milford, MA, USA), Chromolith Performance RP-18e (4.6 mm  $\times$  100 mm, Merck, Darmstadt, Germany), Chromolith Flash RP-18e (4.6 mm  $\times$  25 mm, Merck, Darmstadt, Germany) and Onyx Monolithic  $C_{18}$  (4.6 mm  $\times$  100 mm, Phenomenex, Torrance, CA, USA).

#### 2.2.2. Oxytetracycline

The LC apparatus consisted of a 600E LC pump (Waters), a SpectraSeries AS 100 auto injector (20  $\mu$ L injection) (San Jose, CA, USA) and a UV-vis detector model Spectra 100 (Thermo Separation Products, San Jose, CA, USA) at 280 nm. The columns were maintained at 30 °C in a water bath, heated by means of a Julabo EC thermostat. The same columns as for the analysis of tetracycline were used (see Section 2.2.1).

#### 2.2.3. Chlortetracycline

The LC apparatus consisted of a L-6200 Intelligent pump, a LaChrom Elite L-2200 auto injector (20  $\mu$ L injection) and

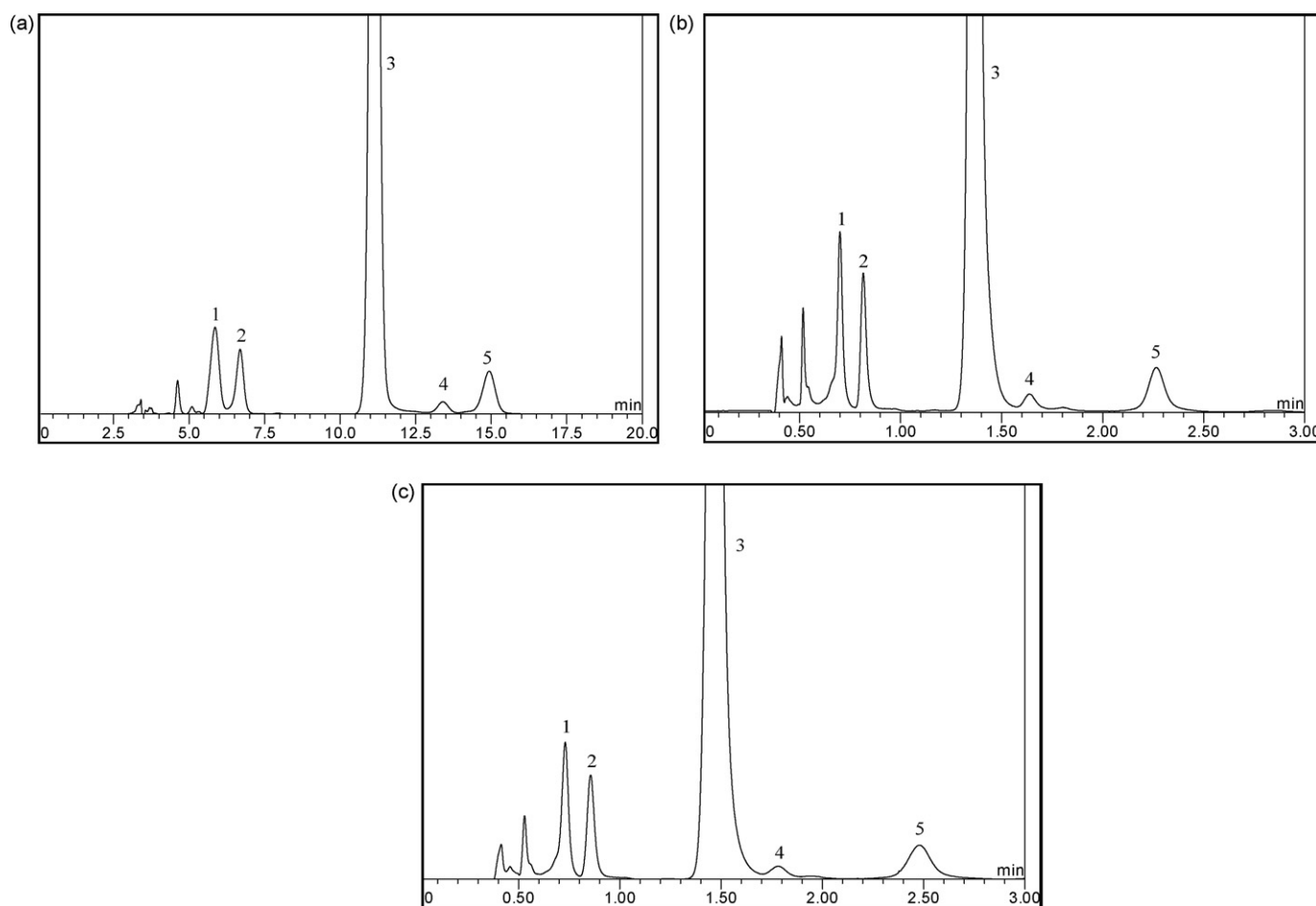


**Fig. 2.** Separation of OTC and its fast eluted impurities on: (a) XTerra RP18; (b) Chromolith Performance; (c) Onyx: (1) EOTC, (2) ETC, (3) OTC, (4) ADOTC and (5) TC.

a LaChrom Elite UV–vis detector model L-2400 (Merck Hitachi) at 280 nm. In addition to the columns used for the tetracycline analysis (see Section 2.2.1), a Zorbax RX-C<sub>8</sub> (4.6 mm × 250 mm, 5 μm, Agilent Technologies, Waldbronn, Germany) was also used. The columns were maintained at 35 °C in a water bath, heated by means of a Julabo EC thermostat.

### 2.3. Sample preparation

#### 2.3.1. Tetracycline

The tetracycline solution consisted of TC, ATC, ADTC, EATC, ETC, OTC, CTC, DMCTC, EDMCTC, isoCTC, ElsoCTC and DMTC in 0.01 mol/L hydrochloric acid (HCl). The solution was prepared at an overall concentration of 1 mg/mL.

#### 2.3.2. Oxytetracycline

The oxytetracycline solution A (containing fast eluted impurities) consisted of OTC, TC, EOTC and ETC in 0.01 mol/L HCl. The oxytetracycline solution B (containing strongly retained impurities) consisted of OTC, β-APOTC, α-APOTC, ADOTC and AOTC in 0.01 mol/L ammonium hydroxide. The overall concentration of solutions was 1 mg/mL.

#### 2.3.3. Chlortetracycline

The chlortetracycline solution consisted of CTC, ECTC, DMCTC, EDMCTC, TC, ACTC, EACTC and IsoCTC in 0.01 mol/L HCl at an overall concentration of 1 mg/mL.

### 2.4. Data processing

The collecting and processing of the data were performed with ChromPerfect 4.4.0 software (Justice Laboratory Software, Fife, England).

## 3. Results and discussion

### 3.1. Monolithic columns versus packed columns

Monolithic columns represent a single piece made of porous cross-linked polymer or porous silica [1]. Columns like the Onyx and Chromolith are produced by sol–gel technology starting from high purity silica. The formed silica rod is enclosed in “polyetheretherketon” (PEEK) shrink-warp tubing to exclude voids. The resulting highly porous skeleton is characterized by a bimodal system, consisting of large macropores (diameter 2 μm) and mesopores (diameter around 12 nm). So far, only C<sub>8</sub> and C<sub>18</sub> silica are commercially available. The length of the straight rods is limited to about 15 cm due to significant shrinkage during formation of the skeleton. However, the separation efficiency can be enhanced by coupling several monolithic columns together [10,11]. These silica-based monolithic columns show remarkable improvements towards conventional columns concerning porosity and the number of theoretical plates.

Particle-based conventional columns show a relatively high backpressure. Monolithic columns, having a total porosity of about 80%, show much lower backpressures in comparison to packed particle-based columns, with a porosity of about 65%. Summarizing,

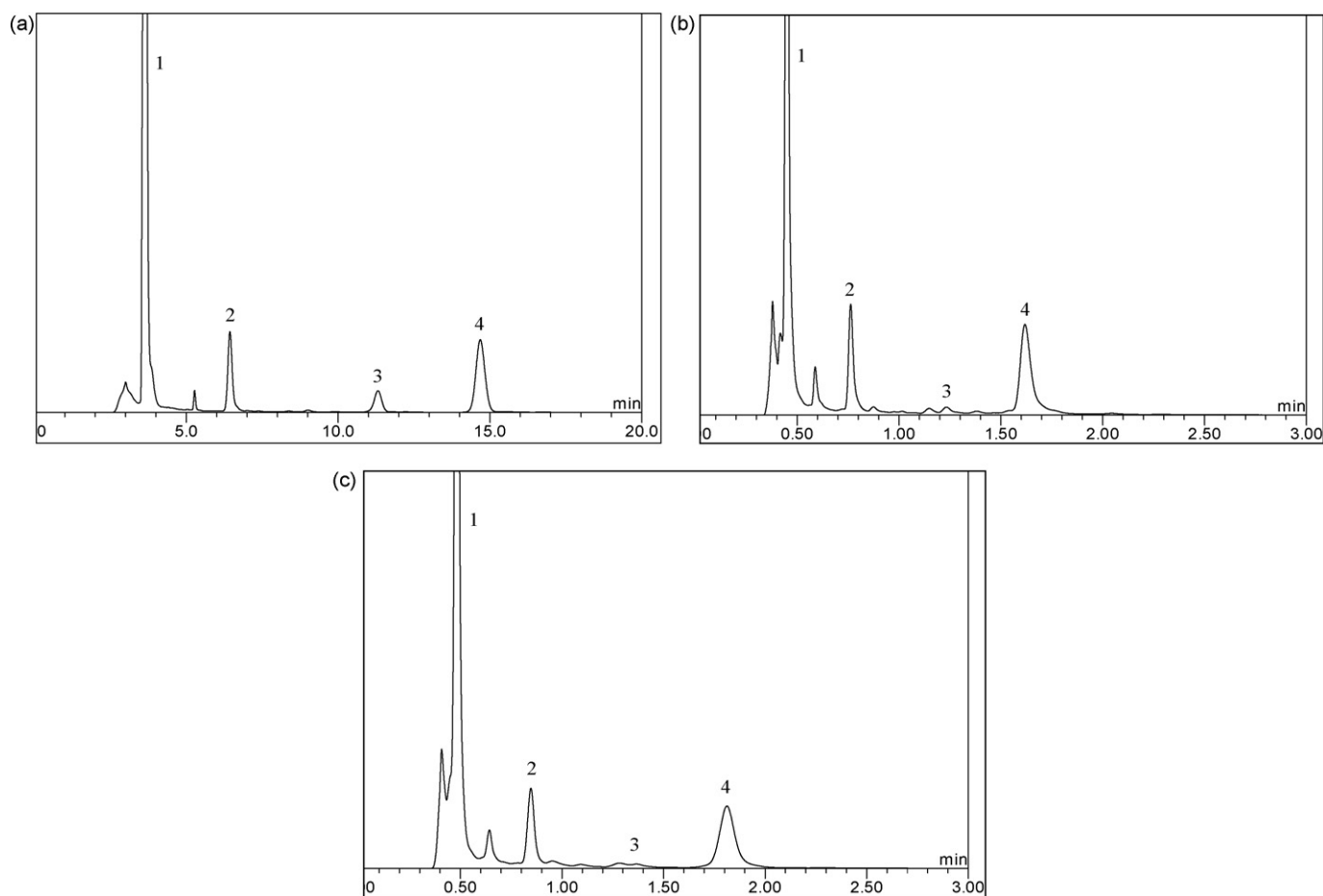


**Fig. 3.** Separation of OTC and its strongly retained impurities on: (a) XTerra RP18; (b) Chromolith Performance; (c) Onyx: (1) OTC, (2)  $\alpha$ -APOTC, (3) AOTC and (4)  $\beta$ -APOTC.

monolithic columns are claimed to be compatible with high flow rates (due to higher porosity), to bring less stress on the system (due to a low backpressure), to have an increased throughput (due to significant shorter run times) and to have an increased reliability and lifetime (due to absence of inlet bed setting). The applicability of these columns for pharmaceutical analysis has not been tested extensively yet.

### 3.2. Practical comparison

#### 3.2.1. Tetracycline

First, the TC mixture was chromatographically separated according to Ref. [7]. The mobile phases consisted of ACN–0.3 mol/L TBA pH 7.5–0.3 mol/L EDTA pH 7.5–water (A) (12:35:35:18, v/v/v/v) and (B) (30:35:35:0, v/v/v/v). Gradient elution at a flow rate of 1.0 mL/min was used: 0–15 min, 5% of B (isocratic); 15–45 min, 5–75% of B (linear gradient) and 45–55 min, 75% of B (isocratic). Fig. 1a shows a chromatogram obtained with the XTerra RP18 column. The flow rate of 1.0 mL/min resulted in a backpressure of 175 bar. Next, the mixture was analysed on the three monolithic columns. Chromatograms obtained with optimised conditions are shown for Chromolith Performance (Fig. 1b), Chromolith Flash (Fig. 1c) and Onyx (Fig. 1d).

As to obtain maximum performance, i.e. baseline separation of the compounds and reduction of the total analysis time, optimisation of the method was performed by changing the flow rate, gradient and solvent ratio of the mobile phases. The new chromatographic circumstances included a slightly different mobile phase A, consisting of ACN–0.3 mol/L TBA pH 7.5–0.3 mol/L EDTA pH 7.5–water (2:35:35:28, v/v/v/v) and an increased flow rate of

1.5 mL/min. The gradient program was adapted for each column and resulted for Chromolith Performance and Onyx in: 0–10 min, 25% of B (isocratic); 10–25 min, 25 to 75% B (linear gradient); 25–35 min, 75% of B (isocratic) and 35–40 min 75–25% B (linear gradient). The backpressure at a flow rate of 1.5 mL/min was 36 bar. For Chromolith Flash a different gradient program was used: 0–10 min, 15% of B (isocratic); 10–25 min, 15–95% B (linear gradient); 25–35 min, 95% of B (isocratic) and 35–40 min 95–15% B (linear gradient). Here, the backpressure was only 22 bar. Using these three columns, three factors of influence were examined. Firstly, monolithic columns versus conventional columns, secondly, the influence of column length (Chromolith Performance versus Flash) and thirdly, the influence of brand (Chromolith Performance versus Onyx).

The columns were compared based on three criteria: (a) the analysis speed (retention time), (b) the separation efficiency (apparent number of theoretical plates and plate height) and (c) the separation quality (resolution).

The most obvious change that was observed for the main peak is the diminished retention time, and as a result, the total analysis time using monolithic columns (Table 1). Amongst the latter, the Chromolith Performance and Onyx showed similar retention times. A column length reduction (Chromolith Performance towards Flash) reduces further the analysis time, as expected.

The  $N$  value of the Chromolith Performance is similar to that of the original XTerra RP18 column, but is lower for the Chromolith Flash (2.5 cm length only) and Onyx. The plate height ( $H$ ), is reciprocally proportional to the apparent number of theoretical plates according to  $H=L/N$  with  $L$ =column length. Based on  $H$ , the Chromolith columns outperform all other columns.

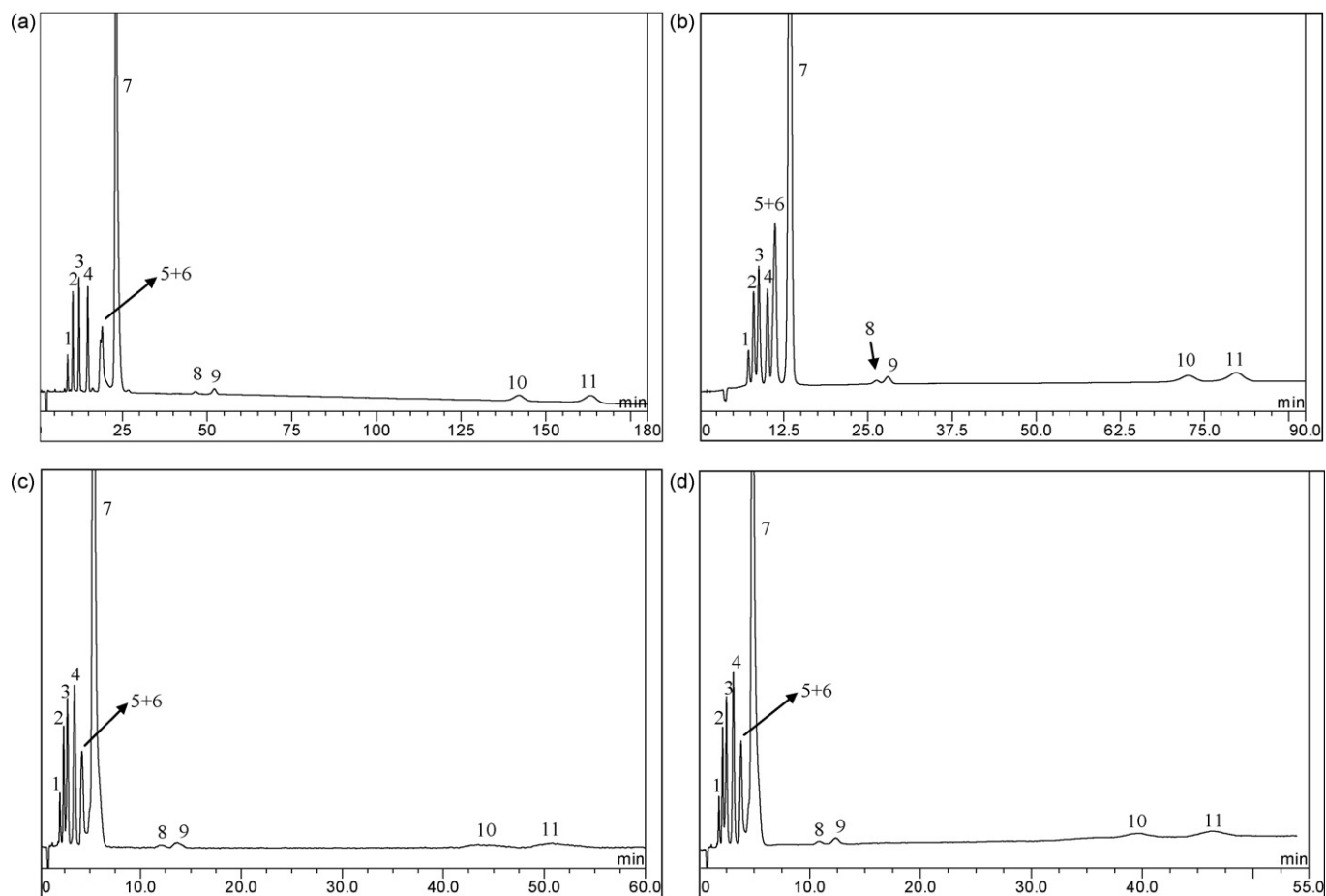


**Fig. 4.** Isocratic separation of CTC and its impurities on: (a) Zorbax RX-C<sub>8</sub>; (b) XTerra RP18; (c) Chromolith Performance; (d) Onyx: (1) ETC, (2) TC, (3) EDMCTC, (4) DMCTC, (5) ECTC, (6) IsoCTC, (7) CTC, (8) EACTC, (9) ATC, (10) EATC and (11) ACTC.

**Table 1**

Overview of the chromatographic data obtained for the main peaks for the separation of tetracycline, oxytetracycline and chlortetracycline from the respective impurities for each of the investigated columns, including the retention time ( $t_R$ ), apparent number of plates ( $N$ ), plate height ( $H$ ) and the resolution for the critical peak pair (pair with the lowest resolution) ( $R_S$ ).

Component	$t_R$ (min)	$N$	$H$ ( $\mu\text{m}$ )	$R_S$
<i>XTerra RP18</i>				
TC	16.2	5092	49	1.3
OTC (f.e. imp)	11.1	6850	37	1.7
OTC (s.r. imp)	3.7	4184	60	6.7
CTC (is)	13.4	4202	60	1.2
<i>Zorbax RX</i>				
CTC (is)	23.1	4072	61	2.5
<i>Chromolith Performance</i>				
TC	9.0	5562	18	1.7
OTC (f.e. imp)	1.4	3697	27	2.4
OTC (s.r. imp)	0.5	4277	23	4.8
CTC (is)	5.4	1152	87	1.1
CTC (grad)	11.3	2298	44	1.4
<i>Chromolith Flash</i>				
TC	3.9	1399	18	1.3
<i>Onyx</i>				
TC	8.0	2636	38	1.6
OTC (f.e. imp)	1.5	2324	43	2.0
OTC (s.r. imp)	0.5	2487	40	1.7
CTC (is)	4.9	1563	64	1.7
CTC (grad)	11.6	1507	66	1.1

f.e. imp: fast eluted impurities; s.r. imp: strongly retained impurities; is: isocratic program; grad: gradient program.

Finally, the quality of the separations was compared using the resolution ( $R_S$ ). For each pair of peaks, the resolution was calculated. The lowest value observed on each column is mentioned in Table 1. It can be seen that the monolithic columns show results similar to the XTerra RP18.

It can be concluded that, using Chromolith columns, similar separation can be obtained in less time and at lower backpressure.

### 3.2.2. Oxytetracycline

The OTC mixture was separated according to reference [8]. The conditions include a flow rate of 1.0 mL/min and mobile phases: ACN–0.25 mol/L TBA pH 7.5–0.25 mol/L EDTA pH 7.5–water (A) (115:360:160:365, v/v/v/v) for fast eluted impurities and (B) (340:360:160:140, v/v/v/v) for strongly retained impurities. Gradient elution showed baseline problems and therefore, two separate isocratic methods were used, differing solely in the amount of ACN.

Separations of the fast eluted impurities are shown in Fig. 2(a, b, c) on XTerra RP18, Chromolith Performance and Onyx, respectively. Similarly, separations of the strongly retained impurities are shown in Fig. 3(a, b, c). The Chromolith Flash, being too short, resulted in co-elution of several peaks and was not further used here.

The chromatograms shown for the monolithic columns were obtained at a flow rate of 4.0 mL/min.

Also here, method optimisation for the monolithic columns was done, and led to faster separation. The backpressure on XTerra RP18 with a flow of 1.0 mL/min was 154 bar while on Chromolith Performance and Onyx it was 68 and 80 bar, respectively, at a flow rate of 4.0 mL/min.



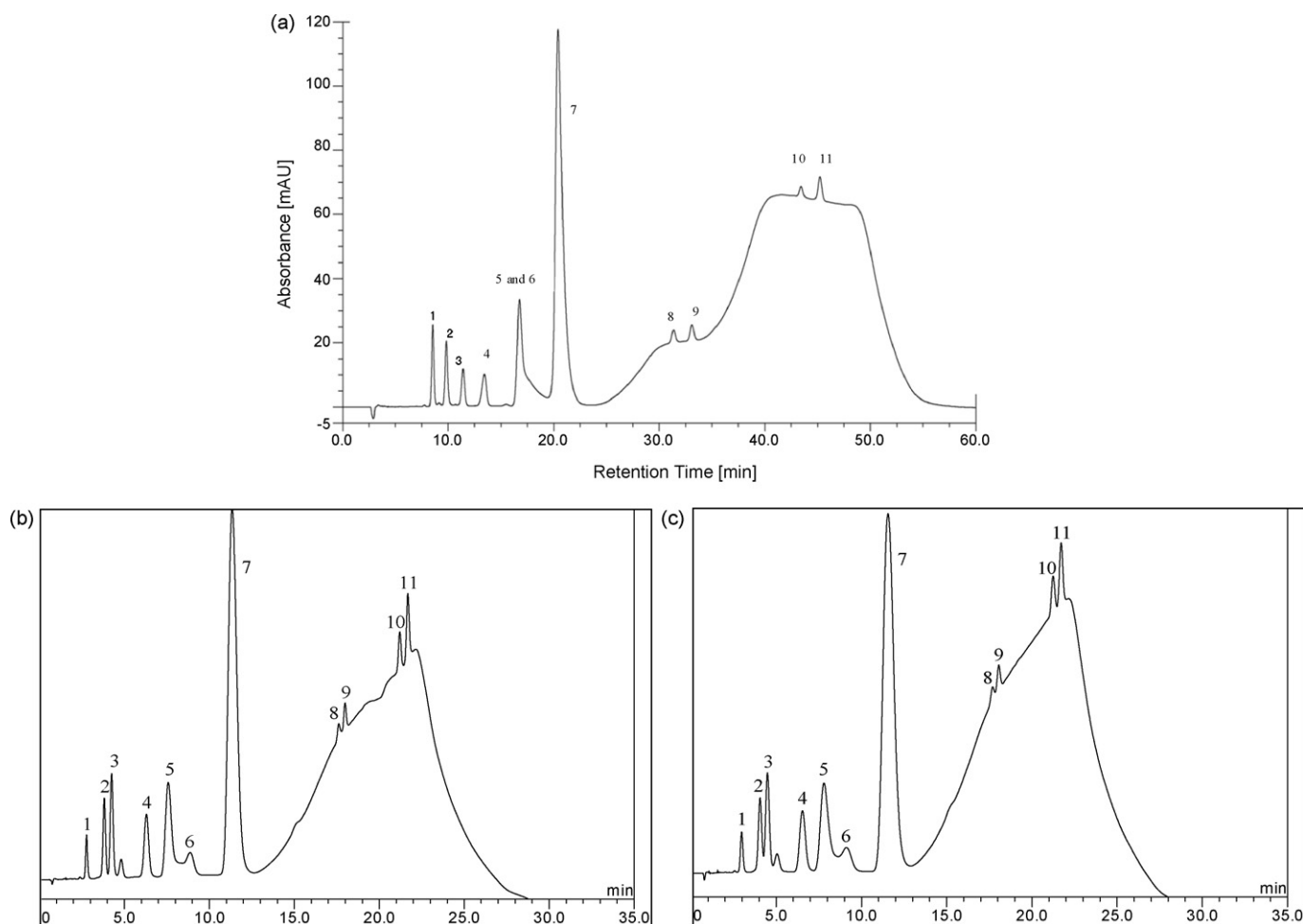


**Fig. 5.** Gradient separation of CTC and its impurities on: (a) Zorbax RX-C<sub>8</sub> column; (b) Chromolith Performance; (c) Onyx: (1) ETC, (2) TC, (3) EDMCTC, (4) DMCTC, (5) ECTC, (6) IsoCTC, (7) CTC, (8) EATC, (9) ATC, (10) EATC and (11) ACTC.

Quantitative results are reported in Table 1. AOTC is unstable [12] and so this peak was not taken into account for resolution. The values mentioned in Table 1 result from the resolution between peaks 1 and 2 in Fig. 3. For OTC also, it can be concluded that, using monolithic columns, similar separations are obtained in a shorter time and at low pressure. The analysis time is shortened by about a factor of 7. Although the flow rate is high, the total mobile phase consumption is reduced.

Again, the Chromolith Performance performs better than the Onyx.

### 3.2.3. Chlortetracycline

**3.2.3.1. Isocratic separation of the CTC mixture.** The CTC mixture was separated according to Ref. [9] on a Zorbax RX-C<sub>8</sub> (25 cm × 4.6 mm i.d., 5 μm). The flow rate was 1.0 mL/min and the mobile phase consisted of DMSO–1 mol/L perchloric acid–water (500:50:450, v/v/v). A typical chromatogram is shown in Fig. 4a. The peak pair IsoCTC–ECTC in peak 5 is not separated and baseline separation between this peak and the main peak of CTC is not obtained. The latter separation is better on a XTerra RP18 column, which also gives a faster elution, as shown in Fig. 4b.

The CTC mixture was then separated on the monolithic columns under the same conditions, except that the flow rate was 2.0 mL/min on the Chromolith Performance (Fig. 4c) and Onyx (Fig. 4d). The backpressure on Zorbax RX-C<sub>8</sub> and XTerra RP18 was 220 and 226 bar, respectively while on Chromolith Performance it was 96 bar and on Onyx 114 bar. The use of the Chromolith Flash resulted

again in co-elution of several peaks and was not further considered.

Fig. 4 and Table 1 show that the conventional columns give a similar separation, but the XTerra RP18 column is faster.

Again, the monolithic columns are faster but less so than observed for OTC. In this case, the total mobile phase consumption is not better than for XTerra RP18.

Contrary to what was observed for TC and OTC, the N values for Chromolith are not higher than for Onyx.

**3.2.3.2. Gradient elution of the CTC mixture.** To elute the strongly retained anhydro derivatives faster and to increase the sensitivity, gradient elution was used by increasing the % DMSO in the mobile phase. Fig. 5a shows the chromatogram of a CTC mixture on a Zorbax RX-C<sub>8</sub> column, with flow rate of 1.0 mL/min and mobile phase: DMSO–1 mol/L perchloric acid–water (A) (450:50:500, v/v/v) and (B) (700:50:250, v/v/v). The gradient program is as follows: 0–18 min, 0% of B (isocratic); 18–23 min, 0–40% of B (linear gradient); 23–28 min, 40% of B (isocratic); 28–33 min, 40–80% of B (linear gradient); 33–43 min, 80% of B (isocratic); 43–48 min, 80–0% of B (linear gradient); 48–60 min, 0% of B (isocratic).

The chromatographic method was optimised for the monolithic columns at flow rate of 2.0 mL/min. The mobile phase consisted of DMSO–1 mol/L perchloric acid–water (A) (225:50:775, v/v/v) and (B) (700:50:250, v/v/v). The gradient program was as follows: 0–10 min: 20% B, 10–15 min: 70% B, 15–20 min: 90% B, 20–25 min: 0% B.

**Table 2**

Overview of the repeatability data expressed as relative standard deviation (R.S.D., %) ( $N=6$ ) for the separation of oxytetracycline and its impurities. Percentages of each compound in mixture are given in brackets. The R.S.D. was determined for the retention time ( $t_R$ ) and the peak area ( $A$ ) for both Chromolith Performance and Onyx, according to the methods of fast eluted or strongly retained compounds.

	Chromolith Performance		Onyx	
	R.S.D. ( $t_R$ )	R.S.D. ( $A$ )	R.S.D. ( $t_R$ )	R.S.D. ( $A$ )
<i>Fast eluted compounds</i>				
EOTC (5.5%)	0.00	0.07	0.55	0.14
ETC (3.8%)	0.65	0.27	0.59	0.26
OTC (86%)	0.00	0.04	0.00	0.17
ADOTC (0.7%)	0.29	4.99	0.29	4.01
TC (4%)	0.33	0.73	0.33	0.47
<i>Strongly retained compounds</i>				
OTC (75%)	1.10	1.09	0.85	0.60
AOTC (2%)	0.65	0.25	0.00	0.31
$\beta$ -APOTC (15%)	0.46	7.90	0.32	1.15
$\alpha$ -APOTC (8%)	0.37	0.41	0.35	0.16

Fig. 5(b) and (c) shows that the analysis time is reduced by about 50% and also that the separation of the peaks IsoCTC–ECTC is improved. There is no considerable gain in mobile phase consumption.

The plate number is somewhat higher for Zorbax RP.

### 3.2.4. Quantitative aspects

The OTC analysis was selected to determine some quantitative aspects, since it has the shortest analysis time.

The limit of detection (LOD), for OTC, corresponding to a signal to noise ratio of 3, was determined by injecting reference solutions with different concentrations. An LOD value of  $9.4 \times 10^{-5}$  mg/mL was found. The limit of quantification (LOQ) was found to be  $3.0 \times 10^{-4}$  mg/mL (6 ng injected), based on a signal to noise ratio of 10. This is close to the LOQ value reported for XTerra RP18: 3.2 ng injected [8].

The repeatability of the methods for fast and late eluted impurities was tested by injecting 6 times OTC mixture A and B, respectively on the Onyx and Chromolith Performance column. The R.S.D. values of the retention time and peak area can be seen in Table 2.

The linearity for OTC was also investigated in the range from 0.03 to 120% (1 mg/mL = 100%). The results found were  $y = 1.826x + 0.161$ ,  $r^2 = 0.999$ ,  $n_c = 9$  and  $n_i = 3$  with  $y$  the peak area,  $x$  the concentration in %,  $r^2$  the coefficient of determination,  $n_c$  the number

of concentrations studied and  $n_i$  the number of analyses per concentration.

These results for repeatability and linearity on monolithic columns were similar to the results obtained on XTerra RP18 [8].

## 4. Conclusion

In this study, the transferability of methods, originally developed on a conventional XTerra RP18 or Zorbax RX column, onto monolithic columns was investigated for TC, OTC and CTC. While the conventional columns showed longer analysis times and higher backpressures, the monoliths showed an increased analysis speed at lower backpressures while maintaining or even improving the separation quality. Regardless the higher flow rates, the total mobile phase consumption did not increase and the sensitivity did not decrease. As for conventional columns, different brands of monoliths (Chromolith Performance and Onyx) gave slightly different results. For the columns tested, the Chromolith Performance performed somewhat better than the Onyx, but it has to be remarked that only one specimen of each column was examined in this study and no data of inter-batch variability were available. The results with the short Chromolith Flash were good for TC, but poor for OTC and CTC. This indicates that a minimum column length may be required for certain separations.

## Acknowledgement

E. Adams is a post-doctoral fellow of the Fund for Scientific Research (FWO)—Flanders, Belgium.

## References

- [1] K.K. Unger, R. Skudas, M.M. Schulte, J. Chromatogr. A 1184 (2008) 393.
- [2] F. Rabel, K. Cabrera, D. Lubola, Am. Lab. 32 (2000) 20.
- [3] W. Gao, G. Yang, J. Yang, H. Liu, Turk. J. Chem. 28 (2004) 379.
- [4] K. Cabrera, J. Sep. Sci. 27 (2004) 843.
- [5] D. Lubola, K. Cabrera, W. Kraas, C. Schaefer, LC–GC Eur. (December) (2001) 2.
- [6] K. Cabrera, D. Lubola, H.M. Eggenweiler, H. Minakuchi, K. Nakanishi, J. High Resol. Chromatogr. 23 (2002) 93.
- [7] R. Capote, J. Diana, E. Roets, J. Hoogmartens, J. Sep. Sci. 25 (2002) 399.
- [8] J. Diana, G. Ping, E. Roets, J. Hoogmartens, Chromatographia 56 (2002) 313.
- [9] J. Diana, L. Vandenbosch, B. De Spiegeleer, J. Hoogmartens, E. Adams, J. Pharm. Biomed. Anal. 39 (2005) 523.
- [10] S. El Deeb, L. Preu, H. Wätzig, J. Pharm. Biomed. Anal. 44 (2007) 85.
- [11] F. Svec, LC–GC Eur. (June) (2003) 24.
- [12] N.H. Khan, E. Roets, J. Hoogmartens, H. Vanderhaeghe, J. Chromatogr. 405 (1987) 229.



## Short communication

# Selective electrochemical sensing of calcium dobesilate based on the nano-Pd/CNTs modified pyrolytic graphite electrode

Guangzhi Hu<sup>a,c</sup>, Long Chen<sup>b,c</sup>, Yong Guo<sup>a</sup>, Shijun Shao<sup>a,\*</sup>, Xiaolai Wang<sup>b,\*</sup>

<sup>a</sup> Key Laboratory for Natural Medicine of Gansu Province, Lanzhou Institute of Chemical Physics, Chinese Academy of Sciences, Lanzhou 730000, PR China

<sup>b</sup> State Key Laboratory for Oxo Synthesis and Selective Oxidation, Lanzhou Institute of Chemical Physics, Chinese Academy of Sciences, Lanzhou 730000, PR China

<sup>c</sup> Graduate School of the Chinese Academy of Sciences, Beijing 100039, PR China

## ARTICLE INFO

## Article history:

Received 8 October 2008

Received in revised form 21 December 2008

Accepted 23 December 2008

Available online 23 January 2009

## Keywords:

Palladium functionalized multi-wall carbon nanotube

Calcium dobesilate

Pyrolytic graphite electrode

Electrochemical sensor

## ABSTRACT

A new palladium nanoparticle functionalized multi-wall carbon nanotubes (nano-Pd/CNTs) modified pyrolytic graphite electrode (PGE) has been fabricated for electrochemical sensing of calcium dobesilate (CD) in pharmaceutical capsules. The nano-Pd/CNTs were characterized by transmission electron microscopy (TEM) and X-ray diffraction (XRD). The nano-Pd/CNTs composite showed a strong electrocatalytic property for CD. The anodic peak current is 6-fold than that obtained in bare PGE and the oxidation potential has an obvious shift to negative. The anodic peak current is proportional to the concentration of CD in the range of  $1.0 \times 10^{-7}$  to  $7.0 \times 10^{-4}$  mol L<sup>-1</sup>, with a linear relative coefficient  $r = 0.999$  and a detection limit  $4.0 \times 10^{-8}$  mol L<sup>-1</sup> ( $S/N = 3$ ). This kind of electrode shows good stability, sensitivity, reproducibility, large linear range and low detection limit towards electrochemical determination of CD. The proposed method provides a selective and sensitive electrochemical sensor of calcium dobesilate.

© 2009 Elsevier B.V. All rights reserved.

## 1. Introduction

As a potent angioprotective reagent, calcium dobesilate (CD) was firstly used for stabilizing blood-retinal barrier in patients with diabetic retinopathy from 1970s [1,2]. Now it is also widely applied for treating peripheral microvascular disease, chronic venous insufficiency and improving blood rheological properties [3,4]. With an increased risk of an adverse effect with CD [5], it is very important to develop rapid, sensitive and low-cost methods to detect CD in pharmaceutical capsule or body fluid.

Traditional CD determination methods comprise with mainly high performance liquid chromatography (HPLC) [6], spectrophotometry [7], chemiluminescence [8]. But these detection methods need expensive equipment and/or complicated treatment procedure. As an electroactive molecule, CD can also be detected via electrochemical method, which is very sensitive, rapid, low-cost and potentially used in laboratory and clinic analysis. Yang et al. reported an electrochemical determination of CD with differential pulse anodic voltammetry [9]. Song et al. reported a flow-injection biamperometric direct determination of CD, with a detection limit of  $4.0 \times 10^{-7}$  mol L<sup>-1</sup> [10]. Unluckily, most conventional solid state electrodes show a weak and/or unstable response towards CD. To improve the electrochemical response of CD at the electrode sur-

face, some chemical modified electrodes have been reported for determination of CD. Wang et al. reported a carbon coated iron nanoparticles modified glassy carbon electrode for CD determination in the range of  $5.0 \times 10^{-7}$  to  $1.0 \times 10^{-5}$  mol L<sup>-1</sup>, with a detection limit  $2.0 \times 10^{-7}$  mol L<sup>-1</sup>. But some electroactive substance such as neurotransmitters, uric acid and ascorbic acid in human fluid, seriously interrupt the accurate determination of CD on this kind of modified electrode [11]. Zheng et al. developed an ionic liquid-type carbon paste electrode for determination of CD with a detection limit  $4.0 \times 10^{-7}$  mol L<sup>-1</sup> [12].

Firstly discovered in 1991, carbon nanotube has various applications in many fields. Wang and co-workers fixed CNTs self-assembled on the surface of SiO<sub>2</sub> for solid-phase extraction of biomacromolecular cytochrome *c* [13]. CNTs were also widely used as electrochemical sensor for determination of some important electroactive biomolecule, such as dopamine [14]. Zhang et al. developed a poly-*o*-phenylenediamine and multi-wall carbon nanotubes composite film modified glassy carbon electrode and applied it for electrochemical determination of CD in 0.1 mol L<sup>-1</sup> H<sub>2</sub>SO<sub>4</sub> [15]. Noble metal nanoparticles (Au, Pt, Ag and Pd) show novel electrocatalytic property, stability and biocompatibility for determination of biomolecule. Guo and Li reported electrochemical synthesis of Pd nanoparticles on functionalized CNTs surfaces for electrochemical oxidation of hydrazine [16]. Li and co-workers fabricated a Pd/CNTs modified glassy carbon electrode and applied it for electrocatalytic oxidation of formaldehyde [17]. To our best of knowledge, applications of Pd/CNTs to detect CD in clinic medication have not been reported up to now.

\* Corresponding authors. Fax: +86 931 8277088.

E-mail addresses: [shaoguo@lzb.ac.cn](mailto:shaoguo@lzb.ac.cn) (S. Shao), [chenlong2000.1984@126.com](mailto:chenlong2000.1984@126.com) (X. Wang).

In the present work, we report a new method for synthesis of Pd nanoparticles functionalized CNTs (nano-Pd/CNTs) modified pyrolytic graphite electrode (nano-Pd/CNTs/PGE) for selective electrochemical determination of CD. This modified electrode showed a good electrocatalytic response to CD and was applied to electrochemical sensing of CD in pharmaceutical capsules, with satisfactory results.

## 2. Experimental

### 2.1. Chemicals and reagents

Calcium dobesilate was purchased from Juye Lingfeng Chemical Materials Limited Corporation (Shandong, China). Calcium dobesilate capsules were supplied by Lijun Pharmaceutical Corp. (Xi'an, China). Other reagents were analytical grade and dissolved with redistilled water for use. Prior to each voltammetric experiment, electrolyte solution was deoxygenated with nitrogen bubbling for 15 min at room temperature.

### 2.2. Synthesis of Pd/CNTs

High quality multi-wall carbon nanotubes were synthesized by chemical vapor deposition method using Co/La<sub>2</sub>O<sub>3</sub> as catalyst and ethylene as carbon source in a tubular quartz reactor. The detailed experimental procedure is given in our earlier report [18]. A sonochemical process was used to treat as-grown CNTs in nitric and sulfuric acids to create surface functional groups for Pd nanoparticles deposition as described previously [19].

Palladium acetate (Pd(OAc)<sub>2</sub>) was used as the palladium precursor, and ethanol as both solvent and reducing agent. Polyvinylpyrrolidone (PVP) was also added to the reaction system. In a typical procedure, 32 mg of Pd(OAc)<sub>2</sub> and 78 mg of PVP were dissolved in 30 mL of ethanol, then 200 mg of functionalized CNTs were added to the above solution. After ultrasonication of the mixture for 1 h, the reaction mixture was then heated to 60 °C in an oil bath and stirred at this temperature for 5 h to ensure completion of the reaction. The product was centrifuged, rinsed several times with ethanol, and dried for future use.

### 2.3. Preparation of the nano-Pd/CNTs/PGE

10 mg nano-Pd/CNTs were dispersed with the aid of ultrasonic agitation in 10 mL of *N,N*-dimethylformamide (DMF) to give a black suspension. The PG electrode was carefully polished with 1.0, 0.3 and 0.05 μm alumina powders, then washed successively in 50% (v/v) nitric acid, ethanol and water in an ultrasonic condition, and then dried in air. The nano-Pd/CNTs/PGE electrode was prepared by

casting 20 μL of nano-Pd/CNTs suspension on the surface of a PG electrode and dried under an infrared lamp.

### 2.4. Apparatus and measurement

Cyclic voltammetry (CV), differential pulse voltammetry (DPV) and amperometric *i*-*t* curve were performed on a CHI660C electrochemical workstation (CHI Instrument Corp. Shanghai) in a conventional three-electrode cell. A bare PG electrode (Tianjin Aidahengsheng Technology Corp., Tianjin) or the nano-Pd/CNTs/PGE electrode was used as working electrode. Platinum wire and saturated calomel electrode (SCE) were used as the counter electrode and reference electrode, respectively. XRD pattern of the sample was recorded with a PANalytical X'Pert PRO X-ray diffractometer with a Ni-filtered Cu Kα X-ray source operating at 40 kV and 50 mA. TEM measurements were carried out on a JEOL JEM-200K transmission electron microscope operated at an accelerated voltage of 200 kV.

## 3. Results and discussion

### 3.1. Characterization of nano-Pd/CNTs

Fig. 1A presents the XRD pattern of Pd/CNTs. Characteristic diffraction peak at 25.8° was observed, which corresponds to the (002) reflection of graphite [20]. Diffraction peaks were also observed at 40.0°, 46.5°, 68.0° and 82.0°, respectively, which could be indexed as the (111), (200), (220) and (311) reflections of crystalline Pd(0) [21]. Thus, metallic Pd was successfully produced in the reaction process. Evaluated from the half-peak width of Pd (111) diffraction peak, the average size of palladium crystalline was 8.4 nm in Pd/CNTs nanocomposite. To reveal the detailed structure of Pd/CNTs nanocomposite, a typical TEM image of Pd/CNTs is shown in Fig. 1B. It can be observed that well dispersed spherical Pd nanoparticles were obtained and most of them were anchored onto the external walls of CNTs. The Pd nanoparticles have a narrow size distribution ranging from 5 to 10 nm, consistent with previous XRD results.

### 3.2. Electrochemical behavior of CD on the nano-Pd/CNTs/PGE

Electrochemistry property of CD on the bare PG electrode and the nano-Pd/MWNT/PG electrode was studied by CV in 0.1 mol L<sup>-1</sup> H<sub>2</sub>SO<sub>4</sub>. The bare PG electrode showed a weak electrochemical response to CD (Fig. 2a). A pair of redox peak of CD ( $E_{pa} = 0.661$  V,  $E_{pc} = 0.208$  V) was observed, with a separation of 0.453 V. However, a strong anodic peak ( $E_{pa} = 0.495$  V) and a relative weak cathodic peak ( $E_{pc} = 0.452$  V) were observed on the nano-Pd/CNTs/PGE elec-

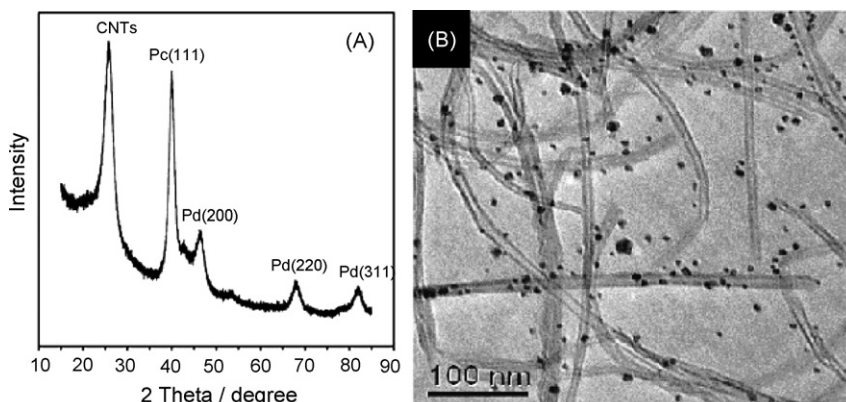
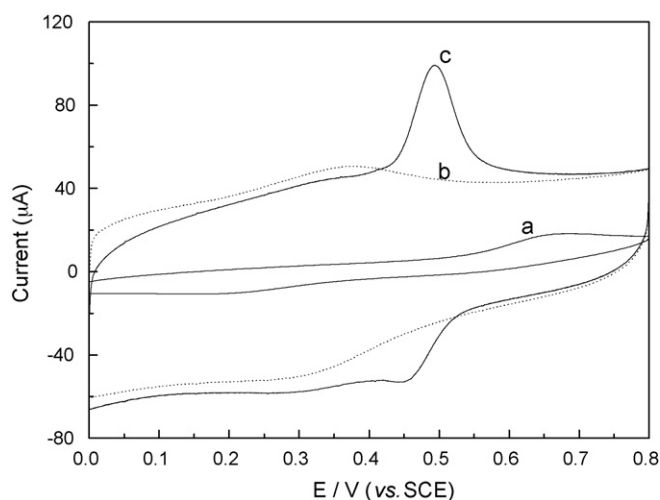


Fig. 1. XRD (A) and TEM image (B) pattern of Pd/CNTs nanocomposite.



**Fig. 2.** CV curves of  $1.0 \times 10^{-4} \text{ mol L}^{-1}$  CD at a bare PGE (curve a) and a nano-Pd/CNTs/PGE (curve c) in  $0.1 \text{ mol L}^{-1} \text{ H}_2\text{SO}_4$ ; Curve b shows cyclic voltammogram of the nano-Pd/CNTs/PGE in the absence of CD. Scan rate:  $100 \text{ mV s}^{-1}$ .

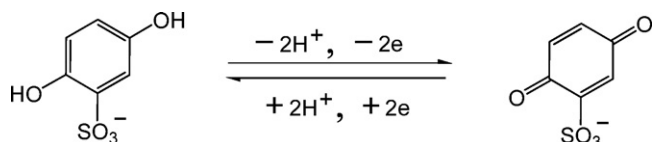
trode, with a peak-to-peak separation of  $0.043 \text{ V}$ . This pair of peaks disappeared in the absence of CD (Fig. 1B), suggesting this couple of redox peak corresponds to the electrochemical redox of CD. And the anodic peak current of CD on the modified electrode is six times than that obtained on the bare PG electrode. The above results indicate that the nano-Pd/CNTs/PGE electrode showed a good electrocatalytic response to CD. The probable reason is that Pd nanoparticles and electroactive group on the CNTs can accelerate the electron transfer between CD and the electrode surface. The anodic and cathodic peak current is linear with the square root of the scan rate ranging from  $20$  to  $200 \text{ mV s}^{-1}$ , indicating that the electrode progress is controlled by diffusion [22].

Cyclic voltammetry was carried out to characterize the effect of solution pH on redox peak potential of CD on the nano-Pd/CNTs composite. It was found that peak potential shifted negatively with the increase of solution pH, indicating that protons take parting in the electrode reaction process [11]. The redox peak potentials of CD was proportional with the solution pH in the range of  $1.0$ – $6.0$ . The linear regression equations were  $E_{\text{pa}}(\text{V}) = 0.529 - 0.047 \text{ pH}$  and  $E_{\text{pc}}(\text{V}) = 0.516 - 0.067 \text{ pH}$ , with the correlation coefficient  $0.998$  and  $0.999$ , respectively, demonstrating that the electrode process is equal proton–electron transfer. As a reversible electrochemical reaction [23]:  $|E_{\text{p}} - E_{\text{p}/2}| = 2.3RT/nF$ , the electron transfer number was calculated to be approximately 2 in this study. So the probable electrochemical mechanism is as follows (Scheme 1).

Stored in the  $0.1 \text{ mol L}^{-1} \text{ PBS}$  (pH 7.0) after every experiment, the modified electrode was used for DPV determination of CD once a day at the same operation conditions. The anodic peak current of CD did not change for at least 12 weeks. This result shows good stability and reproducibility of the nano-Pd/CNTs/PGE.

### 3.3. Electrochemical determination of CD

Determination of CD concentration using the nano-Pd/CNTs modified electrode is performed by DPV. Fig. 3A depicted the DPV



**Scheme 1.** The redox mechanism of calcium dobesilate on the nano-Pd/CNTs/PGE.

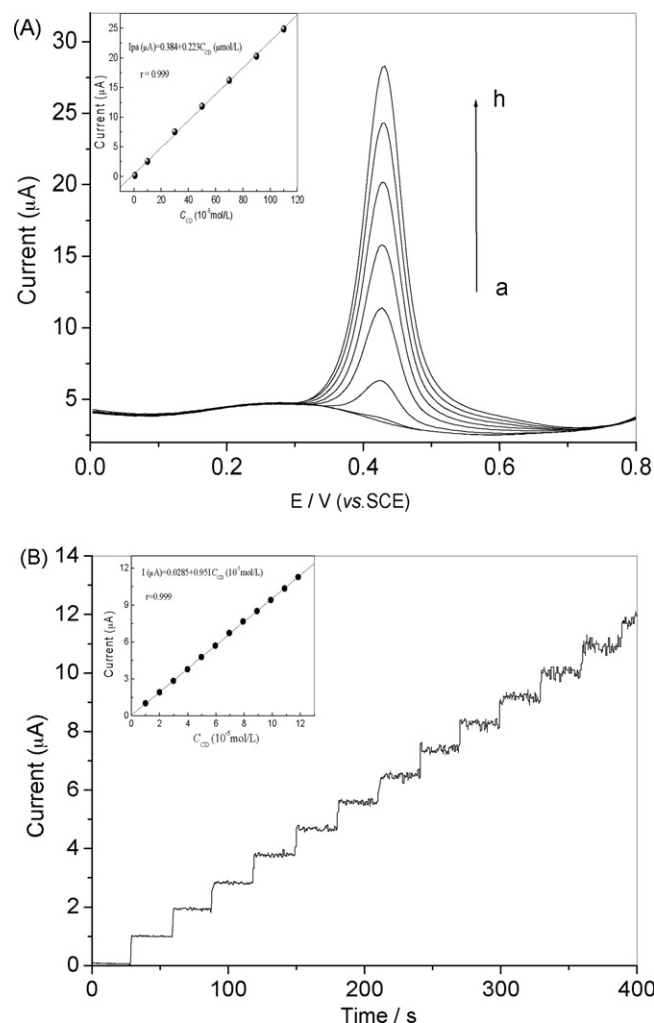


**Fig. 3.** (A) DPV curves of the nano-Pd/CNTs/PGE in different concentrations of CD (a → h:  $0, 5, 10, 30, 50, 70, 90, 110 \times 10^{-6} \text{ mol L}^{-1}$ ), (inset) the plot of peak currents vs. CD concentration; (B) amperometric response of the nano-Pd/CNTs/PGE to the successive additions of  $10 \mu\text{L } 1.0 \times 10^{-2} \text{ mol L}^{-1}$  CD in  $10 \text{ mL } 0.1 \text{ mol L}^{-1} \text{ H}_2\text{SO}_4$  at an applied potential of  $0.5 \text{ V}$ , stirring speed:  $300 \text{ rpm}$ .

curves of different concentration CD at the nano-Pd/CNTs/PGE electrode in  $0.1 \text{ mol L}^{-1} \text{ H}_2\text{SO}_4$ . The results showed that anodic peak current was proportional to the concentration of CD in the range of  $1.0 \times 10^{-7}$  to  $7.0 \times 10^{-4} \text{ mol L}^{-1}$ , the linear equation is obtained:

$$I_{\text{CD}} (10^{-6} \text{ A}) = 0.384 + 0.223 C_{\text{CD}} (10^{-6} \text{ mol L}^{-1})$$

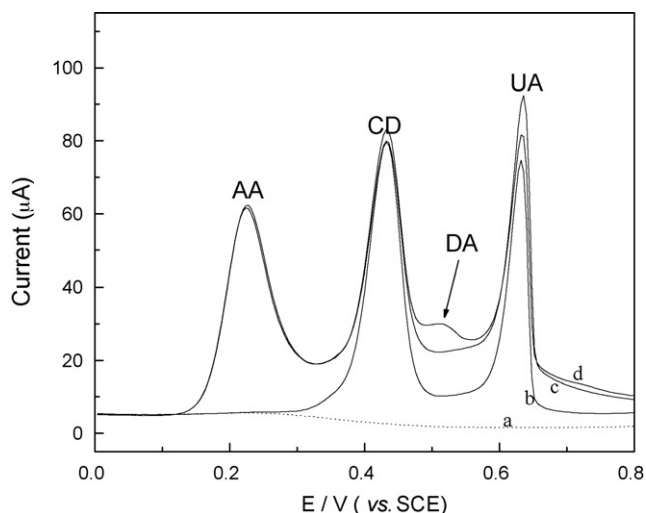
with a linear relative coefficient  $r = 0.999$  and a detection limit  $4.0 \times 10^{-8} \text{ mol L}^{-1}$  ( $S/N = 3$ ).

Fig. 3B shows an amperometric response in oxidation currents caused by adding CD to  $0.1 \text{ mol L}^{-1} \text{ H}_2\text{SO}_4$ . The response current was measured at the potential of  $0.5 \text{ V}$  in a stirred  $10 \text{ mL}$  solution, and  $10 \mu\text{L } 1 \times 10^{-2} \text{ mol L}^{-1}$  CD was added every time. The nearly equal current steps for each addition of CD demonstrated stable and efficient catalytic activity of the nano-Pd/CNTs composite. A linear relationship between CD oxidation currents and concentration was obtained from  $5.0 \times 10^{-7}$  to  $6.0 \times 10^{-4} \text{ mol L}^{-1}$ . The linear equation is also obtained:

$$I_{\text{CD}} (10^{-6} \text{ A}) = 0.0285 + 0.951 C_{\text{CD}} (10^{-5} \text{ mol L}^{-1})$$

with a linear relative coefficient  $r = 0.999$ , and the detection limit is  $2.0 \times 10^{-7} \text{ mol L}^{-1}$  ( $S/N = 3$ ).

Some possible interfering substances were investigated. Glucose, lactose and starch are non-electroactive molecules and have



**Fig. 4.** DPV curves of  $2.0 \times 10^{-4} \text{ mol L}^{-1}$  CD on the nano-Pd/CNTs/PGE successively adding  $1.0 \times 10^{-4} \text{ mol L}^{-1}$  UA (b),  $1.0 \times 10^{-3} \text{ mol L}^{-1}$  AA (c) and  $1.0 \times 10^{-4} \text{ mol L}^{-1}$  DA (d); curve a is the DPV record of the blank solution.

no interference for accurate determination of CD. As uric acid (UA), dopamine (DA) and ascorbic acid (AA) are also electroactive molecules that coexist in a biological system, and can be oxidized at the near oxidation potential of polyphenol compounds CD on bare solid electrodes. Therefore, it is important to eliminate the interference of UA, DA and AA in order to conduct exact CD determination in physiologic condition. Fig. 4 shows that the nano-Pd/CNTs modified electrode resolved the mixed DPV response into three well-defined anodic peaks at potentials 0.225, 0.433 and 0.635 V corresponding to the oxidations of AA, CD, and UA, respectively. The peak-to-peak separation of them is over than 0.2 V, illustrating that UA and AA have no any interference for determination of CD. While the oxidation peak of DA appears at 0.514 V, and experiment results show that 20-fold DA has no interference for accurately detecting CD. The influence of other non-electroactive substances on the CD peak currents was also investigated, and no interference was found to occur in the presence of the following ions: 1000-fold  $\text{K}^+$ ,  $\text{Na}^+$ ,  $\text{NH}_4^+$ ,  $\text{Mg}^{2+}$ ,  $\text{Ca}^{2+}$ ,  $\text{SO}_4^{2-}$ ,  $\text{Cl}^-$ ,  $\text{Br}^-$ , with a deviation below 5%. Both sensitive and selectivity of the proposed method have an obvious improvement to the latest reports [11,15].

In order to evaluate the validity of the proposed method, contents of 30 hard capsules were emptied, weighed and carefully mixed. A portion of the powder equivalent to 500 mg CD was accurately weighed, dissolved into 10 mL  $\text{H}_2\text{SO}_4$  ( $0.1 \text{ mol L}^{-1}$ ) and separated with a centrifugal machine. Further dilution was also performed with  $0.1 \text{ mol L}^{-1}$   $\text{H}_2\text{SO}_4$  to reach the calibration range of CD. A standard addition was used for CD concentration determi-

nation in pharmaceutical capsules. The recoveries were 98–102%, with a relative standard deviation (R.S.D) lower than 1.5% (results not shown). The proposed method was also used for CD determination in urine. The recoveries of the samples solution of the different concentrations of CD were between 97% and 101%, with R.S.Ds lower than 2.4%, illustrating that the proposed method is reliable for CD determination in human urine.

#### 4. Conclusion

A novel Pd nanoparticles functionalized CNTs modified pyrolytic graphite electrode have been fabricated for investigating electrochemical behavior of calcium dobesilate. The nano-Pd/CNTs composite exhibited dramatically electrocatalytic activity for calcium dobesilate. The results of DPV and amperometric determination indicate the feasibility of using the proposed electrode for electrochemical sensing of calcium dobesilate in pharmaceutical formation. Uric acid, ascorbic acid and 20-fold dopamine do not interfere to accurate determination of CD, illustrating the modified electrode can potentially be applied to detect calcium dobesilate in body fluid, which is under investigation.

#### Acknowledgment

The authors thank the financial support of National Nature Science Foundation of China (no. 20672121).

#### References

- [1] B. Nemeth, J. Hudomel, A. Farkas, *Ophthalmologica* 170 (1975) 434.
- [2] P. Berthet, J.C. Farine, J.P. Barras, *Int. J. Clin. Pract.* 53 (1999) 631.
- [3] J. Brunet, J.C. Farine, R.P. Garay, P. Hannaert, *Eur. J. Pharmacol.* 358 (1998) 213.
- [4] E. Marmo, *Eur. Rev. Med. Pharmacol. Sci.* 9 (1987) 1.
- [5] H. Allain, A.A. Ramelet, E. Polard, D. Bentué-Ferrer, *Drug Safety* 27 (2004) 649.
- [6] K. Róna, K. Ary, *J. Chromatogr. B* 755 (2001) 245.
- [7] J. Kracmar, J. Kracmavova, A. Kovarova, Z. Stejskal, *Pharmazie* 43 (1988) 681.
- [8] Z.H. Song, Q.L. Yue, C.N. Wang, *Spectrochim. Acta Part A* 60 (2004) 2377.
- [9] S. Yang, Y. Hei, S. Wu, J. Zheng, *Chin. J. Anal. Lab.* 23 (2004) 4.
- [10] J. Song, J. Chen, *J. Pharm. Biomed. Anal.* 33 (2003) 789.
- [11] S. Wang, Q. Xu, X. Zhang, G. Liu, *Electrochem. Commun.* 10 (2008) 411.
- [12] J. Zheng, Y. Zhang, P. Yang, *Talanta* 73 (2007) 920.
- [13] Z. Du, Y. Yu, X. Yan, J. Wang, *Analyst* 133 (2008) 1373.
- [14] P. Zhang, F. Wu, G. Zhao, X. Wei, *Bioelectrochemistry* 67 (2005) 109.
- [15] X. Zhang, S. Wang, L. Jia, Z. Xu, Y. Zeng, *J. Biochem. Biophys. Methods* 70 (2008) 1203.
- [16] D. Guo, H. Li, *Electrochem. Commun.* 6 (2004) 999.
- [17] G. Gao, D. Guo, H. Li, *J. Power Sources* 162 (2006) 1094.
- [18] L. Chen, H. Liu, K. Yang, J. Wang, X. Wang, *Mater. Chem. Mater. Chem. Phys* 112 (2008) 407.
- [19] Y. Xing, *J. Phys. Chem. B* 108 (2004) 19255.
- [20] A. Cao, C. Xu, J. Liang, D. Wu, B. Wei, *Chem. Phys. Lett.* 344 (2001) 13.
- [21] Z.D. Wei, C. Yan, Y. Tan, L. Li, C.X. Sun, Z.G. Shao, P.K. Shen, H.W. Dong, *J. Phys. Chem. C* 112 (2008) 2671.
- [22] A.J. Bard, L.R. Faulkner, *Electrochemical Methods: Fundamentals and Applications*, Wiley, New York, 1980, p. 218.
- [23] G. Mamantov, D.L. Manning, J.M. Dale, *J. Electroanal. Chem.* 9 (1965) 253.



# A gold nanoparticle labeling strategy for the sensitive kinetic assay of the carbamate–acetylcholinesterase interaction by surface plasmon resonance

Xi Huang, Haiyang Tu, Danhua Zhu, Dan Du, Aidong Zhang\*

Key Laboratory of Pesticide & Chemical Biology of Ministry of Education, College of Chemistry, Central China Normal University, 152 Luoyu Road, Wuhan 430079, PR China

## ARTICLE INFO

### Article history:

Received 17 November 2008  
 Received in revised form 8 January 2009  
 Accepted 9 January 2009  
 Available online 20 January 2009

### Keywords:

Gold nanoparticles  
 Surface plasmon resonance  
 Signal enhancement  
 Acetylcholinesterase  
 Carbamate inhibitors

## ABSTRACT

The article presents a novel strategy for a sensitive investigation of the interaction between acetylcholinesterase (AChE) and its small molecular carbamate inhibitors. Two carbamate inhibitors with different ether linkages and the terminal lipooate were synthesized and labeled with gold nanoparticles (AuNPs). With the signal amplification of AuNPs, the specific interactions between the AuNPs labeled carbamate inhibitors (ALC1 and ALC2) and the immobilized AChE on sensor chip surface were readily examined. The detection sensitivities of ALC1 and ALC2 were 176 and 121 m°/nM, respectively, with the detection limits of 7.0 and 12 pM at a signal-to-noise ratio of 3. The association/dissociation constants for the binding interaction between carbamate inhibitors and AChE were reported for the first time. The affinity constants were estimated to be  $3.13 \times 10^6$  and  $6.39 \times 10^5 \text{ M}^{-1}$  for ALC1 and ALC2 respectively. This AuNPs labeling strategy is versatile and may be applicable for the direct or competitive SPR kinetic assay of the interaction between small molecule inhibitors and their target proteins with a high sensitivity.

© 2009 Elsevier B.V. All rights reserved.

## 1. Introduction

Over the last two decades, surface plasmon resonance (SPR) sensors have been extensively applied for the study of intermolecular interactions [1,2], drug hit identification and lead discovery [3,4], as well as the detection of chemical and biological analytes related to environmental monitoring, food safety and medical diagnostics [5]. The SPR measures changes in refractive index and which are proportional to mass accumulation near the sensor surface; therefore any increase of the mass accumulation on the sensor surface will result in a SPR signal intensity [6]. In the target-based drug candidate screening, small molecular candidates in solution are allowed to flow over the sensor surface immobilizing with receptor proteins such as enzymes for achieving a direct real-time and label-free kinetic measurement. With the improvement of SPR instrumental performance [7], special experiment design is still demanded for obtaining acceptable signals for kinetic analysis, which may be achieved by injecting of a relatively high concentrated analyte solution and employing a sensor surface with a relatively high binding capacity [8]. However, the sensing and kinetic analysis of low molecular weight (LMW) molecules by SPR is generally difficult in the cases of low concentration of LMW molecules and low binding capacity of SPR sensor chip without the extension such as dextran layer used in Biacore techniques [9].

The process in the pesticide discovery possesses the similar pattern as that in the drug discovery [10]. The SPR technique in drug hit identification and lead discovery is applicable to the pesticide discovery. According to our knowledge, at present there is no report concerning the SPR application for the pesticide-like hit identification, lead optimization and screening. The causes possibly lie in two aspects: (1) pesticide-like compound screening conventionally is very convenient with conducting *in vivo* tests on whole organisms or *in vitro* tests on target proteins with fluorescence or other spectroscopic methods [11,12]; (2) well-known pesticide target proteins are usually in complicated polymeric forms with high molecular weight, the direct assay of small pesticide-like compounds with SPR may become impractical. For example, the common and commercial available acetylcholinesterase (AChE) from *Electrophorus electricus* (electric eel) has a molecular weight 480 kDa, with a tetramer composed of four equal subunits of 70 kDa each [13]. The immobilization of this kind of enzyme proteins on a sensor chip may result in a low binding capacity and hence a weak SPR response for the small molecule assay, and the quality of kinetic data will become deteriorated.

Since the kinetic data is more meaningful than affinity data [14], high quality of kinetic data obtained with SPR measurements will be very helpful in the pesticide discovery. Actually there is another SPR assay methodology that may circumvent this difficulty in the direct SPR kinetic assay: the surface competition assay (SCA) [15]. In SCA, the target protein is immobilized to the sensor surface, while the mixture solution of a known large binder and the compound to be screened is injected for a competitive binding to the target,

\* Corresponding author. Tel.: +86 27 67867635; fax: +86 27 67867141.  
 E-mail address: [adzhang@mail.ccnu.edu.cn](mailto:adzhang@mail.ccnu.edu.cn) (A. Zhang).

thus the competitive kinetic can be acquired [16]. In principle, for the surface competition assay, the known large binder with a high molecular weight or a refractive index enhancing tag will result in a SPR kinetic signal with a pronounced sensitivity.

Despite the utility of biological macromolecules as the large binder, the use of gold nanoparticles (AuNPs) labeled small molecules may be an alternative for the surface competition assay. Actually, SPR immunosensors of AuNPs labeled small molecules have been extensively studied [17,18]. Recently, with the combination of AuNPs labeling and the replacement assay, highly sensitive detection of label-free small molecular D-galactose was reported [19]. The amplification mechanism of AuNPs enhanced SPR is the increased apparent mass of the analyte tagged with AuNPs and the coupling of the localized surface plasmon of AuNPs with the propagating plasmon on the SPR gold surface [20]. At present, AuNPs labeling has not been applied to a quantitative or kinetic assay of LMW analytes in solution through the enzyme-based SPR biosensors with respective to the drug or pesticide discovery.

N-Methyl carbamate insecticides target AChE and have been widely used in homes, gardens and agriculture [21]. Highly sensitive assay and screening of N-methyl carbamate insecticides are desired for environmental and health perspectives as well as the drug and pesticide discovery. Since the active site of AChE is accessed by a deep and narrow gorge [22], the N-methyl carbamate group is linked to the lipoate moiety with two different ether linkages, followed by the terminal lipoate moiety (4a and 4b in Fig. 1). 4a and 4b with the terminal lipoate are capable of tagging with a gold nanoparticle to form the expected two AuNPs labeled N-methyl carbamates (ALC1 and ALC2). In our work, AChE is immobilized on the 11-mercaptoundecanoic acid (MUA) self-assembly monolayer through amide bond. When the solutions of ALC1 and ALC2 are allowed to flow over the AChE modified SPR sensor chip surface, SPR angles are intensively changed (Fig. 2), and the binding kinetic data as well as the detection sensitivity can be obtained simultaneously. With this in hand, it is possible to employ this platform for the competitive kinetic assay of any small molecular target-directed inhibitor in a high sensitivity.

## 2. Experimental

### 2.1. Reagents

Acetylcholinesterase (Type C3389, 500 U mg<sup>-1</sup> from electric eel), 11-mercaptoundecanoic acid, bovine serum albumin (BSA), 2,2'-(ethylenedioxy)bis(ethylamine) and 4,7,10-trioxo-1,13-tridecanediamine were purchased from Sigma–Aldrich (St. Louis, USA) and used as received. HAuCl<sub>4</sub>·4H<sub>2</sub>O (Au% > 48%) was obtained from TreeChem. Co. (Shanghai, China). N-Methyl carbamates with ether spacers of different lengths and the terminal lipoate moiety were synthesized in our lab (4a and 4b in Fig. 1). The synthetic steps are available in the [Supplementary data](#) part. Potassium ferrocyanide, potassium ferricyanide, phosphate buffer saline (PBS, pH 7.2), 1-hydroxybenzotriazole (HOBt), N,N'-dicyclohexylcarbodiimide (DCC), 1-ethyl-3-(3-dimethylaminopropyl) carbodiimide hydrochloride (EDC) and other reagents used were of analytical reagent grade. All aqueous solutions were prepared with deionized (DI) water, purified with a Milli-Q system (Millipore).

### 2.2. Apparatus

UV–vis absorption spectra of citrate-capped AuNPs and AuNPs labeled carbamate inhibitors (ALC1 and ALC2) were obtained on an ultraviolet–visible spectrophotometer (Hitachi UV 3310, Japan). The scan wavelength region was from 200 to 700 nm with the interval of

0.5 nm. Contact angles of water on the sensor chip surface at each modification step were measured with a semi-automatic contact angle meter (OCA20, Dataphysics, Germany)

The Autolab SPR system integrated with an electrochemical workstation: Autolab III/FRA (Echo Chemie B.V., The Netherlands) was used in this work. Briefly, the experimental setup was based on the Kretschmann optical configuration and used a monochromatic p-polarized laser ( $\lambda = 670$  nm) as the light resource. The laser light was directed through a hemicylindrical glass prism onto the gold film. The incidence angle ( $\theta_{\text{SPR}}$ ) was obtained by measuring the intensity of reflected light with a photodiode detector among a dynamic range of 4000 m° (4°). The sensor chip with a 50-nm thick gold layer and a 5-nm titanium sublayer as the adhesive layer on glass was attached to the prism using an index-matching oil ( $n_d^{25^\circ\text{C}} = 1.518$ ). Binding curves were acquired and processed with the associated software.

The cuvette in the Autolab SPR instrument contains a three-electrode system and allows for the simultaneous electrochemical measurement. The sensor chip, used as the working electrode (actually electrochemical working area is 2 mm in diameter), was placed on the prism with the index-matching oil and covered with the cuvette. A platinum electrode and a solid Ag/AgCl electrode were used as the counter electrode and the reference electrode, respectively. The electrochemical experiments were conducted with the Autolab III/FRA.

In order to eliminate any possible contamination, the sensor chip was cleaned by dipping into the Piranha (H<sub>2</sub>SO<sub>4</sub>/H<sub>2</sub>O<sub>2</sub>, 7:3, v/v) solution for 3 min, followed by the hydrogen plasma treatment (Harrick plasma cleaner, PDC-32G, USA). The sensor chip was washed with water and ethanol after each cleaning step and dried with a nitrogen stream.

### 2.3. Preparation of colloidal AuNPs and labeling to N-methyl carbamates

The colloidal AuNPs was prepared according to the chemical reduction method [23]. Briefly, 100 mL of 0.01% (w/v) HAuCl<sub>4</sub>·4H<sub>2</sub>O was brought to a boiling, and then 2.0 mL of 1% (w/v) aqueous trisodium citrate was added under vigorous stirring. The color changed to brick-red within a few minutes. The volume was adjusted to 10 mL with pure water, and the concentration of colloidal AuNPs was 480 mg/L. The dispersion was allowed to cool and filtered through a 0.2- $\mu\text{m}$  pore size nylon bottle-top filter system. After characterization with UV–vis spectroscopy, the aqueous solution was diluted into suitable concentrations for the labeling experiments.

N-Methyl carbamates (4a and 4b) were dissolved in ethanol in a proper concentration and slowly added dropwise with an additional funnel to the AuNPs solution at an optimized concentration 24 mg/L with vigorous magnetic stirring. After addition, the mixture solution was kept in a dark place at room temperature overnight, and then centrifuged at 1200 rpm for 10 min. The deposit was collected and re-suspended with PBS. After characterization with UV–vis spectroscopy, the solutions of AuNPs labeled N-methyl carbamates (briefly ALC1 for 4a and ALC2 for 4b, respectively) were ready for use.

### 2.4. Electrochemical characterization of the modification of SPR sensor chips

At each step for the modification of SPR sensor chip, the sensor chip was placed on the prism with the mach oil and covered with the cuvette. The cuvette was charged with a 0.1-M KCl solution containing 10 mM K<sub>4</sub>Fe(CN)<sub>6</sub> and 10 mM K<sub>3</sub>Fe(CN)<sub>6</sub>. Voltammograms were recorded by the voltage sweep between -0.2 and +0.6 V with a sweep rate 0.1 V/s. The impedance spectra were recorded from



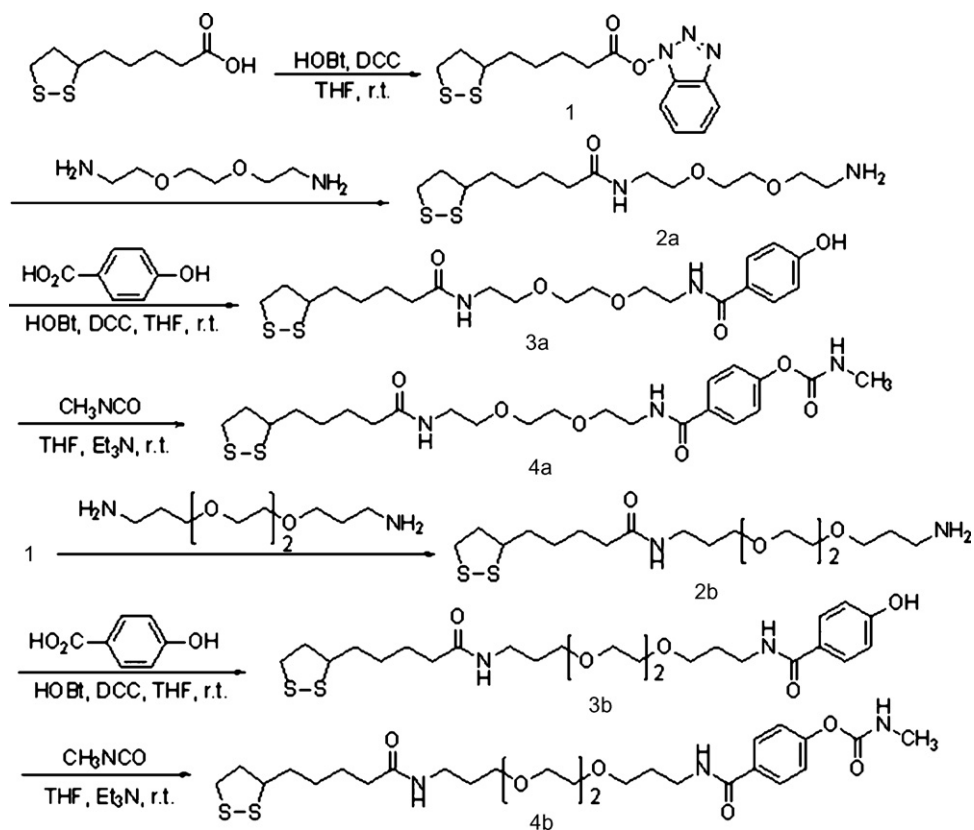


Fig. 1. The synthetic route of N-methyl carbamates with ether spacers of different lengths and the terminal lipioate moiety (4a and 4b).

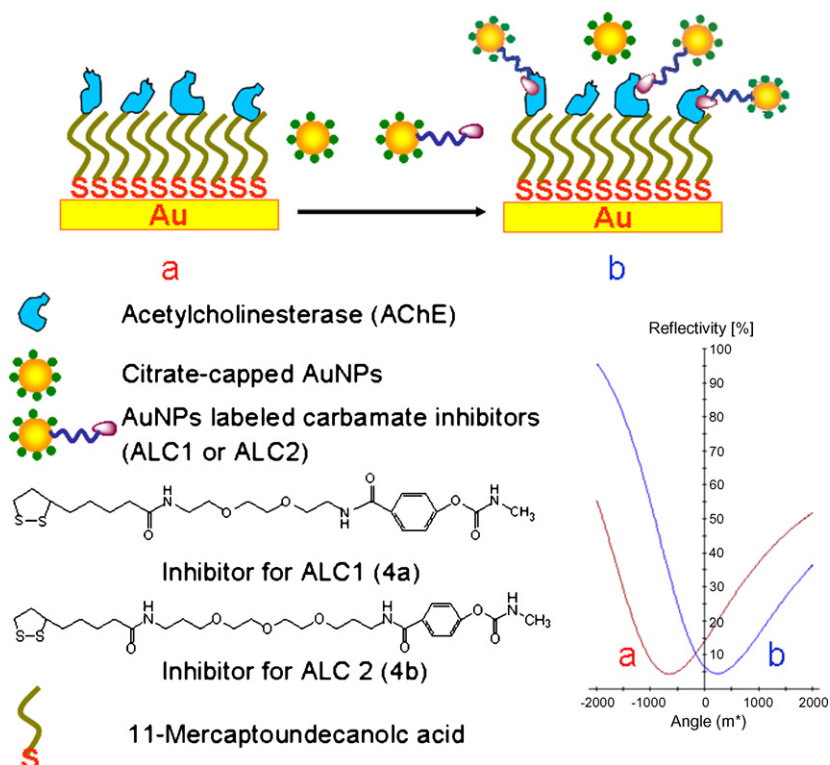


Fig. 2. Schematic illustration of the SPR biosensor based on AuNPs signal enhancement.

100 kHz down to 100 MHz frequency, with the AC amplitude of 5 mV.

### 2.5. Real-time monitoring the preparation of the AChE modified sensor chip and its interaction with AuNPs labeled carbamate with SPR

The cleaned sensor chip was immersed in the 1 mM MUA solution overnight at room temperature. The MUA modified sensor chip was rinsed with ethanol and water for the removal of the residual MUA molecules, followed by drying with a nitrogen stream. Then the sensor chip was mounted on the SPR prism with the matching oil and covered with the cuvette. 50  $\mu$ L of the mixture of 200 mM EDC and 50 mM NHS in PBS was injected into the cuvette for 10 min to activate the terminal carboxyl group of MUA. Afterward, 50  $\mu$ L of 0.004 mg/mL AChE in pH 7.2 PBS was injected onto the activated MUA self-assemble layer to reach an AChE loading response of 120 m°. The remaining active sites on the AChE/MUA sensor chip surface were blocked by injection of 50  $\mu$ L of 1.0 M ethanolamine in PBS (pH 8.5) for 10 min. All the mentioned procedures were followed by rinsing with PBS solution.

To investigate the interaction of modified AChE on sensor chip with ALC1 or ALC2 in solution, 50  $\mu$ L of the corresponding PBS solution of ALC1 or ALC2 with a proper concentration was injected in the cuvette, and the solution was kept in contact with the AChE immobilized sensor chip for association for 10 min. Then the solution was drained out with a peristaltic pump and a 50- $\mu$ L PBS solution was injected for the dissociation measurement. These procedures were controlled with a self-edited semi-automatic program sequence, and the association and dissociation curves were acquired and processed with the associated software.

## 3. Results and discussion

### 3.1. UV–vis characterization of colloid AuNPs and labeling to N-methyl carbamates (4a and 4b)

The reduction of chloroauric acid with citrate salt in aqueous solution is a conventional method for the preparation of colloid

AuNPs with definite particle shapes and sizes. In this respect, the reduction was conducted at a 1:3 chloroauric/citrate molar ratio, colloid AuNPs with the mean diameter of 15 nm in suspension was obtained, and exhibited a surface plasmon absorption maximum at 520 nm, which was similar to other reports [24,25]. Fig. 3a shows the typical maximum absorption of the colloid AuNPs with citrate shell, corresponding to the mean diameter 15 nm. The colloid AuNPs solution was diluted to 24 mg/L with PBS buffer and the final molar particle concentration was estimated to be ca 1.2 nM, based on the AuNP diameter 15 nm.

AuNPs with citrate shell is very stable and can be used for derivatization with various alkylthiol derivatives by the ligand exchange [26]. Herein, the citrate-capped AuNPs was further functionalized by the carbamate 4a and 4b with the citrate–carbamate exchange to form the expected ALC1 and ALC2. A ligand exchange reaction using AuNPs:carbamate in 1:1 molar ratio was employed to achieve monovalent ALC1 and ALC2. The suspensions of ALC1 and ALC2 in PBS buffer were found stable enough and showed a similar surface plasmon absorption maximum centered at 520 nm (for example, Fig. 3b for ALC1), indicating that the functionalized AuNPs retained its own physicochemical properties without aggregation. The peak at around 288 nm is the instinctive absorption of the corresponding carbamate group in 4a (Fig. 3c).

### 3.2. Characterization of modified SPR sensor chips with contact angle measurements and electrochemistry

Immobilization of enzymes through the covalent attachment to the terminal carboxyl group of an alkylthiolate self-assembled monolayer (SAM) on naked gold films is a general procedure for the construction of a SPR sensor chip. The step-by-step construction can be monitored with various analytic techniques including the contact angle measurement, cyclic voltammetry and impedance. The stepwise construction stages are associated with changes in hydrophobic/hydrophilic nature of the surface as well as the different electrochemical barriers. In this study, the average contact angle values were 70° for bare gold disk, 48° for MUA/Au and 38° for AChE/MUA/Au, indicating the formation of MUA SAM with the terminal hydrophilic carboxyl groups, and the subsequent highly hydrophilic feature of AChE protein on the sensor chip surface.

Cyclic voltammetry is a versatile technique for monitoring the construction of enzyme biosensor and for investigating the interaction between the enzyme and its binding partner with the utility of  $[\text{Fe}(\text{CN})_6]^{3-/4-}$  redox probe [27]. As shown in Fig. 4, the formation of the MUA SAM (Fig. 4b) on the sensor chip brings about a substantial decrease in the electrochemical reactivity for the probe molecules, comparing with that of the bare gold electrode (Fig. 4a). This obvious electrochemical blocking effect comes from the negatively charged surface of MUA modified electrode in buffer solution at pH 7.2, which retards the approach of the same negatively charged  $[\text{Fe}(\text{CN})_6]^{3-/4-}$  to the surface and hence the electron exchange with the electrode. The almost total block of the electron transfer between ferricyanide and the electrode indicates a dense package of MUA monolayer on the gold electrode.

After the immobilization of AChE, however, the voltammetric response (Fig. 4c) of AChE/MUA/Au displays an obvious increase, comparing with that of MUA/Au (Fig. 4b). This is probably attributed to the presence of AChE on the MUA interface, which lowers the surface negative charge density of the MUA monolayer and allows the negative charged ferricyanide easier to penetrate the AChE/MUA/Au interface and then access the electrode surface for the occurrence of the electrode reaction [28]. Further binding of the AuNPs labeled N-methyl carbamate (ALC1 or ALC2) to the immobilized AChE leads the formation of the ALC/AChE/MUA/Au interface, which shows a still increase in current response for ALC1 (Fig. 4d) and ALC2 (Fig. 4e), comparing to that of AChE/MUA–Au (Fig. 4c). The still

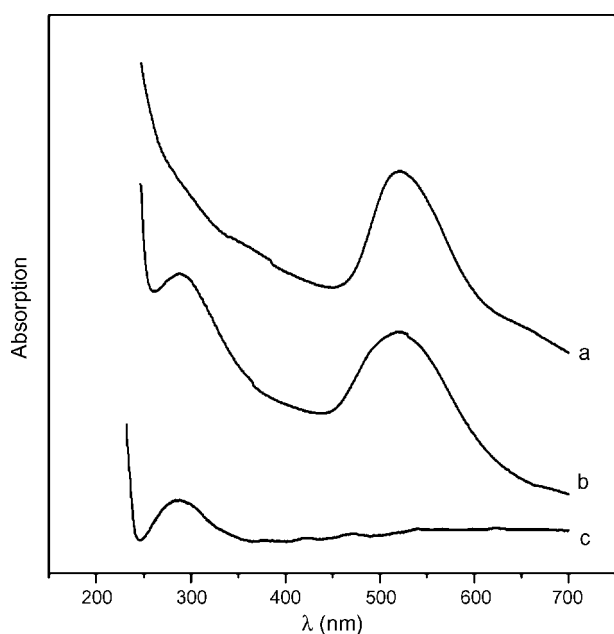
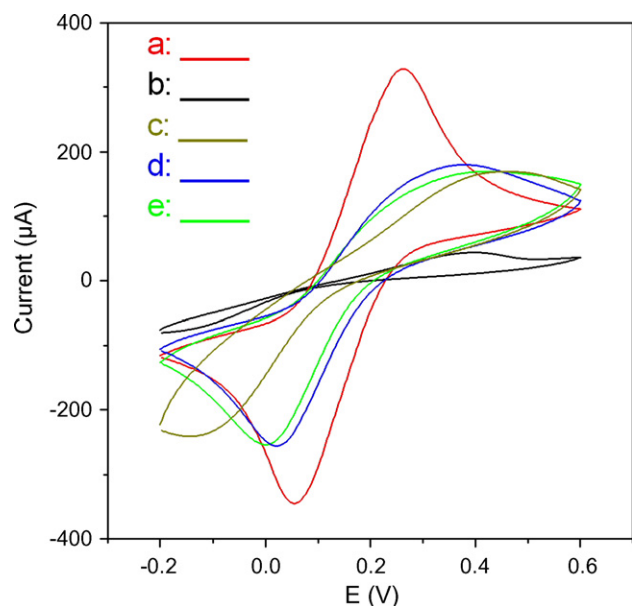


Fig. 3. The UV–vis spectra of 24 mg/L AuNPs (a), ALC 1 (24 mg/L AuNPs) (b) and N-methyl carbamates 4a (c).



**Fig. 4.** Cyclic voltammograms of bare Au (a), MUA/Au (b), AChE/MUA/Au (c), ALC1/AChE/MUA/Au (d) and ALC2/AChE/MUA/Au (e) in 10 mM  $[\text{Fe}(\text{CN})_6]^{3-/4-}$ .

decrease in the redox barrier for ferricyanide may be attributed to the conductive effect of AuNPs resided on the surface [29]. This also demonstrates the firm adsorption resulted from the specific interaction between AChE and the ALC1 or ALC2, because AuNPs with the citrate shell alone cannot produce this pronounced conductive increase in the electrode reaction.

The stepwise assembly of the SPR biosensor and further binding of ALC1 or ALC2 were also confirmed by impedance spectroscopy. Fig. 5 shows the Nyquist plots of the electrochemical impedance spectra for the stepwise assembly stages on sensor chip surface. The charge-transfer resistance ( $R_{ct}$ ) changes in the following order: naked Au film ( $253 \Omega$ ) < ALC1/AChE/MUA-Au ( $655 \Omega$ ) < ALC2/AChE/MUA-Au ( $854 \Omega$ ) < AChE/MUA-Au ( $1154 \Omega$ ) < MUA-Au ( $10870 \Omega$ ), which is well consistent with the results of cyclic voltammetry, indicative of the different conductivity for the redox probe ferricyanide. The slight difference

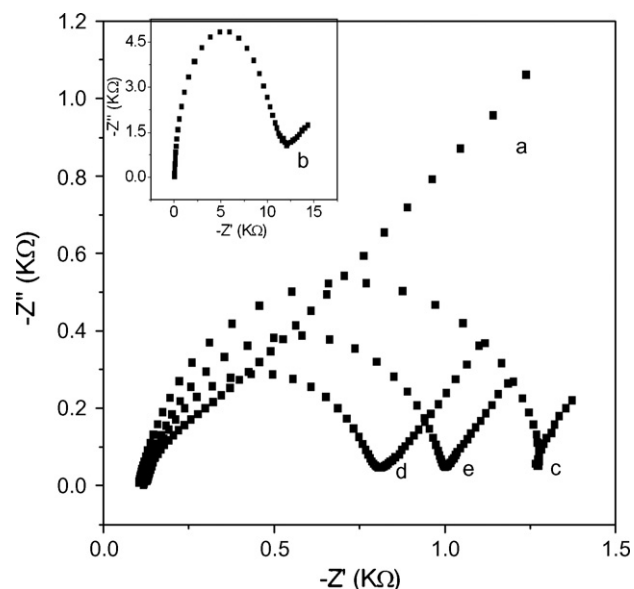


**Fig. 5.** Complex plane impedance plots of bare Au (a), MUA/Au (b), AChE/MUA/Au (c), ALC1/AChE/MUA/Au (d) and ALC2/AChE/MUA/Au (e) in 10 mM  $[\text{Fe}(\text{CN})_6]^{3-/4-}$ .

in  $R_{ct}$  between ALC1 and ALC2 is probably attributed to the different chain lengths of the molecules between the lipoate and the N-methyl carbamate moiety.

### 3.3. SPR evaluation of interaction between AChE and AuNPs labeled carbamates

In a competitive kinetic assay with the SPR technology, a one-to-one binding model for the known binder to its target is a prerequisite for the simplified kinetic analysis. The utility of AuNPs tagged small molecules as a competitive binder implies that each AuNPs should be functionalized with just one small molecule, i.e., a monovalent binder. In this regard, ALC1 or ALC2 was obtained by the citrate-carbamate exchange of AuNPs at a fixed concentration 24 mg/L (1.2 nM) with 4a or 4b at varying concentrations from 0.2 to 1.2 nM. The up limit 1.2 nM of 4a or 4b was chosen to avoid the formation of multivalent ALCs and simplify the kinetic assay of its binding to the immobilized AChE [30]. The choice of the fixed AuNPs concentration 24 mg/L was obtained by the following optimization: AuNPs at varying concentrations from 4.8 to 48 mg/L was functionalized with 4a at a fixed concentration 0.6 nM and its binding to the immobilized AChE was monitored by SPR. A maximum SPR response was obtained for the carbamates functionalized AuNPs at 24 mg/L.

Nonspecific adsorption of AuNPs onto proteins has been considered as a crucial factor for achieving its applications in many fields [31]. In our case, the AuNPs with the citrate shell and the ALC1 or ALC2 with the above mentioned optimization did not show a significant nonspecific adsorption on the protein BSA modified surface at the PBS buffer pH 7.2, which was clearly demonstrated by the SPR measurement.

For the kinetic assays of 4a and 4b binding to the immobilized AChE, the solutions with different concentrations of 4a or 4b that labeled with a fixed concentration of 24 mg/L AuNPs, which were injected on AChE modified SPR chip surface for 10 min. The SPR angle shifts for ALC1 are 21, 83, 112 and 180  $m^\circ$  at varying concentrations of 4a from 0, 0.1, 0.2 and 0.6 nM (Fig. 6b–e). It is worthy mentioning that 0.6 nM of 4a without AuNPs labeling did not cause a perceptible SPR angle shift (Fig. 6a). The SPR angle shift 21  $m^\circ$  (Fig. 6b) for AuNPs without 4a can be attributed to two facets: (1) the existence of nonspecific absorption of AuNPs to the immobi-

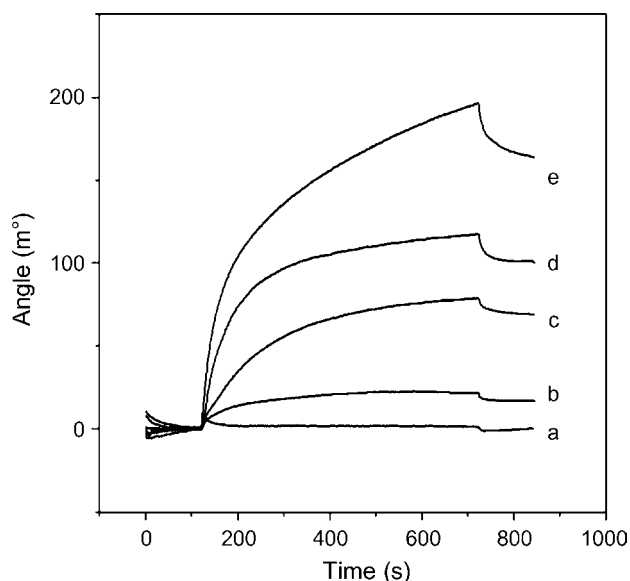


**Fig. 6.** SPR sensorgrams of ALC1 binding to AChE: 0.6 nM 4a without AuNPs (a); 0, 0.1, 0.2 and 0.6 nM 4a with 24 mg/L AuNPs (b–e).

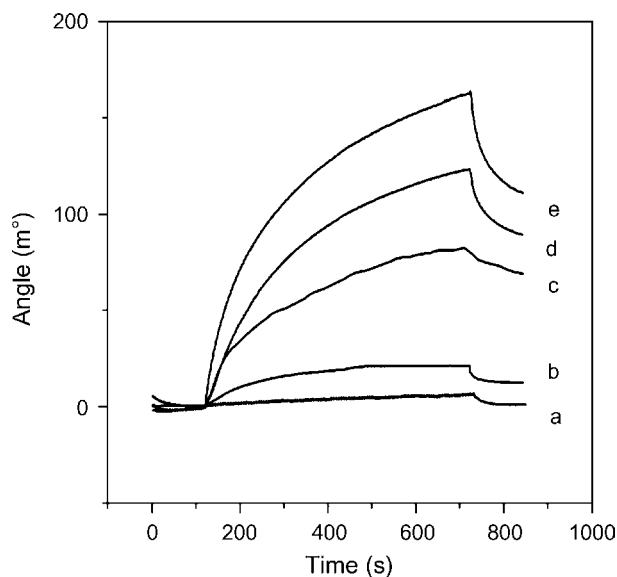


**Fig. 7.** SPR sensorgrams of ALC2 with AChE: 0.6 nM 4b without AuNPs (a); 0, 0.1, 0.2 and 0.6 nM 4b with 24 mg/L AuNPs (b–e).

lized AChE protein [32]; (2) the existence of AuNPs in the solution near to the sensor chip surface, and hence the coupling of the localized surface plasmon of AuNPs with the propagating plasmon on the SPR gold surface [20]. Thus with the AuNPs labeling, the suspension of 0.6 nM 4a (molecular weight 513 Da) resulted in a SPR angle shift 180 m°. A similar binding pattern for the suspensions with 4b various concentrations (0, 0.1, 0.2 and 0.6 nM) was also obtained (Fig. 7b–e), and the suspension with 0.6 nM 4b (585 Da) resulted in a SPR angle shift 144 m°. These angle shift values were obtained by subtracting the angle shift of AuNPs without 4a or 4b. By fitting the binding curves in Figs. 6 and 7 with a 1:1 binding model, the association constants ( $k_a$ ) of 4a and 4b are found to be  $1.46 \times 10^5$  (MS) $^{-1}$  and  $7.73 \times 10^4$  (MS) $^{-1}$ , and their dissociation constants ( $k_d$ ) to be  $4.66 \times 10^{-2}$  and  $1.21 \times 10^{-1}$  s $^{-1}$ , respectively. Thus the affinity constants ( $K_A$ ) of 4a and 4b are estimated to be  $3.13 \times 10^6$  and  $6.39 \times 10^5$  M $^{-1}$ , respectively.

Insecticide carbamates inhibit AChE by binding to the serine residue in the active site, with the inhibition proceeds of the formation of a reversible Michaelis complex followed by the irreversible acylation of the serine residue [33]. The dissociation constants  $K_D$  values, obtained by the spectroscopic measurement of the hydrolytic rate of the substrate p-nitrophenyl acetate, were located around  $10^{-6}$ – $10^{-7}$  M $^{-1}$  for different carbamates [34], corresponding to affinity constants around  $10^5$ – $10^7$  M $^{-1}$ . The affinity data of 4a and 4b are located in this region. On the other hand, the in vivo insecticidal activity test showed that 4a possessed a stronger insecticidal potency against *Rhopalosiphum pseudobrassicae* than 4b, coinciding with the affinity constants of 4a and 4b obtained in our SPR analysis.

#### 3.4. SPR determination of inhibitors concentrations using AuNPs for signal enhancement

The highly sensitive SPR kinetic assay employing the AuNPs labeling leads us to achieve a quantitative detection of N-methyl carbamates with the lipoate moiety, by using various concentrations of 4a and 4b, labeled with a fixed amount of AuNPs, such as 24 mg/L. Interestingly, different maximum SPR angle shifts can be obtained. Fig. 8 shows the linear plot of maximum SPR angular shifts versus the concentrations of N-methyl carbamate 4a and 4b. The linearity range for 4a is 0.01–1.0 nM with a sensitivity of 176 m°/nM (Fig. 8a), whereas for 4b the linearity region is located

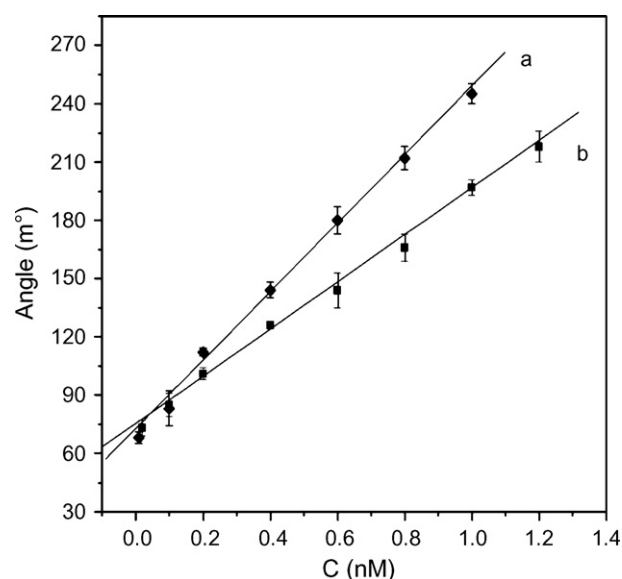


**Fig. 8.** AChE-based SPR detection of different concentrated N-methyl carbamates 4a (a) and 4b (b) with 24 mg/L AuNPs labeling.

in the range from 0.02 to 1.2 nM with a sensitivity of 121 m°/nM (Fig. 8b). The detection limits of 4a and b are estimated to be 7.0 and 12 pM respectively at a signal-to-noise ratio of 3. Comparing with other types of AChE biosensors for the AChE inhibitor analysis, this AuNPs labeling method is more sensitive and has a much lower detection limit [35,36].

#### 4. Conclusions and prospect

The increasing applications of gold nanoparticles have been seen in the conventional SPR analysis for highly sensitive detection of small molecules through the antigen–antibody technique. Tagging of gold nanoparticles to small molecules as the large binders for achieving a sensitive SPR kinetic assay in the direct or competitive format may have an important application for the hit or lead identification in pesticide and drug discovery. This methodology will circumvent the limit of detection (LOD) in the conventional and direct SPR kinetic assay, and be easy to build a desired competitive binder with an enhanced SPR response.

We have shown the strategy for the utilization of AuNPs labeled small molecules for the direct kinetic analysis with the SPR. The strategy is certainly able to circumvent the LOD drawback in a conventional SPR measurement in some special cases. More importantly, if this strategy were used in the surface competitive kinetic assay [15], two advantages would be obvious: (1) easy building of a desired AuNP labeled small molecule as the large competitive binder; (2) convenient SPR kinetic assay with a great signal enhancement through the combination of the increased binder mass and the coupling of the localized surface plasmon of AuNPs with the propagating plasmon on the SPR gold surface [20].

Nevertheless, there are several key factors that should be considered carefully for the application of the AuNP labeling strategy in the direct kinetic assay or in the indirect surface competitive kinetic assay. These factors include the AuNPs stability, monovalent functionalization method, nonspecific adsorption to proteins, as well as experimental parameter optimization in the SPR assay. Recently, the issue concerning the nonspecific interaction of AuNPs has attracted a great attention. Poly(ethylene glycol) (PEG) monolayer protected nanoparticles for eliminating nonspecific binding with biological molecules and the multivalent functionalization of AuNPs for targeted drug delivery are more attractive [37]. Appli-

cation of SPR in surface competitive kinetic assay involving PEG stabilized AuNPs with the monovalent functionalization of small molecules is underway in our laboratory.

### Acknowledgements

The authors are grateful for the financial support from the National Basic Research Program of China (Grant No. 2007CB116302) and the National Natural Science Foundation of China (Grant Nos. 20672043, 20672044, 20705010).

### Appendix A. Supplementary data

Supplementary data associated with this article can be found, in the online version, at doi:10.1016/j.talanta.2009.01.018.

### References

- [1] A.W. Wark, H.J. Lee, A.J. Qavi, R.M. Corn, *Anal. Chem.* 79 (2007) 6697.
- [2] F. Wang, J. Wang, X. Liu, S. Dong, *Talanta* 77 (2008) 628.
- [3] R. Arnell, N. Ferraz, T. Fornstedt, *Anal. Chem.* 78 (2006) 1682.
- [4] R. Karlsson, *J. Mol. Recognit.* 17 (2004) 151.
- [5] J. Homola, *Chem. Rev.* 108 (2008) 462.
- [6] C.D. Primo, I. Lebars, *Anal. Biochem.* 368 (2007) 148.
- [7] D.G. Myszka, *J. Mol. Recognit.* 12 (1999) 279.
- [8] D.G. Myszka, *Anal. Biochem.* 329 (2004) 316.
- [9] R.L. Rich, D.G. Myszka, *Drug Discov. Today: Technol.* 1 (2004) 301.
- [10] M.W. Walter, *Nat. Prod. Rep.* 19 (2002) 278.
- [11] K. Tietjen, M. Drewes, K. Stenze, *Comb. Chem. High Throughput Screen.* 8 (2005) 589.
- [12] S.M. Ridley, A.C. Elliott, M. Yeung, D. Youle, *Pestic. Sci.* 54 (1998) 327.
- [13] P. Taylor, *J. Biol. Chem.* 266 (1991) 4025.
- [14] H. Nordin, M. Jungnelius, R. Karlsson, O.P. Karlsson, *Anal. Biochem.* 340 (2005) 359.
- [15] R. Karlsson, M. Kullman-Magnusson, M.D. Hämäläinen, A. Remaeus, K. Andersson, P. Borg, E. Gyzander, J. Deinum, *Anal. Biochem.* 278 (2000) 1.
- [16] R. Karlsson, *Anal. Biochem.* 221 (1994) 142.
- [17] E. Fu, S.A. Ramsey, P. Yager, *Anal. Chim. Acta* 599 (2007) 118.
- [18] X. Liu, Y. Sun, D. Song, Q. Zhang, Y. Tian, H. Zhang, *Talanta* 68 (2006) 1026.
- [19] S. Takae, Y. Akiyama, Y. Yamasaki, Y. Nagasaki, K. Kataoka, *Bioconjug. Chem.* 18 (2007) 1241.
- [20] L.A. Lyon, M.D. Musick, P.C. Smith, B.D. Reiss, D.J. Pena, M.J. Natan, *Sens. Actuat. B: Chem.* 54 (1999) 118.
- [21] T.R. Fukuto, *Environ. Health Perspect.* 87 (1990) 245.
- [22] J.P. Colletier, B. Sanson, F. Nachon, E. Gabellieri, C. Fattorusso, G. Campiani, M. Weik, *J. Am. Chem. Soc.* 128 (2006) 4526.
- [23] E. Hutter, M.P. Pileni, *J. Phys. Chem. B* 107 (2003) 6497.
- [24] S. Link, M.A. El-Sayed, *J. Phys. Chem. B* 103 (1999) 8410.
- [25] W. Dungchai, W. Siangproh, W. Chaicumpa, P. Tongtawe, O. Chailapakul, *Talanta* 77 (2008) 727.
- [26] C. Mangeney, F. Ferrage, I. Aujard, V. Marchi-Artzner, L. Jullien, O. Ouari, D. El, A. Rékaï, I. Laschewsky, J.W. Vikholm, J. Sadowski, *Am. Chem. Soc.* 124 (2002) 5811.
- [27] E. Katz, I. Willner, *Electroanalysis* 15 (2003) 913.
- [28] S. Liu, K. Wang, D. Du, Y. Sun, L. He, *Biomacromolecules* 8 (2007) 2142.
- [29] L. Su, L. Mao, *Talanta* 70 (2006) 68.
- [30] W.S. Hlavacek, R.G. Posner, A.S. Perelson, *Biophys. J.* 76 (1999) 3031.
- [31] K. Aslan, C.C. Luhrs, V.H. Pérez-Luna, *J. Phys. Chem. B* 108 (2004) 15631.
- [32] S.H. Brewer, W.R. Glomm, M.C. Johnson, M.K. Knag, S. Franzen, *Langmuir* 21 (2005) 9303.
- [33] A. Forsberg, G. Puu, *Eur. J. Biochem.* 140 (1984) 153.
- [34] P.J. Gray, R.M. Dawson, *Toxicol. Appl. Pharmacol.* 91 (1987) 140.
- [35] R.P. Deo, J. Wang, I. Block, A. Mulchandani, K. Joshi, M. Trojanowicz, F. Scholz, W. Chen, Y. Lin, *Anal. Chim. Acta* 530 (2005) 185.
- [36] F. Arduini, F. Ricci, C.S. Tuta, D. Moscone, A. Amineb, G. Palleschi, *Anal. Chim. Acta* 580 (2006) 155.
- [37] J.M. Bergen, H.A. Recum, T.T. Goodman, A.P. Massey, S.H. Pun, *Macromol. Biosci.* 6 (2006) 506.



## Neutral persulfate digestion at sub-boiling temperature in an oven for total dissolved phosphorus determination in natural waters

Xiao-Lan Huang<sup>a,b,\*</sup>, Jia-Zhong Zhang<sup>a</sup>

<sup>a</sup> Ocean Chemistry Division, Atlantic Oceanographic and Meteorological Laboratory, National Oceanic and Atmospheric Administration, Miami, FL 33149, USA

<sup>b</sup> CIMAS, Rosenstiel School of Marine and Atmospheric Science, University of Miami, Miami, FL 33149, USA

### ARTICLE INFO

#### Article history:

Received 17 November 2008

Received in revised form 14 January 2009

Accepted 15 January 2009

Available online 24 January 2009

#### Keywords:

Total dissolved phosphorus

Digestion

Molar absorptivity

Persulfate oxidation

pH

Sample matrix

Spectrophotometry

### ABSTRACT

A simplified, easily performed persulfate digestion method has been developed to process a large number of water samples for routine determination of total dissolved phosphorus. A neutral potassium persulfate solution (5%, w/v, pH ~6.5) is added to the samples (at 10 mg potassium persulfate per mL of sample), which are then digested at 90 °C in an oven for 16 h. This method does not require pH adjustment after digestion because neither an acid nor a base is added to the samples prior to digestion. The full color of phosphoantimonymolybdenum blue from the digested samples develops within 8 min. Compared with the autoclave method, digestion at sub-boiling temperatures in an oven is safer, and a large number of samples can be heated overnight requiring no constant monitoring. The apparent molar absorptivity ( $\epsilon$ ) of nine organic phosphorus compounds and two condensed inorganic phosphates ranged from  $1.17 \times 10^4$  to  $1.82 \times 10^4 \text{ L mol}^{-1} \text{ cm}^{-1}$  in both distilled water and artificial seawater matrixes. The average recovery of these phosphorus compounds was  $94 \pm 11\%$  for the DIW matrix and  $90 \pm 12\%$  for the ASW matrix. No significant difference in molar absorptivity was observed between the undigested and digested phosphate, especially in the seawater matrix. It is, therefore, suggested that a phosphate solution be directly employed without digestion as the calibration standard for routine determination of total dissolved phosphorus. This method was used to study the spatial distribution of total dissolved phosphorus in the surface waters of Florida Bay.

© 2009 Elsevier B.V. All rights reserved.

### 1. Introduction

Phosphorus is an essential nutrient for life on earth and occurs in soil, sediment, water, and organisms. An excess of phosphorus, however, can cause eutrophication of natural waters, which has become a worldwide environmental problem [1,2]. While orthophosphate (IP), the most frequently measured form of phosphorus, is considered to be the only form directly available and rapidly assimilated by bacteria, algae [1], and plants [2,3], the role of organic phosphorus in different ecosystems is still the subject of intensive study [4–8]. This is partly due to a lack of reliable organic phosphorus data because of the complex procedures involved in determining total dissolved phosphorus from which dissolved organic phosphorus is calculated by difference [5,9,10].

Although Inductively Coupled Plasma Optical Emission Spectroscopy (ICP-OES) has been used to directly determine total dissolved phosphorus in soil extracts and runoff water [11–13],

its sensitivity is not suitable for measuring low levels of total dissolved phosphorus in natural waters. Currently, spectrophotometry is the most common method used for determining total dissolved phosphorus, which requires organic phosphorus to be broken down to dissolved phosphate through digestion [14,15]. Several methods, including fusion, dry ashing, and boiling samples in perchloric, sulfuric or nitric acid on a hot plate, have been employed to digest samples for total dissolved phosphorus determination. More recently, autoclaving, ultraviolet (UV) photo-oxidation, and microwave heating have been widely used [15]. However, there are many uncertainties in measuring total dissolved phosphorus [9,10,14–17]. Laboratory performance studies conducted by the Quality Assurance of Information for Marine Environmental Monitoring in Europe (QUASIMEME) project (nutrient section) found that more than half of the laboratories that participated in an inter-comparison study on total dissolved phosphorus could not produce consistent results. It was thus concluded that total dissolved phosphorus was the most problematic parameter in routine water quality monitoring programs [18].

One of the most common and simplest methods to break down organic phosphorus for total phosphorus determination is the autoclave persulfate oxidation technique. This technique was recommended as the standard method for examination of water and

\* Corresponding author at: CIMAS, Rosenstiel School of Marine and Atmospheric Science, University of Miami, Miami, FL 33149, USA. Tel.: +1 305 361 4551; fax: +1 305 361 4447.

E-mail address: [xiaolan.huang@ymail.com](mailto:xiaolan.huang@ymail.com) (X.-L. Huang).

wastewater by the Water Environment Federation (Method 4500-P) [19] and the Environmental Protection Agency (Method 365) [20]. In the original method developed by Menzel and Corwin, samples were autoclaved at 98–137 kPa for 30–40 min [21]. Persulfate digestion in both acidic [22–24] and alkaline matrixes has been used [25–27] for natural water samples. However, various problems have been reported related to the measurement of released phosphate by the molybdenum blue colorimetric method, especially for automated analysis in acidic persulfate digested samples [24,28,29]. Recently, we have found that the intermediate products of persulfate oxidation caused the rate of phosphoantimonymolybdenum blue complex formation to decline in acidic persulfate digested samples, necessitating a pH adjustment to near neutral for both the digested calibration standards and water samples before adding the color reagent [16].

The objective of this study was to explore the feasibility of performing persulfate digestion in a neutral pH medium at 90 °C overnight in an oven. A neutral pH medium was used for digestion to eliminate the tedious process of adjusting the sample pH to neutral after acidic digestion. The use of sub-boiling temperatures for digestion also minimized sample loss due to boiling. Persulfate concentration and digestion time were optimized for the method. Eleven model phosphorus compounds in deionized water and seawater matrixes were digested to estimate the recovery of this method for different phosphorus compounds. The method was used to determine total dissolved phosphorus concentrations in Florida Bay waters.

## 2. Experimental

### 2.1. Apparatus

A Hewlett Packard 8453 UV–visible spectrophotometer with ChemStation software and a high sensitivity gas-segmented continuous flow analyzer were employed in this study [30]. All absorbances were measured at room temperature ( $25 \pm 2$  °C).

### 2.2. Reagents and standards

Deionized water (DIW) used for preparing standards and reagents was first purified by a distilling unit, followed by a Millipore Super-Q Plus Water System that produces water with 18 M $\Omega$  resistance. All samples and reagents were stored in polypropylene bottles which had immersed in a 10% HCl solution overnight, followed by rinsing three times with DIW and then drying at 60 °C in an oven for 5–10 h prior to use. Artificial seawater (ASW) was made following the procedure of Kester et al. [31].

All chemicals used were of analytical grade reagents. Potassium dihydrogen phosphate (KH<sub>2</sub>PO<sub>4</sub>, Aldrich, AR) was used to prepare the stock phosphate (IP) standard solution (1.0 mM), which was stored in a polyethylene bottle at 4 °C in a refrigerator. Working standard solutions were prepared daily from a serial dilution of the

stock solution with DIW. A 5% potassium persulfate solution (20 g potassium persulfate (K<sub>2</sub>S<sub>2</sub>O<sub>8</sub>, Aldrich, AR) in 400 mL of DIW, pH ~6.5) was stored in a brown polyethylene bottle at room temperature. This stock persulfate solution was used within a month.

Determination of released phosphate after digestion was based on the modified method of Murphy and Riley [32] in which the final pH<sub>T</sub> of the sample plus reagent mixture solution was 1.0 (H/Mo = 70) [33]. Two reagents were prepared for phosphate determination. An ammonium molybdate reagent was prepared by mixing 2.4 g of ammonium molybdate ((NH<sub>4</sub>)<sub>6</sub>Mo<sub>7</sub>O<sub>24</sub>·4H<sub>2</sub>O, Merck, GR), 25 mL of concentrated sulfuric acid (H<sub>2</sub>SO<sub>4</sub>, 96–98%, L.T. Baker), and 50 mL of 0.3% antimony potassium tartrate (K(SbO)<sub>4</sub>H<sub>4</sub>O<sub>6</sub>)<sub>2</sub>·H<sub>2</sub>O, Fisher) solution and diluting the mixture to 1 L with DIW. An ascorbic acid solution was prepared daily by dissolving 1 g of ascorbic acid (C<sub>6</sub>H<sub>8</sub>O<sub>6</sub>, Aldrich, AR) in 100 mL of DIW. These two reagents were mixed together in a 1 to 1 (V/V) ratio to form a mixed color reagent.

The recovery of two condensed inorganic phosphate and nine organic phosphorus compounds was examined in the DIW and ASW mediums. The organic phosphorus compounds included phosphate esters (compounds with a C–O–P bond), phosphonates (compounds with a C–P bond), and organic condensed phosphates (compounds with a C–O–P–O–P bond). All of the organic phosphorus compounds were stored in a freezer, as recommended by manufacturers. Details about these phosphorus chemicals are listed in Table 1. A 10 mM phosphorus stock solution was prepared using DIW for each model compound and stored in a polyethylene bottle at 4 °C in a refrigerator. These solutions were used within a week. The lower working concentration solutions for these model phosphorus compounds using the DIW and ASW mediums were prepared daily.

A 10 mL water sample was transferred to an acid-washed 30-mL Teflon (Savillex®) screw-cup vials. A 2 mL of the persulfate solution was added to each sample and mixed. The caps were placed firmly to the Teflon vials and then the vials were placed in an oven. The oven temperature was set at 90 °C for sample digestion. After digestion, a 3 mL of the mixed color reagent was added directly to the cooled 12 mL digested solution (without neutralization), and the color fully developed within 8 min. Its absorbance was then measured at 890 nm by a spectrophotometer with a 5 cm cell.

The amount of persulfate initially varied from 25 to 200 mg for optimization. A set of 5  $\mu$ M P solutions of 2-AEP,  $\beta$ -GLP, ADP, and ATP and 10  $\mu$ M of  $\beta$ -GLP in the DIW matrix were used for this experiment. Four model compounds (2-AEP,  $\beta$ -GLP, ADP, and ATP) in the DIW medium were used to optimize digestion time. The concentration of phosphorus was 5  $\mu$ M, and 100 mg of potassium persulfate was used. The digestion times varied from 1, 2, 4, 8, 16, 24, 40, 48, and 60 h, with two replications at 8–48 h and three replications at 60 h.

The apparent molar absorptivity ( $\epsilon$ ) and recovery of individual organic phosphorus compounds after digestion was measured using a range of phosphorus concentrations (0, 0.5, 1, 2.5, 5, 7.5, and 10  $\mu$ M) in both the DIW and ASW matrixes. The statistical significance of apparent molar absorptivity between different

**Table 1**  
Characteristics of model organic and inorganic phosphorus compounds used in this study.

Name	Abbr	Formula	Manufacturer	MW	nP	Purity (%)
2-Aminoethylphosphonic acid	2-AEP	C <sub>2</sub> H <sub>8</sub> NO <sub>3</sub> P	Aldrich	125.07	1	99
1-Aminoethylphosphonic acid	1-AEP	C <sub>2</sub> H <sub>8</sub> NO <sub>3</sub> P	Aldrich	125.07	1	99
Phosphonoformic acid trisodium salt hexahydrate	PFA	CH <sub>12</sub> Na <sub>3</sub> O <sub>11</sub> P	Aldrich	300.4	1	99
D-Glycose-6-phosphate sodium salt	G6P	C <sub>6</sub> H <sub>12</sub> NaO <sub>9</sub> P	Sigma	282.12	1	99
Glycerol-2-phosphate disodium salt hydrate	$\beta$ -GLP	C <sub>3</sub> H <sub>7</sub> Na <sub>2</sub> O <sub>6</sub> P·xH <sub>2</sub> O	Sigma	216.04	1	99
Adenosine triphosphate	ATP	C <sub>10</sub> H <sub>14</sub> N <sub>5</sub> Na <sub>2</sub> O <sub>13</sub> P <sub>3</sub> ·xH <sub>2</sub> O	Aldrich	551.2	3	99
Adenosine diphosphate	ADP	C <sub>10</sub> H <sub>14</sub> KN <sub>5</sub> O <sub>10</sub> P <sub>2</sub> ·2H <sub>2</sub> O	Sigma	501.3	2	95
Adenosine monophosphate	AMP	C <sub>10</sub> H <sub>14</sub> N <sub>5</sub> O <sub>7</sub> P·xH <sub>2</sub> O	Fluka	391.18	1	99
Phytic acid dipotassium	IP6	C <sub>6</sub> H <sub>16</sub> K <sub>2</sub> O <sub>24</sub> P <sub>6</sub>	Sigma	736.2	6	95
Sodium Tripolyphosphate	Poly-P	Na <sub>5</sub> P <sub>3</sub> O <sub>10</sub> ·6H <sub>2</sub> O	Sigma	475.86	3	98
Pyrophosphate sodium	Pyro-P	Na <sub>2</sub> P <sub>2</sub> O <sub>7</sub> ·10H <sub>2</sub> O	Malinckrodt	446.06	2	99.5

model phosphorus compounds to either IP or digested IP was tested by the analysis of covariance method using R software (version 2.7.2).

This method was used to determine the concentrations of total dissolved phosphorus in Florida Bay. A total of 39 stations were occupied in a survey cruise during February 13–14, 2007. Samples were filtered immediately after collection through a 0.45  $\mu\text{m}$  Nuclepore filter to remove particulate matter and stored in plastic bottles in a cooler at ca. 4 °C. The water samples were then transported to the laboratory and analyzed within a week of their collection. Since the total dissolved phosphorus in Florida Bay is usually below 1  $\mu\text{M}$ , the digested samples were measured by a high sensitivity gas-segmented continuous flow analyzer.

### 3. Results and discussion

#### 3.1. Optimization of the digestion condition

##### 3.1.1. Digestion time

The effect of digestion time on the recovery of different organic phosphorus compounds is presented in Fig. 1. The amount of phosphate liberated from the persulfate oxidation of different organic phosphorus compounds increased rapidly with digestion time within the first 8 h and reached a maxima at 16 h. No significant change in the absorbance of phosphoantimonymolybdenum blue at 890 nm (or the percentage of the full color) was observed between 16 and 60 h. Therefore, a 16-h digestion time was chosen as the standard procedure for routine sample analysis.

In previous studies, 30 min to 3 h of digestion at boiling temperatures was used for acidic persulfate digestion [34,35]. Microwave ovens have also been employed for heating (95 °C, 10–40 min) [27,36,37]. However, the most popular heating technique for persulfate digestion is an autoclave [14,15]. Ridal and Moore [24] found that the liberation of organically bound phosphorus through the use of an autoclave was not completed in 30–60 min; organic phosphorus continually increased between 3 and 6 h. Therefore, Monaghan and Ruttenberg [22] recommended a digestion time of 4 h when using an autoclave. Persulfate thermal decomposition between 50 and 130 °C follows an Arrhenius relationship [38,39], and it has been reported that the half-life of persulfate is about 30 s at 130 °C and 4 h at 75 °C [40]. It is logical to assume that the oxidizable organic phosphorus has been broken down after the sample is digested at 90 °C overnight (16 h). Compared with the autoclave method, digestion at

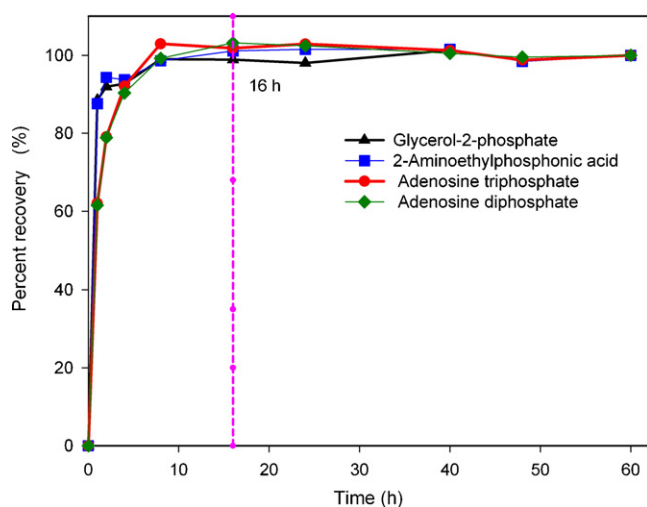


**Fig. 1.** Effect of digestion time (at 90 °C) on the relative recovery of samples containing 5  $\mu\text{M}$  of ADP, ATP, 2-AEP, and  $\beta$ -GLP. The recovery of each phosphorus compound was normalized to its value at 60 h.

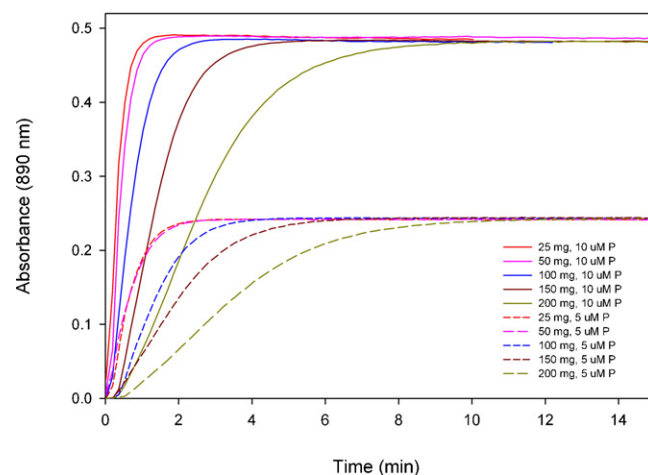


**Fig. 2.** Effect of the amount of potassium persulfate on the formation time of phosphoantimonymolybdenum blue complex in the 5 and 10  $\mu\text{M}$   $\beta$ -GLP solutions, respectively. The absorbances at 890 nm were measured at room temperature ( $25 \pm 2$  °C).

sub-boiling temperatures in an oven is safer, and a large number of samples can be heated overnight requiring no constant monitoring. In fact, the sub-boiling temperature persulfate digestion method has been used for digestion of soil extracts to determine dissolved organic carbon (DOC) and nitrogen (DON) [40].

##### 3.1.2. Persulfate concentration

As expected from our previous results [16], the increased amount of persulfate in the digestion solutions can significantly increase the time required for full color development during phosphate measurement, but the maximum absorbance of phosphoantimonymolybdenum at 890 nm does not increase. In other words, recovery of organic phosphorus does not improve. As shown in Fig. 2, the maximum absorbance of phosphoantimonymolybdenum blue at 890 nm in the 5 and 10  $\mu\text{M}$   $\beta$ -GLP digested solutions did not change when persulfate increased from 50 to 200 mg. However, the time for the digested  $\beta$ -GLP solutions to reach full color varied from 2 to 12 min, and the difference became greater in samples containing lower amounts of organic phosphorus. Because the oxidation residue of the persulfate significantly impedes color development of phosphoantimonymolybdenum blue [16], it is reasonable to assume that the higher the concentration of organic phosphorus in the solution, the less persulfate residue remains in the solution and, therefore, the shorter the time to reach full color.

**Table 2**

Effect of the amount of persulfate on the kinetics of formation of phosphoantimonymolybdenum blue complex from oven digested samples containing 5  $\mu\text{M}$  of ADP, ATP, and 2-AEP, respectively. The formation of the blue complex was measured with its absorbance at 890 nm at reaction time intervals between 3 and 10 min.

P compounds	Time (min)	Persulfate amount (mg)				
		25	50	100	150	200
ADP	3	0.308	0.306	0.298	0.254	0.150
	5	0.309	0.309	0.307	0.299	0.245
	8	0.309	0.307	0.307	0.306	0.298
	10	0.309	0.307	0.307	0.307	0.308
ATP	3	0.353	0.365	0.359	0.302	0.183
	5	0.353	0.365	0.367	0.355	0.295
	8	0.353	0.366	0.367	0.364	0.352
	10	0.354	0.365	0.367	0.365	0.362
2-AEP	3	0.353	0.350	0.343	0.301	0.157
	5	0.353	0.350	0.352	0.347	0.269
	8	0.353	0.351	0.351	0.353	0.336
	10	0.353	0.352	0.351	0.353	0.347



**Table 3**  
Apparent molar absorptivity ( $\epsilon$ , L mol<sup>-1</sup> cm<sup>-1</sup>) and recovery of 11 phosphorus model compounds in the DIW and ASW matrixes. The apparent molar absorptivity was determined from a set of solutions that ranged from 0 to 10  $\mu$ M in the corresponding phosphorus compounds. Samples were digested at 90 °C for 16 h with the addition of 10 mg of potassium persulfate per mL of sample.

P compounds	DIW matrix			ASW matrix		
	Apparent molar absorptivity ( $\epsilon$ )	Recovery (%)		Apparent molar absorptivity ( $\epsilon$ )	Recovery (%)	
		IP	Digested IP		IP	Digested IP
IP	17,432 ± 278	100.0	97.5	17,875 ± 129	100.0	100.9
Digested IP	17,875 ± 84	102.5	100.0	17,720 ± 183	99.1	100.0
$\beta$ -GLP	13,010 ± 168	74.6	72.8	12,580 ± 38	70.4	71.0
G6P	18,201 ± 103	104.4	101.8	15,373 ± 93	86.0	86.8
2-AEP	17,859 ± 48	102.5	99.9	15,774 ± 213	88.2	89.0
1-AEP	17,379 ± 150	99.7	97.2	17,056 ± 94	95.4	96.3
PFA	17,777 ± 94	102.0	99.5	17,932 ± 78	100.3	101.2
AMP	13,569 ± 166	77.8	75.9	13,591 ± 172	76.0	76.7
ADP	13,710 ± 141	78.6	76.7	18,063 ± 137	101.0	101.9
ATP	15,633 ± 112	89.7	87.5	16,639 ± 110	93.1	93.9
IP6	15,605 ± 678	89.5	87.3	11,727 ± 293	65.6	66.2
Poly-P	17,457 ± 86	100.1	97.7	16,906 ± 60	94.6	95.4
Pyro-P	16,442 ± 94	94.3	92.0	18,247 ± 172	102.1	103.0
Min	13,010	74.6	72.8	11,727	65.6	66.2
Max	18,201	104.4	101.8	18,247	102.1	103.0
Average	16,304	93.5	91.2	16,114	90.1	90.9
S.D.	1,836	10.5	10.3	2,196	12.3	12.4

The three other model phosphorus compounds also show a similar pattern (Table 2): the higher concentrations of persulfate do not improve the recovery of organic phosphorus. These results also confirm that organic phosphorus can be oxidized in persulfate solution without initial acidification, as the process of persulfate oxidation produces a hydrogen ion which can lower the digestion solution to a pH of 2–3 [21]. It should be noted that the effect of persulfate in this study differed from the results of acidic persulfate oxidation by the autoclave method [24], in which the recovery of dissolved organic phosphorus from seawater was about 25% higher in high concentrations of persulfate (40 mg mL<sup>-1</sup>) than in low concentrations of persulfate (4 mg mL<sup>-1</sup>).

The results of the experiment with all four model organic phosphorus compounds (Table 2 and Fig. 2) indicate that 100 mg of potassium persulfate (10 mg per mL of sample) was sufficient for 10 mL of sample containing 10  $\mu$ M of organic phosphorus; the phosphoantimonymolybdenum blue complex developed fully within 8 min. Therefore, the recommended amount of potassium persulfate used in digestion was 100 mg for 10 mL of sample, which is similar to the amount used by Menzel and Corwin [21].

Koroleff suggested that the amount of persulfate could be decreased from 1 to 0.3% if the sample was initially acidified [41]. However, an acidic medium can significantly impede color development in phosphate measurement, especially when the pH of the post-digestion solution is less than 1.5. It becomes necessary to adjust the pH of individual samples before the released phosphate can be determined by spectrophotometry [16].

### 3.2. Recovery of model organic phosphorus compounds

#### 3.2.1. Recoveries in the DIW matrix

Traditionally, the recovery of organic phosphorus compounds by digestion has been based on the measured phosphate released from a single concentration of organic phosphorus standard. In this study, the recovery of individual organic phosphorus compounds following digestion was measured with a series of increasing concentrations (0, 0.5, 1, 2.5, 5, 7.5, and 10  $\mu$ M) of given organic phosphorus compound in the DIW matrix. A linear relationship between the absorbances of the digested samples and their known organic phosphorus concentrations was obtained ( $r^2 > 0.99$ ,  $n = 7$ ), and the slope of this linear curve was defined as an apparent molar

absorptivity ( $\epsilon$ ) of the individual organic phosphorus compounds. The “net recovery” of an individual organic phosphorus compound from digestion was calculated as the ratio of its apparent  $\epsilon$  relative to the  $\epsilon$  of IP in the same matrix. The advantage of this approach is not only in averaging the recovery over a wide range of phosphorus concentrations, but also in providing an absolute value of  $\epsilon$  for both IP and organic phosphorus, which might provide additional information when comparing the recovery from different digestion methods.

As shown in Table 3, the measured apparent  $\epsilon$  in DIW ranged from  $1.30 \times 10^4$  L mol<sup>-1</sup> cm<sup>-1</sup> for  $\beta$ -GLP to  $1.82 \times 10^4$  L mol<sup>-1</sup> cm<sup>-1</sup> for G6P with an average of  $1.63 \pm 0.18 \times 10^4$  L mol<sup>-1</sup> cm<sup>-1</sup>. It should be noted that the  $\epsilon$  of the digested IP solution ( $1.79 \times 10^4$  L mol<sup>-1</sup> cm<sup>-1</sup>) is close to that of the undigested IP solution ( $1.74 \times 10^4$  L mol<sup>-1</sup> cm<sup>-1</sup>). No significant differences were observed between IP and digested IP, as well as between IP or digested IP and 1-AEP, 2-AEP, PFA, G6P, and polyphosphate ( $p > 0.05$ ), respectively. However, the difference between IP or digested IP and AMP, ADP, ATP, pyrophosphate, IP6, and  $\beta$ -GLP was very significant ( $p < 0.001$ ). The relatively greater difference in the apparent  $\epsilon$  between organic phosphorus compounds is largely due to the differences in their recovery. For a given organic phosphorus compound, its recovery is usually assumed to be dependent only upon the digestion method and should be constant over a wide range of concentrations. This assumption was verified by measuring the apparent molar absorptivity in mixed phosphorus solutions with varying ratios of organic phosphorus to phosphate. These results indicate that the apparent  $\epsilon$  in the mixed phosphorus solutions increased with the increasing ratio of IP to total phosphorus. As mentioned above, lower absorptivity in the 100% organic phosphorus solutions relative to the 100% phosphate solutions was due to the less than 100% recovery of organic phosphorus compounds following digestion. For any given organic phosphorus mixture, its apparent molar absorptivity can be described by a linear equation as a function of the ratio of IP to total phosphorus (Fig. 3). For the PFA mixture, the apparent  $\epsilon$  was almost constant ( $\epsilon = 1.80 \times 10^4$  L mol<sup>-1</sup> cm<sup>-1</sup>), whereas for the ATP mixture the equation was  $\epsilon = 15,680 + 23.28X$  ( $X$  is the ratio of IP to total phosphorus,  $r^2 = 0.99$ ). For the AMP mixture, the equation was  $\epsilon = 13,246 + 45.529X$  ( $r^2 = 0.96$ ). The linear relationship further confirmed that the recovery of each organic phosphorus compound

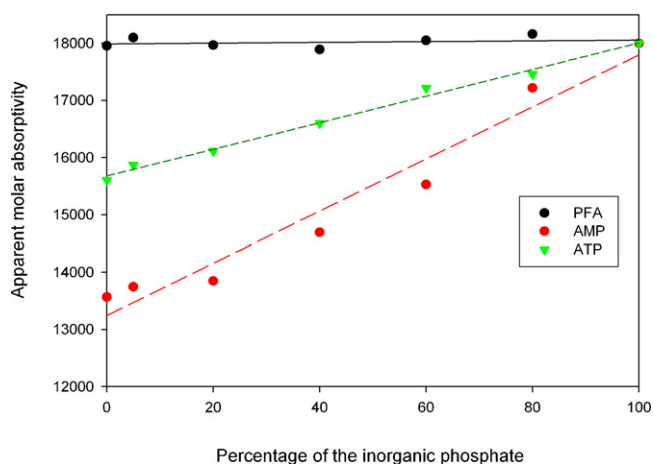


Fig. 3. Effect of the ratio of inorganic phosphate to total phosphorus on the apparent molar absorptivity ( $\text{L mol}^{-1} \text{cm}^{-1}$ ) of the mixed phosphorus solution.

was constant and not dependent upon the amount of phosphate in the mixture.

The recovery calculated from the apparent molar absorptivity in the DIW matrix ranged from 75 to 104%. Similar to other digestion methods [14,15,23,42,43], the recovery of phosphorus was compound specific (Table 3). For the phosphorus compounds containing a C–P bond (1-AEP, 2-AEP, PFA) and a C–O–P bond (G6P), the recoveries were very close to 100%, similar to the values reported using an autoclave with acidic and alkaline persulfate digestion [26,27]. However, the recoveries for the phosphorus compounds containing a C–O–P bond (AMP and IP6) were only 78–90%, lower than the values reported by Kerouel and Aminot [42], but close to our previous results obtained from autoclave acidic persulfate digestion conducted in our laboratory [43]. For phosphorus compounds containing a P–O–P bond (ADP, ATP, polyphosphate, and pyrophosphate), the recoveries were 90–100%, similar to the results obtained by Worsford et al. [14]. On average, recovery of the 11 tested model phosphorus compounds in the DIW matrix was  $94 \pm 11\%$ .

### 3.2.2. Recoveries in the ASW matrix

As shown in Table 3, the measured apparent  $\epsilon$  of organic phosphorus compounds in the ASW matrix ranged from  $1.17 \times 10^4$  for IP6 to  $1.82 \times 10^4 \text{ L mol}^{-1} \text{cm}^{-1}$  for pyrophosphate. The average apparent  $\epsilon$  of the studied phosphorus model compounds in the ASW matrix was  $1.59 \times 10^4 \text{ L mol}^{-1} \text{cm}^{-1}$ . It should be pointed out that there was no significant difference in the  $\epsilon$  of the digested and undigested phosphate solutions in the ASW matrix ( $p = 0.47$ ). Only three model phosphorus compounds (ADP, PFA, and pyrophos-

phate) were found to have no significant difference from either IP or digested IP ( $p > 0.08$ ).

Similar to the behavior of organic phosphorus compounds in the DIW matrix, the recovery of phosphorus was also compound specific in the ASW matrix. However, no apparent correlation between the recovery and compound structures was observed. For phosphorus compounds containing C–O–P bonds, the recoveries were  $70.4 \pm 0.2\%$  for  $\beta$ -GLP and  $86.0 \pm 0.5\%$  for G6P. For the phosphorus compounds containing P–O–P bonds, the recoveries were  $102.1 \pm 1.0\%$  for Pyro,  $94.6 \pm 0.3\%$  for Poly,  $101.0 \pm 0.8\%$  for ADP,  $93.1 \pm 0.6\%$  for ATP, and  $76.0 \pm 1.0\%$  for AMP, respectively. For the phosphorus compounds containing C–P bonds (AEP, PFA, IP6), their recoveries ranged from 66.3 to 101.4%. It is interesting to note the significant difference ( $p < 0.001$ ) in recovery between 1-AEP ( $95.4 \pm 0.5\%$ ) and 2-AEP ( $88.0 \pm 1.2\%$ ) compounds, even though they differ only in structure. The average recovery of the 11 compounds was  $90 \pm 12\%$ , which is similar to previous results from either acidic or alkaline persulfate autoclave methods [14,15,23,42,43]. For example, the recoveries of ATP and G6P using this method were similar to the acidic persulfate autoclave methods of Ormazza-Gonzalez and Statham [23], and the recovery of IP6 was close to Kerouel and Aminot's results [26]. The recoveries of 2-AEP,  $\beta$ -GLP, and Poly-P using this method were slightly higher than the corresponding values obtained from the acidic persulfate autoclave methods [23], and the recoveries of  $\beta$ -GLP, G6P, and 2-AEP were slightly lower than those obtained using alkaline persulfate autoclave methods [23]. In general, the recovery of this method in the ASW matrix was also slightly lower than that in the DIW matrix, which was similar to previous studies that used autoclave digestion [14,15,42].

Traditionally, the calibration standards for determining total dissolved phosphorus in water samples have been prepared from phosphate solutions that have undergone the same procedure as the samples, namely, persulfate digested phosphate solutions [14,15,19,20,23,41–43]. However, there is no systematic study that demonstrates the difference in molar absorptivity of phosphate between persulfate digested IP standard solutions and simple IP solutions (no persulfate addition and digestion). Our results indicate that there is no significant difference in  $\epsilon$  of phosphate in the digested and undigested IP in the DIW and ASW matrixes ( $p > 0.40$ ). To simplify the analytical procedure for this method, it is recommended that a simple phosphate solution prepared in sample matrix, but without involving persulfate digestion as the calibration standard for determining total dissolved phosphorus in natural waters. However, using this simple calibration standard for other methods of total dissolved phosphorus determination requires verification of each individual method. If the matrix effect is also negligible for other methods, using a simple phosphate standard solution has the advantage of making the results of different methods comparable. At present, the concentration of dissolved organic phosphorus remains as an operational definition. Efforts to

Table 4

Method precision estimated from  $2.00 \mu\text{M}$  phosphorus model compounds in the ASW matrix. Samples were digested at  $90^\circ\text{C}$  for 16 h with the addition of 10 mg of potassium persulfate per mL of sample.

P compounds	Concentration ( $\mu\text{M}$ )					Standard deviation ( $\mu\text{M}$ )	CV (%)
	Replication 1	Replication 2	Replication 3	Replication 4	Average		
$\beta$ -GLP	1.374	1.281	1.250	1.335	1.310	0.055	4.21
G6P	1.903	1.908	1.895	1.916	1.906	0.009	0.46
1-AEP	2.085	2.187	2.249	2.164	2.171	0.068	3.13
PFA	2.085	2.159	2.143	2.179	2.141	0.040	1.89
AMP	1.785	1.814	1.831	1.755	1.796	0.033	1.86
ADP	2.059	2.132	2.133	2.052	2.094	0.045	2.13
ATP	1.914	2.074	2.055	2.089	2.033	0.081	3.96
IP6	1.635	1.652	1.683	1.725	1.674	0.040	2.36
Poly-P	1.988	2.134	2.122	2.154	2.100	0.076	3.60
Pyro-P	1.870	1.912	1.904	1.960	1.911	0.037	1.96

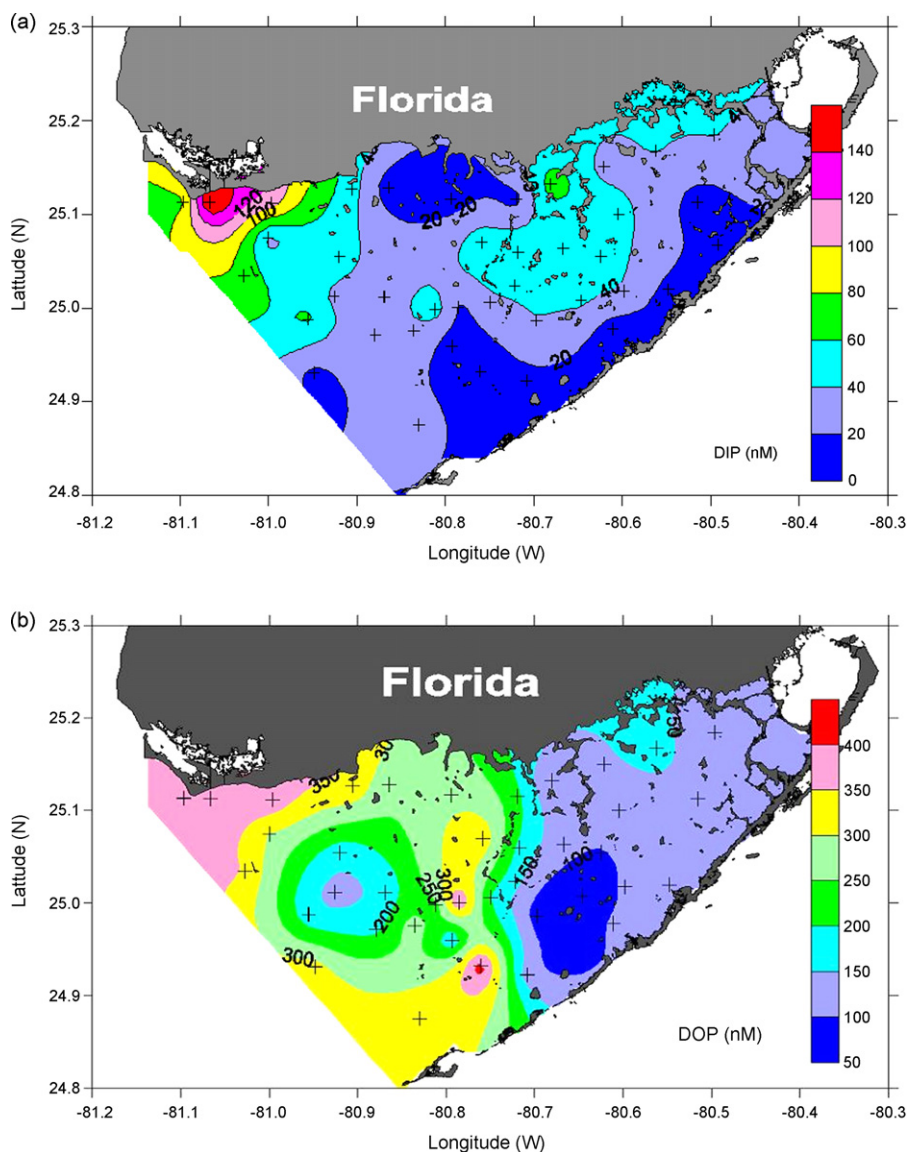


Fig. 4. The spatial distribution of dissolved phosphate (A) and dissolved organic phosphorus (B) in the surface waters of Florida Bay.

improve the accuracy of its determination are mainly hindered by the unknown chemical composition of total dissolved phosphorus pool in natural waters and the variable recovery of different organic phosphorus compounds as shown in this study.

### 3.3. Method precision and its application to natural water samples analysis

The precision of this method was evaluated by sets of  $2.0 \mu\text{M}$  organic phosphorus model compounds in the ASW matrix, and each compound had four replications. After 16 h of digestion, the released phosphate was measured against the undigested phosphate standard in the ASW matrix. The measured concentration of these phosphorus compounds ranged from  $1.31$  to  $2.17 \mu\text{M}$  (Table 4). The coefficient of variation for each phosphorus compound was less than 5% (from 1.9 to 4.2%). This method provides acceptable precision for determination of total dissolved phosphorus in natural water samples.

We used this method to determine the total dissolved phosphorus in Florida Bay waters. The total dissolved phosphorus ranged from 103 to 553 nM, whereas the dissolved phosphate ranged from 9 to 165 nM. It is obvious that the dissolved organic phosphorus in

the water was much higher than that of the inorganic form with a maximum ratio of 49. Similar to the spatial variations of dissolved phosphate in the Bay [30], the dissolved organic phosphorus in the western bay was also much higher than that of the eastern bay and had a spatial gradient decreasing from the west to the east (Fig. 4). The spatial pattern indicates that concentrations of dissolved organic phosphorus in shallow Florida Bay waters are mainly regulated by the phosphorus buffering mechanism of sediments [44,45].

## 4. Conclusion

A method that uses neutral persulfate oxidation at sub-boiling temperatures to determine total dissolved phosphorus has been developed for routine digestion of a large number of samples. It is recommended that 100 mg of potassium persulfate be added to 10 mL of the sample, followed by digestion at  $90^\circ\text{C}$  in an oven overnight (16 h). This method does not require an adjustment of the pH after digestion because neither an acid nor a base is added to the samples prior to digestion. The full color of phosphoantimomolybdenum blue in the digested samples develops within 8 min. The apparent  $\epsilon$  of the 11 phosphorus compounds ranged from

$1.17 \times 10^4$  to  $1.83 \times 10^4$  L mol<sup>-1</sup> cm<sup>-1</sup> in the DIW and ASW matrixes. The average recovery of these phosphorus compounds was  $94 \pm 11\%$  in the DIW matrix and  $90 \pm 12\%$  in the ASW matrix. No significant difference in molar absorptivity was observed between the undigested and digested phosphate, especially in the ASW matrix. It is, therefore, suggested that orthophosphate solution be used directly (without digestion) as the calibration standard for the routine determination of total dissolved phosphorus. This method was used to study the spatial distribution of total dissolved organic phosphorus in surface waters of Florida Bay.

### Acknowledgments

We thank Ms. Xiaosun Lu for her assistance with statistical analysis and Ms. Gail Derr for English editing. Financial support for this study was provided by NOAA's Coastal Ocean Program and Climate and Global Change Program. This research was carried out, in part, under the auspices of the Cooperative Institute for Marine and Atmospheric Studies (CIMAS), a joint institute of the University of Miami and the National Oceanic and Atmospheric Administration, cooperative agreement #NA67RJ0149. The statements, findings, conclusions, and recommendations are those of the authors and do not necessarily reflect the views of NOAA or the U.S. Department of Commerce.

### References

- [1] D.J. Currie, J. Kalff, *Limnology and Oceanography* 29 (1984) 311–321.
- [2] X.L. Huang, Y. Chen, M. Shenker, *Plant and Soil* 271 (2005) 365–376.
- [3] K.G. Raghothama, *Phosphate Acquisition*, Annual Review of Plant Biology, 1999, pp. 665–693.
- [4] B.L. Turner, E. Frossard, D.S. Baldwin, *Organic Phosphorus in the Environment*, CABI Publishing, Wallingford, UK, 2005.
- [5] D.M. Karl, K.M. Björkman, in: D.A. Hansell, C.A. Carlson (Eds.), *Biogeochemistry of Marine Dissolved Organic Matter*, Academic Press, San Diego, 2002, pp. 249–366.
- [6] K.R. Reddy, G.A. O'Connor, C.L. Schelske, *Phosphorus Biogeochemistry in Subtropical Ecosystems*, Lewis, Boca Raton, Florida, 1999.
- [7] B.J. Cade-Menun, J.A. Navaratnam, M.R. Walbridge, *Environmental Science and Technology* 40 (2006) 7874–7880.
- [8] P. Monbet, I.D. McKelvie, A. Saefumillah, P.J. Worsfold, *Environmental Science and Technology* 41 (2007) 7479–7485.
- [9] I.D. McKelvie, in: E.F. Benjamin, L. Turner, D.S. Baldwin (Eds.), *Organic Phosphorus in the Environment*, CABI Publishing, Wallingford, UK, 2005, pp. 1–20.
- [10] P.J. Worsfold, P. Monbet, A.D. Tappin, M.F. Fitzsimons, D.A. Stiles, I.D. McKelvie, *Analytica Chimica Acta* 624 (2008) 37–58.
- [11] A. Cantarero, M.B. Lopez, J. Mahia, M.A. Maestro, A. Paz, *Communications in Soil Science and Plant Analysis* 33 (2002) 3431–3436.
- [12] J.L.M. De Boer, U. Kohlmeier, P.M. Breugem, T. Van Der Velde-Koerts, *Fresenius' Journal of Analytical Chemistry* 360 (1998) 132–136.
- [13] A.P. Rowland, P.M. Haygarth, *Journal of Environmental Quality* 26 (1997) 410–415.
- [14] P.J. Worsfold, L.J. Gimbert, U. Mankasingh, O.N. Omaka, G. Hanrahan, P.C.F.C. Gardolinski, P.M. Haygarth, B.L. Turner, M.J. Keith-Roach, I.D. McKelvie, *Talanta* 66 (2005) 273–293.
- [15] W. Maher, L. Woo, *Analytica Chimica Acta* 375 (1998) 5–47.
- [16] X.L. Huang, J.Z. Zhang, *Talanta* 77 (2008) 340–345.
- [17] I.D. McKelvie, D.M.W. Peat, P.J. Worsfold, *Analytical Proceedings including Analytical Communications* 32 (1995) 437–445.
- [18] A. Aminot, D. Kirkwood, S. Carlberg, *Marine Pollution Bulletin* 35 (1997) 28–41.
- [19] Method 4500-P, in: L.S. Clescerl, A.E. Greenberg, A.D. Eaton (Eds.), *Standard Methods for the Examination of Water and Wastewater*, American Public Health Association, American Water Works Association, Water Environment Federation, Washington, DC, 1998.
- [20] Method 365. 1, in: J.W. O'Dell (Ed.), *Determination of Phosphorus by Semi-Automated Colorimetry*, Environmental Monitoring Systems Laboratory, Office of Research and Development, USEPA, Cincinnati, OH, 1993.
- [21] D.W. Menzel, N. Corwin, *Limnology and Oceanography* 10 (1965) 280–282.
- [22] E.J. Monaghan, K.C. Ruttenberg, *Limnology and Oceanography* 44 (1999) 1702–1714.
- [23] F.I. Ormaza-Gonzalez, P.J. Statham, *Water Research* 30 (1996) 2739–2747.
- [24] J.J. Ridal, R.M. Moore, *Marine Chemistry* 29 (1990) 19–31.
- [25] C.F. D'Elia, P.A. Steudler, N. Corwin, *Limnology and Oceanography* 22 (1977) 760–764.
- [26] F. Koroleff, *Determination of total nitrogen in natural waters by means of persulfate oxidation*, Int. Counc. Explor. Sea (ICES) Paper C.M.C.8, 1970.
- [27] W. Maher, F. Krikowa, D. Wruck, H. Louie, T. Nguyen, W.Y. Huang, *Analytica Chimica Acta* 463 (2002) 283–293.
- [28] F. Koroleff, *Determination of total phosphorus in natural waters by means of persulfate oxidation*, Int. Counc. Explor. Sea (I.C.E.S.) paper C.M./C.33, 1968.
- [29] J.P. Riley, in: J.P. Riley, G. Skirrow (Eds.), *Chemical Oceanography*, Academic Press, London, UK, 1975, pp. 421–428.
- [30] J.-Z. Zhang, J. Chi, *Environmental Science and Technology* 36 (2002) 1048–1053.
- [31] D.R. Kester, I.W. Duedall, D.N. Connors, R.M. Pytkowicz, *Limnology and Oceanography* 12 (1967) 176–179.
- [32] J. Murphy, J.P. Riley, *Analytica Chimica Acta* 27 (1962) 31–36.
- [33] J.Z. Zhang, C.J. Fischer, P.B. Ortner, *Talanta* 49 (1999) 293–304.
- [34] M.E. Gales, E.C. Julian, R.C. Kroner, *Journal of the American Water Works Association* 58 (1966) 1363–1368.
- [35] L.J. Lennox, *Water Research* 13 (1979) 1329–1333.
- [36] R.L. Benson, I.D. McKelvie, B.T. Hart, I.C. Hamilton, *Analytica Chimica Acta* 291 (1994) 233–242.
- [37] S. Hinkamp, G. Schwedt, *Analytica Chimica Acta* 236 (1990) 345–350.
- [38] D.A. House, *Chemical Reviews* 62 (1962) 185–203.
- [39] G.R. Peyton, *Marine Chemistry* 41 (1993) 91–103.
- [40] A. Doyle, M.N. Weintraub, J.P. Schimel, *Soil Science Society of America Journal* 68 (2004) 669–676.
- [41] F. Koroleff, in: K. Grasshoff, M. Ehrhardt, K. Kremling (Eds.), *Determination of phosphorus, Methods of Seawater Analysis*, second, revised and extended edition, Verlag Chemie GmbH, Weinheim, 1983, pp. 125–139.
- [42] R. Kerouel, A. Aminot, *Analytica Chimica Acta* 318 (1996) 385–390.
- [43] J.Z. Zhang, C.J. Fischer, P.B. Ortner, *Method 367.0 Determination of Total Phosphorus in Estuarine and Coastal Waters by Autoclave Promoted Persulfate Oxidation*, National Exposure Research Laboratory, Office of Research and Development, U.S. Environmental Protection Agency, Cincinnati, Ohio 45268, 1998, p. 13.
- [44] J.Z. Zhang, X.L. Huang, *Environmental Science and Technology* 41 (2007) 2789–2795.
- [45] J.Z. Zhang, C.J. Fischer, P.B. Ortner, *Global Biogeochemical Cycles* 18 (2004) 1–14.



# Studies on principal components and antioxidant activity of different Radix Astragali samples using high-performance liquid chromatography/electrospray ionization multiple-stage tandem mass spectrometry

Xin Huang<sup>a,b</sup>, Yan Liu<sup>c</sup>, Fengrui Song<sup>a</sup>, Zhiqiang Liu<sup>a</sup>, Shuying Liu<sup>a,\*</sup>

<sup>a</sup> Changchun Institute of Applied Chemistry, Chinese Academy of Sciences, Changchun Center of Mass Spectrometry, Changchun 130022, PR China

<sup>b</sup> Graduate School of the Chinese Academy of Sciences, Beijing 100039, PR China

<sup>c</sup> School of Chinese Pharmacology, Beijing University of Chinese Medicine, Beijing 100102, PR China

## ARTICLE INFO

### Article history:

Received 6 December 2008

Received in revised form 9 January 2009

Accepted 13 January 2009

Available online 23 January 2009

### Keywords:

Isoflavonoids

Astragalosides

Radix Astragali

HPLC-ESI-MS<sup>n</sup>

Antioxidant activity

## ABSTRACT

The principal components, isoflavonoids and astragalosides, in the extract of Radix Astragali were detected by a high-performance liquid chromatography couple to electrospray ionization ion trap multiple-stage tandem mass spectrometry (HPLC-ESI-IT-MS<sup>n</sup>) method. By comparing the retention time ( $t_R$ ) of HPLC, the ESI-MS<sup>n</sup> data and the structures of analyzed compounds with the data of reference compounds and in the literature, 17 isoflavonoids and 12 astragalosides have been identified or tentatively deduced. By virtue of the extracted ion chromatogram (EIC) mode, simultaneous determination of isoflavonoids and astragalosides could be achieved when the different components formed overlapped peaks. And this method has been utilized to analyze the constituents in extracts of Radix Astragali from Helong City and of different growth years. Then the antioxidant activity of different samples has been successfully investigated by HPLC-ESI-MS method in multiple selected ion monitoring (MIM) mode, applying the spin trapping technology, and the Ferric Reducing Antioxidant Power (FRAP) assay was applied to support the result. The correlations of the isoflavonoids and astragalosides components and the antioxidant activities of Radix Astragali were summarized. The present paper demonstrates that HPLC-ESI-MS<sup>n</sup> is a powerful method for the characterization of the principal components and evaluation of the antioxidant activity of Chinese medicinal herbs.

© 2009 Elsevier B.V. All rights reserved.

## 1. Introduction

Radix Astragali is a commonly used Chinese medicinal herb, derived from the dry roots of *Astragalus membranaceus* (Fisch.) Bge. var. *mongholicus* (Bge.) Hsiao or *Astragalus membranaceus* (Fisch.) Bge. . . Its effects are hepatoprotective, antioxidative, antiviral, anti-hypertensive and immunostimulant activities, etc. [1–3] The major bioactive compounds found in it are isoflavonoids and astragalosides. The crude drugs from different habitat, cultural manner, and harvest time showed different contents of isoflavonoids and astragalosides which will lead to different quality of Radix Astragali. Thus, it appeared important for us to investigate the principal components and bioactivity of Radix Astragali in order to search for the influence of above factors.

So far, several methods have been developed to analyze this Chinese medicinal herb. The detection of isoflavonoids was performed by LC-UV [4–6] and astragalosides were detected using LC-ELSD [7,8] (evaporative light scattering detector) due to their

weak UV absorbance. But UV and ELSD methods appear insufficient with regard to accurate peak identification and are not sensitive for determination of low-content constituents. One of the more important trends in separation-based methodology has been the increasing use of MS as a post-separation detection technique. LC-MS combining the efficient separation capability of LC and great power of structural characterization and high sensitivity of MS, is becoming a standard protocol to analyze the complex components of Chinese medicinal herb extracts [9–12]. Particularly, the well-known LC-ESI-MS<sup>n</sup> is being more and more widely applied in pharmaceutical research [13–16].

Recent findings that many human chronic diseases are associated with radicals have instigated the search for antioxidants and evaluation of antioxidant activity so to reduce the risks of those diseases. Several methods have been described for the detection of radicals, such as electron spin resonance (ESR) [17,18], chemiluminescence (CL) [19], gas chromatography-mass spectrometry (GC-MS) [20], and HPLC coupled with different kinds of detection, including UV detection, electrochemical detection (ED), and MS, etc. [21–25]. As MS technique has many advantages, the application of LC-MS in the study of radicals has begun to receive more attention. Yang et al. [26] have analyzed the hydroxyl radical scavenging

\* Corresponding author. Tel.: +86 431 85262236; fax: +86 431 85262886.  
E-mail address: [mssl@ciac.jl.cn](mailto:mssl@ciac.jl.cn) (S. Liu).

capacity of several phenolic acids by LC–MS. To our knowledge, no previous studies have been published on the LC–ESI–MS applied to evaluate the antioxidant activity of crude extracts of Chinese medicinal herbs.

In the present paper, the identification and elucidation of principal components from extract of Radix Astragali were carried out by LC–ESI–MS<sup>n</sup> in the positive and negative ion modes. By comparing the retention time ( $t_R$ ) and ESI–MS<sup>n</sup> data of the analyzed compounds with the data of reference compounds and the literature, a total of 17 isoflavonoids and 12 astragalosides were unambiguously identified or tentatively characterized. And the constituents of Radix Astragali samples from Helong City and of different growth years were analyzed. Then the LC–ESI–MS method was applied to evaluate the antioxidant activity of different samples in multiple selected ion monitoring (MIM) mode, using 5,5-dimethyl-1-pyrroline N-oxide (DMPO) as spin-trapped agent and N-methyl-2-pyrrolidone (NMP) as the internal standard, and the Ferric Reducing Antioxidant Power (FRAP) assay was applied to support the result. Finally, the effect of growth years on the principal components and antioxidant activity of Radix Astragali were assessed. And the correlations of principal components and antioxidant activity were found. So LC–ESI–MS<sup>n</sup> method is important and useful for controlling and judging Chinese medicinal herb quality.

## 2. Experimental

### 2.1. Instrumentations

The high-performance liquid chromatography system consisted of a Waters (Milford, MA, USA) 2690 HPLC, equipped with photodiode array detection (DAD) and a Millennium 32 software program for analysis of the HPLC data. The components analysis was operated on a Dikma Diamonsil C18 column (250 mm × 4.6 mm, 5 μm). The mobile phase consisted of acetonitrile (A) and 0.5% acetic acid (B). Gradient elution was with 20% A from 0 to 5 min, 20–100% A from 5 to 75 min and 100% A from 75 to 80 min. The mobile phase flow rate was 1.0 mL/min and was reduced to 0.5 mL/min by a split valve just before the eluent entered the ESI–MS. The column temperature was set at 35 °C and the injection volume was 10 μL. The photodiode array detector was set to 190–400 nm.

The mass spectrometry determination was performed on an LCQ<sup>TM</sup> ion trap instrument (Finnigan, San Jose, CA, USA) with an electrospray source in the positive and negative ion mode. The electrospray voltage was set to 5.0 kV, the capillary voltage to 15 V, the tube voltage to 20 V and the capillary temperature at 250 °C. High purity nitrogen (N<sub>2</sub>) was used as the sheath gas and its flow rate was set to 60 arbitrary units. High purity nitrogen (N<sub>2</sub>) was used as the auxiliary gas and its flow rate was set to 10 arbitrary units. HPLC was connected to the mass spectrometer via the UV cell outlet. The mass scale was calibrated using standard compounds according to standard calibration procedure. The isolation width for MS<sup>n</sup> was 1.0 Da and the collision energies for the MS<sup>n</sup> analyses ranged from 30 to 35% depending on the mass of the precursor ions.

The HPLC–ESI–MS experiments of antioxidant activity determination were carried out on 2690 HPLC coupled to LCQ<sup>TM</sup> ion trap instrument in the positive ion mode. The mobile phase consisted of acetonitrile (A) and 0.1% formic acid (B). Isocratic elution was with 90% A and 10% B. The runtime was 5 min. The flow rate was 0.4 mL/min. The analyzed samples were injected directly into photodiode array detection without the column and the UV cell outlet was connected to the mass spectrometer. The ESI–MS conditions were optimized as follows: electrospray voltage, 6.0 kV; capillary voltage, 30 V; tube voltage, 55 V; capillary temperature, 110 °C; sheath gas, 30 arbitrary units; auxiliary gas, 5 arbitrary units.

The FRAP assay was performed on the Tecan GENios ELIASA (Austria), the absorbance readings were taken at 593 nm.

### 2.2. Reference compounds and chemicals

The reference compounds, calycosin (1), formononetin (2) and astragaloside IV (3), were purchased from the Chinese Authenticating Institute of Material Medical and Biological Products (Beijing, China). Acetonitrile (Fisher, USA), formic acid and acetic acid (Tedia, USA) were of HPLC grade and the other solvents were of analytical grade. Distilled deionized water was purified using a Milli-Q water purification system (Millipore, France). 5,5-Dimethyl-1-pyrroline N-oxide (DMPO), N-Methyl-2-pyrrolidone (NMP) and 2,4,6-tripyridyl-s-triazine (TPTZ) were obtained from Sigma Chemical Co. (St. Louis, MO, USA). Ferrous sulfate heptahydrate (FeSO<sub>4</sub>·7H<sub>2</sub>O), ammonium acetate (NH<sub>4</sub>Ac), 30% hydrogen peroxide (H<sub>2</sub>O<sub>2</sub>), ferric chloride (FeCl<sub>3</sub>), L-ascorbic acid, sodium acetate (NaAc) and hydrochloric acid (HCl) were purchased from Beijing Chemical Plant (Beijing, China).

### 2.3. Sample preparation

The roots of Radix Astragali were herborized from Helong City of Jilin Province and were dried in sunlight. The dried roots were pulverized and the powder was screened through 40 mesh sieves. The fine powder (1 g) was accurately weighed and macerated in 25 mL methanol for 30 min. Then, the powder was extracted ultrasonically three times with 25 mL methanol and for 30 min each time at room temperature. The combined extract was concentrated under reduced pressure at 50 °C. After cooling, the condensed extract was transfer to 25 mL volumetric flask and methanol was added to the graduation. The mixture was passed through a 0.45 μm membrane and then 10 μL of the filtrate was injected into the HPLC system for the LC–MS<sup>n</sup> analyses.

## 3. Results and discussion

At first, a suitable HPLC method for Radix Astragali was developed. Parameters were optimized in order to improve the separation. Meanwhile the optimization of MS parameters is also a necessary step to obtain better selectivity. The mass spectral data of the methanol extract of Radix Astragali were obtained in the positive and negative ion mode, which could give more information. Fig. 1 lists some principal components that are discussed in the present paper.

The reference compounds, calycosin, formononetin and astragaloside IV, were investigated by LC–ESI–MS<sup>n</sup> in order to determine their retention time, mass spectra and fragmentation pathways. And subsequently the plausible fragmentation mechanisms of them have been proposed. All the above information was very meaningful, which could be used to identify and characterize the compounds in Radix Astragali methanol extracts.

### 3.1. The LC–ESI–MS<sup>n</sup> investigation of the extract of Radix Astragali

#### 3.1.1. Identification of isoflavonoids by LC–ESI–MS<sup>n</sup>

The retention time of calycosin is at 34.46 min. The [M+H]<sup>+</sup> with high abundance was at  $m/z$  285 and the [M–H]<sup>–</sup> was at  $m/z$  283. The LC–MS<sup>n</sup> data were obtained in the positive ion mode. The product ions at  $m/z$  270 and 253 arose from the eliminations of CH<sub>3</sub> and CH<sub>3</sub>OH, owing to the cleavage of OCH<sub>3</sub> group at C–4'. Similarly, the ion at  $m/z$  241 corresponded to the neutral losses of CO<sub>2</sub> at the C-ring. The important [<sup>1,3</sup>A+H]<sup>+</sup> ion at  $m/z$  137 was formed by the RDA rearrangement procedure. In addition, the other product ions were [M+H–CH<sub>3</sub>–2CO]<sup>+</sup> at  $m/z$  214, [M+H–CH<sub>3</sub>OH–CO]<sup>+</sup> at  $m/z$  225 and [M+H–2CO]<sup>+</sup> at  $m/z$  229 due to the concurrent losses. The retention time of formononetin is at 48.95 min and it gave the [M+H]<sup>+</sup> at  $m/z$  269 and [M–H]<sup>–</sup> at  $m/z$  267. The ions at  $m/z$  254 and 237 were produced by the losses of CH<sub>3</sub> and CH<sub>3</sub>OH at C–4'. The ion at  $m/z$

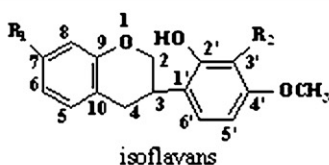
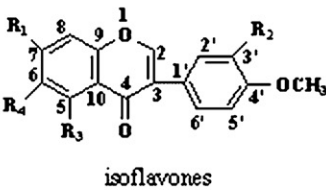
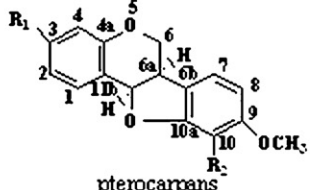
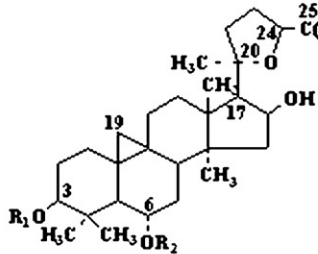
Structure	Compounds	R <sub>1</sub>	R <sub>2</sub>	R <sub>3</sub>	R <sub>4</sub>	NO.
 isoflavans	7,2',3'-trihydroxy-4'-methoxyisoflavan	OH	OH			F1
	2'-hydroxy-3',4'-dimethoxyisoflavan-7-O-β-D-glycoside	glc	OCH <sub>3</sub>			F9
	Astraisoflavanglycoside-6"-O-malonate	glc-6"-O-malonyl	OCH <sub>3</sub>			F14
	7,2'-dihydroxy-3',4'-dimethoxyisoflavan	OH	OCH <sub>3</sub>			F17
 isoflavones	Calycosin-7-O-β-D-glycoside	glc	OH	H	H	F2
	Biocanin-A	OH	H	OH	H	F3
	Calycosin-7-O-β-D-glycoside-6"-O-malonate	glc-6"-O-malonyl	OH	H	H	F5
	Ononin	O-β-D-glc	H	H	H	F6
	5-Hydroxy-4'-methoxyisoflavone-7-O-β-D-glycoside-6"-O-malonate	glc-6"-O-malonyl	H	OH	H	F7
	Calycosin	OH	OH	H	H	F10
	Odoratin	OH	OH	H	OCH <sub>3</sub>	F11
	Formononetin-7-O-β-D-glycoside-6"-O-malonate	glc-6"-O-malonyl	H	H	H	F12
Formononetin	OH	H	H	H	F15	
 pterocarpan	10-Hydroxy-3,9-dimethoxypterocarpan	OCH <sub>3</sub>	OH			F4
	9,10-Dimethoxypterocarpan-3-O-β-D-glycoside	glc	OCH <sub>3</sub>			F8
	Astrapterocarpan-3-O-β-D-glycoside-6"-O-malonate	glc-6"-O-malonyl	OCH <sub>3</sub>			F13
	3-Hydroxy-9,10-dimethoxypterocarpan	OH	OCH <sub>3</sub>			F16
	Cycloastragenol	H	H	H		S1
	Astragaloside I	xyl-2',3'-di-OAc	glc	H		S10
	Astragaloside II	xyl-2'-OAc	glc	H		S8
	Astragaloside IV	xyl	glc	H		S6
	Astragaloside V	xyl-2'-glc	H	glc		S5
	Astragaloside VI	xyl-2'-glc	glc	H		S3
	Astragaloside VII	xyl	glc	glc		S2
	Acetylastragaloside	xyl-2',3',4'-tri-OAc	glc	H		S12
	Isoastragaloside I	xyl-2',4'-di-OAc	glc	H		S11
	Isoastragaloside II	xyl-3'-OAc	glc	H		S9
Agroastragaloside III	xyl-2',3'-di-OAc	glc	glc		S7	
Agroastragaloside IV	xyl-2'-OAc	glc	glc		S4	

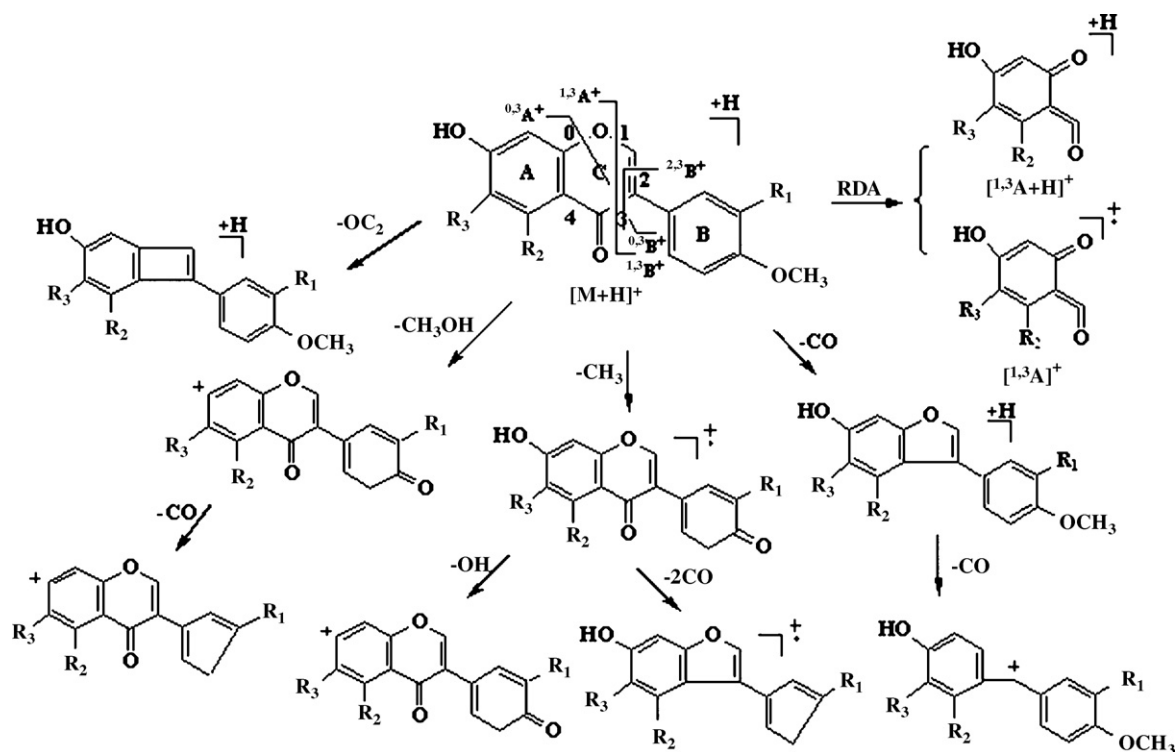
Fig. 1. The isoflavonoids and astragalosides compounds in Radix Astragali.

225 was from the neutral losses of CO<sub>2</sub> at the C-ring. The concurrent losses were also observed, the ions were [M+H-CH<sub>3</sub>-2CO]<sup>+</sup> at *m/z* 198, [M+H-CH<sub>3</sub>OH-CO]<sup>+</sup> at *m/z* 209 and [M+H-2CO]<sup>+</sup> at *m/z* 213, respectively. A characteristic fragment, [<sup>1,3</sup>A]<sup>+</sup> ion at *m/z* 136, was formed by the RDA rearrangement procedure.

Calycosin and formononetin are of isoflavones, so they presented similar fragmentation pathway. The results obtained from LC-MS<sup>n</sup> indicated that the losses of CH<sub>3</sub> and CH<sub>3</sub>OH was predominant, because of the OCH<sub>3</sub> substituents at C-4' in the B-ring. The contraction of C-ring was by the losses of CO and CO<sub>2</sub>. Furthermore, the important difference between calycosin and formononetin was the RDA rearrangement ions, [<sup>1,3</sup>A+H]<sup>+</sup> and [<sup>1,3</sup>A]<sup>+</sup>, which was related to

the 3'-hydroxy in the B-ring. The main fragmentation mechanisms of the isoflavones are summarized in Scheme 1. The above fragmentation behaviors could be extended to identifications of other isoflavonoids.

The LC-UV chromatogram of the isoflavonoids in the methanol extract of Radix Astragali is shown in Fig. 2. The data of retention time (*t<sub>R</sub>*), ESI-MS<sup>n</sup> data and the elucidation of individual peak are listed in Table 1. By comparing the retention time (*t<sub>R</sub>*) and ESI-MS<sup>n</sup> data of analyzed compounds with the data of reference compounds and the literature, a total of 17 isoflavonoids components have been unambiguously identified or tentatively characterized.



Scheme 1. Main MS<sup>n</sup> fragmentation pathways of isoflavones.

The LC–MS data of peak **F10** (Table 1) demonstrated two abundant ions,  $[M+H]^+$  at  $m/z$  285 and  $[M-H]^-$  at  $m/z$  283. So the molar mass of this compound was 284. On the basis of its retention time was at 34.46 min and fragment ions at  $m/z$  270, 214, 253, 225, 229, 241 and 137 were compared with those of reference compounds, the compound of peak **F10** was unambiguously identified as calycosin. Peak **F2** gave an intense  $[M+H]^+$  at  $m/z$  447 and a weak ion at  $m/z$  285. In the LC–MS<sup>2</sup> data, the  $m/z$  447 ion directly gave the product ion at  $m/z$  285 by neutral loss of 162 Da corresponded to losing a hexose residue. The product ions of  $m/z$  285 ion were consistent with that of peak **F10**. Based on the results discussed above, peak **F2** was tentatively identified as calycosin-7-O- $\beta$ -D-glycoside. Similarly, peak **F5** showed an intense ion at  $m/z$  533 and a weak ion at  $m/z$  285 in the LC–MS spectrum. In the LC–MS<sup>2</sup> data, the  $m/z$  533 ion produced the ion at  $m/z$  285 by expelling 248 Da neutral fragments corresponding to malonylglucosyl. The  $m/z$  285 ion

gave rise to the same product ions as that of calycosin. This result indicated that the only difference between peaks **F5** and **F2** was the substituted group at C-7. Thus, it was tentatively identified as calycosin-7-O- $\beta$ -D-glycoside-6'-O-malonate.

For peak **F11**, the first loss observed was a CH<sub>3</sub> group from the  $[M+H]^+$  at  $m/z$  315. In the LC–MS<sup>2</sup> experiment, the loss of a molecule of CH<sub>3</sub>OH could be deduced the existence of an OCH<sub>3</sub> group at C-4' as calycosin. Apart from the above losses,  $m/z$  315 ion also expelled neutral fragments 2CO and CO<sub>2</sub>, and formed the  $[^{1,3}A+H]^+$  ion at  $m/z$  167 from the RDA rearrangement procedure. This result demonstrated that compound of peak **F11** decomposed in a way similar to calycosin. Thus it was identified as odoratin. As described above, compounds of peaks **F2**, **F5**, **F10** and **F11** had similar fragmentation behaviors. According to their structures, they are of the same isoflavones type, have an OH group at C-3' and an OCH<sub>3</sub> group at C-4'.

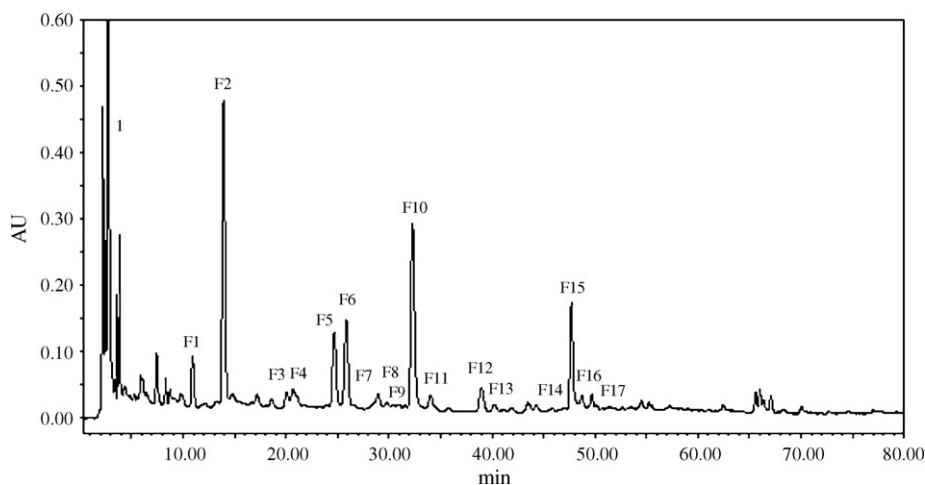


Fig. 2. The LC chromatogram of the isoflavonoids in the methanol extracts of Radix Astragali.



**Table 1**  
The retention time ( $t_R$ ), ESI-MS<sup>n</sup> and elucidation of the isoflavonoids in the methanol extract of Radix Astragali.

No.	$t_R$ (min)	M (+)	M (-)	MS <sup>n</sup> (the boldfaced one is the base peak)	Identification
<b>1</b>	2.48	365	341	203 [M+Na-glc] <sup>+</sup> , 185 [M+Na-glc-H <sub>2</sub> O] <sup>+</sup>	Sucrose
<b>F1</b>	11.76	289		257 [M+H-CH <sub>3</sub> OH] <sup>+</sup> , 167 [ <sup>1,3</sup> B] <sup>+</sup> , 153 [ <sup>2,3</sup> B] <sup>+</sup> , 149 [M+H-ringB] <sup>+</sup> , <b>123</b> [ <sup>1,3</sup> A] <sup>+</sup> , 138 [ <sup>2,3</sup> B-CH <sub>3</sub> ] <sup>+</sup> , 151 [ <sup>0,3</sup> B-CH <sub>3</sub> OH] <sup>+</sup> , 105 [ <sup>1,3</sup> A-H <sub>2</sub> O] <sup>+</sup>	7,2',3'-Trihydroxy-4'-methoxyisoflavan
<b>F2</b>	13.927	285, 447	283	<b>270</b> [M+H-CH <sub>3</sub> ] <sup>+</sup> , 214 [M+H-CH <sub>3</sub> -2CO] <sup>+</sup> , 253 [M+H-CH <sub>3</sub> OH] <sup>+</sup> , 225 [M+H-CH <sub>3</sub> OH-CO] <sup>+</sup> , 229 [M+H-2CO] <sup>+</sup> , 241 [M+H-CO <sub>2</sub> ] <sup>+</sup> , 137 [ <sup>1,3</sup> A+H] <sup>+</sup>	Calycosin-7-O-β-D-glycoside
<b>F3</b>	20.15	285		<b>270</b> [M+H-CH <sub>3</sub> ] <sup>+</sup> , 214 [M+H-CH <sub>3</sub> -2CO] <sup>+</sup> , 253 [M+H-CH <sub>3</sub> OH] <sup>+</sup> , 225 [M+H-CH <sub>3</sub> OH-CO] <sup>+</sup> , 229 [M+H-2CO] <sup>+</sup> , 241 [M+H-CO <sub>2</sub> ] <sup>+</sup> , 152 [ <sup>1,3</sup> A] <sup>+</sup>	Biochanin-A
<b>F4</b>	20.98	301		269 [M+H-CH <sub>3</sub> OH] <sup>+</sup> , 165 [ <sup>1,3</sup> B] <sup>+</sup> , <b>153</b> [ <sup>2,3</sup> B] <sup>+</sup> , 121 [ <sup>2,3</sup> B-CH <sub>3</sub> OH] <sup>+</sup> , 151 [ <sup>0,3</sup> B-CH <sub>3</sub> OH] <sup>+</sup> , 147 [M+H-ringB] <sup>+</sup> , 137 [ <sup>1,3</sup> A] <sup>+</sup> , 106 [ <sup>1,3</sup> A-OCH <sub>3</sub> ] <sup>+</sup>	10-Hydroxy-3,9-dimethoxypterocarpan
<b>F5</b>	24.57	285, 533	283	<b>270</b> [M+H-CH <sub>3</sub> ] <sup>+</sup> , 214 [M+H-CH <sub>3</sub> -2CO] <sup>+</sup> , 253 [M+H-CH <sub>3</sub> OH] <sup>+</sup> , 225 [M+H-CH <sub>3</sub> OH-CO] <sup>+</sup> , 229 [M+H-2CO] <sup>+</sup> , 241 [M+H-CO <sub>2</sub> ] <sup>+</sup> , 137 [ <sup>1,3</sup> A+H] <sup>+</sup>	Calycosin-7-O-β-D-glycoside-6''-O-malonate
<b>F6</b>	26.23	269, 431	267	<b>254</b> [M+H-CH <sub>3</sub> ] <sup>+</sup> , 198 [M+H-CH <sub>3</sub> -2CO] <sup>+</sup> , 237 [M+H-CH <sub>3</sub> OH] <sup>+</sup> , 209 [M+H-CH <sub>3</sub> OH-CO] <sup>+</sup> , 213 [M+H-2CO] <sup>+</sup> , 225 [M+H-CO <sub>2</sub> ] <sup>+</sup> , 136 [ <sup>1,3</sup> A] <sup>+</sup>	Ononin
<b>F7</b>	28.58	285, 533	283	<b>270</b> [M+H-CH <sub>3</sub> ] <sup>+</sup> , 214 [M+H-CH <sub>3</sub> -2CO] <sup>+</sup> , 253 [M+H-CH <sub>3</sub> OH] <sup>+</sup> , 225 [M+H-CH <sub>3</sub> OH-CO] <sup>+</sup> , 229 [M+H-2CO] <sup>+</sup> , 241 [M+H-CO <sub>2</sub> ] <sup>+</sup> , 152 [ <sup>1,3</sup> A] <sup>+</sup>	5-Hydroxy-4'-methoxyisoflavone-7-O-β-D-glycoside-6''-O-malonate
<b>F8</b>	30.62	463, 301	299	269 [M+H-CH <sub>3</sub> OH] <sup>+</sup> , 179 [ <sup>1,3</sup> B] <sup>+</sup> , <b>167</b> [ <sup>2,3</sup> B] <sup>+</sup> , 152 [ <sup>2,3</sup> B-CH <sub>3</sub> ] <sup>+</sup> , 133 [ <sup>0,3</sup> B-2CH <sub>3</sub> OH] <sup>+</sup> , 147 [M+H-ringB] <sup>+</sup> , 123 [ <sup>1,3</sup> A] <sup>+</sup> , 105 [ <sup>1,3</sup> A-H <sub>2</sub> O] <sup>+</sup>	9,10-Dimethoxypterocarpan-3-O-β-D-glycoside
<b>F9</b>	31.58	465, 303	301	271 [M+H-CH <sub>3</sub> OH] <sup>+</sup> , 181 [ <sup>1,3</sup> B] <sup>+</sup> , 167 [ <sup>2,3</sup> B] <sup>+</sup> , 152 [ <sup>2,3</sup> B-CH <sub>3</sub> ] <sup>+</sup> , 133 [ <sup>0,3</sup> B-2CH <sub>3</sub> OH] <sup>+</sup> , 149 [M+H-ringB] <sup>+</sup> , <b>123</b> [ <sup>1,3</sup> A] <sup>+</sup> , 105 [ <sup>1,3</sup> A-H <sub>2</sub> O] <sup>+</sup>	2'-Hydroxy-3',4'-dimethoxyisoflavan-7-O-β-D-glycoside
<b>F10</b>	32.46	285	283	<b>270</b> [M+H-CH <sub>3</sub> ] <sup>+</sup> , 214 [M+H-CH <sub>3</sub> -2CO] <sup>+</sup> , 253 [M+H-CH <sub>3</sub> OH] <sup>+</sup> , 225 [M+H-CH <sub>3</sub> OH-CO] <sup>+</sup> , 229 [M+H-2CO] <sup>+</sup> , 241 [M+H-CO <sub>2</sub> ] <sup>+</sup> , 137 [ <sup>1,3</sup> A+H] <sup>+</sup>	Calycosin
<b>F11</b>	34.53	315		<b>300</b> [M+H-CH <sub>3</sub> ] <sup>+</sup> , 244 [M+H-CH <sub>3</sub> -2CO] <sup>+</sup> , 283 [M+H-CH <sub>3</sub> OH] <sup>+</sup> , 255 [M+H-CH <sub>3</sub> OH-CO] <sup>+</sup> , 259 [M+H-2CO] <sup>+</sup> , 271 [M+H-CO <sub>2</sub> ] <sup>+</sup> , 167 [ <sup>1,3</sup> A+H] <sup>+</sup>	Odoratin
<b>F12</b>	39.00	269, 517	267	<b>254</b> [M+H-CH <sub>3</sub> ] <sup>+</sup> , 198 [M+H-CH <sub>3</sub> -2CO] <sup>+</sup> , 237 [M+H-CH <sub>3</sub> OH] <sup>+</sup> , 209 [M+H-CH <sub>3</sub> OH-CO] <sup>+</sup> , 213 [M+H-2CO] <sup>+</sup> , 225 [M+H-CO <sub>2</sub> ] <sup>+</sup> , 136 [ <sup>1,3</sup> A] <sup>+</sup>	Formononetin-7-O-β-D-glycoside-6''-O-malonate
<b>F13</b>	40.97	301, 549	299	269 [M+H-CH <sub>3</sub> OH] <sup>+</sup> , 179 [ <sup>1,3</sup> B] <sup>+</sup> , <b>167</b> [ <sup>2,3</sup> B] <sup>+</sup> , 152 [ <sup>2,3</sup> B-CH <sub>3</sub> ] <sup>+</sup> , 133 [ <sup>0,3</sup> B-2CH <sub>3</sub> OH] <sup>+</sup> , 147 [M+H-ringB] <sup>+</sup> , 123 [ <sup>1,3</sup> A] <sup>+</sup> , 105 [ <sup>1,3</sup> A-H <sub>2</sub> O] <sup>+</sup>	Astrapterocarpan-3-O-β-D-glycoside-6''-O-malonate
<b>F14</b>	45.82	303, 551	301	271 [M+H-CH <sub>3</sub> OH] <sup>+</sup> , 181 [ <sup>1,3</sup> B] <sup>+</sup> , 167 [ <sup>2,3</sup> B] <sup>+</sup> , 152 [ <sup>2,3</sup> B-CH <sub>3</sub> ] <sup>+</sup> , 133 [ <sup>0,3</sup> B-2CH <sub>3</sub> OH] <sup>+</sup> , 149 [M+H-ringB] <sup>+</sup> , <b>123</b> [ <sup>1,3</sup> A] <sup>+</sup> , 105 [ <sup>1,3</sup> A-H <sub>2</sub> O] <sup>+</sup>	Astraisoflavan-7-O-β-D-glycoside-6''-O-malonate
<b>F15</b>	47.95	269	267	<b>254</b> [M+H-CH <sub>3</sub> ] <sup>+</sup> , 198 [M+H-CH <sub>3</sub> -2CO] <sup>+</sup> , 237 [M+H-CH <sub>3</sub> OH] <sup>+</sup> , 209 [M+H-CH <sub>3</sub> OH-CO] <sup>+</sup> , 213 [M+H-2CO] <sup>+</sup> , 225 [M+H-CO <sub>2</sub> ] <sup>+</sup> , 136 [ <sup>1,3</sup> A] <sup>+</sup>	Formononetin
<b>F16</b>	48.65	301	299	269 [M+H-CH <sub>3</sub> OH] <sup>+</sup> , 179 [ <sup>1,3</sup> B] <sup>+</sup> , <b>167</b> [ <sup>2,3</sup> B] <sup>+</sup> , 152 [ <sup>2,3</sup> B-CH <sub>3</sub> ] <sup>+</sup> , 133 [ <sup>0,3</sup> B-2CH <sub>3</sub> OH] <sup>+</sup> , 147 [M+H-ringB] <sup>+</sup> , 123 [ <sup>1,3</sup> A] <sup>+</sup> , 105 [ <sup>1,3</sup> A-H <sub>2</sub> O] <sup>+</sup>	3-Hydroxy-9,10-dimethoxypterocarpan
<b>F17</b>	49.91	303		271 [M+H-CH <sub>3</sub> OH] <sup>+</sup> , 181 [ <sup>1,3</sup> B] <sup>+</sup> , 167 [ <sup>2,3</sup> B] <sup>+</sup> , 152 [ <sup>2,3</sup> B-CH <sub>3</sub> ] <sup>+</sup> , 133 [ <sup>0,3</sup> B-2CH <sub>3</sub> OH] <sup>+</sup> , 149 [M+H-ringB] <sup>+</sup> , <b>123</b> [ <sup>1,3</sup> A] <sup>+</sup> , 105 [ <sup>1,3</sup> A-H <sub>2</sub> O] <sup>+</sup>	7,2'-Dihydroxy-3',4'-dimethoxyisoflavan

The boldfaced one is the base peak.

Peak **F15** eluted at 48.95 min and showed an intense [M+H]<sup>+</sup> at  $m/z$  269 and [M-H]<sup>-</sup> at  $m/z$  267, which confirmed the molar mass to be 268. It is noteworthy that it also produced ions at  $m/z$  254, 198, 237, 209, 213, 225 and 136. Compared with the information of reference compounds, it was therefore identified as formononetin. Peaks **F6** and **F12** showed the intense [M+H]<sup>+</sup> at  $m/z$  431 and 517. During the LC-MS<sup>2</sup> experiment, these two ions both formed  $m/z$  269 ions required the losses of 162 and 248 Da neutral fragments, respectively. The two  $m/z$  269 ions followed same fragmentation pathway with formononetin (Table 1). So a conclusion can be reached that compounds corresponding to peaks **F6** and **F12**

are ononin and formononetin-7-O-β-D-glycoside-6''-O-malonate, respectively.

The intense [M+H]<sup>+</sup> of peak **F3** was at  $m/z$  285 and it fragmented in a similar way with formononetin in the LC-MS<sup>n</sup> experiment. As the [<sup>1,3</sup>A]<sup>+</sup> ion was at  $m/z$  152, it was identified as biochanin-A. Peak **F7** had the intense [M+H]<sup>+</sup> at  $m/z$  533, which formed  $m/z$  285 ion by the loss of 248 Da fragments. And the  $m/z$  285 ion showed same fragmentation behavior with peak **F3** (Table 1). So it can be concluded that compound of peak **F7** is 5-Hydroxy-4'-methoxyisoflavone-7-O-β-D-glycoside-6''-O-malonate. Consequently, compounds corresponding to peaks

**F3**, **F6**, **F7**, **F12** and **F15** presented the similar fragmentation pathway and the  $[^{1,3}A]^+$  ion is the characteristic of this type isoflavones.

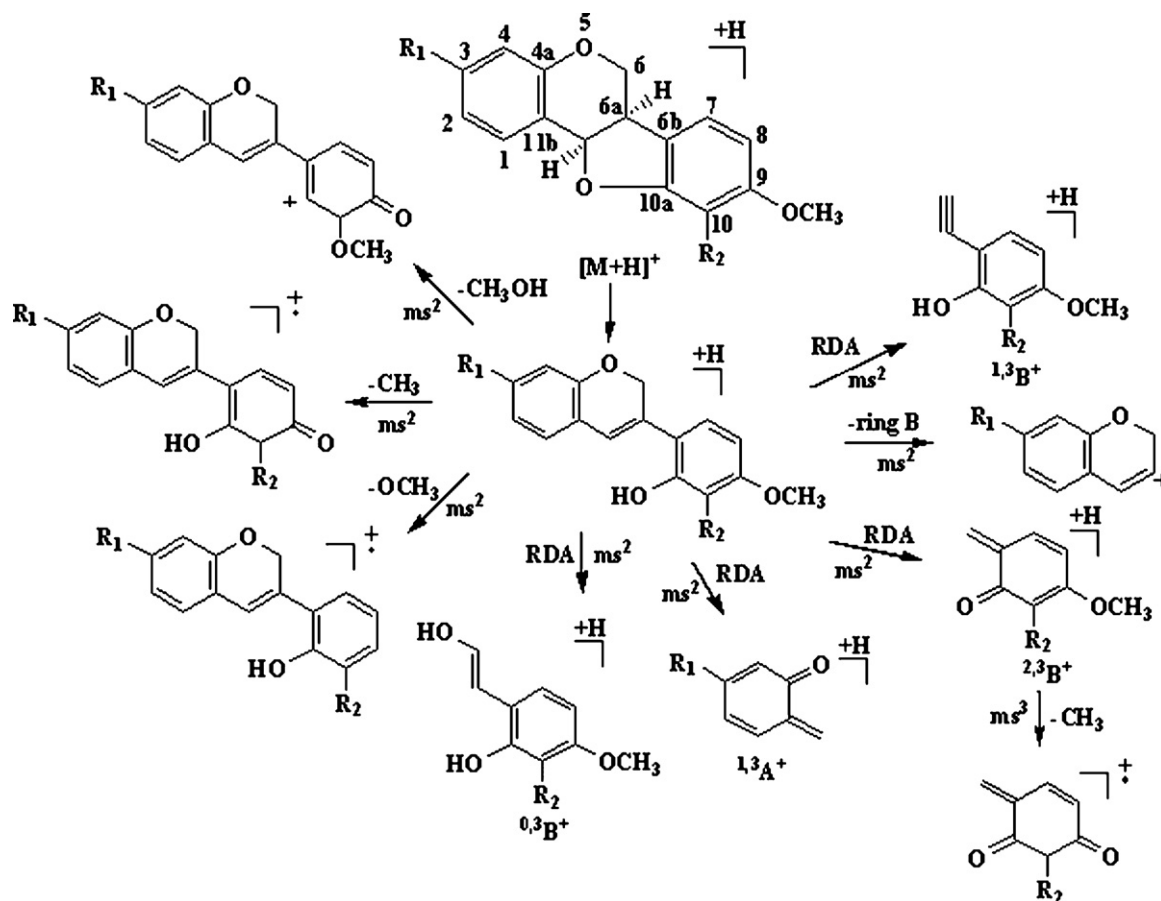
The  $[M+H]^+$  ion of peak **F16** was at  $m/z$  301 and the  $[M-H]^-$  ion was at  $m/z$  299. The product ion at  $m/z$  269 arose from the neutral loss of  $CH_3OH$ , owing to the cleavage of  $OCH_3$  at C-4'. The ion at  $m/z$  147 corresponded to the loss of B-ring, a diagnostic fragment that not presented in the fragmentation of isoflavones. The abundant fragment  $[^{2,3}B]^+$  ion at  $m/z$  167,  $[^{1,3}B]^+$  ion at  $m/z$  179 and  $[^{1,3}A]^+$  ion at  $m/z$  123 were produced in the RDA rearrangement procedure. In addition, the other product ions were  $[^{2,3}B-CH_3]^+$  ion at  $m/z$  152,  $[^{0,3}B-2CH_3OH]^+$  ion at  $m/z$  133 and  $[^{1,3}A-H_2O]^+$  ion at  $m/z$  105 due to the concurrent losses. Comparing the above data with the reference compounds and literatures [9], the compound of peak **F16** presented the characteristic fragmentation pathway of pterocarpan, so it was identified as 3-hydroxy-9,10-dimethoxypterocarpan. Peaks **F8** and **F13** showed the  $[M+H]^+$  at  $m/z$  463 and 549 both directly gave the product ions at  $m/z$  301 by losing hexose residue (162 Da) and malonylglucosyl (248 Da), respectively. The fragment ions of the  $m/z$  301 ion were consistent with that of peak **F16**. Based on the above results, peaks **F8** and **F13** were tentatively identified as 9,10-dimethoxypterocarpan-3-O- $\beta$ -D-glycoside and astrapterocarpan-3-O- $\beta$ -D-glycoside-6''-O-malonate.

The intense  $[M+H]^+$  of peak **F4** was at  $m/z$  301. In the LC-MS<sup>n</sup> experiment, the precursor ion fragmented in a similar way with peak **F16**. The abundant  $[^{2,3}B]^+$  ion was at  $m/z$  153 and the  $[M+H-ringB]^+$  ion was at  $m/z$  147. Therefore, it was identified as 10-hydroxy-3,9-dimethoxypterocarpan. The above analysis demonstrated that compound corresponding to peaks **F4**, **F8**, **F13** and **F16** presented the similar fragmentation pathway. The  $[^{2,3}B]^+$ ,

$[M+H-ringB]^+$  and  $[^{1,3}A]^+$  ions are the characteristics of this type isoflavonoids, pterocarpan.

Peak **F17** showed the  $[M+H]^+$  at  $m/z$  303 with high abundance and fragmented in a same way as pterocarpan. The only difference between them is that pterocarpan yielded the  $[^{2,3}B]^+$  ion as the most predominant fragments, whereas peak **F17** produced  $[^{1,3}A]^+$  ion as the base peak. Comparing the characteristic fragmentation with that of pterocarpan and structures of isoflavonoids, the compound corresponding to peak **F17** was identified of isoflavan type and as 7,2'-dihydroxy-3',4'-dimethoxyisoflavan. Peaks **F9** and **F14** showed the  $[M+H]^+$  at  $m/z$  465 and 551, which directly gave the product ion at  $m/z$  303 by loss of hexose residue (162 Da) and malonylglucosyl (248 Da) fragment, respectively. And the fragment ions of the  $m/z$  301 ion were consistent with that of peak **F17**. On the basis of the above results, peaks **F9** and **F14** were tentatively identified as 2'-hydroxy-3',4'-dimethoxyisoflavan-7-O- $\beta$ -D-glycoside and astraisoflavan-7-O- $\beta$ -D-glycoside-6''-O-malonate. The  $[M+H]^+$  of peak **F1** was at  $m/z$  289, which fragmented in a similar way with peak **F17**. The base peak  $[^{1,3}A]^+$  ion was at  $m/z$  123 and the  $[M+H-ringB]^+$  ion was at  $m/z$  149. Therefore, it was identified as 7,2',3'-Trihydroxy-4'-methoxyisoflavan. The above analysis demonstrated that compound corresponding to peaks **F1**, **F9**, **F14** and **F17** presented the similar fragmentation pathway. The  $[^{1,3}A]^+$ ,  $[M+H-ringB]^+$  and  $[^{2,3}B]^+$  ions are the characteristics of this type isoflavonoids, isoflavans. For clarity, the main fragmentation mechanisms of the pterocarpan and isoflavans are summarized in Scheme 2.

In addition, peak **1** showed an intense  $[M+Na]^+$  at  $m/z$  365 and  $[M-H]^-$  at  $m/z$  341, which confirmed the molar mass to be 342. It is noteworthy that the product ions at  $m/z$  203 and 185 corresponding to  $[hexose+Na]^+$  and  $[hexose-H_2O+Na]^+$ , respectively. Compared



Scheme 2. Main MS<sup>n</sup> fragmentation pathways of pterocarpan.

**Table 2**  
The retention time ( $t_R$ ), ESI-MS<sup>n</sup> and elucidation of the astragalosides in the methanol extract of Radix Astragali.

No.	$t_R$ (min)	M (+)	M (-)	MS <sup>n</sup>	Identification
S1	22.41	491	489	473 [M+H-H <sub>2</sub> O] <sup>+</sup> , 455 [M+H-2H <sub>2</sub> O] <sup>+</sup> , 437 [M+H-3H <sub>2</sub> O] <sup>+</sup> , 419 [M+H-4H <sub>2</sub> O] <sup>+</sup> , 401 [M+H-5H <sub>2</sub> O] <sup>+</sup> , 297 [M+H-3H <sub>2</sub> O-(25-hydroxy-20,24-epoxy residue)] <sup>+</sup>	Cycloastragenol
S2	40.41	947	945	815 [M+H-xyl] <sup>+</sup> , 785 [M+H-glc] <sup>+</sup> , 623 [M+H-2glc] <sup>+</sup> , 643 [M+H-(25-glc-20,24-epoxy residue)] <sup>+</sup> , 605 [M+H-2glc-H <sub>2</sub> O] <sup>+</sup> , 491 [M+H-2glc-xyl] <sup>+</sup> , 473 [M+H-2glc-xyl-H <sub>2</sub> O] <sup>+</sup> , 455 [M+H-2glc-xyl-2H <sub>2</sub> O] <sup>+</sup> , 437 [M+H-2glc-xyl-3H <sub>2</sub> O] <sup>+</sup> , 419 [M+H-2glc-xyl-4H <sub>2</sub> O] <sup>+</sup> , 297 [M+H-2glc-xyl-3H <sub>2</sub> O-(25-hydroxy-20,24-epoxy residue)] <sup>+</sup>	Astragaloside VII
S3	42.00	947	945	785 [M+H-glc] <sup>+</sup> , 623 [M+H-2glc] <sup>+</sup> , 653 [M+H-glc-xyl] <sup>+</sup> , 605 [M+H-2glc-H <sub>2</sub> O] <sup>+</sup> , 491 [M+H-2glc-xyl] <sup>+</sup> , 473 [M+H-2glc-xyl-H <sub>2</sub> O] <sup>+</sup> , 455 [M+H-2glc-xyl-2H <sub>2</sub> O] <sup>+</sup> , 437 [M+H-2glc-xyl-3H <sub>2</sub> O] <sup>+</sup> , 419 [M+H-2glc-xyl-4H <sub>2</sub> O] <sup>+</sup> , 297 [M+H-2glc-xyl-3H <sub>2</sub> O-(25-hydroxy-20,24-epoxy residue)] <sup>+</sup>	Astragaloside VI
S4	46.10	989	987	927 [M+H-CH <sub>3</sub> COOH] <sup>+</sup> , 605 [M+H-CH <sub>3</sub> COOH-2glc] <sup>+</sup> , 685 [M+H-(25-glc-20,24-epoxy residue)] <sup>+</sup> , 629 [M+H-2glc-2H <sub>2</sub> O] <sup>+</sup> , 611 [M+H-2glc-3H <sub>2</sub> O] <sup>+</sup> , 813 [M+H-acetylxy] <sup>+</sup> , 491 [M+H-acetylxy-2glc] <sup>+</sup> , 473 [M+H-acetylxy-2glc-H <sub>2</sub> O] <sup>+</sup> , 455 [M+H-acetylxy-2glc-2H <sub>2</sub> O] <sup>+</sup> , 437 [M+H-acetylxy-2glc-3H <sub>2</sub> O] <sup>+</sup> , 419 [M+H-acetylxy-2glc-4H <sub>2</sub> O] <sup>+</sup> , 297 [M+H-acetylxy-2glc-3H <sub>2</sub> O-(25-hydroxy-20,24-epoxy residue)] <sup>+</sup>	Agroastragaloside IV
S5	46.89	1893, 947	945	785 [M+H-glc] <sup>+</sup> , 623 [M+H-2glc] <sup>+</sup> , 653 [M+H-glc-xyl] <sup>+</sup> , 643 [M+H-(25-glc-20,24-epoxy residue)] <sup>+</sup> , 605 [M+H-2glc-H <sub>2</sub> O] <sup>+</sup> , 491 [M+H-2glc-xyl] <sup>+</sup> , 473 [M+H-2glc-xyl-H <sub>2</sub> O] <sup>+</sup> , 455 [M+H-2glc-xyl-2H <sub>2</sub> O] <sup>+</sup> , 437 [M+H-2glc-xyl-3H <sub>2</sub> O] <sup>+</sup> , 419 [M+H-2glc-xyl-4H <sub>2</sub> O] <sup>+</sup> , 297 [M+H-2glc-xyl-3H <sub>2</sub> O-(25-hydroxy-20,24-epoxy residue)] <sup>+</sup>	Astragaloside V
S6	48.52	1569, 785	783	653 [M+H-xyl] <sup>+</sup> , 623 [M+H-glc] <sup>+</sup> , 605 [M+H-glc-H <sub>2</sub> O] <sup>+</sup> , 491 [M+H-xyl-glc] <sup>+</sup> , 473 [M+H-xyl-glc-H <sub>2</sub> O] <sup>+</sup> , 455 [M+H-xyl-glc-2H <sub>2</sub> O] <sup>+</sup> , 437 [M+H-xyl-glc-3H <sub>2</sub> O] <sup>+</sup> , 419 [M+H-xyl-glc-4H <sub>2</sub> O] <sup>+</sup> , 297 [M+H-xyl-glc-3H <sub>2</sub> O-(25-hydroxy-20,24-epoxy residue)] <sup>+</sup>	Astragaloside IV
S7	50.09	1031	1029	971 [M+H-CH <sub>3</sub> COOH] <sup>+</sup> , 911 [M+H-2CH <sub>3</sub> COOH] <sup>+</sup> , 749 [M+H-2CH <sub>3</sub> COOH-glc] <sup>+</sup> , 587 [M+H-2CH <sub>3</sub> COOH-2glc] <sup>+</sup> , 727 [M+H-(25-glc-20,24-epoxy residue)] <sup>+</sup> , 671 [M+H-2glc-2H <sub>2</sub> O] <sup>+</sup> , 653 [M+H-2glc-3H <sub>2</sub> O] <sup>+</sup> , 815 [M+H-2acetylxy] <sup>+</sup> , 491 [M+H-2acetylxy-2glc] <sup>+</sup> , 473 [M+H-2acetylxy-2glc-H <sub>2</sub> O] <sup>+</sup> , 455 [M+H-2acetylxy-2glc-2H <sub>2</sub> O] <sup>+</sup> , 437 [M+H-2acetylxy-2glc-3H <sub>2</sub> O] <sup>+</sup> , 419 [M+H-2acetylxy-2glc-4H <sub>2</sub> O] <sup>+</sup> , 297 [M+H-2acetylxy-2glc-3H <sub>2</sub> O-(25-hydroxy-20,24-epoxy residue)] <sup>+</sup>	Agroastragaloside III
S8	51.01	1653, 827	825	767 [M+H-CH <sub>3</sub> COOH] <sup>+</sup> , 605 [M+H-CH <sub>3</sub> COOH-glc] <sup>+</sup> , 647 [M+H-glc-H <sub>2</sub> O] <sup>+</sup> , 629 [M+H-glc-2H <sub>2</sub> O] <sup>+</sup> , 653 [M+H-acetylxy] <sup>+</sup> , 491 [M+H-acetylxy-glc] <sup>+</sup> , 473 [M+H-acetylxy-glc-H <sub>2</sub> O] <sup>+</sup> , 455 [M+H-acetylxy-glc-2H <sub>2</sub> O] <sup>+</sup> , 437 [M+H-acetylxy-glc-3H <sub>2</sub> O] <sup>+</sup> , 419 [M+H-acetylxy-glc-4H <sub>2</sub> O] <sup>+</sup> , 297 [M+H-acetylxy-glc-3H <sub>2</sub> O-(25-hydroxy-20,24-epoxy residue)] <sup>+</sup>	Astragaloside II
S9	52.34	1653, 827	825	767 [M+H-CH <sub>3</sub> COOH] <sup>+</sup> , 605 [M+H-CH <sub>3</sub> COOH-glc] <sup>+</sup> , 647 [M+H-glc-H <sub>2</sub> O] <sup>+</sup> , 629 [M+H-glc-2H <sub>2</sub> O] <sup>+</sup> , 653 [M+H-acetylxy] <sup>+</sup> , 491 [M+H-acetylxy-glc] <sup>+</sup> , 473 [M+H-acetylxy-glc-H <sub>2</sub> O] <sup>+</sup> , 455 [M+H-acetylxy-glc-2H <sub>2</sub> O] <sup>+</sup> , 437 [M+H-acetylxy-glc-3H <sub>2</sub> O] <sup>+</sup> , 419 [M+H-acetylxy-glc-4H <sub>2</sub> O] <sup>+</sup> , 297 [M+H-acetylxy-glc-3H <sub>2</sub> O-(25-hydroxy-20,24-epoxy residue)] <sup>+</sup>	Isoastragaloside II
S10	55.19	1737, 869	867	809 [M+H-CH <sub>3</sub> COOH] <sup>+</sup> , 749 [M+H-2CH <sub>3</sub> COOH] <sup>+</sup> , 647 [M+H-CH <sub>3</sub> COOH-glc] <sup>+</sup> , 587 [M+H-2CH <sub>3</sub> COOH-glc] <sup>+</sup> , 689 [M+H-glc-H <sub>2</sub> O] <sup>+</sup> , 671 [M+H-glc-2H <sub>2</sub> O] <sup>+</sup> , 653 [M+H-2acetylxy] <sup>+</sup> , 491 [M+H-2acetylxy-glc] <sup>+</sup> , 473 [M+H-2acetylxy-glc-H <sub>2</sub> O] <sup>+</sup> , 455 [M+H-2acetylxy-glc-2H <sub>2</sub> O] <sup>+</sup> , 437 [M+H-2acetylxy-glc-3H <sub>2</sub> O] <sup>+</sup> , 419 [M+H-2acetylxy-glc-4H <sub>2</sub> O] <sup>+</sup> , 297 [M+H-2acetylxy-glc-3H <sub>2</sub> O-(25-hydroxy-20,24-epoxy residue)] <sup>+</sup>	Astragaloside I
S11	56.39	1737, 869	867	809 [M+H-CH <sub>3</sub> COOH] <sup>+</sup> , 749 [M+H-2CH <sub>3</sub> COOH] <sup>+</sup> , 647 [M+H-CH <sub>3</sub> COOH-glc] <sup>+</sup> , 587 [M+H-2CH <sub>3</sub> COOH-glc] <sup>+</sup> , 689 [M+H-glc-H <sub>2</sub> O] <sup>+</sup> , 671 [M+H-glc-2H <sub>2</sub> O] <sup>+</sup> , 653 [M+H-2acetylxy] <sup>+</sup> , 491 [M+H-2acetylxy-glc] <sup>+</sup> , 473 [M+H-2acetylxy-glc-H <sub>2</sub> O] <sup>+</sup> , 455 [M+H-2acetylxy-glc-2H <sub>2</sub> O] <sup>+</sup> , 437 [M+H-2acetylxy-glc-3H <sub>2</sub> O] <sup>+</sup> , 419 [M+H-2acetylxy-glc-4H <sub>2</sub> O] <sup>+</sup> , 297 [M+H-2acetylxy-glc-3H <sub>2</sub> O-(25-hydroxy-20,24-epoxy residue)] <sup>+</sup>	Isoastragaloside I

Table 2 (Continued)

No.	$t_R$ (min)	M (+)	M (-)	MS <sup>n</sup>	Identification
<b>S12</b>	61.36	1821, 911	909	851 [M+H-CH <sub>3</sub> COOH] <sup>+</sup> , 731 [M+H-3CH <sub>3</sub> COOH] <sup>+</sup> , 689 [M+H-CH <sub>3</sub> COOH-glc] <sup>+</sup> , 551 [M+H-3CH <sub>3</sub> COOH-glc] <sup>+</sup> , 731 [M+H-glc-H <sub>2</sub> O] <sup>+</sup> , 713[M+H-glc-2H <sub>2</sub> O] <sup>+</sup> , 653 [M+H-3acetylxl] <sup>+</sup> , 491 [M+H-3acetylxl-glc] <sup>+</sup> , 473 [M+H-2acetylxl-glc-H <sub>2</sub> O] <sup>+</sup> , 455 [M+H-2acetylxl-glc-2H <sub>2</sub> O] <sup>+</sup> , 437 [M+H-2acetylxl-glc-3H <sub>2</sub> O] <sup>+</sup> , 419 [M+H-2acetylxl-glc-4H <sub>2</sub> O] <sup>+</sup> , 297 [M+H-2acetylxl-glc-3H <sub>2</sub> O-(25-hydroxy-20,24-epoxy residue)] <sup>+</sup>	Acetylastragaloside I

with the information of literature, [27] it was therefore identified as sucrose.

### 3.1.2. Analysis of astragalosides by LC-ESI-MS<sup>n</sup>

Astragaloside IV was analyzed by LC-MS<sup>n</sup> firstly to obtain the retention time and characteristic fragmentation pathway data. Then the LC-MS<sup>n</sup> method was performed on the astragalosides in crude methanol extract of Radix Astragali and the data of retention time ( $t_R$ ), ESI-MS<sup>n</sup> and the elucidation of individual peak are listed in Table 2. By comparing the above data of the analyzed astragalosides with that of reference compound and in the literature, 12 astragalosides have been unambiguously identified or tentatively characterized. The EIC of analyzed astragalosides are shown in Fig. 3.

The retention time of astragaloside IV is at 48.52 min. The [M+H]<sup>+</sup> was at  $m/z$  785, the  $m/z$  1569 ion was the [2M+H]<sup>+</sup> and the [M-H]<sup>-</sup> was at  $m/z$  783. The LC-MS<sup>n</sup> data were obtained in the positive ion mode. The product ions at  $m/z$  653 and 623 arose from the eliminations of xylose (132 Da) and hexose (162 Da) fragments, respectively. The ion at  $m/z$  491 was produced from the simultaneous losses of a xylose and a hexose residue, owing to two different terminal residues were in the structure of astragaloside IV. In addition, the other product ions were at  $m/z$  473, 455, 437 and 419 due to the successive losses of several H<sub>2</sub>O molecules from the aglycone moiety. The ion at  $m/z$  297 corresponded to the loss of 25-hydroxy-20,24-epoxy residue (140 Da) at C-17 from the  $m/z$  437 ion.

As shown in Table 2, peaks **S1** to **S12** all displayed the characteristic ions at  $m/z$  473, 455, 437, 419 and 297, were consisted with astragaloside IV. It demonstrated that all of these astragalosides were of 9,19-cyclolanostane aglycone and the differences of sugar moieties could distinguish them. On the basis of the retention time and MS<sup>n</sup> data of reference compound, peak **S6** was unambiguously identified as astragaloside IV. Peak **S1** did not produce the fragment ion by

losing sugar moieties, so it was identified as cycloastragenol. Peaks **S2**, **S3** and **S5** presented the [M+H]<sup>+</sup> at  $m/z$  947 and [M-H]<sup>-</sup> at  $m/z$  945 in the LC-MS experiment. The  $m/z$  947 ion of Peak **S2** formed the [M+H-132]<sup>+</sup>, [M+H-162]<sup>+</sup> and [M+H-162-162]<sup>+</sup> indicated this compound had a xylose and two glucose terminal residues. The product ion at  $m/z$  643 from loss of 25-glc-20,24-epoxy residue at C-17 demonstrated one glucose residue was at C-25. Thus, compound of peak **S2** was ascribed to astragaloside VII. In the case of peak **S3**, it showed [M+H-162]<sup>+</sup>, [M+H-162-162]<sup>+</sup> and [M+H-162-132]<sup>+</sup>. It concluded that this compound had a xylose and two glucose residues. No [M+H-xy]<sup>+</sup> indicated one glucose residue was linked to the xylose. So compound corresponding to peak **S3** was astragaloside VI. For peak **S5**, the only difference between it and peak **S3** was the [M+H-(25-glc-20,24-epoxy residue)]<sup>+</sup>, so compound of peak **S5** was astragaloside V.

Peaks **S4**, **S7** to **S12** all gave the fragment ions by losing acetic acid, owing to the acetyl group in the structure. According to the fragment ions of peak **S4** (Table 2), it had a xylose and two glucose residues, an acetyl group linked to the xylose and one glucose residue at C-25. The above information coincided with the structure of agroastragaloside IV, so peak **S4** was identified. Take peak **S7** into account, comparing the fragment ions of it with that of peak **S4** and the only difference was peak **S7** had one more acetyl group in the xylose than peak **S4**. So compound of peak **S7** was identified as agroastragaloside III.

Peak **S8** showed the same MS<sup>n</sup> behaviors with peak **S9**. Its full scan mass spectrum presented the [M+H]<sup>+</sup> ion at  $m/z$  827, [2M+H]<sup>+</sup> ion at  $m/z$  1653 and [M-H]<sup>-</sup> ion at  $m/z$  825. The fragmentation of them proved the existence of a xylose linked an acetyl group and a glyucose residue. According to the literature data [11] and the content difference, peaks **S8** and **S9** were tentatively identified as astragaloside II and isoastragaloside II, respectively. Similarly, peaks **S10** and **S11** were tentatively assigned to astragaloside I and isoastragaloside I, respectively. As peak **S12** just had one more acetyl

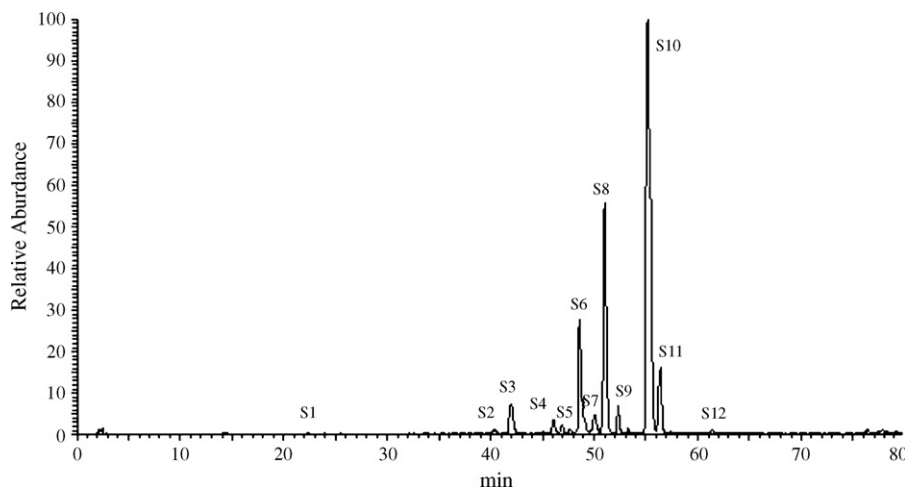
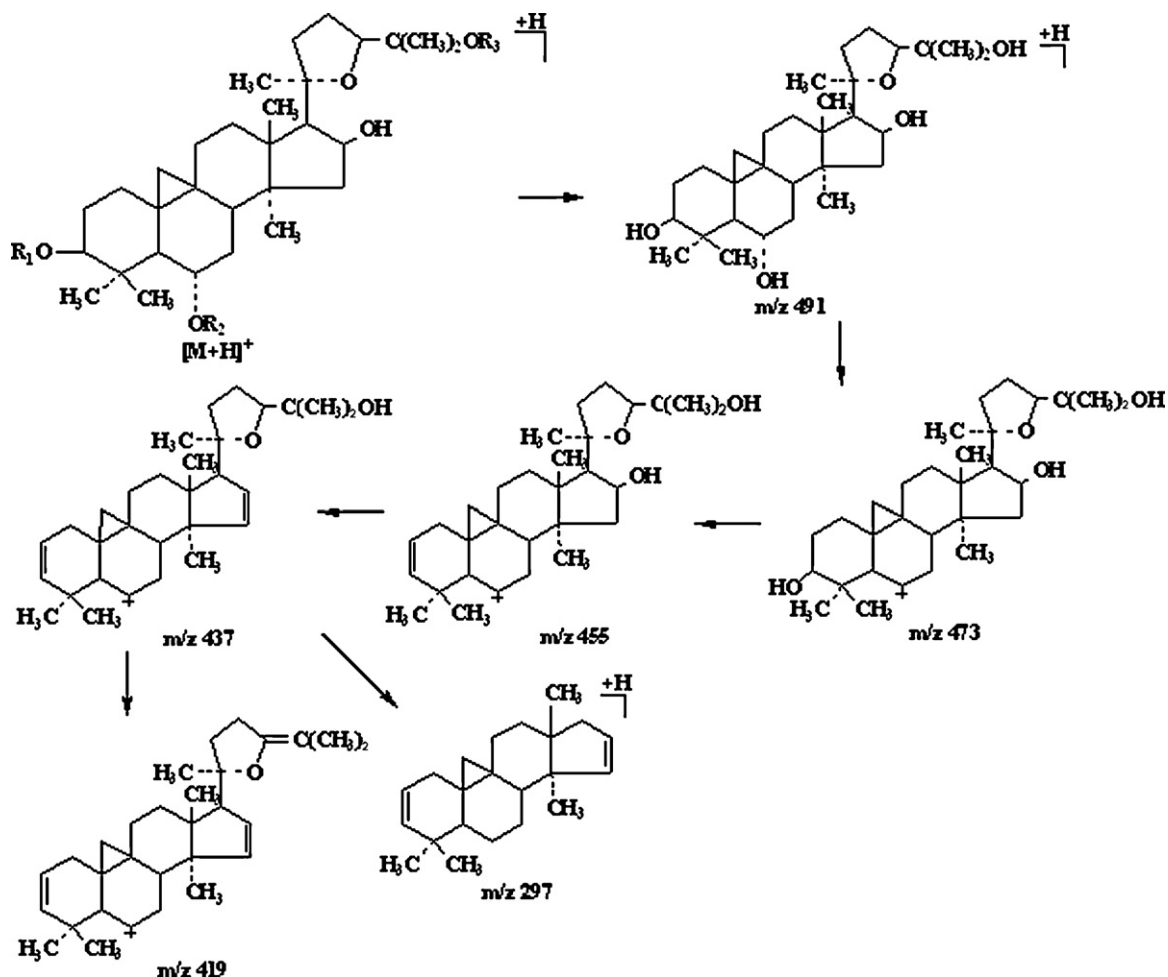


Fig. 3. The EIC chromatogram of the astragalosides in the methanol extracts of Radix Astragali.



Scheme 3. Main MS<sup>n</sup> fragmentation pathways of astragaloside IV.

group in the xylose than peak **S10**, it was therefore ascribed to acetylastragaloside I.

The analyzed astragalosides possessed the same skeletal structure, the 9,19-cyclolanostane aglycone system. The similarity of structure results in similar fragmentation pathway. On the basis of the diagnostic fragment ions, the acetyl group, xylose and glucose residues, identification of those astragalosides can be achieved. For clarity, the main fragmentation mechanisms of the astragalosides are summarized in Scheme 3.

### 3.1.3. Analysis of Radix Astragali samples from different planting area and of different growth years by LC-ESI-MS<sup>n</sup>

The LC-ESI-MS<sup>n</sup> method was applied to qualitative and quantitative analysis of the Radix Astragali samples from Helong City and of different growth years. The information of different samples was shown in Table 3. The LC-UV and LC-TIC spectra were obtained. The relative peak area method was used for the quantitative analyses of the isoflavonoids and astragalosides. Calycosin was used as the reference standard in the analysis of isoflavonoids. The peak area ratio of other isoflavonoids to calycosin is the relative peak area, which could reflect the relative contents of analytes. Similarly, astragaloside IV was used as the standard reference in the analysis of astragalosides and the relative peak areas of them were obtained.

The relative peak areas of the identified isoflavonoids and astragalosides were presented in Table 4. Different samples contained different quantities of isoflavonoids and astragalosides and the results presented some regularity. Among samples 1–16, the relative peak areas of the isoflavonoids **F1**, **F2**, **F5**, **F6**, **F10**, **F12** and

**F15** were in relatively high level and the astragalosides **S3**, **S6**, **S7**, **S8**, **S9**, **S10** and **S11** were more abundant. The major isoflavonoids and astragalosides presented higher content in samples 8–16, relative lower in samples 4–7 and the lowest in samples 1–3. According to the sample information, the growth years are longer and the quantities are better in one to seven years. The different samples of the same growth year showed the similar level of content. Moreover, the relative peak areas of sucrose gave some

Table 3

The information of the Radix Astragali samples from Helong City and of different growth years.

Sample no.	Origins	Growth years
1	Helong City	1
2	Helong City	1
3	Helong City	1
4	Helong City	2
5	Helong City	2
6	Helong City	2
7	Helong City	2
8	Helong City	3
9	Helong City	3
10	Helong City	3
11	Helong City	3
12	Helong City	3
13	Helong City	3
14	Helong City	7
15	Helong City	7
16	Helong City	7

**Table 4**

The relative peak areas of the identified components and the results of antioxidant activity evaluations of different Radix Astragali samples.

Growth years	1	1	1	2	2	2	2	3	3	3	3	3	3	7	7	7
Sample no.	1	2	3	4	5	6	7	8	9	10	11	12	13	14	15	16
<b>1</b>	15.261	15.714	15.485	10.005	10.092	9.425	9.457	7.659	6.422	5.766	7.021	6.988	6.499	4.878	4.950	5.022
<b>F1</b>	0.999	0.962	0.981	1.141	1.816	0.922	0.569	3.013	0.620	1.525	0.708	0.692	0.550	0.662	1.092	0.929
<b>F2</b>	3.572	3.511	3.542	8.614	8.876	8.021	8.220	10.807	11.033	12.295	11.616	11.407	11.353	11.509	10.891	11.386
<b>F3</b>	0.147	0.193	0.170	0.709	0.760	0.612	0.380	0.668	0.114	0.802	0.305	0.477	0.388	0.609	0.692	0.770
<b>F4</b>	0.033	0.025	0.029	0.060	–	–	–	–	0.315	–	–	0.010	0.229	–	–	–
<b>F5</b>	0.423	0.264	0.343	2.011	1.647	3.185	3.487	2.485	6.922	4.417	4.714	3.629	3.359	6.077	5.691	5.593
<b>F6</b>	0.383	0.343	0.363	2.036	2.607	2.401	2.259	3.749	4.327	2.769	3.304	3.021	3.272	3.098	3.211	3.806
<b>F7</b>	0.049	0.048	0.048	0.505	0.356	0.254	0.135	0.549	0.295	0.891	0.056	0.155	0.090	0.910	0.607	0.186
<b>F8</b>	–	–	–	0.308	0.274	0.152	0.121	0.126	1.160	0.442	–	–	0.151	0.005	0.005	0.004
<b>F9</b>	0.054	0.036	0.045	–	0.796	0.450	0.190	1.015	–	1.091	–	0.395	0.305	0.626	0.445	0.462
<b>F10</b>	2.443	2.427	2.435	3.312	2.786	2.152	3.357	6.096	6.322	6.288	6.619	6.489	5.480	5.317	6.302	6.308
<b>F11</b>	0.751	0.740	0.746	0.727	0.742	0.098	0.218	0.156	0.234	0.407	0.405	0.410	0.699	1.413	1.610	1.998
<b>F12</b>	0.130	0.117	0.123	1.271	1.158	1.126	1.631	1.831	0.142	1.624	1.637	0.926	0.334	1.805	1.711	1.853
<b>F13</b>	0.208	0.190	0.199	0.889	0.476	0.321	0.511	0.946	1.104	1.240	0.205	0.591	0.311	1.358	1.198	0.886
<b>F14</b>	0.017	0.067	0.042	0.157	0.032	0.027	0.232	0.163	1.991	0.163	0.021	0.094	0.101	0.406	0.544	0.231
<b>F15</b>	1.374	1.424	1.399	1.328	1.448	1.157	1.041	2.433	1.960	2.430	2.123	2.804	2.863	2.344	2.234	2.104
<b>F16</b>	0.641	0.642	0.641	0.846	0.723	0.244	0.447	0.945	0.450	0.664	0.400	0.297	0.526	1.662	1.297	1.731
<b>F17</b>	0.564	0.585	0.575	0.523	0.428	0.286	0.492	1.548	0.945	1.366	0.694	0.651	1.640	1.318	1.341	1.310
SUM	11.79	11.57	11.68	24.44	24.93	21.41	23.29	36.53	37.93	38.41	32.81	32.05	31.65	39.12	38.87	39.56
<b>S1</b>	0.775	0.644	0.526	0.885	0.789	1.196	0.793	1.082	1.771	1.115	0.421	0.993	0.144	1.213	1.080	1.074
<b>S2</b>	0.638	0.449	0.697	0.601	0.265	0.189	0.299	0.120	0.152	0.140	0.364	0.514	0.364	0.266	0.178	0.111
<b>S3</b>	1.126	1.585	1.643	2.433	2.059	2.498	2.757	4.337	4.310	4.661	4.787	4.738	4.138	6.075	5.497	5.686
<b>S4</b>	0.805	1.041	1.378	1.181	1.252	1.071	1.331	1.248	1.368	1.075	1.157	1.974	1.308	1.919	1.483	1.544
<b>S5</b>	0.896	1.225	0.941	0.379	0.277	0.268	0.422	0.392	0.168	1.797	1.304	0.224	0.406	0.203	0.674	0.491
<b>S6</b>	1.691	1.993	1.067	2.497	2.169	2.164	1.966	4.970	4.225	4.042	4.925	4.941	4.169	5.466	6.269	5.894
<b>S7</b>	1.359	1.298	1.317	2.281	2.389	3.052	1.953	3.043	2.204	7.182	2.433	1.314	0.414	2.808	2.120	2.593
<b>S8</b>	3.737	4.479	4.254	5.951	5.398	5.199	5.788	8.282	8.857	8.004	8.246	8.420	8.451	10.894	10.153	9.895
<b>S9</b>	1.399	1.424	0.998	1.230	1.758	1.271	1.663	2.778	2.312	2.555	2.850	2.232	3.253	2.052	2.473	2.541
<b>S10</b>	12.890	11.789	12.813	15.371	16.010	15.217	15.668	26.712	28.197	24.778	26.252	21.554	23.517	24.115	25.094	25.345
<b>S11</b>	0.277	0.213	0.168	1.085	1.511	1.637	1.141	1.261	1.430	1.100	1.050	1.338	1.369	1.020	1.583	1.877
<b>S12</b>	0.093	0.073	0.090	0.162	0.184	0.264	0.242	0.243	0.215	0.285	0.287	0.146	0.191	0.616	0.347	0.191
SUM	25.69	26.21	25.89	34.06	34.06	34.03	34.02	54.47	55.21	56.73	54.07	48.39	47.72	56.65	56.95	57.24
P (%)	35.13	36.02	35.74	49.90	49.92	42.92	43.14	55.54	55.95	56.39	55.36	55.20	55.10	57.46	58.01	58.75
FRAP Value ( $\mu$ M)	805.84	993.70	879.33	1453.82	1539.89	1089.71	1372.23	2021.53	2162.40	2190.42	1879.86	1861.72	1840.20	2100.49	2297.35	2327.14

difference. The one growth year samples contained the highest content sucrose among the 16 samples. This result indicated that oligosaccharide is concerned with biosynthesis course of glycoside compounds.

#### 4. Investigation of antioxidant activity of Radix Astragali

Firstly, a LC-ESI-MS method for evaluation of antioxidant activity was developed. Then the antioxidant activities data of the methanol extracts of different Radix Astragali samples were obtained. And the Ferric Reducing Antioxidant Power (FRAP) assay was also applied to evaluate the antioxidant activity and support the result of LC-ESI-MS. Finally, the effects of growth years on antioxidant activity of Radix Astragali from Helong City were assessed.

##### 4.1. Evaluation of antioxidant activity using LC-ESI-MS

The hydroxyl radical ( $\cdot\text{OH}$ ) is the most reactive radical among the reactive oxygen species and play an active role in a number of diseases. In general, detection of  $\cdot\text{OH}$  is indirect and trap agents are usually applied, including chemical traps and spin traps.

In this study, the Fenton reaction was used as the  $\cdot\text{OH}$  generator and 5,5-dimethyl-1-pyrroline N-oxide (DMPO) as spin-trapped agent. The spin-adduct DMPO-OH and the internal standard N-methyl-2-pyrrolidone (NMP) were investigated by LC-ESI-MS in multiple selected ion monitoring (MIM) mode. The peak area ratio of DMPO-OH to NMP could indicate the change of  $\cdot\text{OH}$  concentration as they were positively correlated with each other. When the antioxidant was added to the reaction system, part of  $\cdot\text{OH}$  was scavenged and the content of DMPO-OH was reduced. So the decrease percentage ( $P$ , %) of the peak area ratio of DMPO-OH to NMP before and after the antioxidant was added could reflect its activity.

The Fenton reaction is  $\text{Fe}^{2+}$  and  $\text{H}_2\text{O}_2$  give rise to the  $\cdot\text{OH}$ , which can be trapped by trap agents for detection. So the concentrations of reagents, pH value and reaction time were optimized in order to increase the yield of  $\cdot\text{OH}$ . Optimization of LC-MS parameters is a necessary step to obtain better selectivity.

The chromatographic analysis was carried out without column, as the analytes have no retention. The samples were delivered at a flow rate of 0.3 mL/min, an appropriate rate coupled to MS. So the analytes were detected rapidly just within 2.5 min. The mass spectrum of the analytes showed the  $[\text{M}+\text{H}]^+$  ion of DMPO-OH at  $m/z$  130 and that of NMP at  $m/z$  100. The ions at  $m/z$  130 and 100 were monitored in MIM mode to quantify DMPO-OH and NMP, respectively. NMP was selected as the internal standard due to its similar structure to DMPO-OH resulting in similar ionization efficiency and could not trap  $\cdot\text{OH}$  and affect detection. Fig. 4 shows the chromatograms of DMPO-OH and NMP recorded by the LC-MS method in MIM mode.

In the experiment, suitable concentrations of  $\text{Fe}^{2+}$  (2.0 mM), DMPO (2 mM), and  $\text{H}_2\text{O}_2$  (0.01%) were added orderedly in ammonium acetate buffer (pH 5, 10 mM) and incubated at 20 °C for 20 min then NMP (100  $\mu\text{M}$ ) was added and the sample was vortexed for 20 s. Then, a 20  $\mu\text{L}$  of the mixture was injected into the LC-MS system for analysis. All the reaction solutions were freshly prepared every time. When the Radix Astragali sample was determined, it was added into the reaction system just before  $\text{H}_2\text{O}_2$  and operated as above. All treatments were run in five times and the average peak area ratio was obtained. So the decrease percentages of different samples were calculated and were shown in Table 4. Then the reference compounds, calycosin, formononetin and astragaloside IV, were detected as above, the decrease percentages of them were obtained (calycosin 83.90%, formononetin 57.15% and astragaloside IV 64.13%). So the isoflavonoids and astragalosides are the major components presented the antioxidant activities.

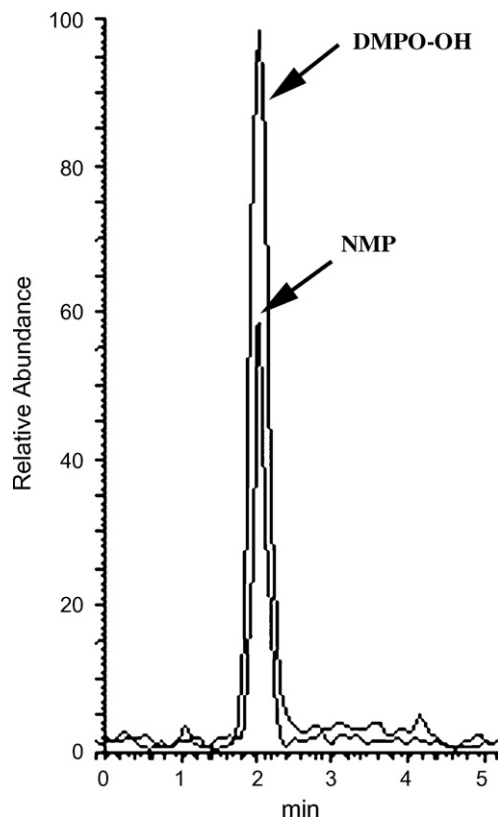


Fig. 4. The LC-MS chromatograms of DMPO-OH and NMP in the MIM mode.

##### 4.2. FRAP assay measure of antioxidant activity

The FRAP assay was applied for measuring the total antioxidant activity, which is based on the reducing power of a compound. A potential antioxidant will reduce the ferric ion ( $\text{Fe}^{3+}$ ) to the ferrous ion ( $\text{Fe}^{2+}$ ) and the latter forms a blue complex with TPTZ ( $\text{Fe}^{2+}/\text{TPTZ}$ ), which increases the absorption at 593 nm.

Briefly, the FRAP reagent was prepared by mixing NaAc buffer (300 mM, pH 3.6), 10 mM TPTZ in 40 mM HCl and 20 mM  $\text{FeCl}_3$  at 10:1:1 (v/v/v). L-ascorbic acid was prepared at 500  $\mu\text{M}$  in methanol and was used as reference standard. The 150  $\mu\text{L}$  FRAP reagent and the 5  $\mu\text{L}$  L-ascorbic acid or sample solutions were added to the well of the microplate. The absorbance readings were taken at 593 nm immediately at 0 min and 4 min after. The plate was incubated at 37 °C for the duration of the reaction. All treatments were run in five times and the average value was obtained. The absorbance changes between 0 and 4 min of the L-ascorbic acid and sample solutions were obtained. So the FRAP values ( $\mu\text{M}$ ) of the samples was calculated on the basis of L-ascorbic acid (Table 4). Then the FRAP values of reference compounds, calycosin, formononetin and astragaloside IV, were obtained (calycosin 698.99  $\mu\text{M}$ , formononetin 161.62  $\mu\text{M}$  and astragaloside IV 193.94  $\mu\text{M}$ ).

The total antioxidant activity of the Radix Astragali crude methanol extracts has never been reported. The results of LC-ESI-MS measure correlated well to those found in the FRAP assay, an indication that the antioxidant activities found in the two model systems supported each other. The antioxidant activities of the reference compounds, calycosin, formononetin and astragaloside IV, were evaluated. The three compounds all presented antioxidant activities, the  $P$  and FRAP value of calycosin was higher than the other two compounds. Astragaloside IV showed higher activity than formononetin. Then different Radix Astragali samples were analyzed. Samples 1–16 from the Helong City with different growth years, the  $P$  and FRAP values of the seven years ones were a little

higher than the three years ones and significantly higher than the other ones. As for the samples of the same growth years ones, the *P* and FRAP values were insignificantly different with each other. Samples of the three years ones, the *P* and FRAP value of them were higher than the two years ones. And the *P* and FRAP values of the two years ones were all higher than the one year ones. So the effect of the growth years on the antioxidant activity was obtained in this study, which was the important influencing factor. In a word, the three years ones presented the best excellent antioxidant quality.

The isoflavonoids and astragalosides are the major bioactivity ingredients of antioxidant activity in Radix Astragali. Comprehensive analysis of the above results, the contents of principal components and antioxidant activities are correlated. So the three years were the optimal growth year for Radix Astragali.

## 5. Conclusions

In the present paper, the structural elucidations of isoflavonoids and astragalosides in the methanol extracts of Radix Astragali have been carried out by means of LC-ESI-MS<sup>n</sup> method. The quality and quantity of different growth year samples from Helong City were analyzed. And then LC-ESI-MS method was performed on the evaluation of antioxidant activity. Meantime, FRAP assay was applied to support the antioxidant activity result of LC-ESI-MS. The experimental results demonstrated that the contents of the principal components and the antioxidant activity of the Radix Astragali are positively correlated. The effect of growth year is significant on the antioxidant activities of Radix Astragali. In short, the LC-ESI-MS<sup>n</sup> method is a powerful and reliable analytical tool for rapidly identifying isoflavonoids and astragalosides and evaluating the antioxidant activity of Radix Astragali.

## Acknowledgments

This work was supported by the National Natural Science Foundation of China (No. 30672600), the key project of Jilin Provincial

Science and Technology (No.20060902) and the Research Project of Changchun Institute of Applied Chemistry, Chinese Academy of Sciences (CX07QZJC-32).

## References

- [1] Z.F. Xie, Z.C. Lou, X.K. Huang, New World Press Beijing, 1999, p. 374.
- [2] J.L. Rios, P.G. Waterman, *Phytother. Res.* 11 (1997) 411–418.
- [3] Z.P. Li, Q. Cao, *Acta Pharmacol. Sin.* 23 (2002) 898–904.
- [4] T. Wu, S.W.A. Bligh, L.H. Gu, Z.T. Wang, H.P. Liu, X.M. Cheng, C.J. Branford-White, Z.B. Hu, *Fitoterapia* 76 (2005) 157–165.
- [5] X.Q. Ma, J.A. Duan, D.Y. Zhu, T.X. Dong, K.W.K. Tsim, *Nat. Med.* 54 (2000) 213–218.
- [6] Z.R. Zheng, C.Q. Song, T. Liu, Z.B. Hu, *Acta Pharm. Sin.* 33 (1998) 148–151.
- [7] F.D. Hu, S.L. Feng, J.X. Zhao, Y. Zhang, L.R. Chen, *Anal. Test. Tech. Instrum.* 9 (2003) 173–177.
- [8] H. Zhang, X.D. Li, S.L. Feng, X. Liu, F.D. Hu, Y. Li, J. Lanzhou Univ. 32 (2006) 64–66.
- [9] H.B. Xiao, M. Krucker, K. Albert, X.M. Liang, *J. Chromatogr. A* 1032 (2004) 117–124.
- [10] W.D. Zhang, C. Zhang, R.H. Liu, H.L. Li, J.T. Zhang, C. Mao, C.L. Chen, *J. Chromatogr. B* 822 (2005) 170–177.
- [11] Q. Xu, X.Q. Ma, X.M. Liang, *Phytochem. Anal.* 18 (2007) 419–427.
- [12] J. Zhao, Q.T. Yu, P. Li, P. Zhou, Y.J. Zhang, W. Wang, *J. Sep. Sci.* 31 (2008) 255–261.
- [13] L.W. Qi, P. Li, M.T. Ren, Q.T. Yu, X.D. Wen, Y.X. Wang, *J. Chromatogr. A* 1203 (2008) 27–35.
- [14] X. Huang, F.R. Song, Z.Q. Liu, S.Y. Liu, *J. Mass Spectrom.* 42 (2007) 1148–1161.
- [15] W. Wu, C.Y. Yan, L. Li, Z.Q. Liu, S.Y. Liu, *J. Chromatogr. A* 1047 (2004) 213–220.
- [16] L. Li, R. Tsaob, J.P. Dou, F.R. Song, Z.Q. Liu, S.Y. Liu, *Anal. Chim. Acta* 536 (2005) 21–28.
- [17] K.Q. Zhou, J.J. Yin, L. Yu, *Food Chem.* 95 (2006) 446–457.
- [18] L.X. Li, Y. Abe, K. Kanagawa, N. Usui, K. Imai, T. Mashino, M. Mochizuki, N. Miyata, *Anal. Chim. Acta* 512 (2004) 121–124.
- [19] T. Sun, Z.S. Jia, Z.D. Xu, *Bioorg. Med. Chem. Lett.* 14 (2004) 1779–1781.
- [20] P. Kumarathasan, R. Vincent, P. Goegan, M. Potvin, J. Guenette, *Biochem. Cell Biol.* 79 (2001) 33–42.
- [21] C. Tai, J.F. Peng, J.F. Liu, G.B. Jiang, H. Zou, *Anal. Chim. Acta* 527 (2004) 73–80.
- [22] E. Kilinc, *Talanta* 65 (2005) 876–881.
- [23] Q. Guo, S.Y. Qian, R.P. Mason, *J. Am. Soc. Mass Spectrom.* 14 (2003) 862–871.
- [24] A. Reis, M.R. Domingues, F.M. Amado, A.J. Ferrer-Correia, P. Domingues, *Biomed. Chromatogr.* 20 (2006) 109–118.
- [25] S.Y. Qian, M.B. Kadiiska, Q. Guo, R.P. Mason, *Free Radic. Biol. Med.* 38 (2005) 125–135.
- [26] F. Yang, R.P. Zhang, J.M. He, Z. Abliz, *Rapid Commun. Mass Spectrom.* 21 (2007) 107–111.
- [27] R. Li, T.J. Fu, Y.Q. Ji, L.S. Ding, S.L. Peng, *Chin. J. Anal. Chem.* 12 (33) (2005) 1676–1680.





# Ratiometric and turn-on monitoring for heavy and transition metal ions in aqueous solution with a fluorescent peptide sensor

Bishnu Prasad Joshi, Junwon Park, Wan In Lee, Keun-Hyeong Lee\*

Bioorganic Chemistry Laboratory, Department of Chemistry, Inha University, 253 Younghyun-Dong, Nam-Gu, Incheon-City, 402-751, South Korea

## ARTICLE INFO

### Article history:

Received 4 November 2008

Received in revised form

29 December 2008

Accepted 29 December 2008

Available online 20 January 2009

### Keywords:

FRET

CHEF

Peptide

Ratiometric

Fluorescent sensor

Cd<sup>2+</sup>

Hg<sup>2+</sup>

## ABSTRACT

A novel fluorescent peptide sensor containing tryptophan (donor) and dansyl fluorophore (acceptor) was synthesized for monitoring heavy and transition metal (HTM) ions on the basis of metal ion binding motif (Cys-X-X-Cys). The peptide probe successfully exhibited a turn on and ratiometric response for several heavy metal ions such as Hg<sup>2+</sup>, Cd<sup>2+</sup>, Pb<sup>2+</sup>, Zn<sup>2+</sup>, and Ag<sup>+</sup> in aqueous solution. The enhancements of emission intensity were achieved in the presence of the HTM ions by fluorescent resonance energy transfer (FRET) and chelation enhanced fluorescence (CHEF) effects. The detection limits of the sensor for Cd<sup>2+</sup>, Pb<sup>2+</sup>, Zn<sup>2+</sup>, and Ag<sup>+</sup> were lower than the EPA's drinking water maximum contaminant levels (MCL). We described the fluorescent enhancement, binding affinity, and detection limit of the peptide probe for HTM ions.

© 2009 Elsevier B.V. All rights reserved.

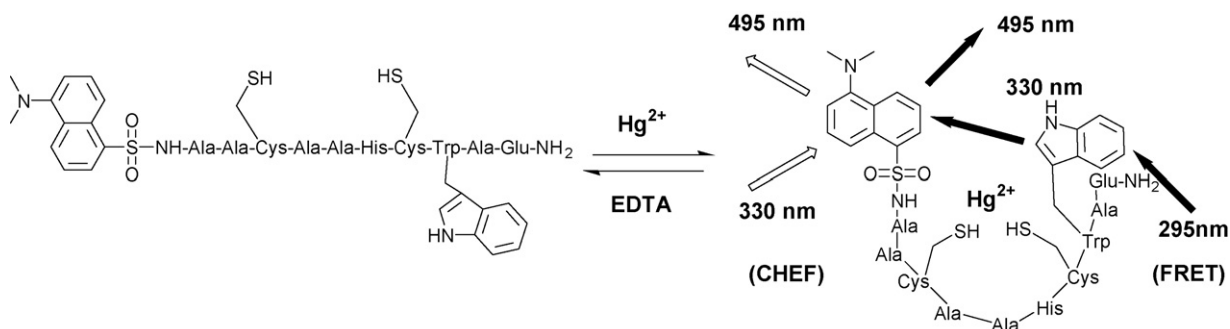
## 1. Introduction

Chemical sensors that monitored metal ions are of current topical interest because a variety of natural and environmental contaminations of heavy and transition metal (HTM) ions causes serious problems for human health and ecology [1–3]. As monitoring of a low level contamination of HTM ions such as Hg<sup>2+</sup>, Cd<sup>2+</sup>, and Pb<sup>2+</sup> has become significant, fluorescent chemical sensors that provide immediate and sensitive responses to HTM ions are particularly valuable. Many kinds of fluorescent chemical sensors for HTM ions such as Hg<sup>2+</sup>, Cd<sup>2+</sup>, and Pb<sup>2+</sup>, have been reported [4–15]. Most of the known fluorescent chemical sensors monitored these cations by fluorescence quenching effects via enhanced spin-orbital coupling (e.g. Hg<sup>2+</sup>) or energy or electron transfer and suffered limitations in aqueous solution due to poor solubility. Thus, the sensors that exhibit turn on response for HTM ions in aqueous solution are required. In addition, ratiometric sensors for heavy metal ions are desirable because they make it possible to measure the analytes more accurately with minimization of background signal [16,17]. However, ratiometric fluorescent probes useful for monitoring HTM ions in aqueous solution were rarely reported [18–20].

Various proteins including metallo-proteins interact with small molecules such as metal ions and this event induces conformational change of the proteins. Several metal binding motifs have been identified in various metallo-proteins [21–25]. Cysteine rich metal ion binding motifs that commonly shared Cys-X<sub>2-4</sub>-Cys sequences have been identified in metallo-proteins such as metallothioneins, Menkes, MerR, and CueR protein [26,27]. Furthermore, the small peptide fragments based on the metal binding motifs showed nanomolar and micromolar affinity for several HTM ions (Group 11 and 12) including Hg<sup>2+</sup>, Cd<sup>2+</sup>, and Zn<sup>2+</sup> [28–30]. Thus, the peptides containing metal binding motifs have potential applications as chemical sensors. In the present study, we focused on the design of ratiometric fluorescent sensors for monitoring HTM ions on the basis of metal binding motifs because peptide sensors have several advantages. Peptides consisting of natural amino acids can be easily synthesized by solid phase synthesis with 9-fluorenylmethoxycarbonyl (Fmoc) or tert-butyloxycarbonyl (Boc) chemistry [31,32]. Peptide sensors are generally working well in aqueous solution or mixed organic-aqueous solution due to their good solubility, and their sensitivity and selectivity can be optimized by further tuning of the amino acid sequences [33–38]. Peptide sensors can be facilely conjugated into solid support in the device for further applications.

Peptides and proteins do not have fluorescent properties to be essential for sensing. Conjugation of a fluorophore group (a signal transduction site) into the peptides is a critical step for developing

\* Corresponding author. Tel.: +82 32 860 7674; fax: +82 32 867 5604.  
E-mail address: [leekh@inha.ac.kr](mailto:leekh@inha.ac.kr) (K.H. Lee).



**Scheme 1.** Structure of **3G** and possible binding mode.

peptide sensors. If the fluorophore site may directly contact bound metal ions, the metal recognition event will be fully monitored. Previously, we and other research groups independently reported the synthesis of fluorescent peptide and chemical probes containing dansyl fluorophore for metal ions [33,35–44] because the sulfonamide of dansyl group has been applied to the chelation enhanced fluorescence (CHEF) system and some of the probes sensed metal ions efficiently by a CHEF [33,35–39] effect. In addition, the emission spectrum of dansyl group is sensitive to its microenvironments [45]. Thus, a short fluorescent peptide sensor consisting of less than 11 amino acids was designed and dansyl group was chosen as a fluorophore group. To design a ratiometric peptide sensor, a Trp residue as a donor and a dansyl group as an acceptor were introduced into the peptide (Scheme 1) [17].

We synthesized a fluorescent peptide probe (**3G**, Dansyl-Ala-Ala-Cys-Ala-Ala-His-Cys-Trp-Ala-Glu-CONH<sub>2</sub>) on the basis of the amino acid sequence of the metal binding motifs. His residue, known to be a heavy metal binding ligand [21], was included in metal ion binding site of the peptide. A Glu residue in the peptide probe was introduced for improving solubility. As shown in Scheme 1, we assume that when the peptide probe interact with metal ions, it may fold and bring the Trp and dansyl closer to each other, resulting in the increase of emission intensity by a fluorescent resonance energy transfer (FRET) effect. In addition, if direct interactions between the dansyl fluorophore and metal ions may occur, enhanced emission intensity will be observed because the complexation of the sulfonamide group of dansyl fluorophore by cations may inhibits photoinduced electron transfer (PET) i.e., that there is a CHEF effect. The synthesized peptide probe successfully exhibited turn on fluorescent response for several heavy metal ions in aqueous solution. The peptide probe showed a ratiometric response with heavy metal ions such as Hg<sup>2+</sup>, Cd<sup>2+</sup>, Zn<sup>2+</sup>, and Ag<sup>+</sup> by FRET and CHEF

effects. We described the fluorescent enhancement, binding affinity, detection limit, and the pH dependent sensitivity of the peptide probes for HTM ions.

## 2. Experimental

### 2.1. Reagents

Fmoc protected amino acids, *N,N'*-diisopropylcarbodiimide, 1-hydroxybenzotriazole, and Rink Amide MBHA resin were from Novabiochem. Other reagents for peptide synthesis including trifluoroacetic acid (TFA), tri-isopropylsilane (TIS), dansyl chloride, triethylamine, diethyl ether, dimethyl sulfoxide (DMSO), *N,N*-dimethylformamide (DMF) and piperidine were purchased from Aldrich.

### 2.2. Peptide synthesis

The peptides were synthesized using Fmoc chemistry by solid phase peptide synthesis with Fmoc chemistry [31]. The coupling of dansyl chloride was performed by applying the following procedure. To the resin bound peptide (65 mg, 0.05 mmol), dansyl chloride (40 mg, 0.15 mmol, 3 eq.) in DMF (3 ml) containing triethylamine (20  $\mu$ l, 0.15 mmol, 3 eq.) were added and kept for 2 h at room temperature. Deprotection and cleavage was achieved by treatment with a mixture of TFA/TIS/H<sub>2</sub>O (9.5:0.25:0.25, v/v/v) at room temperature for 3–4 h. After cleavage of the product from resin, the peptides were purified by preparative-HPLC using a water (0.1% TFA)/acetonitrile (0.1% TFA) gradient (5–50% acetonitrile over 45 min). The peptide mass (**3G** [M + H]<sup>+</sup> calcd. 1263.40; obsd. 1263.17) were characterized by ESI mass spectrometer (Platform II, Micromass, Manchester, UK). The homogeneity (>95%) of

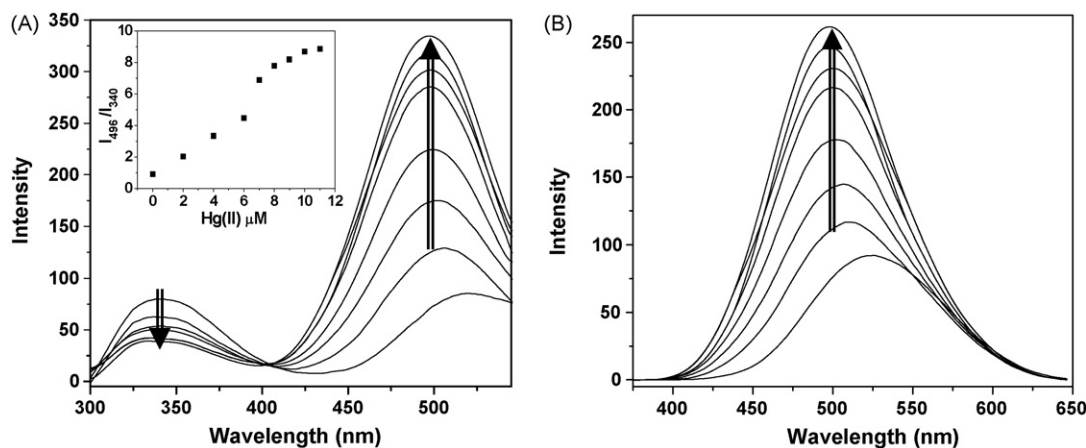


**Fig. 1.** Fluorescence response of **3G** (20  $\mu$ M) to the addition of Hg<sup>2+</sup> at 0, 2, 4, 6, 8, 9, 10, 11  $\mu$ M with an excitation at (A) 295 nm and (B) 330 nm in 10 mM HEPES buffer (pH 7.4).

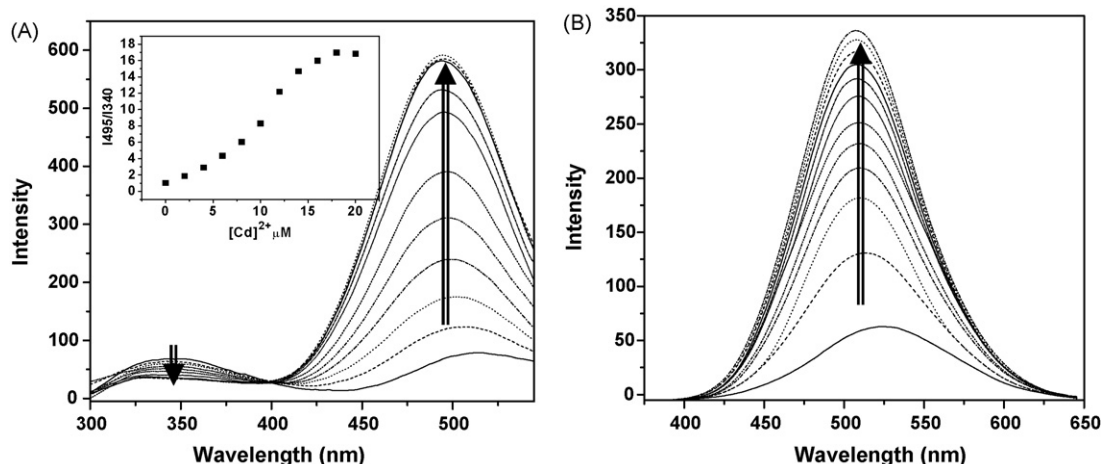


**Fig. 2.** Fluorescence response of **3G** ( $20 \mu\text{M}$ ) to the addition of  $\text{Cd}^{2+}$  at 0, 2, 4, 6, 8, 10, 12, 14, 16, 18, 20  $\mu\text{M}$  with an excitation at (A) 295 nm and (B) 330 nm in 10 mM HEPES buffer (pH 7.4).

the compound was confirmed by analytical HPLC on a  $\text{C}_{18}$  column.

### 2.3. General fluorescence measurements

Fluorescence emission spectrum of a peptide probe in a 10 mm path length quartz cuvette was measured in 10 mM HEPES buffer solution (pH 7.4) using a PerkinElmer luminescence spectrophotometer (model LS 55). Emission spectra (300–650 nm) of the peptide probes ( $20 \mu\text{M}$ ) in the presence of various metal ions ( $\text{Hg}^{2+}$ ,  $\text{Ca}^{2+}$ ,  $\text{Cd}^{2+}$ ,  $\text{Co}^{2+}$ ,  $\text{Pb}^{2+}$ ,  $\text{Ag}^+$ ,  $\text{Mg}^{2+}$ ,  $\text{Cu}^{2+}$ ,  $\text{Mn}^{2+}$ ,  $\text{Ni}^{2+}$ , and  $\text{Zn}^{2+}$  as perchlorate anion; and  $\text{Na}^+$ ,  $\text{Al}^{3+}$ , and  $\text{K}^+$ , as chloride anion) were measured by excitation with 295 nm for FRET measurement or

by excitation with 330 nm for chelation enhanced fluorescence measurement. The slit size for excitation and emission was 6 nm, respectively. The concentration of peptide probe was confirmed by UV absorbance at 330 nm for dansyl group.

### 2.4. Determination of binding stoichiometry and binding constant

The binding stoichiometry of peptides with metal ions was determined by using Job's plot [17,46,47]. A series of solutions with varying mole fraction of metal ions were prepared by maintaining the total peptide and metal ion concentration constant ( $2.5 \mu\text{M}$ ). The fluorescence emission was measured for each sample by exciting at 330 or 295 nm and spectra were measured from 300 to

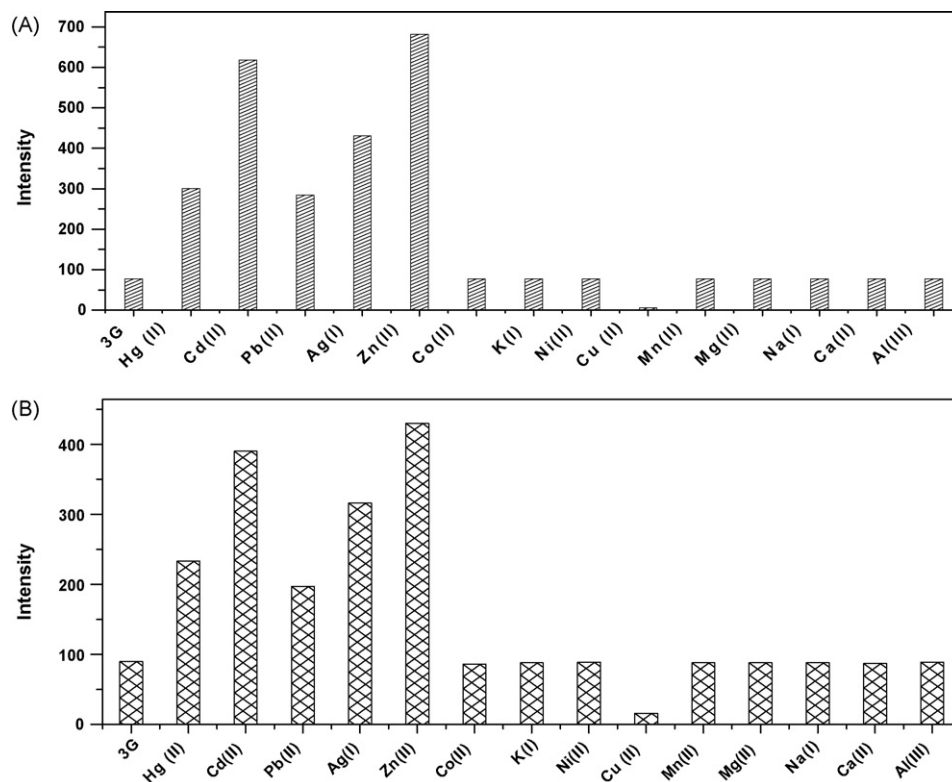


**Fig. 3.** Fluorescence response of **3G** ( $20 \mu\text{M}$ ) in the presence of various metal ions (1 eq.) with an excitation at (A) 295 nm and (B) 330 nm in 10 mM HEPES buffer solution (pH 7.4).

650 nm. The fitting data were acquired by plotting a straight line through the maximum or minimum emission intensity in the titration curve and were plotted against the mole fraction of the metal ion versus emission intensity.

The association constants were calculated based on the titration curve of the probes with metal ions. Association constants were determined by a nonlinear least squares fit of the data with the following equation as referenced elsewhere [48,49].

$$F(x) = \frac{a + b \times cx^n}{1 + cx^n}$$

where  $x$  is the concentration of metal ions,  $F(x)$  is the intensity,  $a$  is the intensity of probe without metal ions,  $b$  is the intensity at the saturation,  $n$  is the binding stoichiometry, and  $c$  is the association constant.

### 2.5. Detection limit

The detection limit was calculated based on the fluorescence titration. To determine the S/N ratio, the emission intensity of **3G** without any metal ions was measured by 10 times and the standard deviation of blank measurements was determined. Three independent duplication measurements of emission intensity were performed in the presence of metal ions and each average value of the intensities was plotted as a concentration of metal ions for determining the slope. The detection limit is then calculated with the following equation.

$$\text{Detection limit} = \frac{3\sigma_{bi}}{m}$$

where  $\sigma_{bi}$  is the standard deviation of blank measurements,  $m$  is the slope between intensity versus sample concentration.

## 3. Results and discussion

### 3.1. Fluorescence response of **3G** to heavy metal ions

As the peptide sensor is fully water soluble, we investigated the fluorescence response of the sensor to HTM ions in 10 mM HEPES buffer solution (pH 7.4). As shown in Scheme 1, fluorescence response of the probe to metal ions might occur via two ways. If metal ions directly interact with a dansyl fluorophore, the emission intensity of a dansyl group will change by a CHEF effect. If the peptides will fold in the presence of metal ions, the distance between Trp (donor) and dansyl (acceptor) may decrease, resulting in the increase of emission intensity by a FRET effect. Thus, fluorescent spectra of **3G** in the presence of HTM metal ions were measured by excitation at a wavelength of 295 nm for the Trp residue or 330 nm for the dansyl fluorophore, respectively.

The fluorescence response of **3G** toward  $\text{Hg}^{2+}$  was measured with a wavelength of 295 nm in HEPES buffer solution (pH 7.4). Fig. 1 showed that **3G** exhibited a fluorescence turn-on response with  $\text{Hg}^{2+}$ . With the increasing concentration of  $\text{Hg}^{2+}$ , a significant increase of the emission intensity around 495 nm and decrease at 340 nm were observed with an isosbestic point at 407 nm. The intensity ratio at 495 and 340 nm increased from 0.9 to 8.9. Upon the addition of 1 eq.  $\text{Hg}^{2+}$ , about 4-fold increase of the intensity at 495 and 30 nm blue shift from 525 to 495 nm of the maximum emission intensity were observed. This result indicated that the sensor (**3G**) showed a ratiometric, turn-on fluorescence response with  $\text{Hg}^{2+}$  by a FRET effect.

When the probe was excited with a wavelength of 330 nm for the dansyl group, **3G** exhibited a fluorescence turn-on response with  $\text{Hg}^{2+}$ . Upon the addition of 1 eq.  $\text{Hg}^{2+}$ , about 3-fold intensity increased and 30 nm blue shift from 525 to 495 nm of the maximum emission intensity were observed. This result indicated that direct

interactions between the dansyl fluorophore with  $\text{Hg}^{2+}$  resulted in the increase of emission intensity by a CHEF effect. The blue shift may be due to the change of circumstances of dansyl fluorophore because the emission intensity of dansyl fluorophore is sensitive to its local environment [45]. The blue shift indicated that when the peptide probe fold in the presence of  $\text{Hg}^{2+}$ , the hydrophilic environment of dansyl group of the free peptide probe was changed into hydrophobic environment.

Fig. 2 indicated that **3G** showed a ratiometric, turn-on response with  $\text{Cd}^{2+}$ . Upon the addition of 1 eq.  $\text{Cd}^{2+}$ , 7.5-fold intensity increase and 30 nm blue shift of the maximum emission intensity were observed with a wavelength of 295 nm. When the probe was excited with a wavelength of 330 nm, 4.3-fold increase and 30 nm blue shift of the maximum emission intensity were observed. In the presence of  $\text{Hg}^{2+}$  and  $\text{Cd}^{2+}$ , the enhancement of emission spectrum measured by excitation with 295 nm was greater than those measured by excitation with 330 nm. To investigate direct interactions between the dansyl fluorophore and metal ions, UV-vis absorption spectra were measured (Fig. S1). In the presence of heavy metal ions, the absorbance maximum blue shift and the extinction coefficient change were observed, which indicated direct interactions between the fluorophore and HTMs. When the lone pair electrons in sulfone amide of dansyl interacted with cations, the resulting reduction of conjugation of the fluorophore could induce a blue shift of the absorption and emission spectrum. Overall results indicated that **3G** exhibited a fluorescence response with  $\text{Hg}^{2+}$  and  $\text{Cd}^{2+}$  via FRET as well as CHEF effects.

### 3.2. Binding stoichiometry and binding affinity

To investigate the response of the peptide to various metal ions, we measured the fluorescence change of the peptide probe in the presence of several metal cations ( $\text{Hg}^{2+}$ ,  $\text{Ca}^{2+}$ ,  $\text{Cd}^{2+}$ ,  $\text{Co}^{2+}$ ,  $\text{Pb}^{2+}$ ,  $\text{Cu}^{2+}$ ,  $\text{Ag}^+$ ,  $\text{Mg}^{2+}$ ,  $\text{Mn}^{2+}$ ,  $\text{Ni}^{2+}$ , and  $\text{Zn}^{2+}$  as perchlorate anion and  $\text{Na}^+$ ,  $\text{Al}^{3+}$ ,  $\text{K}^+$ , as chloride anion). When **3G** was excited with a wavelength of 330 or 295 nm respectively, **3G** exhibited a fluorescence turn-on response with HTM ions including  $\text{Hg}^{2+}$ ,  $\text{Ag}^+$ ,  $\text{Cd}^{2+}$ ,  $\text{Pb}^{2+}$ , and  $\text{Zn}^{2+}$  whereas **3G** exhibited a turn-off response with  $\text{Cu}^{2+}$  (Fig. 3). However, the probe exhibited no response with a representative selection of alkali and alkaline earth metal ions. This selectivity of the peptide sensor for HTM ions would be anticipated because the metal binding motif (CXXXC) of the peptide was reported to bind with several HTM ions including  $\text{Hg}^{2+}$ ,  $\text{Cd}^{2+}$ ,  $\text{Pb}^{2+}$ , and  $\text{Zn}^{2+}$  [25].

We investigated the binding stoichiometry and binding affinities of the peptide sensor for  $\text{Hg}^{2+}$ ,  $\text{Ag}^+$ ,  $\text{Cd}^{2+}$ ,  $\text{Pb}^{2+}$ , and  $\text{Zn}^{2+}$ . In the titration curve, about 10  $\mu\text{M}$  of  $\text{Hg}^{2+}$  was required for the saturation of the emission intensity of **3G** (20  $\mu\text{M}$ ), indicating that the binding ratio between the peptide with  $\text{Hg}^{2+}$  is 2:1 (Fig. 1). Moreover, Job's plot analysis was conducted to determine the binding stoichiometry [17,46,47]. Job's plot of **3G** exhibited a maximum at 0.4 mol fraction of  $\text{Hg}^{2+}$  (Fig. S1). Generally, a Job's plot with a maximum at any other value besides 0.5 reveals that the peptide did not form 1:1 complex. In the titration curve for  $\text{Cd}^{2+}$ ,  $\text{Zn}^{2+}$ ,  $\text{Pb}^{2+}$ , and  $\text{Ag}^+$ , 0.5 eq. of metal ion was required for the saturation of the emission intensity of **3G**. Job's plot exhibited a maximum at 0.35–0.4 mol fraction of  $\text{Cd}^{2+}$ ,  $\text{Zn}^{2+}$ ,  $\text{Pb}^{2+}$ , and  $\text{Ag}^+$  respectively. (Fig. S2). The titration data and a Job's plot analysis indicated that a 2:1 complex might be predominant. It is not surprising that two peptides that contained two Cys residues were required to bind one heavy metal ion because metal binding sites in metallo-proteins often include four Cys residues (i.e. CXXXXC–CXXXXC) and tetrahedral coordination geometries between a protein and a metal ion were frequently observed [30]. The association constants of **3G** for  $\text{Hg}^{2+}$ ,  $\text{Cd}^{2+}$ ,  $\text{Zn}^{2+}$ ,  $\text{Pb}^{2+}$ , and  $\text{Ag}^+$  were calculated by 2:1 complex model. Table 1 summarized the association constants and enhancement

**Table 1**  
Enhancement factors, detection limits, and association constants of **3G**.

Metal	$\lambda_{\text{max}}$ (nm)	Enhancement factor (absorbance = 295 nm)	Enhancement factor (absorbance = 330 nm)	Detection limit ( $\mu\text{g/L}$ )	$K_a$ $M^{-2}$ (2:1 binding)
Hg <sup>2+</sup>	495	4.0	2.6	5.2	$5.5 \pm 0.6 \times 10^{10}$
Cd <sup>2+</sup>	495	7.5	4.3	4.6	$2.6 \pm 0.3 \times 10^{10}$
Pb <sup>2+</sup>	495	3.6	2.2	11.0	$4.5 \pm 0.6 \times 10^{10}$
Ag <sup>+</sup>	495	4.5	3.5	4.3	$3.3 \pm 0.3 \times 10^{10}$
Zn <sup>2+</sup>	495	9.0	4.8	2.8	$4.0 \pm 0.4 \times 10^{10}$

factors for several heavy metal ions. The fitting of titration curve provided less than 15% errors. Even though this error was acceptable, this was larger than those of the reported small chemical sensors [8–13] because the emission intensity increased via FRET as well as CHEF effects and some heavy metal ions showed quenching effect on the emission of Trp (explained later). It is observed that the association constants did not correlate well with the enhancement factors measured by excitation with 295 nm or measured by excitation with 330 nm. The enhancement factors depend on the electron configuration of metal species and the distance between the dansyl fluorophore and the metal ion in the peptide–metal complex. Although  $K_a$  for Zn<sup>2+</sup> is similar to that for Pb<sup>2+</sup>, the enhancement factors measured by excitation with 295 nm are considerably different.

The large difference between the enhancement factors (295 nm) can be explained by several factors such as the secondary structure of peptide–metal complex, and the quenching effect of metal ions. When the peptide folded in the presence of metal ions, the secondary structures would be different depending on metal species. However, the main reason may be the quenching effect of some metal ions. It was reported that if heavy metal ions were close to Trp residue, the emission spectrum of Trp residue was often quenched by some heavy metal ions (Pb<sup>2+</sup> and Hg<sup>2+</sup>) [44,50,51].

To confirm this explanation, we synthesized the peptide containing a Trp residue (Acetyl-Cys-Ala-Ala-His-Cys-Trp-Ala-Glu-CONH<sub>2</sub>) and measured emission intensity in the presence of various metal ions. Noticeably, Pb<sup>2+</sup>, Hg<sup>2+</sup>, Cd<sup>2+</sup>, and Ag<sup>+</sup> among various metal ions showed quenching effects on the emission spectrum of Trp of this peptide (data not shown). The quenching effect of Pb<sup>2+</sup> was the greatest and 1 eq. of Pb<sup>2+</sup> almost completely quenched the emission intensity of the Trp residue. As some of heavy metal ions (Pb<sup>2+</sup>, Hg<sup>2+</sup>, Cd<sup>2+</sup>, and Ag<sup>+</sup>) might have a quenching ability for the emission intensity of the Trp residue of **3G**, we made a titration curve by excitation with 330 nm and calculated  $K_a$  values for Pb<sup>2+</sup>, Hg<sup>2+</sup>, Cd<sup>2+</sup>, and Ag<sup>+</sup>. Except Pb<sup>2+</sup>,  $K_a$  values calculated from the titration curve measured by excitation with 330 nm was similar to those calculated from the titration curve measured with 295 nm. As Pb<sup>2+</sup> showed a strong quenching effect on the emission spectrum of the Trp residue, fluorescence titration curve for Pb<sup>2+</sup> was obtained by excitation with 330 nm and the association constant was calculated.

### 3.3. Detection limit

The binding process of HTM ions to the peptide probe in buffer solution was found to be fast. After adding the metal ions, the emission intensity instantly increased and reached the plateau region

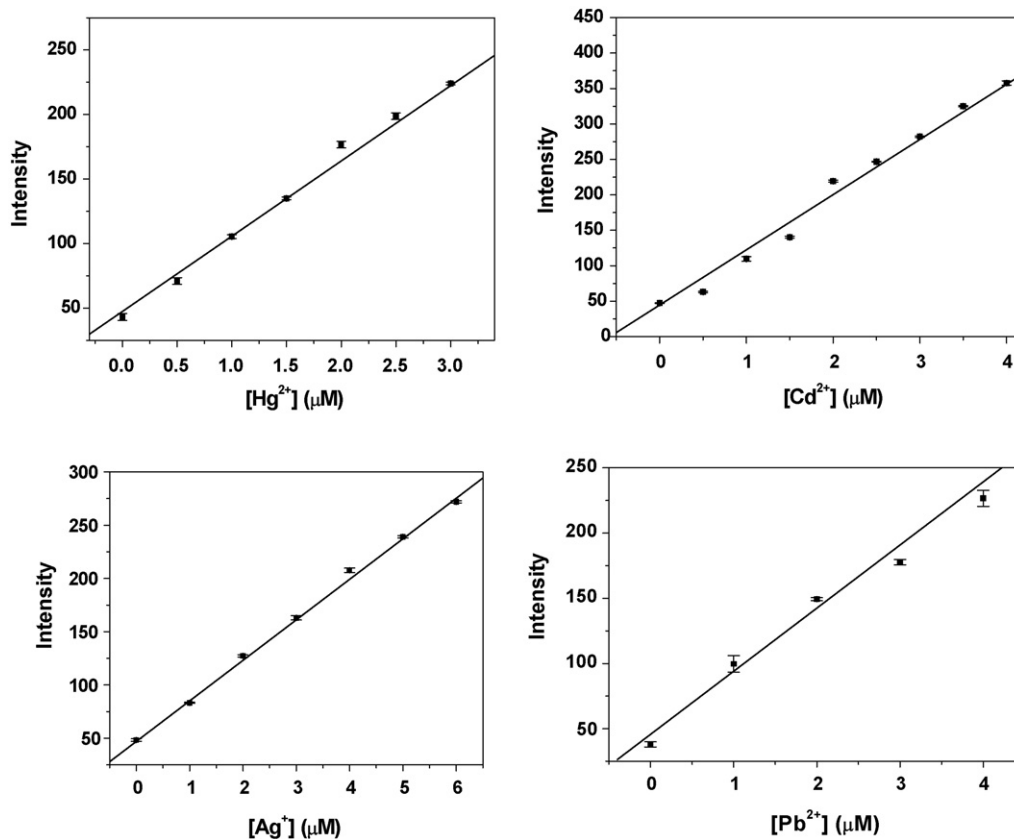


**Fig. 4.** Linear intensity change region as a function of the concentration of HTM ions.

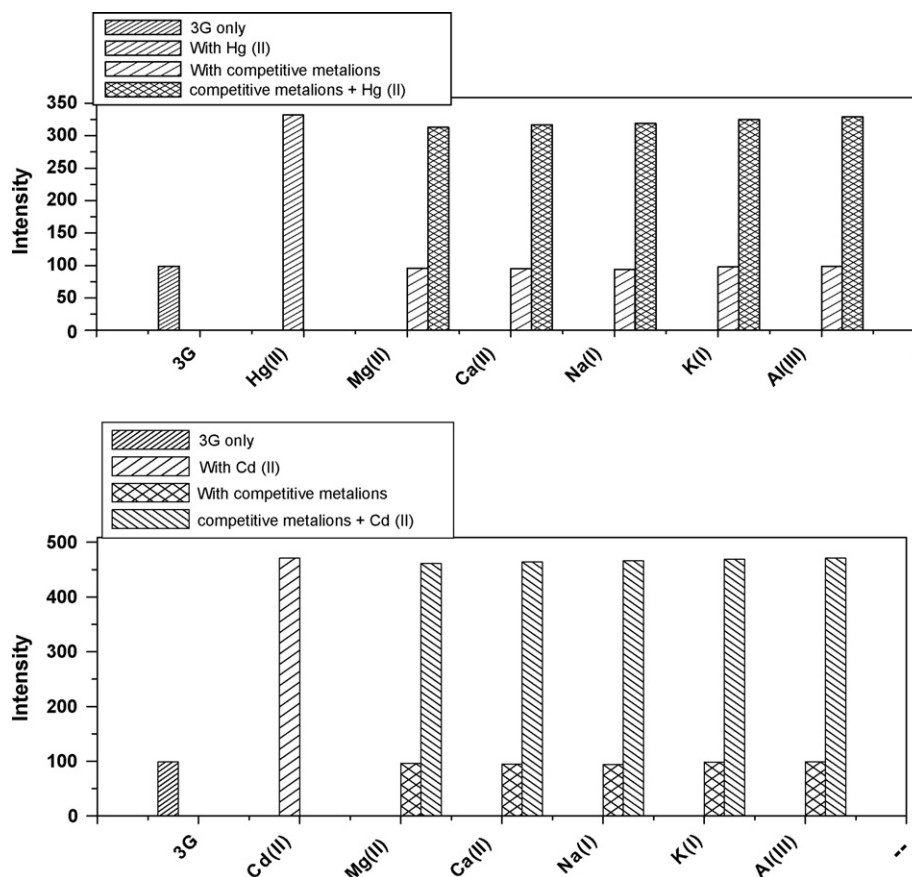


Fig. 5. Emission intensity of **3G** in the presence HTM ions ( $\text{Hg}^{2+}$ ,  $\text{Cd}^{2+}$ , and  $\text{Pb}^{2+}$ ) and additional various metal ions at pH 7.4 (10 mM HEPES buffer). HTM ions ( $\text{Hg}^{2+}$ ,  $\text{Cd}^{2+}$ , and  $\text{Pb}^{2+}$ ) are one equivalent to **3G** (20  $\mu\text{M}$ ) and  $\text{Na}^+$ ,  $\text{K}^+$ ,  $\text{Ca}^{2+}$ , and  $\text{Mg}^{2+}$  are used at 250 eq.

less than 2–3 s, suggesting that equilibrium might reach instantly and the probe has rapid detection ability for HTM ions. The fluorescence response of the probe for HTM ions was reversible because the addition of excess EDTA to the probe–metal complex resulted in the return of the original metal free emission spectrum. Fig. 4 showed a linear response region of the emission intensity as a function of the concentration of metal ions. **3G** showed a linear response of emission intensity to the concentration of HTM ions if the intensity was less than about 80% of maximum emission intensities acquired with excess amounts of HTM ions. The fluorescence sensitivities for HTM ions were calculated on the basis of the lin-

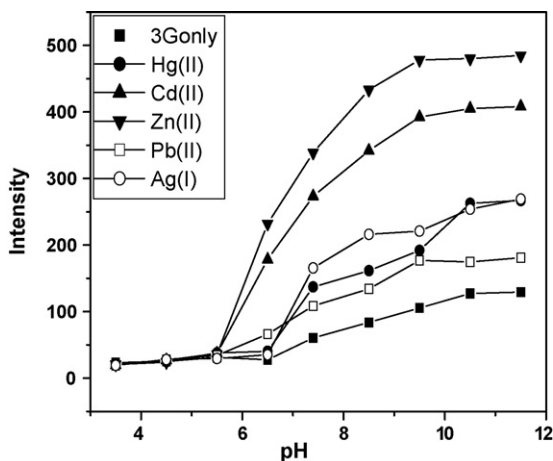


Fig. 6. pH dependence of fluorescence response of **3G** (5  $\mu\text{M}$ ) and **3G**-HTM ions ( $\text{Hg}^{2+}$ ,  $\text{Cd}^{2+}$ ,  $\text{Pb}^{2+}$ ,  $\text{Ag}^+$ , and  $\text{Zn}^{2+}$ ).

ear relationships between the emission intensity and concentration of metal ions, as shown in Fig. 4. The detection limits of **3G** for  $\text{Hg}^{2+}$ ,  $\text{Ag}^+$ ,  $\text{Cd}^{2+}$ ,  $\text{Pb}^{2+}$ , and  $\text{Zn}^{2+}$  were calculated and were summarized in Table 1. The detection limits for  $\text{Zn}^{2+}$  (2.8  $\mu\text{g/L}$ ) and  $\text{Ag}^+$  (4.3  $\mu\text{g/L}$ ) were much lower than the EPA's drinking water maximum contaminant level (MCL) [52] and the detection limits for  $\text{Cd}^{2+}$  and  $\text{Pb}^{2+}$  were also below the EPA's drinking water MCL of 5 and 15  $\mu\text{g/L}$ , respectively. Even though the detection limit for  $\text{Hg}^{2+}$  was slightly higher than the EPA's drinking water MCL of 5.2  $\mu\text{g/L}$ , this value is much lower than the detection limits of the previously reported  $\text{Hg}^{2+}$  chemical and peptide sensors [39,44,53,54]. We expect that this detection limits can be optimized by further tuning of the amino acid sequences and can be improved by optimization techniques such as a more intense light source, a longer integration time, and slit size. Holcombe and co-workers reported a turn-on fluorescent peptide sensor based on the mercury binding protein MerP [44]. The peptide that has a long size (23 mer) showed turn-on response with several heavy metal ions in aqueous solution by a FRET effect. However, the peptide probe has more than two binding sites for HTM ions and the detection limits for several HTM ions were much higher than those of **3G**. For example, the detection limit (103  $\mu\text{g/L}$ ) for  $\text{Cd}^{2+}$  was at least 20 times higher than that of **3G**, whereas the detection limit (496  $\mu\text{g/L}$ ) for  $\text{Ag}^+$  was almost 100 times higher.

#### 3.4. Fluorescence study in the presence of alkali and alkaline earth metal ions and different pH

We investigated the fluorescence response of **3G**- $\text{Hg}^{2+}$ , **3G**- $\text{Cd}^{2+}$ , and **3G**- $\text{Zn}^{2+}$  in the presence of group I, II metal ions, and  $\text{Al}^{3+}$ . The metal-dependent emission intensities of **3G**- $\text{Hg}^{2+}$ , **3G**- $\text{Cd}^{2+}$ , and **3G**-

Zn<sup>2+</sup> complex were not affected by the presence of 5 mM alkali and alkaline earth metal ions (Fig. 5). We investigated the pH influence on the fluorescence intensities of the peptide probe in the absence and presence of heavy metal ions. Fig. 6 indicated that the probe in the presence or absence of HTM ions exhibited little fluorescence intensity at pH lower than 5.5. This might be due to the protonation of the dimethylamino group (pK<sub>a</sub> ~ 4) of the dansyl fluorophore [55]. At pH 6.5, the intensity of **3G** increased by increasing pH and the enhancement factors also increased by increasing pH. Overall results indicated that **3G** was useful for monitoring HTM's in neutral and basic pH.

#### 4. Conclusion

The fluorescent peptide probe containing Trp as a donor and dansyl as an acceptor was synthesized on the basis the amino acid sequences of the metal binding motifs. This peptide probe showed a fluorescent turn-on response for several heavy metal ions by FRET as well as CHEF effects. The peptide probe successfully exhibited a ratiometric response for several heavy metal ions in aqueous solution with a low detection limit. The peptide sensor is useful for monitoring HTM's in neutral and basic pH.

#### Acknowledgment

This work was supported by the grant (R01-2006-000-10956-0) from the Basic Research Program of the Korea Science & Engineering Foundation. B.P. Joshi and J. Park were a recipient of a BK21 (II) fellowship.

#### Appendix A. Supplementary data

Supplementary data associated with this article can be found, in the online version, at doi:10.1016/j.talanta.2008.12.062.

#### References

- [1] H.H. Harris, I. Pickering, G.N. George, *Science* 301 (2003) 1203.
- [2] L. Jarup, *Br. Med. Bull.* 68 (2003) 167.
- [3] P.B. Tchounwou, W.K. Ayensu, N. Ninashvile, D. Sutton, *Environ. Toxicol.* 18 (2003) 149.
- [4] C. Yanke, X. Yang, L. Zang, *Chem. Commun.* 1413 (2008) 1413.
- [5] R.R. Avirah, K. Jyothish, D. Ramaiah, *Org. Lett.* 9 (2007) 121.
- [6] S.K. Kim, S.H. Lee, J.Y. Lee, R.A. Batsch, J.S. Kim, *J. Am. Chem. Soc.* 126 (2004) 16499.
- [7] L. Prodi, F. Bolletta, M. Montalti, N. Zaccheroni, *Coord. Chem. Rev.* 205 (2000) 59.
- [8] E.M. Nolan, S.J. Lippard, *J. Am. Chem. Soc.* 129 (2007) 5910.
- [9] J.S. Wu, I.C. Hwang, K.S. Kim, J.S. Kim, *Org. Lett.* 9 (2007) 907.
- [10] M.H. Lee, J.S. Wu, J.W. Lee, J.H. Jung, J.S. Kim, *Org. Lett.* 9 (2007) 2501.
- [11] J.Y. Kwon, Y.J. Jang, Y.J. Lee, K.M. Kim, M.S. Seo, W. Nam, J. Yoon, *J. Am. Chem. Soc.* 127 (2005) 10107.
- [12] S.H. Kim, J.S. Kim, S.M. Park, S. Chang, *Org. Lett.* 8 (2006) 371.
- [13] X. Peng, J. Du, J. Fan, J. Wang, Y. Wu, J. Zhao, S. Sun, T. Xu, *J. Am. Chem. Soc.* 129 (2007) 1500.
- [14] K. Rurack, *Spectrochim. Acta* A 57 (2001) 2161.
- [15] J. Wang, X. Qian, *Org. Lett.* 8 (2006) 3721.
- [16] M. Xavier, W. Shimon, J. Marcus, *Chem. Rev.* 106 (2006) 1785.
- [17] J.R. Lakowicz, *Principles of Fluorescence Spectroscopy*, Kluwer Academic/Plenum, New York, 1999.
- [18] S.Y. Moon, N.J. Youn, S.M. Park, S.K. Chang, *J. Org. Chem.* 70 (2005) 2394.
- [19] M.H. Lee, H.J. Kim, S. Yoon, N. Park, J.S. Kim, *Org. Lett.* 10 (2008) 213.
- [20] M. Royzen, Z. Dai, J.W. Canary, *J. Am. Chem. Soc.* 127 (2005) 1612.
- [21] J.Y.S. Raina, E.D. Cram, R. Czolij, J.M. Matthews, M. Crossley, J.P. Mackay, *J. Biol. Chem.* 278 (2003) 28011.
- [22] K.O. Pazehoski, T.C. Collins, R.J. Boyle, M.I. Jensen-Seaman, C.T. Dameron, *J. Inorg. Biochem.* 102 (2008) 522.
- [23] P.A. Cobine, G.N. George, C.E. Jones, W.A. Wickramasinghe, M. Solioz, C.T. Dameron, *Biochemistry* 41 (2002) 5822.
- [24] M. Semavina, D. Beckett, T.M. Logan, *Biochemistry* 45 (2006) 12480.
- [25] B.B. Buchanan, Y. Balmer, *Annu. Rev. Plant Biol.* 56 (2005) 187.
- [26] M.J. Stillman, C.F. Shaw, K.T. Suzuki, (Eds.), *Metallothioneins*, VCH, New York, 1992, pp. 55–127.
- [27] A. Changela, K. Chen, Y. Xue, J. Holschen, C.E. Outten, T.V. O'Halloran, *A. Mon-dragon, Science* 301 (2003) 1383.
- [28] G. Veglia, F. Porcelli, T. DeSilva, A. Prantner, S.J. Opella, *J. Am. Chem. Soc.* 122 (2000) 2389.
- [29] Y. Chen, R. Pasquinelli, M. Ataa, R.R. Koepsel, R.A. Kortess, R.E. Shepherd, *Inorg. Chem.* 39 (2000) 1180.
- [30] P. Rousselot-Pailley, O. Seneque, C. Lebrun, S. Crouzy, D. Boturyn, P. Dumy, M. Ferrand, P. Delangle, *Inorg. Chem.* 45 (2006) 5510.
- [31] G.B. Fields, R.L. Nobel, *Int. J. Pept. Protein Res.* 35 (1990) 161.
- [32] J.M. Stewart, *Methods Enzymol.* 289 (1997) 29.
- [33] M.D. Shults, D.A. Pearce, B. Imperiali, *J. Am. Chem. Soc.* 125 (2003) 10591.
- [34] I.A. Rivero, T. Gonzalez, M.E. Diaz-Garcia, *Comb. Chem. High Throughput Screening* 9 (2006) 535.
- [35] H.A. Godwin, J.M. Berg, *J. Am. Chem. Soc.* 118 (1996) 6514.
- [36] S. Deo, H.A. Godwin, *J. Am. Chem. Soc.* 122 (2000) 174.
- [37] B.P. Joshi, W.M. Cho, J.S. Kim, J. Yoon, K.H. Lee, *Bioorg. Med. Chem. Lett.* 17 (2007) 6425.
- [38] A. Torrado, G.K. Walkup, B. Imperiali, *J. Am. Chem. Soc.* 120 (1998) 609.
- [39] Y. Zhao, Z. Zhong, *Org. Lett.* 8 (2006) 4715.
- [40] Y. Zheng, X. Cao, J. Orbulescu, V. Konka, F.M. Andreopoulos, S.M. Pham, R.M. Leblanc, *Anal. Chem.* 75 (2003) 1706.
- [41] T. Kim, J. Park, J. Hong, *J. Chem. Soc. Perkin Trans.* 2 (2002) 923.
- [42] Y. Zhao, Z. Zhong, *J. Am. Chem. Soc.* 128 (2006) 9988.
- [43] B.R. White, J.A. Holcombe, *Talanta* 71 (2007) 2015.
- [44] B.R. White, H.M. Liljestrand, J.A. Holcombe, *Analyst* 133 (2008) 65.
- [45] M.T. Beck, L. Nagypal, *Chemistry of Complex Equilibria*, Halsted Press, New York, 1990, pp. 112–118.
- [46] W.A.E. McBryde, *Talanta* 21 (1974) 979.
- [47] W.D. Likussar, F. Boltz, *Anal. Chem.* 43 (1971) 1265.
- [48] B.D. Wagner, G.J. Mcmanus, *Anal. Biochem.* 317 (2003) 233.
- [49] F.E.O. Suliman, Z.H. Al-Lawati, S.M.Z. Al-Kindy, *J. Fluoresc.* 18 (2008) 1131.
- [50] S.B. Shields, S.J. Franklin, *Biochemistry* 43 (2004) 16086.
- [51] A.I. Anzellotti, M. Sabat, N. Farrell, *Inorg. Chem.* 45 (2006) 1638.
- [52] US Environmental Protection Agency, EPA Office of Water, Washington, DC. (<http://www.epa.gov/ogwdw000/contaminants/index.html#mcls>).
- [53] R. Martinez, A. Espinosa, A. Tarraga, P. Molina, *Org. Lett.* 7 (2005) 5869.
- [54] A. Caballero, R. Martinez, V. Lloveras, I. Ratera, J. Vidal-Gancedo, K. Wurst, A. Tarraga, P. Molina, J. Veciana, *J. Am. Chem. Soc.* 127 (2005) 15666.
- [55] R.P. Haughland, *Handbook of Fluorescent Probes and Research Products*, 8th ed., Molecular Probes, Inc, Eugene, OR, 2001.



# On-line collection/concentration and determination of transition and rare-earth metals in water samples using Multi-Auto-Pret system coupled with inductively coupled plasma-atomic emission spectrometry

Rosi Ketrin Katarina, Mitsuko Oshima, Shoji Motomizu\*

Department of Chemistry, Faculty of Science, Okayama University, 3-1-1 Tsushimanaka, Okayama 700-8530, Japan

## ARTICLE INFO

### Article history:

Received 26 December 2008

Received in revised form 8 January 2009

Accepted 9 January 2009

Available online 20 January 2009

### Keywords:

Multi-Auto-Pret system

Online collection/concentration

Transition metals

Rare-earth metals

Chelating resin

ICP-AES

## ABSTRACT

On-line preconcentration and determination of transition and rare-earth metals in water samples was performed using a Multi-Auto-Pret system coupled with inductively coupled plasma-atomic emission spectrometry (ICP-AES). The Multi-Auto-Pret AES system proposed here consists of three Auto-Pret systems with mini-columns that can be used for the preconcentration of trace metals sequentially or simultaneously, and can reduce analysis time to one-third and running cost of argon gas and labor. A newly synthesized chelating resin, ethylenediamine-*N,N,N'*-triacetate-type chitosan (EDTriA-type chitosan), was employed in the Multi-Auto-Pret system for the collection of trace metals prior to their measurement by ICP-AES. The proposed resin showed very good adsorption ability for transition and rare-earth metal ions without any interference from alkali and alkaline-earth metal ions in an acidic media. For the best result, pH 5 was adopted for the collection of metal ions. Only 5 mL of samples could be used for the determination of transition metals, while 20 mL of samples was necessary for the determination of rare-earth metals. Metal ions adsorbed on the resin were eluted using 1.5 M nitric acid, and were measured by ICP-AES. The proposed method was evaluated by the analysis of SLRS-4 river water reference materials for trace metals. Good agreement with certified and reference values was obtained for most of the metals examined; it indicates that the proposed method using the newly synthesized resin could be favorably used for the determination of transition and rare-earth metals in water samples by ICP-AES.

© 2009 Elsevier B.V. All rights reserved.

## 1. Introduction

Increasing use of metals in industrial activities and agricultural practices can increase the possibility of metals release into the environment. Metal species in the biotic environment pose not only potential ecological risks, but also the possible introduction of these elements in the food chain and severe risks to human health. From this viewpoint, river water is of interest because it can transport metals, and it is also used as drinking water [1].

The attractiveness of the inductively coupled plasma-atomic emission spectrometry (ICP-AES) [2] has increased their use for the determination of trace metals in various kinds of samples, such as waters [3–6], oils [7,8], medicines [9–11], foods [12–14], metrology [15–17], hair and mussel samples [18,19]. However, in such samples as river or seawater, a preconcentration is necessary, especially for the determination of rare-earth elements, since their concentration are usually low and their detection limits are limited and not so good [20–22]. The use of carboxyamino or carboxyimino

resins for the preconcentration of transition metals [4,5,23–25] and rare-earth metals [26–28] in water samples has been well done. In our previous work [29], a new-type chitosan-based chelating resin, ethylenediamine-*N,N,N'*-triacetate-type chitosan (EDTriA-type chitosan) resin was synthesized, and was used in a batch-wise column pretreatment method for multi-element collection/preconcentration of transition and rare-earth metals and for removing the matrix in seawater before measuring the trace metals by inductively coupled plasma-mass spectrometry (ICP-MS). However, the batch-wise method used was very tedious and time consuming. It was much beneficial to perform such procedures on-line and automatically, which could save our labor analysis time, reduce contaminations and errors [30]. However, on-line methods themselves could introduce several problems: mainly, the separation/preconcentration step took more than 10 min, and during this stage, the ICP-AES was idle and waiting for the sample to reach the plasma, thus it wasted expensive resources. To shorten the time for the separation/preconcentration procedure, on-line techniques could be much more efficient.

This work aimed at developing a simple and cost effective ICP-AES detection system which could enable to determine transition and rare-earth metals at ppt (part per trillion) levels, which are

\* Corresponding author.

E-mail address: [motomizu@cc.okayama-u.ac.jp](mailto:motomizu@cc.okayama-u.ac.jp) (S. Motomizu).



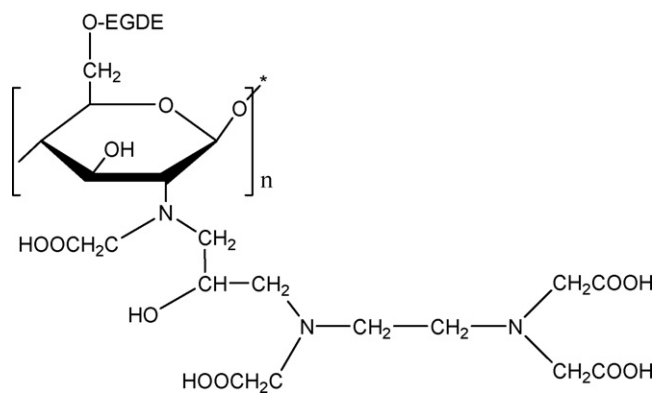


**Fig. 1.** Structure of ethylenediamine *N,N,N'*-triacetate-type chitosan (EDTriA-type chitosan) resin.

comparable to ICP-MS. For such a purpose, an automated on-line pretreatment system with three collection systems (Multi-Auto-Pret AES), which are synchronized, was developed for the rapid determination of trace metals in water samples. The Multi-Auto-Pret AES system consists of three sets of the single Auto-Pret system [23]. Each single Auto-Pret system had one mini-column (40 mm length  $\times$  2 mm i.d.), which was filled with EDTriA-type chitosan resin. Therefore, the Multi-Auto-Pret AES system consisted of three mini-columns that could be used for the preconcentration of trace metals sequentially or simultaneously, which could reduce analysis time and running cost.

## 2. Experimental

### 2.1. Reagents and chemicals

The EDTriA-type chitosan resin was synthesized in the same manner as in the previous work [29]. The chemical structure of the resin was shown in Fig. 1.

A multi-element stock standard solution (57 elements,  $1 \mu\text{g mL}^{-1}$ ) was prepared by diluting analytical multi-element stan-

**Table 1**  
ICP-AES operating conditions.

System	ICP-AES VISTA - PRO
RF generator	Frequency 40 MHz, power 1.1 kW
Plasma gas flow	Ar $15.0 \text{ L min}^{-1}$
Auxiliary gas flow	Ar $1.50 \text{ L min}^{-1}$
Nebulizer gas flow	Ar $0.75 \text{ L min}^{-1}$
Spray chamber	Glass cyclonic spray chamber
Nebulizer	K-style concentric glass nebulizer
Torch	One-piece low flow extended torch in the axial view mode
Measurement mode	Time scan mode

dard solutions, XSTC-13 (Li, Be, Na, Mg, Al, K, Ca, V, Cr, Mn, Fe, Co, Ni, Cu, Zn, Ga, As, Se, Rb, Sr, Ag, Cd, In, Cs, Ba, Hg, Tl, Pb, Bi, Th, and U), XSTC-1 (Ce, Dy, Er, Eu, Gd, Ho, La, Lu, Nd, Pr, Sm, Sc, Tb, Tm, Yb, and Y), purchased from Spex CertiPrep Inc. (Metuchen, NJ, USA), and standard solutions for a single element for AAS (W, Ge, Zr, Pd, Sn, Sb, Te, Hf, Pt, and Au) from Wako Pure Chemicals Industries, Ltd. (Osaka, Japan) in 0.01 M of a nitric acid solution. Working standard solutions were prepared daily by diluting the stock standard solution with nitric acid. All dilution procedures were performed by weight.

Nitric acid for the analysis of poisonous metals with 60–62%, density  $1.38 \text{ g mL}^{-1}$  from Wako Pure Chemicals Industries, Ltd. was used; it was diluted with an ultra-pure water to give a 0.01, a 1.5 or a 2 M solution.

A stock solution of 4 M ammonium acetate buffer solution was prepared by mixing appropriate amounts of concentrated acetic acid and a concentrated ammonia solution, and diluted with ultra-pure water. Both solutions were of electronic industrial reagent grade from Kanto Chemical Co., Inc. (Tokyo, Japan). Buffer solutions of 0.2 and 0.5 M ammonium acetate were prepared by diluting the stock buffer solution and adjusting to pH 3–9 with small amounts of concentrated ammonia or acetic acid.

The ultra-pure water ( $18.3 \text{ M}\Omega \text{ cm}^{-1}$  resistivity) was prepared by an Elix-3/Milli-Q element system, Nihon Millipore (Tokyo, Japan).

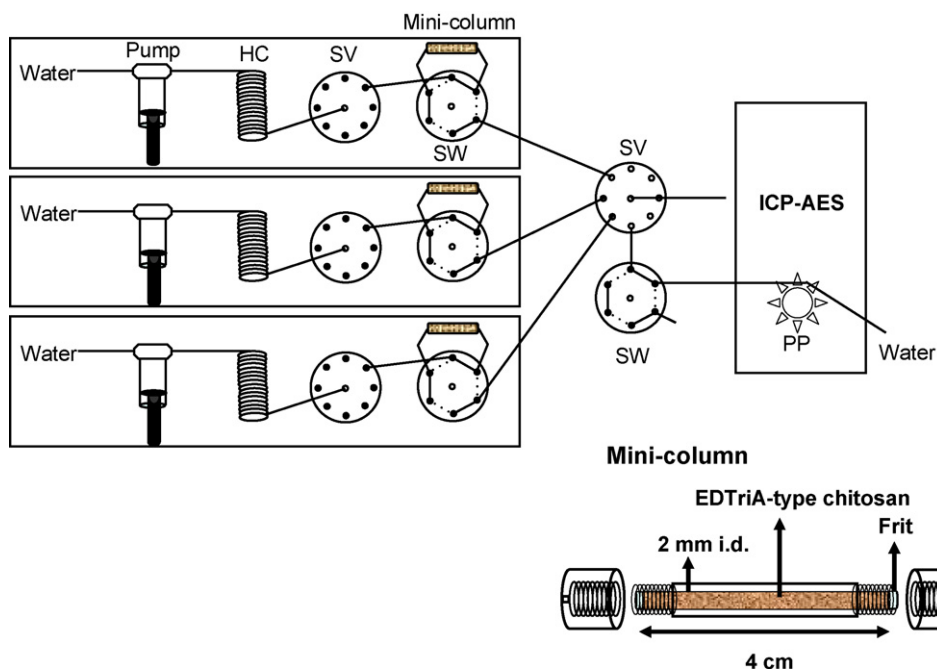


**Fig. 2.** Multi-Auto-Pret AES system. Pump, 10 mL syringe pump; HC, holding coil; SV, 8-port selection valve; SW, 6-port switching valve; PP, peristaltic pump equipped to ICP-AES system.

An artificial river water sample containing  $\text{Na}^+$  ( $2.6 \times 10^{-4}$  M),  $\text{Ca}^{2+}$  ( $3.8 \times 10^{-4}$  M),  $\text{K}^+$  ( $7.0 \times 10^{-5}$  M),  $\text{Mg}^{2+}$  ( $1.7 \times 10^{-4}$  M),  $\text{SO}_4^{2-}$  ( $1.1 \times 10^{-4}$  M) and  $\text{Cl}^-$  ( $2.2 \times 10^{-4}$  M) was prepared by mixing appropriate amounts of salts of sodium sulfate, sodium nitrate, calcium chloride, calcium nitrate, potassium nitrate, and magnesium nitrate in 0.01 M nitric acid solution [31]. All of the reagents were of analytical reagent grade from Wako Pure Chemical Industries, Ltd.

River water samples were collected from Asahi River, Nishi River, and Zasu River, which flow around Okayama City. All of the sample solutions were acidified to pH 2 by adding a small amount of nitric acid and filtered through a 0.45  $\mu\text{m}$  membrane filter made of mixed cellulose ester, Toyo Roshi Kaisha, Ltd. (Tokyo, Japan), before storing [32]. The pH of the sample solutions was adjusted to 5 just before a pretreatment with the Multi-Auto-Pret system by adding small amounts of a concentrated ammonia solution.

SLRS-4 water reference material for trace metals was purchased from Institute for National Measurement Standards, National Research Council of Canada (Ontario, Canada).

## 2.2. Apparatus

Measurements were carried out on a Vista-Pro ICP-AES system Seiko Instruments Co. & Varian Australia Pty. Ltd. (Chiba, Japan – Melbourne, Australia). The operating conditions were listed in Table 1. The ICP-AES was coupled with a Multi-Auto-Pret system. The Multi-Auto-Pret AES system was built from three sets of a single Auto-Pret system [23], an eight-port selection valve and a six-port switching valve, as shown in Fig. 2. Each single Auto-Pret system was equipped with one syringe pump of Hamilton (Reno, NV, USA) with volume capacity of 10 mL, an eight-port selection valve and a six-port switching valve of Hamilton.

## 2.3. Procedure for collection and concentration of trace metals using Multi-Auto-Pret AES system

Before use for the collection and the concentration of trace metals, the EDTriA-type chitosan resin was cleaned to remove any metal impurities in the resin. Ten milliliters of wet resin was transferred to

a plastic beaker; to it, 50 mL of 2 M nitric acid was added. The mixture was carefully stirred at low speed for 6 h. The aqueous solution was decanted, and the resin was rinsed with ultra-pure water until the pH of the effluent was similar to that of the ultra-pure water.

Procedure for the collection/concentration of trace metals using a Multi-Auto-Pret AES system was done in four steps, and an additional step for resin shaking was inserted to restore the resin packing in the column in order to avoid high pressure that might be happened because of resin packing that used on previous cycle.

The preconcentration procedures shown in Table 2 are explained in details as follows. The mini-columns (2.0 mm i.d.  $\times$  40 mm) were filled with EDTriA-type chitosan resin. At the loading stage (switching valve or SW at the position 1), 0.5 mL of 0.5 M ammonium acetate buffer solutions (pH 5) were passed through the columns for conditioning (Step 2). After the pretreatment of the columns, 5 mL of sample solutions at pH 5 was passed through the columns (Step 3) followed by 0.5 mL of 0.2 M ammonium acetate buffer solutions (pH 5) and 0.5 mL of ultra-pure water for eliminating sample matrix (Step 4). Switching valves were moved to the position 2 for the eluting stage, then 1 mL of 1.5 M nitric acid followed by 2 mL ultra-pure water were passed through the columns for eluting metals adsorbed on the resin and for cleaning the resin for the next cycle (Step 5), respectively. At this eluting stage, all of the solutions were flowed to the ICP-AES.

The time required for the whole procedures was 6.3 min for the treatment of 5 mL samples and 15 min for the treatment of 20 mL samples. Since the Multi-Auto-Pret AES system consisted of three sets of the single Auto-Pret system, and the different time of each single system was 2.1 and 5 min, therefore the sample throughput was 28 and 12  $\text{h}^{-1}$  for the treatment of 5 and 20 mL sample, respectively.

## 3. Results and discussion

### 3.1. Adsorption behavior of metal ions on EDTriA-type chitosan resin

The adsorption behavior of 57 elements on the EDTriA-type chitosan at various pHs was investigated by an off-line method using

**Table 2**  
Procedure for preconcentration using Multi-Auto-Pret system.

Step	Operation description	Pump	SV <sup>a</sup>	SW <sup>b</sup>	Flow rate ( $\mu\text{L s}^{-1}$ )	Volume ( $\mu\text{L}$ )	Action of flow	Time required (s)
1	Resin shaking ultra-pure water	In		1	300	100	aspirate	0.3
		Out	5	1	40	100	dispense	2.5
		Out	5	1	40	100	aspirate	2.5
		Out	5	1	40	100	dispense	2.5
		Out	5	1	40	100	aspirate	2.5
		Out	5	1	40	100	dispense	2.5
2	Conditioning 0.5 M buffer	Out	1	1	100	500	aspirate	5
		Out	5	1	40	500	dispense	12.5
3	Sample loading sample	Out	6	1	100	5000	aspirate	50
		Out	5	1	40	5000	dispense	125
4	Matrix removing ultra-pure water 0.2 M buffer	In		1	300	500	aspirate	1.7
		Out	2	1	100	500	aspirate	5
		Out	5	1	40	1000	dispense	25
5	Eluting and cleaning ultra-pure water 1.5 M $\text{HNO}_3$	In		1	300	2000	aspirate	6.7
		Out	3	1	100	1000	aspirate	10
		Out	5	2	40	3000	dispense	75
		Pump/SV/SW moving TOTAL TIME						

<sup>a</sup> SV, position of the selection valve.

<sup>b</sup> SW, position of the switching valve.

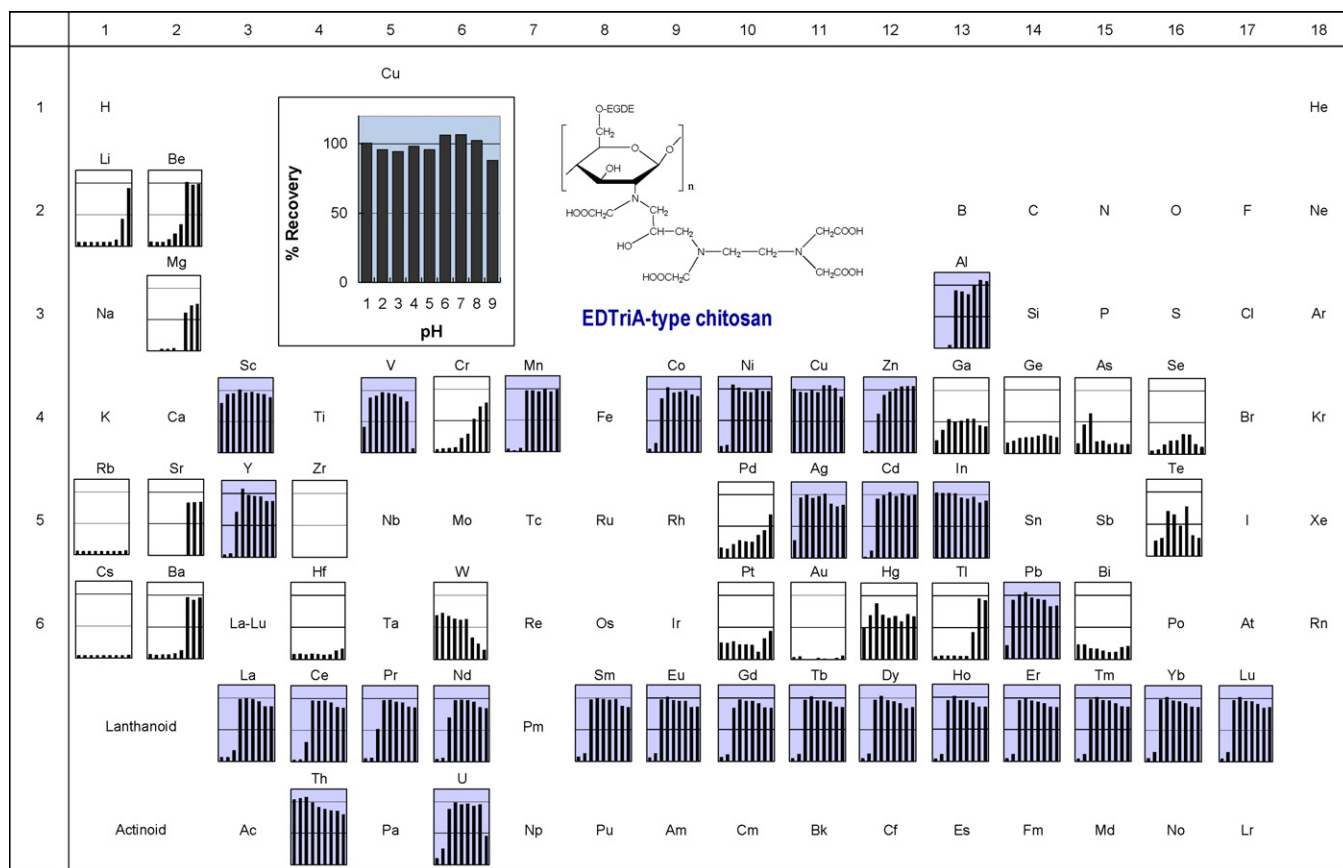


**Fig. 3.** Adsorption behavior of EDTriA-type chitosan for metals at various pH values. Sample volume, 3 mL; concentration of each metal, 20 ng mL<sup>-1</sup>; eluent, 3 mL of 2 M nitric acid.

the Multi-Auto-Pret system, and measured by an ICP-AES. As shown in Fig. 3, most transition and rare-earth metals (29 metal ions) could be collected quantitatively from pH 3 to 7 and recovered at greater than 95% with 3 mL of 2 M nitric acid. The resin did not adsorb both alkali and alkaline-earth metals in acidic media (pH < 6). In

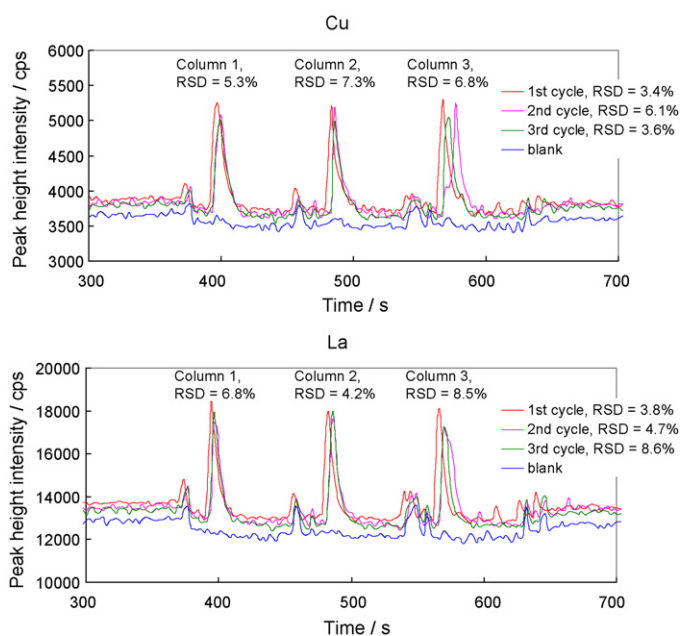


**Fig. 4.** Examples of the repeatability of Multi-Auto-Pret AES system.

Fe(III) and Al(III), the calibration graphs at concentration range of 1–50 ng mL<sup>-1</sup> were not linear. This is probably because the chelations of such metal ions with the resin at pH 5 were weak due to the formation of hydroxo complexes. When Multi-Auto-Pret system was used for on-line collection/concentration, the calibration graphs were linear at least for very important and interesting 24 metal ions. Therefore, in the present study, the proposed resin was used for the collection/concentration of the 24 metal ions, transition and rare-earth metal ions.

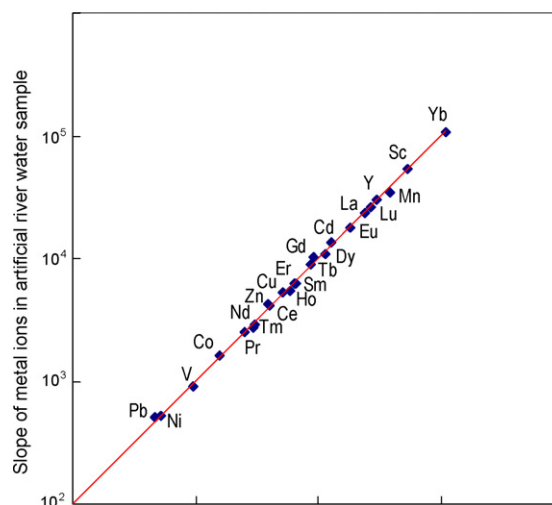


**Fig. 5.** Comparison of slopes of trace metal ions in artificial river water and that in standard samples.

**Table 3**  
Wavelengths, enrichment factors and detection limits.

Elements	Wavelength <sup>a</sup> (nm)	Enrichment factor <sup>b</sup>	LOD (ng mL <sup>-1</sup> )	
			This work <sup>d</sup>	Direct ICP-AES <sup>e</sup>
Cd	226.502	116 <sup>c</sup>	0.002 <sup>c</sup>	0.3
Co	228.615	93 <sup>c</sup>	0.022 <sup>c</sup>	0.8
Cu	324.754	35	0.066	0.3
Mn	257.610	14	0.018	0.7
Ni	231.604	16	0.12	0.9
Pb	220.353	112 <sup>c</sup>	0.080 <sup>c</sup>	3.7
Sc	361.383	30	0.007	0.3
V	292.401	19	0.15	0.8
Zn	213.856	25	0.048	1.2
Y	371.029	25	0.020	0.2
Ce	418.659	120 <sup>c</sup>	0.095 <sup>c</sup>	1.8
Dy	353.171	89 <sup>c</sup>	0.020 <sup>c</sup>	0.3
Er	337.275	92 <sup>c</sup>	0.007 <sup>c</sup>	0.5
Eu	381.967	83 <sup>c</sup>	0.008 <sup>c</sup>	0.3
Gd	342.246	89 <sup>c</sup>	0.022 <sup>c</sup>	0.4
Ho	345.600	90 <sup>c</sup>	0.007 <sup>c</sup>	0.5
La	408.671	93 <sup>c</sup>	0.014 <sup>c</sup>	0.3
Lu	261.541	90 <sup>c</sup>	0.002 <sup>c</sup>	0.08
Nd	401.224	104 <sup>c</sup>	0.081 <sup>c</sup>	2.4
Pr	390.843	110 <sup>c</sup>	0.023 <sup>c</sup>	2.2
Sm	359.259	92 <sup>c</sup>	0.024 <sup>c</sup>	1.6
Tb	350.914	93 <sup>c</sup>	0.050 <sup>c</sup>	0.6
Tm	346.220	92 <sup>c</sup>	0.047 <sup>c</sup>	0.6
Yb	328.937	87 <sup>c</sup>	0.002 <sup>c</sup>	0.07

<sup>a</sup> Emission wavelengths were selected to give the best intensity without any interference [33,34].

<sup>b</sup> Enrichment factor for 5 mL sample, the ratio of peak height obtained by proposed system and that by conventional nebulization of ICP-AES.

<sup>c</sup> Sample volume was 20 mL.

<sup>d</sup> Limit of detection, corresponding to three (S/N).

<sup>e</sup> Instrumental detection limit, corresponding to three SD of blank measured by the conventional nebulization of ICP-AES.

### 3.2. Optimization of the parameters of Auto-Pret system

Basically, the parameters of Auto-Pret system, such as a sample pH, a sample loading flow rate, an eluent flow rate, and an eluent concentration should be optimized in order to obtain a lower background, higher sensitivity and shorter measuring time.

As mentioned before, the EDTriA-type chitosan resin could adsorb a numbers of metal ions at pH 3–7 by the off-line method examined in the previous study [29]. When the Multi-Auto-Pret system was used for on-line measurement, pH 5 gave the highest peak intensity for almost the entire metal ion examined. Therefore, pH 5 was selected for further investigations.

**Table 4**  
Analytical results of trace metals in the SLRS-4<sup>a</sup> (ng mL<sup>-1</sup>).

	This study	Certified	Reference 1 <sup>d</sup>	Reference 2 <sup>e</sup>
Cd	0.013 ± 0.001 <sup>b</sup>	0.012 ± 0.002		
Co	0.034 ± 0.002 <sup>b</sup>	0.033 ± 0.006		
Cu	1.85 ± 0.02	1.81 ± 0.08		
Mn	3.39 ± 0.27	3.37 ± 0.18		
Ni	0.69 ± 0.01	0.67 ± 0.08		
Pb	0.093 ± 0.004 <sup>b</sup>	0.086 ± 0.007		
Sc	(0.028 ± 0.005) <sup>c</sup>	–		
V	0.32 ± 0.03	0.32 ± 0.03		
Zn	0.85 ± 0.08	0.93 ± 0.10		
Y	(0.11 ± 0.01) <sup>b,c</sup>		0.15 ± 0.01	0.14 ± 0.01
Ce	(0.39 ± 0.07) <sup>b,c</sup>		0.36 ± 0.01	0.38 ± 0.01
Dy	(0.026 ± 0.000) <sup>b,c</sup>		0.024 ± 0.002	0.024 ± 0.001
Er	(0.015 ± 0.003) <sup>b,c</sup>		0.013 ± 0.001	0.014 ± 0.001
Eu	(0.009 ± 0.003) <sup>b,c</sup>		0.0080 ± 0.0006	0.0081 ± 0.0006
Gd	(0.038 ± 0.006) <sup>b,c</sup>		0.034 ± 0.002	0.035 ± 0.001
Ho	< 0.007 <sup>b</sup>		0.0047 ± 0.0003	0.0049 ± 0.0001
La	(0.29 ± 0.04) <sup>b,c</sup>		0.29 ± 0.01	0.30 ± 0.01
Lu	(0.004 ± 0.002) <sup>b,c</sup>		0.0019 ± 0.0001	0.0019 ± 0.0001
Nd	(0.29 ± 0.07) <sup>b,c</sup>		0.27 ± 0.01	0.28 ± 0.01
Pr	(0.074 ± 0.003) <sup>b,c</sup>		0.069 ± 0.002	0.074 ± 0.001
Sm	(0.052 ± 0.003) <sup>b,c</sup>		0.057 ± 0.003	0.059 ± 0.001
Tb	< 0.050		0.0043 ± 0.0004	0.0045 ± 0.0002
Tm	< 0.047		0.0017 ± 0.0002	0.0019 ± 0.0001
Yb	(0.010 ± 0.003) <sup>b,c</sup>		0.012 ± 0.000	0.012 ± 0.001

<sup>a</sup> River water reference material for trace metals issued by National Research Council Canada.

<sup>b</sup> Sample volume was 20 mL.

<sup>c</sup> Figure in parentheses was information value.

<sup>d</sup> Cited from Yeghicheyan, et al. [35].

<sup>e</sup> Cited from Lawrence, et al. [36].

Other parameters for Auto-Pret pretreatment were optimized using a 5 mL standard solution containing 1 ng mL<sup>-1</sup> of metal ions. When an eluent flow rate was varied from 10 to 50  $\mu\text{L s}^{-1}$ , a sample loading flow rate was kept constant at 40  $\mu\text{L s}^{-1}$ . Peak height intensity was increased by increasing an eluent flow rate from 10 to 30  $\mu\text{L s}^{-1}$ , and became constant when an eluent flow rate was faster than 30  $\mu\text{L s}^{-1}$ , then decreased after 40  $\mu\text{L s}^{-1}$ . A faster flow rate was preferred to decrease a measuring time and to increase a sample throughput. Therefore, a 35  $\mu\text{L s}^{-1}$  of the eluent flow rate was selected.

A sample loading flow rate was studied by varying from 10 to 50  $\mu\text{L s}^{-1}$ . When the sample loading flow rate was varied, an eluent flow rate was kept constant at 35  $\mu\text{L s}^{-1}$ . There was no significant difference in signal intensity obtained by varying of sample loading flow rates. To avoid the probability of high pressure, the sample loading flow rate of 40  $\mu\text{L s}^{-1}$  was adopted.

As an eluent, a diluted nitric acid was used. At the optimized flow rate, the concentration of nitric acid was varied from 0.5 to 3.0 M. Increase in the nitric acid concentration from 0.5 to 1.5 M increased the peak height intensity. The intensity signal became identical at

**Table 5**  
Analytical results of trace metals in river water samples.

Elements	Spiked (ng mL <sup>-1</sup> )	Asahi River		Nishi River		Zasu River	
		Found (ng mL <sup>-1</sup> )	Recovery (%)	Found (ng mL <sup>-1</sup> )	Recovery (%)	Found (ng mL <sup>-1</sup> )	Recovery (%)
Cd	–	0.025 ± 0.001		0.038 ± 0.004		0.041 ± 0.004	
	0.05	0.079 ± 0.001	108	0.084 ± 0.003	91	0.087 ± 0.005	91
Co	–	0.047 ± 0.008		0.033 ± 0.001		0.034 ± 0.002	
	0.05	0.100 ± 0.009	105	0.089 ± 0.006	110	0.083 ± 0.008	92
Cu	–	1.06 ± 0.05		0.92 ± 0.02		1.18 ± 0.01	
	0.5	1.58 ± 0.02	104	1.40 ± 0.06	97	1.69 ± 0.01	101
Mn	–	4.8 ± 0.1		4.6 ± 0.1		6.8 ± 0.1	
Ni	–	0.34 ± 0.01		0.26 ± 0.04		0.23 ± 0.03	
	0.5	0.83 ± 0.04	98	0.79 ± 0.01	107	0.73 ± 0.05	99
Pb	–	0.14 ± 0.05		0.31 ± 0.02		0.17 ± 0.01	
	0.5	0.69 ± 0.01	108	0.82 ± 0.07	102	0.69 ± 0.02	102
Sc	–	0.025 ± 0.004		0.033 ± 0.001		0.042 ± 0.006	
	0.05	0.074 ± 0.002	98	0.078 ± 0.003	91	0.087 ± 0.004	90
V	–	0.59 ± 0.04		0.50 ± 0.03		0.46 ± 0.01	
	0.5	1.12 ± 0.03	106	1.03 ± 0.02	104	1.00 ± 0.08	108
Zn	–	3.94 ± 0.04		1.4 ± 0.2		1.9 ± 0.1	
	0.5	4.44 ± 0.05	98	2.0 ± 0.2	107	2.4 ± 0.1	106
Y	–	0.050 ± 0.000		0.044 ± 0.002		0.043 ± 0.004	
	0.05	0.097 ± 0.005	94	0.092 ± 0.006	96	0.093 ± 0.004	100
Ce	–	0.16 ± 0.05		0.12 ± 0.00		0.12 ± 0.01	
	0.5	0.67 ± 0.06	102	0.62 ± 0.08	100	0.64 ± 0.02	104
Dy	–	0.047 ± 0.004		0.030 ± 0.000		0.026 ± 0.002	
	0.05	0.093 ± 0.008	93	0.082 ± 0.003	104	0.077 ± 0.008	101
Er	–	0.15 ± 0.01		0.11 ± 0.01		0.078 ± 0.003	
	0.05	0.20 ± 0.01	101	0.16 ± 0.01	99	0.128 ± 0.003	101
Eu	–	0.013 ± 0.001		0.012 ± 0.000		0.013 ± 0.002	
	0.05	0.064 ± 0.003	101	0.062 ± 0.005	100	0.060 ± 0.001	95
Gd	–	0.046 ± 0.003		0.075 ± 0.005		0.021 ± 0.005	
	0.05	0.098 ± 0.002	105	0.121 ± 0.006	91	0.067 ± 0.006	92
Ho	–	0.039 ± 0.004		0.020 ± 0.001		0.008 ± 0.000	
	0.05	0.086 ± 0.006	93	0.074 ± 0.004	109	0.058 ± 0.002	100
La	–	0.104 ± 0.008		0.040 ± 0.000		0.047 ± 0.001	
	0.05	0.156 ± 0.005	103	0.090 ± 0.009	101	0.096 ± 0.001	99
Lu	–	0.002 ± 0.002		0.002 ± 0.001		0.003 ± 0.001	
	0.05	0.056 ± 0.002	106	0.049 ± 0.004	94	0.049 ± 0.004	92
Nd	–	0.29 ± 0.01		0.34 ± 0.05		0.36 ± 0.02	
	0.5	0.76 ± 0.05	95	0.80 ± 0.05	93	0.86 ± 0.01	101
Pr	–	0.049 ± 0.003		0.022 ± 0.004		0.028 ± 0.002	
	0.05	0.098 ± 0.006	98	0.076 ± 0.007	106	0.077 ± 0.003	98
Sm	–	0.049 ± 0.007		0.055 ± 0.003		0.031 ± 0.002	
	0.05	0.103 ± 0.005	109	0.104 ± 0.000	98	0.086 ± 0.004	109
Tb	–	< 0.050		< 0.050		< 0.050	
	0.5	0.51 ± 0.04	101	0.52 ± 0.03	103	0.53 ± 0.02	104
Tm	–	< 0.047		< 0.047		< 0.047	
	0.5	0.53 ± 0.01	106	0.52 ± 0.01	104	0.54 ± 0.05	108
Yb	–	0.009 ± 0.001		0.007 ± 0.001		0.005 ± 0.001	
	0.05	0.059 ± 0.002	101	0.054 ± 0.002	94	0.050 ± 0.000	91

All data were averaged using three replicate measurements.

concentrations higher than 1.5 M. Lower concentrations of the nitric acid was preferable to decrease the amount of nitric acid used and wasted; therefore, a 1.5 M nitric acid solution was employed as an eluent.

### 3.3. Repeatability of the Multi-Auto-Pret AES system

Under the optimized conditions, repeatability of the Multi-Auto-Pret AES system was examined by passing 5 mL standard solutions contained 1 ng mL<sup>-1</sup> of metal ions through the mini-columns filled with EDTriA-type chitosan resin. The repeatability was calculated as a relative standard deviation (RSD) for repeated measurements in same mini-column and single measurement using different mini-column. The repeatability of same mini-column and different mini-column gave similar results, which are less than 10% of RSD for almost all of the metal ions examined. Peak profiles for all elements were very similar, and therefore Cu that is a representative of the transition metal and La that is a representative of the rare-earth metal were selected as examples of signal profiles, as shown in Fig. 4. The results indicate that the Multi-Auto-Pret AES system with EDTriA-type chitosan resin has good repeatability, and could be used for the preconcentration and the determination of trace metals.

### 3.4. Effect of river water matrix on the determination of trace metals

The effect of river water matrix was studied using artificial river water containing alkali and alkaline-earth metal salts that usually present in the river water. The slopes of calibration graphs of trace metal ions in artificial river water were compared with those in standard samples. As shown in Fig. 5 both calibration graphs for metal ions were in good agreement with one another (slope ratio was about 1). It means that the river water matrix did not interfere with the collection of trace metals on the column containing the EDTriA-type chitosan resin.

### 3.5. Enrichment factor and detection limit

The enrichment factors (EF) and the limits of detection (LOD) of metal ions examined at their wavelength under the optimized conditions were shown in Table 3. The emission wavelengths were selected to give the best intensity without any interference [33,34].

The EFs were estimated by comparing the peak heights obtained by the proposed method (using 3 ng mL<sup>-1</sup> of standard solution) with those obtained by a direct nebulization method of ICP-AES (using 30 ng mL<sup>-1</sup> of standard solution). The enrichment factors of the trace metals were in the range of 14 (Mn) to 35 (Cu), when 5 mL of the sample solutions was used. The EF of 120 fold could be obtained for Ce when 20 mL of sample solution was used.

LODs of this work were determined as the concentrations corresponding to three times of the signal-to-noise ratio of the background. LODs of the direct ICP-AES instrument were determined as the concentration corresponding to three times of the standard deviations of the blank solution measured by the conventional nebulization of ICP-AES (for 10 measurement replicates).

From data shown in Table 3, the proposed method with only 5 mL of sample solutions was found to be sensitive enough for determining transition metals in river water samples, while 20 mL of sample solutions was necessary for determining rare-earth metals. Such sensitivity and LODs are almost comparable to those of ICP-MS.

### 3.6. Accuracy

The river water reference material for trace metals, SLRS-4 issued by the National Research Council of Canada (Ottawa, Ontario,

Canada), was used to evaluate the accuracy of the proposed Multi-Auto-Pret AES method. The sample pH was adjusted to 5, and the samples were used in the similar manner to the standard solution.

As shown in Table 4, the results obtained for the transition metals were in good agreement with the certified values. Since there are no certified values for rare-earth metals, the results obtained in this work were compared with the reference values reported by Yeghicheyan et al. [35] and Lawrence et al. [36]. The results for rare-earth metals also were in good agreement with the reference values, except for Tb and Tm, which could not be detected because of lower concentrations than their LODs.

Such a good agreement indicates that the present method will certify a good accuracy and is applicable to the multi-element preconcentration and determination of trace metals in river water samples.

### 3.7. Application to the river water samples

The proposed method was successfully applied to the determination of trace metals in river water samples of Asahi River, Nishi River, and Zasu River, which were collected in Okayama City. The samples were spiked with several concentrations of metal ions; the spiked concentrations were as close as possible to the concentrations found, and the recovery tests were examined.

As shown in Table 5, all of the transition and rare-earth metals in river water samples can be determined with good recovery results in the range of 90–110%, except for Tb and Tm; the LODs of these two metal ions are relatively high compared with their concentrations in river water samples.

## 4. Conclusions

Ethylenediamine *N,N,N'*-triacetate-type chitosan (EDTriA-type chitosan) was developed and used for the collection/concentration of transition and rare-earth metals without any interferences from alkali and alkaline-earth metals.

The Multi-Auto-Pret AES system was developed for a rapid automated on-line pretreatment procedures coupled with ICP-AES. The proposed method is fully automated, and therefore it can be preferably applied to the routine analysis of water samples. The proposed system using EDTriA-type chitosan resin was successfully applied to the simultaneous determination of transition and rare-earth metals in environmental water samples by ICP-AES.

## Acknowledgements

This work was partially supported by a Grant-in-Aid for Scientific Research (B) (no. 19350038) from Japan Society for Promotion of Science (JSPS).

## References

- [1] S. Uchida, K. Tagami, K. Tabei, I. Hirai, J. Alloys Compd. 408 (2006) 525.
- [2] J.M. Mermet, J. Anal. At. Spectrom. 20 (2005) 11.
- [3] T. Shimamura, M. Iwashita, S. Iijima, M. Shintani, Y. Takaku, Atmos. Environ. 41 (2007) 6999.
- [4] T. Sumida, T. Nakazato, H. Tao, M. Oshima, S. Motomizu, Anal. Sci. 22 (2006) 1163.
- [5] E. Vassileva, N. Furuta, Spectrochim. Acta B 58 (2003) 1541.
- [6] M. Chatterjee, E.V. Silva Filho, S.K. Sarkar, S.M. Sella, A. Bhattacharya, K.K. Satpathy, M.V.R. Prasad, S. Chakraborty, B.D. Bhattacharya, Environ. Int. 33 (2007) 346.
- [7] I.J. Cindric, M. Zeiner, I. Steffan, Microchem. J. 85 (2007) 136.
- [8] M. Zeiner, I. Steffan, I.J. Cindric, Microchem. J. 81 (2005) 171.
- [9] G.A. Zachariadis, A.F. Olympiou, J. Pharm. Biomed. 47 (2008) 541.
- [10] S. Raziq, A. Onjia, S. Dogo, L. Slavkovic, A. Popovic, Talanta 67 (2005) 233.
- [11] G.A. Zachariadis, D.C. Kapsimali, J. Pharm. Biomed. 41 (2006) 1212.
- [12] A. Ramesh, B.A. Devi, H. Hasegawa, T. Maki, K. Ueda, Microchem. J. 86 (2007) 124.

- [13] M.D. Ioannidou, G.A. Zachariadis, A.N. Anthemidis, J.A. Stratis, *Talanta* 65 (2005) 92.
- [14] I. Matsushige, E. Oliveira, *Food Chem.* 47 (1993) 205.
- [15] R. Djingova, J. Ivanova, *Talanta* 57 (2002) 821.
- [16] G.V. Ramanaiah, *Talanta* 46 (1998) 533.
- [17] V.Z. Paneva, K. Cundeva, T. Staffilov, *Spectrochim. Acta B* 60 (2005) 403.
- [18] K.S. Rao, T. Balaji, T.P. Rao, Y. Babu, G.R.K. Naidu, *Spectrochim. Acta B* 57 (2002) 1333.
- [19] M.V.B. Krishna, J. Arunachalam, *Anal. Chim. Acta* 522 (2004) 179.
- [20] T.P. Rao, R. Kala, *Talanta* 63 (2004) 949.
- [21] T. Pasinli, A.E. Eroglu, T. Shahwan, *Anal. Chim. Acta* 547 (2005) 42.
- [22] N. Bahramifar, Y. Yamini, *Anal. Chim. Acta* 540 (2005) 325.
- [23] R.K. Katarina, N. Lenghor, S. Motomizu, *Anal. Sci.* 23 (2007) 343.
- [24] S. Hirata, Y. Ishida, M. Aihara, K. Honda, O. Shikino, *Anal. Chim. Acta* 438 (2001) 205.
- [25] K.G. Beck, R.P. Franks, K.W. Bruland, *Anal. Chim. Acta* 455 (2002) 11.
- [26] S.N. Willie, R.E. Sturgeon, *Spectrochim. Acta B* 56 (2001) 1707.
- [27] Y. Zhu, A. Itoh, H. Haraguchi, *Bull. Chem. Soc. Jpn.* 78 (2005) 107.
- [28] O.N. Grebneva, N.M. Kuzmin, G.I. Tsylin, Y.A. Zolotov, *Spectrochim. Acta B* 51 (1996) 1417.
- [29] R.K. Katarina, T. Takayanagi, K. Oshita, M. Oshima, S. Motomizu, *Anal. Sci.* 24 (2008) 1537.
- [30] E.M. Thurman, M.S. Mills, *Solid-Phase Extraction – Principles and Practice*, John Wiley & Sons, New York, NY, United States of America, 1998, pp. 1–23.
- [31] J.M. Murray, Chapter 7-What Controls the Composition of River water and Seawater: Equilibrium versus Kinetic Ocean, University of Washington, 2004, pp. 1–19, [http://www.ocean.washington.edu/courses/oc400/Lecture\\_Notes/CHPT7.pdf](http://www.ocean.washington.edu/courses/oc400/Lecture_Notes/CHPT7.pdf).
- [32] D.P. Bendito, S. Rubio, *Comprehensive Analytical Chemistry*, Vol. XXXII: Environmental Analytical Chemistry, Elsevier Science B. V., The Netherlands, 1999, pp. 97–100.
- [33] EPA Method 200.7 –Trace Elements in Water, Solids, and Biosolids by Inductively Coupled Plasma-Atomic Emission Spectrometry, U.S. Environmental Protection Agency Office of Science and Technology, Washington, 2001.
- [34] T.J. Bruno, P.D.P. Svoronos, *CRC Handbook of Basic Tables for Chemical Analysis*, CRC Press, Inc., United States, 1989, pp. 374–377.
- [35] D. Yeghicheyan, J. Carignan, M. Valladon, M.B.L. Coz, F.L. Cornec, M.C. Rouelle, M. Robert, L. Aquilina, E. Aubry, C. Churlaud, A. Dia, S. Deberdt, B. Dupre, R. Freydier, G. Gruau, O. Henin, A.M.D. Kersabiec, J. Mace, L. Marin, N. Morin, P. Petitjean, E. Serrat, *Geostandard Newslett.* 25 (2001) 465.
- [36] M.G. Lawrence, A. Greig, K.D. Collerson, B.S. Kamber, *Appl. Geochem.* 21 (2006) 839.



# Microfluidic device capable of sensing ultrafast chemiluminescence

Young-Teck Kim<sup>a</sup>, Seok Oh Ko<sup>b,1</sup>, Ji Hoon Lee<sup>c,\*</sup>

<sup>a</sup> Department of Packaging Science, Clemson University, Clemson, SC 29634, USA

<sup>b</sup> Department of Civil Engineering, Kyung Hee University, 1, Seochun-Dong, Giheung-Gu, Yongin-Si 409-701, Republic of Korea

<sup>c</sup> Luminescent MD, LLC, 579 Odendhal Avenue, Gaithersburg, MD 20877, USA

## ARTICLE INFO

### Article history:

Received 28 October 2008

Received in revised form 7 January 2009

Accepted 8 January 2009

Available online 20 January 2009

### Keywords:

1,1'-Oxalyldiimidazole (ODI) derivative  
chemiluminescence

Peroxyoxalate

Liquid core waveguide (LCW)

Microfluidic device

Lab on a chip

## ABSTRACT

Based on the principle of liquid core waveguide, a novel microfluidic device with micro-scale detection window capable of sensing flashlight emitted from rapid 1,1'-oxalyldi-4-methylimidazole (OD4MI) chemiluminescence (CL) reaction was fabricated. Light emitted from OD4MI CL reaction occurring in the micro-dimensional pentagonal detection window (length of each line segment: 900.0  $\mu\text{m}$ , depth: 50.0  $\mu\text{m}$ ) of the microfluidic device with two inlets and one outlet was so bright that it was possible to take an image every 1/30 s at the optimal focusing distance (60 cm) using a commercial digital camera. Peaks obtained using a flow injection analysis (FIA) system with the micro-scale detection window and OD4MI CL detection show excellent resolution and reproducibility without any band-broadening observed in analytical devices having additional reaction channel(s) to measure light generated from slow CL reaction. Maximum height ( $H_{\text{max}}$ ) and area ( $A$ ) of peak, reproducibility and sensitivity observed in the FIA system with the microfluidic device and OD4MI CL detection depends on (1) the mole ratio between bis(2,4,6-trichlorophenyl) oxalate and 4-methyl imidazole yielding OD4MI, (2) the flow rate to mix OD4MI,  $\text{H}_2\text{O}_2$  and 1-AP in the detection window of the microfluidic device, and (3)  $\text{H}_2\text{O}_2$  concentration. We obtained linear calibration curves with wide dynamic ranges using  $H_{\text{max}}$  and  $A$ . The detection limit of 1-AP determined with  $H_{\text{max}}$  and  $A$  was as low as 0.05 fmole/injection (signal/background = 3.0).

© 2009 Elsevier B.V. All rights reserved.

## 1. Introduction

Since the first introduction of capillary electrophoresis on a chip with fluorescence detection [1], an enormous number of microfluidic devices with various optical detections (e.g., UV–vis absorbance [2–4], fluorescence [5–7], chemiluminescence [8–12]) have been developed because of the advantages of these miniaturized devices, including rapid separation of complex sample mixtures, portability, reagent/solvent economy, low cost, and broad applications in diverse fields such as biochemistry, environmental toxicology, genetics, and medical diagnostics.

The primary objective of fabricating microfluidic devices is to develop totally minimized analytical systems capable of diagnosing and monitoring various diseases or quantifying environmental toxic molecules including biological and chemical warfare agents. Thus, appropriate optical detection for microfluidic devices should have good sensitivity and selectivity as well as be cost effective, small and simple. Application of UV/vis absorbance detection for microfluidic devices with very short optical pathlengths (>30  $\mu\text{m}$ )

is generally limited because of the low sensitivity [13]. Laser induced fluorescence (LIF) detection for microfluidic devices is widely applied because of the high sensitivity. However, LIF may not be suitable light source as a detection of the totally minimized analytical systems because it is expensive, complicate and relatively large [13]. Light-emitting diode (LED) fluorescence detection for microfluidic devices has been developed to solve the problems of LIF detection [7,13]. However, sensitivity of LED detection is not as good as that of LIF detection because of a higher level of background signal generated from the wide half-bandwidth of light emitted from LED [13]. Chemiluminescence (CL) emitted by a chemical reaction is more sensitive and selective than UV/vis and fluorescence generated by a light source because of the low background [13]. Thus, various kinds of microfluidic devices with CL detection have been fabricated [8–12]. However, microfluidic devices with CL detection reported so far are more complicate and larger than those with UV/vis and fluorescence detections because the former needs long reactions channels and wide detection windows to measure optimum emission intensity generated by slow CL reactions (e.g., luminol [12], peroxyoxalate [11]). For example, microfluidic devices with extra flow elements to measure CL do not have better resolution due to the wide band-broadening [13]. Also, it is difficult to measure slow and relatively dim CL using micro-scale detection windows. The smallest dimension of detection window for microfluidic device with CL detection was 2.0 mm  $\times$  3.0 mm [13].

\* Corresponding author. Tel.: +1 301 393 9091; fax: +1 301 393 9092.

E-mail address: [jhlee@luminescentmd.com](mailto:jhlee@luminescentmd.com) (J.H. Lee).

<sup>1</sup> Author Seok Oh Ko has equivalently contributed on this paper as a Corresponding Author.



Recently, we reported that the maximum intensity,  $I_{\max}$ , and time required to reach the maximum emission,  $\tau_{\max}$ , for analytical sample monitored in 1,1'-oxalyldiimidazole (ODI) derivative CL reaction are much higher and faster than their values measured in peroxyoxalate (PO) CL reaction [14,15]. For example, values for  $I_{\max}$  and  $\tau_{\max}$  observed with emission of 1-AP in ODI derivative CL reaction are 61.1 times larger and 15.8 times faster than their respective values obtained from emission of 1-aminopyrene (1-AP) in PO-CL reaction [15]. Ultrafast  $\tau_{\max}$  ( $>0.3$  s) measured in ODI derivative CL reaction was apparently independent of physical properties (e.g., oxidation potential, dielectric constant, viscosity) of fluorescent molecules and solvents even though  $\tau_{\max}$  obtained in PO-CL was clearly dependent on the factors [15–17]. Additionally, using the rapid ODI derivative CL reaction, it was possible to quantify analytical molecules dissolved in water without considering critical interferences (e.g., decomposition of CL reagents, side reaction of analytes and CL reagent) observed in relatively slow PO-CL [16,17]. Using the advantages of ODI derivative CL reaction in analytical chemistry, we fabricated a new and simple microfluidic device not having extra flow elements.

1-AP selected as an analyte in this research can emit strong light in ODI derivative CL reaction [15–17]. Also, 1-AP formed under various biological and environmental conditions was quantified and monitored [18–21]. For example, 1-nitropyrene is one of the most mutagenic and carcinogenic nitrated polycyclic hydrocarbons contained in diesel exhaust particulate matter [18,19]. 1-AP, as a biomarker, formed in the *in vivo* metabolism of 1-nitropyrene in living cells was quantified [18,19]. 1-AP formed from the reduction reaction of 1-nitropyrene was quantified to indirectly monitor 1-nitropyrene having poor fluorescence and CL quantum efficiency [20,21]. In this paper, we report that the novel microfluidic device with ODI derivative CL detection can quantify trace level of 1-AP with better resolution and reproducibility.

## 2. Experimental

### 2.1. Chemicals

1-Aminopyrene, bis(2,4,6-trichlorophenyl)oxalate (TCPO), 4-methylimidazole (4MImH), and  $\text{H}_2\text{O}_2$  (50%) were purchased from Aldrich. Spectroscopic grade solvents (acetonitrile, ethyl acetate, and acetone) were purchased from Burdick & Jackson.

### 2.2. Fabrication of lab on a chip

As shown in Fig. 1, we designed a new microfluidic device capable of sensing flash light emitted from ultrafast ODI derivative CL reaction. The microfluidic device has two inlets, one outlet and a pentagonal chamber. The micro-dimensional pentagonal chamber was designed to apply as a high-efficiency mixing and reaction channel as well as a detection window. The microfluidic device we designed was fabricated as follows.

The lab on a chip shown in Fig. 1 was fabricated at the Institute of Advanced Machinery & Design Korea Bio-IT Foundry Center in Seoul, Republic of Korea. Six microchips like that (26.0 mm  $\times$  19.0 mm) shown in Fig. 1(b) were fabricated using two round quartz plates (diameter: 15.2 cm, thickness: 0.5 mm) to observe and quantify OD4ML CL in organic solvent mixture. The diameter and depth of each reservoir on the bottom quartz plate were 2.0 mm and 50.0  $\mu\text{m}$ . Holes (diameter: 0.8 mm) for delivering CL reagents or analyte into each reservoir and taking out waste from the chip were drilled into the cover plate (see Fig. 1(c)). Depth, length, and width of in-flow channel between the reservoir and the pentagonal chamber shown in Fig. 1(d) and (e) were 50  $\mu\text{m}$ , 1.0 cm, and 450  $\mu\text{m}$ , respectively. The depth of the pentagonal chamber, shown in Fig. 1(e), was 50  $\mu\text{m}$ , while its line segment, shown in Fig. 1(f), was 900  $\mu\text{m}$ . Depth, length, and width of out-flow channel between the waste reservoir and the CL detection area shown in Fig. 1(d) were 50  $\mu\text{m}$ , 1.0 cm, and 900  $\mu\text{m}$ , respectively. The surface of the bottom plate mediated with 1% HF was bonded with the cover plate under constant high pressure (0.16 MPa) at room temperature for 24 h. Three PEEK tubings (Inner and outer diameters: 250  $\mu\text{m}$  and 1/32 in., length: 60 cm) purchased from VICI were connected with two inlets and an outlet of the microfluidic device using commercial epoxy glue (Permatex). The other side of the two PEEK tubings connected to the inlets of the microfluidic device was each connected to a 3.0 ml Luer-Lok syringe (BD Medical). Using a high-resolution microscope (Labophot-2, Nikon) with a color video camera (VK-C370, Hitachi) and a syringe pump (975, Harvard Apparatus) having four syringe holders, we confirmed that aqueous and organic solvents inserted through the two inlets (both sides in Fig. 1(b)) were mixed smoothly and completely on the detection area shown in Fig. 1(e) and (f) and flowed out into the outlet (center in Fig. 1(b)) under various flow rates (26.0–390  $\mu\text{l}/\text{min}$ ).

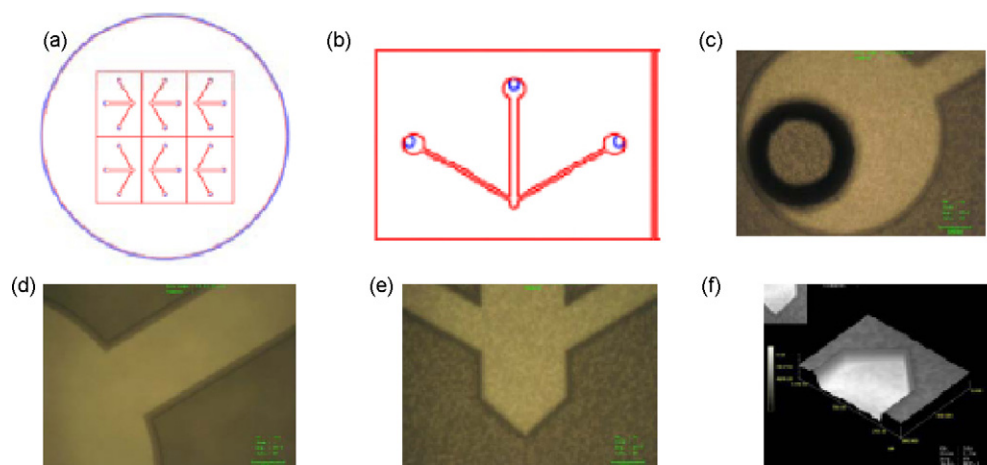


**Fig. 1.** Fabrication of lab on a chip capable of sensing ultrafast ODI derivative CL based on the principle of liquid core waveguide. (a) Design to fabricate 6 microchips on two round quartz plates (diameter: 15.2 cm, thickness: 0.5 mm), (b) design to fabricate microchip (26.0 mm  $\times$  19.0 mm), (c) reservoir (diameter: 2.0 mm, depth: 50.0  $\mu\text{m}$ ) and hole (diameter: 0.8 mm), (d) reservoir and in-flow (width: 450.0  $\mu\text{m}$ , depth: 50.0  $\mu\text{m}$ , length: 1.0 cm) or out-flow (width: 900.0  $\mu\text{m}$ , depth: 50.0  $\mu\text{m}$ , length: 1.0 cm) channel, (e) two in-flow and out-flow channels and pentagonal CL detection area (length of each line segment: 900.0  $\mu\text{m}$ , depth: 50.0  $\mu\text{m}$ ), (f) pentagonal CL detection area.

### 2.3. Measurement CL emission with microfluidic device

Fig. 2 shows the flow injection analysis (FIA) system with the microfluidic device and 1,1'-oxalyldi-4-methylimidazole (OD4MI), one of ODI derivatives, CL detection. It consists of a syringe pump (975, Harvard Apparatus) capable of pumping 1–4 syringes at the same flow rate, an injection valve (D) having 250 nl loop (CN2-4340, Valco Instruments Co, Inc. (VICI)), a microfluidic device (F) we fabricated, detection system (G) having a photomultiplier tube (PTI, Inc.), and a personal computer (H) for data collection and analysis. In order to protect light from the exterior, F and G were placed in a chamber (E, PTI, Inc). One (A) of the two syringes contains acetonitrile and the other syringe (B) has OD4MI formed from the reaction between TCPO and 4MImH in ethyl acetate at room temperature (21–23 °C). 1-AP solution containing H<sub>2</sub>O<sub>2</sub> was injected into D through D-1 with a microsyringe (10.0 μl). Constant loading time for the sample solution was 30 s. The sample solution filled in the 250 nl loop connected between D-3 and D-6 was inserted into the detection area in F through D-5 and one of the two inlets of F. OD4MI was inserted into the detection area in F through the other inlet of F. Flow rate range of CL reagents and sample inserted into the microfluidic device was 26.0–390 μl/min. CL emitted with the fast OD4MI CL reaction in the detection area was detected with G at 427 nm, which is the fluorescence emission wavelength of 1-AP in the solvent of acetonitrile and ethyl acetate mixture. CL measured with G was transferred to H for data collection and analysis. In order to quantify 1-AP under the optimum condition of the FIA system with the microfluidic device and OD4MI CL detection, we observed three parameters (maximum height ( $H_{max}$ ), half-width ( $W_{1/2}$ ), and area ( $A$ )) of each peak under chemical and physical conditions. Experimental results under each reaction condition were analyzed with Origin 7.5 (OriginLab Corporation).

## 3. Results and discussion

### 3.1. Imaging of CL emitted from OD4MI CL reaction in the detection area of the microfluidic device

Using the movie mode (resolution: 640 pixels × 480 pixels, 30 frame/s) of a digital camera (Powershot A640, Canon), instead of the PMT (G) and the computer (H) shown in Fig. 2, we obtained CL images emitted with the ultrafast OD4MI CL reaction in the pentagonal chamber of the microfluidic device. Distance between the

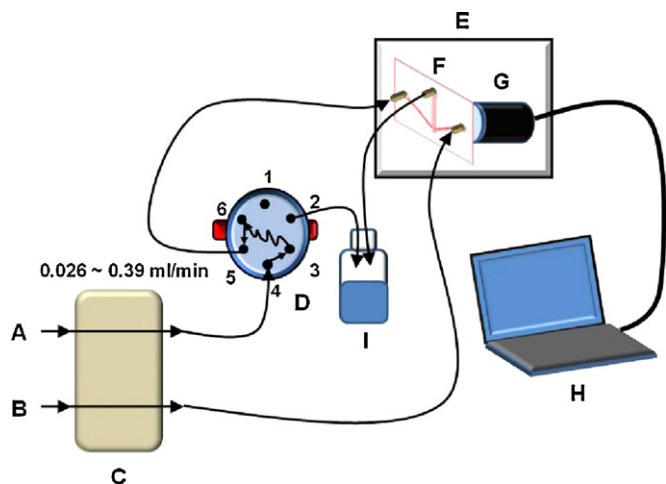


Fig. 2. Diagram of the flow injection analysis (FIA) system with a microfluidic device and OD4MI CL detection. (A) Solvent (acetonitrile), (B) OD4MI, (C) syringe pump, (D) injection valve ((1) sample, (2) vent/waste, (3 and 6) sample loop, (4) carrier/solvent, (5) microfluidic device), (E) chamber, (F) microfluidic device, (G) photomultiplier tube (PMT) and (H) data collection and analysis.

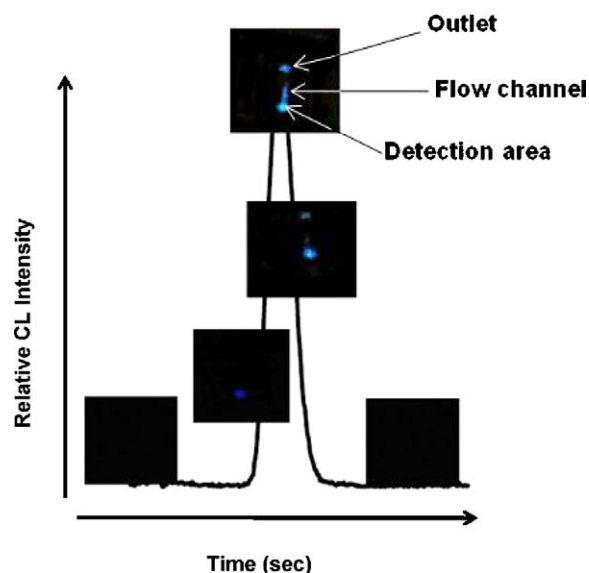


Fig. 3. Images of CL emitted in the detection area of microfluidic device in FIA system. Integration time for each image: 1/30 s, [1-AP] = 20 fmol/injection, [TCPO] = 5.0 mM, [4MImH] = 60.0 mM, [H<sub>2</sub>O<sub>2</sub>] = 1.0 M, Flow rate for 1-AP and OD4MI CL reagents: 100 μl/min.

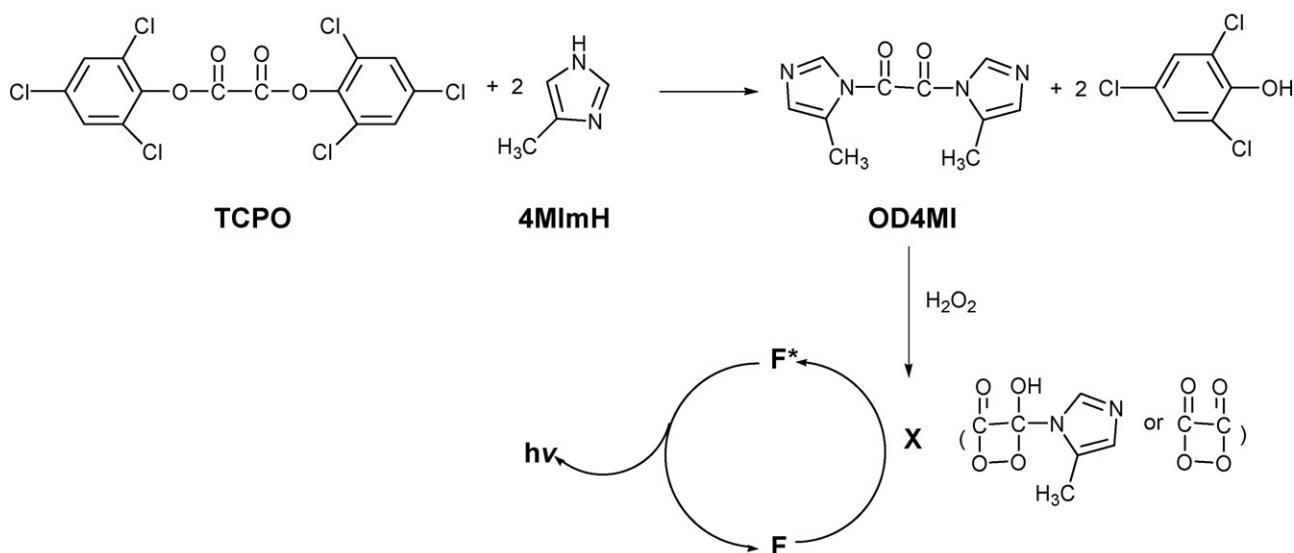
microfluidic device and the camera to maintain optimum focus was 60.0 cm. The peak shown in Fig. 3 was obtained with FIA system shown in Fig. 2, and the experimental condition for obtaining the peak was the same as that for obtaining the images.

As shown in Fig. 3, brightness of CL emitted in the pentagonal chamber was dependent on the concentration of 1-AP. In other words, (1) CL emission was not observed in the absence of 1-AP, (2) brightness of CL was enhanced with the increase of 1-AP concentration, and (3) brightness of CL began to dim with the decrease of 1-AP. The CL emission in the presence of relatively high concentration of 1-AP was observed in the pentagonal chamber as well as outside the pentagonal chamber (out-flow channel and outlet) because the half-life of bright CL emitted in OD4MI CL reaction was as long as 1.7 (±0.2) s [15,16]. The outlet diameter (2.0 mm) of the microfluidic device is wider than the width (900 μm) of the flow channel. As a result, CL was observed in the outlet while CL in the flow channel next to the outlet was not apparent.

Based on the results observed in the section, we studied in detail the effects of OD4MI CL reagents and flow rate in FIA system with PMT instead of a commercial digital camera.

### 3.2. 4MImH effect in FIA system with microfluidic device and OD4MI CL detection

Scheme 1 shows the mechanism of OD4MI CL reaction. High-energy intermediates (X) capable of transferring energy to fluorescent compounds (F) are produced when OD4MI molecules formed from the 1:2 chemical reactions between TCPO and 4MImH react with H<sub>2</sub>O<sub>2</sub> [14,15]. Finally, ultrafast and strong CL emitted from the interaction between X and fluorescent compound (F), based on the chemically initiated electron exchange luminescence (CIEEL) mechanism [18], is observed. Even though OD4MI molecules are formed from the 1:2 reactions between TCPO and 4MImH, as shown in Scheme 1, we reported that appropriate mole ratio in the chemical reaction between TCPO and 4MImH for the fast formation of OD4MI should be larger than 1:2 [14,22]. This is necessary in order to enhance quantum efficiency and sensitivity of OD4MI CL with the elimination of interference effects observed from other PO-CL reactions (e.g., TCPO-CL reaction) occurring competitively with OD4MI CL reaction [14,22]. This is because 4MImH molecules act



Scheme 1. OD4MI CL reaction.

as a reagent to form OD4MI as well as a catalyst. However, maximum CL intensity ( $I_{\max}$ ) observed in the presence of over a certain concentration of 4MImH decreased as excess 4MImH molecules decompose OD4MI quickly before it reacts with  $\text{H}_2\text{O}_2$  to form X [14]. Thus, it is important to determine appropriate mole ratio between TCPO and 4MImH for quantifying trace level of analytes using the FIA system we developed.

We prepared five different 4MImH solutions (20.0–100.0 mM in ethyl acetate) based on the previous research results (observing steady-state OD4MI CL using a stopped-flow injection) [15–17]. Table 1 shows that sensitivity of the FIA system shown in Fig. 2 is dependent on 4MImH concentration used to produce OD4MI. The mixture of 1-AP and  $\text{H}_2\text{O}_2$  was injected into the FIA system after OD4MI was formed from the reaction between TCPO and 4MImH for 1 min in the FIA system. Based on our previous batch experimental results obtained with a stopped-flow system [15–17], we expected that relative  $H_{\max}$  and  $A$  in the presence of 80 or 100 mM 4MImH would be higher and wider than those in the presence of lower 4MImH concentrations, respectively. However, the concentration of 4MImH to obtain the best  $H_{\max}$  and  $A$  observed in the FIA system was 20 mM (TCPO:4MImH = 1:4) and then,  $H_{\max}$  and  $A$  decreased proportionally with the increase of 4MImH concentration. This indicates that environmental condition emitting CL in the detection area of the microfluidic device of FIA system is different from that in the stopped-flow injection system.

The  $W_{1/2}$  of peak as shown in Table 1 was constant in the presence of various concentrations of 4MImH because it is dependent on the fixed flow rate (100.0  $\mu\text{l}/\text{min}$ ) of FIA system. However, the

**Table 1**  
4MImH effect in FIA system with the microfluidic device and OD4MI CL detection at room temperature.

4MImH <sup>a</sup>	$H_{\max}$ ( $\times 10^4$ )	$W_{1/2}$ (s)	$A$ ( $\times 10^5$ )
20.0	4.43 ( $\pm 0.078$ )	7.56 ( $\pm 0.14$ )	3.41 ( $\pm 0.064$ )
40.0	3.38 ( $\pm 0.065$ )	7.42 ( $\pm 0.21$ )	2.63 ( $\pm 0.039$ )
60.0	2.22 ( $\pm 0.059$ )	7.54 ( $\pm 0.26$ )	1.97 ( $\pm 0.041$ )
80.0	1.39 ( $\pm 0.062$ )	7.52 ( $\pm 0.39$ )	1.22 ( $\pm 0.052$ )
100.0	0.96 ( $\pm 0.069$ )	7.66 ( $\pm 0.37$ )	0.76 ( $\pm 0.047$ )

Flow rate: 100.0  $\mu\text{l}/\text{min}$  [1-AP] = 4.34 fmol/injection in acetonitrile, [ $\text{H}_2\text{O}_2$ ] = 1.0 M in acetone, [TCPO] = 5.0 mM in ethyl acetate. Mean value and standard deviation values for  $H_{\max}$  and  $W_{1/2}$  and  $A$  obtained under each experimental condition were determined with values measured with the injection of 1-AP five consecutive times at 30 s intervals.

<sup>a</sup> [mM].

results shown in Table 1 imply that the appropriate mole ratio between TCPO and 4MImH to enhance the sensitivity of OD4MI CL depends on the flow rate of 1-AP and OD4MI CL reagents in FIA system.

### 3.3. Flow rate effect in FIA system with the microfluidic device and OD4MI CL detection

Table 2 shows the results observed under different flow rates of 1-AP and OD4MI CL reagents in the presence of ODI molecules formed under two different mole ratios (1:4 and 1:8) of TCPO and 4MImH. The mixture of 1-AP and  $\text{H}_2\text{O}_2$  was injected into the FIA system after OD4MI was formed from the reaction between TCPO and 4MImH for 1 min in the system.  $H_{\max}$  measured in OD4MI CL reaction in the presence of OD4MI formed from the reaction between TCPO and 4MImH (mole ratio = 1:8) increased with the increase of flow rate up to 100  $\mu\text{l}/\text{min}$  and then began to decrease. One reason is that excess 4MImH acts as a quencher of OD4MI CL emitted in the detection area of microfluidic device when the flow rate is slower than 100.0  $\mu\text{l}/\text{min}$ . The other reason is that 200.0 and 390  $\mu\text{l}/\text{min}$  is so fast that mixture, capable of emitting CL, in the pentagonal chamber flow out to the out-flow channel before attaining the highest CL peak.

**Table 2**  
Flow rate effect in FIA system with the microfluidic device and OD4MI CL detection at room temperature.

Flow rate <sup>a</sup>	$H_{\max}$ ( $\times 10^4$ )	$W_{1/2}$ (s)	$A$ ( $\times 10^5$ )
TCPO:4MImH = 1:8			
26.0	2.42 ( $\pm 0.088$ )	16.78 ( $\pm 0.45$ )	4.67 ( $\pm 0.100$ )
52.0	3.10 ( $\pm 0.073$ )	11.15 ( $\pm 0.24$ )	3.58 ( $\pm 0.074$ )
100.0	3.38 ( $\pm 0.065$ )	7.42 ( $\pm 0.21$ )	2.63 ( $\pm 0.039$ )
200.0	1.63 ( $\pm 0.069$ )	4.83 ( $\pm 0.23$ )	0.83 ( $\pm 0.010$ )
390.0	0.83 ( $\pm 0.015$ )	3.23 ( $\pm 0.14$ )	0.29 ( $\pm 0.007$ )
TCPO:4MImH = 1:4			
26.0	8.29 ( $\pm 0.141$ )	16.48 ( $\pm 0.49$ )	14.19 ( $\pm 0.265$ )
52.0	6.49 ( $\pm 0.105$ )	11.16 ( $\pm 0.24$ )	7.00 ( $\pm 0.134$ )
100.0	4.43 ( $\pm 0.078$ )	7.56 ( $\pm 0.14$ )	3.41 ( $\pm 0.064$ )

[1-AP] = 4.34 fmol/injection in acetonitrile, [ $\text{H}_2\text{O}_2$ ] = 1.0 M in acetone, [TCPO] = 5.0 mM in ethyl acetate, [4MImH] = 40.0 mM in ethyl acetate. Mean value and standard deviation values for  $H_{\max}$  and  $W_{1/2}$  and  $A$  obtained under each experimental condition were determined with values measured with the injection of 1-AP five consecutive times at 30 s intervals.

<sup>a</sup> ( $\mu\text{l}/\text{min}$ ).

**Table 3**

H<sub>2</sub>O<sub>2</sub> effect in FIA system with the microfluidic device and OD4MI CL detection at room temperature.

H <sub>2</sub> O <sub>2</sub> <sup>a</sup>	H <sub>max</sub> (×10 <sup>4</sup> )	W <sub>1/2</sub> (s)	A (×10 <sup>5</sup> )
0.2	1.74 (±0.034)	7.67 (±0.23)	1.23 (±0.011)
0.4	2.12 (±0.028)	7.56 (±0.31)	1.51 (±0.076)
0.6	2.57 (±0.047)	7.54 (±0.28)	1.81 (±0.091)
0.8	3.19 (±0.052)	7.38 (±0.33)	2.47 (±0.081)
1.0	3.17 (±0.046)	7.43 (±0.29)	2.44 (±0.058)

Flow rate: 100.0 μl/min. [1-AP] = 3.20 fmol/injection in acetonitrile, [TCPO] = 5.0 mM in ethyl acetate, [4MImH] = 40.0 mM in ethyl acetate. Mean value and standard deviation values for H<sub>max</sub> and W<sub>1/2</sub> and A obtained under each experimental condition were determined with values measured with the injection of 1-AP five consecutive times at 30 s intervals.

<sup>a</sup> [M].

However, A measured in OD4MI CL reaction in the presence of OD4MI formed from the reaction between TCPO and 4MImH (mole ratio = 1:8) decreased proportionally with the increase of flow rate. This result indicates that A is more dependent on the flow rate than the chemical reaction in the pentagonal chamber while the opposite is true for H<sub>max</sub>.

The effects of flow rate in OD4MI CL reaction under 1:4 mole ratio between TCPO and 4MImH were different from those under 1:8 mole ratio between TCPO and 4MImH. H<sub>max</sub>, W<sub>1/2</sub>, and A increased as flow rate decreased because OD4MI molecules inserted into the pentagonal chamber of microfluidic device at 26.0 μl/min can stably produce high-energy intermediates in the presence of relatively lower 4MImH, predominantly acting as a catalyst instead of quencher [15–17]. The reason why H<sub>max</sub> decreases with the increase of flow rate is that a portion of OD4MI CL reagents flows out from the pentagonal chamber before producing high-energy intermediate.

#### 3.4. H<sub>2</sub>O<sub>2</sub> effect in FIA system with microfluidic device and OD4MI CL detection

Table 3 shows the effects of H<sub>2</sub>O<sub>2</sub> concentration in the FIA system with microfluidic device and OD4MI CL detection. With the increase of H<sub>2</sub>O<sub>2</sub> concentration up to 0.8 M in acetone, H<sub>max</sub> and A increased. And then, H<sub>max</sub> and A measured in the presence of 1.0 M H<sub>2</sub>O<sub>2</sub> concentration were similar to those in the presence of 0.8 M H<sub>2</sub>O<sub>2</sub> because, based on the CIEEL mechanism, excess H<sub>2</sub>O<sub>2</sub> does not act as an activator to form high-energy intermediate capable of transferring energy to 1-AP [18].

#### 3.5. Stability of OD4MI and reproducibility

The results shown in Table 1 and our previous research results [14,16] indicate that the stability and reproducibility of microfluidic device are dependent on the mole ratio between TCPO and 4MImH to form OD4MI. In other words, it is important to identify the optimum ratio between TCPO and 4MImH in order to obtain good results within the statistical error range.

CL peaks of 1-AP (4.3 fmol/injection) measured under the 1:4 mole ratio between TCPO and 4MIm were constant within statistical error range (coefficient of variation (CV): 3.7%) when 1-AP was injected into the FIA system every 2 min for over 30 min at the flow rate of 26 μl/min. We confirmed that H<sub>max</sub>, W<sub>1/2</sub>, and A under the same reaction condition decreased with the increase of flow rate from 26 to 390 μl/min as shown in Table 2. However, the reproducibility for relative CL peaks was not affected by the flow rate.

With the increase of mole ratio between TCPO and 4MImH, the reproducibility for CL peak measured at 2 min intervals for 30 min dropped sharply. This is because excess 4MImH, acting as

a quencher instead of a catalyst, competitively broke down OD4MI formed from the reaction between TCPO and 4MImH within the syringe. For example, relative H<sub>max</sub> measured after 10 min of reaction between TCPO and 4MImH of 1:20 mole ratio was 5.3 times higher than that measured after 30 min of reaction.

#### 3.6. Sensitivity of FIA system with microfluidic device and OD4MI CL detection

Based on the results obtained in this research, we determined the appropriate experimental conditions (e.g., 1:4 mole ratio between TCPO and 4MImH, 100 μl/min flow rate) to quantify 1-AP using the FIA system we developed. As shown in Fig. 4, we obtained linear calibration curves with good R-square values with H<sub>max</sub> and A measured in the presence of 7 different 1-AP concentrations (0.11–2.3 fmol/injection). The background measured in the absence of 1-AP was 483.5 ± 36.5. The detection limit of 1-AP determined with H<sub>max</sub> using signal to background test (signal/background = 3:1) was as low as 0.05 fmole/injection. It was comparable to that determined with A even though the slope (0.7607 ± 0.00414) of calibration curve for A is smaller than that (0.9941 ± 0.0106) for H<sub>max</sub>. Using signal to background test, the detection limits determined with FIA system with OD4MI CL detection are about 30 times lower than that (1.5 fmol/injection) [21] obtained using HPLC with conventional PO-CL detection and about 500 times lower than that (25 fmol/injection) [21] obtained using HPLC with fluorescence detection. Two apparent peaks (signal/background = 2) obtained in the presence of 0.03 fmole/injection 1-AP (see Fig. 4) had good reproducibility even though the concentration of 1-AP was lower than the detection limit (0.05 fmole/injection) determined with FIA system using signal to background test. This indicates that the FIA system with a microfluidic device and OD4MI CL detection has good reproducibility. Also, the lower limit of detection (LOD = 0.018 fmol/injection) and the limit of quantification (LOQ = 0.043 fmol/injection) were determined using the mean value and standard deviation measured in the absence of 1-AP under the experimental condition and the linear calibration curve for H<sub>max</sub> shown in Fig. 4.

Table 2 indicates that 26.0 μl/min is the best flow rate to quantify 1-AP using H<sub>max</sub> and A. The detection limits set with H<sub>max</sub> and A at 26.0 μl/min were about 2 times lower than those at 100.0 μl/min,

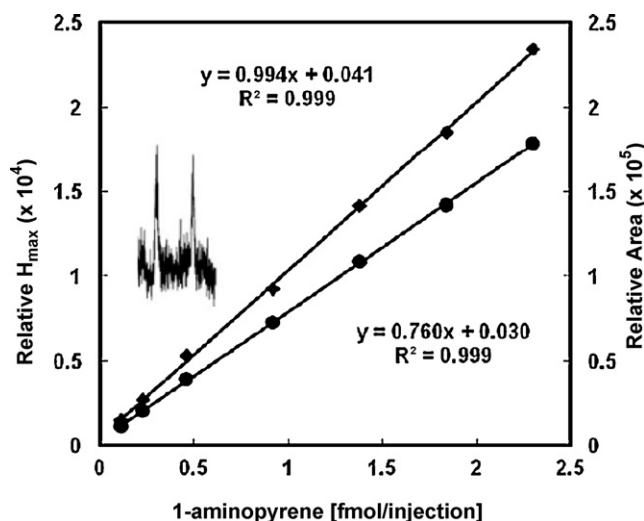


**Fig. 4.** Calibration curves of 1-AP based on relative H<sub>max</sub> (♦) and A (●) in OD4MI CL reaction. Reaction condition: [H<sub>2</sub>O<sub>2</sub>] = 0.8 M in acetone, [TCPO] = 5.0 mM and [4MImH] = 20.0 mM in ethyl acetate, flow rate: 100.0 μl/min. The measurement of H<sub>max</sub> and A at the same concentration of 1-AP were replicated 3 times. The CV for H<sub>max</sub> and A at each concentration of 1-AP were lower than 5.0%.

shown in Fig. 4. However,  $W_{1/2}$  measured in the former was about 2 times longer than that in the latter condition. Thus, for rapid quantification of many analytes without band broadening, 26  $\mu\text{l}/\text{min}$  is not as good as 100.0  $\mu\text{l}/\text{min}$  as the appropriate flow rate of the FIA system we developed.

#### 4. Conclusions

Based on the principle of liquid core waveguide, we fabricated a novel microfluidic device capable of detecting ultrafast OD4MI CL. Peaks obtained in FIA system with the micro-scale pentagonal chamber and OD4MI CL detection showed good resolution as well as excellent reproducibility without band-broadening observed in analytical devices with slow CL detection. As shown in Fig. 1, CL emitted in the micro-scale detection area was so bright that we were able to obtain the integrated CL image within 1/30 s. This indicates that it is possible to monitor and quantify many analytes rapidly and simultaneously using microarray with the OD4MI CL detection. The results shown in Tables 1–3 indicate that amount of 4MImH staying in the pentagonal chamber is in inverse proportion to the flow rate. Also, brightness of CL emitted in the detection area depends on the flow rate of sample and OD4MI CL reagents. In conclusion, based on the results of this research, it will be possible to fabricate advanced microfluidic devices having a smaller detection window, higher efficiency and shorter  $W_{1/2}$  than that shown in Fig. 1. We expect that the FIA system we developed can be applied as a prototype of totally minimized analytical system capable of quantifying environmental toxic chemicals as well as monitoring and diagnosing various diseases.

#### Acknowledgements

This work was funded by LST Korea, Inc. (LST-K8 and LST-K420). This company also provided appropriate microfluidic devices for the research.

#### References

- [1] D.J. Harrison, K. Fluri, K. Seiler, Z. Fan, C.S. Effenhauser, A. Manz, *Science* 261 (1993) 895–897.
- [2] Z.Q. Xu, T. Ando, T. Nishine, A. Arai, T. Hirokawa, *Electrophoresis* 24 (2003) 3821–3827.
- [3] K. Faure, M. Loughran, J.D. Glennon, *Anal. Chim. Acta* 557 (2006) 130–136.
- [4] A.R. Stettler, M.A. Schwarz, *J. Chromatogr. A* 1063 (2005) 217–225.
- [5] S.-H. Lee, S.I. Cho, C.-S. Lee, B.-G. Kim, Y.-K. Kim, *Sens. Actuators B* 110 (2005) 164–173.
- [6] C.F. Duffy, B. MacCraith, D. Diamond, R. O’Kennedy, A. Arriaga, *Lab Chip* 6 (2006) 1007–1011.
- [7] J.B. Edel, N.P. Beard, O. Hofmann, J.C. DeMello, D.D.C. Bradley, A.J. deMello, *Lab Chip* 4 (2004) 136–140.
- [8] B.-F. Liu, M. Ozaki, H. Hisamoto, Q. Luo, Y. Utsumi, T. Hattori, S. Terabe, *Anal. Chem.* 77 (2005) 573–578.
- [9] R.G. Su, J.-M. Lin, K. Uchiyama, M. Yamada, *Talanta* 64 (2004) 1024–1029.
- [10] H. Shen, Q. Fang, Z.-L. Fang, *Lab Chip* 6 (2006) 1387–1389.
- [11] M. Amatongchai, O. Hofmann, D. Nacapricha, O. Chailapakul, A.J. deMello, *Anal. Bioanal. Chem.* 387 (2007) 277–285.
- [12] Y.-X. Guan, Z.-R. Xu, J. Dai, Z.-L. Fang, *Talanta* 68 (2006) 1384–1389.
- [13] S. Gotz, U. Karst, *Anal. Bioanal. Chem.* 387 (2007) 183–192.
- [14] J.H. Lee, J.C. Rock, S.B. Park, M.A. Schlautman, E.R. Carraway, *J. Chem. Soc., Perkin Trans.* (2002) 802–809.
- [15] J.H. Lee, J.T. Je, M.A. Schlautman, E.R. Carraway, *Chem. Commun.* (2003) 270–271.
- [16] J.H. Lee, J. Je, J. Hur, M.A. Schlautman, E.R. Carraway, *Analyst* 128 (2003) 1257–1261.
- [17] J.H. Lee, J. Je, A. Tartaglia, J. Hur, M.A. Schlautman, E.R. Carraway, *J. Photochem. Photobiol. A: Chem.* 182 (2006) 28–32.
- [18] P.C. Howard, M.C. Consolo, L.K. Dooley, F.A. Beland, *Chem. -Biol. Interact.* 95 (1995) 309–325.
- [19] A. Toriba, H. Kitaoka, R.L. Dills, S. Mizukami, K. Tanabe, N. Takeuchi, M. Ueno, T. Kameda, N. Tang, K. Hayakawa, C.D. Simson, *Chem. Res. Toxicol.* 20 (2007) 999–1007.
- [20] K. Hayakawa, R. Kitamura, B.M.N. Imaizumi, M. Miyazaki, *Anal. Sci.* 7 (1991) 573–577.
- [21] K. Hayakawa, N. Terai, P.G. Dinning, K. Akutsu, Y. Iwamoto, R. Etoh, T. Murahashi, *Biomed. Chromatogr.* 10 (1996) 346–350.
- [22] M.M. Rauhut, L.J. Bollyky, B.G. Roberts, M. Loy, *J. Am. Chem. Soc.* 89 (1967) 6515.



## Solid phase extraction of zinc(II) using a PVC-based polymer inclusion membrane with di(2-ethylhexyl)phosphoric acid (D2EHPA) as the carrier

Spas D. Kolev<sup>a,\*</sup>, Yoshinari Baba<sup>b</sup>, Robert W. Catrall<sup>a</sup>, Tsutomu Tasaki<sup>b</sup>, Natalie Pereira<sup>a</sup>, Jilka M. Perera<sup>c</sup>, Geoffrey W. Stevens<sup>c</sup>

<sup>a</sup> School of Chemistry, The University of Melbourne, Victoria 3010, Australia

<sup>b</sup> Department of Applied Chemistry, Faculty of Engineering, University of Miyazaki, 1-1 Gakuen Kinana-dai Nishi, Miyazaki 889-2192, Japan

<sup>c</sup> Department of Chemical and Biomolecular Engineering, The University of Melbourne, Victoria 3010, Australia

### ARTICLE INFO

#### Article history:

Received 4 November 2008

Received in revised form 18 December 2008

Accepted 18 December 2008

Available online 30 December 2008

#### Keywords:

Solid phase extraction

Polymer inclusion membrane

Di(2-ethylhexyl)phosphoric acid (D2EHPA)

Zinc(II) extraction

Zn(II) separation

### ABSTRACT

A polymer inclusion membrane (PIM) is reported consisting of 45% (m/m) di(2-ethylhexyl)phosphoric acid (D2EHPA) immobilized in poly(vinyl chloride) (PVC) for use as a solid phase absorbent for selectively extracting Zn(II) from aqueous solutions in the presence of Cd(II), Co(II), Cu(II), Ni(II) and Fe(II). Interference from Fe(III) in the sample is eliminated by precipitation with orthophosphate prior to the extraction of Zn(II). Studies using a dual compartment transport cell have shown that the Zn(II) flux ( $2.58 \times 10^{-6} \text{ mol m}^{-2} \text{ s}^{-1}$ ) is comparable to that observed for supported liquid membranes. The stoichiometry of the extracted complex is shown to be  $\text{ZnR}_2 \cdot \text{HR}$ , where R is the D2EHPA anion.

© 2008 Elsevier B.V. All rights reserved.

### 1. Introduction

Recently, polymer inclusion membranes (PIMs) have attracted considerable attention for use as solid phase absorbents in separation problems because they eliminate the need for the flammable diluents required in solvent extraction systems while retaining the selectivity associated with the extractant [1]. In addition, when PIMs are incorporated into a transport cell, they allow both extraction and back-extraction to proceed simultaneously at opposite sides of the membrane. This speeds up the separation process compared to conventional adsorption (e.g., ion-exchange resins) or solvent extraction-based separation.

PIMs consist of a carrier immobilized in a base-polymer and our papers using the commercial extraction reagent Aliquat 336 have demonstrated that PIMs can be successfully applied to a variety of separation problems involving metal ions [2–7].

The extraction and separation of Zn(II) from aqueous solutions has achieved great importance because of the widespread industrial use of zinc and its classification as a dangerous substance, particularly in waste streams and saline waters [8]. Some studies on the application of PIMs for Zn(II) extraction and transport have been published [9–11].

Ulewicz and Walkowiak [9] studied the separation of Zn(II), Co(II), Ni(II), Cu(II) and Cd(II) from aqueous chloride solutions using a cellulose acetate (CTA)-based PIM containing di(2-ethylhexyl)phosphoric acid (D2EHPA) as carrier and 2-nitrophenyl pentyl ether as a plasticizer. In another study, Resina et al. [10] studied the transport of Zn(II), Cd(II) and Cu(II) from chloride solutions across CTA/sol-gel hybrid membranes with D2EHPA and di-(2-ethylhexyl)dithiophosphoric acid as carriers and 2-nitrophenyl pentyl ether or tris(2-butoxyethyl)phosphate as plasticizers.

There have also been reports of other solvent extraction reagents being used to extract Zn(II) with PIMs such as basic ion carriers like tri-*n*-octylamine immobilized in CTA [11]. However, to our knowledge, there have been no studies on the membrane extraction of Zn(II) that involve poly(vinyl chloride) (PVC)-based PIMs. PVC-based membranes are more resistant to acidic solutions than CTA-based membranes [1] and this is expected to offer advantages in terms of a wider working pH range and prolonged membrane lifetime.

D2EHPA is an acidic carrier used for the extraction of metal ions [12], which shows good selectivity for the extraction of Zn(II) in the presence of other metal ions (e.g., Co(II), Ni(II), Cu(II), Cd(II), Ca(II) and Mn(II)). The most seriously interfering ion is Fe(III) and this is usually eliminated in solvent extraction by its reduction to Fe(II).

In this paper we report on the use of a PVC/D2EHPA membrane for the solid phase extraction and transport of Zn(II) from acidic chloride solutions. We also demonstrate that the PVC-based

\* Corresponding author. Tel.: +61 3 83447931; fax: +61 3 93475180.

E-mail address: [s.kolev@unimelb.edu.au](mailto:s.kolev@unimelb.edu.au) (S.D. Kolev).

membranes used in this study do not require the inclusion of an additional plasticizer in their composition as has been the case with CTA-based PIMs. This is due to the inherent plasticizing properties of D2EHPA itself towards PVC [1].

## 2. Experimental

### 2.1. Chemical analysis and measurement of membrane thickness

The concentration of Zn(II) in the solutions used in the extraction and transport experiments was determined by atomic absorption spectrometry (AAS) (Shimadzu AA-3600, Japan). The experimental conditions were: slit width—0.7 nm; Zn hollow-cathode lamp (Photron, Australia); current—8 mA; working wavelength—213.9 nm and burner height—7 mm. The flow rates of acetylene and air were 2.0 and 15.0 L min<sup>-1</sup>, respectively.

The concentrations of Co(II), Ni(II), Cu(II), Cd(II), Fe(II), and Fe(III) in the solutions used in the interference studies were determined by inductively coupled plasma-optical emission spectrometry (ICP-OES) (Varian Vista Pro Axial, USA). The measurements were conducted under the following conditions: power level—1.00 kW; coolant flow—15.0 L min<sup>-1</sup>; auxiliary flow—1.50 L min<sup>-1</sup>; nebulizer flow—0.90 L min<sup>-1</sup> and sample aspiration rate—1.50 mL min<sup>-1</sup>.

The pH measurements were conducted with a SmartChem-Lab combined pH/conductivity meter (TPS, Australia).

The thickness of the PIMs was measured along their diameters using an optical microscope (LH50A, Olympus, Japan) with a calibrated Nikon lens (Carton Optical Ind., Japan).

### 2.2. Reagents

The commercial extractant, di(2-ethylhexyl)phosphoric acid (Tokyo Chemical Industry Co. Ltd., Japan), was used as received. High molecular weight PVC (Selectophore, Fluka, Switzerland) was used to prepare membranes. Tetrahydrofuran (THF) (Wako Pure Chemical Industries Ltd., Japan) was of analytical reagent grade and was treated to remove the stabilizer and any peroxides immediately before use by passing through an activated alumina column.

Analytical reagent grade ZnCl<sub>2</sub>, KCl, CH<sub>3</sub>COONa, CH<sub>3</sub>COOH, HNO<sub>3</sub> and HCl (Wako Pure Chemical Industries, Ltd., Japan); FeCl<sub>2</sub> and FeCl<sub>3</sub> (Fluka, Switzerland); NiCl<sub>2</sub> and CoCl<sub>2</sub> (Sigma, USA); CuCl<sub>2</sub> (Ajax Chemicals, Australia); CdCl<sub>2</sub> and Na<sub>2</sub>HPO<sub>4</sub> (BDH, UK) were used in the extraction, transport and interference experiments.

Zinc(II) standards for the atomic absorption measurements were prepared from a 1000 mg L<sup>-1</sup> spectroscopic standard (Wako Pure Chemical Industries Ltd., Japan).

Deionized water (18 MΩ cm, Millipore, Synergy 185, France) was used for the preparation of all solutions.

### 2.3. Membrane preparation

PIMs were prepared by dissolving weighed amounts of D2EHPA and PVC in 10 mL of THF and then pouring the solution into a 7.5 cm diameter glass ring sitting on a glass plate. The THF was allowed to evaporate slowly over 24 h at room temperature to yield a transparent, flexible and mechanically strong membrane. The membrane was then peeled from the glass plate. A square piece with a mass of 114 ± 2 mg was cut out of its central section and subsequently used in the solid/liquid extraction experiments. The average thickness of the membrane studied was 71 μm.

### 2.4. Solid/liquid extraction of zinc(II)

The extraction experiments were conducted in triplicate. The average relative standard deviation for a typical extraction experiment conducted in triplicate was 3.9 ± 1.5%. Each experiment

involved the immersion of a square membrane piece with an average mass of 114 ± 2 mg into a 100 mL solution containing Zn(II) and in some cases also other base metal ions (e.g., Cd(II), Co(II), Cu(II), Ni(II), Fe(II) and Fe(III)). Each solution was mechanically stirred in a water-jacketed beaker thermostated at 30.0 ± 0.1 °C. The stirring rate was maintained at 120 rpm and it was monitored with a digital tachometer (HT-4100, Ono Sokki Co. Ltd., Japan). The PIMs studied contained 15, 20, 25, 30, 40 or 45% (m/m) D2EHPA.

Zinc(II) solutions (15–80 mg L<sup>-1</sup>) were prepared in the pH range 1.0–3.0 using 1.0 M acetic acid/acetate buffer (with addition of HCl where necessary) and all contained 0.2 M KCl for maintaining a constant ionic strength. The solution pH was monitored during the extraction process and 0.1 mL samples were taken at preselected times and replaced with an equal volume of deionized water. The Zn(II) concentration was determined by AAS after appropriate dilution of the original sample with 10 mM HCl solution.

### 2.5. Membrane transport of zinc(II)

Membrane transport studies of Zn(II) were carried out in triplicate in a two compartment transport cell thermostated at 30 ± 0.1 °C (Fig. 1). Each compartment had a volume of 100 mL and the membrane was sandwiched between the two compartments. The solutions in both compartments were mechanically stirred during the transport experiment at 120 rpm. The exposed membrane surface area was 1.25 × 10<sup>-3</sup> m<sup>2</sup>. The source phase consisted of a 22 mg L<sup>-1</sup> Zn(II) solution containing 0.2 M Cl<sup>-</sup> and 1.0 M acetic acid/acetate buffer at pH 3.0 and the receiving phase was 0.1 or 1.0 M HCl. Similarly to the extraction experiments, samples (0.1 mL) from each compartment were taken at preselected time intervals and replaced with equal volumes of deionized water. The Zn(II) concentration was determined as in the extraction experiments outlined above.

The maximum Zn(II) flux ( $J_{max}$ ) at the source solution/membrane interface during the transport experiment involving 1.0 M HCl receiving solution was calculated by Eq. (1).

$$J_{max} = \frac{V}{A} \left( \frac{dC}{dt} \right)_{t=0} \quad (1)$$

where  $V$  is the volume of the source solution (1.00 × 10<sup>-4</sup> m<sup>3</sup>),  $A$  the exposed membrane surface area (1.25 × 10<sup>-3</sup> m<sup>2</sup>),  $C$  the Zn(II) concentration (mol m<sup>-3</sup>) and  $t$  is the time (s).

In the first hour of the transport experiment mentioned above the Zn(II) concentration in the source solution ( $C$ ) was found to decrease linearly with time thus allowing to approximate  $(dC/dt)$  in Eq. (1) by  $(C_t - C_{t=0})/t$ .

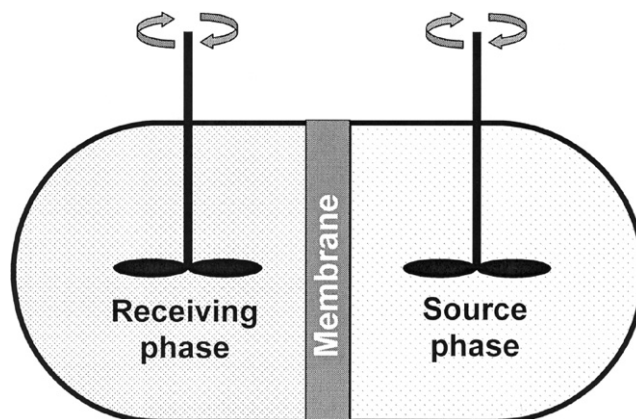


Fig. 1. Schematic of the two compartment transport cell.

## 2.6. Interference studies

The interference studies followed the procedure used in the extraction experiments. A 45% (m/m) D2EHPA membrane with a mass of  $114 \pm 2$  mg was immersed in a 100 mL solution containing  $0.2 \text{ M Cl}^-$  and  $1.0 \text{ M}$  acetic acid/acetate buffer (pH 3.0). The solution also contained  $20 \text{ mg L}^{-1}$  of each of the following ions: Zn(II), Cd(II), Co(II), Cu(II), and Ni(II). Samples (1.0 mL) were taken at pre-selected time intervals and replaced with 1.0 mL of fresh solution. After dilution with 2%  $\text{HNO}_3$ , the concentrations of the metals ions mentioned above were measured by ICP-OES.

The elimination of Fe(III) interference was based on its precipitation with orthophosphate. This approach was applied to aqueous solutions (100 mL) containing  $20 \text{ mg L}^{-1}$  Zn(II) and Fe(III) in concentrations of 20, 50, 100 or  $200 \text{ mg L}^{-1}$ . These solutions were treated with a solution of disodium hydrogen orthophosphate in mole ratio of Fe(III): $\text{Na}_2\text{HPO}_4$  of 1:3. The iron(III) phosphate precipitate was removed by centrifugation and Zn(II) was subsequently extracted into a PVC/D2EHPA membrane as described earlier.

## 3. Results and discussion

### 3.1. Effect of D2EHPA concentration

Membrane pieces (total mass  $114 \pm 2$  mg) containing 15, 20, 25, 30, 40 and 45% (m/m) D2EHPA were studied for their Zn(II) extraction efficiency using an aqueous solution containing  $22 \text{ mg L}^{-1}$  Zn(II) at pH 3.0 and the results are shown in Fig. 2. These membranes were all homogeneous and transparent with an oil free surface and met the requirements of a stable PIM as described in our recent paper [13]. As expected, both the extraction efficiency, determined by the amount of metal extracted, and the rate of extraction increased with increasing the D2EHPA content of the membrane. The 45% (m/m) membrane produced optimum extraction conditions for Zn(II) (Fig. 2). The extraction equilibrium in the corresponding PIM/solution system was established in around 2.5 h. Consequently, the 45% (m/m) PIM was used in all subsequent membrane extraction and transport experiments.

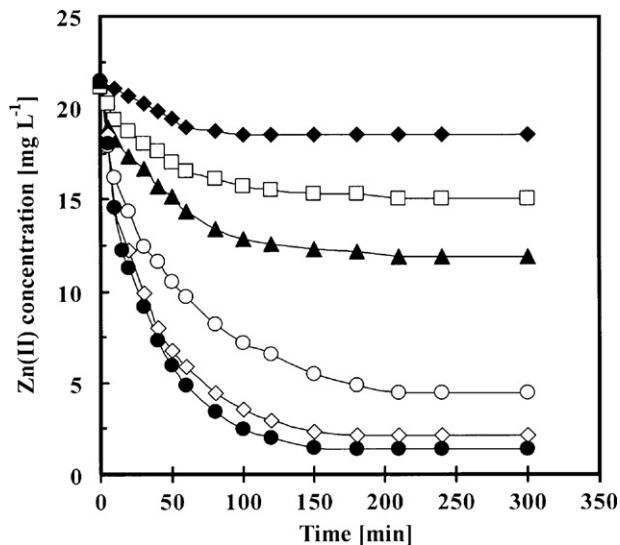


Fig. 2. Effect of the D2EHPA concentration in the membrane ( $\blacklozenge$  15;  $\square$  20;  $\blacktriangle$  25;  $\circ$  30;  $\diamond$  40 and  $\bullet$  45% (m/m)) on the extraction of Zn(II) (100 mL aqueous phase:  $22 \text{ mg L}^{-1}$  Zn(II),  $1.0 \text{ M}$  acetic acid/acetate buffer (pH 3.0) and  $0.2 \text{ M Cl}^-$ ;  $114 \pm 2$  mg PVC/D2EHPA membrane).

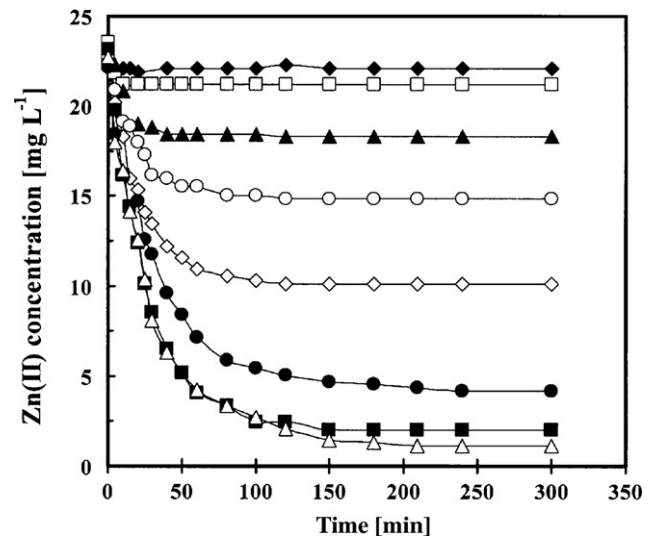


Fig. 3. The effect of pH ( $\blacklozenge$  1.00;  $\square$  1.50;  $\blacktriangle$  1.75;  $\circ$  2.00;  $\diamond$  2.25;  $\bullet$  2.50;  $\blacksquare$  2.75 and  $\triangle$  3.00) on the extraction of Zn(II) ( $400 \text{ mg}$  45% (m/m) PIM) (experimental conditions as in Fig. 2).

### 3.2. Effect of pH

The effect of pH on the Zn(II) extraction efficiency of the 45% (m/m) PVC/D2EHPA PIM is illustrated in Fig. 3. The pH of the acetate buffer solution was adjusted with HCl. It can be seen in Fig. 3 that the extraction increases at higher pH values in accordance with expectations for an acidic extractant like D2EHPA. The pH dependence approaches 100% extraction at pH 3.0 thus resembling very closely that observed for the analogous solvent extraction system for Zn(II) [12]. Therefore, all subsequent experiments were carried out at pH 3.0.

### 3.3. Effect of initial Zn(II) concentration

The effect of the initial Zn(II) concentration on the membrane extraction process involving a 45% (m/m) PIM at pH 3 is shown in Fig. 4. It can be seen that for lower initial Zn(II) concentrations ( $10$ ,  $20$  and  $30 \text{ mg L}^{-1}$ ) virtually all the Zn(II) ion has been extracted. However, this was not the case for higher initial concentrations

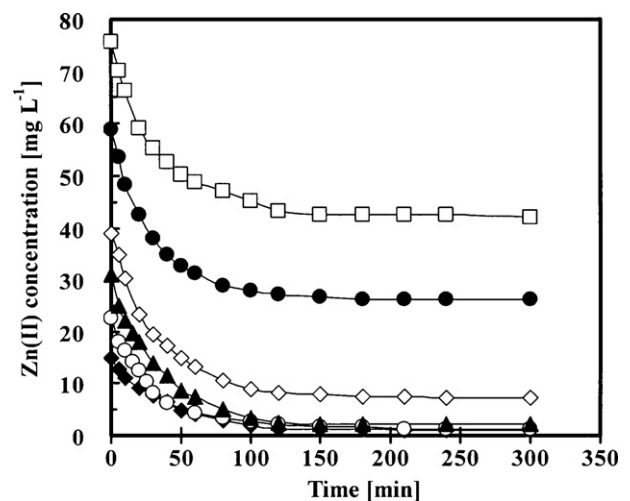


Fig. 4. Effect of initial Zn(II) concentration ( $\blacklozenge$  10;  $\circ$  20;  $\blacktriangle$  30;  $\diamond$  40;  $\bullet$  60 and  $\blacksquare$   $80 \text{ mg L}^{-1}$ ) on the extraction of Zn(II) (experimental conditions as in Fig. 2).



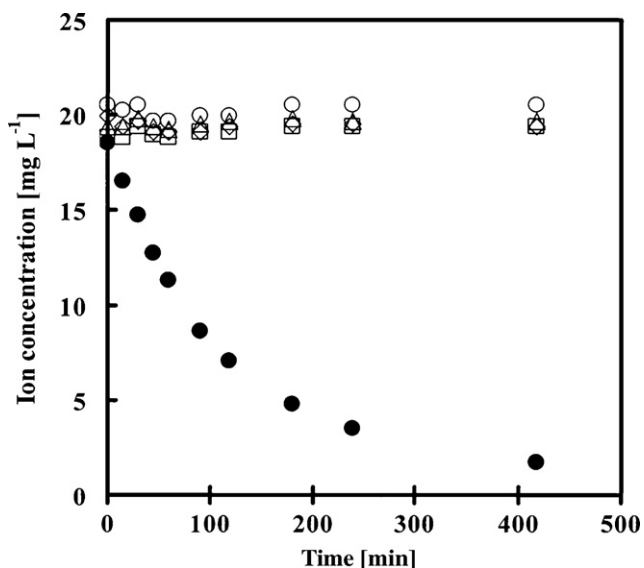


Fig. 5. Extraction of Zn(II) (●) with  $20 \text{ mg L}^{-1}$  initial concentration in the presence of Cd(II) (○), Co(II) (△), Cu(II) (◇) and Ni(II) (□) with the same initial concentrations (experimental conditions as in Fig. 2).

(40, 60, 80  $\text{mg L}^{-1}$ ) due to insufficient D2EHPA in the membrane. For each one of these three initial concentrations the amount of Zn(II) extracted was  $5.1 \times 10^{-5}$  mol, which gives a mole ratio of D2EHPA:Zn(II) of 3.3. It can be assumed that practically all D2EHPA ( $1.7 \times 10^{-4}$  mol) in the membrane has been complexed with Zn(II) thus suggesting a stoichiometry of the extracted complex corresponding to the formula  $\text{ZnR}_2\text{-HR}$ , where R is the D2EHPA anion. This stoichiometry is the same as that found for the Zn(II)–D2EHPA complex in solvent extraction systems [14,15].

### 3.4. Interferences

Common base metal ions expected to be present in samples requiring treatment with the PIM to extract Zn(II) either for its determination or its recovery are Cd(II), Co(II), Cu(II), Ni(II), Fe(III) and possibly Fe(II). From the solvent extraction behaviour of D2EHPA towards these ions [12] only Fe(III) is expected to co-extract with Zn(II) at pH 3.0. Extraction experiments were carried out with the 45% (m/m) membrane immersed in a solution at pH 3 that contained  $20 \text{ mg L}^{-1}$  of each of the following ions: Zn(II), Cd(II), Co(II) and Cu(II). Fig. 5 shows that only Zn(II) was extracted in the presence of Cd(II), Co(II), Cu(II) and Ni(II) which demonstrated that the PVC/D2EHPA PIM studied could be used to selectively extract Zn(II) in the presence of these frequently encountered base metal ions.

The extraction of Zn(II) was also studied in the presence of Fe(II) and Fe(III). As expected, the interference effect of Fe(III) was found to be severe because it readily extracted into the membrane thus substantially decreasing the extraction of Zn(II). Fe(II) did not extract if  $\text{O}_2$  was excluded from the system. The solution was bubbled with nitrogen for 15 min and then the extraction vessel was sealed from the ambient atmosphere. However, excluding  $\text{O}_2$  from the membrane extraction system for prolonged periods of time proved difficult and impractical and it was decided to overcome the Fe(II)/(III) interference by removing Fe(III) from the extraction equilibrium. Attempts to mask the Fe(III) by complexation with  $\text{F}^-$  failed as Zn(II) was also complexed. Attempts were also made to reduce Fe(III) to Fe(II) by the addition of ascorbic acid and continuously bubbling  $\text{N}_2$  through the solution during the extraction process. While this succeeded initially, the relatively long extraction time made these protection measures impractical

and did not allow the efficient isolation of the extraction system from ambient oxygen and some Fe(II) was subsequently reoxidized to Fe(III). Thus, it was decided to investigate possibilities for the removal of Fe(III) from the sample prior to the membrane extraction of Zn(II). This was carried out by the addition of  $\text{Na}_2\text{HPO}_4$  to the sample containing Fe(III), Cd(II), Co(II), Cu(II) and Ni(II). The mole ratio of Fe(III): $\text{Na}_2\text{HPO}_4$  was 1:3 and the amount of Fe(III) was varied from 20 to  $200 \text{ mg L}^{-1}$ . The pH of these solutions varied between 6.5 and 6.8. Under these conditions Fe(III) was precipitated quantitatively as its insoluble phosphate salt, which was removed by centrifugation. The subsequently conducted PIM extraction of Zn(II) resulted in its quantitative recovery.

### 3.5. Transport study

The results of the Zn(II) transport study using a source phase containing  $20 \text{ mg L}^{-1}$  Zn(II) at pH 3.0 and 1.0 or 0.1 M HCl as receiving phase are shown in Fig. 6a and b. In both cases fast and virtually complete transport of Zn(II) took place. However, as expected, the transport process was completed much faster for a receiving phase containing a higher concentration of the stripping reagent, i.e., HCl (Fig. 6b).

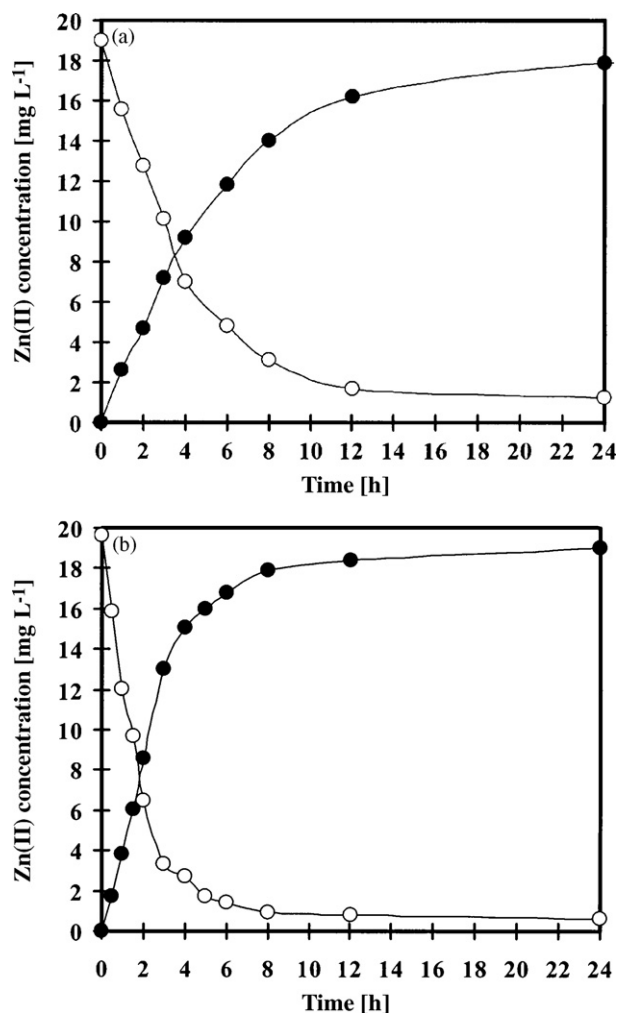
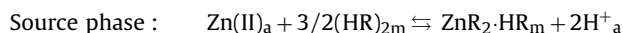


Fig. 6. Transport of Zn(II) across a 45% (m/m) PIM (source phase (○):  $22 \text{ mg L}^{-1}$  Zn(II), 1.0 M acetic acid/acetate buffer, pH 3.0,  $0.2 \text{ M Cl}^-$ ; receiving phase (●): (a) 0.1 M HCl and (b) 1.0 M HCl).

The extraction and back-extraction processes can be described by the following stoichiometric equations:



where *a* and *m* refer to the aqueous and membrane phases.

The maximum flux for Zn(II) at the source solution/membrane interface when the receiving solution was 1.0 M HCl (Fig. 6b) was calculated as  $2.85 \times 10^{-6} \text{ mol m}^{-2} \text{ s}^{-1}$ . This flux value is comparable to those reported for supported liquid membrane systems [1].

#### 4. Conclusions

The results presented in this paper demonstrate that Zn(II) can be selectively and quantitatively extracted into a polymer inclusion membrane of composition 45% (m/m) D2EHPA and 55% (m/m) PVC from aqueous solutions at pH 3.0 which may contain other base metals ions, such as Cd(II), Co(II), Cu(II), Ni(II) and Fe(II). Potential interference from Fe(III) can be removed by precipitation with orthophosphate prior to the membrane extraction of Zn(II). The stoichiometric formula of the extracted Zn(II) complex has been shown to be  $\text{ZnR}_2 \cdot \text{HR}$ , where R is the D2EHPA anion.

The membrane can also be used to selectively transport Zn(II) from a pH 3.0 source phase to an HCl receiving phase and the rate of this transport assessed on the basis of the initial Zn(II) flux value in the source phase is comparable to those reported for supported liquid membrane systems.

The PVC/D2EHPA membrane studied shows a considerable promise for the separation and pre-concentration of Zn(II) prior

to its analytical measurement. It also has potential use in the removal of Zn(II) contamination from waste streams and saline waters.

#### Acknowledgement

We are grateful to the Australian Research Council for financial support under its Discovery Project scheme.

#### References

- [1] L.D. Nghiem, P. Mornane, I.D. Potter, J.M. Perera, R.W. Cattrall, S.D. Kolev, J. Membr. Sci. 281 (2006) 7.
- [2] G. Argiropoulos, R.W. Cattrall, I.C. Hamilton, S.D. Kolev, R. Paimin, J. Membr. Sci. 138 (1998) 279.
- [3] S.D. Kolev, G. Argiropoulos, R.W. Cattrall, I.C. Hamilton, R. Paimin, J. Membr. Sci. 137 (1998) 261.
- [4] S.D. Kolev, R.W. Cattrall, R. Paimin, I.D. Potter, Y. Sakai, Anal. Chim. Acta 413 (2000) 241.
- [5] L. Wang, R. Paimin, R.W. Cattrall, S. Wei, S.D. Kolev, J. Membr. Sci. 176 (2000) 105.
- [6] Y. Sakai, R.W. Cattrall, R. Paimin, I.D. Potter, S.D. Kolev, Sep. Sci. Technol. 35 (2000) 1979.
- [7] A.H. Blitz-Raith, R. Paimin, R.W. Cattrall, S.D. Kolev, Talanta 71 (2007) 419.
- [8] S.D.W. Comber, M.J. Gardner, Int. J. Environ. Anal. Chem. 73 (2) (1999) 145.
- [9] M. Ulewicz, W. Walkowiak, Environ. Protect. Eng. 31 (2005) 73.
- [10] M. Resina, J. Macanas, J. de Gyves, M. Munoz, J. Membr. Sci. 268 (2006) 57.
- [11] C. Kozłowski, W. Apostoń, A. Walkowiak, A. Kita, Physicochem. Prob. Min. Process. 36 (2002) 115.
- [12] M. Cox, in: J. Rydberg, C. Musikas, G.R. Choppin (Eds.), Solvent Extraction in Hydrometallurgy. Principles and Practices of Solvent Extraction, Marcel Dekker, Inc, New York, 1992, Chapter 10, p. 374.
- [13] N. Pereira, A. St John, R.W. Cattrall, J.M. Perera, S.D. Kolev, Desalination 236 (2009) 327.
- [14] A. Mellah, D. Benachour, Chem. Eng. Process. 45 (2006) 684.
- [15] M.-S. Lee, J.-G. Ahn, S.-H. Son, Mater. Trans. 42 (2001) 2548.



## Fabrication and nanoindentation properties of TiN/NiTi thin films and their applications in electrochemical sensing

Ashvani Kumar<sup>a</sup>, Devendra Singh<sup>b</sup>, Rajendra N. Goyal<sup>c,\*</sup>, Davinder Kaur<sup>a</sup>

<sup>a</sup> Department of Physics and Center of Nanotechnology, Indian Institute of Technology Roorkee, Roorkee 247667, India

<sup>b</sup> Metallurgy and Materials Engineering Department, Indian Institute of Technology Roorkee, Roorkee 247667, India

<sup>c</sup> Department of Chemistry, Indian Institute of Technology Roorkee, Roorkee 247667, India

### ARTICLE INFO

#### Article history:

Received 13 October 2008

Received in revised form 5 January 2009

Accepted 5 January 2009

Available online 20 January 2009

#### Keywords:

TiN/NiTi heterostructures

Nanoindentation

Sensors

Corrosion resistance

### ABSTRACT

Nanocrystalline TiN/NiTi thin films have been grown on silicon substrate by dc magnetron sputtering to improve the corrosion and mechanical properties of NiTi based shape memory alloys without sacrificing the phase transformation effect. Interestingly, the preferential orientation of the TiN films was observed to change from (1 1 1) to (2 0 0) with change in nature of sputtering gas from 70% Ar + 30% N<sub>2</sub> to 100% N<sub>2</sub>. In present study the influence of crystallographic orientation of TiN on mechanical and corrosion properties of TiN/NiTi thin films was investigated. TiN (2 0 0)/NiTi films were found to exhibit high hardness, high elastic modulus, and thereby better wear resistance as compared to pure NiTi and TiN (1 1 1)/NiTi films. Electrochemical test revealed that TiN coated NiTi film exhibits better corrosion resistance in 1 M NaCl solution as compared to uncoated NiTi film. The application of TiN/NiTi films in the electrochemical sensing of dopamine, which has a critical physiological importance in Parkinson's disease, has been demonstrated. A comparison of voltammetric response of dopamine at silicon based electrodes modified with different nanocrystalline coatings indicated that these films catalyze the oxidation of dopamine.

© 2009 Elsevier B.V. All rights reserved.

### 1. Introduction

It has been demonstrated that NiTi shape memory alloy (SMA) thin films are promising materials to fabricate micro devices for micro-electro-mechanical systems (MEMS) and bio-MEMS such as micropumps, microwrappers and stents for neurovascular blood vessels [1–3]. However, there are still some concerns for the wide application of SMA thin films because of their unsatisfactory mechanical and tribological performances, chemical resistance and biological reliability. High nickel content in NiTi alloys often stimulated suspicion for their medical use because of nickel toxicity [4,5]. The limited hardness and wear resistance of NiTi make it difficult to be used in orthodontic and MEMS applications. In order to improve surface properties, corrosion resistance and suppression of Ni ions release of NiTi shape memory alloys, many techniques such as nitrogen ion implantation [6], laser surface treatment [7], thermal and anodic oxidation [8,9], have been employed. The problems of these surface treatments are high cost, possible surface or ion induced damage, amorphous phase formation, or degradation of shape memory effects. The magnetron sputtering has important specific advantages such as low levels of impurities and easy control of the deposition rate and also enables the production of

thin films of various morphology and crystallographic structure. The deposition of nanocrystalline and nanocomposite thin films via magnetron sputtering has been reported in literature [10,11].

The present study explored the insitu deposition of hard and adherent nanocrystalline titanium nitride (TiN) protective coating on NiTi thin films by dc magnetron sputtering. TiN is chosen for passivation layer due to its superior mechanical properties, excellent corrosion, wear resistance and good biocompatibility and TiN coatings are often used to modify the orthopedic implant materials to extend their life span [12,13]. The purpose of the present study is to examine the effect of crystallographic orientation of TiN on mechanical and corrosion properties of TiN/NiTi heterostructure thin films. The investigation revealed better mechanical and corrosion properties in case of TiN (2 0 0)/NiTi films as compared to TiN (1 1 1)/NiTi and pure NiTi films. The present study also explores the utility of TiN (2 0 0), TiN (2 0 0)/NiTi, TiN (1 1 1)/NiTi nanocrystalline coatings over Si (1 0 0) substrate as working electrode material for electroanalytical purpose.

In recent years the electrodes modified with various nanomaterials have been used for the electrochemical sensing of biologically important compounds as the surface modification has been found to exhibit electrocatalytic effect [14–18]. As electrochemical methods have distinct advantages [19,20] over other conventional methods for determination of dopamine (DA), a catecholamine neurotransmitter generated in various parts of central and peripheral nervous system, hence, careful monitoring of dopamine

\* Corresponding author. Tel.: +91 1332 285794.

E-mail address: [rngcyfcy@iitr.ernet.in](mailto:rngcyfcy@iitr.ernet.in) (R.N. Goyal).

concentration is considered necessary. Parkinson's disease, associated with tremor, rigidity, bradykinesia and postural instability, is one of the most dreadful neurodegenerative disorders of central nervous system (CNS). The disease occurs when dopaminergic neurons decrease or malfunction which is accompanied by a sharp decline in dopamine level [21,22]. Therefore, in the present investigation, the prepared nanocrystalline thin films have been tested for first time as working electrode for dopamine sensing.

## 2. Experimental

Pure NiTi and TiN/NiTi thin films were deposited on (100) silicon substrate of dimensions 1.5 cm × 2 cm by dc magnetron sputtering system (Excel Instruments). High purity (99.99%) titanium and nickel metal targets of 50 mm diameter and 3 mm thickness were used. Substrate holder was rotated at 20 rpm in a horizontal plane to achieve a uniform film composition. All the NiTi films of approximately 2 μm thickness were prepared at substrate temperature of 823 K in an argon (99.99% pure) atmosphere. The target to substrate distance was fixed at approximately 5 cm. No postannealing was performed after deposition. For the deposition of TiN passivation layer, two different sputtering gas mixtures were used: 70% Ar + 30% N<sub>2</sub> (referred henceforth as Ar + N<sub>2</sub>); and 100% N<sub>2</sub>.

The orientation and crystallinity of the films were studied using a Bruker advanced diffractometer of CuKα (1.54 Å) radiations in  $\theta$ -2 $\theta$  geometry at a scan speed of 1°/min. X-ray diffraction (XRD) studies revealed that the NiTi film exhibits austenite phase with (1 1 0) reflection at room temperature and the orientation of protective TiN layer was found to change from (1 1 1) to (2 0 0) with change in sputtering gas from 70% Ar + 30% N<sub>2</sub> to 100% N<sub>2</sub>. The surface morphology of these films was studied using field emission scanning electron microscope (FEI Quanta 200F) and atomic force microscope (NT-MDT: NTEGRA Model). The film thickness was measured using a surface profilometer and cross sectional field emission scanning electron microscopy (FESEM). The resistivity of the films was measured by a four probe resistivity method using a liquid nitrogen cryocooler and Keithley instruments over a temperature range 90–450 K. The values of martensite start temperature and austenite final temperature were found to be 290 K, 320 K for pure NiTi; 260 K, 326 K for TiN (1 1 1)/NiTi and 242 K, 326 K for TiN (2 0 0)/NiTi films, respectively.

A Hysitron Triboindenter was used to perform nanoindentation tests. Sixteen nanoindentation tests were performed on each sample using a diamond Berkovich indenter probe to determine the hardness and reduced modulus. Each test consisted of a 5-s linear loading segment to a peak load, followed by a 2-s holding segment at the peak load, and finally a 5-s linear unloading segment. The testing temperatures were 298 K, 323 K and 380 K. The maximum load was set at 5 mN.

The electrochemical experiments were performed with BAS (Bioanalytical Systems, West Lafayette, IN, USA) CV-50W Voltammetric analyzer. A conventional three electrode glass cell was used with a platinum wire as an auxiliary electrode, Ag/AgCl electrode as reference (model MF-2052 RB-5B) and TiN or TiN/NiTi coated silicon as working electrodes. The nanocrystalline thin film deposited on silicon substrate was connected to a thin copper strip (5 mm × 60 mm) and molded between two pieces of scotch tape of size 50 mm × 18 mm. One side of the tape was punched for 3 mm diameter hole to provide the contact of films with the solution. The electrode was then ready for use and was kept in air with contact side upwards. All measurements were carried out at room temperature. Dopamine was purchased from Sisco Research Laboratory, India. All other reagents used were of analytical grade. All solutions were prepared in double distilled water. Phosphate buffer

**Table 1**

A comparison of hardness and reduced elastic modulus for nanocrystalline thin films at different temperatures.

Sample	Temperature (K)	Hardness <sup>a</sup> (GPa)	pcReduced modulus <sup>a</sup> , E <sub>r</sub> (GPa)	H/E <sub>r</sub> <sup>a</sup>
NiTi	298	7.3 ± 0.6	134.8 ± 6.4	0.054 ± 0.002
	323	8.0 ± 1.2	123.2 ± 8.9	0.065 ± 0.004
	380	7.8 ± 1.1	102.6 ± 7.4	0.076 ± 0.004
TiN (1 1 1)/NiTi	298	5.9 ± 0.7	123.6 ± 8.7	0.047 ± 0.003
	323	6.1 ± 0.9	126.1 ± 8.9	0.048 ± 0.003
	380	6.6 ± 1.1	128.7 ± 10.3	0.051 ± 0.004
TiN (2 0 0)/NiTi	298	12.0 ± 0.8	139.8 ± 4.0	0.086 ± 0.003
	323	12.2 ± 1.0	140.2 ± 7.2	0.087 ± 0.004
	380	12.7 ± 0.9	142.6 ± 9.7	0.089 ± 0.004

<sup>a</sup> The values are mean ± root mean square deviation (RSD) for  $n = 16$ .

solutions were prepared according to the method of Christian and Purdy [23] and the final pH of the solutions was recorded with the pre-calibrated digital pH meter. Stock solution of DA was prepared in doubly distilled water. Required amount of the stock solution was added to 2 ml of phosphate buffer solution ( $\mu = 1.0$  M, pH 7.2) and the total volume was made to 8.0 ml with double distilled water. The electrochemical measurements were then carried out with voltammetric analyser. Differential pulse voltammetry employed had the following parameters: initial  $E$ : 0 mV, final  $E$ : 750 mV, sweep rate: 20 mV/s, sensitivity: 10 μA/V. The corrosion behaviour of pure NiTi and TiN/NiTi films were recorded in 1 M NaCl solution. Before measurement, each sample was immersed in to the electrolyte for 20 min. The sample area exposed to the electrolyte was 0.0707 cm<sup>2</sup> (3 mm diameter).

## 3. Results and discussion

### 3.1. Structural properties

The surface morphology of the TiN/NiTi films prepared in different gas environment were studied using FESEM and is shown in Fig. 1. Pure NiTi film shows uniform, fine and homogenous microstructures with grain size of 96 nm (Fig. 1(a)). Fig. 1(b) and (c) clearly shows the change in grain morphology from strongly faceted pyramid like grains to nonfaceted spherical grains in case of TiN/NiTi films, with change in crystallographic orientation of TiN from (1 1 1) to (2 0 0). The average surface roughness of the pure NiTi, TiN (1 1 1)/NiTi and TiN (2 0 0)/NiTi was measured using atomic force microscopy (AFM) and found to be 10.84, 7.44 and 4.75 nm, respectively.

### 3.2. Mechanical properties

Fig. 2 shows the normalized indentation load–depth curves for NiTi, TiN (1 1 1)/NiTi, TiN (2 0 0)/NiTi thin films at three different temperatures of 298 K, 323 K and 380 K. Fig. 2(b) and (c) exhibits a deflection in load–displacement curve at the contact depth of ~80 nm (shown by the circle), which could be due to the transition from upper TiN layer to underneath NiTi layer. Hardness, reduced modulus and wear behaviour were evaluated using these curves and are summarized in Table 1. The indentation induced superelastic energy recovery ratio ( $\eta_w$ ) was also calculated using following relation [24]:

$$\eta_w = \frac{W_e}{W_t} = \frac{\int_0^{h_r} F dh}{\int_0^{h_{\max}} F dh}$$

where  $W_e$  is the reversible work and  $W_t$  is the total work done. Superelastic energy recovery ratio at room temperature was found

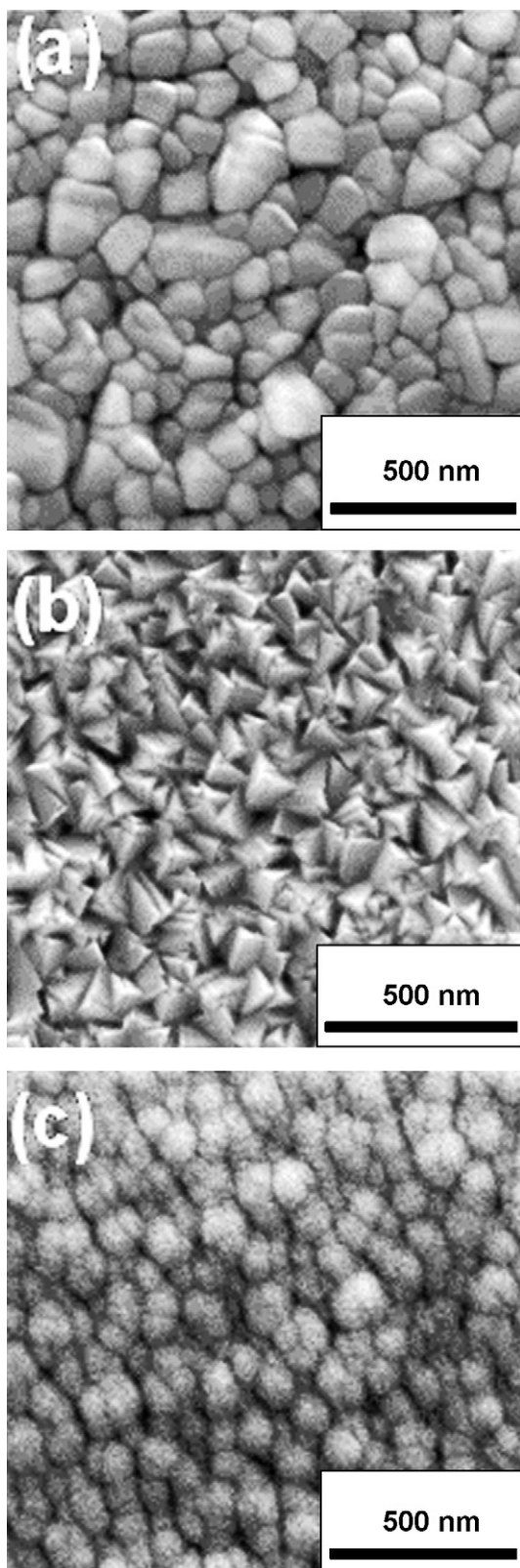


Fig. 1. FESEM images of (a) NiTi film (b) TiN(1 1 1)/NiTi (c) TiN(2 0 0)/NiTi thin films.

to be 0.44, 0.42 and 0.49 for pure NiTi, TiN(1 1 1)/NiTi and TiN(2 0 0)/NiTi films, respectively. Low values of superelastic recovery under Berkovich tip were expected due to the generation of high peak strain levels below the tip that generates high density of dislocations through the conventional plastic deformation. High

dislocation density stabilizes the parent phase and prevents its transformation to martensite thus the high peak strains under a sharp indenting tip inhibit the superelastic recovery. The highest value of indent depth recovery ratio in NiTi using Berkovich indenter has been reported to be 45% at low loads [24]. Inset of Fig. 2 depicts the temperature dependence of superelastic energy recovery ratio ( $\eta_w$ ). It was observed that TiN/NiTi films also exhibit SE energy recovery ratio as comparable to pure NiTi film, which could be due to combined composite properties from top nanocrystalline TiN layer and underneath NiTi layer.

The average hardness ( $H$ ) and reduced elastic modulus ( $E_r$ ) were calculated for each sample from indentation load–depth curves at room temperature and are summarized in Table 1. TiN(2 0 0)/NiTi films were found to exhibit maximum hardness ( $12.0 \pm 0.8$ ) and elastic modulus ( $139.8 \pm 4.0$  GPa). Hardness ( $H$ ) to Young modulus ( $E$ ) ratio has been proposed as the key factor to measure the behaviour of wear resistance of bilayer coatings. It has been reported that the deformation around the indenter surface exhibits piling-up and sinking-in and the tendency of sinking-in increases with increasing  $H/E$  ratio [25]. A relative low value of  $H/E$  ratio (0.054) for pure NiTi films indicate that more fraction of work is consumed in plastic deformation and large plastic strain is expected when contacting a material. In case of TiN(2 0 0)/NiTi film the  $H/E$  ratio (0.086) was found to be higher as compared to NiTi and TiN(1 1 1)/NiTi, which indicate that the TiN(2 0 0) passivated NiTi exhibit better wear resistance.

### 3.3. Electrochemical properties

#### 3.3.1. Voltammetric behaviour of dopamine

It was observed that TiN(2 0 0), TiN(2 0 0)/NiTi and TiN(1 1 1)/NiTi coated silicon electrode exhibit a sharp oxidation peak for dopamine at  $E_p \sim 400, 380,$  and  $365$  mV, respectively which is much lesser than oxidation peak potential observed at bare silicon (800 mV) as shown in Fig. 3(a) and (b). On the contrary, NiTi coated silicon does not show any oxidation peak for dopamine in the potential range 0–1000 mV (Fig. 3(a)). Since both the TiN/NiTi coated silicon electrodes showed better response for dopamine oxidation, a systematic concentration study of the dopamine was carried out at TiN(2 0 0)/NiTi coated silicon electrode in the concentration range 1–10  $\mu$ M. The peak current as found to increase with the increase in concentration of dopamine is shown in Fig. 4. The linear dependence of peak current on concentration (Fig. 5) can be represented by the relation

$$i_p = 5.059[\text{DA}] + 6.874$$

where  $i_p$  is the current in nA and [DA] is the concentration of dopamine in  $\mu$ M. The correlation coefficient for the linear relation was 0.995. It was observed that TiN/NiTi exhibit dominant catalytic behaviour as compared to TiN/Si film. One of the reasons for this behaviour could be the fact that these films are deposited at high substrate temperature ( $T_s = 823$  K), hence, there are favourable chances of silicon diffusion in TiN film that can be responsible for the suppression of catalytic activity of TiN. While in the case of TiN/NiTi, NiTi is acting as a buffer layer and prevent the silicon diffusion to upper TiN film. Also the calculated value of lattice mismatches for TiN(1 1 1)/NiTi and TiN(2 0 0)/NiTi and was found to be 0.5% and 0.2%, respectively. Therefore, it is concluded that NiTi does not exhibit catalytic activity but acts as a good buffer layer and prevents the silicon diffusion to upper TiN layer.

#### 3.3.2. Interference effect

Biological samples contain many electroactive metabolites, which can interfere in voltammetric determination of any compound. Among these ascorbic acid and uric acid are most

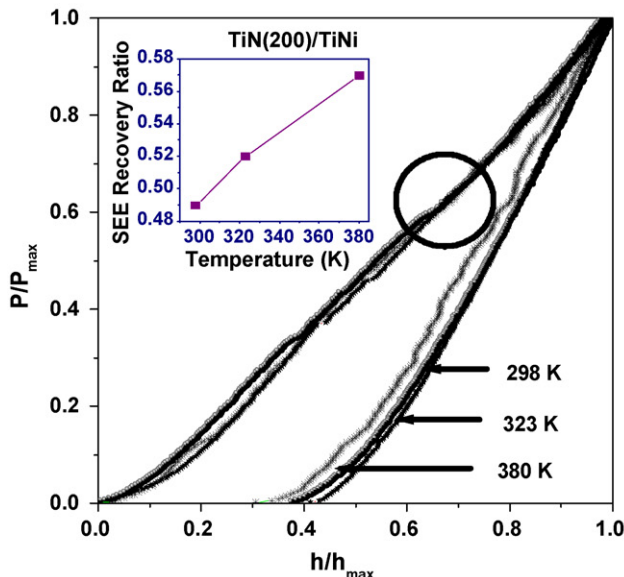
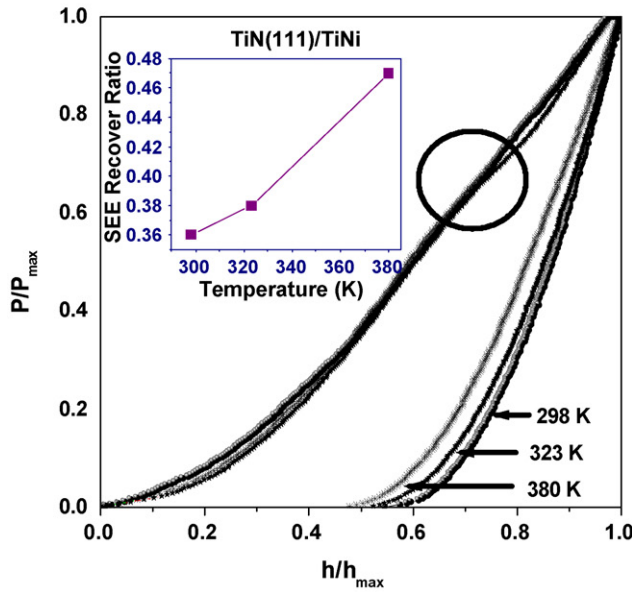
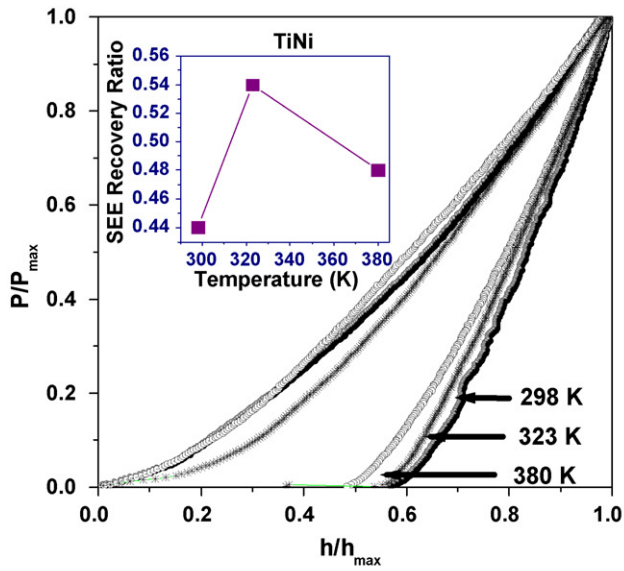


Fig. 2. Normalized indentation load vs. depth curves of (a) NiTi film (b) TiN (111)/NiTi and (c) TiN (200)/NiTi thin films.

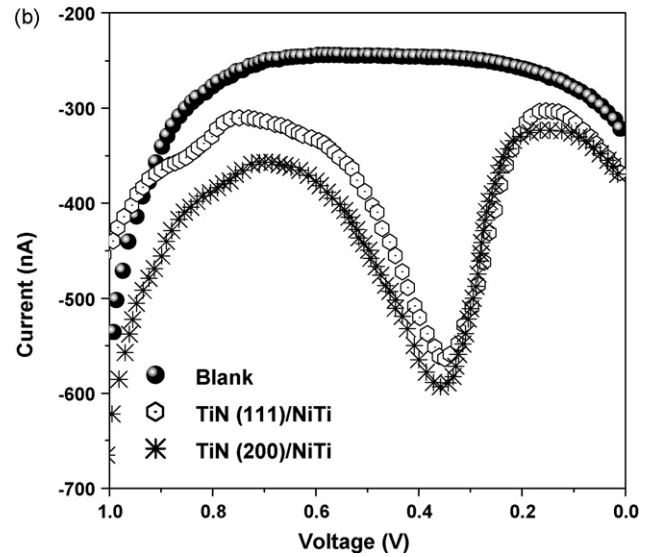
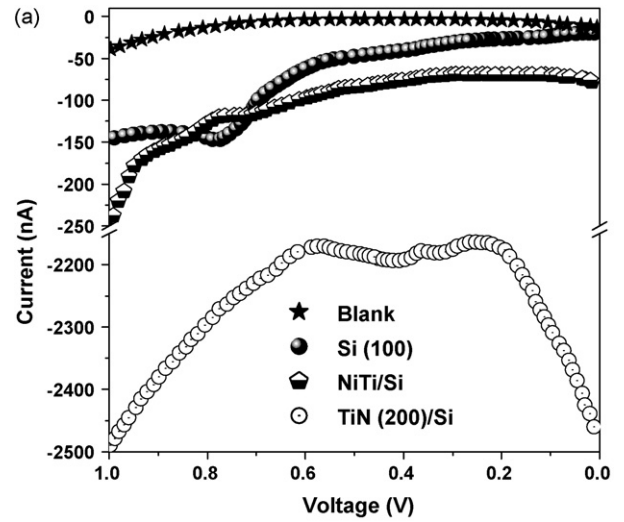


Fig. 3. A comparison of voltammogram of dopamine at pH 7.2 at different working electrodes (a) Si (100), NiTi and TiN (200); (b) TiN (111)/NiTi and TiN (200)/NiTi.

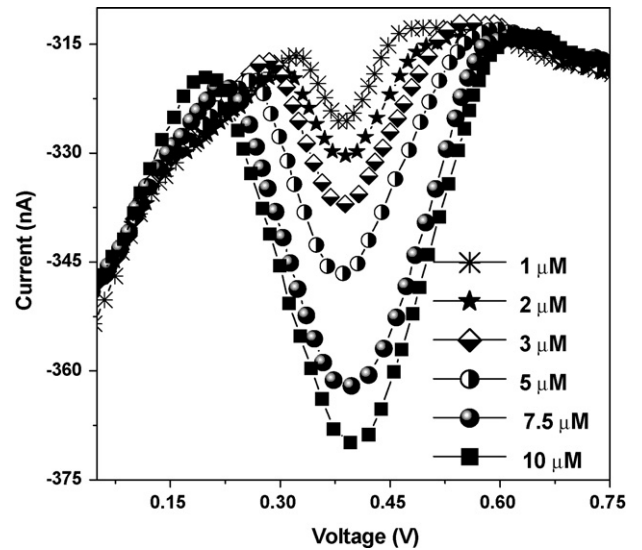


Fig. 4. Voltammograms of dopamine at different concentration using TiN (200)/NiTi as working electrode.

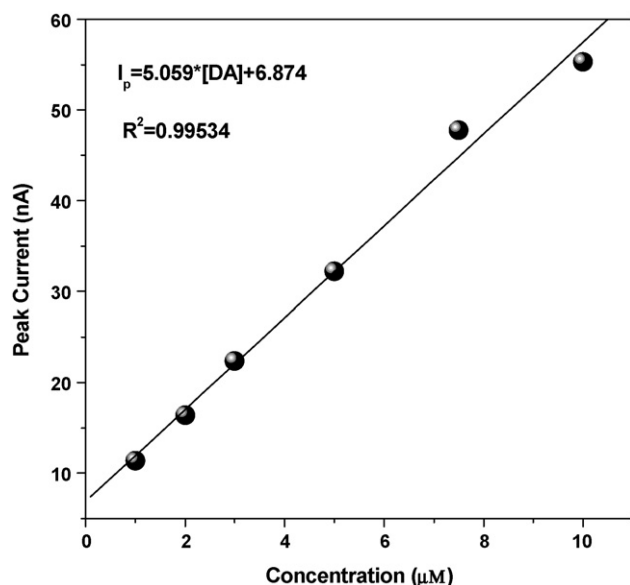


Fig. 5. Observed dependence of peak current on concentration of dopamine at TiN (200)/NiTi working electrode at pH 7.2.

abundantly present in biological samples. Hence, the effect of these two common interferents, which may interfere with determination of dopamine in blood or urine samples was also studied using TiN (200)/NiTi coated silicon electrode. It was found that ascorbic acid and uric acid showed well-defined peaks at modified electrode with  $E_p \sim 608$  and  $812$  mV vs. Ag/AgCl, respectively at pH 7.2. To check the interference of these two compounds, voltammograms were recorded at fixed concentration of dopamine ( $5 \mu\text{M}$ ) with varying concentration of ascorbic acid and uric acid. It was found that peak current of dopamine remained practically unaffected when ascorbic acid and uric acid were added in the concentration range  $50$ – $500 \mu\text{M}$  as shown in Table 2.

On the basis of the observations presented in Table 2, it can be concluded that ascorbic acid and uric acid do not interfere with voltammetric determination of dopamine even when they are in 100-fold excess with respect to dopamine. However, further increase in concentration of ascorbic acid beyond 100 times excess, causes a tendency to merge oxidation peak of ascorbic acid with oxidation peak of dopamine.

### 3.3.3. Stability of modified electrode

Stability and reproducibility of an electrode are the two important features which should be evaluated for analytical purpose. TiN (111)/NiTi and TiN (200)/NiTi coated silicon electrodes were tested for both the features so that a time period can be recommended for assured and accurate use of modified electrode. The variation in current response was observed for six successive

Table 2  
Effect of interferents on peak current of  $5 \mu\text{M}$  dopamine at pH 7.2.

Interferent	Concentration of interferents ( $\mu\text{M}$ )	Peak current ( $i_p$ ) of dopamine ( $\mu\text{A}$ )	Change in $i_p$ of dopamine	
			( $\mu\text{A}$ )	(%)
Ascorbic acid	50	0.351	+0.005	1.4
	125	0.353	+0.007	2.1
	250	0.356	+0.010	2.8
	500	0.363	+0.017	4.9
Uric acid	50	0.349	+0.003	1.1
	125	0.341	-0.005	1.4
	250	0.355	+0.009	2.6
	500	0.360	+0.014	4.2

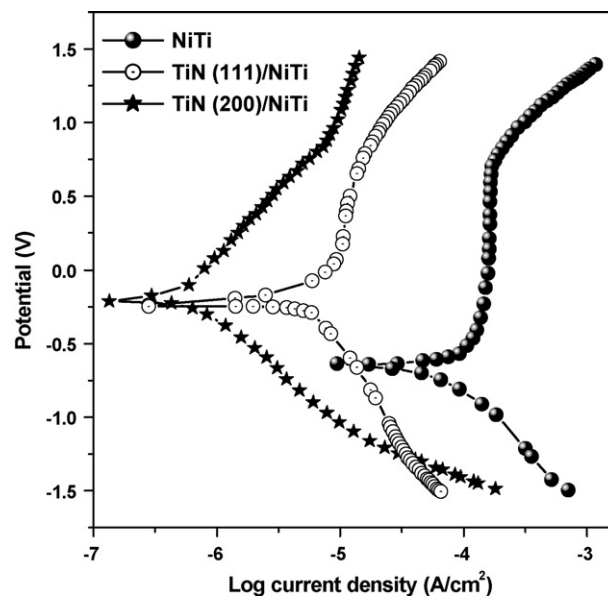


Fig. 6. Potentiodynamic polarization curves of NiTi, TiN (111)/NiTi and TiN (200)/NiTi films.

sweeps in a solution of fixed concentration to check the reproducibility of the electrode. It was noticed that the current was within 97–99% of the  $i_p$  observed for the first sweep. To determine long-term stability of TiN/NiTi coated silicon electrode, current response of dopamine was monitored daily for one week. The electrode was kept in dry conditions after use and it was found that the electrode retained 96–99% current for first three days. After three days, a considerable decline in the peak current was observed and only 91–95% of initial  $i_p$  was recorded. Thus, the electrode can be used for approximately three days without any significant error.

### 3.3.4. Corrosion resistance

Potentiodynamic polarization curves of NiTi, TiN (111)/NiTi and TiN (200)/NiTi films are shown in Fig. 6. The corrosion resistance of TiN coated NiTi films was found to be improved, which can be observed by a shift of whole polarization curve towards the region of lower current density and higher potential. The values of corrosion potential and corrosion current density were found to be  $0.635$  V and  $1.1 \times 10^{-5} \text{ A cm}^{-2}$  for pure NiTi film,  $0.248$  V and  $2.8 \times 10^{-7} \text{ A cm}^{-2}$  for TiN (111)/NiTi film and  $0.212$  V and  $1.4 \times 10^{-7} \text{ A cm}^{-2}$  for TiN (200)/NiTi film, respectively. High corrosion potential and low corrosion current density of the TiN coated NiTi films suggests that these films exhibit a low corrosion rate and a good corrosion resistance. TiN (200)/NiTi film exhibited better corrosion resistance than that of TiN (111)/NiTi film, which could be due to the fact that TiN (200) coated film exhibit higher real surface area/projected area and lower inhomogeneous surface. The real surface area is likely to be in the order, TiN (200)/NiTi > TiN (111)/NiTi > NiTi because, the grain size of these films follow the trend like TiN (200)/NiTi < TiN (111)/NiTi < NiTi. Therefore, smaller the grain size, higher will be the real surface area. The lower surface area and inhomogeneities might be responsible for weak points on the surface cause corrosive attacks.

## 4. Conclusions

A systematic study was performed to see the influence of crystallographic orientation of TiN passivation layer on mechanical and corrosion properties of NiTi thin films. The preferred orientation of the TiN films was observed to change from (111) to (200) with change in nature of sputtering gas. The shape of the crystallite

was also observed to change from a faceted pyramid to nonfaceted spherelike structure with change in crystallographic orientation of nanocrystalline TiN from (1 1 1) to (2 0 0). Nanoindentation studies revealed that the TiN (2 0 0)/NiTi films exhibit high hardness, high reduced elastic modulus and thereby better wear resistance as compared to pure NiTi and TiN (1 1 1)/NiTi. Electrochemical test reveals that TiN coated NiTi film exhibited better corrosion resistance as compared to pure NiTi film. It was also observed that TiN (2 0 0)/NiTi coated silicon electrode showed better response as compared with NiTi coated silicon with straight line calibration in dopamine concentration range 1–10  $\mu$ M. One of the probable reasons for this observation is that as TiN (2 0 0)/NiTi film exhibits higher real surface area due to small grain size as compared to NiTi film, TiN (2 0 0)/NiTi film showed better oxidation peak even at low concentration of dopamine. A significant decrease in peak potential was also observed at modified electrode. An advantage of using these nanocrystalline films in comparison to conventional films used for surface modification is that the films are sufficiently stable and do not require frequent replacements. Such replacement not only requires sufficient time but may also lead to change in the area of the electrode. In addition the films exhibit excellent electrocatalytic behaviour. Thus, it is concluded that use of nanocrystalline TiN layer with preferred (2 0 0) orientation on NiTi thin films improves mechanical, corrosion and electrocatalytic properties and hence can be successfully used as working electrode in voltammetric determination of biomolecules.

#### Acknowledgements

Financial support for carrying out this work was provided by Ministry of Communications and Information Technology, DIT, New Delhi vide grant No. 20(II)/2007-NANO under nanotechnology initiatives scheme. One of the authors (AK) is thankful to DIT for Senior Research Fellowship and to Dr. Sudhanshu P. Singh, Senior Research

Fellow, Department of Chemistry, IIT Roorkee for his help in electrochemical studies. Authors are thankful to Prof. A.K. Raychaudhary, SNBNCBS, India and Prof. Jan. Humbuck, Leuven University, Belgium for helpful discussions.

#### References

- [1] D. Xu, L. Wang, G. Ding, Y. Zhou, A. Yu, B. Cai, *Sens. Actuators A: Phys.* 93 (2001) 87.
- [2] B. O'Brien, W.M. Carroll, M.J. Kelly, *Biomaterials* 231 (2002) 739.
- [3] J.J. Gill, D.T. Chang, L.A. Momoda, G.P. Carman, *Sens. Actuators A: Phys.* 93 (2001) 148.
- [4] G.C. McKay, R. Macnair, C. MacDonald, M.H. Grant, *Biomaterials* 17 (1996) 1339.
- [5] D.J. Wever, A.G. Veldhuizen, J. Vries de, H.J. Busscher, J.R. van Horn, *Biomaterials* 19 (1998) 761.
- [6] X. Zhao, W. Cai, L. Zhao, *Surf. Coat. Technol.* 155 (2002) 236.
- [7] Z.D. Cui, H.C. Man, X.J. Yang, *Surf. Coat. Technol.* 192 (2005) 347.
- [8] G.S. Firstov, R.G. Vitchev, H. Kumar, B. Blanpain, J. Van, *Biomaterials* 23 (2002) 4863.
- [9] P. Shi, F.T. Cheng, H.C. Man, *Mater. Lett.* 61 (2007) 2385.
- [10] P. Singh, D. Kaur, *J. Appl. Phys.* 103 (2008) 043507.
- [11] R. Chandra, D. Kaur, A.K. Chawla, N. Phinichka, Z.H. Barber, *Mater. Sci. Eng. A* 423 (2006) 111.
- [12] S.A. Shabalovskaya, *Bio-Med. Mater. Eng.* 12 (2002) 69.
- [13] A. Thompson, *Int. Endo. J.* 33 (2000) 297.
- [14] R.N. Goyal, N. Bachheti, A. Tyagi, A.K. Pandey, *Anal. Chim. Acta* 605 (2007) 34.
- [15] R.N. Goyal, M. Oyama, S.P. Singh, *J. Electroanal. Chem.* 611 (2007) 140.
- [16] Y. Tao, Z. Lin, X. Chen, X. Huang, M. Oyama, X. Chen, X. Wang, *Sens. Actuators B: Chem.* 129 (2008) 758.
- [17] R.N. Goyal, V.K. Gupta, S. Chatterjee, *Talanta* 76 (2008) 662.
- [18] J. Zhang, M. Oyama, *J. Electroanal. Chem.* 577 (2005) 273.
- [19] R.N. Goyal, S.P. Singh, *Carbon* 46 (2008) 1556.
- [20] R.N. Goyal, V.K. Gupta, M. Oyama, N. Bachheti, *Talanta* 72 (2007) 976.
- [21] T.M. Dawson, *Science* 302 (2003) 819.
- [22] M.C. Shih, M.Q. Hoexter, L.A.F. Andrade, *Revista Paulista de Medicina* 124 (2006) 168.
- [23] G.D. Christian, W.C. Purdy, *J. Electroanal. Chem.* 3 (1962) 363.
- [24] W. Ni, Y.T. Cheng, D.S. Grummon, *Appl. Phys. Lett.* 82 (2003) 2811.
- [25] W. Ni, Y.T. Cheng, M.J. Lukitsch, A.M. Weiner, L.C. Lev, D.S. Grummon, *Appl. Phys. Lett.* 85 (2004) 4028.





# A sensitive, label free electrochemical aptasensor for ATP detection

Wang Li, Zhou Nie\*, Xiahong Xu, Qinpeng Shen, Chunyan Deng, Jinhua Chen\*, Shouzhao Yao

State Key Laboratory of Chemo/Biosensing and Chemometrics, College of Chemistry and Chemical Engineering, Hunan University, Changsha, 410082, PR China

## ARTICLE INFO

### Article history:

Received 3 October 2008

Received in revised form 4 January 2009

Accepted 5 January 2009

Available online 20 January 2009

### Keywords:

ATP detection

Aptasensor

Gold nanoparticles

Chronocoulometry

## ABSTRACT

A sensitive, label free electrochemical aptasensor for small molecular detection has been developed in this work based on gold nanoparticles (AuNPs) amplification. This aptasensor was fabricated as a tertiary hybrid DNA–AuNPs system, which involved the anchored DNA (ADNA) immobilized on gold electrode, reporter DNA (RDNA) tethered with AuNPs and target-responsive DNA (TRDNA) linking ADNA and RDNA. Electrochemical signal is derived from chronocoulometric interrogation of  $[\text{Ru}(\text{NH}_3)_6]^{3+}$  (RuHex) that quantitatively binds to surface-confined DNA via electrostatic interaction. Using adenosine triphosphate (ATP) as a model analyte and ATP-binding aptamer as a model molecular reorganization element, the introduction of ATP triggers the structure switching of the TRDNA to form aptamer–ATP complex, which results in the dissociation of the RDNA capped AuNPs (RDNA–AuNPs) and release of abundant RuHex molecules trapped by RDNA–AuNPs. The incorporation of AuNPs in this strategy significantly enhances the sensitivity because of the amplification of electrochemical signal by the RDNA–AuNPs/RuHex system. Under optimized conditions, a wide linear dynamic range of 4 orders of magnitude (1 nM–10  $\mu\text{M}$ ) was reached with the minimum detectable concentration at sub-nanomolar level (0.2 nM). Those results demonstrate that our nanoparticles-based amplification strategy is feasible for ATP assay and presents a potential universal method for other small molecular aptasensors.

© 2009 Elsevier B.V. All rights reserved.

## 1. Introduction

Detecting and quantifying small molecular substances such as drugs, hormones and adenosine phosphorylated derivatives are increasingly needed in environmental analysis and clinical assay [1–4]. Great progress has been achieved in the development of analytical assays of small molecules with different detection techniques (optical [5], electrochemical [6], piezoelectric [7], electrochemiluminescent (ECL) [8], chromatographic [9], surface-enhanced Raman scattering (SERS) [10], etc.). Among them, electrochemical detection methods became a popular technology because of their numerous merits, including high sensitivity, simple instrumentation, low production cost, fast response and portability [11,12]. Electrochemical affinity sensors, an important part of electrochemical sensors, commonly rely on the immobilization of a biological recognition element (antibodies or aptamers) onto the transducer surface. In recent years, electrochemical affinity sensors for the detection of small molecules, especially non-redox small molecules, have attracted much attention because of good affinity to their target elements [7,12,13].

Aptamers [14,15] are single-stranded DNA or RNA sequences artificially selected through systematic evolution of ligands by

exponential enrichment (SELEX). They are used to bind various targets, such as small molecules [12,16], proteins [6,17] and even viruses and cells [18], with high specificity and affinity. In despite of the similar identification principle for targets with antibodies, aptamers can provide several advantages over antibodies such as simple synthesis, easy labeling, good stability, wide applicability, and high sensitivity. In addition, aptamers are readily applicable to the identification of small molecules that make them superior to antibodies when used as sensing elements for small molecular sensors [19]. Antibodies are applied hardly and complicatedly to the small molecules which are toxic to the host animal or trigger a minimal immunogenic response [19], whereas aptamers could be applied to various small molecules with no limitation. The nucleic acid nature and intrinsic advantages of aptamers, integrated with the previously well-developed nucleic acid sensor technologies, promoted small molecular aptasensor technologies growing rapidly in recent years [18–21].

Although aptamers are the promising small molecular recognition elements, a major disadvantage of aptamers is their relatively low association constants with the small molecules, which leads to a rather poor detection limit. Due to this drawback, the high sensitivity requested in aptamer-based assay for the detection of small molecules is hardly to be reached by simple “direct” binding protocols. Therefore, developing effective amplification paths for small molecular aptasensor is important. With this aim, several methods have been employed to amplify the signal, such as DNAzyme

\* Corresponding authors. Tel.: +86 731 8821961; fax: +86 731 8821848.

E-mail addresses: [niezhou.hnu@gmail.com](mailto:niezhou.hnu@gmail.com) (Z. Nie), [chenjinhua@hnu.cn](mailto:chenjinhua@hnu.cn) (J. Chen).

[22], rolling cycle amplification (RCA) [23], and strand displacement amplification (SDA) [24]. However, the sensitivity of these amplification methods was still not satisfactory (millimolar level). These methods might be hampered by the relatively low catalytic activity of DNA peroxidase or suffer from high cost, time-consuming and complex reaction system for the nucleic acid amplification (RCA or SDA). In recent years, taking the advantage of their high stability, low cost, and labeling convenience, inorganic nanoparticles were employed as signal amplification elements in various DNA or protein electrochemical assays [25–27].

Using gold nanoparticles (AuNPs) as the signal amplification elements, Fan and co-workers [27] reported a novel inorganic nanoparticle-based electrochemical DNA sensor that could sensitively detect femtomolar target DNA. The electrochemical signals of this sensor were generated by chronocoulometric interrogation of  $[\text{Ru}(\text{NH}_3)_6]^{3+}$  (RuHex) through electrostatic adsorption, which was better than labeled methods. In this paper, this sensitive and label free electrochemical strategy is extended to the small molecular detection and is used to detect adenosine triphosphate (ATP). It is well-known that ATP is the mediator of energy exchanges that occur in all living cells, in both catabolic and anabolic processes and is widely used as an index for biomass determinations in clinical microbiology, food quality control and environmental analyses [4,28]. Therefore, in this work, it is chosen as a model analyte and ATP-binding aptamer is taken as a model molecular reorganization element. The proposed ATP aptasensor is based on the DNA–AuNPs hybrid system containing three functional components: AuNPs functionalized with 5'-thiol-modified reporter DNA (RDNA), 3'-thiol-modified anchored DNA (ADNA) immobilized on electrode, and a target-responsive DNA (TRDNA). Here, TRDNA acts as both the recognized element specific for ATP and the linker connecting RDNA and ADNA. The TRDNA is composed of three segments: first, the segment (12 nucleotides) hybridized with ADNA, second, the segment hybridized with the last five nucleotides of RDNA, and third, the segment (the aptamer sequence for ATP) hybridized with the other seven nucleotides on the RDNA. When an aptamer immobilized on the electrode surface captures two ATP molecules, the binding-induced conformational changes lead to the release of the DNA–AuNPs as well as the numerous binding RuHex molecules, resulting in the transduction and amplification of the ATP-binding signal. Based on this strategy, we found this sensor can sensitively detect sub-nanomolar ATP, and provide a universal and sensitive method for small molecular assay.

## 2. Experimental

### 2.1. Materials and apparatus

All oligonucleotides were synthesized and purified by Sangon Inc. (Shanghai, China). The sequences of the single-stranded oligonucleotides are as follows:

ADNA: 5'-TCA CAG ATG AGT TT-SH-3'

RDNA: 5'-HS-CCC AGG TTC TCT-3'

TRDNA: 5'-ACT CAT CTG TGA AGA GAA CCT GGG GGA GTA TTG CGG AGG AAG GT-3'

AuNPs were synthesized according to the published protocol [29]. Mercaptohexanol (MCH), hexaamineruthenium(III) chloride ( $[\text{Ru}(\text{NH}_3)_6]^{3+}$ , RuHex), and tris(2-carboxyethyl)phosphine hydrochloride (TCEP) were purchased from Sigma (St. Louis, MO). ATP, GTP, UTP and CTP were from BBI (Canada). Tris-(hydroxymethyl)aminomethane (Tris) was obtained from Oumay Biotech Co. Ltd. (Changsha, China). All the reagents mentioned above were used without further purification. All solutions were

prepared with Milli-Q water (18.25 M $\Omega$  cm) from a Millipore system.

Electrochemical measurements were performed with a CHI 660a electrochemical workstation (Shanghai Chenhua Instrument Corporation, China). A conventional three-electrode cell was employed, which involved a gold working electrode (2 mm in diameter), a platinum foil counter electrode, and a saturated calomel reference electrode (SCE). All the potentials in this paper were with respect to SCE. The electrolyte buffer was thoroughly purged with nitrogen before experiments.

### 2.2. Functionalization of AuNPs with reporter DNA

The RDNA functionalized AuNPs (RDNA–AuNPs) were prepared as reported in the literature [27]. Briefly, RDNA–AuNPs were synthesized by incubating RDNA (3.0  $\mu\text{M}$ ) in 1 mL of 13 nm AuNPs solution (1.2 nM) for 16 h. Then, the RDNA–AuNPs conjugates were “aged” in salt condition (0.1 M NaCl) for 40 h. Excess reagents were removed by centrifuging at 15,000 rpm for 30 min. The red precipitate was washed, re-centrifuged, and then dispersed in 1 mL solution (0.25 M NaCl, 10 mM phosphate buffer, pH 7.0).

### 2.3. Preparation of the aptasensor and ATP detection

Gold electrode was polished sequentially with 0.3 and 0.05  $\mu\text{m}$  alumina powder followed by ultrasonic cleaning with distilled water, ethanol, and distilled water for 5 min each. Then the electrode was electrochemically cleaned to remove any remaining impurities. Finally, the electrode was washed with distilled water and dried in a mild nitrogen stream.

RDNA–AuNPs/TRDNA/ADNA modified gold electrode was earned by placing 4  $\mu\text{L}$  of the ADNA solution (10 mM Tris–HCl, 1 mM EDTA, 10 mM TCEP, and 0.1 M NaCl (pH 7.4)) on gold electrode, and further treated with 1 mM MCH for 2 h to obtain well aligned DNA monolayers. Then, 4  $\mu\text{L}$  of 10  $\mu\text{M}$  TRDNA solution was placed on electrode for 2 h. At last 4  $\mu\text{L}$  of RDNA–AuNPs was dropped on the electrode for 2 h.

For the ATP detection, 4  $\mu\text{L}$  of ATP solution (a series of concentrations from  $0.2 \times 10^{-9}$  to  $1.0 \times 10^{-3}$  M) was placed onto the modified electrode. Each process was followed with washing and drying. Chronocoulometry (CC) was carried out in Tris buffer (10 mM Tris–HCl, pH 7.4) containing 50  $\mu\text{M}$  RuHex.

The surface density of DNA ( $\Gamma_{\text{ss}}$ ) was measured with CC as described in literature [30],  $\Gamma_{\text{ss}} = [(Q_{\text{total}} - Q_{\text{dl}})N_A/nFA](z/m)$ . Where  $Q_{\text{total}}$  stands for the total charge flowing through the electrode, comprising both Faradaic (redox) and non-Faradaic (capacitive) charges;  $Q_{\text{dl}}$  the capacitive charge;  $n$  the number of electrons in the reaction;  $A$  the surface area of the working electrode;  $m$  the number of nucleotides in the DNA;  $z$  the charge of the redox molecules and  $N_A$  the Avogadro's number.

### 2.4. Preparation of urine samples

Fresh urine samples were obtained from healthy volunteers. Each sample was filtered through a 0.2-mm membrane to remove particulate matter. The human-urine samples were diluted separately by a factor of 100 with the buffer solution and then were equilibrated for 30 min at room temperature.

## 3. Results and discussion

### 3.1. Design strategy of the nanoparticles-based ATP aptasensor

In this work, the electroactive complex, RuHex, serves as the signal molecule, since the RuHex cations can associate with anionic

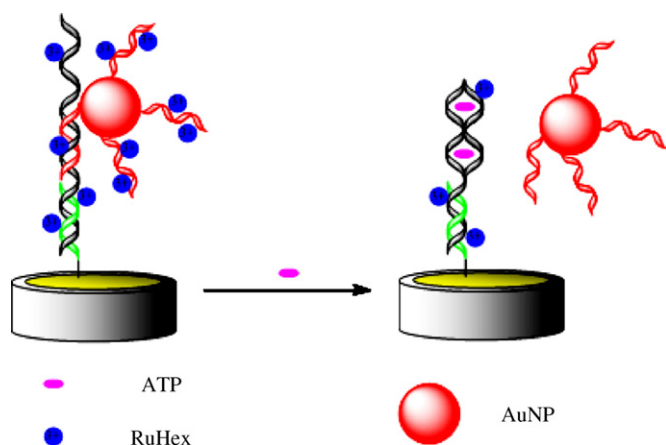


**Fig. 1.** The representation of the aptasensor based on nanoparticles amplification for ATP detection. The color of DNA: ADNA–green, TRDNA–black, RDNA–red. (For interpretation of the references to color in this figure legend, the reader is referred to the web version of the article.)

phosphates of DNA strands as counterions [27]. It has been demonstrated that binding of RuHex to DNA is totally through electrostatic interaction with intrinsic stoichiometric ratio. Thus redox charge of the trapped RuHex is a direct function of the amount of the DNA strands confined to the electrode surface [30]. Based on this strategy, DNA functionalized AuNPs, loaded with hundreds of DNA strands per particle, are used as the signal amplification element in electrochemical assay by absorbing thousands of RuHex molecules. Compared with the covalent redox-labeling technique broadly used in existing electrochemical aptasensors [12,16], the redox probe (RuHex) electrostatic binding strategy is relatively convenient, time-saving and without requirement of purification.

Fig. 1 shows the principle of the nanoparticles-based electrochemical ATP aptasensor for ATP detection. In the absence of ATP, ADNA and RDNA are assembled with TRDNA to form tertiary complex, which brings the RDNA–AuNPs proximate to the electrode surface. The RDNA–AuNPs localized at electrode surface can electrostatically absorb abundant redox charge of numerous RuHex molecules close to the electrode surface. When the ATP is introduced, the aptamer switches its structure to bind ATP and prefers to form an ATP–aptamer complex rather than an aptamer–DNA duplex [31]. As a result, only five base pairs are left to hybridize with RDNA, which is unstable at room temperature [32] and results in the dissociation of RDNA–AuNPs. The release of RDNA–AuNPs is accom-

panied with the extrication of the abundant RuHex molecules, which offers a significant amplification in the capture event. The design relies on the structure-switching properties of aptamers upon binding to their target molecules. Because there are no special requirements on the aptamer part, this strategy is generally applicable to many small molecular aptamers.

### 3.2. Characterization of the sensor

Electrochemical impedance spectroscopy (EIS) was employed for the electrochemical characterization of the modified electrode in 10 mM  $[\text{Fe}(\text{CN})_6]^{4-/3-}$  and 0.1 M KCl aqueous solution and the corresponding results are shown in Fig. 2(A). The electron-transfer resistance increases in the order of the bare electrode (a), TRDNA/ADNA modified electrode (b) and RDNA–AuNPs/TRDNA/ADNA modified electrode (c). Because the negative charge of DNA hinders  $[\text{Fe}(\text{CN})_6]^{4-/3-}$  from reaching to the electrode surface, and the change of resistance reflects the amount of immobilized DNA, the increase in electron-transfer resistance indicates that the TRDNA and RDNA–AuNPs are successfully immobilized on the electrode surface. After the electrode was treated with  $1 \mu\text{M}$  ATP (d), the electron-transfer resistance of the electrode decreases obviously (from 1.7 k $\Omega$  to 1 k $\Omega$ ). This result demonstrates that the aptamer sequences were successfully attached with ATP and DNA–AuNPs were dissociated from the surface of the electrode.

On the other hand, differential pulse voltammetry (DPV) was employed to characterize the electrochemistry of RuHex. As shown in Fig. 2(B), two peaks (peaks I and II) can be observed when the DNA/MCH modified electrode (TRDNA/ADNA or RDNA–AuNPs/TRDNA/ADNA modified gold electrode) is immersed in a solution containing RuHex at a low ionic strength. Peak I, observed for the DNA/MCH modified electrode and also the MCH only modified electrode (data not shown), should be ascribed to the diffusion-based redox process of RuHex (RuHex diffused to the electrode). The other peak (peak II), observed at about  $-0.34 \text{ V}$ , is due to the surface-confined redox process of RuHex electrostatically bound to the phosphate backbone of DNA [27]. Since the surface-confined redox signal can reflect the amount of DNA strands located at the electrode surface, the RDNA–AuNPs loaded on electrode surface can be definitely indicated by the change of the current intensity of peak II. It is noted that a small peak current (peak II) is observed at the TRDNA/ADNA electrode (a), and a significant enhancement of peak II can be found after the formation of the RDNA–AuNPs/TRDNA/ADNA complex (b). This suggests that the On/Off switch of the localization of RDNA–AuNPs on electrode

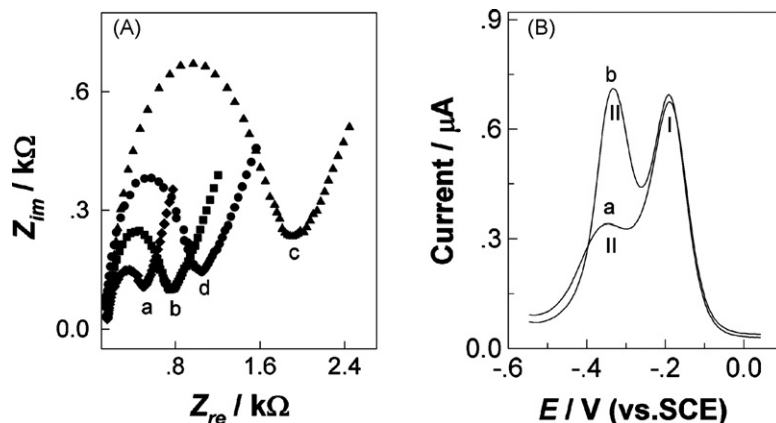


**Fig. 2.** Characterization of the aptasensor: (A) The electrochemical impedance spectra of bare (a), TRDNA/ADNA modified (b) and RDNA–AuNPs/TRDNA/ADNA modified (c) gold electrodes in 10 mM  $[\text{Fe}(\text{CN})_6]^{4-/3-}$  and 0.1 M KCl aqueous solution. (d) is (c) treated with  $1 \mu\text{M}$  of ATP. The frequency changed from 0.1 Hz to 100,000 Hz and the amplitude was 5.0 mV. (B) Differential pulse voltammograms of the (a) TRDNA/ADNA modified and (b) RDNA–AuNPs/TRDNA/ADNA modified gold electrodes in 10 mM Tris buffer containing  $50 \mu\text{M}$  RuHex.

**Table 1**

The effect of the surface density of ADNA on the detection efficiency of the electrode. The standard deviations of measurements were taken from four independent experiments.

ADNA concentration ( $\mu\text{M}$ )	Surface density of ADNA (molecule/ $\text{cm}^2$ )	$\Delta Q$ ( $\mu\text{C}$ )
5	$4.0 \times 10^{12}$	$0.16 \pm 0.01$
1	$2.3 \times 10^{12}$	$0.24 \pm 0.01$
0.2	$1.0 \times 10^{12}$	$0.38 \pm 0.03$
0.04	$4.9 \times 10^{11}$	$0.21 \pm 0.02$
0.02	$3.9 \times 10^{11}$	$0.10 \pm 0.02$

surface can remarkably amplify the variation of surface-confined redox signal.

Fan and co-workers have demonstrated that chronocoulometry is more accurate for detecting the signal of electrostatically trapped redox marker than other electrochemical methods, and RuHex–DNA–electrode system can be used to generate an intense signal in CC [33]. Hence, the CC technique was employed for the subsequent ATP detection experiments.

### 3.3. Optimization of surface density of anchored DNA for effective ATP detection

In order to obtain a perfect sensitivity, an appropriate surface density of the immobilized ADNA is needed. In this work, five kinds of ADNA self-assembled monolayers (SAMs) with different surface density of ADNA ( $4.0 \times 10^{12}$ ,  $2.3 \times 10^{12}$ ,  $1.0 \times 10^{12}$ ,  $4.9 \times 10^{11}$  and  $3.9 \times 10^{11}$  molecule/ $\text{cm}^2$ ) were prepared by placing ADNA solution with different concentration (5.0, 1.0, 0.2, 0.04 and 0.02  $\mu\text{M}$ ) in the same self-assemble time (60 min). After the preparation of ADNA SAMs, TRDNA and RDNA–AuNPs were assembled on the ADNA SAMs successively in sufficient hybridization time. The detection efficiency of the resulting electrodes was investigated in the presence of 10  $\mu\text{M}$  ATP. As shown in Table 1, the largest CC signal change ( $\Delta Q = Q_{\text{total}} - Q_{\text{dl}}$ ) occurred at the surface density of ADNA  $1.0 \times 10^{12}$  molecule/ $\text{cm}^2$ . The CC signal change increases with the decrease of the surface density of ADNA when the density is larger than  $1.0 \times 10^{12}$  molecule/ $\text{cm}^2$ . This phenomenon is probably caused by the too dense ADNA–TRDNA on electrode that cannot fully hybrid with RDNA–AuNPs. The ADNA–TRDNA without RDNA–AuNP hybridization could lead to lose the signal amplification after ATP catching, resulting in sensitivity decrease. However, the CC signal change decreases with the decrease of the surface density of ADNA when the density of ADNA is less than  $1.0 \times 10^{12}$  molecule/ $\text{cm}^2$ . It is probably because the ADNA–TRDNAs can fully

hybrid with RDNA–AuNPs when the surface density of ADNA is less than  $1.0 \times 10^{12}$  molecule/ $\text{cm}^2$ . The high surface density of the ADNA–TRDNA–RDNA–AuNP element could increase the efficiency of ATP capture and the sensitivity of the sensor. Therefore, this clearly shows that control of DNA assembly density is essential for the improvement of sensitivity, and the optimized DNA monolayer ( $1.0 \times 10^{12}$  molecule/ $\text{cm}^2$ ) was adopted in the following experiments.

### 3.4. Detection of ATP

The detection performance of the ATP sensor was evaluated by exposing the sensor to a series of ATP concentrations (from 0.2 nM to 1.0 mM) under the same experimental condition. As shown in Fig. 3(A), the increase in ATP concentration induces a monotonous decrease in CC signal ( $\Delta Q$ ). The plot of the CC signal as a function of ATP concentrations is illustrated in Fig. 3(B). It is found that the value of  $\Delta Q$  is logarithmically related to the ATP concentration. The linear range is from 1 nM to 10  $\mu\text{M}$ . The calibration equation was  $\Delta Q = 0.0808 \log C + 0.0558$  with a correlation coefficient of 0.993. The minimum detectable ATP concentration is at sub-nanomolar level (0.2 nM). The results indicate that the present method can successfully detect the ATP with high sensitivity and low detection limit. Recently, Shao and co-workers reported an electrochemical approach for ATP detection by using the similar CC protocol but without amplification by nanoparticles [21]. They reported that the detection range was from 0.1  $\mu\text{M}$  to 1 mM and detection limit is below 0.1  $\mu\text{M}$ , which are about 2 orders of magnitude higher than those of our method. The high sensitivity of our sensor is contributed to the presence of AuNPs. In our amplification strategy, gold nanoparticle loaded with a few hundred DNA strands was introduced instead of only one complementary DNA strand as leaving group responded in the aptamer–ATP-binding event. It is worth to note that the detection limit of this aptasensor with nanoparticles-based amplification is more than 3 orders of magnitude lower than that of the aptasensor based on nucleic acid amplification strategy. The sub-nanomolar sensitivity of the present sensor is much better than other ATP aptasensors reported in the literatures, including luminescent [34], electrochemical [12,21], SERS [10] and colorimetric [5] aptasensors.

### 3.5. Selectivity and nonspecific adsorption of the sensor

Besides sensitivity, selectivity is also an important feature for biosensors. CTP, UTP, and GTP, which belong to the nucleoside triphosphate family, are usually coexisting with ATP in real biolog-

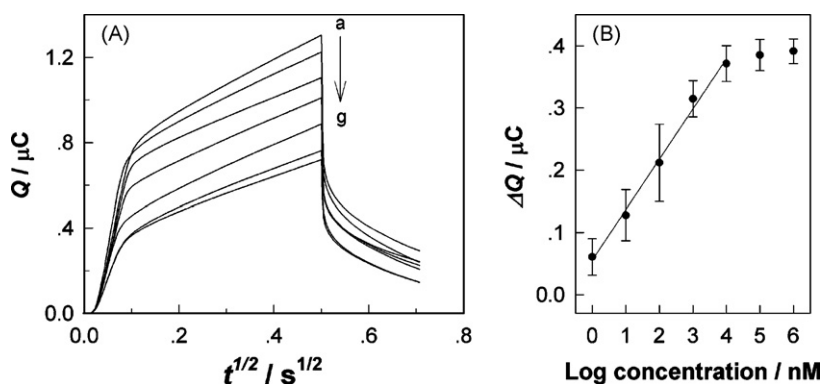


**Fig. 3.** (A) Chronocoulometry curves for electrodes exposed to ATP solution with a series of concentrations (from a to g: 1 nM, 10 nM, 100 nM, 1  $\mu\text{M}$ , 10  $\mu\text{M}$ , 100  $\mu\text{M}$  and 1 mM). The electrolyte is 10 mM Tris buffer containing 50  $\mu\text{M}$  RuHex. Pulse period: 250 ms; pulse width: 700 mV. Intercepts at  $t=0$  in chronocoulometric curves represent redox charges of RuHex bound to DNA. (B) Calibration curve for the detection of ATP. Error bars show the standard deviations of measurements taken from four independent experiments.

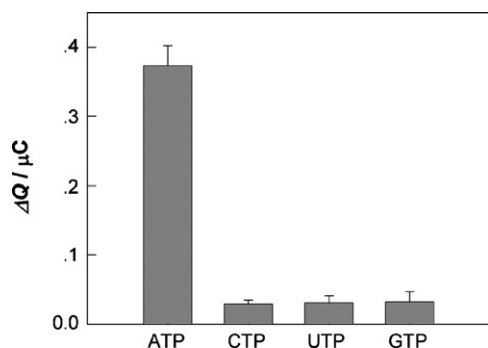


**Fig. 4.** The selectivity of the aptasensor. The sensor was treated with 10  $\mu\text{M}$  (ATP, CTP, UTP, or GTP) sample solution for 60 min. Other conditions are the same as those described in Fig. 3(A). Error bars show the standard deviations of measurements taken from four independent experiments.

**Table 2**

Recovery of ATP assays in real biological samples. The standard deviations of measurements were taken from four independent experiments.

Sample	Added (nM)	Found (nM)	Recovery
1	45.5	51.8 $\pm$ 8.1	114%
2	200	190 $\pm$ 23	95%
3	500	440 $\pm$ 54	88%
4	2000	1816 $\pm$ 225	91%
5	5000	4650 $\pm$ 660	93%

ical samples. Differentiation of the other nucleoside triphosphate from ATP is of significant importance for sensing ATP in biochemical assay. Fig. 4 exhibits that only small signal changes took place after the addition of 4  $\mu\text{L}$  of 10  $\mu\text{M}$  GTP, UTP, or CTP compared to the addition of 4  $\mu\text{L}$  of 10  $\mu\text{M}$  ATP. It was found that the  $\Delta Q$  for 10  $\mu\text{M}$  GTP (UTP, or CTP) equals to that for 1 nM ATP. Furthermore, the  $\Delta Q$  for 1 mM GTP (UTP, or CTP) equals to that for 4 nM ATP (not shown in the figure). This indicates that the proposed strategy has sufficient selectivity in ATP detection, and is able to discriminate ATP in complex samples from its analogues. The excellent selectivity of the sensor arises not only from the high selectivity of ATP aptamer but also from the additional stringency due to the competition between the aptamer-complementary strand duplex and the aptamer-ATP structure.

It was reported that the nonspecific binding of DNA-conjugated AuNPs to solid surfaces is much more severe than that of DNA [35]. Therefore, we investigated the nonspecific adsorption of RDNA-AuNPs onto the electrode surface by dropping 4  $\mu\text{L}$  of RDNA-AuNPs (1.2 nM) onto the ADNA modified electrode for 2 h. We found that a small amount of AuNPs could be nonspecifically adsorbed onto the electrode surface and the respective signal arising was only 18.3  $\pm$  6.6 nC, which was much less than the signal of 0.2 nM ATP ( $\Delta Q = 33 \pm 8$  nC).

### 3.6. Recovery test

The recovery experiment of different ATP concentrations was carried out to evaluate applicability and reliability of the developed electrochemical aptasensors in complex system. Urine samples were employed in this work as the model complex system. Three ATP added samples were prepared and the results are shown in Table 2. The recoveries for the added ATP with 45.5 nM, 200 nM, 500 nM, 2  $\mu\text{M}$ , and 5  $\mu\text{M}$  are 114%, 95%, 88%, 91%, and 93%, respectively.

## 4. Conclusion

We developed a novel, label free small molecular chronocoulometric aptasensor based on gold nanoparticles signal-amplified mechanism. DNA capped gold nanoparticles are demonstrated as potent amplifier for the aptamer-analyte binding event, which causes significant chronocoulometric signal change of surface-confined RuHex. As a model system, ATP was chosen as the model analyte and ATP-binding aptamer was taken as the model molecular reorganization element. This aptasensor can detect as low as sub-nanomolar ATP, which is 3 orders of magnitude more sensitive than the existing aptasensors based on nucleic acid amplification. Furthermore, this novel ATP sensor showed fairly good selectivity. This aptamer sensing strategy based on nanoparticles amplification is versatile and has great potential in the construction of aptamer-based biosensors for the detection of various small molecules.

## Acknowledgments

This work was financially supported by NSFC (No. 20805013, 20675027, 20575019, 20335020) and the SRF for ROCS, SEM, China (2001-498).

## References

- Z. Peng, Y. Bang-Ce, J. Agric. Food Chem. 54 (2006) 6978.
- K. Kerman, N. Nagatani, M. Chikae, T. Yuhi, Y. Takamura, E. Tamiya, Anal. Chem. 78 (2006) 5612.
- B. Liu, M. Ozaki, H. Hisamoto, Q. Luo, Y. Utsumi, T. Hattori, S. Terabe, Anal. Chem. 77 (2005) 573.
- H. Agteresch, P. Dagnelie, J. van den Berg, J. Wilson, Drugs 153 (1999) 211.
- S.J. Chen, Y.F. Huang, C.C. Huang, K.H. Lee, Z.H. Lin, H.T. Chang, Biosens. Bioelectron. 23 (2008) 1749.
- R.Y. Lai, K.W. Plaxco, A.J. Heeger, Anal. Chem. 79 (2007) 229.
- A. Bini, M. Minunni, S. Tombelli, S. Centi, M. Mascini, Anal. Chem. 79 (2007) 3016.
- R. Wilson, C. Clavering, A. Hutchinson, Anal. Chem. 75 (2003) 4244.
- V. Kiemen, W.F. Costa, J.V. Visentainer, N.E. Souza, C.C. Oliveira, Talanta 75 (2008) 141.
- J.W. Chen, X.P. Liu, K.J. Feng, Y. Liang, J.H. Jiang, G.L. Shen, R.Q. Yu, Biosens. Bioelectron. 24 (2008) 230.
- A.E. Radi, J.L.A. Sánchez, E. Baldrich, C.K. O'Sullivan, J. Am. Chem. Soc. 128 (2006) 117.
- X. Zuo, S. Song, J. Zhang, D. Pan, L. Wang, C. Fan, J. Am. Chem. Soc. 129 (2007) 1042.
- Y. Luo, X. Mao, Z.F. Peng, J.H. Jiang, G.L. Shen, R.Q. Yu, Talanta 74 (2008) 1642.
- A.D. Ellington, J.W. Szostak, Nature 346 (1990) 818.
- C. Tuerk, L. Gold, Science 249 (1990) 505.
- B.R. Baker, R.Y. Lai, M.S. Wood, E.H. Doctor, A.J. Heeger, K.W. Plaxco, J. Am. Chem. Soc. 128 (2006) 3138.
- L.S. Green, D. Jellinek, R. Jenison, A. Ostman, C. Heldin, N. Janjic, Biochemistry 35 (1996) 14413.
- C.D. Medley, J.E. Smith, Z. Tang, Y. Wu, S. Bamrungsap, W. Tan, Anal. Chem. 80 (2008) 1067.
- I. Willner, M. Zayats, Angew. Chem. Int. Ed. 46 (2007) 6408.
- J. Liu, Y. Lu, J. Am. Chem. Soc. 129 (2007) 629.
- L. Shen, Z. Chen, Y. Li, P. Jing, S. Xie, S. He, P. He, Y. Shao, Chem. Commun. (2007) 2169.
- D. Li, B. Shlyahovskiy, J. Elbaz, I. Willner, J. Am. Chem. Soc. 129 (2007) 5804.
- J.H. Choi, K.H. Chen, M.S. Strano, J. Am. Chem. Soc. 128 (2006) 1149.
- B. Shlyahovskiy, D. Li, Y. Weizmann, R. Nowarski, M. Kotler, I. Willner, J. Am. Chem. Soc. 129 (2007) 3814.
- P. He, L. Shen, Y. Cao, D. Li, Anal. Chem. 79 (2007) 8024.
- N.L. Rosi, C.A. Mirkin, Chem. Rev. 105 (2005) 1547.
- J. Zhang, S. Song, L. Zhang, L. Wang, H. Wu, D. Pan, C. Fan, J. Am. Chem. Soc. 128 (2006) 8575.
- F. Yu, L. Li, F. Chen, Anal. Chim. Acta 610 (2008) 257.
- G. Fens, Nat. Phys. Sci. 241 (1973) 20.
- A.B. Steel, T.M. Herne, M.J. Tarlov, Anal. Chem. 70 (1998) 4670.
- R. Nutiu, Y. Li, J. Am. Chem. Soc. 125 (2003) 4771.
- H. Yang, H. Liu, H. Kang, W. Tan, J. Am. Chem. Soc. 130 (2008) 6320.
- R. Lao, S. Song, H. Wu, L. Wang, Z. Zhang, L. He, C. Fan, Anal. Chem. 77 (2005) 6475.
- J. Wang, Y. Jiang, C. Zhou, X. Fang, Anal. Chem. 77 (2005) 1789.
- J. Das, C.H. Huh, K. Kwon, S. Park, S. Jon, K. Kim, H. Yang, Langmuir 25 (2009) 235.



# A visual test paper for extremely strong concentrated acidity with a new synthesized isoindole reagent

Chun Mei Li<sup>a</sup>, Yuan Fang Li<sup>a</sup>, Cheng Zhi Huang<sup>b,\*</sup>, Yun Fei Long<sup>c</sup>

<sup>a</sup> College of Chemistry and Chemical Engineering, Education Ministry Key Laboratory on Luminescence and Real-Time Analysis, Southwest University, Chongqing 400715, China

<sup>b</sup> College of Pharmaceutical Sciences, Education Ministry Key Laboratory on Luminescence and Real-Time Analysis, Southwest University, Chongqing 400715, China

<sup>c</sup> Institute of Chemistry and Chemical Engineering, Hunan University of Science and Technology, Hunan 411201, China

## ARTICLE INFO

### Article history:

Received 10 October 2008

Received in revised form 16 January 2009

Accepted 20 January 2009

Available online 30 January 2009

### Keywords:

Test paper

Visual

Strong concentrated acidity

Isoindole reagent

## ABSTRACT

A visual test paper by taking common filter paper as solid support for extremely strong concentrated acidity has been developed in this contribution with a new synthesized isoindole compound starting from *p*-phenylenediamine and the coupled fluorogenic reagent of *o*-phthaldialdehyde- $\beta$ -mercaptoethanol. It was very easy for semiquantitative detection of acidity in the range of 0.2–18 M ( $[H^+]$ ) in extreme acidic solution based on the color changes of the solution or the visual test paper prepared by immersing filter paper slides into the solution of the new synthesized reagent. Quantitative detection of concentrated strong acids could be successfully constructed through the linear relationship exists between the absorbance of the chromogenic reagent at 510 nm and the acid concentrations.

© 2009 Elsevier B.V. All rights reserved.

## 1. Introduction

Concentrated strong acids, like vitriol and hydrochloric acid are highly toxic and corrosive, and the harmful properties confine their measurements of acidity on-site and quality control [1,2]. Classical acid–base titrimetry, although precise, are generally time-consuming. Electrochemical methods, on the other hand, usually cause large errors when applied to concentrated strong acids [3]. pH-dependent fluorescent properties for extreme pH measurement [4] and the new prepared nano-pH sensor, which has proved powerful in the range of pH 3–14 [5], would be broken down when meeting concentrated strong acids. Recently, Xue and co-workers developed a fast and reversible acid optical sensor for highly acidic solutions of 1–11 M ( $[H^+]$ ) with thin films of silica sol–gels doped with an acid indicator [6–9]. This optical sensor for strong acids holds the advantages of stability and fast response, and might act as a good herald for accurately predicting the acidity of concentrated strong acid solutions even if in high ionic strength medium up to 5.5 M salt [8–9]. These sol–gels methods, although have been commonly used as substrates for optical analyses because they are transparent in the visible region [6–13], suffer from comparatively time-consuming preparation of sol–gel. Researchers have developed a highly flexible method for direct and quantitative determination of surface Brønsted acidity of solids in terms of

number, type and strength of the acid sites based on quantitative H/D exchange kinetics between the acid solid and gaseous  $D_2O$ . To our knowledge, there have been no reports about the colorimetric detection of the acidity in concentrated strong acids. On the other hand, it's very important and necessary to develop a fast and simple method to determine the acidity of concentrated strong acid solutions [14].

Herein we report a visual method for extremely strong concentrated acid with our newly prepared visual test paper by starting from the synthesis of a new isoindole compound with a common fluorogenic reaction of *o*-phthaldialdehyde (OPA) and  $\beta$ -mercaptoethanol (MERC) that react with a primary amine to form a 1-alkylthio-2-alkylisoindole in alkaline medium [15–17]. It was found that the new synthesized isoindole is visually sensitive to the concentrated strong acid in the range of 0.2–18 M ( $[H^+]$ ) and thus could be applied to develop a sensitive extreme acid sensor based on the color change. It is convenient and easy for semiquantitative detection of the extreme acidity of the concentrated strong acid solutions such as HCl,  $HNO_3$  and  $H_2SO_4$  solutions.

## 2. Experimental

### 2.1. Materials

*p*-Phenylenediamine, *o*-phthaldialdehyde and  $\beta$ -mercaptoethanol were purchased from Sigma. Hydrochloric acid, perchloric acid, vitriol and nitric were purchased from Chongqing Chemical Reagent Co. Ltd. All chemicals were analytical reagents and were

\* Corresponding author. Tel.: +86 23 68254659; fax: +86 23 68254000.  
E-mail address: [chengzhi@swu.edu.cn](mailto:chengzhi@swu.edu.cn) (C.Z. Huang).

**Table 1**  
IR features of OPA, *p*-phenylenediamine and the chromogenic reagent ( $\text{cm}^{-1}$ ).

Type of vibration	$\nu_{\text{N-H}}$	$\nu_{\text{OH}}$	$\nu_{\text{Ar-H}}$	$\nu_{\text{CHO}}$	$\nu_{\text{C=O}}$	$\nu_{\text{C=C, Ar}}$	$\nu_{\text{C-N}}$	$\nu_{\text{Ar-N}}$	$\delta_{\text{Ar-H}}$
OPA	–	–	3035	2861, 2760	1687	1593, 1575	–	–	765
<i>p</i> -Phenylenediamine	3374	–	3009	–	–	1629, 1516	–	1262	829
Chromogenic reagent	–	3368	3046	–	–	1677, 1514	1380	1333	733

used without further purification. Mili-Q purified water (18.2 M $\Omega$ ) was used for all sample preparations.

## 2.2. Apparatus

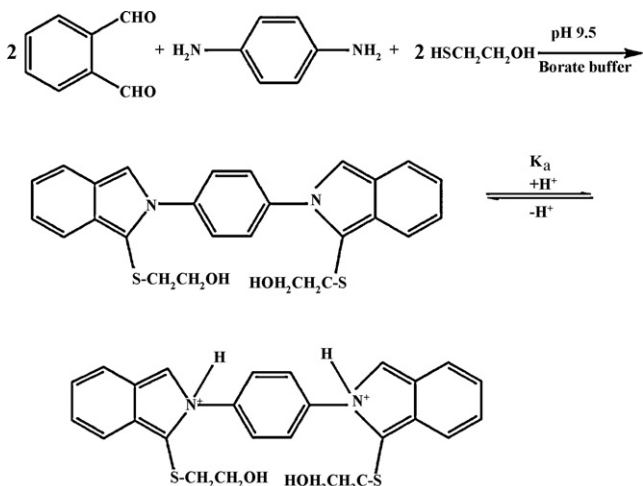
UV-visible spectra were recorded with a Hitachi UV-3010 spectrophotometer (Hitachi, Tokyo, Japan), while IR spectra were obtained with a Spectrumgx spectrophotometer (PerkinElmer). Mass spectra was acquired in a Trace DSQ GC-MS system (Thermo Finnigan, USA). Photographs were taken with COOLPIX4500 digital camera (Nikon, Tokyo, Japan). A vortex mixer QL-901 (Haimen, China) was used to blend the solution. Qualitative filter paper, with medium speed and 0.15% of the ash content, were used as the solid support to load the chromogenic reagent.

## 2.3. Synthesis of the chromogenic reagent

Scheme 1 shows the route to prepare such an isoindole compound starting from *p*-phenylenediamine and the coupled fluorogenic reagent of *o*-phthaldialdehyde- $\beta$ -mercaptoethanol in borate buffer of pH 9.5. 0.5 g of *o*-phthaldialdehyde was at first dissolved into 15 ml of methanol, then 0.9 ml of  $\beta$ -mercaptoethanol and 15 ml of borate buffer were added in under vigorous stirring. It was found that the solution maintained colorless and clear even if the reaction lasted for 50 min at room temperature. However, if 0.2 g *p*-phenylenediamine dissolved in 15 ml of borate buffer was dropwise added into the solution, the solution turned to light red, and gradually changed from clear to milky cloudy. After stirring for 3 h at room temperature, the solution changed to clear again and some yellow-brown oil solid turned out. The resulted yellow-brown oil could be purified with dichloromethane, and become into a yellow powder product after the evaporation of the solvent. The chromogenic reagent was characterized on the basis of IR and MS spectral data.

## 2.4. Preparation of test paper for strong concentrated acidity

23 mg of above prepared chromogenic reagent was dissolved in several drops of DMF, and then diluted to 5 ml with ethanol (0.01 M).



**Scheme 1.** Synthesis of new isoindole chromogenic reagent and the equilibrium of the protonated forms of the chromogenic reagent.

By immersing slides of filter paper into the ethanol solution about 10 h in order to load enough amount of reagent on the slides, light yellow test papers were then prepared for strong concentrated acidity and got ready after taking out from the solution and drying in air.

## 3. Results and discussion

### 3.1. Spectral features of the synthesized reagent

By comparing the IR features of pure OPA and *p*-phenylenediamine and the chromogenic reagent (shown in Fig. 1 and Table 1), we could find a loss of the aldehyde carbonyl stretching vibration ( $\nu_{\text{CHO}}$ ) at 2861  $\text{cm}^{-1}$  and 2760  $\text{cm}^{-1}$  and the loss of a carbonyl stretching vibration ( $\nu_{\text{C=O}}$ ) at 1687  $\text{cm}^{-1}$  in OPA, with the hydroxy stretching vibration ( $\nu_{\text{OH}}$ ) at 3368  $\text{cm}^{-1}$  coming into being in the chromogenic reagent. Concordantly, the spectra shows the amine stretching vibration ( $\nu_{\text{N-H}}$ ) at 3374  $\text{cm}^{-1}$  in *p*-phenylenediamine disappeared and the amidocyanogen stretching vibration ( $\nu_{\text{C-N}}$ ) at 1380  $\text{cm}^{-1}$  came into being in the synthetic product, validating the formation of chromogenic reagent. The data suggest that one of the aldehyde group of OPA might react with the -SH group of  $\beta$ -mercaptoethanol to yield a hemiacetal, while the other forms a Schiff base with the -NH of *p*-phenylenediamine. Whereas, the Ar-H stretching and bending vibrations indicate that the benzene ring still exist in the synthetic product. Thus, we could draw the reaction principle shown in Scheme 1.

Correspondingly, the MS spectra displays three apparent peaks at  $m/z$  405.6, 406.7 and 407.6 that correspond to the fragment ions of  $[\text{M}-\text{SCH}_2\text{CH}_2\text{OH}+\text{Na}]^-$  ions, on account of the effect of carbon isotope. Meanwhile the peaks at  $m/z$  461.5 was assigned to be the  $[\text{M}+\text{H}]^-$  ions. (The formula weight of the chromogenic reagent is about  $M = 460.1$ ).

Fig. 2 shows that the absorption spectra of the chromogenic reagent in the solution of different concentrations of HCl up to 2.0 M. As can be seen from the spectra, the absorption maxima is located at about 510 nm, and following the protonation of the chromogenic reagent (Scheme 1), corresponding colour changes

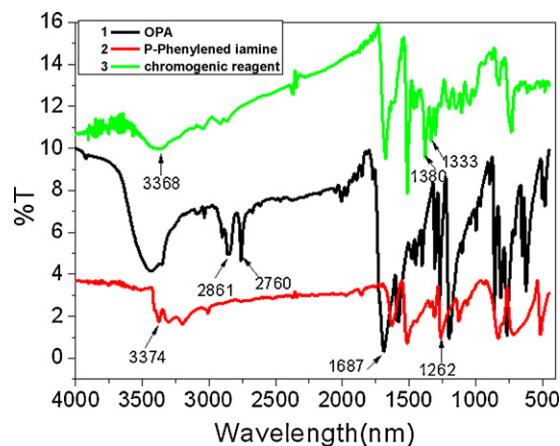


**Fig. 1.** The infrared spectrum of OPA (black), *p*-phenylenediamine (red) and the resulting chromogenic reagent (green). (For interpretation of the references to color in this figure legend, the reader is referred to the web version of the article.)

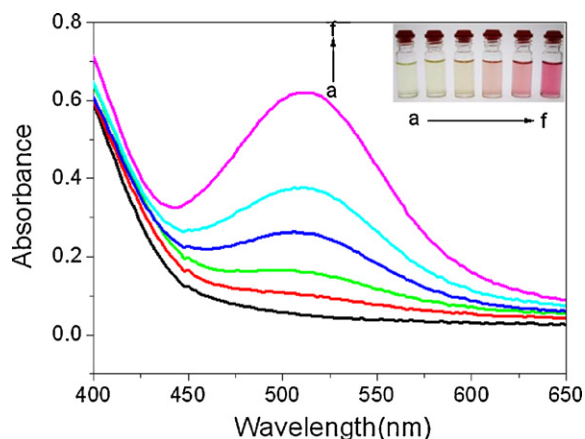


**Fig. 2.** Absorption spectra of the chromogenic reagent in solutions of various concentrations of HCl. (a) Reagent control, (b) 0.04 M, (c) 0.2 M, (d) 0.6 M, (e) 1.0 M and (f) 2.0 M HCl solution. Concentration of chromogenic reagent,  $1.0 \times 10^{-4}$  M.

occur correlated to the acid concentration. The inset picture shows the noticeable transition of color occurred from light yellow to red with the increase of HCl concentrations. These changes were found to follow a linear relationship between the absorbance at 510 nm and the HCl concentrations in the range of 0.04–2.0 M, which could be expressed as  $A = 0.088 + 0.272c_{H^+}$  ( $n=6$ ) with the relative coefficient of  $r^2 = 0.9948$ . It was found that the color develops immediately after the solution mixed and the changed colour could be maintained for 5 h at least without fading. We take the measurement of the spectra after 15 min of the color development. In our later work, we could also observe a noticeable transition occurred from light yellow to red with the increase of HCl concentrations ranging from 0 to 6.0 M. So it is possible to act as an alkaline indicator for the concentrated strong acids.

We have also tried an experiment on other acids. Interestingly, the color changed from yellow to fuchsia noticeably and the absorbance increased concordantly when the acidity of  $HNO_3$  ranging from 0 to 1.0 M, but it gradually faded to rosiness and the absorbance reduced concordantly when the acidity of  $HNO_3$  gets increased continually to 6.0 M (Fig. 3). We suppose the reason is that the dissociative  $H^+$  is gradually decreased in the concentrated  $HNO_3$ , as a result of the intermolecular and intramolecular hydrogen bond forming in the solutions.

However, we found that it was difficult to observe the changes of the colour and the absorbance with the increasing of concentration of organic acids like acetic acid  $CH_3COOH$ . It is probably

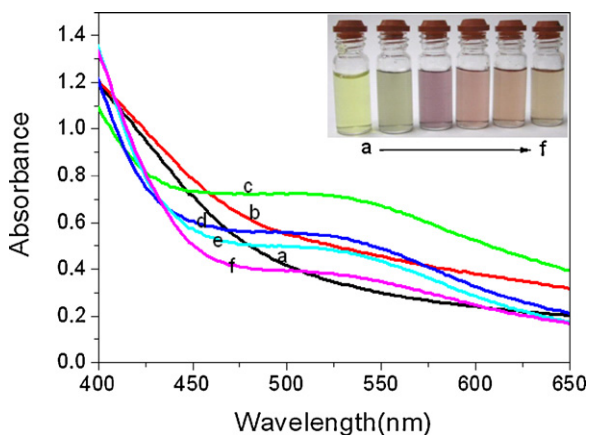


**Fig. 3.** Absorption spectra of the chromogenic reagent in the solutions of various concentrations of  $HNO_3$ . (a) Reagent control, (b) 0.2 M, (c) 1.0 M, (d) 2.0 M, (e) 4.0 M and (f) 6.0 M  $HNO_3$  solution. Concentration of chromogenic reagent,  $3.0 \times 10^{-4}$  M.

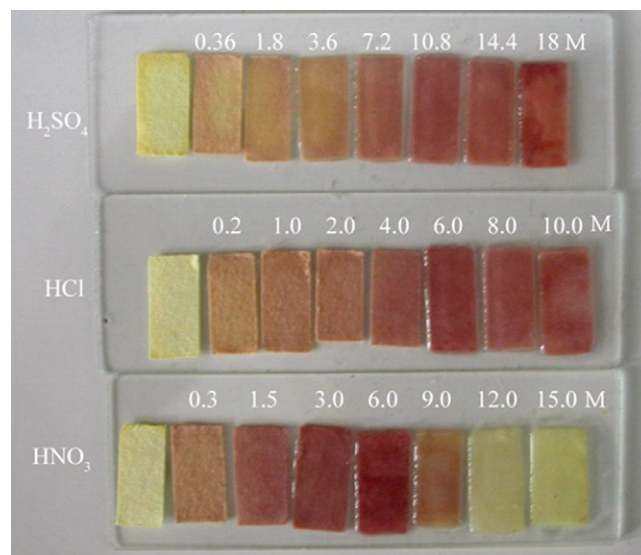


**Fig. 4.** Colorimetric detection of  $H_2SO_4$ , HCl,  $HNO_3$  solutions with different concentrations, the photographs were taken immediately after the test paper taken out from the different acid solutions.

because they are weakly ionized in water and give very weak transfer tendency of hydrogen ion from the acids to the neutral organic molecule of the base indicator and make the chromogenic reagent positive in these solvents of low dielectric constant.

### 3.2. Colorimetric detection of extreme acidity in filter paper

When detecting the acidity of strong concentrated acids, we could immerse the as-prepared test paper slides into acid solutions and then immediately take them out. Fig. 4 shows the color changes of the test paper slides after they were soaked into different concentrations of acids including  $H_2SO_4$  (0.36–18 M), HCl (0.2–10 M) and  $HNO_3$  (0.3–15 M). It was found that a noticeable transition occurred from light yellow to carmine with increasing HCl concentration from 0.2 to 10 M. The colors of the visual paper change very soon, and could maintain for at least ten minutes. So it could be used for semiquantitative detection of HCl solutions in the range of 0.2–10 M. Contrastively, We found that the filter paper that has not load chromogenic reagent on the slides did not cause color change when suffering with the strong acid. Meanwhile the color changed slightly when the acidity of the solution is very low.

It was found that the test paper slides could be regenerated and reused at least three cycles since the colour could change back to light yellow again by soaking into NaOH solution, as the hydrogen protons on the sensor could be neutralized by  $OH^-$ . Therefore, the test paper slides could be employed for visual detection of extreme acidity with the advantages of easy and simple operation, low cost and reproducibility.

It is known that the acidity of a solution determined by means of a simple basic indicator is in fact that the tendency of hydrogen ion from the acids transfers to the neutral organic molecule of the base indicator, making the base indicator positive [18]. So we infer that the color changes are mainly because of the diffusion of the hydrogen proton through the pore structure of the test paper, then the colored complex formed by the chromogenic reagent loading on the test paper and the dissociative  $H^+$ , where the nitrogen atoms of the chromogenic reagent can serve as  $H^+$  receptors. Thus, we presume that the chromogenic reagent in concentrated strong acid solutions exists in protonation/deprotonation forms (see Scheme 1) and so takes on color changes. However, we have to consider a question, which is the issue that addressed by the Hammett indicator



acidity functions, namely, how proton activity varies in concentrated acid [18,19]. In fact, it is insufficient to completely obtain the diprotonated form of the indicator [20]. So, it would be difficult to determine the  $pK_a$  of the chromogenic reagent and it was not clear whether the chromogenic reagent exists in the fully protonated form in highly concentrated HCl or not.

Fig. 4 shows a practical application of the test paper for different acids. After the test paper slides into  $H_2SO_4$  or  $HNO_3$  solutions, they could experience color changes from yellow to red with increasing acidity. What's different is that the test paper gradually changes to carmine when the acidity of  $HNO_3$  reaches to 6.0 M, and fades to light yellow gradually when the concentration of  $HNO_3$  gets increased continually. This is consistent with the changes in Fig. 3. We suppose the reason is the same as before: the intermolecular and intramolecular hydrogen bond forming in the  $HNO_3$  solutions result for the dissociative  $H^+$  is gradually decreased. It should be noted that the strong oxidization property of  $HNO_3$  might have little effect on the fading, as there is not any fading in concentrated  $H_2SO_4$  and  $HClO_4$  solutions, which are also strong oxidized. In addition, as mentioned above, the test paper is not suit for the organic acids as they are weakly ionized in water and release less hydrogen ion in water.

#### 4. Conclusions

In summary, it is convenient and easy with our newly synthesized isoindole compound starting from a common reaction to prepare a test paper for extremely strong concentrated acidity in the extent of semiquantitative detection just by color changes. It is fast and simple to operate, low to cost as the test paper is regenerable after a simple washing with the basic solutions such as NaOH solution. Besides, it could also be used for quantitative detection of concentrated strong acids through the linear relationship exists between the absorbance of the chromogenic reagent and the acid concentration. Since the determination of acidity may be of great importance of catalytic properties by acids and bases in organic reactions, we expect that the test paper could offer a considerable chance for small and innovative business and so there will be a development in the commercial application.

It should be pointed out that Brønsted has shown that the only logically consistent general measurement of acidity is hydrogen-ion potential or the closely related hydrogen-ion activity. Therefore, it is probable that the acidity as measured by a basic indicator does not run parallel to hydrogen-ion activity when there is a change in dielectric constant. In such case, we need to know much about diffusion potentials before we can measure the hydrogen-ion activities directly [18–19]. So it is necessary to make further investigations theoretically.

#### Acknowledgements

This research gets the supports from the National Natural Science Foundation of China (No. NSFC 90813019) and the Chongqing Science and Technology Commission (2006CA8006).

#### References

- [1] E. Wang, K.-F. Chow, W. Wang, C. Wong, C. Yee, A. Persad, J. Mann, A. Bocarsly, *Anal. Chim. Acta* 534 (2005) 301.
- [2] D.K. Nordstrom, C.N. Alpers, C.J. Ptacek, D.W. Blowes, *Environ. Sci. Technol.* 34 (2000) 254.
- [3] O.S. Wolfbeis, *Fresenius J. Anal. Chem.* 337 (1990) 522.
- [4] M.H. Su, Y. Liu, H.M. Ma, Q.L. Ma, Z.H. Wang, J.L. Yang, M.X. Wang, *Chem. Commun.* 11 (2001) 960.
- [5] J.-P. Ndobbo-Epoy, E. Lesniewska, J.-P. Guicquero, *Anal. Chem.* 79 (2007) 7560.
- [6] L.R. Allain, K. Sorasaene, Z.-L. Xue, *Anal. Chem.* 69 (1997) 3076.
- [7] L.R. Allain, Z.-L. Xue, *Anal. Chim. Acta* 433 (2001) 97.
- [8] L.R. Allain, T.A. Canada, Z.-L. Xue, *Anal. Chem.* 73 (2001) 4592.
- [9] T.A. Canada, L.R. Allain, D.B. Beach, Z.-L. Xue, *Anal. Chem.* 74 (2002) 2535.
- [10] T.L. Yost Jr., B.C. Fagan, L.R. Allain, C.E. Barnes, S. Dai, M.J. Sepaniak, Z.-L. Xue, *Anal. Chem.* 72 (2000) 5516.
- [11] B.C. Fagan, C.A. Tipple, Z.-L. Xue, M.J. Sepaniak, P.G. Datskos, *Talanta* 53 (2000) 599.
- [12] L.R. Allain, Z.-L. Xue, *Anal. Chem.* 72 (2000) 1078.
- [13] T.A. Canada, D.B. Beach, Z.-L. Xue, *Anal. Chem.* 77 (2005) 2842.
- [14] N. Keller, G. Koehl, F. Garin, V. Keller, *Chem. Commun.* 2 (2005) 201.
- [15] M. Roth, *Anal. Chem.* 43 (1971) 880.
- [16] J.R. Benson, P.E. Haret, *Proc. Natl. Acad. Sci. U.S.A.* 72 (1975) 619.
- [17] S.S. Simons Jr., D.F. Johnson, *J. Org. Chem.* 43 (1978) 2886.
- [18] L.P. Hammett, A.J. Deyrup, *J. Am. Chem. Soc.* 54 (1932) 2721.
- [19] L.P. Hammett, *J. Am. Chem. Soc.* 50 (1928) 2666.
- [20] M.C. Aragoni, A. Massimiliano, C. Guido, M.N. Valeria, R. Silvagni, *Talanta* 42 (1995) 1157.



# Highly sensitive and reproducible cyclodextrin-modified gold electrodes for probing trace lead in blood

Wei Li, Guiying Jin, Hui Chen, Jilie Kong\*

Department of Chemistry & Institutes of Biomedical Sciences, Fudan University, Handan Rd. 220#, Shanghai 200433, PR China

## ARTICLE INFO

### Article history:

Received 28 September 2008  
Received in revised form 10 December 2008  
Accepted 12 December 2008  
Available online 24 December 2008

### Keywords:

Detection of Pb  
6-(2-Mercapto-ethylamino)-6-deoxy- $\beta$ -cyclodextrin (MEA- $\beta$ -CD)  
Gold modified electrode  
Stripping voltammetry

## ABSTRACT

A highly sensitive and reproducible lead sensor based on a cyclodextrin-modified gold electrode was created. A self-assembled monolayer (SAM) of thiolated  $\beta$ -cyclodextrin (6-(2-mercapto-ethylamino)-6-deoxy- $\beta$ -cyclodextrin (MEA- $\beta$ -CD)) was prepared and modified on a gold electrode (MCGE) for specific Pb<sup>2+</sup>-sensing. Thus the mercury-free sensors for Pb<sup>2+</sup> assay based on MCGE were established. A linear calibration response for Pb<sup>2+</sup> was found in the range of  $1.7 \times 10^{-8}$  M to  $9.3 \times 10^{-7}$  M. The detection limit was  $7.1 \times 10^{-9}$  M (with S/N > 3), which was 10 times lower than other reported methods of detection Pb<sup>2+</sup> with CD. The measurement results via this method for real blood samples were well agree with those obtained by ICP-AES, and thus presented a novel strategy in design of specific lead sensors with high sensitivity and stability for analysis of trace Pb<sup>2+</sup> in real blood samples.

© 2009 Elsevier B.V. All rights reserved.

## 1. Introduction

The lead poisoning is the most common disease of environmental origin in the world [1,2]. Children begin to exhibit permanent neurological and behavioral dysfunctions at low blood lead levels (Balls), with significant neurological damage occurring over the 5–10  $\mu\text{g/dL}$  (0.25–0.5  $\mu\text{M}$ ) range [3,4]. At high Balls ( $\geq 40$   $\mu\text{g/dL}$ ), adults experience fertility problems (lowered sperm count and abnormal sperm for men; infertility and miscarriage for women), as well as neurological dysfunction and anemia.

A number of electrochemical techniques have been mostly used to determine Pb<sup>2+</sup> [5–7]. The anodic stripping voltammetry (ASV) in combination with either a hanging mercury drop electrode (HMDE) or mercury-film or polymer-coated electrodes [8–20] allows the determination of concentrations as low as  $10^{-10}$  M and beyond in favorable cases. However, Hg<sup>2+</sup> is a highly toxic heavy metal ion and is considered to be a dangerous polluting agent. In view of such considerations, it has been fundamental to search for effective alternatives to obtain compatible sensitivity but avoiding the use of mercury.

It is known that cyclodextrins (CDs) belong to the family of cyclic oligosaccharides formed by various D-glucopyranose units, held together by (1–4)-glucosidic bonds. The better-known members of the family are the  $\alpha$ -,  $\beta$ - and  $\gamma$ -CDs, which have six, seven

and eight D-glucopyranose units, respectively. Thus they are widely employed in host–guest recognition of diverse substrates [21,22]. The molecular structure resembling of CDs, i.e. a hollow truncated cone or basket with a cavity that displays receptor-like features provides unique features such as selectivity and sensitivity and can interact with other chemical species to form inclusion complexes due to their different cavity sizes. Hence they have wide range of applications in the pharmaceutical and food industries [23].

Previous work reported that it was possible to form inclusion complexes between the CDs and metal ions, like Pb<sup>2+</sup>, Cu<sup>2+</sup> and Ni<sup>2+</sup> [24,25], especially between the  $\beta$ -CD and Pb<sup>2+</sup> [26]. The  $\beta$ -CD and its derivatives have been used for the removal of polluting species from wastewater. The use of water-insoluble  $\beta$ -CD immobilized on polymeric matrices or solid supports has led to the development of novel decontaminating agents. Undoubtedly the immobilization of  $\beta$ -CD on a surface of insoluble supports (silica, alumina, and aluminosilicates) offers advantages relative to CD attached to polymers. The most important one is that related to the fast kinetics of the process in the former relative to the latter due to the absence of internal diffusion. In those research works, they seldom mentioned the stability of the system.

Further, it has been observed that the functionalized  $\beta$ -CDs display improved solubility and selectivity. Recent research showed that the Langmuir–Blodgett films of amphiphilic CD could be prepared [21,27], while the self-assembled monolayers (SAMs) of thiolated CD derivatives has constructed by Rojas et al. [28], Nelles et al. [29] and Henke et al. [30] on the surface of Au electrodes,

\* Corresponding author. Tel.: +86 21 65642138; fax: +86 21 65641740.  
E-mail address: [jlkong@fudan.edu.cn](mailto:jlkong@fudan.edu.cn) (J. Kong).

producing a modified electrode selective towards electrochemical reactions characterized by cyclic voltammetry.

With the methods mentioned above, the sensitive films for detection of  $\text{Pb}^{2+}$  via MEA- $\beta$ -CD modified gold electrodes were developed. For the case of heavy metals, apparently there are no references to be linked to the study of  $\text{Pb}^{2+}$  with the thiolated CD modified gold electrodes. Therefore, this work aims at developing a gold electrode modified with MEA- $\beta$ -CD to establish an innovative way to measure  $\text{Pb}^{2+}$  in real blood samples, which offers a high selectivity derived from the stable MEA- $\beta$ -CD film. In this study, the application of the MCGE was examined to the determination of lead by adsorptive DPSV, and a practical method was established which was suited to the measurement of ultra-trace lead concentrations in blood.

## 2. Experimental

### 2.1. Reagents and apparatus

$\beta$ -Cyclodextrin ( $\beta$ -CD) and phenylethylamine were purchased from Fluka, USA. Standard metal ion ( $\text{Na}^+$ ,  $\text{K}^+$ ,  $\text{Ca}^{2+}$ ,  $\text{Cu}^{2+}$ ,  $\text{Cd}^{2+}$ ,  $\text{Co}^{2+}$ ,  $\text{Ni}^{2+}$ ,  $\text{Zn}^{2+}$  and  $\text{Cr}^{2+}$ ) solutions of 100 mg/L (analytical grade) were purchased from Shanghai Chemical Co. Inc. A stock solution of 1.00 mg/L  $\text{Pb}(\text{NO}_3)_2$  in 10 mM  $\text{HNO}_3$  was purchased from Shanghai Chemical Co. Inc. and diluted step by step to an adequate concentration immediately prior to use. All solutions were prepared in Typel reagent grade water.

Electrochemical measurements were performed on CHI-1030 Electrochemical Workstation (CH Instrument, Shanghai, China). EIS (electrochemical impedance spectra) measurements were performed on CHI-660 Electrochemical Workstation (CH Instrument, Shanghai, China). FT-IR measurements were performed on NEXUS 470 FT-IR spectrometer (Nicolet Company, USA).  $^1\text{H}$  NMR measurements were performed on Bruker 500 MHz spectrometer. A conventional three-electrode cell was applied, with saturated calomel electrode (SCE) as the reference electrode, a Pt wire electrode as the counter electrode and the modified gold electrode as the working electrode.

All the electrochemical cell was precleaned by soaking in 20% nitric acid, and washed with demineralised water.

### 2.2. Preparation and characterization of thiolated $\beta$ -cyclodextrin

Thiolated  $\beta$ -cyclodextrin, 6-(2-mercapto-ethylamino)-6-deoxy- $\beta$ -cyclodextrin (MEA- $\beta$ -CD), was prepared and identified as follows: "firstly, the tosylated  $\beta$ -CD (6-ots- $\beta$ -CD) was substituted.  $\beta$ -Cyclodextrin (60.0 g, 52.9 mmol) was dissolved with stirring in

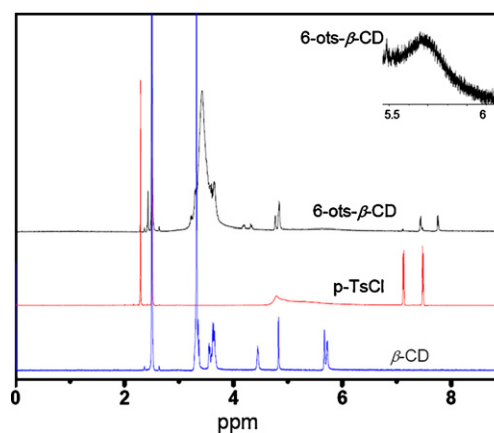


Fig. 2. The NMR spectra for  $\beta$ -CD, p-TsCl and 6-ots- $\beta$ -CD. Inset graph shows the spectra part from 5.5 ppm to 6.0 ppm of 6-ots- $\beta$ -CD.

500 mL of water. To this solution was carefully added NaOH (6.57 g, 164.0 mmol) in 20 mL of water over 6 min. p-Toluenesulfonyl chloride (10.08 g, 52.9 mmol) in 30 mL of acetonitrile was then added dropwise over 8 min to this homogeneous and slightly yellow solution, causing immediate formation of a white precipitate. The precipitate was stirred at 23 °C for 2 h. Then the precipitate was removed by suction filtration and the filtrate refrigerated overnight at 4 °C. The resulting white precipitate was recovered by suction filtration and dried for 12 h (0.005 mmHg). 6-ots- $\beta$ -CD (7.18 g) was recovered as a pure white solid [31].

The IR spectrum of  $\beta$ -CD and 6-ots- $\beta$ -CD were shown in Fig. 1. As  $\beta$ -CD and 6-ots- $\beta$ -CD both were carbohydrates, they had some similar groups at 3340  $\text{cm}^{-1}$  and 1030  $\text{cm}^{-1}$ . In the IR spectra of 6-ots- $\beta$ -CD, the characteristic peak of benzene cycle backbone (Ts groups) vibration appeared at 1600  $\text{cm}^{-1}$  and the symmetrical stretching vibration of sulfonate appeared at 1370  $\text{cm}^{-1}$ . These evidences indicated  $\beta$ -CD had reacted with TsCl.

The NMR experiment for the 6-ots- $\beta$ -CD (Fig. 2):  $^1\text{H}$  NMR (500 MHz,  $\text{DMSO}-d_6$ )  $\delta$  7.74 (2H), 7.42 (2H), 5.87–5.58 (14H), 4.82 (4H), 4.76 (3H), 4.55–4.13 (6H), 3.74–3.43 (28H), 2.42 (3H) ppm.  $^1\text{H}$  NMR spectra and the IR spectra confirmed the 6-ots- $\beta$ -CD had been synthesized.

Secondly, the thiolated MEA- $\beta$ -CD was prepared by a reduction with mercaptoethanol at room temperature overnight after a substitution of tosylated  $\beta$ -CD with excess amount of cystamine in pyridine at 40 °C for 2 days. After evaporation of the solvent, an oily reaction mixture was put into cold acetone, and a white precipitate was obtained. The precipitate was dissolved in MeOH:water = 3:1

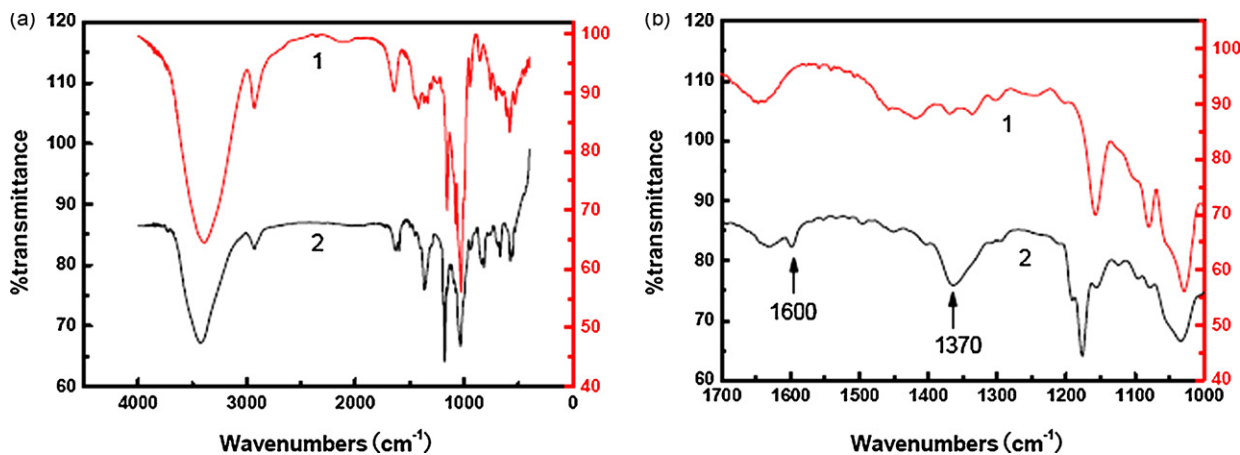
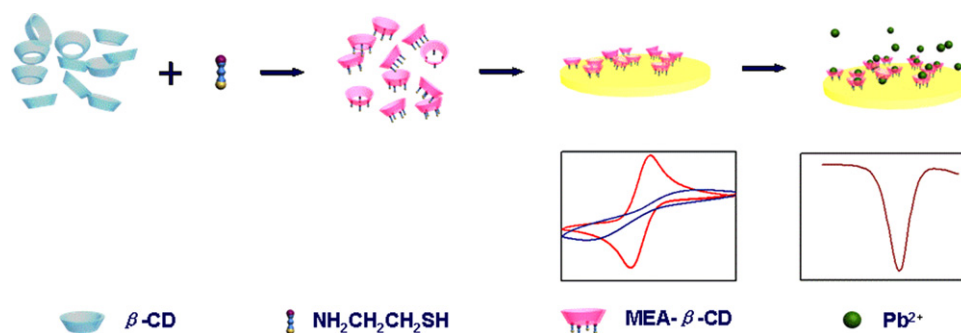


Fig. 1. The whole (a) and part (b) of IR spectra for  $\beta$ -CD (1) and 6-ots- $\beta$ -CD (2).



**Scheme 1.** Illustration of self-assembled monolayer of MEA- $\beta$ -CD on the gold electrode for the detection of  $\text{Pb}^{2+}$  via voltammetry.

and recrystallized in cold acetone. The precipitate was finally filtered and dried in vacuum.

### 2.3. Self-assembled monolayer of MEA- $\beta$ -CD on a gold electrode

A gold electrode ( $3.14 \text{ mm}^2$ ) was polished with alumina powder (with the diameter of first  $1 \mu\text{m}$ , then  $0.3 \mu\text{m}$ , finally  $0.05 \mu\text{m}$  powder) and rinsed with pure water by ultrasonication. After that, the electrode was further washed by dipping in a  $0.1 \text{ M H}_2\text{SO}_4$  and subsequent scanning from  $-0.4 \text{ V}$  to  $+1.5 \text{ V}$  20 times (scan rate,  $100 \text{ mV/s}$ ). The gold electrode was immersed in a  $1.0 \text{ mM}$  aqueous solution of MEA- $\beta$ -CD for 12 h or more under a  $\text{N}_2$  gas atmosphere. The modified electrode obtained was washed alternately more than five times with water and MeOH, and cyclic voltammetric (CV) measurements were performed with CHI-1030 (CH Instrument, Shanghai, China). A Pt electrode and KCl-saturated calomel electrode were used as counter and reference electrodes, respectively [32].

### 2.4. Procedures for the measurement of $\text{Pb}^{2+}$

Scheme 1 illustrates the preparation and measurement steps of the whole experiment. The accumulation of the metal ions on the modified electrode was carried out in  $1 \text{ M HClO}_4$  solution by applying the potential in the preconcentration solution. The conditions for the preconcentration step were  $E_d = -0.9 \text{ V}$  vs. SCE;  $30 \text{ s} \leq t_d \leq 240 \text{ s}$ . After a rest period of 10 s, a differential pulse stripping voltammetry programme (DPSV) was recorded. Finally, a period of time was imposed under the potential of  $0.5 \text{ V}$ , to make the remnant Pb on the electrode surface dissolute. DPSV exhibited the oxidation of Pb to  $\text{Pb}^{2+}$  at about  $-0.43 \text{ V}$  at modified electrode surface.

### 2.5. Blood sample treatment

$2 \text{ mL}$  of whole blood was mixed with  $5 \text{ mL}$  of  $65\%$  (w/v) nitric acid [33]. Then, the contents were heated gently to near dryness in a water bath at  $100^\circ\text{C}$ . After cooling,  $2 \text{ mL}$  of ion-free water was added.

## 3. Results and discussions

### 3.1. Formation of SAM on a gold electrode

Fig. 3 shows the cyclic voltammetric responses of an Au electrode modified with MEA- $\beta$ -CD which compared with those of a bare Au electrode to confirm the formation of a SAM. The potential difference ( $\Delta E$ ) between anodic and cathodic peaks of the redox reaction of the  $\text{Fe}(\text{CN})_6^{3-/4-}$  measured with the modified Au electrode ( $389 \text{ mV}$ ) was larger than that of bare Au ( $88 \text{ mV}$ ). Since the

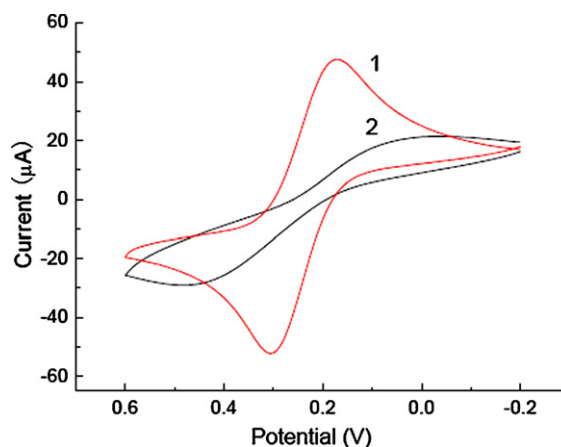


**Fig. 3.** CV curves of gold electrode in the solution of  $5 \text{ mM K}_3[\text{Fe}(\text{CN})_6]/\text{K}_4[\text{Fe}(\text{CN})_6]$  before (1) and after (2) the modification of MEA- $\beta$ -CD. Scan rate was  $100 \text{ mV/s}$ .

size of  $\text{Fe}(\text{CN})_6^{3-/4-}$  is larger than the cavity of  $\beta$ -CD, it cannot be included. The larger value of  $\Delta E$  for the modified electrode indicates that the distance between  $\text{Fe}(\text{CN})_6^{3-/4-}$  and the Au surface is larger on the modified electrode than on the bare electrode [34].

Fig. 4 shows the EIS spectra of bare gold electrode and MEA- $\beta$ -CD/Au modified electrode in the given solution. The resistor of the modified electrode ( $R'_{ct}$ ) was much larger than the bare electrode ( $R_{ct}$ ), also suggesting that the MEA- $\beta$ -CD layer had strong hindrance to the transfer of  $\text{Fe}(\text{CN})_6^{3-/4-}$ . According to the impedance of the two electrodes in high frequency range, the coverage ( $\theta$ ) of the MEA- $\beta$ -CD layer was estimated to be  $99\%$  ( $R_{ct} = 2.5 \text{ k}\Omega$ ,  $R'_{ct} = 279 \text{ k}\Omega$ ,  $\theta = 1 - R_{ct}/R'_{ct}$  [35]), indicating the MEA- $\beta$ -CD layer was quite dense.

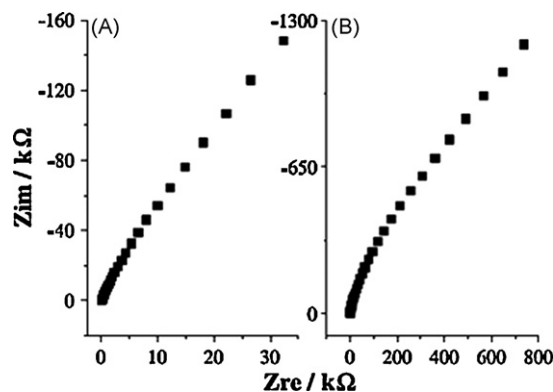


**Fig. 4.** EIS spectra of Au (A) and MEA- $\beta$ -CD/Au (B). Frequency used:  $0.1\text{--}100 \text{ kHz}$ . Solution:  $2 \text{ mM K}_3[\text{Fe}(\text{CN})_6]/\text{K}_4[\text{Fe}(\text{CN})_6]$  containing  $0.1 \text{ M KNO}_3$ .

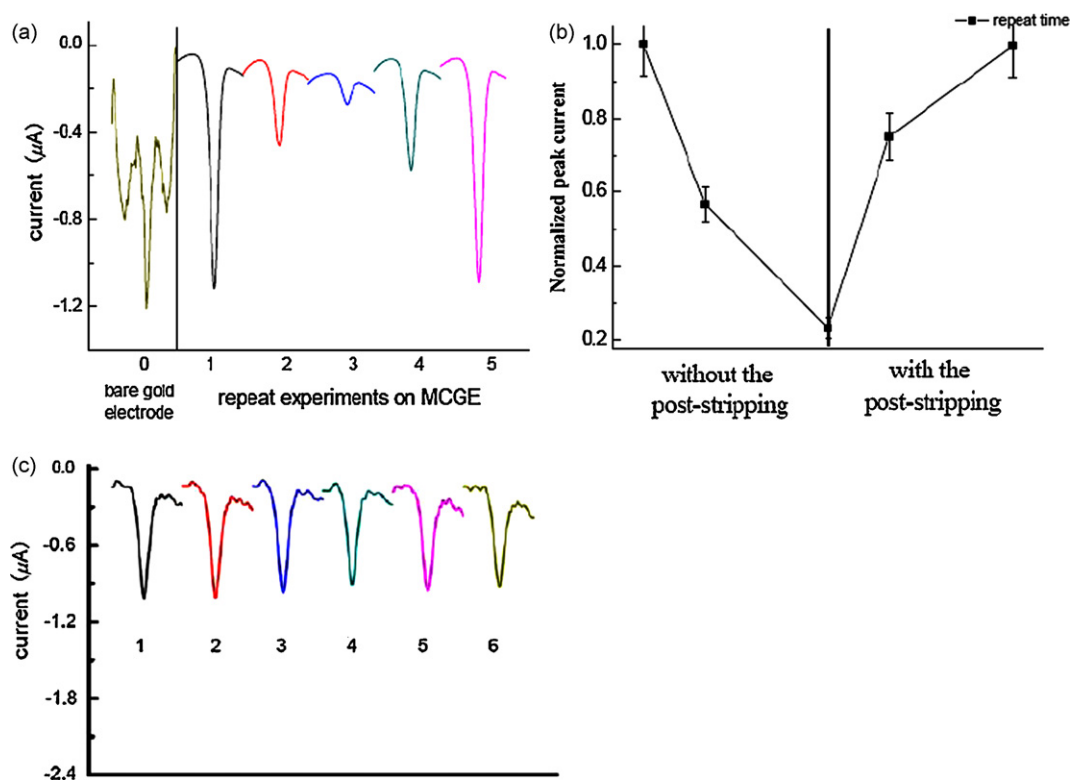


**Fig. 5.** The DPSV curves (a and c) and normalized peak current (b) with and without the post-stripping experiments. The symbol 0 represents DPSV curve of bare gold electrode. The symbols 1–5 represent values for the first, second, third, fourth, and fifth run of the experiments on the MCGE, respectively. Rounds 1–3 in (a) were the DPSV curves without the post-stripping experiments. Rounds 4 and 5 in (a) were the DPSV curves with the post-stripping experiments.  $[\text{Pb}^{2+}] = 7.8 \times 10^{-7}$  M, post-stripping potential: 0.5 V. The data were the average of three measurements. The symbols 1–6 represent values for the first, second, third, fourth, fifth and sixth run of the experiments on the MCGE, respectively (c).

### 3.2. Optimization of conditions

Deposition time ( $t_d$ ) and potential ( $E_d$ ), scan rate ( $\nu$ ), pulse amplitude ( $W_p$ ), post-stripping sweep ( $S_p$ ) and electrolyte's pH were experimental parameters which might have effect on the results. But only two of them were actually selected during the present experimental setup, as they were considered the most important ones (i.e.  $t_d$  and  $S_p$ ). The  $\text{Pb}^{2+}$  concentration used for this set of experiments was  $7.8 \times 10^{-7}$  M, while the deposition potential ( $E_d$ ) chosen for both electrodes was  $-0.9$  V vs. SCE.

#### 3.2.1. Effect of post-stripping sweep

A potential of 0.5 V for a period of time was imposed to the sensors after the DPSV stage. Such experimental procedure was named as post-stripping step, which made the remnant  $\text{Pb}^{2+}$  removal from the electrode surface to gain increased stability and reproducibility. Fig. 5 displays the voltammetric responses of the bare gold electrode and MEA- $\beta$ -CD modified gold electrode, and plot of average normalized peak current with and without the post-stripping. As indicated in Fig. 5a, the S/N of the DPSV curves (Fig. 5a, curves 1–5) was obviously increased with the modified gold electrodes compared to the bare gold electrode (Fig. 5a, curve 0). As a comparison, the stripping peak current value decreased (Fig. 5a, curves 1–3) when no post-stripping was applied. After a certain period of post-stripping potential was imposed, the peak current value was restored. To investigate the reproducibility of the MEA- $\beta$ -CD modified gold electrode, the processes were repeated for six cycles (Fig. 5c, curves 1–6). The R.S.D. was 8.5%.

$\text{Pb}^{2+}$  in the  $\text{HClO}_4$  solution was reduced on the surface of the electrode through the cavity of CD. But part of them would not be oxidized as the differentials potential inflicted, which caused that the rest  $\text{Pb}^{2+}$  in the solution could not be reduced through the cavity

to the electrode surface. It resulted in the decline in the peak current value. Through the imposition of certain oxidation potential, the reproducibility of the sensors was obviously increased, which proved the post-stripping step did remove the residual Pb remained on the electrode surface. Taking account of the stability and reproducibility together, the post-stripping was set at 0.5 V for 40 s.

#### 3.2.2. Effect of deposition time

Fig. 6 shows the effect of the deposition time on the peak current, which was examined using DPSV in 1 M  $\text{HClO}_4$ . The lead deposition time was changed in the range of 30–240 s. As depicted in Fig. 5, the oxidation current increased linearly with the deposition time

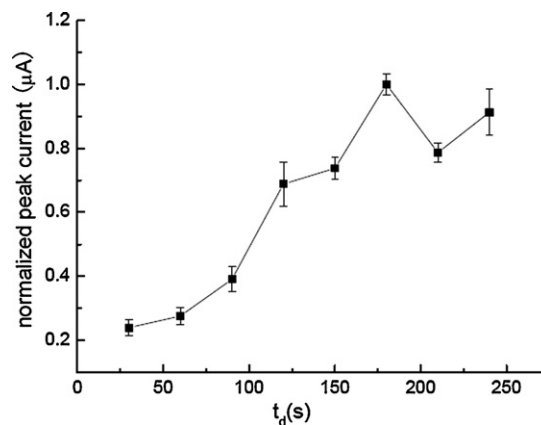


**Fig. 6.** Plot of average normalized peak current vs. deposition time 30 s, 60 s, 90 s, 120 s, 150 s, 180 s, 210 s, 240 s.  $[\text{Pb}^{2+}] = 7.8 \times 10^{-7}$  M, deposition potential:  $-0.9$  V. The data were the average of three measurements.

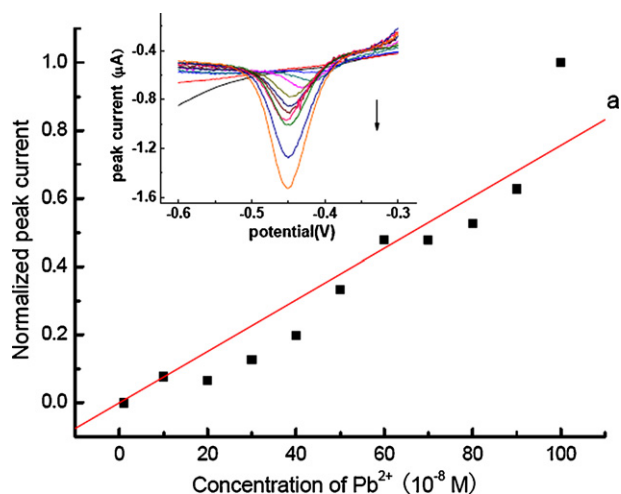


**Fig. 7.** The linear response of the lead sensor and the fitted curve, concentration of  $\text{Pb}^{2+}$ :  $1 \times 10^{-8}$  M to  $1 \times 10^{-6}$  M. Deposition potential:  $-0.9$  V. The direction of arrow shows the increase of concentration for spiked lead.

over the range of 30–180 s, and after that, no further increase was observed. Taking account of the sensitivity and efficiency, 180 s was employed as the incubation time.

### 3.3. Linearity and detection limits

The linear range of the DPSV response for lead was determined with a deposition time of 180 s and a strip potential from  $-0.9$  V to  $0.2$  V. The peak current of blank sample was removed before the other peak current values were normalized. There was a linear relationship between peak currents and concentrations. Stripping curves of lead were presented in Fig. 7. Under proper experimental conditions, linearity between the normalized peak current and concentration was observed in concentration range of  $1.7 \times 10^{-8}$  M to at least  $9.3 \times 10^{-7}$  M  $\text{Pb}^{2+}$ . The linear correlation coefficient was 0.96. The linear response was fitted as the following equation:

$$y = 0.00756x$$

$y$ : normalized peak current value and  $x$ : concentration of lead ( $10^{-8}$  M).

The detection limit was  $0.71 \times 10^{-9}$  M (with  $S/N > 3$ ) for a 3-min electrodeposition, which was 10 times lower than those reports by other methods with CD [24,26]. Compared to the coating or mixed carbon paste to prepare the electrode, this method was more effective to control the conformation of cyclodextrin on the gold electrode surface. It had been proved that the inclusion complexes between the cyclodextrins and metal ions [25,26] had

**Table 1**

Variation of  $i_p$  for  $4.0 \times 10^{-7}$  M  $\text{Pb}^{2+}$ , in the presence of other ions at  $4.0 \times 10^{-7}$  M.

Cation	Na(I)	K(I)	Ca(II)	Cd(II)	Ni(II)	Zn(II)	Cu(II)	Co(II)	Cr(II)
$i_p$ $\text{Pb(II)} = 100\%$	-5.3	-2.7	-3.4	11.9	-7.4	<1	<1	-2.9	-3.3
Contribution (%)									

great dealings with the cavity which displays receptor-like features. Therefore, the site-specific assembly for cyclodextrin was extremely favorable, and therefore improving the sensitivity. On the other hand, the post-stripping sweep removed the residual Pb on the electrode surface, which decreased the blank signal of DPSV and did increase the reproducibility of the sensors.

### 3.4. Selectivity of the MCGE and interference effects

The goal in obtaining a modified electrode is to get better sensitivity and selectivity to determine species of interest; therefore, it is necessary to know the analytical response variation as a function of the presence of other ions. For the present case various cations were considered like  $\text{Na}^+$ ,  $\text{K}^+$ ,  $\text{Ca}^{2+}$ ,  $\text{Cu}^{2+}$ ,  $\text{Cd}^{2+}$ ,  $\text{Co}^{2+}$ ,  $\text{Ni}^{2+}$ ,  $\text{Zn}^{2+}$  and  $\text{Cr}^{2+}$ . The  $\text{Pb}^{2+}$  solution to be used contained  $4.0 \times 10^{-7}$  M; the same DPSV conditions of work were as before, while the concentration for all the other ions in the  $\text{Pb}^{2+}$  solutions was  $4.0 \times 10^{-7}$  M. Table 1 presents the results obtained for the modified electrodes used to determine  $\text{Pb}^{2+}$  in the presence of other ions. As indicated in Table 1, The DPSV peak currents of  $\text{Cu}^{2+}$  and  $\text{Zn}^{2+}$  were very tiny and only about 1% of that of  $\text{Pb}^{2+}$ . It was important to underline that there were cations such as  $\text{Cd}^{2+}$  which interfered with the  $\text{Pb}^{2+}$  signal in the modified electrodes, causing an increment in the peak current. A comparison of the results obtained with  $\text{Na}^+$ ,  $\text{K}^+$ ,  $\text{Ca}^{2+}$ ,  $\text{Co}^{2+}$ ,  $\text{Ni}^{2+}$  and  $\text{Cr}^{2+}$  showed that the behavior was the inverse to that given by  $\text{Cd}^{2+}$ . Such changes could be attributed to the cavity size of  $\beta$ -cyclodextrin's networks.

### 3.5. Real sample analysis

MCGE was applied successfully for the determination of lead in blood. 500  $\mu\text{L}$  of treated blood sample was added to the 5 mL solution of 1 M  $\text{HClO}_4$  to be measured. The obtained data was compared with the results measured by ICP-AES (IRIS Intrepid, Thermo Elemental Co., USA).

As shown in Table 2, the average recovery of MCGE system for blood lead was 104.8%, which demonstrated good agreement with the results by ICP-AES. It could be seen that the MCGE system had shown enough sensitivity to detect  $\text{Pb}^{2+}$  in real blood samples. This made it possible for the determination of blood lead with gold electrodes in mercury-free solution.

**Table 2**

Concentrations ( $1 \times 10^{-7}$  M) of blood lead measured by ICP-AES and MCGE.

No.	ICP-AES value ( $1 \times 10^{-7}$ M)	Added concentration ( $1 \times 10^{-7}$ M)	MCGE calculated value ( $1 \times 10^{-7}$ M)	Recovery (%) ( $1 \times 10^{-7}$ M)
1	$4.23 \pm 0.13$	3	$4.42 \pm 0.43$	104.5
2	$3.49 \pm 0.24$	3	$3.30 \pm 0.09$	94.6
3	$3.17 \pm 0.15$	3	$3.40 \pm 0.35$	107.3
4	$3.78 \pm 0.13$	3	$4.38 \pm 0.36$	115.9
5	$3.18 \pm 0.16$	3	$3.73 \pm 0.23$	117.3
6	$3.28 \pm 0.21$	3	$3.62 \pm 0.43$	110.4
7	$2.84 \pm 0.08$	3	$2.65 \pm 0.40$	93.3
8	$3.21 \pm 0.17$	3	$3.44 \pm 0.25$	107.2
9	$2.54 \pm 0.14$	3	$2.85 \pm 0.38$	112.2
Average				106.9

Recovery was the ratio percent between blood sample value obtained with ICP-AES and that calculated according to the added  $\text{Pb}^{2+}$  concentration to blood sample.

#### 4. Conclusions

A sensitive film was generated via site-specific MEA- $\beta$ -CD modified gold electrodes for trace  $Pb^{2+}$  probing. The MCGE exhibited good analytical response in determining  $Pb^{2+}$  by means of DPSV. One of the advantages was the  $7.1 \times 10^{-9}$  M detection limit (with  $S/N > 3$ ) which was very close to what obtained by the well-known Hg-based DPSV approach [36]. Another advantage of the MCGE was only 180 s were used for deposition, which were undoubtedly less than other works (namely 6 min) [37–39]. The linear range for the determination of lead using the MCGE was found as  $1.7 \times 10^{-8}$  M to at least  $9.3 \times 10^{-7}$  M  $Pb^{2+}$ . The MCGE was also applied to determine  $Pb^{2+}$  in practical samples and showed a good agreement with the result obtained with ICP-AES. The modified electrodes certainly are an effective choice for the simultaneous determination of  $Pb^{2+}$ , as its resolution is ideal for the cations studied, and also an environmentally friendly alternative to substitute the HDME.

#### Acknowledgements

The authors are grateful for the funding provided by the National Natural Science Foundation of China (Grant No. 90606014 and 20525519), MOE of China and the Shanghai Leading Academic Discipline Project B109, 08XD14009 & 0852nm03800.

#### References

- [1] P.J. Landrigan, A.C. Todd, *Western J. Med.* 161 (1994) 153.
- [2] A.C. Todd, J.G. Wetmur, J.M. Moline, J.H. Godbold, S.M. Levin, P.J. Landrigan, *Environ. Health Perspect.* 104 (1996) 141.
- [3] Y. Finkelstein, M.E. Markowitz, J.F. Rosen, *Brain Res. Rev.* 27 (1998) 168.
- [4] R.L. Canfield, C.R. Henderson, D.A. Cory-Slechta, C. Cox, T.A. Jusko, B.P. Lanphear, *N. Engl. J. Med.* 348 (2003) 1517.
- [5] L.T. Viyannalage, S. Bliznakov, N. Dimitrov, *Anal. Chem.* 80 (2008) 2042.
- [6] T. Shtoyko, A.T. Maghasi, J.N. Richardson, C.J. Seliskar, W.R. Heineman, *Anal. Chem.* 75 (2003) 4585.
- [7] A.T. Maghasi, S.D. Conklin, T. Shtoyko, A. Piruska, J.N. Richardson, C.J. Seliskar, W.R. Heineman, *Anal. Chem.* 76 (2004) 1458.
- [8] J.H. Pei, M.L. Tercier-Waeber, J. Buffle, *Anal. Chem.* 72 (2000) 161.
- [9] J. Wang, J.M. Lu, S.B. Hocevar, P.A.M. Farias, B. Ogorevc, *Anal. Chem.* 72 (2000) 3218.
- [10] I. Turyan, D. Mandler, *Anal. Chem.* 65 (1993) 2089.
- [11] B.J. Feldman, J.D. Osterloh, B.H. Hata, A. Dalessandro, *Anal. Chem.* 66 (1994) 1983.
- [12] H.P. Wu, *Anal. Chem.* 68 (1996) 1639.
- [13] Kh.Z. Brainina, A.M. Bond, *Anal. Chem.* 67 (1995) 2586.
- [14] Z.Q. Gao, K.S. Siow, *Talanta* 43 (1996) 727.
- [15] L.Y. Cao, J.B. Jia, Z.H. Wang, *Electrochim. Acta* 53 (2008) 2177.
- [16] F. Heppeler, S. Sander, G. Henze, *Anal. Chim. Acta* 319 (1996) 19.
- [17] L. Baldrianova, I. Svancara, M. Vlcek, A. Economou, S. Sotiropoulos, *Electrochim. Acta* 52 (2006) 481.
- [18] L. Baldrianova, I. Svancara, S. Sotiropoulos, *Anal. Chim. Acta* 599 (2007) 249.
- [19] O. Bagel, G. Lagger, H.H. Girault, D. Brack, U. Royall, H. Schafer, *Electroanalysis* 13 (2001) 100.
- [20] G. Kefala, A. Economou, A. Voulgaropoulos, M. Sofoniou, *Talanta* 61 (2003) 603.
- [21] K. Odashima, M. Kotato, M. Sugawara, Y. Umezawa, *Anal. Chem.* 65 (1993) 927.
- [22] L.A. Godinez, J. Lin, M. Muñoz, W. Coleman, S. Rubin, A. Parikh, T.A. Zawodzinski, D. Loveday, J.P. Ferraris, E.A. Karifer, *Langmuir* 14 (1998) 137.
- [23] L.A. Belyakova, K.A. Kazdoba, V.N. Belyakov, S.V. Ryabov, A.F. Danil de Namor, *J. Colloids Interf. Sci.* 283 (2005) 488.
- [24] C.R. Raj, R. Ramaraj, *Electrochim. Acta* 44 (1999) 2685.
- [25] K. Harata, *Chem. Rev.* 98 (1998) 1803.
- [26] G. Roa, M.T. Ramírez-Silva, M.A. Romero-Romo, L. Galicia, *Anal. Bioanal. Chem.* 377 (2003) 763.
- [27] A. Yabe, Y. Kawabata, H. Niino, M. Tanaka, A. Ouchi, H. Takahashi, S. Tamura, W. Tagaki, H. Nakahara, K. Fukuda, *Chem. Lett.* 1 (1988) 1.
- [28] M.T. Rojas, R. Königer, J.F. Stoddart, A.E. Kaifer, *J. Am. Chem. Soc.* 117 (1995) 336.
- [29] G. Nelles, M. Weisser, R. Back, P. Wohlfart, G. Wenz, S. Mittler-Neher, *J. Am. Chem. Soc.* 118 (1996) 5039.
- [30] C. Henke, C. Steinem, A. Janshoff, G. Steffan, H. Luftmann, M. Sieber, H.J. Galla, *Anal. Chem.* 68 (1996) 3158.
- [31] R.C. Petter, J.S. Salek, C.T. Sikorski, G. Kumaravel, F.T. Lin, *J. Am. Chem. Soc.* 112 (1990) 3860.
- [32] H. Kitano, Y. Taira, H. Yamamoto, *Anal. Chem.* 72 (2000) 2976.
- [33] X.P. Yan, M. Sperling, B. Welz, *Anal. Chem.* 71 (1999) 4216.
- [34] Y. Maeda, T. Fukuda, H. Yamamoto, H. Kitano, *Langmuir* 13 (1997) 4187.
- [35] M.L. Tercier, N. Parthasarathy, J. Buffle, *Electroanalysis* 7 (1995) 55.
- [36] S.V. Prabhu, R.P. Baldwin, L. Kryger, *Electroanalysis* 1 (1989) 13.
- [37] M. Connor, E. Dempsey, M.R. Smyth, D.H. Richardson, *Electroanalysis* 3 (1991) 331.
- [38] Z.M. Hu, C.J. Seliskar, W.R. Heineman, *Anal. Chim. Acta* 369 (1998) 93.
- [39] K. Bandyopadhyay, K. Vijayamohan, G.S. Shekhawat, R.P. Gupta, *J. Electroanal. Chem.* 447 (1998) 11.



# A novel multiwalled carbon nanotubes bonded fused-silica fiber for solid phase microextraction–gas chromatographic analysis of phenols in water samples

Hongmei Liu<sup>a,b</sup>, Jubai Li<sup>a</sup>, Xia Liu<sup>a</sup>, Shengxiang Jiang<sup>a,\*</sup>

<sup>a</sup> Key Laboratory for Natural Medicine of Gansu Province, Lanzhou Institute of Chemical Physics, Chinese Academy of Sciences, Lanzhou 730000, China

<sup>b</sup> Graduate University of the Chinese Academy of Sciences, Beijing 100049, China

## ARTICLE INFO

### Article history:

Received 4 November 2008

Received in revised form

23 December 2008

Accepted 30 December 2008

Available online 20 January 2009

### Keywords:

Multiwalled carbon nanotubes

Solid phase microextraction

Gas chromatography

Phenols

## ABSTRACT

The present work reports on the synthesis of chemically bonded multiwalled carbon nanotubes (MWCNTs)/fused-silica fibers and their use in solid phase microextraction of seven phenols from water samples coupled with gas chromatography (GC). The synthetic strategy was verified by infrared (IR) spectroscopy and field emission scanning electron microscopy. Adsorption factors (pH, ionic strength, stirring rate, adsorption time and temperature) and desorption factors (time and temperature) of the fibers were systematically investigated. Detection limits to seven phenols were less than  $0.05 \mu\text{g L}^{-1}$ , and their calibration curves were all linear ( $R^2 \geq 0.9984$ ) in the range from 0.05 to  $5000 \mu\text{g L}^{-1}$ . This method was then utilized to analyze two real water samples from Yellow River and sanitary wastewater, resulting in satisfactory results. Compared with normal solid phase materials, this MWCNTs-bonded fused-silica fibers showed a number of advantages: wide linear range and low detection limit for extracting phenols couple with GC, and good stability in acid, alkali, organic solvents and at high temperature.

© 2009 Elsevier B.V. All rights reserved.

## 1. Introduction

Recently, a new extraction technology, solid phase microextraction (SPME), is being developed and has attracted considerable attentions due to its high sensitivity, rapidity, simplicity and free of solvents. SPME can extract trace amount of organic chemicals from environmental [1–3], biologic [4,5] and food samples [6–8]. The core technique of SPME is to develop novel coating materials of SPME fibers. So far, many coating materials have been developed and commercialized including carbowax/templated resin (CW-TPR), polydimethylsiloxane/divinylbenzene (PDMS-DVB), polyacrylate (PA), etc. However, polymeric coatings have a number of drawbacks including relatively low operating temperature (generally in the range 240–280 °C), instability and swelling in organic solvents, which greatly restricts their applications [9]. The nanomaterials, having large surface area and being mechanically robust and chemically inert, have added new opportunities for improving the performance of SPME fibers [10,11].

Carbon nanotubes (CNTs), as a kind of effective sorbent nanomaterials [12–17], have been successfully used as the SPME fiber coating for analysis of organic compounds, such as phenols [18],

polybrominated diphenyls [19], organochlorine pesticides [20] and so on. Presently, agglutinate method is a common preparation technology of CNTs fibers, but the prepared fibers possesses some inherent defects, such as weak stabilities in high temperature, organic solvent, strong acidic and basic solution owing to the usage of organic agglomerants [18], and thus limiting their lifetime. Surface modification can afford CNTs some new functions, such as –OH, –COOH, –NH<sub>2</sub> and so on [21–24]. This is also true for fused-silica fibers [25]. So we anticipate that it is feasible to fabricate CNTs-bonded SPME fibers using the method of chemical modification, and some unique properties in SPME can be achieved.

In this study, we reported a chemical bonding method for fabricating multiwalled carbon nanotubes (MWCNTs)/fused-silica fiber based on the surface modification of both MWCNTs materials and fused-silica fibers. Then the fiber coupled with gas chromatography (GC) was used for solid phase microextraction of seven common phenols from water samples, which are largely used in our daily lives and industrial productions, and also are polluting our environment. The relationships of the adsorption factors and desorption factors with the extraction efficiency of seven phenols from water samples using GC were investigated in detail. Analysis of seven phenols in two different source waters (Yellow River and sanitary wastewater) gave satisfactory results. The stability of the MWCNTs/SPME fiber in acid, alkali and organic solvents was evaluated.

\* Corresponding author. Tel.: +86 931 4968266; fax: +86 931 8277088.

E-mail address: [sxjiang@lzb.ac.cn](mailto:sxjiang@lzb.ac.cn) (S. Jiang).



## 2. Experimental

### 2.1. Chemicals and materials

Phenol (P), *o*-methylphenol (*o*-MP), *p*-methylphenol (*p*-MP), 2,5-bimethylphenol (2,5-BMP) were obtained from the Shanghai Chemical Reagent Corporation (China); *o*-ethylphenol (*o*-EP), *p*-ethylphenol (*p*-EP), 2,3-bimethylphenol (2,3-BMP) were obtained from Sigma–Aldrich; 3-aminopropyltriethoxysilane (APTES) was from the Chemical Industrial Corporation of Gaizhou (China); sodium dodecyl sulfate (SDS), from Beijing Donghuan Chemical Industrial Corporation (China). All the reagents are of analytical grade except SDS, which is chemical grade.

The standard mixtures of the seven phenols were prepared by dissolving 10.0 mg of each compound in 10.0 mL of ethanol. The stock solution (1 mg mL<sup>-1</sup>) was stored at 4 °C and diluted with ultrapure water to give the required concentration.

Fused-silica fibers (140 mm × 0.25 mm o.d.) were purchased from Xinnuo Photoconductive Fiber Corporation (Handan, China). MWCNTs were prepared by the decomposition of ethylene over a Co–La–O catalyst, as described in Ref. [26].

### 2.2. Instrument

An Agilent 7890A series gas chromatograph (Agilent Technologies, USA) equipped with a flame ionic detector was used. The separation was carried out on a HP-5 capillary column (30 m × 0.32 mm i.d. × 0.25 μm film thickness). Separation and detection parameters were optimized. In brief, the column temperature was initially hold at 50 °C, and programmed at 5 °C min<sup>-1</sup> to 75 °C, then at the rate of 1 °C min<sup>-1</sup> to 100 °C, finally programmed at 10 °C min<sup>-1</sup> to 250 °C, which was then held for 30 min. Ultrapure nitrogen (>99.999%) was used as the carrier gas (1 mL min<sup>-1</sup>) and make-up gas (30 mL min<sup>-1</sup>). The injector temperature was fixed at 280 °C, and the detector one was fixed at 300 °C. The injection was performed in the splitless mode.

SEM micrographs of MWCNTs-covered fibers were obtained on a field emission scanning electron microscope (FESEM, JSM-6701F, Japan). IR spectra were obtained on an IFS 66v/s IR spectrometer (Bruker, Germany).

### 2.3. Environmental sample collection

The river water sample was collected from the Yellow River (Lanzhou, China). The wastewater (untreated) was sampled from the sanitary wastewater in Lanzhou. These samples were all filtered through a 0.45 μm filter and stored at 4 °C.

### 2.4. Preparation procedures

#### 2.4.1. Oxidation of MWCNTs

Predetermined quantities of pristine MWCNTs and mixed acid (concentrated H<sub>2</sub>SO<sub>4</sub>/HNO<sub>3</sub> = 3/1) were added into a beaker, and then were subjected to an ultrasonic bath for 14 h. Then the unreacted acid solution was removed, and MWCNTs was diluted with ultrapure water until pH 7. Finally, the separation of the oxidized MWCNTs from the solution was carried out using a 0.45 μm filter, and dried in a vacuum desiccator.

#### 2.4.2. Silanization of fiber surface

The silanization of the fiber surface was similar to the silanization procedure of fused-silica capillary in Refs. [27,28]. The primary steps were as followed: one end of the fused-silica fiber (2 cm) was in turn burnt with a spirit lamp to remove the protective polyimide layer, and then this part was dipped in a 1.0 M NaOH solution and heated in a hot water bath (70 °C) for 30 min. After that, the fiber

was put in a dry tube and kept at 120 °C for another 30 min in an oven. Thereafter, it was rinsed with ultrapure water until pH 7, and then dried at room temperature.

The hydroxylated part of the fiber was dipped in an APTES solution for 12 h, and then it was put in an oven at 120 °C for 30 min to react with APTES. These two operations were repeated for six cycles to form a silanized layer on the fiber. Finally, it was rinsed with toluene and ethanol, and dried at room temperature.

#### 2.4.3. Chemical bonding of MWCNT layer to fiber

10 mg oxidized MWCNTs were dispersed in a 5 mL SDS solution (1%) for 30 min ultrasonically bath to prepare the MWCNTs suspension. The pretreated fiber section was put into the MWCNTs suspension for 4 h in a hot water bath (70 °C), and then it was heated in a 120 °C oven for 30 min. This procedure was repeated until the coating reached a required thickness (~20 μm). Finally, the coated fiber was aged at 280 °C for 12 h under the protection of dry nitrogen before the SPME experiments.

### 2.5. SPME

A modified 5 μL-syringe was used as an SPME device as similar as that in Ref. [29]. A 0.04 mL stock solution was diluted with ultrapure water to 8 mL (5 μg mL<sup>-1</sup>). After the homogenization, the needle of the SPME device was stuck the septum of the vial containing the analytes. The sample was extracted though the direct immersion in the solution with a constant depth under the optimum time and temperature. The pH value and ionic strength were adjusted with HCl/NaOH and KCl, respectively; a magnetic stirrer was used with the stirring rate was controlled at 300–1200 rpm.

### 2.6. Stability test of the present coating in acid, base and organic solvents

The tip of the fiber was immersed in four PTFE sealed vials loaded with ethanol (polar), *n*-hexane (nonpolar), HCl (0.1 M) and NaOH (0.1 M) solutions in the room temperature, successively. After 48 h, the fiber was taken out for the extraction experiment coupled with GC. The peak areas of analytes (500 μg L<sup>-1</sup>) before and after dipping in different solutions were compared.

## 3. Results and discussion

### 3.1. Preparation of MWCNTs/SPME fibers

Fig. 1 shows the preparation process of MWCNTs/SPME fibers. The MWCNTs were oxidized by mixed acids (H<sub>2</sub>SO<sub>4</sub>/HNO<sub>3</sub> = 3/1) to create –COOH groups at the sidewall of the MWCNTs. This activation process was verified by IR spectrum as shown in Fig. 2, in which an extra peak at 1720 cm<sup>-1</sup> corresponding to C=O appeared for the oxidized MWCNTs while absent in pristine MWCNTs. The silica fibers were firstly hydroxylated by NaOH solution to break the Si–O–Si bonds to form Si–OH groups which were then transformed to –NH<sub>2</sub> group by reacting with silanizing agents. MWCNTs/SPME fibers were formed by reaction between –COOH and –NH<sub>2</sub> groups upon heat treatment. The generation of amide was confirmed by the peak at 1530 cm<sup>-1</sup> in the IR spectrum (Fig. 2). Apart from covalent bonding, strong van der Waals interactions are also present in MWCNTs [30], which would promote the MWCNTs in the dispersed solution adsorbing spontaneously on the MWCNTs on the fiber. Thus a multilayer-MWCNTs coating can be finally formed on the fiber surface.

Fig. 3a shows the FESEM micrograph of the as-prepared MWCNTs/SPME fiber. It can be observed that a coating uniformly covered on the fiber surface, implying success of the synthetic strategy. The

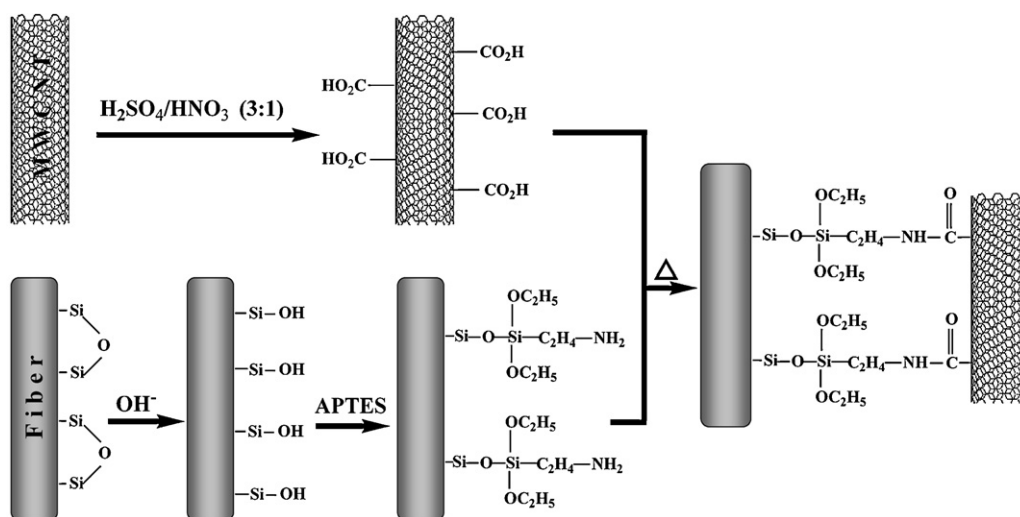


Fig. 1. Schematic illustration of the preparation process of the MWCNTs/fiber.

magnified image in Fig. 3b indicates that the coating is made up of cross-linked CNTs.

### 3.2. Optimization of SPME

The as-prepared MWCNTs/fibers coupled with GC were used for solid phase microextraction of seven phenols from water samples. To achieve the best extraction efficiency, the effects of extracting parameters, such as the adsorption temperature and time, stirring rate, solution ionic strength, pH and desorption conditions were systematically studied.

#### 3.2.1. Effect of extraction parameters

It is generally accepted that the temperature has adverse effects on the extraction: on one hand, an elevated temperature could enhance the mobility of molecules and so the extraction rate; on the other hand, it would decrease the distribution coefficient of the analytes between solid phase coating and sample solution [31]. Therefore, the selection of a proper temperature is necessary for extraction processes. In our experiments, we found a temperature above 70 °C could easily produce air bubbles in the aqueous matrix, which has adverse actions on the adsorption of analytes. So the

temperature effects on the extraction efficiency of analytes were studied in a range of 30–70 °C. Fig. 4 shows the variation of the extraction efficiency with the extraction temperature. The extraction efficiency increased monotonously as the increment of the

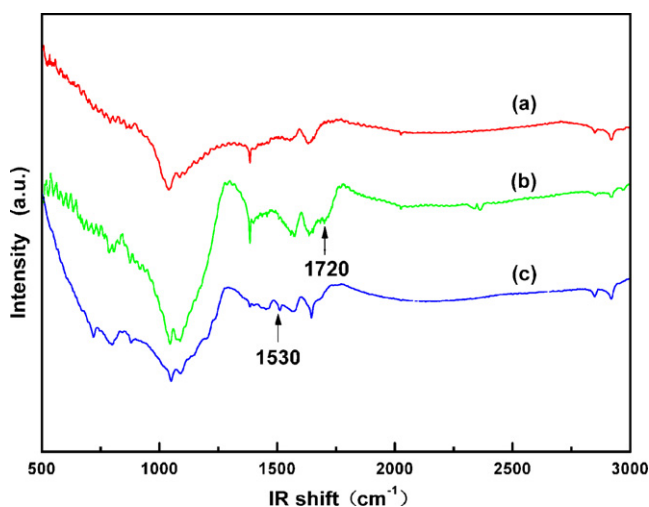


Fig. 2. FT-IR spectra of the MWCNTs: (a) pristine, (b) after oxidation, and (c) after chemical bonding with the fiber.

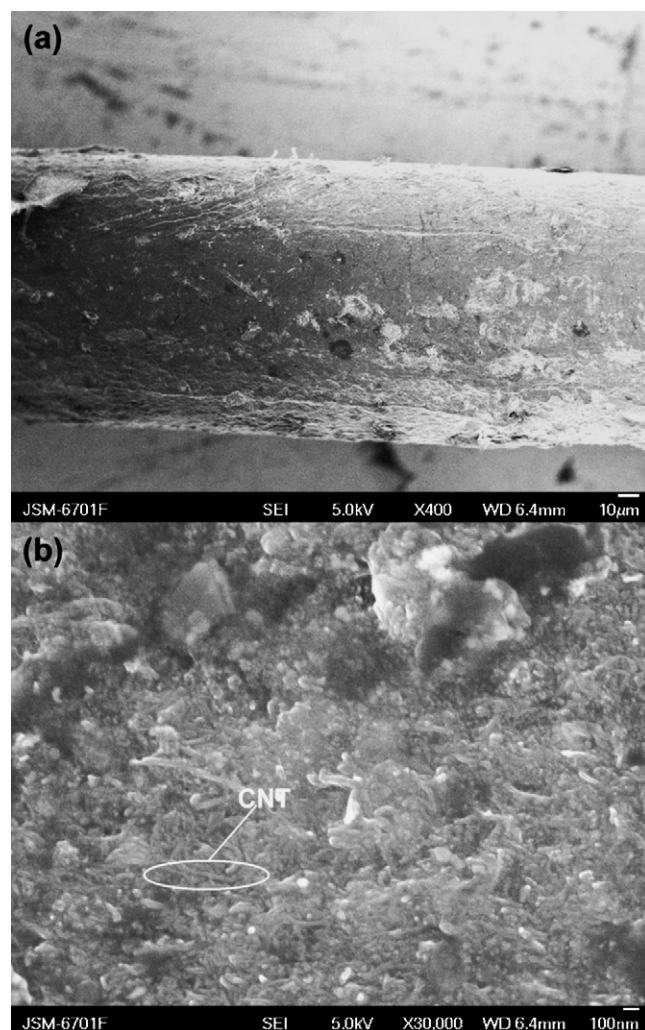
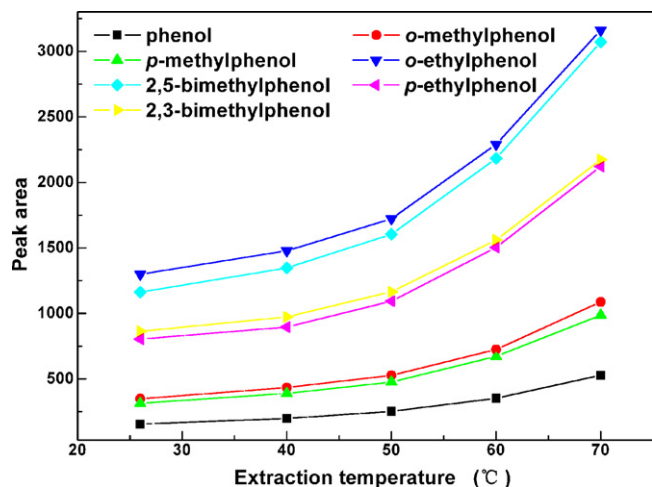


Fig. 3. FESEM images of the MWCNTs-bonded SPME fiber at a magnification of (a) 400 and (b) 30,000.



**Fig. 4.** Effect of extraction temperature on peak area of phenols extracted by the as-prepared MWCNTs/fiber. SPME conditions: extraction time, 50 min; salt concentration, 30% KCl; pH 6.0; stirring rate, 600 rpm; desorption temperature, 280 °C; desorption time, 5 min; phenols concentration, 5  $\mu\text{g mL}^{-1}$ .

extraction temperature. So the 70 °C was chosen for subsequent experiments.

Magnetic stirring is most commonly used in SPME experiments to accelerate the extraction. It was revealed that the chromatographic peak areas of the analytes increased as the stirring rate increased from 0 to 600 rpm, and then decreased from 600 to 1200 rpm. So the 600 rpm stirring rate was chosen.

It is known that adding a salt (KCl) into the solution can have two contrary outcomes. It may help with the extraction by the 'salt out effect' or deteriorate extraction due to the competitive adsorption of  $\text{K}^+$  and  $\text{Cl}^-$ . The extraction efficiency as a function of salt concentration from 0% to 30% (30% is the saturated solubility of KCl) was studied. It was found that the chromatographic peak areas for all the analytes increased monotonously when increasing salt concentration, indicating the 'salt out effect' played a dominant role. Therefore, a concentration of 30% (w/v) was selected as the optimized salt concentration.

The pH value of the solution is another important factor for extracting pH sensitive compounds. It did not only influence the dissociation of functional groups in analytes, but also influence the surface charge density of MWCNTs [32]. The effects of the pH value of the solution on the extraction efficiency for the phenolic compounds were studied up to pH 10 (2–10). It is known that the lowest  $\text{pK}_a$  in these target compounds was 10 (phenol) so that these compounds would not dissociate. As shown in Fig. 5, the chromatographic peak areas increased with the increase of the pH value in the range of 2–6, and then decreased as the pH value increased further. So this result was mainly ascribed to the different surface charge density between the internal and external surfaces. When the pH value was 6, the external surface of CNTs was negatively charged, and the internal surface was positively charged. Such a condition might offer a preferential environment to adsorb phenolic compounds on the surface. However, at high pH values, both the external and internal surfaces were negatively charged; at very low pH values, both the external and internal surfaces presented in positive charge, all these conditions may deteriorate the adsorption of phenols [32]. Therefore, the optimized pH value of the solution is 6 for extracting the phenols.

Generally speaking, extraction time is dependent on the equilibrium time of the analyte distribution between fiber and sample solution. The long extraction time is advantageous to reach the best equilibrium. The extraction time profile of the seven alkylphenols is shown in Fig. 6. The amount of the extracted analytes (correspond-

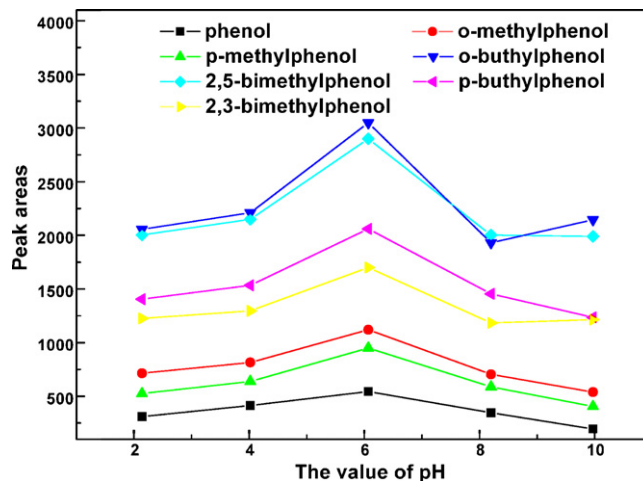


**Fig. 5.** Effect of pH on peak area of phenols extracted by the as-prepared MWCNTs/fiber. SPME conditions: extraction time, 50 min; extraction temperature, 70 °C; salt concentration, 30% KCl; stirring rate, 600 rpm; desorption temperature, 280 °C; desorption time, 5 min; phenols concentration, 5  $\mu\text{g mL}^{-1}$ .

ing to the resulting peak areas) greatly increased as the extraction time increased from 0 to 70 min. A 50-min extraction time was sufficient to achieve satisfactory extraction efficiency, though the equilibrium was not reached. Considering the total operation time, the extraction time was set at 50 min.

### 3.2.2. Effects of desorption parameters

To reach the highest sensitivity, the desorption temperature and time were evaluated to ensure the analytes were completely desorbed from the fiber. The desorption temperature was evaluated at 220, 240, 260, 280 and 300 °C for 5 min. The result indicated that the temperature of 280 °C was sufficient to achieve the complete desorption as shown in Fig. 7. Subsequently, the desorption time was evaluated at 1, 3, 5 and 7 min. Experiments showed that the peak areas of all the studied seven analytes increased with prolongation of the desorption time at 1–5 min, and then they kept invariable at 5–7 min. So the desorption condition was chosen at 280 °C for 5 min.

Fig. 8a was a typical chromatogram of spiked seven phenols (5  $\mu\text{g mL}^{-1}$ ) in ultrapure water under optimal conditions.

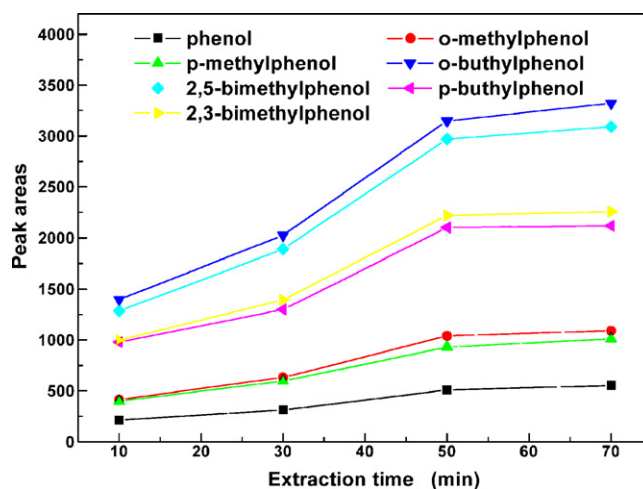


**Fig. 6.** Effect of extraction time on peak area of phenols extracted by the as-prepared MWCNTs/fiber. SPME conditions: extraction temperature, 70 °C; salt concentration, 30% KCl; pH 6.0; stirring rate, 600 rpm; desorption temperature, 280 °C; desorption time, 5 min; phenols concentration, 5  $\mu\text{g mL}^{-1}$ .

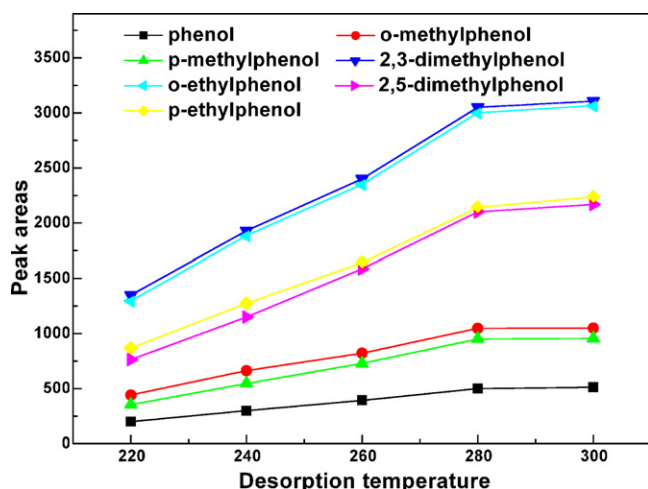


Fig. 7. Desorption-time profile for the as-prepared MWCNTs/fiber. SPME conditions: extraction time, 50 min; extraction temperature, 70 °C; salt concentration, 30% KCl; pH 6.0; stirring rate, 600 rpm; desorption time, 5 min; phenols concentration, 5  $\mu\text{g mL}^{-1}$ .

### 3.3. Detection limit, precision and accuracy

The analytical parameters including the linearity, accuracy and precision, and detection limits for the extraction of seven phenols in ultrapure water with the as-prepared MWCNTs/fiber were listed in Table 1. Under optimized conditions, the linearity of the SPME–GC method was investigated with a serial of mixed standard solutions of P, *o*-MP, *p*-MP, *o*-EP, 2,3-BMP, *p*-EP, 2,5-BMP. The results indicated that all of them could be determined quantitatively in wide ranges. As shown in Table 1, good linearities were achieved in the range of 0.05–5000  $\mu\text{g L}^{-1}$  for all phenols with satisfactory correlation coefficients except for P, *o*-MP and *p*-MP whose linearity range was 0.5–5000  $\mu\text{g L}^{-1}$ . The detection limits for seven phenols were in the range of 0.005–0.05  $\mu\text{g L}^{-1}$ , which was determined by gradually decreasing the concentrations of analytes until signals still could be discerned at a signal-to-noise ratio of 3 ( $S/N=3$ ). The precision of the method for three duplicate measurements of seven phenols mixed standard solution (500  $\mu\text{g L}^{-1}$ ) was investigated, and the relative standard deviation (R.S.D.) varied from 0.97% to 7.96%. Simultaneously, it is worth noting that this MWCNTs-bonded fiber couple with GC possesses the wider linearity range and lower LODs as compared with the agglutinate MWCNTs/fiber coupled with high-performance liquid chromatography (HPLC) [18], two kinds of commercial fibers [33] and the two other new fibers couple with GC [34,35] for extracting the same phenols as shown in Table 1. The effectiveness of the present fiber can be ascribed, on one hand to the high adsorptive ability of CNTs, on the other hand, to a less compact structure as compared with agglutinate ones, which may result in the larger surface area and so larger adsorption amount.

### 3.4. Application to real samples

The established SPME–GC method was used to determine the content of the seven phenols in Yellow River and sanitary wastewater samples. Fig. 8b and c illustrates the chromatograms of the phenols in Yellow River and wastewater samples with the previously established conditions, respectively. Phenols were identified according to the relative retention time calibrated with the standard samples. The analytes of *o*-EP and *p*-EP were found in the two samples. They could not be quantified in the Yellow River sample, while in the wastewater, the concentration of *o*-EP and *p*-EP were found to be 1.24 and 22.9  $\mu\text{g L}^{-1}$ , respectively. In order to demonstrate the applicability and reliability, the recoveries of the target

Table 1  
Characteristic data of the established MWCNTs/fiber-SPME–GC method for determination of phenols and compared with other methods ( $n=3$ ).

Compounds	As-prepared MWCNTs/fiber		Commercial fiber-GC-FID [33]		Agglutinate MWCNTs–HPLC–UV [18]		Silicone oil coated fiber-GC-FID [34]		Polyaniline coated fiber-GC-FID [35]	
	Linearity range ( $\mu\text{g L}^{-1}$ )	Linearity	LODs ( $\mu\text{g L}^{-1}$ )	R.S.D. <sup>a</sup> (%)	LODs of PDMS ( $\mu\text{g L}^{-1}$ )	LODs of PA ( $\mu\text{g L}^{-1}$ )	Linear range ( $\mu\text{g L}^{-1}$ )	LODs ( $\mu\text{g L}^{-1}$ )	Linear range ( $\mu\text{g L}^{-1}$ )	LODs ( $\mu\text{g L}^{-1}$ )
P	0.5–5000	0.9984	0.05	7.02	–	–	0.01–5	12.8	2–20,000	1.65
<i>o</i> -MP	0.5–5000	0.9999	0.05	7.96	75	5	0.01–5	5.3	2–2000	1.67
<i>p</i> -MP	0.5–5000	0.9999	0.05	1.11	59	5	0.01–5	4.0	20–20,000	1.92
<i>o</i> -EP	0.05–5000	0.9999	0.005	2.35	–	–	–	–	–	–
2,5-BMP	0.05–5000	0.9999	0.005	0.97	–	–	–	–	–	–
<i>p</i> -EP	0.05–5000	0.9999	0.005	1.03	–	–	–	–	–	–
2,3-BMP	0.05–5000	0.9995	0.005	1.46	–	–	0.01–5	5.4	–	–

<sup>a</sup>  $n=3$ .

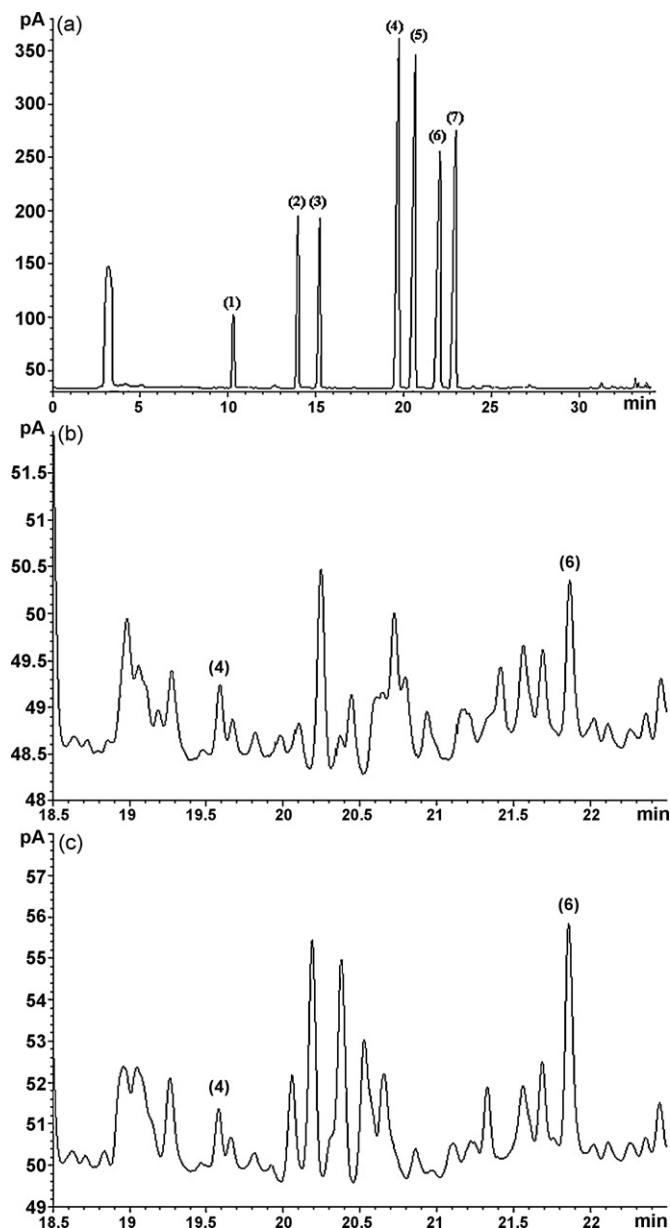


**Fig. 8.** Typical chromatogram of phenols in different water samples using as-prepared MWCNTs fiber under the optimal conditions: (a) ultrapure water with spiked seven phenols ( $5 \mu\text{g mL}^{-1}$ ), (b) Yellow River water, and (c) wastewater samples. Peaks: (1) *P*, (2) *o*-MP, (3) *p*-MP, (4) *o*-EP, (5) 2,5-DMP, (6) *p*-EP, and (7) 2,3-DMP.

**Table 2**  
Recoveries of seven alkylphenols for spiked Yellow River and wastewater samples.

Compounds	Recovery, R.S.D. (%)			
	Yellow River		Wastewater	
	Spiked $5 \mu\text{g L}^{-1}$	Spiked $500 \mu\text{g L}^{-1}$	Spiked $5 \mu\text{g L}^{-1}$	Spiked $500 \mu\text{g L}^{-1}$
<i>P</i>	94.38(±3.25)	88.57(±5.21)	98.91(±2.97)	70.83(±6.34)
<i>o</i> -MP	73.48(±8.32)	106.03(±1.57)	100.54(±5.55)	75.35(±3.21)
<i>p</i> -MP	93.77(±1.60)	96.54(±3.49)	115.36(±2.87)	82.33(±7.59)
<i>o</i> -EP	98.52(±7.22)	109.28(±3.98)	145.62(±8.11)	89.60(±6.48)
2,5-DMP	85.44(±4.19)	109.37(±3.44)	128.10(±6.09)	80.87(±3.04)
<i>p</i> -EP	104.20(±6.44)	103.01(±8.01)	142.12(±3.22)	85.47(±7.77)
2,3-DMP	80.66(±6.12)	106.52(±5.23)	106.04(±1.97)	83.25(±3.21)

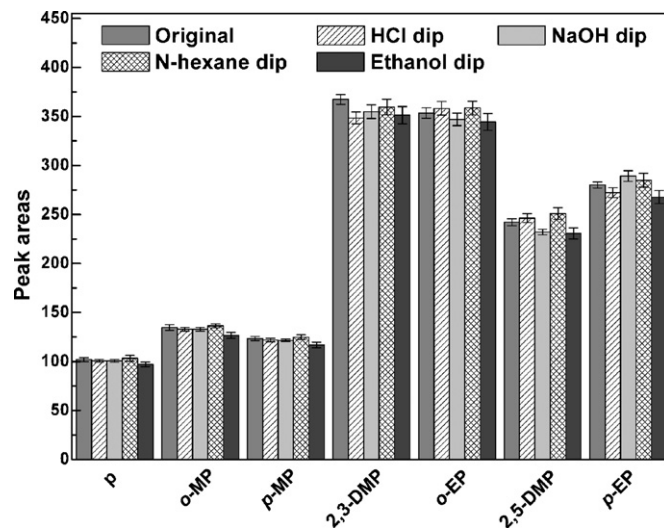


**Fig. 9.** Comparison of chromatographic peak area of extracted phenols before and after dipping the tip of the MWCNTs/fiber into four different solutions for 48 h.

compounds were determined in the two water samples spiked at two concentration levels ( $5$  and  $500 \mu\text{g L}^{-1}$ ). The recoveries were 70.83–148.10% for all analytes in the two water samples, and the recovery in the wastewater sample exhibited larger deviations compared with that in Yellow River sample as shown in Table 2. This can be ascribed to the fact that sanitary wastewater contained a large number of other pollutants such as cleanser, additive, pesticide and so on, which makes extraction of phenols more complicated.

### 3.5. Stability

The lifetime of coating is very important parameter for the practical application. The coating is damaged mainly by high temperature of injection port of a gas chromatograph and/or acidic, alkali solutions or organic solvents in the matrix. Firstly, it should be noted that the highest desorption temperature in the optimized process studied in present work was  $300^\circ\text{C}$ . That is to say, the as-prepared MWCNTs/fiber could function with high thermal stability at least at  $300^\circ\text{C}$ , which greatly expands the application range of the present fiber toward high boiling-point compounds. In addition, covalent bonding allows high stability to organic solvent, strong acidic and alkali solutions. Fig. 9 shows that the extraction ability had no obvious decline after the fiber was dipped in different solutions: *n*-hexane, ethanol, HCl (0.1 M) and NaOH (0.1 M) for 48 h, respectively. The R.S.D.s of the extraction peak areas determined at the concentration of  $500 \mu\text{g mL}^{-1}$  were less than 5% (for three duplicate measurements). The character makes the fiber suitable for the coupling of SPME with many more techniques, such as HPLC and supercritical fluid chromatography (SFC), and also prolongs the lifetime of the fiber for hundreds of times.

#### 4. Conclusion

MWCNTs-covered SPME fibers were produced by covalent bonding based on the surface modification of both multiwalled carbon nanotube and the fused-silica fibers. This novel SPME fiber was then used to extract seven phenols from water samples coupled with GC, and applied to two real water samples, achieving satisfactory results. Having an incompact structure, which brought forth by the chemical bonding design, and combining with the inherent stability of MWCNTs, the MWCNT/SPME fiber possesses some special properties such as good stability at high temperature, in organic solvent (polar and nonpolar), acid and alkali solutions, wide linearity range and low LODs for extracting phenols couple with GC.

#### Acknowledgment

We would like to thank Dr. Long Chen for providing the MWCNTs and participating in many lively discussions.

#### References

- [1] J.L.R. Junior, N. Re-Poppi, *Talanta* 72 (2007) 1833.
- [2] L. Araujo, J. Wild, N. Villa, N. Camargo, D. Cubillan, A. Prieto, *Talanta* 75 (2008) 111.
- [3] V. Pino, J.H. Ayala, V. Gonzalez, A.M. Afonso, *Talanta* 73 (2007) 505.
- [4] H.F. Fang, M.M. Liu, Z.R. Zeng, *Talanta* 68 (2006) 979.
- [5] M.L. Musteata, F.M. Musteata, J. Pawliszyn, *Anal. Chem.* 79 (2007) 6903.
- [6] S. Diez, J.M. Bayona, *Talanta* 77 (2008) 21.
- [7] N. Fidalgo-Used, M. Montes-Bayon, E. Blanco-Gonzalez, A. Sanz-Medel, *Talanta* 75 (2008) 710.
- [8] K.H. Lu, C.Y. Chen, M.R. Lee, *Talanta* 72 (2007) 1082.
- [9] A. Kumar, A.K. Malik Gaurav, D.K. Tewary, B. Singh, *Anal. Chim. Acta* 610 (2008) 1.
- [10] D.D. Cao, J.X. Lv, J.F. Liu, G.B. Jiang, *Anal. Chim. Acta* 611 (2008) 56.
- [11] A. Mehdinia, M.F. Mousavi, M. Shamsipur, *J. Chromatogr. A* 1134 (2006) 24.
- [12] A.F. Barbosa, M.G. Segatelli, A.C. Pereira, A.S. Santos, L.T. Kubota, P.O. Luccas, C.R.T. Tarley, *Talanta* 71 (2007) 1512.
- [13] W.D. Wang, Y.M. Huang, W.Q. Shu, J. Cao, *J. Chromatogr. A* 1173 (2007) 27.
- [14] Z. Du, Y.L. Yu, X.W. Chen, J.H. Wang, *Chem. Eur. J.* 13 (2007) 9679.
- [15] A.H. El-Sheikh, J.A. Sweileh, Y.S. Al-Degs, A.A. Insisi, N. Al-Rabady, *Talanta* 74 (2008) 1675.
- [16] H. Sone, B. Fugetsu, T. Tsukada, M. Endo, *Talanta* 74 (2008) 1265.
- [17] S. Wang, P. Zhao, G. Min, G.Z. Fang, *J. Chromatogr. A* 1165 (2007) 166.
- [18] X.Y. Liu, Y.S. Ji, Y.H. Zhang, H.X. Zhang, M.C. Liu, *J. Chromatogr. A* 1165 (2007) 10.
- [19] J.X. Wang, D.Q. Jiang, Z.Y. Gu, X.P. Yan, *J. Chromatogr. A* 1137 (2006) 8.
- [20] J.X. Lv, J.F. Liu, Y. Wei, K.L. Jiang, S.S. Fan, J.Y. Liu, G.B. Jiang, *J. Sep. Sci.* 30 (2007) 2138.
- [21] V.N. Popov, P. Lambin, *Carbon Nanotubes: From Basic Research to Nanotechnology*, Springer, Amsterdam, Netherlands, 2006, p. 187.
- [22] M.J. O'Connell, *Carbon Nanotubes: Properties and Applications*, Taylor & Francis Group, New York, USA, 2006, p. 275.
- [23] C.N.R. Rao, A. Govindaraj, *Nanotubes and Nanowires*, RSC, Cambridge, UK, 2005, p. 48.
- [24] C.N.R. Rao, A. Muller, A.K. Cheetham, *Nanomaterials Chemistry: Recent Developments and New Directions*, Wiley-VCH, Darmstadt, German, 2007, p. 45.
- [25] G.Q. Liu, Z.L. Yu, *The Technology of Chromatographic Column*, 2nd ed., Chemical Industry Press, Beijing, China, 2005, p. 125.
- [26] L. Chen, H.T. Liu, K.L. Yang, J.K. Wang, X.L. Wang, *Mater. Chem. Phys.* 112 (2008) 407.
- [27] W.D. Qin, S.F.Y. Li, *J. Chromatogr. A* 958 (2003) 447.
- [28] W.D. Qin, S.F.Y. Li, *J. Chromatogr. A* 1048 (2004) 253.
- [29] J.F. Liu, N. Li, G.B. Jiang, J.M. Liu, J.A. Jonsson, M.J. Wen, *J. Chromatogr. A* 1066 (2005) 27.
- [30] M. Sano, A. Kamino, J. Okamura, S. Shinkai, *Nano Lett.* 2 (2002) 531.
- [31] J.G. Hou, Q. Ma, X.Z. Du, H.L. Deng, J.Z. Gao, *Talanta* 62 (2004) 241.
- [32] C. Moreno-Castilla, J. Rivera-Utrilla, M.V. Lopez-Ramon, F. Carrasco-Marin, *Carbon* 33 (1995) 845.
- [33] S.D. Huang, C.P. Cheng, Y.H. Sung, *Anal. Chim. Acta* 343 (1997) 101.
- [34] M. Mousavi, E. Noroozian, M. Jalali-Heravi, A. Mollahosseini, *Anal. Chim. Acta* 581 (2007) 71.
- [35] F.R. Zhou, X.J. Li, Z.R. Zeng, *Anal. Chim. Acta* 538 (2005) 63.



# Determination of nitrite based on its quenching effect on anodic electrochemiluminescence of CdSe quantum dots

Xuan Liu, Liang Guo, Lingxiao Cheng, Huangxian Ju\*

Key Laboratory of Analytical Chemistry for Life Science (Ministry of Education of China), Department of Chemistry, Nanjing University, Nanjing 210093, PR China

## ARTICLE INFO

### Article history:

Received 7 July 2008

Received in revised form 10 December 2008

Accepted 12 December 2008

Available online 24 December 2008

### Keywords:

Quantum dots

Electrochemiluminescence

CdSe

Sensitizing effect

Quenching

Nitrite

## ABSTRACT

A novel method for electrochemiluminescent (ECL) detection of nitrite was proposed based on its quenching effect on anodic ECL emission of CdSe quantum dots (QDs). The ECL emission could be greatly enhanced by sulfite and dissolved oxygen in a neutral system and occurred at a relatively low potential in comparison with traditional anodic ECL emitter, leading to high sensitivity and good selectivity. The quenching mechanism followed an “electrochemical oxidation inhibition” process, which was completely different from those of some analytes on the ECL emission of QDs. The coincidence of photoluminescence and ECL spectra of the QDs indicated that the ECL emission resulted from the redox process of QDs core and the sulfite acted as a coreactant. The nitrite quenched ECL emission could be analyzed according to the treatment of Stern–Volmer equation with a linear range from 1  $\mu\text{M}$  to 0.5 mM for detection of nitrite. This work presented a new efficient ECL methodology for quencher-related detection.

© 2008 Elsevier B.V. All rights reserved.

## 1. Introduction

Electrochemiluminescence (ECL) technique has been widely used in many fields [1]. The ECL processes of quantum dots (QDs) have attracted considerable interest due to their reproducible [2] and size-dependent properties [3]. These QDs provide potential alternatives for developing new ECL emitters [2,4–11] and preparing new ECL sensors. Recently, some biosensors based on the cathodic ECL emission of II–VI QDs film immobilized on electrode surfaces have been developed using  $\text{O}_2$  [4],  $\text{H}_2\text{O}_2$  [5–7] and  $\text{S}_2\text{O}_8^{2-}$  [8,9] as coreactants. The anodic ECL emission produced from water soluble CdTe QDs in presence of dissolved oxygen [10] and amines [11] has also been reported. These ECL biosensors and anodic ECL emission have been used for detection of several analytes, including oxidase substrates [4], hydrogen peroxide [5], thiol compounds [7], proteins [8,9], dopamine [10] and amines [11]. Compared with cathodic ECL emission of QDs, the anodic ECL emission is relatively weak, and only the anodic ECL emission of CdTe QDs was studied [10,11]. Thus the overwhelming majority of anodic ECL luminophores are still focused on  $\text{Ru}(\text{bpy})_3^{2+}$  derivatives in presence of reductive coreactant [12], and most of the reported anodic ECL systems undergo high-excited potentials, which was unfavorable for analytical application.

Our previous work observed the sensitizing effect of sulfite on the anodic ECL emission of CdTe QDs, which led to a relatively low

anodic potential for sensitive detection of tyrosine by combining an enzymatic cycle with a quenching effect based on an energy transfer process [13]. Another work also observed the sensitizing effect of sulfite on the anodic ECL emission of CdSe QDs, producing a novel method for dopamine detection with the same quenching mechanism [14]. This work further studied the sensitizing mechanism and observed a quenching effect of nitrite on the sensitized ECL emission. The quenching process followed a completely different mechanism from dopamine, producing a method for ECL detection of nitrite.

Nitrite detection is of great importance in environmental and public health fields, and various methods based on spectrophotometric [15], chromatographic [16], chemiluminescent [17] and electrochemical techniques [18,19] have been developed for determination of nitrite ions. Some of them are complex, time consuming and require tedious sample pretreatment [18]. Although enzyme electrode can be utilized for nitrite detection [20], this technique has not been widely accepted yet due to its expensive cost and instability under operation conditions [21]. Thus, development of new analytical methods for selective and sensitive detection of nitrite by combining with multifarious techniques is still an attracted object. Herein, the strong anodic ECL emission of CdSe QDs in the presence of sulfite could be produced at a relatively low potential. The quenching effect of nitrite on the ECL emission via an “electrochemical oxidation inhibition” mechanism made it be able to be detected at relatively low potential, which inhibited greatly the interference from the oxidation of some electroactive compounds. To our best knowledge, this is the first ECL method for nitrite detection, thus extending the application field of QDs.

\* Corresponding author. Tel.: +86 25 83593593; fax: +86 25 83593593.

E-mail address: [hxju@nju.edu.cn](mailto:hxju@nju.edu.cn) (H. Ju).

## 2. Experiments

### 2.1. Chemicals

Thioglycolic acid (TGA), Se powder,  $\text{CdCl}_2 \cdot 2.5\text{H}_2\text{O}$ , sodium sulfite and  $\text{NaBH}_4$  were of analytical grade. Tris(hydroxymethyl)-aminomethane hydrochloride and Tris(hydroxymethyl)aminomethane (Tris, reagent grade) were purchased from Sigma. Doubly distilled water and 0.1 M HCl–Tris buffer containing 0.1 M  $\text{KNO}_3$  was used throughout the work. 1 M HCl and 0.1 M Tris were used to adjust solution pH.

### 2.2. Preparation of water-soluble CdSe QDs

The water-soluble CdSe QDs were prepared using TGA as stabilizing agent according to the previous report [7]. The Se source was obtained from the reaction between Se powder and  $\text{NaBH}_4$  in air-free doubly distilled water. After refluxed at  $100^\circ\text{C}$  for 4 h the product was purified by ultrafiltration at 6000 rpm for 5 min, and the upper phase was decanted and kept at  $4^\circ\text{C}$  for ECL detection. The obtained QDs solution could be stable for 3 months, and its concentration and the size of CdSe QDs were detected with UV–vis absorption spectroscopy.

### 2.3. Apparatus and analytical procedures

The electrochemical and ECL measurements were carried out on a MPI-A multifunctional analytical system (Xi'an Remex Analytical Instrument Ltd. Co.) at room temperature with a configuration consisting of an indium tin oxide (ITO) working electrode, a platinum counter electrode, and an Ag/AgCl (saturated KCl solution) reference electrode. The observation window for ECL was placed in front of the photomultiplier tube biased at  $-1000\text{ V}$ .

ECL spectrum was obtained by collecting the ECL data at  $+0.927\text{ V}$  during cyclic potential sweep with six pieces of filters at 490, 535, 550, 580, 600 and 630 nm. Their transparent efficiency was around 88%. UV–vis absorption spectrum was recorded with UV-3600 UV–vis–NIR photospectrometer (Shimadzu Co., Japan). Photoluminescence (PL) spectrum was obtained on a Jasco FP 820 fluorometer (Jasco Co.).

## 3. Results and discussion

### 3.1. Characterization of TGA-modified CdSe QDs

The PL spectrum of 20-times diluted QDs solution showed a maximum intensity at 560 nm, and the UV–vis absorption peak occurred at 424 nm (Fig. 1). From the absorption peak the size and concentration of CdSe QDs product were estimated to be 1.75 nm and  $5.76\ \mu\text{M}$  [22].

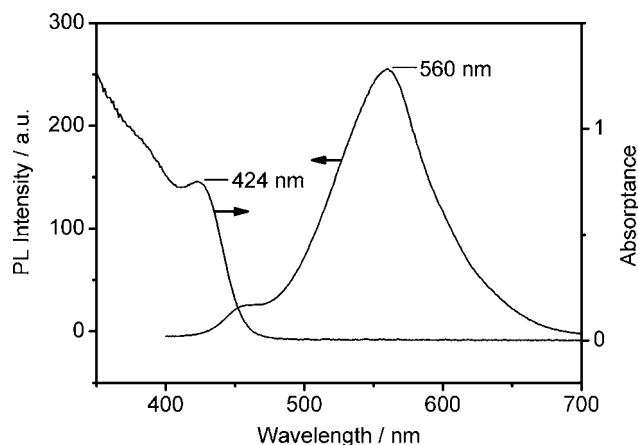


Fig. 1. UV–vis absorption and PL spectra of as-prepared TGA-modified CdSe QDs solution with 20-times dilution.

### 3.2. Electrochemical and ECL behaviors of CdSe QDs solution

In air-saturated pH 7.0 HCl–Tris buffer, the cyclic voltammogram of CdSe QDs at an ITO electrode showed an irreversible anodic peak at  $+0.919\text{ V}$ , while no any ECL emission could be observed (curve a, Fig. 2). After 0.2 mM sulfite was added into the solution, an intensive ECL emission peaked at  $+0.927\text{ V}$  occurred, accompanied with an increase of anodic peak current (curve b, Fig. 2). Sulfite itself could be oxidized at potentials more than  $+0.461\text{ V}$ , but did not show any ECL signal at the same concentration (curve c, Fig. 2). A control experiment showed that HCl–Tris buffer did not produce any observable response (curve d, Fig. 2). Although the anodic wave of CdSe QDs in presence of sulfite could be approximately considered as the sum of the anodic waves of CdSe QDs and sulfite, the anodic ECL emission of this system was obviously produced from the interaction of CdSe QDs and sulfite. The ECL intensity of this system was weaker than those of the most popular  $\text{Ru}(\text{bpy})_3^{2+/3+}/\text{TPRA}$  systems, however, it was strong enough for analytical purpose, and the ECL emission peak potential of  $\sim+0.9\text{ V}$  was about 200 mV lower than that of  $\text{Ru}(\text{bpy})_3^{2+/3+}/\text{TPRA}$  system, indicating a superiority for analysis.

To confirm what was the light emitter of this intensive ECL signal, excited  $\text{QDs}^*$  or  $\text{SO}_2^*$ , the ECL and PL spectra were carried out using the same detection solution. The ECL and PL spectra of CdSe QDs showed the peaks at 560.0 and 560.7 nm (Fig. 3), respectively, which were far from the emission range of  $\text{SO}_2^*$  light-emitter from 300 to 450 nm [23]. The good coincidence in peak position of ECL with that of PL emission confirmed that the light-emitter of the enhanced ECL system was the same as that of PL procedure, i.e. excited  $\text{QDs}^*$ . The same peak position and different emission processes of ECL from PL of QDs with core/shell structure indicated the surface of CdSe

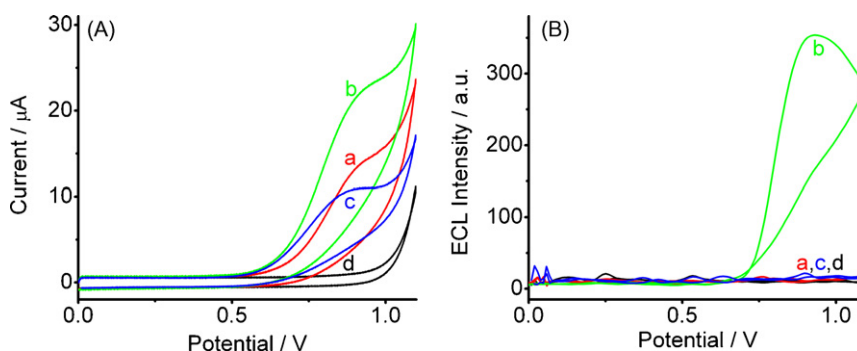
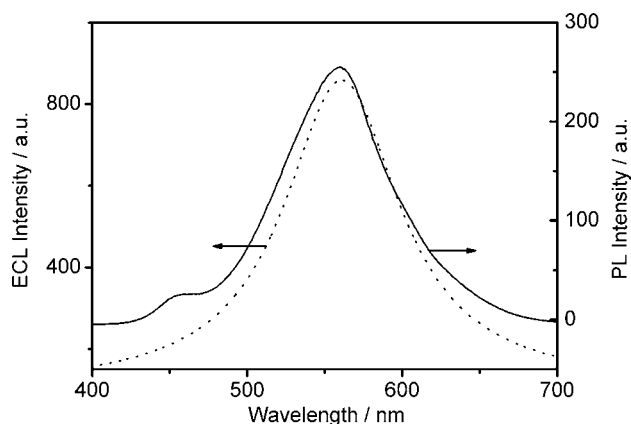


Fig. 2. Cyclic voltammograms (A) and ECL curves (B) of (a)  $5.76\ \mu\text{M}$  QDs, (b)  $5.76\ \mu\text{M}$  QDs + 0.2 mM sulfite, (c) 0.2 mM sulfite and (d) control in pH 7.0 air-saturated HCl–Tris buffer at ITO electrode. Scan rate:  $100\text{ mV s}^{-1}$ .





**Fig. 3.** Coreactant enhanced anodic ECL (dot line) and PL (solid line) spectra of TGA-modified CdSe QDs solution in presence of 0.6 mM sulfite. ECL data were collected at +0.927 V.

QDs was efficiently passivated [24]. During the anodic scanning sulfite as a coreactant could be oxidized to produce  $\bullet\text{SO}_3^-$  species that then reacted with dissolved oxygen to form  $\bullet\text{O}_2^-$  radical [13], which was a key species to produce electron injected QDs ( $\text{QDs}(e^-)$ ) [10]. The formed  $\text{QDs}(e^-)$  collided with hole injected QDs ( $\text{QDs}(h^+)$ ), electro-oxidation product of QDs, to produce the excited  $\text{QDs}^*$ . When  $\text{QDs}^*$  returned to the ground state the ECL emission occurred.

### 3.3. Effects of solution components on ECL emission

The anodic ECL intensity of CdSe QDs depended on the concentration of coreactant and pH value of HCl–Tris buffer. The maximum intensity occurred in pH 7.0 solution containing 0.6 mM sulfite, which was used in following work.

The components of buffer also affected the ECL emission of TGA-modified CdSe QDs. In air-saturated pH 7.0 phosphate buffer containing 0.6 mM sulfite and 5.76  $\mu\text{M}$  QDs the ECL emission peak occurred at +1.16 V, 230 mV more positive than that in HCl–Tris buffer (Fig. 4) and close to that of CdTe QDs in PBS [10]. This was possibly due to the absorption of phosphate on ITO surface, which made the electrode surface more negatively charged [25]. So a lower potential for anodic ECL emission was easily achieved by using HCl–Tris buffer, leading to an ECL analytical protocol at a relatively low-anodic potential.

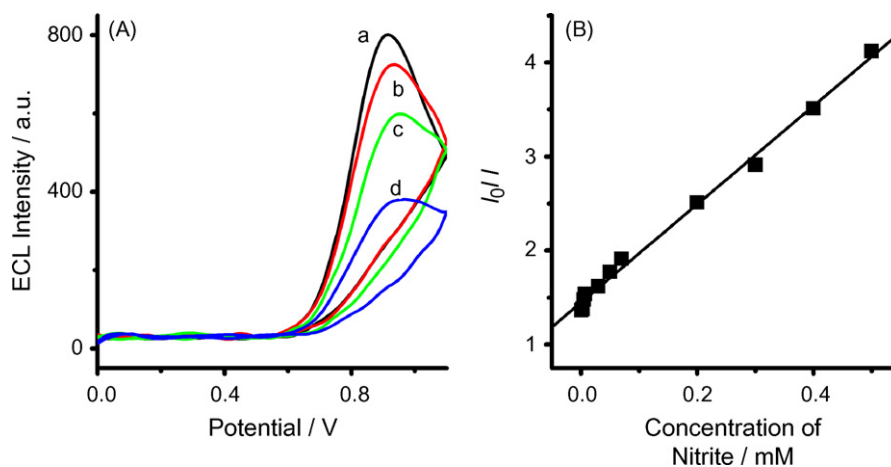


**Fig. 5.** Cyclic ECL curves of TGA-modified CdSe QDs in air-saturated pH 7.0 solution containing 0.6 mM sulfite and 0 (a), 0.1 (b), 1 (c) and 100 (d)  $\mu\text{M}$  nitrite at ITO electrode at 100  $\text{mV s}^{-1}$  (A) and calibration plot for nitrite detection (B).

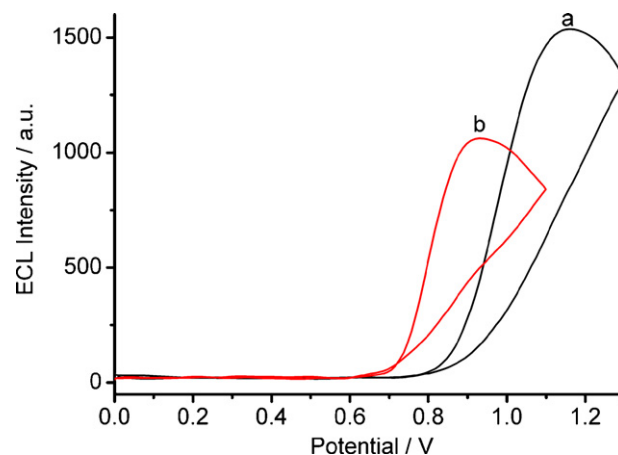


**Fig. 4.** Cyclic ECL curves of 5.76  $\mu\text{M}$  TGA-modified CdSe QDs in air-saturated pH 7.0 phosphate (a) and HCl–Tris (b) buffer in presence of 0.6 mM sulfite at ITO electrode. Scan rate: 100  $\text{mV s}^{-1}$ .

### 3.4. Nitrite detection based on its quenching effect on the anodic ECL emission

Some compounds such as nitrite have been proved to be electroactive ECL quenchers in  $\text{Ru}(\text{bpy})_3^{2+}$  system via an “electrochemical oxidation inhibition” mechanism [26]. The presence of these compounds produces larger IR drop and makes the practical potential  $E_w$  less than the applied potential  $E$  [26]:

$$E_w = E - IR = E - (I_q + I_{\text{emitter}})R \quad (1)$$

where  $I_q$  and  $I_{\text{emitter}}$  are the oxidation currents of the quencher and light-emitter. The lower  $E_w$  decreases the oxidation of light-emitter, leading to weaker ECL emission. Upon addition of nitrite into the detection solution, the ECL intensity at +0.927 V was attenuated (Fig. 5A), indicating an efficient quenching effect.

Based on the quenching effect on the anodic ECL emission of CdSe QDs, a rapid analytical method for nitrite detection could be developed. Under the optimal conditions, the plot of the ratio of initial ECL intensity  $I_0$  to the intensity  $I$  at a given nitrite concentration vs. nitrite concentration ranging from 1  $\mu\text{M}$  to 0.5 mM showed a linear relation ( $R=0.997$ ,  $n=11$ , Fig. 5B). The limit of detection (LOD) was 0.1  $\mu\text{M}$  at a quenching degree of 3 times noise. The relative standard deviation for five measurements at the nitrite concentration of 0 and 10  $\mu\text{M}$  was 2.20% and 3.84%, respectively, indicating accept-

**Table 1**  
Comparison of the proposed method with some electrochemical sensors.

Technique	Linear range ( $\mu\text{mol/L}$ )	LOD ( $\mu\text{mol/L}$ )	Precision	Ref.
Toluidine blue-based sensor	2.94–2110	1.76	1.8%	[18]
CdS QDs-based sensor	0.30–182	0.08	4.2%	[27]
Oxovanadium(IV)-4-methyl salophen-based sensor	3.90–4050	0.61	–	[19]
Nile blue-based sensor	0.5–100	0.1	3.53%	[28]
ECL technique	1–500	0.1	3.84%	This work

able reproducibility of the ECL system and this analytical method for nitrite detection.

The interference experiments were carried out under the same conditions as the nitrite detection. Common anions of  $\text{NO}_3^-$ ,  $\text{Cl}^-$  and cations of  $\text{Na}^+$ ,  $\text{K}^+$  and  $\text{NH}_4^+$  at the concentration of 20 mM did not cause any interference to the determination of 20  $\mu\text{M}$  nitrite, indicating an acceptable selectivity for this method. However, 0.1 mM  $\text{I}^-$  caused a great interference, where ECL intensity decreased by five times. According to the “electrochemical oxidation inhibition”, all coexisted electroactive species with lower oxidation potential than light emitter [26] would act as interferents in nitrite detection when the  $IR$  drop could not be neglected. Thus, the detection of practical samples should be carried out by combining with effective separation techniques.

As shown in Table 1, the proposed method had lower LOD and wider linear range than several reported electrochemical sensors. Moreover, the detection medium tended to be neutral, which would greatly benefit its application in bioanalytical filed.

#### 4. Conclusions

The mechanism of coreactant sulfite induced anodic ECL of CdSe QDs is studied in neutral system. Not only the concentration of sulfite and solution pH but also the components of buffer play important roles for obtaining the sensitive ECL emission at a relatively low potential. The ECL emitter has been proved to be the excited QDs, which is produced from the collision of hole and electron injected QDs. The electron injected QDs result from the reaction of QDs with  $\text{O}_2^-$  formed in presence of oxidized sulfite and dissolved oxygen. The anodic ECL emission can be quenched by electroactive quenchers such as nitrite via an “electrochemical oxidation inhibition” mechanism, producing the first ECL method for detection of nitrite, with rapid speed, acceptable sensitivity and selectivity. By combined with effective separation techniques, this method could be further developed for detection of nitrite in complex practical samples. The CdSe QDs provide a potential alternative

for developing new ECL emitters. This work significantly extends the application of QDs for constructing new rapid analytical methods of electroactive quenchers.

#### Acknowledgements

We gratefully acknowledge the support of the National Science Fund for Creative Research Groups (20521503), the Key Program (20535010) and Major Research Plan (90713015) from the National Natural Science Foundation of China.

#### References

- [1] S. Kulmala, J. Suomi, Anal. Chim. Acta 500 (2002) 21.
- [2] Z. Ding, B.M. Quinn, S.K. Haram, L.E. Pell, B.A. Korgel, A.J. Bard, Science 296 (2002) 1293.
- [3] A.P. Alivisatos, Science 271 (1996) 933.
- [4] H. Jiang, H.X. Ju, Chem. Commun. (2007) 404.
- [5] G.Z. Zou, H.X. Ju, Anal. Chem. 76 (2004) 6871.
- [6] S.N. Ding, J.J. Xu, H.Y. Chen, Chem. Commun. (2006) 3631.
- [7] H. Jiang, H.X. Ju, Anal. Chem. 79 (2007) 6690.
- [8] G.F. Jie, B. Liu, H.C. Pan, J.J. Zhu, H.Y. Chen, Anal. Chem. 79 (2007) 5574.
- [9] G.F. Jie, H.P. Huang, X.L. Sun, J.J. Zhu, Biosens. Bioelectron. 23 (2008) 1896.
- [10] X. Liu, H. Jiang, J.P. Lei, H.X. Ju, Anal. Chem. 79 (2007) 8055.
- [11] L.H. Zhang, X.Q. Zou, E. Ying, S.J. Dong, J. Phys. Chem. C 112 (2008) 4451.
- [12] M.M. Richter, Chem. Rev. 104 (2004) 3003.
- [13] X. Liu, H.X. Ju, Anal. Chem. 13 (2008) 5377.
- [14] X. Liu, L.X. Cheng, J.P. Lei, H.X. Ju, Analyst 133 (2008) 1161.
- [15] A. Aydin, O. Ercan, S. Tascioglu, Talanta 66 (2005) 1181.
- [16] I.M.P.L.V.O. Ferreira, S. Silva, Talanta 74 (2008) 1598.
- [17] P. Mikuška, Z. Večeřa, Anal. Chim. Acta 495 (2003) 225.
- [18] K. Thenmozhi, S.S. Narayanan, Electroanalysis 19 (2007) 2362.
- [19] M.A. Kamyabi, F. Aghajanloo, J. Electroanal. Chem. 614 (2008) 157.
- [20] Z.H. Wen, T.F. Kang, Talanta 62 (2004) 351.
- [21] M.G. Almeida, C.M. Silveira, J.J.G. Moura, Biosens. Bioelectron. 22 (2007) 2485.
- [22] W.W. Yu, L.H. Qu, W.Z. Guo, X.G. Peng, Chem. Mater. 15 (2003) 2854.
- [23] H.W. Sun, L.Q. Li, X.Y. Chen, Anal. Chim. Acta 576 (2006) 192.
- [24] N. Myung, Y. Bae, A.J. Bard, Nano Lett. 3 (2003) 1053.
- [25] B.P. Nelson, R. Candal, R.M. Corn, M.A. Anderson, Langmuir 16 (2000) 6094.
- [26] Y.W. Chi, Y.Q. Dong, G.N. Chen, Anal. Chem. 79 (2007) 4521.
- [27] Z.H. Dai, H.Y. Bai, M. Hong, Y.Y. Zhu, J.C. Bao, J. Shen, Biosens. Bioelectron. 23 (2008) 1869.
- [28] X.W. Chen, F. Wang, Z.L. Chen, Anal. Chim. Acta 623 (2008) 213.



# Inorganic arsenic speciation analysis of water samples by trapping arsine on tungsten coil for atomic fluorescence spectrometric determination

Rui Liu<sup>a</sup>, Peng Wu<sup>b</sup>, Maoyang Xi<sup>a</sup>, Kailai Xu<sup>a</sup>, Yi Lv<sup>a,\*</sup>

<sup>a</sup> Key Laboratory of Green Chemistry & Technology, Ministry of Education, College of Chemistry, Sichuan University, Chengdu, Sichuan 610064, China

<sup>b</sup> Analytical & Testing Center, Sichuan University, Chengdu, Sichuan 610064, China

## ARTICLE INFO

### Article history:

Received 28 August 2008

Received in revised form 24 December 2008

Accepted 24 December 2008

Available online 20 January 2009

### Keywords:

Hydride trapping

Atomic fluorescence spectrometry

Tungsten coil

Rhodium chemical modifier

Arsenic

Speciation analysis

## ABSTRACT

Arsine trapping on resistively heated tungsten coil was investigated and an analytical method for ultra-trace arsenic determination in environmental samples was established. Several chemical modifiers, including Re, Pt, Mo, Ta and Rh, were explored as permanent chemical modifiers for tungsten coil on-line trapping and Rh gave the best performance. Arsine was on-line trapped on Rh-coated tungsten coil at 640 °C, then released at 1930 °C and subsequently delivered to an atomic fluorescence spectrometer (AFS) by a mixture of Ar and H<sub>2</sub> for measurement. In the medium of 2% (v/v) HCl and 3% (m/v) KBH<sub>4</sub>, arsine can be selectively generated from As(III). Total inorganic arsenic was determined after pre-reduction of As(V) to As(III) in 0.5% (m/v) thiourea–0.5% (m/v) ascorbic acid solution. The concentration of As(V) was calculated by difference between the total inorganic arsenic and As(III), and inorganic arsenic speciation was thus achieved. With 8 min on-line trapping, the limit of detection was 10 ng L<sup>-1</sup> for As(III) and 9 ng L<sup>-1</sup> for total As; and the precision was found to be <5% R.S.D. (*n* = 7) for 0.2 ng mL<sup>-1</sup> As. The proposed method was successfully applied in total arsenic determination of several standard reference materials and inorganic arsenic speciation analysis of nature water samples.

© 2009 Elsevier B.V. All rights reserved.

## 1. Introduction

Gas-phase trapping of volatile hydrides/atoms has advantages of efficient enrichment, simple operation [1,2], and the alleviation/elimination of gas-phase interference in hydride atomization for analytical atomic spectrometry. In the past century, graphite furnace is the predominant trapping device, thanks to the development of chemical modifiers in graphite furnace atomic absorption spectrometry. Recently, several novel trapping materials have also been used: quartz tube [3,4], silica trap [5], molybdenum foil strip [6], tungsten tube [7], tungsten coil [8–14], and gold wire [15]. These novel traps offer substantial advantages over conventional graphite furnace, such as smaller size and lower power requirement. Among these traps, tungsten coil is more attractive due to its broad availability and fast heating rate [16,17].

Arsenic is a ubiquitous element that ranks the 20th in abundance in the earth's crust, the 14th in the seawater, and the 2nd in the human body [18]. Many epidemiological evidences show that arsenic in drinking water causes diseases such as skin cancer and several internal cancers, especially lung, bladder and kidney cancers [19]. Besides, recent irregular anthropogenic activities have

resulted in worldwide arsenic contamination problems, especially in Southeast Asian countries [20]. Inorganic arsenicals are the major species found in water samples, and the trivalent species poses more significant threats to human beings [21]. Being aware of the toxicity of the arsenicals, worldwide authorities have already set 10 µg L<sup>-1</sup> as the limit in drinking water [21]. The low concentration of arsenic together with the requirement for arsenic speciation to address the exact toxicity of arsenicals in drinking water has posed significant challenge to scientific community [22–28].

Atomic fluorescence spectrometry (AFS) is a great technique for trace elemental analysis, and especially advantageous for those elements, such as As and Se, that can easily form volatile hydrides for sample introduction. Recently, tungsten coil electrothermal vaporization has also been successfully used for sample introduction into AFS [29,30] in our laboratory. In order to further increase the sensitivity for arsenic determination, we combined the use of tungsten coil for arsine trapping and ETV sample introduction for AFS determination for the purpose of inorganic arsenic speciation.

## 2. Experimental

### 2.1. Instrumentation

A model AFS-2202 non-dispersive atomic fluorescence spectrometer (Beijing Haiguang Instrument Co., Beijing, China) was

\* Corresponding author. Tel.: +86 28 85412798; fax: +86 28 85412798.  
E-mail address: [lvvy@scu.edu.cn](mailto:lvvy@scu.edu.cn) (Y. Lv).

**Table 1**  
AFS working parameters.

Parameter	Setting
As hollow cathode lamp	193.7 nm, 80 mA
Negative voltage of photomultiplier tube	320 V
Observation height	7 mm
Read mode	Peak area
Shield gas flow rate	1200 mL min <sup>-1</sup>
Carrier argon flow rate	200 mL min <sup>-1</sup>
Carrier hydrogen flow rate	60 mL min <sup>-1</sup>

used in this work. The instrument is equipped with a programmable intermittent reactor and two gas–liquid separators to facilitate hydride generation and gas–liquid separation. Arsenic high-intensity hollow cathode lamp (HCL, Research Institute of Non-Ferrous Metals, Beijing, China) was used as the radiation source. The working parameters of HG-AFS were optimized and summarized in Table 1.

The tungsten coil electrothermal trapper and its connection to AFS have been described previously [30]. A tungsten coil was extracted from a commercially available slide projector bulb (HLX 64633, OSRAM, Munich, Germany) and assembled to the laboratory-constructed ETv glass cell. The coil temperature in Celsius was based on voltamperometric measurement. A mixture of Ar and H<sub>2</sub> was employed as carrier gas, and Ar was served as shield gas.

A common microwave oven (Model PJ17C-M, Midea Corporation, Guangdong, China) with a full power of 700 W was used for the closed-vessel (70 mL Teflon containers) microwave sample digestion. An electric hot plate (Model EH20A, LabTech Corporation, Beijing, China) with a controllable temperature range of 40–250 °C was used for the evaporation of the digests.

## 2.2. Reagents

All reagents used were of analytical-reagent grade, except hydrochloric acid (Beijing Chemical Research Institute, China) was Metal-oxide semiconductor (MOS) grade (with lower blank arsenic levels than analytical grade ones). High purity doubly distilled water (DDW) was used throughout the whole work. All solutions were stored in high-density polyethylene bottles. Plastic bottles and glassware materials were cleaned by soaking in 10% (v/v) HNO<sub>3</sub> for 24 h, rinsing five times with DDW and dried in a clean oven.

Standard stock solution of As(III) (1000 mg L<sup>-1</sup>) was purchased from the National Center for Reference Material (Beijing, China). As(V) (1000 mg L<sup>-1</sup>) standard stock solution, was prepared by dissolving 0.416 g Na<sub>2</sub>HAsO<sub>4</sub> (Merck) with 100 mL double-distilled water. Arsenic working solutions in the µg L<sup>-1</sup> and sub-µg L<sup>-1</sup> range were obtained by stepwise dilution from the stock solution. Solution of KBH<sub>4</sub> was stabilized with 3 g L<sup>-1</sup> KOH.

Several certified reference materials were purchased from National Center for Reference Material (Beijing, China) to validate the accuracy of the proposed method: GBW 07601, human hair; GBW 07605, tea leaf; and GBW(E) 08390 and GBW(E) 08391, simulated water. GBW 07601 and GBW 07605 were decomposed using microwave-assisted digestion. Briefly, 0.2 g of the sample powder was added to Teflon vessels containing 2 mL HNO<sub>3</sub> and 2 mL H<sub>2</sub>O<sub>2</sub>. The Teflon vessels were closed tightly and put into the microwave oven for digestion. The heating program was 200 W for 3 min, 400 W for 5 min, 700 W for 3 min, and 400 W for 3 min. After cooling to ambient temperature, the digests were then quantitatively transferred into Teflon crucibles and heated to almost dry on the electric hot plate at 200 °C. The residues were diluted with DDW and adjusted to the final composition containing 6% (v/v) hydrochloric acid, 0.5% (m/v) thiourea and 0.5% (m/v) ascorbic acid. 30 min pre-reduction time was used before total arsenic analysis. Water

samples were collected from the Hehua Lake on campus and Funan River in Chengdu, China. The water samples were filtered through a 0.45 µm filter prior to speciation analysis.

## 2.3. Coating tungsten coils

A newly extracted tungsten coil was subjected to the following heating program for noble-metal coating: 3.8 A, 60 s; 4.2 A, 30 s; 0 A, 5 s; and 7.0 A, 5 s. For all the metal solutions (Re, Pt, Mo, Ta and Rh, 1 g L<sup>-1</sup>), a 20 µL-aliquot was manually pipetted onto the coil surface for several trials, resulting in different amount of noble metal coated onto the coil surface. During the coating process, H<sub>2</sub> and Ar flow rates were kept constant at 40 and 300 mL min<sup>-1</sup>, respectively.

## 2.4. Procedure

For arsine generation, the reductant and the analyte solutions were pumped at a flow rate of 5 and 6 mL min<sup>-1</sup>, respectively, and mixed in a 3-way PTFE connector. Arsenic in 2% (v/v) hydrochloric acid and the reductant of 3% (m/v) KBH<sub>4</sub> solution was used for selective generation of arsine from As(III). For total As determination, pre-reduction of As(V) to As(III) with 0.5% (m/v) thiourea and 0.5% (m/v) ascorbic acid was carried out for 30 min. Arsenic in 6% (v/v) hydrochloric acid and the reductant of 3% (m/v) KBH<sub>4</sub> solution was used as optimum arsine generation medium of the pre-reduced solution.

The generated arsine was subjected to a two-step gas–liquid separation in order to ensure efficient elimination of moisture in the gas mixture, and trapped on the metal-coated tungsten coil. The on-line trapping procedure consisted of two steps: firstly, arsine was transported by a mixture of Ar (200 mL min<sup>-1</sup>) and H<sub>2</sub> (60 mL min<sup>-1</sup>) and trapped on the heated tungsten coil (640 °C, 5.0 A), and secondly, the enriched arsenic species was released by increasing the tungsten coil temperature to 1930 °C (8.0 A) and further swept to AFS detector for the measurement of arsenic.

## 3. Results and discussion

### 3.1. Separation of arsenic species and optimization of hydride generation parameters

Because of the difference of pK<sub>1</sub> between arsenic acid and arsenous acid at ambient conditions (2.3 for arsenic acid and 9.2 for arsenous acid), As(V) can react with KBH<sub>4</sub> with lower reaction kinetics than As(III), that is, differentiation of As(III) and As(V) could be achieved simply by exploiting the concentration dependency of the KBH<sub>4</sub> and HCl reaction [31]. Though such an approach is limited for inorganic arsenicals, it is applicable for the arsenic speciation in natural waters where inorganic arsenic species are dominant. In this work, the selective generation of arsine from As(III) was simply accomplished based on the use of appropriate concentration of HCl and KBH<sub>4</sub>. Then As(V) was reduced upon the pre-reduction with thiourea and ascorbic acid and total amount of As was subsequently obtained. The concentration of As(V) was obtained via subtraction of As(III) from the total As.

The effect of HCl concentration on the atomic fluorescence intensity of As(III) and As(V) was investigated and the results were shown in Fig. 1a. The signal intensity rises significantly with the concentration of HCl for both As(III) and As(V), and this corresponds to an improvement in the hydride generation efficiency from the two species. The signal intensity of As(III) and As(V) tended to level off when further increasing the HCl concentration after 6% (v/v). The influence of KBH<sub>4</sub> concentration on the generation of arsine from As(V) and As(III) was also studied with the results shown in Fig. 1b. An increase of KBH<sub>4</sub> concentration produces an increase of As(III) signal intensity and a decrease of As(V) signal intensity until

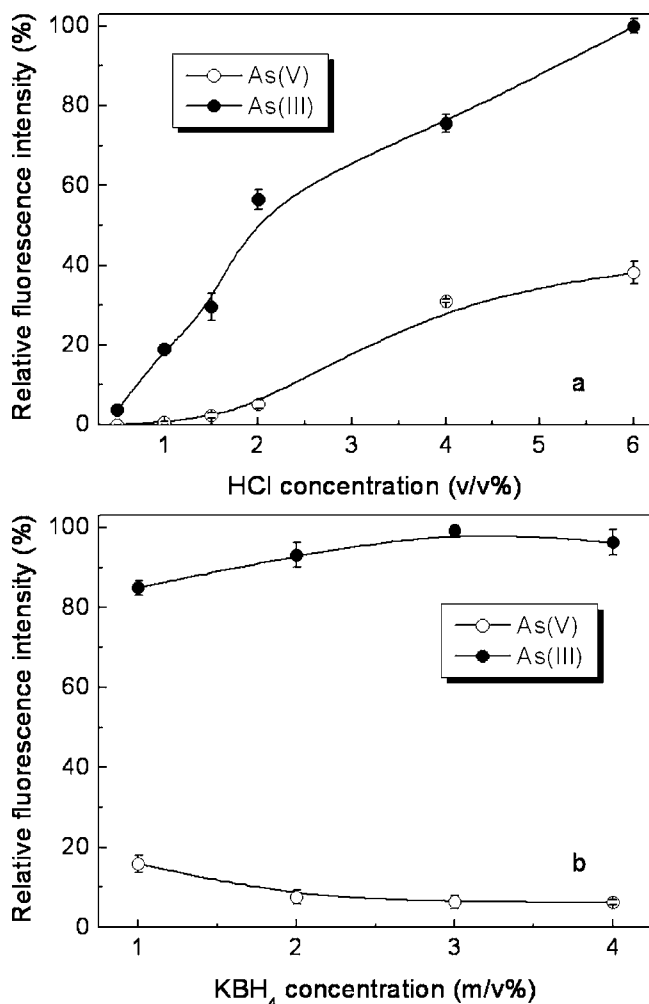


**Fig. 1.** As(III) and As(V) fluorescence signal intensity dependence on HCl concentration and KBH<sub>4</sub> concentration: (a) effect of HCl concentration with 2% (m/v) KBH<sub>4</sub> and (b) effect of KBH<sub>4</sub> concentration with 2% (v/v) HCl. The error bars indicate the S.D. of three replicates. The 100% fluorescence intensity represents the maximum signal intensity during the optimization of the corresponding parameter.

3% (m/v), and then the decrease of both As(III) and As(V) signal intensity was observed after that probably because of the analyte dilution caused by excessive produced hydrogen. Therefore, 2% (v/v) HCl and 3% (m/v) KBH<sub>4</sub> were selected for the selective arsine generation from As(III). Although partial overlap of the reduction of As(III) and As(V) to arsine exist (about 6% at the same concentration), this hydride generation condition was only selected for systematic optimization considering both separation efficiency and sensitivity. For higher concentration ratios of As(V) to As(III), the resolution between As(III) and As(V) should be increased by lowering the HCl concentration, as indicated by Kumar and Riyazuddin [31].

It was found that upon pre-reduction for 30 min with 0.5% (m/v) of thiourea and 0.5% (m/v) of ascorbic acid at room temperature, As(V) was successfully converted to As(III). Total amount of As was thus determined at the optimal HCl and KBH<sub>4</sub> condition, i.e., 6% (v/v) HCl and 2% (m/v) KBH<sub>4</sub>.

### 3.2. Optimization of tungsten coil trapping conditions

#### 3.2.1. Evaluation of permanent modifier coating

Permanent chemical modifier was firstly introduced to tungsten coil hydride trapping by Barbosa et al. for selenium hydride trapping [14], later they have investigated the trapping of arsine with rhodium-coated coil [11]. Generally, the use of permanent chemical

modifiers in tungsten coil trapping was inherited from the knowledge of hydride trapping in graphite furnace. Bare tungsten coil can trap bismuth hydride [30], as tungsten is also an important chemical modifier in graphite furnace. However, this is not applicable for Se, As and Sb and thus further coating of the tungsten coil with a thin layer of noble metal was indispensable. We also demonstrated that the noble metal coating was more effective than the bare tungsten coil, resulting in 60% increase of trapping efficiency [30]. Preliminary experiments in this work showed that trapping of arsine was not successful with un-coated tungsten coil. Since, several potential chemical modifiers, i.e., Pt, Rh, Re, Ta and Mo (200 μg), were coated on tungsten coil for trapping of arsine. As shown in Fig. 2a, all these metals pose the ability for arsine trapping, but their performances are varied. Ta coating exhibits a best trapping efficiency but the signal intensity was highly unstable. Finally, Rh coating was chosen for the further studies considering both trapping efficiency and stability.

The suitable amount of Rh coated on tungsten coil was investigated in the range of 50–400 μg. As shown in Fig. 2b, for routine trapping, 50 μg amount is enough. Several former studies have shown the coated amount has a close relationship with the lifetime of the coating [11,30,32]. And considering the tedious operation of the metal coating, 400 μg amount was selected. In this work, each coating (400 μg Rh) remained stable for about 300 firings, and up to 10% signal intensity loss could be observed thereafter, thus recoating was needed.

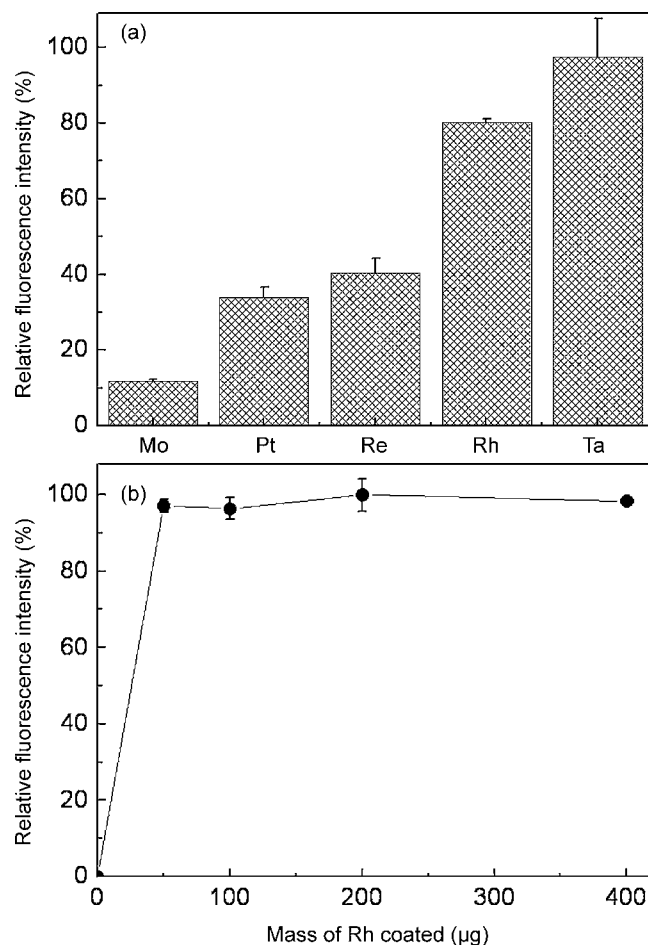


**Fig. 2.** Effect of W-coil permanent chemical modifiers: (a) comparison of different metal modifiers and (b) comparison of different amounts of Rh modifier. The error bars indicate the S.D. of three replicates. The 100% fluorescence intensity represents the maximum signal intensity during the optimization of the corresponding parameter.

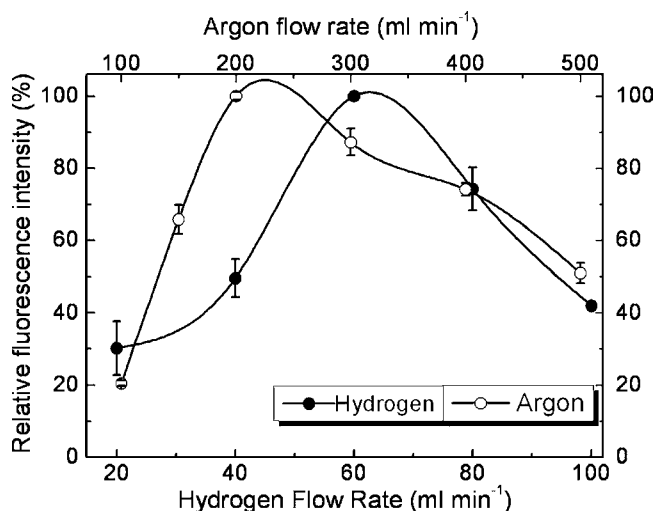


**Fig. 3.** Effect of carrier hydrogen and argon gas flow rates: trapping time 120 s,  $1.0 \text{ ng mL}^{-1}$  As; argon flow rate was  $200 \text{ mL min}^{-1}$  as the hydrogen flow rate was varied; hydrogen flow rate was  $60 \text{ mL min}^{-1}$  as the argon flow rate was varied. The error bars indicate the S.D. of three replicates. The 100% fluorescence intensity represents the maximum signal intensity during the optimization of the corresponding parameter.

### 3.2.2. Effect of trapping temperature and vaporization temperature

Coil temperature was a key parameter for W-coil hydride trapping. The optimum trapping temperature of tungsten coil was found to be  $640^\circ\text{C}$  (5.0 A), while Barbosa et al. reported a maximum arsenic trapping efficiency at the temperature of  $520^\circ\text{C}$  on Rh-coated tungsten coil [11] and Dočekal and Marek [7] found  $700\text{--}900^\circ\text{C}$  was the best for arsenic trapping on Rh-coated tungsten tube. The difference in trapping temperature between these works probably lies in a comprehensive effect of carrier gas composition and flow rate, mass of Rh modifier as well as the construction of trapping device, which affects the interaction between arsenic hydride and tungsten surface. In order to determine the optimum vaporization temperature, the trapping temperature was set to  $640^\circ\text{C}$  (5.0 A) and the vaporization temperature was varied between  $1630$  and  $2060^\circ\text{C}$  (7.0–8.5 A). The fluorescence signal intensity increased with temperature up to  $1930^\circ\text{C}$  (8.0 A) and stayed constant between  $1930$  and  $2060^\circ\text{C}$  (8.0–8.5 A); therefore,

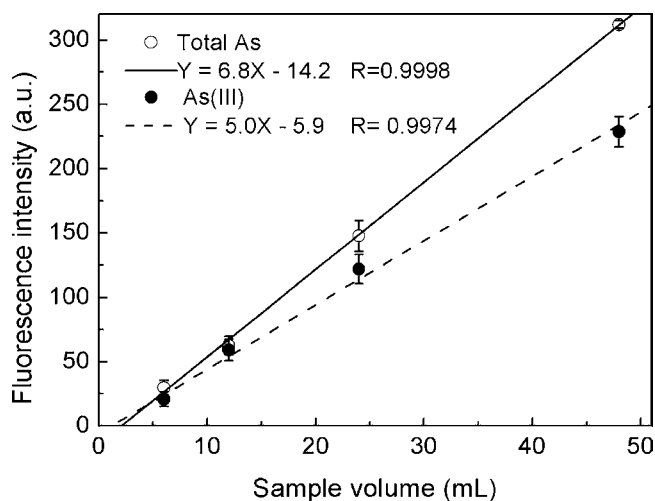


**Fig. 4.** Analytical signal intensity versus sample volume for  $0.2 \text{ ng mL}^{-1}$  As(III) and total As: sampling rate,  $6 \text{ mL min}^{-1}$ . The error bars indicate the S.D. of three replicates.

**Table 2**  
Analytical figures of merit of the proposed method.

Parameter	W-coil trap AFS	
	As(III)	Total As
Sample volume (mL)	48	48
Trapping time (min)	8	8
Calibration function	$I_f = 1118 C (\mu\text{g L}^{-1}) + 4.943$	$I_f = 1673 C (\mu\text{g L}^{-1}) - 3.120$
Correlation coefficient (R)	0.9995	0.9994
Limit of detection ( $\text{ng L}^{-1}$ ) ( $3\sigma$ )	10	9
Absolute limit of detection (ng) ( $3\sigma$ )	0.5	0.4
Precision (R.S.D., %)	4.9 ( $0.2 \mu\text{g L}^{-1}$ , $n=7$ )	4.2 ( $0.2 \mu\text{g L}^{-1}$ , $n=7$ )

$1930^\circ\text{C}$  (8.0 A) was selected as the vaporization temperature. With vaporization temperature lower than  $1930^\circ\text{C}$  (8.0 A), instability of the signal intensity caused by memory effects was also observed as was reported in our previous work of bismuth trapping [30].

Although the exact mechanism for arsine trapping was absent presently, we can still get some knowledge from the well-known Marsh test used in toxicology for detection of arsenic that arsenic atoms may be the eventual trapped species. After gas–liquid separation, the gaseous phase contains considerable amount of oxygen as an impurity [33]. As indicated by Dočekal [6], very fast reaction of hydrogen with oxygen can be induced upon contact of gaseous species with heated trapping device with catalysts such as noble metals. Accordingly, hydrides may be converted to corresponding atoms and subsequently trapped by the tungsten coil. In our previous work of tungsten coil electrothermal vaporization-AFS [29], the best vaporization temperature for arsenic was  $1730^\circ\text{C}$ , it is expected arsenic atoms were sputtered from the tungsten coil at the vaporization stage. Similar vaporization temperature in these two works may confirm that the analyte species vaporized from tungsten coil in the current work is probably arsenic atoms. However, further study concerning the trapping mechanism is still needed.

### 3.3. Effect of the gas flow rate

#### 3.3.1. Effect of hydrogen and argon carrier gas flow rates

Carrier gas flow rate was another key parameter for W-coil as was reported in graphite furnace hydride trapping [2]. The effects of the flow rates of Ar and  $\text{H}_2$  on the trapping of arsenic hydride are shown in Fig. 3. When the W-coil atomizer was used, an addi-

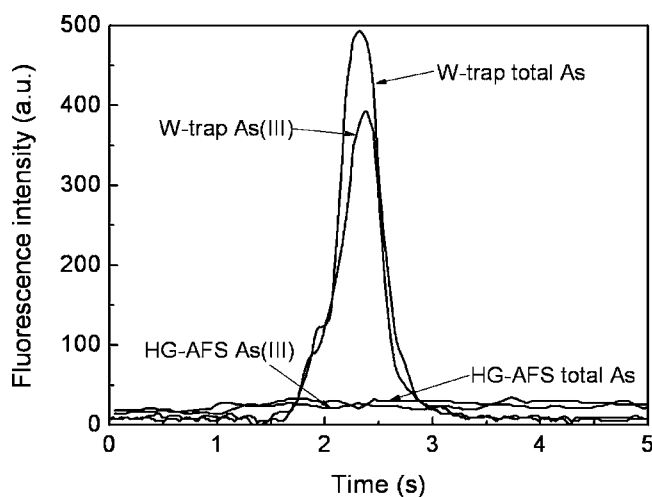


**Fig. 5.** The analytical signal obtained from  $1 \text{ ng mL}^{-1}$  As by the W-trap HG-AFS with 120 s trapping and conventional HG-AFS. The parameters used for conventional HG-AFS are the same with W-trap HG-AFS except tungsten coil conditions.

**Table 3**  
Comparison of the LODs by similar methods.

Method	Total As		As(III)		Sample volume (mL)	Ref.
	Relative LODs ( $\mu\text{g L}^{-1}$ )	Absolute LODs (pg)	Relative LODs ( $\mu\text{g L}^{-1}$ )	Absolute LODs (pg)		
W-trap HG-AFS	0.009	430	0.01	480	48	This work
HG-AFS	0.07	70	0.09	90	1	This work
W-coil ETV-AFS	10	200	– <sup>a</sup>	– <sup>a</sup>	0.02	[29]
W-trap HG-AAS	0.11	160	– <sup>a</sup>	– <sup>a</sup>	1.5	[11]
In situ trapping tungsten tube atomizer-AAS	0.15	150	– <sup>a</sup>	– <sup>a</sup>	1	[7]
In situ trapping HG-GF-AAS	0.0043	43	– <sup>a</sup>	– <sup>a</sup>	10	[36]
Hydride trapping ETV-ICP-MS	0.014	7	– <sup>a</sup>	– <sup>a</sup>	0.5	[37]
In situ Trapping FAAS	4	40000	– <sup>a</sup>	– <sup>a</sup>	10	[38]
Fl on-line sorption HG-AFS	0.023	140	0.023	140	6	[39]
HG-cryotrapping-AAS	0.135	80	0.100	60	0.6	[40]

<sup>a</sup> No data available.**Table 4**  
Analytical results of standard reference materials in comparison with the certified values ( $n = 3$  for each sample).

Samples	Certified ( $\mu\text{g g}^{-1}$ )	Found ( $\mu\text{g g}^{-1}$ )
GBW 07601 Human hair	0.28 ± 0.05	0.26 ± 0.01
GBW 07605 Tea leaf	0.28 ± 0.04	0.27 ± 0.02
GBW(E) 08390 Simulated water	0.50 ± 0.02	0.48 ± 0.01
GBW(E) 08391 Simulated water	4.0 ± 0.1	4.0 ± 0.2

tional hydrogen gas is necessary in order to avoid oxidation of the W-coil [16]. Besides,  $\text{H}_2$  also serves as the build-up of the miniature Ar– $\text{H}_2$  flame in AFS. The hydrogen gas flow rate was varied between 20 and 100  $\text{mL min}^{-1}$ . When  $\text{H}_2$  flow rates were lower than 60  $\text{mL min}^{-1}$ , the oxidation of the W-coil can be observed visually after a few firings as vaporization cell became cloudy, and this would cause serious scattering due to the co-vaporization of the tungsten oxide [29]. The Ar flow rates were studied in the range of 100–500  $\text{mL min}^{-1}$ . At  $\text{H}_2$  flow rates higher than 60  $\text{mL min}^{-1}$  and Ar higher than 200  $\text{mL min}^{-1}$ , the fluorescence signal intensity decreases probably due to dilution of the analyte in the atom cell as well as purge effect to the adsorbed analyte on the tungsten coil surface. It is shown in Fig. 3 that lower flow rates of either Ar or  $\text{H}_2$  caused a sharp decrease of fluorescence signal intensity, which is different from bismuthine trapping in our previous work [30], probably because higher carrier gas flow rate is needed for the effective transportation of arsine [34]. In both trapping and vaporization steps, the same carrier gas flow rate was used for convenience consideration.

### 3.3.2. Effect of argon shield gas flow rate

Similar with the flame-in-gas-shield atomizer employed in hydride atomization developed by Dédina et al. [33,35], argon shield gas is used to prevent extraneous air from entering the current miniaturized Ar/ $\text{H}_2$  flame to ensure its stability. Thus the contamination from oxygen in extraneous air may result in reaction of free atoms with oxygen and hence decrease the free atom popula-

tion. In this work, higher signal intensity was obtained with higher shield gas flow rates; finally the shield gas flow rate was set to be 1200  $\text{mL min}^{-1}$  in the further studies, which is the upper limit of the instrument settings. The use of high shield gas flow rate also implied that arsine atomization was sensitive to extraneous oxygen interference.

## 3.4. Analytical figures of merit

### 3.4.1. Trapping time

The relation between the analytical signal intensity and the sample volume was investigated with a 0.2  $\text{ng mL}^{-1}$  As(III) solution using the hydride generation parameters for As(III) and total arsenic as shown in Fig. 4. In the current study, the sampling rate was 6  $\text{mL min}^{-1}$ . Good linearity of sample volume versus analytical signal intensity was found when the sample volume varied from 6 mL (60 s) to 48 mL (480 s). The reagent blank of As(III) and total arsenic was calculated to be about 0.04 and 0.1  $\text{ng mL}^{-1}$  respectively, which was a limitation for the LOD improvement for the proposed new technique. Reagent blank was thought to be brought by HCl used in the analyte solution.

### 3.4.2. Signal profile, calibration plots, precision and LOD

After selecting the optimum parameters for W-coil trap system, analytical figures of merit of the W-coil trap AFS for inorganic arsenic speciation are shown in Table 2. The reproducibility of the measurements was <5% R.S.D. ( $N=7$ ) for 8 min trapping of 0.2  $\text{ng mL}^{-1}$  As solution. A comparison of AFS signal profile shown in Fig. 5 was obtained for 1  $\text{ng mL}^{-1}$  As standard with and without W-trap, sensitivity improvement can be directly visualized. Without W-coil trap, no obvious signal peak was present; while with 120 s trapping, the signal peak for 1  $\text{ng mL}^{-1}$  is clearly visible. Temporal width of atomic fluorescence peak is as short as 2 s, in comparison, in conventional HG-AFS, signal width is at least 12 s because it accumulates sensitivity from a large sampling volume and thus relatively longer time is needed for delivering the sample to react with  $\text{KBH}_4$ . The calculated LOD ( $3\sigma$ ) for the determination is 10  $\text{ng L}^{-1}$  for

**Table 5**  
Determination of inorganic arsenic species in natural water samples.

Samples	Added ( $\mu\text{g L}^{-1}$ )		Found ( $\mu\text{g L}^{-1}$ ) <sup>a</sup>		Recovery %	
	As(III)	As(V)	As(III)	As(V) <sup>b</sup>	As(III)	As(V) <sup>b</sup>
Lake water	0	0	0.70 ± 0.01	0.10 ± 0.07	–	–
	0.50	0.50	1.22 ± 0.02	0.65 ± 0.02	104	110
	1.00	1.00	1.76 ± 0.06	1.02 ± 0.04	106	92
River water	0	0	0.23 ± 0.01	0.80 ± 0.03	–	–
	0.50	0.50	0.70 ± 0.02	1.32 ± 0.03	94	104
	1.00	1.00	1.27 ± 0.03	1.78 ± 0.03	104	98

<sup>a</sup> Mean of three determinations.<sup>b</sup> Calculated value.

As(III) and  $9 \text{ ng L}^{-1}$  for total As with 480 s trapping time. The limit of detection of the proposed method is compared with the literature values in Table 3. As seen in Table 3, the concentration limit of detection is comparable with the others or better. Compared with the proposed hyphenation system, either ICP-MS or GF-AAS is much more expensive. Furthermore, even better sensitivity can be easily achieved using longer trapping time, due to the good trapping capacity of the Rh-coated tungsten coil.

#### 3.4.3. Accuracy test

The accuracy of the proposed method for total arsenic determination was verified by analyzing several certified reference materials. The analytical results are given in Table 4 and a *t*-test shows that the analytical results by the proposed method have no significant difference from the certified values at the confidence level of 95%. To further verify the accuracy of the proposed method for inorganic arsenic speciation analysis, lake and river water samples were also analyzed. The water samples were filtered through a  $0.45 \mu\text{m}$  membrane filter and analyzed as soon as possible after sampling. In addition, the recovery experiments of different amounts of As(III) and As(V) were carried out, and the results are shown in Table 5. The results indicated that the recoveries were reasonable for trace analysis, ranging from 92 to 110%.

## 4. Conclusions

W-coil hydride trap was successfully applied in inorganic arsenic speciation analysis of water samples. Using proper reaction medium, arsine is selectively generated from As(III), on-line trapped on an rhodium-coated tungsten coil and subsequently vaporized and determined by AFS. Total inorganic arsenic could be determined after conversion of As(V) to As(III) with a reduction treatment by thiourea and ascorbic acid. The W-coil hydride trap greatly improved the sensitivity and the LOD for the determination of arsenic at ultratrace levels. Due to the great improvements of sensitivity as well as simplicity and cost-effectiveness, the proposed method may be used for the speciation of vapor forming organic arsenic species and speciation analysis of other vapor forming elements.

## Acknowledgements

The authors acknowledge the financial support for this project from the National Natural Science Foundation of China

[No.20835003 and 20875066] and Ministry of Education of China [NCET-07-0579].

## References

- [1] O.Y. Ataman, Spectrochim. Acta Part B 63 (2008) 825.
- [2] H. Matusiewicz, R.E. Sturgeon, Spectrochim. Acta Part B 51 (1996) 377.
- [3] İ. Menemenlioğlu, D. Korkmaz, O.Y. Ataman, Spectrochim. Acta Part B 62 (2007) 40.
- [4] J. Kratzer, J. Dědina, Spectrochim. Acta Part B 63 (2008) 843.
- [5] D.K. Korkmaz, N. Ertaş, O.Y. Ataman, Spectrochim. Acta Part B 57 (2002) 571.
- [6] B. Dočekal, Spectrochim. Acta Part B 59 (2004) 497.
- [7] B. Dočekal, P. Marek, J. Anal. At. Spectrom. 16 (2001) 831.
- [8] S. Titretir, E. Kendüzler, Y. Arslan, İ. Kula, S. Bakırdere, O.Y. Ataman, Spectrochim. Acta Part B 63 (2008) 875.
- [9] İ. Kula, Y. Arslan, S. Bakırdere, O.Y. Ataman, Spectrochim. Acta Part B 63 (2008) 856.
- [10] O. Alp, N. Ertaş, J. Anal. At. Spectrom. 23 (2008) 976.
- [11] S.S. de Souza, D. Santos, F.J. Krug, F. Barbosa, Talanta 73 (2007) 451.
- [12] O. Cankur, O.Y. Ataman, J. Anal. At. Spectrom. 22 (2007) 791.
- [13] O. Cankur, N. Ertaş, O.Y. Ataman, J. Anal. At. Spectrom. 17 (2002) 603.
- [14] F. Barbosa, S.S. de Souza, F.J. Krug, J. Anal. At. Spectrom. 17 (2002) 382.
- [15] X.M. Guo, X.W. Guo, J. Anal. At. Spectrom. 16 (2001) 1414.
- [16] X.D. Hou, B.T. Jones, Spectrochim. Acta Part B 57 (2002) 659.
- [17] P. Wu, Y. Zhang, R. Liu, Y. Lv, X. Hou, Talanta 77 (2009) 1778.
- [18] B.K. Mandal, K.T. Suzuki, Talanta 58 (2002) 201.
- [19] A.H. Smith, P.A. Lopipero, M.N. Bates, C.M. Steinmaus, Science 296 (2002) 2145.
- [20] C.F. Harvey, C.H. Swartz, A.B.M. Badruzzaman, N. Keon-Blute, W. Yu, M.A. Ali, J. Jay, R. Beckie, V. Niedan, D. Brabander, P.M. Oates, K.N. Ashfaq, S. Islam, H.F. Hemond, M.F. Ahmed, Science 298 (2002) 1602.
- [21] X.C. Le, X.F. Lu, X.F. Li, Anal. Chem. 76 (2004) 26A.
- [22] Z.L. Zhu, J.X. Liu, S.C. Zhang, X. Na, X.R. Zhang, Anal. Chim. Acta 607 (2008) 136.
- [23] Z.L. Zhu, S.C. Zhang, Y. Lv, X.R. Zhang, Anal. Chem. 78 (2006) 865.
- [24] D.J. Butcher, Appl. Spectrosc. Rev. 42 (2007) 1.
- [25] Y.L. Yu, Z. Du, M.L. Chen, J.H. Wang, J. Anal. At. Spectrom. 23 (2008) 493.
- [26] D.G. Kinniburgh, W. Kosmus, Talanta 58 (2002) 165.
- [27] X.H. Li, Y.Y. Su, K.L. Xu, X.D. Hou, Y. Lv, Talanta 72 (2007) 1728.
- [28] C.M. Xiong, M. He, B. Hu, Talanta 76 (2008) 772.
- [29] P. Wu, X.D. Wen, L. He, Y.H. He, M.Z. Chen, X.D. Hou, Talanta 74 (2008) 505.
- [30] R. Liu, P. Wu, K.L. Xu, Y. Lv, X.D. Hou, Spectrochim. Acta Part B 63 (2008) 704.
- [31] A.R. Kumar, P. Riyazuddin, Int. J. Environ. Anal. Chem. 87 (2007) 469.
- [32] X.D. Hou, Z. Yang, B.T. Jones, Spectrochim. Acta Part B 56 (2001) 203.
- [33] A. D'Ulivo, J. Dědina, L. Lampugnani, A. Selecká, Spectrochim. Acta Part B 60 (2005) 1270.
- [34] A. Martínez, A. Morales-Rubio, M.L. Cervera, M. de la Guardia, J. Anal. At. Spectrom. 16 (2001) 762.
- [35] J. Dědina, Spectrochim. Acta Part B 62 (2007) 846.
- [36] R.E. Sturgeon, S.N. Willie, G.I. Sproule, P.T. Robinson, S.S. Berman, Spectrochim. Acta Part B 44 (1989) 667.
- [37] J.W. Lam, R.E. Sturgeon, Atom. Spectrosc. 20 (1999) 79.
- [38] H. Matusiewicz, M. Krawczyk, Anal. Sci. 22 (2006) 249.
- [39] X.P. Yan, X.B. Yin, X.W. He, Y. Jiang, Anal. Chem. 74 (2002) 2162.
- [40] T. Musila, T. Matoušek, Spectrochim. Acta Part B 63 (2008) 685.





## Investigation of the nonspecific interaction between quantum dots and immunoglobulin G using Rayleigh light scattering

Jia Liu, Wei Zhao, Rong-Li Fan, Wei-Han Wang, Zhi-Quan Tian, Jun Peng, Dai-Wen Pang, Zhi-Ling Zhang\*

College of Chemistry and Molecular Sciences and State Key Laboratory of Virology, Wuhan University, Luojiashan, Wuhan 430072, Hubei, PR China

### ARTICLE INFO

#### Article history:

Received 16 August 2008

Received in revised form 11 December 2008

Accepted 12 December 2008

Available online 24 December 2008

#### Keywords:

Quantum dots

Immunoglobulin G

Nonspecific interaction

Rayleigh light scattering

### ABSTRACT

Quantum dots (QDs) have been used as a new class of bioprobes in medical imaging in recent years. The study of interaction between QDs and biomacromolecules is important for interpreting biological data. In this work, Rayleigh light scattering (RLS) was employed to investigate the nonspecific interaction between mercaptoacetic acid modified CdSe/ZnS quantum dots (MAA-QDs) and human immunoglobulin G (IgG). The conjugation processes between QDs and IgG in different conditions including addition sequence, pH were carefully studied. The addition of IgG to QDs solution was found to form a fixed size of QDs-IgG conjugate, with the QDs-to-IgG ratio of  $\sim 13$ , while the addition of QDs to IgG solution resulted in a gradually increased conjugate size, with variable QDs-to-IgG ratio till the binding saturation was reached.

© 2008 Elsevier B.V. All rights reserved.

### 1. Introduction

Quantum dots (QDs), a class of luminescent inorganic nanoparticles, have found their application as bioprobes in many fields such as cellular imaging with multicolour [1,2], monitoring protein movement *in vitro* [3], sensitive detection of some dangerous toxins [4,5] and bacteria [6,7], and live animal targeting and imaging [8–10], owing to their superior optical properties. Although a high sensitivity has been achieved by the use of QDs comparing with some traditional organic probes, some problems still need to be resolved, among which the nonspecific interaction between QDs and protein is an urgent one. In order to overcome its nonspecific adsorption, many methods have been developed, among which the modification of QDs with polyethylene glycol, a kind of biocompatible material, has been reported frequently [11,12]. However, the detailed investigation of the nonspecific interaction between QDs and protein, which involves the nature of this interaction and the nonspecific binding ratio of QDs to protein, is rarely reported.

Mainly two methods have been used to investigate the binding ratio of QDs to protein at present. One is to measure the diameter of QDs, QDs-protein conjugate and protein molecules, respectively, calculate the proportion of the diameter corresponding to QDs-protein conjugate in a visual field, then estimate the conjugation efficiency and ratio [13]. The high resolution of Atomic Force Microscopy (AFM) renders itself an unmatched tool in this job

[13]. However, the broad effect [14] of AFM tip and the limited size of the visual field in AFM measurement could add errors to the final result. Moreover, the manipulation of AFM usually depends on skills and is time-consuming, hampering the wide use of AFM. Another widely used method is the combination of chromatography separation and fluorescence detection, in which human immunoglobulin G (IgG) is labeled with a fluorescent dye [15]. Compared with AFM, fluorescence spectrometer is easy to operate and can realize the fast detection, and, because of the large size of visual field, the final result is more comprehensive and accurate. However, the influence of the fluorescent dye on the conjugation efficiency of QDs with IgG cannot be neglected and is not easy to estimate.

Rayleigh light scattering (RLS) is a new and attractive method for the analysis of micro-amount of biomacromolecules in recently years due to its simplicity, rapidness and high sensitivity [16]. Resonance-enhanced RLS was first brought forward by Pasternack in 1993 [17,18], and was further used for quantitative study of the interaction between DNA and some organic fluorescent dyes [19,20]. Although the conditions for resonance-enhanced RLS are not easily met, that is the enhanced scattering peak should be close to the absorption band [21], the applications of general RLS to biochemical analysis, in which RLS peaks appear around the least absorption, have also been reported [22–24]. Recently, some nanoparticles have shown their power in the analysis of biomacromolecules by RLS [25,26]. For example, highly sensitive and selective detection of standard proteins and the study of their functionality have been achieved by attachment of gold nanoparticles followed by silver enhancement and RLS detection [25]. In another study, gold RLS particles were used for sensitive detec-

\* Corresponding author. Tel.: +86 27 68756759; fax: +86 27 68754685.

E-mail address: [zhang@whu.edu.cn](mailto:zhang@whu.edu.cn) (Z.-L. Zhang).

tion of DNA hybridization on cDNA microarrays [26]. As the RLS enhancement is greatly influenced by the electric coupling effect and the aggregated particle size [16,17], which are both important factors in the conjugation of QDs to proteins, this technique was employed here to investigate the nonspecific interaction between mercaptoacetic acid modified CdSe/ZnS quantum dots (MAA-QDs) and IgG. The study mainly focuses on the interaction nature, conjugation efficiency, and the ratio of QDs conjugated to IgG in different conditions.

## 2. Experimental

### 2.1. Instruments

UV-vis absorbance spectra were taken on UV-VIS Spectrometer TU-1901 (Beijing Purkinje General). Fluorescence spectra were taken on fluorescence spectrometer LS55 (PerkinElmer). Fluorescence images of QDs (0.255  $\mu\text{M}$ , calculated according to Ref. [27]) and QDs-IgG conjugates (prepared by adding 6  $\mu\text{L}$  of 6.25  $\mu\text{M}$  IgG in 3 mL of 0.255  $\mu\text{M}$  QDs) were obtained using a Hg lamp with excitation wavelength of 365 nm and an oil objective (100 $\times$ ) on an inverted fluorescence microscope (FM) (Olympus IX70). For transmission electron microscopy (TEM) measurement, the QDs solution and QDs-IgG solution (both the same as for FM) were dropped directly onto copper grids coated with carbon film, and dried under a lamp. TEM were carried out on a JEOL-JEM 2010 microscope operated at 200 kV with the accelerating voltage of 200 kV. The RLS measurement was realized on a common fluorescence spectrometer (PerkinElmer, LS55) by choosing the mode of synchronous fluorescence ( $\Delta\lambda=0$ ) with appropriate widths for excitation slit and emission slit, and setting the scanning range from 200 to 700 nm. Dynamic light scattering (DLS) measurement was carried out on a Nano-ZS ZEN 3600 (MALVERN). To study the influence of pH on RLS of QDs-IgG conjugate system, 6  $\mu\text{L}$  of IgG solution (1 mg/mL, prepared in 0.1 M pH 7.0 phosphate buffer) was added in 3 mL of QDs solution (0.3  $\mu\text{M}$ , prepared in 0.1 M phosphated buffer with different pH values). Zeta potential of QDs (1  $\mu\text{M}$ ) and IgG (125  $\mu\text{M}$ ) (both prepared in pure water) was determined by a Zetasizer Nano ZS90 (Malvern Instruments), with three measurements for each solution.

### 2.2. Preparation of MAA modified QDs

CdSe/ZnS QDs were synthesized in our lab as previously reported [28]. For the purpose of water solubility, QDs were modified with MAA (Sigma-Aldrich). Briefly, tri-*n*-octylphosphine oxide (TOPO, Sigma-Aldrich)-capped CdSe/ZnS core-shell nanoparticles (1.5 mL), were first washed several times using ethanol to remove the TOPO molecules on the surface of the QDs. Then, the CdSe/ZnS core-shell nanoparticles were dispersed in 1 mL of *N,N'*-dimethylformamide using ultrasonic power before adding equivalent volume of MAA. After a 30-min shaking of the mixture, tetramethylammoniumhydroxide (Sigma-Aldrich) was added to deprotonate the terminal mercaptoacetic carboxyl group. At last, the MAA modified QDs were precipitated with 1 mL of tetrahydrofuran and redispersed in water.

## 3. Results and discussion

### 3.1. Spectra of QDs, IgG and QDs-IgG

In a typical resonance RLS, a special elastic scattering, could occur when the wavelength of Rayleigh scattering is located at or close to the molecular absorption band. The frequency of the electromagnetic wave absorbed by the electron is equal to its scattering frequency. Due to the rescattering caused by the intensive absorp-

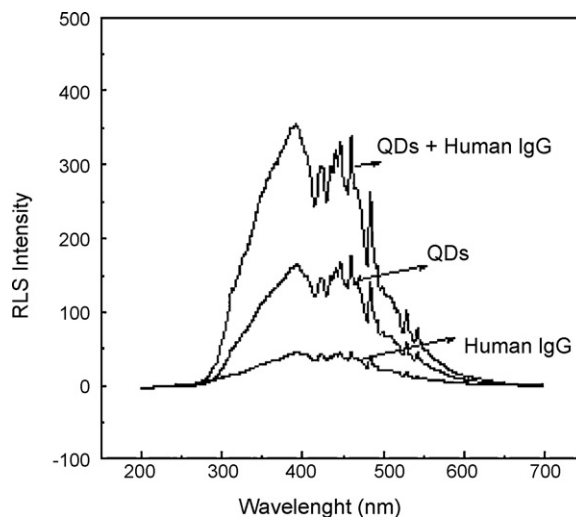


**Fig. 1.** RLS spectra of 0.255  $\mu\text{M}$  QDs, 6.25  $\mu\text{M}$  human IgG, and the solution containing both QDs and IgG (6  $\mu\text{L}$  of 6.25  $\mu\text{M}$  IgG added to 3 mL of 0.255  $\mu\text{M}$  QDs).

tion of light energy of the electron, the scattering intensity is greatly enhanced. Fig. 1 shows the RLS spectra of QDs, human IgG and the solution containing both QDs and IgG. Those RLS spectra are strong and wide, ranging from 300 to 600 nm. This is different from that of traditional organic dyes [16–20], the peak of which in resonance RLS spectrum is much narrower, with the peak near their maximum absorption in UV-vis spectrum. While for QDs, their RLS intensity and UV-vis absorption both cover a very wide wavelength range. The broad peak is not centered on the 380 nm QDs main absorption, and seems to be a combined result of (i) the strong absorption of the main UV feature of QDs, (ii) the low energy of the Xe lamp in the UV region and (iii) in general the instrument transfer function. In this case, the RLS observed in the present study is probably not a typical resonance RLS, but a conventional RLS, which occurs when the particle size is much smaller than the wavelength of the incidence light even when there is no strong absorption of light on the particle. However, even for a conventional RLS, an enhanced light scattering (LS) could still be generated when a dye interacts with some macromolecules [22,23].

In our study, a sharp increase of RLS signal was observed when mixing the human IgG solution with QDs solution (Fig. 1). Only an addition of 6  $\mu\text{g}$  (37.5 pmol, assuming molecular weight of human IgG is 160 kD) of IgG to 3 mL of QDs (0.255  $\mu\text{M}$ ) solution resulted in a twofold increase of RLS intensity. As the intensity of RLS signal is relative to the particle diameter [17,18], this increase reflects an interaction between QDs and human IgG, namely the formation of QDs-IgG clusters. This is also illustrated in the images taken by FM and TEM (Fig. 2). Fig. 2A and B shows that, after the addition of human IgG to the QDs solution, the dispersed nanoparticles came into agglomerates. This phenomenon was also confirmed by TEM. The interaction between QDs and IgG also caused a little red-shift for quantum confining peak in UV-vis absorption spectra (Fig. 3A) and fluorescence peak (Fig. 3B). The decrease of fluorescence intensity is probably because that, when several QDs nanoparticles in a QDs-IgG cluster are only isolated from each other by a distance not much larger than the size of one particle, fluorescence of those QDs would be significantly quenched due to re-absorption and Forster energy transfer [29,30].

### 3.2. Interaction nature between QDs and IgG

In our study, there were no activated or cross-linking reagents in the system, and under common conditions the terminal carboxyl group of MAA on QDs surface cannot combine with amino

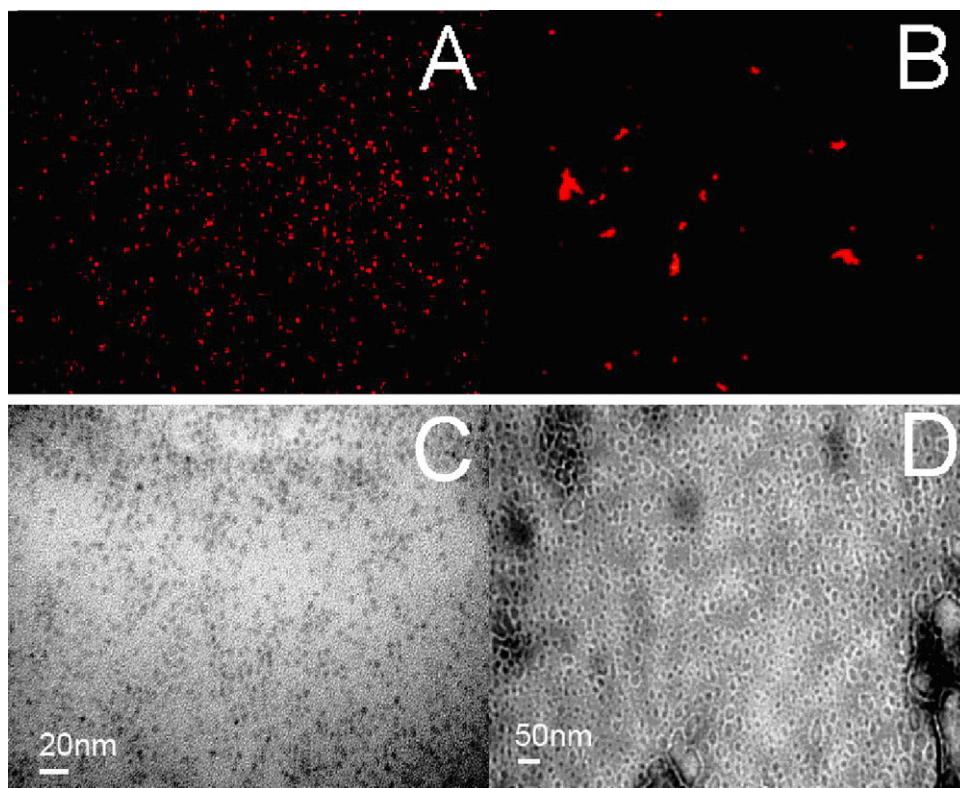


**Fig. 2.** Fluorescence microscopy images of MAA modified QDs (0.255  $\mu\text{M}$ ) (A) and QDs-IgG (6  $\mu\text{L}$  of 6.25  $\mu\text{M}$  IgG added to 3 mL of 0.255  $\mu\text{M}$  QDs) (B); TEM images of MAA modified QDs (0.255  $\mu\text{M}$ ) (C) and QDs-IgG (6  $\mu\text{L}$  of 6.25  $\mu\text{M}$  IgG added to 3 mL of 0.255  $\mu\text{M}$  QDs) (D).

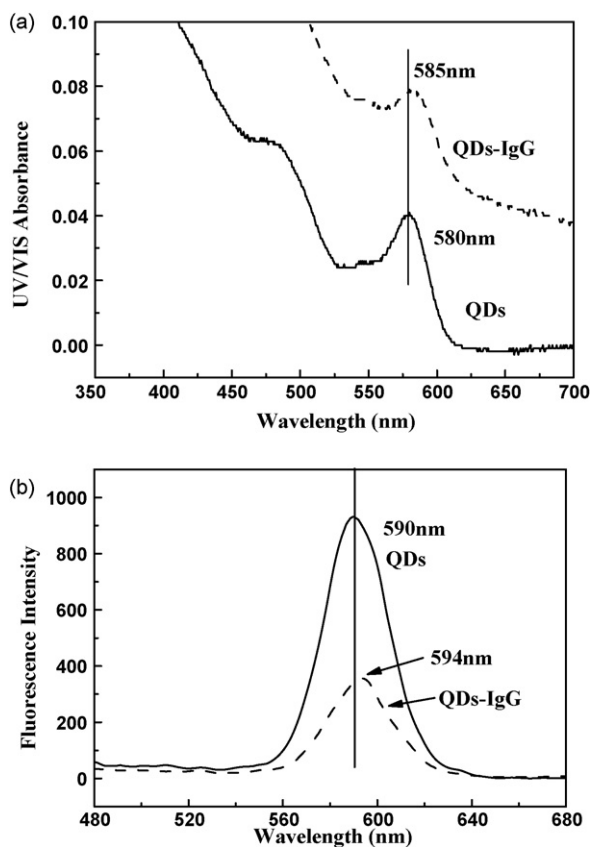


**Fig. 3.** The absorption spectra of QDs and QDs-IgG (A) and fluorescence spectra of QDs and QDs-IgG (B). The concentration of QDs was 0.255  $\mu\text{M}$ , and the QDs-IgG solution was prepared by adding 6  $\mu\text{L}$  of 6.25  $\mu\text{M}$  IgG to 3 mL of 0.255  $\mu\text{M}$  QDs.

acid of IgG in the manner of chemical bond. Therefore, the interaction between QDs and IgG in our research could be classified into noncovalent interaction, such as electrostatic interaction.

The influences of pH value of QDs solution on RLS intensity have been investigated to study this noncovalent interaction. Fig. 4 shows that, the RLS intensity at 380 nm does not fluctuate too much from pH 6.5 to 8.0, while a sharp increase of RLS intensity appears below pH 6.5. As the surface of QDs is negatively charged at pH values above the  $pK_a$  of MAA, 5.20, and human IgG is positively charged when pH is below its  $pI$  (6.0–7.0 [31]), the intensive electrostatic interaction between the two species could be the main reason of the increase of RLS intensity from pH 6.5 to 5.0. An increase in pH

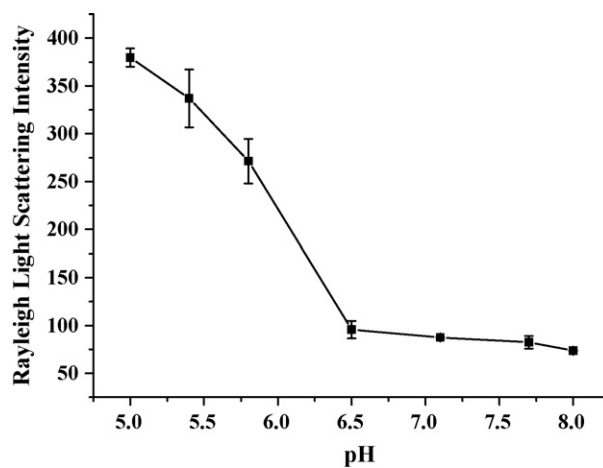


**Fig. 4.** The influence of pH values (0.1 M phosphate solution) on the RLS intensity of QDs-IgG conjugate solution. The concentrations of QDs and IgG are 0.3  $\mu\text{M}$  and 0.0125  $\mu\text{M}$ , respectively. Each dot represents the average of three measurements at a pH value, with the error bars showing the standard deviations.

leads to a decrease of positive charge on IgG, which can weaken the binding of QDs to IgG. The zeta potential of QDs and IgG in pure water was measured to be  $-12.6 \pm 0.3$  and  $-0.450 \pm 0.223$  mV, respectively. The weak negative charge of IgG in pure water is due to its 6.0–7.0 pI value, and could explain the relatively weak RLS intensity of QDs–IgG solution near pH 7.0 (Fig. 4).

### 3.3. Influence of addition sequence of QDs and IgG on conjugate formation

A simple and efficient method for evaluating the nonspecific interaction between QDs and IgG, such as the conjugation efficiency and the ratio of QDs conjugated to IgG was developed based on RLS. Previous studies have shown that, the sequence for mixing proteins and dyes result in different RLS intensities [23,24], suggesting an addition-sequence related interaction nature between biomacromolecules and nanoparticles. Therefore, the present study was carried out in two different conditions: one is adding human IgG solution to the QDs solution (QDs in excess), while the other is adding QDs solution to the human IgG solution (human IgG in excess). The relation between RLS intensity (at 380 nm) and the addition of human IgG in the first condition is shown in Fig. 5A. It can be seen that, with the addition of human IgG, RLS intensity increases linearly first and then levels off. According to Refs. [23,24], when all the other conditions are kept constant, the change of RLS intensity is related to two factors: one is the change of the particle size, and the other is the amount of particle formed. The linear increase of RLS intensity relative to the addition of IgG suggests a constant size variation. In other words, the particles investigated change from a fixed size (single QDs) to another fixed size (QDs–IgG conjugates), and the increase of RLS reflects an increased number of QDs–IgG conjugates, instead of the increased size of QDs–IgG conjugate. Therefore, in this situation, the size of QDs–IgG conjugates formed is kept almost constant. This was further confirmed by DLS experiments (Fig. 6A), in which the size distribution of QDs–IgG conjugates was kept in a narrow range. In Fig. 5A, the intersection point (P1) of two tangents could be regarded as the ideal conjugation saturation point, where the amount of human IgG added is 9.35  $\mu$ g, which amounts to 58.4 pmol, assuming that the molecular weight of human IgG is 160 kD. At the same time, there are 0.771 nmol of QDs in solution (calculated according to Ref. [27]). Therefore, the average number of QDs conjugated to a single human IgG molecule is 13.2. Although this QDs-to-IgG ratio seems very high considering the size of single QD and IgG, a similar result has been reported by other group [32], in which QDs were conjugated to IgG by covalent interaction instead of noncovalent interaction. The actual RLS intensity (dots in Fig. 5A) is lower than the ideal intensity probably owing to the equilibrium between the formation and dissociation of QD–IgG conjugate. The gap between the P1 and P2 could be attributed to the amount of free QDs and IgG. The conjugation efficiency (84%) is thus calculated by dividing the RLS intensity of P2 by that of P1.

In the second condition, QDs solution was added to human IgG solution in portions (3  $\mu$ L for each), with the recording of LS intensity after each addition. As shown in Fig. 5B, the slope of the left part of the curve (left of Q) decreases with the addition of QDs, reflecting a variable particle size owing to the unfixed QD–IgG ratio. This process does not end until a linear increase of LS appears (right side of Q). This is a different conjugation process compared with the first addition method. In the first method, the newly added free IgG molecules did not bind to the existed QDs–IgG conjugate (which carried an extra negative charge owing to the modification with MAA) efficiently due to the low positive charge density of IgG. In the second condition, however, when new QDs were added to the solution containing QDs–IgG conjugates (IgG wrap QD), the free QDs probably binded to not only the free IgG molecules but also the IgG

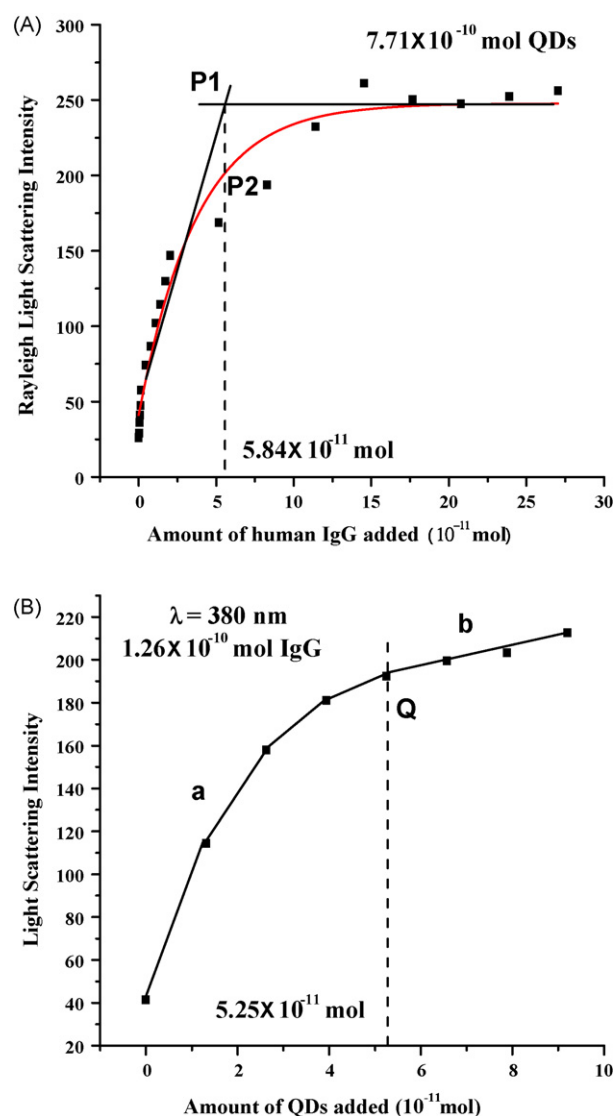
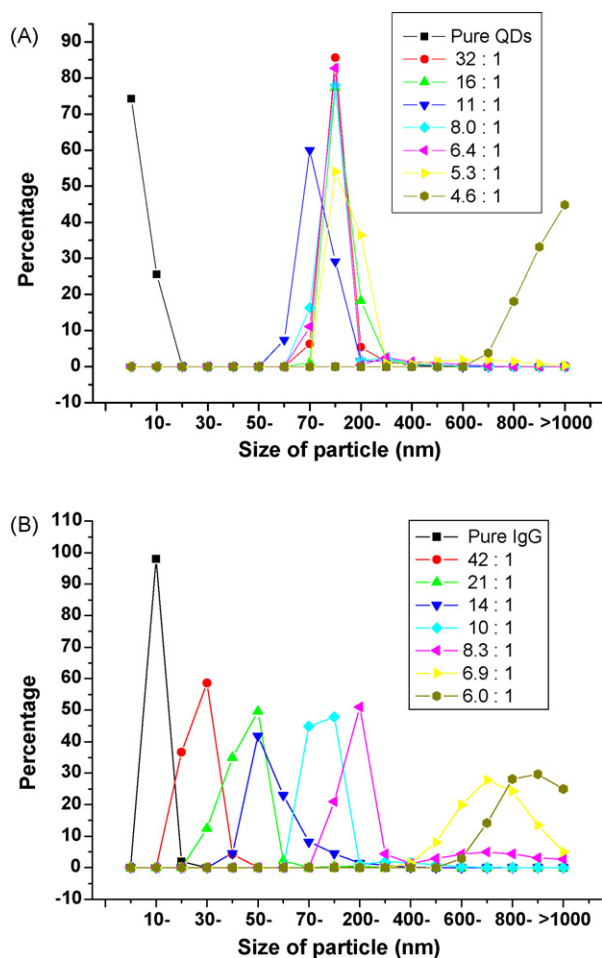


Fig. 5. The relationship between RLS intensity and the addition of human IgG, with the concentration of QDs kept constant (A); and the relationship between light scattering (LS) intensity with the addition of QDs, with the concentration of human IgG kept constant (B).

species on the surface of QDs–IgG conjugate due to the relatively high electric field of negatively charged QDs, resulting in a continuous increase of conjugate size in this process. The DLS signal (Fig. 6B) confirmed the continuously increased average particle size, which could be attributed to an increased number of QDs conjugated to IgG in this process. During the addition of QDs, the average size of particles in solution increased quickly, and finally surpassed the wavelength of the maximum absorption of QDs (380 nm), which is the upper limit for RLS. In this case, the total LS intensity probably include not only Rayleigh scattering on free QDs, free IgG and small-size QDs–IgG conjugates, but also non-RLS on large-size QDs–IgG conjugates. This led to a ruleless increased LS intensity for the left part of the curve in Fig. 5B. Once the saturation of conjugate size was reached (which was estimated to occur after addition of 52.5 pmol QDs in total, shown by Q in Fig. 5B), the LS showed a linear increased intensity, which is probably attributed to the increase of pure RLS on the newly added free QDs. However, further addition of QDs into the solution resulted in precipitation of QDs or QDs–IgG conjugates, which is unfavorable for biological application.



**Fig. 6.** Dynamic light scattering (DLS): (A) 5  $\mu$ L of IgG (6.25  $\mu$ M) solution was added to 1 mL of MAA-QDs solution (1  $\mu$ M) sequentially and (B) 3  $\mu$ L of MAA-QDs (1  $\mu$ M) was added to 1 mL of human IgG solution (0.125  $\mu$ M) sequentially. Different mole ratios of QDs-to-IgG and IgG-to-QDs are labeled in (A) and (B), respectively.

#### 4. Conclusions

In the present study, we developed a simple method for the investigation of nonspecific interaction between QDs and human IgG. By using RLS technique, not only the estimation of the ratio of QDs conjugated to IgG (IgG added to QDs solution) was obtained, but the whole process of the electrostatic conjugation between QDs and IgG could be observed in different conditions.

Comparing the results obtained from two addition sequences, the different behaviors in conjugation deserve paying attention. In the first condition, in which IgG was added to QDs solution, QD-IgG conjugates were formed with a relatively fixed size when new IgG was added to the QDs solution. This leads to a determinate QDs-to-IgG ratio of  $\sim$ 13. While in the second condition, the average size of QD-IgG conjugate continuously increase with the addition of QDs in IgG solution, resulting in an unpredictable particle size, till the binding saturation occurs.

The conclusion drawn from this study is essentially important for the interpretation of biological data labeled with QDs. Accord-

ing to our result, adding IgG to MAA labeled QDs could generate a constant QDs-IgG conjugate size, which is suitable for further application after purification of this QDs-IgG conjugate. While the addition of QDs to IgG solution could lead to errors in interpreting biological data. However, as this work is an initial study of the noncovalent interaction between QDs and IgG using RLS, which is an indirect method for quantifying the QDs-to-IgG ratio, other techniques are still needed to confirm the ratio determined in this work, as well as to explain the unclear situation in the second condition. Due to the advantages of RLS, e.g. convenience and sensitivity, we believe that more problems concerning the surface chemistry of QDs may be better understood by using this technique.

#### Acknowledgements

This work was supported by the National Key Scientific Programs-Nanoscience and Nanotechnology (2006CB933100), the Science Fund for Creative Research Groups (20621502), the 863 Program (2006AA03Z320), the National Natural Science Foundation of China (20505001 and 30570490), and the Ministry of Education (nos. 306011 and IRT0543).

#### References

- [1] X.Y. Wu, H.J. Liu, J.Q. Liu, K.N. Haley, A. Joseph, J.P. Larson, N.F. Ge, F. Peale, P.B. Marcel, *Nat. Biotechnol.* 21 (2003) 41.
- [2] Q. Ma, X. Wang, Y. Li, Y. Shi, X. Su, *Talanta* 72 (2007) 1446.
- [3] F. Pinaud, D. King, H.P. Moore, S. Weiss, *J. Am. Chem. Soc.* 126 (2004) 6115.
- [4] E.R. Goldman, G.P. Anderson, P.T. Tran, H. Mattoussi, P.T. Charles, J.M. Mauro, *Anal. Chem.* 74 (2002) 841.
- [5] B.M. Lingerfelt, H. Mattoussi, E.R. Goldman, J.M. Mauro, G.P. Anderson, *Anal. Chem.* 75 (2003) 4043.
- [6] X.L. Su, Y. Li, *Anal. Chem.* 76 (2004) 4806.
- [7] M.A. Hahn, J.S. Tabb, T.D. Krauss, *Anal. Chem.* 77 (2005) 4861.
- [8] S. Kim, Y.T. Lim, E.G. Soltész, A.M. De Grand, J.Y. Lee, A. Nakayama, J.A. Parker, T. Mihajljevic, R.G. Laurence, D.M. Dor, L.H. Cohn, M.G. Bawendi, J.V. Frangioni, *Nat. Biotechnol.* 22 (2004) 93.
- [9] M.K. So, C.J. Xu, A.M. Loening, S.S. Gambhir, J.H. Rao, *Nat. Biotechnol.* 24 (2006) 339.
- [10] Y. Shan, L. Wang, Y. Shi, H. Zhang, H. Li, H. Liu, B. Yang, T. Li, X. Fang, W. Li, *Talanta* 75 (2008) 1008.
- [11] E.L. Bentzen, I.D. Tomlinson, J. Mason, P. Gresch, M.R. Warnement, D. Wright, E. Sanders-Bush, R. Blakely, S.J. Rosenthal, *Bioconjugate Chem.* 16 (2005) 1488.
- [12] J. Lee, J. Kim, E. Park, S. Jo, R. Song, *Phys. Chem. Chem. Phys.* 10 (2008) 1739.
- [13] B.J. Nehilla, T.Q. Vu, T.A. Desai, *J. Phys. Chem. B* 109 (2005) 20724.
- [14] W. Liao, F. Wei, M.X. Qian, X.S. Zhao, *Sens. Actuators B* 101 (2004) 361.
- [15] E.R. Goldman, G.P. Anderson, P.T. Tran, H. Mattoussi, P.T. Charles, I.M. Mauro, *Anal. Chem.* 74 (2002) 841.
- [16] K.A. Li, C.Q. Ma, Y. Liu, F.L. Zhao, S.Y. Tong, *Chin. Sci. Bull.* 45 (2000) 386.
- [17] R.F. Pasternack, C. Bustamante, P.J. Collings, A. Giannetto, E.J. Gibbs, *J. Am. Chem. Soc.* 115 (1993) 5393.
- [18] R.F. Pasternack, P.J. Collings, *Science* 269 (1995) 935.
- [19] C.Z. Huang, K.A. Li, S.Y. Tong, *Anal. Chem.* 69 (1997) 514.
- [20] C.Z. Huang, K.A. Li, S.Y. Tong, *Anal. Chem.* 68 (1996) 2259.
- [21] W. Lu, B.S.F. Band, Y. Yu, Q.G. Li, J.C. Shang, C. Wang, Y. Fang, R. Tian, L.P. Zhou, L.L. Sun, Y. Tang, S.H. Jing, W. Huang, J.P. Zhang, *Microchim. Acta* 158 (2007) 29.
- [22] C.Q. Ma, K.A. Li, S.Y. Tong, *Analyst* 122 (1997) 361.
- [23] H. Zhong, K. Wang, H.Y. Chen, *Anal. Biochem.* 330 (2004) 37.
- [24] H. Zhong, K. Wang, H.Y. Chen, *Microchim. Acta* 148 (2004) 99.
- [25] Z. Wang, J. Lee, A.R. Cossins, M. Brust, *Anal. Chem.* 77 (2005) 5770.
- [26] P. Bao, A.G. Frutos, C. Greef, J. Lahiri, U. Muller, T.C. Peterson, L. Warden, X. Xie, *Anal. Chem.* 74 (2002) 1792.
- [27] W.W. Yu, L. Qu, W. Guo, X. Peng, *Chem. Mater.* 15 (2003) 2854.
- [28] H.Y. Xie, J.G. Liang, Y. Liu, Z.L. Zhang, D.W. Pang, Z.K. He, Z.X. Lu, W.H. Huang, *J. Nanosci. Nanotechnol.* 5 (2005) 880.
- [29] G.P. Mitchell, C.A. Mirkin, R.L. Letsinger, *J. Am. Chem. Soc.* 121 (1999) 8122.
- [30] C.B. Murray, C.R. Kagan, M.G. Bawendi, *Science* 24 (1995) 1335.
- [31] H. Ai, M. Fang, S.A. Jones, Y.M. Lvov, *Biomacromolecules* 3 (2002) 560.
- [32] S. Pathak, M.C. Davidson, G.A. Silva, *Nano Lett.* 7 (2007) 1839.



# Simultaneous determination of pseudoephedrine, pheniramine, guaifenesin, pyrilamine, chlorpheniramine and dextromethorphan in cough and cold medicines by high performance liquid chromatography

M.R. Louhaichi<sup>a</sup>, S. Jebali<sup>a</sup>, M.H. Loueslati<sup>a</sup>, N. Adhoum<sup>b</sup>, L. Monser<sup>b,\*</sup>

<sup>a</sup> Laboratoire National de Contrôle des Médicaments, 11 bis Rue Jebel Lakhdar Bab Saadoun, 1006 Tunis, Tunisie

<sup>b</sup> Institut National des Sciences Appliquées et de Technologie, Centre Urbain Nord, B.P. No. 676, 1080 Tunis Cedex, Tunisie

## ARTICLE INFO

### Article history:

Received 13 November 2008

Received in revised form 6 January 2009

Accepted 6 January 2009

Available online 20 January 2009

### Keywords:

High performance liquid chromatography

Pseudoephedrine

Pheniramine

Guaifenesin

Pyrilamine

Chlorpheniramine

Dextromethorphan

Sodium benzoate

Methylparaben

Cough–cold pharmaceutical preparations

## ABSTRACT

A new simple, rapid and sensitive liquid chromatographic method has been developed and validated for the simultaneous determination of pseudoephedrine, pheniramine, guaifenesin, pyrilamine, chlorpheniramine and dextromethorphan in cough and cold pharmaceuticals. The separation of these compounds was achieved within 13 min on a Kromasil C18 column using an isocratic mobile phase consisting of methanol–dihydrogenphosphate buffer at pH 3 (45:55, v/v). The analysis was performed at a flow rate of 1 mL min<sup>-1</sup> and at a detection wavelength of 220 nm. The selectivity, linearity of calibration, accuracy, within and between-days precision and recovery were examined as parts of the method validation. The concentration–response relationship was linear over a concentration range of 5–50 µg mL<sup>-1</sup> for pseudoephedrine, pheniramine, chlorpheniramine and 50–600 µg mL<sup>-1</sup> for guaifenesin, pyrilamine, dextromethorphan, methylparaben and sodium benzoate with correlation coefficients better than 0.998. The standard deviations of the intraday and interday were all less than 2%. The proposed liquid chromatographic method was successfully applied for the routine analysis of these compounds in different cough and cold pharmaceutical preparations such as syrups, capsules, tablets and sachets. The presence of preservatives (sodium benzoate and methylparaben) and other excipients did not show any significant interference on the determination of these compounds.

© 2009 Elsevier B.V. All rights reserved.

## 1. Introduction

Cough and cold pharmaceutical preparations are one of the most extended formulations in the world and have got many pharmaceutical forms: syrup, suspension, sachets, capsules and tablets [1]. These preparations represent complex formulations containing several active ingredients and a broad spectrum of excipients such as flavoring agents, saccharose or aspartame, acidulants, natural or artificial coloring and flavoring agents, dyes, sweeteners and preservatives [2,3]. The majority of these ingredients are present as a mixture of basic nitrogenous amino compounds and their separation in pharmaceutical forms is quite complicated due to similarities of their physical and chemical properties [4]. The combination of antihistamine such as pyrilamine maleate (PA) and chlorpheniramine maleate (CLP) is used to overcome the allergic effects and reduce or relieve cold symptoms [5]. Pheniramine maleate (PHEN) and pseudoephedrine hydrochloride (PE) are

widely used in combination with other drugs for the clinical treatment of common cold, sinusitis, bronchitis and respiratory allergies [6]. Dextromethorphan hydrobromide (DEX) and guaifenesin (GUA) were used as cough suppressants antitussive for the relief of non-productive cough and cold preparations [7]. The most common formulation can be either liquid or suspension that requires the addition of preservatives such as sodium benzoate (SB) or methylparaben (MP). All these components have different polarities and exist in very different proportion. Due to these characteristics and because of diverse properties inherent to their formulation, these preparations offer an analytical problem [8].

Several methods are reported in the literature for the determination of these compounds in pharmaceuticals and in physiological fluids [9–18]. High performance liquid chromatography (HPLC) with UV or fluorescence or mass detection, is the most used techniques [1–3,5,6,9,11,14,15,17–24]. Other techniques including ultraviolet–visible (UV–vis) spectroscopy, thin layer chromatography, gas chromatography, GC/MS, capillary electrophoresis and multivariate spectrophotometric method [4,23–27], have been used to determine few of these compounds. However, to the best of our knowledge, no analytical methods have been reported for the simultaneous determination of all compounds in the presence of

\* Corresponding author. Tel.: +216 71703717; fax: +216 71704329.

E-mail address: [lotfi.monser@insat.rnu.tn](mailto:lotfi.monser@insat.rnu.tn) (L. Monser).

preservatives and excipients, which might interfere with the analysis of the active ingredients.

In addition, the majority of the published HPLC methods use an ion pairing agent, in order to reduce peak tailing and enhance separation of basic drugs on silica-based columns. These chromatographic systems are highly suitable but require the use of hydrophobic additives either cationic, such as trimethylamine, hexylamine or anionic, such as the alkyl sulfonate. However, these additives are costly and tend to adsorb very strongly on the stationary phase, leading to difficulty in recovering initial column properties. Furthermore, the use of ion pairing agents in the mobile phase will enhance the retention time of most compounds and as a consequence an increase in the analysis time will be observed.

The aim of this study was to develop a new, rapid, accurate and selective isocratic HPLC method for the simultaneous determination of six of the most commonly used active ingredients found in cough and cold medicines (PE, PHEN, GUA, PA, CLP and DEX) as well as the preservatives (SB and MP) in the presence of other recipients without using ion pairing additives.

## 2. Experimental

### 2.1. Chromatographic conditions

A HP Agilent liquid chromatograph Model 1200, equipped with a quaternary pump, an auto-sampler, a vacuum degasser, a diode-array UV-detector, a column thermostat and a data station (HP Chemstation) was used. The detection of analytes was monitored at 220 nm by a diode-array UV-detector. The separation was achieved on a Kromasil LC18 column (150 mm × 4.6 mm I.D., 5 μm particle size) using a mobile phase containing 45:55 (v/v) methanol/0.1 mol L<sup>-1</sup> KH<sub>2</sub>PO<sub>4</sub> buffer. The analysis was performed at a flow rate of 1 mL min<sup>-1</sup>. The pH of the buffer was adjusted with orthophosphoric acid or sodium hydroxide. Prior to any analysis, the mobile phase was degassed and filtered using 0.45 μm filters. The system was equilibrated with the mobile phase before injection.

### 2.2. Reagents and chemicals

Working reference standard of guaifenesin (GUA), chlorpheniramine maleate (CLP), pheniramine maleate (PHEN), pseudoephedrine hydrochloride (PE), dextromethorphan hydrobromide (DEX), pyrilamine maleate (PA), sodium benzoate (SB) and methylparaben (MP) were purchased from Sigma–Aldrich. HPLC grade methanol (MeOH) was obtained from Prolabo (Paris, France). Ultrapure water was drawn from a Diamond Reverse Osmosis System (United Kingdom). Analytical grade potassium dihydrogenphosphate, orthophosphoric acid and sodium hydroxide were obtained from Prolabo (Paris, France).

The commercialized pharmaceutical products used are detailed below:

*Nortussine syrup for children* (400 mg GUA, 100 mg DEX, 100 mg PA and 50 mg MP for 100 mL) and *nortussine syrup for adult* (200 mg DEX, 200 mg PA and 200 mg SB for 100 mL) were manufactured by Pharmagreb, Tunisia.

*Tussipax syrup cough suppressant for children* (400 mg GUA, 100 mg DEX and 150 mg MP for 100 mL) was manufactured by Opalia, Tunisia.

*Rhinostop syrup* (1 mg CLP, 20 mg PE, and 100 mg paracetamol for 100 mL) was manufactured by Simed.

*Sudafed syrup* (600 mg PE for 100 mL) was manufactured by LABORATOIRE GlaxoSmithKline, France.

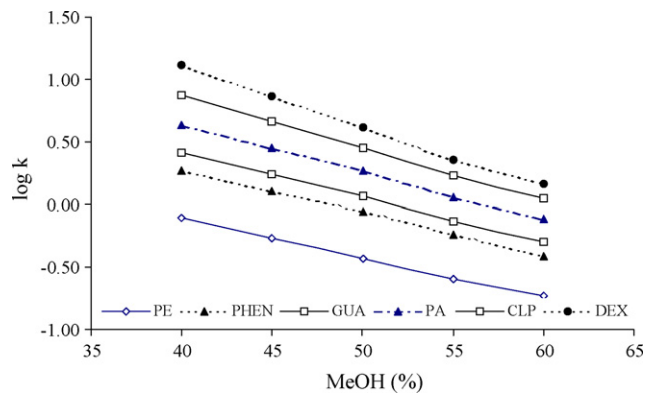


**Fig. 1.** Effect of methanol concentration on the retention of pseudoephedrine (PE), pheniramine (PHEN), guaifenesin (GUA), pyrilamine (PA), chlorpheniramine (CLP), and dextromethorphan (DEX). Mobile phase: methanol:phosphate buffer (0.1 mol L<sup>-1</sup>); column: Kromasil C18; detector = 220 nm; flow rate: 1 mL min<sup>-1</sup>.

*Fervex granuled powder for oral solution* (25 mg CLP, 500 mg paracetamol, and 200 mg ascorbic acid per sachet) was manufactured by Bristol–Myers–Squibb, UPSA, Tunisia.

*Gripex powder for oral solution* (25 mg CLP, 500 mg paracetamol, and 200 mg ascorbic acid per sachet) was manufactured by Galpharma, Tunisia.

*Rhinofebral capsule* (3.2 mg CLP, 240 mg acetaminophen, and 100 mg ascorbic acid per tablet) was manufactured by Crepharm Bessay McNeil SAS, France.

*Rhinostop tablet* (2.5 mg CLP, 60 mg PE, and 250 mg paracetamol for one tablet) was manufactured by SAIPH, Tunisia. All these medicines were kindly provided by local manufactured or purchased at local drug stores.

### 2.3. Preparation of solutions

Stock standard solutions of PE, PHEN, CLP (200 μg mL<sup>-1</sup> each) and of GUA, PA, DEX, SB, MP (1000 μg mL<sup>-1</sup> each) were prepared in ultrapure water. Working standard solutions (5–50 μg mL<sup>-1</sup> for PE, PHEN, CLP and 50–600 μg mL<sup>-1</sup> GUA, PA, DEX, SB and MP) were freshly prepared by serial dilutions of the stock standard solutions.

Commercialized pharmaceutical samples were prepared as follows:

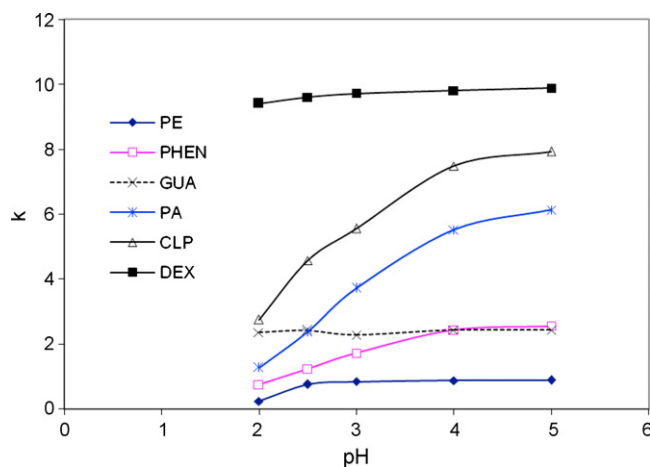


**Fig. 2.** Variation of the retention of pseudoephedrine (PE), pheniramine (PHEN), guaifenesin (GUA), pyrilamine (PA), chlorpheniramine (CLP), and dextromethorphan (DEX) with the pH of the mobile phase. Mobile phase: 45:55 (v/v) methanol:phosphate buffer (0.1 mol L<sup>-1</sup>); column: Kromasil C18; detector = 220 nm; flow rate: 1 mL min<sup>-1</sup>.

**Table 1**

Linearity details of: PE, pseudoephedrine; GUA, guaifenesin; PHEN, pheniramine; PA, pyrillamine; CLP, chlorpheniramine; DEX, dextromethorphan; SB, sodium benzoate; MP, methylparaben using peak areas.

Name	Concentration range ( $\mu\text{g mL}^{-1}$ )	Slope	Intercept	Correlation coefficient
PE	5–50	7.94	0.551	0.999
PHEN	5–50	23.38	9.199	0.999
GUA	50–600	39.91	383.9	0.999
PA	50–600	29.31	-72.27	0.999
CLP	5–50	34.53	-16.57	0.999
DEX	50–600	25.20	-67.59	0.999
SB	50–600	59.71	-274.3	0.998
MP	50–600	40.22	404.7	0.999

### 2.3.1. Syrup samples

An appropriate amount of sample was diluted with ultrapure water to have a concentration ranging between 5 and 50  $\mu\text{g mL}^{-1}$  for PE, PHEN, CLP and between 50 and 600  $\mu\text{g mL}^{-1}$  for GUA, PA, DEX, SB and MP. The resulting solution was sonicated for 10 min and a portion of the sample was filtered with a 0.45  $\mu\text{m}$  filter before injection in the HPLC. The amounts of the commercial cough and cold liquid were varied depending on the drug concentration of the various products and some times further dilution was carried out with ultrapure water.

### 2.3.2. Sachet samples

The content of 10 sachets powder was thoroughly homogenized and an accurately weighted amount of the mixed powder equivalent to the active drug content of one sachet was transferred to a 250 mL volumetric flask. After 30 min of mechanical shaking, 10 mL of the suspension was diluted in a 25 mL flask with ultrapure water and after shaken the sample was filtered with 0.45  $\mu\text{m}$  filter.

### 2.3.3. Tablets and capsules

The contents of 20 tablets or 20 capsules were accurately weighed and powdered separately in a mortar. A weight equivalent to the content of one tablet was dissolved in 50 mL and that equivalent to one capsule was dissolved in 250 mL purified water. After 15 min of mechanical shaking, the solution was filtered through a 0.45  $\mu\text{m}$  Millipore filter. All preparations were performed in three replicates.

## 2.4. Validation procedure

The linearity was tested at three levels of concentrations ranging from 5 to 50  $\mu\text{g mL}^{-1}$  for PE, PHEN and CLP and 10 levels of concentrations ranging from 50 to 600  $\mu\text{g mL}^{-1}$  for GUA, PA, DEX, SB and MP.

The precision was tested at three level concentrations of the standard mixture. The intermediate precision was obtained by repeating intra-assay experiment on different days. The accuracy of the method was evaluated by calculating the percent recoveries and the R.S.D.

## 3. Results and discussion

### 3.1. Chromatography

In an attempt to optimize the separation of PE, PHEN, GUA, PA, CLP, DEX and the preservatives SB and MP in cough and cold pharmaceutical formulations, the effects of some chromatographic parameters such as mobile phase composition and pH of the buffer solution were investigated.

#### 3.1.1. Effect of the mobile phase composition

In order to study the effect of the percentage of the organic fraction in the separation of PE, PHEN, GUA, PA, CLP, DEX, SB and MP, different percentages of methanol (from 40 to 60%) was investigated. The logarithmic evolutions of the capacity factors of GUA, CLP, PHEN, PE, DEX and PA as a function of the percentage of methanol are shown in Fig. 1. The variation of solutes retention with the mobile phase composition follows the usual trend and showed a faster elution of all studied compounds upon increasing methanol percentage. The observed effect is expected, since an increase in the organic modifier concentration leads to a decrease in the dielectric constant of the mixture and consequently to a decrease in the retention factor. The decrease in the retention of DEX was steeper than other compounds, which indicates that the retention of DEX is more dependent on the concentration of methanol ( $t_R = 21.2$  min at 40% MeOH and  $t_R = 3.7$  min at 60% MeOH). When the percentage of methanol was more than 50% the separation of the PHEN and GUA does not occur. The best separation was obtained at a percentage of 40% MeOH but the analysis time was longer than 23 min. Therefore, a percentage of 45% MeOH was selected as an optimum as it offers a compromise between resolution ( $R_s > 3.0$ ) and analysis time ( $\sim 13$  min).

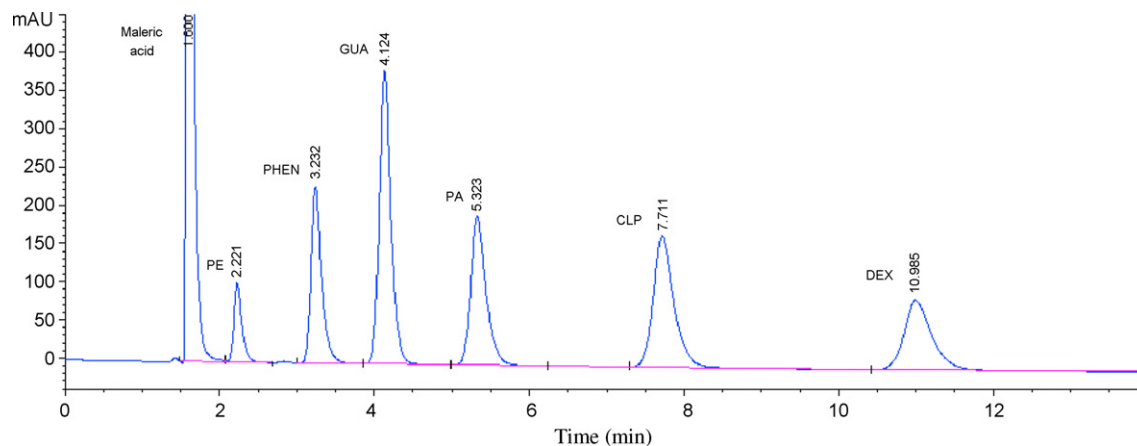


**Fig. 3.** Representative chromatogram of standard active ingredients. Active compounds: PE, pseudoephedrine; GUA, guaifenesin; PHEN, pheniramine; PA, pyrillamine; CLP, chlorpheniramine; DEX, dextromethorphan. Mobile phase: 45:55 (v/v) methanol:phosphate buffer (0.1 mol L<sup>-1</sup>) at pH 3; column: Kromasil C18; detector = 220 nm; flow rate: 1 mL min<sup>-1</sup>.



### 3.1.2. Effect of mobile phase pH

In an attempt to investigate the effect of the mobile phase pH on the retention and resolution of GUA, DEX, PA, CLP, PHEN and PE, the pH was carefully investigated over the range of 2.0–5.0. The changes in the retention as a function of the pH, results from the changes in the ionization form of these solutes, which is  $pK_a$  dependent. The acid base behavior of these compounds involves the protonation of the ethylamine group ( $pK_a \approx 9$ ) and the pyridinic nitrogen ( $pK_a \approx 4$ ) group of these solutes [27]: PE ( $pK_a = 9.9$ ), PHEN ( $pK_a = 9.3$ ), GUA ( $pK_a = 7.9$ ), PA ( $pK_a = 4.0$  and  $8.9$ ), CLP ( $pK_a = 4.0$  and  $9.2$ ), DEX ( $pK_a = 8.3$ ), SB ( $pK_a = 4.2$ ) and MP ( $pK_a = 8.4$ ).

As shown in Fig. 2, the plots of the variation of the retention of these solutes with the mobile phase pH follow the usual trend of basic and acidic compounds except for GUA and DEX. A change in mobile phase pH from 2.0 to 5.0 has caused an increase in the retention of PHEN, PA and CLP. However, the retention of GUA and DEX remained almost unchanged over the studied pH range due to their high  $pK_a$  values (7.9 and 8.3 respectively). The retention of DEX defined the analysis time because it is the last eluting solute. A pH 3 was selected as optimum, as it resulted in the best compromise between peak shape, resolution ( $R_s \geq 3$ ) and analysis time ( $t_R \sim 13$  min).

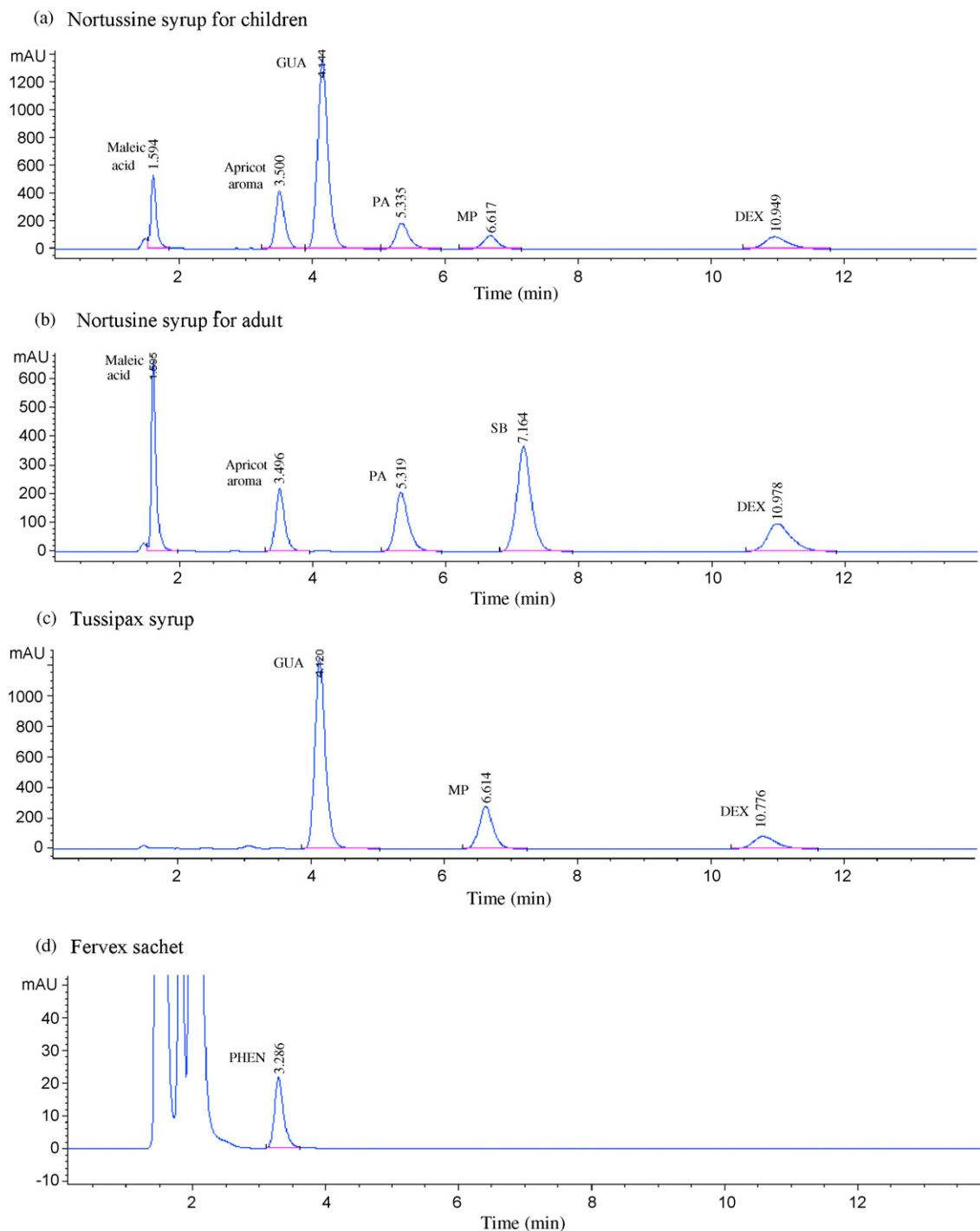


**Fig. 4.** Representative chromatogram of real samples: (a) nortussine syrup for children, (b) nortussine syrup for adult, (c) tussipax syrup, (d) fervex sachet, (e) gripex sachet, (f) rhinofebral capsule and (g) rhinostop syrup. Mobile phase: 45:55 (v/v) methanol:phosphate buffer (0.1 mol L<sup>-1</sup>) at pH 3; column: Kromasil C18; detector = 220 nm; flow rate: 1 mL min<sup>-1</sup>.

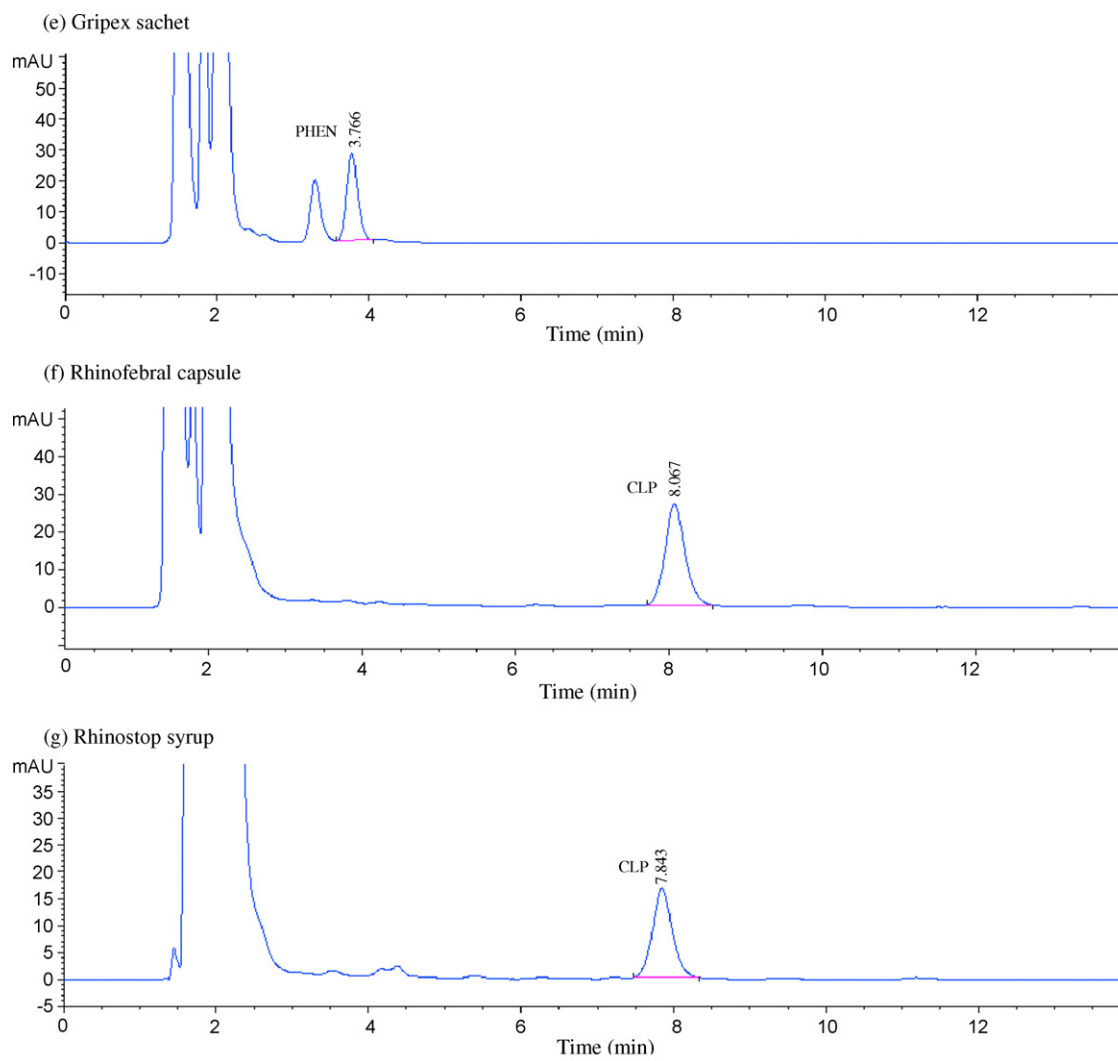


Fig. 4. (Continued).

### 3.2. Validation of the method

The essential parameters to ensure the acceptability of the performance of an analytical method are linearity, repeatability, reproducibility, precision and recovery. Linearity, accuracy and precision were determined within and between three different days and the recovery was determined at three different concentration levels.

#### 3.2.1. Specificity

Specificity is the ability to assess unequivocally the target compound in the presence of components, which may be expected to be present. The specificity of the method was established by studying the resolution factors among all peaks in standard solution (without placebo) and in real samples (in the presence of placebo). As shown in Fig. 3, the resolution of all these compounds was adequate. The selectivity of the method was further assessed by analyzing these compounds in the presence of placebo. Fig. 4(a–g) shows the presence of other peaks in addition to the studied peaks with no interference from placebo components. Peaks of the placebo components were adequately separated from active compounds. Therefore, the proposed method is applicable to selective determination of these compounds.

#### 3.2.2. Linearity

Under the optimum conditions, linearity was studied using two concentration ranges from 5 to 50  $\mu\text{g mL}^{-1}$  for PE, PHEN and CLP and from 50 to 600  $\mu\text{g mL}^{-1}$  for GUA, PA, DEX, SB and MP. The calibration curves exhibit satisfactory linearity with correlation coefficients higher than 0.99. The data were analyzed by the linear least squares fit method and the results are presented in Table 1. The equation of the line was used to calculate the concentration of these compounds in cough–cold medicines.

The detection limit, based on a signal-to-noise ratio of 3:1, was found to be 0.2  $\mu\text{g mL}^{-1}$  for PE, 0.03  $\mu\text{g mL}^{-1}$  for PHEN and PA, 0.04  $\mu\text{g mL}^{-1}$  for GUA, 0.1  $\mu\text{g mL}^{-1}$  for CLP and 0.06  $\mu\text{g mL}^{-1}$  for DEX. The limit of quantification with a signal-to-noise of 10:1 was found to be 0.66  $\mu\text{g mL}^{-1}$  for PE, 0.1  $\mu\text{g mL}^{-1}$  for PHEN and PA, 0.13  $\mu\text{g mL}^{-1}$  for GUA, 0.33  $\mu\text{g mL}^{-1}$  for CLP and 0.2  $\mu\text{g mL}^{-1}$  for DEX.

#### 3.2.3. Precision

The precision of the analytical procedure expresses the closeness of agreement (degree of scatter) between a series of measurements obtained from multiple sampling of the same homogeneous sample under the prescribed conditions. Precision was considered at two levels: repeatability (intradays) and intermediate precision (interdays). The corresponding results were expressed as the relative

**Table 2**  
Data on method precision (intra- and interdays) for standard solutions.

Compound	Concentration ( $\mu\text{g mL}^{-1}$ )	Intraday mean R.S.D. (%)	Interday mean R.S.D. (%)
PE	10	0.76	1.62
	20		
	30		
PHEN	10	1.40	0.63
	20		
	30		
PA	75	1.28	1.45
	100		
	125		
GUA	300	1.41	0.57
	400		
	500		
CLP	10	0.60	0.46
	20		
	30		
DEX	75	1.37	0.74
	100		
	125		
SB	75	0.77	0.77
	100		
	125		
MP	75	1.34	0.86
	100		
	125		

standard deviation and mean recovery of a series of measurements. The mean R.S.D. values for intra- and interday precision were varied from 0.76 to 1.43% and from 0.46 to 1.62%, respectively. The mean recovery values were ranged between 97.13 and 101.98% for the repeatability and between 97.76 and 102.35% for the intermediate precision. The data for the repeatability and intermediate precision are presented in Table 2.

### 3.2.4. Accuracy and recovery

The accuracy of an analytical procedure expresses the closeness of agreement between the value, which is accepted either as a conventional true value or an accepted reference value and the value found. It is determined by calculating the percentage relative error between the measured mean concentrations and added concentrations of analytes. Table 2 shows the results obtained for intra- and interday accuracy.

**Table 4**  
Content of industrial cough syrup with respect to label amount claimed.

Samples	Compounds	Labeled	Found	Relative error (%)
Nortussine children syrup	GUA	400 mg 100 mL <sup>-1</sup>	393.75 mg 100 mL <sup>-1</sup>	-1.56
	PA	100 mg 100 mL <sup>-1</sup>	101.58 mg 100 mL <sup>-1</sup>	1.58
	DEX	100 mg 100 mL <sup>-1</sup>	95.62 mg 100 mL <sup>-1</sup>	-4.37
	MP	50 mg 100 mL <sup>-1</sup>	49.73 mg 100 mL <sup>-1</sup>	-0.53
Nortussine adult syrup	PA	200 mg 100 mL <sup>-1</sup>	206.29 mg 100 mL <sup>-1</sup>	3.14
	DEX	200 mg 100 mL <sup>-1</sup>	207.58 mg 100 mL <sup>-1</sup>	3.79
	SB	200 mg 100 mL <sup>-1</sup>	199.02 mg 100 mL <sup>-1</sup>	-0.49
Tussipax children syrup	GUA	400 mg 100 mL <sup>-1</sup>	397.39 mg 100 mL <sup>-1</sup>	-0.65
	DEX	100 mg 100 mL <sup>-1</sup>	101.58 mg 100 mL <sup>-1</sup>	1.58
	MP	150 mg 100 mL <sup>-1</sup>	150.33 mg 100 mL <sup>-1</sup>	-0.22
Fervex sachet	PHEN	25 mg/sachet	23.94 mg/sachet	-4.22
Gripex sachet	PHEN	25 mg/sachet	23.36 mg/sachet	2.29
Rhenofebral capsule	CLP	3.2 mg/capsule	3.25 mg/capsule	1.57
Rhinostop tablet	CLP	2.5 mg/tablet	2.52 mg/capsule	1.05
Rhinostop syrup	CLP	1 mg 5 mL <sup>-1</sup>	1.01 mg 5 mL <sup>-1</sup>	0.68
Sudafed syrup	PE	600 mg 100 mL <sup>-1</sup>	603.23 mg 100 mL <sup>-1</sup>	0.54

**Table 3**  
Accuracy for the recovery of PE, PHEN, GUA, PA, CLP and DEX.

Samples	Compounds	Amount added ( $\mu\text{g mL}^{-1}$ )	Amount found ( $\mu\text{g mL}^{-1}$ )	Recovery (%)
Nortussine children syrup	GUA	40	39.68	99.20
		80	79.16	98.95
		120	120.28	100.23
	PA	25	24.83	99.35
		50	49.10	98.20
		75	74.81	99.75
	DEX	25	24.71	98.85
		50	50.64	101.28
		75	74.06	98.78
Nortussine adult syrup	PA	25	25.08	100.33
		50	49.59	99.19
		75	75.71	100.95
	DEX	25	25.13	100.52
		50	50.28	100.57
		75	75.46	100.62
Tussipax syrup	GUA	40	39.68	99.2
		80	79.16	98.95
		120	120.28	100.24
	DEX	25	25.27	101.07
		50	49.58	99.16
		75	75.85	101.14
Fervex sachet	PHEN	2.5	2.47	98.66
		5.0	4.95	98.96
		7.5	7.46	99.49
Gripex sachet	PHEN	2.5	2.48	99.26
		5.0	4.98	99.62
		7.5	7.60	101.31
Rhenofebral capsule	CLP	2.5	2.48	99.10
		5.0	4.95	99.09
		7.5	7.42	98.95
Rhinostop tablet	CLP	2.5	2.53	101.13
		5.0	5.04	100.75
		7.5	7.62	101.71
Rhinostop syrup	CLP	2.5	2.48	99.43
		5.0	4.91	98.37
		7.5	7.36	98.21
Sudafed syrup	PE	5.0	4.93	98.51
		8.0	7.93	99.11
		11.0	10.87	98.83

Recovery studies for the accuracy of the method were performed by spiking different samples at three levels with known concentrations of PE, PHEN, GUA, PA, CLP and DEX standards (from 2.5 to 120  $\mu\text{g mL}^{-1}$ ). The mean percentage recoveries of these compounds

were varied between 98.2 and 101.7% (Table 3). The higher values of recoveries and the lower values of the R.S.D. of the assay indicate that the method is precise and accurate. Also, the results depicted that the present method is useful for bulk drug analysis as well as commercial pharmaceutical in different forms and with different types of formulations.

### 3.3. Application of the method

The method was applied to different industrial cough and cold pharmaceutical formulations (five types of syrups, two types of sachets, one type of capsules and one type of tablets) to determine their content in PE, PHEN, CLP, GUA, PA, DEX, SB and MP. The amount of each compound was calculated using calibration curve method. Satisfactory results were obtained for each compound in good agreement with label claims (Table 4). The obtained results demonstrate that the content of drug corresponds to the drug label, which confirms the good accuracy of the proposed method. Indeed, the recovery percentages with respect to the label claims were ranged between 95.63 and 103.79%, indicating the good accuracy of the proposed method. To further assess the accuracy of the proposed method and to evaluate the possible interaction with excipients, recovery experiments were carried out by spiking the drug solutions with known amounts of standard target compounds solutions.

The typical chromatograms for the separation of the nine finish products are illustrated in Fig. 4(a–g). The peaks were identified by comparison of the retention time of the separated compounds and standards. No interfering peak was observed in the chromatograms of the commercial formulation under the conditions described. Therefore the recipients present in the commercial preparations have no interference on the analysis of PE, PHEN, GUA, PA, CLP, DEX, SB and MP. The excipients that are detected in the syrup formulation are a combination of a sweetener and a coloring agent. Analgesics such as acetaminophen and vitamin C eluted near the solvent front and were easily separated from the amine drugs of interest. Therefore the proposed method is precise and accurate and could be applied to the determination of all studied compounds in pharmaceutical formulations.

### 4. Conclusion

A reliable and rapid liquid chromatography method for the simultaneous determination of PE, PHEN, CLP, GUA, PA, DEX, SB and MP in nine pharmaceutical preparations has been developed.

The method avoids the use of ion pairing agents, which are costly and tend to adsorb very strongly on the stationary phase, leading to difficulty in recovering initial column properties. This method is capable of separating a wide range of amine drugs commonly found in cough and cold liquids from the dyes, preservatives and flavoring which are normally associated with cough and cold medicines. In addition, the results indicate that the method is sensitive, precise, accurate and applicable to various commercial cough and cold pharmaceutical preparations: syrups, sachets, capsules and tablet containing PE, PHEN, CLP, GUA, PA, DEX, SB and MP. Therefore the method can be applied to the quality control of cough and cold medicines.

### References

- [1] I. Caraballo, M. Fernandez-Arevalo, M.A. Holgado, J. Alvarez-Fuentes, A.M. Rabasco, *Drug Dev. Ind. Pharm.* 21 (1995) 605.
- [2] G. Halstead, *J. Pharm. Sci.* 71 (1982) 1108.
- [3] V. Galli, C. Barbas, *J. Chromatogr. A* 1048 (2004) 207.
- [4] Y. Dong, X. Chen, Y. Chen, X. Chen, Z. Hu, *J. Pharm. Biomed. Anal.* 39 (2005) 285.
- [5] A.I. Gasco-Lopez, R. Izquierdo-Hornillos, A. Jimenez, *J. Chromatogr. A* 775 (1997) 179.
- [6] M. Kompany-Zareh, S. Mizaei, *Anal. Chim. Acta* 526 (2004) 83.
- [7] United States Pharmacopoeia, 25th Review, The National Formulary, 19th Review, The United States Pharmacopoeia Convention, Rockville, MD, 2002, p. 975.
- [8] G. Goodman, *The Pharmacological Basis of Therapeutics*, 9th edition, McGraw-Hill, New York, 1996, 904 p.
- [9] İ. Palabıyık, F. Onur, *Chromatographia* 66 (2007) 93.
- [10] R.G. Hendrickson, R.L. Cloutier, *J. Emerg. Med.* 32 (2007) 393.
- [11] A. Marin, E. Garcia, A. Garcia, C. Barbas, *J. Pharm. Biomed. Anal.* 29 (2002) 701.
- [12] M. Parsons, C. Ganellin, *Brit. J. Pharmacol.* 147 (2006) 12.
- [13] A. El-Gindy, S. Emara, M. Mesbah, G. Hadad, *Anal. Lett.* 39 (2006) 2699.
- [14] M. Caude, L.X. Phan, *Chromatographia* 9 (1976) 20.
- [15] A. El-Gindy, S. Emara, M. Mesbah, G. Hadad, *J. AOAC Int.* 88 (2005) 1069.
- [16] Y. Chen, P. Wang, Y. Ching, C. Ber-Lin, *J. Food Drug Anal.* 7 (1999) 13.
- [17] M. Paciola, S. Jansen, S. Martellucci, A. Osei, *J. Pharm. Biomed. Anal.* 26 (2001) 143.
- [18] S. Stavchansky, S. Demirbas, L. Reyderman, C. Chai, *J. Pharm. Biomed. Anal.* 13 (1995) 919.
- [19] T.D. Wilson, W.G. Jump, W.C. Neumann, T. San Martin, *J. Chromatogr.* 641 (1993) 241.
- [20] J. Hoskins, G. Shenfield, A. Gross, *J. Chromatogr. B* 696 (1997) 81.
- [21] S. Lin, C. Chen, H. Ho, H. Chen, M. Sheu, *J. Chromatogr. B* 859 (2007) 141.
- [22] J. Rauha, H.S. Alomies, M. Aalto, *J. Pharm. Biomed. Anal.* 15 (1996) 287.
- [23] A. Marin, C. Barbas, *J. Pharm. Biomed. Anal.* 35 (2004) 1035.
- [24] L.A. Shervington, *Anal. Lett.* 30 (1997) 927.
- [25] A.S. Amin, R. El-Sheikh, F. Zahran, A.A. Gouda, *Spectrochim. Acta Part A* 67 (2007) 1088.
- [26] V. Tantishaiyakul, C. Poeaknapo, P. Sribum, K. Sirisuppanon, *J. Pharm. Biomed. Anal.* 17 (1998) 237.
- [27] M. Gil-Agusti, M.C. Garcia-Alvarez-Coque, J. Esteve-Romero, *Anal. Chim. Acta* 421 (2000) 45.



## Simultaneous voltammetric determination of paracetamol and caffeine in pharmaceutical formulations using a boron-doped diamond electrode

Bruna Cláudia Lourenção<sup>a</sup>, Roberta Antigo Medeiros<sup>b</sup>, Romeu C. Rocha-Filho<sup>b</sup>,  
Luiz Henrique Mazo<sup>a</sup>, Orlando Fatibello-Filho<sup>a,b,\*</sup>

<sup>a</sup> Instituto de Química de São Carlos, Universidade de São Paulo, C.P. 780, 13560-970 São Carlos, SP, Brazil

<sup>b</sup> Departamento de Química, Universidade Federal de São Carlos, C.P. 676, 13560-970 São Carlos, SP, Brazil

### ARTICLE INFO

#### Article history:

Received 20 October 2008

Received in revised form 15 December 2008

Accepted 16 December 2008

Available online 30 December 2008

#### Keywords:

Paracetamol

Caffeine

Simultaneous determination

Differential pulse voltammetry

Boron-doped diamond electrode

### ABSTRACT

A simple and highly selective electrochemical method was developed for the single or simultaneous determination of paracetamol (N-acetyl-p-aminophenol, acetaminophen) and caffeine (3,7-dihydro-1,3,7-trimethyl-1H-purine-2,6-dione) in aqueous media (acetate buffer, pH 4.5) on a boron-doped diamond (BDD) electrode using square wave voltammetry (SWV) or differential pulse voltammetry (DPV). Using DPV with the cathodically pre-treated BDD electrode, a separation of about 550 mV between the peak oxidation potentials of paracetamol and caffeine present in binary mixtures was obtained. The calibration curves for the simultaneous determination of paracetamol and caffeine showed an excellent linear response, ranging from  $5.0 \times 10^{-7}$  mol L<sup>-1</sup> to  $8.3 \times 10^{-5}$  mol L<sup>-1</sup> for both compounds. The detection limits for the simultaneous determination of paracetamol and caffeine were  $4.9 \times 10^{-7}$  mol L<sup>-1</sup> and  $3.5 \times 10^{-8}$  mol L<sup>-1</sup>, respectively. The proposed method was successfully applied in the simultaneous determination of paracetamol and caffeine in several pharmaceutical formulations (tablets), with results similar to those obtained using a high-performance liquid chromatography method (at 95% confidence level).

© 2008 Elsevier B.V. All rights reserved.

### 1. Introduction

Paracetamol (N-acetyl-p-aminophenol, acetaminophen) (Fig. 1A) is a long-established substance, being one of the most extensively employed drugs in the world. It is noncarcinogenic and an effective substitute for aspirin for patients with sensitivity to it [1–4]. Paracetamol is an acylated aromatic amide that was firstly introduced in medicine by Von Mering in 1893 as an antipyretic/analgesic; it has been in use as an analgesic for home medication for over 50 years. Moreover, it is accepted as a very effective drug for the relief of pain and fever in adults and children [5].

Because paracetamol is being increasingly used for therapeutic purposes, its determination and quality control are of vital importance [6]. Many methods for determining paracetamol have been recently reported, such as chromatographic [7–13], spectrofluorimetric [14–17], chemiluminescent [18,19], spectrophotometric [20–22], and electrochemical techniques [2,5,6,23–33]. Wang-fuengkanagul and Chailapakul [34] studied the electrochemistry of

paracetamol at a boron-doped diamond thin film electrode using cyclic voltammetry, hydrodynamic voltammetry, and flow injection with amperometric detection. The diamond electrode provided a linear dynamic range from 0.1 mmol L<sup>-1</sup> to 8.0 mmol L<sup>-1</sup> and a detection limit of 10.0 μmol L<sup>-1</sup> for voltammetric measurement. ShangGuan et al. [35] studied the electrochemical determination of paracetamol using differential pulse voltammetry (DPV) at a carbon ionic liquid electrode. The peak oxidation current at this electrode was linear with the paracetamol concentration in the range 1.0–2.0 μmol L<sup>-1</sup> ( $R^2 = 0.9992$ ), with a detection limit of 0.3 μmol L<sup>-1</sup> [35]. The mechanism for paracetamol electrooxidation involves two electrons and two protons to generate N-acetyl-p-quinoneimine [36,37].

Caffeine (3,7-dihydro-1,3,7-trimethyl-1H-purine-2,6-dione) (Fig. 1B) is an alkaloid N-methyl derivative of xanthine widely distributed in natural products, commonly used in beverages. It has many physiological effects, such as gastric acid secretion, diuresis, and stimulation of the central nervous system [38]. Caffeine is used therapeutically in combination with ergotamine in the treatment of migraine or in combination with nonsteroidal anti-inflammatory drugs in analgesic formulations. Sometimes it is included in analgesic preparations because of its diuretic action [39]. Thus, various methods for analyzing caffeine have been developed, including spectrophotometric [40–42] and chromatographic [43,44] ones. These methods are generally more expensive,

\* Corresponding author at: Departamento de Química, Universidade Federal de São Carlos, C.P. 676, 13560-970 São Carlos, SP, Brazil. Tel.: +55 16 33518098; fax: +55 16 33518350.

E-mail address: [bello@ufscar.br](mailto:bello@ufscar.br) (O. Fatibello-Filho).

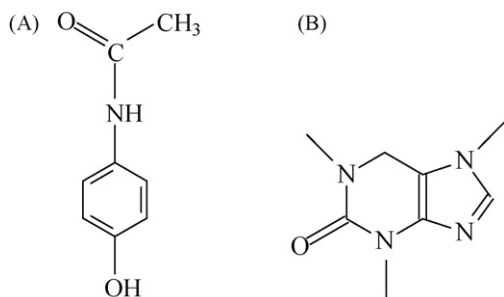


Fig. 1. Chemical structure of paracetamol (A) and caffeine (B).

time-consuming, and complicated than electroanalytical ones. In spite of this, electroanalytical methods have rarely been used for the analysis of caffeine [45–48], mainly because its oxidation occurs at a very positive potential, which overlaps with that for the discharge of the electrolytic solution [45].

Brunetti et al. [46] developed a simple differential pulse voltammetric method based on a Nafion-covered glassy carbon electrode for the quantitative determination of caffeine in cola beverages. This method allows quantifying this analyte in the  $9.95 \times 10^{-7}$  to  $1.06 \times 10^{-5}$  mol L<sup>-1</sup> range, with a detection limit of  $7.98 \times 10^{-7}$  mol L<sup>-1</sup>. The mechanism for caffeine electrooxidation involves four electrons ( $4e^-$ ) and four protons ( $4H^+$ ) [38,47]. The first step is a  $2e^-$ ,  $2H^+$  oxidation of the C-8 to N-9 bond to give the substituted uric acid, followed by an immediate  $2e^-$ ,  $2H^+$  oxidation to the 4,5-diol analogue of uric acid, which rapidly fragments.

Only a few methods have been reported for the simultaneous determination of paracetamol and caffeine [49–51]. Yet, such methods require a long time for extracting and purifying the active principles before analysis. Zen and Ting [52] used a Nafion<sup>®</sup>/ruthenium oxide pyrochlore chemically modified electrode for the simultaneous determination of caffeine and paracetamol in drug formulations by square wave voltammetry (SWV), obtaining detection limits of  $2.2 \times 10^{-6}$  mol L<sup>-1</sup> and  $1.2 \times 10^{-6}$  mol L<sup>-1</sup>, respectively; however, the supporting electrolyte used was perchloric acid, a high cost reagent with controlled sale.

The use of boron-doped diamond (BDD) as an electrode substrate is now well established, mainly due to properties such as: a wide potential window in aqueous solutions, low background currents, long term stability, and low sensitivity to dissolved oxygen [53]. These properties make BDD particularly suitable for electrochemical studies of analytes with a high oxidation potential [54,55]. In BDD, the replacement of approximately one carbon atom in a thousand by a boron atom yields a material with metallic conductivity. The properties of BDD are commonly affected by the quantity and kind of doping agent, morphologic factors and defects in the film, presence of impurities ( $sp^2$  carbon), crystallographic orientation, surface termination (hydrogen or oxygen), and electrochemical pre-treatments of its surface [56,57]. Suffredini et al. [57] called to attention that a cathodic pre-treatment of the BDD electrode dramatically increased the electroanalytical detection limit for chlorophenols. Recently, a BDD electrode was used for acetylsalicylic acid (ASA) determination in pharmaceutical formulations [58], as well as for aspartame and cyclamate determination in dietary products, individually [59,60] or simultaneously [61].

In this paper we describe the use of a cathodically pre-treated BDD electrode for the selective and sensitive determination of paracetamol (by SWV) and caffeine (by DPV) individually as well as simultaneously (by DPV). The obtained results are compared with those from a high-performance liquid chromatography (HPLC) method.

## 2. Experimental

### 2.1. Apparatus

All the electrochemical experiments were conducted in a three-electrode single compartment glass cell. An Ag/AgCl (3.0 mol L<sup>-1</sup> KCl) electrode was used as reference and the counter electrode was a Pt wire. The working electrode (0.72-cm<sup>2</sup> exposed area) was a boron-doped (8000 ppm) diamond film on a silicon wafer from Centre Suisse de Electronique et de Microtechnique SA (CSEM), Neuchat el, Switzerland [56,57]. Prior to the experiments, the BDD electrode was cathodically pre-treated by applying  $-1.0$  A cm<sup>-2</sup> for 180 s in a 0.5 mol L<sup>-1</sup> H<sub>2</sub>SO<sub>4</sub> solution. The voltammetric measurements were carried out using an Autolab PGSTAT-30 (Ecochemie) potentiostat/galvanostat controlled with the GPES 4.0 software.

The paracetamol and caffeine determinations by high-performance liquid chromatography (HPLC) were carried out using a LC-10 AT Shimadzu system, with an ultraviolet-vis detector (SPD-M10-AVP) set at 273 nm. A Shim-Pack CLC-ODS (6.0 mm × 150 mm, 5 μm) chromatographic column was used. The mobile phase was an acetonitrile/water mixture (25/75, v/v) at a flow rate of 0.8 mL min<sup>-1</sup>, while the injection volume was 40 μL [62].

### 2.2. Reagents and standards

All reagents were of analytical grade: paracetamol and caffeine, from Sigma; sodium acetate and acetic acid, from Aldrich. Paracetamol and caffeine  $1.0 \times 10^{-3}$  mol L<sup>-1</sup> standard aqueous solutions were prepared in a 0.2 mol L<sup>-1</sup> acetate buffer solution (pH 4.5). All solutions were prepared using ultra-purified water supplied by a Milli-Q system (Millipore<sup>®</sup>) with resistivity above 18 MΩ cm.

### 2.3. Measurement procedures

After optimizing the experimental parameters for the proposed methods, the analytical curves were constructed by adding small volumes of concentrated standard solutions of the two analytes. The detection limit was calculated as three times the standard deviation for the blank solution divided by the slope of the analytical curve.

Ten tablets of each analyzed pharmaceutical formulation were accurately weighed and finely powdered in a mortar. An adequate amount of the powders was weighed and transferred to a 25-mL calibrated flask, which was completed to volume with the 0.2 mol L<sup>-1</sup> acetate buffer solution (pH 4.5). The standard addition method was used for analyzing the pharmaceutical samples.

## 3. Results and discussion

### 3.1. Investigation of the electrochemical behavior

The electrochemical behavior of paracetamol and caffeine on the BDD electrode was studied by cyclic voltammetry (CV), SWV, and DPV. Various supporting electrolytes for both compounds were investigated using CV: phosphate buffer, Britton–Robinson buffer, acetate buffer, sulfuric acid, and sodium nitrate. The best results were obtained with the acetate buffer at pH 4.5; peak oxidation potentials of 0.80 V and 1.37 V vs. Ag/AgCl (3.0 mol L<sup>-1</sup> KCl) were obtained for paracetamol and caffeine, respectively.

Voltammograms obtained for paracetamol and caffeine at the BDD electrode presented an irreversible chemical behavior for caffeine and a quasi-reversible behavior for paracetamol (results not shown), in good agreement with data previously reported in the literature for caffeine [38] and paracetamol [34].

A linear plot of the peak current vs. the square root of the scan rate was obtained for both drugs, with a 0.998 correlation

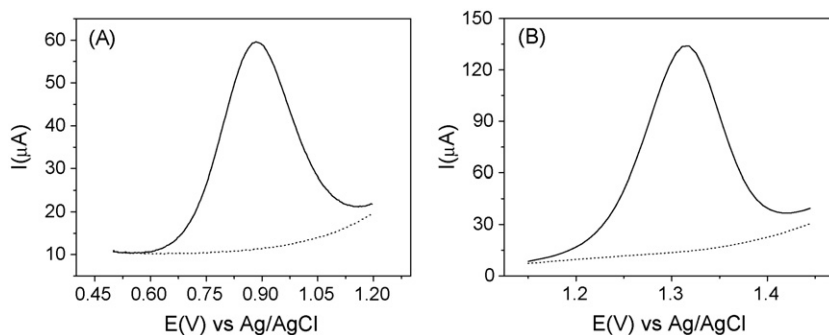


**Fig. 2.** (A) Square wave voltammetric curve (frequency, 70 Hz; amplitude, 50 mV; scan increment, 4 mV) obtained at the BDD electrode for the oxidation of  $5.0 \times 10^{-5} \text{ mol L}^{-1}$  paracetamol in a  $0.2 \text{ mol L}^{-1}$  acetate buffer solution (pH 4.5). (B) Differential pulse voltammetric curve (scan rate,  $70 \text{ mV s}^{-1}$ ; modulation amplitude, 100 mV; modulation time, 7 ms) obtained at the BDD electrode for the oxidation of  $5.0 \times 10^{-5} \text{ mol L}^{-1}$  caffeine in a  $0.2 \text{ mol L}^{-1}$  acetate buffer solution (pH 4.5).

**Table 1**

Investigated square wave voltammetry (SWV) parameters and their optimum values obtained for the determination of paracetamol

Parameters	Studied range	Optimum value
Frequency (Hz)	10–150	70
Amplitude (mV)	10–100	50
Scan increment (mV)	1–7	4

coefficient for both drugs, indicating that the electrode process is controlled by mass transport [25,63].

### 3.2. Determination of paracetamol or caffeine individually

For paracetamol, the best results were obtained using SWV (Fig. 2A), as indicated by figures of merit such as detection limit and sensitivity. The development of this electroanalytical procedure involved a systematic study and optimization of the experimental parameters that affect the SWV response (value of peak oxidation current for  $1.0 \times 10^{-4} \text{ mol L}^{-1}$  paracetamol): square wave frequency ( $f$ ), pulse amplitude ( $a$ ), and scan increment ( $\Delta E_S$ ); the corresponding optimum values are shown in Table 1. The plot of the peak oxidation current vs. paracetamol concentration was linear in the concentration range  $6.0 \times 10^{-7} \text{ mol L}^{-1}$  to  $8.3 \times 10^{-5} \text{ mol L}^{-1}$ ; the corresponding equation ( $R=0.9998$ ) was  $i_{pa}/\mu\text{A}=0.37+0.57 \times 10^6[c/(\text{mol L}^{-1})]$ , with a detection limit of  $4.6 \times 10^{-7} \text{ mol L}^{-1}$ .

For caffeine, the best detection limit and sensitivity values were obtained using DPV, as shown in Fig. 2B. The influence of the instrumental DPV parameters on the value of the peak oxidation current for  $1.0 \times 10^{-4} \text{ mol L}^{-1}$  caffeine in acetate buffer solution (pH 4.5) was also investigated. Table 2 shows the stud-

**Table 2**

Investigated differential pulse voltammetry (DPV) parameters and their optimum values obtained for the determination of caffeine

Parameters	Studied range	Optimum value
Modulation time (ms)	5–20	7
Modulation amplitude (mV)	25–150	100
Scan rate ( $\text{mV s}^{-1}$ )	2.5–100	70

ied range and the optimum obtained values. The plot of the peak oxidation current vs. caffeine concentration shows excellent linearity over a wide concentration range ( $3.0 \times 10^{-7} \text{ mol L}^{-1}$  to  $9.1 \times 10^{-5} \text{ mol L}^{-1}$ ); the corresponding equation ( $R=0.9995$ ) is  $i_{pa}/\mu\text{A}=4.24+2.40 \times 10^6[c/(\text{mol L}^{-1})]$ , with a detection limit of  $1.4 \times 10^{-7} \text{ mol L}^{-1}$ .

### 3.3. Determination of paracetamol and caffeine simultaneously

DPV experiments were carried out for the simultaneous determination of paracetamol and caffeine in the acetate buffer solution (pH 4.5), due to the best values obtained for figures of merit such as sensitivity and precision. The used DPV parameters are the optimum values presented in Table 2.

The DPV curves presented peak oxidation potentials at 0.80 V for paracetamol and 1.35 V for caffeine; this good peak potential separation of about 0.55 V clearly allows the simultaneous determination of the compounds. To further investigate the electrochemical response when both substances are present in solution, DPV curves were obtained in the presence of a large excess of paracetamol (or caffeine) in the acetate buffer solution (pH 4.5). The separate determination of paracetamol in the concentration range  $6.0 \times 10^{-7} \text{ mol L}^{-1}$  to  $1.7 \times 10^{-4} \text{ mol L}^{-1}$  was accomplished

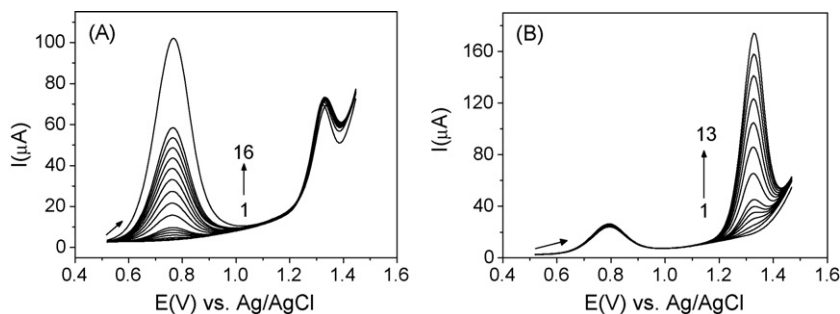


**Fig. 3.** Differential pulse voltammetric curves (scan rate,  $70 \text{ mV s}^{-1}$ ; modulation amplitude, 100 mV; modulation time, 7 ms) obtained at the BDD electrode for: (A) paracetamol at different concentrations in the presence of  $1.7 \times 10^{-5} \text{ mol L}^{-1}$  caffeine in a  $0.2 \text{ mol L}^{-1}$  acetate buffer solution (pH 4.5): (1)  $6.0 \times 10^{-7}$ , (2)  $2.0 \times 10^{-6}$ , (3)  $3.9 \times 10^{-6}$ , (4)  $5.8 \times 10^{-6}$ , (5)  $7.8 \times 10^{-6}$ , (6)  $9.7 \times 10^{-6}$ , (7)  $1.9 \times 10^{-5}$ , (8)  $2.9 \times 10^{-5}$ , (9)  $3.8 \times 10^{-5}$ , (10)  $4.7 \times 10^{-5}$ , (11)  $5.6 \times 10^{-5}$ , (12)  $6.4 \times 10^{-5}$ , (13)  $7.3 \times 10^{-5}$ , (14)  $8.1 \times 10^{-5}$ , (15)  $8.9 \times 10^{-5}$ , and (16)  $1.7 \times 10^{-4} \text{ mol L}^{-1}$ . (B) caffeine at different concentrations in the presence of  $3.8 \times 10^{-5} \text{ mol L}^{-1}$  paracetamol in a  $0.2 \text{ mol L}^{-1}$  acetate buffer solution (pH 4.5): (1)  $8.0 \times 10^{-7}$ , (2)  $1.9 \times 10^{-6}$ , (3)  $3.8 \times 10^{-6}$ , (4)  $5.7 \times 10^{-6}$ , (5)  $7.6 \times 10^{-6}$ , (6)  $9.5 \times 10^{-6}$ , (7)  $1.9 \times 10^{-5}$ , (8)  $4.6 \times 10^{-5}$ , (9)  $5.4 \times 10^{-5}$ , (10)  $7.1 \times 10^{-5}$ , (11)  $8.0 \times 10^{-5}$ , (12)  $8.8 \times 10^{-5}$ , and (13)  $1.6 \times 10^{-4} \text{ mol L}^{-1}$ .

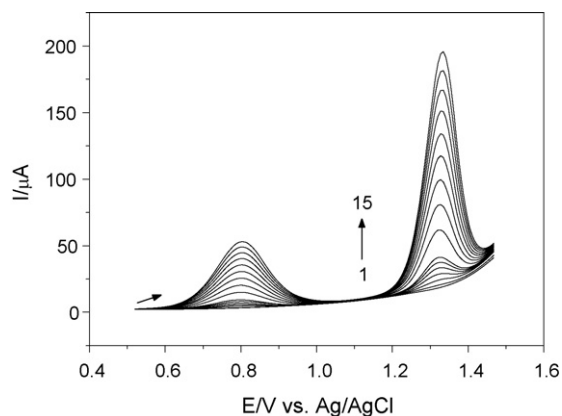


**Fig. 4.** Differential pulse voltammograms (scan rate,  $70 \text{ mV s}^{-1}$ ; modulation amplitude,  $100 \text{ mV}$ ; modulation time,  $7 \text{ ms}$ ) obtained for the oxidation of paracetamol and caffeine at equal concentrations in a  $0.2 \text{ mol L}^{-1}$  acetate buffer solution (pH 4.5): (1)  $5.0 \times 10^{-7}$ , (2)  $2.0 \times 10^{-6}$ , (3)  $4.0 \times 10^{-6}$ , (4)  $5.9 \times 10^{-6}$ , (5)  $7.9 \times 10^{-6}$ , (6)  $9.8 \times 10^{-6}$ , (7)  $1.9 \times 10^{-5}$ , (8)  $2.8 \times 10^{-5}$ , (9)  $3.7 \times 10^{-5}$ , (10)  $4.5 \times 10^{-5}$ , (11)  $5.4 \times 10^{-5}$ , (12)  $6.1 \times 10^{-5}$ , (13)  $6.9 \times 10^{-5}$ , (14)  $7.6 \times 10^{-5}$ , and (15)  $8.3 \times 10^{-5} \text{ mol L}^{-1}$ .

in solutions containing caffeine at the fixed concentration of  $2.0 \times 10^{-5} \text{ mol L}^{-1}$ . On the other hand, the separate determination of caffeine in the concentration range  $8.0 \times 10^{-7} \text{ mol L}^{-1}$  to  $2.0 \times 10^{-4} \text{ mol L}^{-1}$  was accomplished in solutions containing paracetamol at the fixed concentration of  $3.8 \times 10^{-5} \text{ mol L}^{-1}$  (Fig. 3). An examination of Fig. 3A allows concluding that the peak oxidation current for paracetamol increases regularly as its concentration is increased at a fixed concentration of caffeine (its peak oxidation current remains fairly constant). Similarly, as shown in Fig. 3B, the peak oxidation current for caffeine increases regularly as its concentration is increased at a fixed concentration of paracetamol (its peak oxidation current remains constant).

After this previous study, paracetamol and caffeine were determined by simultaneously changing their equal concentrations. Fig. 4 shows the DPV voltammograms obtained for solutions containing paracetamol and caffeine in the acetate buffer solution (pH 4.5).

The calibration curves for paracetamol and for caffeine (Fig. 5) present a good linear response in the concentration range  $5.0 \times 10^{-7} \text{ mol L}^{-1}$  to  $8.3 \times 10^{-5} \text{ mol L}^{-1}$ . The corresponding calibration equations are  $i_{pa}/\mu\text{A} = 0.34 + 0.60 \times 10^6 [c/(\text{mol L}^{-1})]$  and  $i_{pa}/\mu\text{A} = 2.03 + 2.11 \times 10^6 [c/(\text{mol L}^{-1})]$ , both with a 0.9999 correlation coefficient. The calculated detection limits are  $4.9 \times 10^{-7} \text{ mol L}^{-1}$  and  $3.5 \times 10^{-8} \text{ mol L}^{-1}$ , respectively. These detection limits are quite lower than the ones obtained by Zen and Ting [52] using a Nafion<sup>®</sup>/ruthenium oxide pyrochlore chemically modified electrode.

The repeatability was determined by successive measurements ( $n=5$ ) of a  $5.0 \times 10^{-5} \text{ mol L}^{-1}$  paracetamol and caffeine solution;

corresponding relative standard deviations of 0.3% and 1.8% were obtained. The reproducibility was evaluated by measuring the oxidation current values for similar fresh solutions over a period of 5 days. Compared to the obtained original oxidation current values, discrepancies of only 5.1% and 1.4%, respectively, were observed in the measurements with the fresh solutions prepared daily.

It is worthy noting that by comparing these results with the ones obtained for the determination of paracetamol and caffeine separately, the obtained detection limits are of the same magnitude, indicating that the simultaneous determination of paracetamol and caffeine can be considered as efficient as their separate determinations.

### 3.4. Effect of interferences

The effect of some possible interferences was investigated by addition of the compounds to a solution containing  $1.5 \times 10^{-4} \text{ mol L}^{-1}$  paracetamol and caffeine in the acetate buffer (pH 4.5). Saccharin, sodium carbonate, citric acid, and acetylsalicylic acid, all of which can be present in pharmaceutical samples, were tested at the concentration ratios (to paracetamol) of 10:1, 1:1, and 1:10; the obtained results were compared with that obtained using the paracetamol and caffeine standard solution. The analysis of the obtained responses allowed concluding that these compounds do not significantly interfere with the here proposed method.

### 3.5. Application of the voltammetric method to pharmaceutical products

Commercial pharmaceutical samples (tablets) containing paracetamol and caffeine were analyzed to simultaneously determine both substances in order to evaluate the validity of the herein proposed method. Recovery experiments carried out to evaluate matrix effects after standard-solution additions yielded a good average recovery for both substances (97.7% for paracetamol and 99.0% for caffeine), indicating that there were no important matrix interferences for the samples analyzed by the proposed DPV method.

Table 3 presents the values of the amounts of paracetamol and caffeine simultaneously determined in the pharmaceutical formulations employing the proposed DPV method or an HPLC method [62] for comparison. As it can be seen in this table, no significant differences were observed between the values found with the DPV and HPLC techniques for the amounts of paracetamol and caffeine in the tablets. Applying the paired *t*-test [64] to the results obtained using both methods, the calculated *t* values (2.54 for paracetamol and 2.63 for caffeine) were smaller than the critical value (3.18,  $\alpha=0.05$ ). These results indicate that there are no important differences between the obtained results at the 95% confidence level.

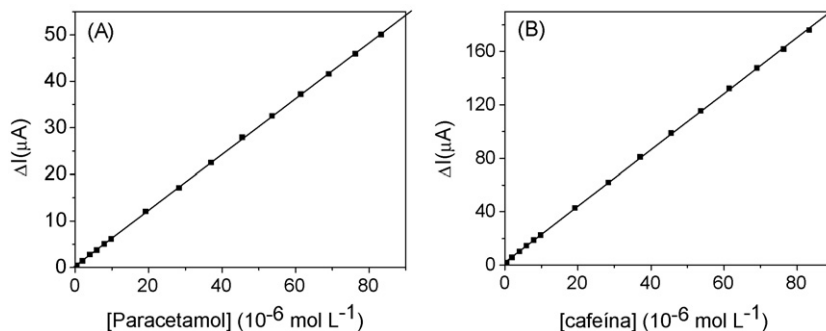


**Fig. 5.** Analytical curves for paracetamol (A) and caffeine (B).



**Table 3**  
Results obtained in the simultaneous determination of paracetamol and caffeine in pharmaceutical formulations (tablets) using the DPV (proposed) and HPLC methods

Samples	Compound	Tablet label value (mg)	HPLC <sup>a</sup> value (mg)	DPV <sup>a</sup> value (mg)	E <sub>1</sub> <sup>b</sup> (%)	E <sub>2</sub> <sup>c</sup> (%)
A	Paracetamol	500	525 ± 1	528 ± 9	5.6	1
	Caffeine	65	67 ± 2	64 ± 1	-2	-4
B	Paracetamol	500	483 ± 18	483 ± 21	-3.4	0
	Caffeine	65	61 ± 2	62 ± 4	-5	2
C	Paracetamol	150	142 ± 5	145 ± 16	-3	2
	Caffeine	50	48 ± 2	51 ± 1	2	6
D	Paracetamol	500	479 ± 28	486 ± 15	-2.8	1
	Caffeine	65	65 ± 3	64 ± 2	-2	-2

<sup>a</sup> Average of 3 measurements.

<sup>b</sup> Relative error 1 (%) = 100 × (voltammetric value – label value)/label value.

<sup>c</sup> Relative error 2 (%) = 100 × (voltammetric value – HPLC value)/HPLC value.

#### 4. Conclusions

The obtained results allow concluding that SWV and DPV along with a cathodically pre-treated BDD electrode can be used with some benefits for the quantitative determination of paracetamol and caffeine, alone or mixed as commonly found in pharmaceutical formulations. When applied to these mixtures, the developed method is easier to be adopted and yields lower detection limits than the voltammetric method reported by Zen and Ting [52]. As it is quite common, the here proposed electroanalytical method has the advantages of being considerably less time-consuming and less expensive than other analytical methods that also apply to the determination of these substances, especially HPLC.

#### Acknowledgements

The authors gratefully acknowledge the financial support from Brazilian funding agencies (FAPESP, CNPq, and CAPES); B.C. Lourenção is also grateful to FAPESP for a M.Sc. scholarship (proc. no. 2007/05894-9).

#### References

- [1] M.E. Bosch, A.J.R. Sanches, F.S. Rojas, C.B. Ojeda, J. Pharm. Biomed. Anal. 42 (2006) 291.
- [2] C. Wang, C. Li, F. Wang, C. Wang, Microchim. Acta 155 (2006) 365.
- [3] R.M. de Carvalho, R.S. Freire, S. Rath, L.T. Kubota, J. Pharm. Biomed. Anal. 34 (2004) 871.
- [4] Q. Chu, L. Jiang, X. Tian, J. Ye, Anal. Chim. Acta 606 (2008) 246.
- [5] R.N. Goyal, V.K. Gupta, M. Oyama, N. Bachheti, Electrochem. Commun. 7 (2005) 803.
- [6] N. Pejic, L. Kolar-Anic, S. Anic, D. Stanisavljevic, J. Pharm. Biomed. Anal. 41 (2006) 610.
- [7] M.J. Gómez, M. Petrovic, A.R. Fernández-Alba, D. Barceló, J. Chromatogr. A 1114 (2006) 224.
- [8] E. McEvoy, S. Donegan, J. Power, K. Altria, J. Pharm. Biomed. Anal. 44 (2007) 137.
- [9] C. Martínez-Algaba, J.M. Bermúdez-Saldanã, R.M. Villanueva-Camañas, S. Sagrado, M.J. Medina-Hernández, J. Pharm. Biomed. Anal. 40 (2006) 312.
- [10] D. Satinsky, I. Neto, P. Solish, H. Sklenarova, M. Conceição, B.S.M. Montenegro, A.N. Araújo, J. Sep. Sci. 27 (2004) 529.
- [11] L.S. Jensen, J. Valentine, R.W. Milne, A.M. Evans, J. Pharm. Biomed. Anal. 34 (2004) 585.
- [12] F. Hiroyuki, Y. Hideyuki, N. Hitoshi, Y. Masatoshi, Anal. Sci. 21 (2005) 1121.
- [13] D. Bose, A. Durgbanshi, A. Martinavarro-Dominguez, M.E. Capella-Peiro, S. Carda-Broch, J.S. Esteve-Romero, M.T. Gil-Agusti, J. Chromatogr. Sci. 43 (2005) 313.
- [14] A.B. Moreira, H.P.M. Oliveira, T.D.Z. Atvars, I.L.T. Dias, G. Oliveira-Neto, E.A.G. Zagatto, L.T. Kubota, Anal. Chim. Acta 539 (2005) 257.
- [15] E.J. Llorent-Martínez, D. Satinsky, P. Solich, P. Ortega-Barrales, A. Molina-Díaz, J. Pharm. Biomed. Anal. 45 (2007) 318.
- [16] H.M. Abdel-Wadood, N.A. Mohamed, F.A. Mohamed, J. AOAC Int. 88 (2005) 1626.
- [17] B. Dejaegher, M.S. Bloomfield, J. Smeyers-Verbeke, Y.V. Heyden, Talanta 75 (2008) 258.
- [18] W. Ruengsitagoon, S. Liawruangrath, A. Townshend, Talanta 69 (2006) 976.
- [19] S. Zhao, W. Bai, H. Yuan, D. Xiao, Anal. Chim. Acta 559 (2006) 195.
- [20] J.F. Chiou, S.L. Chen, S.M. Chen, S.S. Tsou, C.Y. Wu, J.S. Chu, T.Z. Liu, J. Food Drug Anal. 16 (2008) 36.
- [21] A.R. Sirajuddin, A. Khaskheli, M.I. Shah, A. Bhangar, S. Niaz, Mahesar, Spectrochim. Acta Part A 68 (2007) 747.
- [22] H. Filik, I. Sener, S.D. Cekiç, E. Kiliç, R. Apak, Chem. Pharm. Bull. 54 (2006) 891.
- [23] S.J.R. Prabakar, S.S. Narayanan, Talanta 72 (2007) 1818.
- [24] L.S. Duan, F. Xie, F. Zhou, S.F. Wang, Anal. Lett. 40 (2007) 2653.
- [25] F.S. Felix, C.M.A. Brett, L. Angnes, J. Pharm. Biomed. Anal. 43 (2007) 1622.
- [26] S.F. Wang, F. Xie, R.F. Hu, Sens. Actuators B 123 (2007) 495.
- [27] R.N. Goyal, S.P. Singh, Electrochim. Acta 51 (2006) 3008.
- [28] L. Ozcan, Y. Sahin, Sens. Actuators B 127 (2007) 362.
- [29] M. Li, L. Jing, Electrochim. Acta 52 (2007) 3250.
- [30] A. Gómez-Caballero, M.A. Goicolea, R.J. Barrio, Analyst 130 (2005) 1012.
- [31] F.Y. He, A.L. Liu, X.H. Xia, Anal. Bioanal. Chem. 379 (2004) 1062.
- [32] C. Li, G. Zhan, Q. Yang, J. Lu, Bull. Korean Chem. Soc. 27 (2006) 1854.
- [33] V.A. Pedrosa, D. Lowinsohn, M. Bertotti, Electroanalysis 18 (2006) 931.
- [34] N. Wangfuengkanagul, O. Chailapakul, J. Pharm. Biomed. Anal. 28 (2002) 841.
- [35] X. ShangGuan, H. Zhang, J. Zheng, Anal. Bioanal. Chem. 391 (2008) 1049.
- [36] D.J. Miner, J.R. Rice, R.M. Riggan, P.T. Kissinger, Anal. Chem. 53 (1981) 2258.
- [37] J.J.V. Benschoten, J.Y. Lewis, W.R. Heineman, J. Chem. Educ. 60 (1983) 772.
- [38] N. Spätaru, B.V. Sarada, D.A. Tryk, A. Fujishima, Electroanalysis 14 (2002) 721.
- [39] J. Sawynok, Drugs 49 (1995) 37.
- [40] M.Z. Ding, J.K. Zou, Chin. J. Anal. Chem. 36 (2008) 381.
- [41] Y. Yamauchi, A. Nakamura, I. Kohno, M. Kitai, K. Hatanaka, T. Tanimoto, Chem. Pharm. Bull. 56 (2008) 185.
- [42] N.H. Ishler, T.P. Finucane, E. Borker, Anal. Chem. 20 (1948) 1162.
- [43] R.L. Evans, P.H. Siitonen, J. Chromatogr. Sci. 46 (2008) 61.
- [44] Y. Yamauchi, A. Nakamura, I. Kohno, K. Hatanaka, M. Kitai, T. Tanimoto, J. Chromatogr. A 1177 (2008) 190.
- [45] S.Y. Ly, Y.S. Jung, M.H. Kim, I.K. Han, W.W. Jung, H.S. Kim, Microchim. Acta 146 (2004) 207.
- [46] B. Brunetti, E. Desimoni, P. Casati, Electroanalysis 19 (2007) 385.
- [47] B.H. Hansen, G. Dryhurst, J. Electroanal. Chem. 30 (1971) 407.
- [48] J.M. Zen, Y.S. Ting, Y. Shih, Analyst 123 (1998) 1145.
- [49] E. Dinç, J. Pharm. Biomed. Anal. 21 (1999) 723.
- [50] A.B. Moreira, I.L.T. Dias, G.O. Neto, E.A.G. Zagatto, L.T. Kubota, Anal. Lett. 39 (2006) 349.
- [51] A. Wang, J. Sun, H. Feng, S. Gao, Z. He, Chromatographia 67 (2008) 281.
- [52] J.M. Zen, Y.S. Ting, Anal. Chim. Acta 342 (1997) 175.
- [53] M. Hupert, A. Muck, J. Wang, J. Stotter, Z. Cvakova, S. Haymond, Y. Show, G.M. Swain, Diamond Relat. Mater. 12 (2003) 1940.
- [54] Y.V. Pleskov, Russ. J. Electrochem. 38 (2002) 1275.
- [55] N.S. Lawrence, M. Pagels, A. Meredith, T.G.J. Jones, C.E. Hall, C.S.J. Pickles, H.P. Godfried, C.E. Banks, R.G. Compton, L. Jiang, Talanta 69 (2006) 829.
- [56] G.R. Salazar-Banda, L.S. Andrade, P.A.P. Nascente, P.S. Pizani, R.C. Rocha-Filho, L.A. Avaca, Electrochim. Acta 51 (2006) 4612.
- [57] H.B. Suffredini, V.A. Pedrosa, L. Codognato, S.A.S. Machado, R.C. Rocha-Filho, L.A. Avaca, Electrochim. Acta 49 (2004) 4021.
- [58] E.R. Sartori, R.A. Medeiros, R.C. Rocha-Filho, O. Fatibello-Filho, J. Braz. Chem. Soc., in press.
- [59] R.A. Medeiros, A.E. de Carvalho, R.C. Rocha-Filho, O. Fatibello-Filho, Anal. Lett. 40 (2007) 3195.
- [60] R.A. Medeiros, A.E. de Carvalho, R.C. Rocha-Filho, O. Fatibello-Filho, Quim. Nova 31 (2008) 1405.
- [61] R.A. Medeiros, A.E. de Carvalho, R.C. Rocha-Filho, O. Fatibello-Filho, Talanta 76 (2008) 685.
- [62] J.T. Franeta, D. Agbaba, S. Eric, S. Pavkov, M. Aleksic, S. Vladimirov, Farmaco 57 (2002) 709.
- [63] P. Monk, Fundamentals of Electroanalytical Chemistry, Wiley and Sons, New York, 2001.
- [64] R.L. Anderson, Practical Statistics for Analytical Chemists, Van Nostrand Reinhold, New York, 1987.



## Development of an ICP-MS immunoassay for the detection of anti-erythropoietin antibodies

Yanyan Lu<sup>a</sup>, Wenjun Wang<sup>a</sup>, Zhi Xing<sup>a</sup>, Shidong Wang<sup>b</sup>, Po Cao<sup>b</sup>,  
Sichun Zhang<sup>a</sup>, Xinrong Zhang<sup>a,\*</sup>

<sup>a</sup> Department of Chemistry, Key Laboratory for Atomic and Molecular Nanosciences of the Education Ministry, Tsinghua University, Beijing 100084, PR China

<sup>b</sup> Dongzhimen Hospital affiliated to Beijing University of Chinese Medicine, Beijing 100700, PR China

### ARTICLE INFO

#### Article history:

Received 27 October 2008

Received in revised form

22 December 2008

Accepted 23 December 2008

Available online 20 January 2009

#### Keywords:

rhEPO

Anti-EPO antibody

Immunoassay

Inductively coupled plasma mass spectrometry

### ABSTRACT

A sandwich-type immunoassay linked with inductively coupled plasma mass spectrometry (ICP-MS) has been developed for the detection of anti-erythropoietin antibodies (anti-EPO Abs). Recombinant human erythropoietin (rhEPO) was immobilized on the solid phase to capture anti-rhEPO Abs specifically. After the immunoreactions with Au-labeled goat-anti-rabbit IgG, a diluted HNO<sub>3</sub> (2%) was used to dissociate Au nanoparticles which was then introduced to the ICP-MS for measurements. Under the optimized conditions, the calibration graph for anti-EPO Abs was linear in the range of 35.6–500 ng mL<sup>-1</sup> with a detection limit of 10.7 ng mL<sup>-1</sup> ( $3\sigma$ ,  $n=9$ ). The relative standard deviation (R.S.D.) for three replicate measurements of 30.9 ng mL<sup>-1</sup> of anti-EPO Abs was 8.43%. The recoveries of anti-EPO Abs in sera at the spiking level of 50, 100, 150, 200 and 400 ng mL<sup>-1</sup> were 99.2%, 101.5%, 95.0%, 94.0% and 102.9%, respectively. For the real sample analysis, 26 samples from healthy people and 53 samples from patients with rhEPO treatments were studied. One sample from patients showed significantly higher anti-EPO Abs from other samples, indicating a possibility of immune response of this patient.

© 2009 Elsevier B.V. All rights reserved.

### 1. Introduction

Recombinant human erythropoietin (rhEPO), just as its biological equivalent EPO, is a hormone which can stimulate the proliferation of red cells [1]. For this reason, rhEPO is widely used to treat patients with anemia due to renal failure or systemic lupus erythematosus (SLE) [2,3]. However, some patients receiving rhEPO therapy were reported to endure sudden severe anemia or pure red cell aplasia (PRCA), demonstrating the presence of anti-erythropoietin antibodies (anti-EPO Abs) [4–8]. Thus, the assay for anti-EPO Abs is of interest for the studying of anemia caused by rhEPO treatment. In addition, detections and measurements of anti-EPO Abs may also become a supplementary approach of confirming rhEPO drug abuse among athletes.

Currently, several types of assays have been developed to detect anti-EPO Abs, including radioimmunoprecipitation (RIP) [6,9], and enzyme-linked immunosorbent assay (ELISA) [10–15]. Although the RIP method offers high sensitivity and specificity, the performance of radioactive isotopes may cause damage both to the people who handle the whole process and to the environment. ELISA is a popular method to detect antibodies bound to protein antigens either directly or indirectly. Various modifications have

been employed to improve the sensitivity, for example, the applying of avidin–biotin complexes [16–19].

Inductively coupled plasma mass spectrometry (ICP-MS), which is the extensively applied trace and ultra-trace analysis tool today, provides several advantages over other analytical methods including simple spectra, a wide linear dynamic range, low limits of detection, high speed of analysis and the ability of multi-elements analysis [20]. ICP-MS has been widely used in the analysis of bio-samples, for example, metal-binding proteins, selenium-containing proteins [21–24]. In our previous researches, several ICP-MS-based immunoassays have been successfully established [25–28]. The multi-element detection ability has also been demonstrated by using laser ablation technique for sample introduction [29]. The performance of ICP-MS immunoassay on samples for multiple surface biomarkers has been described by other groups as well [30–32]. Compared with traditional immunoassays, ICP-MS immunoassay deals with element-tagged instead of isotope-tagged or enzyme-conjugated antibodies, making it free of radioactive isotope or toxic enzyme substrate reagents. Recently, immunoassays employing Au nanoparticles labeled antibodies have been developed with varieties of detection methods, for instance, electrochemical and ICP-MS methods [20,27,29,33].

In this work, we developed a sandwich-type ICP-MS immunoassay method to detect anti-EPO Abs in human sera. RhEPO was first immobilized to the solid phase. Afterward, the bound RhEPO was allowed to capture anti-rhEPO Abs specifically. The captured

\* Corresponding author. Tel.: +86 10 62787678; fax: +86 10 62781690.  
E-mail address: [xrzhang@chem.tsinghua.edu.cn](mailto:xrzhang@chem.tsinghua.edu.cn) (X. Zhang).

anti-rhEPO Abs reacted with Au-labeled goat-anti-rabbit IgG antibody followed by detection with ICP-MS after the dissociation of the immunocomplex. With this procedure a rapid and simple method for the detection of anti-EPO Abs in human sera was established.

## 2. Experimental

### 2.1. Apparatus

A Thermo X Series ICP-MS (Thermo Fisher Scientific, Bremen, Germany) was used in all experiments. A standard glass concentric nebulizer and a standard glass conical impact bead spray chamber were employed with an uptake rate of round  $1 \text{ mL min}^{-1}$ . The nickel sampling cone and nickel skimmer cone were equipped. The experimental parameters were optimized using 1%  $\text{HNO}_3$  solution containing  $10 \text{ ng mL}^{-1}$  Rh and Tb and adjusted through the detection of Au-labeled goat-anti-rabbit IgG solution. The optimized parameters are listed in Table 1.

### 2.2. Reagents and materials

RhEPO was obtained from Roche Diagnostics (Penzberg, Germany). Rabbit polyclonal anti-EPO antibody (anti-EPO pAb) was purchased from Millipore Corp (Milford, MA, USA). Bovine serum albumin (BSA) and goat-anti-rabbit IgG was purchased from Bo'ao sen Chemical Reagents Co. (Beijing, China). Tween 20 was purchased from Sigma–Aldrich Chemical Co. (St. Louis, MO, USA). Colloidal Au nanoparticles were synthesized in our laboratory. Goat-anti-rabbit colloidal Au conjugates were either bought from Bo'ao sen Chemical Reagents Co (Beijing, China) (for studying the influence of label size) or made in our lab. Unless otherwise stated, all the other reagents used in this study were of analytical grade and obtained from Sinopharm Chemical Reagent Beijing Co. Ltd. (Beijing, China). 96-wells ELISA microplates were of “high binding” grade and purchased from NUNC, Denmark.

### 2.3. Buffers

The buffers and solutions used were: (1) phosphate buffer: saline (PBS) 8.0 g of NaCl, 2.9 g of  $\text{Na}_2\text{HPO}_4$ , 0.2 g of  $\text{KH}_2\text{PO}_4$  and 0.2 g of KCl dissolved in 1 L distilled water (pH 7.4); (2) coating buffer:  $50 \text{ mmol L}^{-1}$   $\text{Na}_2\text{CO}_3\text{--NaHCO}_3$  (pH 9.6) in distilled water; (3) blocking buffer: 3% (w/v,  $\text{g L}^{-1}$ ) BSA in PBS. The blocking solution was stored at  $4^\circ\text{C}$  and used within a week; (4) washing solution (PBST): 0.05% Tween 20 (v/v) in PBS; (5) assay solution: 0.3% (w/v,  $\text{g L}^{-1}$ ) BSA in PBST. All buffers were prepared using water ( $18.3 \text{ M}\Omega \text{ cm}^{-1}$ ) from a Milli-Q water purification system (Millipore Milford, MA, USA).

**Table 1**  
Operating parameters for ICP-MS.

Parameter	Description
ICP RF power	1200 W
Coolant gas flow	$14 \text{ L min}^{-1}$
Nebulizer gas flow	$0.93 \text{ L min}^{-1}$
Auxiliary gas flow	$0.70 \text{ L min}^{-1}$
Sample uptake rate	$1 \text{ mL min}^{-1}$
Sample uptake time	40 s
Washout time	60 s
Acquisition mode	Pulse counting
Dwell time	30 ms
Sweeps per reading	70
Replicates	3
Isotope used	$^{197}\text{Au}$
Internal standard used	$^{159}\text{Tb}$



**Fig. 1.** TEM photograph of colloidal Au.

### 2.4. Preparation of colloidal gold nanoparticles

Colloidal Au nanoparticles were prepared according to the protocol from the literature with slight modification [34,35]. Briefly, 0.01%  $\text{HAuCl}_4$  and 0.05% trisodium citrate were boiled in aqueous solutions for about 30 min. Then, the resulting suspension was cooled and filtered through a  $0.45 \mu\text{m}$  Millipore membrane. The diameter of particle was  $\sim 15 \text{ nm}$  (Fig. 1) as confirmed by Hitachi H-800 transmission electron microscopy.

### 2.5. Preparation of colloidal gold-antibody conjugate

Colloidal gold-antibody conjugates were also prepared according to reported protocols with slight modification [34,36,37]. Briefly, goat-anti-rabbit IgG (10% more than the minimum amount, which was determined using a flocculation test) was added to pH-adjusted colloidal Au suspension. After incubation at room temperature for 1 h, the conjugate was centrifuged at  $5000 \times g$  for 1 h at  $4^\circ\text{C}$ . The soft sediment was then resuspended in  $0.01 \text{ mol L}^{-1}$  Tris-buffered saline. Adding glycerol to a final concentration of 50% allowed storage of the conjugate at  $-20^\circ\text{C}$  for several months.

### 2.6. Assay protocol

$100 \mu\text{L}$  of rhEPO at selected concentration was immobilized by absorption on each wall of the high binding polystyrene 96-well plates. The plates were placed at  $4^\circ\text{C}$  overnight. After washing three times and adding  $250 \mu\text{L}$  blocking solution, the plates were incubated for 1 h. Then  $100 \mu\text{L}$  serum samples or anti-erythropoietin antibody standards were added to each well. We used polyclonal rabbit anti-EPO antibody as a standard because a human anti-EPO antibody standard was not available. The plates were incubated for 1 h. After that,  $100 \mu\text{L}$  Au-labeled goat-anti-rabbit IgG solution was added and incubated for another 1 h. All incubations were carried out at  $37^\circ\text{C}$ . Between steps the plates were washed three times with the washing buffer to remove unbound antibody or antigen.

After the final incubation, liquid in the well was discarded before  $200 \mu\text{L}$  2%  $\text{HNO}_3$  was added. The plate was shaken at room temper-

ature for 15 min, diluted to 1.5 mL with 2% HNO<sub>3</sub> and then samples were introduced to the ICP-MS system.

The calibration curves were established by plotting normalized ICP count values of anti-EPO Abs standards against the concentrations of anti-EPO Abs.

### 2.7. Analysis of spiked serum samples

The recovery of ICP-MS immunoassay was evaluated by spiking anti-EPO Abs to diluted negative human serum in the established working range and analyzing with the protocol as described in Section 2.6.

### 2.8. Human serum sample

Blood samples of rhEPO-treated patients with chronic renal failure (CRF) were from Dongzhimen Hospital (Beijing, China) and the Chinese PLA General Hospital (Beijing, China). Control blood samples from healthy persons were provided by School Hospital of Tsinghua University (Beijing, China). Serum samples were prepared from whole blood by centrifuging at 10,000 × g for 5 min in a serum separation vial and then stored as aliquots at −20 °C until analysis.

## 3. Results and discussion

### 3.1. Optimization

#### 3.1.1. Selection of ICP-MS operational parameters with Au-labeled IgG

The operational parameters for ICP-MS were optimized using 1% HNO<sub>3</sub> solution containing 10 ng mL<sup>−1</sup> Rh and Tb and adjusted through the detection of Au-labeled goat-anti-rabbit IgG solution. Before immunoassay, Au-labeled goat-anti-rabbit IgG solution was serially diluted with 2% HNO<sub>3</sub> and detected by ICP-MS. A linear relationship existed even when the solution was 25,000 times diluted (Fig. 2). Linear response of ICP-MS signals to tagged proteins indicates that ICP-MS can be employed for the determination of antibodies labeled with Au nanoparticles, which is proportional to the anti-EPO Abs in the sample after immunoassay. ICP-MS detection parameters were finely tuned to detect Au-labeled IgG. Optimized parameters can be found in Table 1.

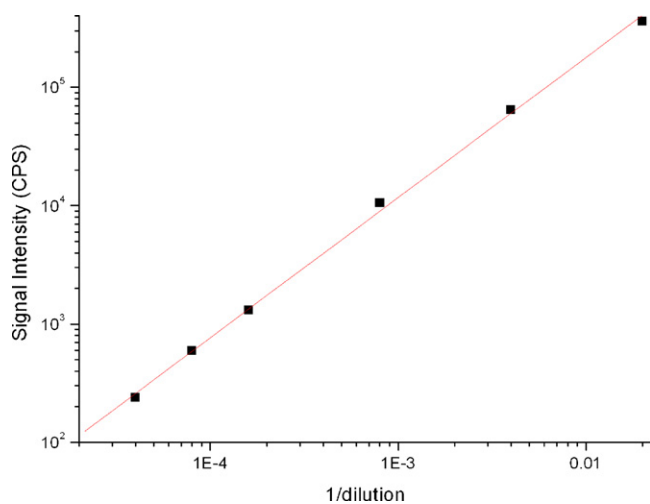


Fig. 2. Serial dilutions of Au-labeled goat-anti-rabbit IgG. The Au-labeled IgG solution was 50; 250; 1250; 6250; 12,500; 25,000 times diluted.

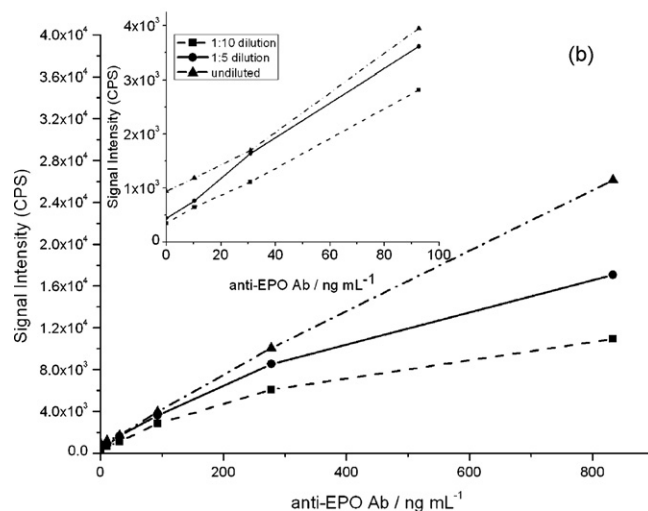
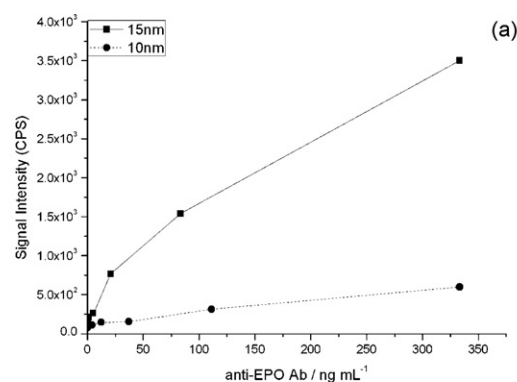


Fig. 3. Optimization of size and concentration of Au nanoparticle labels. (a) Comparing of two different sized Au nanoparticles labeled IgG solution, 10 and 15 nm, respectively. (b) Three concentrations of colloidal Au-labeled goat-anti-rabbit IgG solution including undiluted, 1:5 and 1:10 dilutions with PBS were analyzed. The inset was a zoom in of graph (b) with anti-EPO Ab concentrations from 0 to 92.6 ng mL<sup>−1</sup>. For these experiments, coating concentration of rhEPO was 1 ng mL<sup>−1</sup> while 3% BSA in PBS was used as the blocking buffer.

#### 3.1.2. Size and concentration of Au nanoparticle labels

Two types of goat-anti-rabbit IgG labeled with different sized Au nanoparticles were tested at the same dilution (1:100) while other experimental conditions were the same. Fig. 3a shows that higher response was achieved when applying larger nanoparticles (with a diameter of 15 nm) as the label. This may be explained by more Au element contained in a bigger Au nanoparticle. 15 nm Au nanoparticles labeled IgG solution was used in later experiments.

As ICP-MS signal is determined by contents of the element Au in the sample solutions, the quantity of colloidal Au-labeled goat-anti-rabbit IgG added is crucial. For optimization, undiluted and different dilutions of prepared colloidal Au-labeled goat-anti-rabbit IgG (1:5 and 1:10) were analyzed with a coating concentration (of rhEPO) of 1 ng mL<sup>−1</sup> and 3% BSA in PBS as the blocking buffer. Fig. 3b shows that signal intensity for each analyte concentration increases in the order of 1:10 dilution, 1:5 dilution, and undiluted solution. However, with a further investigation of signal intensity at low analyte level (inset of Fig. 3b), a 1:5 dilution was used throughout the experiment for a relative low nonspecific adsorption compared with undiluted solution though the latter present higher response at each anti-EPO Abs level.

#### 3.1.3. Blocking buffer

To minimize nonspecific binding, a blocking step is necessary after coating and washing away the free antigen. Blocking buffer

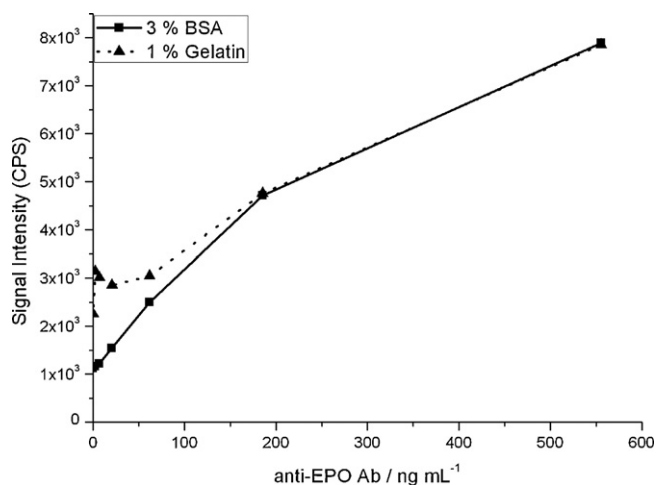


**Fig. 4.** Optimization of the blocking buffer: 3% BSA and 1% gelatin in PBS were analyzed while other conditions were the same. The coating concentration of rhEPO was  $1 \text{ ng mL}^{-1}$  while the Au-labeled IgG solution was five times diluted before use.

can occupy the free sites on the 96-wells plate and thus guarantee a low detection limit of the immunoassay. Two blocking buffers were considered: 3% BSA and 1% gelatin (Fig. 4) while the coating concentration of rhEPO was  $1 \text{ ng mL}^{-1}$  and dilution of Au-labeled IgG was 1:5. Results indicated that the former possessed a better blocking effect. When using 1% gelatin as the blocking buffer, unstable ICP-MS signals appeared at low anti-EPO Ab concentrations (approximately from 0 to  $20 \text{ ng mL}^{-1}$ ). As a result, 3% BSA was chosen as the blocking buffer and 0.3% BSA in PBST was used as assay solution.

### 3.1.4. Coating concentration of rhEPO

Coating is the first step of an immunoassay. Although the coating buffer is also influential (pH value affects antigen binding), we just skipped the optimization process by adopting  $\text{Na}_2\text{CO}_3\text{-NaHCO}_3$  (pH 9.6) buffer following a former experimental result without further discussion [38]. Still, we optimized the coating concentration of rhEPO (Fig. 5). 3% BSA in PBS was the blocking buffer and a 1:5 dilution of Au-labeled IgG was used for those assays with different coating concentrations of 0.5, 1, 5 and  $10 \mu\text{g mL}^{-1}$ , respectively. When the coating concentration was  $0.5 \mu\text{g mL}^{-1}$ , it was less responsive to the increasing anti-EPO Ab concentrations. And for

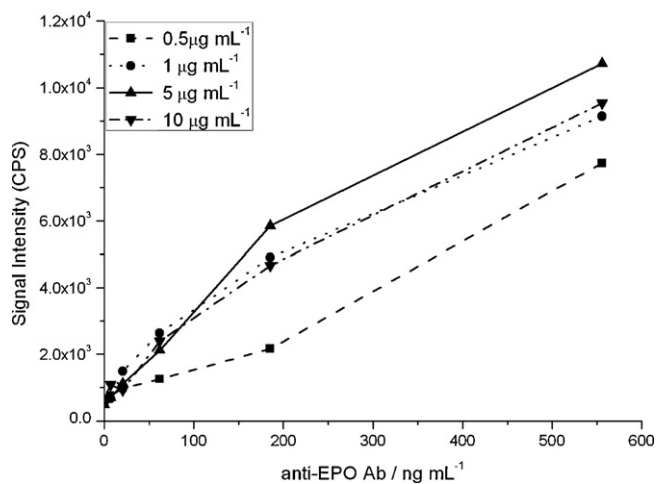


**Fig. 5.** Optimization of coating concentration: rhEPO concentrations of 0.5, 1, 5 and  $10 \mu\text{g mL}^{-1}$  were analyzed. Other experimental conditions were the same: 3% BSA in PBS was used as the blocking buffer and the self-made Au-labeled IgG solution was five times diluted before use.

**Table 2**

Recovery of spiked anti-EPO Abs in serum samples.

Added ( $\text{ng mL}^{-1}$ )	Found, mean $\pm$ S.D. <sup>a</sup> ( $\text{ng mL}^{-1}$ )	Relative recovery (%)
50	$49.6 \pm 4.7$	99.2
100	$101.5 \pm 13.4$	101.5
150	$142.5 \pm 19.2$	95.0
200	$189.7 \pm 8.1$	94.0
400	$411.6 \pm 11.2$	102.9

<sup>a</sup> Standard deviation ( $n=3$ ).

the other coating concentrations, the immunoassay reacted much more similar. For the coating concentration of  $5 \mu\text{g mL}^{-1}$ , it had the least signal intensity value for blank, with the value of  $483.8 \pm 55.2$  compared to  $632.1 \pm 177.4$ ,  $566.0 \pm 144.2$  and  $665.9 \pm 126.7$  for the coating concentrations of 0.5, 1,  $10 \mu\text{g mL}^{-1}$ , respectively. We selected  $5 \mu\text{g mL}^{-1}$  of rhEPO in  $\text{Na}_2\text{CO}_3\text{-NaHCO}_3$  (pH 9.6) buffer as the coating solution.

### 3.2. Analytical characteristics

Under the optimum conditions described above, a calibration curve for anti-EPO Abs was established. The detection limit of anti-EPO Abs for this ICP-MS linked immunoassay method was  $10.7 \text{ ng mL}^{-1}$  ( $3\sigma$ ,  $n=9$ ). The calibration graph was linear in the concentration range of  $35.6\text{--}500 \text{ ng mL}^{-1}$  ( $R^2=0.9882$ ). The relative standard deviation (R.S.D.) for three replicate measurements of  $30.9 \text{ ng mL}^{-1}$  anti-EPO Abs was 8.43%.

### 3.3. Application

For the analysis of spiked serum samples, anti-EPO Abs were added to 20 times diluted serum samples and reached final concentrations of 50, 100, 150, 200 and  $400 \text{ ng mL}^{-1}$ , separately. Recovery for each adding concentration is listed in Table 2.

Serum samples both from healthy donors (control) and patients were 20 times diluted and analyzed in triplicate, of which 26 were obtained from healthy people and the other 53 were from rhEPO-treated patients with chronic renal failure. Independent-Samples *t*-test for those experiment results was then carried out utilizing statistical software, SPSS 11.5 (SPSS, USA). No significant differences were found between patients (53 samples) and the healthy people (26 samples). However, one patient gave signal intensity of  $845.4 \pm 27$  (approximately  $11.4 \text{ ng mL}^{-1}$ ), which was significantly higher than the average of control (with signal inten-

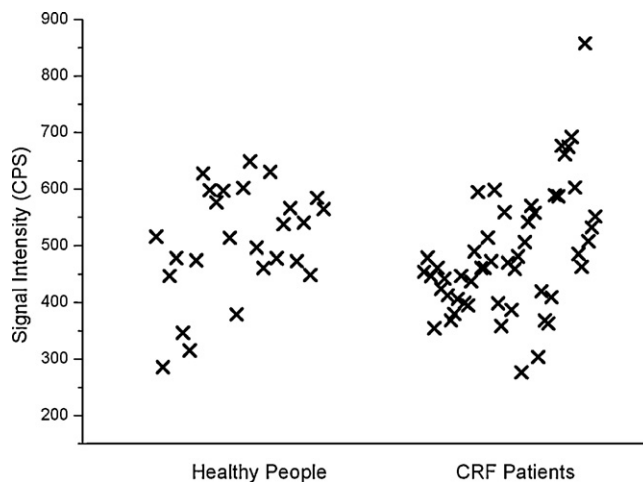


**Fig. 6.** Distribution of ICP-MS signal intensity (CPS) of anti-EPO Abs in healthy people and CRF patients treated with EPO.

sity of  $500.0 \pm 74.7$ ) (Fig. 6). All these experimental results might be explained by the fact that patients treated with rhEPO could only occasionally suffer from PRCA.

#### 4. Conclusion

We have developed a new ICP-MS immunoassay for anti-EPO antibodies in human serum. The detection of spiked serum samples proved that this method possesses good analyzing ability. No significant differences of serum samples from healthy people and patients were observed. Further optimization, changing of the elemental tags or employing of a low sample flow nebulizer (thus a smaller sample size) is encouraged to perform a more sensitive ICP-MS immunoassay for anti-EPO Abs.

#### Acknowledgement

This work was financially supported by the National Natural Science Foundation of China (Project Nos. 20535020; 20635002).

#### References

- [1] B. Berglund, B. Ekblom, *J. Intern. Med.* 229 (1991) 125.
- [2] Y. Beguin, *Leuk. Lymphoma* 18 (1995) 413.
- [3] C.J. Dunn, A. Markham, *Drugs* 51 (1996) 299.
- [4] N. Casadevall, E. Dupuy, P. Molho-Sabatier, G. Tobelem, B. Varet, P. Mayeux, *New Engl. J. Med.* 334 (1996) 630.
- [5] N. Casadevall, *Nephrol. Dial. Transplant* 17 (Suppl. 5) (2002) 42.
- [6] N. Casadevall, J. Nataf, B. Viron, A. Kolta, J.J. Kilagjian, P. Martin-Dupont, P. Michaud, T. Papo, V. Ugo, I. Teysandier, B. Varet, P. Mayeux, *N. Engl. J. Med.* 346 (2002) 469.
- [7] G. Weber, J. Gross, A. Kromminga, H.H. Loew, K.U. Eckardt, *J. Am. Soc. Nephrol.* 13 (2002) 2381.
- [8] The Pure Red Cell Aplasia Global Scientific Advisory Board (GSAB), *Eur. J. Clin. Invest.* 35 (Suppl. 3) (2005) 95.
- [9] R. Tacey, A. Greway, J. Smiell, D. Power, A. Kromminga, M. Daha, N. Casadevall, M. Kelley, *J. Immunol. Methods* 283 (2003) 317.
- [10] J.M. Urrea, M. de la Torre, R. Alcazar, R. Peces, *Clin. Chem.* 43 (1997) 848.
- [11] N.V. Sipsas, I.K. Styliani, J.P. Ioannidis, D. Kyriaki, A.G. Tzioufas, T. Kordossis, *J. Infect. Dis.* 180 (1999) 2044.
- [12] G. Castelli, A. Famularo, C. Semino, A.M. Machi, A. Ceci, G. Cannella, G. Melioli, *Pharmacol. Res.* 41 (2000) 313.
- [13] M. Voulgarelis, S.I. Kokori, J.P. Ioannidis, A.G. Tzioufas, D. Kyriaki, H.M. Moutsopoulos, *Ann. Rheum. Dis.* 59 (2000) 217.
- [14] G. Schett, U. Firbas, W. Füreder, H. Hiesberger, S. Winkler, D. Wachauer, M. Köller, S. Kapitotis, J. Smolen, *Rheumatology* 40 (2001) 424.
- [15] W. Hoesel, J. Gross, R. Moller, B. Kanne, A. Wessner, G. Müller, A. Müller, E. Gromnica-Ihle, M. Fromme, S. Bischoff, A. Haselbeck, *J. Immunol. Methods* 294 (2004) 101.
- [16] M. Suter, J.E. Butler, *Immunol. Lett.* 13 (1986) 313.
- [17] I. Willner, F. Patolsky, Y. Weizmann, B. Willner, *Talanta* 56 (2002) 847.
- [18] J.T. Hea, Z.H. Shi, J. Yan, M.P. Zhao, Z.Q. Guo, W.B. Chang, *Talanta* 65 (2005) 621.
- [19] J. Gross, R. Moller, W. Henke, W. Hoesel, *J. Immunol. Methods* 313 (2006) 176.
- [20] V.I. Baranov, Z. Quinn, D.R. Bandura, S.D. Tanner, *Anal. Chem.* 74 (2002) 1629.
- [21] T. Lindemann, H. Hintelmann, *Anal. Chem.* 74 (2002) 4602.
- [22] J.R. Encinar, L. Ouerdane, W. Buchmann, J. Tortajada, R. Lobinski, J. Szpunar, *Anal. Chem.* 75 (2005) 3765.
- [23] L. Tastet, D. Schaumöffel, B. Bouysiessere, R. Lobinski, *Talanta* 75 (2008) 1140.
- [24] J.S. Becker, S. Mounicoua, M.V. Zoriy, J.S. Becker, R. Lobinskia, *Talanta* 76 (2008) 1183.
- [25] C. Zhang, F.B. Wu, Y.Y. Zhang, X. Wang, X.R. Zhang, *J. Anal. At. Spectrom.* 16 (2001) 1393.
- [26] C. Zhang, F.B. Wu, X.R. Zhang, *J. Anal. At. Spectrom.* 17 (2002) 1304.
- [27] C. Zhang, Z.Y. Zhang, B.B. Yu, J.J. Shi, X.R. Zhang, *Anal. Chem.* 74 (2002) 96.
- [28] S.C. Zhang, C. Zhang, Z. Xing, X.R. Zhang, *Clin. Chem.* 50 (2004) 1214.
- [29] S.H. Hu, S.C. Zhang, Z.C. Hu, Z. Xing, X.R. Zhang, *Anal. Chem.* 79 (2007) 923.
- [30] O.I. Ornatsky, V. Baranov, D.R. Bandura, S.D. Tanner, J. Dick, *J. Immunol. Methods* 308 (2006) 68.
- [31] X.D. Lou, G.H. Zhang, I. Herrera, R. Kinach, O. Ornatsky, V. Baranov, M. Nitz, M.A. Winnik, *Angew. Chem. Int. Ed.* 46 (2007) 6111.
- [32] O.I. Ornatsky, R. Kinach, D.R. Bandura, X.D. Lou, S.D. Tanner, V.I. Baranov, M. Nitz, M.A. Winnik, *J. Anal. At. Spectrom.* 23 (2008) 421.
- [33] A. Ambrosi, M.T. Castañeda, A.J. Killard, M.R. Smyth, S. Alegret, A. Merkoçi, *Anal. Chem.* 79 (2007) 5232.
- [34] A.J. Verkleij, J.L. Leunissen, *Immuno-gold-labeling in Cell Biology*, CRC Press, Boca Raton, FL, 1989.
- [35] G. Frens, *Nat. Phys. Sci.* 241 (1973) 20.
- [36] J. Ni, R.J. Lipert, G.B. Dawson, M.D. Porter, *Anal. Chem.* 71 (1999) 4903.
- [37] L.A. Lyon, M.D. Musick, M.J. Natan, *Anal. Chem.* 70 (1998) 5177.
- [38] W.J. Wang, Y.Y. Lu, S.C. Zhang, S.D. Wang, P. Cao, Y.P. Tian, X.R. Zhang, *Luminescence* 24 (2008) 55–61.



# Simultaneous spectrofluorimetric determination of levodopa and propranolol in urine using feed-forward neural networks assisted by principal component analysis

Tayyebeh Madrakian\*, Abbas Afkhami, Masoumeh Mohammadnejad

Faculty of Chemistry, Bu-Ali Sina University, Hamadan, Iran

## ARTICLE INFO

### Article history:

Received 12 November 2008  
Received in revised form 12 January 2009  
Accepted 12 January 2009  
Available online 20 January 2009

### Keywords:

Spectrofluorimetry  
Levodopa  
Propranolol  
Feed-forward neural network  
Urine

## ABSTRACT

The simultaneous determination of levodopa (LD) and propranolol (PRO) using fluorescence spectrometric technique is described. The method involves measuring the natural fluorescence of these drugs in the micellar media of sodium dodecyl sulfate (SDS) using principal component analysis-feed-forward neural networks (PC-FFNNs). Experimental conditions such as effect of pH and SDS concentration were optimized. Under the optimum conditions, the linear determination ranges of LD and PRO are  $2.0 \times 10^{-8}$  to  $1.0 \times 10^{-5} \text{ mol L}^{-1}$  and  $3.6 \times 10^{-9}$  to  $1.8 \times 10^{-6} \text{ mol L}^{-1}$ , respectively. A set of synthetic binary mixtures of LD and PRO was prepared and their concentrations were predicted by the proposed method. Satisfactory results were obtained by the combination of fluorescence technique with chemometrics methods. The method was successfully applied to the determination of LD and PRO in tap water and in urine samples.

© 2009 Elsevier B.V. All rights reserved.

## 1. Introduction

Levodopa ((S)-2 amino-3-(3,4-dihydroxyphenyl)propionic acid, LD) is a precursor of the neurotransmitter dopamine used in the treatment of Parkinson's disease. It is a progressive neurological disorder that occurs when the brain fails to produce enough dopamine [1]. Propranolol (1-(isopropylamino)-3-[1-naphthylthoxy]-2-propanol, PRO) is member of heterogeneous group of drugs classified as beta-adrenergic receptor blockers and are generally prescribed in the treatment of hypertension, angina pectoris, cardiac arrhythmias and hypertrophic subaortic stenosis, but are also sometimes used as doping agents in sport [2]. Parkinsonism is a syndrome characterized by a combination of cardinal features including resting tremor, bradykinesia, rigidity, and loss of postural reflexes. Levodopa is the most effective medication for treating tremor in Parkinson's disease (PD). At least 50% of patients experience a significant reduction in tremor with levodopa treatment [3]. The efficacy of levodopa is firmly established from over 30 years of use in clinical practice [4]. Propranolol, a nonselective  $\beta$ -blocker, has been used for tremor reduction in a variety of tremor subtypes, including essential tremor and the resting tremor of PD [3]. Therefore it seems that it is important to determine these drugs in biological samples simultaneously.

Levodopa can be slowly titrated starting with one-fourth a tablet three times per day, which can be increased by one-fourth a tablet per dose every week to optimum symptom relief up to a maximum of 1000–1200 mg per day. Dosing schedule for commonly used tremor medication (propranolol) is 10–20 mg with maximum dose 320 mg [3].

In the literature review, due to strong pharmaceutical impact, these drugs have received particular attention. Many methods such as kinetic-spectrophotometry [5–8], capillary electrophoresis [9,10], spectrofluorimetry [11–14] and synchronous spectrofluorimetric methods [15,16] were used for the determination of these drugs in the presence of other components. The determination of levodopa in clinical samples was also reported. Segar and Smyth [17] and Baranowska and Plonka [18] reported the amount of this drug in urine samples in the range 0.5–2 and 3.73–46.80  $\mu\text{g mL}^{-1}$ , respectively, as determined by HPLC. To our knowledge, there is no report on the simultaneous spectrofluorimetric determination of levodopa and propranolol.

Fluorescence spectrometry is widely used in quantitative analysis because of its great sensitivity and selectivity as well as its relatively low cost. This technique has not, however, been widely applied to the simultaneous direct determination of several fluorescent components in mixtures, mainly because the fluorescence spectra of individual substances contain broad bands which often overlap. Several methods have been proposed to resolve such problems without manipulation of the samples or using time-consuming and highly expensive separation techniques [15]. Due

\* Corresponding author. Tel.: +98 811 8272404; fax: +98 811 8272404.  
E-mail address: [madrakian@basu.ac.ir](mailto:madrakian@basu.ac.ir) (T. Madrakian).

to the ability of chemometrics methods for resolving the complex systems, they were developed for simultaneous determination of various mixtures. The chemometric methods such as factor analysis and artificial intelligence, including principal component regression (PCR) and partial least squares (PLS), have found increasing applications for multi component determinations. In these methods, generally, a set of calibration samples with known compositions is first prepared and the measurements are carried out, after which, the mathematical models are established by processing the measured data. Subsequently, the mathematical models are used for the prediction of unknown samples under the same experimental conditions.

Multivariate calibration methods (partial least squares or principal component regression) can be applied to the multi-component determination [19,20]. These methods are not suitable when non-linearity is observed in the system. Artificial neural networks (ANNs) approach has several advantages over the multivariate calibration of data including easy programming of the network architecture, no necessity for any priori assumption on the behavior of the data, ability to process input data containing some degree of uncertainty and handling nonlinearity due to analyte–analyte interaction, the synergistic effects and so on. Due to these advantages ANNs have attracted the interest of many researchers in the field of chemistry as modeling tools for multivariate calibrations [19–22].

The most popular method for data compression in chemometrics is principal component analysis (PCA). In practice, principle components (PCs) are often successfully used as inputs. Even if there is some nonlinearity in data set, all relevant information is usually contained in the first PCs [23]. PCA became ideal tool to remove possible complications caused by multicollinearity from the independent variables. Reducing the number of inputs to a network reduces the training time and repetition in the input data [24–26]. The application of an ANN model with data pretreatment method, such as autoscaling and compressing data into scores with the use of PCA (PC-FFNNs) as input data to quantify mixtures in different kinetic situations has been reported [5,23].

Several reports have been published on the application of chemometrics methods such as mean centering of ratio spectra, PLS, ANNs and continuous wavelet transformation for the analysis of pharmaceutical products and biological samples [5,6,27–30].

In the present work, the applicability of artificial neural networks assisted by principal component analysis was examined. The procedure was based on the recording of fluorescence spectra of drugs in the micellar media and using ANN for simultaneous determination of two components. This method is very precise, sensitive and applicable to the simultaneous determination of LD and PRO over wide ranges. With this approach simultaneous determination can be performed without decreasing the signal-to-noise ratio, and any need to carefully control the experimental conditions. Several synthetic mixtures were estimated and the method validated using water and biological sample.

## 2. Experimental

### 2.1. Apparatus

A PerkinElmer luminescence spectrometer model LS-30, equipped with a xenon lamp, a 7  $\mu\text{L}$  fused silica flow cell and a peristaltic pump was used for recording spectra and fluorescence measurements. A model 713 Metrohm pH meter was used for pH measurement of the solutions and a Heidolf rotary evaporator was used for drying the sample. A short program was written in MATLAB 7.1 for performing principal component analysis of the data and the networks calculations were performed using nnet–Toolbox for MATLAB 7.1.

**Table 1**

Concentration data for the different mixtures used in the calibration set and prediction set for the simultaneous determination of LD and PRO.

Sample no.	Calibration set ( $\text{mol L}^{-1}$ )		Prediction set ( $\text{mol L}^{-1}$ )	
	LD	PRO	LD	PRO
1	$2.00 \times 10^{-8}$	$1.80 \times 10^{-6}$	$1.00 \times 10^{-7}$	$1.80 \times 10^{-6}$
2	$2.00 \times 10^{-7}$	$1.00 \times 10^{-6}$	$6.00 \times 10^{-6}$	$3.60 \times 10^{-8}$
3	$1.00 \times 10^{-6}$	$1.80 \times 10^{-6}$	$8.00 \times 10^{-6}$	$1.80 \times 10^{-7}$
4	$1.00 \times 10^{-5}$	$3.60 \times 10^{-9}$	$1.00 \times 10^{-6}$	$1.00 \times 10^{-6}$
5	$8.00 \times 10^{-6}$	$1.80 \times 10^{-8}$	$6.00 \times 10^{-6}$	$3.60 \times 10^{-7}$
6	$1.00 \times 10^{-6}$	$1.80 \times 10^{-7}$	$6.00 \times 10^{-6}$	$1.00 \times 10^{-6}$
7	$4.00 \times 10^{-6}$	$1.80 \times 10^{-7}$	$2.00 \times 10^{-6}$	$1.45 \times 10^{-6}$
8	$2.00 \times 10^{-6}$	$7.20 \times 10^{-7}$	$2.00 \times 10^{-6}$	$1.80 \times 10^{-7}$
9	$8.00 \times 10^{-6}$	$7.20 \times 10^{-7}$		
10	$4.00 \times 10^{-6}$	$3.06 \times 10^{-7}$		
11	$2.00 \times 10^{-6}$	$1.00 \times 10^{-6}$		
12	$1.00 \times 10^{-5}$	$3.60 \times 10^{-8}$		
13	$8.00 \times 10^{-6}$	$1.00 \times 10^{-6}$		
14	$2.00 \times 10^{-8}$	$1.80 \times 10^{-8}$		
15	$1.00 \times 10^{-7}$	$3.60 \times 10^{-9}$		
16	$1.00 \times 10^{-6}$	$3.60 \times 10^{-7}$		

### 2.2. Reagents

All chemicals were of the analytical grade purchased from Merck Company (Darmstadt, Germany). Stock solutions of  $1.00 \times 10^{-3} \text{ mol L}^{-1}$  of LD and  $1.80 \times 10^{-3} \text{ mol L}^{-1}$  of PRO were prepared by dissolving appropriate amounts of them in doubly distilled water. A solution of  $0.2 \text{ mol L}^{-1}$  SDS was prepared by dissolving appropriate amount of reagent in water and diluting to the mark in a 100 mL volumetric flask. A pH 4.0 acetate buffer solution ( $0.2 \text{ mol L}^{-1}$ ) was prepared from acetic acid and sodium acetate [31].

### 2.3. Procedure

Two sets of standard solutions containing the analytes were prepared as calibration and prediction sets. The correlation between concentrations of the two drugs was avoided. Each set was selected so that the concentrations of the analytes were approximately covered the entire ranges of the analytes. Appropriate amounts of LD and PRO solutions, 1.0 mL of buffer and 0.5 mL of  $0.2 \text{ mol L}^{-1}$  SDS solutions were added to a 5.0 mL volumetric flask. The flask was made up to the mark with water and the fluorescence spectra were recorded in the emission wavelength range 300–450 nm (with excitation at 282 nm). Calibration and prediction sets contained 16 and 8 samples, respectively. Table 1 shows the two sample sets.

#### 2.3.1. Preparation of urine sample

A urine specimen from a volunteer was collected in 10 mL of  $6.0 \text{ mol L}^{-1}$  hydrochloric acid over a 24-h period. Ten milliliter of such urine sample was taken out and evaporated to dryness in vacuum at room temperature using a rotary evaporator; the residue is dissolved in 2 mL methanol. This solution was used as a sample solution [12].

## 3. Results and discussion

### 3.1. Spectral characteristics

Fig. 1 shows the fluorescence emission spectra of LD and PRO in the optimal conditions at  $\lambda_{\text{ex}} = 282 \text{ nm}$ . As Fig. 1 shows, the emission spectra of LD and PRO have strongly overlapped. The maximum emission of them was at 325 and 340 nm, respectively. Therefore the analysis of mixtures of the compounds is not feasible by conventional spectrofluorimetry at their wavelength maxima.



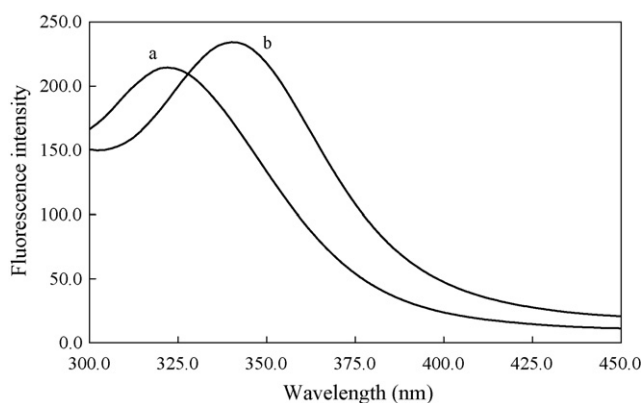


**Fig. 1.** Fluorescence spectra of  $2.00 \times 10^{-6} \text{ mol L}^{-1}$  LD (a) and  $3.60 \times 10^{-7} \text{ mol L}^{-1}$  PRO (b), in the presence of  $0.02 \text{ mol L}^{-1}$  SDS, pH 4.0 buffer solution. Excitation wavelength was 282 nm.

### 3.2. Synchronous fluorescence spectra of levodopa and propranolol

Synchronous spectrometry consists essentially of the simultaneous scanning of both monochromators, while maintaining a constant wavelength interval ( $\Delta\lambda$ ) between them. The simplification of the spectral profile together with the reduction of band width is its main characteristics [15]. The selection of  $\Delta\lambda$  is an important parameter to obtain a good selectivity and sensitivity as it can affect not only the synchronous fluorescence intensity but also the shape of spectrum and the width of the half-wide spectral band. This parameter is usually selected empirically. The fluorescence intensity is maximum when the excitation wavelength corresponds to the maximum of the excitation spectrum and when the emission wavelength corresponds to the maximum of the emission spectrum. In this case, however, this definition was not useful because greater sensitivity does not always mean high selectivity [32]. In this study  $\Delta\lambda$  was changed between 0 and 200 nm with 10 nm intervals. The best result was obtained at  $\Delta\lambda = 80 \text{ nm}$  (Fig. 2).

Experimental results indicated that this method was not suitable for simultaneous determination of LD and PRO as spectral interference occurred in both cases. According to these results, we applied a chemometrics method for the simultaneous determination of these drugs based on their natural fluorescence in the presence of surfactant at pH 4. The artificial neural network was selected for simultaneous determination of these components.

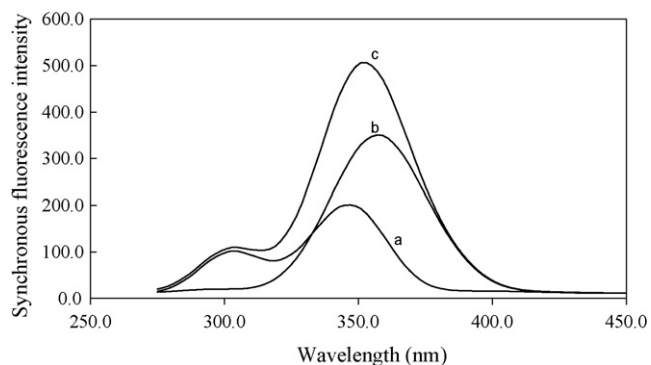


**Fig. 2.** Synchronous fluorescence spectra of  $2.00 \times 10^{-6} \text{ mol L}^{-1}$  levodopa (a) and  $1.00 \times 10^{-6} \text{ mol L}^{-1}$  propranolol (b) and their mixture solution (c), pH 4.0,  $0.02 \text{ mol L}^{-1}$  SDS,  $\Delta\lambda = 80 \text{ nm}$ .

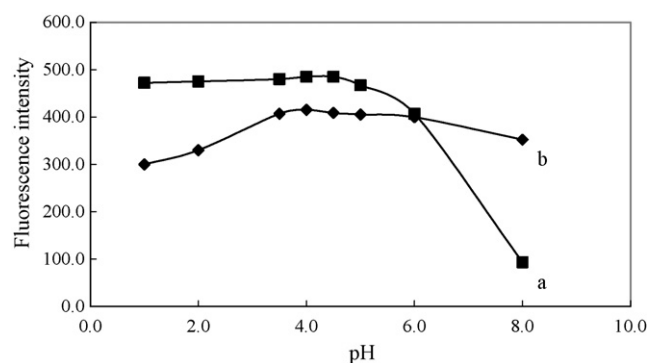


**Fig. 3.** Effect of pH on the determination of  $5.00 \times 10^{-6} \text{ mol L}^{-1}$  levodopa (a) and  $7.00 \times 10^{-7} \text{ mol L}^{-1}$  propranolol (b),  $0.02 \text{ mol L}^{-1}$  SDS solution,  $\lambda_{\text{ex}} = 282 \text{ nm}$ .

### 3.3. Influence of experimental factors

The fluorescence spectra are influenced by pH of the solution and concentration of SDS. So, the various experimental parameters affecting the measurements were carefully studied and optimized.

#### 3.3.1. Effect of pH

LD and PRO showed strong native fluorescence signals at acidic pH. It was observed that their fluorescent emission decreases in alkaline media. Fig. 3 resumes the effect of pH on the fluorescence signals. Analysis of spectrofluorimetric data for LD in water showed that the fluorescence intensity remained constant in the pH range 1.0–5.0 and decreased at higher pH. For PRO, the fluorescence intensity increased by increasing pH over the range 1.0–3.0, remained constant up to pH 6.0 and decreased at higher pH. Therefore, pH 4.0 was selected as working pH due to the higher fluorescence intensity. An acetate buffer solution was used to adjust the pH.

#### 3.3.2. Fluorescence characteristics of levodopa and propranolol in micellar media

The fluorescence properties of LD and PRO in various surfactant media were studied: anionic surfactant (SDS,  $0.00$ – $0.06 \text{ mol L}^{-1}$ ) and non-ionic surfactant (TX-100,  $0.00$  to  $1.00 \times 10^{-3} \text{ mol L}^{-1}$ ). Experimental data showed that the fluorescence intensities of LD and PRO in SDS micellar media are 2.4 times higher than those in water media. TX-100 caused an increase in blank signal and a decrease in the fluorescence intensity of the sample. Thus, the anionic surfactant SDS was chosen for further works. Fig. 3 shows the effect of SDS concentration on the fluorescence intensity of LD and PRO. As Fig. 3 shows,  $0.02 \text{ mol L}^{-1}$  SDS was selected as optimal.

The fluorescence spectra of levodopa and propranolol in pure water and in SDS solution revealed that the fluorescence intensity increased with SDS concentration (above the cmc,  $2.30 \times 10^{-3} \text{ mol L}^{-1}$ ), and that this increase was more evident at  $0.02 \text{ mol L}^{-1}$  (Fig. 4). The increase in the fluorescence intensity in micellar media was attributed to the stabilization/protection of the singlet excited state that hinders decay by quenching and other non-radiative deactivation processes [33,34].

#### 3.4. Optimizing the network variables in PC-FFN network

ANNs are mathematical or computational models based on biological neural networks. They consist of an interconnected group of artificial neurons and process information using a connectionist approach to computation. For the optimization of a neural network, a trial and error method has to be used to find the best neural network architecture. One layer of nodes in the output layer is a common topological suggestion, when an ANN is used as a model of calibration. In this study some factors such as number of principal

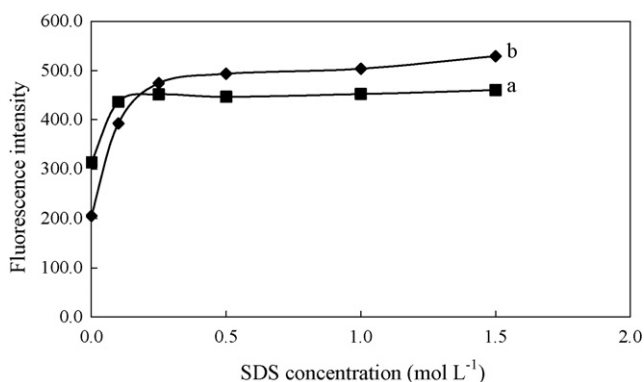


Fig. 4. Effect of SDS concentration on the determination of  $5.00 \times 10^{-6}$  mol L<sup>-1</sup> levodopa (a) and  $7.00 \times 10^{-7}$  mol L<sup>-1</sup> propranolol (b) pH 4.0,  $\lambda_{\text{ex}} = 282$  nm.

components, number of nodes (neurons) in hidden layer, learning function and number of epochs were optimized.

Performance of methods were tested with root mean square errors of prediction (RMSEP), using synthetic solutions of metal ions as prediction set. The results obtained in the quantification of the samples in the training and prediction sets are expressed as

$$\text{RMSEP} = \sqrt{\frac{\sum_{i=1}^n (\hat{y}_i - y_i)^2}{n}} \quad (1)$$

where  $\hat{y}_i$  and  $y_i$  are the desired output and the actual output sets, respectively, and  $n$  is the number of prediction set samples. Reducing the data volume before using ANNs for multivariate calibration was suggested as a preprocessing step in many of the previous studies [23].

If the number of weights exceeds the number of samples for the training of ANN to some extent, “over fitting” may be caused [35]. Also, in the case of a high number of input variables meaningful variables could be hidden [36], the probability of chance correlation increases [37], and may prevent ANN from finding optimized models [38]. Therefore, PCA input selection is necessary in order to improve the predicted results of different ANN.

In this work, spectrofluorimetric data were employed in ANN to predict the concentrations of the corresponding analytes. The spectrofluorimetric data, before building the ANNs models, were subjected to the principal component analysis and decomposed to PC scores. The numbers of input nodes were selected as optimal numbers of PC scores. The PC-FFNN including one to ten PC scores was trained. The lowest RMSEP% values were obtained with three input factors for LD and PRO, respectively. In order to determine the optimal number of hidden layer networks, neural networks with different numbers of hidden nodes were trained. The number of hidden nodes varied from one to ten to train the networks. According to RMSEP% values versus the number of hidden layer nodes, the best numbers of hidden layer nodes were five and three for LD and PRO, respectively. To get the best network architecture, different transfer functions in hidden and output layer were also tested. The best transfer functions as well as some other parameters such as number of epochs, learning rate and momentum are summarized in Table 2. In order to predict drugs concentrations in prediction set, ten times replications were performed in optimum conditions and finally the RMSEP% values were calculated and applied for comparing the applicability of the methods. Table 3 shows the prediction results obtained with a model having optimized parameters.

Table 2

Optimized parameters used for construction of PC-FFNNs for LD and PRO determination.

Parameter	LD	PRO
Number of PCs	3	3
Input nodes	3	3
Hidden nodes	5	3
Output nodes	1	1
Learning rate	0.01	0.05
Number of iteration (epoch)	100	100
Hidden layer transfer function	Logsig	Logsig
Output layer transfer function	Logsig	Tansig

### 3.5. Validity of the method

#### 3.5.1. Linearity and sensitivity

A set of sample solutions with different drugs concentrations was prepared and measurements were carried out under the optimum conditions. The calibration curves of two analytes were linear in the ranges  $2.00 \times 10^{-8}$  to  $1.00 \times 10^{-5}$  mol L<sup>-1</sup> and  $3.60 \times 10^{-9}$  to  $1.80 \times 10^{-6}$  mol L<sup>-1</sup> for LD and PRO, respectively. The triplicate signals demonstrated good reproducibility. Equations for calibration graphs were obtained versus analyte concentrations as:  $F = 8.0 \times 10^7 C + 76.8$  for LD and  $F = 5.0 \times 10^8 C + 51.3$  for PRO where  $F$  is the relative fluorescence intensity and  $C$  is the concentration of analyte in mol L<sup>-1</sup>. Correlation coefficients for LD and PRO were 0.994 and 0.993, respectively. The limit of detection (LOD) and limit of quantification (LOQ) were defined as the compound concentration that produced a signal-to-noise ratio of 3 and 10, respectively. Based on these criteria LOD values were  $4.83 \times 10^{-9}$  mol L<sup>-1</sup> ( $0.95 \mu\text{g L}^{-1}$ ),  $7.76 \times 10^{-10}$  mol L<sup>-1</sup> ( $0.20 \mu\text{g L}^{-1}$ ) and LOQ values were  $1.61 \times 10^{-8}$  mol L<sup>-1</sup> ( $3.17 \mu\text{g L}^{-1}$ ) and  $2.60 \times 10^{-9}$  mol L<sup>-1</sup> ( $0.67 \mu\text{g L}^{-1}$ ) for LD and PRO, respectively.

#### 3.5.2. Interferences of foreign substances

A systematic study was carried out on the effects of foreign species on the determination of  $2.00 \times 10^{-7}$  mol L<sup>-1</sup> LD and  $1.00 \times 10^{-6}$  mol L<sup>-1</sup> PRO. The tolerance limit of a compound was taken as the maximum amount of species causing an error not greater than  $\pm 5\%$ . 1000-fold excess of K<sup>+</sup>, Na<sup>+</sup>, Ca<sup>2+</sup>, Mg<sup>2+</sup>, Ba<sup>2+</sup>, Cd<sup>2+</sup>, Ni<sup>2+</sup>, Al<sup>3+</sup>, Cl<sup>-</sup>, F<sup>-</sup>, S<sup>2-</sup>, glycine, lactose, fructose, starch. 500-fold excess of CO<sub>3</sub><sup>2-</sup>, HCO<sub>3</sub><sup>-</sup> and 50-fold excess of Cu<sup>2+</sup>, NO<sub>3</sub><sup>-</sup>, Pb<sup>2+</sup>, Hg<sup>2+</sup>, did not interfere with the determination of drugs. The interference effect of Fe<sup>3+</sup> was eliminated up to 5-fold excess by addition of 0.05 mol L<sup>-1</sup> ascorbic acid.

For better therapeutic effect and lower toxicity, carbidopa (CBD) is administered in association with levodopa. In pharmaceutical formulations drugs contain 10–25% of CBD. The interference effect of this component was studied and observed that it did not interfere when presented at the same concentration of LD.

Table 3

Prediction results obtained with PC-FFNNs for LD and PRO.

Sample no.	Added (mol L <sup>-1</sup> )		Found (mol L <sup>-1</sup> )	
	LD	PRO	LD	PRO
1	$1.00 \times 10^{-7}$	$1.80 \times 10^{-6}$	$9.99 \times 10^{-8}$	$1.73 \times 10^{-6}$
2	$6.00 \times 10^{-6}$	$3.60 \times 10^{-8}$	$5.99 \times 10^{-6}$	$3.40 \times 10^{-8}$
3	$8.00 \times 10^{-6}$	$1.80 \times 10^{-7}$	$8.00 \times 10^{-6}$	$1.80 \times 10^{-7}$
4	$1.00 \times 10^{-6}$	$1.00 \times 10^{-6}$	$9.99 \times 10^{-7}$	$9.98 \times 10^{-7}$
5	$6.00 \times 10^{-6}$	$3.60 \times 10^{-7}$	$6.01 \times 10^{-6}$	$3.65 \times 10^{-7}$
6	$6.00 \times 10^{-6}$	$1.00 \times 10^{-6}$	$5.99 \times 10^{-6}$	$1.00 \times 10^{-6}$
7	$2.00 \times 10^{-6}$	$1.45 \times 10^{-6}$	$2.00 \times 10^{-6}$	$1.49 \times 10^{-6}$
8	$2.00 \times 10^{-6}$	$1.80 \times 10^{-7}$	$2.00 \times 10^{-6}$	$1.80 \times 10^{-7}$
RMSEP%			0.05	0.08

**Table 4**

The application of the proposed method for simultaneous determination of LD and PRO in real samples.

Sample	Spiked (mol L <sup>-1</sup> )		Found (mol L <sup>-1</sup> )		Recovery (%)		R.S.D. (%)	
	LD	PRO	LD	PRO	LD	PRO	LD	PRO
Tap water	0	0	ND <sup>a</sup>	ND	–	–		
	2.00 × 10 <sup>-7</sup>	1.00 × 10 <sup>-6</sup>	1.98 × 10 <sup>-7</sup>	9.98 × 10 <sup>-7</sup>	99.32	99.85		
	6.00 × 10 <sup>-7</sup>	4.00 × 10 <sup>-8</sup>	5.99 × 10 <sup>-6</sup>	4.04 × 10 <sup>-8</sup>	99.96	101.01		
				99.64 <sup>b</sup>	100.43 <sup>b</sup>	1.35 <sup>b</sup>	1.93 <sup>b</sup>	
Urine	0	0	ND	ND	–	–		
	2.00 × 10 <sup>-6</sup>	7.20 × 10 <sup>-7</sup>	2.05 × 10 <sup>-6</sup>	7.49 × 10 <sup>-7</sup>	102.50	104.13		
	1.00 × 10 <sup>-6</sup>	3.60 × 10 <sup>-7</sup>	1.03 × 10 <sup>-6</sup>	3.68 × 10 <sup>-7</sup>	103.10	102.31		
	4.00 × 10 <sup>-6</sup>	1.00 × 10 <sup>-6</sup>	3.91 × 10 <sup>-6</sup>	9.95 × 10 <sup>-7</sup>	97.73	99.57		
				101.71 <sup>b</sup>	102.00 <sup>b</sup>	1.97 <sup>b</sup>	2.42 <sup>b</sup>	

<sup>a</sup> ND: not detected.<sup>b</sup> Mean of measurements.

### 3.6. Applications

In order to evaluate the analytical applicability of the proposed method, it was applied to the determination of LD and PRO in tap water. Known amount of these drugs were added to the water sample and their concentrations were estimated with the proposed method. Simultaneous determination of drugs in the urine sample prepared according to the procedure was also performed. The sample was found to be free from LD and PRO. Therefore different amounts of LD and PRO were spiked to the sample and analyzed by the proposed method. The results for determination of the two species in real samples are given in Table 4. Satisfactory recovery of the experimental results was found for LD with a range of 99.3–103.1% and for PRO with a range of 99.6–104.1%. The reproducibility of the method was demonstrated by the mean relative standard deviation (R.S.D.). The results obtained indicate that the R.S.D. values for LD and PRO in water were 1.35 and 1.93% and in urine sample were 1.97 and 2.42%, respectively.

### 4. Conclusion

In this paper, we investigated the chemistry, analytical methodology and the chemometrics interpretation of the results for the determination of levodopa and propranolol in water and human urine sample by the spectrofluorimetric method in the micellar media using artificial neural network. The use of SDS micellar system provides a simple mean to enhance the fluorescence intensity of levodopa and propranolol. This phenomenon can be explained by the protection/stabilization of lowest excited state of fluorophore in micellar microenvironment from non-radiative processes that normally readily occur in bulk aqueous solutions.

The simultaneous determination of these drugs was done with neural networks. The system was modeled with neural networks and the model was validated with the use of synthetic binary mixtures of levodopa and propranolol and the figures of merit, RMSEPs% and recoveries% were evaluated. Finally, the most successful ANNs calibration model was applied for the prediction of the levodopa and propranolol in water and human urine sample with satisfactory results. To the best of our knowledge this is the first report for simultaneous determination of these drugs. Moreover the calculated results proved that the proposed neural networks approach

based on the PCA input selection is suitable for the simultaneous determination of LD and PRO in complex mixtures.

### References

- [1] D.B. Clane, N. Engl. J. Med. 329 (1993) 1021.
- [2] T.P. Ruiz, C.M. Lozano, V. Tomás, J. Carpena, Talanta 45 (1998) 969.
- [3] Sh. Chitnis, Neurol. Clin. 26 (2008) S29.
- [4] M. Horstink, E. Tolosa, U. Bonuccelli, G. Deuschl, A. Friedman, P. Kanovsky, J.P. Larsen, A. Lees, W. Oertel, W. Poewe, O. Rascol, C. Sampaio, Eur. J. Neurol. 13 (2006) 1170.
- [5] M. Chamsaz, A. Safavi, J. Fadaee, Anal. Chim. Acta 603 (2007) 140.
- [6] E. Dinc, S. Kayab, T. Doganay, D. Baleanu, J. Pharm. Biomed. Anal. 44 (2007) 991.
- [7] J. Karpińska, J. Smyk, E. Wołyniec, Spectrochim. Acta Part A 62 (2005) 213.
- [8] M. Grünhut, M.E. Centurión, W.D. Fragoso, L.F. Almeida, M.C.U. de Araújo, B.S.F. Banda, Talanta 75 (2008) 950.
- [9] Sh. Zhao, W. Bai, B. Wang, M. He, Talanta 73 (2007) 142.
- [10] W.W. He, X.W. Zhou, J.Q. Lu, Chin. Chem. Lett. 18 (2007) 91.
- [11] L.C. Silva, M.G. Trevisan, R.J. Poppib, M.M. Sen, Anal. Chim. Acta 595 (2007) 282.
- [12] H.Y. Wang, Y. Sun, B. Tang, Talanta 57 (2002) 899.
- [13] H.Y. Wang, Q.Sh. Hui, L.X. Xua, J.G. Jiang, Y. Sun, Anal. Chim. Acta 497 (2003) 93.
- [14] R.A. Silva, Ch.Ch. Wang, L.P. Fernández, A.N. Masi, Talanta 76 (2008) 166.
- [15] J.A.M. Pulgarín, A.A. Molina, P.F. López, Anal. Chim. Acta 370 (1998) 9.
- [16] Z.Q. Cai, Y.X. Zhub, Y. Zhang, Spectrochim. Acta Part A 69 (2008) 130.
- [17] K.A. Sagar, M.R. Smyth, J. Pharm. Biomed. Anal. 22 (2000) 613.
- [18] I. Baranowska, J. Plonka, J. Chromatogr. Sci. 46 (2008) 30.
- [19] Y. Akhlaghi, M. Kompany-Zareh, Anal. Chim. Acta 537 (2005) 331.
- [20] P.J. Gemperline, J.R. Long, V.G. Gregoriou, Anal. Chem. 63 (1991) 2313.
- [21] F. Despagne, D.L. Massart, Analyst 123 (1998) 157R.
- [22] T.B. Blank, S.D. Brown, Anal. Chim. Acta 277 (1993) 273.
- [23] A. Afkhami, M. Abbasi-Tarighat, H. Khanmohammadi, Talanta 77 (2009) 995.
- [24] S.M. Al-Alawi, S.A. Abdul-Wahab, C.S. Bakheit, Environ. Model. Softw. 23 (2008) 396.
- [25] A. Afkhami, M. Abbasi-Tarighat, Anal. Sci. 24 (2008) 779.
- [26] Y.X. Zhang, Talanta 73 (2007) 68.
- [27] T. Madrakian, M. Mohammadnejad, Chem. Pharm. Bull. 55 (2007) 865.
- [28] H. Goicoechea, B.C. Roy, M. Santosa, A.D. Campiglia, S. Mallikb, Anal. Biochem. 336 (2005) 64.
- [29] L. Lvova, E. Martinell, F. Dinic, A. Bergaminid, R. Paolessea, C.D. Natale, A. D'Amico, Talanta 77 (2009) 1097.
- [30] M.L. Luis, J.M.G. Fraga, A.I. Jiménez, F. Jiménez, O. Hernández, J.J. Arias, Talanta 62 (2004) 307.
- [31] J.A. Dean, Analytical Chemistry Handbook, McGraw-Hill Inc., 1995, pp. 14–33.
- [32] A.A. Eiroa, E.V. Blanco, P.L. Mahía, S.M. Lorenzo, D.P. Rodríguez, Analyst 123 (1998) 2113.
- [33] C.D. Tran, T.A. Van Fleet, Anal. Chem. 60 (1988) 2478.
- [34] H. Singh, W.L. Hinze, Anal. Lett. 15 (1982) 221.
- [35] I.V. Tetko, A.I. Luik, G.I. Poda, J. Med. Chem. 36 (1993) 811.
- [36] M.B. Seasholtz, B. Kowalski, Anal. Chim. Acta 277 (1993) 165.
- [37] D.J. Livingstone, D.T. Manallack, Stat. J. Med. Chem. 36 (1993) 1295.
- [38] D. Broadhurst, R. Goodacre, A. Jones, J.J. Rowland, D.B. Kell, Anal. Chim. Acta 348 (1997) 71.



# A piezoelectric immunosensor for the determination of pesticide residues and metabolites in fruit juices

C. March<sup>a</sup>, J.J. Manclús<sup>a</sup>, Y. Jiménez<sup>b</sup>, A. Arnau<sup>b</sup>, A. Montoya<sup>a,\*</sup>

<sup>a</sup> Instituto de Investigación e Innovación en Bioingeniería, Universidad Politécnica de Valencia, Camino de Vera s/n, 46022 Valencia, Spain

<sup>b</sup> Grupo de Fenómenos Ondulatorios (GFO), Departamento de Ingeniería Electrónica, Universidad Politécnica de Valencia, Camino de Vera s/n, 46022 Valencia, Spain

## ARTICLE INFO

### Article history:

Received 10 July 2008

Received in revised form 20 December 2008

Accepted 22 December 2008

Available online 15 January 2009

### Keywords:

Piezoelectric immunosensor

QCM

Self-assembled monolayer

Monoclonal antibody

Carbaryl

TCP

## ABSTRACT

A quartz crystal microbalance (QCM) immunosensor was developed for the determination of the insecticide carbaryl and 3,5,6-trichloro-2-pyridinol (TCP), the main metabolite of the insecticide chlorpyrifos and of the herbicide triclopyr. The detection was based on a competitive conjugate-immobilized immunoassay format using monoclonal antibodies (MAbs). Hapten conjugates were covalently immobilized, via thioctic acid self-assembled monolayer (SAM), onto the gold electrode sensitive surface of the quartz crystal. This covalent immobilization allowed the reusability of the modified electrode surface for at least one hundred and fifty assays without significant loss of sensitivity. The piezoelectrode showed detection limits (analyte concentrations producing 10% inhibition of the maximum signal) of 11 and 7  $\mu\text{g l}^{-1}$  for carbaryl and TCP, respectively. The sensitivity attained ( $I_{50}$  value) was around 30  $\mu\text{g l}^{-1}$  for both compounds. Linear working ranges were 15–53  $\mu\text{g l}^{-1}$  for carbaryl and 13–83  $\mu\text{g l}^{-1}$  for TCP. Each complete assay cycle took 20 min. The good sensitivity, specificity, and reusability achieved, together with the short response time, allowed the application of this immunosensor to the determination of carbaryl and TCP in fruits and vegetables at European regulatory levels, with high precision and accuracy.

© 2009 Elsevier B.V. All rights reserved.

## 1. Introduction

Increasing awareness about the presence of pesticide residues in the environment has been urging the search for simple detection methods. Classical chromatographic analysis (liquid or gas chromatography) are very sensitive and standardized techniques. Nevertheless they often are too laborious and time-consuming. Furthermore, they need complex and expensive instrumentation often available only in very well equipped and centralized laboratories [1].

Immunochemical methods, such as enzyme-linked immunosorbent assays (ELISAs), have already gained a place in the analytical benchtop as alternative or complementary methods for routine pesticide analysis. They are fast, economic, and at least as sensitive as usual chromatographic techniques. The number of pesticides for which immunoassays have been developed is constantly increasing worldwide. The contribution of our group includes immunoassays for pesticides belonging to different chemical families, such as organophosphorous, organochlorine, N-methylcarbamates and fungicides [2–5].

Currently, ELISAs and immunosensors are the most popular immunoassays. The analyte detection in ELISAs is always indirect because one of the immunoreagent is labelled. In immunosensors the detection is direct: one of the immunoreagents is immobilized on the surface of the transducer, and a direct physical signal is produced when the immunochemical interaction occurs. This label-free direct detection represents an essential advantage of immunosensors as compared to label-dependent immunoassays [6]. Immunosensors, which combine the selectivity provided by immunological interactions with the high sensitivity achieved by electronic or opto-electronic signal transducers, are also being proposed and proving to be powerful analytical devices for the monitoring of organic pollutants in food and the environment [7,8].

Immunochemical interactions can be detected as a variation of mass at the transducer surface. Among all the physical transducers that can measure surface mass changes, produced by formation of biocomplexes at their sensitive area, piezoelectric systems represent a cost-effective alternative to advanced optical devices [9]. Piezoelectric immunosensors use a quartz crystal, working in a microgravimetric mode, as the transducer element (QCM, Quartz Crystal Microbalance). When brought into resonance, the quartz crystal is able to oscillate by the application of an external alternating electric field. Piezoelectric transducers are being used as chemical sensors since the discovery of the relationship between mass deposited/adsorbed on the crystal surface and the resonant

\* Corresponding author. Tel.: +34 963877093; fax: +34 963877093.

E-mail address: [amontoya@eln.upv.es](mailto:amontoya@eln.upv.es) (A. Montoya).

frequency variations. This relationship is expressed by Sauerbrey's equation:

$$\Delta f = -\frac{C_f \Delta m}{A} \quad (1)$$

where the measured frequency change ( $\Delta f$ ) is linearly proportional to the ratio of the mass load ( $\Delta m$ ) to the crystal exposed surface ( $A$ ) [10].

This equation is applied when working in air phase. Kanazawa and Gordon [11] found the relationship which account for the variations in resonance frequency when the crystal works in liquid environment. This equation assumes that the surface of the piezoelectric crystal behaves as a rigid film; otherwise, the quartz response depends not only on the mass placed on it but also on its viscoelastic properties [12]. The changes in viscosity produce resistance shifts ( $\Delta R$ ). For suitable QCM immunosensor applications, the properties of the surrounding liquid on the sensitive surface should not significantly change during the measurements: i.e.,  $\Delta R \approx 0$ .

Because of their simplicity, low cost, and real-time response, piezoelectric quartz crystal sensors are gaining an increasing importance as competitive tools for bioanalytical assays and for the characterization of biomolecular interactions [9]. Since the earliest piezoelectric quartz crystal immunoassay was reported in 1972 by Shons et al. [13], QCM immunosensors have been proposed for a wide variety of analysis such as food and biomedical analysis, veterinary diagnosis, environmental monitoring, etc. The target analytes include bacteria and eukaryotic cells [8,14], viruses [7,15], proteins [16], nucleic acids [17], and small molecules as drugs, hormones and pesticides [18,19].

In the present work, the development of a monoclonal antibody-based piezoelectric immunosensor for carbaryl and TCP (3,5,6-trichloro-2-pyridinol), and its application to fruit juice samples, is described. Carbaryl, an acetyl-cholinesterase inhibitor, is a broad-spectrum N-methyl carbamate insecticide [20]. TCP is the major degradation product of the widely used insecticides chlorpyrifos and chlorpyrifos-methyl and the herbicide triclopyr. TCP has been demonstrated to be toxic to some aquatic organisms. In studies of human exposure to pesticides, it has also been detected in urine samples, which is consistent with the high occurrence of the parent pesticides in food [21].

## 2. Experimental

### 2.1. Chemicals and immunoreagents

Bovine serum albumin (BSA) fraction V was purchased from Roche Diagnostics (Mannheim, Germany). Tween 20 was supplied by Fluka-Aldrich Chemie (Buchs, Switzerland). All other chemicals were of analytical grade.

#### 2.1.1. Reagents for covalent immobilization

1-Ethyl-3-(3-dimethyl-amino-propyl)carbodiimide hydrochloride (EDC) and N-hydroxysuccinimide (NHS) were purchased from Pierce (Rockford, IL); thioctic acid (TA) was supplied by Sigma-Aldrich Chemie (Steinheim, Germany); ethanolamine blocking agent was obtained from Sigma (St. Louis, MO).

#### 2.1.2. Analytical pesticide standards

Carbaryl, 1-naphthol, methiocarb, bendiocarb, carbofuran and propoxur were purchased from Dr. Ehrenstorfer (Augsburg, Germany). TCP and chlorpyrifos were generously provided by DowElanco (Midland, MI). Triclopyr was obtained from Riedel-de Haën (Seelze, Germany). 2,4,5-Trichlorophenol, 2,4-dichlorophenol and 2,5-dichlorophenol were supplied by Fluka-Aldrich Química (Madrid, Spain).

### 2.1.3. Immunoreagents

For carbaryl assay, BSA–CNH, BSA–CNA, BSA–1NAH, OVA–1NAH and OVA–CPNU protein–hapten conjugates, as well as LIB–CNH45, LIB–CNH36 and LIB–CNA36 monoclonal antibodies (MAbs), were produced in our laboratory as previously described [24]. For TCP assay, BSA–TS1 protein–hapten conjugate and LIB–MC2 MAb were previously prepared as described [21].

## 2.2. Covalent immobilization

### 2.2.1. Clean up of crystals

Crystal gold-coated electrodes were first cleaned by immersion into piranha solution (concentrated  $H_2SO_4$ : 30%  $H_2O_2$ , 3:1 v/v) for 2 min at room temperature, followed by subsequent rinses with distilled water and ethanol. Finally, the surface of the crystals was blown dry with a stream of nitrogen gas.

### 2.2.2. Immobilization via thioctic acid self-assembled monolayers (SAM)

Hapten conjugates were immobilized on the sensor surface through the formation of SAM, which provide the covalent attachment of the analyte derivatives to the functionalized surface in a controlled way [22]. Freshly cleaned crystals were dipped overnight into 0.2% thioctic acid ethanolic solution with gentle shaking [23], followed by a three times ethanol washing. The activation of alkanethiol carboxylic groups to a reactive intermediate reagent (N-hydroxy-succinimide ester) took place by subsequently immersion of the modified crystals into an ethanolic solution of EDC/NHS (0.2/0.05 M) for 4 h. In the reaction, EDC converts the carboxylic acid of the alkanethiol into an N-hydroxysuccinimide ester, which covalently reacts with lysine amine groups of the hapten conjugates. After washing the reagent excess with ethanol, crystals were dried with nitrogen gas. Then, 60  $\mu$ l of 10 mg  $ml^{-1}$  BSA- or OVA-hapten conjugates in 0.1 M sodium phosphate buffer, pH 7.5 was placed on one face of the gold electrode active surface for 4 h. After washing with sodium phosphate buffer, 60  $\mu$ l of 1 M ethanolamine in 0.1 M sodium borate buffer, pH 8.75, was added and incubated for 1 h. This way, the unreacted NHS-esters remaining on the sensor surface were deactivated. Thereafter, crystals were washed three times with sodium borate buffer and another three more times with double distilled water. Finally, crystals were air-dried and stored at 4 °C. All the procedures took place at room temperature. Negative controls were prepared in the same way but using pure BSA instead of BSA-hapten conjugates.

### 2.3. Immunoassay format

The immunoassays developed to determine carbaryl and TCP were binding inhibition tests, based on the conjugate coated format. For the inhibition assays, a fixed amount of the respective monoclonal antibody was mixed with standard solutions of the analyte, and the mixture was pumped over the sensor surface. Since analyte inhibits antibody binding to the respective immobilized conjugates, increasing concentrations of analyte will reduce the frequency decrease of the piezoelectric (microgravimetric) sensor. Standard solutions of carbaryl and TCP, in the  $10^{-3}$  to  $10^3 \mu g l^{-1}$  range, were prepared daily by serial dilutions in PBS (10 mM phosphate buffer solution, pH 7.45) containing 0.005% Tween 20 (PBST), from 1 mM stock solutions in dimethylformamide stored at  $-20^\circ C$  in dark vials. The standards were mixed with a fixed concentration of LIB–CNH45 or LIB–MC2 MAbs (15.6 or 20.0  $\mu g ml^{-1}$  in PBST for carbaryl or TCP, respectively). Analyte–antibody solutions were incubated for 1 h at room temperature and then injected and brought onto the sensor surface. The resonance frequency of the piezoelectric crystal was monitored in real time as the binding between free antibody and the immobilized conjugate took place.

Regeneration of the functionalized surface was accomplished with 0.1 M HCl to break the antibody–hapten conjugate association.

#### 2.4. QCM immunosensor setup

Gold coated AT-cut 9 MHz quartz crystals (0.167 mm thickness, 14 mm diameter, 0.196 cm<sup>2</sup> active area) were purchased from International Crystal Manufacturing Company Inc. (ICM) (Oklahoma City, OK).

Once biochemically functionalized, the piezoelectric quartz crystal was placed and sealed with two O-rings, in a homemade Arnite flow-through cell (internal volume 50  $\mu$ l) (Fig. 1). Only one face of the crystal was allowed to be in contact with the reagents during the assays. The flow cell was included in a flow-through system controlled by a Minipuls 3 peristaltic pump from Gilson (Villeurbanne, France).

The frequency and resistance measurements during the assays were made with a Research Quartz Crystal Microbalance (RQCM) from Maxtek ([www.maxtekinc.com](http://www.maxtekinc.com)). This instrument is a crystal measurement system based on the capacitance cancellation technique, designed for research applications.

Samples were delivered to the flow cell by means of the peristaltic pump at a constant flow rate of 60  $\mu$ l min<sup>-1</sup>. Two different types of Rheodyne (Supelco, Bellefonte, PA) valves were used: a low-pressure injection valve (5020 model) for injection of a precise volume of 250  $\mu$ l and a 6-port rotary valve (5011 model) for switching from working to washing buffers. Teflon tubing (Supelco, Bellefonte, PA), internal diameter 0.8 mm, was used for connections.

Before the first assay on every freshly immobilized crystal, 5 min flow of PBST, followed by 5 min flow of the blocking buffer (PBS containing 0.5% BSA), at 60  $\mu$ l min<sup>-1</sup>, was applied to block non-specific MAb adsorption to the electrode gold surface. At this stage, only very low variations of frequency ( $\Delta f \leq 10$  Hz) were obtained when crystals were immobilized properly, and signal baseline quickly recovered with PBST. Tween 20 surfactant was included in the working buffer to avoid non-specific binding of proteins. The assay procedure was as follows:

- (1) 5 min flow of the working buffer (PBST) to stabilize the baseline signal.
- (2) Sample injection (250  $\mu$ l) and 10 min flow of working buffer.
- (3) Regeneration for 5 min with 0.1 M HCl.

The flow rate was 250  $\mu$ l min<sup>-1</sup> except for step (2), where it was lowered to 60  $\mu$ l min<sup>-1</sup>. A complete assay cycle, including regeneration, takes 20 min. Everyday after the last assay, crystals were washed with double distilled water, air-dried and stored at 4 °C.

#### 2.5. Data analysis

All standards and samples were run at least in duplicate. Standard curves were obtained by plotting the frequency decrease versus the logarithm of analyte concentration. The experimental points were fitted to the four-parameter logistic equation:

$$y = \frac{D + (A - D)}{1 + (x/C)^B} \quad (2)$$

where  $A$  is the asymptotic maximum (maximum signal in the absence of analyte,  $S_{\max}$ ),  $B$  is the curve slope at the inflection point (related to the analyte concentration giving 50% inhibition of  $S_{\max}$ :  $C$ ,  $I_{50}$ ) and  $D$  is the asymptotic minimum (background signal).

Mean standard curves were obtained by averaging several individual standard ones. These curves were normalized by expressing the frequency decrease provided by each standard concentration as the percentage of the maximum response (maximum signal,  $S_{\max} = 100\%$ ) in the absence of analyte.

#### 2.6. Cross-reactivity assays

The ability of the immunosensor to recognize several carbaryl or TCP related compounds was tested by performing standard curves with the potential cross-reactants and determining their respective  $I_{50}$  values. Cross-reactivity (CR) was calculated as:

$$CR = \left[ \frac{I_{50}(\text{target analyte})}{I_{50}(\text{related compound})} \right] \times 100 \quad (3)$$

where both  $I_{50}$  values are expressed in molar units.

#### 2.7. Analysis of spiked fruit juice samples

Commercial orange and apple juices were purchased from a local supermarket. They were daily spiked at 1, 2, 5 and 10  $\mu$ g ml<sup>-1</sup> carbaryl or TCP from a 1 mM stock solution, and stored at -20 °C in the dark. For assays, samples were diluted 50 and 200 times in PBST and kept at 4 °C.

### 3. Results and discussion

#### 3.1. QCM immunoassay optimization

Low molecular weight compounds, like carbaryl and TCP, should be measured using competitive immunoassays. As antibody immobilization often leads to impaired regeneration capability and poor immunoassay reproducibility of immunosensors, the conjugate-coated assay format was chosen because of its excellent performance in terms of stability and reliability. Furthermore, covalent binding via SAM ensures highly ordered protein immobilization, which provides numerous advantages, e.g. as improvement of detection limits, reproducibility and reusability, and prevention of non-specific binding of biomolecules [7].

##### 3.1.1. Carbaryl immunosensor

For QCM immunoassay optimization, carbaryl was chosen as model analyte. To select the conjugate-MAb combination pro-

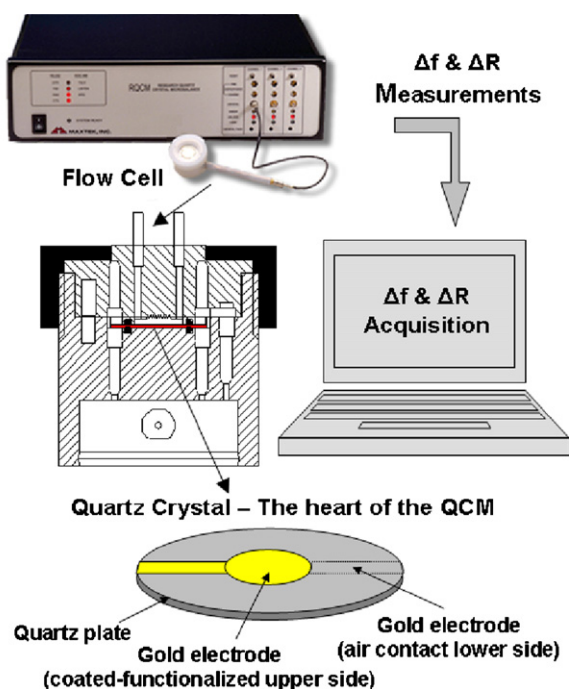
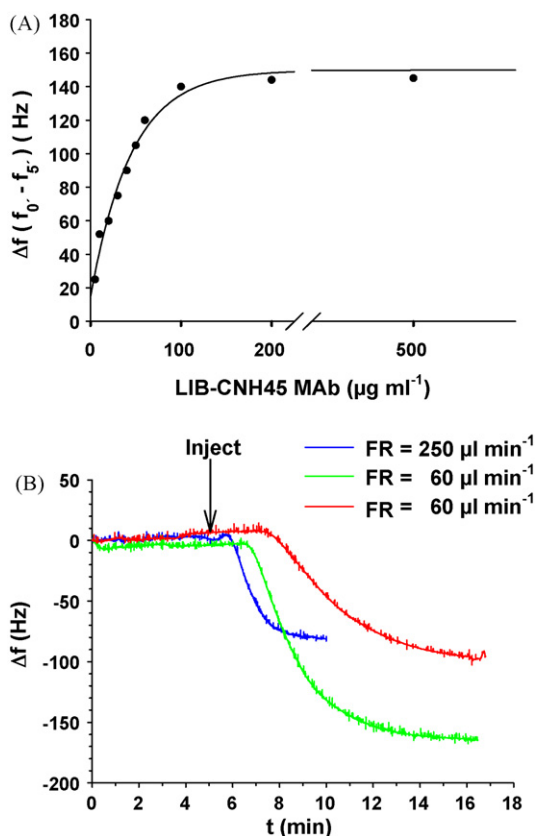


Fig. 1. Scheme of the flow cell and measurement device.



**Fig. 2.** Optimization of the carbaryl QCM immunosensor assay. (A) Signal variation ( $\Delta f$  in 5 min at 250  $\mu\text{l min}^{-1}$ ) as a function of LIB-CNH45 MAB concentration. (B) Influence of the flow rate (FR) on the signal ( $\Delta f$ ) obtained with two LIB-CNH45 MAB concentrations: 31.2 (blue and green) and 15.6  $\mu\text{g ml}^{-1}$  (red). (For interpretation of the references to color in this figure legend, the reader is referred to the web version of the article.)

viding the best assay performance, LIB-CNA36, LIB-CNH36, and LIB-CNH45 MABs were assayed with BSA-CNH as the immobilized protein-hapten conjugate. MABs were chosen because of their availability and/or their high sensitivity for carbaryl in ELISAs [24]. A suitable BSA-CNH concentration (10  $\text{mg ml}^{-1}$ ) was used for conjugate immobilization, following the protocol described in Section 2. MAB solutions at 100  $\mu\text{g ml}^{-1}$  in PBST were assayed with a flow rate of 250  $\mu\text{l min}^{-1}$ . Under these conditions, maximum frequency shifts were produced in 5 min. LIB-CNA36 MAB yielded the highest signals but it required a long time for regeneration. LIB-CNH36 MAB gave the lowest signals and also required long regeneration times. Finally, signals produced by LIB-CNH45 MAB were higher enough, in combination with the shortest regeneration times. Fig. 2A shows the frequency shifts obtained with LIB-CNH45 MAB assayed in the 5–500  $\mu\text{g ml}^{-1}$  concentration range. The influence of MAB concentration on the variation of frequency reached an asymptotic maximum at around 100  $\mu\text{g ml}^{-1}$ . To provide a reasonable signal with minimum MAB wasting, a preliminary concentration of 30  $\mu\text{g ml}^{-1}$  was chosen for further experiments.

With regard to the protein-hapten conjugate selection, carbaryl conjugates of BSA with CNH, CNA, and 1NAH haptens, and of OVA with 1NAH, and CPNU haptens, were immobilized on different crystal gold electrodes as described in the immobilization protocol. Assays were performed with a fixed concentration of LIB-CNH45 MAB (30  $\mu\text{g ml}^{-1}$ ) in PBST. After 5 min, the highest signals obtained were provided by BSA-CNH (80 Hz), OVA-1NAH (92 Hz) and OVA-CPNU (88 Hz). The two OVA-conjugates showed an evident signal leakage after a few complete assay cycles, whereas BSA-CNH did not show any significant signal change for the same

number of assays (data not shown). This fact could be attributed to a less effective covalent attachment of OVA-conjugates to the SAM-modified gold electrode, because of having less amine groups than BSA-conjugates available to produce amide bonds. Therefore, BSA-CNH was chosen as the hapten conjugate for carbaryl competitive assays. In negative controls, performed by passing 40–200  $\mu\text{g ml}^{-1}$  MAB solutions through crystals where pure BSA was immobilized, no significant variations of frequency were found.

Finally, in order to ascertain the combination of flow rate and immunoreagent concentration that produced the maximum signal (highest frequency variation), different flow rates were assayed at two LIB-CNH45 MAB concentrations. As shown in Fig. 2B, when a 31.2  $\mu\text{g ml}^{-1}$  MAB solution was delivered through the sensor at 250  $\mu\text{l min}^{-1}$  (blue line), the maximum signal (82 Hz) was obtained in about 5 min. The same MAB concentration at 60  $\mu\text{l min}^{-1}$  (green line) resulted in a maximum frequency change of 164 Hz in 10 min. Therefore, by diminishing the flow rate, both maximum signal and binding time were duplicated. Employing half a MAB concentration (15.6  $\mu\text{g ml}^{-1}$ ) at 60  $\mu\text{l min}^{-1}$  (red line), the frequency shift produced was similar to that obtained in the first case (96 Hz), whereas 10 min was required to allow the extensive binding of the MAB to the immobilized conjugate. In consequence, 60  $\mu\text{l min}^{-1}$  was chosen as the optimum flow rate, because it assured a sufficiently high maximum signal in combination with a low MAB consumption (15.6  $\mu\text{g ml}^{-1}$ ) and a reasonably short response time (10 min).

In summary, as regards immunoreagents, the optimal conditions chosen were 10  $\text{mg ml}^{-1}$  of BSA-CNH conjugate for immobilization and 15.6  $\mu\text{g ml}^{-1}$  of LIB-CNH45 MAB in PBST, at a flow rate of 60  $\mu\text{l min}^{-1}$ , for binding. For baseline stabilization and regeneration, the flow rate was raised to 250  $\mu\text{l min}^{-1}$ .

In the same way, previous assays for TCP immunoassay optimization were carried out, leading to similar results: BSA-TS1 conjugate at 10  $\text{mg ml}^{-1}$  for immobilization and LIB-MC2 MAB at 20  $\mu\text{g ml}^{-1}$  in PBST, at a flow rate of 60  $\mu\text{l min}^{-1}$ .

### 3.2. Immunosensor characterization

#### 3.2.1. Standard curves and assay sensitivity

3.2.1.1. Carbaryl. Fig. 3 depicts a real screen-print of the signals obtained in a carbaryl competitive curve experiment. As shown, under optimized conditions, the piezoelectric immunosensor was working in the micro-gravimetric mode, since the signal corresponding to the resistance was nearly constant (lower record). Therefore, the obtained decreases of frequency (upper record) could be attributed to changes in the mass deposited (i.e., antibody bound) onto the sensor surface. In order to determine the carbaryl concentrations in sample analysis, these frequency decreases were used to generate the standard calibration curves.

The representative standard curve for the carbaryl assay (Fig. 4A) was obtained by averaging seven 8-point individual curves, in which each point was run in duplicate. Each point is therefore the mean value of 14 assays. The experimental points were fitted to the mathematical function according to Eq. (2). In order to be properly averaged, frequency shifts were normalized by expressing experimental frequency changes as  $100 \times \Delta f / \Delta f_0$ , where  $\Delta f_0$  is the frequency decrease at zero analyte concentration (maximum signal). As expected for binding inhibition immunoassays, the standard curve shows the typical decreasing sigmoidal shape, i.e., the signals provided by the piezoelectric immunosensor are inversely proportional to pesticide concentrations. Carbaryl standards were assayed in the  $10^{-2}$  to  $10^3 \mu\text{g l}^{-1}$  range. The  $I_{50}$  value, which is generally accepted as an estimate of the immunosensor sensitivity, was 30  $\mu\text{g l}^{-1}$ . The limit of detection (LOD), calculated as the pesticide concentration that provided 90% of the maximum signal ( $I_{90}$  value), was 11  $\mu\text{g l}^{-1}$ . The quantification range (linear working

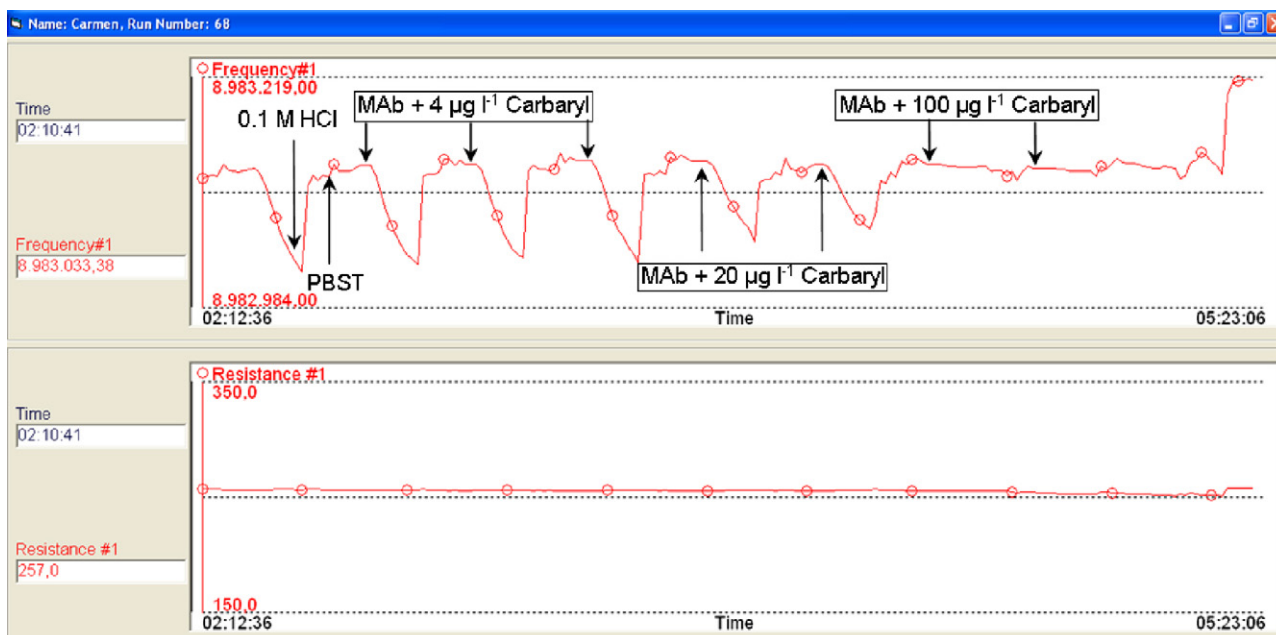


**Fig. 3.** QCM immunosensor response to analyte concentration. Upper record: real-time frequency monitoring of consecutive carbaryl immunoassays. Increasing carbaryl concentrations were assayed with a constant LIB-CNH45 MAb concentration ( $15.6 \mu\text{g ml}^{-1}$ ). Regeneration (0.1 M HCl + PBST) is indicated only between the first two assays. Lower record: real-time monitoring resistance in the same experiment.

range, in which analyte concentrations produced signals between 80 and 20% of the maximum) was between  $15$  and  $53 \mu\text{g l}^{-1}$ .

**TCP:** A representative 8-point standard curve for this analyte, corresponding to the average of seven individual ones, is shown in Fig. 4B. Frequency shifts for TCP concentrations in the  $10^{-2}$  to  $10^3 \mu\text{g l}^{-1}$  range were very similar to those obtained for carbaryl. The  $I_{50}$  value, LOD and working range were  $31$ ,  $7$  and  $13$ – $83 \mu\text{g l}^{-1}$ , respectively.

On the basis of these analytical parameters, this immunosensor can be considered as ten times less sensitive than those previously reported for the same compounds, using nearly the same immunoreagents but employing different transduction principles: flow injection immunoassay [25] and surface plasmon resonance [26,27]. Nevertheless, the analytical performance achieved by the piezoelectric immunosensor for both carbaryl and TCP ( $I_{50}$  value around  $30 \mu\text{g l}^{-1}$  and LOD around  $10 \mu\text{g l}^{-1}$ ) should allow the detection of these compounds in fruits and vegetables at European regulatory levels.

### 3.2.2. Cross-reactivity

The selectivity of the QCM immunosensor was evaluated by assessing its response to several analyte-related compounds. Cross-

**Table 1**

Cross-reactivity (CR) of the QCM immunosensor in comparison with FIA and ELISA.

Compound	CR (%)		
	QCM	FIA <sup>a</sup>	ELISA <sup>b</sup>
Carbaryl	100	100	100
1-Naphtol	0.18	<0.10	<0.10
Methiocarb	0.43	<0.10	0.10
Bendiocarb	<0.10	nd <sup>c</sup>	nd <sup>c</sup>
Carbofuran	<0.10	<0.10	<0.10
Propoxur	<0.10	<0.10	<0.10
TCP	100	100	100
Chlorpyrifos	0.48	<0.10	0.20
Trichlopyr	<0.10	<0.10	<0.10
2,4,5-Trichlorophenol	23.24	9.28	2.00
2,4-Dichlorophenol	1.14	0.55	0.10
2,5-Dichlorophenol	1.08	0.36	<0.10

<sup>a</sup> Ref. [25] (carbaryl), Ref. [28] (TCP).

<sup>b</sup> Ref. [29] (carbaryl), Ref. [21] (TCP).

<sup>c</sup> Not determined.

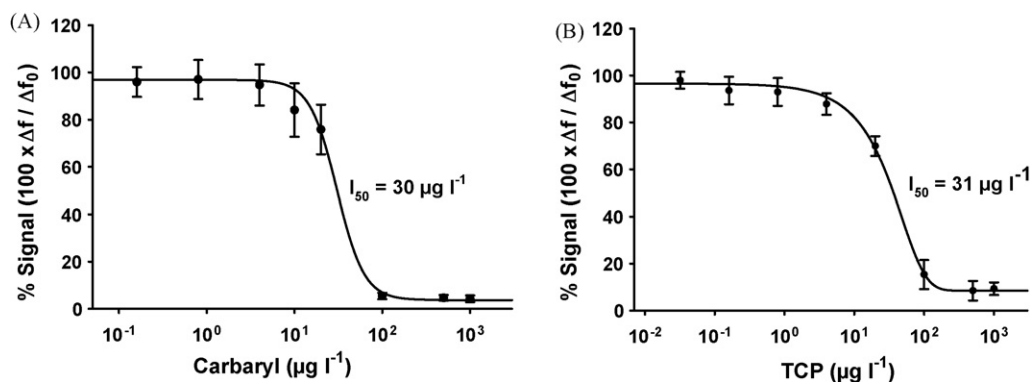


**Fig. 4.** Standard calibration curves of carbaryl (A) and TCP (B). Each curve is the mean of 7 different ones run in duplicate.



**Table 2**  
Recoveries of carbaryl and TCP from spiked orange and apple juice samples.

Juice	Added ( $\mu\text{g ml}^{-1}$ )	Dilution factor	Carbaryl			TCP			
			Found <sup>a</sup> ( $\mu\text{g ml}^{-1}$ )	CV (%)	Recovery (%)	Found <sup>a</sup> ( $\mu\text{g ml}^{-1}$ )	CV (%)	Recovery (%)	
Orange	1.0	200 <sup>b</sup>	1.9	12	194	1.7	27	173	
		50	1.2	5	120	0.8	9	76	
	2.0	200	2.6	19	131	3.3	22	165	
		50	1.7	18	85	2.0	12	98	
	5.0	200	6.3	5	125	4.0	2	79	
		50 <sup>b</sup>	5.3	28	105	2.1	17	43	
	10.0	200	8.1	3	81	8.5	17	85	
		50 <sup>b</sup>	4.7	48	47	– <sup>c</sup>	–	–	
	Apple	1.0	200 <sup>b</sup>	3.0	6	298	1.2	63	116
			50	0.8	5	81	0.9	19	90
2.0		200	2.7	12	137	2.1	23	104	
		50	2.0	3	101	2.1	13	103	
5.0		200	6.1	12	122	4.6	6	92	
		50 <sup>b</sup>	2.9	11	58	3.2	29	64	
10.0		200	11.4	12	114	12.7	27	127	
		50 <sup>b</sup>	3.2	16	32	– <sup>c</sup>	–	–	

<sup>a</sup> Mean from at least four determinations.

<sup>b</sup> Out of range.

<sup>c</sup> Asymptotic minimum (background signal).

reactivity was defined as the percentage ratio between the  $I_{50}$  value of the target analyte (carbaryl or TCP) and the  $I_{50}$  value of the cross-reacting compound. As shown in Table 1, none of the carbaryl related compounds gave cross-reactivities higher than 0.5%, and three of them gave values lower than 0.1%. These results indicate a very specific assay for carbaryl. As regards TCP, the immunosensor was quite selective since only the chlorophenolic compounds tested showed cross-reactivity values higher than 0.5%, 2,4,5-trichlorophenol being in turn the best recognized one (23.24%). This is consistent with the fact that 2,4,5-trichlorophenol is the compound chemically closer to TCP. It should be pointed out that cross-reactivity values of the piezoelectric immunosensor for the same combination of immunoreagents, in spite of being higher, are in complete agreement with those of ELISA for TCP [21] and FIHA for carbaryl and TCP [25,28]. Moreover, cross-reactivity values for the carbaryl immunosensor were very similar to those obtained in ELISA with antibodies raised from the CNH hapten [29]. Therefore, the cross-reactivity seems to be an intrinsic property of the immunoreagents, regardless of the immunoassay technique or configuration used. Since the selectivity of the immunosensor relies on the specificity of the MAb used, highly specific MAbs lead to very selective immunoassays.

The selectivity of the immunochemical interaction in the QCM immunosensor was also proved with the non-related LA-4 monoclonal antibody. This MAb, previously obtained and characterized in our laboratory, and used for the selective immunodetection of beer spoilage lactic acid bacteria [30], did not interact at all with carbaryl and TCP hapten conjugates at the QCM immunosensor.

### 3.2.3. Reusability

One of the main advantages of immunosensors upon other immunological techniques relies on their ability to be reused as many assay cycles as possible. Therefore, the reliability and stability of an immunosensor greatly depends on its regeneration capability.

After testing several regeneration agents, 0.1 M HCl was selected for carbaryl and TCP piezoelectric immunosensors. This reagent assured the complete desorption of both LIB-CNH45 and LIB-MC2 MAbs from their respective monoclonal antibody–assay conjugate complexes. For both analytes, the QCM immunosensor suffered a 30% and a 45% decrease of the maximum signal after 100 and 150 assay cycles, respectively. Nevertheless, no significant loose of sensitivity ( $I_{50}$  value) was found, thus allowing the piezoelectric immunosensors to be reused for at least one hundred and fifty

assay cycles. The reusability achieved is in the same range as those reported for other immunosensors [25–27], which confirms the predicted stability and reliability of the conjugate-coated immunosensor format when covalent attachment of the conjugate to the transducer surface is provided.

### 3.2.4. Analysis of spiked fruit juice samples

Commercial orange and apple juices were spiked with carbaryl or TCP at concentrations ranging from 1 to 10  $\mu\text{g ml}^{-1}$ . Then, samples were analyzed with the QCM immunosensor without any pretreatment other than dilution. Assay signals produced by samples were interpolated in their respective standard curves run in the same experiment. Results obtained for carbaryl and TCP spiked juices are shown in Table 2. For both analytes, when only samples within the assay working ranges were considered, accurate and precise results were produced. In these samples, average coefficients of variation (CV) of 11 and 13% and average recovery values of 104 and 107% were obtained for orange and apple juice, respectively.

Analyte concentrations lower than LOD ( $5 \mu\text{g l}^{-1}$ , i.e.,  $1 \mu\text{g ml}^{-1}$  at 1/200 dilution) were generally overestimated. Concentrations above linear working range such as 100 and  $200 \mu\text{g l}^{-1}$  (5 and  $10 \mu\text{g ml}^{-1}$  at 1/50 dilution) were underestimated, except for orange juice spiked with carbaryl at  $5 \mu\text{g ml}^{-1}$  (105% recovery). In general, concentrations out of range also gave the less precise results.

Carbaryl-spiked apple juice samples were previously analyzed by ELISA and FIHA. In ELISA, 8% mean CV and 101% mean recovery were reported [31], whereas 11% mean CV and 112% mean recovery was found in FIHA [25]. These results are comparable with those obtained with the QCM immunosensor for the same kind of juice, spiked at concentrations within the assay working range of carbaryl (9% mean CV and 111% mean recovery).

## 4. Conclusions

The word immunosensor usually refers to devices based on the non-competitive immunoassay format, where the antibody is the immobilized immunoreagent [32,33]. However, for small analytes such as pesticides, immunosensors are usually developed in the competitive inhibition format, with immobilized hapten conjugates and monoclonal antibodies as specific recognition immunoreagents [26]. This assay configuration results in very good analytical performance in terms of sensitivity, selectivity and

reproducibility. Moreover, this configuration offers the additional advantage of an extended reusability, whereas in the antibody-immobilized formats the immunoreagent usually remains active for only a few assay cycles.

We have developed a novel piezoelectric immunosensor for the determination of the pesticide carbaryl and the TCP metabolite. It is based on hapten conjugate immobilization and monoclonal antibodies. The sensitivity ( $I_{50}$  value) achieved was around  $30 \mu\text{g l}^{-1}$  for both compounds. The determination of these analytes in spiked fruit juice samples was carried out with high precision and accuracy. This piezoimmunosensor, in spite of being ten times less sensitive than other immunosensors developed for the same analytes, would allow the determination of carbaryl and TCP in fruits and vegetables at European regulatory levels. Other reported QCM biosensors for carbaryl [34,35], which are not based on immunoassay but on acetylcholinesterase enzyme inhibition, are ten to one hundred times less sensitive than the present QCM immunosensor.

The properties and potential of advanced piezoelectric immunosensors have been recently reviewed [36–38]. In particular, QCM represents an economical alternative to the overpriced optical systems as SPR [9], and a significant promise in terms of simplicity of use and portability for on-line analysis [39]. However, their sensitivity still remains lower than that achieved by other immunosensor devices. To meet the requirements of the strict European regulations for the presence of pesticide residues in drinking water, further studies to improve the QCM immunosensor sensitivity are in progress. Our work is now being focused on the employment of crystals with higher resonance frequency [40], in combination with better oscillators, to achieve highly stable and sensitive frequency signals.

#### Acknowledgement

We wish to thank the Spanish “Ministerio de Ciencia y Tecnología” for financial support (project AGL2006-12147/ALI).

#### References

- [1] S. Rodríguez-Mozaz, M.J. López de Alda, M.P. Marco, D. Barceló, *Talanta* 55 (2005) 291.
- [2] J.J. Manclús, J. Primo, A. Montoya, *J. Agric. Food Chem.* 44 (1996) 4052.
- [3] A. Abad, M.J. Moreno, R. Pelegrí, M.I. Martínez, A. Sáez, M. Gamón, A. Montoya, *J. Chromatogr. A* 833 (1999) 3.
- [4] J.J. Manclús, A. Abad, M.Y. Lebedev, F. Mojarrad, B. Micková, J.V. Mercader, J. Primo, M.A. Miranda, A. Montoya, *J. Agric. Food Chem.* 52 (2004) 2776.
- [5] M.J. Moreno, E. Plana, A. Montoya, P. Caputo, J.J. Manclús, *Food Addit. Contam.* 24 (2007) 704.
- [6] A. Janshoff, H.-J. Galla, C. Steinem, *Angew. Chem. Int.* 39 (2000) 4004.
- [7] X. Su, S.F.Y. Li, W. Liu, J. Kwang, *Analyst* 125 (2000) 725.
- [8] Y.S. Fung, Y.Y. Wong, *Anal. Chem.* 73 (2001) 5302.
- [9] P. Skládal, *J. Braz. Chem. Soc.* 14 (2003) 491.
- [10] G. Sauerbrey, *Z. Phys.* 155 (1959) 206.
- [11] K.K. Kanazawa, J.G. Gordon, *Anal. Chim. Acta* 175 (1985) 99.
- [12] R. Lucklum, P. Hauptman, *Sens. Actuators B* 70 (2000) 30.
- [13] A. Shons, F. Dorman, J. Najarian, *J. Biomed. Mater. Res.* 6 (1972) 565.
- [14] Z. Fohlerová, P. Skládal, J. Turánek, *Biosens. Bioelectron.* 22 (2007) 1896.
- [15] J.-S. Yu, H.-X. Liao, A.E. Gerdon, B. Huffman, R. Scerce, M. McAdams, S.M. Alam, P.M. Popernack, N. Sullivan, D. Wright, D.E. Cliffel, G. Nabel, B.F. Haynes, *J. Virol. Methods* 137 (2006) 219.
- [16] G. Shen, H. Wang, S. Tan, J. Li, G. Shen, R. Yu, *Anal. Chim. Acta* 540 (2005) 279.
- [17] K. Feng, J. Li, J.-H. Jiang, G.-L. Shen, R.-Q. Yu, *Biosens. Bioelectron.* 22 (2007) 1651.
- [18] H. Sun, Y. Fung, *Anal. Chim. Acta* 576 (2006) 67.
- [19] N. Kim, I.S. Park, D.K. Kim, *Biosens. Bioelectron.* 22 (2007) 1593.
- [20] J.J. D'Amico, F.G. Bollinger, ACS Symposium Series 443, American Chemical Society, Washington, DC, 1991, 300.
- [21] J.J. Manclús, A. Montoya, *J. Agric. Food Chem.* 44 (1996) 3703.
- [22] S. Ferretti, S. Paynter, D.A. Russell, K.E. Sapsford, D.J. Richardson, *TrAC: Trends Anal. Chem.* 19 (2000) 530.
- [23] X. Su, F.T. Chew, S.F.Y. Li, *Anal. Biochem.* 273 (1999) 66.
- [24] A. Abad, J. Primo, A. Montoya, *J. Agric. Food Chem.* 45 (1997) 1486.
- [25] M.A. González-Martínez, S. Morais, R. Puchades, A. Maqueira, A. Abad, A. Montoya, *Anal. Chem.* 69 (1997) 2812.
- [26] E. Mauriz, A. Calle, A. Abad, A. Montoya, A. Hildebrandt, D. Barceló, L.M. Lechuga, *Biosens. Bioelectron.* 21 (2006) 2129.
- [27] E. Mauriz, A. Calle, J.J. Manclús, A. Montoya, L.M. Lechuga, *Anal. Bioanal. Chem.* 387 (2007) 2757.
- [28] M.A. González-Martínez, R. Puchades, A. Maqueira, J.J. Manclús, A. Montoya, *Anal. Chim. Acta* 392 (1999) 113.
- [29] A. Abad, A. Montoya, *J. Agric. Food Chem.* 45 (1997) 1495.
- [30] C. March, J.J. Manclús, A. Abad, A. Navarro, A. Montoya, *J. Immunol. Methods* 303 (2005) 92.
- [31] A. Abad, A. Montoya, *Anal. Chim. Acta* 311 (1995) 365.
- [32] D.M. Disley, D.C. Cullen, H.-K. You, C.R. Lowe, *Biosens. Bioelectron.* 13 (1998) 1213.
- [33] E. Briand, M. Salmain, J.M. Herry, H. Perrot, C. Compère, C.-M. Pradier, *Biosens. Bioelectron.* 22 (2006) 440.
- [34] J.M. Abad, F. Pariente, L. Hernández, H.D. Abruña, E. Lorenzo, *Anal. Chem.* 70 (1998) 2848.
- [35] N.G. Karousos, S. Aouabdi, A.S. Way, S.M. Reddy, *Anal. Chim. Acta* 469 (2002) 189.
- [36] E.R. Hirst, Y.J. Yuan, W.L. Xu, J.E. Bronlund, *Biosens. Bioelectron.* 23 (2008) 1759.
- [37] M. Ávila, M. Zougagh, A. Escarpa, Á. Ríos, *Trends Anal. Chem.* 27 (2008) 54.
- [38] K. Reimhult, K. Yoshimatsu, K. Risveden, S. Chen, L. Ye, A. Krozer, *Biosens. Bioelectron.* 23 (2008) 1908.
- [39] A.E. Gerdon, D.W. Wright, E. Cliffel, *Anal. Chem.* 77 (2005) 304.
- [40] S. Kurosawa, J.-W. Park, H. Aizawa, S.-I. Wakida, H. Tao, K. Ishihara, *Biosens. Bioelectron.* 22 (2006) 473.



## Determination of phytoplankton composition using absorption spectra

R. Martínez-Guijarro<sup>a,\*</sup>, I. Romero<sup>a</sup>, M. Pachés<sup>a</sup>, J.G. del Río<sup>a</sup>, C.M. Martí<sup>a</sup>, G. Gil<sup>a</sup>,  
A. Ferrer-Riquelme<sup>b</sup>, J. Ferrer<sup>a</sup>

<sup>a</sup> Institute for Water Engineering and the Environment [Polytechnic University of Valencia], Camino de Vera s/n 46022 Valencia, Spain

<sup>b</sup> Department of Statistics and Applied Operative Research and Quality [Polytechnic University of Valencia], Camino de Vera s/n 46022 Valencia, Spain

### ARTICLE INFO

#### Article history:

Received 9 May 2008

Received in revised form 18 December 2008

Accepted 22 December 2008

Available online 23 January 2009

#### Keywords:

Absorption spectra

Phytoplankton classes

Partial Least Squares

Phytoplankton pigments

### ABSTRACT

Characterisation of phytoplankton communities in aquatic ecosystems is a costly task in terms of time, material and human resources. The general objective of this paper is not to replace microscopic counts but to complement them, by fine-tuning a technique using absorption spectra measurements that reduces the above-mentioned costs. Therefore, the objective proposed in this paper is to assess the possibility of achieving a qualitative determination of phytoplankton communities by classes, and also a quantitative estimation of the number of phytoplankton cells within each of these classes, using spectrophotometric determination.

Samples were taken in three areas of the Spanish Mediterranean coast. These areas correspond to estuary systems that are influenced by both continental waters and Mediterranean Sea waters. 139 Samples were taken in 7–8 stations per area, at different depths in each station. In each sample, the absorption spectrum and the phytoplankton classes (Bacillariophyceae (diatoms), Cryptophyceae, Chlorophyceae, Chrysophyceae, Prasinophyceae, Prymnesophyceae, Euglenophyceae, Cyanophyceae, Dynophyceae and the *Synechococcus* sp.) were determined.

Data were analysed by means of the Partial Least Squares (PLS) multivariate statistical technique. The absorbances obtained between 400 and 750 nm were used as the independent variable and the cell/l of each phytoplankton class was used as the dependent variable, thereby obtaining models which relate the absorbance of the sample extract to the phytoplankton present in it. Good results were obtained for diatoms (Bacillariophyceae), Chlorophyceae and Cryptophyceae.

© 2009 Elsevier B.V. All rights reserved.

### 1. Introduction

Phytoplankton is one of the organic components of natural waters and, therefore, phytoplankton diagnosis is important to assess the ecological condition of coastal waters [2].

As explained in Millán-Núñez et al. [8], the light absorption by particulate matter, including phytoplankton in the ocean, is of great significance, since the absorption and dispersion of light cause colouring of the sea. The particle variability allows to determine the attenuation of light, the primary productivity and the biomass of phytoplankton pigments. Moreover, some authors (Yentsch and Phinney [12], Nelson and Prezelin [10], Cleveland [1]) showed that changes in the optical characteristics of masses of water were related to cellular biochemical processes inherent in the consumption of energy by photosynthesis. Many of them concluded that there is a non-linear relationship between the light absorption coefficient by phytoplankton and the chlorophyll

*a* concentration. This relationship is complicated due to phytoplankton properties, such as, size, particles shape and accessory pigments.

Phytoplankton contains pigments (chlorophylls *a*, *b* and *c*, carotenoids and phycobiliproteins) in different proportions; thus, phytoplankton identification on the basis of the absorption spectrum depends on pigment composition in cells. Pigment composition in the chloroplasts provides a way to classify the algae group. For example, coloured chloroplasts in diatoms (Bacillariophyceae) are usually yellow-brown due to xanthophylls, whereas blue-green colours (cyanophytes) are variable, within a range that encompasses from blue-green to red due to phycobiliproteins, phycoerythrins (red) and phycocyanins (blue).

Pigments that form the basis for chemical taxonomical discrimination absorb light in wavelengths in the visible spectrum [9]. Therefore, an alternative way to obtain qualitative information about phytoplankton composition is to analyse samples absorption through the visible spectrum. Qualitative information about phytoplankton classes and photoadaptation is included in such spectrum data, but the key is the interpretation thereof [9]. In general, it is better to interpret or evaluate the spectrum data

\* Corresponding author. Tel.: +34 96 3877616; fax: +34 96 3877618.

E-mail address: [mmarting@hma.upv.es](mailto:mmarting@hma.upv.es) (R. Martínez-Guijarro).

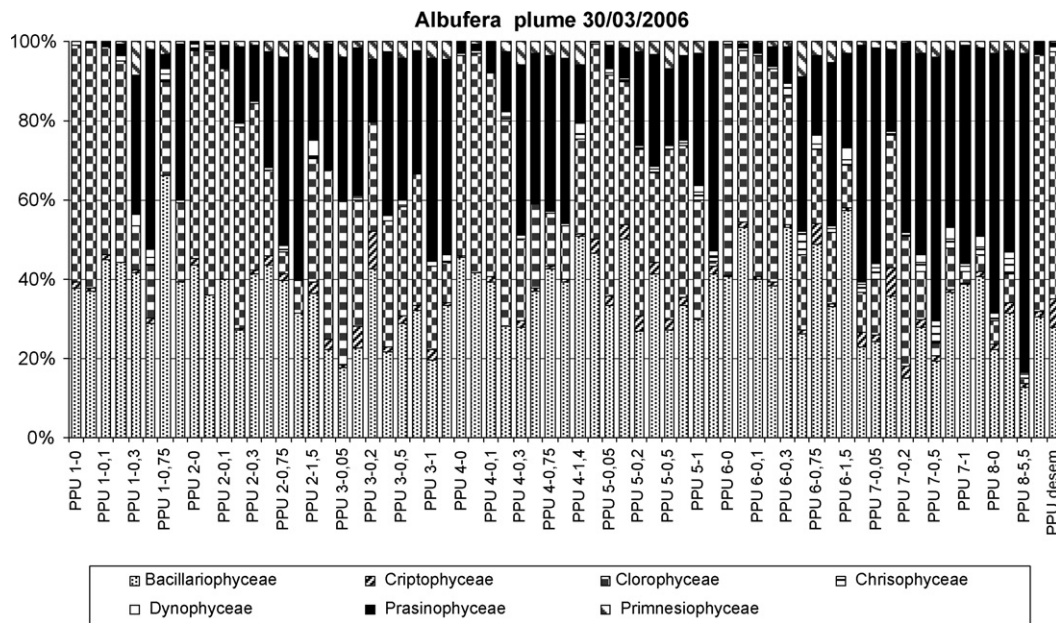


Fig. 1. Phytoplanktonic composition (eukaryota) of the Albufera plume samples.

by means of chemometrics, a branch of chemistry devoted to extracting information from large sets of data.

Furthermore, if the presence of blooms or toxic species of phytoplankton (such as some dinoflagellates) is detected in advance in the phytoplankton population, the harmful effects produced could be mitigated and even prevented [6]. Microscopic examination of water samples is the main method used to detect such toxic groups. Unfortunately, this method is slow, laborious and intermittent. For this reason, optical detection methods and automated methods have been developed to determine the presence of these species in the phytoplankton population in a quick and continuous manner.

Some laboratory works suggest that it is possible to perform group discrimination on the basis of cellular absorption. For example, Johnsen et al. [5] used discriminant analysis to classify the absorption spectrum amongst 31 bloom-formers (which represent the four main groups of phytoplankton with respect to accessory chlorophylls, for example Cl *b*, Cl *c*<sub>1</sub> and/or Cl *c*<sub>2</sub>, Cl *c*<sub>3</sub> and non-accessory chlorophylls), thereby distinguishing dinoflagellates and toxic prymnesiophytes which contain Cl *c*<sub>3</sub> from taxa that do not have this pigment.

It could be argued that, if the absorption spectrum of each individual pigment is known, the absorption spectrum of the phytoplankton may be easily reconstructed from the concentration of pigments. However, the relation between pigments concentration and phytoplankton absorption coefficients is not linear, due to the “package effect”. This effect is caused by the fact that pigments are not in solution, but rather, packed inside the cells (and in cells inside chloroplasts). The package effect varies with cell size, with intracellular concentration of several pigments and with wavelength. Due to these sources of variation (which depend on environmental factors), it is difficult, if not impossible, to precisely model and predict this effect for natural populations. Given the complexity of this effect, it is expected that neuronal network techniques will make it possible to approach the relation model between pigment concentrations and absorption spectra using current measurements that implicitly take the package effect into consideration.

As explained in Perry and Darling [11], phytoplankton, other particles and chromophoric dissolved organic matter are susceptible to radiometric optical sensors because they absorb, disperse, attenuate and fluoresce light with optical pattern characteristics (models).

Phytoplankton, as a photosynthetic organism, absorbs electromagnetic radiation primarily within the blue, blue-green and red bands of the visible spectrum and absorption coefficient is determined by pigment composition. Because they are particles, phytoplankton disperse light. The manner in which dispersion of the spectrum takes place is dependent on size (of the phytoplankton), composition and absorption spectrum. Other non-algal organic particles, such as bacteria and detritus, are relatively weak absorbers, with the maximum absorption in the UV region. As is the case of phytoplankton, the way in which dispersion of the spectrum takes place is dependent on the size distribution. Suspended sediments generally disperse more than they absorb, although a strong absorption has been observed in mineral sediments, particularly in iron-rich minerals.

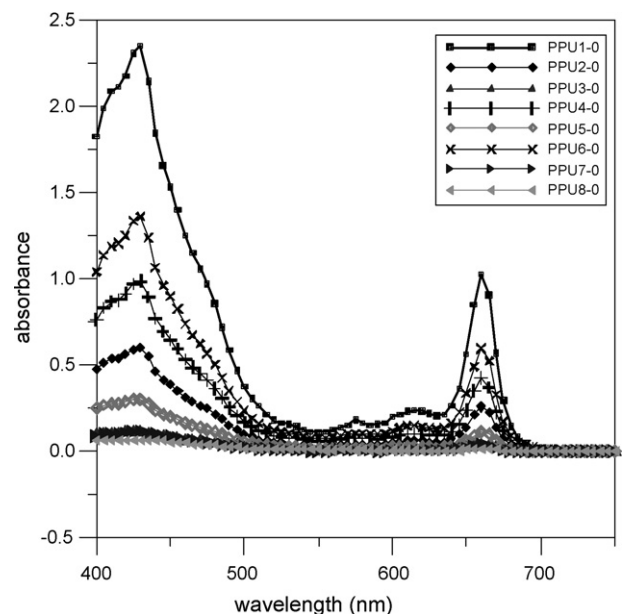


Fig. 2. Absorption spectrum of superficial samples from the Albufera plume.

## 2. Experimental

### 2.1. Sampling

The study was performed in three areas of the Eastern coast of Spain. These areas correspond to estuarine systems which are formed when the fresh/brackish waters of the continental systems flow into the Mediterranean Sea. Samplings campaigns were performed on 29 March 2006 at the area called Almenara plume, on 30 March 2006 at the Albufera plume in Valencia and on 17 May 2006 at the Estany plume in Cullera.

Water samples were collected in 2-l polyethylene bottles and 250-ml glass bottles. They were kept refrigerated until arrival at the laboratory, which never took longer than 12 h. A total of 139 samples were collected, corresponding to 7–8 stations per area, and in each station samples were taken at different depths.

### 2.2. Analytical techniques

Determination of the absorption spectrum was performed on a 90% acetone extract obtained filtering water samples through a cellulose acetate membrane (Millipore 0.45  $\mu\text{m}$  HAWP04700). Subsequently, they were frozen to break the cells and to facilitate the pigments release. Filters with the retained particulate material were introduced in 6 ml of 90% acetone. On this extract absorbance

was determined at 1-nm intervals, at wavelengths between 400 and 750 nm. A 1-cm quartz cuvette and a PerkinElmer Lambda 35 spectrophotometer were used. Absorbance values obtained at 750 nm were subtracted from the values between 400 and 749 nm, in order to eliminate the absorbance which is not caused by the pigments.

In order to analyse phytoplankton communities, epifluorescence microscopic count method was used. Samples contained in a 250-ml glass bottle were fixated with glutaraldehyde until a final concentration of 2%. They were filtered with 0.2- $\mu\text{m}$  membranes (Millipore GTTP), filters were washed with distilled water to eliminate the retained salt and, subsequently, they were dehydrated with successive washes with 50%, 80%, 90% and 99% ethanol. Each dried filter was placed onto a drop of immersion oil in the centre of a slide and two more drops were added on the top side of the filter. Finally, a coverglass was placed on the top of the filter [3]. Phytoplankton counts were performed by epifluorescence microscopy with a Leica DM2500, using the 100 $\times$ -oil immersion objective. A minimum of 300 cells was counted and at least 100 cells of the species or genera more abundant were counted with an error lower than 20% [7].

### 2.3. Statistical techniques

Statistical technique called PLS (Partial Least Squares) was used for the multivariate analysis of the experimental data obtained [4]. To develop the model that relates absorbances to phytoplankton

**Table 1**  
PLS results of model 1 and model 2 with X filtered variables (OSC).

A	R <sup>2</sup> X	R <sup>2</sup> X(cum)	Eigenvalues	R <sup>2</sup> Y	R <sup>2</sup> Y(cum)	Q <sup>2</sup>	Limit	Q <sup>2</sup> (cum)	Significance	Iterations
Model 1										
0	Cent			Cent						
1	0.878	0.878	81.70	0.369	0.369	0.303	0.05	0.303	R1	3
2	0.0788	0.957	7.33	0.026	0.395	0.00295	0.05	0.305	R2	9
3	0.0123	0.969	1.14	0.036	0.431	-0.0144	0.05	0.295	R2	25
Model 2 (OSC)										
0	Cent			Cent						
1	0.999	0.999	92.9	0.373	0.373	0.303	0.05	0.303	R1	2
2	0.000452	1	0.0421	0.0608	0.434	0.0545	0.05	0.341	R1	9
3	9.05e-005	1	0.00842	0.0806	0.515	0.0832	0.05	0.396	R1	11

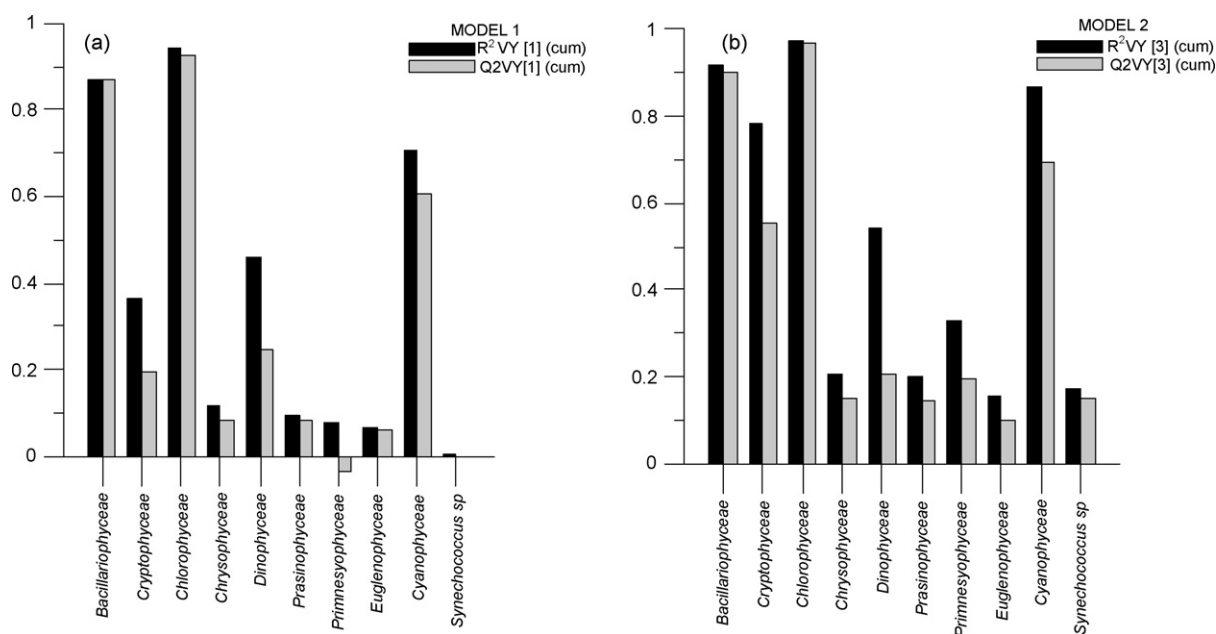


**Fig. 3.** Statistical adjustment ( $R^2$ ) and prediction capacity ( $Q^2$ ) for each individual responses. (a) Model with 1 component; (b) model with 3 components (OSC filter).

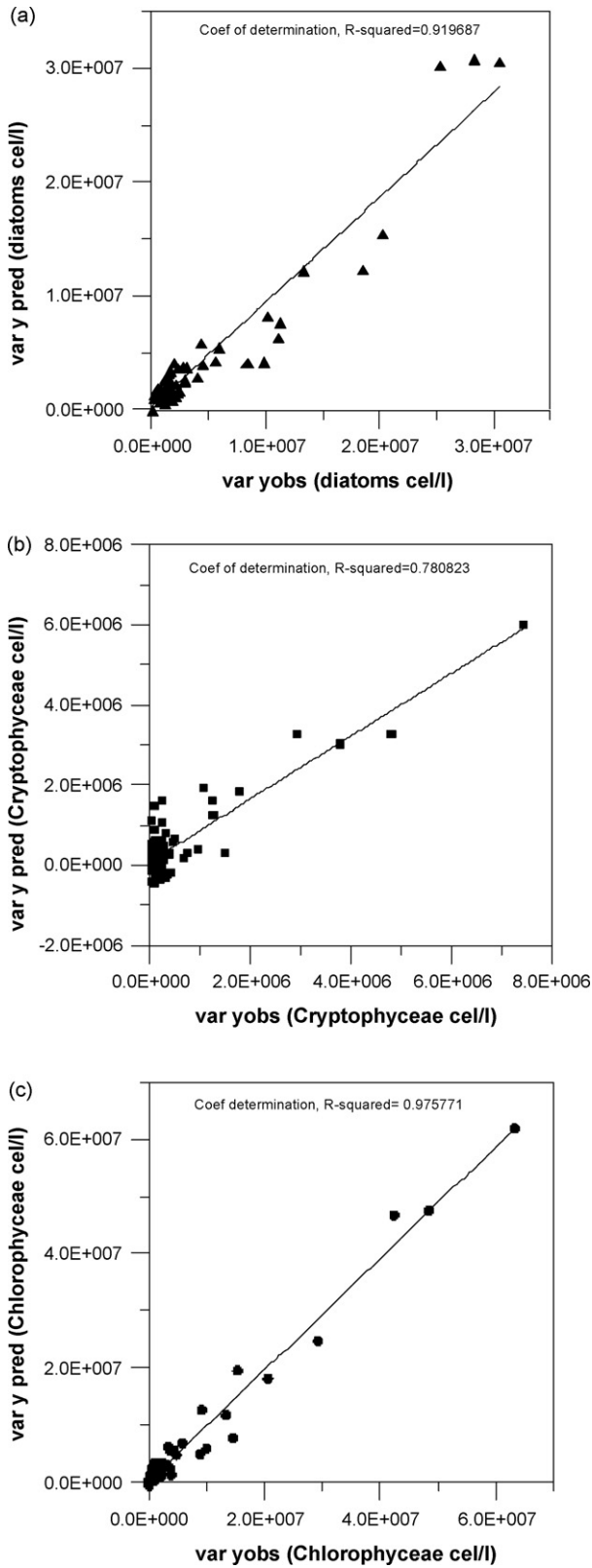


Fig. 4. Graphical representation of the observed values versus the predicted values from model 2 with samples used for the adjustment of the model. (a) Diatoms (Bacillariophyceae); (b) Cryptophyceae; (c) Chlorophyceae.

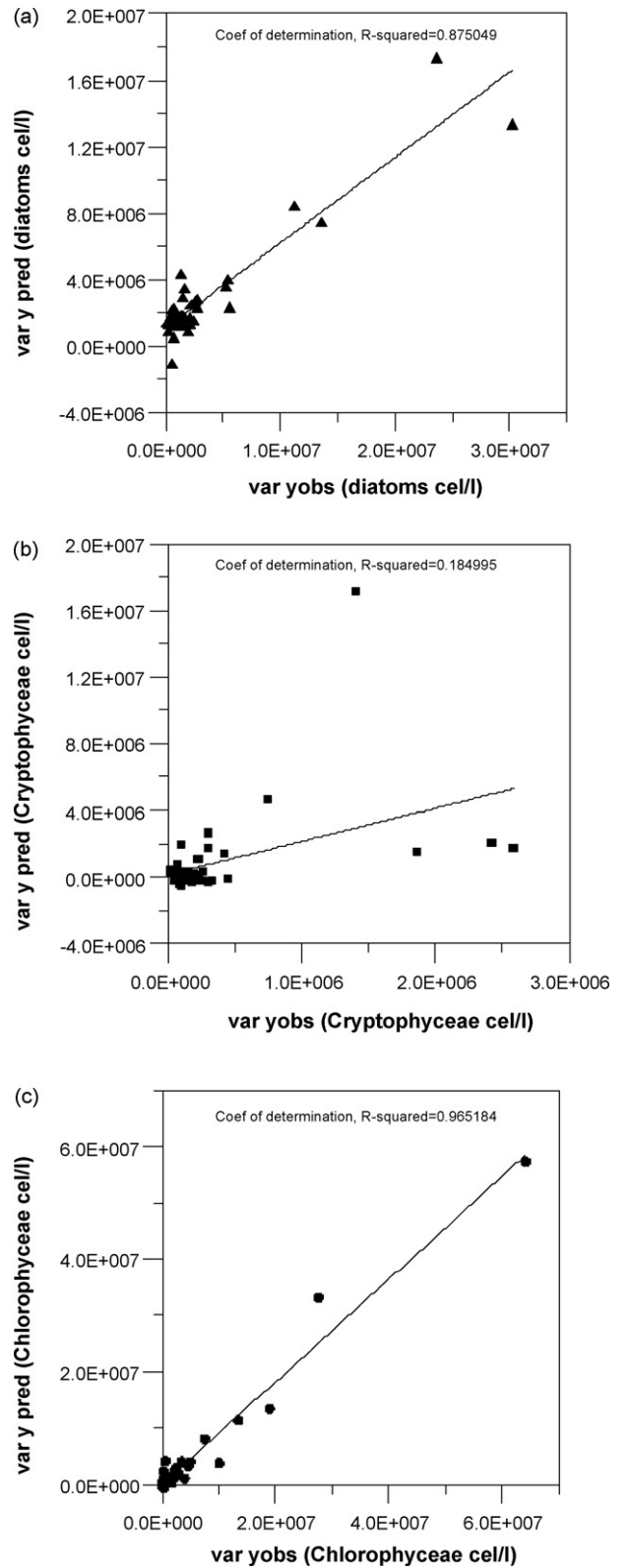


Fig. 5. Graphical representation of the observed values versus the predicted values from model 2 for an external group of samples. (a) Diatoms (Bacillariophyceae); (b) Cryptophyceae; (c) Chlorophyceae.

classes, 2/3 of the total number of samples (139) were used to fit the model, and the remaining one-third of samples (46) were used to validate it. Even though the statistical programme used, SIMCAP 9.0, makes an internal estimation of the model prediction ability by means of “cross-validation”, the only way to be absolutely sure regarding a model prediction ability is to make external predictions, that is, to make predictions for an independent system of observations.

After developing this first model, a second model was developed which made it possible to verify that the results improved when a filter called OSC (Orthogonal Signal Correction) was applied to the X variables (absorbances). The purpose of this method was to correct the matrix of X data by removing the information that was orthogonal to the Y response matrix, that was, the information which was not related to the response of interest. This preliminary pre-processing method was jointly applied to all the spectra in the calibration set. Subsequently, the correction made on the X matrix was applied to the external set of data in order to verify the true prediction ability of the model built from the corrected data.

### 3. Results and discussion

At the three sampled areas, it was found that the closest stations to the continental water outflow exhibited a vertical salinity and chlorophyll *a* gradient, due to freshwater surface layer present in those stations. This layer was not very thick; in most cases it was less than 40 cm thickness, for that reason practically all the samples analysed were saline ( $36.84 \pm 1.68$  g/kg) (salinity and chlorophyll *a* data are not showed).

Samples had a phytoplankton composition with a high content of diatoms, Prasinophyceae and Chlorophyceae as compared to the rest of eukaryotes cells, as it is shown in Fig. 1 for the Albufera plume. Although we have not included prokaryotes (colonial Cyanophyceae and *Synechococcus* genus) in Fig. 1, it is worth mentioning that at the Albufera plume area there are Cyanophyceae which are not present in the other two areas.

Absorption spectra of the pigment-containing extracts in each sample had a similar shape, with peaks at 440 and 664 nm, which correspond to chlorophyll *a*, the main pigment present in phytoplankton cells. An example is shown in Fig. 2 for the Albufera plume. Differences should be studied in the accessory pigments (chlorophylls *b* and *c*, carotenoids, etc.); for that reason the area between 400 and 500 nm would have to be enlarged, since these pigments maximum absorption peaks are in this region.

A first model that related the absorption spectra of the sample extract to phytoplankton composition (model 1) was developed. Subsequently, in order to improve the results obtained with model 1, a second model was developed, but in this case the OSC filter was applied to the X variables (absorbances).

To decide the adequate number of components for model 1, it must be taken into account the general model fit, which is defined by parameter  $R^2$ , and the prediction ability thereof, which is defined by parameter  $Q^2$ . Table 1 shows that the eigenvalue of the first component (81.7) is greater than the one from the other two components; furthermore,  $Q^2$ (cum) values decrease for the third component and, consequently, the model ability prediction. Also, when components 2 and 3 are used, the increase in  $R^2$  is very small. For all these reasons, it is sufficient to use only one component in this model. Results obtained with model 1 are shown in Fig. 3a, where it can be observed that very good results for the individual model responses for phytoplankton classes are achieved for diatoms (Bacillariophyceae), Chlorophyceae and Cyanophyceae, both in terms of the model fit ( $R^2$ ) and its ability to predict these phytoplankton classes content ( $Q^2$ ). However, results for Cyanophyceae were discarded because the presence of this class

was only significant in samples from the Albufera plume area, whereas in the remaining samples most of the Cyanophyceae values were equal to the technique detection limit.

As previously discussed, model 2 was obtained by applying the OSC filter to the X variables previous to performing the PLS analysis. Results obtained with this model improve the former. Table 1 shows that eigenvalue of the first component (92.9), as was the case with model 1, is very large by comparison to the following ones. In this case, it was decided to use three components because, in addition to taking into consideration the  $R^2$  and  $Q^2$  values (Table 1), this was the number of components that led to the best individual response results. Fig. 3b shows that this model produced adequate results also for Cryptophyceae.

Fig. 4 shows diatoms, Cryptophyceae and Chlorophyceae values predicted with model 2 against the real contents of the samples. In this figure, it can be observed that good predictions were obtained, since the  $R^2$  of the linear fit between predicted and real values was 0.9197 for diatoms, 0.7808 for Cryptophyceae, and 0.9758 for Chlorophyceae.

Once obtained model 2, it was validated by means of the external set of samples, which were used to make predictions of the phytoplankton content. As in the case of the calibration set, the OSC filter was first applied to the absorbances. This set corresponded to one-third of the total samples taken, which were not used for the model fit. Prediction results for these samples can be seen in Fig. 5. In this case, good predictions were still obtained for diatoms and Chlorophyceae, but not for Cryptophyceae (Fig. 5a–c, respectively), since the predicted values obtained were not acceptable.

### 4. Conclusions

In this paper, the absorption spectra of the sample extracts led to good results in determining of diatoms and Chlorophyceae content. An acceptable model was also obtained for Cryptophyceae, although in this case, in order to obtain good results, the absorbance values must be processed prior to applying the multivariate statistical technique. Phytoplankton classes for which good results were not obtained were due to either they had a limited presence in most of the samples studied or they had low pigments cellular quota.

In order to improve this work, a study should be performed on samples with different phytoplankton abundance and composition to the samples already studied, since it is possible that the majority presence of certain classes makes it difficult to determine other classes with type and pigments content that have overlapping or masking spectra.

Phytoplankton determination through extract samples absorption spectra is a simple and cheap method that, albeit having limitations, may be used to complement microscopic counts.

### Acknowledgements

This research work has been supported by the Regional Ministry of the Environment, Water, Urban Planning and Housing.

### References

- [1] J.S. Cleveland, J. Geophys. Res. 100 (7) (1995) 13333–13344.
- [2] V.V. Fadeev, D.V. Maslov, D.N. Matorin, R. Reuter, T.I. Zavyalova, 2000. Some peculiarities of fluorescence diagnostics of phytoplankton in coastal waters of the Black sea. Available in: [http://las.physik.uni-oldenburg.de/eProceedings/vol01\\_1/01\\_1\\_fadeev1.pdf](http://las.physik.uni-oldenburg.de/eProceedings/vol01_1/01_1_fadeev1.pdf) [checked 13-04-2007].
- [3] R. Fournier, in: A. Sournia (Ed.), Phytoplankton Manual. Monographs on oceanographic Methodology, Unesco, 1978, pp. 197–201.
- [4] P. Geladi, B.R. Kowalski, Anal. Chim. Acta 185 (1986) 1–17.
- [5] G. Johnsen, O. Samset, L. Granskog, E. Sakshaug, Mar. Ecol. Prog. Ser. 105 (1994) 149–157.

- [6] G.J. Kirkpatrick, D.F. Millie, M.A. Moline, O. Schofield, *Limnol. Oceanogr.* 45 (2) (2000) 467–471.
- [7] J.W.G. Lund, G. Kipling, E.D. Le Cren, *Hydrobiologia* 11 (2) (1958) 143–170.
- [8] E. Millán-Núñez, M.E. Sieracki, R. Millán-Núñez, J.R. Lara-Lara, G. Gaxiola-Castro, C.C. Trees, *Deep-Sea Res. II* 51 (2004) 817–826.
- [9] L. Moberg, B. Karlberg, K. Sørensen, T. Källqvist, *Talanta* 56 (2002) 153–160.
- [10] N.B. Nelson, B.B. Prezelin, *Mar. Ecol. Prog. Ser.* 94 (1993) 217–227.
- [11] M.J. Perry, I.C. Darling, 2003. Optical sensors. Available in: [http://www.geoprose.com/ALPS/white\\_papers/perry.doc](http://www.geoprose.com/ALPS/white_papers/perry.doc) [checked 22-03-2007].
- [12] C.S. Yentsch, D.A. Phinney, *Limnol. Oceanogr.* 34 (1989) 1694–1705.





# On-line ionic liquid-based preconcentration system coupled to flame atomic absorption spectrometry for trace cadmium determination in plastic food packaging materials

Estefanía M. Martinis<sup>a,b</sup>, Roberto A. Olsina<sup>b,d</sup>, Jorgelina C. Altamirano<sup>a,b,c</sup>, Rodolfo G. Wuilloud<sup>a,b,c,\*</sup>

<sup>a</sup> Laboratory of Environmental Research and Services of Mendoza (LISAMEN) (CCT – CONICET – Mendoza), Av. Ruiz Leal S/N Parque General San Martín, CC. 131, M 5502 IRA Mendoza, Argentina

<sup>b</sup> Consejo Nacional de Investigaciones Científicas y Técnicas (CONICET), Argentina

<sup>c</sup> Instituto de Ciencias Básicas, Universidad Nacional de Cuyo, Mendoza, Argentina

<sup>d</sup> INQUISAL-CONICET, Departamento de Química Analítica, Facultad de Química, Bioquímica y Farmacia, Universidad Nacional de San Luis, Argentina

## ARTICLE INFO

### Article history:

Received 30 September 2008

Received in revised form 15 December 2008

Accepted 22 December 2008

Available online 15 January 2009

### Keywords:

1-Butyl-3-methylimidazolium

hexafluorophosphate

Room temperature ionic liquid

Cadmium

On-line preconcentration

Plastic food packaging material

## ABSTRACT

A novel on-line preconcentration method based on liquid–liquid (L–L) extraction with room temperature ionic liquids (RTILs) coupled to flame atomic absorption spectrometry (FAAS) was developed for cadmium determination in plastic food packaging materials. The methodology is based on the complexation of Cd with 2-(5-bromo-2-pyridylazo)-5-diethylaminophenol (5-Br-PADAP) reagent after sample digestion followed by extraction of the complex with the RTIL 1-butyl-3-methylimidazolium hexafluorophosphate ([C<sub>4</sub>mim][PF<sub>6</sub>]). The mixture was loaded into a flow injection analysis (FIA) manifold and the RTIL rich-phase was retained in a microcolumn filled with silica gel. The RTIL rich-phase was then eluted directly into FAAS. A enhancement factor of 35 was achieved with 20 mL of sample. The limit of detection (LOD), obtained as IUPAC recommendation, was 6 ng g<sup>-1</sup> and the relative standard deviation (R.S.D.) for 10 replicates at 10 µg L<sup>-1</sup> Cd concentration level was 3.9%, calculated at the peak heights. The calibration graph was linear and a correlation coefficient of 0.9998 was achieved. The accuracy of the method was evaluated by both a recovery study and comparison of results with direct determination by electrothermal atomic absorption spectrometry (ETAAS). The method was successfully applied for Cd determination in plastic food packaging materials and Cd concentrations found were in the range of 0.04–10.4 µg g<sup>-1</sup>.

© 2009 Elsevier B.V. All rights reserved.

## 1. Introduction

Nowadays polymer packages are used preferentially in packaging foodstuffs. They are able to retard or even prevent detrimental changes in the food due to various external influences such as oxygen, light and microorganisms. They are also capable of reducing the loss in compounds such as water or flavour from the food [1]. Resulting from this protection, polymer packages enable consumers to store foodstuffs over an extended period of time. However, polymers contain additives such as plasticizers, lubricants, stabilizers and antioxidants [2], all chemicals which are necessary either for the processing or to maintain the stability of the final polymer package [3,4]. Recently, numerous studies showed that there is a

potential migration of additives from the packaging material into food [5–7]. Thus, packaging might pose a problem because of some of the additives used are extremely toxic. Cadmium is one of the toxic elements used extensively in the manufacturing of plastics [3]. Recently, the content of Cd in packaging materials undergoes European Community (EC) regulations. The EC Directive (94/62/EC) limits the concentration of Cd to 100 mg kg<sup>-1</sup> [8]. Due to its low excretion rate (biological half-life = 10–30 years) [9], Cd can be accumulated in the body and therefore, the presence of this metal is a problem even at low concentration levels [10]. Thus, sensitive, accurate, and fast analytical methods for trace metal determination in a variety of plastic materials are required.

Elemental analysis by spectrophotometric techniques involve the elution of target metal ions from polymer samples into the aqueous solution [11], before sensitive analytical techniques are needed for trace levels evaluation. Inductively coupled plasma-mass spectrometry (ICP-MS) has been used for the determination of Cd in plastics [12]; however, the cost of such instrumentation may still be prohibitive to many laboratories. Although flame atomic absorption spectrometry (FAAS) or electrothermal atomic absorption spectrometry (ETAAS) are the most commonly used techniques

\* Corresponding author at: Laboratory of Environmental Research and Services of Mendoza (LISAMEN) (CCT – CONICET – Mendoza), Av. Ruiz Leal S/N Parque General San Martín, CC. 131, M 5502 IRA Mendoza, Argentina. Tel.: +54 261 5244064; fax: +54 261 5244001.

E-mail address: [rwuilloud@mendoza-conicet.gov.ar](mailto:rwuilloud@mendoza-conicet.gov.ar) (R.G. Wuilloud).

URL: <http://www.cricyt.edu.ar/lisamen/> (R.G. Wuilloud).

to determine Cd, FAAS is widely applied in routine laboratories due to its low cost and greater simplicity as compared to ETAAS. However, conventional FAAS has a detection limit, which is not low enough to determine Cd at trace levels in plastics. In order to achieve accurate, sensitive and reliable results at trace levels; preconcentration and separation steps are needed prior to analyte determination by FAAS.

The use of room temperature ionic liquids (RTILs) as an alternative to other techniques for separation and preconcentration has attracted considerable attention in recent years [13,14]. RTIL are salts resulting from combinations of organic cations and various anions [15]. The unique physicochemical properties of RTILs, including air and moisture stability, non-volatility, good thermal stability, tunable viscosity and miscibility with water and organic solvents, the fact that they remain liquid at room temperature, make their use particularly attractive in separation processes [16]. Recently, numerous studies have shown their good extractability for various organic compounds and metal ions [17]. However, up to date all the extraction/preconcentration methodologies based on RTIL involve batch procedures [14,18] and no on-line system has been developed so far for RTIL phase separation. It is well known that when preconcentration methods are applied in a batch mode, the risk of contamination is very high and the operation is usually too time-consuming. On the other hand, 2-(5-bromo-2-pyridylazo)-5-diethylaminophenol (5-Br-PADAP) forms stable complexes with numerous metal ions [19–22], and is therefore a suitable reagent for Cd extraction/preconcentration with a RTIL [23].

In this work, a novel on-line RTIL-based preconcentration system for Cd determination at trace levels in plastic food packaging materials is presented. The on-line coupling of a FI preconcentration and separation system to FAAS represents an efficient and simple methodology for routine analysis. Cadmium preconcentration was mediated by chelation with the 5-Br-PADAP reagent, followed by extraction with the RTIL 1-butyl-3-methylimidazolium hexafluorophosphate ( $[C_4mim][PF_6]$ ) [24]. On-line retention and separation of the RTIL phase was achieved with a microcolumn filled with silica gel. The method was successfully applied to Cd determination in plastic materials, demonstrating the possibility of using RTILs for metal extraction from complex matrices.

## 2. Experimental

### 2.1. Apparatus

The experiments were performed using a PerkinElmer 5100PC atomic absorption spectrometer (PerkinElmer, Norwalk, CT, USA), equipped with a FIAS 200 flow injection analysis system (PerkinElmer). A Cd electrodeless discharge lamp (PerkinElmer) operated at a current of 240 mA and a wavelength of 228.8 nm with a spectral band width of 0.7 nm was used. A deuterium background corrector was used. All instrumental parameters are listed in Table 1.

The flow injection system is shown in Fig. 1. Tygon-type pump tubes (Gilson) were employed to propel the sample and reagent. On the other hand, solvent-resistant pump tubes (PerkinElmer) were employed for the organic eluent. A microbore glass column (40 mm length; 2 mm internal diameter) filled with the retention material and fitted with porous 25  $\mu\text{m}$  glass frits, was used for on-line retention of the RTIL phase.

### 2.2. Reagents

All the reagents were of analytical grade and the presence of Cd was not detected within the working range. A  $10^{-2} \text{ mol L}^{-1}$  5-Br-PADAP (Aldrich, Milwaukee, WI, USA) solution was prepared in

**Table 1**  
Instrumental and experimental conditions for Cd determination.

Instrumental conditions	
Wavelength (nm)	228.8
Spectral band width (nm)	0.7
Lamp current (mA)	240
Type of flame	Air/C <sub>2</sub> H <sub>2</sub>
Fuel flow (L min <sup>-1</sup> )	2
Oxidant flow (L min <sup>-1</sup> )	10
Extraction conditions	
Working pH	9
Sample volume (mL)	20
Cd <sup>2+</sup> concentration ( $\mu\text{g L}^{-1}$ )	10
5-Br-PADAP concentration ( $\times 10^{-6} \text{ mol L}^{-1}$ )	7.5
Buffer concentration ( $\times 10^{-6} \text{ mol L}^{-1}$ )	4
Surfactant concentration (w/v)	0.1%
Amount of RTIL (g)	0.7
Eluent	Acidified EtOH
Loading flow rate (mL min <sup>-1</sup> )	4
Elution flow rate (mL min <sup>-1</sup> )	6

ethanol (Merck, Darmstadt, Germany). Lower concentrations were prepared by serial dilution with ethanol. A  $1000 \text{ mg L}^{-1}$  Cd<sup>2+</sup> stock solution was prepared from Cd(II) nitrate (Merck) in  $0.1 \text{ mol L}^{-1}$  nitric acid (Merck). Lower concentrations were prepared by diluting the stock solution with  $0.1 \text{ mol L}^{-1}$  nitric acid. The buffer solution was  $2.0 \text{ mol L}^{-1}$  ammonium hydroxide (Merck) adjusted to pH 9.0 with hydrochloric acid (Merck). A surfactant solution containing 5% (w/v) Triton X-100 (Merck) was employed to avoid RTIL phase sticking onto the Tygon tube walls. Silica gel (100 Å pore size, 70–230 mesh particle size, Aldrich) was used to fill in the microcolumn. The RTIL  $[C_4mim][PF_6]$  was purchased from Solvent Innovation GmbH (Köln, Germany) and it was stored in contact with ultrapure water to equilibrate the water content in the RTIL phase. Ultrapure water (18 M $\Omega$  cm) was obtained from a Millipore Continental Water System.

### 2.3. Sample conditioning

A range of materials commonly used in the food industry were studied, including polyethylene terephthalate (PET), high density polyethylene (HDPE), polyvinyl chloride (PVC), low density polyethylene (LDPE) polypropylene (PP) and polystyrene (PS). Packages representative of different applications were selected: bottles, cups and plastic bags. The samples were cut into small pieces. A wet

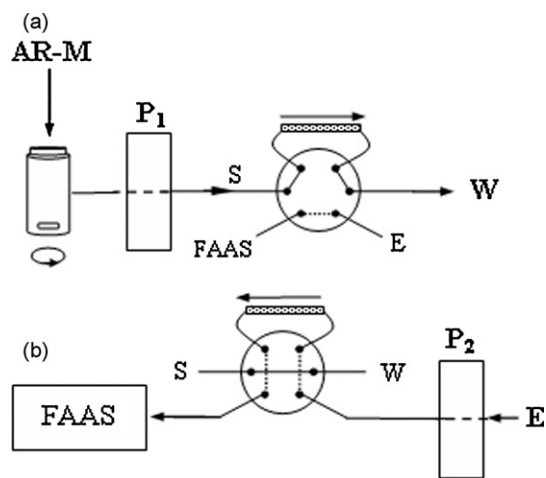


**Fig. 1.** Schematic diagram of the instrumental setup. AR-M: reagents adding and mixing; S: sample and reagents; E: eluent; W: waste; P: peristaltic pump; M: microcolumn; V: load-injection valve. (a) Preconcentration step (load position) and (b) elution step (injection position).

**Table 2**  
Operation sequence for FI on-line preconcentration and separation system.

Step	Time (s)	Valve position	Pump active	Medium pumped	Flow rate (mL min <sup>-1</sup> )	Function
1	10	Fill	P <sub>1</sub>	Buffer-diluted solution	4	pH conditioned
2 (Fig. 1(a))	300	Fill	P <sub>1</sub>	Sample reagent RTIL	4	Load sample
3	10	Fill	P <sub>1</sub>	Buffer-diluted solution	4	Remove sample present in the line, vial and column
4 (Fig. 2)	6	Inject	P <sub>2</sub>	Acidified EtOH	6	Elute analyte into the flame
5	5	Inject	P <sub>2</sub>	Acidified EtOH	6	Remove residual solutions

digestion procedure was followed for all packaging material, 0.5 g of sample was weighted and 5 mL sulfuric acid, 5 mL nitric acid and 5 mL perchloric acid were added in a glass beaker. The mixture was kept boiling on a heating plate for 1 h. The mixture was partially covered with a watch glass to avoid total evaporation. After cooling, the solution was transferred to a 100 mL volumetric flask and diluted to the mark with water. An aliquot of 20 mL of the resulting solution was used for the determination.

#### 2.4. On-line separation and preconcentration procedure

A schematic diagram of the preconcentration and determination system is shown in Fig. 1. The operation sequence for FI on-line preconcentration and separation system is listed in Table 2. In the preconcentration stage (Fig. 1(a)), 20 mL of sample solution, 0.15 mL of 10<sup>-3</sup> mol L<sup>-1</sup> 5-Br-PADAP solution, 0.4 mL of 5% (w/v) Triton X-100, 0.4 mL of 2 mol L<sup>-1</sup> (pH 9.0) buffer solution and 0.7 g of [C<sub>4</sub>mim][PF<sub>6</sub>] were placed in a vial. The resultant system was shaken for about 5 s with a stirring bar before and during the loading of the mixture into the column at a flow rate of 4 mL min<sup>-1</sup>. The RTIL phase containing the Cd–5-Br-PADAP complex was thus retained by the filling material of the column. It has to be pointed out that, before loading, the column was conditioned for preconcentration at the correct pH with a buffer-diluted solution. After loading, further washing with buffer-diluted solution served to remove any sample still present in the lines and in the column. In the elution step (Fig. 1(b)), the injection valve was switched on and the retained RTIL rich-phase was eluted with ethanol acidified with 0.5 mol L<sup>-1</sup> nitric acid at a flow rate of 6 mL min<sup>-1</sup> directly into the nebulizer of FAAS instrument and Cd was determined under the conditions shown in Table 1.

Calibration was performed against aqueous standards submitted to the same preconcentration procedure. Likewise, blank solutions were analyzed in the same manner as standard and sample solutions. For optimizing the preconcentration and determination system, 20 mL of 1 µg L<sup>-1</sup> Cd<sup>2+</sup> standard solution was used instead of the samples.

### 3. Results and discussion

#### 3.1. Column manufacturing and on-line RTIL phase collection

It was supposed that, the high viscosity of the RTIL [C<sub>4</sub>mim][PF<sub>6</sub>] (352.2 mPa s) in combination with a controlled loading flow rate of the RTIL–aqueous mixture through the column, would lead to RTIL phase retention. Therefore, home-made columns packed with a potentially suitable filtering material such as, cotton, polyurethane foam or silica gel [25], were tested to pursue on-line collection and separation of the RTIL phase. For soft filling materials, such as cotton and polyurethane foam, the RTIL phase was not completely retained in the column. In fact, the RTIL phase passed through the cotton fibers or holes in the foam, making difficult its retention. On the other hand, silica gel proved to be highly effective for retention whereas keeping the RTIL phase in a more localized region inside the column. This yielded sharper and well-defined peaks as compared to the other filling materials.

Column design is a critical parameter for defining peak form of transient signals originated in a FI on-line preconcentration system. The sharper the peaks, the higher will be the sensitivity when analyte quantification is performed based on peak height. Therefore, inner diameter and length of the column were important variables to be considered in this work. It was observed that a minimal length of 40 mm was necessary for total RTIL phase retention. Shorter columns did not show good retention as the RTIL phase was not completely entrapped by the filling material. On the other hand, longer columns did not bring further enhancement of the analytical signal and a higher back pressure was generated within the FI system. Another variable considered in the column design was the inner diameter. Thus, a reduced inner diameter was preferred in order to achieve low dispersion of the peak signal. A 2-mm inner diameter was found to be effective for RTIL phase retention.

#### 3.2. Optimization of the loading variables

Several variables were studied in order to optimize Cd–5-Br-PADAP complex formation and extraction, as well as retention of the RTIL phase into the column. Among them, pH, surfactant and chelating agent concentration, RTIL amount and loading flow rate were studied. Additionally, the conditions for suitable elution of the analyte from the column were studied.

The optimal pH values were in the range of 7.8–10.2. This phenomenon is understandable, since the best complexation of Cd with the 5-Br-PADAP reagent occurs within this range [20,23]. According to these results, the selected pH was 9.0. The minimum reagent to metal ion molar ratio necessary to reach the optimum response was 100. Above this ratio, no variation in the analytical response was observed. Therefore, a 150 5-Br-PADAP to metal ion molar ratio was selected for further work. It corresponds to 7.5 × 10<sup>-6</sup> mol L<sup>-1</sup> 5-Br-PADAP concentration.

In order to avoid the precipitation of the complexing agent and Cd–5-Br-PADAP complex in aqueous medium prior to the extraction, Triton X-100 was added to the sample solution. Moreover, the surfactant also reduced the adherence of the RTIL on the inner walls of the tubes, thus improving the flowing ability of the RTIL throughout the FI system and forcing the sole retention into the column. In the presence of a non-ionic surfactant such as Triton X-100, the fine droplets of RTIL are surrounded by their molecules. Hence, RTIL interactions with the inner walls of the lines decrease and consequently, RTIL phase do not stick on it [26]. Although the presence of a surfactant facilitates the flowing of the RTIL phase, it can negatively affect the retention of the RTIL phase by the filling material of the column. Therefore, the effect of Triton X-100 on Cd–5-Br-PADAP extraction and later RTIL phase retention into the column was studied within a surfactant concentration range of 0.01–2.0% (w/v). This study showed that both the complexing agent and the metallic complex remained in solution within range studied. A 0.1% (w/v) surfactant concentration was chosen for further work as yielded high extraction efficiency while keeping the complex in solution (Fig. 2). Higher surfactant concentrations led to inefficient retention into the column, and hence non-reproducible results. Moreover, the greatest analyte enhancement factor was reached at 0.1% (w/v) surfactant concentration.

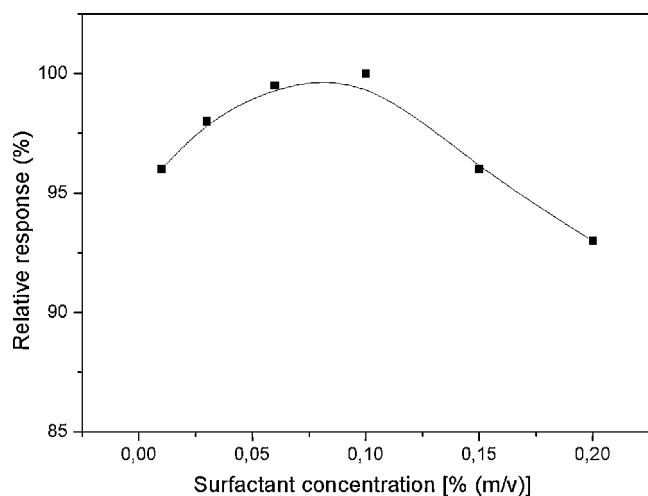


Fig. 2. Effect of Triton X-100 concentration on the efficiency of the preconcentration system. Experimental conditions are listed in Table 1.

Optimization of the minimal sample volume required to be injected into FI-FAAS is crucial in order to reach a suitable response. Therefore, it is highly important to establish the minimal volume of RTIL that leads to total complex extraction while achieving the highest signal. The variation of the analyte signal upon the RTIL amount was examined within the range: 0.4–1.2 g. It was observed that the extraction efficiency of the system and the signal were remarkably affected by the RTIL amount. Quantitative extraction and higher signal was observed for a minimal RTIL amount of 0.6 g. No significant changes were observed on the extraction efficiency by adding higher RTIL amounts. On the other hand, it was considered the effect of RTIL amount on the retention capacity of the column. Experiments performed with different RTIL amounts showed that effective retention of the phase was achieved up to 0.7 g RTIL. A significant reduction in the RTIL retention was observed for higher RTIL amounts. Thus, in order to achieve the best enhancement factor, 0.7 g RTIL amount was chosen as optimal. Under these conditions, a final RTIL volume of 500  $\mu\text{L}$  was obtained.

The sample flow rate through the column is an important parameter, since this is one of the steps that controls the time of analysis. Moreover, the effect of sample flow rate through the column was a critical variable to achieve high retention of the RTIL phase. The influence of the sample loading flow rate on the analytical response was not critical between 1 and 5  $\text{mL min}^{-1}$ . The response decreased at flow rate values higher than 5  $\text{mL min}^{-1}$ , and even none retention of the RTIL phase was observed when the flow rate was as high as 20  $\text{mL min}^{-1}$ . This phenomenon allows us to state that retention of the RTIL phase into the column is mainly produced due to a filtering-like process, rather than a chemical one. In fact, the high viscosity of the RTIL  $[\text{C}_4\text{mim}][\text{PF}_6]$  could be the main reason for allowing the sample to pass through the ionic liquid plug and the column [27]. The capacity of retention of the column was 90%. The dependence of the percent of recovery of Cd on sample loading flow rate is shown in Fig. 3. A flow rate of 4  $\text{mL min}^{-1}$  was chosen for further work.

### 3.3. Elution of the RTIL phase from the column

To elute the RTIL phase retained within the column, a group of solvents miscible with  $[\text{C}_4\text{mim}][\text{PF}_6]$  were studied. Therefore, common organic solvents such as ethanol, methanol, and acetone were chosen. The selection of these solvents was made based on the high solubility that  $[\text{C}_4\text{mim}][\text{PF}_6]$  shows in these media [28–30]. Both acetone and ethanol resulted to be the most effective for RTIL phase and Cd–5-Br-PADAP complex removal from the column. However,

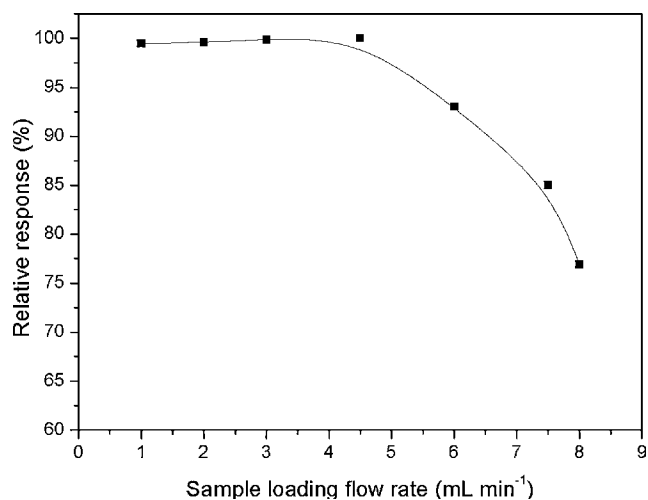


Fig. 3. Dependence of recovery of Cd on loading sample flow rate. Experimental conditions are listed in Table 1.

it was preferred ethanol to acetone due to major compatibility of the alcohol with tubes and valve materials used in the FI system. Likewise, sharper peaks were observed with ethanol. Finally, the eluent was acidified with nitric acid in order to induce dissociation of Cd–Br-PADAP complex and further releasing of Cd into solution. A nitric acid concentration of 0.5  $\text{mol L}^{-1}$  was chosen.

The effect of flow rate of eluent on analyte signal is shown in Fig. 4. As can be seen, the optimum flow rate of eluent was 6  $\text{mL min}^{-1}$ . Therefore, the elution flow rate was compatible with the aspiration flow of the FAAS instrument [31]. Additionally, elution of the analyte through the column was developed in counter-current, which was especially favorable to obtain sharp and well-defined peaks.

The combination of  $[\text{C}_4\text{mim}][\text{PF}_6]$  with other “green” solvent such as ethanol, avoided the use of hazardous toxic and flammable solvents, while increasing FAAS sensitivity with respect to an aqueous solvent. The analyte was completely eluted from the column in 6 s.

### 3.4. Extraction and analytical performance

An extraction percentage higher than 99.9% was achieved when the procedure was carried out under the optimal experimental con-

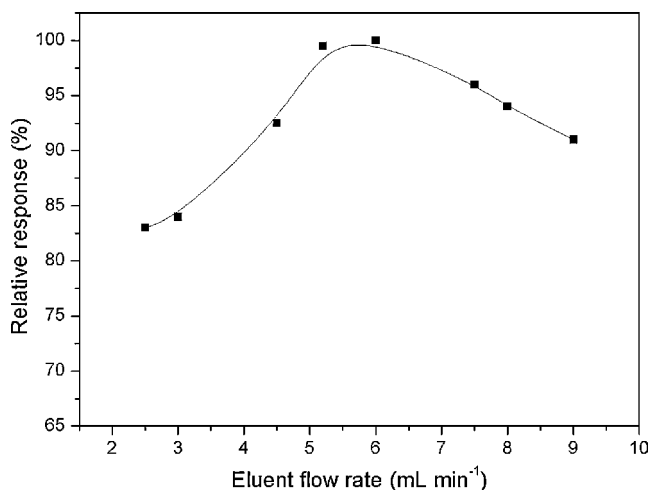


Fig. 4. Dependence of recovery of Cd on elution flow rate. Experimental conditions are listed in Table 1.

**Table 3**  
Accuracy of the proposed method (95% confidence interval;  $n = 6$ ).

Sample	Base value ( $\mu\text{g L}^{-1}$ )	Quantity of $\text{Cd}^{2+}$ added ( $\mu\text{g L}^{-1}$ )	Quantity of $\text{Cd}^{2+}$ found ( $\mu\text{g L}^{-1}$ )	Recovery (%) <sup>a</sup>
PET	1.0	–	$1.0 \pm 0.08$	–
	1.0	5	$6.1 \pm 0.29$	102
	1.0	10	$11.1 \pm 0.47$	101
HDPE	0.61	–	$0.61 \pm 0.06$	–
	0.61	5	$5.7 \pm 0.32$	102
	0.61	10	$10.5 \pm 0.45$	99
PVC	25.0	–	$25.0 \pm 0.98$	–
	25.0	5	$30.0 \pm 1.29$	100
	25.0	10	$35.1 \pm 1.45$	101
LDPE	0.55	–	$0.55 \pm 0.06$	–
	0.55	5	$5.45 \pm 0.37$	98
	0.55	10	$10.5 \pm 0.49$	100
PP	0.70	–	$0.68 \pm 0.07$	–
	0.70	5	$5.6 \pm 0.28$	98
	0.70	10	$10.6 \pm 0.44$	99
PS	1.1	–	$1.1 \pm 0.10$	–
	1.1	5	$6.1 \pm 0.31$	100
	1.1	10	$11.3 \pm 0.49$	102

<sup>a</sup>  $100 \times [(\text{Found} - \text{base})/\text{added}]$ .

ditions (Table 1). The obtained enhancement factor for a sample volume of 20 mL was 35. The enhancement factor was obtained as the ratio of the slopes of the calibration curves for Cd with and without the preconcentration step.

The relative standard deviation (R.S.D.) resulting from the analysis of 10 replicates of 20 mL solution containing  $10 \mu\text{g L}^{-1}$   $\text{Cd}^{2+}$  was 3.9%. The calibration graph was linear with a correlation coefficient of 0.9998 at levels near the detection limits and up to at least  $50 \mu\text{g L}^{-1}$ . The regression equation was  $A = 0.0219C + 0.007$ , where  $A$  is the absorbance and  $C$  is the concentration of Cd in  $\mu\text{g L}^{-1}$ . The limit of detection (LOD), calculated based on three times the standard deviation of the background signal ( $3\sigma$ ), was  $6 \text{ ng g}^{-1}$ . The frequency of analysis was nine samples per hour.

### 3.5. Accuracy of the method and cadmium determination in real samples

To demonstrate the accuracy of the proposed method, a recovery study was performed evaluating any matrix interferences and/or possible analyte losses during the sample pre-treatment of different food packaging materials: PET, HDPE, PVC, LDPE, PP and PS. Thus, the method was applied to six portions of 0.5 g for each plastic material. All the samples were digested and analyzed following the procedure described before. The average concentration of Cd found was taken as a base value. Then, increasing quantities of Cd were added to the other aliquots of sample and the analyte was determined by the same method. As shown in Table 3, analyte recoveries were all around 100%.

The method was applied for Cd determination in different food packaging plastic materials collected from the local market. Cadmium concentrations were in the range of n.d.– $0.20 \text{ mg kg}^{-1}$  for PET; n.d.– $0.12 \text{ mg kg}^{-1}$  for HDPE;  $5.1$ – $10.4 \text{ mg kg}^{-1}$  for PVC; n.d.– $0.11 \text{ mg kg}^{-1}$  for LDPE; n.d.– $0.14 \text{ mg kg}^{-1}$  for PP and n.d.– $0.22 \text{ mg kg}^{-1}$  for PS, at 95% confidence interval ( $n = 6$ ). The proposed method was also validated by comparison of the results obtained by a different technique (Table 4). Determinations by ETAAS were performed by measuring direct aliquots of the digested samples. This was possible due to the low LOD that are possible to reach for Cd with ETAAS. The results were compared by applying the  $F$ -test and no significant differences at the 95% confidence level were observed.

**Table 4**  
Concentration of Cd in food packaging materials (95% confidence interval;  $n = 6$ ).

Sample	Proposed method ( $\text{mg kg}^{-1}$ )	ETAAS ( $\text{mg kg}^{-1}$ )
PET	$0.05 \pm 0.01$	$0.07 \pm 0.01$
	$0.20 \pm 0.02$	$0.19 \pm 0.02$
	n.d. <sup>a</sup>	n.d. <sup>a</sup>
HDPE	$0.12 \pm 0.01$	$0.12 \pm 0.01$
	n.d. <sup>a</sup>	n.d. <sup>a</sup>
	n.d. <sup>a</sup>	n.d. <sup>a</sup>
PVC	$5.1 \pm 0.22$	$5.1 \pm 0.32$
	$10.4 \pm 0.42$	$10.5 \pm 0.51$
	$8.4 \pm 0.40$	$8.4 \pm 0.49$
LDPE	$0.05 \pm 0.01$	$0.07 \pm 0.01$
	$0.11 \pm 0.02$	$0.14 \pm 0.02$
	n.d. <sup>a</sup>	n.d. <sup>a</sup>
PP	n.d. <sup>a</sup>	n.d. <sup>a</sup>
	$0.09 \pm 0.01$	$0.10 \pm 0.01$
	$0.14 \pm 0.02$	$0.12 \pm 0.01$
PS	$0.22 \pm 0.03$	$0.21 \pm 0.03$
	$0.04 \pm 0.01$	$0.05 \pm 0.01$
	n.d. <sup>a</sup>	n.d. <sup>a</sup>

<sup>a</sup> Non-detectable.

## 4. Conclusion

In this work, an original FI system with on-line RTIL phase separation coupled to FAAS detection for Cd determination in plastic materials is proposed. Thus, the excellent extraction efficiency associated with RTILs in combination with the possibility of performing an on-line procedure opens up an attractive alternative in the area of automated separation and preconcentration methodologies. The on-line retention of the RTIL phase by using a silica gel-packed column simplifies the preconcentration methodology while reducing manual operation and risk of contamination. Furthermore, the effect of several variables, including physical, chemical and hydrodynamic characteristics, on the on-line retention of the RTIL phase has been studied. A sensitivity enhancement factor of 35 was achieved. The use of the 5-Br-PADAP–[C<sub>4</sub>mim][PF<sub>6</sub>] extraction system allowed the reliable and accurate determination of Cd in food packaging material.

## Acknowledgements

This work was supported by Consejo Nacional de Investigaciones Científicas y Técnicas (CONICET) and Agencia Nacional de Promoción Científica y Tecnológica (FONCYT) (PICT-BID) (FONTAR – NO PMT II – CAI/073) (Argentina).

## References

- [1] K. Marsh, B. Bugusu, *J. Food Sci.* 72 (2007) R39.
- [2] A.W. Birley, *Food Chem.* 8 (1982) 81.
- [3] D.O. Hummel, *Atlas of Plastics Additives—Analysis by Spectrometric Methods*, Springer, Germany, 2002.
- [4] I.D. Rosca, J.M. Vergnaud, *Polym. Test* 25 (2006) 532.
- [5] D. Thompson, S.J. Parry, R. Benzing, *J. Radioanal. Nucl. Chem.* 213 (1996) 349.
- [6] M.W. Kadi, *Asian J. Chem.* 17 (2005) 40.
- [7] W. Shotyky, M. Krachler, *Environ. Sci. Technol.* 41 (2007) 1560.
- [8] A. Ritter, E. Michel, M. Schmid, S. Affolter, *Polym. Test* 23 (2004) 467.
- [9] R.B. Hayes, *Cancer Causes Contr.* 8 (1997) 371.
- [10] T. Nawrot, M. Plusquin, J. Hogervorst, H.A. Roels, H. Celis, L. Thijs, J. Vangronsveld, E. Van Hecke, J.A. Staessen, *Lancet Oncol.* 7 (2006) 119.
- [11] H. Sakurai, J. Noro, A. Kawase, M. Fujinami, K. Oguma, *Anal. Sci.* 22 (2006) 225.
- [12] E. Skrzydlewska, M. Balcerzak, *Chem. Anal. Wars.* 48 (2003) 909.
- [13] F. Kubota, M. Goto, *Solvent Extr. Res. Dev.* 13 (2006) 23.
- [14] Z. Li, J. Chang, H. Shan, J. Pan, *Rev. Anal. Chem.* 26 (2007) 109.
- [15] G. Singh, A. Kumar, *Indian J. Chem. A* 47 (2008) 495.
- [16] H. Zhao, S. Xia, P. Ma, *J. Chem. Technol. Biotechnol.* 80 (2005) 1089.
- [17] J.F. Liu, G.B. Jiang, J.A. Jönsson, *TrAC, Trends Anal. Chem.* 24 (2005) 20.

- [18] S. Pandey, *Anal. Chim. Acta* 556 (2006) 38.
- [19] M.A. Taher, A. Mostafavi, S.Z.M. Mobarake, D. Afzali, *Bull. Chem. Soc. Ethiopia* 20 (2006) 1.
- [20] R.F. Lara, R.G. Wuilloud, J.A. Salonia, R.A. Olsina, L.D. Martinez, *Anal. Bioanal. Chem.* 371 (2001) 989.
- [21] P.R. Aranda, R.A. Gil, S. Moyano, I.E. De Vito, L.D. Martinez, *Talanta* 75 (2008) 307.
- [22] J.C.A. De Wuilloud, R.G. Wuilloud, M.F. Silva, R.A. Olsina, L.D. Martinez, *Spectrochim. Acta, Part B* 57 (2002) 365.
- [23] E.M. Martinis, R.A. Olsina, J.C. Altamirano, R.G. Wuilloud, *Anal. Chim. Acta* 628 (2008) 41.
- [24] S. Carda-Broch, A. Berthod, D.W. Armstrong, *Anal. Bioanal. Chem.* 375 (2003) 191.
- [25] J. Nan, Y. Jiang, X.P. Yan, *J. Anal. At. Spectrom* 18 (2003) 946.
- [26] M. Baghdadi, F. Shemirani, *Anal. Chim. Acta* 613 (2008) 56.
- [27] M. Cruz-Vera, R. Lucena, S. Cárdenas, M. Valcárcel, *J. Chromatogr. A* 1202 (2008) 1.
- [28] K.A. Fletcher, S. Pandey, *J. Phys. Chem. US* 107 (2003) 13532.
- [29] J. Zhang, W. Wu, T. Jiang, H. Gao, Z. Liu, J. He, B. Han, *J. Chem. Eng. Data* 48 (2003) 1315.
- [30] M.T. Zafarani-Moattar, R. Majdan-Cegincara, *J. Chem. Eng. Data* 52 (2007) 2359.
- [31] H. Chen, J. Liu, X. Mao, *Anal. Chim. Acta* 370 (1998) 151.



## Anti-fouling characteristics of surface-confined oligonucleotide strands bioconjugated on streptavidin platforms in the presence of nanomaterials

Mònica Mir<sup>a,b,\*</sup>, Petra J. Cameron<sup>c</sup>, Xinhua Zhong<sup>d</sup>, Omar Azzaroni<sup>a,e,\*</sup>, Marta Álvarez<sup>a</sup>, Wolfgang Knoll<sup>a</sup>

<sup>a</sup> Max-Planck-Institut für Polymerforschung, Ackermannweg, 10, 55128 Mainz, Germany

<sup>b</sup> Nanobioengineering Group, Institute for Bioengineering of Catalonia (IBEC), Josep Samitier 1-5, 08028 Barcelona, Spain

<sup>c</sup> Department of Chemistry, University of Bath, Bath BA2 7AY, United Kingdom

<sup>d</sup> Department of Chemistry, East China University of Science and Technology, 200237 Shanghai, China

<sup>e</sup> INIFTA-CONICET-UNLP, C.C. 16 Suc. 4 (1900) La Plata, Argentina

### ARTICLE INFO

#### Article history:

Received 10 October 2008

Received in revised form 8 January 2009

Accepted 14 January 2009

Available online 23 January 2009

#### Keywords:

Anti-fouling

Non-specific binding

DNA biosensor

Streptavidin SAM

Surface plasmon fluorescence spectroscopy (SPFS)

Surface acoustic wave (SAW)

Quantum dots (QDs)

Surface plasmon resonance (SPR)

CdSe nanoparticles

Thiol-biotin

### ABSTRACT

This work describes our studies on the molecular design of interfacial architectures suitable for DNA sensing which could resist non-specific binding of nanomaterials commonly used as labels for amplifying biorecognition events. We observed that the non-specific binding of bio-nanomaterials to surface-confined oligonucleotide strands is highly dependent on the characteristics of the interfacial architecture. Thiolated double stranded oligonucleotide arrays assembled on Au surfaces evidence significant fouling in the presence of nanoparticles (NPs) at the nanomolar level. The non-specific interaction between the oligonucleotide strands and the nanomaterials can be sensitively minimized by introducing streptavidin (SAv) as an underlayer conjugated to the DNA arrays. The role of the SAv layer was attributed to the significant hydrophilic repulsion between the SAv-modified surface and the nanomaterials in close proximity to the interface, thus conferring outstanding anti-fouling characteristics to the interfacial architecture. These results provide a simple and straightforward strategy to overcome the limitations introduced by the non-specific binding of labels to achieve reliable detection of DNA-based biorecognition events.

© 2009 Elsevier B.V. All rights reserved.

### 1. Introduction

The fields of nanobiotechnology and nanomedicine are becoming increasingly important in research and industry. Within this growing research field, the ability to control the adsorption of biomolecules, nanomaterials and bio-inorganic hybrids to solid supports plays a key role in achieving reliable and competitive devices. For example, deposition of proteins, cells or bacteria on the surface of an implant or an *in vivo* biosensor usually leads to failure of these devices [1]. Health problems can be caused due to surface-fouling by microorganisms during the food preparation process. Electrochemical analysis is also affected by the adsorption of biomolecules on the surface, where the unwanted molecules result in the passivation of the electrode surface [2]. The diffusion of reagents in devices containing microfluidic circuits can change

drastically if the surface of the channels is affected by fouling [3]. The undesirable non-specific adsorption of different materials on surfaces must be eliminated in effective biosensors as it leads to a reduction in the sensitivity and specificity of the device. For applications such as biosensing, affinity chromatography, biocatalysis or microfluidics it is important not only to build a non-fouling surface, but also to have suitable recognition sites on the non-fouling surface in order to attach specific ligands with desired orientation and coverage, and to ensure a reproducible and reliable response. Thus, the molecular design of a biosensing platform that exhibits: (a) a reproducible and stable surface with resistance to non-specific binding and (b) good control over ligands immobilization is not a trivial task as is of high priority in biosensing community.

Within the great variety of biosensing platforms, of particular relevance is that one concerning to the detection of DNA hybridization. The most common interfacial architecture consists of monolayers of thiolated oligonucleotide probes assembled on gold surfaces forming a brush-like layer [4–6]. However, during last years the use of streptavidin (SAv) as an anchoring layer received increasing attention [7,8]. This is due to the fact that the SAv platform

\* Corresponding author at: Institute for Bioengineering of Catalonia (IBEC), Josep Samitier 1-5, 08028 Barcelona, Spain.

E-mail address: [mmir@ibec.pcb.uib.es](mailto:mmir@ibec.pcb.uib.es) (M. Mir).

enables an optimized distribution and spacing of the probe strands on the Au electrode, thus facilitating the hybridization process. Moreover, depending on the characteristics of the read out system, it is a common practice to use labeled-biomolecules, enzymes, fluorophores or nanoparticles (NPs) to enhance the detection of the biorecognition process [9].

Fluorescence-based transduction is probably one of the most sensitive strategies to detect DNA or oligonucleotide hybridization. Quantum dots (QDs) are nanomaterials that represent a very interesting type of fluorescent nanoparticles [10]. At present, they constitute the greatest promise as labels in fields like biosensing or biological imaging [10]. This is based on their remarkable photostability, high fluorescence yield, low rates of photobleaching and extinction coefficients comparable to conventional organic fluorophores, which render them outstanding candidates for fluorescent labeling of biomolecules. In spite of the widespread use of QDs combined with DNA in biosensing [11] and design of functional materials [12], little is known about the interaction and non-specific binding interactions between these nanomaterials and oligonucleotide strands at solid-liquid interfaces.

In this work we studied with particular emphasis the non-specific adsorption of QDs on surface-confined oligonucleotide strands formed by assembly of thiolated strands and by bioconjugation of biotinylated strands on SAV platforms. Our studies show notable differences between both platforms, indicating that the commonly used thiolated DNA assemblies are prone to non-specific binding of QDs. In contrast, the SAV-based did not evidence any non-specific adsorption of the nanomaterials. These results were also extended to the use of biomolecules, like streptavidin, as labels obtaining similar differences between both platforms.

## 2. Experimental

### 2.1. Materials

The oligonucleotide sequences; 18-mer thiol labeled capture probe (SH-C<sub>6</sub>-5'-TTTTGTACATCACA-3'), 18-mer biotinylated capture probe (biotin-5'-TTTTGTACATCACA-3') and 15-mer target (5'-TAGTTGTGATGTACA-3') used in this work were purchased from MWG Biotech AG. All stock oligonucleotide solutions were 100  $\mu$ M prepared with milliQ water and stored at -20 °C. Streptavidin, mercaptoundecanol, 2-mercaptoethanol, phosphate buffered saline, polyethylene glycol sorbitan monolaurate (tween 20), trioctylphosphine (TOP), oleylamine, oleic acid, 1-octadecene (ODE), CdO, Se powder and 3-mercaptopropionic acid (MPA) were purchased from Sigma. Biotin-terminated thiol was obtained from Roche Diagnostics.

### 2.2. Synthesis of MPA-Capped CdSe nanoparticles

Oil-soluble CdSe nanoparticles were prepared according to a literature method [13]. Typically, 5.0 mL of oleylamine and 0.15 mL of Se stock solution (2.1 M in TOP) were loaded in a 50 mL three neck round-bottom flask, and the mixture was heated to 300 °C in a flow of argon. 1.0 mL of Cd stock solution (0.3 M, obtained by dissolving CdO in 6-fold of oleic acid and ODE at elevated temperature) was injected quickly into the reaction flask. The temperature was then set at 280 °C for the subsequent growth and annealing of nanocrystals. After completion of particle growth, the reaction mixture was allowed to cool to ~60 °C, and 10 mL of methanol was added. The obtained CdSe nanocrystals were precipitated by adding methanol into the toluene solution and further isolated and purified by repeated centrifugation and decantation. MPA-Capped water-soluble QDs were obtained by a ligand replacement reaction [14]. Due to the carboxylic group in the MPA

ligand, the obtained MPA-capped CdSe QDs are negative charged in aqueous solutions. The mean size of the CdSe QDs used for the following experiment is  $\sim 4.5 \pm 0.3$  nm with emission wavelength  $\lambda = 620$  nm.

### 2.3. Biomolecules immobilization

Both interfacial architectures involving thiolated oligonucleotides (DNA-SH) and biotinylated oligonucleotides bioconjugated on SAV monolayers (DNA-SAV) were assembled onto gold surfaces. The DNA-SH architecture was prepared by incubating the gold films in a 1  $\mu$ M solution of thiolated capture probe in 1 M KH<sub>2</sub>PO<sub>4</sub> for 2 h, the slide then was placed in a 1 mM solution of mercaptoethanol in milliQ water for 1 h to backfill any empty spaces between the capture probe strands. It is worth mentioning that the backfilling also improves the orientation of the oligonucleotide strands leading to an improvement of the hybridization process.

The DNA-SAV architectures were constructed by chemisorbing a mixed self-assembled monolayer of 12-mercaptododecanoic (-8-biotinoylamido-3,6-dioxaoctyl)amide and 11-mercapto-1-undecanol in ethanol in a 1:9 ratio [15]. Then, the biotinylated surface was incubated in a 1  $\mu$ M streptavidin solution in 10 mM PBS, 100 mM NaCl at pH 7.4, leading to a compact monolayer evenly distributed on the Au surface [16,17]. Considering that SAV has unique properties as an adapter for the binding of a second layer of biotinylated molecules and the extremely high and very specific interaction with biotin ( $K = 10^{15}$  L mol<sup>-1</sup>), the resulting protein layer acts as stable platform for supramolecularly anchoring the biotinylated capture probes. Both surface architectures were hybridized with a 1  $\mu$ M ss-DNA target solution and afterwards 1  $\mu$ M solution of streptavidin or QDs respectively were left to interact with both platforms in order to investigate the effect of non-specific binding.

In both platforms, the unbounded molecules on the surface sensor were rinsed away after each immobilization step with the buffer used in the immobilization step.

### 2.4. Surface acoustic wave (SAW) measurements

The non-specific adsorption of SAV on both platforms was measured by acoustic wave sensor spectroscopy (SAW) (S-sens<sup>®</sup> k5, Nanofilm Surface Analysis). The sensor chip array consists of five gold sensors with a sensing area of 6.3 mm<sup>2</sup> each. The chips were cleaned before use by plasma treatment for 5 min at 300 W under argon atmosphere. All incubations were programmed and injection was done automatically at a flow rate of 20  $\mu$ L min<sup>-1</sup>. After each experiment an injection of 5% glycerol solution was required for calibration purposes [18].

### 2.5. Surface plasmon fluorescence spectroscopy (SPFS)

The binding of QDs on both interfacial architectures was monitored by surface plasmon fluorescence spectroscopy (SPFS) [19–21]. Laser light at  $\lambda = 594.6$  nm was used to excite surface plasmons in the gold film (coupled in the Kretschmann configuration). The QDs located near the gold–dielectric interface can be excited by the surface plasmon that propagates along this interface. Photons emitted from the QDs were monitored with a photomultiplier. To avoid collection of scattered and transmitted laser light, a  $\lambda = 611$  nm narrow band pass filter was placed in front of the photomultiplier. The sensor chip was a ~50 nm evaporated gold film on BK7 glass with ~2 nm of chromium being evaporated just prior to the gold deposition to improve adhesion between the gold and glass. All incubations were done at a flow rate of 20  $\mu$ L min<sup>-1</sup>.



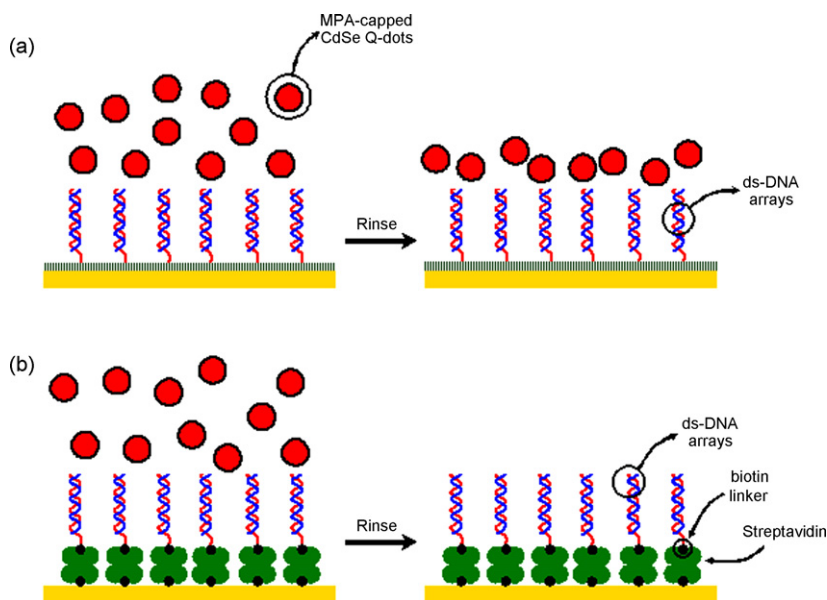


**Fig. 1.** Simplified cartoon describing the interaction of the CdSe QDs with both interfacial architectures: (a) thiolated oligonucleotide strands, DNA-SH; (b) biotinylated oligonucleotide strands assembled on streptavidin platforms, DNA-SAv.

### 3. Results and discussion

Our experimental studies were carried out in two different interfacial architectures: (a) thiolated oligonucleotides (DNA-SH) and (b) biotinylated oligonucleotides bioconjugated on SAV monolayers (DNA-SAv) (Fig. 1).

The non-specific binding of QDs on both platforms was measured by SPFS. The binding curves in Fig. 2 display the striking differences between both interfacial architectures. The injection of the MPA-capped CdSe QDs into the SPFS chamber containing the DNA-SAv platform is evidenced as an increase in the fluorescence signal,  $\sim 1.5 \times 10^6$  cps. This is as a consequence of the excitation of the QDs in the surroundings of the solid–liquid interface [22]. The fluorescence signal was monitored over a period of 1 h displaying good stability after the injection. This fact indicates that the maximum concentration of QDs is achieved during the early stages of the immobilization and no significant changes in the population of QDs occur in the surroundings of the interface. Thereafter, the sensor surface was rinsed by flushing buffer solution through the SPFS chamber. Immediately, the fluorescence signal decayed to the original background signal obtained prior to injecting the

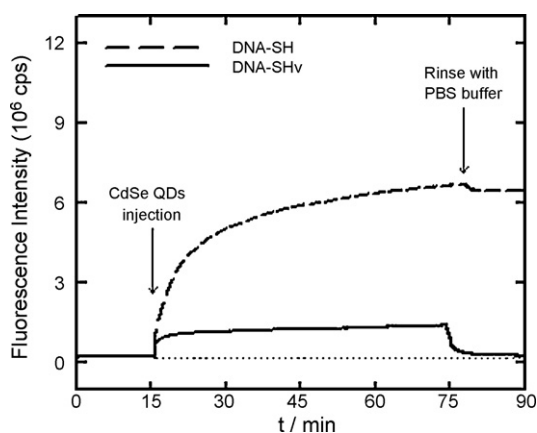


**Fig. 2.** Surface plasmon fluorescence spectroscopy sensorgrams describing the binding of the CdSe QDs to the DNA-SH (dashed line) and DNA-SAv (solid line) platforms.

QDs-containing solution, thus giving a clear indication that the interfacial architecture is not fouled by the nanoparticles.

A different scenario was observed when the same experiment was repeated in the presence of the DNA-SH. After injecting the MPA-capped CdSe QDs into the SPR chamber, the fluorescence signal evidenced a continuous increase reaching values larger than those previously obtained in the presence of DNA-SAv,  $\sim 6.5 \times 10^6$  cps. Rinsing the sensor surface with buffer only promoted a slight change in the fluorescence signal, evidencing that most of the fluorescent nanomaterials remained at the interface, and consequently the sensor surface was heavily fouled by the CdSe QDs.

In principle, this experimental observation is counterintuitive. The hybridized oligonucleotide strands on the DNA-SH/Au platform represent a negatively charged interface where the phosphate groups are responsible for the anionic charges. The interaction with the negatively charged QDs should be repulsive, thus leading to a facile removal of the nanomaterials after rinsing. The experimental evidence indicates the opposite case, where the dominant interactions between the oligonucleotides and the nanoparticles are attractive. This observation is in line with recent results reported by Sandström et al. [23] working on the non-specific binding of citrate-stabilized Au nanoparticles to double stranded oligonucleotides. These authors reported a detailed study describing how negatively charged nanoparticles significantly bind non-specifically to double stranded DNA. Even if the non-specific binding of single-stranded oligonucleotides to Au nanoparticles has been reported by Mirkin and co-workers [24], the case involving double stranded oligonucleotides is a completely different scenario. Single stranded DNA binds non-specifically to flat Au surfaces and Au NPs by means of interactions provided by their bases. However, in the case of double stranded DNA these functional groups are not available for interacting with the nanomaterials. One explanation for this interesting phenomenon was proposed by Sandström et al. [23] suggesting that a possible mechanism could be ion-induced dipole dispersive interactions, where the negatively charged phosphate groups on the DNA induce dipoles in the highly polarizable NPs. This fact would explain why the CdSe QDs remain at a large extent on the sensor surface.

Another possible reason for the non specific adsorption of these negatively capped QDs on the negative DNA surface is the existence

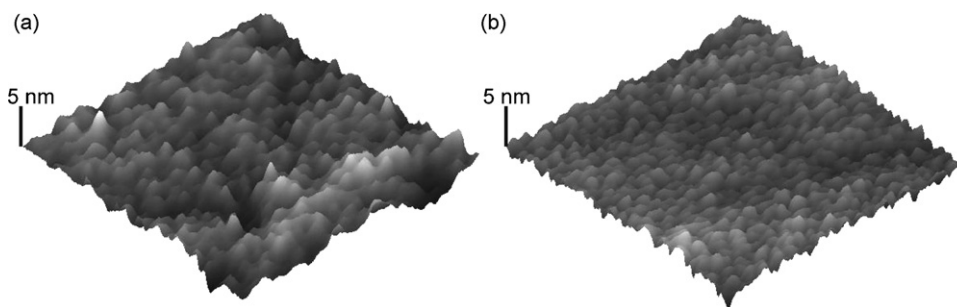


Fig. 3. . 500  $\mu\text{m} \times 500 \mu\text{m}$  AFM topography images for the DNA SAM (a) and SA SAM (b) platforms.

of holes in the DNA layer film, which allow the penetration of these molecules in lower charge repulsion areas. Previous studies carried out with these two sensor platforms showed a higher capture probe packing in the system with the DNA directly immobilised on the surface. In the DNA SAM configuration a surface coverage of  $0.05 \text{ mol mm}^{-2}$  was reported, while in the SA SAM configuration lower capture probe coverage of  $0.035 \text{ mol mm}^{-2}$  was detected. However, the number of target molecules hybridised in the SA SAM system is higher comparing with the hybridisation in the DNA SAM platform. The lower hybridization efficiency of the DNA SAM platform was explained as a consequence of the high capture probe density in this system, which hindrance the access of the target to the probe [25]. These results show a highly packed DNA SAM platform, where is improbable to find holes on the film. In order to assure the lack of defects on both platforms, where the molecules could non specifically be adsorbed, surface topographic studies of both platforms were carried out with AFM. Simultaneous tapping mode topographic and phase imaging were carried out on modified gold mica substrates. Different distribution of the biomolecules on the surface was observed by comparing the phase images of both systems (Fig. 3). However, in both surfaces no holes were observed on the film, showing uniform and homogeneous distribution of the biomolecules on the surface.

On the other hand, we also observed that double stranded oligonucleotide brushes presenting SAV as an underlying platform describe a completely different interfacial behavior, i.e. no binding is observed. Considering the similarities and differences between both platforms it is plausible to ascribe these non-fouling characteristics to the presence of SAV in the interfacial architecture. Recently, van Oss and co-workers [26] discussed the macroscopic-scale surface properties of SAV and their influence on the non-specific interactions with biopolymers. The use of SAV-coated glass substrates presenting a high surface hydrophobicity prevented the fouling of biomolecules like immunoglobulins (IgG) or human serum albumin (HSA). The hydrophilic repulsion between the planar SAV-coated surface and the IgG or HSA precluded the non-specific binding to the surface, to which biotinylated molecules can be easily and firmly attached. In accordance to van Oss et al., this anti-fouling behavior is governed by (non-electrostatic) polar macroscopic-scale hydrophilic repulsion between the SAV-coated surface and the biomolecules. In our case, the SAV underlayer would confer similar properties to the interfacial architecture, where a strong hydrophilic repulsion would prevent the non-specific binding of the nanomaterials.

To further extend of use of the SAV underlayer in DNA sensing platforms we studied the interfacial behavior of SAV molecules in solution interacting with DNA-SH and DNA-SAV. The reason for choosing SAV interacting with the different sensor architectures lies in the fact that it is commonly used as a linker for labeling biotinylated oligonucleotides [27–29] and, in some cases, it has been reported that it non-specifically binds to different substrates [30]. These interfacial studies were carried out using an acous-

tic waveguide device (SAW) [31–34]. The principle of operation of SAW is based on an electric potential applied to a piezoelectric substrate via interdigitated transducers which creates a surface-localized acoustic wave. The phase and amplitude of the surface wave are monitored with time through electrical connections to the output transducers. All sensing occurs within an interfacial region where significant acoustic displacement is detected. This is given by the thickness of the penetration depth which is a function of the viscosity of the surface medium and operating frequency of the device. In particular, phase response is very sensitive to both mass and viscoelastic properties and is commonly the parameter of choice for monitoring the immobilization of biomolecules [35].

Fig. 4 shows the SAW sensorgrams for  $1 \mu\text{M}$  SAV in contact with both interfacial architectures forming brush-like oligonucleotide assemblies at the solid-liquid interface. The DNA-SH assembly described a sudden increase in phase signal after injecting the SAV solution into the chamber. After 10 min the sensor surface was flushed with PBS buffer and the SAW device monitored only a slight decrease in phase signal. This fact evidences that the proteins remain in the surroundings of the interfacial region (within the penetration depth) where the SAW detects their presence. In other words, the DNA-SH interface is sensitively fouled in contact with the proteins.

The same experiment with the DNA-SAV sensor displayed a significant increase in phase signal, larger that in the case of DNA-SH. This could be attributed to the fact that the DNA-SAV sensor presents an interfacial architecture that could be more sensitive to interfacial viscoelastic changes. Phase changes are extremely sensitive to viscous water and mass loading, which are determined by the characteristics of the interfacial architecture [31].

After rinsing with buffer the phase values returned to approximately the original background signal obtained before injecting the

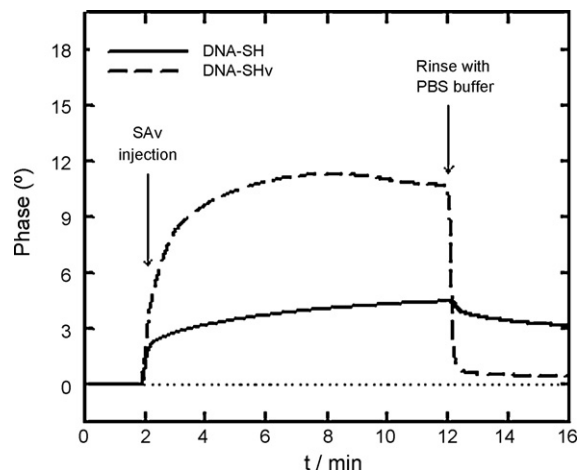


Fig. 4. . Phase response of the surface acoustic wave device monitoring the binding of the CdSe QDs to the DNA-SAV (dotted line) and DNA-SH (solid line) platforms.

SAv solution, thus indicating that the DNA-SAv sensor surface was not fouled by the biomolecules. These results are in agreement with the experimental results obtained working with negatively charged QDs where the presence of the SAv underlayer confers outstanding non-fouling properties to the sensor surface.

#### 4. Conclusions

The goal of our work was to investigate new strategies for designing DNA sensing interfaces which could resist non-specific binding of bio-nanomaterials commonly used as labels. These results evidence the key role played by the SAv underlayer in the creation of interfacial architectures capable of minimizing the non-specific binding of negatively charged nanoparticles and streptavidin. The main role attributed to the SAv layer lies in the significant polar hydrophilic repulsion between the SAv-modified surface and the nanomaterials in solution, which confers the interface anti-fouling characteristics. In many cases, oligonucleotide brushes were assembled onto SAv platforms with the aim of controlling the grafting density and interspacing between DNA strands. This led to the creation of highly reproducible interfaces displaying rapid hybridization kinetics in comparison to thiolated DNA brushes [35]. The experimental evidence discussed in this work adds another key advantage of using SAv-based DNA platforms, which relies on their capabilities to strongly resist the non-specific binding of labeling materials. The different fouling characteristics of DNA-SAv and DNA-SH interfacial architectures is an important aspect that should be taken into account when choosing a platform for biosensing applications.

#### Acknowledgements

We thank Dr. Ulrich Schlecht (Caesar Research Center, Germany) and Dr. Peter Thiesen (Nanofilm, Germany) for helpful assistance with SAW equipment and measurements. O.A. acknowledges financial support from the Alexander von Humboldt Stiftung (Germany).

#### References

- [1] W. Reichert, A. Sharkawy, in: A. Von Recum (Ed.), *Handbook of Biomaterials Evaluation*, Taylor & Francis, Washington D.C., 1999, p. 439.
- [2] M. Kyrolainen, S.M. Reddy, P.M. Vadgama, *Anal. Chim. Acta* 353 (1997) 2813.
- [3] S. Woodward, *Diabetes Care* 5 (1982) 278.
- [4] M. Mir, I. Katakis, *Mol. Biosys.* 3 (2007) 620.
- [5] (a) M. Cardenas, J. Barauskas, K. Schillen, J.L. Brennan, M. Brust, T. Nylander, *Langmuir* 22 (2006) 3294;  
(b) H. Kimura-Suda, D.Y. Petrovykh, M.J. Tarlov, L.J. Whitman, *J. Am. Chem. Soc.* 125 (2003) 9014.
- [6] M. Mir, I. Katakis, *Talanta* 75 (2008) 432.
- [7] C.L. Smith, J.S. Milea, G.H. Nguyen, *Top. Curr. Chem.* 261 (2006) 63.
- [8] W. Knoll, M. Liley, D. Piscevic, J. Spinke, M.J. Tarlov, *Adv. Biophys.* 34 (1997) 231.
- [9] I. Willner, E. Katz (Eds.), *Angew. Chem. Int.* 43 (2004) 6042.
- [10] (a) S.K. Shin, H.J. Yoon, Y.J. Jung, J.W. Park, *Curr. Opin. Chem. Biol.* 10 (2006) 423;  
(b) A.P. Alivisatos, W. Gu, C. Larabell, *Annu. Rev. Biomed. Eng.* 7 (2005) 55;  
(c) L. Pasquato, P. Pengo, P. Scrimin, *Nanoparticles, Building Blocks for Nanotechnology*, Springer Science, New York, 2004, p. 251 (Chapter 10);  
(d) M. Murcia, C.A. Naumann, *Biofunctionalization of Nanomaterial*, Wiley-VCH, Weinheim, 2005, p. 15 (Chapter 1).
- [11] (a) J. Wang, *Small* 1 (2005) 1036;  
(b) J. Wang, G. Liu, A. Merkoci, *J. Am. Chem. Soc.* 125 (2003) 3214;  
(c) E. Katz, I. Willner, *Nanobiotechnology*, VCH-Wiley, Weinheim, 2004, p. 200 (Chapter 14).
- [12] (a) R. Gill, F. Patolsky, E. Katz, I. Willner (Eds.), *Angew. Chem. Int.* 44 (2005) 4554;  
(b) R. Freeman, R. Gill, M. Beissenhirtz, I. Willner, *Photochem. Photobiol. Sci.* 6 (2007) 416.
- [13] X. Zhong, Y. Feng, Y. Zhang, *J. Phys. Chem. C* 111 (2007) 526.
- [14] W.C.W. Chan, S. Nie, *Science* 281 (1998) 2016.
- [15] J. Spinke, M. Liley, F.J. Schmitt, H.J. Guder, L. Angermaier, W. Knoll, *J. Chem. Phys.* 99 (1993) 7012.
- [16] O. Azzaroni, M. Mir, W. Knoll, *J. Phys. Chem. B* 111 (2007) 13499.
- [17] O. Azzaroni, M. Mir, M. Alvarez, L. Tiefenauer, W. Knoll, *Langmuir* 24 (2008) 2878.
- [18] K. Saha, F. Bender, A. Rasmussen, E. Gizeli, *Langmuir* 19 (2003) 1304.
- [19] S. Ekgasit, G. Stengel, W. Knoll, *Anal. Chem.* 76 (2004) 4747.
- [20] S. Ekgasit, F. Yu, W. Knoll, *Langmuir* 21 (2005) 4077.
- [21] T. Neumann, M.L. Johansson, D. Kambhampati, W. Knoll, *Adv. Funct. Mater.* 12 (2002) 575.
- [22] S. Joseph, T.M.M. Gronewold, M.D. Schlensog, C. Olbrich, E. Quandt, M. Famulok, M. Schirner, *Biosens. Bioelectron.* 20 (2005) 1829.
- [23] P. Sandström, M. Boncheva, B. Akerman, *Langmuir* 19 (2003) 7537.
- [24] J.J. Storhoff, R. Elghanian, C.A. Mirkin, R.L. Letsinger, *Langmuir* 18 (2002) 6666.
- [25] M. Mir, M. Alvarez, O. Azzaroni, W. Knoll, *Langmuir* 24 (2008) 13001.
- [26] C.J. Van Oss, R.F. Giese, P.M. Bronson, A. Docoslis, P. Edwards, W.T. Ruyechan, *Colloids Surf. B* 30 (2003) 25.
- [27] J. Liu, S. Tian, L. Tiefenauer, P.E. Nielsen, W. Knoll, *Anal. Chem.* 77 (2005) 2756.
- [28] J. Wang, J. Li, A.J. Baca, J. Hu, F. Zhou, Y. Wan, D.W. Pang, *Anal. Chem.* 75 (2003) 3941.
- [29] F. Lucarelli, G. Marrazza, M. Mascini, *Langmuir* 22 (2006) 4305.
- [30] M.J.W. Ludden, A. Mulder, R. Tampe, D.N. Reinhoudt, J. Huskens (Eds.), *Angew. Chem. Int.* 46 (2007) 4104.
- [31] E. Gizeli, *Anal. Chem.* 72 (2000) 5967.
- [32] M.D. Schlensog, T.M.A. Gronewold, M. Tewes, M. Famulok, E. Quandt, *Sens. Actuators B* 101 (2004) 308.
- [33] T.A.M. Gronewold, A. Baumgartner, E. Quandt, M. Famulok, *Anal. Chem.* 78 (2006) 4865.
- [34] E. Gizeli, *Biomolecular Sensors*, Taylor & Francis, London, 2002, p. 176 (Chapter 7).
- [35] X. Su, Y.J. Wu, W. Knoll, *Biosens. Bioelectron.* 21 (2005) 719.



## Self-assembled monolayer of nickel(II) complex and thiol on gold electrode for the determination of catechin

Sally Katiuce Moccelini<sup>a</sup>, Suellen Cadorin Fernandes<sup>a</sup>, Tiago Pacheco de Camargo<sup>b</sup>, Ademir Neves<sup>b</sup>, Iolanda Cruz Vieira<sup>a,\*</sup>

<sup>a</sup> Departamento de Química, LaBios - Laboratório de Biossensores, Universidade Federal de Santa Catarina, CEP 88040-900 Florianópolis, SC, Brazil

<sup>b</sup> Departamento de Química, LABINC - Laboratório de Bioinorgânica e Cristalografia, Universidade Federal de Santa Catarina, CEP 88040-900 Florianópolis, SC, Brazil

### ARTICLE INFO

#### Article history:

Received 25 September 2008

Received in revised form

28 November 2008

Accepted 13 January 2009

Available online 24 January 2009

#### Keywords:

Self-assembled monolayer

Gold electrode

Nickel(II) complex

Catechin

### ABSTRACT

Self-assembled monolayers of a nickel(II) complex and 3-mercaptopropionic acid on a gold electrode were obtained for determination of catechin by square wave voltammetry. The complex  $[\text{Ni}^{\text{II}}\text{L}]$  with  $\text{L} = [\text{N}-(\text{methyl})-\text{N}'-(2\text{-pyridylmethyl})-\text{N},\text{N}'\text{-bis}(3,5\text{-di-tert-butyl-2-hydroxybenzyl})\text{-1,3-propanediamine}[\text{nickel}(\text{II})]$  was synthesized and characterized by  $^1\text{H}$  NMR, IR, and electronic spectroscopies and electrochemical methods. The optimized conditions obtained for the electrodes were  $0.1 \text{ mol L}^{-1}$  phosphate buffer solution (pH 7.0), frequency of 80.0 Hz, pulse amplitude of 60.0 mV and scan increment of 10.0 mV. Under these optimum conditions, the resultant peak current on square wave voltammograms increases linearly with the concentration of catechin in the range of  $3.31 \times 10^{-6}$  to  $2.53 \times 10^{-5} \text{ mol L}^{-1}$  with detection limits of  $8.26 \times 10^{-7} \text{ mol L}^{-1}$ . The relative standard deviation for a solution containing  $1.61 \times 10^{-5} \text{ mol L}^{-1}$  catechin solution was 2.45% for eight successive assays. The lifetime of the Ni(II) complex-SAM-Au electrode was investigated through testing every day over 4 weeks. The results showed apparent loss of activity after 20 days. The results obtained for catechin in green tea samples using the proposed sensor and those obtained by electrophoresis are in agreement at the 95% confidence level.

© 2009 Elsevier B.V. All rights reserved.

### 1. Introduction

The formation of self-assembled monolayers (SAMs) of alkanethiols on gold surfaces continues to be a focus for research interests due to their importance in chemistry, biology and supramolecular nanotechnology. The chemisorption of thiolates on gold is the most important class of SAM from the electrochemical point of view. Among the reasons why gold is the preferred metal are its relative inertia and the fact that it has a strong specific interaction with sulfur that allows the formation of monolayers in the presence of many other functional groups. The SAM technique is simple, reproducible and the molecules are chemically bound to the electrode. The SAM-modified electrodes have advantages such as selectivity, sensitivity, stability, short response time, the possibility of introducing different chemical functionalities, ease of preparation and highly ordered molecules on the electrode [1,2]. The advantages of SAM-gold electrodes using different metallophthalocyanine complexes have been reported by Nyokong's research group for the determination of several analytes [3–7].

Several mimetic complexes have been prepared to produce a system capable of mimicking enzymatic catalysis and used in the construction of biomimetic sensors [8–13]. Recently, Caovilla et al. [8] studied the catalytic oxidation of limonene,  $\alpha$ -pinene and  $\beta$ -pinene by the complex  $[\text{Fe}^{\text{III}}(\text{BPMP})\text{Cl}(\text{m-O})\text{Fe}^{\text{III}}\text{Cl}_3]$ , a biomimetic for the methane monooxygenase enzyme. In a study described by Sotomayor et al. [9], an iron tetrapyrrolineporphyrin complex was used as a biomimetic catalyst of the P450 enzyme and applied in the construction of a sensor for paracetamol determination in pharmaceutical samples. Wollenberger et al. [10] developed a sensor based on the combination of a screen-printed peroxidase electrode and an iron porphyrin complex iron(III)-meso-tetrakis-(penta-fluorophenyl)- $\beta$ -tetra sulfonatoporphyrin chloride for aliphatic hydrocarbons. Santhiago et al. [11] developed a biomimetic sensor based on a heterodinuclear  $\text{Fe}^{\text{III}}\text{Zn}^{\text{II}}$  mimetic complex which mimics the active site of the hydrolytic enzyme red kidney bean purple acid phosphatase and employed it in the determination of rosmarinic acid. Oliveira et al. [12,13] developed biomimetic sensors based on an  $\text{Fe}^{\text{III}}\text{Fe}^{\text{II}}$  and a dinuclear copper(II) complex for the determination of dopamine in pharmaceutical products and hydroquinone in cosmetics, respectively.

Green tea, a plant of Asiatic origin, is produced from *Camellia sinensis* belonging to the Theaceae family [14] and is popular in

\* Corresponding author. Tel.: +55 48 3721 6844; fax: +55 48 3721 6850.  
E-mail address: [iolanda@qmc.ufsc.br](mailto:iolanda@qmc.ufsc.br) (I.C. Vieira).

China, Japan, Korea and Morocco. This tea is rich in antioxidants and may have a protective role in human health. Traditional Chinese medicine has recommended this plant to prolong life and for headaches, body aches and pains, digestion disorders, depression, detoxification, and as an energizer. Among the components which have beneficial properties are xanthic bases, essential oils and, particularly, polyphenolic compounds (mainly gallic acid and catechin) [15].

The interest in the quantification of catechin is related to its potential benefits in terms of human health, as it has been extensively reported to have various biological and pharmacological effects, including antioxidant, anticarcinogenic, antimutagenic, anti-inflammatory, and antimicrobial activities. Also, it can combat free radicals which damage human cells under oxidative conditions causing grave disturbances in cell metabolism [16–18]. Several analytical methods have been reported in the literature for the determination of catechin [16–33]. The most widely used methods are based on liquid chromatography including HPLC [16,20–23], and others have been proposed, such as spectrophotometry [17], capillary electrophoresis [22,24–26] and electrochemistry [27–31].

Electrochemical methods for the determination of phenolic compounds (e.g., catechin) are preferred over other methods because of their fast response time, low detection limit and relatively low cost [27–31]. Roy et al. [27] developed a biosensor containing laccase from *Trametes versicolor* crystallized, cross-linked and lyophilized with  $\beta$ -cyclodextrin. This biosensor was used to detect several phenols in the concentration range of 50–1000  $\mu\text{mol L}^{-1}$ . Jarosz-Wilkolazka et al. [28] immobilized the laccase from *Cerrena unicolor* on the surface of a graphite electrode and introduced it into a flow-injection system. The linear dynamic range for catechin was 4.0–40  $\mu\text{mol L}^{-1}$ . El-Hady's group constructed two electrodes for the determination of catechin in tea and biological fluids: (I) a modified carbon paste electrode with beta-cyclodextrin [29], the catechin concentration being linear up to 70.0  $\mu\text{g mL}^{-1}$  (cathodic voltammetry) and up to 45.0  $\mu\text{g mL}^{-1}$  (anodic voltammetry); the other (II) containing hydroxypropyl-beta-cyclodextrin [30] with a linear range up to 7.2 and 4.20  $\mu\text{g mL}^{-1}$ . Recently, our research group [31] developed a biomimetic sensor containing a copper(II) complex for determination of catechin in green tea. The analytical curve was linear from  $4.95 \times 10^{-6}$  to  $3.27 \times 10^{-5}$   $\text{mol L}^{-1}$ .

In this study, we present the synthesis and characterization of a mononuclear Ni(II) complex containing the pentadentate  $\text{H}_2\text{L}$  ligand, in which the phenolate groups are suitably protected by bulky substituents (*tert*-butyl) in the *ortho*- and *para*-positions, which through electrochemical oxidation generate the one- and two-electron oxidized phenoxyl species in solution. Finally, and most importantly, we report the construction, optimization and use of self-assembled monolayers of the Ni(II) complex and 3-mercaptopropionic acid on a gold electrode for determination of catechin by square wave voltammetry. The results obtained in the determination of catechin in green tea samples using the Ni(II) complex-SAM-Au electrode compared favorably with those obtained using the capillary electrophoresis method.

## 2. Experimental

### 2.1. Chemicals

All reagents used in this study were of analytical grade and all solutions were prepared with water from a Millipore (Bedford, MA, USA) Milli-Q system (model UV Plus Ultra-Low Organic Water). 3-Mercaptopropionic acid (MPA), cyanamide, sulfuric acid, ethyl alcohol, chloroform and hydrogen peroxide were supplied by Sigma. The substances caffeine, epicatechin, epigallocatechin,

epicatechin gallate, epigallocatechin gallate, gallic acid, guaiacol, ferulic acid, *p*-coumaric acid, syringic acid, vanillic acid, sucrose, glucose, fructose, benzoic acid, citric acid, tartaric acid and fumaric acid standards were also acquired from Sigma and used in the interference study. Chloroform ( $\text{CDCl}_3$ ), sodium dodecylsulfate (SDS) and triethylamine (TEA) were obtained from Merck. For the capillary electrophoresis analysis a stock solution of SDS and TEA was prepared at 1.0  $\text{mol L}^{-1}$ , and the internal standard (propylparaben) was prepared in methanol at 120  $\text{mg L}^{-1}$ . Green tea samples were purchased from a local market and the supporting electrolyte was 0.1  $\text{mol L}^{-1}$  phosphate buffer. The alumina slurry (0.05 and 0.3  $\mu\text{m}$ ) was obtained from Arotec.

### 2.2. Nickel(II) complex characterization instrumentation

$^1\text{H}$  NMR analysis of the ligand was carried out with a Bruker 200 MHz spectrometer in chloroform at 25 °C. Infrared spectra were measured in KBr pellets, using a Perkin Elmer 781 spectrometer. Chemical shifts were reported in ppm as  $\delta$  values downfield from an internal standard of tetramethylsilane ( $\text{SiMe}_4$ ). Elemental analysis was performed with a Carlo Erba E1110 analyzer.

### 2.3. Electrochemical and capillary electrophoresis instrumentation

Cyclic voltammetry measurements of the nickel(II) complex in chloroform solution were performed in an EG&G PAR, model 273A, potentiostat/galvanostat. The electrochemical cell employed was a standard three-electrode configuration: glassy carbon (working), Ag/AgCl (reference) and platinum wire (auxiliary).

Square wave and cyclic voltammetry measurements using the sensor were obtained with an Autolab PGSTAT12 potentiostat/galvanostat (Eco Chemie, Utrecht, The Netherlands) connected to data processing software (GPES, software version 4.9.006, Eco Chemie). All measurements were carried out in a 15 mL glass cell at room temperature ( $25.0 \pm 0.5$  °C). The working electrode used was a gold electrode (surface area 2.0  $\text{mm}^2$ ) modified with the nickel(II) complex. A platinum wire was used as the counter electrode, and Ag/AgCl (3.0  $\text{mol L}^{-1}$  KCl) as the reference. A Unique 1400A ultrasonic bath was used to clean the electrode surfaces.

Electropherograms were obtained with an Agilent Technologies HP<sup>3D</sup>CE capillary electrophoresis automated apparatus (Palo Alto, CA, USA), equipped with a diode array detector. The measurements were performed at 25 °C on an uncoated fused-silica capillary (48.5 cm  $\times$  50  $\mu\text{m}$  I.D.  $\times$  375  $\mu\text{m}$  O.D. 40 cm of effective length) obtained from Polymicro Technologies (Phoenix, AZ, USA). The acquisition software for data treatment was HP Chemstation<sup>®</sup>.

### 2.4. Synthesis and characterization of the ligand and nickel(II) complex

The ligand *N*-(methyl)-*N'*-(2-pyridylmethyl)-*N,N'*-bis(3,5-di-*tert*-butyl-2-hydroxybenzyl)-1,3-propanediamine ( $\text{H}_2\text{L}$ ) was prepared and characterized by  $^1\text{H}$  NMR spectroscopy as described in the literature [32].  $^1\text{H}$  NMR (200 MHz); solvent ( $\text{CDCl}_3$ ); standard ( $\text{SiMe}_4$ ),  $\delta$  (ppm): 8.5 (1H, s), 6.8–7.7 (7H, m), 3.6–3.8 (8H, d), 2.1–2.7 (4H, t), 1.43 (3H, s), 1.38 (18H, s), 1.27 (18H, s).

The neutral  $[\text{Ni}^{\text{II}}\text{L}]$  complex was prepared by adding  $[\text{Ni}(\text{OH}_2)_6](\text{ClO}_2)_2$  ( $1.0 \times 10^{-3}$   $\text{mol L}^{-1}$ ) to a methanolic solution of  $\text{H}_2\text{L}$  ( $1.0 \times 10^{-3}$   $\text{mol L}^{-1}$ ), in the presence of triethylamine. The complex was isolated as a microcrystalline green solid and the yield was 73%. CHN calculated for  $\text{NiC}_{24}\text{H}_{29}\text{N}_3\text{O}_3$  (MM = 466.20  $\text{g mol}^{-1}$ ): C: 69.6%; H: 8.9%; N: 6.1%. Found C: 71.2%; H: 9.5%; N: 6.2%.

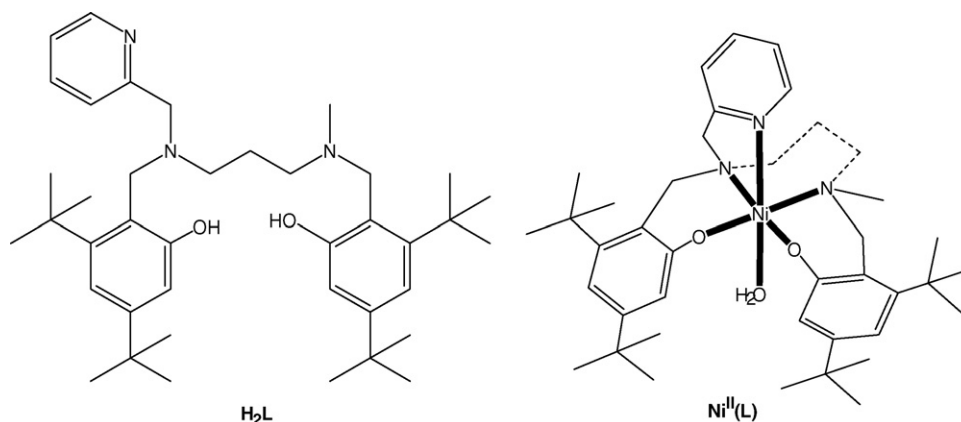


Fig. 1. Schematic representation of the  $H_2L$  ligand and the  $[Ni^{II}(L)]$  complex.

### 2.5. Pre-treatment of the Au electrode and obtainment of the Ni(II) complex–SAM–Au electrode

Prior to surface modification, the working gold electrode was mechanically polished with aqueous slurries of alumina (0.3 and 0.05  $\mu\text{m}$ ), for 2 min each, on a flat pad and then rinsed ultrasonically with absolute ethanol to remove residual alumina particles from the surface. Subsequently, it was cleaned with a piranha solution ( $H_2O_2:H_2SO_4 = 1:3$ , v/v) [3,4,33] for 10 min. An electrochemical cleaning process was carried out using a cyclic voltammetry technique performed from 0.0 to +1.7 V vs. Ag/AgCl ( $KCl\ 3.0\ \text{mol L}^{-1}$ ) in 0.5  $\text{mol L}^{-1}$  sulfuric acid solution using a scan rate of 100  $\text{mV s}^{-1}$  until a stable cyclic voltammogram was obtained. This procedure avoids structural changes to the gold surface.

SAM was formed by immersing the clean gold electrode in an ethanolic solution of  $10.0 \times 10^{-3}\ \text{mol L}^{-1}$  MPA for 1 h at room temperature. The SAM–Au electrode was then rinsed with ethanol in order to remove the unbonded thiol and it was immersed in cyanamide solution containing 0.36  $\text{mol L}^{-1}$  in phosphate buffer (pH 7.0) for another period of 1 h. An aliquot of 15  $\mu\text{L}$  of  $2.0 \times 10^{-2}\ \text{mol L}^{-1}$  of Ni(II) complex solution in dichloromethane was deposited on the SAM electrode surface and dried at room temperature.

### 2.6. Preparation of green tea samples and measurements

Three types of commercial green tea samples with a common trade mark (A = Bioslim, B = Leão and C = Chileno) were purchased from the local market in Florianópolis, SC, Brazil. The samples were prepared by extracting 2.0 g of the tea with 40 mL of the 0.1  $\text{mol L}^{-1}$  phosphate buffer solution (pH 7.0) at 35 °C, incubating for 20 min, shaking for 2 min, filtering and centrifuging. An aliquot of 100  $\mu\text{L}$  of green tea extract was transferred to an electrochemical cell containing 15 mL of non-de-aerated phosphate buffer solution (pH 7.0) and analyzed after successive additions of the reference catechin solution. After each addition of the catechin or sample solution, and stirring for 60 s for homogenization, square wave voltammograms were obtained applying a sweep potential between +0.4 to –0.1 V, under the optimal values of frequency, pulse amplitude, and scan increment (80.0 mV, 60.0 Hz and 10.0 mV, respectively). All measurements were performed in triplicate and all currents were measured at room temperature ( $25 \pm 0.5\ ^\circ\text{C}$ ) and reported vs. Ag/AgCl ( $3.0\ \text{mol L}^{-1}$  KCl).

The capillary electrophoresis method was also used for the determination of catechin in the green tea samples. These samples were diluted, 1:4:1 (v/v/v) sample:distilled water:internal standard (propylparaben), before injection. For the quantifica-

tion, the calibration curve for concentrations of catechin between 15 and 60  $\text{mg L}^{-1}$  and a constant internal standard concentration (20.0  $\text{mg L}^{-1}$ ), was used. Each concentration was prepared and injected in triplicate. The standard solutions and samples were injected hydrodynamically at 50 mbar for 3 s and the applied separation voltage was 25 kV (negative polarity). The detector wavelength was fixed at 206 nm. The background electrolyte (BGE) consisted of a mixture of  $50.0 \times 10^{-3}\ \text{mol L}^{-1}$  sodium dodecylsulfate and  $10.0 \times 10^{-3}\ \text{mol L}^{-1}$  triethylamine at pH 2.5 adjusted with phosphoric acid. At the start of each new working session, the capillary was conditioned at 25 °C and flushed with 1.0  $\text{mol L}^{-1}$  sodium hydroxide for 10 min, followed by deionized water for 5 min and finally with the BGE for 10 min. Between runs with the same buffer, the capillary was rinsed for 2 min with BGE. At the end of the analysis, the capillary was rinsed for 5 min with 1.0  $\text{mol L}^{-1}$  sodium hydroxide and 10 min with deionized water.

## 3. Results and discussion

### 3.1. Characterization of the ligand and of the Ni(II) complex

The ligand N-(methyl)-N'-(2-pyridylmethyl)-N,N'-bis(3,5-di-tert-butyl-2-hydroxybenzyl)-1,3-propanediamine ( $H_2L$ ) was prepared according to the method described in the literature [32] and it was unequivocally characterized by  $^1\text{H}$  NMR spectroscopy.  $H_2L$  reacts readily with nickel(II) perchlorate in methanol solution, in the presence of triethylamine to generate the mononuclear  $[Ni^{II}(L)]$  complex. The octahedral coordination environment around the Ni(II) center in  $[Ni^{II}(L)]$  (Fig. 1) is proposed based on elemental analysis, conductivity, IR, UV–vis and electrochemical measurements.

Fig. 2 shows the cyclic voltammograms of  $[Ni^{II}(L)]$  recorded in dichloromethane under argon atmosphere at a scan rate of 100–400  $\text{mV s}^{-1}$ . The voltammograms showed two quasi-reversible oxidation processes at +0.64 and +0.43 V. There were no cathodic processes detected in the applied potential range (–1.0 to +1.0 V vs. Ag/AgCl), and the anodic processes can be attributed to the quasi-reversible formation of two-coordinated phenoxyl radicals. These potentials are in agreement with nickel(II)–phenoxyl radical systems as described in the literature [34]. As reported by Neves and co-authors [32], the copper and zinc complexes with the same ligand showed a distorted square pyramidal geometry coordinated by two amine and one pyridine nitrogen and two phenolate groups.

The electronic spectrum of the  $[Ni^{II}(L)]$  complex shows an intense charge transfer peak at 403 nm ( $2100\ \text{L mol}^{-1}\ \text{cm}^{-1}$ ) typical of  $O_{\text{phenolate}}\text{–Ni(II)}$  systems and a band at 634 nm ( $49\ \text{L mol}^{-1}\ \text{cm}^{-1}$ )

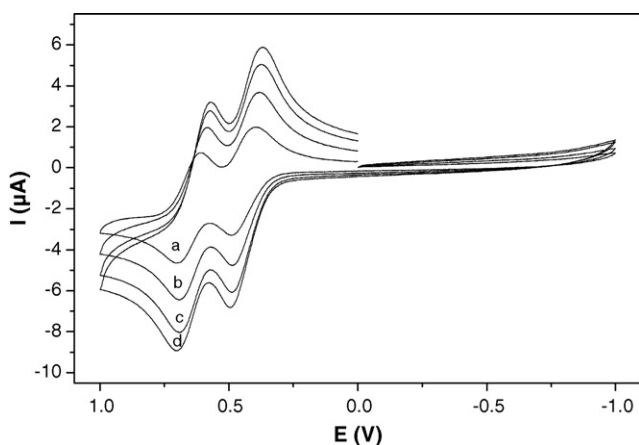


**Fig. 2.** Cyclic voltammograms for  $5.0 \times 10^{-4} \text{ mol L}^{-1}$  Ni(II) complex in dichloromethane and  $0.1 \text{ mol L}^{-1}$  tetrabutylammonium hexafluorophosphate performed by scanning the potential between +1.0 and -1.0 vs. Ag/AgCl at a scan rate of: (a) 100; (b) 200; (c) 300 and (d) 400  $\text{mV s}^{-1}$ .

attributed to d-d internal transitions of the Ni(II) ion. Addition of an equimolar amount of  $(\text{NH}_4)_2\text{Ce}(\text{NO}_3)_6$  to the complex in dichloromethane caused a color change from light green to dark brown. The oxidized complex showed some new intense absorption bands at 400 and 478 nm and broad peaks at 680 and 982 nm. The intense transition band at 398–403 nm may be partly assigned to a  $\pi\text{-}\pi^*$  transition of the phenoxyl radical, and the spectral features are in good agreement with those previously reported for Ni(II)–phenoxyl radical complexes [34,35]. The molar conductivity measurements were obtained in a  $1.0 \times 10^{-3} \text{ mol L}^{-1}$  acetonitrile solution of  $[\text{Ni}^{\text{II}}\text{L}]$  and the value for the complex was  $13.4 \mu\text{S cm}^{-1}$ , which suggests a neutral form of the complex.

### 3.2. Formation and performance of the Ni(II) complex–SAM–Au electrode

Fig. 3A shows a proposed scheme for the immobilization of the Ni(II) complex on the SAM–Au electrode surface. Initially, the surface of the gold electrode was chemically modified with 3-mercaptopropionic acid (a) to form ordered molecular assemblies. Subsequently, it was immersed in a cyanamide solution (b), reacting with the hydroxyl groups of MPA. The Ni(II) complex (c) was immobilized covalently on this monolayer. Transition metal complexes, like nickel, are labels, changing their ligands rapidly because of their kinetics as well as the thermodynamic effect. In the interaction with cyanamide, the nickel complex probably coordinates with the amine group to complete its octahedral coordination sphere, allowing a greater stability than if it were bound to water. The Ni(II) complex catalyzes the oxidation of catechin to its respective quinone and, subsequently, the quinone produced at the sensor surface is electrochemically reduced to catechin at a potential of +0.18 V (Fig. 3B).

Initially, the effect of the concentration of the substances employed in the construction of the Ni(II) complex–SAM–Au electrodes were determined. The MPA ( $1.0 \times 10^{-2}$  to  $1.0 \times 10^{-4} \text{ mol L}^{-1}$ ) and cyanamide ( $0.12$ – $1.12 \text{ mol L}^{-1}$ ) were investigated to obtain the highest response and best performance of the proposed electrodes. The responses of the sensors were based on the cathodic peak currents for a  $1.61 \times 10^{-5} \text{ mol L}^{-1}$  catechin solution and square wave voltammetry. Higher current peaks were observed for the sensor when constructed using  $1.0 \times 10^{-3}$  and  $0.35 \text{ mol L}^{-1}$  of the MPA and cyanamide, respectively. Thus, these concentrations were used for further construction of the electrodes.

### 3.3. Optimization of the pH and SWV parameters

The optimum performance of a self-assembled electrode is directly related to the pH dependence of the Ni(II) complex–SAM–Au electrode response. The effect of pH on the proposed sensor responses were investigated over the pH range of 5.0–9.0 in phosphate buffer solution containing a catechin concentration of  $1.61 \times 10^{-5} \text{ mol L}^{-1}$ . The catalytic current increased up to a value of pH 7.0, and decreased gradually after that. Thus, this pH value was selected for the subsequent experiments.

The influence of square wave voltammetry parameters, like, frequency, pulse amplitude and scan increment offers high sensitivity and well-shaped waves with relatively narrow peaks. In the investigation process, each variable was changed while the other two were kept constant. The effects of frequency (10–120 Hz), pulse amplitude (10–120 mV) and scan increment (0.5–12.0 mV) on the Ni(II) complex–SAM–Au electrode response to a  $1.61 \times 10^{-5} \text{ mol L}^{-1}$  catechin solution were studied.

The maximum sensitivity of the sensor response to the frequency parameter was obtained at 80.0 Hz, remaining constant thereafter and this value was selected for the subsequent tests. The effect of varying pulse amplitude on the current response of Ni(II) complex–SAM–Au electrodes was also investigated. The current response increased up to 60.0 mV, where it stabilized, and this value was used in all experiments employing the proposed electrode. In addition, the scan increment parameter was studied in the range of 0.5–12.0 mV. The scan increment of 10.0 mV was chosen as the highest and applied in the subsequent tests.

### 3.4. Repeatability and stability of Ni(II) complex–SAM–Au electrode

The repeatability of the Ni(II) complex–SAM–Au electrodes was evaluated by measuring the current response in a phosphate buffer solution ( $0.1 \text{ mol L}^{-1}$ ; pH 7.0) containing  $1.61 \times 10^{-5} \text{ mol L}^{-1}$  of catechin, taking several separate measurements using the same sensor. The relative standard deviation (R.S.D.) was 2.45% for eight successive assays.

The long-term stability of the Ni(II) complex–SAM–Au electrodes were investigated by measuring the voltammetric current response to  $1.61 \times 10^{-5} \text{ mol L}^{-1}$  catechin in a  $0.1 \text{ mol L}^{-1}$  phosphate buffer solution (pH 7.0) every day over 4 weeks. The results showed apparent loss of activity after 20 days. The reproducibility was also investigated and a relative standard deviation of 3.5% was obtained. The stability of the Ni(II) complex–SAM–Au electrode can be attributed to the high level of organization of the thiols on gold electrodes.

### 3.5. Interference study

To evaluate the selectivity of the Ni(II) complex–SAM–Au electrode the influence of some common, possibly interfering, substances found in green tea were investigated, i.e., caffeine, epicatechin, epigallocatechin, epicatechin gallate, epigallocatechin gallate, gallic acid, guaiacol, ferulic acid, p-coumaric acid, syringic acid, vanillic acid, sucrose, glucose, fructose, benzoic acid, citric acid, tartaric acid and fumaric acid. The ratios of the concentrations of catechin to those of the excipient substances were fixed at 1.0 and 10.0. None of the substances studied interfered with the proposed procedure, that is, the Ni(II) complex–SAM–Au electrode was able to determine the amount of catechin in the presence of the potential interferences with good selectivity. These data were in agreement with those reported recently by Fernandes et al. [31] using a biomimetic sensor.

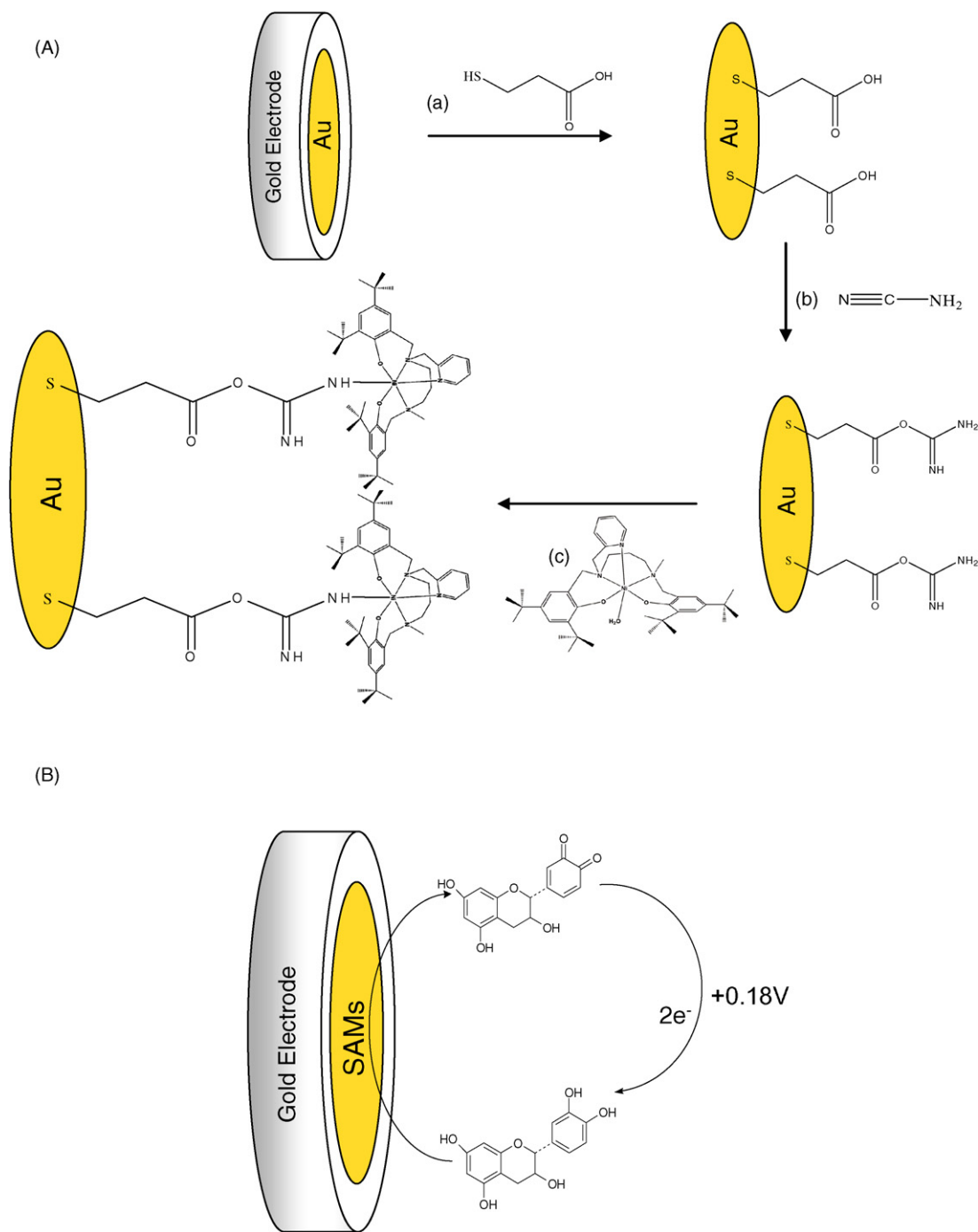


**Fig. 3.** (A) Schematic representation of the immobilization of Ni(II) complex on the SAM-Au electrode and (B) catechin oxidation/reduction on the sensor surface.

### 3.6. Square wave voltammetry, analytical curve, recovery and determination of the catechin

Under the optimum conditions established above, the analytical curve obtained was linear from  $3.31 \times 10^{-6}$  to  $2.53 \times 10^{-5} \text{ mol L}^{-1}$  of catechin and the corresponding regression equation was found to be  $(-\Delta I = 1.846 + 6.70 \times 10^5 [\text{catechin}]; r = 0.9987)$ , where  $\Delta I$  is the resultant peak current in  $\mu\text{A}$ , and  $[\text{catechin}]$  is the catechin concentration in  $\text{mol L}^{-1}$ . Fig. 4 shows these voltammograms and the analytical curve can be seen in the inset. Detection limits of  $8.26 \times 10^{-7} \text{ mol L}^{-1}$  for catechin could be estimated for the SAM-Au electrode considering three times the signal blank/slope.

Recoveries of 98.2–105.0% for catechin present in the green tea samples (A, B and C) were obtained using the Ni(II) complex-SAM-Au electrode. In this study 2.48, 4.64 and  $7.26 \text{ mg L}^{-1}$  of catechin solutions were successively added to each sample and the resultant peak current analyzed. The recovery results obtained were satisfactory, indicating an absence of matrix effects in the catechin determinations using the proposed sensor.

Finally, the green tea samples: A, B and C, were used for the determination of catechin employing the Ni(II) complex-SAM-Au electrode and the values compared with those obtained using the capillary electrophoresis method. The results for the two methods were found to be close (Table 1) applying the paired *t*-test, and are in



**Table 1**  
Determination of catechin in green tea using the Ni(II) complex–SAM–Au electrode and capillary electrophoresis.

Sample	Catechin (mg L <sup>-1</sup> )		Relative error, Re (%)
	Capillary electrophoresis <sup>a</sup>	Ni(II) complex–SAM–Au electrode <sup>a</sup>	
A	159.1 ± 0.1	159.8 ± 0.2	-0.44
B	93.0 ± 0.1	90.6 ± 0.2	+2.58
C	88.2 ± 0.1	87.0 ± 0.1	+1.36

Re = nickel(II) complex–SAM–Au electrode vs. capillary electrophoresis.

<sup>a</sup> n = 4; confidence level of 95%.

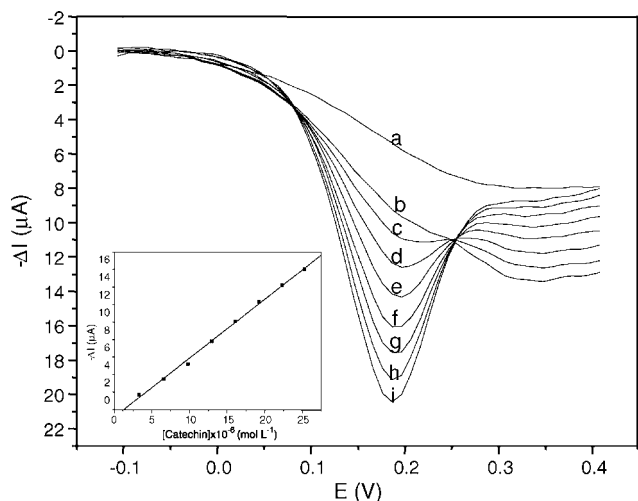


**Fig. 4.** Square wave voltammograms obtained using the Ni(II) complex–SAM–Au electrode for: (a) blank in phosphate buffer solution, and catechin solutions at the following concentrations: (b)  $3.31 \times 10^{-6}$ ; (c)  $6.58 \times 10^{-6}$ ; (d)  $9.80 \times 10^{-6}$ ; (e)  $1.30 \times 10^{-5}$ ; (f)  $1.61 \times 10^{-5}$ ; (g)  $1.92 \times 10^{-5}$ ; (h)  $2.23 \times 10^{-5}$ ; (i)  $2.53 \times 10^{-5}$  mol L<sup>-1</sup> at pulse amplitude 60.0 mV, frequency 80.0 Hz and increment 10.0 mV. Inset: the analytical curve of catechin.

agreement at the 95% confidence level, within an acceptable range of error.

The good performance for the proposed sensor can be attributed to the successful immobilization of the Ni(II) complex using self-assembled monolayers on a gold electrode. Complexes have shown excellent performance in the development of novel sensors [3–13,31]. In addition, the models have an extraordinary advantage in relation to the natural enzyme, that is, high stability in relation to several factors (e.g., temperature, pH, and others) and, consequently, they offer a longer lifetime and greater number of determinations than other biosensors [27,28].

#### 4. Conclusions

A new mononuclear nickel(II) complex containing the pentadentate H<sub>2</sub>L ligand, in which the phenolate groups are suitably protected by bulky substituents (*tert*-butyl) in the *ortho*- and *para*-positions, which through electrochemical oxidation generate the one- and two-electron oxidized phenoxyl species in solution, was synthesized and characterized. This Ni(II) complex was successfully immobilized on a SAM gold electrode for selective determination of catechin in green tea. The gold electrode modified using MPA was used for catechin determination, along with capillary electrophoresis. Since there is no significant difference between the two methods, it can be concluded that the Ni(II) complex–SAM–Au electrode can be used for catechin determination without suffering matrix problems from the green tea samples. This modified

electrode also offers other advantages including good linear range, stability, low cost and rapid response time

#### Acknowledgments

The authors thank CNPq (Processes 472169/2004-1 and 472541/2006-4), MCT/CNPq/PADCT for the financial support of this study, and also CNPq and CAPES for the scholarships granted to SKM, TPC and SCF.

#### References

- [1] D. Chen, L. Jinghong, Surf. Sci. Rep. 61 (2006) 445.
- [2] J.J. Gooding, D.B. Hibbert, Trends Anal. Chem. 18 (1999) 525.
- [3] B. Agboola, P. Westbroek, K.I. Ozoemena, T. Nyokong, Electrochem. Commun. 9 (2007) 310.
- [4] B. Agboola, T. Nyokong, Talanta 72 (2007) 691.
- [5] F. Matemadombo, T. Nyokong, Electrochim. Acta 52 (2007) 6856.
- [6] B. Agboola, K.I. Ozoemena, P. Westbroek, T. Nyokong, Electrochim. Acta 52 (2007) 2520.
- [7] K.I. Ozoemena, T. Nyokong, D. Nkosi, I. Chambrier, M.J. Cook, Electrochim. Acta 52 (2007) 4132.
- [8] M. Caovilla, A. Caovilla, S.B.C. Pergher, M.C. Esmelindro, C. Fernandes, C. Dariva, K. Bernardo-Gusmão, E.G. Oestreicher, O.A.C. Antunes, Catal. Today 133 (2008) 695.
- [9] M.D.P.T. Sotomayor, A. Sigoli, M.R.V. Lanza, A.A. Tanaka, L.T. Kubota, J. Braz. Chem. Soc. 19 (2008) 734.
- [10] U. Wollenberger, B. Neumann, F.W. Scheller, Electrochim. Acta 43 (1998) 3581.
- [11] M. Santhiago, R.A. Peralta, A. Neves, G.A. Micke, I.C. Vieira, Anal. Chim. Acta 613 (2008) 91.
- [12] I.R.W.Z. Oliveira, A. Neves, I.C. Vieira, Sens. Actuators B 129 (2008) 424.
- [13] I.R.W.Z. Oliveira, R.E.H.M.B. Osório, A. Neves, I.C. Vieira, Sens. Actuators B 122 (2007) 89.
- [14] H. Lorenzi, F.J.A. Matos, Plantas Medicinas no Brasil: Nativas e Exóticas, 1st ed., Nova Odessa: Instituto Plantarum, São Paulo, 2002, p. 512.
- [15] C.D. Wu, G.X. Wei, Nutr. Oral Health 18 (2002) 443.
- [16] Y. Masukawa, Y. Matsui, N. Shimizu, N. Kondou, H. Endou, M. Kuzukawa, T. Hase, J. Chromatogr. B 834 (2006) 26.
- [17] D. Ozyurt, B. Demirata, R. Apak, Talanta 71 (2007) 1155.
- [18] D.A. El-Hady, N.A. El-Maali, Talanta 76 (2008) 138.
- [19] J.J. Dalluge, B.C. Nelson, J. Chromatogr. A 881 (2000) 411.
- [20] H. Wang, G.J. Provan, K. Helliwell, Food Chem. 81 (2003) 307.
- [21] E. Nishitani, Y.M. Sagesaka, J. Food Compos. Anal. 17 (2004) 675.
- [22] B.L. Lee, C.-N. Ong, J. Chromatogr. A 881 (2000) 439.
- [23] S. Khokhar, D. Venema, P.C.H. Hollman, M. Dekker, W. Jongen, Cancer Lett. 114 (1997) 171.
- [24] L. Arce, A. Ríos, M. Valcárcel, J. Chromatogr. A 827 (1998) 113.
- [25] K. Tsukagoshi, T. Taniguchi, R. Nakajima, Anal. Chim. Acta 589 (2007) 66.
- [26] Z. Chen, L. Zhang, G. Chen, J. Chromatogr. A 1193 (2008) 178.
- [27] J.J. Roy, T.E. Abraham, K.S. Abhijith, P.V.S. Kumar, M.S. Thakur, Biosens. Bioelectron. 21 (2005) 206.
- [28] A. Jarosz-Wilkolazka, T. Ruzgas, L. Gorton, Enzyme Microb. Technol. 35 (2004) 238.
- [29] D.A. El-Hady, N. El-Maali, Microchim. Acta 161 (2008) 225.
- [30] D.A. El-Hady, Anal. Chim. Acta 593 (2007) 178.
- [31] S.C. Fernandes, R.E.H.M.B. Osório, A. dos Anjos, A. Neves, G.A. Micke, I.C. Vieira, J. Braz. Chem. Soc. 19 (2008) 1215.
- [32] A. dos Anjos, A.J. Bortoluzzi, R.E.H.M.B. Osório, R.A. Peralta, G.R. Friedermann, A.S. Mangrich, A. Neves, Inorg. Chem. Commun. 8 (2005) 249.
- [33] Z. Wang, Y. Tu, S. Liu, Talanta 77 (2008) 815.
- [34] Y. Shimazaki, F. Tani, K. Fukui, Y. Naruta, O. Yamauchi, J. Am. Chem. Soc. 125 (2003) 10512.
- [35] J. Muller, A. Kikuchi, E. Bill, T. Weyhermüller, P. Hildebrandt, L. Ould-Moussa, K. Wieghardt, Inorg. Chim. Acta 297 (2000) 265.



# Headspace solid-phase microextraction using a dodecylsulfate-doped polypyrrole film coupled to ion mobility spectrometry for the simultaneous determination of atrazine and ametryn in soil and water samples

Abdorreza Mohammadi, Akram Ameli, Naader Alizadeh\*

Department of Chemistry, Faculty of Science, Tarbiat Modares University, P.O. Box 14115-175, Tehran, Iran

## ARTICLE INFO

### Article history:

Received 12 October 2008

Received in revised form 13 January 2009

Accepted 14 January 2009

Available online 23 January 2009

### Keywords:

Headspace solid-phase microextraction

Polypyrrole

Triazine

Herbicides

Ion mobility spectrometry

Soil and water samples

## ABSTRACT

A simple and rapid headspace solid-phase microextraction (HS-SPME) based method is presented for the simultaneous determination of atrazine and ametryn in soil and water samples by ion mobility spectrometry (IMS). A dodecylsulfate-doped polypyrrole (PPy-DS), synthesized by electrochemical method, was applied as a laboratory-made fiber for SPME. The HS-SPME system was designed with a cooling device on the upper part of the sample vial and a circulating water bath for adjusting the sample temperature. The extraction properties of the fiber to spiked soil and water samples with atrazine and ametryn were examined, using a HS-SPME device and thermal desorption in injection port of IMS. Parameters affecting the extraction efficiency such as the volume of water added to the soil, pH effect, extraction time, extraction temperature, salt effect, desorption time, and desorption temperature were investigated. The HS-SPME-IMS method with PPy-DS fiber, provided good repeatability (RSDs < 10%), simplicity, good sensitivity and short analysis times for spiked soil (200 ng g<sup>-1</sup>) and water samples (100 and 200 ng mL<sup>-1</sup>). The calibration graphs were linear in the range of 200–4000 ng g<sup>-1</sup> and 50–2800 ng mL<sup>-1</sup> for soil and water respectively ( $R^2 > 0.99$ ). Detection limits for atrazine and ametryn were 37 ng g<sup>-1</sup> (soil) and 23 ng g<sup>-1</sup> (soil) and 15 ng mL<sup>-1</sup> (water) and 10 ng mL<sup>-1</sup> (water), respectively. To evaluate the accuracy of the proposed method, atrazine and ametryn in the three kinds of soils and two well water samples were determined. Finally, comparing the HS-SPME results for extraction and determination of selected triazines using PPy-DS fiber with the other methods in literature shows that the proposed method has comparable detection limits and RSDs and good linear ranges.

© 2009 Elsevier B.V. All rights reserved.

## 1. Introduction

Triazine herbicides and some of their transformation products are considered one of the most important classes of chemical pollutants owing to their widespread use and toxicity. These compounds are applied in agriculture as selective pre- and post-emergence weed control for corn, wheat, barley, sorghum and sugar cane, but they are also widely employed for non-agricultural usage (railways and roadside verges). Triazines and their degradation products have caused concern because they are toxic and persistent in water, soil, and organisms. Moreover, atrazine, one member of the triazine family, has also been classified as a possible human carcinogen.

Their half-lives vary from few weeks to several months and they are usually transformed into more polar compounds, with more tendencies to stay in aquatic media [1]. A variable amount of triazines can also remain strongly sorbed onto the soil, depending on

the characteristics of the matrix (e.g. cation-exchange capacity, pH, surface area, mineralogical composition, clay content). The study and survey of the widespread distribution of triazine herbicides in the environment require the availability of efficient analytical methods for monitoring both agricultural and non-agricultural areas [2].

Usually, gas chromatography (GC) with mass spectrometric (MS) detection, electron capture or nitrogen-phosphorus detection is a common tool for the identification and quantification of triazines [3–5]. Also, high-performance liquid chromatography (HPLC), particularly reversed-phase liquid chromatography, and also capillary electrophoresis in combination with diode array detection have been used for triazines determination [6,7]. The separation and determination of triazines with sensitive and rapid instrumental techniques would simplify the method and as a result, the analysis time would be reduced.

Ion mobility spectrometry (IMS) is an ambient pressure ion separation technique that characterizes chemical substances using gas-phase mobilities of ions in weak electric fields. In the past two decades, IMS has become a powerful technique for the rapid

\* Corresponding author. Fax: +98 21 882883455.

E-mail address: [alizaden@modares.ac.ir](mailto:alizaden@modares.ac.ir) (N. Alizadeh).

and sensitive detection of trace substances, including residues and breakdown products of explosives [8–10], illicit drugs [11–13], and chemical warfare agents (CWA) [14–16]. In addition, IMS has been implemented for environmental monitoring [17,18]. Advances in technology, design, and commercialization of IMS instruments are some of the reasons that facilitated the successful development of this technique. These instruments have low cost and power requirements, rugged design, and small size. IMS provides fast, reliable, and sensitive response for many pollutants.

As is already known, determination of triazines by instrumental techniques requires an extensive and time consuming step of sample preparation that usually includes an extraction step and a cleanup procedure in order to obtain a final extract fully compatible with the instrumental determination. In the last few years, several papers can be found dealing with some of the new trends in chemical residue analysis, focused mainly in the reduction of sample preparation as this is the main source of errors and the most time consuming [19]. In this way, several authors [20–22] indicate the need for a simplification in the sample preparation accounting for a miniaturization in scale which will also result in a reduction of time and solvent consumption [23].

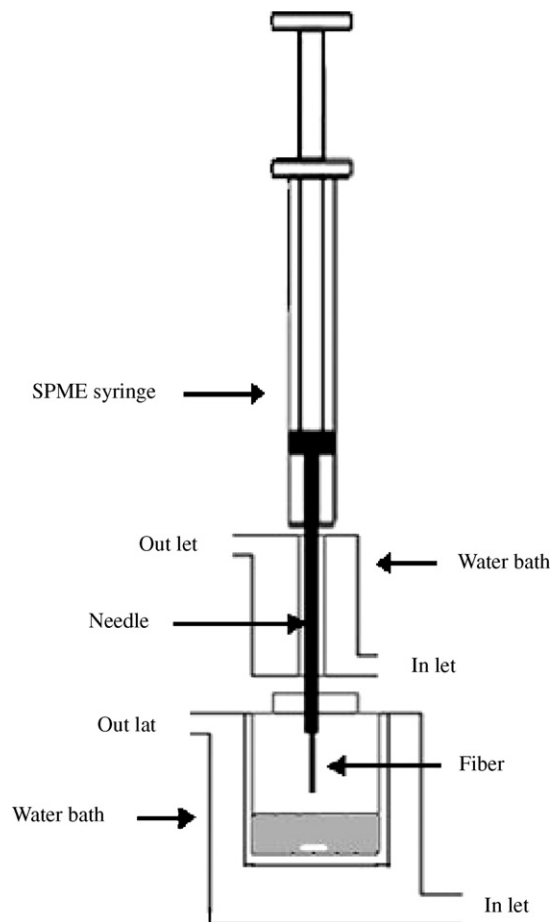
Solid-phase microextraction (SPME) appears to be solvent-free extraction technique that presents some of the characteristics outlined before as primordial in new sample preparation strategies. SPME integrates sampling, extraction, concentration and sample introduction into a single step. The initial concepts on SPME application were published in 1989 by Belardi and Pawliszyn [24], and the following rapid development resulted in first SPME device in 1990 [25]. Finally, the SPME device based on a reusable microsyringe was commercialized in 1993 by Supelco, together with the coated fibers used for extraction, which were initially polydimethylsiloxane (PDMS) and polyacrylate (PA), and that have now extended to other coatings as Carbowax–divinylbenzene, PDMS–divinylbenzene and Carboxen–PDMS. SPME can present flexible extraction ability by changing different fiber coatings.

Since 1995, the soil concentration of 21 compounds from five herbicide families has been determined using SPME methods. Originally, researchers used a soil/water suspension that was sampled either by direct insertion (DI) or headspace solid-phase microextraction (HS-SPME) [26–29]. HS-SPME with sampling from the headspace above the sample can especially offer a high potential in soil/water suspension analysis, for producing neat spectra and protecting the fiber from irreversible damages by non-volatile concomitants present in the soil matrix.

The coupling of SPME to IMS combines rapid sampling with rapid detection while improving sensitivity and selectivity. SPME provides several benefits as a sampling method including the pre-concentration of analytes and the decreases of the extraction time. IMS offers simplicity, high sensitivity and short analysis times for volatile compounds. Both SPME and IMS have been used in independent analyses but very few papers have reported the direct coupling of these two techniques [10,16,29,30].

To achieve more selective determination of different classes of compounds, the number of available coating materials has increased in recent time. In our previous studies [13,31,32], the electrochemical fiber coating (EFC) technique was used for the preparation of dodecylsulfate-doped polypyrrole (PPy-DS), and applied as a new fiber for SPME procedures. In continuation of our research activities, for the first time, the efficiency of PPy-DS as a new fiber for extraction and determination of triazines by HS-SPME device coupled with IMS is described.

Due to the ability of HS-SPME to effective and rapid sampling of triazines from different matrices, and the success of IMS as a method for the separation and quantitative determination of organics in the gas phase, the present study combines HS-SPME with IMS to analyze triazines in soil and water samples. It offers



**Scheme 1.** Diagram of the HS-SPME apparatus.

further evidence of the applicability of HS-SPME–IMS to the analysis of these compounds in soils and water, reveals a successful extraction of triazines by PPy-DS fiber. Some important parameters on the extraction efficiency were investigated. Analytical parameters of the method, i.e. linearity, detection limits, recovery and repeatability were established at low level of concentration ( $\mu\text{g g}^{-1}$  for soil and  $\text{ng mL}^{-1}$  for water). The optimized method is proposed as an efficient alternative to more expensive, time consuming conventional methods. The influence of these different matrices (soil and water) on HS-SPME analysis was evaluated using spiked samples.

**Table 1**  
IMS operation parameters.

Parameter	Setting
Corona voltage	2.5 kV
Drift field	7.5 kV
Drift gas flow ( $\text{N}_2$ )	$500 \text{ mL min}^{-1}$
Carrier gas flow ( $\text{N}_2$ )	$150 \text{ mL min}^{-1}$
Cell oven temperature	$180^\circ \text{C}$
Injection temperature	$220^\circ \text{C}$
Drift tube length	11 cm
Calibrant ion	$(\text{H}_2\text{O})_n\text{H}^+$
Shutter grid pulse	$200 \mu\text{s}$
Scan time	40 ms
Number of scan average for a spectrum	12

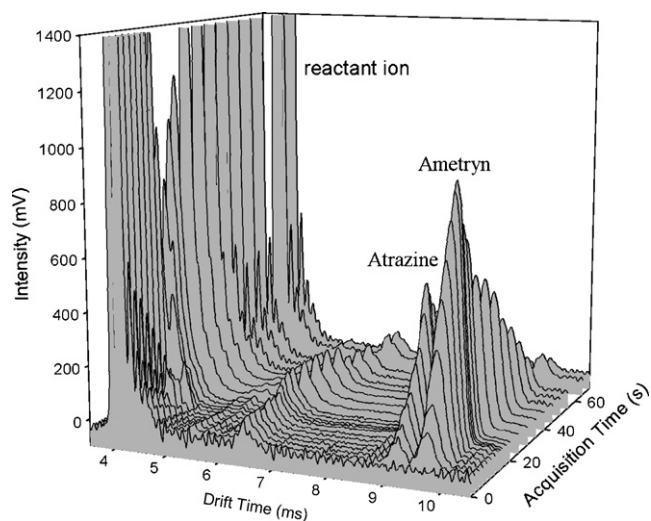


**Fig. 1.** The section of the watershed 3D plot of the ion mobility spectrum obtained by HS-SPME-IMS using a PPy-DS fiber for water sample spiked with both atrazine and ametryn ( $200 \text{ ng mL}^{-1}$ ) IMS at  $220^\circ\text{C}$ .

## 2. Experimental

### 2.1. Reagents

Atrazine and ametryn were obtained from Sigma–Aldrich (Steinheim, Germany). The stock solution of these compounds was prepared with concentration of  $1 \text{ mg mL}^{-1}$  in methanol. These stock standard solutions were diluted with methanol to prepare a mixed standard solution with concentration of  $10 \mu\text{g mL}^{-1}$  for each compound. The model samples containing the required amount of each analyte ( $100\text{--}6000 \text{ ng g}^{-1}$  for soil and  $5\text{--}3000 \text{ ng mL}^{-1}$  for water) were prepared by addition of mixed standard solution. Stock and working standards were stored at  $4^\circ\text{C}$  in the refrigerator. Pyrrole from Fluka (Buchs, Switzerland) was distilled before the use. Double-distilled water was used for preparation of soil/water suspension. The pH of water was adjusted with sodium bicarbonate to saturate the samples, sodium chloride and methanol used in this study all were obtained from Merck (Darmstadt, Germany) with analytical reagent grade. Sodium dodecylsulfate (SDS) was of maximum purity available and obtained from Sigma–Aldrich.

### 2.2. Apparatus

The SPME holder for manual sampling is obtained from Azar Electrode (Ourumieh, Iran). Stirring of the solution was carried out with a magnetic stirrer (Heidolph MR 3001 K) and a  $6 \text{ mm} \times 9 \text{ mm}$  stirring bar. Circulating water bathes (Frigomix B. Braun UM-S) were used for adjusting the temperature of sample suspension with accuracy of  $\pm 0.1^\circ\text{C}$ . Also, a two-compartment recirculating tube laboratory-made from stainless steel was used for cooling of SPME needle. In order to reach a temperature very close to that of the cooling bath, the internal surface of the inner tube was just touching the external surface of the syringe needle (Scheme 1).

Electrochemical polymerization of pyrrole was carried out using Behpajuh (BHP 2061-C model) potentiostat (Isfahan, Iran). An electrochemical cell including a platinum (Pt) working electrode ( $2 \text{ cm} \times 200 \mu\text{m}$  o.d.), a Pt counter electrode and a double junction saturated calomel electrode (dj-SCE), as reference electrode was used for preparation of the polymer.

The ion mobility spectrometer that was utilized for all experiments was constructed at Isfahan University of Technology. The main parts of the instrument are: the IMS cell, the needle for producing the corona, two high-voltage power supplies, a pulse

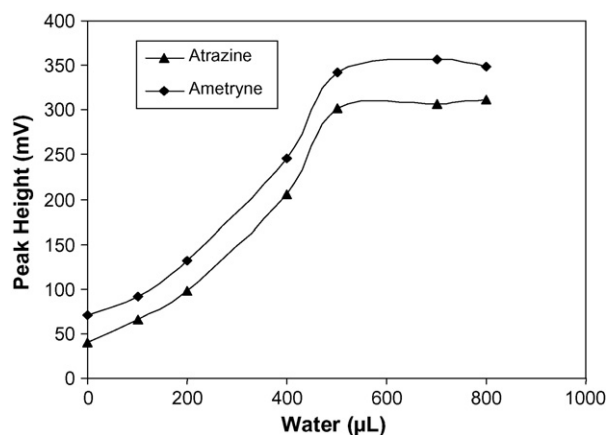


**Fig. 2.** Effect of distilled water added on the extraction efficiency of atrazine and ametryn in soil using PPy-DS fiber. SPME conditions:  $1 \text{ g}$  standard soil ( $1 \mu\text{g g}^{-1}$ ); pH 10; extraction time, 45 min; extraction temperature,  $65^\circ\text{C}$ ; stirring speed, 300 rpm.

generator, an analog to digital converter and a computer. Corona discharge ionization source with positive mode was used in these experiments. The drift length was 11 cm and an electric field of  $7.5 \text{ kV cm}^{-1}$  was used. The shutter grid is made of two series of parallel wires biased to a potential, creating an orthogonal field relative to the drift field, to block ion passage to the drift tube. The grid potential is removed for a short period of time by the pulse generator, to admit an ion pulse to the drift region. Generally, this period of time was selected  $200 \mu\text{s}$ . The IMS cell was housed in a thermostated oven in which temperature was controlled within  $\pm 1^\circ\text{C}$ .

The sample introduction was performed by thermal desorption of analytes over the SPME fiber in injection port. The drift and carrier gas were both, nitrogen and passed through a  $13\times$  molecular sieves (Fluka) trap to remove water vapor and other possible contaminations before entering into the IMS cell. The optimized experimental conditions for obtaining the ion mobility spectra of the compounds are listed in Table 1.

### 2.3. Preparation of spiked soil and water samples

The soil samples were air-dried at room temperature for more than 2 weeks and sieved to a particle size of less than  $0.3 \text{ mm}$ . These samples were spiked as follows:  $1 \text{ g}$  of each soil was spiked with a mixed standard solution of atrazine and ametryn to obtain a final concentration of  $1 \mu\text{g g}^{-1}$  of each analyte. The spiked soil was then placed in a  $4 \text{ mL}$  screw cap glass vial. To evaporate the organic solvent from the soil matrix, the spiked sample was held at room temperature ( $25^\circ\text{C}$ ) for 24 h before analysis, in order to obtain a dry and homogenous sample.

Standard solutions or water samples were adjusted to pH 10 with concentrated phosphate buffer and the ionic strength was fixed at  $4.8 \text{ mol L}^{-1}$  using sodium chloride. A  $7 \text{ mL}$  volume of sample was placed in a  $12 \text{ mL}$  glass vial with a magnetic stirring bar, then the vials were closed with a PTFE/silicon septum and tightly sealed with an aluminum cap to prevent sample loss due to evaporation.

### 2.4. Electrochemical fiber coating

Polypyrrole film was prepared electrochemically using a three-electrode system. In order to ensure film reproducibility, all PPy-DS films were synthesized using the identical electrochemical cyclic voltammetric procedure in a three-electrode cell. Platinum working and auxiliary electrodes were submerged in aqueous solution containing  $7 \times 10^{-3} \text{ mol L}^{-1}$  SDS and  $0.1 \text{ mol L}^{-1}$  pyrrole monomer, and bubbled with nitrogen for about 10 min. The cyclic voltammet-

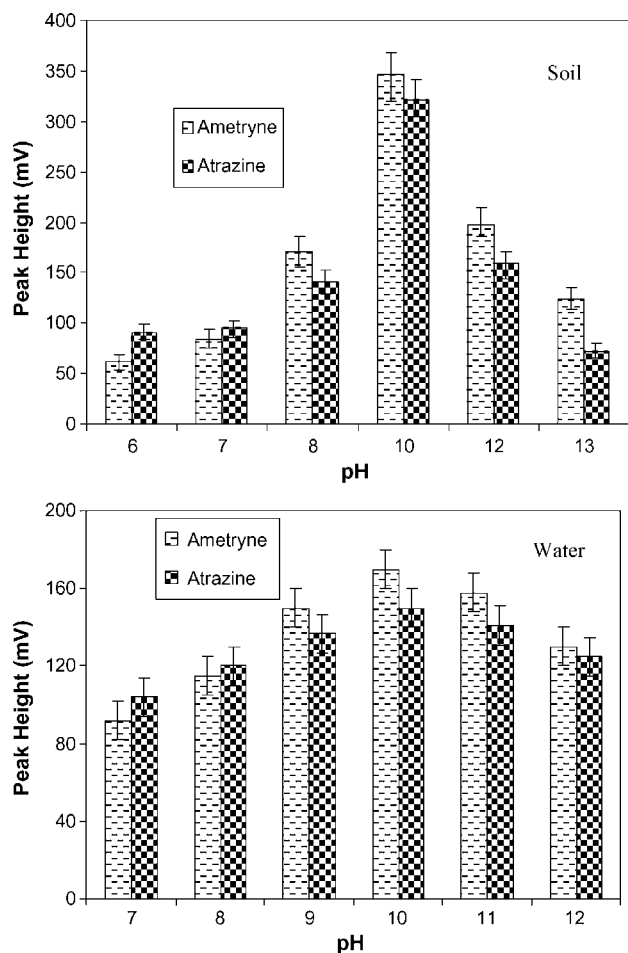


**Fig. 3.** Influence of the pH on the HS-SPME-IMS responses of atrazine and ametryn in soil and water samples using PPy-DS fiber, NaCl 4.8 mol L<sup>-1</sup>, extraction temperature, 65 °C, extraction time 45 min. For soil: concentration of atrazine and ametryn, 1 μg g<sup>-1</sup> respectively; the water added, 500 μL; stirring speed, 300 rpm. For water sample: concentration of atrazine and ametryn, 170 and 140 ng mL<sup>-1</sup> respectively; stirring speed, 700 rpm.

ric scanning (10 cycles) from 0.5 to 1.2 V at a scan rate of 20 mV s<sup>-1</sup> was performed. The thickness of the PPy-DS coating obtained under this condition was 16 μm according to the SEM study. The PPy fiber is connected to a stainless steel tubing of SPME holder. It was heated at 100 °C for 20 min in oven and finally conditioned at 280 °C in a GC injection port under helium gas for an hour, before it was used for SPME experiment.

### 2.5. HS-SPME/IMS of atrazine and ametryn

All extractions were performed in 4 mL amber vials with polytetrafluoroethylene lined silicone septa screw top caps for soil samples. A 500 μL of double-distilled water saturated out with NaCl was added to the spiked soil. The volume of water added to the soil was large enough to form slurry. After the addition of a magnetic stirring bar, the vial was tightly enclosed by septa screw top cap, to prevent sample loss due to evaporation. The vial was stirred by magnetic stirring and thermostated using a heated circulating water bath at 65 °C, for 10 min before HS-SPME, to reach equilibrium. The PPy fibers housed in manual SPME holder were used. Fibers were conditioned prior to use by inserting them into the IMS injection port for 5 min. The needle of the SPME syringe was first passed through the cooling tube, and then the septum of the vial was pierced with the SPME device. The fiber was pushed out of the needle into the headspace above the sample for 10–100 min, depending

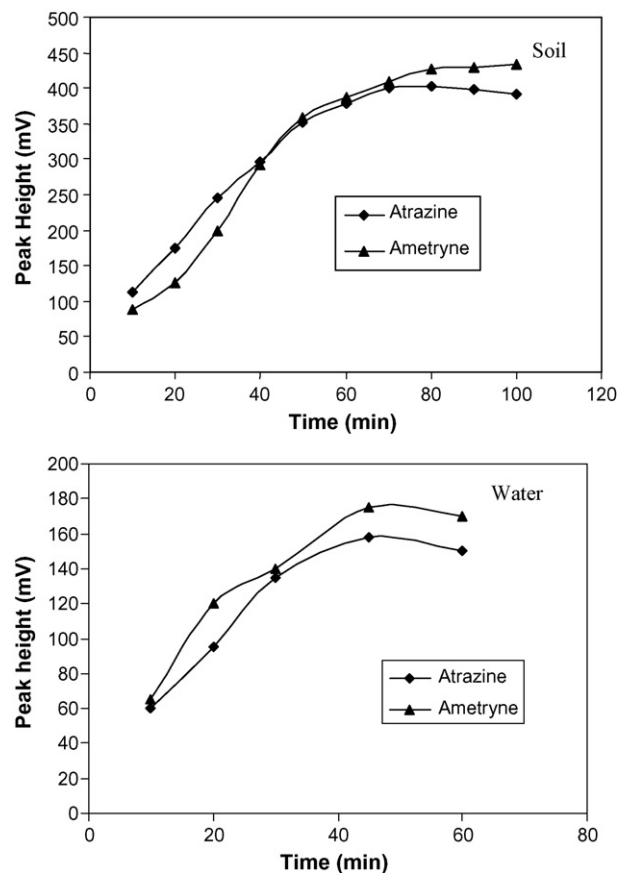


**Fig. 4.** Influence of extraction time on the HS-SPME-IMS responses of atrazine and ametryn in soil and water samples using PPy-DS fiber, NaCl 4.8 mol L<sup>-1</sup>, extraction temperature, 65 °C. For soil: concentration of atrazine and ametryn, 1 μg g<sup>-1</sup> respectively; the buffered water added (pH 10) 500 μL; stirring speed, 300 rpm. For water sample: concentration of atrazine and ametryn, 170 and 140 ng mL<sup>-1</sup> respectively; stirring speed, 700 rpm.

on the experiment. After completion of sampling step, the fiber was withdrawn into the needle and removed from the sample vial. The fiber was then immediately inserted into the injection port of the IMS.

## 3. Result and discussion

### 3.1. IMS conditions

In IMS, ion drift times are often reported as reduced mobility constants for identification purposes. This metric provides a basis for comparison of results by correcting for varying environmental and instrumental experimental conditions. Reduced mobilities are calculated for positive ion mode using (H<sub>2</sub>O)<sub>n</sub>H<sup>+</sup> as the calibrant. The reduced mobility is normalized to a standard pressure (760 Torr) and temperature (273 K). Reduced mobility can be calculated using Eq. (1),

$$K_o(\text{unknown}) = K_o(\text{standard}) \times t_d(\text{standard})/t_d(\text{unknown}) \quad (1)$$

where  $K_o$  is the reduced mobility with the units of (cm<sup>2</sup> V<sup>-1</sup> s<sup>-1</sup>), and  $t_d$  is the drift time. Direct sampling of standard atrazine and ametryn was used in order to determine the characteristic drift times and the reduced ion mobilities used for identification of triazines in the samples. The reduced mobilities obtained for the atrazine and ametryn were 1.185 and 1.141 cm<sup>2</sup> V<sup>-1</sup> s<sup>-1</sup>, respectively. The correlation between ionic mass and reduced mobility values can be described by mass-to-mobility correlation curves

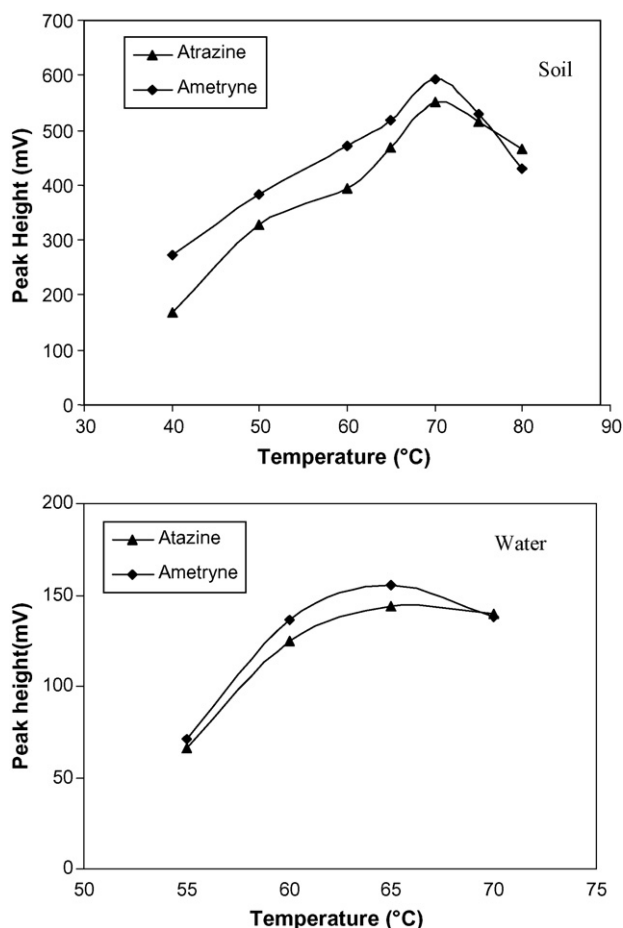


**Fig. 5.** Effect of extraction temperature on the HS-SPME-IMS responses of atrazine and ametryn in soil and water samples using PPy-DS fiber, NaCl 4.8 mol L<sup>-1</sup>. For soil: concentration of atrazine and ametryn, 1 μg g<sup>-1</sup> respectively; the buffered water added (pH 10) 500 μL; extraction time, 60 min; stirring speed, 300 rpm. For water sample: concentration of atrazine and ametryn, 170 and 140 ng mL<sup>-1</sup> respectively; extraction time, 45 min; pH 10; stirring speed, 700 rpm.

[33,34]. The regression equation of the mass-to-mobility correlation curve for corona discharge IMS is as shown in Eq. (2)

$$\log m = -0.52K_0 + 2.95 \quad (2)$$

where  $m$  is mass of product ions or clustering with water. The mass-to-mobility of the atrazine and ametryn peaks was calculated as 215 and 226, respectively which could be interpreted as the protonated molecular ion. The mass-to-mobility values are clearly in

good agreement with the reported mass spectrometry data in literature [35,36].

### 3.2. Optimization of HS-SPME process

Development of a particular procedure for determination of triazines using the HS-SPME technique requires the optimization of the variables related to both extraction and desorption steps, pH effect, extraction time, extraction temperature, salt effect, desorption time, desorption temperature and including the volume of water added for the soil samples. The maximum of peak heights of atrazine and ametryn as the IMS response were used to evaluate the extraction efficiency under different conditions. Three replicate extractions and determinations were performed for each level.

The watershed 3D plot of the ion mobility spectra of atrazine and ametryn are shown in Fig. 1. This figure shows that the corona discharge ionization source with positive mode permits the simultaneous detection of target compounds. The peak heights are changed during the acquisition time (from the injection time until the sample peaks disappear). The product ion peaks appear after a short time, reach a maximum and decay almost exponentially.

Fig. 1 shows the time profile of desorption process of atrazine and ametryn in IMS at 220 °C from the PPy-DS during the 60 s desorption period. The desorption time that produces the maximum analyte response, defined as  $T_{Dmax}$  [11] occurs at 35 s for ametryn and 40 s for atrazine. The 5 s difference in  $T_{Dmax}$  can be attributed to the difference in boiling points of the two analytes. After the maximum desorption time points, the responses tail off as less analyte remains in the PPy-DS fiber.

The desorption temperature is a major parameter affecting SPME efficiency. A temperature study of desorption profile of triazines was conducted by desorbing the analytes at 150, 180, 200, 220, 240 and 260 °C, with all other parameters remaining constant. The desorption temperature rises, the maximum peak height also increases, which enhances the sensitivity of the method (figure not show). The carry over was measured with one blank injection following the initial desorption. At the desorption temperature of 220 °C, analytes are fully desorbed from the fiber coating after 60 s and no carry over effect was observed in blank injection.

The degree of partitioning of semi-volatile organic compounds between the soil and the headspace is generally low, and the addition of small amounts of water can facilitate the desorption and vaporization of analytes, as indicated by Zhang and Pawliszyn [37,38], due to the release of volatile organic compounds from their absorption sites in the soil by the polar water molecules. Responses obtained when different amounts of water solution ranging from 0 to 800 μL were added into the 1 g spiked soil system using HS-SPME-IMS procedure are given in Fig. 2. As can be seen from the Fig. 2, the response obtained in the dry soil system is rather low

**Table 2**

Dynamic linear range (DLR), correlation coefficient ( $R^2$ ), repeatability (RSD%,  $n = 7$ ) and limit of detections for the analysis of atrazine and ametryn in soil and water samples with HS-SPME-IMS using PPy-DS fiber and comparison with other methods.

Analyte	Matrix	DLR (ng g <sup>-1</sup> )	$R^2$	LOD (ng g <sup>-1</sup> )	RSD%	Method
Atrazine	Soil	200–4000	0.992	37	9.2	HS-SPME-IMS
Ametryne	Soil	200–4000	0.996	23	8.3	This work
Atrazine	Soil	–	–	30	11	SPME-GC-ECD [39] <sup>a</sup>
Atrazine	Soil	–	–	10	10	SPME-GC-MS [40] <sup>b</sup>
Atrazine	Tap water	0.5–30	0.999	0.1	25	SPME-GC-MS [3] <sup>c</sup>
Ametryne	Tap water	–	0.991	0.2	–	
Atrazine	Surface water	0.006–40	0.9951	0.006	8.1	SPME-GC-MS [41] <sup>d</sup>
Ametryne	Surface water	0.01–50	0.9974	0.01	7	
Atrazine	Well water	70–2100	0.9954	15	9.7	HS-SPME-IMS
Ametryne	Well water	50–2800	0.9964	10	8.8	This work

Fiber type: (a) polydimethylsiloxane (PDMS), (b) Carbowax/divinylbenzene CW/DVB, (c) polyacrylate (PA), (d) polydimethylsiloxane/divinylbenzene (PDMS/DVB).

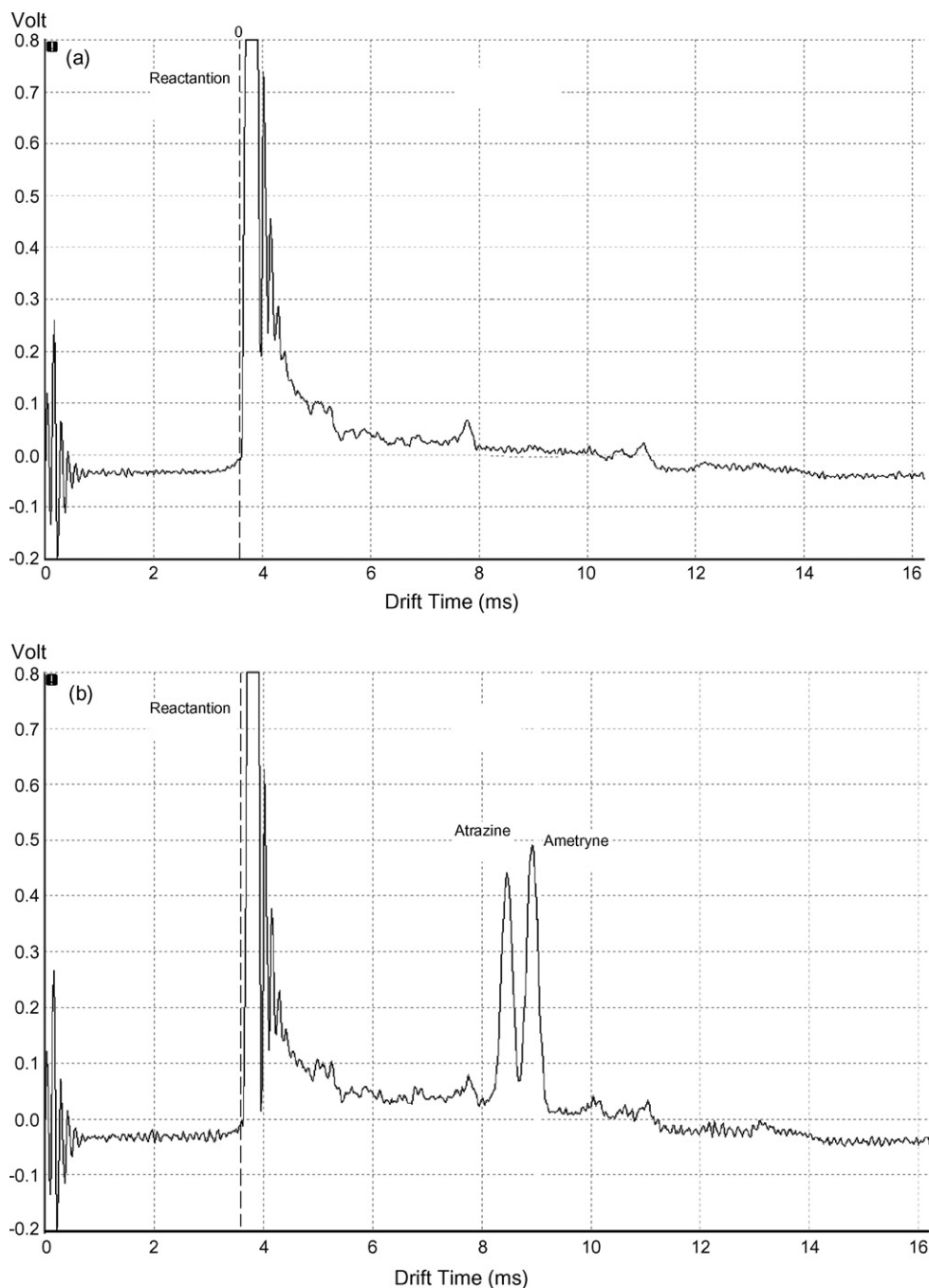


**Fig. 6.** The ion mobility spectrum obtained by HS-SPME-IMS using a PPy-DS fiber for soil sample under optimum conditions: (a) non-spiked and (b) spiked with  $600 \text{ ng g}^{-1}$  of atrazine and ametryn.

in contrast to that obtained in the wet soil system. An important increase in the response for triazines can be observed with the addition of 0–800  $\mu\text{L}$  of water. The response reached the maximum when 500  $\mu\text{L}$  of water was added into the soil, which is large enough to form slurry. An improvement in sensitivity against the dry sample occurred, because the addition of higher amounts of water would dilute the concentration of the analytes and increase the diffusion barrier of triazines from aqueous phase to gaseous phase.

The sample pH is an important factor, which may affect the recovery of triazines from water. To study the effect of sample pH on the extraction of atrazine and ametryn from samples, the fiber was exposed to the headspace of samples at different pH values (6–13). All results were obtained in three replicates to ensure reproducibility.

**Fig. 3** shows the IMS responses obtained at each pH and clearly, the maximum recovery is obtained at pH 10 for both soil and water samples.

Equilibrium time depends on the mass transfer of the analytes through the three-phase system: coating, headspace and matrix. It is generally accepted that the reduction of the diffusion layer is essential in order to reach equilibrium faster, which is easily achieved by sample agitation. Therefore, magnetic stirring was applied during the extraction step. **Fig. 4** shows a typical time profile for SPME process. The time to reach equilibration is about 80 and 45 min for soil and water respectively.

**Fig. 5** represents the extraction temperature profile for HS-SPME analysis. The amount of triazines extracted increased

**Table 3**  
HS-SPME–IMS determination of atrazine and ametryn in soil and water samples.

Sample		Concentration (ng g <sup>-1</sup> )		RSD% (n = 5)	Relative error %
		Added	Found		
Soil I	Atrazine	200	188	6.7	6.0
	Ametryn	200	196	5.4	2.0
Soil II	Atrazine	200	191	7.2	4.5
	Ametryn	200	193	6.1	3.5
Soil III	Atrazine	200	189	6.5	5.5
	Ametryn	200	198	4.9	1.0
Well water I	Atrazine	200	201	6.3	0.5
	Ametryn	200	199	7.3	0.5
Well water II	Atrazine	200	197	6.5	1.5
	Ametryn	100	98	10	2.0

with the increase in temperature, and decreased above 70 and 65 °C for soil and water matrix. This is mainly because the extraction temperature has two opposing effects on the SPME technique. Increasing temperature enhances the diffusion coefficient of analytes, which effectively transfer from the matrix to the fiber coatings; on the other hand, as the adsorption is an exothermic process, increasing temperature reduces the distribution constant of the analytes, resulting in a diminution in the equilibrium amount of analytes extracted. Finally, the extraction temperatures were selected at 70 and 65 °C as an optimized value of this parameter for soil and water samples.

The addition of NaCl to the sample increases the extraction efficiency of triazines.

The amount of triazines extracted greatly enhanced with the increase of salt concentration. The addition of salt increases the ionic strength of the samples. This makes triazines less soluble and forces them to migrate. Therefore, a higher equilibrium concentration of triazines can be achieved in the PPy-DS fiber. A NaCl concentration of 4.8 mol L<sup>-1</sup> was thus chosen to ensure maintaining high analyte responses.

### 3.3. Quantitative analysis

The optimized HS-SPME procedures of spiked soil and water samples were evaluated with respect to dynamic linear range, reproducibility and limit of detection (LOD).

The HS-SPME procedure with PPy-DS fiber for atrazine and ametryn showed excellent linearity in concentrations ranging from 200 to 4000 ng g<sup>-1</sup> and 50 to 2800 ng mL<sup>-1</sup> in soil and water samples, respectively with correlation coefficient of 0.992–0.996. The repeatability expressed as relative standard deviation (RSD) was found to be satisfactory for the proposed method, with a RSD of ≤9.7% and ≤8.8%, for atrazine and ametryn, respectively. Owing to the high sensitivity of the HS-SPME–IMS, low detection limit, about 23 and 37 ng g<sup>-1</sup>, was achieved for atrazine and ametryn in soil matrix, respectively, at a signal-to-noise ratio (S/N) of 3. The limits of detection for atrazine and ametryne in water, when using the optimized conditions, were determined to be 15 and 10 ng mL<sup>-1</sup>, respectively.

The resulting HS-SPME–IMS liner range and detection limits using PPy-DS as a new fiber were compared with those obtained using commercial fibers previously reported in literature [39,40,3,41], Table 2. The HS-SPME–IMS procedure showed a satisfactory linear behavior in the tested range, with correlation coefficients >0.99 for extraction and determination of triazines in soil and water samples.

### 3.4. Environmental soil and water samples analysis

The reliability of the proposed method to the real samples was investigated for three agricultural soils and two well water samples. HS-SPME of non-spiked samples provided an ion mobility spectrum without any peaks which is related to atrazine and ametryn. Thus, the samples were spiked with 200 ng g<sup>-1</sup> of atrazine and ametryne, and five replicate analyses were performed for each sample using HS-SPME followed by IMS at optimal conditions. The ion mobility spectrum obtained of non-spiked and spiked soil samples is shown in Fig. 6. The results obtained by the proposed method and amounts added are in satisfactory agreement. The analytical results are summarized in Table 3.

## 4. Conclusion

A simple and sensitive HS-SPME–IMS method with dodecylsulfate-doped polypyrrole film as a new fiber was introduced and evaluated to quantify atrazine and ametryne in soil and water samples. The use of HS-SPME as a sample preparation step allows the easy and fast extraction and very good recovery values of triazines, whereas IMS offers simplicity and short analysis times as a detector. The method proposed in this study showed high linearity, low detection limit, satisfactory precision and accuracy. Therefore, the experimental results demonstrated the potential of the HS-SPME–IMS method with PPy-DS fiber for the simultaneous determination of atrazine and ametryn in soil and water samples (since analytes are separated in the drift tube of the IMS), which requires just a few milliseconds versus 30–40 min needed for their chromatographic separation with GC or LC based techniques.

## Acknowledgements

The financial support of the Research Council of Tarbiat Modares University and the Iran National Science Foundation (INSF) are gratefully acknowledged.

## References

- [1] C.M. Aelion, P.P. Mathur, Environ. Toxicol. Chem. 20 (2001) 2411.
- [2] C. Crescenzi, in: R.A. Meyers (Ed.), Encyclopedia of Analytical Chemistry, Wiley, West Sussex, 2000, p. 6582.
- [3] C. Aguilar, S. Penalver, E. Pocrull, F. Borrull, R.M. Marce, J. Chromatogr. A 795 (1998) 105.
- [4] A. Navalon, A. Prieto, L. Araujo, J.L. Vilchez, J. Chromatogr. A 946 (2002) 239.
- [5] J. Beltran, F.J. Lopez, O. Cepria, F. Hernandez, J. Chromatogr. A 808 (1998) 257.
- [6] R. Carabias-Martinez, E. Rodriguez-Gonzalo, M.E. Fernandez-Laespada, L. Calvo-Seronero, F.J. Sanchez-San Roman, Water Res. 37 (2003) 928.
- [7] S. Frias, M.J. Sanchez, M.A. Rodriguez, Anal. Chim. Acta 503 (2004) 271.
- [8] T. Khayamian, M. Tabrizchi, M.T. Jafari, Talanta 59 (2003) 327.
- [9] J. Yinon, Trends Anal. Chem. 21 (2002) 292.
- [10] J.K. Lokhnauth, N.H. Snow, J. Chromatogr. A 1105 (2006) 33.
- [11] N. Takayama, R. Iio, S. Tanaka, S. Chinaka, K. Hayakawa, Biomed. Chromatogr. 17 (2003) 74.
- [12] L.M. Matz, H.H. Hill, Anal. Chim. Acta 457 (2002) 235.
- [13] N. Alizadeh, A. Mohammadi, M. Tabrizchi, J. Chromatogr. A 1183 (2008) 21.
- [14] K. Tuovinen, H. Paakkanen, O. Hanninen, Anal. Chim. Acta 440 (2001) 151.
- [15] W.E. Steiner, B.H. Clowers, L.M. Matz, W.F. Siems, H.H. Hill, Anal. Chem. 74 (2002) 4343.
- [16] P. Rearden, P.B. Harrington, Anal. Chim. Acta 545 (2005) 13.
- [17] G.A. Eiceman, Z. Karpas, Ion Mobility Spectrometry, CRC Press, Boca Raton, 1994.
- [18] H. Borsdorf, A. Rammner, J. Chromatogr. A 1072 (2005) 45.
- [19] J. Sherma, J. AOAC 82 (1999) 561.
- [20] A. Balinova, J. Chromatogr. A 754 (1996) 125.
- [21] C.F. Poole, S.K. Poole, Anal. Commun. 33 (1996) 11.
- [22] S.K. Poole, C.F. Poole, Anal. Commun. 33 (1996) 15.
- [23] H.B. Wan, M.K. Wong, J. Chromatogr. A 754 (1996) 43.
- [24] R.P. Belardi, J. Pawliszyn, Water Pollut. Res. J. Canada 24 (1989) 179.
- [25] C.L. Arthur, J. Pawliszyn, Anal. Chem. 62 (1990) 2145.
- [26] A.A. Boyd-Boland, J.B. Pawliszyn, J. Chromatogr. A 704 (1995) 163.
- [27] A.A. Boyd-Boland, S. Magdic, J.B. Pawliszyn, Analyst 121 (1996) 929.
- [28] M. Moder, P. Popp, R. Eisert, J. Pawliszyn, Fresenius J. Anal. Chem. 363 (1999) 680.
- [29] C. Wu, B. Abraham, J. Wronka, Abstr. Pap. Am. Chem. Soc. 219 (2000) 230.



- [30] X. Liu, S. Nacson, A. Grigoriev, P. Lynds, J. Pawliszyn, *Anal. Chim. Acta* 559 (2006) 159.
- [31] A. Mohammadi, Y. Yamini, N. Alizadeh, *J. Chromatogr. A* 1063 (2005) 1.
- [32] N. Alizadeh, H. Zarabadipour, A. Mohammadi, *Anal. Chim. Acta* 605 (2007) 159.
- [33] H. Borsdorf, H. Schelhorn, J. Flachowsky, H.R. Döring, J. Stach, *Anal. Chim. Acta* 403 (2000) 235.
- [34] S.E. Bell, R.G. Ewing, G.A. Eiceman, *J. Am. Soc. Mass Spectrom.* 5 (1994) 177.
- [35] G. Shen, H.K. Lee, *J. Chromatogr. A* 985 (2003) 167.
- [36] H. Bagheri, F. Khalilian, *Anal. Chim. Acta* 537 (2005) 81.
- [37] Z. Zhang, J. Pawliszyn, *J. High Resolut. Chromatogr.* 16 (1993) 389.
- [38] Z. Zhang, J. Pawliszyn, *Anal. Chem.* 67 (1995) 34.
- [39] A. Bouaid, L. Ramos, M.J. Gonzalez, P. Fernandez, C. Camara, *J. Chromatogr. A* 939 (2001) 13.
- [40] F. Hernandez, J. Beltran, F.J. Lopez, J.V. Gaspar, *Anal. Chem.* 72 (2000) 2313.
- [41] S. Frias, M.A. Rodriguez, J.E. Conde, J.P. Perez-Trujillo, *J. Chromatogr. A* 1007 (2003) 127.



## Evaluation of biodiesel–diesel blends quality using $^1\text{H}$ NMR and chemometrics

Marcos Roberto Monteiro<sup>a,\*</sup>, Alessandra Regina Pepe Ambrozin<sup>a</sup>, Maiara da Silva Santos<sup>b</sup>,  
Elisângela Fabiana Boffo<sup>b</sup>, Edenir Rodrigues Pereira-Filho<sup>b</sup>, Luciano Moraes Lião<sup>c</sup>,  
Antonio Gilberto Ferreira<sup>b</sup>

<sup>a</sup> Laboratório de Combustíveis, Centro de Caracterização e Desenvolvimento de Materiais, Departamento de Engenharia de Materiais, Universidade Federal de São Carlos, Rodovia Washington Luiz, km 235, 13560-971 São Carlos, SP, Brazil

<sup>b</sup> Departamento de Química, Universidade Federal de São Carlos, 13560-905 São Carlos, SP, Brazil

<sup>c</sup> Instituto de Química, Universidade Federal de Goiás, Campus Samambaia, 74001-970 Goiânia GO, Brazil

### ARTICLE INFO

#### Article history:

Received 19 August 2008

Received in revised form 9 December 2008

Accepted 10 December 2008

Available online 24 December 2008

#### Keywords:

Biodiesel–diesel blends

Adulteration

NMR

Chemometrics

PLS

PCR

### ABSTRACT

In this work, the use of  $^1\text{H}$  NMR spectroscopy and statistical approach to the evaluation of biodiesel–diesel blends quality is described. Forty-six mixtures of oil–diesel, biodiesel–diesel, and oil–biodiesel–diesel were analyzed by  $^1\text{H}$  NMR and such data were employed to design four predictive models. Thirty-six mixtures were used in the calibration set and the others in the validation. The PCR and PLS models were evaluated through statistical parameters.

Briefly, PLS and PCR models were suitable for the prediction of biodiesel and oil concentration in mineral diesel. Specially, in higher concentration the predicted values were quite similar to the real ones. This fact was evidenced by the low relative errors of high concentrated samples; this means that the prediction of low concentrated samples will probably show high deviation. Therefore,  $^1\text{H}$  NMR-PLS and  $^1\text{H}$  NMR-PCR methods are fairly useful for the quality control of biodiesel–diesel blends, particularly they are suitable for prediction of concentrations greater than 2%.

© 2008 Elsevier B.V. All rights reserved.

### 1. Introduction

The use of ethanol and biodiesel, called alternative fuels or bio-fuels, has increased in the last few years due to environmental, economical, and social issues [1,2]. Biodiesel is basically composed of fatty acid mono-alkyl esters, which are in general obtained through the base-catalyzed transesterification reaction of vegetable oils or animal fats with a short chain alcohol, such as methanol or ethanol. This biofuel is the major substitute for petroleum-derived diesel since its physical properties are very similar to diesel, allowing the use of pure or blended biodiesel without any modification in the diesel engine and in the existing fuel distribution and storage infrastructure [1,3]. Recently, blends of biodiesel with mineral diesel became commercial all over the world. In the United States of America, the utilization of B20 (20% of biodiesel in diesel) is usual, while Europe and Brazil employ B2 blends [4–6].

Besides mono-alkyl esters, the final transesterification mixture could contain glycerol, alcohol, catalyst, free fatty acids, tri-, di- and monoglycerides [7–9]. An uncovered biodiesel and insufficient purification steps afford a bad-quality biodiesel, whose contami-

nants will probably lead to severe operational and environmental problems. Moreover, inadequate transport, handling and storage, or even adulteration with vegetable oils can affect the quality of biodiesel–diesel blends. In fact, the quality control of such mixtures is greatly significant to their successful commercialization and market acceptance.

The most important quality parameters of biodiesel (fatty mono-alkyl esters, fatty acids, glycerol and their acyl derivatives) are commonly analyzed by chromatography, mainly gas chromatography (GC) and high performance liquid chromatography (HPLC). Spectroscopic methods are most employed for monitoring the transesterification reaction and for the determination of blend level. However, biodiesel and its mixtures with diesel could be also analyzed by procedures based on physical properties [10]. Recently, several analytical methods have been developed to determine the concentration of biodiesel in mixtures with diesel [4,10–21], but few investigations have been done in order to detect impurities in these blends [22,23].

Nuclear magnetic resonance (NMR) is a versatile spectroscopic method that has become one of the most powerful techniques for the elucidation of the structure of chemical compounds. Especially, this technique is a powerful tool for fuel analysis without the need of any physical separation or pretreatment. Also,  $^1\text{H}$  NMR measurements are fast, can be easily automated, allowing the analysis of a large number of samples in a short period of time.

\* Corresponding author. Tel.: +55 16 3351 8843; fax: +55 16 3351 8850.  
E-mail address: [monteiro@ccdm.ufscar.br](mailto:monteiro@ccdm.ufscar.br) (M.R. Monteiro).

Frequently chemometric analysis is applied to NMR to extract desired information, since a huge amount of data is produced. In fact, chemometrics, a multivariate data analysis field that uses mathematical, statistical and logical–mathematical methods for extracting chemical information, is capable of treating large quantities of information [24,25]. Recently, the emerged interest in quantitative NMR has increased the number of applications of chemometrics to NMR [25].

Although  $^1\text{H}$  NMR is frequently used for monitoring the biodiesel synthesis and its quality [26–33], there are no reports regarding its use for determining the contamination of biodiesel–diesel blends. In the last few years, our group has developed some analytical methods, employing different techniques and chemometrics, to evaluate the quality of different fuels and biofuels. In this way, the utilization of NMR spectroscopy in combination with chemometric analysis to evaluate the quality of biodiesel–diesel blends is proposed herein. Therefore, in the present study, partial least squares regression (PLS) and principal components regression (PCR) algorithms were applied to the  $^1\text{H}$  NMR data in order to verify the quality of biodiesel–diesel samples.

## 2. Experimental

### 2.1. Chemicals and materials

Soybean oil was obtained from commercial source and two petroleum diesel samples were acquired in different gas stations in São Paulo and Goiás states (Brazil).

Methyl biodiesel from soybean oil was prepared in scale-laboratory according to a procedure described by Oliveira et al. [12]. Briefly, soybean oil was added to a solution of KOH in MeOH and such mixture was maintained under stirring for 2 h at room temperature. After this time, the phases were separated and the excess of MeOH was removed from the phase rich in methyl esters through rotatory evaporation. After that, this phase was purified using aqueous phosphoric acid solution (5%, v/v) and a saturated NaCl solution.

Both biodiesel and diesel samples were previously analyzed by  $^1\text{H}$  NMR. No significant contaminants (glycerides, glycerol, MeOH, among others) were observed in the spectrum of biodiesel. Despite the fact that the biodiesel was not composed by 100% of fatty acid

methyl esters, we did this assumption. So, the biodiesel was considered as 100% pure. The  $^1\text{H}$  NMR analyses of diesel samples allowed to verify that biodiesel was not present in them. Besides that, sulphur content, distillation profile, flash point, and specific mass of these samples were evaluated according to ASTM D 4294, ASTM D 86, NBR 14598, and NBR 14065 standards, respectively. Both diesel from São Paulo and Goiás met specifications established by Brazilian National Agency of Petroleum, Natural Gas and Biofuels (ANP) in the resolution  $n^\circ$  15 from July 19, 2006.

### 2.2. Blends preparation

Binary and ternary blends were prepared by mixing diesel with methyl soybean biodiesel and/or soybean oil to define the blend levels described in Table 1. Thirty-six blends were used in the calibration set and 10 mixtures (in bold and underlined letters in Table 1) were randomly chosen for the validation group.

### 2.3. $^1\text{H}$ NMR analyses

All  $^1\text{H}$  NMR experiments were acquired, in triplicate and at room temperature, on a Bruker DRX 400–9.4 Tesla spectrometer, using a 5 mm inverse-detection probehead with a z-gradient. The spectra were obtained at 400.21 MHz for  $^1\text{H}$ , using  $\text{CDCl}_3$  as solvent, and TMS as internal standard. For each determination, 300  $\mu\text{L}$  of the pure or blended sample was dissolved in the same volume of solvent. Sixteen pulses were employed to the acquisition of the spectra, with acquisition time of 6 s, spectral width of 5208 Hz, and relaxation delay of 1 s. Spectra were processed with 64,000 data points and using an exponential weighing factor corresponding to a line broadening of 0.3 Hz. The phase was manually corrected and the baseline was automatically corrected.

### 2.4. PCR and PLS analyses

All calculations were carried out using the Pirouette<sup>®</sup> software (v. 3.11, InfoMetrix, Woodinville, WA, USA). First of all, the  $^1\text{H}$  NMR spectra were transformed into ASCII files and the resulting data matrices were imported into the Origin software (v. 5.0, Microcal, USA) and, thus to the Pirouette<sup>®</sup>. The mean values of triplicates were used to construct the matrix. Thirty-six samples were employed for

**Table 1**  
Biodiesel–diesel blends used to design the PCR and PLS models.

Sample	Diesel (%)	Oil (%)	Biodiesel (%)	Sample	Diesel (%)	Oil (%)	Biodiesel (%)
do1	99.0	1.0	–	dob2	98.0	1.0	1.0
<b>do2</b>	98.5	1.5	–	<b>dob3</b>	98.0	1.5	0.5
do3	98.0	2.0	–	dob4	95.0	0.5	4.5
do4	97.5	2.5	–	<b>dob5</b>	95.0	1.0	4.0
<b>do5</b>	97.0	3.0	–	dob6	95.0	2.0	3.0
do6	96.5	3.5	–	dob7	95.0	3.0	2.0
<b>do7</b>	96.0	4.0	–	dob8	95.0	4.0	1.0
<b>do8</b>	95.5	4.5	–	dob9	95.0	4.5	0.5
do9	95.0	5.0	–	<b>dob10</b>	90.0	8.0	2.0
do10	94.5	5.5	–	dob11	90.0	7.0	3.0
<b>do11</b>	94.0	6.0	–	dob12	90.0	6.0	4.0
do12	93.0	7.0	–	dob13	90.0	5.0	5.0
<b>do13</b>	92.0	8.0	–	dob14	90.0	4.0	6.0
do14	91.0	9.0	–	dob15	90.0	3.0	7.0
do15	90.0	10.0	–	dob16	90.0	2.0	8.0
do16	85.0	15.0	–	dob17	80.0	18.0	2.0
do17	80.0	20.0	–	dob18	80.0	15.0	5.0
do18	75.0	25.0	–	dob19	80.0	12.0	8.0
db1	98.0	–	2.0	dob20	80.0	10.0	10.0
<b>db2</b>	95.0	–	5.0	dob21	80.0	8.0	12.0
db3	90.0	–	10.0	dob22	80.0	5.0	15.0
db4	80.0	–	20.0	dob23	80.0	2.0	18.0
dob1	98.0	0.5	1.5	d	100	–	–

Samples in bold and underlined: validation group; concentration expressed as volume %.

the calibration and 10 were used in the validation set (Table 1). Initially, an exploratory analysis was carried out, employing principal component analysis (PCA). This allowed the optimization of pre-processing and transformation parameters, which would be applied to the development of PLS and PCR calibration models. The best parameters for both were obtained using autoscaling, normalization to 100 and first order derivative (each 25 data points). The choice of number of principal components (PCs) in the calibration models was based on some statistical parameters, mainly in the low values of SEC (standard error of calibration), SEV (standard error of validation), PRESS Cal (predicted residual error sum of squares of calibration), and PRESS Val (PRESS of validation). Cross-validation and the prediction of validation set of samples were used to evaluate the models.

### 3. Results and discussion

NMR is a valuable technique for evaluation of biodiesel quality and quantification of biodiesel in mixtures with mineral diesel. A typical  $^1\text{H}$  NMR spectrum of diesel (Fig. 1) shows peaks of aromatic and aliphatic hydrogens at 8.8–6.5 ppm and 3.3–0.4 ppm. Methyl biodiesel (Fig. 1) shows a singlet near 3.6 ppm, relates to the methoxy group, which allows biodiesel quantification in diesel samples as well as the monitoring of biodiesel synthesis [4]. Biodiesel production can also be followed through the decrease of peaks at 4.4–4.0 ppm, which are assigned to hydrogens of glycerol moiety of vegetable oils (Fig. 1). So, these characteristic peaks from methyl biodiesel and oils can be used for their quantification in mineral diesel and they could be a practical manner to evaluate the quality of commercial biodiesel–diesel blends. In this way, the goal of the present work was to obtain a method for the quality assurance of biodiesel–diesel blends employing  $^1\text{H}$  NMR spectroscopy and chemometrics. For such, 46 mixtures of oil–diesel, biodiesel–diesel and oil–biodiesel–diesel (Table 1) were analyzed through  $^1\text{H}$  NMR. Besides peaks relate to aliphatic hydrogens (3.3–0.4 ppm), methoxy group (3.6 ppm), and glycerol moiety (4.4–4.0 ppm), the region of olefin hydrogens (near 5.3 ppm) was selected to design PLS and PCR models (Fig. 2). The choice of such regions was based on their significance and also on loadings plots; noise and non-informative ranges were excluded. The correct choice of spectral region in PLS and PCR design will determine both the precision and accuracy of the analytical method [34]. Previously, PLS and PCR applied to several analytical data were suitable to evaluate the quality of some fuels [35–42]. In the present work, PLS and PCR algorithms were applied to the selected spectral data of 36 samples (Table 1). Four models were designed: two for prediction of biodiesel concentration and two for oil prediction.

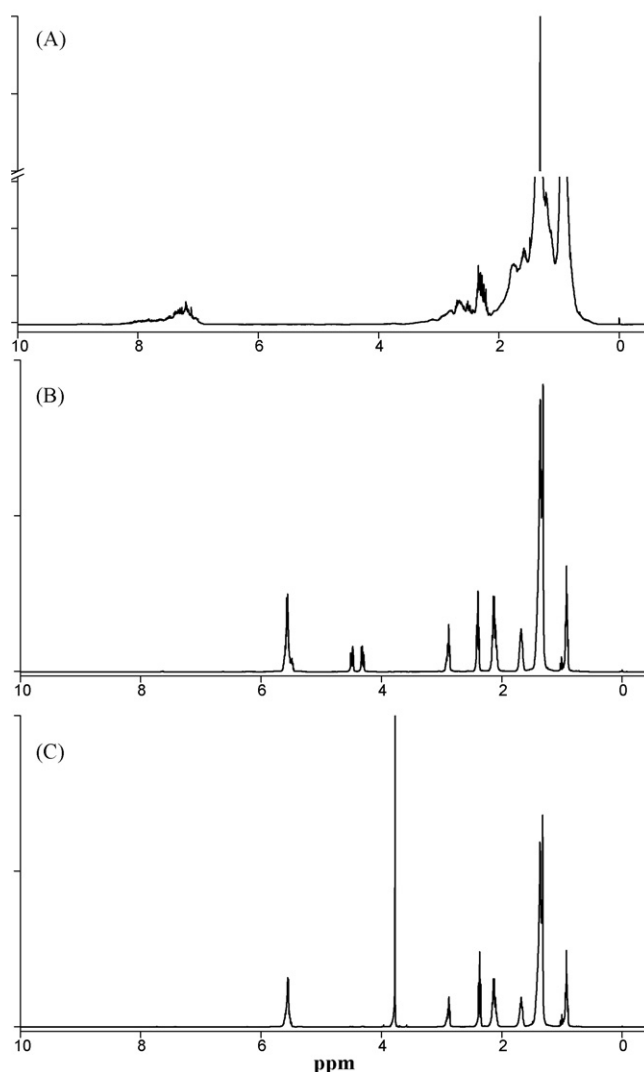


Fig. 1.  $^1\text{H}$  NMR spectra (400 MHz,  $\text{CDCl}_3$ ) of (A) mineral diesel, (B) soybean oil, and (C) methyl biodiesel from soybean oil.

Some statistical parameters were obtained for the models (Table 2), namely: principal components (PCs); variance percent in X matrix (Var %); standard error of validation (SEV); predicted residual error sum of squares of validation (PRESS Val); coefficient of correlation between the real concentration and the concentration predicted during the validation (r Val); SE of calibration

Table 2  
Some statistics related to classification models.

Model	PCs <sup>a</sup>	Var % <sup>b</sup>	SEV <sup>c</sup>	PRESS Val <sup>d</sup>	r Val <sup>e</sup>	SEC <sup>f</sup>	PRESS Cal <sup>g</sup>	r Cal <sup>h</sup>	SEC/SEV <sup>i</sup>	bias <sup>j</sup>
PCR-oil	4	79.34	0.80	23.05	0.9914	0.60	11.32	0.9957	0.75	−0.07
PCR-biodiesel	4	79.34	1.04	39.25	0.9809	0.78	18.75	0.9907	0.75	−0.12
PLS-oil	3	68.66	0.68	16.60	0.9938	0.46	6.78	0.9974	0.68	−0.11
PLS-biodiesel	3	68.65	0.82	24.20	0.9882	0.55	9.82	0.9951	0.67	0.04

<sup>a</sup> Principal components.

<sup>b</sup> Variance percent in X matrix.

<sup>c</sup> Standard error of validation.

<sup>d</sup> Predicted residual error sum of squares of validation.

<sup>e</sup> Coefficient of correlation between the real concentration and the concentration predicted during the validation.

<sup>f</sup> Standard error of calibration.

<sup>g</sup> Predicted residual error sum of squares of calibration.

<sup>h</sup> Coefficient of correlation between the real concentration and the concentration predicted during the calibration.

<sup>i</sup> Similarity criterion.

<sup>j</sup> Medium value obtained from the difference between real and predicted concentration of validation samples set (described in Table 3).

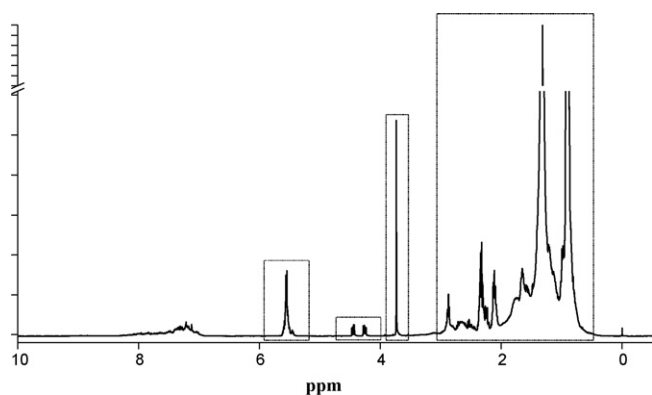


Fig. 2. Selected spectral regions to design PLS and PCR models.

(SEC); PRESS of calibration (PRESS Cal); coefficient of correlation between the real concentration and the concentration predicted during the calibration ( $r$  Cal); the similarity criterion obtained from the SEC/SEV relationship, and bias calculated according to Braga and Poppi [43] and Olivieri et al. [44]. The number of PCs for each model was chosen through the lowest obtained PRESS values.

In Table 2, the lowest values of the statistical parameters of PLS models indicate that they were better than PCR ones, although these have also showed excellent parameters. The values of  $r$  Cal and  $r$  Val near to 0.99 for all models showed that there are a good concordance between the real and predict concentrations (Figs. 3 and 4). In general, these values must be greater than 0.9 [45]. Moreover, the SEC/SEV relationships indicated that all models were well adjusted, since the values were comprised in the 0.5–1 range [45]. These models were also evaluated according to relative errors of validation and calibration, which showed that the lowest the concentration, the highest the errors; this means that the models will probably predict low concentrations with high deviation. This feature was also observed in the prediction of the 10 validation set samples (Table 3). As expected, high deviations were observed specially for low concentrated samples, although there was good correlation between the predicted values and the real ones for all models. PLS models seem to have a slightly prediction ability, but PCR also predicted very well.

Therefore, the use of  $^1\text{H}$  NMR and chemometrics is very suitable for the prediction of biodiesel and oil concentration especially in more concentrated samples ( $>2\%$ ). In this way, the combination of these tools can be used for the quality control of biodiesel–diesel

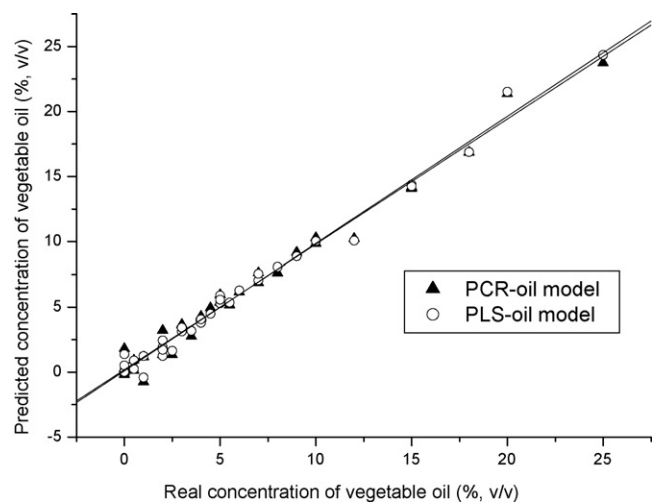


Fig. 3. Results obtained for calibration set using PLS and PCR-oil models.

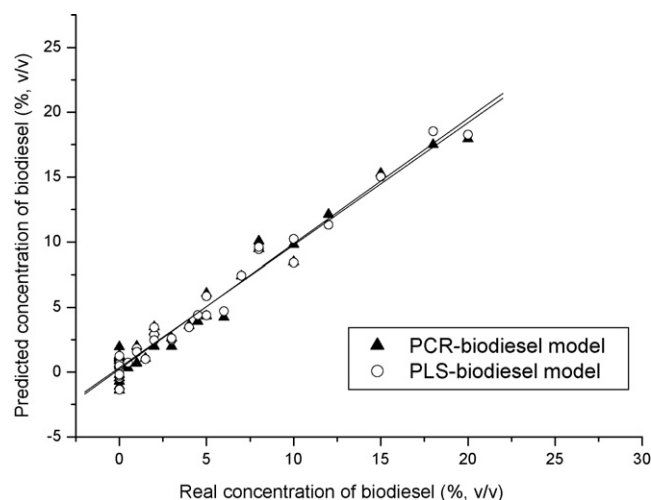


Fig. 4. Results obtained for calibration set using PLS and PCR-biodiesel models.

Table 3

Predicted concentrations for validation set.

Sample	Prediction by PCR		Prediction by PLS		Real concentrations	
	Oil (%)	Biodiesel (%)	Oil (%)	Biodiesel (%)	Oil (%)	Biodiesel (%)
do2	0.7	0.2	1.0	0.2	1.5	0.0
do5	3.3	0.0	3.1	0.0 <sup>a</sup>	3.0	0.0
do7	4.6	0.2	4.4	0.0	4.0	0.0
do8	4.6	0.0 <sup>a</sup>	4.6	0.0 <sup>a</sup>	4.5	0.0
do11	6.2	0.1	6.2	0.0	6.0	0.0
do13	8.0	0.6	8.2	0.0	8.0	0.0
db2	0.1	5.1	0.2	5.1	0.0	5.0
dob3	1.4	0.4	1.4	0.3	1.5	0.5
dob5	0.9	4.4	1.0	4.0	1.0	4.0
dob10	8.4	2.1	8.5	1.8	8.0	2.0

Results expressed as volume %.

<sup>a</sup> Predicted concentration below SEV value (described in Table 2).

blends, whose commercialization has increased in the last few years.

#### 4. Conclusion

In this work, PLS- $^1\text{H}$  NMR and PCR- $^1\text{H}$  NMR showed to be quite useful for the quantification of both biodiesel and vegetable oil in mixtures with mineral diesel. Therefore, the use of  $^1\text{H}$  NMR and chemometrics is very suitable to evaluate the quality of biodiesel–diesel blends that are commercialized all over the world.

#### Acknowledgments

The authors are grateful to Centro de Caracterização e Desenvolvimento de Materiais (CCDM, UFSCar/UNESP), Fundação de Amparo à Pesquisa do Estado de São Paulo (FAPESP), Conselho Nacional de Desenvolvimento Científico e Tecnológico (CNPq), and Financiadora de Estudos e Projetos (FINEP) for the financial support.

#### References

- [1] A.K. Agarwal, Prog. Energy Combust. Sci. 33 (2007) 233.
- [2] A. Demirbas, Prog. Energy Combust. Sci. 33 (2007) 1.
- [3] M.E. Tat, J.H. Van Gerpen, J. Am. Oil Chem. Soc. 76 (1999) 1511.
- [4] G. Knothe, J. Am. Oil Chem. Soc. 78 (2001) 1025.
- [5] European Biodiesel Board, <http://www.ebb-eu.org>.
- [6] Brazilian National Agency of Petroleum, Natural Gas and Biofuels, <http://www.anp.gov.br>.
- [7] A.C. Pinto, L.L.N. Guarieiro, M.J.C. Rezende, N.M. Ribeiro, E.A. Torres, W.A. Lopes, P.A.P. Pereira, J.B. de Andrade, J. Braz. Chem. Soc. 16 (2005) 1313.
- [8] L.C. Meher, D.V. Sagar, S.N. Naik, Renew. Sust. Energy Rev. 10 (2006) 248.
- [9] F. Ma, M.A. Hanna, Bioresour. Technol. 70 (1999) 1.

- [10] M.R. Monteiro, A.R.P. Ambrozini, L.M. Lião, A.G. Ferreira, *Talanta* 77 (2008) 593.
- [11] M.A. Aliske, G.F. Zagonel, B.J. Costa, W. Veiga, C.K. Saul, *Fuel* 86 (2007) 1461.
- [12] J.S. Oliveira, R. Montalvão, L. Daher, P.A.Z. Suarez, J.C. Rubim, *Talanta* 69 (2006) 1278.
- [13] M.F. Pimentel, G.M.G.S. Ribeiro, R.S. da Cruz, L. Stragevitch, J.G.A. Pacheco Filho, L.S.G. Teixeira, *Microchem. J.* 82 (2006) 201.
- [14] I. Eide, K. Zahlsten, *Energy Fuels* 21 (2007) 3702.
- [15] R.C.M. Faria, M.J.C. Rezende, C.M. Rezende, A.C. Pinto, *Quim. Nova* 30 (2007) 1900.
- [16] G.S.R. Sastry, A.S.R.K. Murthy, P.R. Prasad, K. Bhuvaneshwari, P.V. Ravi, *Energy Source Part A* 28 (2006) 1337.
- [17] T.A. Foglia, K.C. Jones, J.G. Phillips, *Chromatographia* 62 (2005) 115.
- [18] L.L.N. Guarieiro, A.C. Pinto, P.F. de Aguiar, N.M. Ribeiro, *Quim. Nova* 31 (2008) 421.
- [19] B. Diehl, G. Randel, *Lipid Technol.* 19 (2007) 258.
- [20] M.R. Monteiro, A.R.P. Ambrozini, L.M. Lião, A.G. Ferreira, *Fuel* 88 (2009) 691.
- [21] F. Adam, F. Bertocini, V. Coupard, N. Charon, D. Thiebaut, D. Espinat, M.C. Hennion, *J. Chromatogr. A* 1186 (2008) 236.
- [22] F.C.C. Oliveira, C.R.R. Brandão, H.F. Ramalho, L.A.F. da Costa, P.A.Z. Suarez, J.C. Rubim, *Anal. Chim. Acta* 587 (2007) 194.
- [23] C.N.C. Corgozinho, V.M.D. Pasa, P.J.S. Barbeira, *Talanta* 76 (2008) 479.
- [24] B.K. Lavine, *Anal. Chem.* 72 (2000) 91.
- [25] H. Winning, F.H. Larsen, R. Bro, S.B. Engelsen, *J. Magn. Reson.* 190 (2008) 26.
- [26] P.R. Costa Neto, M.S.B. Caro, L.M. Mazzuco, M.G. Nascimento, *J. Am. Oil Chem. Soc.* 81 (2004) 1111.
- [27] G. Gelbard, O. Bres, R.M. Vargas, F. Vielfaure, U.F. Schuchardt, *J. Am. Oil Chem. Soc.* 72 (1995) 1239.
- [28] G.F. Ghesti, J.L. de Macedo, I.S. Resck, J.A. Dias, S.C.L. Dias, *Energy Fuels* 21 (2007) 2475.
- [29] F. Jin, K. Kawasaki, H. Kishida, K. Tohji, T. Moriya, H. Enomoto, *Fuel* 86 (2007) 1201.
- [30] G. Knothe, *J. Am. Oil Chem. Soc.* 77 (2000) 489.
- [31] M. Morgenstern, J. Cline, S. Meyer, S. Cataldo, *Energy Fuels* 20 (2006) 1350.
- [32] G. Knothe, *Eur. J. Lipid Sci. Technol.* 108 (2006) 493.
- [33] M.G. Trevisan, C.M. Garcia, U. Schuchardt, R.J. Poppi, *Talanta* 74 (2008) 971.
- [34] F.C.C. Oliveira, A.T.P.C. de Souza, J.A. Dias, S.C.L. Dias, J.C. Rubim, *Quim. Nova* 27 (2004) 218.
- [35] J.J. Kelly, C.H. Barlow, T.M. Jinguji, J.B. Callis, *Anal. Chem.* 61 (1989) 313.
- [36] J.M. Andrade, S. Guarrigues, M. de la Guardia, M. Gómez-Carracedo, D. Prada, *Anal. Chim. Acta* 482 (2003) 115.
- [37] M. Gómez-Carracedo, J.M. Andrade, D.N. Rutledge, N.M. Faber, *Anal. Chim. Acta* 585 (2007) 253.
- [38] P. Felizardo, P. Baptista, J.C. Menezes, M.J.N. Correia, *Anal. Chim. Acta* 595 (2007) 107.
- [39] S. Guarrigues, J.M. Andrade, M. de la Guardia, D. Prada, *Anal. Chim. Acta* 317 (1995) 95.
- [40] L.S.G. Teixeira, F.S. Oliveira, H.C. dos Santos, P.W.L. Cordeiro, S.Q. Almeida, *Fuel* 87 (2008) 346.
- [41] M.A. Al-Ghouti, Y.S. Al-Degs, M. Amer, *Talanta* 76 (2008) 1105.
- [42] H.L. Fernandes, I.M. Raimundo Jr., C. Pasquini, J.J.R. Rohwedder, *Talanta* 75 (2008) 804.
- [43] J.W.B. Braga, R.J. Poppi, *J. Pharm. Sci.* 93 (2004) 2124.
- [44] A.C. Olivieri, N.K.M. Faber, J. Ferré, R. Boqué, J.H. Kalivas, H. Mark, *Pure Appl. Chem.* 78 (2006) 633.
- [45] M.F. Ferrão, C.W. Carvalho, E.I. Muller, C.U. Davanzo, *Cienc. Tecnol. Aliment* 24 (2004) 333.



## Simultaneous determination of inorganic and organic antimony species by using anion exchange phases for HPLC–ICP–MS and their application to plant extracts of *Pteris vittata*

Karsten Müller<sup>a,1</sup>, Birgit Daus<sup>b</sup>, Jürgen Mattusch<sup>a</sup>, Hans-Joachim Stärk<sup>a</sup>, Rainer Wennrich<sup>a,\*</sup>

<sup>a</sup> UFZ Helmholtz Centre for Environmental Research, Department of Analytical Chemistry, Permoserstrasse 15, 04318 Leipzig, Germany

<sup>b</sup> UFZ Helmholtz Centre for Environmental Research, Department Groundwater Remediation, Permoserstrasse 15, 04318 Leipzig, Germany

### ARTICLE INFO

#### Article history:

Received 3 July 2008

Received in revised form 18 December 2008

Accepted 22 December 2008

Available online 15 January 2009

#### Keywords:

Antimony species

HPLC–ICP mass spectrometry

Aqueous extracts

Plant material

*Pteris vittata*

### ABSTRACT

Antimony is a common contaminant at abandoned sites for non-ferrous ore mining and processing. Because of the possible risk of antimony by transfer to plants growing on contaminated sites, it is of importance to analyze antimony and its species in such biota. A method based on high performance liquid chromatographic separation and inductively coupled plasma mass spectrometric detection (HPLC–ICP–MS) was developed to determine inorganic antimony species such as Sb(III) and Sb(V) as well as possible antimony–organic metabolisation products of the antimony transferred into plant material within one chromatographic run. The separation is performed using anion chromatography on a strong anion exchange column (IonPac AS15/AG 15). Based on isocratic optimizations for the separation of Sb(III) and Sb(V) as well as Sb(V) and trimethylated Sb(V) (TMSb(V)), a chromatographic method with an eluent gradient was developed. The suggested analytical method was applied to aqueous extracts of Chinese break fern *Pteris vittata* samples. The transfer of antimony from spiked soil composites into the fern, which is known as a hyperaccumulator for arsenic, was investigated under greenhouse conditions. Remarkable amounts of antimony were transferred into roots and leaves of *P. vittata* growing on spiked soil composites. Generally, *P. vittata* accumulates not only arsenic (as shown in a multiplicity of studies in the last decade), but also antimony to a lower extent. The main contaminant in the extracts was Sb(V), but also elevated concentrations of Sb(III) and TMSb(V) (all in  $\mu\text{g L}^{-1}$  range). An unidentified Sb compound in the plant extracts was detected, which slightly differ in elution time from TMSb(V).

© 2009 Elsevier B.V. All rights reserved.

### 1. Introduction

Antimony is widely distributed in the environmental compartments. In general, the abundance of Sb is low (about  $0.3 \text{ mg kg}^{-1}$  in earth crust [1]). In natural environments it originates from both geological and anthropogenic sources. Over the years, anthropogenic emission of Sb as a result of the widespread use of antimony compounds, e.g. as flame retardant additives and tire vulcanization additives, in batteries, brake linings, ammunition, alloys, semi-conductors, pigments [2,3], led to an increasing burden for the environment. Other sources for the anthropogenic impact are mining and the processing of non-ferrous ores [4,5].

It is well-known that antimony compounds show geochemical behaviours similar to those of arsenic. Antimony and arsenic co-

occur in the environment. Both exist in identical oxidation states  $-3, 0, +3$ , and  $+5$ . Of special relevance as regards the environmental and biogeochemical aspects are the redox pairs Sb(III)/Sb(V) and As(III)/As(V). This means the oxidation state and form of metalloids themselves can be changed under environmental conditions. These transformations primarily affect the mobility and the fate of these elements and also their possible bio-availability. Both elements and their species are also comparable in toxicity [6]. While arsenic has been in the spotlight of environmental concern for decades, elevated concentrations of antimony in polluted mining areas have become of interest in the last 10 years. Antimony and its compounds were considered as pollutants of high priority interest by U.S. Department of Health and Human Services in the ATSDR list 2007 [7] and by WHO Guidelines for Drinking-Water Quality [8].

Considerable efforts have been undertaken during the last decade to improve the performance of analytical methods to study the mobilization behaviour of Sb in and between different matrices. However, most of these studies were based on the determination of total Sb concentrations [9,10]. As considerable differences exist, in part, between the toxicity levels of different Sb species [11,12] and

\* Corresponding author. Tel.: +49 341 235 1215; fax: +49 341 235 1443.

E-mail address: [rainer.wennrich@ufz.de](mailto:rainer.wennrich@ufz.de) (R. Wennrich).

<sup>1</sup> Present address: Fraunhofer Institute for Process Engineering and Packaging IVV, Giggenhauserstrasse 35, 85354 Freising, Germany.

the environmental behaviour is changing depending on the chemical form of Sb [13,14], determination of Sb species is necessary. However, determination of Sb species in environmental samples can be problematic due to the very low, but relevant concentrations often present.

As has already been shown by a multiplicity of studies regarding the determination of arsenic species, the coupling of chromatographic separation with ICP-MS or atomic fluorescence spectrometry (AFS) as very sensitive detectors, e.g. [15], appears to be most suitable for the determination of antimony species. Despite the accepted similarity of arsenic and antimony it is not possible to adapt directly the chromatographic methods for determination of arsenic species to those of antimony species. There is a relatively high degree of different retention behaviours between the species of these two elements applying liquid chromatographic separation. Thus, analytical methods for the determination of inorganic and organic Sb species with a good resolution and suitable detection limits have to be employed.

HPLC separation methodologies for the determination of antimony species in aqueous solutions have been developed for the last 10 years (see reviews [11,13,14,16]). Most of them focused on the determination of the inorganic forms with valence states Sb(III) and Sb(V) in aqueous solutions (groundwater, sea water, extracts from sediments and soils) using anion exchange separation.

There is a growing interest in the speciation of antimony regarding environmental aspects. In particular, the mobility, bio-availability and biological effects of antimony, e.g. the uptake of Sb by biota, depend considerably on their chemical forms and types of binding. Transformation into organic species is very likely in biota. Therefore, it is important to determine both inorganic and organic Sb species. One aspect of the investigations is the formation of volatile antimony species in the presence of bacteria. Here, different analytical procedures based on gas chromatographic separation combined with atomic fluorescence or ICP-MS detections had also been developed [17]. On the other hand a large interest exists in the determination of inorganic and organic Sb species in liquid samples, such as water, biological fluids (urine, etc.), and extracts from soils, sediments and biota.

The separation of Sb(III), Sb(V) and methylated Sb species using a single chromatographic system is problematic due to variations in chemical structure and charge of these species as stated in Ref. [18]. However, some analytical methodologies for the species analysis of Sb in aqueous extracts have been described. Most of them based on the utilization of HPLC separation by means of anion exchange columns and subsequent ICP-MS or AFS detections (see e.g. [19–22]). Foster et al. [23] showed the existence of different Sb species in non-aqueous extracts ( $\text{CCl}_4 + \text{CH}_3\text{OH}$ ) of algae and moss samples which had been collected at polluted sites. Analytical techniques and methods used for Sb speciation analysis in biota were discussed recently by Hansen and Pergantis [24].

Nash et al. [18] describes an improved analytical procedure based on a chromatographic separation with strong anion exchange stationary phases for the determination of aqueous antimony species. Based on optimization, a method was to be created determining inorganic and organic Sb species in one chromatographic run. The objective of this work was to characterize the transfer of antimony into terrestrial plants based on the reported phyto-availability of Sb (total concentration) by plants growing in Sb mining areas [5,9,25–30] by antimony species analysis. In a first trial the method should be applicable for speciation of Sb in extracts of fern samples, *P. vittata* cultivated on antimony spiked composite in greenhouse experiments. Attention was focussed on a sufficient resolution of the anion separation with the possibility to determine additionally unknown Sb species.

## 2. Experimental

### 2.1. Chemicals and reagents

All chemicals used in this study were of analytical-grade, or higher, purity. De-ionized water ( $18.2 \text{ M}\Omega \text{ cm}^{-1}$ ) was obtained from a Direct-Q<sup>TM</sup> 5 system (Millipore). Nitric acid (suprapur, 65% (v/v), Merck) and hydrogen peroxide (suprapur, 30% (v/v), Merck) were used for microwave digestion solutions to determine the total concentration of Sb in the plant material.

The eluent mixtures of differently molar ethylenediaminetetraacetate (EDTA) were prepared by dissolving appropriate amounts of  $(\text{NH}_4)_2 \text{ EDTA}$  (Fluka) in de-ionized water. The pH values were adjusted by ammonia solution (25%, Merck). The resulting solutions were de-gassed and handled under a helium atmosphere.

Stock solutions of antimony species were prepared from  $\text{KSbOH}(\text{C}_4\text{H}_4\text{O}_6) \cdot \text{H}_2\text{O}$  (Sigma–Aldrich, 99.95%),  $\text{KSb}(\text{OH})_6$  (Riedel–de Hën, p.a.) and  $(\text{CH}_3)_3\text{SbCl}_2$  (Sigma–Aldrich, 96%) with a concentration of  $1 \text{ g L}^{-1}$  (as Sb) of the individual compounds in de-ionized water and stored in the dark at  $4^\circ \text{C}$  until use.

### 2.2. Speciation analysis

Speciation analysis of Sb was performed by anion exchange chromatography–ICP mass spectrometry. The chromatographic system (BECKMAN, System Gold, Fullerton, USA) equipped with an autosampler and a binary pump was coupled via a peek capillary to a Meinhard nebulizer of an ICP-MS system (PQ Excell, THERMO) for element selective detection.

A Dionex IonPac AS15 analytical column ( $250 \text{ mm} \times 4 \text{ mm}$ ;  $9 \mu\text{m}$ ) with an IonPac AG15 guard column ( $50 \text{ mm} \times 4 \text{ mm}$ ) was chosen. The Hamilton PRP-X 100 column, which is often used (see reviews [18,24]), was not used to avoid influences by phthalate on the ICP stability. The separation was optimized using the commercially available standards Sb(III), Sb(V) and  $\text{TMSb}(\text{V})$ . In earlier work these species had been detected also in aqueous extracts [31,32]. The existence of  $\text{TMSb}(\text{V})$  was also evidenced by Dodd et al. [33] analysing freshwater plant extracts by HG–GC–MS.

The chromatographic optimization was focused on one hand to accelerate the separation and on the other hand also to leave retention time windows for analyzing additional Sb species assumed in the plant extracts as reported in Ref. [23].

The optimized ICP-MS experimental parameters are the following: forward power:  $1350 \text{ W}$ ; plasma gas flow:  $13 \text{ L min}^{-1}$ ; nebulizer gas flow:  $0.90 \text{ L min}^{-1}$ ; auxiliary gas flow:  $1.0 \text{ L min}^{-1}$ , and detection at  $m/z$  121.

### 2.3. Cultivation and pre-treatment of Chinese break fern—*P. vittata*

Six-month-old Chinese break fern (*P. vittata*) were replanted in antimony contaminated composites. This composite of different particle size of quartz sand (85% sand, 10% silt, 5% potter's clay) was spiked with different concentrated Sb(V) solutions, resulting in final Sb concentration of  $<2 \text{ mg kg}^{-1}$ ,  $5 \text{ mg kg}^{-1}$ ,  $10 \text{ mg kg}^{-1}$  and  $16 \text{ mg kg}^{-1}$  in the substrate (after drying), which were determined by EDXRF (XLAB 2000, SPECTRO A.I.) running the software package X-LAB Pro 2.2.

Six-months old *P. vittata* seedlings were cultivated in greenhouse ( $25^\circ \text{C}$ ; 75–80% air moisture) over 7 weeks on these composites before harvesting.

After harvesting the plants were divided into old fronds, new (renewal) fronds and roots. Each of these portions was divided into sub-samples for determination of moisture content, total antimony and for species analysis. The plant material was washed gently with de-ionized water and afterwards carefully dried with blot-



ting paper. The material for moisture content and total antimony determination was dried at 60 °C for 48 h and afterwards milled to a fine powder (Retsch). The samples for species analysis were ground under liquid nitrogen and stored at –80 °C until analysis.

#### 2.4. Microwave digestion for total analysis

Approximately 0.3 g of fine dry powder plant material was weighed in 50-mL digestion vessels, 4 mL of concentrated HNO<sub>3</sub> (65%, v/v) was added and reacted overnight. After the addition of 0.5 mL H<sub>2</sub>O<sub>2</sub> (30%, v/v) the digestion was performed using a microwave device ultraCLAVE (MLS, Germany). After cooling to room temperature, the resulting solutions were centrifuged, the supernatant was filtered (0.45 µm; cellulose acetate membrane, Sartorius), transferred into 50-mL polyethylene bottles and filled to volume with de-ionized water. The final solutions were stored at 4 °C until analyzing with ICP-MS within a day. The extracts were analyzed with an inductively coupled plasma mass spectrometer (ICP-MS) ELAN 6100 DRC-e (PerkinElmer, Sciex) by measuring the signal intensity at *m/z* 121.

Several reference materials of plants (GBW 08504, GBW 08505, BCR 060, BCR 679, IC-STA-OTL-1, NIST 1573a, NIST 1575) were digested with the same procedure to check the extraction yields.

#### 2.5. Extraction of Sb species from fern samples

Contrary to leaching procedures aimed in high extraction efficiency of Sb using solvent mixtures, e.g. methanol/water, chloroform/methanol, or sequential extraction procedures, e.g. [23] a mild extraction was favoured using water to minimize side reactions between Sb species and the solvents.

An amount of about 0.8 g of the frozen break fern samples was crushed and afterwards shaken horizontally with 7 mL de-ionized water (190 rpm) in 15 mL polyethylene bottles for 2 h under gaseous N<sub>2</sub>. These conditions were chosen to avoid any oxidation in the samples. The resulting suspensions were centrifuged. The supernatant was transferred into HPLC vials and analyzed under optimized conditions for the Sb speciation analysis. Three parallel experiments at each concentration were executed. Additionally the concentration of Sb was determined in the aqueous extracts and in HNO<sub>3</sub> + H<sub>2</sub>O<sub>2</sub> extracts (microwave assisted) of the plant samples by means of ICP-MS to compare the efficiency of the chromatographic method related to these two procedures.

### 3. Results and discussion

#### 3.1. Optimization of separation conditions for Sb speciation analysis

Separation of Sb(III), Sb(V) and methylated Sb species using a single chromatographic run had been characterized as notoriously problematic due to the difference in chemical characteristics of these species as stated by Nash et al. [18]. They reported that a separation of Sb(III), Sb(V) and TMSb(V) could be realized using an HAAX column with secondary and tertiary amine groups (Alltec) and 100 mM ammonium tartrate as a mobile phase with a gradient from pH 3 to pH 1.2, although a system peak co-elutes with TMSb(V). Therefore, it was further necessary to create an improved analytical method for separation of these three Sb species.

Although the investigations by Krachler and Emons [34] using a Dionex IonPac AS14 (with AG14) had shown that the separation of all the three commercially available antimony species Sb(III), Sb(V) and TMSb(V) was not successful, we started the investigations with a similar separation system using an anion exchange column Dionex IonPac AS15 in these studies. The separation was optimized according to the available standards Sb(III), Sb(V) and TMSb(V).

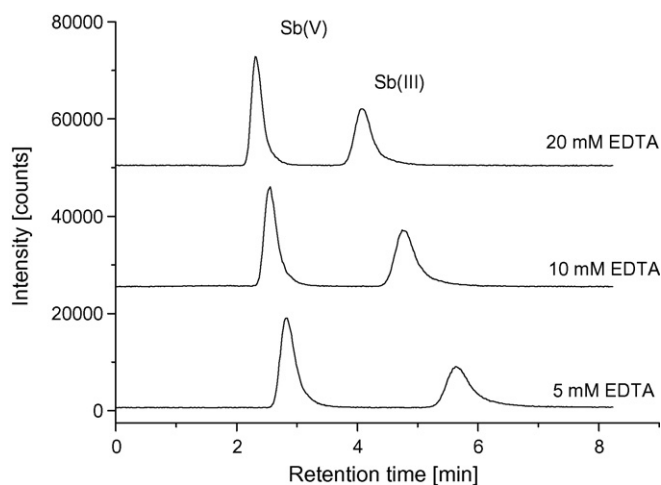


Fig. 1. Chromatograms of Sb(V) and Sb(III) (each 10 µg L<sup>-1</sup>); isocratic elution; variation of EDTA concentration at pH 4.5.

#### 3.1.1. Isocratic elution of Sb(III) and Sb(V) with acidic mobile phase

In a first trial the separation of Sb(III) and Sb(V) was optimized under isocratic conditions. Based on the findings by Lintschinger et al. [35] EDTA was used as a mobile phase with complexing properties for an acceptable separation of the inorganic Sb(III) and Sb(V) species. As demonstrated in Fig. 1 increasing EDTA concentrations at constant pH 4.5 (adjusted with HNO<sub>3</sub>) leads to shorter retention times and improved peak shapes of Sb(III) under isocratic elution.

A proper separation of these two species can be achieved with shortening the retention times for Sb(V) and Sb(III). However, these conditions are not suitable to carry out the elution of TMSb(V).

#### 3.1.2. Isocratic elution of Sb(V) and TMSb(V) with alkaline mobile phase

The separation of inorganic Sb(V) and TMSb(V) was investigated under different pH conditions using NH<sub>4</sub>OH by isocratic elution (without EDTA). The influence of the pH of the eluent can be seen in Fig. 2.

A pH value of ≥ 10 is necessary to separate the two species effectively. The retention time of Sb(V) can be shortened up to 3 min under these conditions by enhancing the pH up to 11.5. However, it was impossible to elute Sb(III) at this pH range.

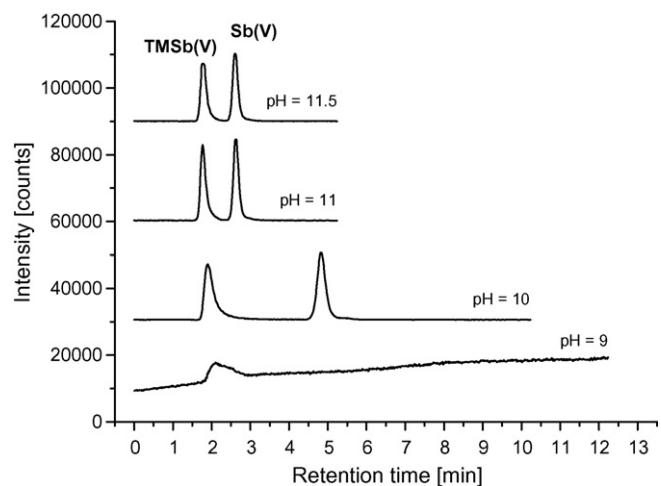
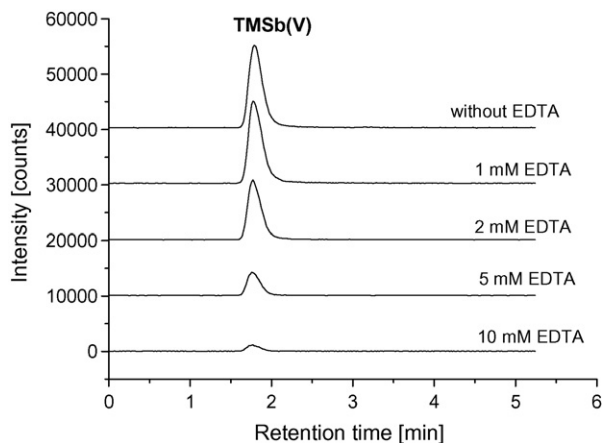


Figure 2. Chromatograms of TMSb(V) and Sb(V) (each 10 µg L<sup>-1</sup>) working with isocratic elution; variation of pH value with ammonia.



**Fig. 3.** Influence of EDTA concentrations on the response of the ICP-MS for TMSb(V) column IonPac AS15/AG15, mobile phase:  $\text{NH}_4\text{OH}$  (at pH 11); TMSb(V) concentration  $10 \mu\text{g L}^{-1}$  (as Sb).

### 3.1.3. Gradient elution for the separation of Sb(III), Sb(V) and TMSb(V)

Based on the results presented before, a chromatographic separation of all three Sb species seems to be possible by combination of both separations by means of a gradient technique.

To avoid possible interferences (e.g. ghost peaks, shifting of the background intensities) in the ICP-MS detection by significant changing of the eluent composition, the influence of varying EDTA concentrations on the determination of TMSb(V) was investigated. As demonstrated in Fig. 3, the intensity of the  $^{121}\text{Sb}$  signal in ICP-MS decreased with increasing concentration of EDTA in the  $\text{NH}_4\text{OH}$  eluent (pH 11) employing IonPac AS15/AG15.

Because of the equality of the peak heights eluting without EDTA and with a concentration of 1 mM EDTA, the following investigations were carried out with 1 mM EDTA as the complexing agent. The gradient profile given in Fig. 4 was found to be optimal for the separation of Sb(V), Sb(III) and TMSb(V) in one run within 7 min. The optimized ion chromatographic conditions can be summarized as follows: column: Dionex IonPac AS15 ( $250 \text{ mm} \times 4 \text{ mm}$ ;  $9 \mu\text{m}$ ) with guard column IonPac AG15 ( $50 \text{ mm} \times 4 \text{ mm}$ ); flow rate:  $1.5 \text{ mL min}^{-1}$ ; injection volume:  $50 \mu\text{L}$ ; eluent A: 20 mM EDTA (pH 4.5); eluent B:  $\text{NH}_4\text{OH}$  (pH 11) + 1 mM EDTA; gradient program: see Fig. 4.

In Fig. 5 the separation of the three Sb species using this gradient is illustrated. In the chromatogram one can recognize that the

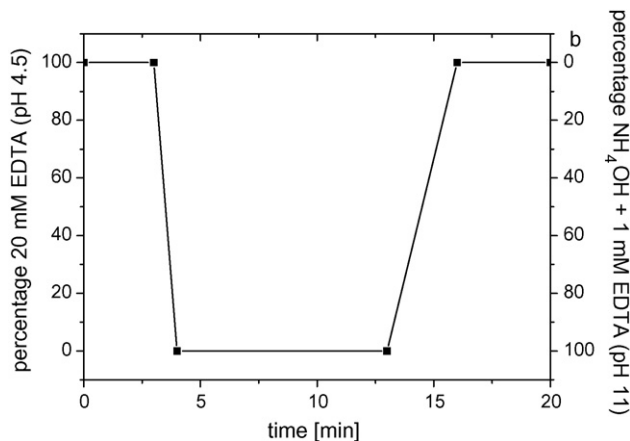


**Fig. 4.** Gradient profile for simultaneous determination of Sb(III), Sb(V) and TMSb(V).

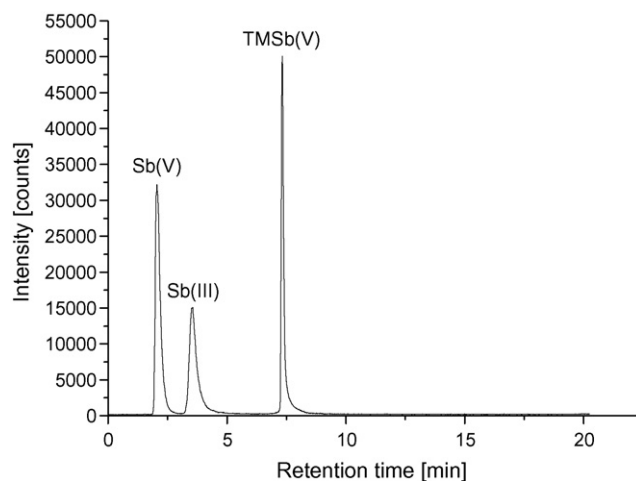


**Fig. 5.** Separation of Sb(III), Sb(V) and TMSb(V) under optimized elution conditions concentration each of species  $10 \mu\text{g L}^{-1}$  (as Sb).

form of the signal for TMSb(V) is somewhat different than for the other peaks. We attribute to that by the change of the flow conditions (and the plasma conditions) if the eluent changes. Since a clear dependence of the peak height (and peak area) with the concentration of TMSb(V) exists, we are sure that this peak is caused by TMSb(V).

The linear working range for the determination of the three Sb species was in the range from  $0.1 \mu\text{g L}^{-1}$  to  $100 \mu\text{g L}^{-1}$  (as Sb) as shown in Fig. 6.

### 3.1.4. Quantification of Sb species

To calibrate the method sets of solutions of the mixed Sb species (Sb(V), Sb(III) and TMSb(V) in water in the concentration range  $1\text{--}10 \mu\text{g L}^{-1}$  (7 levels;  $n = 3$ ) were prepared and measured under the optimized IC-ICP-MS condition. The calibration plots using peak areas vs. concentrations are presented in Fig. 6.

As one can see the coefficient of determination ( $R^2$ ) for all the three linear plots are good. The slope of the calibration curves do not differ very strongly depending on the Sb species. The sensitivities are in the following order Sb(V) > TMSb(V) > Sb(III).

### 3.2. Determination of total antimony in the fern samples (*P. vittata*)

The acid soluble antimony concentration in roots and leaves of the milled fern samples, which had been cultivated as described

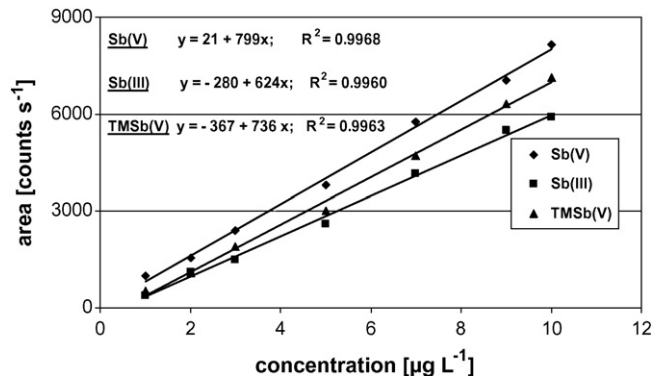


**Fig. 6.** Calibration plots of different Sb species using gradient chromatography (mean values,  $n = 3$ ).

**Table 1**  
Sb concentration in selected reference materials digested with HNO<sub>3</sub>/H<sub>2</sub>O<sub>2</sub> (microwave assisted).

Reference material		Concentration of Sb (μg kg <sup>-1</sup> )	
		Certified	Found in HNO <sub>3</sub> /H <sub>2</sub> O <sub>2</sub> leachate (n = 3)
GBW 08504	Cabbage	20.6 ± 1.4	10.3 ± 0.4
GBW 08505	Tea	37 ± 3	25.4 ± 3.7
BCR 060	Lagarosiphon major	400 <sup>a</sup>	198 ± 1
BCR 060 + 950 ng g <sup>-1</sup> (spiked as Sb(V) <sup>b</sup> )		(1350) <sup>c</sup>	586 ± 22
BCR 679	White cabbage	20.6 ± 2.6	15.9 ± 1.3
IC-STA-OTL-1	Oriental tobacco	75 <sup>a</sup>	41.3 ± 3.1
NIST 1573a	Tomato leaves	63 ± 6	36.3 ± 1.5
NIST 1573a + 950 ng g <sup>-1</sup> (spiked as Sb(V) <sup>b</sup> )		(1010) <sup>c</sup>	648 ± 10
NIST 1575	Pine needles	200 <sup>a</sup>	146 ± 10

<sup>a</sup> Information value.

<sup>b</sup> Spiked CRM before HNO<sub>3</sub>–microwave assisted digestion.

<sup>c</sup> Assumed concentration (certificate + spike).

above, was determined after microwave assisted digestion with HNO<sub>3</sub> and H<sub>2</sub>O<sub>2</sub> by ICP-MS as described above. In Table 2 (column 3) these concentrations of Sb in different plant samples (dry weight) were summarized. (Because of the low concentration of Sb in the plant material it was impossible to determine the total concentration by XRF.)

Certified reference plant materials were analyzed following the above procedure to ensure the accuracy and precision of the analytical procedure (mineralization and ICP-MS determination). The digestion procedures were performed as used for the fern materials (that means without hydrofluoric acid or tetrafluoroboric acid in contrast to the work done by Krachler et al. [26] and Foster et al. [23]) in order to receive comparable results with the plant materials under study for speciation analysis. The data presented in Table 1 show that the recovery using HNO<sub>3</sub> + H<sub>2</sub>O<sub>2</sub> extraction is significantly decreased compared with the certified or indicative values. One has to consider that the reference values base on the neutron activation analysis (NIST 1573a, BCR 679, GBW 08505) and/or on determination after dissolution with hydrofluoric acid addition (BCR 679). Additional investigations resulted in the fact, that the recovery of Sb(V) spikes (added to the reference material in HNO<sub>3</sub> + H<sub>2</sub>O<sub>2</sub> before microwave digestion) is also only about 60% (BCR 060) and about 70% (NIST 1573a) as shown in Table 1. This indicates that – despite the fact that the digestion of Sb in plant material is not complete [23,26] when working without fluoride – the stability of Sb in the HNO<sub>3</sub> solutions (after leaching) seems to be also a serious problem.

These low recoveries have to be keeping in mind for the discussion of the results for the fern samples.

As can be seen from data in Table 2, antimony is transferred into the plant materials, e.g. the extract of 'old' leaves, when the plants were cultivated on the composite containing 16 mg kg<sup>-1</sup> Sb (total), contained a HNO<sub>3</sub>/H<sub>2</sub>O<sub>2</sub> extractable concentration of 8 mg kg<sup>-1</sup> (d.w.) of antimony. The concentration in the roots is higher than even in the composites at which the ferns were cultivated – despite the fact that the total Sb contents in the composites were determined by XRF, while for the analysis of the plant material the HNO<sub>3</sub> extract (with incomplete extraction) was used. This means that the fern *P. vittata* accumulates not only arsenic (as shown in a multiplicity of studies in the last decade [36–38]), but also antimony.

The antimony concentration in leaves is substantially lower than in the roots. There seems to be a barrier for antimony in contrast to arsenic. The transfer of Sb into the roots and inside the plant compartments are the subject of further investigations.

However, the water extractable amounts were rather small. In general, depending on the kind of samples – roots, new or old leaves – between 5% and 20% of the HNO<sub>3</sub>/H<sub>2</sub>O<sub>2</sub> extractable amount of antimony was extracted by the aqueous leaching applied (Table 2).

### 3.3. Determination of Sb species in aqueous extracts of *P. vittata*

In a first trial aqueous extracts of *P. vittata* had been used for speciation analysis. The species analysis was done by the optimized procedure (Section 3.1.3).

In such 'species gentle' extracts four antimony species could be separated and detected as shown in Fig. 7. Three Sb species could also be identified on the basis of their retention time.

The main component of Sb found in this aqueous extract was Sb(V). Beside Sb(V) considerable concentrations of Sb(III), TMSb(V) and a further (so far not identified) Sb species was detected in the extract.

Because of the differences regarding sensitivity with the determination of the different Sb species (IC-ICP-MS) quantification took place only for Sb species, for which standards were available, Sb(V), Sb(III) and TMSb(V) as described in Section 3.1.4.

The quantification of the 'not identified' Sb species was not reasonable. Therefore only an estimation of the concentration of this compound based on the Sb(V)–calibration plot is given in Table 2. The concentration of the antimony species in the aqueous extracts of the *P. vittata* cultivated on Sb spiked substrate were in the μg L<sup>-1</sup> range.

Generally, taking into account the standard deviations of the single analysis, the sum of the quantified Sb species – (Sb(V), Sb(III) and TMSb(V)) is between 70% and 100% of the Sb concentration in the aqueous extracts analysed as total by ICP-MS. Considering the estimated concentration of the 'not identified Sb species' the mean

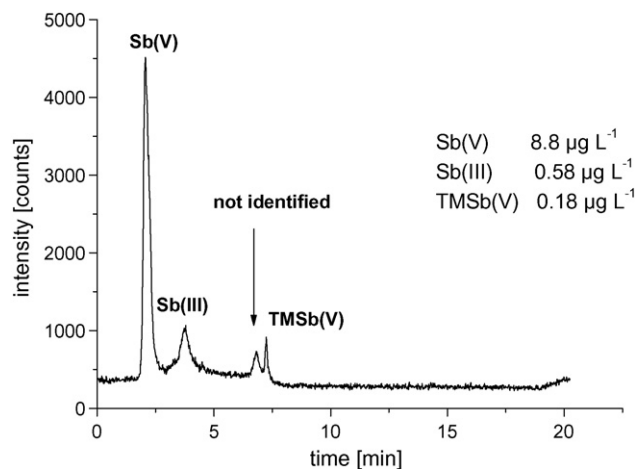


**Fig. 7.** Chromatogram of an aqueous extract of old leaves (*Pteris vittata*, substrate 16 mg kg<sup>-1</sup> Sb). Gradient chromatography, ICP-MS detection at *m/z* 121.

**Table 2**  
Results of total Sb determination and species analysis in *Pteris vittata* (mean of 3 replicates  $\pm$  standard deviation).

Sb in composite (mg kg <sup>-1</sup> ) <sup>a</sup>	Fern material	Sb in HNO <sub>3</sub> + H <sub>2</sub> O <sub>2</sub> extract (mg kg <sup>-1</sup> d.w.)	Sb <sub>total</sub>	Sb concentration in aqueous extract (μg L <sup>-1</sup> )	Sb(V)	TMSb(V)	Not identified <sup>b</sup>	ΣSb <sub>species</sub> /Sb <sub>total</sub> (%) <sup>c</sup>	ΣSb <sub>species</sub> /Sb <sub>HNO<sub>3</sub></sub> (%)
<2	New leaves	0.01 ± 0.003	0.04 ± 0.01	<LOD	<LOD	<LOD	<LOD		
	Old leaves	0.02 ± 0.002	0.07 ± 0.04	<LOD	<LOD	<LOD	<LOD		
	Roots	0.07 ± 0.02	0.07 ± 0.02	<LOD	<LOD	<LOD	<LOD		
5	New leaves	0.5 ± 0.2	3.1 ± 1.0	0.4 ± 0.2	1.5 ± 1.2	0.6 ± 0.01	~0.3	78	20
	Old leaves	3.4 ± 2.4	4.9 ± 2.8	0.6 ± 0.4	3.2 ± 2.2	<LOD	~0.6	79	5
	Roots	49 ± 12	29 ± 3.5	3.3 ± 0.3	25 ± 7.1	0.6 ± 0.1	~0.9	100	8
10	New leaves	0.7 ± 0.4	3.6 ± 1.6	0.4 ± 0.2	1.7 ± 1.0	0.5 ± 0.02	~0.3	70	15
	Old leaves	2.7 ± 1.2	5.1 ± 1.8	0.4 ± 0.3	3.4 ± 1.0	<LOD	~0.4	74	5
	Roots	68 ± 32	75 ± 54	2.9 ± 0.9	61 ± 45	1.0 ± 0.6	~6	86	13
16	New leaves	1.5 ± 0.1	6.1 ± 1.3	0.6 ± 0.1	3.5 ± 1.1	0.5 ± 0.1	~0.4	76	13
	Old leaves	8.1 ± 3.9	12 ± 4.3	0.6 ± 0.1	8.9 ± 2.5	0.2 ± 0.2	~1	78	5
	Roots	63 ± 77	58 ± 20	3.1 ± 0.9	43 ± 34	1.1 ± 0.3	~6	81	8

<sup>a</sup> XRF values.

<sup>b</sup> Semiquantitative.

<sup>c</sup> Σ[Sb(V) + Sb(III) + TMSb(V)]/Sb<sub>total</sub>; <LOD below limit of detection.

values of all recoveries growing up to 90 ± 8%. In all extracts (roots, old and new leaves) Sb(V) was the dominant detected species. Consequently, antimony particularly occurs as Sb(V) in the roots as it was added to the substrate. Sb(V) is in the extracts of the new sheets smallest contained (about 50%).

#### 4. Conclusion

A transfer of antimony from Sb spiked substrate to Chinese break fern *P. vittata* was found. At elevated concentration of Sb in the composite applied for cultivation total antimony is accumulated in both roots and leaves in the mg kg<sup>-1</sup> range. To investigate the accumulation capability of Sb in the plant material, a method for the determination of Sb(V) an Sb(III) as well as TMSb(V) was developed and proven for the analysis of antimony compounds extracted by water from such cultivated fern. The fast hyphenated method (one run in 20 min including conditioning of the chromatographic system) allows a sensitive detection of antimony compounds in aqueous plant extracts.

Substantially to be impaired the investigations thereby that only a small portion of Sb accumulated by the fern is extractable with water under the chosen 'mild' conditions. This indicates that antimony in *P. vittata* forms water-insoluble species. Such species could be inorganic slightly soluble sulfides or high-molecular antimony containing biomolecules.

Based on these preliminary results, the ongoing work is focussed on both more efficient techniques to improve yield of the water extractable Sb species and on the digestion procedures for non-aqueous soluble Sb species.

#### Acknowledgements

We are indebted to Ursula Winkler and Jutta Froehlich (both UFZ) for the technical assistance and Dr. Doris Vetterlein and Ines Krieg (UFZ) for mentoring by cultivation of *P. vittata*. Deutsche Bundesstiftung Umwelt DBU (Contract No. 20004/703) is greatly appreciated for the financial support.

#### References

- [1] M. Filela, N. Belzile, Y.W. Chen, Earth Sci. Rev. 57 (2002) 125.
- [2] W. Shoty, M. Krachler, B. Chen, Met. Ions Biol. Syst. 44 (2005) 171.
- [3] D. van Velzen, H. Langenkamp, G. Herb, Waste Manag. Res. 16 (1998) 32.
- [4] J. Gal, A.S. Hursthouse, S.J. Cuthbert, Environ. Chem. Lett. 3 (2006) 149.
- [5] J. Pratas, M.N.V. Prasad, H. Freitas, L. Conde, J. Geochem. Explor. 85 (2005) 99.
- [6] T.W. Gebel, R.H.R. Suchenwirth, C. Bolten, H.H. Dunkelberg, Environ. Health Persp. 106 (1998) 33.
- [7] <http://www.atsdr.cdc.gov/cercla/07list.html>.
- [8] [http://www.who.int/water\\_sanitation\\_health/dwq/chemicals/antimony.pdf](http://www.who.int/water_sanitation_health/dwq/chemicals/antimony.pdf).
- [9] A. Murciego Murciego, A. Garcia Sanchez, M.A. Rodriguez Ganzalez, E. Pinilla Gil, C. Toro Gordillo, J. Cabezas Fernandez, T. Buyolo Triguero, Environ. Pollut. 145 (2007) 15.
- [10] K. Müller, B. Daus, P. Morgenstern, R. Wennrich, R. Water, Air Soil Pollut. 183 (2007) 427.
- [11] N. Ulrich, in: R. Cornelis, et al. (Eds.), Handbook of Elemental Speciation, John Wiley & Sons, Chichester, 2005, pp. 47–68.
- [12] E. Dopp, L.M. Hartmann, A.M. Florea, A.W. Rettenmeier, A.V. Hirner, Crit. Rev. Toxicol. 34 (2004) 301.
- [13] P. Smichowski, Y. Madrid, C. Camara, Fresen. J. Anal. Chem. 360 (1998) 623.
- [14] M.J. Nash, J.E. Maskall, J.S. Hill, J. Environ. Monit. 2 (2000) 97.
- [15] K. Francesconi, D. Kuehnelt, Analyst 129 (2004) 373.
- [16] M. Krachler, H. Emons, J. Zheng, Trends Anal. Chem. 20 (2001) 79.
- [17] I. Koch, J. Feldmann, J. Lintschinger, S.V. Serves, W.R. Cullen, K.J. Reimer, Appl. Organomet. Chem. 12 (1998) 129.
- [18] M.J. Nash, J.E. Maskall, J.S. Hill, Analyst 131 (2006) 724.
- [19] N. Ulrich, Fresen. J. Anal. Chem. 360 (1998) 797.
- [20] J. Lintschinger, O. Schramel, A. Ketttrup, Fresen. J. Anal. Chem. 361 (1998) 484.
- [21] N. Ulrich, Anal. Chim. Acta 359 (1998) 245.
- [22] A. Guy, P. Jones, S.J. Hill, Analyst 123 (1998) 1513.
- [23] S. Foster, W. Maher, F. Krikowa, K. Telford, M. Ellwood, J. Environ. Monit. 7 (2005) 1214.
- [24] H.R. Hansen, S.A. Pergantis, J. Anal. Atom. Spectrom. 23 (2008) 1328.
- [25] N. Ainsworth, J.A. Cooke, M.S. Johnson, Environ. Pollut. 65 (1999) 77.
- [26] M. Krachler, M. Burow, H. Emons, Environ. Monit. 1 (1999) 477.

- [27] W. Hammel, R. Debus, L. Steubing, *Chemosphere* 41 (2000) 1791.
- [28] F. Baroni, A. Boscagli, G. Protano, F. Riccobono, *Environ. Pollut.* 109 (2000) 347.
- [29] M. Casado, H.M. Anwar, A. Garcia-Sanchez, I. Santa Regina, *Commun. Soil Sci. Plant Anal.* 30 (2007) 1255.
- [30] J. Gal, A. Hursthouse, S. Cuthbert, *J. Environ. Sci. Health, Part A* 42 (2007) 1263.
- [31] R. Miravet, E. Bonilla, J.F. Lopez-Sanches, R. Rubio, *J. Environ. Monit.* 7 (2005) 1207.
- [32] R. Miravet, E. Bonilla, J.F. Lopez-Sanches, R. Rubio, *Appl. Organomet. Chem.* 20 (2006) 12.
- [33] M. Dodd, S.A. Pergantis, W.R. Cullen, H. Li, G.K. Eigendorf, K.J. Reimer, *Analyst* 121 (1996) 223.
- [34] M. Krachler, H. Emons, *J. Anal. Atom. Spectrom.* 15 (2000) 281.
- [35] J. Lintschinger, I. Koch, S. Serves, J. Feldmann, W.R. Cullen, *Fresen. J. Anal. Chem.* 359 (1997) 484.
- [36] L.Q. Ma, K.M. Komar, W.H. Zhang, Y. Cai, E.D. Kennelley, *Nature* 409 (2001) 579.
- [37] J. Wang, F.J. Zhao, A.A. Mehard, A. Raab, J. Feldmann, S.P. McGrath, *Plant Physiol.* 130 (2002) 1552.
- [38] B. Daus, R. Wennrich, P. Morgenstern, H. Weiss, H.E.L. Palimieri, H.A. Nalini, V. Leonel, R.P.G. Monteiro, R.M. Moreira, *Microchim. Acta* 151 (2005) 175.



# Fractionation analysis of oxyanion-forming metals and metalloids in leachates of cement-based materials using ion exchange solid phase extraction

Mesay Mulugeta<sup>a</sup>, Grethe Wibetoe<sup>a,\*</sup>, Christian J. Engelsen<sup>b</sup>, Walter Lund<sup>a</sup>

<sup>a</sup> Department of Chemistry, University of Oslo, P.O. Box 1033, Blindern, N-0315 Oslo, Norway

<sup>b</sup> SINTEF Building and Infrastructure, P.O. Box 124, Blindern, N-0314 Oslo, Norway

## ARTICLE INFO

### Article history:

Received 3 October 2008

Received in revised form 12 December 2008

Accepted 16 December 2008

Available online 25 December 2008

### Keywords:

Fractionation analysis

Ion-exchange SPE

Oxyanions

pH dependent leaching

## ABSTRACT

A simple and versatile solid phase extraction (SPE) method has been developed to determine the anionic species of As, Cr, Mo, Sb, Se and V in leachates of cement mortar and concrete materials in the pH range 3–13. The anionic fractions of these elements were extracted using a strong anion exchanger (SAX) and their concentrations were determined as the difference in element concentration between the sample and the SAX effluent. Inductively coupled plasma mass spectrometry (ICP-MS) was used off-line to analyse solutions before and after passing through the SAX. The extraction method has been developed by optimizing sorbent type, sorbent conditioning and sample percolation rate. Breakthrough volumes and effect of matrix constituents were also studied. It was found that a polymer-based SAX conditioned with a buffer close to the sample pH or in some cases deionised water gave the best retention of the analytes. Optimal conditions were also determined for the quantitative elution of analytes retained on the SAX. Extraction of the cement mortar and concrete leachates showed that most of the elements had similar distribution of anions in both leachate types, and that the distribution was strongly pH dependent. Cr, Mo and V exist in anionic forms in strongly basic leachates (pH > 12), and significant fractions of anionic Se were also detected in these solutions. Cr, Mo, Se and V were not determined as anions by the present method in the leachates of pH < 12. Anionic As and Sb were found in small fractions in most of the leachates.

© 2008 Elsevier B.V. All rights reserved.

## 1. Introduction

The environmental properties of cement-based materials are normally evaluated by assessing the release of toxic elements using leaching tests [1,2]. Emphasis is given to the determination of the total concentration of elements released from such materials. More information about the various forms of the elements, as obtained from speciation analyses, is required to study the release mechanism, bioavailability and potential impact of the elements. Determination of the individual forms of elements is, however, highly demanding when applied to trace elements, where even the determination of the total concentration of elements might be difficult. In such cases, a possible simplified approach is to determine the species in distinct groups according to their size, mass, charge, affinity or hydrophobicity. This approach is termed “fractionation analysis” [3]. Various methods are known for the fractionation analysis of elements [4]. Solid phase extraction (SPE) on ion exchange sorbents is one of the methods, which separates species based on their charge. The technique can also be used to concentrate analytes and remove interfering matrix compo-

nents before analysis. Studies have been reported on the use of ion exchange SPE for the fractionation of elements in water [5], dietary samples [6] and landfill leachates [7–9]. Application of this method to the types of samples considered in this study has not been reported.

The elements studied in this work are As, Cr, Mo, Sb, Se and V. The leachability of these elements depends mainly on their oxyanionic forms [1,10,11]. Very few experimental studies have been done on the determination of oxyanions in leachates of alkaline wastes and none has been reported for leachates of cement mortar and concrete materials [11]. In the present work, the use of strong anion exchangers (SAX) has been studied for the determination of the anionic species of the above-mentioned elements in leachates of cement mortar and concrete materials in the pH range 3–13. The species were retained by SAX and their concentrations were determined as the difference in element concentration between the leachates and their SAX effluents. The extraction method has been developed by optimizing sorbent type, sorbent conditioning and sample percolation rate. Breakthrough volumes and the effect of matrix constituents were studied, and conditions were established for the effective elution of analytes retained on the SAX. The elemental concentration of the leachates and the SAX effluents were determined off-line using inductively coupled plasma mass spectrometry (ICP-MS).

\* Corresponding author. Tel.: +47 22855516; fax: +47 22855441.

E-mail address: [grethe.wibetoe@kjemi.uio.no](mailto:grethe.wibetoe@kjemi.uio.no) (G. Wibetoe).

**Table 1**  
Types and properties of the SAX sorbents.

SAX	Manufacturer	Sorbent container	Resin	Counter ion	Ion exchange capacity <sup>a</sup>	Mean porosity (Å)	Particle size (μm)	Reservoir volume (mL)
Bond Elut JR	Varian	Cartridge <sup>b</sup>	Silica	Cl <sup>-</sup>	0.7–0.9 meq g <sup>-1</sup>	60	47–60	3
Extract-Clean™ EV	Alltech	Syringe barrel <sup>c</sup>	PSDVB <sup>d</sup>	CH <sub>3</sub> COO <sup>-</sup>	1.2 meq mL <sup>-1</sup>		75–150	10
PL-HCO <sub>3</sub> MP SPE	Stratospheres	Syringe barrel <sup>c</sup>	PSDVB <sup>d</sup>	HCO <sub>3</sub> <sup>-</sup>	1.8–2.0 mmol g <sup>-1</sup>	100	150–300	6

<sup>a</sup> All SPE cartridges/barrels contained 500 mg of sorbent having quaternary amine active sites.

<sup>b</sup> The cartridge has Female (inlet) and Male (outlet) Luer.

<sup>c</sup> The barrel has a Male (outlet) Luer.

<sup>d</sup> PSDVB: Polystyrene divinylbenzene.

## 2. Experimental

### 2.1. Instrumentation

A PerkinElmer ELAN 5000 ICP-MS (Norwalk, CT, USA) with cross-flow nebulizer and double pass spray chamber was used. Leachates of high matrix composition were analysed after appropriate dilution. When the dilution lowered the concentration of As and Sb below the detection power of the instrument, the solutions were analysed by a dual-mode ICP-MS method which improves the detection limit of As and Sb by providing hydride generation along with normal nebulization [12].

### 2.2. Sorbent materials and sample application

One silica-based and two polymer-based SAX sorbents were studied for their efficiency in retaining the target anionic species. The relevant properties of the sorbents are given in Table 1. All the SAX cartridges/barrels contained 500 mg of sorbent. The sorbents have quaternary amine active sites, which are positively charged at all pH values between 1 and 14. In the experiments performed using the silica-based sorbent packed in cartridge, sample solutions were delivered by a peristaltic pump (Minipuls 3, Gilson, Paris). When the polymer-based SPE sorbents packed in syringe barrel were used, solutions were loaded manually, and sucked from the barrels using a peristaltic pump.

### 2.3. Chemicals, reagents and working solutions

The following salts were used to prepare stock standard solutions of the oxyanions of As, Cr, Mo, Sb, Se and V: Na<sub>2</sub>HAsO<sub>4</sub>·7H<sub>2</sub>O, Na<sub>2</sub>CrO<sub>4</sub>, and K<sub>2</sub>SbO<sub>4</sub>·4H<sub>2</sub>O·0.5H<sub>2</sub>O (Merck), Na<sub>2</sub>MoO<sub>4</sub>·2H<sub>2</sub>O and K<sub>2</sub>Sb(OH)<sub>6</sub> (Sigma), NaAsO<sub>2</sub> and Na<sub>2</sub>SeO<sub>3</sub> (Fluka), Na<sub>2</sub>SeO<sub>4</sub>·10H<sub>2</sub>O (BDH) and Na<sub>3</sub>VO<sub>4</sub> (Aldrich). All the stock solutions were 1000 mg L<sup>-1</sup> with respect to each target element (As, Cr, Mo, Sb, Se or V). Ultrapure water (18.2 MΩ cm, Millipore, Bedford, USA) was used throughout. The solutions were prepared in polyethylene containers and stored at 4 °C. Fresh working standard solutions were prepared on the day of the analysis by appropriate dilution of the stock solutions. Suprapur HNO<sub>3</sub> (65% m/m, Merck) and pro-analysis NaOH (Fluka) were used.

Two optimization solutions, I and II, were prepared with the following compositions: **I** – As (V), Mo (VI), Sb (V), Se (IV), V (V) and **II** – As (III), Cr (VI), Sb (III) and Se (VI). Both solutions were 10.0 μg L<sup>-1</sup> with respect to each of the target elements if not otherwise stated. In order to simulate the leachate samples to be analysed by the proposed methods, optimization experiments were done with solutions I and II after adjusting their pH to 4, 7, 10 and 13. pH adjustments of the solutions were made by the addition of HNO<sub>3</sub> and NaOH.

The buffer solutions used to condition the SAX sorbents were prepared as follows (reagents were from Merck). The phosphate buffers were prepared from H<sub>3</sub>PO<sub>4</sub> (85%) and NaH<sub>2</sub>PO<sub>4</sub>·H<sub>2</sub>O

(pH 4.0), NaH<sub>2</sub>PO<sub>4</sub>·H<sub>2</sub>O and Na<sub>2</sub>HPO<sub>4</sub> (pH 7.0), Na<sub>2</sub>HPO<sub>4</sub> and Na<sub>3</sub>PO<sub>4</sub>·12H<sub>2</sub>O (pH 10.0) and Na<sub>3</sub>PO<sub>4</sub>·12H<sub>2</sub>O (pH 13.0) [13]. A pH 4.0 acetate buffer was prepared from glacial CH<sub>3</sub>COOH and CH<sub>3</sub>COONa·3H<sub>2</sub>O. Acetate buffer of pH 7.0 was prepared from CH<sub>3</sub>COONH<sub>4</sub>. 25% NH<sub>3</sub> and NH<sub>4</sub>NO<sub>3</sub> were used to prepare a pH 10.0 buffer. The concentrations of the buffer components were in the range 0.001–0.01 M in all the solutions.

KNO<sub>3</sub>, NaOH, Na<sub>2</sub>CO<sub>3</sub>, Na<sub>3</sub>PO<sub>4</sub>·12H<sub>2</sub>O, Al<sub>2</sub>(SO<sub>4</sub>)<sub>3</sub>·18H<sub>2</sub>O, and Na<sub>2</sub>Si<sub>3</sub>O<sub>7</sub> (all from Merck) were used to assess the possible interference from NO<sub>3</sub><sup>-</sup>, OH<sup>-</sup>, CO<sub>3</sub><sup>2-</sup>, PO<sub>4</sub><sup>3-</sup>, SO<sub>4</sub><sup>2-</sup>, Al(OH)<sub>4</sub><sup>-</sup> and Si(OH)<sub>6</sub><sup>-</sup> on the retention of the analytes.

### 2.4. Cement mortar and concrete samples

The mortar and concrete samples used for the leaching tests were prepared from Norcem AS Anleggsement and Norcem AS Industriselement cements, respectively. These cement types are classified according to EN 197-1 [14] as CEM I 52.5 R and CEM I 42.5 R, which contain 95–100% Portland cement clinker, and belong to the strength class of 52.5 and 42.5 rapid hardening (R), respectively. The mortar was prepared by mixing CEN standard sand (1350 g), cement (450 g) and water (225 g) whereas the concrete was prepared by mixing Norstone AS aggregates (83.4 kg), cement (14.6 kg), water (7.3 kg) and Scancem SSP 2000 super plasticizer (0.088 kg). The mixes were filled into steel mould cubes, and cured and hardened for 150 days in a climate chamber at 20 °C and 90% relative humidity. Finally, the mortar and concrete were de-moulded and kept in air tight polyethylene containers. The samples were tested for their physical properties (not shown) according to EN 196-1 [15].

### 2.5. Leaching procedure

Leachate solutions were prepared from the cement mortar and concrete materials according to a standard pH-dependent leaching test [16]. The test assesses the release of elements in terms of their equilibrium concentrations at different pH values. Cement based materials are strongly alkaline. However, the leachability of elements from these materials is assessed at different pH values to evaluate the effect of external factors such as acidic soil water, carbonation and sulphide oxidation, which could change the materials' pH and affect the leachability and speciation of the elements.

In the leaching tests, 60 g portions of the crushed mortar and concrete samples (less than 1 mm particle size) were put in a series of 1 L polyethylene containers. Pre-determined volumes of 3.6 M HNO<sub>3</sub> or 3.0 M NaOH solutions were added to each container and the mixtures were diluted with water to final volumes of 600 mL. The predetermined volumes of HNO<sub>3</sub> or NaOH solutions were added to achieve final leachate pH values between 3 and 13 (see Figs. 5 and 6). The suspensions were agitated in an end-over-end rotor for 48 h. After measuring their pH, the suspensions were filtered through a 0.45-μm membrane filter and the filtrates were preserved in a deep freeze.

**Table 2**  
pK<sub>a</sub> values of the analyte species at 25 °C.

Species	Formula	Protonated form	pK <sub>a</sub>	Reference
Arsenite, As (III)	AsO <sub>2</sub> <sup>-</sup>	HAsO <sub>2</sub>	9.29	[23]
Arsenate, As (V)	AsO <sub>4</sub> <sup>3-</sup>	H <sub>3</sub> AsO <sub>4</sub>	2.24, 6.69, 11.50	[23]
Chromate, Cr (VI)	CrO <sub>4</sub> <sup>2-</sup>	H <sub>2</sub> CrO <sub>4</sub>	-0.20, 6.51	[24]
Molybdate, Mo (VI)	MoO <sub>4</sub> <sup>2-</sup>	H <sub>2</sub> MoO <sub>4</sub>	4.24, 8.24	[24]
Antimonite, Sb (III)	SbO <sub>2</sub> <sup>-</sup>	HSbO <sub>2</sub>		
Antimonate, Sb (V)	SbO <sub>3</sub> <sup>-</sup>	HSbO <sub>3</sub>	2.7	[25]
Selenite, Se (IV)	SeO <sub>3</sub> <sup>2-</sup>	H <sub>2</sub> SeO <sub>3</sub>	2.27, 7.78	[24]
Selenate, Se (VI)	SeO <sub>4</sub> <sup>2-</sup>	H <sub>2</sub> SeO <sub>4</sub>	<0, 1.7	[24]
Vanadate, V (V)	VO <sub>4</sub> <sup>3-</sup>	H <sub>3</sub> VO <sub>4</sub>	4.0, 8.5, 14.3	[24]

## 2.6. Optimized SPE procedure

The optimum extraction conditions used the Extract-Clean EV resin conditioned with deionised water, acetate buffer, ammonia buffer and phosphate buffer (or deionised water) to extract the analytes from moderately acidic (pH 4–6), neutral (pH 6–8), moderately basic (pH 8–10) and strongly basic (pH 11–13) solutions, respectively. 10.0 mL of the conditioning solution was passed through the SPE sorbent at 5.0 mL min<sup>-1</sup> and 10 mL of the sample solution was applied at the same flow rate. After the solution had passed through the SPE package, the sorbent was washed with 1.0 mL of water. In some experiments, the retained anionic species were eluted with 10 mL of 1.0 mol L<sup>-1</sup> HNO<sub>3</sub> at 2.0 mL min<sup>-1</sup> flow rate. The effluents and eluates were collected for subsequent analysis by ICP-MS.

## 2.7. Quantification of analyte fractions

The elemental concentration of the original sample solutions, SPE effluents and eluates were determined by ICP-MS with conventional nebulization or nebulization combined with hydride generation (dual-mode) sample introduction. The quantification was based on external calibration, using standard solutions that had reagent composition similar to that of the samples. For the quantification of analytes in the leachate solutions, procedural blanks were prepared in accordance with the standard pH-dependent leaching test [16]. In the dual-mode ICP-MS, the standard and sample solutions contained 1.0 mol L<sup>-1</sup> HNO<sub>3</sub> and 0.2 mol L<sup>-1</sup> thiourea, and the hydrides were generated using 1.0% (w/v) NaBH<sub>4</sub>. Details of the operating conditions of both ICP-MS methods, and the mass-to-charge ratios (*m/z*) used are given elsewhere [12]. The element fractions retained on the ion exchanger were calculated as the difference in element concentration between the original solution and the SAX effluent. However, in some experiments the analytes retained on the sorbent were eluted and quantified, for comparison (see Section 2.6).

## 3. Results and discussions

### 3.1. Analyte species and their pK<sub>a</sub> values

The target elements in the following oxidation states exist as oxyanions: As (III), As (V), Cr (VI), Mo (VI), Sb (III), Sb (V), Se (IV), Se (VI) and V (V) [17]. The pK<sub>a</sub> values of the protonated forms of these species are given in Table 2. According to these values, the protonated forms of the oxyanions will be ionised at all pH values considered in the method optimization (pH 4–13) except H<sub>2</sub>MoO<sub>4</sub> and H<sub>3</sub>VO<sub>4</sub>, which will be about 50% ionised at pH 4 and HAsO<sub>2</sub> which will be about 50% ionised at pH 9 and almost not ionised below pH 7. However, it should also be noted that these equilibria could be affected by side reactions which may occur in the sample solutions.

### 3.2. Method optimization

The efficiency of SPE is influenced by several factors [18] including type of sorbent, conditioning solution (type, ionic strength, pH and volume), sample pH, volume and loading rate, type and concentration of matrix constituents and analyte breakthrough volume. All these experimental factors were studied when optimizing the extraction method.

#### 3.2.1. Conditioning the SAX sorbents

Preliminary studies were made to evaluate the retention of analyte species on “dry” (unconditioned) SAX sorbents by loading the optimization solutions (I and II prepared at pH 4, 7, 10 and 13, see Section 2.3) onto the three SAX sorbents. The results showed that the retention of most of the analytes was not quantitative, suggesting the need for conditioning the sorbents. The conditioning exchanges the counter ion of the sorbent with an ion that has a lower affinity towards the active sites. Moreover, this step enables removal of air from the sorbent pack. It is usually recommended to condition ion exchange sorbents with deionised water or low

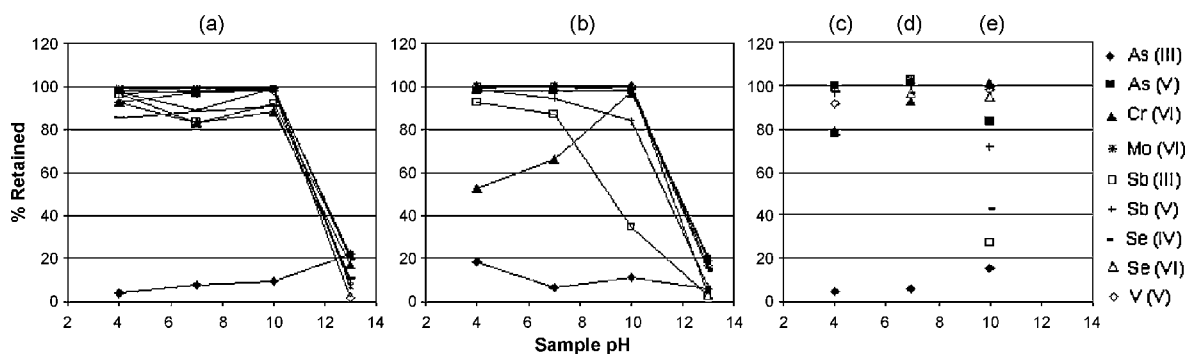


**Fig. 1.** Percentage of analytes retained on the Bond Elut JR SAX sorbent conditioned with (a) deionised water, (b) phosphate buffers (pH 4, 7, 10, 13), (c) pH 4 acetate buffer, (d) pH 7 acetate buffer and (e) pH 10 ammonia buffer. Each data point is the average of three extractions. The RSD values were in the range 1.2–4.9%.



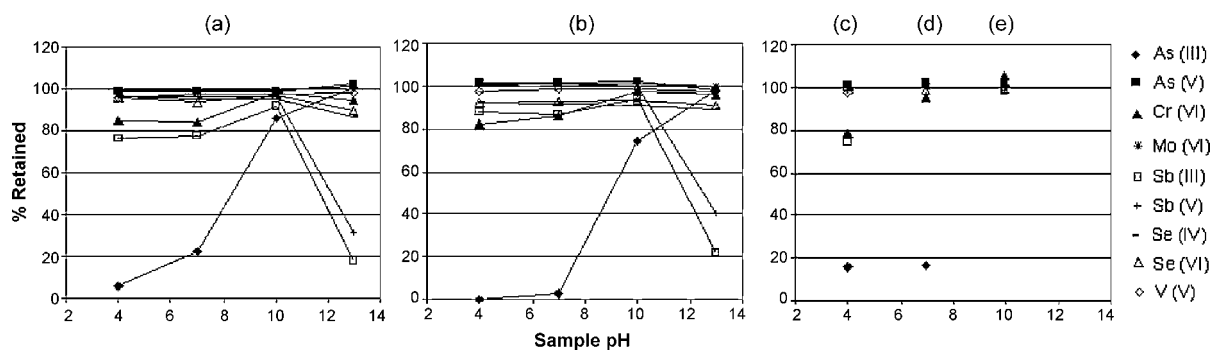


**Fig. 2.** Percentage of analytes retained on the Extract-Clean EV SAX sorbent conditioned with (a) deionised water, (b) phosphate buffers (pH 4, 7, 10, 13), (c) pH 4 acetate buffer (d) pH 7 acetate buffer and (e) pH 10 ammonia buffer. Each data point is the average of three extractions. The RSD values were in the range 0.8–3.6%.

ionic strength (0.001–0.01 M) buffer solution [19]. Conditioning sorbents with buffer having pH close to that of the sample helps to preserve the integrity of chemical species [7,20,21]. In the present work, deionised water and various buffer solutions (with pH close to that of the samples) were examined to condition the silica- and polymer-based SAX materials and to get better retention of analytes. Sorbents were conditioned with 10 mL of the reagent at a flow rate of  $5 \text{ mL min}^{-1}$ . The composition of the buffer solutions used for sorbent conditioning is described in Section 2.3.

**3.2.1.1. Conditioning the silica-based SAX sorbent.** The effects of the different conditioning solutions for the Bond Elut JR SAX sorbent are shown in Fig. 1. All the analytes except As (III) showed >80% retention at pH 4, 7 and 10 when the sorbent was conditioned with deionised water (see Fig. 1(a)). The sorbent conditioned with pH 4 and 7 acetate buffers gave retention of analytes similar to that obtained using the water-conditioned material (Fig. 1(c) and (d)). The low retention of As (III) is probably related to its presence as un-dissociated species ( $\text{HAsO}_2$ ,  $\text{pK}_a$  9.3). As can be seen from Fig. 1(b), conditioning the SAX material with phosphate buffers lowered the retentions of Cr (VI) at pH 4 and 7, and Sb (III) at pH 10. Most of the analytes were poorly retained on this sorbent at pH 10 when it was conditioned with ammonia buffer (Fig. 1(e)). It can also be seen from Fig. 1(a) and (b) that all the analytes were poorly retained on this sorbent at pH 13. This could be due to the instability of the silica resin at high pH values [18].

**3.2.1.2. Conditioning the polymer-based SAX sorbents.** The effect of the different conditioning solutions for the two polymer-based SAX sorbents, Extract-Clean EV SAX and PL- $\text{HCO}_3$  MP SPE are shown in Figs. 2 and 3, respectively. Polymeric sorbents have higher sorption capacity and better tolerance towards strongly acidic (pH < 2) and basic (pH > 10) solutions than silica-based materials [22].

Fig. 2(a) and (b) shows that similar analyte retention patterns were obtained when the Extract-Clean EV SAX was conditioned with deionised water and phosphate buffer, respectively. The sorbent conditioned with pH 4 acetate buffer also gave results similar to the water and phosphate buffer (pH 4) conditioned sorbent (see Fig. 2(c)). In all cases,  $\geq 80\%$  of each analyte was retained except As (III). Lower retention was also observed for Sb (III) and Sb (V) at pH 13. Fig. 2(d) and (e) show that the Extract-Clean EV SAX sorbent provided even better retention for all analytes at pH 7 (except As (III)) and pH 10 after being conditioned with pH 7 acetate buffer and pH 10 ammonia buffer, respectively. The results given in Fig. 2 also demonstrated the superiority of this polymer-based SAX over the silica-based material on retaining analytes from strongly alkaline solutions (pH 13). Only Sb (III) and Sb (V) were poorly retained on the sorbent at pH 13. To check if the other analytes had effect on the retention of the Sb species, Sb (III) and Sb (V) were extracted from their separate solutions prepared at pH 13. No improved retention was observed for either of the species.

The PL- $\text{HCO}_3$  MP SPE sorbent was conditioned in the same way as the Extract-Clean EV sorbent. It showed similar retention for most of the analytes as was observed for the Extract-Clean EV at pH 4, 7 and 10, with slightly lower retention for Cr (VI) and Sb (III) (see Fig. 3). However, the retention of most of the analytes on this sorbent was lowered significantly at pH 13 as shown in Fig. 3(a) and (b), compared to the Extract-Clean EV SAX.

The conditioning experiments clearly showed that the efficiency of analyte extraction depends on the type of sorbent and its conditioning. Based on the results of these studies, the SAX sorbent and conditioning solutions which provided the best retention of analyte species were selected and used for the rest of the experiments. The selected conditions used the Extract-Clean EV SAX conditioned with deionised water, acetate buffer, ammonia buffer and phosphate buffer to extract the analytes from moderately acidic (pH

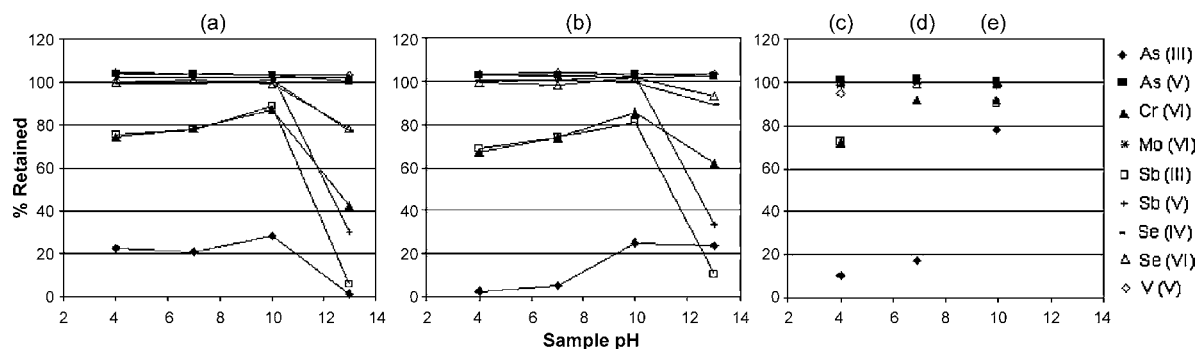


**Fig. 3.** Percentage of analytes retained on the PL- $\text{HCO}_3$  MP SPE sorbent conditioned with (a) deionised water, (b) phosphate buffers (pH 4, 7, 10, 13), (c) acetate buffer (pH 4), (d) acetate buffer (pH 7) and (e) ammonia buffer (pH 10). Each data point is the average of three extractions. The RSD values were in the range 1.7–9.2%.

4–6), neutral (pH 6–8), moderately basic (pH 8–10) and strongly basic (pH 11–14) solutions, respectively.

### 3.2.2. Effect of sample flow rate on analytes retention

In SPE processes, the effect of the rate at which the sample solution passes through the sorbent bed should be evaluated to ensure quantitative retention of analytes along with minimizing the time required for sample extraction. In optimizing the flow rate, 10.0 mL of solution I and II (see Section 2.3), both adjusted to pH 7, were loaded manually onto separate Extract-Clean EV barrels and sucked from the sorbents at different flow rates using a peristaltic pump. It was observed that increasing the flow rate up to 10 mL min<sup>-1</sup> did not affect the retention of any of the analyte species.

### 3.2.3. Elution of retained analytes

Elution of retained substances from ion extraction sorbents can be achieved using solutions that neutralize the functional group of the sorbent or the analyte. If analytes are present at low concentration, they can be recovered in a small volume of eluent to achieve their preconcentration. In the present case, retained analytes were eluted from the resin by protonating them using HNO<sub>3</sub>. HNO<sub>3</sub> is the preferred acid for ICP-MS analyses as it will not cause polyatomic spectral interferences for elements like As. Different concentrations of the acid were tested for the effective elution of the analytes, after the application of 10 mL of solution I and II. The results showed quantitative elution of the analytes with 10.0 mL of  $\geq 0.5$  mol L<sup>-1</sup> HNO<sub>3</sub> at a flow rate of 2 mL min<sup>-1</sup>.

### 3.2.4. Effect of matrix components on analytes retention

The retention of analytes on ion exchangers depends on the type and concentration of other sample constituents which might compete for the active sites of the sorbent. In the present work, the interference from matrix anions which commonly exist in samples of the type studied in this work was examined. Solutions I and II, containing 25.0  $\mu\text{g L}^{-1}$  of each of the target elements, were spiked with the following matrix ions; NO<sub>3</sub><sup>-</sup>, OH<sup>-</sup>, CO<sub>3</sub><sup>2-</sup>, PO<sub>4</sub><sup>3-</sup>, SO<sub>4</sub><sup>2-</sup>, Al<sup>3+</sup> and Si<sup>4+</sup> in the concentration range 0.01 to 1000 mg L<sup>-1</sup> (see Section 2.3). 10 mL of the spiked solutions were extracted on separate barrels after adjusting their pH to 12 (Al and Si exist as hydroxy complexes at this pH). As the two Sb species were less retained from strongly basic solutions, the effect of matrix interferences on their extraction was evaluated after adjusting the pH of the solutions to 9.

The results showed that the presence of these matrix ions up to 100 mg L<sup>-1</sup> had no effect on the retention of the analyte species except for Sb (III), whose retention was lowered as the concentrations of the matrix ions exceeded 10 mg L<sup>-1</sup>. Retention of most of the analyte ions decreased rapidly as the concentrations of the matrix ions increased above 100 mg L<sup>-1</sup>. This is due to the competition of the highly concentrated matrix ions for the ion exchange sites of the sorbent, because at this point the total amount of anions introduced was almost equal to the ion exchange capacity of the cartridge (see Table 1).

### 3.2.5. Breakthrough volume of analytes on the Extract-Clean EV sorbent

The breakthrough volume ( $V_B$ ) refers to the maximum sample volume that passes through a given mass of sorbent until analyte retention is no longer quantitative [22].  $V_B$  depends on the nature of the sorbent material and the type and concentration of sample constituents. The analyte capacity of a sorbent, i.e. the maximum amount of an analyte that can be retained on the sorbent from a particular matrix, can be determined from the breakthrough volume.

To address the effect of matrix constituents of the samples to be analysed in this study, the  $V_B$  of the analytes on the Extract-Clean EV resin were determined using a leachate prepared from a concrete

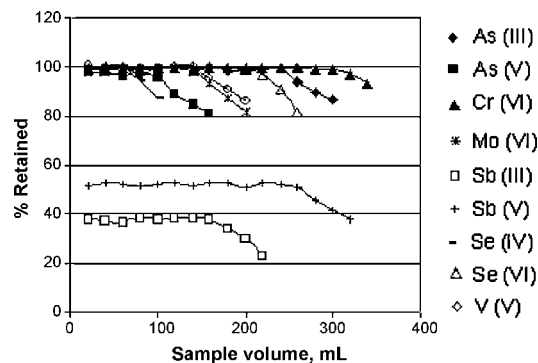


**Fig. 4.** Breakthrough curves for analytes extracted on the Extract-Clean EV SAX sorbent. A concrete leachate sample of pH 12.7 was divided in two portions and spiked with the following analyte concentrations. 1st portion: 7  $\mu\text{g L}^{-1}$  As (V), 60  $\mu\text{g L}^{-1}$  Mo (VI), 4  $\mu\text{g L}^{-1}$  Sb (V), 12  $\mu\text{g L}^{-1}$  Se (IV), 40  $\mu\text{g L}^{-1}$  V (V). 2nd portion: 7  $\mu\text{g L}^{-1}$  As (III), 610  $\mu\text{g L}^{-1}$  Cr (VI), 4  $\mu\text{g L}^{-1}$  Sb (III) and 12  $\mu\text{g L}^{-1}$  Se (VI). The two sample portions were extracted on separate barrels.

material. The leachate (pH 12.7) was divided into two portions; the first portion was spiked with 7  $\mu\text{g L}^{-1}$  As (V), 60  $\mu\text{g L}^{-1}$  Mo (VI), 4  $\mu\text{g L}^{-1}$  Sb (V), 12  $\mu\text{g L}^{-1}$  Se (IV), 40  $\mu\text{g L}^{-1}$  V (V) and the second portion with 7  $\mu\text{g L}^{-1}$  As (III), 610  $\mu\text{g L}^{-1}$  Cr (VI), 4  $\mu\text{g L}^{-1}$  Sb (III) and 12  $\mu\text{g L}^{-1}$  Se (VI). These concentrations reflect the maximum concentration of the respective elements (except Cr) found in the leachate samples analysed in this study. After conditioning the resin with phosphate buffer of pH 13, the spiked samples were passed through the sorbent at a flow rate of 5 mL min<sup>-1</sup> and every 10 mL effluent were collected and analysed.

As can be seen from the breakthrough curves given in Fig. 4, no saturation of the sorbent material was observed until the volume loaded onto the resin reaches a total of 80 mL. As the sample volume exceeded 80 mL some of the analytes were detected in the effluent in the order Se (IV), As (V), Mo (VI) and V (V) until 140 mL of the sample was loaded. The retention of Se (VI), As (III) and Cr (VI) became no longer quantitative for sample volumes higher than 200 mL. As this study was performed using a strongly basic leachate solution (pH 12.7), only a lower fraction of the two Sb species were retained. Attempts to improve the retention of these species by lowering the pH of the sample did not give better results. This might be due to the effect of matrix components of the leachate solution.

## 4. Analysis of leachates of cement mortar and concrete materials

This study aimed to develop a method for the fractionation analysis of oxyanion-forming metals and metalloids in leachates prepared from cement mortar and concrete materials. In the cement mortar leachates the total element concentrations varied as a function of pH in the ranges ( $\mu\text{g L}^{-1}$ ) 1.0–7.0 (As), 4.0–700 (Cr), 0.5–50 (Mo), 0.5–3.0 (Sb), 2.0–13.0 (Se) and 0.5–40.0 (V). The concrete leachates contained these elements in the ranges ( $\mu\text{g L}^{-1}$ ) 0.1–5.5 (As), 2.0–2100 (Cr), 1.0–40.0 (Mo), 0.05–1.5 (Sb), 1.0–8.0 (Se) and 0.2–35.0 (V). The pH dependent release of most of the elements from both materials corresponded to a typical leaching curve for oxyanion-forming elements with a higher release at neutral and mild alkaline pH [1,2,10].

The anionic species of the target elements were extracted from 10.0 mL of the leachates by Extract-Clean EV SAX using the optimum extraction conditions established in this study. The total concentration and the anionic fraction of each element found in the leachates are given in Figs. 5 and 6. The results for the anionic fractions were obtained by subtracting the concentration found in the SPE effluent from the total concentration measured in the leachate. However,

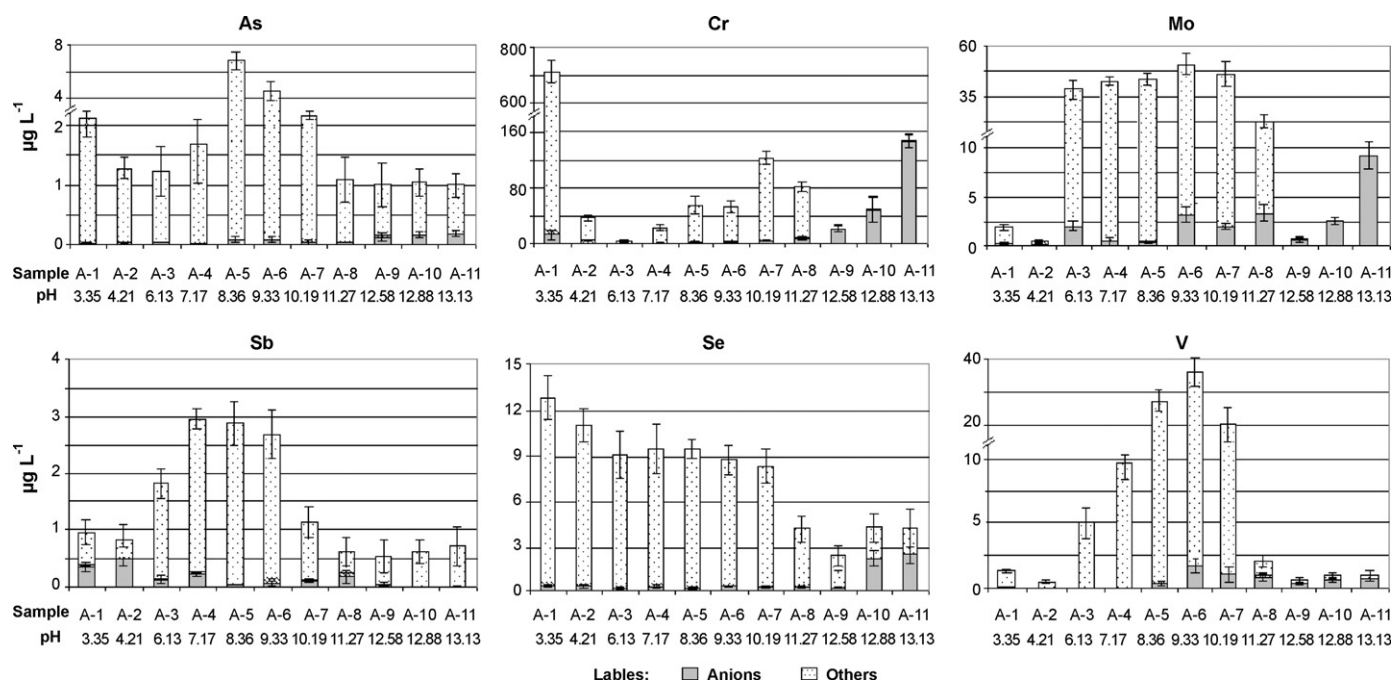


Fig. 5. Total concentrations and anionic fractions of elements in solutions leached from a cement mortar material. Leachate A-9 was prepared without acid/base addition.

the retained anionic species were also eluted from the sorbent with 10.0 mL of 1.0 mol L<sup>-1</sup> HNO<sub>3</sub> and quantified. It was found that the concentrations obtained by elution agreed with those found by subtraction; the concentrations of analytes measured in the elutes were in the range 94–106% of the corresponding anionic fractions given in Figs. 5 and 6.

Figs. 5 and 6 show that the fractions of anionic species of most of the elements were similar for both leachate types (mortar and concrete). Cr, Mo and V were almost entirely present as anions in the strongly basic leachates (pH > 12). Significant proportions (>50%) of Se were detected as anions in the leachates of pH > 12.8. The proportions of anionic Cr, Mo, Se and V were significantly lower in the samples with pH below 12. A small fraction of

anionic As and Sb was detected in most of the leachates regardless of pH.

For the cement mortar and concrete materials, the equilibrium pH of the leachates prepared without acid or base addition were around 12.5 (samples A-9 and B-9, see Figs. 5 and 6). When the leachant pH is lowered below 10.5, most of the cement hydrate phases undergo degradation which results in the release of oxyanionic species, which were incorporated in the hydrated cement. In the leachates analysed in this study, the anionic elemental fractions detected in the neutral and mild alkaline leachates of both materials were low. Possibly, redox processes occurring in the leachate solutions affected the oxidation states of the elements, resulting in the formation of cationic and/or neutral species. An ongoing exper-

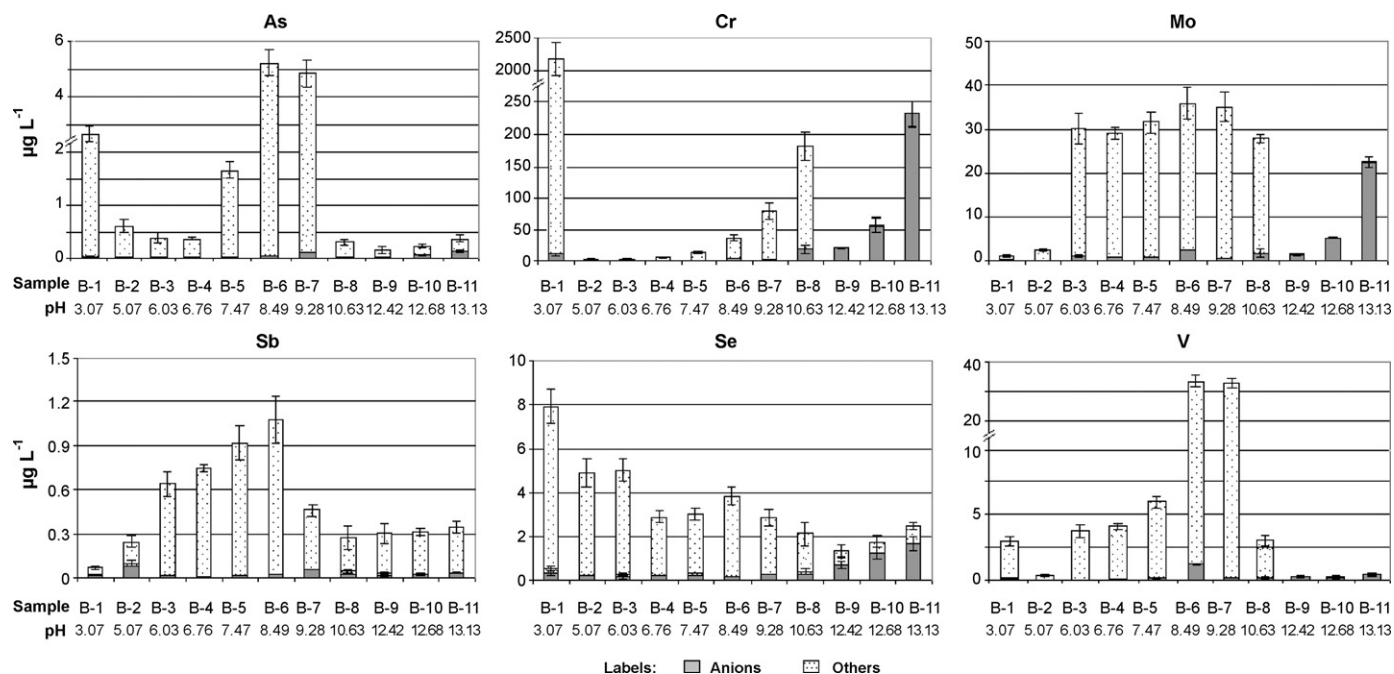


Fig. 6. Total concentrations and anionic fractions of elements in solutions leached from a concrete material. Leachate B-9 was prepared without acid/base addition.

imental study on the cationic species of the leachates showed the retention of a high fraction (>70%) of V on a strong cation exchanger from leachates at pH 6–10. In addition, the anionic species might form neutral ion associates with cationic species which exist in the solutions. Further investigations should be performed to study the speciation of the elements and to identify the factors which control their stability in the leachate solutions.

## 5. Conclusions

The work presented in this paper has demonstrated the use of ion exchange SPE for the determination of the anionic fractions of As, Cr, Mo, Sb, Se and V in leachates of cement mortar and concrete materials. This simple, fast and cost effective procedure is based on the retention of the analytes by a polymer-based SAX sorbent conditioned with a buffer of pH close to that of the sample or in some cases with deionised water. The work has provided valuable information regarding the presence and pH dependence of the anionic forms of the target elements in the leachate solutions which will be helpful in the release mechanism and availability studies of the elements based on the processes occurring in the solid materials and the leachate solutions. Further investigations, however, should be made to identify the chemical species of the elements and the factors which control their stability in the leachates. The present method could be used to determine the anionic species of other elements than those studied in this work.

## Acknowledgements

The authors would like to gratefully acknowledge the Norwegian Quota Scholarship Program for financial support and Anne-Marie Skramstad for skilful technical assistance.

## References

- [1] H.A. van der Sloot, *Cem. Concr. Res.* 30 (2000) 1079.
- [2] D.S. Kosson, H.A. van der Sloot, F. Sanchez, A.C. Garrabrants, *Environ. Eng. Sci.* 19 (2002) 159.
- [3] D.M. Templeton, F. Ariese, R. Cornelis, L.-G. Danielsson, H. Muntau, H.P. Van Leeuwen, R. Lobinski, *Pure Appl. Chem.* 72 (2000) 1453.
- [4] A.M. Ure, C.M. Davidson, *Chemical Speciation in the Environment*, Blackie Academic and Professional, Glasgow, 1995.
- [5] P. Pohl, *Trends Anal. Chem.* 25 (2006) 31.
- [6] P. Pohl, *Trends Anal. Chem.* 26 (2007) 713.
- [7] J.K. Øygard, E. Gjengedal, O. Røyset, *Water Res.* 41 (2007) 47.
- [8] M. Majone, P.M. Papini, E. Rolle, *Environ. Technol.* 17 (1996) 587.
- [9] P.M. Papini, M. Majone, E. Rolle, *Water Sci. Technol.* 44 (2001) 343.
- [10] H.A. van der Sloot, *Waste Manage.* 22 (2002) 181.
- [11] G. Cornelis, C.A. Johnson, T. van Gerven, C. Vandecasteele, *Appl. Geochem.* 23 (2008) 955.
- [12] M. Mulugeta, G. Wibetoe, C.J. Engelsens, A. Asfaw, *Anal. Bioanal. Chem.* 393 (2009) 1015.
- [13] G.D. Christian, W.C. Purdy, *J. Electroanal. Chem.* 3 (1962) 363.
- [14] EN-197-1, Composition, specifications and conformity criteria for common cements CEN TC 51, 2000.
- [15] EN-196-1, Test methods for cement, CEN TC 51, 2005.
- [16] CEN/TS14429:2005, Characterization of waste – leaching behaviour tests – influence of pH on leaching with initial acid/base addition, 2005.
- [17] C.F. Baes, R.E. Mesmer, *The Hydrolysis of Cations*, John Wiley & Sons, Inc., Toronto, 1976.
- [18] V. Camel, in: D. Barcelo (Ed.), *Comprehensive Analytical Chemistry*, vol. 37, Wilson & Wilson's, Amsterdam, 2003, p. 393.
- [19] Solid Phase Extraction Products: Data Sheet 205000U, Alltech Associates Inc., 2002.
- [20] G. Tangen, T. Wickstrøm, S. Lierhagen, R. Vogt, W. Lund, *Environ. Sci. Technol.* 36 (2002) 5421.
- [21] S.B. Erdemoglu, K. Pyrzyniska, S. Gücer, *Anal. Chim. Acta* 411 (2000) 81.
- [22] M.-C. Hennion, *J. Chromatogr. A* 856 (1999) 3.
- [23] A.E. Martell, R.M. Smith, *Critical Stability Constants: First Supplement*, Plenum Press, New York, 1982.
- [24] A.E. Martell, R.M. Smith, *Critical Stability Constants: Inorganic Complexes*, Plenum Press, New York, 1976.
- [25] J. Lintschinger, I. Koch, S. Serves, J. Feldmann, W.R. Cullen, *Fresen. J. Anal. Chem.* 359 (1997) 484.



## Determination of light-absorbing layers at inner capillary surface by cw excitation crossed-beam thermal-lens spectrometry

D.A. Nedosekin<sup>a,\*</sup>, W. Faubel<sup>b</sup>, M.A. Proskurnin<sup>a</sup>, U. Pyell<sup>c</sup>

<sup>a</sup> Analytical Chemistry Division, Chemistry Department, Moscow State University, Moscow, Russia

<sup>b</sup> Research Center Karlsruhe, Institute of Technical Chemistry, Water Technology and Geotechnology Division, Karlsruhe, Germany

<sup>c</sup> Department of Chemistry, University of Marburg, Marburg, Germany

### ARTICLE INFO

#### Article history:

Received 6 October 2008

Received in revised form 6 December 2008

Accepted 11 December 2008

Available online 24 December 2008

#### Keywords:

Thermal-lens detection

Capillary surface

Adsorption study

Heat transfer

### ABSTRACT

A thermal-lens spectrometric unit suitable for selective quantitative measurements of light-absorbing layers adsorbed onto the inner surface of a quartz glass capillary is described. The quantitative description of the thermal-lens signal generated in a quartz glass capillary with a light-absorbing layer at the inner surface of capillary is developed, which is based on the description for the thermal-lens experiment in the layered solids presented elsewhere. The accuracy of calculations is demonstrated by the comparison of predicted results with the experimental data and those predicted by the conventional theory. The data achieved prove the accuracy of calculations both for the time dependent thermal-lens signal and for the lock-in amplifier signal under variation of the spectrometer configuration for capillaries having an adsorbed layer. The proposed technique is used for the investigation of chromate/2,10-ionene and 4-aminoazobenzene adsorption at capillary walls. The estimates of the minimum light absorption detectable at capillary walls are at a level of  $1 \times 10^{-5}$  abs. units; the linear range of the thermal-lens signal from the inner surface layer no less than three orders of magnitude is predicted.

© 2008 Elsevier B.V. All rights reserved.

### 1. Introduction

The use of highly sensitive photothermal (thermo-optical) detection schemes in capillary electrophoresis and chemical-microchip separation methods, in particular thermal-lens detection, becomes a topical alternative to the UV–vis spectrophotometric absorbance detection in these areas [1–6]. A number of studies dedicated to the use of thermo-optical detectors in microchips or capillary electrophoresis expose an important question: of prime significance are not only the detection aspects resulting from a limited size and volume of the sample [3,7], but also other factors appearing from complex on-interface energy-transfer processes in the detection zone [7]. Kim et al. demonstrated the significance of the sample geometry in the case of adsorption studies [8] indicating that a tube of the same size and dimensions as the laser beams in the detection scheme affect the results of absorbance measurements. On the other hand, the interface of a quartz capillary and adsorption processes are also topical subjects for investigations [8,9]; however, there are no direct techniques sensitive enough to determine parameters of an inner capillary surface layer in the course

of experiment or at least without sample destruction. The direct determination of the adsorbed layers would obviously simplify accounting the adsorption in capillary zone electrophoresis [9], investigation of the interaction between the solution and enzyme-linked immunosorbent [10], etc.

From our point of view, the near-field thermal-lens spectrometer with a crossed-beam mode-mismatched schematics could have all the features needed for interface studies in a closed system like a capillary [7]. The crossed-beam optical design provides thermal-lens measurements in small-volume samples without a loss in the sensitivity [7]; this would obviously advantage interface studies alike in photothermal-deflection spectroscopic techniques. Thermal lensing as compared to fluorescence microspectroscopy provides a wider range of detectable substances; as compared to conventional UV-spectroscopy it provides both sufficient spatial resolution and high sensitivity. The use of laser-based absorption methods in this case is not possible as soon as the laser beam will deflect at a curved capillary surface. The preliminary data achieved [11,12] show that the results of the thermal-lens experiment in a surface-absorbing capillary could be attributed to the concentration of light-absorbing substances deposited at a capillary surface. However interesting, these data lack a theoretical description and cannot be used “as is”.

In order to describe the thermal-lens effect at a capillary surface, the knowledge on the temperature profile in the capillary is essential. The complex geometry of laser beams in capillaries

\* Corresponding author at: Moscow State University, Analytical Chemistry Division, Chemistry Department, Vorob'evy Hills d. 1 str. 3, Moscow 119991, Russian Federation. Tel.: +7 495 939 3514; fax: +7 495 939 4675.

E-mail address: [tanarek@mail.ru](mailto:tanarek@mail.ru) (D.A. Nedosekin).

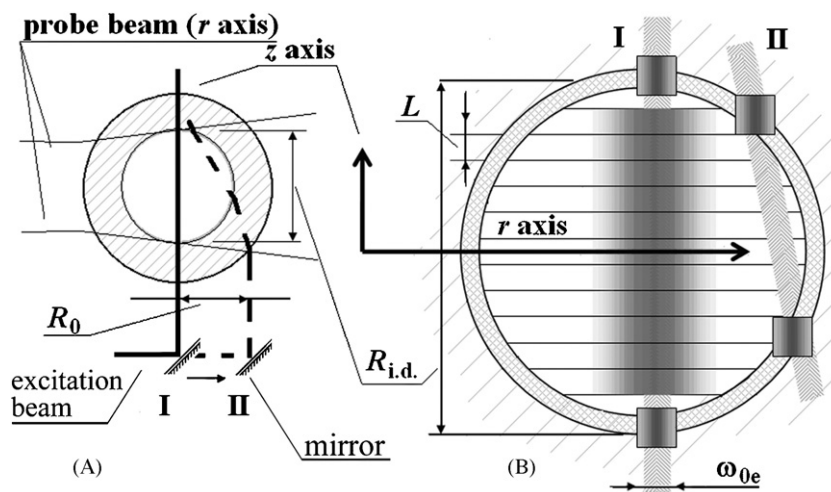


**Fig. 1.** Scheme of the “central” and “marginal” configurations of the spectrometer (marked as I and II, respectively). (A) The scheme of excitation beam path through the spectrometer and capillary. (B) The representation of the inner capillary volume fragmentation for the calculation of temperature profiles in the solution and at a capillary surface upon the absorption of the excitation beam (the quartz part of the capillary is out of the picture frames).

requires the consideration of heat generation at a capillary surface with due account for the geometrical configuration and spatial distribution of light-absorbing substances. Hence, theoretical descriptions developed for the medium with heterogenous light-absorbing structures are required. From our point of view, the approach to the thermal-lens experiments in such complex samples introduced previously for the calculation of the temperature profiles in layered solids [13,14] and further spread to the case of multiple light-absorbing particles [15] could be used to describe thermal lensing at a capillary surface. In this work, this approach is extended to quantitatively describe the thermal-lens signal from layers at an inner capillary surface. The theoretical description is compared to the conventional description of the thermal-lens experiment in a solution-filled capillary. A special emphasis is given to the estimation of the analytical parameters of the technique proposed.

## 2. Theoretical background

In the following section we describe the formation of a thermal lens at the inner surface of a round capillary with an inner diameter of 75  $\mu\text{m}$ .

### 2.1. Initial specifications

The thermal-lens spectrometric unit suitable for the selective quantitative measurement of light-absorbing layers adsorbed onto the inner surface of a quartz glass capillary has the crossed-beam schematics (Fig. 1). It is known that the best analytical parameters of such a spectrometer correspond to a mode-mismatched scheme introduced by Snook [13,16–18]. To implement this, the excitation beam is made narrower than the sample (to diminish the influence from sample boundaries on the thermal diffusion); the size of the beam is constant within the sample [19]. The size of the probe beam is usually equal to the inner size of the capillary [1,2,4] to provide the maximum sensitivity: at cw excitation repetition (chopping) rates of 10–100 Hz, the thermo-optical element fills the whole inner volume of the capillary [19]. In this work, the detection scheme optimal for solutions is kept intact; thus, all the spectrometer parameters including the excitation beam with the waist size of 7.5  $\mu\text{m}$  are used (beam waist is tenfold smaller than the common capillary i.d. of 75  $\mu\text{m}$ ).

The thickness of adsorbed layers at a quartz capillary surface ranges from a sub-nanometer level (adsorption of the analyte or co-ions) to several micrometers (adsorption of electroosmotic-flow modifiers) [20]. In general, for the theoretical description of thermal lensing in a layered system [12,14] the thickness of a layer is less important than the amount of heat generated. This will allow simplifying the description of the thermal-lens experiment [13]. Thus, the thickness of the surface layer in further calculations is always 5  $\mu\text{m}$ ; this corresponds to the maximum thickness of the EOF modifier layer reported elsewhere [20].

### 2.2. Beam propagation through a capillary

The optimization of spectrometer configuration to determine light-absorbing layer at a capillary surface seems to be essential. The position of the probe beam could hardly become a subject of optimization in the presence of a layer at capillary surface as soon as in the mode-mismatched scheme the whole capillary is inside the probe beam. On the other hand, a shift in the position of the relatively narrow excitation beam out of the center of the capillary can lead to drastic changes in system parameters. Considering two possible locations of the light absorption—the solution and the surface layer—two different configurations of the excitation beam–capillary geometry are useful: the conventional schematics, where the excitation beam goes through the center of the capillary (for in-solution measurements); and the configuration important for surface studies, where the excitation beam passes in the vicinity of the capillary wall, Fig. 1. From this point on, in order to distinguish between these schematics, we will refer to them as “central” and “marginal”, respectively.

Obviously, a parallel shift in the excitation beam from the center of capillary would drastically change the location of the irradiated zone at a capillary surface [11,21]. The calculation of the ray-intersection coordinates for the outer and inner capillary interfaces in the  $(r, z)$  plane, Figs. 1 and 2, could be done either in the frames of a simple descriptive geometry (Snell’s laws, ray tracing) [7,21,22] or with the use of a diffraction approach [21]. As the excitation laser beam in the capillary is small enough compared to the dimensions of capillary and a change in the beam waist does not affect the quantity of the heat generated, we used the main law of light refraction [21,22].

It is a parallel shift of excitation beam,  $R_0$ , from the axis ( $z=0$ ) outside the capillary that determines the initial angle of incidence

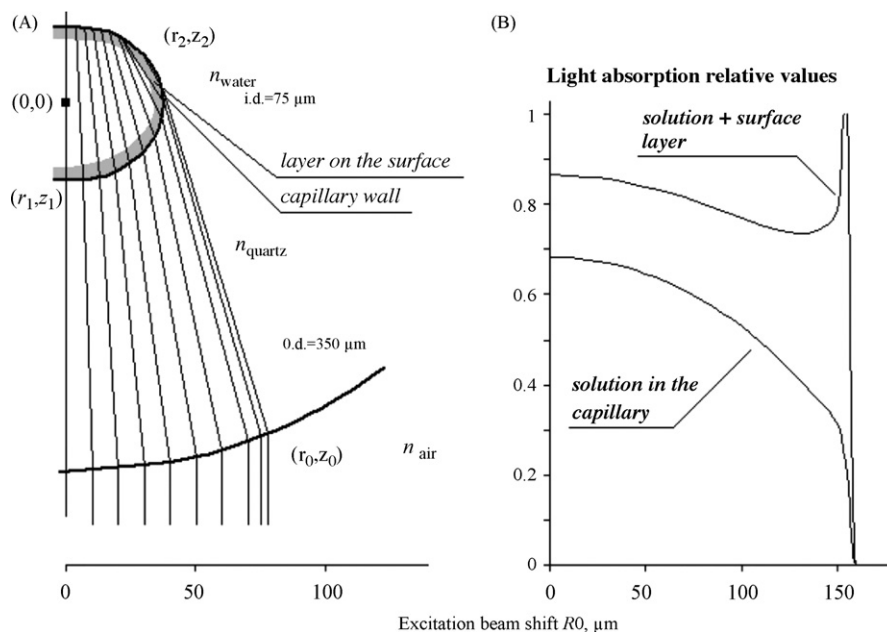


**Fig. 2.** Ray tracing in a capillary. (A) Excitation beam propagation as a function of beam shift value  $R_0$ .  $n_{\text{air}}$ ,  $n_{\text{quartz}}$  and  $n_{\text{water}}$  are the refractive indices for the materials considered. (B) Total light absorption of solution and surface layer (thickness of layer,  $5 \mu\text{m}$ ,  $\alpha_{\text{lay}}/\alpha_{\text{sol}}$  linear light absorption coefficients ratio is  $5/1$ ) calculated according to Eq. (1).

between the beam and the capillary outer surface, and, respectively, coordinates of the intersection points at capillary inner surfaces ( $r_1, z_1$ ) and ( $r_2, z_2$ ). Further, this parameter,  $R_0$ , defines the configuration of spectrometer. An example of ray propagation for a typical capillary with i.d. of  $75 \mu\text{m}$  and o.d. of  $360 \mu\text{m}$  is presented in Fig. 2(a).

### 2.3. Light absorption of the surface layer

To expose the significance of ray tracing in capillary, the total light absorption for a plain water-filled capillary and for a water-filled capillary with a  $5 \mu\text{m}$  thick light-absorbing layer is presented in Fig. 2(b). The light absorption was calculated from the light path length in solution  $l_{\text{sol}}$  and light path length through the layer  $l_{\text{lay}}$ . Consequently,  $\alpha_{\text{sol}}$  and  $\alpha_{\text{lay}}$  are the light absorption coefficients for the solution and the surface layer. If the layer exists,  $\alpha_{\text{lay}}$  is higher than  $\alpha_{\text{sol}}$  and the total light absorption of capillary is:

$$A = l_{\text{sol}}\alpha_{\text{sol}} + l_{\text{lay}}\alpha_{\text{lay}}. \quad (1)$$

As it comes from Fig. 2(b), even a primitive ray tracing in the capillary exposes that the contribution of the layer is important. The “central” configuration  $R_0 = 0 \mu\text{m}$  appears when the excitation beam goes through the center of the capillary and the laser beam mainly is in the solution. The “marginal” configuration corresponds to the significant shift of the beam as the beam goes near the wall through the adsorbed layer, Figs. 1 and 2. For the capillaries considered (i.d.,  $75 \mu\text{m}$  and o.d.,  $360 \mu\text{m}$ ) the beam shift,  $R_0$ , is more than  $50 \mu\text{m}$ , Fig. 2(b). The increase in the total light absorption for the “marginal” configuration calculated is rather close to the experimental data obtained for 2,10-ionene adsorption at capillary inner surface [11]. However, our data on spectrometer optimization for strongly absorbing surface layers of 4-aminoazobenzene [12] show that consideration of temperature profile bloomed at capillary surface [12] is essential for a correct interpretation of the experiment.

### 2.4. Thermo-optical element in a surface-modified capillary

Temperature profiles in a capillary bloomed upon the adsorption of laser radiation were calculated based on the model developed for

thermal lensing in layered solids [12,13]. In the “central” configuration, the capillary and surface layers are on the same axis orthogonal to the probe-beam axis, Fig. 1, that is exactly the situation for layered solids [13]. However, a shift in the excitation beam breaks the central symmetry. In this case, Fig. 1 (the “marginal” configuration), the approach previously tested for gold nanoparticles [15] could be used for the calculation of asymmetrical temperature profiles. Thus, the calculations are split into two parts: one for the “central” configuration and another for the “marginal” one.

In the “central” configuration, a set of layers to describe the heat generation consists of ten layers for the solution plus two for the surface layers: one at the beginning and one at the end of the set. The requirements for layer selection were given elsewhere [13]. For each layer, the linear light absorption coefficients  $\alpha$  could be assigned; thus, it is possible to describe a light-absorbing solution in the capillary (all the layers have the same light absorption,  $\alpha_{\text{sol}} = \alpha_{\text{lay}} > 0$ ); light absorption by surface layers only ( $\alpha_{\text{sol}} \rightarrow 0, \alpha_{\text{lay}} > 0$ ); and the light absorption of the surface-modified capillary filled with a light-absorbing solution ( $\alpha_{\text{sol}} > 0, \alpha_{\text{lay}} > 0$ ). As shown in the Section 2.1, the surface-layer thickness is  $5 \mu\text{m}$  and the assumed thickness of a hypothetical layer in solution is  $(75 - 2 \times 5)/10 = 6.5 \mu\text{m}$ .

The “marginal” configuration requires describing the thermal lens from surface layers for different configurations of the excitation beam, i.e. for different values of the beam shift parameter,  $R_0$ . In accordance with the approach for gold nanoparticles [15], the calculation specifications are the following: firstly, a single layer at the surface of capillary is represented by several light-absorbing layers. Thus, a  $5 \mu\text{m}$  thick surface layer should be simulated at least by three hypothetical layers with a thickness of  $5/3 = 1.66 \mu\text{m}$ . The light absorption coefficient  $\alpha_{\text{lay}}$  for all hypothetical layers should be identical. Details of the calculation specifications are given elsewhere [13]. Next, the temperature profile bloomed upon the absorption of the laser radiation by this set of layers is calculated as a function  $\Delta T = f(r, z, t)$ , where  $r$  and  $z$  are the coordinates in a cylindrical coordinate system and  $t$  is time. This function is transferred in space by substituting coordinates with the new ones,  $r' = r + R$ ,  $z' = z + Z$ . The shift vector  $(R, Z)$  was calculated from the ray tracing data made for excitation beam, Fig. 2(b). A duplicate of the initial function is transferred into the second point of intersection with

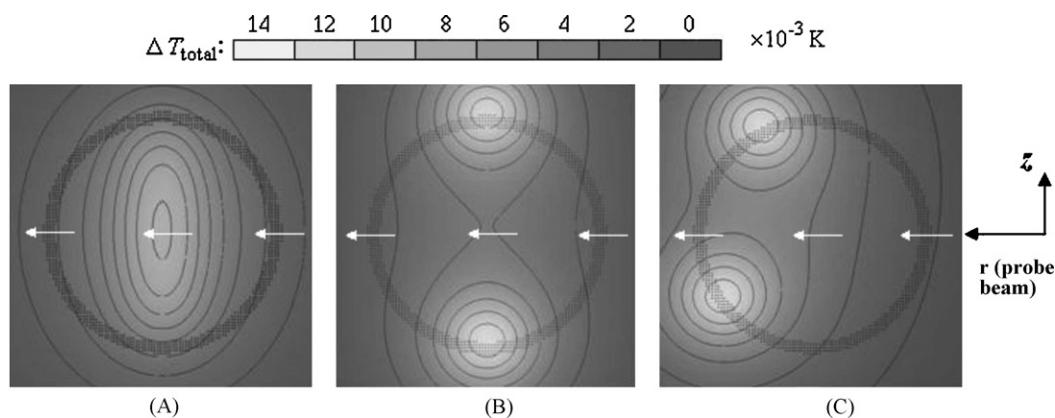


**Fig. 3.** Temperature profiles: (A) Solution in capillary, the “central” configuration, light absorption is  $1 \times 10^{-4}$  abs. units,  $\Delta T_{\max} = 8 \times 10^{-3}$  K; (B) and (C) Surface layers, the “central” and “marginal” configurations, respectively. Light absorption is  $3 \times 10^{-5}$  abs. units,  $\alpha_{\text{lay}} = 6 \text{ m}^{-1}$ ,  $l = 5 \times 10^{-6} \text{ m}$ ,  $\Delta T_{\max} = 1.5 \times 10^{-2}$  K. Black dots denote the layer on capillary surface; white arrows show probe-beam direction. Capillary diameter is 75  $\mu\text{m}$ . Heating duration is 0.01 s. Other parameters are summarized in Table 1.

the capillary inner surface in the same way. The resulting temperature profile corresponds to the selective heating of the capillary surface in accordance with the spectrometer configuration.

Fig. 3 shows three shapes for heat profiles typical for the configurations of the spectrometer–capillary layer. As it was expected, the temperature profiles bloomed at capillary surface change the symmetry of the original temperature profile in solution. In the case of the crossed-beam thermal lensing, formation of the temperature profiles like Fig. 3(b) or (c) could lead to decrease in the thermal-lens signal as soon as the probe beam does not go through the maximum of the temperature profile.

The calculated temperature profiles were additionally characterized by a width (size) parameter. Gaussian trend was fitted for the temperature profile section along the probe-beam axis. The width at the half-height of the Gaussian peak  $\sigma$  was considered as a size parameter.

### 2.5. Thermal-lens signal

The relative probe-beam intensity change in the center of the beam expanded by bloomed thermal-lens element is an instrumental signal  $\vartheta(t)$  [7]:

$$\vartheta(t) = \frac{I_p(0) - I_p(t)}{I_p(t)} \quad (2)$$

where  $I_p(t)$  is the intensity of the probe beam at the detection plane in the time  $t$ , and  $I_p(0)$  is the initial probe-beam center intensity (before thermal-lens excitation). For a homogeneous solution or a bulk solid analytical signal  $\theta$  is defined as following [7]:

$$\theta = 2.303EP_e\epsilon lc \quad (3)$$

where  $P_e$  is the excitation power,  $\epsilon$  is molar absorptivity,  $l$  is the length of the light path in the sample,  $c$  is the molar concentration of the light-absorbing substance, and  $E_0$  is the enhancement factor of thermal lensing for unit excitation power. The instrumental and the analytical signal are related to each other as:

$$\vartheta = KB\theta. \quad (4)$$

where  $K$  is a constant which depends on the electronic amplifier of the detection system and  $B$  is the spectrometer configuration parameter defined differently for paraxial [7] and diffraction models [23] of thermal lensing.

In the frames of the paraxial approach [7,24], the time-dependent thermal-lens signal  $\vartheta(t)$  can be calculated from the known temperature profile as a function of the thermal-lens focal strength  $f$  [7,13,24]. Thus, the focal strength of the thermo-optical element  $f(t)$  in the capillary is obtained by the integration across the

probe-beam propagation path for the second spatial temperature derivative calculated along the direction tangent to the probe-beam axis:

$$\frac{1}{f(t)} = - \int \frac{d^2 n(r, z, t)}{dz^2} dr = - \left( \frac{dn}{dT} \right) \int_{-R}^R \frac{d^2 \Delta T(r, z, t)}{dz^2} dr. \quad (5)$$

Next, expressing the spectrometer dimensions through the constants:  $z_0$  (the probe laser confocal distance);  $z_w$  (the distance between the waist of the probe beam and the sample); and  $z_d$  (the distance between the sample and the detector plane) the thermal-lens signal can be calculated as [7,12,22]:

$$\vartheta(t) = - \left[ \frac{2z_d}{f(t)} \right] \frac{z_w^2 + z_0^2 + z_d z_w}{(z_w + z_d)^2 + z_0^2} + \left[ \frac{z_d}{f(t)} \right]^2 \frac{z_w^2 + z_0^2}{(z_w + z_d)^2 + z_0^2}. \quad (6)$$

The lock-in amplifier constant  $K$  that links the analytical to the instrumental thermal-lens signal, Eq. (4) was determined by comparing experimental data with calculated values for several solutions with different light adsorption. The resulting constant for the “central” configuration of spectrometer was also used for the interpretation of experimental data in the “marginal” configuration of the spectrometer.

### 2.6. Conventional description of thermal lens in the capillary

In order to validate the theoretical description used, the calculations according to the existing theoretical models of thermal lensing in the capillary were undertaken. The temperature magnitude on-axis of the excitation beam in the capillary (relative to the ambient temperature) for the excitation duration  $t$  is the following [7]:

$$\Delta T_{\text{cw}}(0, 0, t) = \frac{P_e \alpha}{4\pi k} \ln \frac{t_c + 2t}{t_c}. \quad (7)$$

here,  $t_c$  is the characteristic time of thermal lens  $t_c = w_{0e}^2/4D$ ;  $k$  is the thermal conductivity of the medium;  $\alpha$  is linear light absorption coefficient. With the use of the paraxial thermal-lens approach the focal strength of the bloomed thermal lens in the center of the probe beam in the case of the crossed-beam cw thermal lensing can be expressed as [7]:

$$\frac{1}{f_{\text{cw}}(t)} = \left( \frac{dn}{dT} \right) \frac{2^{1/2} P_e \alpha}{\pi^{1/2} k \omega_{0e}} \left[ 1 - \frac{1}{(1 + 2t/t_c)^{1/2}} \right]. \quad (8)$$

In order to take into consideration the size of the thermal-lens element in the capillary (i.e. the light path of the probe beam through the thermo-optical element that is thin at the beginning of the cycle and maximum at the end at time  $t_{\text{chop}}$ ) Eq. (8) was mod-



**Table 1**  
Spectrometer parameters and medium constants used in the calculations [7].

Spectrometer configuration		
Excitation laser	Wavelength $\lambda_e$ (nm)	325.0
	Spot size at the waist $\omega_{0e}$ ( $\mu\text{m}$ )	7.7
	Laser power at the sample $P_e$ (mW)	50
Probe laser	Wavelength $\lambda_p$ (nm)	681.9
	Laser power at the sample $P_p$ (mW)	30
	Spot size in the sample $\omega_2$ ( $\mu\text{m}$ )	75
	Confocal distance, $z_0$ (mm)	0.90
	Distance between waist of probe beam and sample $z_{\omega}$ (mm)	3.53
Other constants	Chopper jitter	$\pm 1\%$
	Distance between sample and detector plane, $z_d$ (cm)	180
	Chopper frequency (Hz)	40–95
Thermo-optical parameters of the medium		
Aqueous solutions	Thermal diffusion coefficient, $\text{m}^2 \text{s}^{-1}$	$1.43 \times 10^{-7}$
	Thermal conductivity, $k$ ( $\text{W m}^{-1} \text{K}^{-1}$ )	59.8
	Refractive index, $n_0$	1.33
	Temperature derivative of the refraction index, $dn/dT$ ( $\text{K}^{-1}$ )	$1 \times 10^{-4}$
	Characteristic time of thermal lens, $t_c$ , s	$1 \times 10^{-4}$
Air	Refractive index, $n_0$	1.00
Quartz	Refractive index, $n_0$	1.46

ified by means of the calculated thermal-lens width parameter,  $\sigma$  (Section 2.2).

$$\frac{1}{f_{\text{cw}}(t, \sigma)} = \frac{1}{f_{\text{cw}}(t)} \frac{\sigma(t)}{\sigma(t_{\text{chop}})} \quad (9)$$

### 3. Experimental

#### 3.1. Apparatus

The near-field thermal-lens detector with a crossed-beam mode-mismatched optical schematics designed for the detection in capillary electrophoresis was used. The main parameters of this spectrometer are used in the theoretical calculations and are summarized in Table 1. The detailed description of the detection scheme was given elsewhere [1,2,8].

A WaveRunner 6050A digital oscilloscope was used for the recording of the time-resolved thermal-lens data (350 MHz, 4-Channel, 2.5/5 GS/s 2/4 Mpts, LeCroy Corporation, USA). The change in the intensity of the central part of the probe beam was obtained from a photodiode placed behind a pinhole through a lock-in amplifier used to amplify and convert the probe-beam power data. Simultaneously, the steady-state thermal-lens signal was recorded by a PC connected to the lock-in amplifier output port.

All the experiments were carried out in fused-silica capillaries (Polymicro technologies, Phoenix, AZ, USA); capillary dimensions were the following: i.d. 75  $\mu\text{m}$ , o.d. 360  $\mu\text{m}$ , 71.6 cm, total length (41.3 cm to detector). The protection coating at the 5 mm wide zone of the detection window was removed with warm concentrated sulfuric acid.

#### 3.2. Data treatment

All the calculations of the temperature and thermal-lens signals by the model developed were performed by Maple 10.03 software (Maplesoft, Waterloo Maple Inc.) with the use of an Intel Pentium IV 2.0 GHz-based PC. In addition, SigmaPlot 9.01 (Systat Software Inc.) software was used for the data analysis of the experimental results.

#### 3.3. Reagents

The following reagents were used: Mordant Yellow 7 (dye content 65%, Aldrich, Germany); 4-aminoazobenzene (dye content 98%, Aldrich, Germany);  $\text{NaBO}_2 \times \text{H}_2\text{O}_2 \times 3\text{H}_2\text{O}$  (purum p.a., Fluka, Germany). Deionised high-purity water (Milli-Q 185 plus (18.0  $\text{M}\Omega \text{cm}^{-1}$ ), Millipore, Bedford, MA, USA) was used for sample preparation.

#### 3.4. Procedures

In order to produce light-absorbing layers at a capillary surface, solutions of 4-aminoazobenzene were used. This cationic dye is readily adsorbed at negatively charged capillary surfaces and the process of light induced (UV-vis radiation) isomerization of this dye followed by the precipitation of the insoluble isomer mixture was discovered to take place [12]. The main capillary modification techniques are the adsorption in the dark and the precipitation of the dye under the He-Cd laser irradiation.

##### 3.4.1. Adsorption in the dark

A new capillary was flushed with a 0.1 M NaOH solution for 30 min, rinsed with water and filled with a 100  $\mu\text{M}$  4-aminoazobenzene solution in a 25 mM  $\text{NaBO}_2 \times \text{H}_2\text{O}_2$  buffer (pH 9.4). This capillary was left in the dark for 2 h, and then rinsed with water for 10 min and 0.1 M NaOH for 2 min.

##### 3.4.2. Light-induced adsorption

A new capillary was prepared as described above, filled with the same 4-aminoazobenzene solution and installed into the thermal-lens detector. Then the capillary was rinsed for 10 min with a solution of 4-aminoazobenzene while the He-Cd laser beam was focused according to the “central” or the “marginal” configuration of the spectrometer. After this procedure, the capillary was flushed with water and 0.1 M NaOH successively for 20 min.

##### 3.4.3. Thermal-lens measurements

Calibration of the spectrometer is performed with a clean capillary filled with a dye solution (the position of the maximum signal of the solution is to be found). After the capillary surface has been modified with a light-absorbing layer, the spectrometer is shifted to the “marginal” configuration with the laser beam going far away from the inner volume of the capillary. During these measurements, the capillary can be filled with water or a light-absorbing solution.

The beam is shifted back to the center of the capillary in a 5  $\mu\text{m}$  step by rotating the corresponding micro-screw. The thermal-lens signal is to be recorded by the PC connected to the output of the lock-in amplifier. The time-resolved data are obtained by the digital oscilloscope from the corresponding output of the lock-in amplifier. The thermal-lens signal at each step was recorded only for several seconds in order to avoid complete laser-induced desorption of the surface layer.

## 4. Results and discussion

#### 4.1. Validation of the model

The validation of the theoretical description accuracy is performed for thermal lensing in the “central” configuration of spectrometer for capillary with light-absorbing solution, i.e. without light-absorbing surface layers.

##### 4.1.1. Calculation of temperature profile

Calculation of the temperature increase in the center of capillary was performed for a light-absorbing solution according to the

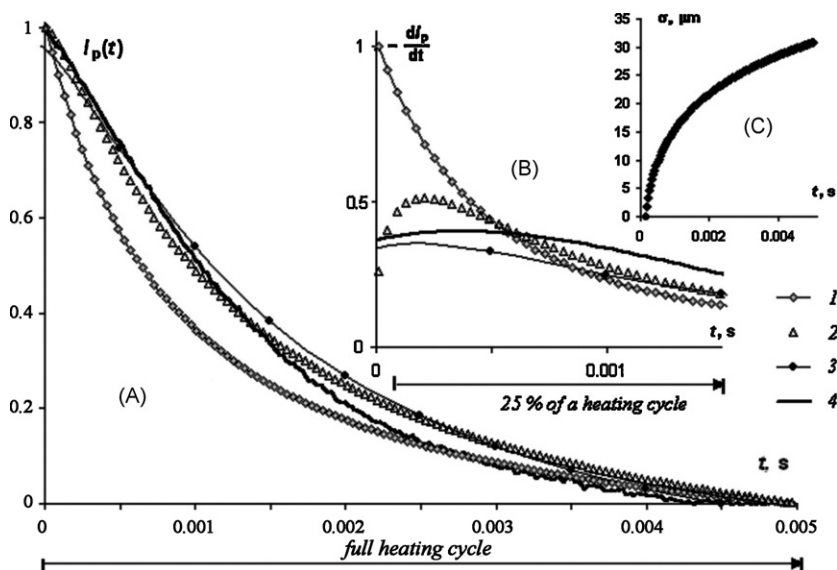


**Fig. 4.** Time-resolved thermal-lens signal, comparison of predicted and experimental values: (A) Thermal-lens experiment in a 50  $\mu\text{M}$  Mordant Yellow 7 solution. Inset (B) shows the time derivative values of the time-resolved signal for a first quarter of heating cycle; inset (C) shows the calculated size of the thermal-lens element. symbol "1", conventional theory, Eqs. (6) and (8); symbol "2", conventional theory modified by the element-size function, Eqs. (6), (8) and (9); symbol "3", the developed model; solid line denotes experimental results.

description proposed and Eq. (7) (conventional approach). Temperature increase in a solution with absorbance of  $1 \times 10^{-4}$  abs. units (the middle of detection range) upon absorption of a laser irradiation for 0.01 s according to conventional approach, Eq. (7) is 0.005 K [4]. Temperature distribution in space obtained according to the model used is given at Fig. 3 (a) and the temperature maximum in the center of capillary is at the level of 0.008 K. From our point of view, these estimates are rather close, which proves the adequacy of our calculations.

#### 4.1.2. Time-resolved thermal-lens experiments

Fig. 4 shows experimental and theoretical data describing development of the thermal-lens effect in time for clean capillary filled with a dye solution (a 50  $\mu\text{M}$  solution of Mordant Yellow 7). In general, the experimental and the predicted data on the probe-beam intensity (inset (A)) are in a good agreement; still, the initial parts

of curves differ noticeably. The evidence of the difference in the curves comes from signal time derivatives, Fig. 4 (inset (B)). The rate of thermal-lens blooming is predicted to be higher in the case of the conventional approach. This could be due to not considering the width of the bloomed thermo-optical element, which at first is small enough (short light path of the probe beam through the formed thermal lens) [7]. This assumption was verified by calculating the thermo-optical element width parameter  $\sigma$ , Fig. 4 (inset (C)), Section 2.2. This data show that in the beginning of the heating cycle thermal lens is smaller than the capillary inner volume. At the end of a heating cycle (for chopper frequencies used in this work), the thermal-lens element has the spatial dimensions of the inner capillary diameter. The time-resolved thermal-lens signal was therefore corrected to consider the size of thermal-lens element according to Eq. (9), Fig. 4 (insets (A) and (B), data marked with the symbol "2"). Now both the calculated time-resolved thermal-lens signal and its

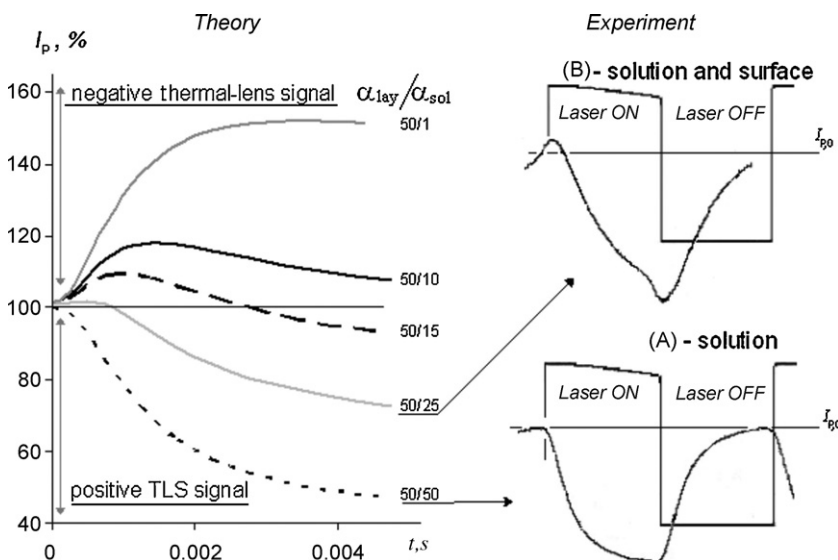


**Fig. 5.** Time-resolved thermal-lens signal, comparison of predicted and experimental values in a capillary with a 5  $\mu\text{m}$  thick surface layer, the "central" configuration. The ratios of surface/solution light absorption coefficients used in the calculations are: (1) 50/1; (2) 50/10; (3) 50/15; (4) 50/25; and (5) 50/50. Inset (A) is for experimental time-resolved signal. Inset (B) is the time-resolved signal for the solution and a surface layer. The square curve marks the time moment when heating starts.

time derivative are in better accordance with the experimental data than the values calculated via the original approach.

Thus, the excellent agreement of calculated and experimental data proves the satisfactory level of model accuracy in description of heat generation in conventional experiments. Hence, the model developed can now be used for describing the spectrometer signal behavior in the case of light-absorbing substances deposited onto the capillary surface.

#### 4.2. Thermal lensing in surface-modified capillaries

The main goal of the section is to expose the differences in blooming of the thermal lens for clean and surface-modified capillaries. This would allow us to correlate the observed thermal-lens signal with the real distribution of the absorbing substances in the capillary. Corresponding changes in the analytical signal are considered both from theoretical and experimental points of view.

##### 4.2.1. “Central” configuration

In the “central” configuration (the excitation beam is in the center of capillary, i.e.  $R_0$  is about zero), the energy absorbed by the solution forms a heated zone with the temperature maximum at the center of capillary (Fig. 3(a)). If heat is generated at a capillary surface, two separate hotspots appear on opposite walls. This results in the formation of a temperature profile with the minimum in the center of capillary where the probe beam passes (Fig. 3(b)). Resulting from the second spatial temperature derivative, Eq. (5), these thermo-optical elements have opposite properties: the first (with a maximum) defocuses the probe beam giving a positive thermal-lens signal, while the second (with a minimum) focuses the probe beam giving a negative thermal-lens signal, Eq. (2). Thus, in the “central” configuration, the resulting signal from a solution and a surface layer could be lower than that for the solution alone or can even reach a negative value. This contradicts the results of total absorbance calculation for surface modified capillary, Eq. (1).

Fig. 5 shows time-resolved signals calculated for surface-modified capillary filled with solutions of different concentrations. In the case when light absorption coefficients are equal for solution and surface layer (curve “50/50” at Fig. 5), the time-resolved curve is identical to the one presented at Fig. 4(a). The superposition of temperature profiles from the surface layer and solution distorts the shape of thermal-lens signal curves; however, the predicted distortion of the curves is in excellent agreement with the experimental data for capillaries with surface layers of 4-aminoazobenzene, Fig. 5(a) and (b).

For a surface-absorbing capillary, the calculated thermal-lens signals  $\vartheta_{\text{sol+lay}}$  for different combinations of the layer and solution absorbances (i.e. the results of imaginary experiments) were fitted as:

$$\vartheta_{\text{sol+lay}} = \vartheta_{\text{sol}} - bLC_{\text{lay}} \quad (10)$$

Here,  $b$  is the slope of the calibration graph for the wall-generated thermal lens in the “central” configuration;  $L$  is the layer thickness.

Thus, experimentally observed changes in thermal-lens signal for the “central” configuration of spectrometer in the case of surface-layer formation are proven by theoretical calculations. The “central” configuration of the spectrometer could be considered disadvantageous for thermal-lens measurements in the case of surface light adsorption due to superposition of temperature profiles formed in the solution and at the capillary surface.

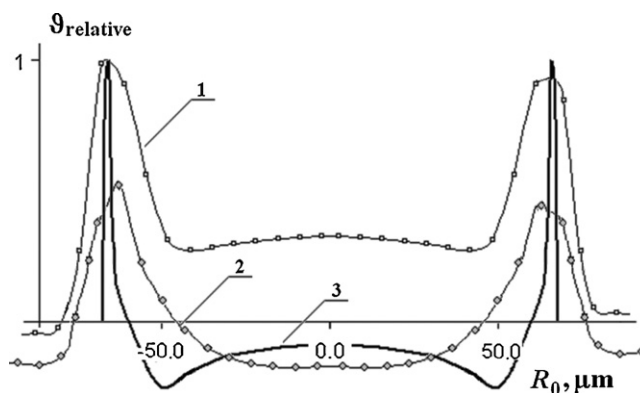


Fig. 6. Relative thermal-lens signal values for a capillary with a thick surface layer as a function of the excitation laser beam position: (1) 100  $\mu\text{M}$  of 4-aminoazobenzene solution in a capillary with a surface layer, experimental data; (2) Water in the capillary and surface layer, experimental data (the signal is scaled relatively to the curve (1)); and (3) theoretical calculations for the surface layer in solution filled capillary (ratio for solution/surface linear absorption coefficients is 1/5, surface layer thickness,  $L$  is 5  $\mu\text{m}$ ).

##### 4.2.2. “Marginal” configuration

Fig. 3(c) shows temperature profile generated at capillary surface in the “marginal” configuration ( $R_0 = 50 \mu\text{m}$  for the capillaries used). Here, the center of the probe-beam, axis  $r$ , does not go through the minimum of temperature profile. Thus, one can expect a positive thermal-lens signal in the “marginal” configuration with the probe beam positioned at the center of the capillary, Eqs. (2) and (5). In the frames of the used model, the following calibration equation was fitted for the “marginal” configuration:

$$\vartheta_{\text{sol+lay}} = \vartheta_{\text{sol}} + dLC_{\text{lay}} \quad (11)$$

Here,  $d$  is the calibration slope for the “marginal” configuration of the spectrometer. The calibration graphs were calculated for the spectrometer (Table 1) by fitting a linear trend to a set of thermal-lens signals calculated for capillaries with surface layers of different light absorption. These data show that value of parameter  $d$  is higher than that of parameter  $b$ , Eqs. (10) and (11), i.e. in the “marginal” configuration of the spectrometer the surface coating produces a thermal lens with a higher impact to the total signal of capillary than in the “central” configuration.

Fig. 6 shows experimental and theoretical thermal-lens signals for a surface-modified capillary at different spectrometer configurations. This figure illustrates the technique developed for capillary surface investigation. The change of spectrometer configurations is made by a parallel shift of the excitation laser beam from one side of capillary to another (the beam shift parameter changes in the range from  $-100$  to  $+100 \mu\text{m}$ ). The thermal-lens signal as a function of the excitation-beam shift could comment the presence of the adsorbed substances at capillary surface itself. The position of the thermal-lens signal maximum correlates with the calculated “marginal” configuration of the spectrometer,  $R_0 \sim 50$  or  $-50 \mu\text{m}$ . Thus, the theoretical description of the thermal-lens experiment for different configurations of spectrometer explains the unusual shape of the thermal-lens signal curve observed in the presence of a surface layer [11].

The theoretical curve, Fig. 6, nicely fits the experiment; however, the calculated width of the zone that corresponds to the “marginal” configuration, is smaller than the experimentally obtained one. This deviation might be due to the limitations of the theoretical model used for the calculation of temperature profiles or it might be related to the use of ray tracing for the excitation beam instead of diffraction pattern calculations.

Fig. 6 exposes another interesting application of the technique proposed. The formation of a strong thermal lens from the sur-

face layer in the “*marginal*” configuration of spectrometer simplifies the investigation of adsorption in the presence of a light-absorbing medium. As mentioned, the thermal-lens signal produced in a solution depends on the spectrometer configuration in the same way as the total absorbance of solution, Fig. 2(b) (the curve for solution only), i.e. the thermal-lens signal from solution in “*marginal*” configuration is almost zero. That means that the surface layer produces maximum thermal-lens signal in such a spectrometer configuration where solution generated signal is minimum.

Thus, the theoretical calculations support our assumptions that light-absorbing substances can be determined directly at the inner capillary surface. The conventional “*central*” configuration of the spectrometer becomes disadvantageous in the case of a layer formation. The theoretical calculations and the experimental data show that the new configuration is well suited for surface layer determinations; while the influence of the thermal-lens formation in solution is minimum. Still, with the theory developed one can estimate the results of the experiment only; the assumptions made to calculate the thermal-lens signal significantly decrease the accuracy of calculations. A check of the theory accuracy is complicated for it is hard to prepare a capillary with an inner surface layer with a known absorbance or to determine the absorbance of the layer in capillary alternatively without its destruction.

#### 4.3. Analytical parameters of the technique proposed

The theoretical description of the thermal-lens experiment in capillary provides a tool for interpretation of the experimental data obtained previously. Preparation of a surface standard is always complicated; thus, in this section the analytical characteristics of the technique proposed are considered on the basis of the estimations made for the previously obtained data [8,11]. The estimation compares the experimental data to the thermal-lens signal calculated *a priori* for an imaginary light-absorbing sample. The calibration plot was constructed *a priori* with the theoretical data only, by the calculation of the thermal-lens signal for various linear light absorption coefficients of the layer at capillary surface with a respect given to the spectrometer configuration. Then, the linear trend was fitted to the calculated data to achieve the calibration plots (similar to Eqs. (10) and (11)) for the “*central*” and “*marginal*” configurations. The coefficients,  $K$  and  $B$ , connecting the analytical and instrumental thermal-lens signals, Eq. (4) were calculated by comparing experimental and theoretical thermal-lens signals for a solution-filled capillary (“*central*” spectrometer configuration) and further used in all the calculations.

On the basis of calibration calculations, it is possible to estimate both the experimental data reported previously for the adsorption of chromate ions in a 2,10-ionene layer on the capillary surface [11] and the data on adsorption of 4-aminoazobenzene at capillary surface [12]. The absorbance of chromate in the surface layer of 2,10-ionene was estimated to be at a level of  $1 \times 10^{-5}$  abs. units (a concentration of chromate of 0.5 M in a 5  $\mu\text{m}$  thick 2,10-ionene layer). This value is by an order of magnitude lower than the one obtained by the direct thermal lensing of quartz plates coated with 2,10-ionene–chromate aggregates [11,20]. On the other hand, the data reported previously concern the maximum capacity of 2,10-ionene layer; thus, the experimental data concerning the adsorption of chromate agree well with those values which would be expected from theoretical considerations.

In the model experiments with the 4-aminoazobenzene, the analyte was precipitating from solution at capillary surface upon adsorption of laser radiation [12] (Section 3.3) that was used to obtain layers of different thicknesses at capillary surface. The range of thermal-lens signals obtained in the “*marginal*” configuration of spectrometer (from the surface layers) was extremely wide (from

$10^4$  to  $10^7$  arb. units) [12]. The estimated range of absorbances for the layers was in the range from  $1 \times 10^{-5}$  abs. units (adsorption in the dark) to  $5 \times 10^{-3}$  abs. units (laser induced precipitation). These calculations were provided for the “*marginal*” configuration of the spectrometer by the use of a calibration Eq. (11) calculated for the spectrometer considered (Table 1). The data observed are plausible and do not contradict with the conditions of the experiment. These data and the previously obtained linear calibration graph [12] for 4-aminoazobenzene precipitation at capillary surface in the flow mode predict the linear range of the technique to be no less than three orders of magnitude.

Estimation of the reproducibility for the technique proposed is a complex task. Mainly this results from the absence of surface standards and from irreproducibility of the layer formation. This parameter is also affected due to photodecomposition and laser-caused desorption of the layer from the surface [12]. Still, the reproducibility was measured for layers of 4-aminoazobenzene formed at a capillary surface by flushing a dye solution through capillary (the “*marginal*” configuration; details of the experiment are given elsewhere [12]; conditions could be considered as an equilibrium between the adsorption and desorption of 4-aminoazobenzene). The relative standard deviation,  $s_r$ , of the thermal-lens signal was from 2 to 6% in the range of signals from  $10^4$  to  $10^7$  arb. units. Correlation coefficient of the calibration graph for 4-aminoazobenzene is 0.992 ( $P=0.95$ ,  $n=6$ ). Therefore, the reproducibility of thermal lensing at an inner capillary surface is high enough to propose the analytical application of the technique.

The locality of the proposed technique earns additional mentioning. There are two separate spots at a surface layer where the excitation beam passes, Figs. 1 and 2(a). Assuming the excitation-beam diameter to be constant in the capillary and ignoring a change in the cross-section size for various coincidence angles, the total capillary surface irradiated with the excitation beam is 44  $\mu\text{m}^2$ . For a thickness of the surface layer of 5  $\mu\text{m}$ , the volume, in which the excitation laser beam is adsorbed, is about  $0.2 \times 10^{-12}$  L. In this case, Fig. 3(c) shows that the thermal lens bloomed at capillary surface occupies more than a half of capillary, i.e. the volume in which analytical signal is generated is much larger.

Thus, the analytical parameters of the technique proposed for the investigation of quartz capillary surface are close to those for solution-absorption detection [1,2,4]. The interpretation of the experimental data estimates the minimum light absorption of the surface layer to be at a level of  $1 \times 10^{-5}$  abs. units.

## 5. Conclusions

The near-field thermal-lens detector with a crossed-beam configuration developed for the detection in capillary electrophoresis could be used to quantify solutes being adsorbed directly onto the capillary surface or being absorbed by a thin layer (about 5  $\mu\text{m}$ ) adsorbed onto the inner surface of a quartz glass capillary. The quantitative determination of the surface layer light absorption requires an excitation beam passing closely to the capillary surface. In this configuration, the determination of the concentration of the adsorbed solute in the surface layer is not disturbed by the presence of a nontransparent solution in the inner capillary volume. The interpretation of the experimental data is realized by comparing the experimental data to the results of theoretical calculations of temperature profile bloomed at the inner surface of quartz glass capillary. The model experiments prove the accuracy of these calculations. The minimum absorbance detectable was estimated to be at a level of  $1 \times 10^{-5}$  abs. units.

The potential applications of the proposed technique include the investigation of adsorption in quartz glass capillaries and study of the interface-transfer or laser-induced processes at the capillary interface. For capillary zone electrophoresis, the direct determina-

tion of the layers at a capillary surface would obviously simplify the description of the adsorption [9] and optimization of separation conditions [25]. It is promising for investigation of reactions in capillary resulting in adsorption of the reaction products at a capillary interface [12].

## References

- [1] B.S. Seidel, E. Steinle, W. Faubel, H.J. Ache, SPIE Proc. 2836 (1996) 283.
- [2] B.S. Seidel, W. Faubel, H.J. Ache, J. Biomed. Opt. 2 (1997) 326.
- [3] T. De Beer, N.H. Velthorst, U.A. Brinkman, C. Gooijer, J. Chromatogr. A 971 (2002) 1.
- [4] M.A. Proskurnin, S.N. Bendrysheva, N. Ragozina, S. Heissler, W. Faubel, U. Pyell, Appl. Spectrosc. 59 (2005) 1470.
- [5] K. Uchiyama, A. Hibara, K. Sato, H. Hisamoto, M. Tokeshi, T. Kitamori, Electrophoresis 24 (2003) 179.
- [6] M. Yamauchi, M. Tokeshi, J. Yamaguchi, T. Fukuzawa, A. Hattori, A. Hibara, T. Kitamori, J. Chromatogr. A 1106 (2006) 89.
- [7] S.E. Bialkowski, Photothermal Spectroscopy Methods For Chemical Analysis, A Wiley-Interscience Publication, New York, 1996, Vol. 134, pp584.
- [8] H.-B. Kim, S. Yoshida, N. Kitamura, Anal. Chem. 70 (1998) 51.
- [9] S.V. Ermakov, M.Y. Zhukov, L. Capelli, P.G. Righetti, J. Chromatogr. A 699 (1995) 297.
- [10] K. Sato, M. Yamanaka, T. Hagino, M. Tokeshi, H. Kimura, T. Kitamori, Lab. Chip 4 (2004) 570.
- [11] D.A. Nedosekin, A.V. Pirogov, W. Faubel, U. Pyell, M.A. Proskurnin, Talanta 68 (2006) 1474.
- [12] D.A. Nedosekin, W. Faubel, M.A. Proskurnin, U. Pyell, Anal. Sci. (2009), in press.
- [13] D.A. Nedosekin, M.A. Proskurnin, M.Y. Kononets, Appl. Opt. 44 (2005) 6296.
- [14] M.A. Schweitzer, J.F. Power, Appl. Spectrosc. 48 (1994) 1054.
- [15] A.V. Brusnichkin, D.A. Nedosekin, M.A. Proskurnin, V.P. Zharov, Appl. Spectrosc. 61 (2007) 1191.
- [16] J. Shen, R.D. Snook, J. Appl. Phys. 73 (1993) 5286.
- [17] R.D. Snook, R.D. Lowe, M.L. Baesso, Analyst 123 (1998) 587.
- [18] R.D. Snook, R.D. Lowe, Analyst 120 (1995) 2051.
- [19] A. Smirnova, M.A. Proskurnin, S.N. Bendrysheva, D.A. Nedosekin, A. Hibara, T. Kitamori, Electrophoresis 29 (2008).
- [20] A.V. Pirogov, W. Buchberger, J. Chromatogr. A 916 (2001) 51.
- [21] A.E. Bruno, E. Gassman, N. Pericles, K. Anton, Anal. Chem. 61 (1989) 876.
- [22] R.E. Synovec, Anal. Chem. 59 (1987) 2877.
- [23] J. Shen, R.D. Lowe, R.D. Snook, Chem. Phys. 165 (1992) 385.
- [24] M.A. Proskurnin, V.V. Kuznetsova, Anal. Chim. Acta 418 (2000) 101.
- [25] L. Fotsing, M. Fillet, P. Chiap, P. Hubert, J. Crommen, J. Chromatogr. A 853 (1999) 391.



# Highly selective preconcentration of Cu(II) from seawater and water samples using amidoamidoxime silica

Wittaya Ngeontae, Wanlapa Aeungmaitrepirom, Thawatchai Tuntulani, Apichat Imyim\*

Department of Chemistry, Faculty of Science, Chulalongkorn University, Bangkok 10330, Thailand

## ARTICLE INFO

### Article history:

Received 9 December 2008

Received in revised form 8 January 2009

Accepted 8 January 2009

Available online 20 January 2009

### Keywords:

Amidoamidoxime

Silica

Copper

Preconcentration

FAAS

## ABSTRACT

Chemically modified silica containing amidoamidoxime group was studied as a sorbent for solid-phase extraction (SPE) and preconcentration of Cu(II) prior to determination by flame atomic absorption spectrometry (FAAS). The sorbent showed an extremely high selectivity towards Cu(II) in the pH range of 4–6, while the extraction of Pb(II), Cd(II), Ni(II) and Co(II) was low. The adsorption isotherm followed the Langmuir model and the maximum sorption capacity of 0.0163 mmol Cu(II) g<sup>-1</sup> was achieved. In the flow system, Cu(II) was completely retained on a column containing 40 mg of the modified silica at the flow rate of 4.0 mL min<sup>-1</sup> and quantitatively eluted by 5 mL of 1% (v/v) HNO<sub>3</sub>. No interference from Na<sup>+</sup>, K<sup>+</sup>, Mg<sup>2+</sup>, Ca<sup>2+</sup>, Cl<sup>-</sup> and SO<sub>4</sub><sup>2-</sup> at 10, 100 and 1000 mg L<sup>-1</sup> was observed. When applied for preconcentration and determination of Cu(II) in tap water, pond water, and seawater, the recoveries were 96, 101, and 95%, respectively, with high precision (% relative standard deviation (R.S.D.) < 4) and low method detection limit (9 µg L<sup>-1</sup>).

© 2009 Elsevier B.V. All rights reserved.

## 1. Introduction

Copper is one of the essential elements that are required to maintain the normal structure, function, and proliferation of cells. However excessive amount of copper can cause abnormal metabolism [1]. Copper ion in the environment can contaminate and accumulate in living system. Thus the selective extraction of copper ion in hydrometallurgy [2,3] as well as its determination in various samples becomes important [4–7].

Many regulations including standard and reference methods for the determination of heavy metals have been announced. A flame atomic absorption spectrometry (FAAS) is widely employed in the determination of heavy metals due to the ease of operation and low instrument and operation cost. However, direct determination of ultratrace level heavy metals presented in environmental samples is difficult because their amount is always lower than the detection limit of instruments and in addition, the problem of nonsuitable matrix occurs. These limitations can be overcome by applying a clean up and/or preconcentration step prior to the determination step [8]. Generally, the separation and preconcentration techniques include liquid–liquid extraction (LLE) [9] and solid-phase extraction (SPE) [10,11]. The SPE technique has been widely used because of many advantages, compared to LLE, such as less waste generation, less matrix effect, higher potential for the reuse of solid phase, higher preconcentration factor and no requirement of toxic solvent.

On the other hand, the drawback of solid sorbents used in SPE is the lack of selectivity [12], which leads to high interference from concomitants. Silica gel has been widely used as a solid support for metal extraction in the SPE technique due to its high porosity, hydrophilicity and ease of surface modification. For this reason, much chemically modified silica has been developed [13].

Silica gel surface can be modified by two ways: organic functionalization [4,11,14–17], where the modifying agent is an organic molecule acting as a chelating ligand and inorganic functionalization [18], in which the group anchored on the surface can be organometallic composite or inorganic compounds such as metallic oxides [19]. From the literature, most inorgano-functionalized silica had low selectivity towards heavy metals [19,20]. Thus, the organo-functionalized silica has attracted greater interests [13]. The most convenient way of chemical modification of silica is achieved by covalently binding of the organic molecule to silica matrix. In order to obtain a selective metal extraction, an appropriate organic chelating ligand should be carefully selected. Many authors reported the use of chelating ligands functionalized onto silica for metal ion extraction and preconcentration; for example, 5-formyl-3-(1'-carboxyphenylazo) salicylic acid was used for Cd(II), Zn(II), Fe(III), Cu(II), Pb(II), Mn(II), Cr(III), Co(II) and Ni(II) extraction from natural water [11]. 1,8-Dihydroxyanthraquinone was used for Pb(II), Cd(II) and Zn(II) extraction from tap, river and underground water samples [14]. 4-Amino-3,5,6-trichloropicolinic acid (picloram) has been used for divalent cations (Cu, Ni, Zn, and Cd) adsorption from aqueous solutions [21]. Quinolinol was immobilized on silica surface for enrichment of trace metal ions like Cu(II), Ni(II), Co(II), Fe(III), Cr(III), Mn(II), Zn(II), Cd(II), Pb(II), and Hg(II) [22]. 2-Aminothiazole

\* Corresponding author. Tel.: +66 2 218 7607; fax: +66 2 2541309.  
E-mail address: [iapichat@chula.ac.th](mailto:iapichat@chula.ac.th) (A. Imyim).

silica was used for preconcentration of Cu(II), Zn(II), Ni(II), and Fe(II) from gasoline [23]. Hydroxyquinoline-functionalized silica was also reported for preconcentration of Mn(II), Co(II), Ni(II), Cu(II), Zn(II), Pb(II), Cr(III) and Cd(II) from seawater sample. Recently, our group reported the use of aminothioamidoanthraquinone for preconcentration of Pb(II), Cu(II), Ni(II), Co(II) and Cd(II) from tap and surface water samples without interfering by natural coexisting cations and anions [24].

However, the literature results showed that the modified silica still have low selectivity towards Cu(II). Some authors have attempted to improve the selectivity of silica gel as follow; da Silva et al. [4] reported the use of 3(1-imidazolyl)propyl silica for the extraction of Cu(II) from potable and surface water in which the concentration of  $K^+$ ,  $Na^+$  and  $Ca^{2+}$  higher than  $100\text{ mg L}^{-1}$  and other elements at  $10\text{ mg L}^{-1}$  affected the extraction efficiency. This research thus focused on the use of the chemically modified silica containing amidoamidoxime group for a highly selective solid-phase extraction and preconcentration of Cu(II) for improving the detection limit of the determination by flame atomic absorption spectrometry. The amidoxime functional group was chosen due to its adsorption capacity and selectivity towards some metal ions [25–29]. The performance was evaluated by applying the proposed method to the determination of Cu(II) in a variety of water samples.

## 2. Experimental

### 2.1. Apparatus

A cross polarization–magic-angle spinning (CP/MAS) nuclear magnetic resonance spectrometer (NMR, DPX-300 Bruker Biospin), a CHNS/O analyzer (PE 2400 Series II PerkinElmer), a Fourier transform infrared spectrometer (FT-IR, Nicolet Impact 410), a simultaneous thermal analyzer (STA, 409 Netzsch) and a specific surface area analyzer (Thermofinnigan Sorptomatic1990 using the BET equation) were used for the characterization of the modified silica products.

A flame atomic absorption spectrometer (PerkinElmer model AAnalyst100) equipped with hollow cathode lamps was used with the recommended condition. The instrumental parameters are the following: the wavelengths used were 324.8, 228.8, 240.7, 283.3, and 232.0 nm with the hollow cathode lamp current 15, 4, 30, 10 and 25 mA for Cu, Cd, Co, Pb, and Ni, respectively, the slit widths were 0.7 nm for Cu, Cd and Pb, and 0.2 nm for Ni and Co, the air flow rate was  $10\text{ L min}^{-1}$  and the acetylene flow rate was  $3\text{ L min}^{-1}$ . The limit of detection values are 0.02, 0.02, 0.02, 0.45, and  $0.06\text{ mg L}^{-1}$  for Cu, Cd, Co, Pb, and Ni, respectively. The pH measurements were conducted by a pH meter Hanna instruments model pH 211 calibrated against two standard buffer solutions, pH 4.0 and 7.0. The column system consisted of an ISMATEC peristaltic pump furnished with Tygon tubes R 3607 (2.79 mm i.d., 0.86 mm wall thickness) and a laboratory-made adsorption minicolumn (2.79 mm i.d., 2.0–3.5 cm length) packed with 40 mg of sorbent.

### 2.2. Materials and reagents

All solutions were prepared using  $18\text{ M}\Omega\text{ cm}^{-2}$  ultrapure water. Standard and working metal solutions (BDH Laboratory Supplies) were prepared by stepwise dilution of  $1000\text{ mg L}^{-1}$  stock standard solution. All reagents were of analytical grade and used without further purification.

### 2.3. Preparation of sorbent

Amidoamidoxime-functionalized silica (Ami-SiO<sub>2</sub>) was prepared by our on-solid-phase synthesis method. A portion of 25 g of silica gel (Merck, 60 mesh) was placed in a 250 mL

two-neck round bottom flask, dried toluene (150 mL) and then 3-aminopropyltriethoxysilane (10 mL) were added. The mixture was refluxed under nitrogen atmosphere for 24 h. The solid was separated and washed with dichloromethane ( $250\text{ mL} \times 3$ ). The product was notated as AP-SiO<sub>2</sub>. The AP-SiO<sub>2</sub> (20 g) was then transferred into a new 250-mL round bottom flask, and dried toluene (150 mL) and methyl cyanoacetate (6.2 g, 62.8 mmol) were added. The mixture was refluxed under nitrogen atmosphere for 24 h. The solid was separated and washed with ethanol ( $100\text{ mL} \times 3$ ) and dichloromethane ( $200\text{ mL} \times 2$ ). The product was notated as CA-SiO<sub>2</sub>. The CA-SiO<sub>2</sub> (20 g) was transferred into a new 250-mL round bottom flask; ethanol (75 mL) and hydroxylamine hydrochloride solution (4.6 g, 67.15 mmol, H<sub>2</sub>NOH-HCl + 2.7 g, 67.2 mmol NaOH in 75 mL distilled water, pH adjustment by conc. HCl to pH 7) were added. The mixture was refluxed under nitrogen atmosphere for 24 h. The solid was separated and washed with water ( $250\text{ mL} \times 3$ ), ethanol ( $250\text{ mL} \times 2$ ), and dichloromethane ( $250\text{ mL} \times 3$ ), and finally air-dried for 3 h at ambient temperature. The Ami-SiO<sub>2</sub> was obtained.

Starting silica gel, AP-SiO<sub>2</sub>, CA-SiO<sub>2</sub>, and Ami-SiO<sub>2</sub> were vacuum dried, kept in a desiccator and characterized by elemental analysis, <sup>13</sup>C NMR, FT-IR, thermogravimetric analysis and specific surface area analysis.

### 2.4. Extraction procedure

Two extraction methods, i.e. batch and column were used to optimize the operational parameters. The batch method was used to evaluate thermodynamic parameters, while the column method was used to investigate kinetic parameters.

#### 2.4.1. Batch method

The effect of solution pH, extraction time and adsorption isotherm were evaluated by batch method. A suspension of 20 mg of Ami-SiO<sub>2</sub> in 5 mL of each metal ion solution previously adjusted the pH to 1–6 ( $5.0\text{ mg L}^{-1}$  of Cu(II), Co(II), Ni(II),  $10.0\text{ mg L}^{-1}$  of Pb(II), and  $2.0\text{ mg L}^{-1}$  of Cd(II)) was mechanically stirred at room temperature for 5–60 min. Before extraction, the solution pH was adjusted by using 1% (v/v) HNO<sub>3</sub> and 1% (w/v) KOH. The adsorption isotherm experiment was conducted at  $25 \pm 1\text{ }^\circ\text{C}$ . After the extraction, the suspension was separated by centrifugation at 3500 rpm for 5 min. The residual metal concentration in the supernatant was determined by FAAS. All experiments were performed with three replicates of each item.

#### 2.4.2. Column method

The column method was used to define an optimum condition for the sorption and desorption of the metals ions. The eluate was collected and then injected to FAAS. The effect of loading flow rate, concentration of stripping solution, sample volume and interfering ions were evaluated in triplicate. The minicolumn was prepared by using 40 mg of Ami-SiO<sub>2</sub>. The Cu(II) solutions were adjusted to pH range 4–5 before passing through the minicolumn at a controlled flow rate. The sample volume was 5.0 mL for the study of the effect of loading flow rate and it varied from 5 to 100 mL for the study of the effect of sample volume. The sorbed Cu(II) ions were desorbed by passing 5 mL of 1% (v/v) HNO<sub>3</sub> at flow rate  $0.5\text{ mL min}^{-1}$ . The amount of Cu(II) in the eluate was determined by FAAS.

### 2.5. Application to real sample

Tap water was collected and used without filtration from tap water supply at Mahamakut Building, Chulalongkorn University. Surface water and seawater samples were collected from Chulalongkorn University Pond and Bangsan Sea, Chonburi Province,

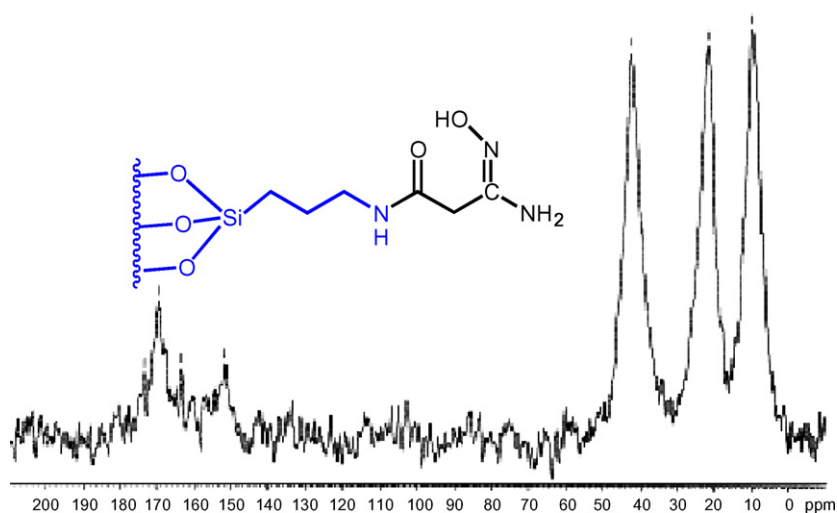


Fig. 1.  $^{13}\text{C}$  NMR spectrum and structure of Ami-SiO<sub>2</sub>.

respectively, by grab sampling method in a 5-L polyethylene bottle (10 cm depth from the surface). The samples were first filtrated through glass fiber, followed by 0.45  $\mu\text{m}$  cellulose nitrate membranes (Millipore). The accuracy of the method was evaluated by spiking 5  $\mu\text{g}$  of Cu(II) in to 100 mL of sample volume (6 replicates). The solution flow rate was 4.0 mL min<sup>-1</sup>. The sorbed Cu(II) was eluted with 1% (v/v) HNO<sub>3</sub> at flow rate 0.5 mL min<sup>-1</sup>.

### 3. Results and discussion

#### 3.1. Characterization of the sorbent

In the modification stage, starting silica gel was initially activated with 3-aminopropyltriethoxysilane. Then, the amine group reacted with methyl cyanoacetate to form amide linkage. The cyano group could be readily reduced by using hydroxylamine hydrochloride to form amidoxime group. The product was called amidoamidoxime silica (Ami-SiO<sub>2</sub>). The novel modified silica was characterized by solid-state  $^{13}\text{C}$  NMR to confirm that the structure of organic moieties being present on the silica surface (Fig. 1). The  $^{13}\text{C}$  NMR signals are: 170 (NCOCH<sub>2</sub>), 163 (CH<sub>2</sub>CNH<sub>2</sub>), 151 (OCCH<sub>2</sub>CN), 42 (HNCH<sub>2</sub>CH<sub>2</sub>), 21 (CH<sub>2</sub>CH<sub>2</sub>CH<sub>2</sub>), and 10 ppm (CH<sub>2</sub>CH<sub>2</sub>OSi). The elemental analysis in each synthetic step is shown in Table 1. The results from Table 1 show the difference of %C, %H and %N in each step indicating the variation of the organic moieties. The C, H and N content appeared in AP-SiO<sub>2</sub> indicating the successful aminopropylation reaction. The increase of C and N content in CA-SiO<sub>2</sub> indicated that the cyano group (-C≡N) was attached to AP-SiO<sub>2</sub>. In the final step, the increase of H content and the decrease of C and N content in Ami-SiO<sub>2</sub> indicated that the cyano moiety was converted to amidoxime group (-C(NH<sub>2</sub>)NOH). The absorption bands of Ami-SiO<sub>2</sub> by FT-IR (KBr disk) exhibit as follows (Fig. 2):  $\nu(\text{cm}^{-1}) = 3000\text{--}3400$  (O-H and -NH<sub>2</sub> stretching), 1660 (C=N stretching), 1552 (N-H bending, C-N stretching), 1081 (Si-C stretching), and 800 (Si-O stretching). The TGA curve of the

Table 1  
Elemental analysis.

Sample	C (%)	H (%)	N (%)
SiO <sub>2</sub>	0.05	0.01	0.06
AP-SiO <sub>2</sub>	5.89	0.98	2.35
CA-SiO <sub>2</sub>	9.07	1.06	3.85
Ami-SiO <sub>2</sub>	5.97	1.57	2.76

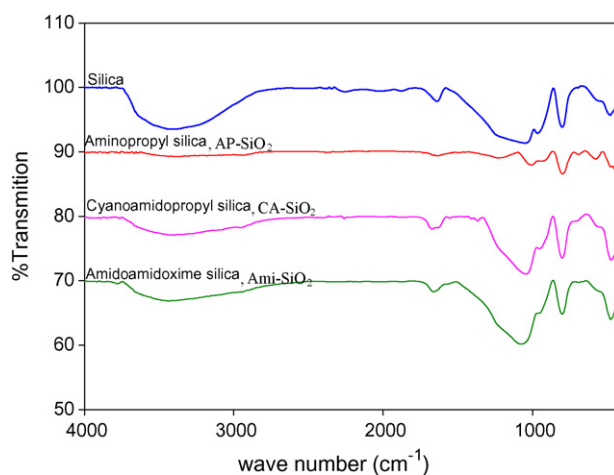


Fig. 2. FT-IR spectra of silica and derivative silica.

starting silica shows only one mass change around 25–210 °C. This mass loss becomes the loss of the remaining absorbed water. The TGA curves of AP-SiO<sub>2</sub> and Ami-SiO<sub>2</sub> are showed in Fig. 3. Ami-SiO<sub>2</sub> shows three stages of weight loss. The first one is similar to that of pure silica with 5% weight loss, following by 12% weight loss around 210–620 °C corresponding to the loss of the organic groups which are aminopropyl and amidoamidoxime groups. This

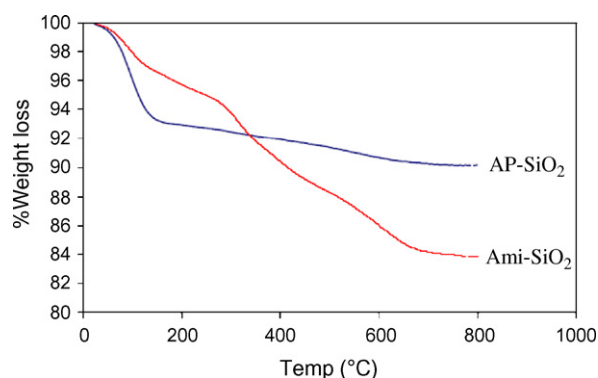


Fig. 3. TGA curves of AP-SiO<sub>2</sub> and Ami-SiO<sub>2</sub>.



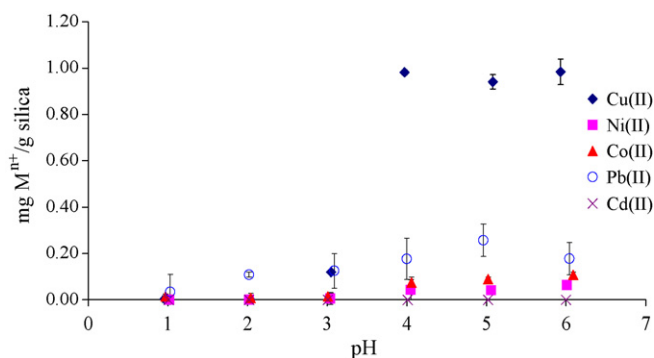


Fig. 4. Effect of pH solution on sorption efficiency of Ami-SiO<sub>2</sub> ( $n=3$ ).

observation shows that the organic part was immobilized on the silica.

The specific surface area ( $S_{\text{BET}}$ ) of silica was obtained by nitrogen adsorption method. The  $S_{\text{BET}}$  of Ami-SiO<sub>2</sub> of 300.3 m<sup>2</sup> g<sup>-1</sup> is smaller than that of non-functionalized silica gel ( $S_{\text{BET}}=421.1$  m<sup>2</sup> g<sup>-1</sup>). A decrease in  $S_{\text{BET}}$  is probably due to the presence of the organic moieties that can block the access nitrogen to the silica base. The BJH average pore diameter of Ami-SiO<sub>2</sub> is 57.1 Å.

## 3.2. Extraction study

### 3.2.1. Batch method

The solution pH and the contact time are ones of the most important factors controlling the limit of extractability of metal ions. The effect of pH and contact time on sorption was studied by batch method. The adsorption efficiency is reported in term of the amount of sorbed metal per weight unit of sorbent (mg M/g silica).

**3.2.1.1. Effect of pH on metal extraction.** The solution of Cu(II) 5 mg L<sup>-1</sup>, Pb(II) 10 mg L<sup>-1</sup>, Cd(II) 2 mg L<sup>-1</sup>, Co(II) 5 mg L<sup>-1</sup> and Ni(II) 5 mg L<sup>-1</sup> was adjusted to appropriate pH with the range of 1–6 with 30 min extraction time. The results are shown in Fig. 4. Only Cu(II) was retained on the sorbent at pH ≥ 4, on the other hand Pb(II), Cd(II), Co(II) and Ni(II) were less retained at a small amount in the interval pH range of 1–6. This result indicated that amidoamidoxime silica had a highly specificity towards Cu(II) at pH 4–6. However, in strong acid solutions (pH ≤ 3), the sorbent surface could be positively charged due to the protonation of N atoms, which cannot bind with metal cations. The possible reason for such a high selectivity for Cu(II) is mainly based on the Cu–amidoamidoxime complex is more stable than other metal–amidoamidoxime complexes. From Fig. 3, the other transition metal ions do not interfere the extraction of Cu(II) if the pH of the solution are controlled at pH 4–6. This observation agrees with the Irving–William series,  $K(\text{Mn}^{2+}) < K(\text{Fe}^{2+}) < K(\text{Co}^{2+}) < K(\text{Ni}^{2+}) < K(\text{Cu}^{2+}) > K(\text{Zn}^{2+})$ , that originates from a combination of ligand–field effects and the Jahn–Teller

distortion of d<sup>9</sup> Cu(II) ion [30]. Compared to our previous publication [24], this Ami-SiO<sub>2</sub> is apparently more selective towards Cu(II) than aminothioamidoanthraquinone-functionalized silica which has two possible binding sites (N<sub>2</sub>S and OS moieties). We propose that two amidoamidoxime moieties could hydrogen bond to form a pseudomacrocyclic system and Cu(II) would form a dimeric pseudomacrocyclic complex with N<sub>2</sub>O<sub>2</sub> donor accompanied by ligand deprotonation as shown in Fig. 5. In addition our proposed mode of chelation is similar to the N<sub>2</sub>O<sub>2</sub>-type Schiff base extractants, reported by Fathi et al. [2], which are selective for Cu(II). This will allow Cu(II) to be back-extracted from the complex; indeed extraction into acidic solution protonates the ligand and releases Cu(II) ions, known as pH-swing method. Therefore, pH range 4–6 was chosen for further extraction experiments and the sorbed Cu(II) would be back-extracted in a pH ≤ 3 solution.

**3.2.1.2. Effect of extraction time.** In this study, the extraction time was varied from 5 to 60 min. A model solution consisting of 5 mL of 5 mg L<sup>-1</sup> Cu(II) at pH 4.5 was used for all experiments. The extraction time required for reaching extraction equilibrium was fairly rapid. The fast extraction rate indicates that the sorbent is highly suitable for the preconcentration of trace Cu(II) from aqueous solution. This behavior indicates that Cu(II) ion has a good accessibility through the chelating sites on the modified silica and the binding constant between the metal ion and the amidoamidoxime group immobilized on the silica surface is possibly high [19]. According to this result, it is suitable for applying the sorbent in a flow system where shorter extraction time or faster adsorption is required.

**3.2.1.3. Adsorption isotherms.** In this experiment, adsorption thermodynamic parameters of Cu(II) ion onto the sorbent surface were investigated. The adsorption behavior of the metal ions by Ami-SiO<sub>2</sub> at equilibrium condition can reveal the adsorption mechanism. Sorption is a physical and/or chemical process in which a substance is accumulated at an interface between liquid and solid phases. A number of different equations can be used to predict theoretical adsorption capabilities for different adsorbents. Among the adsorption models, Langmuir isotherm equations have widely been used to predict adsorption capabilities of metals on the solid sorbent [20].

Langmuir proposed the first isotherm model which assumed monolayer coverage of the adsorbent surface. The most commonly used expression of the Langmuir equation for describing adsorption data for solid–liquid systems is the following equation:

$$N_f = \frac{bN_f^s C}{1 + bC} \quad (1)$$

The linearized expression of this equation is

$$\frac{C}{N_f} = \frac{1}{bN_f^s} + \frac{C}{N_f^s} \quad (2)$$

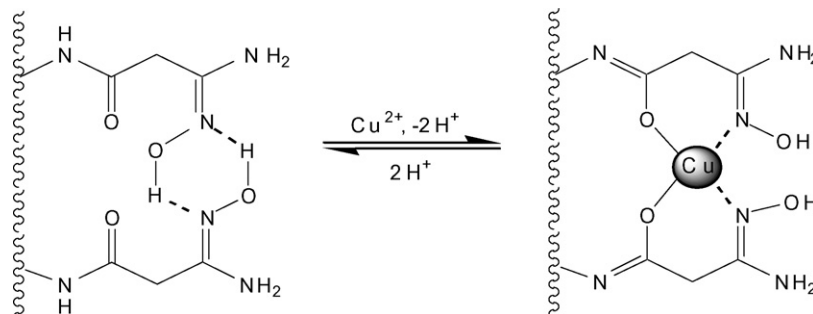


Fig. 5. Proposed extraction of Cu(II) by forming a dimeric pseudomacrocyclic complex with the amidoamidoxime moiety.

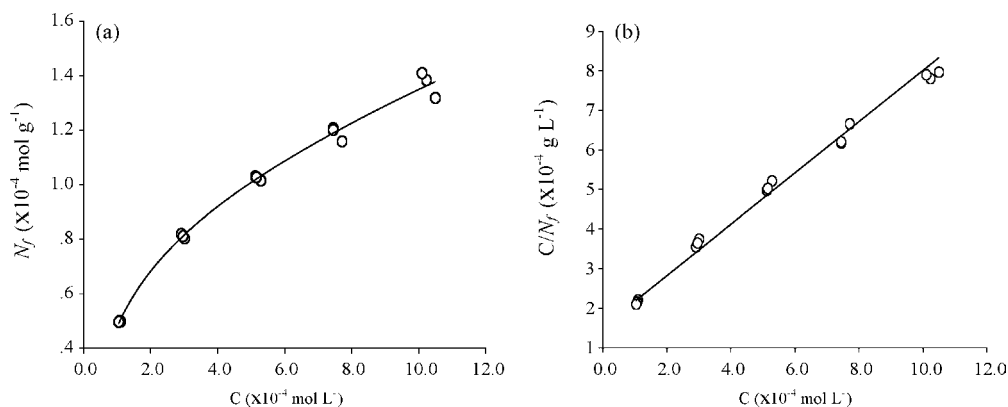


Fig. 6. (a) Adsorption isotherm and (b) Langmuir adsorption plot of Cu(II) on Ami-SiO<sub>2</sub>.

This equation is called the “Double-Reciprocal Langmuir Equation” and more suitable for situations in which the distribution of equilibrium concentrations tends to be skewed towards the lower end of the range of the equilibrium concentrations. Given that  $N_f$  is the amount or concentration of the solute adsorbed (mol) per gram of modified silica,  $C$  is the equilibrium concentration of the metal ion in mol L<sup>-1</sup>,  $b$  is equal to  $K_{eq}/a$ , where  $a$  represents the activity of the solvent in solution and  $N_f^s$  is the maximum sorption capacity of the sorbent.

The working condition was evaluated at the optimum pH and extraction time at  $25 \pm 1^\circ\text{C}$  in batch method. The concentration of Cu(II) was varied from 5 to 100 mg L<sup>-1</sup>. The plot of  $C$  versus  $N_f^s$  and  $C$  versus  $C/N_f^s$  is shown in Fig. 6. The linear least square fit gave a correlation coefficient ( $r$ ) of 0.9964,  $b$  value =  $0.36 \times 10^4$  L mol<sup>-1</sup> and  $N_f^s = 1.6 \times 10^{-4}$  mol g<sup>-1</sup>. These results indicated the adsorption of Cu(II) ion followed Langmuir-type adsorption mechanism, chemisorptions occurred from directly coordination of Cu(II) on amidoamidoxime moiety [21]. The main characteristic of the experiment corresponding with Langmuir model was monolayer coverage of metal ions on the silica surface. Other mechanisms such as precipitation and second adsorption on the first layer did not occur. The  $N_f^s$  value of our sorbent is greater the  $N_f^s$  values of unmodified silica gel, which are  $3.6 \times 10^{-5}$  and  $8.2 \times 10^{-6}$  mol g<sup>-1</sup>, reported by Chiron et al. [31] and Tran et al. [32], respectively. In addition, our sorbent has a greater affinity for Cu(II) than unmodified silica gel.

### 3.2.2. Column method

Cu(II) solution was passed through a minicolumn packed with certain amount of Ami-SiO<sub>2</sub> and equipped with a peristaltic pump to control the solution flow rate. The effects of loading flow rates, sorbent amount, eluent concentration, sample volume, and interfering ions were investigated and discussed as follows.

**3.2.2.1. Effect of loading flow rates and sorbent amount.** In the flow system, solution flow rate is a critical parameter [22]. The time must be enough for complete extraction of the metal ions but should be short enough for an efficient preconcentration step in sample processing. The extraction of 5.0 mL of 5.0 mg L<sup>-1</sup> Cu(II) solution by Ami-SiO<sub>2</sub> column was studied at different flow rates ranging from 0.5 to 6.0 mL min<sup>-1</sup>. The results are illustrated in Fig. 7. In the experiment using 20 mg of Ami-SiO<sub>2</sub> (upper curve), the extraction efficiency was decreased rapidly while increasing the solution flow rate. When the silica amount was increased to 40 mg, the extraction capacity was independent from the solution flow rate in the study range (see Fig. 7, lower curve). Therefore, the flow rate in the range of 4.0 mL min<sup>-1</sup> and 40 mg of Ami-SiO<sub>2</sub> was chosen for next experiments.

**3.2.2.2. Effect of eluent concentration.** Nitric acid was chosen as a stripping or back-extraction solution. An acid solution has been widely used for the elution of metal ions from a sorbent due to the protonation at a chelating site of the sorbent. Nitric acid is commonly suitable and hence replaces the metal ions from binding sites; moreover this acid does not interfere in the subsequent determination by FAAS. The suitable acid concentration is another important factor. Too dilute concentration may not be enough for complete protonation. On the other hand, high concentration may contaminate the sample and cause the problem in determination step.

The solution of 2.5 mg L<sup>-1</sup> Cu(II) was passed through a minicolumn at flow rate 4.0 mL min<sup>-1</sup>. The minicolumn was desorbed by 5.0 mL of 1, 3, 5 and 7% (v/v) of ultrapure HNO<sub>3</sub> solution with a flow rate of 0.5 mL min<sup>-1</sup>. This flow rate was chosen to ensure the elution equilibrium. The experimentally observed recoveries (mean value  $\pm$  confidence interval at 95%,  $n = 3$ ) were  $96 \pm 1$ ,  $97 \pm 2$ ,  $97 \pm 1$ , and  $95 \pm 4\%$  when using 1, 3, 5 and 7% (v/v) HNO<sub>3</sub>, respectively. The overall stripping efficiencies were not significantly different (pair  $t$ -test,  $\alpha = 0.05$ ). Therefore, 1% (v/v) HNO<sub>3</sub> was chosen as a stripping solution.

**3.2.2.3. Effect of sample volume.** An important parameter in SPE is the breakthrough volume, which is the maximum sample volume that should percolate through a given mass of sorbent after which an analyte starts to elute from the sorbent resulting in non-quantitative recoveries. In other words, breakthrough volume is the maximum solution volume that the analyte can be retained with the acceptable recovery range [33]. The breakthrough volume was experimentally evaluated by using the model solutions containing a constant amount of Cu(II) at 12.5  $\mu\text{g}$  in different volumes of solution varying from 5 to 100 mL with the loading flow rate

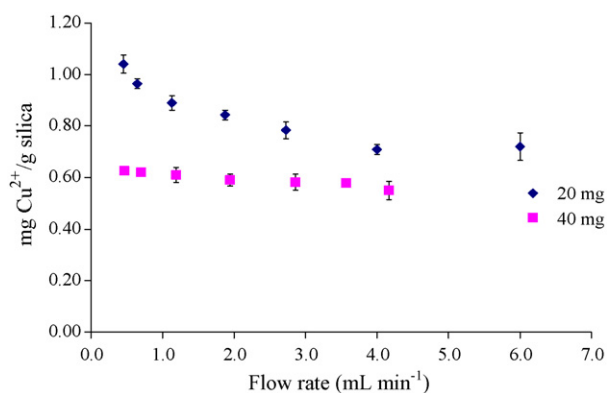


Fig. 7. Effect of solution loading flow rate using modified silica 20 and 40 mg ( $n = 3$ ).

**Table 2**  
Effect of interfering ions on % extraction<sup>a</sup>.

	Concentration (mg L <sup>-1</sup> )		
	10	100	1000
No interfering ion	88 ± 5		
Interfering ions			
Na <sup>+</sup>	91 ± 12	97 ± 2	107 ± 2
K <sup>+</sup>	92 ± 15	108 ± 7	105 ± 2
Mg <sup>2+</sup>	92 ± 5	107 ± 5	104 ± 2
Ca <sup>2+</sup>	102 ± 3	107 ± 3	103 ± 2
Cl <sup>-</sup>	98 ± 2	100 ± 2	103 ± 2
SO <sub>4</sub> <sup>2-</sup>	101 ± 2	102 ± 3	106 ± 2

<sup>a</sup> Mean value ± confidence interval at 95%, n = 3.

of 4.0 mL min<sup>-1</sup> and 40 mg of Ami-SiO<sub>2</sub>. The extraction percentage (mean value ± confidence interval at 95%, n = 3) were 98 ± 3, 98 ± 5, 90 ± 5, 90 ± 2, and 88 ± 5% when using the sample volume of 5.0, 10.0, 25.0, 50.0, and 100.0 mL, respectively.

The results indicated that good and satisfied recoveries were reached for all the solution volumes in the study range and breakthrough did not occur in this sample volume range.

**3.2.2.4. Effect of interfering ions.** In the view of high selectivity provided by FAAS, the only interferences studied were those related to the preconcentration step. Therefore in this experiment, the specificity of Ami-SiO<sub>2</sub> towards Cu(II) in the presence of the other cations and anions was investigated. The hypothesis was initially that the interferents might decrease the extraction efficiency of the analyte. The choice of cations and anions was based on their major natural abundance. A binary mixture (100 mL) between 12.5 µg of Cu(II) and each interfering ion, i.e. Na<sup>+</sup>, K<sup>+</sup>, Mg<sup>2+</sup>, Ca<sup>2+</sup>, Cl<sup>-</sup>, and SO<sub>4</sub><sup>2-</sup> in three concentration levels (10, 100 and 1000 mg L<sup>-1</sup>) was extracted by the column method. The ionic salts used were nitrate or sodium salts. The results are shown in Table 2. The overall % extractions obtained are in the similar order (ranging from 91 to 108%). These results indicated that all studied interfering ions did not affect the extraction efficiency of Cu(II). In contrast all the % extraction obtained was higher than that obtained in a noninterfering system (88 ± 5%).

### 3.3. Method detection limit and linear range of the proposed method

The linearity of an analytical method is an important parameter for a new or developing method. This parameter allows users to know the working concentration range. The method detection limit is usually determined by decreasing metal concentration following by the SPE process until the signal of FAAS disappears. The lowest

**Table 4**  
Concentration and recovery of Cu(II) in water samples (100 mL).

Sample	Added (µg)	Proposed method			US-EPA method [33]		
		Found <sup>a</sup> (µg)	Recovery <sup>b</sup> (%)	R.S.D. (%)	Found <sup>a</sup> , µg	Recovery <sup>c</sup> (%)	R.S.D. (%)
Tap water	–	ND	–	–	1	–	–
	5	4.8 ± 0.1	96	3	5.4 ± 0.1	107	3
Pond water	–	ND	–	–	ND	–	–
	5	5.0 ± 0.2	101	4	5.2 ± 0.1	104	2
Seawater	–	ND	–	–	ND	–	–
	5	4.7 ± 0.1	95	2	4.8 ± 0.0	96	1

ND = not detectable.

<sup>a</sup> Mean value ± confidence interval at 95%.<sup>b</sup> Mean value, n = 6.<sup>c</sup> Mean value, n = 3.**Table 3**  
Recovery at various initial concentrations.

Initial concentration (µg L <sup>-1</sup> )	% recovery <sup>a</sup>
4	34 ± 29
9	83 ± 25
18	86 ± 14
54	93 ± 8
91	88 ± 6

<sup>a</sup> Mean value ± confidence interval at 95%, n = 3.

concentration that still gives an acceptable recovery is defined as method detection limit.

The linear range of our proposed method was studied in the concentration range of 4–91 µg L<sup>-1</sup> of the solution volume 100 mL. The recoveries were reported in Table 3. At 4 µg L<sup>-1</sup> of Cu(II), this method gave an unacceptable recovery of 34 ± 29%. Thus the method detection limit was proposed at around 9 µg L<sup>-1</sup> with 83% recovery and 12% relative standard deviation (R.S.D.) and preconcentration factor is 20. This method can be applied in the concentration range of 9–91 µg L<sup>-1</sup>.

### 3.4. Determination of Cu(II) in water samples

All of the previously determined optimum parameters were taken into account in the preconcentration of Cu(II) in real samples. Actually, Cu(II) ion is present in a trace level along with various substances such as alkali and alkali earth ions, organic matter, and humic acid. Then these substances were an obstacle in the determination of heavy metal. The performance of the proposed method was evaluated using the recovery of the spiked samples. The recoveries and R.S.D. of six replicates were considered in order to determine the accuracy and precision of the method.

Three kinds of water samples tested were tap water, natural pond water, and seawater. The results were shown in Table 4. The concentrations of Cu(II) in the samples were lower than the method detection limit. The recovery of Cu(II) in tap water, Chulalongkorn University pond water and seawater, were 96, 101, and 95, respectively. All of the recoveries of each sample types were in the acceptable range [33]. The recoveries in all samples are remarkably high. This may indicate the high selectivity of the synthetic sorbent towards Cu(II) ion. Other metal ions as well as other substances present in the sample could probably not compete with Cu(II) ion in adsorption process. The R.S.D. being less than 4% indicates that the developing method is highly precise. The data obtained from the proposed method were compared with those obtained from the US-EPA method [34]. No significant difference was found for pond water and seawater (pair *t*-test, α = 0.05) and for tap water (pair *t*-test, α = 0.01).

#### 4. Conclusions

The newly functionalized silica with amidoamidoxime group (Ami-SiO<sub>2</sub>) was successfully synthesized and applied for the selective preconcentration of Cu(II) ion from aqueous solution. The experimentally observed extraction results confirmed the selectivity of the modified silica towards Cu(II) ion. The effects of parameters influencing the extraction efficiency such as the pH of solution, the contact time, and the sorption capacity were investigated by batch method. The column system was also investigated to obtain the optimum conditions for the extraction and elution of the metal ion. The proposed method can be applicable for the determination of trace Cu(II) ion in a variety of water samples with low method detection limit, high accuracy (% recovery ranging from 96 to 101) and high precision (% R.S.D. ranging from 2 to 4). These results are in accordance with those obtained by the standard method.

#### Acknowledgements

The success of this research can be attributed to Environmental Analysis Research Unit and Supramolecular Chemistry Research Unit, Department of Chemistry, Faculty of Science, Chulalongkorn University. The financial support was obtained from the Graduate School and Ratchadaphiseksomphot Endowment Fund, Chulalongkorn University (GRU51-017-23-008), the Development and Promotion of Science and Technology Talent Project Scholarship (DPST), and National Nanotechnology Center, National Science and Technology Development Agency, Thailand (contact NN49-003 code NN-B-22-m11-10-49-19).

#### References

- [1] Y. Zheng, X.K. Li, Y. Wang, L. Cai, *Hemoglobin* 32 (2008) 135.
- [2] S.A.M. Fathi, M. Parinejad, M.R. Yaftian, *Sep. Purif. Technol.* 64 (2008) 1.

- [3] H.R. Watling, F.A. Perrot, D.W. Shiers, A. Grosheva, T.N. Richards, *Hydrometallurgy* 95 (2009) 302.
- [4] E.L. da Silva, A.O. Martins, A. Valentini, V.T. de Favere, E. Carasek, *Talanta* 64 (2004) 181.
- [5] H.S. Ferreira, A.C.N. Santos, L.A. Portugal, A.C.S. Costa, M. Miro, S.L.C. Ferreira, *Talanta* 77 (2008) 73.
- [6] A. Shokrollahi, M. Ghaedi, O. Hossaini, N. Khanjari, M. Soyylak, *J. Hazard. Mater.* 160 (2008) 435.
- [7] S.A.N. Rocha, A.F. Dantas, H.V. Jaeger, A.C.S. Costa, E.S. Leao, M.R. Goncalves, *Spectrochim. Acta A* 71 (2008) 1414.
- [8] A. Goswami, A.K. Singh, *Anal. Chim. Acta* 454 (2002) 229.
- [9] A.N. Anthemidis, G.A. Zachariadis, C.G. Farastelis, J.A. Stratis, *Talanta* 62 (2004) 437.
- [10] P. Daorattanachai, F. Unob, A. Imyim, *Talanta* 67 (2005) 59.
- [11] M.A.A. Akl, I.M.M. Kenawy, R.R. Lasheen, *Microchem. J.* 78 (2004) 143.
- [12] P.K. Jal, S. Patel, B.K. Mishra, *Talanta* 62 (2003) 1005.
- [13] V. Camel, *Spectrochim. Acta B* 58 (2003) 1177.
- [14] A. Goswami, A.K. Singh, *Talanta* 58 (2002) 669–678.
- [15] W.X. Ma, F. Lui, W. Chen, S.Y. Tong, *Anal. Chim. Acta* 416 (2000) 191.
- [16] M.E. Mahmoud, M.M. Osman, M.E. Amer, *Anal. Chim. Acta* 415 (2000) 33.
- [17] Q. Pu, Q. Sun, Z. Hu, Z. Su, *Analyst* 123 (1998) 139.
- [18] H.F. Maltez, E. Carasek, *Talanta* 65 (2005) 537.
- [19] F. Unob, B. Wongsiri, N. Phaeon, M. Puanngam, J. Shiowatana, *J. Hazard. Mater.* 142 (2007) 455.
- [20] A. Scheidegger, M. Borkovec, H. Sticher, *Geoderma* 58 (1993) 43.
- [21] A.G.S. Prado, A.H. Tosta, C. Airoidi, *J. Colloid Interf. Sci.* 269 (2004) 259.
- [22] P.K. Jal, S. Patel, B.K. Mishra, *Talanta* 62 (2004) 1005.
- [23] P.S. Roldan, I.L. Alcantara, C.C.F. Padilha, P.M. Padilha, *Fuel* 84 (2005) 305.
- [24] W. Ngeontae, W. Aeungmaitrepirom, T. Tuntulani, *Talanta* 71 (2007) 1075.
- [25] L. Weiping, L. Yun, Z. Hanmin, *React. Polym.* 17 (1992) 255.
- [26] W.P. Lin, Y. Lu, H.M. Zeng, *J. Appl. Polym. Sci.* 49 (1993) 1635.
- [27] Y. Lu, R.W. Fu, H.M. Zeng, *Polym. Sci.* 35 (1993) 489.
- [28] I.N. Voloschik, M.L. Litvina, B.A. Rudenko, *J. Chromatogr. A* 671 (1994) 51.
- [29] L. Weiping, F. Ruowen, L. Yun, Z. Hanmin, *React. Polym.* 22 (1994) 1.
- [30] E.C. Constable, *Coordination Chemistry of Macrocyclic Compounds*, Oxford University Press Inc., New York, 1999, pp. 91.
- [31] N. Chiron, R. Guilet, E. Deydier, *Water Res.* 37 (2003) 3079.
- [32] H.H. Tran, F.A. Roddick, J.A. O'Donnell, *Water Res.* 33 (1999) 2992.
- [33] L. Huber, *Validation and Qualification in Analytical Laboratories*, Interpharm Press Inc., Illinois, 1999, pp. 344.
- [34] United States Environmental Protection Agency, *Determination of Metals and Trace Elements in Water and Wastes by ICP-AES (US EPA Method 200.7 Revision 4.4)*, 1994.



## Comparison of UV and charged aerosol detection approach in pharmaceutical analysis of statins

Lucie Nováková<sup>a,\*</sup>, Sořía Arnal Lopéz<sup>b</sup>, Dagmar Solichová<sup>c</sup>, Dalibor Šatínský<sup>a</sup>,  
Bohumila Kulichová<sup>d</sup>, Aleš Horna<sup>d,e</sup>, Petr Solich<sup>a</sup>

<sup>a</sup> Department of Analytical Chemistry, Faculty of Pharmacy, Charles University, Heyrovského 1203, 500 05 Hradec Králové, Czech Republic

<sup>b</sup> Faculty of Chemistry, University of Valencia, Valencia, Spain

<sup>c</sup> Department of Metabolic Care and Gerontology, Charles University, Faculty of Medicine and University Hospital in Hradec Králové, Sokolská 581, 500 05 Hradec Králové, Czech Republic

<sup>d</sup> Radanal Ltd., Okružní 613, 530 03 Pardubice, Czech Republic

<sup>e</sup> Tomas Bata University in Zlín, University Institute, T.G. Masaryka 5555, 760 01 Zlín, Czech Republic

### ARTICLE INFO

#### Article history:

Received 23 July 2008

Received in revised form 17 December 2008

Accepted 22 December 2008

Available online 15 January 2009

#### Keywords:

Atorvastatin

Lovastatin

Simvastatin

HPLC

CAD

Pharmaceutical analysis

### ABSTRACT

CAD (charged aerosol detector) has recently become a new alternative detection system in HPLC. This detection approach was applied in a new HPLC method for the determination of three of the major statins used in clinical treatment—simvastatin, lovastatin and atorvastatin.

The method was optimized and the influence of individual parameters on CAD response and sensitivity was carefully studied. Chromatography was performed on a Zorbax Eclipse XDB C18 (4.6 mm × 75 mm, 3.5 μm), using acetonitrile and formic acid 0.1% as mobile phase. The detection was performed using both CAD (20 pA range) and DAD (diode array detector—238 nm) simultaneously connected in series. In terms of linearity, precision and accuracy, the method was validated using tablets containing atorvastatin and simvastatin.

The CAD is designated to be a non-linear detector in a wide dynamic range, however, in this application and in the tested concentration range its response was found to be perfectly linear. The limits of quantitation (0.1 μg/ml) were found to be two times lower than those of UV detection.

© 2009 Elsevier B.V. All rights reserved.

### 1. Introduction

The CAD (charged aerosol detector) belongs among universal detectors and it operates independent of the physiochemical and spectral properties of non-volatile analytes. The eluent of the chromatographic system is first nebulized using a flow of nitrogen. Created droplets are dried in a drift tube to remove mobile phase, producing analyte particles. A secondary stream of nitrogen becomes positively charged as it passes through a high-voltage, platinum corona wire. The charged nitrogen is then mixed with the stream of analyte particles where the charge migrates to analyte. Charged analyte particles proceed to a collector region where a highly sensitive electrometer produces a signal that is proportional to the weight of sample present, independent of chemical structure [1,2]. Recently CAD has been used in the analysis of triacylglycerols [3], synthetic polymers [4] in analysis of squalene, cholesterol and ceramide [5] and in analysis of lipids [6]. Phar-

maceutical applications of CAD are very rare, it appears only two papers have been published [7,8]. Brunelli et al. coupled CAD to supercritical fluid chromatography in the analysis of a model standard mixture of theophylline, testosterone, cortisone, naproxen, sulfadimidine, sulfamerazine, sulfamethoxazole, sulfaquinolaxine and sulfamethizole [7]. The CAD has been found to achieve a higher level of sensitivity than other universal detectors, such as ELSD or RI. The second paper compared the performance of ELSD and CAD in pharmaceutical analysis, also using standard mixtures of azole derivatives and some other compounds [8]. Practical applications in the field of pharmacy, using CAD on drug formulations, are still missing.

Statins drugs are commonly used for the treatment of several forms of hypercholesterolemia. They possess high effectiveness in reducing total cholesterol and low-density lipoprotein (LDL) cholesterol levels in human body. Statins are able to significantly reduce the morbidity and mortality associated with coronary heart disease, as demonstrated in numerous clinical trials [9–12]. Statins include natural (lovastatin), semi-synthetic (simvastatin, and pravastatin) as well as synthetic compounds (fluvastatin, atorvastatin, cerivastatin, rosuvastatin and pitavastatin). They are potent specific and competitive inhibitors of 3-hydroxy-3-methylglutaryl coenzyme A

\* Corresponding author. Tel.: +420 495067345; fax: +420 495067164.  
E-mail address: [novakoval@faf.cuni.cz](mailto:novakoval@faf.cuni.cz) (L. Nováková).

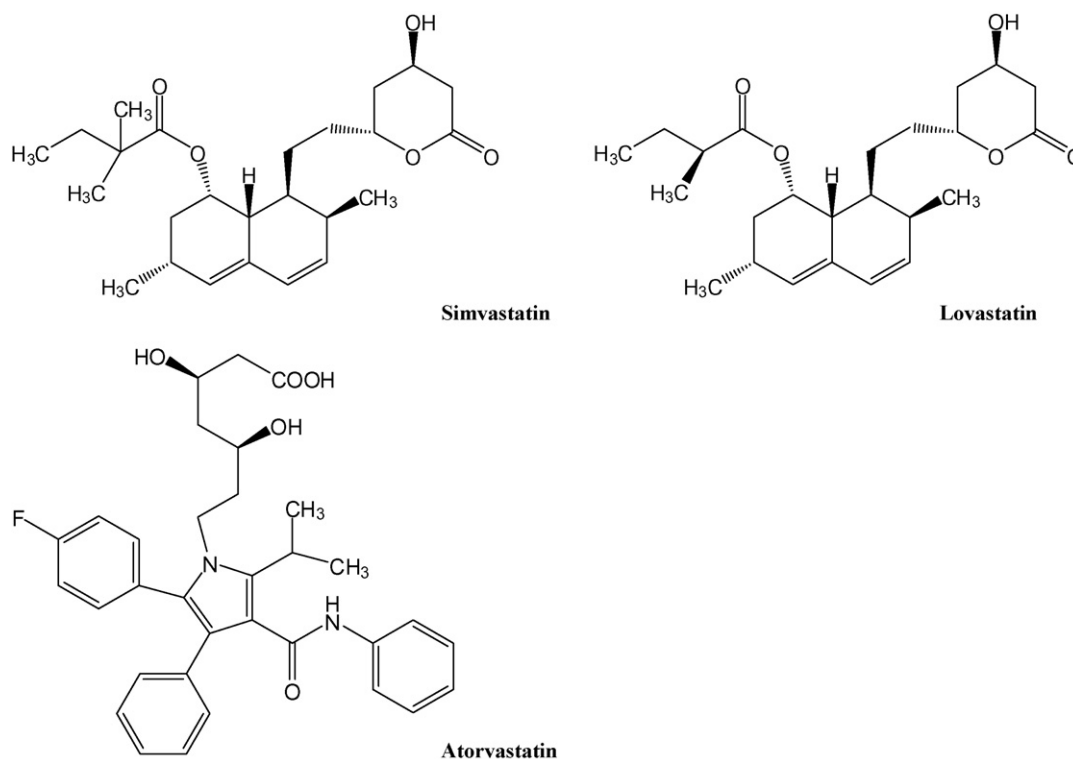


Fig. 1. Chemical structures of simvastatin, lovastatin and atorvastatin.

(HMG-CoA) reductase, which is a key enzyme that catalyzes the conversion of HMG-CoA to mevalonate. This is an early rate-limiting step in the cholesterol biosynthetic pathway [9,13,14].

Simvastatin and atorvastatin are two of the most commercially common drugs available as pharmaceutical formulations used for the clinical treatment of hypercholesterolemia. Structures can be seen in Fig. 1. The determination of drugs is a multi-disciplinary task. During the drug manufacturing process there is a need for analytical methods of quality control to discover any impurities. Bio-analytical methods are necessary for the clinical trials, for therapeutic drug monitoring and individual dosage scheme adjustment. Recently there has been a lot interest in monitoring pharmaceutical residuals in the environment, outlining a need for environmentally focused analytical methods. It is important to note, that higher sensitivity and selectivity is needed for the majority of bio-analytical or environmental methods.

High performance liquid chromatography (HPLC) together with various types of detection – UV (ultraviolet), FD (fluorescence detection) and MS (mass spectrometry) – is the technique of choice during pharmaceutical QC method development. Analytical methods, used for the determination of simvastatin and atorvastatin, were recently reviewed by our group [15]. In pharmaceutical applications UV detection was most commonly used. Identification of impurities in simvastatin the bulk drug and tablets was done by Vuletic et al. [16] using LC–MS/MS approach. The simvastatin assay in the tablets was determined by HPLC–UV by Malenovic et al. using microemulsion eluent [17]. The analytical method for HPLC–UV determination of group of five statins (atorvastatin, lovastatin, pravastatin, rosuvastatin and simvastatin) was developed by Pasha et al. [18]. Erturk et al. used a simple HPLC–UV method to determine atorvastatin and impurities in both the bulk drug and tablets forms [19]. A similar method to determine atorvastatin without impurities was achieved by Altuntas et al. [20]. Atorvastatin together with amlodipine, in combined commercial tablets was also determined by HPLC–UV by Mohammadi et al. [21]. CAD coupled to

HPLC however, has not yet been used in pharmaceutical applications with drug formulations. The aim of this study was to develop and validate a new method for the determination of atorvastatin and simvastatin in real tablet samples using CAD. The results generated would then be compared with those obtained using UV detection.

## 2. Experimental

### 2.1. Chemicals and reagents

Working standards of simvastatin (97%, HPLC), lovastatin (98%, HPLC) and atorvastatin were used during this study. The first two were obtained from Sigma–Aldrich (Prague, Czech Republic), while atorvastatin was obtained from Zentiva (Prague, Czech Republic).

The composition of drug formulations was as follows: simvastatin (excipients: butylhydroxyanisole, ascorbic acid, citric acid, microcrystalline cellulose, magnesium stearate, lactose, hypromellose, titanium oxide, talc and ferric oxide). Atorvastatin drug formulation contained excipients as follows: calcium carbonate, microcrystalline cellulose, lactose, polysorbate, hypromellose and magnesium stearate.

Both the formic acid, reagent grade, and the acetonitrile, HPLC gradient grade, were purchased from Sigma–Aldrich. HPLC grade water was prepared by Milli-Q reverse osmosis Millipore (Bedford, MA, USA) and it meets European Pharmacopoeia requirements.

### 2.2. Chromatography

A Shimadzu Prominence LC 20 system (Shimadzu, Kyoto, Japan) was used to perform all of the analyses. The instrument was equipped with a column oven SIL-20 AC enabling temperature control. The built-in auto-sampler CTO-20 AC also enabled cooling. Chromatographic software Lab Solution was used for data collection and processing. Detection of statins was accomplished using a

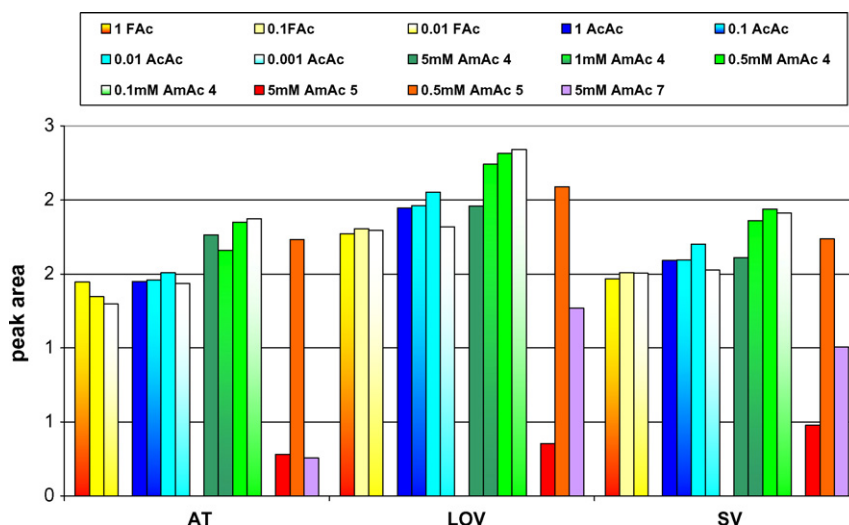


Fig. 2. The influence of various additives to CAD response.

diode array detector SPD-M20A. A Corona CAD detector (ESA, USA) was connected in series.

A Zorbax Eclipse XDB C18 (75 mm × 4.6 mm, 3.5 μm) analytical column (Agilent, Czech Republic), was used for the HPLC separation of the three statins. The column oven temperature was kept at 30 °C. The binary mobile phase, which composed of acetonitrile and 0.1% formic acid (70:30), was pumped at flow-rate 1.0 ml/min. DAD detection was performed at 238 nm. The injection volume was 10 μl and the autosampler was cooled to 4 °C. Optimal CAD detection was performed using a nitrogen pressure of 35 psi and range of 20 pA.

### 2.3. Preparation of standard solutions and samples

The stock solutions of standards were prepared by dissolving 1.0 mg of each statin standard into 1.0 ml of either acetonitrile, for simvastatin and lovastatin, or a mixture of acetonitrile and water (50:50) for atorvastatin due to solubility reasons. Stock solutions were further diluted by acetonitrile to achieve a concentration 10 μg/ml for SST (system suitability test) measurements, and to get individual points of calibration curve in the range 50–0.1 μg/ml, using nine calibration points (50, 25, 10, 5, 2.5, 1.0, 0.5, 0.25 and 0.1 μg/ml).

Tablet samples were prepared by dissolution into 5.0 ml of 5 mM of an ammonium acetate buffer pH 4.0 (stability reasons) using an ultra-sonic bath. Subsequent dilutions of the simvastatin preparations used acetonitrile. A mixture of water and acetonitrile (50:50) was used for the atorvastatin tablets. The samples were filtrated through 0.45 μm PTFE membrane prior to injection into HPLC system.

### 2.4. System suitability test and validation

An important part of method validation is the SST, details of which are usually given in pharmacopoeias [22,23]. The SST was performed under optimized chromatographic conditions, using both UV and CAD detection approaches. Theoretical plates, peak asymmetry, resolution of individual compounds and the repeatability of reference standard solution injections have been established (retentions times and peak areas were checked).

Calibration curves of all statins in the concentration range 50–0.1 μg/ml were measured. The applicability of the method was verified on real samples of pharmaceutical tablets containing simvastatin and atorvastatin at 10 and/or 20 mg levels. Method

precision, accuracy and the assay of statins was established. For precision, six samples of tablets were tested for each preparation at 100% level of simvastatin (10 and 20 mg) and atorvastatin (20 mg) content, which corresponds to ICH (International Conference on Harmonization) requirements. Accuracy was determined by spiking samples by known amount of statin (10 μg/ml).

## 3. Results and discussion

### 3.1. Chromatographic conditions—UV detection and charged aerosol detection

The separation of the three statins, atorvastatin, simvastatin and lovastatin was not a difficult analytical task. The percentage at least of 30 of water part in the mobile phase had to be kept to get a good resolution of all compounds within reasonable time period. Volatile additives are recommended for the coupling with CAD, thus this approach was respected and volatile additives were used during the method development and further experiments. DAD detection was achieved at 238 nm, which was determined from the absorbance spectra of the individual compounds.

The individual parameters which could influence the response of CAD were tested as follows: the range on CAD, the ratio of water/organic part of mobile phase, the flow-rate changes and various additives including formic acid, acetic acid and ammonium acetate buffers at pH 4.0, 5.0 and 7.0 at different concentrations—see Figs. 2 and 3.

The range set-up is a key parameter which influences the sensitivity of the CAD. It was tested as follows: 1, 2, 5, 10, 20, 50, 100, 200, and 500 pA. A difference could be seen in the response according to range as well as comparing to the response of UV detection. The best responses were obtained within the 1 and 2 pA range, however these values are practically impossible to use due to the very high signal to noise ratio. The value of 20 pA was chosen for further experiments because of the best S/N ratio.

The influence of mobile phase additives including formic acid, acetic acid and ammonium acetate buffer at various concentrations and pH values were tested—see Fig. 2. Neither formic nor acetic acid in mobile phase and their changing concentrations (0.01–1%) was found to have a significant influence on CAD response. The ammonium acetate buffer pH 4.0, at all concentrations, showed a small amount of influence. However, increasing the buffer's pH to 5.0 demonstrated a much stronger influence on the CAD response. Higher concentrations of buffer (5 mM) resulted in a much lower

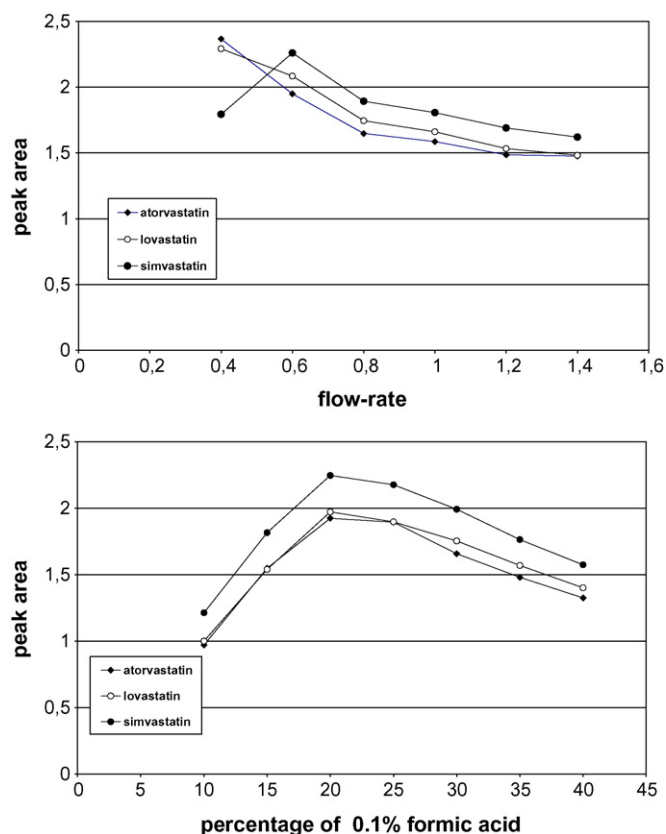


Fig. 3. The influence of flow-rate to CAD response. The influence of composition of mobile phase to CAD response.

response of CAD. At pH 7, a lower response and lower signal to noise ratio were observed as well as very low quality data.

The influence of the mobile phase was tested by changing the ratio of organic/water content. The range of 10–40% of formic acid 0.1% in the mixture with acetonitrile was tested. The best results were obtained using 20% formic acid in the mobile phase. The difference comparing to 10% of formic acid was about 50% of detector response, the difference comparing to the content of 40% of formic acid was about 30% of detector response—see Fig. 3. A mobile phase containing 30% formic acid 0.1% was found to demonstrate a higher

**Table 1**  
System suitability results—analysis of three statins using UV and CAD detection approach.

	Atorvastatin	Lovastatin	Simvastatin	Limits
SST				
Theoretical plates <sup>a</sup>				
UV	944	1534	1623	$N > 900$
CAD	900	1595	1717	
HETP <sup>a</sup>				
UV	158.81	97.77	92.41	Not given
CAD	166.80	94.05	87.35	
Asymmetry <sup>a</sup>				
UV	1.31	1.31	1.42	$As < 1.5$
CAD	1.18	1.27	1.37	
Resolution <sup>a</sup>				
UV	–	7.08	2.72	$R_{ij} > 1.5$
CAD	–	6.85	2.71	
Repeatability- $t_r$ <sup>a</sup> [% R.S.D.]				
UV	0.08	0.05	0.05	R.S.D. < 1%
CAD	0.04	0.07	0.08	
Repeatability- $A$ <sup>a</sup> [% R.S.D.]				
UV	0.17	0.32	0.19	R.S.D. < 1%
CAD	0.88	0.45	0.73	

UV = UV detection; CAD = charged aerosol detection; HETP = height equivalent of the theoretical plates.

<sup>a</sup> Made in 10 replicates.

degree of resolution between peaks of the simvastatin and lovastatin.

The response of the CAD was found to have a slightly dependence on the mobile phase flow-rate. It was higher with lower flow-rates, such as 0.6 ml/min. The difference was about 25% of peak area comparing to 1.0 ml/min flow-rate or almost 40% of peak area comparing to the flow-rate 1.4 ml/min—see Fig. 3.

### 3.2. System suitability test and validation

The SST was performed by 10 subsequent injections of mixed solutions of all statins which were analyzed under optimum conditions. A typical chromatogram could be seen in Fig. 4. Parameters such as number of theoretical plates, peak asymmetry, resolution of individual compounds and the repeatability of reference standard solution injection (retentions times and peak areas were checked,

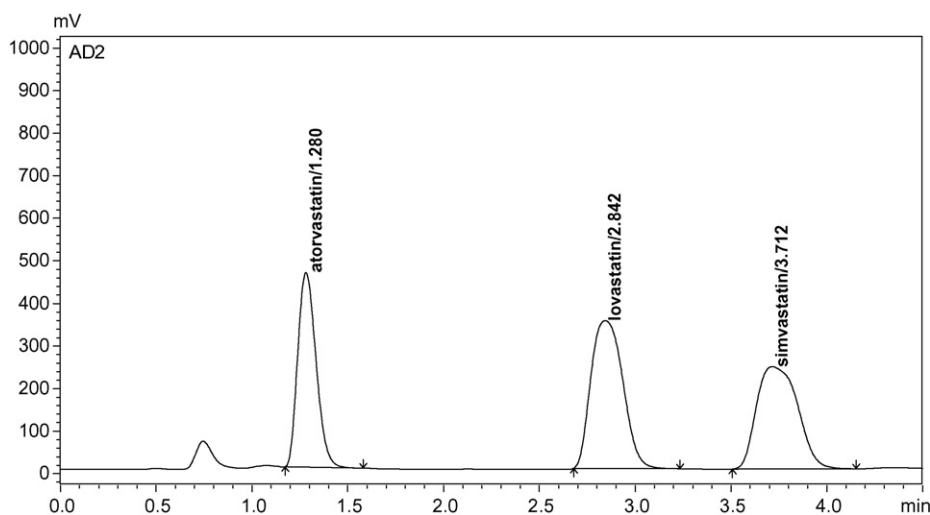
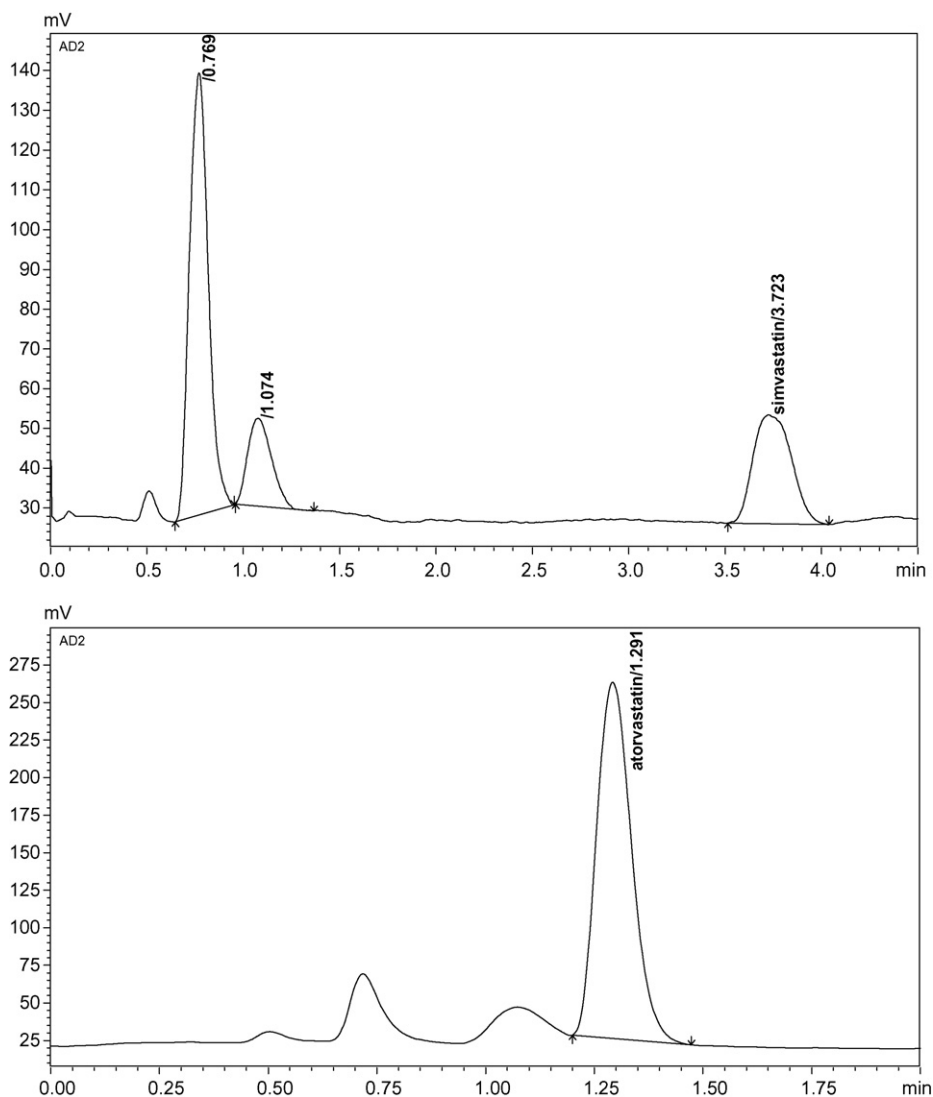


Fig. 4. Typical chromatogram of the separation of standard mixture of statins—CAD.





**Fig. 5.** Analysis of drug formulations: atorvastatin and simvastatin tablets—CAD (top chromatogram the analysis of simvastatin tablets 10 mg, bottom chromatogram the analysis of atorvastatin tablets 20 mg).

the repeatability was expressed as R.S.D. in %) were established. SST results were compared for UV and CAD detection approach—Table 1.

Both the UV and CAD measurements produced results which met the requirements of the appropriate authorities (see the last column in Table 1) concerning all SST parameters. Excellent repeatability of injection, noted by the peak retention time and peak area, was observed for both detectors (R.S.D. < 1%).

### 3.2.1. Linearity—calibration range

Calibration curves for the three statins in the concentration range 0.1–50 µg/ml were measured. Results can be seen in Table 2. Nine calibration points were obtained for simvastatin and lovastatin (0.50 µg/ml) and seven calibration points were obtained for atorvastatin (0.1–50 µg/ml). The calibration curves were linear in the defined range, so it can be concluded that the method was appropriate for quantitative purposes for both UV and CAD detection approach in spite of statement, that CAD is not universally linear detector.

### 3.2.2. Accuracy and precision

Method accuracy and precision were tested using tablet samples of atorvastatin and simvastatin containing 10 or 20 mg of

active substance. Six samples of tablets were prepared for each experiment. Precision was expressed as % R.S.D. of six determinations. Accuracy was established by spiking of statin tablets with a known amount of statin standard and was expressed as % of recovery—see Table 2. All the results were in correspondence with the requirements for method validation in pharmaceutical application.

### 3.2.3. Assay

The assay of the active substance, atorvastatin and simvastatin, in atorvastatin and simvastatin tablets was determined (Fig. 5). The amounts of  $100 \pm 5\%$  of declared assay were found by CAD, the amounts  $100 \pm 10\%$  of declared assay were found by UV detector, which corresponds to the requirements (up to  $100 \pm 10\%$  of declared assay) [23], see Table 2.

### 3.2.4. Limits of detection and quantitation

Limits of detection and quantitation were established for both detection approaches. They were found to be two times higher than the UV detection approach, see Table 2, which is advantageous comparing to ELSD or RI detectors.

**Table 2**

Method validation results for simvastatin and atorvastatin pharmaceutical formulations using UV and CAD detection approach.

Validation	Atorvastatin		Simvastatin		Limits
	Level	20 mg	Level		
Assay <sup>a</sup> [% of declared content]	UV	90.2%	20 mg 10 mg	100.5 94.5	Declared amount ±10%
Assay <sup>a</sup> [% of declared content]	CAD	95.7%	20 mg 10 mg	97.4 97.8	Declared amount ±10%
Accuracy <sup>a</sup> [%]	UV			97.9	Recovery = 100 ± 5%
Accuracy <sup>a</sup> [%]	CAD			105.1	Recovery = 100 ± 5%
Precision <sup>a</sup> [% R.S.D.]	UV	3.47	20 mg 10 mg	3.80 3.80	R.S.D. < 5%
Precision <sup>a</sup> [% R.S.D.]	CAD	2.11	20 mg 10 mg	4.43 4.79	R.S.D. < 5%
Linearity <sup>b</sup> (correlation coefficient)	UV	0.9991		0.9999	R > 0.9990
Linearity <sup>b</sup> (equation)	UV	y = 2E+07x - 9905.9		y = 3E+07x - 6090.5	-
Linearity <sup>b</sup> (correlation coefficient)	CAD	0.9996		0.9995	Non linear detector!
Linearity <sup>b</sup> (equation)	CAD	y = 1E+08x - 28415		y = 3E+07x - 12809	-
LOQ	UV	0.50 µg/ml		0.25 µg/ml	-
LOD	UV	0.17 µg/ml		0.08 µg/ml	-
LOQ	CAD	0.25 µg/ml		0.10 µg/ml	-
LOD	CAD	0.08 µg/ml		0.03 µg/ml	-

<sup>a</sup> Made in six replicates.<sup>b</sup> Nine calibration levels for simvastatin, seven calibration levels for atorvastatin, each injected in three replicates.

#### 4. Conclusions

The new analytical methods were developed for the determination of three statins—atorvastatin, lovastatin and simvastatin using UV and CAD detection approaches, which were compared in this study. Using a Zorbax Eclipse XDB C18 stationary phase, the separation was completed in 4.5 min with a simple volatile mobile phase, composed of acetonitrile and formic acid 0.1% (70:30) at the flow-rate 1.0 ml/min. DAD detection was performed at 238 nm, CAD worked in the 20 pA range.

The results obtained in method optimization showed an influence of the mobile phase flow-rate about 25–40% decrease of detector response, the influence of the composition of mobile phase about 30–40% of the decrease of the detector response and a strong negative impact was demonstrated when using higher concentration of buffers at pH > 4.

The SST and validation results were in good agreement with validation requirements for both detectors. The method repeatability in the frame of SST showed a R.S.D. lower than 1%. Both detectors gave linear response in the tested range, CAD in spite of belonging among non-linear detectors. The sensitivity of CAD detection was two times greater than the UV detection when applied to simvastatin, atorvastatin and lovastatin analysis.

#### Acknowledgements

The authors gratefully acknowledge the financial support of IGA MZ CR No. 1A/8689-4 and MSM 0021620822.

#### References

- [1] R.W. Dixon, D.S. Peterson, *Anal. Chem.* 74 (2002) 2930.
- [2] I. Sinclair, R. Gallagher, *Chromatogr. Today* 1 (2008) 5.
- [3] M. Lísá, F. Lynen, M. Holčápek, P. Sandra, *J. Chromatogr. A* 1176 (2007) 135.
- [4] K. Takahashi, S. Kinugasa, M. Senda, K. Kimizuka, K. Fukushima, T. Matsumoto, Y. Shibata, J. Christensen, *J. Chromatogr. A* 1193 (2008) 151.
- [5] A. Hazzotte, D. Libong, M. Matoga, P. Chaminade, *J. Chromatogr. A* 1170 (2007) 52.
- [6] R.A. Moreau, *Lipids* 41 (2006) 727.
- [7] C. Brunelli, T. Gorecki, Y. Zao, P. Sandra, *Anal. Chem.* 79 (2007) 2472.
- [8] N. Vervoort, D. Daemen, G. Torok, *J. Chromatogr. A* 1189 (2008) 92.
- [9] Y. Shitara, Y. Sugiyama, *Pharmacol. Ther.* 112 (2006) 71–105.
- [10] World Health Organization, *World Health Report, Report of the Director-General*, Geneva, WHO, 1998.
- [11] F.M. Sacks, *Am. J. Cardiol.* 88 (Suppl.) (2001) 14N.
- [12] S. Bertolini, G.B. Bon, L.M. Campbell, M. Farnier, J. Lagan, G. Mahla, *Atherosclerosis* 130 (1997) 191–197.
- [13] L.Y. Ye, P.S. Firby, M.J. Moore, *Ther. Drug Monit.* 22 (2000) 737.
- [14] K.J. Williams, I. Tabas, *Atheroscler. Thromb. Vasc. Biol.* 15 (1995) 551.
- [15] L. Nováková, D. Šatínský, P. Solich, *Trends Anal. Chem.* 27 (2008) 352.
- [16] M. Vuletic, M. Cindric, J.D. Koružnjak, *J. Pharm. Biomed. Anal.* 37 (2005) 715.
- [17] A. Malenovic, M. Medenica, D. Ivanovic, B. Jancic, *Chromatography (Suppl.)* 63 (2006) S95.
- [18] M.K. Pasha, S. Muzeeb, S.J.S. Basha, D. Shashikumar, R. Mullangi, N.R. Srinivas, *Biomed. Chromatogr.* 20 (2006) 282.
- [19] S. Erturk, E.S. Aktas, L. Ersoy, S. Ficicioglu, *J. Pharm. Biomed. Anal.* 33 (2003) 1017.
- [20] T.G. Altuntas, N. Erk, *J. Liq. Chromatogr. Relat. Technol.* 27 (2004) 83.
- [21] A. Mohammadi, N. Rezanour, M.A. Dogahen, F.G. Bidkorbeh, M. Hashem, R.B. Walker, *J. Chromatogr. B* 846 (2007) 215.
- [22] *European Pharmacopoeia 5 edition (Ph. Eur. 5)*, Council of Europe, Strasbourg, 2004.
- [23] *United States Pharmacopoeia 30*, United States Pharmacopoeial Convention, Rockville, MD 20852, United States, 2007.



# Noncovalently galactose imprinted polymer for the recognition of different saccharides

Burcu Okutucu\*, Seçil Önal, Azmi Telefoncu

Ege University, Faculty of Science, Department of Biochemistry, 35100 Bornova-İzmir, Turkey

## ARTICLE INFO

### Article history:

Received 14 October 2008

Received in revised form 21 January 2009

Accepted 23 January 2009

Available online 4 February 2009

### Keywords:

Molecular imprinting

Molecularly imprinted polymer

Galactose imprinting

Carbohydrate

Shape selectivity

## ABSTRACT

Molecularly imprinted polymers (MIPs) represent a new class of materials possessing high selectivity and affinity for the target molecule. The main goal of this study was to prepare a galactose imprinted polymer and its potential application for the recognition of different saccharides. The selectivity of galactose imprinted polymer for several saccharides; glucose, mannose, fructose, maltose, lactose, sucrose and raffinose was investigated. Macroporous polymer was prepared utilizing ethyleneglycoldimethacrylate as a crosslinking agent, in the presence of galactose as a template molecule with acrylamide as a functional monomer. After the synthesis of polymer, galactose was removed by methanol:acetic acid washing. The selectivity of galactose imprinted polymer for other saccharides was utilized by batch rebinding assay. The arrangement of functional groups within cavities versus shape selectivity is discussed. The results showed that, the orientation of the functional groups was the dominating factor for the selectivity of galactose imprinted polymer. The dissociation constants of polymer were determined by Scatchard analysis.

© 2009 Elsevier B.V. All rights reserved.

## 1. Introduction

Carbohydrates are very important group of compounds due to their roles as structural materials, sources of energy, biological functions and environmental analytes. The molecular recognition of carbohydrates in water is an intriguing subject in view of the important role of saccharides especially in biological activities; intracellular recognition, signal transduction, cell–cell communication, molecular and cellular targeting. Because of their selectively recognition in their natural environment is difficult, the mimicking of carbohydrate recognition by synthetic receptors has attracted much attention, especially in supramolecular chemistry [1–3].

Molecular imprinting has proved to be an effective technique for the creation of artificial recognition sites within synthetic polymers. The technique is very simple that involves the construction of the sites of specific recognition, commonly within synthetic polymers. These sites are made in situ by copolymerization of functional monomers and crosslinkers around the template molecules. A molecular imprint is generally formed either by strong covalent interactions or weak noncovalent interactions between functional monomers and the template. After the formation of prepolymerization complex, the polymerization reaction usually occurs by free radical initiation in the presence of a crosslinker and an appropriate solvent. The functional monomer contains spe-

cific chemical structures designed to interact with the template. The print molecules are then subsequently extracted from the polymer, leaving accessible binding sites with specific shape and functional group complementarily to original print molecule in the polymeric network. These binding sites not only maintain the ordered arrangement of complimentary chemical functionalities of the template, but also the overall spatial configuration of the target molecule is maintained [4–8]. According to the initial formation of the prepolymerization complex (template–polymer complex) there are two types of molecularly imprinted polymer (MIP); covalent and noncovalent. Covalent imprinting is considered to be a less flexible method since the interactions between print molecule and functional monomers are limited to rapidly reversible covalent interactions e.g., boronate ester formation. However noncovalent imprinting has no such restrictions, so the range of compounds which can be imprinted is much larger. Besides of this, this method is considered to be much simpler than the covalent approach and therefore, most of the research in this area involves this technique. Providing hydrogen or covalent bonds between functional monomer and carbohydrate during polymerization are demonstrated to lead to carbohydrate imprinted polymers, which are suitable for separation analysis and chromatography [9–13].

Taking the advantage of noncovalent imprinting approach for the preparation of sugar binding polymers, galactose was used as a template molecule, acrylamide was a monomer and dimethylsulfoxide (DMSO) as a porogen. To explore binding specificity of the resulting polymer sites different monosaccharides, disaccharides and polysaccharides were tested. The quantity of binding sites of the

\* Corresponding author. Tel.: +90 232 3438624; fax: +90 232 3438624.

E-mail address: [burcu.okutucu@ege.edu.tr](mailto:burcu.okutucu@ege.edu.tr) (B. Okutucu).

galactose MIP (GAL-MIP) was examined by using Scatchard analysis.

## 2. Experimental

### 2.1. Materials

Acrylamide (ACM), ethyleneglycoldimethacrylate (EGDMA), dimethylsulfoxide, methanol, acetic acid, glucose, galactose, fructose, mannose, maltose, lactose, sucrose and raffinose were obtained from Sigma Chem. Co. (St. Louis, MO, USA). Azobisisobutyronitrile (AIBN) was purchased from Wako Pure Chem. Ind. (Osaka, Japan). All other chemicals and reagents were of the highest available purity and used as purchased.

### 2.2. Synthesis of galactose imprinted polymer

Molecularly imprinted polymer was synthesized by free radical solution polymerization. Typically 1 mmol galactose, 4 mmol acrylamide and 20 mmol of EGDMA were dissolved in 10 ml of DMSO until homogenous solution was obtained. Appropriate amount of AIBN was dissolved in this solution and then the solution was purged with nitrogen to remove oxygen which acts as a free radical scavenger. The polymerization was carried out at 50 °C for 12 h. Control polymer without galactose (non-imprinted polymer; NIP) was prepared at the same time under identical conditions. The polymers (GAL-MIP and NIP) were dried in vacuum at 40 °C for 12 h and then ground to particles of 50 μm diameter or smaller. Galactose molecules were extracted by washing the MIP with methanol:acetic acid (4:1, v/v) for three rounds and then with methanol until 95% of galactose was removed from the MIP. The amount of galactose extracted from MIP was assayed by the 3,5-dinitrosalicylic acid (DNS) assay [14].

### 2.3. Batch rebinding assay

The binding efficiency of polymer towards galactose was assessed in the batch rebinding experiments. Briefly, 10 mg of the each polymer GAL-MIP and NIP was placed in an eppendorf tube which is including a known concentration of galactose (defined as galactose initial 3 μmol) in 1 ml of water and then it was mechanically shaken at room temperature for 4 h. After that, the polymers were centrifuged and the concentration of the substrate remaining in the solution (defined as galactose free) was determined by DNS assay. These rebinding experiments were repeated for three times both for imprinted and non-imprinted polymers with different concentrations of galactose (0.03–3 μmol). The NIP was used as control to determine the non-specific binding. The amount of galactose bound to the polymers ( $Q$ ) was calculated by subtracting the amount of free substrate from the initial concentration. To a comparison for imprinting effect, we define the specific adsorption values as  $\Delta Q = Q_{\text{MIP}} - Q_{\text{NIP}}$ , where  $Q_{\text{MIP}}$  and  $Q_{\text{NIP}}$  were the amounts of bound template on the imprinted and non-imprinted polymer.

### 2.4. Selectivity of galactose MIP in comparison to some carbohydrates

The substrate selectivity of GAL-MIP and NIP was carried out using series of different concentrations the equimolar amount of di- and polysaccharides of carbohydrate moieties (galactose, mannose, glucose, fructose, lactose, maltose, sucrose and raffinose) as substrates by incubating with 10 mg of polymer in 1 ml of water for 4 h at room temperature. After this incubation period, the mixture was centrifuged and the concentration of the substrate remaining in the solution for fructose, mannose, maltose, lactose and glucose

was determined with DNS assay and for the sucrose and raffinose were assayed by phenol–sulfuric acid method [15].

## 3. Results and discussion

Two main approaches for carbohydrate imprinting have been developed; the covalent and the noncovalent approach. The noncovalent molecular imprinting approach is much more flexible in terms of preparation because of the absence of complicated synthetic chemistry as well as the broad selection of functional monomers and possible target molecules available, it is thus being more commonly used. In addition, imprinted polymers prepared by the noncovalent imprinting show much faster rebinding kinetics than those prepared by the covalent approach, making them particularly suitable for applications involving their use as stationary phases in HPLC system and as sensors [10,16–20]. Covalent imprinting of saccharides with boronate esters has been quite successful for racemic resolution. The spatial arrangement of the hydroxyl functions responsible for the interaction with boronic acid binding sites at the polymer. In order to achieve good recognition by covalent imprinting two pairs of cis diols are required on the sugar ring, restricting the range of sugars can be imprinted. The problem is for biologically interesting saccharides are tackled, since the incidence of cis diols will be reduced due to branching. Also enantiomeric selectivity of covalent MIPs strongly dependent on the nature and amount of crosslinker [21–23]. Therefore it is not easy to make molecular imprinting using water soluble or highly hydrophilic templates such as sugars or aminoacids. When water was used as a porogen, the hydrogen bonding or ionic interaction can be disturbed. To solve this problem many researchers were prepared sugar imprinted polymers with metal ions especially  $\text{Cu}^{+2}$  [11,24].

As reported before; the main approach for saccharide imprinting is covalent imprinting. However, this approach needs more chemicals, detailed optimization of polymerization and rebinding conditions. So that, we have synthesized the galactose MIP by noncovalent imprinting. In the preparation of GAL-MIP, acrylamide was chosen as a monomer hence the amide group of acrylamide is a stronger hydrogen bonding functional group and it is also important to note that by using acrylamide instead of basic or acidic monomers, polymers could be made without the existence of charged groups and thus the non-specific, background ionic interactions could be reduced [25]. The DMSO was chosen because of its solubility and polarity required to promote interactions. Selection of EGDMA as a crosslinker was based on previous reports [26].

### 3.1. Determination of association constant by Scatchard analysis

One strategy to investigate the binding performance of MIPs is based on saturation experiments and subsequent Scatchard analysis. Usually, this is done by serial incubation of known amount of imprinted polymer with different concentration of the template during a period of time necessary to reach equilibrium (the time required for 90% of template bind). In our study, we have found that, galactose was reached equilibrium in 4 h.

The Scatchard plot is the easiest way to see multiple classes of binding sites [27]. This is done by plotting the binding isotherm in a Scatchard format as bound/free template ratio (μmol/mM) versus bound template (μmol). Each linear region of the binding isotherm is fitted with a straight line. The dissociation constant and binding site density were calculated from the slope and the y-intercepts, respectively, according to the following equation:

$$\frac{B}{[F]} = \frac{B_{\text{max}}}{K_D} - \frac{B}{K}$$

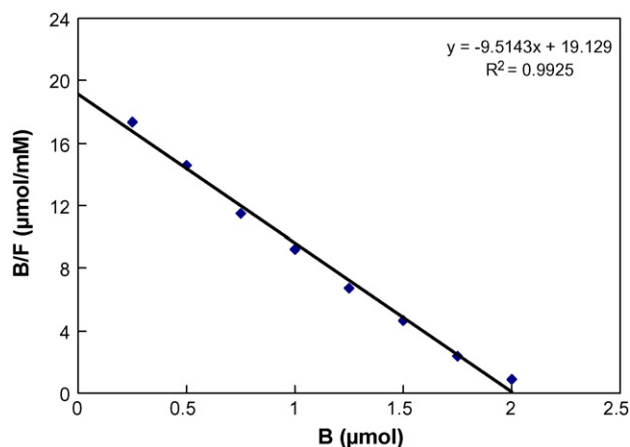


Fig. 1. Binding isotherm of galactose.

where  $B$  is the amount of galactose bound to the polymer,  $[F]$  is the concentration of free galactose (approximated by the analytical concentration of galactose),  $K_D$  is the equilibrium-dissociation constant and  $B_{max}$  is the apparent maximum number of binding sites.

Linear regression of the Scatchard plot gave a  $K_D$  value of 10.5 mM for galactose (Fig. 1). The linearity of the Scatchard plot indicates that the binding sites are identical and independent.

According to previous reports, different polymers (covalently and noncovalently imprinted) with glucose were tested for saccharides and  $K_D$  of glucose was varied from 1 to 5 mM [22,24].

### 3.2. Selectivity of galactose imprinted polymer for different saccharides

The substrate selectivity of the GAL-MIP and NIP was studied with glucose, mannose, fructose, maltose, lactose, sucrose and raffinose as substrates in water. The binding amount bound to MIPs and NIPs was determined by batch method. The distribution coefficient ( $k$ ) was utilized to evaluate the molecular selectivity of polymers [28].

$k$  is defined as follows:

$$k = \frac{C_p}{C_s}$$

where  $C_p$  ( $\mu\text{mol g}^{-1}$ ) is the amount of saccharides adsorbed on polymers and  $C_s$  ( $\mu\text{mol ml}^{-1}$ ) is the equilibrium concentration of saccharides in solution.

As is seen from Table 1, monosaccharides and polysaccharides existed different  $k$  values. Binding could be correlated with the degree of similarity to the original print molecule and these results were depended on their chemical structure. As reported before the high selectivity observed is believed on mainly due to the shape of

Table 1

The  $k$  values of saccharides on galactose MIP and NIP.<sup>a</sup>

Saccharides	MIP	NIP
Galactose	4.7	0.006
Glucose	1.07	0.008
Fructose	0.06	0.020
Mannose	0.14	0.090
Maltose	0.009	0.004
Lactose	0.004	0.001
Sucrose	0.007	0.004
Raffinose	0.005	0.008

<sup>a</sup> Polymer amount, 10 mg; binding time, 4 h; initial concentration of saccharides, 3  $\mu\text{mol}$ ; volume, 1 ml; solvent, water.

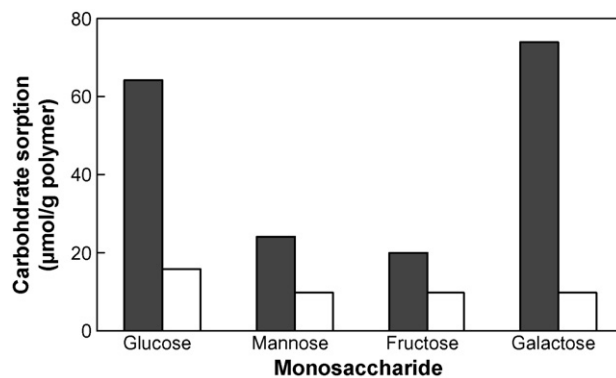
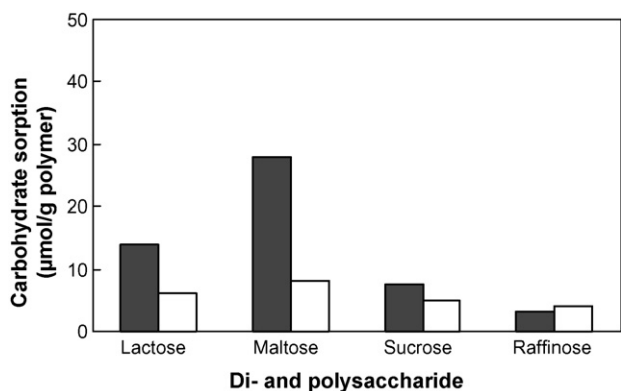


Fig. 2. Selective recognition of some monosaccharides by a galactose imprinted polymer (white bar: control polymer, black bar: galactose imprinted polymer).

cavity and the binding sites within the cavity which are primarily responsible for the driving force to bring the substrates inside the cavity. The other factor which is due to the molecular recognition was the spatial arrangement of the functional groups (binding sites) within the cavity [29]. According to previous studies, the shape of cavity plays an important role for the templates which is binded only hydrogen bonds. The attractive forces (polyfunctional hydrogen bonding between carbohydrate and polymer backbone, or the increase of entropy by freeing ordered water molecules from the solvation shell of the carbohydrate into the solution upon binding) is less important and the hydrophilic disaccharides did not bind the polymer backbone effectively. In aqueous solutions carbohydrates were existed, several equilibria between different tautomeric and hydrated forms and an enol, a keto, an endiol and a hydrated diol form [30–32].

For the monosaccharides, the results were shown that the spatial arrangement of the hydroxyl functions were responsible for the interaction with monomer binding sites at the polymer. Although the chemical composition within a class of saccharides, such as the aldohexopyranose sugars, is identical ( $C_6H_{12}O_6$ ), the orientation of hydroxyl groups can differ across stereoisomers [25]. Galactose differs from its epimer (glucose) in the configuration of carbon atom C4 and mannose differs from its epimer (glucose) only in its configuration of carbon atom C2. The positions of OH groups were different on fructose. The high hydroxyl content of carbohydrates is important to consider when explaining the interactions these molecules make with solvent. Hydroxyl orientation and intramolecular H-bonding influence the structural properties of the aldohexopyranose stereoisomers. According to our results the dominated hydrogen bonds could be between the C1, C2 and C4 carbon atoms and the polymer. Because of this reason the selectivity observed in the galactose imprinted polymer for glucose, fructose and mannose is mainly due to the orientation of the functional groups while the shape of the cavity is less important (Fig. 2). It is interesting that the monosaccharides common to biology are those containing both a hydrophobic patch and limited intramolecular H-bonding; namely, glucose, galactose, mannose.

For the disaccharides, the results showed that the maltose and lactose could not be recognized by the galactose imprinted polymer because of  $\alpha$ - or  $\beta$ -glycosidic linkage. The position of glycosidic linkages was effected the position of effective hydroxyl groups which is important for the recognition. C4 carbon atom has effective hydrogen bond capacity and if it belongs to the glycosidic linkage the binding capacity of these saccharides was effected negatively. We can attribute the lack of selectivity for sucrose and raffinose because of their large chemical structure than the galactose so that they did not fit into the polymer cavity (Fig. 3).



**Fig. 3.** Selective recognition of some polysaccharides by a galactose imprinted polymer (white bar: control polymer; black bar: galactose imprinted polymer).

As a result, the recognition of saccharides by the galactose imprinted polymer the main forces due to was the position of functional groups in the polymer cavity for monosaccharides and the pore structure of cavity for di- and polysaccharides.

#### 4. Conclusion

Recognition and separation of saccharides have been focus of much recent attention MIPs having saccharide binding affinity can be synthesized by copolymerization of functional monomers, excess crosslinker and galactose as a template. Saccharide binding affinity evaluated by the Scatchard analysis was dependent on the composition of the functional monomers, as well as on the degree of crosslinking. The development of such molecular imprinted polymers, which are operational in aqueous solution may open new applications in the fields of life sciences. In conclusion the orientation of hydroxyl groups is primarily responsible for molecular recognition of monosaccharides and shape selectivity is for di- and polysaccharides. The results presented in this paper demonstrate the potential of noncovalently imprinting technique for the

development of molecularly imprinted saccharide recognition. The binding sites with high affinity to functional groups of saccharides are shown that this polymer can be used for the analysis of saccharides from the various synthetic or biological sources.

#### References

- [1] P. Sears, C.H. Wong, *Angew. Chem. Int. Ed.* 38 (1999) 2300.
- [2] P. Sears, C.-H. Wong, *Cell. Mol. Life Sci.* 54 (1998) 223.
- [3] A. Varki, *Glycobiology* 3 (1993) 97.
- [4] B. Okutucu, A. Telefoncu, *Talanta* 76 (2008) 1153.
- [5] C.C. Hwang, W.C. Lee, *J. Chromatogr. A* 962 (2002) 69.
- [6] A.P. Davis, R.S. Wareham, *Angew. Chem. Int. Ed.* 38 (1999) 2979.
- [7] F.G. Tamayo, E. Turiel, A. Martin-Esteban, *J. Chromatogr. A* 1152 (2007) 32.
- [8] R. Rajkumar, A. Warsinke, H. Möhwald, F.W. Scheller, M. Katterle, *Biosens. Bioelectron.* 22 (2007) 3318.
- [9] S. Striegler, E. Tewes, *Eur. J. Inorg. Chem.* 2 (2002) 487.
- [10] A.G. Mayers, L.I. Adersson, K. Mosbach, *Anal. Biochem.* 222 (1994) 483.
- [11] S. Striegler, *Bioseparation* 10 (2002) 307.
- [12] T. Ishii, R. Iguchi, S. Shankai, *Tetrahedron* 55 (1999) 3883.
- [13] T. Ishii, R. Iguchi, S. Shankai, G.H. Chen, Z.B. Guan, C.T. Chen, L.T. Fu, V. Sundaresan, F.H. Arnold, *Nat. Biotechnol.* 15 (1997) 354.
- [14] G.L. Miller, *Anal. Chem.* 31 (1959) 426.
- [15] M. Dubois, K.A. Gilles, J.K. Hamilton, P.A. Rebers, F. Smith, *Anal. Chem.* 28 (1956) 350.
- [16] B. Sellergren, in: B. Sellergren (Ed.), *Molecularly Imprinted Polymers*, Elsevier, Amsterdam, 2001, pp. 113–184.
- [17] K.G.I. Nilsson, K. Sakaguchi, P. Gemeiner, K. Mosbach, *J. Chromatogr. A* 707 (1995) 199.
- [18] S. Wei, B. Mizaikoff, *J. Sep. Sci.* 30 (2007) 1794.
- [19] C. Yu, K. Mosbach, *J. Mol. Recognit.* 11 (1998) 69.
- [20] Q. Liu, R.K. Schmidt, B. Teo, P.A. Karplus, J.W. Brady, *J. Am. Chem. Soc.* 119 (1997) 7851.
- [21] R. Rajkumar, A. Warsinke, H. Möhwald, F.W. Scheller, M. Katterle, *Talanta* 76 (2008) 1119.
- [22] K. Tsukaoshi, R. Kawasaki, M. Maeda, M. Takagi, *Anal. Sci.* 12 (1996) 721.
- [23] W. Wang, S. Gao, B. Wang, *Org. Lett.* 1 (1999) 1209.
- [24] A. Ersöz, A. Denizli, A. Özcan, R. Say, *Biosens. Bioelectron.* 20 (2005) 2197.
- [25] J. Dashnau, K.A. Sharp, J.M. Vanderkooi, *J. Phys. Chem. B* 109 (2005) 24152.
- [26] F. Sineriz, Y. Ikeda, E. Petit, L. Bultel, K. Haupt, J. Kovensky, D. Papy-Garcia, *Tetrahedron* 63 (2007) 1857.
- [27] J.A. Garcia-Calzon, M.E. Diaz-Garcia, *Sens. Actuators B* 123 (2007) 1180.
- [28] H. Guo, X. He, *Fresen. J. Anal. Chem.* 368 (2000) 763.
- [29] B. Leroux, H. Bizot, J.W. Brady, V. Tran, *Chem. Phys.* 216 (1997) 349.
- [30] J. Behler, D.W. Price, M.G.B. Drew, *Phys. Chem. Chem. Phys.* 3 (2001) 588.
- [31] G. Wulff, S. Schauhoff, *J. Org. Chem.* 56 (1991) 395.
- [32] J.L. Dashnau, K.A. Sharp, J.M. Vanderkooi, *J. Phys. Chem. B* 109 (2005) 24152.



## Estimation of uncertainty in size-exclusion chromatography with a double detection system (light-scattering and refractive index)

Alexis Oliva\*, Matías Llabrés, José B. Fariña

Dpto. Ingeniería Química y Tecnología Farmacéutica, Facultad de Farmacia, Universidad de La Laguna, Avda. Fco. Sanchez, s/n, La Laguna, 38200, La Laguna, Tenerife, Spain

### ARTICLE INFO

#### Article history:

Received 16 June 2008

Received in revised form 16 December 2008

Accepted 18 December 2008

Available online 30 December 2008

#### Keywords:

Light-scattering

Uncertainty

Peptides and proteins

Validation

Method reproducibility

### ABSTRACT

Size-exclusion chromatography (SEC) coupled with online laser light-scattering (LS) and refractive index (RI) detection provides an excellent approach to determine the molecular weights (Mw) of proteins by the “two-detector” approach. Mw is determined only at the maximum of a peak, using either peak heights or area ratio from the two detectors. However, proper calibration of the SEC/LS/RI system is critical to obtain high precision.

Today, an essential part of any analysis is to evaluate the uncertainty associated with the method. Basically, it is possible to distinguish between factors related to signal nature, precision and those due to signal processing. Given the signal of interest is the peak height or area ratio from two detectors, the signal ratio uncertainty was calculated using the random propagation of error formula. In this case, the effect of signal correlation was evaluated to avoid the uncertainty overestimation. In the second case, the sources of uncertainty affecting analytical measurement were estimated with the information from the precision assessment. For this, two designs with two-factor fully nested were followed for each method. Finally, the contributions from various uncertainty sources related with calibration are also analysed in detail. There are in fact only three main sources of measurement uncertainty: intermediate precision, calibration and repeatability. Of these, method precision is always the greatest, regardless of approach.

For all proteins and peptides studied, the Mw calculated using both methods are close to the theoretical results, independently of the design, but the contributions of individual terms to combined uncertainty depend on both the design and method used. For example, the combined uncertainty varied between 223 and 813.2 Da for carbonic anhydrase, although higher values were found for human insulin and ovalbumin dimer. Other considerations that can have a significant impact on the results are discussed.

The reproducibility of the two methods versus that based on ASTRA software used as reference method was performed using the concordance correlation coefficient. The methods' reproducibility depends on the permitted losses in precision and accuracy.

© 2008 Elsevier B.V. All rights reserved.

### 1. Introduction

Recombinant proteins intended for clinical use must be extensively characterized with regard to their molecular and biological properties and monitored for structural and biological integrity during manufacturing and storage. Various analyses are used to characterize the biomolecules. Molecular weight, conformation, size and shape, and state and extent of aggregation are a few of the physicochemical properties studied. Recent technological advances have significantly increased the speed of characterizing proteins. It is now feasible to measure the LS, RI and intrinsic viscosity (IV), along with UV-absorption characteristics of protein component peaks separated on a SEC column in real time by coupling four detectors online with HPLC equipment. A combination of two or

more of these four detectors online with chromatographic systems has been used in several laboratories for determination of protein Mw, hydrodynamic radius, protein aggregation, and protein glycosylation [1–5].

Size-exclusion chromatography (SEC) coupled with online laser light-scattering (LS) and refractive index (RI) detection provides an excellent approach to determine the molecular weights (Mw) of proteins by the “two-detector” approach [1,3]. Mw is determined only at the maximum of a peak when using peak heights, or for a selected portion of the eluting peak, if using peak areas ratio from the two detectors. This approach circumvents the need to know the specific refractive index for the protein, a parameter that is otherwise needed to determine Mw using the commercial available software for LS data analysis e.g. ASTRA (Wyatt Corp., Santa Barbara, CA). However, proper calibration of the SEC/LS/RI system is crucial to obtain high precision since the experimentally determined Mw depends on the precision of the instrument calibration constant, and Mw of the calibration standard [1–5]. To obtain precise

\* Corresponding author. Tel.: +34 922 318 452; fax: +34 922 318 514.  
E-mail address: [amoliva@ull.es](mailto:amoliva@ull.es) (A. Oliva).

Mw estimates, the system must be calibrated using various standard proteins; whereas for the values of LS and RI signals, either peak height or peak area methods may be used. The theory behind the use of LS and RI signals for calculation of Mw distribution is described in detail in several of the earlier reports and reviews [6–8].

In order to correctly interpret results of an analytical procedure, their reliability should be demonstrated. Validation is a first step to achieve this, but is not enough if one aims to interpret and compare results correctly. Correct interpretation of a measurement requires its uncertainty to be known. One major advantage of the validation method is that it can give an estimation of uncertainty of measurements without any additional experiments. Broadly speaking, there are two approaches, namely the “Top-Down” and “Bottom-Up” methods [9,10]. For the first, the procedure is considered as a whole and the major sources of uncertainty are identified and evaluated. The total uncertainty is calculated from the results obtained in an inter-laboratory study. In the second approach, the combined uncertainty is calculated from the individual uncertainty of each operation of the analytical process; these individual values can be obtained theoretically or experimentally using a nested experimental design.

The purpose of the present paper is to provide an estimation of the uncertainty associated with Mw determination by the two-detector-method, and an appropriate identification and evaluation of each uncertainty source that affects the measurement process. Two double-factor fully nested designs were used and evaluated for each method. For this, different peptides and proteins were used as model molecules. Additionally, the concordance correlation coefficient proposed by Lin [11,12], which evaluates the agreement of paired samples, was also used to verify whether the new methods can reproduce the results based on a reference method.

## 2. Experimental

### 2.1. Measurement of molecular weight of model proteins

#### 2.1.1. Materials

The following proteins were used, and their Mw calculated from amino-acid sequences using the Swiss-Prot/TrEMBL databases indicated within parenthesis: bovine serum albumin (66433), human serum albumin (67300), lysozyme (14313),  $\beta$ -lactoglobulin (18281), ovalbumin (42750), carbonic anhydrase (29114), and bovine insulin (5814) were purchased from Sigma Chemical Co. (St. Louis, MO, USA), the recombinant human growth hormone (22120) and human insulin (5706) were purchased from Novo Nordisk (Bagsvaerd, Denmark), and the Spf66 peptide (4642) was synthesized at the Instituto de Inmunología San Juan de Dios, Bogotá, Colombia under GMP conditions. Deionized water was purified in a Milli-Q Plus system from Millipore (Molsheim, France) prior to use. All other chemicals and reagents were HPLC grade.

#### 2.1.2. Apparatus

SEC was performed using an HPLC pump (600E Multisolvant Delivery System from Waters, Milford, MA, USA) and an autosampler (700 Wisp Model, Waters). Elution was at room temperature on a Shodex Protein KW 803 column (8 mm  $\times$  300 mm, Waters), and column effluent monitored sequentially with a miniDawn light-scattering detector (Wyatt Technology, Santa Barbara, CA, USA) and a Waters model 410 differential refractometer. The miniDawn was placed downstream of the column and upstream of the differential refractive-index (DRI) detector to avoid the possibility of backpressure on the DRI cell. To reduce baseline noise a pulse dampener (Alltech Associates, USA) was connected downstream of the pump and two 25 mm high-pressure filters with 0.22 and 0.1  $\mu$ m

pores (Millipore) respectively, were used for on-line filtration of the mobile phase.

The LS detector was calibrated according to the protocol provided by the manufacturer; the calibration remains valid for a couple of years unless changes are made in the laser or photodiodes (provided the flow cell is kept clean). The RI detector was calibrated to convert changes in voltage (volts) to changes in refractive index ( $dn$ ); this calibration remains valid for 1 year. For this, five sodium chloride standards prepared in duplicate over a linear concentration range of 1–5 mg/ml were used.

The mobile phase was a phosphate-buffered saline (0.12 M NaCl, 0.025 M phosphate, pH 7.0) at a flow-rate 1.0 ml/min. and injection volume 100  $\mu$ l. All solvents were filtered with 0.45  $\mu$ m pore size filters (Millipore). The mobile phase was filtered and degassed. Samples were prepared by direct dilution with the mobile phase to obtain a concentration of 0.1 mg/ml and analysed the same day, in duplicate unless otherwise indicated.

#### 2.1.3. Data analysis

Data acquisition and Mw calculations were performed using the ASTRA software, version 4.2 (Wyatt Technology). In the two-detector approach [1,3], we have that the LS is proportional to the Mw, concentration, and square of the refractive index increment ( $dn/dc$ ) in the equation

$$(LS) = K_{LS}(c)Mw \left( \frac{dn}{dc} \right)^2 \quad (1)$$

and that the RI is proportional to  $dn/dc$  and concentration in the equation

$$(RI) = K_{RI}(c) \left( \frac{dn}{dc} \right) \quad (2)$$

Combining Eqs. (1) and (2), the Mw can be determined from the ratio of the signals (as peak height or area) from two detectors (LS and RI):

$$Mw = K' \left( \frac{LS}{RI} \right) \quad (3)$$

where  $K' = K_{RI}/[K_{LS}(dn/dc)]$ .

In this method, the signals from two detectors were processed with Mathematica<sup>®</sup> software for Windows [13] to estimate the peak area and height. In all the calculations, we used only the data for scattering at 90° (even though data are available at other angles), both for simplicity and because the 90° data usually have the highest signal/noise ratio.

### 2.2. Signal analysis

At first, it is necessary to describe those aspects of the procedure that are to be considered before actually making any measurements. For example, instrumental precision, such as that associated with each photodiode of the LS detector (this term is given by the ASTRA software) or detector calibration does not have to be taken into account. Only the factors related with the LS and RI signals processing (e.g. peak height or area) were considered.

Many analytical techniques rely on measuring a single variable, such as the light intensity in photometry. For other methods, however, the analytical response is embedded in ratios of two variables. In our case, the ratio of two signal intensities ( $x$  and  $y$ ) is the variable measured to obtain the Mw. Information regarding the uncertainty of the  $x/y$  ratio is often available from repeated measurements of both  $x$  and  $y$ , which can be directly estimated using the following



expression:

$$s_{x/y} = \sqrt{\frac{1}{n-1} \sum_{i=1}^n (x_i/y_i - \bar{x}/\bar{y})^2} \tag{4}$$

or by calculating the uncertainty propagated from the signal ratio,  $x/y$ , using the statistical information of both signal intensities,  $x$  and  $y$ . In this case, random error propagation from a two variable ratio,  $x/y$ , is conventionally carried out via the first-order Taylor series approximation [14]:

$$\left(\frac{s_{x/y}}{x/y}\right) \approx \left(\frac{s_x}{x}\right)^2 + \left(\frac{s_y}{y}\right)^2 \tag{5}$$

The above expression, known as the law of random error propagation, can only be used when  $x$  and  $y$  are uncorrelated random variables as clearly indicated in the Guide to the Expression of Uncertainty in Measurement [15] If the two variables are correlated, we need to consider the generalization of Eq. (5) where the two variables  $x$  and  $y$  need not necessarily be independent, and therefore, the following expression is used:

$$\left(\frac{s_{x/y}}{x/y}\right) \cong \left(\frac{s_x}{x}\right)^2 + \left(\frac{s_y}{y}\right)^2 - 2 \text{cor}(x, y) \cdot \frac{s_x s_y}{xy} \tag{6}$$

where the  $\text{cor}(x, y)$  is the correlation coefficient between the variable  $x$  and  $y$ . Note that the term  $\text{cor}(x, y) \cdot s_x s_y$  is covariance between  $x$  and  $y$ , i.e.  $\text{cov}(x, y) = \text{cor}(x, y) \cdot s_x s_y$ . Thus, Eq. (6) turns into Eq. (5), commonly found in the literature, when  $\text{cor}(x, y) = 0$  [15].

### 2.3. Estimation of uncertainty

The uncertainty derived from estimating  $M_w$  from the calibration curve ( $u(M_w)$ ) is a combination of the uncertainties associated with transformation of the chromatographic signals (peak height or area ratio) in  $M_w$  ( $u^2(\text{cal})$ ) and with the repeatability of the measurements ( $u^2(\text{repeat})$ ). This combination is calculated as

$$u(M_w) = \sqrt{u^2(\text{cal}) + u^2(\text{repeat})} \tag{7}$$

#### 2.3.1. Estimation of $u^2(\text{cal})$

This is the uncertainty of predicting a  $M_w$  for the routine sample with a standard curve, applying the expression for the linear regression of least squares of residuals and considers the uncertainty associated with precision ( $u_{\text{precision}}$ ) [16].

$$u(\text{cal}) = \frac{1}{b_1} \sqrt{u^2(\text{pred}) + u^2(\text{precision})} \tag{8}$$

where  $b_1$  is the slope of the calibration curve.

The uncertainty arising from prediction,  $u^2(\text{pred})$ , is calculated as

$$u(\text{pred}) = \sqrt{s_{\text{resid}}^2 \left( \frac{1}{n} + \frac{(M_{w_{\text{estimated}}} - \bar{M}_w)^2}{\sum (M_{w_i} - \bar{M}_w)^2} \right)} \tag{9}$$

where  $M_{w_{\text{estimated}}}$  is the  $M_w$  estimated by the analytical procedure after having converted the instrumental response into  $M_w$  using a standard curve,  $s_{\text{resid}}^2$  denotes the standard deviation of residuals,  $M_{w_i}$  is the  $M_w$  of the standard  $i$ ,  $n$  denotes the number of standards, and  $\bar{M}_w$  represents the mean  $M_w$  of all the standards analysed.

The uncertainty in the precision,  $u^2(\text{precision})$ , is given by the expression

$$u(\text{precision}) = \sqrt{s_i^2 + u_{\text{conditions}}^2} \tag{10}$$

where  $s_i^2$  represents the intermediate variance obtained when the standards are analysed under intermediate precision conditions,

and  $u_{\text{conditions}}$  denotes the uncertainty associated with how the standards of the calibration curve are analysed. If they are analysed under intermediate conditions,  $u_{\text{conditions}} = 0$  [16].

In research or other small laboratories where analyses are performed by the same operator on a single instrument, the overall precision,  $s_i^2$ , corresponds to time-different intermediate precision:

$$s_i^2 = s_m^2 + s_{\text{day}}^2 \tag{11}$$

where  $s_m^2$  is the measurement variance, i.e. the random error in every measurement under repeatability conditions, and  $s_{\text{day}}^2$  is the between-day variance.

#### 2.3.2. Estimation of $u^2(\text{repeat})$

This term considers the uncertainty associated with the assessment of precision when the routine samples are analysed in repeatability conditions. This uncertainty is given by the expression

$$u(\text{repeat}) = \sqrt{\frac{s_s^2}{n_s}} \tag{12}$$

where  $s_s^2$  represents the standard deviation of the analyses performed on the routine sample and  $n_s$  the number of replicates of each sample analysed in routine analysis.

### 2.4. Reproducibility of the methods

When a new method is developed, it is of interest to evaluate if the new method can reproduce the results based on a reference method. The concordance correlation coefficient can be used to validate the reproducibility of a new method [11,12]. The concordance correlation coefficient ( $p_c$ ) consists of a measure of precision ( $p$ ), normally the Pearson correlation coefficient (not correctable), multiplied by a measure of accuracy ( $C_b$ ), which is correctable, for example by calibration ( $p_c = p \times C_b$ ). This bias consists of a shift (ratio of two standard deviations, denoted by  $v$ ) and a location shift (squared difference in means relative to the product of two standard deviations, denoted by  $u^2$ ).

Then

$$C_b = 2 \left[ v + \left( \frac{1}{v} \right) + u^2 \right]^{-1} \tag{13}$$

where  $v = \sigma_1/\sigma_2$  and  $u^2 = (\mu_1 - \mu_2)/(\sigma_1\sigma_2)$

For  $n$  independent pairs of samples, it is natural to use the sample counterparts of  $p_c$ .

$$p_c = \frac{2S_{12}}{S_1^2 + S_2^2 + (\bar{Y}_1 - \bar{Y}_2)^2} \tag{14}$$

where

$$\bar{Y}_j = \frac{1}{n} \sum_{i=1}^n Y_{ij}; \quad S_j^2 = \frac{1}{n} \sum_{i=1}^n (Y_{ij} - \bar{Y}_j)^2, \quad j = 1, 2;$$

and

$$S_{12} = \frac{1}{n} \sum_{i=1}^n (Y_{i1} - \bar{Y}_1)(Y_{i2} - \bar{Y}_2)$$

The Z-transformation approach was used to calculate the confidence interval for  $p_c$ , yields a distribution asymptotically normal with mean

$$Z_c = \frac{1}{2} \text{Ln} \frac{1+p_c}{1-p_c} \tag{15}$$

and variance

$$\sigma_z^2 = \frac{1}{n-2} \left\{ \frac{(1-p^2)p_c^2}{(1-p_c^2)p^2} + \frac{4p_c^3(1-p_c)u^2}{p(1-p_c^2)^2} - \frac{2p_c^4u^4}{(1-p_c^2)p^2} \right\} \tag{16}$$

**Table 1**  
Comparison of the signal ratio uncertainties: measured versus propagated.

Signal (height)	Average signal	Measured uncertainty <sup>a</sup>	Propagated uncertainty <sup>b</sup>		Signal correlation
			cor(x, y) = 0	cor(x, y) ≠ 0	
LS	0.1190	0.0002768			cor(x, y) = 0.0031, n = 15
RI	0.07663	0.0001101			
LS/RI	1.553	0.004137	0.0027335	0.0027329	
Signal (area)					cor(x, y) = 0.0015, n = 15
LS	0.05010	0.00031121			
RI	0.03846	0.00020884			
LS/RI	1.302	0.01097185	0.0082496	0.0082494	

<sup>a</sup> Uncertainty expressed as 1 standard deviation.

<sup>b</sup> Propagation of the LS/RI uncertainty with the cor(x, y) = 0 assumption is done using Eq. (5), while the cor(x, y) ≠ 0 case is according to Eq. (6).

### 3. Results and discussion

#### 3.1. Signal analysis

As a preliminary step, the signal ratio uncertainty was calculated from repeated measurements of LS and RI signals in accordance with Eq. (4). Alternatively, one can obtain the average ratio by dividing the two signal averages. As the uncertainties of both signal averages are known, that of the average signal ratio can easily be obtained using the uncertainty propagation formula (see Table 1). The signal variance is lower than the variance of the signal averages ratio, regardless of the signal type, whereas the uncertainty of the signal ratio calculated using Eq. (5) is the smallest. In this last case, it is necessary to evaluate the effect of signal correlation since the magnitude of error in signal ratio uncertainty estimates caused by the omission of signal correlation may be higher. For this, a  $\beta$ -lactoglobulin sample was analysed 15 times and the LS and RI signals as peak height or area were estimated. A simple way to present signal correlation is to plot two signals against each other. In our case, the signals are not correlated since a random distribution was observed (Fig. 1), the correlation coefficient ( $R$ ) being lower than 0.06 ( $p > 0.05$ ). This fact can be seen in the propagated uncertainties obtaining values very closest for both approaches. This result clearly demonstrates the need to use appropriate propagation of error formulas since uncertainty may be overestimated, for example, a value of 33.9% for the peak height and 24.8% for the peak area were observed, respectively in comparison with the measured uncertainty using Eq. (4). Therefore, any uncertainty deriving from the signal ratio will be calculated using Eq. (5).

#### 3.2. Estimation of methods uncertainty

As is well known the usual analytical procedure consists of the following main steps: sampling, sub-sampling, sample treatment, measurement and quantification.

Sampling is usually performed out of the laboratory and as its uncertainty is not easy to calculate, it is not specifically considered. The sub-sampling, sample treatment and measurement uncertainties are usually obtained as a whole during reproducibility studies [17]. For this, the data obtained according to the set-up of Fig. 2 were analysed by means of an ANOVA in accordance with Maroto et al. [16]. From this, the variance between measurements ( $s_m^2$ ) and the variance between days ( $s_{day}^2$ ) were calculated to be  $6.061 \times 10^{-5}$  and  $1.767 \times 10^{-4}$ , respectively. The ratio between the day and the measurement variance is about three times, which can be considered normal. Notice that in this expression  $s_{day}^2$  is not a pure variance component due to time, since besides the effect of changes in time it also includes effects due to the solutions and mobile phase being newly prepared each day. However, it must be pointed out that the estimation of the  $s_{day}^2$  may not be as good as would have been obtained if all the important sources of variation

like analyst, time, instrument, calibration, are included as factors in the experimental design. However, in this latter case, the cost in terms of work increases considerably. It follows from Eq. (11) that the time-different intermediate precision is estimated to be  $S_T^2 = 2.374 \times 10^{-4}$ . Thus, the  $u(\text{precision})$  is 198.4.

The quantification step, frequently performed by interpolation from the calibration graph, (LS/RI) signals ratio versus standard proteins molecular weight, is known to be the main source of uncertainty in some situations [18]. The parameters affecting the uncertainty due to quantification are: (a) the number of standards used (b) the amplitude of the linear response range, and (c) the relation between the sample Mw and that of the centroid of the calibration line, i.e. if the interpolation is performed close to or far from the centroid as seen in Eq. (9) [17].

In general, the number of standards used ranges between 3 and 10 [19,20]; in this case, the short working calibration for routine

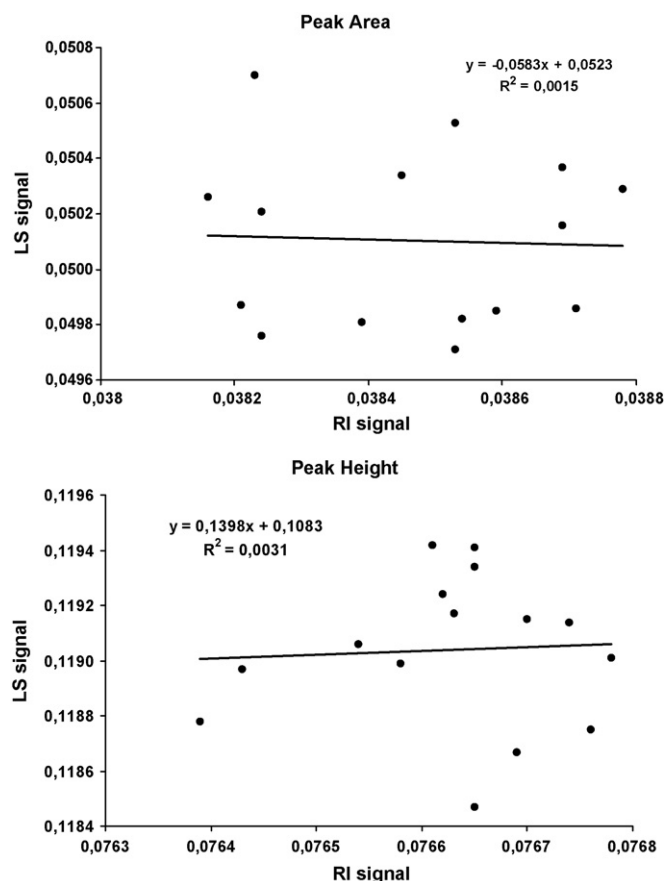


**Fig. 1.** Correlation of the LS/RI signal ratio expressed as peak height and area.

**Table 2**  
Estimates of measurement uncertainties for the different peptides and proteins studied using the peak height method.

Source	Spf66 peptide	Human insulin (M) <sup>a</sup>	Human insulin (D) <sup>b</sup>	$\beta$ -Lactoglobulin	rHGH	Carbonic Anhydrase	Human Serum Albumin (M) <sup>a</sup>	Ovalbumin (D) <sup>b</sup>
<b>Design A</b>								
<i>u</i> (repeatability)	71.0	43.4	43.7	48.1	51.2	46.4	89.7	93.7
<i>u</i> (prediction)	136.7	133.0	116.1	100.9	98.2	90.7	158.1	208.5
<i>u</i> (precision)	198.4	198.4	198.4	198.4	198.4	198.4	198.4	198.4
<i>u</i> (calibration)	240.9	238.9	229.9	222.6	221.4	218.1	253.7	287.8
<i>u</i> (Mw)	251.2	242.8	234.0	227.7	227.2	223.0	269.1	302.7
Mw estimated	4657	6004	12,539	19,883	21,523	28,498	67,217	82,752
<i>U</i> (Mw) <sup>c</sup>	502.3	485.5	468.0	455.5	454.4	446.1	538.2	605.4
<b>Design B</b>								
<i>u</i> (repeatability)	71.0	43.4	43.7	48.1	51.2	46.4	89.7	93.7
<i>u</i> (prediction)	289.1	281.2	244.1	205.6	198.2	169.7	230.1	319.4
<i>u</i> (precision)	283.4	283.4	283.4	283.4	283.4	283.4	283.4	283.4
<i>u</i> (calibration)	404.8	399.2	374.0	350.1	345.8	330.3	365.1	427.0
<i>u</i> (Mw)	411.0	401.6	376.6	353.4	349.6	333.6	375.9	437.2
Mw estimated	4656	6002	12,534	19,876	21,515	28,498	67,192	82,721
<i>U</i> (Mw) <sup>c</sup>	822.0	803.2	753.1	706.8	699.2	667.1	751.8	874.3
Mw (ASTRA) <sup>d</sup>	4688	5805	12,600	21,800	23,100	29,550	67,300	87,500

<sup>a</sup> M = monomer.

<sup>b</sup> D = dimer.

<sup>c</sup> Expanded uncertainty for  $k=2$ .

<sup>d</sup> Mw estimated using ASTRA software.

analysis also called “continuing calibration” [21] was used, i.e. four calibration standards in duplicate, analysed on three different days (Fig. 2, Design A). For this, the bovine insulin (Mw = 5814), lysozyme (Mw = 14,313), ovalbumin (Mw = 42,750) and bovine serum albumin monomer (Mw = 66,433) were used as calibration standards.

To determine the Mw, we used either the peak height or area ratio from two detectors. In the peak height case, the analysis of variance (ANOVA) of the linear regression “height peak ratio versus calibration standard Mw” confirmed the linearity of the method through rejection of the null hypothesis of lack of fit for a significance level of 0.05 ( $\alpha = 0.05$ ); the relative standard deviation (R.S.D.) was 1.36%. A *t*-test was also carried out to determine whether the intercept can be considered zero. The *t*-values are calculated and compared with tabled values, usually at the 5% significance level.

Since the calculated value ( $t = 1.93$ ) is smaller than the tabled value ( $t = 2.07$ ), we can say that on the basis of observed data, the intercept is equal to zero. Therefore, the equation of the regression line was:

$$\text{Peak height ratio} = 7.765 \times 10^{-5} \times \text{Mw}; \quad r = 0.9998; \quad (n = 24)$$

and the root mean square error ( $S_{yx}$ ) was  $3.407 \times 10^{-2}$ .

To estimate the uncertainty due to the interpolation in the calibration line, a recombinant human growth hormone (rHGH) sample was analysed in triplicate, the estimated mean Mw being 21,523, whereas the  $u^2(\text{pred})$  for this mean value calculated in accordance with Eq. (9) was 98.2. Substituting these values in Eq. (8), the  $u(\text{cal})$  for the rHGH was 221.4. The uncertainty when this sample is analysed in repeatability conditions,  $u(\text{repeat})$  was 51.2 ( $n = 3$ ). Normally, this result is obtained with only one analysis or at most as the mean of three replicates. In our case,  $s_y^2$  is the standard deviation obtained from the mean value of one sample analysed in triplicate ( $n_s = 1$ ).

Following the estimation of individual (or groups of) components of the uncertainty and expressing them as standard uncertainties, the next stage was to calculate the combined standard uncertainty  $u(\text{Mw})$  applying Eq. (7), arriving at 227.2. To provide a level of confidence for the final result, the expanded uncertainty  $U(x)$  is obtained by multiplying the overall standard uncertainty by a coverage factor  $k$ , for which a value of 2 usually is chosen to obtain a confidence level of 95% [8]. The expanded uncertainty, using  $k = 2$ , is then:  $U(\text{Mw}) = 454.4$  Da, so the calculated Mw is  $21,523 \pm 454.4$  Da.

To reduce the  $u(\text{Mw})$ , the easier option is to increase the number of replicates in the repeatability measurements. This fact suppose a decrease of around 10–20% in the repeatability measurements using six instead of three replicates, but this only implies a decrease in combined uncertainty of less than 1%. For example, for an rHGH sample the  $u(\text{repeat})$  expressed as peak height ratio was 46.1 ( $n = 6$ ) against a value of 51.2 ( $n = 3$ ) which involves a variation of 9.0%, whereas this value supposes only a 0.5% reduction in the combined standard uncertainty  $u(\text{Mw})$ . However, this fact involves extra work both time and cost, whose effect on the final result will be minimal.

Table 2 shows the relative uncertainties and expanded uncertainty obtained for the different proteins following design A.

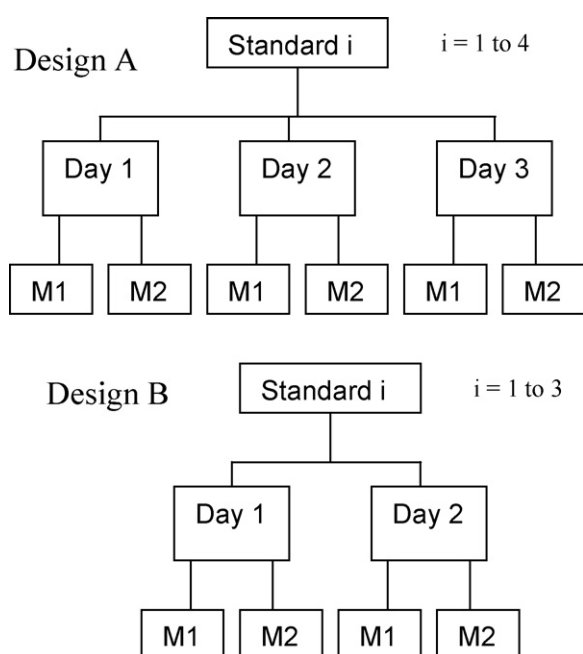


**Fig. 2.** Experimental designs used for determining intermediate precision.

**Table 3**  
Estimates of measurement uncertainties for the different peptides and proteins studied using the peak area method.

Source	Spf66 peptide	Human insulin (M) <sup>a</sup>	Human insulin (D) <sup>b</sup>	β-Lactoglobulin	rHGH	Carbonic Anhydrase	Human Serum Albumin (M) <sup>a</sup>	Ovalbumin (D) <sup>b</sup>
<b>Design A</b>								
<i>u</i> (repeatability)	206.5	126.2	168.0	157.4	163.5	178.4	227.5	236.6
<i>u</i> (prediction)	199.6	194.3	170.6	151.2	142.1	132.1	238.2	311.1
<i>u</i> (precision)	605.2	605.2	605.2	605.2	605.2	605.2	605.2	605.2
<i>u</i> (calibration)	637.3	635.7	628.8	623.8	621.7	619.5	650.4	680.5
<i>u</i> (Mw)	669.9	648.1	650.9	643.4	642.8	644.7	689.1	720.5
Mw estimated	4990	6295	12,551	18,774	22,569	30,311	68,494	83,662
<i>U</i> (Mw) <sup>c</sup>	1339.8	1296.1	1301.8	1301.8	1285.7	1289.3	1378.1	1440.9
<b>Design B</b>								
<i>u</i> (repeatability)	206.6	126.3	168.2	157.6	163.6	205.3	290.0	236.8
<i>u</i> (prediction)	442.8	431.0	376.2	315.9	298.2	252.2	366.4	502.1
<i>u</i> (precision)	745.4	745.4	745.4	745.4	745.4	745.4	745.4	745.4
<i>u</i> (calibration)	867.0	861.0	834.9	809.6	802.8	786.9	830.6	898.7
<i>u</i> (Mw)	891.3	870.2	851.7	824.8	819.3	813.2	879.7	929.4
Mw estimated	4994	6300	12,562	18,790	22,589	30,318	68,602	83,734
<i>U</i> (Mw) <sup>c</sup>	1782.6	1740.5	1703.4	1649.5	1638.7	1626.5	1759.5	1858.8
Mw (ASTRA) <sup>d</sup>	4688	5805	12,600	21,800	23,100	29,550	67,300	87,500

<sup>a</sup> M = monomer.

<sup>b</sup> D = dimer.

<sup>c</sup> Expanded uncertainty for  $k = 2$ .

<sup>d</sup> Mw estimated using ASTRA software.

The uncertainty associated with repeatability of routine samples,  $u(\text{repeat})$ , is similar in all proteins studied, although a higher value was obtained for the Spf66 peptide due to poor peak resolution, including baseline noise which blurs the base of peaks making it difficult for the integrator to identify the beginning and end of peaks [22]. However, there are some differences between  $u(\text{cal})$  values for those samples situated at the extremes of the calibration range. This can be attributed to the larger contribution arising from the prediction step, since  $u(\text{precision})$  is constant. Thus, low values of uncertainty are obtained when the interpolation is around the centroid. Thus, the carbonic anhydrase sample presents the smaller value. However, when the interpolation is performed far away from the centroid, the  $u(\text{pred})$  quickly increases as can be seen in Table 2.

To evaluate the different parameters affecting uncertainty due to quantification, a second design, called "B", was used (Fig. 2). In this case, 3 calibration standards (lysozyme, ovalbumin and bovine serum albumin monomer) were analysed for 2 days in duplicate. With this design, the number of standards is lower and the residual standard deviation higher; the linear response range is shorter and the centroid thus moves to higher values (32327.5–41165).

When applying this design to the rHGH sample, the estimated Mw was very close to those obtained with design A (Mw = 21,515 Da), since the slope did not differ from the value found for the first method, but the precision of the analytical procedure is the main source of uncertainty; the higher the uncertainty due to intermediate precision (283.4), the higher the uncertainty due to prediction (198.2), since this value depends on the amplitude of the linear range considered (Table 2). The expanded uncertainty, for  $k = 2$ , was 699.2 Da. This result implies a 53.9% increase in the 95% confidence limits with respect to design A, and that a decrease in the number of points on the calibration graph leads to a considerable increase in uncertainty. Also, the interpolations close to the limits of the calibration range produce a higher uncertainty  $u(\text{pred})$  than those obtained with the first procedure. For example, its relative contribution increased to 6.21% against an initial value of 2.93% for the Spf66 peptide.

When the peak areas ratio from two detectors was used to determine Mw, the ANOVA of the linear regression "peak area ratio versus calibration standard Mw" also confirmed the linearity of the method through rejection of the null hypothesis of lack of fit for  $\alpha = 0.05$ ; the R.S.D. was 1.99%. On the basis of the

experimental data, we can also say that the intercept is equal to zero ( $t(\text{calculated}) < t(\text{table})$  value). Therefore, the equation of the regression line was:

$$\text{Peak area ratio} = 6.868 \times 10^{-5} \times \text{Mw}; \quad r = 0.9993; \quad (n = 24)$$

and the root mean square error ( $S_{yx}$ ) was  $4.429 \times 10^{-2}$ .

At first, all the Mw estimated by this procedure are very close to those obtained using the peak height ratio, with no significant differences in comparison to the absolute Mw estimated by ASTRA software. Table 3 shows the contributions of the different uncertainty sources to the combined standard uncertainty when the results are expressed as peak area ratio. The main source is calibration, where the contribution of  $u(\text{pred})$  to the combined uncertainty is similar to those for the above method, whereas the uncertainty due to intermediate precision contributes most to the combined uncertainty. In this case, the time-different intermediate precision estimated in accordance with Eq. (11) was  $1.728 \times 10^{-3}$ , which is approximately seven times larger than the intermediate precision by peak heights. A more detail analysis shows that the variance between days obtained for both methods is of the same order of magnitude, whereas variance between measurements is 17 times greater by peak areas than heights.

This is to be expected since the peak area is significantly affected by flow-rate fluctuations, and especially by peak integration, introducing additional variability. Barwick has published two detailed reviews on factors affecting peak areas and heights in HPLC and its sources of uncertainty [23,24]. This was investigated by recording peak height and area for five replicate injections of a human serum albumin (HSA) sample, analysed over a short-time interval where variations in flow-rate can be negligible. In our situation, the definition of a baseline across the peak region can present a problem in estimating peak area since it was not perfectly resolved and therefore, the perpendicular drop and tangent-skin methods were used (Fig. 3). The peak area was obtained by summation, and the peak height from the maximum value with respect to the baseline (Table 4). The precision of the peak height measurements is better than that of peak area measurements, resulting in a loss of approximately 45%. In contrast, the precision of peak area measurements obtained using the drop method was significantly better than that obtained using the tangent-skin method, approximately by a factor

**Table 4**

Effect of the limits of integration on the peak area and height measured for the human serum albumin sample.

Sample	Integration limits (min)	Peak area by drop method			Peak area by tangent-skin method			Peak heights			
		LS signal	RI signal	Ratio	LS signal	RI signal	Ratio	Integration limits (min) <sup>a</sup>	LS signal	RI signal	Ratio
1	9.20–10.90	0.1452	0.03084	4.710	0.1278	0.02715	4.708	7.20–11.0	0.3447	0.06615	5.210
2	9.30–10.90	0.1435	0.03057	4.695	0.1235	0.02631	4.695	7.25–10.95	0.3453	0.06620	5.216
3	9.30–10.85	0.1449	0.03077	4.709	0.1252	0.02661	4.705	7.20–11.0	0.3465	0.06658	5.205
4	9.25–10.85	0.1442	0.03068	4.700	0.1261	0.02655	4.750	7.20–10.95	0.3473	0.06629	5.240
5	9.2–10.95	0.1462	0.03082	4.745	0.1254	0.02684	4.671	7.25–11.0	0.3452	0.06659	5.184
Mean		0.1448	0.03074	4.712	0.1256	0.02669	4.706		0.3458	0.06636	5.211
S.D.		$1.031 \times 10^{-3}$	$1.112 \times 10^{-4}$	0.0195	$1.557 \times 10^{-3}$	$3.179 \times 10^{-4}$	0.0288		$1.094 \times 10^{-3}$	$2.091 \times 10^{-4}$	0.0202
C.V. (%)		0.71	0.36	0.41	1.24	1.19	0.61		0.32	0.31	0.39

<sup>a</sup> Integration limits used to establish the baseline.

of 2, although the relative error in peak area estimated was less than 13.5%. Thus, the decision of when to start and stop the integration has a greater effect on the recorded area.

This variability in peak area measurements is also transferred to  $u(\text{repeat})$ , since a value of 163.5 Da was obtained for the rHGH sample ( $n=3$ ). The combined uncertainty of the result is 642.8 Da, the intermediate precision uncertainty (605.2) being the major contributing factor, whereas the expanded uncertainty, using a coverage factor  $k=2$ , is then:  $U(\text{Mw})=1285.7$  Da, so the Mw calculated is  $22569.5 \pm 1285.7$  Da.

On the other hand, design B provides almost the same results. Fig. 4 shows the relative contributions of the different sources of uncertainty to the combined uncertainty for the rHGH and human insulin monomer samples, where the uncertainty due to precision is greater. This gives the combined uncertainty a high value with regard to the rest of the conditions, although the uncertainty due to prediction is still significant. The expanded uncertainty calculated for  $k=2$  was 1638.7; so the Mw calculated for rHGH was  $22,589 \pm 1638.7$  Da. This result was not unexpected since the results obtained using different methods are strongly correlated with each

other most of the uncertainty components influence both results in the same direction but with different magnitude, according to the nature of the design used.

### 3.3. Reproducibility of the methods

A study was conducted to assess the reproducibility of the peak height method, denoted by “new method”, and to compare it to ASTRA, denoted by “reference method”. The proposed guidelines for such validation require the specification of permissible losses in precision and accuracy. Thus, the reproducibility can be accepted for the studied proteins if the  $100(1-\alpha)\%$  lower confidence limit is greater than or equal to  $p_{c.a.}$ , namely the least acceptable  $p_{c.a.}$  [12]. This value is calculated in function of the precision ( $p$ ), assuming a  $100x\%$  loss in precision and accuracy ( $C_b$ ).

$$p_{c.a.} = \sqrt{p^2 - x} \cdot C_b \quad (17)$$

The sample concordance correlation coefficient was 0.9987 with the 95% lower confidence limit of 0.9970. Given the small amount of

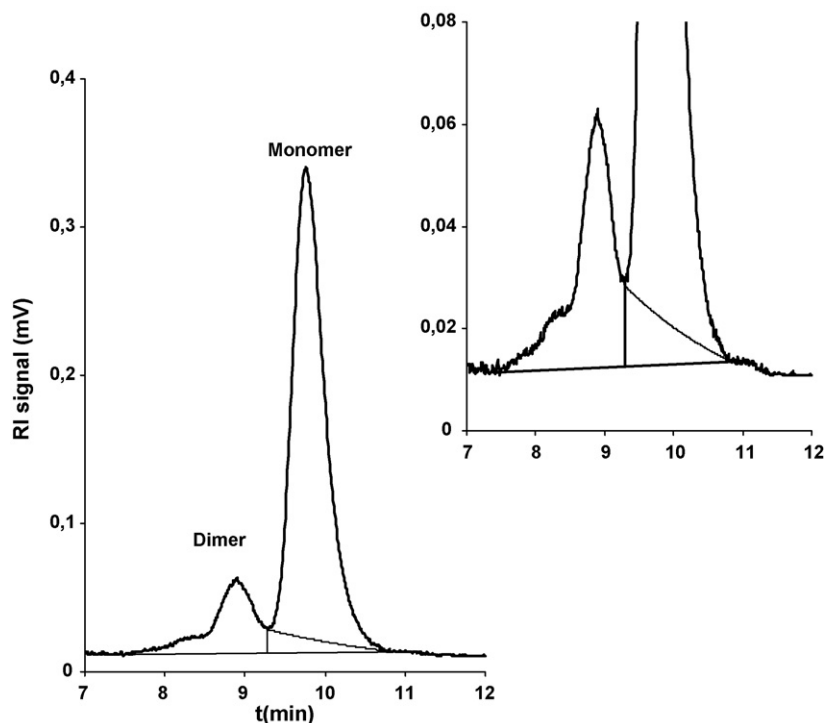


**Fig. 3.** Effect of definition of the baseline in measured peak area. The mean difference between the tangent-skin and perpendicular drop methods for human serum albumin sample was around 12%.

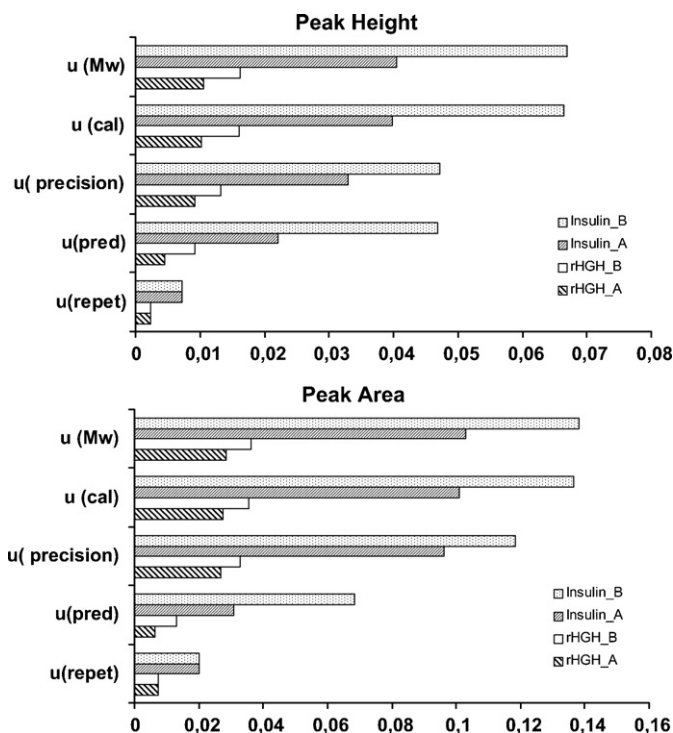


**Fig. 4.** Relative contribution of the different sources of uncertainty to the combined uncertainty as a function of both the method and design used. The parameters affecting the uncertainty due to calibration and from assessment of accuracy were higher for the peak area method than for peak height especially for those samples situated at the calibration range extremes, e.g. human insulin.

within-sample variation in both methods, the peak height method was assumed to explain 99% ( $p = 0.995$ ) of ASTRA (precision), and without loss in precision ( $x = 0.0$ ), these conditions yield the least acceptable  $p_{c.a.}$  of 0.9946. This result shows the reproducibility of both methods since the 95% lower confidence limit was much greater than the least acceptable  $p_{c.a.}$  Also, an excellent precision ( $p = 0.9991$ ), with minimum location shift ( $u = 3.335 \times 10^{-3}$ ) and scale shift ( $v = 1.011$ ) were observed, the coefficient of variation being 3.88%.

Only when a precision of 99% ( $p = 0.995$ ) and a 1% loss in precision ( $x = 0.01$ ) were assumed, the peak area method was judged to reproduce ASTRA since its 95% lower confidence limit is much greater than the least acceptable  $p_{c.a.}$  ( $0.9925 > 0.9885$ ). Also, the coefficient of variation was slightly greater than 5%, although one might decide that a CV of 5.42% is acceptable or not.

In a second study, the peak area method is compared to the peak height method used as reference method; the results clearly show high reproducibility in all terms, as seen in Table 5.

**Table 5**  
Statistical analysis to evaluate the reproducibility of different methods using the concordance correlation coefficient.

Parameter	ASTRA/height	ASTRA/area	Height/area
$p_c$	0.9987	0.9968	0.9992
95% CI <sup>a</sup>	0.9994–0.9970	0.9986–0.9925	0.9997–0.9982
$u^b$	$3.335 \times 10^{-4}$	$1.623 \times 10^{-3}$	$4.664 \times 10^{-4}$
$v$	1.022	1.038	0.9854
$C_b$	0.9996	0.9985	0.9997
$p$	0.9991	0.9983	0.9996
C.V.	3.88%	5.42%	2.66%
$p_{c.a.}$	0.9946 <sup>b</sup>	0.9885 <sup>c</sup>	0.9946 <sup>b</sup>

<sup>a</sup> Confidence interval for  $p_c$ .

<sup>b</sup> Assuming a precision ( $p$ ) = 99% and a precision loss ( $x$ ) = 0%.

<sup>c</sup> Assuming a precision ( $p$ ) = 99% and a precision loss ( $x$ ) = 1%.

## 4. Conclusions

This paper analyses uncertainty in size-exclusion chromatography in the two-detector method using LS and RI detection. The uncertainty in Mw values obtained from use of the ratio of peak height or area from two detectors was contrasted. For this, the main uncertainty sources associated with the two approaches used to determine Mw were identified, quantified and combined. Given the measurement of interest is not measured directly, but it is calculated from peak height or area ratio from two detector, the signal ratio uncertainty must be calculated using the random propagation of error formula. In this case, the effect of signal correlation was evaluated in order to avoid uncertainty overestimation when the correlation is neglected due to any signal ratio is not just a function of signal variance but of their covariance too. The information generated in assessing the precision of analytical procedures is used to calculate the uncertainty without involving extra work. The intermediate precision uncertainty contributed most significantly to the combined uncertainty, followed by that arising from calibration (more specifically from prediction) and then repeatability.

The Mw estimated by the peak area ratio procedures are very close to those obtained using the peak height ratio, although the combined uncertainty is higher ( $\approx 3$  times) due to the peak area is significantly affected by peak integration form, introducing additional variability which is transferred to other uncertainty sources such as repeatability and precision.

The reproducibility of both methods was evaluated and verified using the concordance correlation coefficient. The reproducibility of both methods was accepted by assuming a precision of 99% and a 1% loss in precision using ASTRA as reference.

The main benefits of these methods are therefore their practical simplicity, and universal application to estimate the peptides and proteins Mw containing carbohydrates or not, providing similar results to those obtained with the ASTRA method with the advantages that it is not necessary to know the specific refractive index for the protein and instruments calibration constants, parameters that are otherwise needed to determine Mw using commercial software.

## Acknowledgment

This work was financed by the Fondo de Investigación de la Seguridad Social, Spain as part of project PI 061804.

## References

- [1] J. Wen, T. Arakawa, J.S. Philo, Anal. Biochem. 240 (1996) 155.
- [2] T. Arakawa, J. Wen, Anal. Biochem. 299 (2001) 158.
- [3] E. Foltá-Stogniew, K.R. Williams, J. Biomol. Tech. 10 (1999) 51.
- [4] A. Oliva, M. Llabres, J.B. Fariña, J. Pharm. Biomed. Anal. 25 (2001) 833.
- [5] B.S. Kendrick, B.A. Kerwin, B.S. Chang, J.S. Philo, Anal. Biochem. 299 (2001) 136.
- [6] P.J. Wyatt, Anal. Chim. Acta 272 (1993) 1.
- [7] G. Dollinger, B. Cunico, M. Kunitani, D. Johnson, R. Jones, J. Chromatogr. 592 (1992) 215.
- [8] A. Oliva, J.B. Farina, M. Llabres, Anal. Chim. Acta 512 (2004) 103.
- [9] S.L.R. Ellison, M. Rösslein, A. Williams (Eds.), EURACHEM/CITAC Guide, Quantifying Uncertainty in Analytical Measurement, second ed., 2000.
- [10] EN ISO/IEC 17025, General requirements for the competence of testing and calibration laboratories, CEN Management Centre, Brussels, 2005.
- [11] L.I.-K. Lin, Biometrics 45 (1989) 255.
- [12] L.I.-K. Lin, Biometrics 48 (1992) 599.
- [13] S. Wolfram, MATHEMATICA: A System for Doing Mathematics by Computer, Addison-Wesley, Redwood City, CA, 1988.
- [14] J.R. Taylor, An Introduction to Error Analysis, 2nd ed., Univ. Science Books, Sausalito, CA, 1997.
- [15] Guide to the Expression of Uncertainty in Measurement, 2nd ed., International Organization for Standardization, Geneva, 1995.
- [16] A. Maroto, R. Boqué, J. Riu, F.X. Rius, Anal. Chim. Acta 446 (2001) 131.
- [17] J. Galbán, C. Uribe, Talanta 71 (2007) 1339.
- [18] G. Bagur, M. Sánchez-Viñas, D. Gázquez, M. Ortega, R. Romero, Talanta 66 (2005) 1168.
- [19] M. Thompson, S.L.R. Ellison, R. Wood, Harmonized Guideline for Single-Laboratory Validation of Methods of Analysis, IUPAC Technical Report, Pure Appl. Chem. 74 (2002) 835.

- [20] ISO 8466, Calibration and Evaluation of Analytical Methods and Estimation of Performance Characteristics (I & II), International Organization for Standardization (ISO), Geneva, 1990 and 1993.
- [21] L. Cuadros-Rodríguez, M.G. Bagur-González, M. Sánchez-Viñas, A. González-Casado, A.M. Gómez-Sáez, J. Chromatogr. A 1158 (2007) 33.
- [22] A. Santoveña, A. Oliva, F. Guzman, M.E. Patarroyo, M. Llabres, J.B. Fariña, J. Chromatogr. B 766 (2002) 3.
- [23] V.J. Barwick, J. Chromatogr. A 849 (1999) 13.
- [24] V.J. Barwick, S.L.R. Ellison, C.L. Lucking, M.J. Burn, J. Chromatogr. A 918 (2001) 267.



## Reductive decomposition of a diazonium intermediate by dithiothreitol affects the determination of NOS turnover rates

Indika N. Perera, Talal Sabbagh, Jean A. Boutros, Mekki Bayachou\*

Department of Chemistry SR 397, Cleveland State University, 2399 Euclid Avenue, Cleveland, OH 44115, United States

### ARTICLE INFO

#### Article history:

Received 24 June 2008

Received in revised form 24 December 2008

Accepted 30 December 2008

Available online 23 January 2009

#### Keywords:

Griess assay

Diazonium

Dithiothreitol

Nitric oxide synthase

Turnover

External calibration

Standard addition

### ABSTRACT

Accurate determination of nitrite either as such or as the breakdown product of nitric oxide (NO) is critical in a host of enzymatic reactions in various settings addressing structure–function relationships, as well as mechanisms and kinetics of molecular operation of enzymes. The most common way to quantify nitrite, for instance in nitric oxide synthase (NOS) mechanistic investigations, is the spectrophotometric assay based on the Griess reaction through external standard calibration. This assay is based on a two-step diazotization reaction, in which a cationic diazonium derivative of sulfanilamide is formed as intermediate before the final absorbing azo-product. We show that this intermediate is very sensitive to reducing agents that may be transferred from the reaction media under investigation. The interaction of this vital intermediate with the reducing agent, dithiothreitol (DTT), which is widely used in NOS reactions, is characterized by both electrochemical and spectroscopic means. The effect of DTT on the performance of external calibration, both in sample recovery studies and in actual NOS reactions, is presented. Finally an alternative method of standard additions, which partially compensates for the accuracy and sensitivity problems of external calibration, is proposed and discussed.

© 2009 Elsevier B.V. All rights reserved.

### 1. Introduction

Determination of trace amounts of nitrite is crucial in a number of mechanistic and kinetic investigations addressing structure–function of enzymes. Examples include investigations addressing mechanisms and kinetics of the molecular function of enzymes such as Nitrite Reductases (NiR) [1] and nitric oxide synthases (NOS) [2]. In the latter case, accurate determination of nitrite ( $\text{NO}_2^-$ ) as a breakdown product of nitric oxide (NO) is of particular importance in current investigations, which aim to understand the molecular function of NOS enzymes. Nitric oxide synthases are heme enzymes that catalyze the *in vivo* synthesis of nitric oxide, a diatomic molecule that was found to mediate numerous physiological processes and is involved in the development of a host of pathological states [3]. NO is involved in vasodilation, neurotransmission, cytotoxicity, and cytoprotective processes [4,5]. It is biosynthesized by enzymatic oxidation of one terminal guanidine-nitrogen of the amino acid *L*-arginine through the *N*-hydroxy-*L*-arginine intermediate, yielding *L*-citrulline as a co-product (Scheme 1).

Although several methods have been developed to determine the NOS turnovers [6–8], NO is often quantified in the form of

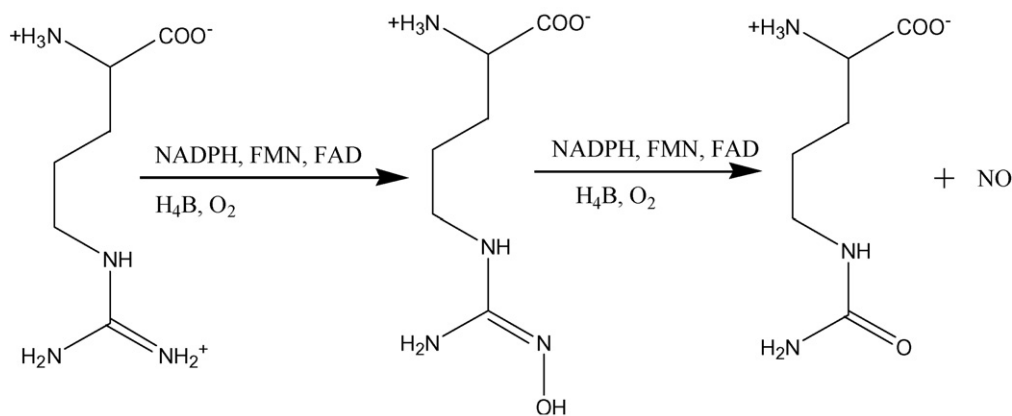
nitrite ( $\text{NO}_2^-$ ), a stable breakdown product of NO in aerobic reaction media. Various methods are employed to quantify nitrite accurately especially in biological samples [9–13]. The most commonly used technique to quantify nitrite in NOS mechanistic investigations is using a spectrophotometric assay based on the Griess reaction through a standard calibration curve [14,15]. This assay is based on a two-step diazotization reaction in which acidified nitrite produces a nitrosating agent which reacts with sulfanilamide to produce the diazonium derivative. The diazonium ion is then coupled to *N*-1-naphthylethylenediamine dihydrochloride (NED) to stoichiometrically form the final azo-product which absorbs at 540 nm (Supporting information, Scheme S1). The Griess assay is widely used to determine nitrite in a variety of biological and experimental matrices such as plasma, serum, urine, and tissue culture media [16–18]. However, serious accuracy problems may arise in the presence of interfering agents, especially if these are not taken into account during the external calibration. It has been already reported that the NOS enzyme itself spectrally interferes with the final product of Griess assay [19]. The NADPH, an essential cofactor in NOS reaction, is also a known interferent in the Griess assay [20]. John Moody and Shaw recently published a reevaluation study of the Griess assay in terms of the extent of interference brought by nicotinamide nucleotides in the assay medium [21]. A prior review by Fox and Suhre documented interferences by a number of agents including thiols [22].

Accurate quantification of nitrite is critical for reliable determination of NOS turnover and other kinetic aspects; it thus can affect

\* Corresponding author. Tel.: +1 216 875 9716; fax: +1 216 687 9298.

E-mail address: [m.bayachou@csuohio.edu](mailto:m.bayachou@csuohio.edu) (M. Bayachou).





**Scheme 1.** Enzymatic synthesis of nitric oxide by NOS enzymes; the reaction uses L-arginine as a substrate and oxygen as co-substrate. NADPH, FAD, FMN, and tetrahydropterin are also necessary for the NOS function.

all derived mechanistic/kinetic interpretations. The cationic diazonium intermediate that forms during the first step of the Griess assay is vulnerable towards most reducing agents in the assay medium, especially dithiothreitol (DTT), which is widely used in NOS reactions. The interaction between diazonium intermediate and DTT, especially when present in high concentrations (0.5 mM or higher), results in a critically low yield for final azo-compound, which seriously affects the sensitivity of the method. This, in turn, leads to serious limitations for nitrite determination especially in the low concentration range (i.e. 2.5–10  $\mu\text{M}$ ), where important mechanistic information is usually derived through measurement of initial rates.

In this work, we probe the nature of critical interaction of the diazonium intermediate with DTT as a reducing agent using electrochemical and spectrophotometric techniques. The study also explores how DTT concentration affects the sensitivity of the Griess assay for nitrite determination, even when matrix correction (i.e. using DTT in standards) is used in the external calibration method. The study further investigates possibilities to minimize the matrix difference to achieve high accuracy and sensitivity using standard addition method.

## 2. Experimental

### 2.1. Reagents

All the chemicals used were of analytical grade. Nanopure deionized water (specific resistance > 18.2  $\Omega\text{ cm}$ ) used in all experiments was supplied by a Barnstead water purification system. All working solutions of nitrite were prepared using 0.1 M standard nitrite solution. Dithiothreitol and NADPH were purchased from Sigma. The Griess reagent kit was purchased from Promega (Madison, WI) and was used following the technical instructions provided. Briefly, the analyte solution is incubated with sulfanilamide first for 10–15 min, followed by the addition of NED (10–15 min), and the absorbance of the final azo dye ( $\lambda_{\text{max}}$  at 540 nm) is recorded. It is worth mentioning the concentration of the Griess ingredients in the stock solutions of the kit. Based on the chemical specifications on the Promega kit, the concentration of sulfanilamide solution is 58 mM while the NED solution is at 3.9 mM. These concentrations ensure that the Griess assay ingredients are always in excess compared to the nitrite analyte.

### 2.2. Apparatus

UV–vis absorbance spectra were recorded on Agilent 8453 spectrophotometer. Spectra were collected between 400 and 650 nm.

Cyclic voltammetry was performed in a standard three-electrode cell using a BAS100W electrochemical workstation (Bioanalytical Systems Inc.). A gold working electrode (CHI, Area = 0.0314  $\text{cm}^2$ ) was polished with alumina slurry (successively with 0.3 and 0.05  $\mu\text{m}$ ), and cleaned in ultrasound bath in deionized water.

### 2.3. Electrochemical measurements

All electrochemical measurements were carried out in nitrogen purged 0.05 M NaCl solution. The solutions were stirred between the cyclic voltammetric experiments; all potential are reported versus the Ag/AgCl reference electrode. After each scan in solutions of diazonium ions, the working electrode was cleaned with piranha solution (70%  $\text{H}_2\text{SO}_4$  and 30%  $\text{H}_2\text{O}_2$ ) and polished as described above.

### 2.4. Procedure for calibration curves

The Griess assay used widely is a two-step process. First the analyte aliquot is incubated for 15 min with an excess sulfanilamide to generate the diazonium cation. NED (in excess of the diazonium cation formed) is then added to the assay medium and the color is allowed to develop. Absorbance is recorded after exactly 15 min of reaction time. Calibration curves were constructed for the range of 2.5–15  $\mu\text{M}$  nitrite; standards were prepared using 0.1 M nitrite stock solution. 500  $\mu\text{L}$ -aliquots of standards are incubated for 15 min each with 100  $\mu\text{L}$  sulfanilamide and 100  $\mu\text{L}$  NED. Deionized water is added up to 1.00 mL and absorbance measurement taken at 540 nm.

To evaluate the matrix effect, samples for recovery studies are prepared by mixing various amounts of nitrite and DTT (from 1 mM working solutions) and diluting with deionized water to 1.00 mL. 500  $\mu\text{L}$  aliquots of each unknown were incubated for 15 min with 100  $\mu\text{L}$  sulfanilamide followed by 100  $\mu\text{L}$  NED and diluted with deionized water to 1.00 mL. The absorbance is then measured and the nitrite amount is quantified using a suitable calibration curve.

### 2.5. Procedure for standard addition method

Samples containing two different concentrations of nitrite (3 and 6  $\mu\text{M}$ , prepared from a 0.1 M stock solution just as we did for the regular calibration method) in the presence of three representative concentrations of DTT (0.0, 0.4, and 1.0 mM) were prepared, giving a total of six test solutions. The total volume of each sample analyzed was 3.00 mL. The range of nitrite concentration in these working samples was selected based on actual ranges used in NOS reaction investigations. Each test solution was divided into

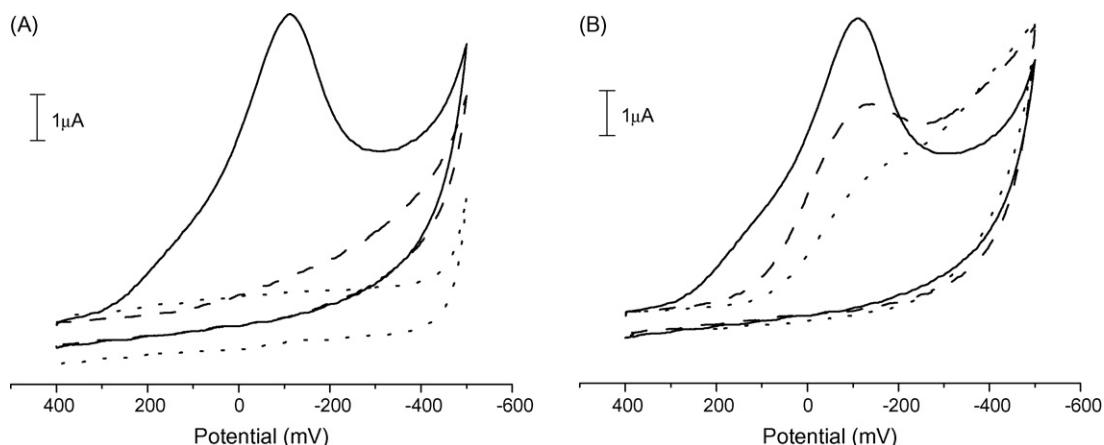


**Fig. 1.** (A) Comparison of cyclic voltammograms obtained for diazonium intermediate formed *in situ* by adding 0.5 mM nitrite to 0.5 mM sulfanilamide. (...) Background voltammogram of sulfanilamide only; (—) 1st voltammetric scan after addition of nitrite; (---) 2nd scan after addition. (B) Voltammetric response of 0.5 mM diazonium ion formed *in situ* in absence (—) and presence of 0.5 mM DTT (---) and 1.0 mM DTT (...); all voltammograms are first scans.

six 0.50-mL aliquots. Then known amounts of nitrite standard were successively spiked into each vial followed by appropriate amounts of the Griess assay reagents (i.e. sulfanilamide and NED solutions). The mixtures were incubated for 15 min. The resulting solutions are then diluted to 1.00 mL with deionized water. Nitrite concentration in each sample was then quantified using known procedures of standard addition method by measuring the absorbance at 540 nm. All results presented, unless otherwise mentioned, are averages of triplicate trials. Results are reported as averages of replicate trials  $\pm$  standard deviation.

## 2.6. NOS assays

The second step of the NOS reaction, i.e. the conversion of *N*-hydroxy-*L*-arginine (NHA) to *L*-citrulline and NO, is generally used in NOS mechanistic investigations and was similarly used here to test the performance of various methods in nitrite quantification. The NOS reaction of this step is facilitated by addition of H<sub>2</sub>O<sub>2</sub>. For validation, three different test samples with three different DTT concentrations, 0, 0.4 and 1 mM, were prepared in pH 7.4 HEPES buffer, each containing 0.1 mM NHA and 10  $\mu$ M H<sub>2</sub>B. 300- $\mu$ L aliquots of each test solution were put in small reaction tubes fitted on a heating block; the tubes were kept 15 min at 37 °C. 5  $\mu$ L of purified iNOS-oxygenase domain (iNOSoxy, 22  $\mu$ M) were then added to the reaction vials. The solutions were kept for another 5 min at 37 °C. The NOS reaction is started by adding 0.25  $\mu$ L of 50 wt.% H<sub>2</sub>O<sub>2</sub> and allowed to proceed for 20 min at 37 °C. The reactions were quenched by adding 100  $\mu$ L ice-cold deionized water into the reaction vessels and stored in ice for calibration and standard addition measurements. All results presented, unless otherwise mentioned, are averages of triplicate trials. Results are reported as averages of replicate trials  $\pm$  standard deviation.

## 3. Results and discussions

### 3.1. Electrochemical results

In the first step of the Griess assay, sulfanilamide, under acidic conditions, reacts with nitrite to form *sulphanilamide-diazonium* intermediate. Most diazonium derivatives can be reduced electrochemically within the potential window of +300 to -500 mV versus Ag/AgCl [23–25].

Fig. 1A shows the cyclic voltammogram for the reduction of *sulphanilamide-diazonium* ion formed *in situ*. The voltammetric signature in the form of the irreversible reduction peak near -100 mV

shows quantitative formation of the diazonium derivative upon reaction of sulfanilamide with added nitrite under acidic conditions. A number of diazonium derivatives have been shown to form in similar conditions, and can be electrochemically reduced to graft the electrode surface in question [23]. Pure sulfanilamide does not give this electrochemical response. Also, the irreversible reduction wave in Fig. 1A exhibits a general behavior characteristic of the electrochemical behavior of aryl-diazonium derivatives in that the first scan generates highly reactive aryl radicals which attach to the electrode surface and prevent direct electrochemical reduction during subsequent cycles. As a result, and unless the electrode surface is thoroughly cleaned and polished, second and subsequent cycles do not show any reduction (Fig. 1A). This typical behavior is another indicator pointing to the formation of the sulfanilamide diazonium derivative upon nitrite addition.

The diazonium intermediate that forms during the first step of the Griess assay is vulnerable towards most reducing agents, especially dithiothreitol, which is widely used in media for NOS reactions [16,26]. Fig. 1B shows the effect of DTT concentrations on the *sulphanilamide-diazonium* intermediate. All scans in Fig. 1B are first scans only, after which the electrode is thoroughly cleaned and polished. Increasing the concentration of DTT from 0.5 to 1.0 mM significantly decreases the diazonium reduction current. The addition of a large excess (>10 mM) of DTT destroys completely the diazonium intermediate as evidenced by total disappearance of its reduction peak (results not shown).

### 3.2. UV-vis spectroscopic results

Diazonium intermediates frequently absorb at or around 375 nm [19]. Fig. 2A shows the location of the absorption band corresponding to the *sulphanilamide-diazonium* ion formed *in situ* upon addition of 0.1 mM nitrite to sulfanilamide; the absorbance was measured at regular time intervals. An absorption band at 365 nm appears within 5 min of nitrite addition. The absorption continues to increase steadily through the first 15 min and then stabilizes as a result of nitrite depletion.

The interaction of DTT with the diazonium intermediate of the Griess assay can also be monitored using absorbance spectroscopy. Addition of 0.5 mM DTT to the diazonium derivative first gives rise to a transient peak that is slightly red-shifted, which then decays over few minutes with an isosbestic point at 406 nm (Fig. 2B). The transient peak corresponds likely to a preliminary association complex between DTT and the diazonium ion, an association that serves as a preamble to internal electron transfer which then decom-

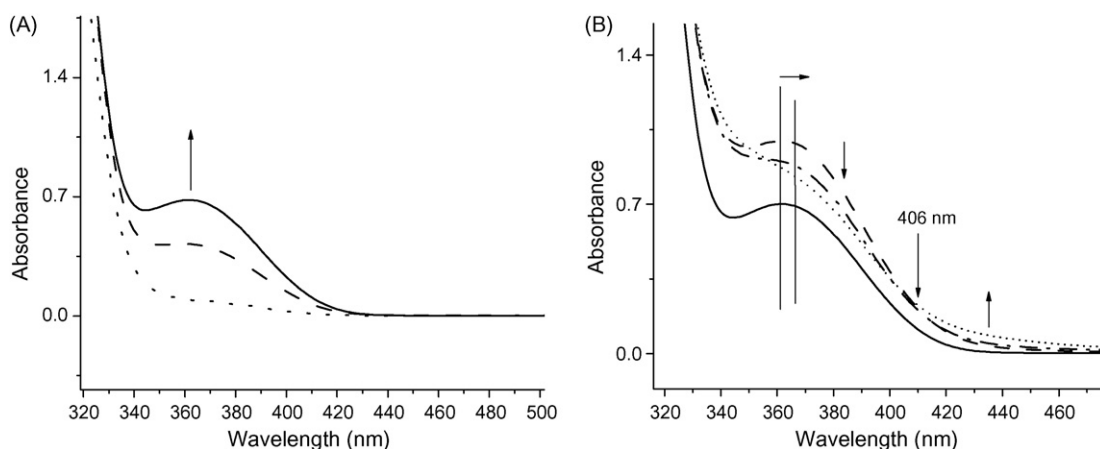


**Fig. 2.** (A) Formation of the sulfanilamide-diazonium derivative *in situ* as a function of time at 20 s (· · ·), 5 min (---) and 15 min (—). (B) Diazonium derivative in absence (—) and presence of DTT immediately at 30 s (---) and after 1 min (· · ·), and 5 min (— · —); note the slightly red-shifted transient peak that appears upon addition of DTT.

poses the diazonium derivative. The decomposition observed with absorbance spectroscopy is consistent with our electrochemical results, which show decrease of the diazonium derivative upon addition of DTT. The decomposition of the diazonium derivative is the result of electron transfer from the reducing thiol (DTT).

### 3.3. Effect of DTT on the slope of the calibration curve

Fig. 3 shows how the sensitivity of the Griess assay using external calibration is affected by the presence of increasing amounts of DTT in nitrite standards. The series of curves unequivocally show that as the concentration of DTT increases, a marked decrease in the slope of the linear calibration results. The presence of DTT greatly affects the level of absorptivity at 540 nm of the final azo-compound produced by the Griess reagents in the presence of nitrite. The decrease in absorptivity is proportional to the concentration of DTT present as shown by the inset in Fig. 3. The effect of DTT on the slope of the Griess calibration curve is rationalized in terms of its effect on the initial cationic diazonium derivative of the two-step assay. However, we need to point out at this point that it is conceivable that DTT, as a dithiol species, may react directly with nitrite to form a mono- and/or di-nitroso-DTT derivatives, which may also contribute to the decreased absorbance of the final azo-compound. To test for this possibility, we have conducted experiments in which we varied the order and the time of addition of DTT (i.e. before or

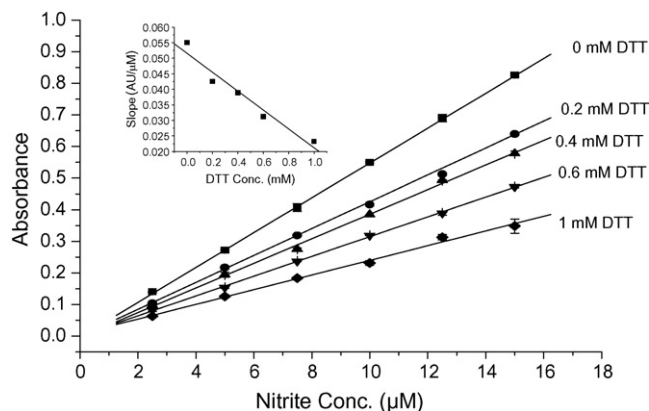


**Fig. 3.** Effect of DTT concentration on the slope of the calibration curve of the Griess assay. Numbers next to the curves indicate the corresponding DTT concentration in the assay medium; Data points reported as averages  $\pm$  standard deviation. Inset: plot of assay sensitivity (absorbance units per  $\mu\text{M}$  of nitrite) as a function of DTT concentration.

after formation of the cationic intermediate) and comparing final absorbances in both cases, we unequivocally show that this reaction, if any, does not contribute to the loss of the final absorbing compound in the Griess assay (Supporting information, Figure S1). In addition, we show that the reaction of a simpler diazonium cation (para-nitrobenzene diazonium) formed and purified in conditions similar to the first step of the Griess (i.e. reaction of the amine form with nitrite under acidic conditions) takes place quantitatively with added DTT and yields the disulfide (i.e. the oxidized) form (Supporting information, Figure S2).

It is important to note that varying times (10, 15, 20 min) of interaction of DTT (with nitrite and with the Griess cationic intermediate) do not change the conclusion of our findings, and always show that the primary interaction of DTT that accounts for the loss of the final azo dye is with the cationic intermediate of the first step of the Griess assay.

These observations are consistent with our electrochemical and spectroscopic results pointing to the reductive decomposition of the initial diazonium-sulfanilamide cation upon addition of the reducing agent DTT. It is important to mention that the concentrations of DTT in NOS reaction media that we used here are typical

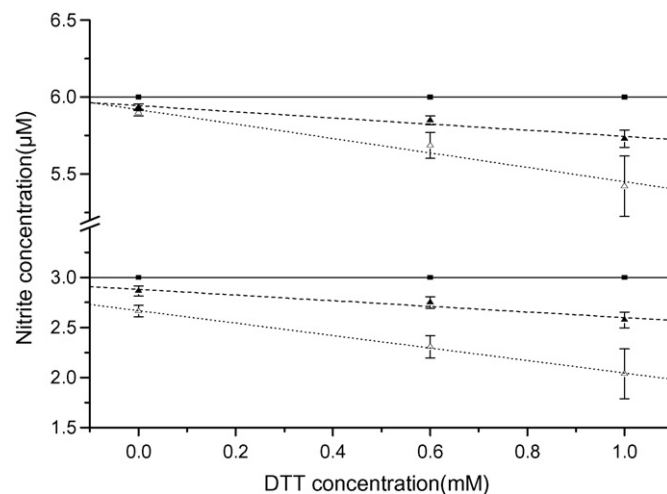


**Fig. 4.** Comparison of values obtained from calibration and standard addition methods for two levels of nitrite as working “unknowns” in the presence of different DTT concentrations. Expected values for the two concentrations (solid line with solid squares) are to be compared with recovered values using standard addition (dashed line with solid triangles) and calibration (dotted line with open triangles). Data points reported as averages of triplicate trials  $\pm$  standard deviation.

concentrations used in NOS investigations [16,26]. These observations indicate that the response of the Griess assay is compromised as the concentration of DTT increases. This effect is significant with concentrations of DTT as small as 0.2 mM for the micromolar range of nitrite (or nitric oxide) routinely encountered in NOS investigations. In addition, the series shows that the 1-mM concentration level of DTT, usually used in reaction media supporting NOS reactions, depresses the response of the assay by over 44%.

The decrease of the response of the Griess assay as a result of DTT presence in reaction media results in significant discrepancy between true nitrite concentrations and quantities determined from the Griess assay using blind external calibration curves, even when DTT is taken into account. In fact, the concentration of DTT, being a sacrificial reducing agent in the enzyme buffer medium, is generally not known accurately at the time of the assay. In addition, even if the concentration can be estimated, as we show in Fig. 3, the sensitivity of the assay (slope of the linear curve) is seriously depressed at higher DTT concentration which will affect the evaluation of lower nitrite concentrations (or NO in the case of NOS reaction) encountered in experiments at limited enzyme turnovers, where lower nitrite (or nitric oxide) concentrations are encountered. Other differences between media used to construct calibration curves for the Griess assay and the samples matrix also affect the accuracy of the results. For instance, in the case of the NOS reaction, slight differences in the concentration of NADPH, another reducing agent that can interact with the diazonium intermediate [21], also result in noticeable discrepancies in analyte recovery tests. Together, these results show that blind external calibrations yield large errors in the determination of nitrite and, thus, of nitric oxide in the case of NOS reaction, particularly at low concentrations such as those encountered under initial rates settings. The large concentration errors caused by DTT would significantly affect derived kinetic and mechanistic interpretations.

#### 3.4. Comparison of the performance for calibration and standard addition methods

Because the presence of DTT changes the accuracy and sensitivity of the Griess assay, we examined whether the method of standard additions would better reproduce nitrite concentrations compared to the method using external calibration [19].

The calibration method shows significant deviations from actual sample values at 3.0 and 6.0  $\mu\text{M}$  levels in the presence of increasing concentrations of DTT. It is important to note that the working

solutions of nitrite mixed with DTT are prepared fresh and used on the spot for the calibration and standard additions [27]. The poor analyte recovery is particularly worse for high DTT concentrations and/or low nitrite concentrations (Fig. 4). As for standard addition method, although it does not entirely eliminate the matrix effect, it has a remarkable performance compared to external calibration, especially if one considers the level of DTT interference present in the assay. One of the attributes of the procedure of standard addition, because it uses spiked analyte samples, is the fact that it averages the depressing effect of DTT at various nitrite concentrations, and actually gives weight to the relatively lower effect of DTT observed at higher nitrite concentrations. The resulting observed effect of DTT present in the analyte sample is smaller than in the original non-spiked sample. However, this method, although it decreases the effect of DTT, will not completely eliminate it because there will be always a finite level of reaction of DTT with the diazonium cation generated in the first step of the Griess assay. Methods aiming at eliminating the interference by background thiols in cases such as measurement of S-nitrosothiols in biological samples are known; these include an alkylation step of interfering thiols in the medium by *N*-ethylmaleimide (NEM) during sample preparation [28,29]. Conceivably, this alkylation method can also be used here to minimize or eliminate the reducing effect of thiols such as DTT in the Griess assay. However, this extra step is not typically used in Griess assays performed in the context of investigation of NOS enzymatic reactions. The standard additions method as shown here significantly minimizes the DTT interference. Despite a certain level of observed deviations from actual concentrations, the method is still far more reliable than blind external calibration when DTT and other potential interferences are involved. In addition, contrary to matrix-corrected external calibration (i.e. with the attempt to compensate for a known level of DTT), the exact level of DTT in the test solution does not need to be known for standard additions method [19].

#### 3.5. Effect of DTT on the determination of NOS turnover using the Griess assay

In this section we wanted to evaluate the effect of various levels of DTT on actual NOS turnover rates through measurements of NO produced. The catalytic oxidation of *N*-hydroxy-L-arginine by inducible NOS oxygenase (iNOSoxy) results in nitric oxide production which is measured under the conditions described in Section 2. The NO produced is evaluated through measurement of nitrite

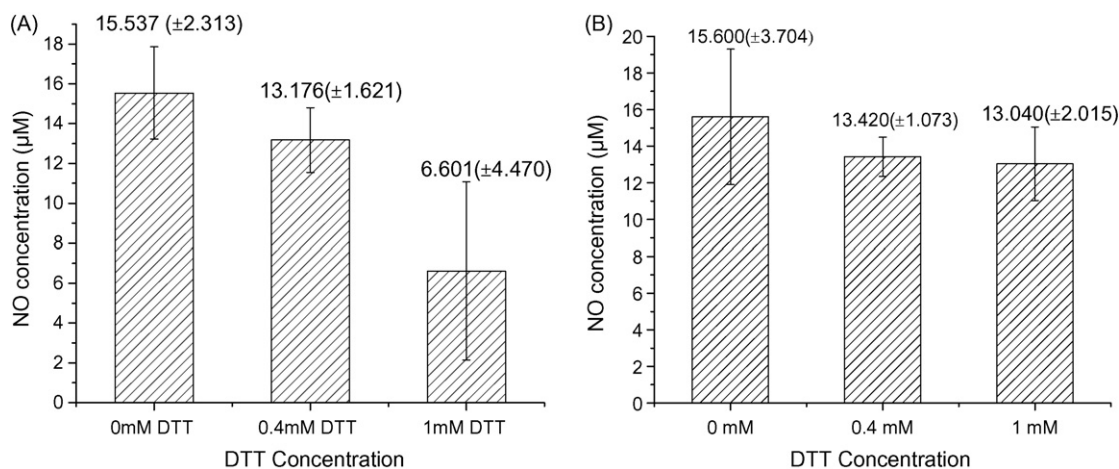


**Fig. 5.** (A) NO production by iNOSoxy after 20-min reaction periods in the presence of different DTT concentrations. NO levels were calculated from external calibration curves using the Griess assay. Error bars indicate  $\pm$  standard deviation. (B) NO production by iNOSoxy after 20-min reaction periods in the presence of different DTT concentrations. NO levels were measured using standard addition method and the Griess assay. Error bars indicate  $\pm$  standard deviation.

using the Griess assay and suitable calibration curves. Fig. 5A shows that the level of DTT in the enzymatic reaction medium affects seriously the findings of the Griess assay and, thus, NOS turnover determination. The amount of NO measured becomes significantly lower as the concentration of DTT in the NOS reaction medium increases (Fig. 5A).

The increasing levels of DTT transferred from the reaction medium to the assay medium likely contribute to greater degradation of the sulfanilamide diazonium intermediate of the Griess assay, which, in turn, results in lower apparent NO concentrations. In addition to accuracy, the standard deviation of nitric oxide determination is also affected (see error bars on chart, Fig. 5A) at high levels of DTT (~1 mM), where the concentration of the absorbing azo-product of the Griess reaction becomes critically low. Assays of nitric oxide from iNOSoxy reactions containing 0 mM DTT and 0.4 mM DTT resulted in relatively close concentrations of 15.537 ( $\pm 2.313$ )  $\mu\text{M}$  and 13.176 ( $\pm 1.621$ )  $\mu\text{M}$ , respectively (for the enzyme amount and reaction time as described in Section 2). This suggests that, at least for this typical reaction setting, the 0.4 mM DTT level does not severely compromise the Griess assay. NOS reaction media with DTT concentration levels of 0.5 mM or higher give extremely low apparent NO concentrations when using external calibration, which can greatly underestimate corresponding NOS turnover rates.

Because the method of standard addition performed much better than the method of external calibration in terms of analyte (NO) recovery (Section 3.4), we examined if this can still hold true when measuring NO produced by NOS in reaction media with various levels of DTT. Fig. 5B shows NO concentrations measured from NOS reaction media with 0.0, 0.4 and 1.0 mM DTT. Here again, the standard addition method shows improved NO recoveries compared to the method of external calibration, even at DTT levels as high as 1.0 mM (Fig. 5B). The standard addition method has been previously shown to correct for the poor performance of external calibration in a multiple-step assay, developed for the determination of banned azo dyes in different leather types [30]. In our case, the standard addition method, due to its inherent use of spiked samples, may be benefiting from a positive contribution of higher concentrations where the DTT effect on the assay is relatively repressed.

#### 4. Conclusion

Our electrochemical and spectrophotometric analyses indicate that the vital diazonium intermediate of sulfanilamide in the Griess assay reacts with the reducing agent DTT in solution which causes a decrease in the concentration of the final absorbing azo-compound. Therefore, the presence of DTT and other similar reducing agents significantly affects the measurement of nitrite concentration using the traditional Griess assay and blind external calibration methods. The performance of the method is especially poor at low nitrite (or NO) concentrations. The apparent lower-concentrations observed can compromise the interpretation of initial reaction rates and derived structure–function analysis. Our work shows that the 1-mM concentration level of DTT, often used in reaction media of NOS reactions, depresses the response of the Griess assay by over 44%.

The standard addition method, on the other hand, performs better than the conventional external calibration method, both in analyte recovery studies, and in actual measurements of NO production in NOS catalytic reactions. While the accuracy and sensitivity issues of the Griess assay in the presence of reducing agents are presented here in the context of the NOS reaction and NO determinations, this problem is quite general [21], and applies to all cases in which the diazonium intermediate of the Griess reaction is exposed to reducing agents.

#### Acknowledgment

The authors wish to acknowledge financial support by the US DOE-BES through a grant of the “Catalysis Science” program to M.B. (DE-FG02-03ER15462). This research was partially supported by an FRD grant from CSU.

#### Appendix A. Supplementary data

Supplementary data associated with this article can be found, in the online version, at doi:10.1016/j.talanta.2008.12.074.

#### References

- [1] Z. Zhang, D. Naughton, P.G. Winyard, N. Benjamin, D.R. Blake, M.C. Symons, *Biochem. Biophys. Res. Commun.* 249 (1998) 767–772.
- [2] W.K. Alderton, C.E. Cooper, R.G. Knowles, *Biochem. J.* 357 (2001) 593–615.
- [3] C.F. Witteveen, J. Giovanelli, M.B. Yim, R. Gachhui, D.J. Stuehr, S. Kaufman, *Biochem. Biophys. Res. Commun.* 250 (1998) 36–42.
- [4] Y. Chen, K. Panda, D.J. Stuehr, *Biochemistry* 41 (2002) 4618–4625.
- [5] M.A. Marletta, A.R. Hurshman, K.M. Ruscic, *Curr. Opin. Chem. Biol.* 2 (1998) 656–663.
- [6] K.D. Kroncke, K. Fehsel, V. Kolb-Bachofen, *Nitric Oxide* 1 (1997) 107–120.
- [7] W. Wang, N. Inoue, T. Nakayama, M. Ishii, T. Kato, *Anal. Biochem.* 227 (1995) 274–280.
- [8] T.S. Maurer, H.L. Fung, *Nitric Oxide* 4 (2000) 372–378.
- [9] V.B. Kumar, A.E. Bernardo, M.M. Alshaher, M. Buddhiraju, R. Purushothaman, J.E. Morley, *Anal. Biochem.* 269 (1999) 17–20.
- [10] T.P. Misko, R.J. Schilling, D. Salvemini, W.M. Moore, M.G. Currie, *Anal. Biochem.* 214 (1993) 11–16.
- [11] T.E. Casey, R.H. Hilderman, *Nitric Oxide* 4 (2000) 67–74.
- [12] R.W. Nims, R.A. Lubet, J. Toxicol. Environ. Health 46 (1995) 271–292.
- [13] K.M. Miranda, M.G. Espey, D.A. Wink, *Nitric Oxide* 5 (2001) 62–71.
- [14] M.J. Moorcroft, J. Davis, R.G. Compton, *Talanta* 54 (2001) 785–803.
- [15] A. Iannone, A. Tomasi, F. Giovannini, A. Bini, F. Daneri, M. Staffieri, R.R.C. Canali, S. Bergamini, *Biol. Chem.* 5 (2001) 349–360.
- [16] S. Boggs, L. Huang, D.J. Stuehr, *Biochemistry* 39 (2000) 2332–2339.
- [17] T.M. Dawson, V.L. Dawson, *Neuroscientist* 1 (1995) 7.
- [18] D.S. Bredt, S.H. Snyder, *Annu. Rev. Biochem.* 63 (1994) 175.
- [19] P.N. Indika, M. Bayachou, *Anal. Bioanal. Chem.* 379 (2004) 1055–1061.
- [20] C.P. Verdon, B.A. Burton, R.L. Prior, *Anal. Biochem.* 224 (1995) 502–508.
- [21] A. John Moody, F.L. Shaw, *Anal. Biochem.* 356 (2006) 154–156.
- [22] J.B. Fox, F.B. Suhre, *Crit. Rev. Anal. Chem.* 15 (1985) 283–313.
- [23] S. Baranton, D. Belanger, *J. Phys. Chem. B* 109 (2005) 24401–24410.
- [24] S.S.C. Yu, A.J. Downard, e-J. Surf. Sci. Nanotechnol. 3 (2005) 294–298.
- [25] E.H. Seymour, N.S. Lawrence, M. Pandurangappa, R.G. Compton, *Microchim. Acta* 140 (2002) 211–217.
- [26] M. Delgado, E.J. Munoz-Elias, R.P. Gomariz, D. Ganea, *J. Immunol.* 162 (1999) 4685–4696.
- [27] We have found that older stock solutions properly stored within the day give essentially the same results. Authors thank a reviewer for pointing to this detail.
- [28] E.S. Ng, D. Jourdeuil, J.M. McCord, D. Hernandez, M. Yasui, D. Knight, P. Kubes, *Circ. Res.* 94 (2004) 559–565.
- [29] R. Marley, M. Feilisch, S. Holt, K. Moore, *Free Radic. Res.* 32 (2000) 1–9.
- [30] L.H. Ahlstrom, S. Amon, L. Mathiasson, *J. Sep. Sci.* 28 (2005) 2407–2412.



Short communication

## Identification of arsenolipids with GC/MS

Georg Raber\*, Sakda Khoomrung, Mojtaba S. Taleshi, John S. Edmonds, Kevin A. Francesconi

Institute of Chemistry, Karl-Franzens University Graz, Universitaetsplatz 1, 8010 Graz, Austria

### ARTICLE INFO

#### Article history:

Received 11 September 2008

Received in revised form

22 December 2008

Accepted 9 January 2009

Available online 20 January 2009

#### Keywords:

Arsenolipids

Fish oil

GC/MS

### ABSTRACT

Arsenic-containing hydrocarbons have recently been reported as natural constituents of fish oil. We report a simple method for determining these compounds by GC/MS. Application of the methodology will delineate the distribution of these novel arsenic compounds in foods, and facilitate an assessment of the toxicological implications.

© 2009 Elsevier B.V. All rights reserved.

## 1. Introduction

Arsenic is a well known toxic element and its presence in drinking water, from natural geological processes, is a worldwide environmental health problem [1]. Arsenic is also naturally present in many foods, with seafood containing particularly high concentrations [2]. Human health concerns about arsenic exposure have encouraged continuing studies to identify the forms of arsenic present in these foods and to assess their toxicology. The vast majority of this work has focussed on water-soluble arsenic compounds [3], while lipid-soluble arsenic compounds, arsenolipids, which were first reported in fish and fish oils 40 years ago [4], have remained virtually unexplored.

Recent studies, however, have identified several major arsenolipids in fish oils: six arsenic-containing long chain fatty acids in cod liver oil [5], and three arsenic-containing hydrocarbons in oil from capelin [6]. The arsenic species were detected by HPLC/ICPMS and HPLC/ESMS; accurate masses were obtained by matrix assisted laser desorption ionization (MALDI) and Fourier transform-ion cyclotron resonance mass spectrometry (FT/ICRMS). These compounds are of immediate human health interest because they are present in foods and food supplements currently recommended by nutritionists owing to their high content of omega-3 fatty acids. The wider distribution of arsenolipids in foods is currently not known and must await the development of a method able to screen for these compounds. The structures of the arsenic-containing

hydrocarbons (compounds A-C in Fig. 1) found in capelin fish oil suggested that the compounds may be amenable to simple analysis by GC, and prompted the work reported here.

## 2. Experimental

### 2.1. Sample preparation

Oil from capelin (100 g containing  $11.7 \mu\text{g As g}^{-1}$ ), was partitioned between hexane (250 mL) and water/methanol (1+9; 150 mL). The hexane layer was not further examined. The aqueous methanol fraction was evaporated to yield an oil (0.42 g, 0.52 mg As) which was dissolved in methanol/chloroform/water (60+30+8, v/v/v) and applied to a column containing the anion exchange resin DEAE Sephadex A-25 (26 mm × 240 mm). Chromatography was performed with the above solvent mixture. Most of the arsenic (the non-acidic fraction) eluted without interaction with the column at 100–120 mL (column volume 130 mL); this fraction was evaporated to yield an oil (74 mg, 0.34 mg As) which was analysed by GC/MS.

### 2.2. Synthesis of arsenic-containing hydrocarbons

1-Pentadecanol was converted to the triflate which was then treated with sodium dimethylarsenide and the resultant arsine oxidized to yield the desired product 1-dimethylarsinoylpentadecane (compound A) as a waxy solid. Treatment of compound A, an arsine oxide, with  $\text{H}_2\text{S}$  gave the thio-analogue, while treatment of compound A with dithiothreitol yielded the arsine. The identity of the compounds was checked by ES/MS prior to GC/MS measurements.

\* Corresponding author. Tel.: +43 316 380 5305; fax: +43 316 380 9845.

E-mail address: [georg.raber@uni-graz.at](mailto:georg.raber@uni-graz.at) (G. Raber).

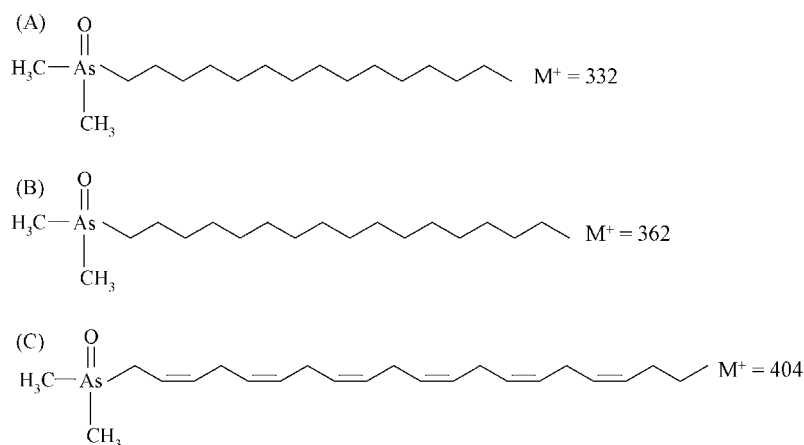


Fig. 1. Arsenic-containing hydrocarbons identified in oil from capelin [1].

### 2.3. Gas chromatography

For GC/MS determinations, a system combining a GC 7890A with a quadrupol MS 5975C (Agilent Technologies, Waldbronn, Germany) was used. The injection volume was 1  $\mu$ l (splitless injection; injection port temperature 280 °C). A (5%-phenyl)methylpolysiloxane column, 30 m  $\times$  0.25 mm i.d., 0.25  $\mu$ m film thickness (DB-5ms from Agilent) was used. Carrier gas was helium. The temperature of the column was started at 50 °C for 1 min, raised to 180 °C at 50 °C/min, raised to 220 °C at 3 °C/min and held for 1 min and then raised to 270 °C at 15 °C/min and held for 4 min. The arsenic-containing hydrocarbons were detected with electronic ionization (70 eV) in scan mode (mass range 20–500), and in selected ion monitoring mode (SIM) at  $m/z$  105, 106, 316, 344, and 388.

### 3. Results and discussion

The feasibility of using GC/MS for the arsenic-containing hydrocarbons was tested using a pure sample of the synthesised compound A ( $(\text{CH}_3)_2\text{As}(\text{O})(\text{CH}_2)_{14}\text{CH}_3$ ;  $M^+ = 332$ ). Direct injection of a solution of compound A in methanol (10  $\mu$ g/mL equivalent to 2.2  $\mu$ g As/mL) gave a single chromatographic peak ( $t_R$  11.54 min). The mass spectrum (Fig. 2) showed two major ions at  $m/z$  106  $[(\text{CH}_3)_2\text{AsH}]^+$ ,  $m/z$  105  $[(\text{CH}_3)_2\text{As}]^+$  and one at  $m/z$  316 which appeared to correspond to the molecular ion of the arsine analogue

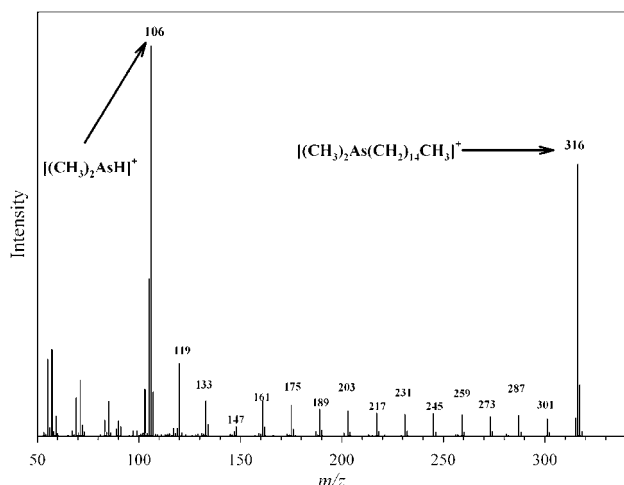


Fig. 2. GC/MS spectrum of synthesised compound A.

of compound A (i.e.  $[(\text{CH}_3)_2\text{As}(\text{CH}_2)_{14}\text{CH}_3]^+$ ). The molecular ion for compound A at  $m/z$  332 was absent.

Two possible explanations were apparent: Either loss of oxygen was taking place during the ionization process; or the arsine oxide was converted to the arsine in the injection port of the GC, and it was the arsine which passed through the column and was being detected as its molecular ion ( $m/z$  316). We presume that the arsine is formed by pyrolysis as reported in early studies performed by Kamai et al. [7,8]. The second of these possible explanations was tested in the following way. The arsine analogue and the thio-analogue  $[(\text{CH}_3)_2\text{As}(\text{S})(\text{CH}_2)_{14}\text{CH}_3$ ,  $m/z$  348] of compound A were synthesised, and the behaviour on GC/MS of both compounds was compared with that of compound A. Arsines are considerably less polar than arsine oxides, and the thio-analogues have intermediate polarity [9]. Accordingly, the three compounds had an anticipated elution order of arsine, thio-analogue, arsine oxide (compound A). However, chromatography of either the arsine or the thio-analogue produced a single peak at  $t_R$  11.54 min, which matched exactly the retention time for compound A. Furthermore, the mass spectrum of this peak was identical for each of the three compounds. From these observations it was concluded that compound A (and its thio-analogue) is converted in the injection port to the corresponding arsine which then passes through the column.

The MS response for the arsine oxide was only 50% that of the arsine, presumably due to incomplete conversion in the injection port. However, no peak was observed for the intact arsine oxide, even after 24 min run-time; probably the arsine oxide is not sufficiently volatile to pass through the column. The thio-analogue gave a comparable response to the arsine indicating that it was quantitatively converted in the injection port. These observations were consistent with the relevant bond enthalpies for As–O and As–S.

The method was then applied to a fish oil to see if it could directly detect the presence of arsenic-containing hydrocarbons. For this purpose,  $m/z$  106  $[(\text{CH}_3)_2\text{AsH}]^+$ ,  $m/z$  105  $[(\text{CH}_3)_2\text{As}]^+$ , and the molecular ion of the arsine analogue of compounds A–C were selected for use as tracers for the qualitative determination of these arsenolipids in a partially purified extract of capelin oil.

The chromatograms obtained from selected ions  $m/z$  106 and of  $m/z$  105 show a clean trace with three peaks at retention times of 11.5, 15.7 and 21.4 min corresponding to compounds A, B, and C, respectively (Fig. 3). The mass spectra (Fig. 4) show the same major characteristic as discussed for the synthesised standard of compound A, i.e. the compounds passed through the GC as their arsine analogues. Additionally, although the fragmentation patterns of the two arsenic-containing alkanes, compound A and B were essentially identical, the fragmentation pattern for the unsaturated compound C showed clear differences. In particular, the dominant fragment for

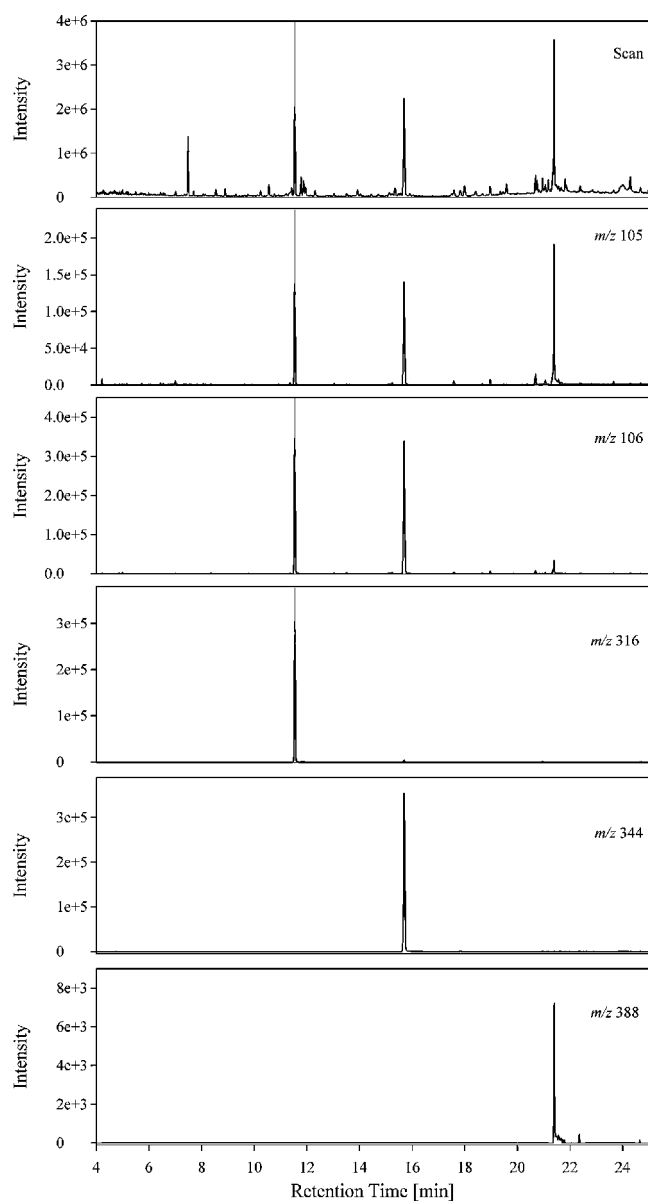


Fig. 3. GC/MS chromatogram of a fraction from capelin oil.

compound C was  $m/z$  106, whereas  $m/z$  105 was the dominant fragment from the two saturated compounds. Another difference lay in the fragmentation pattern of the hydrocarbon chain – whereas the saturated compounds A and B showed the regular loss of the  $\text{CH}_2$  fragments (14 mass units), the unsaturated compound C showed loss of either 14 or 12 mass units. This fragmentation pattern can be used for the assignment of the double bonds within the molecule. Structural identification of unsaturated fatty acids is facilitated by introducing, by derivatisation, a favourable charge site into the molecule [10,11]. In the case of unsaturated arsenic-containing hydrocarbons, however, derivatisation is not required since the arsine group is already a favoured charge site compared with the alkyl chain. Therefore, the GC/MS method appears well suited to the structural analysis of this type of unsaturated arsenolipid.

We also screened (by monitoring the arsenic-containing fragments  $m/z$  105 and 106) for other homologous arsenic-containing alkanes; in the capelin oil none was detected. These results are entirely consistent with the previous study which reported only the three arsenic-containing hydrocarbons, compounds A–C, in capelin

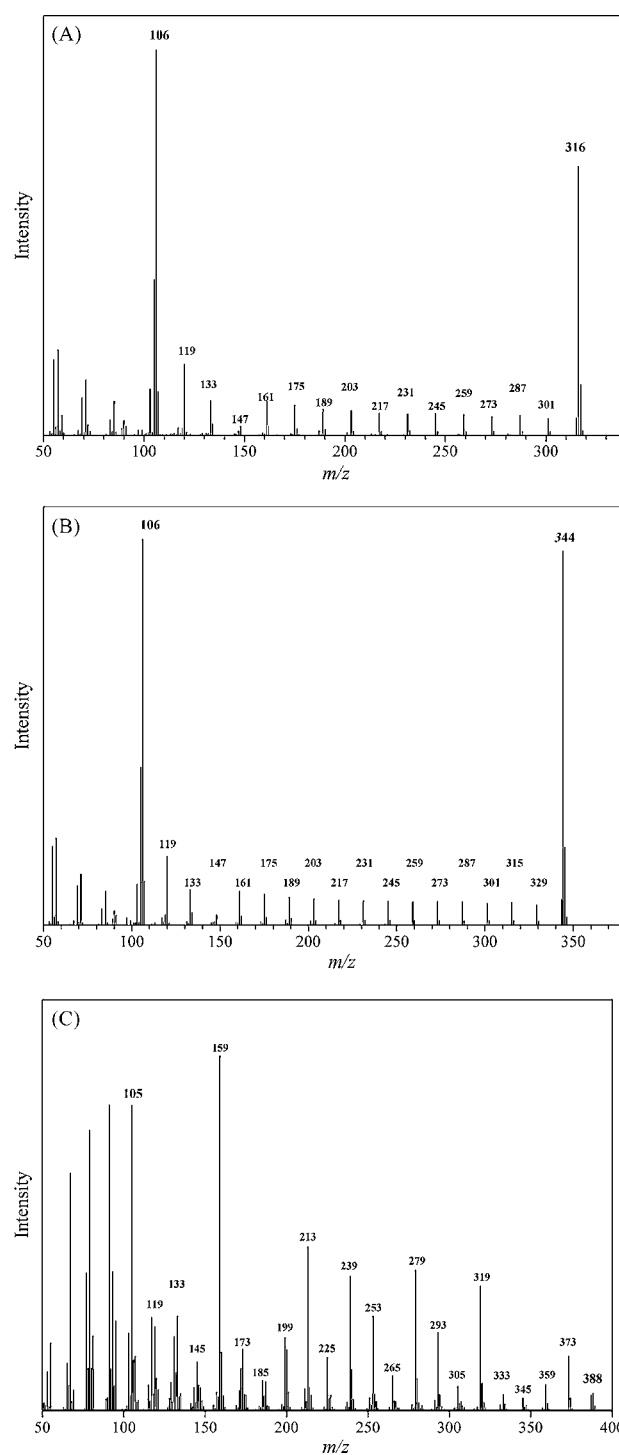


Fig. 4. GC/MS mass spectra of arsenic-containing hydrocarbons from capelin oil.

oil [1]. On that occasion, however, lengthy isolation procedures were necessary to purify the compounds to facilitate their detection by HPLC/electrospray MS and to elucidate their structures by high resolution MS.

In summary, we show that GC/MS can be used to screen for arsenic-containing hydrocarbons in fish oils. The method, in combination with a derivatisation step, might also be suitable for the determination of arsenic-containing fatty acids, which were recently reported in cod liver oil [5]. We are currently investigating the best conditions for preparing methyl esters of these arsenic-containing fatty acids.



## References

- [1] National Research Council, Arsenic in drinking water, National Academic, Washington, DC, 2001.
- [2] K.A. Francesconi, J.S. Edmonds, *Adv. Inorg. Chem.* 44 (1997) 147–189.
- [3] K. Francesconi, D. Kuehnelt, *Analyst* 129 (2004) 373–395.
- [4] G. Lunde, *J. Am. Oil Chem. Soc.* 45 (1968) 331–332.
- [5] A. Rumpler, J.S. Edmonds, M. Katsu, K.B. Jensen, W. Goessler, G. Raber, H. Gunnlaugsdottir, K.A. Francesconi, *Angew. Chem. Int. Ed.* 47 (14) (2008) 2665–2667.
- [6] M.S. Taleshi, K.B. Jensen, G. Raber, J.S. Edmonds, K.A. Francesconi, *Chem. Commun* 39 (2008) 4706–4707.
- [7] G. Kamai, B.D. Chernokal'skii, *Chem. Abstr.* 54 (1960) 23345.
- [8] G. Kamai, B.D. Chernokal'skii, *Chem. Abstr.* 54 (1960) 7538.
- [9] P. Traar, K.A. Francesconi, *Tetrahedron Lett.* 47 (30) (2006) 5293–5296.
- [10] G. Dobson, W.W. Christie, *Trends Anal. Chem.* 15 (3) (1996) 130–137.
- [11] D.V. Kuklev, W.L. Smith, *J. Lipid Res.* 44 (2003) 1060–1066.



# Simultaneous determination of nine flavonoids in *Anaphalis margaritacea* by capillary zone electrophoresis

Zhao-Yan Ren<sup>a</sup>, Yu Zhang<sup>b</sup>, Yan-Ping Shi<sup>a,b,\*</sup>

<sup>a</sup> State Key Laboratory of Applied Organic Chemistry, Lanzhou University, Lanzhou 730000, PR China

<sup>b</sup> Key Laboratory for Natural Medicine of Gansu Province, Lanzhou Institute of Chemical Physics, Chinese Academy of Sciences, Lanzhou 730000, PR China

## ARTICLE INFO

### Article history:

Received 8 October 2008  
Received in revised form 31 December 2008  
Accepted 5 January 2009  
Available online 20 January 2009

### Keywords:

*Anaphalis margaritacea*  
Capillary zone electrophoresis  
Flavonoids

## ABSTRACT

A capillary zone electrophoresis method was developed for simultaneous determination of nine flavonoids, including two rare flavonols, in Tibetan medicine *Anaphalis margaritacea*. Baseline separation was performed at pH 9.6 with 25 mM Na<sub>2</sub>B<sub>4</sub>O<sub>7</sub> and 10 mM NaH<sub>2</sub>PO<sub>4</sub> buffer solution, 20 kV as driving voltage and 275 nm as detection wavelength. Repeatability tests showed that the R.S.D. of both intra- and inter-day migration times and peak areas were less than 5%. Recovery results ranged from 87.9% to 106.1%. Samples of *A. margaritacea* extracts were analyzed using the validated method, which is useful for its quality control.

© 2009 Elsevier B.V. All rights reserved.

## 1. Introduction

Flavonoids have attracted increasing interest in recent years due to their antiplogistic, antiviral and antitumor properties. Several analytical methods, such as HPLC [1], HPLC–MS [2], GC–MS [3] and multidimensional LC [4,5], have been described. And trends in the separation and determination of flavonoids have also been reviewed [6–8]. Among them, capillary electrophoresis (CE) is a very economical technique and it has many advantages such as small injection sample volume, high efficiency, and short analysis time, etc., which can be useful in the rapid and efficient determination of flavonoids in complex systems. Thus many modes have been developed, such as MEKC [9], CGE [10] and CEC [11], etc. Of these, capillary zone electrophoresis (CZE) under the addition of modifiers could provide satisfying resolution of flavonoids in complicated Chinese herbs [12]. Shi and co-workers have studied the determination of flavonoids in *Hippophae rhamnoides* by CZE [13]. Fang and co-workers have also investigated six flavonoids in chrysanthemum by CZE with running buffer modifiers [14].

Tibetan medicine *Anaphalis margaritacea* (Linn.) Benth. et Hook. f. (Compositae) belongs to the *Anaphalis* genus and widely distributed in the northwest and southwest of China. It has long been used by local inhabitants for cough and respiratory problems as well as for colds and rheumatism [15,16]. Chemical investigations

of this plant have resulted in the isolation of main active flavonoids, including rare flavonols with the structures of multi *O*-substituted A-ring and unsubstituted B-ring [17–19]. However, no methods have been reported for the simultaneous determination of these flavonoids.

In this study, we developed a CZE method for the first time to separate and determine nine flavonoids whose structure were shown in Fig. 1, including two rare flavonols (1 and 2 [17]), in *A. margaritacea* extract. These nine analytes could achieve good baseline separation. The results proved that the method was a simple and economical means for the analysis of these flavonoids and can be used for real application in practical samples.

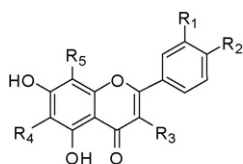
## 2. Experimental

### 2.1. Apparatus

CZE experiments were performed on a Beckman PACE/MDQ capillary electrophoresis instrument equipped with on-column diode-array detection (DAD) (Beckman coulter, Fullerton, CA, USA). A software of 32 Karat system and version 5.0 (Beckman coulter, Fullerton, CA, USA) was used for data acquisition and evaluation. An ultrasonic bath Model KQ-250 (Ultrasonic Co., Ltd. Kunshan China) was used to degas the buffer. PB-10 pH meter (Beijing Sartorius Instrument & System Engineering Co., Ltd.) was used to adjust the pH of background electrolyte (BGE) with 0.1 M NaOH or 0.1 M HCl. Uncoated fused-silica capillaries (Yong-Nian Optical Fiber Factory, Hebei, China) with an inner diameter of 75 μm and a total length of 70.5 cm (effective length of 60 cm) were used.

\* Corresponding author at: Lanzhou Institute of Chemical Physics, Chinese Academy of Sciences, Lanzhou 730000, PR China. Fax: +86 931 8277088.

E-mail address: [shiyp@lzb.ac.cn](mailto:shiyp@lzb.ac.cn) (Y.-P. Shi).



Compounds	R <sub>1</sub>	R <sub>2</sub>	R <sub>3</sub>	R <sub>4</sub>	R <sub>5</sub>
1	H	H	OMe	OMe	OMe
2	H	H	OMe	H	OMe
3	H	H	OMe	H	H
4	H	OH	OGlc	H	H
6	OH	OH	OMe	H	H
7	OH	OGlc	OH	H	H
8	H	OH	H	H	H
9	OH	OH	OH	H	H

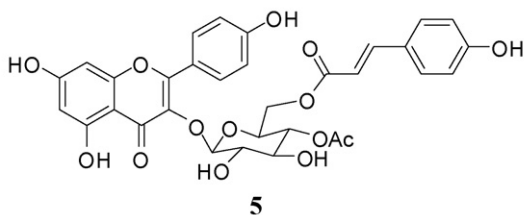


Fig. 1. Molecular structures of nine flavonoids.

## 2.2. Reagents and materials

Standards, 5,7-dihydroxy-3,6,8-trimethoxyflavone (**1**), 5,7-dihydroxy-3,8-dimethoxyflavone (**2**), 5,7-dihydroxy-3-methoxyflavone (**3**), kaempferol-3-*O*- $\beta$ -*D*-glucopyranoside (**4**), tilirosin (**5**), 3-methylquercetin (**6**), spiraein (**7**), apigenin (**8**) and quercetin (**9**) were isolated from this plant in our laboratory and elucidated by MS, <sup>1</sup>H NMR and <sup>13</sup>C NMR spectroscopy [17]. Their purity determined by peak area normalization method with HPLC-PDA was all above 97%. All other chemicals were of analytical grade and purchased from Tianjin Chemical Reagents Co., Ltd. (Tianjin, China). Purified water purchased from Hangzhou Wahaha Group Corporation (Hangzhou, China) was used throughout. *A. margaritacea* was collected in Huzhu County, Qinghai province, China, in August 2005.

## 2.3. Separation performance

CZE experiment was performed at the separation voltage of 20 kV using a 25 mM Na<sub>2</sub>B<sub>4</sub>O<sub>7</sub>–10 mM NaH<sub>2</sub>PO<sub>4</sub> (pH 9.6) running buffer, with a constant temperature of 25 °C. Samples were injected by applying a pressure of 0.5 psi for 5 s. The detection wavelength was set at 275 nm.

Prior to CZE experiments, the capillary was rinsed with 0.1 M NaOH for 15 min, then with purified water for 10 min; it was then conditioned with running electrolyte for 4 min. Before each run in CZE experiments, the capillary was sequentially rinsed with 0.1 M NaOH for 2 min, purified water for 2 min, and finally running buffer for 2 min. Vials of BGE were replaced every 4 injections to keep the same reservoir level of the buffer and avoid the changes of EOF due to the electrolysis of the solutions.

## 2.4. Preparation of standard and samples solutions

Reference standards, **1** (5.5 mg), **2** (4.0 mg), **3** (1.3 mg), **4** (12.0 mg), **5** (14.3 mg), **6** (9.0 mg), **7** (6.0 mg), **8** (1.7 mg), **9** (6.0 mg), were accurately weighed and transferred into 5-mL-volumetric flask, which were then dissolved in methanol to make the standard stock solutions, respectively. A standard mixture solution was prepared by mixing 1 mL of the nine standard stock solutions and then diluted to 25 mL with methanol. Calibration standard working solutions were freshly prepared by appropriate dilution of the stock solutions giving final concentration in the range of 122.2–1.4  $\mu$ g/mL for compound **1**, 88.9–0.7  $\mu$ g/mL for **2**, 86.7–0.2  $\mu$ g/mL for **3**, 266.7–2.2  $\mu$ g/mL for **4**, 316.7–1.2  $\mu$ g/mL for **5**, 200.0–1.5  $\mu$ g/mL for **6**, 133.3–2.2  $\mu$ g/mL for **7**, 113.3–0.2  $\mu$ g/mL for **8**, 133.3–1.1  $\mu$ g/mL for **9**.

The whole plant (2.6 kg) was extracted with 95% EtOH to give 183 g extract [17], of which 0.25 g was dissolved in methanol into a 10.00 mL volumetric flask. Both standard solutions and the sample solution were kept in darkness at 4 °C, and filtered through a 0.45  $\mu$ m membrane filter and degassed by ultrasonication before use.

## 3. Results and discussion

In CZE experiments, borate buffer has been the most often used BGE for analysis of flavonoid due to the formation of borate complexes between the vicinal hydroxyl groups on the aromatic ring of flavonoids and borate ions [20,21]. In addition, all kinds of modifiers were added to improve the separation efficiency, such as  $\beta$ -CD, phosphate, acetate, etc. In this experiment, good effects have been obtained when phosphate was added. Therefore Na<sub>2</sub>B<sub>4</sub>O<sub>7</sub>–NaH<sub>2</sub>PO<sub>4</sub> buffer system was selected

### 3.1. Effect of buffer pH

The effect of buffer pH was studied for a mixture of these nine compounds by varying it from 8.5 to 10.2 at fixed concentration of 25 mM Na<sub>2</sub>B<sub>4</sub>O<sub>7</sub> and 10 mM NaH<sub>2</sub>PO<sub>4</sub>. Fig. 2 shows the change of migration behavior of the nine flavonoids. At pH 8.5, no peaks were detected within 15 min when the nine analytes were introduced in the capillary due to their poor solubility. When pH increased to 9.0, the signal peaks of nine compounds were very weak, and they had poor separation. At pH 9.5, a baseline separation of the nine flavonoids was accomplished with suitable migration time,

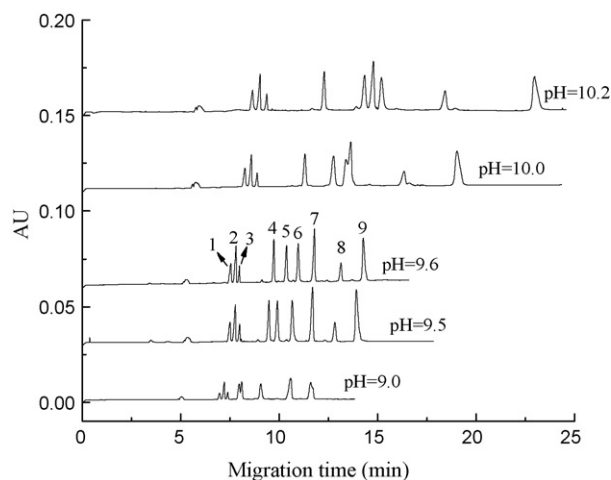
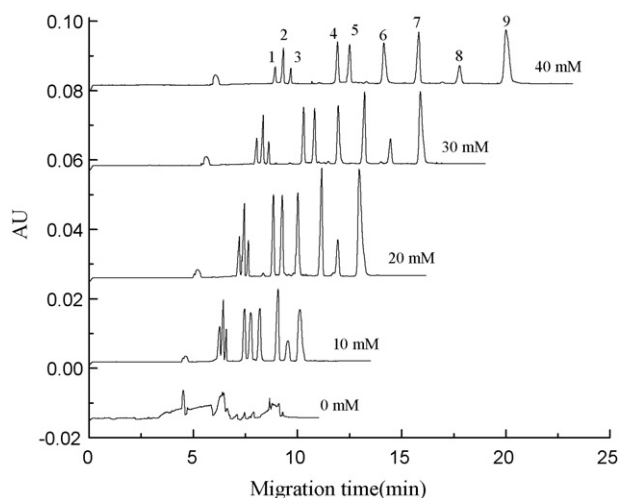


Fig. 2. Effect of buffer pH on the migration behavior. Separation conditions: 25 mM Na<sub>2</sub>B<sub>4</sub>O<sub>7</sub>–10 mM NaH<sub>2</sub>PO<sub>4</sub>; applied voltage, 20 kV; temperature, 25 °C; UV detection, 275 nm.



**Fig. 3.** Effect of  $\text{Na}_2\text{B}_4\text{O}_7$  concentration at pH 9.6 on the migration behavior. Separation conditions: 10 mM  $\text{NaH}_2\text{PO}_4$ , pH 9.6; other conditions as in Fig. 2.

whereas at pH 10.0 the resolution of compounds **6** and **7** was getting worse and at pH 10.2 the migration time was getting longer. Thus pH 9.5 seemed suitable. However, when the real sample was injected into the capillary, compound **6** couldn't be baseline separated from other unknown compounds. While at pH 9.6 the real sample has a good resolution. Therefore pH 9.6 was selected for further experiments.

### 3.2. Effect of borate concentration

As known, the buffer concentration acts directly on the magnitude of the electroosmotic flow, and a higher buffer concentration gives a low EOF and *vice versa* [22,23]. A low EOF produces a long migration time, which just could give a better resolution. Therefore, effect of borate concentration ranging from 0 to 40 mM on the separation of nine compounds was studied. According to the results shown in Figs. 3 and 5A, migration time of the analytes increased and the resolution was significantly improved with increase of the borate concentration. However, higher buffer concentrations led to poor peak shapes and also had negative effect on the detection limits because the effect of Joule heat became more pronounced which increased the baseline noise. Taking into account of the migration time and peak shape, 25 mM borate buffer (pH 9.6) (Fig. 5A), was selected for further experiments.

### 3.3. Effect of $\text{NaH}_2\text{PO}_4$ concentration

Effect of  $\text{NaH}_2\text{PO}_4$  concentration ranging from 0 to 40 mM on the separation was studied at fixed concentration of 25 mM borate buffer at pH 9.6. From the results shown in Fig. 4, it can be seen that the resolutions were obviously improved with the  $\text{NaH}_2\text{PO}_4$

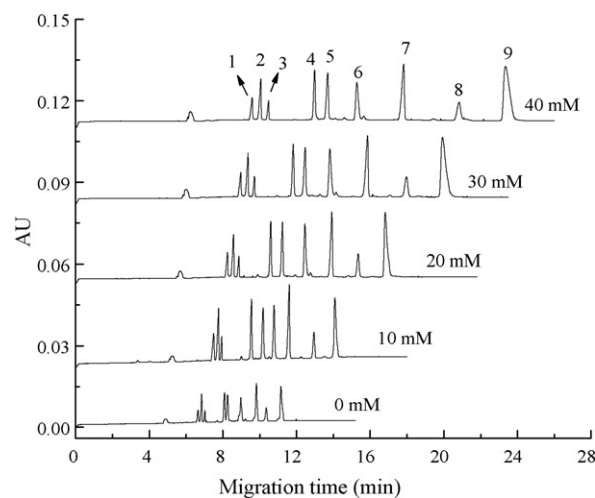


**Fig. 4.** Effect of  $\text{NaH}_2\text{PO}_4$  concentration at pH 9.6 on the migration behavior. Separation conditions: 25 mM  $\text{Na}_2\text{B}_4\text{O}_7$ , pH 9.6; other conditions as in Fig. 2.

**Table 2**

Intra and inter-day R.S.D. of peak areas and migration time ( $n = 5$ ).

Compounds	Concentration ( $\mu\text{g/ml}$ )	Intra-day R.S.D. (%)		Inter-day R.S.D. (%)	
		Peak areas	Migration time	Peak areas	Migration time
<b>1</b>	44.0	2.85	0.96	4.09	1.69
<b>2</b>	32.0	3.89	1.12	3.85	1.72
<b>3</b>	10.4	3.22	1.27	4.26	2.54
<b>4</b>	96.0	3.58	1.20	4.32	1.98
<b>5</b>	114.4	3.02	1.21	3.91	1.62
<b>6</b>	72.0	2.64	1.54	3.79	2.30
<b>7</b>	48.0	3.76	1.49	4.04	2.79
<b>8</b>	13.6	3.13	1.62	3.89	2.01
<b>9</b>	48.0	3.24	1.73	3.77	2.73

concentration increasing. Taking into account of the migration time, 10 mM  $\text{NaH}_2\text{PO}_4$  was chosen. Therefore 25 mM  $\text{Na}_2\text{B}_4\text{O}_7$  and 10 mM  $\text{NaH}_2\text{PO}_4$  (pH 9.6) buffer solution was selected for the experiments.

### 3.4. Method validation

#### 3.4.1. Calibration curve

The calibration curves were plotted using the integrated chromatographic peak areas of the analytes versus the corresponding six different concentrations in three duplicate analyses. The resolution, theoretical plate number ( $N$ ), linear ranges, regression equations and correlation coefficients were listed in Table 1. Good linear relationships of the nine flavonoids were obtained.

**Table 1**

The regression equation, LOD and LOQ of the nine flavonoids.

Compounds	Resolution	$N$	Regression equation ( $y = a + bx^a$ )	Correlation coefficient	Linear range ( $\mu\text{g/ml}$ )	LOD ( $\mu\text{g/ml}$ )	LOQ ( $\mu\text{g/ml}$ )
<b>1</b>	2.6	48,848	$y = 880.3x + 2118.3$	0.9981	1.4–122.2	0.5	1.7
<b>2</b>	2.1	55,546	$y = 1545.8x + 1312.1$	0.9995	0.7–88.9	0.2	0.8
<b>3</b>	21.5	52,598	$y = 5313.1x + 2131$	0.9999	0.2–86.7	0.1	0.3
<b>4</b>	6.7	32,921	$y = 1059.7x + 523.45$	0.9997	2.2–266.7	0.6	2.0
<b>5</b>	5.7	26,534	$y = 695.6x + 9032.1$	0.9890	1.2–316.7	0.4	1.3
<b>6</b>	8.0	21,458	$y = 978.5x + 6634.0$	0.9947	1.5–200.0	0.4	1.3
<b>7</b>	11.4	32,392	$y = 1272.3x + 886.9$	0.9998	2.2–133.3	0.7	2.3
<b>8</b>	8.1	32,187	$y = 5456.4x + 3477.3$	0.9999	0.2–113.3	0.1	0.3
<b>9</b>		21,721	$y = 974.2x + 2522.5$	0.9987	1.1–133.3	0.1	0.3

<sup>a</sup>  $y$  and  $x$  stand for the corrected peak area and the concentration ( $\mu\text{g/mL}$ ) of the analytes, respectively.

**Table 3**  
Recoveries of nine flavonoids ( $n = 3$ ).

Compound	Added amount ( $\mu\text{g}$ )	Found amount ( $\mu\text{g}$ )	Recovery (%)	R.S.D. (%)
1	180.0	158.2	87.9	5.2
2	120.0	111.1	92.6	4.9
3	65.0	62.2	95.7	4.2
4	120.0	124.2	103.5	2.7
5	180.0	169.7	94.3	4.1
6	190.0	201.6	106.1	4.7
7	170.0	161.2	94.8	2.6
8	70.0	66.7	95.3	2.1
9	120.0	117.0	97.5	3.3

### 3.4.2. LOD and LOQ

The limits of detection (LOD) and the limits of quantitation (LOQ) which were defined at an  $S/N$  of 3 and 10, respectively, were also determined. Table 1 showed the data of LOD and LOQ for each investigated compound.

### 3.4.3. Repeatability

The repeatability of the method was examined by performing the intra-day and inter-day assays with five replicate injections of the standard solution mixture. The intra-assay precision was performed with the interval of 4 h in 1 day, while the inter-assay precision was performed on five consecutive days. The RSD values of migration time and peak area for the intra-assay precision were lower than 2.0% and 4.0%, 3.0% and 5.0% for the inter-assay precision, which demonstrated that this method was of good repeatability (Table 2).

### 3.4.4. Accuracy

The accuracy of the developed analytical method was confirmed by recovery test with standard addition method, in order to determine eventual positive or negative interferences produced by the other co-existed chemical constituents in the plant. Accurate amounts of nine standards were added into the real sample with known content of the desired compounds. The mixtures were prepared with the same method as described in Section 2.4, and were analyzed using the developed CZE method mentioned above. Then, the quantity of each compound was subsequently achieved from the corresponding calibration curves. Each set of additions was repeated three times. The results of accuracy, expressed as the percentage of the analytes recovered by the assay, are listed in Table 3. As shown, the recovery of the investigated compound ranged from 87.9% to 106.1%, and their R.S.D. values were all less than 5.5%, which indicates that the method enables the accurate simultaneous determination of the nine analytes.

### 3.5. Application

Sample determinations were carried out using the developed CZE method mentioned above. The nine flavonoids and other unknown compounds in *A. margaritacea* extracts were all baseline-separated successfully within 14 min. The desired compounds in herbal plant samples were identified by comparing both the migration times and the absorption spectra of the flavonoids with those of the reference standards. The analytes were further confirmed by spiking standards in actual samples. To check the peak purity of the compounds, the peaks were monitored with the DAD detector at 200–400 nm. The three spectra corresponding to the upslope, apex and downslope of each peak were normalized and superimposed. Peaks were considered pure when there was an exact coincidence among the three spectra. Typical electropherogram of the standards and sample are shown in Fig. 5. The contents of the nine analytes were calculated as  $1.58 \pm 0.02$ ,  $1.10 \pm 0.02$ ,  $0.44 \pm 0.01$ ,  $3.23 \pm 0.05$ ,  $6.83 \pm 0.06$ ,  $1.29 \pm 0.02$ ,  $5.56 \pm 0.08$ ,  $0.24 \pm 0.01$ ,  $3.67 \pm 0.05$  mg/g (mean  $\pm$  S.D.,  $n = 3$ ) for the nine flavonoids 1–9, respectively.

## 4. Conclusion

In this paper, a CZE method was successfully developed for the simultaneous determination of nine flavonoids, including two rare flavonols, in Tibetan medicine plant *A. margaritacea* extract for the first time. The results demonstrated that this method is of high separation efficiency, short analysis time and convenience of analysis with satisfactory repeatability and good accuracy. This method could be useful in the quality control of *A. margaritacea*.

## Acknowledgements

This work was supported by the Foundation for the National Natural Science Foundation of China (No. NSFC 20621091), the National 863 Program of China (No. 2007AA09Z403), and National Key Technology Research and Development Program of China (No. 2007BAI37B05).

## References

- [1] K. Ishii, T. Furuta, Y. Kasuya, J. Chromatogr. B 794 (2003) 49.
- [2] W. Wu, C.Y. Yan, L. Li, Z.Q. Liu, S.Y. Liu, J. Chromatogr. A 1047 (2004) 213.
- [3] Y.C. Fiamegos, C.G. Nanos, J. Vervoort, C.D. Stalikas, J. Chromatogr. A 1041 (2004) 11.
- [4] T. Hájek, V. Skeříková, P. Česla, K. Vyňuchalová, P. Jandera, J. Sep. Sci. 31 (2008) 3309.
- [5] P. Dugo, F. Cacciola, M. Herrero, P. Donato, L. Mondello, J. Sep. Sci. 31 (2008) 3297.
- [6] J. Vacek, B. Klejdus, L. Lojková, V. Kubán, J. Sep. Sci. 31 (2008) 2054.
- [7] C.D. Stalikas, J. Sep. Sci. 30 (2007) 3268.

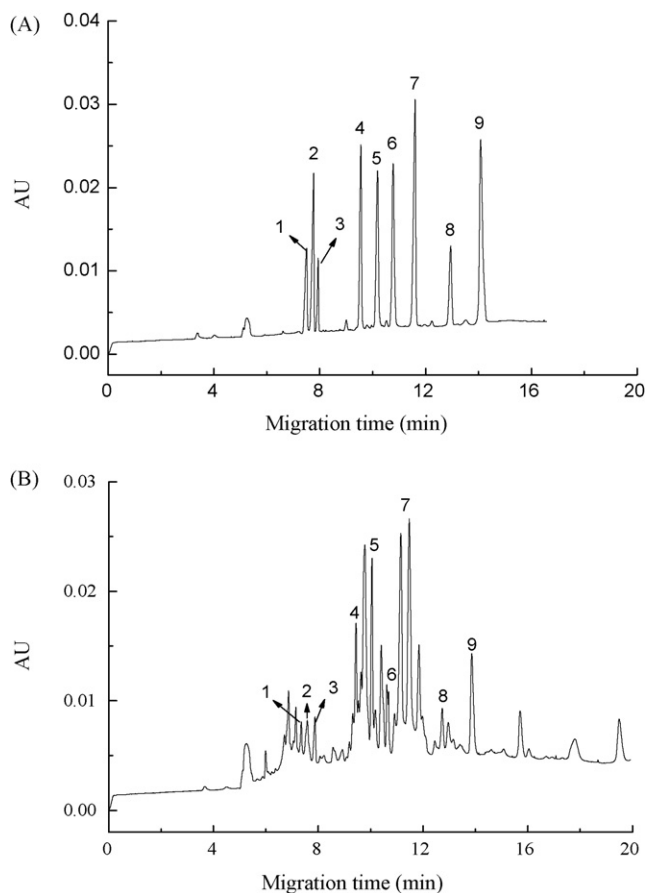


**Fig. 5.** Electropherograms of the nine flavonoids (A) and *A. margaritacea* extract (B). Separation conditions: pH 9.6; other conditions as in Fig. 2.

- [8] E. de Rijke, P. Out, W.M.A. Niessen, F. Ariese, C. Gooijer, U.A.T. Brinkman, J. Chromatogr. A 1112 (2006) 31.
- [9] X. Zhou, L.Y. Fan, W. Zhang, C.X. Cao, *Talanta* 71 (2007) 1541.
- [10] S.Q. Luo, J.M. Feng, H.M. Pang, J. Chromatogr. A 1051 (2004) 131.
- [11] F. Qin, C.H. Xie, S. Feng, J.J. Ou, L. Kong, M.L. Ye, H.F. Zou, *Electrophoresis* 27 (2006) 1050.
- [12] J. Šafra, M. Pospíšilová, J. Honegr, J. Spilková, J. Chromatogr. A 1171 (2007) 124.
- [13] M.E. Yue, T.F. Jiang, Y.P. Shi, *Talanta* 62 (2004) 695.
- [14] S. Zhang, S.Q. Dong, L.Z. Chi, P.G. He, Q.J. Wang, Y.Z. Fang, *Talanta* 76 (2008) 780.
- [15] Beijing Institute of Plant, Chinese Academy of Science, The Picture Index of Senior China Plant, Science Press, Beijing, 1977, p. 468.
- [16] Northwest Institute of Plateau Biology, Chinese Academy of Science, Flora of Qinghai Economic Plants, Qinghai People's Press, Xining, 1987, p. 576.
- [17] Z.Y. Ren, Q.X. Wu, Y.P. Shi, *Chem. Nat. Compd.*, in press.
- [18] A.M. Khattab, Alex. J. Pharm. Sci. 12 (1998) 99.
- [19] E. Wollenweber, H. Fritz, B. Henrich, J. Jakupovic, G. Schilling, J.N. Roitman, Z. Naturforsch. C 48 (1993) 420.
- [20] S. Hoffstetter-Kuhn, A. Paulus, E. Gassmann, H.M. Widmer, *Anal. Chem.* 63 (1991) 1541.
- [21] T. Kaneta, S. Tanaka, H. Yoshida, J. Chromatogr. 538 (1991) 385.
- [22] J. Zukowski, V.D. Biasi, A. Berthod, J. Chromatogr. A 948 (2002) 331.
- [23] J. Pan, S. Zhang, L. Yan, J. Tai, Q. Xiao, K. Zou, Y. Zhou, J. Wu, J. Chromatogr. A 1185 (2008) 117.



# Simultaneous determination of arsenic and selenium species in fish tissues using microwave-assisted enzymatic extraction and ion chromatography–inductively coupled plasma mass spectrometry

Laura Hinojosa Reyes\*, Jorge L. Guzmán Mar, G.M. Mizanur Rahman, Bryan Seybert, Timothy Fahrenholz, H.M. Skip Kingston

Department of Chemistry and Biochemistry, Duquesne University, Pittsburgh, PA 15282, USA

## ARTICLE INFO

### Article history:

Received 30 October 2008

Received in revised form 5 January 2009

Accepted 6 January 2009

Available online 20 January 2009

### Keywords:

Microwave-assisted enzymatic extraction

Arsenic speciation

Selenium speciation

IC–ICP–MS

Fish tissues

## ABSTRACT

A microwave-assisted enzymatic extraction (MAEE) method was developed for the simultaneous extraction of arsenic (As) and selenium (Se) species in fish tissues. The extraction efficiency of total As and Se and the stability of As and Se species were evaluated by analyzing DOLT-3 (dogfish liver). Enzymatic extraction using pronase E/lipase mixture assisted by microwave energy was found to give satisfactory extraction recoveries for As and Se without promoting interspecies conversion. The optimum extraction conditions were found to be 0.2 g of sample, 20 mg pronase E and 5 mg lipase in 10 mL of 50 mM phosphate buffer, pH 7.25 at 37 °C. The total extraction time was 30 min. The speciation analysis was performed by ion chromatography–inductively coupled plasma mass spectrometry (IC–ICP–MS). The accuracy of the developed extraction procedure was verified by analyzing two reference materials, DOLT-3 and BCR-627. The extraction recoveries in those reference materials ranged between 82 and 94% for As and 57 and 97% for Se. The accuracy of arsenic species measurement was tested by the analysis of BCR 627. The proposed method was applied to determine As and Se species in fish tissues purchased from a local fish market. Arsenobetaine (AsB) and selenomethionine (SeMet) were the major species detected in fish tissues. In the analyzed fish extracts, the sum of As species detected was in good agreement with the total As extracted. However, for Se, the sum of its species was lower than the total Se extracted, revealing the presence of Se-containing peptides or proteins.

© 2009 Elsevier B.V. All rights reserved.

## 1. Introduction

Arsenic (As) and selenium (Se) are characterized by their toxicological properties and widespread environmental occurrences. These metalloids are released into the environment through natural and anthropogenic sources, thus exposing humans to increased concentrations of both elements in food, water and other environmental media [1,2]. With respect to As, fish and shellfish diets account for the majority of ingested As, where the total As concentration ranged from 1 to 100 mg kg<sup>-1</sup>. Due to the variable levels of toxicity associated with As species in foods, knowledge of the actual forms present, rather than only the total As, is necessary in order to assess potential harmful contamination [3]. Inorganic As species, such as As(III) and As(V), have been classified as carcinogens and methylated forms, such as monomethylarsonic acid (MMA) and dimethylarsinic acid (DMA), have been labeled as cancer promoters. Arsenobetaine (AsB), the predominant As species

in fish and shellfish, is believed to have negligible toxicity [1,3,4]. Regarding Se, its speciation is of particular interest since it is recognized as both an essential nutrient and a toxin to mammals, and the concentration interval range between essentiality and toxicity is very narrow and strongly dependent on its chemical form [1,2]. Inorganic forms of Se are generally more toxic than organic Se compounds, and inorganic Se(IV) is the most toxic species [2]. Most of the Se in mussel and fish tissues has been associated with organic forms such as selenomethionine (SeMet) [5]. Trimethylselenonium (TMSe<sup>+</sup>) was detected in oyster, mussel and trout, while inorganic Se was found in krill [6]. Although seafood is a significant source of Se, in some cases fish tissue is a poor source of available Se due to the interaction of Se with a number of toxic metals, such as As, which binds to Se forming insoluble inorganic complexes [7,8]. Antagonistic effects between As and Se have been confirmed in many animal species, including humans [9]. Techniques for the simultaneous speciation of As and Se are important to support these findings.

Currently, liquid chromatography (LC) paired with inductively coupled plasma mass spectrometry (ICP–MS) for element selective detection has been predominantly applied for As and/or Se spe-

\* Corresponding author. Tel.: +1 412 396 5564; fax: +1 412 396 5683.

E-mail address: [hinojosalr@gmail.com](mailto:hinojosalr@gmail.com) (L.H. Reyes).

ciation. Ion-exchange has been widely used for separating As or Se compounds in biological materials [6,10–13]. However, a limited number of separation systems for the simultaneous speciation of As and Se in biological samples have been reported. Recently, Wang et al. [14] developed an anion-exchange separation of As(III), As(V), MMA, DMA, AsB, Se(IV) and Se(VI), and the method was applied to the analysis of urine samples and fish extracts.

Sample preparation is the most important and limiting step for speciation analysis in solid dietary matrices. Extraction conditions must be chemically mild but efficient to quantitatively extract analytes from different matrices while maintaining the integrity and the concentration of individual species. Different water/methanol mixtures [15–17] have been commonly used for the extraction of As species from fish tissues. It has been reported, however, that incomplete extraction of inorganic As from biological matrices occurs due to the inability of water/methanol mixtures to break the bonds between As(III) and thiol groups (–SH) in proteins [12]. Alternative methods based on solubilization with tetramethyl ammonium hydroxide (TMAH) for the extraction of As species from marine tissues have been described in the literature [12,18]. Enzymatic extractions with trypsin have also been investigated for As speciation in fish and crustacean samples [19]. Conversely, common extraction methodologies for Se speciation include enzymatic and alkaline extractions, the former being the most widely used. Several enzymes, including protease XIV [20], pronase E [6,10,21], pronase E/lipase mixture [22,23] and trypsin [21], have been applied to Se speciation studies in various biological tissues. Generally, the use of enzymatic hydrolysis has shown better results in the release of Se species from biological solid samples than basic extraction conditions (using TMAH reagent) that lead to Se species degradation [5]. Among the procedures reported in the literature for the extraction of As or Se, enzymatic extraction is of interest due to the use of moderate temperature and pH conditions that prevent elemental losses by volatilization and minimize species degradation. However, the main drawback of enzymatic hydrolysis is the significant time required to complete the hydrolysis process (12–24 h).

In recent years, the use of microwave-assisted extraction (MAE) has gained wide acceptance as a powerful tool for sample preparation of solid matrices for speciation analysis. In contrast with traditional extraction techniques such as mechanical shaking or sonication, sample preparation time and solvent amount are reduced without decreasing the extraction efficiency of the target species [24].

The objective of this study was to evaluate the feasibility of microwave-assisted enzymatic extraction (MAEE) for the simultaneous extraction of As and Se species from fish tissues as an alternative to conventional enzymatic extraction procedures. The combined use of enzymes and closed-vessel microwave-assisted extraction for the multielemental species extraction has not been previously reported. A critical study of the most important parameters involved in the extraction procedure, followed by the comparison of several common extraction procedures used for As or Se in fish tissues, was performed. As and Se species were separated using an anion-exchange chromatography and detected on-line with an inductively coupled plasma mass spectrometer. The results are presented in this article.

## 2. Experimental

### 2.1. Instrumentation

The chromatography system (Metrohm-Peak, LLC, Houston, TX, USA) consisted of two 818 IC Pumps, a 762 IC Interface, and an 838 IC Autosampler. The separation center enclosure included a six-port sample injector equipped with a 100  $\mu$ L sample loop. Ion-

**Table 1**  
ICP–MS instrumental settings and chromatographic separation conditions.

IC	
Column	Metrosep™ Anion Dual 3 column (100 mm $\times$ 4.0 mm, 6 $\mu$ m) and Metrosep™ Anion Dual 3 guard column (1.7 mm $\times$ 3.5 mm, 0.2 $\mu$ m) (Metrohm Peak, LLC.)
Mobile phase	A: 5 mM NH <sub>4</sub> NO <sub>3</sub> , and B: 50 mM NH <sub>4</sub> NO <sub>3</sub> , 2% (v/v) methanol, pH 8.7
Gradient program	1: 0 min, 0% B, 2: 2 min, 0% B, 3: 7 min, 100% B, 4: 9 min, 100% B, 5: 9.5 min, 0% B and 6: 12 min, 0% B.
Flow rate	1 mL min <sup>-1</sup>
Injection volume	100 $\mu$ L
Column temperature	Ambient
SEC	
Column	TSK–gel QC–PAK GFC (200 column, 150 mm $\times$ 7.8 mm, 5 $\mu$ m) (Tosoh Bioscience)
Mobile phase	50 mM phosphate buffer, 2% (v/v) methanol, pH 7.25
Flow rate	0.7 mL min <sup>-1</sup>
Injection volume	100 $\mu$ L
Column temperature	Ambient
ICP–MS	
Rf power	1475 W
Plasma argon flow	15.0 L min <sup>-1</sup>
Auxiliary argon flow	1.0 L min <sup>-1</sup>
Monitoring isotopes	<sup>75</sup> As <sup>a,b</sup> , <sup>77</sup> Se <sup>a,b</sup> and <sup>82</sup> Se <sup>a,b</sup>
Acquisition mode	Spectrum <sup>a</sup> and time-resolved analysis <sup>b</sup>
Integration time per mass (s)	0.30 <sup>a</sup> and 0.20 <sup>b</sup>
Replicates	5 <sup>a</sup> and 1 <sup>b</sup>
Total analysis time (s)	34.45 <sup>a</sup> and 718 <sup>b</sup>

<sup>a</sup> For total As and Se analysis.

<sup>b</sup> For As and Se speciation analysis.

exchange chromatography was performed in a Metrosep Anion Dual 3 analytical column with a Metrosep Anion Dual 3 guard column (Metrohm-Peak, LLC, Houston, TX, USA). A gradient elution of 5 mM and 50 mM NH<sub>4</sub>NO<sub>3</sub>, 2% (v/v) MeOH (pH 8.7) was used. Size exclusion chromatography (SEC) was performed on a TSK–gel QC–PAK GFC 200 column (Tosoh Bioscience LLC, Montgomeryville, PA, USA) with a molecular weight exclusion limit of 150 kDa. The chromatographic system was coupled directly to the nebulizer of the ICP–MS by a small piece of perfluoroalkoxy (PFA) tubing.

The ICP–MS instrument was an Agilent HP–4500 (Palo Alto, CA and Yokogawa Analytical Systems Inc., Tokyo, Japan). The sample introduction system consisted of a concentric nebulizer with a Scott double-pass quartz spray chamber. The operating parameters are summarized in Table 1. The torch position and ion lens voltage settings were optimized daily for optimum sensitivity with a standard solution of 10  $\mu$ g L<sup>-1</sup> Li, Y, Ce, and Tl in 2% (v/v) HNO<sub>3</sub>. Ion intensities at *m/z* 75, 77 and 82 were recorded using spectrum mode for total analysis and time-resolved analysis (TRA) for speciation analysis.

An ETHOS 1 laboratory microwave system [Milestone, Sorisole (BG), Italy] equipped with temperature and pressure feedback controls, magnetic stirring capability and 10 high pressure vessels of 100 mL inner volume, operating at a maximum exit power of 1500 W, was employed for the digestion and extraction processes.

The commercial fish tissues were freeze-dried for 48 h (Freezone 4.5, Labconco Inc., Kansas City, MO). A FAM–40 vacuum unit (Milestone, Sorisole, Italy) was used to filter digest and extracts. A centrifuge (Model 225, Fisher Scientific Co., St. Louis, MO, USA) was employed for the sample preparation.

### 2.2. Reagents and materials

All reagents were of analytical reagent grade. Double-deionized (DDI) water with a resistivity of 18 M $\Omega$ -cm obtained from a Barnstead NANOpure Water System (Dubuque, IA, USA) was used



throughout. Hydrogen peroxide 35% (w/v) in water and ammonium phosphate dibasic were purchased from Acros Organic (New Jersey, USA). TMAH, nitric acid, ammonium bicarbonate and optima grade methanol were obtained from Fisher Scientific (Pittsburgh, PA, USA). Ammonium phosphate monobasic, ammonium nitrate, ammonium hydroxide solution (20–22% NH<sub>3</sub>), trypsin from bovine pancreas, pronase E from *Streptomyces griseus* and lipase VII from *Candida rugosa* were purchased from Sigma–Aldrich Chemical Co. (St. Louis, MO, USA).

Stock standard solutions for As were: As(III) and As(V), 1000 mg As L<sup>-1</sup> from SPEX CertiPrep (Metuchen, NJ, USA); MMA, DMA, and AsB (1000 mg As L<sup>-1</sup>) were prepared by dissolving the appropriate amounts of sodium methylarsonate [CH<sub>3</sub>AsO(ONa<sub>2</sub>)\*6H<sub>2</sub>O] from ChemService (West Chester, PA, USA); sodium cacodylate [C<sub>2</sub>H<sub>6</sub>AsNaO<sub>2</sub>\*3H<sub>2</sub>O] from Sigma (St. Louis, MO, USA); and AsB (AsC<sub>5</sub>H<sub>11</sub>O<sub>2</sub>) from Argus Chemicals (Florence, Italy), in DDI water. Stock standard solutions of Se(IV), Se(VI) and SeMet (1000 mg Se L<sup>-1</sup>) were prepared by dissolving adequate amounts of sodium selenite (Na<sub>2</sub>SeO<sub>3</sub>), sodium selenate (Na<sub>2</sub>SeO<sub>4</sub>) and SeMet (C<sub>5</sub>H<sub>11</sub>NO<sub>2</sub>Se), from Sigma (St. Louis, MO, USA) in DDI water. The standard solutions were stored in amber high density polypropylene containers at 4 °C in a cold room. Analytical working standards were prepared daily by diluting the stock solutions with DDI water prior to analysis.

The following samples were used in this study: certified reference materials DOLT-3 Dogfish Liver [National Research Council of Canada (NRCC), Ontario, Canada] and BCR-627 Tuna Fish Tissue [Institute for Reference Materials and Measurements (IRMM), Geel, Belgium] together with fish tissues purchased at Pittsburgh, PA fish markets (shark, canned tuna in water, and marlin). The certified reference materials were used as received; all other samples were freeze-dried prior to the extraction procedure.

## 2.3. Procedures

### 2.3.1. Microwave-assisted digestion procedure

For the analysis of total As and Se, the samples were digested using EPA Method 3052 [25]. Approximately 500 mg representative samples were weighed into microwave vessels; 9 mL concentrated HNO<sub>3</sub> and 0.5 mL H<sub>2</sub>O<sub>2</sub> along with magnetic stir bar were added into each vessel. Vessels were then sealed and microwave-irradiated at 180 ± 5 °C for 10 min. After digestion, the digests were filtered through 0.22 μm Millipore glass fiber filters (Fisher Scientific, Pittsburgh, PA, USA). The digests were diluted to 30 mL with DDI water and stored in a cold room at 4 °C until analysis (usually within 48 h).

### 2.3.2. MAEE procedure

A 200 mg portion of sample with 20 mg of pronase E and 5 mg of lipase was weighed into individual Teflon digestion vessel; 10 mL of 50 mM phosphate buffer (pH 7.25) were added and a magnetic stir bar was placed into each vessel for thorough mixing of solvent with the sample. The microwave vessels were sealed and irradiated at 37 °C for 30 min and the ramp time was set as 10 min. After

microwave heating, the vessels were allowed to cool to room temperature and the extracts were centrifuged for 10 min at 4000 rpm. The supernatants were filtered through 0.22 μm glass fiber filters followed by a 1 + 3 fold dilution with DDI water. The extracts were stored at 4 °C in a cold room for analysis within 48 h. Blanks were prepared along with the samples in each batch.

### 2.3.3. As and Se species stability

A 200 mg of DOLT-3 was spiked with 100 μL of individual As and Se species [As(III), As(V), MMA, DMA, AsB, Se(IV), Se(VI) and SeMet] standard solution of 10 mg L<sup>-1</sup>, to which the extraction solvent was added. Samples were left for 1 h to equilibrate at room temperature, and then 20 mg of pronase E, 5 mg of lipase and 10 mL of 50 mM phosphate buffer (pH 7.25) were added. Three replicates were prepared in each case. The microwave vessels were sealed and irradiated at 37 °C for 30 min. Finally, the extracts were analyzed by IC–ICP–MS in the same way as the samples to verify As and Se species stabilities during the extraction procedure.

### 2.3.4. Analysis by ICP–MS and IC–ICP–MS

All samples were further diluted and analyzed by ICP–MS and IC–ICP–MS.

**2.3.4.1. Total As and Se determination by ICP–MS.** Total As and Se concentrations in the extracts and digests were determined by ICP–MS in spectrum mode. The isotopes <sup>75</sup>As, <sup>77</sup>Se and <sup>82</sup>Se were monitored. Samples were quantified by external calibration using matrix matching. Calibration was performed by using 0.5–20 μg L<sup>-1</sup> mixture of inorganic As and Se standards in 0.5% (v/v) HNO<sub>3</sub>. The operating conditions are given in Table 1. For Se, the Se isotope *m/z* 82 was used for data evaluation; similar result was obtained using the Se isotope *m/z* 77.

**2.3.4.2. Determination of As and Se species.** The extracts for As and Se species were analyzed by IC–ICP–MS and SEC–ICP–MS. For ICP–MS data acquisition, the time-resolved analysis mode was used. Each sample was analyzed three times. As and Se compounds were quantified by external calibration. Data evaluation was performed using the ChemStation software supplied with the instrument; quantification was performed based on peak areas.

## 3. Results and discussion

### 3.1. Determination of total As and Se in fish tissues

Total As and Se concentrations in DOLT-3, BCR-627 and fish tissues were determined after microwave acid digestion (EPA Method 3052) [25] by ICP–MS under conditions given in Table 1. The analytical results are shown in Table 2 (*n* = 3). The results for As and Se in DOLT-3 and BCR-627 using the proposed digestion procedure were in good agreement with the certified values at 95% confidence level. The content of As in the analyzed fish tissues ranged from 1.11 to 27 mg kg<sup>-1</sup>. The values of As in these fish samples were comparable with other data found in fish [26,27]. Se concentrations in fish

**Table 2**

Total As and Se concentrations (mg kg<sup>-1</sup>) found in fish tissues and the certified reference materials by ICP–MS after microwave digestion (EPA Method 3052).

Sample	Total As (mg kg <sup>-1</sup> )		Total Se (mg kg <sup>-1</sup> )	
	Certified value	Concentration found <sup>a</sup>	Certified value	Concentration found <sup>a</sup>
BCR-627 (IRMM, Belgium)	4.8 ± 0.3	4.8 ± 0.1	-	2.8 ± 0.2
DOLT-3 (NRCC, Canada)	10.2 ± 0.5	10.0 ± 0.2	7.06 ± 0.48	7.6 ± 0.2
Canned tuna (in water)		2.9 ± 0.1		5.6 ± 0.2
Shark		27 ± 1		2.0 ± 0.1
Marlin		1.11 ± 0.04		3.9 ± 0.1

<sup>a</sup> The results are expressed as mean value at 95% CL (*n* = 3).

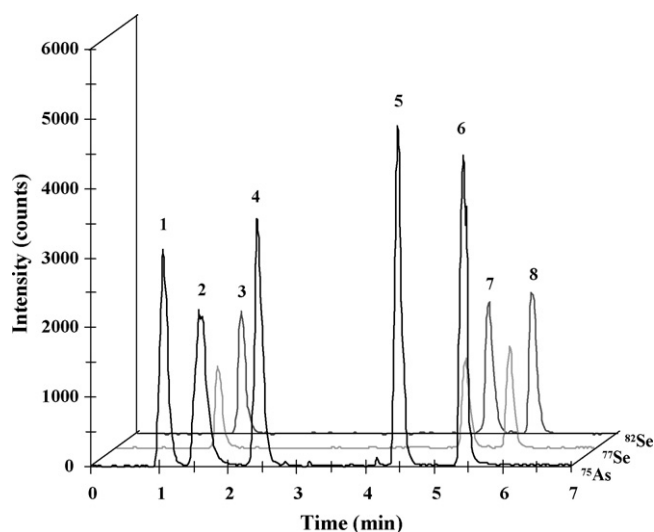


**Fig. 1.** IC-ICP-MS chromatogram of a 100  $\mu\text{L}$  injected standard solution containing 2  $\mu\text{g L}^{-1}$  of each As species and 8  $\mu\text{g L}^{-1}$  of each Se species. Peak identification: (1) AsBet, (2) As(III), (3) SeMet, (4) DMA, (5) MMA, (6) As(V), (7) Se(IV), and (8) Se(VI). The analysis was performed according to the optimum conditions shown in Table 1.

tissues varied between 2  $\text{mg kg}^{-1}$  (shark) and 5.6  $\text{mg kg}^{-1}$  (canned tuna). Se levels were higher than those published in the literature. The reported values were in the range of 0.25–1.02  $\text{mg kg}^{-1}$  [5,27,28]. Such differences could indicate bioaccumulation of Se in the analyzed fish samples.

### 3.2. Ion chromatography separation.

In this study, anion-exchange chromatography was employed for the separation of five As species and three Se species. Ammonium nitrate ( $\text{NH}_4\text{NO}_3$ ) was selected as the mobile phase with concentrations ranging from 5 to 50 mM at pH 8.7 based on a better sensitivity of the species of interest and lower retention times. Additionally, the use of  $\text{NH}_4\text{NO}_3$  as mobile phase has been shown to produce good signal stability on the ICP-MS with minimal salt deposit on the sample and skimmer cones [29]. The ionization of As and Se in the plasma was improved by adding 2% (v/v) methanol to the mobile phase. The chromatographic conditions are listed in Table 1. Fig. 1 shows an IC-ICP-MS chromatogram obtained for a standard solution containing 2.0  $\mu\text{g L}^{-1}$  of As per species [AsB, As(III), DMA, MMA, and As(V)] and 8.0  $\mu\text{g L}^{-1}$  of Se per species [SeMet, Se(IV), and Se(VI)]. Separation of As and Se species was resolved to baseline in less than 7 min. All calibrations were linear for As and Se species over the concentration range of 0.5–40  $\mu\text{g L}^{-1}$  and 1.5–20  $\mu\text{g L}^{-1}$ , respectively. Detection limits ( $S/N=3$ ) with a 100  $\mu\text{L}$  of injection volume were about 0.1  $\mu\text{g L}^{-1}$  for As species and 0.7  $\mu\text{g L}^{-1}$  for Se species. The reproducibility from multiple injections ( $n=5$ ) containing a mixture of As and Se species standard solution of 2.0  $\mu\text{g L}^{-1}$  and 8  $\mu\text{g L}^{-1}$ , respectively, showed that the RSD were less than 5% for all the species investigated.

### 3.3. Optimization of the MAEE procedure of As and Se species

Methods based on enzymatic hydrolysis have been widely used to efficiently extract protein-bound Se species [6,10,21,23] and arsenocompounds [19] in various fish tissues. In this study, the combination of pronase E/lipase mixture and MAE was evaluated for the first time for the simultaneous extraction of As and Se species in fish tissues. Preliminary experiments were carried out to develop the appropriate extraction conditions. The following variables were optimized in DOLT-3 certified reference material:

amount of pronase E and lipase, extraction pH, and irradiation time (Fig. 2). All experiments were carried out in triplicate with 200 mg of a lyophilized reference material. Irradiation temperature was maintained at 37 °C during the extraction (based on information from enzyme supplier). The minimum amount of solvent recommended by the manufacturer of the microwave system, 10 mL, was used in this study. Extraction efficiencies were calculated based on the certified values for As and Se in DOLT-3 sample.

#### 3.3.1. Amount of pronase E

The mass of pronase E was varied from 10, 20 or 40 mg (corresponding to 5:1, 10:1 and 20:1 sample/enzyme mass ratio), and a 10 mg portion of lipase in 10 mL phosphate buffer (pH 7.5) was added to the DOLT-3 reference material. Solutions were irradiated in a closed-vessel microwave oven at 37 °C for 1 h. As can be seen in Fig. 2a, the percent recovery of As increased from 74  $\pm$  1% when the extraction was completed with no pronase E, to 85  $\pm$  1%, in the presence of 40 mg of enzyme. As previously described [30], these results could indicate that As in fish tissue is not linked to proteins. With respect to Se, the amount of pronase E had a pronounced affect on its extraction efficiency. The percent recovery was found to increase from 26  $\pm$  1% without pronase E, to 86  $\pm$  3% using 40 mg of pronase E. Evidently, a high fraction of total Se in fish tissues is associated with proteins. Since there is no statistically significant difference between the extraction recovery of As and Se using either 20 or 40 mg of pronase E, 20 mg of pronase E (10:1 sample/enzyme mass ratio) was chosen for further experiments to minimize reagent consumption, and reduce the cost of the experiment. The sample/enzyme mass ratio of 10:1 has been widely used for the extraction of Se species in different biological materials, such as selenized yeast and fish tissues [6,20,22].

#### 3.3.2. Amount of lipase

Enzymatic extraction using pronase E/lipase mixture has been reported to be the most efficient approach for quantitative extraction of Se in biological samples [22,23]. In order to evaluate the effect of lipase on the extraction of As and Se from DOLT-3 reference material, a 200 mg of sample was treated with 20 mg pronase E and varying amounts of lipase (from 0 to 20 mg). The microwave extraction was performed at 37 °C for 1 h. Results are shown in Fig. 2b. The amount of lipase did not significantly affect the extraction efficiency of As and Se in DOLT-3. A slight increase of the extraction efficiency for both As and Se was observed using 5 mg lipase. Although 20:1 (sample/lipase mass ratio) has been commonly reported for the extraction of Se compounds in biological matrices [22,23], a smaller amount of lipase (sample/lipase mass ratio of 40:1) was required in this study for the simultaneous extraction of As and Se in fish tissues. The percent recovery of As and Se at the aforementioned sample/lipase ratio was 84  $\pm$  1 and 90  $\pm$  3%, respectively.

#### 3.3.3. pH

Typically, enzymatic extraction is carried out in a buffer solution (Tris-HCl or phosphate buffer) under the standard conditions of pH that are recommended by the manufacturer of selected enzymes (pH 7.2 for lipase and 7.5 for pronase E). The application of a buffer solution is recommended in some matrices since the enzymes have optimal pH ranges, rendering necessary careful control of pH when the enzymatic procedure is in progress [31]. The pH range between 7.0 and 7.5 using 50 mM phosphate buffer was evaluated (see Fig. 2c). A modest improvement in the extraction efficiency of As and Se was observed when the pH was  $\geq$  7.25. The extraction recovery for As and Se was 80  $\pm$  1 and 85  $\pm$  3%, respectively, by using pH 7.25. A pH value of 7.25 was selected to comprise a satisfactory extraction recovery for As and Se.

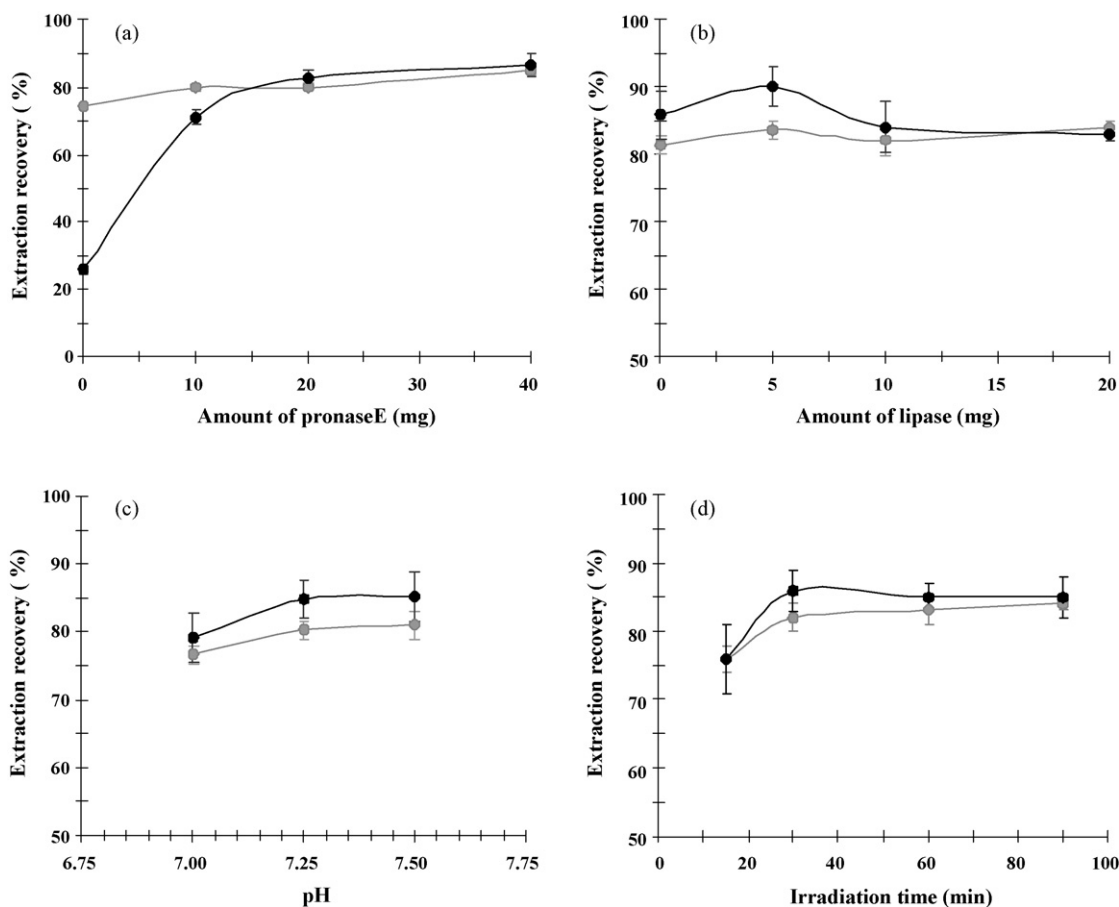


**Fig. 2.** Recovery of As (●) and Se (—●—) from DOLT-3 dogfish liver certified reference material during the evaluation of the following MAEE parameters: (a) amount of pronase E, (b) amount of lipase, (c) pH and (d) irradiation time. Results were expressed as the mean value  $\pm$  standard deviation ( $n = 3$ ).

### 3.3.4. Irradiation time

Irradiation time ranging from 20 to 90 min was investigated at 37 °C. As can be seen from Fig. 2d, a slight increase in the extraction efficiencies of both As and Se was observed for times longer than 30 min. At 30 min irradiation time, the extraction recoveries of As and Se were  $83 \pm 2$  and  $85 \pm 3\%$ , respectively. Since longer extraction times did not further improve percent recovery of As and Se from DOLT-3, an extraction time of 30 min was selected as the optimal time throughout the rest of the study.

The following extraction conditions were adopted for the simultaneous extraction of As and Se in fish tissues: 20 mg pronase E, 5 mg lipase, 10 mL of 50 mM phosphate buffer (pH 7.25) and an extraction time of 30 min. The advantage of this extraction procedure is the shorter extraction time, compared to traditional enzymatic approaches that normally require a treatment period of 20 h. Additionally, the proposed MAEE extraction method offers significant advantages include multielemental speciation extraction capabilities, high sample throughput, adequate temperature control, and minimum risk of contamination or loss of the analyte since the reaction takes place in a closed system.

### 3.3.5. Stability of As and Se species during MAEE

The stability of the As and Se species under the extraction conditions was also determined by spiking individual As [As(III), DMA, MMA, As(V) and AsB] and Se species [Se(IV), Se(VI) and SeMet] into the dogfish liver reference material. Single peaks were identified for all the species following IC-ICP-MS analysis with extraction recoveries in the range 99–106% for As, and 97–104% for Se species of the original spiked standard solutions. The results confirmed the absence of significant losses or

transformations of As and Se species during the MAEE procedure.

### 3.4. Comparison of the developed method with common extraction procedures

The capability of the proposed method for the simultaneous extraction of As and Se was compared with common extraction procedures used for the extraction of As [16,18,19] or Se [6,10,22] in DOLT-3 reference material. The extraction recovery was then calculated based on the certified values of total As and Se in DOLT-3. The comparative results are shown in Table 3. The evaluated extraction procedures were based on the application of the following reagents: 80% (v/v) methanol in water, 8.3% (v/v) TMAH in water and three different enzymes: trypsin, pronase E and pronase E/lipase. The evaluated enzymatic digestion procedures were performed with incubation in a water bath at 37 °C for 12 h (trypsin procedure) and 20 h (pronase E and pronase E/lipase procedures) and with microwave irradiation at 37 °C for 30 min (pronase E/lipase).

Results for total As determination in DOLT-3 (Table 3) showed that the lowest extraction recovery (63% from the certified value) was obtained with aqueous 80% (v/v) MeOH. Lower extraction recoveries of As (76%) have also been reported in dogfish liver reference material (DOLT-1) using 50% (v/v) methanol in water extraction [15]. The conventional enzymatic extraction procedures using trypsin, pronase E, pronase E/lipase provided extraction recoveries between 73 and 76%. The differences in the extracted As were not statistically significant among the three enzymes (one-way ANOVA test,  $P < 0.05$ ) when conventional enzymatic extraction procedures was used. Regarding the enzymatic extraction with the

**Table 3**Total As and Se concentration found in DOLT-3 CRM (dogfish liver) following different extraction procedures ( $n = 3$ , at 95% CL)<sup>a</sup>.

Extraction reagent	Extraction conditions	Concentration found (mg kg <sup>-1</sup> ) <sup>b</sup>		Ref.
		As	Se	
80% (v/v) methanol in water	200 mg of sample and 10 mL of 80% (v/v) methanol in water. MAE at 80 °C for 5 min	6.4 ± 0.1 (63 ± 1)	0.94 ± 0.05 (13 ± 1)	[18]
8.3% (v/v) TMAH in water	300 mg of sample and 9 mL of the mixture containing 3 mL 25% (w/v) TMAH solution and 6 mL DDI water. MAE at 50 °C for 20 min	9.0 ± 0.1 (88 ± 1)	7.6 ± 0.2 (107 ± 2)	[21]
Trypsin	250 mg of sample, 100 mg trypsin and 20 mL 0.1 M carbonate buffer (pH 8). Conventional enzymatic extraction at 37 °C for 12 h	7.7 ± 0.2 (76 ± 2)	5.0 ± 0.1 (70 ± 2)	[22]
Pronase E	200 mg of sample, 20 mg pronase E and 10 mL 50 mM phosphate buffer (pH 7.5). Conventional enzymatic extraction at 37 °C for 20 h	7.6 ± 0.1 (74 ± 1)	5.0 ± 0.3 (71 ± 4)	[6]
Pronase E/lipase	200 mg of sample, 20 mg pronase E, 10 mg lipase and 10 mL 50 mM phosphate buffer (pH 7.5). Conventional enzymatic extraction at 37 °C for 20 h	7.4 ± 0.2 (73 ± 3)	5.4 ± 0.1 (77 ± 1)	[25]
Pronase E/lipase	200 mg of sample, 20 mg pronase E, 5 mg lipase and 10 mL 50 mM phosphate buffer (pH 7.25). MAE at 37 °C for 30 min	8.4 ± 0.1 (82 ± 1)	5.9 ± 0.2 (84 ± 3)	This study

<sup>a</sup> Certified values for total As and Se in DOLT-3 CRM are 10.2 ± 0.5 and 7.06 ± 0.48 mg kg<sup>-1</sup>, respectively.<sup>b</sup> In parentheses, the percent recovery of different extraction methods (%) referred to the certified value.

proteolytic enzyme pronase E, the extraction recovery of As was not enhanced using pronase E/lipase mixture. However, higher extraction recovery for As was obtained using this mixture of enzymes when the extraction procedure involved the action of microwave compared with the conventional enzymatic procedure. The results showed that the extraction recovery of As in DOLT-3 was 82 ± 1%. It is observed from Table 3 that the TMAH procedure using MAE provided the highest extraction recoveries for As (88 ± 1%), although interconversion of As(III) to As(V) was observed during the extraction with TMAH. Results obtained during the current study were in agreement with those from previous studies reported in the literature [12].

With respect to Se, extraction with methanol/water mixture provided the lowest amount of leached Se from DOLT-3 (13%). Similar results were reported by Casiot et al. [22] in selenized yeast using water/methanol extractant. The results for the three enzymatic procedures using incubation in water bath at 37 °C showed statistically significant differences in the extraction recovery of Se (one-way ANOVA test,  $P > 0.05$ ). The extraction recoveries of Se were in the range from 70% (trypsin) to 77% (pronase E/lipase). It is known that trypsin is a specific proteolytic enzyme that breaks peptide bonds at specific regions of the protein chain, while pronase, an unusually non-specific proteolytic enzyme, can act along the entire protein structure [31]. These differences in the mechanism of the two enzymes may explain the higher extraction efficiency of pronase compared to that of trypsin (see Table 3). On the other hand, an increase in the extraction yield was obtained using pronase E/lipase mixture compared with pronase probably due to the significant amount of Se bound to lipids indicating that the use of lipase is justified in this matrix. The application of microwave technology for

the pronase E/lipase mixture increased the extraction recovery of Se from DOLT-3 to 84 ± 3%, compared to 77 ± 1% for the conventional enzymatic procedure using pronase/lipase. The microwave technique appears to provide effective disruption of the sample, thus facilitating enzyme interaction with liberated compounds, resulting in a reduction of sample treatment time from 20 h to 30 min. Although quantitative Se extraction recoveries were achieved using TMAH reagent (107 ± 2%), Se species present in the sample were degraded to inorganic Se during extraction. Conversion of original Se species to Se(VI) in selenized yeast has been reported when alkaline hydrolysis was performed using 25% (v/v) TMAH reagent [22]. Results from this comparative study demonstrate that MAEE procedure using pronase E/lipase mixture is the most suitable method for the simultaneous extraction of As and Se in fish tissues.

### 3.5. Determination of total As and As species in fish tissue extracts after MAEE procedure

The robustness of the optimized extraction MAEE procedure was assessed using two marine certified reference materials (BCR-627 and DOLT-3) and three fish tissues. Following enzymatic extraction, the samples were analyzed for total As by direct ICP-MS and for As species applying the above optimized IC-ICP-MS method. The results are shown in Table 4. For the reference materials, the extraction recoveries of total As were 94 ± 3%, and 82 ± 1% for BCR-627 and DOLT-3. Lower extraction recoveries of total As have been previously published in dogfish liver reference material. Kirby et al. [15] reported an extraction efficiency of 62% in DOLT-1 after water/methanol extraction, and Wahlen et al. [13] reported an extraction efficiency of 55% using water/sonication protocol. The

**Table 4**Analytical results for total As and As species after the proposed MAEE procedure. The results are indicated at 95% CL for  $n = 3$ .

Sample	Total As extracted (mg kg <sup>-1</sup> )	As containing species (mg kg <sup>-1</sup> )					Sum of the species (mg As kg <sup>-1</sup> ) <sup>c</sup>
		AsB	As(III)	DMA	MMA	As(V)	
BCR-627 (IRMM, Belgium) <sup>d</sup>	4.5 ± 0.1 (94 ± 3) <sup>a</sup>	4.17 ± 0.07	ND <sup>e</sup>	0.18 ± 0.01	ND <sup>e</sup>	ND <sup>e</sup>	4.4 ± 0.1 (98 ± 2)
DOLT-3 (NRCC, Canada)	8.4 ± 0.1 (82 ± 1) <sup>a</sup>	7.2 ± 0.1	ND <sup>e</sup>	0.48 ± 0.01	ND <sup>e</sup>	0.08 ± 0.02	7.7 ± 0.1 (92 ± 1)
Canned tuna (in water)	3.1 ± 0.1 (106 ± 2) <sup>b</sup>	2.8 ± 0.2	0.04 ± 0.01	0.03 ± 0.01	0.06 ± 0.01	<LOD <sup>f</sup>	2.9 ± 0.2 (94 ± 6)
Shark	27.4 ± 0.8 (101 ± 3) <sup>b</sup>	25.7 ± 0.4	2.7 ± 0.1	0.03 ± 0.01	ND <sup>e</sup>	0.06 ± 0.01	28.4 ± 0.5 (103 ± 2)
Marlin	0.70 ± 0.01 (63 ± 1) <sup>b</sup>	0.72 ± 0.07	<LOD <sup>f</sup>	ND <sup>e</sup>	ND <sup>e</sup>	0.04 ± 0.01	0.76 ± 0.07 (109 ± 10)

<sup>a</sup> In parentheses, the extraction recovery based on total As certified values.<sup>b</sup> In parentheses, the extraction recovery based on the total As determined by microwave-assisted total digestion (EPA Method 3052).<sup>c</sup> In parentheses, total As speciation recovery based on total As extracted.<sup>d</sup> Certified values for AsB and DMA in BCR-627 reference material are 3.90 ± 0.22 and 0.15 ± 0.02 mg kg<sup>-1</sup>, respectively.<sup>e</sup> Non-detectable.<sup>f</sup> Detection limits for AsB, As(III), DMA, MMA, and As(V) are 0.022, 0.015, 0.016, 0.014 and 0.017 mg kg<sup>-1</sup> in fish tissues.

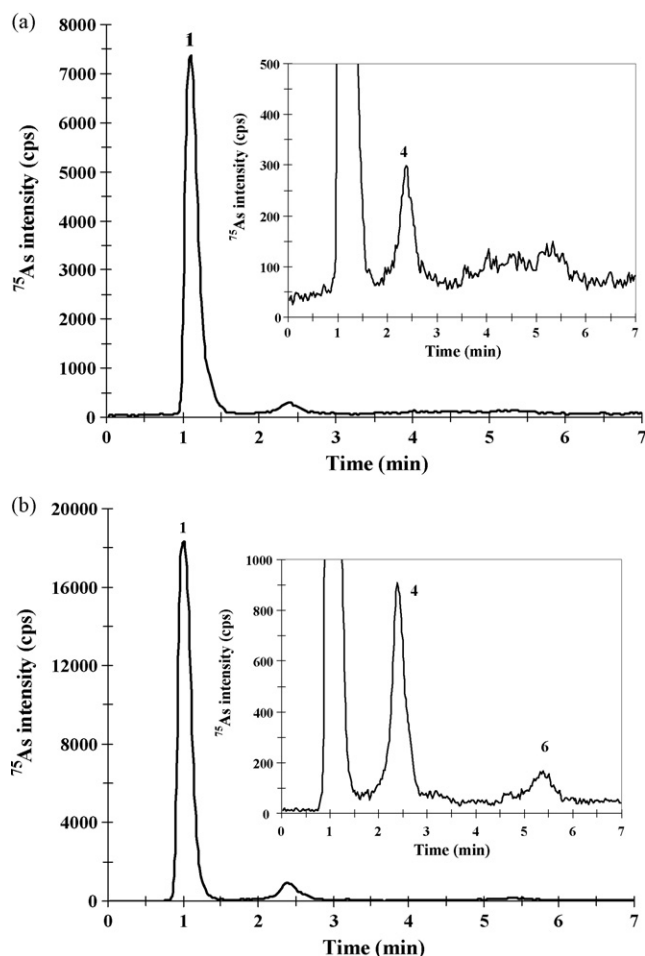


Fig. 3. IC-ICP-MS profile of enzymatic extracts of (a) BCR-627 and (b) DOLT-3 obtained by MAEE. Peak identification: (1) AsBet, (4) DMA, and (6) As(V).

low total As extraction efficiency in this reference material can be partially accounted for by the nature of fish tissue (fibrous with a significant range of particle size) [13].

The method was applied to the analysis of commercial fish tissues showing quantitative recoveries of total As for canned tuna and shark; lower As extraction recovery was obtained for marlin tissue. The percentage of total As extracted in marlin was  $63 \pm 1\%$ . The lower recovery was due to the difficulty of obtaining complete extraction in this fish tissue. It has been reported that the presence of other compounds, such as lipids, can reduce the extraction efficiency of As species in fish tissues [12].

IC-ICP-MS chromatograms of enzymatic extracts of BCR-627 and DOLT-3 obtained by MAEE under the optimized conditions are shown in Fig. 3. Speciation recoveries were calculated by comparing the sum of As species concentrations with the total As extracted. The results of species quantification are shown in Table 4. Results of total As in the extracts and the sum of each As species quantified were in good agreement.

As speciation results were validated by the analysis of BCR-627, which is certified for AsB and DMA (Fig. 3a). No significant differences were found between the certified values and the results obtained by using MAEE during this study at the 95% confidence level (Table 4). In DOLT-3 reference material (Fig. 3b), the major species was AsB (86%), while the levels of DMA and As(V) were much lower. Different relative As distribution among these species was reported in DOLT-2 by Wahlen et al. [13]. The two major species in DOLT-2 tissue extracted by sonication with water were AsB (67%) and DMA (14%). It can be seen from Table 4 that AsB was found to

Table 5

Analytical results for total Se and SeMet after the proposed MAEE procedure. The results are indicated at 95% CL for  $n = 3$ .

Sample	Total Se extracted ( $\text{mg kg}^{-1}$ )	SeMet ( $\text{mg Se kg}^{-1}$ ) <sup>c</sup>
BCR-627 (IRMM, Belgium)	$1.6 \pm 0.2$ ( $57 \pm 9$ ) <sup>a</sup>	$0.6 \pm 0.1$ ( $38 \pm 6$ )
DOLT-3 (NRCC, Canada)	$5.9 \pm 0.2$ ( $84 \pm 3$ ) <sup>b</sup>	$0.5 \pm 0.1$ ( $9 \pm 2$ )
Canned tuna (in water)	$5.5 \pm 0.2$ ( $98 \pm 3$ ) <sup>a</sup>	$1.6 \pm 0.1$ ( $29 \pm 2$ )
Shark	$0.9 \pm 0.1$ ( $46 \pm 5$ ) <sup>a</sup>	$0.5 \pm 0.1$ ( $56 \pm 11$ )
Marlin	$3.5 \pm 0.1$ ( $89 \pm 3$ ) <sup>a</sup>	$1.6 \pm 0.1$ ( $46 \pm 3$ )

<sup>a</sup> In parentheses, the extraction recovery based on the total Se determined by microwave-assisted total digestion (EPA Method 3052).

<sup>b</sup> In parentheses, the extraction recovery based on total Se certified value.

<sup>c</sup> In parentheses, SeMet recovery based on total Se extracted.

be the predominant As species in the commercial fish samples. The amount of As determined in fish tissues varied depending on the type of fish analyzed, but the percentage of AsB was always higher than 87% of the total As extracted. Considerable concentrations of As(III) in shark tissue were detected. The levels of DMA, MMA and As(V) were much lower in the analyzed fish tissues.

### 3.6. Determination of total Se and Se species in fish tissue extracts after MAEE procedure

As can be seen from Table 5, the percentages of extractable Se for the certified reference materials were  $57 \pm 9\%$  for BCR-627 and  $84 \pm 3\%$  for DOLT-3. Díaz Huerta et al. [20] reported total Se recoveries of 63% when conventional enzymatic hydrolysis using protease XIV/lipase was applied to cod muscle BCR-422 reference material. In the commercial fish tissues, the Se recoveries ranged from 46% (shark) to 98% (canned tuna). The extraction recoveries of Se were comparable with other reported data in fish and shellfish samples after enzymatic extraction with proteolytic enzymes. The extraction recoveries were between 65 and 96% [5,21].

It is interesting to observe that the sum of Se species detected by IC-ICP-MS was much lower than the total Se in the resulting enzymatic extracts of all fish tissues studied. SeMet was the only Se compound detected in the samples. Fig. 4a shows a chromatogram of BCR-627 extract after MAEE. Results for speciation analysis in fish tissue extracts are shown in Table 5. In the reference materials BCR-627 and DOLT-3, 38 and 9%, respectively, of the total Se extracted was identified as SeMet. For other analyzed fish tissues, the total amount of SeMet varied depending on type of fish. In shark, 56% of the total Se extracted was SeMet, whereas canned tuna presented lower percentage of SeMet (29% of the total Se extracted). Percentages of SeMet for these fish species were comparable with other reported values in fish tissues between 28 and 93% for tuna and swordfish, respectively [5] and shellfish (35% for Antarctic krill) [10] after enzymatic hydrolysis. It has been demonstrated that during the enzymatic extraction of marine tissues, some Se compounds might remain bound in peptide form, depending on the cleavage specificity of the enzyme and the analyzed fish species [5,6,10,21]. In order to confirm those results, enzymatic extracts of fish tissues were analyzed by SEC-ICP-MS. The chromatographic conditions are listed in Table 1. The chromatographic profile for BCR-627 is shown in Fig. 4b. Two fractions of high molecular weight (fractions II and III) with mass ranges ( $M_r$ ) between 20 and 200 kDa, and a fraction of low molecular weight (fraction I,  $20 \geq M_r \geq 0.2$  kDa) were clearly differentiated after molecular mass calibration of the column (using transferrin, albumin, myoglobin, insulin and SeMet). The low molecular mass range (fraction I) showed the match in retention time of a peak at 8.2 min and SeMet standard, which represented approximately 40% of the total Se in the extract. The results obtained for BCR-627 by SEC were in agreement with the quantitative data of SeMet obtained by IC.

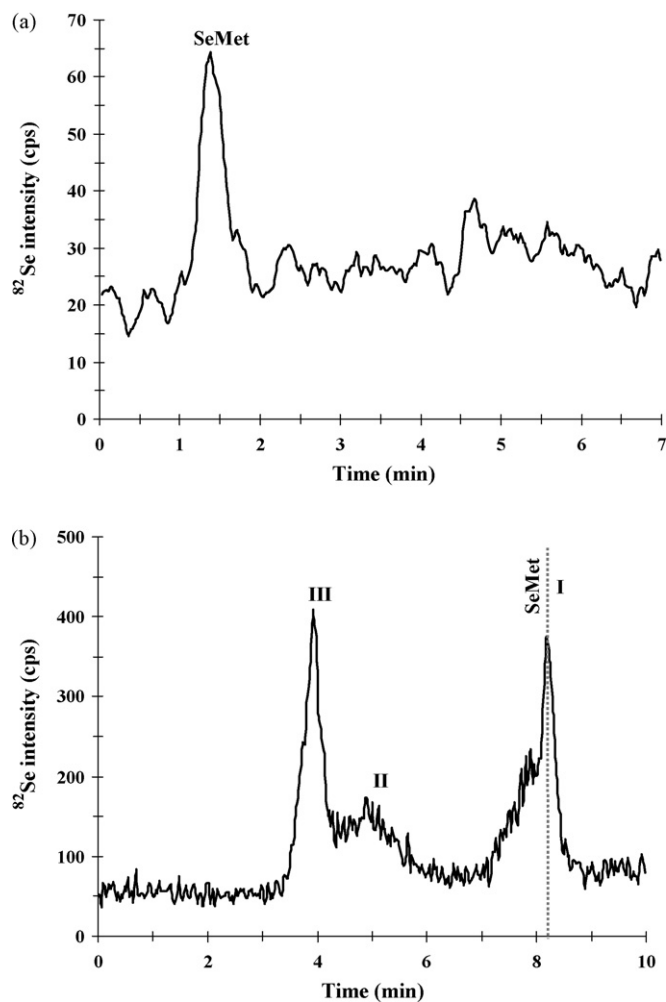


**Fig. 4.** Typical chromatograms obtained by the analysis of BCR-627 extract from MAEE using: (a) anion-exchange chromatography (IC) and (b) size exclusion chromatography (SEC). For Se chromatogram (b), identified fractions were I (20–0.2 kDa), II (150–20 kDa) and III (>150 kDa).

#### 4. Conclusions

The results presented in this study demonstrate for the first time the potential of microwave technology to assist enzymatic extraction of As and Se species from fish tissues prior to their analysis by IC–ICP–MS. MAEE using pronase E/lipase mixture provided, in most of the cases, good extraction efficiencies without chemical alteration of the As and Se species during the extraction process. Additionally, a significant reduction in the extraction time (30 min) was attained using closed vessel MAEE, compared with conventional enzymatic extraction (20 h), simplifying sample preparation steps. Extraction recoveries were in the range of  $63 \pm 1$  to  $106 \pm 2\%$  for As and  $46 \pm 5$  to  $98 \pm 3\%$  for Se.

For As species, good agreement was obtained between the sum of the species quantified and the total As found in the extracts. In

all the fish tissues investigated, the As existed almost exclusively in the form of AsB. For Se, SeMet was the only Se compound found in fish tissues after the enzymatic hydrolysis process. Moreover, SeMet content corresponds to between 29 and 55% of the total Se extracted during the enzymatic extraction since some Se-peptides or Se-containing proteins remained intact.

#### Acknowledgements

The authors are grateful to Milestone, Srl; Metrohm-Peak, LLC; Applied Isotope Technologies, Inc.; and Duquesne University for instrumental and material support. L.H. Reyes thanks Milestone, Srl for financial support. J.L. Guzmán Mar specially acknowledges CONACyT-Mexico for the postdoctoral scholarship.

#### References

- [1] K. Wrobel, K. Wrobel, J.A. Caruso, *Anal. Bioanal. Chem.* 381 (2005) 317–331.
- [2] C. B'Hymer, J.A. Caruso, *J. Chromatogr. A* 1114 (2006) 1–20.
- [3] J. Borak, H. Dean Hosgood, *Regul. Toxicol. Pharmacol.* 47 (2007) 204–212.
- [4] S. McSheehy, J. Szpunar, R. Morabito, P. Quevauviller, *Trends Anal. Chem.* 22 (2003) 191–209.
- [5] A.I. Cabañero, C. Carvalho, Y. Madrid, C. Batoreu, C. Cámara, *Biol. Trace Elem. Res.* 103 (2005) 17–35.
- [6] P. Moreno, M.A. Quijano, A.M. Gutiérrez, M.C. Pérez-Conde, C. Cámara, *Anal. Chim. Acta* 524 (2004) 315–327.
- [7] E.C. Pappa, A.C. Pappas, P.F. Surai, *Sci. Total Environ.* 372 (2006) 100–108.
- [8] M. Sager, *Pure Appl. Chem.* 78 (2006) 111–133.
- [9] H. Zeng, E.O. Uthus, G.F. Combs Jr., *J. Inorg. Biochem.* 99 (2005) 1269–1274.
- [10] M. Siwek, A.B. Noubar, J. Bergmann, B. Niemeyer, B. Galunsky, *Anal. Bioanal. Chem.* 384 (2006) 244–249.
- [11] E. Peachey, N. McCarthy, H. Goenaga-Infante, *J. Anal. Atom. Spectrom.* 23 (2008) 487–492.
- [12] E.H. Larsen, J. Engman, J.J. Sloth, M. Hansen, L. Jorhem, *Anal. Bioanal. Chem.* 381 (2005) 339–346.
- [13] R. Wahlen, S. McSheehy, C. Scriver, Z. Mester, *J. Anal. Atom. Spectrom.* 19 (2004) 876–882.
- [14] R.Y. Wang, Y.L. Hsu, L.F. Chang, S.J. Jiang, *Anal. Chim. Acta* 590 (2007) 239–244.
- [15] J. Kirby, W. Maher, *J. Anal. Atom. Spectrom.* 17 (2002) 838–843.
- [16] K.L. Ackley, C. B'Hymer, K.L. Sutton, J.A. Caruso, *J. Anal. Atom. Spectrom.* 14 (1999) 845–850.
- [17] J.J. Sloth, E.H. Larsen, K. Julshamn, *J. Agric. Food Chem.* 53 (2005) 6011–6018.
- [18] I.B. Karadjova, P.K. Petrov, I. Serafimovski, T. Stafilov, D.L. Tsalev, *Spectrochim. Acta, Part B* 62 (2007) 258–268.
- [19] S. Rattanachongkiat, G.E. Millward, M.E. Foulkes, *J. Anal. Atom. Spectrom.* 6 (2004) 254–261.
- [20] V. Díaz Huerta, M.L. Fernández Sánchez, A. Sanz-Medel, *J. Anal. Atom. Spectrom.* 19 (2004) 644–648.
- [21] M. Siwek, B. Galunsky, B. Niemeyer, *Anal. Bioanal. Chem.* 381 (2005) 737–741.
- [22] C. Casiot, J. Szpunar, R. Lobiski, M. Potin-Gautier, *J. Anal. Atom. Spectrom.* 14 (1999) 645–650.
- [23] J.L. Gómez-Ariza, M.A. Caro de la Torre, I. Giráldez, D. Sánchez-Rodas, A. Velasco, E. Morales, *Appl. Organomet. Chem.* 16 (2002) 265–270.
- [24] K. Srogi, *Anal. Lett.* 39 (2006) 1261–1288.
- [25] US EPA Method 3052: microwave assisted acid digestion of siliceous and organically based matrices, in: *Test Methods for Evaluating Solid Waste, Physical/Chemical Methods SW-846*, US Government Printing Office (GPO), Washington, DC, 1996.
- [26] K. Wrobel, K. Wrobel, B. Parker, S.S. Kannamkumarath, J.A. Caruso, *Talanta* 58 (2002) 899–907.
- [27] J. Burger, M. Gochfeld, *Environ. Res.* 99 (2005) 403–412.
- [28] A.I. Cabañero, Y. Madrid, C. Cámara, *Anal. Chim. Acta* 526 (2004) 51–61.
- [29] Y. Martínez-Bravo, A.F. Roig-Navarro, F.J. López, F. Hernández, *J. Chromatogr. A* 926 (2001) 265–274.
- [30] E. Sanz, R. Muñoz-Olivas, C. Cámara, *J. Chromatogr. A* 1097 (2005) 1–8.
- [31] G. Vale, R. Rial-Otero, A. Mota, L. Fonseca, J.L. Capelo, *Talanta* 75 (2008) 872–884.



## A new method for electrocatalytic oxidation of ascorbic acid at the Cu(II) zeolite-modified electrode

Tahereh Rohani\*, Mohammad Ali Taher

Department of Chemistry, Shahid Bahonar University of Kerman, P.O. Box 76175-133, Kerman, Iran

### ARTICLE INFO

#### Article history:

Received 24 August 2008  
Received in revised form 16 December 2008  
Accepted 16 December 2008  
Available online 30 December 2008

#### Keywords:

Electrocatalytic oxidation  
Modified electrode  
Cu<sup>2+</sup>A/ZCME  
Ascorbic acid

### ABSTRACT

A new method is developed for the catalytic oxidation of ascorbic acid at graphite zeolite-modified electrode, doped with copper(II) (Cu<sup>2+</sup>A/ZCME). Copper(II) exchanged in zeolite type A acts as catalyst to oxidize ascorbic acid. The modified electrode lowered the overpotential of the reaction by ~400 mV. First, the electrochemical behavior of copper(II), incorporated in the zeolite type A modified electrode, was studied. The results illustrate that diffusion can control the copper(II)/copper(0) redox process at the Cu<sup>2+</sup>A/ZCME. Then, the behavior of electrocatalytic oxidation reaction for ascorbic acid was researched. The electrode was employed to study electrocatalytic oxidation of ascorbic acid, using cyclic voltammetry and chronoamperometry as diagnostic techniques. The diffusion coefficient of ascorbic acid was equal to  $1.028 \times 10^{-5} \text{ cm}^2 \text{ s}^{-1}$ . A linear calibration graph was obtained over the ascorbic acid with a concentration range of 0.003–6.00 mmol L<sup>-1</sup>. The detection limit (DL) of ascorbic acid was estimated as  $2.76 \times 10^{-7} \text{ mol L}^{-1}$ . The relative standard deviations of 10 replicate measurements (performed on a single electrode at several ascorbic acid concentrations between 3.0 and 200  $\mu\text{mol L}^{-1}$ ) were measured between 1.0 and 2.4%.

© 2008 Elsevier B.V. All rights reserved.

### 1. Introduction

Vitamin C or L-ascorbic acid is distributed widely in both plant and animal kingdoms. In vegetable cells, it can be found in free form (often bound to protein as “ascorbigen”). Among animal organs, the liver, leukocytes and anterior pituitary lobe show the highest concentration levels of ascorbic acid. Vitamin C, a water-soluble vitamin, which is essential to metabolism and is consumed on a large scale, is electroactive and, therefore, a variety of methods have been developed for its analysis. Spectrophotometric methods have been applied for the analyses of vitamin C in pharmaceutical preparations and fruit juices [1,2]. Enzyme based electrodes [3], polymer based electrodes [4], dye based electrodes [5], etc. have been also proposed for the electrochemical detection and determination of ascorbic acid.

Chemically modified electrodes (CMEs) have recently attracted much attention [6–11]. They are characterized by a chemically altered surface displaying new qualities that can be exploited for electrochemical purposes. Zeolite-modified electrode (ZMEs) which have been widely studied recently, form a subcategory of the chemically modified electrodes [12,13]. There are three major reasons why ZMEs are so important. Firstly, because they combine the advantages of ion-exchange voltammetry with unique molecular-

sieving properties of the zeolite. One can therefore distinguish between the reactants small enough to diffuse freely within the zeolite framework, and excluded from (or occluded in) the structure, and thus, not directly involved in the mass transport reactions. The second reason is linked to the development of new electroanalytical devices (sensors); combining the considerable properties of zeolites (size-selectivity, ion-exchange capacity, high thermal and chemical stability) with the high sensitivity of modern electrochemical techniques, results in more significant improvements compared to the other sensors based on chemically modified electrodes. The third reason for investigating ZMEs is related to their possible use in electrocatalysis. Zeolites attract interest for this application because they offer a selectivity based on the size (and shape) of the reactants, together with a three-dimensional lattice (made of interconnected cages of molecular dimension) coming in a variety of support sites for various catalysts. Although studies of ZMEs focus mainly on preparation methods of the modified electrode, electrochemical characterization of ion exchange and the electrode process, as well as on discussion of electron-transfer mechanism [14,15], only a few articles have emerged on electroanalytical application of ZMEs [16,17].

In particular, substantial efforts have been devoted to the development of voltammetric biosensors based on ZMEs, such as dopamine [18], glucose [19] and phenols [20] biosensors. Zeolite is an interesting material for applications in electroanalytical chemistry; Rolison [21] and Walcarius [22] have published reviews on this subject. A complete comprehension for electrochemical

\* Corresponding author. Tel.: +98 341 3220041; fax: +98 341 3643853.  
E-mail address: [th.rohani@yahoo.com](mailto:th.rohani@yahoo.com) (T. Rohani).

behavior produced by electroactive species in zeolite particles can facilitate the development of sensors. This article reports on studies of the electrochemical behavior of copper(II) incorporated in ZCME and the application of the modified electrode, and can be useful in facilitating the biosensor development based on ZMEs.

## 2. Experimental

### 2.1. Reagents and chemicals

Pure sodium zeolite type A (Na-LTA) powder was synthesized from the raw and accessible materials through a hydrothermal method described in the literature [23]. The synthetic zeolite was characterized by X-ray diffraction (XRD) and infrared (IR) spectroscopy. Then the product was subjected to X-ray fluorescence (XRF) analysis to confirm successful synthesis of zeolite with Si:Al = 1.7 and unit cell formula  $\text{Na}_{12}[(\text{AlO}_2)_{12}(\text{SiO}_2)_{12}]\cdot 27\text{H}_2\text{O}$ .

Graphite powder, ascorbic acid, sodium oxalate, oxalic acid, benzyltrimethyltetradecylammonium chloride-dihydrate, potassium and sodium nitrates, and all other chemicals were of analytical reagent grade from Merck. Doubly distilled, deionized water was used for all experiments. Ascorbic acid solutions were freshly prepared as required and were kept protected against exposure to light during the investigation. Oxalate buffer was prepared from  $0.1 \text{ mol L}^{-1}$  sodium oxalate and the desirable pH was adjusted by addition of sodium hydroxide or oxalic acid solution as appropriate.

### 2.2. Apparatus

Voltammetric experiments were performed using a Metrohm electroanalyzer (Model 757 VA computrace). The measurements were recorded using VA computrace version 2.0 on windows 98 functional system. All voltammograms were recorded with a three-electrode system consisting of an Ag/AgCl reference electrode, a platinum wire as the counter electrode, and a  $\text{Cu}^{2+}$ /ZCME as the working electrode. A Metrohm 710 pH meter was used for pH adjustments. All the electrochemical experiments were carried out under pure nitrogen atmosphere at room temperature ( $23 \pm 1^\circ\text{C}$ ).

### 2.3. Electrode preparation

One gram of zeolite type A was lightly ground and immersed to 100 mL solution of  $0.02 \text{ mol L}^{-1}$   $\text{Cu}(\text{NO}_3)_2\cdot 3\text{H}_2\text{O}$  and was stirred on a magnetic stirrer for 24 h. The exchanged zeolite was washed firstly with dilute  $\text{HNO}_3$  ( $0.01 \text{ mol L}^{-1}$ ) solution to remove occluded material and surface-adherent salt, and then with doubly distilled water until normal pH was obtained and dried in air.

Twenty milligram of zeolite type A loading  $\text{Cu}^{2+}$  was lightly ground together with 18 mg of graphite powder for about 15 min. This product was dispersed in a solution of tetrahydrofuran (1 mL) and PVC (0.04 g). Then  $20 \mu\text{L}$  of this suspension was applied to a clean platinum electrode surface, and was allowed to dry in the air for about 30 min. The CME, used for comparison, was prepared in the same way but omitting the zeolite addition step.

### 2.4. Procedure

For cyclic voltammetric experiments, 20 mL of solution containing  $15 \text{ mL } 0.5 \text{ mol L}^{-1}$   $\text{NaNO}_3$  and  $5 \text{ mL } 0.10 \text{ mol L}^{-1}$  oxalate buffer (pH 4.5), was pipetted into the electrochemical cell and deaerated by purging with high purity nitrogen for 5 min. The inert gas was passed over the solution during all the voltammetric measurements. The modified electrode together with the reference and the counter electrodes were immersed into the solution and after several preliminary scans; the potential was scanned from  $-0.5$  to  $+0.5 \text{ V}$  vs. Ag/AgCl using cyclic voltammetry. The peak current was

appeared at a potential of  $0.023 \text{ V}$  vs. Ag/AgCl. Then different volumes of ascorbic acid solution were added to the voltammetric cell and the potential was scanned from  $-0.5$  to  $+0.5 \text{ V}$  vs. Ag/AgCl. All electrochemical measurements were conducted at room temperature. The modified electrode was kept in open air when not in use. The following results have been obtained.

## 3. Results and discussion

### 3.1. Voltammetric response of the $\text{Cu}(\text{II})$ -A-modified electrode

The voltammograms of the unmodified and  $\text{Cu}^{2+}$ /ZCME were recorded in electrolyte solution ( $15 \text{ mL NaNO}_3$  ( $0.5 \text{ mol L}^{-1}$ ) and  $5 \text{ mL}$  oxalate buffer ( $0.10 \text{ mol L}^{-1}$ ) pH  $\sim 4.5$ ), at a scan rate of  $50 \text{ mV s}^{-1}$ . Fig. 1 shows the resulting voltammograms, recorded after several preliminary scans. No voltammetric response was observed for the unmodified electrode (Fig. 1a). However, a well-defined reduction peak with a peak potential of  $0.023 \text{ V}$  was observed for the  $\text{Cu}(\text{II})$ -A-modified electrode (Fig. 1c). Experimental results showed that the CV voltammetric peak height at the modified electrode depends strongly on the type of supporting electrolyte. Several electrolytes, including benzyltrimethyltetradecylammonium chloride-dihydrate ( $0.02 \text{ mol L}^{-1}$ )  $\text{NaNO}_3$  ( $0.01 \text{ mol L}^{-1}$ ),  $\text{KNO}_3$  ( $0.01 \text{ mol L}^{-1}$ ), and oxalate buffer, pH 4.5 were investigated. There was no wave in the presence of benzyltrimethyltetradecylammonium chloride-dihydrate. However, well-defined reduction peaks were observed in the other electrolytes (Fig. 2).

These observations can be described on the basis of possible mechanisms for the electrochemical processes at zeolite-modified electrodes. Two possible mechanisms have been considered [24]: one where the electrochemical process takes place while the electroactive species is resident inside the zeolite; the other where such a process occurs after the electroactive species exit the zeolite through ion exchange or desorption. These mechanisms are known as intrazeolite and extrazeolite electron transfer processes, respectively [25]. The latter calls for electron transfer to occur at

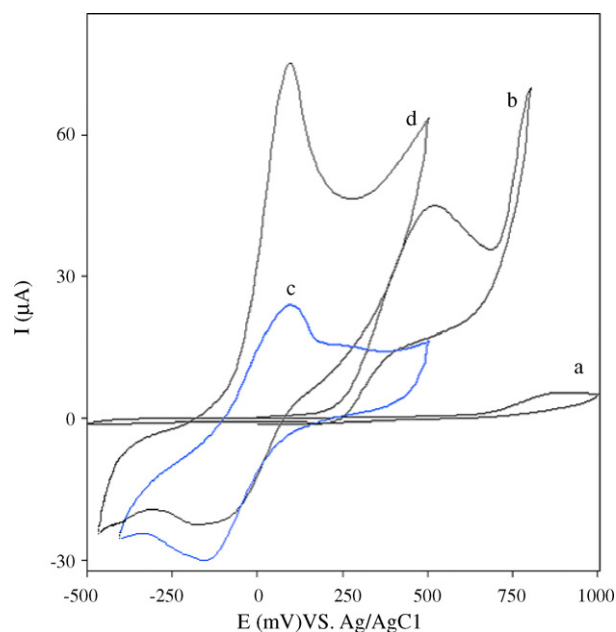


**Fig. 1.** Cyclic voltammograms of (a) bare Pt electrode in supporting electrolyte; (b) bare Pt electrode in solution containing supporting electrolyte and ascorbic acid ( $10.0 \text{ mmol L}^{-1}$ ); (c) modified electrode in solution containing supporting electrolyte; (d) modified Pt electrode in solution containing supporting electrolyte and ascorbic acid ( $3.0 \text{ mmol L}^{-1}$ ). Conditions: supporting electrolyte ( $15 \text{ mL NaNO}_3$  ( $0.5 \text{ mol L}^{-1}$ ) and  $5 \text{ mL}$  oxalate buffer ( $0.10 \text{ mol L}^{-1}$ ) pH  $\sim 4.5$ ), scan rate =  $50 \text{ mV s}^{-1}$ .



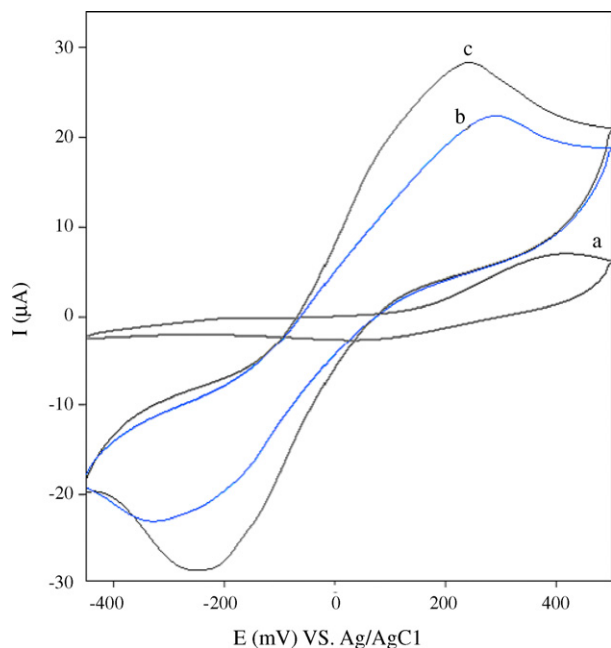
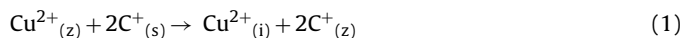


**Fig. 2.** Cyclic voltammograms of  $\text{Cu}^{2+}/\text{A}/\text{ZCME}$  in oxalate buffer (pH 4.5) and different supporting electrolytes: (a) benzyltrimethyltetradecylammonium chloride ( $0.5 \text{ mol L}^{-1}$ ); (b)  $\text{KNO}_3$  ( $0.5 \text{ mol L}^{-1}$ ); (c)  $\text{NaNO}_3$  ( $0.5 \text{ mmol L}^{-1}$ ). Other conditions were the same as Fig. 1.

the electrode-solution interface. This is the mechanism which has been tested to be operative in most cases [24,25]. From Fig. 2, it is clear that no electrochemical reaction occurs in the presence of benzyltrimethyltetradecylammonium chloride electrolyte because the benzyltrimethyltetradecylammonium cation is size excluded from the zeolite type A pore system. Therefore, no ion exchange occurs and all the  $\text{Cu}(\text{II})$  species are located in the interior of the zeolite which is not conductive for the electrochemical reaction to take place. It should be mentioned that no copper species is initially present at the electrode surface, because as described in Section 2, the  $\text{Cu}(\text{II})$ -A-modified zeolite, after preparation, was thoroughly washed with dilute  $\text{HNO}_3$  solution to remove the surface adsorbed species. However, ion exchange occurs between the intrazeolite  $\text{Cu}(\text{II})$  ions and the electrolyte cations in the electrolytes with small cations.

This ion exchange process results in transport of  $\text{Cu}(\text{II})$  to the electrode surface where they can approach the conductive parts of the electrode surface, and therefore, extrazeolite electrochemical mechanism becomes operative. Based on the results presented in Figs. 1 and 2, and in the light of previous works [24,25], the transfer mechanism is in conformity with the extrazeolite electron-transfer mechanism actioned by Bessel and Rolison [14]:



$\text{C}^+$  is an electrolyte cation and the descriptors  $z$ ,  $s$  and  $i$  stand for zeolite, solution and zeolite-solution interface, respectively. When  $\text{Cu}^{2+}_{(i)}$  is reduced at zeolite-solution interface, it will be catalyze the ascorbic acid oxidation process. It is clear that benzyltrimethyltetradecylammonium cation is size excluded from the zeolite type A pore system. The  $\text{Cu}^{2+}$  ions leaving the zeolite pores are reduced at the electrode-solution interface.

As it can be seen in Fig. 2, the response of the electrode depends on the type of cation (size-selectivity) in the supporting electrolyte solution. The current observed for the reduction of  $\text{Cu}(\text{II})$  was highest when the zeolite was exposed to oxalate buffer solution, pH 4.5, containing  $0.1 \text{ mol L}^{-1} \text{ Na}^+$  (Fig. 2c). Stability of the  $\text{Cu}^{2+}/\text{A}/\text{ZCME}$  was long, so that the current response remained almost unchanged

after several determinations, during which the electrode was stored in air. The current produced by  $\text{Cu}(\text{II})$  did not decrease any more when the ion exchange and electroredox attained steady-state. The high stability obtained at the  $\text{Cu}^{2+}/\text{A}/\text{ZCME}$  was due primarily to the strong affinity of zeolite A for  $\text{Cu}^{2+}$  [22].

The current observed in this solution is more than that which had been observed for the neutral  $0.1 \text{ mol L}^{-1} \text{ NaNO}_3$  electrolyte with about the same concentration of  $\text{Na}^+$ . This can be related to cooperation of hydronium ion in displacing  $\text{Cu}(\text{II})$  from zeolite pores. Voltammetric responses of the modified electrodes with 5, 10, 15 and 20% (w/w, with respect to graphite)  $\text{Cu}^{2+}/\text{A}/\text{ZCME}$  were examined by cyclic voltammetry in oxalate buffer, pH 4.5, using the same instrumental parameters. The results of this study revealed that the optimum proportion of zeolite to graphite was 20:80. Lower amounts of the modifier decrease the extent of ion exchange while higher amounts increase the resistance of the electrode; both of which decrease the sensitivity of the electrode response.

The  $\text{Cu}^{2+}/\text{A}/\text{ZCME}$  electrode with the above characteristics was successfully applied for the electrocatalytic oxidation of ascorbic acid, the results of which are presented in the following sections.

### 3.2. Electrocatalytic oxidation of ascorbic acid at the $\text{Cu}(\text{II})$ -A-modified electrode

Electrodes modified with transition metal complexes have the ability to catalyze the oxidation or reduction of solute species. The major effect of the modifier is to lower the potential required for the catalyzed redox systems, which is generally accompanied with a considerable increase in sensitivity. Among the transition metal ions, cobalt and iron complexes show the highest electrocatalytic activity and have shown great promise for the electrocatalytic determination of many organic and biologically important compounds [26–29]. Here, we used the  $\text{Cu}(\text{II})$ -zeolite type A as a modifier in modified electrode as a cyclic voltammetric sensor to study the electrocatalytic oxidation of ascorbic acid. The electrocatalytic function of the  $\text{Cu}^{2+}/\text{A}/\text{ZCME}$  for the electrochemical oxidation of ascorbic acid is demonstrated in Fig. 1d by cyclic voltammograms of  $2.5 \times 10^{-3} \text{ mol L}^{-1}$  ascorbic acid obtained in oxalate buffer, pH 4.5. Under the same experimental conditions, the direct oxidation of ascorbic acid at the unmodified electrode showed relatively weak anodic peak (Fig. 1b).

The corresponding voltammogram for the oxidation of ascorbic acid at the modified electrode gives rise to electrocatalytic responses with an anodic peak current that was greatly enhanced over what had been observed for the unmodified electrode (Fig. 1d). Maximum current for the oxidation of ascorbic acid at the modified electrodes occurred at potentials about 400 mV more negative than those obtained in the absence of the modifier. This behavior, which was observed at several concentrations and at different potential scan rates, clearly demonstrates the electrocatalytic function of the modified electrode toward ascorbic acid oxidation. The influence of pH on the catalytic oxidation of ascorbic acid was investigated in the range 2–8. In all cases the concentration of  $\text{Na}^+$  in the oxalate buffer was maintained at  $0.1 \text{ mol L}^{-1}$  and voltammograms were obtained using  $2.5 \times 10^{-3} \text{ mol L}^{-1}$  ascorbic acid. The highest sensitivity was observed at pH 4.5. Therefore, all subsequent measurements were performed at pH 4.5. Ascorbic acid can be oxidized by dissolved oxygen present as an impurity in solutions [30]; and this effect is intensified under alkaline conditions. Lower electrocatalytic currents observed at  $\text{pH} < 4$  can be related to the formation of undissociated form of ascorbic acid.

Calibration was performed using cyclic voltammetry with increasing concentration of ascorbic acid (Fig. 3). The peak current is linearly related to the concentration of ascorbic acid in the

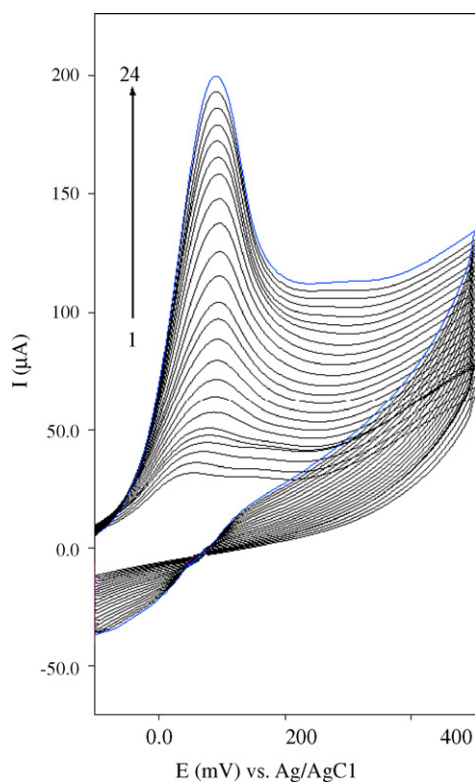


**Fig. 3.** Cyclic voltammograms of  $\text{Cu}^{2+}/\text{ZCME}$  in supporting electrolyte. Ascorbic acid concentrations (1–24): 0.003, 0.054, 0.125, 0.238, 0.476, 0.714, 0.9524, 1.19, 1.42, 1.66, 1.90, 2.14, 2.62, 2.85, 3.095, 3.57, 3.80, 4.05, 4.52, 4.76, 5.00, 5.23, 5.50 and  $6.0 \text{ mmol L}^{-1}$ , respectively. Conditions were the same as Fig. 1.

range  $30\text{--}600 \mu\text{mol L}^{-1}$ , with a least squares fit of  $i (\mu\text{A}) = 34.535 \text{ CAA} (\text{mmol L}^{-1}) + 4.1915$ , and a correlation coefficients of 0.9992. The relative standard deviations of 10 replicate measurements (performed on a single electrode at several ascorbic acid concentrations between  $3.0$  and  $200 \mu\text{mol L}^{-1}$ ) were between 1.0 and 2.4%. The detection limit was  $2.76 \times 10^{-7} \text{ mol L}^{-1}$ .

### 3.3. Interferences and real sample analysis

The effect of various components in the determination of ascorbic acid was studied by applying the method of mixed solutions. When the developed procedure was explored for the determination of  $5 \text{ mmol L}^{-1}$  ascorbic acid with optimum conditions, no interference was encountered for additions of  $10 \text{ mmol L}^{-1}$  of each of uric acid, fructose, cysteine and glucose. However, the presence of  $10 \text{ mmol L}^{-1}$  NADH caused 20% increase in the ascorbic acid peak. In order to demonstrate the capability of this modified electrode for catalytic oxidation of ascorbic acid in the real samples, we examined this ability in the voltammetric determination of ascorbic acid in some pharmaceutical preparations, such as effervescent tablets and chewable tablets available in local pharmacies. Therefore, pharmaceutical tablet solutions were prepared by accurately weighing, grinding of tablets and then dissolving obtained powder in the working buffer solution. The determination of ascorbic acid in pharmaceutical preparations was carried by the standard addition method in order to prevent on any matrix effect. The results were compared with those obtained using the official titration method with 2,6-dichlorophenolindophenol [31]. As it can be seen in the summary of results in Table 1, Student  $t$ -test and the variance-ratio  $F$ -test [32] show that there is no significant difference between the two methods with regard to accuracy and precision.

**Table 1**  
Determination of ascorbic acid in pharmaceutical preparations.

Sample	Ascorbic acid found in powder (%)		$t_{\text{cal}}^{\text{a}}$	$F_{\text{cal}}^{\text{b}}$
	Proposed method <sup>c</sup>	Standard method <sup>c</sup>		
Chewable tablet <sup>d</sup>	$66.98 \pm 2.24$	$65.98 \pm 1.91$	1.23	1.50
Effervescent tablet <sup>e</sup>	$22.89 \pm 1.18$	$25.01 \pm 0.76$	1.82	1.43

<sup>a</sup> Theoretical value of  $t = 2.13$  ( $P = 0.05$ ).

<sup>b</sup> Theoretical value of  $F = 19.00$  ( $P = 0.05$ ).

<sup>c</sup> Average of three determinations  $\pm$  standard deviation.

<sup>d</sup> Darou Pakhsh-Co., Tehran, Iran.

<sup>e</sup> Osveh-Co., Tehran, Iran.

### 3.4. Chronoamperometric measurements

The chronoamperometry as well as the other electrochemical methods was employed for the investigation of electrode processes at chemically modified electrodes. Fig. 4 shows chronoamperometric measurements of ascorbic acid at  $\text{Cu}^{2+}/\text{ZCME}$ . This figure represents the current–time profiles obtained by setting the working electrode potential at  $100 \text{ mV}$  for different concentrations of ascorbic acid. The oxidation current for the electrochemical reaction (under mass transfer control) of an electroactive material with a diffusion coefficient,  $D$  is described through the Cottrell equation:

$$I = \frac{nFAD^{1/2}C^*}{\pi^{1/2}t^{1/2}}$$

where  $D$  and  $C^*$  are the diffusion coefficient  $\text{cm}^2 \text{ s}^{-1}$ , and the bulk concentration  $\text{mol cm}^{-3}$ , respectively. The surface area of the Pt electrode was  $0.0314 \text{ cm}^2$ . The plot of  $I$  vs.  $t^{-1/2}$  for a modified electrode in the presence of ascorbic acid gives a straight line. The plot of  $I$  vs.  $t^{-1/2}$  will be linear, and from the slope, the value of  $D$  can be obtained. Diffusion coefficient of ascorbic acid was found to be  $1.037 \times 10^{-5} \text{ cm}^2 \text{ s}^{-1}$ .

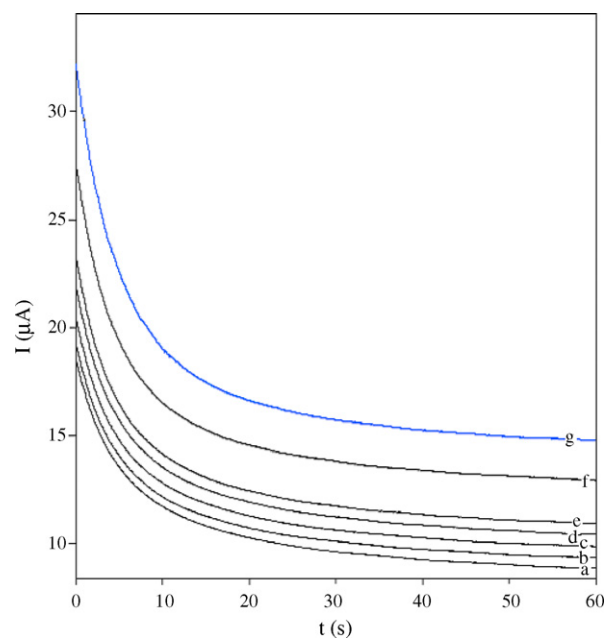


**Fig. 4.** Chronoamperograms obtained at  $\text{Cu}^{2+}/\text{ZCME}$  in the presence of (a)  $0.2 \text{ mmol L}^{-1}$ , (b)  $0.50 \text{ mmol L}^{-1}$ , (c)  $0.8 \text{ mmol L}^{-1}$ , (d)  $1.0 \text{ mmol L}^{-1}$ , (e)  $1.3 \text{ mmol L}^{-1}$ , (f)  $2.3 \text{ mmol L}^{-1}$  and (g)  $3.5 \text{ mmol L}^{-1}$  of ascorbic acid. Other conditions were the same as Fig. 1.

**Table 2**

Comparison of some properties of the present work with other studies.

Type of modification	Technique	Peak potential shift (mV)	LR (mol L <sup>-1</sup> ) <sup>a</sup>	DL (mol L <sup>-1</sup> ) <sup>b</sup>	Refs.
Polyhydroquinone film modified glassy carbon electrode	DPV <sup>c</sup>	–	$3.34 \times 10^{-5}$ – $1.67 \times 10^{-2}$	$3.28 \times 10^{-6}$	[33]
Macrocyclic compounds modified electrode	DPV <sup>c</sup>	~200	$3.41$ – $2.84 \times 10^3$	0.57	[34]
Polypyrrole/ferrocyanide films on a glassy carbon electrode	CV <sup>d</sup>	300	$5 \times 10^{-4}$ – $1.6 \times 10^{-2}$	–	[35]
Polypyrrole/ferrocyanide films modified carbon paste electrode	DPV <sup>c</sup>	540	$4.5 \times 10^{-4}$ – $9.62 \times 10^{-3}$	$5.82 \times 10^{-5}$	[36]
Incorporated ferrocenecarboxylic acid into polypyrrole	CV <sup>d</sup>	300	$0.5 \times 10^{-3}$ – $16 \times 10^{-3}$	–	[37]
Cu(II)-A zeolite-modified electrode	CV <sup>d</sup>	~400	$3 \times 10^{-6}$ – $6.00 \times 10^{-3}$	$2.76 \times 10^{-7}$	This work

<sup>a</sup> Linear range.<sup>b</sup> Detection limit.<sup>c</sup> Differential pulse voltammetry.<sup>d</sup> Cyclic voltammetry.

#### 4. Conclusion

Zeolite was found to have good adsorption characteristics and catalytic capabilities. Therefore, it was of value to explore the use of zeolite as a carrier of catalyst in the electrode. This work demonstrated that Cu(II), loaded in zeolite, can oxidize ascorbic acid catalytically. The kinetic process of the catalytic reaction can be explained using cyclic voltammetry and chronoamperometry. The results obtained for diffusion coefficient of ascorbic acid *D* are in broad agreement with other studies. The Cu<sup>2+</sup>A/ZCME offers the advantages of easy fabrication, fast response time, high sensitivity, low background current and detection limit, which are suitable for routine determinations. This study has been also compared with other studies [33–37] (Table 2).

#### References

- [1] R. Koncki, T. Lenarczuk, S. Glab, *Anal. Chim. Acta* 379 (1999) 69.
- [2] S.P. Arya, M. Mahajan, P. Jain, *Anal. Sci.* 14 (1998) 889.
- [3] G.M. Greenway, P. Ongomo, *Analyst* 115 (1990) 1297.
- [4] Z. Gao, D. Yap, Y. Zhang, *Anal. Sci.* 14 (1998) 1059.
- [5] C. Fang, X. Tang, X. Zhou, *Anal. Sci.* 15 (1999) 41.
- [6] M.J. Gismera, D. Hueso, J.R. Procopio, M.T. Serilla, *Anal. Chim. Acta* 524 (2004) 347.
- [7] Z. Dusun, G. Nisli, *Talanta* 63 (2004) 873.
- [8] M.H. Pournaghi-Azar, H. Dastangoo, *J. Electroanal. Chem.* 523 (2002) 26.
- [9] W. Yantasee, Y. Lin, G.E. Fryxell, B.J. Busche, *Anal. Chim. Acta* 502 (2004) 207.
- [10] H. Razmi-Nerbin, M.H. Pournaghi-Azar, *J. Solid State Electrochem.* 6 (2002) 126.
- [11] A. Abbaspour, M.M. Moosavi, *Talanta* 56 (2002) 91.
- [12] M. Kuronen, R. Harjula, J. Jernstrom, *J. Phys. Chem.* 2 (2000) 2655.
- [13] A. Walcarius, P. Mariaulle, L. Lamberts, *J. Electroanal. Chem.* 463 (1999) 100.
- [14] C.A. Bessel, D.R. Rolison, *J. Phys. Chem.* 101 (1997) 1148.
- [15] F. Bedioui, J. Devynck, *J. Phys. Chem.* 100 (1996) 8607.
- [16] M.D. Baker, C. Senaratne, *Anal. Chem.* 64 (1992) 697.
- [17] B. Chen, N.K. Goh, L.S. Chia, *Electrochim. Acta* 42 (1997) 597.
- [18] G. Wang, A. Walcarius, *J. Electroanal. Chem.* 407 (1996) 183.
- [19] G. Wang, A. Walcarius, *J. Electroanal. Chem.* 404 (1996) 237.
- [20] M.D.C. Rando, I.N. Rodriguez, H.H. Cisneros, *Anal. Chim. Acta* 370 (1998) 231.
- [21] D.R. Rolison, *Chem. Rev.* 90 (1990) 867.
- [22] A. Walcarius, *Anal. Chim. Acta* 384 (1999) 1.
- [23] F.E. Imbert, C. Moreno, A. Montero, B. Fontal, J. Lujano, *Zeolites* 14 (1994) 374.
- [24] B.R. Shaw, K.E. Creasy, C.J. Lanczycki, J.A. Sargeant, M. Tirhado, *J. Electrochem. Soc.* 135 (1988) 869.
- [25] C. Senaratne, J. Zhang, M.D. Baker, C.A. Bessel, D.R. Rolison, *J. Phys. Chem.* 100 (1996) 5849.
- [26] M.J. Aguirre, M. Isaacs, F. Armijo, N. Bocchi, J.H. Zagal, *Electroanalysis* 10 (1998) 571.
- [27] M.K. Amiri, S. Shahrokhian, S. Tangestaninejad, V. Mirkhani, *Anal. Biochem.* 290 (2001) 277.
- [28] J. Ren, Q. Zhang, Q. Ren, C. Xia, J. Wan, Z. Qin, *J. Electroanal. Chem.* 504 (2001) 59.
- [29] R.O. Lezna, S. Juanto, J.H. Zagal, *J. Electroanal. Chem.* 452 (1998) 221.
- [30] A. Lechien, P. Valenta, H.W. Nurnberg, G.C. Partriarche, *Fresen. Z. Anal. Chem.* 311 (1982) 105.
- [31] AOAC Official Methods of Analysis, *J. Official Anal. Chem.* (1990) 1058.
- [32] J.N. Miller, J.C. Miller, *Statistics and Chemometrics for Analytical Chemistry*, 4th ed., Pearson Education Limited, England, 2000.
- [33] C. Xianguang, W. Ren, Z. Guofang, Z. Xiaoyong, *Chin. J. Anal. Chem.* 34 (2006) 1063.
- [34] V.S. Ijeri, P.V. Jaiswal, A.K. Srivastava, *Anal. Chim. Acta* 439 (2001) 291.
- [35] M.H. Pournaghi-Azar, R. Ojani, *J. Solid State Electrochem.* 4 (2000) 75.
- [36] M.H. Pournaghi-Azar, R. Ojani, S.R. Nadimi, *Electrochim. Acta* 49 (2004) 271.
- [37] M.H. Pournaghi-Azar, R. Ojani, *J. Solid State Electrochem.* 3 (1999) 392.



# A blood-assisted optical biosensor for automatic glucose determination

Vanesa Sanz, Susana de Marcos, Javier Galbán\*

Analytical Biosensors Group, Department of Analytical Chemistry, Science Faculty, INA, University of Zaragoza, Zaragoza E-50009, Spain

## ARTICLE INFO

### Article history:

Received 1 September 2008

Received in revised form 17 December 2008

Accepted 22 December 2008

Available online 19 January 2009

### Keywords:

Intrinsic hemoglobin UV–vis

Optical reagentless biosensor

Glucose determination

Blood

Mathematical model

Absolute calibration method

## ABSTRACT

A new approach for glucose determination in blood based on the spectroscopic properties of blood hemoglobin (Hb) is presented. The biosensor consists of a glucose oxidase (GOx) entrapped polyacrylamide (PAA) film placed in a flow cell. Blood is simply diluted with bidistilled water (150:1, v:v) and injected into the carrier solution. When reaching the PAA film, the blood glucose reacts with the GOx and the resulting  $H_2O_2$  reacts with the blood Hb. This produces an absorbance change in this compound. The GOx–PAA film can be used at least 100 times. Lateral reactions of  $H_2O_2$  with other blood constituents are easily blocked (by azide addition). The linear response range can be fitted between 20 and 1200  $mg\ dL^{-1}$  glucose (R.S.D. 4%, 77  $mg\ dL^{-1}$ ). In addition to the use of untreated blood, two important analytical aspects of the method are: (1) the analyte concentration can be obtained by an absolute calibration method; and (2) the signal is not dependent on the oxygen concentration.

A mathematical model relating the Hb absorbance variation during the reaction with the glucose concentration has been developed to provide theoretical support and to predict its application to other compounds after changing the GOx by another enzyme. The method has been applied to direct glucose determination in 10 blood samples, and a correlation coefficient higher than 0.98 was obtained after comparing the results with those determined by an automatic analyzer. As well as sharing some of the advantages of disposable amperometric biosensors, the most significant feature of this approach is its reversibility.

© 2009 Elsevier B.V. All rights reserved.

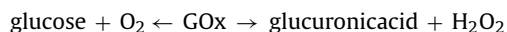
## 1. Introduction

Since research into blood glucose determination methods continues to be particularly important in bioanalytical chemistry, new alternatives are continuously being proposed and tested.

On the one hand, several body fluids such as aqueous humor from the eye [1], saliva [2] and mainly interstitial fluids (ISFs) [3] are being used as alternatives to blood in order to design a less invasive methodology (very important for glycemic control in diabetic patients). The most interesting is ISF; here, technological alternatives currently being tested include transdermal extraction (iontophoresis [4] or ultrasound [5]), direct spectral dermis measurement [6] or subcutaneous puncture [7]. Developments in this field are producing very interesting analytical solutions towards achieving a definitive system. However, the relationship of the glucose levels in these fluids with real blood glucose remains a source of controversy [8,9]. Consequently, improvements in direct glucose determination in blood are still necessary.

On the other hand, the chemical and the transducer parts of the analytical system are simultaneously being developed. Most proce-

dures are based on the use of proteins and enzymes as recognition reagents, given their selectivity. The most commonly used is the classical method based on the glucose oxidase (GOx) reaction:



Several of the previously indicated semi-invasive devices work according to this reaction coupled with  $H_2O_2$  amperometric detection [3–5,7]. Besides the need for frequent recalibration, this method has two main problems [10,11]: the signal dependence with the  $O_2$  concentration and the interference caused by other endogenous substances (uric acid, ascorbic acid) or commonly used pharmaceuticals (acetaminophene). These problems can be partially resolved (but not completely) by using a charge transfer mediator. However, this mediator is usually bio-incompatible and complicates the reversibility of the system, so this methodology is generally used in portable disposable puncture sensors.

In recent years optical detection methods based on the use of the intrinsic and extrinsic optical properties (fluorescence and absorption) of proteins are being considered. These methods represent an attempt to avoid the problem caused by electrochemical detection and to make use of their potential reversibility. The conformational-change-based-fluorescence of binding proteins [12–15], the change in fluorescence originated by cellular signaling (in which regulatory proteins are implied) [16,17], and the optical intrinsic properties

\* Corresponding author. Tel.: +34 976761291; fax: +34 976761292.  
E-mail address: [jgalban@unizar.es](mailto:jgalban@unizar.es) (J. Galbán).

of proteins such as tryptophan [18–20]) or heme groups [21] have proved to be the most interesting bases for these methods. Such methodologies are designed to be selective, reversible, compatible with biological fluids and used as an alternative to synthetic or semi-synthetic organic receptors [22,23]. However, most of these methods require previous steps in order to eliminate interference, and this limits their applicability in future clinical designs. Such previous steps usually involve precipitation or ultra-filtration for the elimination of various blood constituents that can cause interference.

In order to avoid these problems, we have recently developed analytical methods based on the use of the optical properties of hemeproteins [24,25]. These contain heme as the cofactor that shows a molecular absorption spectrum in the visible region which depends on its oxidation state, so that the enzymatic reaction can be followed by means of the absorbance variations during the process. Based on this, we have developed an optical biosensor for the direct glucose determination in blood which uses the horseradish peroxidase (HRP) absorbance variation during the glucose/glucose oxidase/HRP enzymatic reaction [26]. As is known, Hb is a hemeprotein present in the erythrocytes which is made up of two alpha and two beta chains, each containing a heme group with ferrous iron reversibly joined to molecular oxygen (HbII-O<sub>2</sub>). In blood analysis using molecular spectrochemical methods, this protein represents a strong spectral and chemical interference. However, since Hb can react with hydrogen peroxide and this reaction can be followed by the changes in its molecular absorption spectrum, this interference can be converted into a reagent.

Considering the optical transducer qualities of blood Hb [27] and our previous analytical knowledge of the combined glucose oxidase/glucose with Hb/H<sub>2</sub>O<sub>2</sub> reaction mechanism as starting points [28], in this paper we demonstrate that these properties can be used as the basis for reversible optical sensors for glucose determination in blood and that they could also be used for automatic analyzers. Unlike the previously developed sensor [26], this sensor does not require an indicating protein (such as HRP) because it is provided by the sample itself. The linear response range can be properly modified and the precision is similar.

In our opinion, this type of sensor can compete with the current commercially available disposable amperometric glucose sensor or with kit assays used in automatic analyzers [29,30]. With slight modifications, this methodology can be used for the design of optical sensors for other blood components.

## 2. Experimental

### 2.1. Apparatus

The molecular absorption measurements were carried out in a Hewlett-Packard 8452A diode-array spectrometer and in a PerkinElmer Lambda 5 (spectral bandwidth 2 nm) spectrometer. The measurements were performed with a previously described flow cell (300 μL capacity).

### 2.2. Reagents

Buffer solution: 0.1 M citrate buffer of pH 5–6 (from solid sodium citrate, adjusted with NaOH 1 M) and 0.1 M phosphate solution of pH 6 (from solid KH<sub>2</sub>PO<sub>4</sub> and solid Na<sub>2</sub>HPO<sub>4</sub>). Sodium azide from Sigma (S-8032). Glucose solutions prepared from solid β-D-glucose (Sigma G-5250) in buffer solution (the solution is left for 2 h to achieve the equilibrium between β-D-glucose and α-D-glucose). Glucose oxidase was taken from *Aspergillus niger*, EC 1.1.3.4 (Sigma G-7141) was of 245,900 IU/g of lyophilised solid. A<sub>0</sub>

Human Hemoglobin (A<sub>0</sub>) (Sigma H-0267). Blood was taken from 10 volunteers by finger punctation.

### 2.3. GOx film preparation

The preparation of a polyacrylamide (PAA) glucose oxidase film was based on a general enzyme immobilisation procedure described elsewhere [11]. 0.2 mL of a phosphate buffer solution at pH 6.0 containing 0.03 g of acrylamide, 0.002 g of bis-acrylamide and 0.001 g of ammonium persulphate (as a reaction precursor) were mixed with the appropriate amount of the GOx lyophilised solid (about 0.004 g). Dissolved oxygen was eliminated by bubbling nitrogen through the solution. The cocktail was spread in a 0.5 mm hollow, made in a glass film (20 mm × 9 mm × 0.1 mm), covered with a second glass film and irradiated with a UV-lamp (254 nm) for 60 min. The film was then stored in the phosphate buffer solution at 4 °C. The film was located in a flow cell previously described for absorbance measurement [24].

### 2.4. Blood sample preparation

The only sample treatment was dilution in bidistilled water 1/150 (v:v). The mixture was stirred during 30 s until the hemolysis (erythrocyte lyses and Hb liberation) was completed, detected by the disappearance of the turbidity initially observed.

### 2.5. Procedure

The phosphate buffer solution with added azide flowed through the flow cell at 0.84 mL min<sup>-1</sup> and the absorbance at the working wavelength (represented by sub-index λ<sub>w</sub>, 412 nm in most cases) and the reference wavelength (represented by sub-index λ<sub>ref</sub>, 444 nm when 412 nm working wavelength is used) began to be monitored. The initial absorbance of the film was represented by the superscript “film” (Abs<sub>λ<sub>w</sub></sub><sup>film</sup> and Abs<sub>λ<sub>ref</sub></sub><sup>film</sup>, respectively). Then 0.8 mL of the blood sample was injected and the flow stopped when the flow cell was completely filled with the sample (in the designed system at 45 s). At this moment the absorbance measured at both wavelengths is represented by the sub-index “0” (Abs<sub>λ<sub>w</sub></sub><sup>meas,0</sup> and Abs<sub>λ<sub>ref</sub></sub><sup>meas,0</sup>, respectively). The analytical parameters obtained at a given reaction time *t* are:

$$\Delta \text{Abs}_{\lambda_w, t} = \text{Abs}_{\lambda_w, t}^{\text{meas}} - \text{Abs}_{\lambda_w, 0}^{\text{meas}}$$

$$\Delta \text{Abs}_{\lambda_w / \lambda_{\text{ref}}, t} = \frac{\text{Abs}_{\lambda_w, t}^{\text{meas}} - \text{Abs}_{\lambda_w, 0}^{\text{meas}}}{\text{Abs}_{\lambda_{\text{ref}}, 0}^{\text{meas}} - \text{Abs}_{\lambda_{\text{ref}}}^{\text{film}}}$$

Abs<sub>λ<sub>w</sub></sub><sup>meas,0</sup> and Abs<sub>λ<sub>ref</sub></sub><sup>meas,0</sup> being the absorbances at a time *t* at the working and reference wavelengths, respectively.

## 3. Results and discussion

### 3.1. Blood hemoglobin as a transducer reagent

To use Hb as an analytical reagent, lyses induction in erythrocytes without coagulation is required. To achieve this, simple blood dilution in a hypotonic media such as bi-distilled water in an appropriate ratio is sufficient [24,27,28]. In this study, a dilution ratio of 150:1 (v:v) was selected considering the concentrations of glucose in blood, natural hemoglobin concentration and the elimination of possible interferences with the Hb/H<sub>2</sub>O<sub>2</sub> reaction. These diluted solutions are stable during more than 24 h in a closed vessel, away from the light and at room temperature.

Apart from Hb, other proteins (mainly enzymes) present in blood can consume H<sub>2</sub>O<sub>2</sub>. Considering the Hb and glucose concentrations, and the level at which the sample is diluted, only blood catalase

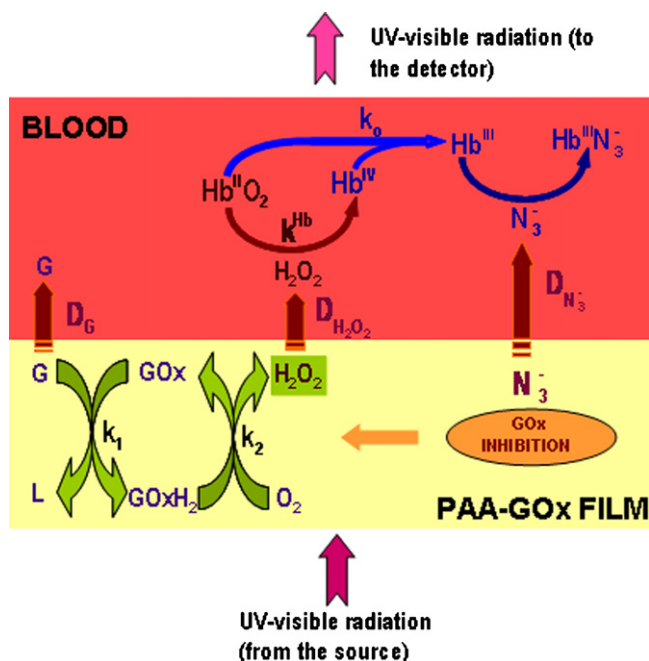


**Fig. 1.** Overall reaction mechanisms occurring in the sensor flow cell. G: glucose; L: gluco lactone; HbII-O<sub>2</sub> (ferrous blood hemoglobin linked to O<sub>2</sub>); HbIII (ferric hemoglobin); HbIII-N<sub>3</sub><sup>-</sup> (azide linked ferric hemoglobine); GOx (glucose oxidase, oxidized form); GOx-H<sub>2</sub> (reduced form); D<sub>G</sub>, D<sub>H<sub>2</sub>O<sub>2</sub></sub> and D<sub>N<sub>3</sub><sup>-</sup></sub>: glucose, H<sub>2</sub>O<sub>2</sub> and azide diffusion coefficients.

can act as a H<sub>2</sub>O<sub>2</sub> scavenger so the H<sub>2</sub>O<sub>2</sub>/catalase reaction must be inhibited. This inhibition can be efficiently performed by azide addition to the carrier [31], which coordinates iron(III) of the catalase heme group blocking its reaction with H<sub>2</sub>O<sub>2</sub>. Obviously, azide also binds ferric hemoglobin (HbIII) to form the HbIII-N<sub>3</sub><sup>-</sup> complex which is unable to react with hydrogen peroxide, but as the Hb/H<sub>2</sub>O<sub>2</sub> reaction mechanism becomes simplified, far from being a problem this fact is an advantage. In Fig. 1 (upper part) a simplified reaction mechanism of Hb with H<sub>2</sub>O<sub>2</sub> in the presence of azide is shown (see Fig. S1 in the Supplementary Material for a full explanation). HbII and HbIII are the hemoglobin in ferrous (Fe<sup>2+</sup>) and ferric (Fe<sup>3+</sup>) states, respectively. HbII-O<sub>2</sub> reacts with hydrogen peroxide giving HbIV, an oxyferryl intermediate with the heme group in an oxidation state of +4, which quickly comproporcionates with HbII-O<sub>2</sub> giving HbIII which in the presence of azide forms HbIII-N<sub>3</sub><sup>-</sup>. The intramolecular and intermolecular reduction of HbIV and the reduction of HbIV by reducer substrate are negligible, so a direct HbII-O<sub>2</sub>/HbIII-N<sub>3</sub><sup>-</sup> transition is observed. As both species have different optical absorption spectra (Fig. S2 in the Supplementary Material) it is possible to follow the reaction through the absorbance variations observed.

### 3.2. Some considerations on sensor design

The sensor film must be as transparent as possible at the working wavelength in order to minimize the background scattering signal. Regarding the flow cell, several aspects have to be considered. The inner volume has to be as small as possible to limit the sample volume consumption (around 300 μL). Furthermore, the thickness of the flow cell has to be as thin as possible (0.12 cm, GOx film thickness 0.03 cm) in order to both concentrate the hydrogen peroxide formed and fit the optical pathway of the system. Regarding the kind of flow, when a non-stop-flow mode is used the H<sub>2</sub>O<sub>2</sub> diffusing to the sample is cleaned out of the flow cell and the sensitivity is low. In this work the flow is stopped when the cell is completely filled with the sample, reaching the maximum sensitivity given that

hemoglobin and glucose concentrations are at a maximum in this condition.

Fig. 2 shows the changes in the absorption spectrum of the GOx film-blood system during the reaction (A: λ < 500 nm; B: λ > 500 nm). Comparing these spectra with those shown in Fig. 2, the following conclusions can be derived: (1) the absorption and scattering in the film due to the GOx remains as a constant during the reaction; (2) absorbance at 412, 538 and 576 decreases during the reaction; these wavelengths correspond to the HbII-O<sub>2</sub> absorption; (3) the isosbestic points at 444, 526 and 586 nm owing to HbII-O<sub>2</sub>/HbIII-N<sub>3</sub><sup>-</sup> remain. This all demonstrates that a HbII-O<sub>2</sub>/HbIII-N<sub>3</sub><sup>-</sup> transition is produced during the reaction, which is very important in order to formulate the correct mathematical model of the system. Maximum sensitivity is obtained at 412 nm.

### 3.3. Mathematical model

According to the overall model given in Fig. 1, the measured absorbance in the flow cell at any wavelength and any time (Abs<sub>λ,t</sub><sup>meas</sup>) is the given by

$$\text{Abs}_{\lambda,t}^{\text{meas}} = \text{Abs}_{\lambda,t}^{\text{film}} + \text{Abs}_{\lambda,t}^{\text{sol}} \quad (1)$$

Abs<sub>λ,t</sub><sup>film</sup> and Abs<sub>λ,t</sub><sup>sol</sup> being the absorbance of the film and the solution (blood sample), respectively. The Abs<sub>λ,t</sub><sup>film</sup> solely depends on the entrapped GOx. The molecular absorption spectrum of GOx depends on whether it is in the initial oxidized form (GOx) or in the reduced form (GOx-H<sub>2</sub>). As has been indicated before [24,27], the oxidized to reduced ratio depends on the O<sub>2</sub> concentration. In our system, since the O<sub>2</sub> concentration is much higher than the glucose concentration, the GOx-H<sub>2</sub> is quickly oxidized, so that the enzyme is mainly in this form (which is consistent with the absorbance variations shown in Fig. 2) and then:

$$[\text{GOx}]_t = [\text{GOx}]_0 \quad (2)$$

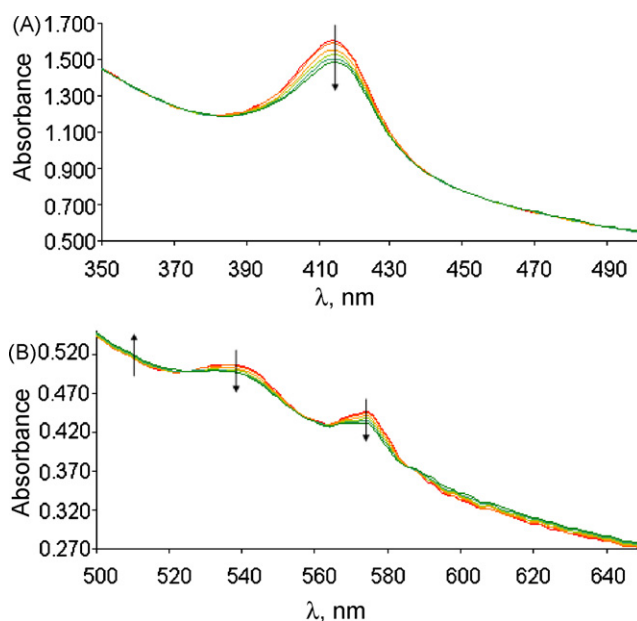


**Fig. 2.** Changes in the molecular absorption spectra of the blood sample-GOx film system. The spectra variations correspond to a HbII-O<sub>2</sub>/HbIII-N<sub>3</sub><sup>-</sup> transition (A, from 350 to 500 nm; B, from 500 to 650 nm). Arrows show increasing time (40 mg mL<sup>-1</sup> GOx concentration in the PAA polymerization mixture; 150:1 (v:v) blood dilution; 10<sup>-3</sup> M azide concentration and 1.38 × 10<sup>-4</sup> M blood glucose concentration).

Thus the  $Abs_{\lambda,t}^{film}$  always remains constant ( $Abs_{\lambda,t}^{film} = Abs_{\lambda}^{film}$ ) and then (1) is given by

$$Abs_{\lambda,t}^{meas} = Abs_{\lambda}^{film} + Abs_{\lambda,t}^{sol} \quad (3)$$

According to (3), when blood fills the flow cell and before the reaction starts, the measured absorbance at the working wavelength ( $\lambda_w$ ) is given by

$$Abs_{\lambda_w,0}^{meas} = Abs_{\lambda_w}^{film} + \varepsilon_{\lambda_w}^{HbII-O_2} L[Hb]_0 \quad (4)$$

$L$  being the optical pathlength of the sensor cell flow. Since  $\varepsilon_{\lambda_w}^{HbII-O_2}$  can be accurately measured, the hemoglobin concentration in blood can be determined. When the reaction starts, the hemoglobin begins to change but, as has been stated before, the only species which are in significant concentrations are  $HbII-O_2$  and  $HbIII-N_3^-$  and the measured absorbance at any time at the working wavelength will be given by

$$Abs_{\lambda_w,t}^{meas} = Abs_{\lambda_w}^{film} + \varepsilon_{\lambda_w}^{HbII-O_2} L[HbII \cdot O_2]_t + \varepsilon_{\lambda_w}^{HbIII-N_3^-} L[HbIII \cdot N_3^-]_t \quad (5)$$

and considering that the mass balance for hemoglobin is

$$[Hb]_0 = [HbII-O_2]_t + [HbIII-N_3^-]_t \quad (6)$$

Eq. (5) gives

$$Abs_{\lambda_w,t}^{meas} = Abs_{\lambda_w}^{film} + \varepsilon_{\lambda_w}^{HbII-O_2} L[Hb]_0 + (\varepsilon_{\lambda_w}^{HbIII-N_3^-} - \varepsilon_{\lambda_w}^{HbII-O_2}) L[HbIII \cdot N_3^-]_t \quad (7)$$

It is very usual to detect slight drifts in the absorbance signals in optical sensors. This can be avoided by measuring the absorbance during the reaction simultaneously at a reference ( $\lambda_{ref}$ ) wavelength for which the absorbance does not change (in this case an isosbestic wavelength for the  $HbII-O_2$  and  $HbIII-N_3^-$  species) and will be given by

$$Abs_{\lambda_{ref},t}^{meas} = Abs_{\lambda_{ref},0}^{meas} = Abs_{\lambda_{ref}}^{film} + \varepsilon_{\lambda_{ref}}^{HbII-O_2} L[Hb]_0 \quad (8)$$

Eqs. ((4), (7) and (8)) can be combined in different forms. In many cases we will use one of the two following analytical parameters:

$$\begin{aligned} \Delta Abs_{\lambda_w,t} &= Abs_{\lambda_w,t}^{meas} - Abs_{\lambda_w,0}^{meas} = (\varepsilon_{\lambda_w}^{HbIII-N_3^-} - \varepsilon_{\lambda_w}^{HbII-O_2}) [HbIII \cdot N_3^-]_t \\ &= \Delta \varepsilon_{\lambda_w} [HbIII \cdot N_3^-]_t \end{aligned} \quad (9a)$$

$$\begin{aligned} \Delta Abs_{\lambda_w/\lambda_{ref},t} &= \frac{Abs_{\lambda_w,t}^{meas} - Abs_{\lambda_w,0}^{meas}}{Abs_{\lambda_{ref},0}^{meas} - Abs_{\lambda_{ref}}^{film}} \\ &= \left( \frac{\varepsilon_{\lambda_w}^{HbIII-N_3^-} - \varepsilon_{\lambda_w}^{HbII-O_2}}{\varepsilon_{\lambda_{ref}}^{HbII-O_2}} \right) \frac{[HbIII \cdot N_3^-]_t}{[Hb]_0} \\ &= \Delta \varepsilon_{\lambda_w/\lambda_{ref}} \frac{[HbIII \cdot N_3^-]_t}{[Hb]_0} \end{aligned} \quad (9b)$$

As can be seen from Fig. 1, the overall reaction includes the diffusion of the glucose from solution to film, the diffusion/reaction of glucose inside the film, diffusion of the  $H_2O_2$  formed from the film to the solution and the reaction of this compound with hemoglobin. Mass transport and reaction kinetic considerations for glucose and  $H_2O_2$  enable us to relate the  $[HbIII-N_3^-]_t$  with glucose and hemoglobin concentrations and thermodynamic constants (see

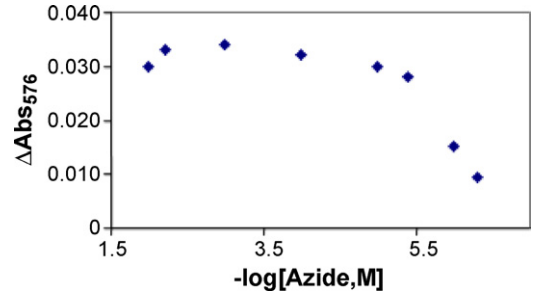


Fig. 3. Effect of azide concentrations (as  $-\log[ ]$ ) on the absorbance variation ( $40 \text{ mg mL}^{-1}$  GOx concentration in the PAA polymerization mixture; 150:1 (v:v) blood dilution).

“Model derivation” section in Supplementary Material for an explanation of the deduction and terms) and the following equation is obtained:

$$[HbIII-N_3^-]_t = K[Hb]_0 t^2 [G]_0 \quad (10a)$$

$K$  being a constant grouping several thermodynamic parameters,  $G$  being the glucose concentration and  $t$  being the reaction time. Eq. (10a) is merely a simplification; in fact the  $[HbIII-N_3^-]_t$  is exponentially related to  $G$  according to:

$$[HbIII \cdot N_3^-] = [Hb]_0 (1 - e^{-2k^{Hb}(D_G^f/LX_f)[G]_0((t^2/2) - (1/6)(D_G^f/LX_s)t^3)}) \quad (10b)$$

(see Eq. (S26) in the Supplementary Material for an explanation), which can be simplified to a straight line for low exponent values. After substitution of (10a) in (9), the global model, working with or without the reference wavelength, is finally found:

$$\Delta Abs_{\lambda_w/\lambda_{ref},t} = \Delta \varepsilon_{\lambda_w/\lambda_{ref}} K t^2 [G]_0 \quad (11)$$

$$\Delta Abs_{\lambda_w,t} = \Delta \varepsilon_{\lambda_w,t} K [G]_0 [Hb]_0 t^2 L \quad (12)$$

Eq. (10) demonstrates that the analytical signal is not dependent on the  $O_2$  concentration.

### 3.4. Mathematical model validation: analytical figures of merit

As stated previously, azide has three effects: (a) it inhibits blood catalase, an enzyme that consumes  $H_2O_2$  which would make the sensitivity lower; (b) it combines with  $HbIII$  to form  $HbIII-N_3^-$  which inhibits the  $HbIII/H_2O_2$  reaction and simplifies the reaction mechanism; (c) it partially inhibits GOx. Effects (a) and (b) play in favour of the method sensitivity while effect (c) works against it, therefore there will be an optimal azide concentration at which the sensitivity is at a maximum (Fig. 3). Taking into account the hemoglobin concentration in the diluted blood sample (minimum dilution for complete hemolysis 50:1 (v:v) and normal hemoglobin levels in blood in the range of 12–18  $\text{g dL}^{-1}$ ) and the experimental data,  $10^{-3} \text{ M}$  was finally chosen.

The GOx concentration in the polyacrylamide film was also studied. Table 1 shows the slopes for four calibration lines  $\Delta Abs_{\lambda_w/\lambda_{ref},t}$  versus the glucose concentration (lineal zone) at different GOx concentrations. As can be seen, and according to the model, the GOx concentration does not affect the method sensitivity (the R.S.D. of the slopes is lower than 2%) in this concentration range and using  $10^{-3} \text{ M}$  azide concentration. This is very important from the point of view of the robustness of the system and permits the biosensor to be easily made. However, for high azide concentrations (about 0.01 M), the signal depends on the GOx concentration as the percentage of GOx inhibition increases.

Hemoglobin is a reagent necessary for the method which is supplied by the sample itself, so the hemoglobin concentration can not be changed by the analyst. Nevertheless, the model predicts the effect of the hemoglobin concentration and checking this

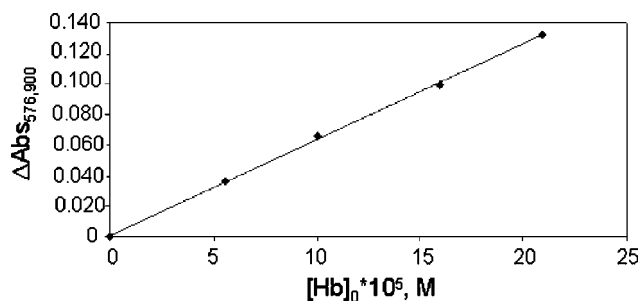


**Fig. 4.** Hb concentration effect of the analytical signal (60 mg mL<sup>-1</sup> GOx concentration in the PAA polymerization mixture; 10<sup>-3</sup> M azide concentration; 3.7 × 10<sup>-5</sup> M blood glucose concentration and 900 s reaction time).

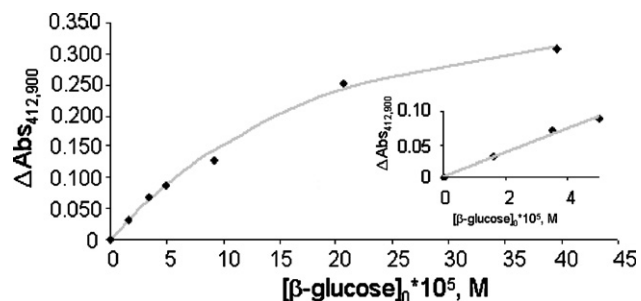


**Fig. 5.** ΔAbs<sub>412,900</sub> versus glucose concentration using a fixed reaction time (900 s). The grey curve corresponds to the theoretical equation:  $\Delta \text{Abs} = 0.3478(1 - e^{-5833.18|G|_{0\beta}})$   $r = 0.994$ . Inset: ΔAbs<sub>412,900</sub> versus glucose concentration in the linear response range (40 mg mL<sup>-1</sup> GOx concentration in the PAA polymerization mixture; 150:1 (v:v) blood dilution; and 10<sup>-3</sup> M azide concentration).

effect is important in order to make corrections. To study this effect, several mixtures of commercial hemoglobin ( $A_0$ , the majority form in blood (>99%)) with a constant glucose concentration were prepared and the absorbance variation in optimal conditions measured. The results obtained (Fig. 4) indicated a linear relationship between  $\Delta \text{Abs}_{\lambda_w,t}$  and the hemoglobin concentration as the model predicts (Eq. (12)). Furthermore, this linear relationship is very interesting because it allows us to omit the dependence of the hemoglobin concentration on the signal as described above (Eq. (11)). We have determined that the percentage of HbII-O<sub>2</sub> consumed during a 1250 s reaction time and with a glucose concentration of 3.73 × 10<sup>-5</sup> M is 60 ± 2%. This value is independent of the hemoglobin concentration, given the linear relationship between  $\Delta \text{Abs}_{\lambda_w,t}$  and  $[\text{Hb}]_0$ .

Fig. 5 shows the representation of the analytical parameter versus glucose concentration. This equation corresponds mathematically to Eq. (10b). For low glucose concentrations, the model (Eqs. (11) or (12)) predicts a linear relationship between the absorbance variation and the analyte concentration. Nevertheless, the method sensitivity expressed as the slope of the calibration line depending of the measuring time (Table 2). The lower the reaction

**Table 1**  
GOx effect on the slope of the calibration line.

[GOx] (mg mL <sup>-1</sup> ) <sup>a</sup>	Slope (M <sup>-1</sup> ) <sup>b</sup>
20	202
40	201
60	205
80	198

Conditions: Blood dilution 150:1 (v:v) in water and azide 10<sup>-3</sup> M, time reaction 900 s.

<sup>a</sup> GOx concentration in the polymerization mixture for polyacrylamide film preparation.

<sup>b</sup> Slope of the calibration line of  $\Delta \text{Abs}_{576,1150}$  versus glucose concentration in the linear range.

**Table 2**

Sensitivity and linear range (lower and upper limit) as a function of the reaction time.

Reaction time (s)	Sensitivity (M <sup>-1</sup> )	Lower limit (mg dL <sup>-1</sup> )	Upper limit (mg dL <sup>-1</sup> )
100	5.9	620	1200
300	28.1	135	950
450	72.1	54	810
700	105	40	675
900	140	25	540
1100	163	20	540

Conditions: GOx concentration in the polymerization mixture for polyacrylamide film preparation 40 mg mL<sup>-1</sup>, blood dilution 150:1 (v:v) in water and azide 10<sup>-3</sup> M. Sensitivity is expressed as the slope for the calibration line; lower limits for the linear range correspond to the detection limit (data for 576 nm).

time, the higher the measuring time where the exponential approximation is fulfilled and thus the higher is the top limit of the linear range. For example, working with 150/1 dilution, the most usual concentrations can be analysed in less than 8 min. It is important to consider that the response range for a given time can be extended using the exponential calibration or modifying the sample dilution. The relative standard deviation for the analytical parameter of a 77 mg dL<sup>-1</sup> glucose was 4% ( $n = 5$ ).

As stated previously, the wavelengths at which the maxima appear were 412, 538 and 576 nm. The sensitivities experimentally obtained (slopes of the calibration lines) for these three wavelengths were 1219, 103 and 166 M<sup>-1</sup>, respectively, which are proportional to  $\Delta \varepsilon_{\lambda_w/\lambda_{ref}}$  (42,132, 4068 and 5833 M<sup>-1</sup> cm<sup>-1</sup>, respectively) as the model predicts (Eq. (12)). The quotient between sensitivity and  $\Delta \varepsilon_{\lambda_w/\lambda_{ref}}$  for the different wavelengths was  $0.028 \pm 0.002$  cm ( $n = 3$ ). The slopes of the calibration lines given can be used for testing the global quality of the model. To do this, Eq. (12) will be considered. In this equation, the following considerations were applied: (a) the  $\Delta \varepsilon_{\lambda_w/\lambda_{ref}}$  were obtained from the spectra; (b) a previously obtained [8] value of 14 M<sup>-1</sup> s<sup>-1</sup> for  $k_{\text{Hb}}$  was taken; (c) the hemoglobin concentration in the sample was calculated from Eq. (2) and the  $\varepsilon_{\text{HbII-O}_2}$  value used [27] was 13,257 M<sup>-1</sup> cm<sup>-1</sup>; (d) the glucose diffusion coefficients in the sample solution ( $D_s^G$ ) and in the film ( $D_f^G$ ) were assumed to be equal. From these considerations the  $K$  value was calculated and from this value it is possible to compare the experimental absorbance variation signals with the theoretical profiles (Eq. (S27) in the Supplementary Data). Fig. 6 compares the experimental with the theoretical (expected) values; as can be seen the model fits very well with the experimental results. A GOx in PAA sensor film lifetime is about 6 months for glucose determination in fruit juices (based on the chemically modified GOx fluorescence) [25]. With this method the same sensor film has been used during 2 months (more than 100 measurements) without damage.

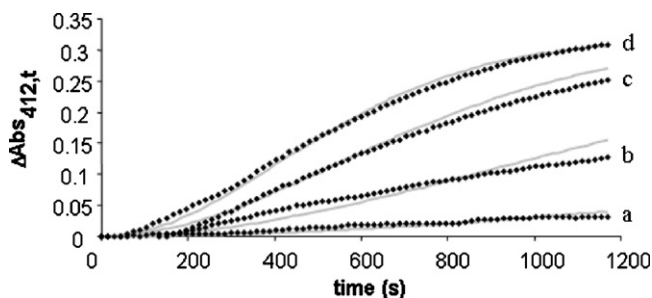


**Fig. 6.** ΔAbs<sub>412,t</sub> versus time for different glucose concentrations: (a) 1.60 × 10<sup>-5</sup> M, (b) 9.20 × 10<sup>-5</sup> M, (c) 2.06 × 10<sup>-4</sup> M and (d) 3.96 × 10<sup>-4</sup> M (40 mg mL<sup>-1</sup> GOx concentration in the PAA polymerization mixture; 150:1 (v:v) blood dilution; and 10<sup>-3</sup> M azide concentration).



### 3.5. Biosensor validation

From the previously reported values the slope of the calibration line can be stated and a self-calibration method for glucose determination in blood can be applied according to the following equation (900 s measurement time):

$$\Delta\text{Abs}_{412/444,900} = 2722[G]_0 \quad (13)$$

This equation was tested in order to be used for direct glucose determination by an absolute calibration method. Ten blood samples were analysed using this method and quantified with both the equation and a Reflotron® instrument (see Fig. S3 in Supplementary Material). The results obtained were submitted to a correlation study and the line obtained was:

$$[\text{Glucose}]_{\text{reference}} = 0.972[\text{Glucose}]_{\text{this method}} + 3.6 \quad r^2 = 0.98 \quad (13)$$

In this equation the slope and the intercept are statistically equal to 1 ( $0.97 \pm 0.14$ , 95% confidence interval) and 0 ( $3.6 \pm 8.5$ , 95% confidence interval), respectively, so both methods give similar results.

## 4. Conclusions

In this paper it has been demonstrated that the molecular absorption properties of blood hemoglobin can be used as an analytical signal for glucose determination in blood, without an additional indicating reaction and without O<sub>2</sub> dependence. The mathematical model developed can be used as a starting point in order to design a methodology for the direct determination of other blood compounds with the appropriate enzyme producing H<sub>2</sub>O<sub>2</sub>. The method can be applied without calibration and can therefore be easily implemented in automatic blood analyzers. These results open the door to new designs for automatic blood glucose analyzers.

## Acknowledgements

This work was supported by the Spanish Ministry of Education and Science (MEC), project CTQ 2005-05761. V.S. thanks the MEC for a grant.

## Appendix A. Supplementary data

Supplementary data associated with this article can be found, in the online version, at doi:10.1016/j.talanta.2008.12.060.

## References

- [1] V.L. Alexeev, S. Das, D.N. Finegold, S.A. Asher, Clin. Chem. 50 (2004) 2353.
- [2] J.K.M. Aps, L.C. Martens, Forensic Sci. Int. 150 (2005) 119.
- [3] K. Rebrin, G.M. Steil, W.P. van Antwerp, J.J. Mastrototaro, Am. J. Physiol. 277 (Endocrinol. Metab. 40) (1999) E561.
- [4] M.J. Tierny, J.A. Tamada, R.O. Potts, L. Jovanovic, S. Cary, Biosens. Bioelectron. 16 (2001) 621.
- [5] J. Kost, S. Mitragotri, R.A. Gabbay, M. Pishko, R. Langer, Nat. Med. 6 (2000) 347.
- [6] K. Maruo, M. Tsurugi, J. Chin, T. Oota, H. Arimoto, Y. Yamada, M. Tamura, M. Ishii, Y. Ozaki, IEEE J. Sel. Top. Quan. Electron. 9 (2003) 322.
- [7] J.J. Mastrototaro, W.P. VanAntwerp, J.H. Mestmann, Diabetologia 39 (1996) 814.
- [8] E. Boland, T. Monsod, M. Delucia, C.A. Brandt, S. Fernando, W.V. Tamborlane, Diabetes Care 24 (2001) 1858.
- [9] G.S. Wilson, R. Gifford, Biosens. Bioelectron. 20 (2005) 2388.
- [10] J.C. Pickup, F. Hussain, N.D. Evans, N. Sachedina, Biosens. Bioelectron. 20 (2005) 1897.
- [11] P. Wang, S. Amarasinghe, J. Leddy, M. Arnold, J.S. Dordick, Polymer 39 (1998) 123.
- [12] J.C. Pickup, F. Hussain, N.D. Evans, O.J. Rolinski, D.J.S. Birch, Biosens. Bioelectron. 20 (2005) 2555.
- [13] R. Hoess, Chem. Rev. 101 (2001) 3205.
- [14] M. Allert, M.A. Dwyer, H.W. Hellinga, J. Mol. Biol. 366 (2007) 945.
- [15] J.E. Noble, P. Ganju, A.E.G. Cass, Anal. Chem. 75 (2003) 2042.
- [16] K. Hakila, M. Maksimow, M. Karp, M. Virta, Anal. Biochem. 301 (2002) 235.
- [17] M. Lepore, M. Portaccio, E. de Tommasi, P. de Luca, U. Bencivenga, P. Maiuri, D.G. Mita, J. Mol. Catal. B 31 (2004) 151.
- [18] E.A. Moschou, B.V. Sharma, S.K. Deo, S. Daunert, J. Fluoresc. 14 (2004) 535.
- [19] V. Scognamiglio, M. Staiano, M. Rossi, S. DiAuria, J. Fluoresc. 14 (2004) 491.
- [20] J. Galbán, Y. Andreu, J.F. Sierra, S. de Marcos, J.R. Castillo, Luminescence 16 (2001) 199.
- [21] V. Sanz, S. de Marcos, J.R. Castillo, J. Galbán, J. Am. Chem. Soc. 217 (2005) 1038.
- [22] V.L. Alexeev, S. Das, D.N. Finegold, S.A. Asher, Clin. Chem. 127 (2004) 2353.
- [23] G. Das, S. Matilde, Chem. Eur. J. 12 (2006) 2936.
- [24] V. Sanz, S. de Marcos, J. Galbán, Biosens. Bioelectron. 22 (2007) 956.
- [25] V. Sanz, S. de Marcos, J. Galbán, Anal. Chim. Acta 607 (2008) 211.
- [26] V. Sanz, S. de Marcos, J. Galbán, Biosens. Bioelectron. 22 (2007) 2876.
- [27] K. Chen, K. Ballas, R.R. Hantgan, D.B. Kim-Saphiro, Biophys. J. 87 (2004) 4113.
- [28] V. Sanz, S. de Marcos, J. Galbán, The Analyst 132 (2007) 59.
- [29] G.B.B. Kristensen, N.G. Christensen, G. Thue, S. Sandberg, Clin. Chem. 51 (2005) 1632.
- [30] M. Du Plessis, J.B. Ubbink, J.H. Vermaak, Clin. Chem. 46 (2000) 1085.
- [31] T. Brittain, J. Inorg. Chem. 81 (2000) 99.



# Separation and determination of benzene, toluene, ethylbenzene and *o*-xylene compounds in water using directly suspended droplet microextraction coupled with gas chromatography-flame ionization detector

A. Sarafraz-Yazdi<sup>a,c,\*</sup>, A.H. Amiri<sup>a</sup>, Z. Es'haghi<sup>b,c</sup>

<sup>a</sup> Department of Chemistry, Faculty of Sciences, Ferdowsi University of Mashhad, Iran

<sup>b</sup> Department of Chemistry, Faculty of Sciences, Payame Noor University, Iran

<sup>c</sup> Biotechnology Research Center of Ferdowsi University, Mashhad, Iran

## ARTICLE INFO

### Article history:

Received 27 November 2008

Received in revised form

28 December 2008

Accepted 30 December 2008

Available online 20 January 2009

### Keywords:

Directly suspended droplet microextraction

(DSDME) technique

BTEX

Water sample

GC-FID

## ABSTRACT

The directly suspended droplet microextraction (DSDME) technique coupled with the capillary gas chromatography-flame ionization detector (GC-FID) was used to determine BTEX compounds in aqueous samples. The effective parameters such as organic solvent, extraction time, microdroplet volume, salt effect and stirring speed were optimized. The performance of the proposed technique was evaluated for the determination of BTEX compounds in natural water samples. Under the optimal conditions the enrichment factors ranged from 142.68 to 312.13, linear range; 0.01–20  $\mu\text{g mL}^{-1}$ , limits of detection; 0.8–7  $\text{ng mL}^{-1}$  for most analytes. Relative standard deviations for 0.2  $\mu\text{g mL}^{-1}$  of BTEX in water were in the range 1.81–2.47% ( $n = 5$ ). The relative recoveries of BTEX from surface water at spiking level of 0.2  $\mu\text{g mL}^{-1}$  were in the range of 89.87–98.62%.

© 2009 Published by Elsevier B.V.

## 1. Introduction

Volatile organic compounds (VOCs) are organic chemical compounds that have high enough vapor pressures under normal conditions to significantly vaporize and enter the atmosphere. The acronym BTEX defines the mixture of benzene, toluene, ethylbenzene and the three xylenes isomers (*ortho*, *meta* and *para*), all being harmful VOCs. The effects of exposure to these substances comprise changes in the liver and damaging effects on the kidneys, heart, lungs, and the nervous system [1]. BTEX are emitted to the environment from an extensive variety of sources including combustion products of wood and fuels, industrial paints, adhesives, degreasing agents and aerosols [2]. Therefore, they are ubiquitous among samples of environmental concern (air, water and soil), the human exposure to these aromatic hydrocarbons occurring by ingestion (consuming contaminated water or food), inhalation or absorption through the skin. In order to reduce the human intake of these hazardous substances a chemical control (and consequently methods of analysis) is desirable.

Historically, liquid–liquid extraction (LLE) and solid-phase extraction (SPE) were often used for the extraction of hazardous compounds from aqueous matrices. However, LLE is time-consuming, generally labor-intensive, and requires large quantities of expensive, toxic, and environmentally unfriendly organic solvents.

In case of SPE, in comparison with LLE, although it requires a smaller volume of toxic organic solvents for the analyte desorption, the small columns or disks used cause “plugging” if the aqueous sample contain fine solid particles. Therefore, nowadays the simplification and miniaturization of the sample preparation methods are recommended, which have the advantages of either none or very little amount ( $\mu\text{L}$ ) of toxic organic solvents used.

Currently, the technique of Solid Phase Microextraction (SPME) is used by some researchers. This technique allows a rapid and solvent-free extraction of organic compounds from aqueous samples by partitioning between the stationary phase and the aqueous medium [3,4]. The technique is commercially available, and is capable of extracting micropollutants in aqueous samples prior to GC analysis. The main drawbacks of SPME are (i) increase in the cost of analysis per sample due to the use of certain special expensive apparatus, (ii) degradation of fibers with increased usage, and (iii) carry-over between extractions [5]. In order to overcome these problems, a simple and inexpensive Liquid-Phase Microextraction (LPME) has been recently introduced.

\* Corresponding author at: Department of Chemistry, Faculty of Sciences, Ferdowsi University of Mashhad, Mashhad, Khorasan 91775, Iran. Tel.: +98 511 8432023; fax: +98 511 8438032.

E-mail address: [asyazdi@ferdowsi.um.ac.ir](mailto:asyazdi@ferdowsi.um.ac.ir) (A. Sarafraz-Yazdi).

In this technique, only several microliters of solvents are required to concentrate analytes from aqueous samples rather than hundreds of milliliters needed in LLE. This technique is not exhaustive and only a small fraction of analytes are preconcentrated for the analysis.

The general idea behind these novel techniques is a great reduction in the volumetric phase ratio of the acceptor-to-donor phase. This can be achieved by using either immiscible liquid phases (solvent microextraction) or a membrane to separate the acceptor–donor phases (membrane extraction). Another important advantage is the integration of extraction and injection into the instrument in one step, thus minimizing the analysis time. Apart from a wide choice of extraction solvents, LPME can be performed with the simplest devices, i.e. a traditional microsyringe and does not suffer from carry-over between extractions that is encountered when using SPME.

One of the main methodologies that evolved from the solvent microextraction approach are the single drop microextraction (SDME) technique [6–8], where the acceptor phase is a microdrop of a water immiscible organic solvent suspended in an aqueous donor solution (two-phase system).

Another version of LPME is membrane extraction and the techniques developed can be divided into two main categories: porous membrane techniques, where the solutions on the both sides of the membrane are in physical contact through the pores of a membrane, and non-porous membrane techniques, where the membrane forms a separate phase (polymeric or liquid) between the donor and the acceptor solutions. The use of membranes presents the advantages of high selectivity, clean extract formation and a high degree of enrichment. One of these membrane techniques was introduced by Pedersen–Bjergaard and Rasmussen [9], which was also termed hollow fiber-based liquid phase microextraction (HF-LPME). It utilized porous, hydrophobic, hollow fibers impregnated with an organic phase. This new extraction methodology proved to be an attractive alternative to other microextraction concepts because, apart from being simple, it is inexpensive, fast and virtually solvent-free.

SDME and HF-LPME require careful and elaborate manual operations, given that problems of organic solvent instability/dissolution have often been reported especially after faster stirring or longer extraction time. Recently, a new mode of LPME named dispersive liquid phase microextraction (DLPME) [10], which is based on a ternary component solvent system such as homogeneous liquid–liquid extraction (HLE) and cloud-point extraction (CPE) were proposed. In this method the phenomenon of separating the phase from a homogeneous solution was used and the target solutes were extracted into a separated phase and then were determined. In DLPME, the appropriate mixture of the extraction and disperser solvents is rapidly injected into the aqueous samples containing analytes. Then, cloudy solution was formed and a drop of organic phase was sedimented in the bottom of the conical tube after centrifugation. This sediment is withdrawn with microsyringe and introduced to an analytical instrument for further analysis.

It has been reported that the main shortcoming of the SDME, is the instability of the droplet when an organic solvent is used as extractant. This fact limits the usable volume of the extracting medium, affecting directly the precision and also the sensitivity of the method.

Ionic liquids, which are ionic media resulting from the combination of organic cations and various anions, have been proposed as an alternative to these organic solvents due to their low vapor pressure and their high viscosity, which allows the use of the larger and more reproducible extracting volumes of solvent [11]. These solvents have other unique properties, including dual natural polarity, or miscibility with water and organic solvents [12]. Additionally, they are regarded as environmentally friendly solvents and are

easily synthesized or commercially available. These characteristics have led to an extensive range of applications and investigations in analytical chemistry [13,14].

Recently, Yangcheng and coworkers have developed a new sampling method termed directly suspended droplet microextraction (DSDME) [15]. In this method, a stirring bar is placed at the bottom of the aqueous sample rotating at a proper speed, which causes a weak gentle vortex or whirlpool in the solution. If a small volume of an immiscible organic solvent is added to the surface of the solution, the motion of the vortex results in the formation of a single microdrop at or near the center of rotation. The droplet itself may also rotate on the surface of the aqueous phase, increasing mass transfer. Compared with the other LPME technique based on droplet system, i.e. single drop microextraction, it provides more flexibility in the choice of the operational parameters, especially for solvent volume and stirring frequency. The possibility of using larger volumes of organic solvent in this method in addition to GC makes it a useful technique comparable to HPLC and UV–vis spectrophotometry.

## 2. Experimental

### 2.1. Reagents and standards

Methanol, 2-octanone and heptanol with Suprasolv quality (for organic trace analysis) were obtained from Merck (Darmstadt, Germany). 1-Octanol was purchased from Fluka (Buchs, Switzerland). Analytical reagents grade benzene, toluene, ethylbenzene and *o*-xylene also were purchased from Merck (Darmstadt, Germany). To prepare stock solutions of BTEX ( $2000 \mu\text{g mL}^{-1}$ ) approximately 23  $\mu\text{L}$  of each of them was transferred into a 10-mL volumetric flask and dissolved with methanol. It was then stored in a refrigerator at 4 °C. Fresh working solutions ( $2 \mu\text{g mL}^{-1}$ ) were prepared daily by diluting the stock solution in distilled water.

### 2.2. Instrumentation

Gas chromatographic analysis was carried out using a Chrompack CP9001 (Middelburg, the Netherlands) fitted with a split/splitless injector and flame ionization detector (FID). Helium (99.999%, Sabalan Co., Tehran, Iran) was used as the carrier gas with a flow rate of  $1.11 \text{ mL min}^{-1}$ . Separations were conducted using a CP-Sil 24CB (50% phenyl, 50% dimethylsiloxane) capillary column, WCOT Fused silica, 30 M  $\times$  0.32 mm i.d. with 0.25  $\mu\text{m}$  stationary film thickness (Chrompack, Middelburg, the Netherlands). The injector temperature was set at 210 °C and all injections were made in the split mode. The column was initially maintained at 60 °C for 1 min; subsequently, the temperature was increased to 100 °C at a rate of  $5 \text{ }^\circ\text{C min}^{-1}$ , then it was increased to 200 °C ( $30 \text{ }^\circ\text{C min}^{-1}$ ). The total time for each GC run was 17 min. The FID temperature was maintained at 250 °C. The flow of Zero Air (99.99%, Sabalan Co., Tehran, Iran) for FID was  $250 \text{ mL min}^{-1}$  and the flow rate of hydrogen was  $30 \text{ mL min}^{-1}$ .

### 2.3. Directly suspended droplet microextraction procedure

The extraction steps are illustrated in Fig. 1. In this extraction procedure, a 3-mL cylindrical sample cell (35 mm  $\times$  13 mm) with a screw cap, a 10- $\mu\text{L}$  syringe (Hamilton Bonaduz AG, Bonaduz, Switzerland) and a 7 mm  $\times$  2 mm stir bar were used.

At first, 2.5 mL sample solution was held in the 3.0-mL sample vial, and a stirring bar was adjusted within the sample solution. The magnetic stirrer was turned on and adjusted to a desired stirring speed. To make a steady and benign vortex, it is important to keep the stirring bar rotating smoothly just at the center of the bottom. A microdroplet of an immiscible organic solvent is placed at the bottom of the vortex, and the syringe removed. The screw cap

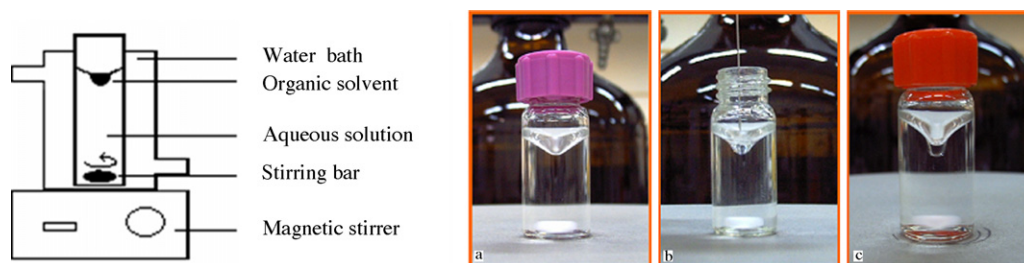


**Fig. 1.** Photography of the different steps in DSDME: (a) magnetic stirrer is on, (b) starting organic solvent addition with a microsyringe and (c) droplet forming while stirring bar is rotating.

should be kept closed during the extraction process. After 25 min., the screw cap was removed and a portion of the organic droplet was withdrawn into a syringe and injected into the GC for further analysis.

### 3. Results and discussion

#### 3.1. Optimization of directly suspended droplet microextraction parameters

Factors affecting the extraction efficiency such as organic solvent, the extraction time, microdroplet volume, stirring speed and salt effect were optimized. The optimization was carried out on water solution of  $2 \mu\text{g mL}^{-1}$  for each BTEX compounds. The chromatographic peak area, which is related to the number of moles of analytes which are extracted into the droplet, was used to evaluate the extraction efficiency under different experimental conditions. Throughout these experiments, the injected volume of the extracted analytes into GC was kept constant at  $1 \mu\text{L}$ .

#### 3.2. Choice of organic solvent

To establish a direct mode LPME technique, it is necessary to choose a proper organic solvent. The choice of the organic solvent needs the following considerations: the solvent should have good affinity for target compounds, low solubility in water such as to prevent the dissolution in the aqueous phase and lower density than water. On the basis of these considerations 1-octanol, 2-octanone and 1-heptanol were tested in the preliminary experiments. The peak area was selected as the extraction efficiency for each solvent. It can be seen from Fig. 2 that 2-octanone gives the best extraction efficiency and is used as the extraction solvent for subsequent extractions.

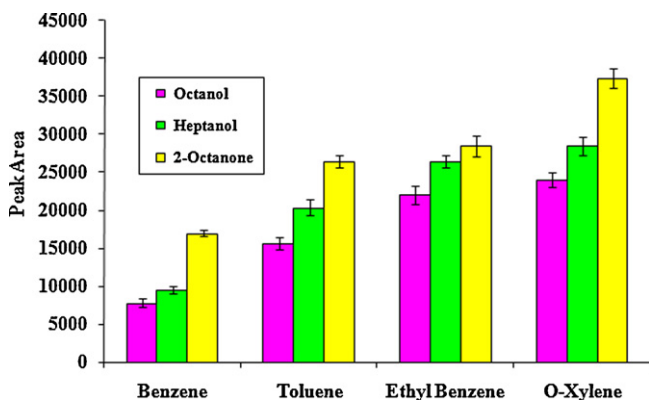


**Fig. 2.** Effect of extraction solvent on DSDME extraction efficiency ( $n=3$ ). Other experimental conditions are as follows: concentration level at  $2 \mu\text{g mL}^{-1}$ , 800 rpm stirring speed, 20 min extraction time, 2.5 mL sample volume, microdroplet volume;  $10 \mu\text{L}$ .

#### 3.3. Effect of the extraction time

Similar to the other LPME procedures, DSDME is a technique which is dependent on equilibrium rather than exhaustive extraction. The amount of analyte extracted into the droplet at a given time depends upon the mass transfer of analyte from the aqueous phase into the organic solvent phase. This procedure requires a period of time for the equilibrium to be established. However, it is not normally practical to use extraction times that are long enough for equilibrium to be established. Fig. 3 shows the effect of extraction time on the method efficiency. By increasing the extraction time the numbers of the moles extracted are increased, therefore the peak area related to the analytes are being increased up to the period of 25 min, and then decreased with the increasing of the extraction time. This may be due to the organic solvent evaporation and dissolution in water solution. Since the extraction here is not an exhaustive one, a reasonable period of time (25 min) is selected for the subsequent experiments.

#### 3.4. Microdrop volume

The volume of the extractor organic droplet has a great effect on the extraction efficiency. The typical injection volume is  $5\text{--}10 \mu\text{L}$  for HPLC and  $50 \mu\text{L}$  or more for UV-vis spectrometer. Both of these volumes are beyond the upper limit of all other droplet microextraction methods reported. DSDME based on free droplets and controlled fluid fields do not fail even when using larger volumes of organic solvent, so DSDME can well match with HPLC and UV-vis spectrometer directly [15].

The effects of the 2-octanone drop size on the extraction were examined in the range of  $7.5\text{--}15 \mu\text{L}$ . The relationship between the volume of organic solvent and extraction efficiency are shown in Fig. 4. Based on this trend, the analytical signals were decreased.

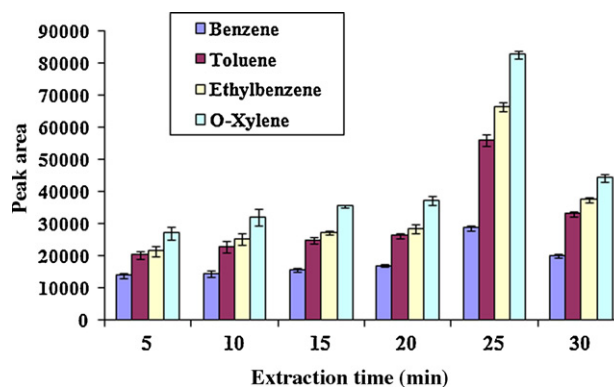


**Fig. 3.** The effect of extraction time on the extraction efficiency of BTEX compounds when using DSDME technique with 2-octanone as solvent. Other extraction conditions: analyte concentration;  $2 \mu\text{g mL}^{-1}$ , stirring speed; 800 rpm, 2.5 mL sample volume, microdroplet volume;  $10 \mu\text{L}$ .

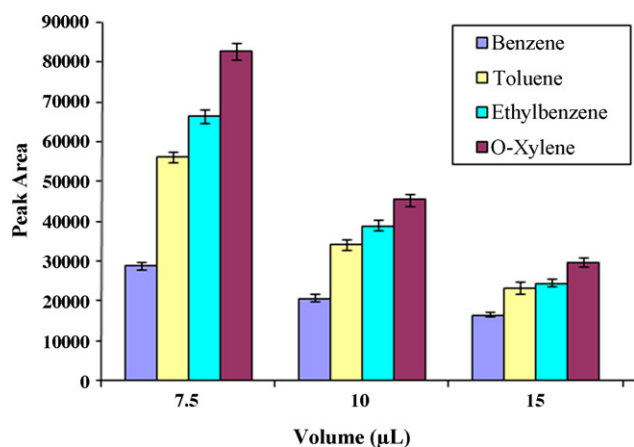


**Fig. 4.** The effect of microdroplet volume on the extraction efficiency of BTEX compounds when using DSDME technique. Extraction conditions: analyte concentration;  $0.2 \mu\text{g mL}^{-1}$ , 2-octanone as organic solvent, extraction time; 25 min, stirring speed; 800 rpm, 2.5 mL sample volume.

In a smaller droplet, the area to volume ratio is greater than in a larger droplet. Therefore, mass transfer could take place more easily in a droplet with a smaller size. This behavior is also expected by considering the enrichment factor equation:

$$E = \frac{C^O}{C_0^{\text{aq}}} = \frac{k_t}{1 + k_t(V^O/V^{\text{aq}})}$$

where  $C^O$  and  $C_0^{\text{aq}}$  are the analyte concentration in organic phase and its initial concentration in the aqueous phase, respectively.  $V^O/V^{\text{aq}}$  is the volume ratio of organic phase to the aqueous one and  $k_t$  is the distribution coefficient (i.e.  $C^O/C^{\text{aq}}$ ) at time  $t$ . As can be seen from this equation, enrichment factor has a reverse correlation with  $V^O/V^{\text{aq}}$  ratio. Thus  $7.5 \mu\text{L}$  microdrop volume was chosen for further work.

### 3.5. Salting effects

The extraction efficiency is related to the ionic strength of the aqueous solution [16]. Usually, depending on the solubility of the target analytes, adding salt to the sample enhances the extraction of the more polar analytes. In the case of DSDME, salt addition was generally limiting the extraction of analytes. It was assumed that apart from the salting-out effect, salt addition causes a second effect named, salting-in effect. This phenomenon leads to changes in the physical properties of the Nernst diffusion film. So, target analyte diffusion rate into the droplet was reduced [17]. In the present work, the effect of NaCl concentration (ranging from 0 to 15%) was investigated and the extraction efficiencies were monitored. The peak area decreased with increasing salt concentration in the aqueous sample (Fig. 5). Therefore, no salt was added to the sample solution in the subsequent extractions.

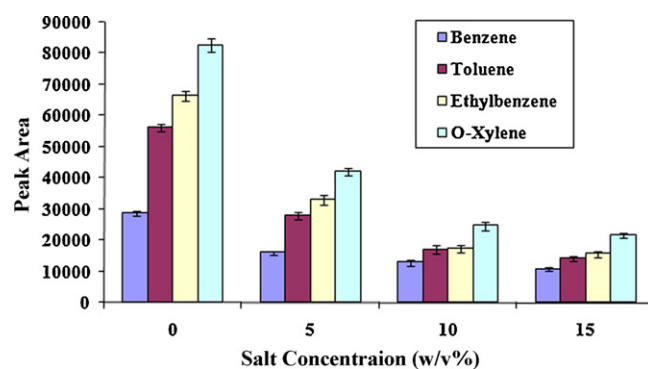


**Fig. 5.** The effect of salt on the extraction efficiency of BTEX compounds. Extraction conditions: analyte concentration;  $2 \mu\text{g mL}^{-1}$ , 2-octanone as organic solvent, stirring rate; 800 rpm, extraction time; 25 min, 2.5 mL sample volume, microdroplet volume;  $7.5 \mu\text{L}$ .

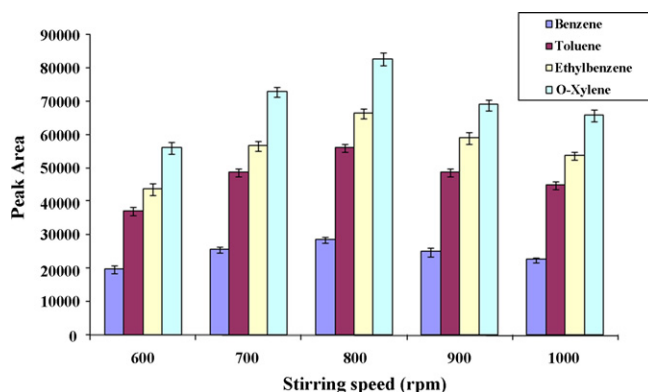


**Fig. 6.** The effect of stirring speed on the extraction efficiency of BTEX compounds. Extraction conditions: analyte concentration  $2 \mu\text{g mL}^{-1}$ , 2-octanone as organic solvent, extraction time 25 min; NaCl concentration 0% (w/v), 2.5 mL sample volume, microdroplet volume  $7.5 \mu\text{L}$ .

### 3.6. Stirring speed

The agitation of the sample solution enhances the microextraction efficiency. In DSDME, the stirring speed has a direct influence on both the shape of the droplet and the mass transfer characteristics in the aqueous sample [15]. In Fig. 6, it is shown that the peak areas of all analytes increase with increasing stirring speed up to 800 rpm. It was also observed that the stirring speed above 800 rpm causes the instability and faster dissolution of the solvent droplet and also decreases the peak area. Hence, the stirring speed of 800 rpm was chosen as the optimum stirring rate.

## 4. Figures of merit of the method

The calibration graphs were drawn using seven spiking levels of all analytes in the concentration range of  $0.01\text{--}20 \mu\text{g mL}^{-1}$ . For each point three replicate extractions were performed. The extraction conditions were as follows: sample solution: 2.5 mL, organic sol-

**Table 1**  
DSDME performance and validation data.

Compound	Enrichment factor	R.S.D. (%) ( $n=5$ )	Linear range ( $\mu\text{g mL}^{-1}$ )	Correlation Coefficient ( $r^2$ )	LOD <sup>b</sup> ( $\text{ng mL}^{-1}$ )
Benzene	142.68	2.21	0.01–20	0.9996	7
Toluene	254.88	2.47	0.01–20	0.9989	3
Ethylbenzene	275.44	1.81	0.01–20	0.9991	1
<i>o</i> -Xylene	312.13	2.45	0.01–20	0.9995	0.8

<sup>a</sup> Water samples spiked at  $0.2 \mu\text{g mL}^{-1}$  for each compound.

<sup>b</sup> Limit of detection for  $S/N=3$  ( $n=5$ ).

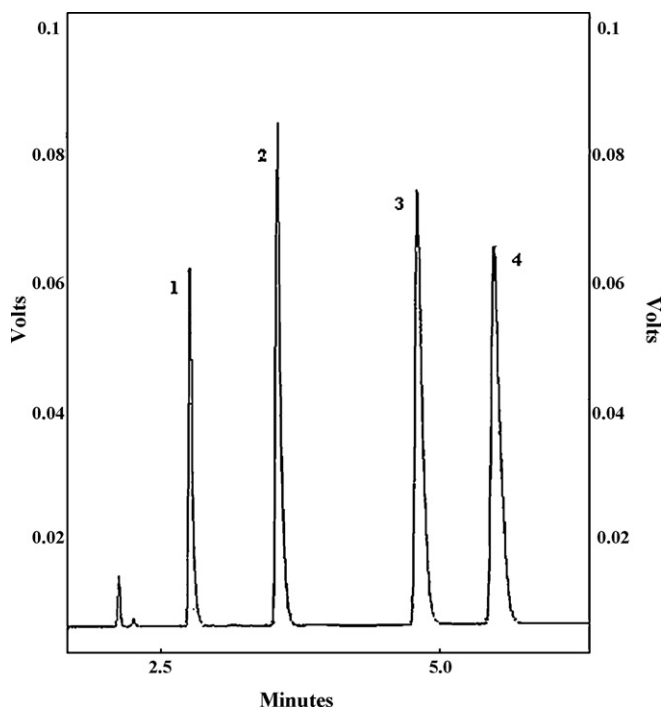


Fig. 7. Chromatogram of BTEX compounds in river water spiked with  $0.2 \mu\text{g mL}^{-1}$  of each analyte: (1) benzene, (2) toluene, (3) ethylbenzene and (4) *o*-xylene.

vent: 2-octanone, extraction time: 25 min, stirring speed: 800 rpm, microdroplet volume:  $7.5 \mu\text{L}$ .

The calculated calibration curves gave a high level of linearity for all target analytes with correlation coefficients ( $r^2$ ) ranging between 0.9989 and 0.9996 as shown in Table 1. The repeatability of the proposed method, expressed as relative standard deviation (R.S.D.%), was evaluated by extracting five consecutive aqueous samples (spiked at  $0.2 \mu\text{g mL}^{-1}$  with each target analyte) and was found to vary between 1.81 and 2.47%. The limits of detections (LODs), based on a signal-to noise ratio ( $S/N$ ) of 3, ranged from 0.8 to  $7 \text{ ng mL}^{-1}$  (Table 1).

## 5. Real water analysis

The DSDME technique was applied for determination of BTEX in river water. These samples were collected from the local river of Mashhad, Iran. No BTEX compounds were detected in river water samples; therefore, these samples were spiked with the BTEX compounds to assess matrix effects (Fig. 7). As it is mentioned above "salting-in effect" causes a decrease in the extraction efficiency, therefore for more complicate matrices the salt interferences must be removed before the extraction or in the critical cases the internal standards or standard addition methods should be used. The DSDME technique is a non-exhaustive extraction procedure and the relative recovery (determined as the ratio of the concentrations found in natural and distilled water samples, spiked with the same amount of analytes) instead of the absolute recovery (used in exhaustive extraction procedures) was employed. Table 2 shows that the relative recovery and relative standard deviation (R.S.D.%) for BTEX compounds in spiked river water sample were between 89.87 and 98.62%.

## 6. Comparison of DSDME with other related methods

Some statistical data of this work for water samples were compared with the other related methods such as: SPME-GC-FID,

Table 2

Relative recoveries and precisions of DSDME technique for river water samples spiked with the analytes.

Analytes	River water		Tap water	
	Relative recovery%	R.S.D. <sup>a</sup> (%)	Relative recovery%	R.S.D. <sup>a</sup> (%)
Benzene	98.62	7.03	96.52	5.3
Toluene	92.65	6.5	89.35	4.78
Ethylbenzene	92.52	6.35	88.27	4.5
<i>o</i> -Xylene	89.87	7.3	88.78	5.68

<sup>a</sup> Precision expressed as R.S.D. at  $0.2 \mu\text{g mL}^{-1}$  level,  $n = 5$  replicates.

Table 3

Comparison of the DSDME-GC-FID method with other related methods for determination of BTEX.

Methods	LOD <sup>a</sup>	R.S.D. (%)	Reference
HF-LPME-GC-FID	7.0–30.0	2.02–4.61	[18]
SPME-GC-FID	0.2–1.0	4–8	[19]
HS-SPME-GC-FID	0.08–0.6	3–7	[19]
DI-SDME-GC-FID	7.2–16.5	10.6–12.2	[20]
Fiber-in-tube LPME-GC-FID	0.3–5.0	3.6–8.1	[20]
DSDME-GC-FID	0.8–7.0	1.81–2.45	This study

<sup>a</sup> LOD, limit of detection in  $\text{ng mL}^{-1}$ .

HS-SPME-GC-FID, DI-SDME-GC-FID, fiber-in-tube LPME-GC-FID and HF-LPME-GC-FID, which are shown in Table 3.

Clearly, the relative standard deviations of DSDME-GC-FID were better than the relative standard deviations of the other methods. The limit of detection values in DSDME-GC-FID is comparable with the other methods. Also this method eliminates the main common problems encountered with SPME, such as carry-over effects between analyses, limited lifetime and fragile nature of the fiber.

## 7. Conclusion

This technique was successfully used for the separation and preconcentration of BTEX from water samples prior to analysis by capillary GC-FID. As compared with the other conventional sample-preparation methods, the DSDME-GC-FID offered advantages such as simplicity, ease of operation, reproducibility and relatively low detection limit. As a conclusion, the proposed method possesses great potential in the analysis of ultra-trace compounds in real aqueous samples.

## Acknowledgement

The authors are grateful to Ferdowsi university of Mashhad, Iran for financial support.

## References

- [1] R.J. Irwin, M. VanMouwerik, L. Stevens, M.D. Seese, W. Basham, Environmental Contaminants Encyclopedia, Fort Collins, Colorado, USA, 1997.
- [2] R.M. Alberici, G.C. Zampronio, R.J. Poppi, M.N. Eberlin, Analyst 127 (2002) 303.
- [3] C. Arthur, J. Pawliszyn, Anal. Chem. 62 (1990) 2145.
- [4] J. Pörschmann, F.D. Kopinke, J. Pawliszyn, J. Chromatogr. A 816 (1998) 159.
- [5] H. Prosen, L. Zupančič-Kralj, Trends Anal. Chem. 18 (1999) 272.
- [6] H. Liu, P.K. Dasgupta, Anal. Chem. 68 (1996) 1817.
- [7] M.A. Jeannot, F.F. Cantwell, Anal. Chem. 68 (1996) 2236.
- [8] M.A. Jeannot, F.F. Cantwell, Anal. Chem. 69 (1997) 235.
- [9] S. Pedersen-Bjergaard, K.E. Rasmussen, Anal. Chem. 71 (1999) 2650.
- [10] M. Rezaee, Y. Assadi, M.R. Millani, E. Aghaee, F. Ahmadi, S. Berijani, J. Chromatogr. A 1116 (2006) 1.
- [11] J.-F. Liu, G.-B. Jiang, Y.-G. Chi, Y.-Q. Cai, Q.-X. Zhou, J.-T. Hu, Anal. Chem. 75 (2003) 5870.
- [12] T. Welton, Chem. Rev. 99 (1999) 2071.
- [13] E. Aguilera-Herrador, R. Lucena, S. Cardenas, M. Valcarcel, Anal. Chem. 80 (2008) 793.

- [14] E. Aguilera-Herrador, R. Lucena, S. Cardenas, M. Valcarcel, J. Chromatogr. A 1201 (2008) 106.
- [15] L. Yangcheng, L. Quan, L. Guangsheng, D. Youyuan, Anal. Chim. Acta 566 (2006) 259.
- [16] R. Eisert, J. Pawliszyn, Crit. Rev. Anal. Chem. 27 (1997) 103.
- [17] E. Psillakis, N. Kalogerakis, Trends Anal. Chem. 21 (2002) 53.
- [18] A. Sarafraz-Yazdi, A.H. Amiri, Z. Es'haghi, Chemosphere 71 (2008) 671.
- [19] J.C. Flórez Menéndez, M.L. Fernández Sánchez, J.E. Sánchez Uría, E. Fernández Martínez, A. Sanz-Medel, Anal. Chim. Acta 415 (2000) 9.
- [20] J.-X. Wang, D.-Q. Jiang, X.-P. Yan, Talanta 68 (2006) 945.



# Laser-induced breakdown spectroscopy for determination of uranium in thorium–uranium mixed oxide fuel materials

Arnab Sarkar, Devanathan Alamelu, Suresh K. Aggarwal\*

Fuel Chemistry Division, Bhabha Atomic Research Centre, Trombay, Mumbai 400 085, India

## ARTICLE INFO

### Article history:

Received 12 November 2008  
Received in revised form 18 December 2008  
Accepted 19 December 2008  
Available online 30 December 2008

### Keywords:

Laser-induced breakdown spectroscopy (LIBS)  
Advanced heavy water reactors (AHWR)  
Uranium  
Thorium  
Nuclear fuel

## ABSTRACT

Laser-induced breakdown spectroscopy (LIBS) has been developed for determining the percentage of uranium in thorium–uranium mixed oxide fuel samples required as a part of the chemical quality assurance of fuel materials. The experimental parameters were optimized using mixed oxide pellets prepared from 1:1 (w/w) mixture of thorium–uranium mixed oxide standards and using boric acid as a binder. Calibration curves were established using U(II) 263.553 nm, U(II) 367.007 nm, U(II) 447.233 nm and U(II) 454.363 nm emission lines. The uranium amount determined in two synthetic mixed oxide samples using calibration curves agreed well with that of the expected values. Except for U(II) 263.553 nm, all the other emission lines exhibited a saturation effect due to self-absorption when U amount exceeded 20 wt.% in the Th–U mixture. The present method will be useful for fast and routine determination of uranium in mixed oxide samples of Th and U, without the need for dissolution, which is difficult and time consuming due to the refractory nature of ThO<sub>2</sub>. The methodology developed is encouraging since a very good analytical agreement was obtained considering the limited resolution of the spectrometer employed in the work.

© 2008 Elsevier B.V. All rights reserved.

## 1. Introduction

The Indian nuclear power program has been conceived bearing in mind the optimum utilization of domestic uranium and thorium reserves with the objective of providing long-term energy security to the country. Keeping in mind that India has to fall back on its vast thorium resources, which account for about one-third of the world's thorium reserves (~300,000 t) [1,2], third stage of the Indian nuclear power program is based on Th–<sup>233</sup>U fuel cycle and developing advanced heavy water reactors (AHWRs). Two different compositions of Th–U mixed oxide have been proposed for AHWR fuel containing 3 and 3.75 wt.% of <sup>233</sup>U [3]. The Th–U mixed oxide pellets are generally prepared by the conventional powder metallurgy route, which has been tested and used for U- and Pu-based fuels. The qualitative as well as quantitative characterization of the fuel materials for major as well as minor constituents is required as a part of chemical quality assurance of nuclear fuels. At present, chemical and mass-spectrometric methods are being employed to determine the composition of major/minor elements in Th–U mixed oxide with the desired accuracy and precision.

Laser-induced breakdown spectroscopy (LIBS) is an emission spectrometric technique with several advantages over the conven-

tional emission spectrometric techniques, especially for nuclear applications [4]. The basic theory of the technique has been described in several reviews [5–7]. However, LIBS has not been extensively used for characterization of nuclear materials. Among the few notable work in the field of nuclear industry by LIBS include the work carried by Fichet et al. which showed the applicability of LIBS for impurity quantification in both UO<sub>2</sub> and in PuO<sub>2</sub> [8]. Shen and Lu have showed the applicability of uranium detection up to 462 ppm in glass samples using laser-induced breakdown spectroscopy in combination with laser-induced fluorescence [9], where as Cremer and co-workers showed a detection limit of 0.1 g L<sup>-1</sup> for uranium in liquid by direct liquid analysis method [10]. With the help of very high-resolution spectrometer, the isotopic ratio of U and Pu had been also determined by LIBS [11–13]. In our laboratory, we have developed LIBS methodology to determine U and Th in aqueous solutions individually as well as in the presence of each other [4]. The applicability of LIBS for the determination of trace constituents in a thoria matrix has also been reported recently by us [14].

Instrumental techniques such as LIBS have huge potential for the determination of uranium in mixed oxides of Th and U. Thoria being a refractory material, the dissolution of sintered thoria pellets or a U–Th mixed oxide pellets is difficult and time consuming which can be avoided in LIBS. However, this is a pre-requisite for chemical as well as mass-spectrometric methods. In the present work, we report the application of LIBS for the rapid determination of U in Th–U mixed oxide samples in the range up to 20% of ura-

\* Corresponding author. Tel.: +91 22 25593740; fax: +91 22 25505151.  
E-mail addresses: [skaggr@barc.gov.in](mailto:skaggr@barc.gov.in), [skaggr2002@rediffmail.com](mailto:skaggr2002@rediffmail.com) (S.K. Aggarwal).



nium. The emission spectra of both Th and U being very complex, proper choice of emission lines of interest is very important. Calibration curves were obtained for four emission lines of U in Th–U mixed oxide. This paper presents details of the work carried out to optimize the experimental parameters like laser fluence and acquisition delay time and gives the results obtained for U determination in two synthetic samples of Th–U mixed oxide.

## 2. Experimental

### 2.1. Instrumentation

A Spectrolaser 1000 M, from M/s. Laser Analysis Technologies Pvt. Ltd. (now known as XRF scientific), Victoria, Australia was employed in this work. The details of the instrument have been described elsewhere [4]. The instrument is equipped with a high-power Q-switched Nd:YAG laser that yields 200 mJ of pulse energy at the fundamental IR wavelength (1064 nm) with a 7 ns pulse width, at a repetition rate of 10 Hz. The laser is focused onto the sample by a plano-convex lens with a focal length of 5 cm. The diameter of the focal spot was 500  $\mu\text{m}$ . The sample is placed in the sample chamber in ambient atmosphere and is mounted on a translation stage so that every laser shot hits on a fresh surface. The emission from plasma is then collected in front of the plasma at a 45° angle with respect to the laser beam direction. Plasma emission was collected by a 15-mm diameter imaging lens at a distance of approximately 50 mm, and focused onto silica optical cable fibers which deliver the plasma light to the entrance slit of spectrographs (Czerny–Turner configuration) equipped with CCDs as detectors.

### 2.2. Sample preparation and analysis

Since certified reference materials (CRMs) for mixed oxide of U and Th are not available commercially, a series of synthetic mixed oxide calibration standards were prepared. Known amount of highly pure ThO<sub>2</sub> and U<sub>3</sub>O<sub>8</sub> powders were weighed and then blended and ground thoroughly for about 30 min. Initially, six Th–U mixed oxide calibration standards with U amount varying from 0 to 32% by weight were prepared. Subsequently two more synthetic samples with U amounts of 4 and 20% were prepared and were treated as unknown to validate the calibration. The powders were mixed with high purity (99.5%) boric acid powder, procured from S.D. Fine-Chem. Ltd., Mumbai, India, in equal-amount ratio for 15 min by blending and grinding thoroughly to obtain homogeneous mixture. Mixed powder samples were then pelletized to 3 cm diameter pellets by applying a pressure of  $2 \times 10^9$  Pa for 5 min. Table 1 gives the compositional data of the calibration standards prepared in this work. The emission lines for U determination were selected from the regions where minimal Th spectral interferences were observed and their intensities were normalized with respect to the B(I) 249.774 nm. Boron was chosen as an internal standard since boric acid was used as the binder and its concentration in the pellet was maintained constant irrespective of the composition of the mixed oxide.

**Table 1**  
Composition of the calibration standards and two synthetically prepared samples.

Standards	U concentration (%)	Th concentration (%)
TU-1-CAL	1.1	98.9
TU-2-CAL	2.1	97.9
TU-3-CAL	3.0	97.0
TU-4-CAL	8.1	91.9
TU-5-CAL	16.0	84.0
TU-6-CAL	32.0	68.0
TU-7-unknown	4.0	96.0
TU-8-unknown	20.3	79.7

**Table 2**

Characteristics of spectral lines employed for determination of U by LIBS.

Element	$\lambda_{ij}$ (nm)	$A_{ij}$ ( $\times 10^8 \text{ s}^{-1}$ )	$E_j$ ( $\text{cm}^{-1}$ )	$E_i$ ( $\text{cm}^{-1}$ )
U(II)	263.553	–	–	–
U(II)	367.007	0.26	914.765	28154.450
U(II)	447.233	–	–	–
U(II)	454.363	–	914.765	22917.451

$\lambda_{ij}$  is the transition wavelength,  $A_{ij}$  the transition probability,  $E_i$  and  $E_j$  are the energies of the upper and lower level, respectively.

Identical conditions of laser fluence, repetition frequency and acquisition delay were used for all analyses. In the present experiment, 1 Hz repetition rate of laser pulse was used. For the LIBS analysis, spectra of 100 shots were averaged. On each pellet including the calibration standards as well as the unknowns, triplicate analyses, i.e., three 100 shot measurements were performed. The stepping motor was fixed with a velocity of 0.2  $\text{mm s}^{-1}$  so that each laser pulse focused on a fresh surface. The emission line intensity can vary due to a variety of reasons that include fluctuations in laser power due to dust in the beam path, time jitter, as well as due to the changes in the focusing and collection optics. In order to reduce these effects and remove them from affecting the results obtained by LIBS, the software is programmed to discard the raw data from analysis where the raw net line intensity is more than  $\pm 10\%$  of the average intensity and then again re-averaging is done to get LIBS spectra.

## 3. Results and discussion

### 3.1. Selection of emission line

The four spectrographs allow simultaneous acquisition of a wide range of spectra, 180–850 nm for each laser shot, which contains almost all the intense emission lines of the two actinide elements under study. Emission spectra of actinides are generally very complex and the situation gets aggravated when two actinides are present in major amount, as in the present case. Presence of a large number of emission lines makes the spectra of mixed oxide as a band of emission lines at the present instrumental resolution (0.6 nm at 300 nm). To select an appropriate emission line for U, spectra of pure U, pure Th and a mixed oxide sample were recorded and compared critically. The pure U pellets were prepared in such a way that the amount of U in the pure U pellets and in the mixed oxide pellets was same. The pure Th pellet was also prepared in the same manner. Fig. 1 shows a comparison of the three spectra under identical conditions of analysis (laser energy of 100 mJ and acquisition delay of 3.5  $\mu\text{s}$ ). By comparison of the emission spectra, four spectral regions where spectral interferences from Th spectrum were minimal in the U emission lines region were identified and the suitable emission lines were selected for U. The emission lines used and their spectroscopic data are listed in Table 2 [15]. Among these four emission lines, U(II) 263.553 nm and U(II) 367.007 nm are among the reported prominent lines in ICP-AES [16].

### 3.2. Effect of laser fluence

To optimize the laser fluence, the calibration standard TU-4-CAL was analysed at different laser fluence. Fig. 2 shows a comparison of the spectra observed at different laser fluence. It is seen that with increasing laser fluence, the U(II) 367.007 nm emission line becomes more and more prominent. At fluence above 56  $\text{J cm}^{-2}$ , the pellet was not intact, and crippled during analysis and hence laser fluence was not increased further.

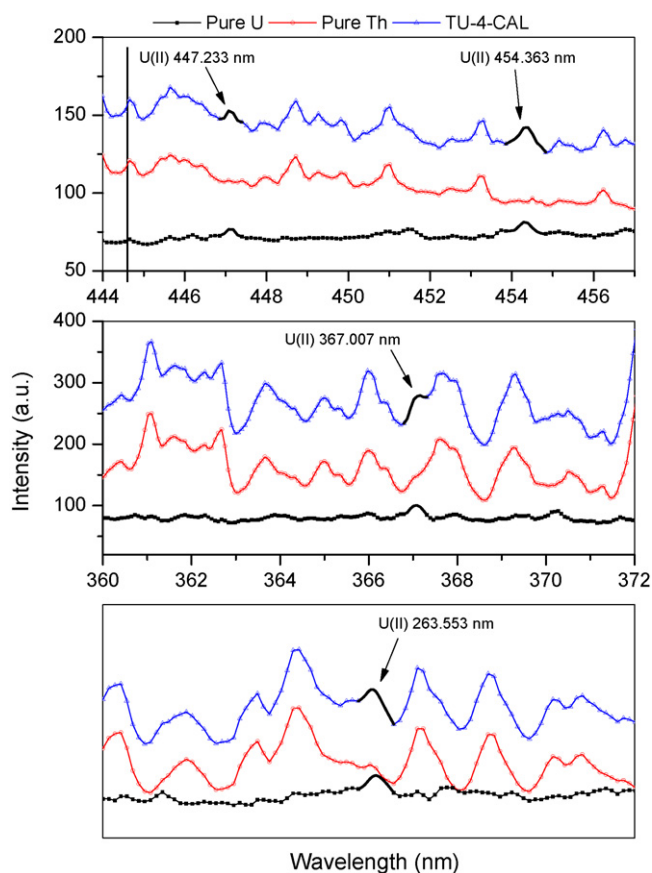


**Fig. 1.** Comparison of the spectra of the individual actinides with the mixed oxide standard under identical conditions of analysis.

### 3.3. Temporal resolution for acquisition

The importance of optimization of the temporal resolution has been discussed in literature [17,18]. A series of measurements were made to determine the optimal time delay between the laser pulse and the start time of the LIBS spectra acquisition. Fig. 3 shows a comparison of emission spectra recorded using TU-4-CAL at different acquisition delays at a laser fluence of  $56 \text{ J/cm}^2$ . For the U(II) 367.007 nm emission line, the best spectral purity with sufficient signal intensity was obtained at an acquisition delay of 3.5  $\mu\text{s}$

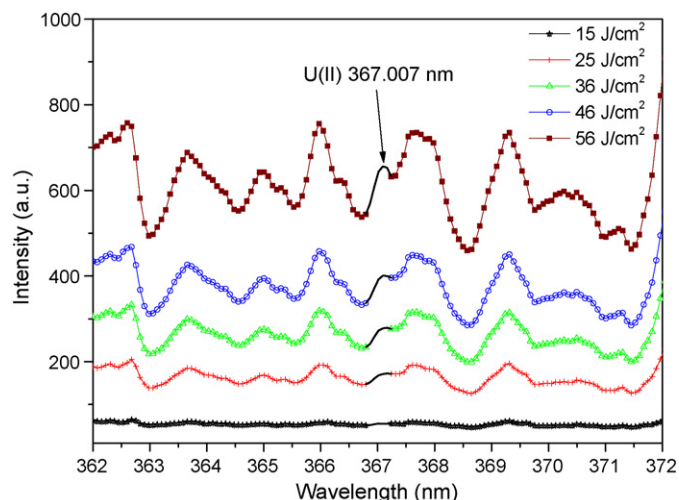


**Fig. 2.** Effect of laser fluence on the U(II) 367.007 nm emission line (TU-4-CAL).

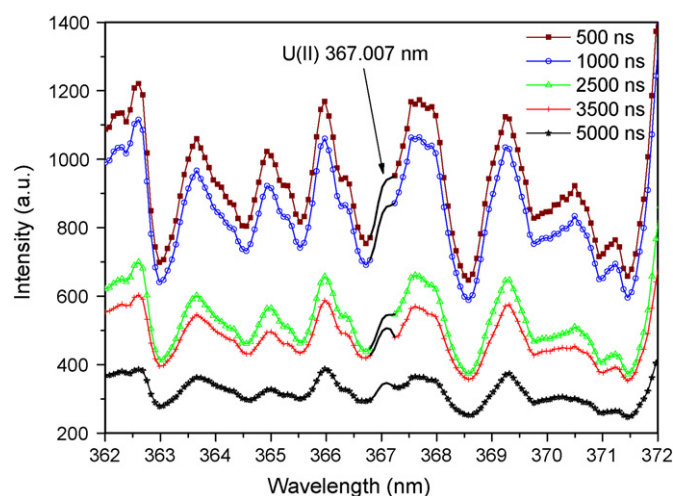


**Fig. 3.** Comparison of the effect of acquisition delay on the U(II) 367.007 nm emission line (TU-4-CAL).

which was selected as optimum acquisition delay for subsequent analyses.

Though for the complete optimization of laser fluence and acquisition delay time, it would be ideal to study the effect on signal to noise ratio (SNR) of each of these parameters keeping the other as constant. In the present work, a rough optimization was carried out in the manner presented above, which provided reasonable good optimization of the experimental parameters with less experimental effort.

### 3.4. Calibration curves and precision

Calibration standards of mixed oxide were used to prepare calibration curves of all the four normalized line intensities of U emission lines with respect to B(I) 249.774 nm versus the corresponding concentration of U, as shown in Fig. 4. Each calibration point corresponds to an average of three measurements at different locations of the corresponding pellet. The practice of discarding spectra with raw line intensity more than  $\pm 10\%$  than the average value was also followed here as discussed in the Section 2.2. The number of spectra that are discarded under this criterion would be useful to determine the statistical significance of the result obtained in this study. Since there is no provision in the present software employed for the spectral analysis to obtain this information, so this detail could not be shown in Fig. 4. The error bars on calibration points are the standard deviations ( $\pm 1\sigma$ ), calculated by measuring the normalized peak intensity of the emission line. Normalization of emission line intensity was done after discarding outlier spectra as stated above. The calibration data were analyzed using the instrument software and applying least squares regression analysis.

The calibration curves show a linear behavior below 8 wt.% U in the Th–U mixed oxide. Above 8 wt.% U, saturation is observed due to self-absorption of the lines in the plasma, a feature commonly observed in laser-induced plasmas at atmospheric pressure [19–21]. For this region, a non-linear equation was used to fit the experimental data, similar to the expression proposed by Aragon et al. [22],

$$y = y_0 + A e^{(-x/t)} \quad (1)$$

where  $x$  denotes wt.% of U and  $y$  stands for normalized emission line intensity. In Eq. (1), the absolute value of “ $t$ ” indicates the concentration where the calibration slope decreases by a factor of  $1/e$  from its value of  $(A/t)$  at  $x=0$ . Hence this value (i.e.,  $x=t$ ) can be regarded as the critical amount above which laser-induced

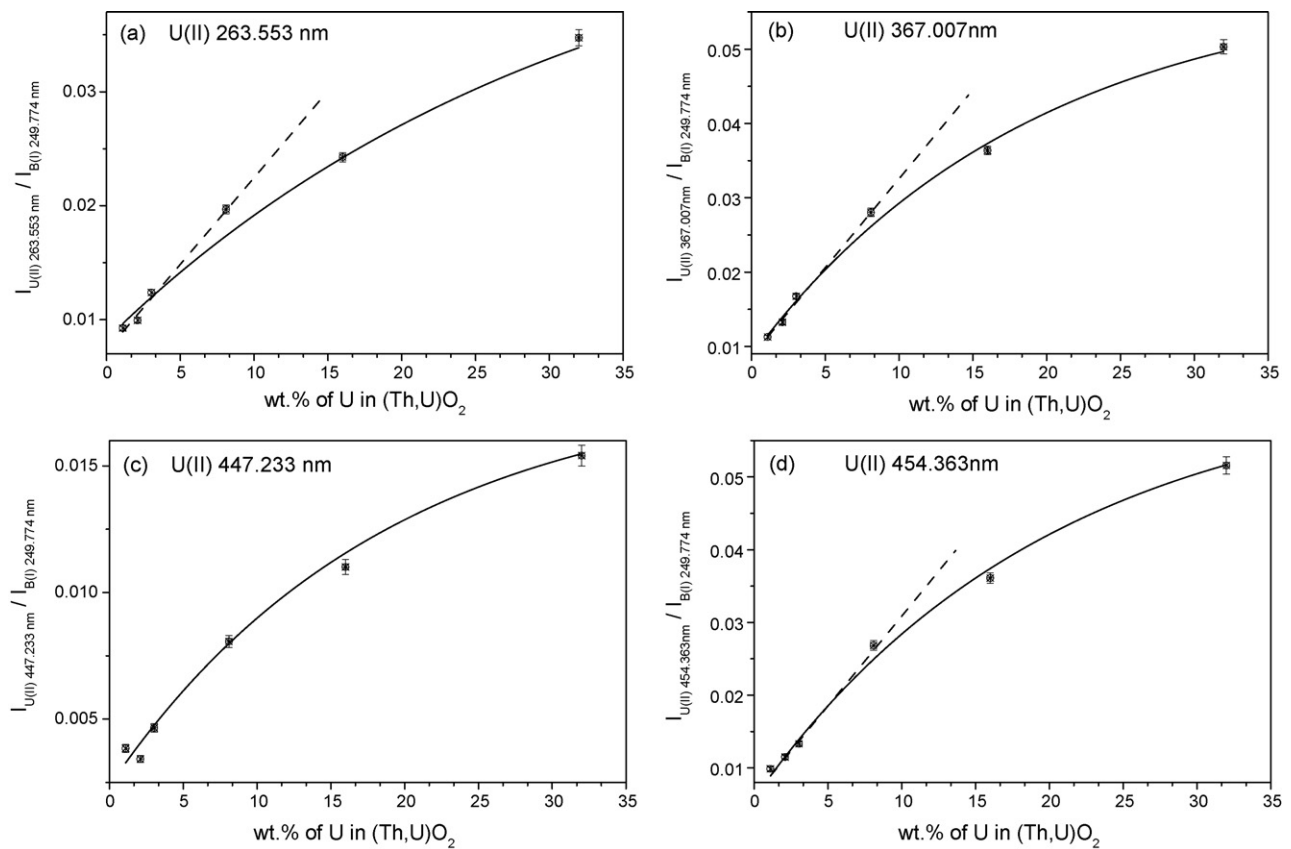


**Fig. 4.** Calibration curves obtained for the lines (a) U(II) 263.553 nm, (b) U(II) 367.007 nm, (c) U(II) 447.233 nm and (d) U(II) 454.363 nm. The broken line corresponds to the linear behavior of optically thin plasma.

self-absorption becomes appreciable and therefore, the analysis of such elements in the sample should be restricted up to this value for using the particular calibration curve. Table 3 gives the data of different parameters in Eq. (1) for the four U emission lines. Except from the U(II) 263.553 nm, the values of “*t*” for the other three emission lines are close to 20. This indicates that the amount of U species in plasma for the Th–U mixed oxide composition with 20 wt.% U is sufficiently high. The value of “*t*” in case of U(II) 263.553 nm is 31.9. Extent of self-absorption is usually high for resonant emission lines or lines having lower energy level close to the ground level.  $E_{\text{lower}}$  for both the U(II) 367.007 nm and U(II) 454.363 nm emission lines is  $914.765 \text{ cm}^{-1}$ , which is very near to the ground level, indicating the possibility of higher degree of self-absorption. The higher value of “*t*” in case of U(II) 263.553 nm is not understood at present, but a proper energy diagram for the above transition might be able to explain the observed effect.

Table 4 show the results obtained for uranium in the two synthetic samples treated as unknown. The wt.% of U determined is in good agreement with the expected value and there is no systematic bias. The calibration curve of U(II) 447.223 nm was not used for unknown synthetic sample with U amount of 4 wt.%, as the cali-

**Table 3**  
Parameters of Eq. (1) obtained by fitting calibrations curves and the correlation coefficients.

Wavelength (nm)	$y_0$	<i>A</i>	<i>t</i>	$R^2$
U(II) 263.553	0.049	−0.04	31.92	0.979
U(II) 367.007	0.059	−0.05	19.08	0.996
U(II) 447.233	0.018	−0.02	18.73	0.994
U(II) 454.363	0.063	−0.06	20.04	0.995

**Table 4**  
Comparison of analytical results for U determination in Th–U mixed oxide samples with expected values.

Sample	Emission wavelength (nm)	Wt.% U		A/B
		LIBS (A)	Expected (B)	
TU-7-unknown	263.553	$3.72 \pm 0.43$	4	0.93
	367.007	$3.82 \pm 0.29$		0.96
	447.233	–		–
	454.363	$3.41 \pm 0.52$		0.85
TU-8-unknown	263.553	$19.4 \pm 1.13$	20.3	0.96
	367.007	$19.4 \pm 0.14$		0.96
	447.233	$20.67 \pm 2.01$		1.02
	454.363	$21.14 \pm 2.44$		1.04

bration curve obtained using this emission line was not sensitive in lower concentration range (Fig. 4).

#### 4. Conclusions

The LIBS method has been developed for the determination of U in mixed oxides of thorium and uranium. The approach will be useful for the rapid determination of U in these samples, avoiding the rigorous dissolution required for other analytical techniques. The reproducibility of the determination is  $\pm 2\%$  ( $1\sigma$ ). Though the addition of boron in nuclear material is undesirable, the result shows the potential of the LIBS method in nuclear industry. The effect of alternative carbon-based binder such as starch, nitrocellulose, can also be explored in these studies. Considering the poor resolution power of the instruments and also the relatively rough optimization procedure employed, the agreement between the expected and experimental results are quite good, which indicated the enormous potential of LIBS and the possibility of using a high-resolution

LIBS for routine industrial work for U–Th mixed oxide characterization. LIBS also provides an independent approach based on different physico-chemical principle for the determination of U in Th–U matrix. This would be useful for the development of certified reference materials for these matrices in thorium-based fuel cycle.

### Acknowledgements

The authors are thankful to Dr. V. Venugopal, Director, Radio-chemistry and Isotope Group, B.A.R.C. for his constant support and encouragement in LIBS work. The authors wish to thank Mr. S. Panja, F.R.D., B.A.R.C. for providing high purity  $U_3O_8$ .

### References

- [1] J.B. Hedrick, U.S. Geological Survey, Mineral Commodity Summaries, January 1998, p. 177.
- [2] <http://www.uic.com.au/nip67.htm>
- [3] R.K. Sinha, A. Kakodkar, Nuclear Eng. Design 236 (2006) 683.
- [4] A. Sarkar, D. Alamelu, S.K. Aggarwal, Appl. Opt. 47 (2008) G58–G64.
- [5] D. Cremers, L. Radziemski, Handbook of Laser Induced Breakdown Spectroscopy, 1st ed., Wiley, West Sussex, 2006.
- [6] V. Majidi, M.R. Joseph, Crit. Rev. Anal. Chem. 23 (1992) 143.
- [7] A.V. Pakhomov, W. Nichols, J. Borysow, Appl. Spectrosc. 50 (1996) 880.
- [8] P. Fichet, P. Mauchien, C. Moulin, Appl. Spectrosc. 53 (1999) 1111.
- [9] X.K. Shen, Y.F. Lu, Appl. Opt. 47 (2008) 1810.
- [10] J. Wachter, D.A. Cremers, Appl. Spectrosc. 41 (1987) 1042.
- [11] H. Liu, Z. Zhang, A. Quentmeier, K. Niemax, Spectrosc. Spectral Analysis 24 (2004) 1244.
- [12] B.W. Smith, A. Quentmeier, M. Bolshov, K. Niemax, Spectrochim. Acta Part B 54 (1999) 943.
- [13] C.A. Smith, M.A. Martinez, D.K. Veirs, D.A. Cremers, Spectrochim. Acta Part B 57 (2002) 929.
- [14] D. Alamelu, A. Sarkar, S.K. Aggarwal, Proceedings of National Laser Symposia—6, Indore, India, 2006, p. 90.
- [15] <http://physics.nist.gov/PhysRefData/Handbook/index.html>.
- [16] R.K. Winge, V.J. Peterson, V.A. Fassel, Appl. Spectrosc. 33 (1979) 206.
- [17] B. Castle, K. Talabardon, B.W. Smith, J.D. Winefordner, Appl. Spectrosc. 52 (1998) 649.
- [18] B. Sallé, D.A. Cremers, S.M. Roger, C. Wiens, Spectrochim. Acta Part B 60 (2005) 479.
- [19] D. Alamelu, A. Sarkar, S.K. Aggarwal, Talanta 77 (2008) 256.
- [20] V. Lazić, R. Barbini, F. Colao, R. Fantoni, A. Palucci, Spectrochim. Acta Part B 56 (2001) 807.
- [21] C. Aragon, J. Bengoechea, J.A. Aguilera, Spectrochim. Acta Part B 56 (2001) 619.
- [22] C. Aragon, J.A. Aguilera, F. Penaiba, Appl. Spectrosc. 53 (1999) 1259.



# An MSFIA system for mercury speciation based on an anion-exchange membrane

A.M. Serra, J.M. Estela, V. Cerdà\*

Department of Chemistry, "Automation and the Environment" Analytical Chemistry Group, University of the Balearic Islands, E-07122 Palma de Mallorca, Spain

## ARTICLE INFO

### Article history:

Received 22 July 2008

Received in revised form 16 December 2008

Accepted 18 December 2008

Available online 31 December 2008

### Keywords:

Mercury speciation

Anion-exchange membrane

MSFIA

Cold vapour atomic fluorescence spectrometry

## ABSTRACT

A new methodology for the in-line preconcentration, clean-up and speciation of mercury by use of an anion-exchange membrane is proposed. The speciation of mercury is based on retention of its tetrachloro complex onto the membrane while organic mercury flows freely through it. A multisyringe is used as a liquid driver and a cold vapour atomic fluorescence detector is employed to ensure a high sensitivity. Organic mercury is decomposed into inorganic mercury by using a UV lamp. The carrier and reductant streams consist of 1.5% (m/v) hydrochloric acid and 2% (m/v) tin chloride, respectively. Certified reference material DORM-2 was digested with 37% hydrochloric acid and analysed directly without the need for extraction. The proposed system is more environmental friendly than the classical liquid–liquid extraction procedure. Mercury recoveries from spiked samples and the reference material were all close to 100%. An LOD of 14 and 16 ng/L was obtained for total and organic mercury, respectively, both with an RSD less than 1.3%.

© 2009 Elsevier B.V. All rights reserved.

## 1. Introduction

The concentrations of pollutants in the environment have increased markedly in parallel to industrial activity. One such pollutant is mercury, which is released into atmosphere mainly as a result of the combustion of coal and other fossil fuels.

The toxic effects of mercury on human health are well documented. Alkylmercury compounds constitute the most toxic form of mercury by effect of their high fat solubility, which facilitates their reaching cells by permeation across biological membranes. Monomethylmercury (MMHg) is the most abundant alkylmercury compound. Mercury methylation occurs mainly in bottom sediments and soils, but is also possible in water. The extent of methylation depends on a number of factors including inorganic mercury availability, microbial activity, redox conditions, pH, temperature, salinity and organic matter content [1].

Several methodologies for speciating mercury have been developed over the past 30 years. Atomic fluorescence, atomic absorption and inductively coupled plasma atomic emission spectrometry in combination with the cold vapour technique are the most sensitive spectrometric choices for its determination. These spectroscopies have been used jointly with powerful chromatographic techniques such ionic chromatography (IC) [2,3], gas chromatography (GC) [4–6] and high performance liquid chromatography (HPLC) [7]; all

afford the speciation of mercury with high resolution and sensitivity.

The GC methods require the prior derivatization of organomercurials into more volatile species. Methylation artifacts arising from the presence of small impurities of methyl groups in the reagents have been detected during the derivatization reaction [8]. Capillary columns have the disadvantage of the generally low sample volumes they can hold [9]. Most HPLC methods for mercury use reversed phase chromatography and a mobile phase containing a buffer, an organic modifier and a chelating or ion-pairing reagent.

However, the complexity and high cost of these techniques has made the use of simple, non-chromatographic approaches an attractive choice for the selective discrimination of mercury species [10]. This has fostered the development of several methodologies for mercury speciation involving non-chromatographic separation. Some rely on the disparate reduction potentials of inorganic and organic mercury compounds [11], while others determine inorganic and total mercury by chemical or UV light oxidation [12,13] and still others employ selective reagents for this purpose [10].

The trace enrichment, matrix simplification and medium exchange capabilities of solid phase extraction (SPE) have fostered its use in flow analysis. SPE methods for mercury speciation rely on the use of selective sorbents (e.g. sulphhydryl cotton fibres [14], 2-mercaptobenzothiazole loaded resin [15]) or non-specific sorbents functionalized with chelating compounds [16–19] or, simply, an anion-exchange resin [20].

In an acid medium containing chloride ions, mercury (II) forms an anionic tetra-chloride complex ( $\text{HgCl}_4^{2-}$ ) while methylmercury remains a neutral species ( $\text{CH}_3\text{HgCl}$ ). Under these conditions, an

\* Corresponding author.

E-mail address: [victor.cerda@uib.es](mailto:victor.cerda@uib.es) (V. Cerdà).

anion-exchange resin can retain the anionic complex and allow methylmercury to flow freely through it with negligible retention.

Worth special note among recent trends in SPE is the use of membrane discs, which afford greater processing expeditiousness and reduced plugging by suspended particles and matrix components; also, using smaller particles and the increased mechanical stability of discs minimize channelling [21]. Moreover, unlike conventional resins, SPE discs can be replaced by unskilled operators [22].

In this work, we assessed the feasibility of preconcentrating mercury onto an anion-exchange membrane with a view to its speciation. To our knowledge, and as of June 2007 (ISI web of knowledge), no similar methodology for this purpose has previously been reported. The reductive elution concept, originally developed by Carrero and Tyson to determine selenium [23], was used here to simplify the determination system by avoiding the use of eluent solutions. Reductive elution was previously used to preconcentrate mercury onto a cation-exchange resin [24], but retention on the resin was found to be interfered with by chloride ion. This led us to use anion-exchange membrane discs instead. An MSFIA system was thus used jointly with a CV-AFS system previously developed by the authors [25] to speciate mercury.

## 2. Experimental

### 2.1. Reagents

The anion-exchange membrane, Anion-SR, was purchased from 3M Empore. Anion-SR is a poly(styrene-divinylbenzene) copolymer modified with quaternary ammonium groups. Note that this resin is not bonded to silica; rather, it is available as 100% copolymer particles that are spherical in shape, porous and cross-linked. The membrane was placed on a methacrylate support reported by Pons et al. [22].

A stock solution containing 1000 mg/L Hg(II) was prepared from HgCl<sub>2</sub> according to Standard Methods (APHA-AWWA-WPCF). A 10 mg/L Hg(II) stock solution containing 1 mL of 37% HCl per 100 mL of total volume was prepared on a weekly basis [26] in order to ensure stability. Mercury (II) working standard solutions were prepared daily in 1.5% (m/v) HCl from this stock solution.

Methylmercury chloride was purchased from Sigma–Aldrich (Steinheim, Germany). A stock solution of this compound was prepared by dissolving the amount of chemical required to obtain a 1000 mg/L Hg concentration. The compound was dissolved in the minimum possible volume of methanol and diluted with Millipore water. A 10 mg/L Hg working stock solution was also made weekly and working standards on a daily basis.

A 2% (m/v) tin chloride solution was prepared daily in 1.5% (m/v) HCl by dissolving the required amount of SnCl<sub>2</sub>·2H<sub>2</sub>O (Merck pro analysis, max. 0.000001% Hg). A 1.5% (m/v) HCl solution was used as carrier. HCl was min. 37% puriss. p.a. and purchased from Riedel-de Haën (Seelze, Germany).

All solutions were made in de-ionized water purified by passage through a Millipore apparatus, and all glassware used to prepare them was soaked in 10% (v/v) nitric acid and then rinsed with Millipore water.

### 2.2. Reagent purification

Diminishing the blank signal entailed removing mercury traces from the carrier and reagents. The amount of mercury impurities contained in the hydrochloric acid was determined by using the standard addition method and found to be  $3.55 \pm 0.28 \mu\text{g/L}$  Hg(II). For removal, a 1.5% (m/v) HCl solution was passed at 1 mL/min through a resin column containing thiol groups in order to retain

mercury. A 75 mm long  $\times$  3 mm diameter methacrylate column filled with porous frit to support Duolite® GT-73 resin from Supelco (Bellefonte, PA) was used. This resin had previously been employed for mercury removal or preconcentration [27–29].

The purified 1.5% HCl solution thus obtained was used to prepare the carrier and standards solutions. Also, the tin chloride reducing solution was purified by passage of a nitrogen stream for 30 min under constant stirring [30].

### 2.3. Apparatus

The liquid driver was a multisyringe burette module with programmable speed (Multiburette 4S, Crison, Alella, Barcelona). A three-way solenoid commutation valve was mounted in the head of each syringe. The proposed system used only two syringes. Syringe S1, connected to valve E1, was used to dispense the sample together with 1.5% (m/v) HCl and the carrier solution. Syringe S3, connected to valve E3, was employed to dispense the reducing solution. Fig. 1 depicts the experimental set-up used.

The multisyringe was equipped with four additional, independent solenoid valves (Takasago Electric, Nagoya, Japan). The valves required using a solenoid protection system (Sciware, Palma de Mallorca, Spain) in order to minimize heat production and extend their useful life.

SV1 was connected to a sample coil and syringe S1 (5 mL) for sample pick-up. In its NC position, it was connected to the sample input, and in its NO position to the manifold. SV2 was connected to syringe S2 (2.5 mL). In its NC position it was connected to SV3 and in its NO position to the UV lamp output in order to facilitate reaction with decomposed methylmercury. SV3 was connected to the membrane in its NO position; this afforded a higher operating pressure than its NC position, where it was connected to the membrane by-pass in order to facilitate injection of the sample and carrier while avoiding passage through the membrane. This afforded total mercury determination. Finally, SV4 was connected to the UV lamp in its NO position and to the lamp by-pass in its NC position.

The manifold used to process samples and reagents was constructed from 1.5 mm i.d. and 0.8 mm i.d. PTFE tubing. The 1.5 mm i.d. tubing was used for the reagent pick-up, sample coil, spray generation coil and gas–liquid separator. A sample–reagent mixer was additionally constructed from 0.8 mm i.d. tubing. A three-channel cross-fitting was used to facilitate mixing of the sample and reagent in the reaction coil. Also, a mixing tee reported in a previous paper [25] was used for gas–liquid mixing and connection with the spray generation coil.

The gas–liquid separator used was Perkin-Elmer model B0507959. An exchangeable PTFE membrane (25 mm diameter, 1  $\mu\text{m}$ , Schleicher and Schuell, Dassel, Germany) placed in the screw cap of the separator was employed to prevent any liquid from reaching the detector cell. The choice of this specific type of separator was dictated by the results of a previous study [31]. Removal of excess liquid from the gas–liquid separator was controlled via a solenoid micropump (Biochem Valve, Inc., Boonton, NJ).

The solenoid micropump was computer controlled via a module available from Sciware (Palma de Mallorca, Spain) and consisting of an I/O digital interface card, eight digital relay output channels and an internal 12V power source required to activate the solenoid micropumps. The module was connected to a PC through an RS485/RS232 interface. A Heraeus Noblelight model TNN 15/32 15W UV lamp was used to decompose methylmercury into inorganic mercury. A gas-dryer unit from Perma Pure (Toms River, NJ) was used for this purpose. The water passed through the membrane wall and evaporated into the surrounding air or gas. This process was driven by the moisture gradient between the inside and outside of the tubing.

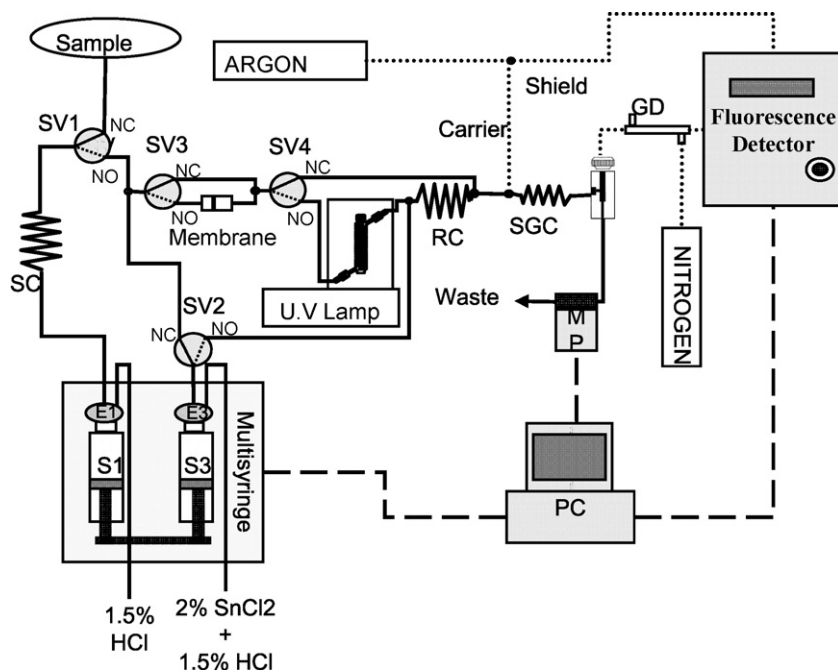


**Fig. 1.** Proposed MSFIA-CV-AFS system. SC: sample coil; GL: gas-liquid separator; RC: reaction coil; MP: micropump; SV: solenoid valve; NC: normally closed position; NO: normally open position; SGC: spray generator coil; PC: personal computer; GD: permature gas dryer.

A model 10.023 mercury atomic fluorescence spectrophotometer from P.S. Analytical (Orpington, UK) was used for detection. This instrument has four internal gains and an external, fine gain, which allows it to operate over a broad concentration range.

System control, data acquisition and processing were all done with the aid of the software package Autoanalysis 5.0 [32], from Sciware (Palma de Mallorca, Spain).

#### 2.4. General procedure

The sample, initially picked up to the holding coil, was propelled through the membrane. In this way, the chloro complex of inorganic mercury was retained onto the membrane while methylmercury was delivered to the UV lamp for decomposition into mercury (II). This facilitated reduction to elemental mercury with tin chloride.

A UV lamp was previously used by some authors to decompose methylmercury [12,26]. We chose UV based oxidation for this purpose as it requires no chemical oxidant such as  $\text{KBr}/\text{KBrO}_3$  or  $\text{KCr}_2\text{O}_7$ , which contain small amounts of mercury and can raise the blank signal.

Valve SV4 was switched when the sample was in the UV lamp coil. While methylmercury was being decomposed by the UV lamp, tin chloride was dispensed through the membrane in order to reduce retained mercury. As a consequence, mercury was released and delivered to the UV lamp by-pass. SV3 was then switched to have the carrier propel the mixture at a flow rate of 12 mL/min. This avoided too high a flow rate through the membrane and extended its useful life as a result.

The liquid phase was merged in a three-way connector through which a continuous stream of argon was passed to obtain a spray. The spray afforded optimal separation of elemental mercury from the liquid phase. The gas-liquid mixture was separated in a gas-liquid separator. The gas phase, containing elemental mercury, left the gas-liquid separator through a PTFE membrane to the mercury detector. Moisture in the carrier gas was removed by passage through a Perma Pure device, which prevented any water vapour from reaching the detection cell and quenching the analytical signal as a result [33]. The liquid phase was removed from the gas-liquid

separator by means of a software controlled micropump. In order to keep a constant liquid volume in the gas-liquid separator, the micropump system was only allowed to operate while the multisyntinge burette was dispensing some liquid. In this way, the gas phase was never removed to waste and the sensitivity preserved. However, overfilling might result in some liquid reaching the detector and causing it to malfunction.

Valves SV2 and SV4 were actuated in order to propel the carrier and reducing solution for the determination of methylmercury. Decomposed methylmercury and tin chloride were merged at the UV lamp output. The flow in the reaction coil was stopped for 30 s in order to increase the reaction yield. Then, the reaction mixture was propelled at 12 mL/min to the spray generation coil and subjected to the same procedure as inorganic mercury.

#### 2.5. Solid samples pre-treatment

The certified reference material used in this study was DORM-2 (dogfish muscle, National Research Council, Canada).

For extraction of mercury compounds, an amount of 0.1 g of sample was leached with 2 mL of 37% HCl overnight, followed by dilution to 25 mL with water. A volume of 2 mL of the resulting solution was diluted to 50 mL with 1.5% HCl and filtered through 0.45  $\mu\text{m}$  mesh prior to analysis. Environmental and digested solid samples required 3 min UV irradiation to ensure acceptable recovery.

### 3. Results and discussion

#### 3.1. Influence of the hydrochloric acid concentration and sample volume

The effect of the concentration of hydrochloric acid used to retain mercury onto the membrane was studied over the range 0.5–2% (m/v). For this purpose, 1% (m/v) tin chloride and 1  $\mu\text{g}/\text{L}$  Hg were prepared at each acid concentration, and variable sample volumes from 0.25 to 1.5 mL of standard solution injected. Fig. 2 shows the signals thus obtained for a 1  $\mu\text{g}/\text{L}$  Hg concentration. As

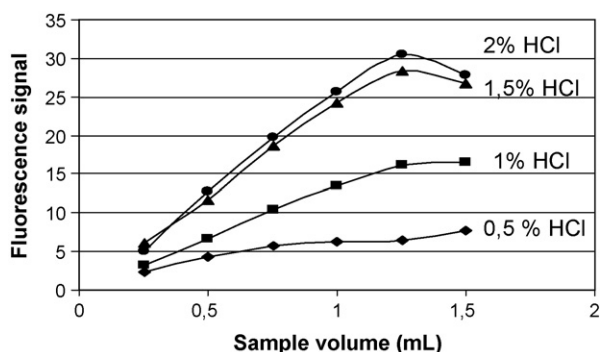


Fig. 2. Influence of the sample volume and hydrochloric acid concentration.

can be seen, raising the acid concentration resulted in stronger retention by formation of an increased amount of chloro complex; however, it also increased the blank signal. This led us to choose a 1.5% hydrochloric acid concentration since a 2% concentration resulted in similar retention.

As can also be seen from Fig. 2 shows, increasing the sample volume up to 1.25 mL increased the analytical signal. With 1.5 mL of 1.5 or 2% HCl, however, the signal decreased through elution of mercury by the carrier. A sample volume of 1 mL was therefore adopted as a compromise between sensitivity and sample throughput; in fact, volumes above 1 mL required inserting an additional pick-up step in the procedure and detracted from throughput as a result.

### 3.2. Influence of the eluted volume

The effect of the volume of reductant was examined over the range 0.125–1 mL. To this end, 1 mL of 1  $\mu\text{g/L}$  Hg(II) in 1.5% (m/v) HCl was preconcentrated onto the membrane and a 1% (m/v) tin chloride solution used to elute mercury. The highest signal was obtained with a volume of 0.25 mL of reducing solution; both smaller and larger volumes resulted in dilution of mercury. With small volumes, the contact time between the membrane and tin chloride was inadequate to elute all retained mercury. Also, lowering the flow rate in order to extend the contact time resulted in decreased throughput.

### 3.3. Influence of the reductant concentration

Once the effect of the reagent volume on the analytical signal was established, the influence of the tin chloride concentration was examined. For this purpose, a volume of 1 mL of 1  $\mu\text{g/L}$  Hg(II) was preconcentrated onto the membrane and mercury eluted from it with variable volumes of tin chloride from 0.25 to 5% (m/v). Based on the results, the signal increased slightly (10%) from 1 to 2% (m/v), but no further with higher concentrations of reductant. In order to ensure the presence of excess tin chloride, a 2% (m/v) concentration was adopted for subsequent testing.

### 3.4. Influence of the preconcentration and elution flow rates

The best flow-rate for mercury preconcentration and elution was found by examining their effect over the range 1.5–8.1 and 1–6 mL/min, respectively. To this end, a volume of 1 mL of a 1  $\mu\text{g/L}$  Hg(II) standard solution in 1.5% (m/v) HCl was preconcentrated and then reduced with 2% (m/v) tin chloride. No relationship between either flow rate and the mercury signal was observed over the studied ranges. This led us to adopt a preconcentration flow rate of 8.1 mL/min and an elution flow rate of 6 mL/min in order to increase the throughput. Pons et al. [22] previously found a chelating membrane disc to exhibit the same response to the flow rates. Thus, unlike resins, retention by membranes is flow rate-independent.

Table 1  
Analytical figures of merit of the proposed method.

	Hg	MeHg
Gain 10		
Slope	17.24	12.48
Intercept	-0.14	-0.26
Linear range ( $\mu\text{g/L}$ )	0.046–11.6	0.054–16.02
RSD (%)	1.14	1.28
LOD (ng/L)	14	16
$r^2$	0.9989	0.9987

### 3.5. Analytical figures of merit

The analytical figures of merit of the proposed method were determined under the previously established optimum operating conditions. Only one of the four internal gains of detector was used for this purpose. Gain 10 provided a wider linear range and similar detection limit as gains 100 or 1000, which exhibited higher sensitivity but also higher noise in the readings. The slopes of the calibration curves obtained with gains 100 and 1000 were calculated as 10 and 100 times, respectively, that for gain 10. The results are shown in Table 1.

The limit of detection (LOD) was calculated as three times the standard deviation of 10 blank signals divided by the slope of the calibration curve ( $3\sigma/S$ ). The relative standard deviations (RSD) for the signals were evaluated from 10 successive injections of a solution containing 8  $\mu\text{g/L}$  Hg and 8  $\mu\text{g/L}$  MeHg. The throughput was 14 injections/h. A preconcentration factor of 1.9 was obtained for inorganic mercury. The reproducibility between membranes was 3.68% as RSD. Finally, the membrane was able to withstand up to 20 injections with RSD values less than 3%.

### 3.6. Interferences

We examined the effect of the presence of nitrate, sulphate and phosphate on the retention of mercury onto the membrane. Based on the results, concentrations up to 1000 mg/L of these anions had no effect on the retention of 1  $\mu\text{g/L}$  Hg.

We also studied the effect of various interfering anions on the reduction of mercury by tin chloride and its retention by the membrane. To this end, we added variable concentrations of  $\text{I}^-$  and  $\text{Br}^-$  to a 1  $\mu\text{g/L}$  solution of Hg and a 1  $\mu\text{g/L}$  solution of MeHg. The maximum tolerated concentrations of  $\text{I}^-$  and  $\text{Br}^-$  were found to be 10 and 100 mg/L, respectively—higher concentrations of either anion reduced the analytical signal. The interfering effect of bromide and iodide was lessened by the membrane; in fact, previous tests without a membrane had revealed the tolerated concentrations of bromide and iodide to be 10 and 1 mg/L, respectively [25].

### 3.7. Analysis of reference materials and environmental samples

The proposed method was validated by analysing solid certified reference material DORM-2 (fish muscle, National Research Council, Canada). The results of the analyses are shown in Table 2.

This procedure requires using no organic solvents to determine methylmercury and thus reduces waste production. The proposed approach is therefore “green” inasmuch as it uses no organic solvents such as toluene or dichloromethane. Use of the alkaline

Table 2  
Analysis of a certified reference material.

Parameter	Certified (mg/kg)	Found (mg/kg)	Recovery (%)
MeHg	4.5 $\pm$ 0.3	4.1 $\pm$ 0.3	92.4
Total Hg	4.6 $\pm$ 0.3	4.2 $\pm$ 0.4 <sup>a</sup>	89.9

The results are expressed as the mean of four replicates  $\pm$  standard deviation ( $n = 4$ ).

<sup>a</sup> Total mercury was calculated as the combination of methylmercury and inorganic mercury.



**Table 3**  
Percent recoveries of mercury from spiked real samples.

Analyte	Seawater	Leachate	Groundwater
Hg	92.4	95.1	101.3
MeHg	99.5	103.3	90.0

digestion procedure of Liang et al. [34], which involves KOH and methanol, with no extraction led to poor recovery; this was possibly a result of the presence of methanol, which quenches the atomic fluorescence signal of mercury [35].

In order to evaluate the usefulness of the proposed system for Hg speciation in environmental samples, we assessed mercury recovery from spiked environmental samples of three different types, namely: seawater, rain leachates from a demolition recycling plant and groundwater. Because the Hg and MeHg levels found were all below the limit of quantitation, the samples were spiked with 1 µg/L Hg and 1 µg/L MeHg. The recoveries obtained with the proposed system are shown in Table 3.

#### 4. Conclusions

The proposed MSFIA system uses an anion-exchange membrane that allows the preconcentration, clean-up and speciation of mercury. Reductive elution of mercury allows its direct released from the membrane, thereby affording elution and reduction in a single step, and minimizing dilution of inorganic mercury. The ensuing method was applied to a certified reference material and spiked real samples, both with good recoveries. The membrane dispenses with the need to use organic solvents for digested solid samples, thereby dramatically reducing waste production. The membrane additionally reduces the interfering effects of iodide and bromide on the reduction of mercury by tin chloride. Also, unlike conventional resins, the membrane can be easily replaced by an unskilled operator and retention of the analyte onto the membrane is not influenced by the particular flow rate used.

#### Acknowledgements

This work was funded by Spain's Ministry of Education and Science (Project CTQ2007-64331) and the Govern de les Illes Balears,

Conselleria de Economia Hisenda i Innovació (Project PROGECIC-5C).

#### References

- [1] L. Broszke, G. Glosinska, J. Siepak, *Pol. J. Environ. Stud.* 11 (4) (2002) 285.
- [2] C. Sarzanini, G. Sacchero, M. Aceto, O. Abollino, E. Mentaste, *Anal. Chim. Acta* 284 (1994) 661.
- [3] Q. Tu, W. Johnson, B. Buckley, *J. Anal. At. Spectrom.* 18 (2003) 696.
- [4] M. Hovart, A.R. Byrne, K. May, *Talanta* 37 (1990) 207.
- [5] M. Hovart, N.S. Bloom, L. Liang, *Anal. Chim. Acta* 281 (1993) 135.
- [6] R. Fischer, S. Rapsomanikis, M.O. Andreae, *Anal. Chem.* 65 (1993) 763.
- [7] C.F. Harrington, *Trends Anal. Chem.* 19 (2000) 167.
- [8] M. Leermakers, W. Baeyens, P. Quevauviller, M. Hovart, *Trends Anal. Chem.* 24 (5) (2005) 383.
- [9] J.E. Sánchez Uría, A. Sanz-Medel, *Talanta* 47 (1998) 509.
- [10] H. Wu, Y. Jing, W. Han, Q. Miao, S. Bi, *Spectrochim. Acta Part B* 61 (2006) 831.
- [11] C.E. Oda, J.D. Ingle, *Anal. Chem.* 53 (1981) 2305.
- [12] H. Morita, M. Sugimoto, S. Shimomura, *Anal. Sci.* 6 (1990) 91.
- [13] P. Cava-Montesinos, A. Domínguez-Vidal, M.L. Cervera, A. Pastor, M. De la Guardia, *J. Anal. At. Spectrom.* 19 (2004) 1386.
- [14] W. Jian, C.W. Macleod, *Talanta* 39 (1992) 1537.
- [15] J. Chwastowska, A. Rogowska, E. Sterlinska, J. Dudek, *Talanta* 49 (1990) 837.
- [16] H. Bagheri, A. Gholami, *Talanta* 55 (2001) 1141.
- [17] J.C.A. de Wuilloud, R.G. Wuilloud, R.A. Olsina, L.D. Martinez, *J. Anal. At. Spectrom.* 17 (2002) 389.
- [18] G.A. Zachariadis, A.N. Anthemidis, E.I. Daftsis, J.A. Stratis, *J. Anal. At. Spectrom.* 20 (2005) 63.
- [19] D.M. Sánchez, R. Martín, R. Morante, J. Martín, M.L. Munuera, *Talanta* 52 (2000) 671.
- [20] J. Sanz, J.C. Raposo, J. Larreta, I. Martinez-Arkarazo, A. de Diego, J.M. Madariaga, *J. Sep. Sci.* 27 (2004) 1202.
- [21] C.F. Poole, *Trends Anal. Chem.* 22 (2003) 362.
- [22] C. Pons, R. Forteza, V. Cerdà, *Anal. Chim. Acta* 542 (2004) 79.
- [23] P.E. Carrero, J.F. Tyson, *Analyst* 122 (1997) 915.
- [24] J.A.G. Neto, L.F. Zara, J.C. Rocha, A. Santos, C.S. Dakuzaku, J.A. Nóbrega, *Talanta* 51 (2000) 587.
- [25] A.M. Serra, J.M. Estela, V. Cerdà, *Talanta* 77 (2008) 556.
- [26] E. Ramalhosa, S. Rio Segade, E. Pereira, C. Vale, A. Duarte, *Anal. Chim. Acta* 448 (2001) 135.
- [27] P. Pohl, B. Prusisz, *Anal. Sci.* 20 (2004) 1367.
- [28] S. Chiarle, M. Ratto, M. Rovatti, *Water Res.* 34 (11) (2000) 2971.
- [29] K.H. Nam, S. Gomez-Salazar, L.L. Tavlarides, *Ind. Eng. Chem. Res.* 42 (2003) 1955.
- [30] S. Mandal, A.K. Das, *At. Spectrosc.* 3 (1982) 56.
- [31] I.D. Brindle, S. Zheng, *Spectrochim. Acta Part B* 51 (1996) 1777.
- [32] E. Becerra, A. Cladera, V. Cerdà, *Lab. Rob. Autom.* 11 (1999) 131.
- [33] C.G. Freeman, M.J. McEwan, R.F.C. Claridge, L.F. Phillips, *Trans. Faraday Soc.* 66 (1970) 2974.
- [34] L. Liang, M. Horvat, E. Cernichiari, B. Gelein, S. Balogh, *Talanta* 43 (1996) 1883.
- [35] C.G. Freeman, M.J. McEwan, R.F.C. Claridge, L.F. Phillips, *Trans. Faraday Soc.* 67 (1971) 67.



# Preparation of colorless ionic liquids “on water” for spectroscopy

Yanfei Shen, Yuanjian Zhang, Dongxue Han, Zhijuan Wang, Daniel Kuehner, Li Niu\*

State Key Laboratory of Electroanalytical Chemistry, Changchun Institute of Applied Chemistry, and Graduate School of the Chinese Academy of Sciences, Chinese Academy of Sciences, Renmin St. 5625, Changchun 130022, PR China

## ARTICLE INFO

### Article history:

Received 4 August 2008

Received in revised form 19 December 2008

Accepted 21 December 2008

Available online 15 January 2009

### Keywords:

Ionic liquids

Colorless

On water

Green chemistry

Spectroscopy

## ABSTRACT

Although colorless ionic liquids (ILs) are most desirable, as synthesized they frequently bear color, despite appearing pure by most analytical techniques. It leads to some uncertainties and limits for the fundamental research and applications of ILs, such as spectroscopy. Using 1-butyl-3-methylimidazolium bromide (BMIMBr), 1-butyl-3-methylimidazolium tetrafluoroborate (BMIMBF<sub>4</sub>) and 1-hexyl-3-methylimidazolium bromide (HMIMBr) as models, we demonstrated that following classic preparing method except that the water was added as solvent, colorless ILs could be facilely prepared. Neither critical pre-treatment of starting materials and pre-cautions during the reaction nor time-consuming and costly post-decolor-purification was needed. The effects of “on water” reaction conditions on preparing colorless IL and the reason why using water as solvent could produce colorless ILs were also preliminary investigated. It was found that the reactant solubility played an important role in the preparation of colorless ILs. Not only as a method to evaluate the quality of as-synthesized ILs, but also as a spectroscopic analytical applications, UV–vis spectra showed that the ILs by this “on water” method was spectral pure and sufficient for future fundamental spectroscopic research and applications.

© 2009 Elsevier B.V. All rights reserved.

## 1. Introduction

Recently room temperature ionic liquids (RTILs) have attracted considerable interest in many fields of chemistry and chemical industry. Their unique physicochemical properties such as negligible vapor pressure, nonflammability, and thermal stability make them as “green” alternatives to conventional organic solvents in a range of synthesis, catalysis, electrochemistry and liquid–liquid extraction [1–4]. Although common ILs should be colorless, they frequently bear color as synthesized [1,5]. After much investigation over the last two decades, the source(s) of color have not been definitely identified [6]. For example, 1,3-dialkylimidazolium halides, typically used as starting ILs to synthesize other ILs bearing other counteranions, are often yellow or even brown, despite appearing pure by most analytical techniques (e.g. NMR, mass spectrometry, HPLC and ion chromatography) other than UV–vis spectroscopy [1,6]. Hence, to date, the chemical structure of the colored impurities is still difficult to be determined. Although until now there is no direct evidence that the colored impurities will affect the chemical or physical properties of ionic liquids, they have a major influence upon measurements containing light absorption or emission. This will lead to many uncertainties and even limitations in various ILs applications such as analytical chemistry [12], photochemistry

[7–11], and *in situ* UV–vis spectroscopy [13–17], thus colorless ILs are most desirable.

There are two general approaches for the preparation of less colored ILs. The first method mainly includes some special purification of starting materials before the synthesis besides simple distillation and controlling the reaction in low temperature (e.g. in ice bath). The special purification of starting materials usually contains extracting the alkyl halide with concentrated sulfuric acid, followed by neutralizing with a concentrated NaHCO<sub>3</sub>-solution and drying with MgSO<sub>4</sub> [17]. The second method is post-treatment of the as-prepared colored ILs, i.e. discolor-purification by charcoal or alumina columns [1,6,18].

In this paper we present a new facile method to prepare colorless ILs by using water as solvent (i.e. in an “on water” reaction system [19–24]) without any special pretreatment of the starting materials. The colored species did not appear during the whole reaction, thus further time-consuming and costly discolor-purification was also excluded. The approach described here would offer a convenient model system to obtain colorless ILs for spectroscopic analytic researches and applications.

## 2. Experimental

### 2.1. Materials

1-Bromobutane (98%), 1-bromohexane (98%) and NaBF<sub>4</sub> (98%) were purchased from Sinopharm Chemical Reagent Co. Ltd., China

\* Corresponding author. Tel.: +86 431 8526 2425; fax: +86 431 8526 2800.

E-mail address: [lniu@ciac.jl.cn](mailto:lniu@ciac.jl.cn) (L. Niu).

**Table 1**  
Preparation conditions and yields of BMIMBr under N<sub>2</sub> protection.

Rxn	Molar ratio <sup>a</sup>	Solvent	v/v <sup>b</sup>	Time (h)	Temp. (°C)	Yield (%)
1	2:1	Water	0.85:1	24	60	61
2	2:1	Water	0.85:1	24	70	96
3	2:1	Water	0.85:1	24	80	98
4	2:1	Water	0.85:1	12	70	72
5	2:1	Water	0.85:1	48	70	97
6	2:1	Water	0.42:1	24	70	94
7	2:1	Water	1.70:1	24	70	87
8	1.2:1	Water	0.85:1	24	70	91
9	2.5:1	Water	0.85:1	24	70	98
10	2	No solvent	–	24	70	99
11	1.2	No solvent	–	24	70	97

<sup>a</sup> Molar ratio of 1-bromobutane to 1-methylimidazole.

<sup>b</sup> v/v (volume ratio) of water to reactant.

and used as-received. 1-methylimidazole (99+%) was obtained from Kaile Chemical Factory (China) and newly distilled before use. All the water used in experiments was purified using a Millipore-Q system.

## 2.2. Preparation of BMIMBr, HMIMBr and BMIMBF<sub>4</sub>

The general procedure for the synthesis of 1-butyl-3-methylimidazolium bromide (BMIMBr) “on water” was similar with previously published procedures [1,25], excepting using water as the solvent. Typically, a mixture of 1-methylimidazole and 1-bromobutane with different ratios was heated under N<sub>2</sub> protection with water as the solvent (Table 1). When the reaction time was completed, the excessive phase-separated 1-bromobutane was first decanted. Then, the residual 1-bromobutane and water were removed under reduced pressure at 70 °C. The preparation of 1-hexyl-3-methylimidazolium bromide (HMIMBr) “on water” was similar to that of BMIMBr.

The general procedure for the synthesis of 1-butyl-3-methylimidazolium tetrafluoroborate (BMIMBF<sub>4</sub>) was according to the references [1]. BMIMBr (21.9 g, 0.1 mol) was dissolved in 100 mL of acetone, to which an equimolar amount of NaBF<sub>4</sub> was added. The mixture was then stirred for about 1 h upon which the white precipitate was formed at the bottom of the beaker. The acetone layer was filtered, and the solvent was evaporated under reduced pressure at 50 °C.

## 2.3. Instruments

UV–vis–NIR spectra and photographs of 1,3-dialkylimidazolium halides in liquid were recorded on a CARY 500 UV–vis–NIR spectrometer and a Kodak DX6340 digital camera, respectively. <sup>1</sup>H NMR spectra were obtained on a Varian Unity-400 (400 MHz) NMR spectrometer with tetramethylsilane (TMS) as an internal standard in per-deuterated dimethyl sulfoxide (DMSO-*d*<sub>6</sub>), where chemical shifts were reported with the indicated solvent as an internal reference. Coupling constants were reported in Hz. The full names of splitting abbreviations were listed as follows: s, singlet; d, doublet; t, triplet; q, quartet; m, multiplet.

## 2.4. NMR results

<sup>1</sup>H NMR (DMSO-*d*<sub>6</sub>, 400 MHz) for BMIMBr prepared without solvents and from “on water” reaction were the same: δ 9.16 (s, 1H), 7.78 (s, 1H), 7.71 (s, 1H), 4.16 (t, *J* = 7.15 Hz, 2H), 3.85 (s, 3H), 1.76 (m, 2H), 1.25 (m, 2H), 0.90 (t, *J* = 7.35 Hz, 3H).

<sup>1</sup>H NMR (DMSO-*d*<sub>6</sub>, 400 MHz) for HMIMBr prepared without solvents and from “on water” reaction were also the same: <sup>1</sup>H NMR (DMSO-*d*<sub>6</sub>, 400 MHz) for HMIMBr prepared without solvents: δ 9.14

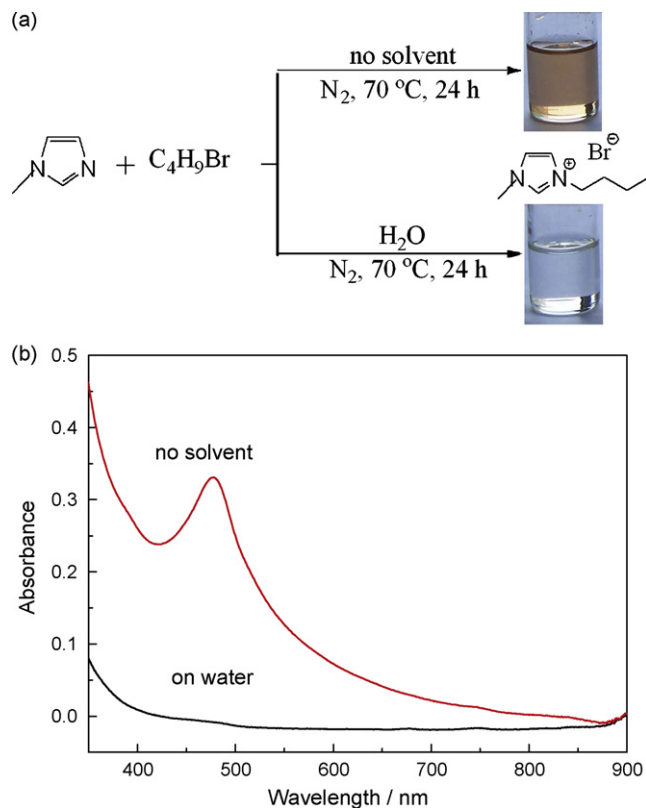


**Fig. 1.** Photographs (a) and UV–vis absorption spectra (b) of BMIMBr in liquid prepared on water (lower) and without any solvent (upper).

(s, 1H), 7.77 (s, 1H), 7.70 (s, 1H), 4.15 (t, *J* = 7.20 Hz, 2H), 3.85 (s, 3H), 1.77 (m, 2H), 1.26 (m, 6H), 0.86 (t, *J* = 6.88 Hz, 3H).

## 3. Results and discussion

In a typical experiment of preparing colorless BMIMBr on water, a conventional oil bath with magnetic stirring bar was used. The biphasic liquid mixture was stirred vigorously under N<sub>2</sub> at 70 °C for 24 h. Because the product BMIMBr was soluble in water, the progress of the reaction could be visually monitored. It was observed that the volume of the 1-bromobutane phase gradually decreased and the mixture became more clarified with time. Excess un-reacted 1-bromobutane phase was colorless and could be easily removed and recycled by the phase split. At last, water and residual 1-bromobutane were removed under reduced pressure at 70 °C. Unlike the conventional synthesis with organic solvents (e.g. toluene) or without solvents (only with excessive alkyl halide), in which the IL is insoluble, our reaction system did not form a viscous product-rich layer, which was favorable to stirring and heat transfer [1].

Both BMIMBr prepared “on water” and that without solvents (the control experiment) were found to be pure by <sup>1</sup>H NMR (see Section 2). However, they appeared distinct in color by naked eye. BMIMBr prepared “on water” was clear and transparent (Fig. 1a, lower), with no appreciable absorption in the visible range (Fig. 1b, lower). The control reaction under similar conditions but without water yielded an orange/yellow product (Fig. 1a, upper) with strong absorption in the range 400–600 nm (Fig. 1b, upper).

To investigate applicability of “on water” reaction to prepare other similar ILs, HMIMBr was also synthesized using water as solvent in a similar way as described above. As shown in Fig. 2, colorless product with no appreciable absorption in the visible range was

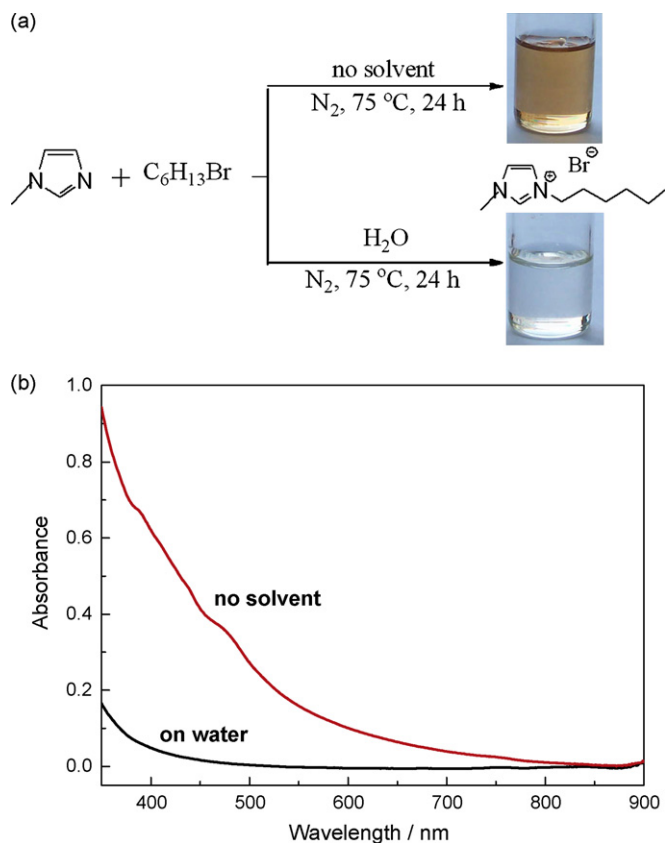


**Fig. 2.** Photographs (a) and UV-vis absorption spectra (b) of HMIMBr in liquid prepared on water (lower) and without any solvent (upper).

again obtained in the “on water” reaction, while the control reaction gave a yellow product.

Because the counteranion-exchange process did not introduce color, via well-developed metathesis method, colorless ILs bearing other counteranions could be facily obtained based on the colorless halide salts as the starting material. For example, colorless BMIMBF<sub>4</sub>, one of most common commercially available ILs, could be obtained from the “on water” colorless BMIMBr via metathesis in NaBF<sub>4</sub>/acetone solution (Fig. 3) [1].

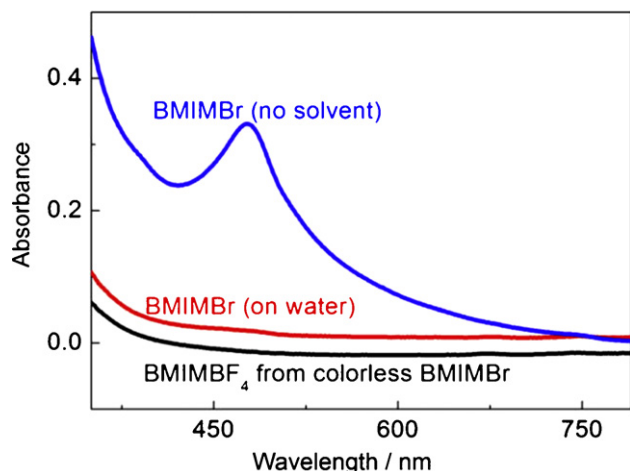


**Fig. 3.** UV-vis absorption of BMIMBr prepared on water (red line) and without any solvent (blue line), and BMIMBF<sub>4</sub> synthesized from BMIMBr (on water) via anion metathesis (black line). (For interpretation of the references to color in this figure legend, the reader is referred to the web version of the article.)

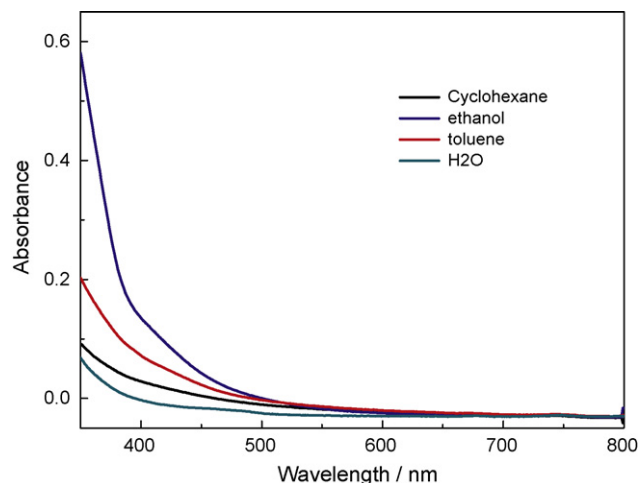


**Fig. 4.** UV-vis absorption of BMIMBr prepared in ethanol, toluene, cyclohexane and water.

It should be noted, for a long time, it has been widely believed that in preparation of ILs, e.g. imidazolium halides, the reaction mixture should be kept dry during the reactions because they are extremely hygroscopic. However, water is usually used in subsequent metathesis or purification of other ILs. It hinted that it was not necessary to absolutely exclude water in the reaction mixture, if the existence of water did not cause unwanted side reactions. Moreover, on the basis of economical and ecological criteria, the use of water as a solvent for organic reactions is highly desirable for organic chemists [19,22–24]. These two facts suggested water might be a suitable solvent to prepare IL. Here <sup>1</sup>H NMR and UV-vis absorption spectra results did surprisingly indicate that water not only could be used as a green solvent (to disperse reactants without causing unwanted side reactions), but also significantly eliminated formation of color impurities. To further understand this surprising result, effects of “on water” reaction conditions on preparing colorless IL, and the reason why using water as solvent could eliminate color were further investigated.

Table 1 lists a series of subsequent reactions, in which parameters were systematically varied to investigate effects on the reaction rate and BMIMBr quality. Twofold dilution of the reactants led to a yield decrease from 96% to 87% (2 and 7, respectively). Concentrating the reactants twofold (6) did not give any increase in yield, and reactions with less than 0.42:1 (v/v) water-to-reactant ratio showed light yellow color. A kinetic study at 70 °C (2, 4, and 5) showed that the reaction was still in progress at 12 h and equilibrates by 24 h. BMIMBr yield improved significantly as temperature increased from 60 °C to 70 °C and further increased only slightly at 80 °C (1, 2, and 3). Below 50 °C, yield was negligible, while above 80 °C, the product again took on light yellow hue. Finally, a concentration study showed that increasing the molar ratio of 1-bromobutane to 1-methylimidazole from 1.2:1 to 2.5:1 led to yield improvement (2, 8, and 9) with most gain realized between 1.2:1 and 2:1. A similar trend was seen in water-free reactions 10 and 11, which, despite having marginally higher yield than the corresponding on-water reactions, gave colored product.

To investigate the reason why using water eliminated color, more control reactions by replacing water with a different protonic solvent (i.e. ethanol) or with one of two nonprotonic solvents (i.e. cyclohexane and toluene) were investigated under similar conditions described above. It was found that IL synthesized in toluene or ethanol was yellow, while that synthesized in cyclohexane was colorless (absorption spectra shown in Fig. 4). This observation indicated that solvents with proton-dissociation equilibria did not prevent the formation of colored product. Moreover, it was noted

that IL was soluble in water or ethanol, but not in cyclohexane or toluene. Thus, it seemed that IL solubility in the solvents had neglected effects on the IL color. Therewith, the effect of reactant solubility in solvents on color formation was further considered. Only one of the reactants was soluble in water (1-methylimidazole) or in cyclohexane (1-bromobutane), and these reaction mixtures contained two liquid phases. However, both reactants were readily soluble in toluene and ethanol, forming a homogenous, single-liquid-phase reaction mixture. Also, in solvent-free reactions, only one liquid phase was present. In single-phase systems, the reactants have higher concentration, i.e. presumably higher reaction rate, than in biphasic systems. This may allow local hot spots (the reaction is mildly exothermic) and formation of trace impurities, which can lead to discoloration of the final product. Therefore, the effect of reactant solubility played an important role in preparation of colorless ILs. As shown, both water and cyclohexane could dissolve only one of the reactants, and they could eliminate the colored impurities. But water was much “greener” than cyclohexane, it was more preferred to be selected as solvent.

Even in the “on water” reaction, it was necessary to exclude oxygen to obtain colorless IL. To investigate whether exposure of reactants to oxygen can cause product coloration, pure 1-methylimidazole or alkyl halide was heated to 70 °C in air for 24 h, respectively. No color developed, indicating that only when both the reactants were present, colored impurities were produced. This result was also in accord with the above-mentioned effect of reactant solubility on color formation, i.e. higher concentration of both reactants in one phase more easily led to colored product.

Characterizations by other methods such as electrochemical method to determine electrochemical window and investigations of physical properties such as melting point and viscosity of ionic liquids from different synthetic methods are very important for their future applications. Our method is similar to classic method to prepare ILs, except that the water was added as solvent, and the purity of as-prepared ionic liquids from our method had been proved by NMR and UV–vis spectroscopy. Thus, if water was removed completely in the final ILs, the electrochemical and physical properties of ILs from this method should not be altered.

In comparison with previous successful examples to prepare colorless ILs, the careful pre-treatment (distill, washing and dry) of starting materials and critical precautions during the reaction [17] or with time-consuming and costly post-decolor-purification [6] were no longer needed by using water as solvent. For example, commercial alkyl-halides (98%) were used as-received and 1-methylimidazole was only fresh distilled, because it was easy to produce color impurities during storing. And the use of organic solvents for reaction and purification was also eliminated. For example, here for preparing imidazolium halides (the starting ILs for other ILs bearing other counteranions), only excessive alkylhalides were used, and moreover, the remainder could be recovered and recycled. Furthermore, the as-produced ionic liquids products in our method were colorless, which did not need further discoloring step, which was somewhat time-consuming and costly. In addition, the reaction steps, time and manpower in our method was similar with the classic method to prepare ILs (without efforts to eliminate colored impurities).

As shown in Figs. 1–3, UV–vis spectra not only prove the quality of the as-prepared ILs, but also shown the examples of applying these colorless ILs in the UV–vis spectroscopic analysis. Moreover, as described aforementioned, colorless ILs from “on water” reaction was more economic. Thus, it would greatly enrich the applications of ILs (especially in large quantity), which were previously hindered by colored impurities.

However, in the current investigation, only the most “popular” colorless imidazolium-based ILs with alkyl group was prepared

without color by “on water” reaction. Investigations of other type of ILs, such as imidazolium-based ILs bearing other halides (e.g. chlorides and iodines) or other cations-based ILs is very important to illustrate whether our method is suitable for all types of ILs. Currently this part of work together with spectroscopic analytic researches and applications of these colorless ILs are ongoing.

#### 4. Conclusion

In conclusion, using 1,3-dialkylimidazolium salts as models, we have demonstrated that water can replace organic solvents for IL preparation and more importantly the “on water” reaction itself did not produce colored impurities, which has been a longstanding challenge in the field. This reaction scheme was relatively green and simple to implement. Besides, the effects of “on water” reaction conditions on preparing colorless IL and the reason why using water as solvent could produce colorless ILs were also preliminary investigated. It was found that the reactant solubility played an important role in the preparation of colorless ILs. It will not only pave the way for economical synthesis of a broad variety of colorless ILs for spectroscopy so as to eliminate the uncertainties and limits, but also motivate theoretical and experimental studies to deepen fundamental understanding of the source(s) of color in ILs and enrich the applications of ILs in spectroscopic analytic researches and applications.

#### Acknowledgments

The authors are most grateful to the National Science Foundation of China (no. 20827004 and no. 20673109), Department of Science and Technology of Jilin Province (no. 20050102) and Ministry of Science and Technology of China (no. 2006BAKB05) for their financial supports.

#### References

- [1] P. Wasserscheid, T. Welton, *Ionic Liquids in Synthesis*, Wiley-VCH, Weinheim, 2002.
- [2] R.D. Rogers, K.R. Seddon, *ACS Symposium Series 856*, American Chemical Society, Washington, DC, 2003.
- [3] T. Welton, *Chem. Rev.* 99 (1999) 2071.
- [4] T. Kakiuchi, T. Yoshimatsu, N. Nishi, *Anal. Chem.* 79 (2007) 7187.
- [5] A. Paul, P.K. Mandal, A. Samanta, *J. Phys. Chem. B* 109 (2005) 9148.
- [6] M.J. Earle, C.M. Gordon, N.V. Plechkova, K.R. Seddon, T. Welton, *Anal. Chem.* 79 (2007) 758.
- [7] T. Nishi, T. Iwahashi, H. Yamane, Y. Ouchi, K. Kanai, K. Seki, *Chem. Phys. Lett.* 455 (2008) 213.
- [8] L. Zhang, Z. Xu, Y. Wang, H. Li, *J. Phys. Chem. B* 112 (2008) 6411.
- [9] Y. Shao, G.C. Bazan, A.J. Heeger, *Adv. Mater.* 19 (2007) 365.
- [10] S. Ito, S.M. Zakeeruddin, R. Humphry-Baker, P. Liska, R. Charvet, P. Comte, M.K. Nazeeruddin, P. Pechy, M. Takata, H. Miura, S. Uchida, M. Gratzel, *Adv. Mater.* 18 (2006) 1202.
- [11] Y. Jeon, J. Sung, C. Seo, H. Lim, H. Cheong, M. Kang, B. Moon, Y. Ouchi, D. Kim, *J. Phys. Chem. B* 112 (2008) 4735.
- [12] J.L. Anderson, D.W. Armstrong, G.T. Wei, *Anal. Chem.* 78 (2006) 2892.
- [13] L. Kavan, L. Dunsch, *ChemPhysChem* 4 (2003) 944.
- [14] A. Stark, O. Braun, B. Ondruschka, *Anal. Sci.* 24 (2008) 681.
- [15] D. Batra, S. Seifert, L.M. Varela, A.C.Y. Liu, M.A. Firestone, *Adv. Funct. Mater.* 17 (2007) 1279.
- [16] Y.H. Pang, H. Xu, X.Y. Li, H.L. Ding, Y.X. Cheng, G.Y. Shi, L.T. Jin, *Electrochem. Commun.* 8 (2006) 1757.
- [17] P. Nockemann, K. Binnemans, K. Driesen, *Chem. Phys. Lett.* 415 (2005) 131.
- [18] A.K. Burrell, R.E. Del Sesto, S.N. Baker, T.M. McCleskey, G.A. Baker, *Green Chem.* 9 (2007) 449.
- [19] U.M. Lindstrom, *Chem. Rev.* 102 (2002) 2751.
- [20] X. Wu, J. Liu, X. Li, A. Zanotti-Gerosa, F. Hancock, D. Vinci, J. Ruan, J. Xiao, *Angew. Chem. Int. Ed.* 45 (2006) 6718.
- [21] B.K. Price, J.M. Tour, *J. Am. Chem. Soc.* 128 (2006) 12899.
- [22] C.J. Li, L. Chen, *Chem. Soc. Rev.* 35 (2006) 68.
- [23] I. Vilotijevic, T.F. Jamison, *Science* 317 (2007) 1189.
- [24] S. Narayan, J. Muldoon, M.G. Finn, V.V. Fokin, H.C. Kolb, K.B. Sharpless, *Angew. Chem. Int. Ed.* 44 (2005) 3275.
- [25] Y.F. Shen, Y.J. Zhang, Q.X. Zhang, L. Niu, T.Y. You, A. Ivaska, *Chem. Commun.* (2005) 4193.



# Haemoglobin immobilized on nafion modified multi-walled carbon nanotubes for O<sub>2</sub>, H<sub>2</sub>O<sub>2</sub> and CCl<sub>3</sub>COOH sensors

Jan-Wei Shie, Umasankar Yogeswaran, Shen-Ming Chen\*

Department of Chemical Engineering and Biotechnology, National Taipei University of Technology, No. 1, Section 3, Chung-Hsiao East Road, Taipei 106, Taiwan, ROC

## ARTICLE INFO

### Article history:

Received 3 November 2008

Received in revised form

25 December 2008

Accepted 29 December 2008

Available online 20 January 2009

### Keywords:

Multiwall carbon nanotubes

Modified electrodes

Electrocatalysis

Hydrogen peroxide

Trichloroacetic acid

Oxygen

## ABSTRACT

A conductive biocomposite film (MWCNTs-NF-Hb) containing multi-walled carbon nanotubes (MWCNTs) incorporated with entrapped haemoglobin (Hb) in nafion (NF) has been synthesized on glassy carbon electrode (GCE), gold (Au), indium tin oxide (ITO) and screen printed carbon electrode (SPCE) separately by potentiostatic methods. The presence of both MWCNTs and NF in the biocomposite film enhances the surface coverage concentration ( $\Gamma$ ), and increases the electron transfer rate constant ( $K_s$ ) to 132%. The biocomposite film exhibits a promising enhanced electrocatalytic activity towards the reduction of O<sub>2</sub>, H<sub>2</sub>O<sub>2</sub> and CCl<sub>3</sub>COOH. The cyclic voltammetry has been used for the measurement of electrocatalysis results of analytes by means of biocomposite film-modified GCEs. The MWCNTs-NF-Hb-modified GCEs' sensitivity values are higher than the values obtained for other film modified GCEs. The surface morphology of the biocomposite films which have been deposited on ITO has been studied using scanning electron microscopy and atomic force microscopy. The studies have revealed that there was an incorporation of NF and immobilization of Hb on MWCNTs. Finally, the flow injection analysis has been used for the amperometric studies of analytes at MWCNTs-Hb and MWCNTs-NF-Hb film modified SPCEs. The amperometric study results have shown higher slope values for MWCNTs-NF-Hb biocomposite film.

© 2009 Elsevier B.V. All rights reserved.

## 1. Introduction

A wide variety of applications of matrices made of carbon nanotubes (CNTs) for the detection of bioorganic and inorganic compounds such as insulin, ascorbic acid, etc. were already reported [1–4]. The rolled-up graphene sheets of carbon, i.e., CNTs, exhibits a  $\pi$ -conjugative structure with a highly hydrophobic surface. This property of CNTs allows them to interact with some organic aromatic compounds through  $\pi$ - $\pi$  electronic and hydrophobic interactions [5–7]. These interactions were used for preparing composite sandwiched films for electrocatalytic studies [8] and in the designing of nanodevices with the help of non-covalent adsorption of enzyme and proteins on the side walls of CNTs. This method resulted in the development of CNT-based nanostructures, which contain biochemical units in them [9]. Some attempts were also made to prepare hydrophilic surface CNTs to overcome the dispersion problems in aqueous medium for bio-electrochemical applications [10]. Electrodes which are modified with composite films are widely used not only in the preparation of capacitors, batteries, fuel cells, chemical sensors and biosensors but also in the field of material science and photoelectrochemistry [11–13].

Even though the electrocatalytic activity of the CNTs with protein matrices individually shows good results; some properties like mechanical stability, sensitivity for different techniques and electrocatalysis for multiple compound detections are poor. Besides CNTs and proteins, there are other interesting polymer materials, and one such material is nafion (NF). Due to the presence of a sulfonated group in NF and its strong acidic character, it has been used as a solid catalyst in organic synthesis. Extensive studies have been already carried out using hybrid thin films of CNTs-NF. These film-modified electrodes are being used for the electrocatalytic oxidation of biochemical compounds [14–16].

Haemoglobin (Hb) consists of four subunits of polypeptide enzymes. A haem (iron porphyrin) group in each subunit acts as an active center. Haemoglobin usually shows slow rates of electron transfer on a bare metal electrode surface. The idea of enhancing the electron transfer rate of haemoglobin using mediators and solid electrodes have been explored, for example, using methylene green [17]. The enhancement of the electron transfer rate of haemoglobin were reported using polyion surfactants of dihexadecylphosphate and poly(diallyldimethylammonium) (DHP and PDDA) [18,19], didodecyldimethylammonium bromide (DDAB) [20,21], poly(ester sulfonic acid) [22], dimyristoylphosphatidylcholine (DMPC) [23], clay films [24,25], etc. [26–30]. Interestingly, the catalytic activity towards different compounds using direct electron transfer between Hb-modified electrode from aqueous

\* Corresponding author. Tel.: +886 2270 17147; fax: +886 2270 25238.  
E-mail address: [smchen78@ms15.hinet.net](mailto:smchen78@ms15.hinet.net) (S.-M. Chen).

solution were already investigated [31,32]. These reports are concerned with analytical applications and the properties of haemoglobin during the electrocatalytic oxidation or reduction of electroactive haemoglobin on electrode surfaces. Further, the literature survey reveals that there were no previous attempts made for the synthesis of biocomposite film composed of CNTs, NF and Hb for sensor applications. In this paper, we report a novel biocomposite film (MWCNTs-NF-Hb) made of multi-walled carbon nanotubes (MWCNTs) incorporated with NF and Hb, its characterization and its enhancement in functional properties, peak current and electrocatalytic activity. We have reported also, its application in the electrocatalysis of  $O_2$ ,  $H_2O_2$  and  $CCl_3COOH$ . The film formation process involves the modification of glassy carbon electrode (GCE) with uniform well dispersed MWCNTs on it and drying it. Then electrodeposition of NF and immobilization of Hb from neutral aqueous solution on the MWCNTs modified GCE have been done subsequently.

## 2. Experimental

### 2.1. Apparatus

Cyclic voltammetry (CV) was performed in an analytical system model CHI-611, CHI-400 and CHI-1205A potentiostat. A conventional three-electrode cell assembly consisting of an Ag/AgCl reference electrode and a Pt wire counter electrode were used for the electrochemical measurements. The working electrode was either an unmodified GCE or GCEs modified with NF-Hb, MWCNTs-NF, MWCNTs-Hb or MWCNTs-NF-Hb biocomposite films. In these experiments, all the potentials have been reported versus the Ag/AgCl reference electrode. The gold working electrode was an 8 MHz AT-cut quartz crystal coated with a gold plating. The diameter of the quartz crystal was 13.7 mm; the gold electrode diameter was 2.4 mm. The flow injection analysis (FIA) of the analytes at screen printed carbon electrode (SPCE) were done using Alltech 426 HPLC pump containing an electrochemical cell. The morphological characterizations of the films were examined by means of SEM (Hitachi S-3000H) and atomic force microscopy (AFM) (Being Nano-Instruments CSPM4000). All the measurements were carried out at  $25^\circ\text{C} \pm 2$ .

### 2.2. Materials

Hb, MWCNTs (OD = 10–20 nm, ID = 2–10 nm and length = 0.5–200  $\mu\text{m}$ ), NF and potassium hydroxide obtained from Aldrich and Sigma–Aldrich were used as received. All other chemicals used were of analytical grade. The preparation of aqueous solution was done with twice distilled deionized water. Solutions were deoxygenated by purging with pre-purified nitrogen gas. Buffer solutions were prepared from  $H_2SO_4$  for the pH 2.5 aqueous solution.

### 2.3. Preparation of MWCNTs and MWCNTs-NF-Hb-modified electrodes

There was an important challenge in the preparation of MWCNTs. Because of its hydrophobic nature, it was difficult to disperse it in any aqueous solution to get a homogeneous mixture. Briefly, the hydrophobic nature of the MWCNTs was converted in to hydrophilic nature by following the previous studies [10,33]. This was done by weighing 10 mg of MWCNTs and 200 mg of potassium hydroxide in to a ruby mortar and grained together for 2 h at room temperature. Then, the reaction mixture was dissolved in 10 ml of double distilled deionized water then precipitated many times in to methanol for the removal of potassium hydroxide. Then, the obtained MWCNTs in 10 ml water were ultrasonicated for 6 h to get a uniform dispersion. This functionalization process of MWCNTs is to get a hydrophilic

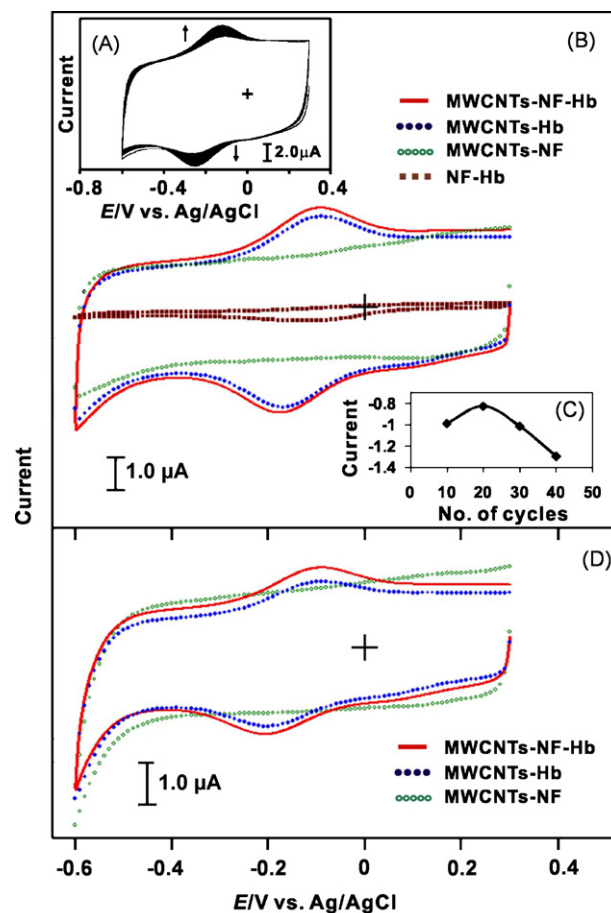
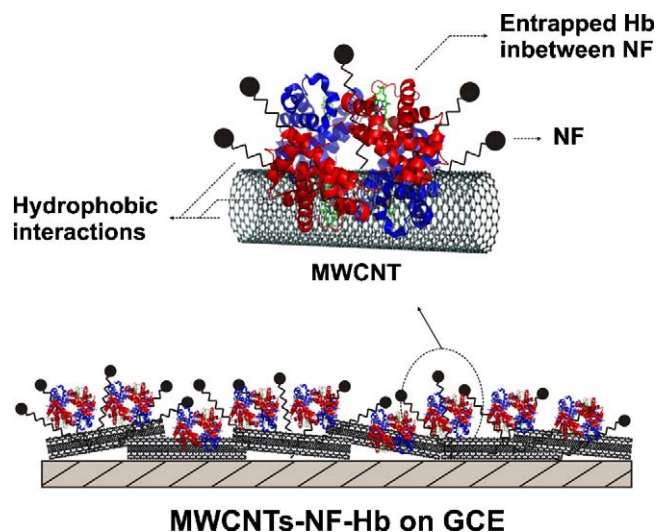


**Fig. 1.** (A) Consecutive CVs of MWCNTs-NF GCE modified from 0.1 mM Hb present in pH 2.5  $H_2SO_4$  aqueous solution, scan rate at  $50\text{ mV s}^{-1}$ . (B) CVs of GCE modified from NF-Hb, MWCNTs-NF, MWCNTs-Hb and MWCNTs-NF-Hb film in pH 2.5  $H_2SO_4$  aqueous solution, scan rate at  $20\text{ mV s}^{-1}$ . (C) Plot of Hb peak current at MWCNTs-NF-modified GCE vs. number of cycles of NF growth by consecutive CVs. (D) CVs of gold electrode modified from MWCNTs-NF-Hb, MWCNTs-Hb and MWCNTs-NF films in pH 2.5  $H_2SO_4$  aqueous solution, scan rate at  $20\text{ mV s}^{-1}$ .

nature for the homogeneous dispersion in water. This process not only converts MWCNTs to hydrophilic nature but this helps to breakdown larger bundles of MWCNTs in to smaller ones too. This was confirmed using SEM, which is not shown in the figures. A homogeneous 0.005 wt% NF solution was used for depositing NF on the electrodes.

Before starting each experiment, GCEs were polished by BAS polishing kit with 0.05  $\mu\text{m}$  alumina slurry and rinsed and then ultrasonicated in double distilled deionized water. The GCEs studied were uniformly coated with  $75\ \mu\text{g cm}^{-2}$  of MWCNTs then dried. The concentration of homogeneously dispersed MWCNTs was exactly measured using a micro-syringe. The electrochemical deposition of NF on MWCNTs modified GCE was performed from the 0.005 wt% NF solution in pH 2.5 by consecutive CV over a suitable potential region of  $-0.6$  to  $0.5\text{ V}$ , 40 cycles and scan rate at  $100\text{ mV s}^{-1}$  (figure not shown). Then, the modified MWCNTs-NF electrode was carefully washed with double distilled deionized water and dried. The immobilization of Hb on the MWCNTs-NF-modified electrode was performed from 0.1 mM Hb in pH 2.5  $H_2SO_4$  aqueous solution by consecutive CV over a suitable potential region of  $-0.6$  to  $0.3\text{ V}$ , 30 cycles and scan rate at  $50\text{ mV s}^{-1}$ . Then, the modified MWCNTs-NF-Hb electrode was carefully washed with double distilled deionized water to perform other studies. Solutions were deoxygenated by purging with pre-purified nitrogen gas for about 1 h. For a detailed comparison of electrocatalysis reac-



**Scheme 1.** Schematic representation of possible interaction between MWCNTs, NF and Hb in the formation of MWCNTs-NF-Hb biocomposite film-modified electrodes.

tions, we studied different types of modified electrodes such as MWCNTs-NF, MWCNTs-Hb and MWCNTs-NF-Hb. In all these experiments, the electrodes were first modified by MWCNTs and then electrodeposited with NF and immobilized with Hb. These comparative characterization studies were done to reveal the obvious necessity of the presence of MWCNTs in the NF-Hb biocomposite film.

The electrocatalytic reduction studies of  $O_2$  were carried out using  $O_2$  saturated aqueous solutions (pH 2.5  $H_2SO_4$ ) at various electrodes mentioned in Section 2.1. The concentration of  $O_2$  in the aqueous solution was varied by de-aerating with pre-purified  $N_2$  gas. The variation of  $O_2$  concentration for each experiment was measured using  $O_2$  meter (Oxi 323-A/set WTW 82362, Germany). In these studies, electrochemical cells were properly sealed with ventilation, and a continuous flow of  $N_2$  gas was maintained over the solution during the electrochemical measurements to avoid the  $O_2$  interference from atmosphere. Similarly, the electrocatalysis studies of  $H_2O_2$  and  $CCl_3COOH$  were also carried out in  $N_2$  atmosphere.

### 3. Results and discussions

#### 3.1. Electrochemical synthesis and its characterization of MWCNTs-NF-Hb biocomposite film

The immobilization of Hb (from 0.1 mM Hb) on MWCNTs-NF modified GCE using pH 2.5  $H_2SO_4$  aqueous solution has been performed by consecutive CVs as shown in Fig. 1(A). In this figure, the redox couple found growing on subsequent cycles, which indicates that during the cycle the immobilization of Hb took place on MWCNTs-NF-modified GCE at suitable potential range of 0.3 to  $-0.6$  V. In the following experiments, each newly prepared biocomposite film on GCE has been washed carefully in deionized water to remove the loosely bounded Hb on the modified GCE, and then

**Table 1**  
Surface coverage concentrations ( $\Gamma$ ) of Hb at different types of modified electrodes using CV technique in  $H_2SO_4$  aqueous solution (pH 2.5).

Electrode type	Modified film	$\Gamma$ (pmol $cm^{-2}$ )
GCE	NF-Hb	96.2
	MWCNTs-Hb	155
	MWCNTs-NF-Hb	169
Gold	MWCNTs-Hb	252
	MWCNTs-NF-Hb	318

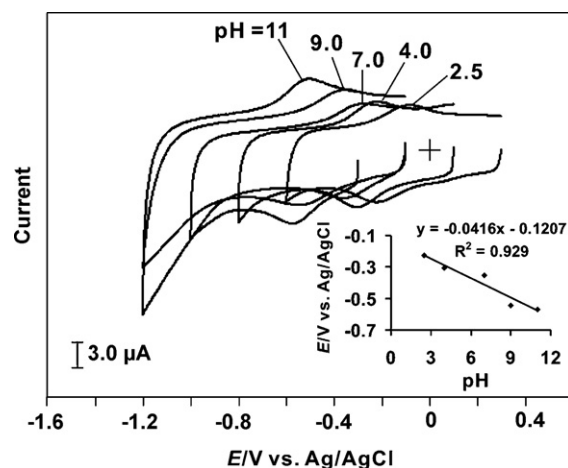


**Fig. 2.** CVs of MWCNTs-NF-Hb film on GCE synthesized at similar conditions and transferred to various pH solutions; scan rate:  $50 \text{ mV s}^{-1}$ . The inset shows the formal potential vs. pH (2.5–11), the slope  $-41 \text{ mV/pH}$  is almost nearer to Nernstian equation for non-equal number of electrons and protons transfer.

transferred to pH 2.5 aqueous solutions for other electrochemical characterizations. Fig. 1(B) shows the electrochemical signal of Hb at  $20 \text{ mV s}^{-1}$  on NF modified GCE with irreversible cathodic peak current at  $E_{pc} = -0.19 \text{ V}$  versus Ag/AgCl in pH 2.5  $H_2SO_4$  aqueous solution. Whereas in MWCNTs and MWCNTs-NF, reversible redox peaks at formal potential  $E^{0'} = -0.13 \text{ V}$  has been obtained for  $Fe^{III/II}$  redox reaction corresponding to the immobilized Hb. Among MWCNTs and MWCNTs-NF, MWCNTs-NF modified GCE shows higher peak current for  $Fe^{III/II}$  redox reaction of the immobilized Hb. The

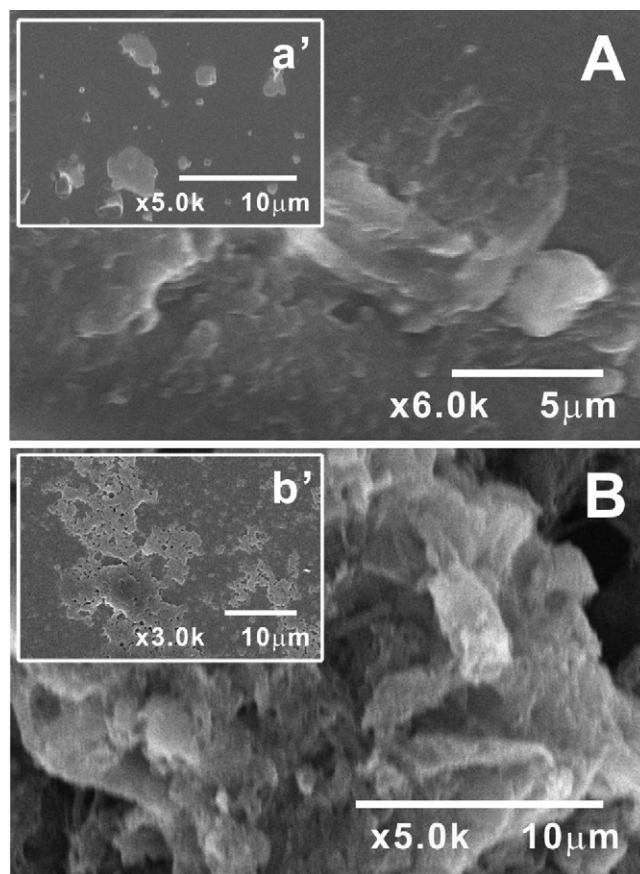


**Fig. 3.** SEM images of (A) NF-Hb and (B) MWCNTs-NF-Hb biocomposite film on ITO electrode. The insets are (a') NF and (b') Hb on ITO electrode.



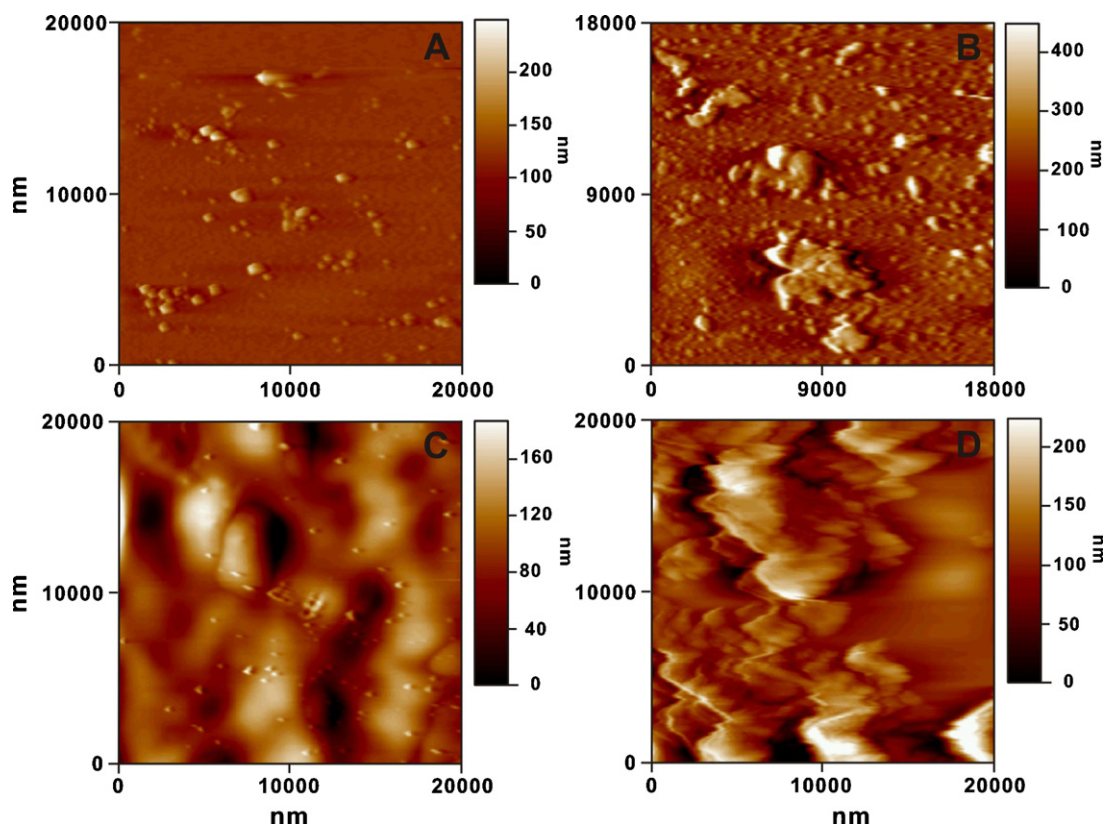


Fig. 4. AFM images of (A) NF, (B) Hb, (C) NF-Hb and (D) MWCNTs-NF-Hb biocomposite film on ITO electrode.

Fig. 1(B) shows no redox peaks at MWCNTs-NF in the absence of Hb. The optimization of the number of cycles for NF deposition has been done using the plots shown in Fig. 1(C). Where, different MWCNTs-NF-Hb films have been synthesized using different cycling of NF deposition, and then the CVs of MWCNTs-NF-Hb have been obtained using pH 2.5 H<sub>2</sub>SO<sub>4</sub> aqueous solution and the peak currents have been plotted against number of cycles. It is obvious that, above and below 20 cycles, the peak current decreases, which shows that the optimum deposition of NF took place at 20 cycles. Similarly, the optimization of NF concentration has also been studied, in which the deposition of NF from 0.005 wt% solution shows higher redox peak current for Hb (figures not shown). The possible interaction between MWCNTs, NF and Hb in the formation of MWCNTs-NF-Hb biocomposite film is given in Scheme 1.

From the CVs in Fig. 1(B), the surface coverage concentration ( $\Gamma$ ) values have been calculated and given in Table 1. In this calculation, the charge involved in the reaction ( $Q$ ) has been obtained from CVs and applied in the equation  $\Gamma = Q/nFA$  where, the number of electron transfer involved in the Hb redox reaction has been assumed as two (one electron for each heme group, that is two Hb molecules) [34]. These values indicate that the presence of MWCNTs increases the surface area of the electrode, which in turn increases the  $\Gamma$  of Hb. The different scan rate studies of MWCNTs-Hb and MWCNTs-NF-Hb biocomposite films on GCE using pH 2.5 H<sub>2</sub>SO<sub>4</sub> aqueous solution (see supplementary data) shows that the redox peak currents of both the films increases linearly with the increase of scan rate. The results demonstrated that the redox process is not controlled by diffusion. Plots from different scan rate results (supplementary data) show that MWCNTs-NF-Hb possesses faster electron transfer rate than MWCNTs-Hb film. Further, the electron transfer rate constant ( $K_s$ ) have been calculated from these different scan rate results based on Laviron theory [35]. Where,  $K_s = 0.08$  and  $0.19 \text{ s}^{-1}$  for MWCNTs-Hb and MWCNTs-NF-Hb bio-

composite film, respectively. From these  $K_s$  values the increase in the ability of electron transfer between the electrode surface and the Hb in presence of NF is  $\approx 132\%$ . These results too show that, there is an enhancement in the functional properties of the biocomposite film at lower scan rates in presence of both NF and MWCNTs [36]. Gold electrodes have also been used to characterize the biocomposite films in pH 2.5 H<sub>2</sub>SO<sub>4</sub> aqueous solution. Fig. 1(D) represents the redox peak of Hb on MWCNTs-NF-Hb, MWCNTs-Hb and MWCNTs-NF-modified gold electrode, where MWCNTs-NF-Hb shows higher redox peak current for Hb than other two films. These results revealed the importance of the presence of both MWCNTs and NF in the biocomposite film, where MWCNTs enhances the electron transfer on different electrodes which in turn widens the sensor-based applications. Fig. 2 shows the CVs of MWCNTs-NF-Hb on GCE in various pH aqueous buffer solutions without the presence of Hb. This shows that the film is stable in the pH range between 2.5 and 11, and the values of  $E_{pa}$  and  $E_{pc}$  depends on pH value of the buffer solution. The inset in Fig. 2 shows the formal potential of MWCNTs-NF-Hb plotted over a pH range of 2.5–11. The response shows a slope of  $-41.6 \text{ mV/pH}$ , which is close to that given by the Nernstian equation for two electron one proton transfer [37].

Four different films; Fig. 3(a') NF, (b') Hb, (A) NF-Hb and (B) MWCNTs-NF-Hb have been prepared on the indium tin oxide (ITO) with similar conditions and potential as that of GCE and were characterized using SEM. From Fig. 3, it is significant that there are morphological differences between all these four films. The morphological structure in (a') shows uniform patches of NF has been formed on ITO. The same uniform patch morphological structure can be seen in (A) and (B). Similarly, (b') shows Hb film with pores as reported previously [38]. When compared (b') with (A) and (B) almost similar morphology could be seen. The presence of MWCNTs is obvious in (B) with highly uneven surface. Comparing all the images, the immobilization of Hb and the incorporation of NF

**Table 2**

Comparison of Epc and Ipc of analytes in electrocatalysis reactions using CV technique at different types of modified electrodes in pH 2.5 H<sub>2</sub>SO<sub>4</sub> aqueous solution.

Analytes	Reaction type	pH	E <sub>p</sub> (mV)		I <sub>p</sub> (μA)	
			Hb <sup>a</sup>	Hb <sup>b</sup>	Hb <sup>a</sup>	Hb <sup>b</sup>
O <sub>2</sub>	Reduction	2.5	−190	−200	4.5	10.6
H <sub>2</sub> O <sub>2</sub>	Reduction	2.5	−210	−200	4.2	5.1
CCl <sub>3</sub> COOH	Reduction	2.5	−240	−250	9.6	11.6

<sup>a</sup> MWCNTs-modified GCE.

<sup>b</sup> MWCNTs-NF-modified GCE.

on MWCNT modified ITO in (B) shows both uniform NF and Hb film pores. It is a well-known fact that the prolonged exposure to the electron beam will damage the Hb films, so, at most care has been taken in measuring these images. The same modified ITO electrodes have been used to measure the AFM topography images, and these measured morphological structures are similar to that of SEM. Fig. 4(A) shows the patches of NF, whereas (B) shows Hb film with pores, (C) and (D) show the NF-Hb and MWCNTs-NF-Hb biocomposite films, respectively. These SEM and AFM results have revealed the formation of a MWCNTs-NF-Hb biocomposite film.

### 3.2. Electrocatalysis studies of oxygen at MWCNTs-NF-Hb biocomposite film

The electrocatalytic reduction of O<sub>2</sub> has been carried out at bare GCE, MWCNTs-NF, MWCNTs-Hb and MWCNTs-NF-Hb biocomposite film modified GCEs at pH 2.5 H<sub>2</sub>SO<sub>4</sub> aqueous solutions. Fig. 5(A) shows the electrocatalytic reduction of O<sub>2</sub> at different modified electrodes. In all the modified electrodes, the cathodic peak current of Hb at the potential of about 0.2 V increases noticeably, as the concentration of O<sub>2</sub> increased. However, for bare GCE the electrocatalytic reduction peak current of O<sub>2</sub> is at −0.6 V. These results show that the MWCNTs-NF-Hb biocomposite film possess higher peak current for O<sub>2</sub> reduction when comparing all other modified GCEs (I<sub>pc</sub> and E<sub>pc</sub> values given in Table 2). The above-mentioned film modified electrodes catalytic phenomenon must be because of the presence of Hb in the modified electrode. From the slopes of the linear calibration curves, the sensitivity of the biocomposite modified GCEs and their correlation coefficient have been calculated and are given in Table 3. From this table, it is clear that the sensitivity of MWCNTs-NF-Hb biocomposite film is higher for O<sub>2</sub> reduction. The electrochemical reduction of the O<sub>2</sub> to H<sub>2</sub>O by Fe<sup>II</sup> present in the MWCNTs-NF-Hb biocomposite film could be given by

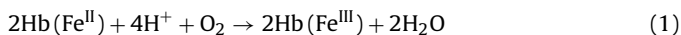
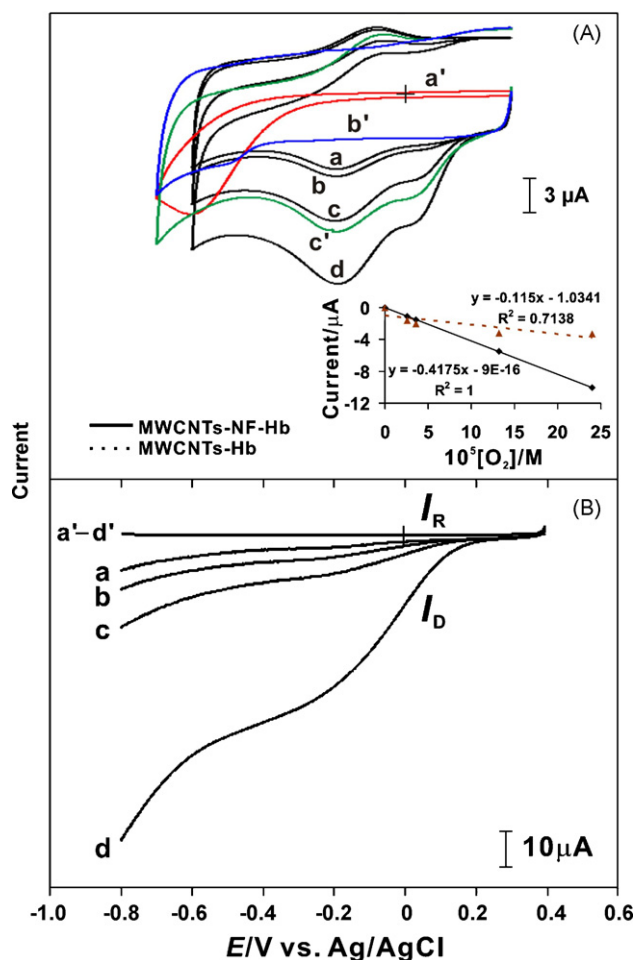


Fig. 5(B) shows the electrochemical reduction of O<sub>2</sub> by MWCNTs-NF-Hb biocomposite film-modified GCE disk electrode (at 0.2 V) and electrochemical oxidation of H<sub>2</sub>O<sub>2</sub> by bare platinum ring electrode (at 0.75 V) in an aqueous buffer solution at pH 2.5. The increase in concentration of O<sub>2</sub> increases the disk current (I<sub>D</sub>). However, the platinum ring current (I<sub>R</sub>), does not show obvious increase during the increase of O<sub>2</sub> concentration, which shows that the reaction in Eq. (2) does not occur at ring electrode. This result shows that H<sub>2</sub>O<sub>2</sub> is not formed during the reduction of O<sub>2</sub>. From this argument, the reduction mechanism of O<sub>2</sub> at the MWCNTs-NF-Hb biocompos-

**Table 3**

Sensitivity and correlation co-efficient of different modified electrodes for various analytes in CV technique.

Analytes	Reaction type	Sensitivity (mA mM <sup>−1</sup> cm <sup>−2</sup> ) [Slope's correlation coefficient]	
		MWCNTs-Hb	MWCNTs-NF-Hb
O <sub>2</sub>	Reduction	−0.14 [0.7138]	−0.52 [1]
H <sub>2</sub> O <sub>2</sub>	Reduction	−0.67 [0.9341]	−0.76 [0.9964]
CCl <sub>3</sub> COOH	Reduction	−0.92 [0.9741]	−1.02 [0.995]



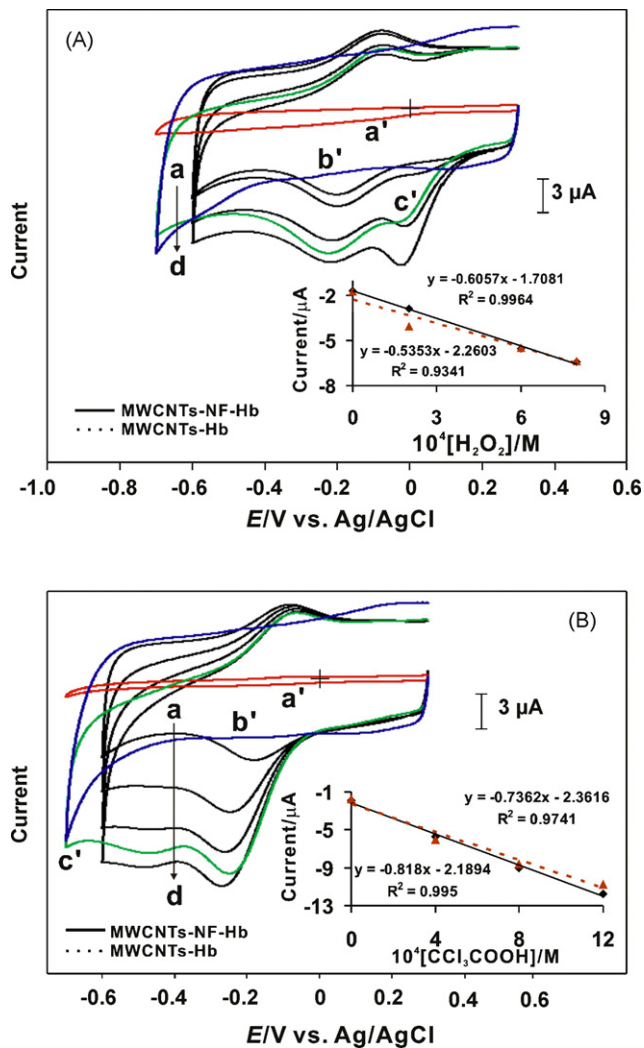
**Fig. 5.** (A) CVs of MWCNTs-NF-Hb biocomposite film in pH 2.5 H<sub>2</sub>SO<sub>4</sub> aqueous solution with various concentration of O<sub>2</sub> = (a) 25.7, (b) 36.2, (c) 131.9 and (d) 240 μM. Where, (a') bare GCE, (b') MWCNTs-NF and (c') MWCNTs-Hb in the highest concentration of the analyte, scan rate at 50 mV s<sup>−1</sup>. The inset in (A) shows the plot of current vs. different concentration of O<sub>2</sub>. (B) RRDE voltammograms of MWCNTs-NF-Hb biocomposite film (at 1600 rpm) in pH 2.5 H<sub>2</sub>SO<sub>4</sub> aqueous solution with various concentration of O<sub>2</sub> = (a) 6.1, (b) 25.3, (c) 48 and (d) 240 μM; scan rate at 15 mV s<sup>−1</sup>. Where, I<sub>D</sub> and I<sub>R</sub> are GC disk electrode and platinum ring electrode currents (E<sub>R</sub> = 0.75 V vs. Ag/AgCl), respectively.

ite could be proposed by Eq. (3).



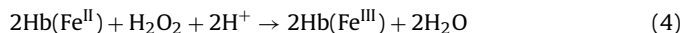
### 3.3. Electrocatalysis studies of H<sub>2</sub>O<sub>2</sub> and trichloroacetic acid at MWCNTs-NF-Hb biocomposite film

Fig. 6(A) and (B) shows the electrocatalytic reduction of H<sub>2</sub>O<sub>2</sub> and trichloroacetic acid (CCl<sub>3</sub>COOH), respectively. The electrolytes used for the electrocatalytic reactions were pH 2.5 H<sub>2</sub>SO<sub>4</sub> aqueous solutions. The CVs have been recorded at the constant time interval of 1 min with nitrogen purging before the start of each experi-



**Fig. 6.** CVs of MWCNTs-NF-Hb biocomposite film in pH 2.5  $\text{H}_2\text{SO}_4$  aqueous solution with various concentration of (A)  $\text{H}_2\text{O}_2$  = (a) 0.0, (b) 0.2, (c) 0.6 and (d) 0.8 mM; (B)  $\text{CCl}_3\text{COOH}$  = (a) 0.0, (b) 0.4, (c) 0.8 and (d) 1.2 mM. Where (a') bare GCE, (b') MWCNTs-NF and (c') MWCNTs-Hb in the highest concentration of the analytes; scan rate at  $50 \text{ mV s}^{-1}$ . The insets in (A) and (B) show the plot of current vs. different concentration of  $\text{H}_2\text{O}_2$  and  $\text{CCl}_3\text{COOH}$ , respectively.

ments. The scan rate used for these electrocatalysis experiments was  $20 \text{ mV s}^{-1}$ . In both the sections of Fig. 6, a' represents bare GCE, b' represents MWCNTs-NF film and c' represents MWCNTs-Hb film-modified GCEs. The CVs of MWCNTs-NF-Hb in Fig. 6(A) and (B) exhibits a reversible redox couple for Hb ( $\text{Fe}^{\text{III/II}}$ ) in the absence of analytes, upon the addition of analytes a new growth in the reduction peak of  $\text{H}_2\text{O}_2$  and  $\text{CCl}_3\text{COOH}$  appeared at  $E_{\text{pc}} = -0.2$  and  $-0.25 \text{ V}$ , respectively. These peak currents show that electrocatalytic reduction of both the analytes took place at Hb ( $\text{Fe}^{\text{II}}$ ) and could be represented by the following equations:



During the electrocatalysis experiments, an increase in the concentration of analytes simultaneously produced a linear increase in the reduction peak currents of the analytes with good film stability as shown in the insets in Fig. 6(A) and (B). It is obvious that, the MWCNTs-NF-Hb shows higher peak current for both the analytes when comparing to all other modified GCEs. The values of  $I_{\text{pc}}$  and  $E_{\text{pc}}$  for the analytes at different films are given in Table 2. From the slopes of the linear calibration curves, the sensitivity of

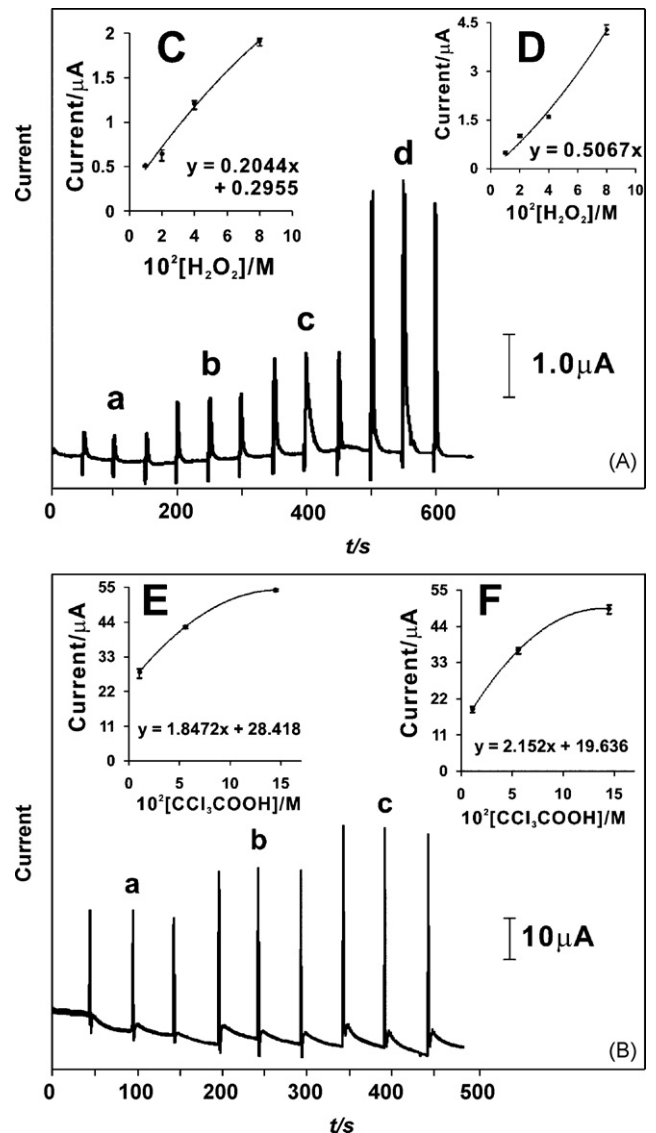


**Fig. 7.** FIA signal of MWCNTs-NF-Hb biocomposite film with various concentration of (A)  $\text{H}_2\text{O}_2$  = (a) 10, (b) 20, (c) 40 and (d) 80 mM; (B)  $\text{CCl}_3\text{COOH}$  = (a) 11, (b) 56 and (c) 145 mM. The potential applied was  $-0.2 \text{ V}$  for  $\text{H}_2\text{O}_2$  and  $-0.25 \text{ V}$  for  $\text{CCl}_3\text{COOH}$ , and the carrier stream used was pH 2.5  $\text{H}_2\text{SO}_4$  aqueous solution; flow rate =  $0.03 \text{ ml s}^{-1}$  and injected volume =  $30 \mu\text{l}$ . (C) and (D) show the plot of current vs. different concentration of  $\text{H}_2\text{O}_2$  at MWCNTs-Hb and MWCNTs-NF-Hb biocomposite films, respectively. Similarly, (E) and (F) show the plot of current vs. different concentration of  $\text{CCl}_3\text{COOH}$  at MWCNTs-Hb and MWCNTs-NF-Hb biocomposite films, respectively.

the biocomposite modified GCEs and their correlation co-efficient have been calculated and given in Table 3. It is clear that, the sensitivity of MWCNTs-NF-Hb is higher for both the analytes and there is no electrocatalysis reaction at MWCNTs-NF-modified GCE. These results clearly show that, the MWCNTs-NF-Hb biocomposite film can be efficiently used for the detection of  $\text{H}_2\text{O}_2$  and  $\text{CCl}_3\text{COOH}$ .

#### 3.4. Flow injection analysis of $\text{H}_2\text{O}_2$ and $\text{CCl}_3\text{COOH}$ at MWCNTs-NF-Hb biocomposite film

Fig. 7(A) and (B) shows the FIA studies of  $\text{H}_2\text{O}_2$  and  $\text{CCl}_3\text{COOH}$ , respectively at MWCNTs-NF-Hb biocomposite films, which have been synthesized on SPCE at similar conditions to that of GCE. Before the start of each experiment, the modified SPCE electrodes have been washed carefully with deionized water to remove the loosely bounded Hb on the modified SPCE. The carrier stream used was pH 2.5  $\text{H}_2\text{SO}_4$  aqueous solution with the flow rate of  $0.03 \text{ ml s}^{-1}$

and the volume of analytes injected at each cycle was 30  $\mu\text{l}$  at the time interval of 50 s. Fig. 7(A) represents the successive addition of  $\text{H}_2\text{O}_2$  in the concentration range from 10 mM to 80 mM at the potential of  $-0.2\text{V}$ ; these are the optimized experimental conditions obtained from CV studies. Similarly, Fig. 7(B) represents the successive addition of  $\text{CCl}_3\text{COOH}$  in the concentration range from 11 mM to 145 mM at the potential of  $-0.25\text{V}$ . In both cases, the rapid amperometric response of the MWCNTs-NF-Hb biocomposite film is proportional to the respective analyte concentrations. For comparative study, MWCNTs-Hb modified SPCEs have also been used for  $\text{H}_2\text{O}_2$  and  $\text{CCl}_3\text{COOH}$  FIA (figures not shown). The results obtained from all the FIA have been plotted as shown in Fig. 7(C–F), where (C) and (D) represents  $\text{H}_2\text{O}_2$  at MWCNTs-Hb and MWCNTs-NF-Hb biocomposite films respectively, whereas (E) and (F) represents  $\text{CCl}_3\text{COOH}$  at MWCNTs-Hb and MWCNTs-NF-Hb biocomposite films, respectively. The slopes obtained from these above-mentioned insets show that MWCNTs-NF-Hb biocomposite film has higher values for both  $\text{H}_2\text{O}_2$  and  $\text{CCl}_3\text{COOH}$  than that of MWCNTs-Hb film. These insets also represent error bars, where each concentration of every analyte was studied three times. These error bars show that the MWCNTs-NF-Hb biocomposite films have good reproducibility for both the analytes.

#### 4. Conclusions

The developed biocomposite material using MWCNTs, NF and Hb (MWCNTs-NF-Hb) at GCE, Au, ITO and SPCE electrodes shows good electrochemical properties in pH 2.5  $\text{H}_2\text{SO}_4$  aqueous solutions. The MWCNTs-NF-Hb biocomposite film for the electrocatalysis combines the advantages of ease of fabrication, high reproducibility and sufficient long-term stability. The SEM and AFM results show the differences between NF-Hb, MWCNTs-Hb, MWCNTs-NF and MWCNTs-NF-Hb biocomposite film's morphological data. Further, it is observed that the MWCNTs-NF-Hb biocomposite film has excellent functional properties with good electrocatalytic activity on  $\text{O}_2$ ,  $\text{H}_2\text{O}_2$  and  $\text{CCl}_3\text{COOH}$ . The experimental methods of CV and FIA with biocomposite film sensor integrated into the GCE and SPCE which are presented in this paper provide an opportunity for a qualitative and quantitative characterization. Therefore, this work establishes and illustrates, in principle and potential, a simple and novel approach for the development of voltammetric and amperometric sensor based on the modified GCE, ITO, Au and SPCE electrodes.

#### Acknowledgement

This work was supported by the National Science Council of the Taiwan (ROC).

#### Appendix A. Supplementary data

Supplementary data associated with this article can be found, in the online version, at [doi:10.1016/j.talanta.2008.12.063](https://doi.org/10.1016/j.talanta.2008.12.063).

#### References

- [1] G. Wu, Y.S. Chen, B.Q. Xu, *Electrochem. Commun.* 7 (2005) 1237.
- [2] J. Wang, M. Musameh, *Anal. Chim. Acta* 511 (2004) 33.
- [3] U. Yogeswaran, S.M. Chen, *Electrochim. Acta* 52 (2007) 5985.
- [4] J. Wang, M. Li, Z. Shi, N. Li, Z. Gu, *Electrochim. Acta* 47 (2001) 651.
- [5] Q. Li, J. Zhang, H. Yan, M. He, Z. Liu, *Carbon* 42 (2004) 287.
- [6] J. Zhang, J.K. Lee, Y. Wu, R.W. Murray, *Nano Lett.* 3 (2003) 403.
- [7] A. Star, T.R. Han, J. Christophe, P. Gabriel, K. Bradley, G. Gruner, *Nano Lett.* 3 (2003) 1421.
- [8] M. Zhang, K. Gong, H. Zhang, L. Mao, *Biosens. Bioelectron.* 20 (2005) 1270.
- [9] R.J. Chen, Y. Zhang, D. Wang, H. Dai, *J. Am. Chem. Soc.* 123 (2001) 3838.
- [10] Y. Yan, M. Zhang, K. Gong, L. Su, Z. Guo, L. Mao, *Chem. Mater.* 17 (2005) 3457.
- [11] G. Han, J. Yuan, G. Shi, F. Wei, *Thin Solid Films* 474 (2005) 64.
- [12] U. Yogeswaran, S. Thiagarajan, S.M. Chen, *Anal. Biochem.* 365 (2007) 122.
- [13] E. Frackowiak, V. Khomenko, K. Jurewicz, K. Lota, F. Béguin, *J. Power Sources* 153 (2006) 413.
- [14] T. Selvaraju, R.R. Ramaraj, *J. Electroanal. Chem.* 585 (2005) 290.
- [15] M. Mao, D. Zhang, T. Sotomura, K. Nakatsu, N. Koshihara, T. Ohsaka, *Electrochim. Acta* 48 (2003) 1015.
- [16] M. Yasuzawa, A. Kunugi, *Electrochem. Commun.* 1 (1999) 459.
- [17] Y. Zhu, S. Dong, *Electrochim. Acta* 35 (1990) 1139.
- [18] H. Liu, L. Wang, N. Hu, *Electrochim. Acta* 47 (2002) 2515.
- [19] P. He, N. Hu, G. Zhou, *Biomacromolecules* 3 (2002) 139.
- [20] Z. Lu, Q. Huang, J.F. Rusling, *J. Electroanal. Chem.* 423 (1997) 59.
- [21] X. Han, W. Cheng, Z. Zhang, S. Dong, E. Wang, *Biochim. Biophys. Acta* 1556 (2002) 273.
- [22] J. Yang, N. Hu, J.F. Rusling, *J. Electroanal. Chem.* 463 (1999) 53.
- [23] J. Yang, N. Hu, *Bioelectrochem. Bioenerg.* 48 (1999) 117.
- [24] Y. Zhou, N. Hu, Y. Zeng, J.F. Rusling, *Langmuir* 18 (2002) 211.
- [25] Y. Zhou, Z. Li, N. Hu, Y. Zeng, J.F. Rusling, *Langmuir* 18 (2002) 8573.
- [26] J.I. Blankman, N. Shahzad, C.J. Miller, R.D. Guiles, *Biochemistry* 39 (2000) 14806.
- [27] C. Fan, H. Wang, S. Sun, D. Zhu, G. Wagner, G. Li, *Anal. Chem.* 73 (2001) 2850.
- [28] H. Huang, N. Hu, Y. Zeng, G. Zhou, *Anal. Biochem.* 308 (2002) 141.
- [29] H. Liu, N. Hu, *Anal. Chim. Acta* 481 (2003) 91.
- [30] H. Wang, R. Guan, C. Fan, D. Zhu, G. Li, *Sens. Actuators B: Chem.* 84 (2002) 214.
- [31] S.M. Chen, C.C. Tseng, *J. Electroanal. Chem.* 575 (2005) 147.
- [32] D. Mimica, J.H. Zagal, F. Bedioui, *Electrochem. Commun.* 3 (2001) 435.
- [33] U. Yogeswaran, S.M. Chen, *Sens. Actuators B: Chem.* 130 (2008) 739.
- [34] S.M. Chen, C.C. Tseng, *Electrochim. Acta* 49 (2004) 1903.
- [35] E. Laviron, *J. Electroanal. Chem.* 101 (1979) 19.
- [36] U. Yogeswaran, S.M. Chen, *Anal. Lett.* 41 (2008) 210.
- [37] J.W. Shie, U. Yogeswaran, S.M. Chen, *Talanta* 74 (2008) 1659.
- [38] Q. Lu, S. Hu, D. Pang, Z. He, *Chem. Commun.* 20 (2005) 2584.



# Microbiosensor based on glucose oxidase and hexokinase co-immobilised on platinum microelectrode for selective ATP detection

O.O. Soldatkin<sup>a</sup>, O.M. Schuvailo<sup>a</sup>, S. Marinesco<sup>b</sup>, R. Cespuaglio<sup>c</sup>, A.P. Soldatkin<sup>a,\*</sup>

<sup>a</sup> Biomolecular Electronics Laboratory, Institute of Molecular Biology and Genetics, National Academy of Sciences of Ukraine, 150 Zabolotny Str., 03143, Kiev, Ukraine

<sup>b</sup> Inserm U628, Université Claude Bernard Lyon I, Lyon, France

<sup>c</sup> EA4170, Université Claude Bernard Lyon 1, 8 Avenue Rockefeller, 69373, Lyon, France

## ARTICLE INFO

### Article history:

Received 3 October 2008  
Received in revised form 30 December 2008  
Accepted 9 January 2009  
Available online 20 January 2009

### Keywords:

Co-immobilised glucose oxidase and hexokinase  
Platinum microelectrode  
Amperometric microbiosensor  
ATP-analysis  
Reproducibility  
Operational and storage stability

## ABSTRACT

ATP determination is of great importance since this compound is involved in a number of vital biological processes. To monitor ATP concentration levels, we have developed a microbiosensor based on cylindrical platinum microelectrode, covered with a layer of poly-m-phenyldiamine (PPD), and layer of co-immobilised glucose oxidase and hexokinase. Conditions for biosensor measurement of ATP (pH, Mg<sup>2+</sup> and substrates concentration) *in vitro* and microbiosensor characteristics such as sensitivity, selectivity, reproducibility, storage stability were studied and optimized. Under optimal conditions the microbiosensor can measure ATP concentrations down to a 2.5 μM detection limit with response time about 15 s. Interferences by electroactive compounds like biogenic amines and their metabolites, ascorbic acid, uric acid and L-cystein are rejected in general by the PPD layer. The microbiosensor developed is insensitive to ATP analogues (or substances with similar structure), such as ADP, AMP, GTP and UTP, too. It can be used for ATP analysis *in vitro* in the reactions consuming or producing macroergic triphosphate molecules to study kinetics of the process and in drug design concerning development of inhibitors specific to target kinases and others target enzymes.

© 2009 Elsevier B.V. All rights reserved.

## 1. Introduction

Adenosine-5'-triphosphate (ATP), a well known macroergic substance in all living organisms, plays a key role in the energy turnover of a cell. Its additional functions (the regulation of muscle contraction and platelet aggregation [1], vascular tone and neurotransmission [2]) have been revealed as a result of extensive research in several branches of biology and biomedicine over the last decades.

ATP determination is of great importance since this compound is involved in a number of vital biological processes. The variation in ATP concentration can exert strong modulatory effects in central nervous system of mammalian. ATP can influence transmitter release, synaptic plasticity, neurone–glia interactions, nociception, sleep–wake cycles, respiratory and locomotor rhythms, anxiety, depression, aggression and addiction (see Ref. [3] and corresponding references from this paper). Moreover, ATP detection can be efficiently used in food industry as a marker of micro-fungal contamination and in drug design at development of inhibitors for specific kinases and others enzymes.

Consequently, there is an actual demand for ATP assays. ATP concentration is usually analyzed using spectrophotometry [4], liquid chromatography [5], fluorescence [6], chemiluminescence [7], bioluminescence [8] methods, potentiometric [9–11] and amperometric [12–18] biosensors. Among these techniques, biosensors seem to be the most promising tools owing to their characteristics (Table 1).

With the help of ATP-biosensors, different biochemical processes can be studied and visualised directly. An analysis of the characteristics presented in Table 1 shows that ATP potentiometric biosensors demonstrated rather low sensitivity to ATP and strong dependence on buffer capacity. These disadvantages do not permit to use them for ATP measurement in real biological fluid samples at its micromolar physiological concentrations. Concerning amperometric biosensors, there are two main approaches to their fabrication: application of the bi-enzyme system based on (1) glycerol oxidase and glycerol kinase (GO/GK) or glycerol kinase and glycerol-3-phosphate oxidase (GK/G-3-PO), and (2) glucose oxidase and hexokinase (GOD/HK). Both approaches give rather good results regarding sensitivity of the developed microbiosensors, however, measurement selectivity and stability presented in Table 1 are not satisfactory enough (unless shown at all). We preferred the development of the GOD/HK microbiosensor since in this case the system needs glucose for ATP detection, which exists practically in all biological samples. So, second approach is used in our work to develop

\* Corresponding author. Tel.: +380 44 2000328; fax: +380 44 5260759.  
E-mail address: [a.soldatkin@yahoo.com](mailto:a.soldatkin@yahoo.com) (A.P. Soldatkin).

**Table 1**  
The main characteristics of developed ATP biosensors.

Enzymatic system	Type of transducer and dimensions	Time of response and sensitivity	Linear dynamic range	Selectivity, interferences	Stability (residual enzyme activity)	Ref.
H <sup>+</sup> -ATPase	ISFET	1–1.5 min	0.2–1.0 mM	Dependence on buffer capacity	10% after 18 day	[9]
Choline kinase	Choline-sensitive membrane electrode	1–2 min, 50 mV/100 μM	10–75 μM	No interferences from ADP, AMP, Na, K	No data presented	[10]
Apyrase (ATP dihydrolyase)	ISFET	5 min, 80 V M <sup>-1</sup>	0.2–1 mM	Dependence on buffer capacity	No data presented	[11]
GOD + HK	Oxygen electrode	2 min	0.2–3.0 mM	Not presented	Not presented	[12]
GOD + HK	Pt electrode, size was not presented	2–3 min, cannot be calculated	50–500 μM	Not presented	30% after 1 week	[13]
GOD + HK	Pt disk electrode Ø 1 mm	5–80 s, 1 A M <sup>-1</sup> cm <sup>-2</sup> <sup>a</sup>	10–200 nM	Not presented	40% after 2 weeks	[14]
GOD + HK	Pt disk electrode Ø 25 μm	150 ms, 100 μA M <sup>-1</sup> cm <sup>-2</sup>	0–1 mM	Not presented	40% after 2 weeks	[14]
GK + G3POx	Pt/Ir electrode (90/10), Ø 25–100 μm	≤10 s, 250 mA M <sup>-1</sup> cm <sup>-2</sup>	200 nM–50 μM	Low <sup>b</sup> , AA, urate, AcPh, 5HT	Not presented	[15]
GOD + HK	Glassy carbon electrode, Ø 3 mm	≤15 s, 85 mA M <sup>-1</sup> cm <sup>-2</sup>	0.5–20 μM	Not presented	65% after 22 days	[16]
EF <sub>0</sub> F <sub>1</sub> -H <sup>+</sup> -ATPase	Au electrode, 2 mm × 2 mm	50 mA M <sup>-1</sup> cm <sup>-2</sup>	2.5–6.0 mM	Not presented	Not presented	[17]
Commercial product, no information about enzyme system	Pt/Ir electrode (90/10), L = 2 mm or 0.5 mm, Ø 50 μm	≤10 s, 0.5 mA M <sup>-1</sup>	0.5–50 μM	Selective vs. UTP, ADP and adenosine, no information concerning electroactive compounds	Shelf-life (dry) ≥6 months	[18]

<sup>a</sup> It seems for us that density of current obtained by the authors [14] is too high and not possible. Authors presented erratum [19] concerning only last Fig. 7 in the paper [14], but it seems for us that all data have to be recalculated.

<sup>b</sup> Measurement in differential mode with null sensor; shortening: G3Pox-glycerol-3-phosphate oxidase; AA, ascorbate; AcPh, acetaminophen; 5HT, serotonin.

the amperometric microbiosensor for ATP measurement in different biological samples. We apply the bi-enzyme system with GOD/HK co-immobilised on the surface of platinum microelectrode preliminarily covered by poly-m-phenylenediamine (PPD) that allows to create microbiosensors with improved main characteristics, i.e. highly sensitive, with good selectivity, reproducibility and long-term stability. Such microbiosensor developed can be used for detection of low micromolar concentration of ATP in small tens microlitre volumes.

## 2. Experimental

### 2.1. Reagents

The following chemicals and preparations were used: glucose oxidase (GOD) from *Aspergillus niger*, EC 1.1.3.4 (190 U mg<sup>-1</sup> solid), hexokinase (HK) from *Saccharomyces cerevisiae*, EC 2.7.1.1 (35.8 U mg<sup>-1</sup> solid), apyrase, grade I from potato (7.7 U mg<sup>-1</sup> solid), bovine serum albumin (BSA), glutaraldehyde (GA) (50% (w/v) aqueous solution), hydrogen peroxide (HP) (3% (w/v) aqueous solution), glucose, magnesium acetate tetrahydrate, sodium and potassium chlorides, m-phenylenediamine (PD), adenosine-5'-triphosphate (ATP), guanosine-5'-triphosphate (GTP) and uracil-5'-triphosphate (UTP). All these chemicals were purchased from Sigma-Aldrich SARL (France). Working HEPES buffer 0.025 M, pH 7.4, was prepared from HEPES [N-(2-hydroxyethyl) piperazine-N'-2-ethanesulfonic acid] (free acid) and deionised water and then was adjusted to needed pH by NaOH.

### 2.2. Microelectrode preparation

Microelectrodes constructed from platinum wire (25 μm in diameter; 90% Pt/10% Ir wire (Goodfellow, Huntington, UK) were developed and manufactured by the authors [20]. The electrodes were then washed 30 min in 0.5 M KOH and 20 min in ethanol.

Poly (phenylenediamine) layer was subsequently deposited on the electrode surface from a quiescent solution of 0.1 M phosphate buffer (pH 7.0) containing 0.1 M PD. The film was grown electrochemically on the platinum surface at a constant potential (+0.7 V)

for 45 min. Before use, PD solutions were deoxygenated by bubbling with argon for 15 min. The modified electrode surface was thoroughly washed with distilled water prior to bioselective membrane creation.

### 2.3. Bioselective-membrane preparation

The bioselective enzymatic membranes of ATP and glucose sensitive microbiosensors were prepared by using a GOD-HK-BSA mixture prepared in a 0.1 M phosphate buffer at pH 7.0. The final concentration of each enzyme was of 40 mg ml<sup>-1</sup> while that of BSA was of 20 mg ml<sup>-1</sup>. For glucose only sensitive biosensor, the same buffer solution was used with the final concentration of GOD 40 mg ml<sup>-1</sup> and BSA 60 mg ml<sup>-1</sup>. In cases of both microbiosensors creation glycerol was also added to each mixture (3% w/v) in order to stabilize the enzymes during their immobilization, to prevent early membrane drying and to improve membrane adhesion to the transducer surface. GA was used as a cross-linker (final concentration at 0.2% w/v). The mixture containing GA was deposited on the sensitive part of the transducer and afterwards cured for 1 h at room temperature. Before use microbiosensors were washed by working buffer.

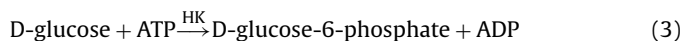
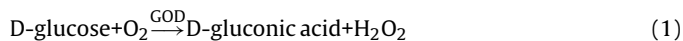
### 2.4. Measurement procedure

Measurements were performed at room temperature using a model solution (25 mM HEPES buffer, pH 7.4, with 127 mM NaCl and 2.7 mM KCl and necessary concentrations of Mg<sup>2+</sup> ions). The required substrates concentrations were obtained by the addition of specific volumes of stock solutions.

Amperometric measurements were performed in open and closed cells filled with working buffer comprising the following conventional three-electrode amperometric system: the platinum working electrode (microbiosensor), an Ag/AgCl reference and a platinum auxiliary electrode. The PalmSens potentiostat equipped with a CH-8 multiplexer device (Palm Instruments BV, the Netherlands) was used in all experiments. The measurements for the ATP biosensor were carried out at a constant potential of +0.6 V.

### 3. Results and discussion

The bioselective element of the amperometric microbiosensor developed consists of two co-immobilized enzymes (GOD and HK). The basic enzymatic reactions are:



As can be seen, this biosensor is sensitive to both the substrates, glucose and ATP, owing to competition between GOD and HK towards substrate glucose. If only glucose is injected in the analyzed medium, reactions (1) and (2) take place, and the electrochemical response proportional within certain range to glucose concentration is generated by the microbiosensor, its value being taken as 100%. When ATP is injected, the reaction (3) takes place resulting in a decrease of the response obtained to glucose injection in the ATP absence, the reduction value being proportional to the ATP concentration in the solution tested.

Therefore, determination of ATP concentration requires the glucose concentration to be kept constant which is possible only under *in vitro* conditions. In the case of biological samples containing unknown glucose concentration the measurements cannot be performed by a single bi-enzyme biosensor since in this case the response depends on both substrates, glucose and ATP. It is though realizable if two microbiosensors are used, one of which is GOD-, another GOD/HK-based. In such set, the first device gives information on glucose concentration, the second shows a difference between the responses to glucose and ATP, thus, the ATP concentration can be evaluated using the data simultaneously obtained from two microbiosensors.

Firstly, the characteristics of the developed bi-enzyme microbiosensor were studied *in vitro* in model solutions. The typical responses of GOD/HK-based microbiosensor to glucose and ATP are presented in Fig. 1. As can be seen, the response to glucose injection was obtained in 20–25 s, while the corresponding responses to ATP were obtained in 15–20 s. The kinetics of generating responses is evidently almost similar in both cases. Addition of apyrase (enzyme hydrolyzing ATP to phosphate and ADP and AMP) in measuring cell shows that ATP responses of microbiosensor directly depend on the ATP concentration.

The calibration curve (Fig. 1B) calculated for ATP measurements from data presented in Fig. 1A shows a possibility to measure ATP starting from 2.5  $\mu\text{M}$  concentration at least.

At the next stage, pH-dependence of the responses of bi-enzyme microbiosensor to glucose and ATP injection was studied. The investigation was carried out in a complex multicomponent buffer (5 mM Tris, 5 mM  $\text{KH}_2\text{PO}_4$ , 5 mM citric acid, 5 mM sodium tetraborate) characterized by identical buffer capacity within a wide pH range (from 5 to 9) [21]. The reason to use such complex buffer in these experiments was to avoid an influence of the buffer composition on different enzymes functioning at various pH values. The results obtained testify the low pH-dependence of the sensor response to glucose with the optimum near pH 7.0 (Fig. 2, curve 1) while in ATP case pH-dependence was more evident and the bell-shaped curve had optimum at pH 7.5–8.0 (Fig. 2, curve 2). This is in very good accordance with the information on pH-dependence of free hexokinase (see Catalog Sigma 2008, Sigma is producer of preparation used in this work). We were afraid that hexokinase co-immobilised with GOD can change pH optimum in comparison to free hexokinase. As the biosensor is supposed for analyses of biological liquids, the 25 mM HEPES buffer, pH 7.4, was utilized in further *in vitro* experiments.

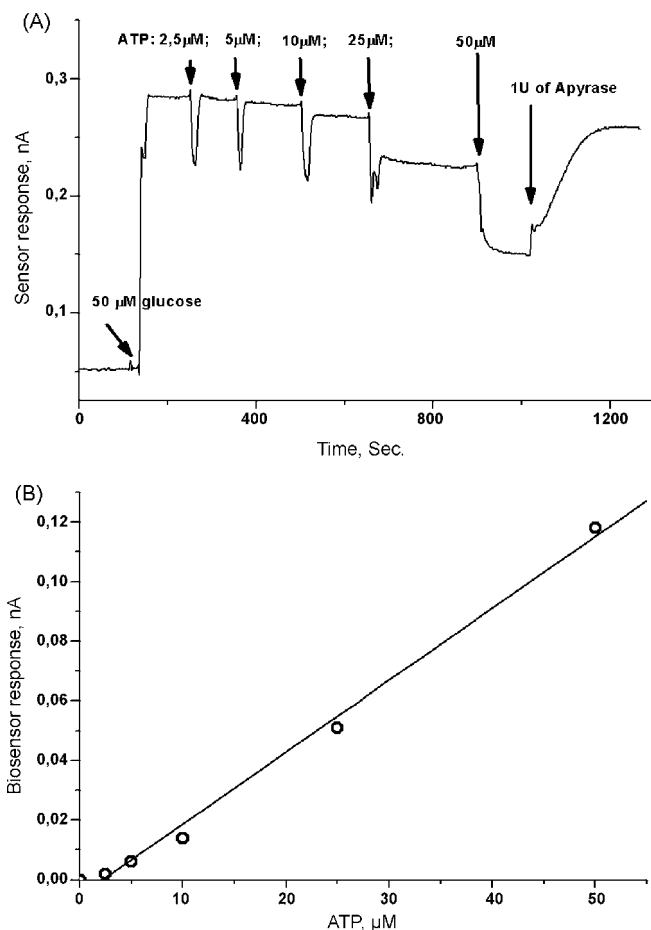


**Fig. 1.** Typical responses of bi-enzyme microbiosensor to glucose and ATP injections in the measuring cell (A) and calibration curve calculated for ATP measurements (B) (final concentrations of glucose and ATP in the cell are marked on the curve). Additionally apyrase (enzyme hydrolyzing ATP to phosphate and ADP and AMP) was added in measuring cell to show that ATP responses of microbiosensor directly dependent on ATP concentration. Measured in 25 mM HEPES buffer, pH 7.4, at constant potential +0.6 V vs. Ag/AgCl reference electrode.

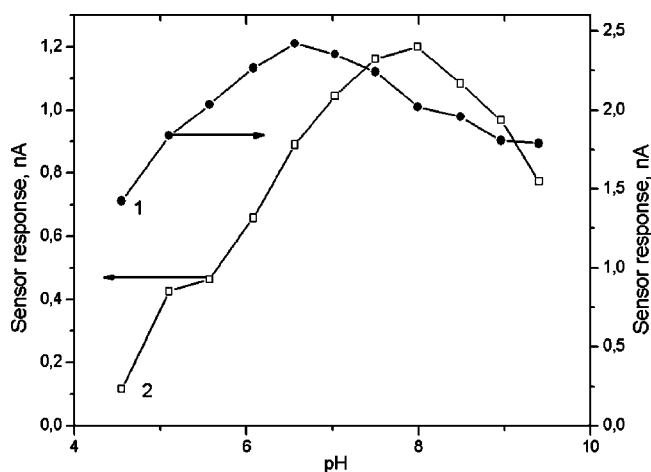


**Fig. 2.** pH-dependence of microbiosensor responses to 0.5 mM glucose (1) and to 0.5 mM ATP (2). Measurements in polymix buffer at constant potential +0.6 V vs. Ag/AgCl reference electrode.

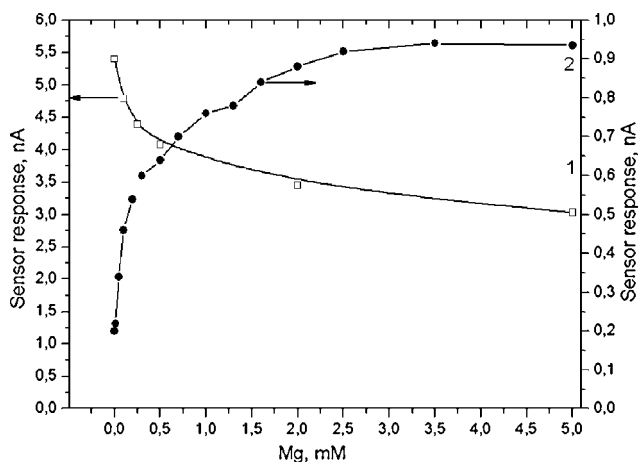


**Fig. 3.**  $Mg^{2+}$ -dependence of bi-enzyme microbiosensor response to 0.5 mM glucose (1) and 0.5 mM ATP (2). Measured in 25 mM HEPES buffer, pH 7.4, at constant potential +0.6 V vs. Ag/AgCl reference electrode.

Since hexokinase is known as an enzyme dependent on the concentration of ions of magnesium which is an enzyme activator ( $K_m = 2.6$  mM for free enzyme, see Catalog *Sigma* 2008 and [22,23]), a number of experiments were carried out to ascertain optimal concentration of magnesium ions as regards the bi-enzyme microbiosensor operation. The value of microbiosensor response to ATP appeared to be actually dependent on magnesium concentration (Fig. 3). An increase in  $Mg^{2+}$  concentration from 0 to 2 mM resulted in 4.5-fold higher response to injection of 250  $\mu$ M ATP.

As to the response of bi-enzyme microbiosensor to glucose, an opposite effect was revealed. An increase in  $Mg^{2+}$  concentration from 0 to 2 mM resulted in decreasing sensor response to injection of 500  $\mu$ M glucose. Further rise of concentration of magnesium ions had no remarkable impact on the biosensor responses to ATP and glucose injection. These results were very unexpected and important for optimisation of glucose and ATP analysis. Subsequent *in vitro* experiments on study of microbiosensor characteristics were performed in working buffer with 2 mM  $Mg^{2+}$ .

The working buffer with optimal values of pH and magnesium ion concentration was used to study the dependence of microbiosensor responses to ATP and glucose at different concentrations (Fig. 4A and B). The slope of linear part of calibration curves and sensitivity of the microbiosensor for ATP detection were regularly the same within the range of glucose concentrations of 0.1–1.6 mM, though it is noteworthy that the linear range differed remarkably (the higher glucose concentration, the wider linear range). However, increase in glucose concentration to more than 1.6 mM resulted in substantially weaker ATP sensitivity (Fig. 4A, curve 5). It can be caused by the saturation of sensor responses to glucose at the concentrations more than 1.6 mM (Fig. 4B) and, consequently, the absence of response/concentration proportionality. At high glucose concentration and low ATP concentrations, HK consumes small amounts of glucose and this does not influence notably the sensor response to glucose since is at excess concentration. Further increase in ATP concentration results in reducing response to glucose and, correspondingly, in higher ATP sensitivity (see Fig. 4A, curve 5). Therefore, *in vitro* determination of ATP requires that glucose concentration would be within the range of linear dependence of the biosensor response on glucose concentration. At physiological glucose concentration in the sample (3.6–6.4 mM and more), the sample should be diluted and glucose should be controlled by the glucose sensor (the second sensor) prior to bi-enzyme (GOD/HEX) biosensor can be used for measurement of ATP concentration. It is obviously that ATP concentration in diluted samples can be assessed if ATP initial value is sufficiently high. For ATP *in vivo*

analysis, the developed bi-enzyme biosensor cannot be used or it should have a wider linear range of glucose measurement covering physiological glucose concentrations. Such microbiosensor is quite feasible by usage of additional polymer membranes in biosensor design [24].

Operational stability and reproducibility are important characteristics of biosensors. The dependence of bi-enzyme microbiosensor responses to ATP and glucose on duration of continuous operation was studied under optimal working conditions, i.e. pH 7.4 and 2 mM  $Mg^{2+}$  (Fig. 5). Reproducibility test for one microbiosensor is presented in Fig. 5A, and for series of microbiosensors—in Fig. 5B. It was shown that during 8.5-h continuous work at 25 °C responses of one microbiosensor are very slightly varied in the case of glucose measurement and for ATP analysis. Reproducibility is very high. Variation of sensor response inside of group of 4 microbiosensors is not so high, but quite good (see Fig. 5B).

To compare sensor responses at room and physiological temperatures (22 and 37 °C) and to understand what enzyme in bi-enzyme system (GOD/HK) is more responsible for stability of developed microbiosensor, the study of temperature dependence of sensor response was done (Fig. 6). It was shown, that at increase temperature from 22 to 45 °C sensor responses to glucose and ATP were increased. Increase of temperature from 22 to 37 °C led to increasing sensor responses to glucose and ATP in almost 2 times. But at subsequent increasing temperature from 45 to 60 °C the response of bi-enzyme microbiosensor to ATP was decreased almost to zero, whereas response to glucose continued to increase

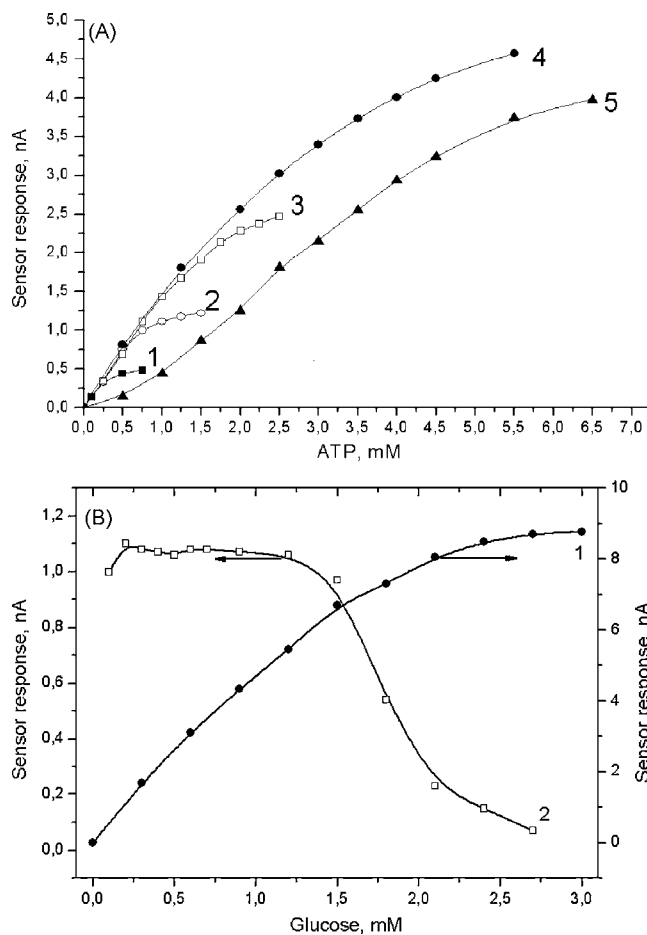


**Fig. 4.** (A) Calibration curves for ATP biosensor at different glucose concentrations: 1–0.1; 2–0.3; 3–0.8; 4–1.6; 5–2.5 mM. (B) Dependence of microbiosensor responses to glucose (1) and to 0.5 mM ATP (2) at different glucose concentration. Measured in 25 mM HEPES buffer with 2 mM Mg, pH 7.4, at constant potential +0.6 V vs. Ag/AgCl.



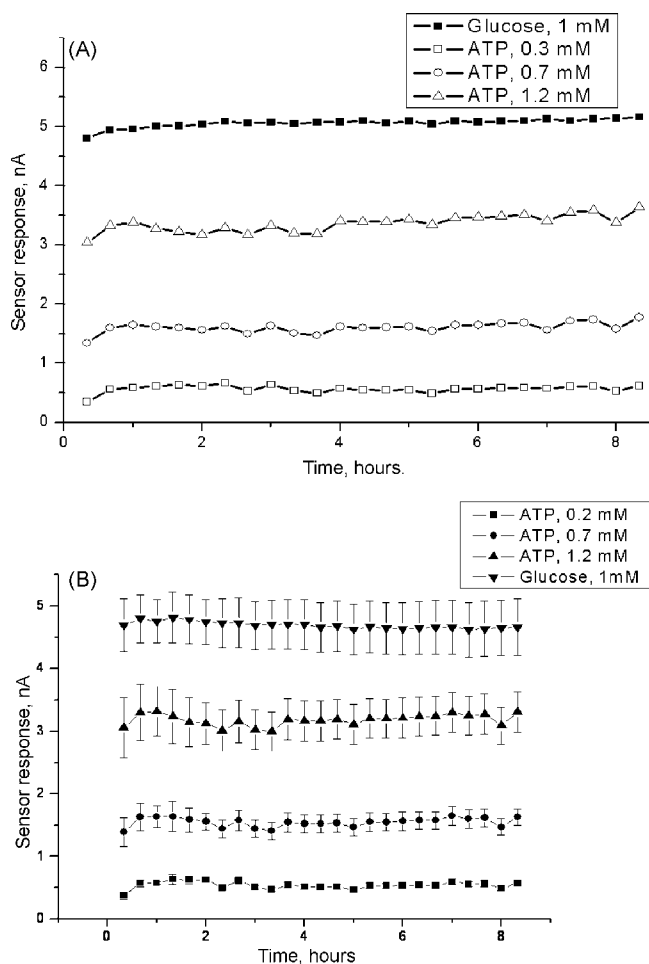


**Fig. 5.** Reproducibility and operational stability test during 8.5 h for one biosensor sensitive to glucose and ATP (A) and for group ( $n=4$ ) biosensors with the same constructions (B). Measurements were done in 25 mM HEPES buffer with 2 mM  $Mg^{2+}$ , pH 7.4, at constant potential +0.6V vs. Ag/AgCl reference electrode.

and only after 65 °C it sharply starts to decrease. It is quite clear, that in this bi-enzyme system GOD is more stable enzyme than HK, and to increase general stability of the system it is necessary to stabilize HK.

As to storage stability of the bi-enzyme microbiosensor, the responses to glucose and ATP did not change at least for 3 months while stored in dry at  $T=-20^{\circ}C$ .

Selectivity is also a vitally important characteristic for any biosensor or sensor device. This characteristic is determined by the transducer selectivity, on the one hand, and the enzyme selectivity—on the other. The selectivity of platinum electrodes, used in our case, toward hydrogen peroxide is not high enough unless special approaches are applied. Special surface modification is required because numerous electroactive substances are oxidized on the electrode surface at a potential of +600 mV generating an electrochemical signal [20,25]. That is why the platinum electrode with a PPD film electrodeposited on its surface was used in this work as a transducer. This procedure allowed to obtain a transducer which was almost insensitive to the presence of electroactive substances (ascorbic acid, uric acid, aspartic acid, dopamine, L-cysteine and acetaminophen) at their physiological concentrations in the medium analyzed (Fig. 7). It is remarkable that PPD film is stable enough and selectivity of microbiosensors covered by such films to electroactive interferences remains unaffected during at least 6-h continuous work [20,25].

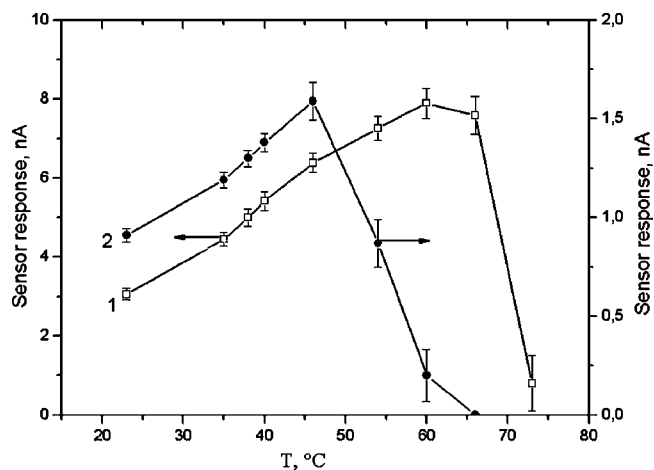


**Fig. 6.** Temperature dependence of microbiosensor responses to 0.5 mM glucose (1) and to 0.5 mM ATP (2). Measurements in 25 mM HEPES buffer, pH 7.4, at constant potential +0.6V vs. Ag/AgCl reference electrode.

As for selectivity of the enzymatic system applied, the bi-enzyme microbiosensors were tested with regard to their sensitivity to ATP analogues (or substances with similar structure), such as ADP, AMP, GTP and UTP. Practically no response was obtained at the concentration of the mentioned interfering substances in the tested medium even as high as 500  $\mu M$  while the response to

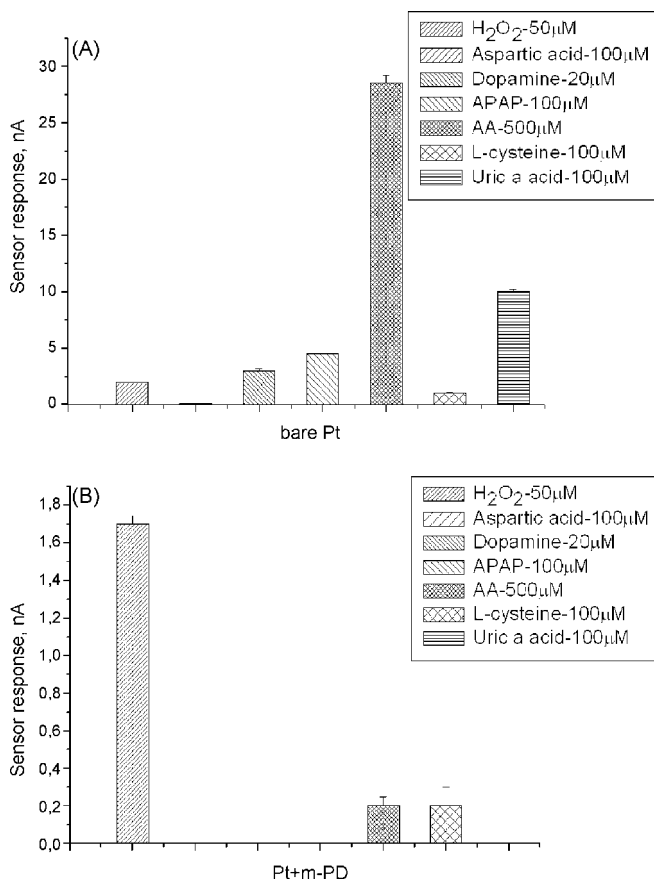


**Fig. 7.** (A) Responses of bare platinum electrode and (B) one covered with poly-m-phenyldiamine to hydrogen peroxide and different electroactive interfering compounds. Microelectrode covered with poly-m-phenyldiamine demonstrated negligible responses to aspartic and uric acids, dopamine and APAP. Measurements in 25 mM HEPES buffer, pH 7.4, at constant potential +0.6V vs. Ag/AgCl reference electrode.

**Table 2**  
Influence of interfering analogues of ATP on the glucose and ATP microbiosensors responses. Measurements were done in 25 mM HEPES buffer, pH 7.4, at a constant potential of +0.6 V vs. Ag/AgCl reference electrode.

Responses of glucose microbiosensor (nA)		Responses of bi-enzyme ATP microbiosensor (nA)			
To 0.5 mM glucose without interfering agents <sup>a</sup>	To 0.5 mM glucose + interfering agents <sup>a</sup>	To 0.5 mM glucose without interfering agents <sup>a</sup>	To 0.5 mM ATP + 0.5 mM glucose without interfering agents <sup>a</sup>	To 0.5 mM glucose + interfering agents <sup>a</sup>	To 0.5 mM ATP + 0.5 mM glucose + interfering agents <sup>a</sup>
3.043 ± 0.045	3.029 ± 0.086	3.026 ± 0.045	1.124 ± 0.023	2.943 ± 0.112	1.149 ± 0.048

<sup>a</sup> Interfering agents: 0.5 mM GTP + 0.5 mM UTP.

500 μM ATP remained the same both in the presence of interfering substances and in their absence (Table 2).

Considering the obtained selectivity results a conclusion can be done that the developed bi-enzyme microbiosensor by its characteristics is suitable for ATP analysis in biological samples. Moreover, in the case of biological samples consisting glucose to measure ATP it is necessary to use two biosensors: based on glucose oxidase (glucose biosensor) and based on glucose oxidase and hexokinase (ATP biosensor).

#### 4. Conclusion

The microbiosensor based on cylindrical platinum microelectrode and co-immobilized glucose oxidase and hexokinase have been developed for *in vitro* analysis of ATP concentrations. The microbiosensor can measure ATP concentrations down to the 2.5 μM detection limit with response time about 15–20 s. The applied PPD layer allows rejecting almost completely interferences caused by electroactive compounds like biogenic amines and their metabolites, ascorbic acid, uric acid and L-cystein. Moreover, the microbiosensor developed is insensitive to ATP analogues, such as GTP and UTP too. Thus, the microbiosensor method is potential for *in vitro* study of ATP concentration in low micromolar range in microvolumes to study kinetics of the process of consumption or production of macroergic triphosphate molecules. Moreover, the ATP microbiosensor developed can be efficiently used in food industry as a tool for detection of micro-fungal contamination as well as in drug design at development of inhibitors for specific kinases and others target enzymes.

#### Acknowledgments

This work was supported by the Claude Bernard University of Lyon (France), National Academy of Sciences of Ukraine and the

NATO Collaborative Linkage Grant (CBP.NUKR.CLG 982788). We also thank N. Polischuk for the technical assistance.

#### References

- [1] A.V. Gourine, E. Llaudet, N. Dale, K.M. Spyer, *J. Neurosci.* 25 (2005) 1211.
- [2] G. Burnstock, *Trends Pharmacol. Sci.* 27 (2006) 166.
- [3] B.G. Frenguelli, G. Wigmore, E. Llaudet, N. Dale, *J. Neurochem.* 101 (2007) 1400.
- [4] H.U. Bergmeyer, *Methods of Enzymatic Analysis*, 3rd edn, VCH Publishers, Deerfield Beach, 1984, 340 pp.
- [5] Y. Kawamoto, K. Shinozuka, M. Kunitomo, J. Haginaka, *Anal. Biochem.* 262 (1998) 33.
- [6] G.P. Foy, G.E. Pacey, *Talanta* 43 (1996) 225.
- [7] T. Perez-Ruiz, C. Martinez-Lozano, V. Tomas, J. Martin, *Anal. Bioanal. Chem.* 377 (2003) 189.
- [8] J.N. Miller, M.B. Nawawi, C. Burgess, *Anal. Chim. Acta* 266 (1992) 339.
- [9] M. Gotoh, E. Tamiya, I. Karube, Y. Kagawa, *Anal. Chim. Acta* 187 (1986) 287.
- [10] T. Katsu, K. Yamanaka, *Anal. Chim. Acta* 276 (1993) 373.
- [11] S. Migita, K. Ozasa, T. Tanaka, T. Haruyama, *Anal. Sci.* 23 (2007) 45.
- [12] F. Scheller, D. Pfeiffer, *Anal. Chim. Acta* 117 (1980) 383.
- [13] D. Compagnone, G.G. Guilbault, *Anal. Chim. Acta* 340 (1997) 109.
- [14] A. Kueng, C. Kranz, B. Mizaikoff, *Biosens. Bioelectron.* 19 (2004) 1301.
- [15] E. Llaudet, S. Hatz, M. Droniou, N. Dale, *Anal. Chem.* 77 (2005) 3267.
- [16] S. Liu, Y. Sun, *Biosens. Bioelectron.* 22 (2007) 905.
- [17] W. Bucking, G.A. Urban, T. Nann, *Sens. Actuators* 104 (2005) 111.
- [18] W.L. Road *sarissaprobe@-ATP*. 2005 [cited; available from: <http://www.sarissa-biomedical.com/index.html>].
- [19] A. Kueng, C. Kranz, B. Mizaikoff, *Biosens. Bioelectron.* 22 (2007) 2774.
- [20] P. Pernot, J.-P. Mothet, O. Schuvailo, A. Soldatkin, L. Pollegioni, M. Pilone, M.-T. Adeline, R. Cespuaglio, S. Marinesco, *Anal. Chem.* 80 (2008) 1589.
- [21] V. Volotovskiy, A.P. Soldatkin, A.A. Shul'ga, V.K. Rossokhaty, V.I. Strikha, A.V. El'skaya, *Anal. Chim. Acta* 322 (1996) 77.
- [22] A. Sols, G. De La Fuente, C. Villarpalasi, C. Asensio, *Biochim. Biophys. Acta* 30 (1958) 92.
- [23] D.C. Hohnadel, C. Cooper, *Eur. J. Biochem.* 31 (1972) 180.
- [24] O.M. Schuvailo, O.O. Soldatkin, A. Lefebvre, R. Cespuaglio, A.P. Soldatkin, *Anal. Chim. Acta* 573–574 (2006) 110.
- [25] S.J. Killoran, R.D. O'Neill, *Electrochim. Acta* 53 (24) (2008) 7303.



# Characterization of As (V), As (III) by selective reduction/adsorption on palladium nanoparticles in environmental water samples

Suvarna Sounderajan, G. Kiran Kumar, Sanjukta A. Kumar, A.C. Udas\*, G. Venkateswaran

Analytical Chemistry Division, Bhabha Atomic Research Center, Mumbai, Maharashtra 400 085, India

## ARTICLE INFO

### Article history:

Received 3 November 2008

Received in revised form 9 January 2009

Accepted 14 January 2009

Available online 24 January 2009

### Keywords:

Arsenic (III)

Arsenic (V)

Speciation

Palladium nanoparticles

Sodium borohydride

Hydrazine

Graphite furnace atomic absorption spectrometry

## ABSTRACT

Hydrazine (HZ) and sodium borohydride (BH) are commonly used reagents for the production of palladium nanoparticles (PdNP) in aqueous solution and also for the reduction of arsenic from higher oxidation state to lower oxidation state. A methodology based on the quantitative adsorption of reduced arsenic species on PdNP generated in situ by BH and HZ is described to characterize As (V) and As (III) in environmental water samples. It was observed that PdNP obtained by BH gave quantitative recovery of As (V) and (III) and the PdNP obtained by HZ could account for As (III). The reduced palladium particles are collected and dissolved in minimum amount of nitric acid. The quantification of arsenic was carried out using GFAAS. Optimization of the experimental conditions and instrumental parameters were investigated in detail. The proposed procedure was validated by applying it for the determination of the content of total As in Certified Reference Material BND 301-02 (NPL, India). The detection limit of arsenic in environmental water samples was  $0.029 \mu\text{g L}^{-1}$  with an enrichment factor of 50. The relative standard deviation (R.S.D.) for 10 replicate measurements of  $5 \mu\text{g mL}^{-1}$  was 4.2%. The proposed method was successfully applied for the determination of sub ppm to ppm levels of arsenic (V), (III) in environmental water samples.

© 2009 Elsevier B.V. All rights reserved.

## 1. Introduction

Ground water is the main source of potable water for a large number of people all over the world. Arsenic is a constituent in some common minerals like arsenopyrite ( $\text{FeAsS}$ ), orpiment ( $\text{As}_2\text{S}_3$ ), ironpyrites ( $\text{FeS}_2$ ) and it has been established that desorption or reductive dissolution of arsenic from arsenic bearing minerals have led to dissolved arsenic concentrations greater than  $50 \mu\text{g L}^{-1}$  in ground water. Under certain conditions some sources have reported aquifers in West Bengal have levels greater than  $300 \mu\text{g L}^{-1}$ . Arsenic is known to be a natural carcinogen and the manifestations of arsenic toxicity in the communities dependent on this ground water for their sustenance have been well documented [1].

Arsenic in ground water exists in two oxidation states: As (V) arsenate, which is predominant in oxidizing condition and As (III) arsenite, under reducing conditions. Generally, inorganic arsenic is more toxic than organic arsenic, and trivalent arsenite is more toxic than pentavalent arsenate and zero-valent arsenic. Arsenic, particularly in its trivalent form, inhibits critical sulfhydryl-containing enzymes. In the pentavalent form, the competitive substitution of arsenic for phosphate can lead to rapid hydrolysis of the high-energy bonds in compounds such as ATP. The carcinogenic effects of

inorganic arsenic in drinking water and the consequent worldwide human health implications have led the environment protection agencies to establish a maximum concentration limit of  $10 \mu\text{g L}^{-1}$  [1,2]. Quantification of total arsenic and the differentiation of As (III) and As (V) in real samples remains a challenge at the lower limit of detection [3,4].

Conventional analytical techniques like spectrochemical, electrochemical, atomic spectroscopic, ED-XRF and mass spectrometric methods have been used for the determination of low concentrations of arsenic. Measurement of the volatile arsine by AAS [5], ICP-AES [6], ICP-MS [7,8] is also commonly used for determinations of trace levels of arsenic.

For the differential quantification of As (V) and As (III), methodologies based on the arsenomolybdate chemistry, ammonium pyrrolidinedithiocarbamate chemistry and arsine formation by As (V) and As (III) at different acidities have been modified and adopted. Measurement based on the gas phase chemiluminescence's (CL) reaction of arsine and ozone [9], purple colour of nanoparticles of ethyl violet with an isopolymolybdate-iodine tetrachloride complex [10] has been reported. Differential estimation of As (V), As (III) using Ag diethyldithiocarbamate (SDEDTC) [11,12], diethyldithiophosphate on C-18 bonded Si-column [13], Ni and Pb pyrrolidinedithiocarbamate [14,15], 12-molybdoarsenic acid [16], Cloud Point Extraction using APDC, Triton X-114 [17], PTFE turnings [18,19], immobilized yeast [20],  $\text{TiO}_2$  nanoparticles immobilized on silica gel [21], mesoporous  $\text{TiO}_2$  [22] has also been

\* Corresponding author. Tel.: +91 22 25595691; fax: +91 22 25505151/19613.  
E-mail address: [acudas@barc.gov.in](mailto:acudas@barc.gov.in) (A.C. Udas).

reported. Recently, a separation of As (V), (III) by adsorption on CTAB modified alkyl silica sorbent has been reported [23]. Chromatographic separation techniques like IC and HPLC hyphenated with AAS, ICP-AES, and ICP-MS have been utilized for identification and quantification of arsenic species; however, the low levels of As (III) and As (V) in environmental samples necessitate preconcentration [24,25].

Transition metal nanoparticles have been widely synthesized and studied due to their applications in the area of catalysis, optoelectronics, etc. [26–29]. Palladium is known to be a versatile catalyst and reducing agents like sodium borohydride (BH) [30], hydrazine (HZ) [31] ascorbic acid (ASA) [32] are used to produce palladium nanoparticles (PdNP). Palladium particles generated in situ have been used as a carrier for the separation and preconcentration of trace elements from a variety of matrices like nickel-based heat resisting superalloys, steels and several metals [33], high purity iron [34] and natural waters [35]. It was seen that, trace elements adsorbed on palladium, depended on the reducing agent used to generate the palladium particles [35]. Recently palladium nanoparticles have been used for the reduction, preconcentration and estimation of Cr (VI), Cr (III) in tested soil and aqueous media [36].

GFAAS is a sensitive technique and is routinely used for the determination of trace impurities in a variety of matrices. The long residence times and efficient sample delivery enable low detection limits [37]. However, this technique is prone to interference from matrix. Also arsenic compounds are known to be volatile hence chemical matrix modifiers are used to stabilize the analyte to higher temperatures to obtain separation from background and obtain reproducible analytical results. Ni, Pd, Pd–Mg modifiers have been investigated and are routinely used in arsenic estimations by GFAAS [38,39].

In this paper we have developed the idea of in situ reduction and adsorption of arsenic on palladium nanoparticles for the characterization and quantification of As (V) and As (III) in environmental samples. It was seen that under our experimental conditions BH, HZ and ASA reduced Pd (II) to Pd (0), however Pd particles generated by BH showed recovery of both As (V) and As (III), and Pd particles generated by HZ and ASA showed recovery of only As (III). Optimization of the experimental conditions including pH of reduction, concentration of reducing agents, amount of palladium, effect of common ions present in sample and instrumental parameters like furnace conditions were investigated in detail. The proposed method has been successfully applied for the quantification of arsenic (V), (III) in environmental water samples. The proposed procedure was validated by applying it for the determination of total As in Certified Reference Material BND 301-02 (National Physical Laboratory, India).

## 2. Experimental

### 2.1. Instrumentation

GBC 906AA AAS unit with deuterium-arc background correction, GF 3000 ElectroThermal Atomizer and an auto sampler PAL-3000 were used in the present investigation. Pyrolytic graphite coated furnace tubes (GBC part no. 99-0059-00) were used in all the studies. All measurements were performed using integrated absorbance (peak area). The elemental hollow cathode lamp of Arsenic  $\lambda$  193.7, GBC, Australia was used.

### 2.2. Reagents

Supra pure nitric acid 65%, Supra pure hydrochloric acid 35% from E. Merck Darmstadt, Germany were used for all sample

treatments. Nanopure water of 18.3 M $\Omega$  delivered from Barnstead Thermolyne Water Purification System was used for all dilutions and washings. Standard solutions of As (V) were prepared by suitable dilution of certified AAS standard solution (1 mg mL<sup>-1</sup>) from E. Merck Darmstadt. Arsenic (III) solution was prepared by dissolving sodium arsenite in 5% hydrochloric acid. Palladium solution was prepared by dissolving weighed quantities of palladium metal (99.99%) in 10 mL conc. nitric acid and making up to volume. 10% sodium borohydride (Riedel-de Haen, AG 96%), 10% ascorbic acid (AR Grade, Thomas Baker, India) and 10% hydrazine nitrate (E. Merck, AG, Darmstadt) were prepared by dissolving weighed quantities and making up to volume.

All containers and glassware were cleaned by soaking successively in three baths of 10%, 1% and 0.1% double distilled nitric acid in nanopure water. All glassware was stored in 0.1% nitric acid baths till further use.

### 2.3. General procedure

#### 2.3.1. Estimation of As (V, III)

A suitable aliquot of sample solution (10–50 mL) was taken in a beaker to which 2 mg Pd (II) was added. The pH of the solution was adjusted to 3 using dilute ammonia and hydrochloric acid. 10% freshly prepared BH was added to reduce palladium completely. The beaker was kept aside for 0.5 h. The contents were transferred to centrifuge tubes and centrifuged. The supernatant solution was discarded and the collected palladium particles were dissolved in 0.1 mL conc. HNO<sub>3</sub> and 0.02 mL HCl and made up to volume (1 mL).

#### 2.3.2. Estimation of As (III)

A similar aliquot of sample solution (10–50 mL) was taken in a beaker to which 1 mg Pd (II) was added. The pH was adjusted to 3 and 10% freshly prepared HZ was added drop wise. The reduced palladium was treated as above and made up to volume (1 mL).

Sample blanks were prepared by running aliquots of deionised water through the sample procedure.

The processed samples, blanks, aqueous standards and modifier were injected into the graphite furnace using an auto sampler. The required amounts were adjusted using the auto mix function of the auto sampler.

## 3. Results and discussion

### 3.1. Optimization of graphite furnace atomic absorption spectrometer

#### 3.1.1. Ashing and atomization temperature

Optimization of furnace conditions was carried out so that effective ashing and atomization temperatures were arrived at, to eliminate any matrix effect and ensure extended life of tube. Arsenic compounds are known to be volatile hence palladium was used to stabilize arsenic to provide a reliable analyte signal. To optimize the pyrolysis temperature the recommended atomization temperature of 2300 °C was chosen and the pyrolysis temperature was varied in steps of 100 °C, starting from 600 °C to 1600 °C showed a decline in absorbance from 600 °C to 1000 °C after which there was a rise which remained constant from 1200 °C to 1400 °C. Pyrolysis temperature of 1300 °C was selected and the atomization temperature was then varied in steps of 100 °C from 2000 °C to 2500 °C. It was observed that in the analyte signal reached a well-defined plateau between 2200 °C and 2400 °C after which a decrease in signal was seen. Though the absorbance in the peak height was higher than in the peak area mode, the results in the area mode showed better

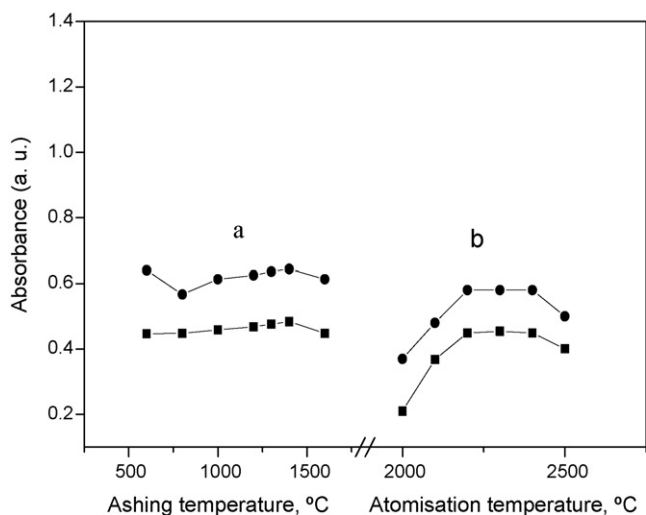


**Fig. 1.** Relationship between (a) ashing and (b) atomization temperature and absorbance of arsenic. Each point represents absorbance for  $0.2 \mu\text{g L}^{-1}$  of arsenic (Pd modifier): (●) peak height; (■) peak area.

precision and linear calibration. Pyrolysis temperature of  $1300^\circ\text{C}$  and atomization temperature of  $2300^\circ\text{C}$  and peak area mode was used in all further studies (Fig. 1).

### 3.1.2. Effect of modifier

In present investigation arsenic was collected by its adsorption on colloidal palladium and hence the samples contained inherently dissolved palladium. Studies were carried out to ascertain that the range of the concentration of modifier did not alter and affect the analyte signal. The amount of Pd (II) added was from  $0 \mu\text{g}$  to  $80 \mu\text{g}$  Pd per atomization cycle. It was observed that there was no change in the absorbance for  $200 \text{ ng mL}^{-1}$  arsenic, when  $10\text{--}25 \mu\text{g}$  Pd (II) was used. Less than  $10 \mu\text{g}$  and more than  $25 \mu\text{g}$  Pd resulted in decrease in absorbance (Fig. 2). The Pd in our experiment varied from  $10 \mu\text{g}$  to  $20 \mu\text{g}$  and hence did not affect the analyte signal.

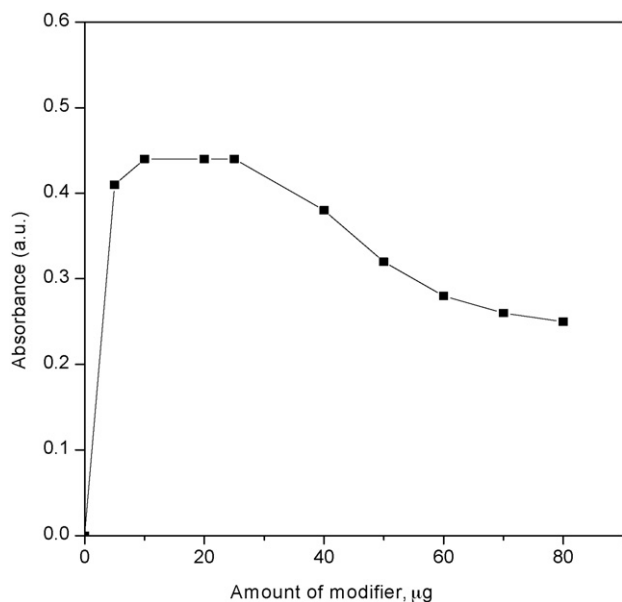


**Fig. 2.** Relationship between concentration of modifier and absorbance of arsenic. Each point represents absorbance for  $0.2 \mu\text{g L}^{-1}$  of arsenic.

**Table 1**  
Effect of reducing agents on recovery of As (V) and As (III).

Reducing agents	Added (ng)		Found
	As (III)	As (V)	
Sodium borohydride, $n = 3$	200	–	$200 \pm 5$
	–	200	$198 \pm 4$
	200	200	$403 \pm 3$
Hydrazine dichloride, $n = 3$	200	–	$203 \pm 6$
	–	200	ND
	200	200	$206 \pm 4$
Ascorbic acid, $n = 3$	200	–	$198 \pm 5$
	–	200	ND
	200	200	$205 \pm 8$

ND = not detected,  $n$  = no. of replicates.

### 3.2. Effect of BH, HZ and ASA on the reduction and adsorption of arsenic on PdNP

A study of the effect of BH, HZ, and ASA on the reduction and adsorption of arsenic on PdNP was carried out using recommended procedure. It was observed that there was quantitative recovery of arsenic (V) and (III) on PdNP from the solutions reduced by BH, while only As (III) was recovered in solution reduced by HZ and ASA (Table 1). Ascorbic acid and hydrazine showed effective reduction of palladium but could not reduce As (V) under the experimental conditions.

### 3.3. Effect of Pd concentration

A study on the effect of the concentration of palladium on the recoveries of As (V), As (III), was carried out. Increasing amount of palladium i.e.  $0.5\text{--}6 \text{ mg}$  was added to solutions containing  $2 \mu\text{g}$  As (V) and  $2 \mu\text{g}$  As (III). 10% BH, 10% HZ and 10% ASA were added to the solutions which were treated as in the recommended procedure. It was found that for the BH reduction quantitative recovery of As (V) started with  $2 \text{ mg}$  Pd and remained constant up to  $6 \text{ mg}$  Pd. For the HZ reduction of As (III) it started from  $0.5 \text{ mg}$  Pd and remained constant up to  $6 \text{ mg}$  Pd and for ASA reduction of As (III) started at  $4 \text{ mg}$  Pd and was constant till  $6 \text{ mg}$  of Pd. There was no recovery of As (V) in solutions reduced by HZ and ASA (Fig. 3). ASA reduction required  $4 \text{ mg}$  Pd for quantitative recovery of As (III) while HZ reduction showed  $100 \pm 2\%$  recovery with  $0.5 \text{ mg}$  Pd.

Adsorption capacity is a surface property and is a function of surface area. The higher adsorption shown by PdNP generated by HZ may be due to a higher active surface area. Adsorption capacity of PdNP (HZ) is  $4 \text{ mg g}^{-1}$ , ASA is  $0.5 \text{ mg g}^{-1}$  while that of PdNP (BH) is  $1 \text{ mg g}^{-1}$ . Since PdNP generated using hydrazine had a higher adsorption capacity than ascorbic acid, hydrazine was used for the estimation of As (III) and BH for the estimation of As (V).

For all subsequent investigations  $1 \text{ mg}$  Pd was used for quantification of As (III) by HZ, and  $2 \text{ mg}$  Pd was used for quantification of As (V) + As (III) using BH.

**Regeneration of palladium:** The sample solutions containing reduced palladium with adsorbed arsenic are acidified with nitric acid and warmed gently. All the arsenic is oxidized to (V). The pH of solution is adjusted to 3 with dilute ammonia and palladium in the solution is reduced by hydrazine. The reduced palladium is reused after washing and dissolving in nitric acid. The regeneration and reuse of palladium greatly reduces the effective cost per analysis and makes it an economical viable procedure.

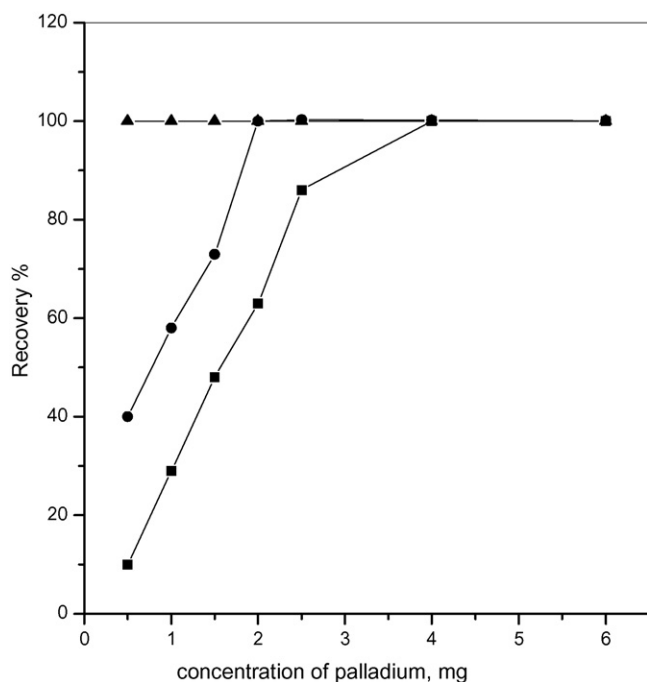


**Fig. 3.** Relation between concentration of palladium and recoveries of As 2  $\mu\text{g}$ : (■) As (V) using sodium borohydride, (▲) As (III) using hydrazine, and (●) As (III) using ascorbic acid.

### 3.4. Characterization of palladium particles

The particles obtained by reduction of palladium by BH and HZ were collected and washed free of reducing agent. These particles were taken in isopropyl alcohol (IPA) and dispersed by ultrasonification. A drop was taken on a glass slide and the sample was coated with 5 nm Au with Baltec-Tec sputter coater model SCD 050. The particles were examined in secondary electron mode at 30 kV beam acceleration. Micrograph (Fig. 4a and b) indicates the presence of agglomerated particles. The BH generated particles had an average size of 50–100 nm (Fig. 4a) while those generated by reduction with hydrazine had an average size of 80–110 nm (Fig. 4b).

### 3.5. Characterization of arsenic adsorbed on PdNP

The particles obtained by reduction of palladium by BH and HZ in the presence of As (V) and As (III) were collected and washed free of reducing agent. XPS measurements were performed on the particles using a Clam-II analyzer equipped with a magnesium anode (Mg K $\alpha$ ) and operating at a pressure of  $10^{-9}$  Torr. It was seen that the PdNP obtained by reduction with HZ in the presence of As (III) (Fig. 5a) and that reduced by BH in the presence of As (V) + As (III) (Fig. 5b) showed a peak corresponding to binding energy 45 eV. Binding energies between 43.4 eV and 45.0 eV have been reported for different oxygen containing As (III) species, the exact value of which depends on the corresponding anions [40–44]. The quantitative recovery of As (V) and As (III) on palladium is explained thus, that BH reduces the As (V) to As (III) which is then chemisorbed on the surface of palladium. This corroborates the experimental findings.

### 3.6. Optimization concentration of reducing agents

To solutions containing appropriate amount of Pd and As (V), As (III) varying amounts of BH and HZ was added. These were then treated as in the general procedure. It was observed that addition of 100 mg of BH (1 mL of 10%) showed recovery of As (V) + As (III)

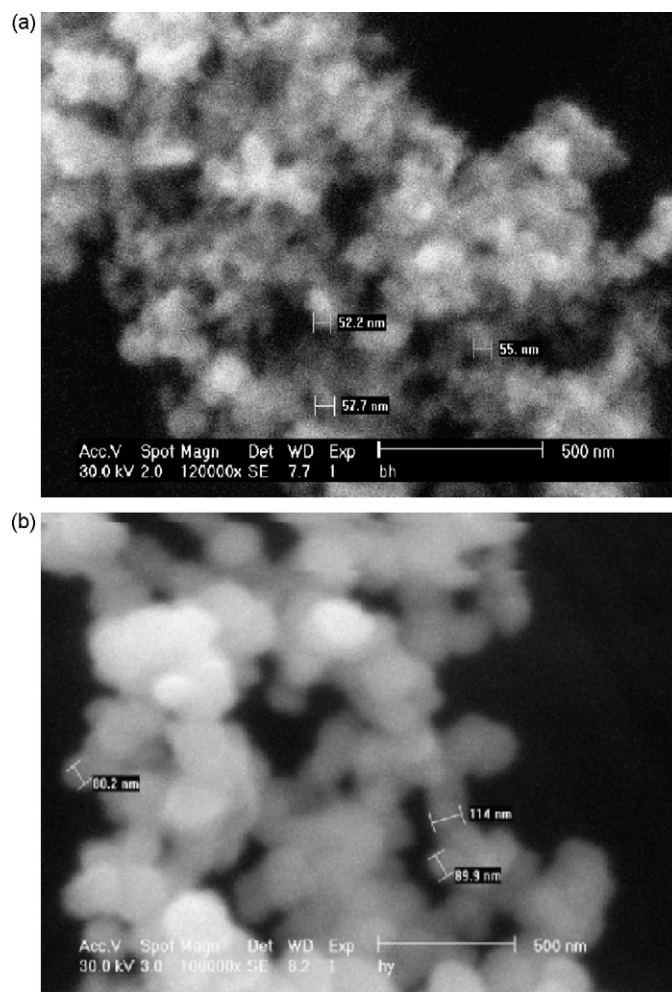


**Fig. 4.** Scanning electron micrograph images of PdNP prepared using (a) sodium borohydride and (b) hydrazine.

while 100 mg HZ (1 mL of 10%) showed recovery of As (III). Based on these results 1 mL of 10% BH and 10% HZ were employed in further investigations.

### 3.7. Effect of pH

Reduction reactions are known to be pH dependent therefore the effect of pH for the quantitative recovery of arsenic was studied adopting the general procedure to the BH and HZ sets after adjusting the pH of the solution from 1 to 9 using dilute ammonium hydroxide or hydrochloric acid. It was observed that As (V) and As (III) were quantitatively recovered by BH reduction from pH 1 to pH 9, while As (III) showed 100% recovery by HZ reduction, from pH 3 to pH 9.

### 3.8. Effect of sample volume

The low levels of arsenic in samples make enrichment of the analyte necessary for quantification. Hence the effect of sample volume on the recovery of arsenic was studied. Two sets of synthetic sample solution, of volume ranging from 10 mL to 1000 mL which contained 1  $\mu\text{g}$  As (V) + 1  $\mu\text{g}$  As (III), were taken and were run through the protocol of the recommended BH and HZ procedure. It was observed that the recovery of As (V), (III) by BH and HZ was 98–100% in sample volumes from 10 mL to 50 mL and decreased in sample solutions from 100 mL to 1000 mL. The reduced palla-

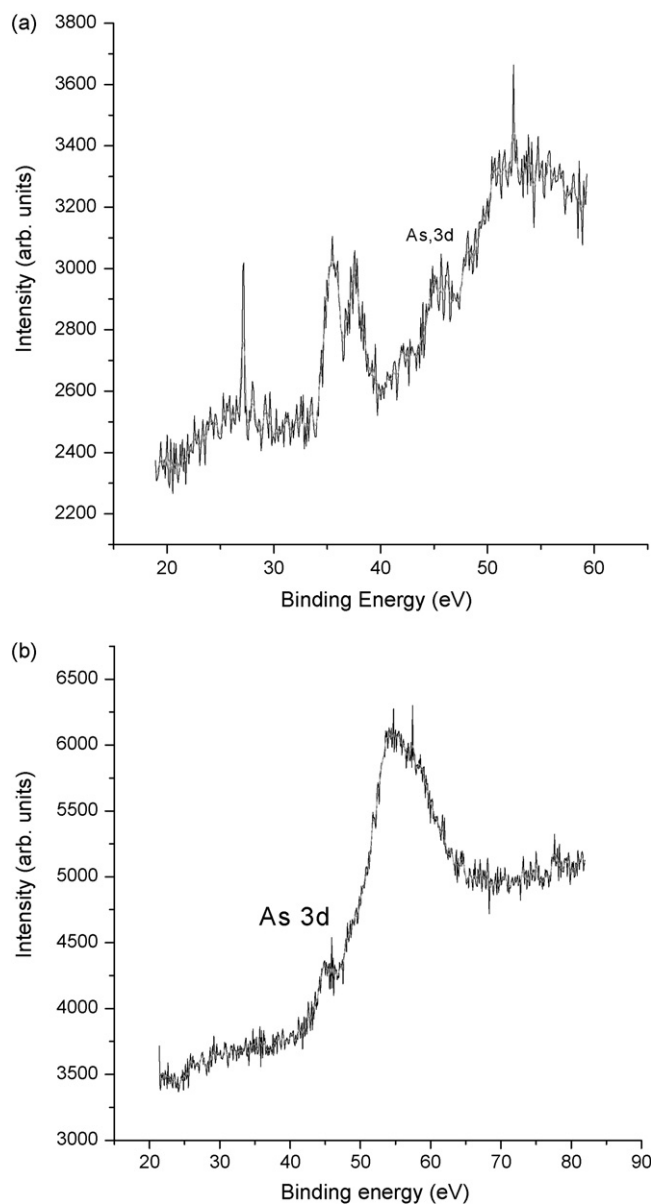


**Fig. 5.** (a) X-ray photoemission spectrum of As (V) on PdNP prepared using sodium borohydride. (b) X-ray photoemission spectrum of As (III) on PdNP prepared using hydrazine.

dium was collected and solution was made up to 1 mL; hence the enrichment factor approached 50.

### 3.9. Effect of time

To establish the minimum time required for quantitative adsorption of arsenic on PdNP, the recommended procedure was applied to sample and the PdNP are collected at time intervals of 0–8 h. It was seen that BH and HZ reduction showed 95–100% recovery at 0.5 h (Fig. 6).

### 3.10. Interferences studies

The effect of common cations and anions present in natural ground water/environmental waters on the uptake of arsenic on palladium particles was carried out by spiking samples with  $\text{Na}^+$ ,  $\text{K}^+$ ,  $\text{Ca}^{2+}$ ,  $\text{Mg}^{2+}$ ,  $\text{Cl}^-$ ,  $\text{NO}_3^-$ ,  $\text{SO}_4^{2-}$ ,  $\text{Fe}^{3+}$ ,  $\text{Cu}^{2+}$ ,  $\text{Zn}^{2+}$ ,  $\text{Mn}^{2+}$ ,  $\text{Al}^{3+}$ ,  $\text{PO}_4^{3-}$  at concentration reported in ground water [45]. It was seen that

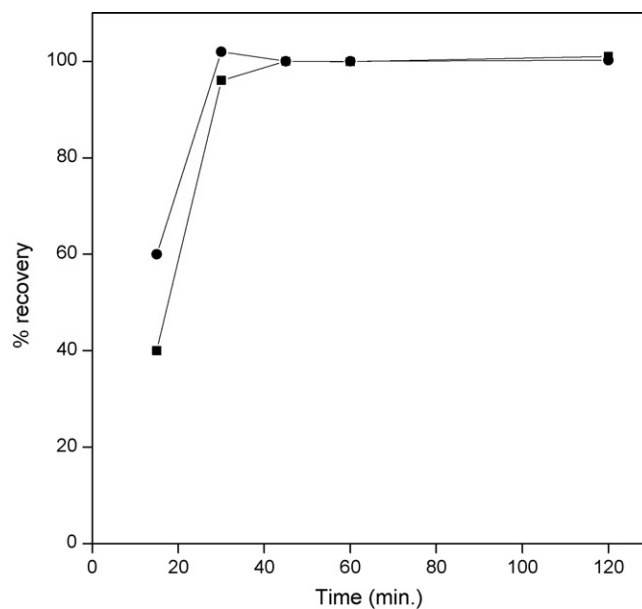


**Fig. 6.** Relationship of time and recovery of arsenic on PdNP. (●) % recovery of As (V, III) using sodium borohydride; (■) % recovery of As (III) using hydrazine.

these extreme concentrations of foreign ions did not interfere in the recovery of trace concentrations of arsenic in groundwater samples (Table 2).

### 3.11. Calibration, precision and figure of merit

Standard arsenic (V) and arsenic (III) solutions were used to obtain the calibration curve for As (V) and As (III). Aliquots containing 5 ng As (V), 5 ng As (III) to 1  $\mu\text{g}$  As (V), and 1  $\mu\text{g}$  As (III) were taken and processed according to the recommended BH and HZ procedure. The processed solutions and aqueous standard solutions were injected into the graphite furnace using an auto sampler. The required amounts of each were adjusted using the auto mix function of the auto sampler. Palladium was used as modifier and optimized furnaces programme was employed for carrying out the analysis.

The calibration curve obtained using processed standards and aqueous standards showed that there was no significant difference in their absorbance values. The graph was linear up to 400  $\text{ng mL}^{-1}$  arsenic. The slopes for aqueous standard and processed standard

**Table 2**  
Effects of foreign ions on the determination of As (V) and As (III).

Ions	( $\text{mg L}^{-1}$ )	Recovery (%) <sup>a</sup> As (III)	Recovery (%) <sup>b</sup> As (III + V)
$\text{Na}^+$	1000	101	99
$\text{K}^+$	10	102	100.5
$\text{Ca}^{2+}$	1000	104	101.0
$\text{Mg}^{2+}$	1000	101	94.5
	( $\mu\text{g L}^{-1}$ )		
$\text{Cu}^{2+}$	200	101	98
$\text{Mn}^{2+}$	200	98	100.5
$\text{Zn}^{2+}$	200	99	102
$\text{Al}^{3+}$	200	103	98
$\text{Fe}^{3+}$	200	102	99
	( $\text{mg L}^{-1}$ )		
$\text{Cl}^-$	1000	101	101
$\text{NO}_3^-$	1000	103	100.5
$\text{SO}_4^{2-}$	1000	96	97
	( $\mu\text{g L}^{-1}$ )		
$\text{PO}_4^{3-}$	250	97	101.5

<sup>a</sup> As (III): 1  $\mu\text{g L}^{-1}$  (HZ).

<sup>b</sup> As (V): 1  $\mu\text{g L}^{-1}$  + As (III): 1  $\mu\text{g L}^{-1}$  (BH).

**Table 3**  
Comparison of the published methods with the proposed method in this work.

Extractant	Detection method	Enrichment factor	Detection limit ( $\mu\text{g L}^{-1}$ )	Reference
Butane-1-ol	GFAAS	20	0.2	[16]
PTFE turnings	GFAAS	44	0.008	[18]
PTFE turnings	HG AAS	10	0.02	[19]
Immobilized nanometer $\text{TiO}_2$	GFAAS	50	0.024	[21]
Modified mesoporous $\text{TiO}_2$	ICP-AES	50	0.11	[22]
CTBA modified alkyl silica microcolumn	ICP-OES	26.7	0.15	[23]
Pd-nanoparticles	GFAAS	50	0.029	This work

**Table 4**  
Determination of arsenic (V), (III) in ground water samples.

Sample	Added ( $\mu\text{g mL}^{-1}$ )		GFAAS ( $\mu\text{g mL}^{-1}$ )		ICP-MS ( $\mu\text{g mL}^{-1}$ )	
	As (III)	As (V)	As (III)	As (III, V)	As (III)	As (III, V)
BND 301-02 <sup>a</sup> , $n = 7^b$	–	–	ND	$1.01 \pm 0.03$	ND	$1.01 \pm 0.02$
Groundwater, $n = 3^b$	–	–	ND	$4.09 \pm 0.03$	ND	$4.3 \pm 0.2$
Groundwater, $n = 3^b$	0.5	0.5	$0.53 \pm 0.02$	$5.08 \pm 0.02$	$0.48 \pm 0.01$	$5.12 \pm 0.02$
Processed water, $n = 3^b$	–	–	$0.23 \pm 0.03$	$0.58 \pm 0.04$	$0.25 \pm 0.02$	$0.61 \pm 0.01$
Processed water, $n = 3^b$	0.5	0.5	$0.74 \pm 0.01$	$1.60 \pm 0.02$	$0.74 \pm 0.02$	$1.62 \pm 0.02$

ND = not detectable.

<sup>a</sup> CRM provided by National Physical Laboratory, India.<sup>b</sup> Number of replicates.**Table 5**  
Determination of arsenic (V), (III) in groundwater samples received from National Institute of Miners Health, Ministry of Mines, Government of India.

Sample code no.	Present method			Ammonium molybdate method [16]		
	Total (As) ( $\mu\text{g mL}^{-1}$ )	As (III) ( $\mu\text{g mL}^{-1}$ )	As (V) ( $\mu\text{g mL}^{-1}$ )	Total (As) ( $\mu\text{g mL}^{-1}$ )	As (V) ( $\mu\text{g mL}^{-1}$ )	As (III) ( $\mu\text{g mL}^{-1}$ )
B-1	$1.20 \pm 0.04$	$0.61 \pm 0.03$	$0.58 \pm 0.03$	$0.98 \pm 0.05$	$0.42 \pm 0.01$	$0.59 \pm 0.04$
B-2	$2.82 \pm 0.3$	$1.35 \pm 0.04$	$1.47 \pm 0.04$	$2.83 \pm 0.02$	$1.51 \pm 0.05$	$1.33 \pm 0.03$
B-3	$1.63 \pm 0.05$	$0.69 \pm 0.01$	$0.95 \pm 0.02$	$1.64 \pm 0.03$	$0.98 \pm 0.02$	$0.63 \pm 0.04$
B-4	$0.64 \pm 0.02$	$0.22 \pm 0.02$	$0.40 \pm 0.03$	$0.63 \pm 0.02$	$0.41 \pm 0.01$	$0.25 \pm 0.03$
B-5	$1.94 \pm 0.05$	$0.47 \pm 0.03$	$1.47 \pm 0.01$	$1.93 \pm 0.04$	$1.52 \pm 0.05$	$0.41 \pm 0.04$
B-6	$<10^{-4}$	$<10^{-4}$	$<10^{-4}$	$<10^{-4}$	$<10^{-4}$	$<10^{-4}$

were 0.00172 and 0.00189, respectively. The regression and standard deviation of the two lines were 0.999 and 0.998, and 0.017 and 0.018, respectively. Since the properties of the calibration curve are similar, aqueous standards were used for quantification of arsenic in all the experiments.

The limit of detection defined as  $C_L = 3S_B/m$  (where  $C_L$  is the limit of detection,  $S_B$  is the standard deviation for 10 replicate measurement of the blank and  $m$  is the slope of the processed calibration curve, respectively) was  $0.029 \mu\text{g L}^{-1}$  for As (III). The relative standard deviation (R.S.D.) for 10 replicate measurements of  $5 \text{ ng mL}^{-1}$  of processed sample was 4.2%. The enrichment factor of present method is 50. The analytical data i.e. enrichment factor and detection limit obtained by the present method compares favorably with those reported in literature [16,18,19,21–23] (Table 3).

### 3.12. Validation of proposed method and application for analysis of samples

To validate the proposed method, the procedure has been applied for the determination of the content of total As in water Certified Reference Material BND 301-02 (National Physical Laboratory, India) The determined value  $1.0 \pm 0.03 \mu\text{g mL}^{-1}$  ( $n = 7$ ) was in good agreement with the certified value of  $1.0 \pm 0.02 \mu\text{g mL}^{-1}$ . The  $t$  value at 95% confidence was 2.1. The critical value of  $t_{0.05,6}$  is 2.45 validating that the estimated value and the certified value are the same.

This protocol was applied to ground water samples received by our laboratory. The samples were filtered through a  $0.45 \mu\text{m}$  membrane filter. Known amounts of As (V) and As (III) were spiked in these samples and run through the BH and HZ protocols. Arsenic

was quantified by GFAAS. The results indicated that the recoveries of spiked As (V) and As (III) obtained were from 98% to 102%. These samples were also analyzed by ICP-MS (Table 4).

The BH and HZ analytical protocol was applied to another set of ground water samples received from National Institute of Miners Health, Ministry of Mines, Government of India, which contained unknown concentrations of As (V) and As (III). Our laboratory has developed a procedure for the analysis of As (V) and As (III) using the ammonium molybdate chemistry which has been published earlier by the same authors [16]. Arsenic (V) is known to form heteropolyacid with ammonium molybdate in acidified aqueous solutions which was quantitatively extracted into butane-1-ol. Sample solutions were gently warmed with nitric acid and As (III) oxidizing to As (V) and total arsenic was estimated. The samples were analyzed applying the present procedure and also the ammonium molybdate procedure. The present method distinguishes As (III) and total arsenic, while the ammonium molybdate protocol estimates As (V) and total arsenic. The analytical results, which are presented in Table 5, establish that the differential determination of As (V) and As (III) using both the protocols are in good agreement with each other.

## 4. Conclusions

We have presented here a novel, simple, economic, sensitive and accurate method for an offline differential determination of trace amounts of arsenic in ground water samples. A methodology based on the quantitative adsorption of reduced arsenic species on PdNP generated in situ by BH and HZ is described to characterize and quantify As (V) and As (III) in environmental water samples. The



quantification of arsenic was carried out using GFAAS. The detection limit of arsenic in environmental water samples was  $0.029 \mu\text{g L}^{-1}$  by GFAAS by the present technique which has an enrichment factor of 50. The proposed method was successfully applied for the determination of arsenic (V), (III) in environmental water samples. It is applicable for the quantification of the maximum concentration limit of  $10 \mu\text{g L}^{-1}$  As established by Environment Protection Agency.

### Acknowledgements

The authors are grateful to Dr. J. Shah and Manisha Tawade BETD, BARC for the Scanning Electron Micrograph and Dr. Jagannath and Niddhi Mithal of TPPED, BARC for carrying out the XPS measurements.

They are grateful to the unknown referees for their valuable suggestions incorporated in the modification of this manuscript.

### References

- [1] WHO, Arsenic Compounds Environmental Health Criteria 224, second ed., World Health Organisation, Geneva, 2003 (Chapter 5).
- [2] U.S. EPA, National Primary Drinking water regulation, Federal Register, vol. 66, 2001, p. 6976.
- [3] P.L. Smedley, D.G. Kinniburgh, *Appl. Geochem.* 17 (2002) 517.
- [4] J. Muller, *Fresenius J. Anal. Chem.* 363 (1999) 572.
- [5] R.M. Camero, R.E. Sturgeon, *Spectrochim. Acta B* 54 (1999) 753.
- [6] M. Thompson, B. Pahlavanpour, S.J. Walton, G.F. Krikbright, *Analyst* 103 (1978) 568.
- [7] A.S. Ribeiro, M.V. Viera, A.J. Curtius, *Spectrochim. Acta B* 59 (2004) 243.
- [8] S.J. Santosa, H. Mokudai, S. Tanaka, *J. Anal. Atom. Spectrom.* 12 (1997) 409.
- [9] A.D. Idowu, P.K. Dasgupta, Z. Genfa, K. Toda, *Anal. Chem.* 78 (2006) 7088.
- [10] K. Morita, E. Kaneko, *Anal. Chem.* 78 (2006) 7682.
- [11] A.G. Howard, M.H. Arbab-Zavar, *Analyst* 105 (1980) 338.
- [12] A. Chatterjee, D. Das, B.K. Mandal, T.R. Chowdhury, G. Samanta, D. Chakraborti, *Analyst* 120 (1995) 643.
- [13] D. Pozebon, V.L. Dressler, J.A.G. Neto, A.J. Curtius, *Talanta* 45 (1998) 1167.
- [14] Q. Zhang, H. Miniami, S. Inoue, I. Atsuya, *Anal. Chim. Acta* 508 (2004) 99.
- [15] L. Zhang, Y. Morita, A. Sakuragawa, A. Isozaki, *Talanta* 72 (2) (2007) 723.
- [16] S. Sounderajan, A.C. Udas, B. Venkatramani, *J. Hazard. Mater.* 149 (2007) 238.
- [17] F. Shemirani, M. Baghdadi, M. Ramezani, *Talanta* 65 (2005) 882.
- [18] P. Herbello-Hermelo, M.C. Barciela-Alonso, A. Bermejo-Barrera, P. Bermejo-Barrera, *J. Anal. Atom. Spectrom.* 20 (2005) 662.
- [19] A.N. Anthemidis, E.K. Martavaltzoglou, *Anal. Chim. Acta* 573 (2006) 413.
- [20] J. Koh, Y. Kwon, Y.N. Pak, *Microchem. J.* 80 (2005) 195.
- [21] P. Liang, R. Liu, *Anal. Chim. Acta* 602 (2007) 32–36.
- [22] C.Z. Huang, B. Hu, Z.C. Jiang, *Spectrochim. Acta B* 62 (2007) 454.
- [23] C. Xiong, M. He, B. Hu, *Talanta* (2008).
- [24] R.T. Gettar, R.N. Garavaglia, E.A. Gautier, D.A. Batistoni, *J. Chromatogr. A* 884 (2000) 211.
- [25] J. Mattusch, R. Wennrich, *Anal. Chem.* 70 (1998) 3649.
- [26] R. Sugano, S. Nishina, S. Ohnishi, *Microclusters*, Springer, Berlin, 1987.
- [27] R. Kubo, *J. Phys. Soc. Jpn.* 17 (1962) 975.
- [28] A. Henglein, *Chem. Rev.* 89 (1989) 1861.
- [29] L.N. Lewis, *Chem. Rev.* 93 (1993) 2693.
- [30] H. Bonnemann, R.M. Richards, *Eur. J. Inorg. Chem.* (2001) 2455.
- [31] M. Moreno-manas, R. Pleixats, *Acc. Chem. Res.* 36 (2003) 638.
- [32] Y. Sun, L. Zhang, H. Zhou, Y. Zhu, E. Sutter, Y. Ji, M.H. Rafailovich, J.C. Sokolov, *Chem. Mater.* 19 (8) (2007) 2065.
- [33] T. Ashino, K. Takada, *JAAS* 11 (1996) 577.
- [34] T. Ashino, K. Takada, *Anal. Chim. Acta* 312 (1995) 157.
- [35] Z. Zhuang, C. Yang, X. Wang, P. Yang, B. Huang, *Fresenius J. Anal. Chem.* 355 (3–4) (1996) 277.
- [36] M.A. Omole, I.O. K'Owino, O.A. Sadiq, *Appl. Catal. B* 76 (2007) 158.
- [37] R.E. Sturgeon, *Fresenius J. Anal. Chem.* 337 (1990) 538.
- [38] E.C. Lima, J.L. Brasil, J.C.P. Vaghetti, *Talanta* 60 (2005) 103.
- [39] B. Welz, M. Sperling, *Atomic Absorption Spectrometry*, third ed., Wiley-VCH, Weinheim, 1999, pp. 485–486.
- [40] C.D. Wagner, W.M. Riggs, L.E. Davis, J.F. Moulder, G.E. Muilenberg, *Handbook of X-ray Photoelectron Spectroscopy*, Perkin Elmer, Eden Pariric, MI, 1979.
- [41] M.K. Bahl, R.O. Woodall, R.L. Watson, K.J. Irgolic, *J. Chem. Phys.* 64 (1976) 1210.
- [42] J.A. Taylor, *J. Vac. Sci. Technol.* 20 (1982) 751.
- [43] W.J. Stec, W.E. Morgan, R.G. Albridge, J.R. Van Wazer, *Inorg. Chem.* 11 (1972) p219.
- [44] W.P. Zhou, L.A. Kibler, D.M. Kolb, *Electrochim. Acta* 49 (27) (2004) 5007.
- [45] ANR Publication 8084, Farm Water Quality Planning Reference Sheet 11.2.



## Electrochemical behaviors of guanosine on carbon ionic liquid electrode and its determination

Wei Sun<sup>a,\*</sup>, Yuanyuan Duan<sup>a</sup>, Yinzhuo Li<sup>a</sup>, Hongwei Gao<sup>b</sup>, Kui Jiao<sup>a</sup>

<sup>a</sup> Key Laboratory of Eco-Chemical Engineering of Ministry of Education, College of Chemistry and Molecular Engineering, Qingdao University of Science and Technology, 53 Zhenzhou Road, Qingdao 266042, China

<sup>b</sup> Shan Dong Entry-Exit Inspection and Quarantine Bureau of People's Republic of China, Qingdao 266002, China

### ARTICLE INFO

#### Article history:

Received 28 July 2008

Received in revised form 10 December 2008

Accepted 12 December 2008

Available online 24 December 2008

#### Keywords:

Guanosine

N-butylpyridinium hexafluorophosphate

Carbon ionic liquid electrode

Cyclic voltammetry

Electrooxidation

### ABSTRACT

The electrochemical behaviors of guanosine on the ionic liquid of N-butylpyridinium hexafluorophosphate (BPPF<sub>6</sub>) modified carbon paste electrode (CPE) was studied in this paper and further used for guanosine detection. Guanosine showed an adsorption irreversible oxidation process on the carbon ionic liquid electrode (CILE) with the oxidation peak potential located at 1.12 V (vs. SCE) in a pH 4.5 Britton–Robinson (B–R) buffer solution. Compared with that on the traditional carbon paste electrode, small shift of the oxidation peak potentials appeared but with a great increment of the oxidation peak current on the CILE, which was due to the presence of ionic liquid in the modified electrode adsorbed the guanosine on the surface and promoted the electrochemical response. The electrochemical parameters such as the electron transfer coefficient ( $\alpha$ ), the electron transfer number ( $n$ ), and the electrode reaction standard rate constant ( $k_s$ ) were calculated as 0.74, 1.9 and  $1.26 \times 10^{-4} \text{ s}^{-1}$ , respectively. Under the optimal conditions the oxidation peak current showed a good linear relationship with the guanosine concentration in the range from  $1.0 \times 10^{-6}$  to  $1.0 \times 10^{-4}$  mol/L by cyclic voltammetry with the detection limit of  $2.61 \times 10^{-7}$  mol/L ( $3\sigma$ ). The common coexisting substances showed no interferences to the guanosine oxidation. The CILE showed good ability to distinguish the electrochemical response of guanosine and guanine in the mixture solution. The urine samples were further detected by the proposed method with satisfactory results.

© 2008 Elsevier B.V. All rights reserved.

### 1. Introduction

Ionic liquids (ILs) are molten salts with the melting point close to or below room temperature. They are composed of two asymmetrical ions of opposite charges that only loosely fit together and have been used as a new class of green solvents, which can be used in different fields of chemistry [1]. RTILs exhibit many virtues such as high chemical and thermal stability, negligible vapor pressure, high conductivity and wide electrochemical windows. Therefore RTILs have been used in different fields of chemistry such as electrochemistry, organic synthesis, catalysis, electrodeposition and separation, etc. [2–8]. Recently, RTILs were proposed as an efficient binder in place of nonconductive organic binders for the preparation of carbon ionic liquid electrodes (CILEs), which was regarded as a new kind of chemical modified electrode with the advantages such as high conductivity, fast electron transfer rate and low overpotential for biomolecules. Several groups had applied different ILs modified electrodes to the detection of electroactive

molecules [9–13] and the protein electrochemistry [14–18]. Maleki et al. [19–21] developed an ionic liquid modified carbon paste electrode with 1-octylpyridinium hexafluorophosphate (OPFP) for the detection of some molecules. Zhao et al. [22] also used single-walled carbon nanotube (SWCNT)-IL gel modified electrode for the *p*-nitroaniline detection. Zhang et al. [23] also applied a 1-amyli-3-methylimidazolium bromide (AMIMBr) modified carbon paste electrode for the sensitive voltammetric detection of rutin. Laszlo et al. [24] had investigated the ability of hemin, microperoxidase-11 and Cytochrome *c* to oxidize 2-methoxyphenol in the different ILs and the results showed markedly higher activities in the IL media compared to molecular solvents.

Guanosine is one of the important nucleosides present in nucleic acids and is important in various biological processes such as the mediation of the RNA splicing process and the protection during brain ischemia [25]. The levels of nucleosides in urine have been shown to be related to carcinoma [26] or as the marker in liver diseases [27]. So it is important to establish sensitive methods for the guanosine detection. Different analytical methods had been proposed for the analysis of guanosine, including high performance liquid chromatography (HPLC) [28], ultra-performance liquid chromatography (UPLC) [29], ion-pair HPLC [30], etc. Elec-

\* Corresponding author. Tel.: +86 532 84023927; fax: +86 532 84023927.  
E-mail address: [sunwei@qust.edu.cn](mailto:sunwei@qust.edu.cn) (W. Sun).

trochemical methods can also be used for the investigation of guanosine. But in general a relatively high oxidation potential is required to accomplish the oxidation reaction, which limits the sensitivity and selectivity. Different kinds of chemical modified electrodes were devised for guanosine detection with the results as the decrease of the electrochemical potential and the enhancement of the sensitivity due to catalytic activity of the modifier. For example Goyal et al. [31,32] used a fullerene-C60-modified glassy carbon electrode and nanogold modified indium tin oxide electrode for the detection of guanosine and adenosine, respectively. Fortin et al. [27] applied a boron doped diamond electrodes to study the direct oxidation process of guanosine.

In this paper an ionic liquid N-butylpyridinium hexafluorophosphate (BPPF<sub>6</sub>) modified carbon paste electrode was fabricated for the investigation of the electrochemical behaviors of guanosine. As indicated in Refs. [19–21], the pyridinium-based ionic liquid modified carbon paste electrode had shown many advantages and displayed very promising electrochemical reactivity toward different compounds. Due to the  $\pi$ - $\pi$  interaction of pyridinium ion with graphite and a layer of cationic pyridinium film present in the electrode, the electrode was stable with the characteristics of ion-exchange and adsorptive ability. The electrochemical behaviors of guanosine on the CILE were carefully studied and the results indicated an adsorption behavior appeared. Based on the electrochemical response of guanosine, a new electrochemical method for guanosine detection was established and further applied to the real urine sample detection.

## 2. Experimental

### 2.1. Apparatus

All the electrochemical measurements were performed with a CHI 1210A electrochemical analyzer (Shanghai CH Instrument, China). Electrochemical studies were performed using a conventional three-electrode system composing of a saturated calomel electrode (SCE) as a reference electrode and a platinum wire as the auxiliary electrode. The working electrode was a home-made N-butylpyridinium hexafluorophosphate (BPPF<sub>6</sub>) modified carbon paste electrode with the diameter of 4 mm. All the experiments were carried out at  $25 \pm 1$  °C.

### 2.2. Chemicals

Guanosine (99%, Sigma), guanine (98%, Sigma), N-butylpyridinium hexafluorophosphate (BPPF<sub>6</sub>, Hangzhou Kemer Chemical Limited Company, China) and graphite powder (average particle size 30  $\mu$ m, Shanghai Colloid Chemical Plant) were used as received. Guanosine and guanine stock solutions were prepared by dissolv-

ing them into 0.1 mol/L NaOH solution. 0.2 mol/L Britton–Robinson (B–R) buffer solution with various pH values was used as supporting electrolyte. Aqueous solutions were prepared with doubly distilled water. All other chemicals are commercially available with analytical grade and used without further purification.

### 2.3. Preparation of modified electrode

The traditional carbon paste electrode was prepared by mixing 1.6 g of graphite powder and 0.5 mL of paraffin in a mortar and grounded homogeneously. The resulting paste was packed into a cavity (4 mm diameter) at one end of a glass tube. The electrical contact was provided by a copper wire connected to the paste in the inner hole of the tube.

The preparation process of the CILE was similar to that of the CPE by mixing 2.1 g of graphite powder with 0.75 g of BPPF<sub>6</sub> together in a mortar and heated at 80 °C. Prior to use, the surface of the well-prepared electrode was smoothed on a weighing paper.

### 2.4. Electrochemical measurements

The three-electrode system was immersed in a 10-mL electrochemical cell containing proper amount of guanosine and 0.2 mol/L B–R buffer solution (pH 4.5). After accumulation at 0.6 V in a still solution for 300 s, cyclic voltammetric experiments were performed in the potential range from 0.50 to 1.30 V with the scan rate as 100 mV/s.

### 2.5. Sample preparation

Urine samples received from laboratory personnel were collected in tubes and then diluted 50 times with 0.2 mol/L B–R buffer solution (pH 4.5). The diluted urine samples were spiked with certain amounts of guanosine standard solution and detected by the proposed method.

## 3. Results and discussion

### 3.1. Cyclic voltammograms of guanosine

Cyclic voltammograms of 50  $\mu$ M guanosine in pH 4.5 B–R buffer solution on the different electrodes were recorded and shown in Fig. 1. On traditional carbon paste electrode (CPE) an irreversible oxidation peak appeared at +1.13 V (vs. SCE) with the oxidation peak current as  $6.644 \times 10^{-6}$  A (curve d), which was contributed to the electrochemical oxidation of guanosine. While on CILE, the oxidation peak located at +1.12 V (vs. SCE) with the oxidation peak current as  $2.780 \times 10^{-4}$  A (curve b), which was 41.84 times higher than that

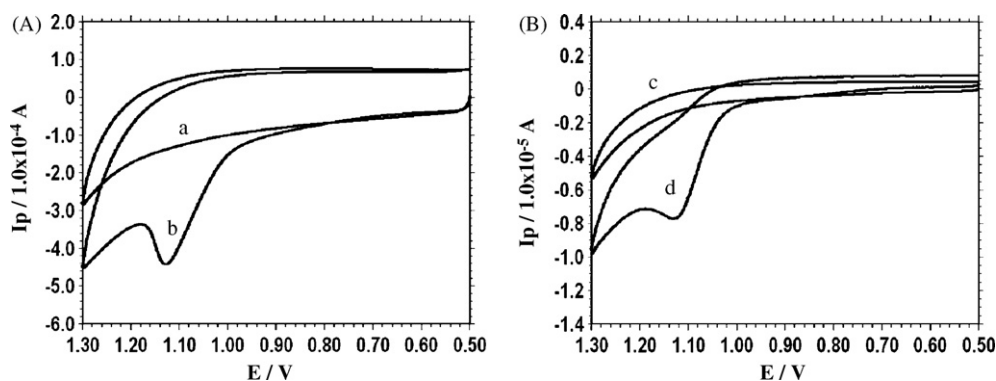
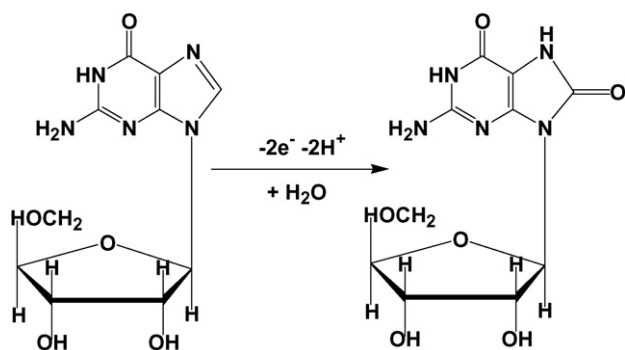


**Fig. 1.** (A) Cyclic voltammograms on CILE for 0.2 mol/L pH 4.5 B–R (a) and  $5.0 \times 10^{-5}$  mol/L guanosine in buffer solution (b); (B) Cyclic voltammograms on CPE for 0.2 mol/L pH 4.5 B–R (c) and  $5.0 \times 10^{-5}$  mol/L guanosine in buffer solution (d). Scan rate: 100 mV/s.



Scheme 1. The proposed electrooxidation mechanism of guanosine.

on CPE. It can be seen that the oxidation peak potential moved a little to the negative direction with a great increase of the oxidation peak current, which was attributed to the presence of ionic liquid as the modifier in the carbon paste electrode. According to the recent reports [19,33], CILE showed the properties such as higher conductivity, fast electron transfer rate, good anti-fouling properties, inherent catalytic ability and adsorptive behaviors. So more guanosine can be accumulated on the surface of CILE and the presence of the IL can act as a very efficient promoter to enhance the kinetics of the electrochemical process. At the same time the background current was increased, which maybe due to the increasing capacitance of the highly viscous IL on the carbon electrode surface [11].

Based on the related Refs. [34,35], the electrochemical oxidation mechanism of guanosine implies an overall four electrons and four protons process in two steps. The primary electrooxidation step including two step of one electron and one proton process with the free radical form involved an oxidation at N7=N8 position to give an 8-hydroxyguanosine, which can be further oxidized into an unstable diimine with the following chemical reaction step. So the proposed mechanism on the CILE may be expressed with the following equation, which involved a two electrons and two protons oxidation process (Scheme 1).

### 3.2. Influence of buffer pH

The influence of the buffer pH on the electrochemical response of guanosine was investigated in the pH range from 3.0 to 6.0 with the results shown in Fig. 2. With the increase of buffer pH, the oxidation peak potential moved to negative direction (curves a–g), indicating protons took part in the electrode reaction. The pH dependence on the oxidation peak potential of guanosine resulted in the linear regression equation as  $E_{pa}(\text{V}) = -0.041 \text{ pH} + 1.257$  ( $n = 7$ ,  $\gamma = 0.998$ ). The buffer pH also showed the influence on the oxidation peak current and the maximum current value was got at pH 4.5. So pH 4.5 buffer solution was selected for all the experiments.

### 3.3. Influence of scan rate

The influences of potential scan rate on the electrochemical responses of guanosine in pH 4.5 B–R buffer were further studied by cyclic voltammetry and the results were shown in Fig. 3. With the increase of the scan rate, the oxidation peak current increased gradually and the oxidation peak potential moved toward more positive values. The oxidation peak current was directly proportional to the scan rate in the range from 10.0 to 300.0 mV/s with the linear regression equation as  $I_{pa}(\mu\text{A}) = 9.311 \nu (\text{V/s}) + 105.7$  ( $n = 13$ ,  $\gamma = 0.996$ ), which indicated that electrode reaction of guanosine on the CILE was an adsorption-controlled process. So the guanosine in the solution was adsorbed and accumulated on the surface of the

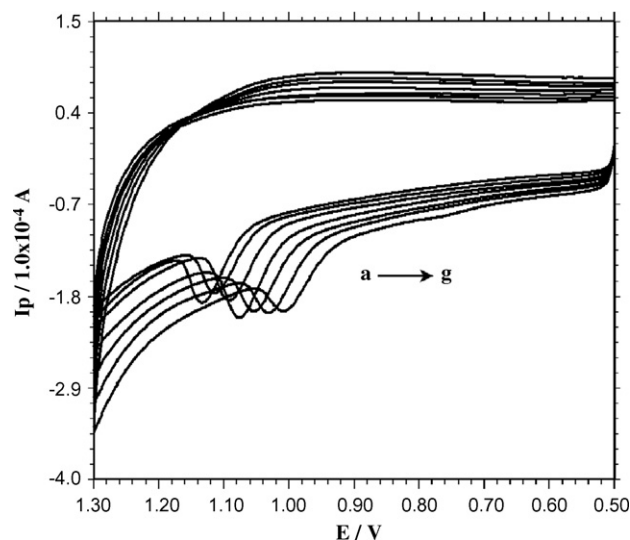


Fig. 2. Influence of buffer pH (from a to g: 3.0, 3.5, 4.0, 4.5, 5.0, 5.5, 6.0) on the cyclic voltammetric response of guanosine at the scan rate of 100 mV/s.

CILE firstly, then the electrochemical oxidation reaction was took place.

The adsorbed amount (maximum surface concentration) of guanosine on the CILE can be calculated according to the following equation [36,37]:

$$I_p = \frac{nFQ\nu}{4RT} = \frac{n^2F^2A\Gamma_T\nu}{4RT}$$

where  $n$  is the number of electron transferred,  $F$  (C/mol) is the Faraday's constant,  $A$  ( $\text{cm}^2$ ) is the area of the electrode,  $\Gamma_T$  ( $\text{mol}/\text{cm}^2$ ) is the surface concentration of the electroactive guanosine,  $Q$  (C) is the quantity of charge consumed during the electrooxidation reaction and  $\nu$  (V/s) is the scan rate.

Based on the relationship of  $I_{pa}$  with  $\nu$  and by integrating the peak area for guanosine oxidation, the values of  $n$  and  $\Gamma_T$  were obtained with the results as 1.9 and  $5.02 \times 10^{-9} \text{ mol}/\text{m}^2$ , respectively. The value of  $n$  indicated that two electrons took part in the oxidation reaction, which was similar with Refs. [34,35].

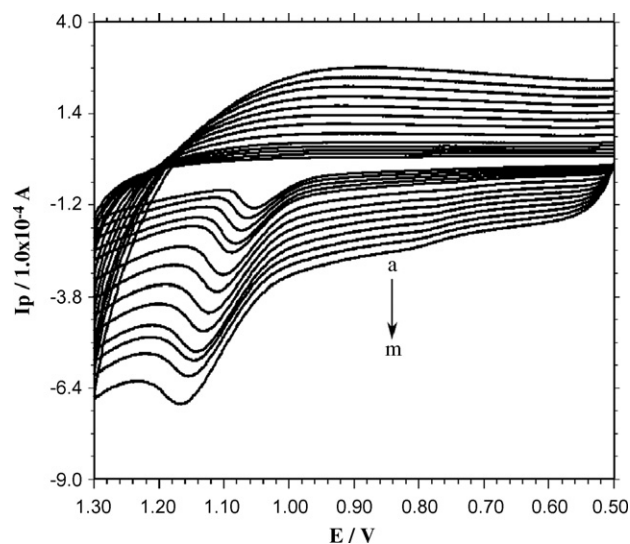


Fig. 3. Cyclic voltammograms of  $5.0 \times 10^{-5} \text{ mol/L}$  guanosine in pH 4.5 B–R buffer solution with different scan rates (from a to m: 20, 30, 40, 50, 60, 80, 100, 120, 140, 160, 180, 200, 220 mV/s).

The relationship of  $E_{pa}$  with  $\ln v$  was further constructed for the calculation of the electrochemical parameters. In the scan rate range from 10.0 to 300.0 mV/s, the linear regression equation was expressed as  $E_{pa}$  (V) = 0.049  $\ln v$  (V/s) + 1.228 ( $n = 13$ ,  $\gamma = 0.991$ ). Based on the Laviron's equations [38]:

$$E_{pa} = E^{0'} + \frac{RT}{(1-\alpha)nF} \ln v$$

$$\log k_s = \alpha \log(1-\alpha) + (1-\alpha) \log \alpha - \log \frac{RT}{nFv} - \frac{(1-\alpha)\alpha nF \Delta E_p}{2.3RT}$$

Then the values of the electron transfer coefficient ( $\alpha$ ) and the electrode reaction standard rate constant ( $k_s$ ) were calculated as 0.74 and  $1.26 \times 10^{-4} \text{ s}^{-1}$ , respectively.

### 3.4. Effect of accumulating conditions

Since the electrode process of guanosine was adsorption-controlled on the CILE, the effect of accumulating conditions for the  $5.0 \times 10^{-5} \text{ mol/L}$  guanosine at the CILE was investigated. With the increase of accumulating time the oxidation peak current increased within 300 s and then leveled off, which indicated that the adsorption of guanosine on the CILE was saturated. The accumulating potential was also investigated in the range from +0.1 to +0.8 V and the maximum peak current was got at +0.6 V. So the accumulating potential of +0.6 V was used for guanosine detection.

### 3.5. Calibration curve

A series of guanosine solutions were measured by cyclic voltammetry in order to test the feasibility of the proposed procedure under the selected conditions. The oxidation peak currents were increased linearly to guanosine concentration in the range from  $1.0 \times 10^{-6}$  to  $1.0 \times 10^{-4} \text{ mol/L}$  with two sections. The linear regression equations were got as  $I_{pa}$  ( $\mu\text{A}$ ) = 12.66C ( $\mu\text{mol/L}$ ) - 5.2 ( $n = 10$ ,  $\gamma = 0.990$ ) in the range of  $1.0 \times 10^{-6}$  to  $1.0 \times 10^{-5} \text{ mol/L}$  and  $I_{pa}$  ( $\mu\text{A}$ ) = 2.58C ( $\mu\text{mol/L}$ ) + 117.1 ( $n = 11$ ,  $\gamma = 0.993$ ) in the range from  $1.0 \times 10^{-5}$  to  $1.0 \times 10^{-4} \text{ mol/L}$ . The detection limit of guanosine with CILE was estimated to be  $2.61 \times 10^{-7} \text{ mol/L}$  ( $S/N = 3$ ) and the relative standard deviation (R.S.D.) for  $1.5 \times 10^{-6} \text{ mol/L}$  guanosine was 3.5% with 7 times parallel determinations.

### 3.6. Interferences

The influences of some foreign substances on the determination of  $1.0 \times 10^{-5} \text{ mol/L}$  guanosine were investigated. The proposed method showed good selectivity for guanosine detection without the interferences from common coexisting compounds. For example,  $1.0 \times 10^{-4} \text{ mol/L}$  of metal ions (e.g.  $\text{Al}^{3+}$ ,  $\text{Mg}^{2+}$ ,  $\text{Cu}^{2+}$ ,  $\text{Zn}^{2+}$ ), uric acid, ascorbic acid and dopamine barely influenced the current response of  $1.0 \times 10^{-5} \text{ mol/L}$  guanosine (signal changes below 5%).

### 3.7. Electrochemical response of guanosine and guanine

The CILE also showed excellent ability to distinguish the electrochemical responses of guanosine and guanine in the mixed solution. Fig. 4 showed the cyclic voltammograms of different concentrations of guanosine with a fixed concentration of guanine on the CILE in 0.2 mol/L pH 4.5 B-R buffer solution. Two well-defined oxidation peaks appeared at 1.12 V and 0.84 V (vs. SCE), respectively, which were corresponded to the oxidation of guanosine and guanine. The peak-to-peak separation was 280 mV, which was large enough for the simultaneous determination. With the increase of the guanosine concentration the oxidation peak currents of guanosine also increased gradually. Thus, electrochemical signals of guanosine and

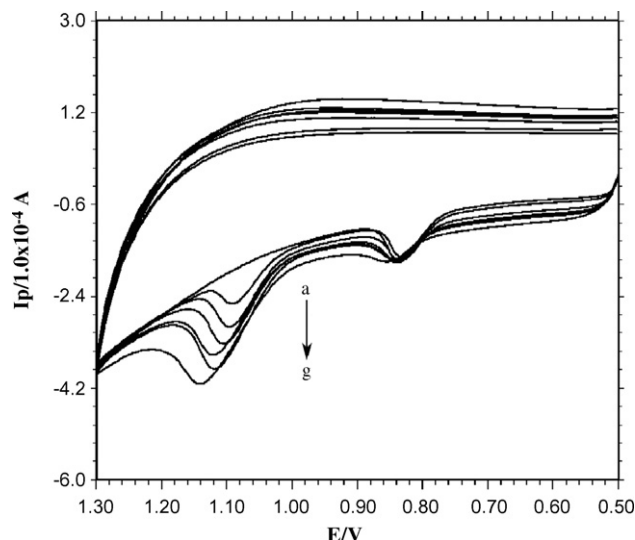


Fig. 4. Cyclic voltammograms of different guanosine concentrations (from a to g: 0, 10, 20, 30, 40, 50, 80  $\mu\text{mol/L}$ ) in the presence of  $1.0 \times 10^{-5} \text{ mol/L}$  guanine in pH 4.5 B-R buffer solution at the scan rate of 100 mV/s.

Table 1

Analytical recovery of guanosine added to urine samples.

	Added ( $\mu\text{M}$ )	Found ( $\mu\text{M}$ )	Recovery (%)
Sample 1	10.0	10.27	102.7
	30.0	29.22	97.4
	50.0	51.90	103.8
	80.0	83.44	104.3
Sample 2	10.0	9.82	98.2
	30.0	30.87	102.9
	50.0	48.25	96.5
	80.0	83.68	104.6

guanine were independent of each other at CILE and hence CILE showed good ability to distinguish the electrochemical response.

### 3.8. Stability and reproducibility of the modified electrode

The stability of the modified electrode was further evaluated. After the modified electrode was stored for 3 weeks, only a small decrease of peak current with a relative standard deviation (R.S.D.) of about 4.7% for  $5.0 \times 10^{-5} \text{ mol/L}$  guanosine was observed, which could be attributed to the excellent stability of the modified electrode. Four modified electrodes were prepared with the same procedure and used for  $5.0 \times 10^{-5} \text{ mol/L}$  guanosine detection. The results showed an acceptable reproducibility with a R.S.D. of 3.2%.

### 3.9. Analytical applications

The practical analytical application of the method was further established by the selective measurement of guanosine in human urine. Two human urine samples obtained from laboratory personnel were preliminary treated according to the general procedure. Then the samples were spiked with certain amounts of guanosine standard solution directly. The results of the determination were listed in Table 1. The recovery of the spiked guanosine was determined and the results were ranged from 96.5 to 104.6%, demonstrating the accuracy of the proposed method.

## 4. Conclusions

In this paper the electrochemical behaviors of guanosine on the N-butylpyridinium hexafluorophosphate (BPPF<sub>6</sub>) modified carbon

paste electrode was investigated carefully. Compared with the traditional CPE, great improvements of the electrochemical response of guanosine on CILE were observed, indicating the superiority of CILE over CPE with IL as the modifier. The presence of IL showed the adsorptive ability and had good promotion to the oxidation of guanosine. The electrochemical parameters of guanosine on CILE were carefully calculated with the electrochemical oxidation mechanism proposed. Under the selected conditions a new electrochemical method for guanosine detection was further established and successfully applied to the human urine sample determination.

### Acknowledgements

We are grateful to the financial support of the National Nature Science Foundation of China (Nos. 20405008 and 20635020) and the Science Foundation of General Administration of Quality Supervision, Inspection and Quarantine of the People's Republic of China (20071K167).

### References

- [1] O. Hiroyuki, *Electrochemical Aspects of Ionic Liquids*, John Wiley & Sons, Inc., 2005.
- [2] G. Maciej, L. Andrzej, S. Izabela, *Electrochim. Acta* 51 (2006) 5567.
- [3] H. Rika, H. Takayuki, T. Tetsuya, I. Yasuhiko, *J. Fluorine Chem.* 105 (2000) 221.
- [4] N. Nishi, S. Imakura, T. Kakiuchi, *Anal. Chem.* 78 (2006) 2726.
- [5] C.M. Lang, K. Kim, L. Guerra, P.A. Kohl, *J. Phys. Chem. B* 109 (2005) 19454.
- [6] A.S. Yazdi, N. Razavi, S.R. Yazdinejad, *Talanta* 75 (2008) 1293.
- [7] J.H. Wang, D.H. Cheng, X.W. Chen, Z. Du, Z.L. Fang, *Anal. Chem.* 79 (2007) 620.
- [8] X.X. Han, D.W. Armstrong, *Acc. Chem. Res.* 40 (2007) 1079.
- [9] J.B. Zheng, Y. Zhang, P.P. Yang, *Talanta* 73 (2007) 920.
- [10] C.M. Li, J.F. Zang, D.P. Zhan, W. Chen, C.Q. Sun, A.L. Teo, Y.T. Chua, V.S. Lee, S.M. Moochhala, *Electroanalysis* 18 (2006) 713.
- [11] H. Liu, P. He, Z. Li, C. Sun, L.J. Shi, Y. Liu, G.Y. Zhu, J.H. Li, *Electrochem. Commun.* 7 (2005) 1357.
- [12] W. Sun, M.X. Yang, K. Jiao, *Anal. Bioanal. Chem.* 389 (2007) 1283.
- [13] W. Sun, Y.Z. Li, M.X. Yang, S.F. Liu, K. Jiao, *Electrochem. Commun.* 10 (2008) 298.
- [14] H. Chen, Y. Wang, Y. Liu, Y. Wang, L. Qi, S. Dong, *Electrochem. Commun.* 9 (2007) 469.
- [15] X. Lu, J. Hu, X. Yao, Z. Wang, J. Li, *Biomacromolecules* 7 (2006) 975.
- [16] W. Sun, R.F. Gao, K. Jiao, *J. Phys. Chem. B* 111 (2007) 4560.
- [17] W. Sun, D.D. Wang, R.F. Gao, K. Jiao, *Electrochem. Commun.* 9 (2007) 1159.
- [18] F. Zhao, X. Wu, M.K. Wang, Y. Liu, L.X. Gao, S.J. Dong, *Anal. Chem.* 76 (2004) 4960.
- [19] N. Maleki, A. Safavi, F. Tajabadi, *Anal. Chem.* 78 (2006) 3820.
- [20] N. Maleki, A. Safavi, F. Sedaghati, F. Tajabadi, *Anal. Biochem.* 369 (2007) 149.
- [21] A. Safavi, N. Maleki, O. Moradlou, F. Tajabadi, *Anal. Biochem.* 359 (2006) 224.
- [22] F.Q. Zhao, L.Q. Liu, F. Xiao, J.W. Li, R. Yan, S.S. Fan, B.Z. Zeng, *Electroanalysis* 19 (2007) 1387.
- [23] Y. Zhang, J.B. Zheng, *Talanta* 77 (2008) 325.
- [24] J.A. Laszlo, D.L. Compton, *J. Mol. Catal. B* 18 (2002) 109.
- [25] J. Yang, G.W. Xu, H.W. Kong, Y.F. Zheng, T. Pang, Q. Yang, *J. Chromatogr. B* 780 (2002) 27.
- [26] H. Lin, D.K. Xu, H.Y. Chen, *J. Chromatogr. A* 760 (1997) 227.
- [27] E. Fortin, J.C. Tune, P. Mailley, S. Szunerits, B. Marcus, J.P. Petit, M. Mermoux, E. Vieil, *Bioelectrochemistry* 63 (2004) 303.
- [28] A.A. Magana, K. Wrobel, Y.A. Caudillo, S. Zaina, G. Lund, K. Wrobel, *Anal. Biochem.* 374 (2008) 378.
- [29] F.Q. Yang, J. Guan, S.P. Li, *Talanta* 73 (2007) 269.
- [30] S. Giannattasio, S. Gagliardi, M. Samaja, E. Marra, *Brain Res. Protoc.* 10 (2003) 168.
- [31] R.N. Goyal, V.K. Gupta, M. Oyamab, N. Bachheti, *Talanta* 71 (2007) 1110.
- [32] R.N. Goyal, M. Oyamab, A. Tyagi, *Anal. Chim. Acta* 581 (2007) 32.
- [33] M. Musameh, J. Wang, *Anal. Chim. Acta* 606 (2008) 45.
- [34] E.E. Ferapontova, *Electrochim. Acta* 49 (2004) 1751.
- [35] R.N. Goyal, N. Jain, D.K. Garg, *Bioelectrochem. Bioenerg.* 43 (1997) 105.
- [36] E. Laviron, *J. Electroanal. Chem.* 101 (1979) 19.
- [37] J. Wang, *Analytical Electrochemistry*, 2nd edn., Wiley–VCH, New York, 2000, p. 37.
- [38] E. Laviron, *J. Electroanal. Chem.* 100 (1979) 263.



## Quantitative extraction of organic tracer compounds from ambient particulate matter collected on polymer substrates

Qinyue Sun<sup>a</sup>, Olga A. Alexandrova<sup>b</sup>, Pierre Herckes<sup>c</sup>, Jonathan O. Allen<sup>a,b,\*</sup>

<sup>a</sup> Department of Chemical Engineering, Arizona State University, Tempe, AZ 85287-6006, United States

<sup>b</sup> Department of Civil and Environmental Engineering, Arizona State University, Tempe, AZ 85287-5307, United States

<sup>c</sup> Department of Chemistry and Biochemistry, Arizona State University, Tempe, AZ 85287-1604, United States

### ARTICLE INFO

#### Article history:

Received 20 November 2008

Received in revised form 13 January 2009

Accepted 14 January 2009

Available online 24 January 2009

#### Keywords:

Particulate matter  
Solvent extraction  
Impactor  
Polyurethane foam  
Polypropylene foam

### ABSTRACT

Organic compounds in ambient particulate matter (PM) samples are used as tracers for PM source apportionment. These PM samples are collected using high volume samplers; one such sampler is an impactor in which polyurethane foam (PUF) and polypropylene foam (PPF) are used as the substrates. The polymer substrates have the advantage of limiting particle bounce artifacts during sampling; however these substrates may contain background organic additives. A protocol of two extractions with isopropanol followed by three extractions with dichloromethane (DCM) was developed for both substrate precleaning and analyte extraction. Some residual organic contaminants were present after precleaning; expressed as concentrations in a 24-h ambient PM sample, the residual amounts were  $1 \mu\text{g m}^{-3}$  for plasticizers and antioxidants, and  $10 \text{ ng m}^{-3}$  for *n*-alkanes with carbon number lower than 26. The quantification limit for all other organic tracer compounds was  $\approx 0.1 \text{ ng m}^{-3}$  in a 24-h ambient PM sample. Recovery experiments were done using NIST Standard Reference Material (SRM) Urban Dust (1649a); the average recoveries for polycyclic aromatic hydrocarbons (PAHs) from PPF and PUF substrates were  $117 \pm 8\%$  and  $107 \pm 11\%$ , respectively. Replicate extractions were also done using the ambient samples collected in Nogales, Arizona. The relative differences between repeat analyses were less than 10% for 47 organic tracer compounds quantified. After the first extraction of ambient samples, less than 7% of organic tracer compounds remained in the extracted substrates. This method can be used to quantify a suite of semi- and non-polar organic tracer compounds suitable for source apportionment studies in 24-h ambient PM samples.

© 2009 Elsevier B.V. All rights reserved.

### 1. Introduction

Airborne particulate matter (PM) has been shown to be harmful to human health [1–4] and the US Environmental Protection Agency (EPA) has set air quality standards for PM concentrations. PM can be emitted directly into the atmosphere (*primary PM*), or formed in the atmosphere by gas-to-particle conversion (*secondary PM*) [5]. Primary PM and PM-precursors are released by a large number of sources and may be extensively transformed in the atmosphere. Identification of the main sources of ambient PM is a first step in the effective and efficient control of ambient PM. Primary organic PM is emitted from natural and anthropogenic sources, including diesel engine exhaust, gasoline engine exhaust, cooking exhaust, cigarette

smoke, road dust, tire wear and vegetative detritus. Primary organic PM contributes approximately 10–30% of the total PM mass present in urban and rural locations in the U.S. [6–9].

Source apportionment is a method for quantifying the contribution that different emission sources make to the PM concentrations at a receptor location [10,11]. Previous studies have demonstrated that organic species quantified using gas chromatography/mass spectrometry (GC/MS) may be used as organic tracer compounds for source apportionment of primary organic PM [7,12–16]. Those organic tracers include polycyclic aromatic hydrocarbons (PAHs) and oxygenated polycyclic aromatic hydrocarbons (OPAHs) from incomplete combustion, *n*-alkanes from vehicle exhaust, and hopanes and steranes from vehicle emissions of lubricant oil [17–24]. Additional organic compounds include 2-(4-morpholinyl) benzothiazole (24MoBT) from tire wear, levoglucosan and retene from wood combustion, and cholesterol and oleic acid from food cooking [25–30].

Organic tracer compounds are present in the atmosphere in concentrations of approximately  $1 \text{ ng m}^{-3}$ , so extended sampling using high volume samplers is usually required to collect quantifiable

\* Corresponding author. Present address: Department of Environmental Health, Harvard School of Public Health, 677 Huntington Avenue, Boston, MA 02115, United States. Tel.: +1 480 2157488.

E-mail addresses: [qinyue.sun@asu.edu](mailto:qinyue.sun@asu.edu) (Q. Sun), [olga.alexandrova@asu.edu](mailto:olga.alexandrova@asu.edu) (O.A. Alexandrova), [pierre.herckes@asu.edu](mailto:pierre.herckes@asu.edu) (P. Herckes), [jon@joallen6.com](mailto:jon@joallen6.com) (J.O. Allen).

amounts of these compounds. Ambient PM samples for organic tracer analysis have usually been collected using a high volume sampler in which particles with aerodynamic diameter,  $D_a$ , larger than 2.5  $\mu\text{m}$  are removed by impaction and particles with  $D_a$  less than 2.5  $\mu\text{m}$  are collected on quartz fiber filters (QFFs) or glass fiber filters (GFFs) [7,12–15].

PM sources emit particles with distinct size distributions, further the behavior and fate of aerosol particles in the atmosphere are strongly dependent on their size [31]. The connection between organic tracer compounds and particle size has motivated the collection of size-segregated PM samples using cascade impactors [32–37]. When impactors are used to collect size-segregated PM samples, particles which strike the impaction substrate may rebound from it, or they may strike built-up deposits and re-entrain previously collected material. These sampling artifacts are indistinguishable and are collectively called “particle bounce”. Turner and Hering [38] demonstrated that for multi-layered solid particle deposits, less than 50% of solid particles were collected on uncoated stages, while more than 90% of solid particles were collected on an impaction substrate impregnated with moderate viscosity (30–300 centistokes) oil. Prior to analysis the organic tracer compounds must then be separated from the oil, for example by high performance liquid chromatography (HPLC) [32].

Demokritou et al. [39] have designed a high volume cascade impactor (ChemVol, Model 2400, Thermo Fisher Scientific, Waltham, MA) suitable for high volume size-segregated PM collection. This impactor has four impaction stages for PM collection in these size ranges: Stage 1:  $D_a > 10 \mu\text{m}$ ; Stage 2:  $D_a = 2.5\text{--}10 \mu\text{m}$ ; Stage 3:  $D_a = 1.0\text{--}2.5 \mu\text{m}$ ; and Stage 4:  $D_a = 0.1\text{--}1.0 \mu\text{m}$ . An after filter (AF) stage is used to collect particles smaller than the final cut-off diameter. Polyurethane foam (PUF) is used as the impaction media and polypropylene foam (PPF) is used as the after filter media. The PUF and PPF are chemically somewhat inert and thus minimize interference with chemical, biological, and toxicological tests [40,41]. Like oil-impregnated membranes, PUF substrates have been shown to efficiently collect particles at high loadings [40,41]. Although no oil or grease coating is required for the PUF substrates, the polymer media contain residual organic species including additives and oligomers which might interfere with later analysis [40]. The PPF filter media also likely contains residual organic species.

Once collected organic tracer compounds are isolated from the substrates by solvent extraction, using either sequential extraction with ultrasonication or Soxhlet extraction. Substrates are usually spiked with isotopically labeled internal standards, extracted, and concentrated; organic compounds are then quantified using GC/MS techniques [27,42–44]. Commonly used solvents include dichloromethane (DCM) [45,14,15]; benzene and isopropanol [46]; hexanes, benzene and isopropanol [7]; hexanes [47]; DCM and methanol [48]; and toluene [49]. The extraction procedures are designed to remove both semi- and non-polar organic tracer species.

The polymer substrates, PUF and PPF, have been used for organic PM sample collection and analysis in previous studies [50,51]. Salonen et al. [52] collected ambient PM on a PUF substrate using a high-volume inertial impactor similar to the ChemVol. They extracted the PUF substrates first using sonication with methanol; these extracts were dried and pooled; the methanol extracts were then Soxhlet extracted using DCM. This technique seems primarily designed to measure organics in doses for toxicological experiments, not organic concentrations in ambient PM. Pennanen et al. [53] used a similar extraction method. Initial extraction using methanol is not expected to quantitatively recover the entire suite of organic tracer compounds, particularly higher molecular weight (MW) non-polar species including *n*-alkanes with carbon number greater than 25 and PAHs with MW larger than pyrene because these have poor solubility in methanol [54].

PUF cartridges have also been used following filters to collect gas-phase semi-volatile organic compounds [55,56,28,21,57,34]. Fraser et al. [55,56] extracted the PUF plugs three times successively with DCM. Schauer et al. [21,28] extracted PUF cartridges twice with hexanes followed by three successive benzene/isopropanol (2:1) extractions. Fernández et al. [34] used Soxhlet extraction with hexanes for 24 h to extract PUF plugs. Dachs and Eisenreich [57] used Soxhlet extraction with petroleum ether for PUF extraction.

In this study, methods for precleaning and extracting a suite of organic tracer compounds from ambient PM collected on PUF and PPF substrates are evaluated. Repeated precleaning extractions, recovery experiments with NIST Standard Reference Material, and repeated analyses of ambient PM samples are used to evaluate the methods. Organic contaminants inherent to PUF and PPF substrates and a range of organic tracer compounds including semi- and non-polar compounds in ambient samples are quantified. We evaluate whether the present analytical methods may be used for the analysis of organic tracer compounds in size-segregated PM samples collected on polymer substrates over 24 h.

## 2. Methods

### 2.1. Polymer substrate preparation

All glassware and laboratory tools were cleaned first using detergent and water, then rinsing three times each with deionized water, isopropanol (Burdick & Jackson, high purity 99.9%) and DCM (Burdick & Jackson, high purity 99.9%).

PUF substrates (Thermo Fisher Scientific, Waltham, MA) were annular pieces approximately 5 mm thick designed to collect PM below the ChemVol slot impingers. Substrates were cleaned as whole annular pieces. Each impactor stage had three slits arranged as segments of a circle; PM samples were collected in three arc sections on the PUF substrates. After sample collection, the PUF substrates were cut into thirds so that the PM collected under each slit was a replicate sample. The PPF substrates were also divided in thirds. In this paper a substrate section refers to one-third of the whole substrate. The mass of whole PUF substrate for Stage 1 was 0.718 g; Stage 2 was 0.662 g; Stage 3 and Stage 4 use the same size substrate and the mass was 0.362 g. The mass for whole PPF substrate was 5.76 g.

PUF substrates were precleaned using sequential solvent extraction to remove both semi- and non-polar organic compounds. The substrates were first put in a cleaned, wide mouth, 2 L glass jar with a Teflon-lined cap. Isopropanol was added to cover and the substrate was sonicated (Branson model 5510R-MTH 42 KHz) at room temperature for 15 min. The solvent was discarded. Cleaning with isopropanol was repeated two times. DCM was then added to cover and the substrates were sonicated for 15 min. Cleaning with DCM was repeated three times. The volume of the isopropanol and DCM added each time depended on the number of substrates cleaned in each batch. Usually six PUF substrates were cleaned at the same time and 15–30 ml of solvent was used per substrate for each cleaning. After each cleaning, substrates were removed from the solvent using precleaned tweezers; the solvent drained easily from the open cell PUF. Substrates were spread flat on a piece of precleaned aluminum foil to maintain shape and covered with a second piece of precleaned aluminum foil to prevent contamination. The PUF substrates were dried in a ventilation hood under atmosphere pressure. The dried substrates were transferred to a precleaned amber jar and stored at  $-20^\circ\text{C}$ .

The PPF preparation procedure was similar to that used for PUF. Different from the PUF substrates, the PPF media was a fiber mat which retained a large solvent volume. Following each cleaning with isopropanol and DCM, PPF substrates were spread on a pre-



cleaned inclined stainless steel plate and a precleaned glass tube was rolled the length of substrate with moderate pressure in order to squeeze out solvent.

Solvents used for substrate cleaning were normally discarded. In order to evaluate the substrate cleaning procedure, cleaning solvents were collected for analysis. For these experiments, two sections of the Stage 2 PUF substrate were cleaned together. Two sections of the PPF substrate were also cleaned together. The entire cleaning procedure (two cleanings with isopropanol followed by three cleanings with DCM) was then repeated a second and third time. Solvents from these repeated cleanings were also collected separately for analysis.

## 2.2. Ambient sample extraction

Organic tracers were extracted from the polymer substrates using sequential solvent extraction analogous to the substrate cleaning procedure. A one-third section of a polymer substrate was cut into pieces of approximately 10 mm × 6 mm using precleaned scissors and the pieces were placed in a precleaned, wide mouth, 200 ml amber jar with a Teflon-lined cap. A 100- $\mu$ l aliquot of a 10-ng  $\mu$ l<sup>-1</sup> solution of perdeuterated internal standards was pipetted evenly to the substrate so that approximately 1  $\mu$ g of each internal standard was added. The internal standards were *n*-decane *D*<sub>22</sub>, *n*-tetracosane *D*<sub>50</sub>, *n*-hexatriacontane *D*<sub>74</sub>, naphthalene *D*<sub>8</sub>, phenanthrene *D*<sub>10</sub>, pyrene *D*<sub>10</sub>, benzo[*e*]pyrene *D*<sub>12</sub>, chrysene *D*<sub>12</sub>, dibenz[*a,h*]anthracene *D*<sub>14</sub>, *n*-decanoic acid *D*<sub>19</sub>, and palmitic acid *D*<sub>31</sub>.

A precleaned stainless steel disk with a stainless steel spring attached was placed on top of the substrate in the jar; when the lid of the jar was closed, the spring was slightly compressed in order to minimize solvent volume and to keep the substrate submerged in the solvent during sonication. Isopropanol was added to cover the substrate; the substrate was sonicated for 15 min and the solvent collected afterwards. The substrate was extracted with isopropanol two times. This was followed by three sequential extractions using the same procedure with DCM. The volume of isopropanol and DCM used for each extraction was 20–40 ml for one-third of a PUF or PPF substrate.

The isopropanol and DCM extracts were combined and concentrated under ultra high purity nitrogen (Air Liquide America) until the extract volume was reduced to approximately 30 ml. The extract was then filtered using a 0.2- $\mu$ m PTFE membrane (Life Science), and concentrated again to a volume between 100  $\mu$ l and 1 ml. During concentration, the extract was placed on a heated plate maintained at approximately 35 °C.

Extracts were analyzed using an Agilent GC/MS (Model 6890) equipped with a quadrupole mass detector system (Agilent MSD 5973 inert). Separation was completed using a 30 m × 250  $\mu$ m × 0.25  $\mu$ m HP-5MS capillary column coated with 5% phenyl methyl siloxane. The temperature program started at 50 °C for 1 min; the column temperature was raised at 4 °C min<sup>-1</sup> to 310 °C; temperature was then held for 15 min at 310 °C.

Authentic standard solutions including internal standards were analyzed using the GC/MS for identification and quantification of organic compounds. Authentic standards were available for all compounds reported here except for bis(2-ethylhexyl) adipate which was identified by comparison with the NIST mass spectrum library. The amounts of organic tracer compounds were calculated relative to the internal standards [44]. The responses of internal standards and tracer compounds were measured as the integrated response for ions of a characteristic and prominent mass-to-charge ratio; e.g., the molecular ion for PAHs and 57 for *n*-alkanes. The relative response factors (*RF*) for each organic tracer were determined from an authentic quantification standard or a standard with similar molecular weight and functionality. The amounts were calculated

as the product of *RF*, tracer compound response, and amount of internal standard added divided by internal standard response.

## 2.3. Ambient PM samples

Recovery of known analytes from standard reference material was measured in order to evaluate the extraction procedures. Approximately 10 mg of NIST Standard Reference Material Urban Dust (1649a) was added to one-third sections of PUF and PPF substrates. Three replicate samples were analyzed for each substrate. These samples were extracted and analyzed as described above.

Ambient PM samples were collected for 24 h on 6 and 10 January 2006 in Nogales, AZ, using a ChemVol 2400 [58]. The sampling site was the air quality monitoring station operated by the Arizona Department of Environmental Quality (ADEQ) at the Nogales Post Office (latitude 31°20.240', longitude 110°56.232'). This site is approximately 1 km north of the US–Mexico border and experiences high PM concentrations in winter. The averaged PM<sub>2.5</sub> and PM<sub>10</sub> concentrations were 19  $\mu$ g m<sup>-3</sup> and 181  $\mu$ g m<sup>-3</sup> on 6 January 2006 and 31  $\mu$ g m<sup>-3</sup> and 257  $\mu$ g m<sup>-3</sup> on 10 January 2006 [59]. The impactor was operated with Stage 1 (S1), Stage 2 (S2), and the after filter (AF) to collect PM with *D*<sub>a</sub> between 2.5  $\mu$ m and 10  $\mu$ m on S2 and PM<sub>2.5</sub> on the AF. One-third sections of the PUF and PPF substrates from each day were extracted in February 2006 and analyzed in June 2006. In February 2008 another one-third section of the PUF and PPF substrates were extracted and analyzed in order to test the reproducibility of the results. The ambient sample substrates which had been extracted were extracted again and the second extracts analyzed to evaluate the efficiency of this extraction method.

## 3. Results and discussion

### 3.1. PPF and PUF preparation

Two sections each of PPF and PUF substrates were cleaned using the above procedure (two cleanings with isopropanol followed by three cleanings with DCM) and this procedure was repeated a second and a third time. The solvents were separately collected and analyzed for organic compounds.

Antioxidants and plasticizers were found in PPF substrates; these were octadecyl 3(3,5-di-tert-butyl-4-hydroxyphenyl) propionate (Irganox 1076, CAS number 2082-79-3), tris(2,4-di-tert-butyl-phenyl)phosphite (Irgafos 168, CAS number 31570-04-4), and bis(2-ethylhexyl)phthalate (DEHP, CAS number 117-81-7) (see Fig. 1). The amount of most polymer additives in the extract from the second cleaning was approximately a factor of 10 lower than the extract from the first cleaning; the extract from the third cleaning contained measureable amounts of polymer additives (see Table 1). One exception was Irgafos 168, the concentration of which was approximately constant in the first and second extracts; these results suggest that that Irgafos 168 was not depleted in the substrate until after the second cleaning. The antioxidant and plasticizer in the blank PUF substrate were Irganox 1076 and DEHP (see Fig. 2). The amount of these polymer additives in the extract from the second cleaning was also approximately a factor of 10 lower than the extract from the first cleaning (see Table 2).

*n*-alkanes with carbon numbers lower than 26 were also found in the PPF substrate and *n*-alkanes with carbon number lower than 24 were found in the PUF substrate. These were likely introduced during manufacture as lubricants. The amount of 13 *n*-alkanes in the extract from the second cleaning of the PPF substrate was approximately a factor of 3 lower than the extract from the first cleaning; the extract from the third cleaning contained approximately the same amount as that from the second cleaning (see Table 1). In PUF the amounts of *n*-alkanes in the extracts from all three cleanings were approximately

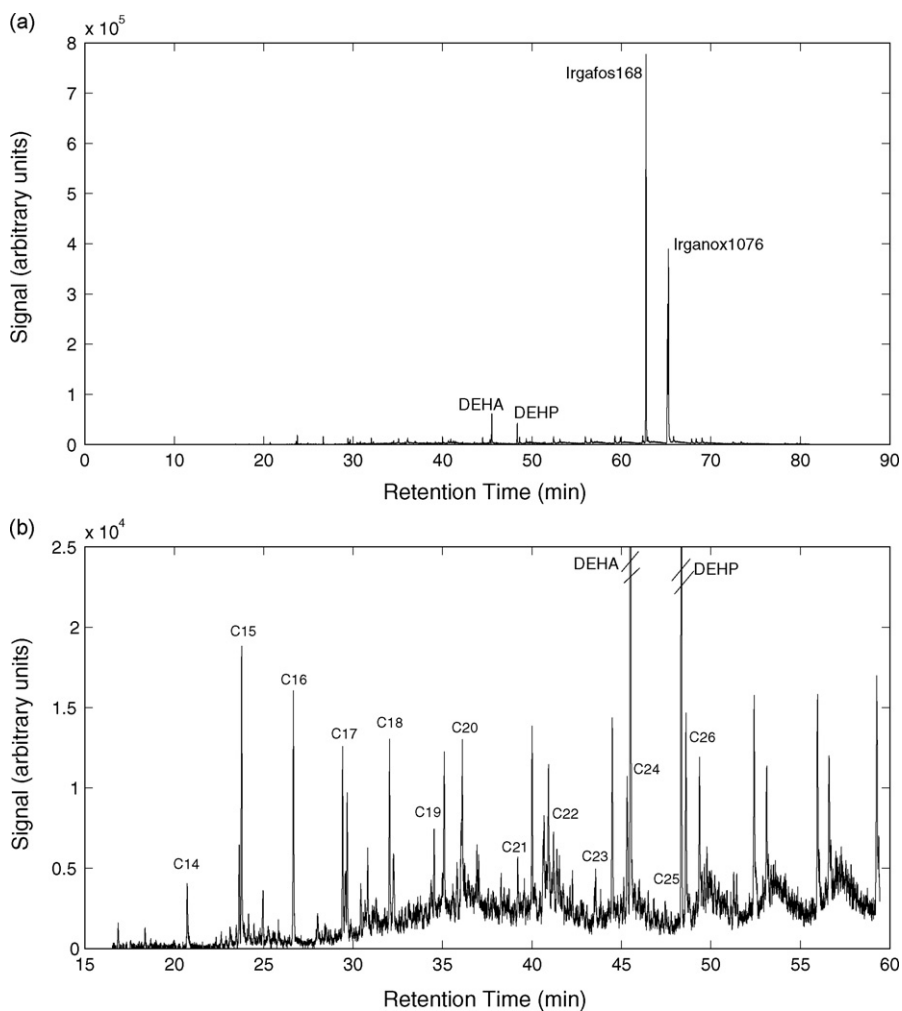


**Fig. 1.** Extracted ion chromatograms for an alkane fragment ion ( $m/z = 57$ ) in second cleaning extract of PPF blank substrate: (a) original chromatogram and (b) chromatogram with expanded scale.

constant (see Table 2). These results suggest that one cleaning cycle removes a large fraction of extractable plasticizers, and that repeated extractions are not effective in reducing the extract polymer additives and *n*-alkanes with low carbon number.

The precleaning of blank PPF and PUF substrates effectively reduced the concentration of organic contaminants in the extract by a factor of approximately 3–10, but the remaining material would interfere with the quantification of these compounds in ambient PM samples. The residual amounts can be expressed in

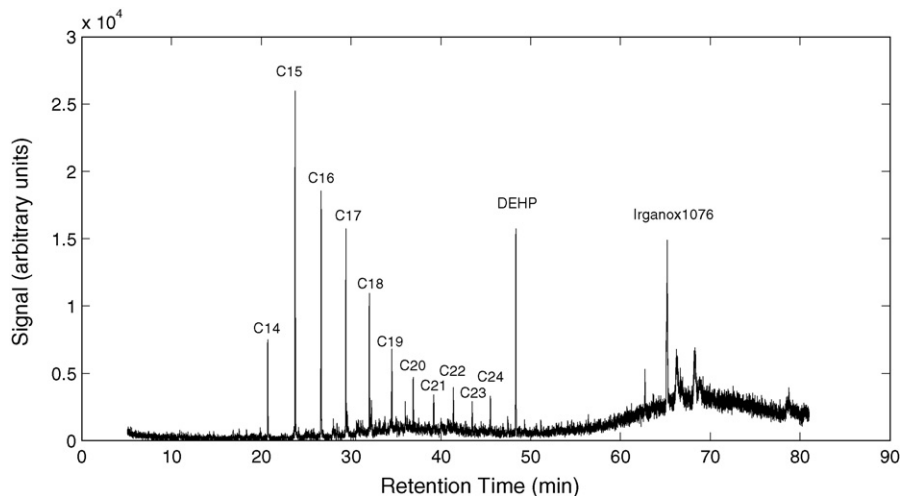


**Fig. 2.** Extracted ion chromatograms for an alkane fragment ion ( $m/z = 57$ ) in second cleaning extract of PUF blank substrate.

**Table 1**Mass fraction of antioxidants, plasticizers, and *n*-alkanes extracted from blank PPF substrates.

Compound	First cleaning (ppm)	Second cleaning (ppm)	Third cleaning (ppm)
Irganox 1076	147	16.1	0.37
Irgafos 168	45.4	45.1	5.31
DEHP	15.7	2.59	0.58
DEHA	15.0	1.82	0.005
C <sub>14</sub> <i>n</i> -alkane	0.63	0.21	0.21
C <sub>15</sub> <i>n</i> -alkane	1.80	0.74	0.70
C <sub>16</sub> <i>n</i> -alkane	2.03	0.66	0.64
C <sub>17</sub> <i>n</i> -alkane	1.84	0.54	0.50
C <sub>18</sub> <i>n</i> -alkane	2.19	0.50	0.41
C <sub>19</sub> <i>n</i> -alkane	0.82	0.23	0.20
C <sub>20</sub> <i>n</i> -alkane	0.31	0.10	0.10
C <sub>21</sub> <i>n</i> -alkane	0.95	0.25	0.18
C <sub>22</sub> <i>n</i> -alkane	1.09	0.24	0.20
C <sub>23</sub> <i>n</i> -alkane	0.08	0.07	0.07
C <sub>24</sub> <i>n</i> -alkane	20.4	0.25	0.19
C <sub>25</sub> <i>n</i> -alkane	0.23	0.11	0.08
C <sub>26</sub> <i>n</i> -alkane	1.87	0.51	0.46

**Table 2**Mass fraction of antioxidants, plasticizers, and *n*-alkanes extracted from blank PUF substrates.

Compound	First cleaning (ppm)	Second cleaning (ppm)	Third cleaning (ppm)
Irganox 1076	300	2.00	0.54
DEHP	12.1	6.02	5.82
C <sub>14</sub> <i>n</i> -alkane	2.94	2.67	2.86
C <sub>15</sub> <i>n</i> -alkane	1.16	1.28	1.07
C <sub>16</sub> <i>n</i> -alkane	7.97	6.91	7.24
C <sub>17</sub> <i>n</i> -alkane	5.85	5.10	5.64
C <sub>18</sub> <i>n</i> -alkane	4.71	4.01	4.17
C <sub>19</sub> <i>n</i> -alkane	1.99	2.29	2.45
C <sub>20</sub> <i>n</i> -alkane	1.22	1.38	1.27
C <sub>21</sub> <i>n</i> -alkane	1.41	1.05	1.14
C <sub>22</sub> <i>n</i> -alkane	1.46	1.33	1.07
C <sub>23</sub> <i>n</i> -alkane	5.46	5.01	5.32
C <sub>24</sub> <i>n</i> -alkane	1.43	1.09	1.32

equivalent ambient PM concentrations calculated as the organic compound mass in the second extract divided by the air volume sampled over 24 h. The equivalent residual amount for plasticizers and antioxidants is  $\approx 1 \mu\text{g m}^{-3}$ , and for *n*-alkanes (carbon number lower than 24 for PUF and 26 for PPF) is  $\approx 10 \text{ ng m}^{-3}$ .

Ambient concentrations of individual *n*-alkanes with carbon numbers between 23 and 26 have been reported: 3.2–11.2  $\text{ng m}^{-3}$  in Los Angeles of California [7]; 1.81–42.3  $\text{ng m}^{-3}$  in the San Joaquin Valley of California [12]; 0.02–4.00  $\text{ng m}^{-3}$  in southeastern United States [13]. These concentrations are of the same magnitude as the 10- $\text{ng m}^{-3}$  equivalent residual amount; thus PUF and PPF substrates are not recommended for measurement in ambient PM of *n*-alkanes with lower carbon numbers. However, *n*-alkanes with carbon number higher than 24 can be measured in PM samples collected on PUF substrates; and those with carbon numbers higher than 26 can be measured in PM samples collected on PPF substrates. In source apportionment studies, *n*-alkanes with carbon numbers higher than 24 are usually used [7,12,13,15]. Thus, despite the *n*-alkane contamination in PUF and PPF substrates, sufficient *n*-alkanes can be measured for source apportionment studies.

Besides the polymer additives and low carbon number *n*-alkanes, no other compounds used as organic tracers were detected in the blank substrate extracts. Without interference from the substrate, the quantification limits for organic tracer compounds is limited by instrument sensitivity; for the present method this is  $\approx 0.5 \text{ ng per } \mu\text{l}$  injection. An extract from a one-third section of PM

**Table 3**

Recovery of PAHs from NIST Standard Material Urban Dust (1649a) on PPF and PUF substrates.

PAH	Recovery from PPF (%)	Recovery from PUF (%)
Benz[ <i>a</i> ]anthracene	121 $\pm$ 2	102 $\pm$ 6
Triphenylene + chrysene	114 $\pm$ 6	99 $\pm$ 20
Benzo[ <i>b</i> + <i>k</i> ]fluoranthene	116 $\pm$ 11	110 $\pm$ 6
Benzo[ <i>e</i> ]pyrene	123 $\pm$ 5	114 $\pm$ 10
Benzo[ <i>a</i> ]pyrene	123 $\pm$ 5	113 $\pm$ 9
Indeno[1,2,3- <i>cd</i> ]pyrene	106 $\pm$ 6	107 $\pm$ 12
Benzo[ <i>ghi</i> ]perylene	119 $\pm$ 2	104 $\pm$ 8

Percentages are relative to NIST-certified concentrations. Means and standard deviations from three replicates are reported.

collected over 24 h and concentrated to 100  $\mu\text{l}$  results in a PM limit of quantification of  $\approx 0.1 \text{ ng m}^{-3}$ .

### 3.2. Recovery experiments

Recoveries of known semi- and non-polar analytes from standard reference material were measured in order to evaluate the extraction procedure. Aliquots of 10 mg NIST Urban Dust Standard Reference Material (SRM 1649a) were added to each of three sections of PUF and PPF substrates. PAHs were quantified in the extracts to estimate recovery (see Table 3). The average PAH recovery from PPF was  $117 \pm 8\%$  and from PUF was  $107 \pm 11\%$ . Extracted amounts of OPAHs were also quantified; note that certified values are not available for OPAHs in SRM 1649a. The concentrations of OPAHs recovered here was within the range published by others (see Table 4) [60–62]. One source of scatter in these results is likely due to the relatively low amounts, approximately 50 ng, of PAHs and OPAHs added here. In contrast, 24-h ambient PM samples contain approximately 1000 ng of individual PAHs and OPAHs as discussed below.

### 3.3. Ambient sample extraction

PM samples were collected using a ChemVol 2400 for 24 h on two days in January 2006 in Nogales, AZ. One section of the PUF and PPF substrates from 6 January 2006 and 10 January 2006 were extracted and analyzed separately; a second section of the PUF and PPF substrates from both days were later extracted and analyzed independently.

The concentration of non- and semi-polar organic tracer compounds [7] were quantified; results from the first analyses for selected analytes are presented in Table 5. These results are consistent with similar ambient measurements of these compounds [7,12,13,63,64]. In addition these organic tracer compounds were quantified: 18  $\alpha$  (H)-22,29,30-trisnorneohopane, 17  $\alpha$  (H)-22,29,30-trisnorhopane, 17  $\alpha$  (H)-21  $\beta$  (H)-29-norhopane, 18  $\alpha$  (H)-30-norhopane, 17  $\alpha$  (H)-21  $\beta$  (H)-hopane, 22S,17  $\alpha$  (H),21  $\beta$  (H)-30-homohopane, 22R,17  $\alpha$  (H),21  $\beta$  (H)-30-homohopane, 22S,17  $\alpha$  (H),21  $\beta$  (H)-30-bishomohopane, 22R,17  $\alpha$  (H),21  $\beta$  (H)-30-bishomohopane, 20S,13  $\beta$  (H),17  $\alpha$  (H)-diacholestane, 20R,13  $\beta$  (H),17  $\alpha$  (H)-diacholestane, 20R,5  $\alpha$  (H),14  $\beta$  (H),17  $\beta$  (H)-cholestane, 20S,5  $\alpha$  (H),14  $\beta$  (H),17  $\beta$  (H)-cholestane, 20R,5  $\alpha$  (H),14  $\beta$  (H),17  $\beta$  (H)-cholestane, 20S,5  $\alpha$  (H),14  $\beta$  (H),17  $\beta$  (H)-ergostane, 20R,5  $\alpha$  (H),14  $\beta$  (H),17  $\beta$  (H)-ergostane, 22R,5  $\alpha$  (H),14  $\beta$  (H),17  $\beta$  (H)-sitostane, and 22S,5  $\alpha$  (H),14  $\beta$  (H),17  $\beta$  (H)-sitostane [58].

Replicate extractions and analyses of organic tracer compounds collected with ambient PM were done in order to evaluate the reproducibility of the present analysis technique. Concentrations of all of the organic tracer compounds (including those not listed on Table 5) measured in two independent analyses agreed to within 10%, except for levoglucosan. Levoglucosan concentrations measured in the second analyses were 2–3 times lower than those in

**Table 4**  
OPAH concentrations ( $\text{ng g}^{-1}$ ) in NIST Standard Material Urban Dust (1649a) extracted from PPF and PUF substrates.

	This work	Fernandez and Bayona [60]	Durant et al. [61]	Albinet et al. [62]
9,10-anthraquinone	2051 (–)	220 (40)	2700 (120)	2238 (363)
Benzo[ <i>a</i> ]anthracene	2145 (128)	1310 (20)	4500 (340)	3715 (872)
Benz[ <i>a</i> ]anthracene-7,12-dione	5588 (1000)	7465 (1100)	2400 (250)	8459 (797)

Means and standard deviations from three replicates are reported.

**Table 5**  
Concentration ( $\text{ng m}^{-3}$ ) of organic tracer compounds from 24-h samples collected in Nogales in January 2006.

Compound	6 January 2006		10 January 2006	
	PM <sub>10–2.5</sub>	PM <sub>2.5</sub>	PM <sub>10–2.5</sub>	PM <sub>2.5</sub>
C <sub>25</sub> <i>n</i> -alkane	0.50	–	1.56	–
C <sub>26</sub> <i>n</i> -alkane	0.27	–	1.08	–
C <sub>27</sub> <i>n</i> -alkane	0.47	0.84	1.36	2.65
C <sub>28</sub> <i>n</i> -alkane	0.41	1.51	1.31	3.77
C <sub>29</sub> <i>n</i> -alkane	1.40	1.67	1.80	2.25
C <sub>30</sub> <i>n</i> -alkane	0.45	5.49	0.75	6.93
C <sub>31</sub> <i>n</i> -alkane	0.67	1.18	1.61	2.10
C <sub>32</sub> <i>n</i> -alkane	0.53	4.83	0.65	8.29
C <sub>33</sub> <i>n</i> -alkane	1.00	3.23	0.81	1.18
Benz[ <i>a</i> ]anthracene	0.25	1.62	0.24	0.18
Triphenylene + chrysene	0.41	1.73	0.23	0.17
Benzo[ <i>b</i> + <i>k</i> ]fluoranthene	0.06	3.49	0.10	3.49
Benzo[ <i>e</i> ]pyrene	–	1.59	0.11	1.49
Benzo[ <i>a</i> ]pyrene	–	2.48	0.09	2.44
Dibenz[ <i>a,h</i> ]anthracene	–	0.34	–	0.33
Indeno[1,2,3- <i>cd</i> ]pyrene	–	0.84	0.10	1.09
Benzo[ <i>ghi</i> ]perylene	–	4.06	0.11	2.78
9H-fluoren-9-one	0.17	0.29	0.33	0.29
9,10-phenanthrenequinone	–	1.78	0.89	0.70
9,10-anthraquinone	–	–	0.42	1.24
Xanthone	–	0.97	0.25	0.42
Benz[ <i>a</i> ]anthracene-7,12-dione	–	0.79	0.15	0.39
1,4-Chrysenequinone	–	–	–	–
Benzo[ <i>a</i> ]anthracene	–	–	0.15	2.60
17 $\alpha$ (H)-21 $\beta$ (H)-hopane	0.21	0.39	0.37	1.40
2-(4-Morpholinyl) benzothiazole	–	–	2.01	3.70
Cholesterol	–	0.13	–	0.14
Levogluconan	–	3.57	0.38	1.17
Retene	0.25	2.02	2.69	7.03
Octadecenoic acid	0.41	0.26	0.07	0.05

Analytes below the limit of quantification are indicated by “–”.

the first set of analyses. This result is consistent with those of Herckes et al. [36] and suggests that the addition of isotopically labeled levoglucosan standard or the derivatization of the extracts would lead to repeatable quantification of this compound.

Ambient PM sample substrates from the second analyses were extracted a second time in order to evaluate the extraction method. The concentrations of PAHs from the second extraction of the PPF media were  $\approx 7\%$  of the concentrations from the first extraction. OPAH concentrations from PPF, and PAH and OPAH concentrations from PUF in the second extraction were all below the GC/MS limit of quantification.

#### 4. Conclusions

The high volume size-segregated PM samples have been collected on PUF and PPF substrates using the ChemVol impactor. The polymer substrates have the advantage of preventing particle bounce during high particle loading, but these do contain extractable organic additives including antioxidants, plasticizers, and *n*-alkanes.

A cleaning and extraction protocol of two extractions with isopropanol followed by three extractions with DCM was developed for the preparation and analysis of the PUF and PPF substrates. These procedures were evaluated for semi- and non-polar organic compounds typically used for PM source apportionment. The clean-

ing procedure reduced the organic additive concentrations in the extracts by up to a factor of 10. The limits of quantification expressed as concentrations in a 24-h ambient PM sample collected on pre-cleaned substrates were  $\approx 1 \mu\text{g m}^{-3}$  for specific antioxidants and plasticizers, and  $\approx 10 \text{ ng m}^{-3}$  for *n*-alkanes with carbon numbers lower than 26 for the PPF substrate and carbon numbers lower than 24 for the PUF substrate. Repeated cleanings did not reduce the limits of quantification for these species to below concentrations typical of urban PM. Therefore additional cleaning cycles are not recommended and the use of these substrates are not recommended for collection of these species.

The extraction procedure is sufficient to recover organic tracer compounds quantitatively. Enough organic compounds can be measured for source apportionment study, including *n*-alkanes with higher molecular weight (carbon number higher than 24). Besides the polymer additives and *n*-alkanes with low carbon number, no other organic tracer compounds were found in the cleaned substrates. The quantification limit for the other organic tracer compounds is  $\approx 0.1 \text{ ng m}^{-3}$ .

Recoveries of PAHs from standard reference material PPF and PUF were  $117 \pm 8\%$  and  $107 \pm 11\%$ , respectively. Replicate extraction and analyses were made of ambient samples collected in Nogales, AZ, during January 2006. The concentration of 47 organic tracer compounds, including *n*-alkanes, PAHs, and OPAHs and excluding levoglucosan, were reproduced with relative errors less than 10%.

After the first extraction less than 7% of organic tracers remained in the extracted substrates. This method can consistently quantify organic tracer compounds needed for source apportionment study.

## Acknowledgments

We thank the staff of the Arizona Department of Environmental Quality, especially Randy Redman, Gerardo Monroy, Peter Hyde, and Leonard Montenegro, for providing access to the sampling site, assisting in the field experiment, and providing air quality data. We also thank the postmaster and staff of the Nogales Post Office for providing access to the field sampling site. This work was funded by the Arizona Department of Environmental Quality.

## References

- [1] D.W. Dockery, C.A. Pope, X. Xu, J.D. Spengler, J.H. Ware, M.E. Fay, B.G. Ferris, F.E. Speizer Jr., *N. Engl. J. Med.* 329 (1993) 1753–1759.
- [2] D. Krewski, R.T. Burnett, M. Goldberg, K. Hoover, J. Siemiatycki, M. Abrahamowicz, W. White, *Inhalation Toxicol.* 17 (2005) 335–342.
- [3] F. Laden, J. Schwartz, F.E. Speizer, D.W. Dockery, *Am. J. Respir. Crit. Care Med.* 173 (6) (2006) 667–672.
- [4] T. Chen, J. Gokhale, S. Shofer, W.G. Kuschner, *Am. J. Med. Sci.* 333 (4) (2007) 235–243.
- [5] N.A. Marley, J.S. Gaffney, *ACS Symp. Ser.* 919 (2006) 1–23.
- [6] L.M. Hildemann, G.R. Markowski, G.R. Cass, *Environ. Sci. Technol.* 25 (4) (1991) 744–759.
- [7] J.J. Schauer, W.F. Rogge, L.M. Hildemann, M.A. Mazurek, G.R. Cass, B.R.T. Simoneit, *Atmos. Environ.* 30 (1996) 3837–3855.
- [8] B.J. Turpin, H.-J. Lim, *Aerosol Sci. Technol.* 35 (2001) 602–610.
- [9] L.M. Russell, *Environ. Sci. Technol.* 37 (2003) 2982–2987.
- [10] J.A. Cooper, J.G. Watson, *J. Air Pollut. Control Assoc.* 30 (10) (1980) 1116–1125.
- [11] G.R. Cass, G.J. MaRae, *Environ. Sci. Technol.* 17 (3) (1983) 129–139.
- [12] J.J. Schauer, G.R. Cass, *Environ. Sci. Technol.* 34 (2000) 1821–1832.
- [13] M. Zheng, G.R. Cass, J.J. Schauer, E.S. Edgerton, *Environ. Sci. Technol.* 36 (2002) 2361–2371.
- [14] M. Zheng, L. Ke, E.S. Edgerton, J.J. Schauer, M. Dong, A.G. Russell, *J. Geophys. Res.* 111 (2006) 1–14.
- [15] L. Ke, X. Ding, R.L. Tanner, J.J. Schauer, M. Zhang, *Atmos. Environ.* 41 (2007) 8898–8923.
- [16] S.G. Riddle, M.A. Robert, C.A. Jakober, M.P. Hannigan, M.J. Kleeman, *Environ. Sci. Technol.* 42 (2008) 6580–6586.
- [17] W.F. Rogge, L.M. Hildemann, M.A. Mazurek, G.R. Cass, B.R.T. Simoneit, *Environ. Sci. Technol.* 27 (4) (1993) 636–651.
- [18] W.F. Rogge, L.M. Hildemann, M.A. Mazurek, G.R. Cass, B.R.T. Simoneit, *Environ. Sci. Technol.* 27 (1993) 1892–1904.
- [19] W.F. Rogge, L.M. Hildemann, M.A. Mazurek, G.R. Cass, B.R.T. Simoneit, *Environ. Sci. Technol.* 27 (4) (1993) 2700–2711.
- [20] W.F. Rogge, L.M. Hildemann, M.A. Mazurek, G.R. Cass, B.R.T. Simoneit, *Environ. Sci. Technol.* 27 (13) (1993) 2736–2744.
- [21] J.J. Schauer, M.J. Kleeman, G.R. Cass, B.R.T. Simoneit, *Environ. Sci. Technol.* 33 (1999) 1578–1587.
- [22] J.J. Schauer, M.J. Kleeman, G.R. Cass, B.R.T. Simoneit, *Environ. Sci. Technol.* 35 (9) (2001) 1716–1728.
- [23] J.J. Schauer, M.J. Kleeman, G.R. Cass, B.R.T. Simoneit, *Environ. Sci. Technol.* 36 (6) (2002) 1169–1180.
- [24] P.M. Fine, G.R. Cass, B.R.T. Simoneit, *Environ. Eng. Sci.* 21 (2004) 705–721.
- [25] H. Kumata, H. Takada, N. Ogura, *Anal. Chem.* 68 (1996) 1976–1981.
- [26] C.M. Reddy, J.G. Quinn, *Environ. Sci. Technol.* 31 (1997) 2847–2853.
- [27] W.F. Rogge, L.M. Hildemann, M.A. Mazurek, G.R. Cass, B.R.T. Simoneit, *Environ. Sci. Technol.* 25 (6) (1991) 1112–1125.
- [28] J.J. Schauer, M.J. Kleeman, G.R. Cass, B.R.T. Simoneit, *Environ. Sci. Technol.* 33 (1999) 1566–1577.
- [29] B.R.T. Simoneit, J.J. Schauer, C.G. Nolte, D.R. Oros, V.O. Elias, M.P. Fraser, W.F. Rogge, G.R. Cass, *Atmos. Environ.* 33 (2) (1999) 173–182.
- [30] J.J. Schauer, M.J. Kleeman, G.R. Cass, B.R. Simoneit, *Environ. Sci. Technol.* 36 (4) (2002) 567–575.
- [31] J.H. Seinfeld, S.N. Pandis, *Atmospheric Chemistry and Physics: From Air Pollution to Global Change*, Wiley-Interscience, New York, 1998.
- [32] J.O. Allen, N.M. Dookeran, K.A. Smith, A.F. Sarofim, K. Taghizadeh, A.L. Lafleur, *Environ. Sci. Technol.* 30 (1996) 1023–1031.
- [33] M.J. Kleeman, J.J. Schauer, G.R. Cass, *Environ. Sci. Technol.* 33 (1999) 3516–3523.
- [34] P. Fernández, J.O. Grimalt, R.M. Vilanova, *Environ. Sci. Technol.* 36 (2002) 1162–1168.
- [35] B. Zielinska, J. Sagebiel, W.P. Arnott, C.F. Rogers, K.E. Kelly, D.A. Wagner, J.S. Lighty, A.F. Sarofim, G. Palmer, *Environ. Sci. Technol.* 38 (2004) 2557–2567.
- [36] P. Herckes, G. Engling, S.M. Kreidenweis, J.L. Collett Jr., *Environ. Sci. Technol.* 40 (2006) 4554–4562.
- [37] M.J. Kleeman, S.G. Riddle, C.A. Jakober, *Environ. Sci. Technol.* 42 (2008) 6469–6475.
- [38] J.R. Turner, S.V. Hering, *J. Aerosol Sci.* 18 (2) (1987) 215–224.
- [39] P. Demokritou, I.G. Kavouras, S.T. Ferguson, P. Koutrakis, *Aerosol Sci. Technol.* 36 (2002) 925–933.
- [40] I.G. Kavouras, S.T. Ferguson, J.M. Wolfson, P. Koutrakis, *Inhalation Toxicol.* 12 (2) (2000) 35–50.
- [41] I.G. Kavouras, P. Koutrakis, *Aerosol Sci. Technol.* 34 (2001) 46–56.
- [42] M.A. Mazurek, B.R.T. Simoneit, G.R. Cass, H.A. Gray, *Int. J. Environ. Anal. Chem.* 29 (1987) 119–139.
- [43] M.A. Mazurek, B.R.T. Simoneit, G.R. Cass, *Aerosol Sci. Technol.* 10 (1989) 408–419.
- [44] ISO, Ambient air—determination of total (gas and particle-phase) polycyclic aromatic hydrocarbons, Collection on sorbent-backed filters with gas chromatographic/mass spectrometric analyses, Technical Report, ISO, 2000.
- [45] M. Zheng, M. Fang, F. Wang, K.L. To, *Atmos. Environ.* 34 (2000) 2691–2702.
- [46] M. Mazurek, M.C. Masonjones, H.D. Masonjones, L.G. Salmon, G.G. Cass, K.A. Hallock, M. Leach, *J. Geophys. Res.* 102 (1997) 3779–3793.
- [47] L. Nizzetto, R. Lohmann, R. Gioia, A. Jahnke, C. Temme, J. Dachs, A.D. Guardo, K.C. Jones, *Environ. Sci. Technol.* 42 (2008) 1580–1585.
- [48] D.A. Azevedo, C.Y. Santos, F.R. Neto, *Atmos. Environ.* 36 (2002) 2383–2395.
- [49] S.-J. Lee, H. Park, S.-D. Choi, J.-M. Lee, Y.-S. Chang, *Atmos. Environ.* 41 (2007) 5876–5886.
- [50] B. Markert (Ed.), *Environmental Sampling for Trace Analysis*, VCH, Weinheim, 1994.
- [51] R.N. Reeve, *Introduction to Environmental Analysis*, John Wiley & Sons, 2002.
- [52] R.O. Salonen, A.I. Hälinen, A.S. Pennanen, M.-R. Hirvonen, M. Sillanpää, R. Hillamo, T. Shi, P. Borm, E. Sandell, T. Koskentalo, P. Aarnio, *Scand. J. Work Environ. Health* 30 (2) (2004) 80–90.
- [53] A.S. Pennanen, M. Sillanpää, R. Hillamo, U. Quass, A.C. John, M. Branis, I. Hunová, K. Meliefste, N.A.H. Janssen, T. Koskentalo, G. Castano-Vinyals, L. Bousou, M.C. Chalbot, I.G. Kavouras, R.O. Salonen, *Sci. Total Environ.* 374 (2007) 297–310.
- [54] E. Swartz, L. Stockburger, L.A. Gundel, *Environ. Sci. Technol.* 37 (2003) 597–605.
- [55] M.P. Fraser, G.R. Cass, B.R.T. Simoneit, R.A. Rasmussen, *Environ. Sci. Technol.* 31 (1997) 2356–2367.
- [56] M.P. Fraser, G.R. Cass, B.R.T. Simoneit, R.A. Rasmussen, *Environ. Sci. Technol.* 32 (1998) 1760–1770.
- [57] J. Dachs, S.J. Eisenreich, *Environ. Sci. Technol.* 34 (2000) 3690–3697.
- [58] J.O. Allen, Q. Sun, J.R. Anderson, H. Xin, P. Herckes, N. Upadhyay, Identification of particulate matter sources in the Nogales border region using electron microscopy and organic tracer compounds, Technical Report, Arizona State University, 2009.
- [59] Arizona Department of Environmental Quality, Personal communication, 2006.
- [60] P. Fernandez, J.M. Bayona, *J. Chromatogr.* 625 (1992) 141–149.
- [61] J.L. Durant, A.L. Lafleur, E.F. Plummer, K. Taghizadeh, W.F. Busby, W.G. Thilly, *Environ. Sci. Technol.* 32 (1998) 1894–1906.
- [62] A. Albinet, E. Leoz-Garziandia, H. Budzinski, E. Villenave, *J. Chromatogr. A* 1121 (2006) 106–113.
- [63] S.G. Brown, P. Herckes, L. Ashbaugh, M.P. Hannigan, S.M. Kreidenweis, J.L. Collett, *Atmos. Environ.* 36 (2002) 5807–5818.
- [64] R.J. Sheesley, J.J. Schauer, E. Bean, D. Kenski, *Environ. Sci. Technol.* 38 (2004) 6491–6500.



## Sensor array data profiling for gas identification

A. Szczurek<sup>a</sup>, M. Maciejewska<sup>a,\*</sup>, Ł. Ochromowicz<sup>b</sup>

<sup>a</sup> Wrocław University of Technology, Wyb. Wyspiańskiego 27, 50-370 Wrocław, Poland

<sup>b</sup> Faculty of Microsystem Electronics and Photonics, Wrocław University of Technology, Wyb. Wyspiańskiego 27, 50-370 Wrocław, Poland

### ARTICLE INFO

#### Article history:

Received 21 August 2008

Received in revised form 17 December 2008

Accepted 22 December 2008

Available online 15 January 2009

#### Keywords:

Gas sensor

Transient response

Classification

Volatile organic compounds

### ABSTRACT

The paper presents a new method of qualitative identification of gas. It is based on a dynamic response of sensor array with the emphasis on the processing of discrete measurement data. The information needed for identification of test samples is obtained in course of profiling the data from calibration measurements. This operation consists of the following steps: classification of data sets, selection of representative data sets, parameterization of classifiers associated with representative data sets and determination of data records. In our work Discriminant Function Analysis was used for data classification. The information saved in data record describes: the sequential number of discrete measurement, combination of gas sensors in this measurement which are best for classification of calibration samples, and the parameters of associated classifier. They are identifiers of gas class. The procedure of data record determination itself is time consuming. However this operation will be performed only at the stage of the development of the measurement instrument and when its malfunction is diagnosed. The routine use of the instrument will be restricted to gas identification task, which only utilizes the results of profiling.

The identification of unknown gas is performed on the base of data records and measurement data obtained for this gas. Data records guide the preparation of data sets, separately for each class of gases. These data sets are used as input of the discriminant functions which have parameter values also indicated by data records. It was shown in the present contribution, that the qualitative identification of nine test gas samples (vapors of ethanol, acetic acid and ethyl acetate in air) with our method was very accurate and fast.

© 2009 Elsevier B.V. All rights reserved.

### 1. Introduction

Among various types of analytical instruments, the devices based on gas sensors offer a number of interesting features. Unfortunately, they suffer also from serious shortcomings such as low selectivity, high sensitivity to humidity, drift and slow response [1]. These disadvantages are still unsolved in spite of extensive studies.

Various attempts are made to improve the measuring characteristics of sensor devices. One approach focuses on perfecting the performance of single gas sensors. This method exploits: chemical properties of the active materials, physical parameters of the sensing layer, surface modification, sensor design, physical and chemical modification of the sample (before it contacts with the chemical sensitive layer) and mode of sensor operation [2–4].

The alternative approach is based on arrays which consist of gas sensors with partially overlapping selectivity to a measured gas. Such arrays yield specific patterns of responses when different gas molecules are in contact with the sensors [5]. These responses can be analysed using well known pattern recognition algorithms.

The analysis of the response signals from the sensor array can provide both qualitative and quantitative information regarding the composition of measured mixture [6].

Usually, the responses of applied sensors (especially commercial ones) to various substances are only slightly different. Therefore, the performance of arrays depends not only on the properties of individual gas sensors, but on their combinations and array size (number of sensing elements) in particular. The inadequate choice of gas sensors can potentially result in insufficient information or it can lead to noise and information redundancy [7]. For these reasons, the selection of the optimal set of gas sensors is necessary for engineers and designers of sensor systems [8–10]. A considerable efforts have been made recently to solve this problem.

Currently developed sensor arrays are mostly dedicated to strictly defined gas mixtures. The selection of gas sensors addresses the particular application and it is performed at the stage of sensor system design. Optimisation takes advantage of statistical methods, which are applied for the analysis of measured calibration data sets. Various multivariate techniques such as principal component analysis, cluster analysis, genetic algorithms, artificial neural networks and others are used to achieve this goal [11–14].

The alternative to sensor arrays dedicated to strictly defined chemical species are devices of more universal applicability. These

\* Corresponding author. Tel.: +48 713203367; fax: +48 713203532.

E-mail address: [monika.maciejewska@pwr.wroc.pl](mailto:monika.maciejewska@pwr.wroc.pl) (M. Maciejewska).

arrays require to use a broad spectrum of sensing elements, so that large number of gases could be measured by one sensor array. Due to progress in sensor technology the construction of relatively cheap arrays, consisting of many sensing elements is already possible. It allows to expand the scope of applicability of measuring systems based on gas sensors. However, a large size of such systems complicates measuring procedure, increases calibration effort and time demand for data collection and processing. Addressing these aspects is very important from the practical point of view.

This paper describes an effective method of qualitative identification of gases using sensor array which consisted of many sensors. They were not selected with a particular application in mind, but they covered as broad range of substances as possible in a partially selective manner. The dynamic mode of sensor array operation was applied in our work, but the conception could be extended to other operation modes. The proposed method was based on the idea of data profiling. The data was obtained during calibration measurements and its profiling was carried out in respect of the classification of measured gases. In course of profiling operation, data records were determined. They were structures, which were designed for the purpose of identification of unknown gas samples based on test measurements.

To show the details of this method an example of array consisting of 15 gas sensors was considered for identification of several unknown gas samples. These were vapors of one of the following substances: ethanol, acetic acid or ethyl acetate in air. Concentrations of volatile organic compounds (VOCs) in tested gases were various. We believe, that the presented method will provide a useful tool for designers and users of sensor systems.

## 2. Experimental

The schematic diagram of the experimental setup used in our work is presented in Fig. 1. This system was composed of the following elements: (1) pure air generator, (2) system for the preparation of gas mixtures (measured samples), (3) unit containing measurement chambers with gas sensors inside, (4) voltage supplier, (5) interface circuits containing reference resistors, (6) digital multimeter with multiplexer module and data acquisition card, and (7) PC with HP BenchLink Datalogger software.

Pure air generator (Horiba) consisted of compressor and cartridges filled with silica gel, activated carbon, soda lime and molecular sieve. Ambient air passing through these filters was purified and dried. The degree of purification was sufficient that the sensors applied in this work did not detect VOCs in the used air. Gas mixtures were prepared in the dedicated system by an evaporation method. Ethanol, acetic acid and ethyl acetate were chosen as gas mixture components of interest. Desired amounts of these compounds were continuously injected as a liquid into the heated vessel and then vaporized in a stream of air from Horiba

generator. The flow rate of air was precisely adjusted and controlled by a mass flow controller. The system had the capability of generating different concentrations of volatile organic compounds using two-step dilution. The concentration of these substances in air was determined by dosage, airflow and dilution rate. The sensors were exposed to 38–610 mg/m<sup>3</sup> (18–297 ppm) of ethanol, 47–423 mg/m<sup>3</sup> (18–158 ppm) of acetic acid and 34–490 mg/m<sup>3</sup> (9–125 ppm) of ethyl acetate. In those ranges the concentrations of investigated mixtures followed approximately the geometrical progression with the ratio of two. This method of selection was justified by the logarithmic character of sensor response. Both, pure air generator and system for preparation of gas mixtures were designed for the dynamic and continuous supply of gases. They were connected by teflon tubes with the unit containing gas sensors.

In our work, measurements were performed using a parallel set of sensors with different sensitivities to volatile organic compounds. The array consisted of 15 commercially available Taguchi Gas Sensors made by Figaro Engineering Japan. The following TGS sensors were applied in this work TGS821, TGS822, TGS824, TGS825, TGS826, TGS880, TGS883, TGS800, TGS2201, TGS2201, TGS2106, TGS2104, TGS2602, TGS2620 and TGS2600. These devices were heated to a constant temperature, by applying voltage of 5 V to the sensor heater.

Sensors were placed inside cells with feed-through electrical wires used for electrical supply and measurements. Each sensor had its own small aluminium chamber. Since these elements were connected parallel, all sensors were exposed to the same gas mixture. The chambers were connected to a gas delivery system, voltage supplier and measuring module.

The transient response of gas sensor over time (a resistance change) was measured sequentially and converted into an output electrical signal (a voltage variations on the load resistance connected to the sensor). This operation was performed by means of interface circuits containing a series of reference resistors. The output signal was a sequence of raw voltage measurements that were related by time, used as an ordinal variable. The measured quantities were digitized and stored for further processing and analysis. The data acquisition board from Agilent was used to record the transient output of sensors. The sampling rate during data acquisition was one point per second (1 s<sup>-1</sup>). Output signals generated by the data acquisition board were transmitted to PC.

Before each set of measurements, chambers containing sensors were cleaned with pure air. The measurement process involved two stages: exposition and regeneration. In the first step, the gas sample was allowed to continuously flow through the chambers. The total gas flow was set to 2 dm<sup>3</sup>/min and it was kept constant. The exposition ran for 10 min. This time was sufficient to attain the steady state in signal output. After this step of experiment, regeneration of sensors was performed. In that phase, the whole system was flushed with a stream of pure air until readouts from sensors reached the level as before exposition.

## 3. Methods of measurement data analysis

Identification of test gas by the sensor array can be defined as the procedure that assigns a sensor array output to a class [15]. In other words, it allows to associate unknown mixture with one of the calibration patterns. In this paper, the class was defined as a group of gas mixtures featured by identical qualitative composition (chemical constitution). Substances in mixtures which belonged to one class could have different concentration values. However, quantification was not attempted at this stage of research. It is proposed here to perform the qualitative identification of unknown gas in mixture with air on the basis of dynamic responses of the sensor array and using data records obtained from calibration data profiling.

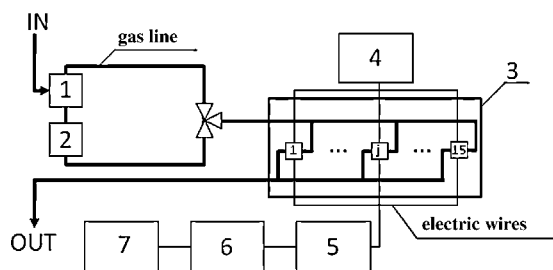


**Fig. 1.** Schematic diagram of the experimental setup. (1) Pure air generator, (2) system for the preparation of gas mixtures, (3) unit containing measurement chambers and gas sensors, (4) voltage supplier, (5) interface circuits containing reference resistors, (6) digital multimeter with multiplexer module and data acquisition card, and (7) PC with HP BenchLink Datalogger software.

### 3.1. Dynamic mode of sensor array operation

In this work, we decided to use dynamic mode of sensor operation. We anticipated it could be a source of information, which improved the discriminating ability of gas sensor array. As a consequence of applied measurement procedure, the output signal was caused by time-dependent gas composition in the atmosphere surrounding sensors. There was a delay between turning on the flow of measured gas through the apparatus and transfer of maximum concentration of tested substances through the sensor array. Therefore gas concentration over sensors was continuously changed until the equilibrium was reached.

It is known, that the conductivity changes in semiconductor sensors are caused by the transport of the reactive species into the sensor, the diffusion of the gas molecules inside pores of the sensing material, adsorption and desorption, the catalysed redox reactions on the surface of the sensing layer (mainly their kinetics) and the electrical/electronic effects in the semiconductor [2]. These processes depend strongly on the properties and concentration of measured substances. For that reason, the transient output signal in our experiment carried information about tested gases. The information content, as well as its change over time was surely not identical for all sensors in the array. Therefore, depending on the time point in the response signal different sensors sets could provide valuable data for the identification and/or quantification of measured gas.

### 3.2. Measurement data matrix

In the dynamic mode of operation the sensor output signal is a function of time and it can be sampled by a sequence of discrete measurements with a defined time step. The dynamic response of sensor array may be presented in the following matrix notation:

$$R = \begin{bmatrix} r_{11} & \dots & r_{1j} & \dots & r_{1n} \\ \dots & \dots & \dots & \dots & \dots \\ r_{k1} & \dots & r_{kj} & \dots & r_{kn} \\ \dots & \dots & \dots & \dots & \dots \\ r_{m1} & \dots & r_{mj} & \dots & r_{mn} \end{bmatrix} \quad (1)$$

where  $k = 1, \dots, m$  and it corresponds to different time points of the exposure interval,  $j = 1, \dots, n$  and it indicates sensors in the array. Single matrix element  $r_{kj}$  is the discrete measurement of gas mixture by the  $j$ th sensor at the  $k$ th time point of exposure. The  $k$ th row in matrix  $R$  describes the state of sensor array in  $k$ th moment of exposure. In our work this data arrangement was considered a fixed template of dynamic sensor array response to a measured gas. Separate data matrix was obtained for each gas which was examined during calibration or test measurements.

The actual size of data matrix  $R$  is determined by the size of sensor array, duration of time response and the sampling rate. Therefore, the amount of data collected in the dynamic mode of sensor array operation may be large. Usually not all the data are necessary to form the distinct pattern of the measured gas. It is advantageous to consider exclusively the data, which is relevant for pattern recognition purpose [7]. A simple elimination of redundant information can be done for example by selecting a subset of the available parameters of time response, e.g. time-to-threshold, transient slope, initial saturation value, deep saturation value [16–18]. They are usually easily measured, time-independent and provide compact representation of the measurement data. Unfortunately, in parametric representation of sensor response part of relevant information about chemical species is lost or inaccessible. Therefore we have chosen another approach. It was based on a specially arranged data records, which referred to the elements of measurement data matrix. In the presented method, they were treated as information units in the identification process.

### 3.3. Data records

In our work, data record was a set, which elements were important for gas identification. It should be noted, that each record was an entity and had a meaning independent of other data records. For the optimum performance of gas identification process, data record was defined as a fixed and consistent structure  $DR = (k, s, c)$ , where  $k$  was the serial number of measurement during single exposure;  $s$  described a combination of sensors and  $c$  were the parameters of classifier associated with the data set indicated by  $k$  and  $s$  in measurement data matrix  $R$ . The objective of this work was to find a method for the determination of data records content, which would be most useful for the identification of unknown gas samples. We have proposed data profiling as the base for this method.

### 3.4. Data profiling

In general, data profiling is the process of auditing (examining and analyzing) data, available in an existing database, and collecting statistics and information regarding its quality. This process also involves the discovery of patterns and insights in data distribution to determine its structure and internal relationships.

In this work, the profiling was performed on the database containing calibration data structured in data matrices  $R$ . The data was used in the form of sets. The data set was a combination of elements  $r_{kj}$  of matrix  $R$ . We assumed that all components of a single data set originate from the same measurement (time point of exposure). The number of data sets associated with a single  $k$ th time point of exposure is given by

$$n_k = \sum_{j=1}^n \frac{j!}{n!(n-j)!} = 2^n - 1 \quad (2)$$

where  $n_k$  are all combinations of  $j$  elements selected from  $n$  elements. The total number of data sets which were obtained from one calibration measurement was  $m \times n_k$ , where  $m$  was the number of time points in the time response of sensor array.

The data profiling proposed in this paper was a multistage process. It included:

- classification of data sets;
- selection of representative data sets;
- parameterization of classifiers associated with representative data sets;
- determination of data records for identification of unknown gas samples.

In course of classification, data sets were categorized in classes corresponding to the various chemical patterns showed by the measured gases. The patterns of interest were associated with classes of measured gases. We used a supervised method, Discriminant Function Analysis (DFA) to indicate pattern grouping. It is a statistical method based on maximum likelihood for determining boundaries that separate the data into categories. Details of the method can be found in [19,20]. On many occasions DFA was shown to have a comparable performance to more sophisticated classifiers like for example ANN, GA [21–23]. In our case the principal reason for the employment of DFA was time efficiency [24]. Considering a great number of data sets which required examination in course of profiling the application of classifiers featured by lengthy training phase could limit the feasibility of proposed approach.

All data sets were examined in respect of classification of measured gases. The aim of classification stage was to find the group of data sets which were most suitable for this task. The data set was considered successful if it allowed for the allocation of all



calibration samples between *the class* and *the others*, without misclassification. The leave one out mode was employed for validation and 100% efficiency of this procedure was required for any of the successful data set.

In our studies, the lowest number of successful data sets for a class of gas mixtures was found several dozen thousands. Therefore, it was impractical to further consider all those data sets for the identification of unknown gas samples. Taking advantage of equal performance of successful data sets it was proposed to select their representative sample. The representativeness of selection was secured by using random drawing. It was assumed on the base of calculation, that the optimum sample size should be  $\mu = 43$ .

After the classification and selection stages were completed, parameters of classifier were determined separately for each representative data set. In our case these were parameters of the discriminant function  $F$ :

$$F = a_0 + \sum_j a_{kj} r_{kj} \quad (3)$$

where  $r_{kj}$  are elements of the representative data set and  $a_0$ ,  $a_{kj}$  are the discriminant function parameters, i.e. the classifier parameters.

Ultimately, the results of classification, selection and parameterization processes provided for determination of data records. They were coupled with classes of gas mixtures and there were 43 data records obtained for each class. In our work, these data records formed the identifier of the gas class. As it was mentioned earlier the information saved in data record described: the serial number of measurement, combination of gas sensors in this measurement which were best from the classification point of view and the parameters of associated classifier. The procedure of data record determination is time consuming. However, to our judgement it is sufficient to carry out this operation relatively rarely.

### 3.5. Identification of test gas samples

The identification process consisted of two steps. In the first step data sets were prepared for the identification of unknown gas mixture. The preparation was performed on the base of data records determined in course of profiling (field  $k$  and  $s$ ) and the measurement data matrix obtained for the tested gas. Separate groups of data sets were prepared for each class of gases. In the next step, they were used as input of the discriminant function (Eq. (3)). Values of parameters of the function were given in the field  $c$  of data record. The greater than zero value of discriminant function  $F$  indicated the match between the identity of tests sample and the class. Actually, the identity check was performed using the identifier of gas class (43 data records). To confirm sample identity 71% success rate was required for the class identifier.

## 4. Results and discussion

The feasibility of data profiling for gas identification was studied using the example of three gas classes named: ethanol, acetic acid and ethyl acetate. Classes were represented by mixtures of those substances and dry air featured by different concentration values. It was proposed here to perform the profiling and identification on the basis of the sensor array responses obtained in the dynamic mode of operation.

Examples of sensor signals obtained in the dynamic mode of sensor array operation are shown in Fig. 2. Our array consisted of 15 sensors, but for the sake of clarity the following sensors TGS824, TGS826, TGS883, TGS2106, TGS2602, TGS2620 were selected for the plot. The presented measurement data were obtained during sensor array exposure to 185 mg/m<sup>3</sup> of ethanol (Fig. 2a), 180 mg/m<sup>3</sup> of acetic acid (Fig. 2b) and 180 mg/m<sup>3</sup> of ethyl acetate (Fig. 2c) in dry

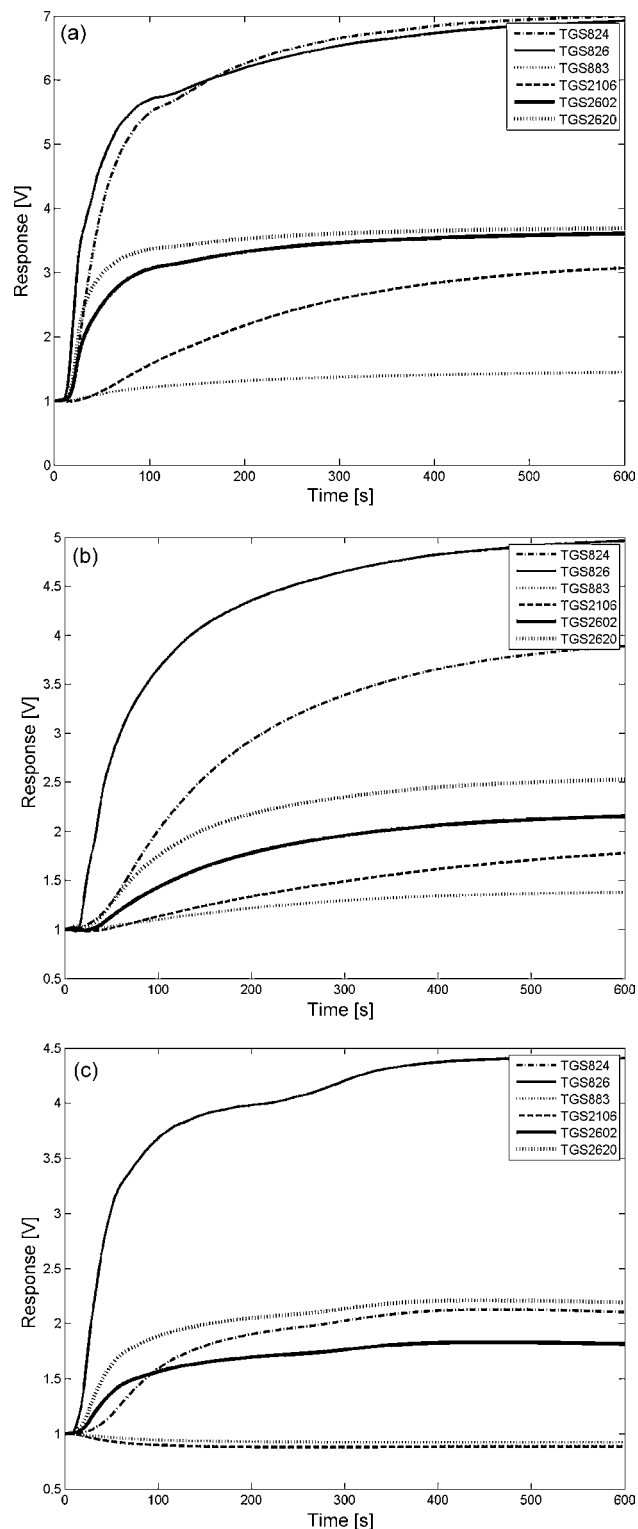


Fig. 2. The preprocessed output signal of selected TGS sensors operating in the dynamic mode upon exposure to: (a) 185 mg/m<sup>3</sup> of ethanol, (b) 180 mg/m<sup>3</sup> of acetic acid, and (c) 180 mg/m<sup>3</sup> of ethyl acetate in dry air.

air. The raw output signal was preprocessed by subtraction of the background (measurement in dry air) and by the subsequent shift of all values by one.

The sensor signals shown in Fig. 2, change in time and they are different for measured gases. The presented data is clearly suitable for discrimination of ethanol, acetic acid and ethyl acetate sam-

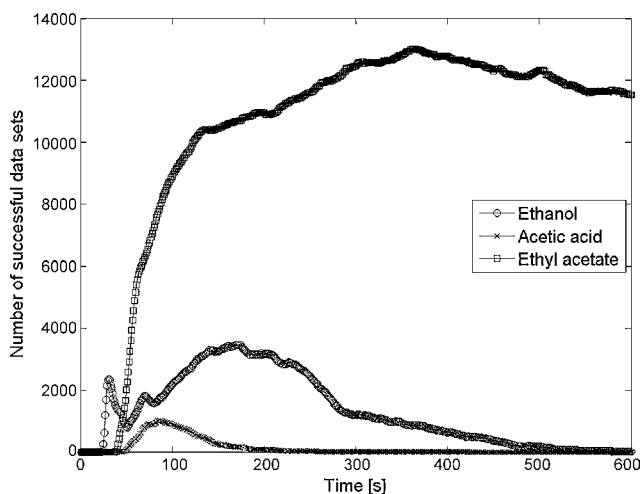


Fig. 3. Number of successful data sets which were found during classification stage of profiling for subsequent measurements (time points in sensor array time response).

ples. It is moreover featured by a considerable redundancy. Based on Fig. 2 many time points could be selected as a base for successful discrimination of these compounds. Also different sets of sensors could be of use. These observations encouraged to focus on a selection of relevant measurements and sensors regarding gas identification. To reach this goal, it was proposed to use the method of data profiling that was earlier described.

The object of profiling was the database of calibration measurements. It was composed of measurement data matrices, which resulted from the dynamic mode of sensor array operation. The calibration measurements were done for samples of ethanol, acetic acid and ethyl acetate in dry air. There were 21 calibration samples of ethanol measured in a concentration range of 38–610 mg/m<sup>3</sup>. They all represented class ethanol. There were 18 samples of acetic acid measured in a concentration range of 47–423 mg/m<sup>3</sup>. They formed the class acetic acid. The ethyl acetate was considered in a range of 34–490 mg/m<sup>3</sup> and there were 24 samples measured. They framed the class ethyl acetate. Concentrations of measured gases were set deliberately at the measurement stage. Using calibration database, data sets were formed as described in Section 3.4. Referring to a single data matrix, we obtained 32,767 data sets for each measurement (Eq. (2)) and 19,660,200 data sets in total (600 measurements per exposure).

During the first stage of profiling all data sets were examined concerning classification of calibration samples by means of DFA. This classifier was chosen because it offered satisfactory time efficiency. A significant number of data sets was found, which supported successful classification of all calibration samples. These data sets were considered successful. The class ethanol was successfully discriminated by 787,591 data sets, which was 4.0% of all. Only 76,430 (0.4%) data sets secured errorless classification of acetic acid. In case of ethyl acetate as much as 6,232,690 (31.7%) data sets were successful. Clearly, ethyl acetate was easiest to identify

and acetic acid was featured by least distinct patterns. Numbers of successful data sets, which were found for subsequent measurements (time points of sensor array response) are presented in Fig. 3.

As shown in Fig. 3 the number of successful data sets changes from measurement to measurement. This provided an argument for the time variability of the amount of useful information that was preserved in sensor signal and could serve pattern recognition purposes. Interestingly, based on Fig. 3 the distribution of this information along the time response of sensor array was compound specific. In case of acetic acid the second minute of time response was most informative. Most of useful information about ethanol occurred between 1st and 6th minute of measurement. Contrarily, ethyl acetate was most distinctly represented in sensor array data since the 2nd minute of measurement.

The successful data sets formed the base for selection of representative data sets in the second step of profiling. It was done by a random drawing from the pools of successful data sets which were found at the classification stage for classes: ethanol, acetic acid and ethyl acetate. There were 43 representative data sets selected for each class.

Representative data sets were used in course of the third stage of profiling. At this stage, parameters of discriminant functions were calculated using representative data sets as classifier input. Discriminant function parameters were obtained separately for each representative data set. They were calculated under supervised grouping of all calibration samples into *the class*, indicated by representative data set, and *the others*.

Finally, data records were determined based on results of classification, selection and classifier parameterization stages. Class identifiers of ethanol, acetic acid and ethyl acetate were formed, which consisted of 43 data records each. The reader is referred to the Supplementary file *ClassIdentifiers.xls* for the complete class identifiers.

The effectiveness of class identifiers was verified in course of qualitative identification of test gas samples. These were three samples of ethanol (74, 300, 500 mg/m<sup>3</sup>), three samples of acetic acid (68, 168, 305 mg/m<sup>3</sup>) and three samples of ethyl acetate (70, 165, 370 mg/m<sup>3</sup>) in dry air. Their choice was guided by the gas classes considered at the stage of calibration data profiling. In the first step of identification, data sets were formed based on data matrices obtained during measurement of test samples and using data records (field *k* and *s*) in class identifiers. Obtained data sets were fed to corresponding discriminant functions, which had parameters as given by data records (field *c*). The match between sample identity and the gas classes was evaluated by each data record separately. The fraction of data records that indicated class membership of studied samples is presented in Table 1.

As shown in Table 1 the identification of nine test samples of gases was very accurate. For each sample there was a class where 100% of data records in class identifier indicated sample membership. Simultaneously, data records associated with other gas classes indicated lack of sample membership. Therefore there was no doubt about identity of samples. There was only one test sample, ethyl acetate at low concentration, which was identified as acetic acid by

Table 1  
Results of identification of test gas samples using identifiers of gas classes.

Gas class	Test samples								
	Ethanol in dry air (mg/m <sup>3</sup> )			Acetic acid in dry air (mg/m <sup>3</sup> )			Ethyl acetate in dry air (mg/m <sup>3</sup> )		
	74	300	500	68	168	305	70	165	370
Ethanol	43/43	43/43	43/43	0	0	0	0	0	0
Acetic acid	0	0	0	43/43	43/43	43/43	1/43	0	0
Ethyl acetate	0	0	0	0	0	0	43/43	43/43	43/43

one data record which was the identifier of acetic acid class. This error does not undermine the presented methodology but it actually is the argument behind the use of multiple data records in class identifier as it is done here. One shall add that, upon the availability of measurement data for test samples, the qualitative identification process itself was immediate.

## 5. Conclusions

This paper presents a new method of qualitative identification of gas. It was based on the dynamic response of sensor array. We have shown that discrete measurements could be directly used for this purpose. In this approach it was necessary to deal with redundant and useless data. It was proposed to use data profiling to solve this problem. Data profiling resulted in data records. They included the information concerning measurement, sensor combination and parameters of classifier. Therefore, in our studies they were considered as the identifier of gas class. It should be mentioned that data records were determined on the base of calibration data.

The identification of test samples was carried out using data sets. Their elements originated from measurement data matrices. Data records obtained in course of profiling provided information for construction of data sets.

Our studies have proved that the proposed method was very accurate and fast when applied for test gas samples identification. It has to be mentioned that data profiling itself is time consuming and computationally intensive. Still the approach is feasible, provided that the time efficient classifier is applied. In this study we worked with DFA. Additionally, it shall be stressed that in practical applications data profiling operation would be performed relatively rarely.

The present contribution is dedicated to the qualitative identification of gases, exclusively. It was the first stage in the development of our data-based approach to sensor array measurements. In the next step our conception will be applied for the quantitative identification of gas mixtures. The related analysis is in progress and first results are very promising.

## Appendix A. Supplementary data

Supplementary data associated with this article can be found, in the online version, at doi:10.1016/j.talanta.2008.12.055.

## References

- [1] P.T. Moseley, J. Norris, D.E. Williams, *Techniques and Mechanisms of Gas Sensing*, IOP Publishing Ltd., New York, 1991.
- [2] J. Itohura, J. Watson, *Stannic Oxide Gas Sensors*, CRC Press, Boca Raton, 1994.
- [3] G. Sberveglieri, *Gas Sensors*, Kluwer Academic Publishers, Dordrecht, 1992, pp. 117–169.
- [4] G. Korotcenkov, *Sens. Actuators B* 107 (2005) 209.
- [5] K.J. Albert, N.S. Lewis, C.L. Schauer, G.A. Sotzing, S.E. Stitzel, T.P. Vaid, D.R. Walt, *Chem. Rev.* 100 (2000) 2595.
- [6] O. Helli, M. Siadat, M. Lumbreras, *Sens. Actuators B* 103 (2004) 403.
- [7] M. Shi, *Electronic Design, Test and Applications, DELTA 2006, Third IEEE International Workshop on 2006*, 2006, p. 448.
- [8] A.N. Chaudry, T.M. Hawkins, P.J. Travers, *Sens. Actuators B* 69 (2000) 236.
- [9] H. Lei, W.G. Pitt, *Sens. Actuators B* 124 (2007) 278.
- [10] D. Ballabio, M.S. Cosio, S. Mannino, R. Todeschini, *Anal. Chim. Acta* 578 (2006) 170.
- [11] Y. Yin, X. Tian, *Sens. Actuators B* 124 (2007) 393.
- [12] M. Penza, G. Cassano, F. Tortorella, *Sens. Actuators B* 81 (2001) 115.
- [13] D.M. Wilson, T. Roppel, R. Kalim, *Sens. Actuators B* 64 (2000) 107.
- [14] M. Aleixandre, I. Sayago, M.C. Horrillo, M.J. Fernandez, L. Ares, M. Garcia, J.P. Santos, J. Gutierrez, *Sens. Actuators B: Chem.* 103 (2004) 122.
- [15] C.D. Natale, F.A.M. Dave, A. D'Amico, A. Hierlemann, J. Mitrovics, M. Schweizer, U. Weimar, W. Göpel, *Sens. Actuators B: Chem.* 24–25 (1995) 808.
- [16] M. Pardo, G. Sberveglieri, *Sens. Actuators B* 123 (2007) 437.
- [17] T. Eklov, P. Martensson, I. Lundstrom, *Anal. Chim. Acta* 381 (1999) 221.
- [18] O. Gualdrón, E. Llobet, J. Brezmes, X. Vilanova, X. Correig, *Sens. Actuators B* 114 (2006) 522.
- [19] P.C. Jurs, G.A. Bakken, H.E. McClelland, *Chem. Rev.* 100 (2000) 2649.
- [20] [www.mathworks.com/access/helpdesk/help/toolbox/stats/index.html?access/helpdesk/help/toolbox/stats/bq.w.hm.html&http://www.mathworks.com/products/statistics/description1.html](http://www.mathworks.com/access/helpdesk/help/toolbox/stats/index.html?access/helpdesk/help/toolbox/stats/bq.w.hm.html&http://www.mathworks.com/products/statistics/description1.html).
- [21] L. Pillonel, U. Batikofer, H. Schlichtherle-Cerny, R. Tabacchi, J.O. Bosset, *Int. Dairy J.* 15 (2005) 557.
- [22] S. Pérez-Magariño, M. Ortega-Heras, M.L. González-San José, Z. Boger, *Talanta* 62 (2004) 983.
- [23] R.M. Alonso-Salces, C. Herrero, A. Barranco, D.M. Lopez-Marquez, L.A. Berrueta, B. Gallo, F. Vicente, *Food Chem.* 97 (2006) 438.
- [24] L.A. Berrueta, R.M. Alonso-Salces, K. HAbberger, *J. Chromatogr. A* 1158 (2007) 196.



# Single-step microwave digestion of food and biological samples for the quantitative conversion of Se into the +4 oxidation state

R. Toniolo, F. Tubaro, S. Bin, A. Pizzariello, S. Susmel, N. Dossi, G. Bontempelli\*

Department of Chemical Science and Technology, University of Udine, via Cottonificio 108, I-33100 Udine, Italy

## ARTICLE INFO

### Article history:

Received 16 September 2008  
Received in revised form 15 December 2008  
Accepted 17 December 2008  
Available online 30 December 2008

### Keywords:

Selenium conversion to Se(IV)  
Microwave digestion  
Hydride generation-induced coupled plasma (HG-ICP)  
Differential pulse cathodic stripping voltammetry (DPCSV)  
Selenium in human blood plasma and food

## ABSTRACT

An improved single step microwave digestion procedure is described for providing the fast and easy exhaustive mineralisation of biological samples concomitantly with the quantitative conversion of any type of selenium compounds into Se(IV). In such a way, digested samples are directly suitable for the subsequent Se analysis at trace and ultratrace levels by both spectrometric methods such as HG-ICP-MS or HG-ICP-OES and differential pulse cathodic stripping voltammetry (DPCSV). It is based on the use, under suitably optimised microwave irradiation conditions, of a digestion mixture with a carefully tailored composition such that its redox potential is made lower than that allowing Se(IV) to be oxidized to Se(VI), but high enough to permit total destruction of biological or, in general, organic matrices. It consists of a nitric acid (65%, w/w) and hydrogen peroxide (30%, w/w) mixture in a volume ratio 5:1, frequently adopted for the mineralisation of organic and biological samples, but added simply with 0.25 g mL<sup>-1</sup> of NaCl. Successful application of the procedure, in terms of both repeatability and accuracy, to the quantification of selenium by the instrumental methods above in standard compounds and in a certified biological sample proved its good performance. The application to the Se determination in human blood plasma and in a wide variety of foods is also reported.

© 2008 Elsevier B.V. All rights reserved.

## 1. Introduction

Selenium was recognized to be essential in the nutrition of animals and humans since about 1950s [1,2]. In fact, it is present in a number of enzymes as the aminoacid Se-cysteine [3,4] and some Se compounds were found to inhibit tumorigenesis in a variety of animal models [5]. In particular, recent studies indicate that supplemental Se in human diets may reduce incidence of different types of carcinoma and prevents cardiovascular disease, male infertility and accelerated brain aging [3].

However, while the presence of Se in biological organisms at low concentration levels is by now considered profitable, fairly little higher contents display toxicity. Thus, a safe daily intake of Se ranging from 55 to 75 µg was estimated and recommended for adult humans and, in particular, an optimal daily intake associated to an average diet was estimated to be 62 µg [6]. Conversely, daily intakes of the order of 350–700 µg are reported to lead to hepatotoxicity and teratogenesis [4]. Moreover, it must be emphasized that, with rare exceptions, Se concentrations falling within less than 10 and not more than few hundreds of µg kg<sup>-1</sup> (or µg L<sup>-1</sup>) are usually found in human tissues and body fluids, as well as in food samples [6].

The monitoring of such low concentrations requires highly sensitive, specific and reliable analytical approaches to be available, together with sample digestion procedures suitable for both an effective mineralisation of biological matrices and the quantitative recovery of Se under the required form. The needs to meet with these requirements has prompted a growing interest in Se analysis at trace levels in biological samples, so that its determination was the subject of several thorough investigations performed over the last two decades. Thus, many analytical approaches have been suggested, such as atomic fluorescence spectrometry (AFS) [7,8], atomic absorption spectrophotometry (AAS) [8,9], inductively coupled plasma spectrometry with either optical (ICP-OES) [10] or mass-spectrometric (ICP-MS) [11,12] detection, all of them used as both independent analytical techniques and hyphenated to gas or liquid chromatography. Moreover, methods based on UV and visible spectrophotometry [13,14], neutron activation analysis [15] and electrochemical measurements [16,17] have also been proposed.

At present, the most effective methods appear to be AAS, ICP-OES and ICP-MS approaches, whose sensitivity is strongly increased by resorting to the hydride generation (HG), consisting in the preliminary conversion of original Se compounds into selenium hydrides, which occurs indeed only whether Se is available in the +4 oxidation state. Also electrochemical methods are rather attractive for selenium analysis, thanks to their intrinsic sensitivity, tunable selectivity and minimal cost instrumentation. Thus, some electroanalytical approaches have been proposed, based on the

\* Corresponding author. Tel.: +39 0432 558842; fax: +39 0432 558803.  
E-mail address: [Gino.Bontempelli@uniud.it](mailto:Gino.Bontempelli@uniud.it) (G. Bontempelli).

use of differential pulse polarography (DPP) or cathodic stripping voltammetry (CSV) [18,19]. Nevertheless, also these electroanalytical techniques require that Se in the samples is available in the +4 oxidation state, in that Se in other oxidation states cannot be determined electrochemically.

Consequently, the mentioned more attractive analytical approaches for Se determination in food and biological samples become practicable only whether a quantitative conversion of total Se to Se(IV) is assured by the preliminary step adopted for transferring the analyte into solutions suitable for the subsequent instrumental analysis.

Pretreatment steps based on extraction, wet and dry sample ashing, oxygen bomb or ultraviolet procedures [20] are almost always tedious, time consuming, not easy to be automatized and suffer from possible contamination. These troubles can be avoided by resorting to microwave (MW) digestion which is a profitable alternative to conventional mineralisation methods for tackling the problem of digesting food samples [21–23]. Unfortunately, complete and reproducible mineralisation of biological samples by microwave digestion requires the use of acid-oxidizing mixtures (typically, concentrated nitric acid and hydrogen peroxide in suitable ratios [23–25]) which lead to extensive oxidation of selenium to Se(VI), which is neither prone to yield selenium hydride for ICP determinations nor suitable for CSV analysis. In order to overcome this drawback and achieving a quantitative reduction to Se(IV) of Se(VI) formed in such a microwave digestion step conducted under usual conditions, a second subsequent MW mineralisation in concentrated HCl of the primary digested sample was suggested in the literature [26,27], thus vanishing however the advantage offered by a typical short-time mineralisation procedure such as MW digestion.

The goal of the present investigation was the development of a fast and easy single step microwave digestion procedure providing the exhaustive mineralisation of biological samples concomitantly with the quantitative conversion of any type of selenium compounds into Se(IV), so as to make digested samples directly suitable for the subsequent Se analysis at trace and ultratrace levels by both spectrometric methods such as HG-ICP-MS or HG-ICP-OES and differential pulse cathodic stripping voltammetry (DPCSV). This paper reports on the proposed procedure and gives illustration of the relevant performance evaluated on both synthetic and real samples, these last consisting of blood plasma as well as of a wide variety of vegetable and animal food.

## 2. Experimental

### 2.1. Chemicals and real samples

All the chemicals used were of analytical reagent grade (Merck Suprapure, Merck, Darmstadt, D) and were used as received. In all instances, high purity deionized water (resistivity  $>18\text{ M}\Omega\text{cm}$ ), purified with an Elgastat<sup>®</sup> UHQ-PS (Elga, High Wycombe, UK) system (“Elgastat water”), was used as the solvent. Stock standard solutions ( $1.49\text{ g L}^{-1} = 12\text{ mmol L}^{-1}$ , equivalent to  $1\text{ g L}^{-1}$  of selenium) of water soluble model compounds containing selenium in different oxidation states (seleno-L-methionine, methyl-seleno-L-cysteine, seleno-L-cystine, sodium selenite, sodium selenate) were prepared by dissolving weighed amounts of these species in Elgastat water. When required, these solutions were diluted to the desired concentration once more with Elgastat water. Zinc selenide was instead used directly in the solid state, owing to its very poor solubility in water. The indium solution used as the internal standard in ICP-MS measurements was prepared by suitably diluting with Elgastat water the corresponding  $1\text{ g L}^{-1}$  standard solution for ICP purchased by Merck.

A BCR certified sample of lyophilized pig kidney from the Community Bureau of Reference (reference material no. 186, Institute for Reference Materials and Measurements, Geel, B), with a certified Se content of  $10.3 \pm 0.5\ \mu\text{g g}^{-1}$  and containing other eight elements too (As, Cd, Cu, Fe, Hg, Mn, Pb and Zn), was used as the reference material.

Vegetable and animal food samples analysed were purchased from local supermarkets, while human blood plasma samples were drawn from volunteers. When necessary, these samples were stored at  $-20\text{ }^\circ\text{C}$ .

Pure argon (transistor quality) was used for ICP determinations, while pure nitrogen was employed for purging solutions subjected to electroanalytical measurements.

### 2.2. Sample microwave digestion

All microwave digestions were run on a Milestone MLS-1200 MEGA (FKV, Bergamo, I) equipped with an EM-45 exhaustor of nitric acid fumes, a control panel and a MDR-1000/6/100/110 rotor, this last being a turntable operating with a maximum of six digestion vessels. Each digestion vessel consisted of a tetrafluoromethoxyl polymer (TFM) sample holder inserted in a hollow polyether-ether-ketone copolymer (PEEK) container. At the top of each vessel, a PEEK relief-valve was present, aimed at allowing vapour release for pressure values exceeding 110 bars. The three-step power program adopted for the microwave digestion was as follows: (i) 2 min with an irradiation power of 250 W; (ii) 2 min with 0 W; (iii) 15 min with 300 W.

Any sample (different amounts of the standard compounds above, containing from 0.06 to 0.30  $\mu\text{mol}$  of Se, or 0.5–2.0 g of both vegetable and animal food ground by a sterilmixer homogenizer (pbi-International, Milan, I), as well as 0.5 mL of blood plasma) was introduced into a digestion vessel and added with controlled volumes (1.2–4.8 mL) of a chloride containing acid oxidizing mixture consisting of a solution prepared by mixing nitric acid (65%, w/w) with hydrogen peroxide (30%, w/w) in a volume ratio 5:1 and adding then  $0.25\text{ g mL}^{-1}$  (4.3 M) NaCl.

After microwave mineralisation, the digestion vessels were cooled and their content was transferred into 100 mL (standard compounds) or 10 mL (real samples) glass volumetric flasks where digested samples were diluted to the mark by 0.1 M HCl, thus achieving the solutions suitable for subsequent analysis. It is worth to underline that digested real samples were less diluted in view of their lower Se contents.

### 2.3. Instrumentation, operative conditions and procedure

ICP-MS and HG-ICP-MS measurements on microwave digested samples were performed by a Spectromass 2000 Type MSDIA10B (Spectro Analytical Instruments, Kleve, D) under the operating conditions reported previously [23,28,29]. All measurements were performed after calibrating these operating conditions, so as to maximize the signal with respect to the background noise for m/z equal to both 82 (Se isotope) and 115 (reference In isotope, only for ICP-MS measurements) amu. <sup>82</sup>Se isotope was exploited for selenium determinations, in spite of its comparatively low abundance (9.2%), owing to the interference provided by argon polyatomic ions <sup>38</sup>Ar<sup>40</sup>Ar<sup>+</sup> and <sup>40</sup>Ar<sup>40</sup>Ar<sup>+</sup>, whose intensity reached some millions counts s<sup>-1</sup>, with major isotopes <sup>78</sup>Se (23.8%) and <sup>80</sup>Se (49.7%).

The nebulization system consisted of a conventional concentric-flow pneumatic nebulizer (Meinhard type, Spectro Analytical Instruments) fed with a nebulizer flow of argon of  $1.1\text{ L min}^{-1}$  which led to a nebulizer gas pressure of 2.8 bars. For HG-ICP-MS measurements a hydride generator module (model 10.006S, Spectro Analytical Instruments) was instead adopted. The gaseous hydride was formed by mixing the sample ( $5\text{ mL min}^{-1}$ ) with a 10 M HCl

solution (1 mL min<sup>-1</sup>) and a solution of NaBH<sub>4</sub> (0.6%, w/w) in 0.12 M NaOH (1 mL min<sup>-1</sup>) by the pump present in the generator equipment.

All signals collected for the Se isotope (counts per second) were normalized to the signal of the In internal standard, whose content was kept carefully constant (8.71 × 10<sup>-4</sup> mol L<sup>-1</sup>, equivalent to 0.1 mg L<sup>-1</sup>) in order to correct for non-spectral interferences and for signal instability. Unless otherwise stated, mean values and standard deviations relative to 10 replicate measurements were always employed. The signals recorded were related to Se concentrations by resorting to suitable calibration plots.

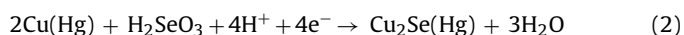
Under these conditions, the response was verified to be linear in the range 5–1000 μg L<sup>-1</sup> of selenium with a correlation coefficient of 0.998 and with sensitivities which turned out to be 5.9 × 10<sup>7</sup> and 2.9 × 10<sup>9</sup> cps L mol<sup>-1</sup> for ICP-MS and HG-ICP-MS measurements, respectively. From these sensitivities, detection limits (LODs) for selenium of 5 and 0.1 μg L<sup>-1</sup> (5.2 × 10<sup>-8</sup> and 1.0 × 10<sup>-9</sup> M), respectively, were evaluated for a signal-to-noise ratio of 3. The relative standard deviation (RSD) characterizing both types of measurements did not go beyond ±9% in 10 replicate measurements.

ICP-OES determinations were performed by a Vista 3000 instrument (Varian Inc., Palo Alto, CA, USA) with a radial configuration, which was equipped with a solid-state segmented-array charge-coupled detector (SCD) and an AS90 autosampler (Varian). All measurements were conducted under the operating conditions already reported in the literature [30]. A Varian VGA-77 Vapour Generation accessory was used for the hydride generation, which was accomplished under the same flow conditions reported above. Selenium was monitored at 196.026 nm, where linear responses were found in the range 10–1000 μg L<sup>-1</sup> with a correlation coefficient of 0.998. From the relevant calibration plots, LODs for selenium of 9 and 0.8 μg L<sup>-1</sup> (9.5 × 10<sup>-8</sup> and 8.4 × 10<sup>-9</sup> M) for ICP-OES and HG-ICP-OES measurements, respectively, were evaluated for a signal-to-noise ratio of 3. The relative standard deviation (RSD) characterizing these types of measurements did not go beyond ±12% in 10 replicate measurements.

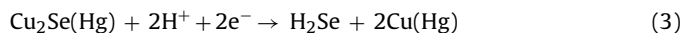
In HG-based measurements, special attention was paid to make the acidity of the analysed samples, standards and blanks very similar with one another, in view of the fact that it is expected to affect significantly the efficiency of the Se conversion into the corresponding hydride [31].

DPCSV measurements were performed by an Autolab PGSTAT30 (Eco Chemie, Utrecht, NL) potentiostat joined to a 663 VA Stand cell (Metrohm, Herisau, Switzerland) consisting of a working hanging mercury drop electrode (HMDE), a glassy carbon tip as the counter electrode and an Ag/AgCl, KCl<sub>sat</sub> reference electrode. This Stand cell was inserted into a 50 mL glass container where all samples were analysed.

A procedure based on the concomitant reduction of Se(IV) and Cu(II) at a HMDE [17,32] was adopted, which was slightly modified as follows, to improve repeatability and accuracy of Se determinations at trace levels. 10 mL of 0.1 M HCl supporting electrolyte solution were introduced into the cell and added with both controlled amounts (usually 0.1–1.0 mL) of 0.1 M HCl solution containing the digested sample and of a standard CuCl<sub>2</sub> solution to achieve a [Cu<sup>2+</sup>] concentration of 1.7 × 10<sup>-5</sup> M. The resulting solution was deaerated for 10 min by bubbling pure nitrogen and then a potential of -0.3 V was applied for 120 s at the HMDE. In this pre-concentration step, elemental copper as soon as deposited onto the mercury surface is chemically oxidized by selenite to yield copper(I) selenide, according to the reaction pathway (1 and 2).



Subsequently, by applying a differential pulse voltammetric scan towards negative potentials (sweep rate 5 mV s<sup>-1</sup>; pulse amplitude 50 mV; pulse duration 50 ms) a cathodic peak is detected at -0.65 V for the reduction of copper(I) (reaction (3)), whose height was linearly dependent on the content of Se present in the analysed sample in the range 0.05–5 μg L<sup>-1</sup> with a correlation coefficient of 0.998.



From the relevant calibration plot, a LOD for selenium of 0.02 μg L<sup>-1</sup> (2.1 × 10<sup>-10</sup> M) was evaluated for a signal-to-noise ratio of 3. The relative standard deviation (RSD) characterizing these measurements did not go beyond ±15% in 10 replicate measurements.

In DPCSV measurements conducted on real samples, the signals recorded were related to Se concentrations not only by the relevant calibration plot, but also by resorting to the standard addition method, in order to check whether current signals suffered from interferences due to the matrix. In all cases, only fairly negligible differences (within ±10%) were found between the results found by the two different approaches.

Turbidimetric-nephelometric measurements were performed by a Thermo Orion AQUAfast IV turbidimeter model AQ4500 (Thermo Scientific, Waltham, MA, USA).

### 3. Results and discussion

#### 3.1. Optimisation of the digestion procedure

As mentioned above, MW digestions of organic or biological materials are in general conducted in strongly oxidant media, usually consisting of nitric acid and hydrogen peroxide mixtures, to attain for certain their exhaustive mineralisation. In any case, the redox potential of these mixtures is conceivably expected to be about 1.3–1.4 V vs. NHE at least, so that their use for digesting Se containing samples leads inevitably to the extensive formation of Se(VI). To avoid this drawback, digestion mixtures should be adopted whose redox potential is buffered in such a way as to range from a maximum of ca. 1.14 V vs. NHE, so as to allow Se(IV) to become stable, to a minimum value of ca. 0.74 V vs. NHE, to prevent reduction of Se(IV) to elemental Se. This is the reason why it is suggested that MW digestions of Se containing samples are performed by a two-step procedure [26,27], the former conducted in a strongly oxidant medium (HNO<sub>3</sub> + H<sub>2</sub>O<sub>2</sub>) aimed at destroying completely the organic matter and the latter, run by using hydrochloric acid as the mineralising medium, performed to exploit the fact that selenate formed in the first step is a sufficiently strong oxidizer to liberate chlorine from chloride ions, being reduced to Se(IV). The need to resort to these two subsequent steps in order to achieve reliable recoveries of Se(IV) makes time expensive even a mineralisation approach such as MW which was instead developed just to perform rapid digestions.

In the view of shortening such a procedure, we have tested the possibility of carrying out the digestion of Se containing samples in a single step by using a suitably optimized power supply program and a digestion mixture containing simultaneously HNO<sub>3</sub>, H<sub>2</sub>O<sub>2</sub> and NaCl in such a ratio as to make its redox potential so buffered as to prevent the formation of Se(VI). With this aim, a series of microwave digestions was conducted under different experimental conditions on synthetic samples (containing from 0.06 to 0.30 μmol of Se) consisting of each of selenium compounds here considered (see Section 2). Each test was replicated in six different digestion vessels, in order to evaluate also the corresponding repeatability.

The power supply program and the digestion mixture initially adopted were those usually employed to achieve a good mineralisation when real biological samples are digested. The heating program

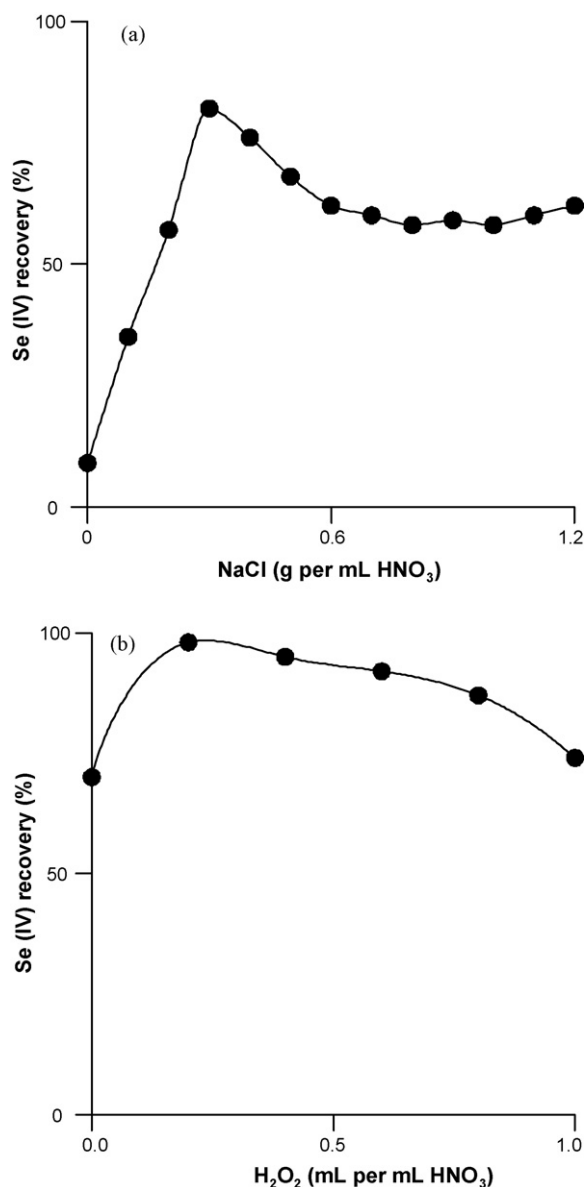


**Fig. 1.** Mean values of selenium(IV) recoveries found by adding increasing amounts of: (a) NaCl to digestion mixtures consisting of  $\text{HNO}_3$  (65%, w/w) +  $\text{H}_2\text{O}_2$  (30%, w/w) in volume ratio 1:1; (b)  $\text{H}_2\text{O}_2$  (30%, w/w) to digestion mixtures consisting of NaCl to  $\text{HNO}_3$  (65%, w/w) in a ratio of 1.3 g per mL. The relative standard deviation, referred to six determinations performed on each selenium compound considered (see Section 2), ranged from 1.2% to 4.6%.

consisted of the following steps: (i) 2 min with an irradiation power of 250 W; (ii) 2 min with 0 W; (iii) 5 min again with 250 W; (iv) 5 min with 400 or 500 W [23]. The composition of the digestion mixture was:  $\text{HNO}_3$  (65%, w/w) +  $\text{H}_2\text{O}_2$  (30%, w/w) in a volume ratio 1:1. Only very poor Se(IV) recoveries (less than 5%) were found under these experimental conditions for all selenium compounds tested.

When these digestions were repeated by adding to mineralisation mixtures increasing amounts of NaCl, to make their redox potential progressively lower than that allowing Se(IV) to be oxidized to Se(VI) but again high enough to permit total destruction of the organic matrix, undoubtedly better but not yet satisfactory results were achieved, as shown in Fig. 1a. Subsequently, on considering that the highest Se(IV) recovery was attained with a NaCl to  $\text{HNO}_3$  ratio of 1.3 g per mL, such a ratio was kept constant and further digestions were run by decreasing progressively the  $\text{H}_2\text{O}_2$

content, in order to decrease the redox potential of the digestion medium, this peroxide being indeed the strongest oxidizing agent. The results found in these digestions are collected in Fig. 1-b which highlights that decreasing contents of  $\text{H}_2\text{O}_2$  are really profitable in that recoveries very close to 100% could be attained for  $\text{H}_2\text{O}_2$  to  $\text{HNO}_3$  volume ratios of about 1:5.

These findings prompted us to consider acid oxidizing mixtures consisting of solutions prepared by mixing nitric acid (65%, w/w) with hydrogen peroxide (30%, w/w) in a volume ratio 5:1 and added with  $0.25 \text{ g mL}^{-1}$  (4.3 M) NaCl quite well tailored to display a redox potential lower than that allowing Se(IV) to be oxidized to Se(VI), but high enough to permit total destruction of the organic matrix. Thus, they were adopted in further assays which were conducted on Se synthetic samples with a series of programs involving different microwave irradiation powers (200–650 W) and irradiation times (2–20 min) in order to improve recoveries and shorten the digestion time.

The whole of these experiments allowed the best performance to be found by carrying out microwave digestions with a three-step power program which was as follows: (i) 2 min with an irradiation power of 250 W; (ii) 2 min with 0 W; (iii) 15 min with 300 W. The first step, conducted with an intermediate irradiation power, was aimed at starting the digestion of organic matter, while the purpose of the second step, run in the absence of microwave irradiation, was to avoid the uncontrolled occurrence of reactions involving the mentioned organic matter. Finally, the third step allowed redox reactions involving selenium compounds to occur without causing high pressure conditions.

The Se(IV) content in all mineralised samples was determined by HG-ICP-MS, HG-ICP-OES and DPCSV. Moreover, in the attempt to check whether not negligible amounts of Se(VI) survived the digestion step, Se(IV) content thus found was also compared with total Se determined by ICP-MS and ICP-OES (i.e. excluding the hydride generation step). Representative examples of typical results found with the different approaches are reported in Table 1, where they are compared with one another as well as with the corresponding theoretical contents.

This Table highlights a good agreement not only among Se(IV) concentrations found by the three analytical approaches suitable for its selective determination (last three columns), but also with total Se, thus proving that digestion conditions adopted were well suited for avoiding the undesired presence of Se(VI) in mineralised samples. However, it is apparent that the worst results were found by ICP-OES, which led in most cases to scarce accuracy and precision, due conceivably to the fact that Se contents involved in these determinations are only slightly higher than its LOD ( $9 \mu\text{g L}^{-1}$ ) and hence lower enough than the corresponding LOQ (about  $30 \mu\text{g L}^{-1}$ ).

### 3.2. Application to real samples

The applicability to real vegetable or animal samples of the single step microwave digestion procedure proposed here was first tested for the determination of selenium in a certified biological material, consisting of lyophilised pig kidney with a selenium content of the order of some  $\mu\text{g g}^{-1}$ , which was used as standard reference sample.

Controlled amounts of this powdered certified sample (ca. 200 mg) were mineralised under the optimised conditions described above and, after digestion, analysed by resorting once again to HG-ICP-MS, HG-ICP-OES and DPCSV for Se(IV) and to ICP-MS and ICP-OES for total selenium. The relevant signals were then related to the Se content by exploiting in all cases the calibration plots constructed for synthetic samples. The results found are summarized in Table 2 where they are compared with one another as well as with theoretical expectations. The good agreement between the selenium content inferred from calibration plots referred to

**Table 1**

Comparison of Se theoretical contents with the results found by the different analytical approaches adopted for controlled amounts of synthetic samples digested by the proposed single-step procedure.

Model compound	Se concentrations ( $\mu\text{g L}^{-1}$ ) <sup>a</sup>					
	Theoretical	ICP-MS (total Se)	ICP-OES (total Se)	HG-ICP-MS (Se(IV))	HG-ICP-OES (Se(IV))	DPCSV (Se(IV))
Seleno-L-methionine	20.0 ± 0.2	21.2 ± 1.3	18.5 ± 3.2	19.1 ± 1.0	19.7 ± 0.5	20.4 ± 0.4
Methyl-seleno-L-cysteine	20.8 ± 0.2	21.1 ± 1.4	22.3 ± 3.5	21.1 ± 0.9	20.7 ± 0.4	21.0 ± 0.3
Seleno-L-cysteine	19.6 ± 0.2	19.4 ± 1.4	18.2 ± 3.0	20.3 ± 1.0	20.2 ± 0.4	19.5 ± 0.4
Sodium selenite	20.7 ± 0.2	20.2 ± 1.3	20.0 ± 3.7	21.7 ± 1.1	21.3 ± 0.4	20.9 ± 0.4
Sodium selenate	20.3 ± 0.2	20.5 ± 1.2	18.2 ± 2.8	19.9 ± 0.8	21.0 ± 0.5	20.5 ± 0.4
Zinc selenide	19.8 ± 0.2	19.7 ± 1.5	18.2 ± 4.1	20.2 ± 0.9	20.6 ± 0.6	19.1 ± 0.8

<sup>a</sup> All recovered amounts were the mean of five replicate digestions. The reported standard deviations were calculated accordingly.

**Table 2**

Comparison of Se theoretical contents with the results found by the different analytical approaches adopted for controlled amounts of a certified lyophilized pig kidney sample digested by the proposed single-step procedure.

Digested amount (mg)	Se concentrations ( $\mu\text{g g}^{-1}$ ) <sup>a</sup>					
	Certified	ICP-MS (total Se)	ICP-OES (total Se)	HG-ICP-MS (Se(IV))	HG-ICP-OES (Se(IV))	DPCSV (Se(IV))
184.2	10.3 ± 0.5	10.5 ± 0.6	9.3 ± 1.7	10.6 ± 0.6	10.5 ± 0.3	10.4 ± 0.2
209.7	10.3 ± 0.5	10.7 ± 0.4	11.3 ± 1.9	10.4 ± 0.3	10.7 ± 0.4	10.3 ± 0.3
238.6	10.3 ± 0.5	10.0 ± 0.8	10.9 ± 2.1	10.2 ± 0.5	10.6 ± 0.6	10.1 ± 0.4

<sup>a</sup> All recovered amounts were the mean of five replicate digestions. The reported standard deviations were calculated accordingly.

synthetic samples and certified data proves that no appreciable interference was caused by matrix effects.

Moreover, it is worth to highlight the good performance provided by DPCSV which, in principle, should be instead expected to suffer more than other approaches from interference caused by the presence in the real sample considered of trace amounts of metal ions mentioned in the experimental section. As a matter of fact, the undesired effect of these possible interferents is avoided thanks to the strategy involved in the procedure adopted. On one hand the preconcentration step is in fact performed at a potential value (−0.3 V) at which they cannot be accumulated onto the electrode surface, they being not reduced, and on the other hand the subsequent potential scan towards negative potentials is run at a Cu-covered Hg electrode where rather appreciable overvoltages are required for the deposition of other metals.

On the basis of these fully satisfactory results, the optimised and validated single step MW digestion procedure was applied to a variety of vegetable and animal food, as well as to human blood

plasma, whose Se contents found turned out to fall in a very wide range (from ca. 5 to 3000  $\text{ng g}^{-1}$ ). In all cases, the efficiency of the mineralisation procedure, in connection with destruction of the biological matrix, was checked by subjecting digested solutions to turbidimetric–nephelometric measurements which pointed out the total absence of solid particles with diameters  $\geq 0.1 \mu\text{m}$ .

Since some of these real matrices were expected to display quite low Se contents, digested samples were analysed by HG-ICP-MS and DPASV alone, in view of their LODs which were found so low as to meet with even trace determinations.

Se content in these real samples was once again inferred from calibration plots constructed for synthetic samples. Their reliability was checked by verifying their full consistence with those found by supplementing Se in the real samples considered. In fact, the data obtained by these two approaches (i.e. calibration plot and standard addition method) differed by about  $\pm 8\%$  at the most, thus highlighting both the satisfactory Se(IV) recovery (and hence good accuracy) achieved by the MW digestion procedure adopted and

**Table 3**

Se content found in food samples and biological fluids.

Sample	Approximate digested amount (g)	Number of different samples analysed	Se content ( $\text{ng g}^{-1}$ ) <sup>a</sup>
Barley	0.5	3	15.38 ± 4.20
Brazil nuts	0.1	3	3182.83 ± 442.06
Bread	0.5	3	112.07 ± 10.86
Carrot	1.0	3	7.04 ± 2.36
Cornmeal	1.0	3	28.33 ± 4.96
Garlic	1.0	3	40.87 ± 3.29
Lettuce	1.0	3	5.77 ± 2.00
Onion	1.0	3	9.60 ± 2.53
Pasta	0.5	3	79.62 ± 2.66
Potato (with peel)	1.0	3	7.36 ± 4.12
Potato (without peel)	1.0	3	10.07 ± 2.46
Potato "Selenella" (with peel)	0.5	3	188.40 ± 12.05
Potato "Selenella" (without peel)	0.5	3	159.43 ± 2.81
Pork loin	0.5	3	88.19 ± 8.07
Raw ham	0.5	3	93.82 ± 2.52
Rice	1.0	3	26.21 ± 5.44
Salami	0.5	3	90.46 ± 7.24
Spelt	0.5	3	53.98 ± 8.91
Human blood plasma	0.5 mL	171 <sup>b</sup>	75.46 ± 24.46

<sup>a</sup> The reported contents are the mean of Se concentrations found in the different samples of the same nature, each subjected to three replicate digestions. The reported standard deviations were hence calculated as pooled standard deviations.

<sup>b</sup> These samples were drawn from volunteers whose age ranged from 20 to 80 (45% male and 55% female).



that the simple use of a regression graph is appropriate for routine work.

The results found for Se contents in the different matrices considered, which are shown in Table 3, agree quite well with mean Se concentrations reported so far by other authors for similar foods from different geographical regions [26,33–38]. In particular, inspection of this Table indicates that most vegetables are poor sources of Se, while products richer in proteins are characterized by higher Se levels. This is in full agreement with the fact that plant species do not require Se for growth and can be hence very low in this element, in contrast to animal species which are unable to survive if tissue levels of this essential nutrient are too low.

#### 4. Conclusions

The suggested single step MW digestion procedure turns out to be well suited for providing concomitantly the exhaustive mineralisation of biological samples and the quantitative conversion of any type of selenium compounds into Se(IV). Digested samples thus obtained in a time very shorter than that required by previously reported mineralisation methods are directly suitable for the subsequent Se analysis at trace and ultratrace levels by both spectrometric methods such as HG-ICP-MS or HG-ICP-OES and differential pulse cathodic stripping voltammetry (DPCSV). The application of this simple approach to standard organic samples and to a certified biological sample allowed precise and accurate results to be achieved, also highlighting its robustness in that it does not require a strict control of the relevant experimental parameters.

#### Acknowledgements

The authors thank Dr. M. Mizzau for her skilful technical and experimental assistance. Financial aid from the Ministry of University and Scientific Research is gratefully acknowledged.

#### References

[1] J. Pinsent, *Biochem. J.* 57 (1954) 10.

- [2] K. Schwarz, C.M. Foltz, *J. Am. Chem. Soc.* 79 (1957) 3292.  
 [3] M.P. Rayman, *Lancet* 356 (2000) 233.  
 [4] H. Tapiero, D.M. Townsend, K.D. Tew, *Biomed. Pharmacother.* 57 (2003) 134.  
 [5] M. Navarro-Alarcon, M.C. Lopez-Martinez, *Sci. Total Environ.* 249 (2000) 347.  
 [6] C. Reilly, *Trends Food Sci. Technol.* 9 (1998) 114.  
 [7] P. Vinas, I. Lopez-Garcia, B. Merino-Merono, N. Campillo, M. Hernandez-Cordoba, *Anal. Chim. Acta* 535 (2005) 49.  
 [8] J.L. Capelo, C. Fernandez, B. Pedras, P. Santos, P. Gonzalez, C. Vaz, *Talanta* 68 (2006) 1442.  
 [9] Y. Zhang, S.B. Adeloju, *Talanta* 76 (2008) 724.  
 [10] N.A.R. Pedro, E. de Oliveira, S. Cadore, *Food Chem.* 95 (2006) 94.  
 [11] K. Jitmanee, N. Teshima, T. Sakai, K. Grudpan, *Talanta* 73 (2007) 352.  
 [12] I.L. Caballero-Arauz, S. Afton, K. Wrobel, J.A. Caruso, J.F. Gutierrez-Corona, K. Wrobel, *J. Hazard. Mater.* 153 (2008) 1157.  
 [13] G. Zhengjun, Z. Xinshen, C. Guohe, X. Xinfeng, *Talanta* 66 (2005) 1012.  
 [14] D. Rekha, K. Suvardhan, K.S. Kumar, G.R.K. Naidu, P. Chiranjeevi, *J. Anal. Chem.* 61 (2006) 1177.  
 [15] T. Ferri, F. Coccioli, C. De Luca, C.V. Callegari, R. Morabito, *Microchem. J.* 78 (2004) 195.  
 [16] P. Zuman, G. Somer, *Talanta* 51 (2000) 645.  
 [17] R. Piech, W.W. Kubiak, *Electrochim. Acta* 53 (2007) 584.  
 [18] O.G. Filichkina, E.A. Zakharova, G.B. Slepchenko, *J. Anal. Chem.* 59 (2004) 541.  
 [19] T. Ferri, G. Favero, M. Frascioni, *Microchem. J.* 85 (2007) 222.  
 [20] D.F. Lambert, N.J. Turoczy, *Anal. Chim. Acta* 408 (2000) 97.  
 [21] M. Miyahara, Y. Saito, *J. Agric. Food Chem.* 42 (1994) 1126.  
 [22] B. Erikson, *Anal. Chim. Acta* 70 (1998) 467A.  
 [23] F. Di Narda, R. Toniolo, G. Bontempelli, *Anal. Chim. Acta* 436 (2001) 245.  
 [24] H.M. Kingston, L.B. Jassie, *Introduction to Microwave Sample Preparation. Theory and Practice*, ACS Professional Reference Book, Washington, DC, 1998.  
 [25] F. Di Narda, R. Toniolo, S. Susmel, A. Pizzariello, G. Bontempelli, *Talanta* 60 (2003) 653.  
 [26] P. Smrkolj, V. Stibilj, *Anal. Chim. Acta* 512 (2004) 11.  
 [27] J. Barciela-Garcia, M. Krachler, B. Chen, W. Shotyk, *Anal. Chim. Acta* 534 (2005) 255.  
 [28] F. Tubaro, F. Barbangelo, R. Toniolo, F. Di Narda, G. Bontempelli, *Ann. Chim. (Rome)* 89 (1999) 863.  
 [29] F. Tubaro, F. Barbangelo, R. Toniolo, F. Di Narda, S. Susmel, G. Bontempelli, *Ann. Chim. (Rome)* 92 (2002) 289.  
 [30] W.T. Buckley, J.J. Budac, D.V. Godfrey, K.M. Koenig, *Anal. Chim. Acta* 64 (1992) 724.  
 [31] P. Pohl, *Trends Anal. Chem.* 23 (2004) 87.  
 [32] L.M. de Carvalho, G. Schwedt, G. Henze, S. Sander, *Analyst* 124 (1999) 1803.  
 [33] M.N.I. Barclay, A. MacPherson, J. Dixon, *J. Food Compos. Anal.* 8 (1995) 307.  
 [34] L. Hussein, J. Bruggeman, *Food Chem.* 65 (1999) 527.  
 [35] J. Murphy, K.D. Cashman, *Food Chem.* 74 (2001) 493.  
 [36] S.A. McNaughton, G.C. Marks, *J. Food Compos. Anal.* 15 (2002) 169.  
 [37] T. Klapeč, M.L. Mandić, J. Grgić, L. Primorac, A. Perl, V. Krstanović, *Food Chem.* 85 (2004) 445.  
 [38] P.P. Sirichakwal, P. Puwastien, J. Polngam, R. Kongkachuichai, *J. Food Compos. Anal.* 18 (2005) 47.



## Determination of human growth hormone in human serum samples by surface plasmon resonance immunoassay

J. Treviño<sup>a,b,\*</sup>, A. Calle<sup>c</sup>, J.M. Rodríguez-Frade<sup>d</sup>, M. Mellado<sup>d</sup>, L.M. Lechuga<sup>a,b</sup>

<sup>a</sup> Grupo de Nanobiosensores y Biofísica Molecular, Centro de Investigación en Nanociencia y Nanotecnología (CIN2: CSIC-ICN), ETSE, Campus UAB, Bellaterra, Barcelona, Spain

<sup>b</sup> Centro de Investigación Biomédica en Red en Bioingeniería, Biomateriales y Nanomedicina (CIBER-BBN), Barcelona, Spain

<sup>c</sup> Instituto de Microelectrónica de Madrid (CNM-CSIC), Madrid, Spain

<sup>d</sup> Departamento de Inmunología y Oncología, Centro Nacional de Biotecnología (CNB-CSIC), Madrid, Spain

### ARTICLE INFO

#### Article history:

Received 22 September 2008

Received in revised form

29 December 2008

Accepted 9 January 2009

Available online 20 January 2009

#### Keywords:

SPR

Immunosensor

Self-assembled monolayer

hGH

Point-of-care device

Serum

### ABSTRACT

A surface plasmon resonance immunoassay has been developed to determine human growth hormone (hGH) directly and without pre-treatment in human serum samples. A binding inhibition immunoassay was employed. Antibody concentration, assay buffer and regeneration solution have been optimized in order to reach the best performance and the lower non-specific binding of the matrix components to the sensor surface. The lowest detection limit was 6 ng/mL, with a working range covering the physiological range. Reproducibility of the assay was excellent with both intra-assay and inter-assay relative standard deviations <5%, while a variation of 2.19% was obtained employing different sensor chips. Reutilization of the sensor surface allows its continuous use over 50 measurements with a signal drop <20%. The SPR immunoassay results were validated using enzyme-linked immunosorbent assay (ELISA) showing an excellent correlation ( $R^2 = 0.985$ ). A portable and fully automated system (Sensia SL) was employed in this work. This is the first SPR biosensor assay capable of detecting relevant concentrations of a clinical analyte in serum. This study shows the potentials of this device as a diagnostic tool for the detection of multiple clinical analytes.

© 2009 Elsevier B.V. All rights reserved.

### 1. Introduction

In the last years diagnostics is starting to leave clinical laboratories to come closer to the patient in point-of-care settings as primary care centres, hospital units and homes [1]. Immunoassay techniques have provided a useful tool for rapid diagnostic and monitoring directly at these locations [2]. Biosensors are ideal for these applications as they can reach similar analytical quality as laboratory methods adding some extra features as a short turnaround time, portability and simple use compared to other analytical techniques [1–3]. Surface plasmon resonance (SPR) biosensors [4] have proven the necessary analytical characteristics as specificity, sensitivity, accuracy and precision. They also provide real-time data avoiding labelling steps, thus fulfilling most of the desirable features for a point-of-care analyzer. However, some disadvantages obstruct the development of all types of optical biosensors for clinical use due to matrix effects produced by non-specific binding of the components of such complex samples.

Blood serum is one of the main sources of clinical analytes and it contains thousands of proteins that provide potential information for disease biomarker detection. But it has the drawback of its complexity as analytical matrix. In fact, 90% of its protein content (60–80 mg/mL) consists in a few high abundant proteins that together with its high lipid content hinder the rest less abundant proteins. The dynamic range of serum proteins is 10 orders of magnitude wide, from sub-pg/mL to above mg/mL. This is a serious obstacle for the development of clinical biosensors handling human serum samples, mainly due to non-specific binding to the sensor surface, which would hinder the specific biological interaction.

Human growth hormone (hGH) is a polypeptide hormone, essential for normal growth and development, secreted by the anterior pituitary gland. Circulating hGH consists of a heterogeneous mixture of proteins including a predominant 22 kDa hGH isoform, and other less abundant variants such as the 20 kDa hGH [5]. Selective assays to define the contribution of the different isoforms could be valuable tools for both clinical diagnostics and basic research. Determination of hGH in serum is essential for the diagnosis of disorders in hGH secretion. hGH excess is commonly caused by pituitary tumours which result in disorders as acromegaly or pituitary gigantism when it occurs in childhood. The main causes of hGH deficiency are pituitary malformations or damages. Detection of hGH is also used by sports authorities in doping detection, as hGH is one

\* Corresponding author at: Centro de Investigación en Nanociencia y Nanotecnología (CIN2: CSIC-ICN), Edificio Q - ETSE, 3ª Planta, Campus UAB, 08193, Bellaterra, Barcelona, Spain. Tel.: +34 93 586 80 12; fax: +34 93 586 80 20.

E-mail address: [juan.trevino@cin2.es](mailto:juan.trevino@cin2.es) (J. Treviño).

of the most habitual substances used to increase performance in some disciplines [6].

Secretion of hGH is pulsatile, resulting in widely fluctuating levels in blood with peaks of 50–100 ng/mL and minimum levels of 0.03 ng/mL [5]. It is widely accepted, for the diagnosis of hGH deficiency, a cut-off value of 10 ng/mL in response to an appropriate provocative test [7]. Clinical assays for the determination of human growth hormone include bioassays, radioreceptor assays and immunoassays. Radioimmunoassays (RIA), immunoradiometric assays (IRMA), enzyme-linked immunosorbent assays (ELISA) and immunofunctional assays (IFA) have been used for hGH determination due to their sensitivity and high sample throughput. Conventional selective assays are time consuming, require fluorescent labels or radioactive probes. In addition, most of these assays require facilities, which obstruct their application in settings out of the lab.

Surface plasmon resonance biosensors allow monitoring of biomolecular interactions as increases in refractive index caused by mass changes at the sensor surface. The coupling of immunoassays with SPR biosensors enables online monitoring of analytes in a fast, simple, direct and reversible way, avoiding labelling and sample preparation steps. In this work, a recently launched commercial sensor,  $\beta$ -SPR (Sensia SL, Spain) based in surface plasmon resonance has been employed to detect hGH in serum samples. This system is portable and incorporates software for data acquisition and instrument control, thus it turns on a useful tool for fast diagnostics in clinical laboratories and point-of-care settings. Recently, this device has proven its usefulness in environmental analysis for the online monitoring of pesticides in natural water samples [8–10].

In this work we report the development and validation of a SPR immunosensor for hGH determination in serum. To our knowledge this is the first biosensor assay for the detection of hGH. Moreover a SPR sensor to detect relevant concentrations of a clinical analyte in serum has not been developed to date [4]. Surface plasmon resonance immunosensor applications that measure clinical samples directly are still unusual, and generally use signal amplification steps, sample pre-treatment or dilution [11–15].

## 2. Experimental

### 2.1. Reagents

Purified monoclonal antibody (mAb) hGH-12, that recognizes all hGH isoforms, was obtained and characterized as described before [16]. Recombinant hGH was obtained from Pfizer (Spain). Rabbit and human sera were purchased from Sigma–Aldrich (Steinheim, Germany). Serum samples from patients undergoing stimulation tests for hGH deficiency diagnostic were kindly provided by Dr. M.D. Rodríguez Arnau. Hospital General Universitario Gregorio Marañón, Madrid, Spain.

Mercaptoundecanoic acid, N-hydroxysuccinimide (NHS) and 1-ethyl-3-(3-dimethyl-amino-propyl)carbodiimide hydrochloride (EDC) were purchased from Sigma–Aldrich (Steinheim, Germany). Organic solvents used in gold chip cleansing process: trichloroethylene, acetone and ethanol, and piranha solution components  $\text{H}_2\text{SO}_4$  and  $\text{H}_2\text{O}_2$  were supplied by Merck (Darmstadt, Germany). Potassium chloride, sodium chloride, disodium hydrogen phosphate and potassium dihydrogen phosphate, used for the preparation of PBST buffer (10 mM phosphate pH 7.4 with 137 mM NaCl, 2.7 mM KCl and 0.05% Tween 20), acetic acid and sodium acetate for the preparation of acetate buffer (10 mM acetate pH 5) and sodium hydroxide and hydrochloric acid, used to adjust the pH of the solutions, were provided by Panreac (Barcelona, Spain). Ethanolamine hydrochloride blocking agent was obtained from Acros Organics (Geel, Belgium). Tween 20 was purchased from Quantum Appligene (Heidelberg, Germany).

### 2.2. Instrumentation

A commercial surface plasmon resonance biosensor, from Sensia SL (Spain) was used for the SPR measurements. The sensor has two flow cells with a volume of 300 nL each. The device incorporates optics and upgradeable electronic modules as well as computer controlled pumps, valves and injection fluidics. All the measurements were performed by sample injection using the flow delivery system incorporated in the platform that assures the injection for analysis of precise volumes of 220  $\mu\text{L}$  while maintaining a continuous flow of buffer between 10 and 40  $\mu\text{L}/\text{min}$ . Further description of this system can be found elsewhere [8].

### 2.3. Preparation of the sensor surface: immobilization procedure

Specific hGH chip surface was prepared with conventional amino coupling on SPR gold chips. Chips were cleaned with trichloroethylene, acetone and ethanol, immersed in piranha solution ( $\text{H}_2\text{SO}_4/\text{H}_2\text{O}_2$ , 3:1) rinsed with water, ultrasonicated for 5 min and dried with  $\text{N}_2$ . Gold chip was then placed over the flow cells and prism was adhered to the chip using matching refractive index oil. A constant flow speed of 10  $\mu\text{L}/\text{min}$  was maintained during the immobilization process. Formation of the carboxyl terminated alkenethiol SAM was carried by adsorption of mercaptoundecanoic acid (0.05 mM solution in ethanol) on the gold sensor surface. After rinse of alkanethiol excess with ethanol, a continuous flow of water was maintained for the next steps of the immobilization process. Then the carboxylic surface was activated with EDC 0.2 M and NHS 0.05 M to form a N-hydroxysuccinimide ester intermediate and immediately after, hGH was covalently coupled via amine groups using two injections with a washing step with HCl 100 mM in between. The unreacted groups remaining on the chip surface were deactivated using ethanolamine 1 M, pH 8.5. Once hGH was immobilized on the sensor surface, a flow of PBST at 20  $\mu\text{L}/\text{min}$  was fixed. This procedure ensures that only covalently bound biomolecules remain on the sensor surface. The selectivity of the monolayer was evaluated by studying possible interactions with non-specific antibodies.

### 2.4. SPR immunoassay format

For calibration curves, a set of triplicate hGH standard concentrations in the  $10^{-4}$  to 100  $\mu\text{g}/\text{mL}$  range in PBST and blank controls were mixed (1:1) with mAb hGH-12 in PBST. Then, solutions were injected sequentially over the hGH sensor surface at 20  $\mu\text{L}/\text{min}$  and SPR signal was monitored in real-time. Calibration curves with mAb hGH-12 concentrations of 0.25, 0.5, 1 and 2  $\mu\text{g}/\text{mL}$  in PBST were evaluated in order to find the one that provides the optimal assay sensitivity. Reutilization of the sensor surface was accomplished by an injection of HCl 5 mM regeneration solution at a flow speed of 30  $\mu\text{L}/\text{min}$ . SPR signal of each standard was expressed as the percentage of the maximum response [ $100 \times (\text{SPR signal}/\text{SPR signal, max})$ ]. The averaged responses of the three standards measured for each concentration were plotted versus the logarithm of hGH concentration and fitted to a four-parameter logistic equation:

$$y = \frac{D + (A - D)}{1 + (x/C)^B}$$

where  $x$  is the concentration,  $y$  is the response,  $A$  is the asymptotic maximum, corresponding to the signal in absence of analyte,  $B$  is the slope at the inflection point,  $C$  is the inflection point, equivalent to the half inhibitory concentration  $I_{50}$  and  $D$  is the asymptotic minimum, corresponding to the background signal.

## 2.5. Sample matrix effects

Experiments to test matrix effects and the conditions to reduce them for improving the regeneration step were carried with rabbit serum, which has similar behaviour in the SPR immunosensor to human serum. Aliquots of rabbit serum were mixed (1:1) with PBST buffer to simulate assay conditions, injected on the sensor without any treatment and recorded the SPR signal.

Twelve PBST buffers were prepared varying simultaneously NaCl concentration (137 and 500 mM), pH (6.5–7.4–8) and Tween 20 concentration (0.05–0.1%). Rabbit serum aliquots were mixed (1:1) with these twelve different assay buffers and were injected on the sensor at 20  $\mu\text{L}/\text{min}$  using the same assay buffer to obtain information of non-specific binding of serum matrix components to the sensor surface. Rabbit serum aliquots were mixed (1:1) with mAb hGH-12 to a concentration in the mixture of 0.25, 0.5, 1 and 2  $\mu\text{g}/\text{mL}$  using those different assay buffers, injected on the sensor at 20  $\mu\text{L}/\text{min}$  and the SPR response was tested to check mAb hGH-12 interaction with the sensor surface in the serum sample matrix. PBST buffer containing 500 mM NaCl, 0.1% Tween 20 and pH 8, hereafter called PBST-S, was maintained as assay buffer for the rest of the measures of serum samples.

Regeneration solutions combining acid or basic pH with a high ionic strength and surfactant Tween 20 were prepared to assess the regeneration of mAb interaction in serum samples. These factors were varied simultaneously, pH (2, 2.3, 3, 11, 11.7, 12), ionic strength (0, 0.5, 1, 2 M NaCl) and Tween 20 (0, 0.05, 0.1%) and were tested to break the interaction after an injection of a (1:1) mixture of rabbit serum with mAb hGH-12 to a concentration of 2  $\mu\text{g}/\text{mL}$  in PBST-S.

## 2.6. Serum sample analysis

To obtain serum calibration curves, triplicate standards of hGH in the  $4 \times 10^{-3}$  to 40  $\mu\text{g}/\text{mL}$  range were prepared in human serum by serial dilution of a stock solution of 1 mg/mL of hGH in PBST-S, mixed (1:1) with mAb hGH-12 to a concentration of 2  $\mu\text{g}/\text{mL}$  in PBST-S and injected on the sensor at 20  $\mu\text{L}/\text{min}$ . Blank controls were prepared equal. Regeneration after the measurement of each sample was accomplished using regeneration solution with 2 M NaCl, 0.1% Tween 20 and pH 11 at 30  $\mu\text{L}/\text{min}$ . Standards were analysed with the SPR immunosensor and calibration curves were calculated as described above.

Serum sample volumes of 110  $\mu\text{L}$  were mixed (1:1) with mAb hGH-12 to a concentration of 2  $\mu\text{g}/\text{mL}$  in PBST-S and injected in the sensor without any further treatment. All samples were analysed with both the immunosensor and ELISA method to validate the immunosensor results. Sandwich ELISA for hGH determination was developed using mAb hGH-27 as a capture antibody and biotinylated mAb hGH-12 as second antibody as described before [16].

## 3. Results and discussion

### 3.1. Characterization of the hGH SPR immunoassay

An inhibition immunoassay format with the antigen immobilized on the biosensor surface was chosen to extend the immunosensor lifespan. Antibody coated surfaces show low performance as antibody affinity could be lost upon immobilization, because they are sensitive to regeneration conditions and due to the random orientation of immobilized antibodies. Inhibition immunoassay allows a direct measure without need of secondary species or fluorescent labels. This format assures immunosensor reusability and stability maintaining its activity intact throughout a long number of measure and regeneration cycles.

Immobilization of the biological receptor involves the formation of a monomolecular film of the biological recognition element in a controlled and stable manner. Self-assembled monolayers (SAMs) provide an excellent method for this purpose, due to the simplicity and reliability of the process, the reproducibility of the surface upon regeneration and to the flexibility for the incorporation of different biomolecules [17]. Covalent attachment of the recognition element to the sensor surface was achieved via carbodiimide coupling between free amino groups in the protein and carboxyl end of the SAM [18].

hGH concentration and immobilization buffer pH were adjusted to obtain the optimal immobilization conditions that produces the best sensor performance. hGH concentrations of 10, 25, 50 and 100  $\mu\text{g}/\text{mL}$  were employed and 10 mM acetate buffer pH was changed from 4, 4.5, 5, 5.5 and 6. Optimal immobilization conditions were found to be hGH 50  $\mu\text{g}/\text{mL}$  in 10 mM acetate buffer pH 5. The response of the immunosensor was assessed using different mAb hGH-12 concentrations: 0.1, 0.5, 1, 2.5 and 5  $\mu\text{g}/\text{mL}$ . Concentrations lower than 0.25  $\mu\text{g}/\text{mL}$  produce signals too low to maintain the desired precision of the assay. The negligible response of non-specific antibodies confirms the selectivity of the monolayer.

The experiments were carried in an inhibitive immunoassay format. This format consists in the addition of a constant amount of antibody to all the samples. Further antibody binding to the immobilized antigen is inhibited by the presence of the analyte, thus producing decreasing SPR signals as the analyte concentration increases. Immunoassay analytical characteristics as detection limit and working range are influenced by antibody concentration, since lower antibody concentrations are saturated by little amounts of the analyte. Therefore, optimization of the immunoassay requires finding a compromise between a low antibody concentration, which provides a better assay sensitivity, and a concentration high enough to generate a quantifiable signal in the SPR immunosensor. A set of calibration curves were obtained using concentrations of 0.25, 0.5, 1 and 2  $\mu\text{g}/\text{mL}$  of mAb hGH-12. Calibration standards including concentrations ranging from  $10^{-4}$  to 100  $\mu\text{g}/\text{mL}$  hGH and blank samples were mixed with the mAb and injected in the sensor. Fig. 1a shows the SPR signal decreases in response to increasing hGH concentrations. Injection of HCl 5 mM solution disrupts completely the interaction, which allows the sensor reutilization as the SPR signal returns to the initial value after each sample measurement. Analysis cycle, including regeneration, takes 20 min. Calibration curves were calculated using mean triplicate measurements of each hGH concentration. The limit of detection was 4 ng/mL, determined as the analyte concentration inhibiting 3 times the standard deviation of blank samples. The linear working range (18–542 ng/mL) comprises the concentrations producing an inhibition from 20 to 80% of the maximum SPR signal and the  $I_{50}$ , 91 ng/mL, is the concentration producing 50% of the maximum SPR signal.

### 3.2. Determination of hGH in human serum samples

The development of optical biosensors for clinical applications has been hindered by matrix effects caused by high molecular weight species present in any complex biological samples. The applications of SPR biosensors using serum are unusual or generally require pre-treatment or dilution of samples. The aim of this work was to achieve hGH determination in serum directly without dilution or any pre-treatment.

Sample matrix components can affect the immunoassay by binding to the sensor surface, producing a non-specific response that hides the real interaction and prevents adequate sensor regeneration, reducing the device shelf-life. These species can additionally interfere the binding of the antibody to the immobilized antigen in such a way that the specific signal is reduced. In inhibition immunoassays, matrix components can affect the interaction

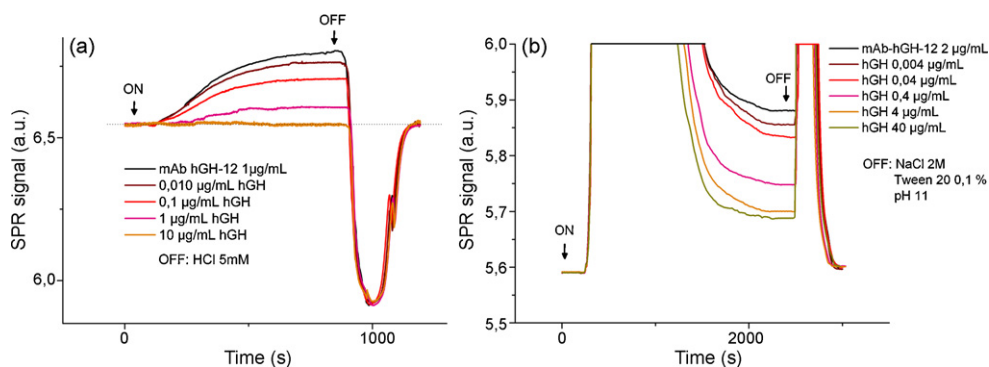


**Fig. 1.** SPR response to the binding of different hGH concentrations and subsequent regeneration cycles during the performance of binding inhibition tests in (a) PBST and (b) serum.

between the antigen and the antibody in the pre-incubated mixture causing a decrease in assay sensitivity. These matrix effects are a challenge not only for SPR biosensors but also for almost any type of biosensor device, so different strategies have been proposed to reduce their impact, among which stand out the development of surface coatings exhibiting high protein resistance [19]. The influence of assay buffer conditions as pH and ionic strength have been studied, and they have proved that an adequate assay buffer can reduce dramatically the non-specific binding from matrix components [20].

Preliminary tests carried to assess non-specific binding of matrix components present in serum show a large non-specific signal which is far exceeding the specific signal and therefore it will mask any result. The effect of assay buffer on non-specific binding of serum proteins to the sensor surface was studied varying three factors: ionic strength, pH and surfactant Tween 20. Non-specific binding was markedly reduced at high pH in all cases, with an additional decrease at high ionic strength. A high concentration of Tween 20 caused a moderated reduction in non-specific binding as well. An elevated ionic strength contributes to minimization of electrostatic interactions and surfactants as Tween 20 prevent protein aggregation and adsorption. PBST buffer containing 500 mM NaCl, 0.1% Tween 20 and pH 8 (PBST-S) produces a reduction in non-specific binding of 88% compared with previous PBST buffer, showing the best behaviour regarding to non-specific binding.

The response in the SPR immunosensor of mAb hGH-12 at concentrations of 0.25, 0.5, 1 and 2 µg/mL was tested to assess the antigen–antibody interaction in those different buffers. PBST-S has demonstrated the best performance in non-specific binding while maintaining 90% of the antibody signal obtained in PBST. Inhibition immunoassay was neither influenced in these buffer conditions.

Regeneration of the sensor surface after each measurement in serum samples was not achieved in the same conditions used in buffer samples. In this case, regeneration comprises disruption of antigen–antibody binding and desorption of non-specific bound serum proteins. Several regeneration solutions were prepared in order to attain the complete regeneration of the surface using mild conditions that make possible its prolonged use over multiple measurement cycles. Complete regeneration was accomplished using a regeneration solution with 2 M NaCl, 0.1% Tween 20 and pH 11 that was maintained for the rest of the measurements carried out in human serum.

Serum samples were measured using the optimal PBST-S buffer. The fixed amount of antibody in the inhibition assay was raised to 2 µg/mL to compensate the signal reduction due to matrix interference and to enhance the response against the matrix residual background. This increase in antibody concentration leads to a

slight decrease in the sensitivity of the assay but it still remains within the physiological concentration range. The measures in serum samples were carried out with the same flow parameters, but after each interaction, the running buffer needs some additional time to wash the surface and to reach a stable signal, enlarging the measure and regeneration cycle to 45 min for the simultaneous determination of two samples. Calibration standards in the  $4 \times 10^{-3}$  to 40 µg/mL range and blank samples were analyzed. Calibration curves were calculated similar to previous experiments. Fig. 1b shows SPR response to different samples containing increasing amounts of hGH and the complete regeneration of the sensor surface. Calibration curve and analytical characteristics of the assay are shown in Fig. 2.

This SPR immunoassay is useful for the determination of a clinical analyte as hGH in serum samples at concentration levels from 6 ng/mL to 1.3 µg/mL that cover the lower part of the physiological range of 30–100 ng/mL, in a direct and fast way without sample pre-treatment or dilution using a small sample volume of 110 µL.

### 3.3. Reproducibility

The immunoassay reproducibility was studied by the assessment of the intra- and inter-day variability. Triplicate samples with hGH concentrations of  $4 \times 10^{-3}$ ,  $4 \times 10^{-2}$ ,  $4 \times 10^{-1}$  and 4 µg/mL were prepared in serum and measured on 3 different days to assess within-day and day-to-day variation. Table 1 shows the intra- and inter-assay coefficients of variation of different samples. Mean intra-assay values were below 3% and inter-assay mean value was

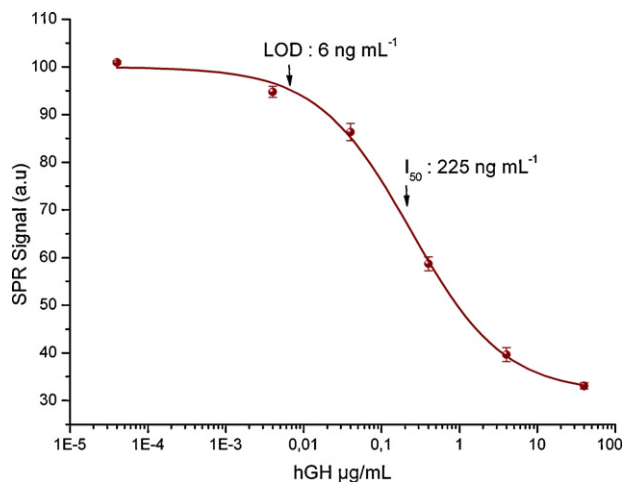


**Fig. 2.** Standard calibration curve of hGH in serum. Each point shows the mean value of three replicate measurements.

**Table 1**

Performance of intra- and inter-assay variations for the SPR determination of triplicate measurements of hGH over a 3-day period.

	hGH concentration ( $\mu\text{g/mL}$ )				Mean
	0.004	0.04	0.4	4	
Intra-assay variation (R.S.D.%)					
Day 1	1.22	2.10	2.52	3.71	2.39
Day 2	0.57	1.22	0.81	3.16	1.44
Day 3	0.37	1.83	3.24	4.92	2.59
Inter-assay variation (R.S.D.%)					
3-Day period	0.24	1.71	2.48	3.06	1.87

1.87%. Furthermore, all the individual coefficients of variations were below 5%. All these values were by far within the accepted variability values for analytical methods.

The variability of the assay using different sensor chips was also tested. Triplicate standard curves were measured under identical conditions using three different sensor surfaces prepared at different times. Fig. 3 shows the three calibration curves for the three sensor chips tested. The chip-to-chip reproducibility is excellent, showing a mean coefficient of variation of 2.19% with  $I_{50}$  values varying from 226 to 235 ng/mL.

### 3.4. Reusability

Together with reproducibility, biosensor reusability is a key point of the immunoassay robustness. The reusability is related to the stability of the sensor surface throughout a number of measurements. Reutilization of an immunosensor is accomplished regenerating the sensing surface by the complete dissociation of the antigen–antibody complex without affecting the affinity of the immobilized molecule. Antigen–antibody interactions are caused by electrostatic, Lewis acid–base and van der Waals forces, which can be disrupted by different strategies. Essentially, regeneration conditions for immunosensors can be guided by experience in affinity chromatography elution conditions. In most cases, regeneration is carried by extreme pH solutions as HCl or glycine pH 1–3 or NaOH pH 10–11, but high ionic strength, detergents and non-polar water-diluted solvents have been used as well. Solutions combining several of these additives can be used to regenerate resistant interactions or to minimize the risk of bioreceptor damage [21].

The stability of the immunosensor upon regeneration was tested by measuring the variation of the maximum SPR signal produced by blank samples introduced in each calibration or sample series.

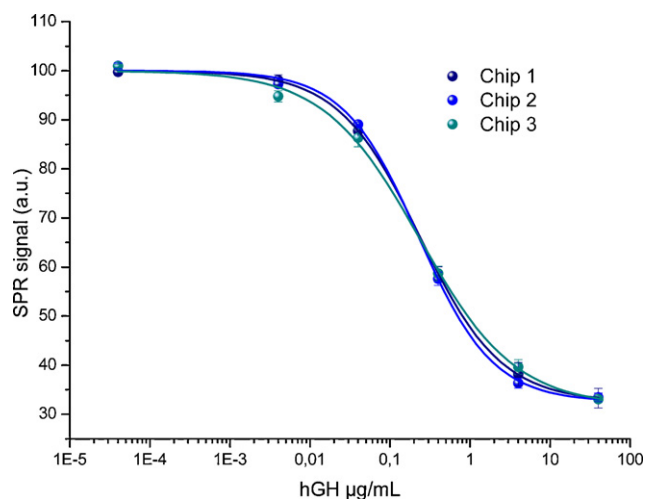


**Fig. 3.** Standard calibration curves of hGH for three different batches of sensor chips. Each point shows the mean value of three replicate measurements.

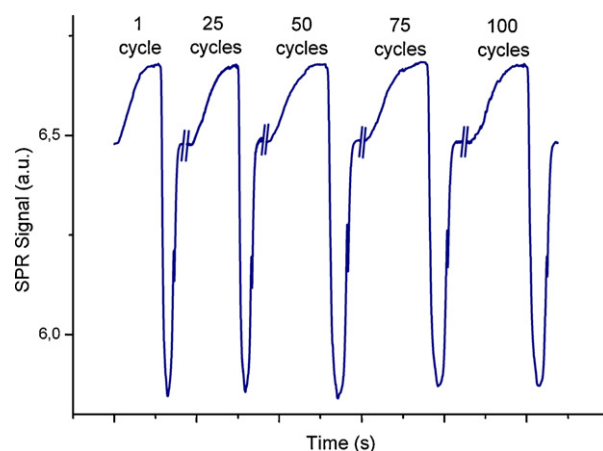


**Fig. 4.** Sensorgram showing the specific SPR response throughout successive measurement and regeneration cycles.

For hGH immunoassay in PBST, mild acid solution HCl 5 mM provides a complete regeneration of the biosensor surface allowing its stable use throughout above 100 measurement cycles within each flow cell. Stability of the sensor was tested in 10 series of daily measurements, making possible its continuous use with a maximum SPR signal drop of 7% of the initial value (Fig. 4). For the measurements carried out with serum samples an inferior reusability is observed as a predictable consequence of the matrix effects described above. Harsher regeneration conditions were employed to disrupt antigen–antibody binding and to desorb non-specific bound serum proteins. Complete regeneration of the biosensor surface is accomplished by the use of a solution containing NaCl 2 M, Tween 20 0.1% at pH 11. Although harsher regeneration conditions were needed, regeneration performance remained appropriate and sensor stability was maintained throughout more than 50 measurement cycles during 5 consecutive days with a maximum SPR signal drop of 17% of the initial value. These slight variations on the signal do not have effect over assay reproducibility since all the measurements are always normalized to the maximum SPR signal.

### 3.5. Comparison with ELISA analysis of real samples

The accuracy of hGH determination by SPR immunoassay was evaluated by comparison with ELISA method. Ten real samples from hGH deficiency provocative tests were analysed by both methods, among them five revealed concentrations under the SPR immunoassay detection limit (6 ng/mL). The five remaining samples above this level showed an excellent agreement between both methods ( $R^2 = 0.985$ ). These data reveal that the SPR immunoassay method proposed here is capable to help hGH deficiency diagnosis identifying the samples under the cut-off value (10 ng/mL) of hGH deficient patients and accurately quantifying the samples above the cut-off level of non-deficient patients.

## 4. Conclusions

The SPR immunoassay method developed in this work demonstrates the usefulness of the  $\beta$ -SPR biosensor for the detection of a relevant clinical analyte as hGH in real serum samples. The method makes possible a fast, label-free and real-time determination using reduced sample volumes. This portable SPR immunosensor is able to determine the analyte directly and without any pre-treatment in serum samples. To our knowledge this is the first biosensor assay for the determination of hGH and the first application of a SPR biosensor for the direct detection of an analyte in serum samples at

relevant concentrations without dilution or sample pre-treatment [4].

The robustness of the method was verified with the excellent reproducibility together with the appropriate regeneration performance. The sensor signal remained stable during more than 50 measurement cycles throughout 5 days of continuous operation. Reproducibility of the method was proven by the low coefficients of variation for intra- and inter-assay precision and low chip-to-chip variation. The validation of hGH determinations in serum samples from stimulation tests for hGH deficiency diagnosis was accomplished by ELISA method. The good correlation of the data demonstrates the application of the method as a valuable tool for fast diagnostics in clinical laboratories and point-of-care settings. This study paves the way for the development of a portable diagnostic tool for the detection of multiple clinical analytes in biological samples and monitoring of protein disease biomarkers.

#### Acknowledgements

The authors gratefully acknowledge the financial support from Fundació La Marató de TV3 and Fundación M. Botín. We thank Dr. M.D. Rodríguez Arnau for the supply of serum samples. The Department of Immunology and Oncology was found and is supported by the Spanish National Research Council (CSIC) and by Pfizer.

#### References

- [1] P. D'Orazio, Clin. Chim. Acta 334 (2003) 41.
- [2] P. von Lode, Clin. Biochem. 38 (2005) 591.
- [3] P. Lippa, L. Sokoll, D. Chan, Clin. Chim. Acta 314 (2001) 1.
- [4] J. Homola, Chem. Rev. 108 (2008) 462.
- [5] V. Popii, G. Baumann, Clin. Chim. Acta 350 (2004) 1.
- [6] A.E. Rigamonti, S.G. Cella, N. Marazzi, L. De Luigi, A. Sartorio, E.E. Muller, Trends Endocrinol. Metab. 16 (2005) 160.
- [7] C.J. Strasburger, Pediatrics 104 (1999) 1024.
- [8] E. Mauriz, A. Calle, A. Abad, A. Montoya, A. Hildebrandt, D. Barcelo, L.M. Lechuga, Biosens. Bioelectron. 21 (2006) 2129.
- [9] E. Mauriz, A. Calle, L.M. Lechuga, J. Quintana, A. Montoya, J.J. Manclus, Anal. Chim. Acta 561 (2006) 40.
- [10] E. Mauriz, A. Calle, J.J. Manclus, A. Montoya, A. Hildebrandt, D. Barcelo, L.M. Lechuga, Biosens. Bioelectron. 22 (2007) 1410.
- [11] C. Cao, J.P. Kim, B.W. Kim, H. Chae, H.C. Yoon, S.S. Yang, S.J. Sim, Biosens. Bioelectron. 21 (2006) 2106.
- [12] J.W. Chung, R.R. Bernhardt, J.C. Pyun, J. Immunol. Methods 311 (2006) 178.
- [13] P. Dillon, S. Daly, B. Manning, R. O'Kennedy, Biosens. Bioelectron. 18 (2003) 217.
- [14] J. Wei, Y. Mu, D. Song, X. Fang, X. Liu, L. Bu, H. Zhang, G. Zhang, J. Ding, W. Wang, Q. Jin, G. Luo, Anal. Biochem. 321 (2003) 209.
- [15] C.Y. Yang, E. Brooks, Y. Li, P. Denny, C.M. Ho, F.X. Qi, W.Y. Shi, L. Wolinsky, B. Wu, D.T.W. Wong, C.D. Montemagno, Lab Chip 5 (2005) 1017.
- [16] M. Mellado, J. Rodríguez-Frade, L. Kremer, C. Martínez-Alonso, J. Clin. Endocrinol. Methods 81 (1996) 1613.
- [17] S. Ferretti, S. Paynter, D. Russell, K. Sapsford, D. Richardson, TrAC Trends Anal. Chem. 19 (2000) 530.
- [18] Z. Grabarek, J. Gergely, Anal. Biochem. 185 (1990) 131.
- [19] E. Ostuni, L. Yan, G.M. Whitesides, Colloids Surf. B 15 (1999) 3.
- [20] M.A. Johansson, K.E. Hellenas, Analyst 129 (2004) 438.
- [21] K. Andersson, M. Hamalainen, M. Malmqvist, Anal. Chem. 71 (1999) 2475.



## A novel electrochemical biosensor based on dynamic polymerase-extending hybridization for *E. coli* O157:H7 DNA detection

Lijiang Wang<sup>a</sup>, Qingjun Liu<sup>b</sup>, Zhaoying Hu<sup>b</sup>, Yuanfan Zhang<sup>b</sup>, Chunsheng Wu<sup>b</sup>, Mo Yang<sup>c</sup>, Ping Wang<sup>b,\*</sup>

<sup>a</sup> Zhejiang California International Nanosystems Institute, Zhejiang University, Hangzhou 310027, PR China

<sup>b</sup> Biosensor National Special Laboratory, Key Laboratory of Biomedical Engineering of Education Ministry, Department of Biomedical Engineering, Zhejiang University, Hangzhou 310027, PR China

<sup>c</sup> Department of Health Technology and Informatics, The Hong Kong Polytechnic University, Hung Hom, Kowloon, Hong Kong

### ARTICLE INFO

#### Article history:

Received 21 October 2008

Received in revised form

26 November 2008

Accepted 1 December 2008

Available online 6 December 2008

#### Keywords:

Electrochemical biosensor  
Polymerase-extending DNA hybridization  
Nanopore membrane  
*E. coli* O157:H7

### ABSTRACT

A novel biosensor based on single-stranded DNA (ssDNA) probe functionalized aluminum anodized oxide (AAO) nanopore membranes was demonstrated for *Escherichia coli* O157:H7 DNA detection. An original and dynamic polymerase-extending (PE) DNA hybridization procedure is proposed, where hybridization happens in the existence of Taq DNA polymerase and dNTPs under controlled reaction temperature. The probe strand would be extended as long as the target DNA strand, then the capability to block the ionic flow in the pores has been prominently enhanced by the double strand complex. We have investigated the variation of ionic conductivity during the fabrication of the film and the hybridization using cyclic voltammetry and impedance spectroscopy. The present approach provides low detection limit for DNA (a few hundreds of pmol), rapid label-free and easy-to-use bacteria detection, which holds the potential for future use in various ss-DNA analyses by integrated into a self-contained biochip.

© 2008 Elsevier B.V. All rights reserved.

### 1. Introduction

Deoxyribonucleic acid (DNA) analysis has become an important tool for genetic diagnostics; identification of disease-causing microorganisms in human body [1], food [2], or environment [3,4], and the assessment of medical treatment [5]. The core of DNA sensing is detecting target ss-DNA fragments by utilizing their hybridization with complementary probe sequences. Traditional methods for identification of the DNA hybridization event, such as membrane blots or gel electrophoresis, are time-consuming and labor intensive. As alternative to the conventional methods, biosensor technique has triggered strong interests for its simpler nucleic acid assays and faster, cheaper process. The transducing elements reported in the literature include optical [6], microgravimetric [7] and electrochemical (EC) devices [8]. Among these methods, EC-transducers have their unique advantages in the detection of DNA hybridization and have arisen considerable interests [9,10]. These sensitive EC devices could be integrated into existing detection schemes, so the EC detection is desirable to realize miniaturization and portability. Moreover, low cost, minimal power requirements, and independence of optical pathway, all make it excellent can-

didate for DNA diagnostics [11]. In addition, electrochemistry provides innovative routes for interfacing the nucleic acid recognition system with signal generating and amplifying elements, which inspired us initially.

Aluminum anodized oxide (AAO) membranes can be synthesized via anodization of metal aluminum [12]. Precise control of pore diameter and length can be achieved [13,14]. Due to these fairly well-defined nanopores, AAO membranes have found popular applications in many areas such as nanostructured materials preparation [15], biological and chemical separations [16], solution flow regulation [17,18], and biosensors [19]. In the studies of Vlassiouk's group, AAO filters modified with covalently linked DNA can be used to detect or separate/purify the target ss-DNA [16,20,21]. They investigated the variation of ionic conductivity in nanopores caused by probe immobilization at the pore walls and its subsequent hybridization with complementary DNA strands. As the target ss-DNA was captured by the DNA probes immobilized on the pore walls, the hybridization events would further block the ionic flow through the pores, which would increase the impedance. This analysis provides a basis for articulating specific recommendations for this DNA biosensor's future use as a convenient combination of detection and separation/purification for unmodified target ss-DNA (and RNA). Compared with other porous membranes adopted in DNA sensors [22,23], the use of AAO filter as a sensing membrane offers several advantages. For instance the fabrication process is

\* Corresponding author. Tel.: +86 571 87952832; fax: +86 571 87951676.  
E-mail address: [cnpwang@zju.edu.cn](mailto:cnpwang@zju.edu.cn) (P. Wang).



correspondingly inexpensive and highly reproducible. In addition, the three-dimensional structure of the AAO membrane provides a much higher surface area available for probe immobilization for the same spot diameter as compared to flat surfaces. Foremost, this matrix is a suitable and protective environment for biomolecule immobilization and can transduce a biorecognition event such as DNA hybridization into an electrical signal.

The *Escherichia coli* O157:H7 is selected as the target bacteria because it is one of the most threatening pathogens in the world. On average, *E. coli* O157:H7 is responsible for 73,000 illnesses, 2100 hospitalizations and 60 deaths annually in the United States alone, and as of September 2006, there was a multistate outbreak of *E. coli* O157:H7 infections associated with consumption of fresh spinach in the country [24,25]. So the exploitation of new methods for rapid and sensitive detection of such microorganism predicates significance to the safety in food or water supplies [26–28]. Especially to the selectivity, DNA is an ideal target for specific detection of pathogenic bacteria, and there is a patent need for more direct and inexpensive sensing of bacteria DNA. In this “proof of concept” report, a novel electrochemical biosensor is proposed for bacteria DNA detection using AAO nanopore membranes ( $73 \pm 7$  nm diameter) by means of cyclic voltammetry (CV) and electrochemical impedance spectroscopy (EIS). This original biosensor could detect the DNA hybridization free of labels, and offer a promising approach for rapid, sensitive and real-time solution monitoring of *E. coli* O157:H7. The critical process in fabricating this DNA biosensor is the specific single strand probe immobilization, while the immobilization efficiency depends on the chemical functionalization in the nanopores. The procedure of probe immobilization comprises three steps: silanization with aminosilane, activation by glutaraldehyde, and covalent attachment of 5'-aminated DNA probe (20-mer in our case), which is specific to the *E. coli* O157:H7 gene *eaeA* [16,29,30]. Commonly, the immobilized probes should hybridize with the target ss-DNA in the sample to induce changes in the electrochemical parameters (e.g. resistance and conductivity). But in this paper, the hybridization process is dynamic and rapid based on the polymerase-extending (PE) method. Once the hybridization event has happened, the probe strand can be extended according to the principle of complementary base pairing in the presence of Taq DNA polymerase and deoxyribonucleotide triphosphates (dNTPs) with the control of reaction temperature. The variation of impedance induced by the complete double strands DNA (ds-DNA) would be much more distinct than that by the routine hybridization complex. To our best knowledge, a dynamic design for DNA hybridization has not been demonstrated, nor has an AAO membrane assisted electrochemical biosensor for bacterial DNA detection ever been reported.

## 2. Materials and methods

### 2.1. Materials and instruments

Free standing AAO nanopore membranes, with a uniform  $73 \pm 7$  nm pore diameter with  $50 \mu\text{m}$  thickness and a high pore density ( $1 \times 10^9/\text{cm}^2$ ), were purchased from Synkera Technologies, Inc. 3-aminopropyltrimethoxysilane (APS) and glutaraldehyde were obtained from Sigma–Fluka. E.Z.N.A.™ Bacterial DNA Kit (Omega Bio-Tek) was used for the bacteria DNA extraction. All other chemicals, such as toluene, propylamine, potassium ferrocyanide, and potassium ferricyanide were analytical pure grade or better quality. Deionized water ( $18.2 \text{ M}\Omega/\text{cm}$ ) produced by a Milli-Q system (Bedford, MA) was used throughout. Electron micrographs of fresh and silanized AAO membranes were taken using Scan Electron Microscope (SEM, Hitachi S-4700). Electrochemical cyclic voltammetric experiments and impedance spectroscopy measurements

were performed using CH Instruments 660A electrochemical analyzer.

### 2.2. Oligonucleotides and PCR amplification

All the oligonucleotides used in sensor development were purchased from TAKARA Biotechnology Co., Ltd. A 20-base oligonucleotide modified at 5' end with  $\text{C}_6\text{-NH}_2$  was used as an ssDNA probe ( $5'\text{-NH}_2\text{-(CH}_2\text{)}_6\text{-CCAAGAGTTGCAGTTCCTGA}$ ), which was specific for *E. coli* O157:H7 *eaeA* gene. A 120-base ss-DNA with 3' end complementary sequence of probe ( $5'\text{-TTCGGCTAAA GCGGATAACGCCGATACCATTACTTATACCGCGACGGTAAAAAGAATGGGGTAGCTCAGGCTAATGTCCCTGTTTCATTTAATATTGTTTCAGGAAGTCAACTCTTGG}$ ), was acted as positive control to characterize the sensor performance, while the negative control with complementary sequence of positive one ( $5'\text{-CCGCC GATTCGCCTATTGCGGCTATGGTAATGAATATGGCGCTGCCACTTTTTCTTACCCCATCGAGTCCGATTACAGGGACAAA-GTAAATTATAACAAAGTCCTTGACGTTGAGAACC}$ ) and the single base mismatch oligonucleotide ( $5'\text{-TTCGGCTAAAGCGGATAACGCCGATACCATTACTTATACCGCGACGGTAAAAAGATGGGGTAGCTCAGGCTAATGTCCCTGTTTCATTTAATATTGTTTCAGGAACTGGAAGTCTTGG}$ ) were adopted to test the specificity of the probe. A short fragment (120 bases) of the *E. coli* O157:H7 *eaeA* gene with the same sequence as the positive control was amplified by asymmetric PCR (forward primer:  $5'\text{-TTCGGCTAAAGCG GATAACG}$ , reverse primer:  $5'\text{-CCAAGAGTTGCAGTTCCTGA}$ ).

Asymmetric PCR, a PCR procedure that predominantly produces ssDNA was utilized to amplify the target DNA for the direct hybridization detection. The concentration ratio of forward primer to reverse primer was 50:1, and the lower concentrated forward primer played a “limiting primer” role. After the limiting primer was consumed, the remaining reverse primer continued to extend the single-stranded *eaeA* gene fragments. The whole asymmetric PCR reaction was executed in a Bio-Rad Thermal Cycler with a temperature profile of  $95^\circ\text{C}$  for 5 min, followed by 40 cycles of 30 s denaturation at  $95^\circ\text{C}$ , 30 s annealing at  $55^\circ\text{C}$ , 45 s extension at  $72^\circ\text{C}$ , and 10 final extension. Regular PCR was also carried out to prove the successful amplification of *eaeA* gene, which was examined by electrophoresis in 2% agarose gel.

### 2.3. Nanopore biosensor setup and data acquisition

The experimental apparatus is illustrated in Fig. 1. A membrane, with an active area of  $0.03 \text{ cm}^2$ , was placed in the middle of two equal volume chambers, which are clamped by four screws. Both chambers were L-shaped and filled with  $10 \text{ mM}$   $[\text{Fe}(\text{CN})_6]^{3-/4-}$  in phosphate buffered saline (PBS, pH 7.0), which was selected to indicate the efficiency of ion blockage. Au electrode was the working electrode, while Pt wire electrode and Ag/AgCl (in saturated KCl) electrode were used as the counter electrode and the reference electrode, respectively. Au and reference electrode were placed in one upward hole of the chamber, and the counter electrode was in the opposite side. The CV rate was  $50 \text{ mV/s}$  and the impedance spectrum was obtained at the equilibrium voltage  $0.20 \text{ V}$  vs. Ag/AgCl by applying  $5 \text{ mV}$  ac voltage.

### 2.4. ss-DNA probe immobilization

After evaluating different methods [21], we found that the most reliable approach which ensures the nanopores unsealed and a high density of covalently linked DNA inside the nanopores is achieved by a glutaraldehyde linker, which joins the amino groups of 5'-aminated DNA and the terminal amino group of aminosilane. Briefly, a fresh AAO filter was washed with 15 min sonication in DI water and dried in oven, then immersed into a 0.5% toluene solution

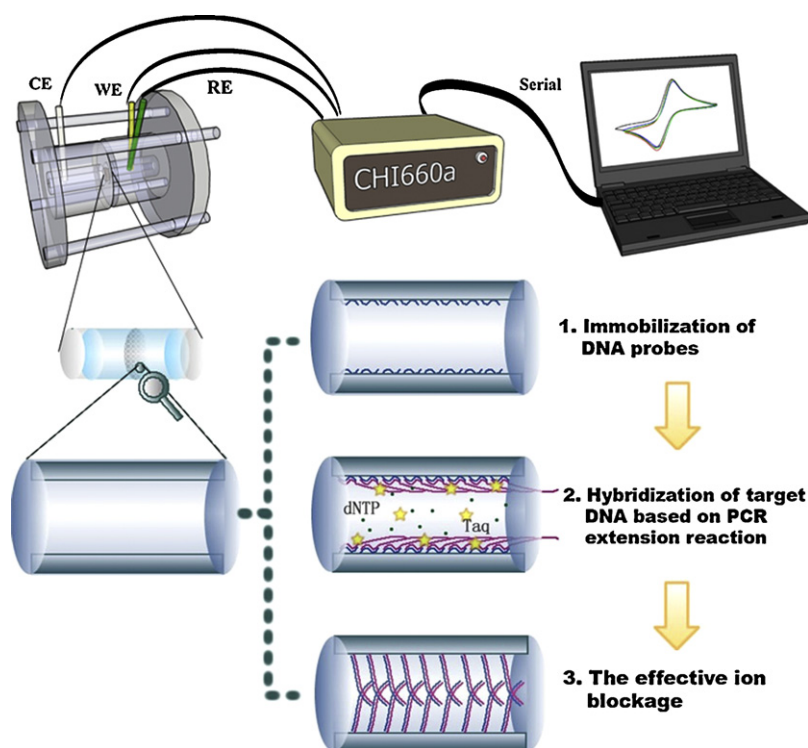


**Fig. 1.** The sketch map of the electrochemical DNA biosensor system and the mechanism of the novel polymerase-extending hybridization method (WE: working electrode; RE: reference electrode; CE: counter electrode).

of APS for 6 h. After sonication washing in toluene (15 min, 3 times) and baking at 120 °C for 4 h, the aminated membrane was activated in an 8% aqueous solution of glutaraldehyde for 12 h. In order to neutralize the unreacted glutaraldehyde, the activated membrane was left overnight in  $10^{-5}$  M aqueous solution of propylamine. Following thorough washing with DI water and drying, the filter was immersed in 50  $\mu$ L of aqueous solution of 5'-aminated ss-DNA (20  $\mu$ M) and kept at high humidity overnight. Finally, the filter was thoroughly washed by DI water and stored at 4 °C for use.

### 2.5. Dynamic polymerase-extending hybridization

Routine hybridization reaction was carried out by immersing the nanopore membrane immobilized with specific probes in 50  $\mu$ L hybridization buffer containing the complementary target ss-DNA for at least 2 h at room temperature [21]. In this study, a novel hybridization process is proposed to improve the effect of ion blockage caused by the hybridization complex. The functionalized AAO filter was dipped into an Eppendorf tube loading 50  $\mu$ L reaction buffer mainly including Taq DNA polymerase, target ss-DNA (5  $\mu$ M), dNTPs,  $Mg^{2+}$  and PCR buffer, and then the whole tube was subjected to the thermal treatment in water bath: 55 °C for 10 min. After the hybridization based on the PE method, the membrane was removed from the EP tube and rinsed with DI water. Finally, CV and EIS measurements were performed to evaluate the efficiency of ion blockage. The scheme of this novel and effective polymerase-extending hybridization method is illustrated in Fig. 1.

## 3. Results and discussion

### 3.1. Biosensor fabrication

Similar to the methods of glass and silica surface modification, we modified the surface of nanopore by the aminosilane-

glutaraldehyde chemistry and found the most reliable concentration of APS was 0.5% after considerable evaluations. From the SEM micrographs of the fresh and silanized membranes (Fig. 2), we can see the open-through nanopore membrane without any treatment contains parallel circular pores with a very tight pore size distribution (about  $73 \pm 7$  nm). This geometry makes it an ideal experimental tool for fundamental studies of ion transfer phenomena in porous support (Fig. 2A). Furthermore, modified by the aminosilane-glutaraldehyde layer, the pores were not occluded, and even the aperture remained the same (Fig. 2B), through which the ss-DNA probes could diffuse into and immobilize on the nanopore wall by condensation reaction.

CV in Fig. 3A clearly shows that both reductive and oxidative current decrease after aminosilane-glutaraldehyde modification of the nanopores, however, after probe immobilization the current increased greatly. When the nanopore wall was covered with a layer of activated aminosilane, the inside diameter of pores should be reduced slightly, which resulted in a lower ion mobility through the pores. As expected, a noticeable current increase was observed after the probe immobilization. It can be explained as a consequence of the increased surface charge density from the negatively charged DNA backbone and possible partial dissolution during the multistep procedure of probe immobilization. Accordingly, the resistance of the pores after immobilization of ss-DNA probes decreased compared to the fresh alumina membrane, which confirmed the results of Takmakov's work [21]. The impedance in Fig. 3B also illustrates the changes accompanying the stepwise modification process.

### 3.2. Target ss-DNA detection by CV and EIS

Synthesized positive control DNAs were applied to hybridize with the probes with PE method originated by ourselves, while another group of hybridization trial was carried out with the routine method. It can be clearly observed that the reductive and oxidative

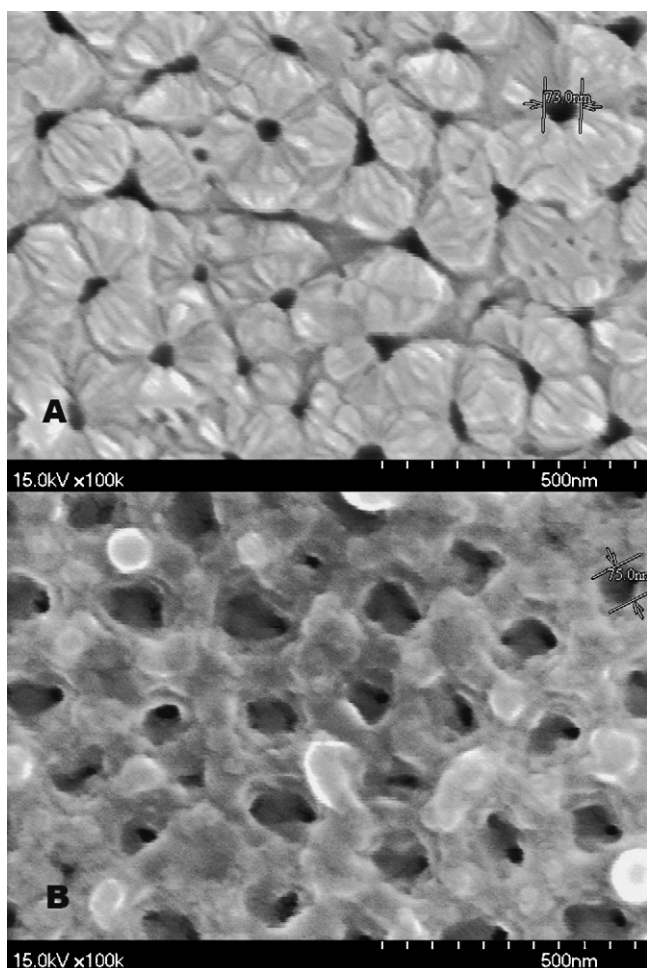


**Fig. 2.** SEM micrographs of (A) untreated nanoporous alumina membrane (top surface) and (B) the aminosilane-glutaraldehyde modified membrane.

currents decreased after these two DNA hybridization methods. However, an obvious current diminishment appeared when PE hybridization method was adopted (Fig. 4A), which verified the PE hybridization more effective for ion blockage. Impedimetric measurement was most sensitive to the ion flow changes accompanying hybridization inside the nanopores. Fig. 4B shows the impedance bode plot of the nanopore membrane based DNA biosensor for the target DNA hybridization with different methods: probe immobilization, PE hybridization and the routine hybridization in the frequency ranging from 1 Hz to 100 kHz with the  $[\text{Fe}(\text{CN})_6]^{3-/4-}$  redox couple in PBS.

To understand and quantitatively analyze the EIS data, it is crucial to construct an equivalent circuit, which must address all relevant physical phenomena and incorporate them correctly. In this study, experiments were conducted with bare gold electrode, solution of ferro/ferricyanide and supporting electrolyte. In this case the equivalent circuit is composed of two parts: the classic Randles circuit and circuit of AAO. The classic Randles circuit contains four elements: the double layer capacitance  $C_{dl}$ , charge transfer resistance of the electrode reaction  $R_{ct}$ , solution resistance  $R_s$  and diffusion impedance  $Z_w$  of the unstirred layer. Circuit of AAO consists of two elements: the resistance of the pores  $R_p$  and the membrane capacitance  $C_m$ . In general, the reaction kinetics is represented by a charge transfer resistance  $R_{ct}$  connected in series with diffusion impedance  $Z_w$ , and  $C_{dl}$  is related to the dielectric features at the electrode/electrolyte interface. Since the changes of ionic flow do not affected by electrode–electrolyte interface in

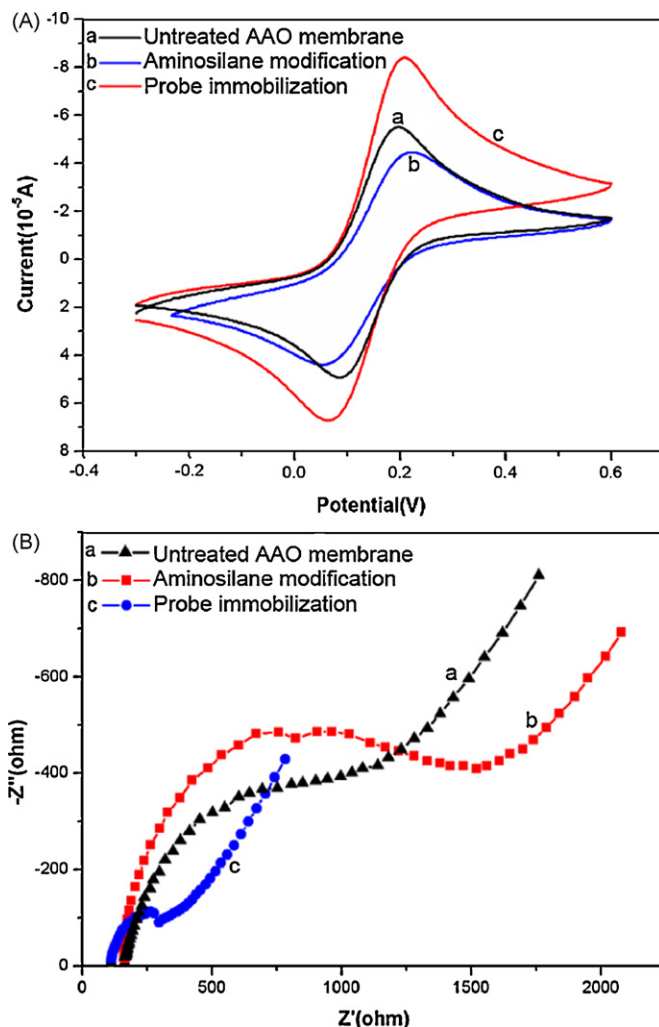


**Fig. 3.** (A) CV in the region for  $[\text{Fe}(\text{CN})_6]^{3-/4-}$  oxidation/reduction for ss-DNA probe immobilization and (B) Nyquist plot ( $Z''$  vs.  $Z'$ ) for membrane impedance at 0.20 V for ss-DNA probe immobilization: a—untreated AAO membrane; b—aminosilane modification; c—probe immobilization.

this study, no further discussion about the Randles circuit would be done here. As shown in Fig. 4B, in the frequency ranging from 1 Hz to 1000 Hz, compared to the probe immobilization (a), the impedance increased after the PE hybridization (b) and the routine hybridization (c), suggesting that the hybridization events happened on the nanopore wall can change the values of these electrical elements in the equivalent circuit.

The results of the fitting of the experimental data to the equivalent circuit by model fitting software are summarized in Table 1, which mainly lists these two pivotal parameters,  $R_p$  and  $C_m$ . Some scatter of the parameter values reflects the inherent irregularities of the membranes enhanced by the small size of the samples and fitting errors. With the routine hybridization method, hybridiza-

**Table 1**

Fitting parameters for the curves in Fig. 4B using the equivalent scheme.

	Pore resistance $R_p(\Omega)$	Membrane capacitance $C_m(\mu\text{F})$
Blank membrane	$297.40 \pm 12.77$	$17.40 \pm 0.57$
Probe immobilization	$99.20 \pm 8.62$	$2.76 \pm 0.20$
Routine hybridization	$127.80 \pm 5.34$	$1.66 \pm 0.10$
PE hybridization	$540.76 \pm 25.55$	$12.03 \pm 0.23$

The value shows means and standard deviation, which is derived from at least 3 independent detections.

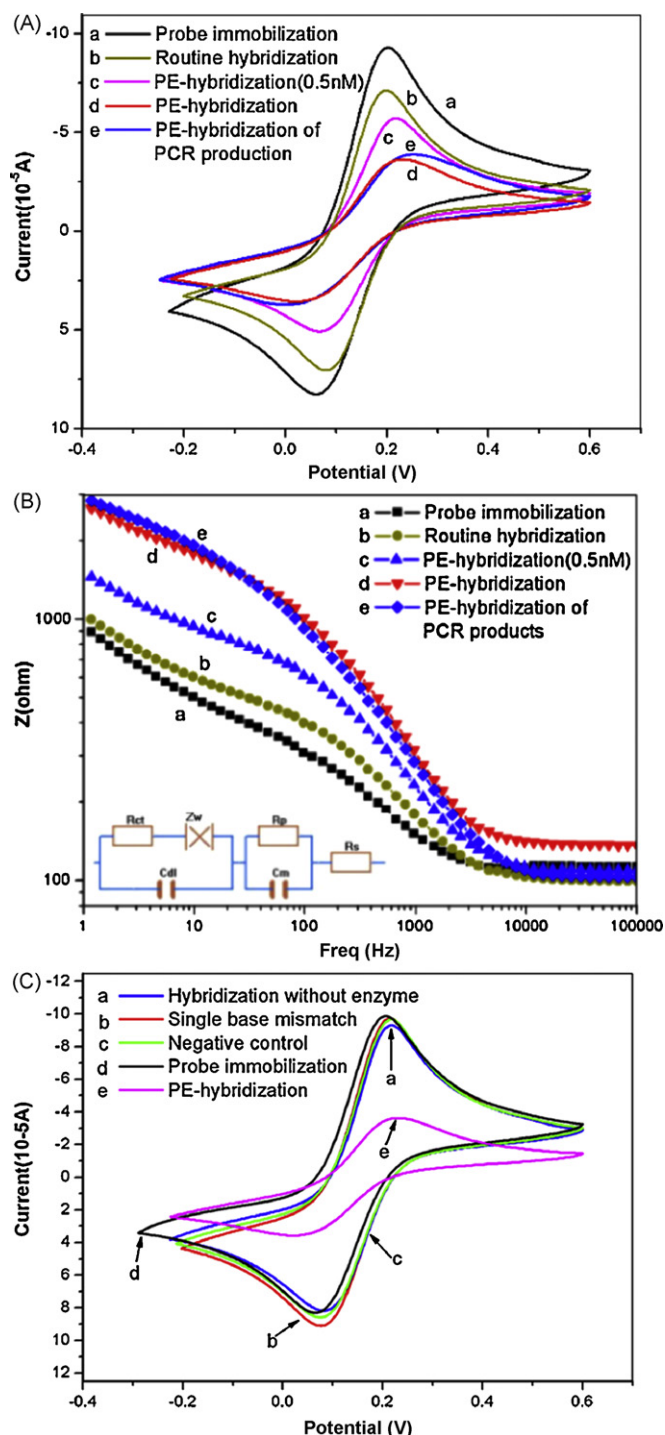


**Fig. 4.** (A) CV in the region for  $[\text{Fe}(\text{CN})_6]^{3-/4-}$  oxidation/reduction for the target DNA hybridization with different methods; (B) impedance bode plots for the target DNA hybridization with different methods; (C) CV in the region for  $[\text{Fe}(\text{CN})_6]^{3-/4-}$  oxidation/reduction for detection of biosensor sensitivity by different control groups.

tion complexes led to an increased  $R_p$  from 99 to 127, which nevertheless was lower than the blank membrane. The effect was similar to the previous report [20], whereas the PE hybridization method changed the nanopore resistance from 99 to 540  $\Omega$  with a net increase of 413  $\Omega$  compared to that by routine hybridization method.

This change was the most significant one among all the electrical elements in the equivalent circuit, indicating that the ion flow was assuredly blocked by the DNA hybridization inside the

nanopores, and the blockage effect was enhanced by PE hybridization method. The ionic conductance through nanopores, which is the pivot of the whole exploration and the foundation of this DNA biosensor development, has a complex nature with contributions from: (a) Volume exclusion due to additional DNA upon hybridization. When analyte binds to the nanopore walls, it will decrease the effective cross-section of the channel, so the current through the nanopores reduces. Particularly, this effect is probably strengthened by a change in DNA orientation with respect to the surface, namely stiffer dsDNA would lift up away from the surface and hinder the ion diffusion to a greater extent. This mechanism is the basis for most DNA detection studies with AAO membrane by routine hybridization method [20]. In our work, we have adopted the Taq DNA polymerase to complete a dynamic and steady hybridization process. The whole course of PE method was similar to the extending step of PCR, and the probe acted as the role of primer. Once the complementary ss-DNA was combined with the immobilized probe, the 3' end of probe would be extended by the polymerase to form a rigid hybridization complex of 120 bp, whereas in routine hybridization, there were only 20 bp stiff dsDNA standing inside the nanopores, and the other soft ss-DNA (100-base) belonging to the target DNA would still be floating in the electrolyte. Therefore, the capability of hindering the ionic current was greatly improved by our PE method (Fig. 4A and C, Table 1). (b) The change in surface charge [31]. Binding of charged analytes to the channel walls in this case affects the ion concentration in the pore and thus the resulting conductance, which reveals the reason for the initial decrease of  $R_p$  and  $C_m$  after immobilization of DNA probes inside the nanopores. In the routine hybridization, the  $C_m$  became smaller than that of probe immobilization (Table 1), which attributes to more negative charge of the floating single strand with 100 bp. However, it is not the case in PE hybridization; the  $C_m$  was increased as a result of the formation of "complete" hybridization complexes [32]. (c) The distribution of pore diameters. It is critical that the pore diameter is comparable to the size of an analyte molecule (for biological molecules it is often nm-grade) in order to have a substantial ion blockage. In our case, the pore diameter (73 nm) was almost double the DNA length (nearly 42 nm for a hybridization complex of 120 bp), thus the PE hybridization was expected to affect the conductance the most.

The asymmetric PCR and regular PCR for *E. coli* O157:H7 *eaeA* gene were carried out in parallel, and the PCR products were first tested by the gel electrophoresis. In Fig. 5, electrophoresis testified the successful amplification of regular PCR products, while single-stranded asymmetric PCR products could not be effectively confirmed on the agarose gel due to the low EtBr staining efficiency for ssDNA [33]. Based on PE hybridization method, the asymmetric PCR product was tested by our DNA biosensor, and showed the same effect on the resistance with the positive DNA control (Fig. 4C). This successful detection is very important for our future work because it indicates that this DNA biosensor has the potential to be integrated into a handheld device for on-site detection of microorganism. This biosensor also shows a good specificity, the CV curve did not change when the negative control or single base mismatch sequences were used, but agreed with the curve of probe immobilization. Based on the results of these control groups, it could be seen that there was no hybridization event happening in the absence of target complementary ss-DNA. To confirm the function of Taq DNA polymerase, the PE hybridization procedure was performed just without the polymerase. As shown in Fig. 4C, there was no obvious variation from the original value before hybridization. It could be explained that if there was no existence of Taq DNA polymerase in the reaction system, the hybridization between the target ss-DNA and probe inside the nanopores was impossible to be completed within 10 min [21]. At present, the sensitivity limit we have reached was 0.5 nM for

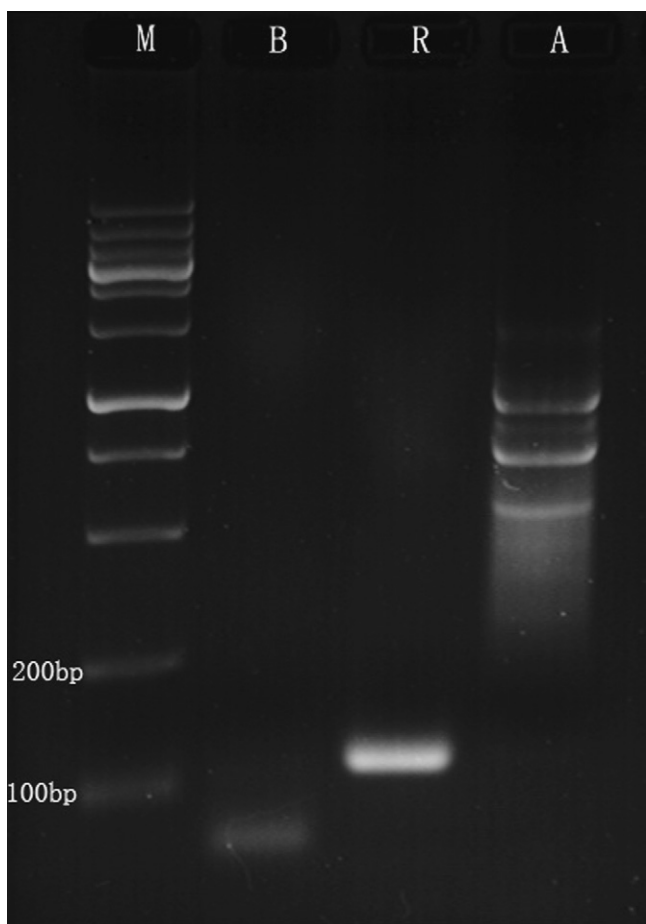


**Fig. 5.** Gel electrophoresis detection of *E. coli* O157:H7 *eaeA* gene PCR products. M, DNA marker; R, regular PCR products; B, blank control (purified water as PCR template); A, *eaeA* asymmetric product.

complementary target DNA by the PE method with this AAO membrane based biosensor (Fig. 4A and B). More efforts are being exerted to achieve better sensitivity.

At present, it is unpractical to utilize a DNA biosensor to directly detect foodborne pathogen with real sample, such as milk, fruit juice and ground beef, because the target is bacteria DNA not the membrane antigen. Many works should be completed before DNA detection, for instance bacteria separation and enrichment, DNA extraction and PCR amplification. It is very difficult to accomplish all these steps in single DNA biosensor now, and an ideal DNA sensor for bacteria detection would be the one that can integrate all of functions mentioned above and can detect the real food or water sample. To further the application of our biosensor, we are proposing a self-contained and fully integrated biochip for sample-to-answer DNA analysis [34]. Sample preparation (including magnetic bead-based cell capture, cell pre-concentration and purification, and cell lysis), polymerase chain reaction, DNA hybridization, and electrochemical detection would be performed in this fully automated and miniature device. In the part of DNA detection, the AAO membrane based DNA biosensor we have studied and demonstrated has been adopted because of its convenience, sensitivity and label-free. In particular, the EC technology will make this biosensor easily integrated into the future handheld nucleic acid testing device for on-site food and water monitoring or point-of-care testing of infectious diseases.

#### 4. Conclusions

In this study, we have shown that the nanopore AAO membrane can be successfully employed to immobilize specific ss-probes by aminosilanes and glutaraldehyde linker, and then be used for electrical detection of complementary target bacteria DNA without additional modification. During the course of hybridization, a novel PE method has been applied to enhance the ion blockage in nanopores by the whole double strand complex, and has greatly improved the sensitivity of the DNA biosensor and makes this system very attractive for further development of various DNA/RNA detections. This new-style AAO membranes based biosensor provides a sensitivity limit of 0.5 nM for complementary target DNA by PE method, which has the potential to be a powerful analytical tool for diagnostic, forensic analysis, and pathogen detection in near future. We are progressing toward experimental realization of this conceivability and hope to achieve even better sensitivity.

#### Acknowledgements

This work was supported by the National Natural Science Foundation of China (Grant No. 60725102), the Natural Science Foundation for the Zhejiang Province of China (Grant No. R205505).

#### References

- [1] J.T. Riordan, S.B. Viswanath, S.D. Manning, T.S. Whittam, J. Clin. Microbiol. 46 (2008) 2070–2073.
- [2] P. Elizaquível, R. Aznar, Food Microbiol. 25 (2008) 705–713.
- [3] O. Koyama, A. Manome, M. Okubo, T. Yokomaku, H. Tanaka, Environ. Microbiol. 22 (2007) 123–127.
- [4] B. Lievens, L. Claes, M.S. Krause, A.C.R.C. Vanachter, B.P.A. Cammue, B.P.H.J. Thomma, Plant Sci. 172 (2007) 505–514.
- [5] M.G. Morshed, M.K. Lee, D. Jorgensen, J.L. Isaac-Renton, FEMS Immunol. Med. Microbiol. 49 (2007) 184–191.
- [6] D.K. Kim, K. Kerman, M. Saito, R.R. Sathulur, T. Endo, S. Yamamura, Y.S. Kwon, E. Tamiya, Anal. Chem. 79 (2007) 1855–1864.
- [7] V.C. Wu, S.H. Chen, C.S. Lin, Biosens. Bioelectron. 22 (2007) 2967–2975.
- [8] E.M. Boon, D.M. Ceres, T.G. Drummond, M.G. Hill, J.K. Barton, Nat. Biotechnol. 18 (2000) 1096–1100.
- [9] H. Chang, F. Kosari, G. Andreadakis, M.A. Alam, G. Vasmatzis, R. Bashir, Nano Lett. 4 (2004) 1551–1556.
- [10] M. Archer, M. Christophersen, P.M. Fauchet, Biomed. Microdev. 6 (2004) 203–211.
- [11] J. Wang, Anal. Chim. Acta 469 (2002) 63–71.
- [12] K. Itaya, S. Sugawara, K. Arai, S. Saito, J. Chem. Eng. Jpn. 17 (1984) 514.
- [13] K.C. Popat, P. Mor, C.A. Grimes, T.A. Desai, Langmuir 20 (2004) 8035–8041.
- [14] F. Matsumoto, M. Kamiyama, K. Nishio, H. Masuda, Jpn. J. Appl. Phys. 44 (2005) 355–358.
- [15] S.Y. Zhao, H. Roberge, A. Yelon, T. Veres, J. Am. Chem. Soc. 128 (2006) 12352–12353.
- [16] I. Vlasiouk, A. Krasnoslobodtsev, S. Smirnov, M. Germann, Langmuir 20 (2004) 9913–9915.
- [17] D.J. Odom, L.A. Baker, C.R.J. Martin, J. Phys. Chem. B 109 (2005) 20887–20894.
- [18] W. Chen, J.H. Yuan, X.H. Xia, Anal. Chem. 77 (2005) 8102–8108.
- [19] P. Kohli, M. Wirtz, C.R. Martin, Electroanalysis 16 (2004) 9–18.
- [20] I. Vlasiouk, P. Takmakov, S. Smirnov, Langmuir 21 (2005) 4776–4778.
- [21] P. Takmakov, I. Vlasiouk, S. Smirnov, Analyst 131 (2006) 1248–1253.
- [22] G.S. Christina, P.N. Dimitrios, A.E.P. Paul, J.K. Ulrich, Electroanalysis 9 (1997) 1067–1071.
- [23] N.N. Zhu, Y.F. Gu, Z. Chang, P.G. He, Y.Z. Fang, Electroanalysis 21 (2006) 2107–2114.
- [24] E. Berkenpas, P. Millard, C.M. Pereira, Biosens. Bioelectron. 21 (2006) 2255–2262.
- [25] P. Gerner-Smidt, J.M. Whichard, Foodborne Pathog. Dis. 4 (2007) 1–4.
- [26] M. Varshney, Y. Li, Biosens. Bioelectron. 22 (2007) 2408–2424.
- [27] Y. Li, X.L. Su, J. Rapid Meth. Autom. Microbiol. 14 (2006) 96–109.
- [28] S.H. Chen, V.C. Wu, Y.C. Chuang, C.S. Lin, J. Microbiol. Methods 73 (2008) 7–17.
- [29] V. Szczepanski, I. Vlasiouk, S.J. Smirnov, J. Memb. Sci. 281 (2006) 587–591.
- [30] P. Takmakov, I. Vlasiouk, S. Smirnov, Anal. Bioanal. Chem. 385 (2006) 954–958.
- [31] F. Wei, B. Sun, Y. Guo, X.S. Zhao, Biosens. Bioelectron. 18 (2003) 1157–1163.
- [32] J.J. Gooding, A. Chou, F.J. Mearns, E. Wong, K.L. Jericho, Chem. Commun. 15 (2003) 1938–1939.
- [33] X. Mao, L. Yang, X. Su, Y. Li, Biosens. Bioelectron. 21 (2006) 1178–1185.
- [34] R.H. Liu, J. Yang, R. Lenigk, J. Bonanno, P. Grodzinski, Anal. Chem. 76 (2004) 1824–1831.



## Problems of PAH quantification by GC–MS method using isotope-labelled standards

Lidia Wolska\*, Monika Gdaniec-Pietryka, Piotr Konieczka, Jacek Namieśnik

Department of Analytical Chemistry, Chemical Faculty, Gdansk University of Technology (GUT), 80-952 Gdańsk, 11/12 G. Narutowicz St., Poland

### ARTICLE INFO

#### Article history:

Received 5 June 2008

Received in revised form 10 December 2008

Accepted 16 December 2008

Available online 25 December 2008

#### Keywords:

Sediments

Polycyclic aromatic hydrocarbons

Internal standard

Extraction

Detection

GC–MS system

### ABSTRACT

The gas chromatography–mass spectrometry (GC–MS) system is presently routinely used in environmental analysis of trace organic compounds. With the use of a MS-detector, stable isotope-labelled materials' analogous of the native analyte are convenient internal standard. They can be used for tracing and compensating analytes' losses during the particular stages of analytical procedure, such as cleaning or diluting, and variations in instrument settings and sensitivity. However, the stage of quantitative analysis is connected with numerous problems that result from the necessity of obtaining reliable results of determination. In this article, problems connected with the quantitative analysis of polycyclic aromatic hydrocarbons in sediment samples using GC–MS system were raised. The aim of conducted work was to assess the influence of the following factors on the results obtained: calibration of the GS–MS system, internal standard addition technique and the amount of internal standard added.

© 2008 Elsevier B.V. All rights reserved.

### 1. Introduction

The gas chromatography–mass spectrometry (GC–MS) system is routinely used today in environmental analysis of trace organic compounds.

In the case of every device, work of which is based on the relative principle, suitable standard substances are needed.

With the use of a MS-detector, stable isotope-labelled materials' analogous of the native analyte, are a convenient internal standard. They can be used for tracing and compensating analytes' losses during the particular stages of analytical procedure, such as cleaning or diluting, and variations in instrument settings and sensitivity. In determination of such environmental analytes as polychlorinated-, dibenzo-p-dioxins (PCDD), dibenzofurans (PCDF), biphenyls and polycyclic aromatic hydrocarbons,  $^{13}\text{C}$ ,  $^2\text{H}$  and  $^{37}\text{Cl}$  labeled compounds are frequently used. The labeled standards allow quantification of trace quantities (ng/g to fg/g), of native analytes with a high precision [1–5]. For this purpose a technique known as isotope dilution mass spectrometry (IDMS) is used. This is a modification of internal standard addition technique, which belongs to the primary methods of measurement, thus directly connected with the International System of Units (SI) in the IDMS method, the concentration of analytes are calculated from their ratios to those of the corresponding inter-

nal standards compared with those in the calibration solution [6,7].

The GC–MS system is a suitable tool for studying the distribution of polycyclic aromatic hydrocarbons in various elements of the environment. Determination of diverse physical forms of the same individual chemical species is a typical example of an activity from the scope of physical speciation analysis [8,9]. In this case, required is the determination of analytes present in the following forms:

- dissolved in the aqueous phase;
- associated with suspended particulate matter;
- associated (as result of bioaccumulation) with organs and tissues of living organisms;
- associated with sediments.

Most environmental particulates consist of solid minerals covered with organic matter where the native analyte is sorbed. For this reason numerous mechanisms of sorption of organic substances to particulate matter are possible [10,11]. When the internal standard is added with solvent to the particle surface—being a solid sample, it cannot be assumed that the internal standard is identically associated with corresponding analyte. The reason is that both the analytes and internal standards are transferred to the sample matrix in different way (the internal standard is added with the organic solvent, what is connected with the solvation by solvent molecule, not by water, as it take place in case of native analytes) and the degree of sorption might then differ. Usually the internal standard is (at least partially) more loosely connected with the matrix than the analytes are. Thus, the extraction efficiency of native analyte

\* Corresponding author. Tel.: +48 58 3471010 fax: +48 58 3472694.

E-mail address: [chemanal@pg.gda.pl](mailto:chemanal@pg.gda.pl) (M. Gdaniec-Pietryka).

and internal standard might differ [12]. It is especially significant in case of extraction techniques characterized by low recovery of analytes.

There are several methods of adding internal standard to the examined solid samples known. In guidelines and recommendations available, information about the proper working conditions with biological samples with a relatively high content of lipid matter are included. However, the internal standard recovery from complex samples differs depending on the matrix type and technique of standard addition [13].

Most often, the internal standard is added to the sample in a small (0.1–1 ml) amount of organic solvent. There are also used more complicated systems based on application of rotating equipment for uniform coating and reduction of large solvent volumes [14]. Nevertheless, no method enable adding the internal standard in the way truly imitating association of native analytes with sample matrix, especially in the case of environmental analyses, where samples with very complex matrix are analysed.

In this article, problems connected with the quantitative analysis of polycyclic aromatic hydrocarbons in sediment samples using GC–MS system were raised.

The aim of conducted work was to assess the influence of the following factors on the results obtained: calibration of the GC–MS system, internal standard addition technique and the amount of internal standard added.

## 2. Experimental

### 2.1. Reagents and standards

High-purity HPLC-grade dichloromethane, acetone and methanol were purchased from Sigma–Aldrich (Germany).

A standard mixture of PAHs in methanol was purchased from Restek Corporation, USA, and consisted of: naphthalene, acenaphthylene, acenaphthene, fluorene, phenanthrene, anthracene, fluoranthene, pyrene, benz[a]anthracene, chrysene, benz[b]fluoranthene, benz[k]fluoranthene, benz[a]pyrene, indeno[123-cd] pyrene, dibenzo[ah]anthracene, benz[ghi]perylene. The mixture contained 2000 µg/ml of each PAH.

Certified naphthalene-d8 and benz[a]anthracene-d12 (2000 µg/ml in dichloromethane) standards were from Supelco (USA). Copper powder and silica gel were from J.T Baker. Reference material—river-sediment METRANAL2 was from Promochem (Poland).

### 2.2. Gas chromatographic analysis

All experiments were performed using a TraceGC gas chromatograph (ThermoQuest, Finningan) equipped with a mass spectrometric detector TraceMS (ThermoQuest, Finningan) and cold on-column injector, using a Rtx-5MS column (30 m; 0.25 mm; 0.25 µm). The carrier gas (helium) was maintained at a constant pressure of 70 kPa. The GC temperature was programmed as follows: from 40 to 120 °C at a rate of 40 °C min<sup>-1</sup>; till 280 °C at a rate 5 °C min<sup>-1</sup> where it was held for 12 min. The MS was operated in electron ionization (EI) mode with the ion source temperature of 220 °C. The mass spectrometer was operated in selected ion monitoring mode; the following ions were monitored: (*m/z*) 127, 128, 136, 151, 152, 153, 154, 165, 166, 176, 178, 202, 203, 226, 228, 240, 250, 252, 276, 277, 278, 279.

### 2.3. Procedure of calculation of the amount of analytes introduced to the chromatographic column

In order to perform the calculations of the quantity of analytes in the sample dosed to the chromatographic column, samples were

introduced subsequently:

- first—the standard-solution, wherein the content of analytes and internal standard is well-known;
- second—the investigated sample, containing internal standards in predefined quantity.

During the studies two standard solutions were used. Standard solution I contained analytes from PAH group at concentration of 133 ng/ml as well as deuterated PAHs at concentration of 167 ng/ml; standard solution II contained analytes at concentrations of 53.5 ng/ml and 66.5 ng/ml, respectively.

The quantity of analytes in the investigated sample was calculated on the basis of formula presented below:

$$\frac{pX^{Pr}/mX^{Pr}}{pD^{Pr}/mD^{Pr}} = \frac{pX^{St}/mX^{St}}{pD^{St}/mD^{St}} \quad (1)$$

where  $pX^{Pr}$  is the peak area of a determined substance  $X$  on a chromatogram obtained after injecting extract from a sediment sample into the chromatographic system,  $mX^{Pr}$  is the mass of a determined substance  $X$  on a chromatogram obtained by dosing extract from a sediment sample into the chromatographic system,  $pD^{Pr}$  is the peak area of a deuterated standard  $D$  on a chromatogram obtained by dosing extract from a sediment sample into the chromatographic system,  $mD^{Pr}$  is the mass of a determined deuterated standard  $D$  on a chromatogram obtained by dosing extract from a sediment sample into the chromatographic system;  $pX^{St}$  is the peak area of a determined substance  $X$  on a chromatogram obtained by dosing standard solution into the chromatographic system,  $mX^{St}$  is the mass of a determined substance  $X$  on a chromatogram obtained by dosing standard solution into the chromatographic system,  $pD^{St}$  is the peak area of a determined deuterated standard  $D$  on a chromatogram obtained by dosing standard solution into the chromatographic system and  $mD^{St}$  is the mass of a determined deuterated standard  $D$  on a chromatogram obtained by dosing standard solution into the chromatographic system.

### 2.4. Calibration of the GC–MS system

The standard curves for analytes were prepared by setting the linear dependence between the chromatographic peak area for the given substance and the amount of the substance in the sample introduced into the control-measurement device. The calibration of the GC–MS system was conducted for 16 analytes from PAH group, and for two isotope-labelled analytes (used as an internal standard). Ten solutions of the each standard analyte in dichloromethane were prepared in the following quantity ranges: 1–120 pg and 160–3200 pg of the analyte in the sample dosed.

The standard solution samples were dosed into the chromatographic column in the volume of 2 µl. On the basis of the obtained measuring points (every point was an average from the three independent determinations) the calibration curves were prepared.

### 2.5. Investigation of the influence of standard addition techniques on the result of quantitative analysis of the analytes from PAH group

Investigation of the influence of standard solution addition on the result of quantitative analysis was performed with the use of certified reference material (Metranal 2).

Three different procedures of the standard addition to the investigated samples were applied:

#### Type I:

- samples filled with sediment (each containing approximately 1 g of certificated sediment) were wetted with acetone, 10 or

100 ng of internal standards in methanol solution was added, samples were left until dry at room temperature, and next 3 ml of dichloromethane was added.

*Type II:*

- to samples filled with sediment (each containing approximately 1 g of certificated sediment) 10 or 100 ng of internal standards in methanol solution was added, and next 3 ml of dichloromethane was added.

*Type III:*

- samples filled with sediment (each containing approximately 1 g of certificated sediment) were wetted with solvent (dichloromethane, 3 ml), next 10 or 100 ng of internal standards in methanol solution was added.

The influence of the amount of added standard on the determination results was also investigated. For this purpose 6 series of 5 sediment samples were prepared. The internal standard was added according to the three different procedures (described above). To three series of samples 10 ng of internal standards was added (variant A), and to the next three series 100 ng of internal standards was added (variant B).

Prepared samples were left in automatic shaker for 24 h. Then extracts were purified on the hand-made small glass columns filled with silica gel and a layer of activated copper [15]. The excess of the solvent from final extracts was removed in the stream of the inert gas (nitrogen). Final volume of extract was 1 ml. The extract samples were dosed to the chromatographic column in the volume of 2  $\mu$ l.

### 3. Results and discussion

#### 3.1. Calibration of the GC–MS system

While using deuterated standards to determine PAHs, it is necessary to observe the following:

1. the relative response factor for each of the compounds vs. the deuterated internal standard should be determined individually. In practice, it means injecting standard solution every several or so times of extract from sediment samples injection into the GC–MS system;

2. deuterated standards should be added to sediment in quantities such that their concentrations in the extract are close to the concentration in standard solution;
3. concentrations of deuterated standards in the extract should be close to the concentrations of determined PAHs.

Quantitative calculations in a method using deuterated standards are based on the assumption that Eq. (1) is true. In other words, relative response factors for substances determined in a sample and standard solution are equal.

Calibration curves for deuterated standards and determined PAHs can be described with linear regression equations (Table 1), and they are different for lower (1–120 pg in injection) and higher (160–3200 pg in injection) concentration ranges.

Fig. 1a and b presents calibration curves of deuterated standards (naphthalene-d8 and benz[a]anthracene-d12) and respective PAHs (naphthalene and benz[a]anthracene) for two concentration ranges, the lower and the higher.

Direction coefficients 'a' of calibration curves for deuterated compounds are several times smaller than direction coefficients of respective PAHs (Table 1). Coefficients of direction for naphthalene-d8 are 2.27 (for lower concentrations) and 1.78 (for higher concentrations) times smaller than for naphthalene, while coefficients of direction for benz[a]anthracene-d12 are 4.25 times lower (for lower concentrations) and 7.11 times lower (for higher concentrations) than for benz[a]anthracene. A lower sensitivity of the mass detector with regards to deuterated compounds probably results from the higher ionization energy of the C–D bond than the C–H bond.

So an assumption about the equality of relative response factors in the extract from a sample and standard solution (Eq. (1)) is true only when response coefficients for a deuterated standard and a determined substance are found in the same range of linearity.

#### 3.2. Investigation of the influence of standard addition techniques on the result of quantitative analysis of the analytes from PAH group

For variant A of standard addition (addition of 10 ng of internal standards to the sample) results were calculated on the basis of the

**Table 1**

Comparison of direction coefficients of calibration curves and relative response coefficients of PAHs for lower and higher concentration ranges (a: direction coefficients of calibrations curves; a/w: relative response factor).

Compound	Lower concentration range [1–120 pg in an injector]		Higher concentration range [160–3200 pg in an injector]		correction coefficient
	a	a/w	a	a/w	
<i>1</i>	<i>2</i>	<i>3</i>	<i>4</i>	<i>5</i>	<i>6</i>
Naphthalene	348	1.79	359	1.75	1.02
Naphthalene -d8	195		205		
Acenaphthylene	321	3.69	477	7.34	0.50
Acenaphthene	225	2.59	265	4.08	0.63
Fluorene	196	2.25	295	4.54	0.50
Phenanthrene	312	3.58	416	6.40	0.69
Anthracene	340	3.91	432	6.65	0.59
Fluoranthene	312	3.99	572	8.80	0.45
Pyrene	377	4.34	628	9.66	0.45
Chrysene	293	3.37	490	7.33	0.46
Benz[a]anthracene	293	3.37	490	7.33	0.46
Benz[a]anthracene-d12	87		65		
Benz[b]fluoranthene	249	2.86	546	8.40	0.34
Benz[k]fluoranthene	249	2.86	546	8.40	0.34
Benz[a]pyrene	222	2.56	427	6.57	0.39
Indeno[1,2,3,-cd]pyrene	230	2.64	484	7.44	0.35
Dibenzo[a,h]anthracene	164	1.89	431	6.63	0.28
Benzo[g,h,i]perylene	233	2.67	439	6.75	0.40



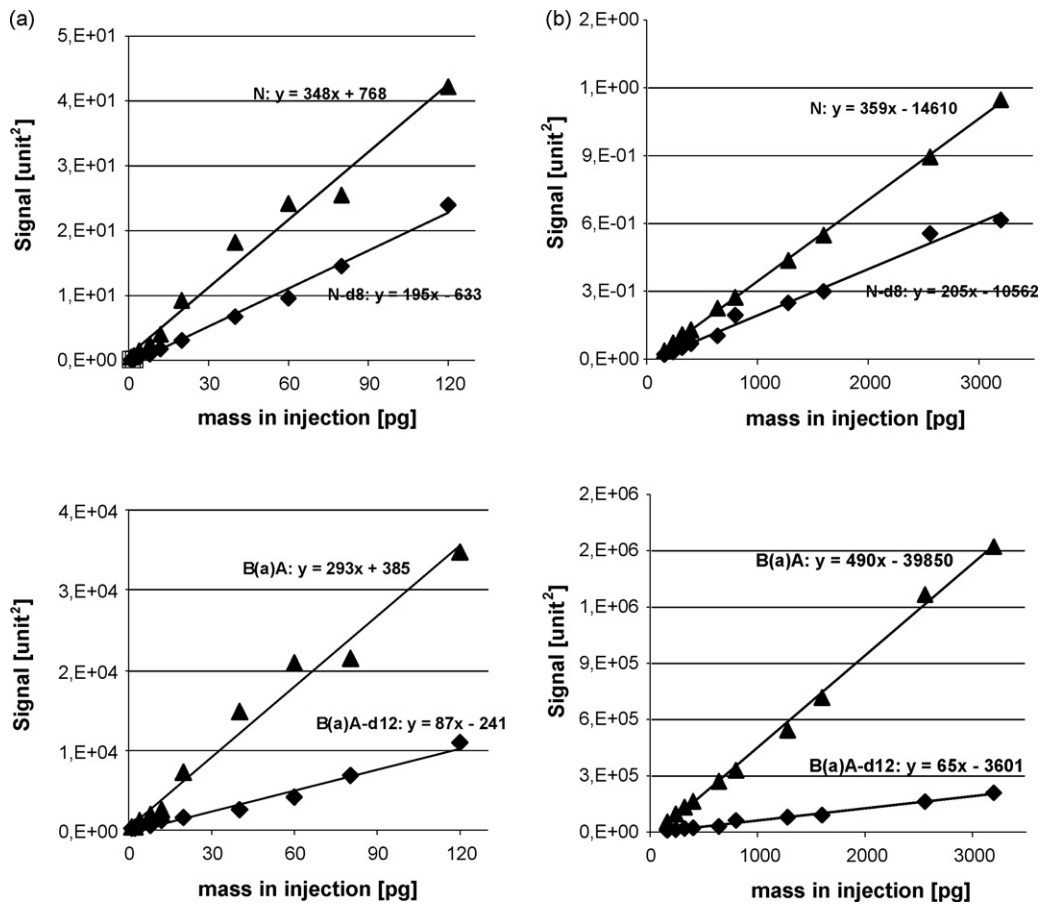


Fig. 1. Calibration curves obtained during the chromatographic analysis of series of standard solutions samples for naphthalene (N) and deuterated naphthalene (N-d8) and for benz[a]anthracene (B(a)A) and deuterated benz[a]anthracene (B(a)A-d12) in lower (a) and higher (b) concentration ranges.

formula (1) using standard solutions I and II, whereas for variant B of standard addition (addition of 100 ng of internal standards to the sample) results were calculated using standard solutions I.

Results obtained are presented in the form of analytes recovery, under assumption that the reference value corresponds to 100%.

Determination results of analytes content from the PAH group in sediment samples obtained using different standard addition techniques are not statistically different among each other (Figs. 2–4). It indicates that in every case the recovery of internal standard is similar, independently on addition technique. However it could be observed that results closer to the certified value were obtained in

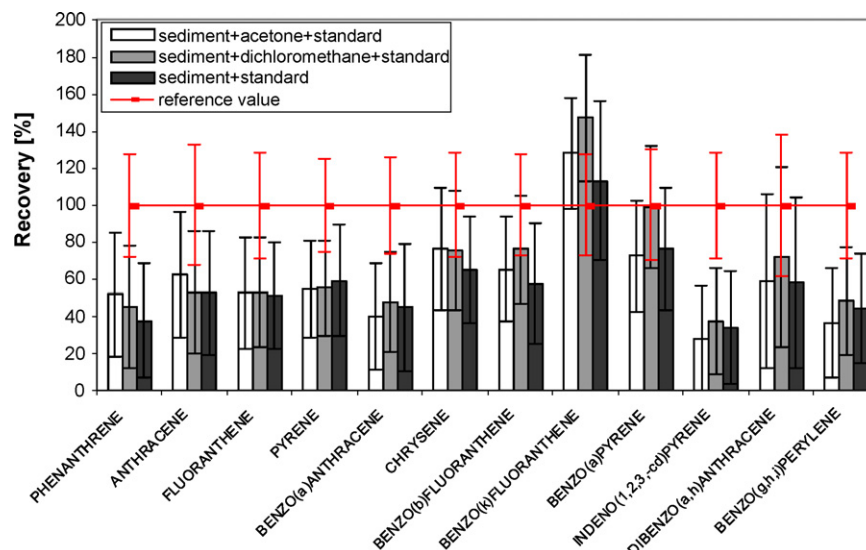
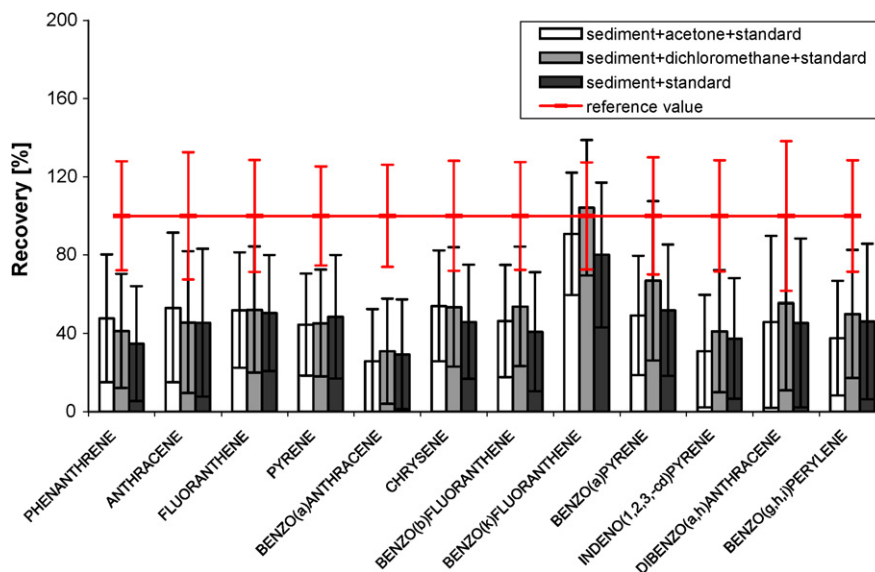


Fig. 2. Comparison of the determination results of analytes from the PAH group in sediment samples, obtained using three different standard addition techniques; variant A (addition of 10 ng of internal standard); results were calculated using standard solution I.



**Fig. 3.** Comparison of the determination results of analytes from the PAH group in sediment samples, obtained using three different standard addition technique; variant A (addition of 10 ng of internal); results were calculated using standard solution II.

variant B (addition of 100 ng of internal standards to the sample), while results obtained in variant A (addition of 10 ng of internal standards to the sample) are lower. Additionally, in case of addition of internal standard in the quantity of 100 ng (variant B), the closest to the certified value results were obtained in case of the I type of the standard addition technique (sediment + acetone + standard).

For variant A (addition of 10 ng of internal standard) no difference were observed during results recalculating to standard solution I and II, what confirms the proper assumption of the formula (1). However it could be observed that results closer to the certified value were obtained during results recalculating to standard solution I, independently on standard addition technique.

Fig. 5 shows results of PAH determination in sediment (reference material: Metranal 2) after dosing 10 and 100 ng of deuterated standards into the sediment sample.

The results of PAH determinations after injecting 100 ng of deuterated standards in methanol solution (all areas, for standard,

deuterated and determined substances were in the higher measurement range) are close to the reference values.

PAH determination results after injecting 10 ng of deuterated standards in methanol solution (areas of deuterated standards were in the lower measurement range) were considerably lower than the reference value (marked in white in the Fig. 5). Correction of determination results for PAHs using a correction coefficient (Table 1) gives results conforming with reference values.

On the basis of the results obtained it can be stated that the technique of internal standard addition does not influence the obtained determination results, whereas the amount of added standard is essential. Additionally, the closest results to the certified value were obtained in case of the addition of 100 ng of standard (variant B) to a sediment wetted with acetone (I type). Therefore, this technique is the best one from all investigated (truly imitates association of analytes with sample matrix, which occurs in aqueous environment). It gives an additional advantage—in case of adding internal stan-

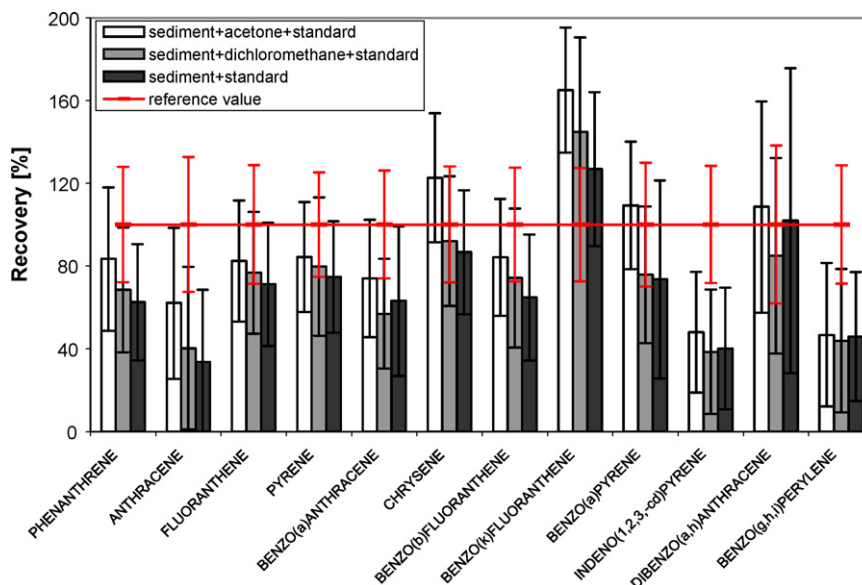


**Fig. 4.** Comparison of the determination results of analytes from the PAH group in sediment samples, obtained using three different standard addition technique; variant B (addition of 100 ng of internal standard); results were calculated using standard solution I.

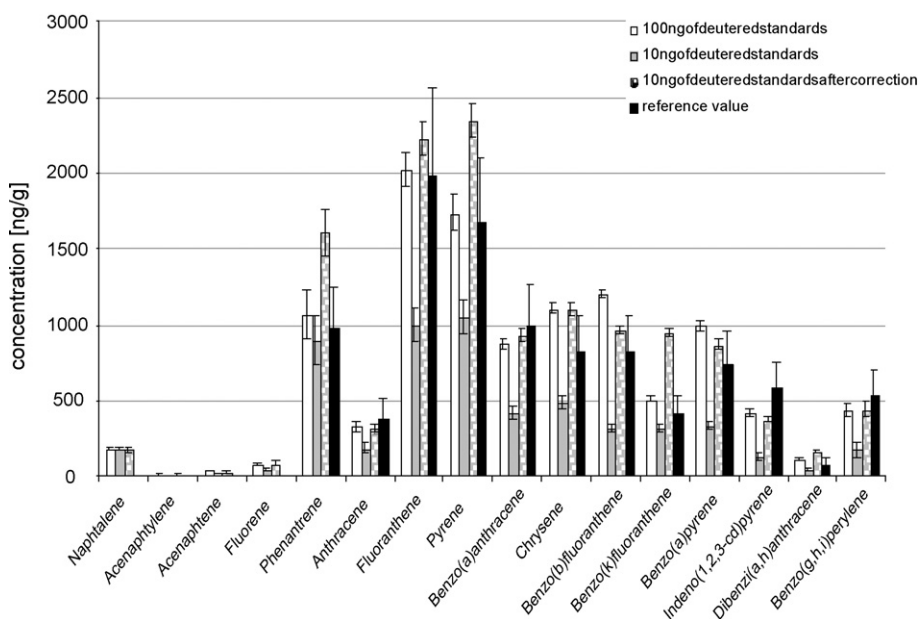


Fig. 5. Comparison reference values with PAH determinations after injecting 10 and 100 ng of deuterated standards in methanol solution, and with corrected results.

dards to sediment sample wetted with acetone it is not necessary to previously dry or freeze-dry a sample.

#### 4. Conclusions

Development of analytical procedures applied in determination of PAHs in sediments was connected with successive trials of solving the problems appearing. The possibility of usage isotope labeled compounds, as recovery standards, in multistage procedure of PAHs isolation and determination, substantially contributed to the improvement of determinations' accuracy and precision. Essential points of procedure based on application of deuterated standards are:

- The lower coefficient of the mass spectrometer's response for deuterated PAHs analogous than for nondeuterated one. Probably it results from the difference in ionization potential of these compounds. Appropriate application of the coefficient of the detector's response for deuterated and nondeuterated analytes in the formula used for quantitative determinations (see formula (1)) allows to obtain correct determination results PAHs, present in the sediment samples.
- Technique of the internal standard addition to the sediment sample. The standard should be added in such a manner that since the sample addition till the final determinations both the analyte and the internal standard behave in the same way, that is, e.g. can be extracted with the same efficiency. In order to meet this condition, it is necessary to add the internal standard in such a way to enable it connecting with the matrix in the closest way to the form of association between the analyte and the sediment. Thank to that, the accuracy of the results obtained is independent on the recovery degree, of course in case, when the value of

the obtained analytical signal is higher than the limit of detection of a given method. Results obtained indicate that wetting of the sediment sample with acetone, spiking of acetone with deuterated standards, intensive stirring of the sample (in order to equalize the concentrations of standards in the sample volume) and undisturbed evaporation of the acetone (for approximately 12 h) allow to achieve a similar binding form between standards added and sediment matter.

#### Acknowledgement

This work has been partially financed in the framework of grant attributed by State Committee of Scientific Research.

#### References

- [1] R. Hengstmann, R. Hamann, H. Weber, A. Kettrup, *Fresenius J. Anal. Chem.* 335 (1989) 982.
- [2] L.O. Kjeller, B. Jonsson, S.E. Kulp, C. Rappe, *Toxicol. Environ. Chem.* 39 (1993) 1.
- [3] A. Filipkowska, L. Lubecki, G. Kowalewska, *Anal. Chim. Acta* 547 (2005) 243.
- [4] W. Jira, *Eur. Food Res. Technol.* 218 (2004) 208.
- [5] A.R. Boden, E.J. Reiner, *Polycyclic Aromat. Compd.* 24 (2004) 309.
- [6] T.J. Quinn, *Metrologia* 34 (1997) 61.
- [7] P. Ellerbe, S. Meiselman, L.T. Sniegoski, M.J. Welch, V.E. White, *Anal. Chem.* 61 (1989) 1718.
- [8] A. Kot, J. Namieśnik, *Trends Anal. Chem.* 19 (2000) 69.
- [9] J. Namieśnik, *Pol. J. Environ. Stud.* 10 (2001) 127.
- [10] S.W. Karickhoff, D.S. Brown, T.A. Scott, *Water Res.* 13 (1979) 241.
- [11] U. Ghosh, J.R. Zimmerman, R.G. Luthy, *Environ. Sci. Technol.* 37 (2003) 2209–2217.
- [12] L.O. Kjeller, *Fresenius J. Anal. Chem.* 361 (1998) 791–796.
- [13] P.W. Albro, Validation of extraction and cleanup procedures for environmental analysis, in: *Environmental Health Chemistry*, The Butterworth Group, 1980, p. 163.
- [14] J.D. Haddock, P.F. Landrum, J.P. Glesy, *Anal. Chem.* 55 (1983) 1197.
- [15] K. Galer, B. Zygmunt, L. Wolska, Namieśnik *J. Chem. Anal.* 45 (2000) 297.



# One-step construction of reagentless biosensor based on chitosan-carbon nanotubes-nile blue-horseradish peroxidase biocomposite formed by electrodeposition

Fengna Xi, Lijun Liu, Zhichun Chen, Xianfu Lin\*

Department of Chemistry, Zhejiang University, Hangzhou 31002, PR China

## ARTICLE INFO

### Article history:

Received 20 October 2008

Received in revised form 10 January 2009

Accepted 13 January 2009

Available online 23 January 2009

### Keywords:

Biosensor

One-step

Electrodeposition

Reagentless

Hydrogen peroxide

## ABSTRACT

A simple and controllable electrodeposition approach was established for one-step construction of novel reagentless biosensors by in situ formation of chitosan-carbon nanotubes-nile blue-horseradish peroxidase (CS-CNTs-NB-HRP) biocomposite film on electrode surface. The mediator effect of NB, conducting performance of CNTs and the biocompatible microenvironment of CS were combined by such one-step non-manual process. NB could interact with CNTs and resulted in good dispersion of CNTs-NB nanocomposites in aqueous solution. Cyclic voltammetry measurements demonstrated that electrons were efficiently shuttled between HRP and the electrode mediated by NB. The developed reagentless biosensor exhibited a fast amperometric response for the determination of  $\text{H}_2\text{O}_2$  and 95% of the steady-state current was obtained within 2 s. The linear response of the reagentless biosensor for the determination of  $\text{H}_2\text{O}_2$  ranged from  $1.0 \times 10^{-6}$  to  $2.4 \times 10^{-4} \text{ mol l}^{-1}$  with a detection limit of  $1.2 \times 10^{-7} \text{ mol l}^{-1}$ . The biosensor exhibited high reproducibility and long-time storage stability. The as-prepared biosensor also showed effective anti-interference capability. The ease of the one-step non-manual technique and the promising feature of the biocomposite could serve as a versatile platform for fabricating electrochemical biosensors.

© 2009 Elsevier B.V. All rights reserved.

## 1. Introduction

Enzyme-based biosensors, which combine the inherent selectivity of enzymatic reactions with the highly efficient electrochemical signal transduction, constitute promising technology in bioanalysis, environmental monitoring and clinical diagnosis due to simplicity, fast response, high sensitivity and selectivity [1,2]. The electrochemical technology based on electron transfer mediator allowed the shuttle of electron from the redox center of enzyme to the surface of working electrode, reduced the operating potential and hopefully avoided the interference from complex samples [3,4]. As compared with solution-phase mediator, immobilization of mediator together with enzyme on an electrode surface using convenient and controllable procedures is of great significance in developing reagentless biosensors for multiple and practical use.

Recently, a series of soluble organic dyes such as methylene blue, nile blue (NB), toluidine blue (Tb) and thionine [3–7] have been proved to be very suitable mediators in horseradish peroxidase (HRP)-based reagentless electrodes due to their high electron transfer efficiency and low cost. It was worth noting that such redox mediators could form stable nanocomposite with car-

bon nanotubes (CNTs) through  $\pi$ - $\pi$  electronic and hydrophobic interactions [5,8–10]. The formed nanocomposites showed good dispersion in water, and could thus be conveniently incorporated into the electrode surface for preparing biosensors. It is well known that CNTs have been widely used as predominant materials for preparing modified electrodes in biosensor applications owing to the high accessible surface area, low electrical resistance and high chemical stability. For biosensors constructed by CNTs-organic dye nanocomposites, organic dye could be used as a mediator for electron transfer and CNTs were excellent conductors and matrices for the enzymatic reaction between enzyme and analytical substrate. The combination of such synergistic effects could produce sensitive reagentless biosensor. For example, Liu et al. [5] used Tb, which adsorbed noncovalently on multiwalled carbon nanotubes (MWCNTs), as a mediator for electric communication between HRP and its substrate to prepare reagentless hydrogen peroxide ( $\text{H}_2\text{O}_2$ ) biosensor. The fabrication of HRP/Tb-MWCNTs-modified electrode, however, was performed by manual casting. Time-consuming and uncontrollable process might be involved. To make the biosensor reproducible, moreover, special and careful attention must be given for controlling the thickness of the resulting composite film. To easily control the fabrication process, non-manual co-immobilization of enzyme and CNTs-mediator nanocomposites in biocompatible matrix is becoming increasingly important.

\* Corresponding author. Fax: +86 571 87952618.

E-mail address: [llc123@zju.edu.cn](mailto:llc123@zju.edu.cn) (X. Lin).

As one of the most promising matrix for enzyme immobilization, the biocompatible polymer, chitosan (CS), remains a focus of study in recent years [11,12]. It was now discovered that CNTs could be dispersed in aqueous solution with the help of CS. Such phenomenon makes CS-CNTs composite materials be attractive for potential applications as biosensing platforms by combination biocompatible microenvironment of CS with excellent conductivity of CNTs [5,13]. Due to the possessing of primary amino groups with a pKa of about 6.3, CS was a unique pH-shift polymer as its solubility and net charge were pH-dependent. Recently, electrochemical deposition of CS was pioneered by Payne and co-workers and Chen and co-workers [14–17] as a simple non-manual method to obtain composite film with controllable thickness under moderate conditions [18,19]. The electrodeposition was performed at reducing potentials and  $H^+$  in the solution was reduced to  $H_2$  at the cathode. Using the locally generated  $H^+$  gradient, acidic side chains of CS were titrated, leading to a change in CS solubility and hence to the controlled deposition of CS film. Moreover, special biocomposites could be easily achieved through effective incorporation of functional substrates in the process [19,20]. Therefore, electrodeposition method could supply a simple and universal way to construct CS-based biocomposite film containing enzyme, mediator and CNTs on conductive bases for developing biosensors.

This work attempts to disclose a simple and controllable electrodeposition method for one-step construction of novel reagentless biosensors by in-situ formation of CS-CNTs-mediator-enzyme biocomposite film on the surface of electrode. HRP was selected as model enzyme. Nile blue (NB), a phenoxiazine dye, which has one positive charge within one molecule and showed promising properties as a redox mediator in HRP system, was selected as model mediator. The carboxylated CNTs could interact with NB and the resulting CNTs-NB nanocomposites possessed good dispersion. The proposed procedure offered simple and convenient methodology for in-situ incorporation of NB, CNTs and HRP into three-dimensional structures of CS hydrogel. Such non-manual approach was direct and facile without complicated and time-consuming manual process. Due to the favorable microenvironment and improved conductivity, the as-prepared reagentless biosensor displayed characteristics of fast response, high sensitivity and good stability for the determination of  $H_2O_2$ .

## 2. Experimental

### 2.1. Reagents

Horseshoe peroxidase (HRP, EC 1.11.1.7, 250 U  $mg^{-1}$ ) was obtained from Shanghai Lizhu Dongfeng Biotechnology Co. Ltd., China. CS (98% deacetylation and an average molecular weight of  $4.8 \times 10^5$  g  $mol^{-1}$ , Yuhuan biomedical Corp., China) and MWCNTs (95%, Shenzhen Nanotech. Port. Co., Ltd., China) were used in this study. All other chemicals were of analytical reagent grade and used without further purification. Hydrogen peroxide ( $H_2O_2$ ) solutions were prepared freshly using a 30%  $H_2O_2$  solution. The 0.1  $mol\ l^{-1}$  phosphate buffer solutions (PBS) at various pH values were prepared by mixing the stock solutions of  $NaH_2PO_4$  and  $Na_2HPO_4$ . Then the pH was adjusted with 0.1  $mol\ l^{-1}$  NaOH or  $H_3PO_4$ .

### 2.2. Apparatus and instrumentations

Electrochemical measurements were performed on a CHI 650 electrochemical analyzer (Shanghai CH Instrument Company, China). A conventional three-electrode system was used. Bare gold electrode or modified gold electrode was used as the working electrode. The reference electrode was Ag/AgCl electrode (saturated with KCl) or saturated calomel electrode (SCE), and platinum disk

was used as auxiliary electrode, respectively. Scanning electron microscopy (SEM) images were obtained at 5.0 kV on a SIRION (FEI, USA) field emission scanning electron microscope.

### 2.3. Preparation of CNTs-NB nanocomposite solution

The MWCNTs were purified by refluxing in 3  $mol\ l^{-1}$  nitric acid for 12 h. The solution was transferred to the polytetrafluoroethylene centrifuge tubes and spun at  $2400 \times g$  for 2 h. After the supernatant acid was decanted off, the resultant solid was ultrasonicated in concentrated  $HNO_3$  and  $H_2SO_4$  (v/v, 1:3) for 6 h followed by extensive washing and filtrating in double deionized water until the filtrate was neutral. Then the pH was adjusted to 8.0 to achieve net negatively charged carboxylate anions [21]. The negatively charged carboxylated-MWCNTs were centrifuged at  $14,000 \times g$  for 30 min to remove the supernatant and dried in vacuum at  $50^\circ C$ . The obtained CNTs ( $1\ mg\ ml^{-1}$ ) were dispersed in 0.05  $mol\ l^{-1}$  PBS containing  $2\ mg\ ml^{-1}$  NB with 5 min ultrasonication to obtain the required CNTs-NB nanocomposites.

### 2.4. Preparation of CS-CNTs-NB-HRP biocomposite film modified electrode

Before each modification, bare gold electrode was successively polished with emery paper and 0.05  $\mu m$   $\alpha-Al_2O_3$  slurry. After being ultrasonicated in double deionized water for 5 min, the electrode was immersed in freshly prepared Piranha solution (30%  $H_2O_2$  and concentrated  $H_2SO_4$ , 3:1, v/v) for 10 min. After being ultrasonicated in double deionized water, the electrode was electrochemically pre-treated by cyclic potential scanning between 1.4 and  $-0.2\ V$  in 0.1  $mol\ l^{-1}$   $H_2SO_4$  until cyclic voltammogram (CV) of clean gold electrode was obtained.

Typically, a homogenous chitosan-carbon nanotubes-nile blue-horseshoe peroxidase (CS-CNTs-NB-HRP) mixture was prepared for electrodeposition by mixing 0.5 wt% CS and  $1\ mg\ ml^{-1}$  HRP with the prepared CNTs-NB solution. CS aqueous solution (0.5 wt%, pH 5.0) was prepared according to the previously reported procedure [16,17,19]. Briefly, CS was dissolved in 0.05  $mol\ l^{-1}$  aqueous HCl solution and the pH of CS solution was adjusted to 5.0 by using a 1.0  $mol\ l^{-1}$  NaOH solution. Then the CS solution was filtered using a 0.45  $\mu m$  cellulose filter film. Afterwards, the prepared CNTs-NB solution was added and the solution was ultrasonicated for 5 min. Then HRP was added and the obtained solution was ultrasonicated for 5 min.

A polished and cleaned gold electrode was dipped into the as-prepared CS-CNTs-NB-HRP solution and was polarized as a negative electrode (the cathode). Deposition was performed by applying a voltage of 1.2 V for 3 min. Consequently,  $H^+$  in the solution was reduced to  $H_2$  at the cathode, and pH near the cathode surface gradually increased. CS became insoluble when pH exceeded its pKa (about 6.3). As a result, the CS hydrogel incorporated with CNTs, NB and HRP was locally electrodeposited onto the cathode surface. After deposition, the modified electrode (Au/CS-CNTs-NB-HRP) was disconnected from the power supply and removed from the solution. Afterwards, the modified electrode was soaked in 0.1  $mol\ l^{-1}$  PBS (pH 8.0) for 10 min. Then the CS coated electrode was stored in 0.1  $mol\ l^{-1}$  PBS (pH 6.5). For comparison with the Au/CS-CNTs-NB-HRP electrodes, Au/CS-NB-HRP electrodes were prepared using the same procedures in CS-NB-HRP solution.

### 2.5. Electrochemical characterization of the reagentless biosensor

Cyclic voltammetric experiments were carried out in quiescent solutions with the scan rate of  $100\ mV\ s^{-1}$ . In steady-state amperometric experiments, the response was obtained at  $-0.4\ V$  versus Ag/AgCl and typical steady-state response of the biosensor

to successive injection of  $\text{H}_2\text{O}_2$  was recorded. EIS was performed in  $5.0 \text{ mmol l}^{-1} \text{ K}_3\text{Fe}(\text{CN})_6/\text{K}_4\text{Fe}(\text{CN})_6$  (1:1) mixture with the frequencies ranging from  $10^4$  to  $10^{-1}$  Hz. Saturated calomel electrode was used as the reference electrode for EIS measurement.

### 3. Results and discussion

#### 3.1. Fabrication of the reagentless biosensor based on one-step electrodeposition

In present investigation, electrodeposition was used for one-step construction of reagentless biosensors by local formation of CS-CNTs-NB-HRP biocomposite film on the surface of electrode. A schematic representation for constructing the reagentless biosensor by one-step formation of CS-CNTs-NB-HRP biocomposite film modified electrode through electrodeposition was illustrated in Fig. 1. It is difficult to disperse CNTs in aqueous water because of their hydrophobic surface. NB is a kind of blue dye and can be easily dissolved in water. As an aromatic compound, NB can easily attach onto CNTs through strong  $\pi$ - $\pi$  stacking force [8–10]. Such interaction greatly improved the dispersion of CNTs due to the hydrophilicity of the adsorbed NB molecules. The mixed solution became dark green when CNTs-NB nanocomposites formed. The CNTs-NB nanocomposites were stable in aqueous solution for at least 15 days, which highly facilitated the application of CNTs in developing biosensors.

CS is a unique polymer and ideally suited for electrodeposition because its net charge and solubility are pH dependent [14–19]. Moreover, it has been proved that CNTs could be dispersed in aqueous solution with the help of CS [5,13]. As a result, CNTs-NB could mix well with CS aqueous solution to form a homogenous solution. The formed CS-CNTs-NB nanocomposites were dispersed and stable in water. The enzyme HRP, as shown in Fig. 1, was also homogeneously dispersed in the CS environment due to the electrostatic interaction between HRP and CS chains. The mechanism for CS deposition at reducing potentials was ascribed to the formation of pH gradient near the cathode surface due to the reduction of water [14–16]. In brief,  $\text{H}^+$  in the solution was reduced to  $\text{H}_2$  at the cathode, and the pH near the cathode surface gradually increased. When pH exceeded the  $\text{pK}_a$  of CS, CS hydrogel incorporated with CNTs, NB and HRP was locally electrodeposited onto the cathode surface (Au/CS-CNTs-NB-HRP).

In summary, the advantages of the proposed strategy for one-step fabrication of reagentless biosensor come from the following four aspects. First, the proposed strategy offered simple and convenient methodology for the preparation of CS-CNTs-NB-HRP biocomposite film. Compared with complicated and time-consuming manual process, the non-manual electrodeposi-

tion approach was simple and controllable. As a result, the thickness of the resulting biocomposite film was controllable and the biosensor fabrication was reproducible. Second, the fabricated biosensor combined the individual benefits of CNTs, NB and CS, as illustrated in Fig. 1. Due to the presence of mediator and the improved conductivity, the biocomposite film might open up new opportunities in biosensors and solid-state electrochemical devices [5,13]. Third, the entrapped HRP could retain its bioactivity due to favorable microenvironment provided by CS. It was well known that CS was one of the most promising matrix for enzyme immobilization [11,12,22]. Fourth, the immobilization of NB by forming CNTs-NB composite could avoid the diffuse of NB from the film, which would lead to significant signal loss and greatly affect the performance and lifetime of the biosensor.

#### 3.2. Morphology characterization of the CS-CNTs-NB-HRP biocomposite film

The morphology of the CS-CNTs-NB-HRP biocomposite film was examined by SEM observation, as shown in Fig. 2. It was found that the CS-CNTs-NB-HRP biocomposite film exhibited a porous surface with three-dimensional network. Moreover, CNTs were symmetrically dispersed in the CS matrix. Such morphological characteristics might result in high loading of enzyme and fast response to the substrate.

#### 3.3. Electrochemical characteristics of the CS-CNTs-NB-HRP biocomposite film modified electrode

The cyclic voltammograms (CVs) of the biosensor, namely Au/CS-CNTs-NB-HRP electrode, give a pair of well defined redox peaks in PBS (pH 6.5) at scan rate of  $100 \text{ mV s}^{-1}$ , as shown in Fig. 3. The peaks represented characteristics of redox couple of NB. With the addition of  $\text{H}_2\text{O}_2$ , reduction peak current increased significantly while oxidation peak current decreased, indicating that a catalytic reaction occurred on this biosensor. These results demonstrated that the response of the biosensor to  $\text{H}_2\text{O}_2$  resulted from only the catalytic activity of HRP immobilized in the biocomposite film. NB incorporated in the film could effectively improve the shuttle of electrons between the electrode and the redox center of HRP. The reduction of  $\text{H}_2\text{O}_2$  catalyzed by HRP and mediated by NB can be described as follows:

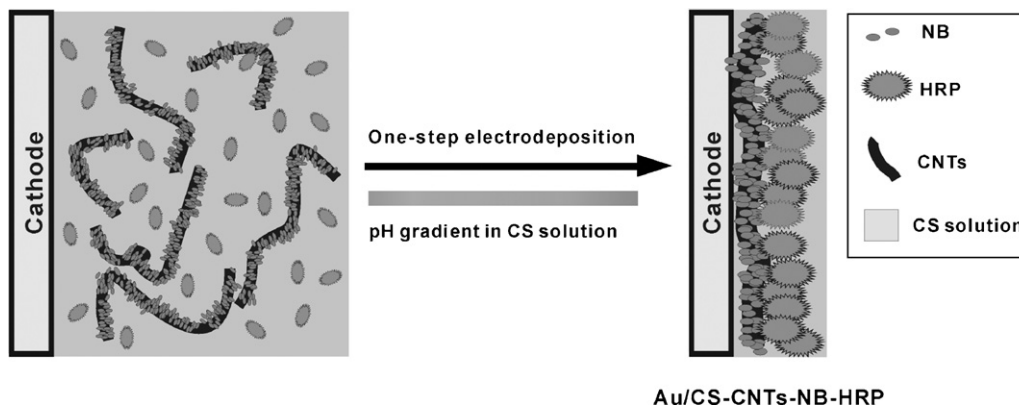
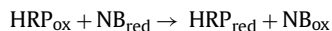


Fig. 1. Schematic representation for construction of the reagentless biosensor by one-step formation of CS-CNTs-NB-HRP biocomposite film modified electrode through electrodeposition.

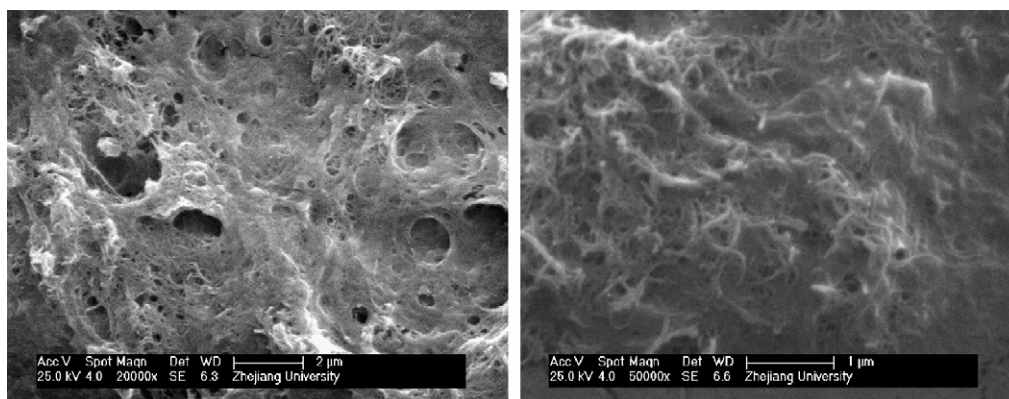
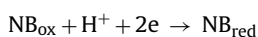


Fig. 2. SEM image of the CS-CNTs-NB-HRP biocomposite film.



where  $\text{HRP}_{\text{ox}}$  and  $\text{HRP}_{\text{red}}$  represent the oxidized and reduced form of HRP, and  $\text{NB}_{\text{ox}}$  and  $\text{NB}_{\text{red}}$  represent the oxidized and reduced form of NB, respectively. In these processes,  $\text{H}_2\text{O}_2$  in solution first diffused to the biocomposite film on electrode where it is reduced by immobilized  $\text{HRP}_{\text{red}}$ . The immobilized  $\text{NB}_{\text{red}}$  reduced the  $\text{HRP}_{\text{ox}}$  produced in the enzymatic reaction. The  $\text{NB}_{\text{ox}}$  was then electrochemically reduced on the electrode surface [6].

The CVs of the Au/CS-CNTs-NB-HRP electrode in  $0.1 \text{ mol l}^{-1}$  PBS at different scan rates were shown in Fig. 4. Inset showed the plots of peak current versus the scan rate. A linear relationship of peak current to scan rate was revealed. For the reduction peak current, a slope of  $0.327 \mu\text{A s mV}^{-1}$  and a correlation coefficient of 0.9983 were revealed. For the oxidation peak current, a slope of  $0.151 \mu\text{A s mV}^{-1}$  and a correlation coefficient of 0.9940 were obtained. The results indicated that the electrode reaction initiated by NB was mainly controlled by surface processes.

EIS has been used to characterize the interface properties of the CS-CNTs-NB-HRP biocomposite modified electrodes. Fig. 5 showed the typical results of AC impedance spectra of Au/CS-CNTs-NB-HRP electrode and Au/CS-NB-HRP electrode, respectively. Significant differences in the impedance spectra were observed. The electron transfer resistance ( $R_{\text{et}}$ ) of Au/CS-NB-HRP was esti-

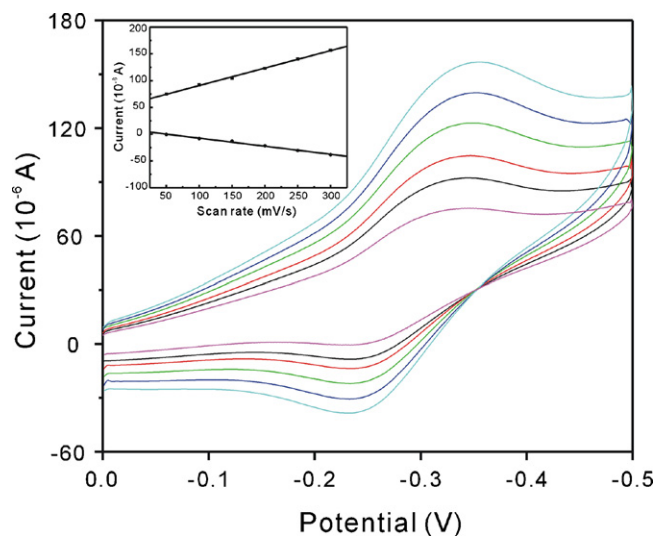


Fig. 4. Typical cyclic voltammograms of the CS-CNTs-NB-HRP biocomposite film modified electrode in  $0.1 \text{ mol l}^{-1}$  PBS (pH 6.5) at different scan rates from 50 to  $300 \text{ mV s}^{-1}$ . Inset showed the plots of peak current versus the scan rate.

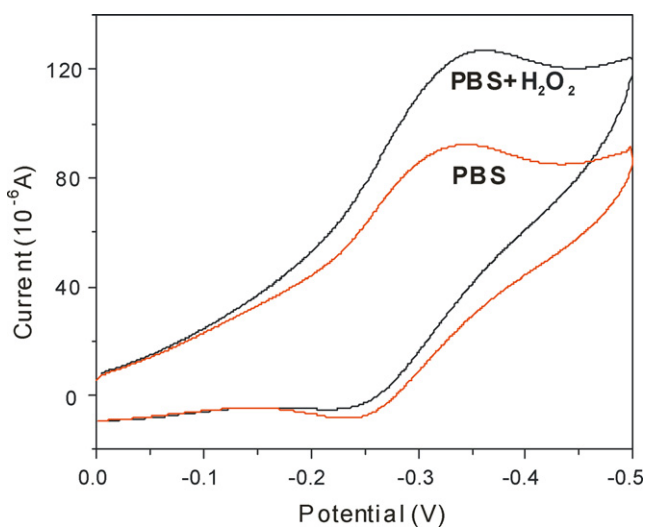


Fig. 3. Cyclic voltammograms of the CS-CNTs-NB-HRP biocomposite film modified electrode in  $0.1 \text{ mol l}^{-1}$  PBS (pH 6.5) at a scan rate of  $100 \text{ mV s}^{-1}$  without  $\text{H}_2\text{O}_2$  and with  $1 \times 10^{-4} \text{ mol l}^{-1}$   $\text{H}_2\text{O}_2$ .

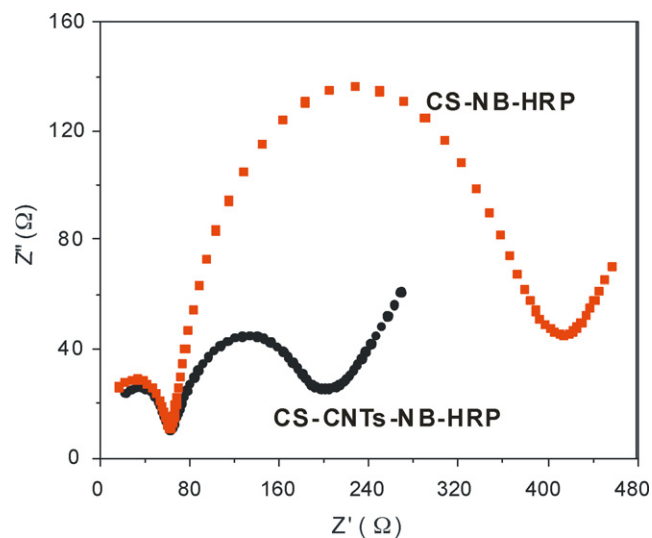
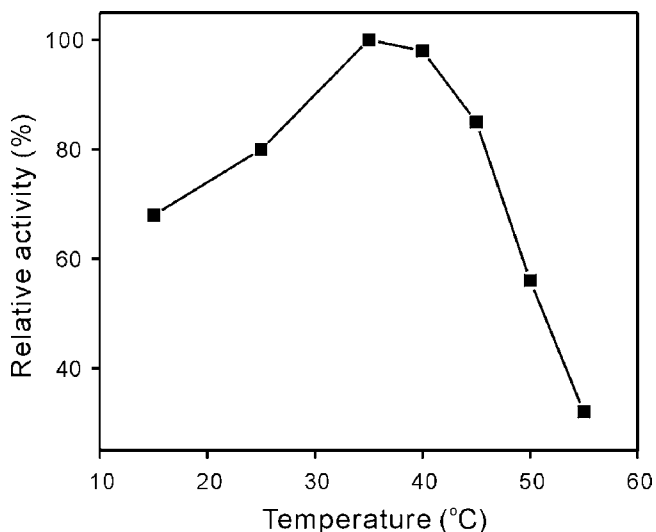


Fig. 5. Electrochemical impedance spectroscopy for Au/CS-CNTs-NB-HRP and Au/CS-NB-HRP in a solution of  $5.0 \text{ mmol l}^{-1}$   $\text{K}_4\text{Fe}(\text{CN})_6/\text{K}_3\text{Fe}(\text{CN})_6$  with SCE as the reference electrode.



**Fig. 6.** Effect of temperature on the response of the biosensor. The maximum response was set as 100%.

mated to be  $334 \Omega$ . For Au/CS-CNTs-NB-HRP, the value of  $R_{\text{et}}$  was found to be  $125 \Omega$ , implying that the incorporation of CNTs greatly facilitated the electron transfer of the electrochemical probe.

#### 3.4. Influence of pH, applied potential and temperature on biosensor response

The conditions of amperometric determination of  $\text{H}_2\text{O}_2$  were optimized. The dependence of the biosensor response on the pH of the measurement solution was investigated. A range of pH values between 5.0 and 8.0 was studied. The current response reached the maximum at pH 6.5. Therefore, the suitable pH with the maximum performance of the biosensor was set at pH 6.5, which was in agreement with that reported for HRP entrapped in CS matrix [22].

Studies to investigate the dependence of the biosensor response on the applied potential were also performed. The amperometric response of the CS-CNTs-NB-HRP biocomposite film modified electrode to  $30 \mu\text{mol l}^{-1}$   $\text{H}_2\text{O}_2$  was investigated over the potential range of  $-0.25$  to  $-0.5$  V. The response increased sharply from  $-0.25$  to  $-0.4$  V, similar to the trend of cyclic voltammetric response. Thus,  $-0.4$  V was selected as the applied potential for detection of  $\text{H}_2\text{O}_2$ .

The current responses at different temperatures were determined from 25 to  $55^\circ\text{C}$ . Results were given in Fig. 6. At relative low temperature, the response increased with the temperature and reached a maximum value at  $35^\circ\text{C}$ . The result was similar with that of native HRP and confirmed the fact that the immobilization of HRP on the biocompatible CS film caused no deformations of its structure [23,24]. When the temperature was higher than  $45^\circ\text{C}$ , the current decreased rapidly. The phenomenon might be ascribed to the denaturation of the enzyme.

#### 3.5. Amperometric response of the developed $\text{H}_2\text{O}_2$ biosensor

Amperometric measurements were performed in a stirred  $0.1 \text{ mol l}^{-1}$  PBS (pH 6.5) at an applied potential of  $-0.4$  V. Fig. 7 showed the typical current–time responses at CS-CNTs-NB-HRP biocompatible film modified electrode for successive addition of  $\text{H}_2\text{O}_2$ . A sharp increase of current was observed after each addition of  $\text{H}_2\text{O}_2$ , and the response reached 95% of the steady-state value within 2 s. Such rapid response could attribute to the presence of CNTs-NB and fast diffusion of substrate in the

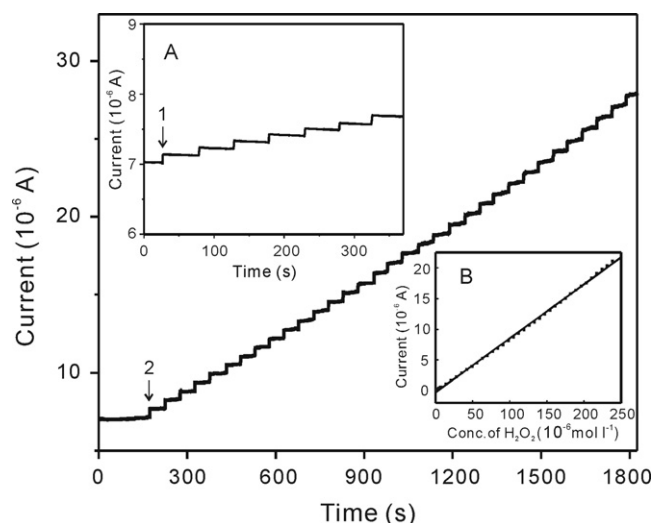


**Fig. 7.** Typical amperometric response of the fabricated biosensor to successive addition of (1)  $1 \mu\text{mol l}^{-1}$   $\text{H}_2\text{O}_2$  and (2)  $7 \mu\text{mol l}^{-1}$   $\text{H}_2\text{O}_2$  in a stirred  $0.1 \text{ mol l}^{-1}$  PBS (pH 6.5). (B) Calibration curve between the current and the concentration of  $\text{H}_2\text{O}_2$ .

porous network of CS-CNTs-NB-HRP biocomposite film. Moreover, well-defined current proportional to the  $\text{H}_2\text{O}_2$  concentration was observed. The inset (Fig. 7B) displayed calibration curve between the amperometric response of the biosensor and the concentration of  $\text{H}_2\text{O}_2$ . The linear range of the developed biosensor for the determination of  $\text{H}_2\text{O}_2$  was found to be  $1.0 \times 10^{-6}$  to  $2.4 \times 10^{-4} \text{ mol l}^{-1}$  with a slope of  $87.9 \mu\text{A ml mol}^{-1}$  and a correlation coefficient of 0.9990 ( $n=40$ ). The detection limit of  $1.2 \times 10^{-7} \text{ mol l}^{-1}$  was estimated at a signal-to-noise ratio of 3.

#### 3.6. Reproducibility and stability of the developed $\text{H}_2\text{O}_2$ biosensor

To prove the precision and practicability of the proposed method, the reproducibility and storage stability of the biosensor were examined. The relative standard deviation (RSD) of the biosensor was 2.8% for twelve successive assays at the  $\text{H}_2\text{O}_2$  concentration of  $30 \mu\text{mol l}^{-1}$ . To evaluate electrode-to-electrode reproducibility, six electrodes were prepared under the same conditions independently. Their response in presence of  $30 \mu\text{mol l}^{-1}$   $\text{H}_2\text{O}_2$  was investigated. The results revealed a RSD of 3.5%. When the electrode was kept by suspending it in above  $0.1 \text{ mol l}^{-1}$  PBS (pH 6.5) at  $4^\circ\text{C}$  in a refrigerator, the long-time storage stability of the fabricated biosensor was examined by intermittent measuring the current response to  $\text{H}_2\text{O}_2$  standard solution every 3 days in 30-day storage. The current response decreased 10% of its initial value after 30 days, showing a long lifetime.

#### 3.7. Selectivity of the developed $\text{H}_2\text{O}_2$ biosensor

The potential interference of some biological substance was investigated. The current in an assay solution containing both  $30 \mu\text{mol l}^{-1}$   $\text{H}_2\text{O}_2$  and a  $0.3 \text{ mmol l}^{-1}$  interfering substance was first obtained. The current in an assay solution containing only  $30 \mu\text{mol l}^{-1}$   $\text{H}_2\text{O}_2$  was then obtained. The interference degree from interfering substances can be evaluated by comparison the above two currents. Glucose, ascorbic acid, uric acid and L-cysteine were investigated. These results indicated that above four tested reagents would not cause observable interference for the determination of  $\text{H}_2\text{O}_2$ . The results indicated that the developed  $\text{H}_2\text{O}_2$  biosensor possessed high sensitivity.



**Table 1**  
H<sub>2</sub>O<sub>2</sub> concentration in real samples tested by the developed H<sub>2</sub>O<sub>2</sub> biosensor.

C <sub>Original</sub> (μmol l <sup>-1</sup> )	C <sub>Added</sub> (μmol l <sup>-1</sup> )	C <sub>Found</sub> (μmol l <sup>-1</sup> )	Recovery (%)
15.00	20.00	34.56	97.8
50.00	30.00	80.71	102.4
100.00	50.00	151.47	102.9

### 3.8. H<sub>2</sub>O<sub>2</sub> determination in real samples

To demonstrate the practical usage of the as-prepared H<sub>2</sub>O<sub>2</sub> biosensor, recovery experiments of three real samples were performed by standard addition method. As listed in Table 1, the recovery rate was in the range 97.8%–102.9%. These results indicate that the biosensor can be directly used to determine H<sub>2</sub>O<sub>2</sub> in real samples. The phenomenon might be ascribed to the high stability and selectivity of the biosensor.

## 4. Conclusion

The one-step electrodeposition of CS-CNTs-NB-HRP biocomposite on electrode surface is shown to be a highly efficient method for the development of new type of reagentless biosensors with sensitivity, stability and reproducibility. The obtained CS-CNTs-NB-HRP biocomposite film possessed unique characteristics for the improvement of the electrochemical performance. Due to the favorable microenvironment and the improved conductivity, enzyme entrapped in such biocomposite possessed high electrocatalytic activity and fast amperometric response to H<sub>2</sub>O<sub>2</sub>. Such non-manual approach offered direct and facile methodology with controllability and reproducibility. The ease of the one-step electrodeposition and the biocompatible matrix endowed the electrode with high reproducibility and storage stability. Both the unique one-step construction method and the promising performance of the developed biosensor enable the construction of an attractive biosensing platform.

## Acknowledgements

This research was supported by the National Natural Science Foundation of China (nos. 20805043, 30800247).

## References

- [1] L.D. Mello, L.T. Kubota, *Talanta* 72 (2007) 335.
- [2] F. Jia, C.S. Shan, F.H. Li, L. Niu, *Biosens. Bioelectron.* 24 (2008) 951.
- [3] L.N. Wu, M. McIntosh, X.J. Zhang, H.X. Ju, *Talanta* 74 (2007) 387.
- [4] Z.J. Wang, M.Y. Li, P.P. Su, Y.L. Zhang, Y.F. Shen, D.X. Han, A. Ivaska, L. Niu, *Electrochem. Commun.* 10 (2008) 306.
- [5] Y. Liu, J.P. Lei, H.X. Ju, *Talanta* 74 (2008) 965.
- [6] S.M. Yang, Z.H. Chen, Y.M. Li, J.X. Ming, X.F. Lin, *Can. J. Anal. Sci. Spectrosc.* 51 (2006) 174.
- [7] X.S. Yang, X. Chen, X. Zhang, W.S. Yang, D.G. Evans, *Sens. Actuators B: Chem.* 129 (2008) 784.
- [8] M.H. Huang, H.Q. Jiang, J.F. Zhai, B.F. Liu, S.J. Dong, *Talanta* 74 (2007) 132.
- [9] J. Zhang, J.K. Lee, Y. Wu, R.W. Murray, *Nano Lett.* 3 (2003) 403.
- [10] Q.W. Li, J. Zhang, H. Yan, M.S. He, Z.F. Liu, *Carbon* 42 (2004) 287.
- [11] J. Abdullah, M. Ahmad, L.Y. Heng, N. Karuppiah, H. Sidek, *Talanta* 70 (2006) 527.
- [12] K.J. Feng, Y.H. Yang, Z.J. Wang, J.H. Jiang, G.L. Shen, R.Q. Yu, *Talanta* 70 (2006) 561.
- [13] G.M. Spinks, S.R. Shin, G.G. Wallace, P.G. Whitten, S.I. Kim, S.J. Kim, *Sens. Actuators B: Chem.* 115 (2006) 678.
- [14] L.Q. Wu, A.P. Gadre, H. Yi, M.J. Kastantin, G.W. Rubloff, W.E. Bentley, G.F. Payne, R. Ghodssi, *Langmuir* 18 (2002) 8620.
- [15] L.Q. Wu, K. Lee, X. Wang, D.S. English, W. Losert, G.F. Payne, *Langmuir* 21 (2005) 3641.
- [16] L.Q. Wu, H. Yi, S. Li, G.W. Rubloff, W.E. Bentley, R. Ghodssi, G.F. Payne, *Langmuir* 19 (2003) 519–524.
- [17] J.J. Xu, X.L. Luo, Y. Du, H.Y. Chen, *Electrochem. Commun.* 6 (2004) 1169.
- [18] Y.H. Song, L. Wang, C.B. Ren, G.Y. Zhu, Z. Li, *Sens. Actuators B: Chem.* 114 (2006) 1001.
- [19] F.N. Xi, L.J. Liu, Q. Wu, X.F. Lin, *Biosens. Bioelectron.* 24 (2008) 29.
- [20] C. Hao, L. Ding, X.J. Zhang, H.X. Ju, *Anal. Chem.* 79 (2007) 4442.
- [21] G.D. Liu, Y.H. Lin, *Anal. Chem.* 78 (2006) 835.
- [22] Q. Lei, X.R. Yang, *Talanta* 68 (2006) 721.
- [23] Y. Zhou, H. Yang, H.Y. Chen, *Talanta* 76 (2008) 419.
- [24] C.L. Xiang, Y.J. Zou, L.X. Sun, F. Xu, *Talanta* 74 (2007) 206.



## Quartz crystal microbalance sensor array for the detection of volatile organic compounds

Xiuming Xu<sup>a,b</sup>, Huaiwen Cang<sup>a</sup>, Changzhi Li<sup>a,b</sup>, Zongbao K. Zhao<sup>a</sup>, Haiyang Li<sup>a,\*</sup>

<sup>a</sup> Dalian Institute of Chemical Physics, Chinese Academy of Sciences, Dalian 116023, PR China

<sup>b</sup> Graduate School of the Chinese Academy of Sciences, Beijing 100039, PR China

### ARTICLE INFO

#### Article history:

Received 25 September 2008

Received in revised form 11 December 2008

Accepted 12 December 2008

Available online 24 December 2008

#### Keywords:

Quartz crystal microbalance

Sensor array

Artificial neural network

Volatile organic compounds

### ABSTRACT

A sensor array system consisting of five quartz crystal microbalance (QCM) sensors (four for measuring and one for reference) and an artificial neural network (ANN) method is presented for on-line detection of volatile organic compounds. Three ionic liquids, 1-butyl-3-methylimidazolium chloride (C<sub>4</sub>mimCl), 1-butyl-3-methylimidazolium hexafluorophosphate (C<sub>4</sub>mimPF<sub>6</sub>), 1-dedocyl-3-methylimidazolium bis(trifluoromethylsulfonyl)imide (C<sub>4</sub>mimNTf<sub>2</sub>), and silicone oil II, which is widely used as gas chromatographic stationary phase, have been selected as sensitive coatings on the quartz surface allowing the sensor array effective to identify chemical vapors, such as toluene, ethanol, acetone and dichloromethane. The success rate for the qualitative recognition reached 100%. Quantitative analysis has also been investigated, within the concentration range of 0.6–6.1 mg/L for toluene, 0.9–7.5 mg/L for ethanol, 2.8–117 mg/L for dichloromethane, and 0.7–38 mg/L for acetone, with a prediction error lower than 8%.

© 2008 Elsevier B.V. All rights reserved.

### 1. Introduction

The detection of volatile organic compounds (VOCs) in environmental protection, health care and food industry has been a challenging task facing analytical workers for decades. Common methods for analyzing VOCs are gas chromatography (GC), mass spectrometry (MS), and fourier transform infrared (FTIR) spectrometry. Although these methods are accurate and reliable, most of them are off-line analyses which are often coupled with solid adsorbent tubes for grabbing samples, and they either need expensive instrumentations or are time-consuming [1,2]. Recently, development of sensors for on-line and *in situ* detection of VOCs has received great attention. As is known, the sensitivity and selectivity of most sensors, such as piezoelectric sensors and metal-oxide gas sensors, depend greatly on the nature of the sensitive layers. However, producing special coatings sensitive to a special analyte, namely, the strict 'lock-and-key' design criterion of traditional sensing devices, is almost unrealizable. Actually, sensors with diverse selectivities, coupled with chemometrics method, are often utilized as a sensor array for on-line VOCs analysis, with higher identification than a single sensor [3–5]. Among all kinds of sensors, quartz crystal microbalance (QCM) sensor has attracted our attention for

its low cost, compact volume, easy portability and high sensitivity. Meanwhile, QCM sensors present preponderance over metal-oxide semiconductor sensors in lower operating temperatures [3,6,7]. QCM is extensively employed in gas analysis since it was first introduced by King in 1964 [8], which is based on the frequency decrease upon mass-increase resulting from adsorption of chemical vapors on the sensor surface. The variation of frequency can be calculated using the Sauerbrey equation [9]

$$\Delta f = -2.26 \times 10^{-6} f_0^2 \frac{\Delta M_s}{A} \quad (1)$$

where  $\Delta f$  is the frequency shift (Hz) when the sensor is exposed to chemical vapors,  $f_0$  is the intrinsic frequency of the piezoelectric crystal (Hz),  $\Delta M_s/A$  is the mass-increase per unit of area (g/cm<sup>2</sup>). Various coating materials for QCM sensor arrays have been reported for recognition of VOCs. Pengchao Si [10] used the principle components analysis (PCA) and an array of eight QCM sensors, each coated with a different conducting polymer, to identify organic vapors, such as toluene, 1-octanol, acetate acid, acetone, acetonitrile, ethanol etc. Gyorgy Barko et al. [11] used a QCM array modified by different gas chromatographic stationary phases to detect VOCs assisted by artificial neural network (ANN) analysis. A sensor system with four piezoelectric detectors has been developed by Ying et al. [12] for the analysis of chemical agents. Munoz et al. [13] has built an odor recognition device using QCM coated with lipids and stationary phase materials of GC for identification of orange and melon flavors.

\* Corresponding author at: Chinese Academy of Sciences, Dalian Institute of Chemical Physics 457, Zhongshan Road, Liaoning, Dalian 116023, China. Tel.: +86 411 84379509.

E-mail address: [hli@dicp.ac.cn](mailto:hli@dicp.ac.cn) (H. Li).

In this work, an array of five QCMs, each of the four measuring QCM coated with a different material and a blank QCM for reference, was used as a sensor system to measure organic compounds. The sensitive coatings included three ionic liquids and a GC stationary phase. Ionic liquids (ILs) are a class of compounds containing organic cations and various anions, which are liquid at ambient temperatures. The unique properties of ILs, such as negligible vapor pressure and high thermal and chemical stability in air, make them well suited for coatings of sensors and detectors [14–17]. Studies on ILs as QCM coatings revealed that ionic liquids composed of different cations and anion had different sensitivities and selectivities towards analytes [18,19]. So we studied the identification property of the sensor array by using an ANN qualitative recognition method for the detection of four typical VOCs of toluene, acetone, ethanol and dichloromethane. Quantitative analyses were carried out by calibration curve-fitting after identification.

## 2. Experimental

### 2.1. Reagents and materials

Toluene, dichloromethane, ethanol, acetone and chloroform were all analytical grade, and they were used as received without further purification.

Ionic liquids 1-butyl-3-methylimidazolium chloride ( $C_4mimCl$ ), 1-butyl-3-methylimidazolium hexafluorophosphate ( $C_4mimPF_6$ ) and 1-dedocyl-3-methylimidazolium bis(trifluoromethylsulfonyl) imide ( $C_4mimNTf_2$ ) were used as QCM sensors' coating materials due to their high sensitivity and selectivity towards VOCs [19], which were prepared according to procedures reported in other literatures [20–22]. Silicone oil II, a widely used gas chromatographic stationary phase (Shanghai Reagent Co., Shanghai, China), was also used as the array's coating material.

### 2.2. Apparatus

The apparatus consisted of five AT-cut piezoelectric quartz crystals (No. 707 factory, Beijing, China) with a fundamental frequency of 10 MHz. They had a 9 mm outer diameter with gold-plated electrodes of 5 mm diameter on both sides. The experimental set-up of the array system was shown in Fig. 1. Each of the four quartz crystals was coated with a different sorbent layer as working sensors, and a fifth blank quartz crystal was used for reference to eliminate the inferences of temperature and pressure. These crystals were located in the same measuring chamber, with a volume of about 5 mL, and

each of them was driven by an independent oscillator circuit so that they worked independently, without mutual interferences. Both of the oscillator circuit and frequency acquisition system were home-built. The resonant frequency of each crystal was recorded every 5 s through the data acquisition system and the data were transferred to a computer via RS232 interface. In this work, the actual frequency and beat frequency of each quartz crystal were recorded in the measurement. The beat frequency is defined as the difference in frequency between the measuring crystal and the reference crystal. In this QCM array system, the beat frequency between each measuring crystal and reference crystal was not achieved by a frequency mixer, but through software approach, namely, by subtracting the frequency of reference from that of corresponding measuring crystal. The beat frequency was saved for later data processing.

### 2.3. Crystal film preparation and experiment procedures

The coating films on quartz crystals were obtained by dip-coating technique. The adsorbent materials were dissolved in chloroform with concentrations of about 10 mg/mL. Dipping the quartz crystal in the coating solution for a certain time, thin film was obtained when the solvent evaporated. Excess coating materials on the edge of the quartz wafer outside the gold electrodes were wiped off by using a chloroform-soaked filter paper. An appropriated film thickness could be obtained by controlling the coating time.

Before each measurement, the array system was purged with pure  $N_2$  until frequency equilibrium was established. Various concentrations of analytes were introduced into the measuring chamber, and each sensor responded in its characteristic way. After adsorption equilibrium was established, the analyte was wiped off by  $N_2$ , which made the frequency of each sensor back to the initial baseline, and the sensor system was ready for the next measurement. The measured analytes were obtained through the gas generation and dilution system which has been described in our previous work [19]. 136 samples of four analytes within the range from 2% to 100% of the saturated analyte vapors generated with the system were measured with the sensor array system. The saturated vapor concentrations of the four organic vapors generated in our experiment are 38.76 mg/L for acetone, 116.50 mg/L for dichloromethane, 7.29 mg/L for ethanol and 6.07 mg/L for toluene. They were divided into two groups: 120 samples for the training set, other 16 samples for the testing set. All measurements were carried out at room temperature with a gas flow rate of 30–90 mL/min.

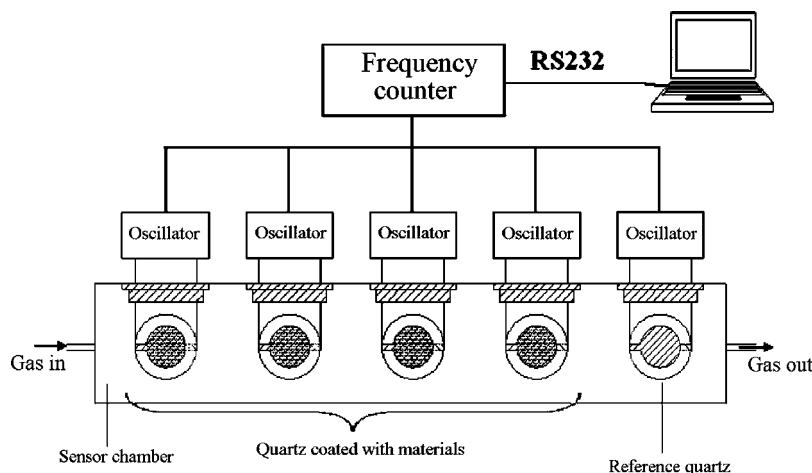


Fig. 1. Schematic diagram of the sensor array system.

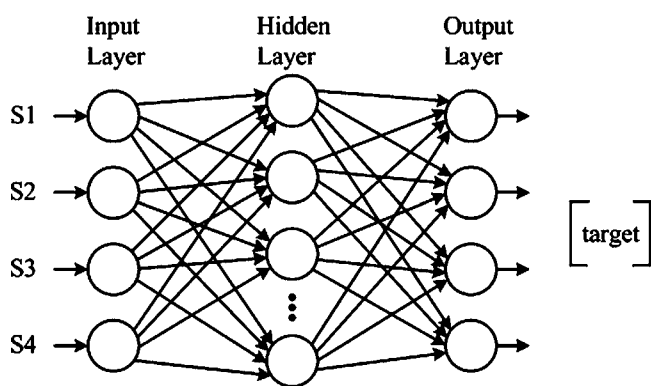


Fig. 2. Topological structure of three-layer back-propagation neural network.

#### 2.4. Artificial neural network

Artificial neural networks (ANNs) are widely used for the identification of analytes measured through sensor array system. In this work, a simple feed forward networks using back propagation learning algorithm was used to handle the frequency signals of the QCM sensor array [11], which were composed of three layers: input layer, hidden layer and output layer. The topological structure of the ANN was shown in Fig. 2. The first (input) layer consisted of four neurons, which was equal to the number of chemical sensors. The number of output neurons was tied to the number of analytes and the number of hidden neurons was generally estimated empirically and was decided through the experiment. In this work, the number of neurons in the input, hidden and output layers were 4, 6 and 4, respectively. The ANN was implemented using software developed in the MATLAB 7.0 environment.

### 3. Results and discussion

#### 3.1. Optimization of film thickness on quartz crystal

Film thickness on the surface of quartz crystal has an important effect on the sensor performance. The optimum amount of IL coated on the QCM surface was investigated. Fig. 3 shows the frequency change as a function of coated  $C_4mimCl$  mass when exposed to 1000 ppm ethanol vapor. Negative frequency change means that adsorption of organic vapors caused a frequency decrease in the QCM sensor. The response of  $C_4mimCl$  coated QCM showed an increase with an increase in coated mass below  $8.5 \mu g$  (correspond-

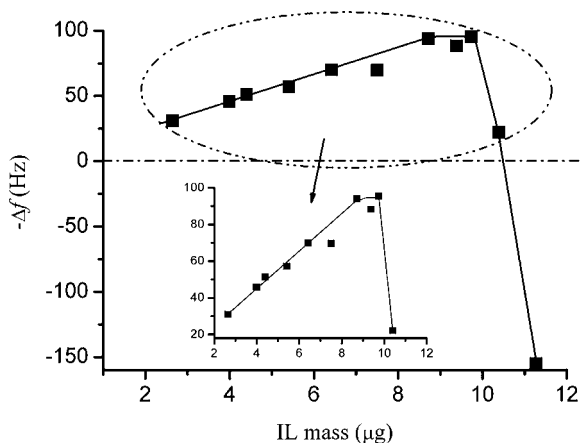


Fig. 3. Frequency change of QCM sensor versus different mass of  $C_4mimCl$  on exposure to 1000 ppm ethanol.

ing to film thickness of 200 nm, the density of  $C_4mimCl$  is  $1.08 \text{ g/mL}$  [23]). However, the response declined sharply when the thickness was more than 229 nm (corresponding to  $9.7 \mu g C_4mimCl$ ). Frequency response of QCM even increased, instead of decreasing, on exposure to ethanol vapor when the coated mass exceeded  $10.5 \mu g$  (shown in Fig. 3). This phenomenon is likely due to the two opposite effects on the frequency shifts of an IL coated QCM sensor on exposure to gases, namely, the mass-increase in the IL film resulting in a decrease in the frequency and the viscosity decrease resulting in an increase in the QCM frequency [15,17]. When the film was thin enough ( $<200 \text{ nm}$  for  $C_4mimCl$ ), the viscosity effect could be ignored, and the Sauerbrey equation (Eq. (1)) worked well [24]. When the coated IL film was specially thicker ( $>10.5 \mu g$  for  $C_4mimCl$ ), the viscosity decrease was the main factor that influenced the QCM performance, which has been utilized as the sensing mechanism for vapor sensing of QCM/IL sensor by Liang et al. [15]. So, the mass of film coatings within the range of  $3.5\text{--}7.0 \mu g$  was used in the following study.

#### 3.2. Characteristic of the QCM sensor array

The oscillating frequency of the piezoelectric crystal is temperature dependent because the material properties of the substrate are temperature dependent [25,26]. When the piezoelectric crystal is coated with sensitive material to make a sensor, the temperature dependence becomes more complicated. However, the temperature effect can be partly eliminated by using an identical piezoelectric crystal to generate a reference frequency. Besides the temperature effect, the buoyancy effect [27], resulted from a change in gas density due to introducing analyte vapor, could also be corrected by the use of reference crystal. Fig. 4 shows the beat frequency responses of the array system to  $5.51 \text{ mg/L}$  toluene vapor. Excellent reversibility for adsorption of gas in the coated materials and rapid response was observed in the sensorgram of Fig. 4, which conformed that the array system could be easily regenerated and could be used for continuous measurement. Rapid response attributed to the higher diffusion rate of gas molecules in relatively low viscosity of ionic liquids and silicone oil than the diffusion rate of gas molecules in solid coating materials [28,29]. Besides, due to the negligible vapor pressure of ILs, there was no coating loss when the array was used for measurement, which ensured the stability of the system. Due to the high stability of the sensor coatings, and the excellent reversibility of the sensor system, the sensor array could have a long life-time theoretically. Frequency changes, calculated from the frequency difference between gas exposure and purging shown in Fig. 4, were used as eigenvalues for data process, e.g. 89,

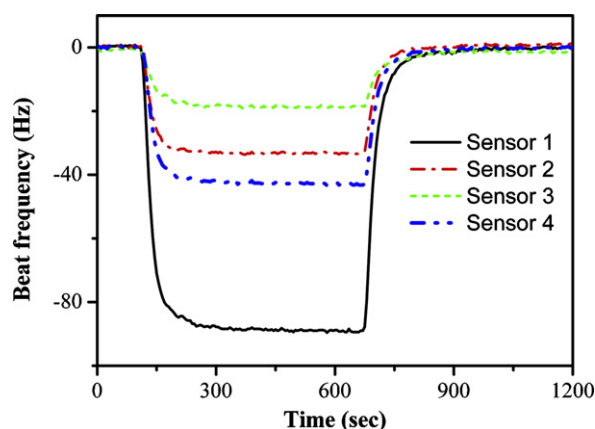


Fig. 4. Sensor array response towards  $5.51 \text{ mg/L}$  toluene vapor. Sensor coating materials: sensor 1,  $C_{12}mimNTf_2$ ; sensor 2,  $C_4mimPF_6$ ; sensor 3,  $C_4mimCl$ ; sensor 4, silicone oil IL.

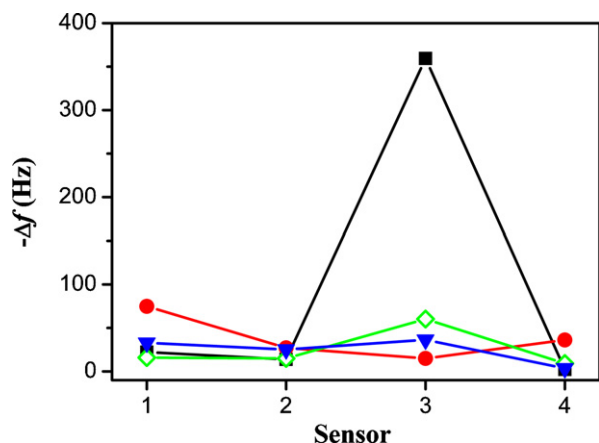


Fig. 5. Sensor array response patterns for (■) ethanol (6.6 mg/L); (●), toluene (4.8 mg/L); (◇), dichloromethane (17.5 mg/L); and (▼), acetone (7.8 mg/L). Sensor coating materials: 1, C<sub>12</sub>mimNTF<sub>2</sub>; 2, C<sub>4</sub>mimPF<sub>6</sub>; 3, C<sub>4</sub>mimCl; 4, silicone oil II.

33, 18 and 43 Hz for each sensor of the array towards 5.51 mg/L toluene.

### 3.3. Qualitative analysis of the sensor array system

Fig. 5 shows the sensor array response to various VOCs. It is clear that each QCM sensor coated with a different coating in the array had quite different response intensities towards the same analyte, e.g. when 4.8 mg/L toluene was measured, signal intensity for each sensor of the array decreased in the sequence of sensor 1 > sensor 4 > sensor 2 > sensor 3; while the array showed quite different response pattern towards other analytes (such as ethanol: sensor 3 > sensor 1 > sensor 2 > sensor 4). On the other hand, the same sensor presented different sensitivities to different VOCs, e.g. response sensitivity decreased in order of ethanol > dichloromethane > acetone > toluene on sensor 3 coated with C<sub>4</sub>mimCl, which has been reported in our previous work [19]. Due to the different response patterns of sensor array system, the analyte can be identified through pattern recognition algorithms.

In the pattern recognition process, the level of inputs to the ANN should be arranged between 0 and 1 [30]. As is shown in Figs. 4 and 5, frequency shift outputs of the QCM array were in the range from a few to several hundred Hertz. So the values of

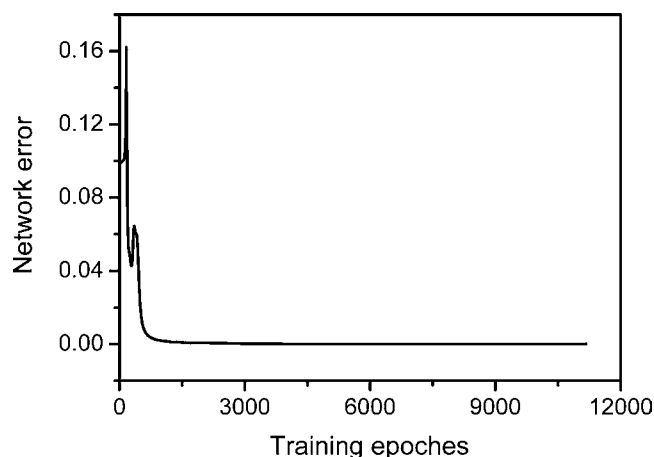


Fig. 6. Convergence curve of the three-layer back-propagation networks.

these outputs must be normalized for the ANN training and testing process. A normalization process for each sensor response was performed according to Eq. (2):

$$X_{ij} = \frac{\Delta f_{ij}}{[\sum_i (\Delta f_{ij})^2]^{1/2}} \quad (2)$$

where  $X_{ij}$  is the normalized value of sensor  $j$  for sample  $i$ ;  $\Delta f_{ij}$  is the frequency change of sensor  $j$  for sample  $i$ . The normalized array outputs,  $X_{ij} = \{X_{i1}, X_{i2}, X_{i3}, \dots, X_{ij}\}$ , were used as inputs of the ANN recognition system. For training the network, the learning process was repeated until the network error reached 0.0001 with 6 neurons in the hidden layer, and the convergence curve was shown in Fig. 6.

After training the network with 120 samples in the training set, 30 samples in each category, the prediction results for the 16 testing samples, 4 samples in each category, of the ANN were listed in Table 1. It can be seen that outputs generated during testing were typically above 0.9, which is the output element value customarily adopted to show the presence of an analyte, compared with the ideal output value of 1.0; and other output elements were below 0.1, compared with an ideal output value of 0 to show the absence of an analyte. Excellent identification was seen, with the largest output error less than 0.02. These results show that the network discriminates well between these chemical species. In addition, the

Table 1  
Prediction results of artificial neural networks.

Sample No.	Output 1		Output 2		Output 3		Output 4		Predicted gas	Actual gas
	Actual	Target	Actual	Target	Actual	Target	Actual	Target		
1	0.9968	1	0.0000	0	0.0000	0	0.0039	0	T	T
2	0.9968	1	0.0000	0	0.0000	0	0.0040	0	T	T
3	0.9967	1	0.0000	0	0.0000	0	0.0042	0	T	T
4	0.9965	1	0.0000	0	0.0000	0	0.0044	0	T	T
5	0.0000	0	0.9891	1	0.0108	0	0.0001	0	E	E
6	0.0000	0	0.9890	1	0.0108	0	0.0001	0	E	E
7	0.0000	0	0.9898	1	0.0099	0	0.0001	0	E	E
8	0.0000	0	0.9904	1	0.0093	0	0.0001	0	E	E
9	0.0000	0	0.0055	0	0.9874	1	0.0102	0	D	D
10	0.0000	0	0.0093	0	0.9874	1	0.0068	0	D	D
11	0.0000	0	0.0107	0	0.9871	1	0.0061	0	D	D
12	0.0000	0	0.0117	0	0.9868	1	0.0057	0	D	D
13	0.0082	0	0.0000	0	0.0030	0	0.9925	1	A	A
14	0.0071	0	0.0000	0	0.0035	0	0.9931	1	A	A
15	0.0032	0	0.0000	0	0.0090	0	0.9933	1	A	A
16	0.0039	0	0.0000	0	0.0069	0	0.9933	1	A	A

Note: T, toluene; E, ethanol; D, dichloromethane; and A, acetone.

**Table 2**

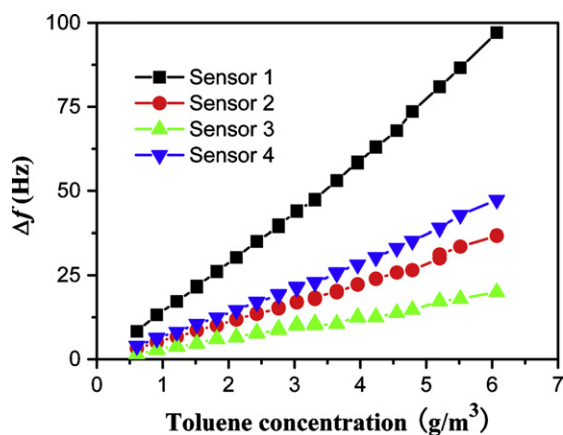
Fitting equations of each QCM sensor in the array towards toluene vapor.

	Fitting equation	Correlation coefficient, $R^2$
Sensor 1	$\Delta f(\text{Hz}) = 15.78C(\text{g/m}^3) - 2.78$	0.996
Sensor 2	$\Delta f(\text{Hz}) = 5.92C(\text{g/m}^3) - 0.73$	0.995
Sensor 3	$\Delta f(\text{Hz}) = 3.22C(\text{g/m}^3) - 0.18$	0.990
Sensor 4	$\Delta f(\text{Hz}) = 7.69C(\text{g/m}^3) - 1.51$	0.996

**Table 3**

Results of quantity analysis for the testing samples.

No.	Sample	Actual concentration ( $C_r$ , mg/L)	Predicted concentration ( $C_t$ , mg/L)	Error (%) <sup>a</sup>
1	Toluene	5.20	5.30	1.9
2	Toluene	3.96	3.91	-1.3
3	Toluene	2.76	2.70	-2.2
4	Toluene	0.91	0.97	6.6
5	Ethanol	6.56	6.55	-0.2
6	Ethanol	4.37	4.42	1.1
7	Ethanol	2.93	2.99	2.0
8	Ethanol	1.46	1.43	-2.1
9	Dichloromethane	98.52	96.50	-2.1
10	Dichloromethane	23.30	23.25	-0.2
11	Dichloromethane	5.83	5.77	-1.0
12	Dichloromethane	34.95	36.06	3.2
13	Acetone	32.99	32.92	-0.2
14	Acetone	19.38	18.99	-2.0
15	Acetone	5.81	5.80	-0.2
16	Acetone	1.94	2.10	8.2

<sup>a</sup> Error was calculated by  $\% = \frac{C_t - C_r}{C_r} \times 100$ **Fig. 7.** Response characteristics of the array system towards various concentrations of toluene vapor. Sensor coating materials: sensor 1,  $C_{12}\text{mimNTf}_2$ ; sensor 2,  $C_4\text{mimPF}_6$ ; sensor 3,  $C_4\text{mimCl}$ ; sensor 4, silicone oil II.

recognition process was very fast, within a second, and the training process took only 2 min.

### 3.4. Quantitative analysis of the sensor array system

Generally, QCM sensors respond linearly to the concentrations of analytes [18,19,31]. When an analyte has been identified by the neural network, the quantity analysis of chemicals can be carried out through the calibration curves of sensors responses versus chemical concentrations. In this work, all sensors responded proportionally to chemicals within the measured concentration ranges. They were 0.6–6.1 mg/L for toluene, 0.9–7.5 mg/L for ethanol, 2.8–117 mg/L for dichloromethane, and 0.7–38 mg/L for acetone. Fig. 7 shows the calibration curves of the QCM sensor array to different concentrations of toluene vapor for representative. The fitting equations towards toluene for each sensor in the array system are listed Table 2, with the correlation coefficient of  $R^2 > 0.99$ . Based on the four calibration curves (or parts of them), the concentration of samples in the test-

ing group can be obtained by averaging the concentration values calculated from the fitting equations, which are shown in Table 3, together with all other testing samples. It showed that analytes could be quantified precisely, with the prediction errors lower than 8%. So, when an analyte was identified, its concentration could be estimated with the calibration curve-fitting method.

## 4. Conclusions

Ionic liquids, due to their unique properties of negligible vapor pressure, tunable selectivity, and high stability, are being widely used as sensitive coatings for chemical sensors. An array of quartz crystal microbalance, each quartz coated with a different ionic liquid or gas chromatographic stationary phase, was presented as a suitable sensor for identifying selected compounds of organic vapors, with rapid response speed. This paper presented that an array of quartz crystal microbalances plus a three-layer neural network was very effective to identify organic vapors. Results showed that it could recognize selected compounds correctly, i.e. the success rate of the system in identifying compounds was 100%. Once an analyte has been identified, quantitative analysis can be carried out due to the linear response characteristic of QCM sensors, with a prediction error lower than 8%.

## References

- [1] M.A. Jochmann, X. Yuan, T.C. Schmidt, Anal. Bioanal. Chem. 387 (2007) 2163.
- [2] M. Schellin, P. Popp, J. Chromatogr. A 1103 (2006) 211.
- [3] A.K. Srivastava, Sens. Actuators B: Chem. 96 (2003) 24.
- [4] R. Dutta, K.R. Kashwan, M. Bhuyan, E.L. Hines, J.W. Gardner, Neural Netw. 16 (2003) 847.
- [5] A. Szczurek, P.M. Szecowka, B.W. Licznarski, Sens. Actuators B: Chem. 58 (1999) 427.
- [6] S. Ampuero, J.O. Bosset, Sens. Actuators B: Chem. 94 (2003) 1.
- [7] K.J. Albert, N.S. Lewis, C.L. Schauer, G.A. Sotzing, S.E. Stitzel, T.P. Vaid, D.R. Walt, Chem. Rev. 100 (2000) 2595.
- [8] W.H. King, Anal. Chem. 36 (1964) 1735.
- [9] G. Sauerbrey, Z. Phys. 155 (1959) 206.
- [10] P.C. Si, J. Mortensen, A. Komolov, J. Denborg, P.J. Møller, Anal. Chim. Acta 597 (2007) 223.
- [11] G. Barko, J. Hlavay, Talanta 44 (1997) 2237.

- [12] Zhihua Ying, Yadong Jiang, Xiaosong Du, Guangzhong Xie, Junsheng Yu, H. Tai, *Eur. Polym. J.* 44 (2008) 1157.
- [13] S. Munoz-Aguirre, A. Yoshino, T. Nakamoto, T. Moriizumi, *Sens. Actuators B: Chem.* 123 (2007) 1101.
- [14] J.-f. Liu, G.-b. Jiang, J.-f. Liu, J.A. Jonsson, *TrAC, Trends Anal. Chem.* 24 (2005) 20.
- [15] C.D. Liang, C.Y. Yuan, R.J. Warmack, C.E. Barnes, S. Dai, *Anal. Chem.* 74 (2002) 2172.
- [16] L. Yu, D. Garcia, R.B. Rex, X.Q. Zeng, *Chem. Commun.* (2005) 2277.
- [17] T. Schafer, F. Di Francesco, R. Fuoco, *Microchem. J.* 85 (2007) 52.
- [18] X.X. Jin, L. Yu, D. Garcia, R.X. Ren, X.Q. Zeng, *Anal. Chem.* 78 (2006) 6980.
- [19] X.M. Xu, C. Li, K.M. Pei, Z.B.K. Zhao, H.Y. Li, *Sens. Actuators B: Chem.* 134 (2008) 258.
- [20] C.Z. Li, Z.B.K. Zhao, *Adv. Synth. Catal.* 349 (2007) 1847.
- [21] P.A.Z. Suarez, J.E.L. Dullius, S. Einloft, R.F. DeSouza, J. Dupont, *Polyhedron* 15 (1996) 1217.
- [22] J.G. Huddleston, H.D. Willauer, R.P. Swatloski, A.E. Visser, R.D. Rogers, *Chem. Commun.* (1998) 1765.
- [23] J.G. Huddleston, A.E. Visser, W.M. Reichert, H.D. Willauer, G.A. Broker, R.D. Rogers, *Green Chem.* 3 (2001) 156.
- [24] R. Michael, K. Bengt, *Sens. Actuators A: Phys.* 54 (1996) 448.
- [25] X.M. Xu, J.D. Wang, H.Y. Li, *Prog. Chem.* 17 (2005) 876.
- [26] Falconer, *Sens. Actuators B: Chem.* 24–25 (1995) 54.
- [27] R.E. Baltus, B.H. Culbertson, S. Dai, H.M. Luo, D.W. DePaoli, *J. Phys. Chem. B* 108 (2004) 721.
- [28] C. Wang, F. Chen, X.W. He, S.Z. Kang, C.C. You, Y. Liu, *Analyst* 126 (2001) 1716.
- [29] L.M. Dorozhkin, I.A. Rozanov, *J. Anal. Chem.* 56 (2001) 399.
- [30] E. Llobet, J. Brezmes, X. Vilanova, J.E. Sueiras, X. Correig, *Sens. Actuators B: Chem.* 41 (1997) 13.
- [31] X.L. Chen, X.W. He, X.B. Hu, H. Xu, *Analyst* 124 (1999) 1787.



# A low-cost light-emitting diode induced fluorescence detector for capillary electrophoresis based on an orthogonal optical arrangement

Feng-Bo Yang, Jian-Zhang Pan, Ting Zhang, Qun Fang\*

*Institute of Microanalytical Systems, Zhejiang University, Hangzhou 310058, China*

## ARTICLE INFO

### Article history:

Received 6 November 2008  
Received in revised form 15 January 2009  
Accepted 18 January 2009  
Available online 24 January 2009

### Keywords:

Light-emitting diode  
Fluorescence detection  
Miniaturization  
Orthogonal optical arrangement  
Capillary electrophoresis

## ABSTRACT

In this work, a simple and low-cost miniaturized light-emitting diode induced fluorescence (LED-IF) detector based on an orthogonal optical arrangement for capillary electrophoresis (CE) was developed, using a blue concave light-emitting diode (LED) as excitation source and a photodiode as photodetector. A lens obtained from a waste DVD-ROM was used to focus the LED light beam into an  $\sim 80 \mu\text{m}$  spot. Fluorescence was collected with an ocular obtained from a pen microscope at  $45^\circ$  angle, and passed through a band-pass filter to a photodiode detector. The performance of the LED-IF detector was demonstrated in CE separations using sodium fluorescein and fluorescein isothiocyanate (FITC)-labeled amino acids as model samples. The limit of detection for sodium fluorescein was  $0.92 \mu\text{M}$  with a signal-to-noise ratio (S/N) of 3. The total cost of the LED-IF detector was less than \$ 50.

© 2009 Elsevier B.V. All rights reserved.

## 1. Introduction

In recent years, the combination of laser-induced fluorescence (LIF) detection with capillary electrophoresis (CE) provides a lot of advantages including rapidity, high resolution, high efficiency, high sensitivity, as well as low sample and reagent consumption. Lasers are commonly used as excitation sources in fluorescence detection systems due to their high emitting intensity and good spatial property, which allow the light to be focused to a very small area. However, the LIF detectors suffer from a number of limitations, such as high cost, large size and limited lifetime ( $\sim 3000$  h). Light-emitting diodes (LEDs) with advantages of a long lifetime ( $>10,000$  h), small size, low cost, stable intensity, high efficiency and multiple emitting wavelengths ranging from red to blue [1], have become an attractive alternative light source for fluorescence detection. Various LEDs have been used to build miniaturized and low-cost fluorescence detection systems for various analytical applications, especially for portable CE instruments.

A number of different types of LED induced fluorescence (LED-IF) detectors for conventional CE [2–16] and microfluidic chip-based CE [17–22] systems have been reported because of those advantages mentioned above. Yang et al. reported a fluorescence detector based on collinear scheme using a bright LED as excitation source,

which was assembled by all-solid-state optical-electronic components and coupled with CE using on-column detection mode [8]. A limit of detection (LOD) of 10 nM for fluorescein isothiocyanate (FITC)-labeled phenylalanine was obtained. Uchiyama et al. developed a polymer CE chip with an LED-IF detector using a LED as light source and an optical fiber placed perpendicular to the LED for fluorescence collecting [18]. LODs of  $160 \mu\text{M}$  and  $90 \mu\text{M}$  were obtained for valine and phenylalanine, respectively. In most of the above-mentioned work, photomultiplier tubes (PMTs) were used as detectors to obtain high detection sensitivities, which in turn resulted in relatively large size and high cost of the whole detection system.

Due to the larger light-emitting angles of LEDs compared with laser light, one of the limitations of using LEDs in CE detection systems lies in the difficulty to focus LED light into a spot with a diameter less than  $100 \mu\text{m}$ , which is required in most of CE systems to ensure the separation efficiency. Slusznay et al. reported a LED-IF detection system for CE separation of native proteins using a continuous-wave 280-nm LED as the excitation source [9]. A spot of approximately  $200 \mu\text{m}$  was obtained by using a set of two ball lenses. The emitted fluorescence was collected with a ball lens at  $90^\circ$  angle, passed through a band-pass filter onto a PMT. A LOD of 20 nM for conalbumin was obtained. Novak and Neuzil presented a miniaturized fluorescence detection system for microfluidic chips based on confocal optical arrangement [21]. Geltech molded glass aspheric lenses were used for both light collimating and focusing on the sample. Light emitted from a blue LED was collimated by the lens, and the collimated light was filtered by an excitation filter, reflected twice by a dichroic and a conventional mirror, and

\* Corresponding author at: Institute of Microanalytical Systems, Chemistry Experiment Building, Room 101, Zhejiang University (Zijingang Campus), Hangzhou 310058, China. Tel.: +86 571 88206771; fax: +86 571 88273572.

E-mail address: [fangqun@zju.edu.cn](mailto:fangqun@zju.edu.cn) (Q. Fang).



focused on the sample of interest by the second lens, forming a spot with a diameter of 480  $\mu\text{m}$ . The fluorescence light passed through the dichroic mirror, was filtered by an emitter filter, and collected by a silicon photodiode. A LOD of 1.96 nM sodium fluorescein was obtained using lock-in amplifier technique to increase the signal/noise (S/N) ratio. In addition to lens or objective, other methods were also developed to improve the focusing performance of LED light by using miniaturized liquid-core waveguide devices [3], aperture [8,14], and optical fiber [22]. However, the use of these assemblies may result in the complicated structure of the detection system or the energy loss of excitation light.

In this work, a miniaturized and low-cost LED-IF detector for CE system was developed based on orthogonal optical arrangement. A concave LED and a lens used in commercial DVD-ROM were employed to obtain small focusing spot (<100  $\mu\text{m}$  diameter) required by CE systems. The performance of the detector was evaluated by using sodium fluorescein and demonstrated in the CE separation of a mixture of FITC-labeled amino acids.

## 2. Experimental

### 2.1. Reagents and chemicals

All reagents were of analytical grade, and demineralized water was used throughout. A 10 mM sodium tetraborate buffer (pH 9.2) was used as working electrolyte for CE separation. NaOH solution (0.1 M) was used for capillary washing. Sodium fluorescein was obtained from Sangon Biotechnology Co. (Shanghai, China). The stock solution of 10 mM sodium fluorescein was prepared by dissolving 37 mg of the dye in 10 mL 10 mM sodium tetraborate buffer (pH 9.2). A series of standard solutions of sodium fluorescein was prepared by sequentially diluting the stock solution with the buffer solution. A solution containing a mixture of 50  $\mu\text{M}$  fluorescein isothiocyanate (FITC, Sigma, St. Louis, USA) labeled L-arginine and D,L- $\beta$ -phenylalanine was prepared as previously described elsewhere [23]. The solutions were stored in a refrigerator at 4  $^{\circ}\text{C}$ .

### 2.2. Apparatus and equipment

Round LEDs (peak wavelength, 470 nm), columnar LEDs (peak wavelength, 470 nm), and concave LEDs (peak wavelength, 470 nm) were purchased from Hangke Electronics Co. (Hangzhou, China). Before use, the LEDs were undergone continuous working under 20 mA current at least for 150 h to eliminate the initial low-frequency noise [1]. The optical setup is shown in Fig. 1. The light beam emitted from the LED was focused at the channel center of the capillary using a lens taken down from a waste DVD-ROM (Pioneer Electronic Co., Japan). The fluorescence emitted from the

capillary channel was collected by a 25 $\times$  ocular obtained from a pen microscope (Xiguang Technology Co., Xi'an, China) with an angle of 45 $^{\circ}$  between the capillary and the fluorescence collecting path. The collected fluorescence beam passed through a 535-nm band-pass filter (10-nm band-pass, Shenyang HuiBo Optical Technology Co., Shenyang, China) and through a 1-mm pinhole before being detected by a photodiode (OPT301, Texas Instruments, Dallas, USA). A sheet of translucent paper was used to facilitate alignment of optical components by imaging the fluorescence beam upon the paper placed at the position of the optical component during optimization of the optical system [23]. The output signals from the photodiode were first amplified by using a high gain amplifier AD620 (Analog Devices Instruments, Norwood, USA), and then the signals were recorded by a data collecting card (USB-6008, Fan-Hua Measurement & Control Technology Co., Beijing, China) and processed using a program written with a LabVIEW 7.0 (National Instruments, Austin, USA). All data were filtered by a Butterworth 5 Hz lowpass filter and smoothed using a 5000 point adjacent averaging smoothing. The entire whole detection system was masked from ambient light using black plastic tubing and plasticine.

A stereo microscope (SZ-45B3, Sunny Instruments Co., Ningbo, China) equipped with a CCD camera (DCMT130, Huaxin IC Technology Inc., Hangzhou, China) was used to observe and evaluate the focused spot of the LED beam.

The CE setup was built using a 7.5-cm-long fused-silica capillary (75- $\mu\text{m}$  i.d., 365- $\mu\text{m}$  o.d., Reafine Chromatography Co., Yongnian, China). A homemade programmable high-voltage power supply, variable in the range of 0–1500 V, was used to perform sample injection and separation. A detection window was made by removing a 1-cm section of polyimide coating on the detection position of the capillary.

### 2.3. CE separation

Prior to use, the capillary was treated with 0.1 M NaOH solution for 30 min. Then the capillary was rinsed sequentially with water and working electrolyte for 2 min. Samples were injected into the capillary with an injection time of 1 s and voltage of 1300 V. The separation voltage was 1300 V. The capillary was conditioned with the working electrolyte for 5 min at 1300 V after each run.

## 3. Results and discussion

### 3.1. Focusing of LED light

In this work, a focusing lens obtained from a waste DVD-ROM, instead of an objective used in most LED-IF systems [6,10–13,20] was employed for LED light focusing to reduce the size and cost of the fluorescence detection system. Three types of LEDs with different shapes, including round, columnar and concave LEDs, were coupled to this lens to test their focusing performance using a glass chip with a 75- $\mu\text{m}$ -wide microchannel. The results are shown in Fig. 2. The diameter of the focused spot varied with the focusing distance between the LED and the focusing lens. Focusing spots less than 100  $\mu\text{m}$  diameter were obtained with 8.7, 3.4 and 1.2 cm focusing distances between the LED and the lens for the round, columnar and concave LEDs, respectively. The three types of LEDs showed significant differences in the focusing distances due to the difference in LED light emitting angle. The longer the focusing distance, the more energy loss of the focused light spot, and the more difficult in the miniaturization of the detection system. Therefore, the concave LED was selected to build the LED focusing system (including LED light source and focusing lens) with a system size of 0.5 cm  $\times$  0.5 cm  $\times$  2.5 cm and focusing spot diameter of 80  $\mu\text{m}$ . To the best of our knowledge, this is the first time

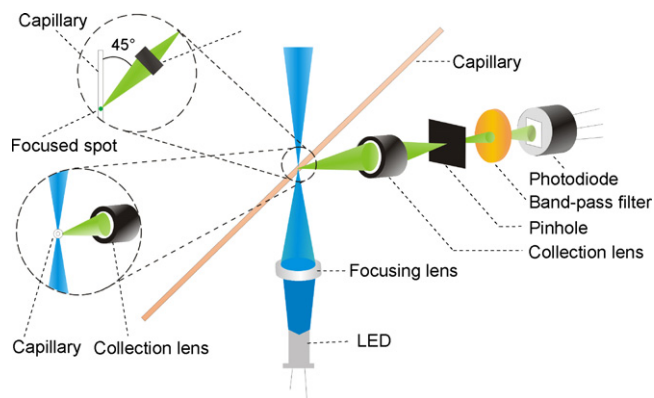
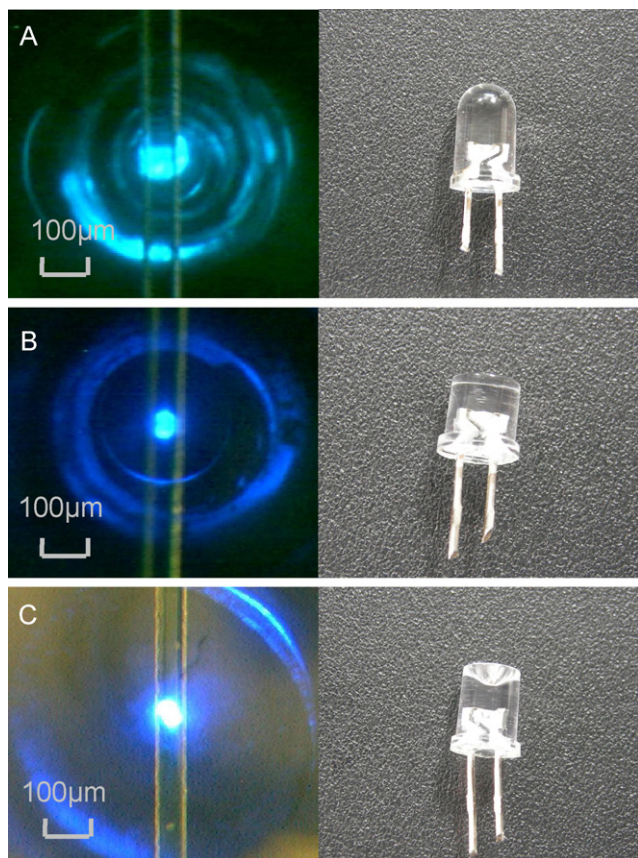


Fig. 1. Schematic diagram of the optical setup of the LED-IF detection system.



**Fig. 2.** Images of the round (A), columnar (B) and concave (C) LEDs and their focused spots on the 75- $\mu\text{m}$ -wide microchannel with the shortest possible distance between the LED and the focused lens of 8.7 cm, 3.4 cm and 1.2 cm, respectively.

that the concave type of LED has been adopted in LED-IF detection system.

### 3.2. Optical arrangement

In the previously reported work, various LED-IF detection systems based on different optical arrangements were developed and have been broadly applied in the CE analysis systems. The confocal arrangement, which has proved effective in LIF detection systems, was also applied in some of LED-IF detection systems. These systems were successfully used in conventional CE [7,8] as well as chip-based CE systems [17,19–21]. However, it is difficult to achieve the miniaturization of LED-IF detection system with confocal arrangement due to its complicated structure and large light-emitting angles of LEDs. Some LED-IF systems based on non-confocal optical arrangement, such as orthogonal arrangement, have also been reported [2,15,18]. In such systems, the scattered light interference from the LED source could be effectively reduced by detecting fluorescence from the direction orthogonal to the incident LED beam. In 2006, we developed a LIF detection system for microchip based on orthogonal arrangement, in which the fluorescence light emitted in the microchannel was detected through the sidewall of the chip with a fluorescence collection angle of 45° in the orthogonal plane [23]. The scattered light interference from the

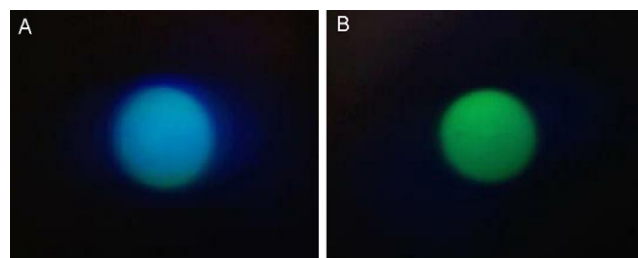


**Fig. 3.** CCD images of the capillary sidewall with the fluorescence spot produced by excitation of 0.5 mM sodium fluorescein at different collection angles of 90° (A) and 45° (B).

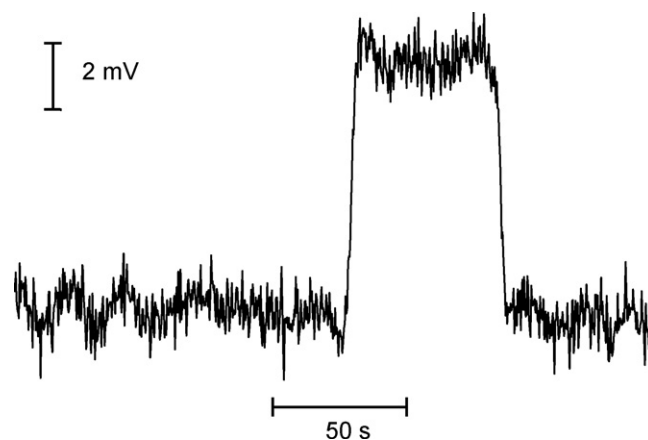


**Fig. 4.** Electropherogram of 4  $\mu\text{M}$  sodium fluorescein for measurement of limit of detection. Working electrolyte, 10 mM sodium tetraborate buffer (pH 9.2); injection voltage, 1300 V; injection time, 50 s; separation voltage, 1300 V; effective separation length, 3.7 cm.

laser source was significantly reduced and high detection sensitivity comparable to those in confocal LIF systems was obtained.

In this work, this technique was applied in LED-IF detection for CE system. Two fluorescence collection angles of 90° and 45° were tested in the LED-IF detection system. A 0.5 mM sodium fluorescein solution was filled in the capillary, and the LED-excited fluorescence beam collected by the ocular was imaged on a sheet of translucent paper with collection angles of 90° and 45°, respectively. The results are shown in Fig. 3. A significant difference between the colors of the fluorescence spots could be observed. The fluorescence spot observed at a collection angle of 90° appeared predominantly blue from the scattered LED light instead of the green color of the fluorescence. The fluorescence spot observed at a collection angle of 45° showed relatively green, which qualitatively demonstrated the intensity of the scattered light could be significantly reduced at this collection angle. This result agrees well with that of the previously reported LIF system for microchip [23]. Therefore, a collection angle of 45° was employed in the present LED-IF detection system.

### 3.3. Performance of the LED-IF detection system

Sodium fluorescein was used as the model sample to demonstrate the performance of the fluorescence detection system. A LOD of 0.92  $\mu\text{M}$  sodium fluorescein ( $S/N=3$ , as shown in Fig. 4) was

**Table 1**  
The cost of the LED-IF detection system.

	LED	Photodiode	Focusing lens	Collection lens	Band-pass filter	Others
Cost (\$)	0.04	12	0.5	12	22	0.5
Total cost (\$)				47		

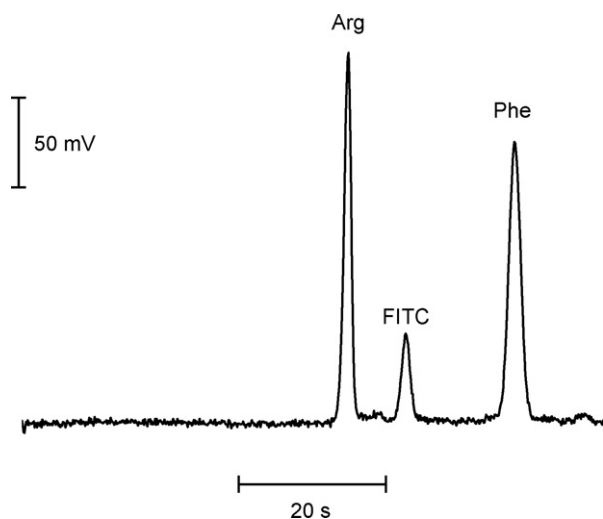


Fig. 5. Electropherogram of a mixture of 50  $\mu$ M FITC-arginine and 50  $\mu$ M FITC-phenylalanine solution. Injection time, 1 s; other conditions as in Fig. 4.

obtained. Although the LOD achieved is much higher than those obtained in LIF detection systems using lasers and PMTs, the total cost of the fluorescence detection system was greatly reduced to \$ 47 (as shown in Table 1). The system was also miniaturized to a total size of only 4 cm  $\times$  13 cm  $\times$  6 cm (width  $\times$  length  $\times$  height). The stability of the detection system was tested by measuring the response of continuously flowing 10  $\mu$ M fluorescein solution in the capillary for 1.5 h. A signal relative standard deviation (RSD) of 3.7% was obtained, which demonstrated the good stability of the present system. The performance of the present LED-IF system was further demonstrated in the CE separation of FITC-labeled amino acids. Fig. 5 shows a typical electropherogram of a mixture of 50  $\mu$ M fluorescein thiocarbonyl (FITC)-arginine and 50  $\mu$ M FITC-phenylalanine solution.

#### 4. Conclusion

In the past decade, miniaturization and integration have become one of the main trends in the development of analytical instruments. In this work, an extremely low-cost and miniaturized LED-IF detection system for CE has been developed. The other advantages

of the system included simple optical structure and ease in building. Based on the optical structure used in the present system, a portable fluorescence detection instrument could be developed, which is especially important for extending the application of miniaturized instruments in routine analysis.

Although the detection sensitivity of the system is lower than those in most of LIF detection systems, it could still be applied in the CE separations of amino acids, peptides, proteins and nucleic acids with high concentration. In addition, the detection sensitivity of the present system is expected to be further improved by using higher intensity LEDs and more sensitive photodiodes.

#### Acknowledgements

Financial supports from National Natural Science Foundation of China (Grant 20775071, 20825517 and 20890020), Ministry of Science and Technology of China (Grant 2007CB714503), and National Education Ministry (Grant NCET-05-0511) are gratefully acknowledged.

#### References

- [1] W. Tong, E.S. Yeung, *J. Chromatogr. A* 718 (1995) 177.
- [2] P.K. Dasgupta, Z. Genfa, J. Li, C.B. Boring, S. Jambunathan, R. Al-Horr, *Anal. Chem.* 71 (1999) 1400.
- [3] S.L. Wang, X.J. Huang, Z.L. Fang, P.K. Dasgupta, *Anal. Chem.* 73 (2001) 4545.
- [4] S. Hillebrand, J.R. Schoffen, M. Mandaji, C. Termignoni, H.P.H. Grieneisen, T.B.L. Kist, *Electrophoresis* 23 (2002) 2445.
- [5] B.C. Yang, Y.F. Guan, *Talanta* 59 (2003) 509.
- [6] A.K. Su, C.H. Lin, *J. Chromatogr. B* 785 (2003) 39.
- [7] L.J. Yu, L.L. Yuan, H.T. Feng, S.F.Y. Li, *Electrophoresis* 25 (2004) 3139.
- [8] B.C. Yang, F. Tan, Y.F. Guan, *Talanta* 65 (2005) 1303.
- [9] C. Slusznzy, Y. He, E.S. Yeung, *Electrophoresis* 26 (2005) 4197.
- [10] E.P. de Jong, C.A. Lucy, *Anal. Chim. Acta* 546 (2005) 37.
- [11] Y.S. Chang, C.M. Shih, C.H. Lin, *Anal. Sci.* 22 (2006) 235.
- [12] S.L. Zhao, H.Y. Yuan, D. Xiao, *Electrophoresis* 27 (2006) 461.
- [13] C.L. Wang, S.L. Zhao, H.Y. Yuan, D. Xiao, *J. Chromatogr. B* 833 (2006) 129.
- [14] B.C. Yang, H.Z. Tian, J. Xu, Y.F. Guan, *Talanta* 69 (2006) 996.
- [15] J. Xu, B.C. Yang, H.Z. Tian, Y.F. Guan, *Anal. Bioanal. Chem.* 384 (2006) 1590.
- [16] S. Hapuarachchi, G.A. Janaway, C.A. Aspinwall, *Electrophoresis* 27 (2006) 4052.
- [17] S.C. Wang, M.D. Morris, *Anal. Chem.* 72 (2000) 1448.
- [18] K. Uchiyama, W. Xu, J.M. Qiu, T. Hobo, *Fresenius J. Anal. Chem.* 371 (2001) 209.
- [19] F.Q. Dang, L.H. Zhang, H. Hagiwara, Y. Mishina, Y. Baba, *Electrophoresis* 24 (2003) 714.
- [20] J.S. Kuo, C.L. Kuyper, P.B. Allen, G.S. Fiorini, D.T. Chiu, *Electrophoresis* 25 (2004) 3796.
- [21] L. Novak, P. Neuzil, J. Pipper, Y. Zhang, S. Lee, *Lab Chip* 7 (2007) 27.
- [22] C.C. Liu, D.F. Cui, X. Chen, *J. Chromatogr. A* 1170 (2007) 101.
- [23] J.L. Fu, Q. Fang, T. Zhang, X.H. Jin, Z.L. Fang, *Anal. Chem.* 78 (2006) 3827.



# Electrochemistry and biosensing of glucose oxidase based on mesoporous carbons with different spatially ordered dimensions

Chunping You, Xin Xu, Bozhi Tian, Jilie Kong, Dongyuan Zhao\*, Baohong Liu\*

Department of Chemistry and Institutes of Biomedical Sciences and Novel Materials, Fudan University, Shanghai 200433, PR China

## ARTICLE INFO

### Article history:

Received 23 September 2008

Received in revised form 10 December 2008

Accepted 12 December 2008

Available online 24 December 2008

### Keywords:

Mesoporous carbon

Electron transfer

Enzyme

Glucose Oxidase

Biosensor

Electrochemistry

## ABSTRACT

A strategy of protein entrapment within mesoporous carbon matrices is demonstrated to probe the electrochemistry of glucose oxidase. Large surface area and remarkable electro-catalytic properties of carbon mesoporous materials make them suitable candidates for high loading of protein molecules and the promotion of heterogeneous electron transfer. In this work, two kinds of mesoporous carbon nanocomposite films were designed and prepared with highly ordered two-dimensional (2D) and three-dimensional (3D) structures for the immobilization of glucose oxidase, in which the quasi-reversible electron transfer of the redox enzyme was probed, and the apparent heterogeneous electron transfer rate constants ( $k_{et}^0$ ) are 3.9 and 4.2 s<sup>-1</sup>, respectively. Furthermore, the associated biocatalytic activity was also revealed. Highly ordered 3D-mesoporous carbon material exhibited larger adsorption capacity for glucose oxidase and the immobilized enzymes retained a higher bioactivity compared with 2D-mesoporous carbons. The preparation of protein-entrapped mesoporous carbon nanocomposites expands the scope of carbon-based electrochemical devices and opens a new avenue for the development of biosensors.

© 2009 Elsevier B.V. All rights reserved.

## 1. Introduction

Probing electron transfer (ET) of redox proteins is crucial for the fundamental research on redox properties of proteins and the development of the biosensing devices. In order to promote the effective ET between proteins and electrodes, a large amount of efforts have been made, among which carbon nanotubes (CNTs) have drawn increasing attention and thus have been extensively investigated [1–4]. However, in the absence of mediators, only a few redox proteins performed direct ET at CNT-modified electrodes [2,4]. Besides, it is well known that two factors seriously affect the redox behavior and bioactivity of the immobilized proteins. One is the biocompatibility and the electro-catalytic performance of the matrix; the other is the protein-loading capability of the material (basically relevant to the specific area). However, the single dimension and narrow channel size of CNTs inevitably limit the protein-loading amount and complicate the immobilizing process, limiting their development in the immobilization of the larger biomolecules and the study of corresponding heterogeneous ET.

Ordered carbon mesoporous materials (CMM) [5,6], a new type of nanostructured carbons different from CNTs, composed of carbon nanorods with highly ordered arrays and large porosity, not only retain good electronic properties and chemical stability, but

also show many unique properties, such as highly ordered and tailored meso-structures, much narrow pore size distributions, high specific surface areas (up to ca. 2000 m<sup>2</sup> g<sup>-1</sup>), and large pore volume (up to ca. 1.5 cm<sup>3</sup> g<sup>-1</sup>) [7–10], making them more promising in the realm of heterogeneous ET than CNTs. Thus CMMs have attracted growing interest in diverse fields from catalyst carriers, absorbents to electronic devices [9–12]. All the advantages make it possible to design the selectivity of substrates for immobilizing biomolecules, by varying pore diameters, mesoscopic topologies and charges of CMMs, in which the pores or channels behave as individual nanocells so that electrochemical reactions are confined to occur inside the pores or near the doors.

In this paper, we demonstrate a strategy for the preparation of glucose oxidase-entrapped CMMs nanocomposite films, in which the quasi-reversible ET for glucose oxidase is probed and the associated high biocatalytic activity is revealed. Furthermore, highly ordered three-dimensional (3D) open framework CMM is demonstrated a more suitable candidate for the immobilization of proteins and shows a larger ET promotion compared with low-dimensional carbon materials (such as 2D-CMM and 1D-CNTs).

## 2. Experimental

### 2.1. Reagents

Glucose oxidase (GOx, Type X-S, EC 1.1.3.4, from *Aspergillus niger*, 157,500 units g<sup>-1</sup>), flavin adenine dinucleotide (FAD, 95%) and

\* Corresponding authors. Tel.: +86 21 65642405.

E-mail addresses: [dyzhao@fudan.edu.cn](mailto:dyzhao@fudan.edu.cn) (D. Zhao), [bhliu@fudan.edu.cn](mailto:bhliu@fudan.edu.cn) (B. Liu).

Nafion® perfluorinated ion-exchange resin, 5 wt% solution were purchased from Sigma–Aldrich. Ferrocenecarboxylic acid (Fc, 97%) was purchased from Fluka. All other reagents were of analytical grade. Phosphate buffer solution (PBS, 0.05 M) was prepared by mixing the stock solution of  $\text{NaH}_2\text{PO}_4$  and  $\text{Na}_2\text{HPO}_4$ . The freshly prepared D-glucose ( $[\alpha]_D^{20} = 52.5\text{--}53.0^\circ$ ) solution was allowed to come to mutarotation equilibrium by standing overnight. Deionized water was used in all experiments.

## 2.2. Syntheses of CMMs

The syntheses of 2D- and 3D-CMMs were performed using SBA-15 and FDU-5 mesoporous silicas [13,14] as the templates, respectively and sucrose as the carbon source. Herein 2D-CMM was prepared as reported previously [7], and 3D-CMM was prepared as follows. Typically 0.5 g of FDU-5 sample was dispersed in 1.0 g of  $\text{H}_2\text{O}$ . Then 0.5–0.6 g of sucrose and 0.05 g of  $\text{H}_2\text{SO}_4$  were added ordinarily. After stirring for 0.5 h, the mixture was dried at 353 K for 2–10 h and subsequently at 433 K for 8–24 h. The impregnating/drying steps were repeated once by consuming another 0.3–0.4 g of sucrose. The obtained black samples were carbonized at 1173 K under nitrogen or argon flow for 6 h. The silica framework was finally removed by HF (5–10 wt%) etching.

## 2.3. Preparation of GOx/CMMs-modified electrode

A glassy carbon electrode (GCE, 3 mm in diameter) was successively polished to a mirror finish with 0.3- and 0.05- $\mu\text{m}$  alumina particles, rinsed thoroughly with deionized water, and successively sonicated in 1:1 nitric acid, acetone and deionized water. Then the GCE was coated by casting an aliquot of 10  $\mu\text{L}$  Nafion suspension uniformly dispersed with 0.5  $\text{mg mL}^{-1}$  CMM samples (2D or 3D) and dried under ambient conditions.

Enzyme immobilization was achieved by matrix adsorption method by immersing CMM modified GCE in 5  $\text{mg mL}^{-1}$  GOx solution at 4 °C for 48 h. Prior to all measurements, the GOx/CMM electrodes were rinsed in phosphate buffer solution (PBS, pH 7.0) to remove non-immobilized protein.

## 2.4. Apparatus

Electrochemical measurements were performed with a CHI 1030 Electrochemical Workstation (CHI, USA) using a three-electrode system, with either a CMM- or GOx/CMM-modified electrode as the working electrode, a platinum plate as the counter electrode, and a saturated calomel electrode (SCE) as the reference, in a thermostated, stirred electrochemical glass cell containing 10 mL 0.05 M PBS (pH 7.0). All experimental solutions (except particular illustration) were deoxygenated by bubbling nitrogen through them for 30 min before measurements and maintained under nitrogen atmosphere during measurements.

A NanoSTAR system (Bruker SAXS) was used for the small-angle X-ray scattering (SAXS) measurements. Transmission electron microscopy (TEM) experiments were conducted on a JEOL 2010 microscope at 200 kV. Nitrogen adsorption/desorption isotherms were measured at 77 K on a Quantachrome Autosorb-1 Adsorption Apparatus after degassing samples at 453 K for 5 h.

## 3. Results and discussion

### 3.1. Characterization of CMMs and GOx immobilization

TEM image including Fourier diffractogram, and SAXS pattern (Fig. 1) feature highly ordered 3D-intertwined carbon nanostructures of 3D-CMM, which has basically two types of mesoscopic

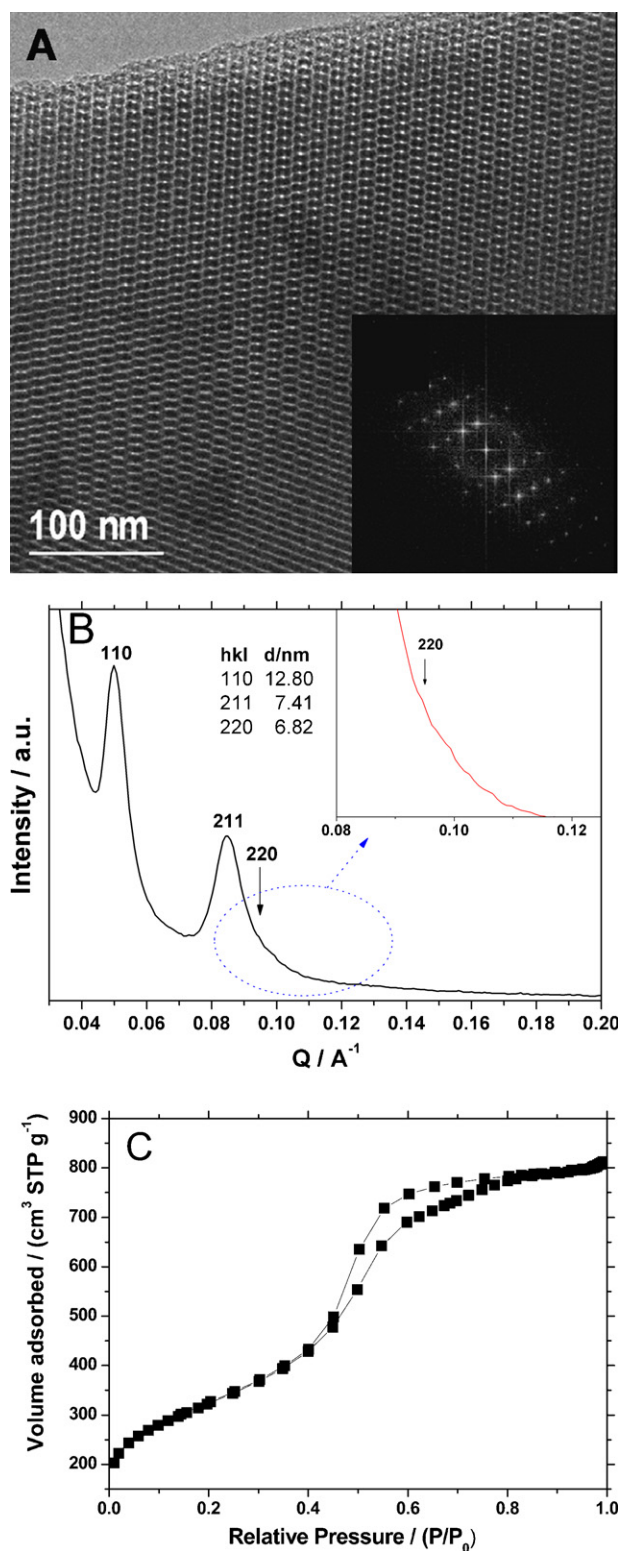


Fig. 1. (A) TEM image, (A, inset) corresponding Fourier diffractogram, (B) SAXS pattern and (C)  $\text{N}_2$  adsorption/desorption curves of 3D-CMM prepared by using FDU-5 as a template.

structures—undisplaced and displaced carbon frameworks. TEM image (Fig. 1A) shows exactly the (3 1 1) projection plane of the undisplaced gyroidal phase (Fig. 1B) further confirms the ordered meso-structure, and the corresponding space groups might be assigned as  $Ia\bar{3}d$  and  $I4_132$  'mixture' [13,15].  $\text{N}_2$  adsorption/desorption isotherms of 3D-CMM (Fig. 1C) show a typical type

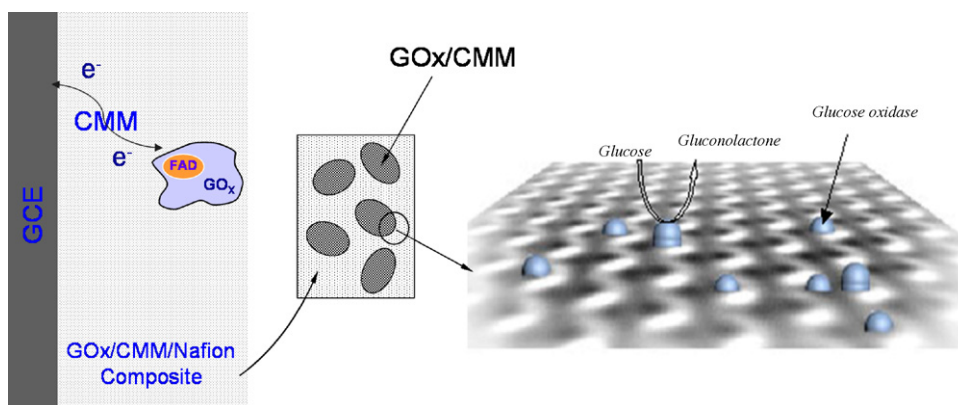


Fig. 2. Schematic diagram of the electron transfer (ET) and the bioelectrocatalytic process of GOx/3D-CMM electrode.

IV curve, suggesting uniform mesopores. 3D-CMM prepared herein has a high surface area of  $1450 \text{ m}^2 \text{ g}^{-1}$ , a total pore volume of  $1.26 \text{ cm}^3 \text{ g}^{-1}$  and a uniform mesopore size of 4.1 nm. While for 2D-CMM, with a 2D-hexagonal p6mm symmetry of the ordered pore system, the above values are  $1430 \text{ m}^2 \text{ g}^{-1}$ ,  $1.28 \text{ cm}^3 \text{ g}^{-1}$ , and 4.2 nm, respectively.

The schematic illustration of GOx/CMM electrode fabricated by the matrix adsorption is shown in Fig. 2. The 2D- or 3D-CMM was readily dispersed in Nafion solution and then deposited on the surface of GCE. GOx molecules are successfully immobilized within the CMM/Nafion composite films, which can enzymatically convert glucose to gluconolactone.

### 3.2. Electrochemistry of GOx on CMMs and related ET kinetics

Fig. 3A shows the cyclic voltammograms of the assembled enzyme at CMMs-modified electrodes. A pair of well-defined and nearly symmetric redox peaks emerges between about  $-0.46$  and  $-0.43 \text{ V}$  for both 2D- and 3D-CMM modified electrodes, while no redox peak is observed for the bare underlying CMM electrode. As shown in Fig. 3B and C, the cathodic and anodic peak potentials of the immobilized GOx show shifts in negative and positive directions, respectively, and the peak currents increase linearly with the scan rate increasing from  $10$  to  $200 \text{ mV s}^{-1}$ , indicating a typical surface-confined redox behavior (current polarity: anodic positive as defined). For GOx/3D-CMM electrode, the peak current is much larger than that for GOx/2D-CMM electrode at the same scan rate, indicating a higher protein-loading capacity of 3D-CMM. The varied protein-loading capacities of 2D- and 3D-CMMs can be concluded from CVs in Fig. 3A. Integration of the areas under the cathodic peaks gives GOx surface coverage ( $\Gamma$ ) [16] of  $(1.9 \pm 0.1) \times 10^{-10} \text{ mol cm}^{-2}$  for 2D-CMM modified electrode, while  $(5.7 \pm 0.2) \times 10^{-10} \text{ mol cm}^{-2}$  for 3D-CMM, much larger than those of gold nanoparticles modified carbon paste electrode ( $9.8 \times 10^{-12} \text{ mol cm}^{-2}$ ) [17], GOx/CdS modified electrode ( $1.54 \times 10^{-11} \text{ mol cm}^{-2}$ ) [18], GOx/SWCNT/PDDA modified electrode ( $2.35 \times 10^{-11} \text{ mol cm}^{-2}$ ) [19] and GOx/SWCNT/chitosan modified electrode ( $1.3 \times 10^{-10} \text{ mol cm}^{-2}$ ) [20]. In addition, this distinct difference in GOx-loading between on 2D-CMM and on 3D-CMM might be due to the textural difference of two such CMMs. With the approximately equal surface area, 3D-CMM shows highly branched intertwined nanostructure which might possess more accessible entrances and channels compared with 2D-CMM, hence resulting in a larger loading of electroactive proteins.

The effect of solution pH on the formal potentials ( $E^0$ ) of GOx/2D-CMM and GOx/3D-CMM electrodes at a scan rate of

$50 \text{ mV s}^{-1}$  was also investigated. The formal potentials of the above two kinds of electrodes depend linearly on the pH value in the range of 5.0–8.0 with a slope of  $(-58.9 \pm 1.9) \text{ mV pH}^{-1}$  ( $r=0.995$ ) and  $(-58.8 \pm 2.1) \text{ mV pH}^{-1}$  ( $r=0.994$ ), respectively, which are close to the theoretical value of  $-59.0 \text{ mV pH}^{-1}$  corresponding to the conversion between GOx (FAD) and GOx (FADH<sub>2</sub>) [17,18,21–23], indicating a two-electron coupled with two-proton reaction process.

For the GOx/2D-CMM,  $E^0$  is  $(-0.446 \pm 0.002) \text{ V}$  at a scan rate of  $10 \text{ mV s}^{-1}$ , while for the GOx/3D-CMM,  $E^0$  is a little positive,  $(-0.440 \pm 0.002) \text{ V}$ , corresponding to the conversion between GOx (FAD) and GOx (FADH<sub>2</sub>) [24]. As shown in Fig. 3B,  $E^0$  is irrelevant to the scan rate. As discussed above, the cathodic and anodic peak potentials of the immobilized GOx shift with the varied scan rate in negative and positive directions, respectively. The peak potential separation ( $\Delta E_p$ ) of GOx/3D-CMM is  $(28 \pm 2) \text{ mV}$ , and considering the electron transfer number ( $n$ ),  $n\Delta E_p$  is close to  $59 \text{ mV}$ . All the above results suggest a quasi-reversible two-electron transfer process. In addition,  $\Delta E_p$  of GOx/3D-CMM is smaller than that of GOx/2D-CMM ( $(33 \pm 2) \text{ mV}$ ), and GOx/1D-SWNT ( $43 \text{ mV}$ ) as reported previously [2], indicating an increasingly quasi-reversible redox process with the increase in the carbons spatial dimensions.

The apparent heterogeneous electron transfer rate constant  $k_{\text{et}}^0$ , was determined from the scan rate dependence of  $\Delta E_p$  by the method of Laviron [25]. The deduced  $k_{\text{et}}^0$  values are  $(3.9 \pm 0.2) \text{ s}^{-1}$  and  $(4.2 \pm 0.2) \text{ s}^{-1}$  for 2D- and 3D-CMM modified electrodes, respectively, larger than that of GOx/CNTs electrode ( $1.7 \text{ s}^{-1}$ ) [2], and GOx/SWCNH ( $3.0 \text{ s}^{-1}$ ) [26], suggesting that the CMMs are more effective electron promoters between the adsorbed GOx and the electrode. Thus, the high surface area and good electro-catalytic property of the CMMs meet the requirement of achieving high capacity for protein assembly and also offers great promise for facilitating ET between entrapped GOx and the electrode, acting as ET tunnels with good conductivity.

### 3.3. Bioelectrocatalytic properties and biosensing applications of GOx/CMMs

The glucose-specific enzyme activities of the fabricated GOx/CMM electrodes were investigated in nitrogen-saturated PBS as shown in Fig. 4A. With the addition of glucose, the cathodic current of GOx(FAD)/GOx (FADH<sub>2</sub>) redox couple decreases with the increase in anodic current, indicating the catalytic reaction occurring between GOx and glucose as Eq. (1):



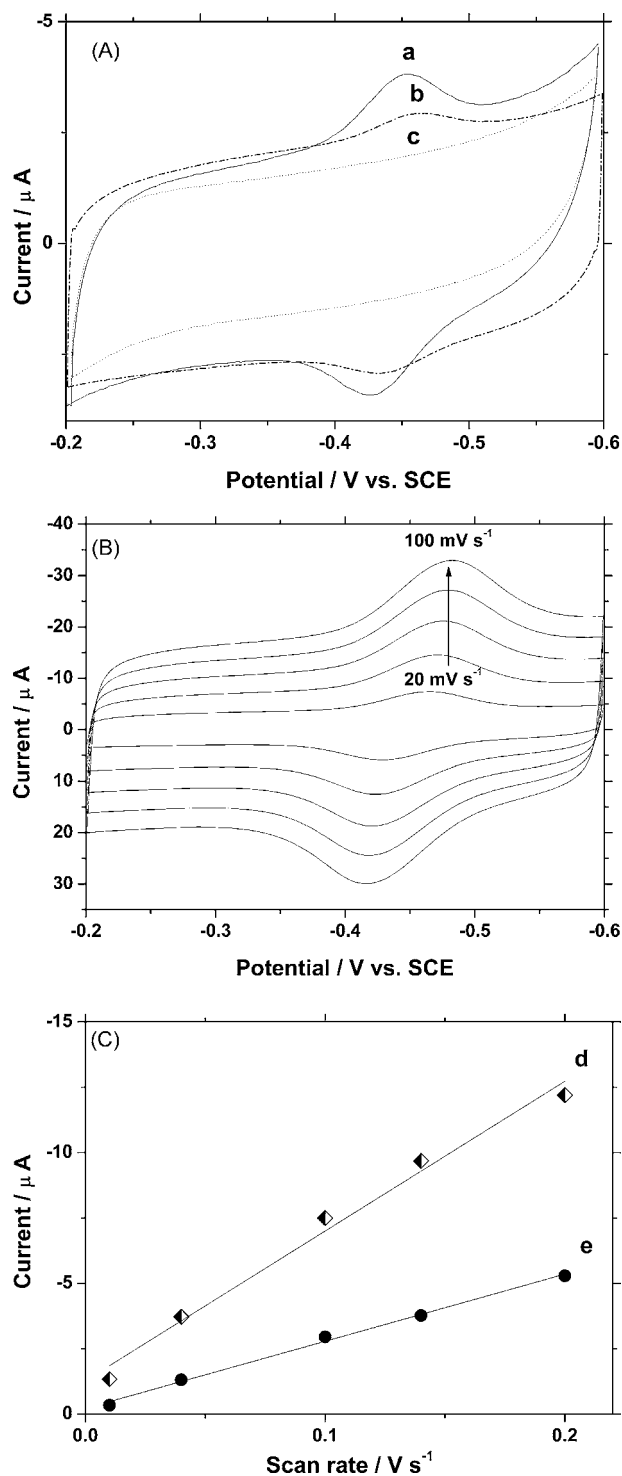


**Fig. 3.** (A) Cyclic voltammograms of the fabricated (a) GOx/3D-CMM, (b) GOx/2D-CMM and (c) bare electrodes in pH 7.0 PBS at a scan rate of  $10 \text{ mV s}^{-1}$ . (B) Cyclic voltammograms of the fabricated GOx/3D-CMM electrode in pH 7.0 PBS at the scan rates of 20, 40, 60, 80 and  $100 \text{ mV s}^{-1}$  at  $30^\circ\text{C}$ . (C) Plot of cathodic peak current versus scan rate for (d) GOx/3D-CMM and (e) GOx/2D-CMM electrodes at the scan rates of 10, 40, 100, 140 and  $200 \text{ mV s}^{-1}$  at  $30^\circ\text{C}$ , respectively.

GOx(FAD) is consumed through being reduced by glucose, while the generated GOx(FADH<sub>2</sub>) is reoxidized on the 2D-CMM/GCE surface, resulting in the decreasing cathodic current and the increasing anodic current. However, such changes cannot be observed for the adsorbed FAD in the 2D-CMM matrix (Fig. 4B). The similar phenomena can be observed for GOx/3D-CMM and FAD/3D-CMM, respectively. Thus it can be concluded that the GOx immobilized into CMMs matrices retains the biocatalytic activity to a certain degree.

The bioactivities of the fabricated GOx/CMM electrodes were further investigated by using some mediators to enhance the electrochemical currents. From cyclic voltammograms in Fig. 4C of the GOx/2D-CMM GCE and FAD/2D-CMM GCE in N<sub>2</sub>-saturated pH 7.0 PBS containing 0.5 mM ferrocenecarboxylic acid (Fc) as a mediator, it should be noted that after the addition of glucose, there is no catalytic current with FAD immobilized into 2D-CMM, while remarkable catalytic currents can be observed with GOx immobilized into 2D-CMM. This result can be explained from the following

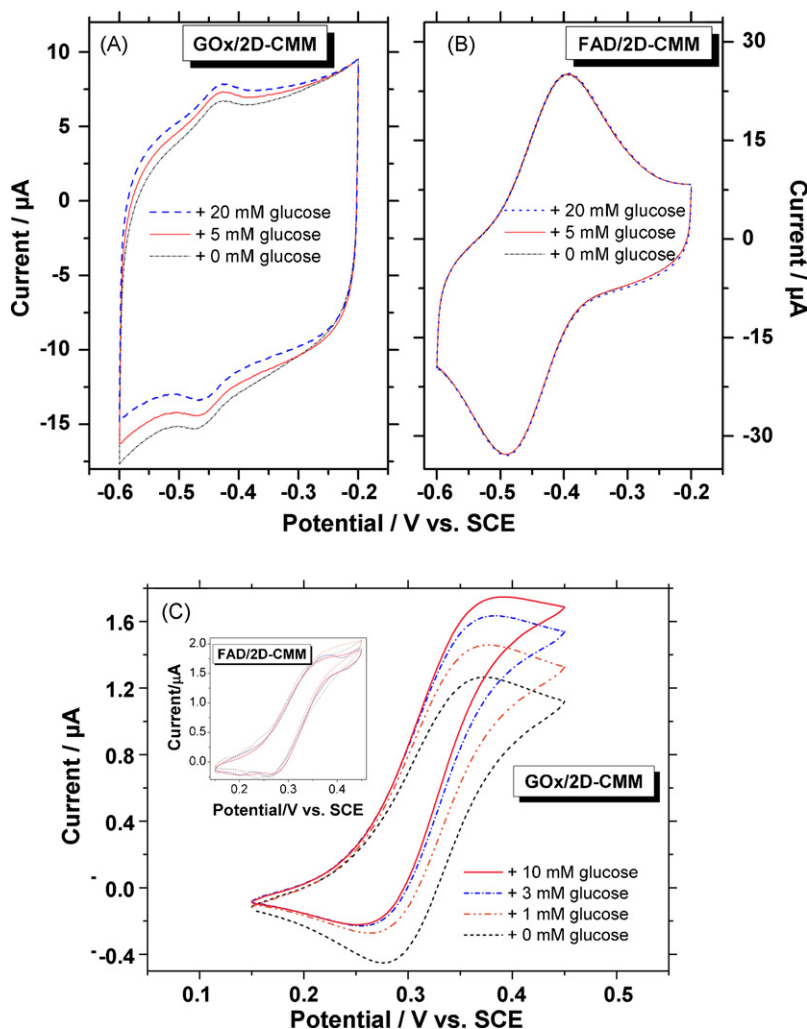
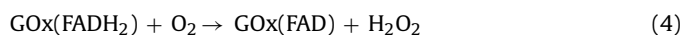
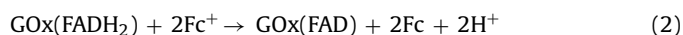


**Fig. 4.** Cyclic voltammograms of (A) GOx/2D-CMM GCE and (B) FAD/2D-CMM GCE at a scan rate of  $50 \text{ mV s}^{-1}$  in the  $\text{N}_2$ -saturated PBS (50 mM, pH 7.0) in the absence of ferrocenecarboxylic acid before and after an addition of glucose at  $30^\circ \text{C}$ . Cyclic voltammograms of the (C) GOx/2D-CMM GCE and (C, inset) FAD/2D-CMM GCE at a scan rate of  $2 \text{ mV s}^{-1}$  in the  $\text{N}_2$ -saturated PBS (50 mM, pH 7.0) in the presence of 0.5 mM ferrocenecarboxylic acid before and after successive additions of glucose at  $30^\circ \text{C}$ .

Eqs. (1)–(3):



which is consistent with the previous report [27]. The similar phenomena can be observed for 3D-CMM.

Moreover, glucose biosensors based on the GOx/CMM electrodes with oxygen in air as a mediator were prepared to detect glucose in PBS. As shown in Fig. 5A and B, the prepared biosensors behave good responses in a broad range of temperatures and pH values. The optimized temperature of  $30^\circ \text{C}$  and pH value of 7.0 was selected in the following experiments. Fig. 5C(a and b) show the amperometric responses of the GOx/3D-CMM electrode to successive additions of glucose into the air-saturated PBS. As expressed by Eqs. ((1) and (4)), in the air-saturated PBS,  $\text{O}_2$  acts as a mediator to facilitate the ET between GOx and the electrode, and the glucose can be measured indirectly by detecting the generated  $\text{H}_2\text{O}_2$  during the oxidation of glucose [28]. The responses of the GOx/2D-CMM electrode to glucose shown in Fig. 5C(c and d) are somewhat smaller compared with that of

GOx/3D-CMM, possibly due to the smaller amount of adsorbed GOx and the lower ET promotion effect of 2D-CMM. The increased current is proportional to the glucose concentration and the linear response is observed up to 9.90 mM (correlation coefficient, 0.993) for GOx/3D-CMM and up to 7.94 mM (correlation coefficient, 0.997) for GOx/2D-CMM, equivalent to the level of glucose in blood. The detection limit is  $1.0 \times 10^{-5} \text{ M}$  for both of the two electrodes. The detection sensitivities of GOx/3D-CMM electrode and GOx/2D-CMM electrode are  $(82.9 \pm 2.3) \text{ nA mM}^{-1}$  and  $(58.8 \pm 1.2) \text{ nA mM}^{-1}$ , respectively. The corresponding apparent Michaelis–Menten constants  $k_m^{\text{app}}$  can be evaluated from Lineweaver–Burk equation [29] to be 4.59 mM and 4.39 mM, respectively, which are smaller than 8.2 mM for GOx/CNT/chitosan [27] and 8.5 mM for GOx/SWCNHs/Nafion [26], indicating that the proposed enzyme electrodes exhibit a higher affinity for glucose and the immobilized GOx retains a higher enzymatic activity.

The fabricated GOx/CMMs electrodes were stored under  $4^\circ \text{C}$  to investigate the reproducibility and stability. The relative standard deviation (RSD) values of the amperometric responses at 0.6 V to 6 times successive additions of 1.0 mM glucose are 6.83% and 2.44% for GOx/3D-CMM electrode and GOx/2D-CMM electrode, respectively. For GOx/3D-CMM electrode, 99.5% of the initial current response to glucose (0.100 mM) remains after a week and 94.8%



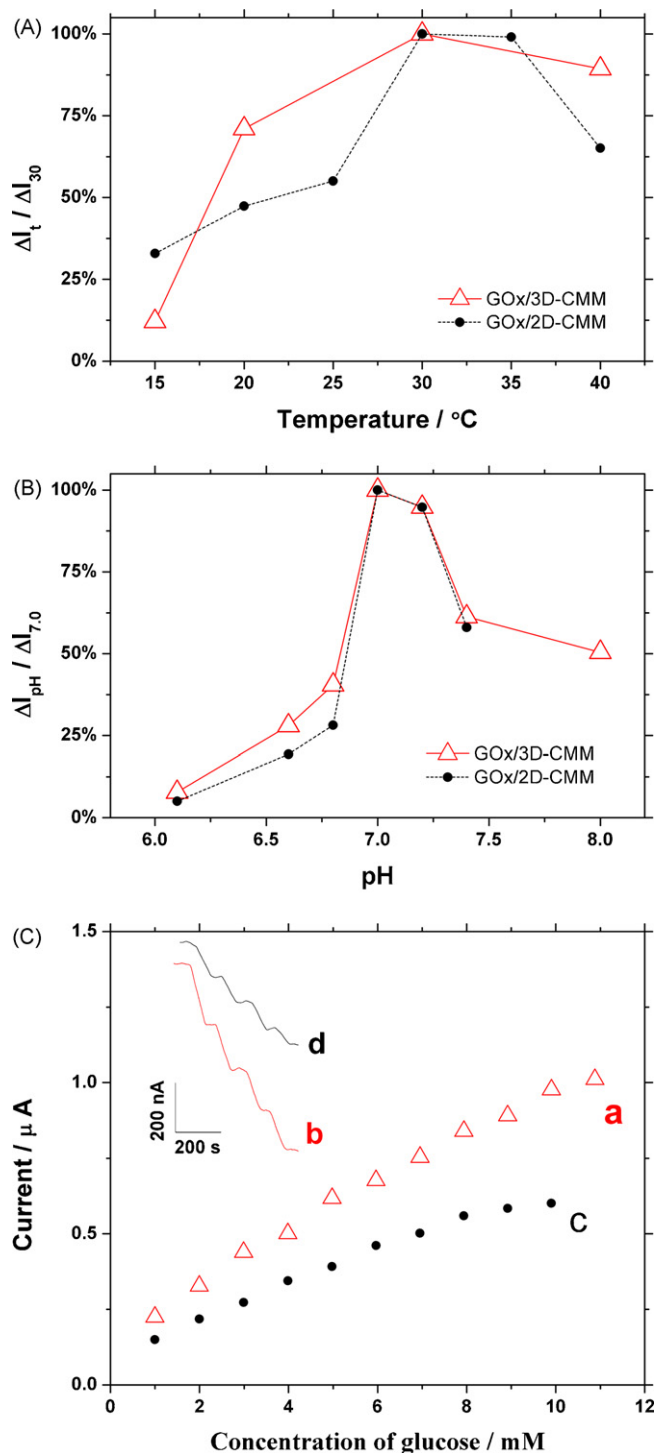


**Fig. 5.** (A) The unitary amperometric responses of GOx/CMMs electrodes at different temperatures with the amperometric response at 30 °C as the reference. (B) The unitary amperometric responses of GOx/CMMs electrodes at different pH with the amperometric response at pH 7.0 as the reference. (C) The calibration curve of the fabricated (a) GOx/3D-CMM and (c) GOx/2D-CMM electrodes for the electrocatalysis of glucose. The dynamic response of (inset b) GOx/3D-CMM and (inset d) GOx/2D-CMM electrodes to successive additions of glucose samples in pH 7.0 PBS saturated by air at the applied potential of 0.6 V.

after 45 days; while for GOx/2D-CMM electrode, 86.3% remains after 45 days, indicating a considerable stability and a long lifetime of the prepared GOx/CMM sensor.

#### 4. Conclusions

We have shown the potential application of ordered mesoporous carbon in the bioelectrochemical research. With the prominent advantages of large surface area, uniform mesopores and remarkable electro-catalytic properties, CMMs were demonstrated as more suitable candidates than CNTs to immobilize glucose oxidase and promote heterogeneous ET. Moreover, enzyme molecules assembled on CMMs still exhibited a high bioactivity. Highly ordered 3D-CMM showed larger adsorption capacity of glucose oxidase and the assembled glucose biosensor showed a broader linear response scale and a higher detection sensitivity than 2D-CMM. All these properties make CMMs valuable in the understanding of the electrochemistry of redox proteins and open a new avenue for the development of biosensors.

#### Acknowledgements

The work was supported by the National Nature Science Foundation of China (20775016), Shanghai Shuguang Project 06SG02 and Leading Academic Discipline Project B109.

#### References

- [1] B.R. Azamian, J.J. Davis, K.S. Coleman, C.B. Bagshaw, M.L.H. Green, *J. Am. Chem. Soc.* 124 (2002) 12664.
- [2] A. Guiseppi-Elie, C.H. Lei, R.H. Baughman, *Nanotechnology* 13 (2002) 559.
- [3] J. Wang, M. Musameh, Y.H. Lin, *J. Am. Chem. Soc.* 125 (2003) 2408.
- [4] M.C. Weigel, E. Tritscher, F. Lisdat, *Electrochem. Commun.* 9 (2007) 689.
- [5] R. Ryoo, S.H. Joo, S. Jun, *J. Phys. Chem. B* 103 (1999) 7743.
- [6] J. Lee, S. Yoon, T. Hyeon, S.M. Oh, K.B. Kim, *Chem. Commun.* (1999) 2177.
- [7] S. Jun, S.H. Joo, R. Ryoo, M. Kruk, M. Jaroniec, Z. Liu, T. Ohsuna, O. Terasaki, *J. Am. Chem. Soc.* 122 (2000) 10712.
- [8] J. Lee, J. Kim, T. Hyeon, *Adv. Mater.* 18 (2006) 2073.
- [9] S.H. Joo, S.J. Choi, I. Oh, J. Kwak, Z. Liu, O. Terasaki, R. Ryoo, *Nature* 412 (2001) 169.
- [10] S. Yoon, J.W. Lee, T. Hyeon, S.M. Oh, *J. Electrochem. Soc.* 147 (2000) 2507.
- [11] A. Vinu, M. Miyahara, K. Ariga, *J. Phys. Chem. B* 109 (2005) 6436.
- [12] H.S. Zhou, S.M. Zhu, M. Hibino, I. Honma, *J. Power Sources* 122 (2003) 219.
- [13] X.Y. Liu, B.Z. Tian, C.Z. Yu, F. Gao, S.H. Xie, B. Tu, R.C. Che, L.M. Peng, D.Y. Zhao, *Angew. Chem., Int. Ed.* 41 (2002) 3876.
- [14] D.Y. Zhao, J.L. Feng, Q.S. Huo, N. Melosh, G.H. Fredrickson, B.F. Chmelka, G.D. Stucky, *Science* 279 (1998) 548.
- [15] T. Wang, X.Y. Liu, D.Y. Zhao, Z.Y. Jiang, *Chem. Phys. Lett.* 389 (2004) 327.
- [16] A.J. Bard, L.R. Faulkner, *Electrochemical Methods: Fundamentals and Applications*, 2nd ed., John Wiley & Sons, New York, 2001.
- [17] S.Q. Liu, H.X. Ju, *Biosens. Bioelectron.* 19 (2003) 177.
- [18] Y.X. Huang, W.J. Zhang, H. Xiao, G.X. Li, *Biosens. Bioelectron.* 21 (2005) 817.
- [19] J. Zhang, M. Feng, H. Tachikawa, *Biosens. Bioelectron.* 22 (2007) 3036.
- [20] Y. Zhou, H. Yang, H.Y. Chen, *Talanta* 76 (2008) 419.
- [21] S.J. Bao, C.M. Li, J.F. Zang, X.Q. Cui, Y. Qiao, J. Guo, *Adv. Funct. Mater.* 18 (2008) 591.
- [22] C.Y. Deng, J.H. Chen, X.L. Chen, C.H. Mao, L.H. Nie, S.Z. Yao, *Biosens. Bioelectron.* 23 (2008) 1272.
- [23] Q. Liu, X.B. Lu, J. Li, X. Yao, J.H. Li, *Biosens. Bioelectron.* 22 (2007) 3203.
- [24] R. Ianniello, J. Lindsay, A. Yacynych, *Anal. Chem.* 54 (1982) 1098.
- [25] E. Laviron, *J. Electroanal. Chem.* 101 (1979) 19.
- [26] X.Q. Liu, L.H. Shi, W.X. Niu, H.J. Li, G.B. Xu, *Biosens. Bioelectron.* 23 (2008) 1887.
- [27] Y. Liu, M.K. Wang, F. Zhao, Z.A. Xu, S.J. Dong, *Biosens. Bioelectron.* 21 (2005) 984.
- [28] J. Wang, *Chem. Rev.* 108 (2008) 814.
- [29] R.A. Kamin, G.S. Wilson, *Anal. Chem.* 52 (1980) 1198.



# Determination of aristolochic acid I and its metabolites in cell culture with a hyphenated high-performance liquid chromatographic technique for cell toxicology

Jinbin Yuan<sup>a,b</sup>, Xizhen Luo<sup>b</sup>, Manli Guo<sup>a</sup>, Jiangang Wu<sup>a</sup>, Wuliang Yang<sup>b</sup>, Riyue Yu<sup>b</sup>, Shouzhuo Yao<sup>a,\*</sup>

<sup>a</sup> State Key Laboratory of Chemo/Biosensing & Chemometrics, Chemistry & Chemical Engineering College, Hunan University, Changsha 410082, China

<sup>b</sup> Key Laboratory of Modern Preparation of TCM, Ministry of Education, Jiangxi University of Traditional Chinese Medicine, Nanchang 330004, China

## ARTICLE INFO

### Article history:

Received 7 October 2008

Received in revised form 16 January 2009

Accepted 18 January 2009

Available online 24 January 2009

### Keywords:

Aristolochic acid I

High-performance liquid chromatography

Determination

L-02 cell

Cell toxicology

## ABSTRACT

Aristolochic acid I (AA I), a major component of the carcinogenic plant extract aristolochic acid (AA), is known to be nephrotoxic, carcinogenic and mutagenic. A simple, rapid and sensitive high-performance liquid chromatography–diode array detection–fluorescence detection (HPLC–DAD–FLD) method was developed and validated for the analysis of AA I and its metabolites in cell culture medium for the first time. The samples were prepared with ethyl acetate liquid–liquid extraction (LLE). Good separation was obtained on an ODS C<sub>18</sub> analytical column with 0.2% HAc/methanol gradient solution. Linearities of about three orders of magnitude were gained with correlation coefficients exceeding 0.9990. The method appears to be a suitable tool for the cellular toxicokinetic study with acceptable precisions and recoveries. Cytotoxicity of AA I on human liver cells (L-02) was investigated with morphological observation and MTT (3-(4,5-Dimethylthiazol-2-yl)-2,5-diphenyltetrazoliumbromide) assay, cytotoxicity increased in AA I concentration-dependent manner. AA I and its metabolites were monitored with the proposed chromatographic analysis, and some preliminary toxicokinetics were investigated.

© 2009 Elsevier B.V. All rights reserved.

## 1. Introduction

Aristolochic acid (AA) analogues are nitrophenanthrene derivatives that occur in *Aristolochiaceae* plants including *Aristolochia* and *Asarum* genera [1,2]. Most of the compounds have been revealed to be nephrotoxic [3–6], carcinogenic [5–9] and mutagenic [10,11]. In which AA I was found to be the most toxic and attracted the most attention [12]. Recent studies have revealed the carcinogenic and mutagenic mechanism of AA analogues [13,14]. As shown in Fig. 1, AA I was reduced by various intrinsic enzymes to active intermediate, aristolactam nitrenium ion, the latter bound to the exocyclic amino group of the DNA bases, then electrophilic attack of the aristolactam nitrenium ion led to the formation of DNA adducts. The metabolites of AA in organisms seem to include the relative aristolactam (AL), N-OH AL, 7-OH AL and DNA adducts. DNA-AA adducts were detected in laboratory rodents [13,14] and in patients [15,16] suffering from aristolochic acid nephropathy (AAN) using <sup>32</sup>P-postlabeling assay. Very recently, a high-performance liquid chromatography coupled with mass spectrometry (LC–MS) method [17] was developed for the detection of the DNA adducts, researchers found that majority of AA I and AA II were reduced to

their corresponding aristolactams. AL I and AL II were also found to be the main metabolites of AA I and AA II after oral administration in experimental mice [18]. Although the nephrotoxicity of AA is well studied, pharmacokinetic studies of AA are still limited [19]. To acquire toxicokinetic or pharmacokinetic data of AA, a sensitive, selective and effective analytical tool for the determination of AA and its metabolites is needed.

Many analytical techniques have been proposed to detect AA in *Aristolochiaceae* and its preparations including thin-layer chromatography (TLC) [20], high-performance liquid chromatography (HPLC) and its hyphenated technique [20–29], and capillary electrophoresis (CE) [30–35]. Most of these methods focus on the analysis of AA I and/or AA II in herbal plants. To the best of our knowledge, no analytical technique for the simultaneous determination of AA and its metabolites in bio-samples can be accessed. In our previous work, a high-performance liquid chromatography–diode array detection–fluorescence detection (HPLC–DAD–FLD) hyphenated technique [29] exhibits the potential with high sensitivity and selectivity for both AA and AL. AA can be analyzed with HPLC–DAD, and their metabolites (various aristolactam derivatives) should have strong fluorescence, thus can be detected in complex matrices with FLD.

Many efforts have been made in order to predict toxicity and reduce or replace animal use in some tests. In vitro evaluation of cytotoxicity effects of chemicals using cultured cells plays an

\* Corresponding author. Tel.: +86 731 8821968; fax: +86 731 8821848.

E-mail address: [kings008@gmail.com](mailto:kings008@gmail.com) (S. Yao).

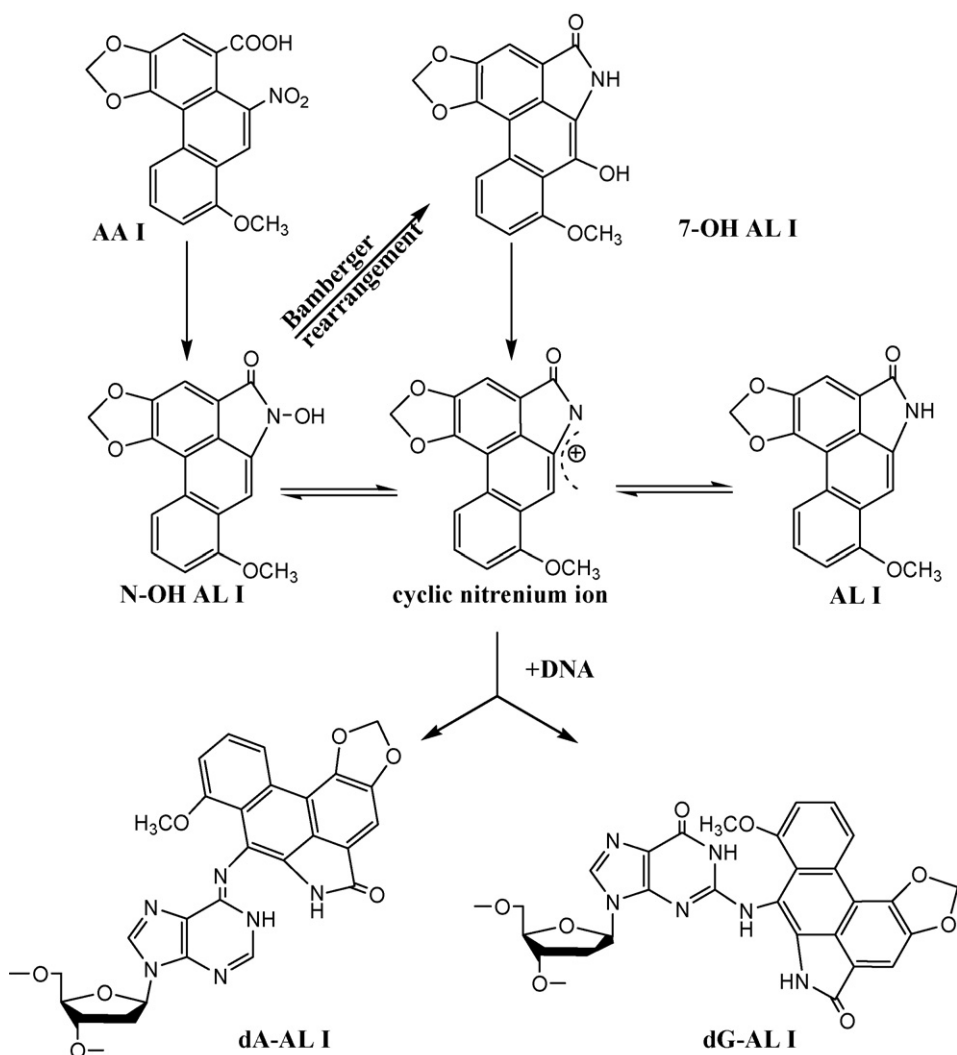


Fig. 1. Metabolic activation and metabolites of AA I.

important role in the discovery of new drug candidates and the assessment of environmental threats. Current techniques for monitoring cell viability and proliferation, including spectrophotometric methods, fluorescent microscopy, flow cytometry and specialized fluorescence instruments such as plate readers, have been widely used in studying the interaction of cells with drugs and toxins [36]. In vitro cytotoxicity and cell viability assays have served to predict acute toxicity for some decades based on various cell-numbering methods, morphology, and metabolic activity [37]. For the cytotoxicity test of AA, proximal tubule epithelial cells such as LLC-PK1 and HKC were often used [38,39]. But recently AA was found to have higher cytotoxicity in liver than in kidney [40]. In the tests [38–40], cytotoxicity was evaluated only according to the structural, morphological changes and apoptosis of cells, and no concentration data for drugs and their metabolites were reported. It is important to detect AA and their metabolites in the culture medium. Then some toxicokinetic data could be acquired.

Based on our previous works [27,29], possible metabolites were identified according to their retention time, UV spectrum, fluorescence characteristics, ESI/MS behaviours and metabolic activation, thus a simple and effective HPLC–DAD–FLD method was developed and validated to determine AA I and its possible metabolites such as AL I in cellular environment. Human liver cells (L-02) were required to carry out cytotoxicity assay. The proliferation and viability of the cells were monitored with microscopy and MTT assay. After the

cells were treated with AA I, the culture medium was extracted to carry out chromatographic analysis at fixed intervals.

## 2. Materials and methods

### 2.1. Instruments and apparatus

Proliferation and morphology of cells were observed with an inverted phase contrast Leica DMI4000B microscope outfitted with a DFC480 digital camera. MTT assay was carried out with a DU800 UV–visible spectrophotometer (Beckman Coulter). Liquid chromatographic system [29] (Shimadzu, Kyoto, Japan) consisted of two LC-20AT pumps, a CTO-10AS VP column oven, a SPD-M20A DAD system and a RF-10AXL FLD system. The two detectors were connected in series. These apparatus were connected *via* a communication module (Model CBM-20A), and controlled by a Shimadzu LCSolution workstation. A Shimadzu Shim-pack vp-ODS column (150L × 4.6) was used. Steady-state fluorescence spectra of AAs were recorded using a fluorescence spectrophotometer (F-4500, Hitachi). MS characteristics were investigated on a Micromass ZQ 4000 electrospray mass spectrometer (Manchester, U.K.) [27].

### 2.2. Materials and reagents

Human liver cell (L-02) was provided by Hunan Normal University. RPMI 1640 medium was purchased from Gibco, and neonatal

bovine serum was from Sijiqing Biological Engineering Materials Co., Ltd (Hangzhou, China). The reference standard of AA I was purchased from National Institute for the Control of Pharmaceutical and Biological Products (Beijing), and AL I was prepared in our lab [29]. HPLC-grade methanol was from Tedia (Fairfield, OH, USA). Distilled water ( $R > 18 \text{ M}\Omega \text{ cm}$ ) was prepared using Aike Purification system (Chengdu, China). Other reagents were of analytical grade.

### 2.3. Cell culture

L-02 cells were cultured in  $25 \text{ cm}^2$  tissue culture flasks at  $37^\circ\text{C}$  in a humidified atmosphere of  $5\% \text{ CO}_2$  in air. RPMI 1640 medium was supplemented with  $13\%$  neonatal bovine serum,  $100 \text{ U/ml}$  penicillin and  $100 \mu\text{g/ml}$  streptomycin. The medium was changed every day. When a single layered cell was formed, the cells were harvested by trypsinization with  $0.25\%$  trypsin– $0.02\%$  EDTA, centrifuged for  $5 \text{ min}$  at  $1000 \text{ rpm}$ , and resuspended in fresh medium. The density of the cell suspension was determined by trypsin blue staining method with a hemacytometer.

AA I ( $2.00 \text{ mg}$ ) dissolved in  $1 \text{ ml}$  of  $1\% \text{ NaHCO}_3$  was used for cytotoxic experiments. The experimental procedures were as follows:

- (1) A  $2 \text{ ml}$  aliquot of cell suspension at a density of  $1 \times 10^5$  cells/ml was added to each well of the 24-well tissue culture plates;
- (2) After  $24 \text{ h}$ ,  $20 \mu\text{l}$  AA I solution ( $2 \text{ mg/ml}$ ) was added and mixed thoroughly but gently;
- (3) Three or six wells of culture medium were taken out for chromatographic analysis at fixed time intervals. The cells were cultured in the  $\text{CO}_2$  incubator during the whole experiments.

### 2.4. MTT assay

Cytotoxicity against cell metabolism was investigated by using MTT assay. After cells were treated for a certain time, the wells were washed twice with phosphate-buffered saline (PBS) to remove non-adherent cells, then  $900 \mu\text{l}$  fresh medium and  $100 \mu\text{l}$  MTT solution (Amresco,  $5 \text{ mg/ml}$ ) were added to each well and the cells were further incubated at  $37^\circ\text{C}$  for  $4 \text{ h}$ . Subsequently the medium was removed, and the formazan crystals were dissolved in  $1 \text{ ml}$  DMSO (Sigma). The amount of absorbed solution was measured at  $570 \text{ nm}$ .

### 2.5. Sample preparation

A  $0.50 \text{ ml}$  of culture medium was taken into a  $10 \text{ ml}$  centrifuge tube, about  $3 \text{ ml}$  of ethyl acetate was added, and the mixture was oscillated for  $1 \text{ min}$ , then the upper layer was collected after delamination. The extraction was repeated twice, and the ethyl acetate solutions were merged. Under the  $\text{N}_2$  atmosphere ethyl acetate was volatilized, and  $200 \mu\text{l}$  methanol was added to dissolve the residues, and the solution can be used for chromatographic analysis directly.

### 2.6. Standard solutions and calibration curves

AA I ( $5.00 \text{ mg}$ ) and AL I ( $2.00 \text{ mg}$ ) were accurately weighed, and dissolved in  $5 \text{ ml}$  methanol as the stock solution. A series of standard solutions with gradient concentration were prepared by diluting the stock solution. A aliquot of  $200 \mu\text{l}$  standard solution at each concentration level was added in  $0.50 \text{ ml}$  culture medium, the same extraction were carried out as that in Section 2.5. Then the obtained series of working calibration solutions were used to construct calibration curves. Calibration curves ( $y = ax + b$ ) were constructed by plotting the peak areas ( $y$ ) against the concentrations ( $x$ ) of the calibration standards.

### 2.7. HPLC–DAD–FLD analysis

Methanol (B) and  $0.2\%$  acetic acid (A) were used as the mobile phase. The gradient was programmed as follows:  $0\text{--}15 \text{ min}$ ,  $40\text{--}80\%$  B;  $15\text{--}20 \text{ min}$ ,  $80\text{--}100\%$  B;  $20\text{--}30 \text{ min}$ ,  $100\%$  B;  $30\text{--}35 \text{ min}$ ,  $100\text{--}40\%$  B. The other analysis conditions were as follows: column temperature,  $30^\circ\text{C}$ ; flow rate,  $1.0 \text{ ml/min}$ ; injection volume,  $20 \mu\text{l}$ ; UV scan,  $210\text{--}600 \text{ nm}$ ; detection wavelength,  $254 \text{ nm}$ . The excitation and emission wavelengths of FLD were  $270$  and  $490 \text{ nm}$ , respectively. Various compounds were selected and went consecutively through the DAD and FLD, the delay was of  $0.20 \text{ min}$  between the two detectors.

## 3. Results and discussion

### 3.1. Optimization of separation and detection conditions

Chromatographic separation of AA analogues (including aristochoic acids and aristolactams) was achieved using a routine C18 column and a linear gradient of methanol against  $0.2\%$  acetic acid [27,29]. In the literature, mass spectrometry (MS) detection [24–27] was developed to replace UV detection [20–23], and similar sensi-

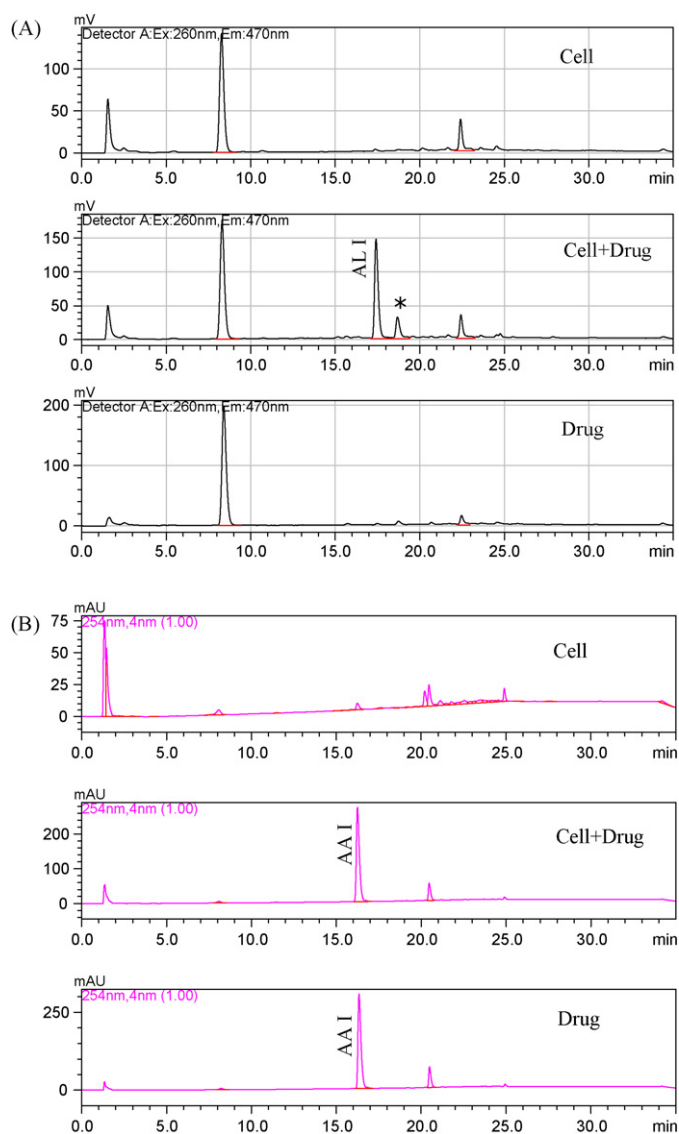


**Fig. 2.** Typical HPLC–FLD (A) and HPLC–DAD (B) chromatograms of samples. Cell–free-of-drug blank sample; Cell+Drug–cellular sample added AA I; Drug–free-of-cell blank sample.

**Table 1**  
Linear ranges, correlation coefficients, quantification and detection limits.

Compound	Linear ranges ( $\mu\text{g/ml}$ )	$r^2$	LOQ (ng/ml)	LOD (ng/ml)
AA I	0.10–200	0.9990	100	30
AL I	0.010–20	0.9992	2.0	0.7

tivity was achieved by UV detection. Then FLD [28] came with high sensitivity, but failed to detect AA without derivatives. In our previous study [29], the hyphenated DAD and FLD was verified to be an optimum tool for the simultaneous analysis of both AA and AL, especially when the content of AA is not too low and AL is at trace level. In this work, the gradient program was further improved to lessen the analysis time. As shown in Fig. 2, the retention time of AA I, AL I and the peak marked with “\*” are 16.25, 17.43 and 18.70 min, respectively, and the determination of the analysis was not interfered by endogenous substances in the cellular environment.

For AA I, 254 nm was a suitable detection wavelength with DAD. It can be seen from Fig. 1, the metabolites of AA I are AL I and its derivatives, seem to have good fluorescence response. According to the previous study [29], 270 and 490 nm were selected as the excitation ( $\lambda_{\text{ex}}$ ) and emission wavelengths ( $\lambda_{\text{em}}$ ).

### 3.2. Extraction method

Sample preparation is a critical step for the accuracy and sensitivity of an analytical method. Liquid–liquid extraction (LLE) with ethyl acetate was found to be a suitable sample preparation method with suitable extraction recovery. Several solvents including ethyl acetate, *n*-hexane, dichloromethane and ethyl acetate acidified by hydrochloric were evaluated. Ethyl acetate and the acidified ethyl acetate were found to be optimal according to the recovery. But no significant differences were found between the two methods. To simplify the procedure, ethyl acetate was selected as extraction solvent. With the LLE method, the concentration and cleaning procedures of the complex samples were completed.

### 3.3. Method validation

The standard curves were constructed via least-squares regression with six concentration levels and three parallels at each level. Good linear relationship was obtained with the correlation coefficients ( $r^2$ ) higher than 0.9990. Limit of detection (LOD) and limit of quantification (LOQ) were estimated as the minimum concentration giving S/N ratios of 3 and 10, respectively. The data are listed in Table 1.

The reliability of the assay was evaluated. Small coefficient of variation and good recovery were achieved. The precision and accuracy were confirmed by five replicate determinations. The mean recovery was studied by spiking the known content of the standards into the culture media. The overall recoveries of three concentrations were above 86.2% for AA I, and 74.8% for AL I (see Table 2). The data proved the suitability of the assay for used in cellular environment.

**Table 2**  
Precision and recovery of the method ( $n=5$ ).

Compound	Added ( $\mu\text{g/ml}$ )	Founded ( $\mu\text{g/ml}$ ) (mean $\pm$ SD)	Precision, RSD (%)	Recovery (%)
AA I	4.00	3.45 $\pm$ 0.28	8.1	86.2
	40.0	35.6 $\pm$ 2.7	7.5	89.0
	100	88.1 $\pm$ 6.8	7.7	88.1
AL I	0.20	0.158 $\pm$ 0.018	11.0	78.8
	2.00	1.53 $\pm$ 0.15	10.2	76.4
	10.0	7.48 $\pm$ 0.86	11.5	74.8

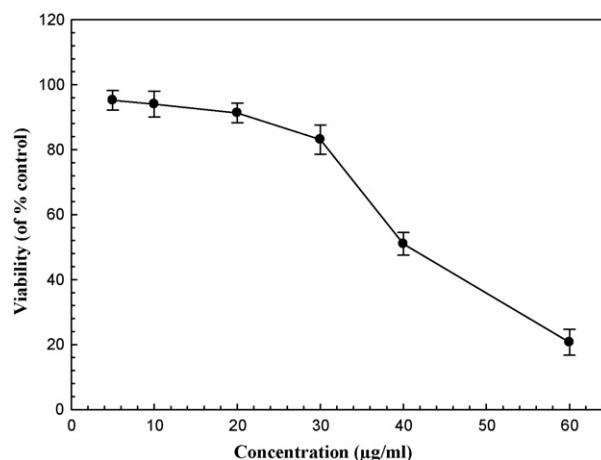


**Fig. 3.** Cytotoxicity of AA I in L-02 cells. Cells were treated for 24 h with different concentration and viability was assessed by MTT assay. Results are expressed as percent of the drug group and the control group ( $n=3$ ).

### 3.4. Cytotoxic effects of AA I

AA I is known to be nephrotoxic, carcinogenic, and mutagenic. In the cytotoxicity assay [12], AA I was found to be the most toxic and attracted the most attention. To assess the cytotoxic effect of AA I on L-02 cells, the proliferation and viability of cells were investigated by morphological observation and MTT assay. For comparison, cells were classified into two groups: the control group, and the drug group.

Dose–time relationship was studied by comparing the proliferation status of cells in different concentration levels (5.0, 10.0, 20.0, 30.0, 40.0, 60.0  $\mu\text{g/ml}$  AA I). No significant differences were found between the control group and the drug group when the drug concentration was lower than 5.0  $\mu\text{g/ml}$ . When the concentration was above 10.0  $\mu\text{g/ml}$ , significant morphological changes of the cells in the drug group occurred, some cells began to die within 24 h. The viabilities of cells cultured for 24 h in the presence of AA I with different concentrations are exhibited in Fig. 3. The viability of cells decreased in AA I concentration-dependent manner. In addition, the cell viability of the drug group (20.0  $\mu\text{g/ml}$ ) is about 50% of the control group after 48 h. To observe the cytotoxicity of a 48 h exposure, 20.0  $\mu\text{g/ml}$  was determined to be the optimal dose.

The typical cell morphologies are shown in Fig. 4 at different time after cell seeding. The cells of the control group gradually proliferated with incubation period, until the whole plate wall was reached. On the contrary, the living cells of the drug group gradually decreased. MTT assay was also performed to investigate cell viability and its proliferation. As shown in Fig. 5, the cell viability of the control group increases with culture time, which indicates that cells proliferate well. However, the viability of the drug group witnesses a course of increase to decrease. The “increase” indicates the cell proliferation can still be in progress and the cytotoxicity of AA I is not enough to induce the cell apoptosis in a short time. The “decrease” after 30 h means the cytotoxic effects of AA I surpasses the cell proliferation, and the number

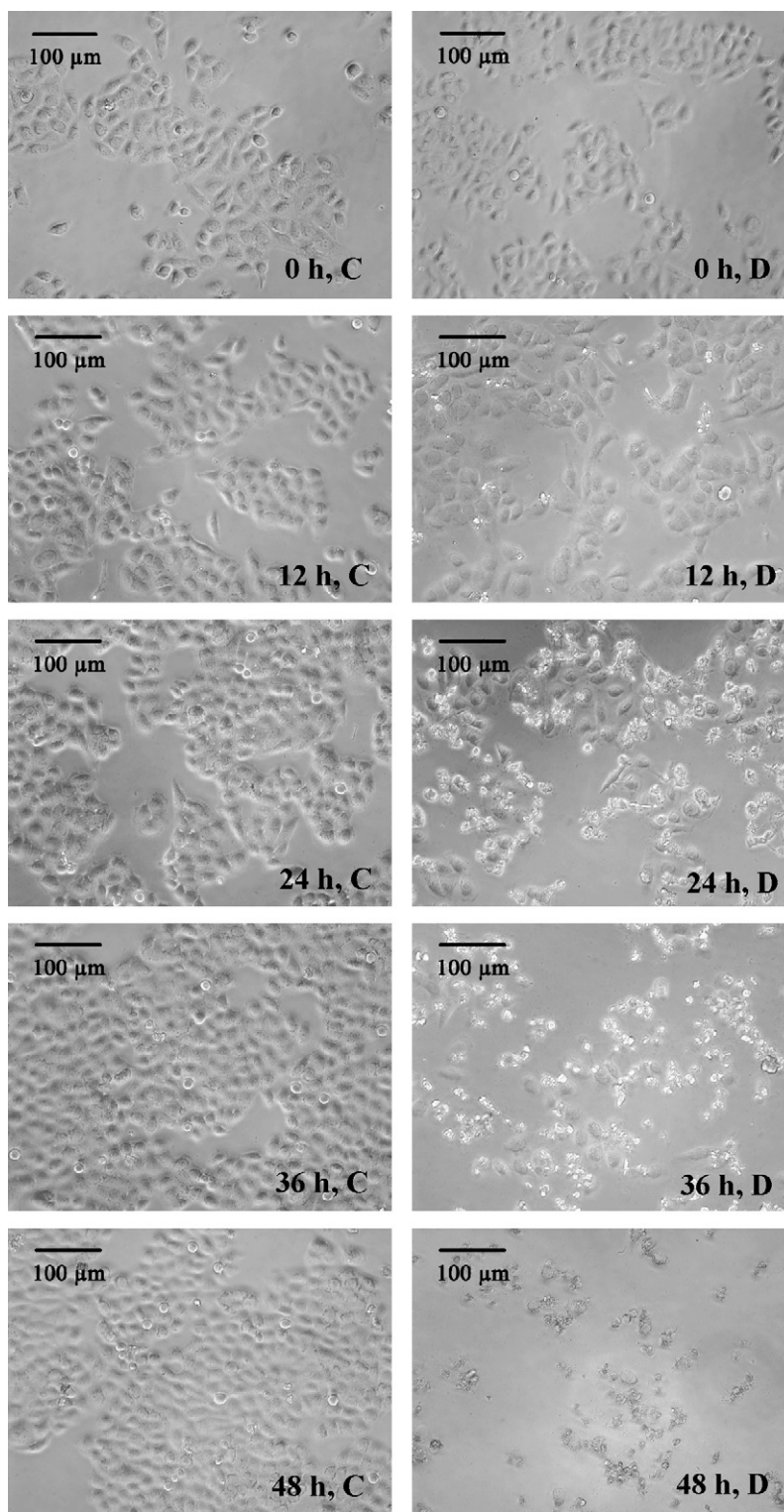


**Fig. 4.** Microscope images of cells during the culture course at different intervals. Cell inoculation density:  $1.0 \times 10^5$  cells/ml. C—the control group, D—the drug group. The initial time was recorded when cells had been cultured for 24 h, and AA I was added at 0 h with a final concentration of 20.0  $\mu\text{g/ml}$ .

of the dead cells exceeds the number of the new proliferated cells.

### 3.5. Sample analysis

In this work, qualitative analyses were based on the retention time, UV spectrum, fluorescence characteristics, ESI/MS and

metabolic activation. It can be seen from the FLD view in Fig. 2A, two peaks appeared in the chromatograph of the drug groups. According to the activation mechanism of AA I, their UV and FL characteristics, the two peaks should be identified as AL derivatives [29]. AL I was easily identified by comparing the chromatographic retention (17.43 min) of the unknown peak with that of the reference standard. As for another unknown peak (marked with “\*”) in

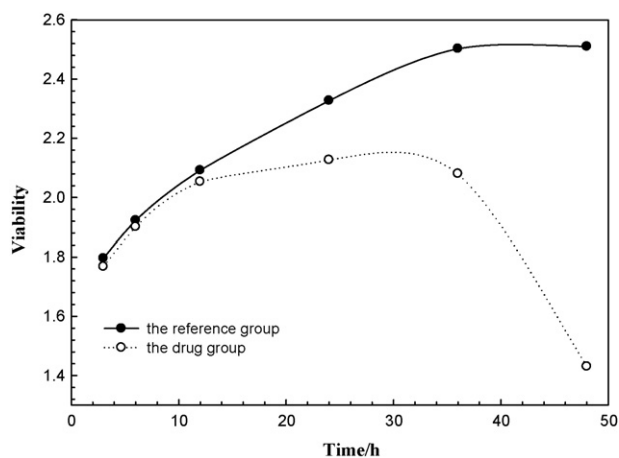


**Fig. 5.** Cytotoxicity of AA I in L-02 cells. Cells were treated with 20.0  $\mu\text{g/ml}$  AA I. Viability was assessed by MTT assay, and expressed as the absorbance at 570 nm ( $n=3$ ).

Fig. 2A, 18.70 min), it is certainly not 7-OH AL I, whose retention time should be less than that of AA I. Both dA-AL I and dG-AL I may or may not exist simultaneously, so they cannot be identified to the unknown metabolite. To find and identify the metabolites, HPLC–DAD–ESI/MS analysis has also been carried out as the previous work [27]. When the samples were further concentrated, a peak can be found with SIR (selective ion recording) mode at the relative retention time (Fig. 6, SIR: 324 for AL I, and SIR 310 for unknown peak). But, there are several AL (such as AL IVa and N-OH AL I, etc) corresponding to 310  $m/z$  [27]. Moreover, the qualitative power of ESI/MS is often not sufficient because it can not provide fragment ion for AL (see Fig. 6B). Therefore, we are not sure which AL the unknown metabolite is. According to the metabolic activation of AA I, it may be N-OH AL I.

The proposed HPLC–DAD–FLD method was applied to determine the AA I and its metabolites in the cell culture. The samples were prepared and analyzed according to the details in Section 2. The typical chromatograms of various samples are shown in Fig. 2. AA I can easily be quantified with HPLC–DAD. AL I, one of its metabolites, can be sensitively determined with HPLC–FLD.

### 3.6. Preliminary cellular toxicokinetic study

During the course of cytotoxicity tests, the proliferation and viability of L-02 cells were monitored with the microscopy and MTT assay. At predetermined intervals after cell seeding, three sets of culture media were taken out for chromatographic analysis with the developed HPLC–DAD–FLD method. AA I and its other two metabolites (AL I and an unknown metabolite) were detected. The concentration–time curve of AA I and the two metabolites were obtained (Fig. 7). The concentration changes of AA I and the metabolites can be explained from the reaction of the cells and the drug. At the beginning, AA I was taken up and metabolized by the cells, so the concentration of AA I in culture media decreased rapidly, and the metabolites appeared and increased. At the same time, the cytotoxicity of AA I affected the viability of the cells, some cells began to die. The dead cells released from the metabolites and some AA I. So the concentration of AA I increased a little at the last part of the test.

Although the concentration variation were in accordance with the proliferation and viability of the cells, no further toxicokinetic parameters can be found. It is because the concentrations came from two parts, metabolized by the living cells and then released by the apoptotic cells. The former can be useful in toxicokinetic study, but the latter may interfere with the detection. The deficiency can be compensated by the kinetics of AL I. The concentration of AL I increasing rapidly during the first 12 h according to a one-phase exponential association process, reaching near saturation after approximately 12 h and a maximal intracellular concentration reached at about 36 h.

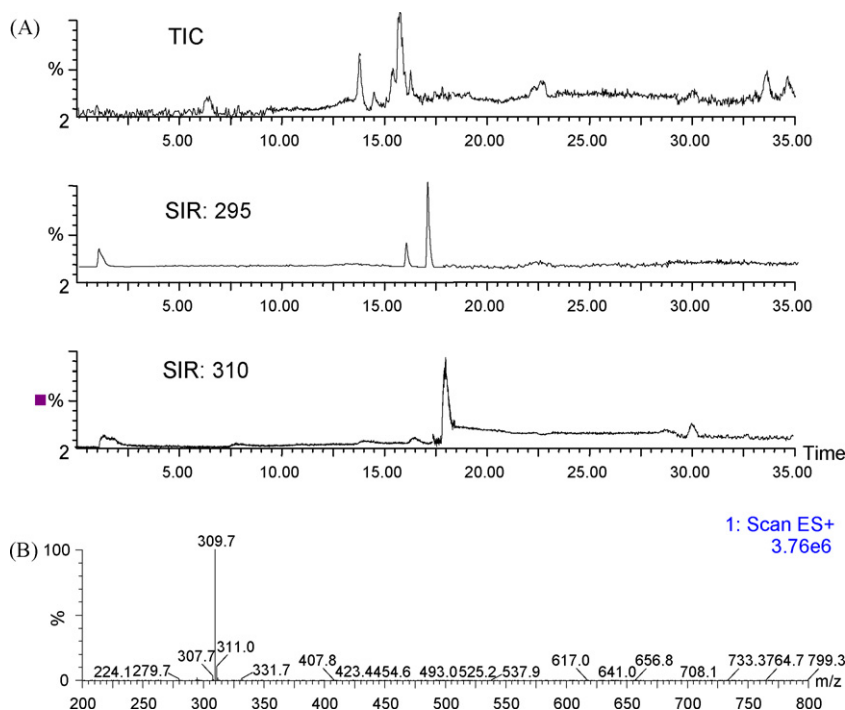


**Fig. 6.** Typical chromatograms (A) of the sample and mass spectrum (B) of AL I. TIC—total ion current; SIR—selective ion recording.

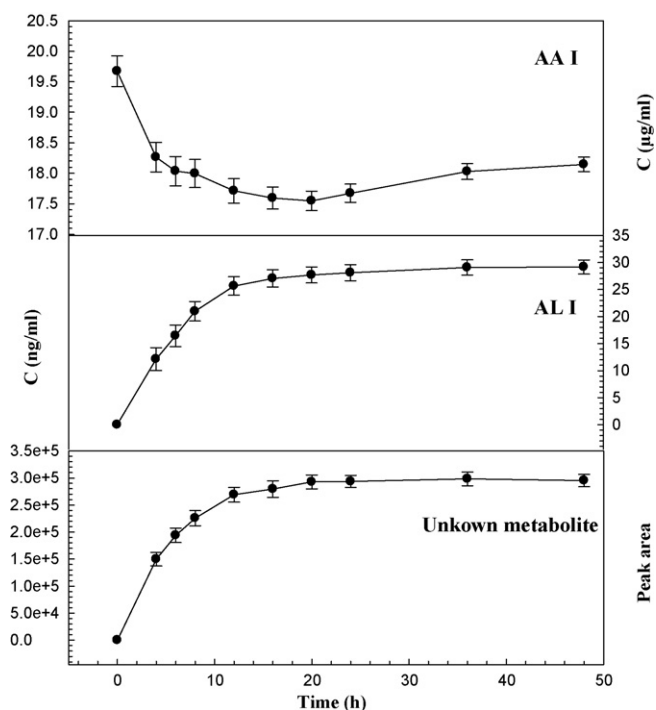


Fig. 7. Time course of AA I and its metabolites ( $n=6$ ). C—short for concentration.

#### 4. Conclusions

The sample preparation procedure (LLE) with ethyl acetate as extraction solvent concentrated and cleaned out. The proposed HPLC–DAD–FLD hyphenated technique was selective and sensitive enough to detect AA analogues and their trace metabolites in complex matrices without laborious sample preparations.

For the first time, AA I and some of its metabolites were simultaneously determined in cellular environment with the developed method. The preliminary cellular toxicokinetics was in accordance with the cytotoxicity assay. The assay could be used for further cellular toxicokinetic study of AAs in cells.

#### Acknowledgements

This work was financially supported by the National Basic Research Program (973 Program) (No. 2006CB504701), the National Natural Science Foundation of China (No. 20575019) and Jiangxi Province Office of Education (No. GJJ09277). Thanking Liang Tan of Hunan Normal University for providing the L-02 cell line. Thanking Xilin Xiao, Xubin Run, Chunfeng Pan of Hunan University for cell culturing. Thanking Zhou Nie of State Key Laboratory

of Chemo/Biosensing & Chemometrics, Hunan University for discussing cell biochemistry.

#### References

- [1] D.B. Mix, H. Guinaudeau, M. Shamma, *J. Nat. Prod.* 45 (1982) 657.
- [2] Y. Wang, J.X. Pan, Z.J. Jia, *Nat. Prod. Res. Dev.* 12 (2000) 84.
- [3] J.L. Vanherweghem, M. Depierreux, C. Tielemans, D. Abramowicz, M. Dratwa, M. Jadoul, C. Richard, D. Vandervelde, D. Verbeelen, R. Vanhaelen-Fastre, M. Vanhaelen, *Lancet* 341 (1993) 387.
- [4] C.S. Yang, C.H. Lin, S.H. Chang, H.C. Hsu, *Am. J. Kidney Dis.* 35 (2000) 313.
- [5] J.L. Nortier, J.L. Vanherweghem, *Toxicology* 181–182 (2002) 577.
- [6] C.L. Cheng, K.J. Chen, P.H. Shih, L.Y. Lu, C.F. Hung, W.C. Lin, J.Y. Gu, *Cancer Lett.* 232 (2006) 236.
- [7] U. Mengs, *Arch. Toxicol.* 52 (1983) 209.
- [8] J.L. Nortier, M.C. Munz Martinez, H.H. Schmeiser, V.M. Arlt, C.A. Bieler, M. Petein, M.F. Depierreux, L. De Pauw, D. Abramowitz, P. Vereerstraeten, J.L. Vanherweghem, *New Eng. J. Med.* 342 (2000) 1686.
- [9] M. Stiborova, E. Frei, A. Breuer, C.A. Bieler, H.H. Schmeiser, *Exp. Toxicol. Pathol.* 51 (1999) 421.
- [10] H.H. Schmeiser, B.L. Pool, M. Wiessler, *Carcinogenesis* 7 (1986) 59.
- [11] A. Kohara, T. Suzuki, M. Honma, T. Ohwada, M. Hayashi, *Mutat. Res.* 515 (2002) 63.
- [12] P. Balachandran, F. Wei, R.C. Lin, I. Khan, D.S. Pasco, *Kidney Int.* 67 (2005) 1797.
- [13] H.H. Schmeiser, K.B. Schoepe, M. Wiessler, *Carcinogenesis* 9 (1988) 297.
- [14] M. Stiborova, R.C. Fernando, H.H. Schmeiser, E. Frei, W. Pfau, M. Wiessler, *Carcinogenesis* 15 (1994) 1187.
- [15] C.A. Bieler, M. Stiborova, M. Wiessler, J.P. Cosyns, C.V. Destrihou, H.H. Schmeiser, *Carcinogenesis* 18 (1997) 1063.
- [16] V.M. Arlt, A. Pfohl-Loszkowicz, J.P. Cosyns, H.H. Schmeiser, *Mutat. Res.* 494 (2001) 143.
- [17] W. Chan, Y.F. Zheng, Z.W. Cai, *J. Am. Soc. Mass Spectrom.* 18 (2007) 642.
- [18] G. Krumbiegel, J. Hallensleben, W.H. Mennicke, *Xenobiotica* 17 (1987) 981.
- [19] S.M. Chen, M.Y. Fan, C.C. Tseng, Y. Ho, K.Y. Hsu, *Toxicol.* 50 (2007) 180.
- [20] J.R. Ioset, G.E. Raelison, K. Hostettmann, *Food Chem. Toxicol.* 41 (2003) 29.
- [21] B.T. Schanegger, I.A. Khan, *J. Ethnopharmacol.* 94 (2004) 245.
- [22] C.Y. Zhang, X. Wang, M.Y. Shang, J. Yu, Y.Q. Xu, Z.G. Li, L.C. Lei, X.M. Li, S.Q. Cai, T. Namba, *Biomed. Chromatogr.* 20 (2006) 309.
- [23] J.B. Yuan, L.H. Nie, D.Y. Zeng, X.B. Luo, F. Tang, L. Ding, Q. Liu, M.L. Guo, S.Z. Yao, *Talanta* 73 (2007) 644.
- [24] G.C. Kite, M.A. Yule, C. Leon, M.S.J. Simmonds, *Rapid Commun. Mass Spectrom.* 16 (2002) 585.
- [25] S.A. Chan, M.J. Chen, T.Y. Liu, M.R. Fuh, J.F. Deng, M.L. Wu, S.J. Hsieh, *Talanta* 60 (2003) 679.
- [26] T.T. Jong, M.R. Lee, S.S. Hsiao, J.L. Hsai, T.S. Wu, S.T. Chiang, S.Q. Cai, *J. Pharm. Biomed. Anal.* 33 (2003) 831.
- [27] J.B. Yuan, Q. Liu, G.B. Wei, F. Tang, L. Ding, S.Z. Yao, *Rapid Commun. Mass Spectrom.* 21 (2007) 2332.
- [28] W. Chan, K.C. Lee, N. Liu, Z.W. Cai, *J. Chromatogr. A* 1164 (2007) 113.
- [29] J.B. Yuan, Q. Liu, W.F. Zhu, L. Ding, F. Tang, S.Z. Yao, *J. Chromatogr. A* 1182 (2008) 85.
- [30] E.S. Ong, S.O. Woo, *Electrophoresis* 22 (2001) 2236.
- [31] W. Li, S.X. Gong, D.W. Wen, B.Q. Che, Y.P. Liao, H.W. Liu, X.F. Feng, S.L. Hu, *J. Chromatogr. A* 1049 (2004) 211.
- [32] S.C. Hsieh, M.F. Huang, B.S. Lin, H.T. Chang, *J. Chromatogr. A* 1105 (2006) 127.
- [33] Z.D. Zhai, X.P. Luo, Y.P. Shi, *Anal. Chim. Acta* 561 (2006) 119.
- [34] W. Li, Z. Chen, Y.P. Liao, H.W. Liu, *Electrophoresis* 27 (2006) 837.
- [35] S.H. Shi, W. Li, Y.P. Liao, Z.W. Cai, H.W. Liu, *J. Chromatogr. A* 1167 (2007) 120.
- [36] M.L. Guo, J.H. Chen, X.B. Yun, K. Chen, L.H. Nie, S.Z. Yao, *Biochim. Biophys. Acta* 1760 (2006) 432.
- [37] L. Pohjala, P. Tammela, S.K. Samanta, J. Yli-Kauhuoma, P. Vuorela, *Anal. Biochem.* 362 (2007) 221.
- [38] R.T. Gao, F.L. Zheng, Y.X. Liu, D.X. Zheng, X.M. Li, Y.H. Bao, Y. Liu, *Chin. J. Nephrol.* 15 (1999) 162.
- [39] H. Li, Z.H. Liu, H.P. Chen, M.Y. Zhu, L.S. Li, *J. Nephrol. Dial. Transplant* 10 (2001) 242.
- [40] L.J. Zhang, X.Q. Mu, J.L. Fu, Z.C. Zhou, *Toxicol. in Vitro* 21 (2007) 734.





# Spectrophotometric and spectrodensitometric determination of Clopidogrel Bisulfate with kinetic study of its alkaline degradation

Hala E. Zaazaa<sup>a</sup>, Samah S. Abbas<sup>a</sup>, M. Abdelkawy<sup>a</sup>, Maha M. Abdelrahman<sup>b,\*</sup>

<sup>a</sup> Analytical Chemistry Department, Faculty of Pharmacy, Cairo University, Kasr El-Aini St., 11562 Cairo, Egypt

<sup>b</sup> Analytical Chemistry Department, Faculty of Pharmacy, Beni-Suef University, Beni-Suef, Egypt

## ARTICLE INFO

### Article history:

Received 29 October 2008

Received in revised form

22 December 2008

Accepted 23 December 2008

Available online 20 January 2009

### Keywords:

Clopidogrel Bisulfate

Derivative spectrophotometry

Kinetic study

Bivariate calibration

Spectrodensitometry

Stability indicating method

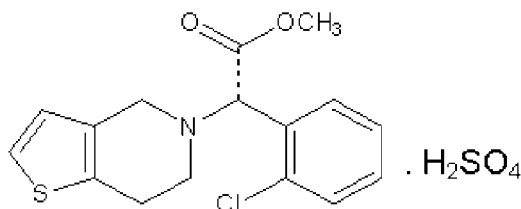
## ABSTRACT

Four sensitive, selective and precise stability-indicating methods for the determination of Clopidogrel Bisulfate (CLP) in presence of its alkaline degradate and in pharmaceutical formulations were developed and validated. Method A is a second derivative ( $D^2$ ) spectrophotometric one, which allows the determination of CLP in presence of its alkaline degradate at 219.6, 270.6, 274.2 and 278.4 nm (corresponding to zero-crossing of the degradate) over a concentration range of 4–37  $\mu\text{g mL}^{-1}$  with mean percentage recoveries  $99.81 \pm 0.893$ ,  $99.72 \pm 0.668$ ,  $99.88 \pm 0.526$  and  $100.46 \pm 0.646$ , respectively. CLP can be determined in the presence of up to 65% of its degradate.  $D^2$  method was used to study the kinetic of CLP alkaline degradation that was found to follow a first-order reaction. The  $t_{1/2}$  was 6.42 h while  $K$  (reaction rate constant) was 0.1080 mol/h. Method B is the first derivative of the ratio spectra ( $DD^1$ ) spectrophotometric method, by measuring the peak amplitude at 217.6 and 229.4 nm using acetonitrile and CLP can be determined in the presence of up to 70% of its degradate. The linearity range was 5–38  $\mu\text{g mL}^{-1}$  with mean percentage recoveries  $99.88 \pm 0.909$  and  $99.70 \pm 0.952$ , respectively. Method C based on the determination of CLP by the bivariate calibration depending on simple mathematic algorithm which provides simplicity and rapidity. The method depends on quantitative evaluation of the absorbance at 210 and 225 nm over a concentration range 5–38  $\mu\text{g mL}^{-1}$  with mean percentage recovery  $99.27 \pm 1.115$ . CLP can be determined in the presence of up to 70% of its degradate. Method D is a TLC-densitometric one, where CLP was separated from its degradate on silica gel plates using hexane:methanol:ethyl acetate (8.7:1:0.3, v/v/v) as a developing system. This method depends on quantitative densitometric evaluation of thin layer chromatogram of CLP at 248 nm over a concentration range of 0.6–3  $\mu\text{g}/\text{band}$  with mean percentage recovery  $99.97 \pm 1.161$ . CLP can be determined in the presence of up to 90% of its alkaline degradate. The selectivity of the proposed methods was checked using laboratory prepared mixtures. The proposed methods have been successfully applied to the analysis of CLP in pharmaceutical dosage forms without interference from other dosage form additives and the results were statistically compared with the official method.

© 2009 Elsevier B.V. All rights reserved.

## 1. Introduction

Clopidogrel hydrogen sulfate (CLP) is methyl (+)-(S)- $\alpha$ -(2-chlorophenyl)-6,7-dihydrothieno [3,2-c] pyridine-5(4H)-acetate hydrogensulfate [1]. The structural formula of CLP is shown below.



Clopidogrel Bisulfate

Mol. Formula  $\text{C}_{16}\text{H}_{16}\text{ClNO}_2\text{S} \cdot \text{H}_2\text{SO}_4$

Mol. Wt. 419.83

Clopidogrel Bisulfate is a new thienopyridine derivative chemically related to ticlopidine. It has been shown to prevent ischemic

\* Corresponding author. Tel.: +20 106599687; fax: +20 822317950.

E-mail address: [maha.m.abdelrahman@yahoo.com](mailto:maha.m.abdelrahman@yahoo.com) (M.M. Abdelrahman).

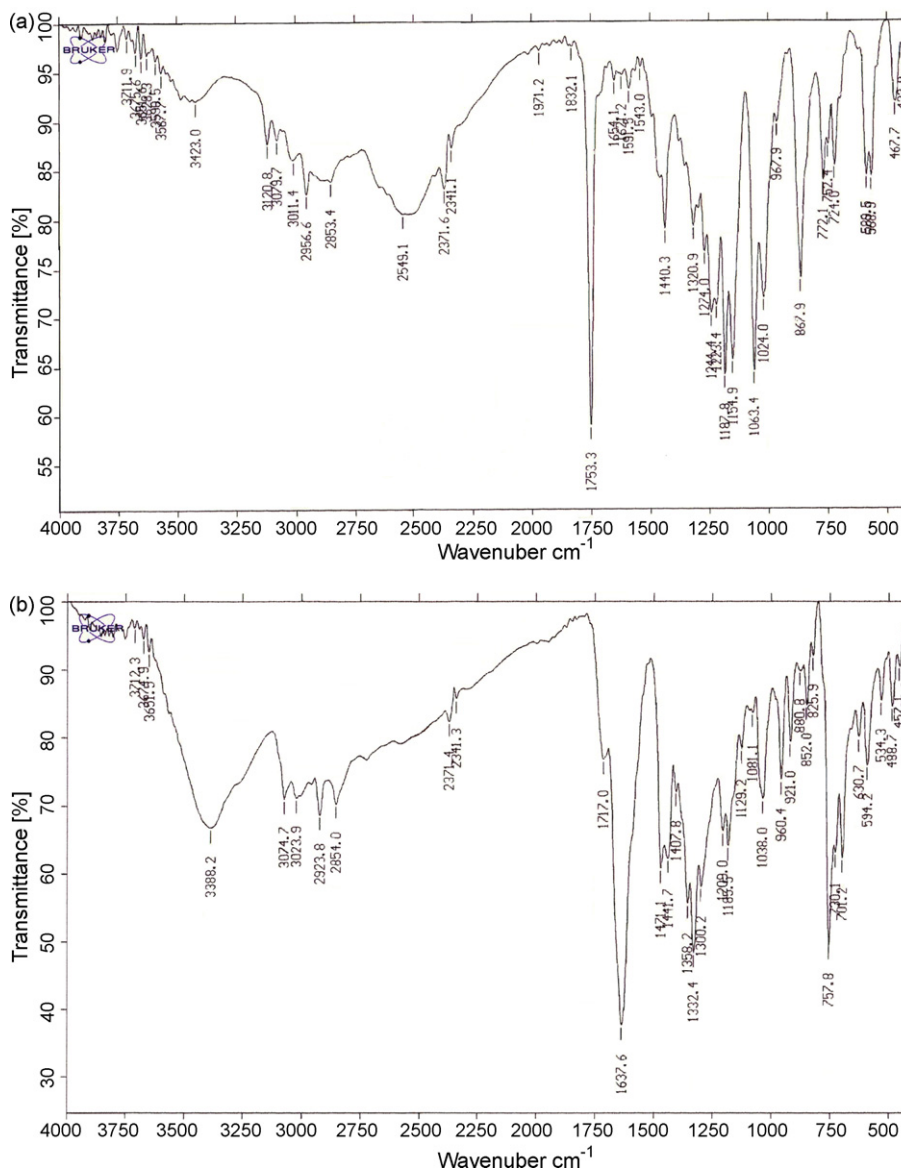


Fig. 1. IR-spectra of Clopidogrel Bisulfate (a) and its alkaline degradate (b).

stroke, myocardial infraction and vascular disease and demonstrated clinical efficacy superior to that of aspirin, in a large phase III trial [2]. Thus, CLP is indicated for the reduction of atherosclerotic events in patients with atherosclerosis documented by recent stroke, recent myocardial infraction or cardiovascular disease [2].

Clopidogrel Bisulfate is an enantiopure carboxylic ester of S-configuration. The R-enantiomer is devoid of antithrombotic activity and can evoke convulsions at high doses of animals [3]. It is rapidly absorbed and undergoes extensive metabolism and metabolic activation, as evidenced by the absence of detectable amounts of unchanged drug in plasma [4,5]. The parent compound is inactive *in vitro*, while its active metabolite inhibits platelet aggregation via selective binding to adenylate cyclase-coupled ADP receptors on the platelet surface [6,7]. The major circulating compound is the inactive carboxylic acid derivative, which is formed by hydrolysis of the ester function by carboxylesterase [8].

Few methods for the determination of CLP have been reported in literature. Recently, the non-enzymatic and enzymatic chiral inversion of Clopidogrel has been investigated *in vitro* using  $^1\text{H}$  NMR and a chiral HPLC procedure [9]. Moreover, in the same article,

a nonstereospecific HPLC assay method was also used to monitor the hydrolysis of CLP. The possible *in vivo* chiral inversion of carboxylic acid metabolite of CLP in rats was also studied using (S)- $\alpha$ -(1-naphthyl) ethylamine as a derivatization reagent and an HPLC method with spectrofluorimetric detection [9] and LC method for determination of CLP [10]. Identification and isolation of oxidation impurity of CLP using HPLC also reported [11]. HPLC determination of carboxylic acid metabolite of CLP in Wistar rat plasma [12] and in human plasma with application to a bioequivalence study [13]. For the analysis of the carboxylic acid metabolite of CLP in plasma and serum a GC-MS method has also been reported [14] and its determination by liquid chromatography-electrospray ionization mass spectrometry [15]. Also, a bioanalytical method for determination of CLP in human plasma [16] was reported. A stability indicating spectrodensitometric method for determination of CLP was also reported [17].

The scientific novelty of the present work is that the methods used are simple, rapid, selective and less expensive and less time-consuming compared with other published LC methods.

The focus of the present study was to develop and validate simple stability-indicating methods for the determinations of CLP in

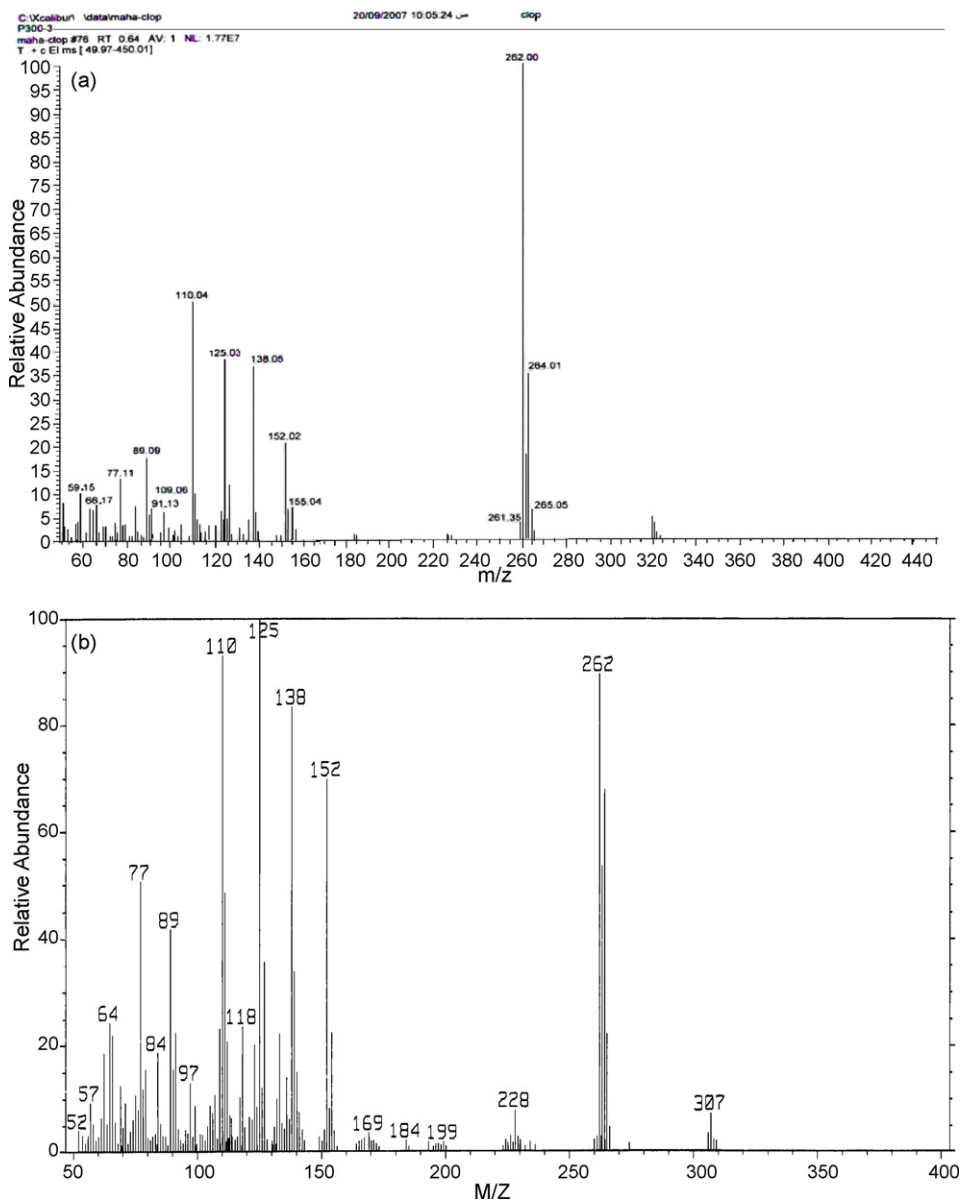


Fig. 2. Mass spectra of Clopidogrel Bisulfate (a) and its alkaline degradate (b).

presence of its alkaline degradate (which is pharmacologically inactive) for the quality control of CLP in pharmaceutical preparations.

## 2. Experimental

### 2.1. Instruments

1. A double beam UV–visible spectrophotometer (SHIMADZU, Japan) model UV-1601 PC with quartz cell of 1 cm pathlength, connected to IBM compatible computer. The software was UVPC personal spectroscopy software version 3.7. The spectral bandwidth was 2 nm and wavelength-scanning speed 2800 nm/min.
2. UV lamp with short wavelength 254 nm (USA).
3. TLC scanner 3 densitometer (Camag, Muttentz, Switzerland).

The following requirements are taken into consideration:

- Slit dimensions: 5 mm × 0.2 mm.
- Scanning speed: 20 mm/S.
- Spraying rate: 10 s  $\mu\text{L}^{-1}$ .
- Data resolution: 100  $\mu\text{m}/\text{step}$ .

4. TLC plates (20 cm × 10 cm) coated with silica gel 60F<sub>254</sub> (Merck, Germany).
5. Sample applicator for TLC Linomat IV with 100  $\mu\text{L}$  syringe (Camag, Muttentz, Switzerland).

### 2.2. Materials

#### 2.2.1. Pure standard

Clopidogrel Bisulfate was kindly supplied from ADWIA Co. S.A.E., 10th of Ramadan city, Egypt. Its purity was found to be 99.86% according to the official HPLC method [26].

#### 2.2.2. Pharmaceutical dosage forms

1. Myogrel<sup>®</sup> tablets are labeled to contain Clopidogrel Bisulfate equivalent to 75 mg of Clopidogrel manufactured by ADWIA Co. S.A.E., 10th of Ramadan city, Egypt. Batch No. 060729.
2. Stroka<sup>®</sup> tablets are labeled to contain Clopidogrel Bisulfate equivalent to 75 mg of Clopidogrel manufactured by Multi-APEX Pharma Co. S.A.E., Badr City, Cairo, Egypt. Batch No. 230/206.

### 2.2.3. Degraded sample

0.5 g of CLP powder was transferred into 250-mL stoppered flask, dissolved in 25 mL methanol, completed to 100 mL with 1N NaOH and refluxed for 8 h with magnetic stirring. Complete hydrolysis was followed via TLC using hexane:methanol:ethyl acetate (8.7:1:0.3, v/v/v) as a developing system. The solution was neutralized with 2N HCl solution till pH 3, then the degradate was extracted with multiple fractions of chloroform (6 × 20 mL). The extract was evaporated at room temperature and collected the degradate. The degradate powder was elucidated by IR and mass spectrometry.

### 2.2.4. Chemicals and reagents

All chemicals used throughout this work were of analytical grade, and the solvents were of spectroscopic grade.

1. Acetonitrile of HPLC grade (E. Merck, Germany).
2. Methanol, hexane, ethyl acetate and chloroform (El-Nasr Pharmaceutical Chemicals Co., Abu-Zabaal, Cairo, Egypt).
3. 2N HCl and 1N NaOH solutions (El-Nasr Pharmaceutical Chemicals Co., Abu-Zabaal, Cairo, Egypt).

### 2.3. Standard solutions

- Stock standard solutions of CLP and its alkaline degradate, 1 mg mL<sup>-1</sup> in acetonitrile (for D<sup>2</sup>, DD<sup>1</sup> and bivariate spectrophotometric methods) and in methanol (for spectrodensitometric method).
- Working solutions of CLP and its alkaline degradate, 100 μg mL<sup>-1</sup> in acetonitrile (for D<sup>2</sup>, DD<sup>1</sup> and bivariate spectrophotometric methods). They were prepared by suitably diluting the stock standard solutions with the suitable solvent.

### 2.4. Kinetic study

Two sets of working standard solutions of CLP ( $5.95 \times 10^{-3}$  and  $8.34 \times 10^{-3}$  mol L<sup>-1</sup>) were prepared by dissolving in 10 mL methanol into 100-mL volumetric flask and diluting to 100 mL with 1N NaOH.

### 2.5. Laboratory prepared mixtures

Solutions containing different ratios of CLP and its alkaline degradate were prepared to contain 10–90% of alkaline degradate of CLP.

## 3. Procedures

### 3.1. Construction of calibration curve for D<sup>2</sup> spectrophotometric method

Aliquots of CLP working solution (100 μg mL<sup>-1</sup> in acetonitrile) equivalent to 40–370 μg were accurately transferred into a series of 10-mL volumetric flasks, the volume was completed to the mark with acetonitrile. The second derivative absorption spectra of the UV-spectrum of each solution against acetonitrile as a blank were recorded. D<sup>2</sup> curves were recorded at Δλ = 4 and scaling factor = 100. Calibration curve was obtained by plotting the peak amplitude at 219.6, 270.6, 274.2 and 278.4 nm (corresponding to zero-crossing of the degradate) of D<sup>2</sup> spectra versus the corresponding concentrations of CLP and the regression equations were computed.

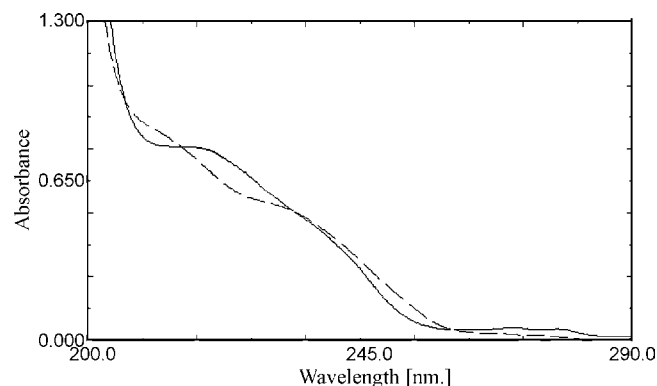


Fig. 3. Zero-order absorption spectra of 25 μg mL<sup>-1</sup> of Clopidogrel Bisulfate (—) and 25 μg mL<sup>-1</sup> of its alkaline degradate (---) using acetonitrile as a solvent.

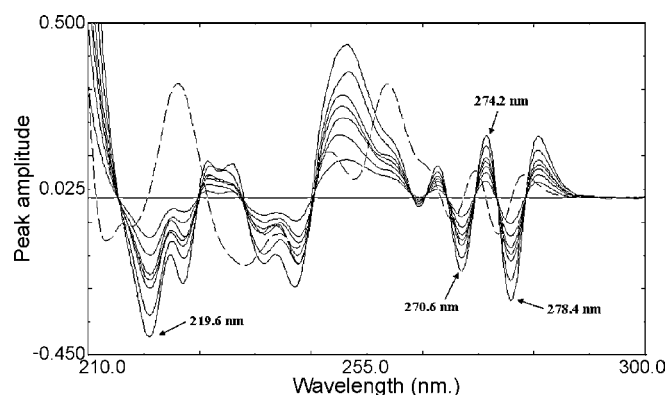


Fig. 4. Second derivative absorption spectra of 4–37 μg mL<sup>-1</sup> of Clopidogrel Bisulfate (—) and 25 μg mL<sup>-1</sup> of its alkaline degradate (---) using acetonitrile as a solvent.

### 3.2. Construction of calibration curve for DD<sup>1</sup> spectrophotometric method

Different aliquots equivalent to 50–380 μg of CLP working solution (100 μg mL<sup>-1</sup> in acetonitrile) were accurately transferred into a series of 10-mL volumetric flasks then diluted to volume using acetonitrile. DD<sup>1</sup> curves were recorded at Δλ = 4 and scaling factor = 10. The absorption spectra of these solutions were divided by the absorption spectrum of 15 μg mL<sup>-1</sup> of the degradate (as a divisor), and then the obtained ratio spectra were differentiated with respect to wavelength. The peak amplitude at 217.6 and 229.4 nm were recorded. The calibration curves representing the relationship between the measured amplitudes and the corresponding concentrations of the drug were constructed.

### 3.3. Construction of calibration curve for bivariate spectrophotometric method

Into two separate sets of 10-mL volumetric flasks, aliquots equivalent to 50–380 μg of CLP and its alkaline degradate were transferred from their working solutions (100 μg mL<sup>-1</sup> in acetonitrile). The volume was completed with acetonitrile. The regression equations at 210 and 225 nm for CLP and its alkaline degradate were computed.

### 3.4. Kinetic study

Two sets of working solutions of CLP ( $5.95 \times 10^{-3}$  and  $8.34 \times 10^{-3}$  mol L<sup>-1</sup>) were prepared in 1N NaOH and inserted as rapidly as possible in a thermostatic water bath set at 80 °C and

**Table 1**  
Determination of Clopidogrel Bisulfate in presence of its alkaline degradate in laboratory prepared mixtures by the proposed methods.

Degradate%	Recovery% <sup>a</sup> of CLP							
	D <sup>2</sup> spectrophotometric method				DD <sup>1</sup> spectrophotometric method		Bivariate calibration method	TLC-densitometric method
	219.6 nm	270.6 nm	274.2 nm	278.4 nm	217.6 nm	229.4 nm		
10	101.28	98.17	100.50	98.94	99.83	100.89	97.61	98.85
20	99.25	98.25	100.50	99.50	101.31	101.00	101.00	99.14
30	99.07	97.93	99.57	98.00	98.29	98.21	97.57	99.80
40	101.92	100.00	100.00	97.42	101.92	100.25	100.25	101.31
50	104.58 <sup>b</sup>	100.30	102.00	101.70	100.20	101.20	100.40	97.93
60	107.88 <sup>b</sup>	99.75	104.77 <sup>b</sup>	99.92	101.00	104.31 <sup>b</sup>	99.75	100.89
65	108.92 <sup>b</sup>	100.86	106.20 <sup>b</sup>	100.50	100.57	105.93 <sup>b</sup>	102.21	101.98
70	110.45 <sup>b</sup>	104.12 <sup>b</sup>	108.57 <sup>b</sup>	95.88 <sup>b</sup>	98.44	108.11 <sup>b</sup>	100.67	102.00
80	115.11 <sup>b</sup>	107.75 <sup>b</sup>	110.32 <sup>b</sup>	92.17 <sup>b</sup>	103.88 <sup>b</sup>	111.78 <sup>b</sup>	94.22 <sup>b</sup>	97.17
90	120.32 <sup>b</sup>	110.15 <sup>b</sup>	115.55 <sup>b</sup>	89.80 <sup>b</sup>	108.60 <sup>b</sup>	117.50 <sup>b</sup>	90.45 <sup>b</sup>	101.55
Mean ± S.D.	100.38 ± 1.435	99.32 ± 1.182	100.51 ± 0.917	99.43 ± 1.464	100.20 ± 1.301	100.31 ± 1.227	99.93 ± 1.612	100.06 ± 1.738

<sup>a</sup> Average of three experiments.

<sup>b</sup> Rejected values.

0.1 mL from the reflux solutions were quantitatively transferred into 10-mL volumetric flask for 8 h at 1 h time interval. The flasks were completed to volume with acetonitrile and measured. By applying in the previously described D<sup>2</sup> method at 278.4 nm for the determination of the remaining intact CLP from its corresponding regression equation, a plot of log the remaining concentration versus time in hours was then performed to determine the kinetic order of alkaline degradation process.

#### 3.4.1. Effect of sodium hydroxide concentration on the reaction rate

The mentioned procedure was followed using 0.5N and 1N NaOH in the degradation of  $8.34 \times 10^{-3} \text{ mol L}^{-1}$  of CLP.

#### 3.5. Construction of calibration curve for TLC-densitometric method

Into a series of 10-mL volumetric flasks, aliquots equivalent to 6–30 µg were accurately transferred from the standard stock solution of CLP ( $1 \text{ mg mL}^{-1}$  in methanol), then the volume was completed with methanol. 10 µL of each solution was spotted as bands of 5 mm width on TLC plates (20 cm × 10 cm with 250 µm thickness) using a Camag Linomat IV applicator. The bands were applied at 5 mm interval and 15 mm from the bottom and sides. Linear ascending chromatogram developing to a distance of 8 cm was performed in a chromatographic tank previously saturated for 1 h with the developing mobile phase consisted of hexane:methanol:ethyl acetate (8.7:1:0.3, v/v/v) at room temperature. CLP was scanned at 248 nm. The peak area was recorded and the calibration curve was constructed by plotting the integrated peak area versus the corresponding concentrations of the drug and the regression equation was computed.

#### 3.6. Application to pharmaceutical formulations

Ten tablets of each of Myogrel<sup>®</sup> tablets and Stroka<sup>®</sup> tablets were powdered and mixed well; an accurately weighed amount of the powder equivalent to 0.1 g of CLP of each was transferred into two separate 100-mL volumetric flasks, 75 mL of the appropriate solvent added (acetonitrile for D<sup>2</sup>, DD<sup>1</sup> and bivariate methods and methanol for spectrodensitometric method), stirred well then cooled and completed to the volume to obtain  $1 \text{ mg mL}^{-1}$  stock solutions, then filtered. The solutions were diluted to the same concentrations of the appropriate working solutions and proceeded according to the procedure of each method mentioned above.

## 4. Results and discussion

Following an oral administration in human, the plasma levels of CLP are very low due to extensive metabolism. The main circulating metabolite is the carboxylic acid derivative which is pharmacologically inactive [8].

Clopidogrel Bisulfate was subjected to oxidation using hydrogen peroxide, giving many oxidative degradation products which were difficult to be separated.

Upon refluxing CLP with acid or alkali, the carboxylic acid degradate was obtained, and being inactive. So the determination of CLP in presence of its alkaline (or acidic) degradate was essential.

The International Conference on Harmonization (ICH) guideline entitled “stability testing of new drugs substances and products” requires the stress testing to be carried out to elucidate the inherent stability characteristics of the active substance [18]. An ideal stability indicating method is one that quantifies the standard drug alone and also resolves its degradation products.

The structure of the alkaline (also obtained by acid hydrolysis) degradate was elucidated by IR and mass spectrometry, where IR spectrum of CLP showed a characteristic band at  $1753.3 \text{ cm}^{-1}$  indicating the presence of carbonyl group. While the IR spectrum of the degradate showed the same band but shifted to  $1637.6 \text{ cm}^{-1}$  and a new broad band at  $3388.2 \text{ cm}^{-1}$  indicating the presence of a hydroxyl group of carboxylic acid (due to hydrolysis). The electron impact showed mass ion peak at  $m/z$  321 corresponding to the intact drug, while the mass ion peak of the degradate was at  $m/z$

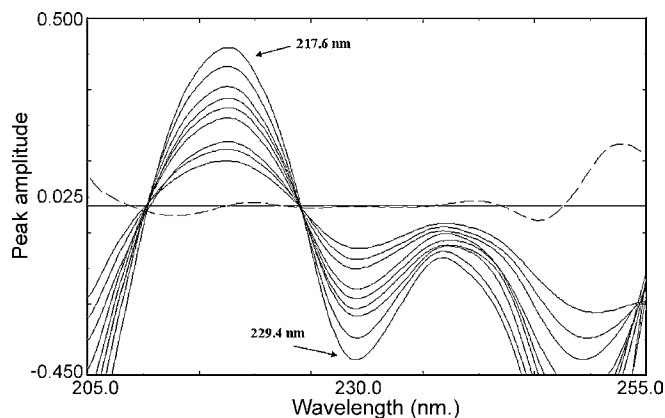
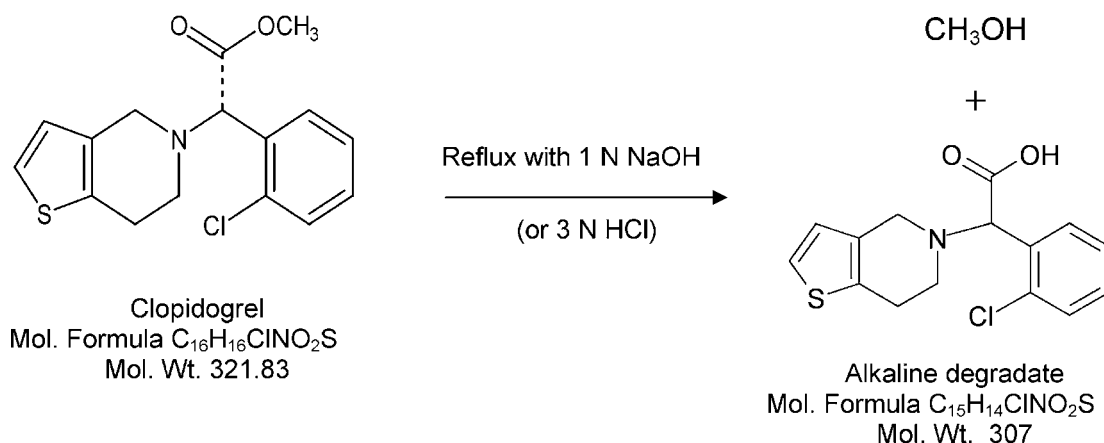


**Fig. 5.** First derivative of the ratio spectra of 5–38 µg mL<sup>-1</sup> of Clopidogrel Bisulfate (—) and 25 µg mL<sup>-1</sup> of its alkaline degradate (---) using 15 µg mL<sup>-1</sup> of the degradate as a divisor and acetonitrile as a blank.

307 as shown in Figs. 1 and 2. Therefore one can conclude that carrying out the alkaline (or acidic) hydrolysis of CLP may proceed as shown below.



The focus of the present work was to develop accurate, specific, reproducible and sensitive stability indicating methods for the determination of CLP in pure form or in pharmaceutical formulations in the presence of its alkaline degradation product.

The zero-order absorption spectra of CLP and its alkaline degradate showed severe overlapping, Fig. 3, which interfere with the direct determination of CLP. Derivative spectrophotometry is an analytical technique of great utility for extracting both qualitative and quantitative information from spectra composed of unresolved bands, and for eliminating the effect of baseline shifts and baseline tilts by using the first or higher derivatives of absorbance with respect to wavelength [19]. A rapid, simple and low cost spectrophotometric method based on measuring the peak amplitude of  $D^2$  spectrum of CLP at 219.6, 270.6, 274.2 and 278.4 nm (corresponding to zero-crossing of the degradate) was developed with good selectivity without interference of alkaline degradate as shown in Fig. 4.

Different solvents were tried to resolve their overlapping, e.g. methanol, ethanol, butanol, acetonitrile, 0.05N NaOH and 0.05N HCl, in each of these solvents derivatization was done. Zero-crossing of degradate corresponding to peak of CLP was obtained by applying  $D^2$  technique using acetonitrile as a solvent.

In order to optimize  $D^2$  method, different smoothing and scaling factors were tested, where a smoothing factor  $\Delta\lambda = 4$  and a scaling factor = 100 showed a suitable signal to noise ratio and the spectra showed good resolution.

A linear correlation was obtained between peak amplitude at 219.6, 270.6, 274.2 and 278.4 nm and the corresponding concentration in the range of 4–37  $\mu\text{g mL}^{-1}$ , from which the linear regression equations were computed and found to be

$$\begin{aligned}
 Y_1 &= 0.0120C - 0.0064, & r &= 0.9999 \text{ at } 219.6 \text{ nm} \\
 Y_2 &= 0.0066C - 0.0145, & r &= 0.9999 \text{ at } 270.6 \text{ nm} \\
 Y_3 &= 0.0056C - 0.0135, & r &= 0.9999 \text{ at } 274.2 \text{ nm} \\
 Y_4 &= 0.0089C - 0.0201, & r &= 0.9999 \text{ at } 278.4 \text{ nm}
 \end{aligned}$$

where  $Y_1, Y_2, Y_3$  and  $Y_4$  are the peak amplitude at 219.6, 270.6, 274.2 and 278.4 nm, respectively,  $C$  is the concentration of CLP in  $\mu\text{g mL}^{-1}$  and  $r$  is the correlation coefficient.

The proposed method is valid for the determination of CLP in presence of up to 65% of its alkaline degradate in different laboratory prepared mixtures as presented in Table 1, where at 270.6 and 278.4 nm showed higher selectivity with mean percentage recovery  $99.32 \pm 1.182$  and  $99.43 \pm 1.464$ , respectively.

In order to improve the selectivity of the analysis of CLP in presence of its alkaline degradate,  $DD^1$  spectrophotometric method

was established. The main advantage of the method is that the whole spectrum of interfering substance is canceled. Accordingly,

the choice of the wavelength selected for calibration is not critical as in the second derivative  $D^2$  method. The spectra are presented in Fig. 5.

In order to optimize  $DD^1$  method, several divisor concentrations 5, 10, 15 and 20  $\mu\text{g mL}^{-1}$  of the degradate were tried, the best result was obtained when using 15  $\mu\text{g mL}^{-1}$  of the degradate as a divisor. Different smoothing and scaling factors were tested, where a smoothing factor  $\Delta\lambda = 4$  and a scaling factor = 10 were suitable to enlarge the signal of CLP to facilitate its measurement and to diminish error in reading the signal.

Dividing the absorption spectra of CLP in the range of 5–38  $\mu\text{g mL}^{-1}$  by the absorption spectrum of 15  $\mu\text{g mL}^{-1}$  of the degradate (as a divisor); the obtained ratio spectra were differentiated with respect to wavelength.

$DD^1$  values showed good linearity and reproducibility at 217.6 and 229.4 nm, the linear regression equations were found to be

$$\begin{aligned}
 Y_1 &= 0.0172C - 0.0155, & r &= 0.9999 \text{ at } 217.6 \text{ nm} \\
 Y_2 &= 0.0152C - 0.0167, & r &= 0.9999 \text{ at } 229.4 \text{ nm}
 \end{aligned}$$

where  $Y_1$  and  $Y_2$  are the peak amplitude at 217.6 and 229.4 nm, respectively,  $C$  is the concentration of CLP in  $\mu\text{g mL}^{-1}$  and  $r$  is the correlation coefficient.

The method was checked by analysis of laboratory prepared mixtures of CLP and its alkaline degradate in different ratios as presented in Table 1. At the wavelength 217.6 nm, CLP could be determined in presence of up to 70% of degradate with mean percentage recovery  $100.20 \pm 1.301$ , giving higher selectivity than at 229.4 nm.

The third method was the bivariate calibration technique, in this work, CLP was determined and resolved from its alkaline degradate by using the bivariate calibration spectrophotometric method [20,21]. This method is based on a simple mathematic algorithm, in which the data used derives from four linear regression calibration equations: two calibrations for each component at two wavelengths selected using the method of Kaiser [22]. The method has been successfully applied to resolve different binary mixtures, such as: metronidazole/furazolidone and metronidazole/diiodohydroxyquinoline [23]. The advantage of bivariate calibration method is its simplicity and the fact that derivatization procedures are not necessary. Unlike other chemometric techniques, there is no need for full spectrum information and no data processing is required.

The linear calibration regression function for the spectrophotometric determination of an analyte A at a selected wavelength ( $i$ ) is

**Table 2**  
Application of the method of Kaiser for the selection of the wavelength set for the determination of Clopidogrel Bisulfate.

$\lambda_1/\lambda_2$	205	210	215	220	225	230	235	245
205	0	16.53	7.79	8.57	13.06	15.25	5.83	10.47
<b>210</b>		0	7.56	14.35	<b>21.64</b>	11.25	4.19	9.20
215			0	11.64	12.34	5.40	6.59	5.50
220				0	3.72	3.50	8.10	9.58
225					0	6.05	9.80	10.04
230						0	3.90	6.10
235							0	3.20
245								0

The absolute values of determinants of sensitivity ( $K \times 10^{-5}$ ). The bold value represents the highest matrix determinant value obtained at the wavelength set 210 and 225 nm.

given by

$$A_{Ai} = m_{Ai} \cdot C_A + e_{Ai}$$

where  $m_{Ai}$  is the slope of linear regression,  $C_A$  is the concentration of analyte A and  $e_{Ai}$  is the intercept value. If the measurements of the binary mixture (A, B) are performed at two selected wavelengths ( $\lambda_1, \lambda_2$ ), we have a two equations set:

$$A_{AB1} = m_{A1}C_A + m_{B1}C_B + e_{AB1}$$

$$A_{AB2} = m_{A2}C_A + m_{B2}C_B + e_{AB2}$$

The resolution of such equations set allows the evaluation of  $C_B$  (concentration of CLP) value:

$$C_B = \frac{m_{A2}(A_{AB1} - e_{AB1}) + m_{A1}(e_{AB1} - A_{AB2})}{m_{A2}m_{B1} - m_{A1}m_{B2}}$$

These simple mathematic algorithms allows the resolution of the two components by measuring the absorbance of CLP and degradate at the two wavelengths and using the parameters of the linear regression functions evaluated individually for each component at the same wavelengths. The method of Kaiser [22] was used for the selection of optimum wavelength set which assured the best sensitivity for the quantitative determination of the cited drug.

In order to apply this method, select the signals of the two components located at eight wavelengths: 205, 210, 215, 220, 225, 230, 235 and 245 nm.

**Table 3**  
Kinetic data of Clopidogrel Bisulfate–alkaline degradation.

Concentration ( $\text{mol L}^{-1}$ )	$K$ (mol/h)	$t_{1/2}$ (h)	Regression equation <sup>a</sup>
$5.95 \times 10^{-3}$	0.1085	6.39	$Y = -0.0471C - 9.2724r = 0.9937$
$8.34 \times 10^{-3}$	0.1080	6.42	$Y = -0.0469C - 8.9475r = 0.9933$

<sup>a</sup>  $Y$  = the peak amplitude at 278.4 nm.  $C$  = the remaining CLP concentration ( $\text{mol L}^{-1}$ ).

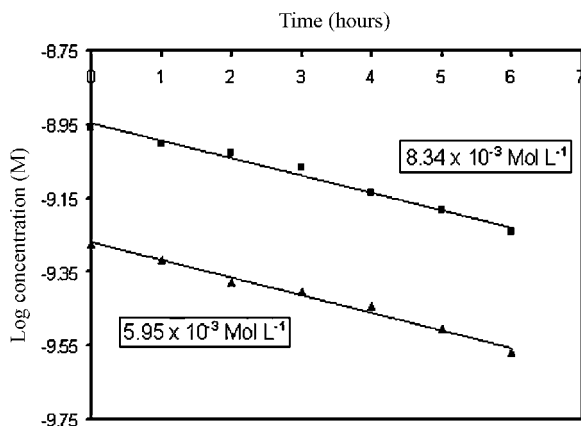


**Fig. 6.** Kinetic plots of the alkaline degradation for  $8.34 \times 10^{-3} \text{ mol L}^{-1}$  and  $5.95 \times 10^{-3} \text{ mol L}^{-1}$  of Clopidogrel Bisulfate using 1N NaOH.

The calibration curve equations and their respective linear regression coefficients are obtained directly with the aim of ensuring the linearity between the signal and the concentrations. The slope values of the linear regression were estimated for both the drug and its alkaline degradate at the selected wavelengths and used for determination of the sensitivity matrices  $K$ , proposed by Kaiser's method [22]. A series of sensitivity matrices  $K$ , were created for each binary mixture and for every pair of pre-selected wavelengths:

$$K = \begin{pmatrix} m_{A1} & m_{B1} \\ m_{A2} & m_{B2} \end{pmatrix}$$

A = Alkaline degradate; B = CLP.

Where  $m_{A1,2}$  and  $m_{B1,2}$  are the sensitivity parameters (slope) of the regression equations of A and B at the two selected wavelengths ( $\lambda_1$  and  $\lambda_2$ ). The determinants of these matrices were calculated as shown in Table 2. The wavelength set was selected for which the highest matrix determinant value was obtained.

For bivariate determination of CLP in presence of its degradate wavelengths 210 and 225 nm were used. At these selected wavelengths, the one-component calibration curves were obtained in the range of  $5\text{--}38 \mu\text{g mL}^{-1}$  for CLP and  $5\text{--}25 \mu\text{g mL}^{-1}$  for alkaline degradate using the following linear regression calibration formula:

$$\begin{aligned} \text{For CLP} \quad & A = 0.0307C + 0.0213, \quad r = 0.9999 \quad \text{at } \lambda_1 = 210 \text{ nm} \\ & A = 0.0271C + 0.0068, \quad r = 0.9999 \quad \text{at } \lambda_2 = 225 \text{ nm} \\ \text{For degradate} \quad & A = 0.0354C - 0.0092, \quad r = 0.9999 \quad \text{at } \lambda_1 = 210 \text{ nm} \\ & A = 0.0242C - 0.0053, \quad r = 0.9999 \quad \text{at } \lambda_2 = 225 \text{ nm} \end{aligned}$$

where  $A$  is the absorbance at the selected wavelength,  $C$  is the concentration in  $\mu\text{g mL}^{-1}$  and  $r$  is the correlation coefficient.

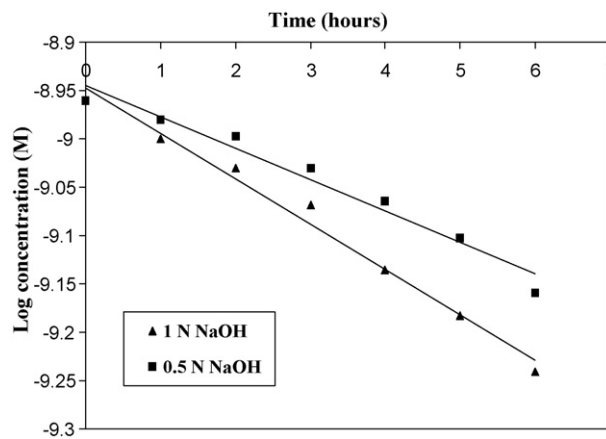


**Fig. 7.** Plot for the effect of sodium hydroxide concentration on the rate of degradation of  $8.34 \times 10^{-3} \text{ mol L}^{-1}$  of Clopidogrel Bisulfate.

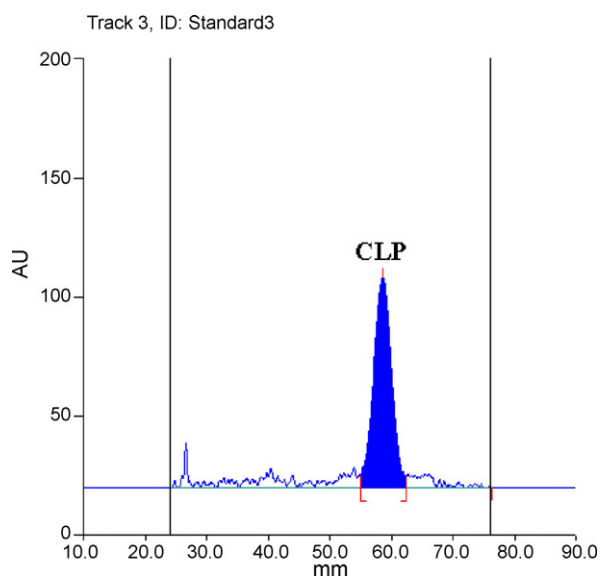


**Fig. 8.** Thin layer chromatogram of standard Clopidogrel Bisulfate (1  $\mu\text{g}/\text{band}$ ) at  $R_f = 0.646 \pm 0.05$  using a mobile phase hexane:methanol:ethyl acetate (8.7:1:0.3, v/v/v).

#### 4.1.1. Analysis of laboratory prepared mixtures

The absorption spectra of different laboratory prepared mixtures were measured at 210 and 225 nm. The concentration of CLP was calculated using the parameters of the linear regression func-

**Table 4**

Parameters of system suitability of the developed TLC-densitometric method for the determination of Clopidogrel Bisulfate.

Parameters	Clopidogrel Bisulfate	Alkaline degradate
Symmetry factor	0.98	0.92
Resolution ( $R_s$ ) <sup>a</sup>		5.32
Capacity factor ( $K'$ )	0.354	0.247
Selectivity ( $\alpha$ ) <sup>a</sup>		2.615

<sup>a</sup> The parameters were calculated using Clopidogrel Bisulfate as reference.

tion evaluated for CLP and its degradate at the same wavelengths and substituting in the following equation:

$$C_{\text{CLP}} = \frac{m_{A2}(A_{AB1} - e_{AB1}) + m_{A1}(e_{AB1} - A_{AB2})}{m_{A2}m_{B1} - m_{A1}m_{B2}}$$

where  $e_{AB1}$  and  $e_{AB2}$  are the sum of intercepts of the linear calibrations at the two wavelengths ( $e_{AB1} = e_{A1} + e_{B1}$ ), 1 and 2 are the wavelengths 210 and 225 nm,  $m_A$  and  $m_B$  are the slopes of the linear regressions and C is the concentration of CLP.

Results obtained in Table 1 showed that the method is valid for the determination of CLP in different laboratory prepared mixtures in presence of up to 70% of its alkaline degradate with mean percentage recovery of  $99.93 \pm 1.612$ .

#### 4.2. Kinetic investigation

$D^2$  method was used to determine the order of the alkaline degradation rate of reaction by following the decrease in concentration of CLP within 8 h at 1 h time interval. Two different concentrations  $5.95 \times 10^{-3}$  and  $8.34 \times 10^{-3} \text{ mol L}^{-1}$  were used for

**Table 5**

Quantitative determination of Clopidogrel Bisulfate in Myogrel<sup>®</sup> tablets by the proposed methods and application of standard addition technique.

The proposed method	Myogrel <sup>®</sup> tablets 75 mg (Batch No. 060729) Recovery% <sup>a</sup> $\pm$ S.D.	Standard addition technique		
		Pure added ( $\mu\text{g mL}^{-1}$ )	Pure found <sup>b</sup> ( $\mu\text{g mL}^{-1}$ )	Recovery%
<b><math>D^2</math> Spectrophotometric method</b>				
At 270.6 nm	98.80 $\pm$ 1.155	10	9.86	98.60
		15	14.73	98.20
		20	19.88	99.40
		25	24.58	98.32
		Mean $\pm$ S.D.		
At 278.4 nm	100.20 $\pm$ 0.982	10	9.92	99.20
		15	14.84	98.93
		20	20.17	100.85
		25	24.62	98.48
		Mean $\pm$ S.D.		
<b><math>DD^1</math> Spectrophotometric method at 217.6 nm</b>	100.20 $\pm$ 1.216	10	10.04	100.40
		15	15.10	100.67
		20	19.95	99.75
		25	24.78	99.12
		Mean $\pm$ S.D.		
<b>Bivariate calibration method</b>	99.10 $\pm$ 0.930	10	10.11	101.10
		15	14.70	98.00
		20	19.98	99.90
		25	24.60	98.40
		Mean $\pm$ S.D.		
<b>TLC-densitometric method</b>	100.50 $\pm$ 2.082	0.8	0.785	98.13
		1	1.011	101.10
		1.2	1.226	102.17
		1.4	1.425	101.79
		Mean $\pm$ S.D.		

<sup>a</sup> Average of six experiments.

<sup>b</sup> Average of three experiments.



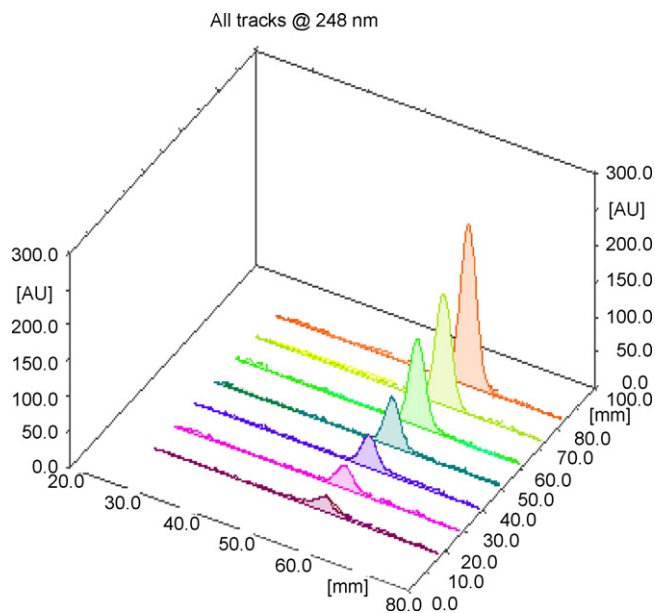


**Fig. 9.** Thin layer chromatogram of Clopidogrel Bisulfate in the concentration range 0.6–3  $\mu\text{g}/\text{band}$  ( $R_f=0.646 \pm 0.05$ ) using a mobile phase hexane:methanol:ethyl acetate (8.7:1:0.3, v/v/v).

the study. Fig. 6 is a plot of log of the remaining concentrations versus time. The slope ( $S$ ) of the obtained curves was nearly the same and the linear relationship obtained indicates that the reaction follows first order kinetics.

**Table 6**

Quantitative determination of Clopidogrel bisulfate in Stroka® tablets by the proposed methods and application of standard addition technique.

The proposed method	Stroka® tablets 75 mg (Batch No. 230/206) Recovery% <sup>a</sup> $\pm$ S.D.	Standard addition technique		
		Pure added ( $\mu\text{g mL}^{-1}$ )	Pure found <sup>b</sup> ( $\mu\text{g mL}^{-1}$ )	Recovery%
<b>D<sup>2</sup> spectrophotometric method</b>				
At 270.6 nm	100.80 $\pm$ 0.802	10	10.03	100.30
		15	15.18	101.20
		20	19.88	99.40
		25	25.18	100.72
Mean $\pm$ S.D.				100.41 $\pm$ 0.764
At 278.4 nm	101.60 $\pm$ 1.030	10	10.01	100.10
		15	15.30	102.00
		20	20.07	100.35
		25	24.62	98.48
Mean $\pm$ S.D.				100.23 $\pm$ 1.441
<b>DD<sup>1</sup> spectrophotometric method at 217.6 nm</b>				
	100.70 $\pm$ 1.342	10	10.01	100.10
		15	14.98	99.87
		20	19.84	99.20
		25	25.39	101.56
Mean $\pm$ S.D.				100.18 $\pm$ 0.995
<b>Bivariate calibration method</b>				
	100.66 $\pm$ 1.530	10	9.89	98.90
		15	14.89	99.27
		20	20.27	101.35
		25	25.32	101.28
Mean $\pm$ S.D.				100.20 $\pm$ 1.297
<b>TLC-densitometric method</b>				
	101.40 $\pm$ 1.887	0.8	0.798	99.75
		1	0.989	98.90
		1.2	1.226	102.17
		1.4	1.414	101.00
Mean $\pm$ S.D.				100.46 $\pm$ 1.432

<sup>a</sup> Average of six experiments.

<sup>b</sup> Average of three experiments.

Alkaline catalyzed hydrolysis is a bimolecular reaction, but one of the reactants is water, which is present in large excess, so the change in concentration is negligible. Such reactions where one of the reactants is present in large excess are considered to follow pseudo-first order kinetics and all equations describing first order can be applied for it. The rate of degradation ( $K$ ) and the  $t_{1/2}$  of the reaction were calculated from the equation  $S=K/2.303$ , while  $t_{1/2}=0.693/K$  [24] and the results are presented in Table 3.

To study the effect of NaOH concentration on the reaction rate, experiments were performed using 0.5N and 1N NaOH. Fig. 7, shows that the reaction rate was increased by elevating the sodium hydroxide concentration. Temperature was essential for complete alkaline degradation.

The last method is a TLC-densitometric method. This technique offers a simple way to quantify directly on TLC plate by measuring the optical density of the separated bands. The amounts of compounds are determined by comparing to a standard curve from reference materials chromatographed simultaneously under the same condition [25].

To improve separation of bands, it was necessary to investigate the effect of different variables. Studying the optimum parameters for maximum separation was carried out as following:

### 1. Mobile phase

Different developing systems of different composition and ratios were tried for separation, e.g. chloroform–ethyl acetate (9.5:0.5, v/v), chloroform–hexane (5:5, v/v), hexane–methanol (9.5:0.5, v/v) and hexane–ethyl acetate–acetic acid (8:2:0.1, v/v/v). The best mobile phase was hexane–methanol–ethyl acetate in ratio (8.7:1:0.3, v/v/v). This selected mobile phase

**Table 7**  
Assay parameters and method validation obtained by applying the proposed methods for the determination of Clopidogrel Bisulfate.

Parameters	D <sup>2</sup> spectrophotometric method		DD <sup>1</sup> spectrophotometric method at 217.6 nm	Bivariate calibration		TLC-densitometric method
	At 270.6 nm	At 278.4 nm		At 210 nm	At 225 nm	
Range	4–37 µg mL <sup>-1</sup>		5–38 µg mL <sup>-1</sup>	5–38 µg mL <sup>-1</sup>		0.6–3 µg/band
Linearity						
Slope	0.0066	0.0089	0.0172	0.0307	0.0271	0.1867 × 10 <sup>4</sup>
Intercept	-0.0145	-0.0201	-0.0155	0.0213	0.0068	0.1153 × 10 <sup>4</sup>
Correlation coefficient (r)	0.9999	0.9999	0.9999	0.9999	0.9999	0.9996
Accuracy (mean ± S.D.)	99.73 ± 0.634	100.38 ± 1.101	99.90 ± 0.914	100.20 ± 1.058	100.29 ± 1.041	99.97 ± 1.161
Specificity	99.32 ± 1.182	99.43 ± 1.464	100.20 ± 1.301	99.93 ± 1.612	100.06 ± 1.738	
Precision (R.S.D.%)						
Repeatability <sup>a</sup>	0.512	0.457	0.788	0.994	1.322	
Intermediate precision <sup>b</sup>	0.882	0.799	1.003	1.11	1.624	
LOD <sup>c</sup>	0.81 µg mL <sup>-1</sup>	0.75 µg mL <sup>-1</sup>	1.30 µg mL <sup>-1</sup>	1.2 µg mL <sup>-1</sup>	1.4 µg mL <sup>-1</sup>	0.04 µg/band
LOQ <sup>c</sup>	2 µg mL <sup>-1</sup>	2.2 µg mL <sup>-1</sup>	3.50 µg mL <sup>-1</sup>	3.2 µg mL <sup>-1</sup>	3 µg mL <sup>-1</sup>	0.4 µg/band

<sup>a</sup> The intraday ( $n = 3$ ), average of three different concentrations repeated three times within day.

<sup>b</sup> The interday ( $n = 3$ ), average of three different concentrations repeated three times in three successive days.

<sup>c</sup> Limit of detection and limit of quantitation are determined experimentally for TLC-densitometric method and via calculations for the other methods.

**Table 8**  
Statistical comparison of the results obtained by the proposed methods and the official method.

Parameters	The proposed methods				Official method <sup>a</sup>	
	D <sup>2</sup> spectrophotometric method		DD <sup>1</sup> spectrophotometric method at 217.4 nm	Bivariate calibration		TLC-densitometric method
	At 270.6 nm	At 278.4 nm				
Mean	99.72	100.46	99.88	99.27	99.97	99.86
S.D.	0.668	0.646	0.909	1.115	1.161	1.116
R.S.D.%	0.670	0.643	0.910	1.123	1.161	1.118
$n$	8	8	10	8	7	7
Variance	0.446	0.418	0.826	1.243	1.347	1.246
Student's $t$ -test	0.299 (2.160) <sup>b</sup>	1.288 (2.160) <sup>b</sup>	0.050 (2.131) <sup>b</sup>	1.020 (2.160) <sup>b</sup>	0.178 (2.179) <sup>b</sup>	
$F$ -Value	2.79 (3.87) <sup>b</sup>	2.98 (3.87) <sup>b</sup>	1.51 (3.37) <sup>b</sup>	1.00 (3.87) <sup>b</sup>	1.08 (4.28) <sup>b</sup>	

<sup>a</sup> Official HPLC method USP (RP-HPLC using acetonitrile:0.05 M KH<sub>2</sub>PO<sub>4</sub> 25:75, and UV detection at 220 nm, flow rate 1 mL/min).

<sup>b</sup> Figures between parentheses represent the corresponding tabulated values of  $t$  and  $F$  at  $P = 0.05$ .

allows the determination of CLP without interference from its alkaline degradate and without tailing of the separated bands, Fig. 8.

## 2. Band dimensions

Different band dimensions were tested in order to obtain sharp and symmetrical separated peaks. The optimum band width chosen was 5 mm and the inter-space between bands was 5 mm.

## 3. Scanning wavelength

Different scanning wavelengths were tried, although peaks at 220 nm ( $\lambda_{\max}$  of CLP) gave higher sensitivity, but at 248 nm, peaks were more sharp and symmetrical and minimum noise was obtained.

## 4. Slit dimensions of scanning light beam

The slit dimensions of the scanning light beam should ensure complete coverage of band dimensions on the scanned track without interference of adjacent bands. Different slit dimensions were tried, where 5 mm × 0.2 mm proved to be the slit dimension of choice which provides highest sensitivity.

## 5. System suitability

Parameters including resolution ( $R_s$ ), peak symmetry, capacity factor ( $K'$ ) and selectivity factor ( $\alpha$ ) were calculated using 1 µg/band of CLP. The resolution is always above two, the selectivity more than one and an accepted value for symmetry factor was obtained, as shown in Table 4.

This method is based on the difference in the  $R_f$  values of CLP ( $R_f = 0.646 \pm 0.05$ ) and degradate ( $R_f = 0.247 \pm 0.03$ ), as shown in Fig. 9.

The calibration curve was constructed by plotting the integrated peak area versus the corresponding concentration in the range of 0.6–3 µg/band for CLP. The regression equation was calculated and found to be

$$A = 0.1867 \times 10^4 C + 0.1153 \times 10^4, \quad r = 0.9996$$

where  $Y$  is the integrated peak area,  $C$  is the concentration of CLP in µg/band and  $r$  is the correlation coefficient.

Results described in Table 1, showed that this method is specific, valid and applicable for determination of CLP in presence of up to 90% of its alkaline degradate with mean percentage recovery  $100.06 \pm 1.738$ .

As the method could effectively separate the drug from its degradation product, it can be employed as a stability indicating one.

The suggested methods are valid and applicable for the analysis of CLP in Myogrel<sup>®</sup> and Stroka<sup>®</sup> tablets. The validity of the proposed methods was assessed by applying the standard addition technique, which showed accurate results and there is no interference from excipients as shown in Tables 5 and 6.

Method validation was performed according to USP guidelines [26] for all the proposed methods. Table 7 shows results of accuracy, repeatability and intermediate precision of the methods.

Table 8 shows statistical comparison of the results obtained by the proposed methods and the official HPLC method [26]. The calculated  $t$  and  $F$  values are less than the theoretical ones indicating that there is no significant difference between the proposed methods and the official method with respect to accuracy and precision. One-way ANOVA was applied for the

comparison of these methods where There is no significant difference between the proposed methods and the official method as  $F_{\text{calculated}}(2.330) < F_{\text{tabulated}}(1.061)$ .

## 5. Conclusion

The present work is concerned with the determination of CLP in presence of its alkaline degradate. In this paper simple, sensitive and rapid methods are described for determination of CLP in pure form or in pharmaceutical formulations.

Reviewing literature in hand no other spectrophotometric methods concerned with the determination of CLP in presence of its alkaline degradate which is pharmacologically inactive while degradation product was not identified in other published TLC-densitometric method and no synthetic mixtures were prepared to check the specificity of the method.

$D^2$  and  $DD^1$  spectrophotometric methods are well-established techniques that are able to enhance the resolution of overlapping bands. These methods are simple, more convenient, less time consuming and economic stability indicating methods compared to other published LC methods.

Kinetic studies of the decomposition of drugs using stability testing techniques are essential for the quality control of such products. In this work, a kinetic investigation of alkaline degradation of CLP Bisulfate was done.

Bivariate calibration method provided simple and rapid determination of CLP with minimal sample and data manipulation.

The advantages of TLC-densitometric method is that several samples can be run simultaneously using a small quantity of mobile phase unlike HPLC, thus lowering analysis time and cost per analysis and provides high sensitivity and selectivity.

High values of correlation coefficients and small values of intercepts validated the linearity of the calibration graphs and the obedience to Beer's law. The R.S.D. values, the slopes and the intercepts of the calibration graphs indicated the high reproducibility of the proposed methods.

From the results obtained, we concluded that the suggested methods showed high sensitivity, accuracy, reproducibility and specificity and can be used as stability indicating methods. Moreover, these methods are simple and inexpensive, permitting their application in quality control laboratories.

## References

- [1] The Merck Index, in: S. Budavari (Ed.), An Encyclopedia of Chemicals, Drugs and Biologicals, 13th edn., Merck & Co., Inc., 2002.
- [2] K. Moshfegh, M. Redondo, F. Julmy, W.A. Wuillemin, M.U. Gebauer, A. Haeberli, B.J. Meyer, *J. Am. Coll. Cardiol.* 36 (2000) 699.
- [3] S.J. Gardell, *Perspect. Drug Disc. Des.* 1 (1993) 521.
- [4] J. McEwen, G. Strauch, P. Perles, G. Pritchard, T.E. Moreland, J. Necciari, J.P. Dickinson, *Thromb. Haemost.* 25 (1999) 45.
- [5] H. Caplain, F. Donat, C. Gaud, J. Necciari, *Thromb. Haemost.* 25 (1999) 25.
- [6] P. Savi, J. Combalbert, C. Gaich, M.C. Rouchon, J.P. Maffrand, Y. Berger, J.M. Herbert, *Thromb. Haemost.* 72 (1994) 313.
- [7] P. Savi, P. Nurden, A.T. Nurden, S. Levy-Toledano, J.M. Herbert, *Platelets* 9 (1998) 251.
- [8] J.M. Herbert, D. Frehel, E. Vallee, G. Kieffer, D. Gouy, Y. Berger, J. Necciari, G. Defreyn, I.P. Maffrand, *Cardiovasc. Drug Rev.* 11 (1993) 180.
- [9] M. Reist, M. Roy-de Vos, J.P. Montseny, J.M. Mayer, P.A. Carrupt, Y. Berger, B. Testa, *Drug Metab. Dispos.* 28 (2000) 1405.
- [10] A. Mitakos, I. Panderi, *J. Pharm. Biomed. Anal.* 28 (2002) 431.
- [11] A. Mohan, M. Hariharan, E. Vikraman, G. Subbaiah, B.R. Venkataraman, D. Saravanan, *J. Pharm. Biomed. Anal.* 47 (2008) 183.
- [12] S.S. Singh, R. Sharma, D. Barot, P.R. Mohan, V.B. Lohray, *J. Chromatogr. B* 821 (2005) 173.
- [13] G. Bahrami, B. Mohammadi, S. Siskhtnezhad, *J. Chromatogr. B* 864 (2008) 168.
- [14] P. Lagorce, Y. Perez, J. Ortiz, J. Necciari, F. Bressole, *J. Chromatogr. B: Biomed. Appl.* 720 (1998) 107.
- [15] A. Mitakos, I. Panderi, *Anal. Chim. Acta* 505 (2004) 107.
- [16] A. Robinson, J. Hillis, C. Neal, A.C. Leary, *J. Chromatogr. B* 848 (2007) 344.
- [17] H. Agrawal, N. Kaul, A.R. Paradkar, K.R. Mahadik, *Talanta* 61 (2003) 581.
- [18] ICH, *Stability Testing of New Drug Substances and Products International Conference on Harmonization*, Geneva, 1993.
- [19] J.J. Berzas Navado, J. Rodriguez Flores, M.J. Villasenor Lierena, *Anal. Lett.* 27 (1994) 1009.
- [20] P.L. López-de-Alba, L.L. Martinez, K.W. Kaczmarzyc, K. Wróbel, J.A. Hernandez, *J. Anal. Lett.* 29 (1996) 487.
- [21] P.L. López-de-Alba, L.L. Martinez, K.W. Kaczmarzyc, K. Wróbel, J.A. Hernandez, *Bol. Soc. Chilena Quim.* 41 (1996) 111.
- [22] D.L. Massart, B.G.M. Vandeginste, S.N. Deming, Y. Michotte, L. Kaufman, *Chemometrics*, Elsevier, Amsterdam, 1988, p. 124.
- [23] P.L. López-de-Alba, L.L. Martinez, K.W. Kaczmarzyc, K. Wróbel, M.L.Y. Murrieta, M.L.Y. Murrieta, J.A. Hernandez, *J. Pharm. Biomed. Anal.* 16 (1997) 349.
- [24] A. Martin, J. Swarbrick, A. Cammarata, *Physical Pharmacy*, 3rd edn., Lea and Febiger, Philadelphia, 1983, pp. 359–360.
- [25] N. Grinberg, *Modern Thin-layer Chromatography*, Marcel Dekker Inc., New York, 1990, p. 249.
- [26] The United States Pharmacopeia and National Formulary, *The Official Compendia of Standards*, Asian Edition, USP 30-NF 25 The United States Pharmacopeial Convention Inc., Rockville, MD, 2007.



## Direct determination of anabolic steroids in pig urine by a new SPME–GC–MS method

Zhuomin Zhang, Hongbin Duan, Lan Zhang\*, Xi Chen, Wei Liu, Guonan Chen\*

Key Laboratory of Analysis & Detection for Food Safety of Ministry of Education, College of Chemistry and Chemical Engineering, Fuzhou University, Fuzhou, Fujian 350002, PR China

### ARTICLE INFO

#### Article history:

Received 21 October 2008

Received in revised form 9 January 2009

Accepted 13 January 2009

Available online 23 January 2009

#### Keywords:

Anabolic steroids

SPME

GC–MS

Pig urine

### ABSTRACT

A new solid phase microextraction (SPME) method coupled with gas chromatography–mass spectrometry (GC–MS) was developed for rapid determination of four anabolic steroids such as 3 $\alpha$ -hydroxy-5 $\alpha$ -androstane-17-one (HA), dihydrotestosterone (DHT), androstenedione (AD) and methyltestosterone (MT) in pig urine. SPME was used to extract the four anabolic compounds directly without derivatization. The optimum SPME sampling conditions were based on the home-made carbowax-divinylbenzene (CW-DVB) fiber coating during extraction at 40 °C for 50 min with 0.18 g/mL NaCl solution and 750 rpm stirring speed. The linear ranges of the proposed method were in the range of 8–640 pg/mL for HA and DHT and 16–510 pg/mL for AD and MT, respectively. The detection limits (S/N=3) were from 2 to 8 pg/mL for the four anabolic steroids. This SPME method provided very high enrichment factors for the four anabolic steroids, which were 1063-fold and 965-fold for HA and DHT at the concentration of 8 pg/mL and 207-fold and 451-fold for AD and MT at the concentration of 16 pg/mL, respectively. The recoveries ranged from 71.3 to 121%, and the RSDs were lower than 12.9%. The method was sensitive and reliable for determination of trace anabolic steroids in biological samples.

© 2009 Elsevier B.V. All rights reserved.

### 1. Introduction

Until now, anabolic steroids have been used as growth promoters in livestock farming for more than 30 years. The use of anabolic steroids could result in increasing the muscular mass of the animals, but led to change the animal origin at the same time. When anabolic steroids are acted as growth promoters, it would take a greatly potential risk of harming the public health of consumers from possible developmental, neurobiological, genotoxic and carcinogenic effects due to the intake of their residues and metabolites. Therefore, anabolic steroids have been banned as the animal growth promoters in the European Community since 1986 [1]. Moreover, anabolic steroids are on the list of prohibited substances published by the World Anti-Doping Agency (WADA) [2,3]. The residues of anabolic steroids in biological samples such as animal urine and human urine could be considered good biomarkers for evaluating the abuse of anabolic steroids.

Determination of anabolic steroids in biological samples has been carried out by some techniques, such as gas chromatography (GC) [4], high performance liquid chromatography (HPLC) [5,6], gas chromatography–mass spectrometry (GC–MS) [7–17] and high performance liquid chromatography–mass spectrometry (HPLC–MS)

[18–25]. Among them GC–MS is a major suitable technique for the assay of anabolic steroids. However, it always required the complicated sample preparation and derivatization to achieve good GC–MS detection result [7,9,10]. The detection limits of the analyses of anabolic steroids by GC–MS with traditional sample preparation methods usually ranged from microgram to nanogram level [11–17], which could not satisfy the rapid determination of trace anabolic steroids in biological samples nowadays. Thus, the appropriate preconcentration methods have been imperative before development of analytical methods with enough sensitivity for the unambiguous detection and confirmation of these substances.

Conventional preconcentration methods for the determination of trace anabolic steroids in the previous works are mainly liquid–liquid extraction (LLE) [2,6,7,9,18] and solid phase extraction (SPE) [3,26,27]. These methods always required the long extraction time, big solvent amounts and multiple consequent steps. Therefore, seeking simple and efficient preconcentration methods have been one of the greatest challenges for the analysis of anabolic steroids. Solid phase microextraction (SPME), developed by Pawliszyn and co-workers [28,29], is a simple and solvent-saving sampling method, which has been widely used in the environmental [30], biological [31], pharmaceutical [32] and other field analyses [33]. SPME merges the extraction, concentration and introduction in one step, greatly reduces preparation time and increases sensitivity simultaneously over other extraction methods [34]. Especially when SPME is directly coupled to GC–MS,

\* Corresponding author. Tel.: +86 591 87893207; fax: +86 591 87892482.  
E-mail addresses: [zlan@fzu.edu.cn](mailto:zlan@fzu.edu.cn) (L. Zhang), [gnchen@fzu.edu.cn](mailto:gnchen@fzu.edu.cn) (G. Chen).

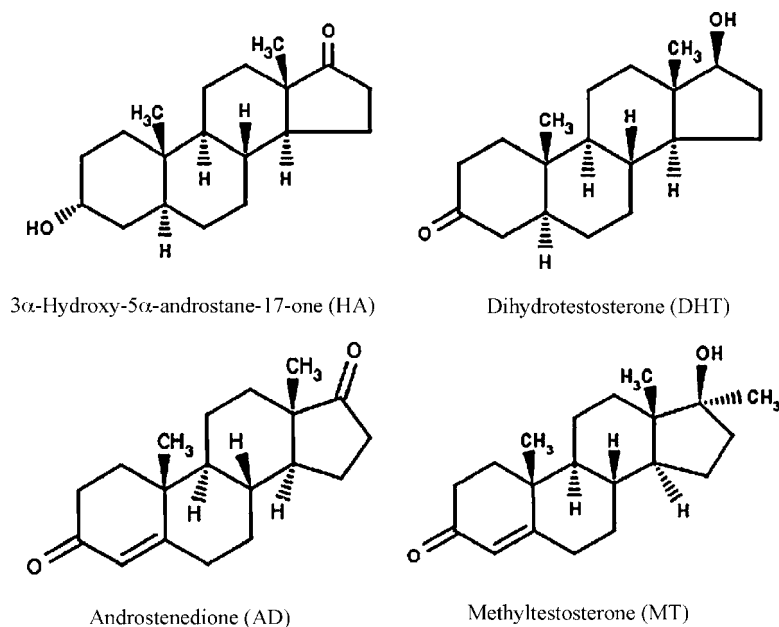
sample preparation, separation, detection and structure interpretation could be inoculated perfectly, which makes the whole analytical procedure simple and fluent. Recently SPME–GC–MS has been used to analyze the single  $\beta$ -agonist clenbuterol [4] and other anabolic steroids such as dehydroisoandrosterone, estrone,  $17\beta$ -estradiol, testosterone, pregnenolone, etc. [8,35]. Although the results suggested the improvement of analytical sensitivity, most works needed the complicated and time-consuming derivatization procedures prior to GC–MS detection. In our work, SPME was used to directly extract the anabolic steroids from the pig urine samples without any derivatization procedures followed by GC–MS detection. This analytical technique possessed the obvious simplicity in comparison with the other techniques mentioned above. Moreover, the analytical targets were different from the present work.

In the present paper, it is the first time to establish a simple and sensitive method for the determination of four anabolic steroids, namely  $3\alpha$ -hydroxy- $5\alpha$ -androstane-17-one (HA), dihydrotestosterone (DHT), androstenedione (AD) and methyltestosterone (MT) in pig urine simultaneously by direct SPME–GC–MS without any complicated derivatization procedures. Some important factors influencing the SPME extraction efficiency were taken into account including the type of SPME fiber coating, thickness of SPME fiber coating, stirring speed, extraction temperature, extraction time, concentration of ionic strength of the sample solution, the pH value of the sample solution, and the thermal desorption temperature and time. SPME and GC–MS conditions were optimized to achieve the good extraction efficiency and distinguishing analytical sensitivity. The detection limits were achieved in picogram/milliliter level, and good recovery and reproducibility were obtained.

## 2. Experimental

### 2.1. Chemicals

HA and AD were obtained from Sigma (St. Louis, MO, USA). DHT was purchased from Tokyo Chemical Industry Co. Ltd. (Tokyo, Japan). MT was purchased from National Institute for the Control of Pharmaceutical and Biological Products (Beijing, China). The structures of the four anabolic steroids are shown in Scheme 1.



Scheme 1. Structures of the four anabolic steroids.

Acetone (HPLC grade), methyl methacrylate (MMA) and benzoyl peroxide (BPO) were purchased from Fucheng Chemical Reagents (Tianjin, China). Methanol (HPLC grade), trifluoroacetic acid and polyethylene glycol 20000 (PEG-20000) were obtained from Sinopharm Chemical Reagent Co. Ltd. (Shanghai, China). Hydroxyl silicone oil (OH-TSO) and polymethylhydrosiloxane (PMHS) were from Santai Organic Silicon Materials (Kaihua, China). Tetramethoxysilane (TMOS) was obtained from Dongou Chemical Reagents (Jintan, China). Divinylbenzene (DVB) was obtained from Shengzhong Fine Chemicals (Shanghai, China). Methyl tert-butyl ether was purchased from Fisher ChemAlert Guide. Silica fiber was purchased from Yongnian Ruifeng Chromatographic Device Co. Ltd. (Hebei, China). C18 SPE column was purchased from Agilent (1000 mg/6 mL, US).

During SPME procedures,  $K_2HPO_4$  and  $NaH_2PO_4$  solution were used to adjust the pH of sample solution.  $K_2HPO_4$  solution (0.067 mol/L) was prepared by dissolving 15.20 g of  $K_2HPO_4 \cdot 2H_2O$  in 1000 mL fresh deionized water.  $NaH_2PO_4$  solution (0.067 mol/L) was prepared by dissolving 10.40 g  $NaH_2PO_4 \cdot 2H_2O$  in 1000 mL of fresh deionized water. All solutions were prepared with fresh deionized ultrapure water. Solid buffering agent for SPE was prepared by mixing  $NaHCO_3$  with  $Na_2CO_3$  (w/w = 8:1, pH 8.8–8.9).

Stock standard solutions of HA, DHT, AD and MT (1 mg/mL) were prepared in methanol and stored at 4 °C in dark. Working solutions were prepared by appropriate dilution of the stock standard solutions with acetone and were stored at 4 °C in dark.

### 2.2. Instrumentation

The Agilent 6890N GC-5973i MS system with 7893 series auto-sampler was used in the study (Agilent Scientific, USA). The home-made SPME device based on the normal GC microsyringe was used to extract the four anabolic steroids in pig urine. Ultrapure water was produced with Milli-Q ultrapure water system (Millipore, Bedford, USA). HGC-24A pressured gas blowing concentrator (Jingyi technologies, Xiamen, China), DF-101S portable heating magnetic whisk (Yuhua instruments, Gongyi, China) and PHS-3C pH Meter (Dapu instruments, Shanghai, China) were used for the preparation of SPME fiber coatings and SPME procedures. 10-Position SPE vacuum manifold instruction sheet was purchased

from Agilent Scientific, USA. The surface property of home-made SPME fiber coatings was monitored by environmental scanning electron microscope (XL30 ESEM, Philips).

### 2.3. GC–MS analysis

Chromatographic separation was performed with an HP-5MS (Agilent Scientific, USA) capillary column (30 m length  $\times$  0.25 mm I.D.  $\times$  0.25  $\mu$ m film thickness). Column flow was volumetric at 1.0 mL/min using ultrapurified helium (>99.999%) as carrier gas. Injection was in splitless mode at 260 °C with a 12 min solvent delay. The transfer line temperature was set at 300 °C. The MS analyzer was set at 70 eV, electron impact source temperature of 230 °C, electron-multiplier voltage 1588 mV. The temperature program was as following: initial 100 °C (5 min) to 250 °C at ramp rate of 25 °C/min, 250 °C for 7 min, from 250 °C to 310 °C at ramp rate of 30 °C/min. The identification of target anabolic steroids was based on the standard mass spectra of the National Institute of Standards and Technology (NIST) MS spectral library, standard compounds and the corresponding references [36–39]. Ions for monitoring HA, DHT, AD and MT at  $m/z$  were the ion fraction groups of (290, 107, 270 and 108), (231, 290, 55 and 163), (286, 124, 148 and 244) and (124, 43, 91 and 302) respectively on the basis of results obtained from an initial scan from 40 to 400 AMU. The quantization was based on the Extracted Ionization Chromatograms (EICs), and the corresponding quantitative ions for HA, DHT, AD and MT at  $m/z$  were 290, 231, 286 and 124, respectively.

### 2.4. Preparation of the home-made SPME fiber coatings

Four fiber coatings with different polarities were prepared by the use of sol–gel method. Prior to sol–gel coating, commercial fiber was immersed in acetone for 15 min to remove the polyimide on its surface, then rinsed with the deionized water and dried. After that, the fiber was immersed in 1 mol/L sodium hydroxide solution for 60 min, then rinsed with the deionized water and dried. Finally, the fiber was immersed in 0.1 mol/L hydrochloric acid for 20 min, then also rinsed with deionized water again and dried. The procedure was repeated three times.

Four kinds of fiber coatings, carbowax-divinylbenzene (CW-DVB) [40], carbowax (CW) [41], hydroxyl silicone oil-polymethyl-hydrosiloxane (OH-TSO-PMHS) [42] and polyacrylate (PA) [43] were prepared according to the procedures in the previous reports with some improvements. For the preparation of CW-DVB fiber coating, 400  $\mu$ L of TMOS, 200  $\mu$ L of OH-TSO, 50  $\mu$ L of PMHS, 300  $\mu$ L of TFA, 200  $\mu$ L of DVB, 200 mg of PEG-20000 and 400  $\mu$ L of acetone were mixed in a 2 mL tube and then shaken by the use of Vortex Shaker (Qilin medical instruments, Haimeng, China) until PEG-20000 was dissolved. The mixture was treated in an ultrasonicator for 5 min and centrifuged at 4000 rpm for 10 min. The top clear sol solution was transferred into a 0.5 mL tube for the consequent preparation of fiber coating. The fiber was immersed vertically into the sol solution for 40 min and then dried naturally. The procedure was repeated 4 times by using of the fresh sol solution each time. Then the fiber was placed in the desiccator at room temperature for 12 h. The sol–gel coated fiber was initially conditioned in the GC inlet set at 230 °C under N<sub>2</sub> protection for 2 h. After cooling to room temperature, the fiber was adjusted again at 250 °C for 10 min. The conditioning procedure was repeated a few times before the experiment until the stable GC baseline was achieved. The surface property of CW-DVB fiber coating was analyzed by ESEM. The sol–gel CW-DVB coatings possessed porous structures, which would significantly increase the available surface area of the fiber coating and further provide enhanced stationary phase loading and extraction capacity. And preparation procedures of other three kinds of fiber coatings were nearly the same as that of CW-DVB.

### 2.5. Sample preparation

For SPME procedure, 20 mL pig urine was put in a 25 mL glass vial followed by adding to 3.50 g NaCl. Under the magnetic agitation, SPME fiber coating was exposed in the sample solution for 50 min. Finally, the target compounds extracted by SPME were thermally desorbed by inserting the fiber directly into the GC injector set at 260 °C in splitless mode for 8 min.

In comparison with SPME, SPE procedures were conducted according to the previous reports [25,44,45]. The SPE column was activated with ultrapure water and methanol. Then, 5 mL pig urine was loaded on the SPE column following by 5 mL water rinsing to remove the impurity and then 5 mL methanol rinsing to elute the target compounds extracted in SPE column. The methanol eluate was dried by the N<sub>2</sub> blow and then dissolved in 1 mL ultrapure water. The pH of solution was adjusted by use of 100 mg solid buffer. After that, the anabolic steroids were extracted with 5 mL methyl-tert-butyl ether on a mechanical shaker for 1 min and then centrifuged for 15 min at 4000 rpm in order to remove precipitated proteins and other particulate matters. After centrifugation, the upper layer was evaporated to dryness under a N<sub>2</sub> flow. The residue was redissolved in the 0.1 mL methanol for the GC–MS analysis.

## 3. Results and discussion

### 3.1. Selection of fiber coatings

During the SPME process, the property of SPME fiber coatings plays a crucial role in the extraction procedure. Some useful and specific factors should be taken into consideration, such as polarity, matrix, etc. Four home-made SPME fiber coatings (CW-DVB, CW, OH-TSO-PMHS and PA) were compared for the good extraction efficiency. Fig. 1 shows the results of the optimization of SPME fiber coatings. It could be seen from the figure that the better detector responses of all target compounds were achieved by use of CW-DVB fiber coatings. According to the “like dissolve like” principle, the polar anabolic steroids have a higher affinity toward the polar CW-DVB fiber coating, so it was selected as the optimized fiber coating. The experiments also demonstrated (see Fig. 1) when the fiber was immersed vertically into the sol solution for 40 min, the best effective was achieved.

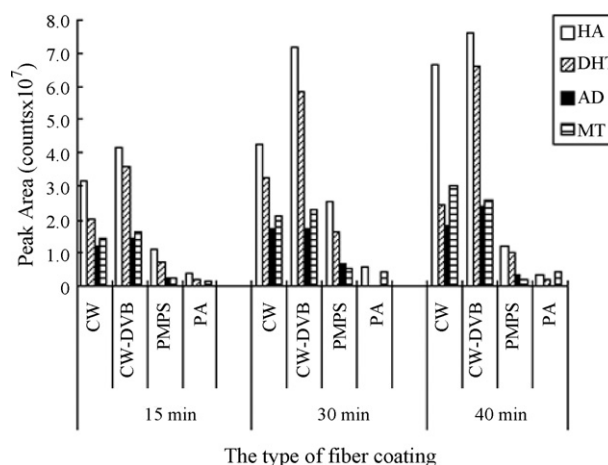


**Fig. 1.** Selection of SPME fiber coatings GC–MS conditions: 100 °C for 5 min, then heated at 25 °C/min to 250 °C, for 7 min, and then heated at 30 °C/min to 310 °C; injection temperature, 260 °C; ion source temperature, 230 °C. SPME conditions: extraction time, 50 min; extraction temperature, 40 °C; stirring speed, 750 rpm; pH 7.00; NaCl concentrations, 0.18 g/mL; desorption temperature, 260 °C; desorption time, 8 min.

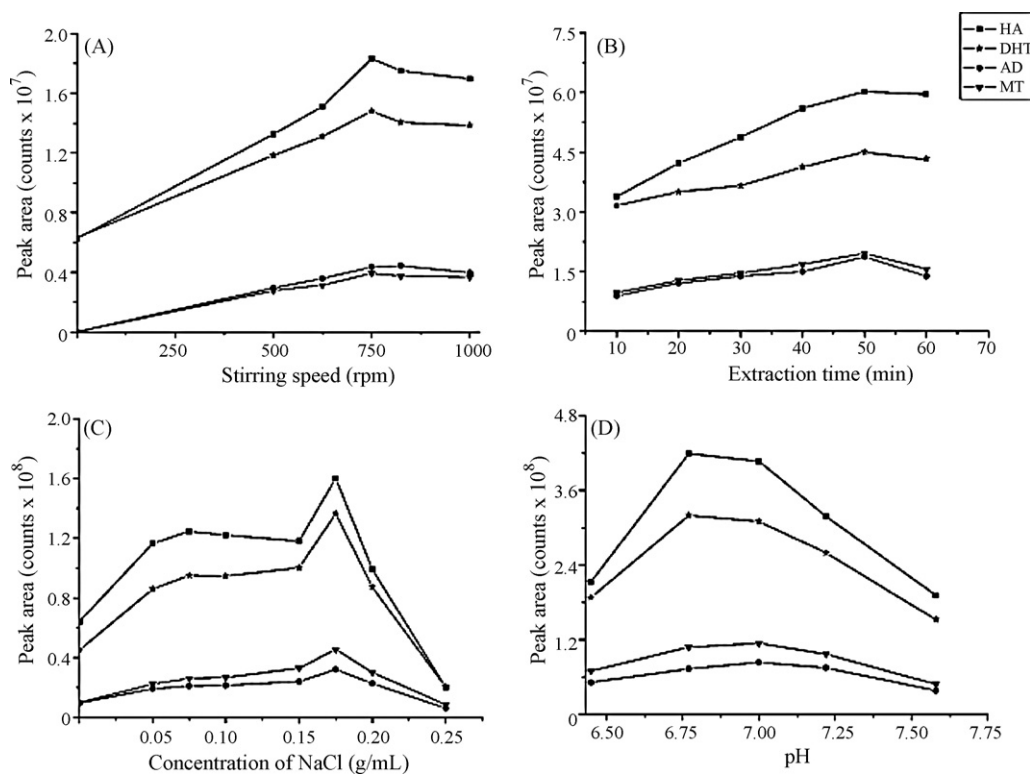


**Fig. 2.** Optimization of SPME conditions (A) optimization of the stirring speed; (B) optimization of the extraction time; (C) optimization of ion strength of the sample solution (expressed as NaCl concentration in sample solution); (D) optimization of the pH of sample solution; SPME and GC-MS conditions as in Fig. 1.

### 3.2. Optimization of SPME conditions

In order to obtain the good extraction efficiency and high analytical sensitivity, the factors influencing SPME samplings were optimized. The results are shown in Fig. 2.

Appropriately stirring the sample solution could accelerate the diffusion of analytes from the water solution to the SPME fiber coatings, reduce the extraction time and improve the extraction efficiency. Fig. 2A shows the results of the stirring speed optimization. It is obvious that the responses of the target compounds increase very much under stirring. Then, the effects of stirring speed on the responses of the target compounds were investigated in detail at the stirring speed ranging from 500 to 1000 rpm. It could be seen from Fig. 2A that the responses of the four anabolic steroids increased with the stirring speed in the range of 500–750 rpm. After the stirring speed exceeded 750 rpm, the extraction reached equilibrium and the responses of the analytes did not increase with the increase in stirring speed. Therefore, 750 rpm was selected as the optimum stirring speed.

Increasing extraction temperature could accelerate the mass transfer and raise the extraction efficiency. The effects of extraction temperature on extraction efficiency were examined at the temperatures of 30, 40, 50 and 60 °C, respectively. The best responses of the target compounds were obtained at the extraction temperature of 40 °C. Therefore, 40 °C was preferred as optimum extraction temperature.

The extraction time is another important factor influencing the SPME efficiency. The extraction time profile of the CW-DVB fiber coating for the four anabolic steroids under the optimized stirring condition (750 rpm, 40 °C) is shown in Fig. 2B. It could be seen from the figure that the responses of all of the target compounds increased with the increase in extraction time until 50 min. At 50 min, the responses of most compounds reached the highest level, thus 50 min was selected as the optimum extraction time.

The ion strength of the sample solution was optimized by spiking a series of NaCl concentrations ranging from 0 to 0.25 g/mL into the sample solution. Fig. 2C shows the results of ion strength optimization. The responses of the anabolic steroids increased with the increasing in NaCl concentration until 0.18 g/mL. Inorganic salts could reduce the affinity of organic compounds in water layer (also call “salting out effect”) and result in the increasing extraction efficiency. However, the high NaCl concentration would make the analytes ionized and dissolved in the matrix solution and reduce the extraction efficiency of the analytes on the contrary. Considering the overall responses of the target compounds, 0.18 g/mL NaCl solution was selected as the optimum level of ion strength.

Generally, weakly acidified sample solution could prevent the organic analytes from dissociating during SPME process and increase the extraction efficiencies [43]. The effects of the pH of the sample solution were examined at pH 6.50–7.60 carefully (adjusted by  $K_2HPO_4$  and  $NaH_2PO_4$ ). Fig. 2D shows that the effects of pH on the responses of MT and AD were insignificant. The responses of HA and DHT increased when the pH of sample solution increased from 6.50 to 6.75, whereas their responses decreased when the pH of sample solution increased from 6.75 to 7.50. However, all the compounds showed the good response of pH 7.00. Considering the analytical responses of all the anabolic steroids and operation convenience, pH 7.00 was selected as the optimum value.

The desorption temperature and time were optimized at last. The experiment showed that the desorption amount of the target compounds increased with the increasing desorption temperature and almost desorbed completely at the temperature of 260 °C. Comparing the responses of target compounds when desorption time ranged from 4 to 12 min, desorption time of 8 min resulted in the best responses of the four anabolic steroids. Considering the overall detector responses and the fiber coating life, 260 °C and 8 min were selected as the optimum desorption temperature and time, respectively.

### 3.3. Validation

On the basis of the experiments discussed above, the optimal SPME conditions for the four anabolic steroids were based on the CW-DVB fiber during extraction at 40 °C for 50 min with 0.18 g/mL NaCl solution and 750 rpm stirring speed. The thermal desorption of analytes from the SPME fiber coating was conducted at 260 °C for 8 min.

In order to clarify the enrichment capacity of SPME, the calibration curves of the standard solutions based on the direct injection and SPME procedures injection were constructed under the optimum experimental conditions by linear curve fitting using the least square linear regression calculation, respectively. The chromatograms of mixed standard solution by direct injection (1.00 µg/mL) and SPME (0.50 ng/mL) procedures are shown in Fig. 3A and B, respectively. The linearity was good for all analytes in the whole range of tested concentrations, as proved by the correlation coefficients ( $R^2$ ) being greater than 0.9935 for all curves. The linear ranges, regression equations, detection limits and enrichment factors of four anabolic steroids by direct injection and SPME procedures are demonstrated in Table 1. The detection limits of SPME sampling projects were 5000 (for HA and DHT) and 6250 (for AD and MT) times lower than those of direct injection projects. The detection limits of four anabolic steroids were at pg/mL level, ranging from 2 to 8 pg/mL. The SPME methods provided very high enrichment factors for the four anabolic steroids, namely 1063-fold for HA and 965-fold for DHA at the concentration of 8 pg/mL and 207-fold for AD and 451-fold for MT at the concentration of 16 pg/mL, respectively. It is obvious that the detection limits and enrichment factors obtained by this direct SPME–GC–MS method are much better than those of conventional methods by use of derivatization.

Under the optimum conditions, the reproducibility of the method was evaluated by five duplicated measurements of the standard mixture solutions of 0.30 µg/mL (by direct injection) and 0.20 ng/mL (by SPME) with the time interval of 60 min. The relative standard deviations (RSDs) of the retention time and the peak area of all the four analytes are also shown in Table 1. The RSDs of the retention time and the peak areas ranged from 0.02 to 0.04% and 2.9 to 5.7%, respectively. All the quantitative parameters suggested the reliability of this new SPME–GC–MS method.

### 3.4. Application

In order to validate the feasibility of this method proposed before, the spiked pig urine samples were prepared according to the procedure described in Section 2.5. The typical chromatograms of the blank and the spiked pig urine samples by SPME are shown

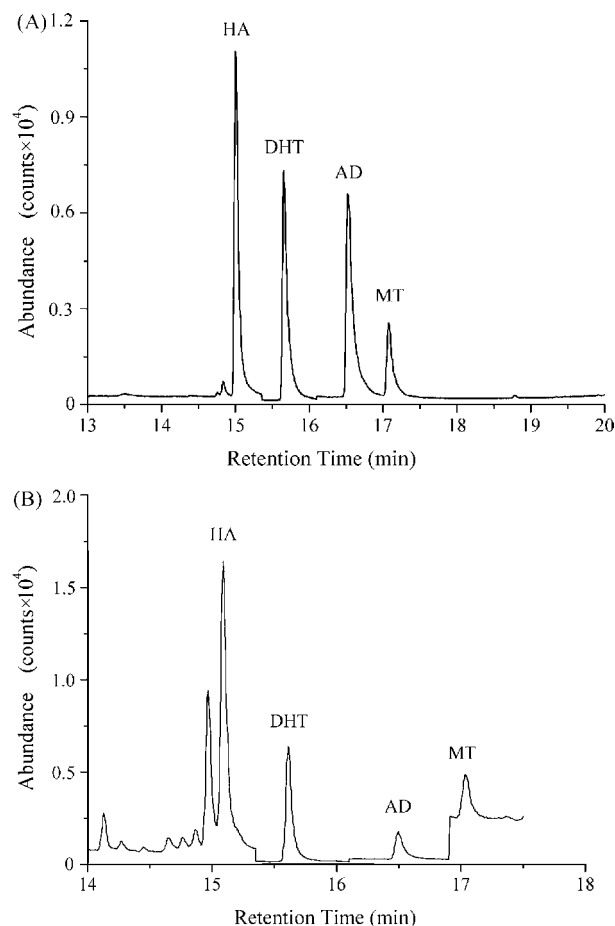


**Fig. 3.** GC–MS analysis of 1.00 µg/mL of four anabolic steroids (A) and SPME–GC–MS analysis of 0.50 ng/mL of four anabolic steroids (B) by use of selected ionization mode (SIM) ions for monitoring HA, DHT, AD and MT at  $m/z$  were based on the ion fraction groups of (290, 107, 270 and 108), (231, 290, 55 and 163), (286, 124, 148 and 244) and (124, 43, 91 and 302), respectively. Other SPME and GC–MS conditions as in Fig. 1.

in Fig. 4. It could be seen from the Fig. 4 that no significant matters in the mixture of body fluids interfered with the determination of the four anabolic steroids. The analytical results of corresponding spiked pig urine samples are illustrated in Table 2. The average recoveries ranged from 71.3 to 121%, and the RSDs ranged from 6.0 to 12.9%.

We also conducted the SPE sampling projects to validate the reliability of the novel SPME method. The typical chromatogram of the spiked pig urine sample by SPE is also shown in Fig. 5. The analyt-

**Table 1**

The regression equations, linear ranges, correlation coefficients, detection limits and reproducibility of the method ( $n = 5$ )<sup>a</sup>.

Compounds	Regression equation $y = ax + b^b$	Linear range (ng/mL)	Enrichment factor <sup>c</sup>	Correlation coefficient ( $R^2$ )	Detection limits (ng/mL)	RSDs (%)		
						Retention time	Peak area	
HA	Direct Injection	$y = 211x - 7122$	50–1000	1063	0.9994	10	3.2	0.02
	SPME	$y = 224269x + 14478$	0.008–0.64		0.9941	0.002	2.9	0.02
DHT	Direct Injection	$y = 220x - 10629$	50–2500	965	0.9997	20	5.0	0.02
	SPME	$y = 212295x + 9857$	0.008–0.64		0.9935	0.004	5.1	0.02
AD	Direct Injection	$y = 241x - 54333$	250–5000	207	0.9962	50	5.2	0.04
	SPME	$y = 49929x + 2027$	0.016–0.51		0.9972	0.008	5.3	0.04
MT	Direct Injection	$y = 127x - 12227$	100–2500	451	0.9985	50	5.6	0.02
	SPME	$y = 57328x + 4534$	0.016–0.51		0.9975	0.008	5.7	0.02

<sup>a</sup> The same experimental conditions as in Fig. 3.

<sup>b</sup> The parameters,  $x$  and  $y$ , refer to the concentration of the target compound (ng/mL) and the corresponding peak area.

<sup>c</sup> Enrichment factor = (the slope of SPME project)/(the slope of direct injection project).



**Table 2**  
Recoveries of spiked urine samples by SPME and SPE ( $n = 3$ )<sup>a</sup>.

Compounds	SPME				SPE			
	Added (pg/mL)	Found (pg/mL)	Recovery (%)	RSD (%)	Added (ng/mL)	Found (ng/mL)	Recovery (%)	RSD (%)
HA	0.5	182	121	7.2	0.5	–	–	–
	300	242	80.7	12.4	500	558	112	16.5
DHT	150	150	100	12.5	0.5	–	–	–
	300	220	73.3	12.9	500	463	92.6	6.8
AD	150	176	117	6.0	0.5	–	–	–
	300	245	81.7	12.7	500	628	126	7.7
MT	150	151	101	9.3	0.5	–	–	–
	300	214	71.3	9.3	500	560	112	4.5

<sup>a</sup> The same experimental conditions as in Fig. 3.

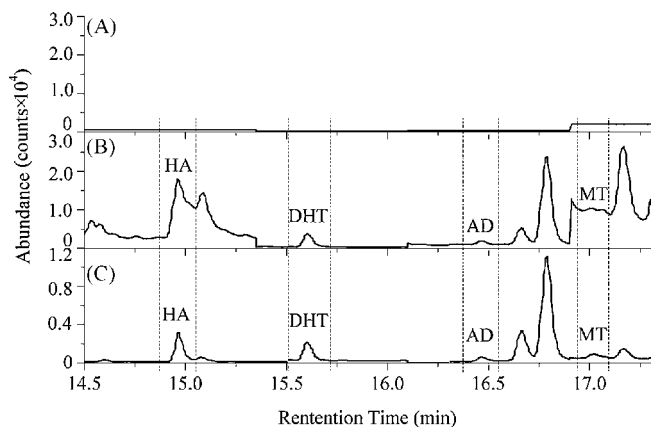


**Fig. 4.** SPME–GC–MS analyses of the blank and spiked urine samples with the 0.30 ng/mL of four anabolic steroids SIM mode is used to monitor the target compounds as MS detection, and the SIM conditions are the same as in Fig. 5. The quantization was based on the EIC, and the corresponding quantitative ions for HA, DHT, AD and MT at  $m/z$  were 290, 231, 286 and 124, respectively. (A) The SIM chromatogram of the blank urine; (B) the SIM chromatogram of the spiked urine sample; (C) the EIC of the spiked urine sample. Other SPME and GC–MS conditions as in Fig. 1.

ical results of corresponding spiked urine samples are illustrated in Table 2. The average recoveries ranged from 92.6 to 126%, and the RSDs ranged from 4.5 to 16.5%, when the concentrations of the added target compounds in the spiked pig urine were at 500 ng/mL. When the concentrations of the added target compounds in the spiked pig urine were 0.5 ng/mL, there were no detector responses

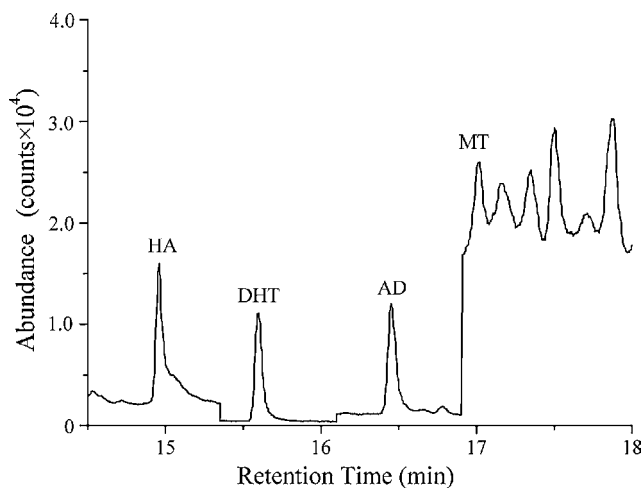


**Fig. 5.** GC–MS analysis of the spiked urine sample with the 0.50 μg/mL of four anabolic steroids by SPE using C18 column GC–MS conditions as in Fig. 1.

of four anabolic steroids by SPE. Comparing the analytical results of SPME and SPE, it could be seen that the SPME method established was reliable and possessed the much higher enrichment capacity than that of SPE. All the analytical results indicate that the simple SPME method proposed is very suitable for the simultaneous and rapid determination of trace HA, DHT, AD and MT in pig urine without derivatization.

#### 4. Conclusion

Monitoring the abuse of anabolic steroids in the livestock farming is a very hot topic for the health of public consumers nowadays. The development of the highly sensitive, simple and rapid method for the simultaneous analysis of the trace anabolic steroids in meat-producing animal's urine is one of crucial aspects for the research. In this work, it is the first time to establish an analytical method based on direct SPME–GC–MS for the simultaneous and rapid determination of four anabolic steroids (HA, DHT, AD and MT) in pig urine without any complicated derivatization procedures. The important SPME conditions were studied in detail to achieve the optimized extraction and analytical results. The optimized SPME conditions were using the home-made CW-DVB fiber during extraction at 40 °C for 50 min with 0.18 g/mL NaCl sample solution and 750 rpm stirring speed. The linear ranges of the method ranged from 8 to 640 pg/mL for HA and DHT, and from 16 to 512 pg/mL for AD and MT, respectively. The corresponding detection limits of SPME projects ranged from 2 to 8 pg/mL ( $S/N = 3$ ). The excellent detection limits obtained by this direct SPME–GC–MS method are much lower than those of conventional methods by use of derivatization. The accuracy and precision have been determined with the recoveries ranging from 71.3 to 121% and the RSDs not exceeding the value of 12.9% for spiked urine samples. Also, we compared the analytical results of SPME and conventional SPE projects to validate the reliability of novel SPME method. The comparison results suggested that the direct SPME method established was reliable and possessed the much higher enrichment capacity than SPE. In a word the SPME-based analytical method is simple, environmental friendly, highly sensitive and very suitable for the simultaneous and rapid determination of trace HA, DHT, AD and MT in pig urine. It is hopeful that the study would facilitate the quality control of meat-producing and food safety.

#### Acknowledgements

The authors are grateful for the National Nature Sciences Foundation of China (20675016, 20735002, 20805008), the Key Program of Science and Technology Department of Fujian Province, China (2007I0020, 2007Y0060), the Key Special Purpose Foundation of Physical Education Bureau of Fujian Province (HX2005-74), the Key Special Funding for Fujian Provincial Colleges and Universities

(2008F5032) and Scientific Research Foundation for Young Talents of Fuzhou University (XRC-0729, 0041826486).

## References

- [1] EC Directive (96/22/EC), Off. J. Eur. Commun. L125 (1996) 3–9.
- [2] M. Thevis, M. Sauer, H. Geyer, et al., *J. Sports Sci.* 26 (2008) 1059.
- [3] D. Barrón, J. Barbosa, J.A. Pascual, et al., *J. Mass Spectrom.* 31 (1996) 309.
- [4] M.D. Engelmann, D. Hinz, B.W. Wenclawiak, *Anal. Bioanal. Chem.* 375 (2003) 460.
- [5] B.H. Ng, K.H. Yuen, *J. Chromatogr. B* 793 (2003) 421.
- [6] P.E. Joos, M.V. Rycckeghem, *Anal. Chem.* 71 (1999) 4701.
- [7] C.S. Aman, A. Pastor, G. Cighetti, et al., *Anal. Bioanal. Chem.* 386 (2006) 1869.
- [8] L.H. Yang, T.G. Luan, C.Y. Lan, *J. Chromatogr. A* 1104 (2006) 23.
- [9] A.A.M. Stolker, S.H.M.A. Linders, L.A.V. Ginkel, et al., *Anal. Bioanal. Chem.* 378 (2004) 1313.
- [10] A.M. Tarrant, C.H. Blomquist, P.H. Lima, et al., *Comp. Biochem. Physiol. B* 136 (2003) 473.
- [11] P. Mikulcikova, S. Ticha, A. Eisner, et al., *Microchim. Acta* 160 (2008) 113.
- [12] Y. Hadeif, J. Kaloustian, H. Portugal, et al., *J. Chromatogr. A* 1190 (2008) 278.
- [13] M. Yamada, S. Aramaki, T. Okayasu, et al., *J. Pharm. Biomed. Anal.* 45 (2007) 125.
- [14] S. Impens, J.V. Loco, J.M. Degroodt, et al., *Anal. Chim. Acta* 586 (2007) 43.
- [15] C. Gambelunghe, M. Somnavilla, C. Ferranti, et al., *Biomed. Chromatogr.* 21 (2007) 369.
- [16] R. Muñoz-Valencia, S.G. Ceballos-Magaña, R. Gonzalo-Lumbreras, et al., *J. Sep. Sci.* 31 (2008) 727.
- [17] M. Mazzarino, M. Oreglia, F. Botrè, *Rapid Commun. Mass Spectrom.* 21 (2007) 4117.
- [18] G. Klamanos, G. Theodoridis, I.N. Papadoyannis, et al., *J. Agric. Food Chem.* 55 (2007) 8325.
- [19] H. Kataoka, E. Matsuura, K. Mitani, *J. Pharm. Biomed. Anal.* 44 (2007) 160.
- [20] O.J. Pozo, P.V. Eenoo, K. Deventer, et al., *Anal. Bioanal. Chem.* 389 (2007) 1209.
- [21] M.W.F. Nielsen, T.F.H. Bovee, M.C.V. Engelen, et al., *Anal. Chem.* 78 (2006) 424.
- [22] O.J. Pozo, P.V. Eenoo, W.V. Thuyne, et al., *J. Chromatogr. A* 1183 (2008) 108.
- [23] N.H. Yu, E.N.M. Ho, D.K.K. Leung, et al., *J. Pharm. Biomed. Anal.* 37 (2005) 1031.
- [24] C.L. Xu, X.G. Chu, C.F. Peng, et al., *J. Pharm. Biomed. Anal.* 41 (2006) 616.
- [25] C. Blasco, C.V. Poucke, C.V. Peteghem, *J. Chromatogr. A* 1154 (2007) 230.
- [26] S.A. Hewitt, M. Kearney, J.W. Currie, et al., *Anal. Chim. Acta* 473 (2002) 99.
- [27] V. Marcos, E. Perogordo, P. Espinosa, et al., *Anal. Chim. Acta* 507 (2004) 219.
- [28] C.L. Arthur, J. Pawliszyn, *Anal. Chem.* 62 (1990) 2145.
- [29] J. Pawliszyn, *Trends Anal. Chem.* 14 (1995) 113.
- [30] A. Peñalve, E. Pocurull, F. Borrull, et al., *Trends Anal. Chem.* 18 (1999) 557.
- [31] G.A. Mills, V. Walke, *J. Chromatogr. A* 902 (2000) 267.
- [32] S. Ulrich, *J. Chromatogr. A* 902 (2000) 167.
- [33] J. Koziel, M.Y. Jia, A. Khaled, et al., *Anal. Chim. Acta* 400 (1999) 153.
- [34] J. Pawliszyn, *Solid Phase Microextraction: Theory and Practice*, Wiley-VCH, New York, 1997, pp. 1–8.
- [35] J. Carpinteiro, J.B. Quintana, I. Rodríguez, et al., *J. Chromatogr. A* 1056 (2004) 179.
- [36] Y.Z. Zhang, X. Liu, L. Ye, et al., *J. Chin. Mass Spectrom. Soc.* 16 (1995) 39.
- [37] G.M. Huang, H. Chen, X.R. Zhang, et al., *Anal. Chem.* 79 (2007) 8327.
- [38] Y.S. Kim, H.J. Zhang, H.Y. Kim, *Anal. Biochem.* 277 (2000) 187.
- [39] J. Muñoz-Guerra, D. Carreras, C. Soriano, et al., *J. Chromatogr. B* 704 (1997) 129.
- [40] H. Bagheria, A. Es-haghia, M.R. Rouini, *J. Chromatogr. B* 818 (2005) 147.
- [41] Y.X. Zheng, The Master Thesis of Sun Yat-Sen University, 2003, pp. 24–44.
- [42] Z.Y. Wang, *Chin. J. Chromatogr.* 17 (1999) 280.
- [43] M.M. Liu, Z.R. Zeng, H.F. Fang, *J. Chromatogr. A* 1076 (2005) 16.
- [44] E.N.M. Ho, D.K.K. Leung, T.S.M. Wan, et al., *J. Chromatogr. A* 1120 (2006) 38.
- [45] G. Pinel, L. Rambaud, G. Cacciatore, et al., *J. Steroid Biochem. Mol. Biol.* 110 (2008) 30.



## Retention properties of novel $\beta$ -CD bonded stationary phases in reversed-phase HPLC mode

Yanyan Zhao<sup>a</sup>, Zhimou Guo<sup>a</sup>, Yongping Zhang<sup>b</sup>, Xingya Xue<sup>a</sup>, Qing Xu<sup>a</sup>,  
Xiuling Li<sup>a</sup>, Xinmiao Liang<sup>a,b,\*</sup>, Yukui Zhang<sup>a</sup>

<sup>a</sup> Key Lab of Separation Science for Analytical Chemistry, Dalian Institute of Chemical Physics, Graduate School of the Chinese Academy of Sciences, Chinese Academy of Sciences, Dalian 116023, China

<sup>b</sup> School of Pharmacy, East China University of Science and Technology, 130 Meilong Road, Shanghai 200237, China

### ARTICLE INFO

#### Article history:

Received 28 September 2008

Received in revised form

29 December 2008

Accepted 30 December 2008

Available online 20 January 2009

#### Keywords:

$\beta$ -CD

Bonded stationary phase

Retention property

LSERs

### ABSTRACT

With the given special structures, the CD bonded stationary phases are expected to have complementary retention properties with conventional C18 stationary phase, which will be helpful to enhance the polar selectivity in RP mode separation. In this work, two  $\beta$ -cyclodextrin ( $\beta$ -CD) bonded stationary phases for reversed-phase HPLC, including 1, 12-dodecyl diol linked  $\beta$ -CD stationary phase (CD1) and olio (ethylene glycol) (OEG) linked  $\beta$ -CD stationary phase (CD2), have been synthesized via click chemistry. The resulting materials were characterized with FT-IR and elemental analysis, which proved the successful immobilization of ligands. The similarities and differences in retention characteristics between the CD and C18 stationary phases have been elucidated by using comparative linear solvation energy relationships (LSERs). The force related to solute McGowan volume has no significant difference, while the hydrogen bonding and dipolar interactions between solutes and CD stationary phases are stronger than between solutes and C18, which is attributed to the special structures (CD and triazole groups) of CD stationary phases. Chemical origins are interpreted by comparison between CD1 and CD2. Similar dispersive interactions of CD1 and CD2 are attributed to their similar length of spacer arms. CD2 which contains OEG spacer arm has relative weaker HBD acidity but stronger HBA basicity. CD stationary phases display no serious different methylene selectivity and higher polar selectivity than in the case of C18. Higher acid selectivity and lower basic selectivity are observed on CD2 than on CD1. Distinctive retention properties and good complementary separation selectivity to C18 make the novel CD bonded stationary phases available for more application in RPLC.

© 2009 Elsevier B.V. All rights reserved.

## 1. Introduction

Cyclodextrins (CDs) are doughnut-shaped cyclic oligosaccharides, containing six to eight glucose units bonded through  $\alpha$ -(1, 4) linkages. CDs are extensively applied in separation science such as capillary electrophoresis and chromatography. This interest can be largely attributed to their special structures. There are 18–24 primary and secondary hydroxyl groups on their upper and lower rims. Meanwhile, inside the CD cavity a hydrophobic environment is provided. The different interactions (hydrogen bonding, hydrophobic and dipolar interactions) of CDs can afford specific selectivity. In the field of liquid chromatography, CDs have been used either as additives in the mobile phase [1–4] or as functionalities bonded to an appropriate solid support [1,4–20]. From the practical viewpoints, more and more attentions have been paid to the exploring

for modified CDs stationary phases and efficient conjugation strategies. Amine, urethane, amide linkages and alkyl, triazine spacer arms were added between CDs and silica beads [9–11,13–15]. Methyl, acetyl, phenylcarbamate, naphthylcarbamate groups were also used to substitute the hydroxyl on CDs [16–20]. Compared with native ones, these modified CDs bonded stationary phases display higher selectivity in the separation of enantiomers, positional isomers, and polar compounds. Various separation modes, such as normal phase, hydrophilic interaction, and reversed-phase, warrant CDs stationary phases of extensive application.

Reversed-phase liquid chromatography (RPLC) as the most commonly used mode of liquid chromatography has been widely applied in pharmaceutical, biochemical, environmental analysis, etc. However, since the retention on ordinary RP stationary phases (alkyl-silica columns) is attributed primarily to solvophobic or hydrophobic interaction, the selectivity for the resolution of polar compounds is often lacked. There are numerous attempts to remedy the problem. Introduction of polar groups on hydrophobic ligands is the most frequent solution [21]. In addition, the strate-

\* Corresponding author. Tel.: +86 411 84379519; fax: +86 411 84379539.  
E-mail address: [liangxm@dicp.ac.cn](mailto:liangxm@dicp.ac.cn) (X. Liang).

gies of introducing novel molecules as functionalities such as calixarene [22–27], poly (ethylene glycol) [28–31], artificial membranes [32,33] have appeared. Although specific selectivity of many solutes have been achieved on these RP stationary phases, it is desirable to develop more stationary phases aiming to the resolution of various solutes.

CDs bonded stationary phases have also been applied in RPLC. Complementary retention properties with conventional C18 stationary phase are expected. In addition to the native CD bonded stationary phases, adding hydrophobic spacer arms between CDs and silica beads is a considerable strategy, which might improve the selectivity of polar solutes as well as maintain hydrophobic selectivity compared with alkyl-silica columns. Selectivity difference and chemical origins could be elucidated through comparison between CD and C18 stationary phases, which is meaningful for chromatography method development. Meanwhile, comprehension of the chemical origins will be helpful to the intentional preparation of CDs stationary phases with expected retention properties.

Since the intermolecular interactions between the stationary phase, the analyte and the mobile phase components play an important role in retention properties, a qualitative and quantitative selectivity evaluation is necessary. However, little attention has been received on the modified CDs stationary phases [34]. Linear solvation energy relationships (LSERs) as an object method is appropriate for the column retention mechanisms investigation [35–40]. By conducting LSER studies, much can be learned about the intermolecular interactions governing the chromatographic process. Different systems (e.g., different stationary phases) can be compared to one another to gain important chemical insight. The contributions to column selectivity for non-ionized solute molecules have been incorporated into the solvation equation model for RPLC retention:

$$\ln k'_w = c + eE + sS + aA + bB + vV \quad (1)$$

Each parameter in the equation accounts for a specific intermolecular interaction:  $E$  is the excess molar refraction,  $S$  is the solute dipolarity/polarizability,  $A$  and  $B$  are the solute overall hydrogen bond donor (HBD) acidity and hydrogen bond acceptor (HBA) basicity, and  $V$  is the solute characteristic volume of McGowan. The constants  $c$ ,  $e$ ,  $s$ ,  $a$ ,  $b$ , and  $v$  in Eq. (1) reflect the corresponding properties of the HPLC system considered.

Herein, we attempt to develop two designed  $\beta$ -CD bonded stationary phases for RPLC via click chemistry (1,2,3-triazole forming reactions), which has been used as a facile, robust and high efficient conjugation strategy in bonded stationary phases synthesis [41–44]. The set of 20 solutes for LSERs is according to the literature [35]. Through LSERs, the different retention properties of CD from that of C18 stationary phases are elucidated. The chemical origins influencing the retention property of the CD stationary phases are also interpreted. Furthermore, the methylene selectivity and polar selectivity are evaluated.

## 2. Experimental

### 2.1. Chemicals

Acetonitrile (HPLC grade) was purchased from Fisher (USA). Water was purified on a Milli-Q system (USA). Silica gel (5  $\mu$ m particle size, 10 nm pore size, 270 m<sup>2</sup>/g surface area) was purchased from Fuji Silysia Chemical (Japan). The reagents which were used for chemical modification of the support material are all identified chemicals. All the evaluation compounds are analytical grade chemicals of various origins and were solved in methanol–water (v/v, 1:1), the concentration is around 1 mg mL<sup>-1</sup>. The injection volume was 1  $\mu$ L. The names of the 20 test solutes are shown in Table 1.

**Table 1**  
Structural descriptors of 20 test solutes in Eq. (1).

No.	Solute	$E$	$S$	$A$	$B$	$V$
1	1,3,5-triisopropylbenzene	0.627	0.40	0	0.22	1.985
2	1,3-diisopropylbenzene	0.605	0.46	0	0.20	1.562
3	1,4-dinitrobenzene	1.13	1.63	0	0.41	1.065
4	3,5-dichlorophenol	1.020	1.10	0.83	0	1.020
5	4-chlorophenol	0.915	1.08	0.67	0.20	0.898
6	4-cyanophenol	0.940	1.63	0.79	0.29	0.930
7	4-iodophenol	1.380	1.22	0.68	0.20	1.033
8	Methyl phenyl ether	0.708	0.75	0	0.29	0.916
9	Benzamide	0.990	1.50	0.49	0.67	0.973
10	Benzene	0.610	0.52	0	0.14	0.716
11	Chlorobenzene	0.718	0.65	0	0.07	0.839
12	Cyclohexanone	0.403	0.86	0	0.56	0.861
13	Dibenzothiophene	1.959	1.31	0	0.18	1.379
14	Phenol	0.805	0.89	0.60	0.30	0.775
15	Hexylbenzene	0.591	0.50	0	0.15	1.562
16	Hexachlorobutadiene	1.019	0.85	0	0	1.321
17	Indazole	1.180	1.25	0.54	0.34	0.905
18	Caffeine	1.500	1.60	0	1.35	1.363
19	Naphthalene	1.340	0.92	0	0.20	1.085
20	Toluene	0.601	0.52	0	0.14	0.716

### 2.2. Preparation of CD bonded stationary phases and column packing

The azide-modified silica gel was prepared according to the procedures in the previous reports [41].

The general procedure for the synthesis of *O,O*-dipropargyl-1, 12-dodecyl diol was as follows: To a solution of 1, 12-dodecyl diol (10.13 g, 50 mmol) in dry THF (100 mL) under Ar at 0 °C, NaH (60% w/w in mineral oil, 5.04 g, 125 mmol) was added. After stirring for 15 min, propargyl bromide (14.85 g, 125 mmol) was added. The ice bath was removed two hours later and the system was kept stirring at room temperature for 5 h. Then the solution was put into 100 mL water and extracted with 300 mL ethyl acetate for 3 times. The ethyl acetate extract was concentrated in vacuo and passed through a silica gel column eluted with ethyl acetate to give yellow oil: yield 6.71 g (50%). <sup>1</sup>H NMR (CDCl<sub>3</sub>)  $\delta$ : 4.12–4.13 (d, 4H,  $J$  = 2.4 Hz), 3.49–3.52 (t, 4H,  $J$  = 6.6 Hz), 2.40–2.41 (t, 2H,  $J$  = 2.4 Hz), 1.55–1.62 (m, 4H,  $J$  = 6.6 Hz).

The procedure for the synthesis of *O,O*-dipropargyltetra (ethylene glycol) was similar to that of *O,O*-dipropargyl-1, 12-dodecyl diol. Yellow liquid was obtained: yield 5.82 g (43%). <sup>1</sup>H NMR (CDCl<sub>3</sub>)  $\delta$ : 4.00–4.21 (d, 4H,  $J$  = 2.4 Hz), 3.61–3.74 (m, 16 H), 2.47–2.48 (t, 2H,  $J$  = 2.4 Hz).

The mono-(6-azido-6-deoxy)- $\beta$ -CD was prepared according to procedures in the literature [45].

CD bonded stationary phases were synthesized over two successive reactions via click chemistry. The general procedures are depicted in Fig. 1. The procedure of CD1 is described in brief as follows: CuSO<sub>4</sub> (0.10 g, 0.6 mmol), sodium ascorbate (0.36 g, 1.8 mmol), and azide-modified silica gel (5.03 g) were added to a solution of *O,O*-dipropargyl-1, 12-dodecyl diol (3.43 g, 12 mmol) in methanol–water (v/v, 9:1, 100 mL). After stirring for 8 h at room temperature, the obtained material was filtrated and washed with 200 mL methanol, 200 mL water, and 200 mL methanol respectively. Then the prepared material, CuSO<sub>4</sub> (0.05 g, 0.3 mmol), sodium ascorbate (0.18 g, 0.9 mmol) were added again to a solution of mono-(6-azido-6-deoxy)- $\beta$ -CD (6.82 g, 6.0 mmol) in methanol–water (v/v, 1:1, 100 mL). The system was then stirred at room temperature. After 72 h the obtained material was filtrated and washed with 200 mL water, 300 mL 0.1 mol L<sup>-1</sup> EDTA, 500 mL water and 200 mL acetone respectively to give CD1 stationary phase. CD2 stationary phase was prepared with the similar procedure. The prepared materials were dispersed into toluene–acetone (v/v, 1:1) and packed into

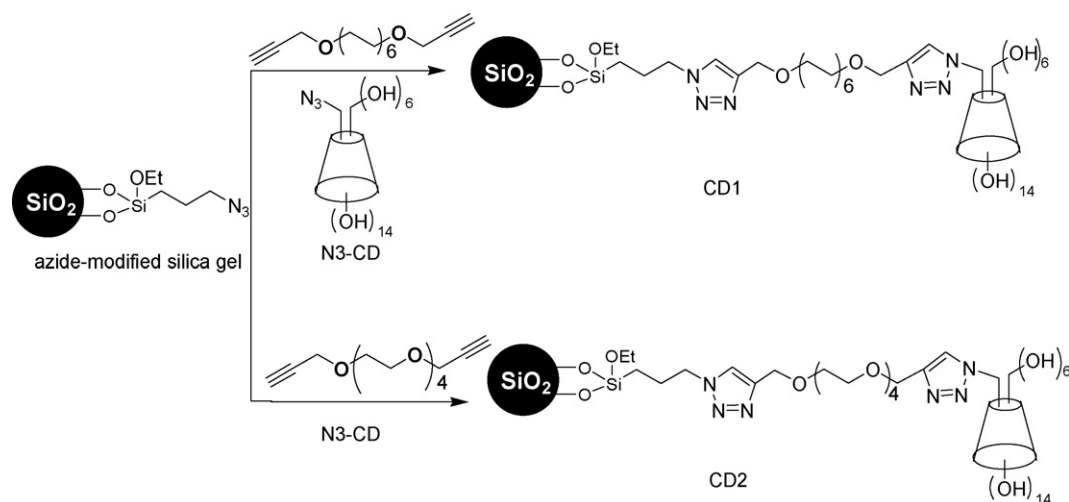


Fig. 1. Scheme for the synthesis of CD1 and CD2, reagents and conditions: CuSO<sub>4</sub> (5 mol%), sodium ascorbate (15 mol%), R.T. 80 h.

stainless-steel column (4.6 mm × 100 mm) by a slurry packing technique.

### 2.3. Instrumentation, columns and condition

FT-IR measurements, before and after the process of click chemistry, were performed on a Nicolet 20 DXB FT-IR (USA) using KBr pellets. Elemental analysis was measured on a Vario EL III elemental analysis system (Germany). <sup>1</sup>H NMR spectra were recorded on a Bruker DRX-400 instrument and were referenced to TMS.

The HPLC system (Agilent 1100, USA) consisted of a quaternary pump, an autosampler, a degasser, an automatic thermostatic column compartment and a diode array detector. The stationary phase for comparison was XTerra MS C18 column (5 μm, 2.1 mm × 150 mm, Waters, USA).

The flow rate for CD stationary phases was 1.0 mL min<sup>-1</sup> and that for C18 was 0.2 mL min<sup>-1</sup>. The mobile phases used for the LSERs were water (A) and acetonitrile (B). The test solutes on CD stationary phases were eluted at 3 different gradients: (1) 12% B - 30 min - 55% B - 5 min - 55% B, (2) 7% B - 40 min - 55% B - 5 min - 55% B, (3) 2% B - 50 min - 55% B - 5 min - 55% B. Three gradients for C18 were: (1) 30% B - 30 min - 100% B, (2) 20% B - 35 min - 100% B, (3) 10% B - 40 min - 100% B. The column temperatures were held constantly at 25 °C during the analysis. The detection wavelengths were 254 and 280 nm for all the compounds.

The mobile phases used for methylene selectivity and polar selectivity evaluations were water and acetonitrile. The components of acetonitrile in mobile phases are shown in Table 5, which were different on columns to obtain similar toluene retention factors (5.5 < k<sub>T</sub> < 6.5).

### 2.4. Data analysis

To start LSERs, the observation of ln k'<sub>w</sub> of 20 test solutes was prerequisite. The structural descriptions of the 20 test compounds are listed in Table 1. We used method and CSASS software developed in our group for obtaining retention equations under gradient conditions aiming to improve the analysis efficiency [45–50]. The retention equation is:

$$\ln k = a + cCB \quad (2)$$

where *k* is the retention factor, *CB* is the acetonitrile content in the mobile phase, *a* and *c* are constants. The retention parameter *a* is

Table 2

Natural logarithms of retention factors corresponding to 100% water eluent determined on the CD and C18 stationary phases.

No	Solute	ln k' <sub>w</sub> (CD1)	ln k' <sub>w</sub> (CD2)	ln k' <sub>w</sub> (C18)
1	1,3,5-triisopropylbenzene	7.481	8.060	9.096
2	1,3-diisopropylbenzene	6.167	6.655	10.088
3	1,4-dinitrobenzene	1.936	2.226	4.134
4	3,5-dichlorophenol	4.450	6.396	6.704
5	4-chlorophenol	2.768	3.916	4.632
6	4-cyanophenol	1.845	3.888	2.898
7	4-iodophenol	3.937	5.003	6.361
8	Methyl phenyl ether	2.103	2.651	4.682
9	Benzamide	0.967	1.227	1.924
10	Benzene	1.771	2.582	4.241
11	Chlorobenzene	2.921	3.691	7.022
12	Cyclohexanone	1.327	1.833	2.223
13	Dibenzothiophene	6.328	6.655	14.509
14	Phenol	1.253	2.135	–
15	Hexylbenzene	6.992	7.608	9.229
16	Hexachlorobutadiene	6.304	7.023	9.543
17	Indazole	2.409	–	3.398
18	Caffeine	1.383	0.330	2.449
19	Naphthalene	4.466	5.529	7.789
20	Toluene	2.455	3.243	6.970

Missing values mean that ln *k'* was poorly correlated to percent acetonitrile and the calculated ln *k'*<sub>w</sub> was unreliable.

equal to the natural logarithm of retention factors corresponding to 100% water (ln k'<sub>w</sub>). Related data are collected in Table 2.

The dead time of each column (1.726 min for CD1; 1.707 min for CD2; 1.931 min for C18) was measured as the first base-line deviation.

The multiple regression analysis was carried out between ln k'<sub>w</sub> and all the structural descriptors with Microsoft Excel software.

## 3. Results and discussion

### 3.1. Preparation and characterization of CD stationary phases

Alkyne groups could be readily introduced to the functional spacers on both ends and react with the azide-silica and the azide group of CD derivative via click chemistry. Two CD stationary phases were prepared. It is assumed that the CD stationary phases possess specific selectivity to solve problems in chromatography through their various available interactions. The CD guarantees the hydrogen bonding, hydrophobic, and dipolar interactions. Further-

**Table 3**  
Characteristics of the CD stationary phases and modified silica gel.

Elemental analysis	CD1	CD2	Azide-modified silica gel
P <sub>C</sub> (%)	11.79	8.39	5.99
P <sub>N</sub> (%)	3.28	2.90	2.48

more, the triazole group which is the product of click chemistry is also available for the dipolar and hydrogen bonding interactions. Two kinds of spacers (OEG and alkyl groups) were used. An OEG molecule has a long chain contributing to hydrophobic interactions and the ether groups on OEG are available for hydrogen bonding and dipolar interactions with polar molecules [44]. To eliminate the influence of spacer length, an alkyl group with the similar length to that of OEG group is used as spacer arm of the other CD stationary phase.

The materials, before and after the immobilization process, were characterized with FT-IR. Azide group has strong absorption at about 2110 cm<sup>-1</sup> on FT-IR spectrum. For CD1 and CD2 the distinct peak at 2110 cm<sup>-1</sup> for azide group on the IR spectra disappeared after the immobilization processes, which indicated that the azide group on the silica support was exhausted (data not shown). The elemental analysis results are showed in Table 3. The increase in carbon content of CD stationary phases than that of azide-modified silica gel indicates the successful immobilization.

### 3.2. Intercorrelations between the stationary phases

Intercorrelations were carried out between the observed retention parameters ( $\ln k'_{w}$ ) of the test solutes on the stationary phases, which are described by the coefficients. The differences in retention properties are demonstrated with relatively low coefficients. The coefficients between the CD stationary phases are relative high ( $R=0.924$ ), indicating their similar retention properties which might results from the common  $\beta$ -CD structure and conjugation strategy. The low coefficients between C18 and CD stationary phases also clearly illustrate that the specific intermolecular interactions, different from that of C18, affect the retention properties of CD stationary phases. However, dissimilarity may still exist between CDs stationary phases due to the effect of different spacer arms. Significant difference between the retention properties of CD1 and CD2 is observed according to their coefficients with C18. Lower intercorrelation between CD2 and C18 ( $R=0.695$ ) than that between C18 and CD1 ( $R=0.779$ ) means that the retention property of CD1 is closer to C18, which may be caused by the different kinds of forces provided by alkyl groups on CD1 from the forces provided by OEG groups on CD2.

### 3.3. Comparison of LSERs coefficients between the stationary phases

It appears interesting which and to what extent intermolecular interaction affects the retention properties of CD stationary phases after the intercorrelation evaluation. The LSERs was used to evaluate the retention mechanisms of CD and C18 stationary phases. From the multiple regression analysis between the retention data

of the 20 test solutes ( $\ln k'_{w}$ ) and the solute descriptors, the coefficients of LSER equations were derived (Table 4). The intercorrelation coefficients of C18 ( $R=0.952$ ), CD1 ( $R=0.984$ ) and CD2 ( $R=0.974$ ) between the observed  $\ln k'_{w}$  and the corresponding  $\ln k'_{w}$  calculated theoretically by Eq. (1) showed no serious outliers. Furthermore, high correlation coefficient ( $R>0.950$ ) was observed on the equation of each stationary phase.

The magnitudes of coefficients  $\nu$ ,  $e$ ,  $a$ ,  $b$ , and  $s$  vary substantially with the type of stationary phases. The negative  $\nu$ ,  $e$ ,  $a$ ,  $b$ , and  $s$  values for the columns denote that the corresponding interactions are stronger between the mobile phase and solutes than between the stationary phase and solutes, while the positive values have the contrary meaning.

The structural parameter of the solute,  $V$  as well as  $E$ , are the solute size (bulkiness)-related descriptors. They can be treated as measures of the ability of solute molecules to participate in dispersive interactions. The  $\nu$  coefficient is a measure of solute characteristic volume of McGowan. The  $e$  coefficient reflects the tendency of the system to interact with the solute through  $\pi$ - and  $n$ -electron pairs. Positive  $\nu$  and  $e$  coefficients are obtained on CD and C18 stationary phases. Since both CD and C18 stationary phases have the “bulky” chains, certainly the dispersive interactions will be stronger between a solute molecule and stationary phases than between the same solute and the small molecules of eluent. As expected, CD1 and CD2, both have spacer arms with similar length, display only slightly different  $\nu$  and  $e$  coefficients, which indicates their similar dispersive interaction. That, in turn, proves that the length of hydrophobic spacer arms is the main factor of dispersive interaction of CD stationary phases. The  $\nu$  values of CD and C18 stationary phases display no serious difference, indicating that the force related to solute volume of McGowan has no significant difference on CD from that on C18 stationary phases, which is attributed to the long chain in common.

In the case of structurally specific intermolecular interactions, two important descriptors are  $B$  and  $A$  which are reflected by  $b$  and  $a$  coefficients accordingly. The coefficients  $b$  and  $a$  are used to measure the difference between the stationary and mobile phases in HBD acidity and HBA basicity, respectively. A larger negative  $a$  and  $b$  can be obtained for the less basic and acidic stationary phases, whereas smaller negative constants reveal the increasing column basicity and acidity. Among the CD stationary phases, CD2 has larger negative  $b$  value and larger  $a$  value than CD1, which indicates the weak HBD acidity interaction and stronger HBA basicity interaction of CD2. The proton acceptor performance of OEG spacer on CD2 is chemical origin of the difference retention property. Significant dissimilarity is observed between CD and C18 stationary phases. Although both C18 and CD stationary phases have negative  $b$  coefficients, smaller negative  $b$  value of CD stationary phases indicates their stronger HBD acidity over C18. The outstanding acidity of CD stationary phases is a consequence of their HB donor hydroxyls on CD. Negative  $a$  value is obtained on C18, while both CD1 and CD2 have positive  $a$  values. Stronger HBA basicity of CD stationary phases is probably caused by the triazole groups on the stationary phases.

The  $s$  coefficient indicates the differences in the dipolarity/polarizability interaction between the mobile and stationary

**Table 4**  
Result of retention parameters of stationary phases on LSERs.

$\ln k'_{w}$	$c$	$e$	$s$	$a$	$b$	$\nu$	$n$	$R$	$F$	$s^b$	$p$
CD1	-1.083	1.517	-1.222	0.042	-3.430	4.844	20	0.984	82.967	0.450	$\leq 6.7 \times 10^{-10}$
CD2	-0.032	1.039	-0.773	0.849	-5.505	4.812	19	0.976	56.738	0.579	$\leq 8.5 \times 10^{-9}$
C18	1.772	5.061	-2.591	-2.307	-6.151	3.987	19	0.953	25.289	1.187	$\leq 2.9 \times 10^{-6}$

$c$ ,  $e$ ,  $s$ ,  $a$ ,  $b$ ,  $\nu$  are retention parameters;  $n$  is the number of the dependent variable data points used to derive the regression;  $R$  is the multiple correlation;  $s^b$  is the standard errors of the estimated of the equations;  $p$  is the significant levels of each term and of whole equations;  $F$  is the values of the  $F$ -test of significance.

**Table 5**  
Methylene selectivity and polar selectivity of stationary phases.

Phase	ACN (%)	$k_T$	$\alpha_{EB/T}$	$\alpha_{PCR/T}$	$\alpha_{CAF/T}$
CD1	30	5.930	1.696	0.466	0.181
CD2	20	6.337	1.806	0.651	0.038
C18	42	5.950	1.727	0.192	0.036

phases. All the studied stationary phases have negative  $s$  values. Smaller negative  $s$  value of CD2 than that of CD1 is caused by the stronger dipolar force of OEG spacer than that of alkyl spacer. In addition, smaller negative  $s$  values of CD stationary phases than C18 indicate stronger dipolar interaction between solutes and CD stationary phases than that is with C18. Triazole groups and CD structure are responsible for the dipolar interaction on CD stationary phases.

The LSERs results and interpretations prove that a solute undergoes different reversed-phase liquid chromatographic retention process on CD and C18 stationary phases. The distinct retention properties of CD stationary phases will contribute to their complementary separation selectivity to C18 in RPLC.

### 3.4. Methylene selectivity and polar selectivity

It is well recognized that solute selectivity is chromatographically important for a given stationary phase. In this work, methylene selectivity and polar selectivity were evaluated between three solute pairs: (1)  $\alpha_{EB/T}$ , relative retention of ethylbenzene to toluene; (2)  $\alpha_{PCR/T}$ , relative retention of *p*-cresol to toluene; (3)  $\alpha_{CAF/T}$ , relative retention of caffeine to toluene [51,52]. Similar toluene retention factors ( $5.5 < k_T < 6.5$ ) between stationary phases were obtained (Table 5) aiming to evaluate the selectivities in a comparable level. Methylene selectivity was measured by  $\alpha_{EB/T}$ , which has been the most extensively studied property to characterize RP stationary phase hydrophobicity. Based on the  $\alpha_{EB/T}$  values, practically no difference is detected in the methylene selectivity of CD and C18 stationary phases, which is the consequence of their common long hydrophobic chain. Acid selectivity and basic selectivity were measured by  $\alpha_{PCR/T}$  and  $\alpha_{CAF/T}$  respectively. Higher  $\alpha_{PCR/T}$  ( $>0.460$ ) and  $\alpha_{CAF/T}$  ( $>0.036$ ) of CD stationary phases than  $\alpha_{PCR/T}$  (0.192) and  $\alpha_{CAF/T}$  (0.036) of C18 demonstrate higher polar selectivity of CD stationary phases than C18. Compared with C18, the notably higher polar selectivity of CD stationary phases is a consequence of their higher hydrogen bonding and dipolar interactions. Among the CD stationary phases, CD2 has larger  $\alpha_{PCR/T}$  values and smaller  $\alpha_{CAF/T}$  values ( $\alpha_{PCR/T} = 0.651$ ,  $\alpha_{CAF/T} = 0.038$ ) than that of CD1 ( $\alpha_{PCR/T} = 0.466$ ,  $\alpha_{CAF/T} = 0.181$ ). Consequently, CD2 displays higher acid selectivity and lower basic selectivity than CD1. The reason is that CD2 have weaker HBD acidity and stronger HBA basicity than in the case of CD1. The selectivity evaluation clearly shows that while hydrophobic selectivity is similar, polar selectivity has been improved on CD stationary phases than alkyl-silica column (C18).

## 4. Conclusion

Two  $\beta$ -CD bonded stationary phases were synthesized via click chemistry and evaluated under reversed-phase mode. The LSERs model was used to evaluate the presence and extent of various interactions of the stationary phases with a series of 20 structurally diverse test solutes. Through LSERs, the differences in the intermolecular interactions of CD and C18 stationary phases were found to be significant. Stronger dipolar and HB interactions are obtained on CD stationary phases than C18. Meanwhile, the chemical origins of the different retention mechanisms were assessed. The contribution of CD structure, the length and structure of the spacers and the

triazole groups produced from conjugation process to the retention process is significant. Separation selectivity evaluation shows that CD stationary phases possess similar methylene selectivity and higher polar selectivity than C18. We believe that the CD RP stationary phases will become useful in many fields and be complement to C18. Further investigations are now in progress in our group.

## Acknowledgements

Financial support from Natural Science Foundation of China (Grant: 20775079) and the grant of the project of the Knowledge Innovation Program of DICP, CAS (Grant: K2006A3) are gratefully acknowledged.

## References

- [1] N. Grobuschek, L. Sriphong, M.G. Schmid, T. Lorand, H.Y. Aboul-Enein, G. Gubitzi, *J. Biochem. Biophys. Methods* 53 (2002) 25.
- [2] O. Lecnik, M.G. Schmid, C.O. Kappe, G. Gubitzi, *Electrophoresis* 22 (2001) 3198.
- [3] Y.Q. Cheng, L.Y. Fan, H.L. Chen, X.G. Chen, Z.D. Hu, *J. Chromatogr. A* 1072 (2005) 259.
- [4] A.R.M. Aucejo, M.L. Estelles, M.E. Carrasco, R.M. Saez, *Anal. Lett.* 39 (2006) 183.
- [5] A. Berthod, S.S.C. Chang, J.P.S. Kullman, D.W. Armstrong, *Talanta* 47 (1998) 1001.
- [6] N.T. McGachy, N. Grinberg, N. Variankaval, *J. Chromatogr. A* 1064 (2005) 193.
- [7] H. Riering, M. Sieber, *J. Chromatogr. A* 728 (1996) 171.
- [8] D.D. Schumacher, C.R. Mitchell, T.L. Xiao, R.V. Rozhkov, R.C. Larock, D.W. Armstrong, *J. Chromatogr. A* 1011 (2003) 37.
- [9] I.W. Muderawan, T.T. Ong, S.C. Ng, *J. Sep. Sci.* 29 (2006) 1849.
- [10] C.H. Lin, C.Y. Chen, S.W. Chang, J.C. Wu, C.E. Lin, *Anal. Chim. Acta* 576 (2006) 84.
- [11] F.T.K.S. Ahmed, A.Y. Badjaj-Hadj-Ahmed, B.Y. Meklati, *Chromatographia* 62 (2005) 571.
- [12] D.W. Armstrong, U.S. Patent 4,539,399 (1985).
- [13] Y. Kawaguchi, M. Tanaka, M. Nakae, K. Funazo, T. Shono, *Anal. Chem.* 55 (1983) 1852.
- [14] K. Fujimura, S. Suzuki, K. Hayashi, S. Masuda, *Anal. Chem.* 62 (1990) 2198.
- [15] K. Fujimura, T. Ueda, T. Ando, *Anal. Chem.* 55 (1983) 446.
- [16] C. Mitchell, M. Desai, R. McCulla, W. Jenks, D.W. Armstrong, *Chromatographia* 56 (2002) 127.
- [17] X.H. Lai, Z.W. Bai, S.C. Ng, C.B. Ching, *Chirality* 16 (2004) 592.
- [18] L.F. Zhang, Y.C. Wong, L. Chen, C.B. Ching, S.C. Ng, *Tetrahedron Lett.* 40 (1999) 1815.
- [19] Y.F. Poon, I.W. Muderawan, S.C. Ng, *J. Chromatogr. A* 1101 (2006) 185.
- [20] Y. Wang, Y. Xiao, T.T.Y. Tan, S.C. Ng, *Tetrahedron Lett.* 49 (2008) 5190.
- [21] S. Kowalska, K. Krupczynska, B. Buszewski, *Biomed. Chromatogr.* 20 (2006) 4.
- [22] Y.K. Lee, Y.K. Ryu, J.W. Ryu, B.E. Kim, J.H. Park, *Chromatographia* 46 (1997) 507.
- [23] R. Meyer, T. Jira, *Curr. Anal. Chem.* 3 (2007) 161.
- [24] J.H. Park, Y.K. Lee, N.Y. Cheong, M.D. Jang, *Chromatographia* 37 (1993) 221.
- [25] T. Sokoliess, U. Menyes, U. Roth, T. Jira, *J. Chromatogr. A* 948 (2002) 309.
- [26] L.S. Li, S.L. Da, Y.Q. Feng, M. Liu, *J. Liq. Chromatogr. Relat. Technol.* 27 (2004) 2167.
- [27] L.S. Li, S.L. Da, Y.Q. Feng, L. Min, *Prog. Chem.* 17 (2005) 523.
- [28] A. Garcia, F.J. Ruperez, A. Marin, A. de la Maza, C. Barbas, *J. Chromatogr. B* 785 (2003) 237.
- [29] F. Cacciola, P. Jandera, Z. Hajdu, P. Cesla, L. Mondello, *J. Chromatogr. A* 1149 (2007) 73.
- [30] F. Pellati, S. Benvenuti, M. Melegari, *J. Chromatogr. A* 1088 (2005) 205.
- [31] F. Pellati, S. Benvenuti, F. Yoshizaki, M. Melegari, *J. Sep. Sci.* 29 (2006) 641.
- [32] C. Pidgeon, S.W. Ong, H.S. Choi, H.L. Liu, *Anal. Chem.* 66 (1994) 2701.
- [33] B. Buszewski, M. Jezierska, M. Welniak, R. Kalisz, *J. Chromatogr. A* 845 (1999) 433.
- [34] T.H. Nah, E.H. Cho, M.D. Jang, Y.K. Lee, J.H. Park, *J. Chromatogr. A* 722 (1996) 41.
- [35] L.R. Snyder, J.W. Dolan, P.W. Carr, *J. Chromatogr. A* 1060 (2004) 77.
- [36] B. Buszewski, R.M. Gdzala-Kopciuch, M. Markuszewski, R. Kalisz, *Anal. Chem.* 69 (1997) 3277.
- [37] M. Michel, T. Baczek, S. Studzinska, K. Bodzioch, T. Jonsson, R. Kalisz, B. Buszewski, *J. Chromatogr. A* 1175 (2007) 49.
- [38] K. Heberger, *J. Chromatogr. A* 1158 (2007) 273.
- [39] Q.Y. Huai, J.M. You, Q. Wang, Y.M. Zuo, *Chromatographia* 57 (2003) 709.
- [40] M. Vitha, P.W. Carr, *J. Chromatogr. A* 1126 (2006) 143.
- [41] Z.M. Guo, A.W. Lei, X.M. Liang, Q. Xu, *Chem. Commun.* 43 (2006) 4512.
- [42] Z.M. Guo, A.W. Lei, Y.P. Zhang, Q. X. Xue, F.F. Zhang, X.M. Liang, *Chem. Commun.* 24 (2007) 2491.
- [43] Y.P. Zhang, Z.M. Guo, J.X. Ye, Q. Xu, X.M. Liang, A.W. Lei, *J. Chromatogr. A* 1191 (2008) 188.
- [44] Z.M. Guo, Y.F. Liu, J.Y. Xu, Q. Xu, X.Y. Xue, F.F. Zhang, Y.X. Ke, X.M. Liang, A.W. Lei, *J. Chromatogr. A* 1191 (2008) 78.
- [45] R.C. Petter, J.S. Salek, C.T. Sikorski, G. Kumaravel, F.T. Lin, *J. Am. Chem. Soc.* 112 (1990) 3860.

- [46] P.Z. Lu, Y.K. Zhang, X.M. Liang, High Performance Liquid Chromatography and Its Expert System, Publishing Company of Liaoning Technology, Shenyang, 1992, p. 318.
- [47] C.Z. Dai, P.Z. Lu, Chin. Sci. Bull. 39 (1994) 1458.
- [48] H.F. Zou, Y.K. Zhang, M.F. Hong, Y.Y. Shy, P.Z. Lu, Acta Chim. Sin. 53 (1995) 269.
- [49] X.Y. Xue, Q. Zhang, X.M. Liang, K. Oxynos, A. Kettrup, P.C. Lu, J. Chromatogr. A 957 (2002) 37.
- [50] D.Y. Zhou, Q. Xu, X.Y. Xue, F.F. Zhang, X.M. Liang, J. Pharm. Biomed. Anal. 42 (2006) 441.
- [51] A. Sandi, L. Szepeszy, J. Chromatogr. A 818 (1998) 19.
- [52] A. Sandi, L. Szepeszy, J. Chromatogr. A 845 (1999) 113.





# D.C. voltammetry of ionic liquid-based capacitors: Effects of Faradaic reactions, electrolyte resistance and voltage scan speed investigated using an electrode of carbon nanotubes in EMIM-EtSO<sub>4</sub>

J.P. Zheng<sup>a</sup>, C.M. Pettit<sup>b</sup>, P.C. Goonetilleke<sup>a</sup>, G.M. Zenger<sup>a</sup>, D. Roy<sup>a,\*</sup>

<sup>a</sup> Department of Physics, Clarkson University, Clarkson Ave, Potsdam, NY 13699-5820, USA

<sup>b</sup> Department of Physics, Emporia State University, Emporia, KS 66801-5087, USA

## ARTICLE INFO

### Article history:

Received 14 November 2008

Received in revised form 9 January 2009

Accepted 12 January 2009

Available online 20 January 2009

### Keywords:

Carbon nanotube

Cyclic voltammetry

Double layer capacitance

Ionic liquid

## ABSTRACT

Carbon nanotube (CNT) electrodes in combination with ionic liquid (IL) electrolytes are potentially important for energy storage systems. We report electrochemical investigation of such a system involving a paper-electrode of multi-wall CNT (MWCNT) in the IL of 1-ethyl-3-methyl imidazolium ethylsulfate (EMIM-EtSO<sub>4</sub>). Our study concentrates on the analytical aspects of cyclic voltammetry (CV) to probe the double layer capacitance of these relatively unconventional systems (that involve rather large charge–discharge time constants). Both theoretical and experimental aspects of CV for such systems are discussed, focusing in particular, on the effects of Faradaic side-reactions, electrolyte resistance and voltage scan speeds. The results are analyzed using an electrode equivalent circuit (EEC) model, demonstrating a method to account for the typical artifacts expected in CV of CNT–IL interfaces.

© 2009 Elsevier B.V. All rights reserved.

## 1. Introduction

Recent advancements in electrochemical double layer capacitors for energy storage indicate considerable interest in the utilization of carbon nanotube (CNT) electrodes with ionic liquid (IL) electrolytes [1–5]. However, owing mostly to the complex electrochemistry of CNT–IL systems, several facets of both the experimental designs and the data analysis protocols necessary to study these systems have remained relatively underexplored. Factors that affect electrochemical characterization of these systems include the intrinsic porosity and in-homogeneity of CNT [1,2] as well as the significantly departing properties of ILs [1,6,7] from those commonly described by classical electrochemical models. Consequently, the analysis of experimental results in such studies can often become a nontrivial task. For instance, frequency dispersion effects can complicate various measurements involving the A.C. techniques. Likewise, the relatively large time constants associated with charging/discharging of these systems can affect the results of D.C. cyclic voltammetry (CV). The present work explores the general aspects of CNT–IL double layer capacitance ( $C_{dl}$ ) measurements based on the CV technique.

The experiments reported here demonstrate how certain complex features of a CNT–IL interface can be detected using

CV. The working principle of these measurements is discussed using an electrode equivalent circuit (EEC) model. The experimental system involves a paper-electrode of multi-wall carbon nanotubes (MWCNT) in the IL, 1-ethyl-3-methyl imidazolium ethylsulfate (EMIM-EtSO<sub>4</sub> or, [EtMelm]<sup>+</sup>[C<sub>2</sub>H<sub>5</sub>SO<sub>4</sub>]<sup>−</sup>). This non-halide (C<sub>8</sub>H<sub>16</sub>N<sub>2</sub>O<sub>4</sub>S) IL has a low melting point (−65 °C), as well as a relatively high conductivity (3.76 mS cm<sup>−1</sup> at room temperature) [8]. The electrochemical window of this CNT–IL interface is examined with CV, and the same experimental framework is used to determine the voltage-dependent double layer capacitance and polarization resistance of the charged interface. The discussion also addresses the experimental artifacts typically associated with such measurements, as well as a relatively straightforward procedure for resolving these effects.

## 2. Theory

A strictly nonFaradaic CNT–IL interface should behave like an ideal non-leaking capacitor [2,9,10], and the analysis of CV under this condition is relatively straightforward [11]. Quite frequently, however, the voltammetric response of such a system within its (apparent) electrochemical window is associated with Faradaic side reactions arising from intrinsic impurities of both the electrode and the electrolyte [3,12,13]. In addition, the rather sizable solution resistance of viscous IL electrolytes can affect the CV measurements. Voltage scan rate-dependent CV (which typically is necessary for D.C. measurement of double layer capacitances [14,15]) is particu-

\* Corresponding author. Tel.: +1 315 268 6676; fax: +1 315 268 6610.  
E-mail address: [samoy@clarkson.edu](mailto:samoy@clarkson.edu) (D. Roy).

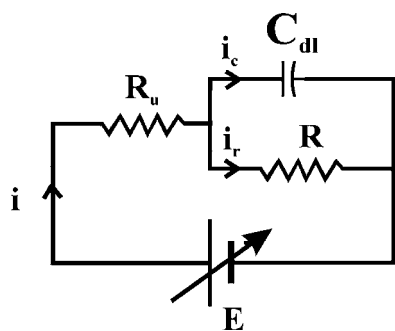


Fig. 1. A typical circuit model for a CNT-IL interface under the conditions of D.C. cyclic voltammetry.

larly prone to these types of effects [11]. The following discussion briefly outlines how these various effects can be accounted for in the analysis of the experimental CV data by using EEC models.

Although EECs most commonly are used in the context of A.C. electrochemical impedance spectroscopy (EIS) [11,16], their utility in D.C. electrochemical studies have also been noted in earlier studies [17–19]. For our present analysis, we refer to the EEC in Fig. 1. This circuit represents a “D.C. version” of the relatively familiar EEC often found in EIS of CNT-IL interfaces [20].  $R_u$  and  $R$  represent the uncompensated electrolyte resistance and the polarization (charge transfer) resistance of Faradaic processes, respectively. The applied D.C. voltage is  $E$ , which leads to the D.C. current  $i$ . Here,  $i = i_c + i_r$ , with  $i_c$  and  $i_r$  representing the current components for double layer charging and Faradaic side reactions, respectively. For CV,  $E$  is scanned at a rate,  $v_{dc} = (dE/dt)$ , starting from an initial potential  $E_i$ , and it is assumed that the value of  $v_{dc}$  is moderate enough to leave the double layer free of dispersion effects in the time domain [16,21–23].

Applying Kirchhoff's voltage rule to Fig. 1, and assuming that  $i_r \neq 0$  at  $E \neq E_{oc}$ , we obtain  $E - E_{oc} - iR_u = (q/C_d) = i_r R$ . Here  $q$  is the charge stored at the double layer capacitor, and  $E_{oc}$  is the open circuit potential (OCP). Combining these identities:

$$i_r = \left( \frac{1}{R_u + R} \right) \left[ E - E_{oc} - R_u \left( \frac{dq}{dt} \right) \right]. \quad (1)$$

By using the standard condition for CV [11], namely,  $E = E_i \pm v_{dc}t$ , and by noting from above that  $i_r \equiv [q/(RC_d)]$ , Eq. (1) can be rearranged as

$$\frac{dq}{dt} + \frac{q}{\tau} = A_1 + A_2 t, \quad (2)$$

where  $t$  is the time measured from the beginning of the voltage scan in a given (positive or negative) direction.  $A_1$  and  $A_2$  are constants at a fixed scan rate of CV;  $A_1 = [(E_i - E_{oc})/R_u]$ ;  $A_2 = \pm(v_{dc}/R_u)$ ; the (+) and (–) signs correspond to positive and negative voltage sweeps, respectively;  $\tau$  is the effective time constant of the electrochemical cell in the presence of Faradaic processes;  $\tau = R_t C_{dl}$ . The total resistance  $R_t$  represents a combination of  $R$  and  $R_u$ ;  $(1/R_t) = (1/R_u) + (1/R)$ . The solution to Eq. (2) has the form [19]:

$$q = \tau[A_1 + A_2(t - \tau)] + k_0 \exp\left(-\frac{t}{\tau}\right), \quad (3)$$

where  $k_0$  is a constant. By using the definition,  $i_c = (dq/dt)$  in Eq. (3):

$$i_c = \pm v_{dc} C_{dl} \left( \frac{R_t}{R_u} \right) \left[ 1 - \exp\left(-\frac{t}{\tau}\right) \right]. \quad (4)$$

where we have incorporated the result,  $k_0 = \pm(v_{dc} \tau^2 / R_u)$ , obtained according to the initial condition,  $i_c = 0$  at  $t = 0$ . For  $R \gg R_u$  (weak or negligible Faradaic reactions), Eq. (4) simplifies to the previously published result [14,15,18].

The Faradaic reaction current  $i_r$  should be voltage-dependent, so that the net current  $i$  in CV would depend on both  $E$  and  $v_{dc}$ :

$$i = i_r(E) \pm v_{dc} C_{dl} \left( \frac{R_t}{R_u} \right) B, \quad (5)$$

$$B = 1 - \exp\left(-\frac{|E - E_i|}{v_{dc} \tau}\right), \quad (6)$$

where we have taken the expression of  $i_c$  from Eq. (4), and used the condition of CV,  $t = |E - E_i|/v_{dc}$ . The term  $B$  indicates how fast the double layer charge–discharge process can follow the voltage variations in CV; this process is instantaneous for  $B = 1$ . Depending on the relative strengths of the cathodic and anodic reactions  $i_r$  can be positive or a negative. As the direction of the voltage scan is reversed,  $i_c$  passes through zero at  $E = E_i$ . In the early stages ( $t \ll \tau$ ) of the given scan, where  $|E - E_i| \approx 0$ , we have:  $\exp[-|E - E_i|(v_{dc} \tau)^{-1}] \approx 1 - [|E - E_i|(v_{dc} \tau)^{-1}]$ . Under this condition,  $i$  defined in Eq. (5) becomes independent of  $v_{dc}$ :

$$i = i_r(E) \pm [|E - E_i|(R_u)^{-1}]. \quad (7)$$

As the value of  $|E - E_i|$  increases during the CV scan, eventually the condition specified in Eq. (8) below is satisfied, and Eq. (5) then takes the form of Eq. (9):

$$|E - E_i| \gg (v_{dc} \tau), \quad (8)$$

$$i = i_r(E) \pm v_{dc} C'_{dl}. \quad (9)$$

$C'_{dl}$  is a scaled value of the double layer capacitance;  $C'_{dl} = [R/(R + R_u)]C_{dl}$ , and for

$$R \gg R_u, \quad (10)$$

one has  $C'_{dl} \equiv C_{dl}$ . This criterion is always met in the absence of Faradaic reactions, when  $R$  is infinitely large.

The above calculations illustrate how the determination of  $C_{dl}$  for CNT-IL systems using the general framework of Eq. (5) can be difficult using CV measurements alone. Two specific issues are identified in this regard. The first one arises because both  $R_u$  for ILs and  $C_{dl}$  for CNTs are rather large, which make the time constant  $\tau$  large, and consequently forces the experimental system to deviate from the condition specified in Eq. (8). In this case, it is difficult to extract the value of  $C_{dl}$  in a straightforward manner from experimental  $i$  vs.  $v_{dc}$  plots. Even if the experimental conditions are favorable to the requirements of Eq. (8), the capacitance term obtained from Eq. (9) is the scaled capacitance  $C'_{dl}$  and not  $C_{dl}$ . This is the second issue in CV-based measurement of the double layer capacitance of CNT-IL systems, and it arises whenever Eq. (10) is not satisfied.

The task of measuring the double layer capacitance for CNT-IL systems is somewhat simplified if the condition of Eq. (8) is met. If a series of voltammograms are recorded at different values of  $v_{dc}$  under this condition, then a plot of  $i$  (ordinate) vs.  $v_{dc}$  (abscissa) at each voltage explored in CV should be linear according to Eq. (9), with an ordinate-intercept of  $i_r(E)$  and a slope of  $C'_{dl}$ . In such cases  $C'_{dl}$  can be determined as a function of  $E$  from the slopes of a series of voltage-dependent  $i - v_{dc}$  graphs recorded at different values of  $v_{dc}$ . Subsequent determination of  $C_{dl}$  from  $C'_{dl}$  would involve measurement of the resistances  $R$  and  $R_u$ . If  $i_r \approx 0$  (weak Faradaic current, or large polarization resistance), then Eq. (10) (which yields  $C_{dl} \approx C'_{dl}$ ) also is satisfied simultaneously. In this latter case, Eq. (9) further simplifies as

$$C_{dl} = |i(v_{dc})^{-1}|. \quad (11)$$

Eq. (11) also follows directly from the conventional definition of  $C_{dl}$  [11], if  $i$  originates exclusively from  $E$ -dependent variations of the surface charge density  $q$ . In other words,  $C_{dl} = (dq/dE) = (dq/dt)(dE/dt)^{-1}$ , with  $i_r = 0$ ,  $i = (dq/dt)$ , and  $v_{dc} = (dE/dt)$  [25]. In the simple case of Eq. (11),  $i$  vs.  $E$  voltammograms of CV can be converted directly to  $C_{dl}$  vs.  $E$  plots [2].

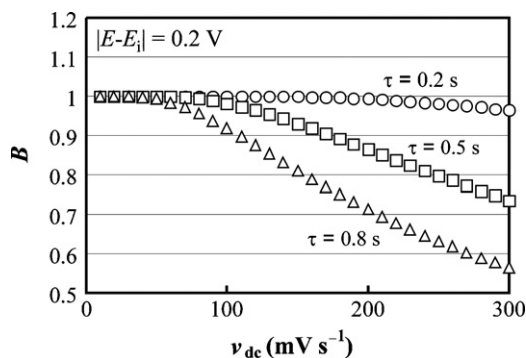


**Fig. 2.** Calculated results for the parameter  $B$ , defined in Eq. (6), describing temporal response characteristics of a CNT-IL interface to D.C. voltage-induced charge–discharge during CV scans. Variation of  $B$  is shown as a function of the voltage sweep rate,  $v_{dc}$ . Only the early stage of the (positive or negative) voltage sweep, within 0.2 V from the initial voltage, is considered for three typical values of the time constant,  $\tau$ , of the electrode–electrolyte interface.

Calculated results for the parameter  $B$  are shown in Fig. 2 as functions of  $v_{dc}$  and for  $\tau = 0.1, 0.5$  and  $0.8$  s (expected values of  $\tau$  for the CNT-IL system considered here), using  $|E - E_i| = 0.2$  V. This figure demonstrates the experimental limits on the voltage scan speeds necessary to validate Eq. (8). For instance, with  $\tau < 0.5$  s,  $v_{dc}$  should be kept below  $200 \text{ mV s}^{-1}$  and at the same time, voltammogram data within  $\sim 0.2$  V of each voltage bound of the CV scan should be excluded from any quantitative analysis to fully justify the use of Eq. (9) (that is, to maintain the value of  $B$  reasonably close to 1). As the value of  $\tau$  and/or that of  $v_{dc}$  increases, the central voltage region (the electrochemical sub-window, with  $|E - E_i|$  subtracted from its both ends) that can be used with Eq. (9) also becomes narrower.

We briefly note in this context that, if the EEC of Fig. 1 is subjected to EIS, the circuit branches/elements are likely to change, because the D.C. and A.C. response characteristics of porous, spatially inhomogeneous interfaces generally are quite different [16–18,21–24]. For instance, circuit branches that only contain D.C. blocking elements (like the Warburg impedance, and adsorption pseudo-capacitance) are not detectable if the electrochemical interface is probed only with D.C. CV [11,16,25] (and hence are excluded from Fig. 1). These additional elements are likely to be found in A.C. EIS, and at the same time, the double layer signature would appear in the EIS data as a constant phase element (CPE), rather than as  $C_{dl}$  [20–24]. Although  $C_{dl}$  can be determined for certain simple  $R$ -CPE combinations [26,27], such analyses of EIS data can be difficult if multiple A.C.-allowing circuit branches and elements are present in the detected EEC. This subject of EIS for CNT-IL interfaces will be addressed in a future report, while our present discussion will center only on D.C. CV.

### 3. Experimental

Commercial MWCNT, BuckyPaper™ was obtained from Nanolab. Preparation and properties, including scanning electron microscope (SEM) images of this material are provided on Nanolab website [28]. The free-standing MWCNT film was about  $100 \mu\text{m}$  thick and 50% dense, containing CNTs with a typical average diameter of 40 nm. Carbon-content of the paper was 95.93%, and Fe represented the highest impurity component (1.65%). The MWCNT paper electrode ( $0.06 \text{ cm}^2$  area exposed to the electrolyte) was fixed in a Teflon holder, and electrical connection to the electrode was made using Ag paste and a Cu current collector. The MWCNT electrode was soaked for several hours in the IL electrolyte prior to all experiments to allow complete wetting of its internal pores. The OCP ( $\approx 0$  V vs. Ag wire) of the system was allowed to stabilize prior to all electrochemical measurements.

The air-tight, three-electrode cell containing 0.5 ml of electrolyte used a silver wire quasi-reference electrode and a Pt wire counter electrode (2 and 1 mm diameters, respectively, both from Alfa Aesar). Several measurements involving IL electrolytes and different working electrodes have already been reported in the literature that used the Ag wire reference [4,10,29–31]. The present choice of Ag reference is based on considerations for comparison of our results with those reported earlier for similar systems. Commercially available EMIM-EtSO<sub>4</sub> (ECOENG 212™), obtained from Solvent Innovation [8], was kept at  $80^\circ\text{C}$  in a vacuum oven for 24 h and was used without further processing or dilution. The solvent-free electrolyte was degassed before the experiments by bubbling ultrahigh purity Ar for 1 h.

CV was performed in the true-analog ramp mode; staircase CV was avoided due to its problematic transient effects on capacitive current measurements. The uncompensated electrolyte resistance ( $R_u$ ) was evaluated following the standard procedure of EIS. A Solartron 1287A potentiostat/galvanostat, coupled with a model 1252A frequency response analyzer was employed for this purpose, using 10 mV A.C. signals between 0.5 Hz and 100 KHz. CV data were recorded at different voltage scan speeds varied between 10 and  $300 \text{ mV s}^{-1}$ .

## 4. Results and discussion

### 4.1. Electrochemical window of the CNT-[EMIM-EtSO<sub>4</sub>] system

Electrochemical windows of ILs commonly are determined using CV. The reported voltage scan speeds used in such measurements vary between 2 and  $100 \text{ mV s}^{-1}$ , with the maximum Faradaic currents often allowed up to  $\pm 20 \text{ mA cm}^{-2}$  [32–35]. Fig. 3 shows voltammograms obtained for a CNT-paper electrode in EMIM-EtSO<sub>4</sub> using experimental parameters similar to those mentioned above. The relatively larger Faradaic currents observed in the end-regions of the voltage range explored in Fig. 2 most likely are generated by oxidation of  $[\text{C}_2\text{H}_5\text{SO}_4]^-$  and reduction of  $[\text{EtMeIm}]^+$  at positive and negative voltages, respectively [36]. The “width” of the voltammograms (that is, the difference between the currents recorded with positive and negative voltage scans) is attributed to the term,  $(v_{dc}C_{dl})$  considered in Eq. (4). This feature is typical of electrochemical interfaces associated with relatively large values of  $C_{dl}$  [11].

The overall voltage range where the electrode current remained approximately confined within  $\pm 5 \text{ mA cm}^{-2}$  was found to extend

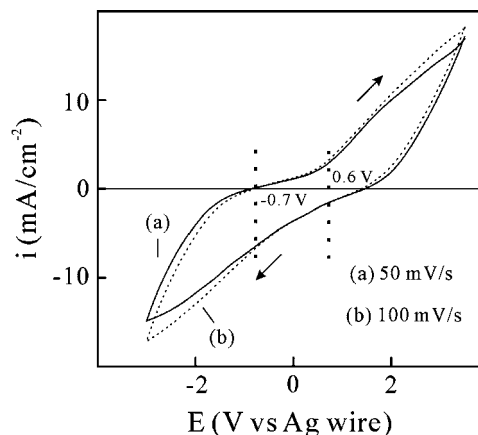


**Fig. 3.** Cyclic voltammograms of a CNT-paper electrode in EMIM-EtSO<sub>4</sub>, recorded in the voltage range between  $-3.5$  and  $3.0$  V at scan rates of (a)  $50 \text{ mV s}^{-1}$  and (b)  $100 \text{ mV s}^{-1}$ . The arrows represent the direction of voltage scan, and the two vertical lines indicate the electrochemical sub-window where  $|i| < 5 \text{ mA cm}^{-2}$ . The currents are normalized with respect to the geometric surface area of the electrode.

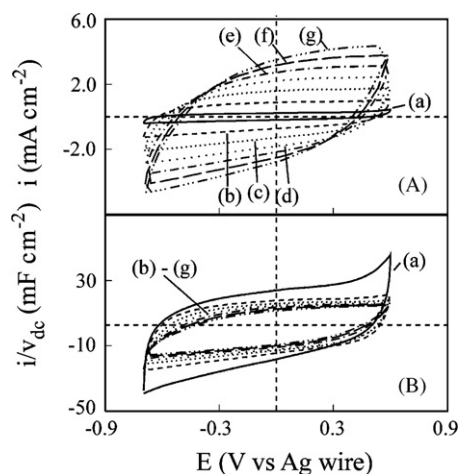


**Fig. 4.** (A) D.C. cyclic voltammograms and (B) scan-speed normalized electrode currents ( $i/v_{dc}$ ) of a paper electrode of CNT in EMIM-EtSO<sub>4</sub> at different voltage scan speeds ( $v_{dc}$ ), recorded with CV within the electrochemical window of the interface. In both (A) and (B)  $v_{dc}$  = (a) 10 mV s<sup>-1</sup>, (b) 50 mV s<sup>-1</sup>, (c) 100 mV s<sup>-1</sup>, (d) 150 mV s<sup>-1</sup>, (e) 200 mV s<sup>-1</sup>, (f) 250 mV s<sup>-1</sup> and (g) 300 mV s<sup>-1</sup>. In (B), the labels (a)–(g) apply sequentially from the outermost to the innermost plot.

from 0.6 to  $-0.7$  V. This “sub-window” (indicated with the two vertical dotted lines in Fig. 3) is somewhat smaller than the earlier published electrochemical windows for a number of ILs [4]. However, most of these earlier data were recorded using Pt working electrodes, and as seen in Xu et al.’s report [9], a noticeable narrowing of the nonFaradaic window of an IL can occur if CNT is used instead of Pt as the working electrode. The results in Fig. 2 are consistent with this observation, as well as with the general trends of CNT electrodes in ILs [1,5,9].

#### 4.2. Analysis of scan rate-dependent voltammograms

In Fig. 2, we have identified a voltage region, 0.6 to  $-0.7$  V, where the electrode currents were minimal. Fig. 4A shows voltammograms that explore this voltage region with  $v_{dc}$  varied between 10 and 300 mV s<sup>-1</sup>. The right hand side of Eq. (11), evaluated using the data from Fig. 4A, is plotted against  $E$  in Fig. 4B. In Fig. 4A, the magnitude of the current increases with increasing  $v_{dc}$ , since  $i_c$  (and hence  $i$ ) is proportional to  $v_{dc}$ . The  $E$  vs. ( $i/v_{dc}$ ) plots for different values of  $v_{dc}$  in Fig. 4B are not coincident, showing a noticeable departure from the simple description of Eq. (11). Nonzero values of  $i_r$  are likely to dictate this effect.

To test for the presence of Faradaic effects, the cathodic ( $i_{rc}$ ) and anodic ( $i_{ra}$ ) components of  $i_r$  should be separated from the measured  $i$ , and this can be done by plotting  $i$  (at different voltages) as a function of  $v_{dc}$ . These plots for the anodic and cathodic current components (extracted from Fig. 4A) are presented in Fig. 5A and B, for different voltages during the negative and positive voltage scans, respectively. In view of the discussion of Eq. (5) and Fig. 2, the data recorded with  $v_{dc} > 200$  mV s<sup>-1</sup> are excluded from Fig. 5 to avoid the scan range associated with strong effects of  $\tau$ . The plots in Fig. 5 are predominantly linear as expected in the description of Eq. (9). However, the slopes of the plots recorded (at 0.6 and  $-0.5$  V) close to the outer voltage limits of the CV scans are rather small, implying that the currents become nearly independent of  $v_{dc}$  at such voltages. This situation corresponds to the initial stage of the voltage scan, as described in Eq. (7). All the linear plots in Fig. 5 have finite intercepts on the current axis, and according to Eq. (9), these intercepts imply  $i_r \neq 0$ . Thus, due to the second term in the quantity  $C_{dl}' + (i_r/v_{dc})$ , the value of ( $i/v_{dc}$ ) obtained from Eq. (9) should increase with decreasing  $v_{dc}$ , and this trend is exhibited in Fig. 4B.

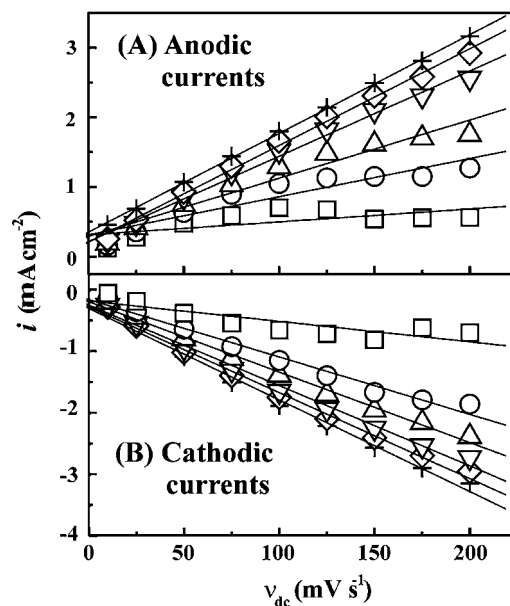


**Fig. 5.** (A) Anodic and (B) cathodic D.C. currents at the CNT-IL interface, measured at different voltage scan rates ( $v_{dc}$ ) using CV in positive- and negative-going voltage sweeps, respectively. The results only for selected D.C. voltages are shown to preserve the clarity of the collective plots. The graphs employing squares, circles, triangles, inverted triangles, diamonds and crosses correspond to  $E = -0.5, -0.4, -0.3, -0.1$  and  $0.1$  and  $0.6$  V in panel (A), respectively. In panel (B), the same sequence of symbols correspond to  $E = 0.4, 0.1, -0.1, -0.3, -0.4$  and  $-0.5$  V, respectively. The lines are linear fits to the data using Eq. (9).

Faradaic side reactions in CNT-IL systems typically arise from impurities. For instance, under voltage polarization, the Fe impurity sites [28] of the CNT electrode may anodically react with the H<sub>2</sub>O impurity in the electrolyte:  $\text{Fe} + 2\text{H}_2\text{O} = \text{Fe}(\text{OH})_2 + 2\text{H}^+ + 2\text{e}^-$ . Furthermore, during their aqueous processing and purification, the nanotubes are acid-treated and slightly functionalized [28,37]. Oxygen-containing functional groups (such as carboxylic, sulphonic, phenolic and ketone groups) are formed on/within the CNTs in this process [37–40]. Most of these functional groups are electroactive [38,39], and as noted by Musso et al. [37], tend to covalently bond to defect sites on the walls and open ends of the CNTs. These electro-active sites on the CNT walls can support both anodic and cathodic reactions, for instance, those indicated in Eqs. (12) and (13) for carboxylic and ketone groups on the CNT surface, respectively [38,40]:



The H<sup>+</sup> (or, H<sub>3</sub>O<sup>+</sup> in the presence of water impurities) generated in reaction (12) can form an ion-pair with the anion of the IL [41].

#### 4.3. Polarization resistance from voltage scan rate-dependent CV

In view of the above results, Eq. (9) provides an acceptable representation of the D.C. response of the CNT-IL system studied here. In order to determine  $C_{dl}$ , using this description, however, it is also necessary to determine the polarization resistance  $R$ . In conventional D.C. measurement (Stern Geary method) [11,16] of the equilibrium polarization resistance, the measured current is analyzed only in a small voltage region near the OCP of the system [19]. We adapt a different approach in the present work, because (i) we seek to determine  $E$ -dependent values of  $R$ , and not just the equilibrium polarization resistance, and (ii) the net current measured for the CNT-IL system is dominated by its capacitive component  $i_c$  (Fig. 5), whereas  $R$  is strictly associated with the Faradaic current  $i_r$ .

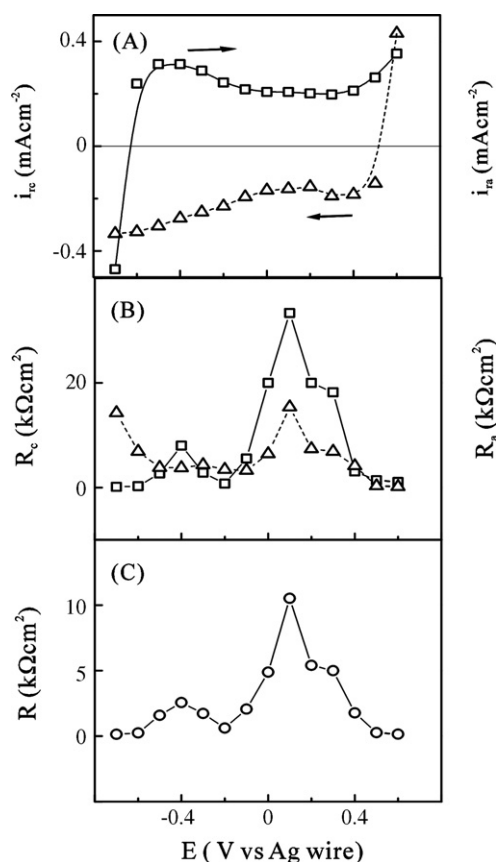


**Fig. 6.** (A) Faradaic reaction currents,  $i_{rc}$  (triangles) and  $i_{ra}$  (squares), given by the y-axis intercepts of the linear plots for positive and negative voltage scans from Fig. 5, respectively. The arrows indicate the voltage-scan direction. (B) Components of the polarization resistance for cathodic ( $R_c$ ) and anodic ( $R_a$ ) reactions, calculated using the local slopes of the  $i_{rc}$  and  $i_{ra}$  plots from panel (A), respectively. (C) Net polarization resistance,  $R$ , of the cathodic and anodic side reactions, calculated from the data of part (B) using Eq. (14).

To proceed with the calculation of  $R$ , first we plot in Fig. 6A the D.C. voltage-dependent values of  $i_{ra}$  and  $i_{rc}$ , obtained as y-intercepts of the linear graphs of Fig. 5A and B, respectively. The squares and the triangles in Fig. 6A correspond to data points recorded in positive and negative voltage scans ( $i_{ra}$  and  $i_{rc}$ ), respectively. The line shows the overall trend of the data. In the EIS formalism, the different sequential steps of a given reaction generally are modeled in terms of series connected circuit elements representing the different steps [16]. Similarly, if multiple reactions occur simultaneously at different sites of the same electrode surface, the circuit branches for the different reactions should be connected in parallel with each other. In the present study, at a given applied voltage, the anodic and cathodic Faradaic steps could be operative at the same time, because these steps represent different reactions having different activation polarizations. Therefore, we consider  $R$  as a net resistance of a parallel combination of the anodic and cathodic reactions, including the ones considered in Eqs. (12) and (13). Thus, defining the polarization resistances for anodic and cathodic reactions as  $R_a$  and  $R_c$ , respectively, we write:  $(1/R) = (1/R_a) + (1/R_c)$ , or

$$\frac{1}{R} = \left| \frac{di_{ra}}{dE} \right| + \left| \frac{di_{rc}}{dE} \right|, \quad (14)$$

where  $R_a = |di_{ra}/dE|^{-1}$  and  $R_c = |di_{rc}/dE|^{-1}$ . When more than one anodic steps are active, the individual polarization resistances for all these steps can be lumped in a mutually parallel connection, and then  $R_a$  will represent the resulting value of these combined resistances. A similar situation will apply to  $R_c$ . The terms  $|di_{ra}/dE|$  and

$|di_{rc}/dE|$  represent the  $E$ -dependent magnitudes of the local slopes of the ( $i_{ra} - E$ ) and ( $i_{rc} - E$ ) plots of Fig. 6A, respectively. It is useful to note here, that even at small values of  $|E - E_i|$  (where Eqs. (8) and (9) are not valid), the y-axis intercepts of the plots in Fig. 5 represent the reaction current  $i_r$  (according to Eqs. (5) and (7)). Therefore, the determination of  $R$  based on Eq. (14) should not be significantly affected by departure from the criterion of Eq. (9).

Fig. 6B shows the voltage-dependent values of  $R_a$  (squares) and  $R_c$  (triangles) calculated by applying the above expressions to the data of Fig. 6A. Fig. 6C presents the values of  $R$  obtained by applying Eq. (14) to the graphs in Fig. 6B. Both  $R_a$  and  $R_c$  in Fig. 6B have maximum values between  $-0.1$  and  $0.2$  V, and consequently, the net polarization resistance  $R$  in Fig. 6C also has maximum values in this region. This is an expected result, considering that the aforementioned voltage range falls in the mid-region of the electrochemical window (Fig. 2), where the Faradaic effects are minimal.

#### 4.4. Double layer capacitance from voltage scan rate-dependent CV

The D.C. voltage-dependent values of  $C'_{dl}$  (that is the slopes of the linear graphs of Fig. 5) are plotted in Fig. 7A. The squares and the triangles represent positive and negative voltage scans, respectively. The positive and negative signs of  $C'_{dl}$  simply indicate increasing and decreasing voltages for charging and discharging the double layer, respectively. Because these data are based on composite graphs constructed from a range ( $10$ – $200$   $\text{mV s}^{-1}$ ) of  $\nu_{dc}$ , the voltage scan rate-dependent effects within this range are essentially “averaged” in the processed data of Fig. 7.

The electrolyte resistance,  $R_u$ , measured using EIS (detailed data not included here), is found to be voltage independent with a value of  $55 \Omega \text{ cm}^2$ . Compared to this value,  $R$  is considerably large ( $2$ – $10 \text{ K}\Omega \text{ cm}^2$ ) in the mid-sector of the experimental voltage window, where  $R/(R+R_u) \approx 1$ , and  $C'_{dl} \approx C_{dl}$ . In the end-regions of the voltage window, however,  $R$  drops to smaller values ( $100$ – $250 \Omega \text{ cm}^2$ ) where the values of  $C'_{dl}$  deviate from those of  $C_{dl}$ . Using the aforementioned  $R_u$  and  $R$  from Fig. 6, we obtained  $C_{dl}$  as shown in Fig. 7B. This plot is similar to those published previously for similar systems [30,31,40].

For the present system, the central voltage region (estimated from the results of Fig. 2) available for straightforward measurement of  $C_{dl}$  extends between  $0.3$  and  $-0.4$  V (bounded by the two vertical dashed lines in Fig. 7). Outside this region, Eq. (8) no longer serves as an adequate working equation for the determination of  $C_{dl}$  or  $C'_{dl}$  using CV. The general form of the scaled capacitance in this “outside-region” (denoted here as  $C'_{dl}(\text{gen})$ ) can be obtained from Eq. (5):  $C'_{dl}(\text{gen}) = [(i - i_r)/\nu_{dc}]/B$ , which is different from the definition obtained from Eq. (9):  $C'_{dl} = [(i - i_r)/\nu_{dc}]$ , for  $B \approx 1$ . Therefore, evaluation of  $C'_{dl}$  based on Eq. (9) in the outside-region would be inaccurate, and the fractional error in this measurement can be estimated phenomenologically as:  $(\Delta C'_{dl}/C'_{dl}) = (1 - B)/B$ , where  $\Delta C'_{dl} = [C'_{dl}(\text{gen}) - C'_{dl}]$ . As expected, this error is minimal for  $B \approx 1$ .  $(\Delta C'_{dl}/C'_{dl})$  for a given time constant depends on both the voltage and the voltage scan speed. For instance, according to Fig. 2, if  $\tau = 0.5$  s, the uncertainty in  $C'_{dl}$  at a voltage  $0.2$  V away from each turn-around point of CV is about 16% (with  $B \approx 0.86$ ) at  $\nu_{dc} = 200 \text{ mV s}^{-1}$ . By dropping  $\nu_{dc}$  down to  $100 \text{ mV s}^{-1}$  ( $B \approx 0.98$  in Fig. 2), while keeping the other experimental parameters unchanged, this uncertainty in  $C'_{dl}$  can be reduced to 2%.

Within the central voltage region of the electrochemical window, where  $\Delta C'_{dl}$  is negligible (but  $C'_{dl} \neq C_{dl}$ ), one may consider the difference between the values of  $C'_{dl}$  and  $C_{dl}$  as the error in  $C_{dl}$  introduced by the relative values of  $R$  and  $R_u$  deviating from the conditions of Eqs. (10) and (11). In this case, the fractional error in the value of  $C_{dl}$  is voltage-dependent through  $R$ , and can be calculated, once again, from phenomenological considerations,

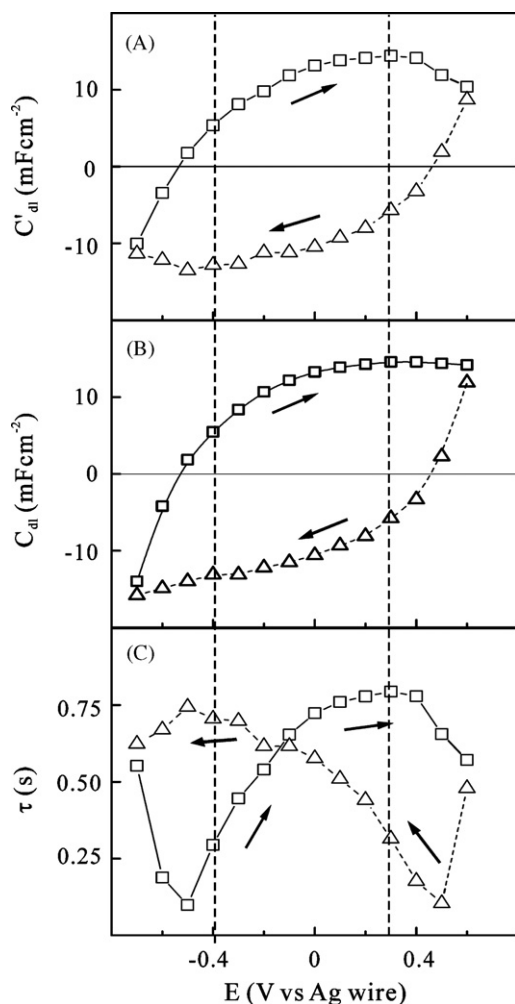


**Fig. 7.** (A) Scaled double layer capacitance ( $C'_{dl}$ ) as a function of the applied voltage of CV, obtained from the slopes of the linear plots of Fig. 5. (B) Double layer capacitance ( $C_{dl}$ ) as a function of the applied voltage of CV, obtained from panel (A) and using the values of  $R$  from Fig. 6C. (C) Voltage-dependent time constant,  $\tau$ , of the CNT working electrode, affected by Faradaic side reactions during charge–discharge in EMIM-EtSO<sub>4</sub>. In all three panels, the triangles and the squares represent positive and negative voltage scans, respectively. Experimental artifacts that tend to alter the formulation of Eqs. (8) and (9) are minimal in the voltage region bounded by the two dashed vertical lines.

by writing:  $(\Delta C_{dl}/C_{dl}) = [(C_{dl} - C'_{dl})/C_{dl}] = R_u/(R + R_u)$ . The minimum value of  $R$  found within the central window (between 0.3 and  $-0.4$  V in Fig. 6C) is about  $2.5 \text{ k}\Omega \text{ cm}^2$ . By combining this  $R$  with the measured  $R_u$  ( $55 \Omega \text{ cm}^2$ ) in the above formula, we estimate that the maximum error in  $C_{dl}$  within the limits of applicability of Eq. (9) is only about 2%. As a result, the overall shape of the plot in Fig. 7B is similar to that in Fig. 7C, and the values also are rather comparable between the two cases.

At and within  $\pm 0.1$  V of the OCP ( $\approx 0$  V), the positive and negative values of  $C_{dl}$  in Fig. 7B are equally separated from the voltage axis with a magnitude of  $\approx 12 \text{ mF cm}^{-2}$ . At these voltages, the net Faradaic current ( $i_r = i_{rc} + i_{ra}$ ) is equal or close to zero ( $|i_{rc}| \approx |i_{ra}|$ ). Thus, the double layer capacitance values of the CNT–IL interface measured here using CV should be most reliable at and near the OCP. Consistent with recently reported results for CNT electrodes [1,2,6] this value is about three orders of magnitude higher than those typically found for flat metal electrodes in traditional aqueous electrolytes [11,16,21]. This high capacitance of the CNT–IL systems is relevant for charge storage devices.

By combining  $C_{dl}$  from Fig. 7B with  $R$  from Fig. 6C, we obtain the voltage-dependent time constant  $\tau$  plotted in Fig. 7C. The symbols

are associated with their corresponding experimental conditions indicated in Fig. 7A and B. In the mid-region of this window, the Faradaic effects are minimized ( $R \gg R_u$ ) where  $\tau \approx R_u C_{dl}$ . The values of  $\tau$  observed here are considerably larger than those typically found (0.1–1 ms) for metal electrodes in aqueous electrolytes [13,18]. The large time constant of the cell is caused by the relatively large solution resistance of the viscous IL, as well as by the large double layer capacitance of the porous CNT electrode.

## 5. Conclusions

We have used voltage scan rate-dependent CV to study the double layer characteristics of a CNT-paper electrode in an IL electrolyte of EMIM-EtSO<sub>4</sub>. The results demonstrate that the measurement of the double layer capacitance for such CNT–IL systems using CV is complicated by two main factors: (i) presence of Faradaic side reactions within the electrochemical window, and (ii) a relatively large time constant for charge/discharge of the CNT–IL double layer. We have demonstrated a relatively simple method of CV that helps to address these issues, as well as to identify and account for the associated experimental artifacts. The theoretical basis of this experimental approach has been discussed. The measured currents of the Faradaic reactions are strongly masked by the charge–discharge current of the double layer. The results reported here also demonstrate how the polarization resistance can be determined in the presence of strong capacitive currents. The double layer capacitance for the CNT–EMIM-EtSO<sub>4</sub> system has also been obtained in the mid-region of the experimentally obtained electrochemical window. The analytical approach discussed in this work can be readily extended to studies of other IL electrolytes in combination with CNT electrodes.

## Acknowledgement

The authors thank the School of Arts and Sciences of Clarkson University for supporting this work.

## References

- [1] M. Ue, in: H. Ono (Ed.), *Electrochemical Aspects of Ionic Liquids*, Wiley, New York, 2005, pp. 205–223.
- [2] E. Frackowiak, *J. Braz. Chem. Soc.* 17 (2006) 1074.
- [3] M. Lazzari, M. Mastragostino, F. Soavi, *Electrochem. Commun.* 9 (2007) 1567.
- [4] M. Galiński, A. Lewandowski, I. Stepniak, *Electrochim. Acta* 51 (2006) 5567.
- [5] J.N. Barisci, G.G. Wallace, D.R. MacFarlane, R.H. Baughman, *Electrochem. Commun.* 6 (2004) 22.
- [6] A.A. Kornyshev, *J. Phys. Chem. B* 111 (2007) 5545.
- [7] K.B. Oldham, *J. Electroanal. Chem.* 613 (2008) 131.
- [8] <http://www.solvent-innovation.com/index.overview.htm>.
- [9] B. Xu, F. Wu, R. Chena, G. Cao, S. Chena, G. Wang, Y. Yang, *J. Power Sources* 158 (2006) 773.
- [10] M.C. Buzzeo, R.G. Evans, R.G. Compton, *Chem. Phys. Chem.* 5 (2004) 1107.
- [11] A.J. Bard, L.R. Faulkner, *Electrochemical Methods*, 2nd ed., Wiley, New York, 2001.
- [12] C.E. Banks, A. Crossley, C. Salter, S.J. Wilkins, R.G. Compton, *Angew. Chem.* 118 (2006) 2595.
- [13] N. Alexeyeva, K. Tammeveski, *Electrochem. Solid-State Lett.* 10 (2007) F18.
- [14] L. Austin, E.G. Gagnon, *J. Electrochem. Soc.* 251 (1973) 120.
- [15] K.B. Oldham, *Electrochem. Commun.* 6 (2004) 210.
- [16] E. Barsoukov, J.R. Macdonald (Eds.), *Impedance Spectroscopy*, Wiley, New York, 2005.
- [17] S. Åberg, *J. Electroanal. Chem.* 419 (1997) 99.
- [18] J.E. Garland, C.M. Pettit, M.J. Walters, D. Roy, *Surf. Interface Anal.* 31 (2001) 492.
- [19] C.M. Sulyma, P.C. Goonetilleke, D. Roy, *J. Mater. Process. Technol.* 209 (2009) 1189.
- [20] J.N. Barisci, G.G. Wallace, D. Chattopadhyay, F. Papadimitrakopoulos, R.H. Baughman, *J. Electrochem. Soc.* 150 (2003) E409.
- [21] P. Zoltowski, *J. Electroanal. Chem.* 443 (1998) 149.
- [22] J.-P. Jorcin, M.E. Orazem, N. Pébère, B. Tribollet, *Electrochim. Acta* 51 (2006) 1473.
- [23] A. Sadkowsky, *J. Electroanal. Chem.* 481 (2000) 232.
- [24] G. Lang, K.E. Heusler, *J. Electroanal. Chem.* 481 (2000) 227.
- [25] S.B. Emery, J.L. Hubble, D. Roy, *Electrochim. Acta* 50 (2005) 5659.
- [26] P.S. Germain, W.G. Pell, B.E. Conway, *Electrochim. Acta* 49 (2004) 1775.

- [27] G.J. Brug, A.L.G. van Eeden, M. Sluyters-Rehbach, J. Sluyters, *J. Electroanal. Chem.* 176 (1984) 275.
- [28] <http://www.nano-lab.com/carbonnanotubeproducts.html>.
- [29] M.C. Buzzeo, C. Hardacre, R.G. Compton, *Chem. Phys. Chem.* 7 (2006) 176.
- [30] A. Saheb, M. Josowicz, *Electroanalysis* 18 (2006) 405.
- [31] J. Zhang, A.M. Bond, *Analyst* 130 (2005) 1132.
- [32] M. Yoshizawa-Fujita, D.R. MacFarlane, P.C. Howlett, M. Forsyth, *Electrochem. Commun.* 8 (2006) 445.
- [33] Q. Zhu, Y. Song, X. Zhu, X. Wang, *J. Electroanal. Chem.* 601 (2007) 229.
- [34] M. Taggougui, M. Diaw, B. Carre, P. Willmann, D. Lemordant, *Electrochim. Acta* 53 (2008) 5496.
- [35] A. Lewandowski, M. Galiński, *J. Phys. Chem. Solids* 65 (2004) 281.
- [36] P. Hapiot, C. Lagrost, *Chem. Rev.* 108 (2008) 2238.
- [37] S. Musso, S. Porro, M. Vinante, L. Vanzetti, R. Ploeger, M. Giorcelli, B. Possetti, F. Trotta, C. Pederzoli, A. Tagliaferro, *Diamond Rel. Mater.* 16 (2007) 1183.
- [38] M. Toupin, D. Bélanger, I.R. Hill, D. Quinn, *J. Power Sources* 140 (2005) 203.
- [39] E. Frackowiaka, F. Béguin, *Carbon* 39 (2001) 937.
- [40] N.P. Blanchard, R.A. Hatton, S.R.P. Silva, *Chem. Phys. Lett.* 434 (2007) 92.
- [41] E.I. Izgorodina, M. Forsyth, D.R. MacFarlane, *Aust. J. Chem.* 60 (2007) 15.



# Study on the interaction of nucleic acids with silver nanoparticles—Al(III) by resonance light scattering technique and its analytical application

Haiping Zhou, Xia Wu\*, Jinghe Yang

Key Laboratory of Colloid and Interface Chemistry (Shandong University), Ministry of Education, School of Chemistry and Chemical Engineering, Shandong University, Shanda Nanlu 27#, Jinan 250100, PR China

## ARTICLE INFO

### Article history:

Received 1 September 2008  
Received in revised form 17 December 2008  
Accepted 21 December 2008  
Available online 15 January 2009

### Keywords:

Nucleic acids  
Resonance light scattering  
Silver nanoparticles  
Al(III)

## ABSTRACT

It is found that Al(III) can further enhance the intensity of resonance light scattering (RLS) of the silver nanoparticles (AgNPs) and nucleic acids system. Based on this, a novel method of determination of nucleic acids is proposed in this paper. Under optimum conditions, there are linear relationships between the enhancing extent of RLS and the concentration of nucleic acids in the range of  $1.0 \times 10^{-9}$ – $1.0 \times 10^{-7}$  g mL<sup>-1</sup>,  $1.0 \times 10^{-7}$ – $2.0 \times 10^{-6}$  g mL<sup>-1</sup> for fish sperm DNA (fsDNA),  $1.0 \times 10^{-9}$ – $7.0 \times 10^{-8}$  g mL<sup>-1</sup> for calf thymus DNA (ctDNA) and  $1.0 \times 10^{-9}$ – $1.0 \times 10^{-7}$  g mL<sup>-1</sup> for yeast RNA (yRNA). The detection limits ( $S/N=3$ ) of fsDNA, ctDNA and yRNA are  $4.1 \times 10^{-10}$  g mL<sup>-1</sup>,  $4.0 \times 10^{-10}$  g mL<sup>-1</sup> and  $4.5 \times 10^{-10}$  g mL<sup>-1</sup>, respectively. The studies indicate that the RLS enhancement effect should be ascribed to the formation of AgNPs–Al(III)–DNA aggregations through electrostatic attraction and adsorption bridging action of Al(III). And the sensitivity and stability of the AgNPs–fsDNA system could be enhanced by Al(III).

© 2009 Elsevier B.V. All rights reserved.

## 1. Introduction

Metal nanoparticles such as AgNPs have attracted considerable interest because of their particular optical, magnetic, electronic and catalytic properties. AgNPs are widely utilized in material science, physics and chemistry fields [1]. Moreover, they also has important curatorial function in inflammation, antiviral, anti-AIDS and especially in anticancer [2,3]. As we know, DNA is an attractive template because of its large aspect ratio (length/diameter), well-defined sequences of DNA base, a variety of superhelix and a high affinity for metal cations. So with chemical reduction, many metal cations could form metallic nanowires following the contour of the DNA template [4–10], for example, silver [4], copper [7], gold [8] and so on. Recently, it has been demonstrated that silver nanocluster [11] and silver nanoring [12] can be formed through a DNA-templated process. And the determination of nucleic acids using AgNPs has aroused abroad interest and attention [13,14].

In this paper, a new method for nucleic acids determination was developed using the system of AgNPs–Al(III)–nucleic acids. The experiments indicated that the enhanced intensity of RLS was in proportion to the concentration of nucleic acids. The interaction mechanism of the system was also studied by the transmission

electronic microscopy (TEM), circular dichroism spectra (CD), zeta potentials and UV spectrometry.

## 2. Experimental

### 2.1. Chemicals

Stock solutions of nucleic acids ( $100 \mu\text{g mL}^{-1}$ ) were prepared by dissolving commercial fsDNA (Sigma), ctDNA and yRNA (Beijing Baitai Co., China) in  $0.05 \text{ mol L}^{-1}$  sodium chloride solutions. Silver nanoparticles prepared: a stock solution of silver nanoparticles ( $2.0 \times 10^{-4} \text{ g mL}^{-1}$ ) was prepared by dissolving 0.0158 g of AgNO<sub>3</sub> in 40 mL of 0.22  $\mu\text{m}$ -filtered doubly distilled water, 2 mL sodium citrate (1%) was added slowly in above AgNO<sub>3</sub> solution by heating at 86 °C with stirring for 30 min, the solution color changed gradually from colorless to olivine, diluting to 50 mL finally. Above solutions were stored at 0–4 °C. A  $0.01 \text{ mol L}^{-1}$  potassium hydrogen phthalate (KHP)–NaOH buffer solution was prepared by dissolving 0.5106 g KHP in distilled water and adjusting the pH to 5.6 with  $0.2 \text{ mol L}^{-1}$  NaOH. A stock solution of aluminium nitrate ( $2.0 \times 10^{-2} \text{ mol L}^{-1}$ ) was prepared by dissolving 0.7503 g Al(NO<sub>3</sub>)<sub>3</sub> in 100 mL volumetric flask with water. All the chemicals used were of analytical reagent grade and double-distilled water was used throughout.

### 2.2. Apparatus

The RLS spectra and the intensity of RLS were performed on a LS-55 spectrofluorimeter (PE, USA). All CD spectra were collected

\* Corresponding author. Tel.: +86 531 88365459; fax: +86 531 88564464.  
E-mail address: [wux@sdu.edu.cn](mailto:wux@sdu.edu.cn) (X. Wu).



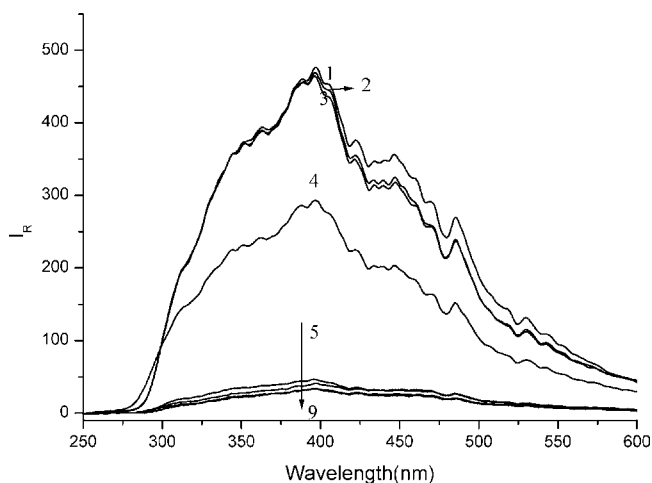


**Fig. 1.** Resonance light scattering spectra. (1) AgNPs–Al(III)–ctDNA; (2) AgNPs–Al(III)–fsDNA; (3) AgNPs–Al(III)–yRNA; (4) AgNPs–fsDNA; (5) Al(III)–fsDNA; (6) AgNPs; (7) AgNPs–Al(III); (8) Al(III); (9) fsDNA. Conditions: AgNPs:  $1.4 \times 10^{-6}$  g mL $^{-1}$ ; Al(III):  $2.0 \times 10^{-3}$  mol L $^{-1}$ ; fsDNA:  $1.0 \times 10^{-6}$  g mL $^{-1}$ ; ctDNA:  $1.0 \times 10^{-6}$  g mL $^{-1}$ ; yRNA:  $1.0 \times 10^{-6}$  g mL $^{-1}$ ; KHP:  $8.0 \times 10^{-4}$  mol L $^{-1}$  (pH 5.6).

on a J-810S Circular Dichroism Spectrometer (JASCO, Japan). All absorption spectra were measured on a U-4100 spectrophotometer (Hitachi, Japan). TEM images were measured on JEM-100 CXII Transmission Electron Microscope (JEOL, Japan). Zeta potentials ( $\zeta$ ) were measured with a JS94H micro-television electrophoretic instrument (Powereach, Shanghai). All pH measurements were made with a Delta 320-S acidity meter (Mettler Toledo, Shanghai).

### 2.3. Procedure

To a 10 mL colorimetric tube, the solutions were added in the following order: buffer, AgNPs, Al(III) and nucleic acids. The mixture was diluted to 5 mL with water and allowed to stand for 10 min. The RLS spectra were obtained by simultaneously scanning the excitation and emission monochromators over the range of 250–600 nm (i.e.  $\Delta\lambda = 0$  nm). The intensity of resonance light scattering was measured at the maximum wavelength (398 nm) in a 1 cm quartz cell, with the slit width at 10 nm for the excitation and emission. The enhanced RLS intensity of AgNPs–Al(III)–nucleic acids system was represented as  $\Delta I = I_R - I_R^0$ , where  $I_R$  and  $I_R^0$  were the RLS intensities of the systems with and without nucleic acids.

## 3. Results and discussion

### 3.1. Light scattering spectra

Fig. 1 shows the RLS spectra of AgNPs–Al(III)–ctDNA, AgNPs–Al(III)–fsDNA, AgNPs–Al(III)–yRNA, AgNPs–fsDNA, Al(III)–fsDNA, AgNPs, AgNPs–Al(III), Al(III) and fsDNA systems. As can be seen, nucleic acids can increase the RLS intensity of AgNPs and Al(III). Additionally, when AgNPs, Al(III) and nucleic acids are mixed together, the RLS intensity is further enhanced and reaches a maximum at 398 nm, which indicates that there are interactions between AgNPs–Al(III) and nucleic acids. We think that the RLS of the system at 398 nm is ascribed to the absorption of AgNPs in the range of 250–280 nm. In comparison with AgNPs, the system of AgNPs–Al(III) has lower intensity of RLS in the detected wavelength range.

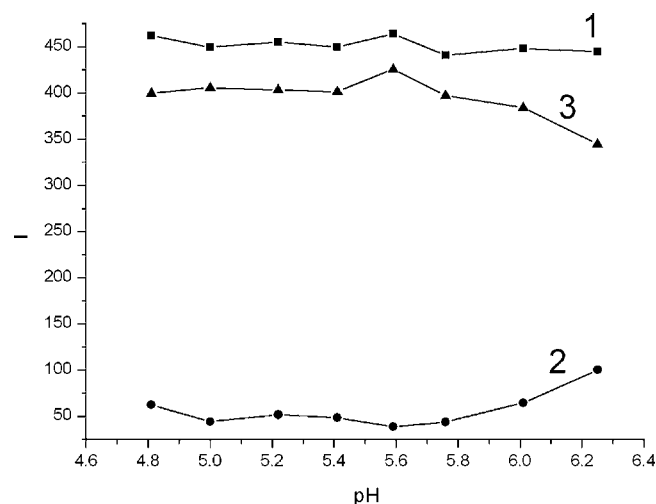


**Fig. 2.** Effect of pH. (1)  $I_R$ ; (2)  $I_R^0$ ; (3)  $\Delta I$ . Conditions: AgNPs:  $1.4 \times 10^{-6}$  g mL $^{-1}$ ; Al(III):  $2.0 \times 10^{-3}$  mol L $^{-1}$ ; fsDNA:  $1.0 \times 10^{-6}$  g mL $^{-1}$ ; KHP:  $8.0 \times 10^{-4}$  mol L $^{-1}$ .

### 3.2. Effects of pH and buffers

The effect of pH on the RLS intensity of this system is shown in Fig. 2. It can be seen that  $\Delta I$  value reaches the maximum at the pH 5.61, so pH 5.61 is used for subsequent work. The buffer also have a large effect on the intensity of the system. The  $\Delta I$  (%) for hexamethylenetetramine (HMTA)–HCl, NaAc–HAc, KHP–HCl, succinic acid–NaOH, BR and citric acid–K $_2$ HPO $_4$  are 3.7, 94.8, 100, 84.3, 95.4 and 94.6, respectively. Further experiments indicate that 0.4 mL of 0.01 mol L $^{-1}$  KHP–NaOH is the most suitable buffer.

### 3.3. Effect of AgNPs concentration

From Fig. 3 it can be seen that the  $\Delta I$  value of this system reaches a maximum when the concentration of AgNPs is  $1.8 \times 10^{-6}$  g mL $^{-1}$ . At the same time, the RLS intensity of the system of AgNPs–Al(III) is high, too. As can be seen that when the concentration of AgNPs is  $1.4 \times 10^{-6}$  g mL $^{-1}$ ,  $I_R/I_R^0$  (%) value of this system reaches a maximum and the value of  $I_R^0$  is lower. Considering the effect of the system reagent blank,  $1.4 \times 10^{-6}$  g mL $^{-1}$  AgNPs is chosen for further experiment.

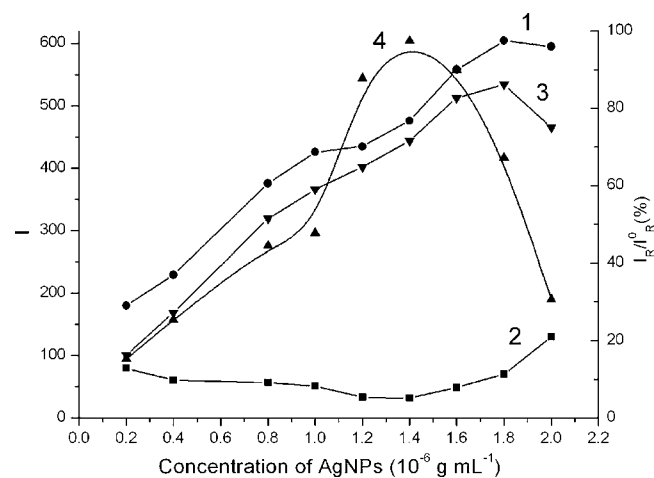


**Fig. 3.** Effect of the concentration of AgNPs. (1)  $I_R$ ; (2)  $I_R^0$ ; (3)  $\Delta I$ ; (4)  $I_R/I_R^0$ . Conditions: Al(III):  $2.0 \times 10^{-3}$  mol L $^{-1}$ ; fsDNA:  $1.0 \times 10^{-6}$  g mL $^{-1}$ ; KHP:  $8.0 \times 10^{-4}$  mol L $^{-1}$  (pH 5.6).

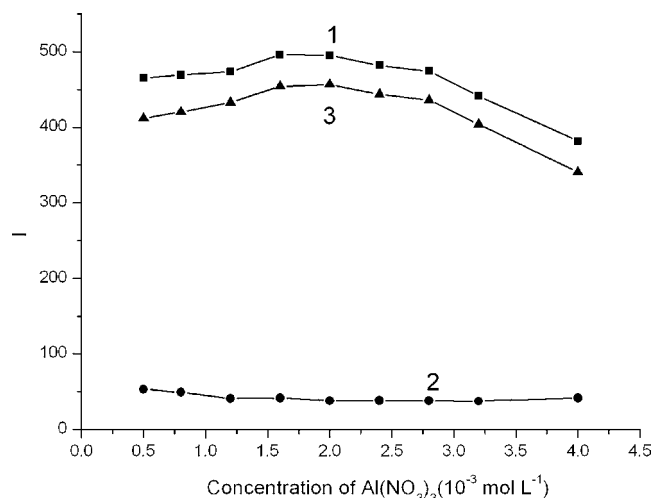


**Fig. 4.** Effect of the concentration of Al(III). (1)  $I_0$ ; (2)  $I_R^0$ ; (3)  $\Delta I$ . Conditions: AgNPs:  $1.4 \times 10^{-6} \text{ g mL}^{-1}$ ; fsDNA:  $1.0 \times 10^{-6} \text{ g mL}^{-1}$ ; KHP:  $8.0 \times 10^{-4} \text{ mol L}^{-1}$  (pH 5.6).

### 3.4. Effect of Al(III) concentration

The effect of the concentration of Al(III) is tested as shown in Fig. 4. It can be seen that the  $\Delta I$  value of this system reaches a maximum when the concentration of Al(III) is  $2.0 \times 10^{-3} \text{ mol L}^{-1}$ . So  $2.0 \times 10^{-3} \text{ mol L}^{-1}$  is chosen for further experiment. A further test indicates that in presence of Al(III), the sensitivity and stability of the AgNPs–fsDNA system can be obviously enhanced.

### 3.5. The addition order and stability of this system

The effect of the adding order is investigated. The results indicate that the order of buffer–AgNPs–Al(III)–fsDNA is the best. Under the optimum condition, the effect of time on the RLS intensity is studied. The results show that the  $\Delta I$  reaches a maximum at 10 min after all the reagents added, and it remains stable for over 2.5 h. Therefore, this system exhibits good stability.

### 3.6. Effect of foreign substances

The interference of foreign substances is shown in Table 1. It is found that most metallic ions, protein, amino acids and nucleotides had not or had little effect on the determination of fsDNA within  $\pm 5\%$  relative error.

## 4. Analytical applications

### 4.1. Calibration graphs and detection limits

Under the optimum conditions defined, the calibration graphs for fsDNA, ctDNA and yRNA are constructed. All the analytical parameters are presented in Table 2. The results show that the limits are down to  $10^{-10} \text{ g mL}^{-1}$ .

**Table 2**  
Analytical parameters of this method.

Nucleic acids	Linear range ( $\text{g mL}^{-1}$ )	Linear regression equation ( $\text{g mL}^{-1}$ )	$r^a$	Limit of detection ( $\text{g mL}^{-1}$ )
fsDNA	$1.0 \times 10^{-9}$ – $1.0 \times 10^{-7}$	$\Delta I = 25.3 + 3.83 \times 10^{-9}C$	0.988	$4.1 \times 10^{-10}$
	$1.0 \times 10^{-7}$ – $2.0 \times 10^{-6}$	$\Delta I = 311.5 + 5.32 \times 10^{-7}C$	0.997	
ctDNA	$1.0 \times 10^{-9}$ – $7.0 \times 10^{-8}$	$\Delta I = 35.0 + 3.85 \times 10^{-9}C$	0.990	$4.0 \times 10^{-10}$
yRNA	$1.0 \times 10^{-9}$ – $1.0 \times 10^{-7}$	$\Delta I = 31.9 + 3.46 \times 10^{-9}C$	0.992	$4.5 \times 10^{-10}$

<sup>a</sup> Correlation coefficient.

**Table 1**  
Interference from foreign substances.

Foreign substance	Concentration coexisting ( $\times 10^{-6} \text{ mol L}^{-1}$ )	Change of $\Delta I$ (%)
$\text{K}^+$ , $\text{Cl}^-$	350	−5.2
$\text{Na}^+$ , $\text{Cl}^-$	180	−3.8
$\text{Mg}^{2+}$ , $\text{SO}_4^{2-}$	200	−4.5
$\text{Ca}^{2+}$	230	+3.8
$\text{Fe}^{3+}$	25	+4.1
$\text{NH}_4^+$ , $\text{Cl}^-$	50	−3.8
CMP	4.0	+4.8
TMP	8.0	+4.0
GMP	4.0	+4.5
AMP	10	−3.8
Phe	40	−4.0
Cys	10	+6.2
L-His	320	+4.6
Pro	40	−5.8
BSA	$30 \mu\text{g mL}^{-1}$	−4.1
HSA	$45 \mu\text{g mL}^{-1}$	−3.7

Conditions: AgNPs:  $1.4 \times 10^{-6} \text{ g mL}^{-1}$ ; Al(III):  $2.0 \times 10^{-3} \text{ mol L}^{-1}$ ; fsDNA:  $6.0 \times 10^{-7} \text{ g mL}^{-1}$ ; KHP:  $8.0 \times 10^{-4} \text{ mol L}^{-1}$  (pH 5.6).

### 4.2. Recovery test and determination of actual sample

The standard addition method is used for both recovery test and the determination of fsDNA in synthetic samples which include fsDNA  $6.0 \times 10^{-7} \text{ g mL}^{-1}$ , KCl  $5.0 \times 10^{-6} \text{ g mL}^{-1}$ ,  $\text{MgSO}_4$   $3.0 \times 10^{-6} \text{ g mL}^{-1}$  and L-His  $1.0 \times 10^{-6} \text{ mol L}^{-1}$ . The recovery ratio for fsDNA is 96–106.5% ( $n=3$ ). The content of plasmid DNA in the real sample is  $700 \text{ ng } \mu\text{L}^{-1}$ , obtained by using a Biophotometer (Eppendorf Co.). The sample is diluted by 7000-fold with water and determines by this proposed method, the mean value of three measurements is  $741 \text{ ng } \mu\text{L}^{-1}$  and the relative standard deviation is 0.50% ( $n=3$ ). Hence, the proposed method is suitable for the determination of trace amount of nucleic acids in this sample.

## 5. Interaction mechanism of the system

### 5.1. Interaction of AgNPs, Al(III) and fsDNA

The interaction between AgNPs, fsDNA and Al(III) can be examined by the  $\zeta$  of the system at different concentration of Al(III). From Fig. 5, it can be seen that the  $\zeta$  of AgNPs–fsDNA is about  $-39 \text{ mV}$  in KHP–NaOH buffer. With the addition of Al(III) to this system, the  $\zeta$  increases and reaches 0 when the concentration of Al(III) is up to  $2.8 \times 10^{-3} \text{ mol L}^{-1}$ , then increases to a positive  $\zeta$ , which is attributed to the neutralization of negatively charged AgNPs–fsDNA with positive charged Al(III). This indicates that there exists electrostatic interaction between AgNPs–fsDNA and Al(III).

### 5.2. Formation of AgNPs–Al(III)–DNA aggregates

The RLS theory [15,16] indicated that the increase of particle aggregation extent was a main reason for the RLS enhancement. From Fig. 1, it can be seen that the RLS intensity of AgNPs–Al(III) is greatly enhanced in the presence of DNA. So we presume that the AgNPs, Al(III) and DNA can form the larger aggregates.

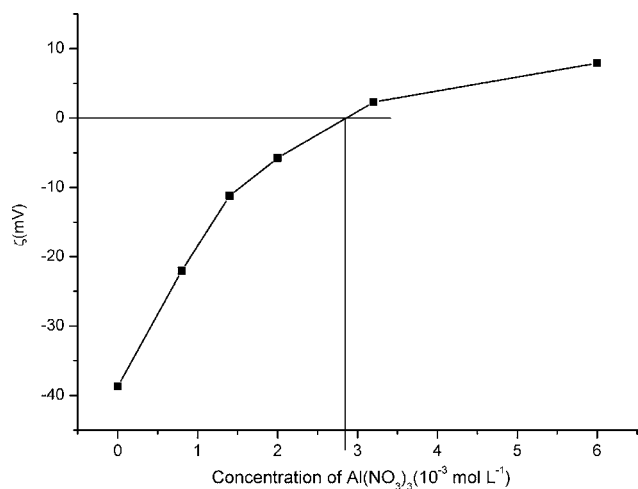


**Fig. 5.**  $\zeta$  of AgNPs–fsDNA against concentrations of Al(III). Conditions: AgNPs:  $1.4 \times 10^{-6}$  g mL $^{-1}$ ; fsDNA:  $1.0 \times 10^{-6}$  g mL $^{-1}$ ; KHP:  $8.0 \times 10^{-4}$  mol L $^{-1}$  (pH 5.6).

A direct evidence for forming the AgNPs–Al(III)–fsDNA aggregates is obtained by TEM images (as shown in Fig. 6). Fig. 6a reveals that AgNPs are spherical in shape with a diameter of 10–15 nm, and they are well dispersed. As we know, DNA has large aspect ratio (length/diameter), well-defined sequences of DNA base, a variety of superhelix and a high affinity for metal cations. With the addition of fsDNA to the AgNPs solution, AgNPs could follow the template of fsDNA and form AgNPs–fsDNA aggregates (Fig. 6b). Owing to strong adsorption bridging action of Al(III) and electro-

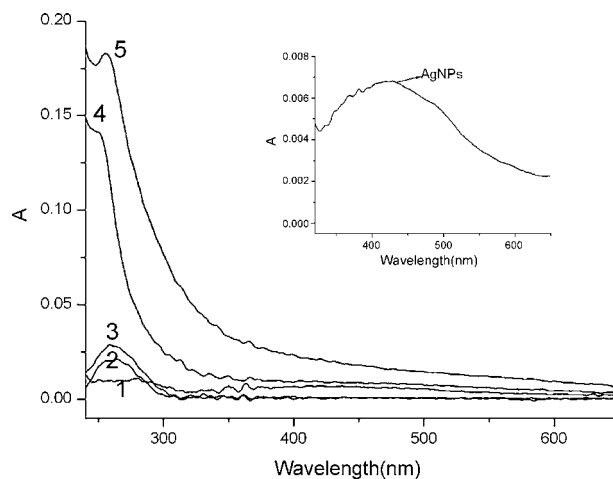


**Fig. 7.** Absorption spectra of the system. (1) AgNPs; (2) Al(III)–fsDNA vs. Al(III); (3) fsDNA; (4) AgNPs–fsDNA vs. fsDNA; (5) AgNPs–Al(III)–fsDNA vs. Al(III)–fsDNA. Conditions: AgNPs:  $1.4 \times 10^{-6}$  g mL $^{-1}$ ; Al(III):  $2.0 \times 10^{-3}$  mol L $^{-1}$ ; fsDNA:  $1.0 \times 10^{-6}$  g mL $^{-1}$ .

static interactions among AgNPs, Al(III) and fsDNA, they could form netlike AgNPs–Al(III)–DNA aggregates (Fig. 6c), causing the RLS enhancement of the system. At the same time, the electron diffraction pattern of AgNPs–Al(III)–DNA confirms that the polycrystalline structure forms.

From the ultraviolet absorption spectra (Fig. 7), it can be seen that AgNPs has weak absorption peak at 420 nm corresponding to its plasmon resonance absorption and another absorption peak

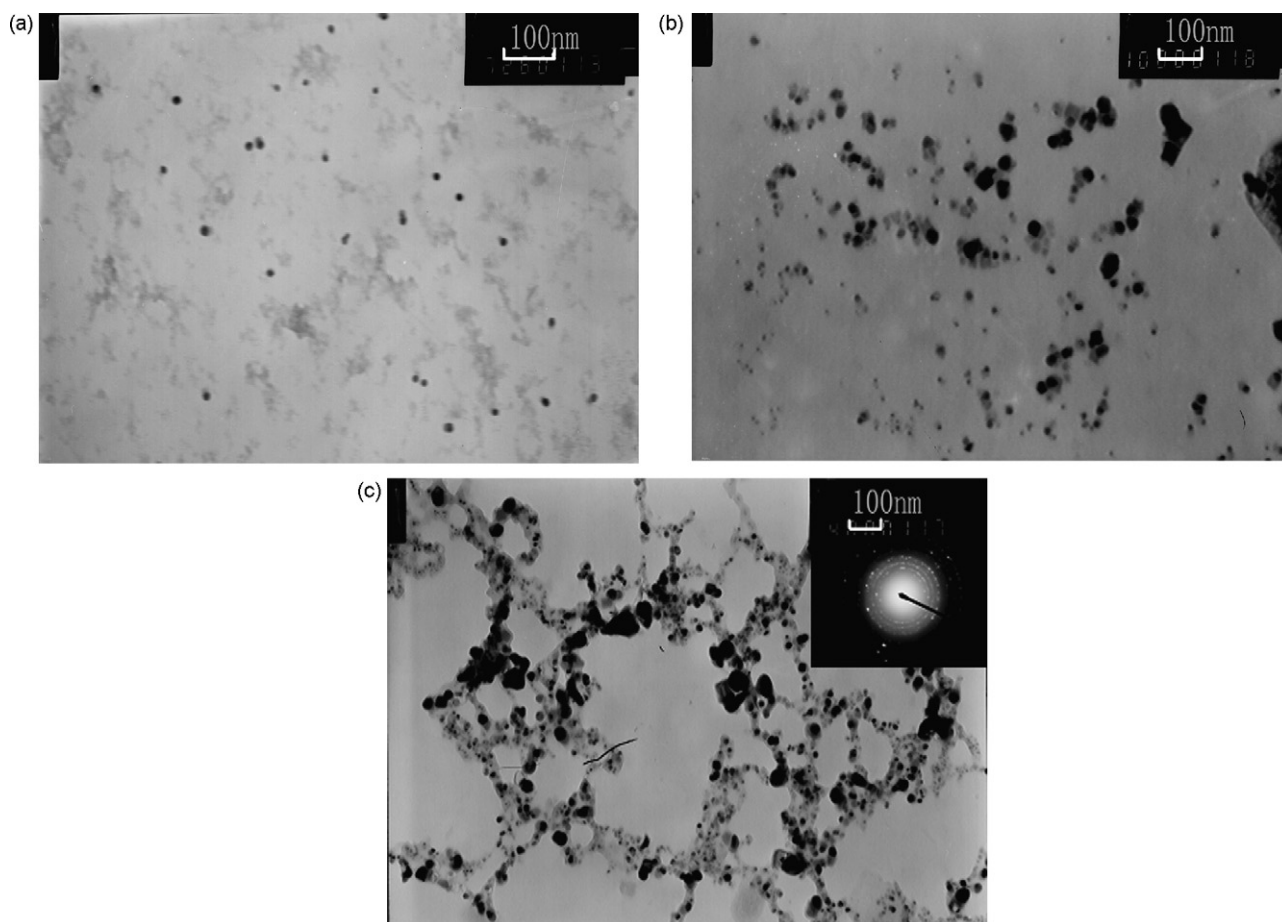


**Fig. 6.** Transmission electronic microscopy (a–c). Conditions: AgNPs:  $1.4 \times 10^{-5}$  g mL $^{-1}$ ; fsDNA:  $1.0 \times 10^{-5}$  g mL $^{-1}$ ; Al(III):  $4.0 \times 10^{-3}$  mol L $^{-1}$ ; KHP:  $8.0 \times 10^{-4}$  mol L $^{-1}$  (pH 5.6).

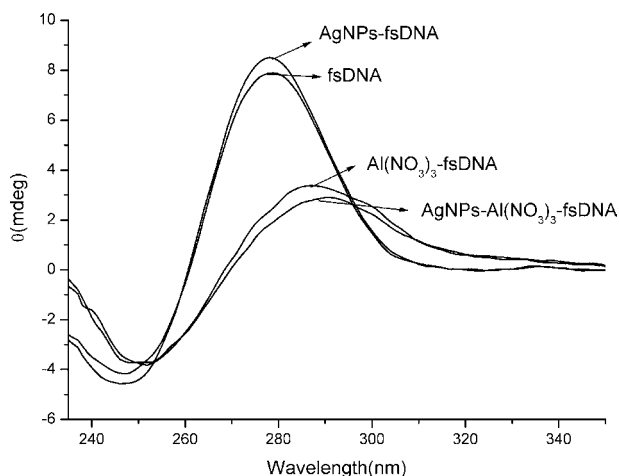


**Fig. 8.** CD spectra of the system. Conditions: AgNPs:  $1.4 \times 10^{-6}$  g mL $^{-1}$ ; fsDNA:  $5.0 \times 10^{-5}$  g mL $^{-1}$ ; Al(III):  $2.0 \times 10^{-3}$  mol L $^{-1}$ .

at 260 nm corresponding to new, overlapping, electronic bands for small silver nanoclusters. When Al(III) is added to fsDNA solution, the absorption spectrum of Al(III)–fsDNA (against Al(III) as reference) system decrease in intensity without obvious shift. With addition fsDNA to AgNPs system, the absorption peak at 260 nm (against fsDNA as reference) shifts to shorter wavelength changing to a shoulder at 248 nm with the peak height increasing. We think it may be caused by the formation of AgNPs–fsDNA aggregates. The absorption intensity of AgNPs–Al(III)–fsDNA system (against fsDNA–Al(III) as reference) increases and the peak shifts from 248 nm to 255 nm. We think that the results are attributed to the formation of netlike aggregates.

### 5.3. Circular dichroism study of the system

The CD-spectra in the UV range can be used to monitor the conformational transition of nucleic acids [17,18]. The CD spectra of system are studied and shown in Fig. 8. It is known that a strong positive cotton effect at 278 nm corresponding to base stacking, and a weak negative cotton effect at 246 nm corresponding to helicity in the CD spectrum of nucleic acid. After adding AgNPs to the fsDNA solution, the positive peaks and the negative peaks all increase a little without obviously shift. We presume that AgNPs have association with the nucleobases of fsDNA, which induces the change of nonplanar and tilted orientations of fsDNA bases, resulting in change of the helicity structure of fsDNA [14]. Furthermore, when Al(III) is added into AgNPs–fsDNA system, the positive peaks decrease more obviously than the negative peaks and their peaks all shift to longer wavelengths. The phenomena indicate that Al(III)

could induce the structural change of base stacking and helicity of fsDNA, and base stacking has a larger change. We think that the formation of AgNPs–Al(III)–DNA aggregations result in the conformational transition of fsDNA.

## 6. Conclusions

In this paper, it is found that the further enhancement effect of resonance light scattering of AgNPs–fsDNA by Al(III). Based on this, a simple and sensitive method for the determination of nucleic acids has been established. Under optimum conditions, the enhanced intensity of RLS is in proportion to the concentration of nucleic acids (e.g. fsDNA, ctDNA and yRNA), with detection limits at the  $10^{-10}$  g mL $^{-1}$  level. The results for the determination of plasmid DNA in actual samples are satisfactory. The interaction mechanism investigation indicates that fsDNA and AgNPs combine with Al(III) through electrostatic attraction and adsorption bridging action and form the netlike AgNPs–Al(III)–DNA aggregations, which result in a remarkable RLS enhancement of the system. This method is very simple, rapid and effective for determination of nucleic acids, which may be suggested for further uses in biology and nanoscience.

## Acknowledgments

This work is supported by Natural Science Foundations of China (20575035) and Shandong Province (Z2008B04).

## References

- [1] A.G. Wu, W.L. Cheng, Z. Li, J.G. Jiang, E. Wang, Talanta 68 (2006) 693.
- [2] J.L. Elechiguerra, J.L. Burt, J.R. Morones, A. Camacho-Bragado, X.X. Gao, H.H. Lara, M.J. Yacaman, J. Nanobiotechnol. 3 (2005) 6.
- [3] E. Braun, Y. Eichen, U. Sivan, G. Ben-Yoseph, Nature 391 (1998) 775.
- [4] Y.J. Xiong, Y. Xie, C.Z. Wu, J. Yang, Z.Q. Li, F. Xu, Adv. Mater. 15 (2003) 405.
- [5] R. Seidel, L.C. Ciacchi, M. Weigel, W. Pompe, M.J. Mertig, J. Phys. Chem. B 108 (2004) 10801.
- [6] J. Richter, R. Seidel, R. Kirsch, M. Mertig, W. Pompe, J. Plaschke, H.L. chackert, Adv. Mater. 12 (2000) 507.
- [7] C.F. Monson, A.T. Woolley, Nano Lett. 3 (2003) 359.
- [8] K. Keren, M. Krieger, R. Gilad, G.B. Yoseph, U. Sivan, E. Braun, Science 297 (2002) 72.
- [9] M. Mertig, L.C. Ciacchi, R. Seidel, W. Pompe, A. De Vita, Nano Lett. 2 (2002) 841.
- [10] W.E. Ford, O. Harnack, A. Yasuda, J.M. Wessels, Adv. Mater. 13 (2001) 1793.
- [11] J.T. Petty, J. Zheng, N.V. Hud, R.M. Dickson, J. Am. Chem. Soc. 126 (2004) 5207.
- [12] L.L. Sun, G. Wei, Y.H. Song, Z.G. Liu, L. Wang, Z. Li, Appl. Surf. Sci. 252 (2006) 4969.
- [13] Q. Pan, R.Y. Zhang, Y.F. Bai, N.Y. He, Z.H. Lu, Anal. Biochem. 375 (2008) 179.
- [14] J.H. Zheng, X. Wu, M.Q. Wang, D.H. Ran, W. Xu, J.H. Yang, Talanta 74 (2008) 526.
- [15] C.Z. Huang, K.A. Li, S.Y. Tong, Anal. Chem. 69 (1997) 514.
- [16] Q.E. Cao, Y.K. Zhao, X.J. Yao, Z.D. Hu, Q.H. Xu, Spectrochim. Acta A 56 (2000) 1319.
- [17] Z.L. Zhang, W.M. Huang, J.L. Tang, E.K. Wang, S.J. Dong, Biophys. Chem. 97 (2002) 7.
- [18] Y.L. Zhou, Y.Z. Li, Biophys. Chem. 107 (2004) 273.



## Determination of REEs in seawater by ICP-MS after on-line preconcentration using a syringe-driven chelating column

Yanbei Zhu<sup>a,b,\*</sup>, Tomonari Umemura<sup>b</sup>, Hiroki Haraguchi<sup>b</sup>,  
Kazumi Inagaki<sup>a</sup>, Koichi Chiba<sup>a</sup>

<sup>a</sup> National Metrology Institute of Japan (NMIJ), National Institute of Advanced Industrial Science and Technology (AIST), 1-1-1, Umezono, Tsukuba, Ibaraki 305-8563, Japan

<sup>b</sup> Department of Applied Chemistry, Graduate School of Engineering, Nagoya University, Furo-cho, Chikusa-ku, Nagoya 464-8603, Japan

### ARTICLE INFO

#### Article history:

Received 10 November 2008  
Received in revised form 24 December 2008  
Accepted 24 December 2008  
Available online 23 January 2009

#### Keywords:

Rare earth elements  
On-line  
Preconcentration  
Syringe-driven chelating column  
ICP-MS

### ABSTRACT

A syringe-driven chelating column (SDCC) was applied to develop an on-line preconcentration/inductively coupled plasma mass spectrometry (ICP-MS) method for preconcentration and determination of rare earth elements (REEs) in seawater samples. The present on-line preconcentration system consists of only one pump, two valves, an SDCC, an ICP-MS, several connectors, and Teflon tubes. Optimizations of adsorption pH condition, sample loading flow rate, and integration range were carried out to achieve optimum measurement conditions for REEs in seawater sample. Six minutes was enough for a preconcentration and measurement cycle using 10 mL of seawater sample, where the detection limits for different REEs were in the range of 0.005 pg mL<sup>-1</sup> to 0.09 pg mL<sup>-1</sup>. Analytical results of REEs in a seawater certified reference material (CRM), NASS-5, confirmed the usefulness of the present method. Furthermore, concentrations of REEs in Nikkawa Beach coastal seawater were determined and discussed with shale normalized REE distribution pattern.

© 2009 Elsevier B.V. All rights reserved.

### 1. Introduction

Because of the unique chemical properties of rare earth elements (REEs), they are useful in marine geochemistry as water-mass tracers [1] and as probes for oxidation–reduction reactions [2]. In recent years, there are increasing reports on Gd anomaly in REE distribution pattern for coastal seawater, which is caused by discharge of Gd compounds used as magnetic resonance imaging (MRI) contrast reagents. Because of the high stability of such Gd compounds, Gd anomaly is considered as one of the possible indicators of anthropogenic impacts on the water environment [3,4]. Taking into consideration these facts, determination of REEs in seawater is necessary for marine geochemistry and environmental chemistry.

Inductively coupled plasma mass spectrometry (ICP-MS), with its high sensitivity and wide linear dynamic range, is one of the powerful instruments compatible for simultaneous determination of REEs. However, determination of REEs in seawater by ICP-MS is still a difficult work, which may be attributed to two facts. One is

the extremely low natural concentrations of REEs, which are generally at sub pg mL<sup>-1</sup> level and are difficult to determine directly by ICP-MS. The other is the high salt content (*ca.* 3%) in seawater, which results in the clogging of introduction systems and causes serious interferences with REE measurement. In order to overcome these difficulties, co-precipitation [5,6], solvent extraction [7,8], and solid phase extraction [9–18] techniques were developed for enrichment of REEs and removal of salt contents prior to measurement of REEs. In these works, solid phase extraction techniques using chelating resins were the most accepted ones, which could be attributed to the merit of selectivity and lack of harmful organic solvent.

Preconcentration methods using chelating resin can be generally classified to two major groups. One is off-line batch method group, which has benefits of simultaneous multi-sample pretreatment; the other is on-line method group, which can improve the sensitivity and reproducibility of measurement. In recent years, syringe-driven chelating columns (SDCCs) were developed for preconcentration of REEs and other trace metals [13,19–27], all of which were carried out off-line. As a matter of fact, SDCCs are convenient both for off-line and for on-line pretreatment of samples. However, on-line preconcentration techniques for trace metals using SDCC have scarcely been reported until now.

Therefore, this paper presents an on-line technique using SDCC for preconcentration of REEs prior to the determination by ICP-MS,

\* Corresponding author at: National Metrology Institute of Japan (NMIJ), National Institute of Advanced Industrial Science and Technology (AIST), 1-1-1, Umezono, Tsukuba, Ibaraki 305-8563, Japan. Tel.: +81 29 861 4130; fax: +81 29 861 6889.

E-mail address: [yb-zhu@aist.go.jp](mailto:yb-zhu@aist.go.jp) (Y. Zhu).

**Table 1**  
Typical operating conditions of ICP-MS instrument.

Plasma conditions:		
Incident power		1.35 kW
Coolant gas flow rate		Ar 16.0 L min <sup>-1</sup>
Auxiliary gas flow rate		Ar 0.90 L min <sup>-1</sup>
Sample gas flow rate		Ar 0.85 L min <sup>-1</sup>
Additional 1 gas flow rate		Ar 0.28 L min <sup>-1</sup>
Chamber: Cinnabar cyclonic spray chamber (20 mL)		
Nebulizer: PFA $\mu$ flow nebulizer		
Sample uptake rate		0.5 mL min <sup>-1</sup>
Data acquisition (low resolution, $m/\Delta m = 300$ ):		
Mass window		100
Integration window		80
Samples per peak		3

**Table 2**  
Major parts for construction of on-line preconcentration system.

Part	Model	Producer
Pump	LC-10Ai	Shimadzu Corp., Kyoto, Japan
6-port rotation valve	TFR-6	GL Sciences Inc., Tokyo, Japan
4-port switching valve	TF-4	GL Sciences Inc., Tokyo, Japan
SDCC	NOBIAS CHELATE-PB1M	Hitachi High-Technologies Corp., Tokyo, Japan
ICP-MS	Finnigan Element2	Thermo Fisher Scientific, GA, USA

which helps to achieve good analytical reproducibility and to lower the risk of contamination.

## 2. Experimental

### 2.1. Instrumentation

A double focusing single collector ICP-MS instrument of model Finnigan Element2 (Thermo Fisher Scientific, Germany) was used for the measurement of REEs. The operating conditions of the ICP-MS instruments are summarized in Table 1. These operating conditions were chosen after the optimization of each instrumental parameter.

Major parts used to construct the on-line preconcentration system are summarized in Table 2. The SDCC is commercially available and is packed with 150 mg of divinylbenzene–methacrylate copolymeric resin containing polyaminopolycarboxylic acid groups (PAPC), in other words ethylenediaminetriacetic acid and iminodiacetic acid groups. The ethylenediaminetriacetic functional group is an analogue of ethylenediaminetetraacetic acid (EDTA), which makes the present resin more effective at adsorbing trace metals in seawater than the resins with iminodiacetic acid and 8-hydroxyquinoline functional groups [28]. The LC-10Ai pump was used in the on-line preconcentration and measurement system for continuous loading of solutions, which provided a maximum flow rate of 10 mL min<sup>-1</sup>. In addition, a syringe pump (model KDS200, KD Scientific, MA, USA) was used for off-line high-speed sample

**Table 3**  
Operating procedure for preconcentration and determination of REEs in seawater sample.

Step	Rotation valve position	Switching valve position	ICP-MS measurement	Time (min)	Flow rate (mL min <sup>-1</sup> )	Purpose
1	1	I	Off	1	5	Column regeneration
2	2	I	Off	0.5	5	pH conditioning
3	4	I	Off	2 <sup>a</sup>	5	Sample loading
4	5	I	Off	0.5	5	Washing
5	6	II	On	2	0.5	Elution and measurement

<sup>a</sup> Depend on sample volume.

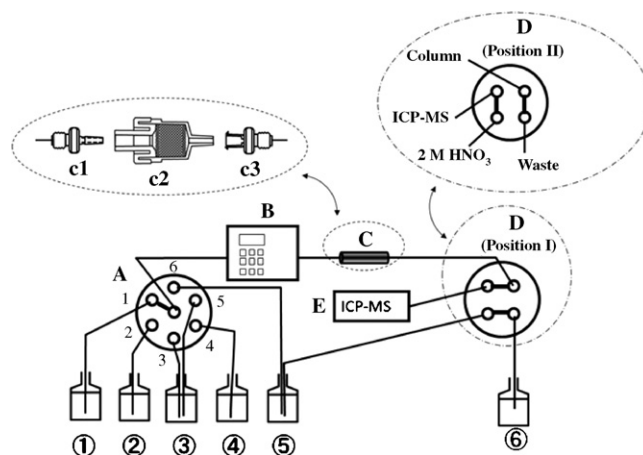


**Fig. 1.** Structure of on-line preconcentration system. (A) 6-port rotation valve; (B) pump; (C) column; (D) 4-port switching valve; (E) ICP-MS (c1, male Luer connector; c2, syringe-driven chelating column; c3, female Luer connector). ① 3 M HNO<sub>3</sub>, ② 1 M AcNH<sub>4</sub>, ③ MilliQ water, ④ Sample, ⑤ 2 M HNO<sub>3</sub> (consists of Cs and Tl, 1 ng mL<sup>-1</sup> each) and ⑥ waste.

loading during optimization of sample loading flow rate. A non-contact type pH meter (Twin pH meter B212; Horiba, Kyoto, Japan) was used for pH adjustment.

### 2.2. Chemicals and samples

Ultrapure grade nitric acid, acetic acid and aqueous ammonia solution were purchased from Kanto Chemicals (Tokyo, Japan). Three REE stock standard solutions (1000  $\mu$ g mL<sup>-1</sup> each: Standard I, La, Ce, and Pr; Standard II, Nd, Sm, Eu, Gd, and Tb; Standard III, Dy, Ho, Er, Tm, Yb, and Lu) for making the working calibration curves were purchased from Wako Pure Chemicals (Osaka, Japan). Standard solutions of 1 ng mL<sup>-1</sup> REEs were prepared for making calibration curves. A standard solution of 10 ng mL<sup>-1</sup> Ba was also prepared to check polyatomic interference with REEs. At the same time, Cs and Tl (1 ng mL<sup>-1</sup> each) was added to standard solutions for monitoring signal drift of ICP-MS. Pure water used throughout the present experiment was prepared by a Milli-Q purification system of model Element A-10 (Nihon Millipore Kogyo, Tokyo, Japan).

Coastal seawater sample collected near the shore of Nikkawa Beach (Kamisu, Ibaraki, Japan) was used for optimizing the experimental conditions of the present preconcentration method. It was filtered with a membrane filter (pore size 0.45  $\mu$ m, Nihon Millipore Kogyo, Tokyo, Japan) immediately after sampling and acidified to approximately pH 1.0 with *conc.* nitric acid. A seawater certified reference material (CRM), NASS-5, was purchased from the National Research Council of Canada (NRCC) and analyzed to confirm the usefulness of the present method.

All bottles, test tubes and pipette tips used in the present experiment were soaked in 6 M nitric acid for a week and then rinsed three times with pure water.

### 2.3. On-line preconcentration system and operating procedure

Structure of the present on-line preconcentration system is shown in Fig. 1. It consists of only one pump, two valves, an SDCC, an ICP-MS, several connectors, and Teflon tubes. All the Teflon tubes (o.d. 1.5 mm, i.d. 0.5 mm) were cut as short as possible to achieve high throughput measurement of REEs in seawater sample. It is noted that a pair of Luer connectors not only permitted the direct connection of the SDCC in the preconcentration system but also made it convenient to exchange SDCC. It is also noted that inert flow path (poly ether–ether ketone, PEEK) of the present pump permitted introduction of high concentration nitric acid solution without contamination of REEs from pump flow path.

The operating procedure is summarized in Table 3. From step 1 to step 4, the switching valve was in position I. Solutions passed through the SDCC were collected in the waste bottle, while 2 M HNO<sub>3</sub> was introduced to the ICP-MS. In step 1, SDCC regeneration was carried out by passing through 5 mL of 3 M HNO<sub>3</sub>. In step 2, pH conditioning of the SDCC was performed by passing through 2.5 mL of 1 M AcNH<sub>4</sub>. In step 3, 10 mL of sample solution was loaded to the SDCC. In step 4, 2.5 mL of Milli-Q water was passed to wash sample residual. In step 5, 2 M HNO<sub>3</sub> solution was passed to the SDCC for elution of REEs. At this step, the switching valve was changed to position II. Consequently, eluate from the SDCC was introduced to ICP-MS and the signals of REEs were monitored. A typical preconcentration–measurement cycle using 10 mL sample lasted for 6 min. In the present experiment, all operations were carried out manually. The results of durability tests showed that an SDCC could be used at least 30 times after on-line regeneration.

It is noted that removal of matrix elements was not carried out by passing AcNH<sub>4</sub> solutions through the SDCC after loading the sample. The reason is that the functional group of PAPC could effectively exclude matrix elements such as Na, Mg, K, and Ca. The result of a preliminary test showed that the total concentration of Na, Mg, K, and Ca in a 10-fold concentrated solution of seawater sample was less than 300 µg mL<sup>-1</sup>, which was low enough for measurement of REEs.

A spiked sample solution added with 10 pg mL<sup>-1</sup> of each REE was used for recovery test of the preconcentration and measurement procedure.

## 3. Results and discussion

### 3.1. Polyatomic interference in REEs' measurement

Most REEs have more than one isotope, except for Pr, Tb, Ho, and Tm. In the present experiment, <sup>139</sup>La, <sup>140</sup>Ce, <sup>141</sup>Pr, <sup>143</sup>Nd, <sup>147</sup>Sm, <sup>153</sup>Eu, <sup>157</sup>Gd, <sup>159</sup>Tb, <sup>163</sup>Dy, <sup>165</sup>Ho, <sup>166</sup>Er, <sup>169</sup>Tm, <sup>173</sup>Yb, and <sup>175</sup>Lu were selected for measurement of REEs taking into consideration the isotope abundance, isobaric interference of adjacent elements, and polyatomic interference. Polyatomic interference ratios of <sup>141</sup>Pr<sup>16</sup>O, <sup>150</sup>Nd<sup>16</sup>O (<sup>150</sup>Sm<sup>16</sup>O), <sup>157</sup>Gd<sup>16</sup>O, and <sup>159</sup>Tb<sup>16</sup>O with the measurement of <sup>157</sup>Gd, <sup>166</sup>Er, <sup>173</sup>Yb, and <sup>175</sup>Lu were approximately 13%, 1.4%, 1.1%, and 1.1%, respectively. Correction of polyatomic interference was carried out to obtain results of these elements. Polyatomic interferences, including BaO species, with other elements were negligible, *i.e.*, interference ratio was less than 0.5%.

### 3.2. Optimization of pH condition

In order to achieve high recoveries for REEs, optimization of pH condition was carried out with a batch method using disposable plastic syringe. The sample and the spiked sample, 20 mL each, were respectively adjusted to the same pH condition and loaded to the SDCC at a flow rate of 2 mL min<sup>-1</sup>. After washing with 5 mL of Milli-

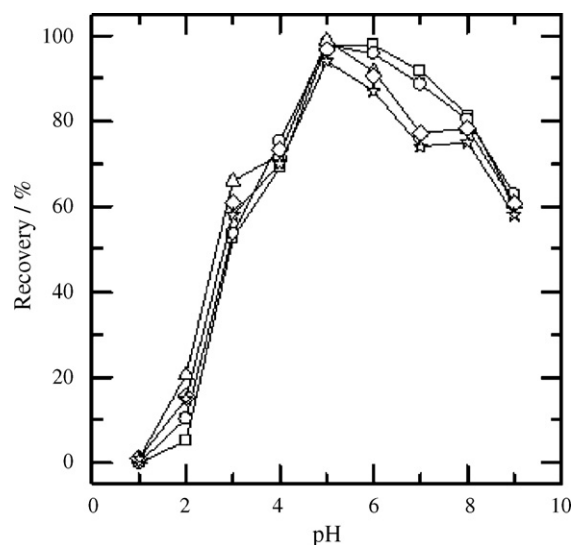


Fig. 2. Dependence of recovery on pH condition. (□) La; (○) Nd; (△) Dy; (◇) Tm; (☆) Lu.

Q water, 5 mL of 2 M HNO<sub>3</sub> was passed through the SDCC to elute REEs and collected in a plastic test tube. Concentrations of REEs in the eluates were measured by ICP-MS and used to calculate recoveries. The results for La, Nd, Dy, Tm, and Lu obtained at different pH conditions are illustrated in Fig. 2. Because the highest recoveries for all REEs were obtained at pH 5.0, samples used in the following experiment were adjusted to pH 5.0.

### 3.3. Dependence of REEs' recoveries on sample loading flow rate

In order to investigate the dependence of the REEs' recovery on the sample loading flow rate, off-line sample loading was carried out using the KDS200 syringe pump. Samples and spiked samples adjusted to pH 5.0 were loaded to the SDCC at 2, 5, 10, 15, and 20 mL min<sup>-1</sup>, respectively. The results showed that recoveries of REEs obtained at 5 mL min<sup>-1</sup> were almost equal to those obtained at 2 mL min<sup>-1</sup>. When the sample loading flow rate increased to 10, 15, and 20 mL min<sup>-1</sup>, the recoveries of REEs decreased approximately 3%, 5%, and 10%, respectively. Therefore, 5 mL min<sup>-1</sup> was selected as the optimum sample loading flow rate in the present experiment.

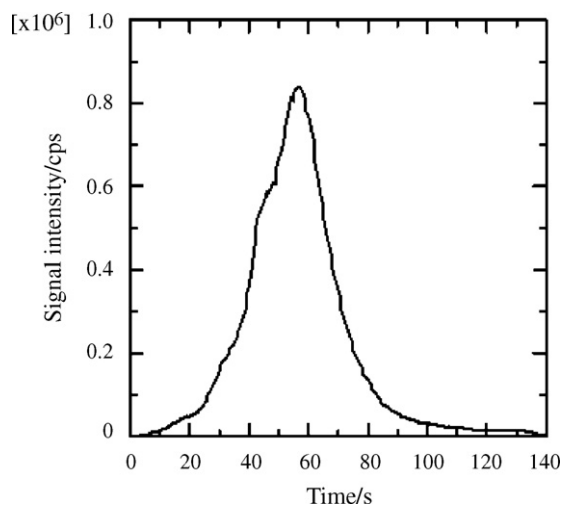


Fig. 3. Elution profile of <sup>139</sup>La from the SDCC.

**Table 4**  
Detection limits and blank values.

Element	m/z	Recovery <sup>a</sup> (%)	Blank value <sup>a</sup> (pg mL <sup>-1</sup> )	ADL <sup>b</sup> (pg mL <sup>-1</sup> )
La	139	99.4 ± 1.4	0.15 ± 0.01	0.04
Ce	140	97.4 ± 0.6	0.11 ± 0.03	0.09
Pr	141	97.7 ± 0.7	0.015 ± 0.004	0.011
Nd	143	98.9 ± 1.9	0.08 ± 0.03	0.08
Sm	147	98.2 ± 0.9	0.014 ± 0.006	0.017
Eu	153	95.0 ± 0.6	0.007 ± 0.002	0.007
Gd	157	98.0 ± 1.1	0.009 ± 0.005	0.014
Tb	159	98.2 ± 0.9	0.009 ± 0.003	0.008
Dy	163	94.2 ± 1.4	0.008 ± 0.004	0.013
Ho	165	96.6 ± 1.1	0.004 ± 0.002	0.005
Er	166	96.7 ± 1.0	0.005 ± 0.003	0.008
Tm	169	94.0 ± 0.7	0.004 ± 0.002	0.005
Yb	173	92.6 ± 1.2	0.007 ± 0.003	0.009
Lu	175	94.2 ± 0.9	0.008 ± 0.003	0.009

<sup>a</sup> Mean ± standard deviation, n = 5.<sup>b</sup> Analytical detection limit.

### 3.4. On-line data processing

Elution profile of <sup>139</sup>La from the SDCC is shown in Fig. 3, which was obtained after loading 10 mL of seawater sample to the SDCC. It can be seen that complete elution of La was obtained in approximately 120 s, which correspond to 1 mL of 2 M HNO<sub>3</sub> solution (flow rate, 0.5 mL min<sup>-1</sup>). When signal intensities equal to 0.5%, 1.0%, 1.5%, 2.0%, 3.0% and 5.0% of the peak top were used as the limit for integration range, the peak covered 136 s, 129 s, 125 s, 104 s, 87 s, and 79 s, respectively. The peak areas were 100.0%, 99.8%, 99.6%, 98.3%, 96.8%, and 95.6%, respectively, where the peak area using 0.5% of the peak top as the limit was regarded as 100%. In the present experiment, 1.5% of the peak top was selected as the limit for integration range. In this condition, the integration range covered approximately 125 s (corresponding to 1.04 mL of elution solution). Therefore, concentration factor (CF) of REEs was approximately 9.6-fold when 10 mL seawater sample was loaded. Besides, for making calibration curves, standard solutions were continuously introduced to ICP-MS at 0.5 mL min<sup>-1</sup> to achieve REEs' signals.

### 3.5. Recoveries, blank values, and detection limits of REEs

Recoveries, blank values, and analytical detection limits are summarized in Table 4. Recovery test and blank test were carried out by using spike sample solution and 0.1 M HNO<sub>3</sub>, respectively. The results given in Table 4 were obtained by loading 10 mL of test solutions, i.e., CF was approximately 9.6-fold. Analytical detection limits (ADL) are given as 3-fold standard deviation of blank values. Taking into consideration the natural concentrations of REEs in seawater, these recoveries, blank values, and analytical detection limits were good enough for determination of REEs in seawater samples. This fact was confirmed by the following experiments. It is noted that all the following results were obtained after recovery correction and blank value correction. Consequently, "standard deviations" of the following results were obtained taking into consideration the standard deviations of recovery, blank value, and concentration in the sample.

### 3.6. Analytical results of REEs in seawater samples

Analysis of seawater CRM with certified values of REEs is the best choice for confirming the usefulness of an analytical method for determining REEs in seawater samples. However, such seawater CRM is still not commercially available, which might be attributed to the extremely low concentration of REEs in natural seawater. Taking into consideration the fact that NASS-5 was developed for analysis of trace metals in seawater, its homogeneity and

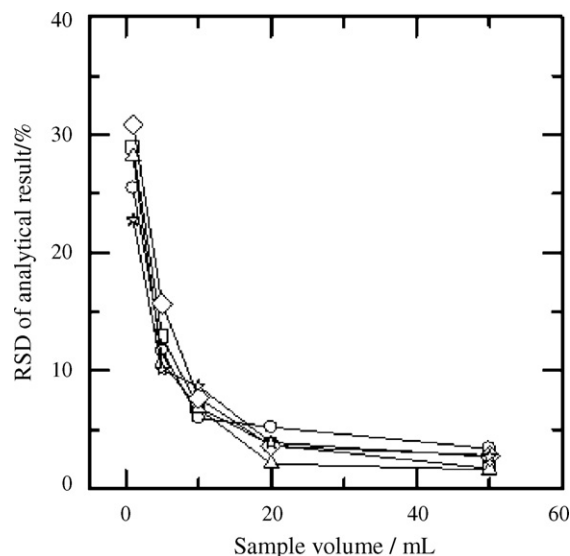
**Table 5**  
Analytical results of REEs in NASS-5 and Nikkawa Beach coastal seawater (unit, pg mL<sup>-1</sup>).

Element	m/z	NASS-5, observed <sup>a</sup>	NASS-5, compiled <sup>b</sup>	Nikkawa Beach <sup>a</sup>
La	139	12.0 ± 0.3	12.2 ± 0.8	4.7 ± 0.3
Ce	140	5.26 ± 0.16	4.58 ± 0.53	3.8 ± 0.2
Pr	141	1.96 ± 0.02	1.78 ± 0.17	0.83 ± 0.04
Nd	143	8.7 ± 0.7	8.8 ± 1.1	4.2 ± 0.2
Sm	147	4.50 ± 0.14	4.33 ± 0.31	0.90 ± 0.07
Eu	153	0.27 ± 0.02	0.27 ± 0.04	0.25 ± 0.02
Gd	157	1.77 ± 0.09	1.57 ± 0.17	1.46 ± 0.10
Tb	159	0.37 ± 0.04	0.25 ± 0.04	0.25 ± 0.02
Dy	163	1.86 ± 0.05	1.73 ± 0.16	1.86 ± 0.13
Ho	165	0.44 ± 0.04	0.39 ± 0.04	0.49 ± 0.03
Er	166	1.49 ± 0.08	1.35 ± 0.13	1.60 ± 0.06
Tm	169	0.19 ± 0.02	0.16 ± 0.03	0.25 ± 0.02
Yb	173	1.40 ± 0.17	1.14 ± 0.15	1.59 ± 0.11
Lu	175	0.21 ± 0.02	0.19 ± 0.03	0.28 ± 0.02

<sup>a</sup> Mean ± standard deviation, n = 5.<sup>b</sup> Mean ± σ, n = 3 (based on the results obtained in refs. [6,10,28]).

chemical stability permitted it as a candidate CRM for REEs measurement. On the other hand, multiple reports on REEs in NASS-5 were available, which could serve as valuable reference data for REEs in NASS-5. Therefore, NASS-5 was analyzed to confirm the usefulness of the present method. The results were summarized in Table 5, along with compiled reference data based on previous reports [6,10,29]. The "mean" and "standard deviation" of reference data were obtained as the average of each reported mean value and the root mean square of each reported standard deviation. It is seen in Table 5 that the present results were coincident with compiled reference data considering the standard deviations. This fact indicates that the present method was useful for determination of REEs in seawater sample.

Determination of REEs in coastal seawater from Nikkawa Beach was carried out as application of the present method. The results are also summarized in Table 5, which were obtained by loading 10 mL of seawater sample for each measurement. Although all REEs were less than 5 pg mL<sup>-1</sup>, the results were replicable with relative standard deviation less than 10%. Furthermore, measurement of REEs was carried out by loading 1, 5, 20, 50 mL of this coastal seawater sample. Dependence of analytical standard deviation on sample volume was shown in Fig. 4, in which the results of La, Nd, Dy, Tm, and Lu were selected as the representative ones. The results were

**Fig. 4.** Dependence of analytical standard deviation on sample volume. (□) La; (○) Nd; (△) Dy; (◇) Tm; (☆) Lu.



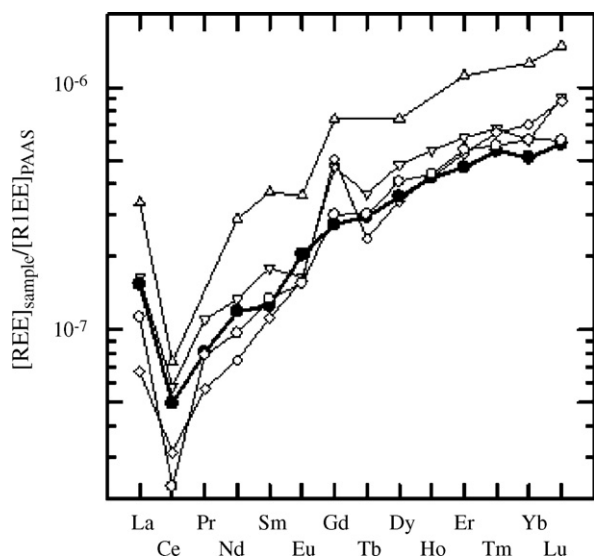


**Fig. 5.** Shale normalized REE distribution pattern of coastal seawater samples. ( $\Delta$ ) Osaka Bay (Ogata et al. [33]); ( $\nabla$ ) Ise Bay (Zhu et al. [34]); ( $\diamond$ ) Tokyo Bay (Tazoe et al. [32]); ( $\circ$ ) Average seawater close to the Japanese mainland (Yabutani et al. [31]); ( $\bullet$ ) Nikkawa Beach (present work).

coincident with those obtained by loading 10 mL of sample, but the standard deviations increased with the decrease of sample volume.

### 3.7. Shale normalized REE distribution pattern of seawater samples

Shale normalized REE distribution pattern of Nikkawa Beach coastal seawater is plotted in Fig. 5. The concentrations of REEs in the sample were normalized to those in post-Archean Average Australian Shale (PAAS) [30]. In Fig. 5, seawater close to the Japanese mainland is given as the representative of open-area coastal seawater in Pacific Ocean [31], while seawater samples from Tokyo Bay [32], Osaka Bay [33], and Ise Bay [34] are given as the representatives of confined-area coastal seawater.

It can be seen in Fig. 5 that the present results of REEs in Nikkawa Beach coastal seawater were generally coincident with the results of REEs in seawater close to the Japanese mainland; significant Gd anomalies were not observed in these seawater samples. By contrast, significant positive Gd anomalies were observed for results of REEs in seawater of Tokyo Bay, Osaka Bay, and Ise Bay, which are close to Tokyo, Osaka, and Nagoya, respectively, the three biggest cities in Japan. The significant positive Gd anomalies in these areas could be attributed to the discharge of Gd compounds due to their medical use as MRI contrast reagent [32–34]. It is noted that the water masses of Tokyo Bay, Osaka Bay, and Ise Bay are relatively confined, which encouraged the accumulation of positive Gd anomaly. Coastal seawater sample in the present work was collected in an open-area of Pacific Ocean close to the Japanese mainland, where the population density (ca. 600/km<sup>2</sup>) is much less than Tokyo (ca. 13,700/km<sup>2</sup>), Osaka (ca. 11,800/km<sup>2</sup>), and Nagoya (ca. 6800/km<sup>2</sup>). These results support the suggestion that Gd anomaly can be used as a geochemical tracer of anthropogenic impacts on natural seawater, especially for water masses in confined areas.

## 4. Conclusion

An SDCC was applied to construct an on-line preconcentration system for determination of REEs in seawater by ICP-MS. After

optimization of each operating condition, a 6-min procedure was suggested for measurement of REEs using 10 mL of seawater sample. The analytical results of REEs in NASS-5 confirmed the usefulness of the present method. The present method was applied to determination of REEs in Nikkawa Beach coastal seawater, in which positive Gd anomaly was not observed.

The present work applied SDCC in an on-line preconcentration system. In fact, SDCC is convenient both for off-line and for on-line pretreatment of samples. Therefore, it permits the development of a method that takes advantage of off-line multi-sample processing and that of on-line continuous measurement, too. Based on the present technique, development of such a method is in progress and will be reported in the future.

## Acknowledgements

The present research was supported partly by a Grant-in-Aid (no. 16002009) of the Specially Promoted Research and by COE Formation Basic Research of “Isotopes for the Prosperous Future” (2003–2007) from the Ministry of Education, Culture, Sports, Science and Technology, Japan. The present authors express sincere gratitude to Mr. Ben. Ahmady (The University of Sheffield) for preliminary grammatical check of the manuscript.

## References

- [1] H. Elderfield, M.J. Greaves, *Nature* 296 (1982) 214.
- [2] H.J.W. De Baar, M.P. Bacon, P.G. Brewer, *Nature* 301 (1983) 324.
- [3] P. Moller, P. Dulski, M. Bau, A. Knappe, A. Pekdeger, C. Sommer-von Jarmstedt, *J. Geochem. Explor.* 69 (2000) 409.
- [4] G. Strauch, M. Moder, R. Wennrich, K. Osenbruck, H.R. Glaser, T. Schladitz, C. Muller, K. Schirmer, F. Reinstorf, M. Schirmer, *J. Soil Sed.* 8 (2008) 23.
- [5] M.J. Greaves, H. Elderfield, G.P. Klinkhammer, *Anal. Chim. Acta* 218 (1989) 265.
- [6] T.J. Shaw, T. Duncan, B. Schmetger, *Anal. Chem.* 75 (2003) 3396.
- [7] J. Zhang, Y. Nozaki, *Geochim. Cosmochim. Acta* 60 (1996) 4631.
- [8] M.B. Shabani, T. Akagi, H. Shimizu, A. Masuda, *Anal. Chem.* 62 (1990) 2709.
- [9] T. Yabutani, S. Ji, F. Mouri, H. Sawatari, A. Itoh, K. Chiba, H. Haraguchi, *Bull. Chem. Soc. Jpn.* 72 (1999) 2253.
- [10] S.N. Willie, R.E. Sturgeon, *Spectrochim. Acta* 56B (2001) 1707.
- [11] L. Halicz, I. Gavrieli, E. Dorfman, *J. Anal. At. Spectrom.* 11 (1996) 811.
- [12] T.-H. Zhang, X.-Q. Shan, R.-X. Liu, H.-X. Tang, S.-Z. Zhang, *Anal. Chem.* 70 (1998) 3964.
- [13] Y. Zhu, A. Itoh, E. Fujimori, T. Umemura, H. Haraguchi, *J. Alloys Comp.* 408–412 (2006) 985.
- [14] B. Wen, X.-Q. Shan, S.-G. Xu, *Analyst* 124 (1999) 621.
- [15] S. Hirata, T. Kajiya, M. Aihara, K. Honda, O. Shikino, *Talanta* 58 (2002) 1185.
- [16] T. Kajiya, M. Aihara, S. Hirata, *Spectrochim. Acta Spectroscop.* 59 (2004) 543.
- [17] Y. Sohrin, S. Iwamoto, S. Akiyama, T. Fujita, T. Kugii, H. Obata, E. Nakayama, S. Goda, Y. Fujishima, H. Hasegawa, K. Ueda, M. Matusi, *Anal. Chim. Acta* 363 (1998) 11.
- [18] Q. Fu, L.-M. Yang, Q.-Q. Wang, *Talanta* 72 (2007) 1248.
- [19] A. Alexandrova, S. Arpadjan, *Anal. Chim. Acta* 307 (1995) 71.
- [20] M. Okumura, Y. Seike, K. Fujinaga, K. Hirao, *Anal. Sci.* 13 (1997) 231.
- [21] J.P. Pancras, B.K. Puri, *Anal. Sci.* 16 (2000) 1271.
- [22] N. Tokman, S. Akman, M. Ozcan, U. Koklu, *Anal. Bioanal. Chem.* 374 (2002) 977.
- [23] S. Akman, N. Tokman, *Talanta* 60 (2003) 199.
- [24] N. Tokman, S. Akman, M. Ozcan, *Talanta* 59 (2003) 201.
- [25] K.-H. Lee, Y. Muraoka, M. Oshima, S. Motomizu, *Anal. Sci.* 20 (2004) 183.
- [26] Y. Bakircioglu, D. Bakircioglu, Tokman, *Anal. Chim. Acta* 547 (2005) 26.
- [27] S.H. Babu, K.S. Kumar, K. Suvaradhan, K. Kiran, D. Rekha, L. Kirtishnaiah, K. Janardhanam, P. Chiranjeevi, *Environ. Monit. Assess* 128 (2007) 241.
- [28] Y. Sohrin, S. Urushihara, S. Nakatsuka, T. Kono, E. Higo, T. Minami, K. Norisuye, *Anal. Chem.* 80 (2008) 6267.
- [29] D. Rahmi, Y. Zhu, E. Fujimori, T. Umemura, H. Haraguchi, *Talanta* 72 (2007) 600.
- [30] S.R. Taylor, S.M. McLennan, *The Continental Crust: Its Composition and Evolution. An examination of the Geochemical Record Preserved in Sedimentary Rocks*, Blackwell, 1985.
- [31] T. Yabutani, F. Mouri, A. Itoh, H. Haraguchi, *Anal. Sci.* 17 (2001) 399.
- [32] H. Tazoe, H. Obata, H. Amakawa, Y. Nozaki, T. Gamo, *Mar. Chem.* 103 (2007) 1.
- [33] T. Ogata, Y. Terakado, *Geochim. J.* 40 (2006) 463.
- [34] Y. Zhu, M. Hoshino, H. Yamada, A. Itoh, H. Haraguchi, *Bull. Chem. Soc. Jpn.* 77 (2004) 1835.



# Study on mechanism of stacking of zwitterion in highly saline biologic sample by transient moving reaction boundary created by formic buffer and conjugate base in capillary electrophoresis

Wei Zhu<sup>a</sup>, Wei Zhang<sup>a</sup>, Liu-Yin Fan<sup>a,\*</sup>, Jing Shao<sup>a</sup>, Si Li<sup>a</sup>, Jin-Lian Chen<sup>b</sup>, Cheng-Xi Cao<sup>a,\*\*</sup>

<sup>a</sup> Laboratory of Analytical Biochemistry & Bioseparation, Key Laboratory of Microbiology of Educational Ministry, School of Life Science and Biotechnology, Shanghai Jiao Tong University, 800 Dongchuan RD, Shanghai 200240, PR China

<sup>b</sup> Shanghai No 6 People Hospital, Shanghai Jiao Tong University, 600 Yishan RD, Shanghai 200233, PR China

## ARTICLE INFO

### Article history:

Received 4 November 2008

Received in revised form 23 January 2009

Accepted 26 January 2009

Available online 5 February 2009

### Keywords:

Capillary electrophoresis

Electromigration

Moving reaction boundary

Salt

Sample stacking

## ABSTRACT

The reason why a moving reaction boundary (MRB) can stack analyte in highly saline sample in capillary electrophoresis [C.X. Cao, Y.Z. He, M. Li, Y.T. Qian, S.L. Zhou, L. Yang, Q.S. Qu, Anal. Chem. 74 (2002) 4167] is still unclear. To illuminate the mechanism of such stacking, three MRBs formed by formic acid-NaOH buffer and sodium formate as well as 40, 80 and 120 mmol/L sodium chloride in matrixes were studied. The computation with MRB theory shows that sodium chloride in matrix has weak effect on the stacking efficiency, whether the concentration of sodium chloride is set at 40, or 80, or 120 mmol/L. The conclusion has been highly manifested by numerous experiments. Furthermore, the computer simulation and theoretical analyses depict that this kind of stacking is induced by the mechanism of MRB, rather than that of electrostacking or isotachopheresis (ITP) under the given electrolytic system. Finally, the application of the sample condensation was achieved for the stacking of analyte(s) in highly saline biological sample of *skeletonema costatum* culture with up to 527 mmol/L total salt and health human urine with 150–320 mmol/L inorganic ions (Cl<sup>-</sup>, Na<sup>+</sup>, K<sup>+</sup>, PO<sub>4</sub><sup>3-</sup>, etc.). The results herein have a clear significance to the design on stacking of analyte in highly saline biological sample.

© 2009 Elsevier B.V. All rights reserved.

## 1. Introduction

Numerous biological sample matrixes, such as serum, urine and zymosis, contain high salt. The salt in these matrixes ought to be removed, otherwise it brings about some harmful action to sample stacking in capillary electrophoresis (CE). For example, salt in a matrix breaks down sample pre-concentration by electrostacking [1–3] or field-amplified sample injection (FASI) [4–7] in CE. The removal of salt from matrix is troublesome. Thus, it is great interesting that sample with high salt can be directly stacked to achieve good improvement of detection sensitivity without loss of separative efficiency of CE.

Numerous methods have been developed for stacking of saline sample in CE. The first method is isotachopheresis (ITP) induced sample stacking. In the last two decades [8–10], the theoretical and experimental studies on transient ITP were widely performed for stacking analytes in saline matrix. The second method is the “acetonitrile addition” idealized by Shihabi [11], the relevant mech-

anism is considered to be a transient ITP/or FASI. The existence of acetonitrile in sample matrix can reduce the ionization of salt and overcome the harmful effect of the salt on sample stacking by FASI.

The third is the “pH-mediated-induced sample concentration” described mainly by Lunte’s group [12–14]. In this method, the sample is dissolved in a weakly acidic (or basic) buffer with salt; conversely the running buffer is just the conjugate base (or acid). A moving reaction boundary (MRB) is formed between the weak acid (or base) and the conjugate base (or acid), if an electric field is applied. The MRB results in a low conductivity zone in the original matrix. The zone further leads to a FASI. The fourth is the “dynamic-pH-junction-induced stacking” developed by Britz-Mckibbin et al. [15–17]. In the method, the analyte velocity is greatly regulated by pH value, but the velocity of the unwanted analyte cannot be adjusted due to its insensitivity to pH. Hence, a selective preconcentration can be achieved in this kind of stacking. The computer simulation revealed that the pH junction-induced stacking was relied on ITP mechanism [17]. The fifth is the sweeping technique for analyte in salt matrix in micellar electrokinetic chromatography [18–22]. The sweeping method cannot only stack neutral analyte, but also condensate ionic solutes in highly saline matrix.

\* Corresponding author. Tel.: +86 21 3420 5820; fax: +86 21 3420 5820.

\*\* Corresponding author. Fax: +86 21 3420 5820.

E-mail addresses: [lyfan@sjtu.edu.cn](mailto:lyfan@sjtu.edu.cn) (L.-Y. Fan), [cxcao@sjtu.edu.cn](mailto:cxcao@sjtu.edu.cn) (C.-X. Cao).

**Table 1**  
 $pK_a$  values and some mobilities of some ions in sample matrix and 32.8 mmol/L pH 2.85 buffer.

Ions	$pK_a$	Mobility ( $10^{-8} \text{ m}^2 \text{ V}^{-1} \text{ s}^{-1}$ )		
		Phase $\alpha$ (formic buffer)	Phase $\beta$ (matrix)	Phase $\gamma$ (formic buffer)
Hydrogen	–	36.5	–	36.5
Sodium	–	5.19	5.19	5.19
Hydroxyl	–	–	–20.9	–
Chloride	–	–	–7.91	–
Formic acid	3.75	–0.63	–5.66	–0.63
Trp	9.13 ( $pK_2$ )	1.22 <sup>a</sup>	–0.32 <sup>b</sup>	1.22 <sup>a</sup>

<sup>a</sup> The mobility was computed from the  $pK_1$  (Trp)=2.83 and Trp mobility ( $+2.49 \times 10^{-8} \text{ m}^2 \text{ v}^{-1} \text{ s}^{-1}$ ) carrying one positive charge [29].

<sup>b</sup> The computation procedure was given in the appendix.

The sixth is the stacking method induced by MRB developed mainly by Cao et al. [23–25]. The stacking could be used for the condensation of analytes in highly saline matrix [23]. Recently, the theoretical procedure was developed for the quantitative design on stacking condition and selective stacking by using the theory of MRB [24,25]. Furthermore, the relevant MRB theory, methods and relevant applications have been reviewed [25]. Even so, the reason why MRB-based stacking can condense analyte in highly saline biological matrix is still unclear.

Thus, the purposes herein are to (i) show the theoretic prediction of weak impact of salt on the MRB-based stacking, (ii) report experiments proving the prediction, (iii) show simulation results revealing non-ITP or non-FASI mechanism in the MRB-based stacking system, and (iv) unveil reason why MRB can stack analyte in highly saline biological matrix without loss of stacking efficiency. In addition, the application of the method was briefly tested for some solute(s) in highly saline culture liquor and health human urine.

## 2. Theoretical computation

The mechanism of sample stacking by the MRB system of formic buffer and sodium formate without salt has been well investigated in the previous work [24,25]. Hence, the paper studies three kinds of MRBs with high salt in the sample matrix. Below are the three MRBs:

*Boundary 1:* 32.8 mmol/L pH 2.85 formate buffer (+,  $\alpha$ ) || [→]

8.2–82.5 mmol/L sodium formate + 40 mmol/L NaCl (–,  $\beta$ ).

*Boundary 2:* 32.8 mmol/L pH 2.85 formate buffer (+,  $\alpha$ ) || [→]

8.2–82.5 mmol/L sodium formate + 80 mmol/L NaCl (–,  $\beta$ ).

*Boundary 3:* 32.8 mmol/L pH 2.85 formate buffer (+,  $\alpha$ ) || [→]

8.2–82.5 mmol/L sodium formate + 120 mmol/L NaCl (–,  $\beta$ ).

where “||” implies a boundary, the symbol of “[→]” indicates the direction of MRB, “+” and “–” imply the anode and cathode, respectively, and “ $\alpha$ ” and “ $\beta$ ” mean phase  $\alpha$  and  $\beta$ , respectively. The three MRBs have been used for the stacking of analytes in saline matrix [23]. In the three MRBs, the boundary velocity should be computed with the following equation [24,25]

$$V^{\alpha\beta} = \left( \frac{\bar{m}_{\text{H}^+}^{\alpha} \bar{c}_{\text{H}^+}^{\alpha}}{\kappa^{\alpha}} - \frac{\bar{m}_{\text{OH}^-}^{\beta} \bar{c}_{\text{OH}^-}^{\beta}}{\kappa^{\beta}} \right) \frac{i}{c_{\text{H}^+}^{\alpha} - c_{\text{OH}^-}^{\beta}} \quad (1)$$

where  $c$  is the equivalent concentration ( $\text{equiv. m}^{-3}$ ), the bar “–” over  $c$  means the constituent concentration, the subscripts  $\text{H}^+$  and  $\text{OH}^-$  indicate the hydrogen and hydroxyl ions, respectively, the superscripts  $\alpha$  and  $\beta$  imply phase  $\alpha$  and  $\beta$ , respectively;  $m$  is the mobility ( $\text{m}^2 \text{ V}^{-1} \text{ s}^{-1}$ ), the bar “–” over  $m$  indicates the constituent mobility;  $i$  is the electric current intensity ( $\text{A m}^{-2}$ ) in capillary;  $V^{\alpha\beta}$  is the velocity ( $\text{m s}^{-1}$ ) of MRB;  $\kappa$  is the specific conductivity ( $\text{S m}^{-1}$ ). The constituent mobility and concentration are, respec-

tively, defined as [24,25]

$$\bar{m} = \sum a_i m_i \quad (2)$$

$$\bar{c} = \sum c_i \quad (3)$$

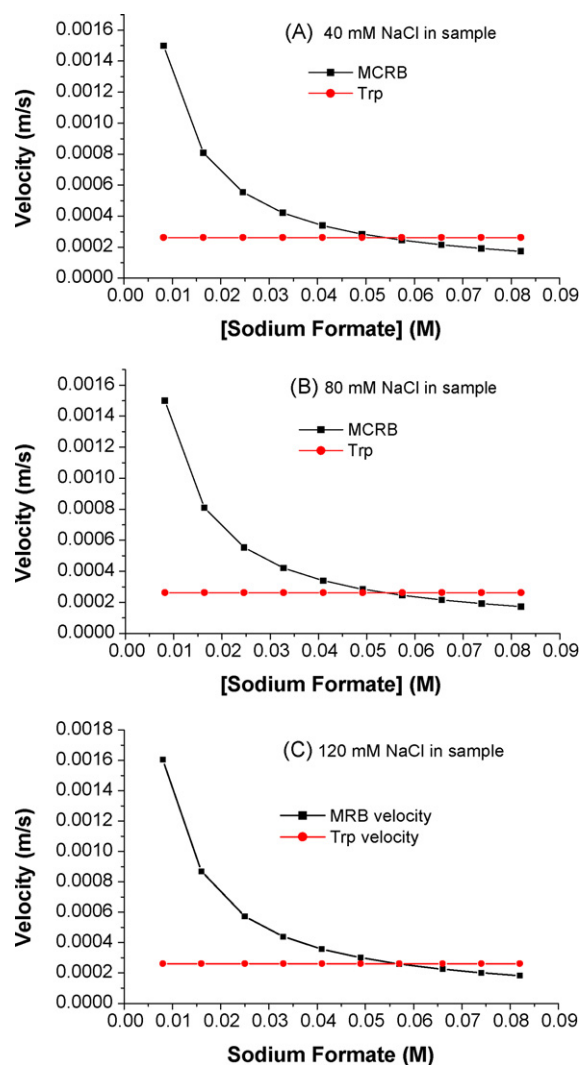


**Fig. 1.** Velocities of Trp and MRB of 32.8 mmol/L pH 2.85 formate buffer (+,  $\alpha$ ) || 8.2–82.5 mmol/L sodium formate + A: 40 mmol/L, B: 80 mmol/L and C: 120 mmol/L NaCl (–,  $\beta$ ). Conditions: Current density  $-2265 \text{ A/m}^2$ ,  $\kappa$  values in sodium formate solutions with different concentration sodium chloride are given in Table S1.

where  $m_i$  is the mobility of subspecies  $i$ ,  $a_i$  is the fraction of subspecies  $i$  with mobility  $m_i$ , viz.,

$$a_i = \frac{c_i}{\bar{c}} = \frac{c_i}{\sum c_i} \quad (4)$$

The absolute mobilities of  $H^+$  and  $OH^-$  in Table 1 at 25 °C were cited from ref. [26]. Before the computation of boundary velocity with Eq. (1), the absolute mobilities were corrected with the empirical equation of ionic mobility [27,28]

$$m_{act} = m_0 \exp(-0.67\sqrt{I}) \quad (5)$$

where  $m_{act}$  and  $m_0$  are the actual and absolute mobilities, respectively,  $I$  the ionic strength. The velocity ( $m s^{-1}$ ) of analyte in phase  $\alpha$  can be computed with the following equation [24,25]

$$V_a^\alpha = \bar{m}_a^\alpha \frac{i}{\kappa^\alpha} \quad (6)$$

where  $V_a^\alpha$  is the velocity ( $m s^{-1}$ ) of analyte in phase  $\alpha$ ,  $\bar{m}_a^\alpha$  is the constituent mobility ( $m^2 V^{-1} s^{-1}$ ) [27].

Numerous data, including pH value, ionic strength and specific conductivity, are needed for the computations of boundary and analyte's velocities. The ionic strength and specific conductivity of 32.8 mmol/L pH 2.85 formic buffer are 3.30 mmol/L and 0.075 S/m, respectively. The ionic strength and specific conductivity of Boundaries 1–3 are given in Table S1. With the data above, we computed the velocities of the MRBs and Trp in the formic buffer. The velocities of Boundaries 1–3 and Trp were, respectively, shown in Fig. 1.

### 3. Experimental

#### 3.1. Chemicals

Acetic acid (analytical reagent grade, AR), sodium acetate (AR), NaCl (AR),  $MgCl_2$  (AR),  $MgSO_4$  (AR),  $CaCl_2$  (AR), KCl (AR),  $NaHCO_3$  (AR),  $NaNO_3$  (AR),  $NaH_2PO_4$  (AR), formate acid (AR), sodium formate (AR), hydrochloric acid (AR), dimethyl sulfoxide (DMSO, AR), 37% hydrochloric acid (Guaranteed Reagent grade, GR) and L-tryptophan (Trp, Chrom pure) were purchased from the Shanghai Chemical Reagent Company (Shanghai, China). Sodium hydroxide (GR) was from the Shanghai Zhongong Reagent Factory (Shanghai, China). An ultra-pure water with 0.055 S/cm conductivity was produced by a pure water system (Ultra Clear system, SG Wasser-aufbereitung und Regenerierstation GmbH, Germany).

#### 3.2. Apparatus

A high performance capillary electrophoresis (HPCE) (ACS 2000, Beijing Cailu Instrumental Co., Beijing, China) was used. The HPCE was equipped with a power supply (up to constant voltage 30 kV), a HW-2000 Chromatography Workstation and an UV-vis detector (double light beams,  $\lambda = 190$ –720 nm, set at 214 nm). A fused-silica capillary with total length 51 cm, effective length 42 cm and i.d. 75  $\mu m$  was used (the Factory of Yongnian Optical Fiber, Hebei, China). The runs were carried out with air-cooled capillary at  $21 \pm 1$  °C. The new capillary was conditioned by rinsing with 1.0 M NaOH for 20 min, ultra-pure water for 10 min, 1.0 M HCl for 20 min and running buffer for 30 min, in order. A UV-vis spectrophotometer (UV mini 1240, Shimadzu Co., Japan) was used for the detection of *skeletonema costarum*'s culture.

#### 3.3. *Skeletonema costarum*'s culture

*Skeletonema costarum*'s cells were cultured at  $30 \pm 1$  °C on the culture medium with 450 mmol/L NaCl, 25 mmol/L  $MgCl_2$ , 8.0 mmol/L  $MgSO_4$ , 10 mmol/L  $CaCl_2$ , 10 mmol/L KCl, 2.4 mmol/L

$NaHCO_3$ , 0.88 mmol/L  $NaNO_3$ , 0.36 mmol/L  $NaH_2PO_4$ . The concentration of total salt is up to 526.64 mmol/L. During the culture, continuous illumination at intensities of 80  $\mu mol m^{-2} s^{-1}$  was provided by cool white fluorescent tubes. Aeration was given by bubbling air at regular pressure. Cell growth was detected by monitoring the optical density of the culture at 730 nm using a Shimadzu UV mini 1240 UV-vis spectrophotometer. The specific growth rate was defined as an increase of  $OD_{730}$  during the time indicated.

#### 3.4. Buffer and sample matrix

32.8 mmol/L pH 2.85 formic acid-NaOH was used as the running buffer. Three kinds of sample matrixes with salt were prepared. The first contains 8.2–82.5 mmol/L sodium formate + 40 mmol/L NaCl + 5.0  $\mu g/mL$  Trp. The second holds 8.2–82.5 mmol/L sodium formate + 80 mmol/L NaCl + 5.0  $\mu g/mL$  Trp. And the third was a matrix comprising 8.2–82.5 mmol/L sodium formate + 120 mmol/L NaCl + 5.0  $\mu g/mL$  Trp. The buffer and samples were degassed and centrifuged at 5000 rpm for 10 min if necessary.

The *skeletonema costarum*'s culture was centrifuged at 10,000 rpm for 20 min, then the upper liquor was filtrated with 0.45  $\mu m$  durapore membrane filters. The filtered liquor was diluted with equal volume 32.8 mmol/L pH 2.85 formic buffer with or without 1.0  $\mu g/mL$  Trp spiked, or diluted with equal volume 120 mmol/L sodium formate with or without 1.0  $\mu g/mL$  Trp spiked.

#### 3.5. General stacking procedure by MRB

The procedure is similar to that in ref. [24] but with some modifications. The stacking procedure by MRB was performed in accordance with the following manner. One of the alkaline sample matrixes was injected into the capillary under the conditions of 15 mbar and 120, or 180, or 240 s injection time. After that, the two ends of the capillary were, respectively, inserted into the anodic and cathodic vials holding the running buffer. When the electric field was applied, a MRB was created between the running buffer and conjugate base (see Fig. 2). The MRB can be used to stack the tested Trp. As shown in Fig. 2, the MRB is designed to move towards the cathode with a velocity of  $V^{\alpha\beta}$  and the velocity of a zwitterion in phase  $\alpha$  is  $V_z^\alpha$ . Under the condition of  $V^{\alpha\beta} \leq V_z^\alpha$ , the zwitterion with positive charge(s) in phase  $\alpha$  can catch up with the MRB and can be completely stacked. At the same time, the zwitterion in phase  $\beta$  migrates towards the anode due to partial negative charge. This can further enhance the stacking efficiency.

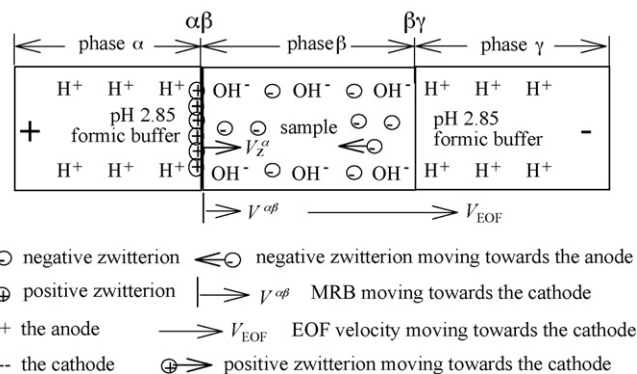


**Fig. 2.** The mechanism of zwitterion stacking by a slow cathodic-direction movement MRB formed with formic buffer at the left side of capillary (viz., phase  $\alpha$ ) and the sample (viz., phase  $\beta$ ) containing 8.2–82.5 mmol/L sodium formate due to  $V^{\alpha\beta} \leq V_z^\alpha$ .

**Table 2**

Initial distributions of pH, conductivity and compounds used for computer simulation.

	Phase $\alpha$	Phase $\beta^a$	Phase $\gamma$
pH	2.85	8.07	2.85
Conductivity (mS/m)	77.35	1891.54	77.35
[Formic] (mmol/L)	30	60	30
[Chloride] (mmol/L)	0	40	0
[Trp] (mmol/L)	0	0.03	0
[Sodium] (mmol/L)	1.9	100	1.9

<sup>a</sup> The conductivities of sample and BGE were automatically computed by Gas' software [29–31]. If 40, 80 and 120 mmol/L sodium chloride existed in the sample matrixes, the conductivities of matrixes were 1385.95, 1638.74 and 1891.54 mS/m, respectively (computed by Gas' software).

### 3.6. Computer simulation

The software SIMUL 4.0 written by Prof. Gas was well used for the simulation of ITP-based stacking [17,29]. The data used are shown in Table 1. The initial simulation conditions of conductivity, pH and compounds in the catholyte, sample and analyte are given in Table 2. The capillary length used for the simulation was set at 10 mm, the plug length was 2 mm. The current density was  $-2265 \text{ A/m}^2$  being equal to that used in Fig. 1. The simulation was continued up to 50 s in migration time, which was enough for the simulation with 10 mm capillary. The time and spaced steps were set at 0.02 s and  $7.5 \mu\text{m}$ , respectively. EOF velocity in capillary was omitted. All of simulations were performed with a HP parilion computer (u808cl, HP Co., USA). It took about  $\sim 30$  min to run a single simulation on stacking of Trp in saline sample matrix.

## 4. Results and conclusions

### 4.1. Prediction to stacking by MRB with high salt

Fig. 1 shows the velocities of Trp and MRB formed with the running buffer and sodium formate as well as 40/80/120 mmol/L sodium chloride in the matrix. Fig. 1 indicates that if the sample matrix is prepared with 50–80 mmol/L sodium formate and 40/80/120 mmol/L sodium chloride, the velocity of Trp in the matrix is very near or higher than that of MRB formed with the buffer and 50–80 mmol/L sodium formate. According to the previous studies [24,25], this result implies that the created MRB can tightly stack the Trp in the sample matrix whether the matrix holds 40, or 80 or 120 mmol/L sodium chloride. In other words, the sodium chlo-

ride in matrix has weak influence on stacking of Trp by the MRB investigated herein. The theoretical prediction will be proved by the following experiments.

### 4.2. Demonstration to prediction

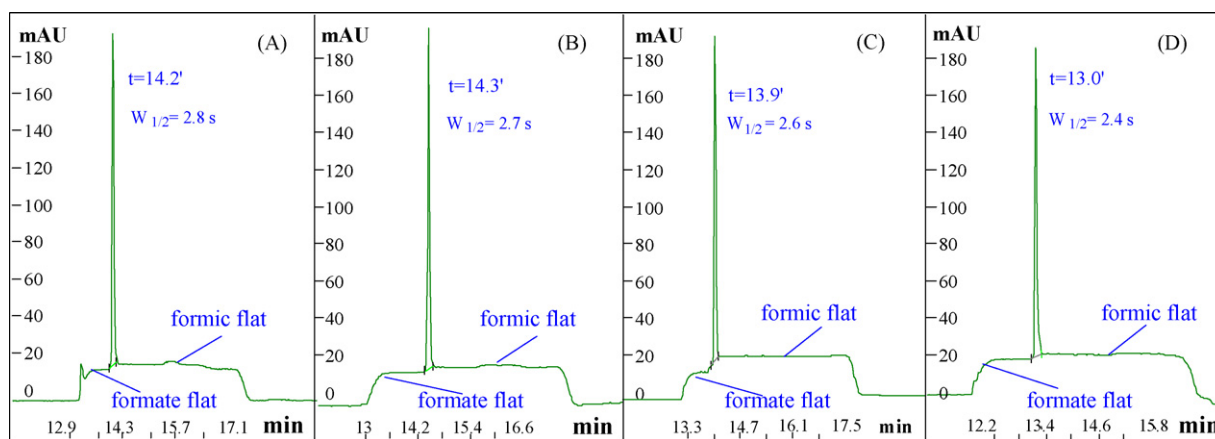
It has been indicated by the experiments of Figs. 5 and 6 in Ref. [24] that the stacked Trp peak became very sharp and was merged with the formate flat if high concentration sodium formate was used as the sample solution. Our unpublished data shows that if 240 s 15 mbars sample injection was used the sharp Trp peak was also merged with the formate flat completely. The merged Trp peak implies that the analyte of Trp is focusing when passing through the UV detector. Thus, the tightly stacked peak of Trp is very useful for the investigation on the real-time stacking efficiency of Trp plug by the MRB investigated herein.

Fig. 3 reveals the real-time stacking efficiency of Trp in the sample matrix with 40 mmol/L sodium chloride by the MRBs formed with 50/60/70/80 mmol/L sodium formate. As shown in Fig. 3, the Trp sample plugs are tightly stacked by these MRBs, the peak heights of Trp are almost equal to each other. Evidently, the results in Fig. 3A–D are in good agreement with the prediction of Fig. 1A. It is also manifested in Fig. S1 that if 80 mmol/L sodium chloride exists in the sample matrix, a good stacking of Trp can be also achieved. In Fig. S2, the concentration of sodium chloride is increased to 120 mmol/L (up to 200 mmol/L sodium ion). Even with such high content salt, the real-time MRB-induced stacking efficiency of Trp is almost the same as that in Fig. 3. Manifestly, the experiments of Fig. S1 and S2 are in coincidence with the predictions of Fig. 1B and C, respectively.

Therefore, the results in Fig. 3 and Figs. S1 and S2 as well highly demonstrate the predictions of Fig. 1, viz., the weak influence of sodium chloride on the real-time MRB-induced stacking efficiency to Trp sample plug. We will show below the stacking of Trp is induced by the mechanism of MRB, rather than that of electrostacking, or FASI or ITP.

### 4.3. Non-FASI- or non-ITP-induced stacking

Evidently, the sample stacking in Fig. 3 herein is not induced by the mechanism of electrostacking or FASI due to highly saline content existing in the sample matrix. Possibly, the stacking in Fig. 3 is induced by an ITP mechanism, because high salt in matrix can lead to transient ITP-based stacking [17,30,31]. To investigate the possibility of the transient ITP, Gas' simulator is



**Fig. 3.** Real-time stacking of 5.0  $\mu\text{g/mL}$  Trp in the 15 mbar 240 s sample plug with 40 mmol/L sodium chloride by MRB created with 32.8 mmol/L pH 2.85 formic buffer and A: 50 mmol/L, B: 60 mmol/L, C: 70 mmol/L and D: 80 mmol/L sodium formate. Conditions: 51 cm total length (42 cm effective length) and  $75 \mu\text{m}$  i.d. capillary; 25 kV and 20–30  $\mu\text{A}$ , detection at 214 nm,  $20^\circ\text{C}$  air-cooling. The formic flats exist in panel A–D. The migration time and width ( $W_{0.5}$ ) of Trp peak are also given in individual panel.

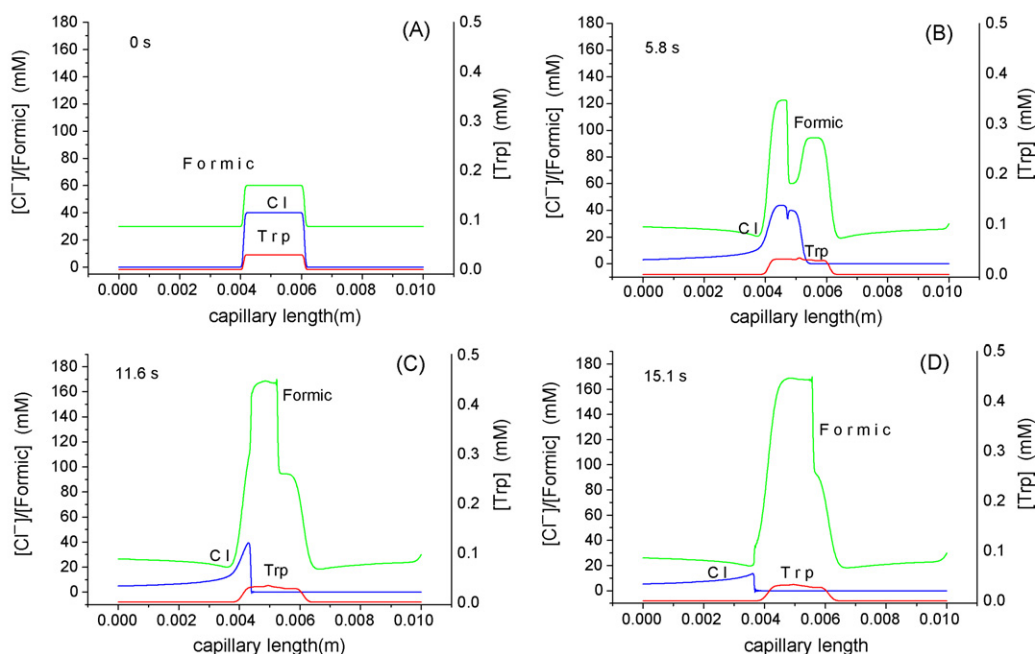


**Fig. 4.** Simulated concentration profiles of chloride, formate and Trp in 60 mmol/L sodium formate + 40 mmol/L sodium chloride at different simulation times of A: 0 s (initial); B: 5.8 s; C: 11.6 s and D: 15.1 s (finishing). The composition of the sample zone was 40 mmol/L chloride, 60 mmol/L formate, 100 mmol/L sodium and 0.03 mmol/L Trp, the BGE is 32.8 mmol/L pH 2.85 formate buffer. Conditions: Simulated current density:  $-2265 \text{ A m}^{-2}$ , 10 mm capillary and 0.2 s edge thickness.

used for the investigation. We firstly computed the mobilities of compounds in the anolyte (viz., phase  $\alpha$ ), the matrix (viz., phase  $\beta$ ) and the running buffer in capillary (viz., phase  $\gamma$ ) with the given data in Table 1. As clearly shown by the data in Table 1, there is the following relation in the matrix: mobility of macro-component (chloride herein =  $7.91 \times 10^{-8} \text{ m}^2 \text{ v}^{-1} \text{ s}^{-1}$ ) > mobility of BGE ion (formate =  $5.66 \times 10^{-8} \text{ m}^2 \text{ v}^{-1} \text{ s}^{-1}$ ) > mobility of Trp ( $0.32 \times 10^{-8} \text{ m}^2 \text{ v}^{-1} \text{ s}^{-1}$ ). Evidently, this relation indicates that there is neither leading-type nor terminating-type ITP-induced stacking to Trp sample plug in Fig. 3. Table 1 also shows that even in the boundary formed by phase  $\beta$  and  $\gamma$  there is still no ITP-induced stacking to Trp sample due to the mobilities of chloride ( $-7.91 \times 10^{-8} \text{ m}^2 \text{ v}^{-1} \text{ s}^{-1}$ ), Trp ( $+1.22 \times 10^{-8} \text{ m}^2 \text{ v}^{-1} \text{ s}^{-1}$ ) and formate ( $-0.63 \times 10^{-8} \text{ m}^2 \text{ v}^{-1} \text{ s}^{-1}$ ). The theoretical conclusion is in high agreement with the simulation in Fig. 4.

Thus, the stacking of Trp in highly saline sample of Fig. 3 is not induced by the mechanism of electrostacking, or FASI or ITP, but is induced by that of MRB. The previous investigations [24,25] have proved that the stacking of Trp can be quantitatively predicted with the theory of MRB. The prediction of Fig. 1 has also been proved by the results in Fig. 3 and Figs. S1 and S2. The following results will explain the essential reason why Trp sample plug with as high as 200 mmol/L sodium ion can be tightly focused by the MRB investigated herein.

#### 4.4. Essence why high salt has weak effect on stacking

In Eq. (1), we can define the following expressions,

$$J_{\text{H}^+}^{\alpha} = \frac{\bar{m}_{\text{H}^+}^{\alpha} \bar{c}_{\text{H}^+}^{\alpha}}{\kappa^{\alpha}} i \quad (7)$$

$$J_{\text{OH}^-}^{\beta} = \frac{\bar{m}_{\text{OH}^-}^{\beta} \bar{c}_{\text{OH}^-}^{\beta}}{\kappa^{\beta}} i \quad (8)$$

where  $J$  is the ionic flux under the electric field (equiv.  $\text{s}^{-1} \text{ m}^2$ ). The mobility of zero charged constituent is can be considered to be zero [25]. For example, in the pH 2.85 formic buffer, there are two hydro-

gen constituents. The first hydrogen constituent is free hydrogen ion ionized from formic acid and the second is hydrogen bonded with formic acid (HFc), which cannot move due to zero charge. Thus, there is

$$m_{\text{HFc}}^{\alpha} = 0 \quad (9)$$

Thus, in the pH 2.85 formic acid-NaOH buffer, we have

$$\bar{m}_{\text{H}^+}^{\alpha} \bar{c}_{\text{H}^+}^{\alpha} = m_{\text{H}^+}^{\alpha} c_{\text{H}^+}^{\alpha} + m_{\text{HFc}}^{\alpha} c_{\text{HFc}}^{\alpha} = m_{\text{H}^+}^{\alpha} c_{\text{H}^+}^{\alpha} \quad (10)$$

due to  $m_{\text{HFc}}^{\alpha} c_{\text{HFc}}^{\alpha} = 0$ . Similarly, there is

$$\bar{m}_{\text{OH}^-}^{\beta} \bar{c}_{\text{OH}^-}^{\beta} = m_{\text{OH}^-}^{\beta} c_{\text{OH}^-}^{\beta} \quad (11)$$

Therefore, Eqs. (7) and (8) are actually re-expressed as Eqs. (12) and (13), respectively,

$$J_{\text{H}^+}^{\beta} = \frac{m_{\text{H}^+}^{\alpha} c_{\text{H}^+}^{\alpha}}{\kappa^{\alpha}} i \quad (12)$$

$$J_{\text{OH}^-}^{\beta} = \frac{m_{\text{OH}^-}^{\beta} c_{\text{OH}^-}^{\beta}}{\kappa^{\beta}} i \quad (13)$$

The division of Eq. (13) by Eq. (12) yields

$$\text{Ratio} = \frac{J_{\text{H}^+}^{\alpha}}{J_{\text{OH}^-}^{\beta}} = \frac{m_{\text{H}^+}^{\alpha} c_{\text{H}^+}^{\alpha}}{m_{\text{OH}^-}^{\beta} c_{\text{OH}^-}^{\beta}} \frac{\kappa^{\beta}}{\kappa^{\alpha}} \quad (14)$$

For the boundaries investigated herein, Eq. (1) can be actually rewritten as

$$v^{\alpha\beta} = \frac{J_{\text{H}^+}^{\alpha} - J_{\text{OH}^-}^{\beta}}{c_{\text{H}^+}^{\alpha} - \bar{c}_{\text{OH}^-}^{\beta}} \quad (15)$$

With Eqs. (12)–(15), we can easily reveal the essential reason why salt in the sample matrix has weak influence on the stacking induced by the boundaries investigated here, whether the concentration of salt in alkaline matrix is low, or middle or high.

Let us omit the influence of salt on MRB. In Boundary 1, the pH value of phase  $\alpha$  is equal to 2.85, the value of  $[\text{H}^+]$  in phase  $\alpha$  is  $1.41 \times 10^{-3} \text{ mol/L}$ . The pH value of phase  $\beta$  is 8.23 and the value

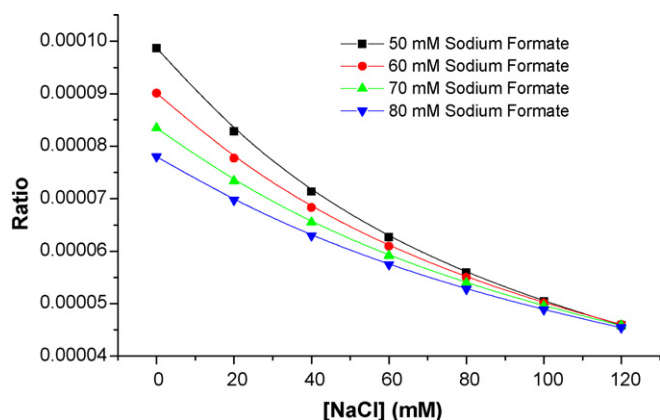


**Fig. 5.** Ratio between the fluxes of hydrogen in phase  $\alpha$  and hydroxyl ions in phase  $\beta$  as a function of concentration of sodium chloride for MBSs formed by formic acid-NaOH buffer and sodium formate.

of  $[\text{OH}^-]$  in phase  $\beta$  is  $1.68 \times 10^{-6}$  mol/L. But the constituent concentration of hydroxyl ion (50 mmol/L) in phase  $\beta$  is much high. Evidently, the concentration of  $\text{OH}^-$  in phase  $\beta$  is nearly lower 3 order degree than that of  $\text{H}^+$  in phase  $\alpha$ . This result leads to the value of Ratio in phase  $\beta$  is very small (0.000099) as shown in Fig. 5. In other words, there is the following expression

$$J_{\text{H}^+}^{\alpha} \gg J_{\text{OH}^-}^{\beta} \quad (16)$$

Now let consider the effect of salt on MRB. The addition of sodium chloride into the matrix, viz., phase  $\beta$ , makes great contribution to the specific conductivity of matrix as shown in Table S1, but has no evident influence on the pH value of matrix, viz., the concentration of free hydroxyl or hydrogen ion. Thus, expression (16) is always present as shown in Fig. 5, whether the concentration of salt is 40, or 80 or 120 mmol/L. Under the conditions defined by Eq. (16), Eq. (14) or (15) can be approximately changed as

$$V^{\alpha\beta} \approx \frac{J_{\text{H}^+}^{\alpha}}{c_{\text{H}^+}^{\alpha} - \bar{c}_{\text{OH}^-}^{\beta}} \quad (17)$$

The above results from Eqs. (16) to (17) indicate that the existence of salt in matrix has weak effect on the boundary velocity, thus has weak influence on the stacking of zwitterion by MRB.

From the theoretical calculations above, it is clear that weak influence of salt on the stacking efficiency is mainly originated from the following three reasons. Firstly, much low concentration of free

hydroxyl ion is present in high concentration conjugate base of phase  $\beta$  and quite high concentration of free hydrogen ion exists in the weak acidic buffer of phase  $\alpha$ . Secondly, the first reason results in the existence of Eqs. (16) and (17). Thirdly, the salt in the conjugate base principally affects the specific conductivity of phase  $\beta$ , rather than pH values of running buffer and sample matrix; thus there is only the negative impact of salt on the flux of hydroxyl ion as shown in Fig. 4, this further strengthen the existences of Eqs. (16) and (17).

#### 4.5. Applications

The actual application of MRB-based stacking for some analyte(s) in biological matrixes with high salt concentration was performed. The first bio-matrix is *skeletonema costarum* culture in which there is as much as 527 mmol/L total salt. Fig. 6 shows the results of Trp spiked into the *skeletonema costarum* culture. Panel A reveals that no Trp peak exists if the analyte is not spiked into the culture. Panel B proves that a much low Trp peak is detected in a capillary zone electrophoresis if 1.0  $\mu\text{g}/\text{mL}$  Trp exist in the culture. Panel C shows there is no stacked Trp peak in the mode of MRB-based stacking followed by CZE if no Trp is added into the culture. Panel D manifests that a sharp focused Trp appears in the mode of MRB-based stacking if 1.0  $\mu\text{g}/\text{mL}$  Trp is spiked into the culture. In Panel D, the limit of detection (LOD) of Trp in the culture is decreased down to 4.23 ng/mL ( $S/N=3$ ).

The second biological matrix is health human urine that contains 150–320 mmol/L total inorganic ions ( $\text{Cl}^-$ ,  $\text{Na}^+$ ,  $\text{K}^+$ ,  $\text{PO}_4^{3-}$ , etc.). Fig. S3 shows the results of urine profiles in CE. Panel A of Fig. S3 is the electrophoregram of CZE of human urine. In Panel A, the urine metabolites are separated in 60 mmol/L pH 11.0 Gly-NaOH running buffer, the urine is simply diluted with equal volume running buffer. Panel A displays that only about 10 metabolites are detected. In Panel B, the urine metabolites separated in the same running buffer, but the urine sample is diluted with equal volume 20 mmol/L pH 5.5 Gly-HCl sample buffer. Evidently, there is a MRB formed between the running and sample buffer. As shown in Panel B, the MRB-based stacking can generally improve the detection sensitivity of urine metabolites, about 40 metabolite peaks are detected, and the peak heights are greatly higher than those in Panel A (except peak 3). It is compared that about 6–20-fold improvement of sensitivity in Panel B is achieved in contrast to Panel A. The same improvement can also be obtained for other human urines with different salt concentrations.

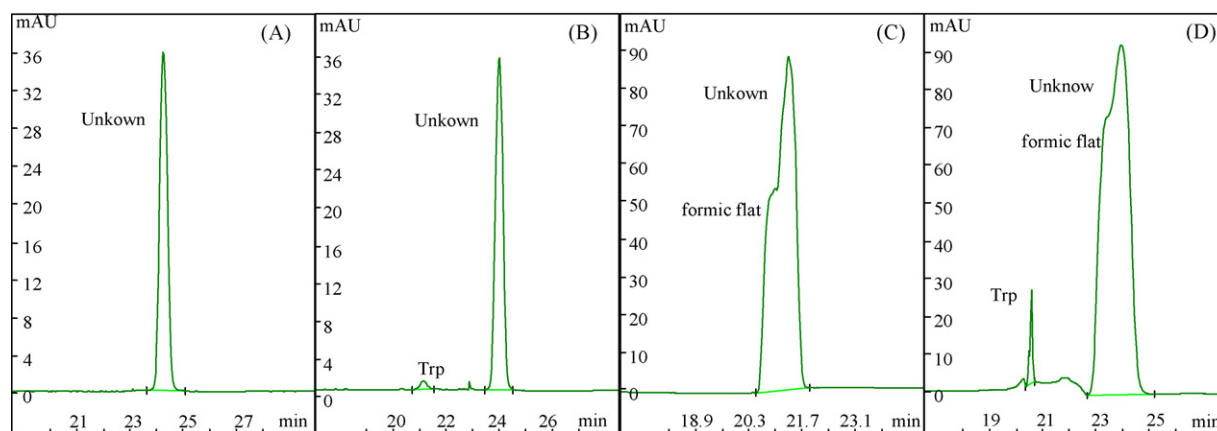


**Fig. 6.** Analysis of real sample of *skeletonema costarum* fermentation liquor of A: no Trp spiked in the sample and diluted with equal volume 32.8 mmol/L pH 2.85 formic buffer as well 10 s 15 mbar sample injection, B: spiked with 1.0  $\mu\text{g}/\text{mL}$  Trp and diluted with equal volume 32.8 mmol/L pH 2.85 formic buffer as well as 10 s 15 mbar sample injection, C: no Trp spiked in the sample and diluted with equal volume 120 mmol/L sodium formate together with 120 s 15 mbar injection, and D: spiked with 1.0  $\mu\text{g}/\text{mL}$  Trp and diluted with equal volume 120 mmol/L sodium formate coupled with 120 s 15 mbar injection. Conditions: 73 cm total length (64 cm effective length) and 75  $\mu\text{m}$  i.d. capillary; 25 kV and 20–30  $\mu\text{A}$ , detection at 214 nm, 20  $^{\circ}\text{C}$  air-cooling. Please note the different calibrations of panels B and D.

## 5. Conclusions

In conclusions, three MRBs formed with formic-acid-NaOH buffer and sodium formate as well as 40, 80 and 120 mmol/L sodium chloride were investigated for the illumination of essential reasons why salt in sample matrix has very weak influence on the MRB-induced stacking. The computations in Fig. 1 firstly show the very weak influence of salt in sample matrix on the stacking of zwitterion by the MRBs, whether the concentration of salt is 40, or 80 or 120 mmol/L. The computations have been well verified by numerous experiments. The theoretical analyses and simulation depict the stacking is relied on mechanism of MRB, rather than that of transient ITP. The applications of MRB-based stacking are well performed for the analyses of Trp spiked into culture liquor (with 527 mmol/L total salt) and urine profiling (with 150–320 mmol/L total inorganic ions).

## Acknowledgements

The project was supported by the National Natural Science Foundation of China (No. 20475036, 20675051 and 20805031) the Shanghai Leading Academic Discipline Project (Approved No. B203) and Shanghai Jiao Tong University. The authors were also grateful to Prof. Zhiyong Li and Prof. Xiaoling Miao for their providing samples.

## Appendix A

The effective mobility of ion can be calculated with

$$m_{\text{eff}} = \alpha m_{\text{act}} \quad (\text{A1})$$

where  $m_{\text{eff}}$  and  $m_{\text{act}}$  are the effective and actual mobilities, respectively,  $\alpha$  is the ionization degree. In alkaline solution, Trp is ionized as anion. There is the following relation between ionization degree and pH value of solution

$$\text{pH} = \text{p}K_2 + \log \frac{\alpha}{1 - \alpha} \quad (\text{A2})$$

In acidic solution, Trp is as cation. Eq. (A2) is changed as

$$\text{pH} = \text{p}K_1 + \log \frac{1 - \alpha}{\alpha} \quad (\text{A3})$$

Hence,  $\alpha$  values of Trp in 50–80 mmol/L sodium formate can be computed with Eq. (A2). The computation is given in Table A1 here.

**Table A1**

Ionization degree and mobility of Trp in sodium formate with actual  $\text{p}K_2$  (9.13).

Sodium formate (mmol/L)	pH value	Mobility ( $10^{-8} \text{ m}^2 \text{ V}^{-1} \text{ s}^{-1}$ )	$\alpha$
50	8.23	0.28	0.11
60	8.27	0.30	0.12
70	8.30	0.33	0.13
80	8.33	0.36	0.14

With the values of ionization degree of Trp in 50–80 mmol/L sodium formate, we can compute the effective mobility of Trp in the sample matrixes, as shown in Table 1.

## Appendix B. Supplementary data

Supplementary data associated with this article can be found, in the online version, at doi:10.1016/j.talanta.2009.01.054.

## References

- [1] M.J. Wojtusik, M.P. Harrold, J. Chromatogr. A 671 (1994) 411.
- [2] A. Sjogren, P.K. Dasgupta, Anal. Chem. 68 (1996) 1933.
- [3] Y.Z. He, M.L. Cervera, A. Pastor, M. de la Guardia, Anal. Chim. Acta 447 (2001) 135.
- [4] D.S. Burgi, R.L. Chien, Anal. Chem. 63 (1991) 2042.
- [5] R.L. Chien, D.S. Burgi, Anal. Chem. 63 (1992) 1046.
- [6] H. Yang, R.L. Chien, J. Chromatogr. A 924 (2001) 155.
- [7] L.Y. Zhu, H.K. Lee, Anal. Chem. 73 (2001) 3065.
- [8] F.M. Everaerts, Jo.L. Becker, E.M. Verheggen, Isotachopheresis: Theory, Instrumentation, and Applications, Elsevier Scientific Publ. Co., 1976, pp. 1–9.
- [9] L. Křivánková, P. Gebauer, W. Thormann, R.A. Mosher, P. Boček, J. Chromatogr. 638 (1993) 119.
- [10] P. Gebauer, L. Křivánková, P. Pantůčková, P. Boček, W. Thormann, Electrophoresis 21 (2000) 2797.
- [11] Z.K. Shihabi, Electrophoresis 23 (2002) 1612.
- [12] M.E. Hadwiger, S.R. Torchia, S.R. Park, M.E. Biggin, C.E. Lunte, J. Chromatogr. B 681 (1996) 241.
- [13] Y.P. Zhao, C.E. Lunte, Anal. Chem. 71 (1999) 3985.
- [14] S.D. Arnett, C.E. Lunte, Electrophoresis 24 (2003) 1745.
- [15] P. Britz-McKibbin, J. Wong, D.D.Y. Chen, J. Chromatogr. A 853 (1999) 535.
- [16] P. Britz-McKibbin, D.D.Y. Chen, Anal. Chem. 72 (2000) 1242.
- [17] J.B. Kim, P. Britz-McKibbin, T. Hirokawa, S. Terabe, Anal. Chem. 75 (2003) 3986.
- [18] J.P. Quirino, S. Terabe, Science 282 (1998) 465.
- [19] J. Palmer, N.J. Munro, J.P. Landers, Anal. Chem. 71 (1999) 1679.
- [20] J.P. Quirino, S. Terabe, P. Boček, Anal. Chem. 72 (2000) 1934.
- [21] Y. Sera, N. Matsubara, K. Otsuka, S. Terabe, Electrophoresis 22 (2001) 3509.
- [22] M.R.N. Monton, J.P. Quirino, K. Otsuka, S. Terabe, J. Chromatogr. A 939 (2001) 99.
- [23] C.X. Cao, Y.Z. He, M. Li, Y.T. Qian, S.L. Zhou, L. Yang, Q.S. Qu, Anal. Chem. 74 (2002) 4167.
- [24] C.X. Cao, W. Zhang, W.H. Qin, S. Li, W. Zhu, W. Liu, Anal. Chem. 77 (2005) 955.
- [25] C.X. Cao, L.Y. Fan, W. Zhang, Analyst 133 (2008) 1139.
- [26] R.L. David, CRC Handbook of Chemistry and Physics, 73rd ed., CRC Press, Boca Raton, 1992–1993, p. D-167.
- [27] W. Friedl, J.C. Reijenga, E. Kennedler, J. Chromatogr. A 709 (1995) 163.
- [28] C.X. Cao, J. Chromatogr. A 771 (1997) 374.
- [29] <http://www.natur.cuni.cz/gas/>.
- [30] L. Křivánková, P. Pantůčková, P. Gebauer, P. Boček, J. Caslavská, W. Thormann, Electrophoresis 24 (2003) 505.
- [31] L. Křivánková, P. Pantůčková, P. Gebauer, P. Boček, Electrophoresis 25 (2004) 3406.





# Luminol chemiluminescence under interaction with heteropoly acids

Oleg Zui<sup>a,\*</sup>, Hiroki Takahashi<sup>b</sup>, Toshitaka Hori<sup>b</sup>, Teruo Hinoue<sup>c</sup>

<sup>a</sup> A.V. Dumansky Institute of Colloid Chemistry and Water Chemistry of the National Academy of Sciences of Ukraine, 03680 Kyiv-142, Vernadsky Prospect 42, Ukraine

<sup>b</sup> Graduate School of Human and Environmental Studies, Kyoto University, Kyoto 606-8501, Japan

<sup>c</sup> Department of Chemistry, Faculty of Science, Shinshu University, 3-1-1 Asahi, Matsumoto, Nagano 390-8621, Japan

## ARTICLE INFO

### Article history:

Received 25 July 2008

Received in revised form 15 January 2009

Accepted 23 January 2009

Available online 4 February 2009

### Keywords:

Heteropoly acids

Luminol

Chemiluminescence

Reaction mechanism

## ABSTRACT

Interaction of luminol with phosphomolybdic, phosphovanadomolybdic and silicomolybdic acids was studied by examination of chemiluminescence spectra, measurement of ESR spectra, investigation of reaction order, and elucidation of inhibition effects. A scheme of the reaction mechanism is proposed.

© 2009 Elsevier B.V. All rights reserved.

## 1. Introduction

Heteropoly acids (HPA) are in a wide class of coordination compounds. HPA molecule consists of a central atom and assemblies of metal–oxygen polyhedrons, including components of molybdenum, tungsten or fragments of oxide crystal grating [1]. Having strong electron-acceptor properties, HPA are readily reduced to form blue products isostructural with the initial acids. Examination of HPA in the reduced state by different methods has shown that they contain some tungsten or molybdenum ions in the (5+) valence state. Chemiluminescence (CL) of luminol with phosphovanadomolybdic and silicomolybdic HPA was first described in 1974 [2], and then determination of germanovanadomolybdic and arsenovanadomolybdic acids was reported via luminol chemiluminescence [3,4]. Later, ion chromatographic separation of phosphate, arsenate, silicate and germanate ions was coupled with CL detection of corresponding HPA in the oxidized state [5]. These chemiluminescence methods gave detection limits at the level of 1–50  $\mu\text{g/L}$  for HPA with central atoms P, As, Ge and Si. Improvement in sensitivity and selectivity was achieved by application of sorption preconcentration of P–V–Mo HPA or its ion associates (IAs) [6], with a detection limit of 20 ng/L for phosphorus. Further, flow-injection methods for phosphate [7,8] and silicate [9] were proposed, based on luminol CL detection of HPA. A flow-through solid-phase-based optical sensor for orthophosphate in water, which also relies on sorption preconcentration of HPA with subsequent CL detection,

was proposed [10]. All methods mentioned include HPA formation (or its ion pair with cationic surfactant) and CL reaction with luminol; however, the oxidation mechanism of luminol by HPA has not been studied up to now. In addition, there are no data on the nature of products of this CL reaction [11], in particular, on reduced heteropoly compounds in the literatures. The main purpose of the present research is to investigate products and intermediates of CL reaction in the system of luminol–HPA by electron spin resonance (ESR) spectroscopy and the chemiluminescence inhibition method.

## 2. Experimental

### 2.1. Reagents

Luminol, osmium tetroxide, 4-aminophenol, methyl isobutyl ketone (MIBK, 4-methyl-2-pentanone, Aldrich, USA), phosphomolybdic acid, sodium hydroxide (Wako Chemicals, Japan), paper filters (ADVANTEC MFS, Japan), phosphovanadomolybdic acid (Nippon Inorganic Color & Chemical Co., Japan), silicomolybdic acid (Strem Chemicals, Japan), tetraethyl orthosilicate (Acros Organics, Japan), catalase from bovine liver (Sigma, USA) were used as received. Ion-exchanged water (Millipore, USA) was used throughout the experiments.

### 2.2. Equipment and procedures

Electron spin resonance spectra were recorded on a JEOL JES-RE3X ESR spectrometer. A solution of HPA was placed on a narrow

\* Corresponding author. Tel.: +380 44 4243175; fax: +380 44 4238224.  
E-mail address: [olegzuy@hotmail.com](mailto:olegzuy@hotmail.com) (O. Zui).

strip of filter paper situated inside a fused silica tube (3–4 mm inner diameter) so that the solution was completely absorbed by the strip in the tube, and then frozen in liquid nitrogen. After a “blank” ESR spectrum was recorded, the fused silica tube was taken out of the instrument cavity and left at room temperature for equilibration. One drop of alkaline luminol solution was put into the tube, allowed to reach the strip of filter paper and to be absorbed on it. After freezing in liquid nitrogen (123 K), the ESR spectrum of luminol–HPA mixture on the strip was recorded. Experimental conditions: X-field sweep; center field, 3300.0 G; sweep width, 500 G; frequency, 9.08900 GHz; power, 1.000 mW; modulation width, 3.2 G; time constant, 0.3 s; sweep time, 5.0 min. The concentration of HPA was 0.05 M, and 0.05 M luminol solution was prepared with 1 M NaOH.

Chemiluminescence spectra were measured on a JASCO FP-750 spectrofluorometer in the range of 350–600 nm without excitation light, using 0.01 M luminol solution in 0.1 M NaOH, and 0.01 M or 0.001 M HPA solution at pH 3.0. As direct measurement of chemiluminescence spectra in aqueous solution was difficult, because of very short-term light emission, a CL spectrum was measured in the following manner. HPA was dissolved in MIBK, and HPA solution was added to an optical cell containing aqueous alkaline luminol solution. Under the condition with a MIBK–water interface, the CL reaction proceeded more slowly. Measurements of CL intensity were carried out using a Triathler luminometer (Finland).

### 3. Results and discussion

#### 3.1. ESR measurements

When one drop of 0.05 M luminol in 1 M NaOH reached the filter paper impregnated with 0.05 M phosphomolybdic acid in the fused silica tube, an intense blue color developed instantly. The ESR spectrum of this blue species at 123 K showed an isotropic signal (Fig. 1). This signal is attributed to a one-electron reduction compound in which one molybdenum atom is in a (5+) valence state [12]. Heating the frozen solution leads to a decrease in signal intensity of the ESR spectrum, and no ESR signal was observed at temperatures higher than 130 K. In Ref. [12], where ESR spectroscopy was used to investigate phosphomolybdic blue obtained from the reduction of phosphomolybdic acid by ethylene in the presence of Pd(II), it was shown that an ESR spectrum of frozen solution of the reduced phosphomolybdic HPA arises from the presence of a solely one-electron reduction compound in aqueous solution. As we obtained an ESR signal identical to that of Ref. [12], phosphomolybdic HPA appears to be one-electron oxidant to luminol. Consequently, the formation of short-lived radical species would be expected to be the intermediate products.

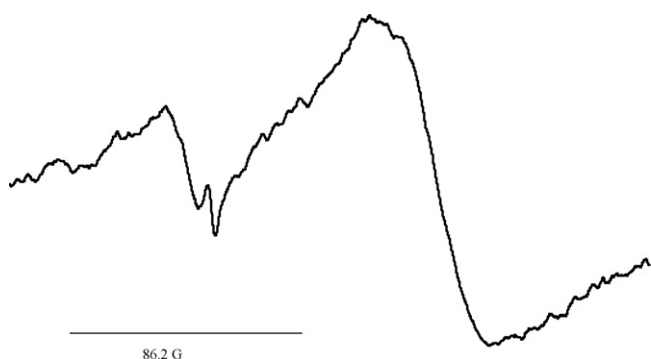


Fig. 1. ESR spectrum obtained during the reaction of phosphomolybdic HPA with luminol in alkaline solution at a temperature of 123 K.

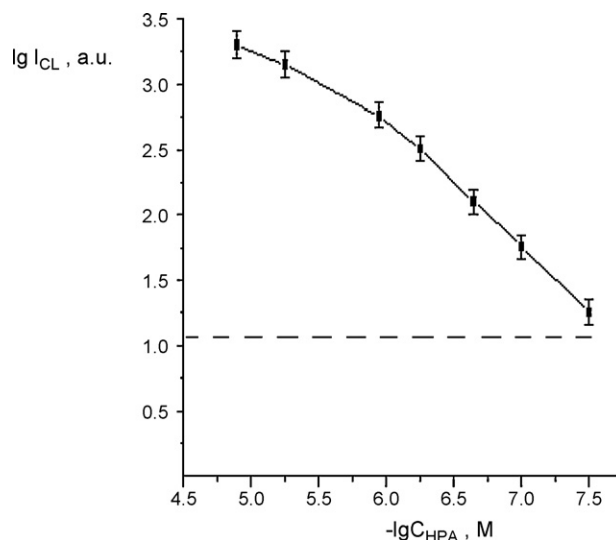


Fig. 2. Dependence of maximum intensity of chemiluminescence in the reaction of phosphomolybdic HPA with luminol on HPA concentration. Luminol concentration is  $2 \times 10^{-4}$  M, pH 12.0. Dashed line shows the value of the blank light emission.

#### 3.2. Examination of dependence of light emission intensity in HPA–luminol reaction on HPA concentration

Optimum pH for the CL luminol–HPA reaction was 12.0, as described later. In order to examine the dependence of CL intensity in the luminol–P–Mo HPA system at pH 12.0 on HPA concentration, CL intensity was plotted against HPA concentration in logarithmic coordinates, as shown in Fig. 2. As can be seen in this figure, the dependence was a straight line in the concentration range of  $1 \times 10^{-7}$  M to  $1 \times 10^{-6}$  M, and at HPA concentrations higher than  $1 \times 10^{-6}$  M, the dependence showed a tendency to level off. The slope of the straight line in the HPA concentration range between  $1 \times 10^{-7}$  M and  $1 \times 10^{-6}$  M was approximately 1, which means that  $I_{\text{CL}}$  is directly proportional to  $C_{\text{HPA}}$ , indicating that a first-order reaction takes place. At HPA concentrations higher than  $1 \times 10^{-6}$  M, it is assumed that the reaction order changes. The reaction order also changed with changing pH. Similar dependences were observed by Seitz and Hercules [13,14] in iodine–luminol and chlorine–luminol reactions.

#### 3.3. Examination of inhibitor effect

In Refs. [15,16], the reaction mechanism was investigated for luminol oxidation by one-electron oxidants. In one-electron oxidation, the formation of superoxide radical and/or hydrogen peroxide is possible as well as semiquinone radical of luminol as intermediate products. As these intermediates are characterized by a very short half-decay period, their direct ESR registration is difficult.

Indirect data on the nature of intermediate products in a reaction between luminol and HPA may be obtained by applying selective inhibitors, i.e., radical scavengers, for example, superoxide radical scavengers such as  $\text{OsO}_4$  and *p*-aminophenol [17,18]. In our experiments,  $\text{OsO}_4$  at a concentration of  $1 \times 10^{-7}$  M or *p*-aminophenol at a concentration of  $1 \times 10^{-6}$  M completely inhibited light emission in the reaction of  $2.2 \times 10^{-6}$  M P–V–Mo HPA or P–Mo HPA with  $2 \times 10^{-4}$  M luminol. The experimental results obtained clearly indicate the formation of superoxide radicals as intermediate products. Further, the effect of catalase on the luminol–HPA reaction was examined: catalase is an enzyme serving as a hydrogen peroxide deactivator which promotes  $\text{H}_2\text{O}_2$  decomposition [19]. Catalase at a concentration of  $1 \times 10^{-6}$  M did not inhibit light emission in

the reaction of  $2.2 \times 10^{-6}$  M HPA and  $2 \times 10^{-4}$  M luminol at pH 12. Hence, it is suggested that hydrogen peroxide is not formed as an intermediate product in this reaction, but only superoxide radical is formed.

The effect of dissolved air oxygen on CL intensity in the luminol–HPA system was examined at pH 12.0. It was found that solutions deoxygenated by bubbling argon of high purity decreased CL intensity, which indicates the participation of oxygen in the reaction. At the same time, the reaction of luminol with oxygen in the absence of HPA also proceeds very slowly. However, this reaction can hardly provide intense luminol chemiluminescence. Consequently, the simultaneous presence of oxygen and HPA is essential to obtain intense luminol chemiluminescence.

### 3.4. Chemiluminescence spectra in luminol–HPA systems

Spectra of chemiluminescence in HPA–luminol systems were not described in the literatures. On mixing aqueous solutions of HPA and luminol, light emission lasts for 7–8 s only, so recording the chemiluminescence spectra was difficult. We obtained the spectra by mixing MIBK solutions of HPA (P–Mo, P–V–Mo and Si–Mo) and aqueous alkaline solution of luminol. In this case, light emission appeared on the interface and lasted for ca. 1 min. The spectra are shown in Fig. 3. As can be seen from this figure,  $\lambda_{\max}$  of the chemiluminescence spectra (curves 1, 2 and 3) is ca. 425 nm, which coincides with that of a fluorescence spectrum of aminophthalate [20]. Consequently, in the HPA–luminol reaction, a light emitter is reasonably assigned to be aminophthalate, as for a number of reactions of luminol oxidation with other oxidants (halogens, hypohalites, peroxyacids, etc.).

It should be pointed out that two peaks were observed in the chemiluminescence spectrum of Si–Mo HPA, shown in Fig. 3, curve 3: the first at 425 nm and the second at 450 nm. When adding tetraethyl orthosilicate dissolved in MIBK into the dark solution, in which Si–Mo HPA in MIBK and aqueous alkaline luminol had already reacted, an increase in the second peak intensity was observed (Fig. 3, curve 4). This experimental fact demonstrates that the second peak ( $\lambda_{\max} = 450$  nm) comes from light emission

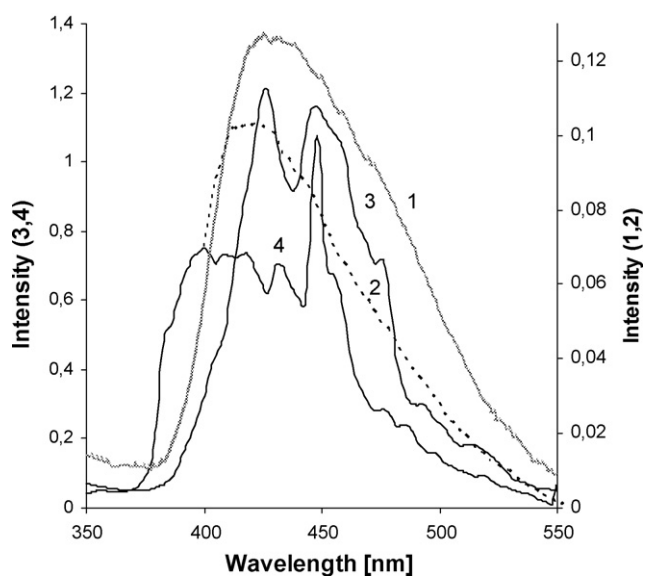


**Fig. 3.** Spectra of chemiluminescence under reaction with  $1 \times 10^{-2}$  M luminol at pH 12.0: (1) phosphovanadomolybdic HPA ( $1 \times 10^{-3}$  M); (2) phosphomolybdic HPA ( $1 \times 10^{-2}$  M); (3) silicomolybdic HPA ( $1 \times 10^{-2}$  M); (4) tetraethyl orthosilicate ( $1 \times 10^{-2}$  M) dissolved in MIBK and added to the dark silicomolybdic HPA–luminol mixture.

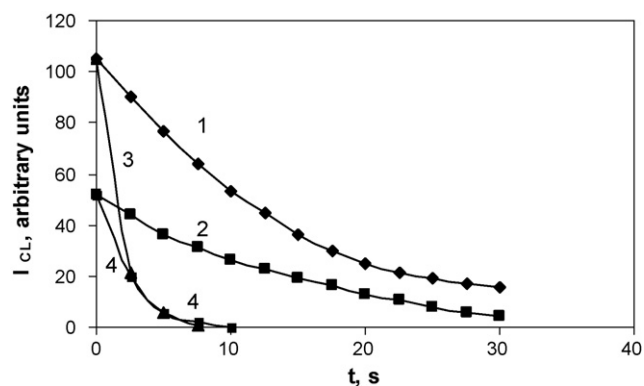


**Fig. 4.** Kinetics of phosphomolybdic HPA decomposition at pH 12.0: (1)  $C_{\text{HPA}} = 5 \times 10^{-6}$  M; (2)  $C_{\text{HPA}} = 5 \times 10^{-7}$  M; and kinetic curves of luminol–phosphomolybdic HPA chemiluminescence at pH 12.0: (3)  $C_{\text{HPA}} = 5 \times 10^{-6}$  M; (4)  $C_{\text{HPA}} = 5 \times 10^{-7}$  M.  $C_{\text{luminol}} = 2 \times 10^{-4}$  M. The temperature was  $20 \pm 1$  °C.

through the reaction of silicate with luminol. Such a CL reaction between  $\text{SiO}_3^{2-}$  and luminol has been reported in Ref. [21]. Obviously, the mechanism of the latter reaction differs from that of HPA–luminol reaction, and its clarification needs additional investigation.

A significant feature of the HPA–luminol CL reaction is specificity to pH conditions. It is well known that luminol is oxidized by heteropoly acids with light emission only in alkaline media. On the other hand, it is also well known that HPA are stable only in acidic media at  $\text{pH} \leq 3$ . Fig. 4 shows the time courses for HPA decomposition (curves 1 and 2) and for chemiluminescence reaction of luminol with HPA (curves 3 and 4) at pH 12. (The procedure for obtaining the time courses for HPA decomposition will be described later.) As can be seen in this figure, the rate of CL reaction of luminol with HPA far exceeds that of HPA decomposition by alkali in the absence of luminol. It is therefore assumed that HPA decomposition has hardly an effect on the chemiluminescence reaction, even at pH 12. From this fact, an optimum pH was chosen from a pH range between 12.0 and 12.5.

### 3.5. Investigation of kinetics of P–Mo HPA decomposition at pH 12.0 and its comparison with kinetics of chemiluminescence HPA–luminol

Kinetics of P–Mo HPA ( $5 \times 10^{-6}$  M and  $5 \times 10^{-7}$  M) decomposition at pH 12.0 was studied by the CL method via registration of the intensity of luminol chemiluminescence. For this purpose, HPA solution was prepared at pH 3.0, 0.5-mL portions were placed into the luminometer cell and 0.5 mL of NaOH solution was added from a syringe to obtain pH 12.0, allowed to stand for a certain period of time (0 s, 5 s, 10 s, 15 s, 20 s and 30 s), and then neutral  $2 \times 10^{-4}$  M luminol solution was added for light emission registration. Kinetics of HPA decomposition in alkaline solution is shown in Fig. 4, curves 1 and 2 correspond to  $5 \times 10^{-6}$  M and  $5 \times 10^{-7}$  M P–Mo HPA, respectively. The curves suggest that the decomposition reaction proceeds according to the first order, namely, the rate of decomposition does not depend on the concentration of HPA. The rate constant and half-life of the HPA decomposition reaction were determined to be  $0.069 \pm 0.004 \text{ s}^{-1}$  and 14.4 s at pH 12.0 at 293 K, respectively. Thus, the kinetics of P–Mo HPA decomposition at pH 12.0 could be successfully examined in a low concentration range of P–Mo HPA using a rapid and sensitive CL detection method. As mentioned previously, kinetics of chemiluminescence of  $5 \times 10^{-6}$  M HPA with luminol ( $2 \times 10^{-4}$  M) at pH 12.0 is represented by curve 3, and that of  $5 \times 10^{-7}$  M HPA by curve 4. These curves indicate that light emission due to the chemiluminescence comes to an end in 7–8 s, namely, the rate

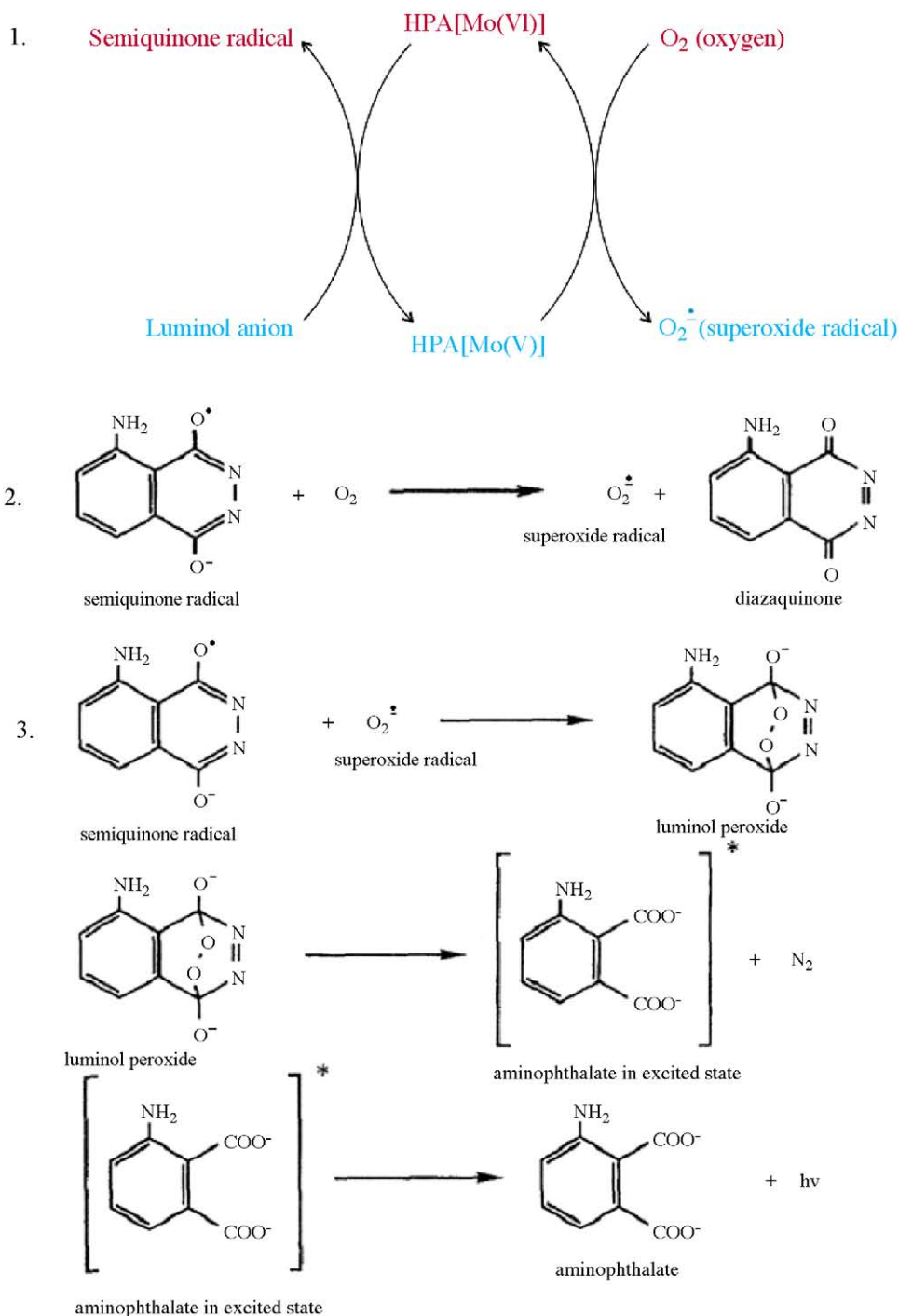


Fig. 5. Scheme of the reactions pathway of luminol with HPA at pH 12.0.

of CL reaction is much higher than the rate of HPA decomposition.

In this connection, when HPA solution is mixed with alkaline luminol solution, only a slight portion of HPA decomposed with the formation of the initial ions (phosphate and molybdate), and most HPA took part in the reaction with luminol. In the course of CL analysis, this factor does not affect the results, because calibration and analysis are carried out under the same conditions. However, a more reasonable version for analysis is the isolation of HPA or the use of its ion associate with cationic surfactant on filter paper, and conducting the reaction with luminol solution directly on the filter paper [6].

### 3.6. Proposed reaction mechanism

From the experimental results obtained, it can be seen that:

- (1) HPA in the presence of luminol and alkali undergoes chemical transformations of two types:
  - (a) Process of decomposition of a part of HPA in alkaline solution with the release of primary anions (PO<sub>4</sub><sup>3-</sup>, MoO<sub>4</sub><sup>2-</sup> and VO<sub>3</sub><sup>-</sup>);
  - (b) participation of most HPA in the CL reaction with luminol.
- (2) CL reaction involving HPA, luminol and ambient dioxygen is a radical process that proceeds with the formation of intermedi-

ate active species, particularly, superoxide radicals,  $O_2^{\cdot-}$ . This is clear from the fact that light emission is inhibited by  $OsO_4$  or *p*-aminophenol.

- (3) The light emitter is aminophthalate, which is the same product formed under luminol oxidation, for example, by  $Cl_2$ ,  $Br_2$  and  $I_2$ . This has been testified by CL spectra in luminol–HPA reactions.
- (4) Both HPA and oxygen are essential for the CL reaction to occur. This is confirmed from the experimental fact that deoxygenation of solutions with argon of high purity lead to substantial reduction of the CL signal.
- (5) It is known that reduced forms of HPA (“blues”) at the moment of formation can be oxidized by air oxygen with the formation of initial oxidized (“yellow”) forms of HPA and superoxide ion-radicals at room temperature [22,23]. Taking into account data [22,23] as well as the fact that presence of oxygen is needed for chemiluminescence of HPA with luminol, it is possible to think that under conditions of CL reaction, luminol reacts with “yellow” HPA to form semiquinone radical (product of one-electron oxidation of luminol) and “blue” HPA; the latter reacts with air oxygen present in solution at the moment of formation to form superoxide radical and initial “yellow” HPA. Thus, HPA acts as a catalyst, accelerating CL reaction of luminol with oxygen through the formation of semiquinone radical and superoxide radical. Such a catalytic reaction proceeds by chemiluminescence pathway, i.e., with formation of aminophthalate and light emission.

Taking into account the factors given above, the following scheme of the CL reaction mechanism is proposed (see Fig. 5). Here stage (1) lies in a catalytic process of oxidation of a luminol anion to a semiquinone radical by air oxygen through an oxidation/reduction cycle of HPA. Reaction (2) indicates oxidation of semiquinone radical by oxygen leading to the formation of diazaquinone and superoxide radical. In reaction (3), the superoxide formed can further oxidize semiquinone radical to luminol peroxide. Under given conditions (luminol concentration  $2 \times 10^{-4}$  M, pH 12.0), the concentration of superoxide radicals in luminol–HPA system is much higher than that of semiquinone radicals. It is known [16] that even during incubation of alkaline luminol solution in the ambient atmosphere under daylight illumination, superoxide radicals are formed in amounts higher than semiquinone radical concentration. Thus, the reaction of semiquinone radical with superoxide radical (reaction (3)) is a first-order reaction. This is just the reaction which leads to chemiluminescence.

Thus, reaction of luminol with oxygen and HPA is a complex multicomponent, multistage process, consisting of a series of sequential and parallel reactions.

#### 4. Conclusion

Reaction of luminol with phosphomolybdic, phosphovanadomolybdic and silicomolybdic acids was studied by examination of chemiluminescence spectra, measurement of ESR spectra, investigation of reaction order, and elucidation of inhibition effects. A scheme of the reaction mechanism is proposed.

#### Acknowledgement

Oleg Zui is indebted to Kyoto University, Graduate School of Human and Environmental Studies, for awarding the grant and for giving an opportunity to carry out experimental work.

#### References

- [1] M.T. Pope, *Heteropoly and Isopoly Oxometalates*, Springer, Berlin, 1983.
- [2] N.M. Lukovskaya, V.A. Bilochenko, *Zh. Anal. Khim.* 40 (1974) 936.
- [3] N.M. Lukovskaya, V.A. Bilochenko, *Zh. Anal. Khim.* 32 (1977) 2177.
- [4] N.M. Lukovskaya, V.A. Bilochenko, *Zh. Anal. Khim.* 34 (1979) 477.
- [5] T. Fujiwara, K. Kurahashi, T. Kumamaru, H. Sakai, *Appl. Organomet. Chem.* 10 (1996) 675.
- [6] O.V. Zui, J.W. Birks, *Anal. Chem.* 72 (2000) 1699.
- [7] M. Yaqoob, A. Nabi, P.J. Worsfold, *Anal. Chim. Acta* 510 (2004) 213.
- [8] Y. Liang, D. Yuan, Q. Li, Q. Lin, *Anal. Chim. Acta* 571 (2006) 184.
- [9] M. Yaqoob, A. Nabi, P.J. Worsfold, *Anal. Chim. Acta* 519 (2004) 137.
- [10] I.P.A. Morais, M. Miró, M. Manera, J.M. Estela, V. Cerdà, M.R.S. Souto, A.O.S.S. Rangel, *Anal. Chim. Acta* 506 (2004) 17.
- [11] I.P.A. Morais, I.V. Tóth, A.O.S.S. Rangel, *Talanta* 66 (2005) 341.
- [12] R.I. Maksimovskaya, L.I. Kuznetsova, K.I. Matveev, *Russ. J. Coord. Chem.* 3 (1977) 685.
- [13] W.R. Seitz, D.M. Hercules, *J. Am. Chem. Soc.* 96 (1974) 4094.
- [14] W.R. Seitz, *J. Phys. Chem.* 79 (1975) 101.
- [15] C. Xiao, D.A. Palmer, D.J. Wesolowski, S.B. Lovits, D.W. King, *Anal. Chem.* 74 (2002) 2210.
- [16] A.L. Rose, T.D. Waite, *Anal. Chem.* 73 (2001) 5909.
- [17] O.M. Zaverukha, Ya.P. Skorobogaty, V.K. Zinchuk, *Dopovidi Akademii Nauk Ukrainy, Series A* 12 (1991) 92.
- [18] J. Zhou, H. Xu, G.-H. Wan, C.-F. Duan, H. Cui, *Talanta* 64 (2004) 467.
- [19] M. Sarıahmetoğlu, R.A. Wheatley, İ. Çakıcı, İ. Kançık, A. Townshend, *Anal. Lett.* 36 (2003) 749.
- [20] A.M. García-Campaña, W.R.G. Baeyens (Eds.), *Chemiluminescence in Analytical Chemistry*, Marcel Dekker, New York-Basel, 2001.
- [21] H. Sakai, T. Fujiwara, T. Kumamaru, *Anal. Chim. Acta* 302 (1995) 173.
- [22] R. Fricke, G. Öhlmann, *J. Chem. Soc., Faraday Trans. 1* (82) (1986) 273.
- [23] R. Fricke, H.-G. Jerschke, G. Öhlmann, *J. Chem. Soc., Faraday Trans. 1* (82) (1986) 3491.